Scientific and Technical Aerospace Reports

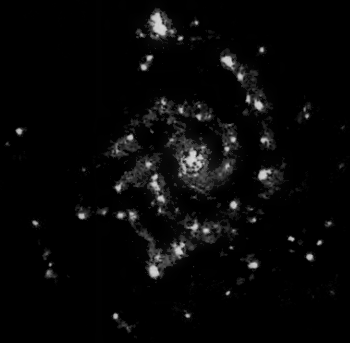

An Abstract Journal

Volume 33, Number 6
June 1995
N95-19883 to N95-22477

The NASA STI Office ... in Profile

Since its founding, NASA has been dedicated to the advancement of aeronautics and space science. The NASA Scientific and Technical Information (STI) Office plays a key part in helping NASA maintain this important role.

The NASA STI Office provides access to the NASA STI Database, the largest collection of aeronautical and space science STI in the world. The Office is also NASA's institutional mechanism for disseminating the results of its research and development activities.

Specialized services that help round out the Office's diverse offerings include creating custom thesauri, translating material to or from 34 foreign languages, building customized databases, organizing and publishing research results ... even providing videos.

For more information about the NASA STI Office, you can:

- **Phone** the NASA Access Help Desk at (301) 621-0390
- **Fax** your question to the NASA Access Help Desk at (301) 621-0134
- **E-mail** your question via the **Internet** to help@sti.nasa.gov
- **Write** to:

NASA Access Help Desk
NASA Center for AeroSpace Information
800 Elkridge Landing Road
Linthicum Heights, MD 21090-2934

Scientific and Technical Aerospace Reports

STAR

Scientific and Technical Aerospace Reports (STAR), is published each month as a major product of the NASA Scientific and Technical Information (STI) Office.

Inside this issue you will find:

- **Front Matter** containing a typical citation and abstract sample explaining the standard format, including codes for ordering reports
- **An Abstract Section** containing citations and abstracts of reports and publications that provide comprehensive coverage of worldwide aerospace-related topics including aeronautics and space science technology. *STAR* lists published and publicly available reports entered into the NASA STI Database during the four weeks preceding publication of this issue. These citations and abstracts are listed by subject categories.
- **An Index Section**
    - Subject
    - Personal author
    - Corporate source
    - Contract number
    - Report number
- **An Appendix** containing a guide for ordering cited reports, registering with the NASA STI Office, and using the available products and services. Additionally, price schedules, phone numbers, and addresses are included in this information packed section.

NASA also sponsors the companion journal, *NASA Open Volumes on Aerospace (NOVA)*, which lists abstracts of the open literature on aerospace subjects available worldwide. *NOVA* is for internal NASA use only, available from the NASA Center for AeroSpace Information (CASI).

Entries found in *STAR* are available through the NASA online retrieval service, RECON.

The NASA STI Office gathers information through national and international agreements and exchanges and makes this information available to the NASA community and to the public in many forms through various outlets.

For additional information on the NASA STI Office, call the NASA Access Help Desk at (301) 621-0390, or write to:

NASA Center for AeroSpace Information
800 Elkridge Landing Road
Linthicum Heights, Maryland 21090-2934

US ISSN 0036-8741

This publication was prepared by the NASA Center for AeroSpace Information,
800 Elkridge Landing Road, Linthicum Heights, MD 21090-2934, (301) 621-0390.

Volume 33 Number 6 / June 1995

TABLE OF CONTENTS

AERONAUTICS For related information see also *Astronautics.*

01 AERONAUTICS (GENERAL) 1199

02 AERODYNAMICS 1199
Includes aerodynamics of bodies, combinations, wings, rotors, and control surfaces; and internal flow in ducts and turbomachinery. For related information see also *34 Fluid Mechanics and Heat Transfer.*

03 AIR TRANSPORTATION AND SAFETY 1202
Includes passenger and cargo air transport operations; and aircraft accidents. For related information see also *16 Space Transportation* and *85 Urban Technology and Transportation.*

04 AIRCRAFT COMMUNICATIONS AND NAVIGATION 1204
Includes digital and voice communication with aircraft; air navigation systems (satellite and ground based); and air traffic control. For related information see also *17 Space Communications, Spacecraft Communications, Command and Tracking* and *32 Communications and Radar.*

05 AIRCRAFT DESIGN, TESTING AND PERFORMANCE 1206
Includes aircraft simulation technology. For related information see also *18 Spacecraft Design, Testing and Performance* and *39 Structural Mechanics.* For land transportation vehicles see *85 Urban Technology and Transportation.*

06 AIRCRAFT INSTRUMENTATION 1208
Includes cockpit and cabin display devices; and flight instruments. For related information see also *19 Spacecraft Instrumentation* and *35 Instrumentation and Photography.*

07 AIRCRAFT PROPULSION AND POWER 1214
Includes prime propulsion systems and systems components, e.g., gas turbine engines and compressors; and onboard auxiliary power plants for aircraft. For related information see also *20 Spacecraft Propulsion and Power, 28 Propellants and Fuels,* and *44 Energy Production and Conversion.*

08 AIRCRAFT STABILITY AND CONTROL 1214
Includes aircraft handling qualities; piloting; flight controls; and autopilots. For related information see also *05 Aircraft Design, Testing and Performance.*

09 RESEARCH AND SUPPORT FACILITIES (AIR) 1215
Includes airports, hangars and runways; aircraft repair and overhaul facilities; wind tunnels; shock tubes; and aircraft engine test stands. For related information see also *14 Ground Support Systems and Facilities (Space).*

ASTRONAUTICS For related information see also *Aeronautics.*

12 ASTRONAUTICS (GENERAL) 1217
For extraterrestrial exploration see *91 Lunar and Planetary Exploration.*

13 ASTRODYNAMICS .... N.A.
Includes powered and free-flight trajectories; and orbital and launching dynamics.

14 GROUND SUPPORT SYSTEMS AND FACILITIES (SPACE) 1218
Includes launch complexes, research and production facilities; ground support equipment, e.g., mobile transporters; and simulators. For related information see also *09 Research and Support Facilities (Air).*

15 LAUNCH VEHICLES AND SPACE VEHICLES 1218
Includes boosters; operating problems of launch/space vehicle systems; and reusable vehicles. For related information see also *20 Spacecraft Propulsion and Power.*

16 SPACE TRANSPORTATION 1219
Includes passenger and cargo space transportation, e.g., shuttle operations; and space rescue techniques. For related information see also *03 Air Transportation and Safety* and *18 Spacecraft Design, Testing and Performance.* For space suits see *54 Man/System Technology and Life Support.*

17 SPACE COMMUNICATIONS, SPACECRAFT COMMUNICATIONS, COMMAND AND TRACKING 1219
Includes telemetry; space communications networks; astronavigation and guidance; and radio blackout. For related information see also *04 Aircraft Communications and Navigation* and *32 Communications and Radar.*

N.A.—No abstracts were assigned to this category for this issue.

18 SPACECRAFT DESIGN, TESTING AND PERFORMANCE 1219
Includes satellites; space platforms; space stations; spacecraft systems and components such as thermal and environmental controls; and attitude controls. For life support systems see *54 Man/System Technology and Life Support.* For related information see also *05 Aircraft Design, Testing and Performance, 39 Structural Mechanics*, and *16 Space Transportation.*

19 SPACECRAFT INSTRUMENTATION 1221
For related information see also *06 Aircraft Instrumentation* and *35 Instrumentation and Photography.*

20 SPACECRAFT PROPULSION AND POWER 1221
Includes main propulsion systems and components, e.g., rocket engines; and spacecraft auxiliary power sources. For related information see also *07 Aircraft Propulsion and Power, 28 Propellants and Fuels, 44 Energy Production and Conversion*, and *15 Launch Vehicles and Space Vehicles.*

CHEMISTRY AND MATERIALS

23 CHEMISTRY AND MATERIALS (GENERAL) 1223

24 COMPOSITE MATERIALS 1224
Includes physical, chemical, and mechanical properties of laminates and other composite materials. For ceramic materials see *27 Nonmetallic Materials.*

25 INORGANIC AND PHYSICAL CHEMISTRY 1233
Includes chemical analysis, e.g., chromatography; combustion theory; electrochemistry; and photochemistry. For related information see also *77 Thermodynamics and Statistical Physics.*

26 METALLIC MATERIALS 1250
Includes physical, chemical, and mechanical properties of metals, e.g., corrosion; and metallurgy.

27 NONMETALLIC MATERIALS 1263
Includes physical, chemical, and mechanical properties of plastics, elastomers, lubricants, polymers, textiles, adhesives, and ceramic materials. For composite materials see *24 Composite Materials.*

28 PROPELLANTS AND FUELS 1281
Includes rocket propellants, igniters and oxidizers; their storage and handling procedures; and aircraft fuels. For related information see also *07 Aircraft Propulsion and Power, 20 Spacecraft Propulsion and Power*, and *44 Energy Production and Conversion.*

29 MATERIALS PROCESSING 1285
Includes space-based development of products and processes for commercial application. For biological materials see *55 Space Biology:*

ENGINEERING For related information see also *Physics.*

31 ENGINEERING (GENERAL) 1285
Includes vacuum technology; control engineering; display engineering; cryogenics; and fire prevention.

32 COMMUNICATIONS AND RADAR 1288
Includes radar; land and global communications; communications theory; and optical communications. For related information see also *04 Aircraft Communications and Navigation* and *17 Space Communications, Spacecraft Communications, Command and Tracking.* For search and rescue see *03 Air Transportation and Safety*, and *16 Space Transportation.*

33 ELECTRONICS AND ELECTRICAL ENGINEERING 1312
Includes test equipment and maintainability; components, e.g., tunnel diodes and transistors; microminiaturization; and integrated circuitry. For related information see also *60 Computer Operations and Hardware* and *76 Solid-State Physics.*

34 FLUID MECHANICS AND HEAT TRANSFER 1337
Includes boundary layers; hydrodynamics; fluidics; mass transfer and ablation cooling. For related information see also *02 Aerodynamics* and *77 Thermodynamics and Statistical Physics.*

35 INSTRUMENTATION AND PHOTOGRAPHY 1363
Includes remote sensors; measuring instruments and gauges; detectors; cameras and photographic supplies; and holography. For aerial photography see *43 Earth Resources and Remote Sensing.* For related information see also *06 Aircraft Instrumentation* and *19 Spacecraft Instrumentation.*

36 LASERS AND MASERS 1368
Includes parametric amplifiers. For related information see also *76 Solid-State Physics.*

37 MECHANICAL ENGINEERING 1377
Includes auxiliary systems (nonpower); machine elements and processes; and mechanical equipment.

38 QUALITY ASSURANCE AND RELIABILITY 1382
Includes product sampling procedures and techniques; and quality control.

39 STRUCTURAL MECHANICS 1384
Includes structural element design and weight analysis; fatigue; and thermal stress. For applications see *05 Aircraft Design, Testing and Performance* and *18 Spacecraft Design, Testing and Performance.*

GEOSCIENCES For related information see also *Space Sciences.*

42 GEOSCIENCES (GENERAL) .... N.A.

43 EARTH RESOURCES AND REMOTE SENSING 1388
Includes remote sensing of earth resources by aircraft and spacecraft; photogrammetry; and aerial photography. For instrumentation see *35 Instrumentation and Photography.*

44 ENERGY PRODUCTION AND CONVERSION 1391
Includes specific energy conversion systems, e.g., fuel cells; global sources of energy; geophysical conversion; and windpower. For related information see also *07 Aircraft Propulsion and Power, 20 Spacecraft Propulsion and Power,* and *28 Propellants and Fuels.*

45 ENVIRONMENT POLLUTION 1400
Includes atmospheric, noise, thermal, and water pollution.

46 GEOPHYSICS 1411
Includes aeronomy; upper and lower atmosphere studies; ionospheric and magnetospheric physics; and geomagnetism. For space radiation see *93 Space Radiation.*

47 METEOROLOGY AND CLIMATOLOGY 1428
Includes weather forecasting and modification.

48 OCEANOGRAPHY 1431
Includes biological, dynamic, and physical oceanography; and marine resources. For related information see also *43 Earth Resources and Remote Sensing.*

LIFE SCIENCES

51 LIFE SCIENCES (GENERAL) 1437

52 AEROSPACE MEDICINE 1441
Includes physiological factors; biological effects of radiation; and effects of weightlessness on man and animals.

53 BEHAVIORAL SCIENCES 1448
Includes psychological factors; individual and group behavior; crew training and evaluation; and psychiatric research.

54 MAN/SYSTEM TECHNOLOGY AND LIFE SUPPORT 1451
Includes human engineering; biotechnology; and space suits and protective clothing. For related information see also *16 Space Transportation.*

55 SPACE BIOLOGY .... N.A.
Includes exobiology; planetary biology; and extraterrestrial life.

MATHEMATICAL AND COMPUTER SCIENCES

59 MATHEMATICAL AND COMPUTER SCIENCES (GENERAL) .... N.A.

60 COMPUTER OPERATIONS AND HARDWARE 1455
Includes hardware for computer graphics, firmware, and data processing. For components see *33 Electronics and Electrical Engineering.*

61 COMPUTER PROGRAMMING AND SOFTWARE 1456
Includes computer programs, routines, algorithms, and specific applications, e.g., CAD/CAM.

62 COMPUTER SYSTEMS 1473
Includes computer networks and special application computer systems.

63 CYBERNETICS **1479**
Includes feedback and control theory, artificial intelligence, robotics and expert systems. For related information see also *54 Man/System Technology and Life Support.*

64 NUMERICAL ANALYSIS **1486**
Includes iteration, difference equations, and numerical approximation.

65 STATISTICS AND PROBABILITY **1497**
Includes data sampling and smoothing; Monte Carlo method; and stochastic processes.

66 SYSTEMS ANALYSIS **1499**
Includes mathematical modeling; network analysis; and operations research.

67 THEORETICAL MATHEMATICS **1500**
Includes topology and number theory.

PHYSICS For related information see also *Engineering.*

70 PHYSICS (GENERAL) **1500**
For precision time and time interval (PTTI) see *35 Instrumentation and Photography*; for geophysics, astrophysics or solar physics see *46 Geophysics, 90 Astrophysics*, or *92 Solar Physics.*

71 ACOUSTICS **1502**
Includes sound generation, transmission, and attenuation. For noise pollution see *45 Environment Pollution.*

72 ATOMIC AND MOLECULAR PHYSICS **1506**
Includes atomic structure, electron properties, and molecular spectra.

73 NUCLEAR AND HIGH-ENERGY PHYSICS **1531**
Includes elementary and nuclear particles; and reactor theory. For space radiation see *93 Space Radiation.*

74 OPTICS **1540**
Includes light phenomena and optical devices. For lasers see *36 Lasers and Masers.*

75 PLASMA PHYSICS **1548**
Includes magnetohydrodynamics and plasma fusion. For ionospheric plasmas see *46 Geophysics*. For space plasmas see *90 Astrophysics.*

76 SOLID-STATE PHYSICS **1563**
Includes superconductivity. For related information see also *33 Electronics and Electrical Engineering* and *36 Lasers and Masers.*

77 THERMODYNAMICS AND STATISTICAL PHYSICS **1579**
Includes quantum mechanics; theoretical physics; and Bose and Fermi statistics. For related information see also *25 Inorganic and Physical Chemistry* and *34 Fluid Mechanics and Heat Transfer.*

SOCIAL SCIENCES

80 SOCIAL SCIENCES (GENERAL) **1583**
Includes educational matters.

81 ADMINISTRATION AND MANAGEMENT **1583**
Includes management planning and research.

82 DOCUMENTATION AND INFORMATION SCIENCE **1586**
Includes information management; information storage and retrieval technology; technical writing; graphic arts; and micrography. For computer documentation see *61 Computer Programming and Software.*

83 ECONOMICS AND COST ANALYSIS **1594**
Includes cost effectiveness studies.

84 LAW, POLITICAL SCIENCE AND SPACE POLICY .... **N.A.**
Includes NASA appropriation hearings; aviation law; space law and policy; international law; international cooperation; and patent policy.

85 URBAN TECHNOLOGY AND TRANSPORTATION **1594**
Includes applications of space technology to urban problems; technology transfer; technology assessment; and surface and mass transportation. For related information see *03 Air Transportation and Safety, 16 Space Transportation,* and *44 Energy Production and Conversion.*

SPACE SCIENCES For related information see also *Geosciences*.

88 SPACE SCIENCES (GENERAL) **1595**

89 ASTRONOMY **1598**
Includes radio, gamma-ray, and infrared astronomy; and astrometry.

90 ASTROPHYSICS **1599**
Includes cosmology; celestial mechanics; space plasmas; and interstellar and interplanetary gases and dust. For related information see also *75 Plasma Physics.*

91 LUNAR AND PLANETARY EXPLORATION **1601**
Includes planetology; and manned and unmanned flights. For spacecraft design or space stations see *18 Spacecraft Design, Testing and Performance.*

92 SOLAR PHYSICS **1602**
Includes solar activity, solar flares, solar radiation and sunspots. For related information see also *93 Space Radiation.*

93 SPACE RADIATION **1604**
Includes cosmic radiation; and inner and outer earth's radiation belts. For biological effects of radiation see *52 Aerospace Medicine.* For theory see *73 Nuclear and High-Energy Physics.*

GENERAL

Includes aeronautical, astronautical, and space science related histories, biographies, and pertinent reports too broad for categorization; histories or broad overviews of NASA programs.

99 GENERAL **1605**

SUBJECT INDEX **I-1**

PERSONAL AUTHOR INDEX **I-185**

CORPORATE SOURCE INDEX **I-207**

CONTRACT NUMBER INDEX **I-237**

REPORT NUMBER INDEX **I-245**

APPENDIX **A-1**

TYPICAL CITATION AND ABSTRACT

NASA SPONSORED ↓↓ **ON MICROFICHE**

ACCESSION NUMBER → **N95-10148*#** National Aeronautics and Space Administration. Lewis ← **CORPORATE SOURCE**
Research Center, Cleveland, OH.

TITLE → **EFFECTS OF A FORWARD-SWEPT FRONT ROTOR ON THE FLOWFIELD OF A COUNTERROTATION PROPELLER**

AUTHORS → M. Nallasamy (NYMA, Inc., Brook Park, OH.) and Gary G. Podboy Aug. ← **PUBLICATION DATE**
1994 19 p Presented at the 30th Joint Propulsion Conference, Indianapolis, IN, 27-29 Jun. 1994; sponsored by AIAA, ASME, SAE, and ASEE

CONTRACT OR GRANT → (Contract NAS3-27186; RTOP 538-03-11)

REPORT NUMBERS → (NASA-TM-106671; E-8994; NAS 1.15:106671; AIAA Paper 94-2694) Avail: ← **AVAILABILITY SOURCE AND PRICE CODE**
CASI HC A03/MF A01; 6 functional color pages

The effects of a forward-swept front rotor on the flowfield of a counterrotation model propeller at takeoff conditions at zero degree angle of attack are studied by solving the unsteady three-dimensional Euler equations. The configuration considered is an uneven blade count counterrotation model with twelve forward-swept blades on the fore rotor and ten aft-swept blades on the aft rotor. The flowfield is compared with that of a reference aft-swept counterrotation geometry and Laser Doppler Velocimeter (LDV) measurements. At the operating conditions considered, the forward-swept blade experiences a higher tip loading and produces a stronger tip vortex compared to the aft-swept blade, consistent with the LDV and acoustic measurements. Neither the solution nor the LDV data indicated the formation of a leading edge vortex. The predicted radial distribution of the circumferentially averaged axial velocity at the measurement station agreed very closely with LDV data, while crossflow velocities showed poor agreement. The discrepancy between prediction and LDV data of tangential and radial velocities is due in part to the insufficient mesh resolution in the region between the rotors and in the tip region to track the tip vortex. The vortex is diffused by the time it arrives at the measurement station. The uneven blade count configuration requires the solution to be carried out for six blade passages of the fore rotor and five passages of the aft rotor, thus making grid refinement prohibitive.

Author

VOLUME 33 NUMBER 6 / June 1995

Scientific and Technical Aerospace Reports

A Monthly Publication of the National Aeronautics and Space Administration

01 AERONAUTICS (GENERAL)

N95-19967# Transportation Research Board, Washington, DC.
PUBLIC-SECTOR AVIATION ISSUES: GRADUATE RESEARCH AWARD PAPERS, 1992-1993 Transportation Research Record
1994 44 p See also PB93-206258
(PB94-217478; TRB/TRR-1428; ISBN-0-309-05506-7) Avail: CASI HC A03/MF A01

The papers in this document reports on research topics chosen by graduate students selected for awards from a nationwide competition under Seventh Graduate Research Award Program on Public-Sector Aviation issues (1992-1993). It has the following contents: Dynamic Analysis of Oligopolistic Behavior in the U.S. Airline Industry; Movements of Domestic Airline Technical Efficiency Scores over Time; Implications for Future Industry Structure; Evaluating Self-Analysis as a Strategy for Learning Crew Resource Management in Undergraduate Flight Training; and Airfoil Performance in Heavy Rain. NTIS

N95-20091 Federal Aviation Administration, Washington, DC. Office of Aviation Policy and Plans.
CENSUS US CIVIL AIRCRAFT CALENDAR YEAR 1993 Annual Report
31 Dec. 1993 444 p Limited Reproducibility: More than 20% of this document may be affected by microfiche quality
(AD-A286309; FAA-APO-94-10) Avail: CASI HC A19

This report presents information about the U.S. civil aircraft fleet. It includes detailed tables of air carrier aircraft and an inventory of registered aircraft by manufacturer and model, and general aviation aircraft by state and county of the owner. DTIC

N95-21640* National Aeronautics and Space Administration, Washington, DC.
AERONAUTICAL ENGINEERING: A CONTINUING BIBLIOGRAPHY WITH INDEXES (SUPPLEMENT 315)
Mar. 1995 84 p
(NASA-SP-7037(315); NAS 1.21:7037(315)) Avail: CASI HC A05

This bibliography lists 217 reports, articles, and other documents introduced into the NASA scientific and technical information system in Mar. 1995. Subject coverage includes: design, construction and testing of aircraft and aircraft engines; aircraft components, equipment, and systems; ground support systems; and theoretical and applied aspects of aerodynamics and general fluid dynamics. Author

N95-22046# Wright Lab., Wright-Patterson AFB, OH.
DAMAGE TOLERANT REPAIR TECHNIQUES FOR PRESSURIZED AIRCRAFT FUSELAGES Final Report, 15 Jun. 1991 - 15 Nov. 1993
Robert S. Fredell 6 Jun. 1994 281 p
(AF Proj. 2401)
(AD-A286298; WL-TR-94-3134) Avail: CASI HC A13/MF A03

Concerns over the safety of the continued use of aging transport aircraft have been voiced in the industry. A key component in the structural integrity of aging aircraft is the damage tolerance of fuselage structural repairs. The investigation focuses on the analysis and testing of contemporary repair methods and develops two improvements. The first technique, known as soft patching, is appropriate for damage tolerant riveted repairs to incidental fuselage damage. Soft patching involves the use of high strength, moderate elastic modulus GLARE 3 fiber metal laminate patches. They extend the fatigue life of riveted repairs to monolithic aluminum fuselages while reducing life cycle costs. The second technique involves bonded crack patching of intact fatigue cracks in fuselage skins. An easy to use analysis program is presented along with analytical and test results of a low cost, high performance patch material known as GLARE 2. The findings demonstrate that GLARE 2 can replace the expensive boron/epoxy composites used in fuselage crack patching applications. DTIC

02 AERODYNAMICS

Includes aerodynamics of bodies, combinations, wings, rotors, and control surfaces; and internal flow in ducts and turbomachinery.

For related information see also *34 Fluid Mechanics and Heat Transfer.*

N95-19913*# National Aeronautics and Space Administration. Langley Research Center, Hampton, VA.
STATIC INVESTIGATION OF TWO FLUIDIC THRUST-VECTORING CONCEPTS ON A TWO-DIMENSIONAL CONVERGENT-DIVERGENT NOZZLE
David J. Wing Dec. 1994 203 p
(RTOP 505-62-30-01)
(NASA-TM-4574; L-17350; NAS 1.15:4574) Avail: CASI HC A10/MF A03

A static investigation was conducted in the static test facility of the Langley 16-Foot Transonic Tunnel of two thrust-vectoring concepts which utilize fluidic mechanisms for deflecting the jet of a two-dimensional convergent divergent nozzle. One concept involved using the Coanda effect to turn a sheet of injected secondary air along a curved sidewall flap and, through entrainment, draw the primary jet in the same direction to produce yaw thrust vectoring. The other concept involved deflecting the primary jet to produce pitch thrust vectoring by injecting secondary air through a transverse slot in the divergent flap, creating an oblique shock in the divergent channel. Utilizing the Coanda effect to produce yaw thrust vectoring was largely unsuccessful. Small vector angles were produced at low primary nozzle pressure ratios, probably because the momentum of the primary jet was low. Significant pitch thrust vector angles were produced by injecting secondary flow through a slot in the divergent flap. Thrust vector angle decreased with increasing nozzle pressure ratio but moderate levels were maintained at the highest nozzle pressure ratio tested. Thrust performance generally increased at low nozzle pressure ratios and decreased near the design pressure ratio with the addition of secondary flow. Author

N95-19946# Aircraft Research Association Ltd., Bedford (England).
INVESTIGATION OF A THERMAL BUOYANCY EFFECT ON THE DRAG OF HALF MODELS TESTED IN THE ARA TRANSONIC WIND TUNNEL
Dennis R. Stanniland, Ian F. Burns, and John E. Green May 1994 12 p Presented at the 19th Congress of the International Council of the Aeronautical Sciences, Anaheim, CA, Sep. 1994
(ARA-Memo-407) Avail: CASI HC A03/MF A01

The demand for improved drag repeatability from wind tunnel measurements, together with the increasing size of models (driven by the requirement for accurate representation of small components), has led to the need for a greater understanding of the flow near the porous walls of the ARA Transonic Wind Tunnel and the implications of very small changes in this flow on the model force measurements. A detailed investigation of the variability of drag measurements on a half model identified a diurnal variation which could be attributed to the small changes in temperature difference between the tunnel shell and the freestream. This paper describes measurements which have been made in the tunnel to identify the cause of this non-repeatability. The results show a variation in the boundary layer development on the tunnel walls caused by differences in the heat transfer in the plenum chamber. This can change the Mach number in the vicinity of a half model afterbody by approximately 0.002 for a temperature increment of 5 deg K, implying a change in drag coefficient 0f 0.0002 for a typical civil aircraft model. An extension to the test section has been designed, which was successful in removing the thermal influence on the boundary layer thickness and centerline Mach number in the empty tunnel. However, some thermal buoyancy remains when a half model is tested in the redesigned section, although this is significantly reduced for a large model. A correction procedure has been developed which has virtually eliminated thermal buoyancy as a source of error, resulting in a drag repeatability of better than 1 count. Author

N95-19991# Aeronautical Systems Div., Wright-Patterson AFB, OH.
OPEN SKIES PROJECT COMPUTATIONAL FLUID DYNAMIC ANALYSIS Final Report, Nov. 1992 - May 1993
James C. Slavey, Mark S. Jurkovich, Robert M. Weyer, and Joseph C. Zuppardo Mar. 1994 130 p
(AD-A285928; ASC-TR-94-5027) Avail: CASI HC A07/MF A02

A Computational Fluid Dynamic (CFD) analysis has been performed on a WC-135B aircraft that has been modified at Wright-Patterson AFB (WPAFB) forming the first Open Skies aircraft designated OC-135B. The studies included the use of panel method, full potential, and Navier-Stokes methods utilizing 2-D/axisymmetric, and 3-D. While providing information useful to the Open Skies program, the studies also provide a good example of how lower order and higher order computational aerodynamic methods can be used together to obtain the maximum benefit from CFD at a minimum cost. Flight test tufting and accelerometer data confirmed the results of the 3-D Full Navier-Stokes results. DTIC

N95-19996* National Aeronautics and Space Administration. Hugh L. Dryden Flight Research Center, Edwards, CA.
F-16XL INTERVIEW WITH MARTA BOHN-MEYER (Videotape)
27 Jul. 1992 Videotape: 30 min. playing time, in color, with sound
(NASA-TM-110505; NONP-NASA-VT-95-41117) Avail: CASI VHS A02/BETA A22

Marta Bohn-Meyer discusses the cooperative research between Rockwell Industries and NASA research facilities in their effort to optimize and maintain the supersonic laminar flow on the F-16XL aircraft. Research on the airfoil design, chord optimization, introduction of a suction feature to maintain pressure distribution, and CFD, both theoretical and actual phenomena, are discussed. Bohn-Meyer discusses the difference between supersonic and subsonic laminar flow, cross flow, reasons behind using this particular F-16 aircraft for this research, and the future of this ongoing research, including the data base that investigators are building from wind tunnel data and in-flight validation. DFRC

N95-20175# California Inst. of Tech., Pasadena, CA. Graduate Aeronautical Labs.
FREE SHEAR LAYERS, BASE PRESSURE AND BLUFF-BODY DRAG
A. Roshko 10 Dec. 1993 19 p
(Contract N00014-94-1-0793)
(AD-A286316) Avail: CASI HC A03/MF A01

Incompressible, non-vortex-shedding bluff-body flows and supersonic base-pressure flows are discussed from a unified viewpoint in which the aspect ratio of the near wake is determined from the balance of shear-stress and pressure forces on the near-wake boundary. The base pressure and drag are then determined from free-streamline theory. The analysis is incomplete, for want of sufficient information about conditions in reattaching supersonic turbulent shear layers. Author (DTIC)

N95-20177 California Inst. of Tech., Pasadena, CA. Graduate Aeronautical Labs.
RESEARCH ON BLUFF BODY VORTEX WAKES
Anatol Roshko, Anthony Leonard, and Morteza Gharib 1994 8 p
Limited Reproducibility: More than 20% of this document may be affected by microfiche quality
(Contract N00014-94-1-0793)
(AD-A286319) Avail: CASI HC A02

The basic approach is to obtain measurements in correlated laboratory experiments and numerical simulations of flows past bluff bodies, especially circular cylinders. Laboratory measurements include flow visualization and digital particle image velocimetry (DPIV). Numerical simulations are based on vortex methods. Interpretation of relations between velocity/vorticity fields and body forces is sought through the generalized Biot-Savart law. The role of Reynolds number, effects of three dimensionality, and effects of body motion are investigated. Relations to the mean near-wake flow and mean force (drag) are also studied, for their basic technological importance and also for insights into the unsteady motion. DTIC

N95-20248# Arnold Engineering Development Center, Arnold AFS, TN.
DESCRIPTION AND FLOW CHARACTERIZATION OF HYPERSONIC FACILITIES Final Report, Jul. 1992 - Jul. 1993
A. Anderson, R. K. Matthews, J. R. Maus, and R. A. Crawford Aug. 1994 59 p
(AD-A284291; AEDC-TR-94-8) Avail: CASI HC A04/MF A01

Hypersonic test facilities will continue to play a major role in the development of hypersonic vehicles. In the past, ground test facilities were often used to perform configuration parametric studies and/or to develop large databases. Future testing will emphasize understanding of fluid physics and validation of codes. Computational fluid dynamics (CFD) has made great progress in the past two decades, but the marriage of CFD and ground testing is clearly a reality today, and will become even more important in the future. One of the challenges for the experimentalist is to develop and utilize facilities that simulate hypersonic flight, and to provide the required data precision to validate CFD codes. This provides a brief review of facility fundamental considerations and simulation issues. It is clear that no one facility will meet the wide variety of test objectives; therefore, the test facilities span a range of size, run time, complexity, and operating cost. Representative facilities are described, as well as their test capabilities, and shortfalls. DTIC

N95-20688*# National Aeronautics and Space Administration. Langley Research Center, Hampton, VA.
THE PERSONAL AIRCRAFT: STATUS AND ISSUES
Scott G. Anders, Scott C. Asbury, Kenneth S. Brentner, Dennis M. Bushnell, Christopher E. Glass, William T. Hodges, Shelby J. Morris, Jr., and Michael A. Scott Dec. 1994 126 p
(RTOP 232-01-04-01)
(NASA-TM-109174; NAS 1.15:109174) Avail: CASI HC A07/MF A02

Paper summarizes the status of personal air transportation with emphasis upon VTOL and converticar capability. The former obviates the need for airport operations for personal aircraft whereas the latter provides both ground and air capability in the same vehicle. Fully automatic operation, ATC and navigation is stressed along with consideration of acoustic, environmental and cost issues. Author

N95-20758# Aircraft Research Association Ltd., Bedford (England).
THE DYNAMIC APPROACH TO ROTOR BLADE RESEARCH: ARA'S OSCILLATORY TEST FACILITY
Caroline M. Humphreys Sep. 1994 12 p Presented at the ICAS 1994, Anaheim, CA, Sep. 1994 Original contains color illustrations
(ARA-Memo-405) Avail: CASI HC A03/MF A01 color page

Helicopters' forward flight performance is limited by the rapid build up in blade and control loads which occur when rotor blades enter stall conditions. Due to a combination of the helicopter forward speed and the rotor rotational velocity the rotor sections experience a wide range of local onset conditions, this leads to vastly different flow characteristics across the span and through the rotational cycle. A great deal of time and effort has been devoted to studying this flow phenomena. Consequently, information covering all aspects of unsteady aerodynamics is easily available. However, one area that needs up-dating is the description of the experimental test facilities that are able to simulate these flow conditions. The dynamic rig at the Aircraft Research Association was designed and built in the 1970's. Since then, as new technology became available, the rig's capabilities have been steadily improved. The paper reports on these amendments. Author

N95-20794*# National Aeronautics and Space Administration. Lewis Research Center, Cleveland, OH.

APPLICATION OF PRESSURE SENSITIVE PAINT IN HYPERSONIC FLOWS

Kenol Jules, Mario Carbonaro (Von Hoerner und Sulger Electronic G.m.b.H., Schwetzingen, Germany.), and Stephan Zemsch (Von Hoerner und Sulger Electronic G.m.b.H., Schwetzingen, Germany.) Feb. 1995 17 p
Sponsored by Von Karman fellowship and AF
(RTOP 466-05-02)
(NASA-TM-106824; E-9373; NAS 1.15:106824) Avail: CASI HC A03/MF A01

It is well known in the aerodynamic field that pressure distribution measurement over the surface of an aircraft model is a problem in experimental aerodynamics. For one thing, a continuous pressure map can not be obtained with the current experimental methods since they are discrete. Therefore, interpolation or CFD methods must be used for a more complete picture of the phenomenon under study. For this study, a new technique was investigated which would provide a continuous pressure distribution over the surface under consideration. The new method is pressure sensitive paint. When pressure sensitive paint is applied to an aerodynamic surface and placed in an operating wind-tunnel under appropriate lighting, the molecules luminesce as a function of the local pressure of oxygen over the surface of interest during aerodynamic flow. The resulting image will be brightest in the areas of low pressure (low oxygen concentration), and less intense in the areas of high pressure (where oxygen is most abundant on the surface). The objective of this investigation was to use pressure sensitive paint samples from McDonnell Douglas (MDD) for calibration purpose in order to assess the response of the paint under appropriate lighting and to use the samples over a flat plate/conical fin mounted at 75 degrees from the center of the plate in order to study the shock/boundary layer interaction at Mach 6 in the Von Karman wind-tunnel. From the result obtained it was concluded that temperature significantly affects the response of the paint and should be given the uppermost attention in the case of hypersonic flows. Also, it was found that past a certain temperature threshold, the paint intensity degradation became irreversible. The comparison between the pressure tap measurement and the pressure sensitive paint showed the right trend. However, there exists a shift when it comes to the actual value. Therefore, further investigation is under way to find the cause of the shift. Author

N95-21031*# Purdue Univ., West Lafayette, IN. Dept. of Aeronautics and Astronautics.

WAKE MEASUREMENTS IN A STRONG ADVERSE PRESSURE GRADIENT

R. Hoffenberg, John P. Sullivan, and S. P. Schneider 1994 13 p
(Grant NAG2-854)
(NASA-CR-197272; NAS 1.26:197272; AIAA Paper 94-2613) Avail: CASI HC A03/MF A01

The behavior of wakes in adverse pressure gradients is critical to the performance of high-lift systems for transport aircraft. Wake deceleration is known to lead to sudden thickening and the onset of reversed flow; this 'wake bursting' phenomenon can occur while surface flows remain attached. Although 'wake bursting' is known to be important for high-lift systems, no detailed measurements of 'burst' wakes have ever been reported. Wake bursting has been successfully achieved in the wake of a flat plate as it decelerated in a two-dimensional diffuser, whose sidewalls were forced to remain attached by use of slot blowing. Pilot probe surveys, L.D.V. measurements, and flow visualization have been used to investigate the physics of this decelerated wake, through the onset of reversed flow. Author

N95-21338*# National Aeronautics and Space Administration. Langley Research Center, Hampton, VA.

APPLICATION OF NAVIER-STOKES CODE PAB3D WITH KAPPA-EPSILON TURBULENCE MODEL TO ATTACHED AND SEPARATED FLOWS

Khaled S. Abdol-Hamid (Analytical Services and Materials, Inc., Hampton, VA.), B. Lakshmanan (Old Dominion Univ., Norfolk, VA.), and John R. Carlson Jan. 1995 43 p
(RTOP 505-59-10-20)
(NASA-TP-3480; L-17354; NAS 1.60:3480) Avail: CASI HC A03/MF A01

A three-dimensional Navier-Stokes solver was used to determine how accurately computations can predict local and average skin friction coefficients for attached and separated flows for simple experimental geometries. Algebraic and transport equation closures were used to model turbulence. To simulate anisotropic turbulence, the standard two-equation turbulence model was modified by adding nonlinear terms. The effects of both grid density and the turbulence model on the computed flow fields were also investigated and compared with available experimental data for subsonic and supersonic free-stream conditions. Author

N95-21343*# Notre Dame Univ., IN. Dept. of Aerospace and Mechanical Engineering.

EXPERIMENTS ON THE FLOW FIELD PHYSICS OF CONFLUENT BOUNDARY LAYERS FOR HIGH-LIFT SYSTEMS Progress Report

Robert C. Nelson, F. O. Thomas, and H. C. Chu [1994] 18 p Original contains color illustrations
(Grant NAG2-905)
(NASA-CR-197318; NAS 1.26:197318) Avail: CASI HC A03/MF A01; 3 functional color pages

The use of sub-scale wind tunnel test data to predict the behavior of commercial transport high lift systems at in-flight Reynolds number is limited by the so-called 'inverse Reynolds number effect'. This involves an actual deterioration in the performance of a high lift device with increasing Reynolds number. A lack of understanding of the relevant flow field physics associated with numerous complicated viscous flow interactions that characterize flow over high-lift devices prohibits computational fluid dynamics from addressing Reynolds number effects. Clearly there is a need for research that has as its objective the clarification of the fundamental flow field physics associated with viscous effects in high lift systems. In this investigation, a detailed experimental investigation is being performed to study the interaction between the slat wake and the boundary layer on the primary airfoil which is known as a confluent boundary layer. This little-studied aspect of the multi-element airfoil problem deserves special attention due to its importance in the lift augmentation process. The goal of this research is is to provide an improved understanding of the flow physics associated with high lift generation. This process report will discuss the status of the research being conducted at the Hessert Center for Aerospace Research at the University of Notre Dame. The research is sponsored by NASA Ames Research Center under NASA grant NAG2-905. The report will include a discussion of the models that have been built or that are under construction, a description of the planned experiments, a description of a flow visualization apparatus that has been developed for generating colored smoke for confluent boundary layer studies and some preliminary measurements made using our new 3-component fiber optic LDV system. Author

N95-21659 Defence Science and Technology Organization, Melbourne (Australia). Aeronautical and Maritime Research Lab.

A PRELIMINARY STUDY OF THE AIRWAKE MODEL USED IN AN EXISTING SH-60B/FFG-7 HELICOPTER/SHIP SIMULATION PROGRAM

Lincoln P. Erm May 1994 44 p
(DSTO-TR-0015; AR-008-644) Copyright Avail: Issuing Activity (DSTO Aeronautical and Maritime Research Lab., GPO Box 4331, Melbourne, Victoria 3001, Australia)

The ship airwake model in a SH-60B/FFG-7 helicopter/ship simulation program is studied in detail. The airwake model is based on wind tunnel measurements obtained for another ship type, with geometric scaling applied to make it suitable for an FFG-7 frigate. Velocities over the flight deck of an FFG-7, predicted using the program, are compared with those obtained from full-scale tests on HMAS Darwin. Differences between predicted and measured velocities are often found to occur, indicating that the model used for prediction should be based on measurements for an FFG-7. Author

N95-21864 Department of the Navy, Washington, DC.

LIFT ENHANCEMENT DEVICE Patent

Samuel Greenhalgh, inventor (to Navy) 9 Aug. 1994 11 p Filed 26 May 1993 Supersedes AD-D016196
(AD-D016522; US-Patent-5,335,886; US-Patent-Appl-SN-067763; US-Patent-Class-244-21) Avail: US Patent and Trademark Office

A lift enhancing device for a solid wing is disclosed. A solid wing with a swept leading edge and unswept trailing edge has a rectangular flap attached along the trailing edge. The flap can be a single segment or can be a plurality of segments joined at contiguous edges. The flap oscillates during air movement and enhances the lift produced. DTIC

N95-21877 Wright Lab., Wright-Patterson AFB, OH.
PRESSURE MEASUREMENTS ON AN F/A-18 TWIN VERTICAL TAIL IN BUFFETING FLOW. VOLUME 1: WIND TUNNEL TEST SUMMARY Final Report, Apr. 1993 - Aug. 1994
Chris Pettit, Michael Banford, Dansen Brown, and Ed Pendleton 31 Aug. 1994 105 p Limited Reproducibility: More than 20% of this document may be affected by microfiche quality
(AD-A279126; WL-TM-94-3039-Vol-1) Avail: Issuing Activity (Defense Technical Information Center (DTIC))

Buffeting pressure measurements were made on the vertical tail surface of a full scale F/A-18 aircraft model in the National Full Scale Aerodynamics Complex at NASA Ames Research Center. Test variables included aircraft angle-of-attack, aircraft sideslip angle, and dynamic pressure. Accelerometers were used to obtain vertical tail accelerations. Pressure transducers were mounted on the starboard vertical tail. Steady and unsteady pressures were obtained. Unsteady pressure data were reduced to power spectral density (PSD) and cross spectral density (CSD) forms. Both steady and unsteady RMS pressure coefficients are also presented. Volume 1 contains the general description of the model, the test program, and highlights of the reduced data. DTIC

N95-21892 Aeronautical Research Labs., Melbourne (Australia).
DERIVED GUST SPECTRA FOR THE MACCHI MB326H
P. Piperias Feb. 1993 41 p
(ARL-TN-3; AR-007-124) Copyright Avail: Issuing Activity (Director, Aeronautical Research Lab., 506 Lorimer St., Fishermens Bend, Victoria 3207, Australia)

Gust spectra for the RAAF Macchi MB326H aircraft fleet have been derived. In-house software has been used with current mission profiles to determine load-exceedence diagrams. Missions exhibiting high exceedences have been identified. Author

N95-22448*# Stanford Univ., CA. Center for Turbulence Research.
UNSTRUCTURED-GRID LARGE-EDDY SIMULATION OF FLOW OVER AN AIRFOIL
Kenneth Jansen *In its* Annual Research Briefs, 1994 Dec. 1994 p 161-173 (For primary document see N95-22437 06-34)
Avail: CASI HC A03/MF A04

03 AIR TRANSPORTATION AND SAFETY

Includes passenger and cargo air transport operations; and aircraft accidents.

For related information see also *16 Space Transportation* and *85 Urban Technology and Transportation.*

N95-20071# Naval Research Lab., Washington, DC.
A REVIEW OF WATER MIST TECHNOLOGY FOR FIRE SUPPRESSION Memorandum Report
P. A. Tatum, C. L. Beyler (Hughes Associates, Inc., Columbia, MD.), P. J. DiNenno (Hughes Associates, Inc., Columbia, MD.), E. K. Budnick (Hughes Associates, Inc., Columbia, MD.), and G. G. Back (Hughes Associates, Inc., Columbia, MD.) 30 Sep. 1994 93 p
(NR Proj. RH2-1-S-22)
(AD-A285738; NRL/MR/6180-94-7624) Avail: CASI HC A05/MF A01

The potential efficacy of water mist fire suppression systems has been demonstrated in a wide range of applications and by numerous experimental programs. These applications have included Class B spray and pool fires, aircraft cabins, shipboard machinery and engine room spaces, shipboard accommodation spaces, and computer and electronics applications. To summarize these experimental efforts, the efficacy of a particular water mist system is strongly dependent on the ability to not only generate sufficiently small droplet sizes but also distribute sufficient mist concentrations throughout the compartment. A widely accepted critical concentration of water droplets required to extinguish a fire is yet to be determined. Factors that contribute to the success or failure of a water mist system for a particular application include droplet size, velocity, the spray pattern geometry as well as the momentum and mixing characteristics of the spray jet, and the geometry and other characteristics of the protected area. At this time, the effect of these factors on system effectiveness is not well known. This will necessitate evaluation of water mist in context of a specific system for unique applications for the reasonable future unless breakthroughs in understanding of mist distribution and flame interaction occur through research. DTIC

N95-20093 Galaxy Scientific Corp., Pleasantville, NJ.
TEST AND EVALUATION REPORT FOR THE MANUAL DOMESTIC PASSIVE PROFILING SYSTEM (MDPPS) Final Report
J. L. Fobes, Ronald J. Lofaro, J. P. Berkowitz, N. J. Dolan, and D. S. Fischer Sep. 1994 55 p Limited Reproducibility: More than 20% of this document may be affected by microfiche quality
(Contract DTFA03-92-C-0035)
(AD-A286312; DOT/FAA/CT-94/86) Avail: CASI HC A04

Presented are a compilation of data collected at Northwest Airlines terminal, General Mitchell International Airport, Milwaukee, Wisconsin, from February 22-24, 1994. The study was conducted in support of the Aviation Security Human Factors Research Program located at the Federal Aviation Administration Technical Center (FAATC), Atlantic City International Airport, New Jersey. Real-time (e.g., at the ticket counter and gate) passenger profiling was conducted February 22-24, 1994 in Milwaukee, Wisconsin. Passengers on twenty-one Northwest Airline flights were profiled according to parameters set forth by the Passenger Profiling Subject Matter Expert panel. One hundred ten passengers (82.7%) were cleared by the profile; twenty-three (17.3%) were not cleared. The mean time to profile was 1 minute 23 seconds. An analysis of variance (ANOVA) and a subsequent least square difference (LSD) multiple comparison showed it took significantly longer to profile passengers who were not cleared (mean = 1 minute 27 seconds) than to profile passengers who were cleared (mean = 1 minute 9 seconds) (F(131, 1) = 36.87, p = .000). Interview and anecdotal data are also summarized. DTIC

N95-20174# Galaxy Scientific Corp., Pleasantville, NJ.
COMMUTER AIRPLANE ACCIDENT DATA ANALYSIS Final Report
G. Wittlin Aug. 1994 34 p
(Contract DTFA03-89-C-00043)
(AD-A286315; DOT/FAA/CT-94/75) Avail: CASI HC A03/MF A01

This report presents the results of a review of data from 120 commuter and air taxi airplane accidents that occurred from 1978 through 1986. The main objectives of this study are (1) to present the severe, but survivable impact condition data from the accident database and (2) to formulate appropriate crash design impact parameters. In 1980 the Federal Aviation Administration Technical Center (FAATC) initiated the Aircraft Crashworthiness Program, which resulted in a compilation of commuter airplane accident data. The program's objectives were (1) to define potentially survivable commuter airplane crash scenarios and (2) to provide impact parameters associated with the appropriate crash scenarios. Based on the data that was received, a crash survivable design envelope was defined for commuter airplanes. DTIC

N95-20275# Galaxy Scientific Corp., Pleasantville, NJ.
COMMUTER/AIR TAXI DITCHINGS AND WATER-RELATED IMPACTS THAT OCCURRED FROM 1979 TO 1989 Final Report, Jun. 1990 - Dec. 1992
Charles C. Chen and Mark Muller Jul. 1994 105 p
(Contract DTFA03-89-C-00043)
(AD-A285691; DOT/FAA/CT-92/4) Avail: CASI HC A06/MF A01

This report documents an investigation of ditchings and water-related impacts for commuter-category aircraft that occurred during the years 1979 through 1989. The main source of accident data was the National Transportation Safety Board (NTSB). Data were also sought from the International Civil Aviation Organization and the U.S. Navy Safety Center. A total of 46 accidents was obtained and examined for this study. Of these, 40 cases satisfied the criteria for inclusion into the database. Impact and post-impact conditions were categorized to assess aircraft behavior and occupant survivability. Two impact scenarios and two post-impact scenarios were established. Special emphasis was placed on examining aircraft flotation behavior and post-impact survivability. In addition, five representative case studies are presented to demonstrate aspects peculiar to the commuter-category aircraft water impact and post-impact sequence that could not be adequately covered by the statistical categorizations alone. DTIC

N95-20706*# National Aeronautics and Space Administration. Langley Research Center, Hampton, VA.

WHY DO AIRLINES WANT AND USE THRUST REVERSERS? A COMPILATION OF AIRLINE INDUSTRY RESPONSES TO A SURVEY REGARDING THE USE OF THRUST REVERSERS ON COMMERCIAL TRANSPORT AIRPLANES

Jeffrey A. Yetter Jan. 1995 65 p
(RTOP 538-05-13-01)
(NASA-TM-109158; NAS 1.15:109158) Avail: CASI HC A04/MF A01

Although thrust reversers are used for only a fraction of the airplane operating time, their impact on nacelle design, weight, airplane cruise performance, and overall airplane operating and maintenance expenses is significant. Why then do the airlines want and use thrust reversers? In an effort to understand the airlines need for thrust reversers, a survey of the airline industry was made to determine why and under what situations thrust reversers are currently used or thought to be needed. The survey was intended to help establish the cost/benefits trades for the use of thrust reversers and airline opinion regarding alternative deceleration devices. A compilation and summary of the responses given to the survey questionnaire is presented. Author

N95-21518# Eagle Ventures, Rockville, MD.

INDEPENDENT REVIEW OF AVIATION TECHNOLOGY AND RESEARCH INFORMATION ANALYSIS SYSTEM (ATRIAS) DATABASE Final Report

Ronald J. Lofaro, L. Hitchcock, S. L. Boggs, and J. E. Mateski Feb. 1994 92 p
(Contract DTFA01-93-P-02265)
(AD-A284049; DOT/FAA/CT-94/12) Avail: CASI HC A05/MF A01

This technical report presents the findings of a critical review of the Aviation Technology and Research Information Analysis System (ATRIAS) for its capability to support the Federal Aviation Administration (FAA)/Aviation Security Research and Development Service's (ACA) Explosive Detection Systems (EDS) programs and Aviation Security Human Factors Program (ASHFP). This review was conducted by an independent consultant selected by the FAA. Section 1 of the report gives a descriptive overview of the ATRIAS analysis and reporting system. The findings of the independent review are contained in sections 2 and 3 of the report. Overall, ATRIAS was found to address many technology application areas relevant to the FAA's aviation security programs. However, the findings did recommend specific modifications to ATRIAS that will provide enhanced information collection and analysis for six topic areas of prime relevance to the FAA's EDS and ASHFP programs. DTIC

N95-21831# Hughes STX, Inc., Lexington, MA.

RADAR STUDIES OF AVIATION HAZARDS

F. I. Harris, Ralph S. Donaldson, Jr., David J. Smalley, and Shu-Lin Tung 31 May 1994 94 p
(Contract F19628-93-C-0054)
(AD-A285845; PL-TR-94-2146; SR-1) Avail: CASI HC A05/MF A01

During the first year of this contract, research was directed toward the development of new techniques to monitor and forecast weather related aviation hazards with Doppler weather radar. Focus was on the characterization of the structure of severe convective storms and of synoptic scale baroclinic fronts. One aspect that was examined is the detection and quantization of the weak echo region usually seen in severe convective storms. Another has been the search for lightning precursors. Finally, considerable effort has been expended on the automated depiction of the wind and precipitation structure associated with baroclinic fronts. DTIC

N95-22318# Federal Aviation Administration, Atlanta, GA.

FUSELAGE BURNTHROUGH FROM LARGE EXTERIOR FUEL FIRES Final Report

Harry Webster Jul. 1994 128 p
(AD-A286295; DOT/FAA/CT-90-10) Avail: CASI HC A07/MF A02

The burnthrough resistance of aircraft fuselages to external fuel fire was investigated in this test series. Three tests were conducted in a wheels-up mode and three in the wheels-down configuration. A comprehensive data base was developed documenting fire entry paths, burnthrough time, and cabin environmental conditions. The overall resistance of the two test intact aircraft fuselages to fire penetration was documented. DTIC

N95-22319# Galaxy Scientific Corp., Pleasantville, NJ.

TEST AND EVALUATION PLAN (TEP) FOR IMPROVISED EXPLOSIVE DEVICE SCREENING SYSTEMS (IEDSS)

James L. Fobes, Ronald J. Lofaro, Robert L. Malone, Douglas S. Fischer, and Jack Berkowitz 14 Aug. 1994 54 p
(Contract DTFA03-89-C-00043)
(AD-A286382; DOT/FAA/CT-94/87) Avail: CASI HC A04/MF A01

This document is the Operational Test and Evaluation Plan (OT&E) to evaluate the effectiveness of X-ray baggage screening equipment for Improvised Explosive Devices (IED's) in cluttered baggage. The Improvised Explosive Device Screening Systems (IEDSS) to be tested during the OT&E consist of standard (black and white) and enhanced (color) display X ray equipment and their operators. The X ray equipment will be used to scan for simulated IEDs in both checked (C) and carry-on (CO) cluttered baggage. The OT&E will be conducted at San Francisco International Airport (SFO). The results will be analyzed and become part of a later document. DTIC

N95-22352# Hughes Associates, Inc., Columbia, MD.

ANALYSIS OF TEST CRITERIA FOR SPECIFYING FOAM FIREFIGHTING AGENTS FOR AIRCRAFT RESCUE AND FIREFIGHTING Final Report

Joseph L. Scheffey and Joseph A. Wright Aug. 1994 96 p Sponsored by FAA
(AD-A286381; DOT/FAA/CT-94/04) Avail: CASI HC A05/MF A01

Foam agent quantities and application rates for FAA certified airports are based on large-scale fire test data of Aqueous Film-Forming Foam (AFFF) and protein-based foams. The philosophy is to control aircraft fuel fires in sixty seconds. Foam agents which are used for aviation applications should demonstrate this level of performance, including a safety factor which assures adequate performance under less than optimum conditions. A review of standard test methods and performance criteria indicates a wide range of requirements. The U.S. Military Specification (MIL SPEC) for AFFF, on which the original agent criteria was developed, is the most stringent in terms of extinguishment application density. However, no direct correlation has been demonstrated between many of the required physical/chemical properties tests and fire extinguishment/burnback performance. It was demonstrated, using comparative data from numerous small and large-scale fire tests, that the small-scale MIL SPEC fire tests correlate with large-scale test results. MIL SPEC agents, which provide a safety factor over minimum FAA requirements, also are formulated to have proportioning, storage, stability, and shelf-life attributes appropriate for crash rescue firefighting applications. Adoption of the MIL SPEC for AFFF agents is recommended. Future work related to foam testing should focus on the use of first principles to establish fundamental foam extinguishment mechanisms. DTIC

N95-22417# Naval Postgraduate School, Monterey, CA.

FORECASTING AIRCRAFT MISHAPS USING MONTHLY MAINTENANCE REPORTS M.S. Thesis

John S. VanHouten Sep. 1994 73 p
(AD-A286049) Avail: CASI HC A04/MF A01

Naval Aviation aircraft mishaps continue to be of great concern due to the high cost of loss of life and aircraft. The goal of this thesis is to develop a predictive statistical model that accurately forecasts Marine Corps AV-8B Harrier aircraft mishaps based on existing monthly maintenance reports. Monthly maintenance reports provide numerous independent variables based on personnel levels and maintenance hours that could possibly be used to forecast aircraft mishaps. These variables were graphically analyzed to determine any relationships that could be exploited in developing the model. Higher order relationships were investigated by the method of principal components and logistic regression. After a thorough analysis, there appears to be no combination of variables in this particular data that could be used to forecast aircraft mishaps. The overall result of the thesis is that there is no relationship between monthly maintenance reports and aircraft mishaps that can be exploited to develop a predictive statistical model. DTIC

04 AIRCRAFT COMMUNICATIONS AND NAVIGATION

Includes digital and voice communication with aircraft; air navigation systems (satellite and ground based); and air traffic control.

For related information see also *17 Space Communications, Spacecraft Communications, Command and Tracking* and *Communications and Radar.*

N95-19950*# McDonnell-Douglas Aerospace, Long Beach, CA.
CREW AIDING AND AUTOMATION: A SYSTEM CONCEPT FOR TERMINAL AREA OPERATIONS, AND GUIDELINES FOR AUTOMATION DESIGN Final Report
John P. Dwyer Dec. 1994 216 p
(Contract NAS1-18028; RTOP 505-64-13-22)
(NASA-CR-4631; NAS 1.26:4631; CRAD-9206-TR-8940) Avail: CASI HC A10/MF A03

This research and development program comprised two efforts: the development of guidelines for the design of automated systems, with particular emphasis on automation design that takes advantage of contextual information, and the concept-level design of a crew aiding system, the Terminal Area Navigation Decision Aiding Mediator (TANDAM). This concept outlines a system capable of organizing navigation and communication information and assisting the crew in executing the operations required in descent and approach. In service of this endeavor, problem definition activities were conducted that identified terminal area navigation and operational familiarization exercises addressing the terminal area navigation problem. Both airborne and ground-based (ATC) elements of aircraft control were extensively researched. The TANDAM system concept was then specified, and the crew interface and associated systems described. Additionally, three descent and approach scenarios were devised in order to illustrate the principal functions of the TANDAM system concept in relation to the crew, the aircraft, and ATC. A plan for the evaluation of the TANDAM system was established. The guidelines were developed based on reviews of relevant literature, and on experience gained in the design effort. Author

N95-20195# Sandia National Labs., Albuquerque, NM.
SAR IMAGE REGISTRATION IN ABSOLUTE COORDINATES USING GPS CARRIER PHASE POSITION AND VELOCITY INFORMATION
S. Burgett and M. Meindl 1994 5 p Presented at the International Symposium on Kinematic Systems in Geodesy, Geomatics, and Navigation, Banff, Alberta, 30 Aug. - 2 Sep. 1994
(Contract DE-AC04-94AL-85000)
(DE94-018738; SAND-94-1417C; CONF-9408163-1) Avail: CASI HC A01/MF A01

It is useful in a variety of military and commercial application to accurately register the position of synthetic aperture radar (SAR) imagery in absolute coordinates. The two basic SAR measurements, range and Doppler, can be used to solve for the position of the SAR image. Imprecise knowledge of the SAR collection platform's position and velocity vectors introduce errors in the range and Doppler measurements and can cause the apparent location of the SAR image on the ground to be in error by tens of meters. Recent advances in carrier phase GPS techniques can provide an accurate description of the collection vehicle's trajectory during the image formation process. In this paper, highly accurate carrier phase GPS trajectory information is used in conjunction with SAR imagery to demonstrate a technique for accurate registration of SAR images in WGS-84 coordinates. Flight test data will be presented that demonstrates SAR image registration errors of less than 4 meters. DOE

N95-20269# Sandia National Labs., Albuquerque, NM.
THE GPS BURST DETECTOR W-SENSOR
Dennis D. McCrady (ITT Aerospace/Communications Div., Clifton, NJ.) and Paul Phipps 1994 10 p Presented at the Ion-GPS 1994, Salt Lake City, UT,21 Sep. 1994
(Contract DE-AC04-94AL-85000)
(DE94-017406; SAND-94-2130C; CONF-9409185-1) Avail: CASI HC A02/MF A01

The NAVSTAR satellites have two missions: navigation and nuclear detonation detection. The main objective of this paper is to describe one of the key elements of the Nuclear Detonation Detection System (NDS), the Burst Detector W-Sensor (BDW) that was developed for the Air Force Space and Missile Systems Center, its mission on GPS Block IIR, and how it utilizes GPS timing signals to precisely locate nuclear detonations (NUDET). The paper will also cover the interface to the Burst Detector Processor (BDP) which links the BDW to the ground station where the BDW is controlled and where data from multiple satellites are processed to determine the location of the NUDET. The Block IIR BDW is the culmination of a development program that has produced a state-of-the-art, space qualified digital receiver/processor that dissipates only 30 Watts, weighs 57 lbs, and has a 12 in. x 14.2 in. x 7.16 in. footprint. The paper will highlight several of the key multilayer printed circuit cards without which the required power, weight, size, and radiation requirements could not have been met. In addition, key functions of the system software will be covered. The paper will be concluded with a discussion of the high speed digital signal processing and algorithm used to determine the time-of-arrival (TOA) of the electromagnetic pulse (EMP) from the NUDET. DOE

N95-20497# Army Topographic Engineering Center, Fort Belvoir, VA.
EVOLUTION OF GROUND LINE OF SIGHT DATA FIELD COLLECTION TECHNIQUES
J. R. Ackeret, L. A. Fatale, J. A. Messmore, and J. C. Walker Sep. 1994 12 p
(AD-A285062; USATEC-R-240) Avail: CASI HC A03/MF A01

Consideration of Line-of-Sight (LOS) conditions has always been an essential aspect of the battlefield. Knowledge of the surrounding terrain and its corresponding elevation has even more implications today in the modern Army. To date, the Defense Mapping Agency's (DMA) Digital Terrain Elevation Data (DTED) Level 1 database, an elevation matrix with 3 arc second or approximately 100-meter post spacing, has been used by most military and DOD users when elevation data was required for modeling, simulations or other applications. Recent advances in weapon systems and combat simulators has brought into question the adequacy of DTED Level 1 for terrain appreciation and threat prediction applications, especially LOS. Consequently, the need for higher resolution terrain data (e.g, greater than 30 meter post spacing) and the ability of differing resolutions of DTED to accurately predict LOS conditions is of great interest to the Army's community. DTIC

N95-21020 Federal Aviation Administration, Atlantic City, NJ.
AN EVALUATION OF AUTOMATIC TERMINAL INFORMATION SERVICE (ATIS) FLIGHT DECK DISPLAY PRESENTATION OPTIONS Technical Report, period ending Dec. 1992
Albert Rehmann Mar. 1994 62 p Limited Reproducibility: More than 20% of this document may be affected by microfiche quality
(AD-A280100; DOT/FAA/CT-TN93/25) Avail: Issuing Activity (Defense Technical Information Center (DTIC))

This document describes the first of three studies relating to human factors aspects in the flight deck display of Automatic Terminal Information Service (ATIS). This research is being conducted by the Federal Aviation Administration (FAA) Technical Center. The first part-task study examined basic format design variables. Its purpose was to begin addressing flight deck design issues pertinent to the design of the tower ATIS workstation and, collect data relevant to standard and certification groups within the FAA. Future studies in an FAA Technical Center high-fidelity mock-up and various aircraft simulators will examine full mission issues, such as procedures, equipment mechanization, and automation. Avionics data link human factors, Automatic Terminal Information Service (ATIS), Aircraft Communications Addressing and Reporting System (ACARS). DTIC

N95-21148# Federal Aviation Administration, Atlantic City, NJ.
MINIMA REDUCTION SIMULATION TEST RESULTS
Barry Billmann, Edward Pugacz, and Carl Everberg Jul. 1994 73 p
(AD-A285626; DOT/FAA/CT-TN92/47) Avail: CASI HC A04/MF A01

This report presents the results of tests conducted in a Beech-200 (B-200) simulator located at the Beech Learning Center in Wichita, Kansas, and operated by Flight-Safety International (FSI). The testing was conducted to examine the feasibility of reducing approach minimums below Category I by utilizing a highly accurate navigation signal, such as the Microwave Landing System (MLS), when standard Category II approach and runway lighting are not available. Results are presented which indicate that properly trained crews using flight director-equipped aircraft can operate to lower approach minima than standard Category I without full Category II approach and runway lighting. Performance in the visual segment and touchdown performance is shown to be equivalent regardless of the availability of touchdown zone or runway centerline lighting. The benefits of a Category II approach lighting system (ALSF-2) are mitigated by the fact that when the aircraft breaks out of weather at the lower decision heights (DH's), i.e., 150 feet above ground level (AGL), most of the approach light system is already behind the aircraft. Recommendations are made for further testing in actual aircraft. DTIC

N95-21369 Eurocontrol Experimental Centre, Bretigny (France).
DATA LINK TERMINAL DLT DOCUMENT
P. Ruault and A. Philippart Mar. 1994 164 p
(PB95-110805; EEC/NOTE-12/94) Avail: Issuing Activity (National Technical Information Service (NTIS))

This note describes the Mode-S Data Link Terminal (DLT) which was developed and assembled by the EUROCONTROL Experimental Center. The DLT is a simplified Multi purpose Control and Display Unit (MCDU). It replaces the aircraft MCDU in the on-board experimental Mode-S installation. Based on the ARINC characteristic 739 the terminal is connected to the Data Link Processor Unit DLPU-C2 via the ARINC 429 bus. The DLT gives the aircrew access to data bases via the Mode-S data link. NTIS

N95-21520# Sandia National Labs., Albuquerque, NM.
ASSESSMENT OF A NON-DEDICATED GPS RECEIVER SYSTEM FOR PRECISE AIRBORNE ATTITUDE DETERMINATION
M. E. Cannon (Calgary Univ., Alberta.), H. Sun, T. E. Owen, and M. A. Meindl 1994 10 p Presented at the Ion-GPS 1994, Salt Lake City, UT, 21 Sep. 1994
(Contract DE-AC04-94AL-85000)
(DE94-019309; SAND-94-1136C; CONF-9409185-2) Avail: CASI HC A02/MF A01

The use of a non-dedicated GPS receiver system for attitude determination was assessed in airborne mode through a test conducted at Sandia National Laboratories. Four independent NovAtel GPSCard(trademark) receivers were installed in Sandia's Twin Engine Otter with two antennas mounted on the fuselage and two on the wing tips at separations of 6 to 18 m. A strapdown INS (Inertial Navigation System) was also on board the aircraft in order to provide an independent attitude reference at rates between 4 and 10 Hz. During the multi-day test, GPS measurements were recorded between 1 and 10 Hz. Carrier phase measurements were post-processed using a double difference approach developed at The University of Calgary in which integer ambiguities were resolved in seconds using the known antenna separations as constraints. The tracking capability of the system is demonstrated under dynamics consisting of roll and pitch angles up to 45 and 12 degrees, respectively. Comparisons between the GPS and INS attitude angles are presented for two of the test days and show agreement at the several arcminute level. Conclusions are made with respect to system accuracy and performance in an operational airborne environment. DOE

N95-21642 Materials Research Labs., Ascot Vale (Australia).
THE DETERMINATION OF STATIC AND TIME VARYING DIPOLE SOURCE. SENSOR GEOMETRY DURING SEA TRIALS USING DIFFERENTIAL GLOBAL POSITIONING SYSTEM
J. Vrbancich, A. Donohoo, L. Scott, S. Turnbull, and M. Andreaus May 1993 37 p
(MRL-TN-631; AR-008-226) Copyright Avail: Issuing Activity (DSTO Materials Research Lab., PO Box 50, Ascot Vale, Victoria 3032, Australia)

Global positioning system (GPS) navigational equipment is used in differential mode to determine the time varying geometry of a boat attached to a submerged dipole source and a sensor positioned on the seafloor which is marked by a surface buoy. The requirement is to track the position of the source relative to the sensor on the seabed in sea depths less than 40 m in the vicinity of Sydney Harbor. A differential GPS (DGPS) system is formed from two or three low cost navigational units, one of which is located at a surveyed reference site and the other is located onboard the vessel. A third unit may be temporarily located at the sea surface above the sensor positioned on the seafloor. The differential system relies on software developed to apply the GPS correction obtained from the reference station to the remote stations after the geographical coordinates have been recorded. Static DGPS measurements using a 7 km baseline between remote and reference datums gave a position accuracy limited by the resolution of the GPS receiver. As a test for kinematic DGPS, the positional accuracy of the moving vessel was checked against the position coordinates derived from the laser tracking facility of the Shark Point Degaussing Range, Sydney Harbor. The agreement was usually found to be better than about 5 m, typical +/- 2 m. DGPS also enabled accurate submarine tracking at periscope depth by interfacing the submarine UHF antenna to the GPS receiver. A discussion of operational issues in the use of DGPS is also included. Author

N95-21891*# California Polytechnic State Univ., San Luis Obispo, CA. Dept. of Aeronautical Engineering.
A REAL-TIME ALGORITHM FOR INTEGRATING DIFFERENTIAL SATELLITE AND INERTIAL NAVIGATION INFORMATION DURING HELICOPTER APPROACH M.S. Thesis
Ty Hoang Apr. 1994 67 p
(Contract NCC2-775)
(NASA-CR-197409; NAS 1.26:197409) Avail: CASI HC A04/MF A01

A real-time, high-rate precision navigation Kalman filter algorithm is developed and analyzed. This Navigation algorithm blends various navigation data collected during terminal area approach of an instrumented helicopter. Navigation data collected include helicopter position and velocity from a global position system in differential mode (DGPS) as well as helicopter velocity and attitude from an inertial navigation system (INS). The goal of the Navigation algorithm is to increase the DGPS accuracy while producing navigational data at the 64 Hertz INS update rate. It is important to note that while the data was post flight processed, the Navigation algorithm was designed for real-time analysis. The design of the Navigation algorithm resulted in a nine-state Kalman filter. The Kalman filter's state matrix contains position, velocity, and velocity bias components. The filter updates positional readings with DGPS position, INS velocity, and velocity bias information. In addition, the filter incorporates a sporadic data rejection scheme. This relatively simple model met and exceeded the ten meter absolute positional requirement. The Navigation algorithm results were compared with truth data derived from a laser tracker. The helicopter flight profile included terminal glideslope angles of 3, 6, and 9 degrees. Two flight segments extracted during each terminal approach were used to evaluate the Navigation algorithm. The first segment recorded small dynamic maneuver in the lateral plane while motion in the vertical plane was recorded by the second segment. The longitudinal, lateral, and vertical averaged positional accuracies for all three glideslope approaches are as follows (mean plus or minus two standard deviations in meters): longitudinal (-0.03 plus or minus 1.41), lateral (-1.29 plus or minus 2.36), and vertical (-0.76 plus or minus 2.05). Author

N95-22161*# Rockwell Space Operations Co., Houston, TX. Flight Design and Dynamics Dept.
THE NAVIGATION TOOLKIT
William F. Rich and Stephen W. Strom Oct. 1994 7 p Presented at OOPSLA 1994, Portland, OR, 23-27 Oct. 1994
(Contract NAS9-18000)
(NASA-CR-197290; NAS 1.26:197290) Avail: CASI HC A02/MF A01

This report summarizes the experience of the authors in managing, designing, and implementing an object-oriented applications framework for orbital navigation analysis for the Flight Design and Dynamics Department of the Rockwell Space Operations Company in Houston, in support of the Mission Operations Directorate of NASA's Johnson Space Center. The 8 person year project spanned 1.5 years and produced 30,000 lines of C++ code, replacing 150,000 lines of Fortran/C. We believe that our experience is important because it represents a 'second project' experience and generated real production-quality code - it was not a pilot. The project successfully demonstrated the use of 'continuous development' or rapid prototyping techniques. Use of formal methods and executable models contributed to the quality of the code. Keys to the success of the project were a strong architectural vision and highly skilled workers. This report focuses on process and methodology, and not on a detailed design description of the product. But the true importance of the object-oriented paradigm is its liberation of the developer to focus on the problem rather than the means used to solve the problem. Author

05 AIRCRAFT DESIGN, TESTING AND PERFORMANCE

Includes aircraft simulation technology.

For related information see also *18 Spacecraft Design, Testing and Performance* and *39 Structural Mechanics.*For land transportation vehicles see *85 Urban Technology and Transportation.*

N95-19963# Defence Science and Technology Organization, Melbourne (Australia). Aeronautical and Maritime Research Lab.

VARIATIONS OBSERVED IN THE AC GENERATOR SIGNAL PERIOD OF A SEA KING HELICOPTER

D. M. Blunt Jun. 1994 25 p
(AD-A284280; DSTO-GD-0004; DODA-AR-008-545) Avail: CASI HC A03/MF A01

The AC generator in the Sea King helicopter can be used as a convenient source of a tachometer signal from the main rotor gearbox, thus enabling synchronous vibration signal averages to be calculated for every shaft in the gearbox. The signal averaging software developed by ARL determines the shaft speeds by measuring the tachometer signal period. Variations in the tachometer signal period not caused by changes in gearbox speed will affect the accuracy of the vibration signal averages. An examination has been made of the AC generator signal of a Sea King helicopter recorded on a Bruel & Kjaer 4 channel FM tape recorder (model 7003). The results show that the signal averaging software measures short term period variations (from one period to the next) in the AC generator signal of up toapp roximately 2% of the mean period. It was found that while most of this variation probably arises from noise present in the recording environment, a considerable proportion comes from noise introduced through the tape recording and filtering processes. DTIC

N95-19994* National Aeronautics and Space Administration. Hugh L. Dryden Flight Research Center, Edwards, CA.

F-15 RESOURCE TAPE (Videotape)

1994 Videotape: 9 min. 25 sec. playing time, in color, with sound
(NASA-TM-110502; NONP-NASA-VT-95-41114) Avail: CASI VHS A02/BETA A22

An F-15 fighter aircraft is portrayed in resource video. A flight test is shown with take-off, touch and go landings, some flight maneuvers, and pilot to control tower communication with references to drag vectors. CASI

N95-20155* National Aeronautics and Space Administration. Hugh L. Dryden Flight Research Center, Edwards, CA.

ACOUSTIC CLIMB TO CRUISE TEST (Videotape)

27 Nov. 1991 Videotape: 9 min. 30 sec. playing time, in color, with sound
(NASA-TM-110504; NONP-NASA-VT-95-41116) Avail: CASI VHS A02/BETA A22

Flight test film footage of three different aircraft testing the acoustical noise levels during take-off, climb, maneuvers, and touch and go landings are described. These sound tests were conducted on two fighter aircraft and one cargo aircraft. Results from mobile test vehicle are shown. DFRC

N95-20181 Naval War Coll., Newport, RI. Dept. of Operations.

BOMBER FORCE 2000: OPERATIONAL CONCEPTS FOR LONG-RANGE COMBAT AIRCRAFT Final Report

Jeffrey K. Beene 8 Feb. 1994 61 p Limited Reproducibility: More than 20% of this document may be affected by microfiche quality
(AD-A279378) Avail: Issuing Activity (Defense Technical Information Center (DTIC))

This research paper seeks to synthesize analyses of air power theory and doctrine, historical insights from major operations, current thinking, and the emerging strategic environment to detail concepts for improved planning and execution of future air operations. These operations would fully integrate bombers as long-range combat aviation assets. The search for a type of aircraft to fit the doctrine derived from early interpretations of air power theory has hindered development of bomber potential. The use of atomic weapons at the end of World War 2 and the ensuing Cold War further obscured understanding of bombers, their real contribution hinging on viewing them as long-range combat aircraft. Today, the bomber is not obsolete, but its traditional nuclear paradigm is. The emergence of regional threats combined with a shrinking defense establishment and the global compression of time and space demand full integration of bomber aircraft into the U.S. air power arsenal. These aircraft provide a theater commander with a unique capability to respond rapidly across the spectrum of conflict from a peacetime show of force to major nuclear or nonnuclear conflict. However, for the operational commander to employ bomber assets effectively requires a full recognition of bomber attributes and a thorough understanding of their capabilities. DTIC

N95-20212# General Accounting Office, Washington, DC. National Security and International Affairs Div.

NAVAL AVIATION: F-14 UPGRADES ARE NOT ADEQUATELY JUSTIFIED. REPORT TO CONGRESSIONAL COMMITTEES

Oct. 1994 12 p
(AD-A286338; GAO/NSIAD-95-12; B-257718) Avail: CASI HC A03/MF A01; GAO, PO Box 6015, Gaithersburg, MD 20884-6015 HC

The implications of the Navy's decision to spend about $2.5 billion between fiscal years 1994 and 2003 for a limited ground attack upgrade and other modifications to about 200 F-14 Tomcat fighters was evaluated. This upgrade was included to add limited ground attack capability and other improvements to 210 F-14 Tomcat fighter aircraft. According to the Navy, the ground attack capabilities were required to partially compensate for the loss in combat capabilities during the period starting in 1997, when all of its A-6E Intruder attack aircraft are scheduled to be retired, to the turn of the century when the F/A-18E/F, the next generation strike fighter, is scheduled to arrive. Although the Navy justified F-14 attack upgrades as necessary to replace some capability that will be lost when it retires all A-6E attack aircraft by fiscal year 1998, planned upgrades will not include an air-to-ground radar for precision ground mapping that would permit crews to locate, identify, and attack targets in adverse weather and poor visibility. In addition, no F-14 will be able to launch current or planned precision munitions or stand-off weapons, except for LGBS. Upgraded F-14's generally have greater range than the F/A-18C and could possibly reach targets beyond the Hornet's range. However, this capability may not be needed with the Navy's shift to a littoral warfare strategy. If greater range is needed, the Navy's Tomahawk cruise missile can attack targets up to a range of about 700 miles, and Air Force bombers have even greater range. Both supplement and complement carrier aviation in striking deep within enemy territory. The Navy has not made a compelling case to proceed with its $2.5 billion plan. DTIC

N95-20329 Department of Defense, Washington, DC.

UNMANNED AERIAL VEHICLES

31 May 1994 135 p Limited Reproducibility: More than 20% of this document may be affected by microfiche quality
(AD-A286190) Avail: CASI HC A07

The Unmanned Aerial Vehicle (UAV) Joint Project Office was officially established in response to Congressional direction by a charter signed by the Director of Defense Research and Engineering on 16 October 1989. This master plan is structured into three parts: an executive summary; a main body providing extensive detail on management, supporting the user, programs, commonality and interoperability, technology, analysis and simulation, integrated logistics support, training, human systems integration, test and evaluation, international programs, and resources; and an appendix of supporting material including discussions of dual uses of UAV's and UAV civil airspace management issues. CASI

N95-20370*# National Aeronautics and Space Administration. Langley Research Center, Hampton, VA.

PARALLEL CALCULATION OF SENSITIVITY DERIVATIVES FOR AIRCRAFT DESIGN USING AUTOMATIC DIFFERENTIATION

C. H. Bischof (Argonne National Lab., IL.), T. L. Knauff, Jr. (Argonne National Lab., IL.), L. L. Green, and K. J. Haigler Jan. 1994 24 p Presented at the 5th AIAA/NASA/USAF/ISSMO Symposium on Multidisciplinary Analysis and Optimization Conference, Panama City, FL, 7-9 Sep. 1994
(Contract W-31-109-eng-38)
(NASA-TM-110103; NAS 1.15:110103; DE94-016894; ANL/MCS/CP-82870; CONF-9409187-1) Avail: CASI HC A03/MF A01

Realistic multidisciplinary design optimization (MDO) of advanced aircraft using state-of-the-art computers is an extremely challenging problem from both the physical modelling and computer science points of view. In order to produce an efficient aircraft design, many trade-offs must be made among the various physical design variables. Similarly, in order to produce an efficient design scheme, many trade-offs must be made among the various MDO implementation options. In this paper, we examine the effects of vectorization and coarse-grained parallelization on the SD calculation using a representative example taken from a transonic transport design problem. DOE

N95-20466 Naval Test Pilot School, Patuxent River, MD.

T-45A HIGH ANGLE OF ATTACK TESTING: US NAVAL TEST PILOT SCHOOL 46TH ANNUAL REUNION AND SYMPOSIUM

Max Rogers and Patrick Perusse 29 Apr. 1994 17 p Symposium was held Limited Reproducibility: More than 20% of this document may be affected by microfiche quality

(AD-A284000) Avail: CASI HC A03

The Symposium provides a forum for the evaluation of high angle of attack (haoa) flying qualities and propulsion system characteristics. Its purpose is to also determine the suitability of T-45A aircraft to perform air combat maneuvering and out-of-control flight training missions. Derived from text

N95-20772# Kaman Sciences Corp., Albuquerque, NM.

TIM-SCT CABLE TESTING PROTOCOL Final Report, 24 Aug. 1992 - 24 Aug. 1993

Kurt H. Coonrod, Karl R. Jurisson, J. T. Hendrickson, and Donald P. McLemore Sep. 1994 40 p

(Contract F29601-92-C-0109)

(AD-A286633; PL-TR-93-1110) Avail: CASI HC A03/MF A01

This document presents a standardized approach for measuring transfer impedance of shielded aircraft cables in-situ. The approach is based on the present Shielded Cable Tester (SCT) and Transfer Impedance Meter (TIM) instruments. DTIC

N95-20860# Technische Hochschule, Aachen (Germany). Inst. fuer Mechanik.

PREDICTION OF ROTOR-BLADE DEFORMATIONS DUE TO UNSTEADY AIRLOADS Interim Report No. 2

Stefan Schlechtriem and Josef Ballmann 31 Jul. 1994 5 p

(Contract N68171-94-C-9068)

(AD-A286593; R/D-7213-AN-01) Avail: CASI HC A01/MF A01

SOFIA, a computer code for aeroelastic computations, was applied to predict the rotor blade deformations due to unsteady airloads caused by BVI and to investigate appropriate control movements to minimize vibration and noise. The computation of the unsteady, compressible, inviscid flow about rotor-blades uses an Euler CFD code, while a quasi one-dimensional structural solver is used to compute the deformation of the rotor blades. DTIC

N95-21186*# National Aeronautics and Space Administration. Ames Research Center, Moffett Field, CA.

SIMULATION OF ROTOR BLADE ELEMENT TURBULENCE

R. E. McFarland and Ken Duisenberg (Systems Consultants, Inc., Falls Church, VA.) Jan. 1995 17 p

(RTOP 505-64-29)

(NASA-TM-108862; A-95028; NAS 1.15:108862) Avail: CASI HC A03/MF A01

A piloted, motion-based simulation of Sikorsky's Black Hawk helicopter was used as a platform for the investigation of rotorcraft responses to vertical turbulence. By using an innovative temporal and geometrical distribution algorithm that preserved the statistical characteristics of the turbulence over the rotor disc, stochastic velocity components were applied at each of twenty blade-element stations. This model was implemented on NASA Ames' Vertical Motion Simulator (VMS), and ten test pilots were used to establish that the model created realistic cues. The objectives of this research included the establishment of a simulation-technology basis for future investigation into real-time turbulence modeling. This goal was achieved; our extensive additions to the rotor model added less than a 10 percent computational overhead. Using a VAX 9000 computer the entire simulation required a cycle time of less than 12 msec. Pilot opinion during this simulation was generally quite favorable. For low speed flight the consensus was that SORBET (acronym for title) was better than the conventional body-fixed model, which was used for comparison purposes, and was determined to be too violent (like a washboard). For high speed flight the pilots could not identify differences between these models. These opinions were something of a surprise because only the vertical turbulence component on the rotor system was implemented in SORBET. Because of the finite-element distribution of the inputs, induced outputs were observed in all translational and rotational axes. Extensive post-simulation spectral analyses of the SORBET model suggest that proper rotorcraft turbulence modeling requires that vertical atmospheric disturbances not be superimposed at the vehicle center of gravity but, rather, be input into the rotor system, where the rotor-to-body transfer function severely attenuates high frequency rotorcraft responses. Author

N95-21425 National Physical Lab., Teddington (England). Div. of Radiation Science and Acoustics.

EFFECT OF ATMOSPHERIC PRESSURE ON MEASURED AIRCRAFT NOISE LEVELS

R. C. Payne Mar. 1994 58 p

(PB95-130423; NPL-RSA(EXT)0048) Copyright Avail: Issuing Activity (National Technical Information Service (NTIS))

Noise certification of subsonic jet airplanes, heavy propeller-driven airplane and helicopters is carried out using the procedures described in the International Civil Aviation Organization (ICAO) document Annex 16. Measured noise levels are corrected to reference atmospheric conditions to allow for differences in air attenuation resulting from variations in ambient temperature and relative humidity. The attenuation is calculated using the Society of Automotive Engineers standard ARP 866A. The procedure does not include the effect of ambient atmospheric pressure. The report discusses the influence of atmospheric pressure on the attenuation of sound transmitted to the ground during noise certification tests carried out using airfields at altitude. ARP 866A and three alternative procedures that include the effect of atmospheric pressure are assessed, and calculations are made of air attenuation rates based on reference atmospheric pressure and pressures that are representative of those that occur at airfields located at altitudes of up to 10000 feet (3048 m). Comparison of these attenuation rates shows differences that are dependent on temperature, relative humidity, frequency and altitude. The effect of these differences on EPNL evaluation is difficult to assess as it is dependent not only on meteorological conditions, but also on spectral shape and propagation distance. NTIS

N95-21730# Sandia National Labs., Albuquerque, NM.

A USER'S GUIDE TO LUGSAN 1.1: A COMPUTER PROGRAM TO CALCULATE AND ARCHIVE LUG AND SWAY BRACE LOADS FOR AIRCRAFT-CARRIED STORES

W. N. Dunn Jul. 1994 202 p

(Contract DE-AC04-94AL-85000)

(DE95-001919; SAND-94-1826) Avail: CASI HC A10/MF A03

LUGSAN (LUG and Sway brace ANalysis) is an analysis and database computer program designed to calculate store lug and sway brace loads from aircraft captive carriage. LUGSAN combines the rigid body dynamics code, SWAY85 and the maneuver calculation code, MILGEN, with an INGRES database to function both as an analysis and archival system. This report describes the operation of the LUGSAN application program, including function description, layout examples, and sample sessions. This report is intended to be a user's manual for version 1.1 of LUGSAN operating on the VAX/VMS system. The report is not intended to be a programmer or developer's manual. DOE

N95-22039 Naval Postgraduate School, Monterey, CA.

EFFECT OF JUNCTURE FILLETS ON DOUBLE-DELTA WINGS UNDERGOING SIDESLIP AT HIGH ANGLES OF ATTACK M.S. Thesis

Wen-Huan Chang Sep. 1994 216 p Limited Reproducibility: More than 20% of this document may be affected by microfiche quality

(AD-A286165) Avail: CASI HC A10

A flow visualization study of the vortical flow over a baseline double-delta wing model and a diamond-fillet double-delta wing model both with sharp leading edges was conducted in the Naval Postgraduate School water tunnel using the dye-injection technique. The main focus of this study was to observe the effect of juncture fillet on the vortex core trajectory, and vortex burst location on the wing surface at high angles of attack with sideslip angles. The results indicate that the strake vortex burst point moves upstream with increasing angle of attack at zero sideslip angle; but at constant angle of attack the windward side strake vortex burst location moves upstream and inboard while the leeward side vortex burst point moves downstream and outboard with increasing sideslip angle. Comparison of test results between the baseline model and the diamond-fillet model indicates a clear delay for the latter model in terms of both vortex core trajectory and breakdown location at high angles of attack with and without sideslip angle. The vortex breakdown data for the diamond-fillet model implies lift augmentation during sideslip motion, thus supporting the concept of flow control using fillets. DTIC

06 AIRCRAFT INSTRUMENTATION

Includes cockpit and cabin display devices; and flight instruments.

For related information see also *19 Spacecraft Instrumentation* and *35 Instrumentation and Photography.*

N95-20032# Federal Aviation Administration, Atlantic City, NJ.
INVESTIGATION OF FLIGHT DATA RECORDER FIRE TEST REQUIREMENTS
Lawrence J. Curran, Jr. Oct. 1994 27 p
(AD-A285832; DOT/FAA/CT-TN94/23) Avail: CASI HC A03/MF A01

This report evaluates fire test methodologies for aircraft flight data and cockpit voice recorders. The current fire test requirement consists of a 30-minute exposure to a propane burner calibrated to the heating conditions created by a jet fuel fire. A comparison was made of the internal temperature of flight recorder models subjected to the propane burner standard and a jet fuel fire. The internal temperature was approximately 40 percent higher during the fuel fire tests which were 6-8 minutes in duration. Although the fuel fire duration was limited, it appears that a 60-minute propane burner test exposure is a feasible and conservative means of evaluating the thermal resistance of a flight recorder subjected to a 30-minute fuel fire. An additional fire test condition (500 F/10 hours) has been proposed to simulate a smoldering fire which may persist for a long period of time at a remote site. A state-of-the-art magnetic tape of the cockpit voice recorder was subjected to this condition in an oven and failed the test, demonstrating the severity of this exposure environment. DTIC

N95-20631# Advisory Group for Aerospace Research and Development, Neuilly-Sur-Seine (France). Avionics Panel.
ADVANCED PACKAGING CONCEPTS FOR DIGITAL AVIONICS [LES TECHNIQUES AVANCEES DE MISE SOUS BOITIER]
Oct. 1994 287 p In ENGLISH and FRENCH Symposium held in San Diego, CA, 6-9 Jun. 1994
(AGARD-CP-562; ISBN-92-836-0004-5) Copyright Avail: CASI HC A13/MF A03

A critical impediment to significantly improving the performance of digital airborne electronics or avionics is the limitation posed by current electronics packaging concepts. This symposium brought together experts from seemingly diverse, but interlocking disciplines ranging from logisticians to digital designers to mechanical engineers to establish the current baseline in digital packaging, failure modes of the electronics and support problems. Trends in both supportability and processing were described for early 21st century application. Along with the projections of asymptotic increase in signal, image and data processing, dramatic increases in thermal densities, chip interconnects, correctors and backplane traffic were described. For individual titles, see N95-20632 through N95-20659.

N95-20632# Wright Lab., Wright-Patterson AFB, OH. Avionics Directorate.
THE IMPACT OF ADVANCED PACKAGING TECHNOLOGY ON MODULAR AVIONICS ARCHITECTURES
Reed Morgan and John Ostgaard *In* AGARD, Advanced Packaging Concepts for Digital Avionics Oct. 1994 12 p (For primary document see N95-20631 06-06)
Copyright Avail: CASI HC A03/MF A03

This paper explores how advances in digital packaging will impact network requirements at the system level. Two main issues connected with modular digital packaging for avionics were investigated: (1) Can conventional electrical designs continue to handle the information network speed and wirability requirements needed at the backplane to efficiently utilize advanced modular data and signal processors? (2) Considering projected network requirements for future sensors, displays, etc., (which are made possible because of digital packaging advances), what type of system architecture will be needed? The paper concludes that: (1) Beyond the module (PCB) interface, a new type of backplane implementation will eventually be needed to support the flexibility and growth needs of modular processing. Several new approaches other than a passive electrical backplane could be employed; however, a switched, photonic-based approach is proposed for information distribution between digital processing modules as well as for interconnection between peripherals. Digital packaging advances will result in I/O speeds of about 2 Gigabits/sec, and (2) advanced integrated RF and EO sensors and display technologies will require network data rates in the range of 2 Gigabits/sec in order to communicate in real time with the high speed signal and graphics processor modules in the common integrated processor racks. Many of these 'peripheral' functions will require virtual point-point links because continuous, streaming data in involved. This resulting system architecture recommended is a switched optical network which interconnects sources and sinks of information to the modular processing assets, as well as providing a network for intermodule intercommunication within the rack. Issues of protocol control of this network remain. Further, several advances in photonic packaging and connectors will be required to make this new architectural approach a reality. Although photonics offers the best long-range solution, significant technology difficulties must be overcome. Author

N95-20633# Naval Air Warfare Center, Indianapolis, IN. Aircraft Div.
STANDARD HARDWARE ACQUISITION AND RELIABILITY PROGRAM (SHARP) ADVANCED SEM-E PACKAGING
Mary H. Mosier and Anthony Hawkins *In* AGARD, Advanced Packaging Concepts for Digital Avionics Oct. 1994 10 p (For primary document see N95-20631 06-06)
Copyright Avail: CASI HC A02/MF A03

The objective of the 'Advanced SEM-E Packaging' is 'to identify existing SEM-E and modular avionics characteristics; delineate where they are not defined; and document consensual requirements and guidance for military and commercial applications to provide a framework for open systems architecture implementation'. SHARP has teamed with the Air Force Modular Avionics Systems Architecture (MASA) Program to bridge Industry and government agencies in defining and documenting Standard Electronic Module (SEM) format E advanced packaging requirements. The baseline for the working group has been identified, but SHARP and MASA are soliciting participation and input from industry, other agencies, and NATO. Author

N95-20634# Dassault Aviation, Saint-Cloud (France).
FASTPACK: OPTIMIZED SOLUTIONS FOR MODULAR AVIONICS DERIVED FROM A PARAMETRIC STUDY. PART 1: PLATFORM FEATURES [FASTPACK: SOLUTIONS OPTIMISEES POUR LE CONDITIONNEMENT DE L'AVIONIQUE MODULAIRE ISSUES D'UNE ETUDE PARAMETRIQUE. PART 1: ASPECTS PORTEUR]
G. Veber, S. Barbageleta (Eurocopter France, Marignane, France.), and P. Helie *In* AGARD, Advanced Packaging Concepts for Digital Avionics Oct. 1994 11 p In FRENCH (For primary document see N95-20631 06-06)
Copyright Avail: CASI HC A03/MF A03

Modular avionics is one of the major concepts to be applied to future avionics systems with the objective of cost (LCC - Life Cycle Cost) containment and improvement of operational performance. The objectives associated with such a concept are numerous: improvement of reliability, standardization, interchangeability, interoperability, etc. To obtain these objectives it is necessary to define characteristics standards for modules (LRM - Line Replaceable Module). The definition of these standards for LRM has a direct impact on the modules and their integration. The choice of the best concept takes place through a careful study of the repercussions of each solution on all levels (racks, bays and platforms), in all the technical fields (thermal, electric, mechanical, electromagnetic protection, connectors). This article presents the results of a parametric platform/system-avionics study and more particularly the possible choices for orientation of the platform on aircraft or helicopters. The method used defines the platform constraints to be parameterized and their interactions. The effects are initially integrated in a model representative of standard missions. Thus the results, field by field, show the importance of the effects of constraints on the platform system. Finally, a process of complete dimensioning of the platform, including the functional reliability aspects leads to the synthesis. This allows both a quantitative and qualitative check of the robustness of the compromises carried out. In conclusion, the control of the platform/avionics-system compromise, by an approach of simultaneous engineering, makes it possible to justify a solution of conditioning of the modular avionics in the optics of a future system. Transl. by CASI

N95-20635# Thomson-CSF, Paris (France).
FASTPACK: OPTIMIZED SOLUTIONS FOR MODULAR AVIONICS DERIVED FROM A PARAMETRIC STUDY. PART 2: AVIONICS
M. Caplot, G. LaBaune, C. Capogna, C. Sarno (Sextant Avionique, Valence, France.), J. Herrewyn (Dassault Electronique, Saint-Cloud, France.), J. C. Dhaussy (Dassault Electronique, Saint-Cloud, France.), and P. Bleicher (Dassault Electronique, Saint-Cloud, France.) *In* AGARD, Advanced Packaging Concepts for Digital Avionics Oct. 1994 13 p Sponsored by Ministry of Defence (For primary document see N95-20631 06-06)
Copyright Avail: CASI HC A03/MF A03

The main requirements for modular avionics have a strong influence on the Packaging solutions for the Line Replaceable Modules (LRM's) and the rack. Packaging is here including: mechanical concepts, cooling, power supplies, interconnections and electromagnetic compatibility. To define the packaging solutions for the next generation of avionics, a parametric study, FASTPACK, has been performed at the platform and avionics levels. The present paper deals with the avionics part and shows how the FASTPACK parametric study has been conducted in order to define a synthesis in each domain, used to derive Packaging concepts. The main results include the choice of a LRM format, called FAST, a distributed power supply network within the rack, conduction and liquid flow through cooling, shielding on the rack against external electromagnetic threats and shielding on the LRM for rack internal interferences and, finally, the first definition of the LRM connector. Author

N95-20636# Naval Air Warfare Center, Warminster, PA. Aircraft Div.
THE ADVANCED AVIONICS SUBSYSTEM TECHNOLOGY DEMONSTRATION PROGRAM
Tim Monaghan, Ghani Kanawati, Jacob Abraham, Daniel Olson, and Ravi Iyer *In* AGARD, Advanced Packaging Concepts for Digital Avionics Oct. 1994 13 p (For primary document see N95-20631 06-06)
Copyright Avail: CASI HC A03/MF A03

The Navy's Advanced Avionics Subsystem Technology (AAST) Fault Tolerant program is clarifying the Navy's fault tolerant avionics specifications methods and acceptance tests. The goal of the program will be to clarify the Specification and Statement of Work language needed in future procurements and to demonstrate fault tolerant validation tools on the avionics design. A set of tool features will then be developed that spans the needs of fault tolerant computer system design from early concept studies to full scale production and operational support, both hardware and software. The paper will give an overview of the AAST Fault Tolerant Demonstration and focus on two tools that are being used in the demonstration: FERRARI - a software fault injector that will be used to validate the fault tolerance of the Common Integrated Processor (CIP), the F-22 Mission Processor, and GRIND - a concept evaluation tool that will be used to evaluate the overall CIP architecture. Author

N95-20637# Rome Lab., Griffiss AFB, NY.
IMPROVING MULTICHIP MODULE (MCM) DESIGN AND RELIABILITY USING THE INTELLIGENT MCM ANALYZER c38
Mark J. Stoklosa, Douglas J. Holzhauer, Dale W. Richards, Peter J. Rocci, and Paul S. Yaworsky *In* AGARD, Advanced Packaging Concepts for Digital Avionics Oct. 1994 6 p (For primary document see N95-20631 06-06)
Copyright Avail: CASI HC A02/MF A03

The Intelligent MCM Analyzer (IMCMA) is a software tool which allows the designer to concurrently assess the reliability of an MCM design based on operational parameters. Traditionally, this type of assessment takes days to accomplish and is performed after the design phase. The Intelligent MCM Analyzer does not require the designer to be a thermal/reliability expert and gives an assessment in minutes depending on the complexity of the design and the speed of the computer. IMCMA assists the designer in achieving a robust design which will improve both quality and reliability. The software uses object-oriented data representation, a blackboard architecture and heuristic expertise to perform lower level reasoning associated with finite element thermal analysis techniques that are normally very tedious and labor intensive. A test case will be presented comparing results from IMCMA with the results from a general purpose finite element code. The ultimate payoff will be the manufacturers' ability to build higher quality, higher reliability MCM's at a lower cost. Author

N95-20638# Texas Instruments, Inc., Dallas, TX. Defense Systems and Electronics Group.
ULTRA-RELIABLE DIGITAL AVIONICS (URDA) PROCESSOR c38
Reagan Branstetter, William Ruszczyk, and Frank Miville *In* AGARD, Advanced Packaging Concepts for Digital Avionics Oct. 1994 10 p (For primary document see N95-20631 06-06)
Copyright Avail: CASI HC A02/MF A03

Texas Instruments Incorporated (TI) developed the URDA processor design under contract with the U.S. Air Force Wright Laboratory and the U.S. Army Night Vision and Electro-Sensors Directorate. TI's approach couples advanced packaging solutions with advanced integrated circuit (IC) technology to provide a high-performance (200 MIPS/800 MFLOPS) modular avionics processor module for a wide range of avionics applications. TI's processor design integrates two Ada-programmable, URDA basic processor modules (BPM's) with a JIAWG-compatible PiBus and TMBus on a single F-22 common integrated processor-compatible form-factor SEM-E avionics card. A separate, high-speed (25-MWord/second 32-bit word) input/output bus is provided for sensor data. Each BPM provides a peak throughput of 100 MIPS scalar concurrent with 400-MFLOPS vector processing in a removable multichip module (MCM) mounted to a liquid-flowthrough (LFT) core and interfacing to a processor interface module printed wiring board (PWB). Commercial RISC technology coupled with TI's advanced bipolar complementary metal oxide semiconductor (BiCMOS) application specific integrated circuit (ASIC) and silicon-on-silicon packaging technologies are used to achieve the high performance in a miniaturized package. A Mips R4000-family reduced instruction set computer (RISC) processor and a TI 100-MHz BiCMOS vector coprocessor (VCP) ASIC provide, respectively, the 100 MIPS of a scalar processor throughput and 400 MFLOPS of vector processing throughput for each BPM. The TI Aladdim ASIC chipset was developed on the TI Aladdin Program under contract with the U.S. Army Communications and Electronics Command and was sponsored by the Advanced Research Projects Agency with technical direction from the U.S. Army Night Vision and Electro-Sensors Directorate. Author

N95-20639# Bell Telephone Labs., Inc., Whippany, NJ.
PACKAGING THE MAMA MODULE c33
J. Dennis Seals *In* AGARD, Advanced Packaging Concepts for Digital Avionics Oct. 1994 7 p Prepared in cooperation with Army Night Vision Labs (For primary document see N95-20631 06-06)
Copyright Avail: CASI HC A02/MF A03

The MAMA (Mixed Arithmetic, Multiprocessing Array) module is being developed to evaluate new packaging technologies and processing paradigms for advanced military processing systems. The architecture supports a tight mix of signal, data,and I/O processing at GFLOP throughput rates. It is fabricated using only commercial-on-the-sehlf (COTS) chips and will provide a high level of durability. Its attributes are largely the result of two new interconnection and packaging technologies. Chip-in-board packaging is used to reduce local x-y communication delays and solder joints, while significantly improving board-level packaging density. A unique 3-D interconnection technology called a cross-over cell has been developed to reduce board-to-board communication delays, drive power, glue logic, and card-edge pin-outs. These technologies enable true 3-D structures that are form, fit and connector compatible with conventional line-replacable modules. The module's design rational, packaging technology, and basic architecture will be presented in this paper. Author

N95-20640# Army Research Lab., Fort Monmouth, NJ.
THE DEMISE OF PLASTIC ENCAPSULATED MICROCIRCUIT MYTHS c33
E. B. Hakim, R. K. Agarwal (Delco Electronics, Kokomo, IN.), and M. Pecht (Maryland Univ., College Park, MD.) *In* AGARD, Advanced Packaging Concepts for Digital Avionics Oct. 1994 7 p (For primary document see N95-20631 06-06)
Copyright Avail: CASI HC A02/MF A03

Production of microelectronic devices encapsulated in solid, molded plastic packages has rapidly increased since the early 1980's. Today, millions of plastic-encapsulated devices are produced daily. On the other hand, only a few million hermetic (cavity) packages are produced per year. Reasons for the increased use of plastic-encapsulated packages include cost, availability, size, weight, quality, and reliability. Markets taking advantage of this technology range from computers and telecommunications to automotive uses. Yet, several industries, the military in particular, will not accept such devices. One reason for this reluctance to use the best available commercial parts is a perceived risk of poor reliability, derived from antiquated military specifications, standards, and handbooks; other common justifications cite differing environments; inadequate screens; inadequate test data, and required government audits of suppliers' processes. This paper describes failure mechanisms associated with plastic encapsulation and their elimination. It provides data indicating the relative reliability of cavity and solid-encapsulated packaging, and presents possible approaches to assuring quality and reliability in the procuring and applying this successful commercial technology. Author

N95-20641# GEC-Marconi Research Centre, Great Baddow (England).
MCMs FOR AVIONICS: TECHNOLOGY SELECTION AND INTERMODULE INTERCONNECTION
N. Chandler, I. R. Croston, S. G. Tyler, T. G. Hamill (GEC-Marconi Avionics Ltd., Rochester, England.), and P. E. Holbourn (GEC-Marconi Avionics Ltd., Edinburgh, Scotland.) *In* AGARD, Advanced Packaging Concepts for Digital Avionics Oct. 1994 15 p Sponsored by European Commission (For primary document see N95-20631 06-06)
Copyright Avail: CASI HC A03/MF A03

There are already several Multi Chip Module (MCM) technologies suitable for avionics applications, and new variations and updates are continually being added. The optimum technology choice for each avionics application will depend on many factors, including the electrical and thermal requirements, the operating environment, size, weight, quantity, cost, etc. This paper will compare the attributes of the various MCM technologies, both at present and future trends, including 3D assembly/packaging and the use of active substrates for MCM-D's. The means of mounting MCM's and interconnecting them into the system using electrical or optical interconnection will also be compared. Some of the methods used to remove very high levels of power dissipation will also be discussed, in relation to the different technologies. The requirements of electronic modules in different parts of avionics systems may be sufficiently different that alternative solutions are optimal for the various parts. The paper will briefly review the range of requirements across military (and comparable civil) avionics systems and, by considering the technology options, indicate how the optimum choice can be decided, both for the MCM's themselves and for the means of interconnection between MCM's and from MCM's to other parts of the system. Author

N95-20642# Naval Air Warfare Center, Indianapolis, IN. Standard Hardware Acquisition and Reliabilty Program.
ADVANCED STANDARD ELECTRONIC MODULES FORMAT-E (SEM-E) PROCESSES FOR RAPID PROTOTYPING c33
Anthony Hawkins *In* AGARD, Advanced Packaging Concepts for Digital Avionics Oct. 1994 11 p (For primary document see N95-20631 06-06)
Copyright Avail: CASI HC A03/MF A03

The objective of the 'Advanced SEM Processes' effort is to simplify the development and qualification processes and reduce the related process times and costs from the current way of doing business. Advanced technology developments and qualifications typically are completed in three to five years from conception. The Standard Hardware Acquisition and Reliability Program (SHARP) is working in conjunction with the Advanced Research Project Agency (ARPA) Application Specific Electronic Modules (ASEM) effort, Raytheon and the Electronics Manufacturing Producibility Facility (EMPF) Manufacturing Technology efforts to define new processes for development and qualification that leverage commercial and military technology in applying 'MultiChip Modules' (MCM's) to Standard Electronic Module format E (SEM-E) packaging. These processes are anticipated to have applicability to the development and qualification of SEM-E packaging, using multiple state of the art technologies in addition to MCM's. The primary objective is to reduce the current cycle time from three - five years to twelve months and costs from $500,000 - $1,000,000 to $100,00 - $250,000, therefore providing a baseline for standardizing electronics hardware acquisition processes into the twenty first century and beyond. Author

N95-20643# Rome Lab., Griffiss AFB, NY.
RELIABILITY ASSESSMENT OF MULTICHIP MODULE TECHNOLOGIES VIA THE TRISERVICE/NASA RELTECH PROGRAM c38
Daniel F. Fayette *In* AGARD, Advanced Packaging Concepts for Digital Avionics Oct. 1994 9 p (For primary document see N95-20631 06-06)
Copyright Avail: CASI HC A02/MF A03

Multichip Module (MCM) packaging/interconnect technologies have seen increased emphasis from both the commercial and military communities as a means of increasing capability and performance while providing a vehicle for reducing cost, power and weight of the end item electronic application. This is accomplished through three basic Multichip module technologies, MCM-L that are laminates, MCM-C that are ceramic type substrates and MCM-D that are deposited substrates (e.g., polymer dielectric with thin film metals). Three types of interconnect structures are also used with these substrates and include, wire bond, Tape Automated Bonds (TAB) and flip chip ball bonds. Application, cost, producibility and reliability are the drivers that will determine which MCM technology will best fit a respective need or requirement. With all the benefits and technologies cited, it would be expected that the use of, or the planned use of, MCM's would be more extensive in both military and commercial applications. However, two significant roadblocks exist to implementation of these new technologies: the absence of reliability data and a single national standard for the procurement of reliable/quality MCM's. To address the preceding issues, the Reliability Technology to Achieve Insertion of Advanced Packaging (RELTECH) program has been established. This program, which began in May 1992, has endeavored to evaluate a cross section of MCM technologies covering all classes of MCM's previously cited. NASA and the Tri-Services (Air Force Rome Laboratory, Naval Surface Warfare Center, Crane IN and Army Research Laboratory) have teamed together with sponsorship from ARPA to evaluate the performance, reliability and producibility of MCM's for both military and commercial usage. This is done in close cooperation with our industry partners whose support is critical to the goals of the program. Several tasks are being performed by the RELTECH program and data from this effort, in conjunction with information from our industry partners as well as discussions with industry organizations (IPC, EIA, ISHM, etc.) are being used to develop the qualification and screening requirements for MCM's. Specific tasks being performed by the RELTECH program include technical assessments, product evaluations, reliability modeling, environmental testing, and failure analysis. This paper will describe the various tasks associated with the RELTECH program, status, progress and a description of the national dual use specification being developed for MCM technologies. Author

N95-20644# Rome Lab., Griffiss AFB, NY.
ASSURING KNOWN GOOD DIE (KGD) FOR RELIABLE, COST EFFECTIVE MCMs c33
Daniel E. Daskiewich *In* AGARD, Advanced Packaging Concepts for Digital Avionics Oct. 1994 7 p (For primary document see N95-20631 06-06)
Copyright Avail: CASI HC A02/MF A03

A key requirement for achieving high yield multichip modules (MCM's) is assuring that the individual dice are known good devices (KGD). A KGD is defined as a bare die available at the same quality and reliability as the equivalent single chip packaged parts. Integrated circuits (IC's) that are Known Good will function over a specified temperature range, are compatible with the MCM approach utilized, and contain no short-term or long-term reliability hazards. The application of reliability and testability techniques at all levels of MCM development, particularly at the chip level, will maximize MCM yield. Today's testing and qualification requirements, defined by MIL-STD-883 Methods 5008 and 2010, are not capable of assuring KGD as defined above. The development of cost effective requirements for achieving 99.9 percent yields poses a challenge which requires new and novel approaches and better methods for bare die testing, wafer level burn-in, tape automated bonding (TAB), temporary packaging, at-speed device testing at the wafer, die, and MCM level. Also of great importance are the methods for built-in self test (BIST), built-in test (BIT), and boundary scan. New standards in very large scale integration (VLSI) device testing must be developed in order for MCM's to be reliable and economical. Rome Laboratory (RL) has funded a program to address and develop these requirements. The objectives of the RL program are to: research and evaluate current and proposed burn-in, electrical and interconnect test techniques for assuring known good VLSI circuits at wafer and die level; and evaluate various methods of incorporating testability features which will decrease test time and cost. In addition, MCM-level reliability and performance assessment procedures will be evaluated to determine appropriate testing concepts and procedures that will assure the procurement of reliable, cost effective MCM's for DOD/NASA applications. The program consists of two phases: Phase One will be a study phase to evaluate, analyze, trade-off, and select best techniques for test and burn-in of wafers, bare die and MCM's. Phase Two will be a demonstration of a cost effective procedure for assuring high quality/reliable production of MCM's based on the KGD methods developed in Phase One. Author

N95-20645# Lucas Electronics, Birmingham (England).

THE DESIGN AND MANUFACTURING DEVELOPMENT OF AN ACTIVE SILICON SUBSTRATE MCM c33

M. G. Roughton and L. Waite *In* AGARD, Advanced Packaging Concepts for Digital Avionics Oct. 1994 7 p Sponsored by DTI (For primary document see N95-20631 06-06)

Copyright Avail: CASI HC A02/MF A03

The demand for engine control systems with reduced weight, size and cost, increased integration, improved reliability and higher temperature operation drives the system designer to the use of advanced hybrid assembly technologies. This paper describes the design and manufacturing development of a silicon based 'D' type multichip module, MCM, containing an active substrate of memory. This CPU module is one of the building blocks for a range of generic engine control systems. The active substrate approach potentially gives higher packing density than wafer scale due to its 3D configuration. The active substrate comprises 12 SRAM 128K x 8 bit of diffused memory arranged in groups of three. The design is organized so that a 'memory manager' ASIC selects pages of good memory from the substrate die thus obtaining the best possible yield. A single wafer contains 4 silicon hybrid substrates, each approximately 40mm sq, which will be processed before separating into discrete circuits. The MCM structure is comprised of four aluminium metallization layers with benzocyclobutene, BCB, as the dielectric. Approximately 16 other devices including a processor, the 'memory manager' ASIC, a Processor Support ASIC and EDPROM, plus resistor network chips and decoupling capacitors will be added to the silicon substrate using adhesive and wire bond interconnection. The 'memory manager' ASIC tests the RAM on power-up, reject areas of bad memory and configures the good areas such that a continuous block of functional RAM is available to the processor. The RAM is configured as a 16 bit wide with both 16 bit and 8 bit read/write accesses being supported. The total module is to be assembled in a high temperature co-fired ceramic package with 200 I/O. After test and any rework that may be necessary the package will be sealed with a Kovar lid ready for final test. Author

N95-20646# Westinghouse Electric Corp., Baltimore, MD.

HIGH DENSITY MONOLITHIC PACKAGING TECHNOLOGY FOR DIGITAL/MICROWAVE AVIONICS c15

Timothy Fertig, Theresa Walter, Eric Gaver, and Kevin Leahy *In* AGARD, Advanced Packaging Concepts for Digital Avionics Oct. 1994 12 p (For primary document see N95-20631 06-06)

Copyright Avail: CASI HC A03/MF A03

There has been a need for generic technologies and common approaches in design, development, and manufacturing of military and commercial products. This need is more pronounced and pressing today than ever before. With the objective to dramatically enhance avionics reliability, maintainability and availability (RM&A), an integrated, generic technology for packaging, cooling, and interconnection of high density and high performance circuits was developed. It is named High Density Monolithic Packaging (HDMP). Under the sponsorship of Wright Laboratory, a two-part complementary program (1990-1994), named Advanced Radio-Frequency Packaging/ARFP was contracted to Westinghouse. Under the ARFP program, the HDMP technology is being applied and its promising capability is being assessed for its ability to reduce the low power RF avionics life-cycle cost. Being better than half way through the program, the results and projections have been extremely promising. The technology assessment is approximately 50 percent complete and initial results have been extremely successful. Although the focus of the development effort has been on RF subsystems, the basic elements of HDMP technology have applications beyond RF/microwave subsystems. As digital processing speeds increase, RF/microwave design techniques must be applied to maintain high speed digital signal integrity. The basic elements of the HDMP technology are: low temperature co-fired ceramic (LTCC), solderless interconnects, multichip modules (MCM's), and composite heatsink materials. The key technology element, in this avionics availability enabling technology, is LTCC. LTCC material technology is a monolithic multilayered ceramic and conductor/metallization structure used as a substrate to support dense co-habitation of high density electronic circuits, their interconnections, and the electromechanical integrity of the integrated constituents. Author

N95-20647# Maryland Univ., College Park, MD. CALCE Electronic Packaging Research Center.

LIQUID FLOW-THROUGH COOLING OF ELECTRONIC MODULES c34

S. Sridhar, M. D. Osterman, J. M. Carbonell (Wright Lab., Wright-Patterson AFB, OH.), and K. E. Herold *In* AGARD, Advanced Packaging Concepts for Digital Avionics Oct. 1994 6 p Sponsored by Westinghouse Electric Corp. and AMRL (For primary document see N95-20631 06-06)

Copyright Avail: CASI HC A02/MF A03

Thermal management of future avionics modules will be a critical design issue. New advances in integrated circuit technology and electronic packaging will allow the design of densely populated electronics modules with potential power dissipation levels in excess of 1.0 W/cm(exp 2). While the module power level trend will be to increase, the maximum allowable junction temperature for integrated circuits may be lowered to provide more benign thermal environment for electronics. This negates the use of conventional thermal management techniques in new avionics applications. A number of trade studies were performed to determine which cooling technique would be best suited to meet the anticipated reliability and performance requirements for the year 2005 and beyond. The approaches to module cooling technologies considered were: edge cooled conduction, immersion, and hollow core flow-through. The technology selected was the hollow core flow-through. This paper discusses the results of flow-through cooling investigations on both single-pass cold plates and SEM-E modules. Author

N95-20648# Naval Air Warfare Center, Indianapolis, IN. Aircraft Div.

IMMERSION/TWO PHASE COOLING c34

Jack Jones and Emmett Perkoski *In* AGARD, Advanced Packaging Concepts for Digital Avionics Oct. 1994 11 p (For primary document see N95-20631 06-06)

Copyright Avail: CASI HC A03/MF A03

Due to increasing heat dissipation requirements, the need for an advanced cooling technique in current military avionics has been recognized. Immersion cooling with phase change has been demonstrated in a Format E clamshell module as an alternative. This module is capable of dissipating more than 700 Watts. From the development of the Format E clamshell module the AAS&T (Advanced Avionics Subsystems and Technology) Program has begun an effort to utilize the clamshell module in the development of a 3/4 ATR Format E Standard Avionics Enclosure utilizing immersion/change of phase cooling. The power dissipation requirement for the enclosure is 6500 Watts minimum. The cooling medium for both efforts is a Fluorinert (FS-72). The FS-72 is an environmentally safe coolant. As the need for greater heat removal and reliability increases, cooling technology must become more advanced to meet the needs of next generation aircraft. Author

N95-20649# Deutsche Aerospace A.G., Munich (Germany). Military Aircraft Div.

MICROCHANNEL HEAT PIPE COOLING OF MODULES c34

G. Moser *In* AGARD, Advanced Packaging Concepts for Digital Avionics Oct. 1994 12 p (For primary document see N95-20631 06-06)

Copyright Avail: CASI HC A03/MF A03

The purpose of this presentation is the proposal of a novel, highly sophisticated cooling technique with a promising performance, but with a very early status of development - the microchannel heat pipe cooling. This technique can be directly adapted to the basic idea of Modular Avionics resulting on the hardware side in a modular packaging design with interchangeable modules. Due to the early status of the development and of the basic research some of the very stringent requirements for military airborne equipment are not met yet (or information is missing) like the impact of acceleration and orientation; nevertheless, the normal performance capability is highly compliant with the dramatically increasing local maximum heat densities and total maximum heat dissipations, which are forecast for future avionic applications. The presentation shall highlight the status of the development and the benefits of this technique; the latter is done by a comparison to the well established cooling methods for the module like Liquid Flow Through (LFT) and conduction cooling, in order to provide a clear impression of the cooling capabilities. Especially if the microchannel heat pipe is combined with a micro heat exchanger for the heat transfer off the module, the performance with respect to the maximum local heat density, the most challenging requirement for the future, is high in excess of the LFT method. Author

N95-20650# Naval Air Warfare Center, Warminster, PA. Aircraft Div.
THE IEEE SCALABLE COHERENT INTERFACE: AN APPROACH FOR A UNIFIED AVIONICS NETWORK
Ralph Lachenmaier and Thomas Stretch (AMPAC, Inc., Norristown, PA.) *In* AGARD, Advanced Packaging Concepts for Digital Avionics Oct. 1994 10 p (For primary document see N95-20631 06-06)
Copyright Avail: CASI HC A02/MF A03

The U.S. Navy Next Generation Computer Resources (NGCR) High Speed Data Transfer Network (HSDTN) program has chosen the IEEE Scalable Coherent Interface (SCI) as one of its baseline standards. This paper proposes to use SCI as a unified avionics network and describes SCI and extensions to it -- particularly an extension known as SCI/ Real Time (SCI/RT). Because SCI can be used in a serial configuration, such a network provides an alternative to the need for ever denser and ever more reliable backplane connectors by reducing the number and size of interconnects and, hence, the need for large numbers of pins. In addition, SCI reduces packaging problems by using a small amount of board real estate and by using distance insensitive links which can extend board to board or box to box, thus facilitating a distributed backplane approach for retrofit aircraft applications. SCI is currently being applied to both parallel and to serial implementations, to both message passing and shared memory computing paradigms, and to both electrical and optical physical layers. SCI/RT is a set of proposed enhancements, developed initially by the Canadian Navy and now being evaluated by the NGGR HSDTN and IEEE working groups, to make SCI more fault tolerant and to provide the determinism and priorities necessary to support Rate Monotonic Scheduling. Addition of these features will allow SCI to perform in a unified and seamless manner, the functions of command and control interconnect, data flow network and sensor/video network. Electrical and optical, and serial and parallel links can be intermixed for the most cost effective solution. As an added benefit, SCI has potential for use interconnecting multiple processing chips on the same board. Author

N95-20651# Naval Air Warfare Center, Warminster, PA. Aircraft Div.
A TECHNIQUE FOR INCREASING THE BANDWIDTH OF HIGH PERFORMANCE ELECTRICAL BACKPLANES **c33**
W. Rosen, S. Rajan, V. Gershman, and M. Shadaram (Texas Univ., El Paso, TX.) *In* AGARD, Advanced Packaging Concepts for Digital Avionics Oct. 1994 4 p (For primary document see N95-20631 06-06)
Copyright Avail: CASI HC A01/MF A03

This paper presents an active matching technique for extending the data rates of electrical backplane interconnects into the gigabit per second (Gb/s) range. In the active matching technique an active bandpass amplifier is used to drive the backplane transmission lines. The gain characteristic of the amplifier is designed to be complementary to that of the transmission line and connectors using standard microwave matching techniques. This technique is suitable for use with conventional stripline and microstrip backplanes as well as newer microcoaxial cables. Using this technique, backplanes operating at serial data rates in excess of 4 Gb/s have been demonstrated and speeds of 10 Gb/s may be possible. These results suggest that electrical backplanes may be competitive with optical backplanes in speed and superior to them in cost, power consumption, and complexity. Author

N95-20652# Deutsche Aerospace A.G., Munich (Germany). Military Aircraft Div.
OPTICAL BACKPLANE FOR MODULAR AVIONICS **c74**
R. Bogenberger and O. Krumpholz *In* AGARD, Advanced Packaging Concepts for Digital Avionics Oct. 1994 6 p (For primary document see N95-20631 06-06)
Copyright Avail: CASI HC A02/MF A03

An experimental study was carried out by DASA and Daimler Benz Research to demonstrate the feasibility of fiber optic technology for use in Modular Avionics. In the first step of the study an inter module communication up to 16 subscribers, with interconnection length of about 1 m was demonstrated. Backplanes being composed of multimode and monomode fibers were tested in a configuration of 4 parallel data channels, each running with 1 GBit/s. This paper will resume results of investigations as: power budget, influence of modal noise with multimode fibers, effects of feedback, as well as optical interference caused by reflections. The paper then goes on to describe the transparency for given protocols (e.g., PI-bus). A prospect of problems arising of optical interconnections of a relatively large number of subscribers and possible solutions by using in-line amplifiers (optically) are reviewed. The backplane implementation is prepared to be arranged as a serial/parallel bus or a part of a switched network. Finally, this paper will give a synopsis of optical backplane solutions. Author

N95-20653# GEC-Marconi Materials Technology, Towcester (England).
HIGH PERFORMANCE BACKPLANE COMPONENTS FOR MODULAR AVIONICS **c33**
C. J. Groves-Kirkby, M. J. Goodwin, J. P. Hall, G. Glynn, J. Hankey, M. D. Salik, R. C. Goodfellow, and D. J. Jibb (GEC-Marconi Avionics Ltd., Chelmsford, England.) *In* AGARD, Advanced Packaging Concepts for Digital Avionics Oct. 1994 6 p (For primary document see N95-20631 06-06)
(ESPRIT 3 Proj. 6276)
Copyright Avail: CASI HC A02/MF A03

The design and development of optoelectronic transceiver and optical pathway components for application in a modular avionics backplane demonstrator system are described and initial performance results are presented. Author

N95-20654# Bell Telephone Labs., Inc., Whippany, NJ.
THE ROC OPTICAL CONNECTOR **c74**
Richard J. Pimpinella and J. Dennis Seals *In* AGARD, Advanced Packaging Concepts for Digital Avionics Oct. 1994 6 p (For primary document see N95-20631 06-06)
(Contract F33615-89-C-1036)
Copyright Avail: CASI HC A02/MF A03

The new multimode connector has been developed that will function under harsh environmental conditions. It meets the military's need for a reliable optical insert that can be integrated into existing electrical, card-edge connectors. Expanded-beam optics and micro-machined silicon sub-assemblies are employed to achieve low optical loss (less than 1 dB) under blind-mate conditions. Low-mass, floating termini and kinematic design make the ROC connector insensitive to high levels of shock and vibration. Self sealing doors protect the optical assemblies from particulate contamination and abusive handling. The connector has performed flawlessly under extensive environmental and durability testing. This paper will describe the ROC design, features, and test results. Author

N95-20655# Thomson-CSF, Paris (France). Div. Radars et Contre-Mesures.
COMPOSITE CASES FOR AIRBORNE ELECTRONIC EQUIPMENT: A TECHNOLOGY STUDY AND EMC [BOITIERS COMPOSITES POUR EQUIPEMENTS ELECTRONIQUES AEROPORTES: UNE ETUDE TECHNOLOGIQUE ET CEM] **c24**
B. Dumont, J. Lecuellet, S. Laforet, G. Labaune, and M. Caplot *In* AGARD, Advanced Packaging Concepts for Digital Avionics Oct. 1994 12 p In FRENCH (For primary document see N95-20631 06-06)
Copyright Avail: CASI HC A03/MF A03

The goal of this paper is to present work related to the development (study, fabrication, qualification) of a box and a bonnet cover out of composite materials intended for airborne electronic equipment on fighter aircraft. Work was undertaken with a double objective: assess mass characteristics compared to a metal case and obtain equivalent electromagnetic shielding performance. The technological step is presented: choice of materials and the processes of fabrication, mechanical and electromagnetic dimensioning. The methods of manufacture are described; they made it possible to obtain the desired characteristics. The metal composite material elements are currently being used on fighter aircraft. Transl. by CASI

N95-20656# Sextant Avionique, Valence (France).
LIGHTWEIGHT ELECTRONIC ENCLOSURES USING COMPOSITE MATERIALS **c24**
C. Sarno *In* AGARD, Advanced Packaging Concepts for Digital Avionics Oct. 1994 12 p Sponsored by Ministry of Defence (For primary document see N95-20631 06-06)
Copyright Avail: CASI HC A03/MF A03

The ever increasing demand in technical and economical performances improvement of aircrafts has a direct incidence for avionics. Except microelectronic integration, the enclosures have a high potential of evolution. The main advantages of composite materials over metals in forming electronic enclosure are: reduction of weight (minimum 30 percent), better resistance to corrosion, improved fatigue and impact resistance, achievement of complex shapes, and low coefficient of thermal expansion. The main problems to be solved in extending the application of the use of composite materials to the field of airborne electronic equipments are to: provide adequate electromagnetic shielding, ensure survival in harsh thermal and mechanical environments, and achieve global competitivity of the final products. Different technologies have been considered: injection molding of short fibers reinforced thermoplastic for small sized equipments (V less than 21), pressure molding of graphite and glass reinforced thermosets for ATR case families, and metal matrix composites. This paper will address the main investigations that have been undertaken in France since 1986 in the first two fields covering both manufacturing and evaluation results. Author

N95-20657# Thomson-CSF, Paris (France). Div. Radars et Contre-Mesures.
MODULAR SUPPLIES FOR A DISTRIBUTED ARCHITECTURE [ALIMENTATIONS MODULAIRES POUR UNE ARCHITECTURE DISTRIBUEE]
A. Moreau, J. M. Rey, M. Caplot, and J. P. Delvinquier *In* AGARD, Advanced Packaging Concepts for Digital Avionics Oct. 1994 12 p In FRENCH (For primary document see N95-20631 06-06)
Copyright Avail: CASI HC A03/MF A03

Future avionics systems will be based on a modular architecture in which each elementary function will correspond to a line replacable module (LRM). Parametric studies, such as FASTPACK, showed that the optimal solution for the supply systems was an architecture distributed on only one level of energy transformation, i.e., a modular supply on each LRM able to deliver 50 W with 100 W directly starting from the main supply system (270 V(dc) or three-phase network 200 V/400 rectified Hz). In order to obtain a coherent level of integration of the digital circuits, it was necessary to develop such modular supplies with a power density of about 1500 W/dm(sup 3) per unit of volume. In addition, so that these supplies can be established directly on a LRM simple face, their thickness had to be limited to 6.8 mm (case included/understood). To achieve this goal, a total integration that guaranteed the performances of the electric supplies, high frequency hybrid converters (of the order of MHz) were developed. After a presentation of the advantages of an architecture of distributed supply and a review of the main technical aims, this article describes the techniques and technologies implemented to achieve these goals. A thorough description of the developed modular supplies is given for delivered powers ranging between 50 W and 100 W and for various output voltages. Finally, the future developments planned to reach a power density of 4000 W/dm(sup 3) per unit of volume are reviewed. Transl. by CASI

N95-20658# Alenia, Turin (Italy). Div. Avionica Apparati Speciali.
ELECTROMAGNETIC COMPATIBILITY EFFECTS OF ADVANCED PACKAGING CONFIGURATIONS **c32**
B. Audone, L. Bolla, and D. Tarducci *In* AGARD, Advanced Packaging Concepts for Digital Avionics Oct. 1994 5 p (For primary document see N95-20631 06-06)
Copyright Avail: CASI HC A01/MF A03

The Electromagnetic Compatibility (EMC) of digital avionic equipments assumes ever larger dimensions especially in the light of the tendency of modern technology aimed at higher data transmission rates and therefore higher clock frequencies and, at the same time, higher component density with reduced consumption. The emission and susceptibility problems commonly encountered in digital circuits are examined indicating critical areas and practicable suggestions to improve design techniques. Author

N95-20659# Rohde and Schwartz, Munich (Germany).
MODULAR CNI AVIONICS SYSTEM
P. H. Reitberger and G. Mey (Ministry of Defence, Bonn, Germany.) *In* AGARD, Advanced Packaging Concepts for Digital Avionics Oct. 1994 11 p (For primary document see N95-20631 06-06)
Copyright Avail: CASI HC A03/MF A03

Today's aircraft contain a multitude of different radio functions for communications, navigation and identification. The individual radio functions, like VHF/UHF, JTIDS/ MIDS, GPS or NIS, are each handled by an individual piece of equipment consisting of several LRU. In the absence of built-in redundancy, the failure of a single LRU can result in a failure of a radio function. In the future, individual radio functions need to be integrated in a modular system concept, the modular CNI system (communication - navigation - identification). Author

N95-22024# Science Applications International Corp., Dayton, OH.
SYSTEMS ENGINEERING DESIGN AND TECHNICAL ANALYSES FOR STRATEGIC AVIONICS CREW-STATION DESIGN EVALUATION FACILITY (SACDEF) Final Report, 15 Jan. 1988 - 14 May 1993
John D. Stengel, Harry Heaton, Steve Finch, James Hopper, and Teresa McKelvey May 1994 71 p
(Contract F33615-87-C-0531)
(AD-A286239; AL/CF-TR-1994-0074) Avail: CASI HC A04/MF A01

This report summarizes all work efforts completed under Contract F33615-87-C-0531, systems engineering design and technical analysis (SEDATA) for the Strategic Avionics Crew Station Design Evaluation Facility (SACDEF). This report consists of four main sections. Section 1 is an overview of SACDEF contract. Section 2 contains descriptions of specific tasks completed under the SEDATA for SACDEF contract. Section 3 contains conclusions and recommendations. Section 4 contains references, which includes reports and documentation produced under specific tasks of the contract. The Armstrong Laboratory has been involved in supporting the development and refinement of Strategic Bomber Crew Systems for almost 25 years. The SACDEF of the CFHI branch within the Human Engineering Division is responsible for research addressing crew station design and areas currently include aircrew workload evaluations, new control/display concepts, display device image quality, and electrophysiological correlates of crew performance. Specific emphasis is directed toward the development of advanced controls and displays for bomber aircraft, employing state-of-the-art, multifunctional display devices and computer programming techniques. An ongoing requirement has been to maintain the SACDEF B-52G Defensive Simulator and the B-1B Engineering Research Simulator (ERS) as designed, developed, tested, and delivered to Armstrong Laboratory under a previous contract. This report documents the work activities completed by Science Applications International Corporation for the SEDATA for SACDEF over the period 15 January 1988 through 14 May 1993. DTIC

N95-22036# PDA Engineering, Costa Mesa, CA.
RESPONSE OF THE B-1B AIR DATA SENSOR TO SIMULATED DUST CLOUD ENVIRONMENTS Technical Report, 17 Sep. 1992 - 15 Aug. 1993
Robert G. Oeding 1 Nov. 1994 106 p
(Contract DNA001-91-C-0021)
(AD-A286134; PDA-TR-1754-02-01; DNA-TR-93-164) Avail: CASI HC A06/MF A02

This report describes an experimental evaluation of the effects of dusty flow environments on the performance of the B-1B air data sensor (ADS). The evaluations were conducted in the DNA dust erosion facility which is located at PDA Engineering laboratories in Santa Ana, CA. The dust erosion facility was modified to provide a high speed dust jet with controlled moisture addition. Full-scale ADS probes were submerged in the dust flow and probe performance was monitored. Performance measurements included total, static, and angle-of-attack pressure outputs. Also pre- and post-test weights of the probes and pressure line dust filters were obtained in order to determine ingested particle mass. Both dry and wet flows included two levels of water addition to simulate cloud precipitation/moisture. The test configurations, procedures, and results are described. DTIC

N95-22232# Naval Postgraduate School, Monterey, CA.
EVALUATION OF THE HAWORTH-NEWMAN AVIONICS DISPLAY READABILITY SCALE M.S. Thesis
Charles F. Chiappetti Sep. 1994 63 p
(AD-A286127) Avail: CASI HC A04/MF A01

This study investigates the suitability of the Haworth-Newman Display Readability Rating Scale as a performance-based test and evaluation tool. This evaluation has been necessary to determine if the scale actually measures display readability, and if consistent, reproducible results are attainable. Background information on the scale's development is presented along with a brief description of display readability characteristics. A technique for systematic degradation of display readability and a method of displaying degraded symbology sets is introduced. A flight simulation experiment was conducted to obtain performance data, Haworth-Newman readability ratings, and participants' written comments for each of the degraded symbology set levels. Five Naval test pilots attempted to maintain specified heading, altitude, and airspeed while utilizing the ten levels of symbology sets and then used the Haworth-Newman scale to rate the display readability for each. Experimental results are discussed and recommendations presented. DTIC

07 AIRCRAFT PROPULSION AND POWER

Includes prime propulsion systems and systems components, e.g., gas turbine engines and compressors; and onboard auxilliary power plants for aircraft.

For related information see also *20 Spacecraft Propulsion and Power, 28 Propellants and Fuels,* and *44 Energy Production and Conversion.*

N95-21243# General Electric Co., Schenectady, NY. Composite and Structural Ceramics Program.
TOUGHENED SILCOMP COMPOSITES FOR GAS TURBINE ENGINE APPLICATIONS Final Report, Apr. 1992 - Jun. 1994
G. S. Corman, K. L. Luthra, M. K. Brun, and P. J. Meschter Jul. 1994 115 p
(Contract DE-FC02-92CE-41000)
(DE95-002851; DOE/CE-41000/2) Avail: CASI HC A06/MF A02

The two main factors driving the development of new industrial gas turbine engine systems are fuel efficiency and reduced emissions. One method of providing improvements in both areas is to reduce the cooling air requirements of the hot gas path components. For this reason ceramic components are becoming increasingly attractive for gas turbine applications because of their greater refractoriness and oxidation resistance. Among the ceramics being considered, continuous fiber ceramic composites (CFCC's) are leading candidates because they combine the high temperature stability of ceramics with the toughness and damage tolerance of composites. The purpose of this program, which is part of DOE's CFCC initiative, is to evaluate the use of CFCC materials as gas turbine engine components, and to demonstrate the feasibility of producing such components from Toughened Silcomp composites. Toughened silcomp is a CFCC material made by a reactive melt infiltration process, and consists of continuous SiC reinforcing fibers, with an appropriate fiber coating, in a fully dense matrix of SiC and Si. Based on the material physical properties, the material/process improvements realized in Phase 1, and the preliminary design analyses from Task 1, they feel the feasibility of fabricating Toughened Silcomp with the requisite physical and mechanical properties for the intended applications has been demonstrated. Remaining work for Phase 2 is to further improve the system for enhanced oxidation resistance, incorporate additional process controls to enhance the reproducibility of the material, transition the fabrication process to the selected vendors for scale-up, develop a more complete material property data base, including long-term mechanical behavior, and fabricate and test preliminary 'representative part' specimens. DOE

N95-21383*# National Aeronautics and Space Administration. Lewis Research Center, Cleveland, OH.
TWO-DIMENSIONAL IMAGING OF OH IN A LEAN BURNING HIGH PRESSURE COMBUSTOR
R. J. Locke (NYMA, Inc., Brook Park, OH.), Y. R. Hicks, R. C. Anderson, K. A. Ockunzzi (Ohio Aerospace Inst., Cleveland, OH.), and G. L. North (Army Research Lab., Cleveland, OH.) Feb. 1995 16 p Presented at the 33rd Aerospace Sciences Meeting and Exhibit, Reno, NV, 9-12 Jan. 1995; sponsored byAIAA Original contains color illustrations
(Contract NAS3-27186; RTOP 537-02-21)
(NASA-TM-106854; E-9444; NAS 1.15:106854; AIAA Paper 95-0173)
Avail: CASI HC A03/MF A01; 5 functional color pages

Planar laser-induced fluorescence (PLIF) images of OH have been obtained from an optically accessible, lean burning high pressure combustor burning Jet-A fuel. These images were obtained using various laser excitation lines of the OH A (reverse arrow) X (1,0) band for several fuel injector configurations with pressures ranging from 1013 kPa (10 atm) to 1419 kPa (14 atm). Non-uniformities in the combusting flow, attributed to differences in fuel injector configuration, are revealed by these images. Contributions attributable to fluorescent aromatic hydrocarbons and complex fuel chemistries are also not evident. Author

N95-22341*# National Aeronautics and Space Administration, Washington, DC.
TURBINE DESIGN AND APPLICATION
Arthur J. Glassman, ed. (National Aeronautics and Space Administration. Lewis Research Center, Cleveland, OH.) Cleveland, OH Jun. 1994 390 p
(NASA-SP-290; E-5666; NAS 1.21:290; LC-94-67487) Avail: CASI HC A17/MF A04

NASA has an interest in turbines related primarily to aeronautics and space applications. Airbreathing turbine engines provide jet and turboshaft propulsion, as well as auxiliary power for aircraft. Propellant-driven turbines provide rocket propulsion and auxiliary power for spacecraft. Closed-cycle turbine engines using inert gases, organic fluids, and metal fluids have been studied for providing long-duration electric power for spacecraft. Other applications of interest for turbine engines include land-vehicle (cars, trucks, buses, trains, etc.) propulsion power and ground-based electrical power. In view of the turbine-system interest and efforts at Lewis Research Center, a course entitled 'Turbine Design and Application' was presented during 1968-69 as part of the In-house Graduate Study Program. The course was somewhat revised and again presented in 1972-73. Various aspects of turbine technology were covered including thermodynamic and fluid-dynamic concepts, fundamental turbine concepts, velocity diagrams, losses, blade aerodynamic design, blade cooling, mechanical design, operation, and performance. The notes written and used for the course have been revised and edited for publication. Such a publication can serve as a foundation for an introductory turbine course, a means for self-study, or a reference for selected topics. Any consistent set of units will satisfy the equations presented. Two commonly used consistent sets of units and constant values are given after the symbol definitions. These are the SI units and the U.S. customary units. A single set of equations covers both sets of units by including all constants required for the U.S. customary units and defining as unity those not required for the SI units. Author

08 AIRCRAFT STABILITY AND CONTROL

Includes aircraft handling qualities; piloting; flight controls; and autopilots.

For related information see also *05 Aircraft Design, Testing and Performance.*

N95-20004# Wright Lab., Wright-Patterson AFB, OH.
SUMMARY OF A JOINT PROGRAM OF RESEARCH INTO AIRCRAFT FLIGHT CONTROL CONCEPTS Final Report, 1983 - 1992
Knut Wilhelm, Robert W. Woodcock, and David B. Leggett May 1993 83 p
(AF Proj. 2403)
(AD-A280012; WL-TR-94-3039) Avail: CASI HC A05/MF A01

The report summarizes the research work into aircraft flight control concepts carried out by WL and DLR under the MoU. Addressed are the methods and scientific approaches used for two subtasks as Pilot vehicle integration and In-Flight Simulation Methodologies. Main emphasis from WL is laid on the different projects performed on the NT-33 and TIFS In-Flight Simulators in order to identify the influence of various system related parameters on longitudinal and lateral handling qualities. The work done by DLR describes the specific technique to be used for ground attack tasks (GRATE) for handling quality research and the development and system identification of DLR's new In Flight Simulator ATTAS. DTIC

N95-21122 Charles River Analytics, Inc., Cambridge, MA.
A NEURAL EXPERT APPROACH TO SELF DESIGNING FLIGHT CONTROL SYSTEMS Final Report, 15 Jul. 1993 - 14 Jan. 1994
Sherif M. Botros, Alper K. Caglayan, and Greg L. Zacharias 21 Apr. 1994 70 p Limited Reproducibility: More than 20% of this document may be affected by microfiche quality
(Contract F49620-93-C-0050)
(AD-A279965; R93081; AFOSR-94-0310TR) Avail: CASI HC A04

Based on the simulations performed in this phase 1 study, we show that Hopfield and RBF feedfoward network architectures may have a great potential in the control of nonlinear systems. In particular, Hopfield implementation of Lagrange multiplier method is suitable for real-time adaptive optimal control. Similarly, RBF feedforward neural network architectures are suitable for learning inverse dynamics and inverse trim in aircraft FCS applications. In addition, RBF feedfoward are easier to train than backpropagation sigmoid networks since RBF formulation results in linear parameters. The initial simulations we performed show very promising results as exemplified by the small control errors in closed-loop Simulations using the nonlinear /A-18 longitudinal dynamics. Further studies are needed to test the applicability of the techniques to real world problems and to study the robustness, stability and general reliability of the proposed neural techniques. Neural networks by themselves cannot be the panacea to all the nonlinear control problems. An effort has to be made to incorporate all the available knowledge about the dynamics system to achieve good performance. DTIC

N95-21214# Wright Lab., Wright-Patterson AFB, OH.
PRESSURE MEASUREMENTS ON AN F/A-18 TWIN VERTICAL TAIL IN BUFFETING FLOW. VOLUME 4, PART 1: BUFFET CROSS SPECTRAL DENSITIES Final Report, 15 Apr. 1993 - 15 Aug. 1994
Chris Pettit, Dansen Brown, Michael Banford, and Ed Pendleton Aug. 1994 695 p See also AD-A285555
(AF Proj. 2401)
(AD-A285593; WL-TM-94-3112-Vol-4-Pt-1) Avail: CASI HC A99/MF A06

Buffeting pressure measurements were made on the vertical tail surface of a full scale F/A-18 aircraft model in the National Full Scale Aerodynamics Complex at NASA Ames Research Center. Test variables included aircraft angle-of-attack, aircraft sideslip angle, and dynamic pressure. Accelerometers were used to obtain vertical tail accelerations. Pressure transducers were mounted on the starboard vertical tail. Steady and unsteady pressures were obtained. Unsteady pressure data were reduced to PSD and CSD forms. Both steady and unsteady RMS pressure coefficients are also presented. Volume 1 contains the general description of the model, the test program, and highlights of the reduced data. Volume 2 contains steady and unsteady RMS data. Volume 3 contains unsteady PSD results. Volume 4 contains unsteady CSD results. DTIC

09 RESEARCH AND SUPPORT FACILITIES (AIR)

Includes airports, hangars and runways; aircraft repair and overhaul facilities; wind tunnels; shock tubes; and aircraft engine test stands.

For related information see also *14 Ground Support Systems and Facilities (Space).*

N95-19931# Army Research Inst. for the Behavioral and Social Sciences, Alexandria, VA.
USING THE BACKWARD TRANSFER PARADIGM TO VALIDATE THE AH-64 SIMULATOR TRAINING RESEARCH ADVANCED TESTBED FOR AVIATION Final Report, Jan. 1993 - Oct. 1993
John E. Stewart, II Sep. 1994 44 p
(AD-A285758; ARI-RR-1666) Avail: CASI HC A03/MF A01

The Simulator Training Research Advanced Testbed for Aviation (STRATA) is a modular simulation system for the AH-64 helicopter. The Adams and McAbee backward transfer of training paradigm was used to determine if AH-64 piloting skills transfer to STRATA. Ten AH-64 pilots participated in the experiment. They were asked to fly a mission scenario consisting of 13 single-pilot aircrew training manual (ATM) tasks. No orientation or practice sessions were given. Most participants rated STRATA as highly similar to the AH-64 in handling, but believed the visual display system had limitations for extremely low-altitude tasks like hovering. Performance ratings during the experiment by a senior instructor pilot (IP) indicated that of the total 130 task events, 88.5% were performed to ATM standards. After the experiment, four independent judges, all aviators, rank-ordered participant performance on the stationary hover task using output from STRATA's automated performance measurement system. Rankings showed agreement between judges and high correlation with IP ratings made during the experiment. DTIC

N95-19955# Army Engineer Waterways Experiment Station, Vicksburg, MS. Geotechnical Lab.
SUPER-HEAVY AIRCRAFT STUDY Final Report
Walter R. Barker and Carlos R. Gonzalez Apr. 1994 73 p
(AD-A279602; WES/TR/GL-94-12) Avail: CASI HC A04/MF A01

The test data for performance of flexible pavements were collected, sorted, and tabularized. The test data were analyzed using Boussinessq and layered elastic pavement models. To assist in the analysis, two computer programs were developed. The first program used the Boussinessq model to compute equivalent single-wheel loads. This program will compute the equivalent single-wheel load considering any selected cutoff distance. The second program used layered elastic theory for the analysis of pavements structures. The program has the capability of determining maximum pavement response for several response parameters, determining allowable loads for selected performance criteria, and computing a new layered elastic aircraft classification number. Several different performance criteria were developed including deflection criteria employing different cutoff distances, and strain criteria determined from the layered elastic pavement model. It was shown that deflection and strain criteria could be developed for the design of heavy multiwheel aircraft which would be independent of the number of tires in the aircraft gear. Performance criteria based on deflection, vertical strain, horizontal shear strain, maximum shear strain, and octahedral strain were incorporated into the layered elastic computer program to give predictions for pavement performance. Comparisons of the strain criteria were made with the current design criteria. DTIC

N95-20080*# National Aeronautics and Space Administration. Langley Research Center, Hampton, VA.
VAPOR GENERATOR WAND Patent Application
David B. Robelen, inventor (to NASA) 28 Nov. 1994 12 p
(NASA-Case-LAR-15058-1; NAS 1.71:LAR-15058-1; US-Patent-Appl-SN-359320) Avail: CASI HC A03/MF A01

In low speed wind tunnels it is often desirable to visualize airflow to augment observations made with instruments such as strain and pressure gages. Current technology devices for delivery of a vapor are bulky and thus disrupt local airflow. It is the object of this invention to provide a device capable of delivering a stream of vapor with a minimal effect on local airflow. The present invention achieves this object by utilizing a narrow tube as a heating device for producing the vapor. Running an electrical current through the tube provides resistive heating to a liquid which produces a vapor when boiled. As the entire heating and delivery portion of the device is simply a small cylinder the disruption to airflow within the tunnel is minimized. this allows an experimenter to place the source of vapor fairly close to a model without causing too much change to the model data. The novelty of the present invention lies in reducing the bulk of current technology devices by combining the acts of heating and delivery. Author

N95-20223# Sandia National Labs., Albuquerque, NM.
CHUNK PROJECTILE LAUNCH USING THE SANDIA HYPERVELOCITY LAUNCHER FACILITY
Lalit C. Chhabildas, Timothy G. Trucano, William D. Reinhart, and Clint A. Hall Jul. 1994 40 p
(Contract DE-AC04-94AL-85000)
(DE94-018494; SAND-94-1273) Avail: CASI HC A03/MF A01

An experimental technique is described to launch an intact 'chunk,' i.e. a 0.3 cm thick by 0.6 cm diameter cylindrical titanium alloy (Ti-6Al-4V) flyer, to 10.2 km/s. The ability to launch fragments having such an aspect ratio is important for hypervelocity impact phenomenology studies. The experimental techniques used to accomplish this launch were similar but not identical to techniques developed for the Sandia Hypervelocity Launcher

(HVL). A confined barrel impact is crucial in preventing the two-dimensional effects from dominating the loading response of the projectile chunk. The length to diameter ratio of the metallic chunk that is launched to 10.2 km/s is 0.5 and is an order of magnitude larger than those accomplished using the conventional hypervelocity launcher. The multidimensional, finite-difference (finite-volume), hydrodynamic code CTH was used to evaluate and assess the acceleration characteristics, i.e., the in-bore ballistics of the chunky projectile launch. A critical analysis of the CTH calculational results led to the final design and the experimental conditions that were used in this study. However, the predicted velocity of the projectile chunk based on CTH calculations was approximately 6% lower than the measured velocity of approximately 10.2 km/s. DOE

N95-20624 Carnegie-Mellon Univ., Pittsburgh, PA. School of Computer Science.

COLLECTED PAPERS OF THE SOAR/IFOR PROJECT, SPRING 1994 Technical Report

W. L. Johnson, Randolph M. Jones, David Keirsey, Frank V. Koss, and John E. Laird 25 Apr. 1994 105 p Limited Reproducibility: More than 20% of this document may be affected by microfiche quality
(Contract N00014-92-K-2015)
(AD-A280063; CMU-CS-94-134; CSE-TR-207-94; ISI/SR-94-379) Avail: CASI HC A06

Since the summer of 1992, the Soar/IFOR research group has been building intelligent automated agents for tactical air simulation. The ultimate goal of this project is to develop automated pilots whose behavior in simulated engagements is indistinguishable from that of human pilots. This technical report is a collection of the research papers that have been generated from this project as of Spring 1994. The research covered in these papers spans a wide spectrum of issues in agent development such as explanation, managing situational awareness, managing multiple interacting goals, coordination between multiple agents, natural language processing, developing believable agents, event tracking, and the infrastructure to support agent development, including knowledge acquisition and use, interfacing to simulation environments, and developing low cost simulators. DTIC

N95-20669*# National Aeronautics and Space Administration. Langley Research Center, Hampton, VA.

16-FOOT TRANSONIC TUNNEL TEST SECTION FLOWFIELD SURVEY

J. A. Yetter and W. K. Abeyounis Dec. 1994 92 p
(RTOP 538-05-13-01)
(NASA-TM-109157; NAS 1.15:109157) Avail: CASI HC A05/MF A01

A flow survey has been made of the test section of the NASA Langley Research Center 16-Foot Transonic Tunnel at subsonic and supersonic speeds. The survey was performed using five five-hole pyramid-head probes mounted at 14 inch intervals on a survey rake. Probes were calibrated at freestream Mach numbers from 0.50 to 0.95 and from 1.18 to 1.23. Flowfield surveys were made at Mach numbers from 0.50 to 0.90 and at Mach 1.20. The surveys were made at tunnel stations 130.6, 133.6, and 136.0. By rotating the survey rake through 180 degrees, a cylindrical volume of the test section 4.7 feet in diameter and 5.4 feet long centered about the tunnel centerline was surveyed. Survey results showing the measured test section upflow and sideflow characteristics and local Mach number distributions are presented. The report documents the survey probe calibration techniques used, summarizes the procedural problems encountered during testing, and identifies the data discrepancies observed during the post-test data analysis. Author

N95-20799# Aircraft Research Association Ltd., Bedford (England).

TESTING IN THE ARA TRANSONIC WIND TUNNEL

Dick Jordan Mar. 1994 48 p Original contains color illustrations
(ARA-Memo-395) Avail: CASI HC A03/MF A01

This note is an overview of the ARA 2.74 x 2.44m Transonic Wind Tunnel facility which covers the full Mach number range M = 0 to 1.4. A description of the main features of the tunnel circuit is given together with operational details. The test capabilities encompass a wide variety of model configurations which can be mounted on interchangeable full or half-span model carts. Load measurements are made using strain-gauge balances in conjunction with an appropriate sting or support strut. Several standard model support arrangements are provided but specialized rigs are frequently developed for particular requirements. High pressure air is available for tests involving propulsion simulation. An advanced data acquisition and data reduction system produces on-line corrected results which are presented on inter-active color graphic displays. Emphasis is placed on the consistently good flow quality in the working section, the high accuracy and repeatability of the aerodynamic measurements, the routine corrections incorporated in the data reduction, and the high productivity of testing in this tunnel. Author

N95-20992 Dayton Univ. Research Inst., OH.

COLOR CONTROL IN A MULTICHANNEL SIMULATOR DISPLAY: THE DISPLAY FOR ADVANCED RESEARCH AND TRAINING Final Report, Jun. 1990 - Jul. 1993

Celeste M. Howard Mar. 1994 35 p Limited Reproducibility: More than 20% of this document may be affected by microfiche quality
(Contract F33615-90-C-0005)
(AD-A279717; AL/HR-TR-1994-0024) Avail: Issuing Activity (Defense Technical Information Center (DTIC))

This report outlines the principles for color-matching of computer-generated imagery in displays made up of sectors served by several display devices. These principles are discussed with reference to a particular multichannel simulator display for which the display devices are projection cathode ray tubes. DTIC

N95-21436*# Purdue Univ., West Lafayette, IN. Aerospace Sciences Lab.

DEVELOPMENT OF QUIET-FLOW SUPERSONIC WIND TUNNELS FOR LAMINAR-TURBULENT TRANSITION RESEARCH Final Report, May 1990 - Dec. 1994

Steven P. Schneider Dec. 1994 55 p
(Grant NAG1-1133)
(NASA-CR-197286; NAS 1.26:197286) Avail: CASI HC A04/MF A01

This grant supported research into quiet-flow supersonic wind-tunnels, between May 1990 and December 1994. Quiet-flow nozzles operate with laminar nozzle-wall boundary layers, in order to provide low-disturbance flow for studies of laminar-turbulent transition under conditions comparable to flight. Major accomplishments include: (1) the design, fabrication, and performance-evaluation of a new kind of quiet tunnel, a quiet-flow Ludweig tube; (2) the integration of preexisting codes for nozzle design, 2D boundary-layer computation, and transition-estimation into a single user-friendly package for quiet-nozzle design; and (3) the design and preliminary evaluation of supersonic nozzles with square cross-section, as an alternative to conventional quiet-flow nozzles. After a brief summary of (1), a description of (2) is presented. Published work describing (3) is then summarized. The report concludes with a description of recent results for the Tollmien-Schlichting and Gortler instability in one of the square nozzles previously analyzed. Author

N95-21719# Test Devices, Inc., Hudson, MA.

PORTABLE STATIC TEST FACILITY FOR SMALL, EXPENDABLE, TURBOJET ENGINES, PHASE 1 Final Report

Borislav Milatovic 28 Oct. 1994 127 p
(Contract DAAH01-94-C-R032)
(AD-A286337) Avail: CASI HC A07/MF A02

Test Devices, Inc. has completed the preliminary design for the Portable Static Test Facility (PSTF) for small, expendable, turbojet engines (50 - 1000 lb thrust) as part of the Phase 1 effort under SBIR contract DAAH01-94-C-RO32. The goal of providing a preliminary design for a development and test facility at a reasonable cost, assembled from standard, transportable modules and requiring minimum setup was achieved. During the Phase 1 activities a detailed analysis was performed that covered the description of engines to be tested, engine test procedures, general test specifications, test facility requirements and design considerations, installation, and engine control and test data requirements. From this a preliminary design for the portable test facility was prepared, plus a conceptual installation design and a preliminary design for the engine control and data system. DTIC

12 ASTRONAUTICS (GENERAL)

For extraterrestrial exploration see *91 Lunar and Planetary Exploration.*

N95-19995* National Aeronautics and Space Administration, Washington, DC.
CHALLENGER'S NIGHT FLIGHT (Videotape)
Aug. 1983 Videotape: 4 min. 30 sec. playing time, in color, with sound
(NASA-TM-110503; NONP-NASA-VT-95-41115; NASA-ASR-222) Avail: CASI VHS A02/BETA A22

STS Mission 8 and its night flight (both launch and landing) are highlighted in this color video. The 5-member crew is introduced and their special assignments for this flight are discussed, along with their continuous weightlessness experiments performed during the flight. The first black astronaut, Guion S. Blufords, Jr., is introduced and file footage of an STS Mission orbiting the earth is shown. CASI

N95-20228# Naval Research Lab., Washington, DC.
A CLEMENTINE COLLECTION: MOONGLOW
Jun. 1994 92 p
(AD-A286360; NRL/PU/1230-94-261) Avail: CASI HC A05/MF A01

The Clementine story began in 1990 when NASA administrator Richard Truly asked the Department of Defense to consider a joint NASA/DOD mission that would achieve goals mutually beneficial to both organizations. That request was given to the then Strategic Defense Initiative Organization (SDIO) to investigate. A mission was conceived to test the latest in space-based imaging components, using the moon and a near-earth asteroid as celestial targets. The Clementine mission is the result of those early investigations. This collection is an early sampling of the 1.8 million images acquired by the Clementine spacecraft. DTIC

N95-20690 Naval War Coll., Newport, RI. Dept. of Operations.
SPACE FUNDAMENTALS FOR THE WAR FIGHTER Final Report
William G. Clapp 8 Feb. 1994 42 p Limited Reproducibility: More than 20% of this document may be affected by microfiche quality
(AD-A279703) Avail: Issuing Activity (Defense Technical Information Center (DTIC))

The quickening space technology revolution is as natural as life itself. Technology leads us to believe that anything is possible and that we are all privileged users. An understanding of some of the limitations of our space assets should moderate our expectations. The purpose of this paper is to provide a short and concise overview of the space environment and a fundamental understanding of space assets in order to understand their capabilities. The paper has been limited to the basic concepts of the atmosphere, rocket propulsion, launch vehicles, communications spectrum, and satellite assets. With the demise of the USSR threat, also gone are sufficient budgets that were going to provide the next generation of bigger and better satellites. We must accept the fact that next generation satellite security systems under development are now too expensive to field. Next generation satellite system funding may someday come again when a new threat diminishes our technological advantage. DTIC

N95-20995 Naval War Coll., Newport, RI. Dept. of Operations.
SPACE TECHNOLOGY: FORCE MULTIPLIER OR FALSE SENSE OF SECURITY Final Report
Jessie W. Canaday 8 Feb. 1994 24 p Limited Reproducibility: More than 20% of this document may be affected by microfiche quality
(AD-A279726) Avail: Issuing Activity (Defense Technical Information Center (DTIC))

The Premise that space technology is a force multiplier is analyzed. Lessons learned from Desert Storm are discussed to show the advantages that space systems can bring to the battlefield and how unprepared the space community and our military forces were to execute a war using space technology. New space technology applications are described to show how space technology can enhance our military forces and the need for space control is discussed as more and more countries acquire space capabilities. Finally, by relying too much on technology and believing that technology will win all wars, we may garner a false sense of security. The paper concludes that space technology can be used as a force multiplier if we integrate space technology into all military operations and exercises, develop space doctrine to drive requirements for technology, educate our people on space systems, develop a coherent space control strategy, win the technology race and carefully assess our military requirements in the 'new world order'. DTIC

N95-21706# Oak Ridge National Lab., TN.
RESTRICTED MASS TRANSPORT EFFECTS ON FREE RADICAL REACTIONS
A. C. Buchanan, III, P. F. Britt, and K. B. Thomas 1994 4 p Presented at the 208th American Chemical Society National Meeting, Washington, DC, 21-26 Aug. 1994
(Contract DE-AC05-84OR-21400)
(DE94-018136; CONF-940813-18) Avail: CASI HC A01/MF A01

Coal possesses a complex chemical and physical structure. The cross-linked, network structure can lead to alterations in normal thermally-induced, free-radical decay pathways as a consequence of restrictions on mass transport. Moreover, in coal liquefaction, access of an external hydrogen donor to a reactive radical site can be hindered by the substantial domains of microporosity present in coals. However, previous work indicates that diffusion effects do not appear to be playing an important role in this coal conversion chemistry. Several possible explanations for this phenomenon were advanced including the potential involvement of a hydrogen hopping/radical relay mechanism recently discovered model systems in the authors' laboratories. The authors have employed silica-anchored compounds to explore the effects of restricted mass transport on the pyrolysis mechanisms of coal model compounds. In studies of two-component systems, cases have been discovered where radical centers can be rapidly relocated in the diffusionally constrained environment as a consequence of rapid serial hydrogen atom transfers. This chemistry can have substantial effects on thermal decomposition rates and on product selectivities. In this study, the authors examine additional surfaces to systematically investigate the impact of molecular structure on the hydrogen atom transfer promoted radical relay mechanism. Silica-attached 1,3-diphenylpropane (approximately Ph(CH2)3Ph, or approximately DPP) was chosen as the thermally reactive component, since it can be considered prototypical of linkages in coal that do not contain weak bonds easily cleaved at coal liquefaction temperatures (ca. 4000 C), but which crack at reasonable rates if benzylic radicals can be generated by hydrogen abstraction. The rate of such hydrogen transfers under restricted diffusion will be highly dependent on the structure and proximity of neighboring molecules. DOE

N95-21894*# National Aeronautics and Space Administration, Washington, DC.
THE PROBLEM OF SPACE TRAVEL: THE ROCKET MOTOR [DAS PROBLEM DER BEFAHRUNG DES WELTRAUMS: DER RAKETEN-MOTOR]
Hermann Noordung, Ernst Stuhlinger, ed., J. D. Hunley, ed., and Jennifer Garland, ed. 1995 174 p Translation into English of Das Problem der Befahrung des Weltraums: Der Raketen-Motor (Berlin, Germany, Richard Carl Schmidt and Co.), 1929 188 p *Its* NASA History Series Prepared by SCITRAN, Inc., Santa Barbara, CA Original contains color illustrations
(NASA-SP-4026; NAS 1.21:4026; LC-94-36645; ISBN-0-16-045462-X)
Avail: CASI HC A08/MF A02; SOD HC; 5 functional color pages

This is an English translation of Noordung's 'Das Problem der Befahrung des Weltraums'. It is a part of the NASA History Series. The book provides Noordung's insight as to how a space station might be constructed. Keep in mind that the author passed away in 1929. It contains ideas that were criticized for faults and those that were acclaimed for their potentially successful ingenuity. CASI

N95-22413# Institute for Defense Analyses, Alexandria, VA.
SPACE SYSTEMS TECHNOLOGY WORKING GROUP: EXECUTIVE REPORT Final Report, Sep. 1993 - Jun. 1994
Raymond V. Wick, Gerald K. Hendricks, and L. K. Lewis Sep. 1994 85 p Revised
(Contract DASW01-94-C-0054)
(AD-A285778; IDA-D-1519-Rev; IDA/HQ-94-45918-Rev; AD-E501845)
Avail: CASI HC A05/MF A01

The speed with which a promising military critical technology becomes available for military use is determined to a great extent by the effort and support focused on that technology. Determining which space technologies deserve this attention requires knowing at what performance level or technical parameter the technology becomes militarily critical. The Space System Technology Working Group (SSTWG) identified and parametrized those space technologies that are militarily critical, space unique, and dual-use and those that should be considered for cooperative agreements with industry and academia and memorandum of understanding (MOU) with other countries. This Executive Report provides government, industry, and academic personnel concerned with space technologies the purpose, methodology, and results of the SSTWG study. It includes tables that identify critical space technologies and their parameters. DTIC

13 ASTRODYNAMICS

Includes powered and free-flight trajectories; and orbital and launching dynamics.

N95-21533*# Jet Propulsion Lab., California Inst. of Tech., Pasadena, CA.

ORBIT DETERMINATION OF HIGHLY ELLIPTICAL EARTH ORBITERS USING IMPROVED DOPPLER DATA-PROCESSING MODES

J. A. Estefan *In its* The Telecommunications and Data Acquisition Report 15 Feb. 1995 p 1-17 (For primary document see N95-21532 06-32)

(RTOP 314-30-11-60-02)

Avail: CASI HC A03/MF A03

14 GROUND SUPPORT SYSTEMS AND FACILITIES (SPACE)

Includes launch complexes, research and production facilities; ground support equipment, e.g., mobile transporters; and simulators.

For related information see also *09 Research and Support Facilities (Air).*

N95-21384*# National Aeronautics and Space Administration. Lewis Research Center, Cleveland, OH.

SPACE POWER FACILITY READINESS FOR SPACE STATION POWER SYSTEM TESTING

Roger L. Smith Feb. 1995 38 p

(RTOP 478-83-00)

(NASA-TM-106829; E-9379; NAS 1.15:106829) Avail: CASI HC A03/MF A01

This document provides information which shows that the NASA Lewis Research Center's Space Power Facility (SPF) will be ready to execute the Space Station electric power system thermal vacuum chamber testing. The SPF is located at LeRC West (formerly the Plum Brook Station), Sandusky, Ohio. The SPF is the largest space environmental chamber in the world, having an inside horizontal diameter of 100 ft. and an inside height at the top of the hemisphere of 122 ft. The vacuum system can achieve a pressure lower than 1 x 10(exp -5) Torr. The cryoshroud, cooled by gaseous nitrogen, can reach a temperature of -250 F, and is 80 ft. long x 40 ft. wide x 22 ft. high. There is access to the chamber through two 50 ft. x 50 ft. doors. Each door opens into an assembly area about 150 ft. long x 70 ft. wide x 80 ft. high. Other available facilities are offices, shop area, data acquisition system with 930 pairs of hard lines, 7 megawatts of power to chamber, 245K gal. liquid nitrogen storage, cooling tower, natural gas, service air, and cranes up to 25 tons. Author

15 LAUNCH VEHICLES AND SPACE VEHICLES

Includes boosters; operating problems of launch/space vehicle systems; and reusable vehicles.

For related information see also *20 Spacecraft Propulsion and Power.*

N95-20770# Department of Defense, Washington, DC.

MILITARY STANDARD: TEST REQUIREMENTS FOR LAUNCH, UPPER-STAGE, AND SPACE VEHICLES

15 Sep. 1994 132 p Supersedes MIL-STD-1540B

(AD-A286627; MIL-STD-1540C; MIL-STD-1540B) Avail: CASI HC A07/MF A02

This Standard establishes the environmental and structural ground testing requirements for launch vehicles, upper-stage vehicles, space vehicles, and for their subsystems and units. In addition, a uniform set of definitions of related terms is established. The formal compliance tests for flight vehicle equipment start at the unit level of assembly and progress at each higher level of assembly until the entire launch system and the on-orbit system can be tested in their operational configurations. In addition, there may be development tests and evaluations at various levels of assembly, and in-process inspections and tests to avoid assembling a defective system. The formal compliance tests addressed in this document are qualification and acceptance at the unit, subsystem, and vehicle level as well as some of the integrated system prelaunch validation tests. Derived from text

N95-20785# Sandia National Labs., Albuquerque, NM.

COMPUTATIONAL DESIGN OF HYPERVELOCITY LAUNCHERS

T. Trucano and L. Chhabildas 1993 23 p Presented at the 1994 Hypervelocity Impact Symposium, Santa Fe, NM, 16-20 Oct. 1994

(Contract DE-AC04-94AL-85000)

(DE95-000744; SAND-93-3909C; CONF-9410131-7) Avail: CASI HC A03/MF A01

The Sandia Hypervelocity Launcher (HVL) uses impact techniques on a two-stage light-gas gun to launch flier plates to velocities in excess of 10 km/s. An important problem in designing successful third stage techniques for impact launching fliers to such velocities is detailed understanding of the interior ballistic performance of the third stage. This is crucial for preventing melt and fracture of the flier plates during the extraordinary accelerations that they undergo (accelerations on the order of 10(exp 9) g are typical on the HVL). We seek to optimize HVL launch conditions in order to achieve two major goals: first, to maximize the potential launch velocity for a given flier; and second, to allow different flier configurations. One tool that we can apply in studying HVL performance is the use of multi-dimensional wave propagation codes. We have used such codes, particularly the Sandia Eulerian code CTH, to study a variety of interior ballistics issues related to gun performance and launcher development for almost ten years. Recently this work has culminated in a major contribution to HVL design, namely the capability to launch 'chunk' fliers. The initial phases of design development were solely devoted to CTH computations that studied potential designs, identified problems, and posed possible solutions for launching chunk fliers on the HVL. Our computations sufficiently narrowed the design space to the point that systematic experimental progress was possible. Our first experiment resulted in the successful launch of an intact 0.33 gram titanium alloy chunk flier to a velocity of 10.2 km/s. The thickness to diameter ratio of this flier was approximately 0.5. DOE

N95-21346*# National Aeronautics and Space Administration. Marshall Space Flight Center, Huntsville, AL.

LAUNCH VEHICLE FLIGHT CONTROL AUGMENTATION USING SMART MATERIALS AND ADVANCED COMPOSITES (CDDF PROJECT 93-05)

C. Barret Washington Feb. 1995 57 p

(NASA-TP-3535; M-770; NAS 1.60:3535) Avail: CASI HC A04/MF A01

The Marshall Space Flight Center has a rich heritage of launch vehicles that have used aerodynamic surfaces for flight stability such as the Saturn vehicles and flight control such as on the Redstone. Recently, due to aft center-of-gravity locations on launch vehicles currently being studied, the need has arisen for the vehicle control augmentation that is provided by these flight controls. Aerodynamic flight control can also reduce engine gimbaling requirements, provide actuator failure protection, enhance crew safety, and increase vehicle reliability, and payload capability. In the Saturn era, NASA went to the Moon with 300 sq ft of aerodynamic surfaces on the Saturn V. Since those days, the wealth of smart materials and advanced composites that have been developed allow for the design of very lightweight, strong, and innovative launch vehicle flight control surfaces. This paper presents an overview of the advanced composites and smart materials that are directly applicable to launch vehicle control surfaces. Author

N95-20646# Westinghouse Electric Corp., Baltimore, MD.

HIGH DENSITY MONOLITHIC PACKAGING TECHNOLOGY FOR DIGITAL/MICROWAVE AVIONICS

Timothy Fertig, Theresa Walter, Eric Gaver, and Kevin Leahy *In* AGARD,

Advanced Packaging Concepts for Digital Avionics Oct. 1994 12 p
(For primary document see N95-20631 06-06)
Copyright Avail: CASI HC A03/MF A03

16 SPACE TRANSPORTATION

Includes passenger and cargo space transportation, e.g., shuttle operations; and space rescue techniques.

For related information see also *03 Air Transportation and Safety* and *18 Spacecraft Design, Testing and Performance.* For space suits see *54 Man/System Technology and Life Support.*

N95-21113* National Aeronautics and Space Administration. Lyndon B. Johnson Space Center, Houston, TX.
STS 63 FLIGHT DAY 4 HIGHLIGHTS/MIR-SHUTTLE RENDEZVOUS (Videotape)
5 Feb. 1995 Videotape: 1 hr. playing time, in color, with sound
(NASA-TM-110512; NONP-NASA-VT-95-42156) Avail: CASI VHS A02/BETA A22

STS 63 Flight, day 4, the MIR-Shuttle rendezvous is highlighted in this video. The six-member team in the Shuttle are introduced and discuss their functions and tests for this day of the flight. There is actual footage of earth from space, of the MIR Space Station, a tour of the Shuttle cockpit, some footage from the MIR of the Space Shuttle, and footage from inside the MIR with the cosmonauts. Mission control communications with the Shuttle, communication between the Shuttle and MIR, and an historic communication between the Shuttle's astronauts and President Bill Clinton are included. President Clinton interviews each of the six-member team and discusses the upcoming space walk by Dr. Bernard Harris, the first black astronaut to walk in space. This video was recorded on February 6, 1995. CASI

N95-21558* National Aeronautics and Space Administration. Lyndon B. Johnson Space Center, Houston, TX.
STS 63: POST FLIGHT PRESENTATION (Videotape)
27 Feb. 1995 Videotape: 42 min. 33 sec. playing time, in color, with sound
(NASA-TM-110514; NONP-NASA-VT-95-42494) Avail: CASI VHS A02/BETA A22

At a post flight conference, Captain Jim Wetherbee, of STS Flight 63, introduces each of the other members of the STS 63 crew (Eileen Collins, Pilot; Dr. Bernard Harris, Payload Commander; Dr. Michael Foale, Mission Specialist from England; Dr. Janice Voss, Mission Specialist; and Colonel Vladimir Titor, Mission Specialist from Russia), gave a short autobiography of each member and a brief description of their assignment during this mission. A film was shown that included the preflight suit-up, a view of the launch site, the actual night launch, a tour of the Space Shuttle and several of the experiment areas, several views of earth and the MIR Space Station and cosmonauts, the MIR-Space Shuttle rendezvous, the deployment of the Spartan Ultraviolet Telescope, Foale and Harris's EVA and space walk, the retrieval of Spartan, and the night entry home, including the landing. Several spaceborne experiments were introduced: the radiation monitoring experiment, environment monitoring experiment, solid surface combustion experiment, and protein crystal growth and plant growth experiments. This conference ended with still, color pictures, taken by the astronauts during the entire STS 63 flight, being shown. CASI

N95-22295* National Aeronautics and Space Administration. Lyndon B. Johnson Space Center, Houston, TX.
STS FLIGHT 64 MISSION HIGHLIGHTS (Videotape)
21 Feb. 1995 Videotape: 1 hr. 4 min. 16 sec. playing time, in color, with sound
(NASA-TM-110515; NONP-NASA-VT-95-42495) Avail: CASI VHS A02/BETA A22

The pre-launch, launch, in-flight, and landing activities of STS Flight 64 are highlighted in this video. Footage of the astronauts (Richard, Hammond, Lee, Helms, Meade, and Linenger) suiting up, the payload activities with the Shuttle arm, the deployment of the Spartan satellite, the untethered spacewalk of Lee and other in-space experiments with Lee and Meade (including a body roll), the pre-landing shots and actual landing, and some footage of the Mission Operations Control Room watching the Space Shuttle maneuvers are included. CASI

17 SPACE COMM., SPACECRAFT COMM., COMMAND & TRACKING

Includes telemetry; space communications networks; astronavigation and guidance; and radio blackout.

For related information see also *04 Aircraft Communications and Navigation* and *32 Communications and Radar.*

N95-20567# Sandia National Labs., Albuquerque, NM.
DIGITAL FILTERING FOR DATA COMPRESSION IN TELEMETRY SYSTEMS
R. M. Bell 1994 6 p Presented at the ICSPAT 1994: Signal Procession Applications and Technology, Dallas, TX, 18-21 Oct. 1994
(Contract DE-AC04-94AL-85000)
(DE94-016611; SAND-94-8613C; CONF-9410164-3) Avail: CASI HC A02/MF A01

There are many obstacles to using data compression in a telemetry system. Non-linear quantization is often too lossy, and the data is too highly structured to make variable-length entropy codes practical. This paper describes a lossless telemetry data compression system that was built using digital FIR filters. The method of compression takes advantage of the fact that the optimal Nyquist sampling rate is rarely achievable due to two factors: (1) Sensor/transducers are not bandlimited to the frequencies of interest; and (2) Accurate, high-order analog filters are not available to perform effective band limiting and prevent aliasing. Real-time digital filtering can enhance the performance of a typical sampling system so that it approaches Nyquist sampling rates, effectively compressing the amount of data and reducing transmission bandwidth. The system that was built reduced the sampling rate of 14 high-frequency vibration channels by a factor of two, and reduced the bandwidth of the-data link from 1.8 Mbps to 1.28 Mbps. The entire circuit uses seven function-specific, digital-filter DSP's operating in parallel (two 128-tap FIR filters can be implemented on each Motorola DSP56200), one EPROM and a Programmable Logic Device as the controller. DOE

18 SPACECRAFT DESIGN, TESTING AND PERFORMANCE

Includes satellites; space platforms; space stations; spacecraft systems and components such as thermal and environmental controls; and attitude controls.

For life support systems see *54 Man/System Technology and Life Support.* For related information see also *05 Aircraft Design, Testing and Performance, 39 Structural Mechanics,* and *16 Space Transportation.*

N95-20148# Lawrence Livermore National Lab., Livermore, CA.
ENERGY AND TECHNOLOGY REVIEW
William A. Bookless, ed. and William J. Quirk, ed. Jun. 1994 20 p
(Contract W-7405-eng-48)
(DE94-017686; UCRL-52000-94-6) Avail: CASI HC A03/MF A01

This report discusses: The Clementine satellite, the first US satellite to the Moon in more than two decades, sent back more than 1.5 million images of the lunar surface using cameras designed and calibrated by LLNL. An LLNL-developed laser ranger provided information that will be used to construct a relief map of the Moon's surface; and Uncertainty and the Federal Role in Science and Technology, Ralph E. Gomory was a recent participate in the Director's Distinguished Lecturer Series at LLNL. In his lecture, he addressed some of the tensions, conflicts, and possible goals related to federal support for science and technology. DOE

N95-20800*# National Aeronautics and Space Administration. Langley Research Center, Hampton, VA.
MATHEMATICAL MODELING OF A CLASS OF MULTIBODY FLEXIBLE SPACECRAFT STRUCTURES

Atul Kelkar, G. Dec. 1994 25 p
(RTOP 505-64-52-01)
(NASA-TM-109166; NAS 1.15:109166) Avail: CASI HC A03/MF A01

A mathematical model for a general multibody flexible spacecraft is obtained. The generic spacecraft considered consists of a flexible central body to which a number of flexible multibody structures are attached. The coordinate systems used in the derivation allow effective decoupling of the translational motion of the entire spacecraft from its rotational motion about its center of mass. The derivation assumes that the deformations in the bodies are only due to elastic motions. The dynamic model derived is a closed-form vector-matrix differential equation. The model developed can be used for analysis and simulation of many realistic spacecraft configurations. Author

N95-21026# Helsinki Univ. of Technology, Espoo (Finland). Lab. of Space Technology.
PRELIMINARY STUDY OF HUTSAT MICROSATELLITE
Matti Brax, Martti Hallikainen, Reijo Lindgren, Sam Lund, Juha-Pekka Luntama, Mika Pikaenen, Jyri Putkonen, and Simo Tauriainen Oct. 1993 85 p See also AD-A164747 and DE89-002741
(ISSN 0786-8154)
(PB95-127619; ISBN-951-22-1783-X) Avail: CASI HC A05/MF A01

The Helsinki University of Technology Satellite (HUTSAT) project started with the funding of the Academy of Finland and Helsinki University of Technology in January 1992. This is the first ever Finnish project concerning an orbiting satellite. The background, objectives and funding of the project are introduced. Then the subsystems of HUTSAT are described, each in its own chapter. Key design parameters are analyzed and then constraints to the other systems and payloads are discussed. The particle detector payload is presented. Product assurance (PA) aspects are discussed and HUTSAT PA principles are drawn. Finally, a short executive summary presents the key parameters of HUTSAT and its payload. NTIS

N95-21147# Maryland Univ., College Park, MD. Systems Research Center.
CONTROL OF COMPLEX MULTIBODY SPACECRAFT Final Report, 15 Jan. 1990 - 14 Jan. 1994
P. S. Krishnaprasad 20 Jul. 1994 33 p
(Grant AF-AFOSR-0105-90)
(AD-A285623; AFOSR-94-0488TR) Avail: CASI HC A03/MF A01

The Project C-MULTICS (Control of Complex Multibody Spacecraft) is a center of excellence at the University of Maryland. The work supported by this project is concerned with the modeling, analysis, control and simulation of large scale complex multibody spacecraft with rigid and flexible components. DTIC

N95-21190*# TRW Space Technology Labs., Redondo Beach, CA. Space and Electronics Group.
TWO-MICRON LASER ATMOSPHERIC WIND SOUNDER (LAWS) POINTING/TRACKING STUDY
Scott Manlief Jan. 1995 149 p
(Contract NAS1-19291; RTOP 233-01-01-03)
(NASA-CR-195012; NAS 1.26:195012) Avail: CASI HC A07/MF A02

The objective of the study was to identify and model major sources of short-term pointing jitter for a free-flying, full performance 2 micron LAWS system and evaluate the impact of the short-term jitter on wind-measurement performance. A fast steering mirror controls system was designed for the short-term jitter compensation. The performance analysis showed that the short-term jitter performance of the controls system over the 5.2 msec round-trip time for a realistic spacecraft environment was = 0.3 micro rad, rms, within the specified value of less than 0.5 micro rad, rms, derived in a 2 micron LAWS System Study. Disturbance modes were defined for: (1) the Bearing and Power Transfer Assembly (BAPTA) scan bearing, (2) the spacecraft reaction wheel torques, and (3) the solar array drive torques. The scan bearing disturbance was found to be the greatest contributing noise source to the jitter performance. Disturbances from the fast steering mirror reaction torques and a boom-mounted cross-link antenna clocking were also considered but were judged to be small compared to the three principal disturbance sources above and were not included in the final controls analysis. Author

N95-21634# Army Research Lab., Adelphi, MD.
REENTRY VEHICLE ON-SITE INSPECTION TECHNOLOGY STUDY Technical Report, 6 Mar. 1992 - 19 May 1993
Mary C. Abe 1 Nov. 1994 116 p
(Contract DNA-MIPR-92-610)
(AD-A285960; DNA-TR-94-22) Avail: CASI HC A06/MF A02

A study group was tasked to develop possible reentry vehicle on-site inspection (RVOSI) scenarios and to recommend research into technologies that could address these scenarios. The task was accomplished by identifying RVOSI technology candidates and evaluating their advantages or disadvantages to compare to the visual protocol for RVOSI prescribed by the Strategic Arms Reduction Treaty (START) on the Reduction and Limitation of Strategic Offensive Arms. RVOIS technologies were evaluated with regard to inspection confidence, cost, intrusiveness, operational impact, and inspector burden. The RVOSI Technology Study identified no technology that readily solves the problems associated with START-prescribed visual inspection protocols. Recommendations for (1) further research in analytic modeling, (2) experimental studies to support this analytic work, and (3) data processing resulted from this study. Technology development for RVOIS appears to be primarily of interest if the technology provides enhanced confidence or additional inspection capability over visual inspections. DTIC

N95-21858* National Aeronautics and Space Administration. Lyndon B. Johnson Space Center, Houston, TX.
TETHERED SATELLITE: FORCES AND MOTION (Videotape)
21 Oct. 1994 Videotape: 21 min. 11 sec. playing time, in color, with sound
(NASA-TM-110518; NONP-NASA-VT-95-42566) Avail: CASI VHS A02/BETA A22

In this 'Lift off to Learning' series, Loren Shriver, commander of STS 46, and the other members of the mission (Claude Nicollier, Marsha Ivins, Andrew Allen, Jeffrey Hoffman, Franklin Chiang-Diaz, and Franco Maerba) use computer graphics, and physical experiments to explain how the tethered satellite to be deployed during their mission will be raised, how it works, the influence of the Shuttle on the satellite and the satellite's influence on the Shuttle's orbit, the gravitational effects, and other effects concerning the Theoretical Physics used to plan this mission (gravity gradient force, center of mass, angular momentum, centrifugal force, and coriolis effect). This video ends with a discussion of the technology transfer and utilization of this tethered satellite concept and design. CASI

N95-22204# Wright Lab., Wright-Patterson AFB, OH.
NONLINEAR DYNAMICS OF THE PLANAR PITCH ATTITUDE MOTION FOR A GRAVITY-GRADIENT SATELLITE Final Report, Jun. 1990 - Jun. 1994
Harry A. Karasopoulos Aug. 1994 220 p
(AD-A286407; WL-TR-94-3123) Avail: CASI HC A10/MF A03

The nonlinear dynamics of the planar pitch attitude motion for a gravity-gradient satellite in an elliptical orbit about a central body are investigated using phase diagrams, Poincare' maps, bifurcation plots, spectral density plots, Lyapunov exponents, and chaos diagrams. The satellite is assumed to be a rigid body influenced only by torques from an inverse-square gravitational field, and its major axis is assumed to be normal to the orbit plane. The resultant planar pitching motion is either periodic, quasiperiodic, or chaotic, depending upon the values of the system parameters, eccentricity and satellite inertia ratio. The relationships of the system parameters to the nonlinearity of the system are explored with chaos diagrams, which incorporate the results of the Lyapunov exponent calculations into a useful tool for predicting the onset of chaotic motion in parameter space. The border between regular and chaotic motion in the chaos diagrams is shown to be fractal. The dynamics of the basic problem supplemented by the addition of damping terms and an oblate, axially symmetric central body are also investigated. Strange attractors are found and the validity of Melnikov's method to predict the border between chaos and regular motion is examined. DTIC

N95-20533*# National Aeronautics and Space Administration. Lewis Research Center, Cleveland, OH.
STATIC STABILITY OF A THREE-DIMENSIONAL SPACE TRUSS
John F. Shaker *In its* Proceedings of the 13th Space Photovoltaic

Research and Technology Conference (SPRAT 13) Sep. 1994 p 299-312 (For primary document see N95-20502 06-33)
Avail: CASI HC A03/MF A04

19 SPACECRAFT INSTRUMENTATION

For related information see also *06 Aircraft Instrumentation* and *35 Instrumentation and Photography.*

N95-22436# Los Alamos National Lab., NM.
IMAGING DESIGN OF THE WIDE FIELD X-RAY MONITOR ONBOARD THE HETE SATELLITE
Jean J. M. IntZand, E. E. Fenimore, N. Kawai (Institute of Physical and Chemical Research, Saitama, Japan.), A. Yoshida (Institute of Physical and Chemical Research, Saitama, Japan.), M. Matsuoka (Institute of Physical and Chemical Research, Saitama, Japan.), and M. Yamauchi (Miyazaki Univ., Japan.) 1994 6 p Presented at the Imaging in High Energy Astronomy Conference, Capri (Italy), 26-30 Sep. 1994
(Contract W-7405-eng-36)
(DE95-002750; LA-UR-84-3645; CONF-9409245-1) Avail: CASI HC A02/MF A01

The High Energy Transient Experiment (HETE), to be launched in 1995, will study Gamma-Ray Bursts in an unprecendented wide wavelength range from Gamma and X-ray to UV wavelengths. The X-ray range (2 to 25 keV) will be covered by 2 perpendicularly oriented 1-dimensional coded aperture cameras. These instruments cover a wide field of view of 2 sr and thus have a relatively large potential to locate GRB's to a fraction of a degree, which is an order of magnitude better than BATSE. The imaging design of these coded aperture cameras relates to the design of the coded apertures and the decoding algorithm. The aperture pattern is to a large extent determined by the high background in this wide field application and the low number of pattern elements ((approximately)100) in each direction. The result is a random pattern with an open fraction of 33%. The onboard decoding algorithm is dedicated to the localization of a single point source. DOE

20 SPACECRAFT PROPULSION AND POWER

Includes main propulsion systems and components, e.g., rocket engines; and spacecraft auxilliary power sources.

For related information see also *07 Aircraft Propulsion and Power, 28 Propellants and Fuels, 44 Energy Production and Conversion,* and *15 Launch Vehicles and Space Vehicles.*

N95-19962# Defence Science and Technology Organization, Melbourne (Australia). Aeronautical and Maritime Research Lab.
INVESTIGATION OF ROCKET MOTORS 3 INCH NUMBER 1 Mk 4
L. M. Barrington May 1994 18 p
(AD-A284278; DSTO-TR-0017; DODA-AR-008-648) Avail: CASI HC A03/MF A01

In 1992, Aircraft Research and Development Unit (ARDU), RAAF, experienced two misfires with Rocket Motors, 3 in., No. 1, Mk 4, during a series of firings at Woomera. These motors were sampled from a batch manufactured in 1957, and subsequent to the misfires this batch was withdrawn from use. An alternate batch of motors manufactured in 1966 was available to ARDU. Tests were conducted on a number of these motors to advise on their suitability for use, and as a result, a further five years life was assigned with a recommendation to retest after that period. DTIC

N95-20059*# Massachusetts Inst. of Tech., Cambridge, MA. Plasma Fusion Center.
PROPULSION RESEARCH ON THE VARIABLE TANDEM MIRROR PLASMA ROCKET Final Report, 1 Feb. 1992 - 31 Jan. 1994
T. F. Yang and F. R. Chang-Diaz 7 Feb. 1994 90 p
(Contract NAS9-18372; AF-AFOSR-0345-89; AF Proj. 2308)
(NASA-CR-196310; NAS 1.26:196310; AD-A280009; PFC/RR-94-1; AFOSR-94-0319TR) Avail: CASI HC A05/MF A01

This report describes the progress made in the past two years as well as the overall picture of this research. In the past years, several-milestones have been achieved towards the realization of a practical space plasma thruster from the tandem mirror rocket experiment, i.e. the specific impulse, thrust, energy conversion efficiency, and mass flow-rate have been determined. The experiment operates at 9.4 kW of input power at an RF-to-plasma efficiency of 68%; The ion temperature is 172 eV (2,000,000 K) which gives an I(sub sp) of 12,852 s. The thrust is 76 mN (milli Newton) which is a high value for a low input power (9.4 kW) and very high I(sub sp), (12,852 s). The radiation loss was found to be very low. Most important, these results fall within our prediction. DTIC

N95-20076# Space Power, Inc., San Jose, CA.
SPACE-R THERMIONIC SPACE NUCLEAR POWER SYSTEM: DESIGN AND TECHNOLOGY DEMONSTRATION
1994 16 p
(Contract DE-AC03-92SF-19441)
(DE95-000713; DOE/SF-19441/T15) Avail: CASI HC A03/MF A01

The objective of this program is to design, develop, demonstrate, and advance the technology for thermionic space nuclear power system (TI-SNPS) to meet key functional requirements with reliable 5(approximately)40 kWe output and 18-month near-term/10-year long-term goals. A 40 kWe TI-SNPS point design will be prepared, and key technologies and critical components supporting that design will be validated. This program will produce an assessed design of a 40 kWe-EOL space nuclear power system. Phase 1 will provide for the performance of parametric trade studies and demonstration of key technologies, resulting in a preferred conceptual design for the TI-SNPS. The focus of the tasks is technology validation drive by the system design. DOE

N95-20124*# SECA, Inc., Huntsville, AL.
RADIATION FROM ADVANCED SOLID ROCKET MOTOR PLUMES Final Report
Richard C. Farmer, Sheldon D. Smith, and Brian L. Myruski Dec. 1994 188 p Original contains color illustrations
(Contract NAS8-39370)
(NASA-CR-196554; NAS 1.26:196554; SECA-FR-94-18) Avail: CASI HC A09/MF A02; 4 functional color pages

The overall objective of this study was to develop an understanding of solid rocket motor (SRM) plumes in sufficient detail to accurately explain the majority of plume radiation test data. Improved flowfield and radiation analysis codes were developed to accurately and efficiently account for all the factors which effect radiation heating from rocket plumes. These codes were verified by comparing predicted plume behavior with measured NASA/MSFC ASRM test data. Upon conducting a thorough review of the current state-of-the-art of SRM plume flowfield and radiation prediction methodology and the pertinent data base, the following analyses were developed for future design use. The NOZZRAD code was developed for preliminary base heating design and Al2O3 particle optical property data evaluation using a generalized two-flux solution to the radiative transfer equation. The IDARAD code was developed for rapid evaluation of plume radiation effects using the spherical harmonics method of differential approximation to the radiative transfer equation. The FDNS CFD code with fully coupled Euler-Lagrange particle tracking was validated by comparison to predictions made with the industry standard RAMP code for SRM nozzle flowfield analysis. The FDNS code provides the ability to analyze not only rocket nozzle flow, but also axisymmetric and three-dimensional plume flowfields with state-of-the-art CFD methodology. Procedures for conducting meaningful thermo-vision camera studies were developed. Author

N95-20708 Johns Hopkins Univ., Columbia, MD. Chemical Propulsion Information Agency.
THE 1993 JANNAF PROPULSION MEETING, VOLUME 2
Debra S. Eggleston, ed. Nov. 1993 405 p Meeting held in Monterey, CA, 15-19 Nov. 1993; sponsored by Joint NASA, Army, Navy, Air Force Interagency Propulsion Committee Limited Reproducibility: More than 20% of this document may be affected by microfiche quality
(Contract N00014-91-C-0001)
(AD-A279569; CPIA-Publ-602-Vol-2) Avail: Issuing Activity (Defense Technical Information Center (DTIC))

This volume, the second of six volumes, is a collection of 30 unclassified/unlimited distribution papers which were presented at the 1993 Joint Army-Navy-NASA-Air Force (JANNAF) Propulsion Meeting, held 15-19 November 1993 at the Hyatt Regency Hotel and Conference Center and the Naval Postgraduate School in Monterey, California. Specific subjects discussed include grain integrity, hybrid motors, liquid engines, turbopumps, reaction control systems, composite motor cases, continuous propellant mixing, nondestructive testing, solar propulsion, combustion chambers, and foreign propulsion technology. DTIC

N95-20853# Martin Marietta Astro Space, Philadelphia, PA.
GPHS-RTGs IN SUPPORT OF THE CASSINI MISSION
20 Oct. 1994 85 p
(Contract DE-AC03-91SF-18852)
(DE95-001492; DOE/SF-18852/T44) Avail: CASI HC A05/MF A01

The progress on the radioisotope generators and ancillary activities is described. This report is organized by program task as follows: spacecraft integration and liaison; engineering support; safety; qualified unicouple fabrication; ETG fabrication, assembly, and test; ground support equipment; RTG shipping and launch support; design, reviews, and mission applications; project management, quality assurance and reliability, contract changes, non-capital CAGO acquisition, and CAGO maintenance; contractor acquired government owned property (CAGO) acquisition. DOE

N95-20906# Prins Maurits Lab. TNO, Rijswijk (Netherlands).
INTEGRAL ROCKET RAMJETS
R. F. Calzone Mar. 1994 49 p
(AD-A285135; PML-1994-B29; TDCK-93-2570) Avail: CASI HC A03/MF A01

A rough overview of the important aspects and problem areas associated with the development of Integral Rocket Ramjet (IRR) technology is given in this report. The IRR is a supersonic air-breathing concept in which the gas generator produces fuel-rich gases. These fuel-rich gases are burnt in the secondary combustion chamber with ambient air captured and decelerated in the inlet. During the boost phase, a solid propellant booster provides the thrust necessary to achieve the velocity at which the ramjet may be operated (about M = 2). The booster is integrated in the secondary combustion chamber. DTIC

N95-21193# Colorado Univ., Boulder, CO. Dept. of Mechanical Engineering.
NONLINEAR ACOUSTIC PROCESSES IN A SOLID ROCKET ENGINE Final Technical Report, 30 Sep. 1991 - 1 Jan. 1994
David R. Kassoy, Kadir Kirkkipn, and Qing Zhao 29 Mar. 1994 154 p
(Grant AF-AFOSR-0023-89)
(AD-A285606; AFOSR-94-0653TR) Avail: CASI HC A08/MF A02

A new formulation for chamber flow dynamics in a model of solid rocket engine shows that vorticity generation and convection are prominent physical features of the flow field. Analytical and fully computational methods are employed to describe a basically inviscid interaction between acoustic disturbances arising from specified boundary disturbances and a sidewall injected flow field which simulates propellant burning. The mathematical model, based on the Navier Stokes equations, is developed in terms of an initial value problem in order to describe the complete, natural chamber flow evolution arising from boundary driven disturbances. The approach is analogous to a direct numerical simulation, although contemporary perturbation methods are employed to extract specific spatial and temporal scales from the equations and boundary conditions. The results show that large unsteady vorticity is created at the injected surface (sidewall) and convects into the cylinder with the radial component of the injection flow velocity. DTIC

N95-21458*# Aerojet Technical Systems Co., Sacramento, CA.
SSME HPOTP POST-TEST DIAGNOSTIC SYSTEM ENHANCEMENT PROJECT Final Report
Timothy W. Bickmore Cleveland, OH NASA Jan. 1995 169 p
(Contract NAS3-25883; RTOP 584-03-11)
(NASA-CR-4643; E-9372; NAS 1.26:4643) Avail: CASI HC A08/MF A02

An assessment of engine and component health is routinely made after each test or flight firing of a space shuttle main engine (SSME). Currently, this health assessment is done by teams of engineers who manually review sensor data, performance data, and engine and component operating histories. Based on review of information from these various sources, an evaluation is made as to the health of each component of the SSME and the preparedness of the engine for another test or flight. The objective of this project is to further develop a computer program which automates the analysis of test data from the SSME high-pressure oxidizer turbopump (HPOTP) in order to detect and diagnose anomalies. This program fits into a larger system, the SSME Post-Test Diagnostic System (PTDS), which will eventually be extended to assess the health and status of most SSME components on the basis of test data analysis. The HPOTP module is an expert system, which uses 'rules-of-thumb' obtained from interviews with experts from NASA Marshall Space Flight Center (MSFC) to detect and diagnose anomalies. Analyses of the raw test data are first performed using pattern recognition techniques which result in features such as spikes, shifts, peaks, and drifts being detected and written to a database. The HPOTP module then looks for combination of these features which are indicative of known anomalies, using the rules gathered from the turbomachinery experts. Results of this analysis are then displayed via a graphical user interface which provides ranked lists of anomalies and observations by engine component, along with supporting data plots for each. Author

N95-21531*# Rockwell International Corp., Canoga Park, CA. Rocketdyne Div.
POWER SYSTEMS FOR FUTURE MISSIONS Final Report
S. P. Gill, P. E. Frye, Franklin D. Littman, and C. J. Meisl Cleveland, OH NASA Dec. 1994 84 p Prepared for Sverdrup Technologies, Inc., Brook Park, OH
(Contract NAS3-25266)
(NASA-CR-195320; E-8735; NAS 1.26:195320) Avail: CASI HC A05/MF A01

A comprehensive scenario of future missions was developed and applicability of different power technologies to these missions was assessed. Detailed technology development roadmaps for selected power technologies were generated. A simple methodology to evaluate economic benefits of current and future power system technologies by comparing Life Cycle Costs of potential missions was developed. The methodology was demonstrated by comparing Life Cycle Costs for different implementation strategies of DIPS/CBC technology to a selected set of missions. Author

N95-21616*# Georgia Inst. of Tech., Atlanta, GA. School of Aerospace Engineering.
MULTIPLE BURN FUEL-OPTIMAL ORBIT TRANSFERS: NUMERICAL TRAJECTORY COMPUTATION AND NEIGHBORING OPTIMAL FEEDBACK GUIDANCE Semiannual Status Report, 7 Jul. 1994 - 6 Jan. 1995
C.-H. Chuang, Troy D. Goodson, and Laura A. Ledsinger 5 Jan. 1995 37 p
(Grant NAG8-921)
(NASA-CR-197317; NAS 1.26:197317) Avail: CASI HC A03/MF A01

This report describes current work in the numerical computation of multiple burn, fuel-optimal orbit transfers and presents an analysis of the second variation for extremal multiple burn orbital transfers as well as a discussion of a guidance scheme which may be implemented for such transfers. The discussion of numerical computation focuses on the use of multivariate interpolation to aid the computation in the numerical optimization. The second variation analysis includes the development of the conditions for the examination of both fixed and free final time transfers. Evaluations for fixed final time are presented for extremal one, two, and three burn solutions of the first variation. The free final time problem is considered for an extremal two burn solution. In addition, corresponding changes of the second variation formulation over thrust arcs and coast arcs are included. The guidance scheme discussed is an implicit scheme which implements a neighboring optimal feedback guidance strategy to calculate both thrust direction and thrust on-off times. Author

N95-21661 Defence Science and Technology Organization, Melbourne (Australia). Aeronautical and Maritime Research Lab.
ULTRAVIOLET EMISSION FROM ROCKET MOTOR PLUMES
David Kilpin Jun. 1994 23 p
(DSTO-TR-0002; AR-008-640) Copyright Avail: Issuing Activity (DSTO Aeronautical and Maritime Research Lab., GPO Box 4331, Melbourne, Victoria 3001, Australia)

Atmospheric limitations on the spectral region of the ultraviolet appropriate for detection of emissions from rocket motor plumes are considered. Origins of ultraviolet emission as spectral continua, bands and lines from the

rocket motor exhaust flow and its atmospheric interaction are discussed. The contrast of infrared emission arising mostly from major products and processes with ultraviolet emissions often resulting from trace constituents and minor pathways, indicates the more detailed knowledge of the rocket motor system required for modeling and prediction of ultraviolet signatures.
Author

N95-21840# Sandia National Labs., Albuquerque, NM.
ISSUES IN THE FLIGHT QUALIFICATION OF A SPACE POWER REACTOR
G. F. Polansky (Phillips Lab., Kirtland AFB, NM.), G. L. Schmidt (New Mexico Univ., Albuquerque, NM.), S. S. Voss (Los Alamos National Lab., NM.), and E. L. Reynolds (Johns Hopkins Univ., Laurel, MD.) 1994 9 p
Presented at the 15th Aerospace Testing Seminar, Manhattan Beach, CA, 11-13 Oct. 1994
(Contract DE-AC04-94AL-85000)
(DE95-001606; SAND-94-2376C; CONF-9410181-2) Avail: CASI HC A02/MF A01

This paper presents an overview of the Nuclear Electric Propulsion Space Test Program (NEPSTP). The program goals, the proposed mission, the spacecraft, and the Topaz II space nuclear power system are described. The subject of flight qualification is examined and the inherent difficulties of qualifying a space reactor are described. The differences between US and Russian flight qualification procedures are explored. A plan is then described that was developed to determine an appropriate flight qualification program for the Topaz II reactor to support a possible NEPSTP launch. Refocusing of the activities of the Ballistic Missile Defense Organization (BMDO), combined with budgetary pressures, forced the cancellation of the NEPSTP at the end of the 1993 fiscal year. DOE

23 CHEMISTRY AND MATERIALS (GENERAL)

N95-19901*# National Aeronautics and Space Administration. Lewis Research Center, Cleveland, OH.
EVALUATION OF PS 212 COATINGS UNDER BOUNDARY LUBRICATION CONDITIONS WITH AN ESTER-BASED OIL TO 300 C
Harold E. Sliney (Aerospace Design and Fabrication, Inc., Brook Park, OH.), William R. Loomis, and Christopher DellaCorte Dec. 1994 19 p
Presented at the International Conference on Metallurgical Coatings and Thin Films, San Diego, CA, 24-25 Apr. 1995; sponsored by American Vacuum Society
(Contract NAS3-25767; RTOP 505-63-5A)
(NASA-TM-106763; E-9206; NAS 1.15:106763) Avail: CASI HC A03/MF A01

High friction and wear of turbine engine components occur during high temperature excursions above the oxidation threshold of the liquid lubricant. This paper reports on research to study the use of a high temperature self lubricating coating, PS 212 for back-up lubrication in the event of failure of the liquid lubricant. Pin on disk tests were performed under dry and boundary-lubricated conditions at disk temperatures up to 300 C. The liquid lubricant was a formulated polyol ester qualified under MIL L-23699. At test temperatures above the oil's thermal degradation level, the use of PS 212 reduced wear, providing a back-up lubricant effect. Author

N95-20033# Rensselaer Polytechnic Inst., Troy, NY. Dept. of Chemistry.
SYNTHESIS AND STUDIES OF ORGANOMETALLIC PRECURSORS FOR CVD OF THIN FILM ELECTRONIC MATERIALS Final Report, Mar. 1991 - Aug. 1994
L. V. Interrante 30 Sep. 1994 12 p
(Contract N00014-91-J-1917)
(AD-A285834) Avail: CASI HC A03/MF A01

Cyclic molecular systems of the type, (A(XX')B(YY'))n (where A, B = Al, N or Si, C; X, X', Y, Y'= H, CH3, etc.; and n = 2 and 3), were studied as potential single-source precursors for the CVD of AlN and SiC films. These compounds provide the required elements for die product film already covalently bound to one another in a single, volatile molecular source and, in the case of the SiC precursors (where n = 2), they contain built-in ring-strain energy to lower the decomposition onset temperature. Efforts have included the study of the ((CH3)2AlNH2)3 yields AlN CVD system by mass spectrometric/time-of-flight (TOF) measurements and the investigation of substituted disilacyclobutanes as single-source SiC precursors. The mass spectrometric/TOF studies have indicated that a slow decomposition of the ((CH3)2AlNH2)3 (1) precursor to produce methane and a series of higher oligomeric products occurs during its vaporization at 75 to 100 C. These oligomeric species are believed to be intermediates formed in the gas-phase thermal decomposition of (1) to AlN. This precursor was used to deposit high quality AlN films up to 2 micrometers thick on Si and sapphire substrates in a LPCVD apparatus and is being tested for use in the deposition of AlN interface layers in Al2O3-reinforced metal matrix composites. Disilacyclobutane, (SiH2CH2)2, was found to yield stoichiometric, crack-free, adherent, polycrystalline SiC films on Si (100) and Si (111) surfaces by LPCVD at temperatures as low as 690 C. DTIC

N95-20264# Department of Energy, Oak Ridge, TN. Office of Scientific and Technical Information.
RESEARCH IN THE CHEMICAL SCIENCES: SUMMARIES OF FY 1994
Dec. 1994 153 p
(DE94-015427; DOE/ER-0144-12) Avail: CASI HC A08/MF A02

This summary book is published annually on research supported by DOE's Division of Chemical Sciences in the Office of Energy Research. Research in photochemical and radiation sciences, chemical physics, atomic physics, chemical energy, separations and analysis, heavy element chemistry, chemical engineering sciences, and advanced batteries is arranged according to national laboratories, offsite institutions, and small businesses. The goal is to add to the knowledge base on which existing and future efficient and safe energy technologies can evolve. The special facilities used in DOE laboratories are described. Indexes are provided (topics, institution, investigator). DOE

N95-20590 Brigham Young Univ., Provo, UT. Dept. of Chemistry.
NEW CHIRAL PYRIMIDINO-CROWN ETHER LIGANDS
J. Ty Redd, Jerald S. Bradshaw, Peter Huszthy, and Reed M. Izatt 11 May 1994 11 p Limited Reproducibility: More than 20% of this document may be affected by microfiche quality
(Contract N00014-91-J-1710)
(AD-A279892; TR-28-ONR) Avail: Issuing Activity (Defense Technical Information Center (DTIC))

Two new chiral macrocyclic ligands containing the pyrimidine subcyclic unit have been prepared. Chiral dimethyl-substituted pyrimidino-crown 1 was prepared from 4-methoxy-5-methyl-2,6-pyrimidinedimethyl ditosylate 3 and chiral dimethyl-substituted tetraethylene glycol. Treatment of dimethyl 4-methoxy-5-methyl-2,6-pyrimidinedicarboxylate 4 with the diamine derivative of chiral dibenzyl-substituted tetraethylene glycol gave the chiral dibenzyl-substituted pyrimidino-crown diamide 2. Starting 4-methoxy-5-methyl-2,6-pyrimidinedimethanol 11 was prepared by a six step process from acetamidine hydrochloride and diethyl oxalpropionate. DTIC

N95-20592 Brigham Young Univ., Provo, UT. Dept. of Chemistry.
THERMODYNAMIC AND NMR STUDIES OF SOLVENT EFFECT ON ENANTIOMERIC RECOGNITION FOR A CHIRAL ORGANIZ AMMONIUM CATION BY CHIRAL DIKETOPYRIDINO-18-CROWN-6 TYPE LIGANDS AT 25.0 C
Xian X. Zhang, Reed M. Izatt, Cheng Y. Zhu, and Jerald S. Bradshaw 11 May 1994 19 p Limited Reproducibility: More than 20% of this document may be affected by microfiche quality
(Contract N00014-91-J-1710)
(AD-A279893; TR-30-ONR) Avail: Issuing Activity (Defense Technical Information Center (DTIC))

Three chiral diketopyridino-18-crown-6 type macrocycles have been shown to exhibit a high degree of enantiomeric recognition toward alpha-(1-naphthyl)ethylammonium perchlorate (NapEt) in various ratios of chloroform/methanol (CDCl3/CD3OD) and 1,2-dichloroethane/methanol (C2H4Cl2/CH3OH) solvent mixtures (from 100% to 10% methanol component). In most cases differences in log K values (delta(log) K) for (R)- and (S)-NapEt complexation with the chiral macrocycles are larger than 0.5. The degree of the enantiomeric recognition indicated by the delta(log) K value changes noticeably with the binary solvent components. The recognition is better in the solvents having a moderate methanol component than in the binary solvents having either a high a low methanol component. The highest degree of recognition is observed in 6/4 (v/v)

CDCl3/CD3OD and C2H4Cl2/CH3OH solvent mixtures and in a 7/3 (v/v) C2H4Cl2/CH3OH mixture for chiral (S,S)-1 macrocycle. Author (DTIC)

N95-20660# New Mexico Univ., Albuquerque, NM. Dept. of Chemistry.
STRUCTURE OF DIBIS(DIETHYLDITHIOCARBAMATO) ZINC (2) Mu-BIS(DIETHYLPHOSPHINO)ETHANE TOLUENE(2) Technical Report No. 14
D. Zeng, M. J. Hampden-Smith, and E. M. Larson 6 May 1994 12 p
(Contract N00014-91-J-1258)
(AD-A279792) Avail: CASI HC A03/MF A01

Dibis(diethyldithiocarbamato) Zinc(2) mu-bis (Diethylphosphino)ethane (2)Toluene ((Et(sub 2) NCSS)2Zn)2 (mu-depe).2C7H8 Mr = 1114.4, monoclinic, P 2(sub l)/c, a = 12.960(1), b = 11.311(2), c = 20.129(5), beta = 96.46(1) deg, V = 2932 A(exp 3), Z = 2, D(sub x) = 1.254 g/cu cm, lambda (MoKa) = 0.070930 A, graphite monochromator, mu = 11.89/cm, F(000) = 1180, T = 298 K, final R = 0.055 (Rw = 0.072) for 2531 observed I greater than 3 sigma(I) reflections. The molecule is positioned symmetrically about an inversion center at the cell origin, which is situated in the center of the bridging diphosphine ligand. Toluene is disordered in this structure such that the rotation between the two positions of the methyl carbon is 36 deg. The geometry about the zinc can be described as distorted trigonal bipyramid. The Zn-P distance is 2.388 A and the zinc-sulphur distances range from 2.320 to 2.653 A. DTIC

N95-21746# Rensselaer Polytechnic Inst., Troy, NY.
CHEMICAL INTERACTIONS BETWEEN PROTEIN MOLECULES AND POLYMER MEMBRANE MATERIALS
J. A. Koehler and G. Belfort 25 Aug. 1994 4 p
(Contract DE-FG02-90ER-14114)
(DE95-001808; DOE/ER-14114/4) Avail: CASI HC A01/MF A01

During the past year, the authors have used the Surface Forces Apparatus (SFA) to measure the intermolecular forces between a model protein (hen egg-white lysozyme) and a model hydrophilic surface (mica), between lysozyme and itself and between lysozyme and a model hydrophobic surface composed of a crosslinked alkoxysilane surfactant (hexadecyltriethoxysilane, HTE). As expected, repulsive forces are dominant between the hydrophilic surfaces with the same charge (lysozyme-lysozyme) while attractive forces are dominant between oppositely charged surfaces (lysozyme-mica) and between the lysozyme and the hydrophobic surface. The DLVO theory for charged surfaces was found to agree with the results of the lysozyme-lysozyme interaction. Efforts also have been focused on trying to create a well-formed, defect-free monolayer of the HTE on the surface of the mica using a Langmuir-Blodgett (LB) apparatus. A smooth, defect-free surface is desired for the intermolecular force studies. Atomic force microscopy has been used to determine the topography of the HTE films. DOE

N95-21911# Westinghouse Science and Technology Center, Pittsburgh, PA.
VIBRATIONAL OVERTONE SPECTROSCOPY OF PYRIDINE AND RELATED COMPOUNDS Technical Report, Sep. 1993 - Jun. 1994
Deanne Snavely and Joyce A. Overly 3 Jun. 1994 14 p
(Contract N00014-91-J-4130)
(AD-A280105; TR-14) Avail: CASI HC A03/MF A01

The vibrational overtone spectra of gaseous pyridine, 3-fluoropyridine, 2,6-difluoropyridine. and pyrazole have been recorded using photoacoustic absorption spectroscopy. The pyridine, 3-fluoropyridine, and 2,6-difluoropyridine overtone spectra exhibit two local mode progressions. These CH local modes are mixed and cannot be assigned to the separate CH oscillators at the 2,6 and 3,4 and 5 positions. The transition wavenumbers and peak widths are compared to those of benzene and pyrrole, both of which exhibit only one overtone peak at each quantum level. The fourth overtone spectrum of gaseous pyrazole displays two peaks. These spectra indicate that the presence of a lone pair perpendicular to the aromatic Pi system in aromatic heterocycles removes the local mode equivalency of the CH oscillators. DTIC

N95-22252# Massachusetts Inst. of Tech., Cambridge, MA. Dept. of Chemistry.
SYNTHESIS AND STRUCTURE OF A NOVEL BIS-STIBOLE
Donald P. Hsu, Benjamin P. Warner, Richard A. Fisher, William M. Davis, and Stephen L. Buchwald 18 Oct. 1994 12 p
(Contract N00014-91-J-1043)
(AD-A286345; TR-6) Avail: CASI HC A03/MF A01

The novel benzobis(stibole) 2a, synthesized from bis(zirconacycle) 1, crystallizes to place all three ring substituents in a syn orientation. Complex 2a stacks in such a manner so that the central phenyl ring of two adjacent Sb2C10 ring systems are nearly perfectly eclipsed. Author (DTIC)

N95-22333 Rijksinstituut voor Volksgezondheid en Milieuhygieene, Bilthoven (Netherlands).
USE OF QUANTUM CHEMICALLY DERIVED DESCRIPTORS FOR QSAR MODELING OF REDUCTIVE DEHALOGENATION OF AROMATIC COMPOUNDS
E. Rorije, J. Richter, and W. J. G. M. Peijnenburg Apr. 1994 47 p
(PB95-132783; RIVM-719101015) Avail: Issuing Activity (National Technical Information Service (NTIS))

Encouraged by the strongly increasing calculative power of the present generation of personal computers, a strong tendency of using quantum-chemically derived descriptors is presently ground in the development of structure-activity relationships for various environmental end-points. In the study, quantum-chemically derived parameters are developed for a limited number of halogenated aromatic compounds to model the anaerobic reductive dehalogenation reaction rate constants of these compounds. It is shown that due to the heterogeneity of the set of compounds used, no single descriptor or combination of descriptors was able to adequately model the reaction under investigation. Thus subsets had to be created out of the group of compounds. NTIS

N95-22474# Giner, Inc., Waltham, MA.
DEVELOPMENT AND DEMONSTRATION OF ADVANCED TECHNOLOGIES FOR DIRECT ELECTROCHEMICAL OXIDATION OF HYDROCARBONS (METHANOL, METHANE, PROPANE) Final Report
J. A. Kosek and A. B. LaConti Jul. 1994 8 p
(Contract DAAL03-92-C-0011)
(AD-A285094) Avail: CASI HC A02/MF A01

Direct methanol fuel cells use methanol directly as a fuel, rather than the reformate typically required by fuel cells, thus eliminating the reformer and fuel processing train. In this program, Giner, Inc. advanced development of two types of direct methanol fuel cells for military applications. Advancements in direct methanol proton-exchange membrane fuel cell (DMPEMFC) technology included development of a Pt-Ru anode catalyst and an associated electrode structure which provided some of the highest DMPEMFC performance reported to date. Scale-up from a laboratory-scale single cell to a 5-cell stack of practical area, providing over 100 W of power, was also demonstrated. Stable stack performance was achieved in over 300 hours of daily on/off cycling. Direct methanol aqueous carbonate fuel cells were also advanced with development of an anode catalyst and successful operation at decreased pressure. Improved materials for the cell separator/matrix and the hardware were also identified. Author (DTIC)

24 COMPOSITE MATERIALS

Includes physical, chemical, and mechanical properties of laminates and other composite materials.

For ceramic materials see *27 Nonmetallic Materials.*

N95-19899# Army Research Lab., Aberdeen Proving Ground, MD.
THE INFLUENCE OF PLY WAVINESS WITH NONLINEAR SHEAR ON THE STIFFNESS AND STRENGTH REDUCTION OF COMPOSITE LAMINATES Final Report, May 1992 - Apr. 1993
Travis A. Bogetti, John W. Gillespie, Jr. (Delaware Univ., Newark, DE.), and Mark A. Lamontia (Du Pont de Nemours, E. I. and Co., Newark, DE.) Oct. 1994 33 p
(Contract MDA972-89-C-0043; DA Proj. 1L1-62618-AH-80)
(AD-A285736; ARL-TR-585) Avail: CASI HC A03/MF A01

The influence of ply waviness with nonlinear shear material response on the mechanical performance of composite laminates is studied. An analytic model, based on a three-dimensional laminated media analysis, is developed to predict the effective nonlinear laminate behavior associated with ply waviness. An undulating 0 ply in a (90/0/90) sublaminate configuration and an undulating (+/- Beta) ply in a (90/ +/- Beta /90) sublaminate configuration are two types of ply waviness considered. An incremental loading strategy is employed wherein piecewise linear solutions are supposed to obtain the overall nonlinear stress/strain response of composite laminates with wavy plies. The analysis also predicts individual ply stress and strain distributions with the wavy ply configuration. The maximum stress failure criteria is used to predict ply failure in local regions with the wavy ply configuration, and a progressive failure methodology is adopted to permit local load redistribution. Results are presented which offer fundamental insight into the dominant mechanisms for stiffness and strength reduction in composite laminates exhibiting ply waviness and nonlinear shear material behavior. DTIC

N95-19919 United Technologies Research Center, East Hartford, CT.
THE ENVIRONMENTAL DURABILITY OF FIBER REINFORCED CERAMIC MATRIX COMPOSITES Annual Report, 6 Jul. 1993 - 6 Jul. 1994
J. J. Brennan 15 Aug. 1994 62 p Limited Reproducibility: More than 20% of this document may be affected by microfiche quality
(Contract N00014-93-C-0065)
(AD-A283750; UTRC-R94-970439-2) Avail: CASI HC A04

The main objective of this program is to investigate the environmental durability of ceramic matrix composites based on glass-ceramic and polymer pyrolysis matrices, with emphasis on the relationship between composite properties, microstructure, and chemistry, and the environment to which the composite is exposed. This environmental exposure will include the effect of oxidation, moisture, and corrosion, under conditions of high temperature and stresses. During the first year of the program, the composite system under study consisted of a barium-magnesium aluminosilicate (BMAS) glass-ceramic matrix reinforced with SiC/BN coated Nicalon SiC fibers. The results of these environmental durability tests on this composite system are discussed. DTIC

N95-19951*# State Univ. of New York, Buffalo, NY. Dept. of Mechanical and Aeronautical Engineering.
ANALYSIS OF THE PROGRESSIVE FAILURE OF BRITTLE MATRIX COMPOSITES Final Report
David J. Thomas Cleveland, OH NASA Feb. 1995 120 p
(Grant NAG3-862; RTOP 537-04-22)
(NASA-CR-195415; E-9337; NAS 1.26:195415) Avail: CASI HC A06/MF A02

This report investigates two of the most common modes of localized failures, namely, periodic fiber-bridged matrix cracks and transverse matrix cracks. A modification of Daniels' bundle theory is combined with Weibull's weakest link theory to model the statistical distribution of the periodic matrix cracking strength for an individual layer. Results of the model predictions are compared with experimental data from the open literature. Extensions to the model are made to account for possible imperfections within the layer (i.e., nonuniform fiber lengths, irregular crack spacing, and degraded in-situ fiber properties), and the results of these studies are presented. A generalized shear-lag analysis is derived which is capable of modeling the development of transverse matrix cracks in material systems having a general multilayer configuration and under states of full in-plane load. A method for computing the effective elastic properties for the damaged layer at the global level is detailed based upon the solution for the effects of the damage at the local level. This methodology is general in nature and is therefore also applicable to (0(sub m)/90(sub n))(sub s) systems. The characteristic stress-strain response for more general cases is shown to be qualitatively correct (experimental data is not available for a quantitative evaluation), and the damage evolution is recorded in terms of the matrix crack density as a function of the applied strain. Probabilistic effects are introduced to account for the statistical nature of the material strengths, thus allowing cumulative distribution curves for the probability of failure to be generated for each of the example laminates. Additionally, Oh and Finney's classic work on fracture location in brittle materials is extended and combined with the shear-lag analysis. The result is an analytical form for predicting the probability density function for the location of the next transverse crack occurrence within a crack bounded region. The results of this study verified qualitatively the validity of assuming a uniform crack spacing (as was done in the shear-lag model). Author

N95-20001*# National Aeronautics and Space Administration. Lewis Research Center, Cleveland, OH.
THIRD INTERMETALLIC MATRIX COMPOSITES SYMPOSIUM, VOLUME 350
J. A. Graves, ed. (General Electric Co., Schenectady, NY.), R. R. Bowman, ed., and J. J. Lewandowski, ed. (Case Western Reserve Univ., Cleveland, OH.) Pittsburgh, PA Materials Research Society 6 Apr. 1994 326 p Symposium held in San Francisco, CA, 4-6 Apr. 1994; sponsored by Materials Research Society
(Contract N00014-94-G-0212) (ISSN 0272-9172)
(NASA-TM-110059; NAS 1.15:110059; AD-A284984; ISBN-1-55899-250-2; LC-94-2659) Avail: CASI HC A15/MF A03

Partial contents include: issues in potential IMC application for aerospace structures; powder metallurgy processing of intermetallic matrix composites; microstructure and properties of intermetallic matrix composites produced by reaction synthesis; combustion synthesis of niobium aluminide matrix composites; ambient temperature synthesis of bulk intermetallics; wear behavior of SHS intermetallic matrix composites; fracture characteristics of metal-intermetallic laminates produced by SHS reactions; and vapor phase synthesis of Ti aluminides and the interfacial bonding effect on the mechanical property of micro-composites reinforced by pyrolized SiC fibers. DTIC

N95-20022# Oak Ridge National Lab., TN.
COMPARISON OF THE DYNAMIC FATIGUE BEHAVIOR OF TWO MONOLITHIC SiC AND AN Al2O3/SiC COMPOSITE
K. Breder and V. J. Tennery 1994 11 p Presented at the 18th Annual Conference on Composites and Advanced Ceramics, Cocoa Beach, FL, 9-14 Jan. 1994
(Contract DE-AC05-84OR-21400)
(DE94-017751; CONF-940135-8) Avail: CASI HC A03/MF A01

Two monolithic silicon carbides, NT230 siliconized SiC from Norton Saint Gobain and sintered (beta)-SiC from Coors, and a silicon carbide particulate reinforced alumina ceramic composite from Lanxide, which all are candidate materials for pressurized heat exchangers in coal-fired power plants have been evaluated. The fast fracture flexure strength was measured as a function of temperature. All candidate materials retained a sufficient strength level up to 1400 C. The susceptibility to slow crack growth (SCG) was evaluated by the dynamic fatigue method at 1100 C and 1400 C. None of the materials exhibited SCG at 1100 C. At 1400 C the siliconized SiC ceramic showed limited SCG and the composite ceramic exhibited creep damage when stressed to 50% of fast fracture strength at the intermediate and slow stressing rates. This prevented the evaluation of the SCG properties of this material at 1400 C. Fractography supported the mechanical observations and with the exception of the specimens which exhibited creep damage, only the siliconized SiC showed a small SCG damage zone at long times at 1400 C. DOE

N95-20023# Oak Ridge National Lab., TN.
THE THERMAL CONDUCTIVITY OF CARBON COATED SILICON CARBIDE FIBERS EMBEDDED IN A SILICON CARBIDE MATRIX
S. C. Beecher, R. B. Dinwiddie, and R. A. Lowden 1993 12 p Presented at the 22nd International Thermal Conductivity Conference, Tempe, AZ, 7-10 Nov. 1993
(Contract DE-AC05-84OR-21400)
(DE94-017758; CONF-9311131-4) Avail: CASI HC A03/MF A01

The room temperature thermal conductivity has been measured for a series of composite materials composed of carbon coated silicon carbide (SiC) fibers embedded in a SiC matrix. The composite samples consisted of 0/30(degree) bi-directional plain weave Nicalon fibers coated with varying thicknesses of pyrolitic carbon and infiltrated with SiC by the forced flow chemical vapor infiltration process to form the matrix. The fiber volume fraction was held constant at 0.423 +/- 0.012 and from 0.03 (mu)m - 0.983 (mu)m, with the fibers of one sample left uncoated. Results transverse to fiber direction show significant differences with the introduction and subsequent increase in the carbon coating thickness. The thermal conductivity decreased for all the coated samples compared to the uncoated sample coating thickness compared to the sample with the thinnest carbon coating. DOE

N95-20027# Argonne National Lab., IL. Energy Technology Div.
ELASTIC ANISOTROPY IN HOT-PRESSED SI3N4 COMPOSITES: ROLE OF IN SITU (BETA)-SI3N4 GRAINS AND ADDED (BETA)-SI3N4 WHISKERS
M. H. Manghnani (Hawaii Univ., Honolulu, HI.), E. S. Fisher (Hawaii Univ., Honolulu, HI.), F. Y. Li (Hawaii Univ., Honolulu, HI.), R. J. Wang (Hawaii Univ., Honolulu, HI.), J. P. Singh, and J. L. Routbort Jun. 1994 14 p Presented at the 96th Annual Meeting of the American Ceramic Society, Indianapolis, IN, 24-28 Apr. 1994
(Contract W-31-109-eng-38)
(DE94-018387; ANL/ET/CP-83963; CONF-940416-25) Avail: CASI HC A03/MF A01

The elastic anisotropy in hot-pressed samples of (beta)-Si3N4 monolithic polycrystalline composites and in composite with 5 to 35% (beta)-Si3N4 whiskers have been investigated at room temperature by high precision acoustic interferometry. All of the samples, including the monolithic Si3N4, show anisotropy characterized as transverse isotropic about the hot-pressing (HP) direction and are described using the five elastic stiffness moduli for hexagonal symmetry. The principal anisotropy is revealed in the shear modulus difference, C(66) - C(44) /C(sub 44), which increases from 7% in the monolithic sample to 15% in samples with 10% or more whiskers. All the stiffness moduli except for C(44) increase with the addition of whiskers. Young's modulus in the HP direction is 5% smaller than in the HP plane in all samples. The whiskers enhance the shear anisotropy produced by the in situ elongated (beta)-grains. DOE

N95-20081# North Dakota State Univ., Fargo, ND.
LOW TEMPERATURE SYNTHESIS OF SEMICONDUCTOR MATERIALS Annual Report, 15 Aug. 1993 - 14 Aug. 1994
Philip Boudjouk 14 Sep. 1994 14 p
(Contract F49620-92-J-0431)
(AD-A285120; AFOSR-94-0600TR) Avail: CASI HC A03/MF A01

This report summarizes the results obtained in the second year of the grant. During this time experiments were conducted which demonstrated that phenyl groups on heavier main group atoms undergo migration with great facility. This mobility has been utilized to prepare novel materials with a broad range of semiconducting and optoelectronic properties. Gallium arsenide and gallium phosphide have been prepared at modest temperatures (approx. 400 C) from easily prepared single source precursors. Work conducted in this time period led to the discovery that ternary compounds composed of tin, sulfur and selenium can be prepared in high yields at approx. 400 C as phase pure materials in nonstoichiometric ratios from readily available compounds. Conventional procedures call for temperatures greater than 1000 C. Also discovered was that pyrolysis of perbenzylated compounds has advantages over the alkylated analogues among which are lower toxicity, faster decomposition times and lower contamination of target products. Author (DTIC)

N95-20092 Pennsylvania Univ., Philadelphia, PA. Dept. of Materials Science and Engineering.
NOVEL ELECTROCHEMICAL MATERIALS PREPARED BY SOL-GEL CHEMISTRY Annual Report
Gregory C. Farrington, John O. Thomas, and Stig Friberg 15 Jul. 1994 12 p Prepared in cooperation with Uppsala Univ., Sweden and Clarkson Univ., Potsdam, NY Limited Reproducibility: More than 20% of this document may be affected by microfiche quality
(Contract N00014-90-J-1156)
(AD-A286310) Avail: CASI HC A03

This program is directed at preparing and characterizing novel gels, xerogels, and aerogels which, because of their conductivity and/or charge storage capability, have unusual electrochemical characteristics. Typical materials of interest are the transition-metal oxides currently being exploited in their polycrystalline forms in the electrodes of the lithium batteries. Characterization involves structural and electrochemical studies, atomic force microscopy, and novel x-ray diffraction and mu-FTIR techniques. One of several novel contributions of this work is the use of molecular dynamics simulation as a powerful source of insight into surface and bulk mechanisms in sol-gel synthesized materials. DTIC

N95-20105# California Univ., Los Angeles, CA. Dept. of Materials Science and Engineering.
INTERNATIONAL COLLABORATION PROGRAM ON INNOVATIVE CHEMICAL PROCESSING OF SUPERIOR ELECTRONIC AND OPTICAL MATERIALS Final Report, 15 Jul. 1991 - 14 May 1994
John D. Mackenzie Jul. 1994 21 p
(Grant AF-AFOSR-0317-91)
(AD-A285122; AFOSR-94-0617TR) Avail: CASI HC A03/MF A01

An international collaborative research project to investigate the preparation and properties of quantum dot materials based on CdS microcrystals in various matrices has been carried out from July 1991 to May 1994. The team consisted of Professor J.D. Mackenzie (P.I.), Professor M. Yamane of the Tokyo Institute of Technology, and Professor N. Peyghambarian of the University of Arizona. Samples were prepared by the Sol-Gel method with sodium borosilicate glass and ormosils (organically modified silicates) as the matrices. The samples showed no photodarkening effect and have chi cubed values up to 10(exp -6) cgs units. Techniques were developed to limit the size distribution of the Cds while maintaining high concentrations (greater than 10%). Waveguides were fabricated by the ion-exchange method. At their present developmental stages, the samples suggested the possibility that they can be made into a new type of laser and also offer the potentials of achieving photochemical hole-burning at room temperature. Author (DTIC)

N95-20125# Oak Ridge National Lab., TN.
THE THERMAL CONDUCTIVITY OF CARBON-FIBER REINFORCED METAL MATRIX COMPOSITES
R. B Dinwiddie, S. C. Beecher, P. V. Arya (Materials and Electrochemical Research Corp., Tucson, AZ.), and J. C. Withers (Materials and Electrochemical Research Corp., Tucson, AZ.) 1993 13 p Presented at the 22nd International Thermal Conductivity Conference, Tempe, AZ, 7-10 Nov. 1993
(Contract DE-AC05-84OR-21400)
(DE94-017767; CONF-9311131-3) Avail: CASI HC A03/MF A01

High thermal conductivity metal matrix composites are being considered for heat sink applications in fusion energy, automotive and aerospace industries. The addition of P-120 carbon fibers was found to enhance the thermal conductivity of both aluminum and copper matrix composites. However, above 60 volume percent loading, the thermal conductivity of the composites tends to decrease. The titanium used as a fiber interface was found to be deleterious to the thermal conductivity of the copper matrix. Small diameter diamond particle additions tend to reduce the thermal conductivity of both the copper and aluminum matrix composites. This is explained in terms of the dominance of thermal boundary resistance due to the large surface to volume ratio of the small diamond particles. DOE

N95-20292 Department of the Navy, Washington, DC.
MULTI-LAYERED TRANSLATED RIB-STIFFENED COMPOSITE HOLLOW CYLINDER ASSEMBLY Patent
Roger M. Crane, inventor (to Navy) and D. M. Bergen, inventor (to Navy) 20 Sep. 1994 13 p Filed 30 Sep. 1993
(AD-D016566; US-Patent-5,348,052; US-Patent-Appl-SN-128785; US-Patent-Class-138-174) Avail: US Patent and Trademark Office

A multiple-layered, translatedly rib-stiffened, composite hollow cylinder and method for fabrication thereof utilizing filament winding techniques known in the art. An inner skin is wound over a mandrel; then, circumferential ribs are wound over the inner skin, pin rings are placed at the axial ends of the mandrel, longitudinal stringers are engaged with the pin rings and wound over the circumferential ribs, circumferential bands are wound near the axial ends over the longitudinal stringers, and another skin is wound over the circumferential bands and longitudinal stringers; these steps, commencing with the winding of circumferential ribs and concluding with the winding of an additional skin, are repeated as many times as desired, each repetition forming an additional layer, with the circumferential ribs for each additional layer being longitudinally staggered in relation to the circumferential ribs for the previous layer. DTIC

N95-20357# Oak Ridge National Lab., TN.
THE IN-SITU FRACTURE AND AUGER ANALYSIS OF NICALON FIBERS
D. N. Braski and M. C. Osborne (Rensselaer Polytechnic Inst., Troy, NY.) 1994 16 p Presented at the 18th Annual Conference on Composites

and Advanced Ceramics, Cocoa Beach, FL, 9-14 Jan. 1994
(Contract DE-AC05-84OR-21400)
(DE94-017771; CONF-940135-10) Avail: CASI HC A03/MF A01

A technique has been developed to fracture irradiated Nicalon SiC fibers in a Scanning Auger Microprobe (SAM) and analyze the fracture surfaces without contaminating the specimen chamber. The technique, which was evaluated using as-received fibers, requires only minor modification of two standard specimen holders and should be applicable to other fibers or materials that can be broken under low loads in bending. The technique is simple, rapid, reduces beam charging, and eliminates the need for ion sputtering. DOE

N95-20412 Georgia Inst. of Tech., Atlanta, GA.
MATERIALS RESEARCH FOR GHz MULTI-CHIP MODULES FY 1993 Letter Report, 1 Oct. 1992 - 30 Sep. 1993
Paul A. Kohl 30 Sep. 1993 7 p Limited Reproducibility: More than 20% of this document may be affected by microfiche quality
(Contract N00014-91-J-4008)
(AD-A279661) Avail: Issuing Activity (Defense Technical Information Center (DTIC))

The goal of this program is to investigate new dielectrics, metals and processes for the fabrication and characterization of multi-chip modules (MCM) which hold the promise of excellent performance, cost and yield for high frequency MCM's. First, the processes for using noble metals (gold and silver) as the interconnection metallization in the module have been investigated. The noble metal process can have fewer processing steps (particularly for gold) than the equivalent copper process and are potentially lower cost, particularly when high reliability is important. A silver process has been developed so that the silver maintains its bulk conductivity (highest of conventional metals) and has low residual stress during high temperature processing. Commercialization of the silver process is being considered. Second, a unique adhesion material has been investigated and is currently being tested for commercial use. We are in the process of evaluating the process with n-Chip and transferring the technology to them. DTIC

N95-20427# Cornell Univ., Ithaca, NY. Dept. of Chemistry.
NOVEL MATERIALS Final Report, 1 Dec. 1990 - 30 Nov. 1993
Francis J. DiSalvo 12 May 1994 4 p
(Contract N00014-91-J-1269)
(AD-A279693) Avail: CASI HC A01/MF A01

This is the final report on a project funded for 3 years by ONR. The project was very successful; it resulted in the discovery of many new solid state ternary nitrides. Since there were so few ternary nitrides known, and since many of the binary nitrides, such as TiN, AlN and Si3N4 are so technologically useful, our aim was to explore the synthesis, structural chemistry and properties of ternary nitrides. Prior to our work very few ternary nitrides, other than those formed by alloying binaries and having simple binary like structures, were known. We have shown that there is indeed a very large class of such ternary nitrides. DTIC

N95-20429# California Univ., Santa Barbara, CA. Dept. of Materials.
THE PROCESSING AND MECHANICAL PROPERTIES OF HIGH TEMPERATURE/HIGH PERFORMANCE COMPOSITES. STRESS REDISTRIBUTION AND NOTCH PROPERTIES, BOOK 2 Annual Report, 1 Mar. 1992 - 28 Feb. 1994
Anthony G. Evans and Frederick A. Leckie 1 Mar. 1994 316 p See also AD-A279738
(Contract N00014-92-J-1808)
(AD-A279737) Avail: CASI HC A14/MF A03

Topics discussed in this document include: (1) Cracking and stress redistribution in ceramic layered composites; (2) Notch sensitivity and stress redistribution in CMC's; (3) Notch-sensitivity and shear bands in brittle matrix composites; (4) On large scale sliding in fiber-reinforced composites; (5) On the tensile strength of a fiber-reinforced ceramic composite containing a crack-like flaw; (6) SiC/CAS: a notch insensitive ceramic matrix composite; (7) On the tensile properties of a fiber reinforced titanium matrix composite; (8) Localization due to damage in two directions for fiber reinforced composites; (9) An elliptical inclusion embedded in an anisotropic body; (10) On the strength of fiber reinforced ceramic composites containing an elliptic hole; (11) On the theoretical toughness and strength of ceramic composites; (12) Microlaminated high temperature intermetallic composites; and (13) Fracture toughness of Al-4%Mg/Al2O3P composites. DTIC

N95-20430# California Univ., Santa Barbara, CA. Dept. of Materials.
THE PROCESSING AND MECHANICAL PROPERTIES OF HIGH TEMPERATURE/HIGH PERFORMANCE COMPOSITES. FATIGUE AND CREEP, BOOK 3 Annual Report, 1 Mar. 1992 - 28 Feb. 1994
Anthony G. Evans and Frederick A. Leckie 1 Mar. 1994 567 p See also AD-A279739
(Contract N00014-92-J-1808)
(AD-A279738) Avail: CASI HC A24/MF A04

This document includes the following topics: (1) Mode I fatigue cracking in a fiber reinforced metal matrix composite; (2) Interfacial crack growth in fiber-reinforced metal-matrix composites; (3) Fatigue crack growth in fiber-reinforced metal-matrix composites; (4) Thermomechanical fatigue cracking in fiber reinforced metal matrix composites; (5) Transverse and cyclic thermal loading of the fiber reinforced metal-matrix composite SCS6/Ti-15-3; (6) Fatigue of ceramic matrix composite; (7) Ductile-reinforcement toughening in gamma gamma/TiAl intermetallic-matrix composites; effects on fracture toughness and fatigue-crack propagation resistance; (8) Creep models for metal matrix composites with long brittle fibers; (9) Models for the creep of ceramic matrix composite materials; (10) Power law creep of ceramic matrix composite materials; (10) Power law creep with interface slip and diffusion in a composite material; (11) Steady state creep of fiber-reinforced composites: Constitutive equations and computational issues; (12) The creep anisotropy of a continuous-fiber-reinforced SiC/CAS composite; (13) Power law creep of a composite material containing discontinuous rigid aligned fibers; and (14) Diffusive void bifurcation in stressed solid. DTIC

N95-20459 Department of the Navy, Washington, DC.
ATTACHMENT METHODOLOGY FOR COMPOSITE CYLINDER ASSEMBLY Patent
Roger M. Crane, inventor (to Navy) and Paul Coffin, inventor (to Navy) 27 Sep. 1994 10 p Filed 30 Sep. 1993
(AD-D016578; US-Patent-5,349,738; US-Patent-Appl-SN-128786; US-Patent-Class-29-434) Avail: US Patent and Trademark Office

Cylinder-to-cylinder attachment method and construction featuring nonutilization of mechanical fasteners or bonding, especially advantageous for attachment of cylinders which are composite or to be subjected to hydrostatic pressure. A fastening ring is interpositionally and rotatively engaged and aligned with a toothed axial end of each cylinder whereby the inwardly radial teeth for each cylinder appropriately mesh with the outer grooved circumferential surface of the fastening ring. The resultant joint is easily detachable and less susceptible than conventional joints to damage, breakage, degradation, stress concentrations and fluid infiltration. DTIC

N95-20583 California Univ., Santa Barbara, CA.
THE PROCESSING AND MECHANICAL PROPERTIES OF HIGH TEMPERATURE/HIGH PERFORMANCE COMPOSITES. BOOK 7: IN-SITU MEASUREMENTS OF STRESS AND DAMAGE Annual Report, Mar. 1993 - Apr. 1994
Anthony G. Evans and Frederick A. Leckie Apr. 1994 135 p Limited Reproducibility: More than 20% of this document may be affected by microfiche quality
(Contract N00014-92-J-1808)
(AD-A279814) Avail: Issuing Activity (Defense Technical Information Center (DTIC))

This document discusses the following topics: Residual Stress Measurement in Sapphire Fiber Composites; Through-Focus and Transmission Fluorescence Spectroscopy; Measurement of Residual Stresses in Sapphire Fiber Composites Using Optical Fluorescence; Luminescence Sensing of Stress in Ti/A2O3 Fiber Reinforced Composites; Optical Fluorescence from Chromium Ions in Sapphire: A Probe of the Image Stress; Residual Stresses in Al2O3-ZrO2 Composites: A Test and Stochastic Stress Models; Stress Measurement Using Optical Fluorescence. DTIC

N95-20584 California Univ., Santa Barbara, CA.
THE PROCESSING AND MECHANICAL PROPERTIES OF HIGH TEMPERATURE/HIGH PERFORMANCE COMPOSITES. BOOK 5: INTERFACE EFFECTS Annual Report, Mar. 1993 - Apr. 1994
Anthony G. Evans and Frederick A. Leckie Apr. 1994 365 p Limited Reproducibility: More than 20% of this document may be affected by microfiche quality
(Contract N00014-92-J-1808)
(AD-A279815) Avail: Issuing Activity (Defense Technical Information Center (DTIC))

This document focuses on the following topics: Mechanics of the Push-Out Process from In-Situ Measurement of the Stress Distribution along Embedded Sapphire Fiber; Relationships Between Hysteresis Measurements and the Constituent Properties of Ceramic Matrix Composites, (theory-Relationships Between Hysteresis Measurements and the Constituent Properties of Ceramic Matrix Composites, and Experimental Studies on Unidirectional Materials); The Effect of Fiber-Matrix Reactions on the Interface Properties in a SCS-6/Ti-24Al-11Nb Composite; Fatigue growth and stress Redistribution at Interface; Dislocations, Steps and Disconnections at Interfaces; On the Directionality of Interfacial Cracking in Bicrystals and the loading phase angle dependence; Models for Metal/Ceramic Interface Fracture; and The Activation Energy for Dislocation nucleation from a Crack Tip. DTIC

N95-20787# Burton Technologies, Inc., Raleigh, NC.
WEAR RESISTANT COMPOSITE STRUCTURE OF VITREOUS CARBON CONTAINING CONVOLUTED FIBERS
R. Gaines Burton and Ralph A. Burton 1 Nov. 1994 27 p
(Contracts DE-FG01-94CE-15613; DE-AC02-88CE-90027)
(DE95-002254; DOE/CE-15613/T2) Avail: CASI HC A03/MF A01

The program goals for the first quarter were to locate and contact potential manufacturers of these components, evaluate their level of interest, and begin discussions of the type and design of the prototypes to be fabricated for their evaluation. Thoughtful discussion at this stage would result in fabricating prototypes which answer the greatest number of questions possible for a given manufacturer at the lowest cost to this program. In the present economy many manufacturing firms have almost no funds for testing and evaluating new materials. This places a greater burden on the data obtained from outside laboratories. In many cases this data will be used to make that first evaluation on MRCC's (metal reinforced carbon composites) suitability for a given application and give firms the confidence to commit to a evaluation program. In Exhibit 1, which is attached to this report the authors have the first set of data from outside laboratories. This has been incorporated into a paper which has been accepted for the annual STLE (Society of Tribologist and Lubrication Engineers) conference in Chicago in the spring of 1995. The authors are in active contact with over 20 companies. Some of these have advanced to the point of requesting prototypes and the drawings have been submitted. In addition two groupings of companies have been formed to pool their resources in combined evaluation programs. These are described. The authors are in the process of manufacturing the first prototypes. DOE

N95-20801 California Univ., Santa Barbara, CA. Dept. of Materials.
THE PROCESSING AND MECHANICAL PROPERTIES OF HIGH TEMPERATURE/HIGH PERFORMANCE COMPOSITES. MECHANISM-BASED CONSTITUTIVE LAWS AND DESIGN, BOOK 1 Annual Report, 1 Mar. 1992 - 28 Feb. 1994
Anthony G. Evans and Frederick A. Leckie 1 Mar. 1994 449 p Limited Reproducibility: More than 20% of this document may be affected by microfiche quality
(Contract N00014-92-J-1808)
(AD-A279736) Avail: CASI HC A19

This document discusses the following: (1) Materials selection and innovation in design; (2) Elasto-plastic analysis of interface layers for fiber-reinforced metal-matrix composites; (3) Modeling of anisotropic behavior of weakly bonded fiber reinforced MMC's; (4) On the tensile properties of a fiber reinforced titanium matrix composite; (5) Control of strength anisotropy of metal matrix fiber composites; (6) Inelastic strains due to matrix cracking in unidirectional fiber-reinforced composites; (7) Location and ultimate tensile strength of fiber-reinforced ceramic-matrix composites; (8) Matrix cracking and debonding of ceramic-matrix composites; (9) Matrix cracking of cross-ply ceramic composites; (10) Transverse cracking in fiber-reinforced brittle matrix, cross-ply laminates; (11) The mechanisms of deformation and failure in carbon matrix composites subject to tensile and shear loading; (12) Uncoupled and coupled approaches to predict crack-initiation in fiber-reinforced ceramic-matrix composites; (13) Stress corrosion cracking in a unidirectional ceramic-matrix composite; (14) Effects of gauge length on the tensile strength of SiC fibers; (15) Tunneling cracks in constrained layers; (16) The effect of interfacial properties on the flow strength of discontinuous reinforced metal matrix composites; (17) On dislocation storage and the mechanical response of fine scale microstructures; and (18) Effect of microstructural parameters on the yield strength of Al-4%Mg/Al2O3p composites. DTIC

N95-20802# California Univ., Santa Barbara, CA. Dept. of Materials.
THE PROCESSING AND MECHANICAL PROPERTIES OF HIGH TEMPERATURE/HIGH PERFORMANCE COMPOSITES. PROCESSING/PROPERTY CORRELATIONS, BOOK 4 Annual Report, 1 Mar. 1992 - 28 Feb. 1994
Anthony G. Evans and Frederick A. Leckie 1 Mar. 1994 408 p See also AD-A279736
(Contract N00014-92-J-1808)
(AD-A279739) Avail: CASI HC A18/MF A04

This document contains the following topics: (1) A fiber fracture model for metal matrix composite monotape consolidation; (2) Effects of composite processing on the strength of sapphire fiber-reinforced composites; (3) On the flexural properties of brittle multilayer materials; (4) The microstructure of SiC/C composites and relationships with mechanical properties; (5) Microstructural observations on constrained densification of alumina powder containing a periodic array of sapphire fibers; (6) Material issues in layered forming; (7) Thermal modelling and experimental testing of Md spray shape deposition processes; (8) Liquid precursor infiltration and pyrolysis of powder compacts; (9) Influence of interparticle force on the rheological behavior of pressure-consolidated alumina particle slurries; (10) Evolution of a metastable FCC solid solution during sputter deposition of Ti-Al-B alloys; (11) Novel ODS copper alloys from rapidly-solidified precursors; (12) Mechanical properties of partially dense alumina produced from powder compacts. DTIC

N95-20805# Advanced Fuel Research, Inc., East Hartford, CT.
DETECTION OF ENVIRONMENTAL DETERIORATION IN FIBER REINFORCED COMPOSITES BY FT-RAMAN SPECTROSCOPY, PHASE 1 Final Report, 30 Jul. 1993 - 30 Apr. 1994
Stuart Farquharson, Anthony Bananno, Rosemary Basilakis, Martin Carangelo, and Marie DiTaranto May 1994 47 p
(Contract DAAL01-93-C-4058)
(AD-A279763) Avail: CASI HC A03/MF A01

A number of advanced fiber reinforced organic matrix composites are being developed and applied in the aerospace industry. In these applications, the composites may be exposed to a variety of harsh environments, which may induce chemical and physical changes in the composite material, and ultimately lead to component failure. The successful use of these composites, therefore, requires methods to reliably detect and assess these changes. During this Phase 1 Program, a fiber optic based Fourier transform Raman spectrometer was specifically developed to perform nondestructive evaluation of environmentally damaged composites. Specifically, graphite and Kevlar reinforced epoxy and polyimide composite samples were subjected to thermal cycling, moisture exposure and ultraviolet irradiation. Three point flexure tests were used to measure flexural strength, flexural modulus, failure strain and failure load to assess induced mechanical property changes in the composites. Reflectance infrared spectra of the sample surfaces, as well as transmission infrared spectra of evolved gas phase chemical species were used to further characterize these changes. DTIC

N95-20808 Army Research Lab., Adelphi, MD.
THE CALCULATION AND MEASUREMENT OF HELMHOLTZ COIL FIELDS Final Report, Oct. 1993 - Oct. 1994
David J. DeTroye and Ronald J. Chase Nov. 1994 20 p Limited Reproducibility: More than 20% of this document may be affected by microfiche quality
(AD-A286081; ARL-TN-35) Avail: CASI HC A03

Helmholtz coils are used to develop uniform magnetic fields for a variety of research applications. Helmholtz coils can be easily constructed, and the fields easily calculated. This makes them especially useful in calibrating sensors and numerous other low frequency magnetic field testing applications. This particular report will discuss the calculation and measurement of Helmholtz coil fields to be used for testing of composite materials to low frequency magnetic fields. DTIC

N95-20840# Argonne National Lab., IL.

TOPOGRAPHY OF NEUTRON SCATTERING FROM DIBLOCK COPOLYMER FILM

Z. Cai and T. P. Russell (International Business Machines Corp., San Jose, CA.) 1994 21 p
(Contract W-31-109-eng-38)
(DE95-001457; ANL/IPNS/PP-79589) Avail: CASI HC A03/MF A01

The surface structure of a multilayered film of symmetric perdeuterated diblock copolymers of polystyrene and polymethylmethacrylate, denoted P(d-S-b-d-MMA), was investigated by neutron scattering at grazing incidence. The film surfaces were covered by islands or holes of uniform height with a lateral size of several micrometers. With the angle of incidence fixed, the off-specular neutron scattering was measured as function of scattering angle and neutron wavelength. The off-specular scattering intensity shows ridges at constant q(sub z), the momentum transfer along the surface normal. The scattering arises from the surface domains. It was found that the off-specular ridges developed from minima in the oscillations in the specular profile corresponding to domain height. The characteristic of the off-specular scattering, which is different from that of the off-specular scattering due to the conformal roughness in a multilayered film, is interpreted in terms of the correlations of the surface domains. DOE

N95-20859# Air Force Inst. of Tech., Wright-Patterson AFB, OH. National Air Intelligence Center.

CERTAIN PHYSICAL PROPERTIES OF LANTHANUM DIGERMANIDE

Yu. B. Paderno, O. B. Goncharuk, and V. M. Makarchenko 3 Oct. 1994 6 p Transl. into ENGLISH from Dopovedi Akademii Nauk Ukrains'Kol RSR (USSR), v. 21, no. 1965 p 56-58
(AD-A286592; NAIC-ID(RS)T-0648-94) Avail: CASI HC A02/MF A01

The authors carried out an investigation of the physical properties of lanthanum digermanide on samples obtained by sintering the components and subsequent smelting in an argon atmosphere. On the basis of the results obtained the conclusion was drawn that lanthanum digermanide possesses semiconductor properties. Author (DTIC)

N95-20912# Argonne National Lab., IL.

ROLE OF INTERNAL STRESSES IN FRACTURE BEHAVIOR OF ENGINEERING COMPOSITES

J. P. Singh, D. Singh, D. S. Kupperman, and S. Majumdar May 1994 15 p Presented at The Metallurgical Society (TMS) Conference on High Performance Composites, Rosemont, IL, 10-15 Oct. 1994
(Contract W-31-109-eng-38)
(DE95-001106; ANL/ET/CP-82224; CONF-9410184-3) Avail: CASI HC A03/MF A01

Microstructure and fracture behavior of SiC(f)/Si3N4 matrix composites, and of Ag-particulate/YBa2Cu3O(x)(YBCO) superconductor matrix composites, together with internal residual strains in composite constituents, have been evaluated as a function of reinforcing-fiber, particulate content, and processing variables. Residual strains were measured by neutron diffraction with the Intense Pulsed Neutron Source and Powder Diffractometer at Argonne National Laboratory. Internal radial strains on SiC fibers in SiC(f)/Si3N4 composites decreased from 0.0015 at 8.4 vol.% fibers to 0.0010 at 23.3 vol.% fibers. This decrease in radial strain with increasing fiber volume fraction is expected to reduce frictional and hence interfacial sliding stresses between SiC fibers and Si3N4 matrix; this is in agreement with interfacial shear strengths measured by the fiber pushout technique. Similar relationships between residual strain and interfacial shear strength was observed for composites hot isostatically pressed (HIPed). For YBCO-AG composites, tensile strain in the Ag phase was as high as 0.085%, whereas compressive strain in the YBCO phase reached 0.09%. The presence of compressive strain (stress) improved the strength of YBCO from 200 to 223 MPa. Implications of the effects of residual stresses on interfacial characteristics and resulting composite mechanical properties and fracture behavior will be discussed. DOE

N95-20913# State Univ. of New York, Buffalo, NY.

CARBON FIBER REINFORCED SUPERCONDUCTOR COMPOSITES

Zheng-Qiang Shi and D. D. L. Chung Nov. 1994 12 p
(Contract DE-FG01-91CE-15520)
(DE95-002504; DOE/CE-15520/T13) Avail: CASI HC A03/MF A01

The sandwiching of YBa2Cu3O(7-delta) by two layers of continuous copper-coated carbon fiber Sn-Pb matrix composite was found to: (1) increase the tensile and compressive strengths in the direction parallel to the fibers, such that both strengths increased with increasing fiber volume fraction; (2) increase the resistance to thermal cycling between room temperature and 77 K; and (3) increase the stability in air. The sandwich composites were made by diffusion bonding at 110 C and 0.34 MPa, or by hot roll bonding at 240 C and 7.0 cm/s. DOE

N95-21008*# National Aeronautics and Space Administration. Langley Research Center, Hampton, VA.

TEST FIXTURE FOR DETERMINATION OF ENERGY ABSORBING CAPABILITIES OF COMPOSITE MATERIALS Patent Application

J. Andre Lavoie, inventor (to NASA) (Virginia Polytechnic Inst., Blacksburg, VA.), Karen E. Jackson, inventor (to NASA) (Army Vehicle Structures Lab., Hampton, VA.), and John Morton, inventor (to NASA) (Virginia Polytechnic Inst., Blacksburg, VA.) 24 Sep. 1994 17 p
(Grant NAG1-343)
(NASA-Case-LAR-15212-1-CU; NAS 1.71:LAR-15212-1-CU; US-Patent-Appl-SN-306556) Avail: CASI HC A03/MF A01

The present invention provides a fixture for supporting an elongated specimen for crush testing. The fixture comprises a base plate, four guiding rods, a sliding plate, four support rods and two collars. The guiding rods connect to the base plate and extend in a direction substantially perpendicular to the base plate. The sliding plate has linear bearings which encircle the guiding rods and enable translation of the sliding plate along the axis of each guiding rod. The four supporting rods mount to the base plate and also extend in a direction substantially perpendicular to the base plate. Each support rod has a keyway for a wedge which contacts the elongated specimen and holds the specimen in place during crushing. Each collar lies above the sliding plate and holds a pair of support rods on their ends opposite the ends connected to the base plate. A spherical bearing sits on top of the sliding plate and transfers an applied load to the sliding plate, which moves downward and crushes the elongated specimen. Author

N95-21149# Materials Sciences Corp., Fort Washington, PA.

IMPLEMENTATION OF THE MILITARY HANDBOOK 17 FOR POLYMER MATRIX COMPOSITES AND METAL MATRIX COMPOSITES Progress Report, 1-30 Sep. 1994

Crystal H. Newton Oct. 1994 15 p Revised
(Contract DAAL01-93-C-4064)
(AD-A285629; MSC-TPR-3458/CA07-Rev) Avail: CASI HC A03/MF A01

Project effort this month concentrated on support of the Coordination Group meeting and data analysis. Information for the meeting booklet was submitted to ARL. Agendas for two working groups were revised based on progress on data analysis and discussions during the briefing meeting in August. These revisions were sent to the chairmen of working groups involved. The log of comments submitted for MIL-HDBK-17 was updated and distributed to the working group of chairmen. The executive session, the meeting of the MIL-HDBK-17 working group chairmen, was held on the afternoon of 19 September 1994. DTIC

N95-21215# Materials Sciences Corp., Fort Washington, PA.

IMPLEMENTATION OF THE MILITARY HANDBOOK 17 FOR POLYMER MATRIX COMPOSITES AND METAL MATRIX COMPOSITES Technical Progress Report, 1-31 Jul. 1994

Crystal H. Newton Oct. 1994 9 p
(Contract DAAL01-93-C-4064)
(AD-A285595; MSC-TPR-3456/CA07) Avail: CASI HC A02/MF A01

Based on the requirements of Contract Modification 0003, preparation of input of handbook from the 27th (Portland), 28th (Alexandria), and 29th (Monterey) meetings has been planned. All figures in the revisions and new sections will be scanned and included as part of the WordPerfect files. Corrections to Volume 1, Chapter 7 have been received from the Structural Joints working group. These corrections will be implemented in the next change notice or revision. The following draft sections from the 29th meeting in Monterey have been approved: Volume 1: Toxicity, Health

Hazards, and Safety; Definitions - new and revised definitions; General (Lamina, Laminate, and Fabric Mechanical Property Tests) - revision; Organization of data in handbook - revision. Volume 3: Polyimides - new; Amorphous Thermoplastics - new material to be appended; Laminate Strength and Failure - revision; Compression postbuckling and crippling - replaces Section 4.7.1.8. DTIC

N95-21363*# Analytical Services and Materials, Inc., Hampton, VA.
TIME-DEPENDENT DEFORMATION OF TITANIUM METAL MATRIX COMPOSITES Final Report
C. A. Bigelow (Federal Aviation Administration, Atlantic City, NJ.), Y. A. Bahei-El-Din (Cairo Univ., Egypt.), and M. Mirdamadi Jan. 1995 32 p
(Contract NAS1-19708; RTOP 505-63-50-04)
(NASA-CR-195030; NAS 1.26:195030) Avail: CASI HC A03/MF A01

A three-dimensional finite element program called VISCOPAC was developed and used to conduct a micromechanics analysis of titanium metal matrix composites. The VISCOPAC program uses a modified Eisenberg-Yen thermo-viscoplastic constitutive model to predict matrix behavior under thermomechanical fatigue loading. The analysis incorporated temperature-dependent elastic properties in the fiber and temperature-dependent viscoplastic properties in the matrix. The material model was described and the necessary material constants were determined experimentally. Fiber-matrix interfacial behavior was analyzed using a discrete fiber-matrix model. The thermal residual stresses due to the fabrication cycle were predicted with a failed interface, The failed interface resulted in lower thermal residual stresses in the matrix and fiber. Stresses due to a uniform transverse load were calculated at two temperatures, room temperature and an elevated temperature of 650 C. At both temperatures, a large stress concentration was calculated when the interface had failed. The results indicate the importance of accuracy accounting for fiber-matrix interface failure and the need for a micromechanics-based analytical technique to understand and predict the behavior of titanium metal matrix composites. Author

N95-21417 National Defence Research Establishment, Stockholm (Sweden). Dept. of Weapons Systems, Effects and Protection.
SIGNIFICANCE OF IMPACT VELOCITY FOR THE EXTENT OF DAMAGE IN CARBON/EPOXY LAMINATES [SPLITTERHASTIGHETENS BETYDELSE FOER SKADEOMFATTNINGEN HOS KOLFIBER/EPOXI-LAMINAT]
L. Svensson May 1994 30 p In SWAHILI
(PB95-133484; FOA-A-20057-2.3) Avail: Issuing Activity (National Technical Information Service (NTIS))

Carbon fiber/epoxy laminates were ballistically damaged. Impact velocity and residual velocity were measured. The extent of damage was estimated and related to impact velocity. An empirical model was adapted to the results to find a relation between laminate thickness, residual velocity and critical velocity. NTIS

N95-21432 National Defence Research Establishment, Stockholm (Sweden). Dept. of Weapon Systems, Effects and Protection.
DAMAGE TOLERANCE OF CARBON FIBRE POLYETHERETHERKETONE LAMINATES [KOLFIBER/POLYETERETERKETON-LAMINATS SKADETALIGHET]
F. Larsson Mar. 1994 20 p In SWAHILI
(PB95-131611; FOA-A-20056-2.4) Avail: Issuing Activity (National Technical Information Service (NTIS))

An investigation has been made of the ballistic damage tolerance of carbon fiber polyetheretherketone laminates (AS4/PEEK,APC-2) with near quasi-isotropic lay-up. The results indicate that a 40% greater compressive stress can be applied to the material compared to a carbon fiber epoxy composite of the first generation (T300/914) without causing collapse when impacted with penetrating steel balls with a diameter of 6,00 mm. Compared with a composite with a toughened epoxy matrix (HTA7/6376) the composite studied has a 20% greater capacity. The ranking order of the composites with respect to ballistic damage tolerance is there-with the same as for low velocity impact damage tolerance. This conclusion is not self evident since there are differences in morphology and composition between the three matrices. Therefore it has been important to find out if an increased impact velocity changes the ranking order of the composites. The ranking order is however unchanged. The delamination energies of the three mentioned composites at high crack propagation velocity have been determined for unidirectional specimens by means of a pendulum impactor. The energy required to delaminate the APC-2 specimens is of the order of three times that of the other composites. NTIS

N95-21445# Northwestern Univ., Evanston, IL.
DEPOSITION AND PROPERTIES OF NOVEL NITRIDE SUPERLATTICE COATINGS Progress Report, 28 Sep. 1990 - Oct. 1994
S. A. Barnett, W. D. Sproul, and M. S. Wong Oct. 1994 3 p
(Contract DE-FG02-90ER-45434)
(DE95-002945; DOE/ER-45434/4) Avail: CASI HC A01/MF A01

The major effort during this report period was to elucidate the hardening mechanisms in polycrystalline superlattices. Since the last progress report, the authors have been working on theoretical modeling of hardening mechanisms in superlattices and have carried out detailed studies of two new polycrystalline superlattice coatings, NbN/VN and CrN/TiN, which were produced using an opposed, dual-cathode, high-rate, reactive, unbalanced-magnetron sputtering system. Significant hardness enhancement the above rule-of-mixture hardness value was found for the CrN/TiN, but not for the NbN/VN. Correlating these results with prior results for TiN/NbN and TiN/VN shows that the major hardening mechanism in polycrystalline superlattices is the difference in layer elastic moduli, which is minimal in the NbN/VN case. The modulus difference provides a barrier to dislocation flow across the layers. In the absence of modulus-difference hardening in NbN/VN, it was found that other hardening mechanisms such as coherency strains and the small grain sizes observed in the superlattices play a minor role. The results achieved in this report period are described in this paper along with publications and presentations. DOE

N95-21481# Oak Ridge National Lab., TN.
PROCESSING AND MECHANICAL PROPERTIES OF LAMINAR Al2O3-Ni3Al COMPOSITES
J. H. Schneibel and K. B. Alexander 1994 7 p Presented at the Spring Meeting of the Materials Research Society, San Francisco, CA, 4-8 Apr. 1994
(Contract DE-AC05-84OR-21400)
(DE94-019332; CONF-940411-53) Avail: CASI HC A02/MF A01

Several compositions of the intermetallic alloy Ni3Al were examined with respect to: (1) their wetting of Al2O3; and (2) their energy absorption capability in Al2O3/Ni3Al laminates. Wetting is enhanced by small additions of carbon (e.g., 0.1 at. %), and bonding by additions of zirconium (e.g., 1 at. %). Chevron-notched laminate specimens were tested in three-point bending to assess the energy absorption due to the presence of a thin layer of Ni3Al. A nickel aluminide with the composition of Ni-22Al-1Zr-0.1C-0.1B was found to have a reasonable combination of wetting, adhesion and energy absorption. Interfacial bonding was found to be weak in all laminates. DOE

N95-21553# General Atomics Co., San Diego, CA.
B4C-SIC REACTION-SINTERED COATINGS ON GRAPHITE PLASMA FACING COMPONENTS
P. G. Valentine, P. W. Trester, and J. Winter (Kernforschungsanlage, Juelich, Germany.) May 1994 24 p Presented at the 11th International Conference on Plasma Surface Interactions in Controlled Fusion Devices, Mito, Japan, 23-27 May 1994
(Contract DE-AC03-89ER-51114)
(DE94-019105; GA-A-21719; CONF-940580-19) Avail: CASI HC A03/MF A01

Boron carbide plus silicon carbide (B4C-SiC) reaction-sintered coatings for use on graphite plasma-facing components were developed. Such coatings are of interest in TEXTOR tokamak limiter-plasma interactions as a means of reducing carbon erosion, of providing a preferred release of boron for oxygen gettering, and of investigating silicon's effect on radiative edge phenomena. Specimens evaluated had: (1) either Ringsdorfwerke EK 98 graphite or Le Carbon Lorraine felt-type AEROLOR A05 CFC substrates; (2) multiphase coatings, comprised of B4C, Sic, and graphite; (3) nominal coating compositions of 69 wt.-% B4C + 31 wt.-% SiC; and (4) nominal coating thicknesses between 250 and 775 (mu)m. Coated coupons were evaluated by high heat flux experiments in the JUDITH (electron beam) test facility at KFA. Simulated disruptions, with energy densities up to 10 MJm(exp -2), and normal operation simulations, with power densities up to 12 MWm(exp -2), were conducted. The coatings remained adherent; at the highest levels tested, minor changes occurred, including localized remelting, modification of the crystallographic phases, occasional microcracking, and erosion. DOE

N95-21736# Ames Lab., IA.
THE ROLE OF MICROCRACKING ON THE CRACK GROWTH RESISTANCE OF BRITTLE SOLIDS AND COMPOSITES
S. B. Biner 1994 10 p
(Contract W-7405-eng-82)
(DE95-001678; IS-M-806) Avail: CASI HC A02/MF A01

A set of numerical analyses of crack growth was preformed to elucidate the influence of microcracking on the fracture behavior of microcracking brittle solids and composites. The random nucleation, orientation and size effects of discrete nucleating microcracks and resulting interactions are fully accounted for in a hybrid finite element model. The results obtained from the finite element analysis are compared with the continuum description of the microcracking. Although continuum description can provide a reasonable estimation of shielding, it fails to resolve the details of micromechanism of toughening resulting from microcracking, since not every shielding event during the course of crack extension corresponds to an increase in the R-curve. Moreover, as seen in the composite cases, the local events leading to toughening behavior may not be associated with the microcracking even in the presence of a large population of microcracks. DOE

N95-21776# Oak Ridge National Lab., TN.
CREEP BEHAVIOR IN SiC WHISKER-REINFORCED ALUMINA COMPOSITE
H. T. Lin and P. F. Becher 1994 12 p Presented at the Engineering Foundation Conference on Plastic Deformation of Ceramics, Snowbird, UT, 7-12 Aug. 1994
(Contract DE-AC05-84OR-21400)
(DE95-001071; CONF-9408175-1) Avail: CASI HC A03/MF A01

Grain boundary sliding (often accompanied by cavitation) is a major contributor to compressive and tensile creep deformation in fine-grained aluminas, both with and without whisker-reinforcement. Studies indicate that the creep response of alumina composites reinforced with SiC whiskers can be tailored by controlling the composite microstructure and composition. The addition of SiC whiskers (less than 30 vol%) significantly increases the creep resistance of fine-grained (1-2 (mu)m) alumina in air at temperatures of 1,200 and 1,300 C. However, at higher whisker contents (30 and 50 vol%), the creep resistance is degraded due to enhanced surface oxidation reactions accompanied by extensive creep cavitation. Densification aids (i.e., Y2O3), which facilitate silica glass formation and thus liquid phase densification of the composites, can also result in degradation of creep resistance. On the other hand, increasing the matrix grain size or decreasing the whisker aspect ratio (increased whisker number density) results in raising the creep resistance of the composites. These observations not only explain the variability in the creep response of various SiC whisker-reinforced alumina composites but also indicate factors that can be used to enhance the elevated temperature performance. DOE

N95-21924# Ames Lab., IA.
THE ROLE OF GRAIN BOUNDARY SLIDING ON CREEP DEFORMATION CHARACTERISTICS OF DISCONTINUOUS REINFORCED COMPOSITES
S. B. Biner 1994 15 p
(Contract W-7405-eng-82)
(DE95-001671; IS-M-807) Avail: CASI HC A03/MF A01

In this study, the grain boundary sliding behavior in discontinuous reinforced composites is investigated numerically. Results indicate that the stress enhancement factor for the composite is much larger than the one observed for the matrix material. In the composite, the increase in the strain rates as a result of grain boundary sliding occurs in a wider stress range in comparison to the matrix. It is shown that the experimentally observed large scale triple point grain boundary cavitation in the composites could occur as a result of large grain rotations resulting from grain boundary sliding and evolution of triaxial stress state. Also, the observed larger creep exponent values or stress dependent creep exponent values for the composites may not be explained solely by the mechanism of grain boundary sliding. DOE

N95-21999# California Univ., Santa Barbara, CA.
THE PROCESSING AND MECHANICAL PROPERTIES OF HIGH TEMPERATURE/HIGH PERFORMANCE COMPOSITES. BOOK 6: DELAMINATION AND COMPRESSIVE BEHAVIOR Annual Report, Mar. 1993 - Apr. 1994
Anthony G. Evans and Frederick A. Leckie Apr. 1994 320 p
(Contract N00014-92-J-1808)
(AD-A279780) Avail: CASI HC A14/MF A03

The general emphasis for 1994 would be on increased software development, testing of subelements and design calculations. For these purposes, the constitutive law coding and development would be coordinated by Nick Aravas, and implemented in ABAQUS. The initial implementation would be the elastic/plastic model for MMC's with interface debonding developed in 1993 (Leckie). This would be extended in 1994 to include creep and some aspects of thermomechanical cycling. The code would be used for design calculations concerned with MMC rotors, actuators and vanes (Leckie). A plan is being formulated to collaborate with Pratt and Whitney to acquire MMC sub-elements representative of these components during 1994. Experimental tests on these subelements would be capable of providing a direct validation of the code capabilities. DTIC

N95-22009# Los Alamos National Lab., NM.
RECENT DEVELOPMENTS IN LOW COST STABLE STRUCTURES FOR SPACE
T. C. Thompson, C. Grastataro, and B. G. Smith 1994 11 p Presented at the Advanced Materials for High Precision Detectors, Geneva, Switzerland, 28 Sep. 1994
(Contract W-7405-eng-36)
(DE95-000857; LA-UR-94-3144; CONF-9409222-1) Avail: CASI HC A03/MF A01

The Los Alamos National Laboratory (LANL) in partnership with Composite Optics Incorporated (COI) is advancing the development of low cost, lightweight, composite technology for use in spacecraft and stable structures. The use of advanced composites is well developed, but the application of an all-composite tracker structure has never been achieved. This paper investigates the application of composite technology to the design and fabrication of an all-composite spacecraft bus for small satellites, using technology directly applicable to central tracking in a high luminosity environment. The satellite program Fast On-Orbit Recording of Transient Events (FORTE) is the second in a series of satellites to be launched into orbit for the US Department of Energy (DOE). This paper will discuss recent developments in the area of low cost composites, used for either spacecraft or ultra stable applications in high energy physics (HEP) detectors. The use of advanced composites is a relatively new development in the area of HEP. The Superconducting Super Collider (SSC) spawned a new generation of Trackers which made extensive use of graphite fiber reinforced plastic (GFRP) composite systems. LANL has designed a structure employing new fabrication technology. This concept will lower the cost of composite structures to a point that they may now compete with conventional materials. This paper will discuss the design, analysis and proposed fabrication of a small satellite structure. Central tracking structures using advanced materials capable of operating in an adverse environment typical of that found in a high luminosity collider could use identical concepts. DOE

N95-22038# Naval Postgraduate School, Monterey, CA.
A TRANSMISSION ELECTRON MICROSCOPE CHARACTERIZATION OF SODIUM SULFATE HOT CORROSION OF SILICON CARBIDE FIBER-REINFORCED LITHIUM ALUMINOSILICATE GLASS-CERAMIC MATRIX COMPOSITE M.S. Thesis
Richard K. Hunt Sep. 1994 84 p
(AD-A286164) Avail: CASI HC A05/MF A01

Sodium sulfate hot corrosion of a SiC/lithium aluminosilicate (LAS) composite was studied using conventional transmission electron microscopy and selected area diffraction. Changes in the morphology, composition, and crystallography of the phases in the glass-ceramic matrix and the fiber/matrix interface were studied. Microchemical analysis using energy dispersive x-ray spectroscopy (EDS) was also performed on all phases detected. Three samples were studied: (1) as-received, (2) no salt coating and annealed in argon, and (3) sodium sulfate coated and annealed in oxygen. Both heat treatments were performed at 900 C for 100 hours. Sample (1) matrix was comprised of small stoichiometric grains of beta-spodumene (Li2O-Al2O3-4SiO2) and mullite (3Al2O3-2SiO2) in a high silica glass (88 wt% SiO_2 and 12 wt% Al_2O_3). The fiber/matrix interface consisted of an amorphous SiO_2 and graphitic carbon layer. Sample (2) showed a substantial decrease in mullite content with a concomitant increase in alumina content of the glass and crystalline phases. Sample (3) suffered considerable hot corrosion. DTIC

N95-22096 National Defence Research Establishment, Stockholm (Sweden). Dept. of Weapon Systems, Effects and Protection.
EFFECT OF LASER RADIATION ON CARBON FIBRE/EPOXY COMPOSITES [INVERKAN AV LASEREXPONERING PA KOLFIBERKOMPOSITER]
O. Dickman, O. Rydlund, and L. Svensson Jun. 1994 18 p In SWAHILI
(PB95-133526; FOA-A-20060-2.4) Avail: Issuing Activity (National Technical Information Service (NTIS))

The effect of laser radiation on carbon fiber/epoxy composites was studied. According to the literature exposure to intensities less than 1 kW/sq cm mainly degrade the matrix whereas intensities greater than 6-7 kW/sq cm degrade both matrix and fibers. The mechanical properties of carbon fiber composites are affected in a similar way as aluminum after exposure to laser. After laser exposure at high intensities the residual tensile strength of the carbon fiber composites was equal to a composite with a drilled hole. The experimental work essentially verified the literature survey at intensities 1 kW/sq cm. After CO_2-laser exposure (1 kW/sq cm) of quasi-isotropic carbon fiber composites no delamination outside the visible damaged area was detected. The reduction in tensile strength after laser exposure was in good agreement with the literature. NTIS

N95-22115# Pacific Northwest Lab., Richland, WA.
HIGH TEMPERATURE CORROSION AND CRACK GROWTH OF SIC/SIC AT VARIABLE OXYGEN PARTIAL PRESSURES
R. H. Jones, C. H. Henager, Jr., and C. F. Windisch, Jr. Jun. 1994 29 p Presented at the Japan-USA Seminar Development and Environmental Characteristics of New Materials, Mount Hood, OR, 7-9 Jun. 1994
(Contract DE-AC06-76RL-01830)
(DE94-018715; PNL-SA-24865; CONF-9406261-1) Avail: CASI HC A03/MF A01

Thermal gravimetric analysis (TGA) and subcritical crack growth (SCG) measurements of chemical-vapor-infiltrated (CVI)-SiC matrix, reinforced with Nicalon fibers and with a 1-micro m-thick C fiber/matrix interface, have been conducted at 1100 C over O_2/Ar mixtures ranging from 0.25% to 20.0% O_2. The TGA and interface recession measurements both gave linear reaction kinetics for O_2 concentrations of 2.0% or less and a reaction order of unity. Subcritical crack-growth measurements demonstrated that crack velocity in the stress intensity-independent Stage 2 regime increases with increasing O_2/Ar ratio. Also, The transition from Stage 2 to the stress intensity-dependent Stage 3 regime is shifted to lower stress intensities with increasing O_2/Ar ratio. A time-dependent crack-growth model that incorporates creep of the bridging SiC fibers and the removal of the C interfacial layer by oxidation successfully explains the subcritical crack-growth characteristics. DOE

N95-22126# Lawrence Livermore National Lab., Livermore, CA.
THE INFLUENCE OF CHEMISTRY AND MICROSTRUCTURE ON THE FRACTURE TOUGHNESS OF V-V3SI IN-SITU COMPOSITES
G. A. Henshall, M. J. Strum, B. P. Bewlay (General Electric Co., Schenectady, NY.), and J. A. Sutliff (General Electric Co., Schenectady, NY.) 19 Aug. 1994 19 p Presented at the 2nd Fatigue and Fracture of Ordered Intermetallic Materials, Rosemont, IL, 3-6 Oct. 1994
(Contract W-7405-eng-48)
(DE94-018997; UCRL-JC-117630; CONF-9410203-1) Avail: CASI HC A03/MF A01

The room temperature fracture behavior is described for ductile-phase toughened V-V3Si in-situ composites produced by arc melting (AM), cold-crucible induction melting (IM), and cold-crucible directional solidification (DS). Composites were produced containing a wide range of microstructures, interstitial impurity contents, and volume fractions of the ductile V-Si solid solution phase, denoted (V). The fracture toughness of these composites generally increases as the volume fraction of (V) increases. For a given volume fraction of (V), the fracture toughness increases with decreasing 'effective' interstitial impurity content, (I)=(N)+1.3(O)+9(H). In eutectic composites, as (I) decreases from 1400 ppm (AM) to 400 ppm (IM), the fracture toughness increases from 10 to 20 MPa radical-m. The fracture toughness of the V-V3Si composites is further correlated with the mechanical properties of the component phases, SEM observations of the fracture surface characteristics, and electron back-scattering pattern measurements of the fracture facet crystallography. These correlations are discussed with respect to conventional ductile phase 'bridging' theories. DOE

N95-22130# Argonne National Lab., IL.
LOW TEMPERATURE TENSILE AND FRACTURE MECHANICAL STRENGTH IN MODE 1 AND MODE 2 OF FIBER REINFORCED PLASTICS FOLLOWING VARIOUS IRRADIATION CONDITIONS
K. Humer (Atominstitut der Oesterreichischen Hochschulen, Vienna, Austria.), H. W. Weber (Atominstitut der Oesterreichischen Hochschulen, Vienna, Austria.), E. K. Tschegg (Technische Univ., Vienna, Austria.), S. Egusa (Japan Atomic Energy Research Inst., Takasaki, Japan.), R. C. Birtcher, H. Gerstenberg (Technische Univ., Munich, Germany.), and B. N. Goshchitskii (Academy of Sciences, USSR, Sverdlovsk, USSR.) Aug. 1994 5 p Presented at the 18th European Symposium on Fusion Technology, Karlsruhe, Germany, 22-26 Aug. 1994 Sponsored by Bundesministerium fuer Wissenschafts und Forschung
(Contract W-31-109-eng-38)
(DE94-019269; ANL/MSD/CP-84144; CONF-940843-8) Avail: CASI HC A01/MF A01

The influence of radiation damage on the mechanical properties of fiber reinforced plastics (FRP's), which are considered as candidate materials for the insulation of superconducting magnets for nuclear fusion reactors, has been investigated. In order to cover the material spectrum produced at present, different types of FRP's (epoxies, polyimides and bismaleimides as resins; two- and three-dimensional E-, S- or T-glass fabrics as reinforcements) have been included in the test program. DOE

N95-22158 Technical Research Centre of Finland, Espoo (Finland). Building Materials Lab.
FIBRE-REINFORCED HIGH-STRENGTH CONCRETE
Sirje Vares and Tarja Haekkinen Dec. 1993 93 p
(PB95-131942; VTT/PUB-160) Copyright Avail: Issuing Activity (National Technical Information Service (NTIS))

The publication comprises two experimental parts. In the first part, 14 different kinds of steel, polypropylene and polyacrylonitrile fibers are studied in order to make high-strength fiber-reinforced concrete. The effect of fiber type and volume on the load-deflection behavior of FRC is studied and discussed. When the steel fiber volume fraction is low there is usually no significant increase in the 'first crack' and flexural strengths, but the toughness of concrete can be significantly increased over that of plane matrix. The relatively high specific surface area of the polymer fibers (PAN and PP) affects advantageously the 'first crack' strength of the composite. In the second part of the report, the influence of aging on the load-deflection behavior of different kinds of FRC is studied. Different matrices reinforced with steel or polypropylene fiber were subjected to aging and temperature and humidity changes. High-strength fiber-reinforced concrete composites, especially those reinforced by steel fibers can withstand large variation of temperature and humidity without the performance of fibers being significantly weakened. NTIS

N95-22211 Pittsburgh Univ., Pittsburgh, PA. Dept. of Chemistry.
NOVEL MATERIALS AND DEVICES FROM SELF-ASSEMBLED PERIODIC STRUCTURES Annual Report, 1 Oct. 1993 - 30 Sep. 1994
Sanford A. Asher 30 Sep. 1994 52 p Limited Reproducibility: More than 20% of this document may be affected by microfiche quality
(Contract F49620-93-1-0008)
(AD-A286499; AFOSR-94-0740TR) Avail: CASI HC A04

The purpose of this work is to develop highly optically nonlinear CdS quantum dot-SiO_2 sphere composites useful for optical switching. The concept is to use these spheres in a BCC array formed from crystalline colloidal arrays. The spheres would normally be refractive index matched to the medium and light would freely transmit. At high light intensities the refractive index of the nonlinear spheres would diverge from the medium and the array would optically pop up to diffract away the high intensity light. The device would act as an optical limiter. Last year's report announced the development of a successful synthesis of these SiO_2-CdS sphere composites. During this report period, we refined our process in order to obtain more homogenous and monodisperse products. We have also extended this synthesis to produce several new materials. DTIC

N95-22395# Materials Sciences Corp., Fort Washington, PA.
IMPLEMENTATION OF THE MILITARY HANDBOOK 17 FOR POLYMER MATRIX COMPOSITES AND METAL MATRIX COMPOSITES Progress Report, 1-31 Aug. 1994
Crystal H. Newton Oct. 1994 27 p
(Contract DAAL01-93-C-4064)
(AD-A285772; MSC-TPR-3457/CA07) Avail: CASI HC A03/MF A01

Changes between the DOD coordination review draft of MIL-HDBK-17-1D, MIL-HDBK-17-2C, and MIL-HDBK-17-3D were reviewed. These changes will be made to the WordPerfect files for the DOD coordination draft. The objective is to provide statistically-based characterization data on current and emerging continuous fiber-reinforced composite materials with guidelines for testing and for the analysis, presentation, and utilization of data. CASI

N95-22399# Vibration Inst., Willowbrook, IL.
ADVANCED MATERIALS AND PROCESS TECHNOLOGY FOR MECHANICAL FAILURE PREVENTION (PROCEEDINGS OF THE 48TH MEETING OF THE MECHANICAL FAILURES PREVENTION GROUP
Henry C. Pusey and Sallie C. Pusey 21 Apr. 1994 495 p Meeting held in Wakefield, MA, 19-21 Apr. 1994
(AD-A285785) Avail: CASI HC A21/MF A04

This document is the proceedings of the 48th Meeting of the Mechanical Failures Prevention Group (MFPG) which was held in Wakefield, Massachusetts on April 19-21, 1994. The proceedings contains featured papers from the Opening Session and a Plenary Session. There are session papers on Machinery Monitoring and Diagnostics, Failure Analysis, Evaluation of Materials Properties, Sensors and Neural Networks, Applications of Diagnostics and Nondestructive Test and Evaluation. Rotating equipment, Machinery, Condition monitoring, Failure analysis, Failure detection, Diagnostics, Sensors, Neural networks, Signature analysis and nondestructive evaluation DTIC

N95-22467 Department of the Navy, Washington, DC.
ACOUSTIC AND VIBRATION ATTENUATION COMPOSITE MATERIAL Patent
Usman A. Sorathia, inventor (to Navy), Joseph W. Killian, inventor (to Navy), and Andrew W. Jarrett, inventor (to Navy) 9 Aug. 1994 15 p Filed 30 Sep. 1992
(AD-D016585; US-Patent-5,337,288; US-Patent-Appl-SN-954805; US-Patent-Class-367-1) Avail: US Patent and Trademark Office

The present invention relates to acoustic and vibration attenuation composite material, particularly to damping tiles of the Type VI class 1, suitable for use in aircraft, ship and submarine applications, that is inexpensive, does not result in an unacceptable weight penalty, and is conformable-in-place to complex curvatures. The present acoustic and vibration attenuation composite comprises a constraining layer of at least one ply of graphite fabric together with curable phenolic resin bonded to a viscoelastic layer. DTIC

N95-20655# Thomson-CSF, Paris (France). Div. Radars et Contre-Mesures.
COMPOSITE CASES FOR AIRBORNE ELECTRONIC EQUIPMENT: A TECHNOLOGY STUDY AND EMC [BOITIERS COMPOSITES POUR EQUIPEMENTS ELECTRONIQUES AEROPORTES: UNE ETUDE TECHNOLOGIQUE ET CEM]
B. Dumont, J. Lecuellet, S. Laforet, G. Labaune, and M. Caplot *In* AGARD, Advanced Packaging Concepts for Digital Avionics Oct. 1994 12 p In FRENCH (For primary document see N95-20631 06-06)
Copyright Avail: CASI HC A03/MF A03

N95-20656# Sextant Avionique, Valence (France).
LIGHTWEIGHT ELECTRONIC ENCLOSURES USING COMPOSITE MATERIALS
C. Sarno *In* AGARD, Advanced Packaging Concepts for Digital Avionics Oct. 1994 12 p Sponsored by Ministry of Defence (For primary document see N95-20631 06-06)
Copyright Avail: CASI HC A03/MF A03

25 INORGANIC AND PHYSICAL CHEMISTRY

Includes chemical analysis, e.g., chromatography; combustion theory; electrochemistry; and photochemistry.

For related information see also *77 Thermodynamics and Statistical Physics.*.

N95-19924# Altamira Instruments, Inc., Pittsburgh, PA.
DIRECT AROMATIZATION OF METHANE
30 May 1994 10 p
(Contract DE-AC22-92PC-92109)
(DE94-017131; DOE/PC-92109/T5) Avail: CASI HC A02/MF A01

The thermal decomposition of methane shows significant potential as a process for the production of higher unsaturated and aromatic hydrocarbons when the extent of the reaction is limited. Preliminary experiments have shown that cooling the product and reacting gases as the reaction proceeds can significantly reduce or eliminate the formation of solid carbon and heavier (C10(+)) materials. Much work remains in optimizing the quenching process and this is one of the goals of this program. We will also study means to lower the temperature of the reaction as this will result in a more feasible commercial process due to savings realized in energy and material of construction costs. The use of free-radical generators and catalysts will be investigated as a means of lowering the reaction temperature thus allowing faster quenching. It is highly likely that such studies will lead to a successful direct methane to higher hydrocarbon process. DOE

N95-19980# Brookhaven National Lab., Upton, NY.
RESONANCE RAMAN SPECTROSCOPY OF VOLATILE ORGANICS: CARBON TETRACHLORIDE
R. E. Barletta and J. T. Veligdan Sep. 1994 21 p
(Contract DE-AC02-76CH-00016)
(DE95-000627; BNL-60755) Avail: CASI HC A03/MF A01

Volatile organic chemicals are a class of pollutants which are regulated at very low levels by the EPA. Consequently a need exists as a part of site remediation efforts within DOE to develop technologies which will allow for the in situ monitoring of these chemicals. Resonance Raman spectroscopy is a potential technique to accomplish this if the resonance enhancement is sufficiently high. Carbon tetrachloride was selected as a test case. Measurements under resonance conditions at 248 nm showed an enhancement factor of 2 x 10(sup 4). Using this value an estimate of the sensitivity for both in situ and remote monitoring of CCl4 was made. It was concluded that resonance Raman could be used to detect these chemicals at levels of regulatory interest. Future effort directed towards the development of a suitable probe as well as a field-portable system would be desirable. Such effort could be directed towards the solution of a particular monitoring problem within a DOE waste remediation project. Once developed, however, it should be easily generalized to the analysis of other VOC's in other environments. DOE

N95-20045# Massachusetts Inst. of Tech., Cambridge, MA. Dept. of Chemical Engineering.
DIRECT CATALYTIC DECOMPOSITION OF NITRIC OXIDE
M. Flytzani-Stephanopoulos, A. F. Sarofim, Y. Zhang, and T. Sun 1994 30 p
(Contract DE-FG22-91PC-91293)
(DE94-018840; DOE/PC-91293/11) Avail: CASI HC A03/MF A01

In this paper, effects of Cu-ZSM-5 catalyst preparation on the activity of over-exchanged copper for NO decomposition are reported. The Cu-ZSM-5 catalysts were prepared by incorporating Cu(2+) cations into ZSM-5 zeolites from an aqueous cupric acetate solution adjusted to different pH values by adding either acetic anhydride or aqueous ammonia in the solution. The Cu(2+) exchange levels in creased with increasing pH level. STEM/EDX analysis identified CuO particles (5-6 nm) on the zeolite surface for the materials exchanged at pHgreater than 6. Conversion and kinetics measurements of NO decomposition to N2 over these catalysts showed that the over-exchanged copper was not active. Short-time wash with aqueous ammonia removed this copper. The catalyst activity correlated very well with the amount of copper remaining in the ZSM-5 channels. DOE

N95-20046# State Univ. of New York, Buffalo, NY. Dept. of Chemical Engineering.
SUPERIOR CATALYSTS FOR SELECTIVE CATALYTIC REDUCTION OF NITRIC OXIDE
J. P. Chen, W. B. Li, M. C. Hausladen, E. S. Kikkinides, and R. T. Yang
1994 20 p
(Contract DE-FG22-93PC-93217)
(DE94-018845; DOE/PC-93217/T3) Avail: CASI HC A03/MF A01

In the last Quarterly Technical Progress Report the authors reported the synthesis and (partial characterization) and SCR (Selective Catalytic Reduction of NO) activity for a delaminated Fe2O3 -pillared clay (Fe2O3)-PILC). The SCR activity for this PILC was substantially higher than that of the commercial-type V2O5 + WO3/TiO2 catalyst. During the past quarter, the authors first completed the characterization of the delaminated Fe2O3-PILC catalyst. Both physical characterization (micropore probing by adsorption and Moessbauer spectroscopy) and chemical characterization (by IR spectroscopy) were performed. Since the synthesis of this PILC sample was undertaken under a specific set of conditions and it is known that the PILC properties depend strongly on the synthesis conditions, they then proceeded to examine in a systematic manner the dependence of the catalytic properties of the PILC on its synthesis conditions. Four parameters in the synthesis were studied: Fe precursors, pH of the pillaring solution, concentration of the pillaring solution, and the starting clay. Finally, the effect of the Cr2O3 promoter on the SCR activity of the pillar clay was studied. Results are reported. DOE

N95-20052# Texas A&M Univ., College Station, TX. Dept. of Chemistry.
CORRELATIONS BETWEEN SURFACE STRUCTURE AND CATALYTIC ACTIVITY/SELECTIVITY
D. W. Goodman Sep. 1994 19 p
(Contract DE-FG05-88ER-13954)
(DE94-019023; DOE/ER-13954/T2) Avail: CASI HC A03/MF A01

The primary focus of this research is to address those issues which are keys to understanding the relationship between surface properties and catalytic activity/selectivity. These issues also impact the understanding of the origins of the enhanced catalytic properties of mixed-metal catalysts. The experimental approach utilizes a microcatalytic reactor contiguous to a surface analysis system, an arrangement which allows in vacuo transfer of the catalyst from one chamber to the other. Surface techniques being used include Auger (AES), ultraviolet and X ray photoemission spectroscopy (UPS and XPS), temperature programmed desorption (TPD), low energy electron diffraction (LEED), high resolution electron energy loss spectroscopy (HREELS), infrared reflection absorption spectroscopy (IRAS), and scanning tunneling and atomic force microscopy (STM and AFM). This research program builds upon previous experience relating the results of single crystal kinetic measurements with the results obtained with supported analogs. As well, the authors are exploiting recent work on the preparation, the characterization, and the determination of the catalytic properties of ultra-thin metal and metal oxide films. Specifically, the program is proceeding toward three goals: (1) the study of the unique catalytic properties of ultrathin metal films; (2) the investigation of the critical ensemble size requirements for principal catalytic reaction types; and (3) the modelling of supported catalysts using ultra-thin planar oxide surfaces. DOE

N95-20100# National Inst. of Standards and Technology, Gaithersburg, MD. Building and Fire Research Lab.
GLOBAL EQUIVALENCE RATIO CONCEPT AND THE PREDICTION OF CARBON MONOXIDE FORMATION IN ENCLOSURE FIRES
W. M. Pitts Jun. 1994 172 p See also PB89-200091 and PB90-209602
(PB94-207511; NIST/Mono-179) Avail: CASI HC A08/MF A02; SOD HC

This report summarizes investigations of the formation of carbon monoxide (CO) in enclosure fires -- the most important factor in fire deaths. It contains the first complete review and analysis of the literature available on the global equivalence ratio (GER) concept. The results of a number of recent investigations (including work during the past fiscal year) which were either supported by the BFRL Grants Program or carried out in-house are then discussed. Based on the findings, two completely new mechanisms for the formation of CO, in addition to the quenching of a fire plume by rich upper layer covered by the GER concept, are identified. The first involves reaction of rich flame gases with air which is entrained directly into the high-temperature upper layer of an enclosure fire. The second results from the pyrolysis of oxygenated polymers (such as wood) which are located in a rich, high-temperature upper layer. The findings of these studies form the basis of an analysis which yields the conditions for which use of the GER concept is appropriate for predicting CO formation in enclosure fires. NTIS

N95-20107# Argonne National Lab., IL.
MERCURY CAPTURE IN BENCH-SCALE ABSORBERS
C. D. Livengood, H. S. Huang, M. H. Mendelsohn, and J. M. Wu 1994 11 p Presented at the 10th Annual Coal Preparation, Utilization and Environmental Control Contractors Conference, Pittsburgh, PA, 18-21 Jul. 1994
(Contract W-31-109-eng-38)
(DE94-016910; ANL/ES/CP-83739; CONF-940780-3) Avail: CASI HC A03/MF A01

This paper gives a brief overview of research being conducted at Argonne National Laboratory on the capture of mercury by both dry sorbents and wet scrubbers. The emphasis in the research is on development of a better understanding of the key factors that control the capture of mercury. Future work is expected to utilize that information for the development of new or modified process concepts featuring enhanced mercury capture capabilities. The results and conclusions to date from the Argonne research on dry sorbents can be summarized as follows: lime hydrates, either regular or high-surface-area, are not effective in removing mercury; mercury removals are enhanced by the addition of activated carbon; mercury removals with activated carbon decrease with increasing temperature, larger particle size, and decreasing mercury concentration in the gas; and chemical pretreatment (e.g., with sulfur or (CaCl2)) can greatly increase the removal capacity of activated carbon. Preliminary results from the wet scrubbing research include: no removal of elemental mercury is obtained under normal scrubber operating conditions; mercury removal is improved by the addition of packing or production of smaller gas bubbles to increase the gas-liquid contact area; polysulfide solutions do not appear promising for enhancing mercury removal in typical FGC systems; stainless steel packing appears to have beneficial properties for mercury removal and should be investigated further; and other chemical additives may offer greatly enhanced removals. DOE

N95-20117# National Renewable Energy Lab., Golden, CO.
PROCEEDINGS OF THE 1994 DOE/NREL HYDROGEN PROGRAM REVIEW
Jul. 1994 477 p Meeting held in Livermore, CA, 18-21 Apr. 1994
(Contract DE-AC36-83CH-10093)
(DE94-011835; NREL/CP-470-6431; CONF-9404194) Avail: CASI HC A21/MF A04

The U.S. Department of Energy has conducted programs of research and development in hydrogen and related technologies since 1975. The current program, conducted in accordance with the DOE Hydrogen Program Plan FY 1993--FY 1997 published in June 1992, establishes program priorities and guidance for allocating funding. The core program, currently under the Office of Energy Management, supports projects in the areas of hydrogen production, storage, and systems research. At an annual program review, each research project is evaluated by a panel of technical experts for technical quality, progress, and programmatic benefit. This Proceedings of the April 1994 Hydrogen Program Review compiles all research projects supported by the Hydrogen Program during FY 1994. For those people interested in the status of hydrogen technologies, we hope that the Proceedings will serve as a useful technical reference. Individual reports are processed separately. DOE

N95-20135# Western Research Inst., Laramie, WY.
NATURAL GAS CLEANUP: EVALUATION OF A MOLECULAR SIEVE CARBON AS A PRESSURE SWING ADSORBENT FOR THE SEPARATION OF METHANE/NITROGEN MIXTURES
R. W. Grimes Jun. 1994 16 p
(Contract DE-FC21-86MC-11076)
(DE94-012263; DOE/MC-11076/3829) Avail: CASI HC A03/MF A01

This report describes the results of a preliminary evaluation to determine the technical feasibility of using a molecular sieve carbon manufactured by the Takeda Chemical Company of Japan in a pressure owing adsorption cycle for upgrading natural gas (methane) contaminated with nitrogen. Adsorption tests were conducted using this adsorbent in two, four, and five-step adsorption cycles. Separation performance was evaluated in terms of product purity, product recovery, and sorbent productivity for all tests. The tests were conducted in a small, single-column adsorption apparatus that held 120 grams of the adsorbent. Test variables included adsorption pressure, pressurization rate, purge rate and volume, feed rate, and flow direction in the steps from which the product was collected. Sorbent regeneration was accomplished by purging the column with the feed gas mixture for all but one test series where a pure methane purge was used. The ratio between the volumes of the pressurization gas and the purge gas streams was found to be an important factor in determining separation performance. Flow rates in the various cycle steps had no significant effect. Countercurrent flow in the blow-down and purge steps improved separation performance. Separation performance appears to improve with increasing adsorption pressure, but because there are a number of interrelated variables that are also effected by pressure, further testing will be needed to verify this. The work demonstrates that a molecular sieve carbon can be used to separate a mixture of methane and nitrogen when used in a pressure swing cycle with regeneration by purge. Further work is needed to increase product purity and product recovery. DOE

N95-20139# Sandia National Labs., Albuquerque, NM. Contamination Free Mfg. Research Center.

FTIR SPECTROSCOPY FOR THE DETERMINATION OF WATER IN CORROSIVE GASES

R. K. Rowe, B. R. Stallard, L. H. Espinoza (New Mexico Univ., Albuquerque, NM.), and T. M. Niemczyk (New Mexico Univ., Albuquerque, NM.) 1994 8 p Presented at the Microcontamination 1994, San Jose, CA, 5-6 Oct. 1994
(Contract DE-AC04-94AL-85000)
(DE94-014658; SAND-94-1554C; CONF-9410132-2) Avail: CASI HC A02/MF A01

Internal corrosion in semiconductor gas delivery systems may lead to increased particle counts in downstream fabrication tools and to catastrophic failure of the delivery system itself. The problem is particularly acute since, once the corrosion begins, it becomes a moisture reservoir to further damage the system. To keep gas systems as moisture free as possible semiconductor manufacturers employ drying filters, usually located just after the source of the process gas. Even so, the piping for corrosive gases may need to be rebuilt every few years. Careful monitoring of the moisture in the process gases can provide valuable information about the state of the gas handling system and its effect on the process integrity. Presently there are several technologies costing $50K or less that are capable of detecting trace water vapor as low as 50 ppb in N2. However, no one type of instrument has achieved universal acceptance. In particular, all have limited compatibility with corrosive gases such as HCl and HBr. The goal of this project is to develop an in-line instrument based on infrared spectroscopy for this purpose. Earlier results leave no doubt that FTIR spectroscopy can be successfully used for trace water detection. However, important questions regarding optimal data analysis and instrument design are not yet fully answered. It is the goal of this research effort to answer these questions and to incorporate the findings into a prototype device suitable for commercialization. DOE

N95-20180*# National Aeronautics and Space Administration. Lewis Research Center, Cleveland, OH.

COMPUTER PROGRAM FOR CALCULATION OF COMPLEX CHEMICAL EQUILIBRIUM COMPOSITIONS AND APPLICATIONS. PART 1: ANALYSIS

Sanford Gordon and Bonnie J. McBride Oct. 1994 58 p
(NASA-RP-1311; E-8017; NAS 1.61:1311) Avail: CASI HC A04/MF A01

This report presents the latest in a number of versions of chemical equilibrium and applications programs developed at the NASA Lewis Research Center over more than 40 years. These programs have changed over the years to include additional features and improved calculation techniques and to take advantage of constantly improving computer capabilities. The minimization-of-free-energy approach to chemical equilibrium calculations has been used in all versions of the program since 1967. The two principal purposes of this report are presented in two parts. The first purpose, which is accomplished here in part 1, is to present in detail a number of topics of general interest in complex equilibrium calculations. These topics include mathematical analyses and techniques for obtaining chemical equilibrium; formulas for obtaining thermodynamic and transport mixture properties and thermodynamic derivatives; criteria for inclusion of condensed phases; calculations at a triple point; inclusion of ionized species; and various applications, such as constant-pressure or constant-volume combustion, rocket performance based on either a finite- or infinite-chamber-area model, shock wave calculations, and Chapman-Jouguet detonations. The second purpose of this report, to facilitate the use of the computer code, is accomplished in part 2, entitled 'Users Manual and Program Description'. Various aspects of the computer code are discussed, and a number of examples are given to illustrate its versatility. Author

N95-20188# Lehigh Univ., Bethlehem, PA. Center for Surface Studies.

SELECTIVE METHANE OXIDATION OVER PROMOTED OXIDE CATALYSTS

K. Klier, R. G. Herman, Chunlei Shi, and Qun Sun Jun. 1994 10 p
(Contract DE-FG21-92MC-29228)
(DE94-012270; DOE/MC-29228/3837) Avail: CASI HC A02/MF A01

Experimental work aiming at developing active catalysts for selective oxidation of methane to methanol was started in this quarter. Some of the experiments used a double catalyst bed design and with H2O as cofeed. The first catalyst bed, which serves as CH3 radical generator, was chosen to be 1 wt % SO4(exp -2)/Sr/La2O3, as this catalyst exhibits remarkable activity and selectivity at lower temperature (500 C to 550 C). A few transition metal oxides were used as the second catalyst bed to react with CH3 to form CH3O(exp -1)M(exp +1) species, which was then hydrolyzed to form CH3OH. It was found that unsupported metal oxides ZrO2, Y2O3, SrO, Fe2O3, MnO2, Cr2O3, CaO, and MgO did not produce CH3OH between 430 C and 600 C when used as the only catalysts, while MoO3 supported on silica produced CH3OH in the temperature range of 430 C to 480 C under the current single-bed reactor configuration. However, when the double-bed configuration was used with the 1 wt % SO4(exp -2)/Sr/La2O3 as the first methyl radical generating catalyst bed, CH3OH was observed when ZrO2 and Y2O3 we re used as the second bed catalysts. Preliminary quantitative analysis showed that the ability of producing CH3OH was in the order of unsupported Y2O3 greater than unsupported ZrO2 greater than MoO3 on silica. For all of these cases, the CH3OH space time yield was within a dozen grams per kilogram catalyst per hour. DOE

N95-20215# Westinghouse Savannah River Co., Aiken, SC.

SAFE CONDITIONS FOR CONTACTING NITRIC ACID OR NITRATES WITH TRI-N-BUTYL PHOSPHATE (TBP)

M. Hyder Jan. 1994 24 p
(Contract DE-AC09-89SR-18035)
(DE95-001243; WSRC-TR-94-059) Avail: CASI HC A03/MF A01

In response to a request from DOE-SR, the current state of knowledge of the reactions between tri-n-butyl phosphate (TBP) and aqueous nitrate solutions is critically reviewed, and recommendations are made for the safe operation of SRS separations equipment in which this combination of chemicals may be present. The existing limits for evaporation are validated. Guidelines are presented for cases in which general limits do not apply. The rate of reaction between nitric acid and TBP appears to be controlled by the rate of TBP hydrolysis. The hydrolysis reaction produces dibutyl phosphate and n-butanol. The hydrolysis rate is a strong function of temperature, and becomes very fast at temperatures in the range 130 to 150 C. The resulting n-butanol is volatile at high temperatures, boiling at 117.5 C, but is also subject to exothermic oxidation by nitric acid or nitrates. If oxidation occurs before the n-butanol evaporates, the heat of oxidation may exceed local cooling by convection. The resulting heating will further accelerate the reaction, leading to an energetic runaway and possibly (in confined systems) an explosion. Extensive experiments and practice have shown that in a well-mixed and well-vented aqueous system such as an evaporator, at moderate acidities and temperatures below 130 C, the heat of reaction is adequately removed by vaporization of steam. In general, the heating will be so slow that natural processes provide adequate cooling at temperatures below 80 C. Above this temperature, care should be taken to ensure that adequate cooling is available for the amount of TBP that may be present. Experiments suggest that in well-ventilated systems n-butanol evaporation and convective cooling are sufficient to control the reaction at temperatures up to 120 C. DOE

N95-20230# Dugway Proving Ground, UT.

TEST OPERATIONS PROCEDURE (TOP) 1-2-616 TROPIC EXPOSURE

TESTING

11 Nov. 1994 26 p
(AD-A286376; TOP-1-2-616) Avail: CASI HC A03/MF A01

This test operations procedure describes general procedures for atmospheric field exposure of materials in a humid tropic environment and for measuring change in physical properties of the materials after exposure. It also describes the various exposure sites available at the U.S. Army Tropic Test Site. DTIC

N95-20256# Helsinki Univ. of Technology, Espoo (Finland). Lab. of Polymer Technology.

ORIENTATION STUDIES OF POLYOLEFINS BY IR-DICHROISM

T. Tjaeder 1994 39 p
(PB95-104386; ISBN-951-22-2080-6) Avail: CASI HC A03/MF A01

The investigation of the structural changes in polymers upon drawing is relevant with respect to their mechanical properties. Although several methods like wide-angle x-ray scattering, birefringence and refractive index measurements exist to analyze the structure of semicrystalline polymers, infrared polarized spectroscopy is the most useful and practical method that yields quantitative information about molecular orientation of the polymer chains in the crystalline and the amorphous phase separately. Infrared dichroism offers also special advantages where multiphase systems such as polymer blends are concerned. The aim of the paper is to present shortly the basics of IR-dichroism and to introduce this method for polyethylene (PE) and polypropylene (PP). Also some hints are given about the practical performance of the method. NTIS

N95-20268# Pacific Northwest Lab., Richland, WA.

FERROCYANIDE SAFETY PROJECT DYNAMIC X-RAY DIFFRACTION STUDIES OF SODIUM NICKEL FERROCYANIDE REACTIONS WITH EQUIMOLAR NITRATE/NITRITE SALTS

J. N. Dodds (Washington State Univ., Pullman, WA.) and W. J. Thomson (Washington State Univ., Pullman, WA.) Jul. 1994 39 p
(Contract DE-AC06-76RL-01830)
(DE94-017396; PNL-10050) Avail: CASI HC A03/MF A01

Dynamic X-ray Diffraction (DXRD) has been to used to identify and quantify the solid state reactions that take place between sodium nickel ferrocyanide, Na2NiFe(CN)6, and equimolar concentrations of sodium nitrate/nitrite, reactions of interest to the continued environmental safety of several large underground waste storage tanks at the Hanford site in eastern Washington. The results are supportive of previous work, which indicated that endothermic dehydration and melting of the nitrates take place before the occurrence of exothermic reactions that being about 300 C. The DXRD results show that a major reaction set at these temperatures is the occurrence of a series reaction that produces sodium cyanate, NaCNO, as an intermediate in a mildly exothermic first step. In the presence of gaseous oxygen, NaCNO subsequently reacts exothermally and at a faster rate to form metal oxides. Measurements of the rate of this reaction are used to estimate the heat release. Comparisons of this estimated heat release rate with heat transfer rates from a hypothetical 'hot spot' show that, even in a worst-case scenario, the heat transfer rates are approximately eight times higher than the rate of energy release from the exothermic reactions. DOE

N95-20277# Los Alamos National Lab., NM.

TESTS OF DIELECTRIC MODEL DESCRIPTIONS OF CHEMICAL CHARGE DISPLACEMENTS IN WATER

G. J. Tawa and L. R. Pratt 1994 12 p Presented at the 208th American Chemical Society National Meeting, Washington, DC, 21-26 Aug. 1994
(Contract W-7405-eng-36)
(DE94-007530; LA-UR-94-431; CONF-940813-1) Avail: CASI HC A03/MF A01

A dielectric model of electrostatic solvation is applied to describe potentials of mean force in water along reaction paths for (1) pairing of sodium and/or chloride ions; (2) the symmetric S(sub N)2 exchange of chloride in methylchloride; (3) nucleophilic attack of formaldehyde by hydroxide anion. For these cases simulation and XRISM results are available for comparison. The accuracy of model predictions varies from spectacular to poor. It is argued that: (1) dielectric models are physical models, even though simplistic and empirical; (2) their successes suggest that second-order perturbation theory is a physically sound description of free energies of electrostatic solvation; and (3) the most serious deficiency of the dielectric models lies in the definition of cavity volumes. Second-order perturbation theory should therefore be used to refine the dielectric models. These dielectric models make no attempt to assess the role of packing effects but for salvation of classical electrostatic interactions the dielectric models appear to perform as well as the more detailed XRISM theory. DOE

N95-20290 National Renewable Energy Lab., Golden, CO.

ASSESSMENT OF LIQUEFACTION AND PYROLYSIS SYSTEMS

Y. Solantausta, J. Diebold, D. C. Elliott, T. Bridgwater, and D. Beckman 1994 206 p Prepared in cooperation with National Renewable Energy Lab., Golden, CO; Battelle Pacific Northwest Labs., Richland, WA; Aston Univ., Birmingham, England; and Zeton, Inc., Burlington, Ontario
(PB95-129797; VTT/RN-1573) Copyright Avail: Issuing Activity (National Technical Information Service (NTIS))

This report summarizes the results of the International Energy Agency (IEA) Biomass Agreement Pyrolysis/Liquefaction activity from 1989 to 1991. A summary of the developments of state of the art direct biomass pyrolysis and liquefaction technology is presented. Results are presented of a technoeconomic analysis of a wood pyrolysis to gasoline process based on experimental work at the National Renewable Energy Laboratory, USA, and of a straw liquefaction to fuel oil process based on experimental work at Manchester University, UK. The potential for chemicals from biomass is also considered. A standard technoeconomic procedure was used for the analysis, with a plant size of 1,000 dry t/d biomass feed. Sensitivity cases covering feedstock costs, capital cost variation and plant capacity are also presented. NTIS

N95-20349# Xavier Univ. of Louisiana, New Orleans, LA.

INVESTIGATION OF SYNGAS INTERACTION IN ALCOHOL SYNTHESIS CATALYSTS

1994 12 p
(Contract DE-FG22-93MT-93010)
(DE94-018784; DOE/MT-93010/2) Avail: CASI HC A03/MF A01

This work presents the progress of the work done during the second quarter on 'Investigation of syngas interaction in Alcohol Synthesis Catalysts'. The essential results have been presented at the second annual Historically Black Colleges and Universities/Private Sector/Energy Research and Development Technology Transfer Symposium. The primary objective of this project is to examine the relations between the catalytic and magnetic properties of the copper-cobalt higher alcohol synthesis catalysts. Since extensive catalytic results are available from the studies of the IFP group, the authors have undertaken to investigate the magnetic character by studying the Zero Field Nuclear Magnetic Resonance (ZFNMR) of cobalt and hysterisis character of the Cu/Co catalysts. The authors have examined three different aspects of these catalysts: (1) effect of metal ratio; (2) effect of method of preparation; and (3) effect of selectivity. DOE

N95-20361# Los Alamos National Lab., NM.

ACTINIDE(IV) AND ACTINIDE(VI) CARBONATE SPECIATION STUDIES BY PAS AND NMR SPECTROSCOPIES

D. L. Clark, S. A. Ekberg, D. E. Morris, P. D. Palmer, and C. D. Tait Sep. 1994 62 p
(Contract W-7405-eng-36)
(DE94-016957; LA-12820-MS) Avail: CASI HC A04/MF A01

Pulsed-laser photoacoustic spectroscopy (PAS) and Fourier-transform nuclear magnetic resonance (NMR) spectroscopy were used to study speciation of actinide(IV) and actinide(VI) ions (Np, Pu, Am) in aqueous carbonate solutions as of pH, carbonate concentration, actinide content, and temperature. PAS focused on Pu(IV) speciation. Stability fields on a pH (8.4 to 12.0) versus total carbonate content (0.003 to 1.0 M) plot for dilute Pu(IV) carbonate species ((Pu)(sub tot) = 1 mM) were mapped. Four plutonium species, with absorption peaks at 486, 492, 500, and 512 nm were found. Loss of a single carbonate ligand does not account for the difference in speciation for the 486 and 492 nm absorption peaks, nor can any of the observed species be identified as colloidal Pu(IV). NMR data have been obtained for UO2(2+), PuO2(2+) and AmO2(2+). This report focuses on results for PuO2(2+). The ligand exchange reaction between free and coordinated carbonate on the PuO2(CO3)3(sup 4-) systems has been examined by variable temperature C-13 NMR spectroscopy. In each of the six different PuO2(CO3)3(sup 4-) samples, two NMR signals are present, one for the free carbonate ligand and one for the carbonate ligand coordinated to a paramagnetic plutonium metal center. The single C-13 resonance line for coordinated carbonate is consistent with expectations of a monomeric PuO2(CO3)3(sup 4-) species in solution. A modified Carr-Purcell-Meiboom-Gill NMR pulse sequence was used for determining of ligand exchange parameters for paramagnetic actinide complexes. Eyring analysis at standard conditions provided activation parameters of (Delta)H = 38 KJ/M and (Delta)S = -60 J/K for the plutonyl triscarbonate system, suggesting an associative transition state for the plutonyl(VI) carbonate complex self-exchange reaction. DOE

N95-20368# Los Alamos National Lab., NM.
KONDO INSULATORS
Z. Fisk (Florida State Univ., Tallahassee, FL.), J. L. Sarrao (Florida State Univ., Tallahassee, FL.), and J. D. Thompson 1994 17 p Presented at the SCES 1994, Amsterdam, Netherlands, Aug. 1994
(Contract W-7405-eng-36)
(DE95-001156; LA-UR-94-2992; CONF-9408113-4) Avail: CASI HC A03/MF A01

The Kondo insulating materials present a particularly simple limiting case of the strongly correlated electron lattice problem: one occupied f-state interacting with a single half-filled conduction band. Experiment shows that the solution to this problem has some remarkably simple aspects. Optical conductivity data display the strong coupling nature of this physics. DOE

N95-20384# Tennessee Univ., Knoxville, TN. Dept. of Chemical Engineering.
THEORETICAL AND EXPERIMENTAL STUDY OF MIXED SOLVENT ELECTROLYTES
P. T. Cummings 1995 10 p
(Contract DE-FG05-94ER-14421)
(DE94-017605; DOE/ER-14421/1) Avail: CASI HC A02/MF A01

The research objectives were: perform Gibbs ensemble Monte Carlo simulation of mixed solvent electrolytes (ethanol/water/NaCl); perform molecular dynamics simulation of supercritical aqueous (electrolyte) solutions; measure experimentally phase equilibria in water/alcohol/organic salt mixtures; and conduct integral equation studies of mixed solvent electrolytes. Progress on all objectives is reported (the most progress was on the molecular dynamics simulation). DOE

N95-20386# Lawrence Livermore National Lab., Livermore, CA.
FABRICATION AND TESTING OF A SILICON IMMERSION GRATING FOR INFRARED SPECTROSCOPY
P. J. Kuzmenko, D. R. Ciarlo, and C. G. Stevens 25 Jul. 1994 12 p Presented at the Annual Meeting of the Society of Photo-Optical Instrumentation Engineers, San Diego, CA, 24-29 Jul. 1994
(Contract W-7405-eng-48)
(DE94-017173; UCRL-JC-117810; CONF-940723-15) Avail: CASI HC A03/MF A01

Recent advances in silicon micromachining techniques (e.g. anisotropic etching) allow the fabrication of very coarse infrared echelle gratings. When used in immersion mode, the dispersion is increased proportionally to the refractive index. This permits a very significant reduction in the overall size of a spectrometer while maintaining the same resolution. We have fabricated a right triangular prism (30 x 60 x 67 mm) with a rectangular entrance face (30 x 38 mm) from silicon with a grating etched into the face of the hypotenuse. The grating covers an area of 32 mm by 64 mm and has a 97.5 PM periodicity with a blaze angle of 63.4 deg. The groove surfaces are very smooth with a roughness of a few manometers. Random defects in the silicon are the dominant source of grating scatter (approximately 12% at 3.39 (mu)m). We measure a grating ghost intensity of 1.2%. The diffraction peak is quite narrow, slightly larger than the Airy disc diameter at F/12. However due to wavefront aberrations, perhaps 15-20% of the diffracted power is in the peak with the rest distributed in a diameter roughly five times the Airy disc. DOE

N95-20438# SRI International Corp., Menlo Park, CA.
NOVEL CATALYSTS FOR METHANE ACTIVATION Quarterly Report No. 7, 1 Apr. - 30 Jun. 1994
A. S. Hirschon, H. J. Wu, R. Malhotra, and R. B. Wilson Sep. 1994 34 p
(Contract DE-AC22-92PC-92112; SRI Proj. 4069)
(DE95-002639; DOE/PC-92112/T7) Avail: CASI HC A03/MF A01

Fullerenes are a recently discovered allotrope of carbon that have been found to possess unusual properties, some of which may be ideal for methane activation. This project is designed to evaluate these carbon based materials for conversion of methane into higher hydrocarbons. The project is divided into three technical tasks: task 1 deals with the synthesis and characterization of the fullerenes and fullerene soots; task 2 with the testing of the catalysts; and task 3 with the evaluation of the results and technical reporting requirements. The results and accomplishments for this quarter are summarized below: soots were prepared either by extraction in toluene or sublimation of the lower fullerenes (such as C 60/C70); a fullerene soot was prepared by adding C60 to an extracted soot; fullerene soot was doped with platinum and nickel by incipient wetness techniques, and a nickel fullerene complex was synthesized using organometallic techniques; soot from three manufactures were tested for methane activation and found to exhibit small but notable differences in reactivity; increasing the surface area of soots by partial oxidation with CO2 did not cause significant changes in the reactivities; the effect of the extraction and sublimation of C60 /C70 was determined to be minor; the effect of added C60 to an extracted MER soot was determined to be beneficial; acetylene black was tested and found to have higher activity and lower selectivity than a Norit-A carbon; and nickel and platinum doped soots were found to be more active than the undoped soots. DOE

N95-20470# Westinghouse Hanford Co., Richland, WA.
QUANTITATIVE AND QUALITATIVE ANALYSIS OF SOME INORGANIC COMPOUNDS BY RAMAN SPECTROSCOPY
D. R. Lombardi (Florida State Univ., Tallahassee, FL.), C. Wang (Florida State Univ., Tallahassee, FL.), B. Sun (Florida State Univ., Tallahassee, FL.), A. W. Fountain, III (Florida State Univ., Tallahassee, FL.), T. J. Vickers (Florida State Univ., Tallahassee, FL.), C. K. Mann (Florida State Univ., Tallahassee, FL.), F. R. Reich, J. G. Douglas, and F. L. Kohlasch Feb. 1994 23 p Presented at the Pittsburgh Conference on Analytical Chemistry and Applied Spectroscopy, Chicago, IL, 28 Feb. - 4 Mar. 1994
(Contract DE-AC06-87RL-10930)
(DE94-009757; WHC-SA-2098; CONF-940209-3) Avail: CASI HC A03/MF A01

Raman spectra have been measured for several nitrates, nitrites, sulfates, ferrocyanides and ferricyanides, both in the solid phase and in aqueous solution. Accurate locations of peak maxima are given. Limits of detection for some of the compounds are given for solutions and for solid mixtures in NaNO3. Preliminary measurements have been made on core material recovered from the storage tanks on the Hanford Site. Representative spectra are presented, showing that it is possible to observe responses of individual components from measurements made directly on untreated cores using a fiber optic sampling probe. DOE

N95-20493# Oak Ridge National Lab., TN.
VISIBLE AND NEAR-IR SPECTROSCOPIC STUDIES OF UC1(4) IN A BASIC AMBIENT TEMPERATURE MELT: THE OBSERVATION OF A POSSIBLE GEOMETRIC DISTORTED UC1(6)(EXP 2-) SPECIES AND THE EVIDENCE FOR THE HYDROGEN-BOND IN THE MELT
S. Dai, L. M. Toth, G. D. DelCul, and D. H. Metcalf 1994 2 p Presented at the 185th Electrochemical Society Meeting, San Francisco, CA, 22-27 May 1994
(Contract DE-AC05-84OR-21400)
(DE94-017764; CONF-940529-24) Avail: CASI HC A01/MF A01

Since high temperatures can lead to broadening of absorption spectra, ambient temperature chloride melts were used; the system used was AlCl3-1-ethyl-3-methyl-imidazolium chloride (EMIC). The uv-visible spectrum of UCl4 in basic melt had many peaks with the most intense (triplet) ones around 2000 nm, similar to these at high temperature and indicating the same species. The electronic transition is allowed by a static rather than a vibronic mechanism. The central peak in the UCl6 (sup 2-) spectrum indicates distortion of geometry from the O(sub h) symmetry by the solvent medium. Very strong hydrogen bonding between UCl6(sup 2-) and solvent EMI is suggested. DOE

N95-20555# George Washington Univ., Washington, DC. Dept. of Chemistry.
ANGLE RESOLVED AUGER ELECTRON SPECTROSCOPY: AN ALTERNATE TOOL FOR IDENTIFYING ELECTRONIC EXCITATION PROCESSES IN SOLIDS Technical Report, Sep. 1993 - Oct. 1994
David E. Ramaker, R. A. Fry, and Y. U. Idzerda Sep. 1994 13 p
(Contract N00014-94-I-0331)
(AD-A285375; TR-67) Avail: CASI HC A03/MF A01

Angle resolved Auger electron spectroscopy (ARAES) is shown to be a useful tool for obtaining unique electronic structure information and identifying satellite excitation processes in solids. Although relatively unexplored, ARAES is an attractive tool which may complement the more conventional energy resolved AES. The ARAES method is successful because the diffraction patterns exhibited in ARAES at fixed energy are strongly dependent on the l-wave of the emitted electron and its magnetic alignment, and each Auger process is generally dominated by a different single l-wave. Potential applications for elucidating satellite excitation processes (resonant excitation, shakeup/shakeoff, and backscattering), one- and two-center decay processes, and electronic structure (directional valence bonds and orbital magnetic moments) at surfaces are discussed. DTIC

N95-20557*# Alabama Univ., Huntsville, AL. In-line Process Control Lab.
SURFACE CHARACTERIZATION AND CONTAMINATION ANALYSIS Annual Progress Report No. 1, period ending 24 Jan. 1995
Gary L. Workman 24 Jan. 1994 12 p
(Grant NAG8-1071)
(NASA-CR-197374; NAS 1.26:197374) Avail: CASI HC A03/MF A01

The research activity for this first year has focussed on three distinct activities: (1) the use of an integrating sphere to improve upon the gathering of spectral data from a variety of surfaces; (2) the use of optical fiber spectrometry to determine levels of contamination from tape residues on critical bonding surfaces; and (3) an exploratory activity in the use of spectroscopic ellipsometry for the analysis of thin films of contaminants on critical surfaces has also begun. Author

N95-20563 Florida Univ., Gainesville, FL. Dept. of Chemistry.
ELECTROSPRAY IONIZATION FOURIER TRANSFORM ION CYCLOTRON RESONANCE MASS SPECTROMETRIC STUDY OF SINGLY AND DOUBLY CHARGED ORGANOMETALLIC COMPLEXES Technical Report, Aug. 1993 - Feb. 1994
R. Ramanathan, D. E. Richardson, J. R. Eyler, C. Stacey, and G. H. Kruppa 27 May 1994 42 p Limited Reproducibility: More than 20% of this document may be affected by microfiche quality
(Contract N00014-87-J-1248)
(AD-A279899; TR-44-ONR) Avail: Issuing Activity (Defense Technical Information Center (DTIC))

An external source electrospray ionization (ESI) Fourier transform ion cyclotron resonance (FTICR) mass spectrometer has been used to study the organometallic complexes Ag2(DPM)2(BF4)2 (where DPM = bis-diphenylphosphino-methane), Ag2(DPM)3(BF4)2 and Ru(II)(bp)3(PF6)2 (where bpy = 2,2'-bipyridyl). The high mass resolution and accurate mass assignment of parent and collisionally induced dissociation (CID) fragment ions provided structural information on these organometallic complexes. CID in the capillary/skimmer region and inside the FTICR analyzer cell were performed on these complexes and results from each type of experiment were compared. Important fragmentation pathways and reaction types, including bond cleavage, ligand loss, and ligand substitution were identified. DTIC

N95-20576# University of Southern California, Los Angeles, CA. Dept. of Chemistry.
COMBUSTION-RELATED STUDIES USING WEAKLY BONDED COMPLEXES
Robert A. Beaudet Oct. 1994 20 p
(Contract DE-FG03-89ER-14053)
(DE95-002801; DOE/ER-14053/T6) Avail: CASI HC A03/MF A01

Binary van der Waals complexes and bimolecular reactions relevant to combustion have been prepared and studied using tunable IR diode laser spectroscopy. The complexes were prepared in supersonic expansions using pulsed slit nozzles. In the first phase, geometries and other molecular properties were determined from vibration-rotation spectra. Two complementary classes of binary complexes were investigated. The first involves molecular oxygen (e.g., O2-HCN, O2-HF, Ob 2-HCl, O2-HBr, O2-HI and O2- hydrocarbons) and the corresponding photoinitiated reactions. The authors obtained spectra O2-HCl in helium. Such complexes involving triplet state molecules have not been studied, and the spectra are more complex than those whose constituents are simple singlet molecules. These complexes are interesting because upon photodissociating the hydride portion, the reaction of H with O2 via the vibrationally excited HO2(+) intermediate can be studied: BrH-O2 + hv(193 nm) (yields) Br-H-O2 (yields) Br + HO2 (+) (yields) Br + OH + O. Also, the authors attempted to study a unique set of species involving oxygen atoms and small molecules such as HF, HCl, HBr, HI, HCN and simple hydrocarbons. A carrier gas was seeded with SO2 and the second constituent O(P-3) is prepared by 193 nm S O2 photodissociation. Because the reactions of O(P-3) with small molecules had a significant activation energies, the complexes survive the expansion: e.g., O + HCl has E(sub act) = 22 kJ/mol, and the oxygen atom will lie in a shallow well just outside the barrier. Unfortunately, the beam temperature after the photolysis was too warm to preserve van der Waals complexes. The authors also developed IR diode laser spectroscopy as a probe to study bimolecular reactions in a pulsed slit supersonic expansion. DOE

N95-20581 Yale Univ., New Haven, CT.
NONLINEAR SPECTROSCOPY OF MULTICOMPONENT DROPLETS AND TWO- AND THREE-DIMENSIONAL MEASUREMENTS IN FLAMES Final Technical Report, 1 Feb. 1991 - 31 Jan. 1994
Richard K. Chang and Marshall B. Long 31 Mar. 1994 36 p Limited Reproducibility: More than 20% of this document may be affected by microfiche quality
(Grant AF-AFOSR-0150-91; AF Proj. 2308)
(AD-A279945; AFOSR-94-0320TR) Avail: Issuing Activity (Defense Technical Information Center (DTIC))

Significant progress has been made in the following two research areas: (A) Nonlinear spectroscopy of micrometer-sized multicomponent droplets; and (B) Two- and three-dimensional scalar and velocity mapping. (A) Chemical species and physical properties of multicomponent liquid droplets in a spray combuster can be determined by a nonintrusive in-situ optical diagnostics techniques. A brief summary of the research accomplishments in the three areas related to the nonlinear optical interactions inside micron-sized droplets and the applications of such spectroscopy to determine the chemical and physical properties of the droplets: (1) Model for nonlinear optical processes in droplets; (2) fluorescence seeding of simulated Raman scattering (SRS) of the Minority Species; and (3) Detection of slight shape distortion by spectroscopic means. (B) A review of the progress in our multi-dimensional scalar and velocity measurements in turbulent flames is also given. Among the accomplishments during the funding period are the following: (1) Scalar field measurements of differential diffusion effects in turbulent flows; (2) Development of a digital particle image velocimetry (PIV) technique for velocity field measurements in reacting and nonreacting flows; (3) Combination of the new digital PIV technique with previously developed fluorescence imaging techniques to allow simultaneous vector and scalar imaging in turbulent flames; and (4) Development of new mixture fraction imaging techniques for studying turbulent nonpremixed hydrocarbon flames. DTIC

N95-20597 Cornell Univ., Ithaca, NY.
MAPPING CLOSURES FOR TURBULENT COMBUSTION Final Report, 15 Feb. 1991 - 14 Feb. 1994
Stephen B. Pope 19 Apr. 1994 12 p Limited Reproducibility: More than 20% of this document may be affected by microfiche quality
(Grant AF-AFOSR-0184-91; AF Proj. 2308)
(AD-A279995; AFOSR-94-0323TR) Avail: Issuing Activity (Defense Technical Information Center (DTIC))

The overall objective of the research program was to develop and test an improved model for the process of molecular diffusion in turbulent reactive flows. In application to turbulent combustion, a major shortcoming of existing models is that they are non-local in composition. A model has been developed, based on the construction of a Euclidean minimum spanning tree (EMST). This model is inspired by the mapping closure, and reduces to it in the case of a single composition. In general, the model is asymptotically local, and hence overcomes a major flaw in previous models.

The model has been tested for decaying scalars in isotropic turbulence and for a mean scalar gradient. Additionally, studies have been made of stochastic Lagrangian mode's for turbulent reactive flows; and an exact expression has been obtained for the probability density function of temperature (or other random quantities) in statistically stationary turbulence. DTIC

N95-20613# Army Research Lab., Aberdeen Proving Ground, MD.
QUANTUM CHEMICAL STUDY OF RARE GAS/HALIDE INTERACTIONS AS A MODEL FOR HIGH ENERGY DENSITY MATERIAL. 1: TRANSITION PROPERTIES IN HCl Final Report, Sep. 1990 - 1991
George F. Adams and Cary F. Chabalowski Nov. 1994 27 p
(DA Proj. 1L1-61102-AH-43)
(AD-A285988; ARL-TR-609) Avail: CASI HC A03/MF A01

As an extension of our earlier studies of rare gas (Rg) atomic and molecular interactions (Chablowski et al. 1989), we begin this preliminary theoretical treatment of the Rg-halide interactions by studying the electronic states and electronic transition probabilities between electronic states in HCl. This information will be necessary to understand the results from future studies where we will explicitly include xenon atoms with the HCl, producing electronic states that are mixtures of xenon and HCl. It is also of interest to determine what effect the use of effective core potentials has on predicting known experimental molecular properties as well as properties predicted by other ab initio studies. Quantum chemical calculations are performed on the ground and excited states of HCl, including Effective Core Potentials (ECPs) (Wadt and Hay 1985), State Averaged-Complete Active Space MCSCF (SA-CASSCF) for generating state averaged molecular orbitals (MOs), and configuration interaction (CI) calculations to obtain the final electronic state wave functions. DTIC

N95-20668# New Orleans Univ., LA. Dept. of Chemistry.
COMPUTATIONAL EVALUATION OF THE FEASIBILITY OF NITRATING PRECURSORS TO C12N12O12
Peter Politzer and M. Edward Grice 20 Oct. 1994 7 p
(Contract N00014-91-J-4057)
(AD-A285976; TR-71) Avail: CASI HC A02/MF A01

In order to determine the feasibility of nitrating the immediate precursors of 1, we have computed the average local ionization energies on their surfaces and compared their minimum values to those of mono-, di- and trinitrobenzene. Our results indicate that there is a reasonable likelihood of being able to nitrate the precursors of C12N12O12. DTIC

N95-20682# State Univ. of New York, Binghamton, NY. Dept. of Chemistry.
PHOTOCHEMISTRY OF INTERMOLECULAR C-H BOND ACTIVATION REACTIONS
A. J. Lees 1994 15 p
(Contract DE-FG02-89ER-14039)
(DE94-018417; DOE/ER-14039/3) Avail: CASI HC A03/MF A01

Goals at the onset were to obtain photophysical and photochemical data on transition-metal organometallic complexes which undergo light-induced intermolecular C-H bond activation reactions with hydrocarbon substrates. The complexes included these of rhodium and rhenium with such as cyclopentadiene, CO, phosphine, pyridines, etc. DOE

N95-20712 New Mexico Univ., Albuquerque, NM. Dept. of Chemistry.
GAS-PHASE GENERATION OF ZINC SULFIDE PARTICLES USING A SINGLE-SOURCE PRECURSOR
Mark J. Hampden-Smith, D. Zeng, A. Datye, Q. Powell, and A. Gurav 6 May 1994 32 p Limited Reproducibility: More than 20% of this document may be affected by microfiche quality
(Contract N00014-91-J-1258)
(AD-A279700; TR-13) Avail: Issuing Activity (Defense Technical Information Center (DTIC))

Nanometer-sized (20 to 40 nm) ZnS particles were produced in a flow reactor by gas-phase reaction of the single-source precursor Zn(S2CNEt(sub2))(sub2)TMEDA), where TMEDA = tetramethylethylenediamine. The precursor was prepared by reaction of the dimer, (Zn(S2CNEt(sub2))(sub 2))(sub 2), with two equivalents of TMEDA. The product was isolated in quantitative yield and characterized by a variety of spectroscopic techniques and by single-crystal X-ray diffraction in the solid state. Transparent, colorless prisms of empirical formula C16H36N4S4Zn crystallized by cooling a warm (60 C), saturated toluene solution to room temperature, in the orthorhombic crystal system, space group P2(1)2(1)2(1) with unit cell dimensions a = 8.785(1) A, b = 11.611(2) A, c = 23.321(2) A, z = 4, with R = 4.64%, Rw = 5.32% for 3262 independent reflections where F is greater than 3.0 sigma(F). The structure of Zn(S2CNEt(sub2))(sub2)(TMEDA) was monomeric and distorted octahedral in the solid state. The precursor was evaporated into the gas phase and reacted in a hot-wall reactor at temperatures of 500, 600, and 700 C resulting in the formation of ZnS particles X-ray diffraction showed phase-pure ZnS particles with crystallite sizes of 15 - 25 nm at all temperature studied. Thermogravimetric analysis, elemental analysis, and transmission electron microscopy suggested that the particles also contained sulfur derived from the precursor. DTIC

N95-20716# Eltron Research, Inc., Boulder, CO.
ELECTROCHEMICAL IMPEDANCE PATTERN RECOGNITION FOR DETECTION OF HIDDEN CHEMICAL CORROSION ON AIRCRAFT COMPONENTS Annual Report, 15 Aug. - 14 Oct. 1994
Anthony F. Sammells and James S. Bowers 14 Oct. 1994 4 p
(Contract F49620-94-C-0043)
(AD-A285998; AFOSR-94-0673TR) Avail: CASI HC A01/MF A01

Progress is presented for the program goal of developing diagnostic instrumentation for both detecting the presence and degree of hidden chemical corrosion on aircraft titanium and aluminum alloy components. DTIC

N95-20736# Universidad Autonoma del Estado de Mexico, Toluca (Mexico). Facultad de Quimica.
DETERMINATIONS OF PHASE TRANSITIONS IN NYLON 6-12, NYLON-6, POLYVINYL CHLORIDE AND POLYETHYLENE TEREPHTHALATE BY POSITRON ANNIHILATION SPECTROSCOPY Ph.D. Thesis [DETERMINACION DE LAS TRANSICIONES DE FASE EN NYLON 6,12, NYLON-6, POLI(CLORURO DE VINILO) Y POLI(TEREFTALATO DE ETILENO) POR ESPECTROSCOPIA DE ANIQUILACION DEL POSITRON]
M. J. CamachoReyes 1993 90 p In SPANISH
(DE94-629992; INIS-MF-13924) Avail: CASI HC A05/MF A01 (US Sales Only)

Positron annihilation lifetime spectroscopy (PALS) was used to investigate the phase transitions, mainly the glass transition, of poly(vinyl chloride) (PVC), Nylon-6,12, Nylon-6, poly(ethylene terephthalate) during the thermal treatment of these polymers. The longest lived component lifetime and intensity, indicative of ortho-Positronium pick-off exhibit thermal dependencies that can be attributed to the anticipated free volume changes associated with structural transitions. Positron lifetime measurements were performed using an E G and G Ortec standard fast-fast coincidence system. Three spectra were collected at each temperature, each consisting of a peak height of approximately 25000 counts. The resulting spectra were consistently modeled with a three component fit using the computer program PATFIT. For nylon-6,12, nylon-6, PVC systems three transitions were obtained in both tau-3 and I-3 as a function of temperature. Changes in the slope of the curves appear for both parameters, these could be attributed to T(sub g1), T(sub g2) and T(sub c), respectively. In the case of PET analysis two transitions were obtained as is shown by the variations of tau-3 as a function of the heating temperature. These transitions can be attributed to T(sub g1) and T(sub g2). Similar changes can be observed for I-3 in relation with temperature. Glass transition behavior was evident in the lifetime behavior of polymers. Increases in slope of the lifetime temperature plots were interpreted free-volume cavity expansion as temperature is increased. The intensity responses in the vicinity of the upper glass transition were consistent with the association of this transition with the reduction of crystalline constraint of segmental mobility in the amorphous phase. DOE

N95-20769 Academy of Sciences (USSR), Moscow (USSR). Inst. Khimicheskoi Fiziki.
PROCEEDINGS OF THE ZEL'DOVICH MEMORIAL INTERNATIONAL CONFERENCE ON COMBUSTION, DETONATION, SHOCK WAVES, VOLUME 2
17 Sep. 1994 534 p Conference held in Moscow, Russia, 12-17 Sep. 1994 Limited Reproducibility: More than 20% of this document may be affected by poor print

(Contract DAJA45-90-C-0053)
(AD-A286626; R/D-7432-AN-02) Avail: Issuing Activity (Defense Technical Information Center (DTIC))

Professor Yakov Borisovich Zel'dovich was one of the most eminent scientists of the 20th century. He made outstanding contributions to the development of the modern theory of combustion and detonation, physics of explosion and shock waves, nuclear physics and physics of elementary particles, theory of gravitation and cosmology, astrophysics and X-ray astronomy. The Technical Program of the Zel'dovich Memorial contained 48 invited plenary lectures and more than 200 poster presentations at 8 Sessions: Kinetics; Ignition and Steady-State Flame Propagation; Diffusion and Heterogeneous Combustion; Turbulent Combustion; Unsteady Combustion; Detonation; Combustion and Detonation Analogies; and Intensive Shock Waves and Extreme States of the Matter. DTIC

N95-20780# Utah Univ., Salt Lake City, UT. Dept. of Chemistry.
TIME-RESOLVED ANALYTICAL METHODS FOR LIQUID/SOLID INTERFACES
Joel M. Harris 31 Oct. 1994 10 p
(Contract DE-FG03-93ER-14333)
(DE95-002255; DOE/ER-14333/T1) Avail: CASI HC A02/MF A01

A number of chemical phenomena that occur at the boundaries between insulating solids and liquids (adsorption, partition, monolayer self-assembly, catalysis, and chemical reactions) are important to energy-related analytical chemistry. These phenomena are central to the development and understanding of chromatographic methods, solid-phase extraction techniques, immobilized analytical reagents, and optical sensors. The goal of this program, therefore, is to develop surface-sensitive spectroscopies by which chemical kinetics at liquid/solid interfaces can be observed on time scales from nanoseconds to seconds. In the second year of this program, the authors used temperature-jump relaxation measurements to monitor adsorption/desorption kinetics at liquid/solid interfaces using Joule heating to compare the adsorption of ions from solution onto C1- and C4-derivatized silica surfaces. They completed a study of rate of migration of covalently-attached ligands on silica surfaces; from the temperature-dependence of the migration, the large energy barrier to migration was estimated. Surface heterogeneity of adsorption sites on silica was characterized by time-resolve fluorescence, and the chemical origins investigated by Si(sup 29) NMR spectroscopy. Surface-enhanced Raman and fluorescence spectroscopies were modified to study adsorption and binding to silica surfaces. Molecular dynamics simulations were started to help better understand kinetic barriers to adsorption; ESR probe measurements were launched to measure and compare the chain mobility of silica-attached alkyl ligands. DOE

N95-20836# Argonne National Lab., IL.
AN IMPROVED AND FACILE METHOD FOR THE SYNTHESIS OF 1,1-BIS(4-HYDROXYPHENYL) 2-PHENYLETHYLENE AND ITS DERIVATIVES
B. Shafii, R. W. Atcher, and E. R. DeSombre (Chicago Univ., Chicago, IL.) 1994 12 p
(Contract W-31-109-eng-38)
(DE95-001125; ANL/CHM/PP-75382) Avail: CASI HC A03/MF A01

The synthesis of 1,1-bis(4-hydroxyphenyl)-2-phenylethylene, which is of biological interest, has been reported by several authors in the past. In this article an improved method is introduced. Different (and commercially available) starting materials are adopted. Also a protective group which is easily attached and removed is used. This procedure provides milder reaction conditions and better yields while the number of steps involved in the synthesis of the compound are reduced. Furthermore, the reactions are clean and formation of byproducts which lead to poorer yields are avoided. DOE

N95-20842# Cornell Univ., Ithaca, NY. Dept. of Chemistry.
GORDON RESEARCH CONFERENCE ON PHYSICAL ELECTROCHEMISTRY Final Report
Hector D. Abruna 30 Mar. 1994 15 p Conference held in New London, NH, 3-7 Aug. 1992
(Contract N00014-92-J-1493)
(AD-A286545) Avail: CASI HC A03/MF A01

The Gordon Research Conference on Physical Electrochemistry was held from August 3-7, 1992 at the Colby Sawyer School in New London, New Hampshire. The program combined researchers in the mainstream of electrochemistry, as well as individuals, who, while not electrochemists, work in areas of relevance to the study and understanding of electrochemical phenomena. The choice of speakers represented a combination of established researchers as well as some younger investigators. This mix gave the conference a sense of what is of current relevance as well as what areas will be forthcoming. The main themes covered in the program were: the use of scanned probe microscopies to the study of electrochemical phenomena with emphasis on STM and AFM. Spectroscopic techniques in the study of electrochemical interfaces with emphasis on synchrotron radiation; Theoretical aspects of the structure of water next to surfaces, electron transfer and superconductivity and their relation to electrochemical phenomena; studies on Langmuir-Blodgett and self-assembling monolayers. DTIC

N95-20865# Naval Research Lab., Washington, DC.
X-RAY SPECTROSCOPY OF XENON
Uri Feldman 19 Jan. 1994 20 p
(Contract DE-FG03-92SF-19202)
(DE95-002132; DOE/SF-19202/T1) Avail: CASI HC A03/MF A01

A high-resolution x ray spectrometer was constructed and fielded at the National Laser Users Facility at the Laboratory for Laser Energetics, University of Rochester. The spectrometer was attached to a streak camera and time-resolved x ray spectra recorded. The targets were irradiated by the 24-beam Omega laser and consisted of CH microballoons filled with DD, argon, and xenon. The x ray spectral lines from Ar and Xe were used to determine the plasma properties of the compressed core region. DOE

N95-20970 Naval Air Warfare Center, Warminster, PA. Air Vehicle and Crew Systems Technology Dept.
ELECTROCHEMICAL IMPEDANCE SPECTROSCOPY OF TRIVALENT CHROMIUM PRE-TREATED ALUMINUM ALLOY Progress Report
Vinod S. Agarwala and Dieter W. Beckert 14 Dec. 1993 21 p Limited Reproducibility: More than 20% of this document may be affected by microfiche quality
(AD-A280093; NAWCADWAR-94014-60) Avail: CASI HC A03

A chemical conversion coating on aluminum alloys was developed using a trivalent chromium bath. Electrochemical impedance spectroscopy (EIS) was made to characterize the corrosion resistant properties of the surface films formed. The results showed a 10 to 100 fold increase in the polarization resistance of the surface films compared to the untreated aluminum alloy. These electrochemical results compared well with the corrosion behavior in salt spray tests. The trivalent chromium-treated surfaces showed no corrosion for up to 200 hours in 5% salt spray. A post-treatment with an oxidizer even further raised the coating's resistance due to an improved corrosion protection. DTIC

N95-21110# Helsinki Univ. of Technology, Espoo (Finland). Lab. of Telecommunications Technology.
INERT GAS PURIFICATION AND MEASURING OXYGEN PARTIAL PRESSURE IN GAS MIXTURES WITH EMF METHOD BASED ON SOLID ELECTROLYTE CELL
Iikka Isomaeki 1994 31 p
(ISSN 0785-5168)
(PB95-127767; TKK-V-B90; ISBN-951-22-1951-4) Avail: CASI HC A03/MF A01

Inert atmospheres are often needed in metallurgical and chemical high-temperature experiments to prevent the sample from undesired reactions such as oxidation. Argon gas is readily available and thus the most commonly used medium for this purpose, so the first task is to secure that this gas is free from unwanted impurities such as oxygen, water and carbon dioxide. For example, AGA Oy supplies three different qualities of argon: (1) Ar 4.8 containing max. 20 ppm impurities; (2) Ar 5.0 containing max, 10 ppm impurities; and (3) Ar 6.0 containing max. 1 pppm impurities. Even if gas which contains max. 1 ppm impurities is used, the actual impurity content of argon in a furnace can be much higher. Gas is easily contaminated if plastic tubes are used. Therefore, it is better to use metallic tubes with brazed or threaded joints. Gas purification can be performed by passing gas through devices between the gas container and the furnace, so it is possible to reach at least the ppb level of impurities. In the report some methods to remove impurities from inert gas, especially from Ar, are discussed, as also the technique for building up the gas tubing, and methods to measure the partial pressure of oxygen, utilizing solid electrolyte based EMF measurements in the experimental atmosphere. NTIS

N95-21123 Florida Univ., Gainesville, FL. Dept. of Chemistry.
HIGH MAGNETIC FIELD GLOW DISCHARGE IONIZATION SOURCE Technical Report, Jul. 1993 - May 19
K. L. Goodner, C. Dejsupa, C. M. Barshick, and J. R. Eyler 27 May 1994 5 p Limited Reproducibility: More than 20% of this document may be affected by microfiche quality
(Contract N00014-87-J-1248)
(AD-A279972) Avail: CASI HC A01

We have modified our 'internal' electrospray source, which operates inside the high magnetic field associated with Fourier transform ion cyclotron resonance (fticr) mass spectrometry, to allow it to serve as a glow discharge (GD) ionization source. Quite reasonable ion signals are obtained with this source, in spite of the fact that the glow discharge ionization is taking place at a magnetic field of about 1.8 tesla. This corresponds to a field at least a factor of 25 higher than has ever been used with glow discharge sources before. One example of an analysis of the (60)Ni(+) signal in a NIST 661 stainless steel signal. Signal-to-noise calculations for the top trace yield a limit of detection of 38 ppm for the peak at m/z 60. The predominant ion is (56)Fe(+), arising from the high concentration of iron in the steel. DTIC

N95-21124# California Univ., Los Angeles, CA.
EXCESS ENERGY AND STRUCTURAL DEPENDENCE OF THE RATE OF ENERGY REDISTRIBUTION DURING THE PHOTODISSOCIATION OF IODOTOLUENES
John E. Freitas, Hyun J. Hwang, and M. A. El-Sayed 27 May 1994 39 p
(Contract N00014-89-J-1350)
(AD-A279997; TR-77) Avail: CASI HC A03/MF A01

The ortho (2-), meta (3-), and para (4-) iodotolunes (C7H7I) are photodissociated at 266 nm and 30.4 nm and studied with state-selective one-dimensional photo-fragment translational spectroscopy. Angular velocity, and translational energy distributions are obtained for the ground state I((2)p(3/2)) and spin-orbit excited state I*((2)P(1/2)) iodine atoms produced photodissociation. As has been observed in iodobenzene, the ground state I channel observed in each isomer of iodotoluene exhibits both a prompt alkyl iodide-like dissociation channel following a parallel excitation to the alkyl iodide (3)Q(zero)(n, sigma*) repulsive state and curve crossing to the (1)Q(1)(n,sigma*) state, and a slower, indirect dissociation channel following a competitive excitation to aromatic charge transfer (pi, pi*) predissociate excited states at both 266 nm and 304 nm. The I* channel observed at both 266 nm and 304 nm for each isomer results from prompt dissociation resulting from parallel absorption to an alkyl iodide type (3)Q(zero)(n, sigma*) state. The rapid I and I* dissociative channels observed for each isomer are found to exhibit strong dependence on the excess excitation. This is discussed in terms of the increase in the density of the vibrational states of the toluene ring. Dissociation times and rates of internal energy redistribution (IER) from the slow dissociative channel (Beta) are estimated for each isomer. For 2-iodotoluene, the rate of IER for the slow I channel increases from 20 kcal/mol-ps at 304 nm to 30 kcal/mol-ps at 266 nm, while the rates of IER for 3- and 4-iodotoluene (16 kcal/mol-ps and 15 kcal/mol-ps, respectively) remain unchanged as the photon energy is increased. DTIC

N95-21168# State Univ. of New York, Cortland, NY. Dept. of Physics.
METHODOLOGY FOR ESCA ANALYSIS OF ELECTROMIGRATION Final Report
Yolanda J. Kime and Peter Grach Oct. 1994 22 p
(Contract F30602-92-C-0084)
(AD-A286229; RL-TR-94-187) Avail: CASI HC A03/MF A01

This preliminary investigation examines the feasibility of using Electron Spectroscopy for Chemical Analysis (ESCA) to monitor electromigration in thin films. Because of the requirements of both the ESCA technique and the requisite in situ electromigration, the experimental methods are quite exacting. We report here designs and experimental methodology to permit the examination of electromigration with ESCA and suggest appropriate avenues for future research. DTIC

N95-21172# Energy International, Inc., Pittsburgh, PA.
TECHNOLOGY DEVELOPMENT FOR COBALT F-T CATALYSTS
A. H. Singleton 31 May 1994 208 p
(Contract DE-AC22-92PC-92108)
(DE94-017363; DOE/PC-92108/T6) Avail: CASI HC A10/MF A03

The goal of this project is the development of a commercially viable, cobalt-based Fischer-Tropsch (F-T) catalyst for use in a slurry bubble column reactor. Cobalt-based catalysts have long been known as being active for F-T synthesis. They typically possess greater activity than iron-based catalysts, historically the predominant catalyst being used commercially for the conversion of syngas based on coal, but possess two disadvantages that somewhat lessen its value: (1) cobalt tends to make more methane than iron does; and (2) cobalt is less versatile with low H2/CO ratio syngas due to its lack of water-gas shift activity. Therefore, the major objectives of this work are: (1) to develop a cobalt-based F-T catalyst with low (less than 5%) methane selectivity; (2) to develop a cobalt-based F-T catalyst with water-gas shift activity; and (3) to combine both these improvements into one catalyst. It will be demonstrated that these catalysts have the desired activity, selectivity, and life, and can be made reproducibly. Following this experimental work, a design and a cost estimate will be prepared for a plant to produce sufficient quantities of catalyst for scale-up studies. DOE

N95-21179# Swedish Inst. for Materials Testing, Boras (Sweden).
FIRE EXPERIMENTS IN A TWO DIMENSIONAL RACK STORAGE: BRANDFORSK-PROJECT 701-917
Haukur Ingason 1993 25 p Sponsored by Swedish Research Board, Lund Univ., and SP
(ISSN 0284-5172)
(PB95-131538; SP-RAPP-1993:56; ISBN-91-7848-441-3) Avail: CASI HC A03/MF A01

Flame heights and air flows in a two dimensional rack storage were investigated. The width of the vertical flue is found to be the predominant geometrical parameter controlling the flue flow. The mass flow rate increases nearly linearly with the width. Variation of the horizontal flue heights was found to have negligible effects on the vertical flue flow. For a certain vertical flue width, the mass flow rate is found to be nearly constant independent of the heat output. Experimental results indicate a linear relationship between the flame height and the ratio of heat output to the vertical flue width. A ratio of entrained air to the stoichiometric air requirements at the flame tip is found to be 7.5. Experiments were carried out using inert boxes and a diffusion propane line burner located at the bottom of the rack. The rack was 0.59 m long and between 1.14 m and 1.34 m in height (4 boxes). The size of the rack is about 1/3 of what can be expected in a real rack storage. NTIS

N95-21217# Pennsylvania State Univ., University Park, PA. Dept. of Chemistry.
LINEAR AND NONLINEAR SPECTROSCOPY WITH THE TUNABLE AC SCANNING TUNNELING MICROSCOPE
S. J. Stranick, L. A. Bumm, M. M. Kamna, and P. S. Weiss 10 Oct. 1994 15 p
(Contract N00014-91-J-1630)
(AD-A285751; TR-20) Avail: CASI HC A03/MF A01

The tunable microwave frequency AC scanning tunneling microscope (ACSTM) has opened the possibility of recording local spectra and local chemical information on insulator surfaces much as the conventional STM has done for metals and semiconductors. We describe the various types of spectroscopies that can be performed with the ACSTM. These include linear spectroscopies where the amplitude at the modulation frequency is measured as well as nonlinear spectroscopies utilizing the amplitudes of the harmonics of the modulation frequency generated in the tunneling junction. Spectroscopy in the microwave frequency range also enables heretofore unrealizable measurements on conducting substrates such as the rotational spectroscopy of a single adsorbed molecule. DTIC

N95-21280# Massachusetts Inst. of Tech., Cambridge, MA. Dept. of Chemical Engineering.
AROMATICS OXIDATION AND SOOT FORMATION IN FLAMES
J. B. Howard 1994 4 p
(Contract DE-FG02-84ER-13282)
(DE95-001803; DOE/ER-13282/10) Avail: CASI HC A01/MF A01

This project is concerned with the kinetics and mechanisms of aromatic oxidation and soot and fullerenes formation in flames. The objective of the aromatics oxidation work is to identify and measure the concentration of important intermediates and products in benzene oxidation, and to determine reaction mechanisms and kinetics properties consistent with the behavior seen in flames. The research on soot formation is concerned primarily with the particle inception stages, but the work includes study of soot structure at all stages of growth in order to obtain mechanistic information from evidence of growth steps recorded in the structure of the particles. The ultimate objective is to understand how nascent soot particles are formed from high molecular weight compounds, including the roles of planar and curved PAH and the relationship between soot and fullerenes. The objective of the proposed research on fullerenes is to develop a more comprehensive understanding of the range of fullerenes formed in flames, the nature of the precursor species, and the mechanisms and kinetics of the formation reactions. DOE

N95-21282# Kauppa-ja Teollisuusministerio, Helsinki, Uudenmaa (Finland). Energy Dept.
LIEKKI COMBUSTION TECHNOLOGY
M. Hupa 1994 140 p
(DE95-700233; KTM/E-B-153) Avail: CASI HC A07/MF A02

The five-year LIEKKI combustion research program (1988-1992) was oriented towards research serving the development of energy production techniques based on combustion. The program was divided into the following five research areas: (1) modeling of combustion processes, (2) combustion chemistry, (3) diagnostics and analytics, (4) pressurized combustion, and (5) applied projects. The first three of these research areas involved theoretical as well as experimental laboratory work carried out at universities or various public research organizations. This research aimed at better understanding of the combustion process and associated phenomena without commitment to any particular combustion technique. The fourth research area was focused at studies associated with the pressurized fluidized bed, using two pilot-size test rigs. The main target in the fifth research area was to reduce the combustion flue gas emissions at existing conventional plants, by affecting the various factors of the combustion process. In the five-year period, the program included 92 projects, whose total costs amounted to FIM 142 million. DOE

N95-21309# Sandia National Labs., Albuquerque, NM.
CHARACTERIZATION OF POLY(TETRAFLUOROETHYLENE) SURFACES BY ATOMIC FORCE MICROSCOPY: RESULTS AND ARTIFACTS
A. J. Howard, R. R. Rye, and K. Kjoller (Digital Instruments, Inc., Santa Barbara, CA.) 1994 12 p Presented at the Atomic Force Scanning Tunneling Microscopy Symposium, Natick, MA, 7-9 Jun. 1994
(Contract DE-AC04-94AL-85000)
(DE95-000742; SAND-94-1129C; CONF-9406268-1) Avail: CASI HC A03/MF A01

The surfaces of virgin and chemically etched poly(tetrafluoroethylene) (PTFE) have been studied using atomic force microscopy (AFM) in both contact and tapping modes. While attempting to perform AFM in contact mode on this relatively soft polymeric material, tip-induced imaging artifacts (presumably due to blunt tips and tip-to-surface interactions) were identified when the results were compared to scanning electron microscopy (SEM) surface images. When subsequent AFM imaging was performed in tapping mode it was apparent that these tip-induced artifacts were eliminated. Comparable tapping mode AFM and SEM images were obtained for even the highly porous, unstable surface that results from sodium naphthalenide etching of PTFE. AFM imaging in tapping mode of virgin and etched PTFE surfaces shows the three-dimensional character of the etched surface necessary for mechanical interlocking and resultant strong adhesion. DOE

N95-21397# Iowa State Univ. of Science and Technology, Ames, IA.
ANODIC OXYGEN-TRANSFER ELECTROCATALYSIS AT IRON-DOPED LEAD DIOXIDE ELECTRODES Ph.D. Thesis
Jianren Feng 1994 134 p
(Contract W-7405-eng-82)
(DE95-001653; IS-T-1713) Avail: CASI HC A07/MF A02

The research illustrated in this thesis was performed under the guidance of Professor Dennis C. Johnson beginning in March 1987. Chapter 2 concentrates on the development and electrocatalytic properties of iron-doped (beta)-PbO2 films on noble-metal substrates. Chapter 3 focuses attention on the preparation and characterization of iron-doped (beta)-PbO2 films on titanium substrates (Fe-PbO2/Ti). Chapter 4 discusses anodic evolution of ozone at Fe-PbO2/Ti electrodes. Chapter 5 describes electrochemical incineration of p-benzoquinone (BQ) at Fe-PbO2/Ti electrodes. In addition, the Appendix includes another published paper which is a detailed study of (alpha)-PbO2 films deposited on various types of stainless steel substrates. DOE

N95-21400# Iowa State Univ. of Science and Technology, Ames, IA.
NOVEL ABSORPTION DETECTION TECHNIQUES FOR CAPILLARY ELECTROPHORESIS Ph.D. Thesis
Y. Xue 27 Jul. 1994 158 p
(Contract W-7405-eng-82)
(DE95-001673; IS-T-1696) Avail: CASI HC A08/MF A02

Capillary electrophoresis (CE) has emerged as one of the most versatile separation methods. However, efficient separation is not sufficient unless coupled to adequate detection. The narrow inner diameter (I.D.) of the capillary column raises a big challenge to detection methods. For UV-vis absorption detection, the concentration sensitivity is only at the (mu)M level. Most commercial CE instruments are equipped with incoherent UV-vis lamps. Low-brightness, instability and inefficient coupling of the light source with the capillary limit the further improvement of UV-vis absorption detection in CE. The goals of this research have been to show the utility of laser-based absorption detection. The approaches involve: on-column double-beam laser absorption detection and its application to the detection of small ions and proteins, and absorption detection with the bubble-shaped flow cell. DOE

N95-21402# California Univ., Los Angeles, CA. Dept. of Materials Science and Engineering.
GRADIENT INDEX LENSES FROM SOL-GEL LAYERING Annual Report, 1 Jul. 1993 - 30 Jun. 1994
John D. Mackenzie 30 Jun. 1994 7 p
(Contract F49620-93-1-0364)
(AD-A285649; AFOSR-94-0657TR) Avail: CASI HC A02/MF A01

The research proposed here is based on the principle of the density gradient column. A liquid (A) of low density is continuously mixed into a liquid (B) of higher density while B is allowed to flow slowly down the wall of a glass cylinder. The feed rate of A is equal to the flow rate of mixture. Thus, a gradient density column is formed. Such columns have been used to measure the density of semiconductors to five (5) significant figures. The gradient is stable for many months at room temperature. We proposed to use this method to prepare gradient index (GRIN) lenses from gels with large axial gradients. The chemical compositions of two sols are selected based on considerations of solubility between the sols; differences in refractive index, density, expansion coefficient and densification temperatures between resulting oxides. DTIC

N95-21426 Selskapet for Industriell og Teknisk Forskning, Trondheim (Norway). Div. of Applied Chemistry.
TECHNICAL AND ECONOMIC EVALUATION OF NATURAL GAS BASED SYNTHESIS GAS PRODUCTION TECHNOLOGIES
J. Sogge, T. Stroem, and T. Sundset 15 Feb. 1994 261 p
(PB95-130597; STF21-A93106) Avail: Issuing Activity (National Technical Information Service (NTIS))

This report describes a conceptual study that has been done on technical and economic evaluation of different synthesis gas production technologies. A literature review on synthesis gas processes and a status on the different technologies and their licensors have been worked out. In addition, 9 different front-end synthesis gas processes supporting a 2500 MTPD methanol plant have been considered: Conventional steam reforming, noncatalytic partial oxidation (POX), catalytic partial oxidation (CPO), autothermal reforming, combined reforming, combined reforming with prereforming, gas heated reforming (GHR), combined autothermal reforming (CAR) and Kellogg reforming exchanger system (KRES). Capital and operating costs were calculated for each process, and sensitivity analysis performed on important cost parameters. The results show that among the commercial processes, autothermal and combined reforming have the best economy with 17-18% lower total cost than steam reforming. Among the new technologies, GHR and KRES both show even better economy, with approximately 22-23% lower total cost than steam reforming. NTIS

N95-21428 National Defence Research Establishment, Stockholm (Sweden). Dept. of Weapon Systems, Effects and Protection.

IGNITION OF SUBMARINE MATERIALS AT VARIOUS OXYGEN CONCENTRATIONS [ANTAENDLIGHETEN HOS MATERIAL I UBAT VID OLIKA SYREKONCENTRATION]

P. O. Werling and B. Onnermark Jun. 1994 22 p In SWAHILI
(PB95-131371; FOA-A-20058-2.4) Avail: Issuing Activity (National Technical Information Service (NTIS))

By an experimental investigation, the ignitability of five 'submarine' materials was studied at thermal irradiations of 0.1 - 10 w/sq cm and oxygen concentrations of 21 and 15% (total pressure 100KPa). The irradiation limit I(sub a) for 'pilot ignition' was found to be larger at 15% and at 21% for three of the materials. The special device, used in the experiments, is described. NTIS

N95-21440# Mound Lab., Miamisburg, OH.

PROPERTIES OF AGED METAL TRITIDES

G. T. McConville, D. A. Menke, D. S. West, and C. M. Woods 22 Jun. 1994 15 p
(Contract DE-AC04-88DP-43495)
(DE95-001787; MLM-3799) Avail: CASI HC A03/MF A01

The interaction of tritium with metals is made complex by two phenomena. The first is that the beta decay in the metal produces He-3. The helium moves to form bubbles. This report shows that growth of the bubbles produces a two-stage swelling of the metal that comes first from the appearance of the helium and second from the relaxation of the lattice disorder. The second phenomena is the steady state ion and free radical concentration in the tritium over gas that interacts with impurities on the metal surface. This report shows that the reaction rates are much faster than for normal hydrogen cleaning. DOE

N95-21447# Pennsylvania State Univ., University Park, PA. Dept. of Chemistry.

CLUSTER REACTIONS: AN APPROACH TO UNDERSTANDING THE FUNDAMENTALS OF HETEROGENEOUS CATALYSIS

A. W. Castleman, Jr. and Evan Pugh 1994 10 p
(Contract DE-FG02-92ER-14258)
(DE95-002947; DOE/ER-14258/2) Avail: CASI HC A02/MF A01

The physical basis for catalysis is not well understood and the motivation for this ongoing research is to provide a basis for unraveling the role which composition, morphology and electronic states have on the functioning of catalysts for various classes of reactions. The work during the first two and one-half year grant period has focused on unsupported clusters of selected composition, charge state, and size. Research has proceeded along three general lines of inquiry: (1) investigation of the reactivity of these cluster materials and determination of the influence of their charged state; (2) determination of the kinetics of association (adsorption) of various reactants and unraveling the mechanisms of certain oxidation reactions known to be catalyzed on metal cluster alloys, oxides and carbides; and (3) thermochemical measurement of the absorption of gaseous species onto alloy and metal oxide and carbide cluster systems. The authors have pursued the role of metal and metal-oxide clusters, and the charge states of these, as they function to influence the reactions of adsorbed species including ammonia, alcohols, water, NO(x), as well as CO and hydrogen. Evidence has been obtained that small positively charged nickel clusters function to catalyze reactions between adsorbed CO and hydrogen. In supportive studies, they have investigated the clustering of ammonia, methanol and water to nickel clusters of varying size. These studies, in conjunction with density functional calculations which are in progress, provide insight into cluster structures and knowledge of adsorption energies. DOE

N95-21472# Oak Ridge National Lab., TN. Instrumentation and Characterization Dept.

OPERATOR'S MANUAL FOR THE MULTISTATION OFFGAS ANALYSIS SYSTEM

A. B. Hayes and J. A. Basford 10 Oct. 1994 18 p
(Contract DE-AC05-84OS-21400)
(DE95-002060; Y/DW-1332) Avail: CASI HC A03/MF A01

The Multistation Offgas Analysis System (MOAS) is a fully automated instrument which can independently measure the gases emitted by up to four samples in containers heated in ovens. A mass spectrometer is used to determine accurately their flow rates. There are six interconnected high vacuum pumping stations, one for each of the sample containers, one for the mass spectrometer, and one for the calibrated leaks which are used to calibrate the mass spectrometer. Quadstar 421(trademark) is the software package marketed by Balzers, the manufacturer of the mass spectrometer. This software used by MOAS is a combination of Quadstar 421(trademark), special routines, called sequences in the Balzers nomenclature, and compiled programs that controls MOAS. Tests are run repeatedly on each of the four oven stations, while stations that are not ready, or do not have a sample are skipped. While the computer is sitting idle between tests, the software monitors the vacuum system. If necessary, the software will shut down a pumping station that is not operating correctly. The status of pumping stations and tests, filenames for data and oven temperatures are stored on disk, so the software can recover from a power failure. The operator can use the software to start or stop testing, load parts, perform calibrations as necessary, and start up or shut down pumping stations. The software aids in routine functions, such as changing an ion gauge, by performing the required valve actuations automatically, and checking the pressure readings and turbopump speeds as necessary. The computer takes mass spectrometer sensitivity calibration data automatically, every week at 12:00AM on Sunday. An operator does not need to be present for these calibrations. The calibration data are saved and may be used or deleted by the operator at a later date. DOE

N95-21473# Westinghouse Hanford Co., Richland, WA.

CONCEPTUAL DESIGN ANALYSES FOR HANFORD SITE DEPLOYABLE REMOTE SPECTROSCOPY SYSTEMS

Barbara L. Philipp and F. R. Reich Sep. 1994 42 p
(Contract DE-AC06-87RL-10930)
(DE95-002078; WHC-SD-WM-TA-158) Avail: CASI HC A03/MF A01

This document identifies potential remote, NIR spectroscopic waste surface moisture monitoring system design alternatives to be operated inside one of the Hanford Site, high level, nuclear waste storage tanks. Potential tank waste moisture data impacts from the remote NIR signal transfer through high humidity vapor space is evaluated. DOE

N95-21500# Oak Ridge National Lab., TN.

PRODUCTION OF S2F10, S2OF10 AND S2O2F10 BY SPARK DISCHARGES IN SF6*

I. Sauers, S. M. Mahajan (Tennessee Technological Univ., Cookeville, TN.), and R. A. Cacheiro (Tennessee Univ., Knoxville, TN.) 1994 8 p Presented at the 7th International Symposium on Gaseous Dielectrics, Knoxville, TN, 24-28 Apr. 1994
(Contract DE-AC05-84OR-21400)
(DE95-001421; CONF-940414-5) Avail: CASI HC A02/MF A01

Measurements have been made of the spark yield of S2F10 and S2OF10 as a function of O2 and H2O concentration. In addition the formation of S2O2F10 is reported. The spark yield of S2F10 is reduced when either oxygen or water is added to SF6. On the other hand the yield of S2OF10 is increased when either oxygen or water is added, oxygen having the greater effect. A simple model is presented based on a common SF5 precursor to S2F10 and S2OF10 showing good agreement with the yields of both byproducts in O2/SF6 and H2O/SF6 mixtures. The yield of S2F10 is found to be greatest when the spark chamber is very dry and the electrodes are well conditioned. DOE

N95-21512# Sandia National Labs., Livermore, CA. Combustion Research Facility.

TEMPORAL EVOLUTION OF TURBULENCE/CHEMISTRY INTERACTIONS IN LIFTED, TURBULENT-JET FLAMES

R. W. Schefer, M. Namazian (Altex Technologies Corp., Santa Clara, CA.), E. E. J. Filtopoulos (Altex Technologies Corp., Santa Clara, CA.), and J. Kelly (Altex Technologies Corp., Santa Clara, CA.) 1994 17 p Presented at the 25th International Symposium on Combustion, Irvine, CA, 31 Jul. - 5 Aug. 1994
(Contract DE-AC04-76DP-00789)
(DE95-002481; SAND-94-8730C; CONF-940711-18) Avail: CASI HC A03/MF A01

Flame ignition, extinction and reignition that control flame stability are time dependent. Two-pulse images of the instantaneous CH/CH4 distributions, with a variable time delay between images, were used to study the temporal evolution of turbulence/chemistry interactions in lifted, turbulent CH4-jet flames. The jet exit velocity was 21 m/s (jet exit Reynolds number 7,000). The results emphasize interactions between turbulence structure and the flame that lead to large fluctuations in experimental flame lift-off height. The results show that the flame envelope curves around semi-organized, large-scale vortical structures formed along the periphery of the jet. Interactions between these vortical structures and the flame cause excessive stretch that leads to local flame extinction. Extinction occurs on both the downstream edges of the structures and on the upstream sides. Once the flame is extinguished by a vortical structure, the flame stabilization point can be carried significant distances downstream by the vortex. The return to an upstream stabilization location occurs through turbulent premixed flame propagation. The images show upstream propagation of the flame within the image plane. Evidence also exists for the importance of flame propagation in the azimuthal direction normal to the image plane. DOE

N95-21517# Columbia Univ., New York, NY. Dept. of Chemistry.
SINGLE-COLLISION STUDIES OF ENERGY TRANSFER AND CHEMICAL REACTION Performance Report, 9 Sep. 1991 - 15 Apr. 1994
James J. Valentini 1994 10 p
(Contract DE-FG02-91ER-14225)
(DE95-002943; DOE/ER-14225/3) Avail: CASI HC A02/MF A01

The work reported here was done during the period September 9, 1991 through April 14, 1994. During this 2 (1/2)-year period this work has been focused on three related efforts: (1) experimental studies of the state-to-state dynamics of the H + RH (yields) H2 + R reactions, where RH is CH4, C2H6, C3H8, and CHCl3; (2) theoretical studies of the H + CH4 (yields) H2 + CH3 reaction; and (3) the development of a single-mode purely pulsed dye laser for Doppler-resolved coherent anti-Stokes Raman scattering (CARS) spectroscopy. A report of the progress the authors have made in each of these efforts is given. DOE

N95-21523# Los Alamos National Lab., NM.
VISIBLE FLUORESCENCE OF WEATHERED LEAD
Alan D. Martin and John L. Lyman 1994 7 p
(Contract W-7405-eng-36)
(DE95-002454; LA-12865) Avail: CASI HC A02/MF A01

This experiment explored the possibility of remotely detecting lead fragments by means of an ultraviolet laser or a handheld spectrometer. Lead oxide has a unique fluorescence spectrum (resolution 18 nm), but it does not phosphoresce. DOE

N95-21524# Sandia National Labs., Albuquerque, NM. Combustion Research Facility.
CORRELATIONS FOR THE OH A(SUP 2)(SIGMA)(SUP +)(V(PRIME)=0) ELECTRONIC QUENCHING CROSS-SECTION
P. H. Paul, C. D. Carter, J. A. Gray, J. L. Durant, Jr., and M. R. Furlanetto (Williams Coll., Williamstown, MA.) Oct. 1994 26 p
(Contract DE-AC04-94AL-85000)
(DE95-002591; SAND-94-8244) Avail: CASI HC A03/MF A01

This report summarizes recent progress in the development of a model for collisional electronic quenching of OH A(sup 2)(Sigma)(sup +)(v(prime)=0) by a number of molecules commonly found in combustion and aerodynamic systems. The model provides a means to reliably extend the measurement data base as well as suggesting simple analytic forms which can be used to provide physically plausible fits to the measurements. This report also contains a partial compilation of the available experimental data for collisional electronic quenching of OH A(sup 2)(Sigma)(sup +)(v(prime)=0). DOE

N95-21549# Oak Ridge National Lab., TN.
RAMAN SPECTRA OF MOCVD-GROWN FERROELECTRIC PbTiO3 THIN FILMS
Z. C. Feng (National Univ. of Singapore,, Singapore.), B. S. Kwak (Georgia Inst. of Tech., Atlanta, GA.), and A. Erbil (Georgia Inst. of Tech., Atlanta, GA.) 1993 13 p Presented at the Fall Meeting of the Materials Research Society (MRS), Boston, MA, 29 Nov. - 3 Dec. 1993
(Contract DE-AC05-84OR-21400)
(DE94-018964; CONF-931108-110) Avail: CASI HC A03/MF A01

Lead titanate (PbTiO3) has been grown on a variety of substrates by using the metalorganic chemical vapor deposition (MOCVD) technique. The substrates employed included Si, GaAs, MgO, fused-quartz, sapphire, and KTaO3. Raman spectra from these heterostructures are presented. All of the films exhibited the strong, narrow spectral features characteristic of PbTiO3 perovskite-oxide crystals and indicative of high crystalline quality. The temperature behavior of the Raman modes, including the so-called 'soft-mode,' was studied. A 'difference-Raman' technique was used to distinguish the contributions of the PbTiO3 film and the KTaO3 single-crystal substrate. DOE

N95-21571# Oak Ridge Y-12 Plant, TN.
SURFACE INSPECTION USING FOURIER TRANSFORM INFRARED SPECTROSCOPY
G. L. Powell (Martin Marietta Energy Systems, Inc., Oak Ridge, TN.), N. R. Smyrl (Martin Marietta Energy Systems, Inc., Oak Ridge, TN.), D. M. Williams (Martin Marietta Energy Systems, Inc., Oak Ridge, TN.), H. M. Meyers, III (Martin Marietta Energy Systems, Inc., Oak Ridge, TN.), T. E. Barber (Oak Ridge Inst. for Science and Education, TN.), and M. Marrero-Rivera (Oak Ridge Inst. for Science and Education, TN.) Aug. 1994 10 p Presented at the Aerospace Environmental Technology Conference, Huntsville, AL, 10-11 Aug. 1994
(Contract DE-AC05-84OS-21400)
(DE95-001699; Y/DZ-1113/R1; CONF-9408174-2) Avail: CASI HC A02/MF A01

The use of reflectance Fourier transform infrared (FTIR) spectroscopy as a tool for surface inspection is described. Laboratory instruments and portable instruments can support remote sensing probes that can map chemical contaminants on surfaces. Detection limits under the best of conditions are in the subnanometer range (i.e., near absolute cleanliness), excellent performance is obtained in the submicrometer range, and useful performance may exist for films tens of microns thick. Identifying and quantifying contamination such as mineral oils and greases, vegetable oils, and silicone oils on aluminum foil, galvanized sheet steel, smooth aluminum tubing, and gritblasted 7075 aluminum alloy and D6AC steel are described. The ability to map in time and space the distribution of oil stains on metals is demonstrated. Techniques for quantitatively applying oils to metals, subsequently verifying the application, and nonlinear relationships between reflectance and the quantity of oil are discussed. DOE

N95-21573# Technische Univ., Eindhoven (Netherlands). Dept. of Mathematics and Computing Science.
ONE-DIMENSIONAL REACTIVE EULER EQUATIONS
A. C. Berkenbosch, E. F. Kaasschieter, and J. H. M. tenThijeBoonkkamp Jun. 1994 26 p
(ISSN 0926-4507)
(PB95-135430; RANA-94-07) Avail: CASI HC A03/MF A01

The reactive Euler equations are derived from the general conservation equations for reacting gas flow. We concentrate on traveling wave solutions of the reactive Euler equations. The Rankine-Hugoniot equations are presented, which relate the upstream and downstream conditions of combustion waves. A classification of combustion waves, based on the Rankine-Hugoniot equations, is given. Finally, the ZND-model is presented and detonation waves are described in more detail. NTIS

N95-21701# North Carolina Univ., Chapel Hill, NC. Dept. of Chemistry.
THE ENERGETICS AND DYNAMICS OF FREE RADICALS, IONS, AND CLUSTERS
T. Baer 1994 12 p
(Contract DE-FG05-88ER-13950)
(DE94-018101; DOE/ER-13950/T3) Avail: CASI HC A03/MF A01

The structure and energetics of free radicals, ions, and clusters have been investigated by photoelectron photoion coincidence (PEPICO) and analyzed with the aid of ab initio molecular orbital and statistical theory (RRKM) calculations. The two major themes are the quantitative analysis of unimolecular reactions with no adjustable parameters, and the study of cluster ion dissociation processes. Molecules (or free radicals) were prepared in a molecular beam so that they are translationally and vibrationally cold. The translational temperature was calculated from the measured time of flight (TOF) peak width, while the vibrational temperature was determined from the shift in the dissociation onset. Free radicals are produced by pyrolysis in the nozzle, and subsequent cooling of the free radicals is demonstrated. Ion dissociation rates in the range from 10(exp 4) to 10(exp 7)/sec are measured from the asymmetric TOF distribution. This method was used to measure the dissociation rates of a number of cold and warm ions, among them HCl (DCl) loss from C2H5Cl(+) (C2D5Cl(+)), a reaction that proceeds via tunneling. The analysis of the butene ion dissociation provided information about the role of angular momentum in dissociation reactions. This dissociative ionization of ethylene clusters demonstrated that ethylene dimerions rearranged to butene ions prior to dissociation. Finally, a new value for the t-butyl ion heat of formation, which corrects a 15 kJ/mol error in the previous value, was obtained from the 0 K breakdown diagram of t-butyl iodide. DOE

N95-21732# Oak Ridge National Lab., TN.

A VISUAL CELL FOR MEASURING THE SOLUBILITY OF PROGRADE SOLUBLE SALTS IN WATER AT HIGH TEMPERATURES AND PRESSURES

R. C. Moore, J. M. Simonson, and R. E. Mesmer Oct. 1994 15 p
(Contract DE-AC05-84OR-21400)
(DE95-002058; ORNL-6829) Avail: CASI HC A03/MF A01

An apparatus has been constructed for measuring the solubility of prograde soluble salts in water at high temperatures and pressures. The apparatus consists of a visually accessible cell thermostated in a rocking furnace. The apparatus allows for rapid, accurate solubility measurements for temperatures over 650 K and pressures up to 170 bars. The cell was constructed of platinum with sapphire windows and gold seals for corrosion resistance. A 3x telescope is used to observe the phase change in the cell. A key feature of the cell is the ability to control the system pressure. A section of small bore platinum tubing is used to connect the cell to an external pressure source. The tubing can remain open to the pressure source or be sealed off during a measurement. To minimize equilibration times, the entire apparatus was mounted to a rocking frame which can operate in the horizontal or vertical position. The apparatus was tested by measuring the solubility of NaCl in water at temperatures between 345 and 516 K at saturation pressure. Results are in good agreement with existing literature values. DOE

N95-21734# Iowa State Univ. of Science and Technology, Ames, IA.

STUDIES OF SELENIUM AND XENON IN INDUCTIVELY COUPLED PLASMA MASS SPECTROMETRY Ph.D. Thesis

T. Bricker 27 Jul. 1994 65 p
(Contract W-7405-eng-82)
(DE95-001676; IS-T-1701) Avail: CASI HC A04/MF A01

Since its development, inductively coupled plasma mass spectrometry (ICP-MS) has been a widely used analytical technique. ICP-MS offers low detection limits, easy determination of isotope ratios, and simple mass spectra from analyte elements. ICP-MS has been successfully employed for many applications including geological, environmental, biological, metallurgical, food, medical, and industrial. One specific application important to many areas of study involves elemental speciation by using ICP-MS as an element specific detector interfaced to liquid chromatography. Elemental speciation information is important and cannot be obtained by atomic spectrometric methods alone which measure only the total concentration of the element present. Part 1 of this study describes the speciation of selenium in human serum by size exclusion chromatography (SEC) and detection by ICP-MS. Although ICP-MS has been widely used, room for improvement still exists. Difficulties in ICP-MS include noise in the background, matrix effects, clogging of the sampling orifice with deposited solids, and spectral interference caused by polyatomic ions. Previous work has shown that the addition of xenon into the central channel of the ICP decreases polyatomic ion levels. In Part 2 of this work, a fundamental study involving the measurement of the excitation temperature is carried out to further understand xenon's role in the reduction of polyatomic ions. DOE

N95-21745# Northwestern Univ., Evanston, IL.

STRONG INTERACTIONS STUDIES WITH MEDIUM ENERGY PROBES

K. K. Seth Sep. 1994 19 p
(Contract DE-FG02-87ER-40344)
(DE95-001800; DOE/ER-40344/8) Avail: CASI HC A03/MF A01

This progress report refers to the period August 1993 to September 1994, which includes the second year of the three year period December 1, 1992 - November 30, 1995 of our existing research contract. The budget proposal for the third year, December 1, 1994 to November 30, 1995 as originally approved, is also presented. As anticipated in our 1992 - 1995 proposal, Fermilab E760/E835 on high precision charmonium spectroscopy has remained a major part of our preoccupation and commitment during the last year, and it will remain so in the forthcoming year. In early 1994 we joined the collaboration of the Brookhaven experiment E852 on the spectroscopy of states with exotic quantum numbers. The first successful three month run of E852 was completed on July 31 and preliminary data analysis has been started. Some new commitments have resulted from this collaboration and a separate proposal for supplemental financial support is being prepared for them. At Los Alamos our experiment (number sign)1274 on search of extremely neutron rich exotic nuclei by pion absorption began making initial measurements a month ago and is expected to take data during the period October 15 - November 30, 1994. In addition to the above on-going programs, our Bates proposal (94-01) for a definitive measurement of the quenching of the longitudinal response in quasi-free scattering of electrons from nuclei has been approved with high priority for 600 hours of beam time, and we expect to start the experiment in late 1995. DOE

N95-21826 Oregon Univ., Eugene, OR. Dept. of Chemistry.

SURFACE SECOND HARMONIC STUDIES OF SI(111)/ELECTROLYTE AND SI(111)/SIO2/ELECTROLYTE INTERFACES Technical Report, Jun. 1993 - May 1994

P. R. Fischer, J. L. Daschbach, and G. L. Richmond 13 May 1994 17 p Limited Reproducibility: More than 20% of this document may be affected by microfiche quality
(Contract N00014-89-J-1261)
(AD-A279450; TR-9) Avail: Issuing Activity (Defense Technical Information Center (DTIC))

The optical second harmonic (SH) response from Si(111) electrode surfaces has been studied and has been found to be highly potential dependent. For both H-terminated Si(111) surfaces in NH4F, and oxide covered surfaces biased in H2SO4, the phase and the amplitude display a potential dependence which we attribute to field effect within the semiconductor space-charge region and at the surface of the Si(111) electrode. The studies are the first to demonstrate that for Si(1110)/oxide samples the potential dependence in the SH phase can be correlated with oxide thickness as demonstrated by examining samples of 0-40 Angstrom thickness. DTIC

N95-21827 Oregon Univ., Eugene, OR. Dept. of Chemistry.

STUDIES OF THE n-ALKANE/WATER INTERFACE BY TOTAL INTERNAL REFLECTION SECOND HARMONIC GENERATION Technical Report, Jun. 1993 - May 1994

J. C. Conboy, J. L. Daschbach, and G. L. Richmond 13 May 1994 12 p Limited Reproducibility: More than 20% of this document may be affected by microfiche quality
(Contract N00014-89-J-1261)
(AD-A279473; TR-11) Avail: Issuing Activity (Defense Technical Information Center (DTIC))

Total internal reflection second harmonic generation (TIRSHG) has made possible the study of a series of neat n-alkane/water interfaces. Analysis of the incident and polarization angular dependent SH response allows for determination of interfacial nonlinear molecular properties. The measured surface nonlinear susceptibilities may be indicative of a high degree of interfacial order. DTIC

N95-21845# Tri-Univ. Meson Facility, Vancouver (British Columbia).

TIME OF FLIGHT SPECTROSCOPY WITH MUONIC HYDROGEN

G. M. Marshall, J. M. Bailey (Liverpool Univ., England.), G. A. Beer (Victoria Univ., British Columbia.), J. L. Beveridge, J. H. Brewer (British Columbia Univ., Vancouver, British Columbia.), M. Fujiwara (British Columbia Univ., Vancouver, British Columbia.), T. M. Huber (Gustavus Adolphus Coll., Saint Peter, MN.), R. Jacot-Guillarmod (Fribourg Univ., Switzerland.), P. Kammel (Academy of Sciences, Vienna, Austria.), and P. E. Knowles (Victoria Univ., British Columbia.) et al 1993 4 p Presented at the International Workshop on Low Energy Muon Science, Santa Fe, NM, 4-8 Apr. 1993 Sponsored in cooperation with NSERC, NATO, and Research Corp.
(Contract DE-FG02-87ER-40333)
(DE94-017056; DOE/ER-40333/142; COO-2197-142; CONF-9304145-4)
Avail: CASI HC A01/MF A01

Time of flight techniques coupled with muonic deuterium and tritium atoms in vacuum can be used to measure parameters important in the understanding of muon catalyzed fusion interactions. Muonic deuterium atomic beams with energy of order 1 eV have been produced via transfer and emission from solid hydrogen containing small deuterium concentrations. Measurements of energy loss in pure deuterium are presented which test calculations of sigma(sub (mu)d+D). Muonic tritium beams should be produced in a similar way, with an energy distribution which overlaps the predicted muonic molecular (d(mu)t) formation resonances. The existence of resonances is crucial for high cycling rates in muon catalyzed fusion, but direct experimental verification of strengths and energies is not yet possible by other means. Results of simulations demonstrate how the resonance structure might be confirmed. DOE

N95-21879# Massachusetts Inst. of Tech., Cambridge, MA. Dept. of Chemistry.

PREPARATION AND X-RAY STRUCTURE OF Cp2Ti(PH2SiH2)(PMe3)

Esther Spaltenstein, Pilar Palma, Kristina A. Kreutzer, Christopher A. Willoughby, and William M. Davis 18 Oct. 1994 11 p
(Contract N00014-91-J-1043)
(AD-A286197; TR-7) Avail: CASI HC A03/MF A01

The synthesis and x-ray structure determination of the novel complex, Cp2Ti(Ph2SiH2)(PMe3), (4), is reported. The spectroscopic and structural data indicate that (4) is best described as being a hybrid between a titanium(4)(silyl)hydride complex and a titanium(2) silane complex. Complex (4) reacts reversibly with N2 to form the bridging dinitrogen complex (5) and, in the presence of norbornene, (4) catalytically dimerizes Ph2SiH2 in quantitative yield. DTIC

N95-21886# Michigan Univ., Ann Arbor, MI. Dept. of Geological Sciences.

APPLICATIONS OF ICP MAGNETIC SECTOR MULTICOLLECTOR MASS SPECTROMETRY TO BASIC ENERGY RESEARCH Progress Report, 1 Dec. 1993 - 31 Aug. 1994

A. N. Halliday and C. M. Hall Sep. 1994 14 p
(Contract DE-FG02-94ER-14412)
(DE95-002600; DOE/ER-14412/1) Avail: CASI HC A03/MF A01

The prototype Inductively-Coupled Plasma (ICP) magnetic sector multicollector mass spectrometer has been installed and commissioned at the University of Michigan. Following performance evaluation and instrument characterization, the absolute abundances of isotopes of tin have been measured with precisions unproved by up to an order of magnitude over those of currently accepted, values. An efficient chemical separation technique for In and Sn in Zn, Cu and Fe sulfides and in silicate matrices has been successfully developed. The predicted Sn-115 anomaly that results from the decay of In-115, has been measured in sulfides. Precise isotopic measurements of molybdenum, tellurium, hafnium, tungsten and platinum have been made. A new ND-YAG laser ablation microsampling device on line to the mass spectrometer for in situ isotopic analysis at high precision has been commissioned and tested with accurate measurements of Sr, W and Pb on standard silicate materials. DOE

N95-21921# Air Products and Chemicals, Inc., Allentown, PA.

DEVELOPMENT OF ACTIVE-TRANSPORT MEMBRANE DEVICES

D. V. Laciak Jul. 1994 144 p
(Contract DE-FC36-89ID-12779)
(DE94-015947; DOE/ID-12779/1) Avail: CASI HC A07/MF A02

This report introduces the concept of Air Products' Active Transport membranes for the separation of NH3 and CO2 from process gas streams and presents results from the first year fabrication concept development studies. DOE

N95-21931 North Carolina State Univ., Raleigh, NC. Dept. of Chemistry.

CHEMISTRY AND ELECTROCHEMISTRY IN LEWIS ACID AND SUPERACID IONIC LIQUIDS Final Report, 1 Jul. 1992 - 31 Dec. 1993

Robert A. Osteryoung 30 Apr. 1994 23 p Limited Reproducibility: More than 20% of this document may be affected by microfiche quality
(Contract F49620-92-J-0326)
(AD-A279396; AFOSR-94-0297TR) Avail: Issuing Activity (Defense Technical Information Center (DTIC))

Studies in an ambient temperature chloroaluminate molten salt composed of aluminum chloride and 1-ethyl-3-methylimidazolium chloride were carried out. A variety of topics were investigated. Work on poly(p-phenylene) and silane based electroactive polymers was carried out. The electrochemistry of several Ru and Co complexes was examined, as was the kinetics of the ferroceneferrocenium couple as a function of melt viscosity. The electrochemistry of anthracene and 9,10 anthraquinone was examined under conditions where protonation of these species was important. Finally, proton speciation and proton equilibrium were examined by NMR and FT-IR spectroscopies. DTIC

N95-21990# California Univ., Berkeley. Lawrence Berkeley Lab, CA. Materials Sciences Div.

BRIDGING THE PRESSURE GAP: IN SITU ATOMIC-LEVEL INVESTIGATIONS OF MODEL PLATINUM CATALYST SURFACES UNDER REACTION CONDITIONS BY SCANNING TUNNELING MICROSCOPY Ph.D. Thesis

Brian James McIntyre May 1994 229 p
(Contract DE-AC03-76SF-00098)
(DE95-002346; LBL-36065) Avail: CASI HC A11/MF A03

Results of this thesis show that STM measurements can provide information about the surfaces and their adsorbates. Stability of Pt(110) under high pressures of H2, O2, and CO was studied (Chap. 4). In situ UHV and high vacuum experiments were carried out for sulfur on Pt(111) (Chap.5). STM studies of CO/S/Pt(111) in high CO pressures showed that the Pt substrate undergoes a stacking-fault-domain reconstruction involving periodic transitions from fcc to hcp stacking of top-layer atoms (Chap.6). In Chap.7, the stability of propylene on Pt(111) and the decomposition products were studied in situ with the HPSTM. Finally, in Chap.8, results are presented which show how the Pt tip of the HPSTM was used to locally rehydrogenate and oxidize carbonaceous clusters deposited on the Pt(111) surface; the Pt tip acted as a catalyst after activation by short voltage pulses. DOE

N95-22000 New Orleans Univ., LA. Dept. of Chemistry.

NON-LOCAL DENSITY FUNCTIONAL CALCULATIONS OF GAS PHASE HEATS OF FORMATION

Dariush Habibollahzadeh, M. E. Grice, Monica G. Concha, Jane S. Murray, and Peter Politzer 3 Nov. 1994 11 p Limited Reproducibility: More than 20% of this document may be affected by microfiche quality
(Contract N00014-91-J-4057)
(AD-A286213) Avail: CASI HC A03

A general procedure is presented for computing the gas phase heats of formation of a wide variety of organic compounds. Delta E for the formation of the molecule from its elements at 0 K is obtained from density functional calculations (Gaussian 92/DFT) for optimized geometries. This result is converted to Delta H at 298 K by assuming ideal behavior and adding the translational, rotational, and vibrational energies. Additive correction terms corresponding to the various coordination states of the carbons, nitrogens, and oxygens were developed using a data base of 54 compounds. The experimental Delta H deg sub f values of these compounds are then reproduced with an average absolute error of 3 kcal/mole and a standard deviation of 4 kcal/mole. For a group of ten test cases that were not part of the data base, the average absolute error is 3.5 kcal/mole and the standard deviation is 4.1 kcal/mole. DTIC

N95-22012# Los Alamos National Lab., NM.

THE APPLICATION OF ELECTRODIALYSIS TO EXTEND THE LIFETIME OF COMMERCIAL ELECTROPLATING BATHS

G. Purdy, C. Zawodzinski, B. Smith, and W. H. Smith 1993 13 p
Presented at the 8th Symposium on Separation Science and Technology for Energy Applications, Gatlinburg, TN, 24-28 Oct. 1993
(Contract W-7405-eng-36)
(DE95-000868; LA-UR-94-3090; CONF-9310360-1) Avail: CASI HC A03/MF A01

Electrodialysis has been investigated as a method to extend the lifetime of industrial electroplating solutions via the selective removal of inert electrolyte salts that build up during electroplating operations. The electrodialysis measurements were made using a commercially available plate-and frame-type cell and various combinations of Nafion cation change and either Tosflex or Neosepta anion exchange membranes. Two commercial plating solutions were studied: a zinc-tin bath in which there is a buildup of excess potassium hydroxide and a nickel-tungsten bath characterized by a buildup of excess sodium sulfate. Potassium hydroxide was effectively removed from the zinc-tin bath with very little loss of the heavy metals. Two configurations were investigated: a three compartment configuration with potassium hydroxide in the anolyte strip and sulfuric acid in the catholyte strip, and a two compartment configuration with sulfuric acid in the catholyte strip and the anode placed directly in the plating solution. In both cases potassium hydroxide was stripped from the plating solution at greater than 94% current efficiency, but at a slightly greater voltage in the three compartment cell due to increased resistance caused by the extra membrane. A three compartment configuration was used to remove sodium sulfate from the nickel-tungsten bath, with acid solution in the catholyte and alkaline solution in the anolyte. Current efficiencies for salt removal were high but with appreciable loss of tungsten and nickel to the strip solutions. DOE

N95-22020# Massachusetts Inst. of Tech., Cambridge, MA. Dept. of Chemistry.
A CATALYTIC METHOD FOR THE CONVERSION OF SILANES TO STANNANES
Benjamin J. Warner and Sephen L. Buchwald 8 Oct. 1994 10 p
(Contract N00014-91-J-1043)
(AD-A286214) Avail: CASI HC A02/MF A01

The transformation of alkynyl-, allyl-, and benzyltrimethylsilanes to the corresponding tributylstannanes is reported. The reaction is initiated by the addition of tetrabutylammonium fluoride to a mixture of the silane and bis(tributyltin)oxide in tetrahydrofuran. The stannanes are isolated in approximately quantitative yields after removal of the volatile bis(trimethylsilyl)oxide in vacuo. DTIC

N95-22049# Oak Ridge National Lab., TN.
CATALYZED REDUCTION OF NITRATE IN AQUEOUS SOLUTIONS
P. A. Haas Aug. 1994 17 p
(Contract DE-AC05-84OR-21400)
(DE94-017660; ORNL/TM-12800) Avail: CASI HC A03/MF A01

Sodium nitrate and other nitrate salts in wastes is a major source of difficulty for permanent disposal. Reduction of nitrate using aluminum metal has been demonstrated, but NH3, hydrazine, or organic compounds containing oxygen would be advantageous for reduction of nitrate in sodium nitrate solutions. The objective of this seed money study was to determine minimum conditions for reduction. Proposed procedure was batch heating of aqueous solutions in closed vessels with monitoring of temperatures and pressures. A simple, convenient apparatus and procedure were demonstrated for observing formation of gaseous products and collecting samples for analyses. The test conditions were 250 C and approximately 1000 psi max. Any useful reduction of sodium nitrate to sodium hydroxide as the primary product was not found. The nitrate present at pHs less than 4 as HNO3 or NH4NO3 is easily decomposed, and the effect of nitromethane at these low pHs was confirmed. When acetic acid or formic acid was added, 21 to 56% of the nitrate in sodium nitrate solutions was reduced by methanol or formaldehyde. With hydrazine and acetic acid, 73 % of the nitrate was decomposed to convert NaNO3 to sodium acetate. With hydrazine and formic acid, 36% of the nitrate was decomposed. If these products are more acceptable for final disposal than sodium nitrate, the reagents are cheap and the conversion conditions would be practical for easy use. Ammonium acetate or formate salts did not significantly reduce nitrate in sodium nitrate solutions. DOE

N95-22150# SRI International Corp., Menlo Park, CA.
NATURAL GAS COMBUSTION CHEMISTRY MECHANISMS RESEARCH Annual Report, 1 Dec. 1992 - 31 Dec. 1993
Gregory P. Smith, David R. Crosley, David M. Golden, Michael Frenklach (Pennsylvania State Univ., University Park, PA.), William C. Gardiner (Texas Univ., Austin, TX.), Ronald K. Hanson (Stanford Univ., CA.), and Craig T. Bowman (Stanford Univ., CA.) 23 Sep. 1994 34 p Prepared for Gas Research Inst., Chicago, IL
(Contract GRI-5092-260-2454; Proj. SRI-PYH4197)
(PB95-111670; MP-94-074; GRI-94/0269) Avail: CASI HC A03/MF A01

An evaluated mechanism of elementary rate constants and thermodynamics for methane combustion was developed. The experimental data set and sensitivity computations for the optimization procedure were selected and completed; the optimization calculations were begun. Important kinetics measurements and analysis were made to aid in this endeavor. Shock tube experiments determined CH3 and OH concentrations in CH4-O2-Ar mixtures for the optimization. Quantum calculations were performed for the CH + N2 reaction. Modeling studies examined the development of reduced and skeletal mechanisms and the prediction of NO and soot levels in diesel engines. NTIS

N95-22207# Army Research Lab., Aberdeen Proving Ground, MD.
AB INITIO POTENTIAL ENERGY SURFACE FOR H + OCS REACTIONS: EXTENDED BASIS SETS AND CORRELATION TREATMENT Final Report, Sep. 1993 - Jun. 1994
Betsy M. Price and Cary F. Chabalowski Nov. 1994 35 p
(DA Proj. 1L1-61102-AH-43)
(AD-A286420; ARL-TR-629) Avail: CASI HC A03/MF A01

Ab initio calculations using extended basis sets are presented for the potential energy surface (PES) of H + OCS. There are two major reaction channels on the PES; Reaction (1) is H(2S) + OCS(1(Sigma)) yields OH(2(Pi)) + CS(1(Sigma)), and Reaction (2) is H(2S) + OCS(1(Sigma)) yields SH(2(Pi)) + CO(1(Sigma)). Results of this study substantiate findings from an earlier quantum chemical study using a lower level of theory, including (1) the existence of 12 transition states and 6 stable 4-body intermediates; (2) the qualitative description of the PES (i.e., geometries, relative barriers, and well depths are similar to those in the earlier study); and (3) the entrance channel transition states leading to (2) are tight, as suggested by experiment. The results presented here also support the explanations of observed product energy distributions for (1) and (2) based on the earlier ab initio study. An additional transition state connecting the cis-HOCS and cis-HSCO minima was located, confirming a previous suggestion that Reaction (2) could result from hydrogen migration after HOCS formation. The current results show a substantial improvement in the quantitative agreement with experiment over the previously calculated values. DTIC

N95-22224# Notre Dame Univ., IN. Dept. of Chemical Engineering.
TRANSIENT STUDIES OF LOW TEMPERATURE CATALYSTS FOR METHANE CONVERSION Quarterly Technical Progress Report, 1 Jul. - 30 Sep. 1994
E. E. Wolf 1994 29 p
(Contract DE-FG22-92PC-92529)
(DE95-003560; DOE/PC-92121/T8) Avail: CASI HC A03/MF A01

This report includes a paper that summarizes the previous work on the Li/LaNiO3 catalysts, and the progress made on the study of the effect of catalyst preparation on the activity and selectivity of a LaRhO3 catalyst toward methane conversion. The latter catalyst has shown earlier an unusually low ignition temperature of about 450C, which deemed further investigation in relation to the production of syngas (CO and H2). DOE

N95-22234# Sandia National Labs., Albuquerque, NM.
ACID-SITE CHARACTERIZATION OF WATER-OXIDIZED ALUMINA FILMS BY NEAR-EDGE X-RAY ABSORPTION AND SOFT X-RAY PHOTOEMISSION
P. J. OHagan (Cornell Univ., Ithaca, NY.), R. P. Merrill (Cornell Univ., Ithaca, NY.), T. N. Rhodin (Cornell Univ., Ithaca, NY.), S. W. Woronick (Cornell Univ., Ithaca, NY.), N. D. Shinn, G. L. Woolery (Mobil Research and Development Corp., Paulsboro, NJ.), and A. W. Chester (Mobil Research and Development Corp., Paulsboro, NJ.) 1994 7 p Presented at the Fall Meeting of the Materials Research Society, Boston, MA, 28 Nov. - 2 Dec. 1994 Prepared in cooperation with BNL, Upton, NY
(Contracts DE-AC04-94AL-85000; DE-AC02-76CH-00016)
(DE95-003355; SAND-94-2716C; CONF-941115-1) Avail: CASI HC A02/MF A01

Hydroxylated alumina films have been synthesized by water oxidation of single crystal Al(110) surfaces. Thermal dehydroxylation results in anion vacancies which produce an Al(3s) defect state 3.5 eV below the conduction band edge. A maximum in the defect-DOS occurs for oxides heated to 350 to 400C, which is where the materials exhibit maximum Lewis acidity with respect to C2H4. Adsorbed C2H4 produces thermally active C2 species which interact covalently with the defect-DOS and nonbonding O(2p) from the top of the valence band. C(1s) binding energies suggest significant charge transfer which is consistent with a carbenium ion. Ni evaporated onto the surface, however, transfers charge directly to Al species and does not interact with O atoms at the defect site. The defect-DOS is regenerated when the C2 species decomposes or when Ni migrates thermally through the oxide layer. DOE

N95-22260# Oak Ridge National Lab., TN.
THE THERMAL CONDUCTIVITY OF SILICON NITRIDE WITH MOLYBDENUM DISILICIDE ADDITIONS
S. C. Beecher, R. B. Dinwiddie, A. M. Abeel, and R. A. Lowden 1993

10 p Presented at the 22nd International Thermal Conductivity Conference, Tempe, AZ, 7-10 Nov. 1993
(Contract DE-AC05-84OR-21400)
(DE94-017757; CONF-9311131-5) Avail: CASI HC A02/MF A01

Room-temperature thermal conductivity has been measured for a series of silicon nitride (Si3N4) matrix composites with molybdenum disilicide (MoSi2) additions of 2, 5, 10, 25 and 50 wt. %. Included in these measurements were a pure MoSi2 sample and a Si3N4 sample containing only sintering aids. Aluminum oxide (Al2O3) and yttrium oxide (Y2O3) were added as the sintering aids, at approximately 6 and 2 respectively. When the amount of MoSi2 was increased to greater than 10 wt. %, the amount of the sintering aids necessary to densify the composite was decreased. No sintering aids were added to the pure MoSi2 sample. Thermal conductivities of the Si3N4 sample without MoSi2 and the pure MoSi2 sample wee 36 W/m.K and 52 W/m.K respectively, which agree very well with the literature values for similar materials. No statistically significant changes were observed in the thermal conductivity for those samples containing up to 10 wt. % MoSi2. However, between 10 and 25 wt. % MoSi2 there was a dramatic decrease in the thermal conductivity from 37 to 20.9 W/m.K. The thermal conductivity then increased steadily with further additions of MoSi2 up to 52 W/m.K for the pure MoSi2 specimen. DOE

N95-22273# Sandia National Labs., Albuquerque, NM.
THE MODIFIED EMBEDDED ATOM METHOD
M. I. Baskes Aug. 1994 27 p
(Contract DE-AC04-94AL-85000)
(DE94-017958; SAND-94-8704) Avail: CASI HC A03/MF A01

Recent modifications have been made to generalize the Embedded Atom Method (EAM) to describe bonding in diverse materials. By including angular dependence of the electron density in an empirical way, the Modified Embedded Atom Method (MEAM) has been able to reproduce the basic energetic and structural properties of 45 elements. This method is ideally suited for examining the interfacial behavior of dissimilar materials. This paper explains in detail the derivation of the method, shows how the parameters of the MEAM are determined directly from experiment or first principles calculations, and examines the quality of the reproduction of the database. Materials with fcc, bcc, hcp, and diamond cubic crystal structure are discussed. A few simple examples of the application of the MEAM to surfaces and interfaces are presented. Calculations of pullout of a SiC fiber in a diamond matrix as a function of applied stress show non-uniform deformation of the fiber. DOE

N95-22321 Army Research Lab., Aberdeen Proving Ground, MD.
QUANTUM CHEMICAL STUDY OF RARE GAS/HALIDE INTERACTIONS AS A MODEL FOR HIGH ENERGY DENSITY MATERIAL. 2: THE INTERACTION OF HYDROGEN CHLORIDE WITH THE RARE GAS XENON Final Report, Sep. 1989 - Sep. 1991
George F. Adams and Cary F. Chabalowski Nov. 1994 41 p Limited Reproducibility: More than 20% of this document may be affected by microfiche quality
(DA Proj. 1L1-61102-AH-43)
(AD-A286385; ARL-TR-621) Avail: CASI HC A03

Electronic transitions from laser excitation have produced charge transfer (CT) reactions in doped xenon solids, which in turn generate spatially separated, long-lived, dipolaron states. These quasi-stable separated charges have been as an energy storage mechanism in the study of high-energy density materials. In a previous study, we performed calculations on selected singlet electronic state of HCl, and in this study we investigate the character of the low-lying singlet electronic states in the systems Cl + Xe and HCl + Xe. The results show at least one excited electronic state which is ionic in nature and could serve as a CT state. It is also known from experimentation that following excitation into the CT state, the H-Cl bond is ruptured. The CT state located in this study is described primarily by a molecular orbital with sigma-antibonding character in the H-Cl bonding region. This CT state would therefore provide both a charge transfer mechanism and a means for weakening or breaking the H-Cl bond consistent with experimental observations. In this report, we also provide potential energy surfaces and electronic transition probabilities as a function of R(HC1...Xe) for a linear arrangement. DTIC

N95-22329# Helsinki Univ. of Technology, Espoo (Finland).
CATALYTIC REACTIONS OF SYNTHESIS GAS. PART 3. DETERMINATION OF REACTION KINETICS
M. Niemelae 1993 44 p See also PB93-179448
(PB95-127759; ISBN-951-22-1902-6) Avail: CASI HC A03/MF A01

The review is aimed at introducing the basic concepts of experimental kinetic procedures relevant in the present characterization and testing of heterogeneous transition metal catalysts in a fixed bed tubular reactor, Carberry spinning basket gradientless reactor, or a batch screening reactor in synthesis gas or methanol homologation reaction. The term differential reactor means a reactor in which the conversion is limited to not more than a few percent. Under these conditions the rate can be calculated directly at fixed concentrations. The obtained rate data may be fit to a reaction rate law, which could provide information on the reaction mechanisms, in order to determine the values of reaction rate constant, activation energy, and individual reaction orders. NTIS

N95-22373# Helsinki Univ. of Technology, Espoo (Finland).
SEPARATION OF PROTEINS BY CONVECTIVE ELECTROPHORESIS THROUGH A POROUS MEMBRANE Ph.D. Thesis
M. Vuoristo 20 Jun. 1994 39 p
(PB95-127130) Avail: CASI HC A03/MF A01

The development of a continuous convective electrophoresis (CCE) method for separation of proteins is presented. The separation in the porous membrane has been modelled by solving the extended Nernst-Planck equations for protein transport. The separation efficiency has been demonstrated by simulations and by experiments with four different mixtures of model proteins: Cytochrome c - Bovine Serum Albumin, Cytochrome c - Lysozyme, Human Serum Albumin - Haemoglobin and pyrogen contaminated Human Serum Albumin. The results of the separation experiments were in good agreement with the predictions of the mathematical model. Relatively high separation efficiency were obtained with all protein pairs studied in a continuous one-step process. NTIS

N95-22385 New Mexico Univ., Albuquerque, NM.
SYNTHESIS AND CHARACTERIZATION OF SINGLE-SOURCE MOLECULAR PRECURSORS TO BINARY METAL SULPHIDES: BIS(DIETHYLDITHIOCARBAMATO) M(2)TRIALKYLPHOSPHINE (M = Zn AND Cd) ADDUCTS
D. Zeng, M. Hampden-Smith, and T. M. Alam 6 May 1994 41 p Limited Reproducibility: More than 20% of this document may be affected by microfiche quality
(Contract N00014-91-J-1258)
(AD-A279746) Avail: CASI HC A03

Monomeric, five-coordinate bis(diethyldithiocarbamato)M(2)-(trialkylphosphine) complexes, 1 (M=Zn, a lkyl=Me), 2 (M=Zn, alkyl=Et), 3 (M=Cd, alkyl=Me), and 4 (M=Cd, alkyl=Et) have been synthesized by addition of trialkylphosphine ligands to toluene solutions of bis(diethyldithiocarbamato)M(II) (M=Zn, and Cd). The bidentate ligand, 1,2-bis(diethylphosphino)ethane (DEPE) reacted with bis(diethyldithiocarbamato)M(II) (M=Zn, Cd) and a 1:1 mixture of (Et2NCS2)2Zn2:(Et2NCS2)2Cd2 in toluene to form five-coordinate, dinuclear DEPE-bridged complexes, (Et2NCS2)2M2(mu-DEPE), 5 (M=Zn), 6 (M=Cd) and 7 (Et2NCS2)2Zn(muEt2PCH2CH2PEt2)Cd(Et2NCS2)2, respectively. The composition and structure of all compounds was confirmed by elemental analyses, infra-red spectroscopy, 1H, 13C (1H) and 31P(1H) nuclear magnetic resonance (NMR) and in selected cases by X-ray crystallography. The solid-state structures of (Et2NCS2)2ZnPMe3(1) and (Et2NCS2)2CdPEt3(4) have been determined by single-crystal X ray diffraction. Thermogravimetric analysis (TGA) of compounds 1-3 showed that the PR3 ligands dissociated prior to thermal decomposition. However, compound 4 exhibited a single weight loss to give crystalline CdS as determined by X ray powder diffraction, electron diffraction and transmission electron microscopy. The homobimetallic species, 5 and 6 also decomposed to give ZnS and CdS, respectively while the heterobimetallic species, 7, thermally decomposed to give crystalline Zn0.5S according to X ray powder diffraction data. DTIC

N95-22433# Los Alamos National Lab., NM.
THE INTERACTION OF LOCALIZED SOLUTIONS IN A SURFACE REACTION
H. R. Brand (Bayreuth Univ., Germany.) and R. J. Deissler 1994 9 p Presented at the NEEDS 1994 Conference, Los Alamos, NM, 12-16 Sep.

1994
(Contract W-7405-eng-36)
(DE95-002736; LA-UR-94-3529; CONF-9409241-1) Avail: CASI HC A02/MF A01

We discuss similarities and differences between spatially localized solutions of the quintic complex Ginzburg-Landau equation applicable near a weakly inverted bifurcation to traveling waves and localized states observed during the catalytic oxidation of CO on Pt(110). It turns out that both, the properties of a single localized state as well as their interaction, share many common features in comparing the two systems. We point out that the experimental results rule out a solitonic mechanism and are only compatible with the picture of a dissipative driven system. DOE

N95-21036*# Escuela Tecnica Superior de Ingenieros Aeronauticos, Madrid (Spain).
EFFECTS OF NON-UNITY LEWIS NUMBERS IN DIFFUSION FLAMES
A. Linan, P. Orlandi (Rome Univ., Italy.), R. Verzicco (Rome Univ., Italy.), and F. J. Higuera *In* Stanford Univ., Studying Turbulence Using Numerical Simulation Databases. 5: Proceedings of the 1994 Summer Program Dec. 1994 p 5-18 (For primary document see N95-21035 06-34)
Avail: CASI HC A03/MF A04

N95-21037*# National Aeronautics and Space Administration. Ames Research Center, Moffett Field, CA.
EFFECT OF CHEMICAL HEAT RELEASE IN A TEMPORALLY EVOLVING MIXING LAYER
F. J. Higuera (Escuela Tecnica Superior de Ingenieros Aeronauticos, Madrid, Spain.) and R. D. Moser *In* Stanford Univ., Studying Turbulence Using Numerical Simulation Databases. 5: Proceedings of the 1994 Summer Program Dec. 1994 p 19-40 (For primary document see N95-21035 06-34)
Avail: CASI HC A03/MF A04

N95-21038*# Sandia National Labs., Livermore, CA.
DIRECT NUMERICAL SIMULATIONS OF TURBULENT NON-PREMIXED METHANE-AIR FLAMES MODELED WITH REDUCED KINETICS
J. M. Card, J. H. Chen, M. Day, and S. Mahalingam (Colorado Univ., Boulder, CO.) *In its* Studying Turbulence Using Numerical Simulation Databases. 5: Proceedings of the 1994 Summer Program Dec. 1994 p 41-54 Sponsored by AWU-DOE faculty fellowship program (For primary document see N95-21035 06-34)
Avail: CASI HC A03/MF A04

N95-21039*# Ecole Centrale de Paris (France).
TRIPLE FLAME STRUCTURE AND DIFFUSION FLAME STABILIZATION
D. Veynante, L. Vervisch (Institut National des Sciences Appliquees, Routen, France.), T. Poinsot (Institut de Mecanique des Fluides de Toulouse, France.), A. Linan (Escuela Tecnica Superior de Ingenieros Aeronauticos, Madrid, Spain.), and G. Ruetsch *In* Stanford Univ., Studying Turbulence Using Numerical Simulation Databases. 5: Proceedings of the 1994 Summer Program Dec. 1994 p 55-73 (For primary document see N95-21035 06-34)
Avail: CASI HC A03/MF A04

N95-21040*# Wisconsin Univ., Madison, WI.
TURBULENT TRANSPORT IN PREMIXED FLAMES
C. J. Rutland and R. S. Cant (Manchester Coll. of Science and Technology, England.) *In* Stanford Univ., Studying Turbulence Using Numerical Simulation Databases. 5: Proceedings of the 1994 Summer Program Dec. 1994 p 75-94 (For primary document see N95-21035 06-34)
Avail: CASI HC A03/MF A04

N95-21041*# Institut Francais du Petrole, Paris.
THE COUPLING BETWEEN FLAME SURFACE DYNAMICS AND SPECIES MASS CONSERVATION IN PREMIXED TURBULENT COMBUSTION
A. Trouve (Institut Francais du Petrole, Paris.), D. Veynante (Ecole Centrale de Paris, France.), K. N. C. Bray (Cambridge Univ., Cambridge, England.), and T. Mantel *In* Stanford Univ., Studying Turbulence Using Numerical Simulation Databases. 5: Proceedings of the 1994 Summer Program Dec. 1994 p 95-124 (For primary document see N95-21035 06-34)
Avail: CASI HC A03/MF A04

N95-21042*# Institut National des Sciences Appliquees, Routen (France).
Pdf MODELING FOR PREMIXED TURBULENT COMBUSTION BASED ON THE PROPERTIES OF ISO-CONCENTRATION SURFACES
L. Vervisch, W. Kollmann (California Univ., Davis, CA.), K. N. C. Bray (Cambridge Univ., Cambridge, England.), and T. Mantel *In* Stanford Univ., Studying Turbulence Using Numerical Simulation Databases. 5: Proceedings of the 1994 Summer Program Dec. 1994 p 125-150 (For primary document see N95-21035 06-34)
Avail: CASI HC A03/MF A04

N95-21043*# Sandia National Labs., Livermore, CA.
PASSIVE TURBULENT FLAMELET PROPAGATION
William T. Ashurst, G. R. Ruetsch (Stanford Univ., CA.), and T. S. Lund (Stanford Univ., CA.) *In* Stanford Univ., Studying Turbulence Using Numerical Simulation Databases. 5: Proceedings of the 1994 Summer Program Dec. 1994 p 151-156 (For primary document see N95-21035 06-34)
Avail: CASI HC A02/MF A04

N95-21044*# Institut Francais du Petrole, Paris.
SIMULATION OF A TURBULENT FLAME IN A CHANNEL
G. Bruneaux, K. Akselvoll (Stanford Univ., CA.), T. Poinsot (Institut de Mecanique des Fluides de Toulouse, France.), and J. H. Ferziger (Stanford Univ., CA.) *In* Stanford Univ., Studying Turbulence Using Numerical Simulation Databases. 5: Proceedings of the 1994 Summer Program Dec. 1994 p 157-174 (For primary document see N95-21035 06-34)
Avail: CASI HC A03/MF A04

N95-21081# Central Inst. of Aviation Motors, Moscow (Russia).
A FLAMELET MODEL FOR TURBULENT UNPREMIXED COMBUSTION
V. R. Kuznetsov *In* AGARD, Application of Direct and Large Eddy Simulation to Transition and Turbulence Dec. 1994 10 p (For primary document see N95-21061 06-34)
Copyright Avail: CASI HC A02/MF A04

N95-21082# Manchester Coll. of Science and Technology (England). Dept. of Mechanical Engineering.
DIRECT NUMERICAL SIMULATION FOR PREMIXED TURBULENT COMBUSTION MODELLING
R. S. Cant *In* AGARD, Application of Direct and Large Eddy Simulation to Transition and Turbulence Dec. 1994 13 p Sponsored by Stanford Univ., Shell Research Ltd., and the UK Science and Engineering Research Council (For primary document see N95-21061 06-34)
Copyright Avail: CASI HC A03/MF A04

N95-22438*# Stanford Univ., CA. Center for Turbulence Research.
CONDITIONAL STATISTICS IN A TURBULENT PREMIXED FLAME DERIVED FROM DIRECT NUMERICAL SIMULATION
Thierry Mantel and Robert W. Bilger (Sydney Univ., Australia.) *In its* Annual Research Briefs, 1994 Dec. 1994 p 3-27 (For primary document see N95-22437 06-34)
Avail: CASI HC A03/MF A04

N95-22439*# Stanford Univ., CA. Center for Turbulence Research.
LEWIS NUMBER AND DAMKOHLER NUMBER EFFECTS IN VORT EX-FLAME INTERACTIONS
Jean-Michael Samaniego *In its* Annual Research Briefs, 1994 Dec. 1994 p 29-43 (For primary document see N95-22437 06-34)
Avail: CASI HC A03/MF A04

N95-22440*# Stanford Univ., CA. Center for Turbulence Research.
FUNDAMENTAL MECHANISMS IN PREMIXED FLAME PROPAGATION VIA VORTEX-FLAME INTERACTIONS: NUMERICAL SIMULATIONS
Thierry Mantel *In its* Annual Research Briefs, 1994 Dec. 1994 p 45-75 (For primary document see N95-22437 06-34)
Avail: CASI HC A03/MF A04

N95-22441*# Stanford Univ., CA. Center for Turbulence Research.
TRIPLE FLAMES AND FLAME STABILIZATION
James E. Broadwell *In its* Annual Research Briefs, 1994 Dec. 1994

p 77-78 (For primary document see N95-22437 06-34)
Avail: CASI HC A01/MF A04

N95-22442*# Stanford Univ., CA. Center for Turbulence Research.
FLAME PROPAGATION UNDER PARTIALLY-PREMIXED CONDITIONS
Gregory R. Ruetsch *In its* Annual Research Briefs, 1994 Dec. 1994
p 79-96 (For primary document see N95-22437 06-34)
Avail: CASI HC A03/MF A04

26 METALLIC MATERIALS

Includes physical, chemical, and mechanical properties of metals, e.g., corrosion; and metallurgy.

N95-19900# Lawrence Livermore National Lab., Livermore, CA.
MIXED-SPUTTER DEPOSITION OF Ni-Ti-Cu SHAPE MEMORY FILMS
P. Krulevitch, P. B. Ramsey, D. M. Makowiecki, A. P. Lee, M. A. Northrup, and G. C. Johnson (California Univ., Berkeley, CA.) May 1994 16 p
(Contract W-7405-eng-48)
(DE94-017296; UCRL-ID-115719) Avail: CASI HC A03/MF A01

Ni-Ti-Cu shape memory films were mixed-sputter deposited from separate nickel, titanium, and copper targets, providing increased compositional flexibility. Shape memory characteristics, examined for films with 7 at.% Cu and 41-51 at.% Ti, were determined with temperature controlled substrate curvature measurements, and microstructure was studied with transmission electron microscopy. The Ni-Ti-Cu films were found to have shape memory properties comparable to bulk materials, with transformation temperatures between 20 and 62 C, a 10-13 C hysteresis, and up to 330 MPa recoverable stress. DOE

N95-19910 Materials Research Labs., Ascot Vale (Australia).
A REVIEW OF MICROBIALLY INDUCED CORROSION (MIC) OF STEEL AND A PRELIMINARY INVESTIGATION TO DETERMINE ITS OCCURRENCE IN NAVAL VESSELS
John F. Upsher May 1993 25 p Original contains color illustrations
(MRL-GD-0048; AR-008-241) Copyright Avail: Issuing Activity

A study was made of the mechanisms of microbially induced corrosion of steels and of influencing factors. The main causative organisms were the sulfate reducing bacteria (SRB) which require little more than a wet situation with depleted oxygen, some small organic molecules and sulfate. The corrosive effect is primarily by cathodic depolarization but local abundance of sulfide and pH change are also involved. SRB were detected at one third of the corrosion sites examined on three Naval ships. They were also present in their oily water wastes which would be a source of infection of any exposed steel surfaces. Based on current information, no special measures to counter microbially induced corrosion of ship steel are recommended but antibacterial treatments warrant further investigation as remedial measures for active microbially induced corrosion (MIC) areas. Author

N95-19979# Brookhaven National Lab., Upton, NY.
CHEMICAL AND ELECTROCHEMICAL INTERACTIONS ON CORRODING METAL SURFACES
H. S. Isaacs and A. J. Aldykiewicz, Jr. 1994 12 p Presented at the Meeting on Electrochemical Methods in Corrosion Research, Lisbon, Portugal, 5-8 Sep. 1994
(Contract DE-AC02-76CH-00016)
(DE95-000624; BNL-60757; CONF-940947-1) Avail: CASI HC A03/MF A01

The corrosion resistance of many metals and alloys depend on their ability to repassivate after breakdown of the passive film. Following breakdown localized corrosion takes place. The consequences of initiation events depends on many factors leading to a dissolution rate of the metal which may be continuous, intermittent or transitory. Major changes in the solution chemistry at the breakdown site must take place to enable active dissolution to take place and prevent repassivation. However, mass transfer of the dissolution products to the bulk environment often plays a decisive role. The composition of the environment is important. Some species inhibit while others stimulate the anodic dissolution. In the presence of particular cations, deposition slowly takes place on cathodic sites. Current density mapping measurements have been used to study pitting processes on iron and aluminum alloys. The effects of phosphate as an anodic inhibitor for steel and cerium as a cathodic inhibitor for aluminum are discussed in conjunction with related chemical processes. DOE

N95-20020# Oak Ridge National Lab., TN.
PROCESSING AND CHARACTERIZATION OF Ni-Al-Fe-B SHAPE-MEMORY ALLOY WIRES PRODUCED BY RAPID SOLIDIFICATION
D. S. Easton, C. T. Liu, J. A. Horton, E. P. George, and J. J. Campbell 1993 4 p Presented at the International Union of Materials Research Societies on Advanced Materials, Tokyo, Japan, 31 Aug. - 4 Sep. 1993
(Contract DE-AC05-84OR-21400)
(DE94-017702; CONF-9308122-19) Avail: CASI HC A01/MF A01

This work describes net-shape ductile wires of Ni-Al-Fe doped with boron produced directly from the melt by in-rotating-liquid (IRL) melt spinning, thus avoiding the difficult and costly problem of fabricating bulk castings. This method produces wires of 0.1 to 0.5 mm dia and lengths to 2 m. X ray diffraction scans showed that the as-spun wires consist of B2, Ll2, and bct martensite phases and that the B2 phase further transforms to bct martensite upon cold working. Shape-memory behavior showed an Ap temperature of (approximately) 180 C as measured by bend recovery tests and by tensile cycling tests. Effects on the wires of IRL processing parameters are discussed. DOE

N95-20043# Oak Ridge National Lab., TN.
Cr2Nb DEVELOPMENT
C. T. Liu, J. A. Horton, and C. A. Carmichael 1994 12 p Presented at the 7th Annual Conference on Fossil Energy Materials, Oak Ridge, TN, 11-13 May 1993
(Contract DE-AC05-84OR-21400)
(DE94-018697; CONF-9305135-10) Avail: CASI HC A03/MF A01

Microstructure and mechanical properties of Cr-Nb alloys containing 5.6 to 17% Nb were studied for high-temperature structural applications. The alloys basically contain the two phases of Cr2Nb and chromium-rich solid solution. Re, Al, Ni, Fe and Co were added to the alloys for control of microstructure and properties. The alloys show excellent strength at temperatures to 1250 C. Among the alloying elements, rhenium is found to be most effective in improving the mechanical properties at room and elevated temperatures. Alloying with greater than or equal to 8% Al, Ni, and Co, on the other hand, lowers the strength and ductility at elevated temperatures. Further development is required to improve the fracture resistance of the alloys at ambient temperatures. DOE

N95-20044# Oak Ridge National Lab., TN.
FABRICATION AND PROPERTIES OF ALUMINA MATRIX COMPOSITES CONTAINING NICKEL ALUMINIDE REINFORCEMENTS
K. B. Alexander, H. T. Lin, J. H. Schneibel, and P. F. Becher 1994 6 p Presented at the Fall Meeting of the Minerals, Metals and Materials Society: Physical Metallurgy and Materials, Pittsburgh, PA, 17-21 Oct. 1993
(Contract DE-AC05-84OR-21400)
(DE94-018703; CONF-931009-30) Avail: CASI HC A02/MF A01

Ductile nickel-aluminide intermetallic alloys have been successfully used to toughen ceramic materials intended for use at a wide range of temperatures. Traditional ceramic processing procedures have been used to produce a variety of microstructures. The fracture toughness increases with increasing particle aspect ratio, however, the flexural strength decreases with increasing particle size. Fracture toughnesses up to 7.6 MPa m(sup 1/2) and flexural strengths up to 550 MPa were observed in an alumina composite containing 10 vol.% nickel aluminide. DOE

N95-20067# Army Research Lab., Watertown, MA. Materials Directorate.
MECHANICAL BEHAVIOR OF 97.2% W ALLOY IN TENSION AT HIGH TEMPERATURES Final Report
John L. Green Sep. 1994 22 p
(AD-A284797; ARL-TR-508) Avail: CASI HC A03/MF A01

The objective was to investigate the behavior of 97.2% tungsten alloy in tension. A modified button head specimen was heated using resistive heating techniques. The affect high temperatures, medium strain rates, and heating rates had on the stress-strain results were observed. A high speed optical pyrometer and an optical clip gage were utilized for temperature and strain measurements. The optical clip gage could measure strain at strain rates up to 11.8/s. The room temperature experiments were at strain rates of 10-(exp 4)/s, 10-(exp 2)/s, and 5/s. The high heating rate experiments were at temperatures of 727 C, and 1097 C, heating rates of 5.4 C/sec and 536 C/sec and a strain rate of 5/s. Increase in yield point and flow stress were observed as the heating rate was increased. A modified Johnson-Cook (MJ+C) material model was proposed to include the effect of heating rate. The constants in the MJ+C model were determined based on the experimental results. DTIC

N95-20068*# National Aeronautics and Space Administration. Marshall Space Flight Center, Huntsville, AL.
HYDROGEN RESISTANT ALLOY - NASA 23 Patent Application
William B. McPherson, inventor (to NASA) and A. K. Kuruvilla, inventor (to NASA) (IIT Research Inst., Huntsville, AL.) 10 May 1994 9 p
(NASA-Case-MFS-26200-1-SB; NAS 1.71:MFS-26200-1-SB; US-Patent-Appl-SN-248611) Avail: CASI HC A02/MF A01

The invention is a high-strength metal alloy that resists hydrogen embrittlement consisting essentially of thirty-seven (37) percent by weight of iron, thirty-two (32) percent by weight of nickel, fifteen (15) percent by weight of cobalt, ten (10) percent by weight of chromium, three (3) percent by weight of niobium, two-and-one-half (2.5) percent by weight of titanium, fifteen hundredths (0.15) percent by weight of aluminum, and an amount of carbon that does not exceed four hundredths (0.04) percent by weight. NASA

N95-20079# Westinghouse Savannah River Co., Aiken, SC.
FRACTURE TOUGHNESS PROPERTIES OF WELDED STAINLESS STEELS FOR TRITIUM SERVICE
M. Morgan 1994 5 p Presented at the 19th Department of Energy Conference on Compatibility, Aging and Service Life, Los Alamos, NM, 28-30 Sep. 1994
(Contract DE-AC09-89SR-18035)
(DE95-000755; SRTC-MTS-94-3017; CONF-9409181-6) Avail: CASI HC A01/MF A01

Studies to determine tritium exposure effects on the properties of welded steels are being conducted. In this investigation, the effects of tritium and decay helium on the fracture toughness properties of high-energy-rate-forged (HERF) Incoloy 903 were measured. Fracture toughness measurements were conducted for tritium-exposed samples in the as-forged condition and compared with welded samples. Tritium-exposed HERF Incoloy 903 had fracture toughness values that were 33% lower than those for unexposed HERF Incoloy 903. Tritium-exposed welded samples had fracture toughness values that were just 8% of the unexposed HERF alloys and 28% of unexposed welded alloys. DOE

N95-20088# Pacific Northwest Lab., Richland, WA.
POST-IRRADIATION DEFORMATION CHARACTERISTICS OF HEAVY-ION IRRADIATED 304L SS
J. I. Cole (Washington State Univ., Pullman, WA.) and S. M. Bruemmer Jun. 1994 12 p Presented at the 17th Symposium on Effects of Radiation on Materials, Sun Valley, ID, 20-23 Jun. 1994
(Contracts DE-AC06-76RL-01830; DE-FG06-89ER-75522)
(DE94-017462; PNL-SA-23641; CONF-940657-5) Avail: CASI HC A03/MF A01

Post-irradiation deformation behavior in Ni-ion-irradiated 304L stainless steel (SS) is examined as a function of radiation dose and deformation temperature. For similar strain levels, specimens exhibit a transition from dislocation slip to deformation-induced twinning at 25 C with increasing radiation dose. At 288 C twinning is no longer observed and highly localized slip occurs by the formation of narrow 'channels' containing a reduced defect density. The observations are discussed in terms of radiation-induced defect character and expected deformation mechanisms. DOE

N95-20090# Pacific Northwest Lab., Richland, WA.
DEVELOPMENT OF SUPERPLASTICITY IN 5083 ALUMINUM WITH ADDITIONS OF Mn AND Zr
C. A. Lavender, J. S. Vetrano, M. T. Smith, S. M. Bruemmer, and C. H. Hamilton (Washington State Univ., Pullman, WA.) May 1994 8 p Presented at the International Conference on Superplasticity in Advanced Materials (ICSAM), Moscow, Russia, 24-26 May 1994
(Contract DE-AC06-76RL-01830)
(DE94-017474; PNL-SA-23032; CONF-9405193-3) Avail: CASI HC A02/MF A01

The superplastic behavior of the 5083 aluminum alloy with additions of Mn and Zr was studied by uniaxial tensile testing and microstructural evaluations. Additions of up to 0.2% Zr and 0.8% Mn were made to a base 5083 aluminum alloy to decrease the grain size and improve superplastic behavior. Constant strain-rate tensile test data were used to determine strain-rate sensitivity (m values) and elongations-to-failure for the alloys at strain rates ranging from 4 x 10(exp -4) to 1 x 10(exp -1) s(exp -1) at temperatures of 450 to 550 C. Elongations-to-failure of up to 400% at 1 x 10(exp -2) s(exp -1) were achieved for the modified alloys. The strain-rate sensitivity for the alloys as a function of strain was determined and two distinct behaviors were observed. For the alloys having composition close to the base 5083 alloy, the m value steadily decreased with increasing strain; however, in alloys with higher levels of Zr, the m value remained stable. A maximum m value of 0.65 was achieved at 0.7 strain for the 1.6% Mn and 0.2% Zr alloy at 1 x 10(exp -3) s(exp -1). DOE

N95-20122# Lawrence Livermore National Lab., Livermore, CA.
DUCTILE-BRITTLE TRANSITION BEHAVIOR OF TUNGSTEN UNDER SHOCK LOADING
D. H. Lassila and G. T. Gray, III (Los Alamos National Lab., NM.) Feb. 1994 8 p Presented at the EURODYMAT 1994: 1st International Conference on Mechanical and Physical Behavior of Materials Under Dynamic Loading, Oxford, England, 26-30 Sep. 1994
(Contract W-7405-eng-48)
(DE94-009913; UCRL-JC-116339; CONF-940956-7) Avail: CASI HC A02/MF A01

The ductile-brittle transition behavior of warm-forged tungsten under shock loading conditions was examined by performing shock/soft-recovery experiments at 22 C and 400 C. The results of a recovery experiment at 22 C indicate that shock (19 GPa)-induced strains were accommodated by fracture processes, i.e. there were no indications of shock-induced plastic deformation, and the test sample was reduced to rubble. At 400 C the test sample was recovered intact and the shock-induced plasticity caused deformation banding and an increase in the dislocation density of the material. The results of these experiments demonstrate the principle of a ductile-brittle transition behavior of tungsten under uniaxial shock loading conditions and indicate that explosively driven deformation of the material studied will likely result in pulverization due to shock loading. DOE

N95-20128# Idaho Univ., Moscow, ID. Dept. of Mechanical Engineering.
MAGNETICALLY CONTROLLED DEPOSITION OF METALS USING GAS PLASMA
D. M. Woodall and E. C. Lemmon Jul. 1994 27 p
(Contract DE-FG07-93ID-13220)
(DE94-018654; DOE/ID-13220/T1) Avail: CASI HC A03/MF A01

Thin layers of secondary material are plated on substrates either by plating or spraying processes. Plating operations produce large amounts of hazardous liquid wastes. Spraying, while one of the less waste intensive methods, produces 'over spray' which is waste that is a result of the uncontrolled nature of the spray stream. In many cases the over spray produces a hazardous waste. Spray coating is a mature process with many uses. Material can be deposited utilizing spraying technology in three basic ways: 'flame spraying,' direct spraying of molten metals, and/or plasma spraying. This project is directed at controlling the plasma spraying process and thereby minimizing the waste generated in that process. Examples of spraying applications that may benefit substantially from this technology are: (1) preparing printed circuit boards and (2) tinning circuit boards with lead in preparation for soldering components. There are many applications of spraying technology that can benefit from a controlled spraying scheme. They include: (1) titanium coating on bio-implants, (2) wear-tolerant ceramic thermal barriers using partially stabilized zirconia (PSZ), (3) alumina and alumina-titania wear resistant-coatings, and (4) ceramic superconductor manufacture using hollow spherical powders. DOE

N95-20178# Pennsylvania State Univ., University Park, PA. Dept. of Engineering Science and Mechanics.
ENHANCEMENT OF CORROSION RESISTANCE AND MECHANICAL PROPERTIES OF LIGHT-WEIGHT METALS THROUGH THE USE OF GRADED NONEQUILIBRIUM MICROSTRUCTURES Technical Report, 1 Jul. 1993 - 30 Jun. 1994

B. A. Shaw and K. A. Kennedy Oct. 1994 65 p
(Contract N00014-93-1-0537)
(AD-A286320) Avail: CASI HC A04/MF A01

Designs for the future will place extreme demands on light-weight materials. In order to meet the challenges of the future it is vital that an emphasis be placed on tailor-making these materials to enhance specific properties. Through the use of rapid solidification processing advances have been made in our ability to engineer materials, but we have yet to be able to tailor-make a light-weight alloy with all of the characteristics we desire. A new approach to tailor-making alloys with the enhanced properties we desire is to use nonequilibrium alloying techniques such as sputter or high-rate vapor deposition to grade the structure and composition of an alloy during processing. Such alloys could be designed to take advantage of recent advances in enhancing both the mechanical properties and the corrosion resistance of Al and Mg. For conventional Al alloys, a combination of high strength and significantly enhanced corrosion resistance are mutually exclusive. In order to achieve high strengths, precipitates are necessary in the microstructure. DTIC

N95-20201 Department of the Navy, Washington, DC.
METHOD OF MAKING COPPER-TITANIUM NITRIDE ALLOY Patent
Harris L. Marcus, inventor (to Navy), Zwy Eliezer, inventor (to Navy), and Morris E. Fine, inventor (to Navy) 16 Aug. 1994 7 p Filed 26 Jul. 1993
(AD-D016582; US-Patent-5,338,374; US-Patent-Appl-SN-104952; US-Patent-Class-148-237) Avail: US Patent and Trademark Office

A process for forming a copper alloy which is strengthened while maintaining good electrical and thermal conductivity by the addition of TiN or ZrN consists of external nitridation of a mechanically alloyed powder mixture followed by further mechanical alloying to break down the surface coating which forms during nitridation. DTIC

N95-20216# Westinghouse Savannah River Co., Aiken, SC.
TRITIUM AND DECAY HELIUM EFFECTS ON THE FRACTURE TOUGHNESS PROPERTIES OF TYPES 316L, 304L AND 21Cr-6Ni-9Mn STAINLESS STEELS
M. J. Morgan and M. Tosten 1994 12 p Presented at the 5th International Conference on Hydrogen Effects on Material Behavior, Moran, WY, 11-15 Sep. 1994
(Contract DE-AC09-89SR-18035)
(DE95-001248; SRTC-MTS-94-3036; CONF-940945-2) Avail: CASI HC A03/MF A01

J-integral fracture mechanics techniques and electron microscopy observations were used to investigate the effects of tritium and its radioactive decay product, He-3, on types 316L, 304L, and 21Cr-6Ni-9Mn stainless steels. Tritium exposed and aged steels had lower fracture toughness values and shallower sloped crack-growth-resistance curves than unexposed steels. Both fracture toughness parameters decreased with increasing concentrations of He-3. The fracture toughness reductions were accompanied by a change in fracture mode from microvoid nucleation and growth processes in control samples to grain and twin boundary fracture in tritium charged and aged samples. Type 316L stainless steel had the highest fracture toughness values and type 21Cr-6Ni-9Mn had the lowest. Samples containing He-3 but degassed of tritium had fracture toughness properties that were similar to uncharged samples. The results indicate that helium bubbles enhance the embrittlement effects of hydrogen by affecting the deformation properties and by increasing localized hydrogen concentrations through trapping effects. DOE

N95-20299# Lynntech, Inc., College Station, TX.
CORROSION OF AIRCRAFT MATERIALS: CORRELATION BETWEEN NANOMETER SCALE AND MACROSCOPIC STRUCTURAL DAMAGE PARAMETERS Annual Report
A. Gonzales-Martin, D. Hodko, C. Andrews, and O. J. Murphy 15 Aug. 1994 8 p
(Contract F49620-94-C-0040)
(AD-A285930; AFOSR-94-0674TR) Avail: CASI HC A02/MF A01

The following work has been carried out during the reporting period: (1) imaging of pitting corrosion initiation in aluminum at the nanometer scale; (2) study of the effects of main atmospheric pollutants on the initiation of the corrosion process; (3) identification of surface regions at an aluminum sample where corrosion is most likely to occur; (4) measurements of the electrochemical impedance spectra on Al sample before and during the pitting process in NaCl; and (5) identification of the impedance parameters characteristic for the pitting the corrosion of the aluminum sample. DTIC

N95-20331# Lawrence Livermore National Lab., Livermore, CA.
PLASMA ARC MELTING OF TITANIUM-TANTALUM ALLOYS
P. Dunn, R. A. Patterson, and R. Haun (Retech, Inc., Ukiah, CA.) 1994 13 p Presented at the Symposium on Liquid Metal Processing and Casting, Santa Fe, NM, 11-14 Sep. 1994
(Contract W-7405-eng-36)
(DE94-016291; LA-UR-94-2409; CONF-940978-1) Avail: CASI HC A03/MF A01

Los Alamos has several applications for high temperature, oxidation and liquid-metal corrosion resistant materials. Further, materials property constraints are dictated by a requirement to maintain low density; e.g., less than the density of stainless steel. Liquid metal compatibility and density requirements have driven the research toward the Ti-Ta system with an upper bound of 60 wt% Ta-40 wt% Ti. Initial melting of these materials was performed in a small button arc melter with several hundred grams of material; however, ingot quantities were soon needed. But, refractory metal alloys whose constituents possess very dissimilar densities, melting temperatures, and vapor pressures pose significant difficulty and require specialized melting practices. The Ti-Ta alloys fall into this category with the density of tantalum 16.5 g/cc and that of titanium 4.5 g/cc. Melting is further complicated by the high melting point of Ta (3020 C) and the relatively low boiling point of Ti (3287 C). Previous electron beam melting experience with these materials resulted in extensive vaporization of the titanium and poor chemical homogeneity. Vacuum arc remelting (VAR) was considered as a melting candidate and discarded due to density and vapor pressure issues associated with electron beam. Plasma arc melting offered the ability to supply a cover gas to deal with vapor pressure issues as well as solidification control to help with macrosegregation in the melt and has successfully produced high quality ingots of the Ti-Ta alloys. DOE

N95-20359# Oak Ridge National Lab., TN.
MICROSTRUCTURES AND TENSILE PROPERTIES OF AS-CAST IRON-ALUMINIDE ALLOYS
S. Viswanathan, C. G. McKamey, P. J. Maziasz, and V. K. Sikka 1994 11 p Presented at the 123th Annual Meeting of the Minerals, Metals and Materials Society, San Francisco, CA, 27 Feb. - 3 Mar. 1994
(Contract DE-AC05-84OR-21400)
(DE94-017868; CONF-940204-8) Avail: CASI HC A03/MF A01

Room-temperature tensile properties of as-cast Fe3Al, Fe3Al with chromium, and Fe3Al-based FA-129 alloy have been investigated. Tensile properties have been obtained in air in the as-cast condition for all three alloys. Samples of FA-129 alloy have also been tested in oxygen and water vapor environments, and after homogenization at 700, 900, and 1200C. Transmission electron microscopy has been used to characterize ordered phases and optical metallography and scanning electron microscopy have been used to characterize the microstructure and fracture morphology. Tensile properties in the as-cast condition exhibited an environmental effect; tensile ductilities in an oxygen atmosphere were greater than those obtained in laboratory air. Homogenized samples of FA-129 alloy exhibited almost twice the ductility of the as-cast condition. Results indicate that the low ductility of as-cast Fe3Al-based alloys may be related to the relatively large grain size in the as-cast condition and the presence of the DO3 ordered phase. Microstructural characterization of the homogenized samples and comparison of the as-cast and homogenized microstructures may provide a clue to the poor ductility in the as-cast condition. DOE

N95-20365# Oak Ridge National Lab., TN.
OXIDE FORMATION ON NbAl3 AND TiAl DUE TO ION IMPLANTATION OF O-18
R. J. Hanrahan, Jr. (Florida Univ., Gainesville, FL.), E. D. Verink, Jr. (Florida Univ., Gainesville, FL.), S. P. Withrow, and E. O. Ristolainen (Helsinki Univ. of Technology, Espoo, Finland.) 1993 6 p Presented at the Fall Meeting of the Materials Research Society (MRS), Boston, MA, 29 Nov. - 3 Dec. 1993
(Contract DE-AC05-84OR-21400)
(DE94-017874; CONF-931108-106) Avail: CASI HC A02/MF A01

Surface modification by ion implantation of O-18 ions was investigated as a technique for altering the high-temperature oxidation of aluminide intermetallic compounds and related alloys. Specimens of NbAl3 and TiAl were implanted to a dose of 1 x 10(exp 18) ions/sq cm at 168 keV. Doses and accelerating energies were calculated to obtain near-stoichiometric concentrations of oxygen. Use of O-18 allowed the implanted oxygen profiles to be measured using secondary ion mass spectroscopy (SIMS). The near surface oxides formed were studied using x ray photoelectron spectroscopy (XPS) and Auger electron spectroscopy. Specimens were also examined using x ray diffraction and SEM. This paper presents results for specimens examined in the as-implanted state. The oxide formed due to implantation is a layer containing a mixture of Nb or Ti and amorphous Al oxides. DOE

N95-20375# Oak Ridge National Lab., TN.
EFFECT OF HEAT TREATMENT TEMPERATURE ON CREEP-RUPTURE PROPERTIES OF Fe3Al-BASED ALLOYS
C. G. McKamey and P. J. Maziasz 1994 12 p Presented at the Metallurgical Society Annual Meeting, San Francisco, CA, 27 Feb. - 3 Mar. 1994
(Contract DE-AC05-84OR-21400)
(DE94-017904; CONF-940286-3) Avail: CASI HC A03/MF A01

The effects of heat treatment at 1100 to 1250 C on the creep-rupture properties of an Fe3Al-based alloy were studied. Tests were conducted at 593 C (1100 F) and 207 MPa (30 ksi) in air. The modes of fracture were identified using optical metallography and scanning electron microscopy. Analytical electron microscopy was also used to study characteristics of the microstructure, including dislocations, ordered domains, and precipitates. The creep results showed maximum creep-rupture resistance with a heat treatment at approximately 1150 C, with significant decreases in rupture life after heat treatments at both lower and higher temperatures. The peak in creep life was associated with fine precipitates that were observed after the 1150 C heat treatment and persisted during prolonged creep at 593 C. Heat treatment at 1150 C appeared to cause dissolution of coarser precipitates which then reprecipitated as new fine particles upon cooling or during creep. These fine precipitates then pinned dislocations and grain boundaries to produce strength during creep. DOE

N95-20417# Ohio State Univ., Columbus, OH. Center for Die Casting.
IMPROVED DIE CASTINGS THROUGH PLASMA SURFACE MODIFICATION, IMPROVED SENSORS AND DIE SOLDERING PREVENTION Quarterly Progress Report No. 1, 1 Jul. - 30 Sep. 1994
C. Mobley and J. Brevick 17 Oct. 1994 35 p
(Contract DE-FC07-94ID-13233; OSURF Proj. 729390)
(DE95-002238; DOE/ID-13233/T1) Avail: CASI HC A03/MF A01

This quarterly report covers activities of the Die Casting Research project during the period July 1, 1994 through September 30, 1994, at The Ohio State University. The objective of the Die Casting Research project is to enhance the competitiveness of the US die casting industry. To accomplish this objective, the Center for Die Casting at The Ohio State University shall perform tasks that focus on three general areas: the application of plasma surface modifications to aluminum and zinc casting dies; the development and evaluation of systems to monitor temperature, pressure, and gas content of die casting cavities; and the determination of causes of die soldering in zinc die castings. This quarterly report covers work on Task 2 -- Commercial Sensor Evaluation. DOE

N95-20447# Lawrence Livermore National Lab., Livermore, CA.
MAGNETIC X RAY CIRCULAR DICHROISM IN Fe Co Pt MULTILAYERS
J. G. Tobin, A. F. Jankowski, G. D. Waddill, and P. A. Sterne (California Univ., Davis, CA.) Apr. 1994 6 p Presented at the Spring Meeting of the Materials Research Society, San Francisco, CA, 4-8 Apr. 1994
(Contract W-7405-eng-48)
(DE94-017522; UCRL-JC-115364; CONF-940411-50) Avail: CASI HC A02/MF A01

Magnetic x-ray circular dichroism in x-ray absorption has been used to investigate the ternary multilayer system, Fe Co Pt. Samples were prepared by planar magnetron sputter deposition and carefully characterized, using a variety of techniques such as grazing-incidence and high-angle x-ray scattering, Auger depth profiling and cross-section transmission electron microscopy. As previously reported, the Fe9.5 Angstrom Pt9.5 Angstrom exhibits a large dichroism in the Fe 2p absorption. Interestingly while the Co9.5 Angstrom Pt9.5 Angstrom has no measurable dichroism, the Fe4.7 Angstrom Co4.7 Angstrom Pt9.5 Angstrom sample has a dichroism at both the Fe 2p and Co 2p absorption edges. These and other results are compared to slab calculation predictions. Possible explanations are discussed. DOE

N95-20481 Eltron Research, Inc., Boulder, CO.
ELECTROCHEMICAL IMPEDANCE PATTERN RECOGNITION FOR DETECTION OF HIDDEN CHEMICAL CORROSION ON AIRCRAFT COMPONENTS Annual Report, 15 Jun. - 14 Aug. 1994
Anthony F. Sammells and James S. Bowers Aug. 1994 4 p Limited Reproducibility: More than 20% of this document may be affected by microfiche quality
(Contract F49620-94-C-0043)
(AD-A284998; AFOSR-94-0608TR) Avail: CASI HC A01

This program is addressing the need for diagnostic instrumentation to detect the presence of hidden chemical corrosion occurring at aircraft titanium and aluminum alloys. The approach is being directed towards development of pattern recognition schemes based upon the initial on-line acquisition of electrochemical impedance spectra using Fast Fourier Transform Electrochemical Impedance Spectroscopy (FFTEIS) instrumentation from the suspect corrosion site. Author (DTIC)

N95-20577 Pennsylvania State Univ., University Park, PA. Dept. of Chemistry.
SCANNING TUNNELING MICROSCOPY STUDIES OF SELF-ASSEMBLED MONOLAYERS OF ALKANETHIOLS ON GOLD
S. J. Stranick, M. M. Kamna, K. R. Krom, A. N. Parikh, and D. L. Allara 5 Apr. 1994 16 p Limited Reproducibility: More than 20% of this document may be affected by microfiche quality
(Contract N00014-91-J-1630)
(AD-A279910; TR-12) Avail: Issuing Activity (Defense Technical Information Center (DTIC))

We have used scanning tunneling microscopy to probe the molecular scale structures of pure and mixed composition self-assembled monolayers of CH3(CH2)15SH and CH3O2C(CH2)15SH on gold. A predominant defect structure is found for both films and is assigned as a void defect in the thiolate overlayer. The mixed composition films are observed to phase segregate into domains of the pure component thiolates. Time-lapse series of scanning tunneling microscope images reveal kink-driven motion at step edges and exchange of thiolate molecules on terraces. DTIC

N95-20673# Oak Ridge National Lab., TN.
PROCESSING AND APPLICATIONS OF IRON ALUMINIDES
V. K. Sikka 1994 16 p Presented at the 123d Annual Meeting of the Minerals, Metals and Materials Society, San Francisco, CA, 27 Feb. - 3 Mar. 1994
(Contract DE-AC05-84OR-21400)
(DE94-017855; CONF-940204-9) Avail: CASI HC A03/MF A01

Iron aluminides are well known for their resistance to high-temperature sulfidizing and oxidizing environments. In order to take advantage of their excellent corrosion resistance, several methods for their processing have been identified. Issues with melting and processing are discussed in detail. Effects of grain size and melting practice on low-temperature ductility are also presented. Many applications for iron aluminides are described. DOE

N95-20676# Oak Ridge National Lab., TN.
THE EFFECT OF OXIDE INCLUSIONS ON THE KINETICS OF THE AUSTENITE TO FERRITE TRANSFORMATION IN LOW ALLOY STEEL WELD METAL
S. S. Babu, S. A. David, J. M. Vitek, and T. DebRoy (Pennsylvania State Univ., State College, PA.) 1994 5 p Presented at the International Conference on Solid-to-solid Phase Transformations in Organic Materials, Pittsburgh, PA, 17-22 Jul. 1994
(Contract DE-AC05-84OR-21400)
(DE94-018131; CONF-940704-2) Avail: CASI HC A01/MF A01

Isothermal transformation kinetics of austenite to acicular ferrite and allotriomorphic ferrite were measured in reheated low alloy steel weld deposits with similar weld compositions and austenite grain size but different inclusion characteristics. Accelerated kinetics of transformation to acicular ferrite were observed in weld metal containing coarser and titanium-rich inclusions. In contrast, kinetics of transformation to allotriomorphic ferrite were not influenced by inclusion characteristics, but, rather, by the austenite grain size and carbon concentration. DOE

N95-20705# Oak Ridge National Lab., TN.

IMPACT BEHAVIOR OF FeAl ALLOY FA-350

D. J. Alexander 1994 11 p Presented at the Metallurgical Society Annual Meeting, San Francisco, CA, 27 Feb. - 3 Mar. 1994
(Contract DE-AC05-84OR-21400)
(DE94-018128; CONF-940286-7) Avail: CASI HC A03/MF A01

The tensile properties and impact behavior of the iron aluminide FeAl-type alloy FA-350 (Fe-35.8Al-0.05Zr-0.24B (at. %) have been studied over the temperature range of -100 to 800 C. Half-size C harpy specimens were either oil quenched from 700 C or furnace cooled. The energy absorbed during the impact test showed a maximum value at 100 to 200 C, with decreasing energy as the temperature wasincreased, for both heat treatments. The furnace-cooled material had greater energy absorption than the oil-quenched material. The tensile tests showed increasing ductility (as measured by total elongation) with increasing temperature. The furnace-cooled material had lower strength and higher ductility than the oil-quenched material. Fractographic examination of the oil-quenched impact specimens revealed that several different fracture modes operated, depending on the test temperature. Fracture occurred by intergranular and quasicleavage fracture at low temperatures, predominantly quasicleavage at intermediate temperatures, and intergranular fracture at 800 C. For the furnace-cooled material fracture was predominantly quasicleavage at all temperatures. The higher ductility and energy absorption for the furnace-cooled material is believed to be the result of softening due to a decrease in the retained vacancy concentration. DOE

N95-20707# Argonne National Lab., IL. Chemical Technology Div.

SPUTTERING OF TIN AND GALLIUM-TIN CLUSTERS

T. Lill, W. F. Calaway, Z. Ma, and M. J. Pellin 1 Aug. 1994 27 p Presented at the 10th International Workshop of Inelastic Ion-surface Collisions, Grand Targhee Resort, WY, 8-12 Aug. 1994
(Contract W-31-109-eng-38)
(DE94-018389; ANL/CHM/CP-83910; CONF-9408150-1) Avail: CASI HC A03/MF A01

Tin and gallium-tin clusters have been produced by 4 keV Ar(+) ion bombardment of polycrystalline tin and the gallium-tin eutectic alloy and analyzed by time-of-flight mass spectrometry. The sputtered neutral species were photoionized with 193 nm (6.4 eV) excimer laser light. Neutral tin clusters containing up to 10 atoms and mixed gallium-tin clusters Ga(sub (n-m))Sn(sub m) with n less than or equal to 4 for the neutrals and N less than or equal to 3 for the sputtered ionic species have been detected. Laser power density dependent intensity measurements, relative yields, and kinetic energy distributions have been measured. The abundance distributions of the mixed clusters have been found to be nonstatistical due to significant differences in the ionization efficiencies for clusters with equal nuclearity but different number of tin atoms. The results indicate that Ga2Sn and Ga3Sn like the all-gallium clusters have ionization potentials below 6.4 eV. In the case of Sn5, Sn6, GaSn and Ga(sub (n-m))Sn(sub m) clusters with n=2 to 4 and m greater than 1, the authors detect species that have sufficient internal energy to be one photon ionized despite ionization potentials that are higher 6.4 eV. The tin atom signal that is detected can be attributed to photofragmentation of dimers for both sputtering from polycrystalline tin and from the gallium-tin eutectic alloy. DOE

N95-20792# Texas Univ., Austin, TX. Dept. of Mathematics.

ON THE SPUTTERING OF METALS AND INSULATORS: A NONLINEAR EVOLUTION PROBLEM WITH NONLINEAR BOUNDARY CONDITION

Hongfei Zhang 1994 17 p
(Contract W-31-109-eng-38)
(DE95-001456; ANL/MCS/PP-71694) Avail: CASI HC A03/MF A01

In this paper the author considers a nonlinear evolution problem denoted in the paper as P. Problem (P) arises in the study of thermal evaporation of atoms and molecules from locally heated surface regions (spikes) invoked as one of several mechanisms of ion-bombardment-induced particle emission (sputtering). Then in the case of particle-induced evaporation, the Stefan-Boltzman law of heat loss by radiation is replaced by some activation law describing the loss of heat by evaporation. The equation in P is the so-called degenerate diffusion problem, which has been extensively studied in recent years. However, when dealing with the nonlinear flux boundary condition, (beta)(.) is usually assumed to be monotone. The purpose of this paper is to provide a general theory for problem P under a different assumption on (beta)(.), i.e., Lipschitz continuity instead of monotonicity. The main idea of the proof used here is to choose an appropriate test function from the corresponding linearized dual space of the solution. The similar idea has been used by many authors, e.g., Aronson, Crandall and Peletier, Bertsch and Hilhorst and Friedman. The author follows the proof of Bertsch and Hilhorst. The paper is organized as follows. They begin by stating the precise assumptions on the functions involved in P and by defining a weak solution. Then, in Section 2 they prove the existence of the solution by the method of parabolic regularization. The uniqueness is proved in Section 3. Finally, they study the large time behavior of the solution in Section 4. DOE

N95-20816# Lawrence Livermore National Lab., Livermore, CA.

THE MATERIALS CORROSION AND ENVIRONMENTAL EFFECTS LABORATORY (MCEL)

D. P. Butt 1994 3 p Presented at the 19th DOE Conference on Compatibility, Aging and Service Life, Los Alamos, NM, 28-30 Sep. 1994
(Contract W-7405-eng-36)
(DE94-018268; LA-UR-94-2731; CONF-9409181-5) Avail: CASI HC A01/MF A01

A new materials corrosion laboratory has been set up, based primarily in the Materials Science Laboratory (MSL) at Los Alamos National Laboratory. The mission of the laboratory is to conduct basic and applied research in order to rapidly evaluate the durability and useful life of materials considered for use in severe environments. The laboratory serves and provides facilities for industry and universities, and researchers from the present and future DOE complex. The primary customers within the DOE complex are those concerned with materials compatibility or durability problems associated with the safety and long term storage of nuclear weapons and waste, transmutation of nuclear waste, and high temperature corrosion and compatibility in energy systems. The general technical objective of MCEL is to identify the causes and mechanisms of corrosion processes or component failures, quantitatively determine corrosion rates or mechanisms, and help the customer adopt appropriate strategies (such as new materials selection, process modification, new inspection methods, anodic or cathodic protection, or the use of coatings or inhibitors) for effective corrosion prevention. To accomplish its technical objectives, MCEL provides both experimental and theoretical analytical approaches to solving corrosion problems. The following is a description of some of the capabilities of the laboratory and personnel. DOE

N95-20822# Oak Ridge National Lab., TN.

MAGNETIC EXCITATIONS IN MODULATED PrNi2Si2

J. A. Blanco (Universidad de Oviedo, Gijon, Spain.), R. M. Nicklow, and D. Schmitt (Centre National de la Recherche Scientifique, Grenoble, France.) 1994 11 p Presented at the International Conference on Magnetism, Warsaw, Poland, 22-26 Aug. 1994
(Contract DE-AC05-84OR-21400)
(DE95-001077; CONF-940819-4) Avail: CASI HC A03/MF A01

The magnetic excitations in a single crystal of PrNi2Si2 have been studied by inelastic neutron scattering. Dispersion curves have been followed through the centered tetragonal Brillouin zone. In the paramagnetic phase, at 39 K, the lowest energy magnetic branch exhibits an important dispersion ranging from 1.9 to 3.5 meV, the minimum energy occuring at the wave vector of the ordered phase; from the observed dispersion the inter-ionic isotropic bilinear exchange parameters are deduced. At 4.2 K, in the modulated phase, the same branch presents a dispersion slightly larger, but not significantly different. DOE

N95-20890# New Energy and Industrial Technology Development Organization, Tokyo (Japan).

FEASIBILITY STUDY OF POWER GENERATION SYSTEM WITH SHAPE MEMORY ALLOYS

Mar. 1994 69 p In JAPANESE
(DE95-714802; NEDO-P-9324) Avail: CASI HC A04/MF A01

The power generation system to use shape memory alloys which operate at temperatures below 100C was conceptually designed and studied in feasibility to amplify the utilization of low temperature energy so far not utilized yet. The energy conversion efficiency of shape memory alloy is

0.7% to 9% per strain of 1% to 8%, so that it has a possibility of being utilized as an energy conversion element. The Ni-Ti alloy excels all the other shape memory alloys in shape recovery stability and corrosion resistivity. The heat engines presently proposed are of four types, i.e., offset crank type, differential pulley turbine type, tilting plate type and piston type. If the deformation strain and life of alloy are taken into consideration, the utilization is highly possible for the piston type heat engine. As a power generation system, engineered is the method in which low temperature waste heat is effectively utilized with an introduction of energy accumulation and storage system. Possibly made structurally compact, the energy conversion part with shape memory alloy is costwise so low that its use has a high feasibility. DOE

N95-20907# Oak Ridge National Lab., TN.

ALCHEMI OF Fe-DOPED B2-ORDERED NiAl ALLOYS WITH DIFFERENT DOPING LEVELS

I. M. Anderson, J. Bentley, and A. J. Duncan 1994 3 p Presented at the Microscopy Society of America and Microbeam Analysis Society Joint Meeting, New Orleans, LA, 31 Jul. - 5 Aug. 1994
(Contract DE-AC05-84OR-21400)
(DE94-017748; CONF-940753-23) Avail: CASI HC A01/MF A01

The ALCHEMI technique yields exact expressions for best-fit parameters in terms of ionization localization constants and site distributions of 3 elements distributed over two sublattices. In this paper, a graphical plotting technique is applied to Fe-doped NiAl B2-ordered alloys Ni(0.5-x)Fe(x)Al(0.5), with x=0.02 or 0.10. The thin foil samples were examined in an electron microscope with an x-ray spectrometer. DOE

N95-20909# China Nuclear Information Centre, Beijing (China).

MOESSBAUER STUDY OF THE SINTERED Mn(0.70)Zn(0.23)Fe(2.07)O4

Dingzhang Li (Shanxi Univ., China.), Yuying Duan (Shanxi Province Inst. of Traditional Chinese Medicine, China.), and Zhenli Zhang (Institute of Magnetic Recording Technology, Taiyuan, China.) Aug. 1993 9 p
(DE94-631462; CNIC-00771; SU-0001) Avail: CASI HC A02/MF A01
(US Sales Only)

The samples of Mn-Zn ferrite having characteristic of low power expense, were obtained. Its structure and phase transformation in pre-sintering process by means of Moessbauer spectroscopy were studied. The conclusions are as follows: (1) The sample sintered at high temperature contains excess iron, has the typical Moessbauer parameters. Its formula can be written as Mn(0.70)Zn(0.23)Fe(2.07)O4. (2) The doublet sub-spectrum arise during thermal transformation varies with the process of the phase transformation. It serves as a mark of the course of the transformation. (3) The pre-sintering temperature 1040 C has primarily approached to the earlier stage of phase transformation to form Mn-Zn ferrite. (4) The breaks in heating and pre-sintering repeatedly at low temperature are unfavorable to phase transformation. (5) The Moessbauer parameters of the raw material Fe2O3 are markedly different from that in literature. There is obvious influence on the samples pre-sintered but little influence on the sample sintered at high temperature. DOE

N95-21108# Helsinki Univ. of Technology, Espoo (Finland). Lab. of Foundry Engineering.

2ND INTERNATIONAL ADI SEMINAR

Julkaisu Orkas, ed., Jouko Poranen, ed., and Jouko J. Vuorinen, ed. Jul. 1994 219 p Conference held in Otaniemi, Finland, June 1-3 1994
(ISSN 0785-1286)
(PB95-127734; ISBN-951-22-2157-8) Avail: CASI HC A10/MF A03

The following topics are addressed: (1) Alloying Elements and Heat Treatment of ADI; (2) The Fatigue Properties of Ductile Irons and Ways of Improving Them; (3) On The Fatigue Properties of ADI; Development of Austempered Ductile Iron for Automobile Applications; (4) The Newest ADI Applications in the USA; (5) Product Development of ADI; and (6) Latest KYMENITE Applications. NTIS

N95-21111# Helsinki Univ. of Technology, Espoo (Finland). Dept. of Materials Science and Rock Engineering.

THERMODYNAMIC ANALYSIS OF STABLE AND METASTABLE EQUILIBRIUM DIAGRAMS OF THE Cu-Cr SYSTEM

Kejun Zeng and Marko Haemaelaeinen 1994 24 p
(ISSN 0785-5168)
(PB95-127775; TKK-V-B87; ISBN-951-22-1923-9) Avail: CASI HC A03/MF A01

The available experimental information is not sufficient to determine the temperature dependence of excess Gibbs energy of the liquid Cu-Cr alloys. The previously optimized excess entropy of mixing of the liquid phase is too positive. A new set of optimized thermodynamic functions of the Cu-Cr system has been obtained from thermodynamic and phase diagram data incorporating the latest ones. The Tanaka-Gokcen-Morita relationship was used to constraint the excess enthalpy and entropy coefficients of the liquid phase. The optimized thermodynamic functions can account very well for the process of precipitation in the supersaturated fcc Cu-Cr alloys. NTIS

N95-21128# Helsinki Univ. of Technology, Espoo (Finland). Dept. of Mechanical Engineering.

NITROGEN ALLOYED MARTENSITIC STEELS

Jyrki Romu, Yong Liu, and Hannu Haenninen May 1994 116 p
(PB95-127791; ISBN-951-22-2135-7) Avail: CASI HC A06/MF A02

The demand of materials having a combination of high strength, good toughness and good corrosion resistance at both low and high temperatures has led to the development of nitrogen alloyed martensitic steels. In these steels carbon is replaced completely or partially with nitrogen. Nitrogen and chromium improve corrosion resistance of martensitic steels. High strength in combination with good toughness is due to the small grain size of the steels and fine and finely distributed nitrides/carbonitrides, which are formed by proper heat treatments of these steels. Nitrides/carbonitrides are formed during tempering heat treatment, when a pronounced secondary hardening effect takes place. Wear resistance of martensitic steels can be improved by proper alloying of nitrogen and nitride forming elements. NTIS

N95-21137# Los Alamos National Lab., NM.

METASTABLE BCC PHASE FORMATION IN THE Nb-Cr-Ti SYSTEM

D. J. Thoma and J. H. Perepezko (Wisconsin Univ., Madison, WI.) 1994 8 p Presented at the ISMANAM-1994, Grenoble, France, 27 Jun. - 1 Jul. 1994
(Contract W-7405-eng-36)
(DE94-016212; LA-UR-94-2528; CONF-9406229-1) Avail: CASI HC A02/MF A01

Metastable disordered bcc phases have been formed from the melt in the Nb-Cr-Ti system where primary Laves phases would develop under equilibrium solidification conditions. Three vertical temperature-composition sections in the ternary system incorporating NbCr, were evaluated: the Nb-Cr binary, the TiCr2-NbCr2 isoplethal section, and the NbCr2-Ti plethal section. In the rapid solidification of NbCr2, metastable bcc phase formation was not observed, but deviations from NbCr2 stoichiometry or alloying with Ti was found to promote bcc phase formation by decreasing the required liquid undercooling to reach the metastable bcc liquidus and solidus. The metastable phases were characterized through x-ray diffraction (XRD), and systematic deviations from Vegard's Rule have been defined in the three plethal sections. The metastable bcc phases decompose at temperatures greater than 800 C to uniformly refined microstructures. As a result, novel microstructural tailoring schemes are possible through the metastable precuror microstrucures. DOE

N95-21238# Los Alamos National Lab., NM.

TRIBOLOGY AND SURFACE MECHANICAL PROPERTIES OF EXCIMER LASER NITRIDED TITANIUM

T. R. Jervis, J. P. Hirvonen (Technical Research Centre of Finland, Espoo, Finland.), T. G. Zocco, and J. R. Tesmer 1994 11 p Presented at the Fall Meeting of the Materials Research Society, Boston, MA, 28 Nov. - 2 Dec. 1994
(Contract W-7405-eng-36)
(DE95-002751; LA-UR-94-3656; CONF-941144-1) Avail: CASI HC A03/MF A01

The authors have nitrided Ti-6Al-4V alloys using excimer laser pulses at 1.2 J/sq cm in high purity N2 at approximately one atmosphere. Substantial nitrogen and some oxygen incorporation resulted from multiple pulse processing. Formation of a TiN surface film was not observed. They have examined the tribological and mechanical properties of these surfaces using pin-on-disk and nanoindenter techniques respectively. Nitrogen alloying results in reduced friction and torque noise in the pin-on-disk measurements.

At higher N concentrations, very little wear is observed, even after the friction behavior suggests surface deterioration. This is consistent with the formation of a transfer film at the sliding interface. Nanoindenter measurements of the surfaces show increasing hardness proportional to nitrogen incorporation. The tribological improvements can therefore be ascribed to a combination of increased surface hardness and tribochemical effects. DOE

N95-21260# California Univ., Berkeley. Lawrence Berkeley Lab, CA.
METHODS OF MEASURING ADHESION FOR THERMALLY GROWN OXIDE SCALES
P. Y. Hou and A. Atkinson (AEA Technology, London, England.) Jun. 1994 25 p Presented at the Workshop on Mechanical Properties of Protective Oxide Scales, Teddington, England, 20-22 Jun. 1994
(Contract DE-AC03-76SF-00098)
(DE94-018177; LBL-35741; CONF-9406247-1) Avail: CASI HC A03/MF A01

High temperature alloys and coatings rely on the formation of adherent scales to protect against further oxidation, but scale spallation is often problematic. Despite the technical importance of the problem, 'practical adhesion', which refers to the separation of the oxide from the metal, has mainly been treated qualitatively in the past. Various techniques now exist such that the subject can be assessed in quantitative or semiquantitative terms. Some of the techniques are described, and their weakness and strength are discussed. The experimental methods addressed here include: tensile pulling, micro-indentation, scratch test, residual stress induced delamination, laser or shock wave induced spallation, double cantilever beam and several four-point beam bending approaches. To date, there is not a universal, easy test for oxide adhesion measurement that can provide reproducible information on interfacial fracture energy for a variety of oxide/metal systems. Much experimentation is still needed to increase confidence in many of the existing tests, and the fundamental mechanics for some present techniques also require further development. DOE

N95-21265# Oak Ridge National Lab., TN.
PLASTIC DEFORMATION OF ORDERED INTERMETALLIC ALLOYS: FUNDAMENTAL ASPECTS
M. H. Yoo (Max-Planck-Inst. fuer Eisenforschung, Duesseldorf, Germany.) 1994 12 p Presented at the 6th International Symposium on Plasticity of Metals and Alloys, Prague, Czechoslovakia, 5-9 Sep. 1994
(Contract DE-AC05-84OR-21400)
(DE95-001070; CONF-9409227-1) Avail: CASI HC A03/MF A01

Fundamental aspects of plastic deformation in ordered intermetallic alloys are reviewed by directly comparing the temperature-dependent yield stresses of Ni3Al and Ni3Si (the L12 structure), NiAl and FeAl (the B2 structure), and TiAl and Ti3Al (non-cubic L1(sub 0) and D0(sub 19) structures, respectively). While the yield strength anomaly observed in Ni3Al is consistent with the prevailing dislocation models, that found in stoichiometric Ni3Si is not. The strong plastic anisotropy observed in NiAl stems from the high antiphase boundary energy, and that found in two-phase (gamma)-TiAl/(alpha)(sub 2)-Ti3Al is due to the exceptionally high compressive yield strength along the c-axis of Ti3Al. DOE

N95-21270# Michoacana Univ., Morelia Michoacan (Mexico). Inst. de Investigaciones Metalurgicas.
THEORETICAL-EXPERIMENTAL STUDY ON THE ELECTROSLAG REMELTING TECHNOLOGY OF HIGH QUALITY STEELS Ph.D. Thesis [ESTUDIO TEORICO EXPERIMENTAL DE LA TECNOLOGIA DE REFUSION BAJO ESCORIA ELECTROCONDUCTORA DE ACEROS FINOS]
Eduardo Francisco RoblesPiedras 1993 234 p In SPANISH
(DE94-629216; INIS-MF-13927) Avail: CASI HC A11/MF A03 (US Sales Only)

This is a theoretical-experimental laboratory study on the electroslag remelting technology (ESRT) of high quality steels. The objective of this study was to analyze the problems that this technology entails and thus facilitate its industrial application in Mexico. The study was carried out using a 1 kg capacity furnace. The behavior of different fluxes on the remelting of 1018 AISI carbon steel was established and a slag 70F/15/15 was selected for the remelting of H-13 AISI hot work tool steel. From the experimental results it was possible to establish a flux manufacture route, the electrode conditioning necessary for the experiments, and the critical points of the process. It was demonstrated that the crucible and electrode advance system are the more critical points in the furnace manufacture, that the start up is fundamental for the remelting continuity, and that the CaF2 base slags are more recommendable for special steels refining. It has been proven that it is possible to experiment with little laboratory electroslag furnaces. DOE

N95-21286# Sandia National Labs., Albuquerque, NM.
EFFECT OF NEUTRON IRRADIATION ON THE IMPACT PROPERTIES OF A533B STEEL
Lonnie E. Schubert (Missouri Univ., Rolla, MO.), Arvind S. Kumar (Missouri Univ., Rolla, MO.), Stan T. Rosinski, and Margaret L. Hamilton (Pacific Northwest Lab., Richland, WA.) 1994 16 p Presented at the 17th Symposium on Effects of Radiation on Materials, Sun Valley, ID, 20-23 Jun. 1994
(Contract DE-AC04-94AL-85000)
(DE95-001834; SAND-94-1539C; CONF-940657-6) Avail: CASI HC A03/MF A01

A new methodology is proposed to correlate the upper shelf energy (USE) of full size and subsize Charpy specimens of a nuclear reactor pressure vessel plate material, ASTM type A 533 Grade B (A533B) having a low USE (USE less than 100 J). The methodology appears to be more satisfactory than those methodologies proposed earlier. The USE was normalized by a normalization factor involving the dimensions of the Charpy specimen, the elastic stress concentration factor, and the plastic constraint at the notch root. The normalized values of the USE were found to be invariant with specimen size. In addition, it was also found that the ratio of the USE of unirradiated to that of irradiated materials was approximately the same for full, half, and third size specimens. The ductile-to-brittle transition temperature (DBTT) increased due to irradiation at 150 C to a nominal fluence of 1.0 x 10(exp 19) n/sq cm (E greater than 1 MeV) by 78 C, 83 C, and 70 C for full, half, and third size specimens, respectively. These shifts in DBTT appeared to be independent of specimen size and notch geometry. DOE

N95-21298# Oak Ridge National Lab., TN. Metals and Ceramics Div.
COMPUTATIONAL MODELING OF DIFFUSION-CONTROLLED TRANSFORMATIONS IN TERNARY SYSTEMS
J. M. Vitek, S. A. Vitek, and S. A. David 1994 7 p Presented at the International Conference on Solid-to-solid Phase Transformations in Organic Materials, Pittsburgh, PA, 17-22 Jul. 1994
(Contract DE-AC05-84OR-21400)
(DE95-001358; CONF-940704-4) Avail: CASI HC A02/MF A01

The diffusion-controlled solid-state transformation between two phases in a ternary system was modeled using an implicit finite difference method. The one-dimensional system that was modeled was of finite size, and the interface the two phases was allowed to move. Equilibrium at the interface was assumed, and a grid that moved with the interface was utilized. The calculations were applied to the iron-nickel-chromium ternary system to model the growth or dissolution of ferrite in an austenitic stainless steel weld at elevated temperatures. The equilibrium conditions at the interface were specified with the aid of the ThermoCalc(trademark) software program that was used to calculate tie-line compositions as a function of overall alloy composition and temperature. Appropriate parameters for the analysis were chosen based on an earlier parametric study. Calculations were made for the isothermal transformation kinetics over a range of temperatures from 973 to 1573 K, in which the behavior varied from complete dissolution of the ferrite to growth of ferrite at the expense of austenite. The variation in ferrite size and composition often was quite complicated and frequently did not follow a direct path from the initial condition to the final equilibrium. Additional calculations were carried out for non-isothermal aging at constant cooling rates from 1573 to 973 K. The computational routine can be applied to any diffusion-controlled transformation in a ternary system with any thermal history, provided suitable data for the equilibrium at the interface is available. DOE

N95-21300# Allied-Signal Aerospace Co., Kansas City, MO.
COPPER METALLIZATION OF STAINLESS STEELS
B. Z. Rosenblum Sep. 1994 3 p
(Contract DE-AC04-76DP-00613)
(DE95-001496; KCP-613-5435) Avail: CASI HC A01/MF A01

Stainless steel plates were vacuum metallized with pure copper films

0.004 inch thick. Prior to metallization the surfaces were cleaned with EPA-approved detergents. A thin layer of chromium was sputtered for improved adhesion followed by sputtering of the copper. Results showed excellent adhesion of the sputtered films to the substrates. DOE

N95-21303# Westinghouse Savannah River Co., Aiken, SC.
ANALYSIS OF WELDS ON HELIUM-CONTAINING RESTRAINT TEST PLATES
W. R. Kanne, Jr. and G. T. Chandler Sep. 1994 30 p
(Contract DE-AC09-89SR-18035)
(DE95-001809; WSRC-TR-94-0449) Avail: CASI HC A03/MF A01

Over the last several years, Savannah River has had the goal of developing a repair process and the technical understanding necessary to make weld repairs on stainless steel containing helium. This report documents the results of a series of test welds made with varying amounts of mechanical restraint on type 304 stainless steel containing helium from tritium decay. This change in restraint produced different states of stress on the weld area during welding. The test welds were either overlay welds or weave beads. The amount of heat affected zone cracking observed in the welds provided the primary, analysis tool for evaluating the tests. Generally, higher restraint produced greater cracking of the welds. These results, along with previous Savannah River data, indicate that in a practical application of a repair method for helium-containing stainless steel, the effect of part configuration must be considered, as well as the type of weld, to reduce stresses that can cause helium embrittlement cracking. DOE

N95-21398# Ames Lab., IA.
THEORETICAL STUDY OF THE NOBLE METALS ON SEMICONDUCTOR SURFACES AND TI-BASE SHAPE MEMORY ALLOYS Ph.D. Thesis
Yungui Ding 27 Jul. 1994 122 p
(Contract W-7405-eng-82)
(DE95-001654; IS-T-1689) Avail: CASI HC A06/MF A02

The electronic and structural properties of the (radical 3 x radical 3) R30 degrees Ag/Si(111) and (radical 3 x radical 3) R30 degrees Au/Si(111) surfaces are investigated using first principles total energy calculations. We have tested almost all experimentally proposed structural models for both surfaces and found the energetically most favorable model for each of them. The lowest energy model structure of the (radical 3 x radical 3) R30 degrees Ag/Si(111) surface consists of a top layer of Ag atoms arranged as 'honeycomb-chained-trimers' lying above a distorted 'missing top layer' Si(111) substrate. The coverage of Ag is 1 monolayer (ML). We find that the honeycomb structure observed in STM images arise from the electronic charge densities of an empty surface band near the Fermi level. The electronic density of states of this model gives a 'pseudo-gap' around the Fermi level, which is consistent with experimental results. The lowest energy model for the (radical 3 x radical 3) R30 degrees Au/Si(111) surface is a conjugate honeycomb-chained-trimer (CHCT-1) configuration which consists of a top layer of trimers formed by 1 ML Au atoms lying above a 'missing top layer' Si(111) substrate with a honeycomb-chained-trimer structure for its first layer. The structures of Au and Ag are in fact quite similar and belong to the same class of structural models. However, small variation in the structural details gives rise to quite different observed STM images, as revealed in the theoretical calculations. The electronic charge density from bands around the Fermi level for the (radical 3 x radical 3) R30 degrees, Au/Si(111) surface also gives a good description of the images observed in STM experiments. First principles calculations are performed to study the electronic and structural properties of a series of Ti-base binary alloys TiFe, TiNi, TiPd, TiMo, and TiAu in the B2 structure. DOE

N95-21399# Ames Lab., IA.
DYNAMIC NMR STUDIES OF RESTRICTED ARENE ROTATION IN THE CHROMIU TRICARBONYL THIOPHENE AND SELENOPHENE COMPLEXES Ph.D. Thesis
M. J. Sanger 27 May 1994 98 p
(Contract W-7405-eng-82)
(DE95-001656; IS-T-1698) Avail: CASI HC A05/MF A02

This thesis contains the results of organometallic studies of thiophene and selenophene coordination in transition metal complexes. Chromium tricarbonyl complexes of thiophene, selenophene, and their alkyl-substituted derivatives were prepared and variable-temperature C-13 NMR spectra of these complexes were recorded in dimethyl ether. Bandshape analyses of these spectra yielded activation parameters for restricted rotation of the thiophene and selenophene ligands in these complexes. Extended Hueckel molecular orbital calculations (EHMO) of the free thiophene and selenophene ligands and selected chromium tricarbonyl thiophene complexes were performed to better explain the activation barriers of these complexes. The structure of Cr(CO)3((eta)(sup 5)-2,5-dimethylthiophene) was established by a single crystal X-ray diffraction study. DOE

N95-21452# Westinghouse Hanford Co., Richland, WA. Materials Engineering.
CORROSION EVALUATION OF FUEL CANISTER CRUSHER RIGGING
Carolyn E. Graves 2 Nov. 1994 20 p
(Contract DE-AC06-87RL-10930)
(DE95-002962; WHC-SD-SNF-ER-004) Avail: CASI HC A03/MF A01

A fuel canister crusher with attached rigging is located in the 105 K-East Basin discharge chute. This equipment is slated to be moved as part of seismic mitigation to prevent a major basin leak through a construction joint located in the base of the chute. This corrosion analysis assessed the load-bearing ability of the rigging, which consists of shackles and thimble-spliced wire rope. The K-East Basin demineralized water results in corrosion rates of less than 2 mil/year (less than 0.05 mm/year) for carbon, low-alloy carbon, and stainless steels. The galvanized carbon steel shackles (with low-alloy steel anchor pins) have experienced negligible corrosion and are judged to be mechanically unaffected by their water exposure. The carbon steel wire rope and stainless steel thimbles have undergone minimal corrosion. Due to the small amount of corrosion products (as seen from video inspection), the absence of wire breakage, and a Factor of Safety calculation, it is judged that the wire rope and thimbles would withstand the proposed relocation activities. DOE

N95-21476# Johns Hopkins Univ., Baltimore, MD. Dept. of Materials Science and Engineering.
SIMULATIONS OF METAL DISSOLUTION AND CORROSION
P. C. Searson 1994 14 p
(Contract DE-FG02-89ER-45388)
(DE94-019295; DOE/ER-45388/T2) Avail: CASI HC A03/MF A01

The control of metal dissolution processes is important in fields ranging from battery technology to corrosion. Nevertheless, metal dissolution remains a poorly understood class of electrochemical reactions. Although the reaction sequences for dissolution of many metals have been elucidated, kinetic descriptions are based on area averaged values of parameters that describe the relationship between the rate of reaction and the activation energy. Theoretical and experimental research on metal dissolution has focused traditionally on macroscopic processes and features. However, in the last few years there has been considerable interest in examining these processes on a microscopic scale. In addition, the growth and formation of rough interfaces is of considerable practical importance in surface science and many similarities can be found between material removal processes (e.g. etching, evaporation, and erosion) and material addition processes (e.g. crystal growth, condensation, vapor deposition, and electrodeposition). Over the next few years, results from theoretical modeling of dissolution processes, in conjunction with new experimental techniques such as in situ scanning tunneling microscopy, are expected to provide a new insight into the processes controlling metal dissolution and corrosion. The objectives of this program were to determine the relationship between dissolution kinetics and surface morphology for metal dissolution and corrosion processes. Specific objectives include determination of: (1) the relationship between surface morphology and applied potential; (2) site population statistics and the contribution of different sites to the total dissolution rate; and (3) the role of surface diffusion in dissolution processes. DOE

N95-21555# Oak Ridge National Lab., TN.
WELDABILITY OF IRON ALUMINIDES
G. M. Goodwin, C. J. McKamey, P. J. Maziasz, and V. K. Sikka 1993 9 p Presented at the 7th Annual Conference on Fossil Energy Materials, Oak Ridge, TN, 11-13 May 1993
(Contract DE-AC05-84OR-21400)
(DE94-019114; CONF-9305135-11) Avail: CASI HC A02/MF A01

Corrosion-resistant, weldable iron-aluminide alloys with improved high-temperature strength are being developed for structural applications, and for weld overlay cladding of conventional structural steels and alloys.

The weld hot cracking of iron-aluminide alloys is highly variable to over a wide range of aluminum content. In general, the higher aluminum content alloys are somewhat more resistant to hot cracking, and by careful choice of alloying additions (and balancing of multiple additions), cracking resistance equivalent to commercial austenitic stainless steels can be achieved. Improved weldability, however, often comes at the expense of high-temperature strength. Delayed cold cracking, presumed to be hydrogen-related, is also an important consideration in welding these alloys, either as monolithic materials, or as weld overlay cladding on stainless or low alloy steel substrates. The authors are employing various combinations of preheat and postweld stress relief heat treatments to assess the severity of this problem, and have determined that heat treatment in excess of 400 C following welding will be required to avoid delayed cracking. Due to the difficulties encountered in fabricating some of the alloy compositions into wire or rod, they are also pursuing the formulation of coated electrodes for use in shielded metal-arc (SMA) welding. Initial attempts have shown very high aluminum losses in the welding arc, and additional batches of electrodes are being formulated and produced. DOE

N95-21560# Battelle Memorial Inst., Columbus, OH.
FINITE ELEMENT MODELLING OF CREEP CRACK GROWTH IN 316 STAINLESS AND 9Cr-1Mo STEELS
P. Krishnaswamy and Frederick W. Brust, Jr. 1994 15 p Presented at the 11th International Invitational Symposium on the Unification of Analytical, Computational, and Experimental Solution Methodologies, Danvers, MA, 18-20 Aug. 1993
(Contract DE-FG02-90ER-14135)
(DE94-018977; CONF-9308138-4) Avail: CASI HC A03/MF A01

The failure behavior of steels under sustained and cyclic loads has been addressed. The constitutive behavior of the two steels have been represented by the conventional strain-hardening law and the Murakami-Ohno model for reversed and cyclic loads. The laws have been implemented into the research finite element code FVP. Post processors for FVP to calculate various path independent integral fracture parameters have been written. Compact tension C(T) specimens have been tested under sustained and cyclic loads with both the load point displacement and crack growth monitored during the tests. FE models with extremely refined meshes for the C(T) specimens were prepared and the experiment simulated numerically. Results from this analysis focus on the differences between the various constitutive models as well as the fracture parameters in characterizing the creep crack growth of the two steels. DOE

N95-21568# Ames Lab., IA.
A NEW UNIVERSAL SOLUTION FOR THE ELECTROFINISHING OF METALLIC MATERIALS
T. W. Ellis, T. A. Lograsso, S. Hilsenbeck, and H. E. Sailsbury 1994 7 p Presented at The Metallurgical Society (TMS) Conference on High Performance Composites, Rosemont, IL, 10-15 Oct. 1994
(Contract W-7405-eng-82)
(DE95-001681; IS-M-795; CONF-9410184-4) Avail: CASI HC A02/MF A01

A new reagent has been applied to the electrofinishing of metallic materials for metallographic preparation and surface cleaning. The development of this reagent was in response to the safety, health, and disposal problems associated with the use of perchloric acid based solutions. This procedure has been applied to metallic materials that are very difficult to electrofinish, e.g., rare earths, Ti, Nd2Fe14B, Pb, and intermetallic alloys. Both the procedure and results of electrofinishing will be discussed. DOE

N95-21575 Martin Marietta Labs., Baltimore, MD.
COLLOCATED TUNABLE WAVENUMBER SENSOR/ACTUATORS FOR SMART STRUCTURES Technical Report, 1-30 Apr. 1994
K. Bridger and L. Jones 4 May 1994 9 p Limited Reproducibility: More than 20% of this document may be affected by microfiche quality
(Contract N00014-92-C-0214)
(AD-A279066; MML-TM-94-10) Avail: Issuing Activity (Defense Technical Information Center (DTIC))

The first full-sized actuator module has been fabricated. The first actuator was sintered using the sintering profile of the 3/4-sized actuator module (5 C/min to 900 C, 1 hour hold, 1 C/min to 1200 C, 3 hour hold, 1 C/min to 500 C to room temperature). This actuator cracked during sintering. The sintering schedule was once again slowed down for the second actuator module (5 C/min to 500 C, 2 C/min to 900 C, hold 1 hour, 1 C/min to 1200 C, hold 3 hours, 1 C/min to room temperature), and as a result, we were able to fabricate our first full-sized actuator module without cracks. One full-sized actuator module is out of burnout and is awaiting sintering. Two 3/4-sized actuator modules have survived sintering without cracks. We plan to use these to help set-up our polishing and testing procedures for the full-sized actuators. DTIC

N95-21600# Oak Ridge National Lab., TN.
CONSEQUENCES OF OSCILLATORY POTENTIALS AND ANGULAR FORCES IN TRANSITION METALS AND THEIR ALUMINIDES
A. E. Carlsson (Washington Univ., Saint Louis, MO.), J. Zou, and R. Phillips (Cornell Univ., Ithaca, NY.) 1994 10 p Presented at the Materials Week 1993, Pittsburgh, PA, 17-21 Oct. 1993
(Contracts DE-AC05-84OR-21400; DE-FG02-84ER-45130)
(DE94-019127; CONF-9310224-3) Avail: CASI HC A02/MF A01

The authors discuss two applications of recently developed potential-energy functions. The first application involves 'constant-volume' type potentials for Al-rich transition-metal compounds and alloys. Using a combination of Green's function analysis and pseudopotential perturbation theory, a set of potentials suitable for atomistic simulations is derived. These are used to study the structural energetics of Al-Co and to analyze the origins of quasicrystallinity and complex phases in Al-Mn. The second type of applications treats the energetics of small atomic clusters using angular forces based on the 'mu(sub 4)' methodology. Calculations using a d-band model fitted to W suggest that the lowest-energy state for a four-body W cluster is a rhombus, rather than the normally expected tetrahedron. DOE

N95-21652 Selskapet for Industriell og Teknisk Forskning, Trondheim (Norway). Dept. for Materials Technology.
RELATIONSHIP BETWEEN DENDRITE COHERENCY AND CASTABILITY OF SOME COMMERCIAL FOUNDRY ALLOYS
A. K. Dahle and L. Arnberg 18 Mar. 1994 29 p
(PB95-110243; STF24-A94558) Avail: Issuing Activity (National Technical Information Service (NTIS))

The castability of different commercial Al-Si foundry alloys have been practically evaluated in a foundry. Although some of the alloys were similar in composition, they showed large differences in castability. The dendrite coherency points have been determined from remelted samples of these alloys. A relationship is observed for some alloys, where a decrease in castability is related to a slightly earlier coherency point. The other alloys showed fading, most probable due to loss of a eutectic modifying element, which prevents any conclusions. Metallographic samples have been investigated for verification. NTIS

N95-21653 Selskapet for Industriell og Teknisk Forskning, Trondheim (Norway). Dept. for Materials Technology.
SHEET METAL FORMABILITY
O. Daaland 12 Apr. 1994 28 p
(PB95-110250; STF24-A94572) Avail: Issuing Activity (National Technical Information Service (NTIS))

By definition, sheet metal forming is the process of converting a flat sheet of metal into a part of desired shape without fracture or excessive localized thinning. The ability to produce a variety of shapes from flat sheets of metal at high rates of production has been one of the real technological advances of the twentieth century. This transition from hand-forming operations to mass-production methods has been an important factor in the great improvement in the standard of living which occurred during the period. The production of useful shapes by plastic deformation is presented in this lecture. NTIS

N95-21676# Oak Ridge National Lab., TN.
FRACTURE BEHAVIOR OF THE Fe-8Al ALLOY FAP-Y
D. J. Alexander 1994 11 p Presented at the 8th Annual Conference on Fossil Energy Materials, Oak Ridge, TN, 10-12 May 1994
(Contract DE-AC05-84OR-21400)
(DE95-000956; CONF-9405143-8) Avail: CASI HC A03/MF A01

The tensile and impact properties of two heats of the reduced aluminum alloy FAP-Y have been measured and compared to the Fe3Al alloy FA-129. The FAP-Y material has similar yield strengths up to 400 C, and much better ductility and impact properties, as compared to the FA-129. Despite excellent room-temperature ductility, the ductile-to-brittle transition temperature is still quite high, around 150 C. The material is found to be strain-rate sensitive, with a significant increase in the yield strength at strain rates of about 10(exp 3) s(exp -1). It is believed that this strain-rate sensitivity is responsible, at least in part, for the high ductile-to-brittle transition temperature. DOE

N95-21687 Battelle Columbus Labs., OH.
AIRCRAFT CORROSION STUDY Final Report
J. T. Stropki and R. D. Smith Dec. 1993 62 p Limited Reproducibility: More than 20% of this document may be affected by microfiche quality
(Contract F09603-90-D-2217)
(AD-A279527; CGR/DC-01/94; USCG-D-05-94) Avail: Issuing Activity (Defense Technical Information Center (DTIC))

A comparison of the test results obtained for the unaged French and 2024-T3 (bare and hard anodized) alloys suggests that the resistance of all materials to raindrop erosion is identical. Superior performance of the hard anodized Alloy 2024-T3 sample was not observed during the erosion testing. Post-test examinations of the hard anodized 2024-T3 sample indicate that the performance of the coating was limited by spalling of the coating from the substrate. A review of the literature suggests that this condition is due to abnormal surface roughness of the anodic coating. This condition, which can be minimized with the application of silicone waxes (or similar surface treatments) to the coated surfaces, does contribute to poor chemical and impact resistance. No pretest surface characterizations were performed on this material. In summary, the results of this program suggest that Alloy 2024-T3 be considered as a candidate replacement material for the French alloy that is currently being used on the outer wing slats of the HU-25A aircraft. DTIC

N95-21707# California Univ., Berkeley. Lawrence Berkeley Lab, CA.
HYDROGENATION OF NITRILES ON A WELL-CHARACTERIZED NICKEL SURFACE: FROM SURFACE SCIENCE STUDIES TO LIQUID PHASE CATALYTIC ACTIVITY MEASUREMENTS Ph.D. Thesis
D. E. Gardin Dec. 1993 187 p
(Contract DE-AC03-76SF-00098)
(DE94-018184; LBL-35914) Avail: CASI HC A09/MF A02

Nitrile hydrogenation is the most commonly used method for preparing diverse amines. This thesis is aimed at the mechanism and factors affecting the performance of Ni-based catalysts in nitrile hydrogenations. Surface science techniques are used to study bonding of nitriles and amines to a Ni(111) surface and to identify surface intermediates. Liquid-phase hydrogenations of cyclohexene and 1-hexene on a Pt foil were carried out successfully. Finally, knowledge about the surface structure, surface chemical bond, dynamics of surface atoms (diffusion, growth), and reactivity of metal surfaces from solid-gas interface studies, is discussed. DOE

N95-21737# Ames Lab., IA.
METHODS AND OPPORTUNITIES IN THE RECYCLING OF RARE EARTH BASED MATERIALS
T. W. Ellis, F. A. Schmidt, and L. L. Jones 1994 8 p Presented at The Metallurgical Society (TMS) Conference on High Performance Composites, Rosemont, IL, 10-15 Oct. 1994
(Contract W-7405-eng-82)
(DE95-001680; IS-M-796; CONF-9410184-5) Avail: CASI HC A02/MF A01

Rare Earth based materials are increasingly being utilized in industrial and commercial practice. Large volume production of permanent magnet materials, $Nd_2Fe_{14}B$, $SmCo_5$, Sm_2Co_{17}, and rechargeable Ni/Metal Hydride batteries, $LaNi_5$, has increased the amount of rare earth based materials in the waste stream. Both for economic and environmental reasons, recycling and reuse of all materials is desirable. Unfortunately, the recycling methodology for these materials is in its infancy. In this paper the present 'state of the art', in recycling of rare earth based materials will be discussed. Additionally, new methods which alleviate many of the concerns of present aqueous based recycling technology will be presented. DOE

N95-21739# Tennessee Valley Authority, Muscle Shoals, AL.
CORROSION RESISTANCE AND BEHAVIOR OF CONSTRUCTION MATERIALS EXPOSED TO DILUTE SULFURIC ACID AT ELEVATED TEMPERATURES UNDER STATIC CONDITIONS
D. T. Nguyen 1994 18 p
(DE95-001723; Z-332) Avail: CASI HC A03/MF A01

Laboratory investigation has been undertaken to determine the electrochemical behavior and corrosion resistance of various construction materials in a simulated hydrolysis environment (5 wt % sulfuric acid) at temperatures ranging from 90 to 220C. Tests were performed in an autoclave-type electrochemical cell. The corrosion behavior of the test materials was determined using computer-controlled DC potentiodynamic polarization. Corrosion rates of the test materials were determined using AC impedance techniques. Among the stainless steels tested, only alloy N08026 (Carpenter 20Mo-6) performed satisfactory up to a temperature of 100C. The alloy passivated spontaneously in the environment and corroded at a rate of less than 2 mpy. None of the stainless steels tested could be used at 120C or above. A number of nickel-based alloys tested had good corrosion resistance up to 100C, but their corrosion rate exceeded 2 mpy at higher temperatures. Zirconium alloys were satisfactory up to 180C. Only tantalum and a tantalum-niobium alloy were satisfactory up to 220C. DOE

N95-21740 Tennessee Valley Authority, Muscle Shoals, AL.
CORROSION RESISTANCE AND BEHAVIORAL CHARACTERISTICS OF METALS EXPOSED TO 70 PERCENT BY WEIGHT SULFURIC ACID AT ELEVATED TEMPERATURES
D. T. Nguyen and G. E. Farina 1994 13 p Limited Reproducibility: More than 20% of this document may be affected by microfiche quality
(DE95-001724; Z-333) Avail: CASI HC A03

The development of a concentrated acid hydrolysis process may necessitate the storage, handling, and processing of concentrated solution of sulfuric acid at temperatures in excess of 70C. Due to the corrosivity of the sulfuric acid at elevated temperatures, a series of corrosion tests was conducted to determine the corrosion performance and behavior of various construction materials using immersion and electrochemical techniques. Test results showed that among the stainless steels tested, only Carpenter 20Mo-6 performed satisfactorily up to 70C. It passivated spontaneously and corroded at a rate less than 40 (mu)m/yr (1.6 mpy). Among numerous nickel-based alloys tested, only Hastelloy B-2 had excellent corrosion resistance up to 100C with a corrosion rate less than 50 (mu)/yr (2 mpy), although the alloy did not passivate. Zirconium alloy Zr 702 provided excellent corrosion resistance to 100C. The alloy passivated spontaneously, but its passive range decreased, evidently with increase in temperature. Tantalum and KBI-40 provided excellent corrosion protection at all test temperatures. The materials passivated spontaneously with a wide passive range. DOE

N95-21838# Sandia National Labs., Albuquerque, NM.
PLASMA-INDUCED-DAMAGE OF GaAs DURING ETCHING OF REFRACTORY METAL CONTACTS
R. J. Shul, M. L. Lovejoy, A. G. Baca, J. C. Zolper, D. J. Rieger, M. J. Hafich, R. F. Corless, and C. R. Vartuli (Florida Univ., Gainesville, FL.) 1994 18 p Presented at the 41st Annual American Vacuum Society Symposium, Denver, CO, 24-28 Oct. 1994
(Contract DE-AC04-94AL-85000)
(DE95-001525; SAND-94-1318C; CONF-941001-1) Avail: CASI HC A03/MF A01

The effect of plasma-induced-damage on the majority carrier transport properties of GaAs has been studied by monitoring changes in sheet resistance (R(sub s)) of thin conducting layers under various plasma conditions including etch conditions for refractory metal contacts. R(sub s) determined from transmission line measurements are used to evaluate plasma-induced-damage for electron cyclotron resonance (ECR) and reactive ion etch (RIE) conditions by varying the thickness of doped epitaxial layers. The authors speculate that plasma-induced-damage in the near surface region plays a major role in explaining the damage mechanism observed in this study. Very consistent trends have been observed where R(sub s) increases with increasing ECR and RIE dc-bias, increasing microwave power, and decreasing pressure, thus showing R(sub s) increases as either the ion energy or ion flux increases. The authors have also observed that R(sub s) is lower for samples exposed to the RIE than the ECR, possibly due to higher ion and electron densities generated in the ECR and higher pressures in the RIE. It has also been observed R(sub s) dependence on ECR plasma chemistry where, R(sub s) is lower in SF_6/Ar plasmas than Ar and N_2 plasmas possibly related to interactions of F or S atoms with the GaAs surface. Moderate anneal temperatures (200 to 500 C) have shown significant R(sub s) recovery. DOE

N95-21841# Iowa State Univ. of Science and Technology, Ames, IA.
SELENOPHENE TRANSITION METAL COMPLEXES Ph.D. Thesis
C. J. White 27 Jul. 1994 134 p
(Contract W-7405-eng-82)
(DE95-001675; IS-T-1699) Avail: CASI HC A07/MF A02

This research shows that selenophene transition metal complexes have a chemistry that is similar to their thiophene analogs. Selenophene coordination has been demonstrated and confirmed by molecular structure in both the (eta)(sup 5)- and the (eta)(sup 1)(Se)-coordination modes. The reaction chemistry of selenophene complexes closely resembles that of the analogous thiophene complexes. One major difference, however, is that selenophene is a better donor ligand than thiophene making the selenophene complexes more stable than the corresponding thiophene complexes. The Se(77) NMR chemical shift values for selenophene complexes fall within distinct regions primarily depending on the coordination mode of the selenophene ligand. In the final paper, the C-H bond activation of (eta)(sup 1)(S)-bound thiophenes, (eta)(sup 1)(S)-benzothiophene and (eta)(sup 1)(Se)-bound selenophenes has been demonstrated. The deprotonation and rearrangement of the (eta)(sup 1)(E)-bound ligand to the carbon bound L-yl complex readily occurs in the presence of base. Reprotonation with a strong acid gives a carbene complex that is unreactive towards nucleophilic attack at the carbene carbon and is stable towards exposure to air. The molecular structure of (Cp(NO)(PPh(sub 3))Re(2-benzothioenylcarbene))O(sub 3)SCF(sub 3) was determined and contains a Re-C bond with substantial double bond character. Methyl substitution for the thienylcarbene or selenylcarbene gives a carbene that rearranges thermally to give back the (eta)(sup 1)(E)-bound complex. Based on these model reactions, a new mechanism for the H/D exchange of thiophene over the hydrodesulfurization catalyst has been proposed. DOE

N95-21855# International Centre for Theoretical Physics, Trieste (Italy).
ELECTRONIC STRUCTURE AND RELATIVE STABILITY OF ICOSAHEDRAL SUPERATOMS IN Al-TRANSITION-METAL ALLOYS
X. G. Gong and V. Kumar Oct. 1993 14 p
(DE94-628996; IC-93/352) Avail: CASI HC A03/MF A01 (US Sales Only)

The electronic structure and relative stability of icosahedral Al12TM superatoms in Al-transition-metal (TM) alloys have been studied using the density functional theory within the local spin density approximation. Our calculations predict large binding energies for superatoms with TM atom in the middle of a d-series in agreement with the occurrence of Al12W phase in these alloys and provide an insight into the understanding of the stability of Al-TM quasicrystal. DOE

N95-21923# Ames Lab., IA.
THE LOW TEMPERATURE PROPERTIES OF (Dy(1-x)Er(x))Ni2 ALLOYS Ph.D. Thesis
M. Gailloux 27 Jul. 1994 72 p
(Contract W-7405-eng-82)
(DE95-001657; IS-T-1691) Avail: CASI HC A04/MF A01

The study of rare earth magnetic properties is undertaken to further the understanding of critical phenomena and the mechanism of magnetic ordering in solids. There is a great variety of magnetic ordering observed in the rare earth compounds, thus providing an insight to phenomena such as heat capacity, magnetostriction and crystal fields. Studies began on the magnetic properties of the rare earths and their compounds in the 1950's. DOE

N95-21926# Los Alamos National Lab., NM.
OXIDATION BEHAVIOR OF ALUMINUM NANOPOWDERS
Christopher E. Aumann, Gretchen L. Skofronick, and Joe A. Martin 1994 18 p Presented at the 41st Annual American Vacuum Society Symposium, Denver, CO, 24-28 Oct. 1994 Submitted for publication Sponsored by DOD
(Contract W-7405-eng-36)
(DE95-002721; LA-UR-94-3499; CONF-941001-6) Avail: CASI HC A03/MF A01

Rutherford backscattering spectrometry, thermogravimetric analysis, and high-resolution transmission electron microscopy were used to investigate the oxidation behavior of ultrafine grain aluminum powder. Fractional change in mass of Al powder samples were obtained as a function of temperature and exposure time for samples with different particle size distributions. Activation energy for oxidation is found to depend on average Al particle size and to be much smaller than that known for flat Al samples. DOE

N95-21986 Army Research Lab., Watertown, MA. Materials Directorate.
THE DEVELOPMENT OF A SUPER-ALPHA2 TITANIUM ALUMINIDE ALLOY CONSOLIDATED BY RAPID OMNIDIRECTIONAL COMPACTION Final Report
Wego Wang and Martin G. Wells Mar. 1994 46 p Limited Reproducibility: More than 20% of this document may be affected by microfiche quality
(AD-A279254; ARL-TR-341) Avail: Issuing Activity (Defense Technical Information Center (DTIC))

Six super-alpha 2 titanium aluminide 'pancakes' were produced by rapid omnidirectional compaction of prealloyed Ti-25Al-1ONb-3V-1Mo (at%) powder. The beta-transus temperature was found to be about 1,090 C (1,990 F). The alloy was heat-treated with four different schedules to develop various structure combinations of alpha(sub 2) and beta, and followed by a series of microstructural analyses and mechanical property determinations. The highest ultimate tensile and yield strengths attained at room temperatures were 1,174.9 and 977.7 MPa (170.4 and 141.8 ksi), respectively. However, the elongation was less than 2%. The alloy also showed good stress rupture resistance. It was observed that, under otherwise similar conditions, ductility increased with the aspect ratio of the alpha(sub 2) phase but the tensile strength is inversely related to the aspect ratio. During the tensile and stress rupture tests, multiple transverse cracks nucleated in the longitudinal direction on the specimen surface and within the specimen simultaneously. DTIC

N95-22006# Los Alamos National Lab., NM.
PLASMA ARC MELTING OF A 80 WEIGHT PERCENT TANTALUM -20 WEIGHT PERCENT TITANIUM ALLOY
P. S. Dunn and R. A. Patterson 1994 13 p Presented at the 1994 International Conference on Tungsten and Refractory Metals, McLean, VA, 17-19 Oct. 1994
(Contract W-7405-eng-36)
(DE95-000846; LA-UR-94-3283; CONF-9410213-2) Avail: CASI HC A03/MF A01

An alloy of 80wt% tantalum-20wt% titanium is being considered for use in an oxidizing and highly corrosive liquid metal application. The high melting point of the alloy, 2400 C, and other physical properties narrowed the possible melting techniques. Previous melting experience with these materials by electron beam resulted in extensive vaporization of the titanium during the melt and poor chemical homogeneity. A technique has been developed using plasma arc melting to melt refractory alloys with very dissimilar densities and vapor pressures. The 80Ta--20Ti alloy falls into this category with the density of tantalum 16.5 g/cc and that of titanium 4.5 g/cc. The melting of these materials is further complicated by the high melting point of tantalum (3020 C) and the relatively low boiling point of titanium (3287 C). The plasma arc melting technique described results in good chemical homogeneity with ingot size quantities of material. DOE

N95-22013# Massachusetts Inst. of Tech., Cambridge, MA. Plasma Fusion Center.
INCOLOGY ALLOY 908 DATA HANDBOOK
L. S. Toma, M. M. Steeves, and R. P. Reed (Cryogenic Materials, Inc., Boulder, CO.) Mar. 1994 89 p
(Contract DE-FC02-93ER-54186)
(DE95-001818; PFC/RR-94-2; DOE/ER-54186/T3) Avail: CASI HC A05/MF A01

This handbook is a compilation of all available properties of Incoloy alloy 908 as of March, 1994. Data included in this paper cover mechanical, elastic, thermal and magnetic characteristics. The mechanical properties include tensile, fracture toughness, fatigue, and stress-rupture for both the base metal and related weld filler metals. Elastic properties listed are Young's, shear and bulk moduli and Poisson's ratio. Thermal expansion, thermal conductivity and specific heat and magnetization are also reported. Data presented are summarized in the main body and presented in detail in the supplements. Areas of ongoing research are briefly described, and topics for future research are suggested. The data have been compiled to assist in the design of large-scale superconducting magnets for fusion reactors. DOE

N95-22035# Syracuse Univ., NY. Dept. of Chemistry.
SPECTROSCOPIC ASSESSMENT OF THE RELIABILITY OF METAL/METAL OXIDE INTERFACES Final Report, Oct. 1990 - Sep. 1991
Joseph Chaiken Oct. 1994 47 p
(Contract F30602-88-D-0028)
(AD-A286131; RL-TR-94-189) Avail: CASI HC A03/MF A01

There is considerable interest in understanding the source of the electromigration resistance of the well-known interconnect material, titanium tungsten (Ti:W). Measures of electromigration can be obtained with respect to a variety of parameters/physical properties. The variation of some parameters over time can presumably be associated with the increase in the probability of an electromigration related interconnect failure. In the simplest analysis, we immediately note that any metal in contact with the atmosphere oxidizes. Furthermore, the process is accelerated by increasing the temperature as is the rate of electromigration related failures. Therefore, a rational basis exists to suspect that oxidation related chemistry can be related to electromigration related failure processes. This study probes the oxidation chemistry in this alloy on native oxide coated silicon. We report physical and chemical measurements on the interface between a ceramic and metal phase. DTIC

N95-22048# Bettis Atomic Power Lab., West Mifflin, PA.
A NEW METALLOGRAPHIC PROCEDURE FOR EDGE RETENTION OF ENCLOSED SURFACES
O. M. Katz 1994 10 p Presented at the 27th Annual International Metallographic Society Meeting, Montreal, Quebec, 24-27 Jul. 1994
(Contract DE-AC11-93PN-38195)
(DE94-017549; WAPD-T-3033; CONF-940793-3) Avail: CASI HC A02/MF A01

Utilization of a low melting point, metallic alloy that expands on solidification has provided a reproducible means of preserving edges and accurately measuring deposits on surfaces mounted for metallographic study. In normal laboratory practice the electrically conducting mounting material generates no hazardous waste, needs no special equipment to prepare and is available commercially at a relatively reasonable price. Previous standard edge preservation techniques were found to be 90% inefficient from a time utilization view compared with the new procedure. This new mounting procedure has greatly improved the quality and efficiency of microstructural studies of all materials, especially those on the inside diameters of heat exchanger components. These studies have included reaction products, shallow creep cracks and deposits on tubing, for which the procedure has proved indispensable. DOE

N95-22119# Sandia National Labs., Albuquerque, NM.
LOWER ACTIVE METALS LOADING FOR HYDROTREATING CATALYSTS
S. E. Lott, T. J. Gardner, L. I. McLaughlin, and J. B. Oelfke 1994 9 p Presented at the US/Japan Meeting on Coal Energy Research, Albuquerque, NM, 26-30 Sep. 1994
(Contract DE-AC04-94AL-85000)
(DE94-018907; SAND-94-2222C; CONF-9409207-1) Avail: CASI HC A02/MF A01

Hydrous metal oxides (HMO's) are chemically synthesized materials which contain a homogeneous distribution of ion exchangeable alkali cations that provide charge compensation to the metal-oxygen framework. Both the presence of these alkali cations and the resulting high cation exchange capacities (4-5 meq/g) clearly set these HMO materials apart from conventional precipitated hydrous oxides. For catalyst applications, the HMO material serves as an ion exchangeable support which facilitates the uniform incorporation of catalyst precursor species. Following catalyst precursor incorporation, an activation step is required to convert the catalyst precursor to the desired active phase. Considerable process development activities at Sandia National Laboratories related to HMO materials have resulted in bulk silica-doped hydrous titanium oxide (HTO:Si)-supported NiMo catalysts that are more active in model compound reactions than commercial NiMo catalysts. These reactions, e.g. pyrene hydrogenation, simulate direct coal liquefaction. However, extension of this process to produce NiMo/HTO:Si catalyst coatings on commercial supports is of interest for liquefaction applications since overall catalyst cost can be reduced and bulk HTO:Si mechanical limitations can be circumvented. In the present effort, NiMo/HTO:Si has been evaluated for hydrodesulfurization (HDS) and hydrodenitrogenation (HDN) of coal derived liquids. NiMo/HTO:Si catalysts have been evaluated in both bulk (unsupported) form and a supported form on commercial alumina extrudates. DOE

N95-22123# Oak Ridge National Lab., TN. Metals and Ceramics Div.
IRRADIATION CREEP IN STRUCTURAL MATERIALS AT ITER OPERATING CONDITIONS
M. L. Grossbeck 1994 8 p Presented at the Materials Issues for Severe Environments Meeting, San Diego, CA, 23-25 Jun. 1993
(Contract DE-AC05-84OR-21400)
(DE94-018946; CONF-9306367-1) Avail: CASI HC A02/MF A01

Irradiation creep is plastic deformation of a material under the influence of irradiation and stress. Below the regime of thermal creep, there remains a deformation mechanism under irradiation that is weakly temperature dependent and clearly different from thermal creep. This is irradiation creep. Both stress and irradiation are required for irradiation creep. Irradiation creep studies for applications in the past focused mostly on liquid metal fast breeder reactors where temperatures are usually above 400 C. Fusion reactors, especially nearterm devices such as the ITER will have components operating at temperatures as low as 100 C exposed to high neutron fluxes. Theories of irradiation creep based on steady-state point defect concentrations do not predict significant irradiation creep deformation at these temperatures; however, data from research reactors show that irradiation creep strains at 60 C are as high or higher than at temperatures above 300 C for austenitic stainless steels. Irradiation creep of nickel has also been observed at cryogenic temperatures. DOE

N95-22127# Oak Ridge National Lab., TN.
ATOM PROBE FIELD ION MICROSCOPY OF TYPE 308 CRE STAINLESS STEEL WELDS
S. S. Babu (Pennsylvania State Univ., University Park, PA.), S. A. David, J. M. Vitek, and M. K. Miller 1994 15 p Presented at the International Field Emission Symposium, Rouen, France, 15-17 Jul. 1994
(Contract DE-AC05-84OR-21400)
(DE94-019162; CONF-9407132-1) Avail: CASI HC A03/MF A01

Additions of controlled residual elements (CRE) such as titanium, boron and phosphorus, to the commercial 308 type stainless steel welds have been found to improve the creep-rupture properties. In both conventional and CRE-type stainless steel welds, during high temperature service, various microstructural changes take place such as the formation of M23C6 carbide networks along austenite(gamma)-ferrite (delta) interface, the formation of sigma phase, and the dissolution of ferrite. Boron-containing CRE welds exhibit similar microstructural evolution as that of conventional types 308 stainless steel welds. As boron may segregate to ferrite-austenite interface and thereby modify the austenite-M23C6 carbide interface, the distribution of boron was measured with an atom probe field ion microscope. Atom probe analysis revealed significant boron and carbon enrichments along the ferrite-austenite boundary in the as-welded state. The ratio of carbon to boron concentration at the interface was found to be approximately 4. DOE

N95-22132# Naval Air Warfare Center, Warminster, PA. Air Vehicle and Crew Systems Technology Dept.
CORROSION BEHAVIOR OF LANDING GEAR STEELS
Eun U. Lee 29 Oct. 1993 24 p
(AD-A285862; NAWCADWAR-94001-60) Avail: CASI HC A03/MF A01

A study was conducted on the corrosion behavior of an AerMet 100 steel and a 300M steel. This study included investigations of stress corrosion cracking (SCC), immersion corrosion, salt spray corrosion, and humidity corrosion of both steels. For the SCC investigation, double cantilever beam (DCB) specimens were employed, and for the immersion, salt spray, and humidity corrosion investigations, sheet specimens were used. The SCC rate is less and the threshold stress intensity for stress corrosion (K(sub ISCC)) is greater in the AerMet 100 steel (33 ksi*in(exp 1/2)) than in the 300M steel (19 ksi*in(exp 1/2)), indicating better SCC resistance of the AerMet 100 steel. In the AerMet 100 steel, the stress corrosion crack grows along an intergranular and transgranular path in the direction of forging deformation. The immersion corrosion and salt spray corrosion rates of the AerMet 100 steel is 33 - 40% and 13 - 20% of those for the 300M steel, respectively. Evidence of humidity corrosion is not detectable in the AerMet 100 steel within the employed test period 110 days, whereas it is substantial (2.0413 mpy or 0.0447 mdd) in the 300M steel. The overall results indicate that the AerMet 100 steel is superior to the 300M steel with respect to the corrosion resistance as well as the mechanical properties. DTIC

N95-22174 Technical Research Centre of Finland, Espoo (Finland).

SURFACE TECHNOLOGY PROGRAMME

S. P. Hannula and J. P. Hirvonen 23 Mar. 1994 145 p
(PB95-132866; VTT/SYMPOSIUM-140) Copyright Avail: Issuing Activity (National Technical Information Service (NTIS))

Included in this report are partial contents regarding the Surface Technology Program: (1) VTT'S research program on surface engineering; (2) Improvement of a C:H film adhesion to different substrate materials by intermediate layer; (3) Tribological characteristics of diamond-like carbon coatings; (4) Polycrystalline diamond coatings made by high pressure technique; (5) The potential of diamond for applications in microelectronics; (6) Studying localized corrosion using scratch technique in a modified Avesta cell; (7) Surface film characterization by contact electric resistance method; (8) Surface sensitive analyzing methods in the investigation of localized corrosion; (9) Surface films and corrosion of stainless steels in sulphur containing paper mill environments; and (10) Mechanical performance and microstructure of PM and cast SiCp-Al alloy composites. NTIS

N95-22289# Los Alamos National Lab., NM.

CHARACTERIZATION OF A TEXTURE GRADIENT IN TANTALUM PLATE

S. I. Wright and G. T. Gray, III 1994 7 p Presented at the 3d International Symposium on Structural and Functional Gradient Materials, Lausanne, Switzerland, 10-12 Oct. 1994
(Contract W-7405-eng-36)
(DE95-002704; LA-UR-94-3413; CONF-9410244-1) Avail: CASI HC A02/MF A01

Clark et al. have shown that significant texture gradients can be produced in rolled tantalum plate and that the strength of the gradient is dependent on the processing path. Texture gradients are often ignored because they are time consuming to characterize and add significant complexity to materials modeling. The variation in texture through the thickness of rolled materials is most commonly measured by sectioning samples to different depths through the thickness of the plate and then measuring the texture from these section planes by X-ray diffraction. A new technique based on automatic indexing of electron backscatter diffraction patterns in the scanning electron microscope enables spatially specific orientations to be measured in a practical manner. This technique allows spatial variations in texture to be measured directly enabling gradients in texture to be investigated in more detail than previously possible. This data can be used directly in coupled finite-element/ polycrystal-plasticity models to simulate the effects of variations in texture on the plastic behavior of polycrystals. This work examines the variation in texture through the thickness of a tantalum plate and its resultant effect on the compressive deformation of samples prepared from the plate. The characterization of the texture gradient using the automatic point-by-point measurement technique mentioned above is described in detail. The effect of the gradient on the plastic response of through-thickness compression tests is also discussed. DOE

N95-22291# Argonne National Lab., IL. Chemistry and Material Science Div.

STUDIES OF THE MICROWAVE RESISTIVITY OF KAPPA-(BEDT-TTF)2Cu(N(CN)2)Cl

M. Dressel (California Univ., Los Angeles, CA.), G. Gruener (California Univ., Los Angeles, CA.), K. D. Carlson, H. H. Wang, and J. M. Williams 1994 3 p Presented at the International Conference on Science and Technology of Synthetic Metals, Seoul, Republic of Korea, 24-29 Jul. 1994 Submitted for publication Sponsored in cooperation with Alexander von Humbolt Foundation
(Contract W-31-109-eng-38)
(DE95-002980; ANL/CHM/CP-84363; CONF-9407117-4) Avail: CASI HC A01/MF A01

The authors have performed temperature dependent measurements of the surface impedance of kappa-(BEDT-TTF)2Cu(N(CN)2)Cl in both directions, parallel and perpendicular to the highly conducting planes. In both orientations the microwave resistivity basically follows the dc behavior for T greater tha n 15 K: the crystal undergoes a broad metal-insulator transition at around 50 K. While there are no indications of superconductivity at ambient pressure found in the dc resistivity and by ac susceptibility, the microwave resistivity clearly drops at 13 K and again at 5 K, indicating two superconducting phases. When pressure is applied by embedding it in grease, only the well known superconducting phase transition at (Tc) = 13 K remains. DOE

N95-22308# Los Alamos National Lab., NM.

EFFECT OF ANNEALING TEMPERATURE ON THE TEXTURE OF ROLLED TANTALUM AND TANTALUM-10 WT % TUNGSTEN

Stuart I. Wright, Sherri R. Bingert, and Melissa D. Johnson 1994 8 p Presented at the 1994 International Conference on Tungsten and Refractory Metals, McLean, VA, 17-19 Oct. 1994
(Contract W-7405-eng-36)
(DE95-002702; LA-UR-94-3431; CONF-9410213-3) Avail: CASI HC A02/MF A01

The effect of annealing temperature on crystallographic texture was investigated on straight- and cross-rolled Ta and cross-rolled Ta-10wt%W sheets. Textures were measured on coupons cut from rolled sheets and annealed for one hour at 800 to 1550 C. In particular the effect of annealing temperature on volume fraction of grains having (111) and (100) crystal directions nearly aligned with the plate normal was investigated. In the pure tantalum sheets, increased annealing temperature lead to increased fractions of the (111) component. The same was true for the Ta-10wt%W but much higher temperatures were required to change the texture from a (100) type texture to a more (111) type texture. In addition, the influence of the annealing temperature on the sharpness of the texture; on the surface to centerline texture gradient; and on the in-plane symmetry of the texture was investigated. DOE

N95-22313# Lawrence Livermore National Lab., Livermore, CA.

A MULTISITE INTERACTION EXPANSION OF THE TOTAL ENERGY IN METALS

E. C. Sowa and A. Gonis 21 Jul. 1994 6 p Presented at the 2nd International Conference on Computer Simulation of Radiation Effects, Santa Barbara, CA, 24-29 Jul. 1994
(Contract W-7405-eng-48)
(DE94-017175; UCRL-JC-117584; CONF-940731-2) Avail: CASI HC A02/MF A01

The local-density approximation provides a proper setting for the decomposition of total energy into many-body (many-atom) contributions. Multiple scattering theory in turn provides a convenient framework for carrying out this process. We illustrate this concept with calculations on a linear chain of atoms in bulk copper. DOE

N95-22344# Oak Ridge National Lab., TN.

BULK AND DEFECT PROPERTIES OF ORDERED INTERMETALLICS

C. L. Fu and M. H. Yoo 1993 10 p Presented at the Fall Meeting of the Minerals, Metals and Materials Society: Physical Metallurgy and Materials, Pittsburgh, PA, 17-21 Oct. 1993
(Contract DE-AC05-84OR-21400)
(DE94-017706; CONF-931009-29) Avail: CASI HC A02/MF A01

First-principles calculations based on the local-density-functional theory have been used to investigate the factors governing strength of ordered intermetallic alloys. Unlike Ni3Al, calculated elastic constants and shear fault energies indicate anomalous yield strength behavior is not likely to occur in Ni3Si. This suggests the inadequacy of cross-slip-pinning model to explain the strength anomaly in the L1(sub 2) structure. For strongly ordered NiAl, the defect structure is dominated by two types of defects - monovacancies on the Ni sites and substitutional antisite defects on the Al sites. By contrast, for Ni3Al, absence of structural vacancies and deviations from stoichiometry are accommodated by substitutional antisite defects on both sublattices. Intrinsic strengthening mechanisms in TiAl are discussed in terms of calculated elastic constants and shear fault energies. Because of reduced fault energies at the gamma/(alpha 2) interface, slip and twinning contribute significantly to high shear deformation of the lamellar structure. DOE

N95-22345# Oak Ridge National Lab., TN.
PROCESSING OF INTERMETALLIC MATERIALS BY REACTION SYNTHESIS
C. T. Liu 1994 9 p Presented at the Workshop on Solidification and Processing, Boston, MA, 18-22 Jul. 1994
(Contract DE-AC05-84OR-21400)
(DE94-017710; CONF-9407122-1) Avail: CASI HC A02/MF A01

This paper provides a brief summary of recent work on reaction synthesis of Ni3Al/NiAl powder compacts at Oak Ridge National Laboratory. Both reaction extent and densification process depend strongly on heat accumulation and heat transfer, which can be effectively controlled by exerting compressive stresses, as well as aluminum concentration and compact thickness. Three distinct stages are observed, corresponding to (1) initial reaction to (no formation of transient liquid phases); (2) partial reaction (occurrence of self-propagating combustion reaction); and (3) full reaction (combustion reaction + conversion reaction). A nearly full density product was obtained in both the fully reacted zone and partially reacted zones during reaction synthesis under compressive stresses. DOE

N95-22346# Oak Ridge National Lab., TN.
TENSILE AND IMPACT PROPERTIES OF IRON-ALUMINUM ALLOYS
D. J. Alexander and V. K. Sikka 1993 16 p Presented at the Fall Meeting of the Minerals, Metals and Materials Society: Physical Metallurgy and Materials, Pittsburgh, PA, 17-21 Oct. 1993
(Contract DE-AC05-84OR-21400)
(DE94-017750; CONF-931009-28) Avail: CASI HC A03/MF A01

Tensile and impact tests have been conducted on specimens from a series of five heats of iron-aluminum alloys. These results have been compared to data for the iron aluminide alloy FA-129. The transition temperatures of all of the Fe3Al-based alloys were similar, but the simple ternary alloy had a much higher upper-shelf energy. The reduced aluminum alloys (based on Fe-8Al (wt %)) had lower transition temperatures and higher upper-shelf energy levels than the Fe3Al-type alloys. The reduced aluminum alloy with yttrium showed excellent tensile properties, with a room temperature total elongation of 40%, and a very high upper-shelf energy level. Despite the high tensile ductility at room temperature, the transition temperature of the yttrium-containing alloy was still about 150 C, compared to approximately 300 C for FA-129. In general, the microstructures were coarse and anisotropic. The fracture processes were dominated by second-phase particles. DOE

N95-22374# Helsinki Univ. of Technology, Espoo (Finland).
NEW THERMODYNAMIC DESCRIPTION OF THE Cu-Zr SYSTEM
K. Zeng and M. Haemaelaeinen 1994 36 p
(PB95-127189; TKK-V-B88) Avail: CASI HC A03/MF A01

An optimized set of thermodynamic functions for the Cu-Zr system has been obtained by the least squares method from phase diagram and thermodynamic data available in the literature. The excess free energies of the solution phases, liquid and three terminal solid solutions, were described by the Redlich-Kister formula. All the intermediate compounds were treated as stoichiometric phases. The calculated phase diagram, as well as the thermodynamic properties vs. compositions, agree well with the experimental values. The reliability of the optimized parameters have been examined using mu-T plots. NTIS

N95-22396# Tennessee Valley Authority, Muscle Shoals, AL. Chemical Development Dept.
AN UPDATE OF CORROSION INHIBITORS FOR MILD STEEL EXPOSED TO 32-0-0 UAN SOLUTION
D. T. Nguyen, D. E. Nichols, and E. J. Lohry (Nutra-Flo Co., Sioux City, IA.) 1994 21 p Presented at the 206th American Chemical Society (ACS) National Meeting, Chicago, IL, 22-27 Aug. 1993
(DE95-001715; CONF-930802-22; Z-337) Avail: CASI HC A03/MF A01

This is a continuation of corrosion studies on the effectiveness of commercial and newly-developed corrosion inhibitors for use with mild steel exposed to urea-ammonium nitrate (UAN) solution. This paper provides updated information on five newly-developed corrosion inhibitors. Tests were conducted with mild steel exposed to 32-0-0 UAN solution containing each corrosion inhibitor at ambient temperature and under static conditions. Real-time corrosion of the test specimens was monitored using AC impedance techniques. Corrosion performance of the inhibitors was evaluated based on comparison of the corrosion rate of specimens exposed to 32-0-0 UAN solution with and without a corrosion inhibitor. DOE

N95-22408# Lawrence Livermore National Lab., Livermore, CA.
FRACTURE BEHAVIOR OF LAMINATED DISCONTINUOUSLY REINFORCED ALUMINUM MATERIAL
T. M. Osman (Case Western Reserve Univ., Cleveland, OH.) and J. J. Lewandowski (Case Western Reserve Univ., Cleveland, OH.) May 1994 10 p Presented at the 4th International Conference of Aluminum Alloys, Atlanta, GA, 11-16 Sep. 1994
(Contract W-7405-eng-48)
(DE94-017307; UCRL-JC-117162; CONF-9409179-3) Avail: CASI HC A02/MF A01

Laminated metallic composites are being developed for applications which require high specific stiffness and fracture resistance. Recent work with laminated discontinuously reinforced aluminum (DRA) materials has demonstrated the potential for marked improvements in stable crack growth resistance via extrinsic toughening. The purpose of this work is to compare the fracture mechanisms and fracture resistance of laminated DRA materials to unlaminated DRA materials. In particular, the production of extensive stable crack growth and the associated improvement in damage tolerance in DRA laminates is documented. DOE

27 NONMETALLIC MATERIALS

Includes physical, chemical, and mechanical properties of plastics, elastomers, lubricants, polymers, textiles, adhesives, and ceramic materials.

For composite materials see *24 Composite Materials.*

N95-19893# Texas Univ., Austin, TX. Dept. of Chemical Engineering.
REACTIVE COMPATIBILIZATION OF POLYMER BLENDS Final Report, 1 Jul. 1991 - 30 Jun. 1994
D. R. Paul 1 Aug. 1994 18 p
(Contract DAAL03-91-G-0128)
(AD-A284836) Avail: CASI HC A03/MF A01

This research has examined the use of functionalized polymers that react at the interfaces in polymer blends to form block or graft copolymers during melt processing. These grafts act as 'compatibilizers' that strengthen the interface and provide a powerful means of controlling blend phase morphology. Consequently, this approach provides an effective means of controlling the properties of multiphase polymeric materials. Most of the work involved the use of various polyamides as one component in the blend. The other component was a reactive elastomer, an acrylonitrile-butadiene-styrene (ABS) material, a core-shell impact modifier, or polypropylene. The end group configuration of the polyamide was shown to be an important consideration in morphology development. Functionalized additives are most efficient when both physical and chemical interactions are optimized. A variety of approaches for producing super-tough polyamide blends with low ductile-brittle transition temperatures are described. Cavitation of the rubber phase was shown to be an important part of the roughening mechanism in certain cases. DTIC

N95-19926# Sandia National Labs., Albuquerque, NM.
A TEST OF THE ARRHENIUS EXTRAPOLATION ASSUMPTION FOR A NITRILE RUBBER
K. T. Gillen, J. Wise, and R. L. Clough 1994 4 p Presented at the 19th Department of Energy Conference on Compatibility, Aging and Service Life, Los Alamos, NM, 28-30 Sep. 1994
(Contract DE-AC04-94AL-85000)
(DE94-017337; SAND-94-2035C; CONF-9409181-2) Avail: CASI HC A01/MF A01

The Arrhenius relation predicts a linear relation between log of time to property change and inverse absolute temperature, with the Arrhenius activation energy E(sub a) given from the slope. For a nitrile rubber, Arrhenius behavior is observed for elongation versus air-oven aging temperature, with a E(sub a) of 22 kcal/mol. Confidence in extrapolation to low temperatures can be increased by measuring oxygen consumption. From 95 to 52 C, the E(sub a) for oxygen consumption is identical to that for elongation; however, below 52 C, the E(sub a) for oxygen consumption drops slightly to 18 kcal/mol, indicating that the extrapolation assumption probably overestimates the tensile property lifetime by a factor of about two at 23 C. DOE

N95-19972 Exxon Research and Engineering Co., Annandale, NJ.
TECHNICAL SUMMARY FOR 1993 FALL MRS SYMPOSIUM O, COMPLEX FLUIDS
19 Aug. 1994 4 p Limited Reproducibility: More than 20% of this document may be affected by microfiche quality
(Contract N00014-94-1-0129)
(AD-A283722) Avail: Issuing Activity (Defense Technical Information Center (DTIC))

The fall 1993 Symposium 'O', Complex Fluids, consisted of 24 invited talks, 60 contributed papers, and over 40 contributed posters, covering the static and dynamic properties of complex fluids in bulk and at interfaces. The subject matter of 'complex fluids' comprises a wide variety of materials outside conventional condensed matter physics, including colloidal suspensions, gels, polymer melts or solutions, and surfactant-containing phases. These diverse systems have in common a number of features, including self-assembly. Many complex fluids contain mesoscopic structures that assemble spontaneously from constituent molecules, which are often specially designed to result in a particular self-assembled structure. Amphiphilic or surfactant molecules, with polar and non-polar regions on the same molecule, aggregate into a huge variety of structures, including micelles, monolayers, and bilayers. Block copolymers, consisting of chemically dissimilar polymer chains covalently joined together, behave in analogous ways. From the mesoscopic self-assembled building blocks, a wide variety of phases are formed, including many phases with crystalline or liquid crysalline order. Complex fluids also have a complex rheology and a broad application in common. DTIC

N95-20016# Argonne National Lab., IL. Energy Technology Div.
RECOGNITION OF SUBSURFACE DEFECTS IN MACHINED CERAMICS BY APPLICATION OF NEURAL NETWORKS TO LASER SCATTER PATTERNS
Michael C. Stinson (University of Central Michigan, Mount Pleasant, MI.), Owen W. Lee (California Univ., Los Angeles, CA.), J. Scott Steckenrider, and William A. Ellingson 1994 4 p Presented at the 18th Annual Conference on Composites and Advanced Ceramics, Cocoa Beach, FL, 9-14 Jan. 1994
(Contract W-31-109-eng-38)
(DE94-018373; ANL/ET/CP-80540; CONF-940135-11) Avail: CASI HC A01/MF A01

Laser scatter has shown promise as a method to characterize damage microstructural variations as well as a method to characterize surfaces in optical translucent ceramics. Because large volumes of data need to be handled (and sorted) quickly, automated pattern recognition methods using neural networks have been implemented to recognize differences in patterns. A He-Ne laser (lambda)=0.632(mu) has been used to obtain scatter patterns from hot pressed Si3N4 with various microstructur al variations. By use of a backpropagation neural network running on an IBM PC clone 486/33 machine, a correlation was established between subsurface microstructure and position in Si3N4 b all bearings. The data were confirmed by destructive analysis. DOE

N95-20024# Oak Ridge National Lab., TN.
PROPERTIES OF WHISKER-REINFORCED CERAMICS
P. F. Becher, C. H. Hsueh, H. T. Lin, K. B. Alexander, T. N. Tiegs, W. H. Warwick, and S. B. Waters 1994 25 p Presented at the 96th Annual Meeting of the American Ceramic Society, Indianapolis, IN, 24-28 Apr. 1994
(Contract DE-AC05-84OR-21400)
(DE94-017759; CONF-940416-24) Avail: CASI HC A03/MF A01

The paper summarizes studies of SiC whisker-reinforced alumina composites, their properties and the influence of composition and microstructure. Both steady-state toughness and R-curve response increase with whisker content and diameter. Room temperature flexure strength of aluminas with different grain sizes also increases with whisker content. Resistance to slow crack growth under both monotonic and cyclic loading is improved by whisker reinforcement compared to alumina and other ceramics. The thermal conductivity and electrical resistivity exhibit a substantial increase and decrease, respectively, with whisker loadings above 10 vol %. Thermal expansion coefficients decrease in a systematic fashion with increase in whisker content. However, the expansion coefficients are greater parallel to hot pressing axis compared to perpendicular direction owing to internal stresses and preferred orientation of whiskers. The changes in mechanical and thermal properties due to SiC whisker additions result in substantial improvement in thermal shock resistance for samples of various sizes. At elevated temperatures, tests in air show that improvements in strength and resistance to strength degradation are associated with SiC whisker reinforcement. The limiting factors in elevated temperature mechanical response of the composite at 1200C and above are related to surface oxidation-reaction processes and creep. On the other hand, the creep resistance of the composite is far greater than alumina with a similar fine grain size at temperatures less than or equal to 1200C. Furthermore by increasing the grain size of the alumina matrix, creep resistance of the composite can be increased. In essence, SiC whisker reinforced alumina composites provide an example of a system whose properties can be tailored through control of microstructure and composition. DOE

N95-20047# Sandia National Labs., Albuquerque, NM.
SOL-GEL-DERIVED SILICA FILMS WITH TAILORED MICROSTRUCTURES FOR APPLICATIONS REQUIRING ORGANIC DYES
M. N. Logan, S. Prabakar (New Mexico Univ., Albuquerque, NM.), and C. J. Brinker 1994 7 p Presented at the Spring Meeting of the Materials Research Society, San Francisco, CA, 4-8 Apr. 1994
(Contract DE-AC04-94AL-85000)
(DE94-018886; SAND-93-4010C; CONF-940411-52) Avail: CASI HC A02/MF A01

A three-step sol-gel process was developed to prepare organic dye-doped thin films with tailored porosity for applications in chemical sensing and optoelectronics. Varying the acid- and base-catalyzed hydrolysis steps of sols prepared from tetraethoxysilane with identical final H2O/Si ratios, dilution factors and pH resulted in considerably different distributions of the silicate polymers in the sol (determined by Si-29 NMR) and considerably different structures for the polymer clusters (determined by SAXS). During film formation these kinetic effects cause differences in the packing and collapse of the silicate network, leading to thin films with different refractive indices and volume fraction porosities. Under conditions where small pore-plugging species were avoided, the porosities of as-deposited films could be varied by aging the sol prior to film deposition. This strategy, which relies on the growth and aggregation of fractal polymeric clusters, is compatible with the low temperature and near neutral pH requirements of organic dyes. DOE

N95-20078# Air-Conditioning and Refrigeration Technology Inst., Inc., Arlington, VA.
ACCELERATED SCREENING METHODS FOR DETERMINING CHEMICAL AND THERMAL STABILITY OF REFRIGERANT-LUBRICANT MIXTURES. PART 2: EXPERIMENTAL COMPARISONS AND VERIFICATION OF METHODS
R. Kauffman (Dayton Univ., OH.) Jul. 1994 52 p
(Contract DE-FG02-91CE-23810)
(DE95-000743; DOE/CE-23810/38C-Pt-2) Avail: CASI HC A04/MF A01

The research reported herein continued to concentrate on in situ conductivity measurements for development into an accelerated screening method for determining the chemical and thermal stabilities of refrigerant/lubricant mixtures. The work reported herein was performed in two phases. In the first phase, sealed tubes were prepared with steel catalysts and mixtures of CFC-12, HCFC-22, HFC-134a, and HFC-32/HFC-134a (zeotrope 30:70) refrigerants with oils as described in ANSI/ASHRAE Method 97-1989. In the second phase of work, modified sealed tubes, with and without steel catalysts present, were used to perform in situ conductivity measurements on mixtures of CFC-12 refrigerant with oils. The isothermal in situ conductivity measurements were compared with conventional tests, e.g., color measurements, gas chromatography, and trace metals to evaluate the capabilities of in situ conductivity for determining the chemical and thermal stabilities of refrigerant/lubricant mixtures. Other sets of tests were performed using ramped temperature conditions from 175 C 347 F to 205 C 401 F to evaluate the capabilities of in situ conductivity for detecting the onset of rapid degradation in CFC-12, HCFC-22 and HFC-134a refrigerant mixtures with naphthenic oil aged with and without steel catalysts present. DOE

N95-20094 University of Southern Mississippi, Hattiesburg, MS. Dept. of Polymer Science.
THIANTHRENE CONTAINING POLYIMIDES WITH MONOMER FORMATION VIA NUCLEOPHILIC AROMATIC SUBSTITUTION
Masaru Yoneyama, Randy A. Johnson, and Lon J. Mathias 7 Nov. 1994 29 p Limited Reproducibility: More than 20% of this document may be affected by microfiche quality
(Contract N00014-89-J-1225)
(AD-A286313; TR-75) Avail: CASI HC A03

Thianthrene-2,3,7,8 - tetracarboxylic dianhydride was synthesized via nucleophilic aromatic substitution of N-phenyl-4,5-dichlorophthalimide with thiobenzamide, thioacetamide, and sodium sulfide. This monomer was then polymerized with aromatic diamines by the conventional low temperature technique in N, N-dimethylacetamide (DMAc) to yield soluble poly(amic acid)s. Polyimides were obtained by thermal cyclization of the poly(amic acid) films. Polymers obtained formed creasable thin films and had excellent thermal stability in air and nitrogen. The bent thianthrene structure limited crystallization and chain-packing as indicated by x-ray analysis. The highly amorphous thianthrene containing polyimides were only soluble in H2SO4. DTIC

N95-20115# Northwestern Univ., Evanston, IL. Dept. of Physics and Astronomy.
ENERGETICS, BONDING MECHANISM AND ELECTRONIC STRUCTURE OF CERAMIC/CERAMIC AND METAL/CERAMIC INTERFACES
A. J. Freeman 1994 5 p
(Contract DE-FG02-88ER-45372)
(DE95-000601; DOE/ER-45372/7) Avail: CASI HC A01/MF A01

New efforts have been directed toward understanding the electronic structure and properties of the metal/ceramic interface. The authors studied the structure and electronic structure properties of the Ag/CdO (100) interface employing the total energy FLAPW thin film method. In addition, the structural, electronic, and magnetic properties of the metal-ceramic interfaces between palladium, rhodium, or ruthenium and magnesium oxide were investigated by the FLAPW method. DOE

N95-20121# Sandia National Labs., Albuquerque, NM.
THE ELECTRONIC PROPERTIES OF POLYSILANES
R. G. Kepler and Z. G. Soos (Princeton Univ., NJ.) 1994 22 p Presented at the International Conference on Polymers for Microelectronics, Kawasaki, Japan, 14-19 Nov. 1994
(Contract DE-AC04-94AL-85000)
(DE94-006464; SAND-94-0198C; CONF-941132-1) Avail: CASI HC A03/MF A01

Results of recent studies of the electronic properties of polysilanes are reviewed. The electronic states can be described by the Hueckel model if coulomb interactions are included using the Pariser-Parr-Pople approximation. The long polymer chains appear to be divided into random length, short, ordered segments by conformational defects, with the energy of the excited states depending on the length of the segments. In isolated polymer chains energy is transferred from high-energy, short segments to longer, lower energy segments but the distance and time during which transfer take place is very limited. In solid films the excitons become highly mobile and remain mobile throughout their lifetime, even at low temperatures. Holes are quite mobile in solid films and the characteristics of transport are the same as those of charge carrier transport in molecularly doped polymer films. DOE

N95-20138# Sandia National Labs., Albuquerque, NM.
REACTIONS AND MICROSTRUCTURE AT CERAMIC/METAL INTERFACES
A. P. Tomsia (California Univ., Berkeley. Lawrence Berkeley Lab, CA.) and R. E. Loehman 1993 19 p Presented at the 7th International Conference on Surface Modification Technology, Nagaoka, Japan, 1-3 Nov. 1994
(Contract DE-AC04-94AL-85000)
(DE94-014287; SAND-93-1306C; CONF-941181-1) Avail: CASI HC A03/MF A01

Reactions of Ti and Zr with AlN, Al2O3 and mullite were studied. The substrates were selected to represent a simple nitride (AlN), a simple oxide Al2O3, and a complex oxide (mullite). The activities of the Ti and Zr were varied by dissolving them at 1 and 5 wt.% in the 72Ag-28Cu eutectic composition, which is otherwise unreactive with the ceramics. Reactions were studied by measuring the variation of the alloy contact angle on the ceramic with time at temperature and by determining the compositions of interfacial reaction products. The reaction products were determined by SEM-EDS, EPMA and XRD hose analysis. Contact angles were lower for Ti alloys than for those containing Zr. Reaction products were primarily the nitrides of Zr and Ti for reaction with AlN and the respective oxides for reaction with Al2O3. Complex alloy phases were found in the metal away from the ceramic-metal reaction zone. DOE

N95-20176# National Materials Advisory Board, Washington, DC.
HIERARCHICAL STRUCTURES IN BIOLOGY AS A GUIDE FOR NEW MATERIALS TECHNOLOGY
1994 142 p
(Contract MDA972-92-C-0028)
(AD-A286317; NMAB-464; LC-94-69232; ISBN-0-309-04638-6) Avail: CASI HC A07/MF A02

Hierarchical structures are assemblages of molecular units or their aggregates that are embedded or intertwined with other phases, which in turn are similarly organized at increasing size levels. The multilevel architectures are capable of conferring unique properties to the structure. Hierarchical structures are found in practically all complex systems, particularly naturally occurring ones. Synthetic hierarchical structures can be prepared from metals, ceramics, or polymers, or from hybrids of various classes of these materials. DTIC

N95-20183# Pennsylvania State Univ., University Park, PA. Dept. of Chemistry.
SYNTHESIS AND CHARACTERIZATION OF POLY(ORGANOPHOSPHAZENE) INTERPENETRATING POLYMER NETWORKS
Karyn B. Visscher, Ian Manners, and Harry R. Allcock 17 May 1994 49 p
(Contract N00014-91-J-1194)
(AD-A279872; TR-17) Avail: CASI HC A03/MF A01

Polyphosphazenes are a broad, novel class of inorganic-organic macromolecules. The physical properties of polyphosphazenes can be understood in terms of a highly flexible backbone, with various physical or chemical characteristics tailored by the incorporation of specific side groups. As part of our program to synthesize new materials with hybrid macromolecular properties, the synthesis and characterization of several IPN's containing phosphazene polymers is described. DTIC

N95-20220# Oak Ridge National Lab., TN.
ENHANCEMENT OF CREEP RESISTANCE OF A SINTERED S3N4 CERAMIC BY MICROWAVE ANNEALING
K. C. Liu, C. O. Stevens, C. R. Brinkman, K. L. More, J. D. Kiggans, and T. N. Tiegs 1994 4 p Presented at the 5th International Symposium on Ceramic Materials and Components for Engines, Shanghai, China, 29 May - 1 Jun. 1994
(Contract DE-AC05-84OR-21400)
(DE94-017698; CONF-9405187-2) Avail: CASI HC A01/MF A01

Creep behavior was investigated for a sintered Si3N4 ceramic following microwave annealing at 1400 and 1500C for 20 h. Results of creep tests at 1200C showed that microwave annealing can enhance the creep resistance in terms of lowering creep rate and, hence, extending creep rupture life, but the 1400C annealing was most effective. X-ray diffraction analyses showed that the crystalline second phase was transformed as a result of microwave annealing from single phase Y10Al2Si3O18N4 to several different phases. The situation was further complicated by evolution of additional phases during high temperature creep experiments. DOE

N95-20226# Oak Ridge National Lab., TN.
MICROWAVE SINTERING OF ZrO2-12 MOL% CeO2
Mark A. Janney, Mitchell L. Jackson, and Hal D. Kimrey 1993 8 p Presented at the 95th Annual Meeting of the American Ceramic Society, Cincinnati, OH, 18-22 Apr. 1993
(Contract DE-AC05-84OR-21400)
(DE94-018709; CONF-930438-32) Avail: CASI HC A02/MF A01

Sintering of ZrO2-12 mol% CeO2 was accelerated by microwave processing at 2.45 GHz as compared with conventional firing. However, the size of the 'microwave effect' was significantly smaller than that which was previously observed for microwave sintering of ZrO2-8 mol% Y2O3. The difference in the effect that the microwave field had on the two zirconia systems is interpreted in terms of their ionic conductivities. DOE

N95-20227# University of Southern Illinois, Carbondale, IL.
PROCEEDINGS OF THE 4TH INTERNATIONAL CONFERENCE ON ELECTRORHEOLOGICAL FLUIDS
Rongja Tao and Gabriel D. Roy 1994 686 p Conference held in Feldkirch, Austria, 20-23 Jul. 1993
(Contract N00014-93-1-0582)
(AD-A286341) Avail: CASI HC A99/MF A06

A total of 58 papers are presented which describe the cutting edge of research in electrorheological (ER) fluids and which cover materials technology, physical mechanisms, properties, and applications of ER fluids. Topics discussed include: the polarization, structuring, and rheology of ER fluids; first experiments on magnetoelectrorheological fluids (MERF's); light scattering studies of a model ER fluid; simulation of solid structure formation in an ER fluid; viscoelasticity of ER fluids: role of electrostatic interactions; fluid flow and falling ball experiments in ER fluids; ER catch/clutch: inertial simulations; and dielectrophoretic assembly: a novel concept in advanced composite fabrication. CASI

N95-20251 Wright Lab., Wright-Patterson AFB, OH. Materials Directorate.
THE PREPARATION OF ALL PARA-POLYPHENYLS WITH INCREASED SOLUBILITY AND ENHANCED THIRD ORDER NLO ACTIVITY Final Report
Marilyn R. Unroe and Bruce A. Reinhardt Jun. 1994 37 p Limited Reproducibility: More than 20% of this document may be affected by microfiche quality
(AF Proj. 2303)
(AD-A284301; WL-TR-94-4070) Avail: Issuing Activity (Defense Technical Information Center (DTIC))

A series of all para-polyphenyenes up to heptaphenyl were prepared with solubilizing n-decyloxy pendants. The n-alkoxy pendants allow solubility in tetrahydrofuran for evaluation by femtosecond degenerate four-wave mixing. The physical, chemical, and electro-optical measurements are summarized. The oligomers corresponding to monomer and trimer have increased second hyperpolarizability due to purely extended pi-conjugation effects. However, the pentamer and heptamer evaluations indicated large increases in hyperpolarizability which were not solely attributable to conjugation increases. Furthermore, two-photon resonance enhancement was confirmed in the heptamer by an upconverted blue emission of the heptamer solution at 602nm. Two photon resonance was suspected in the pentamer because of less intense blue emission. DTIC

N95-20281# Sandia National Labs., Livermore, CA.
EFFECTS OF AMBIENT CONDITIONS ON THE ADHESION OF CUBIC BORON NITRIDE FILMS ON SILICON SUBSTRATES
G. F. Cardinale (California Univ., Davis, CA.), D. G. Howitt (California Univ., Davis, CA.), P. B. Mirkarimi, K. F. McCarty, E. J. Klaus, and D. L. Medlin 1994 14 p Presented at the International Conference on Metallurgical Coatings and Thin Films, San Diego, CA, 25-29 Apr. 1994
(Contract DE-AC04-76DP-00789)
(DE94-016779; SAND-94-8620C; CONF-940440-4) Avail: CASI HC A03/MF A01

Effect of environmental conditions on cubic boron nitride (cBN) film adhesion to silicon substrates was studied. cBN films were deposited onto (100)-oriented silicon substrates by ion-assisted pulsed laser deposition. Irradiating ions were mixtures of nitrogen with argon, krypton, and xenon. Under room-ambient conditions, the films delaminated in the following time order: N/Xe, N/Kr, and N/Ar. cBN films deposited using N/Xe ion-assisted deposition were exposed to four environmental conditions for several weeks: a 1-mTorr vacuum, high humidity, dry oxygen, and dry nitrogen. Films exposed to the humid environment delaminated whereas those stored under vacuum or in dry gases did not. Films stored in dry nitrogen were removed after nearly two weeks and placed in the high-humidity chamber; these films subsequently delaminated within 14 hours. DOE

N95-20291 Department of the Navy, Washington, DC.
CERAMICS FORMED BY PYROLYSIS OF EITHER LINEAR OR THERMOSETTING CARBORANE (SILOXANE OR SILANE) ACETYLENE BASED PRECURSOR POLYMERS Patent
Teddy M. Keller, inventor (to Navy) and Leslie J. Henderson, Jr., inventor (to Navy) 20 Sep. 1994 15 p Filed 8 Feb. 1993 Supersedes AD-D015747
(AD-D016563; US-Patent-5,348,917; US-Patent-Appl-SN-014928; US-Patent-Class-501-92) Avail: US Patent and Trademark Office

Ceramics that are formed from high temperature oxidatively stable thermosetting polymers which, in turn, are formed from linear polymeric materials having repeat units that contain at least one alkynyl group for cross-linking purposes and at least one bis(silyl or siloxanyl)carboranyl group. DTIC

N95-20293 Department of the Navy, Washington, DC.
POLYURETHANE-EPOXY INTERPENETRATING POLYMER NETWORK ACOUSTIC DAMPING MATERIAL Patent
Usman A. Sorathia, inventor (to Navy), William L. Yeager, inventor (to Navy), and Timothy L. Dapp, inventor (to Navy) 19 Jul. 1994 8 p Filed 28 Aug. 1991
(AD-D016567; US-Patent-5,331,062; US-Patent-Appl-SN-752248; US-Patent-Class-525-454) Avail: US Patent and Trademark Office

Improved acoustic damping materials comprise interpenetrating polymer networks having a soft polymer component and a hard polymer component. The soft polymer component, constituting from 50 to 90 percent by weight of the material, is a polyurethane made by polymerization of a diisocyanate with a polyether glycol, and the hard polymer component is made by polymerization of bisphenol A diglycidyl ether, with boron trichloride amine complex as a curing agent. DTIC

N95-20294 Department of the Navy, Washington, DC.
POLYURETHANE-ACRYLIC INTERPENETRATING POLYMER NETWORK ACOUSTIC DAMPING MATERIAL Patent
Usman A. Sorathia, inventor (to Navy) and Timothy L. Dapp, inventor (to Navy) 12 Jul. 1994 6 p Filed 28 Aug. 1991
(AD-D016572; US-Patent-5,328,957; US-Patent-Appl-SN-758972; US-Patent-Class-525-123) Avail: US Patent and Trademark Office

Improved acoustic damping materials comprise interpenetrating polymer networks having a soft polymer component and a hard polymer component. The soft polymer component, constituting from 50 to 90 percent by weight of the material, is made by polymerizing an aromatic diisocyanate with a polyalkylene ether glycol, and the hard polymer component is an acrylic polymer made by polymerization of the alkyl esters and alkylene diesters of acrylic and/or methacrylic acid, e.g. n-butyl methacrylate and tetramethylene glycol dimethacrylate. The curing of the mixture is carried out at room temperature. DTIC

N95-20316# Lawrence Livermore National Lab., Livermore, CA. Dept. of Chemistry and Materials Science.
OVERVIEW ON SUPERPLASTICITY RESEARCH ON SMALL-GRAINED MATERIALS
Oleg D. Sherby (Stanford Univ., CA.), T. G. Nieh, and J. Wadsworth Jul. 1994 12 p Presented at the International Conference on Superplasticity in Advanced Materials (ICSAM), Moscow, Russia, 24-26 May 1994
(Contract W-7405-eng-48)
(DE94-016550; UCRL-JC-117600; CONF-9405193-2) Avail: CASI HC A03/MF A01

Superplasticity is generally associated with fine grains, grain boundary sliding, and high tensile ductility at elevated temperature. This paper reviews some of the recent important findings in fine-grained superplasticity, including the areas of superplastic ceramics and bf-high-strain-rate superplasticity (HSRS). Deformation mechanism maps are shown to be powerful tools for predicting the conditions where HSRS can be expected. Ultrafine grained materials, processed economically, remain an important objective in achieving HSRS. Threshold stresses, observed in fine-grained superplastic materials, are shown to be functions of temperature and grain size but their origin, however, remains obscure. Quasi-superplastic materials, with a strain-rate-sensitivity exponent of $m = 0.33$, are shown to have high elongations, and have considerable promise for netshape isothermal forming of sheet and bulk components. DOE

N95-20317# Lawrence Livermore National Lab., Livermore, CA.
RATE CONTROLLED SYNTHESIS OF COMPOSITION MODULATED, METAL-OXIDE THIN FILMS
A. F. Jankowski Jul. 1994 7 p Presented at the Annual Meeting of the Society of Photo-Optical Instrumentation Engineers, San Diego, CA, 24-29 Jul. 1994
(Contract W-7405-eng-48)
(DE94-016596; UCRL-JC-117604; CONF-940723-7) Avail: CASI HC A02/MF A01

The development of advanced deposition technologies is continuously evolving for the synthesis of oxide coatings used in optical applications. Recent progress is made in the use of magnetron sputtering to reactively deposit metal-oxide thin films. Sputter deposition parameters are chosen to vary the composition along the film growth direction. The key process parameter to control is the sputtering rate of the target. The shape of the composition profile directly corresponds to the preselected variation of deposition rate. By simply varying the sputtering rate using a working gas that consists of an inert-oxygen mixture, structures are synthesized with composition profiles which can be either abrupt or graded in the growth direction. The result is a compositionally modulated structure of the metal-oxide system. This procedure for composition modulated synthesis is demonstrated for metals which are highly reactive with oxygen as well as for those metals which are not. The development of this deposition methodology will facilitate the design of metal oxide films for optical applications, as in gradient-index filters for example. Results are presented for the reactive sputter deposition of metal oxide coatings in the Y-O, Mo-O, and Cu-O systems. DOE

N95-20323# Oak Ridge National Lab., TN.
MICROSTRUCTURAL CONTRIBUTIONS TO THE FRACTURE RESISTANCE OF SILICON NITRIDE CERAMICS
P. F. Becher, S. L. Hwang, H. T. Lin, and T. N. Tiegs 1994 12 p Presented at the International Conference on Silicon Nitride-Based Ceramics, Stuttgart, Germany, 4-6 Oct. 1993
(Contract DE-AC05-84OR-21400)
(DE94-018955; CONF-931030-1) Avail: CASI HC A03/MF A01

There is a need to understand the parameters that influence the fracture resistance and strength response in self-reinforced silicon nitride ceramics. This paper attempts to address a few of the microstructural factors that are found to influence crack wake processes and the fracture resistance response in self-reinforced silicon nitride ceramics and similar systems. DOE

N95-20328 Massachusetts Inst. of Tech., Cambridge, MA. Dept. of Materials Science and Engineering.
THE SYNTHESIS AND CHARACTERIZATION OF NEW MESOGENIC DIACETYLENE MONOMERS AND THEIR POLYMERS Technical Report, Jun. 1993 - Jun. 1994
Paula T. Hammond and Michael F. Rubner Jun. 1994 44 p Limited Reproducibility: More than 20% of this document may be affected by microfiche quality
(Contract N00014-91-J-1381)
(AD-A286188) Avail: CASI HC A03

A series of three functionalized semirigid aromatic thermotropic diacetylene liquid crystals were prepared: an aromatic diacid containing tetramethylene spacers on either side of the diacetylene group (5,7 DODBA), and aromatic diols with four and nine methylene spacers (5,7 DHDP and 10,12 DHDP). This paper addresses the design and synthesis of the monomers, their liquid crystalline behavior, and the reactivity of their diacetylene groups. 5,7 DODBA and 5,7 DHDP each exhibited smectic phases. For the 5,7 DODBA diacid, in particular, hydrogen bonding is thought to play a significant role in the mesogenic behavior and the high stability of the mesophase. The mesogenic nature of 10,12 DHDP was inconclusive, though a liquid crystalline phase may exist within a narrow temperature range. Each of the monomers was photoreactive, producing deeply colored, conjugated polydiacetylene chains via topochemical polymerization upon exposure to UV or electron beam irradiation. The degree of reactivity in the solid state was much greater for the 10,12 DHDP monomer than for the 5,7 monomers due to the added flexibility of the longer methylene spacer. On the other hand, thermally induced liquid state polymerization appeared to be much faster in 5,7 DHDP and DODBA, due perhaps to the more rigid nature of these molecules in the melt. Polymers obtained from the liquid crystalline monomers are polydiacetylenes with functionalized mesogenic side chains. The partially polymerized diacetylene of 10,12 DHDP monomer exhibited clear mesogenic melt behavior based on thermal analysis, optical microscopy, and wide angle x-ray diffraction. DTIC

N95-20350# University of Southern Mississippi, Hattiesburg, MS. Dept. of Polymer Science.
RESPONSIVE COPOLYMERS FOR ENHANCED PETROLEUM RECOVERY
C. McCormick and R. Hester 1994 14 p
(Contract DE-AC22-92BC-14882)
(DE94-018822; DOE/BC-14882/8) Avail: CASI HC A03/MF A01

In this report, the authors consider the synthesis of copolymers of interest in the enhanced recovery of petroleum. Acrylamide and N,N-dimethyl-N-dodecyl-N-(2-amidoethyl) ammonium bromide copolymers were synthesized and characterized by various instrumental methods. The rheological properties of this copolymer were investigated using a porous media elongation rheometer. DOE

N95-20373# Oak Ridge National Lab., TN.
THE EFFECT OF FIBER COATING THICKNESS ON THE INTERFACIAL PROPERTIES OF A CONTINUOUS FIBER CERAMIC MATRIX COMPOSITE
E. Lara-Curzio, M. K. Ferber, and R. A. Lowden 1994 15 p Presented at the 18th Annual Conference on Composites and Advanced Ceramics, Cocoa Beach, FL, 9-14 Jan. 1994
(Contract DE-AC05-84OR-21400)
(DE94-017886; CONF-940135-7) Avail: CASI HC A03/MF A01

The interfacial properties (coefficient of friction, residual clamping stress, residual axial stress, and debond stress) of a continuous fiber ceramic composite were determined by means of single-fiber push-out tests. The composite consisted of Nicalon(trademark) fibers, that had been coated prior to matrix infiltration with carbon layers ranging in thickness from 0.03 to 1.2 micrometers, and a SiC matrix. It was found that the effective interfacial frictional stress decreased as the thickness of the carbon layer increased, from 24.6 +/- 9.9 MPa for a thickness of 0.03 Jim to 5.8 +/- 1.4 MPa for a thickness of 1.25 micrometers. It was also found that both the coefficient of friction and the residual clamping stress decreased as the thickness of the carbon layer increased. These results are explained in terms of the state of residual stresses in this composite and the role of the fiber surface topography during fiber sliding. DOE

N95-20390# Pennsylvania State Univ., University Park, PA. Applied Research Lab.
THERMO-MECHANICAL FATIGUE OF POLYMER MATRIX COMPOSITES
L. H. Strait Oct. 1994 133 p
(Contract N00039-92-C-0100)
(AD-A285931; ARL/PSU/TR-94-12) Avail: CASI HC A07/MF A02

Thermo-mechanical fatigue occurs when a component is exposed to thermal cycling under mechanical constraint and or superimposed mechanical loading. Thermo-mechanical loading is an increasingly common service condition for polymer matrix composite materials. Unfortunately, little or no information is available regarding the behavior of polymer composites subject to this loading condition. The present thesis research program was undertaken to evaluate the effects of mechanical constraint on the response of polymer matrix composites during thermal cycling. Analytical and experimental techniques were used to characterize the response of carbon fiber reinforced cyanate ester (IM6/BT3008) and bismaleimide (IM7/5240-4) composites. Cross-ply laminates were subjected to thermal cycles from 24 to 177 C in the unconstrained, fully-constrained and over-constrained conditions. Laminate response, damage mechanisms and residual compressive properties were characterized for each material and degree of constraint. Predicted ply stress distributions are significantly different for the various degrees of constraint and are highly sensitive to temperature-dependent lamina properties and laminate stress free temperature. Predictions of laminate response correlate well with experimental results. Deviations are apparent at elevated temperature which are attributed to the effects of time-dependent deformation. DTIC

N95-20392# Bristol Univ. (England). Physics Lab.
HIERARCHICAL STRUCTURE IN ADVANCED POLYMERS. PHASE BEHAVIOUR, ORIENTATION, PROPERTIES Final Report
A. Keller and J. A. Odell 1994 168 p
(Contract DAJA45-89-C-0021)
(AD-A285938; R/D-6011-MS-01) Avail: CASI HC A08/MF A02

The original proposal was a broad front investigation of the structure hierarchy in advanced materials embracing phase behaviour, orientation, and properties. We can state that all these objectives have been pursued in the course of the project leading to substantial amount of new knowledge in the respective fields, as testified also by the publication list appended. Derived from text

N95-20396# Sandia National Labs., Albuquerque, NM.
THE ROLE OF HIGH PRESSURE IN THE STUDY AND APPLICATIONS OF THE FERROELECTRIC POLYMER POLYVINYLIDENE FLUORIDE AND ITS COPOLYMERS
G. A. Samara, R. A. Graham, and F. Bauer (Institut Franco-Allemand de Recherches, Saint-Louis, France.) 1994 6 p Presented at the 8th International Symposium on Electrets, Paris, France, 12 Jul. 1994
(Contract DE-AC04-94AL-85000)
(DE94-015742; SAND-94-1926C; CONF-9407105-1) Avail: CASI HC A02/MF A01

Effects of frequency, temperature and hydrostatic pressure on dielectric properties, molecular relaxations, and phase transitions of PVDF and a copolymer with 30 mol % trifluoroethylene are discussed. Pressure causes large slowing down of the beta molecular relaxations as well as large increases in the ferroelectric transition temperatures and melting points, but the magnitudes of the effects are different for the different transitions. These effects can be understood in terms of pressure-induced hindrance of the molecular motions and/or reorientations. A unique application of these polymers as time-resolved dynamic stress gauges based on PVDF studies under very high pressure shock compression is discussed. DOE

N95-20407*# National Aeronautics and Space Administration. Langley Research Center, Hampton, VA.
A DIRECT PROCESS FOR PREPARING SEMI-CRYSTALLINE POLYIMIDES Patent Application
Alice C. Chang, inventor (to NASA) (Lockheed Engineering and Sciences Co., Hampton, VA.) and Terry L. St.Clair, inventor (to NASA) 1 Sep. 1994 16 p
(NASA-Case-LAR-15020-1; NAS 1.71:LAR-15020-1;
US-Patent-Appl-SN-299385) Avail: CASI HC A03/MF A01

The invention is a direct process for preparing semi-crystalline polyimides. This process comprises the steps of: providing a polar aprotic solvent, adding a dianhydride and a diamine to the solvent to form a mixture, stirring the mixture at ambient temperature, and adding glacial acetic acid to the mixture to provide a ratio of polar aprotic solvent to glacial acetic acid which ranges from about 90 to 10 to about 75 to 25 by volume to form a solution. The solution was heated to a range from about 110 C to about 140 C to form a polyimide precipitate. The polyimide precipitate was recovered as a semi-crystalline polyimide powder. NASA

N95-20410*# National Aeronautics and Space Administration. Langley Research Center, Hampton, VA.
VACUUM HOLDING FIXTURE AND METHOD FOR FABRICATING PIEZOELECTRIC POLYMER ACOUSTIC SENSORS Patent Application
E. Thomas Hall, Jr., inventor (to NASA) and Timothy D. Bryant, inventor (to NASA) (Army Vehicle Structures Lab., Hampton, VA.) 4 Oct. 1994 25 p
(NASA-Case-LAR-14240-1; NAS 1.71:LAR-14240-1;
US-Patent-Appl-SN-319142) Avail: CASI HC A03/MF A01

An apparatus and method for bonding a first film to a second film to form a sensor. The first and second films are piezoelectric films. A base section has a mating surface for holding the first film. A top section has a mating surface for holding the second film, the top section and base section being mateable together to form a cavity between the top section mating surface and the base section mating surface with the first film and the second film pressed together inside the cavity to bond the first film to the second film. An internal connection port forming mechanism forms an internal connection port between the first film and the second film when the base section and top section are mated together with the first film and the second film pressed together inside the cavity. Alternately, an internal connection tab forming mechanism can be used to form a sensor having an internal connection tab between the first and second film, instead of having an internal connection port. Author

N95-20428# Pennsylvania State Univ., University Park, PA. Dept. of Chemistry.
RADIATION-INDUCED MODIFICATIONS OF ALLYLAMINO-SUBSTITUTED POLYPHOSPHAZENES
M. F. Welker, H. R. Allock, G. L. Grune, R. T. Chern, and V. T. Stannett 17 May 1994 20 p
(Contract N00014-91-J-1194)
(AD-A279694; TR-18) Avail: CASI HC A03/MF A01

A review describing efforts to synthesize allylamino-substituted polyphosphazenes and characterize their sensitivity to radiation, and determine the value of using such polymers as new and better resist materials for microlithographic applications. DTIC

N95-20442# Pittsburgh Univ., Pittsburgh, PA. Dept. of Chemistry.
THE SYNTHESIS AND CHARACTERIZATION OF SMALL MOLECULE AND PHOTO-CROSS-LINKABLE HIGH POLYMERIC PHOSPHAZENES BEARING CINNAMATE GROUPS
Kenneth J. Wynne 18 May 1994 37 p
(Contract N00014-91-J-1194)
(AD-A279782; TR-21) Avail: CASI HC A03/MF A01

Cyclic trimeric and high polymeric phosphazenes bearing cinnamate groups were synthesized and characterized. Cyclic trimers with the general formula N3P3R(sub y)R'(sub x), where R=OC6H4OC(O)CH=CHPh, R'=OCH2CF3 (y=1, x=5 and y=6, x=O), and R=(OCH2CH2)2OC(O)CH=CHPh (y=l, x=5 and y=6, x=O) were synthesized. Also synthesized were high polymeric phosphazenes NPR(sub x)R'(sub y)(sub n), where R=OC6H4OC(O)CH=CHPh, R'=OCH2CF3 (y=x=1 and y=O, x=2) and R=(OCH2CH2)2OC(O)CH=CHPh (y=x=l and y=O, x=2). The photo-cross-linking of a representative polymer was studied by UV spectroscopy. DTIC

N95-20460 Department of the Navy, Washington, DC.
COMPOSITIVE PIEZOELECTRICS UTILIZING A NEGATIVE POISSON RATIO POLYMER Patent
Wallace A. Smith, inventor (to Navy) 2 Aug. 1994 12 p Filed 4 Dec. 1992
(AD-D016579; US-Patent-5,334,903; US-Patent-Appl-SN-985988;
US-Patent-Class-310-358) Avail: US Patent and Trademark Office

A piezoelectric composite which can be used as a transducer is constructed of parallel piezoelectric ceramic rods set in a passive polymer matrix which has a negative Poisson ratio whereby the electromechanical coupling of the transducer is greatly increased. DTIC

N95-20468# Sandia National Labs., Albuquerque, NM.
SPECTROSCOPIC STUDIES OF GLASS STRUCTURE
R. K. Brow 1994 8 p Presented at the Kreidl Symposium, Malbun (Liechtenstein), 3-8 Jul. 1994
(Contract DE-AC04-94AL-85000)
(DE94-016551; SAND-94-1929C; CONF-9407112-1) Avail: CASI HC A02/MF A01

Today's understanding of the molecular-level structure of inorganic glasses has been transformed by the availability of a wide range of sensitive spectroscopic probes. Today we can relate glass composition to quantitative distributions of glass-forming cations and to changes in oxygen bonding and modifying cation geometries. Future spectroscopic studies will result in improved descriptions of anion and cation geometries and should provide glass scientists with the capability to optimize atomic arrangements for specific optical, electrical, and thermal properties. DOE

N95-20472# National Renewable Energy Lab., Golden, CO.
NOVEL THIN-FILM CuInSe2 FABRICATION
A. M. Gabor (Colorado Univ., Boulder, CO.) and A. M. Hermann (Colorado Univ., Boulder, CO.) Aug. 1994 18 p
(Contract DE-AC36-83CH-10093)
(DE94-011874; NREL/TP-451-7055) Avail: CASI HC A03/MF A01

This report describes work exploring a new technique for the formation of CuIn(x)Ga(1-x)Se2 thin films. The Cu deposition was separated from the

Ga+In deposition such that precursor films with compositions of either Cu(x)Se or (In(x)Ga(1-x))2Se3 were formed. These precursors were exposed to either (1) In+Ga+Se or (2) Cu+Se at substrate temperatures greater than 500 C to form GaIn(x)Ga(1-x)Se2. Films made from the Cu(x)Se precursors were unexceptional, but films made from the (In(x)Ga(1-x))2Se3 precursors were of exceptional smoothness and density. During the period covered in this report, a device made from one of these films resulted in what, at the time, was the highest total-area efficiency measured for any non-single-crystal, thin-film solar cell, at 15.9%. DOE

N95-20486# Army Research Lab., Watertown, MA. Materials Directorate.

FRACTURE ANALYSIS OF AN ALL-CERAMIC BEARING SYSTEM Final Report

Jeffrey A. Swab and Mary P. Sweeney Sep. 1994 40 p
(AD-A285056; ARL-TR-512) Avail: CASI HC A03/MF A01

The report summarizes the fracture mechanism of an all-ceramic duplex spin bearing which was tested to failure to establish a design load margin. This bearing is part of a gyro-optics assembly being developed for use in an infrared seeker. The analysis revealed that machining-induced microcracks grew in the inner raceways beneath a ball. These microcracks coalesced to form macrocracks which led to fracture of the inner race and the failure of the bearing system. DTIC

N95-20548# Carnegie-Mellon Univ., Pittsburgh, PA.

PHYSICAL-CHEMICAL STUDIES ON RODLIKE POLYMER COMPOSITIONS Final Report

G. C. Berry 20 Sep. 1994 65 p
(Contract F49620-92-J-0281)
(AD-A285361; AFOSR-94-0634TR) Avail: CASI HC A04/MF A01

Third harmonic generation (THG) is used to study the third-order nonlinear optical properties of nematic and isotropic solutions of poly(phenylene benzobisthiazole), PBZT, and related small molecule model compounds. Maker fringe patterns (MFP) for isotropic preparations are analyzed in terms of postulated surface layers comprising regions in which the rodlike chains tend to have their axes parallel to the plane of the surface, creating a negatively birefringent uniaxial nematic layer. The THG with the nematic solution exhibits intensity with polarization components unexpected for uniaxial nematic symmetry, along with other unexpected features in the MFP. This behavior is attributed to the effects of surface layers, postulated to exhibit biaxial nematic symmetry, in which the uniaxial nematic symmetry is broken in regions on the scale of a wavelength. Features of the texture of the nematic phase of PBZT solutions are discussed. The nature of twist-loop defects in the texture is described, along with certain defects in the form of an ellipsoid of revolution, postulated to result from a molecular weight fractionation in the heterodisperse polymer. Light scattering studies on dilute solutions of a poly(n-dodecyl thiophene) are given to elucidate supramolecular structure that leads to a thermochromic effect. The supramolecular structure may play a role in the molecular organization in the solid state, with influence on electronic and nonlinear optical behavior. DTIC

N95-20551# Materials Research Society, Pittsburg, PA.

BIOMOLECULAR MATERIALS BY DESIGN, VOLUME 330

Mark Alper, Hagan Bayley, David Kaplan, and Manuel Navia 3 Dec. 1993 356 p Symposium held in Boston, MA, 29 Nov. - 3 Dec. 1993
(AD-A285369) Avail: CASI HC A16/MF A03

The purpose of Symposium S, Biomolecular Materials by Design, was to bring together the materials scientists who use biological approaches with the chemists, biochemists, and molecular geneticists responsible for recent breakthroughs in organic synthesis, surface chemistry, and protein engineering. As the latter may have been unaware of potential applications of their work in the world of materials, the interactions between the participants were intended to be reciprocating. The combination of presentations on new techniques with those on materials applications was a tremendous success. This week's program was so striking and varied that it is impossible to single out highlights. DTIC

N95-20570# General Atomics Co., San Diego, CA.

BORON CARBIDE-BASED COATINGS ON GRAPHITE FOR PLASMA FACING COMPONENTS

P. G. Valentine, P. W. Trester, J. Winter (Kernforschungsanlage, Juelich, Germany.), J. Linke (Kernforschungsanlage, Juelich, Germany.), R. Duwe Kernforschungsanlage, Juelich, Germany.), E. Wallura (Kernforschungsanlage, Juelich, Germany.), and V. Philipps (Kernforschungsanlage, Juelich, Germany.) Jan. 1994 23 p Presented at the 6th International Conference on Fusion Reactor Materials, Stresa, Italy, 27 Sep. - 1 Oct. 1993 Submitted for publication
(Contract DE-AC03-89ER-51114)
(DE94-017976; GA-A-21295; CONF-930928-30) Avail: CASI HC A03/MF A01

In the effort to evaluate boron-rich coatings as plasma facing surfaces in fusion devices, a new process for applying boron carbide (B4C) coatings to graphite was developed. The process entails eutectic melting of the carbon (C) substrate surface with a precursor layer of B4C particles. Adherent coatings were achieved which consisted of two layers: a surface layer and a graded penetration zone in the outer portion of the substrate. The surface-layer microstructure was multiphase and ranged from reaction-sintered structures of sintered B4C particles in an eutectic-formed matrix to that of hypereutectic carbon particles in a B4C-C eutectic matrix. Because of high surface energy, the coating generally developed a nonuniform thickness. Quantitative evaluations of the coating were performed with limiters in the TEXTOR fusion device and with coupons in electron beam tests. Test results revealed the following: good adherence of the coating even after remelting; and, during remelting, diagnostics detected a corresponding interaction of boron with the plasma. DOE

N95-20578 Army Research Lab., Watertown, MA. Materials Directorate.

THE 29TH MIL-HDBK-17 POLYMER MATRIX COMPOSITES COORDINATION GROUP MEETING

31 Mar. 1994 162 p Meeting held in Monterey, CA, 29-31 Mar. 1994 Limited Reproducibility: More than 20% of this document may be affected by microfiche quality
(AD-A279917) Avail: CASI HC A08

This article relates the meeting minutes and workgroup sessions during the 29th Military Handbook-17 Polymer Matrix Composites Coordination Meeting. Various composites and structures were discussed, along with guidelines, materials available and processes, testing, and statistics reported. CASI

N95-20580 Pennsylvania State Univ., University Park, PA. Dept. of Chemistry.

WATER-SOLUBLE POLYPHOSPHAZENES AND THEIR HYDROGELS

Harry R. Allcock 18 May 1994 53 p Limited Reproducibility: More than 20% of this document may be affected by microfiche quality
(Contract N00014-91-J-1194)
(AD-A279695; TR-20) Avail: Issuing Activity (Defense Technical Information Center (DTIC))

Water-soluble polymers and hydrogels are important in areas as varied as biomedicine adhesion, membranes, and viscosity enhancement. They are possible replacements in technology and medicine for many naturally-occurring polymers. Unfortunately, relatively few of the hundreds of known synthetic polymers are soluble in water. Thus, the design and synthesis of new water-soluble polymers or hydrogels is a subject of considerable interest. This chapter is a review of an approach to this problem. DTIC

N95-20582 Massachusetts Inst. of Tech., Cambridge, MA. Dept. of Chemical Engineering.

MORPHOLOGY OF HIGHLY TEXTURED E/EP DIBLOCK COPOLYMERS

P. Kofinas and R. E. Cohen 26 May 1994 35 p Limited Reproducibility: More than 20% of this document may be affected by microfiche quality
(Contract N00014-91-J-1045)
(AD-A279813) Avail: Issuing Activity (Defense Technical Information Center (DTIC))

A series of semicrystalline triblock copolymers E/EP/E, of poly(ethylene) (E) and poly(ethylene-propylene) (EP) were subjected to high levels of plane strain compression using a channel die. The processing was carried out at 150 C, a temperature which lies well above both the E block melting points (99-103 C) and the quiescent order-disorder transitions (ca. 106 C) for these samples. The lamellar orientation relative to the specimen boundaries was determined using two dimensional small-angle X-ray scattering. Using a 2.4 MPa applied stress on the channel die, the lamellae orient parallel to the plane of shear, while processing at an applied stress of 8.0 MPa causes the lamellae to orient perpendicular to the plane of shear. Gas permeability coefficients P for He and carbon dioxide were measured at 25 C for E/EP/E 25/50/25 specimens and compared to modeling predictions. The upper bound (lamellae aligned in parallel with respect to the permeation direction) and lower bound (series lamellar alignment) models were compared to experimental permeation data on the corresponding oriented triblock specimens. DTIC

N95-20596 Michigan Molecular Inst., Midland, MI.
EFFECT OF EXTERNAL STRESS ON THE TRANSPORT OF FLUIDS IN THERMOPLASTIC RESIN SYSTEMS Final Report, 1 Mar. 1993 - 28 Feb. 1994
Clarence T. Wolf Apr. 1994 89 p Limited Reproducibility: More than 20% of this document may be affected by microfiche quality
(Contract F49620-93-1-0196)
(AD-A279993; AFOSR-94-0314TR) Avail: Issuing Activity (Defense Technical Information Center (DTIC))

The transport properties of liquid penetrants into the thermoplastic resin, poly aryl ether ether ketone (PEEK) were investigated. The primary objective of this work was to study the effect of external applied stress on the diffusion and solubility/swelling of fluids with PEEK. The solubility and rate of penetration, i.e., diffusion, into the resin system are greatly increased by the application of stress: we call this phenomenon SEDS (stress enhanced diffusion and solubility/swelling). All eight fluids studied, benzene, toluene, methylene chloride, chloroform, carbon disulfide, methanol, acetone, and even water exhibit SEDS. The effect is particularly striking for crystalline PEEK where the solubility is markedly increased and the time to reach saturation, i.e., the induction period is reduced when the applied stress exceeds a critical value. For example, at 22 C the solubility of toluene into 29% crystalline PEEK increases from 9 wt% to almost 40 wt% upon the application of a tensile stress of 35 MPa. Furthermore, the time for 0.25 mm thick crystalline PEEK film to reach its saturation value was reduced from 1000's of hours to less than 10 hours. DTIC

N95-20603 Naval Command, Control and Ocean Surveillance Center, San Diego, CA. Research, Development, Test and Evaluation Div.
STRUCTURAL PERFORMANCE OF CYLINDRICAL PRESSURE HOUSINGS OF DIFFERENT CERAMIC COMPOSITIONS UNDER EXTERNAL PRESSURE LOADING. PART 1: ISOSTATICALLY PRESSED ALUMINA CERAMIC Final Report
R. P. Johnson, R. R. Kurkchubasche, and J. D. Stachiw Aug. 1993 99 p Limited Reproducibility: More than 20% of this document may be affected by microfiche quality
(AD-A279669; NCCOSC/RDT/E-TR-1590-Pt-1) Avail: Issuing Activity (Defense Technical Information Center (DTIC))

Ten monocoque cylinders, 18-inches (length) by 12-inches (outer diameter, OD) by 0.412 inches (thickness), fabricated from 96-percent alumina ceramic were assembled into external pressure housings and experimentally evaluated under short-term, static, and cyclic pressure loadings. This study was undertaken as part of a program to promote the application of ceramics to large external pressure housings for underwater vehicles. Pressure testing was performed to generate structural performance data that could be used to establish design criteria for external pressure housings constructed by using 96-percent alumina ceramic as the primary hull material. Design curves for 96-percent alumina-ceramic housings are presented that relate the maximum number of operational dive cycles to the maximum allowable stresses in the ceramic housing during each dive cycle. The 96-percent alumina ceramic has been found to be a reliable structural material for the fabrication of cylindrical external pressure housings with a minimum fatigue life of 1,000 dive cycles to nominal design stresses of - 160,000 psi in the hoop direction. DTIC

N95-20664# American Ceramic Society, Westerville, OH.
FERROIC MATERIALS: DESIGN, PREPARATION AND CHARACTERISTICS. CERAMIC TRANSACTIONS, VOLUME 43
A. S. Bhalla, K. M. Nair, I. K. Lloyd, H. Yanagida, and D. A. Payne 10 Nov. 1993 437 p Symposium held in Honolulu, HI, 7-10 Nov. 1993
(Contract N00014-93-1-0366)
(AD-A285937) Avail: CASI HC A19/MF A04

Ferroic materials have found application in both sensing and actuating devices such as detectors, high- and low-frequency transducers, capacitors, optical modulators, shutters, and photorestrictive and electrostrictive devices. The application areas of ferroics in single-crystal, bulk ceramics, thin-film, and composite forms have been expanding quite rapidly in recent years. As a result, new materials design and fabrication techniques are needed to satisfy the new emerging applications of these 'smart' materials and structures. With the drive of new national and international initiatives in the areas of advanced materials and technology, smart structures and systems, environmental benefication programs, etc., it is highly desirable to review and project the direction in materials design, preparation, and sensing properties. DTIC

N95-20671 Pennsylvania State Univ., University Park, PA. Dept. of Chemistry.
INORGANIC-ORGANIC POLYMERS AND THEIR ROLE IN MATERIALS SCIENCE
Harry L. Allcock 18 May 1994 39 p Limited Reproducibility: More than 20% of this document may be affected by microfiche quality
(Contract N00014-91-J-1194)
(AD-A279715; TR-19) Avail: Issuing Activity (Defense Technical Information Center (DTIC))

The design and synthesis of new materials are two of the key steps in the advancement of technology. Significant advances in nearly all fields of advanced technology depend almost completely on the rate at which useful new materials can be devised and synthesized. One of the most promising approaches to the development of new materials that combine the advantages of organic polymers with those of inorganic solids is to devise polymers that have a backbone of inorganic atoms to which are attached organic or organometallic groups. Some inorganic-organic polymer systems are discussed. DTIC

N95-20680# Georgia Inst. of Tech., Atlanta, GA. School of Chemistry and Biochemistry.
THE ORGANIC CHEMISTRY OF CONDUCTING POLYMERS
L. M. Tolbert 19 Aug. 1994 16 p
(Contract DE-FG05-85ER-45194)
(DE94-018216; DOE/ER-45194/2) Avail: CASI HC A03/MF A01

This paper is divided into: solitons in a box (polyacetylene), cyanines as molecular switches/beyond the cyanine limit, low band-gap heteropolymers, 'dimeric' and 'trimeric monomers', and electrically conductive polymeric interconnects. DOE

N95-20689 Applied Data Research, Inc., New York, NY.
AEROSOL-ASSISTED CHEMICAL VAPOR DEPOSITION OF COPPER: A LIQUID DELIVERY APPROACH TO METAL THIN FILMS
Thomas S. Corbitt, Mark J. Hampden-Smith, T. T. Kodas, and C. Roger 6 May 1994 14 p Limited Reproducibility: More than 20% of this document may be affected by microfiche quality
(Contract N00014-91-J-1258)
(AD-A279702; TR-12) Avail: Issuing Activity (Defense Technical Information Center (DTIC))

Aerosol-Assisted Chemical Vapor Deposition (AACVD) has been used to attain high deposition rates (1000 A/min, up to 800 A/min at 140 C) of Cu films at low temperatures (120-200 C) from toluene solutions of (hfac)Cu(1,5-COD) in a warm-wall reactor. The films are crystalline and exhibit resistivities close to bulk (1.7-3.5 micro omega cm). Activation energies calculated from the deposition rate as a function of the preheating temperature and the substrate temperature (varying also the nozzle-substrate distance) were 6.8, 8.9 (0.7 cm) and 9.1 (1.7 cm) kcal/mol, respectively. DTIC

N95-20694*# National Aeronautics and Space Administration. Marshall Space Flight Center, Huntsville, AL.
GUIDELINES FOR QUALIFYING CLEANING AND VERIFICATION MATERIALS
D. Webb Washington Jan. 1995 9 p
(NASA-TM-108474; NAS 1.15:108474) Avail: CASI HC A02/MF A01

This document is intended to provide guidance in identifying technical issues which must be addressed in a comprehensive qualification plan for materials used in cleaning and cleanliness verification processes. Information presented herein is intended to facilitate development of a definitive checklist that should address all pertinent materials issues when down selecting a cleaning/verification media. Author

N95-20700# Oak Ridge National Lab., TN.

EFFECT OF FIBER FABRIC ORIENTATION ON THE MONOTONIC AND FATIGUE BEHAVIOR OF A CONTINUOUS FIBER CERAMIC COMPOSITE

N. Chawla (Tennessee Univ., Knoxville, TN.), P. K. Liaw (Tennessee Univ., Knoxville, TN.), E. Lara-Curzio, R. A. Lowden, and M. K. Ferber 1994 16 p Presented at the The Metallurgical Society (TMS) Conference on High Performance Composites, Rosemont, IL, 10-15 Oct. 1994
(Contract DE-AC05-84OR-21400)
(DE94-018121; CONF-9410184-1) Avail: CASI HC A03/MF A01

The monotonic fast fracture and fatigue behavior of a Nextel(trademark) 312 reinforced SiC matrix composite was investigated. Effect of fabric orientation with respect to the loading axis on the monotonic and fatigue behavior of the composite was examined. Two geometries were investigated: transverse, where fiber fabric is perpendicular to loading direction; and edge-on where the fabric is parallel to the loading axis. The edge-on geometry showed higher flexure strengths than the transverse orientation. The different deformation mechanisms between the edge-on and transverse orientations were due to strong in-plane shearing of the fiber fabric and weak interlaminar shear of the plies, respectively. In cyclic fatigue, stress versus cycles (S-N) curves showed high fatigue endurance limits in both orientations, although the transverse orientation survived more cycles than the edge-on orientation at stresses slightly above the endurance limit. DOE

N95-20704# Oak Ridge National Lab., TN.

APPROACHES TO THE DESIGN OF STRUCTURAL CERAMICS INCORPORATING WHISKERS AND PARTICULATE PHASES

P. F. Becher, H. T. Lin, C. H. Hsueh, K. B. Alexander, W. H. Warwick, and S. B. Waters 1994 4 p Presented at the 3d Conference on Ceramic-Ceramic Composites, Mons, Belgium, 18-20 Oct. 1994
(Contract DE-AC05-84OR-21400)
(DE94-018126; CONF-941059-1) Avail: CASI HC A01/MF A01

Advances in the technologically and commercially important areas of energy production and conversion, transportation, chemical processing, manufacturing, electronics, and communications are predicted upon the development of materials with greatly improved performance. Many of these components will be exposed to tensile stresses, and possibly quite high temperatures, which will require that the materials be designed to (1) achieve greater fracture resistance, (2) resist deformation at elevated temperatures, and (3) achieve the main component function. Here, theoretical modeling and observations of crack propagation in ceramics and composites are combined to identify and characterize mechanisms that contribute to fracture resistance and strength. Materials processing studies can then be employed to (1) develop the microstructural features suggested by the models and (2) understand the mechanisms involved in the generation of such microstructures. In this paper, the authors address how these various aspects can be used to enhance the mechanical performance of zirconia toughened ceramics (specifically involving transformation toughening) and whisker-reinforced ceramics with comments on other composites incorporating other discontinuous phases. DOE

N95-20709 Pennsylvania State Univ., University Park, PA. Dept. of Chemistry.

CROSS-LINKING REACTIONS FOR THE CONVERSION OF POLYPHOSPHAZENES INTO USEFUL MATERIALS

Harry R. Allcock 18 May 1994 98 p Limited Reproducibility: More than 20% of this document may be affected by microfiche quality
(Contract N00014-91-J-1194)
(AD-A279696; TR-23) Avail: Issuing Activity (Defense Technical Information Center (DTIC))

The conversion of phosphazene high polymers to useful materials depends on the development of methods to cross-link the macromolecular chains. A number of cross-linking routes have been used, including chemical, photochemical, and high energy radiation techniques. The relationship of the cross-linking processes to electrochemical-, electrooptical-, elastomer-, structural-, membrane-, surface-, and biomedical properties is discussed. DTIC

N95-20761# Oak Ridge National Lab., TN.

MATERIALS PROCESSING USING A VARIABLE FREQUENCY MICROWAVE FURNACE

R. J. Lauf, D. W. Bible, S. R. Maddox, C. A. Everleigh (Microwave Labs., Inc., Raleigh, NC.), R. J. Espinosa (Microwave Labs., Inc., Raleigh, NC.), and A. C. Johnson (Microwave Labs., Inc., Raleigh, NC.) 1993 9 p Presented at the 95th Annual Meeting of the American Ceramic Society, Cincinnati, OH, 18-22 Apr. 1993
(Contract DE-AC05-84OR-21400)
(DE95-001420; CONF-930438-33) Avail: CASI HC A02/MF A01

We describe a materials processing system that uses a high power traveling wave tube (TWT) as the microwave source. The TWT provides approximately one octave bandwidth and variable power levels up to 2 kW into a multimode cavity. By controlling the frequency, efficient coupling to the load can be maintained even as the load's dielectric properties change. Alternatively, frequency sweeping can be used as a means of mode stirring at rates far beyond those attainable through mechanical stirring. The system has been tested for sintering alumina ceramics, annealing a tungsten penetrator alloy, curing epoxy resin, and depositing diamond films from a microwave plasma. DOE

N95-20788# Sandia National Labs., Albuquerque, NM.

THE NUMERICAL INTEGRATION AND 3-D FINITE ELEMENT FORMULATION OF A VISCOELASTIC MODEL OF GLASS

R. S. Chambers Aug. 1994 66 p
(Contract DE-AC04-94AL-85000)
(DE95-002588; SAND-94-1607) Avail: CASI HC A04/MF A01

The use of glasses is widespread in making hermetic, insulating seals for many electronic components. Flat panel displays and fiber optic connectors are other products utilizing glass as a structural element. When glass is cooled from sealing temperatures, residual stresses are generated due to mismatches in thermal shrinkage created by the dissimilar material properties of the adjoining materials. Because glass is such a brittle material at room temperature, tensile residual stresses must be kept small to ensure durability and avoid cracking. Although production designs and the required manufacturing process development can be deduced empirically, this is an expensive and time consuming process that does not necessarily lead to an optimal design. Agile manufacturing demands that analyses be used to reduce development costs and schedules by providing insight and guiding the design process through the development cycle. To make these gains, however, viscoelastic models of glass must be available along with the right tool to use them. A viscoelastic model of glass can be used to simulate the stress and volume relaxation that occurs at elevated temperatures as the molecular structure of the glass seeks to equilibrate to the state of the supercooled liquid. The substance of the numerical treatment needed to support the implementation of the model in a 3-D finite element program is presented herein. An accurate second-order, central difference integrator is proposed for the constitutive equations, and numerical solutions are compared to those obtained with other integrators. Inherent convergence problems are reviewed and fixes are described. The resulting algorithms are generally applicable to the broad class of viscoelastic material models. First-order error estimates are used as a basis for developing a scheme for automatic time step controls, and several demonstration problems are presented to illustrate the performance of the methodology. DOE

N95-20815# Northeastern Univ., Boston, MA.

NOVEL REAGENTS FOR CHEMICAL VAPOR DEPOSITION OF INTERMETALLIC ALLOYS Final Report, Apr. 1991 - Aug. 1994

Rein U. Kirss 31 Oct. 1994 11 p
(Grant AF-AFOSR-0207-91)
(AD-A286562; AFOSR-94-0723TR) Avail: CASI HC A03/MF A01

Reactions of Hf(CH2SiMe3)4 with AlMe3 were proceeded by formation of covalently bonded heterobimetallic intermediates with no alkyl exchange. Reaction with A1H3.NMe3 yielded A1(Ch2SiMe3)3.NMe3 and 'Hf(CH2SiMe3)H3'. Carbon blocks coated with this mixture produced a HfAlC2 coating which was effective in protecting the substrate from air oxidation at high temperatures. DTIC

N95-20821# Oak Ridge National Lab., TN.

FABRICATION OF CERAMIC COMPOSITES: FORCED CVI

T. M. Besmann, J. C. McLaughin, and Hua-Tay Lin 1994 15 p Presented at the 96th Annual Meeting of the American Ceramic Society, Indianapolis, IN, 24-28 Apr. 1994

(Contract DE-AC05-84OR-21400)
(DE95-001076; CONF-940416-30) Avail: CASI HC A03/MF A01

Forced chemical vapor infiltration (CVI) is being developed as an efficient means for producing thick-wall ceramic matrix components. Recent efforts focussed on process scale-up, modeling and the properties of the resultant material. Disks 24.6 cm in diameter and 1.27 cm thick have been produced. Composites of Nicalon(trademark) fibers and SiC matrix have exhibited 480 MPa strength in flexure. DOE

N95-20856# Fraunhofer-Gesellschaft zur Foerderung der Angewandten Forschung e.V., Munich (Germany).
EXPERIMENTAL INVESTIGATION OF WAVE AND FRACTURE PHENOMENA IN IMPACTED CERAMICS Final Report
E. Strassburger and H. Senf Jun. 1994 55 p
(Contract DAJA45-90-C-0053)
(AD-A286589; R/D-6472-MS-01) Avail: CASI HC A04/MF A01

Four types of glass which differ in their chemical composition, hardness and material density and tiles of SiC, TiB2, and Al2O3 were impacted edge-on with blunt steel projectiles at striking velocities between 20 m/s and 1000 m/s. The propagation of shock waves, of primary and secondary cracks and crack systems and the growing of crack systems from nucleated centers were visualized by means of a Cranz-Schardin high-speed camera within the first twenty microseconds, before the projectile penetrated the target more than a few millimeters. The concept of damage velocity was introduced to describe the different damage processes quantitatively. All four types of glass reveal a similar behavior. The damage velocity equals terminal crack velocity at low loadings. Other than in glass, in the ceramics different types of cracks are generated and different fracture velocities were observed at one impact velocity of continuously growing cracks, including the secondary cracks with sharp edges, fuzzy crack traces and crack fronts. In each of the ceramics the damage velocity increases with increasing striking velocity and approaches the longitudinal wave velocity at high loadings. A terminal crack velocity was found for one type of fracture in SiC. Ceramographical investigations of TiB2 fragments have shown that cracks within large grains as well as intercrystalline cracks are generated by coalescence of voids. DTIC

N95-20889# Sandia National Labs., Albuquerque, NM. Chemical Processing Sciences.
CHARACTERIZATION AND ELECTRICAL PROPERTIES OF COPPER FILMS GROWN VIA DIRECT LIQUID COINJECTION OF (hfac)Cu(TMVS) AND TMVS
John E. Parmeter, Gary A. Petersn, Christopher A. Apblett, and Paul Martin Smith Oct. 1994 30 p
(Contract DE-AC04-94AL-85000)
(DE95-002957; SAND-94-1716) Avail: CASI HC A03/MF A01

This report documents the characterization of thin copper films grown at Sandia as part of on-going research in copper CVD involving Sandia and Schumacher, Inc. The films have been grown using the copper (1) CVD precursor (hfac)Cu(TMVS), which was first developed by Schumacher and has been supplied to Sandia by that company. The CVD was performed using a novel technique in which direct liquid coinjection of (hfac)Cu(TMVS) and TMVS (trimethylvinylsilane) into a commercial reactor is utilized. Films were deposited onto silicon nitride substrates at temperatures in the range of 220C-250C, with growth rates in the range of 400A-800A/min. These films have been analyzed by a variety of techniques, with an emphasis on factors that may influence the resistivity, including thickness, purity, density, grain size, and stress. The authors show that these films have as-deposited resistivities of 1.86 +/- 0.1 microohm-cm, or 1.82 +/- 0.1 microohm-cm after accounting for surface scattering effects. The latter value is only 0.14 microohm-cm above the value for high purity bulk copper. The authors discuss factors that may account for this residual resistivity. They also discuss the effects of film surface roughness on film thickness and resistivity measurements, noting some potential problems associated with the commonly used surface profilometry technique. These results help to establish (hfac)Cu(TMVS) as one of the most promising available copper CVD precursors for metallization applications. DOE

N95-20892# Lawrence Livermore National Lab., Livermore, CA.
SPUTTER DEPOSITION OF MULTILAYER THERMOELECTRIC FILMS: AN APPROACH TO THE FABRICATION OF TWO-DIMENSIONAL QUANTUM WELLS
J. C. Farmer, T. W. Barbee, Jr., G. C. Chapline, Jr., R. J. Foreman, L. J. Summers, M. S. Dresselhaus (Massachusetts Inst. of Tech., Cambridge, MA.), and L. D. Hicks (Massachusetts Inst. of Tech., Cambridge, MA.) Jul. 1994 11 p Presented at the 13th International Conference on Thermoelectrics, Kansas City, MO, 30 Aug. - 1 Sep. 1994
(Contract W-7405-eng-48)
(DE95-002396; UCRL-JC-117602; CONF-940830-2) Avail: CASI HC A03/MF A01

The relative efficiency of a thermoelectric material is measured in terms of a dimensionless figure of merit, ZT. Though all known thermoelectric materials are believed to have ZT less than or equal to 1, recent theoretical results predict that thermoelectric devices fabricated as two-dimensional quantum wells (2D QW's) or one dimensional (1D) quantum wires could have ZT greater than or equal to 3. Multilayers with the dimensions of 2D QW's have been synthesized by alternately sputtering Bi0.09Sb0.1 and PbTe0.8Se0.2 onto a moving single-crystal sapphire substrate from dual magnetrons. These materials have been used to test the thermoelectric quantum-well concept and gain insight into relevant transport mechanisms. If successful, this research could lead to thermoelectric devices that have efficiencies close to that of an ideal Carnot engine. Ultimately, such devices could be used to replace conventional heat engines and mechanical refrigeration systems. DOE

N95-20894# Brookhaven National Lab., Upton, NY.
INFLUENCE OF OXIDATION ON RADIATION HARDNESS OF SILICON DETECTORS
H. W. Kraner, Z. Li, S. Lazanu (Bucharest Univ., Romania.), U. Biggeri (Florence Univ., Italy.), E. Borchi (Florence Univ., Italy.), and M. Bruzzi (Florence Univ., Italy.) Dec. 1993 9 p Presented at the 1st International Conference on Large Scale Applications and Radiation Hardness of Semiconductor Detectors, Florence, Italy, 7-9 Jul. 1993
(Contract DE-AC02-76CH-00016)
(DE95-002466; BNL-60905; CONF-9307163-4) Avail: CASI HC A02/MF A01

The energy levels induced by fast neutron irradiation in high energy silicon detectors produced by different oxidations are analyzed, utilizing TSC (totally self-checking) measurements and a method of deconvolution of the compound experimental spectrum. Conclusions are drawn regarding the influence of the temperature and ambient during oxidation on their radiation hardness. DOE

N95-20895# Sandia National Labs., Livermore, CA.
ENHANCEMENTS IN THE LIVERMORE SPECTRUM ANALYSIS PACKAGE PIXEF
A. J. Antolak, M. L. Hildner, and G. S. Bench (Lawrence Livermore National Lab., Livermore, CA.) 1994 10 p Presented at the Conference on Application of Accelerators in Research and Industry, Denton, TX, 7-10 Nov. 1994
(Contracts DE-AC04-94AL-85000; W-7405-eng-48)
(DE95-002487; SAND-95-8424C; CONF-941129-6) Avail: CASI HC A02/MF A01

A number of enhancements have been incorporated into the Livermore particle-induced x-ray emission (PIXE) spectral fitting program PIXEF (PIXE-Fit) in order to improve our quantitative analysis capability for data collected with Si(Li) detectors. Some of the new features include an improved description for the background which takes into account x-ray absorption effects, a better representation of the line shapes using Voigtian distributions, and a better treatment of peak fitting in regions of poor counting statistics. The implementation of these improvements into PIXEF is described. DOE

N95-20962 Physical Optics Corp., Torrance, CA.
POLYMER BASED ALL-OPTIC RECONFIGURABLE INTERCONNECTS Final Report, 1 Jul. - 31 Dec. 1993
Tomasz Jannson 28 Feb. 1994 45 p Limited Reproducibility: More than 20% of this document may be affected by microfiche quality
(Contract F49620-93-C-0046)
(AD-A279976; AFOSR-94-0313TR) Avail: CASI HC A03

In Phase 1 of this project, POC successfully implemented a prototype all-optic reconfigurable polymer-based crossbar switch. POC's all-optic reconfigurable polymer-based crossbar switch represents a unique combination of polymer techniques, simple geometry optics, and waveguide technology. These three essential technologies are original POC developments. POC's crossbar switch will provide reconfigurability, large fan-out, and radiation hardening. This is a new technology for both parallel and distributed processing and communication networks. The Phase 1 results have shown that POC's crossbar switch can offer a number of important advantages not achievable by either electronic interconnects or currently existing all-optic reconfigurable interconnects. These advantages include: (1) very low power sources (-100 mW); (2) relatively high interconnect reconfigurability time; (3) high data rates over 1 Gb/sec; (4) low bit error rate (less than 10(exp -10)); (5) very large fan-out capability (less than 1000 channels); (6) very low manufacturing cost; and (7) very high erasability. It is expected that POC's crossbar switch performance will be superior to existing electronic and optical interconnection approaches. In Phase 1, POC also demonstrated the feasibility of commercialization in the area of multimedia, video conferencing, and other communication applications. DTIC

N95-20976 Technische Univ., Delft (Netherlands). Dept. of Mechanical Engineering and Marine Technology.

MICROMECHANICAL APPROACH TO TRANSFORMATION TOUGHENING IN CERAMICS Ph.D. Thesis

G. Stam 12 Sep. 1994 61 p Limited Reproducibility: More than 20% of this document may be affected by microfiche quality
(PB95-135422; ISBN-90-370-0106-8) Avail: CASI HC A04

In the thesis, the authors have presented numerical studies of transient crack growth in ceramic composites exhibiting transformation-plasticity based on the recent model of Sun et al. (1991) that includes the effect of transformation-induced dilatation as well as shear. The authors' analyses supplement those of Hom and McMeeking (1990) who considered only dilatational transformations. The finite element results obtained here with the Sun et al. (1991) model show a very significant influence of the transformation shear strains on the transformation zone size and shape, as well as on the toughness development during crack growth. An increasing influence of the shear effect, as governed in the model by the parameter h(sub 0), roughly speaking, leads to larger and more diffuse transformation zones. The increase of toughness with increasing value of h(sub 0) has been found to be quite substantial as compared with the toughness increase that is obtained by purely dilatational transformation only. For values of h(sub 0) between 1 and 1.5, which are representative for ZrO2 composites, the authors have found increases in toughness that are 4 to 8 times larger than without transformation-induced shear strains. Since, so far, dilatant transformation-based theory has underestimated the toughness enhancement found in experiments, the present results with transformation-induced shear effects contribute to explaining this difference. NTIS

N95-20978 Pittsburgh Univ., Pittsburgh, PA. Dept. of Chemistry.

MACROMOLECULAR AND MATERIALS DESIGN USING POLYPHOSPHAZENES

Harry R. Allcock 18 May 1994 27 p Limited Reproducibility: More than 20% of this document may be affected by microfiche quality
(Contract N00014-91-J-1194)
(AD-A279781; TR-22) Avail: CASI HC A03

Polyphosphazenes are among the most versatile of all polymers. This is a consequence of the unique properties of the phosphorus-nitrogen backbone and the ease with which a wide range of different side groups can be introduced mainly by macromolecular substitution, but also by the polymerization of different monomers. This field has reached a stage where the fundamental chemistry now allows the design and synthesis of a broad range of new materials that are valuable for properties such as elasticity, high refractive index, liquid crystallinity, ferroelectric-, NLO-, and photochromic attributes, and for uses as solid ionic conductors, biomedical microencapsulation polymers, and materials with controlled surface properties. DTIC

N95-21000# Army Research Lab., Fort Belvoir, VA.

VOC COMPLIANT WASH PRIMER Progress Report, Oct. 1993 - Sep. 1994

Kestutis G. Chesonis and Christopher E. Miller Sep. 1994 10 p
(AD-A286034; ARL-MR-190) Avail: CASI HC A02/MF A01

DOD-P-15328 Wash Primer is a unique coating that passivates metal surfaces against corrosion and enhances adhesion of primers/topcoats. However, the chromate and high solvent content subject it to strict EPA regulations. This report evaluated a waterborne substitute with the desired properties. Laboratory evaluations revealed a film softening effect when topcoated with solvent type epoxy primers due to trapped solvents in the wash primer. DTIC

N95-21011# Harvard Univ., Cambridge, MA.

MICROBIAL DEGRADATION OF POLYMERS USED IN ELECTRONICS Annual Report

Ralph Mitchell Oct. 1994 4 p
(Contract F49620-92-J-0254)
(AD-A286526; AFOSR-94-0724TR) Avail: CASI HC A01/MF A01

In a continuation of our work on the biodegradation of polyurethane we are identifying and classifying new organisms isolated from enrichment cultures of polyurethane-contaminated soil from disposal sites. During the past year we have isolated in pure culture a number of bacteria and fungi capable of degrading polyurethane. We are in the process of identifying these microorganisms. DTIC

N95-21014# McDonnell-Douglas Aerospace, Saint Louis, MO.

CONDUCTING THERMOSET POLYMERS Annual Technical Report, 1 Oct. 1993 - 30 Sep. 1994

I. M. Brown, D. J. Leopold, and T. C. Sandreczki 20 Oct. 1994 44 p
(Contract F49620-92-C-0074)
(AD-A286541; MDC-94X0025; AFOSR-94-0711TR) Avail: CASI HC A03/MF A01

Continuing efforts to develop conducting thermoset polymers in which the Pi-conjugation extends along the backbone and through the crosslink are described. Acetylene terminated Schiff bases, acetylene-terminated polythiophenes and acetylene-terminated polyanilines are being investigated. Two different approaches to get these thermosets conducting are being pursued: in the AT-Schiff bases and AT-polythiophenes the monomers are first cured then doped with iodine, whereas in the AT-polyanilines the oligomers are first doped with protonic acids then cured. Electron spin resonance, photoluminescence and photo-absorption data suggest that polarons can form in the doped and undoped forms of the AT-Schiff bases and AT-polythiophenes. The dependences of the ESR lineshape parameters of the AT-Schiff bases and amine-cured epoxies on iodine content can be explained in terms of a model involving equilibria between polymeric radical cation complexes containing different stoichiometric amounts of iodine. Several AT-polyanilines oligomers containing either alkoxy substituents or meta substitution in the backbones were synthesized in order to improve the possibility of thermosets. These oligomers were doped with different organic acids. The maximum conductivity value measured was 2 x 10 (exp -2) S/cm. DTIC

N95-21152# Lehigh Univ., Bethlehem, PA. Dept. of Materials Science and Engineering.

MICROSTRUCTURAL DESIGN FOR TOUGH CERAMICS Final Report

Helen M. Chan and Brian R. Lawn Oct. 1994 144 p
(Contract F49620-92-J-0039)
(AD-A285634; AFOSR-94-0652TR) Avail: CASI HC A07/MF A02

Results of a program on the influence of microstructure on the toughness and fatigue properties of ceramics are presented. A theoretical analysis of toughness-curve behavior in two-phase ceramics has been completed. This analysis identifies particle size, volume fraction, and internal thermal expansion anisotropy stress as key microstructural variables in the toughness response. A simple contact fatigue methodology for investigating the accumulation of damage at stress concentrations in tough ceramics, using the Hertzian indentation test in cyclic loading, has been developed. This methodology offers several advantages over traditional long-crack fatigue testing, and relates directly to the stress states that occur in contact bearings. Optical and acoustic emission tests reveal fundamental departures from the classic cone fractures that form in homogeneous brittle materials. Instead, a new kind of damage, shear-initiated microfractures in a distributed zone directly beneath the contact area is observed. The damage thereby occurs in the short-crack region, and is most severe in those ceramics that show the highest long-crack toughness, underlying the need for compromise in materials design. The results bear strongly on such practical properties as bearing fatigue, and strength, wear and erosion of structural ceramics. DTIC

N95-21154 Department of the Navy, Washington, DC.
POLYURETHANE SELF-PRIMING TOPCOATS Patent Application
Charles R. Hegedus, inventor (to Navy), Donald J. Hirst, inventor (to Navy), and Anthony T. Eng, inventor (to Navy) 7 Mar. 1994 23 p Limited Reproducibility: More than 20% of this document may be affected by microfiche quality
(AD-D016204; US-Patent-Appl-SN-207445) Avail: Issuing Activity (Defense Technical Information Center (DTIC))

A corrosion-resistant polyurethane coating for application directly to a surface as self-priming topcoat comprising major amount of a polyurethane binder and minor amount of a combination of pigments consisting essentially of an aluminum phosphate, zinc salts of benzoic acids, and an alkaline earth metal phosphate such as zinc-barium phosphate. In addition, the coating contains up to about 30 parts by weight of a titanium dioxide pigment, up to about 2.0 parts by weight of an oil soluble surface active agent and up to about 50 parts by weight of at least one organic solvent. DTIC

N95-21155 Department of the Navy, Washington, DC.
POLYURETHANE SELF-PRIMING TOPCOATS Patent Application
Charles R. Hegedus, inventor (to Navy), Donald J. Hirst, inventor (to Navy), and Anthony T. Eng, inventor (to Navy) 14 May 1993 26 p Limited Reproducibility: More than 20% of this document may be affected by microfiche quality
(AD-D016205; US-Patent-Appl-SN-062864) Avail: Issuing Activity (Defense Technical Information Center (DTIC))

A corrosion-resistant coating which can be applied directly to a surface as a self-priming topcoat comprising a polyurethane resin binder and a combination of pigments consisting essentially of a molybdate-modified zinc phosphate, zinc salts of benzoic acids, and an alkaline earth metal phosphate such as zinc-barium phosphate. In addition, the coating contains up to about 35 parts by weight of a titanium dioxide pigment, up to about 3.0 parts by weight of an oil soluble dispersant agent and, up to about 50 parts by weight of at least one organic solvent. DTIC

N95-21175# Lawrence Livermore National Lab., Livermore, CA.
BERYLLIUM BASED MULTILAYERS FOR NORMAL INCIDENCE EXTREME ULTRAVIOLET REFLECTIVITY
K. M. Skulina, C. Alford, R. M. Bionta, D. M. Makowiecki, J. Kortright (California Univ., Berkeley. Lawrence Berkeley Lab, CA.), R. Soufli (California Univ., Berkeley. Lawrence Berkeley Lab, CA.), E. Gullikson (California Univ., Berkeley. Lawrence Berkeley Lab, CA.), and J. Underwood (California Univ., Berkeley. Lawrence Berkeley Lab, CA.) 26 May 1994 6 p Presented at the Optical Society of America Conference on Extreme Ultraviolet Lithography, Monterey, CA, 19-21 Sep. 1994 Submitted for publication
(Contracts W-7405-eng-48; DE-AC03-76SF-00098)
(DE94-015560; UCRL-JC-117440; CONF-9409177-1) Avail: CASI HC A02/MF A01

The need for normal incidence mirrors maintaining reflectivity greater than 60% for an industrially competitive Extreme Ultraviolet Lithography (EUV) system has been well documented. The Molybdenum/Silicon system has emerged as the de-facto standard, where researchers are now routinely fabricating mirrors demonstrating 63% reflectivity near 130 Angstroms. However, multilayer mirrors using beryllium as the low atomic number (low-Z) spacer could potentially show similar or better reflectivity, and operate at wavelengths down to the beryllium K-edge at 111 Angstroms. Besides offering potentially greater reflectivity, the shorter wavelength light offers increased dissolution depth in photoresists, and offers potentially better resolution and depth of focus. We will report our latest results from beryllium based multilayers. The mirrors were fabricated at the Lawrence Livermore National Laboratory (LLNL) and tested at the Center for X-Ray Optics at Lawrence Berkeley Laboratory (CXRO/LBL). DOE

N95-21234# State Univ. of East Texas, Commerce, TX. Dept. of Chemistry.
AN INVESTIGATION OF THE APPLICABILITY OF THE NEW ION EXCHANGE RESIN, REILLEX(TM)-HPQ, IN ATW SEPARATIONS
Milestone 4 Final Report
Kenneth R. Ashley, Jason Ball, Melissa Grissom, Michelle Williamson, Stephen Cobb, Daniel Young, and Yen-Yuan James Wu 7 Sep. 1993 156 p Sponsored by DOE
(DE94-016576; LA-SUB-94-106) Avail: CASI HC A08/MF A02

The investigations with the anion exchange resin Reillex(TM)-HPQ is continuing along several different paths. The topics of current investigations that are reported here are: (1) The sorption behavior of chromium(6) on Teillex(TM)-HPQ from nitric acid solutions and from sodium hydroxide/sodium nitrate solutions; (2) The sorption behavior of F(-) on Reillex(TM)-HPQ resin in acidic sodium nitrate solution; (3) The sorption behavior of Cl(-) on Reillex(TM)-HPQ resin in acidic sodium nitrate solution; (4) The sorption behavior of Br(-) on Reillex(TM)-HPQ resin in acidic sodium nitrate solution; and (5) The Honors Thesis by one of the students (which is attached to Appendix 2). Author (revised)

N95-21252*# National Aeronautics and Space Administration. Lewis Research Center, Cleveland, OH.
FRICTION AND WEAR PROPERTIES OF AS-DEPOSITED AND CARBON ION-IMPLANTED DIAMOND FILMS
Kazuhisa Miyoshi Feb. 1994 26 p Presented at the Fifth International Conference onthe Science of Hard Materials, Maui, Hawaii, 20-24Feb. 1995; sponsored by ICSHM-5 Organizing Committee
(RTOP 505-63-5A)
(NASA-TM-106759; E-9194; NAS 1.15:106759) Avail: CASI HC A03/MF A01

Recent work on the friction and wear properties of as-deposited and carbon ion-implanted diamond films was reviewed. Diamond films were produced by the microwave plasma chemical vapor deposition (CVD) technique. Diamond films with various grain sizes and surface roughnesses were implanted with carbon ions at 60 ke V ion energy, resulting in a dose of 1.2310(exp 17) carbon ions/cm(exp 2). Various analytical techniques, including Raman spectroscopy, proton recoil analysis, Rutherford backscattering, transmission and scanning electron microscopy, x-ray photoelectron spectroscopy, and x-ray diffraction, were utilized to characterize the diamond films. Sliding friction experiments were conducted with a polished natural diamond pin in contact with diamond films in the three environments: humid air (40 percent relative humidity), dry nitrogen (less than 1 percent relative humidity), and ultrahigh vacuum (10(exp -7) Pa). The CVD diamond films indeed have friction and were properties similar to those of natural diamond in the three environments. The as-deposited, fine-grain diamond films can be effectively used as self-lubricating, wear-resistant coatings that have low coefficients of friction (0.02 to 0.04) and low wear rates (10(exp -7) to 10(exp -8)mm(exp 3)/N-m) in both humid air and dry nitrogen. However, they have high coefficients of friction (1.5 to 1.7) and a high wear rate (10(exp -4)mm(exp 3/N-m) in ultrahigh vacuum. The carbon ion implanation produced a thin surficial layer (less than 0.1 micron thick) of amorphous, nondiamond carbon on the diamond films. In humid air and dry nitrogen, the ion-implanted, fine- and coarse-grain diamond films have a low coefficient of friction (around 0.1) and a low wear rate (10(exp -7)mm(exp 3/N-m). Even in ultrahigh vacuum, the presence of the nondiamond carbon layer reduced the coefficient of friction of fine-grain diamond films to 0.1 or lower and the wear rate to 10(exp -6)mm(exp 3)/N-m. Thus, the carbon ion-implanted, fine-grain diamond films can be effectively used as wear-resistant, self-lubricating coatings not only in air and dry nitrogen, but also in ultrahigh vacuum. The wear mechanism of diamond films is that of small fragments chipping off the surface. The size of wear particles is related to the extent of wear rates. Author

N95-21263# California Univ., Berkeley. Lawrence Berkeley Lab, CA.
NONLINEAR OPTICAL STUDIES OF POLYMER INTERFACES
Y. R. Shen Nov. 1993 19 p Presented at the POLIMEX 1993 Symposium, Cuncum Quintana Roo, Mexico, 1-3 Nov. 1993
(Contract DE-AC03-76SF-00098)
(DE94-018199; LBL-35308; CONF-9311234-1) Avail: CASI HC A03/MF A01

Second-order nonlinear optical processes can be used as effective surface probes. They can provide some unique opportunities for studies of polymer interfaces. Here the author describes two examples to illustrate the potential of the techniques. One is on the formation of metal/polymer interfaces. The other is on the alignment of liquid crystal films by mechanically rubbed polymer surfaces. DOE

N95-21272 Office National d'Etudes et de Recherches Aerospatiales, Chatillon (France).

ZIRCONIA PRECIPITATES AND ZIRCONIA: GeO2 INTERPHASE IN MULLITE MATRIX-SIC WOVEN FABRICS COMPOSITES PREPARED THROUGH A SOL-GEL ROUTE

E. Mouchon and P. Colomban 1994 9 p Conference on Composite Materials High Temperature Ceramic Matrix Composites, Bordeaux, France, Sep. 20-24 1993 Prepared in cooperation with Direction des Recherches, Etudes et Techniques, Paris, France
(PB95-133427) Avail: Issuing Activity (National Technical Information Service (NTIS))

This paper presents a preliminary report on the influence of zirconia addition in the matrix or at the SiC fiber/mullite matrix interface. The composites have been prepared by a new route based on the hydrolysis-polycondensation of alkoxides. This method allows us to tailor the microstructure of both matrix and interface. NTIS

N95-21275 National Defence Research Establishment, Stockholm (Sweden).

COMPATIBILITY TESTING OF EXPLOSIVES AND PAINTS BY CHEMILUMINESCENCE TECHNIQUES [FOERENLIGHETSUNDERSOEKNINGAR FOER NAGRA EXPLOSIVAEMNEN OCH FAERGER MED HAELP AV KEMILUMINISCENS OCH MIKROKALORIMETRI]

M. Hihkioe and G. Aqvist Jun. 1994 21 p In SWAHILI
(PB95-133609; FOA-C-20986-2.3) Avail: Issuing Activity (National Technical Information Service (NTIS))

An equipment developed for analysis of propellants using chemilumescence reaction between nitric oxide and ozone has been used. The high sensitivity of the method makes it possible to carry out measurements at temperature close to normal storing conditions. The work is a preliminary study of compatibility testing of explosives and paints by chemiluminescence techniques. Some results were also compared with microcalorimetric measurements. In the study, compatibility tests have been done with TNT, RDX, PETN, single base propellant and paints. The authors have investigated compatibility with paints because they are in direct contact with explosives in ammunition. Paints prevent ammunition from rusting and improve explosives to adhere to the shell. NTIS

N95-21289# Massachusetts Inst. of Tech., Cambridge, MA. Materials Processing Center.

THE FORMATION OF REACTION BONDED SI3N4 AT LOW TEMPERATURES AND IN SHORT TIMES

B. W. Sheldon and J. S. Haggerty 1994 15 p Presented at the 13th Annual Conference on Composites and Advanced Ceramics, Cocoa Beach, FL, 15-18 Jan. 1989
(Contract DE-FG02-87ER-45313)
(DE95-001990; CONF-890130-6) Avail: CASI HC A03/MF A01

The kinetics and mechanisms of nitriding high purity, SiH4 derived Si powders were investigated. TGA, X-ray diffraction, FTIR spectroscopy, and TEM techniques were employed. Complete nitridation (greater than 99%) was achieved at 1250 C in less than 10 minutes, and nearly complete nitridation (97%) was achieved at 1100 C in less than 5 hours. The effects of temperature, particle diameter, and surface chemistry were studied and results show that the process is principally controlled by the number of Si3N4 nuclei that form. Reduced temperature, increased Si particle diameter, and surface contamination all reduce the conversion rate through direct effects on nucleation. DOE

N95-21354# CeraMem Corp., Waltham, MA.

CERAMEM FILTERS FOR REMOVAL OF PARTICLES FROM HOT GAS STREAMS

Bruce A. Bishop and Robert L. Goldsmith 1994 11 p Presented at the Coal-fired Power Systems: Advances in IGCC and PFBC Review Meeting, Morgantown, WV, 21-23 Jun. 1994
(Contract DE-FG02-90ER-80896)
(DE95-001976; DOE/ER-80896/94/C0379; CONF-9406131-63) Avail: CASI HC A03/MF A01

The need for hot gas cleanup in the power, advanced coal conversion, process and incineration industries is well documented and extensive development is being undertaken to develop and demonstrate suitable filtration technologies. In general, process conditions include: (1) oxidizingor reducing atmospheres; (2) temperatures to 1800 F; (3) pressures to 300 psi; and (4) potentially corrosive components in the gas stream. The most developed technologies entail the use of candle or tube filters, which suffer from fragility, lack of oxidation/corrosion resistance, and high cost. The ceramic membrane filter described below offers the potential to eliminate these limitations. DOE

N95-21470# Rijksinstituut voor de Volksgezondheid, Bilthoven (Netherlands).

MONOMER MAPPING: A PC-BASED SOFTWARE TOOL FACILITATING THE DETERMINATION OF MONOMER COMPOSITIONS FROM MASS SPECTROMETRIC MOLECULAR WEIGHT DATA

D. C. vanSetten and G. vandeWerken Apr. 1994 38 p
(PB95-132155; RIVM-343605002) Avail: CASI HC A03/MF A01

A method to establish the monomer composition of (bio)macromolecules has been developed. The method, to be called monomer mapping, involves the mass spectrometric determination of the molecular weight and a computer program. The program generates monomer compositions corresponding to the measured molecular weight. If more than one monomer composition for the polymer is generated by monomer mapping, a further limitation can be obtained from the determination of the number of exchangeable hydrogens. Monomer mapping can be used to determine the monomer compositions of individual components in mixtures without applying (chromatographic) separation techniques. This is a clear advantage over methods involving monomerization and consecutive determination of the relative amounts of monomers. As a limitation, monomer mapping requires the elemental compositions of all monomer types possibly present in the polymer. NTIS

N95-21482# Oak Ridge National Lab., TN.

LEAD-INDIUM PHOSPHATE GLASSES FOR OPTICAL APPLICATIONS

B. C. Sales, L. A. Boatner, and S. W. Allison 1994 8 p Presented at the Annual Meeting of the Society of Photo-Optical Instrumentation Engineers, San Diego, CA, 24-29 Jul. 1994
(Contract DE-AC05-84OR-21400)
(DE94-019333; CONF-940723-29) Avail: CASI HC A02/MF A01

A new glass system based on a range of lead-indium phosphate compositions has been developed. These glasses have a relatively high index of refraction (1.8-1.9) in the visible region and exhibit moderate dispersion (typical Abbe number of 32). The ultraviolet absorption edge occurs near 300 nm and the glasses strongly absorb in the infrared at wavelengths greater than 2,800 nm. The glasses can be prepared at relatively low temperatures (900-1,000 C) and are easily poured at temperatures near 800 C due to their low melt viscosities. Lead-indium phosphate glasses exhibit good chemical durability and resistance to both weathering and intense gamma-irradiation. These materials have a glass transition temperature of 430 C, and thermal expansion coefficients in the range of 11 to 12 x 10(exp -6)/C. The structure of these glasses consists of a distribution of chains of PO4 tetrahedra held together by bonding between the non-bridging oxygen of the tetrahedra and the metal cations. The polyphosphate chain distribution was determined using the technique of high-performance liquid chromatography. The high index of refraction of lead-indium phosphate glasses makes them attractive for several applications such as high-numerical-aperture optical fibers and specialty lenses. Optical fibers up to 60 m in length have been drawn, and several simple lenses have been designed, ground, and polished. Preliminary results on the ability to directly case optical components of lead-indium phosphate glass are also discussed as well as the suitability of these glasses as a host medium for rare-earth ion lasers and amplifiers. DOE

N95-21501# Oak Ridge National Lab., TN.

COMPARISON OF PROPERTIES OF SINTERED AND SINTERED REACTION-BONDED SILICON NITRIDE FABRICATED BY MICROWAVE AND CONVENTIONAL HEATING

T. N. Tiegs, J. O. Kiggans, Jr., H. T. Lin, and C. A. Willkens (Norton Co., Northboro, MA.) 1994 6 p Presented at the Spring Meeting of the Materials Research Society, San Francisco, CA, 4-8 Apr. 1994
(Contract DE-AC05-84OR-21400)
(DE95-001426; CONF-940411-54) Avail: CASI HC A02/MF A01

A comparison of microwave and conventional processing of silicon nitride-based ceramics was performed to identify any differences between the two, such as improved fabrication parameters or increased mechanical properties. Two areas of thermal processing were examined: (1) sintered silicon nitride (SSN) and (2) sintered reaction-bonded silicon nitride (SRBSN). The SSN powder compacts showed improved densification and enhanced grain growth. SRBSN materials were fabricated in the microwave with a one-step process using cost-effective raw materials. The SRBSN materials had properties appropriate for structural applications. Observed increases in fracture toughness for the microwave processed SRBSN materials were attributable to enhanced elongated grain growth. DOE

N95-21572# Pennsylvania State Univ., University Park, PA. Dept. of Materials Science and Engineering.

THE MECHANICAL BEHAVIOR OF SURFACE-MODIFIED CERAMICS

D. J. Green Sep. 1994 9 p
(Contract DE-FG02-86ER-45252)
(DE95-001704; DOE/ER-45252/T6) Avail: CASI HC A02/MF A01

The work in the project was focused on: indentation fracture of ion-exchanged glasses, strength variability of residually stressed brittle materials, fracture of SiC-coated graphite, and subcritical crack growth in stress-free and ion-exchanged glasses. DOE

N95-21585# Stanford Univ., CA. Physics Labs.

A STUDY OF MECHANICAL PROCESSING DAMAGE IN BRITTLE MATERIALS

B. T. Khuri-Yakub 1994 7 p
(Contract DE-FG03-84ER-45157)
(DE95-002126; DOE/ER-45157/T7) Avail: CASI HC A02/MF A01

During the last year, the authors have continued work on the ultrasonic characterization of machining-induced cracks and residual stresses in brittle materials. Techniques for the analysis of cracks and surface residual stress are being developed simultaneously. Finally, an acoustic microscope is being developed for the study of porosity and velocity variations in green ceramics. DOE

N95-21644# Brookhaven National Lab., Upton, NY.

THE DEVELOPMENT OF A NEW PLASTICIZER FOR POLY(ETHYLENE OXIDE) BASED POLYMER ELECTROLYTE AND THE INVESTIGATION OF THEIR ION-PAIR DISSOCIATION EFFECT

X. Q. Yang, H. S. Lee, L. L. Hanson, J. McBreen, and Y. Okamoto (Polytechnic Univ., Brooklyn, NY.) 1994 22 p Presented at the 7th International Meeting on Lithium Batteries, Cambridge, MA, 15-20 May 1994
(Contract DE-AC02-76CH-00016)
(DE94-016821; BNL-60652; CONF-940568-5) Avail: CASI HC A03/MF A01

One approach to increasing the ionic conductivity of polymer electrolyte is to add plasticizers to the polymer-salt complexes. Recently, we have synthesized a new plasticizer, modified carbonate (MC3), by attaching three ethylene oxide units to the four-position of ethylene carbonate. AC impedance studies showed that an ionic conductivity of 5 x 10(exp -5) S/cm could be achieved at room temperature, by adding 50 wt% of MC3 into PEO-LiCF3SO3 complex. This is two orders of magnitude higher than that found in PEO-LiCF3SO3 electrolyte without a plasticizer, and one order of magnitude higher than that found when using same amount of propylene carbonate (PC) as plasticizer. Temperature dependent conductivity measurement and thermal analysis show that this new plasticizer increased the ionic conductivity throughout the entire complex system, while the conventional plasticizers only create a high conductivity path way through the plasticizer itself. The samples are free standing films with good mechanical properties. When MC3 is used as a plasticizer, the ionic conductivity increase is much higher than using PC as a plasticizer at high temperature (65 C), implying an increase in the number of charge carriers. Therefore, we believe that MC3 has a stronger ion pair dissociation effect than PC, when used as a plasticizer. The ion pair dissociation effect was studied by Raman, FTIR, and near edge x-ray absorption fine structure (NEXAFS) spectroscopy. DOE

N95-21650 Selskapet for Industriell og Teknisk Forskning, Oslo (Norway). Dept. of Ceramics.

DEVELOPMENT AND APPLICATIONS OF FLAT CERAMIC MEMBRANES

C. Simon and R. Bredesen 13 May 1994 20 p
(PB95-110219; STF24-A94025) Avail: Issuing Activity (National Technical Information Service (NTIS))

The mechanical strength of flat ceramic membranes made by tape casting has been investigated and improved. The characteristics of the powders used to cast the substrate have shown to be related to the quality of the tape. The gas permeability of the substrate and the complete three layer membrane configuration have been measured for alumina membranes. It confirms that the porous gamma-Al2O3 top layer made by this technique are defect-free. The cut-off values of the top layer have been determined by using different molecular weight dextrans. The adsorption behavior of these molecules on the membrane surface material have been investigated. Finally, the membranes have been applied in the filtration of metal particles coming from the dissolution of an alumina alloy in butanol. NTIS

N95-21662# Lawrence Livermore National Lab., Livermore, CA.

FORMING OF SUPERPLASTIC CERAMICS

D. R. Lesuer, J. Wadsworth, and T. G. Nieh May 1994 14 p Presented at the 8th International Context on Modern Materials Technologies, Faenza, Italy, 30 Jun. - 4 Jul. 1994
(Contract W-7405-eng-48)
(DE94-017306; UCRL-JC-117168; CONF-9406239-1) Avail: CASI HC A03/MF A01

Superplasticity in ceramics has now advanced to the stage that technologically viable superplastic deformation processing can be performed. In this paper, examples of superplastic forming and diffusion bonding of ceramic components are given. Recent work in biaxial gas-pressure forming of several ceramics is provided. These include yttria-stabilized, tetragonal zirconia (YTZP), a 20% alumina/YTZP composite, and silicon. In addition, the concurrent superplastic forming and diffusion bonding of a hybrid ceramic-metal structure are presented. These forming processes offer technological advantages of greater dimensional control and increased variety and complexity of shapes than is possible with conventional ceramic shaping technology. DOE

N95-21695 David Sarnoff Research Center, Princeton, NJ.

HIGH PERFORMANCE YBCO FILMS Report, 25 Feb. - 25 May 1994

Edgar J. Denlinger 25 May 1994 14 p Limited Reproducibility: More than 20% of this document may be affected by microfiche quality
(Contract N00014-91-C-0216)
(AD-A279560) Avail: Issuing Activity (Defense Technical Information Center (DTIC))

A Bi2O3-based glass composition was found suitable for use under typical YBCO deposition conditions, which is in a vacuum under partial oxygen pressure at about 750 C. It was experimentally determined that a Ag capping layer thickness of about 5 microns is needed for use with this glass. This Ag thickness will prevent any degradation in the silver layer's conducting properties due to Ag/glass interaction during the glass firing operation at 640 C. Lanthanum aluminate samples with YBCO topped with a thin layer of strontium titanate (STO) were prepared by Neocera and had excellent YBCO surface resistance properties as measured with a dielectric resonator test system. These samples will be used to test the compatibility of the YBCO with the silver capping layer deposited over the STO. DTIC

N95-21697 Pennsylvania State Univ., University Park, PA.

DOMAIN PROCESSES IN FERROELECTRIC CERAMICS Final Report, 30 Sep. 1991 - 31 Dec. 1993

Wenwu Cao and L. E. Cross 14 Apr. 1994 78 p Limited Reproducibility: More than 20% of this document may be affected by microfiche quality
(Grant AF-AFOSR-0433-91)
(AD-A279567; AFOSR-94-0308TR) Avail: CASI HC A05

This report outlines the progress achieved during a two year effort sponsored by the AFOSR on the theoretical study of domain and domain wall formation in ferroelectrics. Understanding on domain formation and domain dynamics in ferroelectrics are crucial for developing better functional ceramic materials for transducers and actuators. A continuum model has been developed to describe the polarization profile in ferroelectrics, which takes into account both nonlinear and nonlocal nature of the ferroelectric system. The theory can give rise to twin and twin band solutions under proper boundary conditions. A theoretical model is also developed for the morphotropic phase boundary in PZT system, which provides a new interpretation on the phase coexistence in a complete solid solution system. According to the new definition, the width of the coexistence region is inversely proportional to the volume of the coherent region, such as the particle size for a fine grain system. Theoretical interpretation is provided to the electron interference pattern across a ferroelectric domain wall in holographic electron microscopy, a newly developed technique with much higher magnification than the conventional TEM. The relationship between microscopic lattice dynamics and the continuum theory is also established. DTIC

N95-21714# Shikoku Chemical Research Industries, Inc., Ibaragi (Japan).
INVESTIGATION ON RESEARCH FOR DEGRADABLE PLASTICS
M. Nishiyama, J. Hosokawa, K. Yoshihara, T. Kubo, H. Kabeya, T. Endo, and R. Kitagawa 31 Mar. 1994 108 p
(DE94-796550; ETDE/JP-mf-94796550) Avail: CASI HC A06/MF A02

This paper investigates and reports problems on plastic waste and the measures to solve them, and the developmental trend of main biodegradable plastics in the world. A large quantity of plastic waste neither rots or returns to nature even if reclaimed. A recycling system has not yet been established due to plastics' low price. Therefore, countries are carrying out regulations to prohibit the use of foamed polystyrene, to enforce the compulsory use of degradable plastics, to create a taxation on plastic bottles, etc. Among biodegradable plastics, a type of polyethylene blended with starch is legislated for its use in the U.S., but it has been met with opposition by environmental organizations because it's plastic powder remains in the soil. Contrary to this partial degradability, the following are cited as completely degradable plastics: (1) bioplastics based on microorganism; (2) natural polymer based on plants and animals; and (3) biodegradable synthetic polymer. All of the m, however, are still in the early stages of research and development and commercialization. DOE

N95-21735# Iowa State Univ. of Science and Technology, Ames, IA.
DIRECTIONAL SOLIDIFICATION OF THE ALUMINA-ZIRCONIA CERAMIC EUTECTIC SYSTEM Ph.D. Thesis
C. Boldt 27 Jul. 1994 95 p
(Contract W-7405-eng-82)
(DE95-001677; IS-T-1621) Avail: CASI HC A05/MF A01

It is possible to produce alumina-zirconia ceramic samples through existing solidification techniques. The resulting microstructures typically consist of rods of zirconia in an alumina matrix, although a lamellar structure has been noted in some cases. In nearly all cases, colony growth was present which may possibly result from grain size, repeated nucleation events, and lamellar oscillations. In the same vein, it appears that the amount of impurities within the system might be the underlying cause for the colony growth. Colony growth was diminished through impurity control as the higher purity samples exhibited colony free behavior. In addition to colony formations, faceted alumina dendrites or nonfaceted zirconia dendrites may result in the ceramic if the sample is solidified out of the coupled zone. In all cases, for larger-sized Bridgman samples, a lower limit in the eutectic spacing was noted. The solidification model which includes the kinetic effect has been developed, although the effect appears to be negligible under present experimental conditions. A spacing limit might also occur due to the result of heat flow problems. Heat flow out of the ceramic is difficult to control, often causing radial and not axial growth. This behavior is exaggerated in the presence of impurities. Thus, higher purity powders should always be used. Higher purity samples, in addition to yielding a more microstructurally uniform ceramic, also showed increased directionality. In the future, the kinetic model needs to be examined in more detail, and further research needs to be accomplished in the area of molten ceramics. Once better system constants are in place, the kinetic model will give a better indication of the behavior in the alumina-zirconia system. DOE

N95-21748# Stanford Univ., CA.
APPLICATION OF QUATERNARY PHASE DIAGRAMS TO COMPOUND SEMICONDUCTOR PROCESSING
R. Sinclair 1994 20 p
(Contract DE-FG03-84ER-45085)
(DE95-001813; DOE/ER-45085/T2) Avail: CASI HC A03/MF A01

Isobaric, isothermal phase diagrams are a molar representation of condensed phases in equilibrium with each other at a fixed temperature, pressure, and composition. Since three or four elements are usually involved at a fabricated interface in a semiconductor device, knowledge of the appropriate ternary or quaternary phase diagram is important for optimizing the processing parameters and designing long term stability of devices. While the use of phase diagrams is well-established in the fields of metallurgy, ceramics and mineralogy, only recently have phase diagrams been employed to provide a framework for understanding thin film reactions on a substrate, encountered in semiconductor processing. Even though there are many examples of applications of ternary phase diagrams in the semiconductor literature (for instance, metallization of GaAs, the use of refractory metal silicides for metallization layers in VLSI devices and oxidation of III-V compounds), the same is not true for quaternary phase diagrams. To date, the only application is oxidation of mercury cadmium telluride. This lack of examples is not warranted, as four elements are often involved at a critical interface in compound semiconductor processing and devices. This paper reports on the progress made to remedy this situation by considering the application of quaternary phase diagrams to understanding and predicting the behavior of II-VI thin film interfaces in photovoltaic devices under annealing conditions. Moreover, for the first time, solid solubility is taken into account for quaternary phase diagrams of semiconductor systems. DOE

N95-21861# Oak Ridge National Lab., TN.
TAILORING SUSPENSION FLOW FOR THE GELCASTING OF OXIDE AND NONOXIDE CERAMICS
O. O. Omatete and A. Bleier 1994 8 p Presented at the Spring Meeting of the Materials Research Society, San Francisco, CA, 4-8 Apr. 1994
(Contract DE-AC05-84OR-21400)
(DE95-001351; CONF-940411-55) Avail: CASI HC A02/MF A01

Gelcasting is a forming process in which a concentrated slurry of ceramic powders suspended in a solution of organic monomers is polymerized to form a green body of the powder held in a polymeric gel. The process is suited to the production of near-net-shape complex parts. The slurry should contain high solids loading (approximately 50 vol%) in order to minimize shrinkage and distortion during drying and, thus, to produce a relatively dense green body that facilitates sintering of the green part to full density. To produce complex-shaped bodies, however, the slurry has to be fluid at the high solids loading, to flow, and to fill complex-shaped molds. Consequently, there is the need to study the rheology of the gelcasting slurries of typical ceramic powders in order to understand the factors that govern the flow and pourability of these slurries. The rheology of gelcasting slurries of concentrated (30 - 60vol%) alumina, zirconia, silicon nitride, and sialon powders with isoelectric points varying between pH 5 and 9, was studied by measuring the viscosity and yield stress as functions of pH. Typically, the rheology is non-Newtonian. The lowest values of viscosity and yield stress that permit the highest solids loading were obtained at high and low pH values, where the powders are colloidally stable, far from the isoelectric points. This relationship applies whether or not a polymer dispersant is present. The acrylamide monomer which is used in gelcasting slurries, lowers these non-Newtonian properties permitting the preparation of more concentrated slurries. Fluid and pourable gelcasting slurries of each powder had apparent viscosities and yield stresses less than 2.0 Pa(center dot)s and 50 Pa, respectively. DOE

N95-21873 Selskapet for Industriell og Teknisk Forskning, Trondheim (Norway). Corrosion Center.
PROTECTIVE ORGANIC COATINGS ON STEEL: ACCELERATED CORROSION TEST METHOD FOR PAINT/COATINGS EXPOSED TO WATER WITH LOW CONDUCTIVITY. NORDTEST PROJECT NO. 1010-92. DEGRADATION OF ORGANIC COATINGS IN FRESH WATER
U. Steinsmo 7 Apr. 1994 11 p See also PB93-170728 and PB94-138484
(PB95-134185; STF24-A94568) Avail: Issuing Activity (National Technical Information Service (NTIS))

An accelerated laboratory test method for assessment of the corrosion protective ability of organic coatings is described. The method is applicable to paints/coatings applied on steel structures and exposed to water with low conductivity i.e. fresh water, condensated water. NTIS

N95-21876 Colorado State Univ., Fort Collins, CO. Dept. of Chemistry.
SYNTHESIS OF POLYMERIC MICROCAPSULE ARRAYS AND THEIR USE FOR ENZYME IMMOBILIZATION Interim Report
Ranjani Parthasarathy and Charles R. Martin Apr. 1994 23 p Limited Reproducibility: More than 20% of this document may be affected by

microfiche quality
(Contract N00014-82-K-0612)
(AD-A279125) Avail: Issuing Activity (Defense Technical Information Center (DTIC))

Immobilized enzymes are used in bioreactors and biosensors. Current methods for immobilizing enzymes include adsorption or covalent attachment to a support, microencapsulation, and entrapment within a membrane/film or gel. The ideal enzyme immobilization method would (1) employ mild chemical conditions; (2) allow for large quantities of enzyme to be immobilized; (3) provide a large surface area for enzyme/substrate contact within a small total volume; (4) minimize barriers to mass transport of substrate and product; and (5) provide a chemically and mechanically robust system. This report describes a new method for enzyme immobilization that satisfies all of these criteria. We have developed a template-based synthetic method that yields hollow polymeric microcapsules of uniform diameter and length. These microcapsules are arranged in a high density array in which the individual capsules protrude from a surface like the bristles of a brush. We have developed procedures for filling these microcapsules with high concentrations of enzymes. The enzyme-loaded microcapsule arrays function as enzymatic bioreactors in both aqueous solution and organic solvents. DTIC

N95-21885# International Centre for Theoretical Physics, Trieste (Italy).
MAGNETIC PROPERTIES OF THE THREE-DIMENSIONAL ISING MODEL WITH AN INTERFACE AMORPHIZATION
A. Benyoussef (Mohammed V Univ., Rabat, Morocco.), Y. ElAmraoui (Mohammed V Univ., Rabat, Morocco.), A. ElKenz (Mohammed V Univ., Rabat, Morocco.), and M. Saber (Mohammed V Univ., Rabat, Morocco.) Sep. 1993 20 p
(DE94-628992; IC-93/304) Avail: CASI HC A03/MF A01 (US Sales Only)

A three-dimensional ferromagnetic Ising model with an interface amorphization is investigated with the use of the effective field theory. Phase diagrams and reduced magnetization curves of interface and bulks are studied. We obtain a number of characteristic behaviour such as the possibility of the reentrant phenomena and a large depression of interface magnetization. DOE

N95-21907 Department of the Navy, Washington, DC.
ALIGNED BISMUTH, STRONTIUM, CALCIUM CUPRATE COATINGS ON POLYCRYSTALLINE SUBSTRATES Patent
Louis E. Toth, inventor (to Navy) and J. R. Spann, inventor (to Navy) 20 Sep. 1994 11 p Filed 21 Dec. 1993
(AD-D016512; US-Patent-5,348,937; US-Patent-Appl-SN-170962; US-Patent-Class-505-238) Avail: US Patent and Trademark Office

An article comprises an oriented thick film superconducting coating on a polycrystalline substrate. The coating includes at least two highly oriented platelet components of Bi(a)Sr(b)Ca(c)Cu(d)O(x) (BSCCO) wherein, in one component, a is 2, b is 2, c is 1, d is 2, and x is 8 and, in another component, a is 2, b is 2, c is 0, d is 1, and x is approximately 6, oriented such that said BSCCO platelets are essentially parallel to said substrate. Suitable polycrystalline substrates are MgO and alumina and mullite. DTIC

N95-21909# Oak Ridge National Lab., TN.
COST-EFFECTIVE CERAMICS PROGRAM IN THE UNITED STATES
R. B. Schulz (Department of Energy, Washington, DC.) and D. R. Johnson 1994 6 p Presented at the 5th International Symposium on Ceramic Materials and Components for Engines, Shanghai, China, 29 May - 1 Jun. 1994
(Contract DE-AC05-84OR-21400)
(DE95-001425; CONF-9405187-3) Avail: CASI HC A02/MF A01

The 5-year Cost-Effective Ceramics for Heat Engines program began in 1993. This effort reflects the realization that the problems with reliability of structural ceramics have been largely overcome, but the high cost of structural ceramics has limited their use in commercial applications. The technical causes of high cost were identified, and a technical plan developed. The work elements in the program include the following: economic cost modeling, ceramic machining, powder synthesis, alternative forming and densification processes, yield improvement, standards development, and low-expansion ceramics. DOE

N95-21937# Oak Ridge National Lab., TN.
CERAMIC TECHNOLOGY FOR ADVANCED HEAT ENGINES
D. R. Johnson and R. B. Schulz (Department of Energy, Washington, DC.) 1994 9 p Presented at the Science and Technology Materials Conference, Greensboro, NC, 27-29 Oct. 1993
(Contract DE-AC05-84OR-21400)
(DE95-000950; CONF-9310328-3) Avail: CASI HC A02/MF A01

The Ceramic Technology Project was initiated in 1983 for the purpose of developing highly reliable structural ceramics for applications in advanced heat engines, such as automotive gas turbines and advanced heavy duty diesel engines. The reliability problem was determined to be a result of uncontrolled populations of processing flaws in the brittle, flaw-sensitive materials, along with microstructural features, such as grain boundary phases, that contribute to time dependent strength reduction in service at high temperatures. The approaches taken to develop high reliability ceramics included the development of tougher materials with greater tolerance to microstructural flaws, the development of advanced processing technology to minimize the size and number of flaws, and the development of mechanical testing methodology and the characterization of time dependent mechanical behavior, leading to a life prediction methodology for structural ceramics. The reliability goals of the program were largely met by 1993, but commercial implementation of ceramic engine components has been delayed by the high cost of the components. A new effort in Cost Effective Ceramics for Heat Engines was initiated in 1993 and is expected to develop the manufacturing technology leading to an order of magnitude cost reduction. The program has been planned for a five year period. DOE

N95-21969 Dayton Univ., OH.
LUBRICANT EVALUATION AND PERFORMANCE, 2 Final Technical Report, 1 Jan. 1991 - 12 Jul. 1993
Costandy S. Saba, Michael A. Keller, Kenneth K. Chao, Douglas K. Toth, Mary F. Borchers, and Hoover A. Smith Feb. 1994 475 p Limited Reproducibility: More than 20% of this document may be affected by microfiche quality
(Contract F33615-88-C-2817)
(AD-A279144; UDR-TR-93-81-2; WL-TR-93-2126-2) Avail: Issuing Activity (Defense Technical Information Center (DTIC))

Thermal and oxidative stability, deposition and foaming techniques were developed for predicting the performance of candidate 4 cSt lubricants, polyphenyl ether (PPE), C-ether and other experimental fluids for use in advanced aircraft turbine engines. A novel sealed tube test was developed to study the rate of reaction in both liquid and vapor phase using only microliter quantities of the lubricants. Blending agents and/or diluents were used to improve the low temperature properties and high temperature oxidative stability of PPE. In-line magnetic wear sensors were evaluated as condition monitoring devices for oil systems with sensitivity well below 5 micrometers. Microfiltration effect on wear was investigated with the results showing effective reduction in secondary wear. HP-DSC analysis technique was limited as an oxidative stability screening device for PPE but was effective in demonstrating differences among various PPE formulations. The tribological behavior of high temperature fluids was evaluated and compared in the boundary lubrication regime using various steel and ceramic specimens. A sliding three-ball-on-disk wear test device was developed for reducing sample size, controlling scar geometry and determining lubricant consumption rate and tribochemistry. The effect of soft and hard solid particulates on the fatigue and wear lives of rolling elements was investigated using a recently developed three-ball rolling test. DTIC

N95-21973 Ibis Associates, Inc., Wellesley, MA.
ANALYSIS OF COST: COMBUSTION FLAME CVD DIAMOND DEPOSITION Quarterly Report No. 1
1994 21 p Limited Reproducibility: More than 20% of this document may be affected by microfiche quality
(Contract N00014-93-C-2044)
(AD-A279153) Avail: Issuing Activity (Defense Technical Information Center (DTIC))

IBIS Associates has developed its predictive spreadsheet model of combustion flame chemical vapor deposition (CVD) diamond film fabrication. This report explains the assumptions for combustion flame deposition theory, and shows preliminary results of the economics of this CVD diamond process. For this report and the results contained herein, it is assumed that the transport theory model which predicts growth rates in the CVD diamond technical cost model closely predicts actual growth rates for the combustion flame technology and that the input values for variables such as the gas flow rate and substrate diameter are physically achievable. With this assumption as the basis for cost estimation, the cost of producing 1,000 planarized polycrystalline diamond wafer at one millimeter thick is estimated in the long run to be $73 per square centimeter for the combustion flame technology. DTIC

N95-21976 Southwest Research Inst., San Antonio, TX.
ROBOTIC PAINT STRIPPING CELL Final Technical Report, 1 Apr. 1986 - 1 Aug. 1993
James Lukemeyer Nov. 1993 208 p Limited Reproducibility: More than 20% of this document may be affected by microfiche quality
(Contract F33615-86-C-5044)
(AD-A279158; WL-TR-93-8029) Avail: Issuing Activity (Defense Technical Information Center (DTIC))

The purpose of this work has been to develop a robotic system for stripping paint from F-16 aircraft using non-chemical means and to integrate the system at Ogden Air Logistics Center (OO-ALC). The Robotic Paint Stripping Cell (RPSC) is an automation system consisting chiefly of two large robots developed for removal of paint from fighter size aircraft and aircraft components using the plastic media blast (PMB) process. The system was installed at Hill AFB in the Plastic Media Blast Booth at building 220 and put into production use by the Air Force in September 1992. The technical effort on this project resulted in the development of an automated system incorporating two robots of unique kinematic design especially suited for paint stripping and general surface processing of fighter-size aircraft. A more consistent paint stripping quality is achievable with the sensor-based, computer-controlled robotic plastic media blast system than is possible using manual methods. The sensor-based controls are used for all F-16 substrate materials, including graphite-epoxy composites. The RPSC is a fully automated plastic media blast paint stripping system, providing improvement of operator health and safety conditions by removing them from the blast environment. DTIC

N95-22022 Naval Research Lab., Washington, DC.
EPOXY LINING FOR SHIPBOARD PIPING SYSTEMS Interim Report
Robert F. Brady, Jr. and James D. Adkins 30 Sep. 1994 30 p Limited Reproducibility: More than 20% of this document may be affected by microfiche quality
(AD-A286228; NRL/MR/6120-94-7629) Avail: CASI HC A03

The Naval Research Laboratory has developed an epoxy lining to prevent corrosion and erosion of copper-nickel pipe. Before being approved for use aboard ship, the lining was tested in the laboratory for resistance to chemicals found in sanitary systems and tested in a simulated ship piping system for application viscosity and hardening time. Commercially-available linings were also tested but found to be deficient in one or more critical properties. Entrained air in the applied coating is avoided more easily by control of application parameters than by the use of air-releasing additives in the lining. The process used to install the lining is described in detail. The Navy now uses this lining to restore corroded or eroded ship piping systems rapidly without lengthy disruption of shipboard operations. This technology has been shown to be a proven inexpensive alternative to replacement of pipe. DTIC

N95-22047 Naval Command, Control and Ocean Surveillance Center, San Diego, CA. Research, Development, Technology and Evaluation Div.
STRUCTURAL PERFORMANCE OF CYLINDRICAL PRESSURE HOUSINGS OF DIFFERENT CERAMIC COMPOSITIONS UNDER EXTERNAL PRESSURE LOADING. PART 4: SILICON CARBIDE PARTICULATE REINFORCED ALUMINA CERAMIC Final Technical Report
Ramon R. Kurchubasche, Richard P. Johnson, Jerry D. Stachiw, and Thomas A. Johnson Dec. 1993 134 p Limited Reproducibility: More than 20% of this document may be affected by microfiche quality
(NR Proj. S03-97)
(AD-A286299; NRAD-TR-1594-Pt-4) Avail: CASI HC A07

Twelve 12-inch-OD by 18-inch-long by 0.412-inch-thick silicon-carbide particulate reinforced alumina-ceramic cylinders were fabricated, assembled, and pressure tested to determine their suitability for use as external pressure-resistant housings for underwater applications. The material, designated 90-X-089, is made by Lanxide Corporation (Newark, DE) by a proprietary directed metal oxidation (DIMOX(TM)) process. The primary advantages of this material are its high compressive strength, high elastic modulus, high fracture toughness, low specific gravity, and ability to be cast in near net shapes, eliminating the need for expensive diamond grinding. Pressure test results are presented along with strain gage data, cyclic fatigue-life data, and acoustic emissions. Conclusions regarding the suitability of the material for application to pressure housings for underwater applications are presented along with a comparison to WESGO's AL-600 96-percent alumina ceramic, which was chosen as a base of comparison for various advanced materials being evaluated under the same program. Recommendations for design implementation, nondestructive evaluation, and further research are made. DTIC

N95-22057 Office of Naval Research, Arlington, VA.
SILOXANES WITH STRONG HYDROGEN BOND DONATING FUNCTIONALITIES Patent Application
Jay W. Grate, inventor 27 May 1994 20 p Limited Reproducibility: More than 20% of this document may be affected by microfiche quality
(AD-D016499; US-Patent-Appl-SN-250768) Avail: Issuing Activity (Defense Technical Information Center (DTIC))

It is an object of the present invention to provide novel, viscous, liquid siloxane-based polymers which are useful for rapid reversible vapor sorption. A further object of the present invention is to provide improved coatings and vapor sorption compositions for chemical sensors which are highly sensitive, reversible and have selective absorptions for particular vapors, especially hydrogen bond accepting vapors such as organophosphorus compounds. DTIC

N95-22091# National Renewable Energy Lab., Golden, CO.
THE ROLE OF POINT DEFECTS AND DEFECT COMPLEXES IN SILICON DEVICE PROCESSING
B. Sopori and T. Y. Tan Aug. 1994 171 p Presented at the 2nd Workshop on Role of Point Defects/defect Complexes in Silicon Device Fabrication, Breckenridge, CO, 24-26 Aug. 1992
(Contract DE-AC36-83CH-10093)
(DE94-011876; NREL/TP-413-7064; CONF-9208175-Summ) Avail: CASI HC A08/MF A02

This report is a summary of a workshop hold on August 24-26, 1992. Session 1 of the conference discussed characteristics of various commercial photovoltaic silicon substrates, the nature of impurities and defects in them, and how they are related to the material growth. Session 2 on point defects reviewed the capabilities of theoretical approaches to determine equilibrium structure of defects in the silicon lattice arising from transitional metal impurities and hydrogen. Session 3 was devoted to a discussion of the surface photovoltaic method for characterizing bulk wafer lifetimes, and to detailed studies on the effectiveness of various gettering operations on reducing the deleterious effects of transition metals. Papers presented at the conference are also included in this summary report. DOE

N95-22136# Lockheed Missiles and Space Co., Palo Alto, CA. Research and Development Div.
DEMONSTRATION OF MULTIFUNCTIONAL DNBM CORROSION INHIBITORS IN PROTECTIVE COATINGS FOR NAVAL AIR/WEAPON SYSTEMS Final Report, Sep. 1989 - Jul. 1992
L. J. Bailin Dec. 1993 50 p
(Contract N62269-89-C-0258)
(AD-A285869; LMSC-P000457; NAWCADWAR-60-94128) Avail: CASI HC A03/MF A01

The corrosion protective properties of multifunctional DNBM salts (quaternary ammonium dichromate, nitrate, borate, and molybdate) have been demonstrated on high-strength steel and aluminum alloys found in prototype aerospace weapon systems. The 100% DNBM mixture added to MIL-P-23377 epoxy-polyamide, minus strontium chromate inhibitor, on bare 7075-T6 aluminum alloy resisted 1000 h ASTM B-117 salt spray. However, the coatings were not resistant to hydraulic fluid immersion at the higher concentrations required for the corrosion inhibition. Microencapsulation of the reactive DNBM mixture was adopted as a means to prevent this susceptibility, as well as the destructive oxidation of the hydroxyl groups in the epoxy resin during cure. In the scale-up operation, approximately 20 gallons of DNBM weighing 64 kg (141 lb) was prepared from the four starting quarternary salts synthesized in a chemical process pilot plant. The salts were mixed by dissolving in toluene. Following removal of solvent, the resultant dark-brown liquid, approximating molasses in viscosity, was microencapsulated by the following method: The DNBM was dispersed to form an oil-in-water emulsion in an aqueous colloidal solution of low-viscosity, high-purity methyl cellulose using a Gifford-Wood homogenizer, followed by spray drying in an Anhydro spray dryer. The maximum practicable payload was 75% DNBM. DTIC

N95-22141 Purdue Univ., West Lafayette, IN. School of Chemical Engineering.
HIGH TEMPERATURE POLYMER FOR SECOND ORDER NONLINEAR OPTICS FOR PHOTONIC MATERIALS
Hilary S. Lackritz 12 May 1994 15 p Limited Reproducibility: More than 20% of this document may be affected by microfiche quality
(Contract N00014-92-J-1415)
(AD-A279309) Avail: Issuing Activity (Defense Technical Information Center (DTIC))

We are examining a variety of novel high temperature stable polymers as new materials for second order nonlinear optical (NLO) and photorefractive devices. Current polymers have sufficient optical signal generated by available chromophores, but are not practical for device applications because of limitations in the temporal stability of the dopant orientation in the polymer caused by poor thermal stability of the host. This is a novel approach for developing a new class of photonic materials with superior thermal and temporal stability and is the first attempt to design a second order NLO polymer with controllable, tailorable local physical and electrical properties. A second, equally important goal is to understand the basic polymer physics controlling the thermal and temporal stability of the optical chromophore orientation. This will determine not only the overall efficiency of the materials for device applications, but will generate substantial information about mobility in high temperature stable polymer systems. DTIC

N95-22258# Oak Ridge National Lab., TN.
MATERIALS SUPPORT FOR THE DEVELOPMENT OF HIGH TEMPERATURE ADVANCED FURNACES (HITAF): A COMPARISON OF SELECTED MECHANICAL PROPERTIES FOR THREE SIC-BASED CERAMICS
K. Breder and V. J. Tennery 1994 12 p Presented at the 10th Annual Coal Preparation, Utilization and Environmental Control Contractors Conference, Pittsburgh, PA, 18-21 Jul. 1994
(Contract DE-AC05-84OR-21400)
(DE94-017752; CONF-940780-4) Avail: CASI HC A03/MF A01

The purpose of this project is to compare structural ceramic materials proposed for use in the air heater of a coal fired high temperature advanced furnace (HITAF) for power generation. The work will provide necessary initial strength and statistical material parameters for design of a prototype system. Two teams are currently funded by Pittsburgh Energy Technology Center (PETC) under the Combustion 2000 program to develop such a system. One team is led by the United Technologies Research Corporation, and consists of UTC Turbo Power and Marine Division, Bechtel, Oak Ridge National Laboratory (ORNL) and a Joint Venture of Physical Sciences Inc. (PSI) Technologies, Reaction Engineering International (REI) and University of North Dakota Energy & Environmental Research Center (UNDEERC); the other team is led by Foster Wheeler Development Corporation, and members are AiResearch Division of Allied Signal Aerospace Systems & Equipment, Research Cottrell, TRW, General Electric and Bechtel. DOE

N95-22259# University of Southern Mississippi, Hattiesburg, MS. Dept. of Polymer Science.
TOWARDS TAILORED INTERPHASE FORMATION UTILIZING SURFACE-BOUND BENZYLSULFONIUM SALTS AS CATIONIC INITIATORS
John A. McGowen and Lon J. Mathias 15 Nov. 1994 3 p
(Contract N00014-89-J-1225)
(AD-A286461; TR-78) Avail: CASI HC A01/MF A01

This study centers on designed composite interphases based on using polymer synthesis to chemically link initiating groups to fiber surfaces, promote radial growth of the interphase out from the surface, and finally initiate matrix cure. The approach is based on tailoring interphase formation before matrix cure, and should help to develop very strong interactions between the composite components. Novel benzylsulfonium salts have been synthesized which possess an alkyl ether tether tied to a reactive trialkoxysilane moiety capable of covalently bonding with glass surfaces. Recently it has been shown that benzylic sulfonium salts can be excellent latent initiators for epoxy resins, vinyl ethers, and spiro orthocarbonates or bicyclo orthoesters. Here we report the coupling of these sulfonium salts with high surface area silica gel as a model for glass fibers. High surface area silica was chosen due to the high loadings achievable, allowing for more facile characterization of the degree of functionalization. The surface-bound sulfonium salts will be used to initiate the cationic polymerization of various resins based on epoxy functionality. Characterization of the surface-bound sulfonium salts on silica, cure kinetics of unbound and surface-bound initiator with a commercial epoxy resin system and preliminary composite formation with glass fibers will be presented. DTIC

N95-22266# Oak Ridge National Lab., TN.
STRENGTH TESTING OF TI-VAPOR-COATED SILICON NITRIDE BRAZE JOINTS
M. L. Santella 1994 21 p Presented at the American Society of Mechanical Engineers' Winter Annual Meeting, Chicago, IL, 9-11 Nov. 1994
(Contract DE-AC05-84OR-21400)
(DE94-017858; CONF-941142-18) Avail: CASI HC A03/MF A01

Sintered silicon nitride was vacuum brazed to itself at 1130C with a Au-25Ni-25Pd wt % filler metal. Wetting was obtained by coating the Si3N4 surfaces with titanium prior to brazing by electron beam evaporation. The brazed joints were virtually free of porosity. Metallographic analysis showed that Ti reacted with the Si3N4, to form a TiN reaction layer during brazing. Small amounts of Si and Ti dissolved in the filler metal layers but they did not appear to influence the mechanical properties of the braze layer. Flexure bars were made from the brazed coupons and tested at room temperature, 600C, 700C, and 800C in air. At 700C and below, fracture of the test bars occurred in the Si3N4, either near the brazed surfaces or at some distance into the monolithic material. The measured strength of joint specimens decreased slightly with increasing test temperature, and generally exceeded the intrinsic braze filler metal strength in this temperature range. It was also found that lapping the Si3N4, prior to Ti coating reduced the number of near-surface flaws and produced joints with higher average strength and lower scatter than those left in a ground condition. Specimens tested at 800C had very low strengths, and this behavior was related to the microstructure at the brazed Si3N4 surfaces. DOE

N95-22270# Oak Ridge National Lab., TN.
MEASUREMENT OF RESIDUAL STRESSES ON CERAMIC MATERIALS WITH HIGH SPATIAL RESOLUTION
K. J. Kozaczek, C. O. Ruud (Pennsylvania State Univ., University Park, PA.), and J. D. Fitting (Pennsylvania State Univ., University Park, PA.) 1993 6 p Presented at the 6th International Symposium on Nondestructive Characterization of Materials, Oahu, HI, 7-11 Jun. 1993
(Contract DE-AC05-84OR-21400)
(DE94-017889; CONF-930685-1) Avail: CASI HC A02/MF A01

A fast x-ray diffraction technique has been developed for measuring the residual stresses with high spatial resolution in ceramic materials. This resolution is limited by the mean size of grains and the radiation type. The effective diffraction elastic constants were experimentally determined for alumina as (E/l+(nu))(sub (1016)) = 200 GPa. The accuracy of XRD measurement of residual stresses with the spatial resolution of 170 micro m and precision +/- 15 MPa was verified experimentally by strain gauge measurements. The stress field around a singular Kovar pin brazed to alumina was asymmetric with high tangential stresses in the vicinity of the pin decreasing with the distance from the pin. DOE

N95-22383*# Aerospace Corp., El Segundo, CA. Mechanics and Materials Technology Center.
ABSORPTION OF WATER AND LUBRICATING OILS INTO POROUS NYLON
P. A. Bertrand 10 Jan. 1995 20 p Sponsored in cooperation with NASA. Goddard Space Flight Center and Space and Missile Systems Center
(NASA-CR-197344; NAS 1.26:197344; ATR-95(5826)-1) Avail: CASI HC A03/MF A01

Oil and water absorption from air into sintered porous nylon can be described by infiltration into the pores of the material. This process can be modeled by a diffusion-like mechanism. For water absorption, we find a formal diffusion coefficient of 1.5 x 10(exp -4)sq cm/min when the nylon is initially dry. The diffusion coefficient is 4 x 10(exp -6)sq cm/min when the nylon is oil-impregnated prior to air exposure. In a 52% RH atmosphere, dry nylon absorbs 3% w/w water, and oil-impregnated nylon absorbs 0.6% w/w water. For oil absorption there are three steps: (1) surface absorption and infiltration into (2) larger and (3) smaller pores. Surface absorption is too fast to be measured in these experiments. The diffusion coefficient for the second step is 6 x 10(exp -4)sq cm/min for SRG-60 oil into dry nylon and 4 x 10(exp -4)sq cm/min for air-equilibrated nylon. The diffusion coefficient for the third step is about 1 x 10(exp -6)sq cm/min for both cases. The total amount of oil absorbed is 31% w/w. The interaction between water and nylon is not as strong as that between water and cotton-phenolic: oil can replace water, and only a small amount of water can enter previously oil-impregnated nylon. Author

N95-22387 Naval Postgraduate School, Monterey, CA.
DETERMINATION OF THE COMPLEX ELASTIC MODULI OF MATERIALS USING A FREE-FREE BAR TECHNIQUE M.S. Thesis
David L. Bartlett Mar. 1994 214 p Limited Reproducibility: More than 20% of this document may be affected by microfiche quality
(AD-A279861) Avail: CASI HC A10

The objective of this research is to investigate the dynamic elastic properties of materials and their temperature and frequency dependence using an acoustic resonance based method. In this technique, the torsional, flexural, and/or longitudinal vibrational modes of a 'free-free' bar are selectively excited and tracked as a function of temperature. The resonance frequency of the torsional model is used to obtain the dynamic shear modulus. The dynamic Young's modulus is obtained from either the resonance frequency of the flexural or longitudinal mode of the bar. The quality factor, Q, of each mode is measured to obtain the damping properties of the material. A phase-locked-loop (PLL) is used to track the resonance frequency as a function of changing temperature for the particular vibrational model selected. Using this technique, the storage modulus and loss tangent may be obtained in a continuous fashion. Materials tested in this thesis include: Polyurethane PR-1592, a common sonar encapsulant, Polymethyl Methacrylate (PMMA) or plexiglass, and Polycarbonate. This research encompasses the theory, accuracy, limitations and applications of this measurement technique. DTIC

N95-22428# Los Alamos National Lab., NM.
CHARACTERIZATION AND PERFORMANCE OF DLC FILMS SYNTHESIZED BY PLASMA AND ION BEAM TECHNIQUES
K. C. Walter, H. Kung, T. Levine, P. Kodali, B. P. Wood, D. J. Rej, M. Nastasi, Jarkko Koskinen (Technical Research Centre of Finland, Espoo, Finland.), and J.-P. Hirvonen 1994 18 p Presented at the 4th International Conference on Plasma Surface Engineering, Garmisch-Partenkirchen, Germany, 19-23 Sep. 1994
(Contract W-7405-eng-36)
(DE94-018287; LA-UR-94-2821; CONF-9409196-1) Avail: CASI HC A03/MF A01

Diamond-like carbon (DLC) films have been deposited on dissimilar substrates using three different deposition processes. Two well-studied methods, employing cathodic arcs and RF-plasma self-bias, have been used. These two processes differ in that cathodic arc processes use gas pressures less than 1 mtorr and deposit atomic ions with energies less than 100 eV, while RF-plasma self-bias processes use gas pressures greater than 1 mtorr and deposit molecular ions with energies greater than 100 eV. In addition, DLC films have been deposited using a new plasma-based, pulsed-bias process. The pulsed-bias process uses gas pressures greater than 1 mtorr and deposits molecular ions with energies greater than 1,000 eV. Both the self-bias and pulsed-bias processes utilized hydrocarbon gases as the carbon source. Cathodic arc processes generally rely on the arc between two graphite electrodes as the carbon source. Deposited films from all three processes have been characterized using ion backscattering techniques, Elastic Recoil Spectrometry (ERS), Transmission Electron Microscopy (TEM) and Selected Area Diffraction (SAD). Films deposited using the cathodic arc process are virtually hydrogen free while the self-bias and pulse-bias films contain up to 40% hydrogen. TEM results indicated the films are homogeneous and amorphous. The hardness, elastic modulus, coefficient of friction and wear rate of the films are also reported. DOE

N95-22434# Los Alamos National Lab., NM.
NEUTRON REFLECTIVITY STUDY OF ADSORBED DIBLOCK COPOLYMERS
G. S. Smith, S. M. Baker, S. Wages, W. Hamilton, C. Toprakcioglu (Patras Univ., Greece.), J. B. Field, and L. Dai (Cambridge Univ., Cambridge, England.) 1994 10 p Presented at the Scaling in Complex Fluids Conference, Catanzaro (Italy), 4-8 Jul. 1994
(Contract W-7405-eng-36)
(DE95-002740; LA-UR-94-3552; CONF-9407145-1) Avail: CASI HC A02/MF A01

This paper summarizes our cumulative work on neutron reflectivity studies of polystyrene-poly(vinyl-2-pyridine) (PS-PVP) and polystyrenepolyethylene oxide (PS-PEO) adsorbed at a quartz-solvent interface. Deuterated toluene was chosen as the solvent since it is a good solvent for PS and a poor one for either of the other two blocks. In this case, the polystyrene dangles into the solvent while the other block acts as an anchor. The neutron reflectivity studies reveal that the form of the polymer density profile normal to the substrate may be varied from an extended 'brush' to a condensed 'mushroom' conformation by manipulating the ratio of the molecular weights of the two blocks. In addition, we present new data on the PS-PEO system in a poor solvent, deuterated cyclohexane, under conditions of shear flow in Poiseuille geometry. We find that when the PS-PEO diblock is absorbed from cyclohexane and is allowed to relax, the PS chain takes on a 'mushroom' conformation. However, when the shear is applied, the layer shear thickens due to the PS chains extended to nearly twice their original lengths. DOE

N95-22470# California Univ., Los Angeles, CA. Dept. of Chemistry and Biochemistry.
THE ENHANCEMENT OF METALLIC SILVER MONOMER EVAPORATION BY THE ADHESION OF POLAR MOLECULES TO SILVER NANOCLUSTER IONS
Clifton Fagerquist, Dilip K. Sensharma, Angel Rubio, Marvin L. Cohen, and M. A. El-Sayed 21 Sep. 1994 36 p
(Contract N00014-89-J-1350)
(AD-A284936; TR-78) Avail: CASI HC A03/MF A01

We have compared the metallic evaporation channels from metastable (Ag(sub X=5,7,11)AgI(sub Y=1-4))(+) clusters in the 1st FFR of a double focussing mass spectrometer with that of the corresponding pure metallic clusters, (Ag(sub X=5,7,11))(+). It is found that the presence of the polar AgI molecules increases the rate of silver monomer evaporation relative to that of silver dimer evaporation. Using thermodynamic expressions for the heat of evaporation of the different evaporation processes and assuming the absence of reverse activation energies, an expression for the difference between the activation energy of silver monomer and dimer evaporation is derived. It is shown that dipole/induced-dipole forces resulting from the presence of AgI polar molecules lead to an enhancement of silver monomer evaporation if the polarizability of the pure metallic cluster ions increases with the number of Jellium electrons. Our theoretical calculations of the static polarizabilities of (Ag(sub x))(+) using time dependent density functional theory within the local density approximation, shows a smooth increase in the polarizabilities with the number of the Jellium electrons in these clusters. Finally, we observe that the enhancement of Ag monomer evaporation per AgI added is smaller for clusters with even number of AgI molecules than with odd numbers. This was proposed to result from the contribution of configurations with dipole 'pairing' of the AgI molecules in clusters with even number of AgI molecules. Dipole pairing would decrease the average dipole/induced-dipole interaction between the AgI molecules and the metallic part of these 'mixed' clusters. DTIC

28 PROPELLANTS AND FUELS

Includes rocket propellants, igniters, and oxidizers; their storage and handling procedures; and aircraft fuels.

For related information see also *07 Aircraft Propulsion and Power, 20 Spacecraft Propulsion and Power,* and *44 Energy Production and Conversion.*

N95-19884 Iowa Univ., Iowa City, IA. Dept. of Mechanical Engineering.
HEAT TRANSFER, FOULING, AND COMBUSTION OF SUPERCRITICAL FUELS Final Report, 15 Aug. 1992 - 31 Mar. 1994

L. D. Chen 28 Apr. 1994 67 p Limited Reproducibility: More than 20% of this document may be affected by microfiche quality
(Contract F49620-92-J-0462)
(AD-A279906; AFOSR-94-0321TR) Avail: Issuing Activity (Defense Technical Information Center (DTIC))

The specific objectives of the project were to investigate the dynamics of the vortex and flame interaction in jet diffusion flames and the transport phenomena associated with the injection of supercritical fluids into a sub-critical environment. The vortex-flame interaction in a near-laminar jet diffusion flame was quantified by a planar visualization and the vortex formation in a transitional jet diffusion flame by a line visualization. The measured vortex crossing frequency in transitional jet diffusion flames was used to verify the time-dependent diffusion flame calculations. The experiments also quantified the spray length in two different ambient environments composed of dissimilar species. The mixture pseudo-critical states were calculated for the conditions examined. The spray length, the calculated mixture pseudo-critical states, along with images of instantaneous light scattering and shadowgraph showed that the mixing of dense fluids dictated the spread of mist-like droplets and vapor-phase injector fluid. The supercritical sprays also exhibited flashing-like atomization as concluded from the experiments. Further investigation on the mixing in the super-critical sprays was suggested. DTIC

N95-19920 Army Research Lab., Aberdeen Proving Ground, MD.
HIGH PRESSURE WINDOWED CHAMBER BURNED RATE DETERMINATION OF LIQUID PROPELLANT XM46 Final Report, Oct. 1991 - Sep. 1993
W. F. McBratney and J. A. Vanderhoff Jun. 1994 32 p Limited Reproducibility: More than 20% of this document may be affected by microfiche quality
(AD-A283770; ARL-TR-442) Avail: Issuing Activity (Defense Technical Information Center (DTIC))

A high-pressure windowed strand burner has been used to obtain burning rates for XM46 over the pressure range from 10 to 300 MPa. Burn rates for the liquid XM46 were erratic due to surface irregularities. This burning surface variable was minimized by gelling; two different gelling agents were used. The burn rate (r) vs. pressure (p) can be adequately expressed by an exponential of the form r = Apn. A definite pressure break occurs around 70 MPa for gelled XM46. For pressures below about 70 MPa, n is approximately 0.2 and for pressures between 70 and 300 MPa, the two different gelling agents gave n values of 1.0 and 1.2. DTIC

N95-19922 Tennessee Valley Authority, Norris, TN.
DEGRADATION OF AROMATIC HYDROCARBONS IN AN AQUIFER DURING A FIELD EXPERIMENT DEMONSTRATING THE FEASIBILITY OF REMEDIATION BY NATURAL ATTENUATION Final Technical Report, Oct. 1989 - Sep. 1992
Thomas B. Stauffer, Christopher P. Antworth, Riki G. Young, William G. MacIntyre, and J. M. Boggs Apr. 1994 155 p Limited Reproducibility: More than 20% of this document may be affected by microfiche quality
(AD-A283809; AL/EQ-TR-1993-0007) Avail: Issuing Activity (Defense Technical Information Center (DTIC))

The purpose of this experiment was to perform a controlled field experiment, involving the injection of several aromatic hydrocarbons and a nonreactive tracer into an uncontaminated aquifer. By monitoring the plume development of these solutes, and by measuring a number of physical and chemical characteristics of the aquifer, this study was designed to provide data on those properties which significantly control the propagation of dissolved contaminants in groundwater systems. A secondary objective was to measure the in situ degradation rates of the selected organic compounds. The disappearance and transformation of the organic solutes during this experiment demonstrated that natural degradation processes were able to effectively reduce these levels of dissolved organic contaminants in a reasonable time frame. This represents the most important result of this field study, since active remediation would not be needed in situations where natural degradation rates were sufficient to reduce contaminant concentrations to safe levels. The monetary and environmental cost savings of allowing natural biological restoration of the residual contaminants are potentially enormous. It appears that this study is the first field experiment to prove conclusively that hydrocarbon solute losses were due to chemical degradation rather than physical losses. DTIC

N95-19927# Michigan Biotechnology Inst., Lansing, MI.
BIOCONVERSION OF COAL DERIVED SYNTHESIS GAS TO LIQUID FUELS
M. K. Jain, R. M. Worden, and H. Grethlein 15 Apr. 1994 8 p
(Contract DE-AC22-92PC-92117)
(DE94-017381; DOE/PC-92117/T8) Avail: CASI HC A02/MF A01

The overall objective of the project is to develop an integrated two-stage fermentation process for conversion of coal-derived synthesis gas to a mixture of alcohols. This is achieved in two steps. In the first steps, Butyribacterium methylotrophicum converts carbon monoxide (CO) to butyric and acetic acids. Subsequent fermentation of the acids by Clostridium acetobutylicum leads to the production of butanol and ethanol. DOE

N95-20187# Materials Research Labs., Ascot Vale (Australia).
THE HOT FRAGMENT CONDUCTIVE IGNITION TEST FOR SCREENING LOVA PROPELLANTS
T. T. Nguyen and P. Berry Mar. 1994 12 p
(AD-A284259; MRL-TN-661; DODA-AR-008-629) Avail: CASI HC A03/MF A01

The Hot Fragment Conductive Ignition (HFCI) Test was set up to determine the relative ignitability of propellant grains in response to hot fragments of different masses heated to different temperatures. The minimum temperature at which the propellant ignites gives a measure of the ignitability of the propellant. The test is a rapid screening to evaluate the vulnerability of propellant to an external aggressive stimulus such as spall attack. A number of different types of propellants including CAB/RDX propellants, nitrocellulose (NC)-based propellants and HTPB/RDX composite propellants were tested. The HTPB/RDX and NC-based propellants were found to be more vulnerable than the CAB/RDX propellants. DTIC

N95-20253# Southwest Research Inst., San Antonio, TX.
EFFECT OF PROPANE-AIR ON NGVs AND VEHICLE FUELING STATIONS Topical Report, 1 Jan. - 1 Oct. 1993
W. E. Liss and D. S. Moulton Jun. 1994 181 p
(Contract GRI-5086-293-1848)
(PB94-210085; SWRI-3178-4.8; GRI-94/0158) Avail: CASI HC A09/MF A02

Propane-air (P/A) peakshaving is an important element of peak-load management for some U.S. gas utilities. P/A is used as a supplemental energy medium with natural gas and has been shown to operate satisfactorily in most natural gas applications. The propane levels injected are compatible with the pressures (under 200 psig) and temperatures (over 40 F) found in utility distribution networks. However, P/A can create problems for natural gas vehicles (NGVs) operating on compressed gas as well as NGV fueling stations. This report contains information on P/A peakshaving and its compatibility with NGV's by documenting condensation impacts at nine conditions--i.e., three propane levels and three temperatures. These data portray the depressurization of a vehicle tank, an area selected because it illustrates NGV operation and can discriminate between acceptable and potentially non-acceptable operating points. These analyses show, not surprisingly, a correlation exists between propane level, ambient temperature, and condensation. NTIS

N95-20899# Fermi National Accelerator Lab., Batavia, IL.
AGING TESTS OF ETHYLENE CONTAMINATED ARGON/ETHANE
M. Atac and G. Bauer (Massachusetts Inst. of Tech., Cambridge, MA.) 22 Sep. 1994 15 p
(Contract DE-AC02-76CH-03000)
(DE95-002526; FNAL/C-94/340-E) Avail: CASI HC A03/MF A01

We report on aging tests of argon/ethane gas with a minor (1800 ppM) component of ethylene. The measurements were first conducted with the addition of alcohol to test the suppression of aging by this additive, with exposure up to approximately 1.5 C/cm. Tests have included: a proportional tube with ethanol, another with isopropyl alcohol, and for comparison a tube has also been run with ethanol and argon/ethane from CDF's old (ethylene-free) ethane supply. The aging test with ethanol showed no difference between the ethylene-free and the ethylene tube. Furthermore, raw aging rates of argon/ethane and argon/ethane/ethylene were measured by exposing tubes without the addition of alcohol to about 0.1 C/cm. Again, no significant difference was observed. In conclusion, we see no evidence that ethylene contamination up to 1800 ppM has any adverse effect on wire aging. However, this level of ethylene does seem to significantly suppress the gas gain. DOE

N95-21161# Pratt and Whitney Aircraft, West Palm Beach, FL.
DEVELOPMENT OF AN ADVANCED JP-8 FUEL Final Report, Aug. 1990 - Jan. 1993
Tedd B. Biddle Dec. 1993 45 p
(Contract F33615-90-C-2051)
(AD-A285583; PWA-FR23047; WL-TR-94-2033) Avail: CASI HC A03/MF A01

Technical effort was directed at increasing the design limit of current JP-8 fuel from 325 F (163 C) to 425 F (218 C) at the fuel nozzle. The objective was to accomplish this near-term thermal stability goal solely through the use of a fuel soluble additive package. JP-Thermally stable fuel was considered the thermal stability target since it has the high-temperature properties sought from the significantly more economical JP-8 + 100 formulation. The additives were evaluated in an additive-free Jet A considered typical of fuel most likely to be encountered in the field. DuPont JFA-5, currently the only accepted thermally stability improving additive, was considered state of the art and used as a bench mark. Additive manufacturers were surveyed and solicited for candidate additives that had potential for improving fuel thermal oxidative stability. Test methods were developed and/or refined for use in screening additives. Using the Hot Liquid Process Simulator (HLPS) in conjunction with a LECO Carbon Determinator, 152 additives were screened. Additive performance was ranked based on surface carbon and differential pressure. Additional screening was performed using the Isothermal Corrosion Oxidation Test (ICOT). Additives screened included oxygen, sulfur, and nitrogen-type antioxidants; dispersants; detergents; metal deactivators; antifoulants; and proprietary thermal stability improvers. Twenty-seven experimental blends comprised of various additive combinations were tested. Five baseline fuels were evaluated. DTIC

N95-21211# Brookhaven National Lab., Upton, NY.
THE CARNOL PROCESS FOR METHANOL PRODUCTION AND UTILIZATION WITH REDUCED CO2 EMISSIONS
M. Steinberg and Yuanji Dong Oct. 1993 22 p Presented at the International Conference on Global Climate Change: Science, Policy and Mitigation Strategies, Phoenix, AZ, 5-8 Apr. 1994
(Contract DE-AC02-76CH-00016)
(DE94-016808; BNL-60575; CONF-940426-3) Avail: CASI HC A03/MF A01

A first order comparative mass and energy analysis is made of alternative processes for the production and utilization of methanol. Conventional reforming of natural gas with steam and CO2 indicates a yield of approximately 1 mol of methanol per mol of methane and a net emission of 1 mol of CO2 per mol of methanol. Three new processes called - Carnol I, Carnol II and Carnol III utilize CO2 as a feedstock in conjunction with hydrogen produced from the thermal decomposition of methane can reduce CO2 emission compared to the conventional process by 35%, 88%, and 100% respectively while reducing methanol production by 11%, 35%, and 39% respectively. The carbon from methane decomposition can be sequestered or sold as a commodity. The methanol can be used in the transportation sector as an alternative efficient fuel. A preliminary economic estimate indicates the equivalent cost for reduction of CO2 to be less than estimates for removal, recovery, and disposal of CO2 from power plant stack gas. The Carnol process leverages the CO2 reduction both from central fossil fuel fired power plants and the transportation sector. The Carnol process assists in the reduction of CO2 emission from an otherwise impossible collection of CO2 from highly dispersed heat engine and small scale fuel users. DOE

N95-21356# Bio-Process Innovations, Inc., West Lafayette, IN.
A LOW ENERGY CONTINUOUS REACTOR SEPARATOR FOR THE PRODUCTION OF ETHANOL FROM CORN GRITS/STARCH AND BIOMASS STREAMS Quarterly Report No. 2, 1 Aug. - 15 Oct. 1994
M. Clark Dale 1994 22 p
(Contract DE-FG01-94CE-15594)
(DE95-002256; DOE/CE-15594/T2) Avail: CASI HC A03/MF A01

This project is an attempt to develop and demonstrate an improved reactor for the production of ethanol from starch and ligno-cellulosic streams. Bio-Process Innovations holds a patent on this reactor technology, and is directing the project. A Continuous Stirred Reactor Separator (CSRS) is being built on a pilot plant scale for testing at a small Iowa ethanol plant (Permeate Refining) while bench scale tests on the reactor system are being performed at Purdue University. The CSRS unit combines several operations within the confines of the reactor vessel: (1) complex carbohydrates are reduced to simple sugars by enzymatic breakdown; (2) sugars are converted to ethanol by yeast or bacteria; and (3) the ethanol is separated by a stripping gas stream. The ethanol is removed from the stripping gas in an absorber, and then taken to an extractive distillation column. This unit should allow concentrated feeds to be converted to ethanol, and the use of bottoms recycle will be extensively tested to establish the limits of minimizing net bottoms water production leaving the plant. During the first quarter, a flocculant yeast was selected, a xylose fermenting yeast strain selected, and some experiments on no-cook starch conversion to ethanol completed. During the last (second) quarter, the authors have tested the effect of bottoms water recirculation on the reactor performance, the performance of the lab scale unit on molasses, and done some work on biomass conversion to ethanol. DOE

N95-21513# Sandia National Labs., Livermore, CA. Combustion Research Facility.
THERMAL DECOMPOSITION REACTIONS OF HMX AND RDX AND THEIR IMPORTANCE IN PREDICTING COOKOFF HAZARDS
Richard Jr. Behrens and Suryanarayana Bulusu (Army Armament Research, Development and Engineering Center, Picatinny Arsenal, NJ.) 1994 9 p Presented at the 1994 Joint Army, Navy, NASA, Air Force (JANNAF) Propulsion Systems Hazards Meeting, San Diego, CA, 1-5 Aug. 1994 Sponsored by ARDEC
(Contract DE-AC04-94AL-85000)
(DE95-002486; SAND-94-8709C; CONF-9408123-4) Avail: CASI HC A02/MF A01

Recent work on the decomposition of hexahydro-1,3,5-trinitro-s-triazine (RDX) and octahydro-1,3,5,7-tetranitro-1,3,5,7-tetrazocine (HMX), utilizing simultaneous thermogravimetric modulated beam mass spectrometry (STMBMS), has shown that they undergo significant decomposition in both the solid and liquid phases. Previous studies have determined the mechanisms of several reaction pathways that control the decomposition of these materials. This paper presents a summary of this previous work and how the results can be applied to developing models to predict the response of energetic materials in cookoff situations. DOE

N95-21514# Sandia National Labs., Livermore, CA. Materials Development and Diagnostics Dept.
THE PERMEATION OF BIS(2-FLUORO-2,2-DINITROETHYL) FORMAL (FEFO), ETHYL 4,4-DINITROPENTANOATE (EDNP), ETHYL 4-NITROPENTANOATE (ENP), AND 1,2,4-TRICHLOROBENZENE (TCB) THROUGH BARRIER MEMBRANES
Timothy J. Shepodd, Aaron R. Daniel, George M. Buffleben, and Patricia Foster (Mason Hanger Pantex Plant, Amarillo, TX.) Oct. 1994 23 p
(Contract DE-AC04-94AL-85000)
(DE95-002492; SAND-94-8239) Avail: CASI HC A03/MF A01

In support of the manufacture and storage of paste explosives, several membrane materials were evaluated as barriers to permeation. The permeation was quantified to evaluate leakage of the fluids from paste explosives during long-term storage. Four permeants were evaluated, though not every permeant was evaluated with every material. Mass uptake measurements were made during prolonged submersion of the materials in the permeants. Equilibrium amount absorbed and rate of absorption were used to calculate the diffusivity, and permeability of the given solvent/polymer pair. Permeabilities through membrane materials were judged using a cutoff of 10(exp -10) mol/s/m above which permeation was unacceptably high. None of the materials tested was suitable for containing TCB at 125 deg C. Additionally, PFA was unacceptable at 75 C. Viton showed unacceptable permeation in ENP, but FEP and PFA were effective barriers for ENP. No significant differences were found in the permeabilities of different thicknesses of FEP and PFA with ENP. All of the materials (including the elastomer Kalrez) tested with both the explosive FEFO and the propellant EDNP were adequate barriers to their permeation. Polyethylene is unsuitable for contact with FEFO at elevated temperatures because of chemical reactions that occur with the polymer. DOE

N95-21624 Materials Research Labs., Ascot Vale (Australia).
AN INITIAL ASSESSMENT OF THE PROPERTIES OF 2,5-DIPICRYL-1,3,4-OXADIAZOLE: A SECONDARY EXPLOSIVE WITH HIGH THERMAL STABILITY
Michael Kony, Lucianna Montelli, and Daniel J. Whelan Oct. 1993 14 p
(MRL-TR-93-16; AR-008-281) Copyright Avail: Issuing Activity (DSTO Materials Research Lab., PO Box 50, Ascot Vale, Victoria 3032, Australia)

The preparation and properties, including hazard assessment, of 2,5-dipicryl-1,3,4-ozadiazole (DPO) are discussed and compared to HNS. DPO was observed to have high thermal stability and was found to be less hazardous to electrostatic spark than HNS. Rotter impact sensitiveness data showed DPO to be more impact sensitive than HNS. Consequently DPO is not suitable, without desensitization, for use below the shutter, in the explosive train of fuzes. High specific surface area DPO (14.5 sq m/g) was prepared and its performance in small slapper detonator devices was evaluated and compared to that of HNS. Both DPO and HNS, at similar surface areas, were found to have similar shock initiation energies. Author

N95-21658 Materials Research Labs., Ascot Vale (Australia).
THE APPLICATION OF A STATISTICAL ANALYSIS SOFTWARE PACKAGE TO EXPLOSIVE TESTING
C. Lam Dec. 1993 58 p
(MRL-TR-93-42; AR-008-572) Copyright Avail: Issuing Activity (DSTO Materials Research Lab., PO Box 50, Ascot Vale, Victoria 3032, Australia)

The report describes a user-friendly software package for the analysis and presentation of results from explosive destructive testing. The analysis covers the Bruceton, Probit and Army Material Command Regulation (AMCR) statistical methods. The program is illustrated by its application to several small scale tests for the assessment of explosive sensitivity to various stimuli. They are the Gap test, Jet Sensitivity test, Slapper Detonator test and Cap Sensitivity test. The report includes an overview of the basis of the mathematical equations used in the evaluation of the statistical data, and the menu commands in the computer model are described. Author

N95-21678 Rockwell International Corp., Canoga Park, CA. Rocketdyne Div.
NOVEL FLUORINE OXIDIZERS Final Report, Jul. 1990 - Aug. 1993
Karl O. Christe and William W. Wilson Feb. 1994 48 p Limited Reproducibility: More than 20% of this document may be affected by microfiche quality
(Contract F04611-90-C-0011)
(AD-A279480; RI/RD-93-176; PL-TR-93-3058; AD-E201866) Avail: Issuing Activity (Defense Technical Information Center (DTIC))

This reports the results of a three-year program in novel energetic materials. The majority of the results was summarized in 30 manuscripts which are in various stages of publication. Major achievements include the synthesis of the ClF6(-) anion, the combination of the N(CH3)4(+) cation with powerful halogen fluorine anion oxidizers, the synthesis of truly anhydrous N(CH3)4F which generated a worldwide renaissance in high coordination number chemistry, the synthesis of XeF5(-) which is the first known example of a pentagonal planar species, the synthesis of OsO2F4, the development of a quantitative scale for the strength of oxidizers, and the discovery of a new class of vibrationally stable polynitrogen compound. DTIC

N95-21951 Defence Science and Technology Organization, Melbourne (Australia). Aeronautical and Maritime Research Lab.
DIFFUSE REFLECTANCE SPECTRA OF ENERGETIC MATERIAL
Rodney A. J. Borg Sep. 1994 24 p
(DSTO-TR-0065; AR-008-928) Copyright Avail: Issuing Activity (DSTO Aeronautical and Maritime Research Lab., GPO Box 4331, Melbourne, Victoria 3001, Australia)

The diffuse reflectance spectra of pure, solid HNS, TNT, HMX, RDX and PETN have been recorded. These spectra reveal that all of the high explosives (HE) have strong absorption profiles in the UV region of the spectrum and much weaker absorption in the visible/near infrared. The influence of particle size on the diffuse reflectance spectra has also been investigated. Reducing the particle size leads to a blue shift of the diffuse reflectance spectrum. The strength of the absorption of the pure HE and the UV region obscures details in the absorption profile. Dilution of the HE with a strong reflector was used to reduce the magnitude of the absorption and allow the UV absorption to be revealed in detail. Chemical interaction between the diluent and HE reduces the general applicability of this approach. Author

N95-21966# Southwest Research Inst., San Antonio, TX. Automotive Products and Emissions Research Div.
NATURAL GAS CONVERTER PERFORMANCE AND DURABILITY Topical Report, May 1992 - Jun. 1994
Jeff J. White and James N. Carroll Sep. 1994 61 p See also PB92-101468 and PB92-127059 Prepared for Gas Research Inst., Chicago, IL
(Contract GRI-5086-293-1848)
(PB95-135554; SWRI-3178-4.23; GRI-94/0314; GETA-94-04) Avail: CASI HC A04/MF A01

The objective of this work was to determine the durability performance of stoichiometric dual-bed converters designed for light and medium-duty natural gas vehicle applications. Converters using palladium-only (Pd) rear bricks were to be compared to Chrysler's production intent dual brick platinum/rhodium (Pt/Rh) converter. Durability performance benefits of varying noble metal loadings were to be evaluated. A high severity engine aging procedure was to be developed, where 300 hours would approximate 50,000 or more vehicle miles, and 600 hours would approximate 100,000 or more vehicle miles. NTIS

N95-22114*# National Aeronautics and Space Administration. Lewis Research Center, Cleveland, OH.
NUMERICAL STUDY OF CONTAMINANT EFFECTS ON COMBUSTION OF HYDROGEN, ETHANE, AND METHANE IN AIR
H. T. Lai (NYMA, Inc., Brook Park, OH.) and S. R. Thomas Feb. 1995 14 p Presented at the Sixth International Aerospace Plane and Hypersonics Conference, Chattanooga, TN, 10-14 Apr. 1995; sponsored by AIAA
(Contract NAS3-27186; RTOP 505-62-52)
(NASA-TM-106844; E-9409; NAS 1.15:106844; AIAA Paper 95-6097)
Avail: CASI HC A03/MF A01

A numerical study was performed to assess the effects of vitiated air on the chemical kinetics of hydrogen, ethane, and methane combustion with air. A series of calculations in static reacting systems was performed, where the initial temperature was specified and reactions occurred at constant pressure. Three different types of test flow contaminants were considered: NP, H2O, and a combustion of H2O and CO2. These contaminants are present in the test flows of facilities used for hypersonic propulsion testing. The results were computed using a detailed reaction mechanism and are presented in terms of ignition and reaction times. Calculations were made for a wide range of contaminant concentrations, temperatures and pressures. The results indicate a pronounced kinetic effect over a range of temperatures, especially with NO contamination and, to a lesser degree, with H2O contamination. In all cases studied, CO2 remained kinetically inert, but had a thermodynamic effect on results by acting as a third body. The largest effect is observed with combustion using hydrogen fuel, less effect is seen with combustion of ethane, and little effect of contaminants is shown with methane combustion. Author

N95-22227# Aerospace Corp., El Segundo, CA. Technology Operations.
LAUNCH SAFETY, TOXICITY, AND ENVIRONMENTAL EFFECTS OF THE HIGH PERFORMANCE OXIDIZER CLF(5)
J. A. Syage 31 Mar. 1994 33 p
(Contract F04701-93-C-0094)
(AD-A286095; TR-94(4231)-4; SMC-TR-94-38) Avail: CASI HC A03/MF A01

An assessment is presented for the human toxicity, environmental, and ecological consequences resulting from accidental releases of ClF5 liquid propellant. Various accident scenarios are considered involving instantaneous releases of 2000 kg of propellant. Plume dispersion profiles were calculated using the AFTOX code for typical climate conditions at Vandenberg Air Force Base (VAFB). For a ground-based cold spill or combustion, the area exceeding long-term human exposure levels is less than 1 km square, and the exposure time is well under an hour (typically several minutes). The area exceeding short-term exposure levels is probably less than 0.1 km square. The toxic hazard is is likely to be less important than the combustion and fire hazard to on-site personnel. Plant life damage would be limited to temporary leaf burns and some defoliation within 300 meters of the spill site. Sea life would be unaffected in the vicinity of

VAFB. Further study should consider the complex interplay of aerosol dynamics and heterogeneous chemistry with propellant and by-products as well as ground deposition of propellant and by-products by gaseous (dry) and aerosol (wet) fallout. The stratospheric impact of a post-launch explosion is small. Fluorine is not very destructive of the ozone due to the extreme stability of the sink molecule HF. The amount of chlorine compound resulting from a combustion of 2000 kg of ClF5 is not large enough to have a significant effect on the stratosphere, even on a transient scale. Routine solid rocket motor firings present a far greater chlorine load on the atmosphere than does any credible ClF5 accident scenario. DTIC

29 MATERIALS PROCESSING

Includes space-based development of products and processes for commercial applications.

For biological materials see *55 Space Biology.*

N95-21322*# National Aeronautics and Space Administration, Washington, DC.

MICROGRAVITY: TEACHER'S GUIDE WITH ACTIVITIES FOR PHYSICAL SCIENCE

Gregory L. Vogt (National Aeronautics and Space Administration. Lyndon B. Johnson Space Center, Houston, TX.), Michael J. Wargo, and Carla B. Rosenberg, ed. Jan. 1995 78 p

(NASA-EG-103; NAS 1.19/4:103) Avail: CASI HC A05/MF A01

This guide is an educational tool for teachers of grades 5 through 12. It is an introduction to microgravity and its application to spaceborne laboratory experiments. Specific payloads and missions are mentioned with limited detail, including Spacelab, the International Microgravity Laboratory, and the United States Microgravity Laboratory. Activities for students demonstrate chemistry, mathematics, and physics applications of microgravity. Activity objectives include: modeling how satellites orbit Earth; demonstrating that free fall eliminates the local effects of gravity; measuring the acceleration environments created by different motions; using a plasma sheet to observe acceleration forces that are experienced on board a space vehicle; demonstrating how mass can be measured in microgravity; feeling how inertia affects acceleration; observing the gravity-driven fluid flow that is caused by differences in solution density; studying surface tension and the fluid flows caused by differences in surface tension; illustrating the effects of gravity on the burning rate of candles; observing candle flame properties in free fall; measuring the contact angle of a fluid; illustrating the effects of gravity and surface tension on fiber pulling; observing crystal growth phenomena in a 1-g environment; investigating temperature effects on crystal growth; and observing crystal nucleation and growth rate during directional solidification. Each activity includes a background section, procedure, and follow-up questions. CASI

N95-22261# Oak Ridge National Lab., TN.

GRAVITATIONAL EFFECTS ON THE DEVELOPMENT OF WELD-POOL AND SOLIDIFICATION MICROSTRUCTURES

L. A. Boatner, S. A. David, and G. Workman (Alabama Univ., Huntsville, AL.) 1994 8 p Presented at the Microgravity Materials Science Conference, Huntsville, AL, 24-25 May 1994

(Contract DE-AC05-84OR-21400)

(DE94-017772; CONF-9405220-1) Avail: CASI HC A02/MF A01

This research effort has as its objective the development of a quantitative understanding of the effects of both low- and high-g environments on the solidification microstructures and morphologies that are produced in alloy single crystals during a variety of melting and solidification processes. The overall goal of the effort is to delineate the nature of the roles played by natural convection, surface-tension-driven convection, and mass transport effects due to interactions associated with various heating methods that are used to form melt pools in practical, commercially important alloy systems. The experimental and theoretical investigations comprising this effort encompass the study of configurations in which stationary heat sources are employed as well as melt pools formed by moving heat sources like those frequently used in fusion-welding processes. DOE

31 ENGINEERING (GENERAL)

Includes vacuum technology; control engineering; display engineering; cryogenics; and fire prevention.

N95-20050# Argonne National Lab., IL.

SOLIDIFICATION MODELING OF A SPIRAL CASTING TO DETERMINE MATERIAL FLUIDITY

S. Ahuja, H. M. Domanus, R. C. Schmitt, L. Chuzhoy (Caterpillar Tractor Co., Peoria, IL.), and J. V. Grabel (Caterpillar Tractor Co., Peoria, IL.) Feb. 1994 11 p

(Contract W-31-109-eng-38)

(DE94-018930; ANL-94/11) Avail: CASI HC A03/MF A01

In casting, fluidity is the measure of the distance a metal can flow in a channel before being stopped by solidification. During mold filling, the metal loses heat to the surrounding mold, thereby cooling and becoming more viscous until the leading portion solidifies and no further flow is possible. A coupled heat-transfer and fluid-flow modeling of a spiral, involving the use of thermophysical properties to determine material fluidity, has been conducted. Fluidity experiments were performed by Caterpillar; several spiral test castings were poured. Simulations of these experiments utilized the Casting Process Simulator (CaPS) software developed at Argonne National Laboratory. Two types of spiral geometries with different assumptions were considered: (1) a two-dimensional laterally stretched spiral; and (2) a three-dimensional lateral spiral. The computed extent of mold filling is in good agreement with the experimental results. Time required by the metal/gas interface to attain specific positions in the spiral arm also compared favorably with the experimental results. The influence of process variables, especially pour time, is discussed. The CaPS software has been used as a computational tool to investigate the validity of the dimensionality assumptions and to evaluate the ability of CaPS to model fluidity adequately. DOE

N95-20194# Oak Ridge National Lab., TN.

PROCEEDINGS OF THE 1993 NON-FLUOROCARBON INSULATION, REFRIGERATION AND AIR CONDITIONING TECHNOLOGY WORKSHOP

1994 329 p Workshop held in Wiesbaden, Germany, 27-29 Sep. 1993

(Contract DE-AC05-84OR-21400)

(DE94-018333; ORNL-6805; CONF-9309409) Avail: CASI HC A15/MF A03

Sessions included: HFC blown polyurethanes, carbon dioxide blown foam and extruded polystyrenes, plastic foam insulations, evacuated panel insulation, refrigeration and air conditioning, absorption and adsorption and stirling cycle refrigeration, innovative cooling technologies, and natural refrigerants. Selected papers have been indexed separately for inclusion in the Energy Science and Technology Database. DOE

N95-20288# Los Alamos National Lab., NM.

NUMERICAL CONTROLLED POLISHING PROGRAM, CONTINUED FORCED WEAR AND PART CORRECTION EXPERIMENTS

Philip R. Hannah, Robert D. Day, Douglas J. Hatch, and E. Ray McClure 1994 5 p Presented at the American Society for Precision Engineers (ASPE) Conference, Cincinnati, OH, 2-7 Oct. 1994

(Contract W-7405-eng-36)

(DE94-018084; LA-UR-94-2716; CONF-9410185-1-Extd-Abst) Avail: CASI HC A01/MF A01

This abstract reports the near completion of the first phase of this program. It is the aim of this program to provide the operator of a N/C diamond turning machine or N/C grinding machine (jig grinder) with the wear characteristics necessary to achieve uniform material removal. The second phase of this program addresses a different problem, although solving this problem is highly dependent on the results of the first phase. Diamond turned, or any lathe turned surface, exhibits regular tool marks due to the tool passing over the surface being cut. Changes in depth of cut, feed rate and work rpm will change the character of these grooves, but will not eliminate them. Optical surfaces produced by this process exhibit increased scattering as the light wavelength decreases limiting their use; at least for optical purposes, to IR and some visible applications. Utilizing wear information gathered in the first part of this program we will attempt to reduce these residual tool marks by polishing. The polishing of diamond turned surfaces is not new. Diamond turned metal surfaces, especially in electroless nickel and high phosphorus nickel electroplate have been polished to improve their scatter characteristics. What we believe is unique is the use of a spherical wheel, rotating on axis and being moved over the part in a prescribed manner by numerical control. Over the past year we have made some major changes in our polishing methods and procedures. We have listed below these changes, as a refresher for the reader as to our previous procedures. These changes will be addressed in the body of the text. DOE

N95-20356# Lawrence Livermore National Lab., Livermore, CA.
THE DEVELOPMENT AND EVALUATION OF WATER-MIST FIRE EXTINGUISHING SYSTEMS
D. G. Beason and K. J. Staggs Aug. 1994 3 p
(Contract W-7405-eng-48)
(DE94-019019; UCRL-ID-118068) Avail: CASI HC A01/MF A01

Fire protection for underfloor space is primarily provided by Halon 1301 which has proven to be very effective. However, due to the link between halons and the possible depletion of the stratospheric ozone layer, plans have been implemented to eventually phase out Halon 1301 and 1211. In September 1987 the Montreal Protocol concerning chlorofluorocarbons (CFC) and halons was signed by the United States, the European Economic Community, and 23 other nations. The Montreal Protocol calls for freezing halon production at 1986 levels. Because the majority of underfloor fire protection at Lawrence Livermore National Laboratory (LLNL), as well as other Department of Energy (DOE) sites, is either Halon 1301 or sprinklers, some other means of suppression will have to be developed and verified. The potential loss to facilities housing computer or control rooms damaged by underfloor fires can be extreme. These losses would not only include hardware and software replacement costs, but also lost computing and control capability. Here at LLNL technical research in a facility could be severely affected. Recent studies conducted by the Fire Research Discipline of the Special Projects Division have shown that severe fires fueled by cable insulation can develop within as little as a 6-in-high underfloor space (even with mechanical ventilation shut off). Studies also show that conventional sprinklers may not be effective in preventing this destruction. Therefore, we are investigating the water-mist fire extinguishing system as an alternative to Halon 1301 and sprinklers. DOE

N95-20611# Naval Research Lab., Washington, DC.
TRAINING SIMULANT FOR HALON 1211 PORTABLE EXTINGUISHERS
Joseph T. Leonard, R. Burns (Hughes Associates, Inc., Columbia, MD.), P. Jones (Hughes Associates, Inc., Columbia, MD.), and R. Ouellette (Hughes Associates, Inc., Columbia, MD.) 8 Sep. 1994 31 p
(AD-A285403; NRL/MR/6180-94-7615) Avail: CASI HC A03/MF A01

The Standard Navy portable Halon 1211 extinguisher can be modified to provide an environmentally acceptable simulant for training. The modifications include replacement of the Halon 1211 with pressurized water as the fire fighting agent and insertion of a full cone spray nozzle in the horn of the extinguisher to form a suitable spray pattern. The modified extinguisher has the same physical appearance and discharge characteristics (time, reach, etc.) as the standard Halon 1211 extinguisher and weighs just two pounds less. Since it uses water as the fire fighting agent, the training simulant has zero Ozone Depletion Potential, zero Global Warming Potential and is non-toxic. Also, there is a potential savings of $160,000-$190,000 per year, based on a usage of 20,000 lbs/year of Halon 1211 for training. DTIC

N95-20717# National Inst. of Standards and Technology, Gaithersburg, MD. Fire Science Div.
ANNUAL CONFERENCE ON FIRE RESEARCH: BOOK OF ABSTRACTS
Abstracts Only
Sheilda B. Smith, ed. Oct. 1994 181 p Conference held in Gaithersburg, MD, 17-20 Oct. 1994
(PB95-104964; NISTIR-5499) Avail: CASI HC A09/MF A02

The contents of this conference include: Suppression Using Halocarbons - Laboratory Studies; Fire Hazard, Risk, and Data; Suppression Using Halocarbons - Large-Scale Studies; Suppression Using Water; Pool Fires; Fire-Induced Flows; Chemistry and Physics of Material and Product Combustion; Soot; Fire Signatures; Flame Spread; Fire Plumes. NTIS

N95-21027 Selskapet for Industriell og Teknisk Forskning, Trondheim (Norway). Div. of Production Engineering.
SIMULATION OF THE INJECTION MOULDING PROCESS
J. Hu and T. Christensen 10 Dec. 1993 46 p See also PB94-171147
(PB94-215555; STF20-A93218) Avail: Issuing Activity

Simulation of the injection molding process is a helpful way for the engineers who work with plastics processing. By simulation, they will get some important parameters which sometimes are highly necessary for the mold design and processing. Thus, the engineers will save much time to do experiments for the parameters. Two simulation programs are used in this report, namely CADMOULD and CADMOULD MEFISTO which are designed by Institut fur Kunststoffverarbeitung (IKV) in Aachen, W. Germany. CADMOULD works with 2-D geometry and is specialized for rheological, thermal and mechanical calculation. It is installed on a personal computer, while CADMOULD MEFISTO works in 3-D and is installed on a VAX 8530 computer at SINTEF. A PC version of this program is also available. This report deals with CADMOULD and CADMOULD MEFISTO. The construction of flow lines, balancing of sprue system, the optimizing of injection time, and gate(s) optimizing are mainly included. NTIS

N95-21129# National Inst. of Standards and Technology, Gaithersburg, MD. Building and Fire Research Lab.
FIREDOC USERS MANUAL, 3RD EDITION
Nora H. Jason Dec. 1993 50 p See also 2nd edition, PB91-178830
(PB95-128674; NISTIR-5305) Avail: CASI HC A03/MF A01

FIREDOC is the on-line bibliographic database which reflects the holdings (published reports, journal articles, conference proceedings, books, and audiovisual items) of the Fire Research Information Services (FRIS) at the Building and Fire Research Laboratory (BFRL), National Institute of Standards and Technology (NIST). This manual provides step-by-step procedures for entering and exiting the database via telecommunication lines, as well as a number of techniques for searching the database and processing the results of the searches. This Third Edition is necessitated by the change to a UNIX platform. The new computer allows for faster response time if searching via a modem and, in addition, offers internet accessibility. FIREDOC may be used with personal computers, using DOS or Windows, or with Macintosh computers and workstations. A new section on how to access Internet is included, and one on how to obtain the references of interest to you. Appendix F: Quick Guide to Getting Started will be useful to both modem and Internet users. NTIS

N95-21130# National Inst. of Standards and Technology, Gaithersburg, MD. Building and Fire Research Lab.
SUMMARIES OF BFRL FIRE RESEARCH IN-HOUSE PROJECTS AND GRANTS, 1994
Nora H. Jason, ed. Oct. 1994 213 p See also report for 1993, PB94-121050
(PB95-130845; NISTIR-5504) Avail: CASI HC A10/MF A03

This report describes the fire research projects performed in the Buildings and Fire Research Laboratory (BFRL) and under its extramural grants program during Fiscal Year 1993. Included are research performed both with funds appropriated to the BFRL Fire Research Program and under contract to outside organizations. The BFRL Fire Research Program has directed its efforts under four program thrusts. The in-house priority projects, extramural grants, and externally-funded efforts thus form an integrated, focussed ensemble. This publication is organized along those lines: (1) Performance-based Fire Standards; (2) Fire Safe Materials and Products; (3) Advanced Fire Sensing and Suppression; (4) Large/Industrial Fires. For the convenience of the reader, an alphabetical listing of all grants is contained in the Part 2.0. NTIS

N95-21333 Technical Research Centre of Finland, Espoo (Finland).
DETERMINATION OF LAYER MODULI FROM FALLING WEIGHT DEFLECTOMETER MEASUREMENTS
A. Ruotoistenmaeki 1994 71 p
(PB95-129748; VTT/RN-1552) Copyright Avail: Issuing Activity (National Technical Information Service (NTIS))

Back calculation programs are used for evaluation of pavement layer moduli from falling weight deflectometer (FWD) measurements. A comparison of two programs with different calculation methods, Modulus and Elmod, is made using deflection data derived from 43 SHRP-LTPP (Strategic Highway Research Program, Long-Term Pavement Performance) test sections. Critical strains were calculated using the linear program (BISAR) with layer moduli from the Modulus program as input and with the Elmod program. It was found that calculated strains from the two programs agree very well, even though the calculated moduli are quite different. Calculated strains from FWD loading were compared with measured strains under moving wheel load at Virttaa test site. The differences between the two are most likely due to differences in the loading conditions and in the method of analysis. NTIS

N95-21422 Helsinki Univ. of Technology, Espoo (Finland). Lab. of Konepajatekniikan.

SAFETY ISSUES IN HIGH SPEED MACHINING [SUURNOPEUSJYRSINNAEN TYOETURVALLISUUS]

31 May 1994 74 p In FINNISH Prepared in cooperation with Technical Research Centre of Finland, Espoo, Finland
(PB95-127411; KPT-4/94) Avail: Issuing Activity (National Technical Information Service (NTIS))

There are several risks related to High-Speed Milling, but they have not been systematically determined or studied so far. Increased loads by high centrifugal forces may result in dramatic hazards. Flying tools or fragments from a tool with high kinetic energy may damage surrounding people, machines and devices. In the project, mechanical risks were evaluated, theoretic values for kinetic energies of rotating tools were calculated, possible damages of the flying objects were determined and terms to eliminate the risks were considered. The noise levels of the High-Speed Machining center owned by the Helsinki University of Technology (HUT) and the Technical Research Center of Finland (VTT) in practical machining situation were measured and the results were compared to those after basic preventive measures were taken. NTIS

N95-21559# Oak Ridge National Lab., TN.

NEW CONCEPTS FOR REFRIGERANT LEAK DETECTION AND MIXTURE MEASUREMENT

F. C. Chen, S. L. Allman, and C. H. Chen 1993 8 p Presented at the 1993 International CCFC and Halon Alternatives Conference, Washington, DC, 20-22 Oct. 1993
(Contract DE-AC05-84OR-21400)
(DE94-018967; CONF-9310191-3) Avail: CASI HC A02/MF A01

Since the discovery that chlorofluorocarbons (CFC's) destroy the ozone layer, the need to reduce the release of these refrigerants into the environment has become critical. A total ban of ozone-depleting CFC's is expected within a few years, and hydrofluorocarbons (HFC's) and fluorocarbons (FC's) and their mixtures are expected to be used during a transition period. Several HFC and FC refrigerants are currently being considered as CFC substitutes. The electronic refrigerant leak detectors currently being considered as CFC substitutes. The electronic refrigerant leak detectors currently on the market were developed to detect CFC's and are not as sensitive to HFC's. Although incremental improvement can be made to these devices to detect HFC's, they often lead to increased false signals. Also, there is no simple device available to measure the composition of a refrigerant mixture. The authors present two new concepts to aid in the development of two portable instruments that can be used for HFC leak detection and for quantitative measurement of refrigerant mixture compositions. The development of simple, easy-to-use portable leak detectors and refrigerant mixture meters is essential to the wide use of alternative refrigerants in industry. DOE

N95-21598 Donmar Ltd., Newport Beach, CA.

EVALUATION OF STATE-OF-THE-ART HIGH SPEED DELUGE SYSTEMS PRESENTLY IN SERVICE AT VARIOUS US ARMY AMMUNITION PLANTS Final Report, Jan. - Mar. 1993

A. D. Goedeke and G. A. Fadorsen Sep. 1993 72 p Limited Reproducibility: More than 20% of this document may be affected by microfiche quality
(Contract F08635-91-C-0217)
(AD-A279102; WL-TR-93-3510) Avail: Issuing Activity (Defense Technical Information Center (DTIC))

A brief study was made of ultra high speed deluge systems used in Army ammunition plants for fire protection against pyrotechnic and propellant material-type fires/explosions. The evaluation included both fire detectors and fire suppressant devices and technologies. It was found that the technologies being utilized today have not been optimized for the specific fire application. In general, it was found that there is a lack of information on the properties of the fire events themselves that detectors are supposedly designed to respond to. No data exists on spectral irradiances in the IR or UV spectral bands where the current detectors operate. A need exists to determine the sources that may be responsible for detector false alarms. Tests should be conducted on the performance of current systems and on other detection and suppression techniques, notably, machine vision fire detection. It is recommended that field testing of old and new hardware systems be conducted; modifications be made to optimize currently installed systems; a new system capability be developed which better meets the overall threat, performance, and reliability requirements; and a thorough purchase description/performance specification be developed. DTIC

N95-21625 Materials Research Labs., Ascot Vale (Australia).

COMPARISON OF HFC-134a AND THE TERNARY BLEND, SUVA MP39, AS REPLACEMENTS FOR THE REFRIGERANT, CGC-12

Lyn E. Fletcher Sep. 1993 20 p
(MRL-GD-0051; AR-008-273) Copyright Avail: Issuing Activity (DSTO Materials Research Lab., PO Box 50, Ascot Vale, Victoria 3032, Australia)

The refrigerant gas CFC-12 has been widely used in Royal Australian Navy (RAN) equipment. With the Montreal protocol phase-out of this and other ozone depleting substances, alternative refrigerant gases must be identified. These replacements would ideally have the same efficiency as CFC-12, cause no health and safety risks and allow changeover to proceed with minimal costs. This paper reviews the attributes of two refrigerant gases, HFC-134a and Suva MP39, which are being considered by the RAN. Author

N95-21626 Army Cold Regions Research and Engineering Lab., Hanover, NH.

OPERATING MANUAL FOR HYBRID THERMOSYPHONS AT THE GAKONA POWER PLANT, ALASKA

F. D. Haynes, Frederick C. Crory, Kurt V. Knuth, and William F. Quinn Mar. 1994 27 p Limited Reproducibility: More than 20% of this document may be affected by microfiche quality
(AD-A279068; CRREL-SR-94-3) Avail: Issuing Activity (Defense Technical Information Center (DTIC))

A power plant building was constructed in 1990 at an over-the-horizon radar site in Gakona, Alaska. Since it was built on permafrost, thermal protection between the building and the underlying permafrost was included in the design, which included rigid board insulation and hybrid thermosyphons placed in the gravel fill under the building. Soil temperature is monitored with eight thermistor strings placed under and at the building perimeter. This manual describes the steps that must be taken to ensure foundation stability, including directions on when to use the thermosyphons in the active, mechanical refrigeration mode. A data acquisition system using a computer-controlled datalogger is described. DTIC

N95-21631# Air-Conditioning and Refrigeration Technology Inst., Inc., Arlington, VA.

MATERIALS COMPATIBILITY AND LUBRICANTS RESEARCH ON CFC-REFRIGERANT SUBSTITUTES

S. R. Szymurski, M. Hawley, G. C. Hourahan, and D. S. Godwin Aug. 1994 81 p
(Contract DE-FG02-91CE-23810)
(DE94-018414; DOE/CE-23810/42) Avail: CASI HC A05/MF A01

The Materials Compatibility and Lubricants Research (MCLR) program supports critical research to accelerate the introduction of CFC and HCFC refrigerant substitutes. The MCLR program addresses refrigerant and lubricant properties and materials compatibility. The primary elements of the work include data collection and dissemination, materials compatibility testing, and methods development. The work is guided by an Advisory Committee consisting of technical experts from the refrigeration and air-conditioning industry and government agencies. The Air-Conditioning and Refrigeration Technology Institute, Inc., (ARTI) manages and contracts multiple research projects and a data collection and dissemination effort. Detailed results from these projects are reported in technical reports prepared by each subcontractor. DOE

N95-21633 Technische Univ., Delft (Netherlands). Electronic Instrumentation Lab.
SURFACE MICROMACHINED CAPACITIVE TACTILE IMAGE SENSOR Ph.D. Thesis
M. R. Wolffenbuttel 25 Apr. 1994 136 p
(PB95-108031; ISBN-90-6275-967-X) Copyright Avail: Issuing Activity (National Technical Information Service (NTIS))

An overview of the various available sensing principles for tactile images and the strategies for the fabrication of these structures are presented, starting from the earliest elastomer-based structures and concluding with recently presented silicon-based structures with on-chip instrumentation. Some principal aspects in the mechanical functioning of the sensor structure are discussed. The realization of the tactile image sensor with on-chip transistors is discussed, with the focus on the technological feasibilities. The available principles for the read-out of a sensor capacitance to detect the stretching of silicon diaphragms under mechanical pressures is presented. Other circuit elements which are required to interface a digital processor are described, and a series of simulation and measurement results to examine the agreement with the theoretical models are presented. NTIS

N95-21651 Selskapet for Industriell og Teknisk Forskning, Trondheim (Norway). Dept. for Materials Technology.
EXTRUDATE SWELL AND EXTRUDATE DISTORTION OF HDPE AS A RESULT OF DIFFERENT DEFORMATION MECHANISMS DURING EXTRUSION THROUGH CAPILLARY DIES
S. Eggen and E. L. Hinrichsen 8 Jun. 1994 31 p
(PB95-110227; STF24-A94039) Avail: Issuing Activity (National Technical Information Service (NTIS))

The effect of varying the die entrance angle and the die length on extrudate swell and on the onset of extrudate distortion in capillary extrusion has been studied. Using theory from the literature, the authors have analyzed the contribution to the total pressure drop from the elongational and shear deformation in the entrance region, and from the capillary pressure drop in the land region of the die. From the contribution of the elongational deformation, they obtained an estimate for the elongational viscosity of the polymer. The same analysis was also used to study the influence of the die geometry on the stick-slip instability. The authors also propose a model for predicting extrudate swell. Input to the model are material parameters obtainable from oscillatoric measurements of the loss and storage modulus and parameters calculated from the geometry of the die. Some of the parameters needed in the model are obtained from a silimar analysis as the one used to derive the elongational properties of the polymer based on the contribution to the pressure drop from the different deformation mechanisms the entrance region. The model includes a fitting parameter that sets the overall scale of the swell. NTIS

N95-21978 National Defence Research Establishment, Stockholm (Sweden). Dept. of Weapons Systems, Effects and Protection.
FIRE SMOKE VENTILATION THROUGH SHAFTS: EXPERIMENTS [BRANDVENTILATION GENOM SCHAKT: EXPERIMENT]
K. Nireus, P. O. Werling, S. G. Hansson, and B. Onnermark Jun. 1994 30 p In SWAHILI
(PB95-132247; FOA-A-20061-2.6) Avail: Issuing Activity (National Technical Information Service (NTIS))

An experimental investigation studied the fire smoke filling of a large compartment (6 x 6 x 6 m) ventilated through shafts of various heights (0, 2, 4, 6 m). The fuel was kerosene. The experiments measured the optical smoke density (OD) and the gas temperature (T) at various heights. By visual observation the height of the smoke layer (h) was measured. The result of the investigation was primarily the large collection of data (OD, T, h) to be used in future tests of calculation models. Directly observed was only a weak correlation between the smoke filling and the heights of the ventilation shafts. NTIS

N95-22014# Selskapet for Industriell og Teknisk Forskning, Trondheim (Norway). Div. of Architecture and Building Technology.
FRAME AND EDGE SEAL TECHNOLOGY: A STATE OF THE ART SURVEY
Marit Thyholt, Inger Andresen, Berit Hugdal (Technical Univ. of Norway, Trondheim.), and Oeyvind Aschehoug (Technical Univ. of Norway, Trondheim.) 3 Apr. 1994 64 p
(PB95-110334; STF62-A94004) Avail: CASI HC A04/MF A01

In windows, the glazing is traditionally mounted in an operable or fixed frame, made of wood, metal (steel or aluminum), or PVC. The glazing component in solar collectors and solar walls is also typically mounted in a frame. The purpose of the frame is to protect the vulnerable edge of the glazing and give structural stability, which is especially important in operable windows. Sealed multipane glazings are almost exclusively fabricated with a metal (aluminum or galvanized steel) spacer bar along the edges. New advanced glazings will require new types of frame and edge seal products. As the insulation properties of the glazing itself reach a performance close to that of well-insulated opaque walls, the thermal bridging caused by the spacer bars and the frames will be unacceptable, even for wooden windows. The new glazings will also integrate other functions, which again will influence the design of the frames. There are already quite a few new technological developments in this field. New materials and products for the edge seal and the frame are being developed, and computer calculations gradually take over the manual analysis and laboratory testing of new products. The objective of this IEA Task 18 Case Study is to investigate the influence of the frame and glazing edge seal on the total U-value of a glazing system, to develop improved test and calculation methods, and to design, construct, and test low thermal loss frames for use in advanced glazing applications. NTIS

32 COMMUNICATIONS AND RADAR

Includes radar; land and global communications; communications theory; and optical communications.

For related information see also *04 Aircraft Communications and Navigation* and *17 Space Communications, Spacecraft Communications, Command and Tracking.* For search and rescue see *03 Air Transportation and Safety,* and *16 Space Transportation.*

N95-19890# Technische Univ., Eindhoven (Netherlands). Dept. of Mathematics and Computing Science.
ALGEBRAIC SEMANTICS OF MESSAGE SEQUENCE CHARTS
S. Mauw and M. A. Reniers Apr. 1994 53 p
(PB95-110581) Avail: CASI HC A04/MF A01

Message Sequence Charts is a graphical and textual language for the description and specification of the interactions between system components and their environment. The language is standardized by the ITU-TS (the Telecommunication Standardization section of the International Telecommunication Union, the former CCITT). The main area of application for Message Sequence Charts is as an overview specification of the communication behavior of real-time systems, in particular telecommunication switching systems. Message Sequence Charts may be used for requirement specification, interface specification, simulation and validation, test-case specification and documentation of real-time systems. In the paper the authors present a formal semantics of Message Sequence Charts exploiting techniques from process algebra. The semantics is proposed for standardization within the ITU-TS. The authors start with the semantics of the core language of Message Sequence Charts, Basic Message Sequence Charts, and subsequently add other features such as process creation and termination, refinement and timer handling. NTIS

N95-19932# Defense Systems Management School, Fort Belvoir, VA.
AN ABSTRACT MODEL OF ROGUE CODE INSERTION INTO RADIO FREQUENCY WIRELESS NETWORKS. THE EFFECTS OF COMPUTER VIRUSES ON THE PROGRAM MANAGEMENT OFFICE Ph.D. Thesis
Christopher V. Feudo Apr. 1994 158 p
(AD-A285759; DSMC-TR-4-94) Avail: CASI HC A08/MF A02

This dissertation demonstrates that inadequately protected wireless LANs are more vulnerable to rogue program attack than traditional LANs. Wireless LANs not only run the same risks as traditional LANs, but they also run additional risks associated with an open transmission medium. Intruders can scan radio waves and, given enough time and resources, intercept, analyze, decipher, and reinsert data into the transmission medium. This dissertation describes the development and instantiation of an abstract model of the rogue code insertion process into a DOS-based wireless communications system using radio frequency (RF) atmospheric signal transmission. The model is general enough to be applied to widely used target environments such as UNIX, Macintosh, and DOS operating systems.

The methodology and three modules, the prober, activator, and trigger modules, to generate rogue code and insert it into a wireless LAN were developed to illustrate the efficacy of the model. Also incorporated into the model are defense measures against remotely introduced rogue programs and a cost-benefit analysis that determined that such defenses for a specific environment were cost-justified. DTIC

N95-19973 Naval Postgraduate School, Monterey, CA.
A SIMPLE ANALYTICAL MODEL FOR ASYNCHRONOUS DENSE WDM/OOK SYSTEMS M.S. Thesis
Yun-Yao Huang Jun. 1994 78 p Limited Reproducibility: More than 20% of this document may be affected by microfiche quality
(AD-A283725) Avail: CASI HC A05

We derive the closed form expression for the bit error probability of asynchronous dense WDM systems employing an external OOK modulator. Our model is based upon a close approximation of the optical Fabry-Perot filter in the receiver as a single-pole RC filter for the signals that are bandlimited to a frequency band approximately equal to one sixtieth of the Fabry-Perot filter's free spectral range. Our model can handle bit rates up to 2.5 Gb/s for a free spectral range of 3800 GHz land up to 5 Gb/s when the power penalty is 1 dB or less. DTIC

N95-19997# Naval Air Warfare Center, China Lake, CA. Weapons Div.
EXPERIMENTAL PROOF-OF-CONCEPT OF PHASE DERIVATIVE BASED RANGE PROFILE ENHANCEMENT ATR Interim Report, Oct. 1993 - Mar. 1994
Dave Banks, Eric VanBronkhorst, Dave Gagnon, and Brett Borden Aug. 1994 15 p
(AD-A284921; NAWC-WPNS-TP-8204) Avail: CASI HC A03/MF A01

This report documents an initial effort to experimentally verify a novel automatic target recognition (ATR) technique applicable to airborne radar targets. The method uses the information about the target's cross-range structure, which is statistically encoded in the radar tracking data and is potentially applicable to many existing radar missile systems. DTIC

N95-20065 Naval Postgraduate School, Monterey, CA.
THE DESIGN AND ANALYSIS OF A PHASED ARRAY MICROSTRIP ANTENNA FOR A LOW EARTH ORBIT COMMUNICATION SATELLITE M.S. Thesis
William L. Barfield Jun. 1994 95 p Limited Reproducibility: More than 20% of this document may be affected by microfiche quality
(AD-A284791) Avail: CASI HC A05

A Naval Postgraduate School spacecraft design class proposed a multiple beam, phased array, microstrip antenna as part of the preliminary design of a low earth orbit communication satellite. The antenna must provide coverage over the satellite's entire field of view while both uplink and down-link operate simultaneously on the same 1-band frequency. This thesis assesses the feasibility of the antenna proposed in that preliminary design. Design tradeoffs for a microstrip array constrained by both available surface area and a limited mass budget are examined. Two different substrate materials are considered in terms of weight and performance. Microstrip patch theory is applied to array element design and layout and antenna array theory is applied to determine phase and amplitude coefficients. The focus of the design is on obtaining the desired beam shape and orientation, given antenna size constraints. A corporate feed method is discussed and a general design presented. Antenna performance is predicted through the use of a computer model based on Modal Expansion theory and results are plotted in a series of graphs which demonstrate the limitations of the proposed design. DTIC

N95-20164# Los Alamos National Lab., NM. Biophysics Group.
EVALUATION OF SUPERCONDUCTING QUANTUM INTERFERENCE DEVICES INTERFACED WITH DIGITAL SIGNAL PROCESSING ELECTRONICS FOR BIOMAGNETIC APPLICATIONS
Pang-Jen Kung, Edward R. Flynn, Roger R. Bracht, and Paul S. Lewis 1994 6 p Presented at the ICSPAT 1994: Signal Procession Applications and Technology, Dallas, TX, 18-21 Oct. 1994
(Contract W-7405-eng-36)
(DE94-016186; LA-UR-94-2620; CONF-9410164-2) Avail: CASI HC A02/MF A01

The performances of a dc-SQUID magnetometer driven by both analog electronics and digital signal processors are investigated and compared for biomagnetic applications. Low-noise (less than 5 microns (Phi) (sub 0)/(radical)Hz at 1 Hz) dc-SQUID's were fabricated by Conductus, Inc. using the all-refractory Nb/Al/Al2O3/Nb process on silicon substrates with on-chip modulation coils and integral washer damping resistors. A second-order gradiometer was magnetically coupled to the input coil of the SQUID to maximize the detected signal strength. The readout of this SQUID gradiometer was achieved using a conventional flux-locked loop (FLL) circuit to provide a linearized voltage output that was proportional to the flux applied to the SQUID. A shielded cylinder was constructed to house the magnetometer to reduce ambient field noise. To realize the digital feedback loop, the analog FLL is replaced except for the preamplifier by a digital signal processing board with dual 16-bit A/D and D/A converters. This approach shows several advantages over the analog scheme including operational flexibility, cost reduction, and possibly, the enhancement of dynamic ranges and slew rates. DOE

N95-20191# National Inst. of Standards and Technology, Boulder, CO. Electronics and Electrical Engineering Lab.
MEASUREMENTS OF SHIELDING EFFECTIVENESS AND CAVITY CHARACTERISTICS OF AIRPLANES
D. A. Hill, M. L. Crawford, R. T. Johnk, A. R. Ondrejka, and D. G. Camell Jul. 1994 63 p
(PB94-210051; NISTIR-5023) Avail: CASI HC A04/MF A01

We present measured data for shielding effectiveness, cavity Q, and cavity time constant of three small (twin-engine) airplanes for frequencies from 400 MHz to 18 GHz. Both CW and time-domain measurement methods were used, and the time-domain method yields higher values of cavity Q. Both methods yield Q values below a theoretical upper bound determined by window leakage losses. The measured shielding effectiveness is quite variable, but averages about 15 dB. The measured time constants are also variable and average about 15 ns. This short time constant is a result of the low Q of the aircraft cavities. NTIS

N95-20211# Mitre Corp., Bedford, MA.
RCS CALCULATION CAPABILITY
1994 52 p
(AD-A286329; MP-94B0000087) Avail: CASI HC A04/MF A01

Over several years, the MITRE Sensor Center has developed and used a capability to calculate the radar cross section (RCS) of complex targets rapidly and accurately. A significant number of projects have been supported with this capability. Capabilities include RCS calculations across frequencies, polarizations, and aspect angles of intercept as well as the calculation of targets over the sea and in various terrain conditions. These capabilities are illustrated and summarized. Derived from text

N95-20214# Department of Energy, Washington, DC. Office of Energy Research.
BEYOND TELECOMMUTING: A NEW PARADIGM FOR THE EFFECT OF TELECOMMUNICATIONS ON TRAVEL
J. S. Niles Sep. 1994 87 p
(DE95-001224; DOE/ER-0626) Avail: CASI HC A05/MF A01

Conventional wisdom about social and economic behavior holds that the use of telecommunications is a natural substitute for transportation. For example, telephone calls can replace travel to meetings, and facsimile or electronic-mail transmission of documents substitutes for courier or postal delivery. The moving of information can replace the moving of people and goods. Vehicle traffic on the national transportation infrastructure can be replaced by digital traffic on what is now called the national information infrastructure (NII). A leading example is telecommuting. This means using telecommunications to replace commuting between home and work. Telecommuting is an optional way of expanding employees' work locations in those circumstances where it yields both improved organizational performance and employee satisfaction. Telecommuting accounts for 7.6 million U.S. workers as of early 1993, up 15% from the 6.6 million counted in 1992. The growth of telecommuting has been strong for the past five years. No one has identified any reasons to suggest that this growth will abate in the forseeable future. DOE

N95-20270 Department of the Navy, Washington, DC.
GENERAL PURPOSE SIDELOBE CANCELLER SYSTEM Patent
Frank F. Kretschmer, Jr., inventor (to Navy) and Bernard L. Lewis, inventor

(to Navy) 27 Sep. 1994 7 p Filed 26 Feb. 1979
(AD-D016560; US-Patent-5,351,058; US-Patent-Appl-SN-025952; US-Patent-Class-342-384) Avail: US Patent and Trademark Office

A digital, open-loop, sidelobe canceller system includes an arrangement of auxiliary-channel preprocessing cancellers and a series of main-channel cancellers in which specific cancellers average a different number of samples for cancelling both barrage (continuous) jamming and false-target-repeater jamming, which enter the sidelobes of a radar antenna. The preprocessing cancellers and each of the main-channel cancellers, except the last succeeding main-channel canceller, use long-time averaging (averaging over a large number, n, of samples of the main and auxiliary signals, where n is much greater than 2) for removing barrage jamming from the main signal. The last succeeding main-channel canceller uses short-time averaging (averaging over approximately 2-4 samples) for removing false-target-repeater jamming from the main signal. DTIC

N95-20306# Cornell Univ., Ithaca, NY. Dept. of Computer Science.
A GROUP COMMUNICATION APPROACH FOR MOBILE COMPUTING MOBILE CHANNEL: AN ISIS TOOL FOR MOBILE SERVICES
Kenjiro Cho and Kenneth P. Birman May 1994 18 p
(Contract N00014-92-J-1866)
(AD-A279785; TR-94-1424) Avail: CASI HC A03/MF A01

This paper examines group communication as an infrastructure to support mobility of users, and presents a simple scheme to support user mobility by means of switching a control point between replicated servers. We describe the design and implementation of a set of tools, called Mobile Channel, for use with the ISIS system. Mobile Channel is based on a combination of the two replication schemes: the primary-backup approach and the state machine approach. Mobile Channel implements a reliable one-to-many FIFO channel, in which a mobile client sees a single reliable server; servers, acting as a state machine, see multicast messages from clients. Migrations of mobile clients are handled as an intentional primary switch, and hand-offs or server failures are completely masked to mobile clients. To achieve high performance, servers are replicated at a sliding-window level. Our scheme provides a simple abstraction of migration, eliminates complicated hand-off protocols, provides fault-tolerance and is implemented within the existing group communication mechanism. DTIC

N95-20308 Defence Research Establishment Ottawa, Ottawa (Ontario).
FACSIMILE TRANSMISSION STANDARDS
Andrew Mudry and Brad Poulin Oct. 1993 51 p Limited Reproducibility: More than 20% of this document may be affected by microfiche quality
(AD-A279911; DREO-TN-93-18) Avail: Issuing Activity (Defense Technical Information Center (DTIC))

Modern tactical communications systems are becoming increasingly compatible with existing civilian systems. This compatibility allows the military to take advantage of the equipment available commercially and spare the expense of developing costly customized systems. It also increases the interoperability of various communications systems employed by allies involved in multinational operations. Finally, the compatibility allows the military to augment its telecommunications assets with existing commercial equipment and networks during times of conflict. One civilian communication standard that has recently been adopted by the military for tactical communications is that of facsimile. Facsimile is now commonly used on the battlefield for the transmission of tactical maps and situation reports. This technical note examines the requirements for facsimile transmission. An overview of the various facsimile standards are given, followed by a detailed description of the most commonly used standard; CCITT Group III. The Group III specifications are a composite of various CCITT modulation and encoding standards. These consist of V.21, V.27ter, and V.29 modulations, as well as T.4 image encoding standards, and T.30 signalling specifications. Each of these standards is described in the context of facsimile transmissions. A complete description of the handshaking which occurs between the facsimile transmitter and receiver is given. DTIC

N95-20376# Sparta, Inc., Lexington, MA.
BACKSCAT LIDAR SIMULATION VERSION 4.0: TECHNICAL DOCUMENTATION AND USERS GUIDE
David R. Longtin, Michael G. Cheifetz, James R. Jones, and John R. Hummel 10 Jun. 1994 149 p
(Contract F19628-91-C-0093)
(AD-A285851; LTR94-001; PL-TR-94-2170; SR-8) Avail: CASI HC A07/MF A02

SPARTA's BACKSCAT software package simulates the performance of lidars for remote sensing and other atmospheric applications. The package accommodates a wide range of lidar systems, viewing scenarios, and atmospheric conditions, plus it contains a user-friendly menu interface system for specifying input parameters. This report gives technical documentation and a users guide for BACKSCAT Version 4.0. In this effort, comprehensive and versatile signal-to-noise (SNR) performance models have been introduced into BACKSCAT. The SNR models give performance and range accuracy estimates for direct detection and coherent Doppler lidar systems, plus estimates of the wind speed accuracy for coherent Doppler systems. The models contain all important noise sources inherent in the detection process and allow the user to select from built-in detectors, as well as define their own detector specifications. In response to the user community, five water clouds have been added to BACKSCAT and they can be 'clicked-on' automatically as built-in cloud models. BACKSCAT Version 4.0 also contains an auxiliary software package, MABS, that estimates the molecular absorption profile for a lidar wavelength. MABS generates output that can be used in a simulation. Because MABS performs a broadband calculation, it is not intended to be a complete treatment of the molecular absorption problem. Finally, methods of handling the increased size of the BACKSCAT package have been developed. DTIC

N95-20474# Sandia National Labs., Albuquerque, NM.
A WIDEBAND EMP TEST SYSTEM
G. J. Rohwein, J. F. Aurand, C. A. Frost, L. D. Roose, and S. R. Babcock 1994 4 p Presented at the 21st International Power Modulator Symposium, Costa Mesa, CA, 27-30 Jul. 1994
(Contract DE-AC04-94AL-85000)
(DE94-015283; SAND-94-1781C; CONF-9407102-2) Avail: CASI HC A01/MF A01

A wideband EMP tester consisting of a high voltage modulator, transmission line, high voltage peaking switch, and a TEM test cell has been developed that delivers repetitive high frequency EMP pulses to an RF-sealed double-test volume of about 1 cu ft. The pulse shape is rectangular, has a duration of 4 ns and a risetime of 120 ps. The system can be operated at pulse repetition rates up to 1500 Hz and electric field levels up to 125 kV/m. Both voltage and pulse rate are continuously adjustable over these ranges may be operated in any combination. DOE

N95-20545 Dartmouth Coll., Hanover, NH. Dept. of Mathematics.
APPLICATIONS OF WAVELETS TO RADAR, IMAGING AND RELATED PROBLEMS Final Report, 1 Jul. 1990 - 30 Sep. 1993
Reece Prosser and Dennis M. Healy, Jr. 30 Sep. 1993 14 p Limited Reproducibility: More than 20% of this document may be affected by microfiche quality
(Grant AF-AFOSR-0292-90)
(AD-A279909; AFOSR-94-0333TR) Avail: Issuing Activity (Defense Technical Information Center (DTIC))

A primary concern of this study has been waveform design for active inverse problems of acoustic and electromagnetic variety. We developed several useful results in the specific areas of electromagnetic and acoustic bullets, signal design for doppler ultrasound velocimetry and magnetic resonance imaging, and limited data tomography problems arising in medical imaging and in radar. Another area of proposed research involved the construction of maximum likelihood receivers for various novel signal sources, such as those arising in particular wideband acoustic data, and image data from non-euclidean sources. We have developed efficient algorithms in both of these regimes. In particular, we have studied receivers for application to wideband acoustic signal processing in acoustic velocimetry for the dense target environments occurring in Doppler ultrasound problems, and computationally efficient matched filter processor for the sphere. This has direct application to directional data of various forms, with applications from remote sensing problems to quality assurance for CAD/CAM. DTIC

N95-20556# Naval Air Warfare Center, China Lake, CA. Weapons Div.
A COLOCATED MAGNETIC LOOP, ELECTRIC DIPOLE ARRAY ANTENNA (PRELIMINARY RESULTS) Interim Report, Oct. 1993 - Sep. 1994
P. L. Overfelt, D. R. Bowling, and D. J. White Sep. 1994 38 p
(AD-A285381; NAWC-WPNS-TP-8212) Avail: CASI HC A03/MF A01

We present a detailed electromagnetic analysis of an electrically small colocated electric dipole and magnetic loop antenna array. This antenna is the simplest example of the Grimes multipole class of antenna arrays. We have determined that since the interaction term between the two elements disappears from the radial complex power, we were able to set the radial reactance to zero by choosing appropriate current magnitudes and phases on the array elements. By driving the two elements in quadrature, we obtained a much increased radiation intensity and directivity as well as increased radiated power. DTIC

N95-20599 Massachusetts Inst. of Tech., Lexington, MA. Lincoln Lab.
GPS-SQUITTER CAPACITY ANALYSIS
Vincent A. Orlando and William H. Harman 20 May 1994 46 p Limited Reproducibility: More than 20% of this document may be affected by microfiche quality
(Contracts DTFA01-93-Z-02012; F19628-90-C-0002)
(AD-A280037; ATC-214) Avail: Issuing Activity (Defense Technical Information Center (DTIC))

GPS-Squitter is a system concept that merges the capabilities of Automatic Dependent Surveillance (ADS) and the Mode S beacon radar. The result is an integrated concept for seamless surveillance and data link that permits equipped aircraft to participate in ADS and/or beacon ground environments. This concept offers many possibilities for transition from a beacon to an ADS-based environment. This report provides the details of the techniques used to estimate GPS-Squitter surveillance and data link capacity. Surveillance capacity of airborne aircraft is calculated for the omni and six-sector ground stations. Next, the capacity of GPS-Squitter for surface traffic is estimated. The interaction between airborne and surface operations is addressed to show the independence of these systems. Air ground data link capacity for GPS-Squitter is estimated, together with an estimate of the use of the Mode S link to support other ground surveillance and data link activities as well as TCAS operation. The analysis indicates the low transponder occupancy resulting from the total effect of these activities. Low occupancy is a key requirement in avoiding interference with the operation of the current ATCRBS and future Mode S interrogators. DTIC

N95-20605 Engineering and Economics Research, Inc., Vienna, VA.
ADVANCED COMMAND AND CONTROL (C2) APPLICATIONS INTERFACES TO THE ADVANCED COMMUNICATIONS TECHNOLOGY SATELLITE (ACTS) Final Report
26 Apr. 1994 35 p Limited Reproducibility: More than 20% of this document may be affected by microfiche quality
(Contract DABT65-93-D-0002)
(AD-A279676) Avail: CASI HC A03

This report documents the equipment, software configuration, physical connections, and procedures required to interface advanced C2 applications with the Advanced Communications Technology Satellite (ACTS) Very Small Aperture Terminal (VSAT). This document describes how to interface the PictureTel 4000, Model 200E, video teleconferencing (VTC) system, the Warrior intelligence processor, Multiple Subscriber Equipment (MSE), and multispectral imagery (MSI) with the ACTS VSAT. Additionally, it also details the communications link from the Leader Development Center (LDC) to the Battle Command Battle Lab (BCBL) at Ft. Leavenworth, Kansas. DTIC

N95-20666# Naval Postgraduate School, Monterey, CA.
EMITTER LOCATION VIA KALMAN FILTERING OF SIGNAL TIME DIFFERENCE OF ARRIVAL M.S. Thesis
Richard W. Williamson Sep. 1994 158 p
(AD-A285972) Avail: CASI HC A08/MF A02

A relatively simple time domain method is developed to calculate the time of arrival for radar signals. The error present in the estimate of the time of arrival for a single pulse and a burst of pulses is developed and the effects of SNR, PRF, pulsewidth, and sampling frequency are examined. Time of arrival is used with multiple sensors and the Kalman filter to estimate the location of the emitter. Algorithms estimate the location of an emitter given the Time Difference of Arrival (TDOA) of a single pulse as well as the TDOA of bursts of pulses received as the emitter scans past the receivers. The algorithms were tested on simulated data. DTIC

N95-20692# Organisatie voor Toegepast Natuurwetenschappelijk Onderzoek, The Hague (Netherlands). Fysisch en Elektronisch Lab.
DIFFRACTION COMPUTATION BY MEANS OF THE METHOD OF EQUIVALENT CURRENTS
L. J. VanEwijk May 1994 45 p
(AD-A285347; FEL-94-B195; TDCK-94-1395) Avail: CASI HC A03/MF A01

In this report the derivation of the Method of Equivalent Currents is given. This method can be used to compute the diffraction of plane waves by edges. A computation of this sort is necessary in addition to a scattering computation using Physical Optics or Geometrical Optics, because these last techniques neglect edge effects by definition. The reason that the Method of Equivalent Currents is chosen is because it is a powerful method, valid at almost all incidence and scattering aspects. Some of the few remaining singularities of the method can be removed in a way described in this report as well. Some interesting comparisons with measured data will be given in order to show the capabilities and shortcomings of the method. DTIC

N95-20697# Los Alamos National Lab., NM.
INNOVATIVE USE OF DSP TECHNOLOGY IN SPACE: FORTE EVENT CLASSIFIER
S. Briles, K. Moore, P. Klingner, D. Neagley, M. Caffrey, K. Henneke, W. Spurgen, P. Blain (Edgerton, Germeshausen and Grier, Inc., Idaho Falls, ID.), and R. Jones 1994 8 p Presented at the ICSPAT 1994: Signal Procession Applications and Technology, Dallas, TX, 18-21 Oct. 1994
(Contract W-7405-eng-36)
(DE94-016086; LA-UR-94-2506; CONF-9410164-5) Avail: CASI HC A02/MF A01

The Fast On-Orbit Recording of Transient Events (FORTE) small satellite will field a digital signal processor (DSP) experiment for the purpose of classifying radio-frequency (RF) transient signals propagating through the earth's ionosphere. Designated the Event Classifier experiment, this DSP experiment uses a single Texas Instruments' SMJ320C30 DSP to execute preprocessing, feature extraction, and classification algorithms on down-converted, digitized, and buffered rf transient signals in the frequency range of 30 to 300 MHz. A radiation-hardened microcontroller monitors DSP- abnormalities and supervises spacecraft command communications. On-orbit evaluation of multiple algorithms is supported by the Event Classifier architecture. Ground-based commands determine the subset and sequence of algorithms executed to classify a captured time series. Conventional neural network classification algorithms will be some of the classification techniques implemented on-board FORTE while in a low-earth orbit. Results of all experiments, after being stored in DSP flash memory, will be transmitted through the spacecraft to ground stations. The Event Classifier is a versatile and fault-tolerant experiment that is an important new space-based application of DSP technology. DOE

N95-20771# Kaman Sciences Corp., Albuquerque, NM.
FAULT DETECTION TECHNIQUES FOR COMPLEX CABLE SHIELD TOPOLOGIES Final Report, 24 Aug. 1992 - 24 Aug. 1993
Kurt H. Coonrod, Stuart L. Davis, and Donald P. McLemore Sep. 1994 65 p
(Contract F29601-92-C-0109)
(AD-A286632; PL-TR-93-1111) Avail: CASI HC A04/MF A01

This document presents the results of a basic principles study which investigated technical approaches for developing fault detection techniques for use on cables with complex shielding topologies. The study was limited to those approaches which could realistically be implemented on a fielded cable, i.e., approaches which would require partial disassembly of a cable were not pursued. The general approach used was to start with present transfer impedance measurement techniques and modify their use to achieve the best possible measurement range. An alternative test approach, similar to a sniffer type test, was also investigated. DTIC

N95-20775 Helsinki Univ. of Technology, Espoo (Finland). Electromagnetics Lab.
DC POTENTIAL ANOMALIES CAUSED BY A CONDUCTING BODY IN AN ANISOTROPIC CONDUCTING HALF-SPACE
Mikko J. Flykt, Esko H. Eloranta (Finnish Centre for Radiation and Nuclear Safety, Helsinki, Finland.), Keijo I. Nikoskinen, Ismo V. Lindell, and Ari H. Sihvola Mar. 1994 18 p Limited Reproducibility: More than 20% of

this document may be affected by microfiche quality
(ISSN 0784-848X)
(PB95-127106; ISBN-951-22-1985-9) Avail: CASI HC A03

Image theory for DC problems involving a current source in an anisotropic half-space bounded by either a perfectly magnetically conducting (PMC) or electrically conducting (PEC) plane is being used to get the solution for the potential in integral form. A dipole approximation for a small sphere is developed. NTIS

N95-20825# Army Research Lab., Adelphi, MD.
LOW-COST CONICAL ULTRA-WIDEBAND ANTENNA Final Report, May - Jun. 1994
Eric E. Funk and Stephen E. Saddow Nov. 1994 17 p
(AD-A286569; ARL-TR-302) Avail: CASI HC A03/MF A01

One of the necessary pieces of equipment needed for ultra-wideband (UWB) radio effects measurements is a suitable UWB field probe and radiating antenna. The conical monopole antenna (CMA) is an easy-to-fabricate, inexpensive, and useful UWB device that can be used for both of these applications. In this report we present information that should allow both antenna designers and users to quickly assemble a custom CMA to meet their design goals. A subjective explanation of the theory of operation is presented along with analytical expressions that predict the radiated and received pulse shapes. Experimental results are presented to verify the CMA theory of operation; these results also serve as an example of how UWB radiation can be monitored with a CMA during field measurements. DTIC

N95-20858# Army Tank-Automotive Command, Warren, MI.
ELECTROMAGNETIC INTERFERENCE TESTING AND ELECTRICAL SUBSYSTEM: NON-COMMUNICATION
Dec. 1994 23 p
(AD-A286591; TOP-2-2-613) Avail: CASI HC A03/MF A01

This TOP describes procedures for conducting Electromagnetic Interference (EMI) tests of Non-Communication Electronic Equipment (NCEE) and Mobile Equipment Power (MEP) sources. DTIC

N95-20904# Atmospheric and Environmental Research, Inc., Cambridge, MA.
REAL-DATA TESTS OF A SINGLE-DOPPLER RADAR ASSIMILATION SYSTEM
Thomas Nehrkorn, James Hegarty, and Thomas M. Hamill 30 Jun. 1994 55 p
(Contract F19628-91-C-0011)
(AD-A286638; PL-TR-94-2199; SR-5) Avail: CASI HC A04/MF A01

Real data tests of a single-Doppler radar data assimilation and forecast system have been conducted for a Florida sea breeze case. The system consists of a hydrostatic mesoscale model used for prediction of the preconvective boundary layer, an objective analysis that combines model first guess fields with radar derived horizontal winds, a thermodynamic retrieval scheme that obtains temperature information from the three-dimensional wind field and its temporal evolution, and a Newtonian nudging scheme for forcing the model forecast to closer agreement with the analysis. As was found in earlier experiments with simulated data, assimilation using Newtonian nudging benefits from temperature data in addition to wind data. The thermodynamic retrieval technique was successful in retrieving a horizontal temperature gradient from the radar-derived wind fields that, when assimilated into the model, led to a significantly improved forecast of the seabreeze strength and position. DTIC

N95-20921# Advisory Group for Aerospace Research and Development, Neuilly-Sur-Seine (France). Electromagnetic Wave Propagation Panel.
MULTIPLE MECHANISM PROPAGATION PATHS (MMPPs): THEIR CHARACTERISATION AND INFLUENCE ON SYSTEM DESIGN [LES TRAJETS DE PROPAGATION DES ONDES A MECANISMES MULTIPLES (MMPP): CARACTERES ET INCIDENCES SUR LA CONCEPTION DES SYSTEMES]
Jul. 1994 415 p In ENGLISH and FRENCH Symposium held in Rotterdam, Netherlands, 4-7 Oct. 1993 Original contains color illustrations
(AGARD-CP-543; ISBN-92-835-0750-9) Copyright Avail: CASI HC A18/MF A04

This publication reports the papers presented to a specialists' meeting held by the Electromagnetic Wave propagation Panel at its Fall 1993 meeting. The topics covered on the occasion of that symposium on the subject of 'Multiple Mechanism Propagation Paths (MMPP's): Their Characterization and Influence on System Design' included: (1) propagation and noise aspects; (2) examples of MMPP systems; (3) system design to exploit or reduce the effects of MMPP's; and (4) future work. For individual titles, see N95-20922 through N95-20961.

N95-20922# Shape Technical Center, The Hague (Netherlands). Communications Div.
HIGHLY SURVIVABLE COMMUNICATIONS: COMPLEMENTARY MEDIA PACKET SWITCHED NETWORKS
D. Yavuz, F. Eken, and N. Karavassilis *In* AGARD, Multiple Mechanism Propagation Paths (MMPPs): Their Characterisation and Influence on System Design Jul. 1994 14 p (For primary document see N95-20921 06-32)
Copyright Avail: CASI HC A03/MF A04

The requirement for highly survivable communications (HSC) for essential command functions in military operations does not need any justification. The ability to communicate under extreme jamming levels and adverse propagation conditions, including high altitude nuclear events, is a very important requirement. There are also many natural disaster related requirements that also need such highly survivable communications. The prevalent and in a sense classical, approach to provide highly assured connectivity can be summarized as follows: Take a particular propagation medium and try to obtain the ultimate performance from it. There are many examples of this philosophy some successful, most not. Our approach, on the other hand, is to use complementary multi-media or mixed-media where communication links utilizing essentially commercial-off-the-shelf (COTS) equipment are integrated using packet radio (PR) techniques. There is also, in our view, an even more fundamental, recently discovered consideration why the expectation of continuous incremental refinement of a system using a given single media may be be achievable. This is derived from the theory of 'deterministic uncertainty' or more popularly known as 'theory of CHAOS', systems whose state space behavior has fractal characteristics. We will elaborate on this novel argument. Complementary multi-media approach has been the focus for all HSC communications activities at STC since 1982. The original STC studies and prototypes were in response to requirements of broadcasting (i.e., one-way transmission) information. A high frequency (HF)/meteorburst (MB) system was developed/prototyped/tested demonstrating the cost effectiveness of the approach. These results are reviewed. More recently, in 1992 STC has completed the development/test of an Open Systems Interconnection (OSI) HF packet radio protocol as no such open or non-proprietary protocol exists. This protocol has been fully tested, documented and made available to all NATO nations/industries. These extensive results show that significant improvements in throughput of up to many times are obtained. A similar development for an OSI MB protocol has also been completed and combined with the HF protocol to obtain an OSI HF/MB link layer protocol with unique properties for HSC networks. Description of these protocols and the relevant results are presented. The conclusion is that, HSC networks using standard COTS transceivers/modems with OSI PRO protocols can provide highly survivable connectivity, by providing the most important ingredient of survivability, media diversity. Author

N95-20923# Shape Technical Center, The Hague (Netherlands).
QoS DRIVEN ROUTING IN PACKET SWITCHED NETWORKS OF MULTIPLE TRANSMISSION MEDIA
C. Tamvaclis *In* AGARD, Multiple Mechanism Propagation Paths (MMPPs): Their Characterisation and Influence on System Design Jul. 1994 9 p (For primary document see N95-20921 06-32)
Copyright Avail: CASI HC A02/MF A04

This paper discusses the application of Quality of Service (QoS) driven routing on packet-swtiched, heterogeneous networks. It is assumed that the network makes use of multiple transmission media of different types including narrowband radio based media such as those used in military tactical and emergency networks, e.g. ECCM SATCOM, HF radio, etc. A critical problem in the operation of such networks is the volatile performance of the transmission media, compounded by the fact that each transmission medium may respond differently to stress conditions. QoS driven routing provides an effective way to handle transmission media performance fluctuations and optimizing the use of all the available communication resources. QoS driven routing means that packet routes are selected according to a global optimization criterion that takes into account not only network connectivity, but also the application QoS requirements, and the currently available QoS from the network links. A routing architecture is described for implementing QoS driven routing on a connectionless internetwork of multiple transmission media. This architecture is based on the use of civilian networking standards and it is implementable using commercial off-the-shelf equipment. Author

N95-20924# Hull Univ. (England). Dept. of Electronic Engineering.

A MMPP COMMUNICATIONS SYSTEM FOR THE FREQUENCY RANGE 2-200MHz

M. Darnell, P. Walker, N. Riley, and G. Vongas (Defence Research Agency, Cosham, England.) *In* AGARD, Multiple Mechanism Propagation Paths (MMPPs): Their Characterization and Influence on System Design Jul. 1994 11 p (For primary document see N95-20921 06-32)

Copyright Avail: CASI HC A03/MF A04

This paper describes the work being carried out to realize a robust digital radio communications system, operational over the frequency range 2-200MHz, which will utilize the existence of multiple mechanism propagation paths (MMPP'S) in order to maximize link-availability. The system incorporates a substantial element of PC-based Digital Signal Processing (DSP). This work is essentially a unification of several areas of ongoing research within the Hull-Lancaster Communications Research Group (HLCRG) on the application of PC and DSP technology in radio system design. Author

N95-20925# Hull Univ. (England). Hull-Lancaster Communications Research Group.

MODELLING AND SIMULATION OF HF/VHF MMPPs

N. G. Riley, M. Darnell, and G. Vongas (Defence Research Agency, Cosham, England.) *In* AGARD, Multiple Mechanism Propagation Paths (MMPPs): Their Characterisation and Influence on System Design Jul. 1994 10 p (For primary document see N95-20921 06-32)

Copyright Avail: CASI HC A02/MF A04

Modelling codes exist for many of the propagation mechanisms which may prevail in the frequency range of approximately 2 to 200MHz and many of the models are embodied in CCIR recommendations. Within the past few years, a number of simulation codes have been developed for use within various projects carried out by the Hull-Lancaster Communications Research Group (HLCRG). The proposed paper will describe current work aimed at bringing together the various models and simulation codes in order to produce a realistic simulation of the multiple mechanism propagation path. The multiple mechanisms under consideration conventionally include groundware, ionospheric skywave, sporadic E, ducting and the various scatter modes. In addition, recent work carried out by the HLCRG has revealed that tropospheric reflection may be responsible for stable propagation which is usable in the frequency range 30 to 70MHz for short (up to 400km) over the horizon paths. The development of a propagation model for this mechanism will be included in the presentation. Author

N95-20926# Lancaster Univ. (England). Dept. of Engineering.

ADAPTIVE ERROR-CONTROL SCHEME FOR 2-200 MHz MULTIPLE-MECHANISM PROPAGATION PATHS

B. Honary, M. Darnell (Hull Univ., England.), and G. Vongas (Defence Research Agency, Cosham, England.) *In* AGARD, Multiple Mechanism Propagation Paths (MMPPs): Their Characterisation and Influence on System Design Jul. 1994 6 p (For primary document see N95-20921 06-32)

Copyright Avail: CASI HC A02/MF A04

In automatic repeat request (ARQ) systems, i.e. those that depend on feedback from the receiver as to the state of the received message, relatively low 'overhead' check digits are required for reliable error detection. A properly designed system of this type can be very reliable, but under poor channel conditions the number of repetitions become excessive. Forward error correction techniques that can correct a mixture of burst and random errors are most suitable for predictable real channels. Recently, an adaptive coding technique has been introduced. The main purpose of an adaptive coding scheme is to permit only the necessary degree of error correction to be applied to the transmitted information according to the channel conditions. The concatenated codes, first introduced by Forney, are formed by cascading two encoders, an inner and outer, where the first is usually a linear binary code, or a combination of two linear binary codes, and the outer is usually a multi-level Reed-Solomon (RS) code over GF(2 exp m). It is known, that with choice of inner and outer codes, concatenated codes become very powerful codes for random and burst error correction. The objective of the proposed paper is to investigate adaptive concatenated codes, which can provide a more efficient error protection in channels with different types of errors. Derived from text

N95-20927# Hull Univ. (England). Dept. of Electronic Engineering.

PASSIVE MONITORING FOR AUTOMATED MMPP COMMUNICATION SYSTEMS

N. G. Riley *In* AGARD, Multiple Mechanism Propagation Paths (MMPPs): Their Characterisation and Influence on Systems and Defence Research Agency Jul. 1994 12 p Sponsored by GEC-Marconi Communication Systems and Defence Research Agency (For primary document see N95-20921 06-32)

Copyright Avail: CASI HC A03/MF A04

A recently completed study of passive sensing techniques for hf communication systems has shown that these sensing techniques can yield data which may be of use in the control of adaptive hf communication systems. The aim of this paper is to review work carried out to date on these techniques and to examine the feasibility of applying similar techniques to radio systems utilizing higher carrier frequencies, up to around 200MHz, where many propagation modes other than ionospheric skywave may exist. Whilst inputs for the control of adaptive radio systems may be derived from a number of sources, many techniques, such as pilot-tone soundings and the transmission of training sequences, involve radiation of signals which may be undesirable in a tactical situation. System control information may also be derived by monitoring other signals which are already present in related parts of the radio spectrum, allowing more covert operation and avoiding unnecessary pollution of the radio spectrum. Derivation of such control information for use in hf systems has been studied in some detail, utilizing the following types of radio signals existing in the hf band: swept frequency sounder signals radiated by other uses of the hf spectrum, broadcast signals, standard time signals, meteorological data signals (RTTY), and overall statistical occupancy measurements of the spectrum. Some of these techniques would also be applicable to the multimechanism case, provided that the more complex propagation inversion, which is due to the greater range of propagation mechanisms available, can be taken into account. Additional, higher frequency, sources of RF energy which may provide data through passive monitoring, include aeronautical navigation beacons, amateur beacons and various types of radar signals. Use may also be made of low-orbiting satellite signals, although these present tracking problems in terms of doppler shift and give data mainly related to ionospheric scintillation and hence magnetic storm effects. Author

N95-20928# Defence Research Agency, Malvern (England). Radio Propagation Group.

THE RELATIVE IMPORTANCE OF METEOR BURST AND OTHER DISTANCE POLAR CAP PROPAGATION MODES IN THE LOW VHF BAND

Paul S. Cannon, Jay A. Weitzen (Massachusetts Univ., Lowell, MA.), Jens Ostergaard (Phillips Lab., Hanscom AFB, MA.), and John E. Rasmussen (Phillips Lab., Hanscom AFB, MA.) *In* AGARD, Multiple Mechanism Propagation Paths (MMPPs): Their Characterisation and Influence on System Design Jul. 1994 8 p (For primary document see N95-20921 06-32)

Copyright Avail: CASI HC A02/MF A04

We have analyzed the duty cycle from a very high frequency polar cap path in Greenland. We find that at 35 MHz and 45 MHz the path is often sustained by sporadic E layers rather than by meteor scatter. At the higher frequencies of 65 MHz and 85 MHz we find that the path is generally dominated by meteor scatter modes. The diurnal, seasonal and geomagnetic variations of sporadic E are examined and off line decision aid models are provided to evaluate the magnitude of multiple mechanism propagation on the path. Author

N95-20929# Rennes Univ. (France). Lab. de Radiocommunications.

STUDY OF THE FAST AND SLOW VARIATIONS OF THE POWER RECEIVED AT VHF LINKS BY TROPOSPHERIC DIFFUSION [ETUDE DE VARIATIONS RAPIDS ET LENTES DE LA PUISSANCE RECUE LORS DE LIASONS VHF PAR DIFFUSION TROPOSPHERIQUE]

O. Ravard, F. Chevrier, L. Bertel, and J. C. LeJannic (Centre d'Electronique de l'Armement, Rennes Armees, France.) *In* AGARD, Multiple Mechanism Propagation Paths (MMPPs): Their Characterisation and Influence on System Design Jul. 1994 12 p In FRENCH (For primary document see N95-20921 06-32)
Copyright Avail: CASI HC A03/MF A04

This paper deals with some experimental results. These correspond to radio links operating in the low VHF band (30 - 80 MHz) and in the range 300 - 500 km. For those distances and frequencies, the received signal is affected by fast and slow variations. On the one hand, time-frequency analysis (wavelength transform) shows that the mainly dominant propagation mode is due to partial reflection on random surfaces (sheets). At a given time, only three or four reflections are significant and contribute to the received power. On the other hand, statistics of slow variations are examined and a log-normal distribution is observed. These slow variations are correlated with meteorological data (radiosonde). Best correlations are obtained with atmospheric pressure, refractive index and height of the tropopause. Author

N95-20930# Paris-Sud Univ., Orsay (France). Lab. d'Electronique et de Technologie de l'Informatique.

PROBLEMS OF CODING IN MULTIPATH CHANNELS [LES PROBLEMES DE CODAGE DANS LES CANAUX A TRAJETS MULTIPLES]

C. Goutelard *In* AGARD, Multiple Mechanism Propagation Paths (MMPPs): Their Characterisation and Influence on System Design Jul. 1994 9 p In FRENCH (For primary document see N95-20921 06-32)
Copyright Avail: CASI HC A02/MF A04

Transmission channels are essentially multipaths. Multipaths are introduced by birefringences of the medium as in the ionosphere, by inhomogeneity as in the ionosphere and troposphere, or by reflections on obstacles as in urban or tropospheric links. The multipaths create phenomena of interference which introduce modifications of amplitude and phase of the transfer function of the channel. The stationarity of the channels complicates their use, in particular in numerical telecommunications or in teledetection. Countermeasures for fading problems call upon particular techniques of modulation or coding devices. The choice, a priori, of a modulation to carry out a system of telecommunication often involves a complexity of coding necessary to correct the errors introduced by the channel. A general method for the analysis of the channels and choice of the modulation and coding is proposed in this presentation. It is shown that the optimum choice cannot be done without an analysis of the distribution of the errors which depends on the transfer function of the channel, but also on the noise and the interferences. From the knowledge of the transfer function, interferences and noise, it is shown that a general method can be created resulting in a model of error distribution that can support code selection. The codes to be used are often very complex. The technique of interlacing can be used to avoid packages of errors, however quasi interval fadings which appear in the channels with multipaths often make regular interlacing ineffective and it then becomes necessary to consider random or pseudo-random interlacing. Transl. by CASI

N95-20931# Naval Command, Control and Ocean Surveillance Center, San Diego, CA. Research, Development, Test and Evaluation Div.

TERRAIN AND REFRACTIVITY EFFECTS ON NON-OPTICAL PATHS

Amalia E. Barrios *In* AGARD, Multiple Mechanism Propagation Paths (MMPPs): Their Characterisation and Influence on System Design Jul. 1994 9 p (For primary document see N95-20921 06-32)
Copyright Avail: CASI HC A02/MF A04

The split-step parabolic equation (SSPE) has been used extensively to model tropospheric propagation over the sea, but recent efforts have extended this method to propagation over arbitrary terrain. At the Naval Command, Control and Ocean Surveillance Center (NCCOSC), Research, Development, Test and Evaluation Division, a split-step Terrain Parabolic Equation Model (TPEM) has been developed that takes into account variable terrain and range-dependent refractivity profiles. While TPEM has been previously shown to compare favorably with measured data and other existing terrain models, two alternative methods to model radiowave propagation over terrain, implemented within TPEM, will be presented that give a two to ten-fold decrease in execution time. These two methods are also shown to agree well with measured data. Author

N95-20932# Thomson-CSF, Velizy (France). Centre d'Applications Radars.

METHODS FOR EVALUATING THE EFFECTS OF CONDUITS AT THE SURFACE OF THE SEA [METHODES D'EVALUATION DE L'EFFET DES CONDUITS A LA SURFACE DE LA MER]

Michel Fournier *In* AGARD, Multiple Mechanism Propagation Paths (MMPPs): Their Characterisation and Influence on System Design Jul. 1994 14 p In FRENCH Sponsored by Direction des Recherches, Etudes et Techniques (For primary document see N95-20921 06-32)
Copyright Avail: CASI HC A03/MF A04

The propagation of radio waves in the atmosphere is determined by the index of refraction which is sensitive to the pressure, temperature and moisture of the air. In the vicinity of the surface of the sea, there is a strong gradient of moisture related to the evaporation of water; it gives rise to a fast decrease of the index of the air creating a conduit of propagation in vicinity of surface. A source located in the interior of the conduit (i.e., at an altitude ranging between that of the minimum of the modified index and sea surface) sees most of its energy remaining captive inside this conduit. This has as an operational consequence - a considerable increase in the range of the radio hardware working in the vicinity of the surface of the sea. In addition, the propagation inside the conduit is characterized by the presence of multipaths related to the successive reflection of the electromagnetic wave on the surface of the sea and the boundary of the conduit. What results is a series of reinforcements and attenuations of the field being propagated in the conduit. Taking into account the practical importance of these effects it is advisable to have suitable methods of evaluation. In this talk three methods are examined: (1) parabolic equation method, (2) method of modes, and (3) method of geometrical optics. The parabolic equation method consists of making an approximation of the wave equation by supposing that the field is propagated around a primary direction. Under these conditions one reduces the equation of propagation to a partial derivative equation of parabolic type which leads to an easy algorithm to work with. The method of modes makes it possible to carry out calculations in an entirely analytical way by supposing that the profile of the index follows a simple law. This method constitutes an analytical reference with respect to the two other methods which are numerical. The method of geometric optics is an asymptotic method. It consists of considering the trajectory of the rays resulting from the source by solving the eikonal equation. The intensity of the electromagnetic field can be given in conjunction with the equation of the trajectories; the calculation of the divergence of the wave vector tangent to the ray passing by the point where the field is evaluated. One thus obtains a system of ordinary differential equations which can be solved numerically by the method of Runge-Kutta. Each one of these methods is analyzed and a comparison between them is carried out on a number of concrete examples. In each case the theoretical limits, the advantages, and the limits of use of the three methods are highlighted. Transl. by CASI

N95-20933# Lille-1 Univ., Villeneuve-d'Asoq (France). Dept. Electronique.

PROPAGATION OF HIGH FREQUENCY WAVES IN URBAN AND ROAD TUNNEL ENVIRONMENTS [PROPAGATION DES ONDES HAUTE FREQUENCE EN MILIEU URBAIN ET EN TUNNEL ROUTIER]

M. Lienard, Ph. Mariage, S. Baranowski, and P. Degauque *In* AGARD, Multiple Mechanism Propagation Paths (MMPPs): Their Characterisation and Influence on System Design Jul. 1994 12 p In FRENCH Sponsored by INRETS/CRESTA, SIRTI, ISSEP, ALCATEL Cables, and AEG Kabel (For primary document see N95-20921 06-32)
Copyright Avail: CASI HC A03/MF A04

Telecommunication between a fixed basic station and a vehicle moving on the surface of the ground are subjected to multiple reflections. When the frequency of the carrier is of the order or higher than 1 GHz, the majority of the obstacles located between the emitter and the receiver has dimensions much larger than the wavelength and a predictive model of the conditions of propagation can be based on the theory of rays and in particular on the uniform theory of diffraction (UTD). The first part of this article presents a brief review of the mathematical formalism and the way of introducing the complex permittivity of the ground into the ideal models. In the case of propagation in an urban environment, a comparison between the results obtained using the UTD and those based on approximate models which account for multiple diffractions is carried out. An important geometrical configuration for which the multiple reflections play a very important part relates to the propagations in tunnels. The analysis is undertaken by successively considering the intrinsic propagation in the tunnel, i.e. by supposing that the tunnel is infinitely long, then the free-tunnel transition space. The study is carried out in the frequency domain then temporal domain closely connected to highlight the fluctuations of amplitude of the signal and the delays to the multipaths. The theoretical predictions are then compared with the experimental results. Transl. by CASI

N95-20934# Centre d'Electronique de l'Armement, Bruz (France).

A WIDEBAND PROPAGATION SIMULATOR FOR HIGH SPEED MOBILE RADIO COMMUNICATIONS

P. Busson, J. C. LeJannic, G. ElZein (Institut National des Sciences Appliquees, Rennes, France.), and J. Citerne (Institut National des Sciences Appliquees, Rennes, France.) *In* AGARD, Multiple Mechanism Propagation Paths (MMPPs): Their Characterisation and Influence on System Design Jul. 1994 13 p In FRENCH (For primary document see N95-20921 06-32)

Copyright Avail: CASI HC A03/MF A04

Multipath, jamming, listening and detection are the main limitations for mobile radio communications. Spread spectrum techniques, especially frequency hopping, can be used to avoid these problems. Therefore, a wideband simulation for multipath mobile channels appeared the most appropriate evaluation technique. It also gives useful indications for system characteristic improvements. This paper presents the design and realization of a new UHF-VHF propagation simulator, which can be considered as an extended version of Bussgang's one. This frequency hopping simulator (up to 100,000 hops per second) is wideband thus capable to deal with spread spectrum signals. As it generates up to 16 paths, it can be used in almost all mobile radio propagation situations. Moreover, it is also able to simulate high mobile relative speeds up to 2000km/h such as air-air communication systems. This simulator can reproduce, in laboratory, 16 rays Rician or Rayleigh fading channels with a maximum time delay of about 15 ms. At the highest frequency of 1200 MHz, Doppler rates up to 2 kHz can be generated corresponding to vehicle speeds up to 2000 km/h. Let note that the Bussgang simulator was defined for narrowband and fixed radio communications. In both equipments, in-phase and quadrature signals are obtained using two numerical transversal filters. Simulation results were derived in various situations especially in terrestrial urban and suburban environments, where they could be compared with measurements. The main advantage of the simulator lies in its capacity to simulate the high speed and wideband mobile radio communication channels. Author

N95-20935# Rutherford Appleton Lab., Chilton (England). Radio Communications Research Unit.

COMBINED EFFECTS OF ATMOSPHERE AND TERRAIN ON UHF/MICROWAVE PATHS

M. F. Levy *In* AGARD, Multiple Mechanism Propagation Paths (MMPPs): Their Characterisation and Influence on System Design Jul. 1994 8 p Sponsored by DTI (For primary document see N95-20921 06-32)

Copyright Avail: CASI HC A02/MF A04

Radiowave propagation on mixed land/sea paths is affected by both atmospheric refraction and terrain effects. The parabolic equation method provides a numerical solution for calculation of field-strength in these circumstances. We give a few applications of the finite-difference PE method, which is particularly well-adapted to problems where ground effects are important. A case in point is that of detection of low targets above a rough sea surface. For air-defense applications, PE computing requirements are prohibitive. We describe a novel method, the horizontal PE method, which allows fast computation of signal strength in large domains, and apply it to calculations of radar coverage. Author

N95-20936# Naval Command, Control and Ocean Surveillance Center, San Diego, CA. Research, Development, Test and Evaluation Div.

MODELING TROPOSPHERIC DUCTING EFFECTS ON SATELLITE-TO-GROUND PATHS

Herbert V. Hitney *In* AGARD, Multiple Mechanism Propagation Paths (MMPPs): Their Characterisation and Influence on System Design Jul. 1994 5 p (For primary document see N95-20921 06-32)

Copyright Avail: CASI HC A01/MF A04

Satellite-to-ground propagation paths are frequently affected by tropospheric refraction and ducting at very low elevation angles. Common effects are substantial enhancements of signals at ranges that would normally be beyond the horizon, and severe distortions of the patterns created by the coherent interferences of multiple propagation paths, in particular the direct and sea-reflected signals. Traditional methods to model tropospheric ducting effects, such as waveguide or parabolic equation methods, are difficult to apply to typical satellite heights. This paper will describe a parabolic-equation and ray-optics hybrid method to model these sometimes important effects, and compare modelled and measured results using a 1000-km high satellite transmitting at 1239 and 2891 MHz. Author

N95-20937# Naval Command, Control and Ocean Surveillance Center, San Diego, CA. Research, Development, Test and Evaluation Div.

THE LORENTZ RECIPROCITY THEOREM AS A CONSISTENCY TEST FOR PROPAGATION MODELS

Richard A. Paulus *In* AGARD, Multiple Mechanism Propagation Paths (MMPPs): Their Characterisation and Influence on System Design Jul. 1994 8 p (For primary document see N95-20921 06-32)

Copyright Avail: CASI HC A02/MF A04

Modeling of electromagnetic propagation in the troposphere has been advanced in the last decade to the point where both the vertical and horizontal variation of refractivity can be accommodated readily. In particular, parabolic equation models inherently allow for lateral and vertical inhomogeneities. A hybrid ray-optics/parabolic equation model is utilized to predict propagation loss for a range-varying refractive structure to demonstrate the model obeys the Sommerfeld-Pfrang statement of the Lorentz Reciprocity Theorem. Author

N95-20938# Physics and Electronics Lab. TNO, The Hague (Netherlands).

MODELLING OF MICROWAVE PROPAGATION AND CLUTTER IN A MARITIME ENVIRONMENT

M. H. Vogel *In* AGARD, Multiple Mechanism Propagation Paths (MMPPs:) Their Characterisation and Influence on System Design Jul. 1994 6 p (For primary document see N95-20921 06-32)

Copyright Avail: CASI HC A02/MF A04

For a radar system in a maritime environment, the probability of detection of a target at a low altitude is strongly dependent on the conditions of the atmosphere and the sea surface. In order to determine the detection probability of a target at low altitude, these conditions should be taken into account. This paper presents numerical methods to calculate electromagnetic propagation in an evaporation duct and to calculate sea clutter returns. Author

N95-20939# Universite Catholique de Louvain (Belgium). Microwave Lab.

SIMULATION OF THE IMPACT OF ATMOSPHERIC TURBULENCES ON MILLIMETER-WAVE COMMUNICATIONS SYSTEMS

H. Vasseur and D. Vanhoenacker *In* AGARD, Multiple Mechanism Propagation Paths (MMPPs): Their Characterisation and Influence on System Design Jul. 1994 13 p Sponsored by ESA (For primary document see N95-20921 06-32)

Copyright Avail: CASI HC A03/MF A04

By inducing scintillation of the transmitted signals, atmospheric turbulence affect both satellite and line-of-sight communication systems in the millimeter-waves range. After a characterization of the scintillation effect from theory and experiments, this paper presents two deterministic models developed at the Microwaves Laboratory U.C.L. for the simulation of scintillation. The first model accounts for the physical process of cloud induced turbulence that yields scintillation on satellite links and the second one deals with the turbulence in the lower atmospheric layer that affects terrestrial paths. These models allow to retrieve the turbulent configuration that produce scintillation, to simulate the scintillation effects on various links and finally to predict the impact of scintillation on the performances of communication systems. Author

N95-20940# Industry and Science Canada, Ottawa (Ontario). Communications Research Centre.

PROPAGATION MEASUREMENTS ON A TROPOSCATTER LINK IN THE CANADIAN HIGH ARCTIC

C. Bilodeau and K. S. McCormick *In* AGARD, Multiple Mechanism Propagation Paths (MMPPs): Their Characterisation and Influence on System

Design Jul. 1994 7 p Sponsored by Dept. of National Defence (For primary document see N95-20921 06-32)
Copyright Avail: CASI HC A02/MF A04

Experimental results of radio propagation measurements at 853 MHz are given for a 500 km troposcatter link in the Canadian High Arctic. The experimental data were acquired using a narrow band measurement system that was developed to permit a transmitting power of only 100 Watts while using a 4.5 meter dish at each end of the link. The system includes a digital signal processor (DSP) receiver for signal strength computation and a high stability noise source reference for amplitude calibration. The main characteristics of this system are described in this paper. Detailed fading distributions are presented for examples of slow and fast fading periods and compared with Rayleigh distributions. An estimate of the long term median path loss is made and compared with values predicted using accepted techniques. The results are believed to be the first ever presented for a microwave troposcatter link above the 80th parallel. Author

N95-20941# Northeastern Univ., Boston, MA. Dept. of Electrical and Computer Engineering.

LARGE BISTATIC ANGLE CLUTTER DEPOLARIZATION STUDY

D. J. McLaughlin, E. Boltniew, J. Barclay, R. S. Raghavan, and M. J. Sowa (Rome Lab., Hanscom AFB, MA.) *In* AGARD, Multiple Mechanism Propagation Paths (MMPPs): Their Characterisation and Influence on System Design Jul. 1994 10 p (For primary document see N95-20921 06-32)
Copyright Avail: CASI HC A02/MF A04

A bistatic radar test bed has recently been developed to measure the depolarization behavior of clutter at large bistatic angles in Eastern Massachusetts. Results presented in this paper describe the co- and cross-polarized S-Band NRCS for low resolution (300m by 300m) forested clutter cells viewed at low grazing angles. We also describe the variation in mean scattered power versus linear receiver antenna orientation angle for both vertical and horizontal transmitted polarizations. Measurements of a 20 km by 20 km region of rolling hills show that vertical copolarized NRCS exceeds horizontal copolarized NRCS by an average of 8 dB over a range of bistatic angles from 100 degrees to 160 degrees. The average polarization ratio is minus 12 dB for vertical transmitter polarization and minus 5 dB for horizontal transmitter polarization. For both transmitter polarizations and variable linear receiver antenna polarization, maximum scatter power was observed when transmitter and receiver antennas were copolarized while minimum received power was observed when the antennas were crosspolarized. Power fluctuation statistical distributions are approximately exponential for all linear receiver antenna polarization angles. Author

N95-20942# Centre de Recherches en Physique de l'Environnement, Velizy (France).

TIME BEHAVIOR AND FREQUENCY RESPONSE OF THE MICROWAVE PROPAGATION CHANNEL DURING MULTIPATH PROPAGATION

D. Rana, M. Sylvain, and A. R. Webster (University of Western Ontario, London, Ontario.) *In* AGARD, Multiple Mechanism Propagation Paths (MMPPs): Their Characterisation and Influence on System Design Jul. 1994 12 p Sponsored in part by the Communications Research Centre and the Natural Sciences and Engineering Research Council of Canada (For primary document see N95-20921 06-32)
Copyright Avail: CASI HC A03/MF A04

In this paper, ray-tracing simulation is used to model the dynamic behavior of the propagation channel in presence of a single super-refractive layer. Three typical mechanisms of layer formation and evolution are simulated according to experimental observations. (1) A ground-based layer formed by nocturnal cooling of the Earth's surface, its intensity increasing with time, (2) an elevating layer, that is a ground-based layer which weakens in rising, its intensity decreasing linearly with height, and (3) an elevated layer formed when a warm dry air mass is produced in the upper atmosphere; this layer grows with time. For each of these three types of layer, a ray-tracing program is used to compute the variations with time of the ray parameters and of the received signal level. As the statistics of the speed of layer formation and evolution are not precisely known, the time scale used in this study is somewhat arbitrary. However, this technique allows one to identify three typical fading patterns and to help interpret the physical mechanisms involved in the generation of multipath propagation. The frequency selective nature of the propagation channel bandwidth is then investigated over a 10.7-11.7 GHz in looking for the influence of each type of layer on the transfer function. Some experimental evidence relating to, and confirming, the predicted behavior values is also considered. Author

N95-20943# Communications Research Centre, Ottawa (Ontario).

DEVELOPMENT OF A FAST SAMPLING SYSTEM FOR ESTIMATION OF IMPULSE RESPONSES OF MOBILE RADIO CHANNELS

Pierre Melancon *In* AGARD, Multiple Mechanism Propagation Paths (MMPPs): Their Characterisation and Influence on System Design Jul. 1994 7 p (For primary document see N95-20921 06-32)
Copyright Avail: CASI HC A02/MF A04

This paper describes the features of measurement equipment developed to measure impulse response estimates of mobile radio channels in less than a ms per measurement. The development of such equipment was required to measure mobile radio channels in realistic operating scenarios, in a normal sized vehicle moving at typical speeds in different environments. Up to speeds of 70 km/hr, the measurement period is short enough to assume the equipment is measuring the same channel during the whole sampling interval. AT the transmitter end of the measurement system, a wideband signal (10 MHz) is produced by modulating a carrier frequency with a 511 bit pseudo random sequence at 5 Mb/s and transmitted through the radio channel. The received signal is down-converted to 70 MHz and demodulated by a complex demodulator. The quadrature baseband signals at the demodulator outputs are then filtered and sampled at high speed by two fast digitizers. During this process, the data are stored in large memory banks to allow a fast sampling rate during a long period of time. Data are transferred to laser disks for further processing in the laboratory. Impulse response of radio channels are estimated by performing a software correlation between a measurement system back to back reference and real time measurements. A minivan was modified to hold the receiver, digitizers, memory banks and the computer. A shaft encoder was attached to its rear left wheel to trigger measurements while moving. Features of the system are discussed along with the effects of data block length, signal to noise ratio, sampling rate, memory size and phase stability on the design of the measurement equipment. Finally, some measurement results are presented and discussed. Author

N95-20944# Institut National des Sciences Appliquees, Rennes (France). Lab. Composants et Systemes pour Telecommunications.

LINE-OF-SIGHT MULTIPATH PROPAGATION MEASUREMENTS AT 15 GHz OVER 500 MHz BANDWIDTH

M. Touati, G. ElZein, and J. Citerne *In* AGARD, Multiple Mechanism Propagation Paths (MMPPs): Their Characterisation and Influence on System Design Jul. 1994 10 p (For primary document see N95-20921 06-32)
Copyright Avail: CASI HC A02/MF A04

An experimental wideband grazing radio link at 15 GHz has been set up on a 17.6 Km line-of-sight between Laille and Rennes to measure the variations of the propagation medium characteristics (attenuation and group delay versus frequency) due to meteorological effects. For this, a meteorological system was set up at the receiver station in order to measure the variations of the meteorological parameters (temperatures, pressure, rain precipitation, speed and direction of the wind). Consequently, the atmosphere refractive index is obtained. A particular interest is given to the occurrence of multipath fading in clear air caused by low-level layering in the troposphere. The collecting and recording of the propagation data (attenuation and group delay), from the MLA (microwave Link Analyzer), and that which relates to the meteorological characteristics, from the meteorological station, are executed using a computer program in a sequential manner. The channel impulse response, corresponding to each measured data, is calculated to deduce the number of rays detected and their different delays respectively. Besides this and using the meteorological parameters data acquired, the refractivity gradient is calculated in order to correlate the multipath fading occurrence to the meteorological parameters. Author

N95-20945# Centre de Recherches en Physique de l'Environnement, Velizy (France).

EXPERIMENTAL STUDY OF THE HELICOPTER-MOBILE RADIOELECTRICAL CHANNEL AND POSSIBLE EXTENSION TO THE SATELLITE-MOBILE CHANNEL

V. Blanchetiere-Ciarletti, M. Sylvain, and P. Lemenn *In* AGARD, Multiple Mechanism Propagation Paths (MMPPs): Their Characterisation and Influence on System Design Jul. 1994 12 p (For primary document see N95-20921 06-32)
Copyright Avail: CASI HC A03/MF A04

The use of satellite seems to be an answer to the radioelectrical covering problem for the mobile communications, particularly in the low populated areas. Frequency bands at 1.5 and 2.5 GHz have been dedicated to these future services. Satellite-mobile links will be much more affected by propagation phenomena than the existing links between satellites and fixed stations. The reasons for that are twofold: The probable use of LEO (Low-Earth-Orbit) satellites instead of GEO; such satellites will have to be received at relatively low elevation to limit their number; the use of mobile communication terminals with small and non directive antennas that must work in various environments instead of terrestrian stations located at carefully chosen places and equipped with large diameter paraboloids. These propagation phenomena mainly consist in the fading of the signal level (shadowing of the link), and a frequency selective fading due to multipath propagation. The experience run by C.R.P.E. is aimed at a better understanding of the satellite-mobile propagation channel at fixed frequency as well as on a large band. In this paper, we discuss preliminary results from a series of propagation measurements performed (by lack of any experimental satellite) on an experimental radio link at 1.45 GHz on a of 20 MHz bandwidth between a helicopter flying at a height of 2 km and a mobile receiver. The whole experiment has been run in a rural environment in Brittany (France). In a first part, we illustrate the quality of the data collected during the experiment on a typical case study and give a possible physical interpretation of the observed phenomena. Then we present statistical results concerning the various characteristics (attenuation and delay spreads) of the propagation channel. Finally, we discuss the problem of using a helicopter (flying at a height of 2 km) as a substitute for a satellite at about 1000 km and try to estimate to what extent it is possible to use the data collected during this experiment to characterize the satellite-mobile channel. To do that, both the helicopter-mobile and the satellite-mobile propagation channels are simulated under the same environmental conditions. Author

N95-20946# Rome Lab., Hanscom AFB, MA.

COMPARATIVE STUDY OF C- AND K-BAND PROPAGATION MECHANISMS BEYOND THE HORIZON

Uve H. W. Lammers, Richard A. Marr, Robert K. Crane (Oklahoma Univ., Norman, OK.), and Magnus Wennemyr (Oklahoma Univ., Norman, OK.) *In* AGARD, Multiple Mechanism Propagation Paths (MMPPs): Their Characterisation and Influence on System Design Jul. 1994 7 p (For primary document see N95-20921 06-32)
Copyright Avail: CASI HC A02/MF A04

At intervals over a period of several years, we conducted simultaneous troposcatter measurements at frequencies of 4.95 and 15.73 GHz on a 161 km path in the northeastern United States. This ensured a fair comparison within a largely unspecified but identical propagation medium. Besides signal level, both systems yielded Doppler information on the propagation mechanism. In addition, the Ku-band system provided delay resolution by pseudorandom phase modulation. On the basis of these data, three primary propagation mechanisms could be identified: clear air turbulent scatter, rain scatter, and ducting. Criteria are given for the identification of these mechanisms along with the resulting received signal level and delay spread distributions under each propagation condition. Author

N95-20947# PTT Research, Leidschendam (Netherlands).

ANGLE DIVERSITY ON DIGITAL MICROWAVE LINKS: ANTENNA DESIGN AND EXPERIMENTAL RESULTS

D. Beaufort and L. P. Lighart (Technische Hogeschool, Delft, Netherlands.) *In* AGARD, Multiple Mechanism Propagation Paths (MMPPs): Their Characterisation and Influence on System Design Jul. 1994 7 p (For primary document see N95-20921 06-32)
Copyright Avail: CASI HC A02/MF A04

PTT Research and Delft University of Technology examined the merits of angle diversity for multipath fading reduction on digital microwave links. A dual-polarized hybrid reflector array, suitable for beam switching in the vertical plane, was designed and produced. The antenna specifications were based on extensive propagation studies. The antenna was tested for two years on a 45 km hop in The Netherlands. It was found that switching between the antenna beams is superior to adaptive (maximum power) combining. Switching reduces the time that the Bit Error Ratio (BER) exceeds 10(exp -3) by a factor 27. Author

N95-20948# Naval Command, Control and Ocean Surveillance Center, San Diego, CA. Research, Development, Test and Evaluation Div.

MITIGATION OF EFFECTS OF MULTIPLE PATH NULLS AT SUPER-HIGH FREQUENCIES THROUGH DIVERSITY AND NETWORKING

N. Dave *In* AGARD, Multiple Mechanism Propagation Paths (MMPPs): Their Characterisation and Influence on System Design Jul. 1994 12 p (For primary document see N95-20921 06-32)
Copyright Avail: CASI HC A03/MF A04

The goal of this work is to investigate the design issues implied by multipath effects for a high bandwidth communication network consisting of platforms in a Navy battle group. This communication network is designed to operate using super-high frequency (SHF) or ultra-high frequency (UHF) line-of-sight (LOS) propagation, and must be robust to variations in link quality due to platform motion or deletion, as well as to the effects of multipath propagation. High bandwidth in this context implies data rate in excess of 1.544 megabits per second (Mbps), known as 'TI' in the commercial world. Multipath nulls at the above frequencies can render links useless at certain ranges. In this work, we briefly discuss the well-known methods of height and frequency diversity, as well as a less frequently used but potentially powerful method of 'path diversity' through networking, to alleviate the ill effects of multipath nulls. The communication system configurations discussed are appropriate for expected platform separations in post-Cold War battle group scenarios, which envision most platforms within line-of-sight (LOS) distance from each other, i.e., separated by no more than about 20 nautical miles (nmi). Author

N95-20949# Phillips Lab., Hanscom AFB, MA. Ionospheric Effects Div.

MULTIPATH IMPACT ON GROUND-BASED GLOBAL POSITIONING SYSTEM RANGE MEASUREMENTS: ASPECTS OF MEASUREMENT, MODELING, AND MITIGATION

G. J. Bishop and E. A. Holland (Northwest Research Associates, Inc., Bellevue, WA.) *In* AGARD, Multiple Mechanism Propagation Paths (MMPPs): Their Characterisation and Influence on System Design Jul. 1994 10 p (For primary document see N95-20921 06-32)
Copyright Avail: CASI HC A02/MF A04

Multiple mechanisms propagation paths (multipath) can be the most important error source in ground-based Global Positioning System (GPS) measurement of range to the satellites. This multipath error, arising from a combination of the direct path and reflections from objects relatively close to the receiving antenna, can at times exceed the ionospheric delay error, which the two-frequency (1228 and 1575 MHz) GPS signal format is designed to measure and correct. GPS multipath can seriously degrade Differential GPS (DGPS) navigation, geodetic measurements, ionospheric monitoring, and other GPS applications, yet the source of the problem may not be evident without the use of specialized tests. Several techniques have been proposed to reduce the effects of GPS multipath; these include: improved receiver technology, specialized antenna designs, and various modeling or filtering approaches. This paper illustrates the nature of the two-frequency GPS multipath problem with measurement data from typical ground-based installations, exhibiting variation in multipath conditions, ranging from low to quite high for the varying geometries of the available satellite tracks. Leading mitigation techniques are reviewed, with emphasis on multipath modeling. A new simple modeling approach currently being studied by Phillips Laboratory is discussed. This technique takes advantage of the daily repetition of the GPS observation geometry from a ground station to create a 'multipath template' specific to each satellite pass, and reduce multipath effects on successive days. Data is presented showing significant improvement in a severe multipath environment and contrasting the effectiveness of this approach with all-sky modeling techniques. Mitigation techniques for GPS multipath show potential to enable GPS ground-based range and ionospheric measurement to greatly reduce errors at low elevation angles, leading to improved accuracy and wider coverage area capability. Author

N95-20950# Leeds Univ. (England). Satellite Communications Group.
IMPACT OF PROPAGATION MECHANISMS ON GLOBAL NAVIGATION SATELLITE SYSTEM PERFORMANCE
Stuart Riley, Peter Daly, and Peter Raby *In* AGARD, Multiple Mechanism Propagation Paths (MMPPs): Their Characterisation and Influence on System Design Jul. 1994 11 p (For primary document see N95-20921 06-32)
Copyright Avail: CASI HC A03/MF A04

Propagation mechanisms have a detrimental effect on the accuracy of satellite positioning systems such as GPS and GLONASS. The ionosphere at times of high activity will cause the greatest error due to the propagation medium. This paper describes a dual GPS/GLONASS receiver that is capable of measuring the ionospheric delay in the measured GLONASS pseudo ranges using both the code and carrier phases. This allows the pseudo ranges to be corrected for ionospheric delay and a more accurate position solution to be calculated. This paper describes the receiver architecture and fundamental accuracy; receiver measurement noise and calibration are also discussed before the impact of propagation mechanisms on the measurements are investigated. The measurement of the line of sight ionospheric delay, from a GLONASS satellite, is shown and compared with the GPS transmitted ionospheric model. An example of GLONASS P code navigation is given with and without correction for the ionosphere. Author

N95-20951# Boston Univ., MA. Center for Space Physics.
MITIGATION OF THE EFFECTS OF F LAYER REGULARITIES BY USING MULTIPLE PATHS
Jules Aarons *In* AGARD, Multiple Mechanism Propagation Paths (MMPPs): Their Characterisation and Influence on System Design Jul. 1994 6 p Sponsored by ONR (For primary document see N95-20921 06-32)
Copyright Avail: CASI HC A02/MF A04

In recent military operations trans-ionospheric satellite to ground communications have been utilized in the equatorial region. One problem for the predominantly 250 MHz systems has been fading due to irregularities in the region within plus and minus 20 degrees of the magnetic equator. A similar problem has been encountered at high latitudes. For minimizing the effect of the fading, one might expect that radio links sufficiently separated in frequency and polarization would be effective in combating scintillation. Unfortunately frequency separations would have to be of the order of 100 MHz to obtain an adequate diversity improvement. The use of right and left circular polarization or of orthogonal linear polarizations is not effective. However, time diversity is a demonstrated procedure for overcoming scintillation but there is a loss of using coding or redundancy and a reluctance to complicate the system with modems. If the paths from a single satellite are sufficiently well separated then fading on two links is uncorrelated and diversity gain may be achieved. Unfortunately at equatorial latitudes separations of the order of a kilometer are involved. Another use of 'space diversity' can be effective. If the paths from two satellites with spacing between them are available and there is recognition that scintillation is causing the fading on the path to one satellite, then operators can utilize the path to a second satellite. For equatorial paths the operator must be alert as to the time development of irregularities and the dynamics of plume development. The differences in activity on the paths are due to two aspects of the irregularity plume i.e. the start time as the sunset moves westward and the spacing between plumes on the very active days. Examples of the time difference between the start of equatorial scintillations on one path versus that of another have been recorded in many sectors of the world. The results of these studies as applied to the problem of multiple paths will be shown. At high latitudes during moderate magnetic activity, it is possible to find paths that are not dominated by irregularities. However at auroral latitudes when a magnetic storm commences, the irregularity development moves equatorward with great rapidity and encompasses large areas. It is then difficult to find a path free of irregularities. Author

N95-20952# Maryland Univ., College Park, MD. Dept. of Physics.
ELECTROMAGNETIC WAVE REFLECTION FROM IRREGULAR PLASMA LAYERS
K. Papadopoulos, R. Short (ARCO Power Technologies, Inc., Washington, DC.), and R. Shanny (ARCO Power Technologies, Inc., Washington, DC.) *In* AGARD, Multiple Mechanism Propagation Paths (MMPPs): Their Characterisation and Influence on System Design Jul. 1994 10 p (For primary document see N95-20921 06-32)
Copyright Avail: CASI HC A02/MF A04

The general theory describing reflection of electro-magnetic waves from irregular reflectors was formulated by using path integral techniques. The general formulae reproduce the well known reflection coefficients for wave scattering from random rough surfaces derived by using Kirchhoff's theory or perturbation theory. The theory was used to determine the degradation of an OTH radar signal scattered from irregular Artificial Ionospheric Mirrors (AIM). The cases of density irregularities induced by fluctuations in the ambient neutral density and by fluctuations in the heater power were separately examined. Scaling laws and bounds for minimal signal loss were derived. Author

N95-20953# Phillips Lab., Hanscom AFB, MA. Ionospheric Physics Lab.
THE EFFECTS OF MULTIHOP HF PROPAGATION ON THE PERFORMANCE OF OTH BACKSCATTER RADARS
J. Buchau, S. Dandckar, G. S. Sales (Massachusetts Univ., Lowell, MA.), B. Weijers (Rome Lab., Hanscom AFB, MA.), and D. Reynolds (Radex, Inc., Bedford, MA.) *In* AGARD, Multiple Mechanism Propagation Paths (MMPPs): Their Characterisation and Influence on System Design Jul. 1994 7 p (For primary document see N95-20921 06-32)
Copyright Avail: CASI HC A02/MF A04

Analysis of approximately one year's data from an operational OTH radar shows that equatorial clutter, originating in the ionosphere in regions up to 14,000 km from the radar, directly impacts the radar's performance. The radio wave propagation to these regions often involves from three or more ground hops depending on the radar's azimuth. These phenomena are important to all OTH radar systems in that great circle paths always cross the magnetic equator. The special data processing developed for this program uses both the long range (to 8000 nm) wideband 6 to 28 MHz) backscatter ionograms made routinely at selected azimuths and the radar's amplitude, range and Doppler data format, measuring the frequency of occurence, location and intensity of the clutter as a function of time and azimuth. These data indicate that intense ionospheric irregularities connected with the nighttime equatorial activity produce sufficient Doppler spread scattered energy that directly affects the performance of the radar. With the Parametric Ionospheric Model developed at the Phillips Laboratory and numerical ray tracing the specific interaction regions for the radar signal and the ionospheric irregularities are shown and an explanation for the observed temporal behavior is proposed. Several mechanisms for Doppler spreading of the clutter signal are also reviewed. Author

N95-20954# Paris-Sud Univ., Orsay (France). Lab. d'Electronique et de Technologie de l'Informatique.
TEMPORAL AND SPATIAL COMPORTMENT OF MULTIPLE PATHS IN IONOSPHERIC PROPAGATION IN OBLIQUE INCIDENCE: FRACTAL MEASURES OF PERTURBATIONS [COMPORTEMENT TEMPOREL ET SPATIAL DES TRAJETS MULTIPLES DANS LES PROPAGATIONS IONOSPHERIQUES EN INCIDENCE OBLIQUE MESURE FRACTALE DES PERTURBATIONS]
C. Goutelard, J. Caratori, and L. Barthes *In* AGARD, Multiple Mechanism Propagation Paths (MMPPs): Their Characterisation and Influence on System Design Jul. 1994 17 p In FRENCH Original contains color illustrations (For primary document see N95-20921 06-32)
Copyright Avail: CASI HC A03/MF A04

The electromagnetic wave propagation in the ionosphere is complex; the anisotropy and the inhomogeneity introducing multiple paths and the non stability of the Doppler effects. The ionospheric models usually used make it possible to account for the multiple paths and the Doppler shifts. According to these models, based on ray tracings, it appears that there is only one triplet (amplitude, Doppler, time travel) which makes it possible to plot simple diagrams. The experimental observation shows that, if one finds the signatures envisaged in the classical theory of the ray tracings for the signals of great amplitude, one observes, with systems of measurement of great sensitivity, signals of low amplitude which seem to translate the existence of diffuse propagations. The results of an oblique bistatic survey and of a backscattering study given in this presentation, show the appearance of effects of the second order. A method of characterization of these effects is proposed by the introduction of measurement of fractal dimensions of the functions of scattering, obtained by a method of high resolution spectral analysis. Transl. by CASI

N95-20955# Defence Research Agency, Malvern (England). Radio Propagation Exploitation Group.

DAMSON: A SYSTEM TO MEASURE MULTIPATH DISPERSION, DOPPLER SPREAD AND DOPPLER SHIFT ON MULTI-MECHANISM COMMUNICATIONS CHANNELS

Nigel C. Davies and Paul S. Cannon *In* AGARD, Multiple Mechanism Propagation Paths (MMPPs): Their Characterisation and Influence on System Design Jul. 1994 6 p (For primary document see N95-20921 06-32)

Copyright Avail: CASI HC A02/MF A04

The performance of communications equipment (especially data modems) designed to work over high frequency paths which can propagate by a number of different mechanisms is dependent on their ability to work with a wide range of signal to noise conditions and with varying degrees of frequency and time dispersion. The latter phenomena are a particular problem for systems operating over high latitude paths and yet there appears to be little available data documenting their severity or frequency of occurrence. DAMSON (Doppler And Multipath SOunding Network) is an oblique channel sounding system which has been developed by the UK Defence Research Agency (DRA) to measure a number of real-time channel parameters using low power pulse compression waveform transmissions. Extensive use is made of digital signal processing techniques. The system will allow signal time-of-flight, time dispersion (multipath dispersion), frequency dispersion (Doppler spread and Doppler shift) and signal strength to be measured over point-point communications paths. The DAMSON experiment is to be deployed to make measurements over a number of mid and high-latitude paths. This paper provides an introduction to the DAMSON system, its basic operation and measurement performance. The initial experiments to be conducted and the associated system deployment are presented. Author

N95-20956# Rennes Univ. (France). Lab. Radiocommunications.

IDENTIFICATION OF THE PROPAGATION MODES AND PATHS ON HF LINKS USING A GONIOPOLARIMETER [IDENTIFICATION DES MODES ET TRAJETS DE PROPAGATION SUR DES LIAISONS HF A L'AIDE D'UN GONIOPOLARIMETRE]

A. Edjeou, L. Bertel, and V. Massot *In* AGARD, Multiple Mechanism Propagation Paths (MMPPs): Their Characterisation and Influence on System Design Jul. 1994 12 p In FRENCH (For primary document see N95-20921 06-32)

Copyright Avail: CASI HC A03/MF A04

We present a system which is able to separate the propagation paths and also to identify the type of polarization of the modes. The studied links are between Monterfil (48 deg 05 N latitude, 2 deg W longitude) and all types of known location transmitters which work on carrier. The experimental analysis is performed using a 'goniopolarimeter' which is a device determining both the arrival angles (goniometrical function) and the type of polarization of the corresponding incoming skywaves. We apply a high resolution non linear frequency analysis associated with a reiterated method of filtering matched to this polarization. Author (revised)

N95-20957# Hull Univ. (England). Hull-Lancaster Communications Research Group.

GEOGRAPHICAL DIVERSITY COMBINING TO EXPLOIT MULTI-MECHANISM PROPAGATION

M. Darnell and T. J. Speight *In* AGARD, Multiple Mechanism Propagation Paths (MMPPs): Their Characterisation and Influence on System Design Jul. 1994 18 p Sponsored by UK Science and Engineering Research Council (For primary document see N95-20921 06-32)

Copyright Avail: CASI HC A03/MF A04

The paper introduces the principles of a new macroscopic diversity scheme employing maximum likelihood, symbol-level, diversity combining. The performance of the scheme is compared with that of other classical post-detector diversity combining methods. It is shown that the new scheme has a performance similar to the classical techniques; however, its complexity is significantly lower. The application of macroscopic diversity in the HF band is then described, and the results of practical on-air trials presented. Author

N95-20958# Leeds Univ. (England). Dept. of Electronic and Electrical Engineering.

SUPERRESOLUTION DIRECTION FINDING ALGORITHMS FOR THE CHARACTERISATION OF MULTI-MODED HF SIGNALS

M. A. Zatman and H. J. Strangeways *In* AGARD, Multiple Mechanism Propagation Paths (MMPPs): Their Characterisation and Influence on System Design Jul. 1994 10 p (For primary document see N95-20921 06-32)

Copyright Avail: CASI HC A02/MF A04

In this work three superresolution direction finding algorithms for use with arbitrary array geometries are described, all of which are capable of dealing with coherent signals, as typically found in the multi-path environment. DOSE is a quick single snapshot algorithm developed by the authors which operates on the received data vector. The IMP and Maximum Likelihood (ML) algorithms are used to process time averaged data covariance matrices. All three algorithms attempt in different ways to find a multi-dimensional solution to the inverse problem of direction finding. It is shown that calibration of arrays of identical elements is simplified by the use of these multi-dimensional algorithms when compared to 1 dimensional methods such as MUSIC. A common methodology for the implementation of these multi-dimensional algorithms is presented, and a quick method of implementing the ML algorithm and determining the number of signals present is described. Author

N95-20959# Thomson-CSF, Gennevilliers (France).

MEASUREMENTS OF ANGLES OF ELEVATION OF HF BY A HIGH RESOLUTION METHOD USING POLARIZATION DIVERSITY [MESURES D'ANGLES D'ELEVATION EN HF PAR UNE METHODE HAUTE RESOLUTION UTILISANT LA DIVERSITE DE POLARISATION]

Cedric Demeure, Anne Ferreol, and Jean-Luc Rogier *In* AGARD, Multiple Mechanism Propagation Paths (MMPPs): Their Characterisation and Influence on System Design Jul. 1994 9 p In FRENCH (For primary document see N95-20921 06-32)

(Contract DRET-90-34-473)

Copyright Avail: CASI HC A02/MF A04

In this paper, we present the use of high resolution techniques and polarization diversity in order to analyze HF links in ionospheric propagation, links which are characterized in general by the presence of several modes of propagation giving rise to several incident waves with the reception. These modes are strongly correlated and can have very different polarizations. The high resolution techniques have the capacity to simultaneously measure several incident waves present in a given frequency channel of analysis, and are thus adapted particularly to the situation of jamming where a frequency and/or temporal separation is no longer possible. The use of a network with polarization diversity allows, beyond obtaining certain parameters of polarization, an increase in the resolution of the methods considered, because of the difference in polarization of the modes. A better knowledge of the phenomenon of propagation waves in this medium is the anticipated result of the application of these techniques. For a given connection and at first approximation (one neglects the effects due to the 'tilt', or the rebound on a tilted ground), the modes arrive under the same azimuth with different angles of elevation. In the experiment described in this paper, the measurement of the angles of elevation is made by supposing a knowledge of azimuth. Thus we use a linear network and let us direct it in order to obtain good performances for the estimate of the angles of elevation. The method high resolution with diversity of polarization used is method MUSIC adapted in order to take account of the use of sensors having gains different according to polarization from the received wave. Transl. by CASI

N95-20960# Forschungsinstitut fuer Hochfrequenzphysik, Werthhoven (Germany).

MEASUREMENTS OF RADAR BACKSCATTER FROM THE OCEAN SURFACE AT 94 GHz AS A FUNCTION OF WIND SPEED, DIRECTION AND THE MODULATION BY THE OCEAN WAVES DURING THE SAXON-FPN EXPERIMENT

Hans-Hellmuth Fuchs *In* AGARD, Multiple Mechanism Propagation Paths (MMPPs): Their Characterisation and Influence on System Design Jul. 1994 7 p (For primary document see N95-20921 06-32)

Copyright Avail: CASI HC A02/MF A04

As part of the joint German/US SAXON-FPN remote sensing experiment a series of mm-wave radar backscatter measurements were carried out in the German Bight of the North Sea in November 1990, 1991 and August 1992. The dependence of the reflectivity sigma(sup o) on wind speed and direction was determined by means of a 94 GHz (W-band) radar mounted on the German Research Platform North Sea (FPN). The radar backscattering measurements were performed at an incidence angle of 45 deg and at azimuth angles relative to the wind direction ranging from upwind to crosswind. Based on the data evaluation of the three measurement periods values for the wind speed exponent gamma defined by an empirical relation between the reflectivity sigma(sup o) at vertical polarization and the windspeed U measured at a height of 46 m above mean sea level at the FPN were obtained. The values of gamma range between 2.33 and 2.50 depending on wind direction and the wave spectrum. This result shows that the wind speed exponent at W-band is higher than those at X-, Ku- and Ka-band indicating that either an enhanced generation of higher amplitudes of short waves in the millimeter range or other processes exist like specular scattering from facets reinforcing the backscatter cross section. Author

N95-20961# Centre National d'Etudes des Telecommunications, Lannion (France). Lab. PTI.

SOUNDER CALIBRATION WITH BACKSCATTERING FROM LOSQUET ISLAND IN THE PRESENCE OF MULTIPATHS [CALIBRATION DU SONDEUR A RETRODIFFUSION DE L'ILE LOSQUET EN PRESENCE DE MULTI-TRAJETS]

F. Gauthier, J. Y. LeSaout, and R. Fleury *In* AGARD, Multiple Mechanism Propagation Paths (MMPPs): Their Characterisation and Influence on System Design Jul. 1994 12 p In FRENCH (For primary document see N95-20921 06-32)

Copyright Avail: CASI HC A03/MF A04

The precise localization of the areas of the ionosphere by HF forward-scatter radars depends on the parameters characteristic of the propagation at the time of the survey, and often requires the use of calibration techniques. To gauge the data of the sounder with backscattering data from the Losquet Island, the National Center of Studies of Telecommunications (CNET) implemented a HF mobile monofrequency responder radar. This paper presents the results of surveys obtained in 'scanning of site' mode with this responder and established to approximately 1000 km the Losquet Island; these data are used to calculate the position of the responder. It is shown that the multipaths are the primary source of the statistical error of localization in radial distance and that the use of simple methods of treatment allows the reduction of this error. Transl. by CASI

N95-20972 Helsinki Univ. of Technology, Espoo (Finland). Radio Lab.

LOW NOISE 22 GHz RECEIVER FOR THE RADIOASTRON SATELLITE. PART 1: REQUIREMENTS, DESIGN AND RELIABILITY ANALYSIS

P. Piironen, J. Mallat, and A. Raeisaenen Mar. 1994 93 p Limited Reproducibility: More than 20% of this document may be affected by microfiche quality

(PB95-104410; ISBN-951-22-2047-4) Avail: Issuing Activity (National Technical Information Service (NTIS))

Radioastron project, initiated in 1985, is an international collaborative mission to launch a space research satellite carrying a radio telescope to an elliptical orbit around the Earth. The telescope comprises a 10 meter antenna and four two-channel VLBI (very long baseline interferometry) receivers at different frequencies built by project participants. This report presents principles of interferometry, VLBI system requirements, receiver requirements, principles and solutions for space qualified design and a reliability analysis for the cooled zz GHz receiver. The most important receiver design objectives have been low noise, good phase stability and high reliability. NTIS

N95-20980 Helsinki Univ. of Technology, Espoo (Finland). Lab. of Signal Processing and Computer Technology.

ROUTING OF UNIDIRECTIONAL PACKET RADIO FOR WIDE-AREA PAGING NETWORK CONTROL AND MAINTENANCE

J. Honkanen 1994 67 p Limited Reproducibility: More than 20% of this document may be affected by microfiche quality

(PB95-104428; ISBN-951-22-2062-8) Avail: Issuing Activity (National Technical Information Service (NTIS))

The object of this report is to present ways to design a packet radio system for the paging network control and maintenance. The main interest is laid on the routing of the packet radio, but also other design questions of the packet radio and the paging network systems are considered too. In order to obtain an efficient packet radio network that is also robust against radio path fluctuations and interferences, a new quality controlled packet radio model is presented. Two different routing and scheduling methods that are based on the quality controlled packet radio model are proposed. The first method consists of several heuristic and non-iterative algorithms. The second method is iterative, and it is an implementation of the evolutionary algorithms. NTIS

N95-21029 Technische Univ., Delft (Netherlands).

STUDY ON THE REACTION KINETICS IN PULSED RF DISCHARGES UNDER RIE CONDITIONS Ph.D. Thesis

Jacobus Antonius Gij Baggerman (Philips Research Labs., Eindhoven, Netherlands.) 26 Oct. 1993 133 p

(PB95-107868; ISBN-90-74445-07-1) Copyright Avail: Issuing Activity (National Technical Information Service (NTIS))

In the present-day electronics industry, reactive ion etching (RIE) is a technique widely used to etch thin films anisotropically. The subject of this thesis is the determination of (reaction) kinetics of rf discharges under RIE conditions. Special attention is given to determining quantitatively the rise and decay of densities and energy distributions of plasma particles. A production-type RIE reactor was used for all experiments. In chapter 2 the ion density is determined by LIF spectroscopy in a model (N2) discharge under RIE conditions. Chapter 3 concerns energy-flux density measurements on the various parts of the etch reactor in contact with a 30 Pa nitrogen rf discharge. Chapter 4 concerns the etch mechanism of various organic polymers in oxygen and argon of discharges under RIE conditions studied by performing energy-flux density and ion-flux density measurements on the powered electrode. The polymers of interest are a novolac-based photoresist, polyimide and polymethylmethacrylate (PMMA). The density and the reaction kinetics of ground-state methylidyne (CH radical) are determined by LIF in order to determine whether small molecules in addition to atoms are sputtered from the polymer surface. In chapter 5 a model is set up in which diffusion of CH from the substrate into the gas phase and chemical reactions in the gas phase are taken into account. NTIS

N95-21099 Massachusetts Inst. of Tech., Lexington, MA. Lincoln Lab.

ADAPTIVE DETECTION IN STATIONARY AND NONSTATIONARY NOISE ENVIRONMENTS

Paul Monticciolo 24 Feb. 1994 69 p Limited Reproducibility: More than 20% of this document may be affected by microfiche quality

(Contract F19628-90-C-0002)

(AD-A279581; TR-937; ESC-TR-93-238) Avail: CASI HC A04

This report describes the statistical performance of several radar-based adaptive detection schemes in both stationary and nonstationary noise and interference environments. The detectors under study must be able to correctly determine the presence of a target in a range gate with a high degree of probability given that the probability of misclassification is a fixed small value. The hostile noise environment is assumed to consist of possibly time-varying, spatially correlated interference along with Gaussian background noise. In a typical radar environment, the mean value of the returned radar signal and the noise covariance matrix are unknown parameters; therefore, generalized likelihood ratio test procedures were used to develop decision rules that meet the Neyman-Pearson criterion. Three major cases of interest were examined. First, the single-pulse test developed by Kelly is reviewed. The multiple-pulse return test case is extremely complicated and was divided into distinct detector forms: noncoherent and coherent. The performance of each detector is a function of the signal-to-noise ratio, the number of radar pulse returns used in the decision rule, and the quality of the covariance estimate. DTIC

N95-21104# Helsinki Univ. of Technology, Espoo (Finland). Electromagnetics Lab.

LOW-FREQUENCY IMAGE THEORY FOR A CURRENT DIPOLE IN FRONT OF A PERMEABLE SPHERE

Johan C.-E. Sten May 1994 17 p See also PB93-179075 Sponsored by Academy of Finland

(ISSN 0784-848X)

(PB95-127676; ISBN-951-22-2131-4) Avail: CASI HC A03/MF A01

Image theory, previously developed for a low-frequency current source in front of a dielectric sphere, is formulated for the magnetically permeable sphere. The low-frequency image source corresponding to an electric dipole outside the sphere arises only when the orientation of the dipole is tangential to the surface of the sphere. Two alternative image representations are developed. One is a combination of a magnetic strip current and a bifilar magnetic line current, both flowing between the center of the sphere and the Kelvin inversion point on the axis connecting the sphere and the dipole. The other is a combination of a magnetic strip current and an electric strip current flowing orthogonally to each other. NTIS

N95-21107# Helsinki Univ. of Technology, Espoo (Finland). Lab. of Material Physics.
EIGENMODE METHOD FOR ELECTROMAGNETIC SYNTHESIS OF DIFFRACTIVE ELEMENTS WITH THREE-DIMENSIONAL PROFILES
Eero Noponen and Jari Turunen 1994 13 p
(ISSN 0355-7790)
(PB95-127726; TKK-F-A726; ISBN-951-22-2038-5) Avail: CASI HC A03/MF A01

The authors extend the rigorous eigenmode theory of binary surface-relief gratings to accommodate three-dimensional-modulation profiles, to formulate a synthesis problem for doubly-periodic resonance-domain diffractive elements, and to demonstrate some of its symmetry properties. Several solutions for multiple beam splitters with about 90% transmission-mode diffraction efficiency are obtained by nonlinear parametric optimization. The polarization sensitivity and the required fabrication accuracy are analyzed for some solutions. NTIS

N95-21109# Helsinki Univ. of Technology, Espoo (Finland). Lab. of Telecommunications Technology.
CELL LOSS ANALYSIS OF TWO-CLASS PRIORITY GENERALIZED KNOCKOUT SWITCH
Jian Ma and Kauko Rahko 1994 11 p
(ISSN 1235-8975)
(PB95-127742; ISBN-951-22-1932-8) Avail: CASI HC A03/MF A01

Since services require different quality of service, an asynchronous transfer mode (ATM) switch must be capable of handling the requirements of different services. In this letter, we introduce a two-class priority scheme to Knockout Switch (KS) and Generalized Knockout Switch (GKS). The priority switches achieve much lower loss rate of high-priority cells than no-priority switches. Using the priority scheme in the GKS is more efficient than in the KS to reduce the interconnect complexity of switch. NTIS

N95-21156 Department of the Navy, Washington, DC.
SMALL ANTENNAS FOR COMMUNICATION OVER SEA ICE Patent Application
Paul Mileski, inventor (to Navy) 4 Oct. 1993 13 p Limited Reproducibility: More than 20% of this document may be affected by microfiche quality
(AD-D016206; US-Patent-Appl-SN-130940) Avail: Issuing Activity (Defense Technical Information Center (DTIC))

The invention described herein relates to an antenna system which makes use of the waveguide properties of sea ice. The antenna system broadly includes at least one antenna wire extending along and preferably in contact with a sea ice surface for transmitting and receiving substantially vertically polarized radio waves. In a first embodiment, the antenna system has a single antenna wire connected to a tuner at one end and grounded to seawater at a second end. The antenna system also has a second length of wire attached to the tuner. The second wire passes through a hole in the sea ice and is also grounded to the seawater beneath the sea ice. In an alternative embodiment, only the second wire is grounded to the seawater beneath the sea ice. The single antenna wire in this embodiment is ungrounded. In yet another embodiment, the antenna system comprises a dipole antenna wire laying on the surface of the sea ice and being connected to a radio for transmitting and receiving radio signals. DTIC

N95-21205# Lawrence Livermore National Lab., Livermore, CA.
THREE-DIMENSIONAL GROUND PENETRATING RADAR IMAGING USING MULTI-FREQUENCY DIFFRACTION TOMOGRAPHY
J. E. Mast and E. M. Johansson Jul. 1994 9 p Presented at the Annual Meeting of the Society of Photo-Optical Instrumentation Engineers, San Diego, CA, 24-29 Jul. 1994
(Contract W-7405-eng-48)
(DE94-016687; UCRL-JC-116340; CONF-940723-13) Avail: CASI HC A02/MF A01

In this paper we present results from a three-dimensional image reconstruction algorithm for impulse radar operating in monostatic pulse-echo mode. The application of interest to us is the nondestructive evaluation of civil structures such as bridge decks. We use a multi-frequency diffraction tomography imaging technique in which coherent backward propagations of the received reflected wavefield form a spatial image of the scattering interfaces within the region of interest. This imaging technique provides high-resolution range and azimuthal visualization of the subsurface region. We incorporate the ability to image in planarly layered conductive media and apply the algorithm to experimental data from an offset radar system in which the radar antenna is not directly coupled to the surface of the region. We present a rendering in three-dimensions of the resulting image data which provides high-detail visualization. DOE

N95-21241# Stanford Linear Accelerator Center, CA.
RESONANT PHOTON-GRAVITON CONVERSION IN EM FIELDS: FROM EARTH TO HEAVEN
Pisin Chen Sep. 1994 9 p Presented at the 1st International Conference on Phenomenology of Unification From Present To Future, Rome, Italy, 23-26 Mar. 1994
(Contract DE-AC03-76SF-00515)
(DE95-002784; SU-SLAC-PUB-6666; CONF-9403118-2) Avail: CASI HC A02/MF A01

Gravitational radiation from high energy particles in modern accelerators is reviewed. We point out that the most effective way for laboratory production and detection of gravitons is through resonant photon-graviton conversion in a strong external EM field. Specific example using crystal channels for the (gamma) (yields) g (yields) (gamma) process is given, where the physical parameters needed for such a test appears to be reasonable. As another application of this effect in astrophysics, we show that the coupling between the cosmic microwave background radiation (CMBR) and the primordial magnetic field can induce a frequency-independent fluctuation in the photon flux. Using the observed CMBR fluctuation, we derive a bound on the primordial field strength. The effect can also convert the relic gravitons into photons. For the string cosmology it gives a new bound on the Hubble parameter at the Big Bang. DOE

N95-21277# Sandia National Labs., Albuquerque, NM.
AN OBJECT-ORIENTED IMPLEMENTATION OF THE Xpress TRANSFOR PROTOCOL
W. Timothy Strayer, Simon Gray, and Raymond E. Cline, Jr. 1994 14 p Presented at the 2nd IWACA Workshop, Heidlegerg, Germany, 26-28 Sep. 1994 Sponsored by AT and T Bell Labs.
(Contract DE-AC04-76DP-00789)
(DE95-001506; SAND-94-8718C; CONF-9409236-1) Avail: CASI HC A03/MF A01

Object-oriented design principles map well onto protocol implementations because protocols essentially manipulate two structures - packets and the states of the endpoints. In this paper the authors describe an implementation of the Xpress Transfer Protocol as a user space daemon written in C++. The object-oriented model forces the programmer to properly place functionality and information ownership. The model facilitates porting to various platforms and greatly eases the task of building data delivery services. DOE

N95-21292 Defence Research Establishment Ottawa, Ottawa (Ontario).
OVERVIEW OF DATA FUSION WORK FOR LAND ELECTRONIC WARFARE
J. Hooper Oct. 1993 28 p Limited Reproducibility: More than 20% of this document may be affected by microfiche quality
(AD-A279829; DREO-TN-93-31) Avail: Issuing Activity (Defense Technical Information Center (DTIC))

Electronic warfare (EW) is a land combat function. EW produces tactical intelligence information which, if timely, can affect the outcome of the battle. Automation is required for the EW/intelligence cycle to stay inside the ever-narrowing window of the commander's opportunity to respond to and impact battlefield situations. Data fusion will automate the EW analysis process to provide timely situation assessments. Data Fusion and Correlation Techniques Testbed (DFACTT) is a system designed in Canada to respond to the Canadian EW requirement. It is user verified and field proven. DFACTT is also the vehicle for long term research into the more esoteric

AI aspects of EW analysis including multisensor fusion. DFACTT is made up of a number of workstations which, together, automate the land EW process as practiced by Canada's EW Squadron. DTIC

N95-21305# Sandia National Labs., Albuquerque, NM.

SYNTHETIC APERTURE RADAR PROCESSING WITH POLAR FORMATTED SUBAPERTURES

Armin W. Doerry 1994 6 p Presented at the 28th Annual Asilomar Conference on Signals, Systems, and Computers, Pacific Grove, CA, 31 Oct. - 2 Nov. 1994
(Contract DE-AC04-94AL-85000)
(DE95-001830; SAND-94-1375C; CONF-9410156-2) Avail: CASI HC A02/MF A01

Synthetic Aperture Radar (SAR) uses the motion of a small real antenna to synthesize a larger aperture, and thereby achieve very fine azimuth resolution. Efficient SAR image formation requires modelling the radar echo and compensating (focusing) the delay and phase for various positions in the target scene. Polar-Format processing is one successful algorithm developed to process large scenes at fine resolutions, but is still limited, especially at resolutions near a wavelength. This paper shows how using tiers of subapertures can overcome the limitations of Polar-Format processing and increase the focused scene size substantially while using only efficient vector multiplies and Fast Fourier Transforms. DOE

N95-21324# Naval Postgraduate School, Monterey, CA.

VIBRATION ANALYSIS OF THE AN/SPS-67(V)3 SURFACE SEARCH RADAR M.S. Thesis

Thomas A. Tomaiko Sep. 1994 131 p
(AD-A286050) Avail: CASI HC A07/MF A02

Modern warships rely greatly upon electronic systems for their combat effectiveness, as well as defense. The ability of the U. S. Navy to maintain sea control and to project sea power depends upon the state-of-the-art combat systems equipment. Shipboard combat systems must, therefore, be shock hardened to be capable of operating in the combat shock environment. The structural survivability of the mast and antennae and hence, the shipboard combat systems, is a shock induced vibration problem in which relatively low frequency equipment responses are observed. The structural survivability of combat systems can be 'designed in' through the application of modern digital techniques for measuring and analyzing dynamic phenomena. The purpose of this study was to build and demonstrate the practical value of a finite element model of the AN/SPS-67(V)3 surface search radar which when validated by experimentally obtained shock qualification data can serve as a powerful tool toward improving survivability of combat systems. The finite element model developed may be used to compute predicted shock-induced accelerations, velocities, displacements, and shock spectra resulting from UNDEX in order to evaluate the potential for antenna structural survivability or vulnerability on an existing platform. Furthermore, the antenna finite element model may be used in the design of new mast-antenna systems. DTIC

N95-21405# NTL, Inc., Greenlawn, NY.

CLASSICAL ANALYSIS METHODS FOR DESIGNING AND DEVELOPING DOWNLOOKING RADARS Final Technical Report, Sep. 1992 - Apr. 1994

George Skahill Aug. 1994 96 p
(Contract F30602-92-C-0080)
(AD-A285760; RL-TR-94-113) Avail: CASI HC A05/MF A01

This report describes analytical methods for characterizing the distributions of surface clutter as observed by downlooking radars over spherical planets, taking the classical, pencil and paper, methods of analytic geometry and calculus as far as possible before turning to computer based numerical evaluations. General expressions describing surface clutter power distributions in range and range-rate coordinates are developed in closed form and evaluated for several low PRF, phased array configurations. Information contained in this document formed the subject matter for a series of eight lectures at Rome Laboratory, under this contract, to relative newcomers to the study of clutter limited radar. With the classical analysis tools, they were able to quickly obtain results which compared favorably with those from elaborate simulations evolved by teams of experts over periods of many years. DTIC

N95-21431 Institut National des Sciences Appliquees, Rennes (France).

DESIGN AND IMPLEMENTATION OF A DUAL-BEAM PRINTED ANTENNA FOR A RECEPTION IN ANGULAR DIVERSITY ON A HERTZIEN CLUSTER (OR BUNDLE) Ph.D. Thesis [CONCEPTION ET REALISATION D'UNE ANTENNE BI-FAISCEAUX IMPRIMEE POUR UNE RECEPTION EN DIVERSITE ANGULAIRE SUR UN FAISCEAU HERTZIEN A 15 GHZ]

S. Tessereau 4 Mar. 1993 188 p In FRENCH Sponsored by Direction des Recherches, Etudes et Techniques
(PB95-131603) Avail: Issuing Activity (National Technical Information Service (NTIS))

The purpose of this research was to design and implement an angular-diversity receiving system for a 15-GHz radio-relay system, while favoring low cost and small overall dimensions. It led to the development of a software aid to the design of linear networks of printed antennas powered in series by proximity coupling, and to the validation of the angular diversity achieved thanks to a dual-beam antenna consisting of two linear networks of printed antennas. NTIS

N95-21438 Brown Univ., Providence, RI. Div. of Applied Mathematics.

DIFFUSION APPROXIMATIONS IN COMMUNICATION AND STOCHASTIC THEORY Final Report, 1 Jun. 1993 - 31 May 1994

Paul Dupuis 10 Nov. 1994 10 p Presented at the Workshop on Stochastic Systems and their Applications, Newport, RI, 15-16 Apr. 1994 Limited Reproducibility: More than 20% of this document may be affected by microfiche quality
(Contract F49620-93-1-0279)
(AD-A286440; AFOSR-94-0742TR) Avail: CASI HC A02

The workshop Stochastic Systems and Their Applications was held in Newport, RI on April 15-16, 1994. The main topics of the conference were asymptotic methods in stochastic systems theory and related applications. The goal of the conference was to review recent advances in asymptotic methods and expose some important new application areas where those methods might be useful. DTIC

N95-21448# Sandia National Labs., Albuquerque, NM. Optics and Exploratory Technologies Dept.

LIDAR TECHNOLOGIES FOR AIRBORNE AND SPACE-BASED APPLICATIONS

Tammy D. Henson, Randal L. Schmitt, Tim J. Sobering, Thomas D. Raymond, and David A. Stephenson Oct. 1994 117 p
(Contract DE-AC04-94AL-85000)
(DE95-002954; SAND-94-0024) Avail: CASI HC A06/MF A02

This study identifies technologies required to extend the capabilities of airborne light detection and ranging (lidar) systems and establish the feasibility of autonomous space-based lidars. Work focused on technologies that enable the development of a lightweight, low power, rugged and autonomous Differential Absorption Lidar (DIAL) instruments. Applications for airborne or space-based DIAL include the measurement of water vapor profiles in support of climate research and processing-plant emissions signatures for environmental and nonproliferation monitoring. A computer-based lidar performance model was developed to allow trade studies to be performed on various technologies and system configurations. It combines input from the physics (absorption line strengths and locations) of the problem, the system requirements (weight, power, volume, accuracy), and the critical technologies available (detectors, lasers, filters) to produce the best conceptual design. Conceptual designs for an airborne and space-based water vapor DIAL, and a detailed design of a ground-based water vapor DIAL demonstration system were completed. Future work planned includes the final testing, integration, and operation of the demonstration system to prove the capability of the critical enabling technologies identified. DOE

N95-21456*# Jet Propulsion Lab., California Inst. of Tech., Pasadena, CA.

THE DEEP SPACE NETWORK AS AN INSTRUMENT FOR RADIO SCIENCE RESEARCH

S. W. Asmar and N. A. Renzetti 15 Apr. 1993 76 p Revised
(Contract NAS7-918; RTOP 314-40-31-30-26)
(NASA-CR-197341; JPL-Publ-80-93-Rev-1; NAS 1.26:197341) Avail: CASI HC A05/MF A01

Radio science experiments use radio links between spacecraft and sensor instrumentation that is implemented in the Deep Space Network. The deep space communication complexes along with the telecommunications subsystem on board the spacecraft constitute the major elements of the radio science instrumentation. Investigators examine small changes in the phase and/or amplitude of the radio signal propagating from a spacecraft to study the atmospheric and ionospheric structure of planets and satellites, planetary gravitational fields, shapes, masses, planetary rings, ephemerides of planets, solar corona, magnetic fields, cometary comae, and such aspects of the theory of general relativity as gravitational waves and gravitational redshift. Author

N95-21459# Oak Ridge National Lab., TN.
THREE-DIMENSIONAL EFFECTS FOR RADIO FREQUENCY ANTENNA MODELING
M. D. Carter, D. B. Batchelor, and D. C. Stallings 1993 4 p Presented at the 10th Topical Conference on Radio Frequency Power in Plasmas, Boston, MA, 1-3 Apr. 1993
(Contract DE-AC05-84OR-21400)
(DE94-019125; CONF-9304112-26) Avail: CASI HC A01/MF A01

Electromagnetic field calculations for radio frequency (RF) antennas in two dimensions (2-D) neglect finite antenna length effects as well as the feeders leading to the main current strap. The 2-D calculations predict that the return currents in the sidewalls of the antenna structure depend strongly on the plasma parameters, but this prediction is suspect because of experimental evidence. To study the validity of the 2-D approximation, the Multiple Antenna Implementation System (MAntIS) has been used to perform three-dimensional (3-D) modeling of the power spectrum, plasma loading, and inductance for a relevant loop antenna design. Effects on antenna performance caused by feeders to the main current strap and conducting sidewalls are considered. The modeling shows that the feeders affect the launched power spectrum in an indirect way by forcing the driven RF current to return in the antenna structure rather than the plasma, as in the 2-D model. It has also been found that poloidal dependencies in the plasma impedance matrix can reduce the loading predicted from that predicted in the 2-D model. For some plasma parameters, the combined 3-D effects can lead to a reduction in the predicted loading by as much as a factor of 2 from that given by the 2-D model, even with end-effect corrections for the 2-D model. DOE

N95-21462 New Jersey Inst. of Tech., Newark, NJ. Dept. of Mathematics.
APPLIED MATHEMATICAL PROBLEMS IN MODERN ELECTROMAGNETICS Final Report, 1 Jun. 1991 - 31 May 1994
Gregory Kriegsman 31 May 1994 15 p Limited Reproducibility: More than 20% of this document may be affected by microfiche quality
(Grant AF-AFOSR-0252-91)
(AD-A286448; AFOSR-94-0703TR) Avail: CASI HC A03

We have primarily investigated two classes of electromagnetic problems. The first contains the quantitative description of microwave heating of dispersive and conductive materials. Such problems arise, for example, when biological tissue are exposed, accidentally or purposefully, to microwave radiation. Other instances occur in ceramic processing, such as sintering and microwave assisted chemical vapor infiltration and other industrial drying processes, such as the curing of paints and concrete. The second class characterizes the scattering of microwaves by complex targets which possess two or more disparate length and/or time scales. Spatially complex scatterers arise in a variety of applications, such as large gratings and slowly changing guiding structures. The former are useful in developing microstrip energy couplers while the later can be used to model anatomical subsystems (e.g., the open guiding structure composed of two legs and the adjoining lower torso). Temporally complex targets occur in applications involving dispersive media whose relaxation times differ by orders of magnitude from thermal and/or electromagnetic time scales. For both cases the mathematical description of the problems gives rise to complicated ill-conditioned boundary value problems, whose accurate solutions require a blend of both asymptotic techniques, such as multiscale methods and matched asymptotic expansions, and numerical methods incorporating radiation boundary conditions, such as finite differences and finite elements. DTIC

N95-21464 Department of the Navy, Washington, DC.
METHOD AND APPARATUS FOR CLASSIFYING TARGETS Patent
Roger F. Dwyer, inventor (to Navy) 9 Aug. 1994 14 p Filed 22 Oct. 1993
(AD-D016519; US-Patent-5,337,053; US-Patent-Appl-SN-147238) Avail: US Patent and Trademark Office

A method and apparatus for classifying objects based upon information contained in the fourth order cumulant derived from energy of the object. Successive pulse returns in active systems and samples in passive systems are converted into vectors based upon the fourth order cumulant information for each successive return or sample. The vectors for each such pulse are compared to corresponding class information based upon the corresponding fourth order cumulant information. The comparison uses loglikelihood ratios of the different pairs of classes. Decision making is based upon the value of each loglikelihood ratio in comparison with a class threshold. DTIC

N95-21491 Surveillance Research Lab., Salisbury (Australia).
PASSIVE MILLIMETRE WAVE IMAGING: A REVIEW
Philip J. Picone Feb. 1994 32 p Limited Reproducibility: More than 20% of this document may be affected by microfiche quality
(AD-A279275; SRL-0144-RR; DODA-AR-008-522) Avail: CASI HC A03

The propagation of millimeter waves through the atmosphere is reviewed. Target temperature contrast and ranges possible are calculated for current passive millimeter wave detectors under various atmospheric conditions. Some possible future developments in passive millimeter wave imaging arrays are also discussed. DTIC

N95-21493 Mitre Corp., Bedford, MA.
SEMAPHORE NETWORK ENCRYPTION REPORT
Karen L. Johnson Mar. 1994 42 p Limited Reproducibility: More than 20% of this document may be affected by microfiche quality
(AD-A279294; MP-94B0000022) Avail: Issuing Activity (Defense Technical Information Center (DTIC))

This paper documents the results of a preliminary assessment performed on the commercial off-the-shelf (COTS) Semaphore Communications Corporation (SCC) Network Security System (NSS). The Semaphore NSS is a family of products designed to address important network security concerns, such as network source address authentication and data privacy. The assessment was performed in the INFOSEC Core Integration Laboratory, and its scope was product usability focusing on interoperability and system performance in an existing operational network. Included in this paper are preliminary findings. Fundamental features and functionality of the Semaphore NSS are identified, followed by details of the assessment, including test descriptions and results. A summary of test results and future plans are also included. These findings will be useful to those investigating the use of commercially available solutions to network authentication and data privacy. DTIC

N95-21532*# Jet Propulsion Lab., California Inst. of Tech., Pasadena, CA.
THE TELECOMMUNICATIONS AND DATA ACQUISITION REPORT Progress Report, Oct. - Dec. 1994
Joseph H. Yuen, ed. 15 Feb. 1995 222 p
(NASA-CR-197390; JPL-TDA-PR-42-120; NAS 1.26:197390) Avail: CASI HC A10/MF A03

This quarterly publication provides archival reports on developments in programs managed by JPL's Telecommunications and Mission Operations Directorate (TMOD), which now includes the former Telecommunications and Data Acquisition (TDA) Office. In space communications, radio navigation, radio science, and ground-based radio and radar astronomy, it reports on activities of the Deep Space Network (DSN) in planning, supporting research and technology, implementation, and operations. Also included are standards activity at JPL for space data and information systems and reimbursable DSN work performed for other space agencies through NASA. The preceding work is all performed for NASA's Office of Space Communications (OSC). For individual titles, see N95-21533 through N95-21543.

N95-21533*# Jet Propulsion Lab., California Inst. of Tech., Pasadena, CA.
ORBIT DETERMINATION OF HIGHLY ELLIPTICAL EARTH ORBITERS USING IMPROVED DOPPLER DATA-PROCESSING MODES c13
J. A. Estefan *In its* The Telecommunications and Data Acquisition

Report 15 Feb. 1995 p 1-17 (For primary document see N95-21532 06-32)
(RTOP 314-30-11-60-02)
Avail: CASI HC A03/MF A03

A navigation error covariance analysis of four highly elliptical Earth orbits is described, with apogee heights ranging from 20,000 to 76,800 km and perigee heights ranging from 1,000 to 5,000 km. This analysis differs from earlier studies in that improved navigation data-processing modes were used to reduce the radio metric data. For this study, X-band (8.4-GHz) Doppler data were assumed to be acquired from two Deep Space Network radio antennas and reconstructed orbit errors propagated over a single day. Doppler measurements were formulated as total-count phase measurements and compared to the traditional formulation of differenced-count frequency measurements. In addition, an enhanced data-filtering strategy was used, which treated the principal ground system calibration errors affecting the data as filter parameters. Results suggest that a 40- to 60-percent accuracy improvement may be achievable over traditional data-processing modes in reconstructed orbit errors, with a substantial reduction in reconstructed velocity errors at perigee. Historically, this has been a regime in which stringent navigation requirements have been difficult to meet by conventional methods. Author

N95-21534*# Jet Propulsion Lab., California Inst. of Tech., Pasadena, CA.

SEAMLESS DATA-RANGE CHANGE USING PUNCTURED CONVOLUTIONAL CODES FOR TIME-VARYING SIGNAL-TO-NOISE RATIOS

Y. Feria and K.-M. Cheung *In its* The Telecommunications and Data Acquisition Report 15 Feb. 1995 p 18-28 (For primary document see N95-21532 06-32)
(RTOP 314-30-61-02-05)
Avail: CASI HC A02/MF A03

In a time-varying signal-to-noise ration (SNR) environment, symbol rate is often changed to maximize data return. However, the symbol-rate change has some undesirable effects, such as changing the transmission bandwidth and perhaps causing the receiver symbol loop to lose lock temporarily, thus losing some data. In this article, we are proposing an alternate way of varying the data rate without changing the symbol rate and, therefore, the transmission bandwidth. The data rate change is achieved in a seamless fashion by puncturing the convolutionally encoded symbol stream to adapt to the changing SNR environment. We have also derived an exact expression to enumerate the number of distinct puncturing patterns. To demonstrate this seamless rate change capability, we searched for good puncturing patterns for the Galileo (14,1/4) convolutional code and changed the data rates by using the punctured codes to match the Galileo SNR profile of November 9, 1997. We show that this scheme reduces the symbol-rate changes from nine to two and provides a comparable data return in a day and a higher symbol SNR during most of the day. Author

N95-21535*# Jet Propulsion Lab., California Inst. of Tech., Pasadena, CA.

TURBO CODES FOR DEEP-SPACE COMMUNICATIONS

D. Divsalar and F. Pollara *In its* The Telecommunications and Data Acquisition Report 29-39 (SEE N95-21532 06-32) 15 Feb. 1995 (For primary document see N95-21532 06-32)
(RTOP 315-91-20-20-53)
Avail: CASI HC A03/MF A03

Turbo codes were recently proposed by Berrou, Glavieux, and Thitimajshima, and it has been claimed these codes achieve near-Shannon-limit error correction performance with relatively simple component codes and large interleavers. A required E(b)/N(o) of 0.7 dB was reported for a bit error rate of 10(exp -5), using a rate 1/2 turbo code. However, some important details that are necessary to reproduce these results were omitted. This article confirms the accuracy of these claims, and presents a complete description of an encoder/decoder pair that could be suitable for deep-space applications, where lower rate codes can be used. We describe a new simple method for trellis termination, analyze the effect of interleaver choice on the weight distribution of the code, and introduce the use of unequal rate component codes, which yield better performance. Author

N95-21536*# Jet Propulsion Lab., California Inst. of Tech., Pasadena, CA.

CDMA WITH INTERFERENCE CANCELLATION FOR MULTIPROBE MISSIONS

D. Divsalar and M. K. Simon *In its* The Telecommunications and Data Acquisition Report 15 Feb. 1995 p 40-53 (For primary document see N95-21532 06-32)
(RTOP 315-91-20-20-53)
Avail: CASI HC A03/MF A03

Code division multiple-access spread spectrum has been proposed for use in future multiprobe/multispacecraft missions. This article considers a general parallel interference-cancellation scheme that significantly reduces the degradation effect of probe (user) interference but with a lesser implementation complexity than the maximum-likelihood technique. The scheme operates on the fact that parallel processing simultaneously removes from each probe (user) the total interference produced by the remaining most reliably received probes (users) accessing the channel. The parallel processing can be done in multiple stages. The proposed scheme uses tentative decision devices with different optimum thresholds at the multiple stages to produce the most reliably received data for generation and cancellation of probe/spacecraft interference. The one-stage interference cancellation was analyzed for two types of tentative decision devices, namely, hard and null zone decisions. Simulation results are given for one- and two-stage interference cancellation for equal as well as unequal received power probes. Author

N95-21537*# Jet Propulsion Lab., California Inst. of Tech., Pasadena, CA.

COMBINING IMAGE-PROCESSING AND IMAGE COMPRESSION SCHEMES **c61**

H. Greenspan (California Inst. of Tech., Pasadena, CA.) and M.-C. Lee (Microsoft Corp., Redmond, WA.) *In its* The Telecommunications and Data Acquisition Report 15 Feb. 1995 p 54-76 (For primary document see N95-21532 06-32)
(RTOP 315-91-40-20-36)
Avail: CASI HC A03/MF A03

An investigation into the combining of image-processing schemes, specifically an image enhancement scheme, with existing compression schemes is discussed. Results are presented on the pyramid coding scheme, the subband coding scheme, and progressive transmission. Encouraging results are demonstrated for the combination of image enhancement and pyramid image coding schemes, especially at low bit rates. Adding the enhancement scheme to progressive image transmission allows enhanced visual perception at low resolutions. In addition, further progressing of the transmitted images, such as edge detection schemes, can gain from the added image resolution via the enhancement. Author

N95-21538*# Jet Propulsion Lab., California Inst. of Tech., Pasadena, CA.

A METHOD USING FOCAL PLANE ANALYSIS TO DETERMINE THE PERFORMANCE OF REFLECTOR ANTENNAS

P. W. Cramer, W. A. Imbriale, and S. R. Rengarajan (California State Univ., Northridge, CA.) *In its* The Telecommunications and Data Acquisition Report 15 Feb. 1995 p 78-103 (For primary document see N95-21532 06-32)
(RTOP 314-30-11-00-12)
Avail: CASI HC A03/MF A03

Reflector antenna optimization schemes using array feeds have been used to recover antenna losses resulting from antenna distortions and aberrations and to generate contour coverage patterns. Historically, these optimizations have been carried out using the antenna far-field scattered patterns. The far-field patterns must be calculated separately for each of the array feed elements. For large or complex antennas (which include beam-waveguide antennas), the far-field calculation times can be prohibitive. This article presents a method with which the optimization can be carried out in the antenna focal region, where the scattering calculation needs only to be done once independently of the number of the elements in the array. This article also includes the results of a study, utilizing this unique technique, to determine the capabilities and limitations of using array feeds to compensate for gravitational induced losses in large reflector antennas. Author

N95-21539*# Jet Propulsion Lab., California Inst. of Tech., Pasadena, CA.

ON-WAFER, CRYOGENIC CHARACTERIZATION OF ULTRA-LOW NOISE HEMT DEVICES **c33**

J. J. Bautista, J. Laskar (Hawaii Univ., Honolulu, HI.), and P. Szydlik (State Univ. of New York, Plattsburgh, NY.) *In its* The Telecommunications and Data Acquisition Report 15 Feb. 1995 p 104-120 (For primary document see N95-21532 06-32)
(RTOP 314-30-11-10-02)
Avail: CASI HC A03/MF A03

Significant advances in the development of high electron-mobility field-effect transistors (HEMT's) have resulted in cryogenic, low-noise amplifiers (LNA's) whose noise temperatures are within an order of magnitude of the quantum noise limit (hf/k). Further advances in HEMT technology at cryogenic temperatures may eventually lead to the replacement of maser and superconducting insulator superconducting front ends in the 1- to 100-GHz frequency band. Key to identification of the best HEMT's and optimization of cryogenic LNA's are accurate and repeatable device measurements at cryogenic temperatures. This article describes the design and operation of a cryogenic coplanar waveguide probe system for the characterization and modeling of advanced semiconductor transistors at cryogenic temperatures. Results on advanced HEMT devices are presented to illustrate the utility of the measurement system. Author

N95-21540*# Jet Propulsion Lab., California Inst. of Tech., Pasadena, CA.

RADIO-SCIENCE PERFORMANCE ANALYSIS SOFTWARE

D. D. Morabito and S. W. Asmar *In its* The Telecommunications and Data Acquisition Report 15 Feb. 1995 p 121-152 (For primary document see N95-21532 06-32)
(RTOP 314-30-21-00-06)
Avail: CASI HC A03/MF A03

The Radio Science Systems Group (RSSG) provides various support functions for several flight project radio-science teams. Among these support functions are uplink and sequence planning, real-time operations monitoring and support, data validation, archiving and distribution functions, and data processing and analysis. This article describes the support functions that encompass radio-science data performance analysis. The primary tool used by the RSSG to fulfill this support function is the STBLTY program set. STBLTY is used to reconstruct observable frequencies and calculate model frequencies, frequency residuals, frequency stability in terms of Allan deviation, reconstructed phase, frequency and phase power spectral density, and frequency drift rates. In the case of one-way data, using an ultrastable oscillator (USO) as a frequency reference, the program set computes the spacecraft transmitted frequency and maintains a database containing the in-flight history of the USO measurements. The program set also produces graphical displays. Some examples and discussions on operating the program set on Galileo and Ulysses data will be presented. Author

N95-21541*# Jet Propulsion Lab., California Inst. of Tech., Pasadena, CA.

ANALYSIS OF A MICROSTRIP REFLECTARRAY ANTENNA FOR MICROSPACECRAFT APPLICATIONS

J. Huang *In its* The Telecommunications and Data Acquisition Report 15 Feb. 1995 p 153-173 (For primary document see N95-21532 06-32)
(RTOP 315-91-50-20-04)
Avail: CASI HC A03/MF A03

A microstrip reflectarray is a flat reflector antenna that can be mounted conformally onto a spacecraft's outside structure without consuming a significant amount of spacecraft volume and mass. For large apertures (2 m or larger), the antenna's reflecting surface, being flat, can be more easily and reliably deployed than a curved parabolic reflector. This article presents the study results on a microstrip reflect-array with circular polarization. Its efficiency and bandwidth characteristics are analyzed. Numerous advantages of this antenna system are discussed. Three new concepts using this microstrip reflectarray are also proposed. Author

N95-21542*# Jet Propulsion Lab., California Inst. of Tech., Pasadena, CA.

THE EFFICIENCY CALIBRATION OF THE DSS-24 34-METER BEAM-WAVEGUIDE ANTENNA

L. S. Alvarez, M. J. Britcliffe, M. M. Franco, S. R. Stewart, and H. J. Jackson *In its* The Telecommunications and Data Acquisition Report 15 Feb. 1995 p 174-187 (For primary document see N95-21532 06-32)
(RTOP 314-30-63-02-04)
Avail: CASI HC A03/MF A03

Microwave performance testing of the new Deep Space Station (DSS)-24 34-m-diameter antenna was carried out during the summer of 1994. Efficiency measurements were made at the 8.45 GHz (X-band) and 32-GHz (ka-band) frequencies both at the antenna Cassegrian (f1) and beam-waveguide (f3) focal points. In addition, the antenna f3 efficiencies were measured on the DSS-24 operational 2.295-GHz (S-band) and 8.45-Ghz feeds. This article presents the efficiency determinations as a function of elevation angle along with a corresponding error analysis of the measurements. Peak measured gains and efficiencies are tabulated for all frequencies. Author

N95-21543*# Jet Propulsion Lab., California Inst. of Tech., Pasadena, CA.

ANALYSIS OF A DISK-ON-ROD SURFACE WAVE ELEMENT INSIDE A CORRUGATED HORN USING THE MODE-MATCHING TECHNIQUE

J. C. Chen *In its* The Telecommunications and Data Acquisition Report 15 Feb. 1995 p 188-202 (For primary document see N95-21532 06-32)
(RTOP 314-30-11-00-10)
Avail: CASI HC A03/MF A03

A disk-on-rod inside a corrugated horn is one of the horn configurations for dual-frequency or wide-band operation. A mode-matching analysis method is described. A disk-on-rod inside a corrugated horn is represented as a series of coaxial waveguide sections and circular waveguide sections connected to each other. Three kinds of junctions need to be considered: coaxial-to-coaxial, coaxial-to-circular, and circular-to-circular. A computer program was developed to calculate the scattering matrix and the radiation pattern of a disk-on-rod inside a corrugated horn. The software as verified by experiment, and good agreement between calculation and measurement was obtained. The disk-on-rod inside a corrugated horn design gives an option to the Deep Space Network dual-frequency operation system, which currently is a two-horn/one-dichroic plate system. Author

N95-21576 Massachusetts Inst. of Tech., Cambridge, MA. Digital Signal Processing Group.

NUMERICAL AND SYMBOLIC ALGORITHMS FOR APPLICATION AND SPECIFIC SIGNAL PROCESSING Semiannual Report, 31 Oct. 1993 - 4 Apr. 1994

Alan V. Oppenheim 25 May 1994 11 p Limited Reproducibility: More than 20% of this document may be affected by microfiche quality
(Contract N00014-93-1-0686)
(AD-A279902) Avail: Issuing Activity (Defense Technical Information Center (DTIC))

Efforts have been oriented to impact the RASSP program and objectives in two major ways. One is to identify and develop appropriate classes of emerging as well as more classical signal processing algorithms which will exercise and challenge the RASSP tools and process. In this way we would anticipate being able to identify and define in detail signal processing algorithms that are important but that the current tools can't accommodate well. We are currently envisioning doing this with the iterative and PDE algorithms, 'approximate' algorithms, and algorithms oriented toward fault tolerance. The second is for our research to provide specific input for a real or hypothetical next generation of RASSP tools and process. One phase of this, of course, will follow somewhat from our having identified weaknesses in the currently available tools. In addition, we are developing specific paradigms for environments that incorporate symbolic design and processing and approximate processing. Derived from text

N95-21579 Technische Hogeschool, Delft (Netherlands). Dept. of Electrical Engineering.

SUBSAMPLING METHODS FOR IMAGE SEQUENCE CODING Ph.D. Thesis

R. A. F. Belfor 9 Jun. 1994 146 p
(PB95-107991; ISBN-90-5326-017-X) Copyright Avail: Issuing Activity (National Technical Information Service (NTIS))

Subsampling can be used as a method to compress digital image sequences. The thesis begins with a look at fixed lattice subsampling systems with linear non-adaptive interpolation filters. This system is used to discuss the basics of subsampling. The interpolation process is the only aspect in this subsampling scheme open for improvement. Therefore, some alternatives for the linear non-adaptive interpolation are discussed. The restriction of a fixed subsampling lattice prevents the effective use of all the image characteristics. Thus, adaptive sampling lattices are used instead. First, the sampling lattice is adapted to the local image structure. Then, sub-Nyquist sampling and motion compensated sub-Nyquist sampling is discussed. The problem of combining transform coding with either fixed lattice subsampling or sub-Nyquist sampling is considered. Finally, the different subsampling systems are compared with each other. NTIS

N95-21623 Technische Univ., Twente (Netherlands). Tele-Informatics and Open System Group.

APPLICATION-ORIENTED ARCHITECTURE FOR MULTIMEDIA TELESERVICES

Erwin vanRijssen, Ing Widya, and Eddie Michiels 1994 22 p
(ISSN 0924-3755)
(PB95-135513; Memo-INF-94-26) Copyright Avail: Issuing Activity
(National Technical Information Service (NTIS))

This paper looks into communications capabilities that are required by distributed multimedia applications to achieve relation preserving information exchange. These capabilities are derived by analyzing the notion of 'information exchange' and are embodied in communications functionalities. To emphasize the importance of the users' view, a top-down approach is applied. The revised Open Systems Interconnection (OSI) Application Layer Structure (OSI-ALS) is used to model the communications functionalities and to develop an architecture for composition of multimedia teleservices with these functionalities. This work may therefore be considered an exercise to evaluate the suitability of OSI-ALS for composition of multimedia teleservices. NTIS

N95-21672 Office of Naval Research, Arlington, VA.

BROADBAND PRESSURE BARRIER FOR CIRCULAR WAVEGUIDE Patent Application

David F. Rivera, inventor, Michael J. Josypenko, inventor, and Thomas R. Floyd, inventor 8 Aug. 1994 23 p Limited Reproducibility: More than 20% of this document may be affected by microfiche quality
(AD-D016503; US-Patent-Appl-SN-287023) Avail: Issuing Activity
(Defense Technical Information Center (DTIC))

A broad passband pressure barrier arrangement is provided for insertion in a circular waveguide between a source and a receiver of radio frequency (RF) energy with a spatially circumferential electric field characteristic of the TE 01 mode. At least three abutting cylindrical barrier regions are coaxially aligned and arranged symmetrically in mirror image fashion about a radial plane of the circular waveguide. The cylindrical barrier regions include: at least one solid cylindrical plug region sealed in a cross-section of the circular waveguide and having a longitudinal thickness sufficient to withstand a predetermined pressure load, and at least one solid cylindrical tuning region having a radius less than that of the circular waveguide and further having a longitudinal thickness. Each of the cylindrical barrier regions are defined by a characteristic impedance at opposing end faces thereof and by a characteristic impedance between the opposing end faces. A region-by-region impedance analysis process begins with an end face of the arrangement that is furthest from the source and is completed with an end face of the arrangement that is nearest the source. DTIC

N95-21684 Range Commanders Council, White Sands Missile Range, NM.

NONCOHERENT TRANSPONDER STANDARDS

Apr. 1994 22 p Supersedes N81-132512 Limited Reproducibility: More than 20% of this document may be affected by microfiche quality
(AD-A279512; RCC-254-94; AD-A091282) Avail: Issuing Activity (Defense Technical Information Center (DTIC))

Most of the modern noncoherent pulse transponders available today are the result of commercial development with guidance from the US government in terms of specifications or user requirements. These standards are written to accommodate the present state-of-the-art technology in both the radar and the transponder fields. DTIC

N95-21686 Coast Guard Research and Development Center, Groton, CT.

AN/APS-137 FORWARD LOOKING AIRBORNE RADAR (FLAR) EVALUATION, FALL 1992 EXPERIMENT Interim Report, May 1991 - Oct. 1992

R. Q. Robe, K. OBrien, D. L. Raunig (Analysis and Technology, Inc., New London, CT.), and R. L. Marsee (Analysis and Technology, Inc., New London, CT.) Jan. 1994 127 p Limited Reproducibility: More than 20% of this document may be affected by microfiche quality
(AD-A279526; CGR/DC-04/94; USCG-D-07-94) Avail: Issuing Activity
(Defense Technical Information Center (DTIC))

During April 1992 and September/October 1992, the U.S. Coast Guard R&D Center conducted experiments to determine the sweep width for the AN/APS-137 Forward Looking Airborne Radar (FLAR) when searching for 4-, 6- and 10-person life rafts and small recreational boats. Workboats used to deploy the life rafts during the Fall 1992 experiment were used as targets of opportunity. The experiments were conducted in the coastal waters off the west coast of Florida from Wacussa Bay to Gasparilla Island and on Lake Erie. Realistic radar searches to collect data used unalerted sensor operators and standard search patterns for small waterborne targets. Aircraft and target positions were recorded using a Differential Global Positioning System (DGPS). Target detections were recorded by observers and by computers onboard the aircraft. Environmental conditions were recorded by observers on the workboats. In addition, MINIMET(TM) environmental buoys recorded the sea and wind conditions in the search areas. Environmental conditions represented in the data set included 1.0- to 3.6-foot significant sea heights and 2.9- to 15.2-knot winds. DTIC

N95-21834 Department of the Navy, Washington, DC.

IMPROVED BROADBAND WAVEGUIDE PRESSURE WINDOW Patent Application

David Rodriquez, inventor (to Navy) and Thomas R. Floyd, inventor (to Navy) 8 Aug. 1994 19 p Limited Reproducibility: More than 20% of this document may be affected by microfiche quality
(AD-D016487; US-Patent-Appl-SN-287026) Avail: Issuing Activity
(Defense Technical Information Center (DTIC))

A broad passband pressure barrier arrangement is provided for insertion in a circular waveguide between a source and a receiver of radio frequency (RF) energy with a spatially circumferential electric field characteristic of the TE(sub 01) mode. At least two cylindrical barrier regions are coaxially aligned and arranged symmetrically in mirror image fashion about a radial plane of the circular waveguide. The cylindrical barrier regions include at least one solid cylindrical plug region sealed in a cross-section of the circular waveguide and having a longitudinal thickness sufficient to withstand a predetermined pressure load. Each of the cylindrical barrier regions are defined by a characteristic impedance at opposing end faces thereof and by a characteristic impedance between the opposing end faces. A region-by-region impedance analysis process begins with an end face of the arrangement that is furthest from the source and is completed with an end face of the arrangement that is nearest the source. The permittivities of the barrier regions and the longitudinal thicknesses of barrier regions are optimized across the passband of interest. DTIC

N95-21835 Department of the Navy, Washington, DC.

ELECTROMAGNETIC RADIATION DETECTOR UTILIZING AN ELECTROMAGNETIC RADIATION ABSORBING ELEMENT IN A MACH-ZEHNDER INTERFEROMETER ARRANGEMENT Patent

Lloyd C. Bobb, inventor (to Navy) 20 Sep. 1994 5 p Filed 30 Sep. 1992
(AD-D016507; US-Patent-5,349,437; US-Patent-Appl-SN-954521;
US-Patent-Class-356-345) Avail: US Patent and Trademark Office

Apparatus is provided to detect electromagnetic radiation, in which a radiation-absorbing element is disposed on a short section of an optical waveguide to provide a thermal interface there between. Radiation is absorbed by the element, which thereby heats the waveguide, causing it to change its optical pathlength in proportion to the radiation absorbed. Interferometer apparatus is connected to measure this change in optical pathlength as a change in the interference condition. This device is highly sensitive and can be operated at room temperature. DTIC

N95-21849# International Centre for Theoretical Physics, Trieste (Italy).
ELECTROMAGNETIC WAVES IN AN ULTRARELATIVISTICALLY HOT AND STRONGLY MAGNETIZED ELECTRON-POSITRON PLASMA
U. A. Mofiz (Atomic Energy Research Establishment, Dhaka, Bangladesh.) and Ferdous Khan (Atomic Energy Research Establishment, Dhaka, Bangladesh.) Sep. 1993 6 p
(DE94-628963; IC-93/313) Avail: CASI HC A02/MF A01 (US Sales Only)

Electromagnetic waves in an ultrarelativistically hot and strongly magnetized electron-positron plasma is considered. The dispersion formulae for the circularly polarized waves propagating along the ambient magnetic field is obtained. The linear growth (damping) of these modes is calculated and the nonlinear propagation of Alfven mode is investigated. Spiky Alfven solitons are found and its relationship with the pulsar radiation is discussed. DOE

N95-21883# Naval Postgraduate School, Monterey, CA. Dept. of Electrical and Computer Engineering.
INBAND SCATTERING FROM ARRAYS WITH SERIES FEED NETWORKS Final Report
Seunghoon Lee Sep. 1994 50 p
(AD-A286209) Avail: CASI HC A03/MF A01

Approximate formulas for the inband radar cross section (RCS) of an array with series feed have been derived. The formulas are based on the hypothesis that an incident wave excites forward and backward traveling waves on the main line. The approximate formulas are in good agreement with results obtained using scattering matrices, thereby verifying the assumptions made in the approximate solution. Spikes in the RCS pattern have been identified with specific scattering sources in the array. The parameters affecting the level and location of the lobes have been noted. The main advantage of the approximate method relative to the scattering matrix method is its speed. The scattering matrix method requires that a matrix equation be solved, and its size increases with the number of array elements. DTIC

N95-21890*# National Aeronautics and Space Administration. Lewis Research Center, Cleveland, OH.
COCHANNEL AND ADJACENT-CHANNEL INTERFERENCE IN NONLINEAR MINIMUM-SHIFT-KEYED SATELLITE SYSTEM
John Yu Mar. 1995 9 p
(RTOP 235-01-03)
(NASA-TM-106834; E-9395; NAS 1.15:106834) Avail: CASI HC A02/MF A01

The interference susceptibility of a serial-minimum-shift-keyed (SMSK) modulation system to an interfering signal transmitted through a satellite link with cascaded nonlinear elements was investigated through computer simulation. The satellite link evaluated in this study represented NASA's Advanced Communications Technology Satellite (ACTS) system. Specifically, nonlinear characteristics were used that had specified amplitude-modulation to amplitude-modulation and amplitude-modulation to phase-modulation transfer characteristics obtained from the actual ACTS hardware. Two measurement scenarios were analyzed: degradation of an MSK satellite link from cochannel interference and from adjacent-channel interference. Interference was evaluated in terms of the probability of bit error rate (BER) versus energy per bit over noise power density Eb/No. Author

N95-21904 Department of the Navy, Washington, DC.
FREQUENCY-CODED MONOPULSE MTI Patent
Bernard L. Lewis, inventor (to Navy) and Ben H. Cantrell, inventor (to Navy) 13 Sep. 1994 7 p Filed 23 Jul. 1976
(AD-D016495; US-Patent-5,347,281; US-Patent-Appl-SN-707465; US-Patent-Class-342-160) Avail: US Patent and Trademark Office

A pulse-compression, MTI, doppler-radar system for determining target velocity information from a single, frequency-coded uncompressed target-return pulse includes a coded modulator, two pulse compressors, and a phase-comparison processor. The coded modulator generates for transmission an uncompressed pulse with the first and second halves of the pulse coded with the even and odd harmonic sidebands of a pulse repetition frequency, respectively. The first and second halves of the pulse returning from the target are pulse compressed simultaneously by the two pulse compressors. The phase comparison processor then determines the phase difference between the compressed pulses to obtain the target velocity information. DTIC

N95-21908 Department of the Navy, Washington, DC.
DIRECTIVE OPTIMIZATION OF COHERENT SIDELOBE CANCELLER SYSTEMS Patent
James P. Hansen, inventor (to Navy) 27 Sep. 1994 5 p Filed 25 Nov. 1974
(AD-D016513; US-Patent-5,351,057; US-Patent-Appl-SN-528194; US-Patent-Class-342-378) Avail: US Patent and Trademark Office

A new technique is introduced for improving the operation of a interference suppression system, particularly in a side-lobe canceller system, against multiple interference sources. A plurality of auxiliary receiving antennas, providing interference signals to side-lobe canceller loops, are spaced about a main directional receiving antenna and positioned to preferably form a configuration such that no lines of sight through any two auxiliary antennas are collinear or parallel to a line of sight through any other two auxiliary antennas. The configuration is then arranged relative to the main antenna such that no lines through any two auxiliary antennas are substantially parallel with the primary direction of a multiple jammer attack. DTIC

N95-21910 Department of the Navy, Washington, DC.
PASSIVE SURFACE DEPLOYED VARIABLE INDUCTANCE WIRE ANTENNA STATEMENT OF GOVERNMENT INTEREST Patent Application
Paul Mileski, inventor (to Navy) 4 Oct. 1993 12 p Limited Reproducibility: More than 20% of this document may be affected by microfiche quality
(AD-D016210; US-Patent-Appl-SN-130941) Avail: Issuing Activity (Defense Technical Information Center (DTIC))

An antenna adapted for surface deployment is provided. A coaxial feedline, terminated at one end thereof at a feedpoint, has a center conductor and a shield at ground potential. A continuous length of antenna wire having first and second ends is electrically connected at its first end to the center conductor at the feedpoint. A first portion of the continuous length is spooled adjacent to the first end. A second portion of the continuos length is deployed from the first portion by means of tension at the second end. The second portion extends to the second end along a substantially straight line away from the first portion. The second portion is typically at least as long as the first portion. The first portion serves as a variable tuning inductor for the antenna as the second portion is deployed therefrom. DTIC

N95-21915 Army Armament Research, Development and Engineering Center, Picatinny Arsenal, NJ.
MILLIMETER WAVE FRONT-END FIGURE OF MERIT, PART 1
Gabriel G. Silberman Apr. 1994 16 p Limited Reproducibility: More than 20% of this document may be affected by microfiche quality
(AD-A279093; ARFSD-TR-93046-Pt-1) Avail: Issuing Activity (Defense Technical Information Center (DTIC))

This report outlines a theoretical approach for defining and calculating a meaningful figure of merit for frequency modulated continuous wave radar systems with separate receive/transmit antennas. DTIC

N95-21970 Army Armament Research, Development and Engineering Center, Picatinny Arsenal, NJ.
THERMAL IMAGING SYSTEMS Final Report, Jan. - Dec. 1992
John Antonacos May 1994 26 p Limited Reproducibility: More than 20% of this document may be affected by microfiche quality
(AD-A279146; ARFSD-TR-93051) Avail: Issuing Activity (Defense Technical Information Center (DTIC))

This report examines the basic elements of a thermal imaging system. The four types of thermal imaging systems are described and the advantages and disadvantages of each are indicated. DTIC

N95-21985 Aerospace Corp., El Segundo, CA. Technology Operations.
ATOMIC VELOCITY DISTRIBUTIONS IN A HYDROGEN BEAM EFFUSING OUT OF AN RF DISCHARGE DISSOCIATOR
B. Jaduszliwer and Y. C. Chan 15 Mar. 1994 19 p Limited Reproducibility: More than 20% of this document may be affected by microfiche quality
(Contract F04701-88-C-0089)

(AD-A279253; TR-93(3925)-6; SMC-TR-99-22) Avail: Issuing Activity (Defense Technical Information Center (DTIC))

We have measured atomic hydrogen velocity distributions in an effusive beam coming out of an RF discharge dissociator by using a magnetic deflection technique. Dissociator pressures varied between 0.028 and 0.340 torr. At low dissociator pressures, the measured atomic velocity distributions were narrower than the expected beam-Maxwellians; at higher pressures, they were indistinguishable from beam-Maxwellians at the dissociator wall temperature, indicating full thermalization of the atoms prior to exiting the dissociator. Monte Carlo simulations of the thermalization process within the dissociator reproduce these results and point out the important role of vibrational excitation of the background hydrogen molecules as an energy loss mechanism. Our results are significant when designing magnetic state selectors for spin- or hyperfine-polarized atomic hydrogen beams. DTIC

N95-21988# IIT Research Inst., Chicago, IL.

COMPILATION OF 1993 ANNUAL REPORTS OF THE NAVY ELF COMMUNICATIONS SYSTEM ECOLOGICAL MONITORING PROGRAM. VOLUME 2: TABS C-F Report, Jan. - Sep. 1993

J. E. Zapotosky Apr. 1994 214 p See also AD-A279771

(Contract N00039-93-C-0001)

(AD-A279770; D06209-2-Vol-2) Avail: CASI HC A10/MF A03

During 1993, the U.S. Navy continued to conduct a program to monitor flora, fauna, and their ecological relationships for possible effects from electromagnetic (EM) fields produced by the Navy's Extremely Low Frequency (ELF) Communications System. Physiological, developmental, behavioral, and ecological variables for dominant biota in upland and riverine habitats near the Naval Radio Transmitting Facility at Republic, Michigan (NRTF-Republic) have been monitored since 1982. The NRTF-Republic was intermittently energized at low amperages beginning in early 1986. Electric current and periods of energization were then gradually increased until 1989, when the transmitter became a fully operational facility. A split-plot or blocked strategy was used to examine biological variables for possible effects from EM exposure. Reports compiled in this document present the progress of these studies through 1993. Final results and conclusions are expected after all data have been analyzed in 1994. Investigators for similar studies completed in Wisconsin concluded that there were no EM bioeffects from intermittent or full operation of the transmitter in that state. DTIC

N95-22005# Federal Aviation Administration, Cambridge, MA. National Transportation Systems Center.

RECOMMENDATION ON TRANSITION FROM PRIMARY/SECONDARY RADAR TO SECONDARY-ONLY RADAR CAPABILITY Final Report, Sep. 1993 - Mar. 1994

Janis Vilcans and Richard J. Lay Oct. 1994 137 p

(AD-A286279; DOT-VNTSC-FAA-94-10; DOT/FAA/NR-94-1) Avail: CASI HC A07/MF A02

This recommendation has been prepared to support the FAA decision to deactivate primary long-range radars (LRR) and presents transition strategy and implementation plan for the transformation of the existing primary/secondary en route radar system to a beacon-only system by the year 2002. The estimated cost associated with this transition is $2.1 billion, but the cost directly related to the decision is approximately $138.6 million. Thus, the potential saving of approximately $1.4 billion associated with LRR replacement results in a benefit-to-cost ratio greater than 10. It is therefore recommended that the decision to deactivate the LRR be implemented as rapidly as possible in order to minimize costs necessary to sustain and maintain the existing system; that an orderly transition be accomplished; and that the transition to the beacon-only capability be adopted on a center-by-center basis. It is also recommended that the goal of an en route beacon system, comprising stand-alone beacon radars and backed up with an automatic dependent surveillance (ADS) system be established, but achievement of this goal should not delay implementation of the deactivation decision. DTIC

N95-22021 Army Research Lab., Aberdeen Proving Ground, MD.

INVESTIGATIONS INTO ALTERNATE SPARK GAP SWITCHING TECHNIQUES Final Report

Brian G. Smith Sep. 1994 24 p Limited Reproducibility: More than 20% of this document may be affected by microfiche quality

(AD-A286225; ARL-TR-623) Avail: CASI HC A03

This report documents the design, operation, and experimental results of the evaluation of a new spark gap triggering method. These spark gaps were developed to support ARL's ongoing nuclear electromagnetic pulse (EMP) current injection assessment programs. This trigger method provides operator control, multiple spark gap control with synchronous triggering, and a limited amount of hardware to control the spark gap triggering. A patent application has been started for this device and has been assigned case number HDL No. 94-3. DTIC

N95-22041# Colorado Univ., Boulder, CO. Dept. of Electrical and Computer Engineering.

SIGNAL PROCESSING IN THE LINEAR STATISTICAL MODEL Final Report, 1 Oct. 1991 - 30 Sep. 1994

Louis L. Scharf and Clifford T. Mullis 4 Nov. 1994 10 p

(Contract N00014-89-J-1070)

(AD-A286255) Avail: CASI HC A02/MF A01

This report summarizes work on four general problems during the three-year period of the contract: (1) estimation of frequency-wavenumber, (2) matched subspace filters, (3) maximum likelihood estimation of modes from space-time data, and (4) statistical inference within the wavelet representation. We have generalized the theory of multiwindow estimators of the power spectrum to multiwindow estimators of the frequency wavenumber spectrum and of the related correlation sequence. We are now applying these ideas to the derivation of adaptive filters. We have developed a theory of matched subspace detectors for detecting signals which lie in low-dimensional model subspaces. The theory bridges the gap between generalized likelihood ratio theories and invariance theories. We have generalized the theory of maximum likelihood for identifying time domain modes and space domain directions of arrival. We have characterized subband decompositions for perfect reconstruction, developed filter design algorithms for constructing near perfect reconstruction filterbanks from nonorthogonal analysis filters, and derived algorithms for predicting and filtering in periodically correlated time series. DTIC

N95-22080 Technische Univ., Twente (Netherlands). Tele-Informatics and Open Systems Group.

MODELLING MULTIMEDIA TELESERVICES WITH OSI UPPER LAYERS FRAMEWORK: SHORT PAPER

I. Widya, E. vanRijssen, and E. Michiels 1994 12 p

(PB95-132734; Memo-INF-94-40) Copyright Avail: Issuing Activity (National Technical Information Service (NTIS))

The paper presents the use of the concepts and modelling principles of the Open Systems Interconnection (OSI) upper layers structure in the modelling of multimedia teleservices. It puts emphasis on the revised Application Layer Structure (OSI/ALS). OSI/ALS is an object based reference model which intends to coordinate the development of application oriented services and protocols in a consistent and modular way. It enables the rapid deployment and integrated use of these services. The paper emphasizes further on the nesting structure defined in OSI/ALS which allows the design of scalable and user tailorable/controllable teleservices. OSI/ALS consistent teleservices are moreover implementable on communication platforms of different capabilities. An analysis of distributed multimedia architectures which can be found in the literature, confirms the ability of the OSI/ALS framework to model the interworking functionalities of teleservices. NTIS

N95-22087 Technische Univ., Twente (Netherlands). Tele-Informatics and Open Systems Group.

MODELLING THE REASSEMBLY BUFFER IN A CONNECTIONLESS SERVER

Geert J. Heijenk and Ignas G. Niemegeers 1994 32 p

(ISSN 0924-3755)

(PB95-132908; TIOS-94/13) Copyright Avail: Issuing Activity (National Technical Information Service (NTIS))

One way of providing connectionless services over an asynchronous transfer mode (ATM) network is by means of Connectionless Servers (CLS's), routing and forwarding cells on a per packet basis (message mode). Packets are sent to a CLS over ATM connections (either virtual channel or virtual path connections). These packets come from other CLS's, interworking units, or end systems. The CLS stores cells of a packet in a reassembly buffer until the last one has been received, and forwards all cells of the packet at once. We present a performance model of the reassembly buffer in a CLS operating in message mode. NTIS

N95-22134# Aerospace Corp., El Segundo, CA. Technology Operations.
LADAR DETECTION STATISTICS IN THE PRESENCE OF POINTING ERRORS
Hal T. Yura 15 Dec. 1993 69 p
(Contract F04701-88-C-0089)
(AD-A285865; TR-93(3505)-1; SMC-TR-94-39) Avail: CASI HC A04/MF A01

The probability of detection of optically rough targets by pulsed LADAR systems that employ direct detection is considered here. It is assumed that the LADAR operates under conditions of both unintentional pointing off-set bias (i.e., bore-sight error) and jitter. Under these conditions, the probability of detection of targets in both the near and far field of the collecting aperture (i.e., for resolved, partially resolved, and unresolved targets) and for both large and small photoelectron counts is derived, and, in many cases of practical interest, accurate, elementary analytic approximations that are useful for parametric system studies are obtained. As such, the approximate engineering expressions derived here will be useful, for example, to those performing engineering modeling of space-based LADAR systems. A number of appendices are included to serve as technical references, where some key results employed in the main body of the report are derived. In particular, an interesting new mathematical result involving the complementary incomplete gamma function and an analytic expression for the probability distribution function of a signal photocount obeying Bose-Einstein statistics (such as that arising from unresolved targets) immersed in Poisson noise are derived. DTIC

N95-22215 North Carolina Univ., Charlotte, NC. Dept. of Mathematics.
LOCALIZATION PHENOMENON IN SOME RANDOM CLASSICAL SYSTEMS Final Report, 1 Jun. 1991 - 31 May 1994
Alexander Figotin 20 Jul. 1994 4 p Limited Reproducibility: More than 20% of this document may be affected by microfiche quality
(Grant AF-AFOSR-0243-91; AF Proj. 2304)
(AD-A286514; AFOSR-94-0748TR) Avail: CASI HC A01

For the reported period the researchers focused on several problems on the propagation of electromagnetic and acoustic waves in periodic and disordered media. (1) Localization properties of some discrete models for light, (2) Existence of gaps and exponential localization for the Anderson type models for periodic and disordered acoustic dielectric media, and (3) Band-gap structure for periodic two component dielectric and acoustic media. DTIC

N95-22229# Massachusetts Inst. of Tech., Lexington, MA. Lincoln Lab.
DATA SAMPLING FOR A BURST MODE COMMUNICATIONS SYSTEM
A. G. Rocco 1 Sep. 1994 44 p
(Contract F19628-90-C-0002)
(AD-A286098; MIT-TR-1012) Avail: CASI HC A03/MF A01

A data sampling circuit and method is provided for a burst mode communication system. The circuit is an entirely digital circuit for reliably sampling an incoming stream of data to automatically adjust to variations in data stream clock rates and phase variations in the incoming data. The circuit includes a delay line with a plurality of serially coupled taps, each tap having a variable delay. One aspect of the invention includes increasing the delay time until the delay line captures at least one, but preferably two, full data cells of the incoming data stream (i.e., signal levels over at least one full clock period, defined by two transitions of the data stream), thereby aligning the receiving circuit with the frequency of the data stream clock. A second aspect of the invention includes outputting data from a tap that is selected to be midway between two regions of transitions of the incoming data stream, thereby aligning the receiving circuit with the phase of the data stream clock. The invention can, in alternative embodiments, track changes in the input data stream's phase/frequency. This involves updating the amount of delay in each tap of the delay line as well as picking the output of the appropriate tap to be used as the sampled data stream in response to changes in the input signal as well as changes in propagation delays of the circuits used to implement the delay line, resulting from temperature and voltage variations. DTIC

N95-22230# Naval Postgraduate School, Monterey, CA.
THE APPLICABILITY OF NEURAL NETWORKS TO IONOSPHERIC MODELING IN SUPPORT OF RELOCATABLE OVER-THE-HORIZON RADAR M.S. Thesis
James A. Pinkepank Sep. 1994 44 p
(AD-A286114) Avail: CASI HC A03/MF A01

Ionospheric models have been developed to interpret Relocatable Over-the-Horizon Radar data. This thesis examines the applicability of neural networks to ionospheric modeling in support of Relocatable Over-the-Horizon Radar. Two neural networks were used for this investigation. The first network was trained and tested on experimental ionospheric sounding data. Results showed neural networks are excellent at modeling ionospheric data for a given day. The second network was trained on ionospheric models and tested on experimental data. Results showed neural networks are able to learn many ionospheric models and the modeling network generally agreed with the experimental data. DTIC

N95-22241# Lawrence Livermore National Lab., Livermore, CA.
X-BAND MICROWAVE BACKSCATTERING FROM OCEAN WAVES
P. H. Y. Lee (TRW, Inc., Redondo Beach, CA.), J. D. Barter (TRW, Inc., Redondo Beach, CA.), and K. L. Beach (TRW, Inc., Redondo Beach, CA.) Jan. 1994 53 p Presented at the IGARSS 1994: International Geoscience and Remote Sensing Symposium, Pasadena, CA, 8-12 Aug. 1994 Submitted for publication
(Contract W-7405-eng-48)
(DE94-016719; UCRL-CR-117680; CONF-940814-3) Avail: CASI HC A04/MF A01

Backscattering experiments at microwave frequencies were conducted off the west coast of Scotland in the summer of 1991. Using a dual-polarization, 8-frequency X-band coherent scatterometer mounted on the bow of a boat, we measured time-resolved backscattering from ocean waves at a range of grazing angles from 10 deg to 70 deg. From the grazing-angle-dependent signals and their Doppler spectra, we differentiate Bragg scattering from non-Bragg scattering and resolve 'peak separation' between the vertical and horizontal polarizations. We observe instances of 'super' events, i.e., instances when the horizontal polarization return power equals or exceeds the vertical polarization power. We find that 'super' events occur not only at low grazing angles but at any grazing angle for against-wind viewing directions. Statistics for such occurrences as a function of grazing angle are obtained. We study the coherence properties of scatterers and find strong evidence that at low grazing angles, lifetime-dominated, non-Bragg scattering contributes noticeably to returns of both polarizations, but is dominant in providing returns for the horizontal polarization. We examine 'spiking' events and find that they can be related to, but need not be limited to, breaking wave events. By comparing the data of against-wind runs with cross-wind and circle runs, we obtain wind-direction dependence of Doppler spectra which further assists in the identification of scattering mechanisms. DOE

N95-22245# Naval Postgraduate School, Monterey, CA.
DESIGN AND MODELLING OF A LINK MONITORING MECHANISM FOR THE COMMON DATA LINK (CDL) M.S. Thesis
John W. Eichelberger, III Sep. 1994 257 p
(AD-A286167) Avail: CASI HC A12/MF A03

The Common Data Link (CDL) is a full duplex, point-to-point microwave communications system used in imagery and signals intelligence collection systems. It provides a link between two remote Local Area Networks (LAN's) aboard collection and surface platforms. In a hostile environment, there is an overwhelming need to dynamically monitor the link and thus, limit the impact of jamming. This work describes steps taken to design, model, and evaluate a link monitoring system suitable for the CDL. The monitoring system is based on features and monitoring constructs of the Link Control Protocol (LCP) in the Point-to-Point Protocol (PPP) suite. The CDL model is based on a system of two remote Fiber Distributed Data Interface (FDDI) LAN's. In particular, the policies and mechanisms associated with monitoring are described in detail. An implementation of the required mechanisms using the OPNET network engineering tool is described. Performance data related to monitoring parameters is reported. Finally, integration of the FDDI-CDL model with the OPNET Internet model is described. DTIC

N95-22246# Naval Postgraduate School, Monterey, CA.

PERFORMANCE OF A FAST FREQUENCY-HOPPED NONCOHERENT MFSK RECEIVER OVER RICIAN FADING CHANNELS WITH EITHER PARTIAL-BAND INTERFERENCE OR MULTI-TONE INTERFERENCE M.S. Thesis

Joseph F. Sheltry Sep. 1994 102 p
(AD-A286168) Avail: CASI HC A06/MF A02

An error probability analysis is performed for a conventional noncoherent M-ary orthogonal frequency-shift keying (MFSK) receiver employing fast frequency-hopped (FFH) spread spectrum waveforms transmitted over a frequency-nonselective, slowly fading Ricean channel with partial-band noise interference. Each diversity reception is assumed to fade independently. The partial-band interference is modeled as a Gaussian process. The effects of wideband thermal noise are also included. The energy per hop is held constant; thus, as diversity increases, energy per symbol increases. Previous analyses considered only constant energy per symbol systems, however, practical military systems are likely to employ fixed hop rates. There is some performance enhancement to be obtained from implementing diversity in a conventional FFH/MFSK system with fixed hop rates, but partial band interference still results in significant degradation. Additionally, the performance of this FFH receiver is investigated over the same channel in the presence of partial-band tone jamming without diversity for the case of binary frequency-shift keying (BFSK) when both the signal and the jammer can fade independently. Performance when only a single jamming tone per hop slot is allowed is compared to that obtained when two jamming tones per hop slot are possible. When the jamming signal experiences Rayleigh fading there is very little degradation of the jammer's effectiveness as compared to when the jamming signal is not affected by fading. DTIC

N95-22247# Range Commanders Council, White Sands Missile Range, NM.

GLOSSARY OF FREQUENCY AND TIMING TERMS AND A PICTORIAL REPRESENTATION OF TERMS USED IN THE BEHAVIOR AND ANALYSES OF FREQUENCY STANDARDS

May 1994 49 p
(AD-A286172; RCC-214-94) Avail: CASI HC A03/MF A01

This document is a glossary of frequency and timing terms and is intended for use as a reference, so those within and outside the precision time and time interval (PTTI) field may have a common reference source for acceptable definitions and current terminology and usage of frequency and timing terms. The document should be used as a guide in preparing specifications and requirements for procurement of equipment and for other technical documents. DTIC

N95-22250 Delaware Univ., Newark, DE. Dept. of Mathematical Sciences.

INVERSE AND CONTROL PROBLEMS IN ELECTROMAGNETICS Final Report, 1 Jul. 1991 - 30 Jun. 1994

Ralph E. Kleinman and Thomas S. Angell 14 Oct. 1994 255 p Limited Reproducibility: More than 20% of this document may be affected by microfiche quality
(Grant AF-AFOSR-0277-91)
(AD-A286438; AFOSR-94-0743TR) Avail: CASI HC A12

This report summarizes work carried out in a number of specific areas of investigation in inverse scattering and optimal control problems in electromagnetics. The progress is briefly described and detailed results are included in an appendix. The major accomplishments include: the application of multi-criteria optimization techniques to problems in antenna design; the development of inverse scattering algorithms which use scattered field data in the frequency domain to reconstruct the shape, location and constitutive parameters of a scattering object; establishing the well-posedness of electromagnetic scattering problems with resistive or conductive boundary conditions; and derivation of new boundary integral equations for electromagnetic scattering from local distributions of a plane screen. In addition some new results on low frequency scattering have been found which establish the exact nature of the asymptotic expansion in two dimensions. DTIC

N95-22251# Naval Postgraduate School, Monterey, CA.

PROBABILITY OF DETECTION FOR A GO CFAR RADAR PROCESSOR USING ENVELOPE DETECTION APPROXIMATION M.S. Thesis

Joseph J. Hache Sep. 1994 139 p
(AD-A286211) Avail: CASI HC A07/MF A02

The greatest-of logic for a constant false alarm rate processor (GO CFAR) is a commonly used method for the adaptive setting of a radar detection threshold in the presence of clutter edges. Instead of using a true envelope detector x = I2 + Q2, which is difficult to implement, envelope detection approximations of the form Xe = aMax (I),(Q) + bMin (I),(Q) and xe = a(I) + b(Q) (no Max and Min operators) where a and b are constants, are often used to detect a signal decomposed into its in-phase (I) and quadrature (Q) components. Closed form expressions are derived for the probability density function (pdf) of a radar range cell containing a detected target signal in the presence of noise using both approximations. These can then be used to calculate the probability of detection (PD). They can also be used to calculate the probability of false alarm (PFA) if the means of I and Q are set to zero. Closed form expressions are obtained analytically and by curve-fitting the numerically derived pdf of the target cell. Finally, using Monte Carlo techniques, this thesis also compares the GO CFAR detection performance using envelope detection approximations xe, xe and the true envelope detector x for zero mean white Gaussian noise input samples I and Q. DTIC

N95-22253# BBN Systems and Technologies Corp., Cambridge, MA.

USABLE, REAL-TIME, INTERACTIVE SPOKEN LANGUAGE SYSTEMS Final Report

J. Makhoul and M. Bates Sep. 1994 87 p
(Contract N00014-92-C-0035; ARPA Order 8455)
(AD-A286349) Avail: CASI HC A05/MF A01

The objective of this project was to make the next significant advance in human-machine interaction by developing a spoken language system (SLS) that operates in real-time while maintaining high accuracy on cost-effective COTS (commercial, off-the-shelf) hardware. The system has a highly interactive user interface, is largely user independent and to be easily portable to new applications. The BBN HARC spoken language system consists of Byblos speech recognition system and the Delphi or HUM language understanding system. DTIC

N95-22299# Lawrence Livermore National Lab., Livermore, CA.

CALIOPE AND TAISIR AIRBORNE EXPERIMENT PLATFORM

C. J. Chocol Jul. 1994 11 p Presented at the 1994 Chemical Analysis by Laser Interrogation of Proliferation Effluents (CALIOPE ITR) Interim Technical Review, Livermore, CA, 26-28 Apr. 1994
(Contract W-7405-eng-48)
(DE94-018328; UCRL-JC-118289; CONF-9404162-10) Avail: CASI HC A03/MF A01

Between 1950 and 1970, scientific ballooning achieved many new objectives and made a substantial contribution to understanding near-earth and space environments. In 1986, the Lawrence Livermore National Laboratory (LLNL) began development of ballooning technology capable of addressing issues associated with precision tracking of ballistic missiles. In 1993, the Radar Ocean Imaging Project identified the need for a low altitude (1 km) airborne platform for its Radar system. These two technologies and experience base have been merged with the acquisition of government surplus Aerostats by Lawrence Livermore National Laboratory. The CALIOPE and TAISIR Programs can benefit directly from this technology by using the Aerostat as an experiment platform for measurements of the spill facility at NTS. DOE

N95-22311# Helsinki Univ. of Technology, Espoo (Finland).

IMAGE SOLUTION FOR POISSON'S EQUATION IN WEDGE GEOMETRY

K. I. Nikoskinen and I. V. Lindell Apr. 1994 25 p
(PB95-127171; ISBN-951-22-2094-6) Avail: CASI HC A03/MF A01

Recently a novel static solution appeared for two-dimensional electrostatic field excited by an infinite line charge in the vicinity of a dielectric wedge whose edge was parallel to the source. In the present paper Poisson's equation is studied mainly in three dimensions but the solution for the analog two dimensional problem is also provided. It appears that numerically a simple and efficient method to compute the potential inside and outside the wedge can be found by solving first image sources for the exterior and interior problem that give rise to the potential contribution of the wedge. Both the exterior and interior consist of a line charge that decays exponentially as a function of complex angle and a set of point charges that can be interpreted as a reflection or transmission images of a dielectric plane. All known closed-form solutions in terms of elementary functions are derived for an electrically and magnetically conducting half plane. NTIS

N95-22358 Technische Univ., Delft (Netherlands). Faculteit der Elektrotechniek.
IMAGE AND VIDEO CODING USING A WAVELET DECOMPOSITION Ph.D. Thesis
H. J. Barnard 1994 222 p
(PB95-135067; ISBN-90-5326-016-1) Copyright Avail: Issuing Activity (National Technical Information Service (NTIS))

The thesis discusses the recently developed wavelet theory with respect to its application to image and video coding. The purpose is to evaluate what this theory has contributed to the already existing subband coding method. Further, a new image coding technique is presented that can be viewed as a combination of the wavelet transform and a contour-texture coding technique. The coding performance of the new method is compared to existing methods. NTIS

N95-22363# Helsinki Univ. of Technology, Espoo (Finland).
DIELECTRIC MIXTURES WITH ARBITRARILY ANISOTROPIC COMPONENTS: FOCUS ON SPECIAL GYROTROPIC EFFECTS
A. H. Sihvola and O. P. M. Perkonen Apr. 1994 27 p
(PB95-127015; ISBN-951-22-2051-2) Avail: CASI HC A03/MF A01

The report studies the dielectric properties of mixtures with components that can have arbitrary permittivity dyadic. The anisotropic inclusions are assumed spherical. In the analysis, quasistatic approach is used, and it leads to the general Maxwell Garnett formula. This is represented in many forms, and depending on the orientation distribution of the inclusions, effective permittivity can be dyadic or scalar. Special emphasis is on the case of random orientation of the inclusions. The macroscopic permittivity depends on seven parameters of the mixture, six coming from the symmetric and antisymmetric parts of the inclusion permittivity dyadic, and one from the volume fraction. Numerical illustrations focus on the gyrotropy effects that are shown to lead to sharp maxima and minima in the polarizabilities and macroscopic permittivities. NTIS

N95-22365 Helsinki Univ. of Technology, Espoo (Finland).
IMAGE THEORY FOR THE UNIDIRECTIONALLY CONDUCTING SCREEN
I. V. Lindell Jun. 1994 11 p
(PB95-127031; ISBN-951-22-2184-5) Avail: Issuing Activity (National Technical Information Service (NTIS))

Image theory is developed for electromagnetic sources in front of a planar unidirectionally conducting screen made of ideally conducting parallel wires with thickness and interspace dimensions much smaller than the wavelength. Replacing the screen by the image sources gives the correct reflected and transmitted fields on the respective sides of the screen. The problem is solved through a decomposition of the original source in two parts giving rise to fields TE and TM with respect to the direction of the wires. For the TE and TM source components, the images can be constructed from previous knowledge. For an electric dipole source, the images are seen to involve dipole and transmission-line sources. NTIS

N95-22401# Texas Univ., Arlington, TX. Dept. of Electrical Engineering.
EFFECT OF CELL SIZE ON ELLIPTICALLY POLARIZED RADAR CLUTTER STATISTICS Final Report
Adrian K. Fung Sep. 1994 84 p
(Contract F19628-91-K-0013)
(AD-A285789; RL-TR-94-172) Avail: CASI HC A05/MF A01

In this final report, we summarize the approach used and relevant information for simulation of radar signal statistics from randomly rough surfaces. The total number of cases to be performed in this contract is 60 and is depicted in Table 1. Two sets of cases reported in the past are: (1) 30 cases for receiver orientation angles of 135 degrees, five azimuthal angles, three cell sizes with signal distributions expressed in both field amplitude and power; and (2) 12 cases for receiver orientation angle of 45 degrees at azimuthal angles of 180 and 135 degrees, three cell sizes with signal distributions expressed in both field amplitude and power. Additional calculations to be given in this report are for receiver orientation angle of 45 degrees at azimuthal angles of 90, 45, and 0 degrees corresponding to 18 cases. For the sake of completeness, all results reported earlier are included in Appendix B. DTIC

N95-22407# Sandia National Labs., Albuquerque, NM.
TDX: A HIGH-BANDWIDTH CROSSBAR-SWITCHED COMMUNICATION PARADIGM
P. E. Pierce, D. L. Eilers, and A. L. Schreiber 1994 6 p Presented at the ICSPAT 1994: Signal Procession Applications and Technology, Dallas, TX, 18-21 Oct. 1994
(Contract DE-AC04-94AL-85000)
(DE94-017187; SAND-94-1075C; CONF-9410164-4) Avail: CASI HC A02/MF A01

Digital signal processing systems under development today require scalable and reconfigurable high bandwidth communication resources between processing elements. Shared memory architectures require the ability to transfer data from one processor node to another, as well as maintaining data coherency such as provided by the Scalable Coherent Interface (SCI). Signal processing systems that must move large amounts of data between processor nodes, are best served by a communication system that allows reconfigurable streams of data to flow at deterministic rates with minimal overhead. A Time Domain Crossbar (TDX) communication system providing scalable, programmable, high-bandwidth, streaming communication has been developed and is described in this paper. DOE

N95-22415# Naval Postgraduate School, Monterey, CA.
A PERIODIC SCHEDULING HEURISTIC FOR MAPPING ITERATIVE TASK GRAPHS ONTO DISTRIBUTED MEMORY MULTIPROCESSORS M.S. Thesis
Charles Darwin Kasinger Sep. 1994 52 p
(AD-A286047) Avail: CASI HC A04/MF A01

This thesis investigates the problem of statically assigning the tasks of applications represented by repetitive task graphs (such as sonar or radar signal processing) to the processors of a distributed memory multiprocessor system with the objective of maximizing graph instance throughput. The repetitive nature of these task graphs allows for pipelining and the overlapping of successive graph instances, suggesting a departure from classical directed acyclic graph scheduling techniques. To investigate such a claim, a version of the Mapping Heuristic (MH) ELR 90 is extended for use with iterative applications. Then a new heuristic, Periodic Scheduling (PS), is developed to capitalize on the repetitive nature of these task graphs by overlapping successive graph instances. The PS heuristic assigns tasks to processors in such a way so as to minimize the maximal utilization of the processors and the communications links between them. This maximal utilization figure dictates the interval between successive instances of the task graph. We conduct experiments in which the graph instance throughput of PS is compared to that of MH across a broad range of processor topologies, utilizing several communications/computation ratios. It is shown that, compared to MH, the PS heuristic improves the throughput performance between two and 50 percent. Particularly noteworthy improvement is noted on systems with high average inter-node communications costs. DTIC

N95-20658# Alenia, Turin (Italy). Div. Avionica Apparati Speciali.
ELECTROMAGNETIC COMPATIBILITY EFFECTS OF ADVANCED PACKAGING CONFIGURATIONS
B. Audone, L. Bolla, and D. Tarducci *In* AGARD, Advanced Packaging Concepts for Digital Avionics Oct. 1994 5 p (For primary document see N95-20631 06-06)
Copyright Avail: CASI HC A01/MF A03

33 ELECTRONICS AND ELECTRICAL ENGINEERING

Includes test equipment and maintainability; components, e.g., tunnel diodes and transistors; microminiaturization; and integrated circuitry.

For related information see also *60 Computer Operations and Hardware* and *76 Solid-State Physics.*

N95-19894# Westinghouse Science and Technology Center, Pittsburgh, PA.

PROCESSING, FABRICATION, AND DEMONSTRATION OF HTS INTEGRATED MICROWAVE CIRCUITS Research and Development Status Report No. 12, 25 Apr. - 24 Jul. 1994

G. R. Wagner, S. H. Talisa, and J. Talvacchio 29 Sep. 1994 138 p
(Contract N00014-91-C-0112; ARPA Order 7932)
(AD-A285611; Rept-94-9SL2-LAFIL-R1) Avail: CASI HC A07/MF A02

High temperature superconductor (HTS) devices can and will improve the performance of ESM and shared aperture receiver systems. For the near term the most promising candidate for the reference channelized cued ESM receiver system is an HTS IF Delsy line that can provide 200 nanoseconds of delay across a 3 to 5 GHz band. Such a delay line can improve sensitivity by 1 to 2 dB while providing about a 6 dB improvement in two tone dynamic range. Perhaps even of greater importance is that the low device loss combined with the elimination of multiple amplifiers previously needed to overcome loss can significantly improve the amplitude and phase tracking of the delay lines. In future systems it is unlikely that a single HTS device will be employed. Rather, it is more likely that large portions of the RF architecture will be placed in a cooler as a means of achieving performance and cost advantages. This is thought to include an HTS front-end, conventional IF amplifier, and HTS IF receivers. Looking even further in the future it is likely that entire HTS receivers will be remotely located with their HTS antennas and only digits will be returned to central for processing. DTIC

N95-19909*# Auburn Univ., AL. Dept. of Electrical Engineering.

DESIGN OF POWER ELECTRONICS FOR TVC AND EMA SYSTEMS Final Report

R. Mark Nelms, J. Brett Bell, and Michael T. Shepherd 7 Nov. 1994 41 p
(Contract NAS8-39131)
(NASA-CR-196540; NAS 1.26:196540) Avail: CASI HC A03/MF A01

The Component Development Division of the Propulsion Laboratory at Marshall Space Flight Center (MSFC) is currently developing a class of electromechanical actuators (EMA's) for use in space transportation applications such as thrust vector control (TVC) and propellant control valves (PCV). These high power servomechanisms will require rugged, reliable, and compact power electronic modules capable of modulating several hundred amperes of current at up to 270 volts. MSFC has selected the brushless dc motor for implementation in EMA's. A previous project performed by Auburn University examined the use of the resonant dc link (RDCL) inverter, pulse density modulation (PDM), and mos-controlled thyristors (MCT's) for speed control of a brushless dc motor. The speed of the brushless dc motor is proportional to the applied stator voltage. In a PDM system, the control system determines the number of resonant voltage pulses which must be applied to the stator to achieve a desired speed. The addition of a waveshaping circuit to the front end of a standard three-phase inverter yields a RDCL inverter; the resonant voltage pulses are produced through the action of this wave shaping circuit and the inverter. This project has focused on the implementation of a system which permits zero-voltage switching with the bus voltage clamped at the input voltage level. In the same manner as the RDCL inverter, the inverter selected for this implementation is a combination of waveshaping circuit and a standard three-phase inverter. In addition, this inverter allows a pulse-width modulated (PWM)-like control scheme instead of a PDM scheme. The operation of waveshaping circuit will be described through analysis and waveforms. Design relationships will also be presented. Derived from text

N95-19934# Technical Research Centre of Finland, Espoo (Finland).

PHYSICAL Si(1-x)Ge(x)/Si HETEROJUNCTION BIPOLAR TRANSISTOR MODEL FOR DEVICE AND CIRCUIT SIMULATION

M. Andersson, Z. Xia, P. Kuivalainen, and H. Pohjonen 1994 26 p
Prepared in cooperation with Helsinki Univ. of Technology, Espoo, Finland
(ISSN 0355-5712)
(PB95-110896; ISBN-951-22-2154-3) Avail: CASI HC A03/MF A01

A physical but compact Si(1-x)Ge(x)/Si heterojunction bipolar transistor (HBT) model suited for device design and circuit simulation is presented. The model is based on the de Graaf-Kloosterman formalism for the modeling of the bipolar transistors, but adds important heterostructure device physics as well as physical properties of SiGe material. The model, implemented in the APLAC circuit simulator, shows how currents and charges depend on minority carrier concentrations, which in turn are functions of the heterojunction voltages. In this way the influence of the built-in electric fields due to Ge concentration and doping density gradients, the bias-dependent transit times and the Early effect can be incorporated naturally. Comparisons between the model prediction and the experimental data for the DC current/voltage characteristics and cutoff frequencies in Si(1-x)Ge(x)/Si HBT's are included to demonstrate the model utility and accuracy. NTIS

N95-19935# Helsinki Univ. of Technology, Espoo (Finland). Lab. of Telecommunications Technology.

HIGH-PERFORMANCE PACKET SWITCHING ARCHITECTURE FOR ATM: CONVENTIONAL SOLUTION AND NEURAL NETWORK SOLUTION Ph.D. Thesis

J. Ma Feb. 1994 93 p
(PB95-110920; ISBN-951-22-2146-2) Avail: CASI HC A05/MF A01

The thesis consists of two subjects in a high performance packet switch: the first subject is a conventional solution for design, implementation and performance analysis of an Asynchronous Transfer Mode (ATM) modular switch, and the second subject is a neural network application in a high performance packet switch. The first subject covers the following topics: The design of a modular ATM switch is considered. Two modular switch architectures have been proposed: Nonuniform traffic effect on the switch has been investigated; since services require different quality of service, an ATM switch must be capable of handling the requirements of different services. The second subject covers the following topics: The rearrangeable Clos' packet switch has especially attractive advantage in a nonblocking interconnection with less hardware than a nonblocking network can be realized. In addition, the output queuing rearrangeable Clos' switch proposed in this thesis has the best delay/throughput performance. In the thesis the equations of the neural network for the routing problem have been developed, while simulations of the neural networks have been carried out in computers. NTIS

N95-19958# Martin Marietta Corp., Baltimore, MD.

COLLOCATED TUNABLE WAVENUMBER SENSOR/ACTUATORS FOR SMART STRUCTURES Report, 1 Sep. - 30 Sep. 1993

K. Bridger and L. Jones 6 Oct. 1993 4 p
(Contract N00014-92-C-0214)
(AD-A279608; MML-TM-93-23) Avail: CASI HC A01/MF A01

The first actuator module delaminated during burnout. The module showed evidence (bulging) of pressure build up internally which is usually caused by too rapid burnout schedule. The next module is being fabricated and will be in burnout by the end of this week. The pad of smaller actuators look good and are terminated ready for testing. Plans for September 1993; Electromechanical measurements will be on the first set of small actuator, Electromechanical modelling on the actuators will be conducted. Two actuator module iterations will be conducted. One will use a burnout profile based on a conventional (100-mg sample size) thermogravimetric analysis result; the other will be in a specially rigged furnace to monitor temperature, weight loss and strain during the burnout--this sample will essentially be sacrificed but the amount of information gained will enable us to optimize the burnout cycle for this actuator size. DTIC

N95-19966# Battelle Columbus Labs., OH.

MERCURY USAGE AND ALTERNATIVES IN THE ELECTRICAL AND ELECTRONICS INDUSTRIES Final Report

B. M. Sass, M. A. Salem, and L. A. Smith Jan. 1994 58 p See also

PB92-162569
(Contract EPA-68-C0-0003)
(PB94-165362; EPA/600/R-94/047) Avail: CASI HC A04/MF A01

Many industries have already found alternatives for mercury or have greatly decreased mercury use. However, the unique electromechanical and photoelectric properties of mercury and mercury compounds have made replacement of mercury difficult in some applications. The study was initiated to identify source reduction and recycling options for mercury in the electrical and electronics industry (SIC 36) and measurement and control instrument manufacture (SIC 382). The project identified trends in pollution prevention for mercury use throughout the U.S. economy by a review of the sources and use of mercury in the economy. Regulatory trends encouraging mercury pollution prevention were examined, and current practices in the electrical and electronics industry were reviewed in details to identify potential source reduction and reuse options for mercury. NTIS

N95-20119# Lawrence Livermore National Lab., Livermore, CA.

DESIGN AND PACKAGING ASPECTS OF MICROWAVE BANDWIDTH LITHIUM NIOBATE MODULATORS

C. F. McConaghy, S. Y. Lu, P. Sargis, M. Lowry, and R. A. Becker Jan. 1994 9 p Presented at the 4th Annual Advanced Research Project Agency (ARPA) Symposium on Photonics Systems for Antenna Applications, Monterey, CA, 18-21 Jan. 1994
(Contract W-7405-eng-48)
(DE94-016602; UCRL-JC-115676; CONF-940194-2) Avail: CASI HC A02/MF A01

Packaging of integrated optic modulators can be simplified if the electrodes are 50 ohms impedance. Recently built X-cut lithium niobate velocity matched modulators have a 50 ohm impedance. The interconnection of the modulators to external connectors by on-chip tapers is critical to their performance at frequencies in the 23 to 50 GHz frequency range. The attachment of fibers to the modulators is being enhanced with work on a robotic machine that uses a combination of machine vision and active alignment to both coarse and fine position the fiber to the waveguide. The design goal is to have each fiber attached in under 2 minutes. DOE

N95-20168# Los Alamos National Lab., NM.

DSP CONTROL OF SUPERCONDUCTING QUANTUM INTERFERENCE DEVICES

R. R. Bracht, Pang-Jen Kung, P. S. Lewis, and E. R. Flynn 1994 7 p Presented at the ICSPAT 1994: Signal Procession Applications and Technology, Dallas, TX, 18-21 Oct. 1994
(Contract W-7405-eng-36)
(DE94-016193; LA-UR-94-2639; CONF-9410164-1) Avail: CASI HC A02/MF A01

Superconducting quantum interference devices (SQUIDS) are used to detect very low level magnetic fields. Los Alamos National Laboratory is involved in developing digital signal processing (DSP) based instrumentation for these devices in conjunction with detecting magnetic flux from the human brain. This field of application is known as magnetoencephalography (MEG). The magnetic signals generated by the brain are on the order of a billion times smaller than the earth's magnetic field, yet they can readily be detected with these highly sensitive magnetic detectors. Los Alamos National Laboratory has developed and implemented DSP control of the SQUID system. This has been accomplished by using an AT&T DSP32C DSP in conjunction with dual 18 bit a-to-d and d-to-a converters. The DSP performs the signal demodulation by synchronously sampling the recovered signal and applying the appropriate full wave rectification. The signal is then integrated and filtered and applied to the output. Also, the modulation signal is generated with the DSP system. All of the flux lock loop electronics are replaced except for the low noise analog preamplifier at the front of the recovery components. The system has been tested with both an electronic SQUID simulator and a low temperature thin film SQUID from Conductus. A number of experiments have been performed to allow evaluation of the system improvement made possible by use of DSP control. DOE

N95-20213# Los Angeles City Dept. of Water and Power, CA.

TEST AND EVALUATION OF ELECTRIC VEHICLES

1994 7 p
(Contract DE-FG07-90ID-12942)
(DE95-001153; DOE/ID-12942/1) Avail: CASI HC A02/MF A01

The Los Angeles Department of Water and Power currently operates 11 electric vehicles: 6 G-Vans, 4 Chrysler TEVans, and 1 Hybrid minivan. LADWP's participation in US DOE's site operator program involves the Hybrid electric minivan (manufactured by Unique Mobility, Englewood, CO) and one Chrysler TEVan. The program efforts are described. DOE

N95-20257# Maryland Univ., College Park, MD. Dept. of Electrical Engineering.

TRACKING A DYNAMIC SET OF FEATURE POINTS

Yi-Sheng Yao and Rama Chellappa Jun. 1994 36 p
(Contract DAAH04-93-G-0419; ARPA Order A422)
(AD-A285124; CAR-TR-720; CS-TR-3294) Avail: CASI HC A03/MF A01

This paper presents a model-based algorithm for tracking feature points over a long sequence of monocular noisy images with the ability to include new feature points detected in successive frames. The trajectory for each feature point is modeled by a simple kinematic motion model. A Probabilistic Data Association Filter is first designed to estimate the motion between two consecutive frames. A matching algorithm then identifies the corresponding point to subpixel accuracy and an Extended Kalman Filter (EKF) is employed to continually track the feature point. An efficient way to dynamically include new feature points from successive frames into a tracking list is also addressed. Tracking results for several image sequences are given. DTIC

N95-20262# Sandia National Labs., Albuquerque, NM.

TRIMODE POWER CONVERTER OPTIMIZES PV, DIESEL AND BATTERY ENERGY SOURCES

George OSullivan (Abacus Controls, Inc., Somerville, NJ.), Russell Bonn, and Ward Bower 1994 4 p Presented at the 1st World Conference on Photovoltaic Energy Conversion, Waikoloa, HI, 5-9 Dec. 1994
(Contract DE-AC04-94AL-85000)
(DE94-015014; SAND-94-1775C; CONF-941203-6) Avail: CASI HC A01/MF A01

Conservatively, there are 100,000 localities in the world waiting for the benefits that electricity can provide, and many of these are in climates where sunshine is plentiful. With these locations in mind a prototype 30 kW hybrid system has been assembled at Sandia to prove the reliability and economics of photovoltaic, diesel and battery energy sources managed by an autonomous power converter. In the Trimode Power Converter the same power parts, four IGBT's with an isolation transformer and filter components, serve as rectifier and charger to charge the battery from the diesel; as a stand-alone inverter to convert PV and battery energy to AC; and, as a parallel inverter with the diesel-generator to accommodate loads larger than the rating of the diesel. Whenever the diesel is supplying the load, an algorithm assures that the diesel is running at maximum efficiency by regulating the battery charger operating point. Given the profile of anticipated solar energy, the cost of transporting diesel fuel to a remote location and a five year projection of load demand, a method to size the PV array, battery and diesel for least cost is developed. DOE

N95-20280 Department of the Navy, Washington, DC.

LONG SEQUENCE CORRELATION COPROCESSOR Patent

Douglas W. Gage, inventor (to Navy) 20 Sep. 1994 8 p Filed 27 Jun. 1991
(AD-D016558; US-Patent-5,349,550; US-Patent-Appl-SN-772059; US-Patent-Class-364-728.03) Avail: US Patent and Trademark Office

A long sequence correlation coprocessor (LSCC) accelerates the bitwise correlation of arbitrarily long digital sequences by calculating in parallel the correlation score for 16, for example, adjacent bit alignments between two binary sequences. The LSCC integrated circuit is incorporated into a computer system with memory storage buffers and a separate general purpose computer processor which serves as its controller. Each of the LSCC's set of sequential counters simultaneously tallies a separate correlation coefficient. During each LSCC clock cycle, computer enable logic associated with each counter compares one bit of a first sequence with one bit of a second sequence to increment the counter if the bits are the same. A shift register assures that the same bit of the first sequence is simultaneously compared to different bits of the second sequence to simultaneously calculate the correlation coefficient by the different counters to represent different alignments of the two sequences. DTIC

N95-20286# Sandia Labs., Albuquerque, NM. Electronics Quality/Reliability Center.

LOW ELECTRON BEAM ENERGY CIVA ANALYSIS OF PASSIVATED ICs

Edward I. Cole, Jr., Jerry M. Soden, Bruce A. Dodd, and Christopher L. Henderson 1994 11 p Presented at the International Symposium for Testing and Failure Analysis, Los Angeles, CA, 14-18 Nov. 1994
(Contract DE-AC04-94AL-85000)
(DE94-017421; SAND-94-1167C; CONF-941154-1) Avail: CASI HC A03/MF A01

Low Energy Charge-Induced Voltage Alteration (LECIVA) is a new scanning electron microscopy technique developed to localize open conductors in passivated IC's. LECIVA takes advantage of recent experimental work showing that the dielectric surface equilibrium voltage has an electron flux density dependence at low electron beam energies (less than or equal to 1.0 keV). The equilibrium voltage changes from positive to negative as the electron flux density is increased. Like Charge-Induced Voltage Alteration (CIVA), LECIVA images are produced from the voltage fluctuations of a constant current power supply as an electron beam is scanned over the IC surface. LECIVA image contrast is generated only by the electrically open part of a conductor, yielding, the same high selectivity demonstrated by CIVA. Because LECIVA is performed at low beam energies, radiation damage by the primary electrons and x-rays to MOS structures is far less than that caused by CIVA. LECIVA may also be performed on commercial electron beam test systems that do not have high primary electron beam energy capabilities. The physics of LECIVA signal generation are described. LECIVA imaging examples illustrate its utility on both a standard scanning electron microscope (SEM) and a commercial electron beam test system. DOE

N95-20298 Department of the Navy, Washington, DC.

SEMICONDUCTOR COLD ELECTRON EMISSION DEVICE Patent

Max N. Yoder, inventor (to Navy) 2 Aug. 1994 5 p Filed 29 Sep. 1993
(AD-D016577; US-Patent-5,334,853; US-Patent-Appl-SN-128508; US-Patent-Class-257-10) Avail: US Patent and Trademark Office

A semiconductor cold electron emission device comprising a type I heterojunction formed of a P-type semiconductor mixture of AlN and a N-type semiconductor mixture of SiC which junction is forward biased so that electrons are monoenergetically emitted from the P-type semiconductor mixture. DTIC

N95-20311 Hughes Research Labs., Malibu, CA.

PASOTRON(TM) TECHNOLOGY Final Report, 1 Jan. - 31 Dec. 1993

J. M. Butler, D. M. Goebel, and J. Santoru 1 Feb. 1994 33 p Limited Reproducibility: More than 20% of this document may be affected by microfiche quality
(Contract F49620-92-C-0015)
(AD-A279994; HAC-REF-J4924; AFOSR-94-0311TR) Avail: Issuing Activity (Defense Technical Information Center (DTIC))

This annual report describes research progress made in the second year of the PASOTRON Technology Program. This program is a two year effort sponsored by the Air Force Office of Scientific Research to develop and investigate a single-stage amplifier and a multi-stage oscillator; each based on Hughes' Plasma-Assisted, Slow-Wave Oscillator (PASOTRON) technology. During the program's second year amplifier performance was briefly re-explored to take advantage of system and diagnostic upgrades implemented by HRL under a parallel IR&D Program; and the first stage of the multi-stage oscillator was demonstrated. Data is reported showing improved amplifier performance. Amplifier gains of 10-to-17 dB were maintained; while instantaneous bandwidth was increased from 0.1% to 1.0%. Amplified power levels of several tens to hundred kilowatts were measured to give a factor-of-ten increase in efficiency to levels of a few present. The first phase measurements were completed, and coherent amplifier operation was achieved with phase stability of up to 0.005 deg/V. Additionally, a multi-stage oscillator system was designed and experimental investigations were conducted on the first stage of the three-stage apparatus. Characterization of the second and third stages will be completed during the program's three-month no-cost extension. DTIC

N95-20338# Sandia National Labs., Albuquerque, NM.

PROTON IRRADIATION EFFECTS ON ADVANCED DIGITAL AND MICROWAVE III-V COMPONENTS

G. L. Hash, J. R. Schwank, M. R. Shaneyfelt, C. E. Sandoval, M. P. Connors, T. J. Sheridan, F. W. Sexton, E. M. Slayton, J. A. Heise, and C. Foster (Indiana Univ., Bloomington, IN.) 1994 8 p Presented at the 31st Annual International Nuclear and Space Radiation Effects Conference, Tucson, AZ, 18-22 Jul. 1994
(Contract DE-AC04-94AL-85000)
(DE94-018742; SAND-94-0205C; CONF-940726-14) Avail: CASI HC A02/MF A01

A wide range of advanced III-V components suitable for use in high-speed satellite communication systems were evaluated for displacement damage and single-event effects in high-energy, high-fluence proton environments. Transistors and integrated circuits (both digital and MMIC) were irradiated with protons at energies from 41 to 197 MeV and at fluences from 10(exp 10) to 2 x 10(exp 14) protons/sq cm. Large soft-error rates were measured for digital GaAs MESFET (3 x 10(exp -5) errors/bit-day) and heterojunction bipolar circuits (10(exp -5) errors/bit-day). No transient signals were detected from MMIC circuits. The largest degradation in transistor response caused by displacement damage was observed for 1.0-(mu)m depletion- and enhancement-mode MESFET transistors. Shorter gate length MESFET transistors and HEMT transistors exhibited less displacement-induced damage. These results show that memory-intensive GaAs digital circuits may result in significant system degradation due to single-event upset in natural and man-made space environments. However, displacement damage effects should not be a limiting factor for fluence levels up to 10(exp 14) protons/sq cm (equivalent to total doses in excess of 10 Mrad(GaAs)). DOE

N95-20339# Michigan Biotechnology Inst., Lansing, MI.

BIOCONVERSION OF COAL DERIVED SYNTHESIS GAS TO LIQUID FUELS

M. K. Jain, R. M. Worden, and A. Grethlein 18 Jul. 1994 7 p
(Contract DE-AC22-92PC-92117)
(DE94-018849; DOE/PC-92117/T9) Avail: CASI HC A02/MF A01

The overall objective of the project is to develop an integrated two-stage fermentation process for conversion of coal-derived synthesis gas to a mixture of alcohols. This is achieved in two steps. In the first step, Butyribacterium methylotrophicum converts carbon monoxide (CO) to butyric and acetic acids. Subsequent fermentation of the acids by Clostridium acetobutylicum leads to the production of butanol and ethanol. The tasks for this quarter were: development/isolation of superior strains for fermentation of syngas; evaluation of bioreactor configuration for improved mass transfer of syngas; recovery of carbon and electrons from H2-CO2; initiation of pervaporation for recovery of solvents; and selection of solid support material for trickle-bed fermentation. Technical progress included the following: butyrate production was enhanced during H2/CO2 (50/50) batch fermentation; isolation of CO-utilizing anaerobic strains is in progress; pressure (15 psig) fermentation was evaluated as a means of increasing CO availability; polyurethane foam packing material was selected for trickle bed solid support; cell recycle fermentation on syngas operated for 3 months. Acetate was the primary product at pH 6.8; trickle bed and gas lift fermentor designs were modified after initial water testing; and pervaporation system was constructed (No alcohol selectivity was shown with the existing membranes during initial start-up). DOE

N95-20341# Sandia National Labs., Albuquerque, NM.

OBSERVATION OF EXCITONIC AND BAND-TO-BAND BEHAVIOR IN ORDERED InGaP2 ALLOYS

E. D. Jones, D. M. Follstaedt, H. Lee, J. S. Nelson, R. P. Schneider, Jr., R. G. Alonso (National Renewable Energy Lab., Golden, CO.), G. S. Horner (National Renewable Energy Lab., Golden, CO.), J. Machol (National Renewable Energy Lab., Golden, CO.), and A. Mascarenhas (National Renewable Energy Lab., Golden, CO.) 1994 5 p Presented at the 22nd International Conference on Physics of Semiconductors, Vancouver, British Columbia, 15-19 Aug. 1994
(Contract DE-AC04-94AL-85000)
(DE94-018891; SAND-94-2065C; CONF-9408155-4) Avail: CASI HC A01/MF A01

Photoluminescence measurements on ordered InGaP2 were studied as a function of temperature, laser power density, and magnetic field. The temperature varied between 1.4 and 300 K, the laser power densities ranged from 10 nW/sq cm to 20 W/sq cm, and the maximum magnetic field was 13.6 T. The data show both excitonic and band-to-band behavior, depending upon the incident laser power density. A consistent interpretation of all data leads to a type-II valence-band offset between the ordered domains. DOE

N95-20369# Joensuu Univ. (Finland). Karelian Inst.
ANAEROBIC TREATMENT OF MUNICIPAL SOLID WASTE AND SLUDGE FOR ENERGY PRODUCTION AND RECYCLING OF NUTRIENTS
S. Leinonen, ed. 1993 113 p Workshop held in Joensuu, Finland, 1-2 Oct. 1993
(DE95-700217; JOY/KT-JULK-105; CONF-9310356) Avail: CASI HC A06/MF A02

This volume contains 18 papers presented at a Nordic workshop dealing with application of anaerobic decomposition processes on various types of organic wastes, held at the Siikasalmi Research and Experimental Station of the University of Joensuu on 1-2 Oct. 1992. Subject coverage of the presentations extends from the biochemical and microbiological principles of organic waste processing to descriptions and practical experiences of various types of treatment plants. The theoretical and experimental papers include studies on anaerobic and thermophilic degradation processes, methanogenesis, effects of hydrogen, treatment of chlorinated and phenolic compounds, and process modeling, while the practical examples range from treatment of various types of municipal, industrial, and mining wastes to agricultural and fish farm effluents. The papers provide technical descriptions of several biogas plants in operation. Geographically, the presentations span the Nordic and Baltic countries. DOE

N95-20380# Oregon State Univ., Corvallis, OR.
BRUSHLESS DOUBLY-FED MACHINE SYSTEM DEVELOPMENT PROGRAM, PHASE 3 Final Technical Report, 1 Jan. 1992 - 30 Jun. 1993
G. C. Alexander, R. Spee, and A. K. Wallace 1993 171 p
(Contract DE-BI79-90BP-03362)
(DE94-013095; DOE/BP-03362/T1-Phase-3) Avail: CASI HC A08/MF A02

Since the inception of the Brushless Doubly-Fed Machine (BDFM) System Development Program in 1989, the value of BDFM technology has become apparent. The BDFM provides for adjustable speed, synchronous operation while keeping costs associated with the required power conversion equipment lower than in competing technologies. This provides for an advantage in initial as well as maintenance expenses over conventional drive system. Thus, the BDFM enables energy efficient, adjustable speed process control for applications where established drive technology has not been able to deliver satisfactory returns on investment. At the same time, the BDFM challenges conventional drive technologies in established markets by providing for improved performance at lower cost. BDFM converter rating is kept at a minimum, which significantly improves power quality at the utility interface over competing power conversion equipment. In summary, BDFM technology can be expected to provide significant benefits to utilities as well as their customers. This report discusses technical research and development activities related to Phase 3 of the BDFM System Development Program, including work made possible by supplemental funds for laboratory improvement and prototype construction. DOE

N95-20394# North Carolina State Univ., Raleigh, NC. Dept. of Electrical and Computer Engineering.
SOLID-STATE DYNAMICS AND QUANTUM TRANSPORT IN NOVEL SEMICONDUCTOR NANOSTRUCTURES Annual Report, 1 Oct. 1993 - 30 Sep. 1994
Sep. 1994 50 p
(Contract N00014-90-J-1835)
(AD-A285946) Avail: CASI HC A03/MF A01

The objective of this research program is to study theoretically the underlying principles of solid-state dynamics and quantum mechanical transport of carriers in ultrasmall novel semiconductor devices. The areas of research are: (1) theory of phonon modes in reduced dimensions; (2) effects of band structure on electronic and optical properties of heterostructures; and (3) quantum transport in solids with special emphasis on the non-perturbative role of high-electric fields and many-body effects in dynamical processes. The treatment of these problems is mainly analytical through the development of macroscopic and microscopic physical models with an emphasis on quantum mechanical principles. At the same time, numerical approaches has also been utilized for realistic solutions with accuracy. Specific subjects discussed in this report include the effects of confinement and localization on optical and acoustic phonon modes, band mixing in phonon-assisted transitions, and Bloch electron quantum transport theory under hot-electron conditions. The knowledge developed in this work will be of major importance in explaining the novel phenomena and fundamental questions relating to the breakdown of classical solid-state electronics as device dimensional scales are reduced to the submicron and ultra-submicron regime. DTIC

N95-20436 Department of the Navy, Washington, DC.
MODULE COOLING SYSTEM Patent
Frank E. Altoz, inventor (to Navy) 5 Jul. 1994 6 p Filed 25 Jun. 1993
(AD-D016584; US-Patent-5,325,913; US-Patent-Appl-SN-081712; US-Patent-Class-165-32) Avail: US Patent and Trademark Office

An apparatus is provided for cooling electronic components mounted on a circuit board. The circuit board is placed in thermal contact with a heat sink enclosure that has an interior cavity and a release opening that provides a path from the interior cavity to the external ambient. A meltable pellet blocks the release opening. A wick is bonded to the inside surface of the interior cavity. The device is sealed with a working fluid that permeates the wick. When the components get hot, the heat is transferred through the heat sink enclosure to the working fluid in the wick, causing the working fluid to vaporize. The vapors remain trapped in the interior cavity until the pellet melts, allowing the vapor to be released and the temperature of the heat sink enclosure to be stabilized or lowered. DTIC

N95-20443# Rensselaer Polytechnic Inst., Troy, NY.
THE RELIABILITY OF LASER REFLOWED Sn-Ag SOLDER JOINTS Quarterly Report No. 1
C. H. Raeder, D. L. Millard, and R. W. Messler 4 May 1994 5 p
(AD-A279787) Avail: CASI HC A01/MF A01

This is the first quarterly report of a project aimed at determining the reliability of electronic interconnects made with Sn-3.5wt%Ag solder alloy. The reliability of solder interconnects is primarily determined by two factors: (1) the type of electronic assembly; and (2) the environment to which the assembly is exposed. These two factors (each composed of several variables i.e. assembly thermal expansion coefficients, elastic moduli of assembly members, maximum operating temperature, rate of temperature change, etc.) boil down to three critical parameters; temperature, strain and strain rate (or stress). The interdependence of these variables must first be explored when addressing a creep-fatigue problem such as the case of solder joints. Specific environment (beyond temperature) and state of stress at a propagating crack, which are determined by the specific application and package geometry, are being neglected at this point in time. Little involving the creep or fatigue properties of Sn-3.5Ag is reported in the literature. Prior studies have used unique joint geometries to measure joint properties. DTIC

N95-20488# Applied Science and Technology, Inc., Woburn, MA.
MATERIALS PROCESSING AND MANUFACTURING TECHNOLOGIES FOR DIAMOND SUBSTRATES MULTICHIP MODULES Technical Report, Jan. - Mar. 1994
Evelio Sevillano 15 Aug. 1994 3 p Sponsored by DARPA
(Contract N00014-93-C-2026)
(AD-A285060) Avail: CASI HC A01/MF A01

In this quarter we have continued our baseline program to optimize the throughput of diamond in conventional chemistries, achieving the target 1 g/hr of deposition at 75 kW, completed modifications to the AX6600 substrate stage allowing full power operation on a continuous basis, continued work on release techniques using novel materials for successful production of free standing 6 inch diameter diamond, and constructed a thermal conductivity test stand for quality measurements on free standing diamond films. DTIC

N95-20502*# National Aeronautics and Space Administration. Lewis Research Center, Cleveland, OH.
PROCEEDINGS OF THE 13TH SPACE PHOTOVOLTAIC RESEARCH AND TECHNOLOGY CONFERENCE (SPRAT 13)
Sep. 1994 421 p Conference held in Cleveland, OH, 14-16 Jun. 1994
(Contracts NAS1-19592; NAS3-26703; NAS3-27004; NAG3-1466; RTOP 233-01-0A)
(NASA-CP-3278; E-9083; NAS 1.55:3278) Avail: CASI HC A18/MF A04

The Thirteenth Space Photovoltaic Research and Technology (SPRAT) Conference included 38 technical papers, 6 program reviews and 5 workshop discussions. The effects of shrinking research and development budgets were evident in the focus and tone of this SPRAT. Most attendees appeared to be oriented toward near term, system oriented projects and fewer were involved in long term, high risk research. It was generally agreed that space power requirements would continue to move toward smaller (less than 2kW) power levels. Most future applications are believed to be in traditional orbits (LEO, GEO) although interesting opportunities may be found in high radiation, mid-altitude orbits useful for global communication networks. New solar cell devices and materials will be difficult to introduce unless they are mission enabling, or offer significant cost and/or performance benefits. Many factors influence the selection of type of array. For individual titles, see N95-20503 through N95-20543.

N95-20503*# National Aeronautics and Space Administration. Goddard Space Flight Center, Greenbelt, MD.
GODDARD SPACE FLIGHT CENTER SOLAR ARRAY MISSIONS, REQUIREMENTS AND DIRECTIONS c44
Edward Gaddy and John Day *In* NASA. Lewis Research Center, Proceedings of the 13th Space Photovoltaic Research and Technology Conference (SPRAT 13) Sep. 1994 p 1-12 (For primary document see N95-20502 06-33)
Avail: CASI HC A03/MF A04

The Goddard Space Flight Center (GSFC) develops and operates a wide variety of spacecraft for conducting NASA's communications, space science, and earth science missions. Some are 'in house' spacecraft for which the GSFC builds the spacecraft and performs all solar array design, analysis, integration, and test. Others are 'out of house' spacecraft for which an aerospace contractor builds the spacecraft and develops the solar array under direction from GSFC. The experience of developing flight solar arrays for numerous GSFC 'in house' and 'out of house' spacecraft has resulted in an understanding of solar array requirements for many different applications. This presentation will review those solar array requirements that are common to most GSFC spacecraft. Solar array technologies will be discussed that are currently under development and that could be useful to future GSFC spacecraft. Author

N95-20504*# Ballistic Missile Defense Organization, Washington, DC.
BMDO PHOTOVOLTAICS PROGRAM OVERVIEW c44
Leonard H. Caveny and Douglas M. Allen (Schafer, W. J. Associates, Inc., North Olmsted, OH.) *In* NASA. Lewis Research Center, Proceedings of the 13th Space Photovoltaic Research and Technology Conference (SPRAT 13) Sep. 1994 p 13-21 (For primary document see N95-20502 06-33)
Avail: CASI HC A02/MF A04

This is an overview of the Ballistic Missile Defense Organization (BMDO) Photovoltaic Program. Areas discussed are: (1) BMDO advanced Solar Array program; (2) Brilliant Eyes type satellites; (3) Electric propulsion; (4) Contractor Solar arrays; (5) Iofee Concentrator and Cell development; (6) Entech linear mini-dome concentrator; and (7) Flight test update/plans. Author

N95-20505*# National Renewable Energy Lab., Golden, CO.
AN UPDATE ON THE DEPARTMENT OF ENERGY'S PHOTOVOLTAIC PROGRAM c44
John P. Benner and Mark Fitzgerald *In* NASA. Lewis Research Center, Proceedings of the 13th Space Photovoltaic Research and Technology Conference (SPRAT 13) Sep. 1994 p 31-33 (For primary document see N95-20502 06-33)
Avail: CASI HC A01/MF A04

Funding for the terrestrial photovoltaic's program is $78 million in 1994. This is more than double the minimum level reached in 1989 and runs counter to the general trend of decreasing budgets for Department of Energy (DOE) programs. During the past five years, the program has expanded its mission from research and development to also address manufacturing technology and commercialization assistance. These new activities are directed toward revitalizing the market to reinstate the rapid rate of sales growth needed to attract investment. The program is approaching balance among efforts in each of the three areas. This translates to a reduction in some of the R & D activities of most relevance to the space power community. On the other hand, some of the advancements in manufacturing may finally bring thin-film technologies to reality for space arrays. This talk will describe the status and direction of DOE program with an eye toward highlighting its impact on technology of interest for space. Author

N95-20506*# European Space Agency. European Space Research and Technology Center, ESTEC, Noordwijk (Netherlands).
EUROPE'S SPACE PHOTOVOLTAICS PROGRAMME c44
Klaus P. Bogus *In* NASA. Lewis Research Center, Proceedings of the 13th Space Photovoltaic Research and Technology Conference (SPRAT 13) Sep. 1994 p 35-39 (For primary document see N95-20502 06-33)
Avail: CASI HC A01/MF A04

The current space PV (photovoltaic) technology development program of ESA is described. The program is closely coupled to the European space mission scenario for the next 10 year period and has as its main objective to make the most effective use of the limited resources available for technology in the present economical climate. This requires a well-balanced approach between concentration on very few options and keeping the competition alive if more than one promising technology exists. The paper describes ESA's main activities in the areas of solar array technology, solar cell technology, solar cell assembly technology, and special test and verification activities including the in-orbit demonstration of new technologies. Author

N95-20507*# Research Triangle Inst., Research Triangle Park, NC.
HIGH-EFFICIENCY, DEEP-JUNCTION, EPITAXIAL InP SOLAR CELLS ON (100) AND (111)B InP SUBSTRATES c44
R. Venkatasubramanian, M. L. Timmons, J. A. Hutchby, Robert J. Walters (Naval Research Lab., Washington, DC.), and Geoffrey P. Summers (Naval Research Lab., Washington, DC.) *In* NASA. Lewis Research Center, Proceedings of the 13th Space Photovoltaic Research and Technology Conference (SPRAT 13) Sep. 1994 p 43-51 (For primary document see N95-20502 06-33)
Avail: CASI HC A02/MF A04

We report on the development and performance of deep-junction (approximately 0.25 micron), graded-emitter-doped, n(sup +)-p InP solar cells grown by metallorganic chemical vapor deposition (MOCVD). A novel, diffusion-transport process for obtaining lightly-doped p-type base regions of the solar cell is described. The I-V data and external quantum-efficiency response of these cells are presented. The best active-area AMO efficiency for these deep-junction cells on (100)-oriented InP substrates is 16.8 percent, with a J(sub SC) of 31.8 mA/sq cm, a V(sub OC) of 0.843 V, and a fill-factor of 0.85. By comparison, the best cell efficiency on the (111)B-oriented InP substrates was 15.0 percent. These efficiency values for deep-junction cells are encouraging and compare favorably with performance of thin-emitter (0.03 micron) epitaxial cells as well as that of deep-emitter diffused cells. The cell performance and breakdown voltage characteristics of a batch of 20 cells on each of the orientations are presented, indicating the superior breakdown voltage properties and other characteristics of InP cells on the (111)B orientation. Spectral response, dark I-V data, and photoluminescence (PL) measurements on the InP cells are presented with an analysis on the variation in J(sub SC) and V(sub OC) of the cells. It is observed, under open-circuit conditions, that lower-V(sub OC) cells exhibit higher band-edge PL intensity for both the (100) and (111)B orientations. This anomalous behavior suggests that radiative recombination in the heavily-doped n(sup +)-InP emitter may be detrimental to achieving higher V(sub OC) in n(sup +)-p InP solar cells. Author

N95-20508*# Houston Univ., TX.
CHEMICAL BEAM EPITAXY FOR HIGH EFFICIENCY PHOTOVOLTAIC DEVICES c44
A. Bensaoula, A. Freundlich, M. F. Vilela, N. Medelci, and P. Renaud *In*

NASA. Lewis Research Center, Proceedings of the 13th Space Photovoltaic Research and Technology Conference (SPRAT 13) Sep. 1994 p 53-61 Sponsored in cooperation with the State of Texas advanced technology program and IST, Inc. (For primary document see N95-20502 06-33)
Avail: CASI HC A02/MF A04

InP-based multijunction tandem solar cells show great promise for the conversion efficiency (eta) and high radiation resistance. InP and its related ternary and quanternary compound semiconductors such as InGaAs and InGaAsP offer desirable combinations for energy bandgap values which are very suitable for multijunction tandem solar cell applications. The monolithically integrated InP/In(0.53)Ga(0.47)As tandem solar cells are expected to reach efficiencies above 30 percent. Wanlass, et.al., have reported AMO efficiencies as high as 20.1% for two terminal cells fabricated using atmospheric-pressure metalorganic vapor phase epitaxy (APMOVPE). The main limitations in their technique are first related to the degradation of the intercell ohmic contact (IOC), in this case the In(0.53)Ga(0.47)As tunnel junction during the growth of the top InP subcell structure, and second to the current matching, often limited by the In(0.53)Ga(0.47)As bottom subcell. Chemical beam epitaxy (CBE) has been shown to allow the growth of high quality materials with reproducible complex compositional and doping profiles. The main advantage of CBE compared to metalorganic chemical vapor deposition (MOCVD), the most popular technique for InP-based photovoltaic device fabrication, is the ability to grow high purity epilayers at much lower temperatures (450 C - 530 C). In a recent report it was shown that cost-wise CBE is a breakthrough technology for photovoltaic (PV) solar energy progress in the energy conversion efficiency of InP-based solar cells fabricated using chemical beam epitaxy. This communication summarizes our recent results on PV devices and demonstrates the strength of this new technology. Author (revised)

N95-20509*# National Aeronautics and Space Administration. Lewis Research Center, Cleveland, OH.
STATUS OF DIFFUSED JUNCTION p+n InP SOLAR CELLS FOR SPACE APPLICATIONS **c44**
Mircea Faur (Cleveland State Univ., OH.), C. Goradia (Cleveland State Univ., OH.), Maria Faur (NYMA, Inc., Brook Park, OH.), N. S. Fatemi (NYMA, Inc., Brook Park, OH.), P. P. Jenkins (NYMA, Inc., Brook Park, OH.), D. J. Flood, D. J. Brinker, D. M. Wilt, S. Bailey, and M. Goradia (Cleveland State Univ., OH.) et al *In its* Proceedings of the 13th Space Photovoltaic Research and Technology Conference (SPRAT 13) Sep. 1994 p 63-79 (For primary document see N95-20502 06-33)
Avail: CASI HC A03/MF A04

Recently, we have succeeded in fabricating diffused junction p(sup +)n(Cd,S) InP solar cells with measured AMO, 25 C open circuit voltage (V(sub OC)) of 887.6 mV, which, to the best of our knowledge, is higher than previously reported V(sub OC) values for any InP homojunction solar cells. The experiment-based projected achievable efficiency of these cells using LEC grown substrates is 21.3 percent. The maximum AMO, 25 C internal losses due to date on bare cells is, however, only 13.2 percent. This is because of large external and internal losses due to non-optimized front grid design, antireflection (AR) coating and emitter thickness. This paper summarizes recent advances in the technology of fabrication of p(sup +)n InP diffused structures and solar cells, resulted from a study undertaken in an effort to increase the cell efficiency. The topics discussed in this paper include advances in: (1) the formation on thin p(sup +) InP:Cd emitter layers, (2) electroplated front contacts, (3) surface passivation and (4) the design of a new native oxide/Al2O3/MgF2 tree layer AR coating using a chemically-grown P-rich passivating oxide as a first layer. Based on the high radiation resistance and the excellent post-irradiation annealing and recovery demonstrated in the early tests done to date, as well as the projected high efficiency and low-cost high-volume fabricability, these cells show a very good potential for space photovoltaic applications.
Author

N95-20510*# Astropower, Inc., Newark, DE.
HIGH QUALITY InP-ON-Si FOR SOLAR CELL APPLICATIONS **c44**
Zane A. Shellenbarger, Thomas A. Goodwin, Sandra R. Collins, and Louis C. DiNetta *In* NASA. Lewis Research Center, Proceedings of the 13th Space Photovoltaic Research and Technology Conference (SPRAT 13) Sep. 1994 p 81-89 (For primary document see N95-20502 06-33)
Avail: CASI HC A02/MF A04

InP on Si solar cells combine the low-cost and high-strength of Si with the high efficiency and radiation tolerance of InP. The main obstacle in the growth of single crystal InP-on-Si is the high residual strain and high dislocation density of the heteroepitaxial InP films. The dislocations result from the large differences in lattice constant and thermal expansion mismatch of InP and Si. Adjusting the size and geometry of the growth area is one possible method of addressing this problem. In this work, we conducted a material quality study of liquid phase epitaxy overgrowth layers on selective area InP grown by a proprietary vapor phase epitaxy technique on Si. The relationship between growth area and dislocation density was quantified using etch pit density measurements. Material quality of the InP on Si improved both with reduced growth area and increased aspect ratio (length/width) of the selective area. Areas with etch pit density as low as 1.6 x 10(exp 4) sq cm were obtained. Assuming dislocation density is an order of magnitude greater than etch pit density, solar cells made with this material could achieve the maximum theoretical efficiency of 23% at AMO. Etch pit density dependence on the orientation of the selective areas on the substrate was also studied. Author

N95-20511*# Spire Corp., Bedford, MA.
P/N InP SOLAR CELLS ON Ge WAFERS **c44**
Steven Wojtczuk, Stanley Vernon, and Edward A. Burke (Burke, Edward A., Woburn, MA.) *In* NASA. Lewis Research Center, Proceedings of the 13th Space Photovoltaic Research and Technology Conference (SPRAT 13) Sep. 1994 p 91-98 (For primary document see N95-20502 06-33)
Avail: CASI HC A02/MF A04

Indium phosphide (InP) P-on-N one-sun solar cells were epitaxially grown using a metalorganic chemical vapor deposition process on germanium (Ge) wafers. The motivation for this work is to replace expensive InP wafers, which are fragile and must be thick and therefore heavy, with less expensive Ge wafers, which are stronger, allowing use of thinner, lighter weight wafers. An intermediate InxGs1-xP grading layer starting as In(0.49)Ga(0.51) at the GaAs-coated Ge wafer surface and ending as InP at the top of the grading layer (backside of the InP cell) was used to attempt to bend some of the threading dislocations generated by lattice-mismatch between the Ge wafer and InP cell so they would be harmlessly confined in this grading layer. The best InP/Ge cell was independently measured by NASA-Lewis with a one-sun 25 C AMO efficiently measured by NASA-Lewis with a one-circuit photocurrent 22.6 mA/sq cm. We believe this is the first published report of an InP cell grown on a Ge wafer. Why get excited over a 9 percent InP/Ge cell? If we look at the cell weight and efficiency, a 9 percent InP cell on an 8 mil Ge wafer has about the same cell power density, 118 W/kg (BOL), as the best InP cell ever made, a 19 percent InP cell on an 18 mil InP wafer, because of the lighter Ge wafer weight. As cell panel materials become lighter, the cell weight becomes more important, and the advantage of lightweight cells to the panel power density becomes more important. In addition, although InP/Ge cells have a low beginning-of-life (BOL) efficiency due to dislocation defects, the InP/Ge cells are very radiation hard (end-of-life power similar to beginning-of-life). We have irradiated an InP/Ge cell with alpha particles to an equivalent fluence of 1.6 x 10(exp 16) 1 MeV electrons/sq cm and the efficiency is still 83 percent of its BOL value. At this fluence level, the power output of these InP/Ge cells matches the GaAs/Ge cell data tabulated in the JPL handbook. Data are presented indicating InP/Ge has more power output than GaAs/Ge cells at fluences in excess of this value.
Author

N95-20512*# International Solar Electric Technology, Inglewood, CA.
STATUS OF FLEXIBLE CIS RESEARCH AT ISET **c44**
B. M. Basol, V. K. Kapur, A. Minnick, A. Halani, and C. R. Leidholm *In* NASA. Lewis Research Center, Proceedings of the 13th Space Photovoltaic Research and Technology Conference (SPRAT 13) Sep. 1994 p 101-106 (For primary document see N95-20502 06-33)
(Contract NAS3-26615)
Avail: CASI HC A02/MF A04

Polycrystalline thin film solar cells fabricated on light-weight, flexible substrates are very attractive for space applications. In this work CuInSe2 (CIS) based thin film devices were processed on metallic foil substrates using the selenization technique. CIS deposition method involved reaction of electron-bean evaporated Cu-In precursor layers with a selenizing atmosphere at around 400 C. Several metallic foils such as Mo, Ti, Al, Ni, and Cu were evaluated as possible substrates for these devices. Solar cells with AM1.5 efficiencies of 9.0-9.34 percent and good mechanical integrity were demonstrated on Mo and Ti foils. Monolithic integration of these devices was also demonstrated up to 4 in x 4 in size. Author

N95-20513*# Astropower, Inc., Newark, DE.

DEVELOPMENT OF A LIGHTWEIGHT, LIGHT-TRAPPED, THIN GaAs SOLAR CELL FOR SPACECRAFT APPLICATIONS **c44**

Margaret H. Hannon, Louis C. DiNetta, Michael W. Dashiell, John R. Cummings, and Allen M. Barnett *In* NASA. Lewis Research Center, Proceedings of the 13th Space Photovoltaic Research and Technology Conference (SPRAT 13) Sep. 1994 p 107-114 Sponsored in cooperation with Ballistic Missile Defense Organization and Phillips Lab. (For primary document see N95-20502 06-33)
Avail: CASI HC A02/MF A04

This paper describes ultra-lightweight, high performance, thin, light trapping GaAs solar cells for advanced space power systems. The device designs can achieve 24.5 percent efficiency at AMO and 1X conditions, corresponding to a power density of 330 W/m2. A significant breakthrough lies in the potential for a specific power of 2906 W/kg because the entire device is less than 1.5 microns thick. This represents a 440 percent improvement over conventional 4-mil silicon solar cells. In addition to being lightweight, this thin device design can result in increased radiation tolerance. The attachment of the cover glass support to the front surface has been demonstrated by both silicone and electrostatic bonding techniques. Device parameters of 1.002 volts open-circuit voltage, 80 percent fill factor, and a short-circuit current of 24.3 mA/sq cm have been obtained. This demonstrates a conversion efficiency of 14.4 percent resulting in a specific power of 2240 W/kg. Additionally, this new technology offers an alternative approach for enabling multi-bandgap solar cells and high output space solar power devices. The thin device structure can be applied to any 3-5 based solar cell application, yielding both an increase in specific power and radiation tolerance. Author

N95-20514*# Martin Marietta Corp., Denver, CO.

ADVANCES IN POLYCRYSTALLINE THIN-FILM PHOTOVOLTAICS FOR SPACE APPLICATIONS **c44**

Bruce R. Lanning, Joseph H. Armstrong, and Mohan S. Misra *In* NASA. Lewis Research Center, Proceedings of the 13th Space Photovoltaic Research and Technology Conference (SPRAT 13) Sep. 1994 p 115-123 (For primary document see N95-20502 06-33)
(MM-IRD Proj. D-17R)
Avail: CASI HC A02/MF A04

Polycrystalline, thin-film photovoltaics represent one of the few (if not the only) renewable power sources which has the potential to satisfy the demanding technical requirements for future space applications. The demand in space is for deployable, flexible arrays with high power-to-weight ratios and long-term stability (15-20 years). In addition, there is also the demand that these arrays be produced by scalable, low-cost, high yield, processes. An approach to significantly reduce costs and increase reliability is to interconnect individual cells series via monolithic integration. Both CIS and CdTe semiconductor films are optimum absorber materials for thin-film n-p heterojunction solar cells, having band gaps between 0.9-1.5 ev and demonstrated small area efficiencies, with cadmium sulfide window layers, above 16.5 percent. Both CIS and CdTe polycrystalline thin-film cells have been produced on a laboratory scale by a variety of physical and chemical deposition methods, including evaporation, sputtering, and electrodeposition. Translating laboratory processes which yield these high efficiency, small area cells into the design of a manufacturing process capable of producing 1-sq ft modules, however, requires a quantitative understanding of each individual step in the process and its (each step) effect on overall module performance. With a proper quantification and understanding of material transport and reactivity for each individual step, manufacturing process can be designed that is not 'reactor-specific' and can be controlled intelligently with the design parameters of the process. The objective of this paper is to present an overview of the current efforts at MMC to develop large-scale manufacturing processes for both CIS and CdTe thin-film polycrystalline modules. CIS cells/modules are fabricated in a 'substrate configuration' by physical vapor deposition techniques and CdTe cells/modules are fabricated in a 'superstrate configuration' by wet chemical methods. Both laser and mechanical scribing operations are used to monolithically integrate (series interconnect) the individual cells into modules. Results will be presented at the cell and module development levels with a brief description of the test methods used to qualify these devices for space applications. The approach and development efforts are directed towards large-scale manufacturability of established thin-film, polycrystalline processing methods for large area modules with less emphasis on maximizing small area efficiencies. Author

N95-20515*# TRW Space Technology Labs., Redondo Beach, CA.

AMORPHOUS SILICON THIN FILMS: THE ULTIMATE LIGHTWEIGHT SPACE SOLAR CELL **c44**

G. J. Vendura, Jr., M. A. Kruer, H. H. Schurig, M. A. Bianchi, and J. A. Roth *In* NASA. Lewis Research Center, Proceedings of the 13th Space Photovoltaic Research and Technology Conference (SPRAT 13) Sep. 1994 p 125-134 (For primary document see N95-20502 06-33)
Avail: CASI HC A02/MF A04

Progress is reported with respect to the development of thin film amorphous (alpha-Si) terrestrial solar cells for space applications. Such devices promise to result in very lightweight, low cost, flexible arrays with superior end of life (EOL) performance. Each alpha-Si cell consists of a tandem arrangement of three very thin p-i-n junctions vapor deposited between film electrodes. The thickness of this entire stack is approximately 2.0 microns, resulting in a device of negligible weight, but one that must be mechanically supported for handling and fabrication into arrays. The stack is therefore presently deposited onto a large area (12 by 13 in), rigid, glass superstrate, 40 mil thick, and preliminary space qualification testing of modules so configured is underway. At the same time, a more advanced version is under development in which the thin film stack is transferred from the glass onto a thin (2.0 mil) polymer substrate to create large arrays that are truly flexible and significantly lighter than either the glassed alpha-Si version or present conventional crystalline technologies. In this paper the key processes for such effective transfer are described. In addition, both glassed (rigid) and unglassed (flexible) alpha-Si cells are studied when integrated with various advanced structures to form lightweight systems. EOL predictions are generated for the case of a 1000 W array in a standard, 10 year geosynchronous (GEO) orbit. Specific powers (W/kg), power densities (W/sq m) and total array costs ($/sq ft) are compared. Author

N95-20516*# National Aeronautics and Space Administration. Lewis Research Center, Cleveland, OH.

MODELING OF HIGH EFFICIENCY SOLAR CELLS UNDER LASER PULSE FOR POWER BEAMING APPLICATIONS **c44**

Raj K. Jain and Geoffrey A. Landis (NYMA, Inc., Brook Park, OH.) *In its* Proceedings of the 13th Space Photovoltaic Research and Technology Conference (SPRAT 13) Sep. 1994 p 135-140 (For primary document see N95-20502 06-33)
Avail: CASI HC A02/MF A04

Solar cells have been used to convert sunlight to electrical energy for many years and also offer great potential for non-solar energy conversion applications. Their greatly improved performance under monochromatic light compared to sunlight, makes them suitable as photovoltaic (PV) receivers in laser power beaming applications. Laser beamed power to a PV array receiver could provide power to satellites, an orbital transfer vehicle, or a lunar base. Gallium arsenide (GaAs) and indium phosphide (InP) solar cells have calculated efficiencies of more than 50 percent under continuous illumination at the optimum wavelength. Currently high power free-electron lasers are being developed which operate in pulsed conditions. Understanding cell behavior under a laser pulse is important in the selection of the solar cell material and the laser. An experiment by NAsA lewis and JPL at the AVLIS laser facility in Livermore, CA presented experimental data on cell performance under pulsed laser illumination. Reference 5 contains an overview of technical issues concerning the use of solar cells for laser power conversion, written before the experiments were performed. As the experimental results showed, the actual effects of pulsed operation are more complicated. Reference 6 discusses simulations of the output of GaAs concentrator solar cells under pulsed laser illumination. The present paper continues this work, and compares the output of Si and GaAs solar cells. Author

N95-20517*# Houston Univ., TX.

CALCULATION OF NEAR OPTIMUM DESIGN OF InP/In(0.53)Ga(0.47)As MONOLITHIC TANDEM SOLAR CELLS **c44**

P. Renaud, M. F. Vilela, A. Freundlich, N. Medelci, and A. Bensaoula *In* NASA. Lewis Research Center, Proceedings of the 13th Space Photovoltaic

Research and Technology Conference (SPRAT 13) Sep. 1994 p 141-146 (For primary document see N95-20502 06-33)
Avail: CASI HC A02/MF A04

An analysis of InP/GaAs tandem solar cell structure has been undertaken to allow for maximum AMO conversion efficiencies (space applications) while still taking into account both the theoretical and technological limitations. The dependence of intrinsic and extrinsic parameters such as diffusion lengths and generation-recombination (GR) lifetimes on N/P and P/N devices performances are clearly demonstrated. We also report for the first time the improvement attainable through the use of a new patterned tunnel junction as the inter cell ohmic interconnect. Such a design minimizes the light absorption in the interconnect region and leads to a noticeable increase in the cell efficiency. Our computations predict 27 percent AMO efficiency for N/P tandems with ideality factor gamma = 2 (GR lifetimes approximately equal 1 micron), and 36 percent for gamma = 1 (GR lifetimes approximately equals 100 microns). The method of optimization and the values of the physical and optical parameters are discussed.
Author

N95-20518*# National Aeronautics and Space Administration. Lewis Research Center, Cleveland, OH.

PERFORMANCE, DEFECT BEHAVIOR AND CARRIER ENHANCEMENT IN LOW ENERGY, PROTON IRRADIATED p+nn+ InP SOLAR CELLS **c44**

I. Weinberg, G. C. Rybicki, C. Vargas-Aburto (Kent State Univ., OH.), R. K. Jain (Toledo Univ., OH.), and D. Scheiman (NYMA, Inc., Brook Park, OH.) *In its* Proceedings of the 13th Space Photovoltaic Research and Technology Conference (SPRAT 13) Sep. 1994 p 149-158 (For primary document see N95-20502 06-33)
Avail: CASI HC A02/MF A04

The highest AMO efficiency (19.1 percent) InP solar cell consisted of an n+pp+ structure epitaxially grown on a p+ InP substrate. However, the high cost and relative fragility of InP served as motivation for research efforts directed at heteroepitaxial growth of InP on more viable substrates. The highest AMO efficiency (13.7 percent) for this type of cell was achieved using a GaAs substrate. Considering only cost and fracture toughness, Si would be the preferred substrate. The fact that Si is a donor in InP introduces complexities which are necessary in order to avoid the formation of an efficiency limiting counterdiode. One method used to overcome this problem lies in employing an n+p+ tunnel junction in contact with the cell's p region. A simpler method consists of using an n+ substrate and processing the cell in the p+ nn+ configuration. This eliminates the need for a tunnel junction. Unfortunately, the p/n configuration has received relatively little attention the best cell with this geometry having achieved an efficiency of 17 percent. Irradiation of these homoepitaxial cells, with 1 Mev electrons, showed that they were slightly more radiation resistant than diffused junction n/p cells. Additional p/n InP cells have been processed by some activity aimed at diffusion. Currently, there has been some activity aimed at producing heteroepitaxial p+nn+ InP cells using n+ Ge substrates. Since, like Si, Ge is an n-dopant in InP, use of this configuration obviates the need for a tunnel junction. Obviously, before attempting to process heteroepitaxial cells, one must produce a reasonably good homoepitaxial cell. In the present case we focus our attention on homoepitaxially on an n+ Ge substrate.
Author

N95-20519*# Naval Research Lab., Washington, DC.

ELECTRON-IRRADIATED TWO-TERMINAL, MONOLITHIC InP/Ga0.47In0.53As TANDEM SOLAR CELLS AND ANNEALING OF RADIATION DAMAGE **c44**

H. L. Cotal, Robert J. Walters, Geoffrey P. Summers, and Scott R. Messenger (SFA, Inc., Landover, MD.) *In* NASA. Lewis Research Center, Proceedings of the 13th Space Photovoltaic Research and Technology Conference (SPRAT 13) Sep. 1994 p 159-166 (For primary document see N95-20502 06-33)
Avail: CASI HC A02/MF A04

Radiation damage results from two-terminal monolithic InP/Ga(0.47)In(0.53)As tandem solar cells subject to 1 MeV electron irradiation are presented. Efficiencies greater than 22 percent have been measured by the National Renewable Energy Laboratory from 2x2 sq cm cells at 1 sun, AMO (25 C). The short circuit current density, open circuit voltage and fill factor are found to tolerate the same amount of radiation at low fluences. At high fluence levels, slight differences are observed. Decreasing the base amount of radiation at the Ga(0.47)In(0.53)As bottomcell improved the radiation resistance of J(sub sc) dramatically. This is turn, extended the series current flow through the subcell substantially up to a fluence of 3x10(exp 15) cm(exp -2) compared to 3x10(exp 14) cm(exp -2), as observed previously. The degradation of the maximum power output form tandem device is comparable to that from shallow homojunction (SHJ) InP solar cells, and the mechanism responsible for such degradation is explained in terms of the radiation response of the component cells. Annealing studies revealed that the recovery of the tandem cell response is dictated by the annealing characteristics exhibited by SHJ InP solar cells.
Author

N95-20520*# SFA, Inc., Landover, MD.

RADIATION EFFECTS ON p+n InP JUNCTIONS GROWN BY MOCVD **c44**

Scott R. Messenger, Robert J. Walters (Naval Research Lab., Washington, DC.), M. J. Panunto (Maryland Univ., Baltimore, MD.), and Geoffrey P. Summers (Naval Research Lab., Washington, DC.) *In* NASA. Lewis Research Center, Proceedings of the 13th Space Photovoltaic Research and Technology Conference (SPRAT 13) Sep. 1994 p 167-180 (For primary document see N95-20502 06-33)
Avail: CASI HC A03/MF A04

The superior radiation resistance of InP over other solar cell materials such as Si or GaAs has prompted the development of InP cells for space applications. The early research on radiation effects in InP was performed by Yamaguchi and co-workers who showed that, in diffused p-InP junctions, radiation-induced defects were readily annealed both thermally and by injection, which was accompanied by significant cell recovery. More recent research efforts have been made using p-InP grown by metalorganic chemical vapor deposition (MOCVD). While similar deep level transient spectroscopy (DLTS) results were found for radiation induced defects in these cells and in diffused junctions, significant differences existed in the annealing characteristics. After injection annealing at room temperature, Yamaguchi noticed an almost complete recovery of the photovoltaic parameters, while the MOCVD samples showed only minimal annealing. In searching for an explanation of the different annealing behavior of diffused junctions and those grown by MOCVD, several possibilities have been considered. One possibility is the difference in the emitter structure. The diffused junctions have S-doped graded emitters with widths of approximately 0.3 micrometers, while the MOCVD emitters are often doped with Si and have widths of approximately 300A (0.03 micrometers). The difference in the emitter thickness can have important effects, e.g. a larger fraction of the total photocurrent is generated in the n-type material for thicker emitters. Therefore the properties of the n-InP material may explain the difference in the observed overall annealing behavior of the cells.
Author

N95-20521*# National Renewable Energy Lab., Golden, CO.

DESIGN OF HIGH-EFFICIENCY, RADIATION-HARD, GaInP/GaAs SOLAR CELLS **c44**

Sarah R. Kurtz, K. A. Bertness, A. E. Kibbler, C. Kramer, and J. M. Olson *In* NASA. Lewis Research Center, Proceedings of the 13th Space Photovoltaic Research and Technology Conference (SPRAT 13) Sep. 1994 p 181-186 (For primary document see N95-20502 06-33)
(Contract DE-AC02-83CH-10093)
Avail: CASI HC A02/MF A04

In recently years, Ga(0.5)In((0.5)P/GaAs cells have drawn increased attention both because of their high efficiencies and because they are well suited for space applications. They can be grown and processed as two-junction devices with roughly twice the voltage and half the current of GaAs cells. They have low temperature coefficients, and have good potential for radiation hardness. We have previously reported the effects of electron irradiation on test cells which were not optimally designed for space. From those results we estimated that an optimally designed cell could achieve 20 percent after irradiation with 10(exp 15) cm(exp -2) 1 MeV electrons. Modeling studies predicted that slightly higher efficiencies may be achievable. Record efficiencies for EOL performance of other types of cells are significantly lower. Even the best Si and InP cells have BOL efficiencies lower than the EOL efficiency we report here. Good GaAs cells have an EOL efficiency of 16 percent. The InP/Ga(0.5)In(0.5)As two-junction, two-terminal device has a BOL efficiency as high as 22.2 percent, but radiation results for these cells were limited. In this study we use the previous modeling and irradiation results to design a set of

Ga(0.5)In(0.5)P/GaAs cells that will demonstrate the importance of the design parameters and result in high-efficiency devices. We report record AMO efficiencies: a BOL efficiency of 25.7 percent for a device optimized for BOL performance and two of different designs with EOL efficiencies of 19.6 percent (at 10(exp 15) cm(exp -2) 1MeV electrons). We vary the bottom-cell base doping and the top-cell thickness to show the effects of these two important design parameters. We get an unexpected result indicating that the dopant added to the bottom-cell base also increases the degradation of the top cell. Author

N95-20522*# Wayne State Univ., Detroit, MI.
INVESTIGATION OF THE STABILITY AND 1.0 MeV PROTON RADIATION RESISTANCE OF COMMERCIALLY PRODUCED HYDROGENATED AMORPHOUS SILICON ALLOY SOLAR CELLS c44
Kenneth R. Lord, II, Michael R. Walters, and James R. Woodyard *In* NASA. Lewis Research Center, Proceedings of the 13th Space Photovoltaic Research and Technology Conference (SPRAT 13) Sep. 1994 p 187-196 Sponsored in cooperation with NASA, TRW and Wayne State Univ. Inst. for Mfg. Research (For primary document see N95-20502 06-33)
Avail: CASI HC A02/MF A04

The radiation resistance of commercial solar cells fabricated from hydrogenated amorphous silicon alloys is reported. A number of different device structures were irradiated with 1.0 MeV protons. The cells were annealing at 200 C. The annealing time was dependent on proton fluence. Annealing devices for one hour restores cell parameters or fluences below 1(exp 14) cm(exp -2); fluences above 1(exp 14) cm(exp -2) require longer annealing times. A parametric fitting model was used to characterize current mechanisms observed in dark I-V measurements. The current mechanisms were explored with irradiation fluence, and voltage and light soaking times. The thermal generation current density and quality factor increased with proton fluence. Device simulation shows the degradation in cell characteristics may be explained by the reduction of the electric field in the intrinsic layer. Author

N95-20523*# Naval Research Lab., Washington, DC.
THE USE OF DISPLACEMENT DAMAGE DOSE TO CORRELATE DEGRADATION IN SOLAR CELLS EXPOSED TO DIFFERENT RADIATIONS c44
Geoffrey P. Summers, Edward A. Burke (SFA, Inc., Landover, MD.), Philip Shapiro (SFA, Inc., Landover, MD.), Richard Statler (SFA, Inc., Landover, MD.), Scott R. Messenger (SFA, Inc., Landover, MD.), and Robert J. Walters *In* NASA. Lewis Research Center, Proceedings of the 13th Space Photovoltaic Research and Technology Conference (SPRAT 13) Sep. 1994 p 197-201 (For primary document see N95-20502 06-33)
Avail: CASI HC A01/MF A04

It has been found useful in the past to use the concept of 'equivalent fluence' to compare the radiation response of different solar cell technologies. Results are usually given in terms of an equivalent 1 MeV electron or an equivalent 10 MeV proton fluence. To specify cell response in a complex space-radiation environment in terms of an equivalent fluence, it is necessary to measure damage coefficients for a number of representative electron and proton energies. However, at the last Photovoltaic Specialist Conference we showed that nonionizing energy loss (NIEL) could be used to correlate damage coefficients for protons, using measurements for GaAs as an example. This correlation means that damage coefficients for all proton energies except near threshold can be predicted from a measurement made at one particular energy. NIEL is the exact equivalent for displacement damage of linear energy transfer (LET) for ionization energy loss. The use of NIEL in this way leads naturally to the concept of 10 MeV equivalent proton fluence. The situation for electron damage is more complex, however. It is shown that the concept of 'displacement damage dose' gives a more general way of unifying damage coefficients. It follows that 1 MeV electron equivalent fluence is a special case of a more general quantity for unifying electron damage coefficients which we call the 'effective 1 MeV electron equivalent dose'. Author

N95-20524*# Naval Research Lab., Washington, DC.
ANNEALING OF IRRADIATED n+p InP BURIED HOMOJUNCTIONS c44
Robert J. Walters, Geoffrey P. Summers, M. L. Timmons (Research Triangle Inst., Research Triangle Park, NC.), R. Venkatasubramanian (Research Triangle Inst., Research Triangle Park, NC.), J. A. Hancock (Research Triangle Inst., Research Triangle Park, NC.), and J. S. Hills (Research Triangle Inst., Research Triangle Park, NC.) *In* NASA. Lewis Research Center, Proceedings of the 13th Space Photovoltaic Research and Technology Conference (SPRAT 13) Sep. 1994 p 203-212 (For primary document see N95-20502 06-33)
Avail: CASI HC A02/MF A04

At the last SPRAT conference, the Naval Research Laboratory (NRL) presented results from two experiments. One studied n+p diffused junction (DJ) InP solar cells, and the other studied n+p shallow homojunction (SHJ) InP mesa diodes grown by metalorganic chemical vapor deposition (MOCVD). The former work showed that a DJ solar cell in which the maximum power P(sub max) had been degraded by nearly 80 percent under irradiation recovered completely under short circuit illumination at 450K. The recovery was accompanied by the removal of all but one of the radiation-induced defect levels. The latter work, on the other hand, showed that the radiation-induced defects in the SHJ diodes did not anneal until the temperature reached 650K. These results suggest that an irradiated DJ solar cell, under illumination, will anneal at a temperature 200K lower than an irradiated SHJ cell. This is an unexpected result considering the similarity of the devices. The goal of the present research is to explain this different behavior. This paper investigates two points which arose from the previous studies. The first point is that the DJ cells were annealed under illumination while the SHJ diodes were annealed without bias. The second point investigated here is that the emitters of the DJ and SHJ devices were significantly different. Author

N95-20525*# Optical Coating Lab., Inc., Santa Rosa, CA.
QUALIFICATION TEST RESULTS FOR BLUE-RED REFLECTING SOLAR COVERS c44
W. T. Beauchamp *In* NASA. Lewis Research Center, Proceedings of the 13th Space Photovoltaic Research and Technology Conference (SPRAT 13) Sep. 1994 p 213-222 Presented at the Proceedings of the 23d IEEE Photospecialist Conference, Louisville, KY, May 1994 (For primary document see N95-20502 06-33)
Avail: CASI HC A02/MF A04

Recent market forces and design innovations have spurred the development of solar cell covers that significantly reduce the solar absorptance for a cell array. GaAs cells, using Ge as the substrate host material, can have a significantly higher output if the solar absorptance of the cell array is reduced. New optical coating design techniques have allowed the construction of covers that reflect the ultraviolet energy (below 350 nm) and the near infrared energy (above 900 nm) resulting in the beneficial reduction in absorptance. Recent modeling suggests three or more present output increase due to the lowered temperature with such a device. Within the last several months we have completed the testing of production samples of these new covers in a qualification series that included the usual environmental effects associated with the routine testing of solar cell covers and the combined effects of protons, electrons and solar UV as would be encountered in space. For the combined effects testing the samples were exposed to 300 sun days equivalent UV, 5 x 10(exp 14)/sq cm of 0.5 MeV protons and 10(exp 15)/sq cm of 1.0 MeV electrons. Measurements of the reflectance, transmission, emittance and other appropriate parameters were made before and after the testing. As measured by the averaged transmission over the cell operating band, the change in transmission for the samples was less than or about equal to 1 percent. The details of the testing and the results in terms of transmission, reflectance and emittance are discussed in the paper. Author

N95-20526*# Communications Satellite Corp., Clarksburg, MD.
UV TESTING OF INTELSAT-7, 7A, AND 8 SOLAR CELLS c44
A. Meulenberg *In* NASA. Lewis Research Center, Proceedings of the 13th Space Photovoltaic Research and Technology Conference (SPRAT 13) Sep. 1994 p 223-225 (For primary document see N95-20502 06-33)
Avail: CASI HC A01/MF A04

A 4000 hour experiment, conducted in late 1992 through mid 1993, confirmed earlier results on the ultraviolet damage effects in covered solar cells of various types being used, or proposed for use, in INTELSAT programs. Two different UV test systems were used to identify systematic errors and to study the effects of UV source-bulb age on degradation rate. After correction for contamination and UV source-bulb aging, the extrapolated degradation rates for irradiated and unirradiated INTELSAT-5, -6 single AR(SAR) coated cells and INTELSAT-7, -7A, -8 double layer AR(DAR) coated cells in both the 1993 tests confirm the following hypotheses resulting from the 1992 experiment. (a) Irradiated cells display significantly more UV degradation than do the unirradiated cells for tests exceeding 2000 hours. The new data indicates that degradation effects from electron irradiation are proportional to t(exp 2) (the square of the UV hours), at least for times less than or equal to 3000 hours. (b) This difference does not depend upon entire reflective coating, cell resistivity, or manufacturer within the sensitivity and reproducibility of the experiment. (c) There is a clear difference in degradation rate between single AR coated cells (TiO(x)) and double layer AR coated cells (SiO(x) and Al2O3?). At 100,000 hours (11.4 years) the DAR coated cells display more degradation than do the SAR coated cells, even though at 1,000 hours the DAR cells display less degradation. (d) UV degradation rates, to modern covered silicon solar cells, at the beginning of bulb life drop from approximately 2 times the average rate to near zero after 2000 hours (average end-of-life for the xenon short-arc lamps used in the tests). The effects of 1 MeV electron irradiation (10(exp 15) e(-)/sq cm) prior to UV exposure are clearly indicated in the plot of percent change in cell open circuit voltage (Voc) versus percent change in short circuit current (Isc) during the UV test and post-test cleanup of the cells. Clearly, extended UV testing produces a permanent photo-induced redegradation of previously irradiated cells. However, this photo-induced redegradation may be caused by the long-wavelength light, not the UV light. Author

N95-20527*# Maxwell Labs., Inc., San Diego, CA. S-Cubed Div.
PARASITIC CURRENT COLLECTION BY SOLAR ARRAYS IN LEO c44
Victoria A. Davis and Barbara M. Gardner *In* NASA. Lewis Research Center, Proceedings of the 13th Space Photovoltaic Research and Technology Conference (SPRAT 13) Sep. 1994 p 227-235 Sponsored by AF Materiel Command (For primary document see N95-20502 06-33)
Avail: CASI HC A02/MF A04

Solar cells at potentials positive with respect to a surrounding plasma collect electrons. Current is collected by the exposed high voltage surfaces: the interconnects and the sides of the solar cells. This current is a drain on the array power that can be significant for high-voltage arrays. In addition, this current influences the current balance that determines the floating potential of the spacecraft. One of the objectives of the Air Force (PL/GPS) PASP Plus experiment is an improved understanding of parasitic current collection. As part of the PASP Plus program, we are using computer modeling to improve our understanding of the physical processes that control parasitic current collection. Author

N95-20528*# National Aeronautics and Space Administration. Lewis Research Center, Cleveland, OH.
FINAL RESULTS OF THE ADVANCED PHOTOVOLTAIC EXPERIMENT c44
David J. Brinker and John R. Hickey (Eppley Lab., Inc., Newport, RI.) *In its* Proceedings of the 13th Space Photovoltaic Research and Technology Conference (SPRAT 13) Sep. 1994 p 239-246 (For primary document see N95-20502 06-33)
Avail: CASI HC A02/MF A04

The Advanced Photovoltaic Experiment (APEX) was designed to generate laboratory reference standards as well as to explore the durability of a wide variety of space solar cells. In addition to the cells, it was equipped with an absolute cavity radiometer to measure solar intensity, a spectroradiometer to measure the spectral content of this radiation, and a sun angle sensor. Data from the solar cells and various sensors was obtained on a daily basis during the first eleven months of the 69 month flight. We compare pre-flight and post-flight laboratory measurements with on-orbit calibration data. Pre-flight and post-flight calibration data for the cavity radiometers as well as on-orbit data demonstrated the accuracy and durability of the Eppley Labs instrument flown on APEX. Author

N95-20529*# National Aeronautics and Space Administration. Lewis Research Center, Cleveland, OH.
PRELIMINARY RESULTS FROM THE FLIGHT OF THE SOLAR ARRAY MODULE PLASMA INTERACTIONS EXPERIMENT (SAMPIE) c44
Dale C. Ferguson and G. Barry Hillard *In its* Proceedings of the 13th Space Photovoltaic Research and Technology Conference (SPRAT 13) Sep. 1994 p 247-256 (For primary document see N95-20502 06-33)
Avail: CASI HC A02/MF A04

SAMPIE, the Solar Array Module Plasma Interactions Experiment, flew in the Space Shuttle Columbia payload bay as part of the Office of Aeronautics and Space Technology-2 (OAST-2) mission on STS-62, March, 1994. SAMPIE biased samples of solar arrays and space power materials to varying potentials with respect to the surrounding space plasma, and recorded the plasma currents collected and the arcs which occurred, along with a set of plasma diagnostics data. A large set of high quality data was obtained on the behavior of solar arrays and space power materials in the space environment. This paper is the first report on the data SAMPIE telemetered to the ground during the mission. It will be seen that the flight data promise to help determine arcing thresholds, snapover potentials, and floating potentials for arrays and spacecraft in LEO. Author (revised)

N95-20530*# Air Force Systems Command, Wright-Patterson AFB, OH.
PHOTOVOLTAIC ELECTRIC POWER APPLIED TO UNMANNED AERIAL VEHICLES (UAV)
Jack Geis and Jack H. Arnold (Rockwell International Corp., Canoga Park, CA.) *In* NASA. Lewis Research Center, Proceedings of the 13th Space Photovoltaic Research and Technology Conference (SPRAT 13) Sep. 1994 p 257-268 (For primary document see N95-20502 06-33)
Avail: CASI HC A03/MF A04

Photovoltaic electric-powered flight is receiving a great deal of attention in the context of the United States' Unmanned Aerial Vehicle (UAV) program. This paper addresses some of the enabling technical areas and their potential solutions. Of particular interest are the long-duration, high-altitude class of UAV's whose mission it is to achieve altitudes between 60,000 and 100,000 feet, and to remain at those altitudes for prolonged periods performing various mapping and surveillance activities. Addressed herein are studies which reveal the need for extremely light-weight and efficient solar cells, high-efficiency electric motor-driven propeller modules, and power management and distribution control elements. Since the potential payloads vary dramatically in their power consumption and duty cycles, a typical load profile has been selected to provide commonality for the propulsion power comparisons. Since missions vary widely with respect to ground coverage requirements, from repeated orbiting over a localized target to long-distance routes over irregular terrain, we have also averaged the power requirements for on-board guidance and control power, as well as ground control and communication link utilization. In the context of the national technology reinvestment program, wherever possible we modeled components and materials which have been qualified for space and defense applications, yet are compatible with civilian UAV activities. These include, but are not limited to, solar cell developments, electric storage technology for diurnal operation, local and ground communications, power management and distribution, and control servo design. And finally, the results of tests conducted by Wright Laboratory on ultralight, highly efficient MOCVD GaAs solar cells purchased from EPI Materials Ltd. (EML) of the UK are presented. These cells were also used for modeling the flight characteristics of UAV aircraft. Author (revised)

N95-20531*# European Space Agency. European Space Research and Technology Center, ESTEC, Noordwijk (Netherlands).
POST-FLIGHT INVESTIGATION PROGRAMMES OF RECENTLY RETRIEVED SOLAR GENERATORS c44
Lothar Grelach *In* NASA. Lewis Research Center, Proceedings of the 13th Space Photovoltaic Research and Technology Conference (SPRAT 13) Sep. 1994 p 269-283 (For primary document see N95-20502 06-33)
Avail: CASI HC A03/MF A04

In 1993 two ESA solar power generators were successfully retrieved from space: EURECA with its 10 panel rigid array in August, after 11 months in a 500 km orbit, and one of the two flexible Hubble Space Telescope (HST) arrays in December, after almost 4 years in a 600 km orbit. Both solar generators are undergoing separate post-flight investigation programs (PFIP). These programs cover investigations of all solar array (SA) components and mechanisms. Since both programs have much in common, most of the component and material investigations are the same. Extremely valuable information on numerous essential subjects, such as atomic oxygen, radiation, meteoroid and space debris environment resulting damage, low cycle fatigue, material degradation, etc. are expected to be obtained for both types of arrays. We will also be able to explain and understand the anomalies experienced on both solar arrays in orbit. The paper will outline both post-flight investigation programs and will concentrate on reporting the first results and findings. Author (revised)

N95-20532*# Martin Marietta Corp., Denver, CO.

HIGH-PERFORMANCE, FLEXIBLE, DEPLOYABLE ARRAY DEVELOPMENT FOR SPACE APPLICATIONS

Russell N. Gehling, Joseph H. Armstrong, and Mohan S. Misra *In* NASA. Lewis Research Center, Proceedings of the 13th Space Photovoltaic Research and Technology Conference (SPRAT 13) Sep. 1994 p 287-297 (For primary document see N95-20502 06-33)

Avail: CASI HC A03/MF A04

Flexible, deployable arrays are an attractive alternative to conventional solar arrays for near-term and future space power applications, particularly due to their potential for high specific power and low storage volume. Combined with low-cost flexible thin-film photovoltaics, these arrays have the potential to become an enabling or an enhancing technology for many missions. In order to expedite the acceptance of thin-film photovoltaics for space applications, however, parallel development of flexible photovoltaics and the corresponding deployable structure is essential. Many innovative technologies must be incorporated in these arrays to ensure a significant performance increase over conventional technologies. For example, innovative mechanisms which employ shape memory alloys for storage latches, deployment mechanisms, and array positioning gimbals can be incorporated into flexible array design with significant improvement in the areas of cost, weight, and reliability. This paper discusses recent activities at Martin Marietta regarding the development of flexible, deployable solar array technology. Particular emphasis is placed on the novel use of shape memory alloys for lightweight deployment elements to improve the overall specific power of the array. Array performance projections with flexible thin-film copper-indium-diselenide (CIS) are presented, and government-sponsored solar array programs recently initiated at Martin Marietta through NASA and Air Force Phillips Laboratory are discussed. Author

N95-20533*# National Aeronautics and Space Administration. Lewis Research Center, Cleveland, OH.

STATIC STABILITY OF A THREE-DIMENSIONAL SPACE TRUSS c18

John F. Shaker *In its* Proceedings of the 13th Space Photovoltaic Research and Technology Conference (SPRAT 13) Sep. 1994 p 299-312 (For primary document see N95-20502 06-33)

Avail: CASI HC A03/MF A04

Space station requirements for power have resulted in a need for photovoltaic solar arrays possessing large blanket surface area. However, due to the limited shuttle payload volume solar array designers have been driven to a deployable concept that by nature is extremely flexible. The principal support for this array system is the Folding Articulating Square Truss Mast (FASTMast). In order to accomodate service loads the FASTMast is expected to exhibit nonlinear behavior which could possibly result in structural instability. Presented herein are the results of the Lewis Research Center test and analysis efforts performed in an effort to characterize the FASTMast structural behavior in terms of stability. Results include those obtained from recent nonlinear testing and analysis involving a 1/10 segment of the FASTMast flight article. Implications of these results as they relate to expected behavior of the flight unit will also be discussed. Author

N95-20534*# National Aeronautics and Space Administration. Lewis Research Center, Cleveland, OH.

AN UPDATE ON THE DEVELOPMENT OF A LINE-FOCUS REFRACTIVE CONCENTRATOR ARRAY c44

Michael F. Piszczor, Mark J. ONeill (ENTECH Corp., Dallas-Fort Worth Airport, TX.), and Lewis M. Fraas (JX Crystals, Issaquah, WA.) *In its* Proceedings of the 13th Space Photovoltaic Research and Technology Conference (SPRAT 13) Sep. 1994 p 313-322 (For primary document see N95-20502 06-33)

Avail: CASI HC A02/MF A04

Concentrator arrays offer a number of generic benefits for space (i.e. high array efficiency, protection from space radiation effects, minimized plasma interactions, etc.). The line-focus refractive concept, however, also offers two very important advantages: (1) relaxation of precise array tracking requirements to only a single axis and (2) low-cost mass production of the lens material. The linear refractive concentrator can be designed to provide an essentially flat response over a wide range of longitudinal errors for satellites having only single-axis tracking capability. New panel designs emphasize light weight, high stiffness, storability, and ease of manufacturing and assembly. This paper addresses the current status of the concentrator program with special emphasis on the design implications, and flexibility, of using a linear refractive concentrator lens as well as details recent fabrication of prototype hardware. Author

N95-20535*# Astro Aerospace Corp., Carpinteria, CA.

AN INTRODUCTION TO THE ASTRO EDGE SOLAR ARRAY c44

B. R. Spence and G. W. Marks *In* NASA. Lewis Research Center, Proceedings of the 13th Space Photovoltaic Research and Technology Conference (SPRAT 13) Sep. 1994 p 323-331 (For primary document see N95-20502 06-33)

Avail: CASI HC A02/MF A04

The Astro Edge solar array is a new and innovative low concentrator power generating system which has been developed for applications requiring high specific power, high stiffness, low risk, light modular construction which utilizes conventional materials and technology, and standard photovoltaic solar cells and laydown processes. Mechanisms, restraint/release devices, wiring harnesses, substrates, and support structures are designed to be simple, functional, lightweight, and modular. A brief overview of the Astro Edge solar array is discussed. Author

N95-20536*# National Aeronautics and Space Administration. Lewis Research Center, Cleveland, OH.

RARE EARTH GARNET SELECTIVE EMITTER c76

Roland A. Lowe (Kent State Univ., OH.), Donald L. Chubb, Serene C. Farmer, and Brian S. Good *In its* Proceedings of the 13th Space Photovoltaic Research and Technology Conference (SPRAT 13) Sep. 1994 p 335-339 (For primary document see N95-20502 06-33)

Avail: CASI HC A01/MF A04

Thin film Ho-YAG and Er-YAG emitters with a platinum substrate exhibit high spectral emittance in the emission band (epsilon(sub lambda) approximately equal to 0.74, ((4)I(sub 15/2)) - ((4)I(sub13/2)), for Er-YAG and epsilon(sub lambda) approximately equal to 0.65, ((5)I(sub 7))-((5)I(sub 8)) for Ho-YAG) at excellent candidates for high efficiency selective emitters in the thermophotovoltaics (TPV) systems operating at moderate temperatures (1200-1500K). Spectral emittance measurements of the thin films were made (1.2 less than lambda less than 3.0 microns) and compared to the theoretical emittances calculated using measured values of the spectral extinction coefficient. In this paper we present the results for a new class of rare earth ion selective emitters. These emitters are thin sections (less than 1 mm) of yttrium aluminum garnet (YAG) single crystal with a rare earth substitutional impurity. This paper presents normal spectral emittance, epsilon(sub lambda), measurements of holmium (Ho), and erbium (Er) doped YAG thin film selective emitters at 1500 K, and compares those results with the theoretical spectral emittance. Author

N95-20537*# National Aeronautics and Space Administration. Lewis Research Center, Cleveland, OH.

InGaAs PV DEVICE DEVELOPMENT FOR TPV POWER SYSTEMS c76

David M. Wilt (Essential Research, Inc., Cleveland, OH.), Navid S. Fatemi (Essential Research, Inc., Cleveland, OH.), Richard W. Hoffman, Jr. (Essential Research, Inc., Cleveland, OH.), Phillip P. Jenkins (NYMA, Inc., Brook Park, OH.), David J. Brinker (NYMA, Inc., Brook Park, OH.), David Scheiman (NYMA, Inc., Brook Park, OH.), Roland A. Lowe (Kent State Univ., OH.), and Donald Chubb *In its* Proceedings of the 13th Space Photovoltaic Research and Technology Conference (SPRAT 13) Sep. 1994 p 341-351 See also N95-11587 (For primary document see N95-20502 06-33)

Avail: CASI HC A03/MF A04

Indium gallium arsenide (InGaAs) photovoltaic devices have been fabricated with bandgaps ranging from 0.75 eV to 0.60 on Indium phosphide (InP) substrates. Reported efficiencies have been as high as 11.2 percent (AMO) for the lattice matched 0.75 eV devices. The 0.75 eV cell demonstrated 14.8 percent efficiency under a 1500 K blackbody with a projected efficiency of 29.3 percent. The lattice mismatched devices (0.66 and 0.60 eV) demonstrated measured efficiencies of 8 percent and 6 percent respectively under similar conditions. Low long wavelength response and high rack currents are responsible for the poor performance of the mismatched devices. Temperature coefficients have been measured and are presented for all of the bandgaps tested. Author

N95-20538*# National Aeronautics and Space Administration. Lewis Research Center, Cleveland, OH.

PULSED LASER ILLUMINATION OF PHOTOVOLTAIC CELLS c44

Jane A. Yater, Roland A. Lowe (Kent State Univ., OH.), Phillip P. Jenkins (NYMA, Inc., Brook Park, OH.), and Geoffrey A. Landis (NYMA, Inc., Brook Park, OH.) *In its* Proceedings of the 13th Space Photovoltaic Research and Technology Conference (SPRAT 13) Sep. 1994 p 353-362 See also N95-18572 (For primary document see N95-20502 06-33)

Avail: CASI HC A02/MF A04

In future space missions, free electron lasers (FEL) may be used to illuminate photovoltaic array receivers to provide remote power. Both the radio-frequency (RF) and induction FEL provide FEL produce pulsed rather than continuous output. In this work we investigate cell response to pulsed laser light which simulates the RF FEL format. The results indicate that if the pulse repetition is high, cell efficiencies are only slightly reduced compared to constant illumination at the same wavelength. The frequency response of the cells is weak, with both voltage and current outputs essentially dc in nature. Comparison with previous experiments indicates that the RF FEL pulse format yields more efficient photovoltaic conversion than does an induction FEL pulse format. Author

N95-20539*# National Aeronautics and Space Administration. Langley Research Center, Hampton, VA.

P/N In(Al) GaAs MULTIJUNCTION LASER POWER CONVERTERS c36

Steven Wojtczuk (Spire Corp., Bedford, MA.), Themis Parados (Spire Corp., Bedford, MA.), and Gilbert Walker *In* NASA. Lewis Research Center, Proceedings of the 13th Space Photovoltaic Research and Technology Conference (SPRAT 13) Sep. 1994 p 363-371 (For primary document see N95-20502 06-33)

Avail: CASI HC A02/MF A04

Eight In(Al)GaAs PN junctions grown epitaxially on the semi-insulating wafer were monolithically integrated in series to boost the approximately 0.4V photovoltage per typical In(Al)GaAs junction to over 3 volts for the 1 sq cm laser power converted (LPC) chip. Advantages of multijunction LCP designs include the need for less circuitry for power reconditioning and the potential for lower I(sup 2)R power loss. As an example, these LPC's have a responsivity of approximately 1 amp/watt. With a single junction LPC, 100 watts/sq cm incident power would lead to about 100 A/sq cm short-circuit current at approximately 0.4V open-cicuit voltage. One disadvantage is the large current would lead to a large I(sup 2)R loss which would lower the fill factor so that 40 watts/sq cm output would not be obtained. Another is that few circuits are designed to work at 0.4 volts, so DC-DC power conversion circuitry would be necessary to raise the voltage to a reasonable level. The multijunction LPC being developed in this program is a step toward solving these problems. In the above example, an eight-junction LPC would have eight times the voltage, approximately 3V, so that DC-DC power conversion may not be needed in many instances. In addition, the multijunction LPC would have 1/8 the current of a single-junction LPC, for only 1/64 the I(sup 2)R loss if the series resistance is the same. Working monolithic multijunction laser power converters (LPC's) were made in two different compositions of the In(x)Al(y)Ga(1-x-y)As semiconductor alloy, In(0.53)Ga(0.47)As (0.74 eV) and In(0.5)Al(0.1)Ga(0.4)As (0.87 eV). The final 0.8 sq cm LPC's had output voltages of about 3 volts and output currents up to about one-half amp. Maximum 1.3 micron power conversion efficiencies were approximately 22 percent. One key advantage of multijunction LPC's is that they have higher output voltages, so that less DC-DC power conversion circuitry is needed in applications. Author

N95-20540*# Astropower, Inc., Newark, DE.

HIGH EFFICIENCY GaP POWER CONVERSION FOR BETAVOLTAIC APPLICATIONS

Paul E. Sims, Louis C. DiNetta, and Allen M. Barnett *In* NASA. Lewis Research Center, Proceedings of the 13th Space Photovoltaic Research and Technology Conference (SPRAT 13) Sep. 1994 p 373-382 (For primary document see N95-20502 06-33)

(Grant NSF III-92-61713)

Avail: CASI HC A02/MF A04

AstroPower is developing a gallium phosphide (GaP) based energy converter optimized for radio luminescent light-based power supplies. A 'two-step' or 'indirect' process is used where a phosphor is excited by radioactive decay products to produce light that is then converted to electricity by a photovoltaic energy converter. This indirect conversion of beta-radiation to electrical energy can be realized by applying recent developments in tritium based radio luminescent (RL) light sources in combination with the high conversion efficiencies that can be achieved under low illumination with low leakage, gallium phosphide based devices. This tritium to light approach is inherently safer than battery designs that incorporate high activity radionuclides because the beta particles emitted by tritium are of low average energy and are easily stopped by a thin layer of glass. GaP layers were grown by liquid phase epitaxy and p/n junction devices were fabricated and characterized for low light intensity power conversion. AstroPower has demonstrated the feasibility of the GaP based energy converter with the following key results: 23.54 percent conversion efficiency under 968 muW/sq cm 440 nm blue light, 14.59 percent conversion efficiency for 2.85 muW/sq cm 440 nm blue light, and fabrication of working 5 V array. We have also determined that at least 20 muW/sq cm optical power is available for betavoltaic power systems. Successful developments of this device is an enabling technology for low volume, safe, high voltage, milliwatt power supplies with service lifetimes in excess of 12 years. Author

N95-20541*# NYMA, Inc., Brook Park, OH.

REVIEW OF SOLAR CELL TEMPERATURE COEFFICIENTS FOR SPACE c44

Geoffrey A. Landis *In* NASA. Lewis Research Center, Proceedings of the 13th Space Photovoltaic Research and Technology Conference (SPRAT 13) Sep. 1994 p 385-399 (For primary document see N95-20502 06-33)

Avail: CASI HC A03/MF A04

Energy conversion efficiency is an important parameter for solar cells, and well reported in the literature. However, solar cells heat up in sunlight, and the efficiency decreases. The temperature coefficient of the conversion efficiency is thus also extremely important, especially in mission modeling, but is much less well reported. It is of value to have a table which compiles into a single document values of temperature coefficients reported in the literature. In addition to modeling performance of solar cells in Earth orbit, where operating temperatures may range from about 20 C to as high as 85 C, it is of interest to model solar cells for several other recently proposed missions. These include use for the surface of Mars, for solar electric propulsion missions that may range from Venus to the Asteroid belt, and for laser-photovoltaic power that may involve laser intensities equivalent several suns. For all of these applications, variations in operating temperature away from the nominal test conditions result in significant changes in operating performance. In general the efficiency change with temperature is non-linear, however, in the range from negative 100 C through room temperature to a few hundred degrees C, efficiency is usually quite well modeled as a linear function of temperature (except for a few unusual cell types, such as amorphous silicon, and for extremely low bandgap cells, such as InGaAs). Author

N95-20542*# Ohio State Univ., Columbus, OH.

EFFECTS OF PLASMA HYDROGENATION ON TRAPPING PROPERTIES OF DISLOCATIONS IN HETEROEPITAXIAL InP/GaAs c76

S. A. Ringel and B. Chatterjee *In* NASA. Lewis Research Center, Proceedings of the 13th Space Photovoltaic Research and Technology Conference (SPRAT 13) Sep. 1994 p 401-408 (For primary document see N95-20502 06-33)

(Grant NAG3-1461)

Avail: CASI HC A02/MF A04

In previous work, we have demonstrated the effectiveness of a post-growth hydrogen plasma treatment for passivating the electrical activity of dislocations in metalorganic chemical vapor deposition (MOCVD) grown InP on GaAs substrates by a more than two order of magnitude reduction in deep level concentration and an improvement in reverse bias leakage current by a factor of approximately 20. These results make plasma hydrogenation an extremely promising technique for achieving high efficiency large area and light weight heteroepitaxial InP solar cells for space applications. In this work we investigate the carrier trapping process by dislocations in heteroepitaxial InP/GaAs and the role of hydrogen passivation on this process. It is shown that the charge trapping kinetics of dislocations after hydrogen passivation are significantly altered, approaching point defect-like behavior consistent with a transformation from a high concentration of dislocation-related defect bands within the InP bandgap to a low concentration of individual dislocation related deep levels, before and after passivation. It is further shown that the 'apparent' activation energies of dislocation related deep levels, before and after passivation, reduce by approximately 70 meV as DLTS fill pulse times are increased from 1 microsecond to 1 millisecond. A model is proposed which explains these effects based on a reduction of Coulombic interaction between individual core sites along the dislocation cores by hydrogen incorporation. Knowledge of the trapping properties in these specific structures is important to develop optimum, low loss heteroepitaxial InP cells. Author

N95-20543*# Yale Univ., New Haven, CT.
NUCLEATION, GROWTH, AND STRAIN RELAXATION OF LATTICE-MISMATCHED 3-5 SEMICONDUCTOR EPITAXIAL LAYERS
c76
R. E. Welser and L. J. Guido *In* NASA. Lewis Research Center, Proceedings of the 13th Space Photovoltaic Research and Technology Conference (SPRAT 13) Sep. 1994 p 409-418 (For primary document see N95-20502 06-33)
(Grants NGT-50832; NSF ECS-92-53760)
Avail: CASI HC A02/MF A04

We have investigated the early stages of evolution of highly strained 2-D InAs layers and 3-D InAs islands grown by metal-organic chemical vapor deposition (MOCVD) on (100) and (111)B GaAs substrates. The InAs epilayer/GaAs substrate combination has been chosen because the lattice-mismatch is severe (approximately 7.2 percent), yet these materials are otherwise very similar. By examining InAs-on-GaAs composites instead of the more common In(x)Ga(1-x)As alloy we remove an additional degree of freedom (x) and thereby simplify data interpretation. A matrix of experiments is described in which the MOCVD growth parameters - susceptor temperature, Thin flux, and AsH3 flux - have been varied over a wide range. Scanning electron microscopy, atomic force microscopy, transmission electron microscopy, and electron microprobe analysis have been employed to observe the thin film surface morphology. In the case of 3-D growth, we have extracted activation energies and power-dependent exponents that characterize the nucleation process. As a consequence, optimized growth conditions have been identified for depositing approximately 250 A thick (100) and (111)B oriented InAs layers with relatively smooth surfaces. Together with preliminary data on the strain relaxation of these layers, the above results on the evolution of thin InAs films indicate that the (111)B orientation is particularly promising for yielding lattice-mismatched films that are fully relaxed with only misfit dislocations at the epilayer/substrate interface. Author

N95-20574# M-C Power Corp., Burr Ridge, IL.
MOLTEN CARBONATE FUEL CELL PRODUCT DEVELOPMENT TEST
Dec. 1993 75 p
(Contract DE-FC21-92MC-28065)
(DE95-000005; DOE/MC-28065/3880) Avail: CASI HC A04/MF A01

Advanced fuel cell active components have been developed and scaled up from laboratory scale to commercial scale. Full width components of both the stabilized nickel cathodes and the low chrome anodes have been successfully cast on M-C Power's production tape caster. An improved design for a fuel cell separator plate has been developed. The improved design meets the goals of lower cost and manufacturing simplicity, and addresses performance issues of the current commercial area plate. The engineering that the Bechtel Corporation has completed for the MCFC power plant includes a site design, a preliminary site layout, a Process Flow Diagram, and specification for the procurement of some of the major equipment items. Raw materials for anode and cathode components were ordered and received during the first half of 1993. Tape casting of anodes was started in late summer and continued through August. In addition to the technical progress mentioned above, an environment assessment was prepared in compliance with the National Environmental Policy Act of 1969 (NEPA). As a result, the PDT has received a categorical exclusion from the Air Pollution Control District permit requirements. The PDT is configured to demonstrate the viability of natural gas-fueled MCFC for the production of electricity and thermal energy in an environmentally benign manner for use in commercial and industrial applications. DOE

N95-20587 Colorado State Univ., Fort Collins, CO. Dept. of Chemistry.
CHEMICALLY MODIFIED ELECTRODES Interim Report
Colby A. Foss, Jr. and C. R. Martin 26 May 1994 60 p Limited Reproducibility: More than 20% of this document may be affected by microfiche quality
(Contract N00014-82-K-0612)
(AD-A279821; TR-95) Avail: Issuing Activity (Defense Technical Information Center (DTIC))

We learn that the field of chemically-modified electrodes involves attaching specific molecules to the surfaces of conventional inert electrodes. We also discover the two major reasons for wanting to attach molecules to electrode surfaces. One objective is to obtain fundamental information about the mechanism of electron transfer at electrode surfaces. The second objective is to impart to the electrode surface some chemical specificity not available at the unmodified electrode. For example, the modified electrode might catalyze a specific chemical reaction. Alternatively, the modified electrode might be able to recognize a specific molecule present in a contacting solution phase. DTIC

N95-20610# University of Southern California, Los Angeles, CA. Dept. of Electrical Engineering and Electrophysics.
APPLIED PHYSICS RESEARCH FOR INNOVATION IN PULSED POWER Final Report, 1 Jun. 1990 - 30 Jun. 1994
Martin A. Gundersen 30 Sep. 1994 14 p
(Contract N00014-90-J-4074)
(AD-A285392) Avail: CASI HC A03/MF A01

The program addressed fundamental issues in pulsed power technology, emphasizing new GaAs based solid state switches, and new high power thyratron type switches. Results included demonstration of a fast GaAs-based vertical FET-type switch for power modulator, radar and microwave applications, and development of super-emissive cathode switches. Transition of this research to technology is discussed first, then summaries of some of the recent activity are presented. Technology transitions from the research include initiation of a small business in the area of pulsed power technology, substantial impact on modern high power thyratron technology, and impact on the development of solid state devices, including GaAs-based structures. Ongoing work that is related to technology transfer includes development of electron beams for fusion (electron beam ion trap), accelerator and microlithography applications, and development of cathodes with ultra-high emission properties (super-emissive cathode). DTIC

N95-20626# Sandia National Labs., Albuquerque, NM.
PROGRESS IN THE DEVELOPMENT OF RECYCLING PROCESSES FOR ELECTRIC VEHICLE BATTERIES
R. G. Jungst and R. P. Clark 1994 10 p Presented at the 12th International Electric Vehicle Symposium, Anaheim, CA, 5-7 Dec. 1994
(Contract DE-AC04-94AL-85000)
(DE94-015894; SAND-94-1944C; CONF-941221-1) Avail: CASI HC A02/MF A01

Disposition of electric vehicle (EV) batteries after they have reached the end of their useful life is an issue that could impede the widespread acceptance of EV's in the commercial market. This is especially true for advanced battery systems where working recycling processes have not as yet been established. The DOE sponsors an Ad Hoc Electric Vehicle Battery Readiness Working Group to identify barriers to the introduction of commercial EV's and to advise them of specific issues related to battery reclamation/recycling, in-vehicle battery safety, and battery shipping. A Sub-Working Group on the reclamation/recycle topic has been reviewing the status of recycling process development for the principal battery technologies that are candidates for EV use from the near-term to the long-term. Recycling of near-term battery technologies, such as lead-acid and nickel/cadmium, is occurring today and it is believed that sufficient processing capacity can be maintained to keep up with the large number of units that could result from extensive EV use. Reclamation/recycle processes for midterm batteries are partially developed. Good progress has been made in identifying processes to recycle sodium/sulfur batteries at a reasonable cost and pilot scale facilities are being tested or planned. A pre-feasibility cost study on the nickel/metal hydride battery also indicates favorable economics for some of the proposed reclamation processes. Long-term battery technologies, including lithium-polymer and lithium/iron disulfide, are still being designed and developed for EV's, so descriptions for prototype recycling processes are rather general at this point. Due to the long time required to set up new, full-scale recycling facilities, it is important to develop a reclamation/recycling process in parallel with the battery technologies themselves. DOE

N95-20628# Sandia National Labs., Albuquerque, NM.

DEVELOPMENT OF A TESTER FOR EVALUATION OF PROTOTYPE THERMAL CELLS AND BATTERIES

Ronald A. Guidotti 1994 7 p Presented at the 10th Annual Battery Conference on Applications and Advances, Long Beach, CA, 10-13 Jan. 1995
(Contract DE-AC04-94AL-85000)
(DE95-000540; SAND-94-2472C; CONF-950121-1) Avail: CASI HC A02/MF A01

A tester was developed to evaluate prototype thermal cells and batteries--especially high-voltage units--under a wide range of constant-current and constant-resistance discharge conditions. Programming of the steady-state and pulsing conditions was by software control or by hardware control via an external pulse generator. The tester was assembled from primarily Hewlett-Packard (H-P) instrumentation and was operated under H-P's Rocky Mountain Basic (RMB). Constant-current electronic loads rated up to 4 kW (400 V at up to 100 A) were successfully used with the setup. For testing under constant-resistance conditions, power metal-oxide field-effect transistors (MOSFET's) controlled by a programmable pulse generator were used to switch between steady-state and pulse loads. The pulses were digitized at up to a 50 kHz rate (20 microseconds/pt) using high-speed DVM's; steady-state voltages were monitored with standard DVM's. This paper describes several of the test configurations used and discusses the limitations of each. Representative data are presented for a number of the test conditions. DOE

N95-20661 SRI International Corp., Menlo Park, CA.

FIELD-EMITTER ARRAYS FOR RF VACUUM MICROELECTRONICS Quarterly Technical Report No. 10, 1 Jan. - 31 Mar. 1994

C. A. Spindt 31 May 1994 17 p Limited Reproducibility: More than 20% of this document may be affected by microfiche quality
(Contract MDA972-91-C-0029; ARPA Order 8162)
(AD-A279959) Avail: Issuing Activity (Defense Technical Information Center (DTIC))

SRI International has completed the tenth quarter of a program to develop field-emitter arrays for vacuum microelectronics. We have met the first-phase program goals of 5 mA total emission, with a current density of 5 A/sq cm for at least 2 hours and demonstrated modulation of the emission current at a frequency of 1 GHz. Principal efforts involved the development of a process for forming emitter cones in small diameter apertures and with improved aspect ratios to reduce stress accumulation on film, modification of reactive ion etching chemistry to eliminate sulfur contamination of the cathode, investigation of galvanic etching resulting from a deionized-water rinse, and methods of fabricating emitters arrays with increased geometric field-enhancement factors and higher packaging densities. Variations in emission test results in cathodes at SRI and in cathodes given high-frequency tests at NRL were investigated, and an emission microscope for use in studying emitter array performance, yield, and reliability was assembled. DTIC

N95-20663 Department of the Navy, Washington, DC.

ELASTOMERIC ELECTRICAL CONNECTOR Patent

Joseph E. Laska, inventor (to Navy), John T. Oakley, inventor (to Navy), and Francis R. Reinert, inventor (to Navy) 27 Sep. 1994 8 p Filed 16 Aug. 1993 Supersedes AD-D016340
(AD-D016559; US-Patent-5,350,308; US-Patent-Appl-SN-107431; US-Patent-Class-439-91) Avail: US Patent and Trademark Office

This is an elastic device that provides solderless, pressure contact, electrical connections between leads or leads and terminals at an interface. The elastic device comprises elastomeric material, such as silicone rubber, and has electrical conductive, compressible wires formed of a metal, such as monel, embedded in the silicone. The elastic device is particularly suited to provide electrical connections between an interface that is brought together by a connector and which is separable in response to an impulse that may be created by an explosion produced by a pyrotechnic device. DTIC

N95-20702 Direction des Recherches, Etudes et Techniques, Paris (France). Centre de Documentation de l'Armement.

CHANGES IN THE BEHAVIOR OF MAGNETIC MATERIALS UNDERGOING PROCESSING IN ELECTRICAL ROTATING MACHINES Final Report [CONTRIBUTION A L'ETUDE DE L'EVOLUTION DU COMPORTEMENT DES MATERIAUX MAGNETIQUES AU COURS DE LA MISE EN OEUVRE DANS UNE MACHINE ELECTRIQUE TOURNANTE]

S. DeFoug 1994 60 p In FRENCH
(PB95-104493) Avail: Issuing Activity (National Technical Information Service (NTIS))

The author studied Fe-Si samples featuring non-oriented crystals using an ORTHOPLAN polarizing microscope and a visualization system. The system consisted of a Proxitronics camera with intensifier tubes, a monitor, and image processing. Various increments of current were used to excite the samples. The precision required in magnetic domain observation prompted the author to conduct in-depth optical and vibration studies of the setup, which she describes in this report. She also develops two quantitative methods, and presents an approach to eliminating the Kerr longitudinal effect. NTIS

N95-20715# Naval Postgraduate School, Monterey, CA. Dept. of Electrical and Computer Engineering.

SOFTWARE FOR FLOW DISTRIBUTION IN ELECTRONIC RACK STRUCTURES Final Report, 1 Oct. 1993 - 30 Sep. 1994

Ron J. Pieper 1 Sep. 1994 48 p
(AD-A285994; NPSEC-94-010) Avail: CASI HC A03/MF A01

A FORTRAN CODE has been developed which predicts pressures and flow rates in a piping network for the regimes of laminar, transition, and turbulent flow. A novel and effective scheme for modeling the transition region between laminar and turbulent flow is demonstrated. A proposed linear indicator for the deviation from laminar behavior is introduced into the analysis in order to facilitate the computational task. Although the turbulent flow problem is inherently nonlinear, the method of analysis described herein, typically employed with linear electrical networks, is found to converge rapidly to an approximate solution without user-specified a priori guesses. DTIC

N95-20726 Department of the Navy, Washington, DC.

METHOD OF FABRICATING A MICROELECTRONIC PHOTOMULTIPLIER DEVICE WITH INTEGRATED CIRCUITRY Patent

Randy L. Shimabukuro, inventor (to Navy) and Stephen D. Russell, inventor (to Navy) 12 Jul. 1994 12 p Filed 22 Nov. 1993
(AD-D016530; US-Patent-5,329,110; US-Patent-Appl-SN-156192; US-Patent-Class-250-207) Avail: US Patent and Trademark Office

A microelectronic photomultiplier device is fabricated by discrete procedures to provide a photocathode-anode and dynode chain arrangement which is analogous in operation to conventional photomultiplier tubes. This microelectronic photomultiplier device provides for low level photon detection and realizes the advantages of high reliability, small size and fast response, plus lower cost, weight and power consumption compared to conventional photomultiplier tubes. In addition, the fabrication on an SOI substrate permits integration of logic and control circuitry with detectors. The insulating substrate also permits the integration of an on-chip high voltage supply and may easily be extended to a plurality of detectors offering improved performance and design flexibility. DTIC

N95-20727 Department of the Navy, Washington, DC.

MICRODYNAMIC DEVICES FABRICATED ON SILICON-ON-SAPPHIRE SUBSTRATES Patent

Douglas A. Sexton, inventor (to Navy) 19 Jul. 1994 5 p Filed 19 Aug. 1992
(AD-D016531; US-Patent-5,331,236; US-Patent-Appl-SN-932430; US-Patent-Class-310-40) Avail: US Patent and Trademark Office

Silicon-on-sapphire substrates are provided for the fabrication of micromechanical devices, such as micromotors. The high voltage stand-off characteristics of silicon-on-sapphire thereby provides for the construction of superior electrostatically driven devices and sensors capable of being driven at significantly higher applied potentials since silicon-on-sapphire has demonstrated a capability for building in the range of hundreds of Angstroms, or thick, in the range of microns very high speed, low power, very densely packed integrated circuits using standard silicon processing techniques. As a consequence, the electrostatically driven devices, micromotors, can be incorporated in the integrated circuits and yet be powered at elevated voltages to increase their work potential. DTIC

N95-20729 Department of the Navy, Washington, DC.
HIGH ISOLATION ELECTRONIC SWITCH Patent
Thomas I. Kirkpatrick, inventor (to Navy) 2 Aug. 1994 6 p Filed 19 Mar. 1992
(AD-D016533; US-Patent-5,334,881; US-Patent-Appl-SN-854112; US-Patent-Class-307-241) Avail: US Patent and Trademark Office

A high isolation electronic switch is provided for selectively switching an output line between first and second input lines. Each input line is connected to a respective circuit that has a first current carrying path to connect the respective input line to the output line, and a second current carrying path to connect a portion of the first current carrying path of the respective circuit to a ground potential. Each respective circuit is further selectively operated to conduct along only one of its first or second current carrying paths. A unity gain buffer is connected serially in the first current carrying path of each respective circuit. The switch is selectively operated such that one circuit conducts along its first current carrying path when the other circuit is conducting along its second current carrying path. DTIC

N95-20730 Department of the Navy, Washington, DC.
HYBRID HIGH POWER AMPLIFIER Patent
Russell E. Hammond, inventor (to Navy) and Leopold J. Johnson, inventor (to Navy) 12 Jul. 1994 9 p Filed 28 Jun. 1993
(AD-D016534; US-Patent-5,329,245; US-Patent-Appl-SN-086079; US-Patent-Class-330-251) Avail: US Patent and Trademark Office

The invention provides a high power, low distortion, high efficiency amplifier design incorporating a high efficiency switching amplifier used in conjunction with a linear difference amplifier. The high efficiency switching amplifier, typically of full or half bridge design, is designed to generate a high efficiency, arbitrarily formed, wave portion such as a square wave. The high efficiency waveform is scaled down and is compared to a desired reference, such as a sinusoid. The output of the comparison is the analog difference (mathematical subtraction) between the reference waveform and the scaled-down switch amplifier output wave. This difference signal is then used to drive the linear difference amplifier which simply scales the signal linearly. The two power signals, one from the switching amplifier and the other from the linear difference amplifier, are then summed magnetically. To permit a low harmonic output, the input signals to the switching amplifier and the reference are locked together in frequency. DTIC

N95-20733# Institut National Polytechnique, Toulouse (France).
MAGNETRON POWER SUPPLY AT HIGH STABILITY AND ITS APPLICATION IN PLASMA EXCITATION FOR THE PRODUCTION OF ULTRAVIOLET RADIATION Ph.D. Thesis [ALIMENTATION DU MAGNETRON A HAUTE STABILITE ET APPLICATION A L'EXCITATION DE PLASMAS POUR LA GENERATION DE RAYONNEMENT ULTRAVIOLET]
J. O. PachecoSotelo 1993 143 p In FRENCH
(DE94-629656; INIS-MF-13929) Avail: CASI HC A07/MF A02 (US Sales Only)

This work describes the combination of different disciplines which allow the development of a microwave generator with capacity for power control and stabilization frequency. This generator is used for plasma excitation in partially filled mercury lamps and for the production of ultraviolet radiation. By now, resonance techniques lead to a lot of researches. For our part we used a resonance converter as a magnetron power supply, exploiting its inherent characteristic of current limitation to protect the magnetron. The power is controlled by varying the frequency of the converter. The implementation of several electronic systems for the detection and control of the power and microwave frequency was made, in order to get an optimum dynamic behaviour. For the optimum transfer in energy, from the source (microwave generator) to the load (mercury lamp), a special resonator was implemented. This resonator allow UV radiation, at the same time avoiding the leakage of microwave energy. Finally, this work shows the advantages of the UV radiation through microwave discharge in comparison to conventional methods. DOE

N95-20791# Oak Ridge National Lab., TN. Health Sciences Research Div.
EFFECT OF A SOLID INSULATOR ON THE SPARK YIELD OF S2F10 IN SF6(*)
I. Sauers, S. M. Mahajan, and R. A. Cacheiro 1994 4 p Presented at the IEEE International Symposium on Electrical Insulation, Pittsburgh, PA, 5-8 Jun. 1994
(Contract DE-AC05-84OR-21400)
(DE95-001422; CONF-940671-1) Avail: CASI HC A01/MF A01

Because of its toxicity S2F10 production in SF6 discharges has been the focus of intensive study in recent years. In previous work we have examined the yield of S 2F10 for corona, spark and arc discharges and, in sparks, the effects of water and oxygen have been studied systematically. Here we report the influence of an insulating solid spacer on the production of S2F10 in SF6 when subjected to spark discharges in the energy range 1.6-43 J/spark at a gas pressure of 1 atm. Analyses of the sparked gases were performed using a cryogenic enrichment gas chromatography technique with a sensitivity of less than 10 ppb (parts-per-billion) or 1 in 10(exp 8). With this sensitivity S2F10 can be detected after one or just a few spark(s), minimizing secondary effects of gas contamination, electrode erosion and insulator damage that can influence S2F10 production and make quantitative yield determinations difficult to establish. For these studies Teflon was used as the spacer sandwiched between two stainless steel electrodes. Energy measurements were made after recording the voltage and current waveforms. The amount of S2F10 produced per unit energy deposited into the discharge was found to be greater in the presence of the spacer than for a purely gas gap. Factors which influence S2F10 stability such as surfaces and water will also b e discussed. DOE

N95-20814# California Univ., Berkeley. Lawrence Berkeley Lab, CA. Energy and Environment Div.
NICKEL HYDROXIDE ELECTRODES IN REDUCED-ALKALINITY ELECTROLYTES Ph.D. Thesis
Robert F. Plivelich Apr. 1994 81 p
(Contract DE-AC03-76SF-00098)
(DE95-002333; LBL-35628) Avail: CASI HC A05/MF A01

Nickel oxide electrodes cycled to failure in zinc-nickel oxide cells were studied. These cells incorporated novel electrolytes intended to increase the Zinc electrode cycle life. The Zinc species deposited in the failed Ni electrodes was probably ZnOH2 or ZnO. Evidence was found for a strictly mechanical interpretation of the capacity degradation of the Nickel oxide electrodes. The gas evolution in failure of Nickel electrodes in the zinc-nickel oxide system using a reduced-alkalinity electrolyte, needs to be studied. DOE

N95-20824# David Sarnoff Research Center, Princeton, NJ.
HIGH PERFORMANCE YBCO FILMS Report, 25 Aug. 1994 - 25 Nov. 1995
Edgar J. Denlinger, Aly Fathy, David Kalokitis, Valerie Pendrick, and Barry Thaler 25 Aug. 1994 7 p
(Contract N00014-91-C-0216)
(AD-A286567) Avail: CASI HC A02/MF A01

The focus for the remainder of our program, which will end during the next quarter, is on oxygen annealing the buried YBCO ground plane through the Ag power plane and glass/metal handle as well as making an MCM structure with YBCO being used for only the signal layer. Oxygen annealing of a YBCO-covered lanthanum aluminate through five microns of thermally evaporated silver, after subjecting the sample to glass-firing conditions, recovered the microwave Q of the sample to within 16-18% of its original value (measured before the silver was deposited). The oxygen annealing time was only 4 hours. This Q degradation is believed to be acceptable for the YBCO ground plane of an MCM module. Addition of the STO dielectric layer between the YBCO ground plane and the silver makes the oxygen annealing time very long (greater than 18 hours). DTIC

N95-20827# Army Armament Research, Development and Engineering Center, Picatinny Arsenal, NJ. Precision Munitions Div.
BRIEF TUTORIAL ON THE KALMAN FILTER Annual Report, Sep. - Nov. 1991
John Podesta Nov. 1994 32 p
(AD-A286571; ARFSD-SP-94001) Avail: CASI HC A03/MF A01

A derivation of the Kalman filter equations is presented which should provide a concise introduction to Kalman filter theory for scientists, engineers, and mathematicians alike. An elementary derivation of the basic Kalman filter, the 1-step Kalman predictor, is given first in 1-dimension and then in n-dimension. The well known prediction-correction formulation of the Kalman filter equations are derived for the filtered estimate, or current state estimate. Then, the state prediction is obtained from the filtered estimate. It is assumed that the reader has a background in probability theory and some exposure to stochastic processes. DTIC

N95-20854# Lawrence Livermore National Lab., Livermore, CA.
LLNL/LION PRECISION LVDT AMPLIFIER
D. J. Hopkins Apr. 1994 8 p Presented at the American Society for Precision Engineering (ASPE) Conference, Tucson, AZ, 6-8 Apr. 1994
(Contract W-7405-eng-48)
(DE95-001504; UCRL-JC-116930; CONF-9404131-3) Avail: CASI HC A02/MF A01

A high-precision, low-noise, LVDT amplifier has been developed which is a significant advancement on the current state of the art in contact displacement measurement. This amplifier offers the dynamic range of a typical LVDT probe but with a resolution that rivals that of non contact displacement measuring systems such as capacitance gauges and laser interferometers. Resolution of 0.1 (mu) in with 100 Hz bandwidth is possible. This level of resolution is over an order of magnitude greater than what is now commercially available. A front panel switch can reduce the bandwidth to 2.5 Hz and attain a resolution of 0.025 (mu) in. This level of resolution meets or exceeds that of displacement measuring laser interferometry or capacitance gauge systems. Contact displacement measurement offers high part spatial resolution and therefore can measure not only part contour but surface finish. Capacitance gauges and displacement laser interferometry offer poor part spatial resolution and can not provide good surface finish measurements. Machine tool builders, meteorologists and quality inspection departments can immediately utilize the higher accuracy and capabilities that this amplifier offers. The precision manufacturing industry can improve as a result of improved capability to measure parts that help reduce costs and minimize material waste. DOE

N95-20882# Sandia National Labs., Albuquerque, NM.
COMPLEMENTARY GaAs JUNCTION-GATED HETEROSTRUCTURE FIELD EFFECT TRANSISTOR FABRICATION FOR INTEGRATED CIRCUITS
A. G. Baca, J. C. Zolper, M. E. Sherwin, P. J. Robertson, R. J. Shul, A. J. Howard, D. J. Rieger, and J. F. Klem 1994 10 p Presented at the 186th Meeting of the Electrochemical Society, Miami, FL, 9-14 Oct. 1994
(Contract DE-AC04-94AL-85000)
(DE95-001522; SAND-94-1670C; CONF-941063-7) Avail: CASI HC A02/MF A01

A new GaAs junction-gated complementary logic technology that integrates a modulation doped p-channel heterostructure field effect transistor (pHFET) and a fully ion implanted n-channel JFET has recently been fabricated. High-speed, low-power operation has been demonstrated with loaded ring oscillators that show gate delays of 179 ps/stage for a power-delay product of 28 fJ at 1.2 V operation and 320 ps/stage and 8.9 fJ at 0.8 V operation. The principal advantages of this technology include the ability to independently set the threshold voltage of n- and p-channel devices and to independently design the pHFET for high performance. A self-aligned refractory gate process based on tungsten and tungsten silicide gate metal has been used to fabricate the FETs. Novel aspects of the fabrication include the simultaneous formation of non-alloyed, refractory ohmic contacts for the junction gates and the formation of shallow p-n junctions by ion implantation. DOE

N95-20883# Sandia National Labs., Albuquerque, NM.
TECHNOLOGIES FOR HIGHLY PARALLEL OPTOELECTRONIC INTEGRATED CIRCUITS
K. L. Lear 1994 6 p Presented at the GaAs Symposium, Philadelphia, PA, 16-19 Oct. 1994
(Contract DE-AC04-94AL-85000)
(DE95-001607; SAND-94-2349C; CONF-9410195-2) Avail: CASI HC A02/MF A01

While summarily reviewing the range of optoelectronic integrated circuits (OEIC's), this paper emphasizes technology for highly parallel optical interconnections. Market volume and integration suitability considerations highlight board-to-board interconnects within systems as an initial insertion point for large OEIC production. The large channel count of these intrasystem interconnects necessitates two-dimensional laser transmitter and photoreceiver arrays. Surface normal optoelectronic components are promoted as a basis for OEIC's in this application. An example system is discussed that uses vertical cavity surface emitting lasers for optical buses between layers of stacked multichip modules. Another potentially important application for highly parallel OEIC's is optical routing or packet switching, and examples of such systems based on smart pixels are presented. DOE

N95-20905# Phillips Lab., Kirtland AFB, NM.
DEVELOPMENT OF AN ANNULAR ELECTRON BEAM HPM AMPLIFIER Final Report, Aug. 1991 - Jan. 1994
Kyle J. Hendricks, Walter R. Fayne, Thomas A. Spencer, Lester A. Bowers, and M. J. Arman Sep. 1994 70 p
(AD-A286646; PL-TR-94-1065) Avail: CASI HC A04/MF A01

Experiments and computer simulations of annular electron beam powered microwave devices have been conducted, This work included the generation of an annular electron beam using the IMP pulser, the modulation of this beam via a two-cavity klystron-like amplifier, and the extraction or radiation of the microwave power. Results of computer simulations from several codes used to design the experiments and results of experiments on propagating the electron beam, injecting a magnetron signal into the two-cavity klystron-like amplifier via a vacuum coaxial line, and initial work on modulating the electron beam are presented. DTIC

N95-20966 Institute for Defense Analyses, Alexandria, VA.
THE OPPORTUNITIES FOR AND CHALLENGES OF COMMON INTEGRATED ELECTRONICS Final Report, Jul. - Dec. 1993
J. R. Nelson, Bernard L. Retterer, and Harley A. Cloud Feb. 1994 40 p Limited Reproducibility: More than 20% of this document may be affected by microfiche quality
(Contract MDA903-89-C-0003)
(AD-A279991; IDA-D-1490; IDA/HQ-93-44599; AD-E501787) Avail: CASI HC A03

This document summarizes a portion of IDA's work concerning common integrated electronics and the potential cost savings of using common electronic hardware and software. It addresses trends in avionics costs and recent experiences in applying common electronic standards to weapon programs as a way to reduce costs. The following essential elements of a program to acquire common integrated electronics are explored: (1) integrated system architecture; (2) advanced technology programs; (3) open system standards; (4) standard common modules; and (5) associated management and policies. The principal recommendation is that OSD support and coordinate such a-program by taking a strong leadership role and setting standards policy. DTIC

N95-20967 Illinois Univ., Urbana, IL. Coordinated Science Lab.
PROTOTYPE RULE-BASED RELIABILITY ANALYSIS FOR VLSI CIRCUIT DESIGN Final Report, Oct. 1992 - Oct. 1993
Sung-Mo Kang, Yusuf Leblebici, Weishi Sun, and Chin-Chi Teng Apr. 1994 80 p Limited Reproducibility: More than 20% of this document may be affected by microfiche quality
(Contract F30602-92-C-0069)
(AD-A280065; RL-TR-94-23) Avail: Issuing Activity (Defense Technical Information Center (DTIC))

This report describes the development and application of parametric and geometry based macro-models of hot-carrier induced dynamic degradation in MOS VLSI circuits. Previously, a simulation based approach has been used for reliability analysis, but this is inefficient for reliability assessment of very large scale integrated circuits. Geometry-based macro-models for hot-carrier reliability estimation have been developed. The macro-models express hot-carrier damage as functions of designable parameters such as transistor size (W), output loading capacitance (C1) and the input signal slew rate (a). A prototype rule-based reliability diagnosis tool, iRULE, has been developed. This tool uses the macro-models for designing hot-carrier resistant circuits without the need for transient reliability simulations. This provides the ability to analyze very large circuits with more than one million transistors on a workstation in a short amount of time. This report also describes a fast timing reliability simulation tool, ILLIADS-R, that can accurately estimate hot-carrier degradation while providing several orders of magnitude speed up over traditional transistor-level circuit simulators. DTIC

N95-20997# University of Southern California, Marina del Rey, CA. Information Sciences Inst.
AN AUTOMATIC PLACEMENT TOOL FOR RAPID PROTOTYPING OF PRINTED CIRCUIT BOARDS
John Granacki and Tauseef Kazi Nov. 1993 24 p
(AD-A286029; ISI/RR-93-388) Avail: CASI HC A03/MF A01

This report describes a fully automatic placement tool for PCB's (printed circuit boards), nap (nonhierarchical automatic placement) that combines approaches from different placement heuristics developed both for PCB and VLSI chip placement. Although the problem of placement for a PCB can be abstractly cast into the same formalism as the problem of VLSI cell placement, a practical tool must incorporate many additional features. In this report we describe the impact of incorporating these PCB-specific features as well as other constraints imposed by the CAD environment (that is, the schematic capture system and the automatic routing tools) into an automatic placement tool. Next we discuss the selected heuristics and their associated data structures in detail. Following this discussion, we present the results of using the placement tool on two test cases along with an analysis of the tools performance. Finally, we identify the limitations of the current implementation and we propose some possible solutions and future work. DTIC

N95-21017 SRI International Corp., Menlo Park, CA.
IR MATERIALS PRODUCIBILITY Quarterly Technical Report No. 7, 1 Feb. - 30 Apr. 1994
A. Sher, M. A. Berding, A. T. Paxton, and M. W. Muller 3 Jun. 1994 12 p Limited Reproducibility: More than 20% of this document may be affected by microfiche quality
(Contract MDA972-92-C-0053; ARPA Order 8557)
(AD-A280094) Avail: Issuing Activity (Defense Technical Information Center (DTIC))

The formation energy for mercury vacancy - tellurium antisite pairs is calculated. We developed a method for calculating the ionization energies of the defects in semiconductors. The electron-phonon interaction-induced band-edge shifts in semiconductors are calculated using accurate band structures. The temperature variation of gaps in GaAs (done to validate our method) and Hg(0.78)Cd(0.22)Te have been calculated and are found to agree well with experiments. DTIC

N95-21118 Department of the Navy, Washington, DC.
TRANSDUCERS WITH IMPROVED SIGNAL TRANSFER FIELD OF THE INVENTION Patent Application
Chulo Kim, inventor (to Navy) and Manfred Kahn, inventor (to Navy) 25 Jan. 1994 31 p Limited Reproducibility: More than 20% of this document may be affected by microfiche quality
(AD-D016228; US-Patent-Appl-SN-193686) Avail: CASI HC A03

A transducer includes a rigid resin in the form of a solid block; a plurality of spaced and parallel piezoelectric rods of equal length disposed in the rigid resin and extending at one end thereof beyond the rigid resin; a solid soft resin enveloping the rods; and electrically conducting cover plates disposed against extremities of the rods; the rigid resin block being composed of a plurality of stacked preforms having spaced and parallel upper grooves wherein the rods are disposed. The process for making transducers with extended piezoelectric rods includes the steps of loading the rods into a plurality of spaced and parallel upper grooves of preforms made from a rigid resin; stacking the loaded preforms one on top of another to the desired height, the rods being flush with the preforms at one end and extending beyond the preforms at the other end; infiltrating a soft resin around the rods; curing the soft resin to a solid, compressible state; and applying electrically conducting cover plates against the rod ends. DTIC

N95-21139# Sandia National Labs., Albuquerque, NM.
FIBER-OPTIC CONTROL OF CURRENT FILAMENTS IN HIGH GAIN PHOTOCONDUCTIVE SEMICONDUCTOR SWITCHES
F. J. Zutavern, G. M. Loubriel, W. D. Helgeson, M. W. OMalley, R. R. Gallegos, A. G. Baca, T. A. Plut, and H. P. Hjalmarson 1994 4 p
Presented at the 21st International Power Modulator Symposium, Costa Mesa, CA, 28-30 Jun. 1994
(Contract DE-AC04-94AL-85000)
(DE94-015804; SAND-94-0428C; CONF-940678-7) Avail: CASI HC A01/MF A01

The discovery of current filaments in GaAs photoconductive semiconductor switches (PCSS) raised concerns about the location and density of the current distribution during high gain switching. This paper describes experiments using fiber-optic coupled laser diode arrays (LDA) to control the location and number of current filaments in GaAs PCSS. Infrared (IR) images of the recombination radiation, that is emitted from the surface of the PCSS, show precisely where the current is concentrated. These were recorded as the fiber-optic configuration and switch test parameters were varied. Up to twenty individually-coupled laser diodes and fibers were used to initiate multiple, simultaneous filaments. Fibers were configured in a row both parallel and perpendicular to the direction of current. Two types of experiments were performed: high current; and high voltage. System impedances of 0.25 Omega and 50 Omega were used with switch currents up to 5.2 kA and initial charging voltages up to 100 kV, respectively. Switch sizes were 1 x 5 sq mm and 15 x 38 sq mm (parallel x perpendicular to the current). With the 0.25 Omega system charged to 4 kV (40 kV/cm across the PCSS), individual filaments were triggered with 150 nJ of optical trigger energy. In this case, filaments were triggered at both ends near the contacts with pairs of 250 micro m fibers, each ofwhich delivered 75 nJ in 140 ps. The use of multiple fiber pairs to distribute the current more uniformly across the switch improved switch performance. It allowed higher total currents to be switched with narrower switches. With the 50 Omega system charged to 100 kV (67 kV/cm across the PCSS), individual filaments were triggered with as little as 90 nJ of optical trigger energy. The trigger pulse was delivered in 2 ns through one fiber which was 400 micro m in diameter. DOE

N95-21169# State Univ. of New York, Cortland, NY. Dept. of Physics.
GEOMETRIC CHARACTERIZATION OF ELECTROMIGRATION VOIDS (A STATISTICAL ANALYSIS OF ELECTROMIGRATION VOIDS) Final Report, Jun. 1993 - Sep. 1994
Yolanda J. Kime and Peter Grach Oct. 1994 13 p
(Contract F30602-93-C-0167)
(AD-A286494; RL-TR-94-190) Avail: CASI HC A03/MF A01

The areas, perimeters, lengths, and widths of 998 electromigration induced voids on 38 test stripes have been measured by SEM and digital image analysis. Virtually all of the voids occurred along the passivation-conductor interface on the side of the stripe. A plot of the number of voids on each stripe versus time to failure does not extrapolate to zero at zero time to failure, which suggests there are a certain number of active sites predisposed to voiding. DTIC

N95-21178# Advanced Fuel Research, Inc., East Hartford, CT.
HTS JOSEPHSON TECHNOLOGY ON SILICON WITH APPLICATION TO HIGH SPEED DIGITAL MICROELECTRONICS Monthly Progress Report, 30 Sep. - 29 Oct. 1994
Peter Rosenthal 27 Oct. 1994 1 p
(Contract N00014-94-C-0261)
(AD-A285964) Avail: CASI HC A01/MF A01

A brief summary of the following activities is presented: (1) Josephson junction fabrication and testing; (2) Rapid Single Flux Quantum (RSFQ) modeling and design; and (3) RSFQ circuit fabrication and testing. The growth of two films of YSZ buffered YCBO films on silicon substrates is outlined. Derived from text

N95-21218# Pennsylvania State Univ., University Park, PA. Dept. of Chemistry.
SMALL CAVITY NONRESONANT TUNABLE MICROWAVE-FREQUENCY ALTERNATING CURRENT SCANNING TUNNELING MICROSCOPE
L. A. Bumm and P. S. Weiss 10 Oct. 1994 22 p
(Contract N00014-91-J-1630)
(AD-A285752; TR-21) Avail: CASI HC A03/MF A01

We have developed a broadly tunable microwave frequency alternating current scanning tunneling microscope which employs a cavity with no resonances in the frequency range used. This results in a low flat background for spectroscopic measurements with this instrument. DTIC

N95-21296# Argonne National Lab., IL. Energy Systems Div.
EFFECTS OF BATTERY TECHNOLOGIES, DRIVING PATTERNS, AND CLIMATE COMFORT CONTROL ON THE PERFORMANCE OF ELECTRIC VEHICLES
William W. Marr, Michael Q. Wang, and Danilo J. Santini 15 May 1994 7 p Presented at the Electric, Hybrid and Alternative Fuel Vehicles Conference, Aachen, Germany, 31 Oct. - 4 Nov. 1994
(Contract W-31-109-eng-38)
(DE95-001102; ANL/ES/CP-82395; CONF-9410221-2) Avail: CASI HC A02/MF A01

A computer software package, EAGLES, has been developed at Argonne National Laboratory to analyze electric vehicle (EV) performance. In this paper, we present EAGLES predictions of EV driving range, acceleration rate, and energy consumption under various driving patterns, with different battery technologies, and with assumptions concerning use of air conditioners and/or heaters for climate comfort control. The specifications of a baseline, four-passenger EV for given design performance requirements are established, assuming urban driving conditions represented by the Los Angeles 92 (LA-92) driving cycle and using battery characteristics similar to those of the United States Advanced Battery Consortium (USABC) midterm battery performance goals. To examine the impacts of driving patterns, energy consumption is simulated under three different driving cycles: the New York City Cycle, the Los Angeles 92 Cycle, and the ECE-15 Cycle. To test the impacts of battery technologies, performance attributes of an advanced lead-acid battery, the USABC midterm battery goals, and the USABC long-term battery goals are used. Finally, EV energy consumption from use of air conditioners and/or heaters under different climates is estimated and the associated driving range penalty for one European city (Paris) and two United States cities (Chicago and Los Angeles) is predicted. The results of this paper show the importance of considering various effects, such as battery technology, driving pattern, and climate comfort control, in the determination of EV performances. Electric vehicle energy consumption decreases more than 20% when a battery with characteristics similar to the USABC long-term goals is used instead of an advanced lead-acid battery. DOE

N95-21301# Allied-Signal Aerospace Co., Kansas City, MO.
SURVIVABILITY OF SOLDERED LEADLESS CHIP CARRIERS AFTER TEMPERATURE CYCLING
L. R. Zawicki, B. W. Lenhardt, and F. R. Smith Sep. 1994 6 p Presented at the Meeting on the Revolution in Microelectronics, Boston, MA, 15-17 Nov. 1994
(Contract DE-AC04-76DP-00613)
(DE95-001497; KCP-613-5388; CONF-941199-3) Avail: CASI HC A02/MF A01

Temperature cycling evaluations were conducted on leadless chip carriers (LCC's) soldered to thick film networks (TKN's). Various temperature ranges, rates of change, cycle times, number of cycles, and sizes of LCC's were used. The TKN's were attached to metal backing plates with 63Sn/37Pb solder preforms using an infrared vacuum soldering process. The LCC's were attached to Pt/Au TKN's with 63Sn/37Pb solder paste using a belt reflow process. Visual examination and cross-sectional analysis were used to evaluate the survivability. Results were also correlated with finite elemental analysis. Considering the initial results, possible solutions included changing the solder from 63Sn/37Pb to 50Pb/50In, deleting the metal backplate, changing the rate of change in the temperature cycle, and/or adding leads to the large LCC's. Because of a system requirement, the rate of change in the temperature cycle could not be changed. Since there was no long term reliability information on the Pt/Au TKN with 50Pb/50In solder, this option was also dropped. Additional evaluations showed little difference in the survivability of large LCC solder joints with or without the metal backing plate. The final results indicated that LCC's beyond a certain physical size required compliant leads to survive the temperature cycle requirements. DOE

N95-21326# Helsinki Univ. of Technology, Espoo (Finland). Low Temperature Lab.
EQUIVALENT SOURCE CURRENT FORMULATION IN IMPEDANCE TOMOGRAPHY
Risto J. Ilmoniemi (Helsinki Univ. Central Hospital, Helsinki, Finland.) and Seppo P. Ahlfors Apr. 1994 15 p
(ISSN 0355-7790)
(PB95-127627; TKK-F-A728; ISBN-951-22-2122-5) Avail: CASI HC A03/MF A01

Changes in the conductivity distribution of a body modify the electromagnetic field due to injected current in the same way as an equivalent source current distribution J(sup eq)(r) does. In the limit of small perturbations, it is shown that J(sup eq)(r) = Sigma(sup 1)(r)E(sup 0)(r), where Sigma(sup 1)(r) is a deviation in the conductivity and E(sup 0)(r) is the non-perturbed electric field. A model experiment demonstrates how a conductivity anomaly can be located using the minimum-norm estimate of the equivalent currents. The minimum-norm solution for small perturbation Sigma(sup 1)(r) is derived as well. The equivalent-source formulation allows the direct application of biomagnetic and bioelectric source-determination methods to conductivity imaging. NTIS

N95-21390# Sandia National Labs., Albuquerque, NM.
COMPLEMENTARY GaAs JUNCTION-GATED HETEROSTRUCTURE FIELD EFFECT TRANSISTOR TECHNOLOGY
A. G. Baca, J. C. Zolper, M. E. Sherwin, P. J. Robertson, R. J. Shul, A. J. Howard, D. J. Rieger, and J. F. Klem 1994 4 p Presented at the GaAs Symposium, Philadelphia, PA, 16-19 Oct. 1994
(Contract DE-AC04-94AL-85000)
(DE94-018901; SAND-94-1302C; CONF-9410195-1) Avail: CASI HC A01/MF A01

The first circuit results for a new GaAs complementary logic technology are presented. The technology allows for independently optimizable p- and n- channel transistors with junction gates. Excellent loaded gate delays of 179 ps at 1.2 V and 319 ps at 0.8 V have been demonstrated at low power supply voltages. A power-delay product of 8.9 fJ was obtained at 0.8 V. DOE

N95-21394# Sandia National Labs., Albuquerque, NM.
SPECTROSCOPIC, MORPHOLOGICAL, AND ELECTRICAL CHARACTERIZATION OF PdGe OHMIC CONTACTS TO n-GaAs
A. J. Howard, M. L. Lovejoy, K. R. Zavadil, D. J. Rieger, R. J. Shul, J. C. Zolper, and P. A. Barnes (Auburn Univ., AL.) 1994 6 p Presented at the Topical Conference on the Synthesis and Processing of Electronic Materials, San Francisco, CA, 13-18 Nov. 1994
(Contract DE-AC04-94AL-85000)
(DE95-000738; SAND-94-2201C; CONF-9411132-1) Avail: CASI HC A02/MF A01

Novel material systems such as ZnS(y)Se(1-y) and Zn(x)Cd(1-x)Te that are commonly grown at low temperatures (approximately 300 C), require unique, low temperature processing schemes. For example, ohmic contact formation with the common AuGeNi n-GaAs contact is not appropriate for this application due to its relatively high anneal temperature (approximately 400 C). For this reason, we investigated the effects of anneal temperature (150 to 400 C) and time (5 to 30 min) on the contact resistivity of PdGe to n-GaAs substrates. The contact surface morphology was measured by AFM and the material composition profile was analyzed by XPS. The characteristics of the PdGe contact are compared to the standard AuGeNi n-GaAs contact. DOE

N95-21395# Sandia National Labs., Albuquerque, NM.
DEVELOPMENT STATUS OF AN INTENSE BEAM KLYSTRON
P. D. Coleman, R. W. Lemke, K. J. Hendricks (Phillips Lab., Kirtland AFB, NM.), M. J. Arman (Phillips Lab., Kirtland AFB, NM.), and L. A. Bowers (Phillips Lab., Kirtland AFB, NM.) 1994 11 p Presented at the Pulsed Radio Frequency Sources for Linear Colliders, Long Island, NY, 2-7 Oct. 1994
(Contract DE-AC04-94AL-85000)
(DE95-000745; SAND-94-2542C; CONF-9410218-1) Avail: CASI HC A03/MF A01

Investigations are being performed on a high current (16 kA), mildly relativistic (400kV), L-band klystron source. Experiments are in an early stage, and thus far have progressed to beam modulation studies. This paper discusses general klystron design considerations, beam propagation results, initial modulation results, and various extraction techniques being considered. DOE

N95-21442# Massachusetts Inst. of Tech., Cambridge, MA. Plasma Fusion Center.
THEORY AND MODELLING OF QUENCH IN CABLE-IN-CONDUIT SUPERCONDUCTING MAGNETS Ph.D. Thesis
A. Shajii Apr. 1994 267 p
(Contracts DE-FC02-93ER-54186; DE-AC07-76ID-01570)
(DE95-001819; PFC/RR-94-5; DOE/ER-54186/T4) Avail: CASI HC A12/MF A03

A new simple, self consistent theoretical model is presented that describes the phenomena of quench propagation in cable-in-conduit superconducting magnets. The model (Quencher) circumvents many of the difficulties associated with obtaining numerical solutions in more general existing models. Specifically, a factor of 30-50 is gained in CPU time over the general, explicit time dependent codes used to study typical quench events. The corresponding numerical implementation of the new model is described and the numerical results are shown to agree very well with those of the more general models, as well as with experimental data. Further, well justified approximations lead to the MacQuench model that is shown to be very accurate and considerably more efficient than the Quencher model. The MacQuench code is suitable for performing quench studies on a personal computer, requiring only several minutes of CPU time. In order to perform parametric studies on new conductor designs it is required to utilize a model such as MacQuench because of the high computational efficiency of this model. Finally, a set of analytic solutions for the problem of quench propagation in cable-in-conduit conductors is presented. These analytic solutions represent the first such results that remain valid for the long time scales of interest during a quench process. The assumptions and the resulting simplifications that lead to the analytic solutions are discussed, and the regimes of validity of the various approximations are specified. The predictions of the analytic results are shown to be in very good agreement with numerical as well as experimental results. Important analytic scaling relations are verified by such comparisons, and the consequences of some of these scalings on currently designed superconducting magnets are discussed. DOE

N95-21471# Edgerton, Germeshausen and Grier, Inc., Idaho Falls, ID.
PERFORMANCE TESTING OF THE AC PROPULSION ELX ELECTRIC VEHICLE
W. E. Kramer, R. D. MacDowall, and A. F. Burke Jun. 1994 141 p
(Contract DE-AC07-76ID-01570)
(DE95-002049; EGG-EP-11320) Avail: CASI HC A07/MF A02

Performance testing of the AC Propulsion ELX electric vehicle is described. Test data are presented and analyzed. The ELX vehicle is the first of a series of electric vehicles of interest to the California Air Resources Board. The test series is being conducted under a Cooperative Research and Development Agreement (CRADA) between the US Department of energy and the California Air Resources Board. The tests which were conducted showed that the AC Propulsion ELX electric vehicle has exceptional acceleration and range performance. When the vehicle's battery was fully charged, the vehicle can accelerate from 0 to 96 km/h in about 10 seconds. Energy consumption and range tests using consecutive FUDS and HWFET Driving cycles (the all-electric cycle) indicate that the energy economy of the AC Propulsion ELX electric vehicle with regenerative braking is 97 W(center dot)h/km, with a range of 153 km (95 miles). Computer simulations performed using the SIMPLEV Program indicate that the vehicle would have a range of 327 km (203 miles) on the all-electric cycle if the lead acid batteries were replaced with NiMH batteries having an energy density of 67 W(center dot)h/kg. Comparisons of FUDS test data with and without regenerative braking indicated that regenerative braking reduced the energy consumption of the ELX vehicle by approximately 25%. DOE

N95-21490 Naval Academy, Annapolis, MD. Dept. of Physics.
ELECTRICAL IMPEDANCE STUDIES OF ACID-FORM NAFION MEMBRANES Interim Technical Report, Apr. 1993 - May 1994
J. J. Fontanella, M. G. McLin, M. C. Wintersgill, J. P. Calame, and S. G. Greenbaum 1 May 1994 14 p Limited Reproducibility: More than 20% of this document may be affected by microfiche quality
(AD-A279271; TR-6) Avail: Issuing Activity (Defense Technical Information Center (DTIC))

Electrical conductivity/dielectric relaxation studies of acid form Nafion-117 have been carried out at frequencies from 10 to 10(exp 8) Hz. By direct measurement, it is shown that when standard two terminal measurements are made across the thickness of a 0.18 mm film, it is necessary to use frequencies in excess of 10(exp 7) Hz in order to observe the bulk conductivity of the sample. As a consequence, previous reports of a power law dependence for the electrical conductivity are not associated with the bulk electrical conductivity but rather are due to electrode effects and space charge. As confirmation, it is shown that by changing the geometry of the electrodes, the low frequency electrical response of the material is significantly changed. DTIC

N95-21545# Sandia National Labs., Albuquerque, NM.
GATE OXIDE SHORTS IN nMOS TRANSISTORS: ELECTRICAL PROPERTIES AND LIFETIME PREDICTION METHOD
S. A. Dababneh (New Mexico Univ., Albuquerque, NM.), C. F. Hawkins (New Mexico Univ., Albuquerque, NM.), and J. M. Soden 1994 9 p Presented at the 5th European Symposium on Reliability of Electron Devices, Failure Physics and Analysis (ESREF), Glasgow, Scotland, 4-7 Oct. 1994
(Contract DE-AC04-94AL-85000)
(DE94-018904; SAND-94-2008C; CONF-9410199-1) Avail: CASI HC A02/MF A01

Degradation in nMOS transistors from gate oxide shorts is dependent upon oxide trapping and interface state generation. Three distinct damage mechanisms were identified, including generation of: (1) electron traps in the bulk oxide by the injected holes, N(sub ox,h); (2) electron traps in the bulk oxide by the injected electrons, N(sub ox,e); and (3) interface states, N(sub ss). The three damage mechanisms are incorporated into a device lifetime prediction method. DOE

N95-21554# Oak Ridge National Lab., TN.
MONOLITHIC CIRCUITS FOR LEAD-GLASS CALORIMETRY
A. L. Wintenberg, T. C. Awes, C. L. Britton, Jr., L. G. Clonts (Tennessee Univ., Knoxville, TN.), M. S. Emery, M. N. Ericson, F. Plasil, M. L. Simpson, J. W. Walker, and G. R. Young 1994 18 p Presented at the LeCroy Conference on Electronics for Future Colliders, Montvale, NJ, 10-11 May 1994
(Contract DE-AC05-84OR-21400)
(DE94-019112; CONF-9405199-2) Avail: CASI HC A03/MF A01

Electronics developed for signal processing, digitization, and readout of a 10,000-element lead-glass electromagnetic calorimeter for CERN experiment WA98 are described. Chief among the components developed are two CMOS monolithic circuits. One, known as the 'Preamp' chip, includes eight channels each of integrator, dual gain amplifier, fast shaping amplifier, constant fraction discriminator, and also two 2 by 2 current sums for trigger purposes, and maskable calibration pulsers for the time and energy channels. It also includes three 6-bit DAC's for setting thresholds and calibration values. The other chip, known as the 'ATA' (AMU/TAC/ADC) chip, includes 16 channels of AMU (analog memory unit), 8 channels of TAC, and 24 channels of Wilkinson-type ADC. A description of these chips' design and performance is given, together with a short description of supporting circuitry and of initial system performance as measured with 2- to 20-GeV electrons. DOE

N95-21590 Technische Univ., Delft (Netherlands).
NON-LINEAR A/D CONVERTERS FOR INTEGRATED SILICON SMART SENSORS Ph.D. Thesis [NIET-LINEAIRE A/D OMZETTERS VOOR SMART GEIENTEGREERDE SILICIUM SENSOREN]
K. E. M. Mahmoud 26 Apr. 1994 37 p
(PB94-208402; ISBN-90-6275-976-9) Avail: Issuing Activity (National Technical Information Service (NTIS))

Many sensors have a wide dynamic range and a limited accuracy. The use of a high-resolution A/D converter to cover the sensor dynamic range adds to the cost of the system without any benefit being derived from the high resolution in respect to the system overall accuracy. A nonlinear A/D converter offers an optimal solution for digitizing the output of these sensors. The aim of this research was to develop a non-linear A/D converter that features a wide dynamic range (about 10(exp 15)) and a resolution of about 8 bits. Further, in this research, the effect of the post-processing annealing and the epilayer thickness and doping concentrations on the DC bipolar characteristics were investigated. DTIC

N95-21614*# National Aeronautics and Space Administration. Marshall Space Flight Center, Huntsville, AL.

ROLE OF DIELECTRIC CONSTANT IN ELECTROHYDRODYNAMICS OF CONDUCTING FLUIDS

Percy H. Rhodes, Robert S. Snyder, and Glyn O. Roberts (Roberts Associates, Inc., Reston, VA.) [1992] 23 p Submitted for publication
(NASA-TM-110499; NAS 1.15:110499) Avail: CASI HC A01/MF A01

Electrohydrodynamic (EHD) flows are driven by the interaction of an electric field with variations in electric conductivity or dielectric constant. In reported EHD experiments on the deformation of drops of immiscible dielectric fluids, the role of conductivity has tended to overshadow the role of dielectric constant. Often, large conductivity contrasts were convenient because the conductivities of the dielectric fluid were relatively uncertain. As a result, the observed effects were always qualitatively the same as if there had been no contrast in dielectric constant. Our early experiments studying the EHC deformations of cylindrical streams readily showed the conductivity effect but the dielectric constant effect was not discernible. We have modified our flow chamber and improved our method of observation and can now see an unequivocal dielectric constant effect which is in agreement with the prior theory. In this paper we first give a brief description of the physics of charge buildup at the interface of an immersed spherical drop or flowing cylindrical sample stream and then show how these charge distributions lead to interface distortions and accompanying viscous flows which constitute EHD. We next review theory and experiment describing the deformation of spherical drops. We show that in the reported drop deformation experiments, the contrast in dielectric constant was never sufficient to reverse the deformation due to the conductivity contrast. We review our work describing the deformation of a cylindrical stream of one fluid flowing in a parallel flow of another, and we compare the deformation equations with those for spherical drops. Finally, we show a definite experimental dielectric constant effect for cylindrical stream of aqueous polystyrene latex suspension. The dielectric constant varies with the frequency of the imposed electric field, and the associated EHD flow change is very apparent. Author

N95-21660# Northwestern Univ., Evanston, IL. Dept. of Electrical Engineering and Computer Science.

InTlSb FOR LONG-WAVELENGTH INFRARED PHOTODETECTORS AND ARRAYS Annual Report

Manijeh Razeghi 1993 24 p
(Contract N00014-93-1-0409)
(AD-A280109) Avail: CASI HC A03/MF A01

The heteorepitaxial narrow-gap semiconductors on Si or GaAs substrates offer the possibility of monolithic integration of detectors and readout circuits in the infrared focal plane arrays (IRFPA's). This structure can avoid the problems of a complicated etch-thinning process and indium bump displace in the hybrid case. This structure permits the production of a large-area FPA's with high reliability and low cost. The purpose of this project is to develop III-V IRFPA on InSb, GaAs, Si substrates, special detectors made from In(1-x)Tl(x)Sb material system. The devices are of potential in the long wavelength (8-14 micrometers), particularly in the application of thermal imaging, as MCT materials suffer from poor composition uniform over large areas and thermal stability. As a preliminary step towards InTlSb photovoltaic detectors, it is necessary to establish a reliable procedure to fabricate InSb photovoltaic detectors. DTIC

N95-21667# Los Alamos National Lab., NM.

AN 8-METER-LONG COUPLED CAVITY RFQ LINAC

L. M. Young 1994 4 p Presented at the 17th International LINAC Conference, Tsukuba, Japan, 21-26 Aug. 1994
(Contract W-7405-eng-36)
(DE94-018077; LA-UR-94-2686; CONF-9408125-8) Avail: CASI HC A01/MF A01

A model has been constructed of an 8-m-long high energy (7 MeV) Radio-Frequency Quadrupole (RFQ) to prove the concept of a resonantly coupled RFQ. The model consists of four 2-in-long RFQ segments resonantly coupled together. A small gap (3 mm) between the vane tips, at the segment joints, provides capacitive coupling. This model is of a RFQ designed for a proposed Los Alamos Accelerator Performance Demonstration Facility (APDF). The RFQ, as designed, will operate cw at 350 kHz and accelerate a 100-mA beam of protons to 7 MeV. DOE

N95-21671 Office of Naval Research, Arlington, VA.

COAXIAL HYBRID WIGGLER Patent Application

Robert H. Jackson, inventor, Henry P. Freund, inventor, Dean E. Pershing, inventor, and Jose M. Taccetti, inventor 12 Jul. 1994 28 p Limited Reproducibility: More than 20% of this document may be affected by microfiche quality
(AD-D016501; US-Patent-Appl-SN-274183) Avail: Issuing Activity (Defense Technical Information Center (DTIC))

An electromagnetic wiggler is introduced having a cylindrical member, and a central member disposed axially within the cylindrical member, both of which are formed from alternating cylindrical sections of ferromagnetic and non-ferromagnetic material, each sequential pair of these sections being the length of the wiggler's period Lambda w. The sequence of sections between the inner and outer members is shifted Lambda w/2, so that ferromagnetic sections of the outer member are disposed radially opposite non-ferromagnetic sections of the inner member, and vice versa. The resultant radial magnetic flux density in the cylindrical gap between the members is larger and sharper than the flux density for the same wiggler without the central member, permitting higher radiated power output, at higher radiation frequencies, for the same energy of input electron beam. DTIC

N95-21690 Honeywell, Inc., Bloomington, MN.

RF VACUUM MICROELECTRONICS BASED ON THIN FILM EDGE-EMITTER TECHNOLOGY Final Report, Sep. 1991 - Feb. 1994

Tayo Akinwande Apr. 1994 69 p Limited Reproducibility: More than 20% of this document may be affected by microfiche quality
(Contract MDA972-91-C-0030; ARPA Order 8162)
(AD-A279539) Avail: Issuing Activity (Defense Technical Information Center (DTIC))

We report the design, fabrication, and demonstration of thin-film-edge emitter vacuum diodes and transistors. The two-terminal device uses a thin-film-edge emitter as an electron source whose current density depends on the anode voltage. The three terminal device uses a thin-film-edge emitter as an electron source whose current density depends on the voltage applied to the extraction electrodes (gates). The emitted electrons are collected by the anode. All three electrodes (emitter, gate, and anode) are integrated on the same substrate. The devices have integrated on-chip resistors for bum-out prevention. The 3D microstructure was fabricated using IC and micromachining techniques. Contrasted with the usual vertical FEA structures, the particular vacuum transistor design invokes two dimensional vertical symmetry for the extraction electrodes (gate) using multi-layer thin film deposition techniques. The central thin-film-edge emitter is about 300 A thick and is surrounded by two gate electrodes, one above and one below. DTIC

N95-21693 Westinghouse Science and Technology Center, Pittsburgh, PA.

HIGH TEMPERATURE SUPERCONDUCTING FILMS AND MULTILAYERS FOR ELECTRONICS Final Report, 21 Feb. 1991 - 20 Feb. 1994

John R. Gavaler and John Talvacchio 19 Apr. 1994 209 p Limited Reproducibility: More than 20% of this document may be affected by microfiche quality
(Contract F49620-91-C-0034)
(AD-A279545; WCTC-94-9SL2-Super-R1; AFOSR-94-0307TR) Avail: CASI HC A10

The overall objective of this program was to develop a materials and fundamental device base for high-transition-temperature superconducting (HTS) electronics capable of operating at greater than 50K. Progress is reported on four tasks which address problems fundamental to the understanding of the superconducting state in HTS films, the application of HTS films in passive microwave circuits, the realization of HTS digital electronics, and the development of new superconducting devices. Large-area epitaxial YBCO films with low RF losses developed under this program and techniques for depositing them on both sides of single-crystal substrates were used in other Westinghouse and government-funded programs to develop HTS channelized filterbanks, delay lines, UHF antenna matching networks, and low-phase-noise resonators. An understanding was achieved of the role of oxygenation during film growth and the effect of film microstructure on RF losses. For HTS digital circuit fabrication, both active devices step-edge and edge-type YBCO Josephson junctions and trilayer BKBO junctions and passive structures were developed, such as crossovers, vias, and contacts. These capabilities were transfered to other Westinghouse and government-funded programs which demonstrated the first HTS SFQ circuits and SQUID's with integrated ground planes. DTIC

N95-21725# Massachusetts Inst. of Tech., Cambridge, MA. Plasma Fusion Center.
CURRENT DISTRIBUTION IN CABLE-IN-CONDUIT CONDUCTORS M.S. Thesis
M. A. Ferri May 1994 104 p Prepared for Oak Ridge Inst. for Science and Education, TN
(Contracts DE-FC02-93ER-54186; DE-AC05-76OR-00033)
(DE95-001820; DOE/ER-54186/T5; PFC/RR-94-6) Avail: CASI HC A06/MF A02

A numerical study of the current distribution in Cable-In-Conduit Conductors (CICC's) experiencing linearly ramping transport currents and transverse magnetic fields was conducted for both infinitely long, periodic cables and finite length cables terminated in low resistance joints. The goal of the study was to gain insight into the phenomenon known as Ramp Rate Limitation, an as yet unexplained correspondence between maximum attainable current and the ramp time taken to reach that current in CICC superconducting magnets. A discrete geometric model of a 27 strand multiply twisted CICC was developed to effectively represent the flux linkages, mutual inductances, and resistive contact points between the strands of an experimentally tested cable. The results of the numerical study showed that for fully periodic cables, the current imbalances due to ramping magnetic fields and ramping transport currents are negligible in the range of experimentally explored operating conditions. For finite length, joint terminated cables, however, significant imbalances can exist. Unfortunately, quantitative results are limited by a lack of knowledge of the transverse resistance between strands in the joints. Nonetheless, general results are presented showing the dependency of the imbalance on cable length, ramp time, and joint resistance for both ramping transverse magnet fields and ramping transport currents. At the conclusion of the study, it is suggested that calculated current imbalances in a finite length cable could cause certain strands to prematurely 'quench' - become non-superconducting - thus leading to an instability for the entire cable. This numerically predicted 'current imbalance instability' is compared to the experimentally observed Ramp Rate Limitation for the 27 strand CICC sample. DOE

N95-21729# Allied-Signal Aerospace Co., Kansas City, MO.
PLASTIC ENCAPSULATED PARTS
T. Castillo Oct. 1994 19 p
(Contract DE-AC04-76DP-00613)
(DE95-001876; KCP-613-5432) Avail: CASI HC A03/MF A01

Plastic semiconductor packages were characterized as possible alternatives for canned devices, which are susceptible to internal shorts caused by conductive particles. Highly accelerated stress testing (HAST) as well as electrical and mechanical testing were conducted on plastic technology devices. DOE

N95-21731# Idaho National Engineering Lab., Idaho Falls, ID.
ELECTRIC AND HYBRID VEHICLE PROGRAM: SITE OPERATOR PROGRAM Quarterly Progress Report, Oct. - Dec. 1993
D. M. Kiser and J. F. Warren Mar. 1994 54 p
(Contract DE-AC07-76ID-01570)
(DE95-001925; EGG-EP-11237-Qtr1) Avail: CASI HC A04/MF A01

The DOE Site Operator Program was initially established to meet the requirements of the Electric and Hybrid Vehicle Research, Development, and Demonstration Act of 1976. The Program has since evolved in response to new legislation and interests. Its mission now includes three major activity categories: (1) Advancement of Electric Vehicle (EV) technologies; (2) development of infrastructure elements needed to support significant EV use; (3) increasing public awareness and acceptance of EV's. The 14 Program participants, their geographic locations, and the principal thrusts of their efforts are identified. The EV inventories of each participant are summarized. The topics of this report include participants' experience with EV operation; an appraisal of the overall current status of EV's for transportation; program management; and a program experience overview, the result of analyzing Site Operator inputs, provides an insight into the variables that can affect electric vehicle performance and operating cost. DOE

N95-21738# Department of Energy, Washington, DC. Office of Transportation Technologies.
ELECTRIC AND HYBRID VEHICLES PROGRAM
Aug. 1994 73 p
(DE95-001711; DOE/EE-0026) Avail: CASI HC A04/MF A01

This program, in cooperation with industry, is conducting research, development, testing, and evaluation activities to develop the technologies that would lead to production and introduction of low-and zero-emission electric and hybrid vehicles into the Nation's transportation fleet. This annual report describes program activities in the areas of advanced battery, fuel cell, and propulsion systems development. Testing and evaluation of new technology in fleet site operations and laboratories are also provided. Also presented is status on incentives (CAFE, 1992 Energy Policy Act) and use of foreign components, and a listing of publications by DOE, national laboratories, and contractors. DOE

N95-21742# InnovASIC, Inc., Albuquerque, NM.
DESIGN AND DEVELOPMENT SAWAFE PEAK DETECTOR CHIP Final Report
1994 3 p Prepared for Los Alamos National Lab., NM
(Contract W-7405-eng-36)
(DE95-001745; LA-Sub-94-132) Avail: CASI HC A01/MF A01

InnovASIC, Inc. was placed under contract by Los Alamos National Laboratories to specify, design, and have fabricated an Application Specific Integrated Circuit for the SAWAFE program. The design was completed, and an initial fabrication run was made. The ASIC vendor, under subcontract to InnovASIC, had an error in the initial build of the chip. An investigation of the problem is now under way. A second build is expected to be completed in June. DOE

N95-21774 Northwestern Univ., Evanston, IL. Dept. of Electrical Engineering and Computer Science.
InTlSb FOR LONG-WAVELENGTH INFRARED PHOTODETECTORS AND ARRAYS Annual Report
Manijeh Razeghi 1 Jun. 1994 15 p Limited Reproducibility: More than 20% of this document may be affected by microfiche quality
(Contract N00014-93-1-0931)
(AD-A280108) Avail: CASI HC A03

A number of samples have been grown in the Intervac-EPI solid-source Molecular Beam Epitaxy (MBE) system since it was first commissioned in early May, 1994. The samples have consisted of both undoped and doped InSb, undoped InAs and various calibration layers such as n-type and p-type GaAs doping staircases. The different surface reconstructions and surfaces phase transitions have been investigated using Reflection High Energy Electron Diffraction (RHEED). For example, InSb growth temperature is set relative to a c(4x4) to a(1x3) surface phase transition, corresponding to an actual surface temperature of 390 C. RHEED oscillations were observed for GaAs, InAs and InSb as this is particularly important for determining growth rates and III/V flux radio. The philosophy has been to determine system independent growth parameters so that the technology can be easily transferred to other growth systems. DTIC

N95-21775 Department of the Navy, Washington, DC.
MULTI-PORT TESTER INTERFACE Patent Application
Alvin Botelho, inventor (to Navy) 10 Feb. 1994 19 p Limited Reproducibility: More than 20% of this document may be affected by microfiche quality
(AD-D016240; US-Patent-Appl-SN-194600) Avail: Issuing Activity (Defense Technical Information Center (DTIC))

A multi-port tester interface is coupled between an interface port tester having only one test port and a plurality of interface ports to be tested. The multi-port tester interface includes timing and control logic which provides an initialization signal to the interface port tester. The timing and control logic controls an interface port selector to provide an interface port address to a test signal multiplexer and an input multiplexer. A test signal from the interface port tester is transmitted to the appropriate interface port under test through the test signal multiplexer. A successful test completion signal is received by the appropriate input of the test completion multiplexer as selected by the address provided by the interface port selector, and provided to an input port of the interface port tester. Each interface port to be tested is thus sequentially yet automatically coupled to the interface port tester, and is sequentially tested without

connecting and disconnecting individual interface ports from a tester. Appropriate reset and voltage level signal shifting circuitry is also provided.
DTIC

N95-21865 Department of the Navy, Washington, DC.
MONOLITHIC LOW NOISE PREAMPLIFIER FOR PIEZOELECTRIC SENSORS Patent
Timothy B. Straw, inventor (to Navy) 16 Aug. 1994 6 p Filed 12 Apr. 1993
(AD-D016524; US-Patent-5,339,285; US-Patent-Appl-SN-045143; US-Patent-Class-367-135) Avail: US Patent and Trademark Office

A preamplifier for a piezoelectric sensor requiring a high-impedance, low noise interface circuit is introduced. The preamplifier is a single, monolithic integrated circuit that can be mounted directly onto or inside a miniature sensor without degrading the sensor's performance. The preamplifier performs signal amplification with a full-differential amplifier that includes common-mode feedback. A pair of feedback capacitors together with the sensor capacitance control the voltage gain of the preamplifier over much of it's useful operating range of 100 Hz to 100 kHz. The preamplifier circuit also has feedback resistors that discharge any accumulated DC voltage which might appear on the capacitors. Also the feedback resistors form a high pass filter which rejects low frequency background noise from the sensor. DTIC

N95-21881# Sandia National Labs., Albuquerque, NM.
INTEGRATION OF THIN FILM DECOUPLING CAPACITORS
Terry Garino, Duane Dimos, and Steve Lockwood 1994 6 p Presented at the Meeting on the Revolution in Microelectronics, Boston, MA, 15-17 Nov. 1994
(Contract DE-AC04-94AL-85000)
(DE95-001609; SAND-94-2239C; CONF-941199-2) Avail: CASI HC A02/MF A01

Thin film decoupling capacitors consisting of submicron thick, sol-gel Pb(Zr,Ti)O3 layers between Pt electrodes on a Si substrate have recently been developed. Because the capacitor structure needs to be only (approximately) 3 micrometers thick, these devices offer advantages such as decreased package volume and ability to integrate so that interconnect inductance is decreased, which allows faster IC processing rates. To fully utilize these devices, techniques of integrating them onto packages such as multi-chip modules and printed wiring boards or onto IC dies must be developed. The results of our efforts at developing integration processes for these capacitors are described here. Specifically, we have demonstrated a process for printing solder on the devices at the Si wafer level and reflowing it to form bumps and have developed a process for fabricating the devices on thin (25 to 75 micrometers) substrates to facilitate integration onto IC's and printed wiring boards. Finally, we assessed the feasibility of fabricating the devices on rough surfaces to determine whether it would be possible to fabricate these capacitors directly on multi-layer ceramic substrates. DOE

N95-21900 Department of the Navy, Washington, DC.
THERMAL FIXTURE FOR TESTING AN INTEGRATED CIRCUIT Patent
Walter T. Schneider, inventor (to Navy) 19 Jul. 1994 7 p Filed 10 Apr. 1992
(AD-D016483; US-Patent-5,331,273; US-Patent-Appl-SN-866920; US-Patent-Class-324-158) Avail: US Patent and Trademark Office

An apparatus for controlling the temperature of an integrated circuit is introduced. A thermally conductive block has a vacuum passage connected to a vacuum pump for clamping the block to the top of an integrated circuit housing without mechanical clamping structures. A closed fluid loop including a circulating pump, heater and chiller modulate the temperature of a fluid passing through the conductive block thereby to control its temperature and the temperature of the integrated circuit independently of any other integrated circuit. DTIC

N95-21901 Department of the Navy, Washington, DC.
MAGNETOSTRICTIVE MOTOR SYSTEM Patent
Bruce S. Maccabee, inventor (to Navy) 23 Aug. 1994 7 p Filed 18 Jan. 1991
(AD-D016484; US-Patent-5,341,056; US-Patent-Appl-SN-643632; US-Patent-Class-310-26) Avail: US Patent and Trademark Office

A plurality of drive modules positioned at spaced locations along a drive path of a driven member respectively include two magnetostrictive rod elements in alignment with each other, with adjacent ends thereof in engagement with a third magnetostrictive rod element extending transversely of the drive path to engage the driven member. Simultaneous elongation and contraction of the two rod elements during elongation of the third rod element in the drive modules imparts unidirectional motion to the driven member. DTIC

N95-21906 Department of the Navy, Washington, DC.
THORIATED-TUNGSTEN, SPLIT-RING, HOLLOW-CATHODE ELECTRODE FOR DISCHARGE DEVICES Patent
Edward J. Seibert, inventor (to Navy), Gerald D. Ferguson, inventor (to Navy), and Marie E. Taylor, inventor (to Navy) 27 Sep. 1994 7 p Filed 14 Mar. 1994
(AD-D016508; US-Patent-5,351,260; US-Patent-Appl-SN-209345; US-Patent-Class-372-84) Avail: US Patent and Trademark Office

An electrode assembly for a gas or metal vapor discharge device is disclosed. A pair of electrode assemblies each comprising thoriated tungsten with an alloy composition of tungsten (W) and from about 2% to about 3% of thorium dioxide, ThO2, are located at opposite ends of the discharge chamber of the discharge device. The tip of the electrode preferably has four slots equally spaced around its circumference and a groove at its outermost edge. The tip of the electrode provides mechanical flexibility that inhibits the cracking of the thoriated tungsten electrode when it is mounted in the discharge device. Each electrode assembly further comprises a copper spacer, preferably I-shaped in cross-section, brazed against the base of the electrode and against a vacuum flange. The pair of electrode assemblies confines the discharge of the discharge device between the tips of the electrodes and inhibits the arc condition from finding its way to delicate vacuum seals. DTIC

N95-21917 California Univ., Santa Barbara, CA. Dept. of Materials.
GROWTH AND ELECTRICAL AND FAR-INFRARED PROPERTIES OF WIDE ELECTRON WELLS IN SEMICONDUCTORS Final Technical Report, 15 Feb. 1991 - 14 Feb. 1994
Arthur C. Gossard 15 Apr. 1994 122 p Limited Reproducibility: More than 20% of this document may be affected by microfiche quality
(Grant AF-AFOSR-0214-91)
(AD-A279409; UCSB-08-075892; AFOSR-94-0285TR) Avail: Issuing Activity (Defense Technical Information Center (DTIC))

The thrust of the research carried out under this grant has been the development and study of wide, specially shaped graded quantum wells for electrons in semiconductors, as synthesized by high-precision epitaxial growth. In basic characterization of the wide wells, fundamental measurements of charge density, energy levels, and electron motions in the wells were pursued. The achievement of high-Q solid state electron resonators at Terahertz frequencies in the wide wells was stressed. Highly resonant cavities with electron scattering times nearly two orders of magnitude larger than for electrons in high-purity uniformly doped wells of comparable electron concentration have been grown. Structures were also achieved in which the resonant frequency of the electrons could be changed by application of a potential to a control electrode. Modification of the parabolic potential by superposition of periodic potentials and the extension of the parabolic well concept to remotely doped hole wells were also emphasized. DTIC

N95-21960# Edgerton, Germeshausen and Grier, Inc., Idaho Falls, ID. Idaho National Engineering Lab.
ELECTRIC AND HYBRID VEHICLE PROGRAM SITE OPERATOR PROGRAM
D. M. Kiser and J. F. Warren Aug. 1994 54 p
(Contract DE-AC07-76ID-01570)
(DE95-002042; EGG-EP-11237-Qtr2) Avail: CASI HC A04/MF A01

The Site Operator Program was initially established by the Department of Energy (DOE) to incorporate the electric vehicle activities dictated by the Electric and Hybrid Vehicle Research, Development and Demonstration Act of 1976. The Program currently includes thirteen sites located in diverse geographic, metrological,and metropolitan areas across the United States. Information is shared reciprocally with a fourteenth site, not under Program contract. The vehicles are operator-owned, except for two Griffon vans. The Mission Statement of the Site Operator Program includes three major activities: (1) Advancement of electric vehicle technologies. (2) Development

of infrastructure elements necessary to support significant electric vehicle use; and (3) Increasing the awareness and acceptance of electric vehicles (EVs) by the public. The ultimate thrust of program activities varies among sites, reflecting not only the Operator's business interests but also geographic and climate-related operating conditions. These considerations are identified below for each Program Status entry. This second quarter report (FY-94) will include a summary of activities from the previous three quarters.
DOE

N95-22011# Los Alamos National Lab., NM.
A 500 MW ANNULAR BEAM RELATIVISTIC KLYSTRON
M. V. Fazio, W. B. Haynes, B. E. Carlsten, and R. M. Stringfield 1994 4 p Presented at the 17th International LINAC Conference, Tsukuba, Japan, 21-26 Aug. 1994
(Contract W-7405-eng-36)
(DE95-000867; LA-UR-94-3101; CONF-9408125-34) Avail: CASI HC A01/MF A01

This paper describes the experimental development of a long pulse, high current, annular beam relativistic klystron amplifier. The desired performance parameters are 1 GW output power and 1 (mu)s pulse length with an operating frequency of 1.3 GHz. The electron beam voltage and current are nominally 600 kV and 5 kA. Peak powers approaching 500 MW have been achieved in pulses of 1 (mu)s nominal baseline-to-baseline duration. The half power pulse width is 0.5 (mu)s. These pulses contain an energy of about 160 J. The design of this class of tube presents some unique challenges, particularly in the output cavity. The output cavity must exhibit a very low gap shunt impedance in order to obtain reasonable conversion efficiency from the low impedance modulated electron beam to microwave power, while still maintaining a reasonable loaded Q for mode purity. The physics of this device is dominated by space charge effects which strongly impact the design. Current experimental results and theoretical design considerations for this class of tube, and scaling to higher frequency operation, suitable for the Next Linear Collider are discussed.
DOE

N95-22023# ARC Professional Service Group, Inc., Rome, NY.
CATHODE LIFE TEST FACILITY Final Report
Ronald J. Jardieu Oct. 1994 90 p
(Contract F30602-89-D-0028)
(AD-A286232; RL-TR-94-180) Avail: CASI HC A05/MF A01

The Cathode Life Test Facility (CLTF) has been in operation for ten years and has tested ten different cathode types for a total of approximately 2.0 million hours of life test data. As part of the defense management review (DMR) process, Rome Laboratory (RL) has eliminated internal research efforts pertaining to cathode life testing. Based on this directive, the CLTF was moved to the Naval Surface Warfare Center (NSWC) at Crane, Indiana. This report summarizes the process of moving the CLTF from RL to the NSWC.
DTIC

N95-22030 Department of the Navy, Washington, DC.
UNINTERRUPTED, ENHANCED-RATE EVENT SEQUENCER WITH MIXED-SPEED COUNTER MODULES Patent
Willard M. Cronyn, inventor (to Navy) 5 Apr. 1994 9 p Filed 18 Dec. 1991
(AD-D016255; US-Patent-5,301,219; US-Patent-Appl-SN-809349; US-Patent-Class-377-44) Avail: US Patent and Trademark Office

The invention includes a data memory having sequentially stored N-bit words that are each a binary description of a time at which an event is to occur. Also stored is a K-bit word, associated with each N-bit word, that is a binary description of what the scheduled event is to be. The invention utilizes a free-running clock and clock circuitry to gauge when an event should occur. The clock circuitry tallies an N-bit description of running time. M-bits of the N-bit description of running time are specified by a single fast synchronous counter. The remaining N-M bits are specified by two slow counters each of N-M bit capacity. Because incrementation of slow counters creates count settling times that may significantly affect accurate event sequencing, the slow counters are alternately incremented and a multiplexer is used to switch to the counter that will provide a 'steady state' count at a scheduled event time.
DTIC

N95-22062# EG and G Mound Applied Technologies, Miamisburg, OH.
SEQUENTIAL SHOCK INDUCED SWITCH TESTS FOR EGLIN AIR FORCE BASE
Russell D. Cech 11 Aug. 1994 16 p
(Contract DE-AC04-88DP-43495)
(DE95-001786; MLM-3785) Avail: CASI HC A03/MF A01

Tests were performed at EG&G Mound Applied Technologies to investigate the effect of using the tangential shock wave from detonating Extex explosive to cause shock conduction of a Kapton dielectric. Two voltages (600 and 4000) were switched from a 600 pF capacitor. Timing between four shock switches and four pin switches was found and compared during a single detonation event. Electrical conduction was observed between shock switches and the current paths were found.
DOE

N95-22086# Sandia National Labs., Albuquerque, NM.
SEU AND SEL RESPONSE OF THE WESTINGHOUSE 64K E-2PROM, ANALOG DEVICES AD7876 12-BIT ADC, AND THE INTEL 82527 SERIAL COMMUNICATIONS CONTROLLER
F. W. Sexton, G. L. Hash, M. P. Connors, J. R. Murray, J. R. Schwank, P. S. Winokur, and E. G. Bradley 1994 9 p Presented at the 31st Annual International Nuclear and Space Radiation Effects Conference, Tucson, AZ, 18-22 Jul. 1994
(Contract DE-AC04-94AL-85000)
(DE95-003349; SAND-94-0449C; CONF-940726-16) Avail: CASI HC A02/MF A01

The Westinghouse SA3823 64K E(sup 2)PROM radiation-hardened SONOS non-volatile memory exhibited a single-event-upset (SEU) threshold in the read mode of 60 MeV-sq cm/mg and 40 MeV-sq cm/mg for data latch errors. The minimum threshold for address latch errors was 35 MeV-sq cm/mg. Hard errors were observed with Kr at V(sub p) = 8.5 V and with Xe at Programming voltages (V(sub p)) as low as 7.5 V. No hard errors were observed with Cu at any angle up to V(sub p) = II V. The system specification of no hard errors for Ar ions or lighter was exceeded. No single-event latchup (SEL) was observed in these devices for the conditions examined. The Analog Devices AD7876 12bit analog-to-digital converter (ADC) had an upset threshold of 2 MeV-cm(sup 2)/mg for all values of input voltage (V(sub in)), while the worst-case saturation cross section of approximately 2 x 10(exp -3)sq cm as measured with V(sub in) = 4.49 V. No latchup was observed. The Intel 82C527 serial communications controller exhibited a minimum threshold for upset of 2 MeV-cm(exp 4)/mLi, and a saturation cross section of about 5 x 10(exp-4)sq cm. For latchup the minimum threshold was measured at 17 MeV-sq cm/mg, and cross section saturated at about 3 x10(exp -4)sq cm. Error rates for the expected applications are presented.
DOE

N95-22112*# National Aeronautics and Space Administration. Lewis Research Center, Cleveland, OH.
PERFORMANCE OF Ga(0.47)In(0.53)As CELLS OVER A RANGE OF PROTON ENERGIES
I. Weinberg, R. K. Jain (Toledo Univ., OH.), C. VargasAburto (Kent State Univ., OH.), D. M. Wilt, and D. A. Scheiman (NYMA, Inc., Brook Park, OH.) Jan. 1995 6 p Presented at the First World Conference on Photovoltaic Energy Conversion, Waikoloa, HI, 5-9 Dec. 1994; sponsored by IEEE, PVSEC-Japan and PSEC-Europe
(Contract NAS3-27186; RTOP 233-02-0A)
(NASA-TM-106819; E-9359; NAS 1.15:106819) Avail: CASI HC A02/MF A01

Ga(0.47)In(0.53)As solar cells were processed by OMVPE and their characteristics determined at proton energies of 0.2, 0.5, and 3 MeV. Emphasis was on characteristics applicable to use of this cell as the low bandgap member of a monolithic, two terminal high efficiency InP/GaInAs cell. It was found that the radiation induced degradation in efficiency, I(sub SC), V(sub OC) and diffusion length increased with decreasing proton energy. When efficiency degradations were compared with InP it was observed that the present cells showed considerably more degradation over the entire energy range. Similar to InP, R(sub C), the carrier removal rate, decreased with increasing proton energy. However, numerical values for R(sub C) differed from those observed with InP. The difference is attributed to differing defect behavior between the two cell types. It was concluded that particular attention should be paid to the effects of low energy protons especially when the particle's track ends in one cell of the multibandgap device.
Author

N95-22118# Sandia National Labs., Albuquerque, NM.
DEFECT CLASSES: AN OVERDUE PARADIGM FOR CMOS IC TESTING

C. F. Hawkins (New Mexico Univ., Albuquerque, NM.), J. M. Soden, A. W. Righter, and F. J. Ferguson (California Univ., Santa Cruz, CA.) 1994 13 p Presented at the International Test Conference, Washington, DC, 3-5 Oct. 1994
(Contract DE-AC04-94AL-85000)
(DE94-018905; SAND-94-2009C; CONF-9410194-1) Avail: CASI HC A03/MF A01

The IC test industry has struggled for more than 30 years to establish a test approach that would guarantee a low defect level to the customer. We propose a comprehensive strategy for testing CMOS IC's that uses defect classes based on measured defect electrical properties. Defect classes differ from traditional fault models. Our defect class approach requires that the test strategy match the defect electrical properties, while fault models require that IC defects match the fault definition. We use data from Sandia Labs failure analysis and test facilities and from public literature. We describe test pattern requirements for each defect class and propose a test paradigm. DOE

N95-22144 Hughes Research Labs., Malibu, CA.
SUB-MILLIMETERWAVE SEMICONDUCTOR SIGNAL SOURCES Final Report, Aug. 1990 - Aug. 1993
S. E. Rosenbaum Apr. 1994 38 p Limited Reproducibility: More than 20% of this document may be affected by microfiche quality
(Contract F19628-90-C-0171)
(AD-A279375; HAC-REF-J1881; RL-TR-94-13) Avail: Issuing Activity (Defense Technical Information Center (DTIC))

Research on Indium Phosphide Pseudomorphic High Electron Mobility Transistors (InP PHEMT's) resulted in 155 GHz and 215 GHz monolithic integrated circuit oscillators. These circuits represent the highest frequencies achieved to date for a fundamental signal source using a three terminal device. Advances in epitaxial growth of the pseudomorphic semiconductor structures and the achievement of low-resistance, 50-nm-long self-aligned gates resulted in the highest short circuit current gain cutoff frequency (ft) transistors ever reported. The planar quasi-optical slot oscillators verify the high frequency capabilities of the InP PHEMT. Hughes Laboratories performed the research on materials, device design and processing device characterization and modeling. The University of Michigan designed the oscillator circuits, including the integrated planar antennas, and measured the, oscillator performance. DTIC

N95-22149# Oak Ridge National Lab., TN.
PLASMA PROCESSING FOR INTEGRATED CIRCUITS
L. A. Berry 1994 7 p Presented at the 1993 Fusion Power Associates Annual Meeting, Oak Ridge, TN, 4-6 Oct. 1993
(Contract DE-AC05-84OR-21400)
(DE95-001419; CONF-9310209-2) Avail: CASI HC A02/MF A01

The steady advance of integrated circuit technology is one of the most remarkable technology trends in this era of technological revolution. For example, the 64-k memory chips of the early 1980s are now being replaced by 4-M and even 16-M chips. This trend is expected to continue with chips at the giga-bit level being available in a decade. The needs for ultraviolet and then X-ray lithography to define the submicron features needed for these larger, denser chips have been widely discussed. However, in parallel, the equipment (referred to as tools in the industry) and related processes to carry out the deposition and etching steps needed to actually produce devices in the tenth-micron range also require significant development. This paper summarizes present and anticipated contributions of magnetic fusion plasma theory and diagnostics and plasma production technology at Oak Ridge National Laboratory (ORNL) for the development of integrated circuit production technology. The discussion is introduced with a review of past technology evolution and of the present economic context for manufacturing. DOE

N95-22165# Los Alamos National Lab., NM.
RADIATION CHARACTERIZATION REPORT FOR THE GPS RECEIVER MICROCONTROLLER CHIP
20 Jun. 1994 16 p Prepared in cooperation with Novus Technologies, Inc., Albuquerque, NM
(Contract W-7405-eng-36)
(DE94-019169; LA-SUB-94-122) Avail: CASI HC A03/MF A01

The overall objective of this characterization test was to determine the sensitivity of the Motorola 68332 32-bit microcontroller to radiation induced single event upset and latch-up (SEU/SEL). The microcontroller is a key component of the GPS Receiver which will be a subsystem of the satellite required for the 'FORTE' experiment. Testing was conducted at the Single Event Effects Laboratory at Brookhaven National Laboratory. The results obtained included a latch-up (SEL) threshold LET (Linear Energy Transfer) of 20 MeV-sq cm/mg and an upset (SEU) threshold LET of 5 MeV-sq cm/mg. The SEU threshold is typical of this technology, commercial 0.8 micrometers HCMOS. Some flow errors were observed that were not reset by the internal watchdog timer of the 68332. It is important that the Receiver design include a monitor of the device, such as an external watch-dog timer, that would initiate a reset of the program when this type of upset occurs. The SEL threshold is lower than would be expected for this 12 micrometer epi layer process and suggests the need for a strategy that would allow for a hard reset of the controller when a latch-up event occurs. Analysis of the galactic cosmic ray spectrum for the FORTE orbit was done and the results indicate a worst case latch-up rate for this device of 6.3 x 10(exp -5) latch-ups per device day or roughly one latch-up per 43.5 device years. DOE

N95-22184# European Organization for Nuclear Research, Geneva (Switzerland).
RADIATION TESTS ON SERVICE ELECTRONICS FOR FUTURE MULTI TeV DETECTORS
H. Larsen, H. Schoenbacher, T. Massam (Istituto Nazionale di Fisica Nucleare, Bologna, Italy.), and F. Wulf (Hahn-Meitner-Inst. G.m.b.H., Berlin, Germany.) 12 Oct. 1993 107 p
(DE94-632822; CERN-93-04) Avail: CASI HC A06/MF A02 (US Sales Only)

Irradiation tests of a number of essential components for use in the service electronics of the Leading Proton Spectrometer (LPS) have been undertaken. The components are simple medium-scale integrated circuits such as Transistor Transistor Logic (TTL) buffers from the Advanced Low-power Schottky (ALS), Low-power Schottky (LS), and Fast (F) families, optocouplers, and balanced line drivers and receivers. More complex circuits, such as a Fuse Programmable Array Logic chip, programmed as a 6-bit counter, and a complete switched-mode power supply unit were also tested. Further, monolithic voltage regulators with an output potential of 5 V, and 10 MHz quartz oscillator hybrids were tested. The different radiation fields were X-rays (80 keV), (sup 60)Co gamma rays, electrons (2.5 MeV), and a high-energy proton accelerator environment. Depending on the device degradation, the maximum dose was up to 0.8 MGy. It is shown that the simple choice of circuit family can achieve a hardness level of nearly 1 MGy(Si), provided that one is prepared to make some sacrifices in power consumption, and in speed. It has been found that this radiation hardness can be reached with LS technology. The maximum level of about 1 MGy(Si) was obtained with 2.5 MeV electrons, which is equivalent to a 1 MeV neutron fluence of the order of 6x10(exp 13)/sq cm. DOE

N95-22189# Argonne National Lab., IL.
ESTIMATION OF LIGHTNING STROKE PEAK CURRENT AS A FUNCTION OF PEAK ELECTRIC FIELD AND THE NORMALIZED AMPLITUDE OF SIGNAL STRENGTH: CORRECTIONS AND IMPROVEMENTS
Y. P. Liaw, D. R. Cook, and D. L. Sisterson 1994 18 p
(Contract W-31-109-eng-38)
(DE94-016900; ANL/ER/PP-82416) Avail: CASI HC A03/MF A01

Corrections and improvements have been made to published equations relating return stroke peak current and peak electric field for cloud-to-ground lightning. The original equations were derived from measurements made at the Rocket-Triggered-Lightning Program (RTLP) facility at the Kennedy Space Center in Florida. Some previous articles include errors in the conversion of equations from units of volts per meter, for peak electric field, into lightning location and protection units, representing normalized signal strength amplitude. This article presents the proper conversion procedure and the resultant corrected equations. Furthermore, equations are presented that were produced by converting other published relationships. Finally, we combined 1985-1988 RTLP data to produce equations based on more data than has been used previously; the resulting equation for peak current as a function of normalized signal strength amplitude supports previous evidence that the slope should be near 0.2 for a zero intercept. All relationships are tabulated, and three are graphically compared against the data. DOE

N95-22236# California Univ., Berkeley. Lawrence Berkeley Lab, CA.
REFLECTIVE MASKS FOR EXTREME ULTRAVIOLET LITHOGRAPHY Ph.D. Thesis
Khanh Bao Nguyen May 1994 146 p
(Contract DE-AC03-76SF-00098)
(DE95-003427; LBL-36078) Avail: CASI HC A07/MF A02

Extreme ultraviolet lithographic masks are made by patterning multilayer reflective coatings with high normal incidence reflectivity. Masks can be patterned by depositing a patterned absorber layer above the coating or by etching the pattern directly into the coating itself. Electromagnetic simulations showed that absorber-overlayer masks have superior imaging characteristics over etched masks (less sensitive to incident angles and pattern profiles). In an EUVL absorber overlayer mask, defects can occur in the mask substrate, reflective coating, and absorber pattern. Electromagnetic simulations showed that substrate defects cause the most severe image degradation. A printability study of substrate defects for absorber overlayer masks showed that printability of 25 nm high substrate defects are comparable to defects in optical lithography. Simulations also indicated that the manner in which the defects are covered by multilayer reflective coatings can affect printability. Coverage profiles that result in large lateral spreading of defect geometries amplify the printability of the defects by increasing their effective sizes. Coverage profiles of Mo/Si coatings deposited above defects were studied by atomic force microscopy and TEM. Results showed that lateral spread of defect geometry is proportional to height. Undercut at defect also increases the lateral spread. Reductions in defect heights were observed for 0.15 micro m wide defect lines. A long-term study of Mo/Si coating reflectivity revealed that Mo/Si coatings with Mo as the top layer suffer significant reductions in reflectivity over time due to oxidation. DOE

N95-22254# Howard Univ., Washington, DC. Dept. of Physics.
HIGH TEMPERATURE SUPERCONDUCTING MICROWAVE DEVICE Final Report
Robert M. Catchings Nov. 1993 9 p
(Contract DAAL01-92-K-0200)
(AD-A286351; CT-2-R4921-CT-CT/01; ARL-CR-76) Avail: CASI HC A02/MF A01

Thin films of the high-Tc superconductor Bi-Sr-Ca-Cu-0 were prepared by sputter deposition. The films were deposited at room temperature and then post deposition annealed. A microwave measurement system based on a microstrip resonator was established. X ray diffraction revealed that the films were multi-phase. Resistance of these films did not show a transition when cooled to liquid nitrogen temperatures. DTIC

N95-22271# Oak Ridge National Lab., TN.
DEVELOPMENT OF PRACTICAL HIGH TEMPERATURE SUPERCONDUCTING WIRE FOR ELECTRIC POWER APPLICATIONS
Robert A. Hawsey, Robert S. Sokolowski (Intermagnetics General Corp., Latham, NY.), Pradeep Haldar (Intermagnetics General Corp., Latham, NY.), and Leszek R. Motowidlo (IGC Advanced Superconductors, Inc., Waterbury, CT.) 1994 9 p Presented at the 4th International Conference and Exhibition of the World Congress on Superconductivity, Orlando, FL, 27 Jun. - 1 Jul. 1994
(Contracts DE-AC05-84OR-21400; DE-FG02-92ER-81461)
(DE94-017894; CONF-940627-4) Avail: CASI HC A02/MF A01

The technology of high temperature superconductivity has gone from beyond mere scientific curiosity into the manufacturing environment. Single lengths of multifilamentary wire are now produced that are over 200 meters long and that carry over 13 amperes at 77 K. Short-sample critical current densities approach 5 x 10(exp 4) A/sq cm at 77 K. Conductor requirements such as high critical current density in a magnetic field, strain-tolerant sheathing materials, and other engineering properties are addressed. A new process for fabricating round BSCCO-2212 wire has produced wires with critical current densities as high as 165,000 A/sq cm at 4.2 K and 53,000 A/sq cm at 40 K. This process eliminates the costly, multiple pressing and rolling steps that are commonly used to develop texture in the wires. New multifilamentary wires with strengthened sheathing materials have shown improved yield strengths up to a factor of five better than those made with pure silver. Many electric power devices require the wire to be formed into coils for production of strong magnetic fields. Requirements for coils and magnets for electric power applications are described. DOE

N95-22284# Colorado Univ., Boulder, CO.
PARALLEL NANOMETER SCALE FABRICATION Final Report, 19 Sep. 1989 - 14 Sep. 1992
K. Douglas Sep. 1993 14 p
(Contract DE-FG02-89ER-14077)
(DE95-002122; DOE/ER-14077/T1) Avail: CASI HC A03/MF A01

Our approach to nanotechnology stresses parallel (as opposed to serial) processing and self-assembly techniques and we have demonstrated a basic parallel nanofabrication process that will enable a wide variety of nanometer-scale structures to be made. The process of nanometer molecular lithography employs two-dimensional biomolecular crystals as patterning elements in the parallel fabrication of structures on the 1-10 nm length scale. We have further demonstrated the fabrication of composite biomolecular/solid state heterostructures of nanometer dimension (nanoheterostructures). We are presently pursuing central issues in the development of nanotechnology such as the understanding and control of fluctuations and structural variations as well as applications of our nanofabrication process. An example of the latter is the formation of porous silicon having monodisperse arrays of silicon 'quantum wires' to elucidate the role of quantum confinement in the phenomenon of luminescent silicon. DOE

N95-22382 Technische Univ., Delft (Netherlands). Electronic Instrumentation Lab.
MULTI SIGNAL-DOMAIN MODELING OF SOLID-STATE TRANSDUCERS: A THEORETICAL FRAMEWORK BASED ON IRREVERSIBLE THERMODYNAMICS MIXED FINITE ELEMENTS AND MULTIGRID Ph.D. Thesis
Dave C. vanDuyn 29 Nov. 1993 263 p
(PB95-134995; ISBN-90-6275-932-7) Copyright Avail: Issuing Activity (National Technical Information Service (NTIS))

The more specific aims of this dissertation is the modeling and simulation of the thermoelectric effects in silicon solid-state transducers. This work is roughly split into two main parts. The first part (Chapters 2 and 3) deals with the construction of a physical model of the thermoelectric effects in the continuous space-time domain. The second part (Chapters 4, 5 and 6) deals with the implementation of the thermoelectric model. This work is, therefore, organized as follows: In Chapter 2, the authors discuss some generic aspects of physically based system models that can be used to model the (real-time) behavior of solid-state transducer configurations. In Chapter 3, a concrete example of the considerations presented in Chapter 2 is discussed, which is the modeling of the thermal and electrical energy domain for the case of a generic semiconductor. In Chapter 4, the authors discuss the transformation of the continuous space-time model into its discrete equivalent. In Chapter 5 the authors discuss a rather unconventional method for solving these discrete equations numerically. Chapter 6 deals with some of the practical implementation issues. Finally, in Chapter 7 the authors give illustrative examples. NTIS

N95-22412# Applied Science and Technology, Inc., Woburn, MA.
MATERIALS PROCESSING AND MANUFACTURING TECHNOLOGIES FOR DIAMOND SUBSTRATES MULTICHIP MODULES
Evelio Sevillano 14 Oct. 1994 4 p
(Contract N00014-93-C-2026)
(AD-A285775) Avail: CASI HC A01/MF A01

The previous quarter saw attainment of the target 1g/hr diamond deposition at 75kW, as well as full power continuous operation of the AX6600 system. In this quarter we have focused on process chemistry at full power, exploring the operating range of the AX6600 and process chemistry variables. Specific process conditions we have explored include: deposition rates from 300 mg/hr to over 900 mg/hr, operation from 50 to over 75 kW, deposition on areas from 6 diameter to 12 diameter, deposition on a variety of substrate materials and techniques for intact release of the diamond at the end of the deposition step, deposition of non-uniform films for stress/flatness control. DTIC

N95-22418 Department of the Navy, Washington, DC.
PRE-AMPLIFIER WITH MULTI-STAGE FEEDBACK Patent Application
James D. Hagerty, inventor (to Navy) 25 Mar. 1994 16 p Limited Reproducibility: More than 20% of this document may be affected by microfiche quality
(AD-D016254; US-Patent-Appl-SN-215879) Avail: CASI HC A03

A circuit for amplifying an input signal comprises an operational amplifier, a dual operational amplifier, and a buffering operational amplifier all cascaded in the aforementioned order. The first operational amplifier amplifies the input signal with minimum noise degradation, is set up as a non-inverting amplifier stage, and has a local negative feedback loop comprising a resistor and capacitor in parallel. The dual operational amplifier has two amplifying devices. One device forms a second amplifying stage which increases the gain of the pre-amplified input signal and has a local negative feedback loop comprising a resistor. DTIC

N95-22421# Lawrence Livermore National Lab., Livermore, CA.
DEMONSTRATION OF ZINC/AIR FUEL BATTERY TO ENHANCE THE RANGE AND MISSION OF FLEET ELECTRIC VEHICLES: PRELIMINARY RESULTS IN THE REFUELING OF A MULTICELL MODULE
J. F. Cooper, D. Fleming, L. Keene, A. Maimoni, K. Peterman, and R. Koopman Aug. 1994 9 p Presented at the 29th Intersociety Energy Conversion Engineering Conference, Monterey, CA, 7-12 Aug. 1994
(Contract W-7405-eng-48)
(DE95-004206; UCRL-JC-117946; CONF-940812-23) Avail: CASI HC A02/MF A01

We report progress in an effort to develop and demonstrate a refuelable zinc/air battery for fleet electric vehicle applications. A refuelable module consisting of twelve bipolar cells with internal flow system has been refueled at rates of nearly 4 cells per minute, indicating a refueling time of 10 minutes for a 15 kW, 55 kWh battery. The module is refueled by entrainment of 0.5-mm particles in rapidly flowing electrolyte, which delivers the particles into hoppers above each cell in a parallel-flow hydraulic circuit. The concept of user-recovery is presented as an alternative to centralized service infrastructure during market entry. DOE

N95-22427# Lawrence Livermore National Lab., Livermore, CA.
UNIQUE MICROCHANNEL PLATE PROCESS DOUBLES MCPI RESOLUTION
S. Thomas and G. Power 22 Aug. 1994 7 p Presented at the 21st International Congress on High Speed Photography and Photonics, Taejon, Republic of Korea, 29 Aug. - 2 Sep. 1994
(Contract W-7405-eng-48)
(DE94-017507; UCRL-JC-116838; CONF-9408148-1) Avail: CASI HC A02/MF A01

Applying a dielectric layer to the output of a microchannel plate (MCP) has allowed the screen voltage of a sealed microchannel-plate intensifier tube (MCPI) to be raised to over 10 kV, producing a field strength of 36 kV/mm without any detectable field emission or breakdown of the MCP/screen gap. Tube resolution exceeded 16l p/mm at 50% modulation. Breakdown is higher in a dielectric than in a vacuum. In a concept being patented by Gary Power, a few micrometers thick layer of a dielectric was sputtered onto the output surface of an 18 mm MCP, which was incorporated into a tube under a contract for four tube starts. This process is applicable to any device incorporating a proximity-focused MCP and screen, including streak tubes and gated MCP x-ray imagers. Other improvements discussed include a patented use of a collimator for eliminating the electrons that are elastically scattered from the screen. This method also provides for further improvements in screen gap limited resolution to any desired degree by eliminating electrons with high transverse energy. This occurs at the expense of output brightness, which can be recovered through an appropriate increase in screen voltage. DOE

N95-20639# Bell Telephone Labs., Inc., Whippany, NJ.
PACKAGING THE MAMA MODULE
J. Dennis Seals *In* AGARD, Advanced Packaging Concepts for Digital Avionics Oct. 1994 7 p Prepared in cooperation with Army Night Vision Labs (For primary document see N95-20631 06-06)
Copyright Avail: CASI HC A02/MF A03

N95-20640# Army Research Lab., Fort Monmouth, NJ.
THE DEMISE OF PLASTIC ENCAPSULATED MICROCIRCUIT MYTHS
E. B. Hakim, R. K. Agarwal (Delco Electronics, Kokomo, IN.), and M. Pecht (Maryland Univ., College Park, MD.) *In* AGARD, Advanced Packaging Concepts for Digital Avionics Oct. 1994 7 p (For primary document see N95-20631 06-06)
Copyright Avail: CASI HC A02/MF A03

N95-20642# Naval Air Warfare Center, Indianapolis, IN. Standard Hardware Acquisition and Reliabilty Program.
ADVANCED STANDARD ELECTRONIC MODULES FORMAT-E (SEM-E) PROCESSES FOR RAPID PROTOTYPING
Anthony Hawkins *In* AGARD, Advanced Packaging Concepts for Digital Avionics Oct. 1994 11 p (For primary document see N95-20631 06-06)
Copyright Avail: CASI HC A03/MF A03

N95-20644# Rome Lab., Griffiss AFB, NY.
ASSURING KNOWN GOOD DIE (KGD) FOR RELIABLE, COST EFFECTIVE MCMs
Daniel E. Daskiewich *In* AGARD, Advanced Packaging Concepts for Digital Avionics Oct. 1994 7 p (For primary document see N95-20631 06-06)
Copyright Avail: CASI HC A02/MF A03

N95-20645# Lucas Electronics, Birmingham (England).
THE DESIGN AND MANUFACTURING DEVELOPMENT OF AN ACTIVE SILICON SUBSTRATE MCM
M. G. Roughton and L. Waite *In* AGARD, Advanced Packaging Concepts for Digital Avionics Oct. 1994 7 p Sponsored by DTI (For primary document see N95-20631 06-06)
Copyright Avail: CASI HC A02/MF A03

N95-20651# Naval Air Warfare Center, Warminster, PA. Aircraft Div.
A TECHNIQUE FOR INCREASING THE BANDWIDTH OF HIGH PERFORMANCE ELECTRICAL BACKPLANES
W. Rosen, S. Rajan, V. Gershman, and M. Shadaram (Texas Univ., El Paso, TX.) *In* AGARD, Advanced Packaging Concepts for Digital Avionics Oct. 1994 4 p (For primary document see N95-20631 06-06)
Copyright Avail: CASI HC A01/MF A03

N95-20653# GEC-Marconi Materials Technology, Towcester (England).
HIGH PERFORMANCE BACKPLANE COMPONENTS FOR MODULAR AVIONICS
C. J. Groves-Kirkby, M. J. Goodwin, J. P. Hall, G. Glynn, J. Hankey, M. D. Salik, R. C. Goodfellow, and D. J. Jibb (GEC-Marconi Avionics Ltd., Chelmsford, England.) *In* AGARD, Advanced Packaging Concepts for Digital Avionics Oct. 1994 6 p (For primary document see N95-20631 06-06)
(ESPRIT 3 Proj. 6276)
Copyright Avail: CASI HC A02/MF A03

N95-21539*# Jet Propulsion Lab., California Inst. of Tech., Pasadena, CA.
ON-WAFER, CRYOGENIC CHARACTERIZATION OF ULTRA-LOW NOISE HEMT DEVICES
J. J. Bautista, J. Laskar (Hawaii Univ., Honolulu, HI.), and P. Szydlik (State Univ. of New York, Plattsburgh, NY.) *In its* The Telecommunications and Data Acquisition Report 15 Feb. 1995 p 104-120 (For primary document see N95-21532 06-32)
(RTOP 314-30-11-10-02)
Avail: CASI HC A03/MF A03

34 FLUID MECHANICS AND HEAT TRANSFER

Includes boundary layers; hydrodynamics; fluidics; mass transfer; and ablation cooling.

For related information see also *02 Aerodynamics* and *77 Thermodynamics and Statistical Physics.*

N95-19912*# Detroit Diesel Allison, Indianapolis, IN.
EXPERIMENTAL STUDY OF VANE HEAT TRANSFER AND AERODYNAMICS AT ELEVATED LEVELS OF TURBULENCE Final Report
Forrest E. Ames Cleveland, OH NASA Nov. 1994 125 p
(Contract NAS3-25950; RTOP 505-62-10)
(NASA-CR-4633; E-9203; NAS 1.26:4633) Avail: CASI HC A06/MF A02

A four vane subsonic cascade was used to investigate how free stream turbulence influences pressure surface heat transfer. A simulated combustor turbulence generator was built to generate high level (13 percent) large scale (Lu approximately 44 percent inlet span) turbulence. The mock combustor was also moved upstream to generate a moderate level (8.3 percent) of turbulence for comparison to smaller scale grid generated turbulence (7.8 percent). The high level combustor turbulence caused an average pressure surface heat transfer augmentation of 56 percent above the low turbulence baseline. The smaller scale grid turbulence produced the next greatest effect on heat transfer and demonstrated the importance of scale on heat transfer augmentation. In general, the heat transfer scaling parameter U(sub infinity) TU(sub infinity) LU(sub infinity)(exp -1/3) was found to hold for the turbulence. Heat transfer augmentation was also found to scale approximately on Re(sub ex)(exp 1/3) at constant turbulence conditions. Some evidence of turbulence intensification in terms of elevated dissipation rates was found along the pressure surface outside the boundary layer. However, based on the level of dissipation and the resulting heat transfer augmentation, the amplification of turbulence has only a moderate effect on pressure surface heat transfer. The flow field turbulence does drive turbulent production within the boundary layer which in turn causes the high levels of heat transfer augmentation. Unlike heat transfer, the flow field straining was found to have a significant effect on turbulence isotropy. On examination of the one dimensional spectra for u' and v', the effect to isotropy was largely limited to lower wavenumber spectra. The higher wavenumber spectra showed little or no change. The high level large scale turbulence was found to have a strong influence on wake development. The free stream turbulence significantly enhanced mixing resulting in broader and shallower wakes than the baseline case. High levels of flow field turbulence were found to correlate with a significant increase in total pressure loss in the core of the flow. Documenting the wake growth and characteristics provides boundary conditions for the downstream rotor. Author

N95-19923# Argonne National Lab., IL.

LIQUID-METAL PIN-FIN PRESSURE DROP BY CORRELATION IN CROSS FLOW

Zhibi Wang, T. M. Kuzay, and L. Assoufid 1994 9 p Presented at the International Meeting on Synchrotron Radiation Instrumentation, Stony Brook, NY, 18-22 Jul. 1994
(Contract W-31-109-eng-38)
(DE94-017086; ANL/XFD/CP-82933; CONF-940714-16) Avail: CASI HC A02/MF A01

The pin-fin configuration is widely used as a heat transfer enhancement method in high-heat-flux applications. Recently, the pin-fin design with liquid-metal coolant was also applied to synchrotron-radiation beamline devices. This paper investigates the pressure drop in a pin-post design beamline mirror with liquid gallium as the coolant. Because the pin-post configuration is a relatively new concept, information in literature about pin-post mirrors or crystals is rare, and information about the pressure drop in pin-post mirrors with liquid metal as the coolant is even more sparse. Due to this the authors considered the cross flow in cylinder-array geometry, which is very similar to that of the pin-post, to examine the pressure drop correlation with liquid metals over pin fins. The cross flow of fluid with various fluid characteristics or properties through a tube bank was studied so that the results can be scaled to the pin-fin geometry with liquid metal as the coolant. Study led to two major variables to influence the pressure drop: fluid properties, viscosity and density, and the relative length of the posts. Correlation of the pressure drop between long and short posts and the prediction of the pressure drop of liquid metal in the pin-post mirror and comparison with an existing experiment are addressed. DOE

N95-19933*# National Aeronautics and Space Administration. Lewis Research Center, Cleveland, OH.

AUGMENTED THERMAL BUS Patent Application

Dean S. Schrage, inventor (to NASA) (Aerospace Design and Fabrication, Inc., Brook Park, OH.) 25 Jun. 1993 24 p
(NASA-Case-LEW-15595-1-C; NAS 1.71:LEW-15595-1-C; US-Patent-Appl-SN-081891) Avail: CASI HC A03/MF A01

The present invention is directed to an augmented thermal bus. In the present design a plurity of thermo-electric heat pumps are used to couple a source plate to a sink plate. Each heat pump is individually controlled by a model based controller. The controller coordinates the heat pump to maintain isothermality in the source. NASA

N95-19952*# National Aeronautics and Space Administration. Lewis Research Center, Cleveland, OH.

EFFECT OF MICROGRAVITY ON MATERIAL UNDERGOING MELTING AND FREEZING: THE TES EXPERIMENT

David Namkoong, David Jacqmin, and Andrew Szaniszlo Jan. 1995 12 p Presented at the 33rd Aerospace Sciences Meeting and Exhibit, Reno, NV, 9-12 Jan. 1995; sponsored byAIAA
(RTOP 233-03-0B)
(NASA-TM-106845; E-9414; NAS 1.15:106845; AIAA Paper 95-0614)
Avail: CASI HC A03/MF A01

This experiment is the first to melt and freeze a high temperature thermal energy storage (TES) material under an extended duration of microgravity. It is one of a series to validate an analytical computer program that predicts void behavior of substances undergoing phase change under microgravity. Two flight experiments were launched in STS-62. The first, TES-1, containing lithium fluoride in an annular volume, performed flawlessly in the 22 hours of its operation. Results are reported in this paper. A software failure in TES-2 caused its shutdown after 4 seconds. A computer program, TESSIM, for thermal energy storage simulation is being developed to analyze the phenomena occurring within the TES containment vessel. The first order effects, particularly the surface tension forces, have been incorporated into TESSIM. TESSIM validation is based on two types of results. First is the temperature history of various points of the containment structure, and second, upon return from flight, the distribution of the TES material within the containment vessel following the last freeze cycle. The temperature data over the four cycles showed a repetition of results over the third and fourth cycles. This result is a confirmation that any initial conditions prior to the first cycle had been damped out by the third cycle. The TESSIM simulation showed a close comparison with the flight data. The solidified TES material distribution within the containment vessel was obtained by a tomography imaging process. The frozen material was concentrated toward the colder end of the annular volume. The TESSIM prediction showed the same pattern. With the general agreement of TESSIM and the data, a computerized visual representation can be shown which accurately shows the movement and behavior of the void during the entire freezing and melting cycles. Author

N95-19953*# National Aeronautics and Space Administration. Lewis Research Center, Cleveland, OH.

FLOW COEFFICIENT BEHAVIOR FOR BOUNDARY LAYER BLEED HOLES AND SLOTS

B. P. Willis, D. O. Davis, and W. R. Hingst Jan. 1995 16 p Presented at the 33rd Aerospace Sciences Meeting and Exhibit, Reno, NV, 9-12 Jan. 1995; sponsored by AIAA
(RTOP 505-62-52)
(NASA-TM-106846; E-9420; NAS 1.15:106846; AIAA Paper 95-0031)
Avail: CASI HC A03/MF A01

An experimental investigation into the flow coefficient behavior for nine boundary layer bleed orifice configurations is reported. This test was conducted for the purposes of exploring boundary layer control through mass flow removal and does not address issues of stability bleed. Parametric data consist of bleed region flow coefficient as a function of Mach number, bleed plenum pressure, and bleed orifice geometry. Seven multiple hole configurations and two single slot configurations were tested over a supersonic Mach number range of 1.3 to 2.5 (nominal). Advantages gained by using multiple holes in a bleed region instead of a single spanwise slot are discussed and the issue of modeling an entire array of bleed orifices based on the performance of a single orifice is addressed. Preconditioning the flow approaching a 90 degree inclined (normal) hole configuration resulted in a significant improvement in the performance of the configuration. The same preconditioning caused only subtle changes in performance for a 20 degree inclined (slanted) configuration. Author

N95-20009* Institute for Computer Applications in Science and Engineering, Hampton, VA.

EVALUATION OF REYNOLDS STRESS TURBULENCE CLOSURES IN COMPRESSIBLE HOMOGENEOUS SHEAR FLOW Final Report

C. G. Speziale, R. Abid, and N. N. Mansour Mar. 1994 31 p Submitted

for publication Limited Reproducibility: More than 20% of this document may be affected by microfiche quality
(Contracts NAS1-19480; NAS1-19299; RTOP 505-90-52-01)
(NASA-CR-194892; NAS 1.26:194892; AD-A280141; ICASE-94-17) Avail: Issuing Activity (Defense Technical Information Center (DTIC))

Direct numerical simulation data bases for compressible homogeneous shear flow are used to evaluate the performance of recently proposed Reynolds stress closures for compressible turbulence. Three independent pressure-strain models are considered along with a variety of explicit compressible corrections that account for dilatational dissipation and pressure-dilatation effects. The ability of the models to predict both time evolving fields and equilibrium states is systematically tested. Consistent with earlier studies, it is found that the addition of simple dilatational models allows for the prediction of the reduced growth rate of turbulent kinetic energy in compressible homogeneous shear flow. However, a closer examination of the equilibrium structural parameters uncovers a major problem. None of the models are able to predict the dramatic increase in the normal Reynolds stress anisotropies or the significant decrease in the Reynolds shear stress anisotropy that arise from compressible effects. The physical origin of this deficiency is attributed to the neglect of compressible terms in the modeling of the deviatoric part of the pressure-strain correlation. DTIC

N95-20058# Rutgers - The State Univ., New Brunswick, NJ. Dept. of Mechanical and Aerospace Engineering.

A NUMERICAL INVESTIGATION OF ENERGY TRANSFER AND SUBGRID-SCALE EDDY VISCOSITY IN HOMOGENEOUS, ISOTROPIC AND SHEAR TURBULENCE Final Technical Report, Dec. 1991 - Dec. 1993

Richard B. Pelz 22 Mar. 1994 94 p
(Grant AF-AFOSR-0248-91)
(AD-A280005; AFOSR-94-0339TR) Avail: CASI HC A05/MF A01

Numerical solutions to the Navier-Stokes equations for a 3-D, time-dependent, highly-symmetric flow have been completed. An effective resolution of up to 10243 collocation points (341 modes after dealiasing) is attained within the memory on the 256 MW CRAY-2 at Kirtland AFB and the C90 at the Pittsburgh Supercomputer Center. These simulations constitutes the highest resolution runs made to date. One of the primary purposes of the work was to create a data base from which a detailed energy transfer and triad analysis could be made by Andrzej Domaradzki at USC. The data base has been made, and runs for Reynolds numbers of 500, 1000, 2000 and 5000 have been stored on tape. We shall give some information concerning the turbulent flows later in this report. The other purpose of this work is to try to understand the transition process through which the flow becomes turbulent. Our early-time analysis of the data base of runs was concerned with this problem, and hence most of this report will deal with our findings. We also attach a manuscript on this subject that will be published shortly in The Physics of Fluids. DTIC

N95-20137# Sandia National Labs., Albuquerque, NM.

HINDERED SETTLING COMPUTATIONS USING A PARALLEL BOUNDARY ELEMENT METHOD

M. S. Ingber (New Mexico Univ., Albuquerque, NM.) and D. E. Womble 1994 7 p Presented at the American Society of Mechanical Engineers' Winter Annual Meeting, Chicago, IL, 9-11 Nov. 1994
(Contract DE-AC04-94AL-85000)
(DE94-014286; SAND-94-1396C; CONF-941142-10) Avail: CASI HC A02/MF A01

This paper presents a parallel implementation of the boundary element method (BEM) for multiple instruction multiple data (MIMD) computer architectures to determine the hindered settling function for a suspension of sedimenting rigid particles in Stokes flow. The hindered settling function is a measure of the average sedimentation velocity of the suspension. This function can be determined numerically by performing statistical analyses of several random realizations of a physical system characterized by a set of defining parameters. These defining parameters can include the volume fraction of the solid phase, shape factors, orientation characteristics, and others. The boundary element method is particularly well suited for studying such systems because of the simplification in the discretization associated with the method. However, as the number of solid particles to be modeled is increased so are the computational demands. Parallel computation offers the opportunity to model systems of greater complexity. We discuss a parallel boundary element formulation based on the torus-wrap mapping. In this approach, blocks of the coefficient matrix associated with the discretized boundary element equations are assigned to processors as opposed to more traditional parallel boundary element implementations where rows or columns are assigned to processors. The torus-wrap mapping can be shown to minimize the communication volume between processors during the LU factorization. Therefore, the present formulation scales well with increases in the number of processors. DOE

N95-20166# Los Alamos National Lab., NM.

NONLINEAR DYNAMIC FLUID-STRUCTURE INTERACTION CALCULATIONS WITH COUPLED FINITE ELEMENT AND FINITE VOLUME PROGRAMS

M. W. Lewis, B. A. Kashiwa, R. W. Meier, and S. Bishop (Army Night Vision Lab., Fort Belvoir, VA.) 1994 11 p Presented at the American Society of Mechanical Engineers' Winter Annual Meeting, Chicago, IL, 9-11 Nov. 1994
(Contract W-7405-eng-36)
(DE94-016204; LA-UR-94-2443; CONF-941142-15) Avail: CASI HC A03/MF A01

Two- and three-dimensional fluid-structure interaction computer programs for the simulation of nonlinear dynamics were developed and applied to a number of problems. The programs were created by coupling Arbitrary Lagrangian-Eulerian finite volume fluid dynamics programs with strictly Lagrangian finite element structural dynamics programs. The resulting coupled programs can use either fully explicit or implicit time integration. The implicit time integration is accomplished by iterations of the fluid dynamics pressure solver and the structural dynamics system solver. The coupled programs have been used to solve problems involving incompressible fluids, membrane and shell elements, compressible multiphase flows, explosions in both air and water, and large displacements. In this paper, we present the approach used for the coupling and describe test problems that verify the two-dimensional programs against an experiment and an analytical linear problem. The experiment involves an explosion underwater near an instrumented thin steel plate. The analytical linear problem is the vibration of an infinite cylinder surrounded by an incompressible fluid to a given radius. DOE

N95-20250# Wright State Univ., Dayton, OH. Dept. of Mechanical and Materials Engineering.

CONTINUUM TRANSIENT AND FROZEN STARTUP BEHAVIOR OF CONVENTIONAL AND GAS-LOADED HEAT PIPES Final Report

Amir Faghri Feb. 1994 104 p
(Contract F33615-88-C-2820)
(AD-A284297; WL-TR-94-2044) Avail: CASI HC A06/MF A02

The heat pipe startup process is described physically and mathematically. During most of the heat pipe startup process, the continuum and rarefied vapor flows coexist along the heat pipe length. A two-region model is thereby proposed in which the vapor flow in the continuum region is modeled by the compressible Navier-Stokes equations, and the vapor flow in the rarefied region is modeled by the self-diffusion model. The two vapor regions are linked with appropriate boundary conditions, and the heat pipe wall, wick and vapor flow are solved as a conjugate problem. Both numerical and analytical solutions for the entire heat pipe startup process from the frozen state are compared with the corresponding experimental data with good agreement. DTIC

N95-20297 Department of the Navy, Washington, DC.

LOW FLOW FLUID SEPARATOR Patent

Michael K. Adams, inventor (to Navy) and Thomas H. Hane, inventor (to Navy) 5 Jul. 1994 7 p Filed 13 Nov. 1992
(AD-D016575; US-Patent-5,326,474; US-Patent-Appl-SN-976033; US-Patent-Class-210-519) Avail: US Patent and Trademark Office

A separator for immiscible fluids and particulate matter of differing densities provides a plurality of stages of fluid flow velocity reduction by change of cross-sectional areas between a plurality of flow regions (e.g. conduits and chambers) and separates a fraction of the introduced fluid or suspended particulate matter at each change of velocity whereby flow velocity may be reduced to a degree greater than accounted for by the change of cross-sectional area from stage to stage when significant amounts of materials to be separated are present in the input fluid. Further, a substantial effective length is provided, relative to the footprint of the separator. This length and gradual slowing of the fluids therein provides generally laminar flow and low turbulence. By doing so, overall volume of the passive separator is reduced and separation efficiency is substantially improved. DTIC

N95-20312 Texas A&M Univ., College Station, TX.
STABILIZATION AND CONTROL PROBLEMS IN STRUCTURAL DYNAMICS Final Technical Report, 1 Jan. 1991 - 31 Dec. 1993
Goong Chen and Jianxin Zhou 20 Jan. 1994 10 p Limited Reproducibility: More than 20% of this document may be affected by microfiche quality
(Grant AF-AFOSR-0097-91; AF Proj. 2304)
(AD-A279996; AFOSR-94-0325TR) Avail: Issuing Activity (Defense Technical Information Center (DTIC))

Drs. G. Chen and J. Zhou investigated various problems in the analysis, control, optimization and computation of structural mechanical systems and partial differential equations. Three monographs along with over twenty technical papers have been published/ written over the support period. The PI's research activities, interaction with Air Force laboratory, video production, and efforts in technology transitions are described in this report. Recent progress in shell equations, computation of fluids and nonlinear partial differential equations is also made through the support of this grant. DTIC

N95-20547# Illinois Univ., Urbana, IL.
STRUCTURE AND DYNAMICS OF TURBULENT WALL LAYERS Final Report, 1 Mar. 1990 - 31 May 1994
Ronald J. Adrian 10 Jun. 1994 11 p
(Grant AF-AFOSR-0169-90)
(AD-A285360; AFOSR-94-101TR) Avail: CASI HC A03/MF A01

The three-dimensional structure of the turbulent motion of fluid flowing close to a surface has been studied using the technique of linear mean square stochastic estimation to find estimates of the flow field when certain events occur in the flow. The structures given the velocity at one point have been documented, and their dynamic evolution is being studied. It is shown that they are long-lived. One-point events provide insight into the physical bases of closure approximations in one-point moment closures, and they have been used to provide a new closure approximation for the fast pressure-strain correlation. Stochastic estimation is used as a means of defining three-dimensional, dynamic wall boundary conditions for large eddy simulations. DTIC

N95-20561*# National Aeronautics and Space Administration. Marshall Space Flight Center, Huntsville, AL.
TRANSPORT PHENOMENA IN THE MICROPORES OF PLUG-TYPE PHASE SEPARATORS
M. M. Fazah Washington Feb. 1995 58 p
(NASA-TM-108479; NAS 1.15:108479) Avail: CASI HC A04/MF A01

This study numerically investigates the transport phenomena within and across a porous-plug phase separator. The effect of temperature differential across a single pore and of the sidewall boundary conditions, i.e., isothermal or linear thermal gradient, are presented and discussed. The effects are quantified in terms of the evaporation mass flux across the boundary and the mean surface temperature. A two-dimensional finite element model is used to solve the continuity, momentum, and energy equations for the liquid. Temperature differentials across the pore interface of 1.0, and 1.5 K are examined and their effect on evaporation flux and mean surface temperature is shown. For isothermal side boundary conditions, the evaporation flux across the pore is directly proportional and linear with Delta T. For the case of an imposed linear thermal gradient on the side boundaries, Biot numbers of 0.0, 0.15, and 0.5 are examined. The most significant effect of Biot number is to lower the overall surface temperature and evaporation flux. Author

N95-20619*# National Aeronautics and Space Administration. Langley Research Center, Hampton, VA.
INTERNAL AERODYNAMICS OF A GENERIC THREE-DIMENSIONAL SCRAMJET INLET AT MACH 10
Scott D. Holland Jan. 1995 55 p
(RTOP 506-40-41-02)
(NASA-TP-3476; L-17347; NAS 1.60:3476) Avail: CASI HC A04/MF A01

A combined computational and experimental parametric study of the internal aerodynamics of a generic three-dimensional sidewall compression scramjet inlet configuration at Mach 10 has been performed. The study was designed to demonstrate the utility of computational fluid dynamics as a design tool in hypersonic inlet flow fields, to provide a detailed account of the nature and structure of the internal flow interactions, and to provide a comprehensive surface property and flow field database to determine the effects of contraction ratio, cowl position, and Reynolds number on the performance of a hypersonic scramjet inlet configuration. The work proceeded in several phases: the initial inviscid assessment of the internal shock structure, the preliminary computational parametric study, the coupling of the optimized configuration with the physical limitations of the facility, the wind tunnel blockage assessment, and the computational and experimental parametric study of the final configuration. Good agreement between computation and experimentation was observed in the magnitude and location of the interactions, particularly for weakly interacting flow fields. Large-scale forward separations resulted when the interaction strength was increased by increasing the contraction ratio or decreasing the Reynolds number. Author

N95-20781# Oak Ridge National Lab., TN.
SCALE-UP AND MODELING OF FORCED CHEMICAL VAPOR INFILTRATION
T. M. Besmann, J. C. McLaughlin, and T. L. Starr (Georgia Tech Research Inst., Atlanta, GA.) 1994 11 p Presented at the 18th Annual Conference on Composites and Advanced Ceramics, Cocoa Beach, FL, 9-14 Jan. 1994
(Contract DE-AC05-84OR-21400)
(DE94-017769; CONF-940135-9) Avail: CASI HC A03/MF A01

The forced flow-thermal gradient chemical vapor infiltration (FCVI) process has been scaled-up from a maximum of 7.6 cm dia. disk to fabrication of 24 cm dia. disks, 1.6 cm in thickness. The components are turbine rotor subelements produced from polar weave Tyranno fibers preforms. The disks were subjected to non-destructive testing and spin-tested to high rpm. The processing conditions were modeled with the GTCVI code to aid in optimization. DOE

N95-20796*# Rensselaer Polytechnic Inst., Troy, NY. Dept. of Chemical Engineering.
AN AUGMENTED YOUNG-LAPLACE MODEL OF AN EVAPORATING MENISCUS IN A MICRO-CHANNEL WITH HIGH HEAT FLUX Final Report
P. C. Wayner, Jr., J. Plawsky, J. A. Schonberg, and S. DasGupta [1993] 28 p Submitted for publication
(Grant NAG3-1399)
(NASA-CR-197622; NAS 1.26:197622; RPI/CHE/NASA-5-23390-5) Avail: CASI HC A03/MF A01

High flux evaporations from a steady meniscus formed in a 2 micron channel is modeled using the augmented Young-Laplace equation. The heat flux is found to be a function of the long range van der Waals dispersion force which represents interfacial conditions between heptane and various substrates. Heat fluxes of (1.3-1.6) x 10(exp 6) W/m(exp 2) based on the width of the channel are obtained for heptane completely wetting the substrate at 100 C. Small channels are used to obtain these large fluxes. Even though the real contact angle is 0 deg, the apparent contact angle is found to vary between 24.8 deg and 25.6 deg. The apparent contact angle, which represents viscous losses near the contact line, has a large effect on the heat flow rate because of its effect on capillary suction and the area of the meniscus. The interfacial heat flux is modeled using kinetic theory for the evaporation rate. The superheated state depends on the temperature and the pressure of the liquid phase. The liquid pressure differs from the pressure of the vapor phase due to capillarity and long range van der Waals dispersion forces which are relevant in the ultra think film formed at the leading edge of the meniscus. Important pressure gradients in the thin film cause a substantial apparent contact angle for a complete wetting system. The temperature of the liquid is related to the evaporation rate and to the substrate temperature through the steady heat conduction equation. Conduction in the liquid phase is calculated using finite element analysis except in the vicinity of the thin film. A lubrication theory solution for the thin film is combined with the finite element analysis by the method of matched asymptotic expansions. Author

N95-20831# Sandia National Labs., Albuquerque, NM.
CONSERVATIVE SMOOTHING VERSUS ARTIFICIAL VISCOSITY
C. Guenther (Michigan Technological Univ., Houghton, MI.), D. L. Hicks (Michigan Technological Univ., Houghton, MI.), and J. W. Swegle Aug. 1994 48 p
(Contract DE-AC04-94AL-85000)
(DE95-001108; SAND-94-1853) Avail: CASI HC A03/MF A01

This report was stimulated by some recent investigations of S.P.H. (Smoothed Particle Hydrodynamics method). Solid dynamics computations with S.P.H. show symptoms of instabilities which are not eliminated by artificial viscosities. Both analysis and experiment indicate that conservative smoothing eliminates the instabilities in S.P.H. computations which artificial viscosities cannot. Questions were raised as to whether conservative smoothing might smear solutions more than artificial viscosity. Conservative smoothing, properly used, can produce more accurate solutions than the von Neumann-Richtmyer-Landshoff artificial viscosity which has been the standard for many years. The authors illustrate this using the vNR scheme on a test problem with known exact solution involving a shock collision in an ideal gas. They show that the norms of the errors with conservative smoothing are significantly smaller than the norms of the errors with artificial viscosity. DOE

N95-20843# Army Engineer Waterways Experiment Station, Vicksburg, MS.
HIVEL2D: A TWO-DIMENSIONAL FLOW MODEL FOR HIGH-VELOCITY CHANNELS Final Report
R. L. Stockstill and R. C. Berger Nov. 1994 55 p
(AD-A286556; WES/TR/REMR-HY-12) Avail: CASI HC A04/MF A01

A numerical flow model, HIVEL2D, has been developed as a tool to evaluate high-velocity channels. HIVEL2D is a depth-averaged, two-dimensional flow model designed specifically for flow fields that contain supercritical and subcritical regimes as well as the transitions between the regimes. The model is a finite element description of the two-dimensional shallow-water equations in conservative form. Provided in this report are a description of the numerical flow model and illustrative examples of typical high-velocity flow fields that the model is capable of simulating. Model verification is obtained by comparison of simulation results with data obtained from flume studies. Model assumptions and limitations are also discussed. DTIC

N95-20849# Catholic Univ. of America, Washington, DC. Dept. of Mechanical Engineering.
APPLICATION OF WAVELET-FILTERING TECHNIQUES TO INTERMITTENT TURBULENT AND WALL PRESSURE EVENTS. PART 1: EXPLORATORY RESULTS Progress Report, Oct. 1993 - Oct. 1994
Pablo B. Penafiel, Mario J. Casarella, and Mark Kammeyer 25 Oct. 1994 43 p
(Contract N00014-88-K-0141)
(AD-A286077) Avail: CASI HC A03/MF A01

Large amplitude wall-pressure events, observed beneath a turbulent boundary layer, appear to be the signatures of intermittent organized motions within the turbulent flow. The temporal localization of these events could be applied to the active control of turbulent wall flows. This report presents preliminary results on utilizing time-frequency localization techniques (wavelet transforms) for the detection of these events. The advantage of these methods is that they do not require a priori assumptions regarding the features of the signal. A tutorial overview of these techniques is first presented. This is followed by a discussion of some exploratory results obtained from the application of wavelet filtering to wall pressure and turbulent temporal records acquired from wind tunnel experiments. DTIC

N95-20968 Naval Postgraduate School, Monterey, CA. Dept. of Aeronautics and Astronautics.
LASER ANEMOMETRY AND VISCOUS COMPUTATION OF THE FLOW THROUGH AN ANNULAR TURBINE CASCADE M.S. Thesis
Joseph D. Spitz Mar. 1994 85 p Limited Reproducibility: More than 20% of this document may be affected by microfiche quality
(AD-A280070) Avail: Issuing Activity (Defense Technical Information Center (DTIC))

An annular turbine cascade, designed for laser-Doppler velocimetry, was further modified to provide additional laser and pressure probe access. The purpose of the research was to devise laser anemometry measurement techniques in a confined annulus and improve the ability to compare numerical predictions with experimental results. Flowfield computations were completed using a viscous flow solver, with the numerical exit plane coincident with experimental measurement location. A data reduction program was written to transfer nondimensional numerical output to the experimental coordinate system for comparison of total pressure ratio, Mach number and flow angle. Endwall two-dimensional laser measurements were obtained through a 1.0922 millimeter hole to a depth of approximately three millimeters. DTIC

N95-20981# Helsinki Univ. of Technology, Espoo (Finland). Lab. for Strength of Materials.
MIXED hp FINITE ELEMENT METHODS FOR PROBLEMS IN ELASTICITY AND STOKES FLOW
Rolf Stenberg and Manil Suri (Maryland Univ. Baltimore County, Catonsville, MD.) Feb. 1994 25 p
(Contract F49620-92-J-0100)
(PB95-104444) Avail: CASI HC A03/MF A01

We consider the mixed formulation for the elasticity problem and the limiting Stokes problem. We derive a set of sufficient conditions under which families of mixed finite element spaces are simultaneously stable with respect to the mesh size h and subject to a maximum loss with respect to the polynomial degree k. We obtain asymptotic rates of convergence that are optimal in the displacement/velocity and in the pressure. Several choices of elements are discussed with reference to properties desirable in the context of the hp-version. NTIS

N95-21001# Naval Postgraduate School, Monterey, CA.
A COMPUTER CODE (SKINTEMP) FOR PREDICTING TRANSIENT MISSILE AND AIRCRAFT HEAT TRANSFER CHARACTERISTICS M.S. Thesis
Mary L. Cummings Sep. 1994 64 p
(AD-A286044) Avail: CASI HC A04/MF A01

A FORTRAN computer code (SKINTEMP) has been developed to calculate transient missile/aircraft aerodynamic heating parameters utilizing basic flight parameters such as altitude, Mach number, and angle of attack. The insulated skin temperature of a vehicle surface on either the fuselage (axisymmetric body) or wing (two-dimensional body) is computed from a basic heat balance relationship throughout the entire spectrum (subsonic, transonic, supersonic, hypersonic) of flight. This calculation method employs a simple finite difference procedure which considers radiation, forced convection, and non-reactive chemistry. Surface pressure estimates are based on a modified Newtonian flow model. Eckert's reference temperature method is used as the forced convection heat transfer model. SKINTEMP predictions are compared with a limited number of test cases. SKINTEMP was developed as a tool to enhance the conceptual design process of high speed missiles and aircraft. Recommendations are made for possible future development of SKINTEMP to further support the design process. DTIC

N95-21035*# Stanford Univ., CA. Center for Turbulence Research.
STUDYING TURBULENCE USING NUMERICAL SIMULATION DATABASES. 5: PROCEEDINGS OF THE 1994 SUMMER PROGRAM
Dec. 1994 426 p Program held in Stanford, CA, 5-29 Jul. 1994
(Contract NCC2-460)
(NASA-CR-197362; NAS 1.26:197362) Avail: CASI HC A19/MF A04

Direct numerical simulation databases were used to study turbulence physics and modeling issues at the fifth Summer Program of the Center for Turbulence Research. The largest group, comprising more than half of the participants, was the Turbulent Reacting Flows and Combustion group. The remaining participants were in three groups: Fundamentals, Modeling & LES, and Rotating Turbulence. For the first time in the CTR Summer Programs, participants included engineers from the U.S. aerospace industry. They were exposed to a variety of problems involving turbulence, and were able to incorporate the models developed at CTR in their company codes. They were exposed to new ideas on turbulence prediction, methods which already appear to have had an impact on their capabilities at their laboratories. Such interactions among the practitioners in the government, academia, and industry are the most meaningful way of transferring technology. For individual titles, see N95-21036 through N95-21060.

N95-21036*# Escuela Tecnica Superior de Ingenieros Aeronauticos, Madrid (Spain).

EFFECTS OF NON-UNITY LEWIS NUMBERS IN DIFFUSION FLAMES **c25**

A. Linan, P. Orlandi (Rome Univ., Italy.), R. Verzicco (Rome Univ., Italy.), and F. J. Higuera *In* Stanford Univ., Studying Turbulence Using Numerical Simulation Databases. 5: Proceedings of the 1994 Summer Program Dec. 1994 p 5-18 (For primary document see N95-21035 06-34)
Avail: CASI HC A03/MF A04

The purpose of this work is to carry out direct numerical simulations of diffusion controlled combustion with non-unity Lewis numbers for the reactants and products, thus accounting for the differential diffusion effects of the temperature and concentration fields. We use a formulation based on combining the conservation equations in a way to eliminate the reaction terms similar to the method used by Burke and Schumann (1928) for unity Lewis numbers. We present calculations for an axisymmetric fuel jet and for a planar, time evolving mixing layer, leaving out the effects of thermal expansion and variations of the transport coefficients due to the heat release. Our results show that the front of the flame shifts toward the fuel or oxygen sides owing to the effect of the differential diffusion and that the location of maximum temperature may not coincide with the flame. The dependence of the distribution of the reaction products on their Lewis number has been investigated. Author

N95-21037*# National Aeronautics and Space Administration. Ames Research Center, Moffett Field, CA.

EFFECT OF CHEMICAL HEAT RELEASE IN A TEMPORALLY EVOLVING MIXING LAYER **c25**

F. J. Higuera (Escuela Tecnica Superior de Ingenieros Aeronauticos, Madrid, Spain.) and R. D. Moser *In* Stanford Univ., Studying Turbulence Using Numerical Simulation Databases. 5: Proceedings of the 1994 Summer Program Dec. 1994 p 19-40 (For primary document see N95-21035 06-34)
Avail: CASI HC A03/MF A04

Two-dimensional numerical simulations of a temporally evolving mixing layer with an exothermic infinitely fast diffusion flame between two unmixed reactants have been carried out in the limit of zero Mach number to study the effect of the heat release on the early stages of the evolution of the flow. Attention has been directed to relatively large values of the oxidizer-to-fuel mass stoichiometric ratio typical of hydrocarbon flames, and initial vorticity distributions thicker than the temperature and species distributions have been chosen to mimic the situation at the outlet of a jet. The results show that, during the stages of the evolution covered by the present simulations, enhancement of combustion occurs by local stretching of the flame without much augmentation of its area. The rate of product generation depends strongly on the initial conditions, which suggests the possibility of controlling the combustion by acting on the flow. Rollup and vortex amalgamation still occur in these reacting flows but are very much affected by the production of new vorticity by baroclinic torques. These torques lead to counter rotating vortex pairs around the flame and, more importantly, in thin layers of light fluid that leave the vicinity of the flame when the Kelvin-Helmholtz instability begins to develop. Propelled by the vortex pairs, these layers wind around, split on reaching high pressure regions, and originate new vortex pairs in a process that ends up building large-scale vortices with a vorticity distribution more complex than for a constant density fluid. Author

N95-21038*# Sandia National Labs., Livermore, CA.

DIRECT NUMERICAL SIMULATIONS OF TURBULENT NON-PREMIXED METHANE-AIR FLAMES MODELED WITH REDUCED KINETICS **c25**

J. M. Card, J. H. Chen, M. Day, and S. Mahalingam (Colorado Univ., Boulder, CO.) *In its* Studying Turbulence Using Numerical Simulation Databases. 5: Proceedings of the 1994 Summer Program Dec. 1994 p 41-54 Sponsored by AWU-DOE faculty fellowship program (For primary document see N95-21035 06-34)
Avail: CASI HC A03/MF A04

Turbulent non-premixed stoichiometric methane-air flames modeled with reduced kinetics have been studied using the direct numerical simulation approach. The simulations include realistic chemical kinetics, and the molecular transport is modeled with constant Lewis numbers for individual species. The effect of turbulence on the internal flame structure and extinction characteristics of methane-air flames is evaluated. Consistent with earlier DNS with simple one-step chemistry, the flame is wrinkled and in some regions extinguished by the turbulence, while the turbulence is weakened in the vicinity of the flame due to a combination of dilatation and an increase in kinematic viscosity. Unlike previous results, reignition is observed in the present simulations. Lewis number effects are important in determining the local stoichiometry of the flame. The results presented in this work are preliminary but demonstrate the feasibility of incorporating reduced kinetics for the oxidation of methane with direct numerical simulations of homogeneous turbulence to evaluate the limitations of various levels of reduction in the kinetics and to address the formation of thermal and prompt NO(x). Author

N95-21039*# Ecole Centrale de Paris (France).

TRIPLE FLAME STRUCTURE AND DIFFUSION FLAME STABILIZATION **c25**

D. Veynante, L. Vervisch (Institut National des Sciences Appliquees, Routen, France.), T. Poinsot (Institut de Mecanique des Fluides de Toulouse, France.), A. Linan (Escuela Tecnica Superior de Ingenieros Aeronauticos, Madrid, Spain.), and G. Ruetsch *In* Stanford Univ., Studying Turbulence Using Numerical Simulation Databases. 5: Proceedings of the 1994 Summer Program Dec. 1994 p 55-73 (For primary document see N95-21035 06-34)
Avail: CASI HC A03/MF A04

The stabilization of diffusion flames is studied using asymptotic techniques and numerical tools. The configuration studied corresponds to parallel streams of cold oxidizer and fuel initially separated by a splitter plate. It is shown that stabilization of a diffusion flame may only occur in this situation by two processes. First, the flame may be stabilized behind the flame holder in the wake of the splitter plate. For this case, numerical simulations confirm scalings previously predicted by asymptotic analysis. Second, the flame may be lifted. In this case a triple flame is found at longer distances downstream of the flame holder. The structure and propagation speed of this flame are studied by using an actively controlled numerical technique in which the triple flame is tracked in its own reference frame. It is then possible to investigate the triple flame structure and velocity. It is shown, as suggested from asymptotic analysis, that heat release may induce displacement speeds of the triple flame larger than the laminar flame speed corresponding to the stoichiometric conditions prevailing in the mixture approaching the triple flame. In addition to studying the characteristics of triple flames in a uniform flow, their resistance to turbulence is investigated by subjecting triple flames to different vortical configurations. Author

N95-21040*# Wisconsin Univ., Madison, WI.

TURBULENT TRANSPORT IN PREMIXED FLAMES **c25**

C. J. Rutland and R. S. Cant (Manchester Coll. of Science and Technology, England.) *In* Stanford Univ., Studying Turbulence Using Numerical Simulation Databases. 5: Proceedings of the 1994 Summer Program Dec. 1994 p 75-94 (For primary document see N95-21035 06-34)
Avail: CASI HC A03/MF A04

Simulations of planar, premixed turbulent flames with heat release were used to study turbulent transport. Reynolds stress and Reynolds flux budgets were obtained and used to guide the investigation of important physical effects. Essentially all pressure terms in the transport equations were found to be significant. In the Reynolds flux equations, these terms are the major source of counter-gradient transport. Viscous and molecular terms were also found to be significant, with both dilatational and solenoidal terms contributing to the Reynolds stress dissipation. The BML theory of premixed turbulent combustion was critically examined in detail. The BML bimodal pdf was found to agree well with the DNS data. All BML decompositions, through the third moments, show very good agreement with the DNS results. Several BML models for conditional terms were checked using the DNS data and were found to require more extensive development. Author

N95-21041*# Institut Francais du Petrole, Paris.

THE COUPLING BETWEEN FLAME SURFACE DYNAMICS AND SPECIES MASS CONSERVATION IN PREMIXED TURBULENT COMBUSTION **c25**

A. Trouve (Institut Francais du Petrole, Paris.), D. Veynante (Ecole Centrale de Paris, France.), K. N. C. Bray (Cambridge Univ., Cambridge, England.), and T. Mantel *In* Stanford Univ., Studying Turbulence Using Numerical

Simulation Databases. 5: Proceedings of the 1994 Summer Program Dec. 1994 p 95-124 (For primary document see N95-21035 06-34)
Avail: CASI HC A03/MF A04

Current flamelot models based on a description of the flame surface dynamics require the closure of two inter-related equations: a transport equation for the mean reaction progress variable, (tilde)c, and a transport equation for the flame surface density, Sigma. The coupling between these two equations is investigated using direct numerical simulations (DNS) with emphasis on the correlation between the turbulent fluxes of (tilde)c, bar(pu"c"), and Sigma, (u")(sub S)Sigma. Two different DNS databases are used in the present work: a database developed at CTR by A. Trouve and a database developed by C. J. Rutland using a different code. Both databases correspond to statistically one-dimensional premixed flames in isotropic turbulent flow. The run parameters, however, are significantly different, and the two databases correspond to different combustion regimes. It is found that in all simulated flames, the correlation between bar(pu"c") and (u")(sub S)Sigma is always strong. The sign, however, of the turbulent flux of (tilde)c or Sigma with respect to the mean gradients, delta(tilde)c/delta(x) or delta(Sigma)/delta(x), is case-dependent. The CTR database is found to exhibit gradient turbulent transport of (tilde)c and Sigma, whereas the Rutland DNS features counter-gradient diffusion. The two databases are analyzed and compared using various tools (a local analysis of the flow field near the flame, a classical analysis of the conservation equation for (tilde)(u"c"), and a thin flame theoretical analysis). A mechanism is then proposed to explain the discrepancies between the two databases and a preliminary simple criterion is derived to predict the occurrence of gradient/counter-gradient turbulent diffusion. Author

N95-21042*# Institut National des Sciences Appliquees, Routen (France).

Pdf MODELING FOR PREMIXED TURBULENT COMBUSTION BASED ON THE PROPERTIES OF ISO-CONCENTRATION SURFACES **c25**

L. Vervisch, W. Kollmann (California Univ., Davis, CA.), K. N. C. Bray (Cambridge Univ., Cambridge, England.), and T. Mantel *In* Stanford Univ., Studying Turbulence Using Numerical Simulation Databases. 5: Proceedings of the 1994 Summer Program Dec. 1994 p 125-150 (For primary document see N95-21035 06-34)
Avail: CASI HC A03/MF A04

In premixed turbulent flames the presence of intense mixing zones located in front of and behind the flame surface leads to a requirement to study the behavior of iso-concentration surfaces defined for all values of the progress variable (equal to unity in burnt gases and to zero in fresh mixtures). To support this study, some theoretical and mathematical tools devoted to level surfaces are first developed. Then a database of direct numerical simulations of turbulent premixed flames is generated and used to investigate the internal structure of the flame brush, and a new pdf model based on the properties of iso-surfaces is proposed. Author

N95-21043*# Sandia National Labs., Livermore, CA.

PASSIVE TURBULENT FLAMELET PROPAGATION **c25**

William T. Ashurst, G. R. Ruetsch (Stanford Univ., CA.), and T. S. Lund (Stanford Univ., CA.) *In* Stanford Univ., Studying Turbulence Using Numerical Simulation Databases. 5: Proceedings of the 1994 Summer Program Dec. 1994 p 151-156 (For primary document see N95-21035 06-34)
Avail: CASI HC A02/MF A04

We analyze results of a premixed constant density flame propagating in three-dimensional turbulence, where a flame model developed by Kerstein, et al. (1988) has been used. Simulations with constant and evolving velocity fields are used, where peculiar results were obtained from the constant velocity field runs. Data from the evolving flow runs with various flame speeds are used to determine two-point correlations of the fluctuating scalar field and implications for flamelet modeling are discussed. Author

N95-21044*# Institut Francais du Petrole, Paris.

SIMULATION OF A TURBULENT FLAME IN A CHANNEL **c25**

G. Bruneaux, K. Akselvoll (Stanford Univ., CA.), T. Poinsot (Institut de Mecanique des Fluides de Toulouse, France.), and J. H. Ferziger (Stanford Univ., CA.) *In* Stanford Univ., Studying Turbulence Using Numerical Simulation Databases. 5: Proceedings of the 1994 Summer Program Dec. 1994 p 157-174 (For primary document see N95-21035 06-34)
Avail: CASI HC A03/MF A04

The interaction between turbulent premixed flames and channel walls is studied. Combustion is represented by a simple irreversible reaction with a large activation temperature. Feedback to the flowfield is suppressed by invoking a constant density assumption. The effect of wall distance on local and global flame structure is investigated. Quenching distances and maximum wall heat fluxes computed in laminar cases are compared to DNS results. It is found that quenching distances decrease and maximum heat fluxes increase relative to laminar flame values. It is shown that these effects are due to large coherent structures which push flame elements towards to wall. The effect of wall strain is studied in flame-wall interaction in a stagnation line flow; this is used to explain the DNS results. It is also shown that 'remarkable' flame events are produced by interaction with a horseshoe vortex: burnt gases are pushed towards the wall at high speed and induce quenching and high wall heat fluxes while fresh gases are expelled from the wall region and form finger-like structures. Effects of the wall on flame surface density are investigated, and a simple model for flame-wall interaction is proposed; its predictions compare well with the DNS results. Author

N95-21045*# National Aeronautics and Space Administration. Ames Research Center, Moffett Field, CA.

PRESSURE AND HIGHER-ORDER SPECTRA FOR HOMOGENEOUS ISOTROPIC TURBULENCE

D. I. Pullin (Stanford Univ., CA.) and R. S. Rogallo *In* Stanford Univ., Studying Turbulence Using Numerical Simulation Databases. 5: Proceedings of the 1994 Summer Program Dec. 1994 p 177-187 (For primary document see N95-21035 06-34)
Avail: CASI HC A03/MF A04

The spectra of the pressure, and other higher-order quantities including the dissipation, the enstrophy, and the square of the longitudinal velocity derivative are computed using data obtained from direct numerical simulation of homogeneous isotropic turbulence at Taylor-Reynolds numbers R(sub lambda) in the range 38 - 170. For the pressure spectra we find reasonable collapse in the dissipation range (of the velocity spectrum) when scaled in Kolmogorov variables and some evidence, which is not conclusive, for the existence of a k(exp -7/3) inertial range where k = absolute value of K, is the modulus of the wavenumber. The power spectra of the dissipation, the enstrophy, and the square of the longitudinal velocity derivative separate in the dissipation range, but appear to converge together in the short inertial range of the simulations. A least-squares curve-fit in the dissipation range for one value of R(sub lambda) = 96 gives a form for the spectrum of the dissipation as k(exp 0)exp(-Ck eta), for k(eta) greater than 0.2, where eta is the Kolmogorov length and C is approximately equal to 2.5. Author

N95-21046*# National Aeronautics and Space Administration. Ames Research Center, Moffett Field, CA.

STATISTICS OF PRESSURE AND PRESSURE GRADIENT IN HOMOGENEOUS ISOTROPIC TURBULENCE

T. Gotoh (Nagoya Inst. of Tech., Japan.) and R. S. Rogallo *In* Stanford Univ., Studying Turbulence Using Numerical Simulation Databases. 5: Proceedings of the 1994 Summer Program Dec. 1994 p 189-205 (For primary document see N95-21035 06-34)
Avail: CASI HC A03/MF A04

The statistics of pressure and pressure gradient in stationary isotropic turbulence are measured within direct numerical simulations at low to moderate Reynolds numbers. It is found that the one-point pdf of the pressure is highly skewed and that the pdf of the pressure gradient is of stretched exponential form. The power spectrum of the pressure P(k) is found to be larger than the corresponding spectrum P(sub G)(k) computed from a Gaussian velocity field having the same energy spectrum as that of the DNS field. The ratio P(k)/P(sub G)(k), a measure of the pressure-field intermittence, grows with wavenumber and Reynolds number as -R(sub lambda)(exp 1/2)log(k/k(sub d)) for k less than k(sub d)/2 where k(sub d) is the Kolmogorov wavenumber. The Lagrangian correlations of pressure gradient and velocity are compared and the Lagrangian time scale of the pressure gradient is observed to be much shorter than that of the velocity. Author

N95-21047*# Hong Kong Univ. of Science and Technology, Kowloon (Hong Kong).

THE DECAY OF AXISYMMETRIC HOMOGENEOUS TURBULENCE

J. R. Chasnov *In* Stanford Univ., Studying Turbulence Using Numerical Simulation Databases. 5: Proceedings of the 1994 Summer Program Dec. 1994 p 207-219 (For primary document see N95-21035 06-34)
Avail: CASI HC A03/MF A04

The decay of a homogeneous turbulence generated by an axisymmetric distribution of random impulsive forces acting at the initial instant is considered. The impulsive forces may be either parallel or perpendicular to the symmetry axis. For impulsive forces which result in a kappa(exp 4) low wavenumber energy spectrum of the turbulence, it is determined that the flow approaches isotropy on all scales of motion at long-times provided the Reynolds number is large. However, for the type of impulsive forces originally proposed by Saffman in which a sq kappa low wavenumber energy spectrum is produced, the turbulence approaches isotropy only at the smallest scales and remains significantly anisotropic at the largest and energy-containing scales. Nevertheless, a similarity state of the flow field establishes itself asymptotically, in which the kinetic energy per unit mass of the turbulence decays as t(exp -6/5). Author

N95-21048*# National Aeronautics and Space Administration. Ames Research Center, Moffett Field, CA.

VORTEX RING INSTABILITY AND ITS SOUND

R. Verzicco (Rome Univ., Italy.) and K. Shariff *In* Stanford Univ., Studying Turbulence Using Numerical Simulation Databases. 5: Proceedings of the 1994 Summer Program Dec. 1994 p 221-228 (For primary document see N95-21035 06-34)
Avail: CASI HC A02/MF A04

This work carries earlier finite-difference calculations of the Widnall instability of vortex rings into the late non-linear stage. Plots of energy in azimuthal Fourier modes indicate that low-order modes dominate at large times; their structure and dynamics remain unexplored, however. An attempt was made to calculate the acoustic signal using the theory of Mohring (1978), valid for unbounded flow. This theory shows that only low-order azimuthal modes contribute to the sound. As a check on the effects of axial periodicity and a slip wall at large radius imposed by the numerical scheme, the acoustic integrals were also computed in a truncated region. Half of the terms contributing to the sound have large differences between the two regions, and the results are therefore unreliable. The error is less severe for a contribution involving only the m = 2 mode, and its low frequency is consistent with a free elliptic bending wave on a thin ring. Author

N95-21049*# National Aeronautics and Space Administration. Ames Research Center, Moffett Field, CA.

INSTABILITY OF STREAMWISE VORTICES IN PLANE CHANNEL FLOWS

K. Coughlin (Montreal Univ., Quebec.), J. Jimenez (Stanford Univ., CA.), and R. D. Moser *In* Stanford Univ., Studying Turbulence Using Numerical Simulation Databases. 5: Proceedings of the 1994 Summer Program Dec. 1994 p 229-244 (For primary document see N95-21035 06-34)
Avail: CASI HC A03/MF A04

We present analysis and numerical experiments on the instability of streamwise vortices in 'minimal channel' flows and argue that this instability is a key feature in the observed intermittent cycle of formation, break-up, and re-formation of these structures. The base flow is a three-component, two-dimensional pair of counter-rotating rolls with axes aligned along the direction of the mean shear. While it is not a steady solution to the Navier-Stokes equations, we show numerically that this flow is unstable on a fast time scale to a secondary, three-dimensional Floquet mode. The growth of the secondary instability does not saturate in a new equilibrium, but continues until highly unstable local shear layers form and the entire flow breaks down into turbulence. Our analysis is motivated in part by the strong similarities between the intermittent turbulent cycle in minimal channel flows and one studied, both experimentally and in computations, in Couette-Taylor flow. Author

N95-21050*# Deutsche Forschungsanstalt fuer Luft- und Raumfahrt, Brunswick (Germany).

NUMERICAL INVESTIGATION OF SUPERSONIC TURBULENT BOUNDARY LAYERS WITH HIGH WALL TEMPERATURE

Y. Guo and N. A. Adams (Stanford Univ., CA.) *In* Stanford Univ., Studying Turbulence Using Numerical Simulation Databases. 5: Proceedings of the 1994 Summer Program Dec. 1994 p 245-267 (For primary document see N95-21035 06-34)
Avail: CASI HC A03/MF A04

A direct numerical approach has been developed to simulate supersonic turbulent boundary layers. The mean flow quantities are obtained by solving the parabolized Reynolds-averaged Navier-Stokes equations (globally). Fluctuating quantities are computed locally with a temporal direct numerical simulation approach, in which nonparallel effects of boundary layers are partially modeled. Preliminary numerical results obtained at the free-stream Mach numbers 3, 4.5, and 6 with hot-wall conditions are presented. Approximately 5 million grid points are used in all three cases. The numerical results indicate that compressibility effects on turbulent kinetic energy, in terms of dilatational dissipation and pressure-dilatation correlation, are small. Due to the hot-wall conditions the results show significant low Reynolds number effects and large streamwise streaks. Further simulations with a bigger computational box or a cold-wall condition are desirable. Author

N95-21051*# Johns Hopkins Univ., Baltimore, MD.

A LAGRANGIAN DYNAMIC SUBGRID-SCALE MODEL TURBULENCE

C. Meneveau, T. S. Lund (Stanford Univ., CA.), and W. Cabot (Stanford Univ., CA.) *In* Stanford Univ., Studying Turbulence Using Numerical Simulation Databases. 5: Proceedings of the 1994 Summer Program Dec. 1994 p 271-299 (For primary document see N95-21035 06-34)
Avail: CASI HC A03/MF A04

A new formulation of the dynamic subgrid-scale model is tested in which the error associated with the Germano identity is minimized over flow pathlines rather than over directions of statistical homogeneity. This procedure allows the application of the dynamic model with averaging to flows in complex geometries that do not possess homogeneous directions. The characteristic Lagrangian time scale over which the averaging is performed is chosen such that the model is purely dissipative, guaranteeing numerical stability when coupled with the Smagorinsky model. The formulation is tested successfully in forced and decaying isotropic turbulence and in fully developed and transitional channel flow. In homogeneous flows, the results are similar to those of the volume-averaged dynamic model, while in channel flow, the predictions are superior to those of the plane-averaged dynamic model. The relationship between the averaged terms in the model and vortical structures (worms) that appear in the LES is investigated. Computational overhead is kept small (about 10 percent above the CPU requirements of the volume or plane-averaged dynamic model) by using an approximate scheme to advance the Lagrangian tracking through first-order Euler time integration and linear interpolation in space. Author

N95-21052*# Pratt and Whitney Aircraft, West Palm Beach, FL.

EFFECTS OF TURBULENCE COMPRESSIBILITY AND UNSTEADINESS IN COMPRESSION CORNER FLOW

A. Brankovic and O. Zeman (Stanford Univ., CA.) *In* Stanford Univ., Studying Turbulence Using Numerical Simulation Databases. 5: Proceedings of the 1994 Summer Program Dec. 1994 p 301-311 (For primary document see N95-21035 06-34)
Avail: CASI HC A03/MF A04

The structure of the separated flow region over a 20 degree compression corner at a free-stream Mach number of 2.84 is investigated computationally using a Reynolds averaged Navier Stokes (R.A.N.S.) solver and kappa-epsilon model. At this Mach number and ramp angle, a steady-state recirculation region of order delta(sub o) is observed, with onset of a 'plateau' in the wall pressure distribution near the corner. At lower ramp angles, separation is negligible, while at an angle of 24 degrees, separation regions of length 2 delta(sub o) are expected. Of interest here is the response of the mathematical model to inclusion of the pressure dilatation term for turbulent kinetic energy. Compared with the experimental data of Smits and Muck (1987), steady-state computations show improvement when the pressure dilatation term is included. Unsteady computations, using both unforced and then forced inlet conditions, did not predict the oscillatory motion of the separation bubble as observed in laboratory experiments. An analysis of the separation bubble oscillation and the turbulent boundary layer (T.B.L.) frequencies for this flow suggests that the bubble oscillations are of nearly the same order as the turbulent frequencies, and therefore difficult for the model to separate and resolve. Author

N95-21053*# Old Dominion Univ., Hampton, VA.

ROLE OF PRESSURE DIFFUSION IN NON-HOMOGENEOUS SHEAR FLOWS

A. O. Demuren, S. K. Lele (Stanford Univ., CA.), and P. Durbin (Stanford Univ., CA.) *In* Stanford Univ., Studying Turbulence Using Numerical Simulation Databases. 5: Proceedings of the 1994 Summer Program Dec. 1994 p 313-321 (For primary document see N95-21035 06-34)

Avail: CASI HC A02/MF A04

A non-local model is presented for approximating the pressure diffusion in calculations of turbulent free shear and boundary layer flows. It is based on the solution of an elliptic relaxation equation which enables local diffusion sources to be distributed over lengths of the order of the integral scale. The pressure diffusion model was implemented in a boundary layer code within the framework of turbulence models based on both the kappa-epsilon-(bar)upsilon(exp 2) system of equations and the full Reynolds stress equations. Model computations were performed for mixing layers and boundary layer flows. In each case, the pressure diffusion model enabled the well-known free-stream edge singularity problem to be eliminated. There was little effect on near-wall properties. Computed results agreed very well with experimental and DNS data for the mean flow velocity, the turbulent kinetic energy, and the skin-friction coefficient. Author

N95-21054*# Electricite de France, Chatou (France).

MODELING NEAR WALL EFFECTS IN SECOND MOMENT CLOSURES BY ELLIPTIC RELAXATION

D. Laurence and P. Durbin (Stanford Univ., CA.) *In* Stanford Univ., Studying Turbulence Using Numerical Simulation Databases. 5: Proceedings of the 1994 Summer Program Dec. 1994 p 323-338 (For primary document see N95-21035 06-34)

Avail: CASI HC A03/MF A04

The elliptic relaxation model of Durbin (1993) for modeling near-wall turbulence using second moment closures (SMC) is compared to DNS data for a channel flow at Re(sub t) = 395. The agreement for second order statistics and even the terms in their balance equation is quite satisfactory, confirming that very little viscous effects (via Kolmogoroff scales) need to be added to the high Reynolds versions of SMC for near-wall-turbulence. The essential near-wall feature is thus the kinematic blocking effect that a solid wall exerts on the turbulence through the fluctuating pressure, which is best modeled by an elliptic operator. Above the transition layer, the effect of the original elliptic operator decays rapidly, and it is suggested that the log-layer is better reproduced by adding a non-homogeneous reduction of the return to isotropy, the gradient of the turbulent length scale being used as a measure of the inhomogeneity of the log-layer. The elliptic operator was quite easily applied to the non-linear Craft & Launder pressure-strain model yielding an improved distinction between the spanwise and wall normal stresses, although at higher Reynolds number (Re) and away from the wall, the streamwise component is severely underpredicted, as well as the transition in the mean velocity from the log to the wake profiles. In this area a significant change of behavior was observed in the DNS pressure-strain term, entirely ignored in the models. Author

N95-21055*# National Aeronautics and Space Administration. Ames Research Center, Moffett Field, CA.

MODELING THE TWO-POINT CORRELATION OF THE VECTOR STREAM FUNCTION

M. Oberlack (Technische Hochschule, Aachen, Germany.), M. M. Rogers, and W. C. Reynolds (Stanford Univ., CA.) *In* Stanford Univ., Studying Turbulence Using Numerical Simulation Databases. 5: Proceedings of the 1994 Summer Program Dec. 1994 p 339-352 (For primary document see N95-21035 06-34)

Avail: CASI HC A03/MF A04

A new model for the two-point vector stream function correlation has been developed using tensor invariant arguments and evaluated by the comparison of model predictions with DNS data for incompressible homogeneous turbulent shear flow. This two-point vector stream function model correlation can then be used to calculate the two-point velocity correlation function and other quantities useful in turbulence modeling. The model assumes that the two-point vector stream function correlation can be written in terms of the separation vector and a new tensor function that depends only on the magnitude of the separation vector. The model has a single free model coefficient, which has been chosen by comparison with the DNS data. The relative error of the model predictions of the two-point vector stream function correlation is only a few percent for a broad range of the model coefficient. Predictions of the derivatives of this correlation, which are of interest in turbulence modeling, may not be this accurate. Author

N95-21056*# National Aeronautics and Space Administration. Ames Research Center, Moffett Field, CA.

HOMOGENEOUS TURBULENCE SUBJECTED TO MEAN FLOW WITH ELLIPTIC STREAMLINES

G. A. Blaisdell and K. Shariff (Purdue Univ., West Lafayette, IN.) *In* Stanford Univ., Studying Turbulence Using Numerical Simulation Databases. 5: Proceedings of the 1994 Summer Program Dec. 1994 p 355-371 (For primary document see N95-21035 06-34)

Avail: CASI HC A03/MF A04

Direct numerical simulations are performed for homogeneous turbulence with a mean flow having elliptic streamlines. This flow combines the effects of rotation and strain on the turbulence. Qualitative comparisons are made with linear theory for cases with high Rossby number. The nonlinear transfer process is monitored using a generalized skewness. In general, rotation turns off the nonlinear cascade; however, for moderate ellipticities and rotation rates the nonlinear cascade is turned off and then reestablished. Turbulence statistics of interest in turbulence modeling are calculated, including full Reynolds stress budgets. Author

N95-21057*# Arizona State Univ., Tempe, AZ.

ON THE TRANSITION TOWARDS SLOW MANIFOLD IN SHALLOW-WATER AND 3D EULER EQUATIONS IN A ROTATING FRAME

A. Mahalov *In* Stanford Univ., Studying Turbulence Using Numerical Simulation Databases. 5: Proceedings of the 1994 Summer Program Dec. 1994 p 373-382 (For primary document see N95-21035 06-34)

Avail: CASI HC A02/MF A04

The long-time, asymptotic state of rotating homogeneous shallow-water equations is investigated. Our analysis is based on long-time averaged rotating shallow-water equations describing interactions of large-scale, horizontal, two-dimensional motions with surface inertial-gravity waves field for a shallow, uniformly rotating fluid layer. These equations are obtained in two steps: first by introducing a Poincare/Kelvin linear propagator directly into classical shallow-water equations, then by averaging. The averaged equations describe interaction of wave fields with large-scale motions on time scales long compared to the time scale 1/f(sub o) introduced by rotation (f(sub o)/2-angular velocity of background rotation). The present analysis is similar to the one presented by Waleffe (1991) for 3D Euler equations in a rotating frame. However, since three-wave interactions in rotating shallow-water equations are forbidden, the final equations describing the asymptotic state are simplified considerably. Special emphasis is given to a new conservation law found in the asymptotic state and decoupling of the dynamics of the divergence free part of the velocity field. The possible rising of a decoupled dynamics in the asymptotic state is also investigated for homogeneous turbulence subjected to a background rotation. In our analysis we use long-time expansion, where the velocity field is decomposed into the 'slow manifold' part (the manifold which is unaffected by the linear 'rapid' effects of rotation or the inertial waves) and a formal 3D disturbance. We derive the physical space version of the long-time averaged equations and consider an invariant, basis-free derivation. This formulation can be used to generalize Waleffe's (1991) helical decomposition to viscous inhomogeneous flows (e.g. problems in cylindrical geometry with no-slip boundary conditions on the cylinder surface and homogeneous in the vertical direction). Author

N95-21058*# National Aeronautics and Space Administration. Ames Research Center, Moffett Field, CA.

ON THE ASYMPTOTIC SIMILARITY OF ROTATING HOMOGENEOUS TURBULENCE

K. D. Squires (Vermont Univ., Burlington, VT.), J. R. Chasnov (Hong Kong Univ. of Science and Technology, Kowloon, Hong Kong.), and N. N. Mansour *In* Stanford Univ., Studying Turbulence Using Numerical Simulation Databases. 5: Proceedings of the 1994 Summer Program Dec. 1994 p 383-395 (For primary document see N95-21035 06-34)

Avail: CASI HC A03/MF A04

Asymptotic similarity states at large Reynolds numbers and small Rossby numbers in rotating homogeneous turbulence are investigated using the database obtained from large-eddy simulations of the incompressible Navier-Stokes equations. Previous work has shown that the turbulence kinetic energy and integral length scales are accurately described by simple scaling laws based on the low wavenumbers part of the three-dimensional energy spectrum. The primary interest of the present study is to search for spectrum similarity in the asymptotic state. Four independent energy spectra are defined. It is shown that rescaling of these energy spectra in the asymptotic regime will collapse three out of the four spectra. The spectrum which does not collapse is a function only of the vertical wavenumber and corresponds to two-component motions in the plane normal to the rotation axis. Detailed investigation of the cause of this anomalous behavior reveals the existence of a strong reverse cascade of energy from small-to-large scales of the two-dimensional, two-component motions. This feature of the rotating flow is presumably linked to the lack of a complete similarity state, though further study of this issue is required. Author

N95-21059*# National Aeronautics and Space Administration. Ames Research Center, Moffett Field, CA.

ANISOTROPIC STRUCTURE OF HOMOGENEOUS TURBULENCE SUBJECTED TO UNIFORM ROTATION

C. Cambon (Ecole Centrale de Lyon, France.), N. N. Mansour, and K. D. Squires (Vermont Univ., Burlington, VT.) *In* Stanford Univ., Studying Turbulence Using Numerical Simulation Databases. 5: Proceedings of the 1994 Summer Program Dec. 1994 p 397-420 (For primary document see N95-21035 06-34)

Avail: CASI HC A03/MF A04

Large-eddy simulation results are used to investigate the development of anisotropies and the possible transition towards a quasi two-dimensional state in rotating turbulence at high Reynolds number. The present study demonstrates the existence of two transitions that are identified by two Rossby numbers. The first transition marks the onset of anisotropic effects and corresponds to a macro Rossby number Ro(sup L) (based on a longitudinal integral length scale) near unity. A second transition can be defined in terms of a lower bound of micro-Rossby number Ro(sup w) also near unity (defined in this work as the ratio of the rms fluctuating vorticity to background vorticity) and corresponds to a continued development of anisotropy but with an increasing emergence of those indicators based on the pure two-dimensional component of the flow, e.g., integral length scales measured along the rotation axis. Investigation of the vorticity structure shows that the second transition is also characterized by an increasing tendency for alignment between the fluctuating vorticity vector and the basic angular velocity vector with a preference for corotative vorticity. Author

N95-21060*# National Aeronautics and Space Administration. Ames Research Center, Moffett Field, CA.

SINGLE POINT MODELING OF ROTATING TURBULENT FLOWS

A. H. Hadid (Rockwell International Corp., Canoga Park, CA.), N. N. Mansour, and O. Zeman (Stanford Univ., CA.) *In* Stanford Univ., Studying Turbulence Using Numerical Simulation Databases. V: Proceedings of the 1994 Summer Program Dec. 1994 p 421-432 (For primary document see N95-21035 06-34)

Avail: CASI HC A03/MF A04

A model for the effects of rotation on turbulence is proposed and tested. These effects which influence mainly the rate of turbulence decay are modeled in a modified turbulent energy dissipation rate equation that has explicit dependence on the mean rotation rate. An appropriate definition of the rotation rate derived from critical point theory and based on the invariants of the deformation tensor is proposed. The modeled dissipation rate equation is numerically well behaved and can be used in conjunction with any level of turbulence closure. The model is applied to the two-equation kappa-epsilon turbulence model and is used to compute separated flows in a backward-facing step and an axisymmetric swirling coaxial jets into a sudden expansion. In general, the rotation modified dissipation rate model shows some improvements over the standard kappa-epsilon model. Author

N95-21061# Advisory Group for Aerospace Research and Development, Neuilly-Sur-Seine (France). Fluid Dynamics Panel.

APPLICATION OF DIRECT AND LARGE EDDY SIMULATION TO TRANSITION AND TURBULENCE [L'APPLICATION DE LA SIMULATION DIRECTE ET DE LA SIMULATION DES GROS TOURBILLONS A LA TRANSITION ET A LA TURBULENCE]

Dec. 1994 400 p In ENGLISH and FRENCH The 74th symposium was held in Chania, Greece, 18-21 Apr. 1994 Original contains color illustrations

(AGARD-CP-551; ISBN-92-836-0006-1) Copyright Avail: CASI HC A17/MF A04

The papers prepared for the AGARD Fluid Dynamics Panel (FDP) Symposium on 'Application of Direct and Large Eddy Simulation to Transition and Turbulence', which was held April 1994 in Greece are contained in this report. In addition, a Technical Evaluator's Report assessing the success of the Symposium objectives, and an edited transcript of the General Discussion are also included. In the past two decades significant progress has been made in the numerical simulation of turbulent flows. Vast improvements in speed and memory size of modern supercomputers, and recent progress in simulation algorithms and parallel computation have put us on the threshold of being able to simulate flows in configurations of engineering interest. For individual titles, see N95-21062 through N95-21098.

N95-21062*# National Aeronautics and Space Administration. Ames Research Center, Moffett Field, CA.

DEVELOPMENTS AND APPLICATIONS OF DYNAMIC MODELS FOR LARGE EDDY SIMULATION OF COMPLEX FLOWS

P. Moin, D. Carati, T. Lund, S. Ghosal, and K. Akselvoll *In* AGARD, Application of Direct and Large Eddy Simulation to Transition and Turbulence Dec. 1994 9 p Prepared in cooperation with Stanford Univ., CA Sponsored by ONR and AFOSR (For primary document see N95-21061 06-34)

Copyright Avail: CASI HC A02/MF A04

The dynamic modeling procedure for large eddy simulation of turbulent flows is reviewed and recent developments in the theoretical aspects and applications are described. Methods for inclusion of backscatter of energy from small to large scale motions are presented. New formulations of the dynamic procedure are proposed which are optimized based on the subgrid scale flux vector or the energy dissipation rate instead of the subgrid scale stress tensor. Recent results from application of the model to forced isotropic turbulence with an inertial subrange, flow over a backward facing step at Reynolds number of 28000, and flow over a concave curved surface are presented. Author

N95-21063# Von Karman Inst. for Fluid Dynamics, Rhode-Saint-Genese (Belgium). Dept. of Environmental and Applied Fluid Dynamics.

SUBGRID SCALE MODELS IN FINITE DIFFERENCE SIMULATIONS OF COMPLEX WALL BOUNDED FLOWS

Elias Balaras and Carlo Benocci *In* AGARD, Application of Direct and Large Eddy Simulation to Transition and Turbulence Dec. 1994 6 p (For primary document see N95-21061 06-34)

(Grant EEC-ERBCHDICT930257)

Copyright Avail: CASI HC A02/MF A04

The dynamic subgrid scale model had been used in the Large Eddy Simulation (LES) of turbulent flow in a straight square duct. The Reynolds numbers considered, (based on the friction velocity and the duct halfwidth), are varying from 150 to 1125. The results obtained are in good agreement with the reference Direct Numerical Simulation (DNS) and experimental data. The accuracy and suitability of the model in high Reynolds number finite difference computations of three dimensional non-equilibrium flows is investigated. The influence of approximate wall boundary conditions in such flow cases is also addressed. Author

N95-21064# Maryland Univ., College Park, MD. Dept. of Mechanical Engineering.

LARGE-EDDY SIMULATION OF ROTATING CHANNEL FLOWS USING A LOCALIZED DYNAMIC MODEL

Ugo Piomelli and Junhui Liu *In* AGARD, Application of Direct and Large Eddy Simulation to Transition and Turbulence Dec. 1994 9 p (For primary document see N95-21061 06-34)

(Contract N00014-89-J-1638)
Copyright Avail: CASI HC A02/MF A04

Most applications of the dynamic subgrid-scale stress model use volume- or planar-averaging to avoid ill-conditioning of the model coefficient, which may result in numerical instabilities. A spatially-varying coefficient is also mathematically inconsistent with the model derivation. A localization procedure is proposed here that removes the mathematical inconsistency to any desired order of accuracy in time. This model is applied to the simulation of rotating channel flow, and results in improved prediction of the turbulence statistics. Author

N95-21065*# National Aeronautics and Space Administration. Ames Research Center, Moffett Field, CA.

THE ASYMPTOTIC STATE OF ROTATING HOMOGENEOUS TURBULENCE AT HIGH REYNOLDS NUMBERS

Kyle D. Squires (Vermont Univ., Burlington, VT.), Jeffrey R. Chasnov (Hong Kong Univ. of Science and Technology, Clear Water Bay, Hong Kong.), Nagi N. Mansour, and Claude Cambon (Ecole Centrale de Lyon, France.) *In* AGARD, Application of Direct and Large Eddy Simulation to Transition and Turbulence Dec. 1994 9 p Prepared in cooperation with Stanford Univ., CA Sponsored in part by the American Society for Engineering Education (For primary document see N95-21061 06-34)
Copyright Avail: CASI HC A02/MF A04

The long-time, asymptotic state of rotating homogeneous turbulence at high Reynolds numbers has been examined using large-eddy simulation of the incompressible Navier-Stokes equations. The simulations were carried out using 128 x 128 x 512 collocation points in a computational domain that is four times longer along the rotation axis than in the other directions. Subgrid-scale motions in the simulations were parameterized using a spectral eddy viscosity modified for system rotation. Simulation results show that in the asymptotic state the turbulence kinetic energy undergoes a power-law decay with an exponent which is independent of rotation rate, depending only on the low-wavenumber form of the initial energy spectrum. Integral lengthscale growth in the simulations is also characterized by power-law growth; the correlation length of transverse velocities exhibiting much more rapid growth than observed in non-rotating turbulence. Author

N95-21066# Technische Hogeschool, Twente (Netherlands). Dept. of Applied Mathematics.

COMPARISON OF DNS AND LES OF TRANSITIONAL AND TURBULENT COMPRESSIBLE FLOW: FLAT PLATE AND MIXING LAYER

Bernard Geurts, Bert Vreman, and Hans Kuerten *In* AGARD, Application of Direct and Large Eddy Simulation to Transition and Turbulence Dec. 1994 14 p (For primary document see N95-21061 06-34)
Copyright Avail: CASI HC A03/MF A04

We present a priori and a posteriori test results of LES (large eddy simulation) of compressible flow over a flat plate and in a mixing layer. Through a comparison with filtered DNS (direct numerical simulation) data the 'quality' of subgrid-models for the turbulent stress can be assessed. In particular, the scale similarity model of Bardina and the dynamic mixed model arising from a combination of Bardina's model with the Germano eddy-viscosity model show excellent correlations a priori, and give rise to accurate LES simulations a posteriori. Moreover, the filtering approach close to solid walls is considered and the contribution to the filtered equations arising from the non-commutation of the filter operator with the partial derivatives is calculated. It appears, in a priori tests for 2D simulations, that these non-commutation terms can be comparable to the turbulent stress. The scale similarity hypothesis yields models for these terms which show a good correlation. Author

N95-21067# Technische Univ., Munich (Germany). Lehrstuhl fuer Fluidmechanik.

DIRECT NUMERICAL SIMULATION OF TURBULENT FLOW IN A SUDDEN PIPE EXPANSION

C. Wagner and R. Friedrich *In* AGARD, Application of Direct and Large Eddy Simulation to Transition and Turbulence Dec. 1994 11 p (For primary document see N95-21061 06-34)
Copyright Avail: CASI HC A03/MF A04

Direct numerical simulations (DNS) of fully developed turbulent pipe flow and sudden pipe expansion flow with an expansion ratio of ER = 1.2 have been performed. The former DNS provides inflow conditions for the latter. The upstream Reynolds number, based on friction velocity and pipe diameter is 360 or 6950 based on mean centerline velocity. This is too low a Reynolds number to obtain a universal logarithmic law of the wall. Moreover, transverse curvature effects are observed when the data are compared with DNS data of Kim, Moin, Moser in the plane channel. The reason for these effects is that the streak spacing is of the same order of magnitude as the pipe radius. Hence, the pipe expansion flow will also reflect transverse curvature effects. The mean reattachment length is 10.1 step heights. Instantaneous and statistical flow variables are presented. They give an impression of the complex flow dynamics in the free shear layer, the recirculation and reattachment regions. Author

N95-21068# Office National d'Etudes et de Recherches Aerospatiales, Paris (France).

SIMULATION OF SEPARATED FLOWS [SIMULATION D'ECOULEMENTS DECOLLES]

B. Troff, T. H. Le, P. Sagaut, and Loc TaPhuoc (Centre National de la Recherche Scientifique, Orsay, France.) *In* AGARD, Application of Direct and Large Eddy Simulation to Transition and Turbulence Dec. 1994 10 p In FRENCH Sponsored by DGA/DRET (For primary document see N95-21061 06-34)
Copyright Avail: CASI HC A02/MF A04

Direct Numerical Simulation and Large Eddy Simulations of separated flows have been carried out using the PEGASE code. The incompressible Navier-Stokes equations are solved using a projection method. The spatial discretization is performed via a hybrid finite difference / finite element approach. Results related to the bidimensional backward facing step provided in DNS at Reynolds numbers up to 800 and in LES at a Reynolds number equal to 11,200 are shown. Author

N95-21069# Technical Univ. of Lisbon (Portugal). Dept. of Mechanical Engineering.

LARGE EDDY SIMULATION OF TURBULENT FLOW OVER A CAVITY

J. C. F. Pereira and J. M. M. Sousa *In* AGARD, Application of Direct and Large Eddy Simulation to Transition and Turbulence Dec. 1994 10 p Original contains color illustrations (For primary document see N95-21061 06-34)
Copyright Avail: CASI HC A02/MF A04

Smagorinsky and structure-function models are applied to the large eddy simulation of the turbulent flow over a cavity at a Reynolds number Re = 63,600. The near-wall flow region is modeled by implementing either a logarithmic law-of-the-wall or an exponential damping function. Results obtained with two values of the Smagorinsky constant, C(sub s) = 0.10 and 0.20, have been compared. Further, the results provided by the mentioned subgrid-scale models are compared with those obtained using the standard kappa-epsilon model. As a basis for the comparison, LDV measurements of mean and fluctuating turbulent quantities are also reported. The computational results have demonstrated that the use of large eddy simulation is clearly rewarding in face of kappa-epsilon model computation, yielding better results employing a similar number of grid nodes. Author

N95-21070# Ruhr Univ., Bochum (Germany). Inst. fuer Thermo- und Fluiddynamik.

LARGE-EDDY SIMULATION OF SEPARATED FLOW IN A RIBBED DUCT

Harald Braun, Martin Fiebig, and Nimai Kumar Mitra *In* AGARD, Application of Direct and Large Eddy Simulation to Transition and Turbulence Dec. 1994 9 p Sponsored by Deutsche Forschungsgemeinschaft (For primary document see N95-21061 06-34)
Copyright Avail: CASI HC A02/MF A04

Large-eddy simulation of turbulent channel flows over a one-sided periodically ribbed wall has been performed. Large-scale nonsteady structures have been correlated with the statistical values of the turbulent flow field. It is shown, that high turbulent kinetic energy and vortex shedding appear at the same location. The shedding of vortical structures from the edge of the rib is the dominating turbulent phenomena of the flow. The instantaneous behavior of the large-scale vortical structures is visualized and their interaction with the highly fluctuating recirculation zones is observed. Author

N95-21071*# Georgia Inst. of Tech., Atlanta, GA. School of Aerospace Engineering.

ANALYSIS OF SUBGRID MODELS USING DIRECT AND LARGE-EDDY SIMULATIONS OF ISOTROPIC TURBULENCE

S. Menon and P. K. Yeung *In* AGARD, Application of Direct and Large Eddy Simulation to Transition and Turbulence Dec. 1994 12 p Sponsored by NASA. Ames Research Center (For primary document see N95-21061 06-34)
(Contract N00014-93-1-0342)
Copyright Avail: CASI HC A03/MF A04

Direct and large eddy simulations of forced and decaying isotropic turbulence have been performed using a pseudospectral and a finite-difference code. Subgrid models that include a one-equation subgrid kinetic energy model with and without a stochastic backscatter forcing term and a new scale similarity model have been analyzed in both Fourier space and physical space. The Fourier space analysis showed that the energy transfer across the cutoff wavenumber k(sub c) is dominated by local interaction. The correlation between the exact and the modeled (by a spectral eddy viscosity) nonlinear terms and the subgrid energy transfer in physical space was found to be quite low. In physical space, a similar correlation analysis was carried out using top hat filtering. Results show that the subgrid stress and the energy flux predicted by the subgrid models correlates very well with the exact data. The scale similarity model showed very high correlation for reasonable grid resolution. However, with decrease in grid resolution, the scale similarity model became more uncorrelated, when compared to the kinetic energy subgrid model. The subgrid models were then used for large-eddy simulations for a range of Reynolds number. It was determined that the dissipation was modeled poorly and that the correlation with the exact results was quite low for all the models. In general, for coarse grid resolution, the scale similarity model consistently showed very low correlation while the kinetic energy model showed a relatively higher correlation. These results suggest that to use the scale similarity model relatively fine grid resolution may be required, whereas, the kinetic energy model could be used even in coarse grid. Author

N95-21072# Milan Univ. (Italy). Dipt. di Ingegneria Aerospaziale.

A CHEAP DNS TOOL FOR TURBULENCE MODELS TESTING

A. Baron and M. Quadrio *In* AGARD, Application of Direct and Large Eddy Simulation to Transition and Turbulence Dec. 1994 10 p Sponsored by Ministero dell'Univ. e della Ricerca Scientifica e Tecnologica and Consorzio Interuniv. Lombardo per l'Elaborazione Automatica (For primary document see N95-21061 06-34)
Copyright Avail: CASI HC A02/MF A04

The Narrow Channel (NC) assumption, together with a simple although efficient numerical scheme are adopted in order to perform the Direct Numerical Simulation (DNS) of turbulent channel flows at moderate Reynolds numbers with extremely reduced computational resources. Typical results are presented for a constant property fluid, which certify the reliability of the numerical tool and the quality of the simulations. The closure problem of turbulence modeling is then considered and the transport equations for the Reynolds stresses and for the dissipation rate of the turbulence kinetic energy are solved on the basis of the Narrow Channel data. The comparison of the distributions of the various terms in the transport equations with published full channel DNS data confirms that, although the NC assumption substantially reduces the computational cost of the simulations, it does not affect the accuracy of the numerical predictions. Finally, as an example of the use that can be done of the numerical tool, an algebraic stress model and a one-equation model for the dissipation rate tensor for low Reynolds number flows are considered, and the modeled quantities are compared with their directly computed counterparts. Author

N95-21073# Det Norske Veritas, Hovik (Norway).

DIRECT SIMULATION OF TURBULENT FLOW IN A SQUARE DUCT: REYNOLDS-STRESS BUDGETS

Asmund Huser, Sedat Biringen (Colorado Univ., Boulder, CO.), and Ferhat F. Hatay (Colorado Univ., Boulder, CO.) *In* AGARD, Application of Direct and Large Eddy Simulation to Transition and Turbulence Dec. 1994 12 p Sponsored by Fulbright Foundation, Norwegian Space Agency, and Royal Norwegian Council for Scientific and Industrial Research (For primary document see N95-21061 06-34)
Copyright Avail: CASI HC A03/MF A04

The data base from a direct numerical simulation of turbulent flow in a square duct is used to calculate all the terms in the Reynolds stress transport equations. The simulation of this complex turbulent flow was performed at a Reynolds number of 600 based on the friction velocity and the duct width. The distributions of the Reynolds stress budget terms along the wall bisector show similar dynamics to wall-bounded turbulent flows with one inhomogeneous direction. Budget terms in the vicinity of the corner demonstrate how transport and redistribution of energy and shear stresses between the Reynolds stress components takes place, promoting the turbulence characteristics of secondary flows of the second kind. The redistribution of energy by pressure velocity correlations can be explained by the low pressures at the cores of streamwise vortices. The data base is also used to evaluate a nonlinear turbulence model in its ability to accommodate the anisotropy of the Reynolds stress tensor in this flow. This anisotropy is known to be entirely responsible for the formation of the secondary flow in noncircular ducts and cannot be captured by linear models. Author

N95-21074*# National Aeronautics and Space Administration. Ames Research Center, Moffett Field, CA.

NUMERICAL SIMULATION OF SUPERSONIC BOUNDARY LAYER TRANSITION

Y. Guo (Eidgenoessische Technische Hochschule, Zurich, Switzerland.), N. A. Adams, N. D. Sandham (Westfield Coll., London, England.), and L. Kleiser (Eidgenoessische Technische Hochschule, Zurich, Switzerland.) *In* AGARD, Application of Direct and Large Eddy Simulation to Transition and Turbulence Dec. 1994 12 p Prepared in cooperation with Deutsche Forschungsanstalt fuer Luft- und Raumfahrt, Goettingen, Germany (For primary document see N95-21061 06-34)
Copyright Avail: CASI HC A03/MF A04

The present contribution reviews some of the recent progress obtained at our group in the direct numerical simulation (DNS) of compressible boundary layer transition. Elements of the different simulation approaches and numerical techniques employed are surveyed. Temporal and spatial simulations, as well as comparisons with results obtained from Parabolized Stability Equations, are discussed. DNS results are given for flat plate boundary layers in the Mach number range 1.6 to 4.5. A temporal DNS at Mach 4.5 has been continued through breakdown all the way to the turbulent stage. In addition results obtained with a recently developed extended temporal DNS approach are presented, which takes into account some nonparallel effects of a growing boundary layer. Results from this approach are quite close to those of spatial DNS, while preserving the efficiency of the temporal DNS. Author

N95-21075# Institut de Mecanique de Grenoble (France).

SIMULATION OF LARGE SCALE TRANSITIONAL FLOWS [SIMULATION DES GRANDES ECHELLES D'ECOULEMENTS TRANSITIONNELS]

P. Comte, F. Ducros, J. Silvestrini, E. David, E. Lamballais, O. Metais, and M. Lesieur *In* AGARD, Application of Direct and Large Eddy Simulation to Transition and Turbulence Dec. 1994 12 p In FRENCH (For primary document see N95-21061 06-34)
Copyright Avail: CASI HC A03/MF A04

Two new subgrid-scale models of turbulence are proposed on the basis of a 2nd-order velocity structure function model developed by Metais and Lesieur. They result from two different approaches aimed at preventing fluctuations at large scales from bringing about turbulent viscosity. Simulations of boundary layers at Mach 0.5 are presented showing that these two models make it possible to simulate the transition to a turbulent regime developed at moderate computational costs in appreciably different configurations (adiabatic plate and strongly heated dihedral). Transl. by CASI

N95-21076# Naval Research Lab., Washington, DC. Remote Sensing Div.

LARGE EDDY SIMULATION OF CHANNEL FLOW USING A VORTICITY TRANSPORT SUBGRID MODEL

Amy L. Rovelstad, Robert A. Handler, Peter S. Bernard (Maryland Univ., College Park, MD.), and James M. Thomas (Maryland Univ., College Park, MD.) *In* AGARD, Application of Direct and Large Eddy Simulation to Transition and Turbulence Dec. 1994 7 p Sponsored in part by NAS-NRC (For primary document see N95-21061 06-34)
(Contracts N00014-91-WX-24079; N00014-93-1-0184)
Copyright Avail: CASI HC A02/MF A04

Vorticity transport concepts are applied to large eddy simulation (LES) techniques in two different contexts. In the first example, the LES equations of motion are reformulated by applying a spatial filter to the rotational rather than the momentum form of the Navier-Stokes equation, leading to the introduction of a subgrid-scale (SGS) vorticity flux tensor. A model originally developed using ensemble averaging is proposed and tested locally and instantaneously using simulations of full channel flow and a minimal channel calculation. The modeled and exact vorticity fluxes are found to generally agree, even for vorticity flux terms which are only present locally and instantaneously. The development of a vorticity transport based wall treatment using a deterministic vortex element approach is also outlined. Initial tests comparing the results of this approach to the zero pressure gradient and stagnation point boundary layer are compared to the Blasius and Falkner-Skan solutions and found to be in good agreement. Author

N95-21077# Ecole Centrale de Lyon (France). Lab. de Mecanique des Fluides et d'Acoustique.

MODELLING ANISOTROPY AND BACKSCATTER EFFECTS IN THE SUBGRID SCALE STRESS TENSOR

T. Goutorbe and D. Laurence (Electricite de France, Chatou, France.) *In* AGARD, Application of Direct and Large Eddy Simulation to Transition and Turbulence Dec. 1994 7 p (For primary document see N95-21061 06-34)
Copyright Avail: CASI HC A02/MF A04

A new Subgrid scale (SGS) model used for Large-Eddy Simulation (LES) is developed by extending the scale-similarity hypothesis. Here a conventional Reynolds averaging is used instead of a test filter, resulting using the resolved (large scale) part of the Reynolds stress tensor. This resolved Reynolds stress (RRS) model, without any eddy viscosity assumption, is shown to properly reproduce the drain and backscatter partition of energy exchange between resolved and subgrid scales (for a channel flow at moderate Reynolds numbers). After assessing these properties by a priori tests (filtering DNS results), LES computations are carried out, determining the model constants by an analytical approach and a dynamic approach. In both cases, backscatter effects can lead to instabilities which are finally cured by introducing a transport equation for the SGS energy. This is felt necessary because when backscatter occurs, both SGS production and Kolmogorov dissipation are negative, so SGS energy must vanish, thus ending backscatter. Only a transport equation for the SGS energy can account for this energy conservation principle which is violated by dynamic approaches, that impose an average procedure. Slight discrepancies appear in the buffer layer which may be attributed to the insufficient resolution of streak structures in the spanwise direction. Thus, an adaptation for the buffer-layer appears to be the last obstacle to construct a model accounting for the most important physical properties required for SGS modeling and applicable for practical applications at high Reynolds numbers. Author

N95-21078# Princeton Univ., NJ. Fluid Dynamics Research Center.

SIMULATION OF PIPE FLOW

Y. Zhang, A. Gandhi, A. G. Tomboulides, and S. A. Orszag *In* AGARD, Application of Direct and Large Eddy Simulation to Transition and Turbulence Dec. 1994 9 p Sponsored in cooperation with ARPA (For primary document see N95-21061 06-34)
(Contracts N00014-92-J-1796; N00014-92-C-0216)
Copyright Avail: CASI HC A02/MF A04

In this paper we report simulations of low to moderate Reynolds number turbulent pipe flow, obtained using a 3-D spectral code. Here we describe features of flows at Reynolds numbers Re = 2500 and 4000 and compare with available data. It is noted that simulations with periodic inflow/outflow boundary conditions do not reproduce the turbulent puff and slug flows found in spatially evolving transitional flows. The goal is to coordinate the use of this code with the currently performed SuperPipe experiments now underway at Princeton University. Author

N95-21079*# Aeronautical Research Inst. of Sweden, Bromma.

SIMULATIONS OF BYPASS TRANSITION FOR SPATIALLY EVOLVING DISTURBANCES

A. Lundbladh, P. J. Schmid (Washington Univ., Seattle, WA.), S. Berlin (Royal Inst. of Tech., Stockholm, Sweden.), and D. S. Henningson *In* AGARD, Application of Direct and Large Eddy Simulation to Transition and Turbulence Dec. 1994 13 p Sponsored by NASA. Langley Research Center (For primary document see N95-21061 06-34)
Copyright Avail: CASI HC A03/MF A04

The spatial evolution of disturbances in plane Poiseuille flow and zero pressure gradient boundary layer flow is considered. For disturbances governed by the linearized equations, potential for significant transient growth of the amplitude is demonstrated. The maximum amplification occurs for disturbances with zero or near zero frequencies. Spatial numerical simulations of the transition scenario involving a pair of oblique waves has been conducted for both flows. A fully spectral solver using a simple but efficient fringe region technique allowed the flows to be computed with high resolution into the fully turbulent domain. A modal decomposition of the simulation results indicates that non-linear excitation of the transient growth is responsible for the rapid emergence of low-frequency structures. Physically, this corresponds to streaky flow structures, as seen from the results of a numerical amplitude expansion. Thus, this spatial transition scenario has been found to be similar to the corresponding temporal one. In the boundary layer simulations the streaks are seen to break down from what appears to be a secondary instability. Author

N95-21080# Universidad Politecnica de Madrid (Spain). School of Aeronautics.

DIRECT NUMERICAL DETERMINATION OF THE MINIMUM BYPASS REYNOLDS NUMBER IN BOUNDARY LAYERS

Roque Corral and Javier Jimenez *In* AGARD, Application of Direct and Large Eddy Simulation to Transition and Turbulence Dec. 1994 10 p Sponsored by ESA (For primary document see N95-21061 06-34)
Copyright Avail: CASI HC A02/MF A04

It is argued that bypass transition on a flat plate can be interpreted as a consequence of the subcritical nature of the instability of the boundary layer, and that the minimum bypass Reynolds number should coincide with the one at which the turbulent layer relaminarizes spontaneously. This threshold is found by direct numerical simulation of a spatially periodic turbulent layer in which spatial growth is modeled by a linear normal velocity. The computed mean profiles and integral properties agree well with experimental results at the higher Reynolds numbers, but diverge from them at the lower ones. While experiments turn away from the turbulent correlations below Re(sub theta) approx. equals 300 - 500, the computations follow them until relaminarizing abruptly at Re(sub theta) approx. equals 200. The simulations use relatively small periodic computational boxes, holding only a few boundary layer thickness, and it is argued that this provides enough feedback to prevent the transitional effects observed in experiments and to result in an absolute relaminarization threshold. The Reynolds number obtained in this way agrees with the onset of bypass transition in experiments with very high free stream turbulence levels, or with strong roughness tripping. Author

N95-21081# Central Inst. of Aviation Motors, Moscow (Russia).

A FLAMELET MODEL FOR TURBULENT UNPREMIXED COMBUSTION

c25

V. R. Kuznetsov *In* AGARD, Application of Direct and Large Eddy Simulation to Transition and Turbulence Dec. 1994 10 p (For primary document see N95-21061 06-34)
Copyright Avail: CASI HC A02/MF A04

Combustion theory is an applied science which is syntheses of several fundamental theories such as chemistry, heat and mass transfer theory, hydrodynamics, turbulence, etc. Now the knowledge of these theories is adequate to make calculations for practical purposes. However some difficulties still remain unresolved. The most important one is associated with the steep dependence of chemistry on temperature. As a result chemistry is confined to very thin zones (flamelets). Hence very large memory and speed of computers are needed to resolve flamelets in DNS. This difficulty is aggravated by the large number of intermediate species. The use of turbulence closures does not help since one has to assume that eddy diffusivities of reacting species and their pdf's (which are needed to average chemistry rates) are the same as that of conserved scalar. There are several examples indicating that these assumptions may lead to significant errors. Therefore there is a need to develop some new approach. Author

N95-21082# Manchester Coll. of Science and Technology (England). Dept. of Mechanical Engineering.

DIRECT NUMERICAL SIMULATION FOR PREMIXED TURBULENT COMBUSTION MODELLING c25

R. S. Cant *In* AGARD, Application of Direct and Large Eddy Simulation to Transition and Turbulence Dec. 1994 13 p Sponsored by Stanford Univ., Shell Research Ltd., and the UK Science and Engineering Research Council (For primary document see N95-21061 06-34)
Copyright Avail: CASI HC A03/MF A04

Recent advances in computer power have made it feasible to carry out Direct Numerical Simulation (DNS) of fundamental test problems in turbulent combustion. Nevertheless the requirements in terms of numerical grid resolution remain very severe and engineering computations will remain beyond the reach of DNS for some time to come. Thus there is an undiminished role for statistical modeling using traditional moment-closure techniques and DNS can be used to provide fundamental data in support of such modeling. The present paper describes a specific example of the use of DNS results to improve the quality of a well-established model of premixed turbulent combustion. A brief outline of the model formulation is given, followed by a short description of the DNS and post-processing techniques employed. Some results of immediate utility are presented in order to illustrate the usefulness of the approach, and the parameterization of some further data is discussed in detail. The significance of the main improvements to the modeling is indicated and some remaining limitations are discussed. The prospects for future model refinement by improved DNS are examined and found to be excellent. Author

N95-21083# Stanford Univ., CA. Dept. of Mechanical Engineering.

ENTRAINMENT IN A SHEAR-FREE TURBULENT MIXING LAYER

D. A. Briggs, J. H. Ferziger, J. R. Koseff, and S. G. Monismith *In* AGARD, Application of Direct and Large Eddy Simulation to Transition and Turbulence Dec. 1994 18 p (For primary document see N95-21061 06-34)
(Contract N00014-92-J-1611)
Copyright Avail: CASI HC A03/MF A04

Results from a direct numerical simulation of turbulent mixing layer are presented. The flow evolves without shear and the mixing mechanisms associated with the turbulence are isolated. In the first set of simulations the turbulent mixing layer decays as energy is exchanged between the layers. In the second set, a forced mixing layer is simulated by continuously supplying energy to the higher energy side to maintain a stationary kinetic energy profile. Reynolds numbers based on the Taylor microscale of 28 and 38 are obtained in the decaying and forced simulations, respectively. The intermittency of the mixing layer is quantified by calculating the skewness and kurtosis of the velocity fields: results compare well with the shearless mixing layer experiments. Eddies of size of the integral scale (k(exp 3/2)/epsilon) penetrate the mixing layer intermittently, transporting energy and governing the growth rate. The scalar dissipation rate, a measure of the mixing, peaks in the mixing layer. The triple correlation models are applied to the inhomogeneous mixing layer and evaluated. The isotropic models tend to underpredict these correlations by as much as 60 percent while the more complicated anisotropic models are shown to be significantly more accurate. Both models for the pressure strain tensor are also shown to predict values that are incorrect by as much as 50 percent. Author

N95-21084*# National Aeronautics and Space Administration. Ames Research Center, Moffett Field, CA.

DIRECT SIMULATION OF A SELF-SIMILAR PLANE WAKE

Robert D. Moser and Michael M. Rogers *In* AGARD, Application of Direct and Large Eddy Simulation to Transition and Turbulence Dec. 1994 8 p (For primary document see N95-21061 06-34)
Copyright Avail: CASI HC A02/MF A04

Direct simulations of two time-developing turbulent wakes have been performed. Initial conditions for the simulations were obtained from two realizations of a direct simulation of a turbulent boundary layer at momentum thickness Reynolds number 670. In addition, extra two-dimensional disturbances were added in one of the cases to mimic two-dimensional forcing. The unforced wake is allowed to evolve long enough to attain self-similarity. The mass-flux Reynolds number (equivalent to the momentum thickness Reynolds number in spatially developing wakes) is 2000, which is high enough for a short kappa(exp -5/3) range to be evident in the streamwise one-dimensional velocity spectrum. Several turbulence statistics have been computed by averaging in space and over the self-similar period in time. The growth rate in the unforced flow is low compared to experiments, but when this growth-rate difference is accounted for, the statistics of the unforced case are in reasonable agreement with experiments. However, the forced case is significantly different. The growth rate, turbulence Reynolds number, and turbulence intensities are as much as ten times larger in the forced case. In addition, the forced flow exhibits large-scale structures similar to those observed in transitional wakes, while the unforced flow does not. Author

N95-21085*# National Aeronautics and Space Administration. Ames Research Center, Moffett Field, CA.

THE EFFECT OF INITIAL CONDITIONS ON THE DEVELOPMENT OF TEMPORALLY EVOLVING PLANAR THREE DIMENSIONAL INCOMPRESSIBLE WAKES

Rolf Sondergaard (Stanford Univ., CA.), Nagi N. Mansour, and Brian J. Cantwell (Stanford Univ., CA.) *In* AGARD, Application of Direct and Large Eddy Simulation to Transition and Turbulence Dec. 1994 13 p (For primary document see N95-21061 06-34)
(Contract N00014-90-J-1976)
Copyright Avail: CASI HC A03/MF A04

A set of direct numerical simulations of temporally evolving incompressible plane wakes started from a variety of initial conditions have been performed. The intent is to explore the effect of initial conditions on the development of three dimensionality. It was found that the existence of an oblique disturbance at a streamwise wavelength equal to the two-dimensional subharmonic wavelength plays a very important role in the development of the wake. The Reynolds number and the presence or absence of longer wavelength disturbances were also found to be important at late times in the development of the flow. Disturbance phase was found to have an effect on the details of the structure of the wake, but has relatively little effect on the wake growth. Author

N95-21086# University of West Bohemia, Plzen (Czechoslovakia).

DIRECT SIMULATION OF TRIDIMENSIONAL WAKE OF NACA 0012 PROFILE [SIMULATION DIRECTE DU SILLAGE TRIDIMENSIONNEL DU PROFIL NACA 0012]

J. Dusek and Ph. Fraunie (Universite de Toulon et du Var, France.) *In* AGARD, Application of Direct and Large Eddy Simulation to Transition and Turbulence Dec. 1994 9 p In FRENCH Sponsored by cooperation with the European program CST PECO - Individual Mobility (For primary document see N95-21061 06-34)
(Grant DGA-91/158)
Copyright Avail: CASI HC A02/MF A04

Direct numerical simulation of the tridimensional wake developing downstream from a NACA 0012 wing has been performed using the spectral element code NEKTON. The onset of instability in the wake of an infinite NACA 0012 wing is investigated. The first bifurcation is studied in a two dimensional configuration with a mesh obtained using the numerical experience with a two dimensional unstable cylinder wake. The second bifurcation accompanied by the onset of three-dimensionality is simulated on a three dimensional spectral element mesh obtained by extending the two-dimensional mesh spanwise. The onset of three-dimensionality is characterized by a deformation of the downstream and transverse velocity profiles in the spanwise direction and by the onset of an oscillating spanwise velocity. The critical Reynolds numbers are estimated for both bifurcations. The second bifurcation is shown to be characterized by a period doubling, i.e., the Strouhal frequency of the spanwise velocity is rather precisely equal to half the frequency of the transverse velocity oscillations. This result is in agreement with the numerical results of Karniadakis and Triantafyllou obtained for an infinite circular cylinder and confirms indirectly the experimental results of Williams-Stuber and Gharib showing that to obtain a Ruelle and Takens scenario in a wake, an external forcing is needed. Furthermore, simulations in a geometrically three-dimensional configuration of a finite wing are performed. The development of the tip vortex of a finite wing is investigated. Comparisons are made with available experimental results performed at low Reynolds numbers. The structure of the three dimensional flow is found to be in good agreement with experiments. The simulations are carried out at supercritical Reynolds numbers at which the wake is unstable. The wake oscillations and tip vortex oscillations are evidenced and shown to be characterized by roughly the same Strouhal frequency although the computations could not be pushed until relaxation of transients. Author

N95-21087# Von Karman Inst. for Fluid Dynamics, Rhode-Saint-Genese (Belgium).

NUMERICAL SIMULATION OF SPATIALLY-DEVELOPING PLANAR JETS

Guy Hoffmann and Carlo Benocci *In* AGARD, Application of Direct and Large Eddy Simulation to Transition and Turbulence Dec. 1994 6 p (For primary document see N95-21061 06-34)

Copyright Avail: CASI HC A02/MF A04

The flowfield of an impinging jet is investigated numerically by means of the LES technique. The numerical scheme uses a high order upwind biased formulation for the advective transport. A localized dynamic evaluation of the Smagorinsky constant is employed to avoid an empirical tuning of this value. A critical problem is the formulation of open boundary conditions. The set of boundary conditions presented here allows both the entrainment of fluid into the computational domain as well as the exit of the large vortical structures typical for this flow problem. Author

N95-21088# La Sapienza Univ., Rome (Italy). Dipt. de Meccanica e Aeronautica.

RIB VORTICES IN ROUND JETS: DIRECT AND LARGE EDDY SIMULATION

M. Fatica, R. Verzicco, and P. Orlandi *In* AGARD, Application of Direct and Large Eddy Simulation to Transition and Turbulence Dec. 1994 10 p Sponsored by Agenzia Spaziale Italiana (For primary document see N95-21061 06-34)

Copyright Avail: CASI HC A02/MF A04

Direct and Large Eddy simulations of temporal evolving round jets at low Reynolds numbers have been performed by a second-order finite difference scheme in cylindrical coordinates. The simulations have shown the formation of longitudinal structures whose number increases with the Reynolds number. The role of these structures in the spreading of the jet and in the creation of small scales has been analyzed. LES models (Smagorinsky and dynamic models) permit to have satisfactory results with coarse grids. Author

N95-21089# Ankara Univ. (Turkey). Dept. of Mechanical Engineering.

DIRECT NUMERICAL SIMULATION OF TRANSITION TO TURBULENCE FROM A HIGH-SYMMETRY INITIAL CONDITION

Olus N. Boratav and Richard B. Pelz (Rutgers - The State Univ., Piscataway, NJ.) *In* AGARD, Application of Direct and Large Eddy Simulation to Transition and Turbulence Dec. 1994 9 p (For primary document see N95-21061 06-34)

(Grant AF-AFOSR-0248-91)

Copyright Avail: CASI HC A02/MF A04

The three-dimensional time evolution of a highly symmetrical vortex array is simulated using a Fourier pseudospectral method for Re = 1/nu = 2000 with an effective resolution of 1024(exp 3) collocation points (k(sub max) = 340). It is found that before the peak enstrophy is reached, there is a short stage when the local quantities increase sharply. The velocity derivative skewness and flatness values reach to 0.9 and 80 respectively. It is also found that during this interval, 6 vortex dipoles (at the origin) and 3 dipoles (at the pi/2 corner) collapse towards two separate vorticity null points. The coherent vortices break up afterwards followed by sharp decrease in local quantities possibly due to dissipation. The singularity analysis shows that maximum vorticity scales as (T - T(sub c))(exp -1) shortly before the break up. The temporal evolution of the width of the analyticity strip shows that delta approaches zero but reaches a minimum positive value and starts to increase. This suggests that the solution remains uniformly analytic similar to the viscous Burgers equation. Author

N95-21090*# Arizona State Univ., Tempe, AZ. Dept. of Mechanical and Aerospace Engineering.

DIRECT NUMERICAL SIMULATIONS OF LEADING-EDGE RECEPTIVITY FOR FREESTREAM SOUND

David A. Fuciarelli and Helen L. Reed *In* AGARD, Application of Direct and Large Eddy Simulation to Transition and Turbulence Dec. 1994 8 p Sponsored by NASA. Langley Research Center and NSF (For primary document see N95-21061 06-34)

Copyright Avail: CASI HC A02/MF A04

The objective of this paper is to review our efforts in spatial direct numerical simulations for modeling leading-edge receptivity to freestream sound and vorticity. These results begin to provide the link between the freestream and the initial boundary-layer response and can provide the upstream conditions for further simulations marching through the transition process toward turbulence. Author

N95-21091# Boeing Commercial Airplane Co., Seattle, WA.

NUMERICAL STUDY OF REALISTIC PERTURBATIONS IN THREE-DIMENSIONAL BOUNDARY LAYERS

P. R. Spalart, J. D. Crouch, and L. L. Ng *In* AGARD, Application of Direct and Large Eddy Simulation to Transition and Turbulence Dec. 1994 10 p (For primary document see N95-21061 06-34)

Copyright Avail: CASI HC A02/MF A04

Direct Numerical Simulation is applied to a variety of small perturbations developing in a three-dimensional boundary layer. The basic flow is independent of the spanwise coordinate but incorporates a favorable and an adverse pressure gradient in the chordwise direction, similar to the leading-edge region of a swept wing. The edge velocity is analytically defined. Both Cross-Flow and Tollmien-Schlichting modes are amplified. Results focus on questions that are often open in three-dimensional transition-predictions codes, particularly 'e(exp N)' type codes. They include: non-parallel effects; choice of wave-vector; choice of propagation velocity and direction; and the effect of broad spectra, in either space direction and/or time. For this we survey a range of perturbations from pure waves to wave packets; the latter result from initial perturbations that are local in both space and time, and are arguably the richest type of disturbance. Quantitative results are offered for the validation of stability codes, and some are compared with Orr-Sommerfeld results. Author

N95-21092# Technische Hogeschool Twente, Enschede (Netherlands). Dept. of Applied Mathematics.

ON SUBCRITICAL INSTABILITY OF THE ATTACHMENT LINE BOUNDARY LAYER

Vassilios Theofilis *In* AGARD, Application of Direct and Large Eddy Simulation to Transition and Turbulence Dec. 1994 8 p (For primary document see N95-21061 06-34)

Copyright Avail: CASI HC A02/MF A04

Subcritical instability in the two-dimensional incompressible attachment-line boundary layer remains a topic of debate, after the apparently contradictory results of Hall and Malik (1986) on one hand and Spalart (1988) and Jimenez et al. (1990) on the other. Direct Numerical Simulation (DNS) results are presented, aiming at addressing this question. Extensive numerical experimentation has been performed and all results obtained suggest that the two-dimensional model equations describing leading edge boundary layer (LEBL) flow doe not support solutions growing subcritically in Reynolds number, although the nonlinear neutral loop is seen to bifurcate from its linear counterpart in a manner consistent with the predictions of the theory of Hall and Malik (1986). Nonlinear neutral loops have been obtained suggesting that the two-dimensional model LEBL flow is similar to the classical Blasius boundary layer in terms of the location, in parameter space, of the experimentally observed naturally occurring instability waves. Author

N95-21093# Stuttgart Univ. (Germany). Inst. fuer Aerodynamik und Gasdynamik.

SPATIAL DIRECT NUMERICAL SIMULATION OF BOUNDARY LAYER TRANSITION UNDER STRONG ADVERSE PRESSURE GRADIENT

H. Bestek, M. Kloker, and W. Mueller *In* AGARD, Application of Direct and Large Eddy Simulation to Transition and Turbulence Dec. 1994 12 p Sponsored by Deutsche Forschungsgemeinschaft and Stiftung Volkswagenwerk (For primary document see N95-21061 06-34)

Copyright Avail: CASI HC A03/MF A04

Laminar-turbulent breakdown of a strongly decelerated Falkner-Skan-type boundary layer (Hartree-Parameter beta(sub H)=-0.18) is investigated by direct numerical simulations using the complete Navier-Stokes equations for three-dimensional incompressible flows. The numerical method is based on the so-called spatial model, and allows for simulations of spatially evolving three-dimensional disturbance waves in a two-dimensional growing boundary layer. Transition is initiated by 2-D and a pair of oblique 3-D waves, both with small amplitudes, excited periodically within a narrow disturbance strip at the plate surface. Their streamwise (linear and subsequent nonlinear) evolution resulting in the fundamental breakdown of laminar flow is simulated with high spatial resolution. It is observed that the fundamental breakdown process under adverse pressure gradient is dramatically more complex than the well-known K-breakdown in the Blasius flow: In addition to the (upper) high-shear layer on top of the lambda-vortex, a (lower) characteristic high-shear layer is formed simultaneously in between neighboring lambda-vortices. This shear layer, induced by a secondary vortex system close to the wall, precipitates ultimate breakdown to turbulence. Finally, some results of preliminary studies on the effect of suction on boundary-layer transition are presented that demonstrate the great potential of spatial direct numerical simulations for applied transition research in flows of practical interest. Author

N95-21094*# Arizona Univ., Tucson, AZ. Dept. of Aerospace and Mechanical Engineering.

NAVIER-STOKES SIMULATIONS OF THE EFFECTS OF SUCTION HOLES ON A FLAT PLATE BOUNDARY LAYER

Hubert L. Meitz and Hermann F. Fasel *In* AGARD, Application of Direct and Large Eddy Simulation to Transition and Turbulence Dec. 1994 10 p (For primary document see N95-21061 06-34)
(Grant NAG1-1422)
Copyright Avail: CASI HC A02/MF A04

Direct numerical simulations (DNS) of the Navier-Stokes equations are employed to explore the effects of suction holes on transition in a laminar flat plate boundary layer. The Navier-Stokes equations are cast in vorticity-velocity form. Periodicity is imposed in spanwise direction; all other spatial derivatives are discretized with fourth order compact differences. An explicit fourth order Runge-Kutta scheme is employed for the time-integration of the vorticity transport equations. Suction is applied through a row of holes aligned in spanwise direction. For low suction strengths, each hole generates a pair of stable streamwise vortices. When the suction strength exceeds a critical value, the vortices become unstable. For high suction strengths, vortex shedding occurs right at the suction holes. Our numerical findings agree well with experimental observations. Author

N95-21095# Stuttgart Univ. (Germany). Inst. fuer Aerodynamik und Gasdynamik.

DIRECT NUMERICAL SIMULATION OF 2-D AND 3-D INSTABILITY WAVES IN A LAMINAR SEPARATION BUBBLE

Ulrich Rist and Ulrich Maucher *In* AGARD, Application of Direct and Large Eddy Simulation to Transition and Turbulence Dec. 1994 7 p (For primary document see N95-21061 06-34)
(Contract DFG-Ri-680/1-1)
Copyright Avail: CASI HC A02/MF A04

Direct Numerical Simulations of a laminar separation bubble are presented, where the bubble is generated by prescribing a locally decelerated free-stream velocity along a flat-plate. Controlled disturbances are introduced into the flow field upstream of the bubble by suction and blowing through the wall in order to study the linear and nonlinear stability characteristics of the flow. A number of generic cases with different two-dimensional (2-D) and three-dimensional (3-D) initial disturbance amplitudes are investigated: (1) a linear case; (2) a case subject to secondary instability (strong amplification of 3-D disturbances by resonance with a large amplitude 2-D wave); (3) a 3-D nonlinear case (interaction of two oblique waves); and (4) a nonlinear case combining the interaction of two oblique waves with a 2-D wave. Good quantitative agreement of the numerical results with (local) linear stability theory is observed throughout case (1) and for the initial disturbance development of the priming waves in the other cases despite the nonparallel base flow. For the nonlinear disturbance development development, however, unexpected results are obtained: Secondary instability is hard to distinguish from primary instability and apparently breaks down as soon as the priming 2-D disturbances saturate. However, the nonlinear mechanism identified in cases (3) and (4), is obviously much more likely to produce large amplitude 3-D disturbances necessary for the generation of a transitional laminar separation bubble. The mechanism leads to a nonlinearly saturated regime with reasonably turbulent mean-flow characteristics as well as longitudinal vortices in the reattachment zone. Author

N95-21096# Hellenic Air Force Academy, Athens (Greece). Dept. of Aerodynamics.

INVESTIGATION OF SHEAR LAYER TRANSITION USING VARIOUS TURBULENCE MODELS

J. K. Kaldellis and G. A. Georgantopoulos *In* AGARD, Application of Direct and Large Eddy Simulation to Transition and Turbulence Dec. 1994 11 p (For primary document see N95-21061 06-34)
Copyright Avail: CASI HC A03/MF A04

The accurate prediction of shear layer transition plays an important role in the performance amelioration of modern aero-mechanical devices, since transitional shear layers are frequently observed on axial turbomachine blades and other low Reynolds number airfoils. In the present work some of the most famous existing turbulence models are used in order to analyze a large variety of well documented experimental transitional shear flows. Particular attention is paid to the estimation of the transition length and to the calculation of loss evolution inside the transition area. Finally interesting conclusions of the proposed analysis are summarized in the last part of the paper, where the behavior of several transitional blade shear layers is examined, applying the most reliable of the above tested turbulence models. Author

N95-21097# Groningen Rijksuniv. (Netherlands). Dept. of Mathematics.

DNS OF TURBULENT FLOW IN A DRIVEN CAVITY AND THEIR ANALYSIS USING PROPER ORTHOGONAL DECOMPOSITION

W. Cazemier, R. W. C. P. Verstappen, and A. E. P. Veldman *In* AGARD, Application of Direct and Large Eddy Simulation to Transition and Turbulence Dec. 1994 11 p (For primary document see N95-21061 06-34)
Copyright Avail: CASI HC A03/MF A04

Direct Numerical Simulation (DNS) of 2D and 3D lid-driven cavity flows have been performed. The results have been analyzed using Proper Orthogonal Decomposition (POD). POD has been applied to a 2D driven cavity at Reynolds number 22,000 and to a 3D at Re = 10,000. The POD-basis-functions have been computed using the so-called 'snapshot' method of Sirovich. The 2D basisfunctions are used for a Galerkin projection of the Navier-Stokes equations. This results in a relatively low (20 to 80) dimensional dynamical behavior, that shows (almost) the same dynamical behavior, in short and long term, as the DNS. Moreover, if the Reynolds number is set to 11,000, the 80-dimensional dynamical system has (almost) the same periodic solution as the 2D Navier-Stokes equations have at Re = 11,000. Author

N95-21098# Office National d'Etudes et de Recherches Aerospatiales, Paris (France).

DIRECT SIMULATION AND GRAPHICS POST-PROCESSING OF THREE-DIMENSIONAL TURBULENT FLOWS

J. Ryan, P. Leoncini (Italian Aerospace Research Center, Capua.), U. Berrino (Italian Aerospace Research Center, Capua.), and B. Troff *In* AGARD, Application of Direct and Large Eddy Simulation to Transition and Turbulence Dec. 1994 6 p (For primary document see N95-21061 06-34)
(PAGEIN Proj. R2031)
Copyright Avail: CASI HC A02/MF A04

Direct Simulations involve huge amounts of time dependent data and are expensive to run fully even on supercomputers. A thousand hours of CRAY to obtain valid results is in the order of things. Such costs can be significantly reduced by MIMD machines. To be able to analyze the computed results many and various visualization techniques are also essential. This paper presents work that was done at ONERA to parallelize a Navier-Stokes solver PEGASE and development of an interactive visualization tool at CIRA applied to numerical turbulent flow fields generated by the solver. This work was partly achieved within the framework of the European RACE/PAGEIN project which was aimed at demonstrating the feasibility of Direct Numerical Simulation techniques for future industrial developments, implying modern supercomputer technology, high performance computing networking and massive data transfers between vector and/or parallel supercomputers. The first part of this paper presents the essential characteristics of version 1.0 of PEGASE implemented on a vector machine, the second part describes modifications in algorithms and coding in order to implement it efficiently on the IPSC860 and on a PARAGON. Numerical results and comparisons in costs between the three machines are given. The third part describes the graphics post-processing developed at CIRA. Author

N95-21106 Helsinki Univ. of Technology, Espoo (Finland). Lab. of Aerodynamics.

APPLICATION OF ROE'S FLUX-DIFFERENCE SPLITTING FOR KAPPA-EPSILON TURBULENCE MODEL

T. Silkonen 3 May 1994 37 p
(PB95-127718; SER-A-94-A15) Avail: Issuing Activity (National Technical Information Service (NTIS))

In the paper Roe's flux-difference splitting is applied for the solution of Reynolds-averaged Navier-Stokes equations. Turbulence is modeled using a low-Reynolds number form of the K-epsilon turbulence model. The coupling between the turbulence kinetic energy equation and the inviscid part of the flow equations is taken into account. The equations are solved with a DDADI-factorized implicit time integration method. A multigrid algorithm is used to accelerate the convergence. To improve the stability some modifications are needed in comparison with the application of an algebraic turbulence model. The developed method is applied to three different test cases. These cases show the efficiency of the algorithm, but the results are only marginally better than those obtained with algebraic models. NTIS

N95-21132# National Defence Research Establishment, Stockholm (Sweden). Dept. of Weapon Systems, Effects and Protection.
COMPUTATION OF TRANSONIC FLOW ON COMPOSITE OVERLAPPING GRIDS IN 2 D
Brodd Leif Andersson Apr. 1994 134 p
(ISSN 0347-3694)
(PB95-131348; FOA-C-20972-2.5) Avail: CASI HC A07/MF A02

We study the composite overlapping grid technique by applying it to two cases of transonic flow past an airfoil in two dimensions. A second order accurate explicit time marching finite difference scheme for the pseudo-unsteady Euler equations together with first order nonconservative interpolation at the component grid interfaces has been used. The numerical results indicate that the technique of overlapping grids is very useful if the decomposition of the domain is made carefully. A substantial improvement of the resolution in particular parts of the domain is easily obtained by the use of refined subgrids. NTIS

N95-21146# High Technology Corp., Hampton, VA.
COMPUTATIONAL STUDIES OF LAMINAR TO TURBULENCE TRANSITION Final Report, 15 Dec. 1990 - 14 May 1994
Mujeeb R. Malik and Fei Li 14 Jul. 1994 132 p
(Contract F49620-91-C-0014)
(AD-A285622; AFOSR-94-0488TR) Avail: CASI HC A07/MF A02

Nonlinear evolution of Goertler and crossflow vortices is investigated. The associated secondary instabilities of these streamwise vortices are also studied. The Goertler vortex is found to be subject to two types of secondary modes: a sinuous mode and a varicose mode similar to that observed in the experiments. The growth rate of the sinuous mode is higher initially but the varicose mode becomes more unstable in the downstream. It is also found that crossflow vortices are subject to a high frequency secondary instability prior to breakdown, as found in experiments performed on swept wings. In agreement with the experiments, our calculations show that the frequency of this secondary instability, which resides on top of the crossflow vortex, is an order of magnitude higher than the frequency of the most amplified traveling crossflow disturbances. The interaction of stationary and traveling disturbances is also considered. These studies have been carried out by using parabolized stability equations (PSE) and a two-dimensional (2D) eigenvalue approach. The mathematical nature of PSE approximation is also discussed. DTIC

N95-21182# Lawrence Livermore National Lab., Livermore, CA.
VISUALIZING 3D VELOCITY FIELDS NEAR CONTOUR SURFACES
Nelson Max, Roger Crawfis, and Charles Grant Aug. 1994 10 p
Presented at the Visualization 1994, Washington, DC, 17-21 Oct. 1994
(Contract W-7405-eng-48)
(DE95-000841; UCRL-JC-116231-Rev-1; CONF-941085-1-Rev-1) Avail: CASI HC A02/MF A01

Vector field rendering is difficult in 3D because the vector icons overlap and hide each other. We propose four different techniques for visualizing vector fields only near surfaces. The first uses motion blurred particles in a thickened region around the surface. The second uses a voxel grid to contain integral curves of the vector field. The third uses many antialiased lines through the surface, and the fourth uses hairs sprouting from the surface and then bending in the direction of the vector field. All the methods use the graphics pipeline, allowing real time rotation and interaction, and the first two methods can animate the texture to move in the flow determined by the velocity field. DOE

N95-21258*# National Aeronautics and Space Administration. Langley Research Center, Hampton, VA.
ACOUSTIC RECEPTIVITY DUE TO WEAK SURFACE INHOMOGENEITIES IN ADVERSE PRESSURE GRADIENT BOUNDARY LAYERS
Meelan Choudhari (High Technology Corp., Hampton, VA.), Lian Ng (Analytical Services and Materials, Inc., Hampton, VA.), and Craig Streett Feb. 1995 39 p
(Contracts NAS1-18240; NAS1-18599; RTOP 537-03-23-03)
(NASA-TM-4577; L-17162; NAS 1.15:4577) Avail: CASI HC A03/MF A01

The boundary layer receptivity to free-stream acoustic waves in the presence of localized surface disturbances is studied for the case of incompressible Falkner-Skan flows with adverse pressure gradients. These boundary layers are unstable to both viscous and inviscid (i.e., inflectional) modes, and the finite Reynolds number extension of the Goldstein-Ruban theory provides a convenient method to compare the efficiency of the localized receptivity processes in these two cases. The value of the efficiency function related to the receptivity caused by localized distortions in surface geometry is relatively insensitive to the type of instability mechanism, provided that the same reference length scale is used to normalize the efficiency function for each type of instability. In contrast, when the receptivity is induced by variations in wall suction velocity or in wall admittance distribution, the magnitudes of the related efficiency functions, as well as the resulting coupling coefficients, are smaller for inflectional (i.e., Rayleigh) modes than for the viscous Tollmien-Schlichting waves. The reduced levels of receptivity can be attributed mainly to the shorter wavelengths and higher frequencies of the inflectional modes. Because the most critical band of frequencies shifts toward higher values, the overall efficiency of the wall suction- and the wall admittance-induced receptivity decreases with an increase in the adverse pressure gradient. Author

N95-21268# Technische Univ., Eindhoven (Netherlands). Dept. of Mathematics and Computing Science.
TRANSIENT BEHAVIOUR AND STABILITY POINTS OF THE POISEUILLE FLOW OF A KBKZ-FLUID
A. C. T. Aarts and A. A. F. vandeVen Jun. 1994 29 p
(ISSN 0926-4507)
(PB95-132064; RANA-94-10) Avail: CASI HC A03/MF A01

The Poiseuille flow of a Kaye-Bernstein-Kearsly-Zapas (KBKZ) fluid, being a nonlinear viscoelastic model for a polymeric fluid, is studied. The flow starts from rest and especially the transient phase of the flow is considered. It is shown that under certain conditions the steady flow equation has three different equilibrium points. The stability of these points is investigated. It is proved that two points are stable, whereas the remaining one is unstable, leading to several peculiar phenomena such as discontinuities in the velocity gradient near the wall of the pipe ('spurt') and hysteresis. Our theoretical results are confirmed by numerical calculations of the velocity gradient. NTIS

N95-21317# Los Alamos National Lab., NM.
ACCURATE SOLUTION ALGORITHMS FOR INCOMPRESSIBLE MULTIPHASE FLOWS
William J. Rider, Douglas B. Kothe, S. Jay Mosso, John H. Cerutti, and John I. Hochstein (Memphis State Univ., Memphis, TN.) 19 Oct. 1994 11 p Presented at the 32nd Aerospace Sciences Meeting and Exhibit, Reno, NV, 11-14 Jan. 1994
(Contract W-7405-eng-36)
(DE95-002727; LA-UR-94-3611; CONF-940152-3) Avail: CASI HC A03/MF A01

A number of advances in modeling multiphase incompressible flow are described. These advances include high-order Godunov projection methods, piecewise linear interface reconstruction and tracking and the continuum surface force model. Examples are given. DOE

N95-21340*# Tennessee Univ. Space Inst., Tullahoma, TN.
SUPERSONIC LAMINAR FLOW CONTROL RESEARCH Semiannual Report No. 2, Jul. - Dec. 1994

Ching F. Lo Dec. 1994 65 p
(Grant NAG2-881)
(NASA-CR-196049; NAS 1.26:196049) Avail: CASI HC A04/MF A01

The objective of the research is to understand supersonic laminar flow stability, transition, and active control. Some prediction techniques will be developed or modified to analyze laminar flow stability. The effects of supersonic laminar flow with distributed heating and cooling on active control will be studied. The primary tasks of the research applying to the NASA/Ames Proof of Concept (POC) Supersonic Wind Tunnel and Laminar Flow Supersonic Wind Tunnel (LFSWT) nozzle design with laminar flow control are as follows: (1) predictions of supersonic laminar boundary layer stability and transition, (2) effects of wall heating and cooling for supersonic laminar flow control, and (3) performance evaluation of POC and LFSWT nozzles design with wall heating and cooling effects applying at different locations and various length. Author

N95-21387# Lawrence Livermore National Lab., Livermore, CA.
A MIXED TIME INTEGRATION METHOD FOR LARGE SCALE ACOUSTIC FLUID-STRUCTURE INTERACTION
M. A. Christon, S. J. Wineman, G. L. Goudreau, and J. D. Foch 18 Jul. 1994 14 p Presented at the American Society of Mechanical Engineers' Winter Annual Meeting, Chicago, IL, 9-11 Nov. 1994
(Contract W-7405-eng-48)
(DE94-018327; UCRL-JC-117820; CONF-941142-20) Avail: CASI HC A03/MF A01

The transient, coupled, interaction of sound with structures is a process in which an acoustic fluid surrounding an elastic body contributes to the effective inertia and elasticity of the body. Conversely, the presence of an elastic body in an acoustic medium influences the behavior of propagating disturbances. This paper details the application of a mixed explicit-implicit time integration algorithm to the fully coupled acoustic fluid-structure interaction problem. Based upon a dispersion analysis of the semi-discrete wave equation a second-order, explicit scheme for solving the wave equation is developed. The combination of a highly vectorized, explicit, acoustic fluid solver with an implicit structural code for linear elastodynamics has resulted in a simulation tool, PING, for acoustic fluid-structure interaction. PING's execution rates range from 1 micro s/Element/(delta)t for rigid scattering to 10 micro s/Element/(delta)t for fully coupled problems. Several examples of PING's application to 3-D problems serve in part to validate the code, and also to demonstrate the capability to treat complex geometry, acoustic fluid-structure problems which require high resolution meshes. DOE

N95-21578# Technische Hogeschool, Delft (Netherlands).
INSTABILITIES IN NATURAL-CONVECTION FLOWS IN CAVITIES Ph.D. Thesis [INSTABILITEITEN IN NATUURLIJKE CONVECTIESTROMINGEN IN GESLOTEN RUIMTES]
Roger Joseph Anna Janssen 9 May 1994 188 p Sponsored by the Stichting voor Fundamenteel Onderzoek der Materie
(PB95-107975) Avail: CASI HC A09/MF A02

In the thesis, a study of instabilities occurring in a natural-convection flow is described. Natural-convection flows arise from density differences in a fluid. These density differences, under the influence of the earth's gravity field, result in a buoyant force which causes the heavier fluid particles to descend and the lighter fluid particles to ascend and which thus drives the resulting flow. The adjective natural is used to distinguish these flows from forced-convection flows which are driven by pressure differences. The density differences occurring in natural-convection flows may have their origin in a number of different physical phenomena; they may result from temperature differences, from differences in the concentration of chemical species in the fluid and from the presence of multiple phases in the fluid. In the present study, however, only flows in which the density differences are caused by temperature differences are considered. NTIS

N95-21583# Grenoble Univ. (France). Inst. de Mecanique.
FOURTH INTERNATIONAL SYMPOSIUM ON STRATIFIED FLOWS, VOLUME 1
Emil Hopfinger, Bruno Voisin, and Genevieve Chavand 10 Oct. 1994 329 p Symposium held in Grenoble, France, 29 Jun. - 2 Jul. 1994
(Contract N00014-94-J-9018)
(AD-A286450) Avail: CASI HC A15/MF A03

Papers are presented in four sessions covering shear flow instability, baroclinic vortices, turbulent shear flows, and convection. Contents include: wave packet critical layers in stratified shear flows; multiple instability in a laboratory stratified shear layer; nonlinear oscillatory evolution of baroclinically unstable geostrophic vortex; intense vortex motion in a continuously stratified differentially rotating fluid; a study of plane mixing layer with cross shear; heat and mass transfer in stably stratified flow; modeling deep ocean convection events; penetration convection in rapidly rotating flows; and characteristics of the instability in a surface boundary current. CASI

N95-21584# Grenoble Univ. (France). Inst. de Mecanique.
FOURTH INTERNATIONAL SYMPOSIUM ON STRATIFIED FLOWS, VOLUME 3
Emil Hopfinger, Bruno Voisin, and Genevieve Chavand 10 Oct. 1994 464 p Symposium held in Grenoble, France, 29 Jun. - 2 Jul. 1994
(Contract N00014-94-J-9018)
(AD-A286452) Avail: CASI HC A20/MF A04

Papers presented cover internal waves, lakes and ocean basins, internal wave breaking, and gravity currents. Contents include: laboratory measurements of gravity wave, critical layer interactions; nonlinear internal waves in observations from shelves: manifestations of soliton-like behavior; investigations of the vertical water exchange in the Baltic Sea; turbulent mixing in the oceanic boundary layer due to internal wave reflection from sloping terrain; a numerical study of the breaking of an internal soliton and its interactions with a slope; decay of internal solitary waves and a comparison of timescales of dissipation and dispersion; the dynamics of sedimenting surface-gravity currents; the internal slab-collapse problem; and experimental study of regular background and ship internal waves interaction in the thermocline. CASI

N95-21649 Helsinki Univ. of Technology, Espoo (Finland). Lab. of Materials Processing and Powder Metallurgy.
FLOW AND HEAT TRANSFER SIMULATION IN A FLASH SMELTING FURNACE
T. Ahokainen, A. Jokilaakso, O. Teppo, and Y. Yang 1994 34 p
(PB95-108197; TKK-V-B94) Avail: Issuing Activity (National Technical Information Service (NTIS))

Fluid flow and heat transfer phenomena taking place in an industrial Outokumpu type flash smelting furnace were simulated with CFD software CFD2000 1.0 and PHOENICS 1.6.6. The computational domains and grids are basically the same as described in earlier reports. However, some changes and simplifications are made to the grids, especially in the reaction shaft model. All the two-phase simulations presented in the report are cold and isothermal, where the particles exchange only momentum with the gas phase. As a first attempt, combustion of gaseous sulphur with oxygen was used to represent the heat release from the copper concentrate oxidation reactions. The results presented in the report are preliminary reflecting the different stages of the model development. NTIS

N95-21656 Selskapet for Industriell og Teknisk Forskning, Oslo (Norway). Dept. of Ceramics.
STABILITY OF PRESSURE AND VELOCITY COMPUTATIONS FOR HETEROGENEOUS RESERVOIRS
A. M. Bruaset and B. F. Nielsen 20 Apr. 1994 22 p
(PB95-110284; STF33-A94031) Avail: Issuing Activity (National Technical Information Service (NTIS))

This paper is concerned with the stability of self-adjoint second order elliptic problems with respect to perturbations of the involved coefficient functions. In particular, we study such behavior for the pressure equation related to incompressible or steady state flow in a heterogeneous reservoir. We establish analytical estimates on the changes in the pressure and velocity caused by mobility perturbations measured by suitable norms. This stability analysis is complemented by numerical experiments. NTIS

N95-21675*# National Aeronautics and Space Administration. Marshall Space Flight Center, Huntsville, AL.
NUMERICAL INVESTIGATIONS OF LOW-DENSITY NOZZLE FLOW BY SOLVING THE BOLTZMANN EQUATION
Zheng-Tao Deng, Goang-Shin Liaw (Alabama A & M Univ., Huntsville, AL.), and Lynn Chen Chou (Alabama A & M Univ., Huntsville, AL.) 1995 6 p Presented at the 33rd Aerospace Science Meeting and Exhibit, Reno, NV, 9-12 Jan. 1995

(Grant NAG8-201)
(NASA-TM-110492; NAS 1.15:110492) Copyright Avail: CASI HC A02/MF A01

A two-dimensional finite-difference code to solve the BGK-Boltzmann equation has been developed. The solution procedure consists of three steps: (1) transforming the BGK-Boltzmann equation into two simultaneous partial differential equations by taking moments of the distribution function with respect to the molecular velocity u(sub z), with weighting factors 1 and u(sub z)(sup 2); (2) solving the transformed equations in the physical space based on the time-marching technique and the four-stage Runge-Kutta time integration, for a given discrete-ordinate. The Roe's second-order upwind difference scheme is used to discretize the convective terms and the collision terms are treated as source terms; and (3) using the newly calculated distribution functions at each point in the physical space to calculate the macroscopic flow parameters by the modified Gaussian quadrature formula. Repeating steps 2 and 3, the time-marching procedure stops when the convergent criteria is reached. A low-density nozzle flow field has been calculated by this newly developed code. The BGK Boltzmann solution and experimental data show excellent agreement. It demonstrated that numerical solutions of the BGK-Boltzmann equation are ready to be experimentally validated. Author

N95-21726# Oak Ridge National Lab., TN.

A NEW KRYLOV-SUBSPACE METHOD FOR SYMMETRIC INDEFINITE LINEAR SYSTEMS

R. W. Freund (Bell Telephone Labs., Inc., Murray Hill, NJ.) and N. M. Nachtigal Oct. 1994 16 p
(Contract DE-AC05-84OR-21400)
(DE95-001826; ORNL/TM-12754) Avail: CASI HC A03/MF A01

Many important applications involve the solution of large linear systems with symmetric, but indefinite coefficient matrices. For example, such systems arise in incompressible flow computations and as subproblems in optimization algorithms for linear and nonlinear programs. Existing Krylov-subspace iterations for symmetric indefinite systems, such as SYMMLQ and MINRES, require the use of symmetric positive definite preconditioners, which is a rather unnatural restriction when the matrix itself is highly indefinite with both many positive and many negative eigenvalues. In this note, the authors describe a new Krylov-subspace iteration for solving symmetric indefinite linear systems that can be combined with arbitrary symmetric preconditioners. The algorithm can be interpreted as a special case of the quasi-minimal residual method for general non-Hermitian linear systems, and like the latter, it produces iterates defined by a quasi-minimal residual property. The proposed method has the same work and storage requirements per iteration as SYMMLQ or MINRES, however, it usually converges in considerably fewer iterations. Results of numerical experiments are reported. DOE

N95-21902 Department of the Navy, Washington, DC.

SUPERCONDUCTING ELECTROMAGNETIC THRUSTER Patent

James C. Meng, inventor (to Navy) 2 Aug. 1994 15 p Filed 11 Feb. 1993
(AD-D016485; US-Patent-5,333,444; US-Patent-Appl-SN-016324; US-Patent-Class-60-221) Avail: US Patent and Trademark Office

An electromagnetic thruster for marine vehicles using a jet of water driven by the interaction of a mutually perpendicular intensified magnetic field and an intensified electric field is disclosed. The intensified magnetic field is produced by superconducting coils cooled by a coolant such as liquid helium. An intensified electric field is produced by passing high amperage current across the seawater jet. These interacting fields produce a Lorentz force perpendicular to mutually perpendicular electric and magnetic field vectors which is used to drive the seawater jet. In some embodiments, the force may also be used to draw water into the jet from the boundary layer flow around the vehicle thereby reducing boundary layer turbulence and associated radiated noise. DTIC

N95-21942 Michigan Univ., Ann Arbor, MI. Dept. of Electrical Engineering and Computer Science.

MASSIVELY-PARALLEL COMPUTATIONAL FLUID DYNAMICS Final Technical Report, 15 Oct. 1989 - 14 Jan. 1994

Donald Calahan 10 Mar. 1994 7 p Limited Reproducibility: More than 20% of this document may be affected by microfiche quality
(Grant AF-AFOSR-0020-90)
(AD-A279389; AFOSR-94-0296TR) Avail: Issuing Activity (Defense Technical Information Center (DTIC))

The effort has three major goals: (1) Gain algorithm experience in conversion of a suite of Air Force production (CFD codes to a general format applicable to a variety of such commercial architectures); (2) Examine the feasibility of using workstation networks for such distributed computation (this involves: developing timing models of the communication systems of such networks, projecting performance of the above codes on such networks, and implementing one or more codes, as time permits); and (3) Initiate research on CFD-based low-radar crossection analysis on parallel systems: this effort is in association with Dr. Joseph Shang at WRDC. DTIC

N95-21954*# National Aeronautics and Space Administration. Ames Research Center, Moffett Field, CA.

THE VELOCITY AND VORTICITY FIELDS OF THE TURBULENT NEAR WAKE OF A CIRCULAR CYLINDER Final Report

James Wallace (Maryland Univ., College Park, MD.), Lawrence Ong (Maryland Univ., College Park, MD.), and Parviz Moin Jan. 1995 24 p
(Contract NCC2-5003)
(NASA-TM-110513; NAS 1.15:110513) Avail: CASI HC A03/MF A01

The purpose of this research is to provide a detailed experimental database of velocity and vorticity statistics in the very near wake (x/d less than 10) of a circular cylinder at Reynolds number of 3900. This study has determined that estimations of the streamwise velocity component in flow fields with large nonzero cross-stream components are not accurate. Similarly, X-wire measurements of the u and v velocity components in flows containing large w are also subject to the errors due to binormal cooling. Using the look-up table (LUT) technique, and by calibrating the X-wire probe used here to include the range of expected angles of attack (+/- 40 deg), accurate X-wire measurements of instantaneous u and v velocity components in the very near wake region of a circular cylinder has been accomplished. The approximate two-dimensionality of the present flow field was verified with four-wire probe measurements, and to some extent the spanwise correlation measurements with the multisensor rake. Hence, binormal cooling errors in the present X-wire measurements are small. Derived from text

N95-21957*# National Aeronautics and Space Administration. Lewis Research Center, Cleveland, OH.

HYBRID UPWIND SPLITTING (HUS) BY A FIELD-BY-FIELD DECOMPOSITION

Frederic Coquel and Meng-Sing Liou Jan. 1995 91 p
(Contract NCC3-233; RTOP 505-62-52)
(NASA-TM-106843; ICOMP-95-2; E-9408; NAS 1.15:106843) Avail: CASI HC A05/MF A01

We introduce and develop a new approach for upwind biasing: the hybrid upwind splitting (HUS) method. This original procedure is based on a suitable hybridization of current prominent flux vector splitting (FVS) and flux difference splitting (FDS) methods. The HUS method is designed to naturally combine the respective strengths of the above methods while excluding their main deficiencies. Specifically, the HUS strategy yields a family of upwind methods that exhibit the robustness of FVS schemes in the capture of nonlinear waves and the accuracy of some FDS schemes in the resolution of linear waves. We give a detailed construction of the HUS methods following a general and systematic procedure directly performed at the basic level of the field by field (i.e. waves) decomposition involved in FDS methods. For such a given decomposition, each field is endowed either with FVS or FDS numerical fluxes, depending on the nonlinear nature of the field under consideration. Such a design principle is made possible thanks to the introduction of a convenient formalism that provides us with a unified framework for upwind methods. The HUS methods we propose bring significant improvements over current methods in terms of accuracy and robustness. They yield entropy-satisfying approximate solutions as they are strongly supported in numerical experiments. Field by field hybrid numerical fluxes also achieve fairly simple and explicit expressions and hence require a computational effort between that of the FVS and FDS. Several numerical experiments ranging from stiff 1D shock-tube to high speed viscous flows problems are displayed, intending to illustrate the benefits of the present approach. We assess in particular the relevance of our HUS schemes to viscous flow calculations. Author

N95-21959*# National Aeronautics and Space Administration. Lewis Research Center, Cleveland, OH.

COMPUTATIONS OF UNSTEADY VISCOUS COMPRESSIBLE FLOWS USING ADAPTIVE MESH REFINEMENT IN CURVILINEAR BODY-FITTED GRID SYSTEMS

E. Steinthorsson, David Modiano, and Phillip Colella (California Univ., Berkeley, CA.) Aug. 1994 14 p Presented at the 25th Fluid Dynamics Conference, Colorado Springs, CO, 20-23 Jun. 1994; sponsored by AIAA
(Contract NCC3-233; RTOP 505-90-5K)
(NASA-TM-106704; ICOMP-94-17; E-9066; NAS 1.15:106704; AIAA Paper 94-2330) Avail: CASI HC A03/MF A01

A methodology for accurate and efficient simulation of unsteady, compressible flows is presented. The cornerstones of the methodology are a special discretization of the Navier-Stokes equations on structured body-fitted grid systems and an efficient solution-adaptive mesh refinement technique for structured grids. The discretization employs an explicit multidimensional upwind scheme for the inviscid fluxes and an implicit treatment of the viscous terms. The mesh refinement technique is based on the AMR algorithm of Berger and Colella. In this approach, cells on each level of refinement are organized into a small number of topologically rectangular blocks, each containing several thousand cells. The small number of blocks leads to small overhead in managing data, while their size and regular topology means that a high degree of optimization can be achieved on computers with vector processors. Author

N95-21963 Technische Univ., Delft (Netherlands).

VORTEX ATOMS AND VORTONS Ph.D. Thesis

Alfons Johannes Quir Alkemade 5 Apr. 1994 223 p
(PB95-134599; ISBN-90-370-0103-3) Copyright Avail: Issuing Activity (National Technical Information Service (NTIS))

The thesis deals with two topics which are related to the concept of vorticity. Therefore, it consists of two parts. The 'vortex-atom-part' shows the development of a theory of matter, introduced by the English scientist Lord Kelvin in 1867, which would attract the attention of several 19th century scientists up to the beginning of our century. Kelvin's 'vortex atom theory' can be put into the context of several developments in 19th century physics, especially those with regard to theories of matter and the still developing theory of rotational flow or vorticity. The second part, the 'vorton-part', is an account of the theoretical foundation and the application to numerical simulations of the vorton method. This is one of the many vortex methods, applied nowadays to the (numerical) study of flow phenomena. Vortex methods are based on the fact that vortices play important roles in fluid flows and can be regarded as important applications of the knowledge on vortex motion which has been gathered in the past centuries and of the surging use of numerical techniques in fluid mechanics. The vorton method will be investigated by means of numerical simulation of several test cases. Most of these were already studied by the scientists who occupied themselves with the elaboration of the vortex atom model or who were just incited to research on vortex motion by this model. However, their investigations were largely hindered by mathematical difficulties. Today, the use of vortex methods as computational tools may provide more insight into the kinematics and dynamics of vortex structures. NTIS

N95-22017 Selskapet for Industriell og Teknisk Forskning, Trondheim (Norway). Div. of Applied Thermodynamics.

STATE OF THE ART IN CFD PRE- AND POSTPROCESSING

B. E. Vembe and E. W. M. Hansen 9 Jun. 1994 50 p
(PB95-110391; STF15-A94004) Avail: Issuing Activity (National Technical Information Service (NTIS))

Computational fluid dynamics (CFD) is a generic name for a wide range of numerical techniques that are used for obtaining solutions to the governing equations of thermo-fluid dynamics with or without chemical reactions. The report presents to the state of the art in pre- and postprocessing for CFD codes, both commercial and in-house SINTEF-NTH codes. The objectives of advanced CFD systems are discussed and the techniques for pre- and postprocessing are reviewed. The user friendliness of CFD codes, in general, are highlighted. A common definition of a user friendly computer program is one that is easy to learn, efficient, easy to remember, and satisfactory to use. Most of today's commercial CFD codes could benefit from an enhanced interface. It is desirable to develop standard data formats for input and output of CFD codes and direct-manipulation user interfaces are desirable in CFD applications. Largest potential for improvements of CFD codes and for users is in geometry modeling and grid generation. NTIS

N95-22060 Department of the Navy, Washington, DC.

ELASTIC MICRO-FABRICATED SURFACE LAYER FOR REDUCING TURBULENCE AND DRAG ON AN OBJECT WHILE IT MOVES THROUGH A FLUID MEDIUM Patent

Promode R. Bandyopadhyay, inventor (to Navy) 13 Sep. 1994 8 p Filed 1 Jun. 1993
(AD-D016516; US-Patent-5,346,745; US-Patent-Appl-SN-069820; US-Patent-Class-428-156) Avail: US Patent and Trademark Office

A surface for use in connection with an object in relative motion through a fluid medium includes a plurality of surface elements arranged in rows on the surface, with surface elements of each row being arranged generally orthogonal to the direction of relative motion of the object in a medium. Each surface element includes means defining a cavity, the means including a bottom surface layer, sidewalls, and an upper lip supported along an upstream edge in a cantilevered manner and extending in a downstream direction over the cavity to define a gap permitting fluid communication between the medium and the cavity. The lip is flexible so as to facilitate deflection in response to differentials between pressure inside the cavity and outside the cavity. The cavities of the surface elements in each row are interconnected by means of passageways thereby to facilitate fluid communication therebetween. DTIC

N95-22063 Technische Univ., Delft (Netherlands). Faculty of Technical Mathematics and Information.

ABSORBING BOUNDARY CONDITION FOR FLOATING TWO-DIMENSIONAL OBJECTS IN CURRENT AND WAVES

L. M. Sierevogel and A. J. Hermans 1994 17 p
(ISSN 0922-5641)
(PB95-132882) Copyright Avail: Issuing Activity (National Technical Information Service (NTIS))

In the paper a new absorbing boundary condition for floating two-dimensional objects in current and waves is studied. A numerical algorithm is developed, which computes the velocity potential in the physical time domain, using an artificial boundary to split the infinite fluid domain into a computational and residual part. In the residual part a special Green's function is developed. The condition on the artificial boundary is independent of the wave frequency, hence there is no restriction to harmonic waves. Because of the smaller computational domain and the independence of frequency the time to compute the hydrodynamic coefficients of floating objects will decrease. NTIS

N95-22145 Illinois Univ., Urbana, IL. Inst. for Environmental Studies.

THE MECHANISMS AND EFFECTS OFF THE PLANT-ACTIVATIONS OF CHEMICALS IN THE ENVIRONMENT Annual Report, 30 Apr. 1992 - 29 Sep. 1993

Michael J. Plewa 20 Dec. 1993 23 p Limited Reproducibility: More than 20% of this document may be affected by microfiche quality
(Grant AF-AFOSR-0432-91)
(AD-A279388; AFOSR-94-0286TR) Avail: Issuing Activity (Defense Technical Information Center (DTIC))

Plants can activate promutagens into stable mutagens and these genotoxic agents may be hazardous to the environment and to the public health. Plant systems have been widely employed in classical and environmental mutagenesis. However, the environmental and human health impact of plants exposed to environmental xenobiotics were not well recognized until the presence of pesticide contaminants in food supplies caused alarm. The capability of plants to bioconcentrate environmental agents and activate promutagens into toxic metabolites is significant when one realizes the immense diversity of xenobiotics to which plants are intentionally and unintentionally exposed. Finally, we all must be attentive to the effects that toxic agents may have on the biosphere and the grave global consequences that would result in a disruption in the carbon cycle. DTIC

N95-22148# Northwestern Univ., Evanston, IL.

STUDIES IN NONLINEAR PROBLEMS OF ENERGY

B. J. Matkowsky Sep. 1994 17 p

(Contract DE-FG02-87ER-25027)
(DE95-001387; DOE/ER-25027/8) Avail: CASI HC A03/MF A01

The authors concentrate on modeling, analysis and large scale scientific computation of combustion and flame propagation phenomena, with emphasis on the transition from laminar to turbulent combustion. In the transition process a flame passed through a stage exhibiting increasingly complex spatial and temporal patterns which serve as signatures identifying each stage. Often the transitions arise via bifurcation. The authors investigate nonlinear dynamics, bifurcation and pattern formation in the successive stage of transition. They describe the stability of combustion waves, and transitions to combustion waves exhibiting progressively higher degrees of spatio-temporal complexity. One aspect of this research program is the systematic derivation of appropriate, approximate models from the original models governing combustion. The approximate models are then analyzed. The authors are particularly interested in understanding the basic mechanisms affecting combustion, which is a prerequisite to effective control of the process. They are interested in determining the effects of varying various control parameters, such as Nusselt number, Lewis number, heat release, activation energy, Damkohler number, Reynolds number, Prandtl number, Peclet number, etc. The authors have also considered a number of problems in self-propagating high-temperature synthesis (SHS), in which combustion waves are employed to synthesize advanced materials. Efforts are directed toward understanding fundamental mechanisms. DOE

N95-22160# Technische Univ., Delft (Netherlands). Dept. of Mechanical Engineering and Marine Technology.
FLUID DYNAMICS OF THE FREEBOARD IN A FLUIDIZED BED REACTOR Ph.D. Thesis
Willem Cornelis Verloop 31 May 1994 204 p
(PB95-134029; ISBN-90-370-0107-6) Avail: CASI HC A10/MF A03

The present study focuses on the fluid dynamics of the gas-particle freeboard flow, whereas a subsequent study will cover the chemistry. The objective of the present thesis is to increase the insight in the physical processes that govern the freeboard particle flow. Special attention has to be paid to the lateral transport of particles and the often observed phenomenon of a downflowing wall layer of solids, which has not been explained satisfactorily up to now. In order to achieve this, detailed experiments have to be performed which provide data on the local flow structure. In addition, the freeboard flow has to be modeled at least two-dimensionally, incorporating the essential physical processes. The resulting model of the freeboard flow should firstly be capable of predicting the local properties of both the gas flow and the particle flow. This prediction has to serve as a basis for the subsequent modeling of the freeboard chemistry. Secondly, the model should serve as a basis for studying the consequences of the scaling up a fluidized bed installation from lab scale to industrial size. NTIS

N95-22173*# Arizona Univ., Tucson, AZ. Dept. of Aerospace and Mechanical Engineering.
NONLINEAR INTERACTION BETWEEN A PAIR OF OBLIQUE MODES IN A SUPERSONIC MIXING LAYER: LONG-WAVE LIMIT Final Technical Report
Thomas F. Balsa and James Gartside Feb. 1995 61 p
(Grant NAG3-781)
(NASA-CR-197380; NAS 1.26:197380) Avail: CASI HC A04/MF A01

The nonlinear interaction between a pair of symmetric, oblique, and spatial instability modes is studied in the long-wave limit using asymptotic methods. The base flow is taken to be a supersonic mixing layer whose Mach number is such that the corresponding vortex sheet is marginally stable according to Miles' criterion. It is shown that the amplitude of the mode obeys a nonlinear integro-differential equation. Numerical solutions of this equation show that, when the obliqueness angle is less than pi/4, the effect of the nonlinearity is to enhance the growth rate of the instability. The solution terminates in a singularity at a finite streamwise location. This result is reminiscent of that obtained in the vicinity of the neutral point by other authors in several different types of flows. On the other hand, when the obliqueness angle is more than pi/4, the streamwise development of the amplitude is characterized by a series of modulations. This arises from the fact that the nonlinear term in the amplitude equation may be either stabilizing or destabilizing, depending on the value of the streamwise coordinate. However, even in this case the amplitude of the disturbance increases, though not as rapidly as in the case for which the angle is less than pi/4. Quite generally then, the nonlinear interaction between two oblique modes in a supersonic mixing layer enhances the growth of the disturbance. Author

N95-22206# Army Natick Research and Development Command, MA.
GOVERNING EQUATIONS FOR MULTIPHASE HEAT AND MASS TRANSFER IN HYGROSCOPIC POROUS MEDIA WITH APPLICATIONS TO CLOTHING MATERIALS Final Report, Jan. - Jun. 1994
Phillip Gibson Nov. 1994 68 p
(AD-A286418; NATICK-TR-95/004) Avail: CASI HC A04/MF A01

Whitaker's theory of coupled heat and mass transfer through porous media was modified to include hygroscopic porous materials which can absorb liquid into the solid matrix. The system of equations described in this report should make it possible to evaluate the time-dependent transport properties of hygroscopic and non-hygroscopic clothing materials by including many important factors which are usually ignored in the analysis of heat and mass transfer through textile materials. The set of equations allows for the unsteady capillary wicking of sweat through fabric structure, condensation and evaporation of sweat within various layers of the clothing system, forced gas phase convection through the porous structure of a textile layer, and the swelling and shrinkage of fibers and yarns as they absorb/desorb liquid water and water vapor. DTIC

N95-22208 Naval Undersea Warfare Center, Newport, RI.
DERIVATION OF A WAVENUMBER FILTER DESIGN FOR THE MEASUREMENT OF TURBULENT WALL PRESSURE FLUCTUATIONS Final Report
William L. Keith and Bruce M. Abraham 14 Nov. 1994 32 p Limited Reproducibility: More than 20% of this document may be affected by microfiche quality
(AD-A286421; NUWC-NPT-TR-10693) Avail: CASI HC A03

Measurement of the wavenumber-frequency spectrum o(kl,w) of turbulent wall pressure fluctuations requires a line array (wavenumber filter) of closely spaced sensors. However, the wide range of wavenumbers of the wall pressure fluctuations that contribute to the spectrum imposes constraints on sensor size, spacing, and number. In this study, the Corcos model of the wall pressure field is used in conjunction with recent experimental measurements to determine design parameters expressed in terms of boundary layer length and time scales. For the case of turbulent boundary layers at moderate to high Reynolds numbers, the resulting wavenumber design requires microfabrication technology. DTIC

N95-22212# California Inst. of Tech., Pasadena, CA.
SHOCK WAVE INTERACTIONS IN HYPERVELOCITY FLOW
S. R. Sanderson and B. Sturtevant Aug. 1994 10 p
(Contract F49620-93-1-0338)
(AD-A286507; AFOSR-94-0727TR) Avail: CASI HC A02/MF A01

The impingement of shock waves on blunt bodies in steady supersonic flow is known to cause extremely high local heat transfer rates and surface pressures. Although these problems have been studied in cold hypersonic flow, the effects of dissociative relaxation processes are unknown. In this paper we report a model aimed at determining the boundaries of the possible interaction regimes for an ideal dissociating gas. Local analysis about shock wave intersection points in the pressure-flow deflection angle plane with continuation of singular solutions is the fundamental tool employed. Further, we discuss an experimental investigation of the nominally two-dimensional mean flow that results from the impingement of an oblique shock wave on the leading edge of a cylinder. The effects of variations in shock impingement geometry were visualized using differential interferometry. Generally, real gas effects are seen to increase the range of shock impingement points for which enhanced heating occurs. They also reduce the type 4 interaction supersonic jet width and influence the type 2-3 transition process. DTIC

N95-22264# National Inst. of Standards and Technology, Boulder, CO.
MEASUREMENT OF THE THERMAL PROPERTIES OF ELECTRICALLY CONDUCTING FLUIDS USING COATED TRANSIENT HOT WIRES
R. A. Perkins 1994 9 p Presented at the 12th Symposium on Energy Engineering Sciences, Argonne, IL, 27-29 Apr. 1994
(Contract DE-AI05-89ER-13992)
(DE94-017816; CONF-9404137-6) Avail: CASI HC A02/MF A01

Measurements of fluid thermal properties using the transient hot-wire technique are described. When bare hot wires are used in electrically conducting fluids there are additional measurement uncertainties due to the formation of electric double layers on the surfaces of the wires and the cell wall. If the electrical conductivity of the fluid is large enough there is also significant power generation in the fluid. These measurement uncertainties can be eliminated by electrically insulating the hot wires with a thin film. The use of tantalum hot wires with an anodized layer of tantalum pentoxide is demonstrated with measurements on nonpolar argon and polar 1,1,1,2 tetrafluorethane (R134a). Although coated tantalum hot wires have been used previously in a transient mode to measure the thermal conductivity of liquids, this work is the first demonstration of the use of coated wires to measure thermal conductivity in the liquid, vapor, and supercritical gas phases. DOE

N95-22290# California Inst. of Tech., Pasadena, CA. Dept. of Physics.
FAST PARALLEL TREE CODES FOR GRAVITATIONAL AND FLUID DYNAMICAL N-BODY PROBLEMS
John K. Salmon, Michael S. Warren, and Gregoire S. Winckelmans 1993 14 p
(Contract N00014-92-J-1072)
(AD-A286480) Avail: CASI HC A03/MF A01

We discuss two physical systems from separate disciplines that make use of the same algorithmic and mathematical structures to reduce the number of operations necessary to complete a realistic simulation. In the gravitational N-body problem, the acceleration of an object is given by the familiar Newtonian laws of motion and gravitation. The computational load is reduced by treating groups of bodies as single multipole sources rather than individual bodies. In the simulation of incompressible flows, the flow may be modeled by the dynamics of a set of N interacting vortices. Vortices are vector objects in three dimensions, but their interactions are mathematically similar to that of gravitating masses. The multipole approximation can be used to greatly reduce the time needed to compute the interactions between vortices. Both types of simulations were carried out on the Intel Touchstone Delta, a parallel MIMD computer with 512 processors. Timings are reported for systems of up to 10 million bodies, and demonstrate that the implementation scales well on massively parallel systems. The majority of the code is common between the two applications, which differ only in certain physics modules. In particular, the code for parallel tree construction and traversal is shared. DTIC

N95-22294# Cornell Univ., Ithaca, NY. Lab. of Atomic and Solid State Physics.
FULLY DEVELOPED TURBULENT FLOWS Final Report, 1 Oct. 1990 - 30 Sep. 1994
Eric D. Siggia 30 Sep. 1994 5 p
(Grant AF-AFOSR-0011-91)
(AD-A286496; AFOSR-94-0716TR) Avail: CASI HC A01/MF A01

An analytic theory for the large (passive) scalar derivative skewness for turbulent transport in a mean scalar gradient has been devised using Lie Algebraic methods to solve the Hopf equation. This Reynolds independent skewness strongly contradicts Kolmogorov's theory occurs in shear flows, which are being studied numerically, emphasizing the analogies between scalar and momentum transport. DTIC

N95-22307# Texas Univ., Austin, TX. Dept. of Physics.
1/F NOISE IN TWO-DIMENSIONAL FLUIDS
S. B. Cable (Southwest Research Inst., San Antonio, TX.) and T. Tajima Oct. 1994 10 p Sponsored by NSF
(Contract DE-FG05-80ET-53088)
(DE95-002617; DOE/ET-53088/678) Avail: CASI HC A02/MF A01

We derive an exact result on the velocity fluctuation power spectrum of an incompressible two-dimensional fluid. Employing the fluctuation-dissipation relationship and the enstrophy conversation, we obtain the frequency spectrum of a 1/f form. DOE

N95-22424# Grenoble Univ. (France). Inst. de Mecanique.
FOURTH INTERNATIONAL SYMPOSIUM ON STRATIFIED FLOWS, VOLUME 4
Emil Hopfinger, Bruno Voisin, and Genevieve Chavand 10 Oct. 1994 194 p Symposium held in Grenoble, France, 29 Jun. - 2 Jul. 1994
(Contract N00014-94-J-9018)
(AD-A286453) Avail: CASI HC A09/MF A03

Papers are presented under the headings 'Entrainment and Mixing' and 'Oceanic Processes: Observations and Models.' Topics include: biomass production in stratified waters; persistence theory of stratified entrainment; diapycnal mixing: fluxes and energetics; turbulent penetration and mixing at an interfacial layer in a wind tunnel; direct measurements of the mutual-entrainment velocity at a density interface; turbulence produced by internal waves in the oceanic thermocline at mid and low latitudes; geostrophic adjustment: frontogenesis and energy conversion; laboratory experiments with midlatitude circulation in a two layer ocean; and manifestations of bottom topography on the ocean surface: the physical mechanism and solution of direct and inverse problems on a beta-plane. CASI

N95-22437*# Stanford Univ., CA. Center for Turbulence Research.
ANNUAL RESEARCH BRIEFS, 1994
Dec. 1994 386 p
(Contract NCC2-460)
(NASA-CR-197352; NAS 1.26:197352) Avail: CASI HC A17/MF A04

Briefs of the 1994 annual progress reports of the Research Fellows and students of the Center for Turbulence Research are presented. Subjects covered include turbulence combustion, large eddy simulation, Reynolds-averaged turbulence modeling, turbulence control, postprocessing, sound generation, and turbulence physics. For individual titles, see N95-22438 through N95-22465.

N95-22438*# Stanford Univ., CA. Center for Turbulence Research.
CONDITIONAL STATISTICS IN A TURBULENT PREMIXED FLAME DERIVED FROM DIRECT NUMERICAL SIMULATION **c25**
Thierry Mantel and Robert W. Bilger (Sydney Univ., Australia.) *In its* Annual Research Briefs, 1994 Dec. 1994 p 3-27 (For primary document see N95-22437 06-34)
Avail: CASI HC A03/MF A04

The objective of this paper is to briefly introduce conditional moment closure (CMC) methods for premixed systems and to derive the transport equation for the conditional species mass fraction conditioned on the progress variable based on the enthalpy. Our statistical analysis will be based on the 3-D DNS database of Trouve and Poinsot available at the Center for Turbulence Research. The initial conditions and characteristics (turbulence, thermo-diffusive properties) as well as the numerical method utilized in the DNS of Trouve and Poinsot are presented, and some details concerning our statistical analysis are also given. From the analysis of DNS results, the effects of the position in the flame brush, of the Damkoehler and Lewis numbers on the conditional mean scalar dissipation, and conditional mean velocity are presented and discussed. Information concerning unconditional turbulent fluxes are also presented. The anomaly found in previous studies of counter-gradient diffusion for the turbulent flux of the progress variable is investigated. Derived from text

N95-22439*# Stanford Univ., CA. Center for Turbulence Research.
LEWIS NUMBER AND DAMKOHLER NUMBER EFFECTS IN VORTEX-FLAME INTERACTIONS **c25**
Jean-Michael Samaniego *In its* Annual Research Briefs, 1994 Dec. 1994 p 29-43 (For primary document see N95-22437 06-34)
Avail: CASI HC A03/MF A04

A combined experimental-numerical study of the interaction of a two-dimensional vortex pair with a plane premixed laminar flame has been carried out. The selected geometry is two-dimensional in order to allow for the use of quantitative line-of-sight measurement techniques and for comparisons with two-dimensional direct numerical simulations. The experiment is used to identify possible effects of the Lewis number and of radiative heat losses, and direct numerical simulations reproducing the experimental conditions are used to investigate the role of the Lewis number, of heat losses, and of multi-step kinetics. The heat losses considered in this study are essentially radiative losses from the burnt gases and do not include conductive losses to the walls. This report presents the final results of this study of vortex-flame interactions. The main result is the creation of experimental data sets of vortex-flame interactions, which demonstrate the importance of the Lewis and Damkohler numbers to the flame and which allow for comparison with direct numerical simulations. In turn, the comparison between experimental and numerical results shows that the Lewis number effects and complex chemistry play significant roles, which

can be reproduced using a two-step reaction mechanism.
Derived from text

N95-22440*# Stanford Univ., CA. Center for Turbulence Research.
FUNDAMENTAL MECHANISMS IN PREMIXED FLAME PROPAGATION VIA VORTEX-FLAME INTERACTIONS: NUMERICAL SIMULATIONS c25
Thierry Mantel *In its* Annual Research Briefs, 1994 Dec. 1994 p 45-75 (For primary document see N95-22437 06-34)
Avail: CASI HC A03/MF A04

The goal of the present study is to assess numerically the ability of single-step and two-step chemical models to describe the main features encountered during the interaction between a two-dimensional vortex pair and a premixed laminar flame. In the two-step mechanism, the reaction kinetics are represented by a first chain branching reaction A + X yields 2X and a second chain termination reaction X + X yields P. This paper presents the fundamental mechanisms occurring during vortex-flame interactions and the relative impact of the major parameters encountered in turbulent premixed flames and suspected of playing a role in quenching mechanism: (1) Influence of stretch is investigated by analyzing the contribution of curvature and tangential strain on the local structure of the flame. The effect of Lewis number on the flame response to a strained field is analyzed. (2) Radiative heat losses which are suspected to be partially or totally responsible for quenching are also investigated. (3) The effect of the diffusion of the radicals is studied using a two-step mechanism in which an intermediate species is present. The parameters of the two-step mechanism are entirely determined from physical arguments. (4) Precise quantitative comparisons between the DNS and the experimental results of Samaniego et al are performed. These comparisons concern the evolution of the minimum heat release rate found along the flame front during the interaction and the distribution of the heat release rate along the flame front. Derived from text

N95-22441*# Stanford Univ., CA. Center for Turbulence Research.
TRIPLE FLAMES AND FLAME STABILIZATION c25
James E. Broadwell *In its* Annual Research Briefs, 1994 Dec. 1994 p 77-78 (For primary document see N95-22437 06-34)
Avail: CASI HC A01/MF A04

It is now well established that when turbulent jet flames are lifted, combustion begins, i.e., the flame is stabilized, at an axial station where the fuel and air are partially premixed. One might expect, therefore, that the beginning of the combustion zone would be a triple flame. Such flames have been described; however, other experiments provide data that are difficult to reconcile with the presence of triple flames. In particular, laser images of CH and OH, marking combustion zones, do not exhibit shapes typical of triple flames, and, more significantly, the lifted flame appears to have a propagation speed that is an order of magnitude higher than the laminar flame speed. The speed of triple flames studied thus far exceeds the laminar value by a factor less than two. The objective of the present task is the resolution of the apparent conflict between the experiments and the triple flame characteristics, and the clarification of the mechanisms controlling flame stability. Being investigated are the resolution achieved in the experiments, the flow field in the neighborhood of the stabilization point, propagation speeds of triple flames, laboratory flame unsteadiness, and the importance of flame ignition limits in the calculation of triple flames that resemble lifted flames. Derived from text

N95-22442*# Stanford Univ., CA. Center for Turbulence Research.
FLAME PROPAGATION UNDER PARTIALLY-PREMIXED CONDITIONS c25
Gregory R. Ruetsch *In its* Annual Research Briefs, 1994 Dec. 1994 p 79-96 (For primary document see N95-22437 06-34)
Avail: CASI HC A03/MF A04

This study concentrates on developing a better understanding of triple flames. We relax the assumption of zero heat release, address the issue of stabilization, and, in order to investigate the role that heat release plays in flame propagation in partially premixed combustion, we return to a simple flow field and investigate the behavior of flames in a laminar environment. We solve the compressible Navier-Stokes equations in a two-dimensional domain. At the boundaries, we use an inflow boundary condition on the left and nearly-perfect reflective boundary conditions, required to avoid pressure drift, at the outflow and sides. After the flow and flame are initialized, the mixture fraction is varied at the inlet from its uniform stoichiometric value to a tanh profile varying from zero to one. As the mixture fraction gradient reaches the flame surface only the centerline is exposed to the stoichionetric mixture fraction and locally maintains the planar flame speed and reaction rate. Above this point the mixture is fuel rich, and below fuel lean. As a result, these regions of non-unity equivalence ratio burn less, the reaction rate drops, and the local flame speed is reduced. The excess fuel and oxidizer then combine behind the premixed flame along the stoichiometric surface and burn in a trailing diffusion flame. Thus the 'triple' flame refers to the fuel-rich premixed flame, the fuel-lean premixed flame, and the trailing diffusion flame. Due to heat release, the normal velocity across the flame is increased, whereas the tangential component remains unchanged. Far-field flame speed, local flame speed, and their differences are shown as a function of the local mixing thickness. It was also determined that the lateral position of the flame affects stabilization, and the distribution of the reaction rate along the premixed wings of triple flames affects flame propagation. Derived from text

N95-22443*# Stanford Univ., CA. Center for Turbulence Research.
TURBULENCE MODELING FOR SEPARATED FLOW
Paul A. Durbin *In its* Annual Research Briefs, 1994 Dec. 1994 p 97-105 (For primary document see N95-22437 06-34)
Avail: CASI HC A02/MF A04

Two projects are described in this report. The first involves assessing turbulence models in separated flow. The second addresses the anomalous behavior of certain turbulence models in stagnation point flow. The primary motivation for developing turbulent transport models is to provide tools for computing non-equilibrium, or complex, turbulent flows. Simple flows can be analyzed using data correlations or algebraic eddy viscosities, but in more complicated flows such as a massively separated boundary layer, a more elaborate level of modeling is required. It is widely believed that at least a two-equation transport model is required in such cases. The transport equations determine the evolution of suitable velocity and time-scales of the turbulence. The present study included assessment of second-moment closures in several separated flows, including sharp edge separation; smooth wall, pressure driven separation; and unsteady vortex shedding. Flows with mean swirl are of interest for their role in enhancing mixing both by turbulent and mean motion. The swirl can have a stabilizing effect on the turbulence. An axi-symmetric extension to the INS-2D computer program was written adding the capability of computing swirling flow. High swirl can produce vortex breakdown on the centerline of the jet and it occurs in various combustors. Derived from text

N95-22444*# Stanford Univ., CA. Center for Turbulence Research.
NOTES ON ROTATING TURBULENCE
Otto Zeman *In its* Annual Research Briefs, 1994 Dec. 1994 p 107-114 (For primary document see N95-22437 06-34)
Avail: CASI HC A02/MF A04

This work investigates the turbulent constitutive relation when turbulence is subjected to solid body rotation. Laws regarding spectra and asymptotic decay of rotating homogeneous turbulence were confirmed through large-eddy simulation (LES) computations. Rotating turbulent flows exist in many industrial, geophysical, and astrophysical applications. From Lagrangian analysis a relation between turbulent stress and strain in rotating homogeneous turbulence was inferred. This relation was used to derive the spectral energy flux and, ultimately, the energy spectrum form. If the rotation wavenumber k(sub Omega) lies in the inertial subrange, then for wavenumbers less than k(sub Omega) the turbulence motions are affected by rotation and the energy spectrum slope is modified. Energy decay laws inferred in other reports and the present results suggest a modification of the epsilon model equation and eddy viscosity in k-epsilon models.
Derived from text

N95-22445*# Stanford Univ., CA. Center for Turbulence Research.
A DYNAMIC LOCALIZATION MODEL WITH STOCHASTIC BACKSCATTER
Daniele Carati and Sandip Ghosal *In its* Annual Research Briefs, 1994 Dec. 1994 p 115-125 (For primary document see N95-22437 06-34)
Avail: CASI HC A03/MF A04

The modeling of subgrid scales in large-eddy simulation (LES) has been rationalized by the introduction of the dynamic localization procedure. This method allows one to compute rather than prescribe the unknown coefficients in the subgrid-scale model. Formally, the LES equations are supposed to be obtained by applying to the Navier-Stokes equations a 'grid filter' operation. Though the subgrid stress itself is unknown, an identity between subgrid stresses generated by different filters has been derived. Although preliminary tests of the Dynamic Localization Model (DLM) with k-equation have been satisfactory, the use of a negative eddy viscosity to describe backscatter is probably a crude representation of the physics of reverse transfer of energy. Indeed, the model is fully deterministic. Knowing the filtered velocity field and the subgrid-scale energy, the subgrid stress is automatically determined. We know that the LES equations cannot be fully deterministic since the small scales are not resolved. This stems from an important distinction between equilibrium hydrodynamics and turbulence. In equilibrium hydrodynamics, the molecular motions are also not resolved. However, there is a clear separation of scale between these unresolved motions and the relevant hydrodynamic scales. The result of molecular motions can then be separated into an average effect (the molecular viscosity) and some fluctuations. Due to the large number of molecules present in a box with size of the order of the hydrodynamic scale, the ratio between fluctuations and the average effect should be very small (as a result of the 'law of large numbers'). For that reason, the hydrodynamic balance equations are usually purely deterministic. In turbulence, however, there is no clear separation of scale between small and large eddies. In that case, the fluctuations around a deterministic eddy viscosity term could be significant. An eddy noise would then appear through a stochastic term in the subgrid-scale model and could be the source of backscatter. Author

N95-22446*# National Aeronautics and Space Administration. Ames Research Center, Moffett Field, CA.
LARGE-EDDY SIMULATION OF A PLANE WAKE
Sandip Ghosal (Stanford Univ., CA.) and M. M. Rogers *In* Stanford Univ., Annual Research Briefs, 1994 Dec. 1994 p 127-141 (For primary document see N95-22437 06-34)
Avail: CASI HC A03/MF A04

Previously the theoretical development leading to the dynamic localization model (DLM) for large-eddy simulation (LES) was presented. The method has been successfully applied to isotropic turbulence, channel flow, and the flow over a backward-facing step. Here we apply the model to the computation of the temporally developing place wake. The two main objectives of this project are: (1) Use the model to perform an LES of a time developing plane wake and compare the results with direction numerical simulation (DNS) data to see if important statistical measures can be readily predicted, and to provide a relative evaluation of the several versions of the model in terms of predictive capability and cost; and (2) If the tests in (1) show that the model generates reliable predictions, then use the LES to study various aspects of the physics of turbulent wakes and mixing layers. Derived from text

N95-22447*# Stanford Univ., CA. Center for Turbulence Research.
LOCAL DYNAMIC SUBGRID-SCALE MODELS IN CHANNEL FLOW
William H. Cabot *In its* Annual Research Briefs, 1994 Dec. 1994 p 143-159 (For primary document see N95-22437 06-34)
Avail: CASI HC A03/MF A04

The dynamic subgrid-scale (SGS) model has given good results in the large-eddy simulation (LES) of homogeneous isotropic or shear flow, and in the LES of channel flow, using averaging in two or three homogeneous directions (the DA model). In order to simulate flows in general, complex geometries (with few or no homogeneous directions), the dynamic SGS model needs to be applied at a local level in a numerically stable way. Channel flow, which is inhomogeneous and wall-bounded flow in only one direction, provides a good initial test for local SGS models. Tests of the dynamic localization model were performed previously in channel flow using a pseudospectral code and good results were obtained. Numerical instability due to persistently negative eddy viscosity was avoided by either constraining the eddy viscosity to be positive or by limiting the time that eddy viscosities could remain negative by co-evolving the SGS kinetic energy (the DLk model). The DLk model, however, was too expensive to run in the pseudospectral code due to a large near-wall term in the auxiliary SGS kinetic energy (k) equation. One objective was then to implement the DLk model in a second-order central finite difference channel code, in which the auxiliary k equation could be integrated implicitly in time at great reduction in cost, and to assess its performance in comparison with the plane-averaged dynamic model or with no model at all, and with direct numerical simulation (DNS) and/or experimental data. Other local dynamic SGS models have been proposed recently, e.g., constrained dynamic models with random backscatter, and with eddy viscosity terms that are averaged in time over material path lines rather than in space. Another objective was to incorporate and test these models in channel flow. Author

N95-22448*# Stanford Univ., CA. Center for Turbulence Research.
UNSTRUCTURED-GRID LARGE-EDDY SIMULATION OF FLOW OVER AN AIRFOIL **c02**
Kenneth Jansen *In its* Annual Research Briefs, 1994 Dec. 1994 p 161-173 (For primary document see N95-22437 06-34)
Avail: CASI HC A03/MF A04

Historically, large-eddy simulations (LES) have been restricted to simple geometries where spectral or finite difference methods have dominated due to their efficient use of structured grids. Structured grids, however, not only difficulty representing complex domains and adapting to complicated flow features, but also are rather inefficient for simulating flows at high Reynolds numbers. The lack of efficiency stems from the need to resolve the viscous sublayer, which requires very fine resolution in all three directions near the wall. Structured grids make use of a stretching to reduce the normal grid spacing but must carry the fine resolution in the streamwise and spanwise directions throughout the domain. The unnecessarily fine grid for much of the domain leads to disturbingly high grid estimates. Chapman (1979), and later Moin & Jimenez (1993), pointed out that, in order to advance the technology to airfoils at flight Reynolds numbers, structured grids must be abandoned in lieu of what are known as nested or unstructured grids. The finite element method can efficiently solve the Navier-Stokes equations on unstructured grids. Although the CPU cost per time step per element is somewhat higher than structured grid methods, this effect is more than offset by the reduction in the number of elements. The use of unstructured grids, coupled with the advances in dynamic subgrid-scale modeling such as those made by Germano et al. (1991) and Ghosal et al. (1994), make LES of an airfoil tractable. We have chosen the NACA 4412 airfoil at maximum lift as the first simulation since this flow has not been successfully simulated with the Reynolds-averaged Navier-Stokes equations. Author

N95-22449*# Stanford Univ., CA. Center for Turbulence Research.
LARGE-EDDY SIMULATION OF FLOW THROUGH A PLANE, ASYMMETRIC DIFFUSER
Hans-Jakob Kaltenbach *In its* Annual Research Briefs, 1994 Dec. 1994 p 175-184 (For primary document see N95-22437 06-34)
Avail: CASI HC A02/MF A04

A challenge for traditional turbulence modeling, based on the Reynolds averaged Navier-Stokes equations, remains the accurate prediction of 'mild', adverse pressure-gradient driven separation from a smooth surface. With this study we want to explore the capability of large-eddy simulation to predict the separation which occurs on the deflected wall of an asymmetric, plane diffuser with opening angle of 10 deg. The flow through the plane diffuser exhibits some additional interesting physical phenomena which make it a challenging test case. In addition to 'mild' separation about halfway down the deflected ramp, the flow is characterized by a small backflow zone with stalled fluid in the rear part of the expanding section. The turbulent flow entering the diffuser is subject to combined adverse and radial pressure gradients stemming from the convex curvature. Finally the flow recovers into a developed, turbulent channel flow in the outlet section. Obi et al. provide measurements of mean flow, Reynolds stresses, and pressure recovery, which were obtained by means of LDV in a wind tunnel. The objective of this study is to investigate whether LES with the standard dynamic model is able to accurately predict the flow in the one-sided diffuser and to explore the resolution requirements and associated costs. Author

N95-22450*# Stanford Univ., CA. Center for Turbulence Research.
LARGE-EDDY SIMULATION OF A BOUNDARY LAYER WITH CONCAVE STREAMWISE CURVATURE
Thomas S. Lund *In its* Annual Research Briefs, 1994 Dec. 1994 p 185-195 (For primary document see N95-22437 06-34)
Avail: CASI HC A03/MF A04

Turbulence modeling continues to be one of the most difficult problems in fluid mechanics. Existing prediction methods are well developed for certain classes of simple equilibrium flows, but are still not entirely satisfactory for a large category of complex non-equilibrium flows found in engineering practice. Direct and large-eddy simulation (LES) approaches have long been believed to have great potential for the accurate prediction of difficult turbulent flows, but the associated computational cost has been prohibitive for practical problems. This remains true for direct simulation but is no longer clear for large-eddy simulation. Advances in computer hardware, numerical methods, and subgrid-scale modeling have made it possible to conduct LES for flows or practical interest at Reynolds numbers in the range of laboratory experiments. The objective of this work is to apply ES and the dynamic subgrid-scale model to the flow of a boundary layer over a concave surface. Author

N95-22451*# Stanford Univ., CA. Center for Turbulence Research.
EXPERIMENTAL INVESTIGATIONS OF ON-DEMAND VORTEX GENERATORS
Seyed G. Saddoughi *In its* Annual Research Briefs, 1994 Dec. 1994
p 197-203 (For primary document see N95-22437 06-34)
Avail: CASI HC A02/MF A04

Conventional vortex generators as found on many civil aircrafts are mainly for off-design conditions - e.g. suppression of separation or loss of aileron power when the Mach number accidentally rises above the design (cruise) value. In normal conditions they perform no useful function and exert a significant drag penalty. Recently there have been advances in new designs for passive vortex generators and boundary layer control. While traditionally the generators heights were of the order of the boundary layer thickness (delta), recent advances have been made where generators of the order of delta/4 have been shown to be effective. The advancement of MIcro-Electro-Mechanical (MEM) devices has prompted several efforts in exploring the possibility of using such devices in turbulence control. These new devices offer the possibility of boundary layer manipulation through the production of vortices, momentum jets, or other features in the flow. However, the energy output of each device is low in general, but they can be used in large numbers. Therefore, the possibility of moving from passive vortex generators to active (on-demand) devices becomes of interest. Replacement of fixed rectangular or delta-wing generators by devices that could be activated when needed would produce substantial economies. Our proposed application is not strictly 'active' control: the vortex generators would simply be switched on, all together, when needed (e.g. when the aircraft Mach number exceeded a certain limit). To this extent our scheme is simpler; however, to promote mixing and suppress separation we desire to deposit longitudinal vortices into the outer layer of the boundary layer as in conventional vortex generators. This requires a larger device although an alternative might be an array of smaller devices, for example, a longitudinal row with phase differences in the modulation signals so that the periodic vortices join up. The vortex pair with common flow up has the advantage that it will naturally drift away from the surface, but the disadvantage is that the net vorticity is zero so that the pair is eventually obliterated by turbulent mixing, rather than simply being diffused as in the case of a single vortex. It should be possible to devise alternative shapes of cavity wall so that the jet emerges obliquely and produces net longitudinal vorticity. Author

N95-22452*# Stanford Univ., CA. Center for Turbulence Research.
DIRECT NUMERICAL SIMULATIONS OF ON-DEMAND VORTEX GENERATORS: MATHEMATICAL FORMULATION
Petros Koumoutsakos *In its* Annual Research Briefs, 1994 Dec. 1994
p 205-214 (For primary document see N95-22437 06-34)
Avail: CASI HC A02/MF A04

The objective of the present research is the development and application of efficient adaptive numerical algorithms for the study, via direct numerical simulations, of active vortex generators. We are using innovative computational schemes to investigate flows past complex configurations undergoing arbitrary motions. Some of the questions we try to answer are: Can and how may we control the dynamics of the wake? What is the importance of body shape and motion in the active control of the flow? What is the effect of three-dimensionality in laboratory experiments? We are interested not only in coupling our results to ongoing, related experimental work, but furthermore to develop an extensive database relating the above mechanisms to the vortical wake structures with the long-range objective of developing feedback control mechanisms. This technology is very important to aircraft, ship, automotive, and other industries that require predictive capability for fluid mechanical problems. The results would have an impact in high angle of attack aerodynamics and help design ways to improve the efficiency of ships and submarines (maneuverability, vortex induced vibration, and noise). Author

N95-22453*# Stanford Univ., CA. Center for Turbulence Research.
DRAG REDUCTION STRATEGIES
D. Christopher Hill *In its* Annual Research Briefs, 1994 Dec. 1994
p 215-218 (For primary document see N95-22437 06-34)
Avail: CASI HC A01/MF A04

previously a description was given of an active control scheme using wall transpiration that leads to a 15% reduction in surface skin friction beneath a turbulent boundary layer, according to direct numerical simulation. In this research brief further details of that scheme and its variants are given together with some suggestions as to how sensor/actuator arrays could be configured to reduce surface drag. The research which is summarized here was performed during the first half of 1994. This research is motivated by the need to understand better how the dynamics of near-wall turbulent flow can be modified so that skin friction is reduced. The reduction of turbulent skin friction is highly desirable in many engineering applications. Experiments and direct numerical simulations have led to an increased understanding of the cycle of turbulence production and transport in the boundary layer and raised awareness of the possibility of disrupting the process with a subsequent reduction in turbulent skin friction. The implementation of active feedback control in a computational setting is a viable approach for the investigation of the modifications to the flow physics that can be achieved. Bewley et al. and Hill describe how ideas from optimal control theory are employed to give 'sub-optimal' drag reduction schemes. The objectives of the work reported here is to investigate in greater detail the assumptions implicit within such schemes and their limitations. It is also our objective to describe how an array of sensors and actuators could be arranged and interconnected to form a 'smart' surface which has low skin friction. Author

N95-22454*# McDonnell-Douglas Aerospace, Saint Louis, MO.
OPTIMAL ACTIVE CONTROL FOR BURGERS EQUATIONS
Yutaka Ikeda *In* Stanford Univ., Annual Research Briefs, 1994 Dec. 1994 p 219-224 (For primary document see N95-22437 06-34)
Avail: CASI HC A02/MF A04

A method for active fluid flow control based on control theory is discussed. Dynamic programming and fixed point successive approximations are used to accommodate the nonlinear control problem. The long-term goal of this project is to establish an effective method applicable to complex flows such as turbulence and jets. However, in this report, the method is applied to stochastic Burgers equation as an intermediate step towards this goal. Numerical results are compared with those obtained by gradient search methods. Author

N95-22455*# Stanford Univ., CA. Center for Turbulence Research.
ACOUSTICS OF LAMINAR BOUNDARY LAYERS BREAKDOWN
Meng Wang *In its* Annual Research Briefs, 1994 Dec. 1994
p 225-242 (For primary document see N95-22437 06-34)
Avail: CASI HC A03/MF A04

Boundary layer flow transition has long been suggested as a potential noise source in both marine (sonar-dome self noise) and aeronautical (aircraft cabin noise) applications, owing to the highly transient nature of process. The design of effective noise control strategies relies upon a clear understanding of the source mechanisms associated with the unsteady flow dynamics during transition. Due to formidable mathematical difficulties, theoretical predictions either are limited to early linear and weakly nonlinear stages of transition, or employ acoustic analogy theories based on approximate source field data, often in the form of empirical correlation. In the present work, an approach which combines direct numerical simulation of the source field with the Lighthill acoustic analogy is utilized. This approach takes advantage of the recent advancement in computational capabilities to obtain detailed information about the flow-induced acoustic sources. The transitional boundary layer flow is computed by solving the incompressible Navier-Stokes equations without model assumptions, thus allowing a direct evaluation of the pseudosound as well as source functions, including the Lighthill stress tensor and the wall shear stress. The latter are used for calculating the radiated pressure field based on the Curle-Powell solution of the Lighthill equation. This procedure allows a quantitative assessment of noise source mechanisms and the associated radiation characteristics during transition from primary instability up to the laminar breakdown stage. In particular, one is interested in comparing the roles played by the fluctuating volume Reynolds stress and the wall-shear-stresses, and in identifying specific flow processes and structures that are effective noise generators. Derived from text

N95-22456*# Stanford Univ., CA. Center for Turbulence Research.
SMALL-SCALE BEHAVIOR IN DISTORTED TURBULENT BOUNDARY LAYERS AT LOW REYNOLDS NUMBER
Seyed G. Saddoughi *In its* Annual Research Briefs, 1994 Dec. 1994 p 243-261 (For primary document see N95-22437 06-34)
Avail: CASI HC A03/MF A04

During the last three years we have conducted high- and low-Reynolds-number experiments, including hot-wire measurements of the velocity fluctuations, in the test-section-ceiling boundary layer of the 80- by 120-foot Full-Scale Aerodynamics Facility at NASA Ames Research Center, to test the local-isotropy predictions of Kolmogorov's universal equilibrium theory. This hypothesis, which states that at sufficiently high Reynolds numbers the small-scale structures of turbulent motions are independent of large-scale structures and mean deformations, has been used in theoretical studies of turbulence and computational methods such as large-eddy simulation; however, its range of validity in shear flows has been a subject of controversy. The present experiments were planned to enhance our understanding of the local-isotropy hypothesis. Our experiments were divided into two sets. First, measurements were taken at different Reynolds numbers in a plane boundary layer, which is a 'simple' shear flow. Second, experiments were designed to address this question: will our criteria for the existence of local isotropy hold for 'complex' nonequilibrium flows in which extra rates of mean strain are added to the basic mean shear? Derived from text

N95-22457*# McDonnell-Douglas Aerospace, Saint Louis, MO.
TRANSVERSE VORTICITY MEASUREMENTS IN THE NASA AMES 80 X 120 WIND TUNNEL BOUNDARY LAYER
John F. Foss, D. G. Bhol, F. D. Bramkamp (Technische Hochschule, Aachen, Germany.), and J. G. Klewicki (Utah Univ., Salt Lake City, UT.) *In* Stanford Univ. Annual Research Briefs, 1994 Dec. 1994 p 263-268 (For primary document see N95-22437 06-34)
Avail: CASI HC A02/MF A04

The MSU compact four-wire transverse vorticity probe permits omega(sub z)(t) measurements in a nominally 1 sq mm domain. Note that a conventional coordinate system is used with x and y in the streamwise and normal directions respectively. The purpose of this investigation was to acquire time series data in the same access port at the ceiling of the 80 ft x 120 ft wind tunnel (NASA Ames Research Center) as earlier used by the Wallace group from the University of Maryland and to compare the present results with those of the three-component vorticity probe used in that earlier study. Derived from text

N95-22458*# Stanford Univ., CA.
EXPERIMENTAL AND NUMERICAL STUDY OF THE INTERMITTENCY EXPONENT MU
Alexander Praskovsky *In its* Annual Research Briefs, 1994 Dec. 1994 p 269-286 (For primary document see N95-22437 06-34)
Avail: CASI HC A03/MF A04

After publication of the Kolmogorov refined similarity hypotheses, the small-scale intermittency of the energy dissipation field became a central problem in fully developed turbulence (FDT). This phenomenon has been studied in many different ways, e.g. by searching for corrections to scaling exponents in the inertial range velocity structure functions. A direct measure of this intermittency is, however, available by studying the local rate of energy dissipation, and it may be quantitatively characterized by the intermittency exponent mu. As far as we know, nobody has posed an obvious question: Is the intermittency exponent mu a unique constant, i.e., are the values mu(sub kappa), mu(sub epsilon), mu(sub r), mu(sub b), and mu(sub e) the same at high Reynolds numbers, or do they create a set of different (and perhaps independent) exponents? This paper addresses the above question using the high Reynolds number experiments. Derived from text

N95-22459*# National Aeronautics and Space Administration. Ames Research Center, Moffett Field, CA.
ON THE DYNAMICS OF SMALL-SCALE VORTICITY IN ISOTROPIC TURBULENCE
Javier Jimenez (Stanford Univ., CA.) and A. A. Wray *In* Stanford Univ., Annual Research Briefs, 1994 Dec. 1994 p 287-312 (For primary document see N95-22437 06-34)
Avail: CASI HC A03/MF A04

It was previously shown that the strong vorticity in isotropic turbulence is organized into tubular vortices ('worms') whose properties were characterized through the use of full numerical simulations at several Reynolds numbers. At the time most of the observations were kinematic, and several scaling laws were discovered for which there was no theoretical explanation. In the meantime, further analysis of the same fields yielded new information on the generation of the vortices, and it was realized that even if they had to be formed by stretching, they were at any given moment actually compressed at many points of their axes. This apparent contradiction was partially explained by postulating axial inertial waves induced by the nonuniformity of the vortex cores, which helped to 'spread' the axial strain and allowed the vortices to remain compact even if not uniformly stretched. The existence of such solutions was recently proved numerically. The present report discusses a set of new numerical simulations of isotropic turbulence, and a reanalysis of the old ones, in an effort to prove or disprove the presence of these waves in actual turbulent flows and to understand the dynamics, as opposed to the kinematics, of the vortices. Author

N95-22460*# Stanford Univ., CA. Center for Turbulence Research.
FORCED FREE-SHEAR LAYER MEASUREMENTS
Richard L. LeBoeuf *In its* Annual Research Briefs, 1994 Dec. 1994 p 313-338 (For primary document see N95-22437 06-34)
Avail: CASI HC A03/MF A04

Detailed three-dimensional three-component phase averaged measurements of the spanwise and streamwise vorticity formation and evolution in acoustically forced plane free-shear flows have been obtained. For the first time, phase-averaged measurements of all three velocity components have been obtained in both a mixing layer and a wake on three-dimensional grids, yielding the spanwise and streamwise vorticity distributions without invoking Taylor's hypothesis. Initially, two-frequency forcing was used to phase-lock the roll-up and first pairing of the spanwise vortical structures in a plane mixing layer. The objective of this study was to measure the near-field vortical structure morphology in a mixing layer with 'natural' laminar initial boundary layers. For the second experiment the second and third subharmonics of the fundamental roll-up frequency were added to the previous two-frequency forcing in order to phase-lock the roll-up and first three pairings of the spanwise rollers in the mixing layer. The objective of this study was to determine the details of spanwise scale changes observed in previous time-averaged measurements and flow visualization of unforced mixing layers. For the final experiment, single-frequency forcing was used to phase-lock the Karman vortex street in a plane wake developing from nominally two-dimensional laminar initial boundary layers. The objective of this study was to compare measurements of the three-dimensional structure in a wake developing from 'natural' initial boundary layers to existing models of wake vortical structure. Author

N95-22461*# Stanford Univ., CA. Center for Turbulence Research.
NUMERICAL STUDY OF BOUNDARY LAYER INTERACTION WITH SHOCKS: METHOD AND CODE VALIDATION
Nikolaus A. Adams *In its* Annual Research Briefs, 1994 Dec. 1994 p 339-356 (For primary document see N95-22437 06-34)
Avail: CASI HC A03/MF A04

A major problem in modeling of turbulent supersonic flows is the correct assessment of viscous-inviscid interaction problems. Of particular interest is the interaction of boundary layers with shocks. Present turbulence models give in most cases unsatisfactory results in the region of rapid distortion and in the separation region (if one is present) in particular with regard to mean flow profiles and turbulence quantities. The objective of the present work is the direct numerical simulation of shock boundary layer interaction. This report summarizes the first phase during which a numerical method suitable for this problem has been developed and a computer code has been written and tested. Author

N95-22462*# Stanford Univ., CA. Center for Turbulence Research.
RESOLUTION REQUIREMENTS FOR VELOCITY GRADIENTS IN TURBULENCE
Javier Jimenez *In its* Annual Research Briefs, 1994 Dec. 1994 p 357-364 (For primary document see N95-22437 06-34)
Avail: CASI HC A02/MF A04

Since high resolution numerical simulations of turbulent flows, or experiments at high Reynolds numbers, represent a substantial investment in resources, the estimation of the minimum resolution required for the study of a given property has been the subject of continued interest. Different properties require, in general, different resolutions, and the present paper is dedicated to the requirements for the measurement of the probability distribution functions of the velocity gradients and, in particular, of their low order moments. The deviation of these quantities from the values corresponding to a Gaussian distribution was one of the first indications of the presence of Reynolds number-dependent intermittency and has been the object of recent interest as numerical simulations have become able to explore the distribution of gradients in the low Reynolds number range, while new experiments have extended the range to increasingly high Reynolds numbers. We will use progressive filtering of the results of numerical simulations of isotropic turbulence as a model for the effect of a sensor of finite size. The numerical issues will be addressed first to ensure that the simulations are fully resolved from the point of view of the velocity gradients. This will also give us an estimate for the numerical resolution required for the different quantities. Author

N95-22463*# Stanford Univ., CA. Center for Turbulence Research.
A METHOD FOR OBTAINING A STATISTICALLY STATIONARY TURBULENT FREE SHEAR FLOW
Stephen F. Timson, S. K. Lele, and R. D. Moser *In its* Annual Research Briefs, 1994 Dec. 1994 p 365-371 (For primary document see N95-22437 06-34)
Avail: CASI HC A02/MF A04

The long-term goal of the current research is the study of Large-Eddy Simulation (LES) as a tool for aeroacoustics. New algorithms and developments in computer hardware are making possible a new generation of tools for aeroacoustic predictions, which rely on the physics of the flow rather than empirical knowledge. LES, in conjunction with an acoustic analogy, holds the promise of predicting the statistics of noise radiated to the far-field of a turbulent flow. LES's predictive ability will be tested through extensive comparison of acoustic predictions based on a Direct Numerical Simulation (DNS) and LES of the same flow, as well as a priori testing of DNS results. The method presented here is aimed at allowing simulation of a turbulent flow field that is both simple and amenable to acoustic predictions. A free shear flow is homogeneous in both the streamwise and spanwise directions and which is statistically stationary will be simulated using equations based on the Navier-Stokes equations with a small number of added terms. Studying a free shear flow eliminates the need to consider flow-surface interactions as an acoustic source. The homogeneous directions and the flow's statistically stationary nature greatly simplify the application of an acoustic analogy. Author

N95-22464*# Stanford Univ., CA. Dept. of Aeronautic and Astronautics.
DIRECT NUMERICAL SIMULATION OF INCOMPRESSIBLE AXISYMMETRIC FLOWS
Patrick Loulou *In its* Annual Research Briefs, 1994 Dec. 1994 p 373-378 (For primary document see N95-22437 06-34)
Avail: CASI HC A02/MF A04

In the present work, we propose to conduct direct numerical simulations (DNS) of incompressible turbulent axisymmetric jets and wakes. The objectives of the study are to understand the fundamental behavior of axisymmetric jets and wakes, which are perhaps the most technologically relevant free shear flows (e.g. combuster injectors, propulsion jet). Among the data to be generated are various statistical quantities of importance in turbulence modeling, like the mean velocity, turbulent stresses, and all the terms in the Reynolds-stress balance equations. In addition, we will be interested in the evolution of large-scale structures that are common in free shear flow. The axisymmetric jet or wake is also a good problem in which to try the newly developed b-spline numerical method. Using b-splines as interpolating functions in the non-periodic direction offers many advantages. B-splines have local support, which leads to sparse matrices that can be efficiently stored and solved. Also, they offer spectral-like accuracy that are C(exp O-1) continuous, where O is the order of the spline used; this means that derivatives of the velocity such as the vorticity are smoothly and accurately represented. For purposes of validation against existing results, the present code will also be able to simulate internal flows (ones that require a no-slip boundary condition). Implementation of no-slip boundary condition is trivial in the context of the b-splines. Author

N95-22465*# Stanford Univ., CA. Center for Turbulence Research.
DATABASES POST-PROCESSING IN TENSORAL
Eliot Dresselhaus *In its* Annual Research Briefs, 1994 Dec. 1994 p 379-390 (For primary document see N95-22437 06-34)
Avail: CASI HC A03/MF A04

The Center for Turbulent Research (CTR) post-processing effort aims to make turbulence simulations and data more readily and usefully available to the research and industrial communities. The Tensoral language, introduced in this document and currently existing in prototype form, is the foundation of this effort. Tensoral provides a convenient and powerful protocol to connect users who wish to analyze fluids databases with the authors who generate them. In this document we introduce Tensoral and its prototype implementation in the form of a user's guide. This guide focuses on use of Tensoral for post-processing turbulence databases. The corresponding document - the Tensoral 'author's guide' - which focuses on how authors can make databases available to users via the Tensoral system - is currently unwritten. Section 1 of this user's guide defines Tensoral's basic notions: we explain the class of problems at hand and how Tensoral abstracts them. Section 2 defines Tensoral syntax for mathematical expressions. Section 3 shows how these expressions make up Tensoral statements. Section 4 shows how Tensoral statements and expressions are embedded into other computer languages (such as C or Vectoral) to make Tensoral programs. We conclude with a complete example program. Author

N95-20647# Maryland Univ., College Park, MD. CALCE Electronic Packaging Research Center.
LIQUID FLOW-THROUGH COOLING OF ELECTRONIC MODULES
S. Sridhar, M. D. Osterman, J. M. Carbonell (Wright Lab., Wright-Patterson AFB, OH.), and K. E. Herold *In* AGARD, Advanced Packaging Concepts for Digital Avionics Oct. 1994 6 p Sponsored by Westinghouse Electric Corp. and AMRL (For primary document see N95-20631 06-06)
Copyright Avail: CASI HC A02/MF A03

N95-20648# Naval Air Warfare Center, Indianapolis, IN. Aircraft Div.
IMMERSION/TWO PHASE COOLING
Jack Jones and Emmett Perkoski *In* AGARD, Advanced Packaging Concepts for Digital Avionics Oct. 1994 11 p (For primary document see N95-20631 06-06)
Copyright Avail: CASI HC A03/MF A03

N95-20649# Deutsche Aerospace A.G., Munich (Germany). Military Aircraft Div.
MICROCHANNEL HEAT PIPE COOLING OF MODULES
G. Moser *In* AGARD, Advanced Packaging Concepts for Digital Avionics Oct. 1994 12 p (For primary document see N95-20631 06-06)
Copyright Avail: CASI HC A03/MF A03

35 INSTRUMENTATION AND PHOTOGRAPHY

Includes remote sensors; measuring instruments and gages; detectors; cameras and photographic supplies; and holography.

For aerial photography see *43 Earth Resources and Remote Sensing.* For related information see also *06 Aircraft Instrumentation,* and *19 Spacecraft Instrumentation.*

N95-20031# Federal Aviation Administration, Atlantic City, NJ.
ROUND-ROBIN COMPARISON OF HEAT RELEASE APPARATUS
Richard M. Johnson Sep. 1994 15 p
(AD-A285831; DOT/FAA/CT-TN94/42) Avail: CASI HC A03/MF A01

A series of 150 comparative tests were run by four currently operating laboratories using heat release apparatuses compliant with present FAA/JAR standards and the ATI Russian Institute of Aviation Materials (VIAM) designed heat release apparatus. The evaluation of data showed little or no correlation between the subject apparatus and the four compliant apparatuses. DTIC

N95-20036# Atmospheric Radiation Consultants, Acton, MA.
NOISE MODEL OF THE MSX SPIRIT 3 INTERFEROMETER
Alexander S. Zachor 20 May 1994 32 p Revised
(Contract F19628-93-C-0044)
(AD-A285837; PL-TR-94-2141-Rev; SR-1-Rev) Avail: CASI HC A03/MF A01

A preliminary model for predicting the performance of the MSX SPIRIT 3 interferometer has been implemented as a computer code module that provides estimates of expected total noise and saturation levels. This report gives the theoretical development of the model and includes usage instructions for the code. A later version of the code will be used in the automated analysis of SPIRIT 3 interferometer data at the Phillips Laboratory Data Analysis Center. The model has provided predictions of system performance in planned MSX experiments for remote sensing of atmospheric trace constituents. DTIC

N95-20069 Northeastern Univ., Boston, MA. Dept. of Electrical Engineering.
ADVANCED DETECTOR DEVELOPMENT, LABORATORY SIMULATIONS, DIAGNOSTIC DEVELOPMENT, AND DATA ANALYSIS ON WAKE PHYSICS Final Report, 24 May 1991 - 24 May 1994
John M. Talbet and Chung Chan 30 Jun. 1994 14 p Limited Reproducibility: More than 20% of this document may be affected by microfiche quality
(Contract F19628-91-K-0019)
(AD-A284798; PL-TR-94-2205) Avail: CASI HC A03

We have performed a number of experiments and have developed a theoretical analysis of the current scaling issues of a negatively biased probe in a plasma wake. The end product of the laboratory research performed in the large vacuum chamber JUMBO at Phillips Laboratory can be found in the associated publication. Theoretical assumptions have been analyzed qualitatively and quantitatively by the use of the POLAR computer code. For a plasma with a constant beam energy, the analysis shows that the I-V collection characteristics are unaffected by Mach variations for Mach numbers above the value of two. For the same case, the current was found to scale with the 3/7 power of the density. DTIC

N95-20224# Westinghouse Hanford Co., Richland, WA.
IN SITU VISCOMETER INSTRUMENT ACCEPTANCE TEST REPORT
K. L. Pearce and T. I. Stokes 24 Aug. 1994 56 p
(Contract DE-AC06-87RL-10930)
(DE94-018507; WHC-SD-WM-ATR-089) Avail: CASI HC A04/MF A01

This document presents the results of the acceptance test for the mechanical and electrical features (not specifically addressed by the software acceptance test procedure (ATP)) of the viscometer instrument. This document and the ATP satisfy the requirements in EP-4.1, 'Design Verification Requirements.' The selected mode of design verification is qualification testing. The testing described in this document verifies that the mechanical and electrical features are operating as designed and that the unit is ready for field service. DOE

N95-20233# Phytron Instruments, Inc., Mountain View, CA.
A CHARGE DISTRIBUTION ANALYSIS INSTRUMENT FOR CATALYSIS AND MATERIAL SCIENCE APPLICATIONS
F. Freund Aug. 1994 15 p
(Contract DE-FG49-93CE-15566)
(DE94-016489; DOE/CE-15566/T3) Avail: CASI HC A03/MF A01

Key component in the CDA instrument is the differential capacitive force sensor. The CDA instrument has four basic components: OEM analytical balance, flexure point and capacitor plates, gas confinement tower and high-voltage bias electrodes, and the furnace. Phyton is in position to purchase an OEM analytical balance; negotiations are underway for obtaining the feedback control circuitry for the differential capacitive force sensor. Progress with the differential capacitive force sensor is reviewed. DOE

N95-20320# Pacific Northwest Lab., Richland, WA.
AN EVALUATION OF 915-MHz RADAR WIND PROFILER/RASS BY TOWER AND SODAR MEASUREMENTS
S. Zhong, W. J. Shaw, and J. M. Hubbe Aug. 1994 4 p Presented at the 3rd International Symposium on Tropospheric Profiling: Needs and Technologies, Hamburg, Germany, 30 Aug. - 2 Sep. 1994
(Contract DE-AC06-76RL-01830)
(DE94-018913; PNL-SA-24487; CONF-9408118-3) Avail: CASI HC A01/MF A01

The accuracy and precision of the 915-MHz low-atmosphere wind profiler/RASS have been investigated through comparisons with other better-understood instruments such as rawinsonde (Strauch et al., 1987 and May et al., 1989), sodar (Neff and Wilczak, 1993), and tower instruments (Ye et al., 1993). These studies have provided useful information as well as confidence in the performance of this new technology in boundary-layer research and monitoring. However, because the accuracy of the profiler/RASS measurements depends to a large degree on the strength and homogeneity of small-scale turbulence and the amount of moisture in the atmosphere, the performance of the profiler may change significantly from one environment to another. As the radar wind profiler/RASS technology becomes more widely applied to a variety of research applications and moves toward operational wind, temperature, and eventually flux profiling, it is crucial to quantify its performance under different environmental and meteorological conditions. South-central Washington is a semi-arid shrub-steppe environment with an average annual precipitation of only about 15 cm, which is significantly different from the other locations where comparative studies have been conducted. The performance of the RADIAN 915-MHz wind profiler/RASS in such an environment was evaluated using data from standard instruments mounted on a 120-m meteorological tower and a nearby sodar at the Hanford Meteorological Station. The results of this evaluation are presented in this paper. DOE

N95-20321# Pacific Northwest Lab., Richland, WA.
HYDROSTATIC FORCE SENSOR
M. S. Evans, R. S. Stoughton, and H. Kazerooni (California Univ., Berkeley, CA.) Aug. 1994 5 p Presented at the 5th International Symposium on Robotics and Manufacturing, Maui, HI, 14-18 Aug. 1994
(Contract DE-AC06-76RL-01830)
(DE94-018923; PNL-SA-24676; CONF-940859-26) Avail: CASI HC A01/MF A01

This paper presents a theoretical and experimental investigation of a new kind of force sensor which detects forces by measuring an induced pressure change in a material of large Poisson's ratio. In this investigation we develop mathematical expressions for the sensor's sensitivity and bandwidth, and show that its sensitivity can be much larger and its bandwidth is usually smaller than those of existing strain-gage-type sensors. This force sensor is well-suited for measuring large but slowly varying forces. It can be installed in a space smaller than that required by existing sensors. DOE

N95-20398# Sandia National Labs., Albuquerque, NM.
DEVELOPMENT OF SOLID STATE MOISTURE SENSORS FOR SEMICONDUCTOR FABRICATION APPLICATIONS
K. B. Pfeifer, M. J. Kelly, T. R. Guilinger, D. W. Peterson, J. N. Sweet, and M. R. Tuck 1994 12 p Presented at the SEMATECH: Symposium on Contamination Free Manufacturing, San Jose, CA, 4-6 Oct. 1994
(Contract DE-AC04-94AL-85000)
(DE94-015771; SAND-94-1533C; CONF-9410161-1) Avail: CASI HC A03/MF A01

We describe the design and fabrication of two types of solid state moisture sensors, and discuss the results of an evaluation of the sensors for the detection of trace levels of moisture in semiconductor process gases. The first sensor is based on surface acoustic wave (SAW) technology. A moisture sensitive layer is deposited onto a SAW device, and the amount of moisture adsorbed on the layer produces a proportional shift in the operating frequency of the device. Sensors based on this concept have excellent detection limits for moisture in inert gas (100 ppb) and corrosive gas (150 ppb in HCl). The second sensor is a simple capacitor structure that uses porous silicon as a moisture-sensitive dielectric material. The detection limits of these sensors for moisture in inert gas are about 700 ppb prior to HCl exposure, and about 7 ppm following HCl exposure. DOE

N95-20413 Pennsylvania State Univ., University Park, PA. Dept. of Chemistry.
A LOW TEMPERATURE, ULTRAHIGH VACUUM, MICROWAVE-FREQUENCY-COMPATIBLE SCANNING TUNNELING MICROSCOPE
S. J. Stranick, M. M. Kamna, and P. S. Weiss 1 May 1994 22 p Limited Reproducibility: More than 20% of this document may be affected by microfiche quality
(Contract N00014-91-J-1630)
(AD-A279869; TR-15) Avail: Issuing Activity (Defense Technical Information Center (DTIC))

To expand the capabilities of the microwave frequency alternating current scanning tunneling microscope to include the ability to study isolated adsorbates and highly reactive surfaces, we have developed a low temperature, ultrahigh vacuum alternating current scanning tunneling microscope. In this alternating current scanning tunneling microscope, we employ the reliable beetle-style sample approach mechanism with a number of other components unique to a low temperature scanning tunneling microscope. These include the sample transfer, delivery, retrieval, storage, sputtering, and heating systems. This alternating current scanning tunneling microscope has been operated at 77K and 4K. DTIC

N95-20431 Colorado State Univ., Fort Collins, CO. Dept. of Chemistry.
MECHANISM OF THE AMPEROMETRIC RESPONSE OF A PROPOSED GLUCOSE SENSOR BASED ON A POLYPYRROLE-TUBULE-IMPREGNATED MEMBRANE Interim Report
Susumu Kuwabata and Charles R. Martin May 1994 29 p Limited Reproducibility: More than 20% of this document may be affected by microfiche quality
(Contract N00014-82-K-0612)
(AD-A279836; TR-94) Avail: Issuing Activity (Defense Technical Information Center (DTIC))

Nolte et al recently proposed a new type of amperometric glucose sensor. This sensor is based on a microporous membrane that contains polypyrrole tubules within the pores of the membrane. The procedure for preparing these polypyrrole tubules was developed in this laboratory. Nolte et al claim that glucose oxidase can be irreversible adsorbed to the inside walls of these polypyrrole tubules and that the resulting device functions as a glucose sensor. Indeed, they claim that this device functions via direct electron transfer from the reduced enzyme to the polypyrrole tubule. We have recently explored the response characteristics of this proposed new sensor. Our results suggest that this sensor does not function in the manner proposed by Nolte et al. Instead, our results indicate that the device operates by direct electrochemical oxidation of glucose at the metal (Pt) film that is coated onto one face of the membrane. This is proven by the fact that the sensitivity of the device is improved when polypyrrole and glucose oxidase are not present in the membrane. DTIC

N95-20560*# National Aeronautics and Space Administration. Marshall Space Flight Center, Huntsville, AL.
PRELIMINARY CONTROL SYSTEM DESIGN AND ANALYSIS FOR THE SPACE STATION FURNACE FACILITY THERMAL CONTROL SYSTEM
M. E. Jackson Washington Jan. 1995 39 p
(NASA-TM-108476; NAS 1.15:108476) Avail: CASI HC A03/MF A01

This report presents the Space Station Furnace Facility (SSFF) thermal control system (TCS) preliminary control system design and analysis. The SSFF provides the necessary core systems to operate various materials processing furnaces. The TCS is defined as one of the core systems, and its function is to collect excess heat from furnaces and to provide precise cold temperature control of components and of certain furnace zones. Physical interconnection of parallel thermal control subsystems through a common pump implies the description of the TCS by coupled nonlinear differential equations in pressure and flow. This report formulates the system equations and develops the controllers that cause the interconnected subsystems to satisfy flow rate tracking requirements. Extensive digital simulation results are presented to show the flow rate tracking performance. Author

N95-20604 Naval Command, Control and Ocean Surveillance Center, San Diego, CA. Research, Development, Test and Evaluation Div.
AN AT-SEA EVALUATION OF AN INFRARED/RESISTANCE TEMPERATURE DEVICE FOR AIR/SEA-SURFACE TEMPERATURE MEASUREMENTS Final Technical Report, Oct. 1992 - Sep. 1993
W. L. Patterson Mar. 1994 25 p Limited Reproducibility: More than 20% of this document may be affected by microfiche quality
(AD-A279672; NCCOSC/RDT/E-TR-1639) Avail: Issuing Activity (Defense Technical Information Center (DTIC))

Air and sea-surface temperatures were measured and recorded by the USS Kitty Hawk's meteorological personnel during a 6-month deployment period. Using infrared/resistance temperature devices (IR/RTD) and hand-held psychrometers, air and sea-surface temperature data were compiled. In comparing these data with data collected earlier by the USS Ranger, it became apparent that the shipboard use of the IR/RTD to measure sea-surface and air temperatures was not warranted. The IR/RTD suffered mechanical and electrical failures during both the USS Kitty Hawk and USSR Ranger measurement periods. Since repair and recalibration must be done at the manufacturer's facility, the device is inappropriate for shipboard use. In addition, the design of the battery-recharging unit does not conform to shipboard requirements for electrical grounding. Borne out by both the comments of the USS Kitty Hawk oceanographer and the large number of highly suspicious readings, additional training for observers is justified. Thus, training on the proper use and care of temperature-measuring devices could be made part of the Aerographer's Mate course curriculum and shipboard performance factors. DTIC

N95-20759 Aeronautical Research Labs., Melbourne (Australia).
DYNAMIC RESPONSE OF PRESSURE MEASURING SYSTEMS
M. F. Lee Apr. 1993 23 p
(ARL-TR-32; AR-007-104) Copyright Avail: Issuing Activity (Aeronautical Research Labs., Melbourne, Australia)

The measurement of time varying pressures is limited when a pressure transmission line must be used. The type of pressure transducer can further limit the speed at which pressure changes can be observed. This report investigates these limitations by subjecting commonly used pressure line tubing and pressure transducers to a step pressure input. By spectrally analyzing the response to this step input a frequency response for the system can be determined. Author

N95-20902# Fermi National Accelerator Lab., Batavia, IL.
MECHANICAL DESIGN OF THE DO SILICON DETECTOR
W. E. Cooper Sep. 1994 6 p Presented at the Meeting of the Division of Particles and Fields of the American Physical Society, Albuquerque, NM, 2-6 Aug. 1994
(Contract DE-AC02-76CH-03000)
(DE95-002532; FNAL/C-94/342-E; CONF-940816-45) Avail: CASI HC A02/MF A01

The upgrade of the DO detector for Run II of the Fermilab collider includes the addition of a silicon tracker for vertex determination. The mechanical structure of the silicon tracker is described. DOE

N95-21117 Department of the Navy, Washington, DC.
ELECTRON TUNNELING MAGNETIC FIELD SENSOR Patent Application
Daniel DiLella, inventor (to Navy) and Richard J. Colton, inventor (to Navy) 7 Feb. 1994 30 p Limited Reproducibility: More than 20% of this document may be affected by microfiche quality
(AD-D016227; US-Patent-Appl-SN-193690) Avail: CASI HC A03

The magnetic sensor of this invention is characterized by a magnet suspended on a torsion bar or wire and by a tunneling tip separated from one end of the magnet, a gap between the tip and the magnet that is small enough to support a tunneling current, means for imposing a constant biasing voltage across the gap, means to maintain the magnet and the tip sufficiently close so that a constant tunneling current is maintained therebetween, a feedback circuit to monitor current changes in the gap that result from rotation of the magnet due to changes in the surrounding magnetic field, and recording means to record changes in the magnetic field. DTIC

N95-21138# Westinghouse Hanford Co., Richland, WA.

RADIOACTIVE CHECK SOURCES FOR ALPHA AND BETA SENSITIVE RADIOLOGICAL INSTRUMENTATION

J. M. Barnett and J. E. Kane, II Jun. 1994 13 p Presented at the Health Physics Society Annual Meeting, San Francisco, CA, 27-30 Jun. 1994
(Contract DE-AC06-87RL-10930)
(DE94-016477; WHC-SA-2518; CONF-9406210-3) Avail: CASI HC A03/MF A01

Since 1991, the Westinghouse Hanford Company has examined the construction and use of alpha and beta radioactive check sources for calibrating instruments and for performing response checks of instruments used for operational and environmental radiation detection. The purpose of using a radioactive check source is to characterize the response of a radiation monitoring instrument in the presence of radioactivity. To accurately calibrate the instrument and check its response, the check source used must emulate as closely as possible the actual physical and isotopic conditions being monitored. The isotope employed and the physical methods used to fabricate the check source (among other factors) determine instrument response. Although information from applicable national and international standards, journal articles, books, and government documents was considered, empirical data collected is most valuable when considering the type of source to use for a particular application. This paper presents source construction methods, use considerations, and standard recommendations. The results of a Hanford Site evaluation of several types of alpha and beta sources are also given. DOE

N95-21259*# National Aeronautics and Space Administration. Lewis Research Center, Cleveland, OH.

EVALUATION OF Pd-Cr WIRES FOR STRAIN GAGE APPLICATION

Jih-Fen Lei (NYMA, Inc., Brook Park, OH.), L. C. Greer, III, and L. G. Oberle Feb. 1995 15 p
(Contract NAS3-27186; RTOP 505-62-50)
(NASA-TM-106857; E-9448; NAS 1.15:106857) Avail: CASI HC A03/MF A01

A newly developed alloy, palladium-13 weight percent chromium (Pd13Cr), was identified by United Technologies Research Center under a NASA contract to be the best material for high temperature strain gage applications. An electrical resistance strain gage that can provide accurate static strain measurement to a temperature higher than that of a commercially available gage is urgently needed in aerospace and aeronautics research. A strain gage made of a 25.4 micron (1 mil) diameter Pd13Cr wire has been recently demonstrated to be usable for static strain measurements to 800 C. This compares to the 400 C temperature limit of the commercially available strain gages. The performance of the Pd-Cr gage, however, strongly depends on the quality of the Pd13Cr wire. Four batches of Pd-Cr wires purchased from three different manufacturers were therefore evaluated to determine the best source of the wire for strain gage applications. The three suppliers were Precious Metal Institute in China, Sigmund Cohn Co., and G & S Titanium, Inc. in the United States. Two batches of wires obtained from Previous Metal Institute in 1987 and 1992, respectively are referred to herein as China87 and China92 wires. The mechanical, chemical and electrical properties of these wires, both as-received and after high temperature exposures at 800 C for 50 hours were analyzed. The elastic modulus and the failure strength of the wires were evaluated using a tensile test machine equipped with a laser speckle strain measurement system. The chemical and microstructural properties of the wires were inspected using a plasma atomic emission spectrometer and a scanning electron microscope (SEM) equipped with an energy dispersive X-ray spectroscope (EDS). The electrical stability and repeatability of the wires were determined by measuring the electrical resistance of the wires during three thermal cycles to 1000 C and a ten-hour soak at 1000 C. As a result of this study, the wire which has the highest strength, the least impurities content, the best oxidation resistance and the best electrical stability will be selected for upcoming strain gage applications. Author

N95-21323*# National Aeronautics and Space Administration. Ames Research Center, Moffett Field, CA.

A THREE-DIMENSIONAL ORTHOGONAL LASER VELOCIMETER FOR THE NASA AMES 7- BY 10-FOOT WIND TUNNEL

Stephen E. Dunagan and Donald L. Cooper Feb. 1995 23 p Original contains color illustrations
(RTOP 505-59-54)
(NASA-TM-108864; A-95032; NAS 1.15:108864) Avail: CASI HC A03/MF A01; 1 functional color page

A three-component dual-beam laser-velocimeter system has been designed, fabricated, and implemented in the 7-by 10-Foot Wind Tunnel at NASA Ames Research Center. The instrument utilizes optical access from both sides and the top of the test section, and is configured for uncoupled orthogonal measurements of the three Cartesian coordinates of velocity. Bragg cell optics are used to provide fringe velocity bias. Modular system design provides great flexibility in the location of sending and receiving optics to adapt to specific experimental requirements. Near-focus Schmidt-Cassegrain optic modules may be positioned for collection of forward or backward scattered light over a large solid angle, and may be clustered to further increase collection solid angle. Multimode fiber optics transmit collected light to the photomultiplier tubes for processing. Counters are used to process the photomultiplier signals and transfer the processed data digitally via buffered interface controller to the host MS-DOS computer. Considerable data reduction and graphical display programming permit on-line control of data acquisition and evaluation of the incoming data. This paper describes this system in detail and presents sample data illustrating the system's capability. Author

N95-21391*# National Aeronautics and Space Administration. Lewis Research Center, Cleveland, OH.

DUAL ACTIVE SURFACE HEAT FLUX GAGE PROBE

Curt H. Liebert and Paul Kolodziej (National Aeronautics and Space Administration. Ames Research Center, Moffett Field, CA.) Feb. 1995 14 p Presented at the 41st International Instrumentation Symposium, Denver, CO, 7-11 May 1995; sponsored by Instrument Society of America
(RTOP 763-22-21)
(NASA-TM-106861; E-9466; NAS 1.15:106861) Avail: CASI HC A03/MF A01

A unique plug-type heat flux gage probe was tested in the NASA Ames Research Center 2x9 turbulent flow duct facility. The probe was fabricated by welding a miniature dual active surface heat flux gage body to the end of a hollow metal cylindrical bolt containing a metal inner tube. Cooling air flows through the inner tube, impinges onto the back of the gage body and then flows out through the annulus formed between the inner tube and the hollow bolt wall. Heat flux was generated in the duct facility with a Huels arc heater. The duct had a rectangular cross section and one wall was fabricated from 2.54 centimeter thick thermal insulation rigid surface material mounted onto an aluminum plate. To measure heat flux, the probe was inserted through the plate and insulating materials with the from of the gage located flush with the hot gas-side insulation surface. Absorbed heat fluxes measured with the probe were compared with absorbed heat fluxes measured with six water-cooled reference calorimeters. These calorimeters were located in a water-cooled metal duct wall which was located across from the probe position. Correspondence of transient and steady heat fluxes measured with the reference calorimeters and heat flux gage probe was generally within a satisfactory plus or minus 10 percent. This good correspondence was achieved even though the much cooler probe caused a large surface temperature disruption of 1000K between the metal gage and the insulation. However, this temperature disruption did not seriously effect the accuracy of the heat flux measurement. A current application for dual active surface heat flux gages is for transient and steady absorbed heat flux, surface temperature and heat transfer coefficient measurements on the surface of an oxidizer turbine inlet deflector operating in a space shuttle test bed engine. Author

N95-21453# Argonne National Lab., IL. Energy Technology Div.

AN IN-LINE ULTRASONIC VISCOMETER

S. H. Sheen, H. T. Chien, and A. C. Raptis Oct. 1994 12 p Presented at the 21st Annual Review of Progress in Quantitative Nondestructive Evaluation Conference, Snowmass, CO, 31 Jul. - 5 Aug. 1994; sponsored by Iowa State Univ.
(Contract W-31-109-eng-38)
(DE95-002982; ANL/ET/CP-82855; CONF-9407123-2) Avail: CASI HC A03/MF A01

An in-line nonintrusive viscometer based on ultrasonic technology is described. The viscometer measures both acoustic and shear impedances of the fluid being monitored, from which both density and viscosity of the fluid are derived. The viscometer uses nominal-incidence wedges to transmit ultrasonic waves to the fluid. A simple model calculation is used to estimate the measurement accuracy and resolution. A laboratory prototype was built and tested. Results show that the viscometer can provide an accurate measurement of fluid density and viscosity over a wide viscosity range. Potential application of the viscometer to monitoring of non-Newtonian fluids is discussed. DOE

N95-21478# Lawrence Livermore National Lab., Livermore, CA.
AN ECHELLE GRATING SPECTROMETER (EGS) FOR MID-IR REMOTE CHEMICAL DETECTION
C. G. Stevens, N. Thomas, P. Kuzmenko, and T. Alger Jul. 1994 11 p Presented at the Annual Meeting of the Society of Photo-Optical Instrumentation Engineers, San Diego, CA, 24-29 Jul. 1994
(Contract W-7405-eng-48)
(DE94-019310; UCRL-JC-118226; CONF-940723-28) Avail: CASI HC A03/MF A01

The availability of high performance two-dimensional InSb detectors enables the design and construction of mid-infrared spectrographs capable of obtaining high resolution spectra over extended spectral regions without moving components. Rugged, stable, cryo-cooled spectrographs suitable for remote field operation are now possible using prism-echelle cross dispersion designs. The authors discuss the design, fabrication, and performance of a high resolution mid-IR field spectrograph designed specifically for the detection of atmospheric-borne chemicals from airborne platforms. The instrument design provides maximum optical throughput covering the two atmospheric windows at 2.0-2.5 micron and 3.0-4.2 micron. DOE

N95-21507# Sandia National Labs., Albuquerque, NM.
MICROMACHINED SILICON-BASED ANALYTICAL MICROINSTRUMENTS FOR SPACE SCIENCE AND PLANETARY EXPLORATION
F. J. Grunthaner, R. E. Stalder, S. Boumsellek, T. R. VanZandt, T. W. Kenny, M. H. Hecht, A. Ksendzov, M. L. Homer, R. W. Terhune, and A. L. Lane et al 1994 4 p Presented at the 12th International Conference on Solid State Devices and Materials, Yokohoma, Japan, 23-26 Aug. 1994
(Contract DE-AC04-94AL-85000)
(DE94-019306; SAND-94-2293C; CONF-940857-1) Avail: CASI HC A01/MF A01

For future planetary science missions, the authors are developing a series of microinstruments using the techniques of silicon-based micromachining. Conventional instruments such as chemical sensors, charged particle analyzers and mass spectrometers are reduced in size and effective volume to the dimension of cubic centimeters, while maintaining or enhancing performance. Using wafer/wafer bonding techniques, selective chemical etching, thin Film growth, and high resolution lithography, complex three dimensional structures can be assembled. This paper discusses the design, implementation and performance of two new instruments: The Micromachined Bessel Box Auger Electron Spectrometer, and the Mars Soil Chemistry Experiment (MOx). DOE

N95-21546# Sandia National Labs., Albuquerque, NM.
QUARTZ RESONATOR FLUID MONITORS FOR VEHICLE APPLICATIONS
R. W. Cernosek, S. J. Martin, K. O. Wessendorf, M. D. Terry, and A. N. Rumpf (Ktech Corp., Albuquerque, NM.) 1994 13 p Presented at the Sensors Expo 1994, Cleveland, OH, 20-22 Sep. 1994
(Contract DE-AC04-94AL-85000)
(DE94-018910; SAND-94-1999C; CONF-9409202-1) Avail: CASI HC A03/MF A01

Thickness shear mode (TSM) quartz resonators operating in a new 'Lever oscillator' circuit are used as monitors for critical automotive fluids. These monitors respond to the density and viscosity of liquids contacting the quartz surface. Sensors have been developed for determining the viscosity characteristics of engine lubricating oil, the state-of-charge of lead-acid storage batteries, and the concentration variations in engine coolant. DOE

N95-21638# Brookhaven National Lab., Upton, NY. National Synchrotron Light Source.
SIGNAL TO NOISE IMPROVEMENTS WITH A NEW FAR-IR RAPID-SCAN MICHELSON INTERFEROMETER
C. J. Hirschmugl and G. P. Williams 1994 7 p Presented at the International Meeting on Synchrotron Radiation Instrumentation, Stony Brook, NY, 18-22 Jul. 1994 Submitted for publication
(Contract DE-AC02-76CH-00016)
(DE95-002416; BNL-60892; CONF-940714-36) Avail: CASI HC A02/MF A01

In this paper we discuss signal to noise issues in the infrared spectral region, presenting an update on instrumentation developments that have focused on this topic. We have been able to achieve reproducibilities in the 0.01 % range for spectra measured in around 1 minute on samples with an area of 1 sq mm illuminated with an fl 10 beam. We show how this result is consistent with the synchrotron source intensity and detector noise and we also show a comparison with a conventional globar source. For these new studies, a Nicolet(trademark) Impact 400 rapid scan Michelson Interferometer was modified by Pike Technologies and installed in vacuum at the U41R infrared beamline at the NSLS. The instrument is capable of scanning at an optical retardation rate of 3.2 cm/sec, and of a data collection frequency of 50 kHz triggered by the co-linear reference beam of a HeNe laser. A proprietary Nicolet(trademark) solid state beamsplitter was used to cover the range from 10-2500 cm(exp -1). Spectra were taken in reflection at grazing incidence off a single crystal Cu surface in ultra-high vacuum using liquid helium cooled detectors of the photoconductive type (Cu/Ge) or bolometric type (B/Si). The sample throughput for this system was 0.01 sq mm steradians. DOE

N95-21680 Army Cold Regions Test Center, Fort Greely, AK.
COLD REGIONS INSTRUMENTATION CONSIDERATIONS Final Report
27 May 1994 10 p Supersedes N84-25024 Limited Reproducibility: More than 20% of this document may be affected by microfiche quality
(AD-A279492; TOP-1-1-004; AD-A139805) Avail: Issuing Activity (Defense Technical Information Center (DTIC))

This TOP provides background information on the problems and adaptations associated with instrumentation, photographic and video equipment required for conducting tests in cold regions. Basic information and procedures are presented as general guidelines to planning and using instrumentation systems for cold environments. DTIC

N95-21889*# National Aeronautics and Space Administration. Lewis Research Center, Cleveland, OH.
MULTIWIRE THERMOCOUPLES: FREQUENCY RESPONSE Final Report, Apr. 1992 - Dec. 1994
L. J. Forney (Georgia Inst. of Tech., Atlanta, GA.) and G. C. Fralick Dec. 1994 82 p
(Contract NCC3-302)
(NASA-TM-110510; NAS 1.15:110510; E19-X20-1) Avail: CASI HC A05/MF A01

Experimental measurements are made with a novel two wire thermocouple. Signals from two wires of unequal diameters are recorded from the thermocouple suspended in constant flow with a periodic temperature fluctuation. It is demonstrated that the reconstructed signal from the two wire thermocouple requires no compensation for omega less than or equal to 2 omega(sub 1) where omega is the natural frequency of the smaller wire. A compensation factor is recommended for larger frequencies omega greater than 2 omega(sub 1). Theory and experimental measurements are compared with a novel three wire thermocouple. Signals from three wires of unequal diameters are recorded from the thermocouple suspended in constant flow with a periodic temperature fluctuation. It is demonstrated that the reconstructed signal from the three wire thermocouple requires no compensation for omega less than or equal to 5 omega(sub 1) where omega (sub 1) is the natural frequency of the smaller wire. The latter result represents a significant improvement compared to previous work with two wire thermocouples. A correction factor has also been derived to account for wires of arbitrary diameter. Measurements are recorded for multiwire thermocouples consisting of either two or three wires of unequal diameters. Signals from the multiwire probe are recorded for a reversing gas flow with a periodic temperature fluctuation. It is demonstrated that the reconstructed signal from the multiwire thermocouple requires no compensation provided omega/omega(sub 1) is less than 2.3 for two wires or omega/omega(sub 1) is less than 3.6 for three wires where omega(sub 1) is the natural frequency of the smaller wire based on the maximum gas velocity. The latter results were possible provided Fourier transformed data were used and knowledge of the gas velocity is available. Author

N95-22109*# National Aeronautics and Space Administration. Langley Research Center, Hampton, VA.
EFFECTS OF YAW AND PITCH MOTION ON MODEL ATTITUDE MEASUREMENTS
Ping Tcheng, John S. Tripp, and Tom D. Finley Feb. 1995 11 p
(RTOP 505-59-54-02)
(NASA-TM-4641; L-17381; NAS 1.15:4641) Avail: CASI HC A03/MF A01

This report presents a theoretical analysis of the dynamic effects of angular motion in yaw and pitch on model attitude measurements in which inertial sensors were used during wind tunnel tests. A technique is developed to reduce the error caused by these effects. The analysis shows that a 20-to-1 reduction in model attitude measurement error caused by angular motion is possible with this technique. Author

N95-22143 California Univ., Irvine, CA.
TIME RESOLVED X-RAY DETECTION Final Report, 1 Jul. 1989 - 31 Dec. 1993
Peter M. Rentzepis 20 Apr. 1994 45 p Limited Reproducibility: More than 20% of this document may be affected by microfiche quality
(Contract F49620-89-C-0104)
(AD-A279348; AFOSR-94-0303TR) Avail: Issuing Activity (Defense Technical Information Center (DTIC))

The goal of the project was to design, develop and construct an x-ray detector with high sensitivity and picosecond time resolution. This was achieved. A Ford Aerospace Charged Coupled Device, CCD, was utilized as the x-ray sensitive material around which the design and construction of the picosecond x-ray detector was built. This device has now become a commercial product sold, among other companies, by Photometrics Inc., and Princeton Research Inc. In addition we designed and built the first picosecond x-ray system. This system was utilized for the first ever picosecond x-ray diffraction experiments. The picosecond x-ray system was utilized in the oxidative fuel cell project to measure the decomposition of methanol and the change of the structure of its platinum catalyst. Another direct product of the work is the publication of 36 papers, in major scientific journals, and two patents. DTIC

N95-22256# Air Force Inst. of Tech., Wright-Patterson AFB, OH. National Air Intelligence Center.
APPLICATION OF COMPUTER-GENERATED HOLOGRAMS TO OPTICAL TRANSFORMATIONS
Shanfeng Zheng and Tianji Wang 8 Nov. 1994 11 p Transl. into ENGLISH from Guangxue Xuebao (China), v. 11, no. 7, Jul. 1991 p 620-623
(AD-A286356; NAIC-ID(RS)T-0380-94) Avail: CASI HC A03/MF A01

Ring-to-line, line-to-point and ring-to-point optical transformations by using computer generated holograms as a holographic lens are discussed in this paper. A liquid crystal television spatial light modulator fabricates computer generated holograms in quasi-real time. DTIC

N95-22322# Army Research Lab., Adelphi, MD.
DESIGN AND CONSTRUCTION OF A Ka-BAND SCATTEROMETER Final Report, FY 1990
Michael Zoll Oct. 1994 23 p
(AD-A286296; ARL-TR-364) Avail: CASI HC A03/MF A01

This report provides documentation of a Ka-band scatterometer designed and constructed for the Corps of Engineers Waterways Experiment Station. The system is designed to work in conjunction with a Hewlett-Packard 8510 network analyzer to provide fully polarimetric measurements of back-scatter from terrain. It operates over a 2-GHz bandwidth and can be operated in a monostatic, quasimonostatic, or bistatic configuration. The design, theory of operation, and characteristics are provided as a means to assist the operator or to provide information to others wishing to construct their own. DTIC

36 LASERS AND MASERS

Includes parametric amplifiers.
For related information see also *76 Solid-State Physics.*

N95-19986# Lawrence Livermore National Lab., Livermore, CA.
SCALING OF SOLID STATE LASERS FOR SATELLITE POWER BEAMING APPLICATIONS
H. W. Friedman, G. F. Albrecht, and R. J. Beach Jan. 1994 11 p Presented at the OE/LASE 1994 Conference on Optics, Electro-Optics, and Laser Applications in Science and Engineering, Los Angeles, CA, 22-29 Jan. 1994
(Contract W-7405-eng-48)
(DE94-016366; UCRL-JC-114400; CONF-940142-43) Avail: CASI HC A03/MF A01

The power requirements for a satellite power beaming laser system depend upon the diameter of the beam director, the performance of the adaptive optics system, and the mission requirements. For an 8 meter beam director and overall Strehl ratio of 50%, a 30 kW laser at 850 nm can deliver an equivalent solar flux to a satellite at geostationary orbit. Advances in Diode Pumped Solid State Lasers (DPSSL) have brought these small, efficient and reliable devices to high average power and they should be considered for satellite power beaming applications. Two solid state systems are described: a diode pumped Alexandrite and diode pumped Thulium doped YAG. Both can deliver high average power at 850 nm in a single aperture. DOE

N95-19987# Stanford Univ., CA.
FREE ELECTRON LASER PROGRAM Final Report
Todd Smith 14 Oct. 1994 4 p
(Contract N00014-86-K-0118)
(AD-A285906) Avail: CASI HC A01/MF A01

This final report concerns the Free Electron Laser Program which allowed work on the Superconducting Linear Accelerator at the Stanford facility. A list of the fourteen papers from this research is included. Derived from text

N95-20035# KJT, Inc., Rochester, NY.
FIBER LASER AMPLIFIERS AND OSCILLATORS Final Report, Jan. 1993 - Jan. 1994
Kenneth J. Teegarden Aug. 1994 29 p
(Contract F30602-93-C-0020)
(AD-A285835; RL-TR-94-112) Avail: CASI HC A03/MF A01

This study reports on the experimental development of a passively modelocked fiber laser. It is based on erbium doped fiber, similar to that used successfully in optical amplifiers. The focus of the work is to retain as much signal processing capability in the fiber medium as possible, and to select essential system components for ruggedness and straightforward field integration. The fiber ring laser here described uses the simplest and most compact configuration reported to date. The measured pulse durations are variable from 15 pico seconds to 1 nanosecond and are completely self starting. One self-modulation mechanism proposed and described is nonlinear polarization evolution. The surprising result is that this nonlinear effect is achieved in fiber at the low pump powers available from a compact diode source. This Kerr type effect generates modelocking in the fiber medium, and is somewhat analogous to the mechanism of operation in self-modelocked Ti:sapphire lasers. The construction of one of the fiber lasers is based on commercially available components most of which are integrated, allowing the final package size to be less than that of a notebook computer. Further work involves increased pulse stability control for applications in fiber communication systems and possibly fiber sensors. DTIC

N95-20063# Boston Univ., MA. Dept. of Chemistry.
PHOTODEGRADATION AND PHOTOPHYSICS OF LASER DYES Final Technical Report, Sep. 1989 - May 1992
Guilford Jones, II 30 Jun. 1994 17 p
(Contract DAAL03-89-K-0162)
(AD-A285105) Avail: CASI HC A03/MF A01

The solubilization of laser dyes in water with the aid of the polyelectrolyte, poly(methacrylic acid) (PMAA) has been studied. An important strategy was the isolation of dye species in the 'hypercoils' associated with the polyelectrolyte, as it is found a moderately acidic pH. Polymer-bound dyes in water display markedly enhanced emission yield, lifetime, and polarization. Dye materials are also less susceptible to photodegradation, since they are isolated in polymer domains away from adventitious quenchers. Also examined in the study was the possibility that two dyes could be co-bound within polymer domains and that energy transfer between the two would result in 'downshifting' of output emission wavelengths. Of the various amphiphilic media used for solubilizing organic dyes in water (e.g., detergent micelles, cyclodextrins), PMAA shows the greatest promise in term of fluorescence enhancement and compartmentalization or organized assembly of additives. These studies show promise for the protection of the dyes against undesirable photodegradation under flash excitation. DTIC

N95-20072# Massachusetts Inst. of Tech., Cambridge, MA. Research Lab. of Electronics.
COMPACT FREE ELECTRON LASERS FOR MEDICAL APPLICATIONS Annual Report, 30 Sep. 1993 - 29 Sep. 1994
George Bekefi 19 Oct. 1994 40 p
(Contract N00014-90-J-4130)
(AD-A285739) Avail: CASI HC A03/MF A01

We have designed, constructed, and operated a 70-period microwiggler for free electrons lasers (FEL's). The device is a pulsed ferromagnetic-core electromagnet with a period of 8.8 mm, which generates an on-axis peak magnetic field of 4.2 kG. The pulses, of 0.5 msec duration, are generated at a rate of 0.5 Hz. Each field peak is independently tunable. We employed a novel tuning regimen to reduce the RMS spread in the peak amplitudes to 0.12%, the lowest value thus far attained in a sub-cm-period periodic magnetic field. DTIC

N95-20082# Arizona Univ., Tucson, AZ. Optical Sciences Center.
PROGRAM OF THE 1993 9TH INTERDISCIPLINARY LASER SCIENCE CONFERENCE (ILS-9) Final Report, 1 Mar. - 31 Dec. 1993
N. Peyghambarian Oct. 1993 100 p Conference held in Toronto, Ontario, 3-8 Oct. 1993; sponsored by American Physical Society and Optical Society of America
(Contract N00014-93-1-0316)
(AD-A285131) Avail: CASI HC A05/MF A02

The 1993 Interdisciplinary Laser Science (ILS) Conference-to be held 3-8 October 1993 in Toronto, Canada, at the Metro Toronto Convention Center-is the ninth in the ILS Conference Series. The series was established to survey the core laser-science areas, including lasers and their properties, nonlinear-optical properties of materials and devices, applications of lasers in physics and chemistry, and a selection of laser applications in other areas of science and technology. DTIC

N95-20221# Oak Ridge National Lab., TN.
COMPUTATIONAL MODELING OF PHYSICAL PROCESSES DURING LASER ABLATION
C. L. Liu, J. N. Leboeuf, R. F. Wood, D. B. Geohegan, J. M. Donato, K. R. Chen, and A. A. Puretzky 1994 21 p Presented at the International Conference on Laser Processing of Materials, Palm Coast, FL, 1-6 May 1994
(Contract DE-AC05-84OR-21400)
(DE94-017699; CONF-940586-1) Avail: CASI HC A03/MF A01

A combined theoretical and experimental effort to model various physical processes during laser ablation of solids (silicon) using a variety of computational techniques is described. Currently the focus of the modeling is on the following areas: (1) rapid transformations through the liquid and vapor phases under possibly nonequilibrium thermodynamic conditions induced by laser-solid interactions; (2) breakdown of the vapor into a plasma in the early stages of ablation through both electronic and photoionization processes; (3) hydrodynamic behavior of the vapor/plasma during and after ablation; and (4) effects of initial conditions in the vapor, in particular, the nature of the initial velocity distribution, on the characteristics of subsequent vapor expansion. Results from the modeling are compared with experimental observations where possible. DOE

N95-20225# Sandia National Labs., Albuquerque, NM.
THE EFFECT OF REUSING LASER GAS ON THE FISSION-FRAGMENT PUMPED 1.73 MICRON ATOMIC XENON LASER OUTPUT
G. A. Hebner Aug. 1994 10 p
(Contract DE-AC04-94AL-85000)
(DE94-018512; SAND-94-1998) Avail: CASI HC A02/MF A01

Fission-fragment pumped 1.73 micron atomic xenon laser output was measured without changing the laser gas mixture before each reactor pulse. For a Ar/Xe gas mixture at 260 Torr and 0.3 percent xenon, no degradation in laser output was noted for five reactor pulses. DOE

N95-20335# Lawrence Livermore National Lab., Livermore, CA.
ENHANCED OUTPUT OF SOFT X-RAY LASERS USING DOUBLE SLAB TARGETS
J. C. Moreno, J. Nilsen, and E. Chandler Jun. 1994 6 p Presented at the 4th International Colloquium on X-ray Lasers, Williamsburg, VA, 16-20 May 1994
(Contract W-7405-eng-48)
(DE94-016689; UCRL-JC-116927; CONF-940592-3) Avail: CASI HC A02/MF A01

Double slab neon-like niobium soft x-ray laser experiments have been performed using the Nova laser. The two slabs have their front surfaces facing in opposite directions with either a 300 (mu)m planar separation between them. Separate laser beams irradiate each slab with an intensity on target of 1.3 x 10(exp 14)W/sq cm. Best coupling was observed using a 300 (mu)m separation. The angular divergence of the laser is measured for single slab and double slab configurations. Comparisons to numerical models are discussed. DOE

N95-20378# Cornell Univ., Ithaca, NY.
MODELOCKING AND WAVEGUIDE AMPLIFIERS USING Cr:FORSTERITE AND Cr:YAG Final Report, Dec. 1992 - Dec. 1993
Clifford Pollack, Steven Johns, Michael Hayduk, Douglas Norton, and Mark Krol Aug. 1994 15 p
(Contract F30602-93-C-0003)
(AD-A285857; RL-TR-94-120) Avail: CASI HC A03/MF A01

Solid state laser systems have been demonstrated using Cr:YAG crystals. CW, regenerative modelocking, and self-modelocking have been achieved with pulses as short as 120 femtoseconds being transform limited. Thin film amplifiers based on Cr:forsterite on glass using a sol-gel deposition technique were fabricated and tested. Other techniques such as nanocrystal embedded in an index matching matrix made of polymers were explored. DTIC

N95-20379# Cornell Univ., Ithaca, NY.
SEMICONDUCTOR LASER JOINT STUDY PROGRAM WITH ROME LABORATORY Final Report, Feb. 1993 - Feb. 1994
William J. Schaff, Sean S. OKeefe, and Lester F. Eastman Sep. 1994 36 p
(Contract F30602-93-C-0083)
(AD-A285858; RL-TR-94-163) Avail: CASI HC A03/MF A01

A program to jointly study vertical-cavity surface emitting lasers (VCSEL) for high speed vertical optical interconnects (VOI) has been conducted under an ES&E between Rome Laboratory and Cornell University. Lasers were designed, grown, and fabricated at Cornell University. A VCSEL measurement laboratory has been designed, built, and utilized at Rome Laboratory. High quality VCSEL material was grown and characterized by fabricating conventional lateral cavity lasers that emitted at the design wavelength of 1.04 microns. The VCSEL's emit at 1.06 microns. Threshold currents of 16 mA at 4.8 volts were obtained for 30 microns diameter devices. Output powers of 5 mW were measured. This is 500 times higher power than from the light emitting diodes employed previously for vertical optical interconnects. A new form of compositional grading using a cosinusoidal function has been developed and is very successful for reducing diode series resistance for high speed interconnection applications. A flip-chip diamond package compatible with high speed operation of 16 VCSEL elements has been designed and characterized. A flip-chip device binding effort at Rome Laboratory was also designed and initiated. This report presents details of the one-year effort, including process recipes and results. DTIC

N95-20389# Rome Lab., Griffiss AFB, NY.
GaAs OPTICAL CIRCUITS Report, Oct. 1992 - Sep. 1993
Michael A. Parker, J. S. Kimmet, S. I. Libby, and P. D. Swanson Aug. 1994 43 p

(AF Proj. 4600)
(AD-A285859; RL-TR-94-103) Avail: CASI HC A03/MF A01

This report presents two new smart pixels for use in optical computing and communications. These devices are configurable optical gates (COG's) that form the diode laser logic (DLL) family and spontaneous emission filtered laser amplifiers (SEFLA). DLL is a complete, new logic family comprised of Q-switched lasers and photodetectors. The lasers and detectors are monolithically integrated on multiple quantum well laser heterostructure with semi-insulating substrates. Preliminary results indicate an ON/OFF contrast ratio better than 500:1, gain in excess of 20, and variable 1/0 hysteresis characteristics. As a result, the devices can be cascaded to form more complex optical circuits. In addition to introducing the DLL family, a basic model is presented and the fabrication process is described in detail. The SEFLA combines an optical amplifier with a spontaneous emission filter in order to increase the signal-to-noise ratio by actively filtering out the spontaneous emission from the output signal. The filtering function is accomplished by integrating the amplifier with a semiconductor laser in such a way that the signal in the amplifier suppresses the gain in the laser. Unlike conventional optical amplifiers, these can, in principle, be cascaded without significantly decreasing the performance. DTIC

N95-20484# Colorado Univ., Boulder, CO. Dept. of Chemistry and Biochemistry.
STATE-TO-STATE COLLISIONAL DYNAMICS OF ATMOSPHERIC SPECIES Technical Report, 1 Aug. 1993 - 31 Jul. 1994
David J. Nesbitt 30 Aug. 1994 6 p
(Contract F49620-93-1-0444; AF-AFOSR-0231-93)
(AD-A285053; JILA-153-1236; AFOSR-94-0559TR) Avail: CASI HC A02/MF A01

The AFOSR/AASERT research efforts over this past year have been toward the following two thrusts: (1) state-to-state collisional energy transfer in H2O, HF and CH4 in crossed molecular beams via high sensitivity, direct absorption of a single mode IR probe laser, and (2) development and testing of high resolution IR laser Dopplerimetry methods for measuring velocity and quantum-state resolved Cl + HCl scattering in open shell collision systems. DTIC

N95-20550# Southampton Univ. (England).
LIQUID XENON AS A POTENTIAL LASER HOST MEDIUM Final Report, 30 Sep. 1992 - 30 Mar. 1994
H. N. Rutt 23 Aug. 1994 28 p
(Contract F49620-92-J-0504)
(AD-A285365; EOARD-TR-94-06) Avail: CASI HC A03/MF A01

This report describes preliminary attempts to investigate the feasibility of using liquid xenon as a solvent for novel laser systems. The objective was to see if the wide transparency range and low non radiative relaxation rates of this solvent can be exploited. A novel cell and filling system was successfully constructed. Barium fluoride windows repeatedly failed at a small fraction of their design pressure. They were successfully replaced with sapphire windows, but this severely limited the use of infrared diagnostics. As supplied xenon was found to be contaminated with excessive hydrocarbons (mainly methane) further limiting infrared diagnostics and nullifying the low non-radiative rate advantage of the solvent. Attempts to dissolve Rhodamine 6g and B were unsuccessful; there was limited evidence of p-terphenyl solubility. Overall the program was very seriously restricted by the combined problems of window failure and xenon contamination and the key concepts remain unproven, although methods to overcome these difficulties are identified. DTIC

N95-20569# California Univ., Berkeley. Lawrence Berkeley Lab, CA.
THREE-DIMENSIONAL LASER COOLING
Hiromi Okamoto, Andrew M. Sessler, and Dieter Moehl (European Organization for Nuclear Research, Geneva, Switzerland.) Jun. 1994 3 p Presented at the 4th European Particle Accelerator Conference, London, England, 27 Jun. - 1 Jul. 1994
(Contract DE-AC03-76SF-00098)
(DE94-017963; LBL-35899; CONF-940618-67) Avail: CASI HC A01/MF A01

To realize effective transverse laser cooling simultaneously with longitudinal laser cooling, two possibilities are theoretically studied. The schemes are both based on forced synchro-betatron coupling, which transfer the extremely effective longitudinal laser cooling action to transverse directions. The coupling is provided by an RF-cavity with a transverse variation of the longitudinal electric field (e.g. TM(sub 210) mode) or by a normal RF-cavity located at a position of finite dispersion. It is shown that, when a working point is close to the difference resonance, cooling in all three degrees of freedom is simultaneously obtained. DOE

N95-20572# Brookhaven National Lab., Upton, NY.
INVERSE CERENKOV LASER ACCELERATION EXPERIMENT AT ATF
X. J. Wang, I. Pogorelsky, R. Fernow, K. P. Kusche, Y. Liu, W. D. Kimura (STI Optronics, Inc., Bellevue, WA.), G. H. Kim (STI Optronics, Inc., Bellevue, WA.), R. D. Romea (STI Optronics, Inc., Bellevue, WA.), and L. C. Steinhauer (STI Optronics, Inc., Bellevue, WA.) 1994 3 p Presented at the 16th International Free Electron Laser Conference, Stanford, CA, 21-26 Aug. 1994
(Contract DE-AC02-76CH-00016)
(DE94-017990; BNL-60737; CONF-9408146-6) Avail: CASI HC A01/MF A01

Inverse Cerenkov laser acceleration was demonstrated using an axicon optical system at the Brookhaven Accelerator Test Facility (ATF). The ATF S-band linac and a high power 10.6 MICROMETERSCO2 laser were used for the experiment. Experimental arrangement and the laser and the electron beams synchronization are discussed. The electrons were accelerated more than 0.7 MeV for a 34 MW CO2 laser power. More than 3.7 MeV acceleration was measured with 0.7 GW CO2 laser power, which is more than 20 times of the previous ICA experiment. The experimental results are compared with computer program TRANSPORT simulations. DOE

N95-20600 Duke Univ., Durham, NC.
A URI PROGRAM FOR ULTRAVIOLET/EXTREME ULTRAVIOLET RESEARCH Final Report, 1 Feb. 1990 - 31 May 1993
John M. Madey 15 Apr. 1994 55 p Limited Reproducibility: More than 20% of this document may be affected by microfiche quality
(Grant AF-AFOSR-0112-90)
(AD-A279159; AFOSR-94-0284TR) Avail: Issuing Activity (Defense Technical Information Center (DTIC))

The purpose of the 3-year effort was to facilitate research and training in free electron laser and synchrotron device physics in the UV/XUV portion of the spectrum and to undertake research in those areas of optical technology, materials science, chemistry and physics relevant to the requirements, and capabilities of these devices. As documented here, these objectives were accomplished by: (1) developing the basic instrumentation and operating support required to carry out the research and training objectives of the program; (2) providing direct support for research on selected topics to be carried out using these facilities; (3) encouraging graduate and undergraduate education in the scientific disciplines which form the basis of these technologies; and (4) promoting enhanced contacts with the scientific staff of the DOD laboratories. The successful completion of this effort has provided the FEL Laboratory, its faculty, students and collaborators with the unique resources required for the continuing pursuit of research in these fields. DTIC

N95-20698# Oak Ridge National Lab., TN.
APPLICATION OF DIODE LASERS TO THE ISOTOPICALLY SELECTIVE DETERMINATION OF URANIUM IN OXIDES BY OPTOGALVANIC SPECTROSCOPY
J. P. Young, C. M. Barshick, R. W. Shaw, and J. M. Ramsey 1994 5 p Presented at the 7th International Symposium on Resonance Ionization Spectroscopy and Its Applications, Bernkastel-Kues, Germany, 3-8 Jul. 1994
(Contract DE-AC05-84OR-21400)
(DE94-018045; CONF-940706-1) Avail: CASI HC A01/MF A01

We have observed isotopically selective diode laser-excited optogalvanic effects in uranium at 778.42 and 776.19 nm. The samples were natural abundance uranium oxide, as well as depleted (0.3% U-235), natural (0.7% U-235) and enriched (9.75% U-235) uranium metal or powders. The measurements were carried out in a demountable-cathode glow discharge cell. Preliminary evaluations of precision for uranium isotopic ratios measured using this technique suggest that it should have broad analytical applications for uranium and other amenable actinides or lanthanides. DOE

N95-20757# Japan Atomic Energy Research Inst., Tokyo (Japan).
ON FEL INTEGRAL EQUATION AND ELECTRON ENERGY LOSS IN INTERMEDIATE GAIN REGIME
Masaru Takao (Japan Atomic Energy Research Inst., Tokai, Japan.) Mar. 1994 12 p
(DE94-770631; JAERI-M-94-025) Avail: CASI HC A03/MF A01

The FEL pendulum equation in a intermediate gain small signal regime is investigated. By calculating the energy loss of the electron beam in terms of the solution of the pendulum equation, we confirm the consistency of the FEL equation in intermediate gain regime. DOE

N95-20783# Lawrence Livermore National Lab., Livermore, CA.
COMPUTATIONAL MODEL OF DRILLING WITH HIGH RADIANCE PULSED LASERS
C. D. Boley Aug. 1994 12 p Presented at the Applications of Lasers and Electro-Optics, Orlando, FL, 17-20 Oct. 1994
(Contract W-7405-eng-48)
(DE94-018548; UCRL-JC-117078; CONF-9410189-1) Avail: CASI HC A03/MF A01

This paper describes a model of drilling by high radiance pulsed lasers. The model contains a one-dimensional description of heat transport below the bottom of the hole, hydrodynamic expansion of the vapor and compressed air, and light propagation through the vapor. The pressure and energy of the vapor are taken from a separate Saha equilibrium code. The boundary conditions at the vaporization surface include the formation of a Knudsen layer within which macroscopic fluid conditions are reached. The absorption mechanisms in the pertinent range of densities and temperatures are photoionization and inverse bremsstrahlung. The model has been applied to the case of drilling in stainless steel with green copper laser light, for peak input intensities ranging from 10(exp 8) to 5 x 10(exp 10) W/sq cm. Below 3 x 10(exp 8) W/sq cm , their is negligible absorption in the vapor and ablation increases rapidly with intensity. Above this point, ablation still generally increases with intensity, because of a combination of partially penetrating light and electron thermal conduction to the surface. The predicted ablation rates agree semiquantitatively with experiment. DOE

N95-20786# Los Alamos National Lab., NM.
EFFECTS OF PLASMA PHYSICS ON CAPSULE IMPLOSIONS IN GAS-FILLED HOHLRAUMS
E. L. Lindman, N. D. Delamater, G. R. Magelssen, and A. Hauer 1994 4 p Presented at the ECLIM 23: Laser Interaction With Matter, Oxford, England, 19-23 Sep. 1994
(Contract W-7405-eng-36)
(DE95-000923; LA-UR-94-3165; CONF-9409226-3) Avail: CASI HC A01/MF A01

Initial experiments on capsule implosions in gas-filled hohlraums have been carried out on the NOVA Laser at Lawrence Livermore National Laboratory. Observed capsule shapes from preliminary experiments are more oblate than predicted. Improvements in modeling required to calculate these experiments and additional experiments are being pursued. DOE

N95-20817# Lawrence Livermore National Lab., Livermore, CA.
PERFORMANCE OF THE NIF PROTOTYPE BEAMLET
Bruno M. VanWonterghem, John R. Murray, D. Ralph Speck, and John H. Campbell 20 Jul. 1994 8 p Presented at the 35th Annual Meeting of the American Nuclear Society, New Orleans, LA, 11-16 Jun. 1994 and at the 11th Topical Meeting on the Technology of Fusion Energy, New Orleans, LA, 19-24 Jun. 1994
(Contract W-7405-eng-48)
(DE94-018500; UCRL-JC-115580; CONF-940602-19; CONF-940630-48) Avail: CASI HC A02/MF A01

Beamlet is a full scale single beam prototype laser system, built to demonstrate the laser technology and performance of the 192 beam National Ignition Facility (NIF) fusion laser driver. Both laser systems apply multipass amplifier architectures. By passing the beam four times through the large aperture amplifier sections, the small signal gain during the first few passes is used efficiently to reduce expensive staged amplifier chains. The beamlet prototype laser integrates results of development programs for large aperture components: large aperture optical switch, polarizers, 2 x 2 multisegment amplifiers and new pulse generation and pre-amplification techniques. The authors report on performance test results of the recently completed 1 (omega)-laser section of Beamlet. DOE

N95-20832# Sandia National Labs., Albuquerque, NM.
DETECTION OPTIMIZATION USING LINEAR SYSTEMS ANALYSIS OF A CODED APERTURE LASER SENSOR SYSTEM
S. M. Gentry Sep. 1994 57 p
(Contract DE-AC04-94AL-85000)
(DE95-001112; SAND-94-0349) Avail: CASI HC A04/MF A01

Minimum detectable irradiance levels for a diffraction grating based laser sensor were calculated to be governed by clutter noise resulting from reflected earth albedo. Features on the earth surface caused pseudo-imaging effects on the sensor's detector arrays that resulted in the limiting noise in the detection domain. It was theorized that a custom aperture transmission function existed that would optimize the detection of laser sources against this clutter background. Amplitude and phase aperture functions were investigated. Compared to the diffraction grating technique, a classical Young's double-slit aperture technique was investigated as a possible optimized solution but was not shown to produce a system that had better clutter-noise limited minimum detectable irradiance. Even though the double-slit concept was not found to have a detection advantage over the slit-grating concept, one interesting concept grew out of the double-slit design that deserved mention in this report, namely the Barker-coded double-slit. This diffractive aperture design possessed properties that significantly improved the wavelength accuracy of the double-slit design. While a concept was not found to beat the slit-grating concept, the methodology used for the analysis and optimization is an example of the application of optoelectronic system-level linear analysis. The techniques outlined here can be used as a template for analysis of a wide range of optoelectronic systems where the entire system, both optical and electronic, contribute to the detection of complex spatial and temporal signals. DOE

N95-20866# Brookhaven National Lab., Upton, NY.
APPROACH TO COMPACT TERAWATT CO2 LASER SYSTEM FOR PARTICLE ACCELERATION
I. V. Pogorelsky, W. D. Kimura (STI Optronics, Inc., Bellevue, WA.), C. H. Fisher (STI Optronics, Inc., Bellevue, WA.), F. Kannari (Keio Univ., Yokahama, Japan.), and N. A. Kurnit (Los Alamos National Lab., NM.) 1994 14 p Presented at the Advanced Accelerator Concepts Workshop, Lake Geneva, WI, 13-18 Jun. 1994
(Contract DE-AC02-76CH-00016)
(DE95-002170; BNL-60826; CONF-940681-1) Avail: CASI HC A03/MF A01

A compact table-top 20-GW 50-ps CO2 laser system is in operation for strong-field physics studies at the ATF. We propose scaling up of the picosecond CO2 laser to a terawatt peak power level to meet the requirements of advanced laser accelerators. Computer modeling shows that a relatively compact single-beam picosecond CO2 laser system with a high-pressure x ray picosecond amplifier of a 10-cm aperture is potentially scalable to the (approximately)1-TW peak power level. DOE

N95-20867# Sandia National Labs., Albuquerque, NM.
REACTOR PUMPED LASER RESEARCH AT THE SANDIA NATIONAL LABORATORIES PULSED REACTOR FACILITIES
D. E. Bodette, D. R. Neal, D. A. McArthur, P. S. Pickard, G. Hebner, and R. Michie (Mission Research Corp., Albuquerque, NM.) 1994 9 p Presented at the Winter Meeting of the American Nuclear Society, Washington, DC, 13-18 Nov. 1994
(Contract DE-AC04-94AL-85000)
(DE95-002181; SAND-94-1978C; CONF-941102-31) Avail: CASI HC A02/MF A01

Sandia National Labs has been investigating concepts for high power lasers pumped directly by fission energy. The direct pumping of laser media with fission fragments offers the potential advantages of scaling to high powers and very long run times in a compact, self powered system. To investigate the potential of this concept, extensive experiments have been conducted in the Annular Core Research Reactor (ACRR) and the Sandia Pulsed Reactor (SPR-3). These experiments include laser physics tests, radiation effects tests on optical materials, and experiments to examine the scaling of reactor pumped lasers to high powers. The SPR-3 is a U-10%Mo fast burst reactor which is used for laser physics experiments. SPR-3 is capable of 70 to 1500 micro FWHM pulses generating up to several kW/cc excitation in a liter size laser cavity. The pulse widths greater than a few hundred microseconds are achieved using a pulse stretcher consisting of gram amounts of fissile material surrounded by moderator. The ACRR is a UO2BeO fueled epithermal reactor which is used for larger volume scaling and beam quality experiments. ACRR operates in both steady state and pulsed modes with pulse widths of 7 to 250 ms resulting in excitation rates of (approximately)2 to 100 W/cc in excitation volumes of up to 50 l. Experimental configurations on both reactors have included central cavity and external cavity locations. The experiments on SPR-3 have defined optimum conditions for efficient reactor pumping of rare gas lasers. This information has been used to define scaling experiments now in progress in the ACRR. DOE

N95-20983 Office National d'Etudes et de Recherches Aerospatiales, Paris (France).

CHEMICAL LASERS EMITTING IN THE VISIBLE SPECTRUM: METASTABLE OXYGEN REACTIONS AND YOSHIDA LASER Final Report [LASERS CHIMIQUES EMETTANT DANS LE VISIBLE: REACTIONS DE L'OXYGENE METASTABLE ET LASER YOSHIDA]

1994 35 p In FRENCH Sponsored by Direction des Recherches, Etudes et Techniques

(PB95-104485) Avail: Issuing Activity (National Technical Information Service (NTIS))

The study explored the possibility of producing laser oscillation through the action of metastable oxygen on heated metals. It attempted to reproduce the results of the YOSHIDA experiment, in which an iodine-oxygen chemical laser appeared to produce intense emissions in the visible (red and infrared) spectrum under certain conditions in the laser's reaction area. An extensive analysis of the YOSHIDA reaction enabled the authors to elucidate the main mechanisms of the red and infrared emissions. They were unable to reproduce the laser oscillations in the red region, and their study indicated little likelihood of that being possible, at least in continuous mode. On the other hand, the metastable state that causes infrared emission could be sustained in population inversion of the basic CuCl2 state, as long as the chemically-induced population of the electronic state was efficient enough. NTIS

N95-21009 California Inst. of Tech., Pasadena, CA. Graduate Aeronautical Labs.

LASER-INDUCED THERMAL ACOUSTICS (LITA): FOUR-WAVE MIXING MEASUREMENT OF SOUND SPEED, THERMAL DIFFUSIVITY, AND VISCOSITY

Eric B. Cummings Aug. 1994 11 p Presented at the International Conference of Lasers (SOQUE), McLean, VA, 1993 Limited Reproducibility: More than 20% of this document may be affected by microfiche quality

(Contract F49620-93-1-0338; AF Proj. 3484)

(AD-A286524; AFOSR-94-0738TR) Avail: CASI HC A03

Laser-induced thermal acoustics (LITA) is a promising optical four-wave mixing technique for gasdynamic measurement. The Chi(3) nonlinear process is a sequence of two opto-acoustic effects, electrostriction and absorption/rapid-thermalization, and the acousto-optic effect. The evolution of the laser-induced acoustic structures temporally modulates Chi(3) and thereby the LITA signal. Time resolution of the signal provides the sound speed, thermal diffusivity, and acoustic damping rate, along with information about atomic or molecular energy transfer rates. LITA can also measure spectra of both the real and imaginary gas susceptibility. The physics of LITA is discussed and the derivation is sketched of a simple analytical expression that accurately describes both the magnitude and time history of the LITA signal. Early experimental results are presented. Sound speeds accurate to 0.5% and transport properties accurate to 30% have been measured in a single-shot without calibration. More realistic modeling should dramatically improve transport-property measurement. LITA spectra have been taken of weak spectral lines of NO2 in concentrations less than 50 ppb. Signal reflectivities as high as 0.0001 have been estimated. New applications of LITA, including velocimetry, are suggested. DTIC

N95-21019 Stanford Univ., CA. Physics Lab.

ULTRA-HIGH AGGREGATE BANDWIDTH TWO-DIMENSIONAL MULTIPLE-WAVELENGTH DIODE LASER ARRAYS Final Report, 10 Apr. 1993 - 9 Apr. 1994

Connie Chang-Hasnain 9 Apr. 1994 12 p Limited Reproducibility: More than 20% of this document may be affected by microfiche quality

(Contract N00014-93-1-0558)

(AD-A280098) Avail: Issuing Activity (Defense Technical Information Center (DTIC))

Two-dimensional (2D) multi-wavelength vertical cavity surface emitting laser (VCSEL) arrays is promising for ultrahigh aggregate capacity optical networks. A 2D VCSEL array emitting 140 distinct wavelengths was reported by implementing a spatially graded layer in the VCSEL structure, which in turn creates a wavelength spread. In this program, we concentrated on novel epitaxial growth techniques to make reproducible and repeatable multi-wavelength VCSEL arrays. DTIC

N95-21135# Lawrence Livermore National Lab., Livermore, CA.

ULTRAVIOLET LASER EMISSION PROPERTIES OF Ce(3+)-DOPED LiSrAlF6

C. D. Marshall, S. A. Payne, J. A. Speth, W. F. Krupke, G. J. Quarles (Lightning Optical Corp., Tarpon Springs, FL.), V. Castillo (Lightning Optical Corp., Tarpon Springs, FL.), and B. H. T. Chai (University of Central Florida, Orlando, FL.) Mar. 1994 7 p Presented at the 9th Advanced Solid-State Lasers Meeting, Salt Lake City, UT, 7-10 Feb. 1994

(Contract W-7405-eng-48)

(DE94-016364; UCRL-JC-115148; CONF-940226-9) Avail: CASI HC A02/MF A01

The ultraviolet laser properties of Ce(3+)-doped LiSrAlF6 (Ce:LiSAF) and LiCaAlF6 (Ce:LiCAF) are reported. The polarized absorption, emission and excited state absorption cross sections for both Ce:LiSAF and Ce:LiCAF were determined for the 266 nm pump and 290 nm laser emission wavelengths. The gain was found to be highest when the probe was polarized parallel to the optic axis of the crystal due to the anisotropic nature of the excited state absorption. The excited state absorption is ascribed to a transition from the 5d orbital of Ce(3+) to the conduction band of the host. Laser slope efficiencies of up to 29% and 21% were measured for Ce-LiSAP and Ce:LiCAF when the 266 nm pulsed pump beam was polarized parallel to the optic axis. These are the highest laser slope efficiencies yet observed for any known solid-state ultraviolet laser material. DOE

N95-21144# Stanford Univ., CA. Lab. of Physics.

RESEARCH STUDIES ON SHORT WAVELENGTH LASERS BY SELECTIVE AUGER PROCESSES Final Report, 15 May 1991 - 14 May 1994

S. E. Harris 14 May 1994 27 p

(Contract N00014-87-K-2001)

(AD-A285620) Avail: CASI HC A03/MF A01

We report the observation of a gain of approximately 10(exp 11) at 41.8 run in eight times-ionized xenon. This XUV laser is driven by a 10-Hz, 70-mJ circularly-polarized femtosecond laser pulse. The laser is focused into Xe at pressures ranging from 5 to 12 torr. The laser is collisionally excited, with both the ions and electrons produced by field induced tunneling. DTIC

N95-21173# Lawrence Livermore National Lab., Livermore, CA.

ANALYTIC MODELS FOR BEAM PROPAGATION AND FAR-FIELD PATTERNS IN SLAB AND BOW-TIE X RAY LASERS

E. A. Chandler Jun. 1994 7 p Presented at the 4th International Colloquium on X Ray Lasers, Williamsburg, VA, 16-20 May 1994

(Contract W-7405-eng-48)

(DE94-016607; UCRL-JC-117795; CONF-940592-4) Avail: CASI HC A02/MF A01

Simplified analytic models for beam propagation in slab and bow-tie x ray lasers yield convenient expressions that provide both a framework for guidance in computer modeling and useful approximates for experimenters. In unrefracted bow-tie lasers, the laser shape in conjunction with the nearly-exponential weighting of rays according to their length produces a small effective aperture for the signal. We develop an analytic expression for the aperture and the properties of the far-field signal. Similarly, we develop the view that the far-field pattern of refractive slab lasers is the result of effective apertures that are created by the interplay of refraction and exponential amplification. We present expressions for the size of this aperture as a function of laser parameters as well as for the intensity and position of the far-field lineout. This analysis also yields conditions for the refraction limit in slab lasers and an estimate for the signal loss due to refraction. DOE

N95-21195# Massachusetts Inst. of Tech., Cambridge, MA. Research Lab. of Electronics.
MECHANISMS AND DIAGNOSTICS OF ULTRASHORT PULSE LASER OCULAR EFFECTS Annual Technical Report, 15 Apr. 1993 - 14 Apr. 1994
James G. Fujimoto 30 Sep. 1994 12 p
(Contract F49620-93-1-0301)
(AD-A285610; AFOSR-94-0656TR) Avail: CASI HC A03/MF A01

The objective of our program is to investigate the mechanisms of ultrashort pulse laser retinal injury and to develop and apply new diagnostics for the assessment of retinal injury. During the past contract period, we have focussed on the development of a new diagnostic technique called optical coherence tomography (OCT) for the noninvasive measurement of ocular and retinal structure. DTIC

N95-21210# Lawrence Livermore National Lab., Livermore, CA.
EBIT X RAY SPECTROSCOPY STUDIES FOR APPLICATIONS TO PHOTO-PUMPED X RAY LASERS
S. R. Elliott, P. Beiersdorfer, and J. Nilsen 10 May 1994 7 p Presented at the 4th International Colloquium on X Ray Lasers, Williamsburg, VA, 16-20 May 1994
(Contract W-7405-eng-48)
(DE94-016701; UCRL-JC-116836; CONF-940592-5) Avail: CASI HC A02/MF A01

Several pumping mechanisms have been suggested for x-ray lasers including collisional excitation, recombination, photo-ionization and photo-pumping. The success of photo-pumping as an x-ray laser scheme hinges on sufficient overlap of the emission and adsorption lines. For such a scheme to exhibit gain, the difference of the energies of the two lines must be within the line widths determined by the plasma dynamics, such as Doppler and opacity broadening. Typically, an overlap of a few parts in 10(exp 4) is required. Due to correlation effects, high-n levels of multi-electron ions are difficult to calculate and are reliable to roughly a part in 10(exp 3). These differences are large enough to preclude accurate predictions of successful overlaps. As a result, precise measurements of the overlaps are needed. The continued interest in photo-pumping schemes lies in its potential to improve the laser output. It also allows the excitation of lasing transitions not accessible to other mechanisms and thus to the test laser kinetics from a different perspective. We have studied several such photo-pumping schemes at the LLNL electron beam ion trap. The N-like isoelectronic sequence 3d-5f and 3d-6f transitions were studied for photo-pumping by He-like ions, the Ne-like 2p-4d transitions were studied for photo-pumping by N-like 3d-4f transitions, and Ni-like 3d(sub 5/2)-6f(sub 7/2) transitions were studied for photo-pumping by H-like Ly-alpha transitions. A number of other chance coincidence pairs which do not follow an isoelectronic sequence were also studied. The data were taken with a flat-crystal vacuum spectrometer, a flat-crystal helium atmosphere spectrometer, or a curved-crystal spectrometer in the von Hamos geometry. The advantage of EBIT over laser-produced or tokamak plasmas for such experiments is its ability to control the charge balance and the excitation process. By choosing the electron beam energy, we can select a dominant charge state. DOE

N95-21226 Rutherford Appleton Lab., Oxford (England).
LARGE FACILITIES PILOT PROGRAMME. ACCESS TO THE VULCAN HIGH POWER LASER FACILITIES AT RUTHERFORD APPLETON LABORATORY Final Technical Report
A. Giulietti, V. Biancalana, P. Chessa, D. Giulietti, and L. A. Gizzi Jun. 1994 19 p Prepared in cooperation with Institute of Atomic and Molecular Physics, Pisa, Italy; Ecole Polytechnique, Palaiseau, France; and Imperial Coll. of Science and Technology, London, England
(PB95-130340; RAL-94-060) Avail: Issuing Activity (National Technical Information Service (NTIS))

The funds allocated under this contract were used to operate the VULCAN 5 Terawatt Nd:Glass laser for a major experiment for which special configurations of the laser and diagnostic equipment were required. Complex targets were required, and a special fabrication process was developed. A wide variety of laser beam outputs were provided from Vulcan including beam smoothing by random phase plates (RPP), Induced Spatial Incoherence (ISI) and Smoothing by Spectral Dispersion (SSD). A pulse sequence from the laser was used to generate a pre-formed uniform plasma using four main beams, which was then heated by a delayed interaction beam. This arrangement simulates the plasma conditions of interest to I.C.F. studies. The interaction was studied by emission spectroscopy, and optical probing using a further synchronized laser beam. Optical streak cameras were used to observe the time dependence of spatial and spectral features of the plasma emission, and Nomarski interferometry was used to diagnose plasma density distribution as a function of time during the pulse. Time resolved X-ray diagnostics gave information on the plasma temperature. During four weeks of data taking, 180 full power shots were delivered to target (a record for a single experiment), and all the major objectives of the experiment were achieved. NTIS

N95-21261# California Univ., Berkeley. Lawrence Berkeley Lab, CA.
PROGRESS IN ULTRAFAST SCANNING PROBE MICROSCOPY
S. Weiss, D. Botkin, D. F. Ogletree, M. Salmeron, and D. S. Chemla May 1994 4 p Presented at the Lasers and Electro-Optics Society Annual Meeting, Boston, MA, 31 Oct. - 3 Nov. 1994
(Contract DE-AC03-76SF-00098)
(DE94-018179; LBL-35803; CONF-9410192-1) Avail: CASI HC A01/MF A01

We demonstrate simultaneous picosecond time and atomic space resolution measurements. The room temperature quantum mechanical capacitance of the STM point contract is observed for the first time. The potential for ultrafast movies of surface dynamics on atomic scale is discussed. DOE

N95-21312# Lawrence Livermore National Lab., Livermore, CA. Chemical Science and Technology Div.
CONTINUOUSLY-TUNABLE, NARROW-LINEWIDTH, Q-SWITCHED Cr:LiSAF LASER FOR LIDAR APPLICATIONS
Tsutomu Shimada, James W. Early, Charles S. Lester, C. Robert Quick, Joe J. Tiee, and Nigel J. Cockroft 1994 5 p Presented at the Advanced Solid-state Laser Conference, Memphis, TN, 29 Jan. - 1 Feb. 1995
(Contract W-7405-eng-36)
(DE95-000862; LA-UR-94-3132; CONF-950101-1) Avail: CASI HC A01/MF A01

A continuously-tunable, narrow-linewidth, flashlamp-pumped, Q-switched Cr:LiSAF laser has been developed (energy: 30 mJ, pulsewidth: 40 ns, linewidth: less than 2 GHz) and was used successfully for the DIAL (differential absorption lidar) measurements of atmospheric water vapor. DOE

N95-21393# Sandia National Labs., Albuquerque, NM.
APPLICATIONS FOR REACTOR-PUMPED LASERS
R. J. Lipinski and D. A. McArthur 1994 8 p Presented at the Physics of Nuclear Induced Plasmas and Problems of Nuclear Pumped Lasers, Arzamas, Russia, 26-30 Sep. 1994
(Contract DE-AC04-94AL-85000)
(DE95-000536; SAND-94-2469C; CONF-9409225-2) Avail: CASI HC A02/MF A01

Nuclear reactor-pumped lasers (RPL's) have been developed in the US by the Department of Energy for over two decades, with the primary research occurring at Sandia National Laboratories and Idaho National Engineering Laboratory. The US program has experimentally demonstrated reactor-pumped lasing in various mixtures of xenon, argon, neon, and helium at wavelengths of 585, 703, 725, 1,271, 1,733, 1,792, 2,032, 2,630, 2,650, and 3,370 nm with intrinsic efficiency as high as 2.5%. The major strengths of a reactor-pumped laser are continuous high-power operation, modular construction, self-contained power, compact size, and a variety of wavelengths (from visible to infrared). These characteristics suggest numerous applications not easily accessible to other laser types. The continuous high power of an RPL opens many potential manufacturing applications such as deep-penetration welding and cutting of thick structures, wide-area hardening of metal surfaces by heat treatment or cladding application, wide-area vapor deposition of ceramics onto metal surfaces, production of sub-micron sized particles for manufacturing of ceramics, and 3-D ceramic lithography. In addition, a ground-based RPL could beam its power to space for such activities as illuminating geosynchronous communication satellites in the earth's shadow to extend their lives, beaming power to orbital transfer vehicles, removing space debris, and providing power (from earth) to a lunar base during the long lunar night. DOE

N95-21480# Texas Univ., Austin, TX. Dept. of Physics.

SELF-STARTING FEMTOSECOND PULSE GENERATION FROM A TI:SAPPHIRE LASER SYNCHRONOUSLY PUMPED BY A POINTING-STABILIZED MODE-LOCKED Nd:YAG LASER

Craig W. Siders, Erhard W. Gaul, Michael C. Downer, Alexei Babine (Academy of Sciences, USSR, Nizhny Novgorod, USSR.), and Andrey Stepanov (Academy of Sciences, USSR, Nizhny Novgorod, USSR.) 1994 11 p Presented at the OE/LASE 1994: Conference on Optics, Electro-optics, and Laser Applications in Science and Engineering, Los Angeles, CA, 22-29 Jan. 1994
(Contract DE-FG05-92ER-40739)
(DE94-019319; CONF-940142-47) Avail: CASI HC A03/MF A01

We have constructed a self-starting Kerr-lens mode-locked Ti:sapphire laser pumped synchronously by a mode-locked, LBO-doubled Nd:YAG laser. Using a home-built beam-pointing stabilizer, beam wander of the 532 nm pump is reduced by a factor of 25, thus enabling long term operation of TEM(sub 00) nearly transform limited pulses with amplitude, repetition rate, and pulsewidth fluctuations comparable to or better than those of Ar-pumped Ti3(+):Al2O3 lasers. Interferometric autocorrelation using second harmonic in reflection from GaAs yielded a pulse width of 30 fs, limited by the dispersion of wide bandwidth cavity optics which permit tunability from 0.7 to 1.0 microns. DOE

N95-21528# California Univ., Berkeley. Lawrence Berkeley Lab, CA. Center for Beam Physics.

TIME-RESOLVED STUDY OF SIDEBAND GENERATION AND TRANSITION TO CHAOS ON AN INFRARED FEL

W. P. Leemans, M. E. Conde, R. Govil, B. vanderGeer, M. deLoos, H. A. Schwettman (Stanford Univ., CA.), T. I. Smith (Stanford Univ., CA.), and R. L. Swent (Stanford Univ., CA.) Aug. 1994 12 p Presented at the 16th International Free Electron Laser Conference, Stanford, CA, 21-26 Aug. 1994
(Contract DE-AC03-76SF-00098)
(DE95-002336; LBL-36109; CBP-102; CONF-9408146-10) Avail: CASI HC A03/MF A01

We report observations on sideband generation and transition to chaos in an infrared Free Electron Laser operating at a wavelength (lambda)(sub r) of 4 micrometers with a low loss optical cavity. The temporal evolution of the radiation spectrum through the complete macropulse has been measured on a micropulse to micropulse basis. Stable sidebands are observed for small cavity detuning with frequency offsets in good agreement with calculations. For even smaller cavity detuning, self-oscillations occur with the main laser wavelength varying by up to 2%. Using a wavelength stabilization system based on RF feedback, we have suppressed these wavelength fluctuations without loss of peak power. DOE

N95-21594# Sandia National Labs., Albuquerque, NM. Materials and Processing Technologies.

LASER MATERIALS PROCESSING AT SANDIA NATIONAL LABORATORIES

James L. Jellison and Michael J. Cieslak 1994 10 p Presented at the Applications of Lasers and Electro-optics, Orlando, FL, 17-20 Oct. 1994
(Contract DE-AC04-94AL-85000)
(DE95-002183; SAND-94-2676C; CONF-9410189-5) Avail: CASI HC A02/MF A01

The interest in laser processing has been driven by Sandia's responsibility to design, prototype, manufacture, and steward high reliability defense hardware for the Department of Energy. The system requirements for the hardware generally necessitate hermetic sealing for ensured long life operation. With the advent of miniaturized electronic devices, traditional welding processes were no longer practical choices because of their limited ability to make very small weld closures without heat damage to the hardware. Gas and solid state lasers offered the opportunity to make hermetic closure welds in small, heat sensitive hardware. In order to consistently produce quality product, the Sandia laser materials processing team performed research aimed at identifying those critical parameters which controlled the laser welding process. This has been directed towards both the development of quantitative engineering data needed in product design and process control, and research to achieve fundamental process understanding. In addition, they have developed novel diagnostic systems to measure these important parameters, pioneered the use of calorimetric techniques to measure energy transfer efficiencies, and correlated the occurrence of welding defects with alloy compositions and type of laser welding process. Today, Sandia's laser materials processing team continues to advance the state of laser processing technology in many areas, including aluminum laser welding, the design of novel optics for specific laser processing needs, laser micromachining of silicon and diamond for microelectronics applications, and fluxless laser soldering. This paper will serve to highlight some examples of where Sandia has made contributions to the field of laser materials processing and will indicate the directions where they expect to focus their future efforts. DOE

N95-21630# California Inst. of Tech., Pasadena, CA. Dept. of Applied Physics.

OPTICAL, ELECTRONIC AND OPTOELECTRONIC MATERIAL AND DEVICE RESEARCH Final Report, 1 Nov. 1990 - 31 Oct. 1993

Amnon Yariv 31 Oct. 1993 10 p
(Contract N00014-91-J-1195)
(AD-A280111) Avail: CASI HC A02/MF A01

During the contract period of 1990-1993 we have continued our research effort on semiconductor lasers (SCL's) by investigating the fundamental limits of SCL's, which are often the limiting factors in applications. Our research concentrated on reducing the threshold current, increasing the wavelength tunability, reducing the linewidth, increasing the modulation bandwidth, reducing the chirp under modulation, and generation of ultra short light pulses. DTIC

N95-21663# Lawrence Livermore National Lab., Livermore, CA.

COLLISIONAL REDISTRIBUTION EFFECTS ON X RAY LASER SATURATION BEHAVIOR

J. A. Koch, B. J. MacGowan, L. B. DaSilva, D. J. Matthews, R. W. Lee, R. A. London, S. Mrowka, J. H. Underwood (California Univ., Berkeley. Lawrence Berkeley Lab, CA.), and P. J. Batson (California Univ., Berkeley. Lawrence Berkeley Lab, CA.) Jun. 1994 7 p Presented at the 4th International Colloquium on X Ray Lasers, Williamsburg, VA, 16-20 May 1994
(Contracts W-7405-eng-48; DE-AC03-76SF-00098)
(DE94-017308; UCRL-JC-117793; CONF-940592-7) Avail: CASI HC A02/MF A01

We recently published a detailed summary of our experimental and theoretical research on Ne-like Se x-ray laser line widths, and one of our conclusions was that collisional redistribution rates are likely to have an effect on the saturation behavior of the 206.4 A Se x-ray laser. In this paper we focus on the effects of collisional redistribution on x-ray laser gain coefficients, and discuss ways of including these effects in existing laser line- transfer models. DOE

N95-21694# University of Southern California, Los Angeles, CA. Dept. of Electrical Engineering.

COMPETITION BETWEEN ELECTROMAGNETIC MODES IN A FREE-ELECTRON MASER Final Technical Report, 1 Mar. 1990 - 28 Feb. 1994

Alan H. McCurdy, V. Kasibhotla, R. Liou, and J. S. Plewa 28 Feb. 1994 90 p
(Grant AF-AFOSR-0155-90)
(AD-A279546; AFOSR-94-0305TR) Avail: CASI HC A05/MF A01

A three part report is presented describing the mode competition in a gyrotron oscillator with two competing electromagnetic modes. Part 1 gives the theory of this mode coupling is presented using a quasi-linear assumption which is valid for small power levels. The results are interpreted in terms of the phase plane. These general results are applied to a specific case of mode competition, that between TE101 and TE011 modes in a cavity of rectangular cross section. Part 2 presents the theory of coupling which may occur between any number of cavity modes through finite conductivity in the cavity walls, holes in the conducting cavity walls, or though interaction with an electron beam. Part 3 details the experimental work. The electrodynamic circuit is described as are microwave and electron beam diagnostics. Results of initial tests are also given. DTIC

N95-21743# Illinois Univ., Chicago, IL. Lab. for Atomic, Molecular and Radiation Physics.

MOLECULAR DESIGN CONCEPT FOR MULTI-KILOVOLT X-RAY AMPLIFICATION

C. K. Rhodes, A. McPherson, and K. Boyer 24 May 1994 10 p
(Contract DE-FG02-91ER-12108)
(DE95-001763; DOE/ER-12108/T1) Avail: CASI HC A02/MF A01

The goal of this program is the construction of an X-ray laser in the multi-kilovolt regime which can serve as a vital enabling technology in the broad and fundamental field of materials science. Experimental findings indicate that an entirely new technique for amplification at X-ray wavelengths is feasible. This method involves the combination of: (1) a recently discovered mode of multiphoton coupling to molecules which efficiently yields core excited ions; (2) a new channeled mode of propagation for spatial organization; and (3) an ultrahigh brightness subpicosecond laser technology. The concept of molecular X-ray laser design, which involves matching the conditions of excitation to the molecular structure, enables the inner-shell excitation to be selectively achieved. Basically, the molecular approach enables the copious generation of a highly excited species to occur rapidly in an environment characteristic of dense cold matter, a situation exceptionally conducive to X-ray amplification. High energy efficiency and wavelength tunability also appear as intrinsic features of this method. Experimental data concerning the study of five cases (Xe(N), Xe(M), Xe(L), Kr(M), and Kr(L)), spanning-spectrally from approximately 80 eV to approximately 5 keV, have: (1) established the important role of cluster formation; (2) verified the scaling of this phenomenon into the kilovolt region; (3) demonstrated the production of hollow atoms having multiple inner-shell vacancies; (4) provided evidence for the crucial influence of coherent electronic motions on the strength of the multiphoton coupling; (5) led to the conclusion that a regime of strong-coupling exists in which multi-electron ejection from an inner-shell can occur with high probability; (6) revealed the scaling in atomic number which potently favors heavy atoms; and (7) combined the multiphoton induced X-ray emission from clusters with channeled propagation. DOE

N95-21837 Los Alamos National Lab., NM.
DIRECTED LIGHT FABRICATION
G. K. Lewis, R. Nemec, J. Milewski, D. J. Thoma, D. Cremers, and M. Barbe 1994 11 p Presented at the Applications of Lasers and Electro-Optics, Orlando, FL, 17-20 Oct. 1994 Limited Reproducibility: More than 20% of this document may be affected by microfiche quality
(Contract W-7405-eng-36)
(DE94-018293; LA-UR-94-2845; CONF-9410189-2) Avail: Issuing Activity (Department of Energy (DOE))

Directed Light Fabrication (DLF) is a rapid prototyping process being developed at Los Alamos National Laboratory to fabricate metal components. This is done by fusing gas delivered metal powder particles in the focal zone of a laser beam that is programmed to move along or across the part cross section. Fully dense metal is built up a layer at a time to form the desired part represented by a 3 dimensional solid model from CAD software. Machine 'tool paths' are created from the solid model that command the movement and processing parameters specific to the DLF process so that the part can be built one layer at a time. The result is a fully dense, near net shape metal part that solidifies under rapid solidification conditions. DOE

N95-21903 Department of the Navy, Washington, DC.
METHOD FOR LASER-ASSISTED SILICON ETCHING USING HALOCARBON AMBIENTS Patent
Stephen D. Russell, inventor (to Navy), Douglas A. Sexton, inventor (to Navy), and Richard J. Orazi, inventor (to Navy) 20 Sep. 1994 22 p Filed 25 May 1993
(AD-D016494; US-Patent-5,348,609; US-Patent-Appl-SN-066745; US-Patent-Class-156-345) Avail: US Patent and Trademark Office

An etching process allows a selective single-step patterning of silicon devices in a noncorrosive environment. The etching of silicon relies on a maskless laser-assisted technique in a gaseous halocarbon ambient, such as the gaseous chlorofluorocarbons, dichlorodifluoromethane and chloropentafluoroethane. Laser-assisted photothermal chemical etching reactions on silicon occur in these ambients when the incident fluence from an excimer laser at 248 nm exceeds the melt threshold (approximately 0.75 J/sq cm). When incident fluence exceeds the ablation threshold (approximately 2.2 J/sq cm) an undesirable, increased surface roughness is observed. Etch rates as large as approximately 15 angstroms per pulse are attained within predetermined processing windows. This provides a means for thin membrane formation in silicon, rapid etches and processing of packaged devices or partially fabricated dies. The reduction in processing steps as compared to conventional wet chemical etches provides improvements in yield reliability and cost. DTIC

N95-21919# Los Alamos National Lab., NM.
PERFORMANCE OF CESIUM TELLURIDE PHOTOCATHODES AS AN ELECTRON SOURCE FOR THE LOS ALAMOS FEL
S. H. Kong, J. Kinross-Wright, D. C. Nuguyen, R. L. Sheffield, and M. E. Weber 1994 9 p Presented at the 16th International Free Electron Laser Conference, Stanford, CA, 21-26 Aug. 1994
(Contract W-7405-eng-36)
(DE94-018302; LA-UR-94-2850; CONF-9408146-3) Avail: CASI HC A02/MF A01

The Los Alamos Advanced Free Electron Laser (FEL) was successfully operated with a Cs2Te photocathode driven by a frequency quadrupoled Nd:YLF laser as the electron source. Lasing was achieved at 5-6 microns. Cs2Te photocathodes with quantum efficiencies of 12-18% at 254 nm were fabricated in an ultrahigh-vacuum chamber and transferred under high vacuum to the FEL. 263 nm light from the drive laser was focused to an 8 mm spot on the center of the photocathode. The authors estimated the operational life time of Cs2Te photocathodes to be at least 20 times that for K2CsSb photocathodes. The measured dark current of 0.3 mA in an electric field of 22-24 MV/m is well within the acceptable level. The maximum amount of charge extracted was observed to be limited by space charge to about 3.5 nC per micropulse. The emittance of the beam was estimated by fitting the data from a quadrupole scan. The authors measured an emittance that is comparable with the emittance measured with a K2CsSb photocathode in their system. A pulse length of 9.3 +/- 2 ps for 1.3 +/- 0.2 nC electron micropulses and a pulse length of 7.1 +/- 0.7 ps for the laser pulses were measured with a streak camera. Therefore, the response of the Cs2Te photocathode to the laser pulse is sufficiently fast for FEL applications. DOE

N95-22007# Los Alamos National Lab., NM.
TUNABLE CW BLUE, GREEN, ORANGE AND RED UPCONVERSION FIBER LASERS AT ROOM TEMPERATURE
Ping Xie and T. R. Gosnell 1994 24 p Presented at the Annual Meeting of the Optical Society of America, Dallas, TX, 2-7 Oct. 1994
(Contract W-7405-eng-36)
(DE95-000851; LA-UR-94-3020; CONF-941062-1) Avail: CASI HC A03/MF A01

The authors report tunable CW laser actions at 491-493nm, 517-540nm, 605-622nm and 635-637nm in Pr(3+)/Yb(3+) doped ZBLAN optical fibers. A tunable Ti:Al2O3 laser was used as the pump source to simulate diode laser pumping. With 60 nW launched power, the excitation wavelength of the lasers was in the range of 780nm to 880nm. 300mW Output power has been achieved at 635nm with 760mW launched power at 860nm. With the pump wavelength at 860nm, the authors have also demonstrated stimulated emissions of 45mW at 615 nm with 430mW launched power, 20mW at 520 and 4mW at 493nm with 200mW launched power. DOE

N95-22079# New Energy and Industrial Technology Development Organization, Tokyo (Japan).
RESEARCH ON THE PROMOTION MEASURES TO INTRODUCE NEW ENERGY AND ENERGY-SAVING TECHNOLOGIES WITH A LEASING SYSTEM
Mar. 1994 111 p In JAPANESE
(DE95-714801; NEDO-P-9328) Avail: CASI HC A06/MF A02

Effects of introducing the leasing system were studied in order to promote the introduction of photovoltaic power generation, wind power generation and other new energy technologies, and phosphoric acid fuel cell, regional air conditioning and other energy efficiency-heightening technologies. Judging from the result of investigating its needs, the introduction of leasing system is most effective when the technological reliability and safety have been established with a cost differential made small, to a certain extent, from the existing energy. The introduction of leasing system is considered effective not from the point of view that, in order to reduce the initial introduction cost, the leasing system is the best measures of investment in the facilities for the introduction of new energy and energy-saving technologies, but from the point of view that the addition of leasing system as one of the preferential measures widens the user's selectivity among the debt, self-funds and leasing. The following tasks are raised for the introduction of leasing system: Determination of leasing term, Determination of insurance rate, Study of leasing for the household use, Development of leasing system as commodities fulfilling the user's needs. DOE

N95-22121# Lawrence Livermore National Lab., Livermore, CA.

HIGH AVERAGE POWER DIODE PUMPED SOLID STATE LASERS FOR CALIOPE

B. Comaskey, J. Halpin, and B. Moran Jul. 1994 20 p Presented at the 1994 Chemical Analysis by Laser Interrogation of Proliferation Effluents (CALIOPE ITR) Interim Technical Review, Livermore, CA, 26-28 Apr. 1994
(Contract W-7405-eng-48)
(DE94-019248; UCRL-JC-118148; CONF-9404162-13) Avail: CASI HC A03/MF A01

Diode pumping of solid state media offers the opportunity for very low maintenance, high efficiency, and compact laser systems. For remote sensing, such lasers may be used to pump tunable nonlinear sources, or if tunable themselves, act directly or through harmonic crystals as the probe. The needs of long range remote sensing missions require laser performance in the several watts to kilowatts range. At these power performance levels, more advanced thermal management technologies are required for the diode pumps. The solid state laser design must now address a variety of issues arising from the thermal loads, including fracture limits, induced lensing and aberrations, induced birefringence, and laser cavity optical component performance degradation with average power loading. In order to highlight the design trade-offs involved in addressing the above issues, a variety of existing average power laser systems are briefly described. Included are two systems based on Spectra Diode Laboratory's water impingement cooled diode packages: a two times diffraction limited, 200 watt average power, 200 Hz multirod laser/amplifier by Fibertek, and TRW's 100 watt, 100 Hz, phase conjugated amplifier. The authors also present two laser systems built at Lawrence Livermore National Laboratory (LLNL) based on their more aggressive diode bar cooling package, which uses microchannel cooler technology capable of 100% duty factor operation. They then present the design of LLNL's first generation OPO pump laser for remote sensing. This system is specified to run at 100 Hz, 20 nsec pulses each with 300 mJ, less than two times diffraction limited, and with a stable single longitudinal mode. The performance of the first testbed version is presented. The authors conclude with directions their group is pursuing to advance average power lasers. This includes average power electro-optics, low heat load lasing media, and heat capacity lasers. DOE

N95-22154# Los Alamos National Lab., NM.

RECENT PROGRESS OF THE COMPACT AFEL AT LOS ALAMOS

D. C. Nguyen, S. M. Gierman, J. C. Goldstein, J. M. Kinross-Wright, S. H. Kong, J. G. Plato, S. J. Russell, R. L. Sheffield, F. E. Sigler, and B. A. Sherwood et al 1994 16 p Presented at the 16th International Free Electron Laser Conference, Stanford, CA, 21-26 Aug. 1994
(Contract W-7405-eng-36)
(DE95-002728; LA-UR-94-3624; CONF-9408146-12) Avail: CASI HC A03/MF A01

The Advanced Free Electron Laser (AFEL) is a compact, infrared, RF-linac FEL that uses a high-brightness photoinjector and a short-period permanent-magnet wiggler. Lasing at saturation with and without sidebands has been achieved over the 4-6 micrometer region with a nominally 15-MeV electron beam energy and a 1-cm period, 24-period wiggler. Sideband-free FEL operation was optimized with respect to outcoupling by tuning off the reflectivity curve of the multilayer dielectric mirrors. Sideband operation was achieved using copper mirrors with a 1.1% outcoupling hole. The measured macropulse energy with (approximately)1300 micropulses was approximately 50 mJ per 1 nC of beam, corresponding to an output efficiency of 0.25% and a maximum extraction efficiency of 1.4%. DOE

N95-22164 Academy of Sciences (USSR), Moscow (USSR). General Physics Inst.

INTERNATIONAL SYMPOSIUM ON ADVANCED LASER TECHNOLOGIES

13 Nov. 1993 133 p Sympoosium held in Prague, Czechoslovakia, 8-13 Nov. 1993 Limited Reproducibility: More than 20% of this document may be affected by microfiche quality
(Contract DAJA45-93-M-0461)
(AD-A279849; R/D-7234-EE-02) Avail: Issuing Activity (Defense Technical Information Center (DTIC))

Optical reflectivity and transmissivity measurements have been used to investigate the dynamics of melting and recrystallization of thin films of Si and Ge after laser-annealing with a ns Nd:YAG-laser pulse. We report on temperature dependent changes of the reflectivity of the liquid phase above and below the melting point and on various nucleation and solidification scenarios in thin films, depending on the energy density of the annealing laser. DTIC

N95-22169# Sandia National Labs., Livermore, CA.

CRYOGENIC PELLET LASER PLASMA SOURCE TARGETS

Glenn D. Kubiak, Kevin D. Krenz, Kurt W. Berger, Timothy G. Trucano, Peter W. Fisher (Oak Ridge National Lab., TN.), and Michael J. Gouge (Oak Ridge National Lab., TN.) 1994 8 p Presented at the Optical Society of America Conference on Extreme Ultraviolet Lithography, Monterey, CA, 19-21 Sep. 1994 Sponsored by ARPA Advanced Lithography Program
(Contract DE-AC04-94AL-85000)
(DE95-002488; SAND-95-8426C; CONF-9409177-3) Avail: CASI HC A02/MF A01

We have developed a new laser plasma cryogenic target scheme that achieves high conversion efficiency (CE), but produces no condensable target debris and low vaporized target gas loads. This scheme employs a solidified pellet of a rare gas, such as Xe, which is irradiated in free flight by a focused drive laser. The pellet is made small enough that gas loads produced following target vaporization are manageable, but large enough to fully intercept the laser energy at its focus. To assess the fundamental utility of cryogenic pellet targets, we have examined the conversion efficiency, extreme ultraviolet (EUV) spectroscopy, and fragmentation dynamics of Xe pellets irradiated with a 248 mn KrF laser. DOE

N95-22242# Los Alamos National Lab., NM.

PHOTOCATHODES FOR FREE ELECTRON LASERS

S. H. Kong, J. Kinross-Wright, D. C. Nuguyen, and R. L. Sheffield 1994 16 p Presented at the 16th International Free Electron Laser Conference, Stanford, CA, 21-26 Aug. 1994
(Contract W-7405-eng-36)
(DE94-018305; LA-UR-94-2849; CONF-9408146-5) Avail: CASI HC A03/MF A01

Many different photocathodes have been used as electron sources for Free Electron Lasers (FEL's) and other electron accelerator systems. In choosing one, a compromise between lifetime and quantum efficiency have been unavoidable. High quantum efficiency photocathodes such as CsK2Sb, Cs3Sb, and cesiated GaAs have short operational lifetimes and require an ultrahigh-vacuum environment. Long lifetime photocathodes such as LaB6, Cu, and Y have relatively low quantum efficiencies. However, recently, cesium telluride was found to be an exception. Initial results from CERN and now at Los Alamos have shown that Cs2Te is reasonably rugged with a high quantum efficiency below 270 nm. Further studies were carried out at Los Alamos in determining its performance as an electron source for the Los Alamos Advanced FEL. The Los Alamos Advanced FEL was successfully operated at 5-6 microns with a Cs2Te photocathode driven by a frequency quadrupoled Nd:YLF laser as the electron source. Cs2Te photocathodes with quantum efficiencies of 12-18% at 254 mn were fabricated in an ultrahigh-vacuum chamber and transferred under high vacuum to the FEL. The authors estimated that the operational lifetime of Cs2Te photocathodes to be at least 20 times that for K2CsSb photocathodes. Furthermore, experiments in the fabrication chamber have shown that heating to 150-200 C photocathodes exposed for one hour at 2 x 10(exp -4) torr of air was sufficient to revive the quantum efficiency from below 1% to about 10%. The electron beam for the FEL extracted from a cesium telluride target was also characterized. The emittance, response time, saturation level and dark current of cesium telluride photocathodes was determined to be sufficient for FEL applications. DOE

N95-22301# Lawrence Livermore National Lab., Livermore, CA.

3-D TECATE/BREW: THERMAL, STRESS, AND BIREFRINGENT RAY-TRACING CODES FOR SOLID-STATE LASER DESIGN

R. J. Gelinas, S. K. Doss, and R. G. Nelson 20 Jul. 1994 71 p

(Contract W-7405-eng-48)
(DE95-000330; UCRL-ID-115123) Avail: CASI HC A04/MF A01

This report describes the physics, code formulations, and numerics that are used in the TECATE (totally Eulerian code for anisotropic thermo-elasticity) and BREW (birefringent ray-tracing of electromagnetic waves) codes for laser design. These codes resolve thermal, stress, and birefringent optical effects in 3-D stationary solid-state systems. This suite of three constituent codes is a package referred to as LASRPAK. DOE

N95-22304 Department of the Navy, Washington, DC.
BROADBAND THERMAL OPTICAL LIMITER FOR THE PROTECTION OF EYES AND SENSORS Patent Application
Brian L. Justus, inventor (to Navy), Alan L. Huston, inventor (to Navy), and Anthony J. Campillo, inventor (to Navy) 31 May 1994 34 p Limited Reproducibility: More than 20% of this document may be affected by microfiche quality
(AD-D016493; US-Patent-Appl-SN-251146) Avail: Issuing Activity (Defense Technical Information Center (DTIC))

A broadband thermal optical limiter for protecting a light sensitive object from intense laser beams at all near ultraviolet, visible and near infrared wavelengths is disclosed. The broadband thermal optical limiter comprises: a sample cell containing a solution of broadband absorber material dissolved in a thermal solvent; and a first optical device for converging an incident laser beam into the sample cell. The sample cell is responsive to a converged incident laser beam below a predetermined intensity level for passing therethrough the converged incident laser beam below the predetermined intensity level. The sample cell is also responsive to a converged incident laser beam at or above a predetermined intensity level for thermally defocusing substantially all of the converged incident laser beam in different directions and passing therethrough only a remaining small portion of the converged incident laser beam at or above the predetermined intensity level. The broadband thermal optical limiter further includes a second optical device for focusing substantially all of the laser beam passing through the sample cell into the light sensitive object to be protected. DTIC

N95-22312# Lawrence Livermore National Lab., Livermore, CA.
COHERENCE PROPERTIES OF HIGH ORDER HARMONIC RADIATION
T. Ditmire, K. S. Budil, J. K. Crane, H. Nguyen, M. D. Perry, P. Salieres (Commissariat a l'Energie Atomique, Gif-sur-Yvette, France.), and A. L. Huillier (Commissariat a l'Energie Atomique, Gif-sur-Yvette, France.) May 1994 7 p Presented at the 9th International Conference on Ultrafast Phenomena, Dana Point, CA, 1-5 May 1994
(Contract W-7405-eng-48)
(DE94-016974; UCRL-JC-117330; CONF-940593-13) Avail: CASI HC A02/MF A01

The results of a series of experiments to characterize the coherence properties of XUV (extreme ultraviolet) radiation produced by high-order harmonic generation in helium, neon and argon are reported and compared to predictions from an effective order model. The harmonics exhibit smooth, near Gaussian spatial profiles, and have a divergence that is approximately constant (less than 12 mrad) in the plateau region and decreases (approximately 4 mrad) in the cutoff for f/17 focusing. For a bandwidth limited, 140 fsec incident pulse, we measure a harmonic line width of Delta lambda/lambda approximately 2 x 10(exp -3) at 30.3 nm. By reducing the spectral width of the driving pulse, harmonics with Delta lambda/lambda approximately 2 x 10(exp-4) can be produced. Absolute conversion efficiency as high as 10(exp -7) for harmonic radiation as short as 20 nm has been achieved by using 400 fsec, 526 nm pulses from an Nd:Glass laser. DOE

N95-22343# Lawrence Livermore National Lab., Livermore, CA.
DEFECT GEOMETRIES AND LASER-INDUCED DAMAGE IN MULTILAYER COATINGS
R. J. Tench, M. R. Kozlowski, and R. Chow Jul. 1994 9 p Presented at the Annual Meeting of the Society of Photo-Optical Instrumentation Engineers, San Diego, CA, 24-29 Jul. 1994
(Contract W-7405-eng-48)
(DE94-017695; UCRL-JC-118203; CONF-940723-18) Avail: CASI HC A02/MF A01

A correlation between laser-induced damage and the height of a coating defect was found from an examination of HfO2/SiO2 mirrors made by three different coating vendors. The nodular defects in these reactive e-beam deposited mirrors were studied using the combination of SEM, optical microscopy, FIB and AFM techniques. Each vendor had small defects in common, but characteristically different large defects. Also the majority of seeds that caused the defects were made of hafnia, not silica. The apparent mechanical stability of the defects within the coating plays a major role in the laser resistance (1064 nm and 10ns) of a high damage threshold coating. DOE

N95-22348# Los Alamos National Lab., NM.
FABRICATION AND CHARACTERIZATION OF CESIUM TELLURIDE PHOTOCATHODES: A PROMISING ELECTRON SOURCE FOR THE LOS ALAMOS ADVANCED FEL
S. H. Kong, D. C. Nuguyen, R. L. Sheffield, and B. A. Sherwood 1994 15 p Presented at the 16th International Free Electron Laser Conference, Stanford, CA, 21-26 Aug. 1994
(Contract W-7405-eng-36)
(DE94-018303; LA-UR-94-2851; CONF-9408146-4) Avail: CASI HC A03/MF A01

The Advanced Free Electron Laser (FEL) at Los Alamos embodies a K2CsSb photocathode as an electron source. The photocathode consists of a K2CsSb film deposited on a molybdenum plug that can be inserted into the linac of the FEL. However, because K2CsSb is easily contaminated and has a half-life of less than a day when in use, switching to a more rugged high quantum efficiency (QE) material such as Cs2Te is considered as a means to lengthen the beam time. Cs2Te films were deposited on molybdenum plugs in an ultrahigh-vacuum research chamber. Several Cs2Te films were measured in-situ for their spectral responses with a bias voltage of 90V; the resulting QE's were 12-18% at a wavelength of 254 nm, 0.2-1.2% at 334 nm, 10(exp -4)-10(exp -3) at 365 nm, and 10(exp -7)-10(exp -5) at 546 nm. For this cathode to be useful, the authors need to frequency quadruple the 1052 nm line of the Nd:YLF laser to achieve a wavelength of 263 nm. Initial studies showed that the 251-nm QE of Cs2Te is much less sensitive to contamination than the 526-nm QE of K2CsSb. The authors exposed Cs2Te photocathodes to air at 10(exp -4) torr for five minutes. As a result, the QE's dropped from 16-18% to 1-2% at 254 mn. However, heating the cathode to 165 C revived the QE to about 10%. They conclude that Cs2Te is a very rugged photocathode material for use in an RF photoelectron source. DOE

N95-20539*# National Aeronautics and Space Administration. Langley Research Center, Hampton, VA.
P/N In(Al) GaAs MULTIJUNCTION LASER POWER CONVERTERS
Steven Wojtczuk (Spire Corp., Bedford, MA.), Themis Parados (Spire Corp., Bedford, MA.), and Gilbert Walker *In* NASA. Lewis Research Center, Proceedings of the 13th Space Photovoltaic Research and Technology Conference (SPRAT 13) Sep. 1994 p 363-371 (For primary document see N95-20502 06-33)
Avail: CASI HC A02/MF A04

37 MECHANICAL ENGINEERING

Includes auxiliary systems (nonpower); machine elements and processes; and mechanical equipment.

N95-19984 Naval Postgraduate School, Monterey, CA.
THE ORIGIN OF ACICULAR FERRITE IN GAS METAL ARC AND SUBMERGED ARC WELDS M.S. Thesis
Daniel G. Brothers Mar. 1994 161 p Limited Reproducibility: More than 20% of this document may be affected by microfiche quality
(AD-A286129) Avail: CASI HC A08

The nature of weld metal inclusions in relation to the formation of acicular ferrite was investigated. Gas-metal arc welds (GMAW) on High Strength Low Alloy (HSLA) plate with varying amounts of oxygen and/or carbon dioxide added to the argon cover gas and submerged arc welds (SAW) on HY-100 plate with five different fluxes were analyzed. This analysis determined the effect of weld metal composition on non-metallic inclusion composition and the ultimate effects on the formation of acicular ferrite. Scanning and transmission electron microscopy with energy dispersive x-ray analysis were used to determine inclusion size distribution, concentration and composition. This investigation revealed that the inclusions were complex MnO-Al2O3-SiO2-TiO2 oxides which contain a titanium-rich compound, Pyrophanite (MnTiO3), existing as a faceted particle in those inclusions promoting acicular ferrite formation. From these results and the research of others such as Grong/Matlock and Ramsay/Matlock/Olson it is concluded that the formation of acicular ferrite does depend on non-metallic inclusion composition demonstrating the importance of weld wire composition for achieving welds with optimum mechanical properties. DTIC

N95-20048# Sandia National Labs., Albuquerque, NM.

APPLICATION OF A DIMENSIONLESS PARAMETER MODEL FOR LASER BEAM WELDING

P. W. Fuerschbach 1994 7 p Presented at the Applications of Lasers and Electro-Optics, Orlando, FL, 17-20 Oct. 1994
(Contract DE-AC04-94AL-85000)
(DE94-018902; SAND-94-1205C; CONF-9410189-4) Avail: CASI HC A02/MF A01

A new dimensionless parameter model for continuous wave laser welding that relates the size of the weld to the energy absorbed by the part is described. The model has been experimentally validated previously through calorimetric determinations of the net heat input and metallographic measurements of the weld size. It will be shown that both the melting efficiency and energy transfer efficiency for LBW are quite variable and need to be considered when selecting processing conditions. Specific applications will be detailed in order to observe the simplicity and value of the model in laser weld process development. It will be shown that by using certain dimensionless parameters one can determine the energy transfer efficiency and thereby correctly select processing conditions that more fully utilize the available laser output power. In applications where minimizing heat input to the surrounding weldment is paramount, the dimensionless parameters can be used to select conditions that maximize melting efficiency. DOE

N95-20053# Sandia National Labs., Albuquerque, NM.

FUSION WELDING OF ADVANCED BORATED STAINLESS STEELS

C. V. Robino and M. J. Cieslak Feb. 1994 85 p
(Contract DE-AC04-94AL-85000)
(DE94-019037; SAND-93-3981) Avail: CASI HC A05/MF A01

This work addressed two major areas concerning joining of advanced borated stainless steels. These areas included the development of a understanding of the physical metallurgy of borated stainless steels and the development of welding processes and post-weld heat treatments for these alloys. Differential thermal analysis experiments were conducted on ten heats of borated stainless steel to determine the transformation temperatures and melting behavior of the alloys. On-heating solidus temperatures were measured for all of the alloys and were used to define the temperatures associated with the fusion line during welding. Isothermal heat treatments designed to evaluate the effects of elevated temperature exposures on the toughness of the borated grades were conducted. These tests were used to determine if significant changes in the microstructure or mechanical properties of weld heat-affected zones (HAZ) occur. Specifically, the tests addressed the solid-state region of the HAZ. The test matrix included a variety of alloy compositions and thermal exposures at temperatures near the on-heating solidus (as determined by the DTA experiments). Welding experiments designed to assess the mechanical properties and microstructure of gas-tungsten arc and electron beam welds were conducted. DOE

N95-20085# Oak Ridge National Lab., TN.

MATERIALS/MANUFACTURING ELEMENT OF THE ADVANCED TURBINE SYSTEM PROGRAM

M. A. Karnitz, J. H. Devan, R. S. Holcomb, M. K. Ferber, and R. W. Harrison 1994 6 p Presented at the Joint Contractors Meeting on Advanced Turbine Systems, Fuel Cells and Coal-Fired Heat, Morgantown, WV, 3-5 Aug. 1993
(Contract DE-AC05-84OR-21400)
(DE94-017299; CONF-930893-41) Avail: CASI HC A02/MF A01

One of the supporting elements of the Advanced Turbine Systems (ATS) Program is the materials/manufacturing technologies task. The objective of this element is to address critical materials issues for both industrial and utility gas turbines. DOE Oak Ridge Operations Office (ORO) will manage this element of the program, and a team from DOE-ORO and Oak Ridge National Laboratory is coordinating the planning for the materials/manufacturing effort. This paper describes that planning activity which is in the early stages. DOE

N95-20151*# National Aeronautics and Space Administration. Lyndon B. Johnson Space Center, Houston, TX.

BEVEL GEAR DRIVER AND METHOD HAVING TORQUE LIMIT SELECTION Patent Application

Joseph S. Cook, Jr., inventor (to NASA) 10 Aug. 1994 46 p
(NASA-Case-MSC-22384-1; NAS 1.71:MSC-22384-1;
US-Patent-Appl-SN-288102) Avail: CASI HC A03/MF A01

This invention comprises a torque drive mechanism utilizing axially translatable, mutually engageable transmission members having mating crown gears, driven and driving members with a three-element drive train being biased together by resilient means or by a fluid actuator system, the apparatus being operable to transmit a precisely controlled degree of torque to a driven member. The apparatus is applicable for use in hand tools and as a replacement for impact torque drivers, torque wrenches, motorized screw drivers, or the like, wherein the applied torque must be precisely controlled or limited. The bevel torque drive includes a drive gear which is axially displaceable and rotatable within cylindrical driver housing, a rotatable intermediate gear, and an output gear. Key rotationally secures displaceable gear with respect to input shaft but permits axial movement therebetween. A thrust bearing is preferably connected to the lower end of shaft for support to reduce play and friction between shaft and a transmission joint disc during rotation of the gear train. Coaxially mounted coiled spring is footed against displaceable gear for biasing the displaceable gear toward and into engagement with the intermediate gear for driving intermediate gear and output gear. Torque control is achieved by the use of straight or spiral beveled gears which are of configurations adapted to withdraw from mutual engagement upon the torque exceeding a predetermined limit. The novel, advantageous features of the invention include the configuration of the mating, crown gear sets and the axially translatable, slidable drive gear. The mechanism is capable of transmitting a high degree of torque within a narrow, compact transmission housing. The compact size and narrow, elongated configuration of the housing is particularly applicable for use in hand tools and in multiple torque driver mechanisms in which it is necessary to drive multiple fasteners which are located in close proximity. Prior torque drivers such as 'click-type' torque wrenches do not actually limit torque application but only provide an audible warning that the limit has been reached. Author

N95-20295 Department of the Navy, Washington, DC.

MALONE-BRAYTON CYCLE ENGINE/HEAT PUMP Patent

Thomas A. Gilmour, inventor (to Navy) 12 Jul. 1994 9 p Filed 28 Sep. 1993
(AD-D016573; US-Patent-5,327,745; US-Patent-Appl-SN-127567;
US-Patent-Class-62-467) Avail: US Patent and Trademark Office

A machine, such as a heat pump, and having an all liquid heat exchange fluid, operates over a more nearly ideal thermodynamic cycle by adjustment of the proportionality of the volumetric capacities of a compressor and an expander to approximate the proportionality of the densities of the liquid heat exchange fluid at the chosen working pressures. Preferred forms of a unit including both the compressor and the expander on a common shaft employs difference in axial lengths of rotary pumps of the gear or vane type to achieve the adjustment of volumetric capacity. Adjustment of the heat pump system for differing heat sink conditions preferably employs variable compression ratio pumps. DTIC

N95-20409*# National Aeronautics and Space Administration. Lyndon B. Johnson Space Center, Houston, TX.

DISPLACEABLE SPUR GEAR TORQUE CONTROLLED DRIVER AND METHOD Patent Application

Joseph S. Cook, Jr., inventor (to NASA) 10 Aug. 1994 45 p
(NASA-Case-MSC-22381-1; NAS 1.71:MSC-22381-1;
US-Patent-Appl-SN-288112) Avail: CASI HC A03/MF A01

Methods and apparatus are provided for a torque driver including a laterally displaceable gear support member to carry an output spur gear. A biasing assembly biases the output spur gear into engagement with a pinion to which is applied an input torque greater than a desired output torque limit for a threaded fastener such as a nut or screw. A coiled output linkage connects the output spur gear with a fastener adaptor which may be a socket for a nut. A gear tooth profile provides a separation

force that overcomes the bias to limit torque at the desired torque limit. Multiple fasteners may be rotated simultaneously to a desired torque limit if additional output spur gears are provided. A gauged selector mechanism is provided to laterally displace multiple driver members for fasteners arranged in differing configurations. The torque limit is selectably adjustable and may be different for fasteners within the same fastener configuration.
Author

N95-20627# Los Alamos National Lab., NM.
CONCEPTUAL DESIGN OF AN RTG FACILITY TRANSPORTATION SYSTEM
Stephen J. Black, Robert C. Gentzlinger, and Richard E. Lujan 3 Jun. 1994 6 p Presented at the 12th Symposium on Space Nuclear Power and Propulsion, Albuquerque, NM, 8-12 Jan. 1995
(Contract W-7405-eng-36)
(DE94-014443; LA-UR-94-1938; CONF-950110-1) Avail: CASI HC A02/MF A01

The conceptual design of an Radioisotope Thermoelectric Generator (RTG) Facility Transportation System which is part of the overall RTG Transportation System has been completed and is described in detail. The Facility Transportation System serves to provide locomotion, cooling, shock protection and data acquisition for the RTG package during loading and unloading sequences. The RTG Facility Transportation System consists of a Transporter Subsystem, a Package Cooling Subsystem, and a Shock Limiting Transit Device Subsystem. The Transporter Subsystem is a uniquely designed welded steel cart combined with a pneumatically-driven hand tug for locomotion. The Package Cooling Subsystem provides five kilowatts of active liquid cooling via an on-board refrigeration system. The Shock limiting Transit Device Subsystem consists of a consumable honeycomb transit frame which provides shock protection for the 3855 kg (8500 LB) RTG package. These subsystems have been combined into an integrated system which will facilitate the unloading and loading of the RTG, of the Transport Trailer as well as meet ALARA radiation Package into and out exposure guidelines. DOE

N95-20695# Sandia National Labs., Albuquerque, NM.
INPUT SHAPING FOR VIBRATION-DAMPED SLEWING OF A FLEXIBLE BEAM USING A HEAVY-LIFT HYDRAULIC ROBOT
G. G. Parker, R. Eisler, J. Phelan, and R. D. Robinett 1994 8 p Presented at the 1994 American Control Conference, Baltimore, MD, 29 Jun. - 1 Jul. 1994
(Contract DE-AC04-94AL-85000)
(DE94-015803; SAND-94-1702C; CONF-9406133-3) Avail: CASI HC A02/MF A01

An input shaping scheme originally used to slew flexible beams via a tabletop D.C. motor is modified for use with an industrial-type, hydraulic-drive robot. This trajectory generation method was originally developed to produce symmetric, rest-to-rest maneuvers of flexible rotating rods where the angular velocity vector and gravitational vector were collinear. In that configuration, out-of-plane oscillations were excited due to centripetal acceleration of the rod. The bang-coast-bang acceleration profile resulted in no oscillations in either plane at the end of the symmetric slew maneuver. In this paper, a smoothed version of the bang-coast-bang acceleration is used for symmetric maneuvers where the angular velocity vector is orthogonal to the gravitational vector. Furthermore, the hydraulic robot servo dynamics are considered explicitly in determining the input joint angle trajectory. An instrumented mass is attached to the tip of a flexible aluminum rod. The first natural frequency of this system is about 1.0 Hz. Joint angle responses obtained with encoder sensors are used to identify the servo actuator dynamics.
DOE

N95-20723# Oak Ridge National Lab., TN.
USE OF AN INTEGRATED DESIGN TOOL FOR WELD QUALITY ENHANCEMENT
C. Cheng (Concurrent Technologies Corp., Johnstown, PA.), A. J. Paul (Concurrent Technologies Corp., Johnstown, PA.), and T. Zacharia 1993 8 p Presented at the American Welding Society International Conference on Modeling and Control of Joining Processes, Orlando, FL, 8-10 Dec. 1993
(Contract DE-AC05-84OR-21400)
(DE94-018135; CONF-931234-11) Avail: CASI HC A02/MF A01

It has been shown previously that the use of a mathematical model to predict the inherent fluid flow, heat transfer, free surface profiles and other associated phenomena during welding leads to a better understanding and, therefore, control of the welding process. Unfortunately many of the models available today are primarily research codes and, therefore, do not serve as design tools for the production welding engineer. In the current investigation, WELDER - a three dimensional, transient mathematical model, has been integrated with a framework based on the Rational Product & Process Design (R(center dot)P(sup 2)(center dot)D(sub sm))(sup +) methodology to create a true design tool aimed towards use by engineers. This highly interactive and graphic tool simulates the welding process from the start to finish, and provides the user with capabilities to view the progression of welding and the associated heating and cooling of the base plate. In addition, analysis modules analyze the temperature profiles to predict residual stresses and evolving microstructures. DOE

N95-20795*# Carnegie-Mellon Univ., Pittsburgh, PA. Dept. of Mechanical Engineering.
MODELING THE EFFECT OF SHROUD CONTACT AND FRICTION DAMPERS ON THE MISTUNED RESPONSE OF TURBOPUMPS Final Report, 31 May 1991 - 31 Aug. 1994
Jerry H. Griffin and M.-T. Yang Jan. 1994 79 p
(Contract NAS8-38348)
(NASA-CR-197285; NAS 1.26:197285) Avail: CASI HC A05/MF A01

The contract has been revised. Under the revised scope of work a reduced order model has been developed that can be used to predict the steady-state response of mistuned bladed disks. The approach has been implemented in a computer code, LMCC. It is concluded that: the reduced order model displays structural fidelity comparable to that of a finite element model of an entire bladed disk system with significantly improved computational efficiency; and, when the disk is stiff, both the finite element model and LMCC predict significantly more amplitude variation than was predicted by earlier models. This second result may have important practical ramifications, especially in the case of integrally bladed disks. Author

N95-20984# National Inst. of Standards and Technology, Gaithersburg, MD. Ceramics Div.
ABRASIVE WEAR BY DIESEL ENGINE COAL-FUEL AND RELATED PARTICLES
L. K. Ives Sep. 1994 66 p Sponsored in part by ORNL
(Contract DE-A105-83OR-21322)
(PB95-104915; NISTIR-5461; ORNL/SUB/83-21322/03) Avail: CASI HC A04/MF A01

The purpose of the work summarized in this report was to obtain a basic understanding of the factors which are responsible for wear of the piston ring and cylinder wall surfaces in diesel engines utilizing coal-fuel. The approach included analytical studies using scanning electron microscopy and energy dispersive x-ray analyses to characterize coal-fuel and various combustion particles, and two different wear tests. The wear tests were a modified pin-on-disk test and a block-on-ring test capable of either unidirectional or reciprocating-rotational sliding. The wear tests in general were conducted with mixtures of the particles and lubricating oil. The particles studied included coal-fuel, particles resulting from the combustion of coal fuel, mineral matter extracted during the processing of coal, and several other common abrasive particle types among which quartz was the most extensively examined. The variables studied included those associated with the particles, such as particle type, size, and hardness; variables related to contact conditions and the surrounding environment; and variables related to the type and properties of the test specimen materials. NTIS

N95-20998# Army Research Lab., Aberdeen Proving Ground, MD.
STATISTICAL ANALYSIS OF TURBINE ENGINE DIAGNOSTIC (TED) FIELD TEST DATA Final Report, Aug. 1993 - Jun. 1994
Malcolm S. Taylor and John T. Monyak Nov. 1994 23 p
(AD-A286032; ARL-TR-614) Avail: CASI HC A03/MF A01

During the summer of 1993, a field test of turbine engine diagnostic (TED) software, developed jointly by U.S. Army Research Laboratory and the U.S. Army Ordnance Center and School, was conducted at Fort Stuart, GA. The data were collected in conformance with a cross-over design, some of whose considerations are detailed. The initial analysis of the field test data was exploratory, followed by a more formal investigation. Technical aspects of the data analysis insights that were elicited are reported.
DTIC

N95-21157# Michigan Univ., Ann Arbor, MI. Transportation Research Inst.
ELECTRORHEOLOGY FOR SMART AUTOMOTIVE SUSPENSIONS Final Technical Report
Z. Lou, C. B. Winkler, R. D. Ervin, F. E. Filisko, and P.J. Venhovens Jun. 1994 140 p
(Contract DAAE07-92-C-R078)
(AD-A285543; UMTRI-94-15) Avail: CASI HC A07/MF A02

The purpose of the work reported was to demonstrate the suitability of electrorheological (ER) technology for adaptive control of suspension forces on tracked and wheeled vehicles. The mechanical shear strength properties of ER fluids change in response to the application of an electric field. The change is very rapid and fully reversible. This property was used to create an automotive suspension damper whose resistive force is readily controlled by an external electrical signal. The device was applied in a semiactive suspension system for the Army's high mobility multipurpose wheeled vehicle (HMMWV). The work reported covers a range of development tasks including definition of the semiactive control algorithm, ER fluid formulation, design and fabrication of an ER damper, design of an electrical control circuit, creation of a quarter-HMMWV test stand for the simulation of ride vibrations, laboratory measurement of the ER-damped performance characteristics over a range of physically simulated operating conditions, and computer simulation of the quarter-HMMWV system. The research demonstrated that an ER damper and appropriate control circuits could out-perform the conventional hydraulic shock absorber, but that various complexities tend to impede broad application of electrorheology in automotive devices. DTIC

N95-21171# Instituto Superior Tecnico, Lisbon (Portugal). Dept. of Mechanical Engineering.
PROCEEDINGS OF THE NATO-ADVANCED STUDY INSTITUTE ON COMPUTER AIDED ANALYSIS OF RIGID AND FLEXIBLE MECHANICAL SYSTEMS. VOLUME 1: MAIN LECTURES
Manuel S. Pereira, ed. and Jorge A. C. Ambrosio, ed. 9 Jul. 1993 493 p Meeting held in Troia, Portugal, 27 Jun. - 9 Jul. 1993
(Contract DAJA45-93-M-0233)
(AD-A286062; R/D-7022-MA-02-Vol-1) Avail: CASI HC A21/MF A04

During the last few years, major scientific progress has been achieved in fields related to computer aided analysis of multibody systems. In view of this progress and recent developments of computer hardware and general purpose software, there is a need to access the current state of art and results from different schools of thought, with the objective of focussing trends in future research. Going back to 1983 when an important NATO-NSF-ARO Advanced Study Institute on Computer Aided Analysis and Optimization of Mechanical Systems was held at the University of Iowa, one may notice that less then 10 years ago the state of art was mainly dwelling on rigid body dynamics. The interest in the dynamic simulation of mechanical systems has steadily increased in recent years coming mainly from the aerospace and automative industries. The development of multibody system analysis formulations have been more recently motivated with the need to include several features such as: real-time simulation capabilities, highly non-linear control devices, work space path planing, active control of machine flexibilities and reliability and accuracy in the analysis results. The need for accurate and efficient analysis tools for design of large and lightweight mechanical systems has driven many research groups in the challenging problem of flexible systems with an increasing interaction with finite element methodologies. Basic approaches to mechanical systems dynamic analysis have recently been presented in several new text books. These publications demonstrate that both recursive and absolute methods still have their proponents to resolve the redundancy encountered in most mechanical systems. DTIC

N95-21295# Neste Oy, Helsinki (Finland).
REDUCING EXHAUST GAS EMISSIONS FROM CITYDIESEL BUSSES Final Report
Seppo Mikkonen 1994 20 p In FINNISH
(DE95-700245; NEI-FI-234) Avail: CASI HC A03/MF A01

The effect of fuel composition and exhaust gas aftertreatment on the emissions was measured from truck and bus engines. Possibilities to measure unregulated emissions (aldehydes, polyaromatic hydrocarbons, mutagenicity) were built. A reformulated diesel fuel 'Citydiesel' was developed. Citydiesel was able to reduce emissions compared to standard diesel fuel as follows: particulates by 10 to 30%, nitrogen oxides by 2 to 10%, sulphur dioxide by 97%, polyaromatic hydrocarbons (PAH) over 50%, mutagenicity of the exhaust particulates clearly, odor of the exhaust, and smoke after a cold start. The use of Citydiesel fuel reduces emissions of the existing vehicles immediately which is a remarkable benefit. The very low sulphur content (below 50 ppm) makes it possible to use oxidation. catalytic converters to reduce emissions of diesel vehicles. The new Euro 2 exhaust regulations coming into force during 1996 can be met with a modern diesel engine, Citydiesel fuel, and exhaust gas aftertreatment. Properties of Citydiesel fuel were verified in a three year field test with 140 city buses. Experience was good; e.g., engine oil change interval could be lengthened. Total value of the exhaust was estimated with different fuels and aftertreatment device in order to find out cheap ways to reduce emissions. DOE

N95-21359*# Akron Univ., Akron, OH.
SEEK: A FORTRAN OPTIMIZATION PROGRAM USING A FEASIBLE DIRECTIONS GRADIENT SEARCH Final Report
M. Savage Cleveland, OH NASA Jan. 1995 149 p
(Grant NAG3-1047; RTOP 505-62-36; DA Proj. 1L1-62211-A-47-A)
(NASA-CR-4641; E-9338; NAS 1.26:4641; ARL-TR-645) Avail: CASI HC A07/MF A02

This report describes the use of computer program 'SEEK' which works in conjunction with two user-written subroutines and an input data file to perform an optimization procedure on a user's problem. The optimization method uses a modified feasible directions gradient technique. SEEK is written in ANSI standard Fortran 77, has an object size of about 46K bytes, and can be used on a personal computer running DOS. This report describes the use of the program and discusses the optimizing method. The program use is illustrated with four example problems: a bushing design, a helical coil spring design, a gear mesh design, and a two-parameter Weibull life-reliability curve fit. Author

N95-21416 Central Iron and Steel Research Inst., Beijing (China).
JOINING OF DISSIMILAR MATERIALS. A REVIEW
Zheng Sun and Risto Karppi Mar. 1994 60 p
(ISSN 1235-0605)
(PB95-132999; VTT/RN-1545,; ISBN-951-38-4479-X) Copyright Avail: Issuing Activity (National Technical Information Service (NTIS))

Multimaterial technology is set to become one of the most promising solutions for the design and fabrication of many high performance products and engineering structures. Joining dissimilar materials is a key process in the manufacture of multimaterial products and has hence become a very important and vital field of research and development. This report contains a literature survey on the joining of dissimilar materials. The characteristics of dissimilar material joints are discussed. Theoretical and practical problems encountered in joining dissimilar materials are reviewed with special reference to the joinability of various materials and how they can be combined. Applications of dissimilar material joints are highlighted with reference to industrial requirements. Furthermore, examples are given in order to illustrate the principles of solving specific problems. The survey aims at providing the industrial and research and development (R&D) sectors with identification of the major needs for future development in the joining of dissimilar materials. NTIS

N95-21446 Technical Research Centre of Finland, Espoo (Finland).
JOINING DISSIMILAR STAINLESS STEELS FOR PRESSURE VESSEL COMPONENTS
Zheng Sun and Huai-Yue Han (Central Iron and Steel Research Inst., Beijing, China.) Mar. 1994 33 p Sponsored by China National Nuclear Corp.
(ISSN 1235-0605)
(PB95-133005; VTT/RN-1550; ISBN-951-38-4484-6) Copyright Avail: Issuing Activity (National Technical Information Service (NTIS))

A series of studies was carried out to examine the weldability and properties of dissimilar steel joints between martensitic and austenitic stainless steels - F6NM (OCr13Ni4Mo) and AISI 347, respectively. Such joints are important parts in, e.g. the primary circuit of a pressurized water reactor (PWR). This kind of joint requires both good mechanical properties, corrosion resistance and a stable magnetic permeability besides good weldability. The weldability tests included weld thermal simulation of the martensitic steel for investigating the influence of weld thermal cycles and post-weld heat treatment (PWHT) on the mechanical properties of the heat-affected zone (HAZ); implant testing for examining the tendency for cold cracking of martensitic steel; rigid restraint testing for determining hot crack susceptibility of the multi-pass dissimilar steel joints. The joints were subjected to various mechanical tests including a tensile test, bending test and impact test at various temperatures, as well as slow strain-rate test for examining the stress corrosion cracking tendency in the simulated environment of a primary circuit of a PWR. The results of various tests indicated that the quality of the tube/tube joints is satisfactory for meeting all the design requirements. NTIS

N95-21488# Instituto Superior Tecnico, Lisbon (Portugal). Dept. of Mechanical Engineering.
PROCEEDINGS OF THE NATO-ADVANCED STUDY INSTITUTE ON COMPUTER AIDED ANALYSIS OF RIGID AND FLEXIBLE MECHANICAL SYSTEMS. VOLUME 2: CONTRIBUTED PAPERS
Manuel S. Pereira and Jorge A. Ambrosio 9 Jul. 1993 607 p Meeting held in Troia, Portugal, 27 Jun. - 9 Jul. 1993
(Contract DAJA45-93-M-0233)
(AD-A286063; R/D-7022-MA-02-Vol-2) Avail: CASI HC A99/MF A06

Partial Contents: Dynamics of Constrained Systems Based on Mass-Orthogonal Projections; An Efficient Implementation of the Velocity Transformation Method for Real Time Dynamics with Illustrative Examples; Efficient Object Oriented Programming of Multibody Dynamics Formalisms; Sparse Matrix Generation of Jacobians for the Object-Oriented Modelling of Multibody Dynamics; Minimal Dynamic Characterization of Three-Like Multibody Systems. DTIC

N95-21550# Oak Ridge National Lab., TN.
WELD POOL PHENOMENA
S. A. David, J. M. Vitek, T. Zacharia, and T. DebRoy (Pennsylvania State Univ., University Park, PA.) 1994 29 p Presented at the 46th Annual Meeting of the International Institute of Welding (IIW), Glasgow, Scotland, 28 Aug. - 4 Sep. 1993
(Contract DE-AC05-84OR-21400)
(DE94-018965; CONF-9308247-1) Avail: CASI HC A03/MF A01

During welding, the composition, structure and properties of the welded structure are affected by the interaction of the heat source with the metal. The interaction affects the fluid flow, heat transfer and mass transfer in the weld pool, and the solidification behavior of the weld metal. In recent years, there has been a growing recognition of the importance of the weld pool transport processes and the solid state transformation reactions in determining the composition, structure and properties of the welded structure. The relation between the weld pool transport processes and the composition and structure is reviewed. Recent applications of various solidification theories to welding are examined to understand the special problems of weld metal solidification. The discussion is focussed on the important problems and issues related to weld pool transport phenomena and solidification. Resolution of these problems would be an important step towards a science based control of composition, structure and properties of the weld metal. DOE

N95-21601# Oak Ridge National Lab., TN.
ON THE ORIGINS AND MODELING OF FRICTIONAL BEHAVIOR IN INTERFACIALLY-COMPLEX SLIDING CONTACTS
P. J. Blau 1994 18 p Presented at the American Society of Mechanical Engineers/Society of Tribologists and Lubrication Engineers (ASME/STLE) Joint Tribology Conference, New Orleans, LA, 24-27 Oct. 1993
(Contract DE-AC05-84OR-21400)
(DE94-019129; CONF-9310170-2) Avail: CASI HC A03/MF A01

The magnitude of the kinetic friction force usually varies with time in very clean or marginally-lubricated sliding systems. In some poorly-lubricated tribosystems, this variation can be as large as the nominal value of the friction force itself. Most classical sliding friction models attempt to derive a single value for the friction force or friction coefficient for a given set of materials and conditions, even in the face of numerous experiments and observations of real machine behavior which continue to demonstrate its multivalued, time-dependent nature. The simultaneous frictional processes in complex sliding interfaces are considered in more detail using graphical constructions called friction process diagrams (FPD). These diagrams provide a straightforward technique to account for the changing, relative contributions of mechanisms which explain the variability in friction. Applications of binary and ternary FPD's to metallic and ceramic sliding systems with debris are provided to illustrate their wide applicability. DOE

N95-21692*# Aerojet-General Corp., Sacramento, CA.
MODELING OF ROLLING ELEMENT BEARING MECHANICS. COMPUTER PROGRAM USER'S MANUAL Final Report
Lyn M. Greenhill and David H. Merchant 1 Oct. 1994 65 p
(Contract NAS8-38607)
(NASA-CR-196557; NAS 1.26:196557) Avail: CASI HC A04/MF A01

This report provides the user's manual for the Rolling Element Bearing Analysis System (REBANS) analysis code which determines the quasistatic response to external loads or displacement of three types of high-speed rolling element bearings: angular contact ball bearings, duplex angular contact ball bearings, and cylindrical roller bearings. The model includes the defects of bearing ring and support structure flexibility. It is comprised of two main programs: the Preprocessor for Bearing Analysis (PREBAN) which creates the input files for the main analysis program, and Flexibility Enhanced Rolling Element Bearing Analysis (FEREBA), the main analysis program. This report addresses input instructions for and features of the computer codes. A companion report addresses the theoretical basis for the computer codes. REBANS extends the capabilities of the SHABERTH (Shaft and Bearing Thermal Analysis) code to include race and housing flexibility, including such effects as dead band and preload springs. Author

N95-21705*# Aerojet-General Corp., Sacramento, CA.
MODELING OF ROLLING ELEMENT BEARING MECHANICS. THEORETICAL MANUAL Final Report
David H. Merchant and Lyn M. Greenhill 1 Oct. 1994 98 p
(Contract NAS8-38607)
(NASA-CR-196556; NAS 1.26:196556) Avail: CASI HC A05/MF A02

This report documents the theoretical basis for the Rolling Element Bearing Analysis System (REBANS) analysis code which determines the quasistatic response to external loads or displacement of three types of high-speed rolling element bearings: angular contact ball bearings; duplex angular contact ball bearings; and cylindrical roller bearings. The model includes the effects of bearing ring and support structure flexibility. It is comprised of two main programs: the Preprocessor for Bearing Analysis (PREBAN) which creates the input files for the main analysis program; and Flexibility Enhanced Rolling Element Bearing Analysis (FEREBA), the main analysis program. A companion report addresses the input instructions for and features of the computer codes. REBANS extends the capabilities of the SHABERTH (Shaft and Bearing Thermal Analysis) code to include race and housing flexibility, including such effects as dead band and preload springs. Author (revised)

N95-22034 Department of the Navy, Washington, DC.
ATTACHMENT METHODOLOGY FOR COMPOSITE CYLINDER ASSEMBLY Patent
Roger M. Crane, inventor (to Navy) and Paul Coffin, inventor (to Navy) 22 Feb. 1994 10 p Filed 7 Apr. 1992
(AD-D016256; US-Patent-5,288,114; US-Patent-Appl-SN-864794; US-Patent-Class-285-370) Avail: US Patent and Trademark Office

Cylinder-to-cylinder attachment method and construction featuring nonutilization of mechanical fasteners or bonding, especially advantageous for attachment of cylinders which are composite or to be subjected to hydrostatic pressure, is described. A fastening ring is interpositionally and rotatively engaged and aligned with a toothed axial end of each cylinder whereby the inwardly radial teeth for each cylinder appropriately mesh with the outer grooved circumferential surface of the fastening ring. The resultant joint is easily detachable and less susceptible than conventional joints to damage, breakage, degradation, stress concentrations, and fluid infiltration. DTIC

N95-22268# Oak Ridge National Lab., TN.
MODELING OF FUNDAMENTAL PHENOMENA IN WELDS
T. Zacharia, J. M. Vitek, J. A. Goldak (Carleton Univ., Ottawa, Ontario.), T. A. DebRoy (Pennsylvania State Univ., University Park, PA.), and M. Rappaz (Ecole Polytechnique Federale de Lausanne, Switzerland.) 1993 61 p Presented at the Modeling for Welding Science Workshop, Cocoa Beach, FL, 17-19 Mar. 1993

(Contract DE-AC05-84OR-21400)
(DE94-017859; CONF-9303302-1) Avail: CASI HC A04/MF A01

Recent advances in the mathematical modeling of fundamental phenomena in welds are summarized. State-of-the-art mathematical models, advances in computational techniques, emerging high-performance computers, and experimental validation techniques have provided significant insight into the fundamental factors that control the development of the weldment. The current status and scientific issues in the areas of heat and fluid flow in welds, heat source metal interaction, solidification microstructure, and phase transformations are assessed. Future research areas of major importance for understanding the fundamental phenomena in weld behavior are identified. DOE

N95-22292# Argonne National Lab., IL.
LOW ROTATIONAL DRAG IN HIGH-TEMPERATURE SUPERCONDUCTING BEARINGS
J. R. Hull, T. M. Mulcahy, K. L. Uherka, and R. G. Abboud (Commonwealth Research Corp., Chicago, IL.) 17 Oct. 1994 5 p Presented at the Applied Superconductivity Conference, Boston, MA, 16-21 Oct. 1994
(Contract W-31-109-eng-38)
(DE95-002983; ANL/ET/CP-82119; CONF-941013-8) Avail: CASI HC A01/MF A01

Bearings consisting of permanent magnets stably levitated over high-temperature superconductors exhibit low rotational drag and have the potential to enable high-efficiency flywheel energy storage. The coefficient of friction mu for such storage systems is derived as a function of bearing parameters and is shown to be an appropriate figure of merit to describe bearing losses. Analysis shows that values of mu 10(exp -6) enable flywheel standby losses less than 0.1 %/hr for high-speed flywheels. A vacuum-chamber experimental apparatus has been constructed to measure values of (mu) for various experimental bearing designs. Experimental values for mu at low velocity have been as low as 3 x 10(exp-7) for a 89-mm-diameter ring permanent magnet stably levitated over an array of melt-textured Y-Ba-Cu-O. An important loss mechanism occurs from eddy currents induced in the rotating magnet due to the discrete nature of the superconductor array. DOE

N95-22356# Westinghouse Savannah River Co., Aiken, SC.
WELDING TRITIUM EXPOSED STAINLESS STEEL
W. R. Kanne, Jr. 1994 12 p Presented at the 5th International Conference on Hydrogen Effects on Material Behavior, Moran, WY, 11-15 Sep. 1994
(Contract DE-AC09-89SR-18035)
(DE95-003208; WSRC-MS-94-0101P; CONF-940945-4) Avail: CASI HC A03/MF A01

Stainless steels that are exposed to tritium become unweldable by conventional methods due to buildup of decay helium within the metal matrix. With longer service lives expected for tritium containment systems, methods for welding on tritium exposed material will become important for repair or modification of the systems. Solid-state resistance welding and low-penetration overlay welding have been shown to mitigate helium embrittlement cracking in tritium exposed 304 stainless steel. These processes can also be used on stainless steel containing helium from neutron irradiation, such as occurs in nuclear reactors. DOE

N95-22404*# Toledo Univ., OH.
WAVE JOURNAL BEARING. PART 1: ANALYSIS Final Report
Florin Dimofte Cleveland, OH NASA Jan. 1995 10 p Presented at the Energy and Environmental Expo 1995, Houston, TX, 29 Jan. - 1 Feb. 1995; sponsored by ASME
(Grant NAG3-1370; RTOP 778-32-21)
(NASA-CR-195431-Pt-1; E-9423-Pt-1; NAS 1.26:195431-Pt-1) Avail: CASI HC A02/MF A01

A wave journal bearing concept features a waved inner bearing diameter of the non-rotating bearing side and it is an alternative to the plain journal bearing. The wave journal bearing has a significantly increased load capacity in comparison to the plain journal bearing operating at the same eccentricity. It also offers greater stability than the plain circular bearing under all operating conditions. The wave bearing's design is relatively simple and allows the shaft to rotate in either direction. Three wave bearings are sensitive to the direction of an applied stationary side load. Increasing the number of waves reduces the wave bearing's sensitivity to the direction of the applied load relative to the wave. However, the range in which the bearing performance can be varied decreases as the number of waves increases. Therefore, both the number and the amplitude of the waves must be properly selected to optimize the wave bearing design for a specific application. It is concluded that the stiffness of an air journal bearing, due to hydrodynamic effect, could be doubled and made to run stably by using a six or eight wave geometry with a wave amplitude approximately half of the bearing radial clearance. Author

N95-22405*# National Aeronautics and Space Administration. Lewis Research Center, Cleveland, OH.
WAVE JOURNAL BEARING. PART 2: EXPERIMENTAL PRESSURE MEASUREMENTS AND FRACTIONAL FREQUENCY WHIRL THRESHOLD FOR WAVE AND PLAIN JOURNAL BEARINGS
James F. Walker, Florin Dimofte (Toledo Univ., OH.), and Harold E. Addy, Jr. Jan. 1995 10 p Presented at the Energy and Environmental Expo 1995, Houston, TX, 29 Jan. - 1 Feb. 1995; sponsored by ASME
(Grant NAG3-1370; RTOP 778-32-21)
(NASA-TM-106848-Pt-2; E-9424-Pt-2; NAS 1.15:106848-Pt-2) Avail: CASI HC A02/MF A01

A new hydrodynamic bearing concept, the wave journal bearing, is being developed because it has better stability characteristics than plain journal bearings while maintaining similar load capacity. An analysis code to predict the steady state and dynamic performance of the wave journal bearing is also part of the development. To verify numerical predictions and contrast the wave journal bearing's stability characteristics to a plain journal bearing, tests were conducted at NASA Lewis Research Center using an air bearing test rig. Bearing film pressures were measured at 16 ports located around the bearing circumference at the middle of the bearing length. The pressure measurements for both a plain journal bearing and a wave journal bearing compared favorably with numerical predictions. Both bearings were tested with no radial load to determine the speed threshold for self-excited fractional frequency whirl. The plain journal bearing started to whirl immediately upon shaft start-up. The wave journal did not incur self-excited whirl until 800 to 900 rpm as predicted by the analysis. Furthermore, the wave bearing's geometry limited the whirl orbit to less than the bearing's clearance. In contrast, the plain journal bearing did not limit the whirl orbit, causing it to rub. Author

38 QUALITY ASSURANCE AND RELIABILITY

Includes product sampling procedures and techniques; and quality control.

N95-20414 Southwest Research Inst., San Antonio, TX.
EDDY CURRENT FOR DETECTING SECOND-LAYER CRACKS UNDER INSTALLED FASTENERS Final Report, 30 Sep. 1991 - 31 Oct. 1993
Gary L. Buckhardt, Robert E. Beissner, Edith A. Creek, and Jay L. Fisher Feb. 1994 110 p Limited Reproducibility: More than 20% of this document may be affected by microfiche quality
(Contract F33615-91-C-5661)
(AD-A279871; SWRI-17-4665; WL-TR-93-4125) Avail: Issuing Activity (Defense Technical Information Center (DTIC))

Southwest Research Institute developed an eddy current (EC) laboratory breadboard inspection system to detect second-layer cracks around installed fasteners in two-layer airframe structures with the probe positioned on the first layer (outside surface). Probe design considered both cup and segment-core configurations as exciter coils and various orientations and positions of sensor coils. Highest sensitivity was obtained with a segment-core exciter covering an 85 degree segment with the sensor oriented normal to the specimen surface and placed near the core outer leg. EC data were presented in two-dimensional color images. The goal of detecting a 2.5mm second-layer flaw through a first-layer thickness of 6.4mm was achieved in eight of nine specimen configurations which contained simulated cracks. The specimens included structure geometries containing second-layer edges, first-layer edges, adjacent fasteners, different fastener sizes, different flaw orientations around the hole, and fasteners of different materials (titanium and steel). In fatigue crack specimens supplied by WL/MLLP, where adjacent fasteners were spaced more closely and caused interfering signals, flaw detection was more difficult; however, a

2.5mm flaw was detected through a 4.5mm first layer by comparing the signal patterns from adjacent holes. DTIC

N95-20616*# National Aeronautics and Space Administration. Langley Research Center, Hampton, VA.
APPARATUS AND METHOD FOR DETERMINING THE MASS DENSITY OF A FILAMENT Patent Application
Jeffrey A. Hinkley, inventor (to NASA) and Joseph M. Marchello, inventor (to NASA) (Old Dominion Univ., Norfolk, VA.) 29 Sep. 1994 17 p
(Grant NAG1-1067)
(NASA-Case-LAR-14879-1-CU; NAS 1.71:LAR-14879-1-CU; US-Patent-Appl-SN-316708) Avail: CASI HC A03/MF A01

A method and apparatus for determining the mass density of a moving filament is provided. The method includes the steps of providing a filament across two supports, tensioning the filament, inducing a vibration into the filament segment between the supports, reinforcing the vibration using an amplified feedback signal, detecting the vibrational frequency data, processing the data using a fast-fourier transform analysis, and then displaying the frequency. The use of the feedback signal results in a self-tuning resonant loop. Open loop versions may also be used. The apparatus includes a base supporting a fixed support and a transducer which in turn supports a moveable support. The transducer vibrates the moveable support transversely to the direction of travel of the filament, thereby inducing a transverse vibrational mode. The output of the transducer is amplified and used to drive a second amplifier to produce a self-tuning resonant loop. In the open loop version a signal generator is used to drive the transducer through a frequency range, during which the amplitude peak is identified. NASA

N95-20764*# National Aeronautics and Space Administration. Langley Research Center, Hampton, VA.
FLUX-FOCUSING EDDY CURRENT PROBE AND ROTATING PROBE METHOD FOR FLAW DETECTION Patent Application
Buzz A. Wincheski, inventor (to NASA) (Analytical Services and Materials, Inc., Hampton, VA.), James P. Fulton, inventor (to NASA) (Analytical Services and Materials, Inc., Hampton, VA.), Shridhar C. Nath, inventor (to NASA) (Analytical Services and Materials, Inc., Hampton, VA.), John W. Simpson, inventor (to NASA) (Lockheed Engineering and Sciences Co., Hampton, VA.), and Min Namkung, inventor (to NASA) 22 Nov. 1994 34 p Continuation-in-part of US-Patent-Appl-SN-134444, filed 12 Oct. 1993
(NASA-Case-LAR-15231-1-SB; NAS 1.71:LAR-15231-1-SB; US-Patent-Appl-SN-343740; US-Patent-Appl-SN-134444) Avail: CASI HC A03/MF A01

A flux-focusing electromagnetic sensor which uses a ferromagnetic flux-focusing lens simplifies inspections and increases detectability of fatigue cracks about circular fasteners and other circular inhomogeneities in high conductivity material. The unique feature of the device is the ferrous shield isolating a high-turn pick-up coil from an excitation coil. The use of the magnetic shield is shown to produce a null voltage output across the receiving coil in the presence of an unflawed sample. A redistribution of the current flow in the sample caused by the presence of flaws, however, eliminates the shielding condition and a large output voltage is produced, yielding a clear unambiguous flaw signal. By rotating the probe in a path around a circular fastener such as a rivet while maintaining a constant distance between the probe and the center of a rivet, the signal due to current flow about the rivet can be held constant. Any further changes in the current distribution, such as due to a fatigue crack at the rivet joint, can be detected as an increase in the output voltage above that due to the flow about the rivet head. NASA

N95-21933 Microelectronics and Computer Technology Corp., Austin, TX.
CONSORTIA FOR KNOWN GOOD DIE (KGD), PHASE 1 Final Report, 1 Jan. 1993 - 1 Jan. 1994
Marshall Andrews, David Carey, Mary M. Fellows, Larry Gilg, Cindy Murphy, Chad Noddings, Greg Pitts, Claude Rathmell, and Charles Spooner Feb. 1994 320 p Limited Reproducibility: More than 20% of this document may be affected by microfiche quality
(Contract F33615-93-C-1213; AF Proj. 9316)
(AD-A279407; WL-TR-94-5008) Avail: Issuing Activity (Defense Technical Information Center (DTIC))

This report describes the results of Phase 1 of the Infrastructure for KGD program at MCC. The objective of the work is to resolve the issues for supplying and procuring Known Good Die (KGD) in a way that fosters industry acceptance and confidence in Application Specific Electronic Modules (ASEM's for military systems) and MultiChip Modules (MCM's for commercial systems). This report is divided into four sections. Section 1 describes the technical assessment of proposed industry approaches to KGD implementation. Section 2 of the report contains an outline for the plan for industry and government cooperation for the demonstration, validation, and implementation of KGD methodologies identified in this Phase 1 study. Section 3 of the report contains the industry-generated requirements for KGD implementation. Section IV of the report contains the KGD specifications for TAB and flip chip IC's. DTIC

N95-21961# Vrije Univ., Amsterdam (Netherlands). Dept. of Mathematics and Computer Science.
MINIMAX OPTIMAL STOP RULE IN RELIABILITY CHECKING
Jose M. Gouweleeuw 10 Mar. 1994 25 p Sponsored by Fulbright scholarship
(PB95-134557) Avail: CASI HC A03/MF A01

Consider a machine, that may or may not have a defect, and the probability q that this machine is defective is unknown. In order to determine whether the machine is defective, it is tested. On each test, the defect is found with probability p, if it has not been found yet. Performing n tests costs c(sub n) dollars. There is a fine of 1 dollar, if there is a defect and it is not found on the tests. When should we stop testing, in order to minimize the costs. This problem is treated in a minimax setting: the authors try to find a strategy that works well, even for 'bad' q's. It turns out that the minimax optimal stop rule can be unexpectedly complicated. For example, if p = 1/2 and c(sub n) = cn = 0.25n, then the optimal rule is to perform one test. If a defect is found, then again stop, else toss a coin and stop if this shows heads. If the authors have not stopped, a third and last test is performed. NTIS

N95-22037# Surface Optics Corp., San Diego, CA.
NON-DESTRUCTIVE INSPECTION BY INFRARED IMAGING SPECTROSCOPY, PHASE 1 Final Report, 14 Feb. - 14 Oct. 1994
Mark Dombrowski and Virgil Moore 14 Oct. 1994 140 p
(Contract DAAA21-94-C-0013)
(AD-A286158; SOC-R875-003-1094) Avail: CASI HC A07/MF A02

The objective of the phase 1 effort was to investigate the applicability of infrared imaging spectroscopy to multiple nondestructive inspection (NDI) applications. The program demonstrated object discrimination using an algorithm which post-processes an infrared spectral image of two apparently identical objects by filtering across the spectral radiance distribution of the scene. The project also addressed three major design issues concerning the transition of Surface Optics's existing visible spectral radiometer to an infrared version. DTIC

N95-22202# Sandia National Labs., Albuquerque, NM.
EVALUATION OF SCANNERS FOR C-SCAN IMAGING FOR NONDESTRUCTIVE INSPECTION OF AIRCRAFT Final Report
John H. Gieske Sep. 1994 52 p
(Contract DTFA03-91-A-0018)
(AD-A286398; DOT/FAA/CT-94/79) Avail: CASI HC A04/MF A01

The goal of this project was to produce a document that contains information on the usability and performance of commercially available, fieldable, and portable scanner systems as they apply to aircraft nondestructive inspections. In particular, the scanners are used to generate images of eddy current, ultrasonic, or bond tester inspection data. The scanner designs include manual scanners, semiautomated scanners, and fully automated scanners. A brief description of the functionality of each scanner type, a sketch, and a list of the companies that support the particular design are provided. Vendors of each scanner type provided hands-on demonstrations of their equipment on aircraft samples in the Federal Aviation Administration (FAA) Aging Aircraft Nondestructive Inspection Validation Center in Albuquerque, New Mexico. From evaluations recorded during the demonstrations, a matrix of scanner features and factors and ranking of the capabilities and limitations of the design, portability, articulation, performance, usability, and computer hardware/software was constructed to provide a quick reference to compare the different scanner types. Illustrations of C-scan images obtained during the demonstration are shown. DTIC

N95-20637# Rome Lab., Griffiss AFB, NY.
IMPROVING MULTICHIP MODULE (MCM) DESIGN AND RELIABILITY USING THE INTELLIGENT MCM ANALYZER
Mark J. Stoklosa, Douglas J. Holzhauer, Dale W. Richards, Peter J. Rocci, and Paul S. Yaworsky *In* AGARD, Advanced Packaging Concepts for Digital Avionics Oct. 1994 6 p (For primary document see N95-20631 06-06)
Copyright Avail: CASI HC A02/MF A03

N95-20638# Texas Instruments, Inc., Dallas, TX. Defense Systems and Electronics Group.
ULTRA-RELIABLE DIGITAL AVIONICS (URDA) PROCESSOR
Reagan Branstetter, William Ruszczyk, and Frank Miville *In* AGARD, Advanced Packaging Concepts for Digital Avionics Oct. 1994 10 p (For primary document see N95-20631 06-06)
Copyright Avail: CASI HC A02/MF A03

N95-20643# Rome Lab., Griffiss AFB, NY.
RELIABILITY ASSESSMENT OF MULTICHIP MODULE TECHNOLOGIES VIA THE TRISERVICE/NASA RELTECH PROGRAM
Daniel F. Fayette *In* AGARD, Advanced Packaging Concepts for Digital Avionics Oct. 1994 9 p (For primary document see N95-20631 06-06)
Copyright Avail: CASI HC A02/MF A03

39 STRUCTURAL MECHANICS

Includes structural element design and weight analysis; fatigue; and thermal stress.

For applications see *05 Aircraft Design, Testing and Performance* and *18 Spacecraft Design, Testing and Performance.*

N95-19930# Helsinki Univ. of Technology, Espoo (Finland). Ship Lab.
ANALYSES OF SOME BENCHMARK CASES IN FRACTURE MECHANICS USING BOUNDARY ELEMENT METHOD
J. Tuhkuri 31 May 1994 50 p
(PB95-110888; ISBN-951-22-2162-4) Avail: CASI HC A03/MF A01

The boundary element method and especially the analysis of fracture mechanics problems by using the dual boundary element program Cracker is introduced. This code is especially suitable for studying crack growth in two-dimensional, linear, and elastic problems. Cracker can automatically model an incremental crack extension, and no user made remeshing is needed. Eleven different benchmark cases have been analyzed to verify the results given by Cracker. The stress intensity factors and the crack paths calculated by the program are similar to those given in the literature. NTIS

N95-19975# Sydney Univ. (Australia). School of Civil and Mining Engineering.
INELASTIC BENDING AND TORSION OF STEEL I-BEAMS
Y. L. Pi and N. S. Trahair Nov. 1993 38 p See also PB94-208360
(PB94-208378; R-683) Avail: CASI HC A03/MF A01

The inelastic combined bending and torsion of I-section beams is investigated in this paper using the finite element method. The elastic-plastic load-deformation relationships of beams under combined bending and torsion are determined by taking into account the effects of large deformations, material inelasticity, and initial conditions of residual stresses and geometric imperfections. The interactions between in-plane bending, lateral buckling, and torsion are studied. The effects of secondary bending actions about the minor axis caused by torsional rotations are important for the interaction between bending (with flexural-torsional buckling) and destabilizing torsion. Interaction equations for the design of I-section beams against combined bending and free torsion, and against combined flexural-torsional buckling and destabilizing torsion are proposed. It is found that a commonly quoted circular interaction equation for combined bending and torsion does not always provide a true lower bound for I-section beams. NTIS

N95-20003 Sydney Univ. (Australia). School of Civil and Mining Engineering.
INFLUENCE OF PRIMARY BOUNDARY CONDITIONS ON THE BUCKLING OF SHALLOW CYLINDRICAL SHELLS
H. Showkati and P. Ansourian Jan. 1994 62 p Limited Reproducibility: More than 20% of this document may be affected by microfiche quality
(PB94-208352; R-684) Avail: CASI HC A04

Slender cylinders of intermediate length subjected to external pressure normally buckle into sinusoidal waves in the circumferential and meridional directions; the wave numbers are a function of the edge restraints, aspect ratio L/R and wall slenderness R/t. All instability formulas purporting to evaluate the lowest eigenvalue require minimization with respect to the circumferential wave number n; any 'exact' formulation requires the a-priori evaluation of n. Therefore, in any investigation of the effect of boundary conditions on the buckling pressure q(cr) the evaluation of n is crucial. In this paper, a numerical study is presented of the influence of 11 separate sets of boundary conditions on the circumferential wavenumber n and the buckling pressure q(cr). It is found that, as the restraint of the cylinder edged increases, the meridional wavelength decreases, and the wavenumber n increases. It is also found in the investigation that for the higher wavenumbers, the follower load effect on the buckling mode is small. NTIS

N95-20077# Sandia National Labs., Albuquerque, NM.
A COMPUTATIONAL STUDY OF PROJECTILE SHAPE DEPENDENCE ON PHASE CHANGE PHENOMENA WITH COMPARISONS TO EXPERIMENTAL DATA
E. S. Hertel, Jr., R. L. McIntosh, and B. C. Patterson (Wright Lab., Wright-Patterson AFB, OH.) 1994 8 p Presented at the American Institute of Aeronautics and Astronautics Space Programs and Technologies Conference and Exhibit, Birmingham, AL, 27 Sep. 1994
(Contract DE-AC04-94AL-85000)
(DE95-000740; SAND-94-0060C; CONF-9409211-2) Avail: CASI HC A02/MF A01

To make an estimate of the current state of predictive capabilities of hydrocodes for impacts where phase changes may be important, we have simulated a series of experiments where a zinc sphere, rod, and plate impact thin zinc plates at 5 km/s. The experimental data consists of radiographs of the debris cloud and visual evidence of the damage in an aluminum witness plate. CTH was used to simulate the three experiments noted above. A detailed comparison of the simulated debris structure and subsequent damage will be made with the available data. In general, the CTH predictions match the experimental record. DOE

N95-20101# Sydney Univ. (Australia). School of Civil and Mining Engineering.
INELASTIC TORSION OF STEEL I-BEAMS
Y. L. Pi and N. S. Trahair Sep. 1993 44 p See also PB94-104817, PB94-104825 and PB94-208378
(PB94-208360; R-679) Avail: CASI HC A03/MF A01

A nonlinear inelastic analysis of the non-uniform torsion of I-section beams is presented in this paper. Large twist rotations are included in the geometry non-linearity. The nonlinear equilibrium equations of beams in nonuniform torsion have been derived and a finite element procedure has been developed based on the analysis. The elastic-plastic behavior of beams in non-uniform torsion is studied using the finite element procedure and the results are compared with tests. It is found that I-section beams have much larger torsional capacities than can be predicted by linear plastic collapse analysis, and that torsional failure occurs not by the formation of a mechanism but by the tensile rupture of the flanges. A method is proposed for calculating the full plastic non-uniform torque for practical design purposes. NTIS

N95-20109# National Renewable Energy Lab., Golden, CO.
TURBULENCE DESCRIPTORS FOR SCALING FATIGUE LOADING SPECTRA OF WIND TURBINE STRUCTURAL COMPONENTS
N. D. Kelley Jul. 1994 10 p Presented at the International Energy Agency Meeting on Wind Conditions for Wind Turbine Design, Hamburg, Germany, 27-28 Jun. 1994
(Contract DE-AC36-83CH-10093)
(DE94-011833; NREL/TP-442-7035; CONF-9406223-1) Avail: CASI HC A02/MF A01

The challenge for the designer in developing a new wind turbine is to incorporate sufficient strength in its components to safely achieve a 20- or 30-year service life. To accomplish this, the designer must understand the load and stress distributions (in a statistical sense at least) that the turbine is likely to encounter during its operating life. Sources of loads found in the normal operating environment include start/stop cycles, emergency shutdowns, the turbulence environment associated with the specific site and turbine location, and extreme or 'rare' events that can challenge the turbine short-term survivability. Extreme events can result from an operational problem (e.g., controller failure) or violent atmospheric phenomena (tornadic circulations, strong gust fronts). For the majority of the operating time, however, the character of the turbulent inflow is the dominant source of the alternating stress distributions experienced by the structural components. Methods of characterizing or scaling the severity of the loading spectra (or the rate of fatigue damage accumulation) must be applicable to a wide range of turbulent inflow environments - from solitary isolation to the complex flows associated with multi-row wind farms. The metrics chosen must be related to the properties of the turbulent inflow and independent of the nature of local terrain features. DOE

N95-20179*# National Aeronautics and Space Administration. Lewis Research Center, Cleveland, OH.

APPLICATION OF AN ENERGY-BASED LIFE PREDICTION MODEL TO BITHERMAL AND THERMOMECHANICAL FATIGUE

V. M. Radhakrishnan (Indian Inst. of Tech., Madras.), Sreeramesh Kalluri (NYMA, Inc., Brook Park, OH.), and Gary R. Halford Jul. 1994 18 p
Sponsored by NAS-NRC
(Contract NAS3-27186; RTOP 505-63-5B)
(NASA-TM-106684; E-9038; NAS 1.15:106684) Avail: CASI HC A03/MF A01

The inelastic hysteresis energy applied to the material in a cycle is used as the basis for predicting nonisothermal fatigue life of a wrought cobalt-base superalloy, Haynes 188, from isothermal fatigue data. Damage functions that account for hold-time effects and time-dependent environmental phenomena such as oxidation and hot corrosion are proposed in terms of the inelastic hysteresis energy per cycle. The proposed damage functions are used to predict the bithermal and thermomechanical fatigue lives of Haynes 188 between 316 and 760 C from isothermal fatigue data. Predicted fatigue lives of all but two of the nonisothermal tests are within a factor of 1.5 of the experimentally observed lives. Author

N95-20237# Lawrence Livermore National Lab., Livermore, CA.

A COMPUTATIONAL STUDY OF PROJECTILE MELT IN IMPACT WITH TYPICAL WHIPPLE SHIELDS

M. L. Alme (Alme and Associates, Columbia, MD.) and C. E. Rhoades, Jr. 3 Jun. 1994 23 p Presented at the 1994 Hypervelocity Impact Symposium, Santa Fe, NM, 16-20 Oct. 1994
(Contract W-7405-eng-48)
(DE94-016454; UCRL-JC-116598; CONF-9410131-4) Avail: CASI HC A03/MF A01

This paper presents scaling results based on simulations with the CALE hydrodynamics code of aluminum projectile impacts on typical aluminum Whipple shields at speeds of 6 to 14 km/s. The objective was to determine the extent of projectile and target material melting. The approach was to perform a matrix of computer simulations varying the impact speed from 6 to 14 km/s and varying the areal density of the shield from 5 percent to 80 percent of the centerline areal density of the projectile. The projectile radius was fixed at 9.5 mm (mass = 1.27 grams). The melt state of the projectile material and the shield material was assessed after release of the initial shock. The post-release specific energy in the projectile and in the shield was compared with the enthalpy of incipient melt and the enthalpy of complete melt provided in the Hultgren Tables. Material with specific energy greater than the enthalpy of complete melt was assumed to be fully melted; material with specific energy greater than the enthalpy of incipient melt but less than that of complete melt was assumed to be partially solid and partially melted mixed phase material with no strength; and material with specific energy less than the enthalpy of incipient melt was assumed to be in a solid state with strength. It is likely that this solid material is in a highly fragmented state as a result of the initial shock. DOE

N95-20322# Oak Ridge National Lab., TN.

AN OVERVIEW OF THE HSST FULL-THICKNESS SHALLOW-CRACK CLAD BEAM TESTING PROGRAM

J. A. Keeney, T. J. Theiss, W. J. McAfee, and B. R. Bass 1994 7 p Presented at the 12th Biennial Conference for the International Association for Structural Mechanics in Reactor Technology (SMIRT 12), Stuttgart, Germany, 16-26 Aug. 1993
(Contract DE-AC05-84OR-21400)
(DE94-018940; CONF-930803-32) Avail: CASI HC A02/MF A01

A testing program is described that will utilize full-thickness clad beam specimens to quantify fracture toughness for shallow flaws in material for which metallurgical conditions are prototypic of those found in reactor pressure vessels (RPV's). The beam specimens are fabricated from a section of an RPV wall that includes weld, plate and clad material. Metallurgical factors potentially influencing fracture toughness for shallow flaws in the beam specimen include material gradients due to welding and cladding applications, as well as material inhomogeneities in welded regions due to reheating in multiple weld passes. Fracture toughness tests focusing on shallow flaws in plate and weld material will also provide data for evaluating the relative influence of absolute and normalized crack depth on constraint conditions. Pretest finite-element analyses are described that provide near-tip stress and strain fields for characterization of constraint in the shallow-crack specimens in terms of the Q-stress. Analysis results predict a constraint loss in the shallow-crack clad beam specimen similar to that determined for a previously tested shallow-crack single-edge notch homogeneous bend specimen with the same normalized crack depth. DOE

N95-20374# Oak Ridge National Lab., TN.

RESIDUAL STRESSES IN MATERIAL PROCESSING

K. J. Kozaczek, T. R. Watkins, C. R. Hubbard, Xun-Li Wang, and S. Spooner 1994 7 p Presented at the 1994 Pressure Vessels and Piping Conference, Minneapolis, MN, 19-23 Jun. 1994
(Contract DE-AC05-84OR-21400)
(DE94-017888; CONF-940613-26) Avail: CASI HC A02/MF A01

Material manufacturing processes often introduce residual stresses into the product. The residual stresses affect the properties of the material and often are detrimental. Therefore, the distribution and magnitude of residual stresses in the final product are usually an important factor in manufacturing process optimization or component life prediction. The present paper briefly discusses the causes of residual stresses. It then addresses the direct, nondestructive methods of residual stress measurement by X ray and neutron diffraction. Examples are presented to demonstrate the importance of residual stress measurement in machining and joining operations. DOE

N95-20416# Oak Ridge National Lab., TN.

DYNAMIC MEASUREMENT OF THE HOOP MODULUS OF A COMPOSITE CYLINDER

J. B. Andriulli 1994 11 p Presented at the Annual Winter Meeting of the American Society of Mechanical Engineers, New Orleans, LA, 28 Nov. - 3 Dec. 1993
(Contract DE-AC05-84OR-21400)
(DE94-018958; CONF-931121-39) Avail: CASI HC A03/MF A01

Hoop modulus of a composite cylinder is measured by the impact-hammer modal-test method of a ring-segment specimen suspended in the near free-free boundary condition. The ring segment is cut from one end of the composite cylinder forming a curved bar with curvature equal to the radius of the cylinder. Free-free axial resonances are imposed by striking one end of the curved bar with a hammer. Axial response is measured by a miniature accelerometer on either end of the bar. The axial modulus of the curved bar is determined from the bar material density and the axial resonances in a manner similar to that used to determine modulus from axial resonances of a straight bar. An algorithm is used to correct for the frequency shift of the axial modes due to the bar curvature. The use of higher-axial modes minimizes bar curvature effects on frequency and improves accuracy. The hoop modulus of the composite cylinder is assumed to be the same as that determined from the axial modulus of the curved bar (ring segment). The measurement method has been confirmed by conducting the procedure on straight and curved aluminum bars and ring segments of two different lengths and three different curvatures. The method has been successfully demonstrated with aluminum and composite ring segments having circumferential arc lengths ranging from 60 degrees to 305 degrees. Both measured and computed results are compared and shown to be in good agreement. DOE

N95-20615 Wright Lab., Wright-Patterson AFB, OH. Materials Directorate.
THE MECHANICAL PROPERTY DATA BASE FROM AN AIR FORCE/INDUSTRY COOPERATIVE TEST PROGRAM ON ADVANCED ALUMINUM ALLOYS Final Report, Jul. 1986 - May 1993
Mary Ann Phillips and Steven R. Thompson Dec. 1993 574 p Limited Reproducibility: More than 20% of this document may be affected by microfiche quality
(DA Proj. 2418)
(AD-A280038; WL-TR-94-4014) Avail: CASI HC A24

This report contains a mechanical property data base on aluminum-lithium alloys 2091, 8090, IN905XL, AL905XL, and Weldalite 2095 and a data base on powder metallurgy alloys 7064 and CW67. Basic mechanical property data consist of tension, compression, shear, bearing and fracture toughness properties. Fatigue data were generated from both smooth and notched specimens. Constant amplitude fatigue crack growth rate data and spectrum fatigue test data were generated. Other tests performed on a select number of alloys were ballistic, hardness and conductivity. DTIC

N95-20703# Oak Ridge National Lab., TN.
THE PRODUCTION OF CALIBRATION SPECIMENS FOR IMPACT TESTING OF SUBSIZE CHARPY SPECIMENS
D. J. Alexander, W. R. Corwin, and T. D. Owings 1994 8 p Presented at the Symposium on Pendulum Impact Machine: Procedures and Specimens for Verification, Montreal, Quebec, 18-19 May 1994
(Contract DE-AC05-84OR-21400)
(DE94-018125; CONF-9405223-1) Avail: CASI HC A02/MF A01

Calibration specimens have been manufactured for checking the performance of a pendulum impact testing machine that has been configured for testing subsize specimens, both half-size (5.0 x 5.0 x 25.4 mm) and third-size (3.33 x 3.33 x 25.4 mm). Specimens were fabricated from quenched-and-tempered 4340 steel heat treated to produce different microstructures that would result in either high or low absorbed energy levels on testing. A large group of both half- and third-size specimens were tested at -40 C. The results of the tests were analyzed for average value and standard deviation, and these values were used to establish calibration limits for the Charpy impact machine when testing subsize specimens. These average values plus or minus two standard deviations were set as the acceptable limits for the average of five tests for calibration of the impact testing machine. DOE

N95-20790*# National Aeronautics and Space Administration. Lewis Research Center, Cleveland, OH.
RELIABILITY ANALYSIS OF UNIAXIALLY GROUND BRITTLE MATERIALS
Jonathan A. Salem, Noel N. Nemeth, Lynn M. Powers, and Sung R. Choi Feb. 1995 14 p Presented at the Turbo Expo 1995, Houston, TX, 5-8 Jun. 1995; sponsored by ASME
(Contract RTOP 505-63-5B; DE-AC05-840R-21400)
(NASA-TM-106852; E-9441; NAS 1.15:106852) Avail: CASI HC A03/MF A01

The fast fracture strength distribution of uniaxially ground, alpha silicon carbide was investigated as a function of grinding angle relative to the principal stress direction in flexure. Both as-ground and ground/annealed surfaces were investigated. The resulting flexural strength distributions were used to verify reliability models and predict the strength distribution of larger plate specimens tested in biaxial flexure. Complete fractography was done on the specimens. Failures occurred from agglomerates, machining cracks, or hybrid flaws that consisted of a machining crack located at a processing agglomerate. Annealing eliminated failures due to machining damage. Reliability analyses were performed using two and three parameter Weibull and Batdorf methodologies. The Weibull size effect was demonstrated for machining flaws. Mixed mode reliability models reasonably predicted the strength distributions of uniaxial flexure and biaxial plate specimens. Author

N95-20833# Sandia National Labs., Albuquerque, NM.
GEOMETRIC MOIRE METHOD OF STRAIN ANALYSIS WITH DISPLACEMENT DISCONTINUITIES
S. R. Brown and R. D. Hardy Aug. 1994 57 p
(Contract DE-AC04-94AL-85000)
(DE95-001114; SAND-93-1157) Avail: CASI HC A04/MF A01

Prediction of the deformation behavior of large engineering structures in jointed rock under a specified loading history requires the extensive use of numerical simulation. For example, the evaluation of the stability of the openings for the Exploratory Studies Facility and a potential repository for high-level nuclear waste at Yucca Mountain, Nevada will require computer codes capable of predicting slip on rock joints resulting from changes in thermal stresses. The testing and ultimate validation of these complex finite element computer codes is an important step in their development before their use as a design tool for an engineering structure or for the study of some other practical problem. While field tests may be ultimately necessary, the authors propose a different and more thorough approach where early tests are done on a bench scale with easily characterized materials and geometries. For these bench-scale tests, the basic approach is to construct a laboratory specimen with a known geometry from an easily characterized material. Digital video imaging combined with the geometric moire fringe method of strain analysis is used to measure and derive the displacements on the sample under load. Here the authors present the method of acquiring and analyzing the moire data and give an analysis of its problems and benefits. DOE

N95-21006# Technische Univ., Delft (Netherlands). Geotechnical Lab.
GEOMATERIAL MODELS AND NUMERICAL ANALYSIS OF SOFTENING Ph.D. Thesis
R. B. J. Brinkgreve 24 May 1994 64 p Sponsored by Technology Foundation (STW), Dutch Ministry of Transport, Public Works and Water Management, and Shell Research
(PB95-135380; ISBN-90-9007034-6) Avail: CASI HC A04/MF A01

Since 1960, researchers have been working on constitutive models for geomaterials, i.e. soil and rock. In later years such models have been applied in finite element codes, in particular the simple elastoplastic Mohr-Coulomb model. More refined models exist, but they are not easily applied in practical geotechnical engineering. Even well-known Cam-Clay type models are, as yet, not generally applied for clays, and are subject to criticism. From a practical point of view, the criticism concerns among other things the prediction of lateral stresses in soil layers. From a theoretical point of view, the quite general use of non-conservative elasticity laws is not justified. In fact, a proper potential for the elastic strain-energy is missing. This study is among other things aimed at improving this situation, and some improvements of existing constitutive models are proposed. Another quite different part of this study concerns a new topic of geomechanics, namely non-local material softening. Dense clays and rock show material softening, i.e. negativeness of the second-order work, but classical softening models lead to ill-posed formulations. Numerical calculations with such models produce unreliable results. Recently, some researchers have put forward new ideas for arriving at well-posedness of boundary value problems. Stimulated by some pioneering work in this field, a so-called non-local approach is put into operation. NTIS

N95-21133# Swedish Inst. for Materials Testing, Boras (Sweden).
ACCURACY PROBLEMS IN THE GENERATION OF DISCRETE TIME STOCHASTIC PROCESSES
Thomas Svensson 1994 26 p
(ISSN 0284-5172)
(PB95-131397; SP-RAPP-1994:24; ISBN-91-7848-483-9) Avail: CASI HC A03/MF A01

A method for the generation of discrete time stochastic processes for fatigue testing was previously presented. The generated process is constructed according to user requirements regarding irregularity and level crossings. In the present investigation this type of discrete time stochastic process is further investigated in order to calculate prediction limits for user requirements. These limits can be used to decide the length of sequences that need to be generated in a certain fatigue test. For instance, our results show that irregularity factor errors better than 1% are possible to achieve in fatigue applications. NTIS

N95-21212# Naval Undersea Warfare Center, Newport, RI.
A MODEL OF AN INFINITE LENGTH, AXISYMMETRIC, ISOTROPIC, FORCED THICK SHELL Final Report
Andrew J. Hull 22 Aug. 1994 39 p
(AD-A285586; NUWC-NPT-TR-10719) Avail: CASI HC A03/MF A01

The model described in this report provides an exact solution to the equations of motion for an infinite length, axisymmetric, isotropic, forced thick shell. In this model, the governing equations of motion of an isotropic elastic solid in cylindrical coordinates are first separated into a dilatational wave equation and three distortional wave equations that can be solved with Bessel functions. These general solutions are then inserted into stress-strain constitutive equations at the interior and exterior of the shell. The displacements are next determined from forcing functions that are applied to the shell. In this new model, the shell thickness effects on wave propagation are addressed. The case where the mean radius of the shell is equal to its thickness has been analyzed and compared with thin shell equations of motion. It is shown that, in general, the thin shell equations of motion often underpredict thick shell response. DTIC

N95-21364# Los Alamos National Lab., NM.
TUNGSTEN-URANIUM PENETRATOR TARGET INTERACTION
P. S. Dunn and B. K. Damkroger (Sandia National Labs., Albuquerque, NM.) 1994 14 p Presented at the 1994 International Conference on Tungsten and Refractory Metals, McLean, VA, 17-19 Oct. 1994
(Contracts W-7405-eng-36; DE-AC04-94AL-85000)
(DE95-000847; LA-UR-94-3284; CONF-9410213-1) Avail: CASI HC A03/MF A01

Several studies performed in recent years have been directed at determining the penetration mechanism of long rod kinetic energy penetrators into Rolled Homogeneous Armor (RHA). Much of the work has centered on comparing U-0.75Ti and Tungsten Heavy Alloys (WHA), with the goal being to relate the superior ballistic performance of the uranium materials to a fundamental difference in penetration mechanisms. This has been found to be true, with the dominant mechanisms being adiabatic shear in U-0.75Ti and bulk deformation in WHA. Recent work has sought to achieve improvements in the ballistic performance of the tungsten materials via both mechanical property improvements and alloy modifications designed to bring about adiabatic shear. As an alternative, the authors propose the consideration of materials which utilize mechanisms other than bulk deformation and adiabatic shear to optimize ballistic performance. This paper will present the postmortem analysis of a uranium-20 vol% tungsten composite penetrator fired into RHA at 0 degree obliquity. The analysis shows that the penetration mechanism in this material is bulk heating and extensive co-melting of the target and penetrator at the penetration interface. The results of the analysis will then be compared to a similar analysis made of targets into which U-0.75Ti penetrators had been fired. DOE

N95-21386# Los Alamos National Lab., NM.
STRAIN MEASUREMENT BY DIFFRACTION AT LANSCE
M. A. M. Bourke, J. A. Goldstone, and R. A. Robinson 29 Jul. 1994 7 p Presented at the International Conference on Neutron Scattering, Sendai, Japan, 11-14 Oct. 1994 Submitted for publication
(Contract W-7405-eng-36)
(DE94-018264; LA-UR-94-2736; CONF-9410165-3) Avail: CASI HC A02/MF A01

Residual strains affect the structural integrity of components during both fabrication and service and consequently industrial manufacturers routinely invest considerable effort in their characterization and control. Neutron diffraction has proved to be a unique technique for non-destructive strain measurement within crystalline solids. The technique is achieving recognition but is limited by lack of beam time and compromises involved in using instruments designed for powder diffraction. This paper summarizes its importance, lists the capabilities of the Los Alamos (pulsed) neutron scattering center (LANSCE) and briefly describes a concept for a dedicated instrument. DOE

N95-21396# Sandia National Labs., Albuquerque, NM.
A HYPERVELOCITY EXPERIMENTAL RESEARCH DATABASE (HERD): SUPPORT FOR THE WRIGHT LABORATORY ARMAMENT DIRECTORATE CODE VALIDATION PROGRAM (COVAL)
Scott A. Mullin (Southwest Research Inst., San Antonio, TX.), Charles E. Anderson, Jr. (Southwest Research Inst., San Antonio, TX.), Eugene S. Hertel, Jr., and Ronald D. Hunt (Wright Lab., Eglin AFB, FL.) 1994 11 p Presented at the American Institute of Aeronautics and Astronautics Space Programs and Technologies Conference and Exhibit, Birmingham, AL, 27 Sep. 1994
(Contract DE-AC04-94AL-85000)
(DE95-001628; SAND-94-0378C; CONF-9409211-4) Avail: CASI HC A03/MF A01

The Hypervelocity Experimental Research Database (HERD) described in this paper was developed to aid researchers with code validation for impacts that occur at velocities faster than the testable regime. Codes of concern include both hydrocodes and fast-running analytical or semi-empirical models used to predict the impact phenomenology and damage that results to projectiles and targets. There are several well documented experimental programs that can serve as benchmarks for code validation; these are identified and described. Recommendations for further experimentation (a canonical problem) to provide validation data are also discussed. DOE

N95-21557 Swedish Inst. for Materials Testing, Boras (Sweden).
CRACK CLOSURE AND SEQUENTIAL EFFECTS IN FATIGUE: A LITERATURE SURVEY
M. Holmgren 1994 33 p
(PB95-131637; SP-Rapport-1994:20) Avail: Issuing Activity (National Technical Information Service (NTIS))

A literature survey of the phenomenon of crack closure is reported here. The state of the art is reviewed and several empirical formulas for determining the crack closure are compared with each other. Their properties, advantages and disadvantages are briefly discussed. Experimental techniques for determining the crack closure stress are presented and experimental data from the literature are reported. NTIS

N95-21967 Wright Lab., Wright-Patterson AFB, OH.
INFLUENCE OF FATIGUE CRACK CLOSURE ON THE GROWTH RATE OF SURFACE FLAWS Final Report, Sep. 1982 - May 1988
William A. Troha Feb. 1994 239 p Limited Reproducibility: More than 20% of this document may be affected by microfiche quality
(AF Proj. 3066)
(AD-A279130; WL-TR-92-2032) Avail: Issuing Activity (Defense Technical Information Center (DTIC))

Inconsistent experimental results of fatigue crack closure studies over the past 15 years have caused recent investigators to conclude that the fundamental phenomena controlling the crack driving mechanisms are not understood. A major contributor to this misunderstanding is an inadequate understanding of the complex three-dimensional nature of closure. This is true for two-dimensional thru-the-thickness cracks as well as for three-dimensional part-thru surface cracks. To assess the three-dimensional influences of fatigue crack closure on the growth rate of surface flaws, an experimental investigation was conducted using a rectangular plate of polymethyl methacrylate (PMMA) material loaded in four-point bending. The use of transparent PMMA material and a Newton optical interferometer system with a laser light source provided the capability to simultaneously measure three-dimensional crack opening displacement (COD) profiles and closure loads. DTIC

N95-22025# Army Armament Research, Development and Engineering Center, Watervliet, NY.
PERIMETER-YARDSTICK TECHNIQUE FOR FRACTURE SURFACE FRACTAL ANALYSIS Final Report
Gay Kendall, P. J. Cote, and L. V. Meisel Aug. 1994 15 p
(AD-A286240; ARCCB-TR-94028) Avail: CASI HC A03/MF A01

Local fractal dimensions alpha(chi, epsilon), which are closely related to crowding indices of individual islands and lakes formed by sectioning of fracture surfaces produced in Charpy impact testing of a high-strength and high-toughness steel (ASTM A723) alloy, have been determined by perimeter-yardstick analysis. In this type of analysis, the perimeter of an island or lake on a fracture surface section is measured at several different magnifications, and Richardson's equation is employed to determine the fractal dimension of the island or lake. Perimeter-yardstick analysis, which had not previously been applied to fracture surface analysis, yielded alpha(chi, epsilon) values ranging from 1.17 to 1.40 (mean: 1.28, standard deviation: 0.08) for Charpy fracture islands and lakes in ASTM A723 steel for epsilon-values near 0.00013 cm. The mean alpha(chi, epsilon)-value is consistent with the (global) fractal dimension of 1.25 obtained by slit-island analysis of the same fracture surface sections, a value typical of high-strength steel alloys previously studied. The island-to-island and lake-to-lake variations of the local fractal dimensions reflect real variations analogous to differences in the fractal dimensions of the coastlines of Norway and England. Either the fracture surfaces are fractally inhomogeneous or the range of alpha(chi, epsilon)-values determines limits on the variation of the global multifractal dimensions D(q) and a(q). DTIC

N95-22070# Sandia National Labs., Albuquerque, NM.
EFFECTS OF CYCLIC STRESS DISTRIBUTION MODELS ON FATIGUE LIFE PREDICTIONS
H. J. Sutherland and P. S. Veers Oct. 1994 7 p Presented at the American Society of Mechanical Engineers (ASME) Energy Sources Technology Conference and Exhibition, Houston, TX, 29 Jan. - 1 Feb. 1995
(Contract DE-AC04-94AL-85000)
(DE95-001619; SAND-94-2334C; CONF-950116-1) Avail: CASI HC A02/MF A01

The fatigue analysis of a wind turbine component typically uses representative samples of cyclic loads to determine lifetime loads. In this paper, several techniques currently in use are compared to one another based on fatigue life analyses. The generalized Weibull fitting technique is used to remove the artificial truncation of large-amplitude cycles that is inherent in relatively short data sets. Using data from the Sandia/DOE 34-m Test Bed, the generalized Weibull file technique is shown to be excellent for matching the body of the distribution of cyclic loads and for extrapolating the tail of the distribution. However, the data also illustrate that the fitting technique is not a substitute for an adequate data base. DOE

N95-22093# National Aerospace Lab., Amsterdam (Netherlands). Structures and Materials Div.
COUNTING METHODS FOR THE ANALYSIS OF LOAD TIME HISTORIES
1994 32 p
(PB95-132916; MEMO-SB-80-106-U) Avail: CASI HC A03/MF A01

Signals of a stochastic nature are usually analyzed on their statistical properties (distribution function, moments, etc.). An important tool for the analysis of both deterministic and stochastic signals is the so-called harmonic analysis. These methods, however, will not be discussed in the present document. This memorandum is concentrated on analysis methods which look for the occurrence of specific events in a load-time trace. These events can be for example the exceedance of specific load levels, the occurrence of a load-change of certain magnitude, etc. As the basis of these analysis techniques is to count the number of times the specified events do occur, these methods are usually indicated as 'counting techniques'. NTIS

N95-22097 National Defence Research Establishment, Stockholm (Sweden). Dept. of Information Technology.
ALUMINIUM OXIDE TARGETS AFTER BALLISTIC IMPACT; FRAGMENTATION OF THE CERAMIC AND THE PROJECTILE [ALUMINIUMOXID EFTER BESKJUTNING; FRAGMENTERING AV KERAM OCH PROJEKTIL]
P. O. Olsson Jun. 1994 29 p In SWAHILI
(PB95-133625; FOA-C-20987-2.3) Avail: Issuing Activity (National Technical Information Service (NTIS))

In this report three different alumina targets are studied after ballistic impact with tungsten alloy long rod projectiles. Two of the targets consist of two well confined circular tiles placed on top of each other and the third one in a single less confined quadratic tile. Three projectile velocities have been used: 1,555 m/s, 1,846 m/s and 2,527 m/s. The different crackpatterns formed, the appearance of the projectile fragments and the importance of the confinement for the armor are discussed. This has been done by comparing the experimental results with models given in the literature. NTIS

N95-22320 Army Armament Research, Development and Engineering Center, Watervliet, NY.
RESIDUAL STRESS ANALYSIS IN SWAGE AUTOFRETTAGED THICK-WALLED CYLINDERS BY POSITION-SENSITIVE X-RAY DIFFRACTION TECHNIQUES Final Report
S. L. Lee Aug. 1994 21 p Presented at the ASME International Conference on Pressure Vessels and Piping, Denver, CO, 25-29 Jul. 1993 Limited Reproducibility: More than 20% of this document may be affected by microfiche quality
(AD-A286383; ARCCB-TR-94031) Avail: CASI HC A03

Experimental and theoretical investigations were made for swage autofrettaged partially plastic ASTM A723 steel cylinders with an outside diameter (OD) to inside diameter (ID) ratio of 2.75 and 74 percent overstrain. Residual stress radial distribution and angular stress distribution around the bore were analyzed using two position-sensitive x ray diffraction stress analyzers. Theoretical calculation was made by implementing an interactive, iterative Lotus Works spreadsheet residual stress model on an IBM PC. The model was based on the classical solution to the elastic-plastic deformation problem of a symmetric thickwalled cylinder under internal pressure, including reverse yielding effect. Angular stress distribution data at the ID and OD indicated that non-axisymmetric deformation had occurred during yielding of the cylinders. Excellent agreement was obtained between experimental results and theoretical predictions, including the Bauschinger effect near the bore. By comparing experimental data with theoretical calculations for the 74 percent overstrained cylinders, the Bauschinger factor for the A723 steel was determined to be close to 0.5. Residual stress analysis for the entire cylinder is suggested in the future. DTIC

N95-22411# Naval Command, Control and Ocean Surveillance Center, San Diego, CA. Research, Development, Technology and Evaluation Div.
STRUCTURAL PERFORMANCE OF CYLINDRICAL PRESSURE HOUSINGS OF DIFFERENT CERAMIC COMPOSITIONS UNDER EXTERNAL PRESSURE LOADING. PART 3: SINTERED REACTION BONDED SILICON NITRIDE CERAMIC Final Report
R. R. Kurkchubasche, R. P. Johnson, and J. D. Stachiw Jun. 1994 78 p
(NR Proj. SO3-97)
(AD-A285773; NCCOSC/RDT/E-TR-1592-Pt-3) Avail: CASI HC A05/MF A01

Ten 12-inch-OD by 18-inch-long reaction-bonded sintered silicon-nitride cylinders were fabricated, assembled, and pressure tested to determine their suitability for use as external pressure-resistant housings for underwater applications. The material, designated PSX Si3N4, is made by CERCOM, Inc. (Vista, CA) by a proprietary process. The primary advantages of this material are high compressive strength, high elastic modulus, high fracture toughness, and low specific gravity. Pressure test results are presented along with strain gage data and cyclic fatigue life data. Conclusions regarding the suitability of the material for application to pressure housings for underwater applications are presented along with a comparison to WESGO's AL-600 96-percent alumina ceramic, which was chosen as the base of comparison for various advanced materials being evaluated under the same program. Recommendations for design implementation, nondestructive inspection, and further research are made. DTIC

42 GEOSCIENCES (GENERAL)

No abstracts in this category.

43 EARTH RESOURCES AND REMOTE SENSING

Includes remote sensing of earth resources by aircraft and spacecraft; photogrammetry; and aerial photography.
For instrumentation see *35 Instrumentation and Photography.*

N95-20006# Naval Research Lab., Bay Saint Louis, MS.
ICE PROCESSING SYSTEM SOFTWARE SUPPORT DOCUMENTATION Final Report
Sylvia Seal, Barbara Bassett, Douglas A. May, and Florence Fetterer 3 May 1994 112 p
(AD-A280030; NRL/MR/7240-94-7510) Avail: CASI HC A06/MF A02

The Ice Processing System is a digital image processing function that performs sea-ice lead statistics analysis functions and ice-motion estimations. The menu-driven process permits the user to utilize Advanced Very High Resolution Radiometer and/ or Operational Line Scan infrared or visible satellite imagery. The lead analysis software utilizes a Hough transform technique to determine lead orientation statistics. The function also provides/displays lead size, lead orientation, and lead spacing information in various forms to the user. Ice-motion vectors are obtained automatically from image pairs using a cross-correlation technique. The resultant motion vectors are then displayed over a screen image. Together, these techniques provide analysts with near-real-time indications of sea-ice conditions over regions of interest. DTIC

N95-20156*# Remote Sensing Systems, Inc., Santa Rosa, CA.
DERIVING EARTH SCIENCE PRODUCTS FROM SSM/I Progress Report, Aug. 1993 - Jan. 1995
Frank J. Wentz 3 Jan. 1995 16 p Original contains color illustrations
(Contract NASw-4714)
(NASA-CR-197299; NAS 1.26:197299; RSS-Memo-010395) Avail: CASI HC A03/MF A01; 2 functional color pages

A few of the major accomplishments during the second phase include: (1) all three Special Sensor Microwave Imagers (SSM/I's: F08, F10, and F11) have been cross-calibrated; (2) a very large, quality-controlled, collocated SSM/I and radiosonde data set has been produced; (3) the SSM/I-radiosonde and SSM/I-buoy data sets have been used to calibrate the SSM/I ocean retrieval algorithm; (4) ocean products have been produced for both F10 and F11 SSM/I for 1991-1993; (5) the SSM/I-buoy data set was used to better determine the variation of the ocean T(sub B) with wind direction; and (6) it was demonstrated that under high wind conditions, wind direction information can be obtained from individual SSM/I observations. CASI

N95-20207# Technische Hogeschool, Delft (Netherlands).
INVARIANT MEASURES OF INTERVAL MAPS Ph.D. Thesis
H. P. Bruin 24 Jun. 1994 115 p
(PB95-107835) Avail: CASI HC A06/MF A02

This thesis on unimodal maps is primarily inspired by two questions: How can one construct invariant measures which are absolutely continuous with respect to Lebesgue measure, and to what extent is the existence of such a measure to topological property. Contents: Long-branched maps -- Introduction and statement of the results, Combinatorics and kneading theory, The induced Markov map, Estimates on branches, Proofs of the theorems; Markov extensions -- Preliminaries, Finite measures on the Hofbauer tower, Sigma-finite measures, Absorbing Cantor sets, Martens' tower; Kneading theory -- Definitions, The splitting of itineraries, Admissibility conditions, Restrictive intervals and periodic attractors, Some remarks on omega(c), and Lorenz-like maps. NTIS

N95-20903# Pacific Northwest Lab., Richland, WA.
AIRBORNE MULTISENSOR POD SYSTEM (AMPS) DATA ACCESS CONCEPT
Jiing-Yih J. Jou and W. D. Meitzler Oct. 1994 13 p
(Contract DE-AC06-76RL-01830)
(DE95-002586; PNL-10197) Avail: CASI HC A03/MF A01

The purpose of this document is to provide the conceptual design for accessing data collected under the Airborne Multisensor Pod System (AMPS) program and for accessing data about that data. The purpose of the AMPS program is to provide multisensor data for data fusion research as it applies to arms control treaty verification, non-proliferation surveillance, and related programs. Secondary objectives include sensor development and technology demonstration. The program was established by the U.S. Department of Energy (DOE), Office of Arms Control and Non-proliferation (DOE/AN) and is integrated into the overall DOE AN-10.1 technology development program. The AMPS program interacts with other technology programs of DOE/NN-20. The AMPS program participants include five DOE laboratories. Four will be responsible for collecting and supplying data to AMPS data researchers: (1) Lawrence Livermore National Laboratory (LLNL); (2) Remote Sensing Laboratory (RSL); (3) Sandia National Laboratories (SNL); (4) Savannah River Technology Center (SRTC). The Pacific Northwest Laboratory (PNL), has been assigned data management responsibility for the program, which is defined as the process of planning, acquiring, organizing, qualifying and disseminating data. Data ranges from single sensor readings, to high resolution images, to video. The potential volume of data to be collected under the AMPS program will require considerable management effort. The AMPS program specifies a distributed approach for the sharing and management of AMPS data. This approach shares the burden of data distribution across the DOE laboratories, which will be responsible for AMPS instruments development and implementation and the data those instruments produce. This approach will also provide the laboratories with direct control over the distribution of the data for which they are responsible. DOE

N95-21105# Helsinki Univ. of Technology, Espoo (Finland). Lab. of Space Technology.
INVESTIGATION ON THE BACKSCATTERING PROPERTIES OF FINNISH BOREAL FORESTS AT C- AND X-BAND: A SEMI-EMPIRICAL MODELING APPROACH Ph.D. Thesis
Jouni T. Pulliainen May 1994 128 p
(ISSN 0786-8154)
(PB95-127692; ISBN-951-22-2161-6) Avail: CASI HC A07/MF A02

This study is concerned with the empirical research on microwave radar remote sensing of Finnish boreal forests (C- and X-band signatures). The radar response to forest characteristics, such as the stem volume (or forest biomass), was analyzed, and a semi-empirical model describing the microwave interaction with forests as a function of the forest stem volume was developed. The investigations presented are based on the employment of a high-resolution ranging scatterometer called HUTSCAT (Helsinki University of Technology SCATterometer), and additionally, on the use of satellite-borne ERS-1 Synthetic Aperture Radar (SAR) data. NTIS

N95-21433# Lawrence Livermore National Lab., Livermore, CA.
SOLID STATE FREQUENCY CONVERSION TECHNOLOGY FOR REMOTE SENSING
S. P. Velsko, M. S. Webb, W. M. Cook, and W. A. Neuman Jul. 1994 12 p Presented at the 1994 Chemical Analysis By Laser Interrogation of Proliferation Effluents (CALIOPE ITR) Interim Technical Review, Livermore, CA, 26-28 Apr. 1994
(Contract W-7405-eng-48)
(DE94-019102; UCRL-JC-118150; CONF-9404162-11) Avail: CASI HC A03/MF A01

Long range remote sensing from airborne or other highly mobile platforms will require high average power tunable radiation from very compact and efficient laser systems. The solid state laser pumped optical parametric oscillator (OPO) has emerged as a leading candidate for such high average power, widely tunable sources. In contrast to laboratory systems, efficiency and simplicity can be the decisive issues which determine the practicality of a particular airborne remote sensing application. The recent advent of diode laser pumped solid state lasers has produced high average power OPO pump sources which are themselves both compact and efficient. However, parametric oscillator technology which can efficiently convert the average powers provided by these pump sources remains to be demonstrated. In addition to the average power requirement, many airborne long range sensing tasks will require a high degree of frequency multiplexing to disentangle data from multiple chemical species. A key advantage in system simplicity can be obtained, for example, if a single OPO can produce easily controlled multispectral output. In this paper the authors address several topics pertaining to the conversion efficiency, power handling, and multispectral capabilities of OPO's which they are currently investigating. In Section 2, single pulse conversion efficiency issues are addressed, while average power effects are treated in Section 3. Section 4 is concerned with multispectral performance of a single OPO. The last section contains a short summary and some concluding remarks. DOE

N95-21552# Lawrence Livermore National Lab., Livermore, CA.
OVERVIEW OF REMOTE SENSING LASER DEVELOPMENT AND SEMICONDUCTOR LASER TECHNOLOGY
N. W. Carlson, R. Beach, B. Comaskey, M. Emanuel, T. Scharlemann, J. Skidmore, S. Velsko, B. Krupke, and R. Solarz Jul. 1994 19 p Presented at the 1994 Chemical Analysis By Laser Interrogation of Proliferation Effluents (CALIOPE ITR) Interim Technical Review, Livermore, CA, 26-28 Apr. 1994
(Contract W-7405-eng-48)
(DE94-019103; UCRL-JC-118149; CONF-9404162-12) Avail: CASI HC A03/MF A01

There are many new requirements for remote detection in the atmosphere that have been generated by government agencies. The associated field scenarios anticipated for carrying out the measurements, in many cases, are extremely demanding on the existing technology. Moreover, additional innovations in remote-sensing technology will be needed to satisfy requirements for longer measurement ranges, detection of low concentration levels of target species, new laser wavelengths for a growing list of species, and compact/efficient systems for deployment in airborne platforms. Remote-sensing laser transmitter architectures based on diode-pumped, solid-state lasers offer the most promise in terms of meeting these demanding requirements, although in order to realize this promise, the present level of power performance must be extended by one to two orders of magnitude. The LLNL remote sensing laser development program is aimed at developing those necessary solid-state laser systems with performance characteristics that go well beyond the state-of-the-art. This paper will cover: (1) an overview of the remote sensing laser development program, which includes high-average power solid-state lasers, tunable laser/OPO systems, temperature-insensitive nonlinear materials, and new solid-state/semiconductor laser materials; and (2) a review of the technical progress on semiconductor laser technology development. DOE

N95-21628 Hydrologic Engineering Center, Davis, CA.
REVIEW OF GIS APPLICATIONS IN HYDROLOGIC MODELING
Bruce A. DeVantier and Arlen D. Feldman May 1993 21 p Limited Reproducibility: More than 20% of this document may be affected by microfiche quality
(AD-A279076; HEC-TP-144) Avail: Issuing Activity (Defense Technical Information Center (DTIC))

Geographic information systems (GIS) provide a digital representation of watershed characteristics used in hydrologic modeling. This paper summarizes past efforts and current trends in using digital terrain models and GIS to perform hydrologic analyses. Three methods of geographic information storage are discussed: raster or grid, triangulated irregular network, and contour-based line networks. The computational, geographic, and hydrologic aspects of each data-storage method are analyzed. The use of remotely sensed data in GIS and hydrologic modeling is reviewed. Lumped parameter, physics-based, and hybrid approaches to hydrologic modeling are discussed with respect to their geographic data inputs. Finally, several applications areas (e.g., floodplain hydrology and erosion prediction) for GIS hydrology are described. DTIC

N95-21872 Commission of the European Communities, Brussels (Belgium).
EUROPEAN WORKSHOP ON OPTICAL GROUND TRUTH INSTRUMENTATION FOR THE VALIDATION OF SPACE-BORNE OPTICAL REMOTE SENSING DATA OF THE MARINE ENVIRONMENT
Marcel R. Wernand, ed. 1994 66 p Workshop held on 23-25 Nov. 1993
(ISSN 0923-3210)
(PB95-134144; NIOZ-1994-3) Copyright Avail: Issuing Activity (National Technical Information Service (NTIS))

The primary aims of the workshop were: (1) to define specifications for a multi-band ocean colour ground truth instrument; (2) to design a 'low cost', multi-band ocean colour ground truth instrument to be used from ships and other sea-borne or airborne platforms; and (3) to achieve common procedures for (inter) calibration of marine optical instruments; such procedures are indispendsable to maintain the quality of optical measurements over the years and to ensure compatibility of optical measurement data from different sources. In addition, the possible set-up of a European Optical Databank (ODB) was discussed. Since European coastal waters are largely of Case-2 type, the workshop had its main focus on this type of waters. NTIS

N95-21912 Mitre Corp., Bedford, MA.
COMMON MAPPING SYSTEM MEDIA STUDY
Jeffrey R. Leger Apr. 1994 38 p Limited Reproducibility: More than 20% of this document may be affected by microfiche quality
(Contract F19628-94-C-0001)
(AD-A279086; MTR-93B0000043; ESC-TR-93-312) Avail: Issuing Activity (Defense Technical Information Center (DTIC))

The Common Mapping System (CMS) defines data formats and standard distribution media for the storage, interchange, and retrieval of mapping, charting, geodesy, and imagery (MCG&I) data. A variety of DOD system are expected to adopt the CMS standard, including mission planning, intelligence, and avionics systems. The distribution media types supported by CMS will significantly impact the utility and cost of CMS for these system. This paper presents the results of an investigation into the attributes of candidate distribution media for CMS, describing cost and production time tradeoffs. We conclude that there would be value in adding compact-disk-read-only-memory (CD-ROM) to erasable optical disk (EOD) as supported distribution media to meet the needs of the Air Force Mission Support System (AFMSS). Additional media types may be necessary to support the requirements of other systems. DTIC

N95-22055# Naval Research Lab., Bay Saint Louis, MS.
DIGITAL MAPPING, CHARTING, AND GEODESY ANALYSIS PROGRAM TECHNICAL REVIEW OF VECTOR SMART MAP (VMAP) LEVEL 1
H. V. Miller, Kevin B. Shaw, and Susan V. Carter 9 Sep. 1994 23 p
(AD-A286294; NRL/MR/7441-94-7537) Avail: CASI HC A03/MF A01

The Naval Research Laboratory's Digital Mapping, Charting, and Geodesy Analysis Program (DMAP), in an effort to ensure that naval requirements are being met, has performed a technical review of the specification for Vector Smart Map (VMap) Level 1, as directed by the Defense Mapping Agency (DMA) via the Oceanographer of the Navy. VMap, a DMA product formatted in vector product format, will eventually provide users with an excellent source of medium-resolution map data in digital form. Considering only the written specifications, DMAP discovered errors that could hinder not only the production of authentic VMap database libraries but also the user comprehension as well. DMAP emphasizes that essential changes should be made before prototype production begins. Minor suggested changes are also given. DTIC

N95-22110*# National Aeronautics and Space Administration. Marshall Space Flight Center, Huntsville, AL.
REMOTE-SENSING BASED TECHNIQUE TO ACCOUNT FOR SUB-GRID SCALE VARIABILITY OF LAND SURFACE PROPERTIES
William L. Crosson and Charles A. Laymon (Institute for Global Change Research and Education, Huntsville, AL.) 1995 7 p Presented at the Conference on Hydrology, Annual Meeting, American Meteorological Society, Dallas, TX, 15-20 Jan. 1995
(Contracts NCC8-22; SUB93-216)
(NASA-TM-110501; NAS 1.15:110501) Avail: CASI HC A02/MF A01

A method has been presented for the representation of sub-grid scale variability of surface properties within a land surface processes model. The method uses remotely-sensed data to directly or indirectly estimate probability density functions (PDF's) or key surface variables. Application of this technique in a coupled land surface-atmosphere model requires only grid-scale values of the variables of interest, obtained from low-resolution satellite imagery or surface/remote sensing data assimilation. The PDF's of each controlling surface property are superimposed on the respective grid-scale values to simulate sub-grid scale heterogeneity. Sensitivity studies will be carried out to ascertain the relative importance of the heterogeneity of several variables, and the degree to which non-linear property-process interactions impact large-scale fluxes. Author

N95-22111*# National Aeronautics and Space Administration. Marshall Space Flight Center, Huntsville, AL.
REGIONAL SCALE HYDROLOGY WITH A NEW LAND SURFACE PROCESSES MODEL
Charles Laymon and William Crosson (Institute for Global Change Research and Education, Huntsville, AL.) 1995 7 p Presented at the Conference on Hydrology, Annual Meeting, American Meteorological Society, Dallas, TX, 15-20 Jan. 1995
(Contracts NCC8-22; SUB93-216)
(NASA-TM-110500; NAS 1.15:110500) Avail: CASI HC A02/MF A01

Through the CaPE Hydrometeorology Project, we have developed an understanding of some of the unique data quality issues involved in assimilating data of disparate types for regional-scale hydrologic modeling within a GIS framework. Among others, the issues addressed here include the development of adequate validation of the surface water budget, implementation of the STATSGO soil data set, and implementation of a remote sensing-derived landcover data set to account for surface heterogeneity. A model of land surface processes has been developed and used in studies of the sensitivity of surface fluxes and runoff to soil and landcover characterization. Results of these experiments have raised many questions about how to treat the scale-dependence of land surface-atmosphere interactions on spatial and temporal variability. In light of these questions, additional modifications are being considered for the Marshall Land Surface Processes Model. It is anticipated that these techniques can be tested and applied in conjunction with GCIP activities over regional scales. Author

N95-22131# Army Research Lab., Aberdeen Proving Ground, MD.
SOLVING THE INVERSE PROBLEM IN TERRAIN MODELING Final Report, Nov. 1993 - Jul. 1994
Joseph K. Wald Oct. 1994 19 p
(DA Proj. 1L1-61618-AH-43)
(AD-A285860; ARL-TR-605) Avail: CASI HC A03/MF A01

In the computer simulation of combat over a specific geographical area, the terrain is typically represented using sets of isolated, measured terrain altitudes. The 'inverse' problem is to construct in closed form a smooth surface function that matches these measured values to within a prescribed tolerance. If such a surface could be defined, then at any point on the simulated battlefield, both the terrain altitude and the slope of the terrain in any direction could be obtained simply by evaluating the surface functions and its derivatives. Such a terrain description would allow all calculations related to terrain, from line-of-sight to troop movement, to be done more simply and at any desired resolution. In this report, we will show how to solve the inverse problem. DTIC

N95-22398# Idaho National Engineering Lab., Idaho Falls, ID.
A MULTISPECTRAL SCANNER SURVEY OF THE IDAHO NATIONAL ENGINEERING LABORATORY AND THE HANFORD RESERVATION
S. B. Brewster, Jr., M. E. Howard, and J. E. Shines Sep. 1994 42 p
(Contract DE-AC08-93NV-11265)
(DE95-003922; EGG-11265-1098) Avail: CASI HC A03/MF A01

An airborne multispectral scanner survey of selected sites on the Idaho National Engineering Laboratory and the Hanford Reservation was performed in mid-November 1993. Aerial multispectral scanner and photography data were acquired coincidentally with the Big O experiment at both locations. To illustrate two potential applications, the multispectral scanner data were digitally enhanced to facilitate the detection of soil disturbance and evidence of surface water transport. The main conclusion of this study was that multispectral data acquired under these conditions can be useful for soil disturbance detection. The imagery did not prove as useful, however, for direct indications of surface water transport. It was possible to infer some water transport patterns from dry water beds, but only if surface indications were present. DOE

44 ENERGY PRODUCTION AND CONVERSION

Includes specific energy conversion systems, e.g., fuel cells; global sources of energy; geophysical conversion; and windpower.

For related information see also *07 Aircraft Propulsion and Power, 20 Spacecraft Propulsion and Power,* and *28 Propellants and Fuels.*

N95-20104# Oregon Inst. of Tech., Klamath Falls, OR. Geo-Heat Center.
GEOTHERMAL DIRECT-HEAT UTILIZATION ASSISTANCE
1994 17 p
(Contract DE-FG07-90ID-13040)
(DE94-011546; DOE/ID-13040/T22) Avail: CASI HC A03/MF A01

The Geo-Heat Center provides technical assistance on geothermal direct heat applications to developers, consultants and the public which could include: data and information on low-temperature (less than 1500 C) resources, space and district heating, geothermal heat pumps, greenhouses, aquaculture, industrial processes and other technologies. This assistance could include preliminary engineering feasibility studies, review of direct-use project plans, assistance in project material and equipment selection, analysis and solutions of project operating problems, and information on resources and utilization. The following are brief descriptions of technical assistance provided during the second quarter of the program. DOE

N95-20118# Colorado School of Mines, Golden, CO.
POLYCRYSTALLINE THIN FILM CADMIUM TELLURIDE SOLAR CELLS FABRICATED BY ELECTRODEPOSITION
J. U. Trefny, T. E. Furtak, D. L. Williamson, and D. Kim Jul. 1994 57 p
Prepared for National Renewable Energy Lab., Golden, CO
(Contract DE-AC36-83CH-10093)
(DE94-011848; NREL/TP-451-7046) Avail: CASI HC A04/MF A01

This report describes the principal results of work performed during the second year of a 3-year program at the Colorado School of Mines (CSM). The work on transparent conducting oxides was carried out primarily by CSM students at NREL and is described in three publications listed in Appendix C. The high-quality ZnO produced from the work was incorporated into a copper indium diselenide cell that exhibited a world-record efficiency of 16.4%. Much of the time was devoted to the improvement of cadmium sulfide films deposited by chemical bath deposition methods and annealed with or without a cadmium chloride treatment. Progress was also made in the electrochemical deposition of cadmium telluride. High-quality films yielding CdS/CdTe/Au cells of greater than 10% efficiency are now being produced on a regular basis. We explored the use of zinc telluride back contacts to form an n-i-p cell structure as previously used by Ametek. We began small-angle x-ray scattering (SAXS) studies to characterize crystal structures, residual stresses, and microstructures of both CdTe and CdS. Large SAXS signals were observed in CdS, most likely because of scattering from gain boundaries. The signals observed to date from CdTe are much weaker, indicating a more homogeneous microstructure. We began to use the ADEPT modeling program, developed at Purdue University, to guide our understanding of the CdS/CdTe cell physics and the improvements that will most likely lead to significantly enhanced efficiencies. DOE

N95-20260# National Renewable Energy Lab., Golden, CO.
ERROR ANALYSIS IN WIND TURBINE FIELD TESTING
B. McNiff (McNiff Light Industries, Carlisle, MA.) and D. Simms Aug. 1994 8 p Presented at the Windpower 1992, Seattle, WA, 19-23 Oct. 1992
(Contract DE-AC36-83CH-10093)
(DE94-011864; NREL/TP-441-7079; CONF-921049-11) Avail: CASI HC A02/MF A01

In wind turbine field testing, one of the most important issues is understanding and accounting for data errors. Extended dynamic testing of wind turbines requires a thorough uncertainty analysis and a regimen of quality assurance steps in order to preserve accuracy. Test objectives need to be identified to determine the accuracy requirements of any data measurement, collection, and analysis process. Frequently, the uncertainty analysis reveals that the major sources of error can be allowed for with careful calibration and signal drift tracking procedures. This paper offers a basis for the discussion and development of a repeatable and accurate process to track errors and account for them in data processing. DOE

N95-20263# Sandia National Labs., Albuquerque, NM. Photovoltaic Systems Applications.
ANALYSES OF GROUNDED AND UNGROUNDED PHOTOVOLTAIC POWER SYSTEMS
Ward Bower and John Wiles (New Mexico State Univ., Las Cruces, NM.) 1994 5 p Presented at the 1st World Conference on Photovoltaic Energy Conversion, Waikoloa, HI, 5-9 Dec. 1994
(Contract DE-AC04-94AL-85000)
(DE94-015015; SAND-94-1774C; CONF-941203-5) Avail: CASI HC A01/MF A01

Photovoltaic (PV) modules and photovoltaic balance of systems equipment are designed, manufactured, and marketed internationally. Each country or group of countries has a set of electrical safety codes, either in place or evolving, that guide and regulate the design and installation of PV power systems. A basic difference in these codes is that some require hard (low-resistance) grounding (the United States and Canada) and others opt for an essentially ungrounded system (Europe and Japan). The significant design and safety issues that exist between the two grounding concepts affect the international PV industry's ability to economically and effectively design and market safe, reliable, and durable PV systems in the global market place. This paper will analyze the technical and safety benefits, penalties, and costs of both grounded arid ungrounded PV systems. The existing grounding practice in several typical countries will be addressed. DOE

N95-20332# National Renewable Energy Lab., Golden, CO.
THE FIRST NREL CONFERENCE ON THERMOPHOTOVOLTAIC GENERATION OF ELECTRICITY: PROCEEDINGS
1994 165 p Conference held in Copper Mountain, CO, 24-27 Jul. 1994
(Contract DE-AC36-83CH-10093)
(DE94-011831; NREL/CP-413-6186; CONF-9407100) Avail: CASI HC A08/MF A02

This collection of abstracts from the July 1994 meeting contains various information on thermophotovoltaic (TPV) conversion and converters. Discussed topics include: the current status of TPV conversion, TPV tutorials, heat source and emitter technologies, advanced TPV devices, selective emitter theory and practice, programmatic and systems issues, device fundamentals, and device and material characterization. DOE

N95-20333# National Renewable Energy Lab., Golden, CO.
POLYCRYSTALLINE CuInSe2 AND CdTe SOLAR CELLS
N. G. Dhere (Florida Solar Energy Center, Cape Canaveral, FL.) Aug. 1994 35 p
(Contract DE-AC36-83CH-10093)
(DE94-011875; NREL/TP-451-6637) Avail: CASI HC A03/MF A01

The principal objective is to develop processes for the fabrication of cadmium-telluride, CdTe, and copper-indium-gallium-diselenide, Cu(In(1-x)Ga(x))Se2, polycrystalline thin-film solar cells using techniques that can be scaled-up for economic manufacture on a large scale. The aims are to fabricate CdTe solar cells using Cd and Te layers sputtered from elemental targets; to promote the interdiffusion between Cd/Te layers, CdTe phase formation, and grain growth; to utilize nontoxic selenization so as to avoid the use of extremely toxic H2Se in the fabrication of Cu(In(1-x)Ga(x))Se2 thin-film solar cells; to optimize selenization parameters; to improve adhesion; to minimize residual stresses; and to improve the uniformity, stoichiometry, and morphology of CdTe and Cu(In(1-x)Ga(x))Se2 thin films, and the efficiency of CdTe and Cu(In(1-x)Ga(x))Se2 solar cells. DOE

N95-20439# California Univ., Berkeley. Lawrence Berkeley Lab, CA. Energy and Environment Div.
EXPLORATORY TECHNOLOGY RESEARCH PROGRAM FOR ELECTROCHEMICAL ENERGY STORAGE Executive Summary Report, 1993
Kim Kinoshita, ed. Sep. 1994 13 p
(Contract DE-AC03-76SF-00098)
(DE95-002651; LBL-35566) Avail: CASI HC A03/MF A01

The U.S. Department of Energy's Office of Propulsion Systems provides support for an Electrochemical Energy Storage Program, that includes research and development (R&D) on advanced rechargeable batteries and fuel cells. A major goal of this program is to develop electrochemical power sources suitable for application in electric vehicles (EV's). The program centers on advanced systems that offer the potential for high performance and low life-cycle costs, both of which are necessary to permit significant penetration into commercial markets. The DOE Electrochemical Energy Storage Program is divided into two projects: the Electric Vehicle Advanced Battery Systems (EVABS) Development Program and the Exploratory Technology Research (ETR) Program. The EVABS Program management responsibility has been assigned to Sandia National Laboratories (SNL); Lawrence Berkeley Laboratory (LBL) is responsible for management of the FIR Program. The EVABS and ETR Programs include an integrated matrix of R&D efforts designed to advance progress on selected candidate electrochemical systems. The United States Advanced Battery Consortium (USABC), a tripartite undertaking between DOE, the U.S. automobile manufacturers and the Electric Power Research Institute (EPRI), was formed in 1991 to accelerate the development of advanced batteries for consumer EV's. The role of the FIR Program is to perform supporting research on the advanced battery systems under development by the USABC and EVABS Program, and to evaluate new systems with potentially superior performance, durability and/or cost characteristics. The specific goal of the ETR Program is to identify the most promising electrochemical technologies and transfer them to the USABC, the battery industry and/or the EVABS Program for further development and scale-up. This report summarizes the research, financial and management activities relevant to the ETR Program in CY 1993. DOE

N95-20473# National Renewable Energy Lab., Golden, CO.
THE PHOTOVOLATIC MANUFACTURING TECHNOLOGY PROJECT (PVMaT) AFTER THREE YEARS
C. Edwin Witt, Richard L. Mitchell, Holly Thomas, and Lloyd O. Herwig (Department of Energy, Washington, DC.) Aug. 1994 6 p Presented at the 29th Intersociety Energy Conversin Engineering Conference, Monterey, CA, 7-12 Aug. 1994
(Contract DE-AC36-83CH-10093)
(DE94-011877; NREL/TP-411-6639; CONF-940812-20) Avail: CASI HC A02/MF A01

The Photovoltaic Manufacturing Technology project (PVMaT) is a government/industry research and development (R&D) partnership involving joint efforts between the federal government (through the US Department of Energy (DOE)) and members of the US photovoltaic (PV) industry. The project's goal is to assist US industry in retaining and extending its world leadership role in the manufacture and commercial development of PV components and systems. PVMaT is being carried out in three separate phases, each designed to address separate R&D requirements for achieving PVMaT goals. Phase 1 was a problem identification phase of about 3 months duration. In Phase 1, the status and needs of the US PV manufacturing industry were identified, and the development of a Phase 2 procurement responsive to the industry's needs was begun. Phase 1 was completed in 1991. Problem solution began in 1992, under Phase 2A, when DOE awarded multiyear subcontracts. Technical accomplishments for PVMaT 2A are presented in this paper. Subcontracts were recently awarded for a second, overlapping, and similar process-specific solicitation (PVMaT 2B). The activities of these new subcontracts are also described. Two subcontracts presently comprise the Phase 3 effort. Phase 3 addresses R&D problems that are relatively common to a number of PV companies or the PV industry as a whole. A teamed research approach is being used to improve automated module manufacturing lines and encapsulation materials used in module manufacturing. The first year's work on these subcontracts is also described in this paper. DOE

N95-20480# Argonne National Lab., IL.
MULTIPLY MANIFOLDED MOLTEN CARBONATE FUEL CELLS
M. Krumpelt, M. F. Roche, H. K. Geyer, and S. A. Johnson 1994 4 p Presented at the Fuel Cells 1994, Morgantown, WV, 17-19 Aug. 1994
(Contract W-31-109-eng-38)
(DE94-017074; ANL/CMT/CP-83649; CONF-940883-1) Avail: CASI HC A01/MF A01

This study consists of research and development activities related to the concept of a molten carbonate fuel cell (MCFC) with multiple manifolds. The objective is to develop an MCFC having a higher power density and a longer life than other MCFC designs. The higher power density will result from thinner gas flow channels; the extended life will result from reduced temperature gradients. Simplification of the gas flow channels and current collectors may also significantly reduce cost for the multiply manifolded MCFC. DOE

N95-20685# Tokyo Univ., Tanashi (Japan). Inst. for Nuclear Study.
ACCELERATORS FOR ENERGY PRODUCTION
Takeshi Katayama Nov. 1993 7 p
(DE94-770764; INS-1015) Avail: CASI HC A02/MF A01

A tremendous progress of accelerators for these several decades, has been motivated mainly by the research on subnuclear physics. The culmination in high energy accelerators might be SSC, 20 TeV collider in USA, probably the ultimate accelerator being built with the conventional principle. The technology cultivated and integrated for the accelerator development, can now stably offer the high power beam which could be used for the energy problems. The Inertial Confinement Fusion (ICF) with high current, 10 kA and short pulse, 20 ns heavy ion beam (HIB) of mass number approximately 200, would be the most promising application of accelerators for energy production. In this scenario, the fuel containing D-T mixture, will be compressed to the high temperature, approximately 10 keV and to the high density state, approximately 1000 times the solid density with the pressure of ablative plasma or thermal X ray produced by bombarding of high power HIB. The efficiency, beam power/electric power for accelerator, and the repetition rate of HIB accelerators could be most suitable for the energy production. In the present paper, the outline of HIB ICF (HIF) is presented emphasizing the key issues of high current heavy ion accelerator system. DOE

N95-20778# National Renewable Energy Lab., Golden, CO.
SOLAR RADIATION RESOURCE ASSESSMENT PROJECT
Jun. 1994 16 p
(Contract DE-AC36-83CH-10093)
(DE94-000286; NREL/SP-463-6156) Avail: CASI HC A03/MF A01

The mission of the Solar Radiation Resource Assessment Project is to provide essential information about the solar radiation resource to users and planners of solar technologies so that they can make informed and timely decisions concerning applications of those technologies. The project team accomplishes this by producing and disseminating relevant and reliable information about solar radiation. Topics include: variability of solar radiation, measurements of solar radiation, spectral distribution of solar radiation, and assessment of the solar resource. FY 1993 accomplishments are detailed. DOE

N95-20839# Argonne National Lab., IL.
A FUEL CELL OVERVIEW
M. Krumpelt and C. Reiser 1994 5 p Presented at the Northeast Sustainable Energy Association (NESEA) Symposium, Providence, RI, 3-5 Oct. 1994
(Contract W-31-109-eng-38)
(DE95-001455; ANL/CMT/CP-84205; CONF-9410217-1) Avail: CASI HC A01/MF A01

This paper is an overview of the fuel cell as an efficient and environmentally benign energy conversion technology. The topics of the paper include their physical arrangement, types of fuel cells, status of commercial development, applications of the fuel cell power plants and comparison with existing alternatives, and good design practice for fuel cell safety. DOE

N95-20861# Sandia National Labs., Albuquerque, NM.
RECENT REFLUX RECEIVER DEVELOPMENTS UNDER THE US DOE PROGRAM
C. E. Andraka, R. B. Diver, J. B. Moreno, T. A. Moss, and D. R. Adkins 1994 11 p Presented at the 7th International Symposium on Solar Thermal Concentrating Technologies, Moscow, Russia, 26-30 Sep. 1994
(Contract DE-AC04-94AL-85000)
(DE95-001622; SAND-94-1758C; CONF-940970-3) Avail: CASI HC A03/MF A01

The United States Department of Energy (DOE) Solar Thermal Program, through Sandia National Laboratories (SNL), is cooperating with industry to commercialize dish-Stirling technology. Sandia and the DOE have actively encouraged the use of liquid metal reflux receivers in these systems to improve efficiency and lower the levelized cost of electricity. The reflux receiver uses two-phase heat transfer as a 'thermal transformer' to transfer heat from a parabolic tracking-concentrator to the heater heads of the Stirling engine. The two-phase system leads to a higher available input temperature, lower thermal stresses, longer life, and independent design of the absorber and engine sections. Two embodiments of reflux receivers have been investigated: Pool boilers and heat pipes. Several pool-boiler reflux receivers have been successfully demonstrated on sun at up to 64 kWt throughput at SNL. In addition, a bench-scale device was operated for 7500 hours to investigate materials compatibility and boiling stability. Significant progress has also been made on heat pipe receiver technology. Sintered metal wick heat pipes have been investigated extensively for application to 7.5 kWe and 25 kWe systems. One test article has amassed over 1800 hours of on-sun operation. Another was limit tested at Sandia to 65 kWt throughput. These devices incorporate a nickel-powder thick wick structure with condensate return directly to the wick surface. Circumferential tubular arteries are optionally employed to improve the operating margin. In addition, DOE has begun a development program for advanced wick structures capable of supporting the Utility Scale Joint Venture Program, requiring up to 100 kWt throughput. Promising technologies include a brazed stainless steel powdered metal wick and a stainless steel metal felt wick. Bench-scale testing has been encouraging, and on-sun testing is expected this fall. Prototype gas-fired hybrid solar receivers have also been demonstrated. DOE

N95-20862# Sandia National Labs., Albuquerque, NM.
AN OVERVIEW: COMPONENT DEVELOPMENT FOR SOLAR THERMAL SYSTEMS
T. R. Mancini 1994 14 p Presented at the 7th International Symposium on Solar Thermal Concentrating Technologies, Moscow, Russia, 26-30 Sep. 1994
(Contract DE-AC04-94AL-85000)
(DE95-001623; SAND-94-2431C; CONF-940970-1) Avail: CASI HC A03/MF A01

In this paper, I review the significant issues and the development of solar concentrators and thermal receivers for central-receiver power plants and dish/engine systems. Due to the breadth of the topic area, I have arbitrarily narrowed the content of this paper by choosing not to discuss line-focus (trough) systems and energy storage. I will focus my discussion on the development of heliostats, dishes, and receivers since the 1970s with an emphasis on describing the technologies and their evolution, identifying some key observations and lessons learned, and suggesting what the future in component development may be. DOE

N95-20863# Sandia National Labs., Albuquerque, NM.
HIGHLIGHTS OF RECENT BALANCE OF SYSTEM RESEARCH AND EVALUATION
M. G. Thomas and J. W. Stevens 1994 7 p Presented at the Photovoltaic Performance and Reliability Workshop, Lakewood, CO, 21-23 Sep. 1994
(Contract DE-AC04-94AL-85000)
(DE95-001626; SAND-94-2498C; CONF-9409170-1) Avail: CASI HC A02/MF A01

The cost of most photovoltaic (PV) systems is more a function of the balance of system (BOS) components than the collectors. The exception to this rule is the grid-tied system whose cost is related more directly to the collectors, and secondarily to the inverter/controls. In fact, recent procurements throughout the country document that collector costs for roof-mounted, utility-tied systems (Russell, PV Systems Workshop, 7/94) represent 60% to 70% of the system cost. This contrasts with the current market for packaged stand-alone all PV or PV-hybrid systems where collectors represent only 25% to 35% of the total. Not only are the BOS components the cost drivers in the current cost-effective PV system market place, they are also the least reliable components. This paper discusses the impact that BOS issues have on component performance, system performance, and system cost and reliability. We will also look at recent recommended changes in system design based upon performance evaluations of fielded PV systems. DOE

N95-20864# Sandia National Labs., Albuquerque, NM.
TESTING OF THE SAIC FACETS ON THE STRETCHED-MEMBRANE DISH
J. W. Grossman, W. W. Erdman, R. M. Houser, and R. Davenport (Science Applications International Corp., Golden, CO.) Apr. 1994 14 p Presented at the 1995 American Society of Mechanical Engineers/Japanese Society of Mechanical Engineers/Japan Solar Energy Society (ASME/JSME/JSES) International Solar Energy Conference, Maui, HI, 19-24 Mar. 1994
(Contract DE-AC04-94AL-85000)
(DE95-001831; SAND-94-1245C; CONF-9403170-1) Avail: CASI HC A03/MF A01

A dish structure sized for a 25 kW electric dish/generator system has been installed at the National Solar Thermal Test Facility (NSTTF). The dish is used as an optical test bed for prototype stretched-membrane facets. Sandia procured twelve (12) stretched-membrane facets from Science Applications International Corporation (SAIC) for installation on the dish structure. Individual facet optical performance was measured using the 2f test method under development at Sandia. Four facets were tested on-sun using the test truss at the NSTTF prior to installation on the dish structure. During the final stages of the structure assembly, the facets were installed for testing. A distant light source alignment technique was used to align the facets to a 9 meter focal length. The alignment and focus were optimized with on-sun measurements of individual facet characteristics. On-sun flux maps of the image were made using the Beam Characterization System. Calorimetry tests were performed using a cold water calorimeter. This data was used to create a power intercept curve and predict the power inside apertures of different sizes. The focal plane was moved to 9.95 meters and the alignment, optimization, and on-sun tests repeated. This paper presents the results of the testing on the individual facets as well as the results of testing the dish system. The effects of the change in focal length on the optical performance of the dish are shown in the results. DOE

N95-20870# Sandia National Labs., Albuquerque, NM.
SI CONCENTRATOR SOLAR CELL DEVELOPMENT
D. D. Krut (Spectrolab, Inc., Sylmar, CA.) Oct. 1994 24 p
(Contract DE-AC04-94AL-85000)
(DE95-002314; SAND-94-2453) Avail: CASI HC A03/MF A01

This is the final report of a program to develop a commercial, high-efficiency, low-cost concentrator solar cell compatible with Spectrolab's existing manufacturing infrastructure for space solar cells. The period covered is between 1991 and 1993. The program was funded through Sandia National Laboratories through the DOE concentrator initiative and, was also cost shared by Spectrolab. As a result of this program, Spectrolab implemented solar cells achieving an efficiency of over 19% at 200 to 300X concentration. The cells are compatible with DOE guidelines for a cell price necessary to achieve a cost of electricity of 12 cents a kilowatthour. DOE

N95-20871# Applied Solar Energy Corp., City of Industry, CA.
DEVELOPMENT OF CONCENTRATOR SOLAR CELLS
Aug. 1994 40 p Prepared for Sandia National Labs., Albuquerque, NM
(Contracts DE-AC04-94AL-85000)
(DE95-002316; SAND-94-2068) Avail: CASI HC A03/MF A01

A limited pilot production run on PESC silicon solar cells for use at high concentrations (200 to 400 suns) is summarized. The front contact design of the cells was modified for operation without prismatic covers. The original objective of the contract was to systematically complete a process consolidation phase, in which all of the process improvements developed during the contract would be combined in a pilot production run. This pilot run was going to provide a basis for estimating cell costs when produced at high throughput. Because of DOE funding limitations, the Photovoltaic Concentrator Initiative is on hold, and Applied Solar's contract was operated at a low level of effort for most of 1993. The results obtained from the reduced scope pilot run showed the effects of discontinuous process optimization and characterization. However, the run provided valuable insight into the technical areas that can be optimized to achieve the original goals of the contract. DOE

N95-20896# Department of Energy, Morgantown, WV. Energy Technology Center.
PERFORMANCE AND COST ANALYSIS OF MONOLITHIC SOLID OXIDE FUEL CELLS
Mar. 1994 42 p
(Contract DE-AC21-89MC-26006)
(DE95-002511; DOE/MC-26006/3804) Avail: CASI HC A03/MF A01

This report was prepared by AlliedSignal Aerospace Systems & Equipment (ASE) in partial fulfillment of the statement of work (SOW) for Contract DE-AC21-89MC-26006, specifically, item 3, 'Task 5 - Topical Report' of Section C, 'Deliverables.' It comprises an evaluation and optimization of a 2-Mwe monolithic solid oxide fuel (MSOFC) system operating on natural gas fuel, and an update of the stack manufacturing costs developed under Contract DE-AC21-88MC-25166. The system studies are supported by the stack performance model FCELL developed under 'Task 5.1 - Stack Performance Studies.' The system studies show a clear advantage of stacks that are sealed vs. the current 'seal-less' approaches; the sealed stacks achieve extraordinarily high system efficiencies. A market survey supplemented by key inputs from DOE/METC and EPRI personnel led to the power level and fuel selections. DOE

N95-20915# California Univ., Berkeley. Lawrence Berkeley Lab, CA. Energy and Environment Div.
EXPLORATORY TECHNOLOGY RESEARCH PROGRAM FOR ELECTROCHEMICAL ENERGY STORAGE Annual Report, 1993
Kim Kinoshita, ed. Sep. 1994 52 p
(Contract DE-AC03-76SF-00098)
(DE95-002652; LBL-35567) Avail: CASI HC A04/MF A01

The U.S. Department of Energy's Office of Propulsion Systems provides support for an Electrochemical Energy Storage Program, that includes research and development (R&D) on advanced rechargeable batteries and fuel cells. A major goal of this program is to develop electrochemical power sources suitable for application in electric vehicles (EV's). The program centers on advanced systems that offer the potential for high performance and low life-cycle costs, both of which are necessary to permit significant penetration into commercial markets. The DOE Electrochemical Energy Storage Program is divided into two projects: the Electric Vehicle Advanced Battery Systems (EVABS) Development Program and the Exploratory Technology Research (ETR) Program. The EVABS Program management responsibility has been assigned to Sandia National Laboratories (SNL); Lawrence Berkeley Laboratory (LBL) is responsible for management of the ETR Program. The EVABS and ETR Programs include an integrated matrix of R&D efforts designed to advance progress on selected candidate electrochemical systems. The United States Advanced Battery Consortium (USABC), a tripartite undertaking between DOE, the U.S. automobile manufacturers and the Electric Power Research Institute (EPRI), was formed in 1991 to accelerate the development of advanced batteries for consumer EV's. The role of the FIR Program is to perform supporting research on the advanced battery systems under development by the USABC and EVABS Program, and to evaluate new systems with potentially superior performance, durability and/or cost characteristics. The specific goal of the ETR Program is to identify the most promising electrochemical technologies and transfer them to the USABC, the battery industry and/or the EVABS Program for further development and scale-up. This report summarizes the research, financial and management activities relevant to the ETR Program in CY 1993. DOE

N95-20985# National Renewable Energy Lab., Golden, CO.
ADVANCED WIND TURBINE DESIGN STUDIES: ADVANCED CONCEPTUAL STUDY
P. Hughes and R. Sherwin Aug. 1994 246 p Prepared in cooperation with Atlantic Orient Corp., Norwich, VT
(Contract DE-AC36-83CH-10093)
(DE93-000031; NREL/TP-442-4740) Avail: CASI HC A11/MF A03

In conjunction with the US Department of Energy and the National Renewable Energy Laboratory's Advanced Wind Turbine Program, the Atlantic Orient Corporation developed preliminary designs for the next generation of wind turbines. These 50 kW and 350 kW turbines are based upon the concept of simplicity. By adhering to a design philosophy that emphasizes simplicity, we project that these turbines will produce energy at extremely competitive rates which will unlock the potential of wind energy domestically and internationally. The program consisted of three distinct phases. First, we evaluated the operational history of the Enertech 44 series wind turbines. As a result of this evaluation, we developed, in the second phase, a preliminary design for a new 50 kW turbine for the near-term market. In the third phase, we took a clean-sheet-of-paper approach to designing a 350 kW turbine focused on the mid-1990s utility market that incorporated past experience and advanced technology. DOE

N95-21294# Institute of Energy Conversion, Newark, NJ.
PROCESSING AND MODELING ISSUES FOR THIN-FILM SOLAR CELL DEVICES
R. W. Birkmire, J. E. Phillips, W. A. Buchanan, S. S. Hegedus, B. E. McCandless, W. N. Shafarman, and T. A. Yokimcus Sep. 1994 206 p Prepared for National Renewable Energy Lab., Golden, CO
(Contract DE-AC36-83CH-10093)
(DE94-011895; NREL/TP-451-7056) Avail: CASI HC A10/MF A03

The overall objective of the research presented in this report is to advance the development and acceptance of thin-film photovoltaic modules by increasing the understanding of film growth and processing and its relationship to materials properties and solar cell performance. The specific means toward meeting this larger goal include: (1) investigating scalable, cost-effective deposition processes; (2) preparing thin-film materials and device layers and completed cell structures; (3) performing detailed material and device analysis; and (4) participating in collaborative research efforts that address the needs of PV-manufacturers. These objectives are being pursued with CuInSe2, CdTe, and a-Si based solar cells. DOE

N95-21353# Sandia National Labs., Albuquerque, NM.
RECENT NATIONAL SOLAR THERMAL TEST FACILITY ACTIVITIES, IN PARTNERSHIP WITH INDUSTRY
Cherly Ghanbari, Christopher P. Cameron, Mark E. Ralph, James E. Pacheco, K. Scott Rawlinson, and Lindsey R. Evans (Ewing Technical Design, Albuquerque, NM.) 1994 15 p Presented at the 7th International Symposium on Solar Thermal Concentrating Technologies, Moscow, Russia, 26-30 Sep. 1994
(Contract DE-AC04-94AL-85000)
(DE95-001828; SAND-94-2437C; CONF-940970-5) Avail: CASI HC A03/MF A01

The National Solar Thermal Test Facility (NSTTF) at Sandia National Laboratories in Albuquerque, New Mexico, USA conducts testing of solar thermal components and systems, funded primarily by the US Department of Energy. Activities are conducted in support of Central Receiver Technology, Distributed Receiver Technology and Design Assistance projects. All activities are performed in support of various cost-shared government/industry joint ventures and, on a design assistance basis, in support of a number of other industry partners. DOE

N95-21361# Department of Energy, Morgantown, WV. Power Generation Technology.
SOLID OXIDE FUEL CELLS IN THE UNITED STATES
Diane Traub Hooie 1994 11 p Presented at the 1st European Solid Oxide Fuel Cell Forum: Engineering, Systems, Applications, Lucerne, Switzerland, 3-7 Oct. 1994
(DE95-002405; DOE/METC-C/95/7162; CONF-9410170-1) Avail: CASI HC A03/MF A01

This paper presents an overview of the solid-oxide fuel cell program being undertaken in the US. This program addresses both intermediate and high temperature fuel cells as well as a variety of configurations including planar/monolithic, and tubular. These projects also address a variety of issues such as material compatibility, life/degradation, fuel compatibility, and system scaleup and integration. The primary applications currently being developed is for power generation but a variety of other potential applications, such as transportation, are being considered. The funding for these projects is provided through a variety of sources including the US Government (primarily Departments of Energy, Transportation, and Defense), the Electric Power Research Institute (EPRI), the Gas Research Institute (GRI), and industry. DOE

N95-21409# Georgetown Univ., Washington, DC.
THE PHOTOVOLTAIC HIGHER EDUCATION NATIONAL EXEMPLAR FACILITY (PHENEF)
V. Podbielski and D. Shaff Apr. 1994 65 p
(Contract DE-FG05-80CS-83014)
(DE94-015641; DOE/CS-83014/1) Avail: CASI HC A04/MF A01

In August 1980, the US Department of Energy awarded the proposed grant to Georgetown University. The grant covered the following tasks: Task 1, The Department of Energy would participate in the building of an academic facility that would facilitate the integration of flat plate photovoltaic roof modules with an optimally oriented solar architecture. The completion of the facility to be built on the Georgetown University Campus and known as the Georgetown University Intercultural Center was to be a jointly funded endeavor with the Department of Education funding $9.2M through a grant and a loan, Department of Energy funding a maximum of $4M and Georgetown University funding the residual costs. Task 2, Georgetown University would provide the necessary skills, services, materials, equipment and facilities to design, furnish, install and make operational the Georgetown University Intercultural Center Photovoltaic System. The specific objective of this effort would be to build an exemplar flat plate electrical grid connected photovoltaic (PV) system which would demonstrate integration of PV modules into a watertight roofing surface. The system capability, measured at the input to the inverter, would be a 300 kilowatt peak power system as measured at the normal cell operating temperature and an isolation of 100 milliwatts per square centimeter at the collector surface. DOE funding under the grant for the PV system would be limited to a system cost of $20.00 per peak watt up to maximum of six million dollars. DOE

N95-21508# Toledo Univ., OH.
THIN-FILM CADMIUM TELLURIDE PHOTOVOLTAIC CELLS
A. D. Compaan and R. G. Bohn Sep. 1994 32 p Prepared for National Renewable Energy Lab., Golden, CO
(Contract DE-AC36-83CH-10093)
(DE94-011886; NREL/TP-451-7162) Avail: CASI HC A03/MF A01

This report describes work to develop and optimize radio-frequency (RF) sputtering for the deposition of thin films of cadmium telluride (CdTe) and related semiconductors for thin-film solar cells. Pulsed laser physical vapor deposition was also used for exploratory work on these materials, especially where alloying or doping are involved, and for the deposition of cadmium chloride layers. The sputtering work utilized a 2-in diameter planar magnetron sputter gun. The film growth rate by RF sputtering was studied as a function of substrate temperature, gas pressure, and RF power. Complete solar cells were fabricated on tin-oxide-coated soda-lime glass substrates. Currently, work is being done to improve the open-circuit voltage by varying the CdTe-based absorber layer, and to improve the short-circuit current by modifying the CdS window layer. DOE

N95-21530*# Rockwell International Corp., Canoga Park, CA. Rocketdyne Div.
POWER SYSTEMS FOR FUTURE MISSIONS. APPENDICES A-L Final Report
S. P. Gill, P. E. Frye, Franklin D. Littman, and C. J. Meisl Cleveland, OH NASA Dec. 1994 477 p Prepared for Sverdrup Technologies, Inc., Brook Park, OH
(Contract NAS3-25266)
(NASA-CR-195320-App-A-L; NAS 1.26:195320-App-A-L) Avail: CASI HC A21/MF A04

Selection of power system technology for space applications is typically based on mass, readiness of a particular technology to meet specific mission requirements, and life cycle costs (LCC). The LCC is typically used as a discriminator between competing technologies for a single mission application. All other future applications for a given technology are usually ignored. As a result, development cost of a technology becomes a dominant factor in the LCC comparison. Therefore, it is common for technologies such as DIPS and LMR-CBC to be potentially applicable to a wide range of missions and still lose out in the initial LCC comparison due to high development costs. This collection of appendices (A through L) contains the following power systems technology plans: CBC DIPS Technology Roadmap; PEM PFC Technology Roadmap; NAS Battery Technology Roadmap; PV/RFC Power System Technology Roadmap; PV/NAS Battery Technology Roadmap; Thermionic Reactor Power System Technology Roadmap; SP-100 Power System Technology Roadmap; Dynamic SP-100 Power System Technology Roadmap; Near-Term Solar Dynamic Power System Technology Roadmap; Advanced Solar Dynamic Power System Technology Roadmap; Advanced Stirling Cycle Dynamic Isotope Power System Technology Roadmap; and the ESPPRS (Evolutionary Space Power and Propulsion Requirements System) User's Guide. Derived from text

N95-21611# Pacific Northwest Lab., Richland, WA.
A PROPOSED WIND MEASUREMENT AND ANALYSIS APPROACH FOR EVALUATING A PROSPECTIVE WIND PLANT SITE
L. L. Wendell, J. C. Barnard, and V. R. Morris May 1994 7 p Presented at the American Wind Energy Association Annual Conference and Exhibition, Minneapolis, MN, 9-13 May 1994
(Contract DE-AC06-76RL-01830)
(DE94-019187; PNL-SA-24143; CONF-940548-8) Avail: CASI HC A02/MF A01

On the basis of research results, cooperative efforts with wind energy developers, and work with meteorological consultants, Pacific Northwest Laboratory (PNL) has proposed an approach for performing wind measurement assessments for prospective wind plant sites. The primary goal of this approach is to effectively balance comprehensiveness with expense. The approach begins with the acquisition of high-resolution digital terrain data for the site. These data are used in computational and visual analyses to determine the best locations for a reference tower and several satellite towers used for wind measurements. The reference tower has wind sensors at three levels: 20, 30, and 40 m. The satellite towers have one sensor at 30 m. The sensors measure the vertical wind speed as well as the horizontal speed and direction. The sampling rate must be at least 4 times per second. The data acquisition system keeps track of turbulence statistics that are saved at intervals from ten minutes to one hour. Statistics for the 30-m level at the satellite towers, as well as the reference tower, provide the mean and variance of the total speed and covariances of the component speeds. The data base produced by this approach over 1-2 years should be valuable for both routine and in-depth analyses. This approach takes advantage of some recent technological developments. It is not being proposed as a standard at this time, but as a tool to be refined with experience. DOE

N95-21844# National Renewable Energy Lab., Golden, CO.
NON-H2Se, ULTRA-THIN CuInSe2 DEVICES
A. E. Delahoy (Energy Photovoltaics, Inc., Princeton, NJ.), J. Britt (Energy Photovoltaics, Inc., Princeton, NJ.), F. Faras (Energy Photovoltaics, Inc., Princeton, NJ.), and Z. Kiss (Energy Photovoltaics, Inc., Princeton, NJ.) Sep. 1994 34 p
(Contract DE-AC36-83CH-10093)
(DE94-011894; NREL/TP-413-7165) Avail: CASI HC A03/MF A01

This report describes advances made during Phase 2 (November 10, 1992 - November 9, 1993) of a three-phase, cost-shared subcontract whose ultimate goal is the demonstration of thin film CuInSe2 photovoltaic modules prepared by methods adaptable to safe, high yield, high volume manufacturing. At the end of Phase 1, EPV became one of the first groups to clear the 10% efficiency barrier for CIS cells prepared by non-H2Se selenization. During Phase 2 a total area efficiency of 12.5% was achieved for a 1 cm(exp 2) cell. The key achievement of Phase 2 was the production of square foot CIS modules without the use of H2Se. This is seen as a crucial step towards the commercialization of CIS. Using a novel interconnect technology, EPV delivered an 8.0% aperture area efficiency mini-module and a 6.2% aperture area efficiency 720 cm(exp 2) module to NREL. On the processing side, advances were made in precursor formation and the selenization profile, both of which contributed to higher quality CIS. The higher band gap quaternary chalcopyrite material CuIn(S(x)), Se(1-x)2 was prepared and 8% cells were fabricated using this material. Device analysis revealed a correlation between long wavelength quantum efficiency and the CIS Cu/In ratio. Temperature dependent studies highlighted the need for high V(sub OC) devices to minimize the impact of the voltage drop at operating temperature. Numerical modeling of module performance was performed in order to identify the correct ZnO sheet resistance for modules. Efforts in Phase 3 will focus on increase of module efficiency to 9-10%, initiation of an outdoor testing program, preparation of completely uniform CIS plates using second generation selenization equipment, and exploration of alternative precursors for CIS formation. DOE

N95-21897# Argonne National Lab., IL.

SEAWATER TEST RESULTS OF OPEN-CYCLE OCEAN THERMAL ENERGY CONVERSION (OC-OTEC) COMPONENTS

F. Zangrando (National Renewable Energy Lab., Golden, CO.), D. Bharathan (National Renewable Energy Lab., Golden, CO.), H. Link (National Renewable Energy Lab., Golden, CO.), and C. B. Panchal 1994 23 p
(Contract W-31-109-eng-38)
(DE94-019254; ANL/ES/PP-73762) Avail: CASI HC A03/MF A01

Key components of open-cycle ocean thermal energy conversion systems- the flash evaporator, mist eliminator, passive predeaerator, two surface condenser stages, and two direct-contact condenser stages- have been tested using seawater. These components operate at lower steam pressures and higher inlet noncondensable gas concentrations than do conventional power plant heat exchangers. The rate of heat exchanged between the evaporator and the condenser is on the order of 1.25MW-thermal, requiring a warm seawater flow of about 0.1 cu m/s; the cold seawater flow is on the order of half the warm water flow. In addition to characterizing the performance of the various components, the system has produced potable water from condensation of the steam produced in the evaporator. The information obtained in these tests is being used to design a larger scale experiment in which net power production is expected to be demonstrate for the first time using OC-OTEC technology. DOE

N95-21899 Department of the Navy, Washington, DC.

METHOD OF FORMING A HIGH VOLTAGE SILICON-ON-SAPPHIRE PHOTOCELL ARRAY Patent

Wadad B. Dubbelday, inventor (to Navy), Larry D. Flesner, inventor (to Navy), and George P. Imthurn, inventor (to Navy) 19 Jul. 1994 5 p
Filed 31 Aug. 1992
(AD-D016479; US-Patent-5,330,918; US-Patent-Appl-SN-938920; US-Patent-Class-437-2) Avail: US Patent and Trademark Office

A method is provided for forming a multi-cell photovoltaic circuit on an insulating substrate, comprising the steps of forming a photovoltaic junction between p-type and n-type layers in a silicon wafer; bonding the silicon wafer to an insulating substrate after forming the photovoltaic junction; patterning the silicon wafer to produce isolated photovoltaic cells; and electrically interconnecting the photovoltaic cells. DTIC

N95-21952*# Rockwell International Corp., Canoga Park, CA. Rocketdyne Div.

MARS POWER SYSTEM CONCEPT DEFINITION STUDY. VOLUME 1: STUDY RESULTS Final Report

Franklin D. Littman Dec. 1994 100 p
(Contract NAS3-25808; RTOP 326-84-00)
(NASA-CR-195420-Vol-1; E-9361-Vol-1; NAS 1.26:195420-Vol-1) Avail: CASI HC A05/MF A02

A preliminary top level study was completed to define power system concepts applicable to Mars surface applications. This effort included definition of power system requirements and selection of power systems with the potential for high commonality. These power systems included dynamic isotope, Proton Exchange Membrane (PEM) regenerative fuel cell, sodium sulfur battery, photovoltaic, and reactor concepts. Design influencing factors were identified. Characterization studies were then done for each concept to determine system performance, size/volume, and mass. Operations studies were done to determine emplacement/deployment maintenance/servicing, and startup/shutdown requirements. Technology development roadmaps were written for each candidate power system (included in Volume 2). Example power system architectures were defined and compared on a mass basis. The dynamic isotope power system and nuclear reactor power system architectures had significantly lower total masses than the photovoltaic system architectures. Integrated development and deployment time phasing plans were completed for an example DIPS and reactor architecture option to determine the development strategies required to meet the mission scenario requirements. Author

N95-21953*# Rockwell International Corp., Canoga Park, CA. Rocketdyne Div.

MARS POWER SYSTEM CONCEPT DEFINITION STUDY. VOLUME 2: APPENDICES Final Report

Franklin D. Littman Dec. 1994 276 p
(Contract NAS3-25808; RTOP 326-84-00)
(NASA-CR-195420-Vol-2; NAS 1.26:195420-Vol-2) Avail: CASI HC A13/MF A03

This report documents the work performed by Rockwell International's Rocketdyne Division on NASA Contract No. NAS3-25808 (Task Order No. 16) entitled 'Mars Power System Definition Study'. This work was performed for NASA's Lewis Research Center (LeRC). The report is divided into two volumes as follows: Volume 1 - Study Results; and Volume 2 - Appendices. The results of the power system characterization studies, operations studies, and technology evaluations are summarized in Volume 1. The appendices include complete, standalone technology development plans for each candidate power system that was investigated. Author

N95-22033# Southern California Gas Co., Los Angeles, CA.

ECONOMIC FEASIBILITY ANALYSIS OF DISTRIBUTED ELECTRIC POWER GENERATION BASED UPON THE NATURAL GAS-FIRED FUEL CELL Final Report

Mar. 1994 100 p
(Contract DE-FC21-92MC-29227)
(DE94-012277; DOE/MC-29227/3849) Avail: CASI HC A05/MF A02

The final report provides a summary of results of the Cost of Ownership Model and the circumstances under which a distributed fuel cell is economically viable. The analysis is based on a series of micro computer models estimates of the capital and operations cost of a fuel cell central utility plant configuration. Using a survey of thermal and electrical demand profiles, the study defines a series of energy user classes. The energy user class demand requirements are entered into the central utility plant model to define the required size the fuel cell capacity and all supporting equipment. The central plant model includes provisions that enables the analyst to select optional plant features that are most appropriate to a fuel cell application, and that are cost effective. The model permits the choice of system features that would be suitable for a large condominium complex or a residential institution such as a hotel, boarding school or prison. Other applications are also practical; however, such applications have a higher relative demand for thermal energy, a characteristic that is well-suited to a fuel cell application with its free source of hot water or steam. The analysis combines the capital and operation from the preceding models into a Cost of Ownership Model to compute the plant capital and operating costs as a function of capacity and principal features and compares these estimates to the estimated operating cost of the same central plant configuration without a fuel cell. DOE

N95-22175 Technische Univ., Delft (Netherlands).

HYDROTHERMAL CONVERSION OF CARBOHYDRATES AND RELATED COMPOUNDS Thesis

Gerardus Christianus Luijkx 1994 132 p Sponsored by Koninklijke/Shell-Lab.
(PB95-134011; ISBN-90-407-1002-3) Avail: Issuing Activity (National Technical Information Service (NTIS))

The research described in this thesis was aimed at the (partial) elucidation of the chemistry of the major decarboxylation pathways occurring in the hydrothermal conversion of carbohydrates. Knowledge of the chemical background of this hydrothermal decarboxylation might enable more effective processing of biomass with respect to minimizing the oxygen content of hydrothermolysis products. NTIS

N95-22183# International Centre for Theoretical Physics, Trieste (Italy).
INFLUENCE OF WAVELENGTH ON TRANSIENT SHORT-CIRCUIT CURRENT IN POLYCRYSTALLINE SILICON SOLAR CELLS
B. Ba and M. Kane (Universite Cheikh Anta Diop, Dakar, Senegal.) Oct. 1993 10 p
(DE94-629082; IC-93/348) Avail: CASI HC A02/MF A01 (US Sales Only)

The influence of the wavelength of a monochromatic illumination on transient short-circuit current in an n/p polycrystalline silicon part solar cell junction is investigated. A wavelength dependence in the initial part of the current decay is observed in the case of cells with moderate grain boundary effects. This influence is attenuated in polycrystalline cells with strong grain boundary activity. DOE

N95-22309# New Energy and Industrial Technology Development Organization, Tokyo (Japan).
RESEARCH ON THE POWER GENERATION SYSTEM WITH THERMOELECTRIC CONVERSION ELEMENTS
Mar. 1994 119 p In JAPANESE
(DE95-714804; NEDO-P-9323) Avail: CASI HC A06/MF A02

The semiconductor thermoelectric power generation system was conceptually designed which utilized, as a case study, a high temperature exhaust heat of 2000 kW from 10MW phosphoric acid fuel cells. Technical problems were then raised to put it to practical use. A system in which the thermoelectric power generation was applied to the heat exchanger of high temperature exhaust water was structured, because the high temperature exhaust heat had to be utilized without thermally unbalancing the fuel cell system. Through studying the influence to be given to the power generation performance by the configuration of module with Bi-Te elements, it was indicated that the present element performance generates power of about 100kW, which corresponds to the net power of about 80kW with a deduction of pumping power. Not only is the element performance enhanced, but it is indispensable to evaluate and demonstrate the reliability which is viewed from the thermomechanical point in the module joining and other thermoelectric power generation parts, and from the point of thermal resistance and other power generation performance in the members and pressure-welded parts. It was pointed out that the system experiment is necessary on a small and medium scale. DOE

N95-22335# Sandia National Labs., Albuquerque, NM.
BRIDGING WORLDS/CHARTING NEW COURSES
1994 18 p
(Contract DE-AC04-94AL-85000)
(DE95-003808; SAND-93-0992) Avail: CASI HC A03/MF A01

This report describes the work being done within Sandia's renewable energy program. This work touches on four major disciplines. (1) Photovoltaics. The goal of this project is to develop costeffective, reliable energy system technologies for energy supplies worldwide produced by U.S. industry. It encompasses cell research and development, collector development, technology evaluation, systems engineering, domestic and international applications, and design assistance. (2) Solar Thermal. This project endeavors to develop and increase acceptance of solar thermal electric and industrial technologies as cost-competitive candidates for power generation and to promote their commercialization. Its' major activities are with dish/Stirling systems, the Solar Two power tower, design assistance to industry and users, technology development and research activities. (3) Wind. The wind project impacts domestic and international markets with commercially feasible systems for utility-scale and other applications of wind energy. The project conducts applied research in aerodynamics, structural dynamics, fatigue, materials and controls, and engineering systems, and develops cooperative work with industry. (4) Geothermal. This project is developing technology to increase proven geothermal reserves and is assisting industry in expanding geothermal power on-line. Development work is in stemhole drilling, drilling techniques, instrumentation for geothermal wells, acoustic telemetry, and drilling exploratory wells. DOE

N95-22336*# Jet Propulsion Lab., California Inst. of Tech., Pasadena, CA.
THE LARGE AREA PULSED SOLAR SIMULATOR (LAPSS)
R. L. Mueller 15 Jul. 1994 15 p Revised
(Contract NAS7-1260)
(NASA-CR-197339; JPL-Publ-93-22-Rev-A; NAS 1.26:197339) Avail: CASI HC A03/MF A01

The Large Area Pulsed Solar Simulator (LAPSS) has been installed at JPL. It is primarily intended to be used to illuminate and measure the electrical performance of photovoltaic devices. The simulator, originally manufactured by Spectrolab, Sylmar, CA, occupies an area measuring about 3 m wide x 12 m long. The data acquisition and data processing subsystems have been modernized. Tests on the LAPSS performance resulted in better than plus or minus 2 percent uniformity of irradiance at the test plane and better than plus or minus 0.3 percent measurement repeatability after warm-up. Glass absorption filters reduce the ultraviolet light emitted from the xenon flash lamps. This results in a close match to three different standard airmass zero and airmass 1.5 spectral irradiances. The 2-ms light pulse prevents heating of the device under test, resulting in more reliable temperature measurements. Overall, excellent electrical performance measurements have been made of many different types and sizes of photovoltaic devices. Since the original printing of this publication, in 1993, the LAPSS has been operational and new capabilities have been added. This revision includes a new section relating to the installation of a method to measure the I-V curve of a solar cell or array exhibiting a large effective capacitance. Another new section has been added relating to new capabilities for plotting single and multiple I-V curves, and for archiving the I-V data and test parameters. Finally, a section has been added regarding the data acquisition electronics calibration. Author

N95-22337# Helsinki Univ. of Technology, Otaniemi (Finland).
ADVANCED ENERGY SYSTEMS AND TECHNOLOGIES RESEARCH PROGRAMME Annual Report, 1993
P. Lund and E. Tuominen (Helsinki Univ. of Technology, Otaniemi, Finland.) 1993 46 p
(DE95-717486; TKK-NEMO-25) Avail: CASI HC A03/MF A01

NEMO 2 is a national energy research program for the evaluation, development and promotion of new and renewable forms of energy. NEMO 2 is one of the energy research programs of the Finnish Ministry of Trade and Industry for the years 1993-1998. In NEMO 2 -program, new energy technology is developed as a whole in close collaboration between industry, universities and research institutes, as well as with customers and consumers. The overall budget of NEMO 2 is close to 125 MFIM (1 dollar = 5.7 FIM, Nov. 1993). The main emphasis of the program is on wind and solar energy. DOE

N95-22362 Swedish Inst. for Materials Testing, Boras (Sweden).
ACCELERATED LIFE TESTING OF SOLAR ENERGY MATERIALS: CASE STUDY OF SOME SELECTIVE SOLAR ABSORBER COATING MATERIALS FOR DHW SYSTEMS. A REPORT OF TASK 10 SOLAR MATERIALS RESEARCH AND DEVELOPMENT
Bo Carlsson, Michael Koehl (Fraunhofer-Inst. fuer Solare Energiesysteme, Freiburg, Germany.), Ulrich Frei (Solar Energy Lab., Rapperswil, Switzerland.), and Kenneth Moeller Feb. 1994 264 p Sponsored by International Energy Agency Limited Reproducibility: More than 20% of this document may be affected by microfiche quality
(PB95-132411) Avail: CASI HC A12

Accelerated life testing offers the possibility to forecast material service life prior to installation. For the development of new components and systems it, thus, opens a possibility for systematic life cost analysis and material selection. The present report documents the results of a joint study aimed at establishing the use and limitations of methods for accelerated life testing applicable to materials used in solar heating and cooling applications. The study was conducted as part of the work in Task 10 'Solar Materials Research and Development' of the International Energy Agency Solar Heating and Cooling Program. The work was organized as a case study in which four commercially-available selective absorber materials were selected for study. These materials are used in single-glazed flat plate solar collectors for domestic hot water production. NTIS

N95-22425# Kauppa-ja Teollisuusministerio, Helsinki, Uudenmaa (Finland). Energy Dept.
PRODUCING LIQUID FUELS FROM BIOMASS [POLTTONESTETUOTANTO BIOMASSASTA]
Yrjo Solantausta and Steven Gust (Neste Oy, Porvoo, Finland.) 1994 137 p In FINNISH
(DE95-717458; KTM/E-B-185) Avail: CASI HC A07/MF A02

The aim of this survey was to compare, on techno-economic criteria, alternatives of producing liquid fuels from indigenous raw materials in Finland. Another aim was to compare methods under development and prepare a proposal for steering research related to this field. Process concepts were prepared for a number of alternatives, as well as analogous balances and production and investment cost assessments for these balances. Carbon dioxide emissions of the alternatives and the price of CO2 reduction were also studied. All the alternatives for producing liquid fuels from indigenous raw materials are utmost unprofitable. There are great differences between the alternatives. While the production cost of ethanol is 6 to 9 times higher than the market value of the product, the equivalent ratio for substitute fuel oil produced from peat by pyrolysis is 3 to 4. However, it should be borne in mind that the technical uncertainties related to the alternatives are of different magnitude. Production of ethanol from barley is of commercial technology, while biomass pyrolysis is still under development. If the aim is to reach smaller carbon dioxide emissions by using liquid biofuels, the most favorable alternative is pyrolysis oil produced from wood. Fuels produced from cultivated biomass are more expensive ways of reducing CO2 emissions. Their potential of reducing CO2 emissions in Finland is insignificant. Integration of liquid fuel production to some other production line is more profitable. DOE

N95-22429# Energy Information Administration, Washington, DC. Office of Coal, Nuclear, Electric and Alternate Fuels.
SOLAR COLLECTOR MANUFACTURING ACTIVITY 1993
15 Aug. 1994 82 p
(DE94-017340; DOE/EIA-0174(93)) Avail: CASI HC A05/MF A01

The report presents national and State-level data on the U.S. solar thermal collector and photovoltaic cell and module manufacturing industry. DOE

N95-22468# National Renewable Energy Lab., Golden, CO.
WIND ENERGY PROGRAM OVERVIEW, FISCAL YEAR 1993
May 1994 32 p
(Contract DE-AC36-83CH-10093)
(DE94-000285; DOE/CH-10093/279) Avail: CASI HC A03/MF A01

Wind energy research has two goals: (1) to gain a fundamental understanding of the interactions between wind and wind turbines; and (2) to develop the basic design tools required to develop advanced technologies. A primary objective of applied research activities is to develop sophisticated computer codes and integrate them into the design, testing, and evaluation of advanced components and systems. Computer models have become a necessary and integral part of developing new high-tech wind energy systems. A computer-based design strategy allows designers to model different configurations and explore new designs before building expensive hardware. DOE works closely with utilities and the wind industry in setting its applied research agenda. As soon as research findings become available, the national laboratories transfer the information to industry through workshops, conferences, and publications. DOE

N95-20503*# National Aeronautics and Space Administration. Goddard Space Flight Center, Greenbelt, MD.
GODDARD SPACE FLIGHT CENTER SOLAR ARRAY MISSIONS, REQUIREMENTS AND DIRECTIONS
Edward Gaddy and John Day *In* NASA. Lewis Research Center, Proceedings of the 13th Space Photovoltaic Research and Technology Conference (SPRAT 13) Sep. 1994 p 1-12 (For primary document see N95-20502 06-33)
Avail: CASI HC A03/MF A04

N95-20504*# Ballistic Missile Defense Organization, Washington, DC.
BMDO PHOTOVOLTAICS PROGRAM OVERVIEW
Leonard H. Caveny and Douglas M. Allen (Schafer, W. J. Associates, Inc., North Olmsted, OH.) *In* NASA. Lewis Research Center, Proceedings of the 13th Space Photovoltaic Research and Technology Conference (SPRAT 13) Sep. 1994 p 13-21 (For primary document see N95-20502 06-33)
Avail: CASI HC A02/MF A04

N95-20505*# National Renewable Energy Lab., Golden, CO.
AN UPDATE ON THE DEPARTMENT OF ENERGY'S PHOTOVOLTAIC PROGRAM
John P. Benner and Mark Fitzgerald *In* NASA. Lewis Research Center, Proceedings of the 13th Space Photovoltaic Research and Technology Conference (SPRAT 13) Sep. 1994 p 31-33 (For primary document see N95-20502 06-33)
Avail: CASI HC A01/MF A04

N95-20506*# European Space Agency. European Space Research and Technology Center, ESTEC, Noordwijk (Netherlands).
EUROPE'S SPACE PHOTOVOLTAICS PROGRAMME
Klaus P. Bogus *In* NASA. Lewis Research Center, Proceedings of the 13th Space Photovoltaic Research and Technology Conference (SPRAT 13) Sep. 1994 p 35-39 (For primary document see N95-20502 06-33)
Avail: CASI HC A01/MF A04

N95-20507*# Research Triangle Inst., Research Triangle Park, NC.
HIGH-EFFICIENCY, DEEP-JUNCTION, EPITAXIAL InP SOLAR CELLS ON (100) AND (111)B InP SUBSTRATES
R. Venkatasubramanian, M. L. Timmons, J. A. Hutchby, Robert J. Walters (Naval Research Lab., Washington, DC.), and Geoffrey P. Summers (Naval Research Lab., Washington, DC.) *In* NASA. Lewis Research Center, Proceedings of the 13th Space Photovoltaic Research and Technology Conference (SPRAT 13) Sep. 1994 p 43-51 (For primary document see N95-20502 06-33)
Avail: CASI HC A02/MF A04

N95-20508*# Houston Univ., TX.
CHEMICAL BEAM EPITAXY FOR HIGH EFFICIENCY PHOTOVOLTAIC DEVICES
A. Bensaoula, A. Freundlich, M. F. Vilela, N. Medelci, and P. Renaud *In* NASA. Lewis Research Center, Proceedings of the 13th Space Photovoltaic Research and Technology Conference (SPRAT 13) Sep. 1994 p 53-61 Sponsored in cooperation with the State of Texas advanced technology program and IST, Inc. (For primary document see N95-20502 06-33)
Avail: CASI HC A02/MF A04

N95-20509*# National Aeronautics and Space Administration. Lewis Research Center, Cleveland, OH.
STATUS OF DIFFUSED JUNCTION p+n InP SOLAR CELLS FOR SPACE APPLICATIONS
Mircea Faur (Cleveland State Univ., OH.), C. Goradia (Cleveland State Univ., OH.), Maria Faur (NYMA, Inc., Brook Park, OH.), N. S. Fatemi (NYMA, Inc., Brook Park, OH.), P. P. Jenkins (NYMA, Inc., Brook Park, OH.), D. J. Flood, D. J. Brinker, D. M. Wilt, S. Bailey, and M. Goradia (Cleveland State Univ., OH.) et al *In its* Proceedings of the 13th Space Photovoltaic Research and Technology Conference (SPRAT 13) Sep. 1994 p 63-79 (For primary document see N95-20502 06-33)
Avail: CASI HC A03/MF A04

N95-20510*# Astropower, Inc., Newark, DE.
HIGH QUALITY InP-ON-Si FOR SOLAR CELL APPLICATIONS
Zane A. Shellenbarger, Thomas A. Goodwin, Sandra R. Collins, and Louis C. DiNetta *In* NASA. Lewis Research Center, Proceedings of the 13th Space Photovoltaic Research and Technology Conference (SPRAT 13) Sep. 1994 p 81-89 (For primary document see N95-20502 06-33)
Avail: CASI HC A02/MF A04

N95-20511*# Spire Corp., Bedford, MA.
P/N InP SOLAR CELLS ON Ge WAFERS
Steven Wojtczuk, Stanley Vernon, and Edward A. Burke (Burke, Edward A., Woburn, MA.) *In* NASA. Lewis Research Center, Proceedings of the 13th Space Photovoltaic Research and Technology Conference (SPRAT 13) Sep. 1994 p 91-98 (For primary document see N95-20502 06-33)
Avail: CASI HC A02/MF A04

N95-20512*# International Solar Electric Technology, Inglewood, CA.
STATUS OF FLEXIBLE CIS RESEARCH AT ISET
B. M. Basol, V. K. Kapur, A. Minnick, A. Halani, and C. R. Leidholm *In* NASA. Lewis Research Center, Proceedings of the 13th Space Photovoltaic Research and Technology Conference (SPRAT 13) Sep. 1994 p 101-106 (For primary document see N95-20502 06-33)
(Contract NAS3-26615)
Avail: CASI HC A02/MF A04

N95-20513*# Astropower, Inc., Newark, DE.
DEVELOPMENT OF A LIGHTWEIGHT, LIGHT-TRAPPED, THIN GaAs SOLAR CELL FOR SPACECRAFT APPLICATIONS
Margaret H. Hannon, Louis C. DiNetta, Michael W. Dashiell, John R. Cummings, and Allen M. Barnett *In* NASA. Lewis Research Center, Proceedings of the 13th Space Photovoltaic Research and Technology Conference (SPRAT 13) Sep. 1994 p 107-114 Sponsored in cooperation with Ballistic Missile Defense Organization and Phillips Lab. (For primary document see N95-20502 06-33)
Avail: CASI HC A02/MF A04

N95-20514*# Martin Marietta Corp., Denver, CO.
ADVANCES IN POLYCRYSTALLINE THIN-FILM PHOTOVOLTAICS FOR SPACE APPLICATIONS
Bruce R. Lanning, Joseph H. Armstrong, and Mohan S. Misra *In* NASA. Lewis Research Center, Proceedings of the 13th Space Photovoltaic Research and Technology Conference (SPRAT 13) Sep. 1994 p 115-123 (For primary document see N95-20502 06-33)
(MM-IRD Proj. D-17R)
Avail: CASI HC A02/MF A04

N95-20515*# TRW Space Technology Labs., Redondo Beach, CA.
AMORPHOUS SILICON THIN FILMS: THE ULTIMATE LIGHTWEIGHT SPACE SOLAR CELL
G. J. Vendura, Jr., M. A. Kruer, H. H. Schurig, M. A. Bianchi, and J. A. Roth *In* NASA. Lewis Research Center, Proceedings of the 13th Space Photovoltaic Research and Technology Conference (SPRAT 13) Sep. 1994 p 125-134 (For primary document see N95-20502 06-33)
Avail: CASI HC A02/MF A04

N95-20516*# National Aeronautics and Space Administration. Lewis Research Center, Cleveland, OH.
MODELING OF HIGH EFFICIENCY SOLAR CELLS UNDER LASER PULSE FOR POWER BEAMING APPLICATIONS
Raj K. Jain and Geoffrey A. Landis (NYMA, Inc., Brook Park, OH.) *In its* Proceedings of the 13th Space Photovoltaic Research and Technology Conference (SPRAT 13) Sep. 1994 p 135-140 (For primary document see N95-20502 06-33)
Avail: CASI HC A02/MF A04

N95-20517*# Houston Univ., TX.
CALCULATION OF NEAR OPTIMUM DESIGN OF InP/In(0.53)Ga(0.47)As MONOLITHIC TANDEM SOLAR CELLS
P. Renaud, M. F. Vilela, A. Freundlich, N. Medelci, and A. Bensaoula *In* NASA. Lewis Research Center, Proceedings of the 13th Space Photovoltaic Research and Technology Conference (SPRAT 13) Sep. 1994 p 141-146 (For primary document see N95-20502 06-33)
Avail: CASI HC A02/MF A04

N95-20518*# National Aeronautics and Space Administration. Lewis Research Center, Cleveland, OH.
PERFORMANCE, DEFECT BEHAVIOR AND CARRIER ENHANCEMENT IN LOW ENERGY, PROTON IRRADIATED p+nn+ InP SOLAR CELLS
I. Weinberg, G. C. Rybicki, C. Vargas-Aburto (Kent State Univ., OH.), R. K. Jain (Toledo Univ., OH.), and D. Scheiman (NYMA, Inc., Brook Park, OH.) *In its* Proceedings of the 13th Space Photovoltaic Research and Technology Conference (SPRAT 13) Sep. 1994 p 149-158 (For primary document see N95-20502 06-33)
Avail: CASI HC A02/MF A04

N95-20519*# Naval Research Lab., Washington, DC.
ELECTRON-IRRADIATED TWO-TERMINAL, MONOLITHIC InP/Ga0.47In0.53As TANDEM SOLAR CELLS AND ANNEALING OF RADIATION DAMAGE
H. L. Cotal, Robert J. Walters, Geoffrey P. Summers, and Scott R. Messenger (SFA, Inc., Landover, MD.) *In* NASA. Lewis Research Center, Proceedings of the 13th Space Photovoltaic Research and Technology Conference (SPRAT 13) Sep. 1994 p 159-166 (For primary document see N95-20502 06-33)
Avail: CASI HC A02/MF A04

N95-20520*# SFA, Inc., Landover, MD.
RADIATION EFFECTS ON p+n InP JUNCTIONS GROWN BY MOCVD
Scott R. Messenger, Robert J. Walters (Naval Research Lab., Washington, DC.), M. J. Panunto (Maryland Univ., Baltimore, MD.), and Geoffrey P. Summers (Naval Research Lab., Washington, DC.) *In* NASA. Lewis Research Center, Proceedings of the 13th Space Photovoltaic Research and Technology Conference (SPRAT 13) Sep. 1994 p 167-180 (For primary document see N95-20502 06-33)
Avail: CASI HC A03/MF A04

N95-20521*# National Renewable Energy Lab., Golden, CO.
DESIGN OF HIGH-EFFICIENCY, RADIATION-HARD, GaInP/GaAs SOLAR CELLS
Sarah R. Kurtz, K. A. Bertness, A. E. Kibbler, C. Kramer, and J. M. Olson *In* NASA. Lewis Research Center, Proceedings of the 13th Space Photovoltaic Research and Technology Conference (SPRAT 13) Sep. 1994 p 181-186 (For primary document see N95-20502 06-33)
(Contract DE-AC02-83CH-10093)
Avail: CASI HC A02/MF A04

N95-20522*# Wayne State Univ., Detroit, MI.
INVESTIGATION OF THE STABILITY AND 1.0 MeV PROTON RADIATION RESISTANCE OF COMMERCIALLY PRODUCED HYDROGENATED AMORPHOUS SILICON ALLOY SOLAR CELLS
Kenneth R. Lord, II, Michael R. Walters, and James R. Woodyard *In* NASA. Lewis Research Center, Proceedings of the 13th Space Photovoltaic Research and Technology Conference (SPRAT 13) Sep. 1994 p 187-196 Sponsored in cooperation with NASA, TRW and Wayne State Univ. Inst. for Mfg. Research (For primary document see N95-20502 06-33)
Avail: CASI HC A02/MF A04

N95-20523*# Naval Research Lab., Washington, DC.
THE USE OF DISPLACEMENT DAMAGE DOSE TO CORRELATE DEGRADATION IN SOLAR CELLS EXPOSED TO DIFFERENT RADIATIONS
Geoffrey P. Summers, Edward A. Burke (SFA, Inc., Landover, MD.), Philip Shapiro (SFA, Inc., Landover, MD.), Richard Statler (SFA, Inc., Landover, MD.), Scott R. Messenger (SFA, Inc., Landover, MD.), and Robert J. Walters *In* NASA. Lewis Research Center, Proceedings of the 13th Space Photovoltaic Research and Technology Conference (SPRAT 13) Sep. 1994 p 197-201 (For primary document see N95-20502 06-33)
Avail: CASI HC A01/MF A04

N95-20524*# Naval Research Lab., Washington, DC.
ANNEALING OF IRRADIATED n+p InP BURIED HOMOJUNCTIONS
Robert J. Walters, Geoffrey P. Summers, M. L. Timmons (Research Triangle Inst., Research Triangle Park, NC.), R. Venkatasubramanian (Research Triangle Inst., Research Triangle Park, NC.), J. A. Hancock (Research Triangle Inst., Research Triangle Park, NC.), and J. S. Hills (Research Triangle Inst., Research Triangle Park, NC.) *In* NASA. Lewis Research Center, Proceedings of the 13th Space Photovoltaic Research and Technology Conference (SPRAT 13) Sep. 1994 p 203-212 (For primary document see N95-20502 06-33)
Avail: CASI HC A02/MF A04

N95-20525*# Optical Coating Lab., Inc., Santa Rosa, CA.
QUALIFICATION TEST RESULTS FOR BLUE-RED REFLECTING SOLAR COVERS
W. T. Beauchamp *In* NASA. Lewis Research Center, Proceedings of the 13th Space Photovoltaic Research and Technology Conference (SPRAT

13) Sep. 1994 p 213-222 Presented at the Proceedings of the 23d IEEE Photospecialist Conference, Louisville, KY, May 1994 (For primary document see N95-20502 06-33)
Avail: CASI HC A02/MF A04

N95-20526*# Communications Satellite Corp., Clarksburg, MD.
UV TESTING OF INTELSAT-7, 7A, AND 8 SOLAR CELLS
A. Meulenberg *In* NASA. Lewis Research Center, Proceedings of the 13th Space Photovoltaic Research and Technology Conference (SPRAT 13) Sep. 1994 p 223-225 (For primary document see N95-20502 06-33)
Avail: CASI HC A01/MF A04

N95-20527*# Maxwell Labs., Inc., San Diego, CA. S-Cubed Div.
PARASITIC CURRENT COLLECTION BY SOLAR ARRAYS IN LEO
Victoria A. Davis and Barbara M. Gardner *In* NASA. Lewis Research Center, Proceedings of the 13th Space Photovoltaic Research and Technology Conference (SPRAT 13) Sep. 1994 p 227-235 Sponsored by AF Materiel Command (For primary document see N95-20502 06-33)
Avail: CASI HC A02/MF A04

N95-20528*# National Aeronautics and Space Administration. Lewis Research Center, Cleveland, OH.
FINAL RESULTS OF THE ADVANCED PHOTOVOLTAIC EXPERIMENT
David J. Brinker and John R. Hickey (Eppley Lab., Inc., Newport, RI.) *In its* Proceedings of the 13th Space Photovoltaic Research and Technology Conference (SPRAT 13) Sep. 1994 p 239-246 (For primary document see N95-20502 06-33)
Avail: CASI HC A02/MF A04

N95-20529*# National Aeronautics and Space Administration. Lewis Research Center, Cleveland, OH.
PRELIMINARY RESULTS FROM THE FLIGHT OF THE SOLAR ARRAY MODULE PLASMA INTERACTIONS EXPERIMENT (SAMPIE)
Dale C. Ferguson and G. Barry Hillard *In its* Proceedings of the 13th Space Photovoltaic Research and Technology Conference (SPRAT 13) Sep. 1994 p 247-256 (For primary document see N95-20502 06-33)
Avail: CASI HC A02/MF A04

N95-20531*# European Space Agency. European Space Research and Technology Center, ESTEC, Noordwijk (Netherlands).
POST-FLIGHT INVESTIGATION PROGRAMMES OF RECENTLY RETRIEVED SOLAR GENERATORS
Lothar Grelach *In* NASA. Lewis Research Center, Proceedings of the 13th Space Photovoltaic Research and Technology Conference (SPRAT 13) Sep. 1994 p 269-283 (For primary document see N95-20502 06-33)
Avail: CASI HC A03/MF A04

N95-20534*# National Aeronautics and Space Administration. Lewis Research Center, Cleveland, OH.
AN UPDATE ON THE DEVELOPMENT OF A LINE-FOCUS REFRACTIVE CONCENTRATOR ARRAY
Michael F. Piszczor, Mark J. ONeill (ENTECH Corp., Dallas-Fort Worth Airport, TX.), and Lewis M. Fraas (JX Crystals, Issaquah, WA.) *In its* Proceedings of the 13th Space Photovoltaic Research and Technology Conference (SPRAT 13) Sep. 1994 p 313-322 (For primary document see N95-20502 06-33)
Avail: CASI HC A02/MF A04

N95-20535*# Astro Aerospace Corp., Carpinteria, CA.
AN INTRODUCTION TO THE ASTRO EDGE SOLAR ARRAY
B. R. Spence and G. W. Marks *In* NASA. Lewis Research Center, Proceedings of the 13th Space Photovoltaic Research and Technology Conference (SPRAT 13) Sep. 1994 p 323-331 (For primary document see N95-20502 06-33)
Avail: CASI HC A02/MF A04

N95-20538*# National Aeronautics and Space Administration. Lewis Research Center, Cleveland, OH.
PULSED LASER ILLUMINATION OF PHOTOVOLTAIC CELLS
Jane A. Yater, Roland A. Lowe (Kent State Univ., OH.), Phillip P. Jenkins (NYMA, Inc., Brook Park, OH.), and Geoffrey A. Landis (NYMA, Inc., Brook Park, OH.) *In its* Proceedings of the 13th Space Photovoltaic Research and Technology Conference (SPRAT 13) Sep. 1994 p 353-362 See also N95-18572 (For primary document see N95-20502 06-33)
Avail: CASI HC A02/MF A04

N95-20541*# NYMA, Inc., Brook Park, OH.
REVIEW OF SOLAR CELL TEMPERATURE COEFFICIENTS FOR SPACE
Geoffrey A. Landis *In* NASA. Lewis Research Center, Proceedings of the 13th Space Photovoltaic Research and Technology Conference (SPRAT 13) Sep. 1994 p 385-399 (For primary document see N95-20502 06-33)
Avail: CASI HC A03/MF A04

45 ENVIRONMENT POLLUTION

Includes atmospheric, noise, thermal, and water pollution.

N95-19921 Sorbent Technologies Corp., Twinsburg, OH.
LABORATORY EVALUATION OF A REACTIVE BAFFLE APPROACH TO NOx CONTROL Final Technical Report, Feb. - Apr. 1993
S. G. Nelson, D. A. VanStone, R. C. Little, and R. A. Peterson Sep. 1993 41 p Limited Reproducibility: More than 20% of this document may be affected by microfiche quality
(Contract F08635-90-C-0053)
(AD-A283802; AL/EQ-TR-1993-0017) Avail: CASI HC A03

Vermiculite, vermiculite coated with magnesia, and activated carbon sorbents have successfully removed NOx (and carbon monoxide and particles) from combustion exhausts in a subscale drone jet engine test cell (JETC), but back pressure so generated elevated the temperature of the JETC and of the engine. The objective of this effort was to explore the feasibility of locating the sorbents in the face of the duct or of baffles parallel to the direction of flow within the ducts. Jet engine test cells (JETC's) are stationary sources of oxides of nitrogen (NOx), soot, and unburned or partially oxidized carbon compounds that form as byproducts of imperfect combustion. Regulation of NOx emissions is being considered for implementation under the Clean Air Act Amendments of 1990. Several principles have been examined as candidate methods to control NOx emissions from JETC's. DTIC

N95-19964# Air Force Materiel Command, Brooks AFB, TX. Occupational and Environmental Health Directorate.
CALCULATION METHODS FOR CRITERIA AIR POLLUTANT EMISSION INVENTORIES Final Report, Feb. 1993 - May 1994
Kurt D. Jagielski and Robert J. OBrien Jul. 1994 90 p
(AD-A284675; AL/OE-TR-1994-0049) Avail: CASI HC A05/MF A01

This report serves as a guidance manual for Bioenvironmental Engineering personnel or other, responsible environmentally-related office in the development of installation-level criteria air pollutant emission inventories. Emission inventories are used to assess and document compliance with federal, state, and local environmental statutes and regulations and can serve as a useful pollution management tool. This report may be used in a stand-alone fashion or in conjunction with an Air Staff-approved emissions software database management program tailored for the Air Force community. Source-specific emissions software, available through the U.S. Environmental Protection Agency for some sources such as motor vehicles and fuel storage tanks, may also be used to assist in calculating and managing emissions data. DTIC

N95-19965# National Oceanic and Atmospheric Administration, Research Triangle Park, NC. Atmospheric Sciences Modeling Div.
EFFECTS OF METEOROLOGY ON CONCENTRATIONS OF ACID AEROSOLS
M. P. Zelenka and H. H. Suh (Harvard School of Public Health, Boston, MA.) 1994 8 p
(Contract EPA-CR-816740)
(PB94-209749; EPA/600/A-94/168) Avail: CASI HC A02/MF A01

Ambient air samples of strong acid aerosol, sulfate, ammonia, and ammonium were collected in Pittsburgh and Uniontown, PA during the summer of 1990. High correlations were found for both acid aerosol and sulfate concentrations between Pittsburgh and the semi-rural site in

Uniontown. One possible implication is that acid aerosols and their precursors are regionally transported. To test this hypothesis, air samples from the Uniontown site were statistically analyzed for the meteorological relationships that resulted in episodic events of elevated ambient acid aerosol levels. Standard measures of atmospheric conditions in both Pittsburgh and Uniontown were used; they included temperature, pressure, relative humidity, wind speed and direction. Results show that the episodic events of elevated acid aerosol occurred with the same general set of meteorological conditions. The major meteorological variables which correlated with the episodes were the mean wind speed in Pittsburgh and the mean westerly wind component at Uniontown. These two variables accounted for one-third of the variance. NTIS

N95-20089# Pacific Northwest Lab., Richland, WA.

DUST BOWL MIGRATION AS AN ANALOG FOR POSSIBLE GLOBAL WARMING-INDUCED MIGRATION FROM MEXICO

M. H. Turner, J. D. Longstreth, A. K. Johnson, and N. J. Rosenberg Jun. 1994 40 p Presented at the 19th Annual Conference and Exposition of the National Association of Environmental Professionals (NAEP): Global Strategies for Environmental Issues, New Orleans, LA, 12-15 Jun. 1994
(Contract DE-AC06-76RL-01830)
(DE94-017472; PNL-SA-23891; CONF-940650-9) Avail: CASI HC A03/MF A01

As a result of increases in CO2 and other radiatively important trace gases, scientists have predicted increases in mean worldwide temperatures of 2 to 5 C over the next 50 to 100 years. Such temperature increases may result in climate modifications that would in turn be associated with increases in drought and desertification and could even change the patterns of the monsoons and tropical rains, which are important to agriculture throughout the world. They predicted that the rise in sea level caused by melting and thermal expansion of glaciers and polar icecaps could flood large population centers, destroying habitation and displacing populations. This will result in approximately 50 million 'environmental refugees' worldwide, triple the number of today. The expected shifts in precipitation are also likely to result in (1) increased runoff contaminated with pesticides, salts, garbage, sewage, and eroded soil, and (2) drought also leading to increased soil erosion and salinization, as well as depletion of limited water resources. The total impact of global warming on agriculture and human habitation could considerably slow the economic development of some nations and would particularly affect agricultural production. Loss of homes, the inability to raise food, an increased prevalence of disease and worsened economic conditions may drive people to leave their homelands, seeking entry into countries which have more resources and greater resistance to the economic consequences of climatic change. This report looks at the possible environmental impacts and economic impacts of the greenhouse effect on Mexico while using the American Dust Bowl event as an analog. DOE

N95-20192# Energy and Environmental Research Corp., Irvine, CA.

EXPERIMENTAL INVESTIGATION OF PIC FORMATION DURING THE INCINERATION OF RECOVERED CFC-11 Final Report, Jul. 1993 - Jul. 1994

B. Springsteen, L. Ho, and G. Kryder Sep. 1994 238 p
(Contract EPA-68-CO-0094)
(PB94-214772; EPA/600/R-94/163) Avail: CASI HC A11/MF A03

The report gives results of an investigation of the formation of products of incomplete combustion (PIC's) during 'recovered' trichlorofluoromethane (CFC-11) incineration. Tests involved burning the recovered CFC-11 in a propane gas flame. Combustion gas samples were taken and analyzed for volatile organic compounds as well as polychlorinated dibenzo-p-dioxins and dibenzofurans (PCDD/PCDF). Test results confirm that incineration can be used to effectively destroy recovered CFC-11; CFC destruction efficiencies of greater than 99.9999 were consistently demonstrated for CFC-11-to-propane molar ratios of 0.66-0.6. Additionally, low levels were detected when sampling downstream of the flue gas scrubber. Results of a secondary goal of the study, to determine the fate of chlorine (Cl) and fluorine (F), were inconclusive. NTIS

N95-20193# Oklahoma Univ., Norman, OK. Cooperative Inst. for Mesoscale Meteorological Studies.

SITE SCIENTIFIC MISSION PLAN FOR THE SOUTHERN GREAT PLAINS CART SITE, JULY - DECEMBER 1994

J. M. Schneider, P. J. Lamb, and D. L. Sisterson (Argonne National Lab., IL.) Jul. 1994 65 p
(Contract W-31-109-eng-38)
(DE94-017289; ARM-94-002) Avail: CASI HC A04/MF A01

The Southern Great Plains (SGP) Cloud and Radiation Testbed (CART) site is designed to help satisfy the data needs of the Atmospheric Radiation Measurement (ARM) Program Science Team. This document defines the scientific priorities for site activities during the six months beginning on July 1, 1994, and also looks forward in lesser detail to subsequent six-month periods. The primary purpose of this Site Scientific Mission Plan is to provide guidance for the development of plans for site operations. It also provides information on current plans to the ARM Functional Teams (Management Team, Experiment Support Team, Operations Team, Data Management Team, Instrument Team, and Campaign Team), and it serves to disseminate the plans more generally within the ARM Program and among the Science Team. This document includes a description of the site's operational status and the primary envisaged site activities, together with information concerning approved and proposed Intensive Observation Periods. Amendments will be prepared and distributed whenever the content changes by more than 30% within a six-month period. The primary users of this document are the site operator, the site scientist, the Science Team through the ARM Program Science Director, the ARM Program Experiment Center, and the aforementioned ARM Program Functional Teams. This plan is a living document that will be updated and reissued every six months as the observational facilities are developed, tested, and augmented and as priorities are adjusted in response to developments in scientific planning and understanding. DOE

N95-20234 Argonne National Lab., IL.

PERFORMANCE SPECIFICATIONS FOR TECHNOLOGY DEVELOPMENT: APPLICATION FOR CHARACTERIZATION OF VOLATILE ORGANIC COMPOUNDS IN THE ENVIRONMENT

S. E. Carpenter, P. V. Doskey, M. D. Erickson, and P. C. Lindahl Jul. 1994 109 p Limited Reproducibility: More than 20% of this document may be affected by microfiche quality
(Contract W-31-109-eng-38)
(DE94-016627; ANL/ER/TM-3) Avail: CASI HC A06

This report contains information about technology development for the monitoring and remediation of environmental pollution caused by the release of volatile organic compounds. Topics discussed include: performance specification processes, gas chromatography, mass spectrometer, fiber-optic chemical sensors, infrared spectroscopy, Raman spectroscopy, piezoelectric sensors and electrochemical sensors. These methods are analyzed for their cost efficiency, accuracy, and the ability to meet the needs of the customer. DOE

N95-20238# Oak Ridge National Lab., TN.

WORKSHOP ON UNCERTAINTY AND GLOBAL CLIMATE CHANGE RESEARCH

B. E. Tonn and R. Weiher (National Oceanic and Atmospheric Administration, Silver Spring, MD.) Jun. 1994 45 p Workshop held in Knoxville, TN, 22-23 Mar. 1994
(Contract DE-AC05-84OR-21400)
(DE94-016728; ORNL/M-3704-Summ; CONF-9403147-Summ) Avail: CASI HC A03/MF A01

This report summarizes the results and recommendations of the Workshop on Uncertainty and Global Climate Change Research. The purpose of the workshop was to examine in-depth the concept of uncertainty. From an analytical point of view, uncertainty is a central feature of global climate science, economics and decision making. The magnitude and complexity of uncertainty surrounding global climate change has made it quite difficult to answer even the most simple and important of questions: whether potentially costly action is required now to ameliorate adverse consequences of global climate change or whether delay is warranted to gain better information to reduce uncertainties. A major conclusion of the workshop is that multidisciplinary integrated assessments using decision analytic techniques as a foundation is the key to addressing global change policy concerns. First, uncertainty must be dealt with explicitly and rigorously since it is and will continue to be a key feature of analysis and recommendations on policy questions for years to come. Second, key policy questions and variables need to be explicitly identified, prioritized, and their uncertainty characterized to guide the entire scientific, modeling, and policy analysis process. Multidisciplinary integrated assessment techniques and value of information methodologies are best suited for this task. In terms of timeliness and relevance of developing and applying decision analytic techniques, the global change research and policy communities are moving rapidly toward integrated approaches to research design and policy analysis. DOE

N95-20247# Argonne National Lab., IL.

AN APPLICATION OF WAVELET TRANSFORM FOR DECOMPOSITION OF MILLIMETER-WAVE SPECTROSCOPIC SIGNALS

K. Gopalan (Purdue Univ., Hammond, IN.), N. Gopalsami, S. Bakhtiari, and A. C. Raptis Aug. 1994 9 p Presented at the 1995 IEEE International Conference on Acoustics, Speech and Signal Processing, Detroit, MI, 8-12 May 1994
(Contract W-31-109-eng-38)
(DE94-018366; ANL/ET/CP-83924; CONF-9405229-1) Avail: CASI HC A02/MF A01

Millimeter-wave technique, based on rotational energy transitions of molecules, holds promise for remote monitoring of environmentally hazardous effluents from processes. Argonne National Laboratory is developing a millimeter-wave sensor based on active swept-frequency radar technique in the frequency range of 220-320 GHz. Because the line widths of millimeter-wave spectra of molecules at atmospheric pressure are broad (approximately 4 GHz half-width at half height), the composite spectrum of multicomponent mixtures of chemicals is generally complex and overlapping. This paper presents an application of discrete wavelet transform for efficient representation and decomposition of millimeter-wave spectral data. A two-layer back propagation neural network is trained using multifrequency wavelet coefficients of the signals as input features and the known composition of different chemicals in the mixture as target output vectors. After training, composition of an unknown mixture of the base chemicals is determined using the wavelet representation of its absorption spectra. Simulated and experimental spectral data were used to test the wavelet transform technique. Accurate values of individual chemical compositions resulted for noise-free laboratory data. In addition, the technique showed more robustness than conventional multivariate techniques under noisy conditions. DOE

N95-20353# Lawrence Livermore National Lab., Livermore, CA.

INDIRECT GLOBAL WARMING EFFECTS OF OZONE AND STRATOSPHERIC WATER VAPOR INDUCED BY SURFACE METHANE EMISSION

D. J. Wuebbles, A. S. Grossman, J. S. Tamaresis, K. O. Patten, Jr., A. Jain, and K. A. Grant Jul. 1994 38 p
(Contract W-7405-eng-48)
(DE94-019016; UCRL-ID-118061) Avail: CASI HC A03/MF A01

Methane has indirect effects on climate due to chemical interactions as well as direct radiative forcing effects as a greenhouse gas. We have calculated the indirect, time-varying tropospheric radiative forcing and GWP of O3 and stratospheric H2O due to an impulse of CH4. This impulse, applied to the lowest layer of the atmosphere, is the increase of the atmospheric mass of CH4 resulting from a 25 percent steady state increase in the current emissions as a function of latitude. The direct CH4 radiative forcing and GWP are also calculated. The LLNL 2-D radiative-chemistry-transport model is used to evaluate the resulting changes in the O3, H2O and CH4 atmospheric profiles as a function of time. A correlated k-distribution radiative transfer model is used to calculate the radiative forcing at the tropopause of the globally-averaged atmosphere profiles. The O3 indirect GWP's vary from (approximately)27 after a 20 yr integration to (approximately)4 after 500 years, agreeing with the previous estimates to within about 10 percent. The H2O indirect GWP's vary from (approximately)2 after a 20 yr integration to (approximately)0.3 after 500 years, and are in close agreement with other estimates. The CH4 GWP's vary from (approximately)53 at 20 yrs to (approximately)7 at 500 yrs. The 20 year CH4 GWP is (approximately)20% larger than previous estimates of the direct CH4 GWP due to a CH4 response time (approximately)17 yrs that is much longer than the overall lifetime (10 yrs). The increased CH4 response time results from changes in the OH abundances caused by the CH4 impulse. The CH4 radiative forcing results are consistent with IPCC values. Estimates are made of latitude effects in the radiative forcing calculations, and UV effects on the O3 radiative forcing calculations (10%). DOE

N95-20355# Lawrence Livermore National Lab., Livermore, CA. Global Climate Research Div.

RADIATIVE FORCING CALCULATIONS FOR CH3Cl

Allen S. Grossman, Keith E. Grant, and Donald J. Wuebbles Jun. 1994 8 p
(Contract W-7405-eng-48)
(DE94-019018; UCRL-ID-118065) Avail: CASI HC A02/MF A01

Methyl chloride, CH3Cl, is the major natural source of chlorine to the stratosphere. The production of CHCl is dominated by biological sources from the oceans and biomass burning. Production has a seasonal cycle which couples with the short lifetime of tropospheric CH3Cl to produce nonuniform global mixing. As an absorber of infrared radiation, CH3Cl is of interest for its potential affect on the tropospheric energy balance as well as for its chemical interactions. In this study, we estimate the radiative forcing and global warming potential (GWP) of CH3Cl. Our calculations use an infrared radiative transfer model based on the correlated k-distribution algorithm for band absorption. Global and annual average vertical profiles of temperature and trace gas concentration were assumed. The effects of clouds are modeled using three layers of global and annual average cloud optical properties. A radiative forcing value of 0.0053 W/sq m ppbv was obtained for CH3Cl and is approximately linear in the background abundance. This value is about 2 percent of the forcing of CFC-11 and about 300 times the forcing of CO2, on a per molecule basis. The radiative forcing calculation for CH3Cl is used to estimate the global warming potential (GWP) of CH3Cl. The results give GWP's for CH3Cl of the order of 25 at a time of 20 years (CO2 = 1). This result indicates that CH3Cl has the potential to be a major greenhouse gas if significant human related emissions were introduced into the atmosphere. DOE

N95-20440 Center for Mathematics and Computer Science, Amsterdam (Netherlands). Dept. of Numerical Mathematics.

IMPLEMENTATION AND PERFORMANCE OF A THREE-DIMENSIONAL NUMERICAL TRANSPORT MODEL

B. P. Sommeijer and J. Kok Feb. 1994 35 p
(PB95-135745; CWI-NM-R9402) Copyright Avail: Issuing Activity (National Technical Information Service (NTIS))

We present two numerical solution methods for the time integration of a three-dimensional model for computing transport of salinity, pollutants, suspended material (such as sediment or mud), etc. in shallow seas. The emphasis in this paper is on the performance of the methods when implemented on a vector/parallel, shared memory computer, such as a CRAY type machine. The first method is an explicit time integrator and can straightforwardly be vectorized and parallelized. Although a stabilizing technique has been applied to this method, it still suffers from a severe timestep restriction. The second method is partly implicit, resulting in much better stability characteristics; however, as a consequence of the implicitness, it requires in each step the solution of a large number of tridiagonal systems. When implemented in a standard way, the recursive nature would prevent vectorization, resulting in a very long solution time. Following a suggestion of Golub and Van Loan, this part of the algorithm has been tuned for use on the CRAY Y-MP4/464. On the basis of a large-scale test problem, performance results will be presented for various implementations. NTIS

N95-20441 Army Construction Engineering Research Lab., Champaign, IL.

ENVIRONMENTAL COMPLIANCE ASSESSMENT AND MANAGEMENT PROGRAM Final Report

Carolyn ORourke and Lisa A. Gifford Apr. 1994 243 p Limited Reproducibility: More than 20% of this document may be affected by microfiche quality
(AD-A279605; CERL-SR-EC-94/15) Avail: CASI HC A11

The number of environmental laws and regulations has continued to grow in the United States and worldwide, making compliance with these regulations increasingly difficult. Environmental assessments became a way to determine compliance with current environmental regulations. The U.S. Air Force has adopted an environmental compliance program that identifies compliance problems before they are cited as violations by the U.S. Environmental Protection Agency (USEPA). Beginning in 1984, the U.S. Army Construction Engineering Research Laboratories (USACERL), in cooperation with the Air Force Engineering and Services Center, began research on the U.S. Environmental Compliance Assessment and

Management Program (ECAMP). The concept was to combine Federal, Department of Defense (DOD), and Air Force environmental regulations, along with existing checklists from the USEPA and private industry, and documentation of good management practices and risk-management issues, into a series of checklists that list legal requirements and specify items or operations to review. Each assessment protocol lists a point of contact to help assessors review the checklists as effectively as possible. The Hawaii Supplement was developed to be used in conjunction with the U.S. ECAMP manual, using existing Hawaii state environmental legislation and regulations as well as suggested management practices. DTIC

N95-20456 Kansas State Univ., Manhattan, KS. Dept. of Chemistry.
MONITORING BIOREMEDIATION OF VOLATILE ORGANIC COMPOUNDS (VOCs) USING FOURIER TRANSFORM INFRARED (FT-IR) SPECTROMETRY M.S. Thesis
Vance P. Visser 1994 147 p Limited Reproducibility: More than 20% of this document may be affected by microfiche quality
(AD-A279631) Avail: Issuing Activity (Defense Technical Information Center (DTIC))

Bioremediation has repeatedly been demonstrated to be an innovative and effective technology for a wide variety of chemically contaminated environments. Although, once predominantly used in wastewater treatment, bioremediation technology is now being applied to soils, ground and surface water, and sludges. The contaminates include chemicals such as crude oil, petroleum hydrocarbons, fuels, and solvents. Regardless of the type of contaminant, the success of any bioremediation approach includes these essential elements; site characterization, initial bioassessment testing, detailed laboratory testing, hydrologic modeling, installation and start-up, process monitoring and operation, final sampling and closure, reporting and management. A major expense in bioremediation can be associated with monitoring the degradation of contaminates. This cost may be reduced by applying readily available, simple analytical methods and instrumentation to the monitoring of the bioremediation process. Our research involves the monitoring of the bioremediation of ground water contaminated by low levels of volatile organic compounds (VOC's) by adapted alfalfa plants and their associated rhizosphere bacteria. DTIC

N95-20465 Army Communications-Electronics Command, Fort Monmouth, NJ.
PROCEEDINGS OF THE INTERNATIONAL WIRE AND CABLE SYMPOSIUM
18 Nov. 1993 905 p Symposium held in Saint Louis, MO, 15-18 Nov. 1993 Limited Reproducibility: More than 20% of this document may be affected by microfiche quality
(AD-A279242) Avail: Issuing Activity (Defense Technical Information Center (DTIC))

The International Wire and Cable Symposium provides a forum for the exchange of technical information amongst its suppliers, manufacturers, and users on technological advancements in materials, processes, and products used for voice, data and video transmission systems. Topics covered include the following: (1) fiber optic cables and design; (2) fiber optic cable installation; (3) materials processing and manufacturing; (4) manufacturing and testing of high performance copper cable; (5) coaxial and power cables; future architecture of the outside plant; (6) extended fiber performance and survivability; (7) fire resistance; (8) copper durability; (9) polarization mode dispersion; (10) submarine cables; and (11) fiber optic coating. Derived from text

N95-20478# Argonne National Lab., IL.
ENERGY IMPACTS OF CONTROLLING CARBON DIOXIDE EMISSIONS FROM AN INTEGRATED GASIFICATION/COMBINED-CYCLE SYSTEM
C. D. Livengood, R. D. Doctor, J. C. Molburg, and P. Thimmapuram 1994 10 p Presented at the 10th Annual Coal Preparation, Utilization and Environmental Control Contractors Conference, Pittsburgh, PA, 18-21 Jul. 1994
(Contract W-31-109-eng-38)
(DE94-016878; ANL/ES/CP-83738; CONF-940780-5) Avail: CASI HC A02/MF A01

This paper presents results from a study of the impacts associated with CO2 recovery in integrated gasification/combined-cycle (IGCC) systems which is being conducted for the Morgantown Energy Technology Center by Argonne National Laboratory. The objective of the study is to compare, on a consistent systems-oriented basis, the energy and economic impacts of adding CO2 capture and sequestration to an IGCC system. The research reported here has emphasized commercial technologies for capturing CO2, but ongoing work is also addressing advanced technologies under development and alternate power-system configurations that may enhance system efficiency. DOE

N95-20487# Naval Facilities Engineering Service Center, Port Hueneme, CA.
ENVIRONMENTAL CLEANUP TECHNOLOGY TRANSFER INITIATIVES Technical Report, Jun. - Jul. 1994
Laurel A. Muehlhausen Aug. 1994 57 p
(AD-A285059; NFESC-TR-2023-ENV) Avail: CASI HC A04/MF A01

This white paper provides brief descriptions of environmental cleanup technology transfer initiatives and points of contact for further information. The summaries describe the mission and goals, the modus operandi or actual activities and projects implemented to achieve the goals, the source and amount of funding for the initiative, and other general information. The initiatives are programs, committees, organizations, and demonstration projects that promote development of innovative environmental cleanup technologies and help ensure the transfer of lower cost technologies into full-scale use. Opinions differ on the meaning of innovative technology. Most of the initiative described here consider a technology innovative if it has been demonstrated at the pilot scale but performance and cost data are lacking. Innovative technologies do not get widely used for many reasons such as risk of failure to meet cleanup standards or unknown cost information. Even if the cleanup succeeds, the project could fail if the public or the regulatory agency distrust a new and different technology. Federal and State agencies, legislatures, and private firms are working to reduce the barriers to technology innovations and commercialization through the initiatives described here. Lower cost technologies are needed to meet environmental cleanup standards in a time of shrinking budgets. Federal lands (military bases, defense production and research facilities, park, forest, and range lands) contain thousands of past disposal sites. The Federal government is committed to the environmental cleanup of these sites although estimates of the cleanup cost exceed $250 billion. Adding in the further cleanup costs of state and private waste sites, the nation's total cleanup estimates exceed $750 billion. DTIC

N95-20720# Army Construction Engineering Research Lab., Champaign, IL.
ENVIRONMENTAL COMPLIANCE ASSESSMENT PROTOCOL - CENTERS FOR DISEASE CONTROL AND PREVENTION (ECAP-CDC), WEST VIRGINIA SUPPLEMENT Final Report
Donald H. Wiggins Nov. 1994 95 p
(AD-A286009; CERL-SR-EC-95/01) Avail: CASI HC A05/MF A01

In response to the growing number of environmental laws and regulations worldwide, the Centers for Disease Control and Prevention (CDC) has adopted an environmental compliance program that identifies compliance problems before they are cited as violations by the U.S. Environmental Protection Agency (USEPA). In 1992, the CDC developed a program to maintain compliance with all Federal, state, and local environmental regulations. The goal is to protect human health/safety and the environment. The CDC, headquarters in Atlanta, Georgia, with facilities in several other states, developed and implemented a specific environmental assessment and management program tailored to the type and size of their facilities and operations. The resulting system combines Federal environmental regulations, along with good management practices and risk management information, into a series of checklists that show legal requirements and which specific items or operations to review. The Environmental Compliance Assessment Protocol Centers for Disease Control and Prevention (ECAP-CDC) incorporates existing checklists from USEPA and private industry. The West Virginia Supplement was developed to be used in conjunction with the ECAP-CDC manual, using existing West Virginia environmental legislation and regulations as well as suggested management practices. DTIC

N95-20834# Pacific Northwest Lab., Richland, WA.
CHEMICAL STRUCTURE AND DYNAMICS PROGRAM Annual Report, 1993
S. D. Colson Jul. 1994 58 p

(Contract DE-AC06-76RL-01830)
(DE95-001117; PNL-9445) Avail: CASI HC A04/MF A01

The Chemical Structure and Dynamics program responds to the need for a fundamental, molecular-level understanding of chemistry at the wide variety of environmentally-important interfaces. The research program is built around the established relationship between structure, thermodynamics, and kinetics. This research effort continues to evolve into a program of rigorous studies of fundamental molecular processes in model systems (e.g., well-characterized surfaces, single-component solutions, clusters, and biological molecules), and studies of complex systems found in the environment. Experimental studies of molecular and supramolecular structures and thermodynamics are key to understanding the nature of matter, and lead to direct comparison with computational results. Kinetic and mechanistic measurements, combined with real-time dynamics measurements of atomic and molecular motions during chemical reactions, provide for a molecular-level description of chemical reactions. The anticipated results of this work are the achievement of a quantitative understanding of chemical processes at complex interfaces, the development of new techniques for the detection and measurement of species at such interfaces, and the interpretation and extrapolation of the observations in terms of models of interfacial chemistry. The Chemical Structure and Dynamics research program includes five areas described in detail in this report: Reaction mechanisms at solid interfaces; Solution and solution interfaces; Structure and dynamics of biological systems; Analytical methods development; and atmospheric chemistry. Extended abstracts are presented for 23 studies. DOE

N95-20835# Argonne National Lab., IL.
GLOBAL CHANGE INTEGRATING FACTORS: TROPICAL TROPOPAUSE TRENDS
R. A. Reck 1994 10 p
(Contract W-31-109-eng-38)
(DE95-001121; ANL/ER/PP-79069) Avail: CASI HC A02/MF A01

This research proposes new criteria, shifts in the height and temperature of the tropical tropopause, as measures of global climate change. The search for signs of global warming in the temperature signal near the earth's surface is extremely difficult, largely because numerous factors contribute to surface temperature forcing with only a small signal-to-noise ratio relative to long-term effects. In the long term, no part of the atmosphere can be considered individually because the evolution will be a function of all states of all portions. A large surface greenhouse signal might ultimately be expected, but the analysis of surface temperature may not be particularly useful for early detection. What is suggested here is not an analysis of trends in the surface temperature field or any of its spatial averages, but rather an integrating factor or integrator, a single measure of global change that could be considered a test of significant change for the entire global system. Preferably, this global change integrator would vary slowly and would take into account many of the causes of climate change, with a relatively large signal-to-noise ratio. Such an integrator could be monitored, and abrupt or accelerated changes could serve as an early warning signal for policy makers and the public. Earlier work has suggested that temperature has much less short-term and small-scale noise in the lower stratosphere, and thus the global warming signal at that level might be more easily deconvoluted, because the cooling rate near the 200-mb level is almost constant with latitude. A study of the temperature signal at this pressure level might show a clearer trend due to increased levels of greenhouse gases, but it would yield information about the troposphere only by inference. DOE

N95-20991# Department of Energy, Washington, DC. Ocean Margins Program.
CLOSURE ON THE GLOBAL CARBON CYCLE
Michael R. Riches Aug. 1994 23 p
(DE94-018617; DOE/ER-0620P) Avail: CASI HC A03/MF A01

The Department of Energy's Ocean Margins Program (OMP) is designed to quantitatively assess the importance of coastal ocean systems in the global carbon cycle. Since the beginning of the Industrial Revolution, human energy-related activities have dramatically altered the global carbon cycle, and consequently, this cycle is not presently in a steady-state. To reduce major uncertainties in predicting future global environmental quality, it is imperative to understand the sources and sinks of atmospheric CO2, the role of anthropogenic activities in disrupting the natural carbon cycle, and the effects of, and feedbacks between, these activities and the natural carbon cycle. Due to continuously increased loading of nutrients to the margins, which, globally, is related to the rate of human population growth and high population densities in coastal states, biological carbon fixation has been stimulated. Depending on the fate of the fixed carbon, this stimulation has the potential to mitigate the anthropogenically derived CO2. Determining the factors that control the magnitude of carbon exchanges between the ocean margins and the atmosphere, and the subsequent fate of this carbon, is crucial to predicting the strength and capacity of the oceans to absorb excess anthropogenic atmospheric CO2. The goals of the OMP are to: quantify the ecological and biogeochemical processes and mechanisms that define the cycling, flux, and storage of carbon and other biogenic elements at the land/ocean interface; identify how ocean-margin sources and sinks of carbon change in response to human activities; and determine whether continental shelves are quantitatively significant in removing atmospheric carbon dioxide and isolating it via burial in sediments or export to the interior of the open ocean. DOE

N95-21034 Center for Mathematics and Computer Science, Amsterdam (Netherlands).
EXPLICIT METHODS FOR STIFF ODEs FROM ATMOSPHERIC CHEMISTRY
J. G. Verwer and D. Simpson (Norwegian Meteorological Inst., Blindern, Norway.) Apr. 1994 25 p See also N94-30729 Prepared in cooperation with Norske Meteorologiske Inst., Oslo
(PB95-135794; CWI-NM-R9409) Copyright Avail: Issuing Activity (National Technical Information Service (NTIS))

The subject research is the numerical integration of atmospheric chemical kinetics systems. The application lies in the study of air pollution, modelled by atmospheric chemistry-transport problems. The application puts high demands on the efficiency of the stiff solver. Three explicit methods are discussed and compared for a selected chemical kinetics system which is representative for the state of the art. The first and the second method are of the explicit QSSA type and the third is based on the two-step backward differentiation formula, combined with Gauss-Seidel iteration to approximately solve the implicitly defined solution. This also renders the method explicit. In the comparison the two-step method comes out best. NTIS

N95-21143# Institute of Energy Economics of Japan, (Japan).
ENERGY AND ENVIRONMENTAL ISSUES AND INTERNATIONAL OPPERATION IN ASIA
Mar. 1994 131 p
(DE94-796596; IEE-SR-251) Avail: CASI HC A07/MF A02

Investigation and report were made on the present status of air pollution in major Asian countries except China and their energy and environmental policies. In Asian countries, air pollution has been intensifying because of the progress of industrialization and concentrating population into cities. Pollution, however, is different among countries; SO(x) from the industry in Seoul, suspended particulate matters from transportation in Kuala Lumpur, NO(x) and CO from transportation in Bangkok, SO(x) from power generation and the industry in Jakarta, and soot/smoke in Delhi. Judging from the energy consumption structure, soot/smoke has a connection with coal consumption, SO(x) with coal and petroleum consumption, NO(x) with all fossil fuels. With relation to the environmental legislation and administration system on air pollution, arrangement started in the 1980s, but execution is still poor except for Korea. As for Japan's international cooperation, regarded as important are anti-pollution technology such as desulfurization, thermal efficiency and coal ash treatment, and energy conservation technology. DOE

N95-21150# Aerospace Corp., El Segundo, CA.
COMPUTER MODEL PREDICTIONS OF THE LOCAL EFFECTS OF LARGE, SOLID-FUEL ROCKET MOTORS ON STRATOSPHERIC OZONE
P. F. Zittel 10 Sep. 1994 23 p
(Contract F04701-93-C-0094)
(AD-A285632; TR-94(4231)-9; SMC-TR-94-36) Avail: CASI HC A03/MF A01

The solid-fuel rocket motors of large space launch vehicles release gases and particles that may significantly affect stratospheric ozone densities along the vehicle's path. In this study, standard rocket nozzle and flowfield computer codes have been used to characterize the exhaust gases and particles through the afterburning region of the solid-fuel motors of the Titan IV launch vehicle. The models predict that a large fraction of the HCl gas exhausted by the motors is converted to Cl and Cl2 in the plume afterburning region. Estimates of the subsequent chemistry suggest that on expansion into the ambient daytime stratosphere, the highly reactive chlorine may significantly deplete ozone in a cylinder around the vehicle track that ranges from 1 to 5 km in diameter over the altitude range of 15 to 40 km. The initial ozone depletion is estimated to occur on a time scale of less than 1 hour. After the initial effects, the dominant chemistry of the problem changes, and new models are needed to follow the further expansion, or closure, of the ozone hole on a longer time scale. DTIC

N95-21181# National Defence Research Establishment, Stockholm (Sweden).

ATMOSPHERIC STABILITY AND ITS INFLUENCE ON AIR QUALITY IN SMALL COMMUNITIES IN NORTHERN SWEDEN

Per-Erik Johansson, Edward Karlsson, Lennart Thaning, and Bertil Forsberg (Umea Univ., Sweden.) May 1994 78 p
(ISSN 0347-2124)
(PB95-131652; FOA-C-40323-4.5) Avail: CASI HC A05/MF A01

The relation between air quality and meteorology during winter conditions in the northern parts of Sweden has been studied. Several stability schemes has been tested against the measurements and a new improved one has been developed, in order to take into account conditions with low solar altitude, high albedo and low temperatures. At all sites the stratification was stable during more than half of the period. It is shown that the concentration of black smoke may be higher in the studied communities than in much larger cities, under certain conditions. Furthermore it is concluded that the covariance between pollution levels and meteorological parameters are higher in the northern parts of Sweden that in the south. The highest correlation was obtained between black smoke and temperature. NTIS

N95-21274# National Defence Research Establishment, Umea (Sweden). Dept. of NBC Defence.

ICE BABY: MEASUREMENTS OF CONCENTRATION FLUCTUATIONS IN A FOREST AREA IN WINTER CONDITIONS

K. Nyren, D. J. Ride (Chemical and Biological Defense Establishment, Porton Down, England.), and C. D. Jones (Chemical and Biological Defense Establishment, Porton Down, England.) Jun. 1994 63 p
(ISSN 0347-2124)
(PB95-133468; FOA-C-40320-4.5) Avail: CASI HC A04/MF A01

Outdoor experiments to measure atmospheric concentration fluctuations of a tracer gas at high resolution in winter conditions in wooded terrain were conducted in Umea, northern Sweden, in April 1992. The experiments were useful in testing the performance of the new Ultra Violet Ion Collector (UVIC) sensors in a cold climate. The scope of the experiments was limited, but large fluctuations were detected both within the woodland and outside of it. The nature of the fluctuations appeared similar in both locations. Both instantaneous and continuous clouds of tracer gas, propylene, were used. Two UVIC's were employed; both worked well in temperatures around -5 C. Concentration fluctuation statistics from the measured time series are reported. More comprehensive experiments are recommended to assess atmospheric dispersion in winter conditions. The development of an in-field calibration system for the UVIC is proposed. NTIS

N95-21327 Rijksinstituut voor Volksgezondheid en Milieuhygieene, Bilthoven (Netherlands).

EVALUATION OF THE TECHNICAL PERFORMANCE OF THE DUTTCH NATIONAL AIR QUALITY MONITORING NETWORK IN 1992 [EVALUATIE VAN HET FUNCTIONEREN VAN HET LANDELIJK MEETNET LUCHTKWALITEIT IN 1992]

E. Buijsman, D. vanStraalen, P. Swaan, P. W. deVos, and B. G. vanElzakker Jan. 1994 44 p In DUTCH
(PB95-131892; RIVM-723102003) Avail: Issuing Activity (National Technical Information Service (NTIS))

In the report the results of an evaluation of the technical performance of the Dutch National Air Quality Monitoring Network in 1992 are presented. The average brute component efficiencies, i.e. a measure for the availability of measuring data, are: for the automatically measured components (CO, NOx, O3, SO2) 96%; for the meteorological parameters (global radiation, temperature, wind direction, wind speed) 97%; for aerosols etc. (black smoke, acidifying compounds, metals, tsp) 96%; for the chemical composition of precipitation (i.a. acidifying compounds, heavy metals) 96%. Current Dutch legislation requires the measurement of a number of components in such way that only a minimal loss of data is tolerated. The number of stations which did not meet the legal requirements in 1992 are; two for CO (18% of the total number of stations), seven for NO2 (35%), six for SO2 (7%), two for lead aerosol (50%) and 6 for black smoke (30%). NTIS

N95-21329 Rijksinstituut voor Volksgezondheid en Milieuhygieene, Bilthoven (Netherlands).

OZONE QUALITY CONTROL MEASUREMENTS IN THE DUTCH NATIONAL AIR QUALITY MONITORING NETWORK [KWALITEITSCONTROLEMETINGEN OZON IN HET LANDELIJK MEETNET LUCHTKWALITEIT]

P. Swaan Mar. 1994 25 p In DUTCH
(PB95-131900; RIVM-723101001) Avail: Issuing Activity (National Technical Information Service (NTIS))

From August 1992 until July 1993, ozone quality control measurements were carried out in the Dutch National Air Quality Monitoring Network (LML). Measurement results from 17 LML measurement locations were compared with those from a reference monitor. It can be concluded that on average ozone levels from the LML give an underestimation of 4.9%, which is independent of the absolute measured levels. In some cases, deviations up to 20% are found suggesting the need for further investigation. NTIS

N95-21330 Technische Hogeschool, Delft (Netherlands). Vakgroep Gezondheidstechniek en Waterbeheersing.

DISINFECTION OF PURIFIED WASTE WATER WITH ULTRA VIOLET LIGHT ON A TECHNICAL SCALE [DESINFECTIE VAN GEZUIVERD AFVALWATER MET ULTRAVIOLET LICHT OP TECHNISCHE SCHAAL]

T. J. Nieuwstad and A. H. Havelaar 1994 95 p In DUTCH Prepared in cooperation with Rijksinstituut voor de Volksgezondheid en Milieuhygiene, Bilthoven, Netherlands Sponsored by Rijksinstituut voor Zuivering van Afvalwater
(PB95-131926) Avail: Issuing Activity (National Technical Information Service (NTIS))

In 1976 the Dutch National Institute for the Purification of Waste Water initiated the project 'The disinfection of sewage plant effluents'. At first the project's supervisory committee concentrated mainly on chemical disinfection. Later it was decided that besides chemical disinfection other methods of disinfection, which do not result in the formation of (harmful) by-products, should be included in the research. On the basis of the experimental studies of the disinfection of purified waste water with ultraviolet light, the Technical University in Delft has carried out further research. This report presents the results of this research. NTIS

N95-21350 Rijksinstituut voor Zuivering Afvalwater, Lelystad (Netherlands).

DEFINITION REPORT ON ENVIRONMENTAL INDICES IN FUTURE ENVIRONMENTAL ASSESSMENTS ENVIRONMENTAL BALANCE/ENVIRONMENTAL OUTLOOK [DEFINITIERAPPORT GRAADMETERS ATMOSFEER IN DE MILIEUBALANS/MILIEUVERKENNING]

H. Noordijk, H. S. M. A. Diederen, H. vanderWoerd, and K. vanVelze May 1994 99 p In DUTCH
(PB95-131876; RIVM-723308001) Avail: Issuing Activity (National Technical Information Service (NTIS))

The report includes environmental indices that will be an important tool in future environmental assessments (Milieubalansen en Milieuverkenningen). The report defines the indices for the atmosphere. It describes the state of definition at the start of the year 1994, and it is the result of the project group in the Laboratory of Air Research (LLO) of RIVM, with support of some experts within and outside of RIVM. This definition needs to be discussed by all the parties involved with environmental assessments, in order to improve the definition and to obtain consensus on it. The report serves as a basis for these discussions. The indices are clustered in human exposure, ecosystem exposure, depletion of stratospheric ozone, climatic change, decreasing self-cleaning capability of the atmosphere, and the damage to the cultural inheritance and the economy. The clusters on human and ecosystem exposure are subdivided into exposure to higher concentrations over a short time (smog), and exposure to concentrations averaged over a time-scale of seasons. Exposure of humans in the indoor environment is also treated separately. NTIS

N95-21351 Rijksinstituut voor Volksgezondheid en Milieuhygieene, Bilthoven (Netherlands).

MONITORING ACTIVITIES IN THE FRAMEWORK OF THE DUTCH NATIONAL AIR QUALITY MONITORING NETWORK IN 1994 [MEETACTIVITEITEN IN 1994 IN HET KADER VAN HET LANDELIJK MEETNET LUCHTKWALAITEIT]

P. Swaan and E. Buijsman Apr. 1994 42 p In DUTCH
(PB95-131884; RIVM-723102004) Avail: Issuing Activity (National Technical Information Service (NTIS))

The report presents an overview of monitoring activities in the framework of the Dutch National Air Quality Monitoring Network. The network is one of the responsibilities of the Laboratory for Air Research of the National Institute of Public Health and Environmental Protection. Surveys of the monitoring stations per component are provided, together with maps of their locations. Overviews are presented for: gaseous components (CO, NO(x), O3, SO2, NH3, Volatile Organic Components (VOC)); aerosols etc. (metals, acidifying components, particulate matter); chemical composition of precipitation (a.o. acidifying components, metals); and other monitoringactivities (wind speed, wind direction, measurements for ECE/EMEP, fluoride accumulation). NTIS

N95-21373# Sierra Research, Inc., Sacramento, CA.

ANALYSIS OF INVALID EMISSION TESTING IN THE CALIFORNIA SMOG CHECK PROGRAM

Thomas C. Austin, H. Anthony Ashby, and Thomas R. Carlson 27 Apr. 1994 34 p
(Contract EPA-68-C1-0079)
(PB95-128922; EPA/420/R-94/003) Avail: CASI HC A03/MF A01

The report describes the results of exhaust emissions measurements reported by licensed automotive repair dealerships participation in the California motor vehicle inspection and maintenance (I/M) program called Smog Check. The results have been compared to measurements made on the same vehicles at the California Air Resources Board (ARB) laboratory. Based on an experimental program conducted by ARB the Smog Check station exhaust emission test results appear to be invalid for about 17.5% of the vehicles. The report describes the issues involved. NTIS

N95-21379# Brown Univ., Providence, RI.

SENSITIVITY OF CLIMATE MODELS: COMPARISON OF SIMULATED AND OBSERVED PATTERNS FOR PAST CLIMATES Progress Report, 1 Feb. 1994 - 31 Jan. 1995

J. Kutzbach, R. J. Oglesby, W. L. Prell, and T. Webb, III Oct. 1994 12 p
(Contract DE-FG02-85ER-60304)
(DE95-002257; DOE/ER-60304/10) Avail: CASI HC A03/MF A01

General circulation models of the atmosphere and oceans are key to the prediction of the potential climate changes that may be induced by increased concentrations of greenhouse gases. Confidence in the predictions of these models can be gained by testing of these models in their ability to simulate past climates. Estimates of global mean temperature change show that the magnitude of warming since the last glacial maximum 21,000 calendar years ago match the magnitude of warming currently being predicted for the doubling of carbon dioxide in the atmosphere. Simulations of the climatic changes for the past 21,000 years as well as for warmer-than-present climates at 6000 and 125,000 years ago provide an excellent opportunity to test the models that are being used in global climate change research. Recognition of this opportunity has been central to our DOE research for the past decade and is now central to PMIP (Paleoclimate Modeling Intercomparison Project) to which our research is contributing. DOE

N95-21410# Colorado State Univ., Fort Collins, CO. Dept. of Atmospheric Science.

MONITORING THE RESPONSE OF THE UPPER TROPOSPHERE/LOWER STRATOSPHERE TO A GREENHOUSE GAS SCENARIO

J. M. Davis and S. K. Cox 25 Sep. 1994 26 p
(Contract DE-FG02-90ER-60970)
(DE95-000982; DOE/ER-60970/3) Avail: CASI HC A03/MF A01

A measurement system for examining the possible linkage between an increased concentration of Greenhouse Gases (GG's) and symptoms of climate change has been designed and evaluated. The system consists of a dual port emission interferometer and supporting data analysis algorithms for the remote sensing the upper troposphere/lower stratosphere from a high elevation ground site deployment. Two blackbody systems were designed and tested to provide necessary calibration targets for the interferometer. The interferometer was deployed during four different periods at climatologically distinct locations to test the capabilities of the system. Over two hundred spectra were collected in a variety of conditions ranging from a clear middle latitude atmosphere viewed from mountain site at 3.0 km ASL to sub-tropical marine stratocumulus cloudiness measured at Porto Santo Island near Madeira. The algorithm has been used successfully to retrieve temperature and moisture profiles from both the mountain and sea level deployments. These initial retrievals indicate that ground based systems may only be effective in sensing the temperature and moisture profiles for the first few kilometers above the instrument. The interferometric data have been used to estimate the size of 'equivalent spherical' ice particles in cirrus clouds. The data from the sea level deployment were examined in order to retrieve the absorption coefficients of marine stratocumulus clouds and a double iteration algorithm has been developed to deduce the emittance of cirrus clouds from interferometric spectral measurements. DOE

N95-21487# Pacific Northwest Lab., Richland, WA.

POSSIBLE GLOBAL ENVIRONMENTAL IMPACTS OF SOLID WASTE PRACTICES

M. M. Davis, G. M. Holter, T. J. DeForest, D. C. Stapp, and J. C. Dibari (Heritage Coll., Toppenish, WA.) Sep. 1994 67 p
(Contract DE-AC06-76RL-01830)
(DE95-000830; PNL-10149) Avail: CASI HC A04/MF A01

Pollutants resulting from the management of solid waste have been shown to affect the air, land, oceans, and waterways. In addition, solid wastes have other, more indirect impacts such as reduction in feedstocks of natural resources, because useful materials are disposed of rather than recycled. The objective of this study is to evaluate solid waste management practices that have negative implications on the global environment and develop recommendations for reducing such impacts. Recommendations identifying needed changes are identified that will reduce global impacts of solid waste practices in the future. The scope of this study includes the range of non-hazardous solid wastes produced within our society, including municipal solid waste (MSW) and industrial solid waste (ISW), as well as industry-specific wastes from activities such as construction, demolition, and landclearing. Most solid waste management decisions continue to be made and implemented at very local levels, predominantly with a short-term focus to respond to relatively immediate pressures of landfill shortages, funding problems, political considerations, and the like. In this rush to address immediate local problems, little consideration is being given to potential impacts, either short- or long-term, at the national or global level resulting from solid waste management practices. More and more, the cumulative impacts from local decisions concerning solid waste management are beginning to manifest themselves in broader, longer-term impacts than are being addressed by the decision-makers or, at the very least, are presenting a greater and greater potential for such impacts. DOE

N95-21565# Medical Univ. of South Carolina, Charleston, SC.

ENVIRONMENTAL HAZARDS ASSESSMENT PROGRAM

1994 725 p
(Contract DE-FG01-92EW-50625)
(DE94-019075; DOE/EW-50625/T18-Vol-4) Avail: CASI HC A99/MF A06

The Medical University of South Carolina's (MUSC) vision is to become the premier national resource for medical information and for environmental/health risk assessment. A key component to the success of the many missions of the Environmental Hazards Assessment Program (EHAP) is timely access to large volumes of data. The significant growth in the number of environmental/health information systems that has occurred over the past few years has made data access challenging. This study documents the results of the needs assessment effort conducted to determine the information access and processing requirements of EHAP. The following topics are addressed in this report: immunological consequences of beryllium exposure; assessment of genetic risks to environmental diseases; low dose-rate radiation health effects; environmental risk perception in defined populations; information support and access systems; and environmental medicine and risk communication: curriculum and a professional support network-Department of Family Medicine. DOE

N95-21596 Air Force Engineering and Services Center, Tyndall AFB, FL.
SPECTROSCOPIC STUDIES OF HAZARDOUS FUEL INTERACTIONS WITH SOILS Interim Report, Oct. 1989 - Oct. 1990
Terence L. Tipton and Daniel A. Stone Dec. 1993 180 p Limited Reproducibility: More than 20% of this document may be affected by microfiche quality
(AD-A279099; ESL-TR-90-47) Avail: Issuing Activity (Defense Technical Information Center (DTIC))

This report describes the development and application of techniques for the spectroscopic study of hazardous fuel compounds in soils. The objective is to obtain improved models of bulk pollutant transport through soils. Two approaches have been used for this study: one consists of in-situ measurements of electronic and vibrational interactions via ultraviolet-visible spectroscopy and infrared spectroscopy, respectively; the other incorporates analytical separation techniques to extract contaminants from soils and identify individual reaction products. Initially, montmorillonite clay has been chosen as a prototype soil sample because the structure of this clay is well characterized and spectroscopic results can be readily interpreted. Further simplification has been obtained by exposing the clay samples to individual fuel components rather than mixtures. An interpretation of one clay/fuel system has been accomplished. The plan is to gradually increase the complexity of the samples until typical field conditions can be modeled. DTIC

N95-21608# Oak Ridge National Lab., TN.
THE MESSAGE PASSING VERSION OF THE PARALLEL COMMUNITY CLIMATE MODEL
J. B. Drake, R. E. Flanery, D. W. Walker, P. H. Worley, I. T. Foster (Argonne National Lab., IL.), J. G. Michalakes (Argonne National Lab., IL.), R. L. Stevens (Argonne National Lab., IL.), J. J. Hack (National Center for Atmospheric Research, Boulder, CO.), and D. L. Williamson (National Center for Atmospheric Research, Boulder, CO.) 1994 14 p Presented at the 5th ECMWF Workshop on Parallel Processing in Meteorology, Reading, England, 23-27 Nov. 1992 Sponsored in cooperation with NSF
(Contracts DE-AC05-84OR-21400; W-31-109-eng-38)
(DE94-019158; CONF-9211198-3) Avail: CASI HC A03/MF A01

This paper is a brief overview of a parallel version of the NCAR Community Climate Model, CCM2, implemented for MIMD massively parallel computers using a message-passing programming paradigm. The parallel implementation was developed on an Intel iPSC/860 with 128 processors and on the Intel Delta with 512 processors, and the initial target platform for the production version of the code is the Intel Paragon with 2,048 processors. Because the implementation uses a standard, portable message-passing library, the code can be easily ported to other multiprocessors supporting a message-passing programming paradigm, or run on machines distributed across a network. The parallelization strategy used is to decompose the problem domain into geographical patches and assign each processor to do the computation associated with a distinct subset of the patches. With this decomposition, the physics calculations involve only grid points and data local to a processor and are performed in parallel. Using parallel algorithms developed for the semi-Lagrangian transport, the fast Fourier transform and the Legendre transform, both physics and dynamics are computed in parallel with minimal data movement and modest change to the original CCM2 source code. DOE

N95-21617# Argonne National Lab., IL.
REMOVAL OF CO2 IN CLOSED LOOP OFF-GAS TREATMENT SYSTEMS
M. K. Clemens, P. A. Nelson, and W. M. Swift 1994 23 p Presented at the 6th Emerging Technologies in Hazardous Waste Management, Atlanta, GA, 19-21 Sep. 1994
(Contract W-31-109-eng-38)
(DE94-019259; ANL/CMT/CP-82692; CONF-9409215-1) Avail: CASI HC A03/MF A01

A closed loop test system has been installed at Argonne National Laboratory (ANL) to demonstrate off-gas treatment, absorption, and purification systems to be used for incineration and vitrification of hazardous and mixed waste. Closed loop systems can virtually eliminate the potential for release of hazardous or toxic materials to the atmosphere during both normal and upset conditions. In initial tests, a 250,000 Btu/h (75 kW thermal) combustor was operated in an open loop to produce a combustion product gas. The CO2 in these tests was removed by reaction with a fluidized bed of time to produce CaCO3. Subsequently, recirculation system was installed to allow closed loop operation with the addition of oxygen to the recycle stream to support combustion. Commercially marketed technologies for removal of CO2 can be adapted for use on closed loop incineration systems. The paper also describes the Absorbent Solution Treatment (AST) process, based on modifications to commercially demonstrated gas purification technologies. In this process, a side loop system is added to the main loop for removing CO2 in scrubbing towers using aqueous-based CO2 absorbents. The remaining gas is returned to the incinerator with oxygen addition. The absorbent is regenerated by driving off the CO2 and water vapor, which are released to the atmosphere. Contaminants are either recycled for further treatment or form precipitates which are removed during the purification and regeneration process. There are no direct releases of gases or particulates to the environment. The CO2 and water vapor go through two changes of state before release, effectively separating these combustion products from contaminants released during incineration. The AST process can accept a wide range of waste streams. The system may be retrofitted to existing Facilities or included in the designs for new installations. DOE

N95-21635 Rijksinstituut voor de Volksgezondheid, Bilthoven (Netherlands).
SELECTION OF SUBSTANCES TO BE CONSIDERED IN THE ENVIRONMENTAL BALANCE/ENVIRONMENTAL OUTLOOK IN RELATION TO THE DISSEMINATION THEME [STOFKEUZE VOOR HET THEMA VERSPREIDING IN DE MILIEUBALANS/MILIEUVERKENNING]
W. Slooff Apr. 1994 57 p In DUTCH
(PB95-132197; RIVM-482516002) Avail: Issuing Activity (National Technical Information Service (NTIS))

This report presents a proposal on a selection of substances, to be considered in the Environmental Balance/Environmental Outlook in relation to the Dissemination theme. As a first step in the selection procedure it was decided to exclude new substances, notified prior to their introduction on the market; substances that also are considered within other policy themes, except for those compounds that exceed toxicological risk levels; genetically modified organisms; biological agents; and cleaning up contaminated soils. As a second step a number of criteria (relevance, knowledge, controllability) was applied to policy based lists of substances. NTIS

N95-21666# Los Alamos National Lab., NM.
IMPLEMENTATION OF ELECTRONIC CHAIN-OF-CUSTODY, ANALYSIS REQUESTS, AND DATA VERIFICATION AT LOS ALAMOS NATIONAL LABORATORY
H. C. Pound and J. J. Miglio 1994 13 p Presented at the American Society for Quality Control Energy and Environmental Quality Division Conference, Tucson, AZ, 18-21 Sep. 1994
(Contract W-7405-eng-36)
(DE94-018076; LA-UR-94-2694; CONF-940985-7) Avail: CASI HC A03/MF A01

To improve the efficiency of the entire environmental data collection process from sample collection to reporting to the client, Los Alamos National Laboratory is developing an automated system to carry out as much of the process as possible. The system uses 'off-the-shelf' software. Our program anticipates a drastic reduction of the amount of paper generated throughout the process. The electronic system includes spreadsheets used for field and laboratory chains-of-custody. In addition, the system is used to order analyses and to verify data for compliance. DOE

N95-21683 General Accounting Office, Washington, DC. National Security and International Affairs Div.
ENVIRONMENTAL CLEANUP: TOO MANY HIGH PRIORITY SITES IMPEDE DOD'S PROGRAM. REPORT TO THE CHAIRMAN, COMMITTEE ON GOVERNMENTAL AFFAIRS, US SENATE
Apr. 1994 28 p Limited Reproducibility: More than 20% of this document may be affected by microfiche quality

(AD-A279511; GAO/NSIAD-94-133; B-256676) Avail: Issuing Activity (Defense Technical Information Center (DTIC)); GAO, PO Box 6015, Gaithersburg, MD 20884-6015 HC

Military installations are similar to small cities in term of population, industrial activities, and some types of contaminated sites, However, some cover an area larger than a small state. DOD has operated industrial facilities on its installations for several decades that have generated, stored, recycled, or disposed of hazardous wastes. Many of these activities have contaminated the nearby soil and groundwater. To study and clean up contaminated sites, DOD established the Installation Restoration Program (IRP) in 1975. In 1984, the IRP was made part of the Defense Environmental Restoration Program. DTIC

N95-21685 Mar, Inc., Rockville, MD.

OHMSETT TEST OF NOFI VEE-SWEEP AND NOFI 600S OILBOOM Final Report

Michael J. Goodwin Oct. 1993 122 p Limited Reproducibility: More than 20% of this document may be affected by microfiche quality
(Contract DOT-CG-14-35-0001-30544)
(AD-A279525; USCG-D-04-94; CGR/DC-22/93) Avail: Issuing Activity (Defense Technical Information Center (DTIC))

A NOFI Vee-Sweep and a NOFI 600S Oilboom, both manufactured by NOFI TROMSO A/S of Norway, were tested at the Ohmsett test tank in Leonardo, NJ. The V-Shaped Sweep is an oil boom designed for use with a skimmer at the apex of the V-Shaped configuration. Oil is funneled back to the skimmer by the converging sides of the V and concentrated for more efficient skimming. The 60 meter length of the sweep is doubled over to form the V and held in this shape by cross netting at the bottom of the skirt. The bottom netting is claimed to help stabilize the oil in the sweep. The sweep was towed with a 700 mm skirt depth and mouth opening of 16 meters. The mouth opening was reduced from the designed 19.8 meters to fit in the tow tank without causing excess blockage. The limiting towing speeds of the sweep were determined with and without oil present, in calm water and in small waves. The sweep's ability to conform to waves was also determined. Towing forces were measured. Limited data on oil loss rates were obtained. Testing confirmed the manufacturer's claim that the sweep can be towed at 1.0 and 1.4 knots with oil in calm water, based on the first loss of oil. The critical tow speed was found to be 3.4 to 3.6 knots in calm water. DTIC

N95-21689 Army Construction Engineering Research Lab., Champaign, IL.

ENVIRONMENTAL COMPLIANCE ASSESSMENT AND MANAGEMENT PROGRAM (ECAMP), SOUTH CAROLINA SUPPLEMENT Interim Report

Carolyn ORourke and Lisa A. Gifford Apr. 1994 311 p Limited Reproducibility: More than 20% of this document may be affected by microfiche quality
(AD-A279533; CERL-SR-EC-94/16) Avail: Issuing Activity (Defense Technical Information Center (DTIC))

The number of environmental laws and regulations has continued to grow in the United States and worldwide, making compliance with these regulations increasingly difficult. Environmental assessments became a way to determine compliance with current environmental regulations. The U.S. Air Force has adopted an environmental compliance program that identifies compliance problems before they are cited as violations by the U.S. Environmental Protection Agency (USEPA). Beginning in 1984, the U.S. Army Construction Engineering Research Laboratories (USACERL), in cooperation with the Air Force Engineering and Services Center, began research on the U.S. Environmental Compliance Assessment and Management Program (ECAMP). The concept was to combine Federal, Department of Defense (DOD), and Air Force environmental regulations, along with existing checklists from the USEPA and private industry, and documentation of good management practices and risk-management issues, into a series of checklists that list legal requirements and specify items or operations to review. Each assessment protocol lists a point of contact to help assessors review the checklists as effectively as possible. The South Carolina Supplement was developed to be used in conjunction with the U.S. ECAMP manual, using existing South Carolina state environmental legislation and regulations as well as suggested management practices. DTIC

N95-21696 Army Construction Engineering Research Lab., Champaign, IL.

ENVIRONMENTAL COMPLIANCE ASSESSMENT SYSTEM (ECAS): OREGON SUPPLEMENT Final Report

Carolyn ORourke and Lisa A. Gifford Apr. 1994 55 p Limited Reproducibility: More than 20% of this document may be affected by microfiche quality
(AD-A279565; CERL-SR-EC-94/18) Avail: Issuing Activity (Defense Technical Information Center (DTIC))

In response to the growing number of environmental laws and regulations worldwide, the U.S. Army has adopted an environmental compliance program that identifies compliance problems before they are cited as violations by the U.S. Environmental Protection Agency (USEPA). Beginning in 1985, Major Army Commands (MACOM's) were required to conduct comprehensive environmental assessments at all installations on a 4-year cycle. The installations must also conduct a mid-cycle internal assessment. Because each MACOM was developing a separate assessment system, the Army mandated, through Army Regulation 200-1, one unified Army-wide assessment mechanism. The resulting system combines Federal, Department of Defense (DOD), and Army environmental regulations, along with good management practices and risk management information, into a series of checklists that show legal requirements and specific items or operations to review. Each assessment protocol lists a point of contact to help assessors review the checklist items as effectively as possible. The Environmental Compliance Assessment System (ECAS) manual incorporates existing checklists from USEPA and private industry. The Oregon Supplement was developed to be used in conjunction with the U.S. ECAS manual, using existing Oregon state environmental legislation and regulations as well as suggested management practices. DTIC

N95-21699 IIT Research Inst., Chicago, IL.

COMPILATION OF 1993 ANNUAL REPORTS OF THE NAVY ELF COMMUNICATIONS SYSTEM ECOLOGICAL MONITORING PROGRAM Annual Report, Jan. - Sep. 1993

J. E. Zapotosky Apr. 1994 410 p Limited Reproducibility: More than 20% of this document may be affected by microfiche quality
(Contract N00039-93-C-0001)
(AD-A279575) Avail: Issuing Activity (Defense Technical Information Center (DTIC))

During 1993, the U.S. Navy continued to conduct a program to monitor flora, fauna, and their ecological relationships for possible effects from electromagnetic (EM) fields produced by the Navy's Extremely Low Frequently (ELF) Communications System. Physiological, developmental, behavioral, and ecological variables for dominant biota in upland and riverine habitats near the Naval Radio Transmitting Facility at Republic, Michigan (NRTF-Republic) have been monitored since 1982. The NRTF-Republic was intermittently energized at low amperages beginning in early 1986. Electric current and periods of energization were then gradually increased until 1989, when the transmitter became a fully operational facility. A split-plot or blocked strategy was used to examine biological variables for possible effects from EM exposure. Reports complied in this document present the progress of these studies through 1993. Final results and conclusions are expected after all data have been analyzed in 1994. Investigators for similar studies completed in Wisconsin concluded that there were no EM bioeffects from intermittent or full operation of the transmitter in that state. DTIC

N95-21708# Scripps Institution of Oceanography, La Jolla, CA.

MODELING THE RESPONSE OF THE CALIFORNIA CURRENT SYSTEM TO GLOBAL GREENHOUSE WARMING

A. Pares-Sierra and R. C. J. Somerville 1993 7 p
(Contract DE-FC03-90ER-61010)
(DE94-018253; DOE/ER-61010/T26) Avail: CASI HC A02/MF A01

This is the final report for the project 'Modeling the Response of the California Current System to Global Greenhouse Warming,' supported 1990 and 1991 by NIGEC. The scientists involved are Dr. Richard C.J. Somerville and Alejandro Paries-Sierra of Scripps Institution of Oceanography, UCSD. A copy of papers submitted to the Journal of Physical Oceanography, and Geofisica Internacional that were supported in part or whole by WEST-GEC, as well as a summary of a talk delivered at the 20th General Assembly of the IUGG, Vienna are appended to this report. The objective of the research was to improve the understanding of the response of the California Current system to the large-scale anomalous forcing thought to be associated with greenhouse warming. The authors viewed this as a necessary initial step in the study of the California climate response to global change. DOE

N95-21718 Rijksinstituut voor Volksgezondheid en Milieuhygieene, Bilthoven (Netherlands).

AIR POLLUTION CAUSED BY FIREWORKS DURING THE TURN OF THE YEAR 1992-1993 [LUCHTVERONTREINIGING DOOR VUURWERK TIJDENS DE JAARWISSELING VAN 1992-1993]

H. Noordijk Apr. 1993 56 p In DUTCH
(PB95-135265; RIVM-722103001) Avail: Issuing Activity (National Technical Information Service (NTIS))

Various meteorological conditions, especially the presence of a very low and strong temperature inversion and the absence of wind, caused a sharp increase of atmospheric pollutants during the festivities at the turn of the year 1992. The major components of the particles are carbonates, sulfates and chlorides of potassium. The average concentration of metals in cities in the first hour of the new year is estimated to be about 100 - 1,000 micrograms/cu m. Salts of aluminum and magnesium predominate. Minor contributions are observed for strontium, barium and lead. Contributions of other metals are very low or not observed. Other compounds, such as nitrogen oxides, sulfur dioxide and carbon monoxide, did not noticeably increase after the fireworks. The high concentration of fine particles may have caused acute health effects, such as tightness of the chest. Especially people with chronic lung or pulmonary diseases may have experienced troubles. Visibility was reduced due to scattering by the released particles, in combination with moisture in the air. Visibility in or near domestic areas has been reduced to several tens of meters in the first hours of the new year. Locally, further visibility reductions, due to fireworks and fires, are expected. Extreme visibility reductions have been observed indeed. NTIS

N95-21722# Richland Operations Office (AEC), WA.

OZONE-DEPLETING-SUBSTANCE CONTROL AND PHASE-OUT PLAN

J. M. Nickels and M. J. Brown Jul. 1994 65 p
(DE95-001647; DOE/RL-94-86) Avail: CASI HC A04/MF A01

Title VI of the Federal Clean Air Act Amendments of 1990 requires regulation of the use and disposal of ozone-depleting substances (ODS's) (e.g., Halon, Freon). Several important federal regulations have been promulgated that affect the use of such substances at the Hanford Site. On April 23, 1993, Executive Order (EO) 12843, Procurement Requirements and Policies for Federal Agencies for Ozone-Depleting Substances (EPA 1993) was issued for Federal facilities to conform to the new US Environmental Protection Agency (EPA) regulations implementing the Clean Air Act of 1963 (CAA), Section 613, as amended. To implement the requirements of Title VI the US Department of Energy, Richland Operations Office (RL), issued a directive to the Hanford Site contractors on May 25, 1994 (Wisness 1994). The directive assigns Westinghouse Hanford Company (WHC) the lead in coordinating the development of a sitewide comprehensive implementation plan to be drafted by July 29, 1994 and completed by September 30, 1994. The implementation plan will address several areas where immediate compliance action is required. It will identify all current uses of ODS's and inventories, document the remaining useful life of equipment that contains ODS chemicals, provide a phase-out schedule, and provide a strategy that will be implemented consistently by all the Hanford Site contractors. This plan also addresses the critical and required elements of Federal regulations, the EO, and US Department of Energy (DOE) guidance. This plan is intended to establish a sitewide management system to address the clean air requirements. DOE

N95-21846 Rijksinstituut voor Volksgezondheid en Milieuhygieene, Bilthoven (Netherlands).

DEFINITION REPORT ON TARGET AND RELATED STEERING VARIABLES OF RADIATION AS A PART OF THE ENVIRONMENTAL BALANCE AND ENVIRONMENTAL OUTLOOK INVESTIGATION [DEFINITIERAPPORT: GRAADMETERS STRALING IN DE MILI EUBALANS/MILIEUVERKENNING]

M. J. M. Pruppers, F. J. Aldenkamp, R. O. Blaauboer, G. J. Eggink, and P. J. M. Kwakman Feb. 1994 40 p In DUTCH
(PB95-135471; RIVM-610055001) Avail: Issuing Activity (National Technical Information Service (NTIS))

This definition report describes the elaboration of this approach when it is applied to the complete area of interest 'radiation'. Together with other definition reports it is supposed to be the justification of choices which are made in defining the sequence of subjects and the minimum set of variables. The elaboration is guided by the policy document 'Radiation protection and risk management'. The policy can be characterized as 'risk management by focusing directly on the sources of radiation'. In other words steering at the beginning and setting limits at the end of the source-risk-chain. Therefore, in the report it is concluded that the complete source-risk-chain has to be analyzed and modelled. NTIS

N95-21914 Army Engineer Waterways Experiment Station, Vicksburg, MS. Environmental Lab.

AQUATIC PLANT CONTROL RESEARCH PROGRAM. ECOLOGICAL ASSESSMENT OF KIRK POND Final Report

John D. Madsen, Gary O. Dick, David Honnell, Judy Shearer, and R. M. Smart Mar. 1994 75 p Limited Reproducibility: More than 20% of this document may be affected by microfiche quality
(AD-A279090; WES/MP/EL-A-94-1) Avail: Issuing Activity (Defense Technical Information Center (DTIC))

Kirk Pond is a 24-ha man-made pond adjacent to Fern Ridge Reservoir, OR. It is the central feature of Kirk Park, a multiple day-use park at the project. Kirk Pond supports a naturally reproducing warmwater fishery and a put-and-take trout fishery. For many years, the pond has been impacted by dense growths of Eurasian watermilfoil (Myriophyllum spicatum L.), which has greatly restricted recreational use of the pond and threatens both the native plants and vigor of the fishery. The primary purpose of this study was to provide an ecological assessment of the pond in preparation for an experimental application of the potential biological control agent Mycoleptodiscus terrestris (Mt), marketed as the mycoherbicide Aqua-Fyte. The primary goals of the assessment were to (1) determine the role of environmental factors, such as water depth, sediment and water chemistry, and light availability in affecting the present and future distribution and abundance of submersed aquatic plants (particularly M. spicatum) in Kirk Pond; (2) assess the condition of the Kirk Pond ecosystem, including water quality as well as the distribution, abundance, and species diversity of fish populations; and (3) document the existence of any endemic populations of the pathogenic fungus Mycoleptodiscus terrestris. DTIC

N95-22101 Environmental Protection Agency, Research Triangle Park, NC. Atmospheric Research and Exposure Assessment Lab.

TRANSPORT, RADIATIVE, AND DYNAMICAL EFFECTS OF THE ANTARCTIC OZONE HOLE: A GFDL SKYHI MODEL EXPERIMENT

J. D. Mahlman, J. P. Pinto, and L. J. Umscheid 15 Feb. 1994 24 p See also PB88-168240 Submitted for publication Prepared in cooperation with NOAA, Princeton, NJ Limited Reproducibility: More than 20% of this document may be affected by microfiche quality
(PB94-192754; EPA/600/J-94/308) Avail: Issuing Activity (National Technical Information Service (NTIS))

The Geophysical Fluid Dynamics Laboratory 'SKYHI' general circulation model has been used to simulate the effect of the Antarctic 'ozone hole' phenomenon on the radiative and dynamical environment of the lower stratosphere. Both the polar ozone destruction and photochemical restoration chemistries are calculated by parameterized simplifications of the still uncertain more complete chemical processes. The modeled total column ozone depletions are near 25% in spring over Antarctica, with 1% depletion reaching equatorial latitudes by the end of the 4 and 1/2 year model experiment. In the lower stratosphere, ozone reductions of 5% reach to the equator. Large coolings of about 8 C are simulated in the lower stratosphere over Antarctica in late spring, while a general cooling of about 1-1.5 C is present throughout the Southern Hemisphere's lower stratosphere. The model atmosphere experiences a long-term positive temperature-chemical feedback because significant ozone reductions carry over into the next winter. The overall temperature response to the reduced ozone is essentially radiative in character. However, substantial dynamical changes are induced by the ozone hole effect. The Antarctic middle stratosphere in late spring warms by about 6 C over Antarctica and the lower mid-latitude stratosphere warms by approximately one degree. These warming spots are produced mainly by an increased residual circulation intensity. NTIS

N95-22124 Rijksinstituut voor Volksgezondheid en Milieuhygieene, Bilthoven (Netherlands).

INITIAL ASSESSMENT OF THE HAZARDS AND RISKS OF NEW CHEMICALS TO MAN AND THE ENVIRONMENT, PART 2

T. G. Vermeire, G. W. Kroese, G. R. Meijer, J. Mohn, and W. J. G. M. Notenboom May 1993 79 p See also PB93-178184
(PB95-106407; RIVM-679102018) Avail: Issuing Activity (National Technical Information Service (NTIS))

This report is a continuation of the description of the initial hazard and risk assessment process for new substances at the National Institute of Public Health and Environmental Protection (RIVM) in The Netherlands. The present publication pertains to the post base set assessment, specifically on the basis of tests required at market volumes of 100 to 1000 tons per year or 500 to 5000 tons cumulative (level 1). It has primarily been written as a reference guide for those involved in the hazard and risk assessment process at RIVM, but also for risk managers responsible for the regulation and the overall dossier evaluation of new substances, and for others interested in this subject, e.g. industry, nongovernmental organizations, and the public at large. NTIS

N95-22125# Rijksinstituut voor Volksgezondheid en Milieuhygieene, Bilthoven (Netherlands).

DERIVATION OF PRELIMINARY MAXIMUM PERMISSIBLE CONCENTRATIONS OF VOLATILE COMPOUNDS IN AIR

B. C. Rademaker, E. P. Guinee, and E. J. vandePlassche Jul. 1993 114 p
(PB95-107447; RIVM-679101-009) Avail: CASI HC A06/MF A02

In the sub-project 'Volatile Compounds', part of the project 'Setting integrated environmental quality objectives', maximum permissible concentrations (MPC's) are derived for 46 volatile substances for water, sediment, soil, and air. These MPC's are used for setting integrated environmental quality objectives (i.e., limit and target values). In case of the derivation of MPC's in air a step-wise approach was used. First, preliminary MPC's are derived based on information from reviews only. These preliminary MPC's will be harmonized with the ones for water, sediment, and soil. If it can be concluded that the preliminary MPC in air leads to exceedance of a MPC in another compartment, the preliminary MPC in air will be reevalauted. The present report contains the results of the derivation of these preliminary MPC's. Therefore preliminary MPC's in air were derived aiming at the protection of man as well as the ecosystem: the MPC(sub human) and MPC(sub eco), respectively. Both MPC's are compared and one will be selected as the preliminary MPC in air used for harmonization. NTIS

N95-22142 Army Construction Engineering Research Lab., Champaign, IL.

ENVIRONMENTAL COMPLIANCE ASSESSMENT SYSTEM (ECAS): JAPAN SETTLEMENT Final Report

David A. Krooks and Tina M. Hurt Dec. 1993 228 p Limited Reproducibility: More than 20% of this document may be affected by microfiche quality
(Contract MIPR-0823)
(AD-A279328; CERL-SR-EC-94/05) Avail: Issuing Activity (Defense Technical Information Center (DTIC))

The U.S. Army has adopted an environmental compliance program that identifies compliance problems before they are cited as violations by the U.S. Environmental Protection Agency (USEPA). Major Army Commands (MACOMs) must conduct comprehensive environmental assessments at all installations on a 4-year cycle and conduct a mid-cycle internal assessment. Because each MACOM developed a separate system, the Army mandated a unified, Army-wide assessment mechanism, which combines Federal, Department of Defense (DOD), and Army environmental regulations; good management practices; and risk-management issues into a series of checklists that show requirements and specific items or operations to review. Each protocol lists a point of contact to help assessors review checklist items. The Worldwide Environmental Compliance Assessment System (ECAS) manual incorporates checklists from USEPA and from private industry. It integrates information from the Overseas Environmental Baseline Guidance Document (OEBGD). Worldwide ECAS includes pertinent information from Army Regulations and DOD Directives and Instructions and cites management practices for an overall environmental review. The ECAS JAPAN supplement incorporates Japanese legislation, regulations, and suggested management practices. It was developed for use in conjunction with the Worldwide ECAS manuals (USACERL SR-EC-93/03) and is updated continually to address changes in Japanese laws and regulations. DTIC

N95-22186# Rijksinstituut voor Volksgezondheid en Milieuhygieene, Bilthoven (Netherlands).

ASSESSMENT OF THE ATMOSPHERIC HAZARDS AND RISKS OF NEW CHEMICALS: PROCEDURES TO ESTIMATE HAZARD POTENTIALS

F. A. A. M. deLeeuw Mar. 1993 26 p See also PB93-178168
(PB95-107488; RIVM-679102017) Avail: CASI HC A03/MF A01

A procedure for the assessment of atmospheric hazards and risks of newly introduced chemicals is discussed. However, an assessment of direct effects caused by exposure to expected ambient concentrations or by deposition is not discussed; here emphasis is on the role which new substances might play in the atmosphere. Procedures to estimate 'hazard potentials' to quantify the potential risk of a new substance in atmosphere-related environmental problems are proposed. In particular, hazard potentials for the following topics are defined: global warming; ozone depletion; photochemical smog formation; and acidification and eutrophication. NTIS

N95-22219# Waseda Univ., Tokyo (Japan).

PROCEEDINGS: INTERNATIONAL SYMPOSIUM ON GLOBAL CHANGE (IGBP)

1993 793 p Symposium held in Tokyo, Japan, 27-29 Mar. 1992
(DE94-765351; INIS-JP-019; CONF-9203300) Avail: CASI HC A99/MF A10

Seventy papers were presented at the following sessions: (1) source and sink of greenhouse gases, (2) the role of ocean in global change, (3) joint atmospheric/ocean session, (4) effects of global change on terrestrial ecosystem, and (5) paleoenvironments in monsoon Asia. DOE

N95-22278# National Renewable Energy Lab., Golden, CO.

GAS-PHASE PHOTOCATALYTIC OXIDATION: COST COMPARISON WITH OTHER AIR POLLUTION CONTROL TECHNOLOGIES

Craig S. Turchi, Edward J. Wolfrum, and Richard A. Miller (IT Corp., Knoxville, TN.) Nov. 1994 6 p Presented at the 1st International Conference on Advanced Oxidation Technologies for Water and Air Remediation, London, Ontario, 25-30 Jun. 1994
(Contract DE-AC36-83CH-10093)
(DE95-000241; NREL/TP-471-7014; CONF-9406143-2) Avail: CASI HC A02/MF A01

Gas-phase photocatalytic oxidation (PCO) appears to be particularly well suited for waste streams with low pollutant concentrations (1,000 ppm or less) and low to moderate flow rates (less than 20,000 cu ft/min, cfm). The PCO technology is modular in nature and thus is well suited to treat dispersed or low flow rate streams. This same attribute minimizes the advantages of scale for PCO and makes the technology comparatively less attractive for high volume waste streams. Key advantages for PCO lie in its low operating cost and ability to completely destroy pollutants at ambient temperature and pressure. The photocatalytic oxidation process destroys organic air pollutants at ambient temperature and pressure through the use of a light-excited titanium dioxide catalyst. It is being developed for the treatment of industrial emissions, site remediation, and indoor air quality. The objective of this study is to compare PCO costs to those for other common means of treating volatile organic compounds (VOCs) in air. DOE

N95-22330 Winand Staring Centre, Wageningen (Netherlands).

USE OF THE CARBO-FLO PROCESS TO PURIFY PROCESS WATER CONTAMINATED BY AGRICULTURAL PESTICIDES

M. Maaskant, E. vanDullemen, R. Ronday, A. J. Zweers, and H. Perebolte 1994 156 p
(PB95-127825) Copyright Issuing Activity (National Technical Information Service (NTIS))

The objective of the project is to reduce substantially contamination of surface water by pesticides as a result of the discharge of process water from the agricultural and horticultural sectors. The purification efficiency of the Carbo-Flo process has been studied in nine important agricultural and horticultural sectors. Chemical and toxicological analyses show that a high degree of purification is possible using the Carbo-Flo process. For the collection and storage of unused spray and washings, the infrastructure at farm level needs to be adapted. For large-scale introduction, processing plants with a capacity of 5-10 cubic meters per day are a good option from the point of view of treatment costs, licenses, and quality control. NTIS

N95-22342# Oak Ridge National Lab., TN.

MICROMETEOROLOGICAL METHODS FOR MEASUREMENTS OF MERCURY EMISSIONS OVER CONTAMINATED SOILS

K. H. Kim, S. E. Lindberg, P. J. Hanson, J. Owens, and T. P. Myers (National Oceanic and Atmospheric Administration, Oak Ridge, TN.) 1993 5 p Presented at the 1st Workshop on Emissions and Modelling of Atmospheric Transport of Persistent Organic Pollutants and Heavy Metals, Durham, NC, 6-7 May 1993
(Contract DE-AC05-84OR-21400)
(DE94-017679; CONF-9305320-2) Avail: CASI HC A01/MF A01

As part of a larger study involving development and application of field and laboratory methods (micrometeorological, dynamic enclosure chamber, and controlled laboratory chamber methods) to measure the air/surface exchange of Hg vapor, we performed a series of preliminary measurements over contaminated soils. From March - April 1993, we used the modified Bowen ratio (MBR) method to measure emission rates of mercury over a floodplain contaminated with mercury near Oak Ridge, TN. The mercury emission rates measured from contaminated EFPC soils using the MBR method during early spring show that: (1) in all cases, the contaminated soils acted as a source of mercury to the atmosphere with source strengths ranging from 17 to 160 ng m(exp -2) h(exp -1); and (2) the strengths of mercury emissions can be greatly influenced by the combined effects of surface soil temperature, residence time of air masses over the source area, and turbulence conditions. The mercury fluxes measured in a controlled flow chamber indicate that contaminated soils can exhibit up to an order of magnitude higher emission rates of Hg under conditions of elevated soil temperature, soil structure disturbance, and high turbulence. Mercury emissions from contaminated soils exceeded emissions from background soils by one to two orders of magnitude. DOE

N95-22381# Rijksinstituut voor de Volksgezondheid, Bilthoven (Netherlands).

DERIVATION OF MAXIMUM PERMISSIBLE CONCENTRATIONS FOR SEVERAL VOLATILE COMPOUNDS FOR WATER AND SOIL

E. J. vandePlassche, M. D. Polder, and J. H. Canton May 1993 142 p
(PB95-107454; RIVM-679101-008) Avail: CASI HC A07/MF A02

In this report Maximum Permissible Concentrations (MPC's) for water, sediment and soil were derived for 46 volatile organic compounds in frame of the project 'Volatile compounds'. This project is part of another one called 'Setting integrated environmental quality objectives'. Because most of the 46 compounds are acting by narcosis the QSAR (Quantitative Structure-Activity Relationships) approach from Van Leeuwen et al. (1992) is used in order to derive MPC's for water. This approach uses NOEC values obtained by application of QSAR's for minimum toxicity for 19 different organisms. These NOEC values are used as input data for the extrapolation method of Aldenberg and Slob to calculate a MPC. Toxicity data for soil organisms were gathered from literature. Due to scarcity of data only for 11 compounds a MPC for soil could be derived. In all cases the modified EPA method had to be applied. No toxicity data were available for benthic organisms exposed via contaminated sediment. NTIS

N95-22414# Institute for Defense Analyses, Alexandria, VA.

PROCEEDINGS OF THE 4TH ANNUAL MAJOR RANGE AND TESTFACILITY BASE (MRTFB) ENVIRONMENTAL WORKSHOP Final Report, Jan. 1994 - Jul. 1995

Charles T. Ackerman and Christine M. Jordan Jul. 1994 509 p Workshop held in Alexandria, VA, 26-28 Apr. 1994
(Contract DASW01-94-C-0054)
(AD-A285779; IDA-D-1537; IDA/HQ-94-45640; AD-E501847) Avail: CASI HC A22/MF A04

Rapidly increasing environmental requirements are forcing a shift in the way the DOD test and evaluation community conducts business. In order to promote understanding of environmental requirements and facilitate communication on approaches to meeting these requirements, the Major Range and Test Facility Base Environmental Coordinating Committee (MECC) with the support of the Office of the Under Secretary of Defense (Acquisition and Technology), Deputy Director, Test and Evaluation (Test Facilities and Resources), sponsored the Fourth Annual Major Range and Test Facility Base (MRTFB) Environmental Workshop on 26-28 April 1994. The material contained in this document serves as a record of the workshop. It provides copies of the presentations made and summaries of the MECC subcommittee sessions held during the workshop. DTIC

46 GEOPHYSICS

Includes aeronomy; upper and lower atmosphere studies; ionospheric and magnetospheric physics; and geomagnetism.
For space radiation see *93 Space Radiation.*

N95-19981# Colorado School of Mines, Golden, CO. Center for Wave Phenomena.

VELOCITY ANALYSIS FOR TRANSVERSELY ISOTROPIC MEDIA

T. Alkhalifah and I. Tsvankin Aug. 1994 62 p Presented at the CWP Annual Project Review Meeting, Breckenridge, CO, 11-14 May 1993
(Contract DE-FG02-89ER-14079)
(DE95-000643; DOE/ER-14079/32; CWP-145P; CONF-9305377-2) Avail: CASI HC A04/MF A01

The main difficulty in extending seismic processing to anisotropic media is the recovery of anisotropic velocity fields from surface reflection data. Velocity analysis for transversely isotropic (TI) media can be done by inverting the dependence of P-wave moveout velocities on the ray parameter. P-wave NMO velocity in homogeneous TI media with a vertical symmetry axis depends just on the zero-dip value V(sub nmo) and a new effective parameter (eta) that reduces to the difference between Thomsen parameters (epsilon) and (delta) in the limit of weak anisotropy. It is possible to obtain (eta) and reconstruct the NMO velocity as a function of ray parameter using moveout velocities for two different dips. Moreover, V(sub nmo)(0) and (eta) determine not only the NMO velocity, but also also long-spread (nonhyperbollic) P-wave moveout for horizontal reflectors and time-migration impulse response. Inversion of dip-moveout information allows performance of all time-processing steps in TI media using only surface P-wave data. Isotropic time-processing methods remain entirely valid for elliptical anisotropy (epsilon = delta). Accurate time-to-depth conversion, however, requires the vertical velocity V(sub P0) be resolved independently. If I-P0 is known, then all isotropies (epsilon) and (delta) can be found by inverting two P-wave NMO velocities corresponding to a horizontal and a dipping reflector. If no information is available, all three parameters (V (sub P0), (epsilon), and (delta)) can be obtained by combining inversion results with shear-wave information. such as the P-SV or SV-SV wave NMO velocities for a horizontal reflector. Generalization of Tsvankin's single-layer NMO equation for layered anisotropic media with a dipping reflector provides a basis for extending anisotropic velocity analysis to vertically inhomogeneous media. The influence of a stratified overburden on moveout velocity can be stripped through a Dix-type differentiation procedure. DOE

N95-19982# Colorado School of Mines, Golden, CO. Center for Wave Phenomena.

P-WAVE SIGNATURES AND PARAMETERIZATION OF TRANSVERSELY ISOTROPIC MEDIA: AN OVERVIEW

I. Tsvankin Jul. 1994 51 p Presented at the CWP Annual Project Review Meeting, Breckenridge, CO, 11-14 May 1993
(Contract DE-FG02-89ER-14079)
(DE95-000644; DOE/ER-14079/33; CWP-152P; CONF-9305377-1) Avail: CASI HC A04/MF A01

Progress in seismic inversion and processing in anisotropic media depends on our ability to relate different seismic signatures to the anisotropic parameters. While the conventional notation (stiffness coefficients) is suitable for forward modeling, it is inconvenient in developing analytic insight into the influence of anisotropy on wave propagation. The author gives a consistent description of P-wave signatures in transversely isotropic media with arbitrary strength of the anisotropy, using the notation suggested by Thomsen (1986). The influence of transverse isotropy on P-wave propagation is shown to be practically independent of the vertical S-wave velocity V(sub S0), even in models with strong velocity variations. Therefore, the contribution of transverse isotropy to P-wave kinematic and dynamic signatures is controlled by just two anisotropic parameters, (epsilon) and (delta), with the vertical velocity V(sub P0) being no more than a scaling coefficient in homogeneous models. DOE

N95-19985# Lawrence Livermore National Lab., Livermore, CA.
SIMULATION OF STELLAR SPECKLE IMAGING
E. M. Johansson and D. T. Gavel Apr. 1994 14 p Presented at the Society of Photo-Optical Instrumentation Engineers (SPIE) Conference, Kona Beach, HI, 13-18 Mar. 1994
(Contract W-7405-eng-48)
(DE94-016606; UCRL-JC-115104; CONF-940391-11) Avail: CASI HC A03/MF A01

Standard FFT-based phase screen generation methods do not accurately model low frequency turbulence characteristics. This paper introduces a new phase screen generation technique which uses low frequency subharmonic methods. The structure functions for this new method match very closely the structure functions of Kolmogorov turbulence theory. DOE

N95-20002*# Jet Propulsion Lab., California Inst. of Tech., Pasadena, CA.
A COMPARATIVE SURVEY OF CURRENT AND PROPOSED TROPOSPHERIC REFRACTION-DELAY MODELS FOR DSN RADIO METRIC DATA CALIBRATION Survey and Evaluation Report
J. A. Estefan (State Univ. of New York, Buffalo, NY.) and O. J. Sovers Oct. 1994 62 p
(Contract NAS7-918)
(NASA-CR-197338; JPL-Publ-94-24; NAS 1.26:197338) Avail: CASI HC A04/MF A01

The standard tropospheric calibration model implemented in the operational Orbit Determination Program is the seasonal model developed by C. C. Chao in the early 1970's. The seasonal model has seen only slight modification since its release, particularly in the format and content of the zenith delay calibrations. Chao's most recent standard mapping tables, which are used to project the zenith delay calibrations along the station-to-spacecraft line of sight, have not been modified since they were first published in late 1972. This report focuses principally on proposed upgrades to the zenith delay mapping process, although modeling improvements to the zenith delay calibration process are also discussed. A number of candidate approximation models for the tropospheric mapping are evaluated, including the semi-analytic mapping function of Lanyi, and the semi-empirical mapping functions of Davis, et. al.('CfA-2.2'), of Ifadis (global solution model), of Herring ('MTT'), and of Niell ('NMF'). All of the candidate mapping functions are superior to the Chao standard mapping tables and approximation formulas when evaluated against the current Deep Space Network Mark 3 intercontinental very long baselines interferometry database. Author

N95-20116# State Univ. of New York, Albany, NY. Atmospheric Sciences Research Center.
COMPLETION OF SPECTRAL ROTATING SHADOWBAND RADIOMETERS AND ANALYSIS OF ARM SPECTRAL SHORT-WAVE DATA
J. Michalsky and L. Harrison 18 Jul. 1994 17 p
(Contract DE-FG02-90ER-61072)
(DE95-000602; DOE/ER-61072/9) Avail: CASI HC A03/MF A01

Our ARM goal is to help improve both longwave and shortwave models used in GCM's by providing improved radiometric shortwave data. The inference of cloud cover and optical properties of clouds is another goal of this research effort. At the Atmospheric Sciences Research Center (ASRC) in Albany, New York, we are acquiring downwelling shortwave, including direct and diffuse irradiance, at six wavelengths, plus downwelling longwave, upwelling and downwelling broadband shortwave, and aerosol optical depth that we combine with National Weather Service surface and upper air data as a model test data set for ARM researchers. The major objective of our program has been to develop two spectral versions of the rotating shadowband radiometer (RSR). The multi-filter rotating shadowband radiometer (MFRSR) contains six filtered, narrow-passband detectors, and one unfiltered silicon detector that serves as a surrogate total shortwave sensor. The rotating shadowband spectroradiometer (RSS) contains a 256-channel diode array that spans the wavelengths 350-1050 nm with resolution varying between 0.6 nm and 8 nm. With some of the instrument development complete we are devoting more effort to analysis of the MFRSR data. Progress was made on several fronts this year, resulting in conference papers and submissions to refereed journals. Data from the ASRC roof has been used to develop corrections of the MFRSR shortwave sensor. SGP data has been used to develop and validate a retrieval technique for total column water vapor. Total column ozone has been estimated using MFRSR data, but validation at the SGP was not possible for lack of a suitable ozone column standard. Some progress has been made on cloud cover detection, but it is not yet implemented as a routine classification and reporting procedure. DOE

N95-20171# Argonne National Lab., IL.
A HYPERSPECTRAL IMAGE DATA EXPLORATION WORKBENCH FOR ENVIRONMENTAL SCIENCE APPLICATIONS
M. A. Woyna, J. H. Christiansen, D. G. Zawada, and K. L. Simunich 1994 9 p Presented at the DOD Database Colloquium 1994, San Diego, CA, 29-31 Aug. 1994
(Contract W-31-109-eng-38)
(DE94-016373; ANL/DIS/CP-83606; CONF-9408129-2) Avail: CASI HC A02/MF A01

The Hyperspectral Image Data Exploration Workbench (HIDEW) software system has been developed by Argonne National Laboratory to enable analysts at Unix workstations to conveniently access and manipulate high-resolution imagery data for analysis, mapping purposes, and input to environmental modeling applications. HIDEW is fully object-oriented, including the underlying database. This system was developed as an aid to site characterization work and atmospheric research projects. DOE

N95-20278*# National Aeronautics and Space Administration. Lyndon B. Johnson Space Center, Houston, TX.
AN OVERVIEW OF THE EVALUATION OF OXYGEN INTERACTIONS WITH MATERIALS 3 EXPERIMENT: SPACE SHUTTLE MISSION 46; JULY-AUGUST, 1992
Steven L. Koontz, Lubert J. Leger, James T. Visentine, Don E. Hunton (Phillips Lab., Hanscom AFB, MA.), Jon B. Cross (Los Alamos National Lab., NM.), and Charles L. Hakes (Lockheed Engineering and Sciences Co., Houston, TX.) 1993 44 p Presented at the 3d Long Duration Exposure Flight (LDEF) Symposium, Williamsburg, VA, 8-12 Nov. 1993 Submitted for publication
(Contract W-7405-eng-36)
(NASA-TM-110129; NAS 1.15:110129; DE94-009365; LA-UR-94-897; CONF-9311137-2) Avail: CASI HC A03/MF A01

The flight experiment was developed to obtain benchmark atomic oxygen reactivity data and was conducted during Space Transportation System Mission 46 (STS 46), July 31 to August 7, 1992. In this paper, we present an overview of EOIM-III and the results of the materials reactivity and mass spectrometer/carousel experiments. Mass spectrometer calibration methods are discussed briefly, as a prelude to a detailed discussion of the mass spectrometric results produced during STS-46. Mass spectrometric measurements of ambient O-atom flux and fluence are in good agreement with the values calculated using the MSIS-86 model of the thermosphere as well as estimates based on the extent of O-atom reaction with Kapton polyimide. Mass spectrometric measurements of gaseous products formed by O-atom reaction with C(sup 13) labeled Kapton revealed CO, CO2, H2O, NO and NO2. By operating the mass spectrometer so as to detect naturally occurring ionospheric species, we characterized the ambient ionosphere and detected the gaseous reaction products formed when ambient ions interacted with the C(sup 13) Kapton carousel sector. By direct comparison of the results of on-orbit O-atom exposures with those conducted in ground-based laboratory systems, we have demonstrated the strong translational energy dependence of O-atom reactions with a variety of polymers. A 'line-of-centers' reactive scattering model was shown to provide a reasonably accurate description of the translational energy dependence of polymer reactions with O atoms over a three order-of-magnitude range in translational energy and a four order-of-magnitude range in reaction efficiency. Postflight studies of the polymer samples by x-ray photoelectron spectroscopy and infrared spectroscopy demonstrate that O-atom attack is confined to within 50 to 100 Angstroms of the surface. DOE

N95-20287# Oak Ridge National Lab., TN. Environmental Sciences Div.
INVESTIGATING THE RESOLUTION OF RESISTIVITY ARRAYS USING INVERSE THEORY

L. P. Beard and A. C. Tripp (Utah Univ., Salt Lake City, UT.) 1994 14 p Presented at the Symposium on the Application of Geophysics to Environmental and Engineering Problems, Boston, MA, 27-31 Mar. 1994
(Contract DE-AC05-84OR-21400)
(DE94-017760; CONF-940353-8) Avail: CASI HC A03/MF A01

We used a fast 2-D minimum structure inverse solution to examine the ability of different resistivity arrays to resolve structures given noisy synthetic data. We found that the resistivity models obtained from it inversion of the dipole-dipole data were usually very similar to the estimated models from pole-dipole data, and both were superior to estimated models from pole-pole data. This is because noisy dipole-dipole or pole-dipole data define geoelectric structures much more precisely than an equivalent set of noisy pole-pole data. One structure where the dipole-dipole array appeared decidedly superior was the prism beneath a conductive overburden. The final estimated models from the pole-pole data were more poorly resolved than the final models from the other arrays. Our results show that the pole-pole data is a poor choice if vertical resolution of a geoelectric structure is crucial. Furthermore, if pole-pole data contains even a fraction of a percent of noise, the transformation of such data through superposition to equivalent data of other array types is virtually impossible, and significant information is lost. DOE

N95-20289# Los Alamos National Lab., NM.
INFRASONIC OBSERVATIONS OF THE NORTHRIDGE, CALIFORNIA, EARTHQUAKE
J. Paul Mutschlecner and Rodney W. Whitaker 1994 17 p Presented at the 6th International Symposium on Long Range Sound Propagation, Ottawa, Ontario, 12-14 Jun. 1994
(Contract W-7405-eng-36)
(DE94-018095; LA-UR-94-2770; CONF-9406244-2) Avail: CASI HC A03/MF A01

Infrasonic waves from the Northridge, California, earthquake of 17 January 1994 were observed at the St. George, Utah, infrasound array of the Los Alamos National Laboratory. The distance to the epicenter was 543 kilometers. The signal shows a complex character with many peaks and a long duration. An interpretation is given in terms of several modes of signal propagation and generation including a seismic-acoustic secondary source mechanism. A number of signals from aftershocks are also observed. DOE

N95-20354# Lawrence Livermore National Lab., Livermore, CA.
RADIATIVE FORCING FOR CHANGES IN TROPOSPHERIC O3
A. S. Grossman, D. J. Wuebbles, and K. E. Grant Jun. 1994 7 p
(Contract W-7405-eng-48)
(DE94-019017; UCRL-ID-118063) Avail: CASI HC A02/MF A01

We have evaluated the radiative forcing for assumed changes in tropospheric O3 in the 500-1650 cm(exp -1) wavenumber range. The radiative forcing calculations were performed as a function of latitude as well as for a globally and seasonally averaged model atmosphere, both in a clear sky approximation and in a model containing a representative cloud distribution. The scenarios involved radiative forcing calculations for O3 at normal atmospheric abundance and at a tropospheric abundance depleted by 25 ppbv, at each altitude, for all Northern Hemisphere latitudes. Normal abundances of H2O, CO2, CH4, and N2O were included in the calculations. The IR radiative forcing was calculated using a correlated k-distribution radiative transfer model. The tropospheric radiative forcing values are compared to the IPCC formulae for ozone tropospheric forcing as well as other published values to determine the validity of the correlated k-distribution approach to the radiative forcing calculations. The results for the global average atmosphere show agreement with previous results to the order of 10 percent. We conclude that the O3 forcing is linear in the background abundance and that the radiative forcing for ozone for the globally averaged atmosphere and the latitude averaged radiative forcing in the clear sky approximation are in agreement to within 10 percent. For the case of an atmosphere in which the tropospheric ozone has been depleted by 25 ppbv at all altitudes in the Northern Hemisphere, the mid latitude zone contributes (approximately)50 percent of the forcing, tropic zone contributes (approximately)37 percent of the forcing and the polar zone contributes (approximately)13 percent of the total forcing. Author

N95-20377# New Mexico State Univ., Las Cruces, NM. Dept. of Mathematical Sciences.
MARUSSI HYPOTHESIS IN DIFFERENTIAL GEODESY
J. D. Zund 13 Jun. 1994 27 p
(Contract F19628-89-K-0044)
(AD-A285853; PL-TR-94-2207; SR-7) Avail: CASI HC A03/MF A01

This report contains a detailed discussion of the primary conceptual aspects of the Marussi-Hotine theory of differential geodesy, and how it stands today. In addition to reviewing the Marussi hypothesis and Ansatz, we present a derivation of why Hotine's normal coordinate system is admissible, and a new conjecture on the type of local coordinate systems permitted in the Marussi-Hotine theory. DTIC

N95-20397# Sandia National Labs., Livermore, CA.
DAYTIME RAMAN LIDAR PROFILING OF ATMOSPHERIC WATER VAPOR
J. E. M. Goldsmith and S. E. Bisson 1994 3 p Presented at the 17th International Laser Radar Conference, Sendai, Japan, 25-29 Jul. 1994
(Contract DE-AC04-76DP-00789)
(DE94-015747; SAND-94-8715C; CONF-9407106-2) Avail: CASI HC A01/MF A01

Detailed measurements of the distribution of water vapor in the atmosphere are needed for a variety of scientific inquiries, including global climate change and related issues in radiative processes (water vapor is the major greenhouse gas in the atmosphere), and studies of a variety of atmospheric processes such as cloud formation and atmospheric circulation. The Raman lidar is a leading candidate for an instrument capable of the detailed, time- and space-resolved measurements required by these and other studies. DOE

N95-20453* National Aeronautics and Space Administration. Goddard Space Flight Center, Greenbelt, MD.
LOCATION AND CHARACTERISTICS OF THE RECONNECTION X-LINE DEDUCED FROM LOW-ALTITUDE SATELLITE AND RADAR OBSERVATIONS
M. Lockwood, C. J. Davis, M. F. Smith, T. G. Onsager, and W. F. Denig Jul. 1994 47 p Prepared in cooperation with Rutherford Appleton Lab., Chilton, England; New Hampshire Univ., Durham; and Phillips Lab., Hanscom AFB, MA
(NASA-TM-110114; NAS 1.15:110114; PB95-129805; RAL-94-081) Avail: Issuing Activity (National Technical Information Service (NTIS))

We present an analysis of a cusp ion step observed between two poleward-moving events of enhanced ionospheric electron temperature. From the computed variation of the reconnection rate and the onset times of the associated ionospheric events, the distance between the satellite and the X-line can be estimated, but with a large uncertainty due to that in the determination of the low-energy cut-off of the ion velocity distribution function, f(E). Nevertheless, analysis of the time series f(t) shows the reconnection site to be on the dayside magnetopause, consistent with the pulsating cusp model, and the best estimate of the X-line location is 13 R(E) from the satellite. The ion precipitation is used to reconstruct the field-parallel part of the Cowley-D ion distribution function injected into the open low latitude boundary layer (LLBL) in the vicinity of the X-line. From this the Alfven speed, plasma density, magnetic field, parallel ion temperature, and flow velocity of the magnetosheath near the X-line can be derived. NTIS

N95-20455# Westinghouse Savannah River Co., Aiken, SC.
THE EFFECT OF REGIONAL-SCALE SOIL-MOISTURE DEFICITS ON MESOSCALE ATMOSPHERIC DYNAMICS THAT INFLUENCE FIRE SEVERITY
J. D. Fast 30 Sep. 1994 143 p
(Contract DE-AC09-89SR-18035)
(DE95-002682; WSRC-TR-94-0468) Avail: CASI HC A07/MF A02

This study employs a three-dimensional, nonhydrostatic mesoscale model to evaluate the effects of horizontally heterogeneous soil moisture and vegetation type on the atmosphere during two periods in which wildland fires occurred. Numerical sensitivity simulations demonstrate that evapotranspiration significantly affects the boundary-layer structure embedded in the synoptic-scale circulations. In regions with sufficiently moist soils, evapotranspiration increases the humidity and modifies the diurnally varying temperature near the surface. Occasionally, changes in the humidity and temperature fields can also be seen a significant distance downwind of the moist soil regions. The perturbations in the temperature fields ultimately affect the wind speed and direction over or at the boundaries of the moist-soil regions, but only at certain times during the simulation period. The higher humidity also increases the cloudiness and changes the precipitation amounts, indicating that soil moisture and vegetation may play an important role in modifying the spatial distribution and intensity of precipitation. A lower atmospheric stability index, that is an indicator of the potential for wildland fire, is also calculated from the model results. This index is also sensitive to the horizontal distribution of soil moisture and vegetation, especially in regions with relatively moist soils. While only two periods are examined in this study, the impact of surface inhomogeneities in soil moisture and vegetation type on the atmosphere is expected to be highly dependent on the particular synoptic conditions and upon the distribution of soil moisture. DOE

N95-20498# Boston Univ., MA. Center for Space Physics.
METALLIC IONS AND ATOMS IN THE UPPER ATMOSPHERE Final Report, 1 Jan. 1992 - 31 Dec. 1993
Jeffrey M. Forbes 28 Feb. 1994 10 p
(Contract F49620-92-J-0092)
(AD-A285229; AFOSR-94-0582TR) Avail: CASI HC A02/MF A01

The main focus of research under AFOSR Grant F49620-920-J-0092 is to investigate the global and local transport of metallic ions in the upper atmosphere, in particular the layering of ionization, through use of comprehensive numerical models which account for realistic meteoric sources, chemical conversions and sinks, and transport by molecular and eddy diffusion, winds and electric fields. The ultimate goal is to better understand the mechanisms producing ionization layers, and ultimately the seasonal, latitudinal, local time, and temporal variations in the occurrences of ionization layers. Plasma layering can affect HF communications by introducing new reflection paths thus complicating the propagating modes, and presumably in extreme cases by producing blanketing effects. In addition, plasma irregularities may also accompany the sharp gradients characterizing the plasma layers. DTIC

N95-20591 Utah State Univ., Logan, UT. Center for Atmospheric and Space Sciences.
ANALYSIS OF MESOSPHERIC WINDS AND WAVES Final Report, 1 Sep. 1993 - 31 Dec. 1993
Kent L. Miller and Robert G. Roper 5 May 1994 42 p Limited Reproducibility: More than 20% of this document may be affected by microfiche quality
(Contract F49620-93-1-0460)
(AD-A279956; AFOSR-94-0340TR) Avail: Issuing Activity (Defense Technical Information Center (DTIC))

During the four months this grant was operative, a paper expanding on the Arecibo Initiative in Dynamics of the Atmosphere (AIDA '89) incoherent scatter/imaging Doppler interferometry (ISR/IDI) radar comparisons, which used revised data from both techniques, was prepared, and has subsequently been submitted and accepted for publication in the Journal of Atmospheric and Terrestrial Physics. In this paper, 'Mesospheric Wind Studies During AIDA Act 1989: Morphology and Comparison of Various Techniques,' by R. S. Turek, K. L. Miller, R. G. Roper and J. W. Brosnahan, all of the measured line of sight velocity profiles for which data was available from both techniques, rather than a few selected profiles as previously analyzed, were subjected to a statistical analysis. This resulted in comparison of over 200 profiles, ten times more than the 20 previously published. After establishing that the sum of the prevailing wind, diurnal and semidiurnal tides deduced from the IDI data represented the statistical mean of the ISR data, we determined the morphology of the prevailing winds and tides over Arecibo during the April and May AIDA campaigns. The results are presented in this report. DTIC

N95-20760 Advanced Research Projects Agency, Arlington, VA.
THE NOVAYA ZEMLYA EVENT OF 31 DECEMBER 1992 AND SEISMIC IDENTIFICATION ISSUES: 15TH ANNUAL SEISMIC RESEARCH SYMPOSIUM
10 Sep. 1993 165 p Symposium held in Vail, CO, 8-10 Sep. 1993 Limited Reproducibility: More than 20% of this document may be affected by microfiche quality
(AD-A279847) Avail: CASI HC A08

On December 31, 1992 a small (mb 2.5) event (hereafter '921231') was detected on Novaya Zemlya by the Threshold Monitor (TM) system. The TM system uses data from the on-line array network to continuously monitor seismic amplitude levels for a number of specified experimental target sites, including the Russian nuclear test range on Novaya Zemlya. The method involves continuous beamforming (i.e., time-aligning and summing the traces for each regional array) for the target beam-steering points, to extract parameters of the beams for continuous assessment of the upper magnitude limit of events at the target site that would go undetected by the Scandinavian array network. When events occur that are above the network noise level, they appear as peaks on the TM beams and are thus tagged for detailed off-line analysis. The 921231 event was detected in this way and was identified as an event that might be of particular interest to ARPA. On receipt of the information ARPA decided to use the 921231 event as an example to test the effectiveness of seismic identification tools and systems that are being developed within the nuclear monitoring research community. DTIC

N95-20878# Tech Foundation, Inc., Montgomery, WV.
EPSCoR SUPPLEMENTAL GRANT FOR AN APPLICATION OF NEURAL NETWORKS TO SEISMIC SIGNAL DISCRIMINATION Scientific Report No. 3
James A. Cercone and John R. Martin 11 Apr. 1994 94 p
(Contract F19628-91-K-0039)
(AD-A285846; PL-TR-94-2178; AD-E202187; SR-3) Avail: CASI HC A05/MF A01

The Experimental Program to Stimulate Competitive Research (EPSCoRe) Supplemental Grant for An Application of Neural Networks to Seismic Signal Discrimination was used to fund a Graduate Student for work with a parent ARPA project. The students course and research activities are presented along with a copy of the completed Masters Thesis based on the application of an ARMA model for seismic event discrimination. DTIC

N95-20908# Argonne National Lab., IL. Environmental Research Div.
STATISTICAL PROPERTIES OF GEOLOGIC FRACTALS
C. Loehle 1994 29 p
(Contract W-31-109-eng-38)
(DE94-019272; ANL/ER/PP-79574) Avail: CASI HC A03/MF A01

To use fractal models for geologic data, the statistical properties of fractals need to be clarified. No sampling or estimation theory for fractals currently exists. Several concrete steps in this direction are taken here. First, the information fractal dimension is proposed as a new measure that is relatively robust with respect to sampling error. The information fractal is tested with field data and is shown to be capable of delineating stratified structures and defining the scale of heterogeneity in the data. Comparison to semivariance analysis reveals the superiority of the fractal model for sample data that are nonisotropic and nonstationary. It is argued that approaches using regression to estimate fractal dimensions of spatial patterns are statistically invalid, and alternatives are proposed. Sampling of geologic objects with transects (e.g., wells) is explored. For nonisotropic media, random placement of transects is shown to give an unreliable estimate of pattern. For transects taken perpendicular to a directional pattern (i.e., strata), it is shown that the man of multiple estimates of the multiscale fractal dimensional profile does converge to the true value. Other sampling issues are addressed. DOE

N95-20990# Lawrence Livermore National Lab., Livermore, CA.
FRACTAL NATURE AND SCALING OF NORMAL FAULTS, RIO GRANDE RIFT, NM: IMPLICATIONS FOR GROWTH AND STRAIN
K. E. Carter 1994 4 p Presented at the Faults Populations Meeting, Edinburgh, United Kingdom, 17-21 Oct. 1994
(Contract W-7405-eng-36)
(DE94-018261; LA-UR-94-2739; CONF-9410196-1) Avail: CASI HC A01/MF A01

In this paper I introduce a suite of Quaternary normal faults from within an active continental rift and characterize the nature of the relationship between fault dimensions. I address the statistical and geological significance of the fractal analysis used in that characterization and discuss the tectonic implications. Specifically, I suggest (1) scaling laws for a previously unanalyzed population of young normal faults in rift environment; (2) implications for fault growth models in this area, in particular, addressing self-similar growth implied from the population; and (3) estimates for the total strain in this part of the basin, considering the contribution of small to unobserved faults. DOE

N95-21184# Hercules Defense Electronics Systems, Inc., Clearwater, FL. Defense Electronics Systems.

PROJECT WHITEFEATHER

1994 46 p Prepared for Los Alamos National Lab., NM
(Contract W-7405-eng-36)
(DE94-016575; LA-Sub-94-105) Avail: CASI HC A03/MF A01 (US Sales Only)

Four primary tasks have been carried out in this program. Upon request of LANL, the Eloranta paper was reviewed. It was determined that the correlation solution presented was too computationally complex to execute in the allocated 1 second update time. An alternative algorithm approach was under taken using a simulation baseline. A simulation was developed and applied to generate synthetic LIDAR data from randomized aerosol patches drifting with the wind. Algorithms have been designed and implemented in the simulation to reduce the data and apply it to obtain wind estimates. A substantial effort was completed in reverse engineering the EVIEW data format structure of the supplied data. Finally the collected, LIDAR data has been examined to obtain an assessment of the prospects for successful wind estimation. Unfortunately, the data examination has not shown good prospects for a successful outcome. It is recommended that future data be taken with the procedure previously outlined. Hercules believes that if lidar data is collected using this procedure that wind information will be as successful using the collected data as it was in simulation. DOE

N95-21188*# National Aeronautics and Space Administration. Lewis Research Center, Cleveland, OH.

ELECTROSTATIC NOISE IN THE PLASMA ENVIRONMENT AROUND THE SHUTTLE

Boris V. Vayner and Dale C. Ferguson Feb. 1995 9 p Presented at the 26th Plasmadynamics and Lasers Conference, San Diego, CA, 19-22 Jun. 1995; sponsored by AIAA
(RTOP 233-01-0E)
(NASA-TM-106856; E-9447; NAS 1.15:106856; AIAA Paper 95-1944)
Avail: CASI HC A02/MF A01

The Langmuir probe flown as part of the Solar Array Module Plasma Interactions Experiment (SAMPIE) package aboard the space shuttle flight STS-62 was used to determine plasma potential fluctuations in the vicinity of the shuttle. The broadband noise was observed at frequencies 250 - 20,000 Hz. Measurements were performed in ram conditions; thus, it seems reasonable to believe that the influence of spacecraft operations on plasma parameters was absolutely negligible. The average spectrum of fluctuations is in agreement with theoretical predictions. The influence on the observed spectra of arcing generated by high negative bias voltages applied to solar cell samples is briefly discussed. Author

N95-21308# Tech Foundation, Inc., Montgomery, WV.

APPLICATION OF NEURAL NETWORKS TO SEISMIC SIGNAL DISCRIMINATION RESEARCH FINDINGS Final Report, 12 Dec. 1991 - 11 Apr. 1994

James A. Cercone, W. M. Clark, J. J. Fuller, Stephan Goodman, and Don J. Smith 11 Apr. 1994 110 p
(Contract F19628-91-K-0039)
(AD-A285848; PL-TR-94-2122; AD-E202186) Avail: CASI HC A06/MF A02

Research focused on identification and collection of a suitable database, identification of parametric representation of the time series seismic waveforms, and the training and testing of neural networks for seismic event classification. It was necessary to utilize seismic events that had a high degree of reliability for accurate training of the neural networks. The seismic waveforms were obtained from the Center for Seismic Studies and were organized into smaller databases for training and classification purposes. Unprocessed seismograms were not well suited for presentation to a neural network because of the large number of data points required to represent a seismic event in the time domain. The parametric representation of the seismic events in some cases provided adequate information for accurate event classification, while significantly reducing the minimum size of the neural network. Various networks have achieved classification rates ranging from 88 percent classification of three class problem to 75 percent for the 5 class problem. The results vary dependent on the number of classes and the method of parametric transformations utilized. Multiple tests were performed in order to statistically average the training and classification rates. Test summaries presented and individual test results are given in the appendix. DTIC

N95-21477# Argonne National Lab., IL.

ANATOMY OF THE MIDCONTINENT RIFT BENEATH LAKE SUPERIOR

M. D. Thompson, L. D. McGinnis, C. P. Ervin (University of Northern Illinois, De Kalb, IL.), and M. G. Mudrey (Wisconsin Geological and Natural History Survey, Madison, WI.) 1994 41 p
(Contract W-31-109-eng-38)
(DE94-019298; ANL/ES/PP-76517) Avail: CASI HC A03/MF A01

The structure and geometry of the 1.1-b.y.-old Midcontinent Rift system under Lake Superior is interpreted from 20 seismic reflection profiles recorded during the early and mid-1980s. The seismic data reveal that rift basins under Lake Superior are variable in depth and are partially filled with Keweenawan age sediments to depths of 7 km or more and volcanic flows to depths of 36 km. These rift basins form a continuous and sinuous feature that widens in the Allouez Basin and Marquette Basin in the western and central lake and narrows between White Ridge and the Porcupine Mountains. The rift basin bends southeast around the Keweenaw Peninsula, widens to about 100 km as it extends into the eastern half of Lake Superior, and exists the lake with its axis in the vicinity of Au Sable Point in Pictured Rocks National Lake Shore, about 50 km northeast of Munising, Michigan. The axis of the rift may exit the western end of the lake near Chequamegon Bay in Wisconsin. However, lack of data in that area limits interpretation at this time. Prior to late-stage reverse-faulting, a continuous basin of more uniform thickness was present beneath the lake. Crustal extension during rifting of approximately 50 km was followed by plate convergence and crustal shortening of approximately 30 km, with the major component of thrust from the southeast. Crustal shortening occurred after development of rift grabens and their filling with lava flows, but before deposition of the final sag basin sediments. Integration of information obtained from outcrops with data reported here indicates that the Lake Superior section of the rift is associated with as many as three major boundary faults. DOE

N95-21511# Synapse Science Center/Moscow IRIS Data Analysis Center, Moscow (Russia).

COMPUTER PROGRAMS FOR ANALYSIS OF GEOPHYSICAL DATA

Mikhail Rozhkov and Keith Nakanishi Jun. 1994 119 p
(Contract W-7405-eng-48)
(DE95-002472; UCRL-CR-117756) Avail: CASI HC A06/MF A02

This project is oriented toward the application of the mobile seismic array data analysis technique in seismic investigations of the Earth (the noise-array method). The technique falls into the class of emission tomography methods but, in contrast to classic tomography, 3-D images of the microseismic activity of the media are obtained by passive seismic antenna scanning of the half-space, rather than by solution of the inverse Radon's problem. It is reasonable to expect that areas of geothermal activity, active faults, areas of volcanic tremors and hydrocarbon deposits act as sources of intense internal microseismic activity or as effective sources for scattered (secondary) waves. The conventional approaches of seismic investigations of a geological medium include measurements of time-limited determinate signals from artificial or natural sources. However, the continuous seismic oscillations, like endogenous microseisms, coda and scattering waves, can give very important information about the structure of the Earth. The presence of microseismic sources or inhomogeneities within the Earth results in the appearance of coherent seismic components in a stochastic wave field recorded on the surface by a seismic array. By careful processing of seismic array data, these coherent components can be used to develop a 3-D model of the microseismic activity of the media or images of the noisy objects. Thus, in contrast to classic seismology where narrow windows are used to get the best time resolution of seismic signals, our model requires long record length for the best spatial resolution. DOE

N95-21777*# Lunar and Planetary Inst., Houston, TX.

CONFERENCE ON DEEP EARTH AND PLANETARY VOLATILES Abstracts Only

1994 59 p Conference held in Pasadena, CA, 21-23 Sep. 1994

(Contract NASw-4574)
(NASA-CR-196944; NAS 1.26:196944; LPI-Contrib-845) Avail: CASI HC A04/MF A01

The following topics are covered in the presented papers: (1) rare gases systematics and mantle structure; (2) volatiles in the earth; (3) impact degassing of water and noble gases from silicates; (4) D/H ratios and H2O contents of mantle-derived amphibole megacrysts; (5) thermochemistry of dense hydrous magnesium silicates; (6) modeling of the effect of water on mantle rheology; (7) noble gas isotopes and halogens in volatile-rich inclusions in diamonds; (8) origin and loss of the volatiles of the terrestrial planets; (9) structure and the stability of hydrous minerals at high pressure; (10) recycling of volatiles at subduction zones and various other topics. For individual titles, see N95-21778 through N95-21824.

N95-21778*# Paris VI Univ. (France). Lab. de Geochimie et Cosmochimie.
RARE GASES SYSTEMATICS AND MANTLE STRUCTURE Abstract Only
C. J. Allegre and T. Staudacher *In* Lunar and Planetary Inst., Conference on Deep Earth and Planetary Volatiles 1994 p 1 Prepared in cooperation with Paris VII Univ., France (For primary document see N95-21777 06-46)
Avail: CASI HC A01/MF A01

The following points are emphasized: one of the most important ones is certainly the first set of experimental data on the solubility of noble gases in metal phases at intermediate pressures, since the core was certainly not formed at ultra high pressures, as emphasized by Ahrens and confirmed by trace elements systematics Wanke. The experimental data clearly show that the core can not be a major reservoir for terrestrial rare gases; the second point is a more elaborate reconsideration of the (40)K-(40)Ar budget of the Earth. This shows that (40)Ar contained in continental crust plus upper mantle plus atmosphere is at maximum half of the (40)Ar inventory of the whole earth. This implies the existence of a two layered mantle; the third point is the discovery by the Australian noble gases group of the existence of high (20)Ne/(22)Ne and low (21)Ne/(22)Ne isotopic ratios in Loihi seamount samples. This results which are different to the MORB ratios confirm the idea of a two layered model, but suggest the existence of a primordial solar type Ne reservoir. Several possibilities about the origin of this (20)Ne excess in the mantle will be discussed; The high (40)Ar/(36)Ar, (129)Xe/(130)Xe and (134) Xe/(130)Xe, (136)Xe/(130)Xe are confirmed by new data. The corresponding ratios for the lower mantle will be discussed. (40)Ar/(36)Ar ratios up to 6000 can be accepted and will not modify the general model of the mantle. They confirm the atmosphere chronology, about 85 percent of the atmosphere was formed in the first 50 My and 15 percent later on. Author

N95-21779*# California Inst. of Tech., Pasadena, CA. Seismological Lab.
VOLATILES IN THE EARTH: ALL SHALLOW AND ALL RECYCLED Abstract Only
Don L. Anderson *In* Lunar and Planetary Inst., Conference on Deep Earth and Planetary Volatiles 1994 p 2 (For primary document see N95-21777 06-46)
Avail: CASI HC A01/MF A01

A case can be made that accretion of the Earth was a high-temperature process and that the primordial Earth was dry. A radial zone-refining process during accretion may have excluded low-melting point and volatile material, including large-ion lithophile elements toward the surface, leaving a refractory and zoned interior. Water, sediments and altered hydrous oceanic crust are introduced back into the interior by subduction, a process that may be more efficient today than in the past. Seismic tomography strongly suggests that a large part of the uppermantle is above the solidus, and this implies wet melting. The mantle beneath Archean cratons has very fast seismic velocities and appears to be strong to 150 km or greater. This is consistent with very dry mantle. It is argued that recycling of substantial quantities of water occurs in the shallow mantle but only minor amounts recycle to depths greater than 200 km. Recycling also oxidizes that mantle; ocean island ('hotspot') basalts are intermediate in oxidation state to island-arc and midocean ridge basalts (MORB). This suggests a deep uncontaminated reservoir for MORB. Plate tectonics on a dry Earth is discussed in order to focus attention on inconsistencies in current geochemical models of terrestrial evolution and recycling. Author

N95-21780*# Tokyo Univ. (Japan). Dept. of Earth and Planetary Studies.
IMPACT DEGASSING OF WATER AND NOBLE GASES FROM SILICATES Abstract Only
S. Azuma, H. Hiyagon, Y. Iijima (Nagoya Univ., Aichi, Japan.), and Y. Syono (Tohoku Univ., Sendai, Japan.) *In* Lunar and Planetary Inst., Conference on Deep Earth and Planetary Volatiles 1994 p 3 (For primary document see N95-21777 06-46)
Avail: CASI HC A01/MF A01

Previous shock experiments by Ahrens and his colleagues show that degassing of H2O and CO2 occurs at 8-65GPa from hydrous minerals such as serpentine. In early solar system, the impact degassing would have played an important part in the formation of primary-atmospheres of the terrestrial planets. However, degassing conditions of noble gases are not well-known because there are few experiments for them. We conducted some shock recovery experiments to investigate the degassing condition and to understand the degassing mechanisms of water and noble gases. We used natural richterites (Ri), amphibolites (Am), serpentines (Sep) and orthoclases (or) as target samples. These, except Sep, contain radiogenic noble gases such as (40)Ar. The samples were put in stainless steel containers, and were show by a rail gun at ISAS or single-stage powder guns at Nagoya or Tohoku University, Japan. We used two kinds of containers: 'open' type containers having a ventilating path for released volatiles for most of samples and 'closed' type ones for some samples for comparison. On Ri and Sep, we made shock experiments for pre-heated (at 400-500 C) and unheated targets, and for powdered and uncrushed samples. Water and noble gases were analyzed both for the recovered shocked samples and the unshocked original samples, and the fractions of the degassed volatiles were calculated by comparing them. Water content in the sample was analyzed by thermo-gravimetry. Noble gases were extracted by heating the samples under high vacuum and analyzed with a sector-type mass spectrometer. Author

N95-21781*# Carnegie Institution of Washington, Washington, DC. Geophysical lab.
D/H RATIOS AND H2O CONTENTS OF MANTLE-DERIVED AMPHIBOLE MEGACRYSTS FROM DISH HILL, CALIFORNIA Abstract Only
David R. Bell and T. C. Hoering *In* Lunar and Planetary Inst., Conference on Deep Earth and Planetary Volatiles 1994 p 4 (For primary document see N95-21777 06-46)
Avail: CASI HC A01/MF A01

D/H ratios are, in principle, useful in characterizing reservoirs of mantle hydrogen and as tracers of volatile transfer processes in Earth's interior. In practice, however, interpretation of isotopic measurements on mantle derived H is complicated by surface processes such as contamination and degassing which may alter the primary D/H ratio. Although there are indications that water associated with subduction zones and certain chemically enriched basalts is enriched in D relative to 'typical' upper mantle water, the extent of isotopic heterogeneity of mantle H remains uncertain. Kaersutitic amphibole megacrysts in alkaline basalts are one of the most widespread sources of mantle water and are therefore potentially useful for large-scale regional studies of D/H variation. However, D/H ratios of these amphiboles vary widely (from plus 8 to minus 113 percent), even in samples from the same locality, so that this potential has yet to be realized. In order to investigate the origin of this variability, and to explore the possibility that primary mantle D/H ratios may be deduced from these amphiboles, we analyzed the D/H ratios and chemical compositions of a suite of 17 kaersutitic amphiboles from Dish Hill, California. This work contrasts with previous studies in which sampling is widespread, but representatives from any given locality are few. Samples were collected from a restricted area on the southern flank of the volcanic center and are associated with the basal volcanic breccia. Fourteen of the samples were large single crystals or crystal fragments (megacrysts, 0.4 to 30 grams), believed to derive from pegmatitic veins crystallized from melts in the mantle. Two were coarse-grained intergrowths of amphibole with olivine and spinel, and one was a thin (2 mm) selvage on a peridotite xenolith. Author

N95-21782*# Princeton Univ., NJ. Dept. of Geological and Geophysical Sciences.
THERMOCHEMISTRY OF DENSE HYDROUS MAGNESIUM SILICATES Abstract Only

Kunal Bose, Pamela Burnley (Colorado Univ., Boulder, CO.), and Alexandra Navrotsky *In* Lunar and Planetary Inst., Conference on Deep Earth and Planetary Volatiles 1994 p 5 (For primary document see N95-21777 06-46)
Avail: CASI HC A01/MF A01

Recent experimental investigations under mantle conditions have identified a suite of dense hydrous magnesium silicate (DHMS) phases that could be conduits to transport water to at least the 660 km discontinuity via mature, relatively cold, subducting slabs. Water released from successive dehydration of these phases during subduction could be responsible for deep focus earthquakes, mantle metasomatism and a host of other physico-chemical processes central to our understanding of the earth's deep interior. In order to construct a thermodynamic data base that can delineate and predict the stability ranges for DHMS phases, reliable thermochemical and thermophysical data are required. One of the major obstacles in calorimetric studies of phases synthesized under high pressure conditions has been limitation due to the small (less than 5 mg) sample mass. Our refinement of calorimeter techniques now allow precise determination of enthalpies of solution of less than 5 mg samples of hydrous magnesium silicates. For example, high temperature solution calorimetry of natural talc (Mg(0.99) Fe(0.01)Si4O10(OH)2), periclase (MgO) and quartz (SiO2) yield enthalpies of drop solution at 1044 K to be 592.2 (2.2), 52.01 (0.12) and 45.76 (0.4) kJ/mol respectively. The corresponding enthalpy of formation from oxides at 298 K for talc is minus 5908.2 kJ/mol agreeing within 0.1 percent to literature values. Author

N95-21783*# Potsdam Univ., Potsdam (Germany). General Geophysics Group.

MODELING THE EFFECT OF WATER ON MANTLE RHEOLOGY Abstract Only

Ch. Bounama and S. Franck *In* Lunar and Planetary Inst., Conference on Deep Earth and Planetary Volatiles 1994 p 6 (For primary document see N95-21777 06-46)
Avail: CASI HC A01/MF A01

To study the thermal history of the Earth we use a parameterized model of mantle convection. This model includes a mathematical description of de- and regassing processes of water from the Earth's mantle. The rates of this processes are considered to be directly proportional to the seafloor spreading rate. The kinematic viscosity of the mantle depends on the temperature/pressure as well as on the volatile content. Dissolved volatiles such as water weaken the minerals by reducing their activation energy for solid state creep. Karato and Toriumi showed a power law dependence between creep rate and water fugacity derived from experimental results. Therefore, we use such flow parameters of diffusion creep in olivine under wet and dry conditions to calculate the mantle viscosity as a function of the water content. Because the creep rate is proportional to the concentration of water-related point deflects we assume that the water fugacity is proportional to the water weight fraction. An equation for the steady-state strain rate under wet conditions is established. To assess the unknown constant K in this equation, we use flow law parameters given by Karato and Wu as well as the results of McGovern and Schubert. Author

N95-21784*# Manchester Univ. (England). Dept. of Geology.

NOBLE GAS ISOTOPES AND HALOGENS IN VOLATILE-RICH INCLUSIONS IN DIAMONDS Abstract Only

Raymond Burgess and Grenville Turner *In* Lunar and Planetary Inst., Conference on Deep Earth and Planetary Volatiles 1994 p 7 (For primary document see N95-21777 06-46)
Avail: CASI HC A01/MF A01

Application of the (40)Ar-(39)Ar method and noble gas studies to diamonds has increased our understanding of their age relationships to the host kimberlite or lamproite, and of the source and composition of volatile-rich fluids in the upper mantle. The properties of diamond (inert, high mechanical strength and low gas diffusivities) means they are especially useful samples for studying gases trapped deep within the earth (less than 150 km) as they are unlikely to have undergone loss or exchange of entrapped material since formation. Volatile-rich fluids (H2O-CO2) are important agents for metasomatic processes in the upper mantle, and the noble gases and halogens preferentially partition into this phase leading to a strong geochemical coherence between these groups of elements. The abundances of the halogens in the major reservoirs of the Earth shows a marked progression from chlorine, concentrated in the oceans, through to iodine which, through its affinity to organic material, is concentrated mainly in sediments. Abundances in the upper mantle are low. This is particularly true for iodine which is of special interest in view of its potential significance as an indicator of sediment recycling and by way of its link to (129)Xe amomalies in the mantle through the low extinct isotope (129)I. Extensions of the (40)Ar-(39)Ar technique enable measurements of halogens and other elements (K, Ca, Ba, U) by production of noble gas isotopes from these species during neutron irradiation. Samples analyzed in this way include 15 coated stones from an unknown source in Zaire, 3 boarts from the Jwaneng and 1 boart from the Orapa kimberlites, both in Botswana. Author

N95-21785*# Michigan Univ., Ann Arbor, MI. Dept. of Atmospheric, Oceanic and Space Sciences.

ORIGIN AND LOSS OF THE VOLATILES OF THE TERRESTRIAL PLANETS Abstract Only c91

T. M. Donahue *In* Lunar and Planetary Inst., Conference on Deep Earth and Planetary Volatiles 1994 p 8 (For primary document see N95-21777 06-46)
Avail: CASI HC A01/MF A01

How the terrestrial planets obtained their original endorsement of volatiles and proceeded to lose them selectively is the theme of this paper. Where good and convincing answers to these questions are still not available, the principal issues are becoming better and better understood, and thus many of the decisive measurements and calculations needed to obtain them can be well defined. In this paper our present inventories of volatiles such as the noble gases, hydrogen compounds and atmophiles such as CO2, N2, and O2 will be presented. Careful attention will be given to isotopic ratios and their significance. Escape processes past and present - blow off impact erosion, thermal and non-thermal loss of neutral and ionic species will be discussed, and the contribution of each to volatile loss assessed. It will be argued that our understanding of these processes is adequate to explain the present level of fractionation of many of the noble gases and their isotopes on all the terrestrial planets. It will also be argued that we are close to understanding loss of hydrogen well enough to assess reasonably the early abundance of water on early Venus and Mars. Author

N95-21786*# Carnegie Institution of Washington, Washington, DC. Geophysical Lab.

STRUCTURE AND STABILITY OF HYDROUS MINERALS AT HIGH PRESSURE Abstract Only

T. S. Duffy, Y. Fei, C. Meade, R. J. Hemley, and H. K. Mao *In* Lunar and Planetary Inst., Conference on Deep Earth and Planetary Volatiles 1994 p 9 (For primary document see N95-21777 06-46)
Avail: CASI HC A01/MF A01

The presence of even small amounts of hydrogen in the Earth's deep interior may have profound effects on mantle melting, rheology, and electrical conductivity. The recent discovery of a large class of high-pressure H-bearing silicates further underscores the potentially important role for hydrous minerals in the Earth's mantle. Hydrogen may also be a significant component of the Earth's core, as has been recently documented by studies of iron hydride at high pressure. In this study, we explore the role of H in crystal structures at high pressure through detailed Raman spectroscopic and x ray diffraction studies of hydrous minerals compressed in diamond anvil cells. Brucite, Mg(OH)2, has a simple structure and serves as an analogue for the more complex hydrous silicates. Over the past five years, this material has been studied at high pressure using shock-compression, powder x ray diffraction, infrared spectroscopy, Raman spectroscopy, and neutron diffraction. In addition, we have recently carried out single-crystal synchrotron x-ray diffraction on Mg(OH)2 and Raman spectroscopy on Mg(OD)2 at elevated pressure. From all these studies, an interesting picture of the crystal chemical behavior of this material at high pressure is beginning to emerge. Some of the primary conclusions are as follows. First, hydrogen bonding is enhanced by the application of pressure. Second, layered minerals which are elastically anisotropic at low pressure may not be so at high pressure. Furthermore, the brucite data place constraints on the effect of hydrogen on seismic velocities and density at very high pressure. Third, the stability of hydrous minerals may be enhanced at high P by subtle structural rearrangements that are difficult to detect using traditional probes and require detailed spectroscopic analyses. Finally, brucite appears to be unique in that it undergoes pressure-induced disordering that is confined solely to the H-containing layers of the structure. Author

N95-21787*# California Inst. of Tech., Pasadena, CA. Div. of Geological and Planetary Sciences.

RECYCLING OF VOLATILES AT SUBDUCTION ZONES: NOBLE GAS EVIDENCE FROM THE TABAR-LIHIR-TANGA-FENI ARC OF PAPUA NEW GUINEA Abstract Only

Kenneth Farley, Brent McInnes, and Desmond Patterson *In* Lunar and Planetary Inst., Conference on Deep Earth and Planetary Volatiles 1994 p 10 (For primary document see N95-21777 06-46)

Avail: CASI HC A01/MF A01

Convergent margin processes play an important but poorly understood role in the distribution of terrestrial volatile species. For example, subduction processes filter volatiles from the subducting package, thereby restricting their return to the mantle. In addition, once extracted from the downgoing slab, volatiles become an essential component in the petrogenesis of island arc magmas. The noble gases, with their systematic variation in physical properties and diversity of radiogenic isotopes, should carry a uniquely valuable record of these processes. However, thus far studies of noble gases in arc volcanics have achieved only limited success in this regard. Subduction-related lavas and geothermal fluids carry (3)He/(4)He ratios equal to or slightly lower than those found in the depleted upper mantle source of mid-ocean ridge basalts. Apparently slab-derived helium (which should have (3)He/(4)He much less than MORB) is extensively diluted by MORB-like helium from the mantle wedge, making it difficult to use helium as a tracer of convergent margin processes. Interpretation of the heavier noble gases (Ne-Ar-Kr-Xe) in arc lavas has also proven difficult, because the lavas carry low noble gas concentrations and hence are subject to pervasive atmospheric contamination. The low noble gas concentrations may be a consequence of degassing in the high level magma chambers characteristic of arc stratovolcanos. We have recently initiated a project to better constrain the behavior of volatiles in subduction zones through geochemical studies of the tectonically unusual volcanoes of the Tabar-Lihir-Tanga-Feni (TLTF) arc in the Bismarck Archipelago, Papua New Guinea. Author

N95-21788*# Potsdam Univ., Potsdam (Germany). General Geophysics Group.

MANTLE DEVOLATILIZATION AND RHEOLOGY IN THE FRAMEWORK OF PLANETARY EVOLUTION Abstract Only c91

S. Franck and Ch. Bounama *In* Lunar and Planetary Inst., Conference on Deep Earth and Planetary Volatiles 1994 p 11 (For primary document see N95-21777 06-46)

Avail: CASI HC A01/MF A01

We investigate the thermal history of an Earth-like planet with the help of a parameterized mantle convection model including the volatile exchange between mantle and surface reservoirs. The weakening of mantle silicates by dissolved volatiles is described by a functional relationship between creep rate and water fugacity. We use flow law parameters of diffusion creep in olivine under dry and wet conditions. The mantle degassing rate is considered as directly proportional to the seafloor spreading rate, which is also dependent on the mantle heat flow. To calculate the spreading rate, we assume that the heat flow under the mid-ocean ridges is double the average mantle heat flow. The rate of regassing also depends on the seafloor spreading rate as well as on other factors like the efficiency of volatile recycling through island arc volcanism. Both mechanisms (de- and regassing) are coupled self-consistently with the help of the parameterized convection model under implementation of a temperature and volatile-content-dependent mantle viscosity. Author

N95-21789*# Max-Planck-Inst. fuer Chemie, Mainz (Germany).

SPATIAL VARIATION OF PRIMORDIAL 3-He IN CRUSTAL FLUIDS ALONG THE EAST-AFRICAN RIFT SYSTEM (THE ETHIOPIAN AND THE KENYA RIFT SECTION) Abstract Only

E. Griesshaber, S. Weise, and G. Darling (Geological Survey of Britain, Wallingford, England.) *In* Lunar and Planetary Inst., Conference on Deep Earth and Planetary Volatiles 1994 p 12 (For primary document see N95-21777 06-46)

Avail: CASI HC A01/MF A01

(3)He/(4)He compositions are presented for groundwater samples from the Ethiopian segment of the East-Afrikan Rift and from its northern extension, the adjacent Afar region (Djibuti). Helium isotope data are compared to those obtained previously from the Gregory Rift, south of Ethiopia. The distribution pattern of mantle-derived volatiles along the entire East-African-Rift (-from south Kenya to Djibuti-) is discussed and their sources are identified. Helium isotope ratios (R) for samples from the Ethiopian part of the Rift range from 6.3 to 16.0 times the atmospheric ratio (Ra=1.4 x 10(exp -6) and thus show together with a MOR component a considerable hotspot helium component. These mantle helium concentrations are comparable to those observed in groundwaters and volcanic rocks from the Afar plume region in Djibuti. Here R/Ra values range from 9 to 13 times the atmospheric composition, with mantle-derived helium concentrations being higher than at spreading ocean ridges. R/Ra values from Ethiopia and Djibuti are entirely different from those observed in groundwaters at the southerly extending Gregory Rift in Kenya, where R/Ra values scatter between 0.5 and 6. At the northernmost part of the Gregory Rift, close to Ethiopia mantle helium contents are slightly higher, with R/Ra-values varying between 6.5 and 8.0. Author

N95-21790*# Osaka Univ., Toyonaka (Japan). Dept. of Earth and Space Sciences.

TRANSPORTATION OF VOLATILE ELEMENTS IN THERMALLY EVOLVING PLANETESIMALS: AN IMPORTANT ROLE OF METALLIC IRON Abstract Only c90

K. Hashizume and N. Sugiura (Tokyo Univ., Japan.) *In* Lunar and Planetary Inst., Conference on Deep Earth and Planetary Volatiles 1994 p 13 (For primary document see N95-21777 06-46)

Avail: CASI HC A01/MF A01

Ordinary chondrites are considered to have experienced thermal metamorphism in small bodies. We are interested in behaviors of volatile elements in such a kind of thermally evolving planetesimals. Volatile elements generally have high vapor pressures at high temperature. In porous bodies, with a high gas permeability, volatile elements are transported efficiently over a long range. Behavior of volatile elements transported by permeable gas flow can be handled by an equation whose form is similar to that of the equation of thermal diffusion. We can follow transportation of heats and volatile elements in planetesimals, when parameters in these equations, initial conditions and chemical behavior of volatile elements are given. Recently, we discovered that nitrogen in equilibrated H-chondrites is mainly trapped in taenite (f.c.c. Fe-Ni), probably dissolved in interstitial sites. Fegley suggests that metallic iron cannot trap nitrogen in the solar nebula gas due to its very low nitrogen partial pressure. Approximately 1 bar of nitrogen pressure is required to explain the nitrogen content in taenite. We may expect high nitrogen gas partial pressure (possibly produced by vaporization of nitrogen-bearing solids such as organic materials) at the interior of thermally evolving planetesimals. Kinetic behavior of nitrogen in taenite suggests that it can easily be equilibrated with the ambient nitrogen gas at temperatures of approximately 500 C or higher. We consider that nitrogen is trapped in taenite through a nitrogen redistribution process occurred during the thermal metamorphic event. Author

N95-21791*# Carnegie Institution of Washington, Washington, DC. Geophysical Lab.

HYDROGEN AND RELATED MATERIALS AT HIGH DENSITY: PHYSICS, CHEMISTRY AND PLANETARY IMPLICATIONS Abstract Only

R. J. Hemley, H. K. Mao, T. S. Duffy, A. Goncharov, W. Vos, C. S. Zha, J. H. Eggert, M. Li, and M. Hanfland *In* Lunar and Planetary Inst., Conference on Deep Earth and Planetary Volatiles 1994 p 14 (For primary document see N95-21777 06-46)

Avail: CASI HC A01/MF A01

Recent studies of low-Z molecular materials including hydrogen to multimegabar pressures (less than 300 GPa) have uncovered a range of phenomena relevant to understanding the nature of the interiors of the outer planets and their satellites. Synchrotron x ray diffraction measurements (to 42 GPa) have been used to determine the crystal structure of the solid (hexagonal-close packed) and equation of state. Sound velocities in fluid and solid hydrogen (to 24 GPa) have been inverted to obtain elastic constants and aggregate bulk and shear moduli. In addition, an improved intermolecular potential has been determined which fits both static and shock-wave data. Use of the new potential for the molecular envelope of Jupiter suggests the need for major revisions of existing Jovian models or a reanalysis of reported free oscillations for the planet. Studies at higher pressures (greater than 100 GPa) reveal a sequence of pressure-induced symmetry-breaking transitions in molecular hydrogen, giving rise to three high-pressure phases (1, 2, and 3). Phase 1 is the rotationally disordered hcp phase which persists from low pressure to well above 100 GPa at high temperature (e.g., 300 K). Phase 2 is a low-temperature, high-pressure phase (transition at 100 GPa and 77 K in H2) with spectral features indicative of partial rotational ordering and crystallographic distortion. The transition to Phase 3 at 150 GPa is accompanied by a weakening of the molecular bond, gradual changes in orientational ordering, strong enhancement of the infrared intramolecular vibrational absorption, and strong intermolecular interactions similar to those of ambient-pressure network solids. Studies of the phase diagram reveal a triple point near 130 K and 160 GPa. Higher pressure measurements of vibrational spectra place a lower bound of approximately 250 GPa on the predicted transition pressure for dissociation of molecular hydrogen to form a monatomic metal. Author

N95-21792*# Tokyo Univ. (Japan). Dept. of Earth and Planetary Physics.

LOSS OF SOLAR He AND Ne FROM IDPS IN SUBDUCTING SEDIMENT: DIFFUSION AND THE EFFECT OF PHASE CHANGES Abstract Only

H. Hiyagon *In* Lunar and Planetary Inst., Conference on Deep Earth and Planetary Volatiles 1994 p 15 (For primary document see N95-21777 06-46)

Avail: CASI HC A01/MF A01

The results of the diffusion experiment for solar He and Ne in IDP's in a magnetic separate from Pacific Ocean sediment suggest that solar He and Ne would be easily released from IDP grains and hence lost from subducting slabs at shallow depths. However, since the diffusion experiments was conducted under high vacuum, there may be a possibility that magnetite grains, which are supposedly the main constituent of the magnetic fraction, might be partly reduced to form a metal phase due to low oxygen fugacity in the experimental condition. If this is the case, such a phase change might affect the gas release and hence the results of the diffusion coefficients. In order to examine whether or not such a phase change really occurred in the condition of the diffusion experiment, I conducted a heating experiment for a magnetic separate from Pacific Ocean sediment. In the same condition as in the diffusion experiment, and the run products were examined with an x ray diffraction method. Three samples were prepared: they were wrapped with platinum foil, put in a vacuum line, and heated in a molybdenum crucible for two hours at 500 C, 800 C,and 950 C, respectively. After cooling the furnace, the samples were taken out from the crucible and analyzed with an x ray diffraction method. Author

N95-21793*# Australian National Univ., Canberra (Australia). Research School of Earth Sciences.

SOLAR HELIUM AND NEON IN THE EARTH Abstract Only

M. Honda, I. McDougall, and D. B. Patterson (California Inst. of Tech., Pasadena, CA.) *In* Lunar and Planetary Inst., Conference on Deep Earth and Planetary Volatiles 1994 p 16 (For primary document see N95-21777 06-46)

Avail: CASI HC A01/MF A01

Neon isotopic compositions in mantle-derived samples commonly are enriched in (20)Ne and (21)Ne relative to (22)Ne compared with atmospheric neon ((20)Ne/(22)Ne and (21)Ne/(22)Ne ratios in atmospheric neon are 9.8 and 0.029, respectively), together with significant primordial (3)He. Such results have been obtained on MORB's, intraplate plume-related oceanic island basalts, backarc basin basalts, mantle xenoliths, ancient diamonds and CO2 well gases (e.g., 1 - 8). The highest (20)Ne/(22)Ne ratio observed in MORB glasses (= 13.6 plus or minus 1.3 is close to the solar value (= 13.6, as observed in solar wind). In order to explain the enrichment of (20)Ne and (21)Ne relative to atmospheric neon for samples derived from the mantle, it is necessary to postulate the presence of at least two distinct non-atmospheric components. The two most likely candidates are solar and nucleogenic ((20)Ne/(22)Ne solar = 13.6 (21)Ne/(22)Ne solar = 0.032, (20)Ne/(22)Ne nucleogenic = 2.5 and (21)Ne/(22)Ne nucleogenic = 32). This is because solar neon is the only known component with a (20)Ne/(22)Ne ratio greater than both the atmospheric value and that observed in samples derived from the mantle. Nucleogenic neon is well known to elevate (21)Ne/(22)Ne ratios. Neon isotopic signatures observed in mantle-derived samples can be accounted for by mixing of the three neon end members: solar, nucleogenic and atmospheric. Author

N95-21794*# Arizona Univ., Tucson, AZ. Lunar and Planetary Lab.

ATMOSPHERES OF THE MOON AND MERCURY Abstract Only c91

D. M. Hunten *In* Lunar and Planetary Inst., Conference on Deep Earth and Planetary Volatiles 1994 p 17 (For primary document see N95-21777 06-46)

Avail: CASI HC A01/MF A01

Mercury and the Moon have long been considered to be similar objects, but this view was based on limited information at visible wavelengths. It is now known that real differences exist in the atmospheres and in the rock types as deduced from mid-infrared observations. Lunar Ar and perhaps Ne were observed from Apollo landed experiments in spite of a large local background. An ultraviolet spectrometer (UVS) in orbit placed upper limits on a number of gases including H and O. At Mercury, the UVS on Mariner 10 measured H, He, and perhaps O and again a number of upper limits for other gases. Less than a decade ago, emissions of Na and K were observed from the ground, with abundances 2 orders of magnitude smaller on the Moon than on Mercury. It is likely that impacting meteoroids bring a significant amount of water to Mercury, whose atmosphere should therefore contain water vapor. This notion is supported by the recent discovery of radar-bright polar deposits almost certainly composed of ice. A variety of origins is likely for the different components. Impact of meteoroids could supply water, Na, and K, and could also vaporize surface material; Na, K, and Ar could be degassed from the crust. H is probably from the solar wind, and He could reasonably come from degassing or the solar wind. A substantial loss process for all components is photoionization (or dissociation); ions on one side are swept away into the solar wind and on the other are swept back to the surface. This process is complicated at Mercury by its permanent magnetic field, but there is little doubt that both loss and recycling still occur. Some of the recycling probably occurs by way of the magnetotail through night side auroral precipitation; atoms implanted in the surface will diffuse back into the atmosphere shortly after dawn, an effect that seems to be present for K. Finally the light atoms H and He have high enough velocities to escape directly, an effect that may be enhanced by the suprathermal velocity distributions that are likely to be present. Author

N95-21795*# Hiroshima Univ. (Japan). Dept. of Earth and Planetary Sciences.

PRIMITIVE Xe IN THE ATMOSPHERES OF EARTH AND MARS Abstract Only

G. Igarashi *In* Lunar and Planetary Inst., Conference on Deep Earth and Planetary Volatiles 1994 p 18 (For primary document see N95-21777 06-46)

Avail: CASI HC A01/MF A01

Published data on Xe isotope compositions in primitive carbonaceous meteorites are examined using multidimensional correlation analysis. Distribution of the Xe data in multidimensional data space, except for (129)Xe, can be characterized by a single component, whose isotope composition is identical to 'H plus L minus Xe'. Additional small contributions to the data variations, less than 1 percent of total variations, can be attributed to 'S minus Xe' as well as atmospheric contamination. Isotopic composition of primitive Xe common to the Earth's atmosphere and carbonaceous meteorites are determined with the same assumption as adopted by Pepin and Phinney: primitive Xe is precisely related to fission-free Xe in the Earth's atmosphere by mass fractionation. The determined isotopic composition of primitive Xe is closer to Solar-type Xe, rather than U-Xe (and the primitive Xe estimated from chondrite-achondrite correlation. Hence, the present published data on Xe isotope compositions in meteorites do not seem to require any special component for the primitive Xe common to the Earth's atmosphere and carbonaceous meteorites. Thus Earth's accreting planetesimals would have trapped Xe from the surrounding nebula gases where Xe isotope composition is identical to Solar-type Xe. The trapped Xe was subsequently subject to isotopic fractionation due to gravitational separation as planetesimals grew. Finally fissiogenic Xe from (244)Pu was added to form the present Xe isotope composition of the Earth's atmosphere. The amount of fissiogenic (136)Xe is estimated to be 2.6 percent of the total amount of (136)Xe in the atmosphere, which is about a half of that estimated by Pepin and Phinney (4.65 percent). Author

N95-21796*# Colorado Univ., Boulder, CO. Lab. for Atmospheric and Space Physics.
MARS ATMOSPHERIC LOSS AND ISOTOPIC FRACTIONATION BY PICK-UP-ION SPUTTERING AND PHOTOCHEMICAL ESCAPE Abstract Only **c91**
B. M. Jakosky, R. O. Pepin (Minnesota Univ., Minneapolis, MN.), R. E. Johnson (Virginia Univ., Charlottesville, VA.), and J. L. Fox (State Univ. of New York, Stony Brook, NY.) *In* Lunar and Planetary Inst., Conference on Deep Earth and Planetary Volatiles 1994 p 19 (For primary document see N95-21777 06-46)
Avail: CASI HC A01/MF A01

We examine the effects of loss of constituents of the Martian atmosphere due to sputtering by solar-wind pick-up ions and photochemical escape during the last 3.8 billion years. Sputtering is capable of efficiently removing species from the upper atmosphere to space, including the light noble gases; nitrogen and oxygen are removed by both sputtering ad photochemical processes. Due to diffusive separation (by mass) above the homopause, removal from the top of the atmosphere will fractionate the isotopes of each species, with the lighter isotope being preferentially lost. This allows current measurements of the isotopic ratios to be used as a measure of the atmospheric evolution as integrated over geologic time. For carbon and oxygen, isotopic fractionation is buffered by exchange of atmospheric species with non-atmospheric reservoirs of CO2 and H2O. This allows us to determine the size of the non-atmospheric reservoirs which are capable of mixing with the atmosphere; these reservoirs can be CO2 absorbed in the regolith and/or H2O in the polar ice caps. Such an exchangeable reservoir is required in order to keep the fractionation of the atmospheric gases as low as is observed. Author

N95-21797*# Academy of Sciences (USSR), Moscow (USSR). Inst. of Geochemistry and Analytical Chemistry.
THE PRIMARY CARBON AND THE FORMATION OF CARBON SPECIES IN TERRESTRIAL MAGMAS Abstract Only
A. Kadik and V. I. Vernadsky *In* Lunar and Planetary Inst., Conference on Deep Earth and Planetary Volatiles 1994 p 20 (For primary document see N95-21777 06-46)
Avail: CASI HC A01/MF A01

There is general agreement that primary carbon and redox state of mantle play an important role in the formation of carbon species in the terrestrial basalts as well as in the composition of gases, evacuated by these liquids to the upper layers of the Earth. It is expected, that interaction between native carbon and production of partial melting of the upper mantle : C(graphite,diamond) + O2(-) (melt) + O2 = CO3(2-) (melt) (1) leads to the formation of CO3(2-) (carbonate ion) in melt. Next mechanism, that may control the presence of free carbon and the formation of C-bearing components in magmas, is the carbon solubility in minerals under mantle conditions by participating in point defect equilibria. Author

N95-21798*# California Univ., Los Angeles, CA. Dept. of Earth and Space Sciences.
DYNAMICS OF VOLATILE DELIVERY FROM OUTER TO INNER SOLAR SYSTEM Abstract Only **c90**
W. M. Kaula *In* Lunar and Planetary Inst., Conference on Deep Earth and Planetary Volatiles 1994 p 21 (For primary document see N95-21777 06-46)
Avail: CASI HC A01/MF A01

Owen et al. propose that the Ar excess of Venus compared to Earth was caused by impact of a large icy planetesimal from the outer solar system, where temperatures were low enough for Ar to adhere to ice, about 30 K. A body of solar Ar/Si and C/H similar to Pluto and Triton less than 100 km diameter would suffice. However, direct delivery from the Uranus-Neptune zone to Venus would result in a very high approach velocity, causing erosion rather than accretion of volatiles. It would also be an extremely improbable event. Virtually all icy bodies scattered from the Uranus-Neptune zone to the terrestrial zone were strongly perturbed by Jupiter, but even then arrived at Venus (or Earth) at too-high velocities. What is needed is a 'deboost' of bodies scattered inward from Jupiter by Earth and Venus perturbations, prior to impact into Venus. This has low probability, since the influence radii of Venus and Earth for the high velocities are small compared to that of Jupiter for the lower velocities further out. It is desirable that this problem be examined by an integrator that allows for close approaches, such as developed by Levison and Duncan. However, it would be a long and expensive computation compared to explaining short-period comets to accomplish the third 'deboost' phase. But since close encounters dominate in such distant scattering, an Opik algorithm seems the appropriate reconnaissance tool. Author

N95-21799*# Arizona State Univ., Tempe, AZ. Dept. of Geology.
PHASE E IN A WATER-SATURATED PERIDOTITE SYSTEM AT 9.3 GPa Abstract Only
Tatsuhiko Kawamoto, Kurt Leinenweber, and Richard L. Hervig *In* Lunar and Planetary Inst., Conference on Deep Earth and Planetary Volatiles 1994 p 22 (For primary document see N95-21777 06-46)
Avail: CASI HC A01/MF A01

The stability of hydrous phases in a natural upper mantle system has been investigated at 9.3 GPa using a gel of KLB-1 peridotite composition with brucite which contains 14 wt. percent (30 atom. percent) water. No hydrous mineral was found at 950 (+150 -50) degree C. At 800 degree C, an assemblage of phase A, phase E, enstatite, clinohumite, and garnet is obtained. Although there is a significant thermal gradient over the sample, phase E is found to be surrounded by phase A in the lower temperature part. Electron probe analyses show that phase E has 35.5 SiO2, 4.4 Al2O3, 41.1 MgO and 8.5 wt. percent FeO* (Mg value is 90) with an oxide sum of 89.7 wt. percent, and possesses a stoichiometry similar to that proposed by Kanzaki. CaO and TiO2 are both less than 0.1 wt. percent. Coexisting phase A has 0.5 wt. percent CaO but only 0.4 wt. percent Al2O3 concentration. Phase A coexists with only enstatite in the water-saturated MgO-FeO-SiO2 system at 800 degree C and 9.3 GPa as well as the results in the water-saturated MgO-SiO2 system. Therefore it is suggested that the addition of Al2O3 expands the stability field of phase E to lower than 13 - 17 GPa in the water-saturated MgO-SiO2 system. Author

N95-21800*# California Univ., San Diego, La Jolla, CA. Dept. of Chemistry.
NITROGEN ISOTOPIC COMPONENTS IN THE EARLY SOLAR SYSTEM Abstract Only **c90**
J. F. Kerridge *In* Lunar and Planetary Inst., Conference on Deep Earth and Planetary Volatiles 1994 p 23-24 (For primary document see N95-21777 06-46)
Avail: CASI HC A01/MF A01

It is quite common to take the terrestrial atmospheric value of (15)N/(14)N (0.00366) as typical of nitrogen in the early solar system, but in fact there is little reason to suppose that this value had a nebula-wide significance. Indeed, it is not clear that there was a unique solar-system-wide (15)N/(14)N ratio, of whatever value. Here we review what is known about the distribution of the nitrogen isotopes among those solar-system objects that have been sampled so far and conclude that those isotopes reveal widespread inhomogeneity in the early solar system. Whether the isotopically distinct primordial components implied by this analysis were solid or gaseous or a mixture of both is not known. The isotopic composition of N in the Earth's mantle is controversial: estimates range from a 1.1 percent depletion in (15)N to a 1.4 percent enrichment. (Isotopic compositions will be expressed throughout as percent deviations from the terrestrial atmospheric value.) The present-day Martian atmosphere is characterized by a value of plus 62 percent but this enrichment in (15)N is attributed to selective loss of (14)N from the Martian exosphere. Modelling of this fractionation leads to an estimated primordial composition similar to the terrestrial atmospheric value, through the precision of this model-dependent result is unclear. Author

N95-21801*# Lunar and Planetary Inst., Houston, TX.
VOLATILES, RHEOLOGY, AND MANTLE CONVECTION: COMPARING EARTH, VENUS, AND MARS Abstract Only **c90**
Walter S. Kiefer *In its* Conference on Deep Earth and Planetary Volatiles 1994 p 25 (For primary document see N95-21777 06-46)
Avail: CASI HC A01/MF A01

Silicate rheology is controlled in part by volatile content. The variation of viscosity with position in the mantle will influence the nature of mantle convection; hence, modeling mantle convection and its effect on surface observables such as the geoid places constraints on the viscosity structure of a planet's mantle and may indirectly constrain the volatile distribution. Models of viscous mantle flow and the Earth's geoid indicate that there is roughly a two order of magnitude variation in viscosity between the upper and lower mantles, although there is some disagreement over the depth of the viscosity minimum in the upper mantle. Some studies of post-glacial rebound also support such a viscosity contrast between the upper and lower mantles. On Venus, several highland regions appear to be supported by mantle plumes. Modeling of the geoid and topography of these regions indicates that if these features are plume-related, then the mantle of Venus can not have an Earth-like low viscosity zone in its upper mantle. On Mars, the Tharsis volcanic province has alternatively been explained as supported either by mantle convection or by flexure of a thick lithosphere. If the convective model is correct, then the large geoid anomaly requires that Mars can not have a low viscosity zone in its upper mantle. Author

N95-21802*# Purdue Univ., West Lafayette, IN. Dept. of Earth and Atmospheric Sciences.

SUBDUCTION AND VOLATILE RECYCLING IN EARTH'S MANTLE Abstract Only

S. D. King, J. J. Ita (California Inst. of Tech., Pasadena, CA.), and H. Staudigel (Vrije Univ., Amsterdam, Netherlands.) *In* Lunar and Planetary Inst., Conference on Deep Earth and Planetary Volatiles 1994 p 26 (For primary document see N95-21777 06-46)

Avail: CASI HC A01/MF A01

The subduction of water and other volatiles into the mantle from oceanic sediments and altered oceanic crust is the major source of volatile recycling in the mantle. Until now, the geotherms that have been used to estimate the amount of volatiles that are recycled at subduction zones have been produced using the hypothesis that the slab is rigid and undergoes no internal deformation. On the other hand, most fluid dynamical mantle flow calculations assume that the slab has no greater strength than the surrounding mantle. Both of these views are inconsistent with laboratory work on the deformation of mantle minerals at high pressures. We consider the effects of the strength of the slab using two-dimensional calculations of a slab-like thermal downwelling with an endothermic phase change. Because the rheology and composition of subducting slabs are uncertain, we consider a range of Clapeyron slopes which bound current laboratory estimates of the spinel to perovskite plus magnesiowustite phase transition and simple temperature-dependent rheologies based on an Arrhenius law diffusion mechanism. In uniform viscosity convection models, subducted material piles up above the phase change until the pile becomes gravitationally unstable and sinks into the lower mantle (the avalanche). Strong slabs moderate the 'catastrophic' effects of the instabilities seen in many constant-viscosity convection calculations; however, even in the strongest slabs we consider, there is some retardation of the slab descent due to the presence of the phase change. Author

N95-21803*# California Univ., Berkeley, CA. Dept. of Geology and Geophysics.

VOLATILES IN THE DEEP EARTH: AN EXPERIMENTAL STUDY USING THE LASER-HEATED DIAMOND CELL Abstract Only

Xiaoyuan Li, Raymond Jeanloz, and Jeffrey H. Nguyen *In* Lunar and Planetary Inst., Conference on Deep Earth and Planetary Volatiles 1994 p 27 (For primary document see N95-21777 06-46)

Avail: CASI HC A01/MF A01

Experiments with the laser-heated diamond cell show that H2O and CO2 can be stabilized within crystalline mineral structures of the lower-mantle, and hence can be present at relatively non-volatile components of the Earth's deep interior. Samples quenched from high pressures and temperatures document that the MgCO3-FeCO3 magnesite-siderite solid-solution is stable and coexists with (Mg,Fe)SiO3 perovskite at 30-40 GPa and approximately 1500-2000 K. In contrast, H2O combines with the silicate to form (Mg,Fe)SiH2O4 phase D, coexisting with (Mg,Fe)SiO3 perovskite at these conditions. If enough water is present, phase D can become the predominant phase in the MgSiO3-H2O system at lower-mantle conditions. Our work extends previous studies to Fe-bearing compositions and to the pressures of the mid-lower mantle. Thus, the results of high-pressure experiments suggest that both H2O and CO2 can be abundant in the Earth's lower mantle, being present in stable hydroxisilicate and carbonate phases. Author

N95-21804*# Washington Univ., Saint Louis, MO. Dept. of Earth and Planetary Sciences.

ALKALI ELEMENT DEPLETION BY CORE FORMATION AND VAPORIZATION ON THE EARLY EARTH Abstract Only

K. Lodders and B. Fegley, Jr. *In* Lunar and Planetary Inst., Conference on Deep Earth and Planetary Volatiles 1994 p 28 (For primary document see N95-21777 06-46)

Avail: CASI HC A01/MF A01

The depletion of Na, K, Rb, and Cs in the Earth's upper mantle and crust relative to their abundances in chondrites is a long standing problem in geochemistry. Here we consider two commonly invoked mechanisms, namely core formation, and vaporization, for producing the observed depletions. Our models predict that a significant percentage of the Earth's bulk alkali element inventory is in the core (30 percent for Na, 52 percent for K, 74 percent for Rb, and 92 percent for Cs). These predictions agree with independent estimates from nebular volatility trends and (for K) from terrestrial heat flow data. Our models also predict that vaporization and thermal escape during planetary accretion are unlikely to produce the observed alkali element depletion pattern. However, loss during the putative giant impact which formed the Moon cannot be ruled out. Experimental, observational, and theoretical tests of our predictions are also described. Alkali element partitioning into the Earth's core was modeled by assuming that alkali element partitioning during core formation on the aubrite parent body (APB) is analogous to that on the early Earth. The analogy is reasonable for three reasons. First, the enstatite meteorites are the only known meteorites with the same oxygen isotope systematics as the Earth-Moon system. Second, the large core size of the Earth and the V depletion in the mantle requires accretion from planetesimals as reduced as the enstatite chondrites. Third, experimental studies of K partitioning between silicate and metal plus sulfide show that more K goes into the metal plus sulfide at higher pressures than at one atmosphere pressure. Thus partitioning in the relatively low pressure natural laboratory of the APB is a good guide to alkali elemental partitioning during the growth of the Earth. Author

N95-21805*# Academy of Sciences (USSR), Moscow (USSR). Inst. of Precambian Geology and Geochronology.

THE RATIOS OF CARBON AND NON-RADIOGENIC HELIUM AND ARGON ISOTOPES IN THE MANTLE AND CRUSTAL ROCKS Abstract Only

K. Lokhov and L. Levsky *In* Lunar and Planetary Inst., Conference on Deep Earth and Planetary Volatiles 1994 p 29 (For primary document see N95-21777 06-46)

Avail: CASI HC A01/MF A01

The studies of the relations of carbon and primary isotopes of noble gases were carried out on the natural gases and on the mantle rocks from the mantle M-type sources, which represent the degassed mantle reservoir (MORB's). These works has the aim of estimation of the values of the C/3He ratios in the deep mantle fluids to determine the flux of the mantle CO2 on the basis of known flux of primary mantle 3He. It was found, that in the natural gases the values of the C/3He ratios fall into the range from 1 times E plus 6 to 1 times E plus 15, and in the fluids of MORB's are constant near 2 times E plus 9. We have studied the mantle rocks from the relatively undergassed mantle P minus type sources: continental; Baikal Rift (Siberia), Mongolia, Catalonia (Spain), Pannonia Depression (central Europe) and ocean; Spietzbergen isl., Hawaii isl., Canarian isl. It ws found, that in mantle xenolites and the host alkaline basalts from the continental rifts and ocean islands, the values of the C/3He ratios fall into the range from E plus 11 to E plus 15 (and this result needed to be explained; the higher carbon to helium ratios is relatively undergassed mantle reservoir compared with the degassed one, requires whether hilly compatibility of helium compared with carbon, whether additional flux of 3He to the degassed mantle reservoir). From the other hand it was found that in the mantle rocks from the sources of P minus and M minus types, continental carbonatites, the values of the C/36Ar ratios are constant in the range from E plus 9 to E plus 10, the close values have the MORB's also. Author

N95-21806*# Arizona Univ., Tucson, AZ. Lunar and Planetary Lab.

SOLAR SYSTEM FORMATION AND THE DISTRIBUTION OF VOLATILE SPECIES Abstract Only **c90**

Jonathan I. Lunine *In* Lunar and Planetary Inst., Conference on Deep Earth and Planetary Volatiles 1994 p 30-31 Sponsored by NASA (For primary document see N95-21777 06-46)

Avail: CASI HC A01/MF A01

To understand how the solar system formed we must understand the compositional distribution of the current system. Volatile species are particularly important in that their stability as condensed phases is limited in temperature-pressure space, and hence variations in their distribution at present potentially contain an imprint of processes by which temperature and pressure varied in the solar nebula. In this talk we restrict ourselves to species more volatile than water ice, and address issues related to processes in the outer solar system and the formation of bodies there; others in this conference will cover volatile species relevant to inner solar system processes. Study of the outer solar system is relevant both to understanding the interface between the solar nebula and the progenitor giant molecular cloud (since the chemical links to present-day observables in molecular clouds are species like methane, carbon monoxide, etc.), as well as the origin of terrestrial planet atmospheres and oceans (the latter to be covered by Owen). The wealth of compositional information on outer solar system bodies which has become available from spacecraft and ground-based observations challenges traditional simplistic views of the composition and hence dynamics of the solar nebula. The basic assumption of thermochemical equilibrium, promulgated in the 1950's, in which methane and ammonia dominate nitrogen- and carbon-bearing species, is demonstrably incorrect on both observational and theoretical grounds. However, the kinetic inhibition model which replaced it, in which carbon monoxide and molecular nitrogen dominate a nebula which is fully mixed and hence cycles outer solar system gases through a hot, chemically active zone near the disk center, is not supported either by observations. Instead, a picture of the outer solar system emerges in which the gas and grains are a mixture of relatively unaltered, or modestly altered, molecular cloud material, along with a fraction which has been chemically altered in the solar nebula itself (and perhaps giant planet nebulae). Author

N95-21807*# Tokyo Univ. (Japan). Dept. of Earth and Planetary Sciences.

SOLUBILITIES OF NITROGEN AND NOBLE GASES IN BASALT MELT Abstract Only

A. Miyazaki, H. Hiyagon, and N. Sugiura *In* Lunar and Planetary Inst., Conference on Deep Earth and Planetary Volatiles 1994 p 32 (For primary document see N95-21777 06-46)

Avail: CASI HC A01/MF A01

Nitrogen and noble gases are important tracers in geochemistry and chosmochemistry. Compared to noble gases, however, physicochemical properties of nitrogen, such as solubility in melt or melt/silicate partition, are not well known. Solubility of nitrogen in basalt melt depends on redox condition of the atmosphere. For example, solubility of nitrogen in E chondrite melt under reducing conditions is as high as 2 mol percent at 1500 C, suggesting that nitrogen is chemically dissolved in silicate melts, i.e., being dissolved as free anions or replacing oxygen sites in silicate network. However, the solubility and the dissolution mechanism of nitrogen under oxidizing conditions are not well investigated. To obtain nitrogen solubility in silicate melts under various redox conditions and to understand its mechanism, we are conducting experiments by using (15)N(15)N-labeled nitrogen gas. This makes it easy to distinguish dissolved nitrogen from later contamination of atmospheric nitrogen, and hence enables us to measure the nitrogen solubility accurately. As a preliminary experiment, we have measured solubility of nitrogen in basalt melt under the atmospheric oxygen pressure. Author

N95-21808*# Princeton Univ., NJ. Dept. of Geological and Geophysical Sciences.

SEISMIC EVIDENCE FOR VOLATILES AT LARGE DEPTH IN THE EARTH Abstract Only

Guust Nolet *In* Lunar and Planetary Inst., Conference on Deep Earth and Planetary Volatiles 1994 p 33 (For primary document see N95-21777 06-46)

Avail: CASI HC A01/MF A01

High resolution tomographic images that have been obtained of the subduction zones in the west Pacific do not only show very low P wave velocities above the leading edge of the slab at shallow depth, but also below 300 km. The two zones are generally, but not always, separated by a zone of normal shear velocity near 200 km depth. These findings confirm some earlier inferences from local seismic data in Japan, and similar findings of low Vp and low Q zones beneath South America. Surprisingly, such deep seismic low velocity zones have recently also been discovered beneath the locations of ancient subduction zones. A study of upper mantle shear velocity in Central Europe shows a similar distribution of low velocity zones beneath the Tornquist-Teisseyre line, the former west coast of the old continent of Baltica, and the site of the subducting Tornquist ocean in the early Palezoic. Preliminary results from a Russian-French experiment shows low P velocities below 250 km under the Urals, while an older tomographic study shows such low P velocities beneath the northern Appalachians. Author

N95-21809*# Cambridge Univ., Cambridge (England). Dept. of Earth Sciences.

RATES OF EARTH DEGASSING Abstract Only

R. K. ONions *In* Lunar and Planetary Inst., Conference on Deep Earth and Planetary Volatiles 1994 p 34 (For primary document see N95-21777 06-46)

Avail: CASI HC A01/MF A01

The degassing of the Earth during accretion is constrained by Pu-U-I-Xe systematics. Degassing was much more efficient during the first 100-200 Ma than subsequently, and it was more complete for Xe than for the lighter gases. More than 90 percent of the degassed Xe escaped from the atmosphere during this period. The combination of fractional degassing of melts and rare gas escape from the atmosphere is able to explain the deficit of terrestrial Xe as a simple consequence of this early degassing history. By the time Xe was quantitatively retained in the atmosphere, the abundances of Kr and the lighter gases in the Earth's interior were similar to or higher than the present-day atmospheric abundances. Subsequent transfer of these lighter rare gases into the atmosphere requires a high rate of post-accretion degassing and melt production. Considerations of Pu-U-Xe systematics suggest that relatively rapid post-accretion degassing was continued to ca. 4.1-4.2 Ga. The present-day degassing history of the Earth is investigated through consideration of rare gas isotope abundances. Although the Earth is a highly degassed body, depleted in rare gases by many orders of magnitude relative to their solar abundances, it is at the present-day losing primordial rare gases which were trapped at the time of accretion. Author

N95-21810*# Hawaii Univ., Honolulu, HI. Inst. for Astronomy.

COMETS, IMPACTS, AND ATMOSPHERES Abstract Only c90

Tobias Owen and Akiva Bar-Nun (Tel-Aviv Univ., Ramat-Aviv, Tel-Aviv, Israel.) *In* Lunar and Planetary Inst., Conference on Deep Earth and Planetary Volatiles 1994 p 35 (For primary document see N95-21777 06-46)

Avail: CASI HC A01/MF A01

Studies of element abundances and values of D/H in the atmospheres of the giant planets and Titan have emphasized the important role of icy planetesimals in the formation of these bodies. In these atmospheres, C/H and D/H increase as the relative masses of the 'cores' of the planets increase. N/H appears to deviate from this trend in an interesting way. In the inner solar system, the traditional approach of using carbonaceous chondrites as the source of planetary volatiles is in serious trouble because of the depletion of xenon and the unusual pattern of xenon isotopes found in the atmospheres of Earth and Mars, and because of the solar-type abundance ratios of argon, krypton and xenon and the large amounts of neon and argon on Venus. Recent studies of elemental abundances in comets, especially P/Halley, coupled with laboratory studies of the trapping of gas in ice formed at low temperatures by A. Bar-Nun et al. provide a consistent interpretation of all of these results. This interpretation emphasizes the fundamental importance of icy planetesimals (comets) and the randomness of early impacts in the formation of planetary systems. Cometary delivery by itself will not explain the noble gas abundances on the inner planets. There is good evidence for at least one additional scurce, which presumably consists of the rocky material making up the bulk of the planets. The existence of this rocky reservoir is manifested in the nucleogenic isotopes and in the neon which is found in all these atmospheres and is also present in the Earth's mantle. This neon may well be a relic of the planets' earliest, accretional atmospheres. Author

N95-21811*# California Univ., Los Angeles, CA. Dept. of Earth and Space Sciences.

POLAR VOLATILES ON MERCURY AND THE MOON Abstract Only c91

D. A. Paige, S. E. Wood, and A. R. Vasavada (California Inst. of Tech., Pasadena, CA.) *In* Lunar and Planetary Inst., Conference on Deep Earth

and Planetary Volatiles 1994 p 36 (For primary document see N95-21777 06-46)
Avail: CASI HC A01/MF A01

The possibility that condensed volatiles might be stable in the permanently shadowed polar regions of the Moon and Mercury has been anticipated in a number of theoretical studies. In 1992, VLA-Goldstone and Arecibo observations revealed the presence of bright, depolarized radar features near the poles of Mercury that have been widely interpreted as evidence for the presence of polar ice deposits. Recently acquired high-resolution Arecibo radar images show that the anomalous radar features are concentrated in crater-sized regions whose locations can be made to coincide exactly with the locations of known impact craters in the Mariner-10 images. These new Arecibo images provide an unusual opportunity to learn more about the distribution and history of Mercury's polar ice deposits. We have constructed a thermal model that can predict surface and subsurface temperatures within impact craters on Mercury and the Moon. Included in the calculations are the effects of 1-dimensional subsurface heat conduction, direct sunlight, multiply reflected sunlight within the crater, and re-radiated infrared radiation within the crater. We also use realistic crater topographic profiles for larger flat-floored craters as well as smaller spherical bowl-shaped craters. Author

N95-21812*# California Inst. of Tech., Pasadena, CA. Lunatic Asylum.
MANTLE RARE GAS RELATIVE ABUNDANCES IN A STEADY-STATE MASS TRANSPORT MODEL Abstract Only
D. Porcelli and G. J. Wasserburg *In* Lunar and Planetary Inst., Conference on Deep Earth and Planetary Volatiles 1994 p 37 (For primary document see N95-21777 06-46)
Avail: CASI HC A01/MF A01

A model for He and Xe was presented previously which incorporates mass transfer of rare gases from an undegassed lower mantle (P) and the atmosphere into a degassed upper mantle (D). We extend the model to include Ne and Ar. Model constraints on rare gas relative abundances within P are derived. Discussions of terrestrial volatile acquisition have focused on the rare gas abundance pattern of the atmosphere relative to meteoritic components, and the pattern of rare gases still trapped in the Ear,th is important in identifying volatile capture and loss processes operating during Earth formation. The assumptions and principles of the model are discussed in Wasserburg and Porcelli (this volume). For P, the concentrations in P of the decay/nuclear products 4 He, 21 Ne, 40 Ar, and 136 Xe can be calculated from the concentrations of the parent elements U, Th, K, and Pu. The total concentration of the daughter element in P is proportional to the isotopic shifts in P. For Ar, ((40)Ar/(36)Ar)p - ((40)Ar/(36)Ar)o =Delta (exp 40) p= 40 Cp/(exp 36)C where(i)C(sub j) the concentration of isotope i in j. In D, isotope compositions are the result of mixing rare gases from P, decay/nuclear products generated in the upper mantle, and subducted rare gases (for Ar and Xe). Author

N95-21813*# Carnegie Institution of Washington, Washington, DC. Geophysical Lab.
HYDROGEN STORAGE IN EARTH'S MANTLE AND CORE Abstract Only
Charles T. Prewitt *In* Lunar and Planetary Inst., Conference on Deep Earth and Planetary Volatiles 1994 p 38 (For primary document see N95-21777 06-46)
Avail: CASI HC A01/MF A01

Two different approaches to explaining how hydrogen might be stored in the mantle are illustrated by a number of papers published over the past 25-30 years, but there has been little attempt to provide objective comparisons of the two. One approach invokes the presence in the mantle of dense hydrous magnesium silicates (DHMS) stable at elevated pressures and temperatures. The other involves nominally anhydrous minerals (NAM) that contain hydrogen as a minor constituent on the ppm level. Experimental studies on DHMS indicate these phases may be stable to pressures and temperatures as high at 16 GPa and 1200 C. This temperature is lower than that indicated by a mantle geotherm at 16 GPa, but may be reasonable for a subducting slab. It is possible that other DHMS could be stable to even higher pressures, but little is known about maximum temperature limits. For NAM, small amounts of hydrogen (up to several hundred ppm) have been detected in olivine, orthopyroxene, clinopyroxene, and garnet recovered from xenoliths in kimberlites, eclogites, and alkali basalts; it has been demonstrated that synthetic wadsleyite and perovskite can accommodate significant amounts of hydrogen. A number of problems are associated with each possibility. For NAM originating in the mantle, one would like to assume that the hydrogen measured in samples recovered on Earth's surface was incorporated when the phase-crystallized at high temperatures and pressures, but it could have been introduced during transport to the surface. Major problems for the DHMS proponents are that none of these phases have been found as minerals and little is yet known about their stabilities in systems containing other cations such as Fe, Al, and Ca. Author

N95-21814*# State Univ. of New York, Stony Brook, NY. Center for High Pressure Research.
SUBDUCTION OF HYDRATED BASALT OF THE OCEANIC CRUST: IMPLICATIONS FOR RECYCLING OF WATER INTO THE UPPER MANTLE AND CONTINENTAL GROWTH Abstract Only
R. P. Rapp *In* Lunar and Planetary Inst., Conference on Deep Earth and Planetary Volatiles 1994 p 39 (For primary document see N95-21777 06-46)
Avail: CASI HC A01/MF A01

Subduction zones are presently the dominant sites on Earth for recycling and mass transfer between the crust and mantle; they feed hydrated basaltic oceanic crust into the upper mantle, where dehydration reactions release aqueous fluids and/or hydrous melts. The loci for fluid and/or melt generation will be determined by the intersection of dehydration reaction boundaries of primary hydrous minerals within the subducted lithosphere with slab geotherms. For metabasalt of the oceanic crust, amphibole is the dominant hydrous mineral. The dehydration melting solidus, vapor-absent melting phase relationships; and amphibole-out phase boundary for a number of natural metabasalts have been determined experimentally, and the pressure-temperature conditions of each of these appear to be dependent on bulk composition. Whether or not the dehydration of amphibole is a fluid-generating or partial melting reaction depends on a number of factors specific to a given subduction zone, such as age and thickness of the subducting oceanic lithosphere, the rate of convergence, and the maturity of the subduction zone. In general, subduction of young, hot oceanic lithosphere will result in partial melting of metabasalt of the oceanic crust within the garnet stability field; these melts are characteristically high-Al_2O_3 trondhjemites, tonalites and dacites. The presence of residual garnet during partial melting imparts a distinctive trace element signature (e.g., high La/Yb, high Sr/Y and Cr/Y combined with low Cr and Y contents relative to demonstrably mantle-derived arc magmas). Water in eclogitized, subducted basalt of the oceanic crust is therefore strongly partitioned into melts generated below about 3.5 GPa in 'hot' subduction zones. Although phase equilibria experiments relevant to 'cold' subduction of hydrated natural basalts are underway in a number of high-pressure laboratories, little is known with respect to the stability of more exotic hydrous minerals (e.g., ellenbergite) and the potential for oceanic crust (including metasediments) to transport water deeper into the mantle. Author

N95-21815*# National Aeronautics and Space Administration. Ames Research Center, Moffett Field, CA.
SURFACE ICES IN THE OUTER SOLAR SYSTEM Abstract Only c91
Ted L. Roush and Dale P. Cruikshank *In* Lunar and Planetary Inst., Conference on Deep Earth and Planetary Volatiles 1994 p 40-41 (For primary document see N95-21777 06-46)
(RTOP 151-01-60-01; RTOP 196-41-67-03)
Avail: CASI HC A01/MF A01

Planetary volatile inventories are products of several factors: (1) condensation-accretion of pre-planetary material which determines the bulk volatile inventory; (2) energy history of a planet, including timing, causes, and mechanisms of degassing; (3) the volatile sinks, including temporary, long term, and permanent; and (4) external processes operating on the volatile inventory. Information regarding the current surface compositions provide insight into both internal and surface-atmosphere evolutionary history. Our discussion focuses upon the surface composition of outer solar system planets and satellites as determined by spacecraft and telescopic spectral observations. We provide a review and an update of the recent work by Cruikshank and Brown that includes more recent observations and interpretations. In the context of formation and evolution of solar system bodies, the interesting ices typically considered are simple molecules formed from elements having high cosmic abundances. These mainly include ices of H_2O, NH_3, SO_2, H_2S, CH_4, CO, CO_2, and N_2. In the solid state, these ices have vibrational spectral features, analogous to their gaseous counterparts but rotational transitions are quenched, that lie in the near- and mid-infrared. The overtone and combination modes, occurring in the visible and near-IR region, are of particular importance as standard observational techniques used to identify these ices rely upon reflected solar energy. Table I summarizes the ices found on various bodies in the outer solar system. H2O is most abundant surface material in the inner and middle regions while more volatile species appear to dominate surfaces in the outermost edge of the outer solar system. Author

N95-21816*# Tokyo Univ. (Japan). Geological Inst.
DEGASSING HISTORY AND EVOLUTION OF VOLCANIC ACTIVITY OF TERRESTRIAL PLANETS BASED ON RADIOGENIC NOBLE GAS DEGASSING MODELS Abstract Only **c91**
S. Sasaki and E. Tajika *In* Lunar and Planetary Inst., Conference on Deep Earth and Planetary Volatiles 1994 p 42 (For primary document see N95-21777 06-46)
Avail: CASI HC A01/MF A01

Current abundances of radiogenic noble gases (4-He, 40-Ar, 129-Xe) in the planetary atmospheres provide valuable information on planetary evolution through their degassing histories. Of these, 40-Ar (from 40-K with half life 1.25 Ga) can be used to envisage long-term degassing from their interior. Present amounts of 36 and 40-Ar should have information on timing and degree of degassing from the interior. On the other hand, 129-Xe (from 129-I with half life 17 Ma) is used in discussing early planetary degassing. Because life time of helium in the atmosphere is short, atmospheric 4-He (from 235-U, 238-U, 232-Th) data might be used only for current degassing. The relative abundance of 40-Ar in the Cytherean atmosphere is 0.26 of that in the Earth's atmosphere. We have executed numerical calculation of a 40-Ar degassing model along with mantle evolution and melt migration. Our result shows that the average magma production rate on Venus is about 5 (km(exp 3)/yr). Duration of plate motion on Venus, if existed, would be less than several hundred million years. Author

N95-21817*# Colorado Univ., Boulder, CO. Dept. of Geological Sciences.
A CRYSTALLOGRAPHIC MODEL FOR HYDROUS WADSLEYITE (BETA-Mg2SiO4) Abstract Only
J. R. Smyth *In* Lunar and Planetary Inst., Conference on Deep Earth and Planetary Volatiles 1994 p 43 (For primary document see N95-21777 06-46)
Avail: CASI HC A01/MF A01

Wadsleyite (beta-Mg2SiO4) is believed to be the most abundant phase in the Earth between depths of 400 and about 525km. Because of the unusual crystal chemistry, Smyth suggested that this phase might be a significant host for hydrogen in the transition zone. Indeed, of the nominally anhydrous phases believed to make up the upper mantle and transition zone none has been reported with a greater H content than wadsleyite. Young et al, report the synthesis of hydrous, Fe-bearing wadsleyite with up to 60,000 H per 10(exp 6) Si. Using ionic constraints and maximal subgroup symmetry, a hypothetical, ordered model for hydrous wadsleyite has been created and examined. The model has formula Mg7Si4O14(OH)2, has space group Pmmb, has an ordered vacancy into one of two non-equivalent M2 sites, and contains two different H positions, one on each of the non-equivalent O1 sites. Electrostatic calculations indicate that hydration would relieve the underbonding of O1 as well as the overbonding of the bridging oxygen, O2, so that the hydrous phase may be more stable than the anhydrous phase. This model makes several predictions that may be of significance for the mechanisms and amounts of H that may be stored in the transition zone of the Earth, and by which the model may be tested experimentally. Author

N95-21818*# Arizona Univ., Tucson, AZ. Lunar and Planetary Lab.
SEMI-VOLATILES AT MERCURY: SODIUM (Na) AND POTASSIUM (K) Abstract Only **c91**
A. Sprague *In* Lunar and Planetary Inst., Conference on Deep Earth and Planetary Volatiles 1994 p 44 (For primary document see N95-21777 06-46)
Avail: CASI HC A01/MF A01

Several lines of evidence now suggest that Mercury is a planet rich in moderately-volatile elements such as Na and K. Recent mid-infrared spectral observations of Mercury's equatorial and mid-latitude region near 120 degrees mercurian longitude indicate the presence of plagioclase feldspar. Spectra of Mercury's surface exhibit spectral activity similar to labradorite (plagioclase feldspar with NaAlSi3O8: 30-50 percent) and bytownite (NaAlSi3O8: 10-30 percent). These surface studies were stimulated by the relatively large abundance of Na and K observed in Mercury's atmosphere. An enhanced column of K is observed at the longitudes of Caloris Basin and of the antipodal terrain. Extreme heating at these 'hot' longitudes and severe fracturing suffered from the large impact event could lead to enhanced outgassing from surface or subsurface materials. Alternatively, sputtering from a surface enriched in K could be the source of the observed enhancement. Recent microwave measurements of Mercury also give indirect evidence of a mercurian regolith less FeO-rich than the Moon. An anomalously high index of refraction derived from the whole-disk integrated phase curve of Danjon may also be indicative of surface sulfides contributing to a regolith that is moderately volatile-rich. The recent exciting observations of radar-bright spots at high latitudes also indicate that a substance of high volume scattering, like ice, is present in shadowed regions. Other radar-bright spots have been seen at locations of Na enhancements on the atmosphere. All combined, these pieces of evidence point to a planet that is not severely depleted in volatiles or semi-volatiles. Author

N95-21819*# Arizona Univ., Tucson, AZ. Lunar and Planetary Lab.
IMPLICATIONS OF NOBLE GASES IN A RECENTLY RECOGNIZED MARTIAN METEORITE (ALH84001) FOR THE DEGASSING HISTORY OF MARS Abstract Only **c91**
T. D. Swindle *In* Lunar and Planetary Inst., Conference on Deep Earth and Planetary Volatiles 1994 p 45 (For primary document see N95-21777 06-46)
Avail: CASI HC A01/MF A01

For terrestrial planets, atmospheric compositions are not static, but evolve with time, in part due to degassing of the interior. Unfortunately, the evolution is slow enough that it is usually not observable on human timescales, or even on the timescales of rocks that preserve samples of Earth's ancient atmosphere. Preliminary results on a recently recognized Martian meteorite, ALH84001, indicate that it is a very old rock, and has a relatively high noble gas content suggestive of atmospheric incorporation, but with an isotopic composition slightly inconsistent with currently known Martian reservoirs. Hence, this rock may provide a sample of ancient Martian atmosphere, which can be used to test models of volatile evolution (in particular, degassing) on Mars. ALH84001 is a cumulate orthopyroxenite. Although originally classified as a diogenite, its oxygen isotopes, and several chemical and petrographic features, strong suggest that it is, like the SNC meteorites, Martian. A Sm-Nd crystallization age of 4.5 Ga has been reported. The meteorite is rich in noble gases, compared to most SNC's. In many respects the noble gases are typical of SNC meteorites. However, there are some subtle differences. In particular, the Xe isotopes in SNC meteorites can be explained as a mixture of Martian atmospheric Xe (as represented by glass in EETA 79001), the Xe in the dunite Chassigny (usually assumed to be representative of the Martian interior, and with lower (129)Xe/(132)Xe, (134)Xe/(132)Xe and (136)Xe/(132)Xe ratios), and later additions from known processes like fission, spallation and terrestrial contamination. The isotopic composition of ALH84001 is inconsistent (at greater than 2-3 sigma) with any mixture of those components. Even if no accumulation of fission Xe during the age of the rock is assumed, there is too little (136)Xe and (134)Xe for the amount of (129)Xe measured. Author

N95-21820*# Max-Planck-Inst. fuer Chemie, Mainz (Germany).
WATER ABUNDANCE AND ACCRETION HISTORY OF TERRESTRIAL PLANETS Abstract Only
H. Waenke and G. Dreibus *In* Lunar and Planetary Inst., Conference on Deep Earth and Planetary Volatiles 1994 p 46 (For primary document see N95-21777 06-46)
Avail: CASI HC A01/MF A01

According to a widespread believe, Earth's water was either added in form of a late volatile-rich veneer or as we have argued repeatedly that of all the water which was added to the Earth only that portion remained which was added towards the end of accretion when the mean oxygen fugacity of the accreting material became so high that metallic iron could not exist any longer. Prior to this moment, all the water in the latter scenario would have been used up for the oxidation of iron. Fe + H2O yields FeO + H2. Huge quantities of hydrogen would continuously be produced in this scenario which escaped. In the same moment the hydrogen on its way to the surface would lead to an efficient degassing of the growing Earth's mantle. The fact that - assuming C1 abundances - the amount of iridium in the Earth's mantle agrees, within a factor of two with the total water inventory of the Earth's mantle and crust is taken as evidence for the validity of such a scenario. In both scenarios, the Earth's mantle would remain dry and devoid of other volatiles. Some species soluble in metallic iron like carbon and hydrogen will probably partly enter the core in some portions. It is generally assumed that today a considerable portion of the earth's total water inventory resides in the mantle. It is also clear that over the history of the Earth the water of the Earth's oceans has been recycled many times through the mantle. This is the consequence of plate subduction. In a similar way mantle convection was probably responsible to being water into the originally dry mantle. As a consequence, today the Earth is wet both inside and outside. Author

N95-21821*# California Inst. of Tech., Pasadena, CA. Lunatic Asylum.
He, Xe AND Ne ISOTOPES IN A STEADY-STATE MASS TRANSPORT MODEL AND IMPLICATIONS ABOUT TERRESTRIAL VOLATILES Abstract Only
G. J. Wasserburg and D. Porcelli *In* Lunar and Planetary Inst., Conference on Deep Earth and Planetary Volatiles 1994 p 47 (For primary document see N95-21777 06-46)
Avail: CASI HC A01/MF A01

We present a model of the steady-state transport assuming three reservoirs: a lower mantle (P) with a relatively undepleted inventory of U, Th, Pu, I, He, Ne, Xe, Ar; an upper mantle that has been extensively outgassed (D); and the atmosphere. There is mass transport at a rate M(sub PD) by plumes from the lower mantle, a fraction of which is outgassed directly into the atmosphere, while the remainder feeds matter and associated nuclei into D. D is well outgassed at spreading centers and has material containing atmospheric gases added to it by subduction. In the case of He, there is no subduction component. The approach follows the treatment of Kellogg and Wasserburg. A summary of the pertinent equations and constraints was reported earlier. The U, Th and Pu in P are estimated for Earth models from refractory element abundances in meteorites. In this model the inventory of rare gases in D is governed by the simple mixing of components from P (both radiogenic and original) with distinctive atmospheric components. In addition, alpha decay and spontaneous fission of U, and (alpha, n) reaction on oxygen from energetic alpha particles produce radiogenic/nuclear daughter products in D. These include (4)He, (136)Xe and (21)Ne. (40)K in D generates excess radiogenic (40)Ar. Author

N95-21822*# Bristol Univ. (England). Dept. of Geology.
STORAGE AND RECYCLING OF WATER AND CARBON DIOXIDE IN THE EARTH Abstract Only
Bernard J. Wood *In* Lunar and Planetary Inst., Conference on Deep Earth and Planetary Volatiles 1994 p 48-49 (For primary document see N95-21777 06-46)
Avail: CASI HC A01/MF A01

The stabilities and properties of water- and carbon-bearing phases in the earth have been determined from phase equilibrium measurements, combined with new data on the equations of state of water, carbon dioxide, carbonates and hydrates. The data have then been used to predict the fate of calcite and hydrous phases in subducting oceanic lithosphere. From the compositions of MORB's one can estimate concentrations of water and carbon of around 200 ppm and 80 ppm respectively in the upper mantle. Lower mantle estimates are very uncertain, but 1900 ppm water and 2000 ppm C are plausible concentrations. Measurements of the density of supercritical water to 3 GPa demonstrate that this phase is less compressible than anticipated from the equations of state of Haar et al. or Saul and Wagner and is closer to predictions based on molecular dynamics simulations. Conversely, fugacity measurements on carbon dioxide to 7 GPa show that this fluid is more compressible than predicted from the MRK equation of state. The results imply that hydrates are relatively more stable and carbonates less stable at pressures greater than 5 GPa than would be predicted from simple extrapolation of the low pressure data. Nevertheless, carbonates remain extremely refractory phases within both the upper and lower mantle. Author

N95-21823*# National Aeronautics and Space Administration. Ames Research Center, Moffett Field, CA.
IS XENON ELDEST? Abstract Only
K. Zahnle *In* Lunar and Planetary Inst., Conference on Deep Earth and Planetary Volatiles 1994 p 50 (For primary document see N95-21777 06-46)
Avail: CASI HC A01/MF A01

It is well known that the solubility of noble gases in magmas decreases with increasing atomic weight. Xenon, the weightiest of the stable noble gases, is the least soluble atmospheric gas in magma. It is not unreasonable to suppose that the noble gases should have degassed from (or equilibrated with) a bubbling mantle in order of increasing solubility, such that xenon was the most rapidly degassed and helium the least. The apparent relative ages of the famous radiogenic noble gas isotopes agrees, at least qualitatively, with this premise. When atmospheric loss processes are assigned their proper place, several long-standing xenonological puzzles become added evidence for xenon's relative antiquity. Xenon being the afore-mentioned sense the oldest atmospheric gas, will have been most greatly subject to escape, be it impact-driven or EUV-driven. Nonradiogenic xenon's pronounced isotopic fractionation has already been attributed to escape; why it should be more fractionated than krypton would be assigned to xenon's greater atmospheric age. The small atmospheric inventory of xenon relative to the other nonradiogenic noblegases, known as the 'missing xenon' problem, could easily be explained by differential escape. The relatively tiny atmospheric inventories of the radiogenic daughter products of 129 Iodine and 244 Plutonium, both much smaller than would be expected from the inferred abundances of the parents in meteorites, offer a third and fourth data to support the hypothesis that Earth has lost most of its xenon. Author

N95-21824*# Tokyo Univ. (Japan). Dept. of Earth and Planetary Physics.
DEGASSING MECHANISMS OF NOBLE GASES FROM CARBONADO DIAMONDS Abstract Only
S. Zashu and H. Hiyagon *In* Lunar and Planetary Inst., Conference on Deep Earth and Planetary Volatiles 1994 p 51 (For primary document see N95-21777 06-46)
Avail: CASI HC A01/MF A01

Diamonds are unique samples for inferring ancient mantle conditions, because of their enormous stability, antiquity and also of mantle origin. However, as temperatures in the mantle where diamonds have existed are very high (greater than 1000 C) and residence time of some diamonds could be more than a few billion years, it is imperative to examine whether or not diamonds have retained their pristine characteristics, especially those of noble gases, under such extreme conditions. As discussed in a review article by Ozima, there are rather large variations in the diffusivity of helium in diamonds obtained in the early determinations. The data are also limited to temperatures higher than 1200 C. In the present study, we conducted more refined diffusion experiments for He using carbonado diamonds, which have large amounts of radiogenic (4)He approximately 10(exp -2) cu cm STP/g. On the basis of the experimentally estimated diffusion coefficients, we will discuss retentivity of He in diamonds in the mantle condition. Author

N95-21833# Northwest Research Associates, Inc., Bellevue, WA.
VARIABILITY OF TOTAL ELECTRON CONTENT IN THE HIGH-ALTITUDE IONOSPHERE FOLLOWING SOLAR MAXIMUM
C. C. Andreasen and Elizabeth Holland 9 Mar. 1994 20 p
(Contract F19628-92-C-0162)
(AD-A285849; NWRA-CR-94-R111; PL-TR-94-2078; SR-1) Avail: CASI HC A03/MF A01

Northwest Research Associates (NWRA) is recording a database containing measurements of the differential carrier phase (DCP) and the differential group delay (DGD) between the two L-band signals transmitted by satellites of the Global Positioning System (GPS). Data collection is continuing at Shemya, AK, and Hanscom AFB, MA. Software has been, and continues to be, developed to process these data into measurements of trans-ionospheric total electron content (TEC). This database is being analyzed in order to document the variability of TEC and to specify TEC morphology in the region of Shemya, AK. Studies of multipath mitigation and accurate satellite bias determination have been conducted to insure high data quality. Analysis of these and other data developed by NWRA in other high latitude studies in the Shetland Islands, UK, has yielded ionospheric trough boundary signatures. These data will be compared to Ionosphere, Morphology, Total electron content, Ionospheric trough. DTIC

N95-21836# Argonne National Lab., IL.

STABILITY EFFECTS ON THE PROFILES OF VERTICAL VELOCITY AND ITS VARIANCE IN KATABATIC FLOW

R. L. Coulter and T. J. Martin 1994 7 p Presented at the 7th International Symposium on Acoustic Remote Sensing and Associated Techniques of the Atmosphere and Oceans, Boulder, CO, 3-7 Oct. 1994
(Contract W-31-109-eng-38)
(DE95-001126; ANL/ER/CP-82594; CONF-9410222-1) Avail: CASI HC A02/MF A01

The atmospheric katabatic flow in the foothills of the Front Range of the Rocky Mountains has been monitored by a network of towers and sodars for several years as part of the Atmospheric Studies in Complex Terrain (ASCOT) program. The dependence of the vertical component of motion, its variance, and the mean component of the wind perpendicular to the surface at the mouth of Coal Creek Canyon on surface cooling and channeling by winds above the canyon has been explored by using almost three years of data from the network. The magnitude of the near-surface temperature differences was found to decrease with increasing surface cooling in light winds, apparently because of increasing turbulence resulting when increasing winds interact with surface topography. The variance of vertical velocity exhibits three types of vertical profiles, corresponding to different cooling rates and external wind speeds. The mean variance was found to depend strongly on a locally derived Richardson number. DOE

N95-21874*# National Aeronautics and Space Administration. Marshall Space Flight Center, Huntsville, AL.

POTENTIAL FLOW DOWNSTREAM OF THE HELIOSPHERIC TERMINAL SHOCK: A NON-SPHERICAL SHOCK

Steven Nerney and Steven T. Suess Oct. 1994 12 p Submitted for publication Sponsored by NASA
(NASA-TM-110493; NAS 1.15:110493) Avail: CASI HC A03/MF A01

We have solved for the potential flow downstream of the terminal shock of the solar wind in the limit of small departures from a spherical shock due to a latitudinal ram pressure variation in the supersonic solar wind. The solution connects anisotropic streamlines at the shock to uniform streamlines down the heliotail because we use a non-slip boundary condition on the heliopause at large radii. The rotational velocity about the heliotail in the near-field solution decays as the fourth power of distance from the shock. The polar divergence of the streamlines will have consequences for the previously discussed magnetic pressure ridge that may build-up just inside the heliopause. Author

N95-21875# Los Alamos National Lab., NM.

HIGH RESOLUTION PROPERTIES OF THE EQUATORIAL PACIFIC MARINE ATMOSPHERIC BOUNDARY LAYER FROM LIDAR AND RADIOSONDE OBSERVATIONS

Daniel I. Cooper, William E. Eichinger, Mike V. Hynes, Charles F. Keller, Charles F. Lebeda, and David A. Poling 1994 7 p Presented at the 75th Annual Meeting of the American Meteorological Society: Diamond Anniversary, Dallas, TX, 15-20 Jan. 1995
(Contract W-7405-eng-36)
(DE95-001028; LA-UR-94-3103; CONF-950124-1) Avail: CASI HC A02/MF A01

Water vapor and relative aerosol concentration were measured with two shipboard lidars from the ocean surface to tropospheric and lower stratospheric altitudes in support of the Central Equatorial Pacific Experiment (CEPEX) program. The goal of CEPEX is to evaluate the 'thermostat' hypothesis regarding feedback mechanisms between the tropical ocean and the atmosphere. This paper describes some of the features observed with the first two kilometers of the equatorial troposphere, known as the marine Atmospheric Boundary Layer (ABL), as well as the coupling between the ocean and the atmosphere. This paper will present the initial analysis of the structure of the atmospheric boundary layer. Finally, we will look at the implications of this structure for ocean-atmosphere coupling by comparing the height of the mixing layer with sea surface temperatures and other factors. DOE

N95-21932 Southern Methodist Univ., Dallas, TX. Dept. of Geological Sciences.

SOURCE CONTRIBUTIONS AT FAR-REGIONAL DISTANCES

Karl Koch and Brian Stump 12 Dec. 1993 94 p Limited Reproducibility: More than 20% of this document may be affected by microfiche quality
(Contract F19628-91-K-0016)
(AD-A279405; PL-TR-94-2018; AD-E201929; SR-1) Avail: Issuing Activity (Defense Technical Information Center (DTIC))

In order to investigate source contributions at far-regional distances (as far as 2,000 km), a reliable model of the upper mantle structure is necessary. In many cases successful discriminants are based on the S wave part of far-regional seismograms including Sn, Sg, Lg and surfaces waves. Therefore it is mandatory to place corresponding weight on constraining the upper mantle S wave structure for the region under consideration. This current report hence provides an investigation of the mantle shear structure for the Western U.S. from body and surface wave inversion. Earthquakes on the coast of northern California and off the coast of southern Oregon (5.5 less than Ms less than 7.1) have provided a set of data at LTX showing clear mantle S arrivals that become very impulsive at distances near 2,400 km. The great circle paths for these events to LTX coincide with the LTX-NTS path. These data allow the interpretation of the S velocity structure for the Western U.S. to depths of the upper mantle transition zone from the body waves and give constraints for the shallower structure from surface waves from inversion of Rayleigh and Love waves, summarized in the two papers contained in this report. DTIC

N95-21944 Woods Hole Oceanographic Inst., MA.

SURFACE EXPOSURE GEOCHRONOLOGY USING COSMOGENIC NUCLIDES: APPLICATIONS IN ANTARCTIC GLACIAL GEOLOGY Ph.D. Thesis - MIT

Edward J. Brook Feb. 1994 234 p Sponsored in part by ONR Limited Reproducibility: More than 20% of this document may be affected by microfiche quality
(Grants NSF DPP-91-17458; NSF DPP-88-17406)
(AD-A279392; WHOI-93-50) Avail: Issuing Activity (Defense Technical Information Center (DTIC))

Cosmogenic He(3), Al(26), and Be(10) were measured in Antarctic glacial deposits in the McMurdo Sound-Dry Valleys region to constrain surface exposure ages. Moraines deposited by the Taylor glacier, an outlet glacier of the East Antarctic Ice Sheet, have exposure ages from approx. 120 kyr to 2myr. Be(10), He(3) ages of 122 +/- 29 and 134+ / -54 kyr, respectively, for the Taylor II moraine are consistent with deposition during isotope stage 5e approx. 120 kyr. Mean Be(10) exposure ages for older moraines in the valley of 362 + or - 26 kyr (Taylor III), 1.1 + or 1 0.1 myr (Taylor IVa) and 1.9 + or - 0.1 myr (Taylor IVb) suggest that major ice sheet advances during the last 2 myr were similar in extent to changes during the last glacial-interglacial cycle. Exposure ages for the 'late Wisconsin' Ross Sea Drift, deposited on the coast of McMurdo Sound by the Ross Sea Ice Sheet, range from 8-106 kyr, suggesting that this deposit does not, as previously thought, represent a single ice advance in response to lowered sea level at the last glacial maximum. The data suggest instead that the Ross Sea Ice Sheet may have grounded and advanced on the coast several times during the last glacial period. DTIC

N95-22019# Naval Postgraduate School, Monterey, CA.

A SIMULATION OF PLASMA MOTION IN THE POLAR IONOSPHERE M.S. Thesis

David W. Deist Sep. 1994 52 p
(AD-A286166) Avail: CASI HC A04/MF A01

A model of plasma motion in the polar ionosphere is presented. Plasma motion due to polar convection and corotation above 50 deg N is modeled. The universal time (UT)-dependent corotation electric field (in the geomagnetic frame) is added to a polar convection electric field that is UT-dependent in the geographic frame and the total is displayed in both reference frames. To simulate actual magnetic conditions, varying polar convection patterns may be used by the model we have developed. Trajectories of single plasma parcels and regions of plasma are calculated. The calculated trajectories are displayed in the geographic and magnetic inertial reference frames. The model developed is applied to the study of a region of electron depletion near the pole, a polar hole. Changes in the size and location of the polar hole are explained in terms of a changing convection pattern. The results of this thesis are being used by the Johns Hopkins University Applied Physics Laboratory to further study ionospheric plasma motion. DTIC

N95-22095 Technical Research Centre of Finland, Espoo (Finland).
VTT TEST BOREHOLE FOR BEDROCK INVESTIGATIONS
Olli Okko, Pertti Hassinen, and Kai Front Feb. 1994 42 p
(PB95-132965; VTT/RN-1538) Copyright Avail: Issuing Activity (National Technical Information Service (NTIS))

A borehole of depth 150 m and diameter 56 mm has been drilled in the area adjacent to the premises of the Technical Research Center of Finland (VTT) at Otaniemi, Espoo, for the purposes of calibrating geophysical measurement devices. The report presents the test results obtained so far and illustrates the processing of these, in which the various measurements are plotted as curves and combinations of curves. The interpretations provided so far consist of analyses of lithological variations, bedrock fracturing, the nature and occurrence of fracture zones and groundwater flow patterns. Samples were taken from those parts of the core shown by the borehole measurements to be homogeneous and thin sections made from these for mineralogical determinations. The rock mechanical and petrophysical properties of the same points were examined. The core is in the possession of VTT, and the hole itself is available to outsiders for the calibration and testing of borehole measurement equipment. NTIS

N95-22240# Colorado Univ., Boulder, CO. Lab. for Atmospheric and Space Physics.
CONFIRMATORY ANALYSIS OF SAGE-1, AND -2 DATA Semiannual Progress Report, 30 Jun. - 30 Dec. 1994
David W. Rusch, Stanley C. Solomon, Cora E. Randall, and R. Todd Clancy 1994 3 p
(Contract DE-FG03-94ER-61856)
(DE95-003623; DOE/ER-61856/T1) Avail: CASI HC A01/MF A01

This study is motivated by the need for an independent assessment of the SAGE-1, and -2 data to determine the long-term tenacity of the data set and the inversion procedures used to handle the data. In particular, ozone measurements in the lower stratosphere, where our primary attention is focused, are complicated by the permanent presence of atmospheric aerosols. At times, the natural background aerosol density is complemented or even overwhelmed by volcanic injections which interfere with the normal data processing of instruments such as SAGE. This report summarizes progress on the grant for the first 6 months of the grant period ending 12/30/94. During this period we have collected the relevant SAGE data, purchased needed computers and equipment, designed the database, and outlined the forward model requirements and mathematical procedures. DOE

N95-22249# Aerospace Corp., El Segundo, CA. Technology Operations.
THRESHOLD DETECTION IN THE PRESENCE OF ATMOSPHERIC TURBULENCE
H. T. Yura 15 Oct. 1994 20 p
(Contract F04701-93-C-0094)
(AD-A286175; TR-94(4911)-1; SMC-TR-94-40) Avail: CASI HC A03/MF A01

Recently, there has been increased interest in threats to spacecraft from ground-based lasers. It has been suggested that some spacecraft should employ laser-threat warning receivers. Here, we consider the effects of atmospheric turbulence on threshold detection of optical signals by an exoatmospheric receiver. The present results are applicable to both cw and pulsed optical illumination from ground-based lasers. In particular, we obtain accurate analytical expressions, over a wide range of conditions of practical interest, that give the required signal-to-noise ratio for a given (single-event) probability of detection, false-alarm rate, and turbulence-induced log-intensity variance. The degrading effects of atmospheric turbulence on threshold detection are most important for large zenith angles in the blue-green region of the spectrum. As an illustrative example, a false-alarm rate of one in three years is assumed, and specific numerical results are presented for the required signal-to-noise ratio necessary to obtain a detection probability of at least 95% over a range of opticalwavelengths and propagation conditions of interest. DTIC

N95-22326*# Boston Univ., MA. Center for Space Physics.
SUBSTORM THEORIES: UNITED THEY STAND, DIVIDED THEY FALL
Gary M. Erickson 4 Jan. 1995 11 p Submitted for publication
(Contract NAGw-2627; NAGw-2856; F19628-90-K-0003)
(NASA-CR-197672; NAS 1.26:197672; F19628-90-K-0003) Avail: CASI HC A03/MF A01

Consensus on the timing and mapping of substorm features has permitted a synthesis of substorm models. Within the synthesis model the mechanism for onset of substorm expansion is still unknown. Possible mechanisms are: growth of an ion tearing mode, current disruption by a cross-field current instability, and magnetosphere-ionosphere coupling. While the synthesis model is consistent with overall substorm morphology, including near-Earth onset, none of the onset theories, taken individually, appear to account for substorm expansion onset. A grand synthesis with unification of the underlying onset theories appears necessary. Author

N95-22368 Rutherford Appleton Lab., Oxford (England).
LARGE-SCALE FIELDS AND FLOWS IN THE MAGNETOSPHERE-IONOSPHERE SYSTEM
M. Lockwood Sep. 1994 56 p
(PB95-134664; RAL-94-097) Avail: Issuing Activity (National Technical Information Service (NTIS))

Advances in the author's understanding of the large-scale electric and magnetic fields in the coupled magnetosphere-ionosphere system are reviewed. The literature appearing in the period January 1991-June 1993 is sorted into 8 general areas of study. The phenomenon of substorms receives the most attention in this literature, with the location of onset being the single most discussed issue. However, if the magnetic topology in substorm phases was widely debated, less attention was paid to the relationship of convection to the substorm cycle. A significantly new consensus view of substorm expansion and recovery phases emerged, which was termed the 'Kiruna Conjecture' after the conference at which it gained widespread acceptance. The second largest area of interest was dayside transient events, both near the magnetopause and the ionosphere. It became apparent that these phenomena include at least two classes of events, probably due to transient reconnection bursts and sudden solar wind dynamic pressure changes. The contribution of both types of events to convection is controversial. Several new techniques were introduced including ionospheric observations which yield reconnection rate as a function of time. The magnetospheric and ionospheric behavior due to various quasi-steady interplanetary conditions was studied using magnetic cloud events. NTIS

N95-22423# Boston Univ., MA. Center for Space Physics.
THE EFFECTS OF MAGNETIC STORM PHASES ON F-LAYER IRREGULARITIES FROM AURORAL TO EQUATORIAL LATITUDES Quarterly Report, 1 Jul. - 30 Sep. 1994
Jules Aarons and Michael Mendillo 30 Sep. 1994 4 p
(Contract N00014-89-J-1754)
(AD-A286173) Avail: CASI HC A01/MF A01

Results are presented for the following topics: the global positioning system (GPS) and scintillation; GPS signals and forecasting fading on FLEETSATCOM; middle latitude ionospheric studies; and the ONR AASERT program in upper atmosphere and ionospheric physics. CASI

N95-22477# Los Alamos National Lab., NM.
MAGNETOSPHERIC PLASMA ANALYZER (MPA): PLASMA OBSERVATIONS FROM GEOSYNCHRONOUS ORBIT
D. J. McComas 1994 24 p Presented at the 10th Taos Workshop on the Earth's Trapped Particle Environment, Taos, NM, Aug. 1994
(Contract W-7405-eng-36)
(DE95-002739; LA-UR-94-3554; CONF-9408182-1) Avail: CASI HC A03/MF A01

This paper briefly summarizes the early studies of the Los Alamos Magnetospheric Plasma Analyzer (MPA) observations. The three MPA instruments presently on orbit are returning a unique set of simultaneous, multi-point observations of the geosynchronous plasma environment. So far, MPA studies can be divided into six general topics: (1) morphology and distribution of the plasma regions observed at geosynchronous orbit; (2) the location and shape of the magnetopause when compressed and/or eroded to within geosynchronous orbit; (3) rare geosynchronous lobe encounters, (4) magnetic field line models and field line mapping; (5) outer plasmasphere shape, configuration and dynamics; and (6) local plasma processes. This paper briefly highlights the MPA-related work in each of these areas. In addition, a list of ongoing MPA studies is provided; other collaborative uses of these data are strongly encouraged. DOE

47 METEOROLOGY AND CLIMATOLOGY

Includes weather forecasting and modification.

N95-19948*# Purdue Univ., West Lafayette, IN. Dept. of Earth and Atmospheric Sciences.
RAINFALL RATES AND THE VERTICAL DISTRIBUTION OF DIABATIC HEATING COMPONENTS OVER TROPICAL OCEANS Semiannual Status Report, 1 Sep. 1993 - 28 Feb. 1994
Dayton G. Vincent and Grant W. Petty 28 Feb. 1994 2 p
(Grant NAG8-1031)
(NASA-CR-197603; NAS 1.26:197603) Avail: CASI HC A01/MF A01

During the fall of 1993, nearly all of the emphasis on this project was devoted to the completion of Ph.D. research. In January 1994, a poster summarizing research was presented at the 8th Conference on Atmospheric Radiation held in Nashville, TN. In February 1994, we submitted two papers for publication. Finally, we learned that we have had a paper accepted for poster presentation at the European Conference on the Global Energy and Water Cycle to be held in London, England in July 1994. Titles for all these papers are provided. Derived from text

N95-19989# Army Research Lab., Aberdeen Proving Ground, MD.
COMPARISON OF METEOROLOGICAL DATA WITH FITTED VALUES EXTRACTED FROM PROJECTILE TRAJECTORY Final Report, Jul. 1993 - Jul. 1994
Gene R. Cooper and Kevin S. Fansler Oct. 1994 35 p
(AD-A285921; ARL-TR-603) Avail: CASI HC A03/MF A01

In this report, the atmospheric conditions are found by knowing only the projectile's flight trajectory and its flight coefficients together with the initial atmospheric conditions on the ground. The test trajectories were generated as solutions of the modified point mass (MPM) equations of motion. The correct atmospheric conditions for the generated flight trajectory are obtained from data collected during a weather balloon flight. A nonlinear least squares method was then used to fit the MPM equations to the test trajectory by varying the meteorological parameters. Density, sound speed, and wind profiles agreed well. Further tests of the method involved the flight coefficients, which we perturbed to observe the corresponding variation for the fitted values. Also, Gaussian noise was introduced onto the trajectory values to simulate the uncertainty in trajectory measurements. The results of the analysis shows that the whole trajectory should be fitted, and not small trajectory segments, to obtain accurate atmospheric parameters with the location precision provided by current radar and Global Positioning Satellite System (GPS) techniques. DTIC

N95-20008# Manchester Univ. (England). Dept. of Physics.
THE INITIATION OF LIGHTNING AND THE GROWTH OF ELECTRIC FIELDS IN THUNDERSTORMS Final Report, 1 Nov. 1991 - 31 Mar. 1994
John Latham Dec. 1993 60 p
(Contract F49620-92-J-0020)
(AD-A280033; UMIST/PHYS/2; AFOSR-94-0317TR) Avail: CASI HC A04/MF A01

Further research into the glaciation of convective clouds of-the type that produce lightning has revealed that the early stages of ice formation can be detected by measurement of the supercooled droplet radius - a result which also has climatological implications. Further laboratory experiments have shown that the most effective methods of lightning initiation are likely to involve supercooled raindrops, with threshold fields around 300kV/m. A new model of thundercloud electrification and lightning production has been developed, from which it is possible to deduce the sensitivity of lightning frequency to meteorological and cloud microphysical parameters. DTIC

N95-20099# National Oceanographic Data Center, Washington, DC.
MARINERS WEATHER LOG, VOLUME 38, NUMBER 3, SUMMER 1994
R. M. DeAngelis, ed. and N. ODonnell, ed. 1994 106 p See also PB94-191848
(PB94-209541) Avail: CASI HC A06/MF A02

Contents include: The Black Hole -- or where do those weather observations go; Weather Dampens Sydney to Hobart Yacht Rack; Real-time Oceanographic Data for Ports; GMDSS -- a Safety Net for Mariners; Inmarsat and Beyond; The Admiralty List of Radio Signals; The Broadcasting of Weather Maps by Radio Accomplished; and Weather on the Net. NTIS

N95-20140# Lawrence Livermore National Lab., Livermore, CA.
MONSOONS: AMIP SIMULATIONS OF THE 1987 AND 1988 DROUGHT AND FLOOD REGIMES
K. R. Sperber and T. N. Palmer (European Centre for Medium-Range Weather Forecasts, Reading, England.) Oct. 1993 6 p Presented at the 18th Climate Diagnostics Workshop, Boulder, CO, 1-5 Nov. 1994
(Contract W-7405-eng-48)
(DE94-014789; UCRL-JC-114511; CONF-941193-1) Avail: CASI HC A02/MF A01

The simulation of monsoons, in particular the Indian summer monsoon, has proven to be a critical test of a general circulation models ability to simulate tropical climate and variability (Simulation of Monsoon Variability, WCRP-68, 1992). In an effort to better understand the necessary conditions for the simulation of a phenomenologically correct Indian Monsoon, we present analyses of simulations associated with the Atmospheric Model Intercomparison Project, a coordinated effort to simulate the 1979-88 decade using standardized boundary conditions with approximately 30 atmospheric general circulation models. Diagnostics, such as those performed under the auspices of the Monsoon Numerical Experimentation Group have been evaluated to address questions regarding the predictability of monsoon extremes. Particular attention has been devoted to the 1987 and 1988 Indian monsoon drought and flood regimes associated with El Nino and La Nina conditions in the Pacific. DOE

N95-20186 Colorado Univ., Boulder, CO. Dept. of Astrophysical Planetary and Atmospheric Sciences.
FRONT-BOUNDARY LAYER MODELS FROM STORM-FEST OBSERVATIONS Annual Report, 1 Jun. 1993 - 31 May 1994
William Blumen 2 May 1994 8 p Limited Reproducibility: More than 20% of this document may be affected by microfiche quality
(Contract F49620-93-1-0416)
(AD-A279907; AFOSR-94-0318TR) Avail: Issuing Activity (Defense Technical Information Center (DTIC))

The STORM-FEST field campaign to investigate atmospheric frontal structure and evolution provided data on deformation frontogenesis observed 20-21 February 1992. These data have been analyzed, and the principal features compared with the theoretical predictions of a semigeostrophic, inviscid, adiabatic model. The overall agreement is good, although viscous and thermal diffusion in the planetary boundary layer is omitted from the theoretical model. DTIC

N95-20319# Sandia National Labs., Albuquerque, NM.
SIMULATION OF LARGE SYSTEMS WITH NEURAL NETWORKS
T. L. Paez 1994 10 p Presented at the Shock and Vibration Symposium, San Diego, CA, 31 Oct. 1994
(Contract DE-AC04-94AL-85000)
(DE94-018898; SAND-94-2314C; CONF-9410187-2) Avail: CASI HC A02/MF A01

Artificial neural networks (ANN's) have been shown capable of simulating the behavior of complex, nonlinear, systems, including structural systems. Under certain circumstances, it is desirable to simulate structures that are analyzed with the finite element method. For example, when we perform a probabilistic analysis with the Monte Carlo method, we usually perform numerous (hundreds or thousands of) repetitions of a response simulation with different input and system parameters to estimate the chance of specific response behaviors. In such applications, efficiency in computation of response is critical, and response simulation with ANN's can be valuable. However, finite element analyses of complex systems involve the use of models with tens or hundreds of thousands of degrees of freedom, and ANN's are practically limited to simulations that involve far fewer variables. This paper develops a technique for reducing the amount of information required to characterize the response of a general structure. We show how the reduced information can be used to train a recurrent ANN. Then the trained ANN can be used to simulate the reduced behavior of the

original system, and the reduction transformation can be inverted to provide a simulation of the original system. A numerical example is presented.
DOE

N95-20381# Lawrence Livermore National Lab., Livermore, CA.
EFFECTS OF MICROPHYSICS AND RADIATION ON MESOSCALE PROCESSES OF A MIDLATITUDE SQUALL LINE
Hung-Neng Steve Chin Apr. 1994 6 p Presented at the 6th Conference on Mesoscale Processes, Portland, OR, 18-22 Jul. 1994
(Contract W-7405-eng-48)
(DE94-014732; UCRL-JC-115990; CONF-940769-7) Avail: CASI HC A02/MF A01

The understanding of the essential dynamics of mesoscale convective systems (MCS's) was well addressed in the literature. Effects of different physics on mesoscale processes of MCS's are, however, not well understood at some particular aspects, such as the origins of the rear inflow and the transition zone in the radar reflectivity. Attention is focused on these two aspects for a midlatitude broken-line squall system. The existence of the rear inflow in MCS's has been identified in many observational and modeling studies. Although convincing evidence has shown that physical processes internal to the mesoscale system and pressure gradient effects in the convective and trailing stratiform regions are undoubtedly important in developing the rear inflow, it remains unclear how these internal processes interact with pressure effects to trigger the rear inflow. Moreover, many modeling studies have replicated the bright melting band, but the transition zone has not been successfully simulated. With the enhanced model physics, such as radiation, in a cloud model, we can simulate these features and provide some supplemental evidences, at least in part, to explain them. The modulation of the rear inflow by microphysics, longwave (LW) and shortwave (SW) radiation, and its related cloud-radiative feedback to the modeled squall line system are also discussed. DOE

N95-20391# Pennsylvania State Univ., University Park, PA. Dept. of Meteorology.
THE VERTICAL DISTRIBUTION OF HEATING IN THE TROPICAL ATMOSPHERE Annual Report, 1 Oct. 1991 - 30 Sep. 1994
William M. Frank 30 Sep. 1994 5 p
(Contract N00014-92-J-1069)
(AD-A285934) Avail: CASI HC A01/MF A01

This grant supported research is in two areas. The primary goal of the work was to plan and participate in the TOGA-COARE (Tropical Ocean-Global Atmosphere Couple Ocean-Atmosphere Experiment) program to analyze large-scale heat and moisture budgets with the data from that experiment. The second major goal was to analyze relationships between large-scale tropical circulations and tropical cyclone intensity changes in the Northwest Pacific. Research has gone very well in both areas. DTIC

N95-20395# Pennsylvania State Univ., University Park, PA. Dept. of Meteorology.
BOUNDARY LAYER CLOUD STUDIES IN SUPPORT OF ASTEX
Bruce A. Albrecht 1994 5 p Sponsored by ONR
(AD-A285947) Avail: CASI HC A01/MF A01

The research goals of this project are to investigate the effects of drizzle, diurnal decoupling, entrainment, and mesoscale processes on the type and amount of marine boundary layer cloudiness using surface-based remote and in situ sensors deployed during the Atlantic Stratocumulus Transition Experiment (ASTEX), 1992. Derived from text

N95-20782# Lawrence Livermore National Lab., Livermore, CA.
MESO-SCALE COOLING EFFECTS OF HIGH ALBEDO SURFACES: ANALYSIS OF METEOROLOGICAL DATA FROM WHITE SANDS NATIONAL MONUMENT AND WHITE SANDS MISSILE RANGE
B. Fishman, H. Taha, and H. Akbari 20 May 1994 30 p
(Contract DE-AC03-76SF-00098)
(DE94-018535; LBL-35056) Avail: CASI HC A03/MF A01

Urban summer daytime temperatures often exceed those of the surrounding rural areas. Summer 'urban heat islands' are caused by dark roofs and paved surfaces as well as the lack of vegetation. Researchers at Lawrence Berkeley Laboratory are interested in studying the effects of increasing the albedo of roof tops and paved surfaces in order to reduce the impacts of summer urban heat islands. Increasing the albedo of urban surfaces may reduce this heat island effect in two ways, directly and indirectly. The direct effect involves reducing surface temperature and, therefore, heat conduction through the building envelope. This effect of surface albedo on surface temperatures is better understood and has been quantified in several studies. The indirect effect is the impact of high albedo surfaces on the near surface air temperatures. Although the indirect effect has been modeled for the Los Angeles basin by Sailor, direct field observations are required. The objective of this report is to investigate the meso-scale climate of a large high albedo area and identify the effects of albedo on the near surface air temperature. To accomplish this task, data from several surface weather stations at White Sands, New Mexico were analyzed. This report is organized into six sections in addition to this introduction. The first gives the general geological, topographic, and meteorological background of White Sands. The second is a discussion of the basic surface meteorology of the White Sands region. This section is followed by a general discussion of the instrumentation and available data. The fourth section is a description of the method used for data analysis. The fifth section which presents the results of this analysis. Finally, the last section is the summary and conclusion, where a discussion of the results is presented. DOE

N95-20826# Naval Research Lab., Monterey, CA.
A STUDY OF WESTERLY WIND BURSTS PRECEDING THE 1991-1992 EL NINO Final Report
Patricia A. Phoebus and John C. Kindle Jul. 1994 57 p
(AD-A286570; NRL/FR/7531-94-9450) Avail: CASI HC A04/MF A01

Anomalous westerly wind events in the western equatorial Pacific are of interest because of their potential to generate equatorially trapped ocean Kelvin waves that may be related to the development or enhancement of the El Nino. While a number of ideas have been proposed about the nature and origin of the equatorial westerlies, detection and description of these events is hindered by the lack of observational data in the area of interest (3 deg S-3 deg N, 130 deg E-180 deg E). Under such circumstances, the best tool for obtaining a realistic representation of the atmosphere is a four-dimensional global data assimilation system which continually updates a short-term model forecast using synoptic data to produce meteorological fields that are consistent with known dynamical and physical relationships. Using low-level wind fields from the U.S. Navy's operational global analysis/forecast system for the period October 1990-February 1992, we observed a clear association between significant westerly wind events and tropical cyclone development. In general, there is an eastward and equatorward shift in cyclone activity that is associated with the concentration of westerlies along the equator in the western and central Pacific. The strongest westerlies are associated with the development of dual-hemisphere cyclone pairs, and these events preceded the maximum warming in the eastern Pacific by a couple of months, thus supporting the hypothesis for ocean Kelvin wave contributions to the El Nino. Similar patterns in tropical cyclone activity are observed during other years marking the beginning of the El Nino. DTIC

N95-20857# Federal Aviation Administration, Atlantic City, NJ.
TEST AND EVALUATION MASTER PLAN (TEMP) FOR THE WEATHER MESSAGE SWITCHING CENTER REPLACEMENT (WMSCR)
William Benner, Nannette Gordner, and David Roth Oct. 1994 46 p
(AD-A286590; DOT/FAA/CT-TN94/38) Avail: CASI HC A03/MF A01

The Weather Message Switching Center Replacement (WMSCR) Test and Evaluation Master Plan (TEMP) outlines the Test and Evaluation (T and E) process that will be used to ensure that the WMSCR meets the requirements of both the project specification and the requirements allocated from the National Airspace System (NAS) documents. It provides strategy and guidance for test requirements. The WMSCR TEMP has been prepared in accordance with FAA Order 1810.4B and FAA-STD-024a. The WMSCR TEMP follows the requirements defined in FAA-E-2764c, WMSCR Requirements Specification. This TEMP is a high-level document that related required system characteristics and critical issues to test objectives. It addresses Developmental Test and Evaluation (DT and E), Production Acceptance T and E (PAT and E), Operational T and E (OT and E) for System Shakedown (OT and E Shakedown). The TEMP also outlines procedures to be followed to ensure the successful integration of the WMSCR system into the NAS. Testing is performed to ensure integration of new subsystems will not degrade the current operations of the NAS.
DTIC

N95-20969 North Carolina State Univ., Raleigh, NC. Dept. of Marine Earth and Atmospheric Sciences.
BALLOON TRACKING FOR THE ASTEX/MAGE LAGRANGIAN EXPERIMENT
Steven Businger Apr. 1994 24 p Limited Reproducibility: More than 20% of this document may be affected by microfiche quality
(Contract N00014-92-J-1285)
(AD-A280078) Avail: Issuing Activity (Defense Technical Information Center (DTIC))

The Lagrangian experiments in Atlantic Stratocumulus Transition Experiment/Marine Aerosol Gas Exchange (ASTEX/MAGE) were the first attempt to repeatedly sample the same remote marine air parcel over an extended period (36 to 48 hours), permitting observation of chemical changes in the sulfur budget (in particular, the formation of sulfate aerosol from biogenic DMS gas) while limiting the complication of advection through the sampling area. Our goal in supporting the Lagrangian experiments is to provide tetroon location data and analysis of relevant meteorological data to provide an unambiguous track of a chosen volume of air, estimate the entrainment through the MBL inversion, and estimate the impact of air-mass divergence. Author (DTIC)

N95-20974# Phillips Lab., Hanscom AFB, MA.
PROCEEDINGS OF THE CLOUD IMPACTS ON DOD OPERATIONS AND SYSTEMS 1993 CONFERENCE (CIDOS 1993) Interim Report
D. D. Grantham 1 Jul. 1994 510 p Conference held in Fort Belvoir, VA, 16-19 Nov. 1993
(AD-A286658; PL-TR-94-2188; ERP-1152) Avail: CASI HC A22/MF A04

The Tri-Service Cloud Modeling Program was established by OUSDR&E and is chaired by the Phillips Lab., Geophysics Directorate. As part of this program, the CIDOS conference is held at 18 month intervals. This forum was attended by over 150 researchers and DOD systems designers/users to exchange information on requirements and ongoing research for cloud effects of weapon, communication, and surveillance systems. The theme of CIDOS-93 was Clouds; The First Order Impact-For Defense and Civil Simulations. A Keynote address entitled 'Modeling and Simulation-To Fight the Future...Harness the Power of Simulation' was presented by Lt. Col. David Bartlett, Defense Modeling Simulation Office, United States Marine Corps. Three and a half days of CIDOS-93 were devoted to oral and poster presentations in six sessions: (1) Introduction and Program Reviews, (2A) Simulation Support, (2B) Analysis and Applications, (2C) Forecasting, (3) Systems and Sensors, and (4) Databases. The final session consisted of workshop meetings on two topics; Simulation Support and Cloud Microphysical Impacts Military Systems Support (e.g. Ship/Aircraft Tracks). Summaries of these are included in Part 1 of this document. DTIC

N95-21177# Boston Coll., Chestnut Hill, MA. Inst. for Space Research.
GLOBAL IONOSPHERIC WEATHER
Dwight T. Decker and Patricia H. Doherty 28 Feb. 1994 45 p
(Contract F19628-93-K-0001)
(AD-A285520; PL-TR-94-2147; SR-1) Avail: CASI HC A03/MF A01

In the last year, we have studied several issues that are critical for understanding ionospheric weather. Work on global F-region modeling has consisted of testing the Phillips Laboratory Global Theoretical Ionosphere Model. Comparisons with both data and other theoretical models have been successfully conducted and are ongoing. GPS observations, as well as data analysis, are also ongoing. Data have been collected for a study on the limitations in making absolute ionospheric measurements using GPS. Another study on ionospheric variability is the first of its kind using GPS data. The observed seasonal total electron content behavior is consistent with that determined from the Faraday rotation technique. Work on the FAA's Phase 1 Wide Area Differential GPS (WADGPS) Satellite Navigation Testbed Experiment also continues. Initial results indicate that stations using operational WADGPS should be located no greater than 430 km apart. Work comparing our electron-proton-H atom model to both observations and other models has been generally successful. We have successfully modeled the creation of high-latitude large-scale plasma structures using two separate mechanisms (time-varying global convection and meso-scale convection events). DTIC

N95-21413 Helsinki Univ. of Technology, Espoo (Finland). Radio Lab.
APPLICABILITY OF THE ECMWF RAIN HEIGHT AND RAINFALL RATE DATA TO THE PREDICTION OF LOW-AVAILABILITY RAIN ATTENUATION IN EUROPE
Seppo Karhu, Sakari Uppala (Finnish Meteorological Inst., Helsinki, Finland.), and Erkki Salonen May 1994 63 p Limited Reproducibility: More than 20% of this document may be affected by microfiche quality
(ISSN 0355-5712)
(PB95-127684; ISBN-951-22-2143-8) Avail: Issuing Activity (National Technical Information Service (NTIS))

In this report the purpose is to evaluate the different estimates of the rain height, based on the ECMWF grid data, and to compare them with the results and the models available from the literature. The Rice-Holmberg rainfall rate model and its input parameters from the ECMWF are also assessed in many ways. The objective is to decide whether the Rice-Holmberg model is sufficiently good in the estimation of the rainfall rate statistics for low rainfall rates. Since the rain heights and the Rice-Holmberg input parameters are intended for the prediction of rain attenuation at the low-availability range of annual time percentages in Europe, the ultimate test of their applicability for this purpose is presented in the companion report, where cumulative distributions of the predicted atmospheric attenuation, including attenuation due to rain, are compared with the distributions of the measured atmospheric attenuation. NTIS

N95-21527# Pennsylvania State Univ., University Park, PA.
AN INTEGRATED CLOUD OBSERVATION AND MODELING INVESTIGATION IN SUPPORT OF THE ARM PROGRAM
1994 9 p
(Contract DE-FG02-90ER-61071)
(DE95-002798; DOE/ER-61071/T1) Avail: CASI HC A02/MF A01

Work continued on the development of techniques for defining cloud properties from the 94 GHz cloud radar. Information, in the form of a submitted manuscript, has been developed about the use of radar to determine cloud boundary statistics and cloud structure with specific applications to marine boundary layer clouds, a mid-latitude cyclone, and cirrus. In addition a comparison of the aircraft and radar observations and a description of how data from the radar can be combined with other remote sensing systems is included. Mesoscale numerical modelling within the Penn State DOE-ARM research program has continued. In order to study the response of clouds to various forcing functions, development continues on a detailed numerical model of the microphysical processes known to operate in the atmosphere during the cloud and precipitation formation. DOE

N95-21586 New Mexico State Univ., Las Cruces, NM. Physicai Science Lab.
UNIFIED VERY LOW STRATUS CLOUD/SUBCLOUD MICROPHYSICS MODEL: USER'S GUIDE Final Report
Neal H. Kilmer Jul. 1994 100 p Sponsored by Army Research Lab. Limited Reproducibility: More than 20% of this document may be affected by microfiche quality
(AD-A286454; ARL-CR-96) Avail: CASI HC A05

Use of computer program MACACASM is described. MACACASM is based on the Rachele-Kilmer microphysics model for simulating very low stratus clouds and their associated subcloud regions. This model uses the assumption that the atmosphere contains particles that grow in the presence of moisture as a function of relative humidity, temperature, and the size and chemistry of the particles. Components of this model include droplet growth and evaporation, phase change and mass balance of total water, thermodynamics, and ascent of a cluster of drops enclosed in moist air. User input includes some conventional meteorological values at a reference height near ground level and some parameter values and other specifications. Vertical profiles of drop size distributions can be simulated and used for further analysis. Examples of further use of drop size distribution profiles include simulation of profiles of extinction, backscatter, absorption, and scattering coefficients. The first part of this guide is intended for the scientist-user. The second part has been prepared for the computer programmer who may be developing other programs related to this model. DTIC

N95-22288# Oak Ridge National Lab., TN. Carbon Dioxide Information Analysis Center.

CLIMATOLOGICAL DATA FOR CLOUDS OVER THE GLOBE FROM SURFACE OBSERVATIONS, 1982-1991: THE TOTAL CLOUD EDITION

C. J. Hahn (Colorado Univ., Boulder, CO.), S. G. Warren (Washington Univ., Seattle, WA.), and J. London (Colorado Univ., Boulder, CO.) Oct. 1994 46 p

(Contract DE-AC05-84OR-21400)

(DE95-002537; ORNL/CDIAC-72; NDP-026A) Avail: CASI HC A03/MF A01

Routine, surface synoptic weather reports from ships and land stations over the entire globe, for the ten-year period December 1981 through November 1991, were processed for total cloud cover and the frequencies of occurrence of clear sky, precipitation, and sky-obscured due to fog. Archived data, consisting of various annual, seasonal and monthly averages, are provided in grid boxes that are typically 2.5 deg x 2.5 deg for land and 5 deg x 5 deg for ocean. Day and nighttime averages are also given separately for each season. Several derived quantities, such as interannual variations and annual and diurnal harmonics, are provided as well. This data set incorporates an improved representation of nighttime cloudiness by utilizing only those nighttime observations for which the illuminance due to moonlight exceeds a specified threshold. This reduction in the night-detection bias increases the computed global average total cloud cover by about 2%. The impact on computed diurnal cycles is even greater, particularly over the oceans where is found, in contrast to previous surface-based climatologies, that cloudiness is often greater at night than during the day. DOE

N95-22393 Pennsylvania State Univ., University Park, PA. Dept. of Meteorology.

SAR-RELATED STRESS VARIABILITY IN THE MARINE ATMOSPHERIC BOUNDARY LAYER (MABL) Annual Report

Hampton N. Shirer and George S. Young 1994 12 p Sponsored by ONR Limited Reproducibility: More than 20% of this document may be affected by microfiche quality

(AD-A286462) Avail: CASI HC A03

By variably stressing the sea surface, secondary circulations within the marine atmospheric boundary layer (MABL) can modulate the sea surface wave field and so can produce discernible signatures on synthetic aperture radar (SAR) images of the ocean. Our most immediate goal is to determine how effective these two and three dimensional buoyantly forced MABL circulations are in producing patterns of sea-surface stress variability that can be directly linked to the quasilinear and cellular SAR signatures that were observed during the two HI-RES ARI cruises and by satellite mounted sensors. Our approach is to combine observational and modeling studies of the various secondary circulations in the MABL to determine their contributions to stress variability at the sea surface. Analysis of ship observations and model results suggest that a solenoidal circulation, dynamically akin to the classic sea-breeze circulation, causes the significant MABL wind variations observed in the vicinity of the northwest wall of the Gulf Stream. The preliminary results from the two and three dimensional models indicate that the stress variability patterns at the sea surface are reasonable. CASI

48 OCEANOGRAPHY

Includes biological, dynamic, and physical oceanography; and marine resources.

For related information see also *43 Earth Resources and Remote Sensing.*

N95-19888 Naval Research Lab., Bay Saint Louis, MS.

TESTS OF AN IMPROVED OCEANOGRAPHIC EXPERT SYSTEM Final Report

Matthew Lybanon 4 May 1994 10 p Limited Reproducibility: More than 20% of this document may be affected by microfiche quality

(AD-A280123; NRL/MR/7240-94-7517) Avail: Issuing Activity (Defense Technical Information Center (DTIC))

For 8 years the Naval Research Laboratory's Remote Sensing Applications Branch has been developing an oceanographic expert system (OES) that models some aspects of the kinematics of the Gulf Stream and its associated eddies. The OES uses a rule base to provide ring-motion forecasts and a neural network to forecast Gulf Stream motion. Previous work showed that OES forecasts of ring motion are at least as good as those produced by other methods. Recent work led to improvements in the ring-motion geometry equations, replacement of the Gulf Stream motion logic, and the addition of a natural-language explanation facility. The first two changes required 'retuning' of the OES. The changes were designed to remove linear trends in the mean forecast position errors for noninteracting (with the Gulf Stream) rings. This report presents a comparison of the present system's performance with 'prototype' and improved parameters. For noninteracting rings, the improved system provides ring-motion forecasts that are superior to a no-motion assumption 75% or more of the time for both warm-core rings and cold-core rings, for both 7-day and 14-day forecasts. The forecast ring positions are within 20 km of the true positions. This report provides more complete information on the OES and the test results. DTIC

N95-19895# Coastal Engineering Research Center, Vicksburg, MS.

THE SURFACE WAVE DYNAMICS EXPERIMENT (SWADE): A RETROSPECTIVE LOOK AT THE WAVE MODELING ACTIVITIES

R. E. Jensen Sep. 1994 12 p

(AD-A285612; CERC-94-3) Avail: CASI HC A03/MF A01

Approximately four years ago a group of internationally known researchers in meteorology, air-sea interactions, and wave theory met for the last of many preliminary meetings finalizing their respective tasks for the Surface Wave Dynamics Experiment (SWADE) to commence in October 1990 off the DelMarVa peninsula. Not since the Joint North Sea Wave Project had there been a concentrated measurement program investigating the evolution of wave spectra in deep water. This experiment was timely because new and improved in situ measurement methods and advancement of remote sensing devices had come of age in the estimation of high-resolution directional spectra, providing the basis to support a new generation of spectral wave models under development. Derived from text

N95-19896# Naval Command, Control and Ocean Surveillance Center, San Diego, CA. Research, Development, Technology and Evaluation Div.

RADIANCE OF THE OCEAN HORIZON Final Report

C. R. Zeisse Apr. 1994 103 p

(AD-A285613; NRAD-TR-1660) Avail: CASI HC A06/MF A02

Cox and Munk proposed that the fluctuating surface of the open ocean could be accurately represented by many small mirror-like facets, each of which is randomly tilted with respect to the local horizon. Through aerial photographs of sun glint, they determined the statistical distribution of capillary wave slopes as a function of wind velocity. However, when their equation connecting the slope distribution with sun glint is used on the horizon, an infinite glint is predicted even though it can easily be shown that sun glint should never exceed solar radiance. The objective of this report is to remove the infinite horizon radiance from the Cox-Munk model of the ocean surface. DTIC

N95-19918 Naval Postgraduate School, Monterey, CA. Dept. of Oceanography.

HYDROGRAPHIC DATA FROM EQUATORIAL PACIFIC WATERS NEAR THE GALAPAGOS

Brian H. Miller, Vernon N. Anderson, and Curtis A. Collins Aug. 1994 57 p Limited Reproducibility: More than 20% of this document may be affected by microfiche quality

(AD-A283741; NPS-OC-94-002) Avail: Issuing Activity (Defense Technical Information Center (DTIC))

This data report presents hydrographic (CTD) data from a cruise in an area extending to approximately three hundred kilometers from the Galapagos Islands. A total of 30 CTD casts were made. The report includes remarks concerning data processing and analysis. DTIC

N95-19971 Naval Postgraduate School, Monterey, CA.

A MODAL ANALYSIS OF CURRENTS IN A PACIFIC ATOLL LAGOON M.S. Thesis

Burton T. Palmer Jun. 1994 178 p Limited Reproducibility: More than 20% of this document may be affected by microfiche quality

(AD-A283721) Avail: Issuing Activity (Defense Technical Information Center (DTIC))

The results of an initial quantitative study to define the physical oceanography of Johnston Atoll's lagoon circulation is presented. A bathymetric data base of the Island has been manually digitized from Navigational charts. A numerical model designed to predict the seiche modes of basins in two and three dimensions, in elliptic and Cartesian coordinates is developed, which seems to represent accurately the free modes of oscillation observed in current meter records. The numerical model is suitable for applications using a personal computer equipped with MATLAB (4.0) or later, and has applicability to basins of arbitrary shape in two dimensions, and rectangular, elliptical or circular symmetry in three dimensions. An analysis of currents within the lagoon at Johnston Atoll shows highly polarized tidal flow, phase locked to the diurnal tide. Spectral energy content of current meter records show six fundamental oscillatory modes and harmonics of tidal components. DTIC

N95-19988# Scripps Institution of Oceanography, La Jolla, CA.

OCEANOGRAPHIC ANALYSIS OF THE ACOUSTIC MID-OCEAN DYNAMICS EXPERIMENT Final Report, 1 Nov. 1992 - 30 Jun. 1994

Peter Worcester, Bruce Cornuelle, and David Chester 30 Sep. 1994 6 p
(Contract N00014-93-1-0461)
(AD-A285907) Avail: CASI HC A02/MF A01

Reciprocal acoustic transmissions made in the Northwest Atlantic have been analyzed to determine the general circulation of the region between Bermuda and Puerto Rico. Six tomographic transceivers were moored from March 1991 to March 1992 in the region centered at 25 deg N, 66 deg W during Acoustic Mid-Ocean Dynamics Experiment (AMODE). The goals of the research performed under this contract have been: (1) to study large-scale (300 to 1000 km) circulation and variability in temperature, current, and relative vorticity fields; (2) to study mesoscale eddy kinematics and dynamics; and (3) to study the value of integral constraints on eddy-resolving numerical ocean models. Large-scale range averages (over 300 to 700 km sections) of temperature and velocity and large-scale areal averages (over regions comprising 100,000 sq km of relative vorticity in the upper 3500 m of the water column have been estimated through inversion of the tomographic travel time data. DTIC

N95-20012 Naval Research Lab., Bay Saint Louis, MS.

ATLAS OF SSM/I SATELLITE ICE CONCENTRATION INTERPOLATED TO OPERATIONAL ICE MODEL DOMAINS OF THE ARCTIC FOR 1993 Final Report

G. N. Lundeen, R. H. Preller, P. G. Posey, and A. Cheng 5 May 1994 355 p Limited Reproducibility: More than 20% of this document may be affected by microfiche quality
(NR Proj. X20-08)
(AD-A280183; NRL/MR/7322-94-7524) Avail: Issuing Activity (Defense Technical Information Center (DTIC))

The Navy's Polar Ice Prediction System, which is run daily at the Fleet Numerical Meteorology and Oceanography Center (FNMOC), is initialized once each week from ice concentration data derived by the Navy/National Oceanic and Atmospheric Administration National Ice Center (formerly the Joint Ice Center). Ice concentration data, derived by applying the U.S. Navy's algorithm to the Defense Meteorological Satellite Program Special Sensor Microwave Imager (SSM/I) data, have been collected from FNMOC on a daily basis and archived at the Naval Research Laboratory. These data were then interpolated to the operational ice model grids for possible use as a real-time daily update to the operational forecast systems. Collection of data with coverage from the Pole southward to 20 deg N allows for the observation of ice concentrations for the entire Arctic region and surrounding coastal seas. SSM/I ice concentration data from 1993 are presented for each available day and on each of the operational model grids. DTIC

N95-20040# Hawaii Univ., Honolulu, HI. School of Ocean and Earth Sciences and Technology.

ANALYSIS OF LOW FREQUENCY OCEAN NOISE. 1: FROM A LONG-TERM EXPERIMENT ACROSS THE US EAST COAST. 2: FROM THE WAKE ISLAND HYDROPHONE ARRAY DURING NORTHWEST PACIFIC TYPHOONS

Charles S. McCreery, Frederick K. Duennebier, and Daniel A. Walker 22 Jul. 1994 149 p
(Contract N00014-90-J-1683)
(AD-A284975) Avail: CASI HC A07/MF A02

The East Coast experiment, called the Environmentally Controlled Ocean floor NOise Monitoring Experiment (ECONOMEX), was designed to sample ambient noise in the water column and on the ocean floor across the continental shelf and slope east of Chesapeake Bar. A vertical array of hydrophones in the water column, a horizontal array of hydrophones, and three-component seismometers were deployed for several months in the spring of 1991. The experiment was designed to coincide with the Surface WAve Dynamics Experiment (SWADE) in order to take advantage of their extensive measurements of surface winds and directional ocean wave spectra in the same region. This comprehensive and long-term data set permits the identification of specific noise generation and propagation mechanisms for the continental shelf and slope, and evaluation of their contribution to the noise field under a wide variety of ocean surface conditions. The primary goal of studying data from the Wake Island Hydrophone Array is to quantify changes in the noise field due to the extreme ocean surface conditions produced by typhoons, and to identify mechanisms by which these storms produce noise. DTIC

N95-20209 Mississippi State Univ., Bay Saint Louis, MS. Center for Air Sea Technology.

MISSISSIPPI STATE UNIVERSITY CENTER FOR AIR SEA TECHNOLOGY FY 1993 AND FY 1994 RESEARCH PROGRAM IN NAVY OCEAN MODELING AND PREDICTION Final Technical Report

Lanny A. Yeske and James H. Corbin 30 Sep. 1994 73 p Limited Reproducibility: More than 20% of this document may be affected by microfiche quality
(Contract N00014-92-J-4109)
(AD-A286322; CAST-TR-94-3) Avail: CASI HC A04

The Mississippi State University Center for Air Sea Technology (CAST) began operation on 1 Oct. 1992 under a two-year research grant (N00014-92-J-4109) issued by the Office of Navy Research. This final technical report is submitted in accordance with requirements contained in the grant. Included is a discussion of the FY93 (1 Oct. 1992 - 30 Sep. 1993) research program under the Experimental Center for Mesoscale Ocean Prediction Project with its tasks of ocean model initialization and evaluation data; ocean model verification, evaluation, and transition; and scientific visualization for model evaluation. This is followed by the FY94 (1 Oct. 1993 - 30 Sept. 1994) program which was reorganized into the Coastal and Semi-Enclosed Seas Relocatable Models Project (6.1), the Ocean Model Technology Project (6.2), and the Advanced Development and Transitions Project (6.3). Also included is a discussion of the planned research for FY95 and FY96. This is followed by Appendix 1 which summarizes eight other contracts obtained by CAST with the Naval Research Laboratory, Naval Oceanographic Office, Army Corps of Engineers Coastal Engineering Research Center, Gulf Weather Corporation, Department of Defense, and Office of Naval Research. Finally, Appendix 2 summarizes CAST publications completed during this two year period as well as other CAST accomplishments. DTIC

N95-20303 Massachusetts Inst. of Tech., Cambridge, MA.

AMBIENT NOISE AND SURFACE WAVE DISSIPATION IN THE OCEAN Ph.D. Thesis

Francis C. Felizardo Jun. 1993 221 p Limited Reproducibility: More than 20% of this document may be affected by microfiche quality
(AD-A279650) Avail: Issuing Activity (Defense Technical Information Center (DTIC))

There is a growing consensus that the sound generated by breaking waves is responsible for much of the ambient noise level in the ocean. While numerous field measurements have shown a strong correlation between the ambient noise spectrum level (N) in the range 100 Hz to 25 kHz and wind speed in the ocean, very little has been done to establish a comparable correlation between the ambient noise spectrum level and surface wave field parameters. The difficulty in establishing this relationship is remarkable given that the frequency and intensity of wave breaking are dependent on the characteristics of the wave field. In Fall 1991, an experiment was conducted from the research platform Flip 130 kilometers off the coast of Oregon, where the ambient noise between 2.5 and 25 kHz, the wind speed, and the sea surface elevation using wire wave gauges were measured. The correlation between N and the root mean square wave amplitude (a) was found to be poor but could be improved if the swell was filtered out from the wave elevation time series. The influence of swell on the value of a was disproportionate to the level of ambient noise since its characteristics were not directly due to the local wind-wave conditions. Observations of the dependence of the high frequency wind waves and the directional wave spectrum under turning winds suggested that the high frequency wave components responded more quickly to changes in the wind speed and direction than the energy-containing frequencies. DTIC

N95-20420# Lawrence Livermore National Lab., Livermore, CA.
MODEL-BASED INVERSION FOR A SHALLOW OCEAN APPLICATION
J. V. Candy and E. J. Sullivan (Naval Undersea Warfare Center, Newport, RI.) Mar. 1994 11 p Presented at the Inversion Methods in Ocean and Seismic Acoustics Conference, La Spezia, Italy, 27 Jun. 1994
(Contract W-7405-eng-48)
(DE94-016968; UCRL-JC-115131; CONF-9406241-1) Avail: CASI HC A03/MF A01

A model-based approach to invert or estimate the sound speed profile (SSP) from noisy pressure-field measurements is discussed. The resulting model-based processor (MBP) is based on the state space representation of the normal mode propagation model. Using data obtained from the well known Hudson Canyon experiment, a noisy shallow water ocean environment, the processor is designed and the results compared to those predicted using various propagation models and data. It is shown that the MBP not only predicts the sound speed quite well, but also is able to simultaneously provide enhanced estimates of both modal and pressure-field measurements which are useful for localization and rapid ocean environmental characterization. DOE

N95-20433 Woods Hole Oceanographic Inst., MA.
DATA REPORT: STRESS MEASUREMENTS IN THE BOTTOM BOUNDARY LAYER WITH BASS TRIPODS STRESS 2 1990-1991
Thomas F. Gross, Julie Amft, and Albert J. Williams, III Nov. 1993 44 p Limited Reproducibility: More than 20% of this document may be affected by microfiche quality
(Contracts N00014-89-J-1058; N00014-90-J-1046)
(AD-A279875; WHOI-93-48) Avail: CASI HC A03

Two Benthic Acoustic Stress Sensor (BASS) equipped tripods were deployed in the Sediment TRansport Events on Shelves and Slopes (STRESS) experiment on the California Shelf acquiring data from January to March 1991. They measured velocity profiles in the bottom boundary layer over the lowest 5 meters. Transmissometers, thermistors, and a pressure sensor on each tripod provided suspended sediment concentration, stratification, and wave spectral information, as well. DTIC

N95-20458 Woods Hole Oceanographic Inst., MA. Dept. of Physical Oceanography.
SYNTHESIZING THE GULF STREAM THERMAL STRUCTURE FROM XBT DATA
Melinda M. Hall 14 Feb. 1994 32 p Limited Reproducibility: More than 20% of this document may be affected by microfiche quality
(Contracts N00014-87-K-0001; N00014-88-K-0612; N00014-89-J-1056; NR Proj. 083-004)
(AD-A279665; WHOI-Contrib-8394) Avail: Issuing Activity (Defense Technical Information Center (DTIC))

Thirty-six XBT temperature profiles have been used in a parametric model introduced by Hendry to model the Gulf Stream's thermal structure at 65 deg W between 200 and 1200 dbar, with an rms residual error of 0.56 C. Velocity has been computed geostrophically relative to 1200 dbar, and has been included in calculating potential vorticity analytically from the model. The resulting potential vorticity section for 65 deg W has been compared with the analogous result from Hendry's parametric model at 59 deg W, as well as observed potential vorticity sections from 68 deg to 55 deg W. There is a significant feature in the potential vorticity structure at 65 deg W not found at 59 deg W, namely a relative minimum in potential vorticity along isopycnals, centered at the Gulf Stream's axis and 350 dbar. The modelled potential vorticity sections are consistent with the observations, including the downstream disappearance of this feature. The dynamical implications of these results are briefly discussed. DTIC

N95-20999# Texas Univ., Austin, TX. Applied Research Lab.
MULTIPLE SCATTER THEORY OF OCEAN SEDIMENTS Technical Letter, 1 Feb. - 31 Jul. 1994
Nicholas P. Chotiros 25 Apr. 1994 7 p
(Contract N00014-94-1-0438)
(AD-A286033; TL-AS-94-07) Avail: CASI HC A02/MF A01

The long term goal was to develop a new model of acoustic bottom backscatter from sandy sediments, based on a multiple scattering theory approach, and, hence, properly explain observed phenomena, including Lambert's rule and frequency dependence of backscattering strength, particularly at shallow grazing angles, for which current theories are at a loss. DTIC

N95-21018 Naval Research Lab., Bay Saint Louis, MS.
MONTHLY MEAN SEA ICE DATA FROM THE POLAR ICE PREDICTION SYSTEM, THE REGIONAL POLAR ICE PREDICTION SYSTEM-BARENTS SEA AND THE REGIONAL POLAR ICE PREDICTION SYSTEM-GREENLAND SEA Final Report
P. G. Posey and R. H. Preller 6 May 1994 83 p Limited Reproducibility: More than 20% of this document may be affected by microfiche quality
(NR Proj. X05-13)
(AD-A280095; NRL/MR/7322-94-7525) Avail: Issuing Activity (Defense Technical Information Center (DTIC))

The Polar Ice Prediction System (PIPS), the Regional Polar Ice Prediction System - Barents (RPIPS-B) and the Regional Polar Ice Prediction System - Greenland Sea (RPIPS-G) are all operational sea ice forecasting systems that have been run daily at the Fleet Numerical Meteorology and Oceanography Center (FNMOC) since September 1987, June 1989, and October 1991, respectively. The basis for all three models is the Hibler ice model. A Dynamic Thermodynamic Sea Ice Model. Journal of Physical Oceanography 9. Modeling a Variable Thickness Sea Ice Cover. Monthly Weather Review 108. The ice models are driven by monthly mean ocean currents and deep ocean heat fluxes derived from the Hibler and Bryan A Diagnostic Ice-Ocean Model. Journal Physical Oceanography 17 coupled ice-ocean model. They are also driven by atmospheric forcing from the Navy Operational Global Atmospheric Prediction System (NOGAPS). In Fifth Conference on Numerical Weather Prediction, American Meteorological Society, Boston, Massachusetts, preprint volume, 74-79. The Description of the Navy Operational Global Atmospheric Prediction System's Forecast Model. Naval Research Laboratory, Monterey, California, NOARL Report 13. Each day a 24-h forecast of PIPS, RPIPS-B, and RPIPS-G is submitted and archived by the Naval Research Laboratory. DTIC

N95-21158# University of Southern Mississippi, Bay Saint Louis, MS. Center for Ocean and Atmospheric Modeling.
MODELING OPEN BOUNDARY CONDITIONS BY USING THE OPTIMIZATION APPROACH
James K. Lewis and Igor Shulman Oct. 1994 19 p
(Contract N00014-92-J-4112)
(AD-A285548; COAM-TR-1/95) Avail: CASI HC A03/MF A01

An optimization approach to prescribe open boundary conditions (OBC's) is proposed. Open boundary conditions are chosen by providing the best fit to available observations on the open boundary and to the energy flux through the open boundary. It is shown that many local open boundary conditions widely used in the oceanographic community are special cases of the derived optimized OBC's. Numerically, the proposed methods consist of the integration of the governing equations and solving the optimization problem only on the open boundary for each time step. Results of tidal simulations for a channel and the Louisiana-Texas shelf are presented and discussed. Schemes for coupling limited area coastal models with basin scale coarse models by using optimized OBC's are proposed. Preliminary simulations of coupling a fine resolution model of the Mediterranean Sea are presented and discussed. The use of optimized OBC's is shown to be better in predicting tidal amplitudes and phases compared to the use of local OBC's. DTIC

N95-21291 Dedicated Electronics, Inc., Chester, NH.
DEVELOPMENT OF A PORTABLE ICE-THICKNESS MEASURING INSTRUMENT Final Report, 7 Aug. 1992 - 15 Feb. 1994
John C. Joseph, Dennis P. Glenn, and Philip J. Joseph 14 Mar. 1994 19 p Limited Reproducibility: More than 20% of this document may be affected by microfiche quality
(Contract DACA33-91-C-0030)
(AD-A279472) Avail: Issuing Activity (Defense Technical Information Center (DTIC))

A portable instrument that can be manually placed in contact with the surface of an ice-covered body of water to non-obtrusively measure the ice thickness was developed. The instrument design is based on determining ice thickness from microwave frequency signals which are transmitted through the ice and reflect from the ice/water interface. Prior methods include drilling through the ice to manually measure its thickness and using radar equipment which is costly, time consuming, and which produces data often difficult to interpret. The ice measuring instrument produced under this contract meets its goals for performance and physical characteristics. Measurement range exceeds the required 2 to 24 inches with 1/2 inch accuracy. Ice measurements take 12 seconds on average, thickness processing takes 10 seconds, and calibration is performed in under 30 seconds. The instrument is fully portable; it is powered by an internal, rechargeable battery. The instrument is built into a transit case, which also houses accessories. DTIC

N95-21293 Stanford Univ., CA. Environmental Fluid Mechanics Lab.
THE STRUCTURE OF TURBULENCE AND OTHER MOTIONS BENEATH AN AIR-WATER INTERFACE Final Technical Report, 1 Nov. 1990 - 31 Jan. 1994
Robert L. Street and Stephen G. Monismith 1 Feb. 1994 13 p Limited Reproducibility: More than 20% of this document may be affected by microfiche quality
(Contract N00014-91-J-1200)
(AD-A279838; SU-EFML-94-1) Avail: Issuing Activity (Defense Technical Information Center (DTIC))

This is the final technical report for Grant N00014-91-J-1200, entitled 'The Structure of Turbulence and Other Motions Beneath an Air-Water-Interface.' The grant period was from 1 November 1990 through 31 January 1994. This research couples definitive physical experiments and numerical simulation experiments to study three-dimensional, unsteady, real-fluid flows beneath the air-water interface. The overall goals for the long term are to develop a complete understanding of the flow physics and a numerical simulation tool that allows accurate prediction of the motion from a specified set of initial and boundary conditions. This report covers the early period of the long term project. The numerical tool developed is for the simulation of free-surface flows through the solution of the time-dependent, incompressible, Navier-Stokes equations with non-linear dynamic and kinematic boundary conditions. It is being developed in three dimensions; the two-dimensional version is operational. The physical experiments have focused on developing-accurate maps of the flow fields under the waves with and without a surface piercing body. DTIC

N95-21306 Woods Hole Oceanographic Inst., MA.
MIXING AND DYNAMICS OF THE MEDITERRANEAN OUTFLOW Ph.D. Thesis
Molly O. Baringer Feb. 1994 244 p Limited Reproducibility: More than 20% of this document may be affected by microfiche quality
(Contract N00014-90-J-1474)
(AD-A279803; WHOI-93-52) Avail: Issuing Activity (Defense Technical Information Center (DTIC))

Hydrographic and expendable current profiler (XCP) data taken during the Gulf of Cadiz Expedition in September 1988 are analyzed here to understand the mixing and dynamics of the Mediterranean outflow from the Strait of Gibraltar. Rapid entrainment of fresh North Atlantic water prevents the flow from reaching abyssal depths in the North Atlantic despite its large initial density anomaly. Dynamical ideas about mixing and stress are tested by examining the evolution of momentum and density as the flow adjusts. The flow is found to be unstable to Kelvin-Helmholtz instability in regions where intense mixing occurs. Evaluation of the cross-stream momentum balance shows the importance of advection as the flow makes a 90 degree inertial turn after exiting the Strait. The downstream momentum residuals indicate that large stresses disrupt this rapidly achieved geostrophic balance and enable the flow to cross isobaths. The intense mixing observed suggests rates of entrainment three orders of magnitude larger than typical rates of Ekman pumping in the open North Atlantic. A simple numerical model is used to test these dynamical concepts. The model predicts the evolution of the bulk properties of the Mediterranean outflow using a Froude number dependent entrainment. DTIC

N95-21320# National Defence Research Establishment, Linkoeping (Sweden). Dept. of Information Technology.
SIMULATION OF LASER BATHYMETRY FOR IRREGULAR BOTTOMS
Ove Steinvall, Kurt Koppari, and Ulf Karlsson Apr. 1994 41 p See also PB94-123668
(ISSN 0347-3708)
(PB95-133518; FOA-C-30752-3.1) Avail: CASI HC A03/MF A01

This report deals with simulation of bottom echoes from a depth sounding laser system. The aim is to investigate how detected depths are affected by irregularities in the form of bottom slope, stone on the bottom or a steplike bottom feature. NTIS

N95-21461 Washington Univ., Seattle, WA. Applied Physics Lab.
RESOLVING VELOCITY PROFILES WITH THE MULTI-SCALE PROFILER
D. P. Winkel, M. C. Gregg, B. M. Bell, and T. B. Sanford Oct. 1994 82 p Limited Reproducibility: More than 20% of this document may be affected by microfiche quality
(Contracts N00014-90-J-1188; N00014-90-J-1108; N00014-94-I-0079; N00014-86-K-0690)
(AD-A286446; APL-UW-TR-9414) Avail: CASI HC A05

The multiscale profiler (MSP), a freely falling dropsonde, has been used over the last 12 years to resolve oceanic shear variance at vertical scales from a few hundred meters down to nearly a centimeter. Because MSP yielded the first complete oceanic shear spectra, it is important to document the methods by which they were produced. Large scales are measured by an electromagnetic current meter (ECM), microscales by airfoil probes, and intermediate scales by an acoustic current meter (ACM). The ACM detects velocity relative to the instrument, so the platform motion must be known to determine the water velocity. Primarily, the ACM measurements are affected by tilt oscillations and by the gross (point-mass) motion of the vehicle; the former is inferred from accelerometer data, and the latter is constructed from a model of the vehicle's response to oceanic shear. Horizontal forcing on the array of drag brushes and turning blades at the tail complicates the response by causing MSP to react strongly to fluctuations with scales near the instrument's length of 4.3 m. We examine the effects of this response on spectra of the ACM measurements, noting particularly a deep notch near 0.2 cpm (cycles per meter). To account for such spectral features, the model of Hayes et al. for the TOPS dropsonde was modified so that it correctly parameterized our large tail force. We discuss the dynamics, data processing, and model formulation relevant to production of oceanic velocity profiles from the ACM data, and present analytic transfer functions, derived from Fourier transforms of the model equations, which guide selection of optimal values for the model parameters. DTIC

N95-21657 Materials Research Labs., Ascot Vale (Australia).
UNDERWATER ACOUSTIC GENERATOR PHASE 2: SEA TRIAL, MARCH 1992
R. Alksne Aug. 1993 29 p
(MRL-TN-640; AR-008-268) Copyright Avail: Issuing Activity (DSTO Materials Research Lab., PO Box 50, Ascot Vale, Victoria 3032, Australia)

In support of a joint ALO-SA, DSTO, and industry program to develop a discrete low frequency towed underwater acoustic generator (UAG), a series of sea trials were conducted. These trials were conducted in the Gulf of St. Vincent and the sea west of Kangaroo Island to check the environmental and acoustic performance of a concept UAG. This report describes the UAG Phase 2 evaluation trial held in March 1992. Details and results of the trial are provided along with an assessment of the UAG performance and conclusions and recommendations for further development and tests. Author

N95-21677 Woods Hole Oceanographic Inst., MA.
A SIMPLE OCEAN BOTTOM HYDROPHONE WITH 200 MEGABYTE DATA CAPACITY
K. R. Peal, G. M. Purdy, D. E. Koelsch, and F. B. Wooding Jun. 1993 43 p Limited Reproducibility: More than 20% of this document may be affected by microfiche quality
(Grants NSF OCE-89-17628; NSF OCE-90-19918)
(AD-A279478; WHOI-93-31) Avail: Issuing Activity (Defense Technical Information Center (DTIC))

The Woods Hole Ocean Bottom Hydrophone instrument records the digitized output of a single hydrophone sensor at rates between 250 and 1200 samples per second with a dynamic range of 98 dB and can be deployed at depths to 6000 meters. The unit's 200 megabyte disk recorder allows operation for periods up to 5 days. Designed for typical marine seismic refraction operational the unit is reliable and simple to deploy and recover. A detailed description is provided of the instrument design and application including transfer function, clock accuracy, data format, sample data and power requirements. DTIC

N95-21681 Woods Hole Oceanographic Inst., MA.
CTD CALIBRATION AND PROCESSING METHODS USED AT WOODS HOLE OCEANOGRAPHIC INSTITUTION
Robert C. Millard and Keqi Yang Oct. 1993 87 p Limited Reproducibility: More than 20% of this document may be affected by microfiche quality
(Grant NSF OCE-91-14465)
(AD-A279507; WHOI-93-44) Avail: Issuing Activity (Defense Technical Information Center (DTIC))

Processing methods, programs, and procedures currently used to create CTD data sets at Woods Hole Oceanographic Institution (WHOI) are described. The post-acquisition data processing steps include instrument calibrations in the laboratory and data calibration at sea, CTD data transformation from a time series to a pressure series, and the water sample data processing using the World Ocean Circulation Experiment (WOCE) format guidelines. Processing software has been developed for both the MicroVAX and IBM compatible personal computers. The description of the data processing procedures is restricted to the PC system. The programs are written primarily in FORTRAN with some format-related changes required between computer systems. DTIC

N95-21682 Woods Hole Oceanographic Inst., MA.
LONG TIME SERIES MEASUREMENTS IN THE COASTAL OCEAN: A WORKSHOP
C. L. Vincent (Coastal Engineering Research Center, Vicksburg, MS.), T. C. Royer (Alaska Univ., Fairbanks, AK.), and K. H. Brink Nov. 1993 104 p Workshop held in Washington, DC, 11-12 Mar. 1993 Limited Reproducibility: More than 20% of this document may be affected by microfiche quality
(Grant NSF OCE-92-24824)
(AD-A279509; WHOI-93-49) Avail: Issuing Activity (Defense Technical Information Center (DTIC))

Existing long time series efforts can be readily augmented by addition of existing sensors, enhancing scope and impact. Significant benefits would result from multidisciplinary measurements to document long-term trends in physical as well as other variables. Standard observations as well as a diversity of approaches and measurements should comprise the suite of long-term measurements. Sites for long-term observations should be selected to define processes, represent major and diverse oceanographic systems, and to document pristine as well as stressed systems. The initial rationale for sites and observed properties must be clearly defined to avoid monitoring for monitoring's sake. In the long term, three-dimensional zones ('corridors') of long time series measurements might be created. Long time series measurements should be supplemented with process and modeling studies to ensure appropriate rationale and to provide a regional understanding for the site-specific observations. The Coastal Ocean Processes Program (CoOP) might provide some of these studies. DTIC

N95-21717 Nederlands Inst. voor Onderzoek der Zee, Texel (Netherlands).
LONG TERM CHANGES ON THE CONTINENTAL SHELF OF THE NORTH SEA: INVERTEBRATE TRENDS, 1931-1990 [LANGE TERMIJN VERANDERINGEN OP HET NEDERLANDS CONTINENTAAL PLAT VAN DE NOORDZEE: TRENDS IN EVERTEBRATEN VAN, 1931-1990]
C. G. N. deVooys, J. I. J. Witte, R. Dapper, J. vanderMeer, and H. W. vanderVeer 1993 74 p In DUTCH Prepared in cooperation with Rijkswaterstaat, Rijswijk (Netherlands). North Sea Directorate
(PB95-135224; NIOZ-1993-17) Copyright Avail: Issuing Activity (National Technical Information Service (NTIS))

Alterations in the functioning in the ecosystem of the North Sea can be made visible from long series of observations. At the Netherlands Institute for Sea Research a registration for (epi)benthic invertebrates from 1930 till 1992 exists caught between 52 and 55 degrees North and 3 and 7 degrees East. In this report, data of 15 species of invertebrates were analyzed: the whelk (Buccinum undatum), red whelk (Neptunea antiqua), slender spindle shell (Colus gracillis), common cuttlefish (Sepia officinalis), common European squid (Loligo vulgaris), lesser octopus (Eledone cirrosa), European lobster (Homarus gammarus), Norway lobster (Nephrops norvegicus), edible crab (Cancer pagurus), velvet swimming crab (Macropipes puber), masked crab (Corystes cassivelaunus), green sea urchin (Psammechinus miliaris), purple heart urchin (Spatangus purpureus), dahlia anemone (Tealia felina) and the sea mouse (Aphrodite aculeata). From these data maps for each species were prepared for periods of 10 years between 1930 and 1990, and the pattern in occurrence over the period 1930-1990. Besides, an ecological description is given for each species. First the results are interpreted in connection with the life cycle of the species. Next the patterns are compared with those found earlier for a number of non-commercial fish species. The largest alterations in the North Sea since 1930 relevant to the occurrence of invertebrate species are changes in fishery, pollution and climate. NTIS

N95-21880 Naval Postgraduate School, Monterey, CA. Dept. of Electrical and Computer Engineering.
A NUMERICAL STUDY OF WIND FORCING EFFECTS ON THE CALIFORNIA CURRENT SYSTEM M.S. Thesis
James R. Vann Sep. 1994 230 p Limited Reproducibility: More than 20% of this document may be affected by microfiche quality
(AD-A286205; NPS-OC-94-006) Avail: CASI HC A11

A high-resolution multilevel, primitive equation ocean model is used to examine the response of an idealized, flat-bottom, eastern boundary oceanic regime on a beta-plane to climatological average (1980-1989), individual year, and multiple year wind forcing. The focus of this study is the California Current System along the coastal region, from 35 deg N to 47.5 deg N, off the West Coast of North America. Two types of experiments are conducted. The first type forces the model from rest with climatological, 1981, and 1983 monthly winds to examine the generation phase of features such as currents, upwelling, meanders, eddies, and filaments. The second type continues the forcing from the previous years to examine the maintenance of these features. In the first type of experiments, the following features are observed: a poleward coastal surface current near the start and end of each year, and equatorward surface current, a poleward undercurrent, upwelling, meanders, and eddies. In the second type of experiments, meanders and eddies were already present at the start of the experiment. In addition to the features observed during the first type of experiment, filaments are generated. The results support the hypothesis that wind forcing is an important mechanism for the generation of many of the observed features in the California Current System. DTIC

N95-21918 Woods Hole Oceanographic Inst., MA. Dept. of Applied Ocean Physics and Engineering.
THE ISOTOPE GEOCHEMISTRY OF ABYSSAL PERIDOTITES AND RELATED ROCKS Ph.D. Thesis - MIT
Jonathan E. Snow Jun. 1993 353 p Sponsored by NSF and the Ocean Ventures Fund Limited Reproducibility: More than 20% of this document may be affected by microfiche quality
(AD-A279435; WHOI-93-36) Avail: Issuing Activity (Defense Technical Information Center (DTIC))

The mantle origin of abyssal peridotites and their alteration by hydrothermal solutions and seawater have been the object of intensive study in the scientific community in recent years. Abyssal peridotites from the American-Antarctic and southwest Indian ridges were studied using major elements, trace elements and the isotopic compositions of Nd, Sr and Os. These studies reveal the nature of the mantle these abyssal peridotites were once a part of, and the nature of alteration processes the peridotites have undergone during and after their emplacement on the sea floor. The major conclusions of this dissertation are as follows: Abyssal peridotites have lost significant Mg during their weathering on the seafloor. Abyssal peridotites are altered at low temperatures and high water/rock ratios during this process. The water/rock ratios during alteration are high enough to compromise the Sr, Nd and Os isotopic systems in bulk peridotite. 'Orphan' 87Sr detected in alteration products is due to the mechanical entrainment of sediment particles into the peridotite. Mantle Os and Nd isotopic compositions detected do not conform to current models for the formation of the depleted mantle. DTIC

N95-21943 Woods Hole Oceanographic Inst., MA.
THE DYNAMIC ROLE OF RIDGES IN A BETA-PLANE CHANNEL. TOWARDS UNDERSTANDING THE DYNAMICS OF LARGE SCALE CIRCULATION IN THE SOUTHERN OCEAN Ph.D. Thesis - MIT

Liping Wang Sep. 1993 255 p Limited Reproducibility: More than 20% of this document may be affected by microfiche quality
(Grant NSF OCE-90-17158)
(AD-A279390; WHOI-93-38) Avail: Issuing Activity (Defense Technical Information Center (DTIC))

In this thesis, the dynamic role of bottom topography in a Beta-plane channel is systematically studied in both linear homogeneous and stratified layer models in the presence of either wind stress or buoyancy forcing. In these studies, the structure of the geostrophic contour plays a fundamental role, and the role of bottom topography is looked at from two different angles. It is shown that blocking all the geostrophic contours leads to two different physical processes in which bottom topographic form drag is generated and enables geostrophic flow in a Beta- plane channel to support a net cross-channel volume transport. It is demonstrated that by blocking all the geostrophic contours in the presence of a sufficiently high ridge, the dynamics of both source-sink and wind driven circulations in a Beta-plane is similar to that in a closed basin. DTIC

N95-21987 Washington Univ., Seattle, WA. Applied Physics Lab.
ACOUSTIC THERMOMETRY OF OCEAN CLIMATE (ATOC): SELECTION OF CALIFORNIA SOURCE SITE
Bruce M. Howe Nov. 1993 27 p Limited Reproducibility: More than 20% of this document may be affected by microfiche quality
(Contract MDA972-93-1-0003)
(AD-A279295; APL-UW-TM30-93) Avail: Issuing Activity (Defense Technical Information Center (DTIC))

This report discusses the general criteria for choosing a site for ATOC (Acoustic Thermometry of Ocean Climate) cabled sources. In particular, the process of selecting the California site is reviewed. Two possible locations are considered: Pioneer Seamount and Sur Ridge. The Sur Ridge site has been selected because a requisite marine mammal research program can be conducted there for less cost. DTIC

N95-22028# Naval Research Lab., Bay Saint Louis, MS.
RAPID DETERMINATION OF GEOACOUSTIC PROPERTIES OF THE SEA FLOOR BY SIMULATED ANNEALING Final Report
Dennis Lindwall 9 Sep. 1994 13 p
(AD-A286297; NRL/MR/7432-94-7548) Avail: CASI HC A03/MF A01

The Naval Research Laboratory (NRL) developed and tested a simulated annealing (SA) inversion method for geoacoustic data. Significant improvements in the classical Metropolis SA algorithm improved the speed and accuracy of the SA method. This method solves for compressional and shear wave velocities, layer thicknesses, density, and attenuation when the data are sensitive to these properties. NRL demonstrated the effectiveness of the SA method with a realistic geological case that is a nonlinear problem with several traps that foil other inversion methods. DTIC

N95-22072* Woods Hole Oceanographic Inst., MA. Dept. of Applied Ocean Physics and Engineering.
EXCHANGES BETWEEN HEMISPHERES AND GYRES: A DIRECT APPROACH TO THE MEAN CIRCULATION OF THE EQUATORIAL PACIFIC Ph.D. Thesis - MIT
Susan Elizabeth Wijffels Sep. 1993 263 p Sponsored by NASA Scholarship in Global Change Research and Caltex Graduate Woman National Scholarship Limited Reproducibility: More than 20% of this document may be affected by microfiche quality
(Grant NSF OCE-87-16910)
(NASA-CR-196311; NAS 1.26:196311; AD-A279437; WHOI-93-42) Avail: Issuing Activity (Defense Technical Information Center (DTIC))

The pathways for cross-equatorial and cross-gyre exchange are studied with an extensive set of new high-quality hydrographic data. Use of repeat surveys or comparison with historical data ensured that the data reflect mean conditions. An inverse model adjusts the circulation such that volume, heat and salt are conserved in subthermocline layers. Cross-equatorial flow is achieved in the abyss in a deep western boundary current which transports 10 Sv (1x10(exp 6)/cu m/s) of dense Southern Ocean water into the North Pacific. This flow returns southward as warmer deep water, crossing the equator in the interior by some unknown mechanism. In the upper ocean, subtropical gyre waters flow equatorward and entrain in the eastward equatorial currents which in turn feed the eastern Pacific upwelling system. The upwelled waters supply the South Equatorial Current, accounting for a larger transport than predicted by Sverdrup theory. Surface northward flow across the equator in the western Pacific supplies the North Pacific Ekman flux. The Pacific Ocean does not convert large mounts of abyssal to thermocline water, as required by several theories of the global thermohaline circulation. The Pacific-Indian throughflow is essentially zero, though an error analysis allows a range of 0-8 Sv. DTIC

N95-22073 Woods Hole Oceanographic Inst., MA.
DESCRIPTIONS OF WHOI SEDIMENT CORES, VOLUME 8
P. B. Mills, ed. and J. E. Broda, ed. May 1993 502 p Limited Reproducibility: More than 20% of this document may be affected by microfiche quality
(Grants NSF OCE-88-00693; NSF OCE-91-01734)
(AD-A279444; WHOI-93-19-Vol-8) Avail: Issuing Activity (Defense Technical Information Center (DTIC))

The report contains visual descriptions and smear slide analyses for several suites of cores received in the geological samples collection of the Woods Hole Oceanographic Institution between mid-1984 and late 1989. Approximately 220 sample localities from the North Atlantic, South Atlantic, Mediterranean and Pacific Oceans are represented. Charts of ships tracks for cruises included in this report and updated computer listings of all cores in the W.H.O.I. collection are also presented. DTIC

N95-22187 Hawaii Univ., Honolulu, HI. School of Ocean and Earth Science and Technology.
[SEISMIC ANISOTHROPY AND LARGE-SCALE POROSITY INTHE OCEAN FLOOR] Final Technical Reports
1 Sep. 1994 393 p Limited Reproducibility: More than 20% of this document may be affected by poor print
(Contract N00014-87-K-0181)
(AD-A286580) Avail: Issuing Activity (Defense Technical Information Center (DTIC))

Research goals include a description and modeling of the kinematical structure and dynamical processes of oceanic motions that have horizontal scales from a few meters to a few kilometers, understanding the role that these small-scale motions play in the redistribution and mixing of momentum, potential vorticity heat, and salt. Our objective is to identify the processes that affect the kinematical and dynamical evolution of near-inertial internal gravity waves, especially those processes that can transfer energy out of near-inertial internal waves into the internal wave continuum. DTIC

N95-22209 Woods Hole Oceanographic Inst., MA.
REAL TIME SYSTEM FOR PRACTICAL ACOUSTIC MONITORING OF GLOBAL OCEAN TEMPERATURE Quarterly Report No. 6, Jul. - Sep. 1994
John L. Spiesberger and Daniel E. Frye 4 Nov. 1994 178 p Limited Reproducibility: More than 20% of this document may be affected by microfiche quality
(Contract MDA972-93-1-0004)
(AD-A286435) Avail: CASI HC A09

The acoustic multipaths from the Kaneohe source have been identified at one SOSUS station using a ray tracing algorithm called ZRAY. This is the furthest, 4000 km, that ray theory has been successfully used to understand acoustic propagation in the ocean. This further validates that acoustic thermometry is valid at basin-scales and that changes in the travel time from the Kaneohe source are not due to changes in the multipaths. FSU designed an acoustic tomography assimilation scheme for a reduced gravity model, but with spatially variable density. The goal of this effort is to estimate the time independent density field in the upper northeast Pacific ocean. A second test cruise was conducted at the AUTEC Range in August to verify SSAR performance with a 70 Hz source. This test consisted of the deployment of a normal SSAR (Snubber design) and a moored SSAR. The moored SSAR was deployed on a subsurface mooring, thus removing surface generated noise. A 70 Hz source transmitted an M-sequence signal and both systems recorded data on hard disk. The normal SSAR also telemetered processed data. In addition, the SSAR acoustic navigation system was tested against the AUTEC Range system. All data were successfully collected and processing of this information is ongoing. DTIC

51 LIFE SCIENCES (GENERAL)

N95-19969# Argonne National Lab., IL.
A PHOTOPHYSICAL CONTROL MECHANISM FOR ZEAXANTHIN-ASSOCIATED RADIATIONLESS ENERGY DISSIPATION IN PHOTOSYNTHESIS
Harry A. Frank (Connecticut Univ., Storrs, CT.), Agnes Cua (Connecticut Univ., Storrs, CT.), Andrew Young (Liverpool Univ., England.), David Gosztola, and Michael R. Wasielewski 1994 10 p
(Contract W-31-109-eng-38)
(DE94-018383; ANL/CHM/CP-80107) Avail: CASI HC A02/MF A01

Understanding the way in which excess solar energy is dissipated by photosynthetic membranes under high light stress is a major problem in photosynthesis studies. This paper reports femtosecond time-resolved, fast-transient optical spectroscopic analyses of three important xanthophylls: violaxanthin, antheraxanthin, zeoaxanthin. The results support the notion that the enzymatic reactions that interconvert these xanthophylls act as a kind of 'molecular gear shift' controlling whether the molecules function as light-harvesting pigments performing forward energy transfer or as fluorescence quenchers performing reverse energy transfer. DOE

N95-20185# Massachusetts Inst. of Tech., Cambridge, MA. Artificial Intelligence Lab.
VIEWER-CENTERED OBJECT RECOGNITION IN MONKEYS
Nikos Logothetis, J. Pauls, and Tomaso Poggio Apr. 1994 21 p
(Contract N00014-93-I-0385)
(AD-A279876; AI-M-1473; CBCL-95) Avail: CASI HC A03/MF A01

How does the brain recognize three-dimensional objects? We trained monkeys to recognize computer rendered objects presented from an arbitrarily chosen training view, and subsequently tested their ability to generalize recognition for other views. Our results provide additional evidence in favor of a recognition model that accomplishes view-invariant performance by storing a limited number of object views or templates together with the capacity to interpolate between the templates. DTIC

N95-20208# Technische Hogeschool, Delft (Netherlands). Dept. of Biochemical Engineering.
PROCESS STRATEGIES IN THE ENZYMATIC RESOLUTION OF ENANTIOMERS Ph.D. Thesis
J. L. L. Rakels 1 Jun. 1994 170 p
(PB95-107850) Avail: CASI HC A08/MF A02

Contents: General Introduction; A Simple Method to Determine the Enantiomeric Ration in Enantioselective Biocatalysis; Kinetic Analysis of Enzymatic Chiral Resolution by Progress Curve Evaluation; Kinetics of the Enzymatic Resolution of Racemic Compounds in Bi-bi Reactions; Modification of Enzyme Enantioselectivity by Product Inhibition; Comparison of Enzymatic Kinetic Resolution in a Batch Reactor and a CSTR; Strategies in the Preparation of Homochiral Compounds Using Combined Enantioselective Enzymes; Sequential Kinetic Resolution by two Enantioselective Enzymes; Improvement of Enzymatic Enantioselective Ester Hydrolysis in Organic Solvents; Improved Kinetic Resolution by Enzyme Catalyzed Parallel Reactions. NTIS

N95-20252 Battelle Memorial Inst., Research Triangle Park, NC.
THEORETICAL PREDICTION OF VIBRATIONAL CIRCULAR DICHROISM SPECTRA OF R-GLYCERALDEHYDE, R-ERYTHROSE, AND R-THREOSE. PART 2: DEVELOPMENT OF A PROCEDURE TO SCALE THE FORCE CONSTANT MATRIX EXPRESSED IN TERMS OF INTERNAL COORDINATES Final Report, May - Oct. 1992
Daniel Zeroka, James O. Jensen, and Janet L. Jensen Nov. 1993 43 p Limited Reproducibility: More than 20% of this document may be affected by microfiche quality
(Contract DAAL03-91-C-0034; DA Proj. 1O1-62622-A-553-C)
(AD-A284305; ERDEC-TR-112-Pt-2) Avail: CASI HC A03

A very important objective of the Detection Directorate at the U.S. Army Edgewood Research, Development and Engineering Center is the remote detection of biological materials in the field. One line of thinking, currently being followed, is the recognition that sugars are distinguishing features of biological materials. In Part 1 of this study, the theoretical prediction of the vibrational circular dichroism (VCD) of the 3 and 4 carbon sugars R-glyceraldehyde, R-erythrose, and R-threose is considered. The calculational procedure used involves determination of the frequencies corresponding to the normal modes of vibration. Since calculated frequencies at the Hartree-Fock level are typically 10% too high, some form of scaling of the frequencies or the force constant matrix is required for quantitative agreement with experimental measurements. In Part 2 of this study, a scaling method is described, and three key FORTRAN computer programs are presented. Basically, the force constant matrix in internal coordinates at the 6-31G HF level of calculation is scaled to the calculated 6-31G MP2 level of calculation. The force constant matrix in terms of Cartesian coordinates can be determined from a matrix transformation, originally shown by Pulay, involving the force constant matrix in terms of internal coordinates. The scaling constant for each off-diagonal element of the force constant matrix was determined by using the geometric mean Q(sub ij) = ((Q sub i)(Q sub j))(exp 1/2) of the diagonal scaling constants (Q sub i) and (Q sub j). DTIC

N95-20471# National Renewable Energy Lab., Golden, CO.
ANAEROBIC DIGESTION ANALYSIS MODEL: USER'S MANUAL
M. Ruth and R. Landucci Aug. 1994 79 p
(Contract DE-AC36-83CH-10093)
(DE94-011858; NREL/TP-421-6331) Avail: CASI HC A05/MF A01

The Anaerobic Digestion Analysis Model (ADAM) has been developed to assist investigators in performing preliminary economic analyses of anaerobic digestion processes. The model, which runs under Microsoft Excel(trademark), is capable of estimating the economic performance of several different waste digestion process configurations that are defined by the user through a series of option selections. The model can be used to predict required feedstock tipping fees, product selling prices, utility rates, and raw material unit costs. The model is intended to be used as a tool to perform preliminary economic estimates that could be used to carry out simple screening analyses. The model's current parameters are based on engineering judgments and are not reflective of any existing process; therefore, they should be carefully evaluated and modified if necessary to reflect the process under consideration. The accuracy and level of uncertainty of the estimated capital investment and operating costs are dependent on the accuracy and level of uncertainty of the model's input parameters. The underlying methodology is capable of producing results accurate to within +/- 30% of actual costs. DOE

N95-20559*# Texas Univ., San Antonio, TX. Dept. of Life Sciences.
MONOCLONAL ANTIBODIES DIRECTED AGAINST SURFACE MOLECULES OF MULTICELL SPHEROIDS Semiannual Progress Report, 1 Jul. - 31 Dec. 1994
Andrew O. Martinez 31 Dec. 1994 25 p
(Grant NAG2-819)
(NASA-CR-197367; NAS 1.26:197367) Avail: CASI HC A03/MF A01

The objective of this project is to generate a library of monoclonial antibodies (MAbs) directed against surface molecules of tumor and transformed cells grown as multicell spheroids (MCS). These MCS are highly organized, 3-dimensional multicellular structures which exhibit many characteristics of in vivo organized tissues which are not found in conventional monolayer or suspension culture. In brief, MCS combine the relevance or organized tissues with in vitro methodology making the MCS a good model system to study the interactions of mammalian cells, and thereby provide a functional assay for surface adhesion molecules. This project also involves investigations of cell-cell interactions in a gravity-based environment. It will provide an important base of scientific information for future comparative studies on the effects of hypergravity and simulated microgravity environments on cell-cell interactions. This project also has the potential to yield important materials (e.g. cellular products) which may be useful for the diagnosis and/or treatment of certain human diseases. Moreover, this project supports the training of one undergraduate and one graduate student; thus, it will also assist in developing a pool of future scientists with research experience in gravitational biology research. Author

N95-20711 Texas A&M Univ., College Station, TX.
BACTERIAL LUCIFERASE: DETERMINATION OF THE STRUCTURE BY X-RAY DIFFRACTION Final Report, 1 May 1992 - 31 Dec. 1993
Miriam M. Ziegler and Thomas O. Baldwin 20 May 1994 73 p Limited Reproducibility: More than 20% of this document may be affected by

microfiche quality
(Contract N00014-92-J-1900)
(AD-A279699) Avail: Issuing Activity (Defense Technical Information Center (DTIC))

This project was focused on determination of the three-dimensional structure of bacterial luciferase. The structure of the enzyme is of fundamental importance to the understanding of the catalytic mechanism and the mode of interaction of the enzyme with accessory proteins, and is essential to future plans to develop biosensor technologies. In the course of this project, numerous crystallization trials were carried out and conditions were refined that permitted high resolution data to be collected and interpreted. In collaboration with Dr. Ivan Rayment of the University of Wisconsin, data have been collected from native crystals and 3 derivatives at 2.8 A. Higher resolution data are being collected at this time, and we fully expect to have a high resolution structure within the next few months, certainly by the end of the calendar year 1994. We have also developed crystallization protocols for several mutant luciferases. Structural analysis of the mutant luciferases should enable us to locate the active site in the three-dimensional structure of the wild-type enzyme, permit mechanistic interpretation of numerous experiments that have been reported over the past ca. 25 years, and assist us in designing the next generation of mutant enzymes to test hypotheses regarding the mechanism of light production by this intriguing and important enzyme. DTIC

N95-20806# Texas Univ. Health Science Center, San Antonio, TX. Dept. of Radiology.
IN VIVO DISTRIBUTION OF LIPOSOME ENCAPSULATED HEMOGLOBIN STUDIED WITH IMAGING RADIOTRACERS Final Technical Report, 1 Dec. 1990 - 31 Mar. 1994
William T. Phillips 31 Mar. 1994 117 p
(Contract N00014-91-J-1217)
(AD-A279774) Avail: CASI HC A06/MF A02

The objective of this project was to develop radiotracer imaging technology to follow the in vivo circulation and organ deposition of liposome encapsulated hemoglobin (LEH). A liposome labeling technique based on the most common radioisotope used in nuclear medicine, technetium-99m (99m Tc), was developed and patented. A comparison of this 99mTc-liposome labeling method with previous methods using indium-111 (In-111) was performed. The label LEH was infused into small animals to monitor any in vivo differences between different LEH formulations (bovine hemoglobin, recombinant human hemoglobin, human hemolysate, lyophilized) using gamma scintigraphy and tissue biodistribution determination. These studies were correlated with any hematological and pathological changes associated with LEH treatment such as the interaction of LEH with circulating platelets using indium-111-labeled platelets. DTIC

N95-20917# Georgia Univ., Athens, GA. Dept. of Biochemistry.
MICROBIOLOGY AND PHYSIOLOGY OF ANAEROBIC FERMENTATIONS OF CELLULOSE
H. D. Peck, Jr., L. G. Ljungdahl, L. E. Mortenson, and J. K. W. Wiegel 1994 26 p
(Contract DE-FG09-86ER-13614)
(DE95-002899; DOE/ER-13614/T1) Avail: CASI HC A03/MF A01

This project studies the biochemistry and physiology of four major groups (primary, secondary, ancillary and methane bacteria) of anaerobic bacteria, that are involved in the conversion of cellulose to methane or chemical feedstocks. The primary bacterium, Clostridium thermocellum, has a cellulolytic enzyme system capable of hydrolyzing crystalline cellulose and consists of polypeptide complexes attached to the substrate cellulose with the aid of a low molecular yellow affinity substance (YAS) produced by the bacterium in the presence of cellulose. Properties of the complexes and YAS are studied. Aspects of metabolism are being studied which appear to be relevant for the interactions on consortia and their bioenergetics, particularly related to hydrogen, formate, CO, and CO2. The roles of metals in the activation of H2 are being investigated, and genes for the hydrogenases cloned and sequenced to established structural relationships among the hydrogenases. The goals are to understand the roles and regulation of hydrogenases in interspecies H2 transfer, H2 cycling and the generation of a proton gradient. The structures of the metal clusters and their role in the metabolism of formate will be investigated with the goal of understanding the function of formate in the total synthesis of acetate from CO2 and its role in the bioenergetics of these microorganisms. Additionally, the enzyme studies will be performed using thermophiles and also the isolation of some new pertinent species. The project will also include research on the mechanism of extreme thermophily (growth over 70 deg) in bacteria that grow over a temperature span of 40C or more. These bacteria exhibit a biphasic growth response to temperature and preliminary evidence suggests that the phenomenon is due to the expression of a new set of enzymes. These initial observations will be extended employing techniques of molecular biology. DOE

N95-21112# Helsinki Univ. of Technology, Espoo (Finland). Lab. of Computer and Information Science.
ATTEMPT TO INTERPRET THE SELF-ORGANIZING MAPPING PHYSIOLOGICALLY
Teuvo Kohonen Nov. 1993 24 p
(ISSN 0783-7445)
(PB95-127783; ISBN-951-22-1291-9) Avail: CASI HC A03/MF A01

It is argued that the Self-Organizing Map (SOM) may be implemented in biological neural networks by partly neural, partly chemical mechanisms. For the Winner Take All function a laterally connected network seems proper. The active forgetting relating to the automatic normalization of the synaptic strengths in learning is thought to ensure from competition on postsynaptic resources. The neighborhood function needed in the SOM algorithm is most effectively implemented by chemical agents, which are formed or released in the neighborhood of highly active cells. These agents are thought to control the synaptic plasticity. Such a physiological model then behaves in the same way as the idealized SOM algorithm, which has been found very effective in many information-processing applications. NTIS

N95-21366# Los Alamos National Lab., NM.
POTENTIAL-OF-MEAN-FORCE DESCRIPTION OF IONIC INTERACTIONS AND STRUCTURAL HYDRATION IN BIOMOLECULAR SYSTEMS
G. Hummer, A. E. Garcia, and D. M. Soumpasis (Max-Planck-Inst. fuer Biophysikalische Chemie, Goettingen, Germany.) 1994 18 p Presented at the Non-Linear Exitations in Biomolecules, Houches, France, 30 May - 4 Jun. 1994
(Contract W-7405-eng-36)
(DE95-000859; LA-UR-94-3139; CONF-9405240-2) Avail: CASI HC A03/MF A01

To understand the functioning of living organisms on a molecular level, it is crucial to dissect the intricate interplay of the immense number of biological molecules. Most of the biochemical processes in cells occur in a liquid environment formed mainly by water and ions. This solvent environment plays an important role in biological systems. The potential-of-mean-force (PMF) formalism attempts to describe quantitatively the interactions of the solvent with biological macromolecules on the basis of an approximate statistical-mechanical representation. At its current status of development, it deals with ionic effects on the biomolecular structure and with the structural hydration of biomolecules. The underlying idea of the PMF formalism is to identify the dominant sources of interactions and incorporate these interactions into the theoretical formalism using PMF's (or particle correlation functions) extracted from bulk-liquid systems. In the following, the authors shall briefly outline the statistical-mechanical foundation of the PMF formalism and introduce the PMF expansion formalism, which is intimately linked to superposition approximations for higher-order particle correlation functions. The authors shall then sketch applications, which describe the effects of the ionic environment on nucleic-acid structure. Finally, the authors shall present the more recent extension of the PMF idea to describe quantitatively the structural hydration of biomolecules. Results for the interface of ice and water and for the hydration of deoxyribonucleic acid (DNA) will be discussed. DOE

N95-21376# Argonne National Lab., IL. Genome Structure Group.
PROPOSAL FOR A TUTORIAL ON MINIMAL LENGTH ENCODING (MLE) IN MOLECULAR BIOLOGY
Aleksandar Milosavljevic Mar. 1994 6 p Presented at the 2nd International Conference on Intelligent Systems for Molecular Biology, Stanford, CA, 15-17 Aug. 1994
(Contract W-31-109-eng-38)
(DE94-015076; ANL/CMB/CP-82418; CONF-9408117-1) Avail: CASI HC A02/MF A01

This paper describes a tutorial to introduce the Minimal length encoding

(MLE) method to computational biologists who are designing sequence analysis algorithms, to computer scientists who are interested in learning more about macromolecular sequence analysis, and to biologists who are more advanced users of the sequence analysis programs. An emphasis of the workshop will be on the use of the MLE method as a tool for comparative analysis of inference programs in computational biology, with an ultimate purpose of providing more methodological coherence to the emerging field of computational biology. DOE

N95-21526# Georgia Univ., Athens, GA. Dept. of Botany.
NITROGEN CONTROL OF CHLOROPLAST DIFFERENTIATION
Gregory W. Schmidt 1994 6 p
(Contract DE-FG09-84ER-13188)
(DE95-002797; DOE/ER-13188/9) Avail: CASI HC A02/MF A01

This project was directed toward understanding how the availability of nitrogen affects the accumulation of chloroplast pigments and proteins that function in energy transduction and carbon metabolism. The availability of this nutrient most pervasively limits plant growth and agricultural productivity but the molecular and physiological consequences of nitrogen-deficiency are poorly understood. The model system for our studies of nitrogen-dependent regulation of chloroplast differentiation is the unicellular green alga Chlamydomonas reinhardtii which is grown phototrophically in a continuous culture system. When 150 micrometers nitrogen is provided at a dilution rate of 0.25 volumes of the growth medium per day, the cultures are sustained at a density of less than 10(exp 5) cells/ml and chlorophyll deficiency, the classical symptom of nitrogen-deficiency, becomes quite pronounced. We found that there is a concomitant loss of light-harvesting complexes and reduced levels of Photosystem II reaction center complexes while ATP synthetase and Photosystem I reaction centers are maintained at high levels. Moreover, reduced rates of chloroplast protein synthesis are due to differential effects on mRNA translation. In contrast, the deficiency of light-harvesting genes is due to marked reductions of the nuclear-encoded cab mRNA's. Although there is no significant reduction of the amounts of RuBPCase, we also detected substantial changes in the mRNA abundance of the alga's two small subunit genes. All of the effects of nitrogen-limitation are readily reversible: greening of cells is completed within 24 hours after provision of 10 mM ammonium. During this time, the plastid translational constraints are disengaged and progressive changes in the abundance of nuclear transcripts occur, including a transient 30-fold elevation of (und cab) mRNA's. DOE

N95-21529*# Universities Space Research Association, Columbia, MD.
ANNUAL PROGRAM ANALYSIS OF THE NASA SPACE LIFE SCIENCES RESEARCH AND EDUCATION SUPPORT PROGRAM Report, 1 Dec. 1993 - 30 Nov. 1994
30 Nov. 1994 42 p
(Contract NAS9-18440)
(NASA-CR-197298; NAS 1.26:197298) Avail: CASI HC A03/MF A01

The basic objectives of this contract are to stimulate, encourage, and assist research and education in NASA life sciences. Scientists and experts from a number of academic and research institutions in this country and abroad are recruited to support NASA's need to find a solution to human physiological problems associated with living and working in space and on extraterrestrial bodies in the solar system. To fulfill the contract objectives, a cadre of staff and visiting scientists, consultants, experts, and subcontractors has been assembled into a unique organization dedicated to the space life sciences. This organization, USRA's Division of Space Life Sciences, provides an academic atmosphere, provides an organizational focal point for science and educational activities, and serves as a forum for the participation of eminent scientists in the biomedical programs of NASA. The purpose of this report is to demonstrate adherence to the requirement of Contract NAS9-18440 for a written review and analysis of the productivity and success of the program. In addition, this report makes recommendations for future activities and conditions to further enhance the objectives of the program and provides a self-assessment of the cost performance of the contract. Derived from text

N95-21544*# National Aeronautics and Space Administration. Ames Research Center, Moffett Field, CA.
HYPERVOLEMIA IN MEN FROM DRINKING HYPERHYDRATION FLUIDS AT REST AND DURING EXERCISE
J. E. Greenleaf, R. LooftWilson, P. P. Wisherd, P. P. Fung, A. C. Ertl, C. G. R. Jackson, P. R. Barnes, and L. G. Wong (Shaklee US, Inc., San Francisco, CA.) Dec. 1994 55 p
(RTOP 199-18-12-07)
(NASA-TM-4657; A-94138; NAS 1.15:4657) Avail: CASI HC A04/MF A01

To test the hypothesis that drink composition is more important than drink osmolality (Osm) for maintaining and increasing plasma volume (PV) at rest and during exercise, six men (22-39 yr, 76.84 +/- 16.19 kg, 2.99 +/- 0.45 L/min VO2 peak) each underwent six treatments while sitting for 90 min (VO2 = 0.39 L/min) and then performed upright ergometer exercise for 70 min (VO2 = 2.08 +/- 0.33 1/min, 70% +/- 7% VO2 peak). Drink formulations (10 ml/kg body weight, X = 768 ml) for the sitting period were: P1 (55 mEq Na(+), 365 mOsm/kg H2O), P2 (97.1 mEq Na(+), 791 mOsm/kg), P2G (113 mEqNa(+), 80 ml glycerol, 1,382 mOsm/kg, HyperAde (HA) (164 mEq Na(+), 253 mOsm/kg), and 01 and 02 (no drinking). The exercise drink (10 ml/kg, 768 ml) was P1 for all treatments except 02. Plasma volume at rest increased (p less than 0.05) by 4.7% with P1 and by 7.9% with HA. Percent change in PV during exercise was +1% to +3%0(NS) with HA; -6% to 0% (NS) with P1, P2, P2G, and 01; and -8% to -5% (p less than 0.05) with 02. HyperAde, with the lowest osmolality (253 mOsm/kg), maintained PV at rest and during exercise, whereas the other drinks with lower Na(+) and higher osmolality (365 to 1,382 mOsm/kg) did not. But Performance 1 also increased PV at rest. Thus, drink composition may be more important than drink osmolality for increasing plasma volume at rest and for maintaining it during exercise. Author

N95-21548# Oak Ridge National Lab., TN.
CELL MEMBRANE POTENTIALS INDUCED DURING EXPOSURE TO EMP FIELDS
P. C. Gailey and C. E. Easterly 1994 8 p Presented at the Theater Nuclear Warfare Program, Williamsburg, VA, 16-18 Mar. 1993
(Contract DE-AC05-84OR-21400)
(DE94-018952; CONF-9303304-1) Avail: CASI HC A02/MF A01

Internal current densities and electric fields induced in the human body during exposure to EMP fields are reviewed and used to predict resulting cell membrane potentials. Using several different approaches, membrane potentials of about 100 mV are predicted. These values are comparable to the static membrane potentials maintained by cells as a part of normal physiological function, but the EMP-induced potentials persist for only about 10 ns. Possible biological implications of EMP-induced membrane potentials including conformational changes and electroporation are discussed. DOE

N95-21606# Oak Ridge National Lab., TN.
THE MOLECULAR MECHANICS PROGRAM DUPLEX: COMPUTING STRUCTURES OF CARCINOGEN MODIFIED DNA BY SURVEYING THE POTENTIAL ENERGY SURFACE
B. E. Hingerty and S. Broyde (New York Univ., New York, NY.) 1994 16 p Presented at the 27th Jerusalem Symposium in Quantum Chemistry and Biochemistry, Jerusalem, Israel, 23-26 May 1994
(Contracts DE-AC05-84OR-21400; DE-FG02-90ER-60931)
(DE94-019153; CONF-9405196-2) Avail: CASI HC A03/MF A01

The nucleic acids molecular mechanics program DUPLEX has been designed with useful features for surveying the potential energy surface of polynucleotides, especially ones that are modified by polycyclic aromatic carcinogens. The program features helpful strategies for addressing the multiple minimum problem: (1) the reduced variable domain of torsion angle space; (2) search strategies that emphasize large scale searches for smaller subunits, followed by building to larger units by a variety of strategies; and (3) the use of penalty functions to aid the minimizer in locating selected structural types in first stage minimizations (penalty functions are released in terminal minimizations to yield final unrestrained minimum energy conformations). Predictive capability is illustrated by DNA modified by activated benzo(a)pyrenes. DOE

N95-21884# Rijksinstituut voor Volksgezondheid en Milieuhygieene, Bilthoven (Netherlands).
EFFECTS OF INCREASED UV-B RADIATION ON PHYTOPLANKTON: A PRELIMINARY STUDY AND RESEARCH PROGRAMME
Arnold Veen Feb. 1993 32 p See also DE88-753545 Sponsored by Dutch National Research Programme on Global Air Pollution and Climate Change
(PB95-133732; RIVM-731054001) Avail: CASI HC A03/MF A01

The depletion of the ozone layer through actions of, for instance, chlorine containing catalysts is expected to result in an increased UV-B irradiance. Since phytoplankton is known to be sensitive to this radiation, effects on global primary production cannot be excluded. The preliminary results in semi-continuous culture experiments indicated that algae differ widely in their response to UV-B radiation. Desmid and diatom species were much more sensitive than green algae. Furthermore, the experiments emphasized the importance of an accurate dosimetry, so the next step was to build a continuous culture system with steering software to simulate natural photosynthetic light regimes and UV-B simultaneously, and study the effect on growth rate and other physiological parameters. The culture system was designed to allow for exact quantification of the UV-B exposure. Finally a list of publications is presented that were necessary to build the system and its steering components, and gave background information on reactions of both photosynthetic light and UV-B radiation on phytoplankton. NTIS

N95-22065# Los Alamos National Lab., NM.
LIFE SCIENCES DIVISION AND CENTER FOR HUMAN GENOME STUDIES Progress Report, 1992-1993
Morton Bradbury, comp., Scott Cram, comp., and Carolyn Stafford, comp. Jul. 1994 94 p
(Contract W-7405-eng-36)
(DE94-017796; LA-12754-PR) Avail: CASI HC A05/MF A01

This report summarizes the research and development activities of the Los Alamos National Laboratory's Life Sciences Division and the biological aspects of the Center for Human Genome Studies for the calendar years 1992 and 1993. The technical portion of the report is divided into two parts: (1) selected research highlights; and (2) research projects and accomplishments. The research highlights provide a more detailed description of a select set of projects. A technical description of all projects is presented in sufficient detail to permit the informed reader to assess their scope and significance. Summaries useful to the casual reader desiring general information have been prepared by the group leaders and appear in each group overview. Investigators on the staff of Life Sciences Division will be pleased to provide further information. DOE

N95-22066# Carnegie Institution of Washington, Stanford, CA. Dept. of Plant Biology.
THE USE OF CYANOBACTERIA TO EXPLORE BASIC BIOLOGICAL PROCESSES Abstracts Only
Arthur R. Grossman 1994 113 p Workshop held in Pacific Grove, CA, 30 May - 2 Jun. 1993
(Contract DE-FG02-93ER-20112; NSF MCB-93-04625; USDA-9301106)
(DE94-019238; CONF-9305375-Absts) Avail: CASI HC A06/MF A02

This volume contains the proceedings of The Cyanobacteria Workshop, 1993 held at the Asilomar Conference Center in Pacific Grove, California May 30--June 2, 1993. The volume contains single page abstracts of forty-one presentations made at the meeting organized under the topics addressed by the meeting: (1) Photosynthesis; (2) Nitrogen Metabolism and Heterocyst Differentiation; (3) Nutrient Stress Responses and Metabolic Processes; (4) The Phycobilisome; and (5) Miscellaneous Topics. DOE

N95-22067# Argonne National Lab., IL.
DISCOVERING RELATED DNA SEQUENCES VIA MUTUAL INFORMATION
A. Milosavljevic 1994 17 p
(Contracts W-31-109-eng-38; DE-FG03-91ER-61152)
(DE95-001101; ANL/CMB/PP-81002) Avail: CASI HC A03/MF A01

One of the problems in DNA and protein sequence comparisons is to decide whether the observed similarity should be explained by their relatedness or by the mere presence of some shared internal structure, e.g., shared internal repetitive patterns. Machine discovery of related DNA sequences critically depends on a solution to this problem. In this paper we propose a general solution that is based on minimal length encoding: we measure mutual information between two sequences as the difference between the encoding length of one of the sequences sequence and its encoding length relative to the other sequence; two sequences are considered similar if the mutual information exceeds a threshold of significance; the significance is determined using an extension of the newly proposed algorithmic significance method. We show that mutual information factors out sequence similarity that is due to shared internal structure and thus enables discovery of truly related sequences. In addition to this general method, we also propose an efficient way to compare sequences based on their subword composition that does not require any a priori assumptions about k-tuple length. DOE

N95-22075# Argonne National Lab., IL.
ELECTROSTATIC BASIS FOR MOLECULAR RECOGNITION IN PHOTOSYNTHESIS
D. M. Tiede, A. C. Vashista, and M. R. Gunner (City Coll. of the City Univ. of New York, NY.) 1994 6 p
(Contract W-31-109-eng-38)
(DE95-002979; ANL/CHM/PP-79997) Avail: CASI HC A02/MF A01

An electrostatic basis for molecular recognition in photosynthesis has been found, based upon calculations from the crystal structure of the Rhodobacter sphaeroides photosynthetic reaction center, and supported by experimental measurements of water-soluble c-cytochrome docking on the reaction center. Besides providing a physical explanation for molecular recognition in photosynthesis, this work is significant because it is a starting point for the examination of the role for electrostatics in the incorporation of membrane proteins into crystals and other ordered arrays that have potential for molecular device applications. Solar energy conversion in photosynthesis requires that reactive, bimolecular electron-transfer complexes are formed between the reaction center, the protein that carries out the initial conversion of solar energy to chemical energy, and specific secondary electron donors and acceptors. The molecular basis for recognition between the reaction center and its photosynthetic partners is determined by the charge and chemical properties of the associated proteins. This work identified a likely electrostatic mechanism for assembly of electron transfer complexes between the reaction center from Rb. sphaeroides and a series of structurally homologous water-soluble c-cytochromes by identifying correlations between electron transfer and electrostatic properties of the reaction center and the various c-cytochromes. The kinetics of electron transfer between the reaction center and nine soluble c-cytochromes were analyzed and compared to the patterns of the surface electrostatic potentials for each of the proteins. DOE

N95-22220 Georgia Univ., Athens, GA. Complex Carbohydrate Research Center.
STRUCTURES AND FUNCTIONS OF OLIGOSACCHARINS
P. Albersheim Oct. 1994 12 p Limited Reproducibility: More than 20% of this document may be affected by microfiche quality
(Contract DE-FG09-85ER-13425)
(DE95-003195; DOE/ER-13425/T4) Avail: CASI HC A03

This document contain abstracts of 25 papers published or in preparation describing the structure and function of oligosaccharins. Research is described in the following areas: Phytotoxic effects of microbial pectic enzymes; Fungal enzymes, plant cell wall fragments, and plant cell death; Roles of cell wall constituents in plant-pathogen interactions; The control of morphogenesis in tobacco thin cell-layer explants; Studies of the ability of xyloglucan oligosaccharides to inhibit auxin-stimulated growth; and Oligosaccharins - oligosaccharides that regulate growth, development, and defence responses in plants. DOE

N95-22296# Los Alamos National Lab., NM.
FLOW CYTOMETRY: A POWERFUL TECHNOLOGY FOR MEASURING BIOMARKERS
J. H. Jett 1994 17 p Presented at the Workshop on Development and Application of Biomarkers, Santa Fe, NM, 26-29 Apr. 1994
(Contract W-7405-eng-36)
(DE94-018284; LA-UR-94-2831; CONF-9404178-1) Avail: CASI HC A03/MF A01

A broad definition of a biomarker is that it is a measurable characteristic of a biological system that changes upon exposure to a physical or chemical insult. While the definition can be further refined, it is sufficient for the purposes of demonstrating the advantages of flow cytometry for making quantitative measurements of biomarkers. Flow cytometry and cell sorting technologies have emerged during the past 25 years to take their place alongside other essential tools used in biology such as optical and electron microscopy. This paper describes the basics of flow cytometry technology, provides illustrative examples of applications of the technology in the field of biomarkers, describes recent developments in flow cytometry that have not yet been applied to biomarker measurements, and projects future developments of the technology. The examples of uses of flow cytometry for biomarker quantification cited in this paper are meant to be illustrative and not exhaustive in the sense of providing a review of the field. DOE

N95-22397 American Association for Cancer Research, Philadelphia, PA.
CELLULAR RESPONSES TO ENVIRONMENTAL DNA DAMAGE
1994 245 p Presented at the AACR Conference in Cancer Research: Cellular Responses To Environmental DNA Damage, Banff, Alberta, 1-6 Dec. 1991 Limited Reproducibility: More than 20% of this document may be affected by microfiche quality
(Contract DE-FG02-92ER-61370)
(DE94-015606; DOE/ER-61370/1; CONF-9112182) Avail: CASI HC A11

This volume contains the proceedings of the conference entitled Cellular Responses to Environmental DNA Damage held in Banff, Alberta December 1-6, 1991. The conference addresses various aspects of DNA repair in sessions titled: DNA repair; Basic Mechanisms; Lesions; Systems; Inducible Responses; Mutagenesis; Human Population Response Heterogeneity; Intragenomic DNA Repair Heterogeneity; DNA Repair Gene Cloning; Aging; Human Genetic Disease; and Carcinogenesis. Individual papers are represented as abstracts of about one page in length. DOE

52 AEROSPACE MEDICINE

Includes physiological factors; biological effects of radiation; and effects of weightlessness on man and animals.

N95-19898# Wyoming Univ., Laramie, WY. Dept. of Molecular Biology.
USAF CELLULAR MECHANISM OF TURNOVER OF THE STRESS INDUCED PROTEIN HSP70 Final Report, 15 Apr. 1983 - 14 Apr. 1994
Nancy S. Petersen 14 Apr. 1994 11 p
(Contract F49620-92-J-0234)
(AD-A285618; AFOSR-94-0480TR) Avail: CASI HC A03/MF A01

Because heat shock proteins are made by all organisms in response to environmental stress, it has been proposed that accumulation of these proteins could be useful in environmental monitoring. In order to use the accumulation of heat shock proteins as indicators of environmental stress, it is important to understand how their stability is regulated. This research is concerned with determining the influences that regulate the stability of the major heat shock protein, hsp7O, in rainbow trout (used for environmental monitoring) and in fruit files (a well characterized system used for basic research). During the tenure of this grant progress has been made characterizing the rainbow trout heat shock response, cloning and sequencing the rainbow trout heat shock gene, and in generating antibodies specific for fruit fly and rainbow trout hsp7O. The accumulation of hsp7O in juvenile rainbow trout exposed to heavy metals has been assessed in collaboration with the H. Berman Lab. Commercially available antibodies have been used to identify hsp7O breakdown products in flies, trout, chick, and mouse, and the sequences of the major breakdown fragments of the fly hsp7O generated in vivo have been determined. DTIC

N95-20074# Argonne National Lab., IL.
THORIUM-232 IN HUMAN TISSUES: METABOLIC PARAMETERS AND RADIATION DOSES
A. F. Stehney 1994 58 p
(Contract W-31-109-eng-38)
(DE94-019275; ANL/BIM/PP-70108) Avail: CASI HC A04/MF A01

Higher than environmental levels of Th-232 have been found in autopsy samples of lungs and other organs from four former employees of a Th refinery. Working periods of the subjects ranged from 3 to 24 years, and times from end of work to death ranged from 6 to 31 years. Concentrations of Th-232 in these samples and in tissues from two cases of non-occupational exposure were examined for compatibility with dosimetric models in Publication 30 of the International Commission on Radiological Protection (ICPP 1979a). The concentrations of Th-232 in the lungs of the Th workers relative to the concentrations in bone or liver were much higher than calculated from the model for class Y aerosols of Th and the exposure histories of the subjects, and concentrations in the pulmonary lymph nodes were much lower than calculated for three of the Th workers and both non-occupational cases. Least-squares fits to the measured concentrations showed that the biological half-times of Th in liver, spleen, and kidneys are similar to the half-time in bone instead of the factor of 10 less suggested in Publication 30, and the fractions translocated from body fluids were found to be about 0.03, 0.02, and 0.005, respectively, when the fraction to bone was held at the suggested value of 0.7. Fitted values of the respiratory parameters differed significantly between cases and the differences were ascribable to aerosol differences. Average inhalation rates calculated for individual Th workers ranged from 50 to 110 Bq Th-232 y(sup -1), and dose equivalents as high as 9.3 Sv to the lungs, 2.0 Sv to bone surfaces, and 1.1 Sv effective dose equivalent were calculated from the inhalation rates and fitted values of the metabolic parameters. The radiation doses were about the same when calculated from parameter values fitted with an assumed translocation fraction of 0.2 from body fluids to bone instead of 0.7. DOE

N95-20301 North Dakota State Univ., Fargo, ND.
A PHYSIOLOGICAL NEURAL NETWORK FOR SACCADIC EYE MOVEMENT CONTROL Final Report, 26 Feb. 1991 - 1 Feb. 1994
John D. Enderle Apr. 1994 56 p Limited Reproducibility: More than 20% of this document may be affected by microfiche quality
(Contract F33615-90-D-0606)
(AD-A279599; AL/AO-TR-1994-0023) Avail: CASI HC A04

Based on electrophysiological evidence, eye-movement measurements and systems control theory, a new physiological neural network model of horizontal saccadic control is described. The neural control mechanism is first-order, time-optimal, and is initiated by the deep layers of the superior colliculus and terminated by the cerebellar fastigial nucleus. The neural circuit consists of neurons in the paramedian pontine reticular formation, the vestibular nucleus, abducens nucleus, oculomotor nucleus, cerebellum, substantia nigra, nucleus reticularis tegmenti pontis, the thalamus, the deep layers of the superior colliculus and the oculomotor plant for each eye. Each of the neural sides in the model produce firing rates matching experimental data, and simulate fast eye movements that match the recorded data extremely well for saccades of all sizes. All features of these simulations, including peak velocity, duration, and amplitude conform to published observations. DTIC

N95-20307# Naval Aerospace Medical Research Lab., Pensacola, FL.
BEHAVIORAL EFFECTS OF TYROSINE DURING SUSTAINED WAKEFULNESS
D. L. Wiegmann, D. F. Neri, R. R. Stanny, S. A. Shappell, and A. H. McCardie Dec. 1993 25 p
(NR Proj. MM3-3-P-30)
(AD-A279789; NAMRL-1392) Avail: CASI HC A03/MF A01

The fatigue and cognitive performance deficits associated with sleep loss and stress, like that experienced during sustained flight operations and nighttime flying, have motivated the search for effective nonpharmacological countermeasures. The behavioral effects of the potential countermeasure tyrosine, an amino-acid precursor to dopamine and norepinephrine, were examined during an episode of continuous nighttime work involving one night's sleep loss. Volunteers performed nine iterations of a battery of cognitive and subjective tasks for approximately 13 h, beginning at 1930 and ending at 0820 the following morning. Subjects remained awake throughout the day on which the experiment began and were awake for approximately 24 h by the end of testing. Six hours after the start of the experiment, one-half of the subjects received 150 mg/kg tyrosine in a split dose while the other half received a cornstarch placebo in a double-blind procedure. The tracking-task performance of tyrosine subjects declined less during the night than that of placebo subjects. Tyrosine administration was also associated with nonsignificant trends toward reducing: (1) lapses on a high-event-rate vigilance task; (2) subjective sleepiness; and (3) the intensities of several fatigue-related symptoms. DTIC

N95-20408*# National Aeronautics and Space Administration. Langley Research Center, Hampton, VA.
METHOD AND APPARATUS FOR NON-INVASIVE EVALUATION OF DIAPHRAGMATIC FUNCTION Patent Application
William T. Yost, inventor (to NASA), Juliette L. Wait, inventor (to NASA) (Veterans Administration, Washington, DC.), Patricia A. Nahormek, inventor (to NASA) (Veterans Administration, Washington, DC.), John H. Cantrell, inventor (to NASA), and Pamela D. Hanna-Hawver, inventor (to NASA) (Analytical Services and Materials, Inc., Hampton, VA.) 14 Feb. 1994

21 p
(NASA-Case-LAR-13888-1; NAS 1.71:LAR-13888-1;
US-Patent-Appl-SN-195500) Avail: CASI HC A03/MF A01

A method for non-invasive evaluation of diaphragmatic function in humans measures the thickness of the diaphragm in real time with an ultrasonic device, and displays the variations of diaphragm thickness versus time. Formulae are given for calculating a quantitative value for the reserve fatigue capacity of a patient's diaphragm from data obtained by measuring the time limits for maintaining a constant breathing pattern on the display at two different pressure differentials in series with the patient's airways. An apparatus for displaying the diaphragm thickness in real time is also described. The method can be used both on healthy patients and on patients with so severe breathing dysfunctions that they require breathing support from respirators. Author

N95-20457 Biodynamic Research Corp., San Antonio, TX.
MODELING PLATFORM DYNAMICS AND PHYSIOLOGICAL RESPONSE TO SHORT ARM CENTRIFUGATION Final Report, 7 May - 17 Dec. 1993
David J. Pancratz, John B. Bomar, Jr., and James H. Raddin, Jr. Mar. 1994 182 p Limited Reproducibility: More than 20% of this document may be affected by microfiche quality
(Contract F41624-93-C-6011)
(AD-A279640; AL/CF-TR-1994-0025) Avail: Issuing Activity (Defense Technical Information Center (DTIC))

An analysis is presented for the operation of a short radius centrifuge on an orbiting platform. A review of literature confirms that such a centrifuge could be useful in ameliorating the effects of microgravity deconditioning of astronauts. Our analysis indicates that operation of the centrifuge could generate potentially destabilizing forces and moments. Several ideas for reducing or eliminating the forces and moments are discussed. The use of pedals to drive the centrifuge and exercise the rider is also described. Excess power from pedalling could be stored as electrical energy. A mathematical model of the human cardiovascular system indicates that centrifugation at a short radius would indeed stimulate the heart, even though there is a significant acceleration gradient from head to toe. Consideration of the disorienting effects of short radius centrifugation reveals that discomfort originating in the otoliths from the lack of gravity would probably be alleviated; however, the angular motion of the centrifuge would likely cause disorientation or discomfort through the semicircular canals. DTIC

N95-20485# Georgia Univ., Athens, GA. Dept. of Pharmacology and Toxicology.
INTERSPECIES EXTRAPOLATIONS OF HALOCARBON RESPIRATORY AND TISSUE KINETICS: APPLICATIONS TO PREDICTING TOXICITY IN DIFFERENT SPECIES Annual Report, 15 Jul. 1993 - 14 Jul. 1994
Cham E. Dallas, J. V. Bruckner, R. L. Tacket, and T. Reigle 15 Aug. 1994 167 p
(Grant AF-AFOSR-0356-91)
(AD-A285055; AFOSR-94-0558TR) Avail: CASI HC A08/MF A02

A series of experiments have been conducted to provide a pharmacokinetic data base for interspecies comparisons and for formulation and validation of physiologically-based pharmacokinetic models. The basic experimental design has involved giving equal doses of halocarbons in different species, including mice, rats, and dogs. Perchloroethylene (PCE), tetrachloroethane (TET), trichloroethylene (TCE), and trichloroethane (TRI) have been employed as test chemicals, in order to evaluate the relative importance of the physicochemical property of volatility on the kinetics and toxicity of halocarbons. In order to determine the dose received in target organs and other tissues, serial samples of brain, liver, kidney, lung, heart, skeletal muscle, and adipose tissue have been taken and analyzed for halocarbon content after administration of PCE, TET, and TRI in rats, PCE and TET in dogs, and TRI in mice. For neurobehavioral studies, an operant testing system has been employed for monitoring the central nervous system effects of halocarbons. Neurobehavioral studies have been conducted following oral and inhalation exposure to PCE, and from inhalation exposure to TRI in rats. DTIC

N95-20549# California Univ., San Diego, La Jolla, CA.
SKELETAL MUSCLE ISCHEMIA AND HEAT SHOCK PROTEINS Annual Report, 1 Jul. 1993 - 30 Jun. 1994
Wolfgang H. Dillman 26 Jul. 1994 9 p
(Contract DAMD17-93-J-3027)
(AD-A285364) Avail: CASI HC A02/MF A01

Blood loss resulting in decreased organ perfusion and subsequent ischemic injury of cardiac and skeletal muscle presents a significant problem for the soldier in combat. Recent findings have indicated that different forms of noxious stress including exposure to increased temperature, noxious chemical agents, and ischemia lead to increased expression of heat shock proteins (HSP) which have a protective effect against injury induced by noxious stimuli. We will determine in this proposal if a rat skeletal muscle derived permanent cell line, L6 cells, expressing increased amounts of HSP70 will show protection against damaged induced by simulated ischemia. To generate L6 cells which permanently overexpress the inducible HSP70 proteins, cells will be transfected with a neomycin resistance gene and the inducible HSP70 gene. Stable lines will be selected by growing L6 cells in the presence of neomycin. Cells which have the neomycin resistance gene and the HSP70 gene incorporated into their DNA will survive. Such stably transfected L6 cell lines will then be exposed to simulated ischemia consisting of hypoxia, absence of glucose, low tonicity, and resultant ischemic damage will be determined by quantitating cell viability measured in colony formation assays, the inhibition of protein synthesis and the release of cytoplasmic enzymes like creatine kinase. These studies will determine if inducible HSP70 exerts a protective effect against ischemia mediated muscle injury. Demonstrating a protective effect of HSP70 protein will make it a useful agent to reduce ischemic muscle damage in soldiers exposed to muscle injury in combat. DTIC

N95-20602 Defence Research Establishment Suffield, Ralston (Alberta).
ENHANCEMENT OF CELL MEDIATED IMMUNITY THROUGH NON-SPECIFIC IMMUNOSTIMULATION WITH LIPOSOME ENCAPSULATED GAMMA-INTERFERON
J. P. Wong, B. Kournikakis, E. G. Saravolac, and L. C. Gorton Apr. 1994 24 p Limited Reproducibility: More than 20% of this document may be affected by microfiche quality
(AD-A279667; DRES-SR-584) Avail: Issuing Activity (Defense Technical Information Center (DTIC))

The ability of liposome-encapsulated gamma interferon (LIP-gamma IFN) to stimulate mouse cell-mediated immunity was assessed both in vivo and in vitro. The enhancement of the cell-mediated immune response was demonstrated in vitro by a chemiluminescent assay which measured the phagocytic activity of peritoneal macrophages. Peritoneal macrophages harvested from mice treated with gamma interferon (gamma IFN) or muramyldipeptide showed significant increases in both macrophage yield as well as in ability to phagocytize zymosan particles. However, when treated with gamma IFN encapsulated within liposomes both macrophage yield and phagocytic activity further increased by at least 100% over unencapsulated gamma IFN. Using the in vivo influenza mouse protection model, intranasally administered LIP-gamma IFN resulted in a 70% survival rate to mice challenged intranasally with 10 LD50 doses of influenza A/PR/8 virus compared with a 20% survival rate with free gamma IFN. Together these results suggest that liposome encapsulation increases gamma IFN efficacy in providing non-specific stimulation of the cell-mediated immune system. DTIC

N95-20710 Naval Aerospace Medical Research Lab., Pensacola, FL.
EFFECTS OF BIFOCAL AND PROGRESSIVE-ADDITION CORRECTIVE LENSES ON AVIATOR TARGET-DETECTION PERFORMANCE Interim Report, 1 Oct 1992 - 30 Sep. 1993
M. D. Reddix, A. S. Markovits, P. D. Collyer, and S. R. OConnell Dec. 1993 17 p Limited Reproducibility: More than 20% of this document may be affected by microfiche quality
(NR Proj. M00-96)
(AD-A279698; NAMRL-1390) Avail: Issuing Activity (Defense Technical Information Center (DTIC))

The objective of this project was to determine if the type of presbyopic correction worn by aviators, conventional bifocal versus progressive-addition lenses (PAL's), differentially affects aviator visual search performance. Experienced aviators with tactical fighter aircraft experience searched for high-contrast targets under simulated dawn/dust lighting conditions while wearing either a standard bifocal (ST-25) or PAL spectacle correction. Latency of locating high-contrast targets under these viewing conditions was affected differentially by the type of presbyopic correction used.

Specifically, compared to a standard bifocal (ST-25), a PAL correction (Varilux Infinity) significantly lowered the time needed to locate static targets at a cockpit-instrument viewing distance (83 cm). Accuracy of target-location responses was not affected by the type of correction used. In addition, 7 months post experiment, 7 of the 12 participants (58%) indicated that they used their PAL correction exclusively when flying the T-39 Sabre Liner. Three subjects (25%) used their PAL correction intermittently (primarily at night) when flying, and two subjects preferred not to use the PAL's. These results suggest that: (1) relative to bifocals, speed of responding to static targets at intermediate viewing distances may be improved by wearing PALS; and (2) subjects were able to adapt to PAL lenses quickly in a laboratory setting, using them later in a functional aviation environment.
DTIC

N95-20763*# National Aeronautics and Space Administration. Langley Research Center, Hampton, VA.
ACOUSTIC CALIBRATION APPARATUS FOR CALIBRATING PLETHYSMOGRAPHIC ACOUSTIC PRESSURE SENSORS Patent Application
Allan J. Zuckerwar, inventor (to NASA) and David C. Davis, inventor (to NASA) 11 May 1994 14 p
(NASA-Case-LAR-14977-1; NAS 1.71:LAR-14977-1;
US-Patent-Appl-SN-243665) Avail: CASI HC A03/MF A01

An apparatus for calibrating an acoustic sensor is described. The apparatus includes a transmission material having an acoustic impedance approximately matching the acoustic impedance of the actual acoustic medium existing when the acoustic sensor is applied in actual in-service conditions. An elastic container holds the transmission material. A first sensor is coupled to the container at a first location on the container and a second sensor coupled to the container at a second location on the container, the second location being different from the first location. A sound producing device is coupled to the container and transmits acoustic signals inside the container.
NASA

N95-20811# California Univ., Berkeley, CA. Dept. of Molecular Biology.
COMPUTER BASED ANALYSIS AND SYNTHESIS OF RETINAL FUNCTION Annual Report, 1 Feb. 1992 - 31 Jan. 1993
Frank S. Werblin 27 Jan. 1994 16 p
(Grant AF-AFOSR-0196-91)
(AD-A286084; AFOSR-94-0676TR) Avail: CASI HC A03/MF A01

A fully functional, real time dynamic model of retinal activity has been implemented on a high speed digital image processor. The model uses a complete set of physiciological parameters derived from electrophysiological studies of synaptic transmission, cell coupling, voltage-gated currents and visual function in the retina of the tiger salamander. This model displays the patterns of activity generated at each sheet of retinal cells in real time, in response to any arbitrary stimulus pattern. Recent work measures both the patterns of activity and the activity of single units within the living retina itself at the level of the photoreceptors, horizontal and bipolar cells. These measurements are then correlated with the patterns generated by the model to verify the accuracy of the parameters and functions used to model the retina. For the most part, the correlations are quite close, suggesting that the parameters we have used and the functional relations between elements we have selected are adequate. A recording system using an array of electrodes to constructed and will be used during the next year to record patterns of activity. These patterns will then be compared with those generated by the model.
DTIC

N95-20848# Texas Univ. Health Science Center, San Antonio, TX.
INVESTIGATION OF LASER-INDUCED RETINAL DAMAGE: WAVELENGTH AND PULSEWIDTH DEPENDENT MECHANISMS Final Technical Report, 1 Apr. 1992 - 30 Jun. 1994
Randolph D. Glickman 30 Jun. 1994 19 p
(Grant AF-AFOSR-0208-91)
(AD-A286066; UTHSCSA-OPH-94-01; AFOSR-94-0621TR) Avail: CASI HC A03/MF A01

Although the consequences of excessive light exposure to the eye have been known since ancient times, the actual mechanisms of light damage in biological tissue have only been systematically investigated in this century. The response of tissue to laser or incoherent light depends on the power density, peak power, and wavelength of irradiating energy. At least three light damage mechanisms have been identified. Photochemical damage is produced by short wavelength light (typically less than 550 nm) of long exposure duration, low peak power, and relatively low to moderate power density. Because tissue heating is minimal under these conditions, damage is thought to occur as result of excitation of target molecules to excited triplet states, some of which damage tissues directly through proton or electron transfers. The light-activated molecules may also cause damage indirectly by reacting with molecular oxygen to produce oxygen radicals, which are known agents of cellular damage. Thermal damage may be produced by light exposures of any wavelength capable of being absorbed by the tissue, given a sufficiently high power density and/or moderate to high peak power. Heating occurs by direct absorption of photons by a tissue chromophore which converts this photic energy into increased vibrational modes. The target chromophore, as well as surrounding structures depending on local heat conductivity, may then undergo thermal denaturation. At very high peak power, however, the strength of E-, or electrical, field of the absorbed electromagnetic wave may exceed the dielectric properties of the absorbing tissue, causing optical breakdown, ionization, plasma formation, and other phenomena associated with nonlinear (photodisruptive) damage mechanisms.
DTIC

N95-20850# East Carolina Univ., Greenville, NC. School of Medicine.
EVALUATION OF DRIED STORAGE OF PLATELETS FOR TRANSFUSION: PHYSIOLOGIC INTEGRITY AND HEMOSTATIC FUNCTIONALITY Triannual Report No. 2, 1 Jun. - 30 Sep. 1994
Arthur P. Bode 27 Oct. 1994 7 p
(Contract N00014-92-J-1244)
(AD-A286078) Avail: CASI HC A02/MF A01

The current long term dried storage study was terminated at 8 months in this reporting period. The preparations under study were (1) 0.02% permanganate in 5% BSA, and (2) 1.8% paraformaldehyde in 500 mM Trehalose stored desiccated at RT, 4 C, or at -70 C. Neither prep maintained good morphology at any temperature, and there was minimal ristocetin aggregation or hypotonic shock response remaining. At this 8 month workup, yield of intact platelets upon reconstitution was dependent on the storage conditions: 27-29% for RT, 41-46% for 4 C, 68-78% for -70 C. Our conclusion from this study reinforces what we learned from earlier storage studies: that there is significant deterioration of product at RT. In this particular experiment we found that permanganate-treated platelets, or para-platelets dried in Trehalose are as susceptible to loss of integrity over time as other preps. Our platelet handling techniques have improved since these studies were initiated. Another set of new preparations will be set aside for long-term storage in the next reporting period.
DTIC

N95-20851# East Carolina Univ., Greenville, NC. School of Medicine.
PRECLINICAL INVESTIGATION OF LYOPHILIZED PLATELET PREPARATIONS Annual Report No. 1, 1 Sep. - 31 Aug. 1994
Arthur P. Bode 31 Oct. 1994 9 p
(Contract N00014-93-J-1034)
(AD-A286079) Avail: CASI HC A02/MF A01

We have previously shown that lyophilized platelets (L-Plt) retain properties of adhesion and activatability in the Baumgartner perfusion chamber (Trans 33:72S, 1993). Now we have analyzed L-Plt in two systems directly testing hemostatic function. Study Design: One is a prototype device simulating the Ivy bleeding time in vitro (IVBT) and collagen-induced thrombus formation (CITF) in recalcified whole blood (Xylum Clot Signature Analyzer: CSA); the other is an in vivo bleeding time in dogs on full clinical heart-lung bypass before and after infusion of L-Plt. Results: On the CSA, L-Plt gave an average (n=4) IVBT of 1 min 58 sec and a CITF of 73% versus 2 min 14 sec and 88% respectively for fresh platelets. Expired platelet concentrates gave indeterminate results because aggregates clogged the lines. IVBT greater than 6 min and CITF less than 25% is typical of vWD patients. In two canine heart-lung bypass studies, the in vivo bleeding time improved from greater than 15 min to 5-7 min after infusion of abolus of 2-3 x 1011 L-Plt. The corrected count increments were (1) 88% and (2) 47% based on estimated circulatory volume. Conclusions: These results demonstrate the hemostatic activity of L-Plt and their potential value in transfusion medicine.
DTIC

N95-20971# Helsinki Univ. of Technology, Espoo (Finland). Dept. of Technical Physics.
SEMINAR ON BIOMEDICAL ENGINEERING 1993
T. Katila, ed. and Jyrki Lotjonen, ed. 23 Mar. 1994 123 p Seminar

held in Feb. - Apr. 1993
(ISSN 0355-7804)
(PB95-104402; TKK-F-B151; ISBN-951-22-1612-4) Avail: CASI HC A06/MF A02

Devices that collect 3D data from human beings are nowadays very common diagnostic tools in big hospitals. Magnetic Resonance Imaging (MRI) and Computerized Tomography Imaging (CT) produce very detailed anatomical information of a human being. Those methods collect a series of 2D images. When slices are put one on the other, a 3D image can be created. The finest resolution of modern imaging devices is about one millimeter (MRI and CT techniques). Usually the interslice distance is longer than the pixel distance in the slices. The resolution limits the size of the collected digital images. This problem can be removed by enlarging the image. Because data is in digital form we have to calculate more voxels (3D pixel) between the original points. This is called interpolation. NTIS

N95-20977 Naval Aerospace Medical Research Lab., Pensacola, FL.
BIBLIOGRAPHY OF SCIENTIFIC PUBLICATIONS 1975-1993
K. S. Mayer Mar. 1994 61 p Limited Reproducibility: More than 20% of this document may be affected by microfiche quality
(AD-A279767) Avail: CASI HC A04

This publication lists citations of all unclassified research reports, special reports, monographs, joint reports, journal articles, and proceedings that were published by the Naval Aerospace Medical Laboratory during calendar years 1975 through 1993. Qualified users may request reprints from the Defense Technical Information Center, Cameron Station, Alexandria, VA 22314 (commercial 202/274-7633 or DSN 284-7633). Reports are available to the public from the National Technical Information Service, Department of Commerce, 5285 Port Royal Road, Springfield, VA 22161 (telephone 703/487-4650). DTIC

N95-20979# Environmental Protection Agency, Research Triangle Park, NC. Clinical Research Branch.
CARBOXYHEMOGLOBIN FORMATION DUE TO TRANSIENT EXPOSURE TO HIGH LEVEL CARBON MONOXIDE: EXPERIMENTAL RESULTS AND AN EXPLANATORY MODEL Final Report, 18 Aug. 1987 - 30 Sep. 1994
Milan J. Hazucha (North Carolina Univ., Chapel Hill, NC.), Marjolein V. Smith (Smith, Marjolein V., Raleigh, NC.), Vernon A. Benignus, and Phillip A. Bromberg (North Carolina Univ., Chapel Hill, NC.) Sep. 1994 68 p
(AD-A285476) Avail: CASI HC A04/MF A01

Fifteen men were exposed to 6,683 PPM C18O for 3.1 - 6.6 min. Venous and arterial blood sample were drawn at one-min intervals beginning at the start of exposure and finishing 10 min later. Simultaneously, V(sub A) was calculated from the measured values of V(sub E) and deadspace. V(sub E) was measured by integrating digitized continuous measures of inhaled and exhaled gas. All parameters of the nonlinear Coburn-Forster-Kane equation (CFKE) were measured on the individual subject except for the Haldane affinity ratio. Predictions of venous blood COHb in samples collected ca. two min after cessation of exposure were accurately predicted by the CFKE. Both venous and arterial COHb were inaccurately predicted during COHb formation, however. Venous levels were overpredicted during formation due to delayed appearance of COHb. Individual subjects differed markedly in the delay of COHb appearance in venous blood. Arterial COHB was consistently underestimated either by the CFKE or by predictions based on venous blood samples. Thus, exposure of such organs as brain or heart to COHb can be higher than expected from previous knowledge when transient CO exposure is involved. An explanation is suggested for the observed differences between arterial and venous COHb on the basis of the regional circulation of the forearm, where both samples were taken. Because regional circulation patterns are known to vary with physical training, the differences in physical training between subjects may account for the observed variation. An expanded model was derived from the Coburn-Forster-Kane equation that reflects the above hypothesis. Most of the parameter values for the expanded model were measured on individual subjects. Literature values were used for other parameters. DTIC

N95-21007 Technical Research Centre of Finland, Espoo (Finland).
ANALYSIS OF MUSCULO-SKELETAL LOADING USING ELECTROMYOGRAPHY AND BIOMECHANICAL MODELLING Ph.D. Thesis
Hannu Nieminen 1 Jun. 1994 257 p
(PB95-135828; VTT/PUB-180) Copyright Avail: Issuing Activity (National Technical Information Service (NTIS))

Musculoskeletal disorders of chronic nature are a serious problem in modern society. Two important methods for studying the operation of the musculoskeletal system and indirectly estimating the muscle forces are biomechanical modelling and electromyography (EMG). NTIS

N95-21016 Technische Univ., Delft (Netherlands).
RADIOFREQUENCY HYPERTHERMIA SYSTEMS: EXPERIMENTAL AND CLINICAL ASSESSMENT OF THE FEASIBILITY OF RADIOFREQUENCY HYPERTHERMIA SYSTEMS FOR LOCO-REGIONAL DEEP HEATING Ph.D. Thesis
G. C. vanRhoon 1994 205 p Prepared in cooperation with Daniel den Hoed Cancer Center, Rotterdam, Netherlands
(PB94-206885; ISBN-90-6275-978-5) Copyright Avail: Issuing Activity (National Technical Information Service (NTIS))

Contents are: introduction; loco-regional deep hyperthermia; methods to evaluate the characteristics of hyperthermia applicators; the RCA 27 MHz ridged waveguide system; the HTM3000P capacitive hyperthermia system; a ring applicator system for loco-regional deep hyperthermia; and experimental assessment of electric impedance tomography integrated with the ring applicator. NTIS

N95-21028 Technische Hogeschool, Delft (Netherlands).
INTEGRATION OF SEGMENTATION AND STEREO MATCHING Ph.D. Thesis
Y. Zhang 16 Jun. 1994 187 p
(PB95-107819; ISBN-90-9007256-X) Copyright Avail: Issuing Activity (National Technical Information Service (NTIS))

Segmentation and stereo matching are the two essential steps in stereo vision. The thesis deals with their integration and can be roughly divided into three parts: segmentation, local matching, and global matching. It uses the Minimal Description Length (MDL) principle to encode image intensities and introduce a robust method to estimate the image intensity from raw image data. It also develops an approach for shape constrained image segmentation which integrates region growing and region boundary fitting. The thesis then deals with local matching in which only the local attributes of image regions are considered. It contains a detailed discussion on the integration of segmentation and stereo matching. The introduction of feedback enables the proposed system to send back the matching result to a resegmentation stage to improve the segmentation result and consequently the matching result. It then moves on to discuss global matching whose goal is to get unique matches, taking care of topological and other matching constraints. It formulates the global matching as a relaxation problem. NTIS

N95-21160# Naval Health Research Center, San Diego, CA.
MICROCLIMATE COOLING EFFECT ON PERCEIVED EXERTION IN FOUR HEAT/EXERCISE SCENARIOS Interim Report
Ralph G. Burr, Daniel W. Trone, Robert S. Pozos, Elmer J. Labranch, and Christopher S. Parrish May 1994 16 p
(NR Proj. MM3-3-P-30)
(AD-A285549; NHRC-94-7) Avail: CASI HC A03/MF A01

Operation Desert Storm demonstrated a need for individual microclimate cooling during strenuous activity. Evaluation of a cooling system should not only consider physiological functions but subjective measures of comfort, such as ratings of perceived exertion (RPE). The objectives of this study were evaluate a cooling suit's effect on: (1) subjective RPE, (2) heart rate (HR), and (3) the magnitude of the correlation between RPE and HR. Thirty-one U.S. Marine Corps subjects, wearing chemical defense ensemble, were tested in four separate scenarios of heat/exercise combinations during both cooling suit and control sessions. Results of repeated measures multivariate analysis of variance showed that RPE was significantly lowered by wearing a cooling suit during only the most strenuous of the four scenarios. A decrease in the magnitude of the correlation between RPE and HR during all four cooling suit sessions indicated that a microclimate cooling suit interferred with perception of exertion. DTIC

N95-21180 Naval Aerospace Medical Research Lab., Pensacola, FL.
THE SHARPER IMAGE: IMPLEMENTING A FAST FOURIER TRANSFORM (FFT) TO ENHANCE A VIDEO-CAPTURED IMAGE Special Report
J. E. Parker, W. K. Krebs, J. S. Marsh, D. L. Still, and L. A. Teeme Jan. 1994 35 p Limited Reproducibility: More than 20% of this document may be affected by microfiche quality
(NR Proj. MM3-3130)
(AD-A279790; NAMRL-SR-94-1) Avail: CASI HC A03

The lack of visual information and cues in night vision images has produced a history of in-flight mishaps where night vision devices (NVDS) were used as the primary source of sight. In an effort to produce improved night vision images and thereby reduce in-flight mishaps, a video enhancement technique, the sharper image, was developed to enhance, filter, and study images generated by NVDS. The sharper image technique enhances night vision images by filtering or amplifying the spatial frequencies that are distorted by NVDS. In this report, we describe the necessary methodology and procedures to enhance, filter, or process any visual image. We also discuss other computational image software and review the advantages and disadvantages of each. DTIC

N95-21348# Helsinki Univ. of Technology, Espoo (Finland). Low Temperature Lab.
SOURCE DISTRIBUTION OF VISUAL EVOKED NEUROMAGNETIC RESPONSES
Seppo Ahlfors, Risto J. Ilmoniemi (Helsinki Univ. Central Hospital, Helsinki, Finland.), Matti Kajola, Jukka Knuutila, and Juha Simola May 1994 18 p See also PB85-201036
(ISSN 0355-7790)
(PB95-127643; TKK-F-A729) Avail: CASI HC A03/MF A01

Visual contrast-onset-evoked magnetic fields were measured with a 122-channel magnetometer covering the whole scalp. To facilitate the estimation of the spatial and temporal distribution of cortical generators, the responses were broken into two parts according to the dependence on the visual-field location of the stimulus. Minimum-norm estimates suggested that the generators for the part that was independent of the stimulus position were located in several occipital and extra-occipital regions, whereas the visual-field-dependent generators were predominantly in the occipital cortex. Our results support the view that information about the retinal image, even during passive viewing, is routed to several cortical areas. NTIS

N95-21352# Netherlands Inst. for Brain Research, Amsterdam (Netherlands).
NETHERLANDS INSTITUTE FOR BRAIN RESEARCH PROGRESS REPORT, 1993
R. M. Buijs, O. Pach, and W. T. P. Verweij 1994 117 p
(PB95-135398) Avail: CASI HC A06/MF A02

The central research theme of the Netherlands Institute for Brain Research is 'Development, plasticity and aging of the brain'. The theme has been specified in the following three themes and four research programs. Hypothalamus 1-Life span functions of hypothalamic nuclei in health and disease; Hypothalamus 2-Hypothalamic integration mechanisms; The development and plasticity of the prefrontal cortex (PFC); Significance of structure-function relationships for the development and self-organization of neurons and networks. NTIS

N95-21424 Centre d'Etudes et de Recherches de Medecine Aeronautique, Paris (France). Dept. de Physiologie Analytique.
EFFECT OF INCREASED VENOUS BACKFLOW ON THE RELEASE OF CARDIAC HORMONE. FINE STRUCTURAL, IMMUNOHISTOCHEMICAL, AND BIOCHEMICAL STUDY Final Report [EFFETS DE L'AUGMENTATION DU RETOUR VEINEUX SUR LA LIBERATION DE L'HORMONE CARDIAQUE. ETUDE ULTRASTURCTURALE, IMMUNOHISTOCHIMIQUE ET BIOCHIMIQUE]
X. Holy, E. Zerath, P. Facy, A. Francois, and A. Malouvier Feb. 1993 100 p In FRENCH Sponsored by Direction des Recherches, Etudes et Techniques
(PB95-130399) Avail: Issuing Activity (National Technical Information Service (NTIS))

This study sought to identify the cellular events that occur after a blood shift to the upper part of the body stimulates the release of Atrial Natriuretic Factor (ANF). Eight male rats were placed in antiorthostatic position (-30 deg) to produce right atrial distention for periods ranging from 1/4 hour to 6 hours. Samples of the right atrial appendage were then analyzed. Results showed a significant increase in immunoreactivity inside the granules after 1/2 hour of stimulation. The number of granules rose, but the size of the vesicles did not change. Plasma ANF concentration increased significantly after 1 hour of stimulation. This result indicates that in less than 1/2 hour, heart myocytes can modify their storage of ANF, and that the concentration of the hormone inside secretion vesicles increases at an early stage. The delay between this event and the hormone's peak plasma level is probably linked to the vesicles' release process. Further studies are need to describe the mechanism involved. NTIS

N95-21580 Technische Hogeschool, Delft (Netherlands). Dept. of Mechanical Engineering and Marine Technology.
INTRAMYOCARDIAL BLOOD VOLUME AND OXYGEN EXCHANGE Ph.D. Thesis
C. P. B. VanderPloeg 7 Jun. 1994 142 p
(PB95-108015; ISBN-90-370-0104-1) Copyright Avail: Issuing Activity (National Technical Information Service (NTIS))

Contents include the following: Introduction; Functional Distribution of Coronary Vascular Volume in the Beating Goat Heart; Comparison of Different Oxygen Exchange Models; Heart Rate Influences Gregg's Phenomenon During Flow Controlled Perfusion in Goats; Transients in Myocardial Oxygen Consumption Following Abrupt Changes in Perfusion Pressure in the Goat; Effect of Heart Contraction on the Functional Distribution of Coronary Volume in Goats; and Conclusions. NTIS

N95-21595# Michigan Univ., Ann Arbor, MI.
RADIOPHARMACEUTICALS FOR DIAGNOSIS Progress Report, 1987-1993
Mar. 1994 51 p
(Contract DE-FG02-88ER-60639)
(DE95-002200; DOE/ER-60639/6) Avail: CASI HC A04/MF A01

In the period 1969-1986, this project was directed to the evolution of target-specific labeled chemicals useful for nuclear medical imaging, especially radioactive indicators suited to tracing adrenal functions and localizing tumors in the neuroendocrine system. Since 1986, this project research has focused on the chemistry of positron emission tomography (PET) ligands. This project has involved the evaluation of methods for radiochemical syntheses with fluorine-18, as well as the development and preliminary evaluation of new radiopharmaceuticals for positron emission tomography. In the radiochemistry area, the ability to predict fluorine-18 labeling yields for aromatic substitution reactions through the use of carbon-13 NMR analysis was studied. Radiochemical yields can be predicted for some structurally analogous aromatic compounds, but this correlation could not be generally applied to aromatic substrates for this reaction, particularly with changes in ring substituents or leaving groups. Importantly, certain aryl ring substituents, particularly methyl groups, appeared to have a negative effect on fluorination reactions. These observations are important in the future design of syntheses of complicated organic radiopharmaceuticals. In the radiopharmaceutical area, this project has supported the development of a new class of radiopharmaceuticals based on the monoamine vesicular uptake systems. The new radioligands, based on the tetrabenazine structure, offer a new approach to the quantification of monoaminergic neurons in the brain. Preliminary primate imaging studies support further development of these radioligands for PET studies in humans. If successful, such radiopharmaceuticals will find application in studies of the causes and treatment of neurodegenerative disorders such as Parkinson's disease. DOE

N95-21629 Science Applications International Corp., McLean, VA.
ACUTE RADIATION SICKNESS AMELIORATION ANALYSIS Technical Report, 20 Jul. 1990 - 19 Jul. 1993
Sabina I. Robinson, Alan J. Feister, and Donna L. Bareis 1 May 1994 91 p Limited Reproducibility: More than 20% of this document may be affected by microfiche quality
(Contract DNA001-90-C-0111)
(AD-A279084; DNA-TR-93-131) Avail: Issuing Activity (Defense Technical Information Center (DTIC))

Three tasks were conducted under the acute radiation sickness amelioration analysis in support of the Defense Nuclear Agency (DNA) and

NATO Army Armaments Group (NAAG) Project Group 29 (PG-29) on drugs for the prevention of radiation-induced nausea and vomiting: (1) documents were collected and entered into a data base, (2) data reviews and analyses were performed, and (3) PG-29 and Triservice meetings involving anti-emetic drug development were supported and documented. Approximately 2000 documents were collected, with 1424 complete bibliographic citations entered into a WordPerfect 5.1 data base. Eight reviews and analyses addressing different aspects of the safety and efficacy of the candidate anti-emetic drugs ondansetron and granistron were prepared. Support was provided for seven international PG-29 meetings and two U.S. Triservice meetings in which the efforts of PG-29 were discussed. These tasks have enabled the DNA and PG-29 to make good progress toward the goal of recommending a serotonin type-3 (5-HT3) receptor antagonist anti-emetic drug for use in military personnel. DTIC

N95-21941 Rothe Development, Inc., San Antonio, TX.
THE INFLUENCE OF CORONARY ARTERY DISEASE ON +Gz TOLERANCE: A PRELIMINARY STUDY Final Report, Feb. 1989 - Dec. 1991
John W. Burns, Jemett L. Robinson, John W. Fanton, Harold Davis, and Londe A. Richardson Apr. 1994 7 p Limited Reproducibility: More than 20% of this document may be affected by microfiche quality
(Contract F33615-85-D-4510; AF Proj. 7930)
(AD-A279305; AL/CF-TP-1994-0004) Avail: Issuing Activity (Defense Technical Information Center (DTIC))

Current Air Force policy restricts pilots, with even minimal coronary artery disease (CAD), from flying high-performance aircraft. Liberalization of this policy is being considered, but additional data are needed for more informed decision. Eleven miniature swine (MS) were placed on a high cholesterol/high fat diet for 1 year. Five additional MS were maintained on a standard control swine diet (no cholesterol) over the same time. A vascular access port (VAP) was surgically placed into the superior vena cava. The 16 unanesthetized MS were +Gz-stressed one or two times each, using an alternating 4-8 +Gz simulated aerial combat maneuver (SACM) with 10 sec at each +Gz level. The MS were protected with an abdominal bladder anti-G suit. At the end of the SACM, Tc-99m was infused into the VAP and the MS were scanned for myocardial perfusion approximately 1 h later. Three MS died before data collection, one at 6 mos and two at 9 mos. Histopathology showed moderate-to-severe CAD in the three MS. Control and experimental plasma cholesterol levels (mg%) were: total = 77 and 422; ratio = 2.3 and 8.6; LDL = 35 and 353, respectively. Dysrhythmias and T-wave alterations during +Gz were seen equally in both the control and experimental MS. However, ST-T segment changes during +Gz were observed in all of the cholesterol MS, but not in the control MS. DTIC

N95-21947* National Aeronautics and Space Administration, Washington, DC.
AEROSPACE MEDICINE AND BIOLOGY: A CONTINUING BIBLIOGRAPHY WITH INDEXES (SUPPLEMENT 399)
Mar. 1995 121 p
(NASA-SP-7011(399); NAS 1.21:7011(399)) Avail: CASE HC A06

This bibliography lists 299 reports, articles and other documents introduced into the NASA Scientific and Technical Information System during March 1995. Subject coverage includes: aerospace medicine and physiology, life support systems and man/system technology, protective clothing, exobiology and extraterrestrial life, planetary biology, and flight crew behavior and performance. Author

N95-21989# Naval Aerospace Medical Research Lab., Pensacola, FL.
COMMAND HISTORY, 1993 Final Report, Jan. - Dec. 1993
R. E. Gadolin and K. S. Mayer Apr. 1994 145 p
(AD-A279775) Avail: CASI HC A07/MF A02

This publication is a compilation of significant events that occurred at the Naval Aerospace Medical Research Laboratory during 1993. DTIC

N95-22001 Defence and Civil Inst. of Environmental Medicine, Downsview (Ontario).
THERMAL RESISTANCE OF THE CHEEK IN COLD AIR
R. J. Osczevski Sep. 1994 9 p Limited Reproducibility: More than 20% of this document may be affected by microfiche quality
(AD-A286257; DCIEM-94-47) Avail: CASI HC A02

Some experiments were carried out to characterize the thermal resistance of the tissues of the cheek area. Heat flow and skin temperature in cold air were measured with a heat-flux transducer. The face was cold when the cheek skin temperature was below 15 C and painful when the skin temperature fell below 10 C. Thermal resistance increased as skin temperature fell, reaching a maximum of 0.07 m(exp 2) K/W at a skin temperature between 10 C and 15 C. DTIC

N95-22003# Naval Medical Research Inst., Bethesda, MD.
SOLUBILITIES OF NITROGEN AND HELIUM IN WATER AND BLOOD AT 37 C AND PRESSURES OF UP TO 11 ATA Technical Report, 1990 - 1992
J. Thai and G. Albin Jun. 1994 17 p
(Proj. M00-99)
(AD-A286269; NMRI-94-21) Avail: CASI HC A03/MF A01

The solubilities of N2 and He in water and whole blood were measured at 37 C using a barometric method described in an earlier report. Solubilities have been measured successfully in H2O at approximately 2 ATA and approximately 11 ATA. In addition, protocols for measuring solubilities in whole blood have been explored. Measurements in blood have been unsuccessful thus far (i.e., have disagreed with published results), apparently because efforts have failed to eliminate interphase transport of the metabolic gases O2 and CO2 during the experiment. Blood experiments can resume after the experimental assembly has been modified to allow sampling of the gas phase so that its composition can be determined. This information, in conjunction with the pressure measurements that already are made during each experiment, will enable one to eliminate the confounding effect of O2 and CO2 transport. DTIC

N95-22004# Army Research Inst. of Environmental Medicine, Natick, MA.
SUSTAINING THE HEALTH AND PERFORMANCE OF SOLDIERS/WARFIGHTERS DEPLOYED TO HARSH ENVIRONMENTS Final Technical Note
Beau J. Freund, G. C. Lindsay, and Ross E. Lipton Nov. 1994 27 p
(AD-A286270; USARIEM-TN95-2) Avail: CASI HC A03/MF A01

This report describes the contributions, core competencies, and capabilities of the U.S. Army Research Institute of Environmental Medicine and this institute's commitment to protect, sustain, and enhance the health and performance of soldiers. The institute's mission focuses on two of the four major threats to the warfighter: environmental and occupational. The significance placed upon environmental threats is described in Army FM 100-5, '... U.S. Army forces must be prepared to fight and win on short notice anywhere in the world, from blistering deserts, frigid wastelands, in rain forests, tundra, mountains, jungles and swamps ... ' Environmental threats to the soldier are addressed with militarily relevant discussions of injuries and casualties incurred by military forces operating in harsh environments within the research disciplines of environmental physiology and medicine. Occupational threats are presented in areas of physical capabilities, physical and cognitive performance, and the multi-stressors associated with continuous and sustained operations. The impact of these threats is studied within the research disciplines of occupational physiology and physical performance; occupational medicine; military performance and neuroscience; and military nutrition. The products of this research institute draw heavily upon the knowledge gained by its research staff over the past forty years and by our researchers that have accompanied troops deployed around the world in training, peacekeeping, and combat operations. DTIC

N95-22027# Hilton Systems, Inc., Cherry Hill, NJ.
AGE 60 STUDY. PART 1: BIBLIOGRAPHIC DATABASE Final Report
Oct. 1994 181 p
(Contract DTFA02-90-C-90125)
(AD-A286245; DOT/FAA/AM-RN-94/20-Pt-1) Avail: CASI HC A09/MF A02

As part of their research contract with the FAA to study issues related to the Age 60 Rule for pilot mandatory retirement, Hilton Systems, Inc. in collaboration with Lehigh University faculty and research facilities, compiled this extensive bibliography. Topics included pilot aging, performance, health and physiological factors, as well as other aviation and pilot related topics. Citations were included from a variety of sources including international and military studies. The bibliography was organized in three sections. The

first section presents a bibliographic listing on the above topics. The second section provides a listing of publications by authors active in related fields. Finally, the third section provides citations from the driving literature.
DTIC

N95-22040# Hilton Systems, Inc., Cherry Hill, NJ.
AGE 60 STUDY. PART 2: AIRLINE PILOT AGE AND PERFORMANCE. A REVIEW OF THE SCIENTIFIC LITERATURE Final Report
Diane T. Hyland, Edwin J. Kay, Jim D. Deimler, and Ernest B. Gurman Oct. 1994 139 p
(Contract DTFA02-90-C-90125)
(AD-A286246; RN-8025-1A-Pt-2; DOT/FAA/AM-94/21-Pt-2) Avail: CASI HC A07/MF A02

This review of the literature establishes the scientific foundation for subsequent studies on the Age 60 Rule research conducted under a contract with Hilton Systems, Inc. The scientific literature relevant to the separate scientific approaches required by the contract is reviewed. The document first provides a review of the Age 60 Rule, as well as theoretical and methodological considerations critical to the study of aging and the assessment of individual pilot performance. A proposed model is presented to form a framework for the research. Pilot behaviors affected by aging and/or experience are reviewed. Specific performance assessment batteries are reviewed in detail in Appendix A. Issues related to measuring complex pilot performance are discussed. Recommendations and criteria for developing a performance methodology are presented. The second part of the literature review provides a discussion of the issues related to the analysis of existing data to assess the relationship between pilot age, experience, and accident rates. This section provides a critical review of existing analyses and presents recommendations for an improved analytical methodology.
DTIC

N95-22083 Gezondheidsraad, Hague (Netherlands).
OPTICAL RADIATION: HEALTH BASED EXPOSURE LIMITS FOR ELECTROMAGNETIC RADIATION IN THE WAVELENGTH RANGE FROM 100 NANOMETER TO 1 MILLIMETER [OPTISCHE STRALING: GEZONDHEIDSKUNDIGE ADVIESWAARDEN VOOR BLOOTSTELLING AAN ELEKTROMAGNETISCHE STRALING MET GOLFLENGTEN TUSSEN 100 NANOMETER EN 1 MILLIMETER]
29 Jun. 1993 134 p In DUTCH
(PB95-132767) Avail: Issuing Activity (National Technical Information Service (NTIS))

Optical radiation includes infrared radiation, light and ultraviolet radiation. It is a form of electromagnetic radiation with wavelengths between 1 millimeter and 100 nanometers. The main source of optical radiation is the sun. Examples of artificial sources of optical radiation are electric radiators, halogen heaters and lamps, light bulbs, gas discharge tubes and various types of lasers. Excessive exposure to optical radiation can damage health. The levels at which this happens and the effects that occur are the subject of this report. Possible health-promoting effects of optical radiation are not considered.
NTIS

N95-22285# Inhalation Toxicology Research Inst., Albuquerque, NM.
URBAN AIR CARCINOGENS AND THEIR EFFECTS ON HEALTH
John F. Lechner 1994 13 p Presented at the Health and Environment Meeting, Mexico City, Mexico, 20-21 Oct. 1994
(Contract DE-AC04-76EV-01013)
(DE95-002259; CONF-9410236-2) Avail: CASI HC A03/MF A01

Airborne carcinogens may be relevant especially in metropolitan regions with extreme smog as a primary cause of lung cancer. Lung cancer is most common in urban environs and the incidence directly correlates with the size of the city. In addition, several, but not all formal epidemiological studies also suggest a positive correlation between lung cancer incidence and the intensity of air pollution exposure. There is further support for a role of air pollution; as of 1993, 4.4% of all of the bronchogenic adenocarcinoma cancer cases among Mexicans living in industrialized cities are under 40 years of age. It is plausible that chronic inhalation of automobile combustion products, factory emissions, and/or radon is at least partially responsible for the higher incidence of lung cancer exemplified by the never-smoking urban residents. The exceptionally high incidence of lung cancer cases among never-smokers living in highly industrialized Mexican cities offers a unique opportunity to use molecular epidemiology to test whether chronic inhalation of atmospheric pollutants increases the risk for this disease. Overall, the analysis of the genetic alterations in two cancer genes, and possibly the hprt locus should give new insight as to whether the urban never-smokers developed their cancers because of exposure to environmental pollutants.
DOE

N95-22287# Inhalation Toxicology Research Inst., Albuquerque, NM.
CURRENT CONCEPTS ON AIRBORNE PARTICLES AND HEALTH
Joe L. Mauderly 1994 15 p Presented at the Health and Environment Meeting, Mexico City, Mexico, 20-21 Oct. 1994
(Contract DE-AC04-76EV-01013)
(DE95-002260; CONF-9410236-1) Avail: CASI HC A03/MF A01

Epidemiological evidence of associations between environmental particulate concentrations and both acute and chronic health effects has grown with numerous recent studies conducted in the US and other countries. An association between short-term changes in particulate levels and acute mortality now seems certain. The association is consistent among studies and coherent among indicators of mortality and morbidity. Effects observed at surprisingly low pollution levels have raised concern for current exposures even in modestly polluted cities. Toxicology did not predict the acute mortality effect, and causal mechanisms are difficult to rationalize. Present data suggest that the fine fraction of particulate pollution is more toxic than larger particles, but the contribution of specific particulate species is poorly understood.
DOE

N95-22361 Centre de Recherches du Service de Sante des Armees, La Tronche (France).
STUDY OF PULSED LASER EFFECTS ON LIVING TISSUES Final Report [ETUDE DES EFFETS LASERS PULSES SUR LES TISSUS VIVANTS]
L. Court, D. Courant, D. Dormont, and B. Abadie 1994 59 p In FRENCH Prepared in cooperation with Direction des Recherches, Etudes et Techniques, Paris, France
(PB95-131330) Avail: Issuing Activity (National Technical Information Service (NTIS))

The object of the research was to study the effects of brief laser pulses emitted in the visible spectrum and the near infrared on living tissues, the eye and cell cultures, and human fibroblasts. Within the limits of their experimental conditions, the authors found that the irradiation of human fibroblasts by a laser beam will not alter the range of oncogenes that are normally expressed, their level of expression, and their regulation according to their growth. Because of technical problems, the study of the Ha-ras oncogene will require a more detailed analysis of the messenger RNA of the irradiated cells.
NTIS

N95-22371# Helsinki Univ. of Technology, Espoo (Finland).
TRANSFORMATION OF MULTICHANNEL MAGNETOCARDIOGRAPHIC SIGNALS TO STANDARD GRID FORM
J. Numminen, S. Ahlfors, R. J. Ilmoniemi, J. Montonen, and J. Nenonen Apr. 1994 33 p
(PB95-127114; TKK-F-A727) Avail: CASI HC A03/MF A01

Multichannel magnetocardiographic (MCG) recordings with fixed sensor arrays are not directly comparable with single-channel measurements carried out at standard grid locations. In addition, comparison of data obtained with different types of magnetometers is difficult. The authors present a method for transforming multichannel measurements to the standard-grid format. The minimum-norm estimate (MNE) of the source current distribution in the body is calculated, and the desired field components in standard grid points are then computed from the MNE. The authors measured three subjects with both a 24-channel and a single-channel instrument. The signals extrapolated from the multichannel measurements corresponded quite well to the single-channel data registered at the standard grid locations, especially in those grid points that were covered by the 24-channel device. It was also found that the method is relatively tolerant to errors in the location and orientation of the multichannel magnetometer. The basic advantage of the authors extrapolation method is its physiologic nature: the method is based on the mathematical modeling of the source current distribution rather than on direct constraints applied to the magnetic field.
NTIS

N95-22475# Columbia Univ., New York, NY.
DIFFUSIBLE DRIVING AND COUPLING SIGNALS OF THE BIOLOGICAL CLOCK Final Report, 1 Apr. 1992 - 31 Mar. 1994

Rae Silver 24 Jul. 1994 5 p
(Contract F49620-92-J-0195)
(AD-A285353; AFOSR-94-0591TR) Avail: CASI HC A01/MF A01

The goal of the research has been to determine whether there is evidence of a diffusible coupling signal from the Suprachiasmatic Nucleus. If a diffusible signal is physiologically significant, it has the potential for use as a bioactive agent for exogenous administration. We believe we now have evidence that such a signal exists, and that it can appear in biologically significant amounts in the cerebrospinal fluid. At the present time we are working to complete the most definitive experiments providing such proof. We are also working towards our next goal: to establish the experimental conditions for identifying the diffusible signal. DTIC

N95-22476# Helsinki Univ. of Technology, Espoo (Finland).
MAGNETIC SOURCE IMAGING OF VISUALLY EVOKED AND OSCILLATORY ELECTRICAL ACTIVITY OF THE HUMAN BRAIN Ph.D. Thesis
S. Ahlfors 6 Jun. 1994 148 p See also PB85-201036
(PB95-127205; ISBN-951-22-2150-0) Avail: CASI HC A07/MF A02

The aim of this thesis work was to develop biomagnetic recording and analysis techniques and to apply them to studies of visually-evoked and spontaneous electrical activity in the human brain. The magnetoencephalographic method was applied to studies of the human visual cortex and oscillatory brain activity. Cerebral source currents evoked by simple, passively viewed checkerboard stimuli were found to be distributed over large regions of the cortex, showing complex variations as a function of time. The usefulness of minimum-norm estimates was evident in cases in which a multitude of sources overlap, both when giving a 2D estimate of the primary current distribution and when providing a standard representation of the measured magnetic field. With retinotopically organized stimuli, some of the difficulties inherent in the biomagnetic inverse problem could be overcome. Similar differentiation of the underlying source patterns should be possible in future studies by varying other stimulus properties as well. NTIS

53 BEHAVIORAL SCIENCES

Includes psychological factors; individual and group behavior; crew training and evaluation; and psychiatric research.

N95-19887 Carnegie-Mellon Univ., Pittsburgh, PA. School of Computer Science.
A DATABASE FOR ANALYZING SEQUENTIAL BEHAVIORAL DATA AND THEIR ASSOCIATED COGNITIVE MODELS
Bonnie E. John 15 May 1994 24 p Revised Limited Reproducibility: More than 20% of this document may be affected by microfiche quality
(AD-A280061; CMU-CS-94-127; CMU-HCII-94-101) Avail: Issuing Activity (Defense Technical Information Center (DTIC))

Sequential behavioral data, be it verbal protocols, automatically-recorded keystrokes, or complete videotape protocols, can be analyzed at different levels of detail and from different viewpoints. If raw behavioral data is stored in a powerful database, rather than a simple text file, many domains will allow some automatic interpretation of that data. In addition, the raw data can be compared with traces of an associated computational cognitive model to assess how well the model accounts for the data and, conversely, how much support the behavioral data provides for the components of the model. This report describes a prototype database and user interface, called Trace & Transcription, that is designed to facilitate protocol analysis and cognitive modeling. This research was supported in part by a grant from US West Advanced Technologies Sponsored Research Program. The views and conclusions contained in this document are those of the author and should not be interpreted as representing the official policies, either expressed or implied, of US West. DTIC

N95-19957# Naval Aerospace Medical Research Lab., Pensacola, FL.
TEST RELIABILITY AND EXPERIMENTAL POWER
R. R. Stanny Dec. 1993 15 p
(AD-A279607; NAMRL-SP-93-7) Avail: CASI HC A03/MF A01

The reliability coefficient, rho(sub xx), has long been accepted as an index of the stability, repeatability, and precision of psychological tests. Because rho(sub xx) measures the proportion of the variance in a set of scores attributable to variation among individuals, values of rho(sub xx) are sometimes compared to justify using particular tests in studies of individual differences. Values of rho(sub xx) are also sometimes compared to justify using particular tests in experimental research. The latter practice is usually justified by arguing that larger values of rho(sub xx)) imply greater measurement precision and, therefore, potentially greater sensitivity to experimental treatments. That argument is not generally correct because the individual variation measured by rho(sub xx) is frequently confounded with measurement error in the denominators of significance tests. The effects of this confounding lead to 'paradoxical' situations in which reliability, as measured by rho(sub xx), may be inversely related (or unrelated) to experimental precision, as measured-by the reciprocal of experimental error. Because the power of an experiment increases with precision, as just defined, conditions that invert or negate the relationship between rho(sub xx) and precision also invert or negate the relationship between rho(sub xx) and power. These considerations do not mean that the reliability coefficient is necessarily irrelevant to experimental research. Because experimental designs differ in the degree to which they are influenced by individual variation, a consideration of the value of rho(sub xx)) a specific test yields will sometimes provide information about the best design in which to use that test. DTIC

N95-19970# Air Force Materiel Command, Brooks AFB, TX. Human Resources Directorate.
INTELLIGENT TUTORING SYSTEMS: PAST, PRESENT, AND FUTURE Interim Report, Apr. 1993 - Apr. 1994
Valerie J. Shute and Joseph Psotka May 1994 69 p Submitted for publication
(AF Proj. 2313)
(AD-A280011; AL/HR-TP-1994-0005) Avail: CASI HC A04/MF A01

In this paper, we address many aspects of Intelligent Tutoring Systems (ITS) in our search for answers to the following main questions: (1) What are the precursors of ITS?; (2) What does the term mean?; (3) What are some important milestones and issues across the 20+ year history of ITS?; (4) What is the status of ITS evaluations?; and (5) What is the future of ITS? We start with an historical perspective. DTIC

N95-19998# Harvard Univ., Cambridge, MA. Dept. of Psychology.
INTERMEDIATE LEVELS OF VISUAL PROCESSING Annual Report, 1 Oct. 1992 - 30 Sep. 1993
Ken Nakayama 30 Sep. 1993 3 p
(Contract F49620-92-J-0016)
(AD-A284922; AFOSR-94-0622TR) Avail: CASI HC A01/MF A01

Over the past year we have completed a number of studies on surface perception and visual attention. Although the two have been studied in isolation, during the latter part of our investigation, we have found some surprising relationships between the two. DTIC

N95-20007# South Carolina Univ., Columbia, SC. Dept. of Psychology.
ROLE OF WORKING MEMORY LIMITATIONS OF RETRIEVAL Annual Technical Report, May 1993 - May 1994
Randall W. Engle 12 May 1994 10 p
(Contract F49620-93-1-0336)
(AD-A280032; AFOSR-94-0332TR) Avail: CASI HC A02/MF A01

Over the past year, 11 studies have been completed on the role of working memory limitations on storage retrieval of information. One series demonstrated that, if subjects are highly trained and there is no interference among the items being retrieved, working memory limitations play no role in retrieval. However if there is interference among the information being retrieved, individuals low in working memory capacity suffer in retrieval from active memory compared to high working memory individuals. Regardless of interference condition, however, working memory capacity plays no role in retrieval from inactive or secondary memory. A second series of studies demonstrated that the phonological similarity effect, one of the primary sources of evidence for the articulatory loop, is not found if the words in the lists to be recalled are chosen from an unlimited set and presented silently. This casts doubt on the generality of this code, particularly for silent reading. DTIC

N95-20062# Air Force Materials Lab., Wright-Patterson AFB, OH. Crew Systems Directorate.
THE SPATIOTEMPORAL CHARACTERISTICS OF VISUAL MOTION PRIMING Final Report, Aug. 1991 - Aug. 1992
Alan R. Pinkus Jul. 1994 100 p
(AF Proj. 6893)
(AD-A284782; AL/CF-TR-1994-0084) Avail: CASI HC A05/MF A02

A motion signal that is produced from a sine-wave luminance grating which has undergone an abrupt 90-degree phase shift (frames 1 to 2) can serve as a priming signal that disambiguates motion of a second, 180-degree (counterphase) shift (frames 2 to 3). Four experiments investigated the spatiotemporal characteristics of this phenomenon which is termed visual motion priming (VMP). Experiment 1 varied the phase-shift magnitude of the priming signal from 22.5 through 157.5 degrees. This resulted in an inverted U-shaped half-sine function that peaked at 90 degrees with 93.5% priming. Experiment 2 varied frame 2 duration (192, 384, 768, and 1530 ms), spatial frequency (0.7, 1.4, and 2.8 cycles/degree), and used 19 or 48% contrast for the 3 frames. VMP decreased monotonically from about 94% at 192 ms to near 50% (chance level) at 768 and 1530 ms. Duration and spatial frequency were significant, but contrast had no systematic effect. Experiment 3 varied the ratio of frame 1 contrast (4, 6, 13, 19, 30, 48%) relative to frames 2 and 3, where both of the latter two frames had either 19 or 48% contrast. Several effects were observed. When the ratio of the contrasts between frames 1 and 2 was largest (4-48-48% contrast for frames 1-2-3, respectively), VMP was lowest at 82%. A smaller initial ratio, but a lower overall contrast level (4-19-19% contrast), resulted in a higher VMP of 91.5%. As the priming contrast ratios decreased to 1:4 or less, irrespective of overall contrast level, VMP quickly asymptoted. DTIC

N95-20064 Air Force Inst. of Tech., Wright-Patterson AFB, OH. School of Engineering.
A 3D STEREO DATA VISUALIZATION AND REPRESENTATION M.S. Thesis
Kai-Heng Wang Sep. 1994 110 p Limited Reproducibility: More than 20% of this document may be affected by microfiche quality
(AD-A284788; AFIT/GCE/ENG/94S-01) Avail: CASI HC A06

This thesis investigates a technique for improving the perception and visualization of three dimensional information. This improvement will eventually give physicians the ability to both visualize and understand biomedical image data. Raw data is used to generate a stereo image pair. The raw data must be put in run length encoding (RLE) format and then converted to a stereo pair. Once the stereo pair is generated, they must be displayed on the Silicon Graphics ONYX workstation in stereo mode. This research uses 3D images of planets and satellites. The display information is transmitted across cable and is projected onto a spherical mirror, a real 3D stereo image can be observed. Biomedical data of interest to this research are slices of a volume of tissue. To convert the slice information into volume data a representation that allows meaningful interpolation between the slices for stereo image pair generation is necessary. A second thrust of this thesis is to investigate neural networks and Kriging algorithm for potential use in interpolation of the biomedical volume data. DTIC

N95-20314 California Univ., Santa Cruz, CA. Dept. of Psychology and Psychobiology.
SPACE CONSTANCY ON VIDEO DISPLAY TERMINALS Final Report, 1 Jan. - 31 Dec. 1991
Bruce Bridgeman 28 Apr. 1994 24 p Limited Reproducibility: More than 20% of this document may be affected by microfiche quality
(Grant AF-AFOSR-0095-90; AF Proj. 2313)
(AD-A280015; AFOSR-94-0331TR) Avail: Issuing Activity (Defense Technical Information Center (DTIC))

Flicker of video display terminals (VDT's) has several consequences for visual function: space perception is distorted, and reading is slowed. We first tested the hypothesis that the flicker of VDT's interferes with visual space constancy, the perception that the world remains in the same place despite eye movements. Space constancy was probed by moving targets during eye movements, and noting a difference in movement threshold that depended upon whether a target jumped in the same direction as the eye or the opposite direction. Flicker rates up to 260 Hz distorted perception in a direction that implies breakdown of space constancy. Another experiment investigated the roles of color and luminance mechanisms in space constancy. The conclusion was that perception is actively suppressed during eye movements. The suppression depends on channels in the visual system that are insensitive to chromatic differences. Reading with 60 Hz flicker was 3.05% slower than with 500 Hz flicker. The result is consistent with a hypothesis that under flicker the eye 'parks' following an eye movement, until a new sample of text appears. Processing then proceeds in the usual way. The results allow quantitative predictions of reading speed at an flicker rate. DTIC

N95-20393# Maryland Inst. for Emergency Medical Services, Baltimore, MD.
DEVELOPMENT AND ENHANCEMENT OF A MODEL OF PERFORMANCE AND DECISION MAKING UNDER STRESS IN A REAL LIFE SETTING Annual Report, 1 Oct. 1993 - 30 Sep. 1994
Colin F. Mackenzie Sep. 1994 7 p
(Contract N00014-91-J-1540)
(AD-A285945) Avail: CASI HC A02/MF A01

We have concentrated our analysis on 50 of over 100 videotapes acquired of trauma patient resuscitation and anesthesia. The management of the airway (tracheal intubation) in these 50 videotapes was classified into three types of situations: (1) emergency (less than 10 min after patient admission); (2) semi-emergency (less than 30 min after patient admission); and elective. Such a classification allowed us to contrast the impact of stress on performance and team activity. As a result of this analysis, several factors have been illustrated that may have contributed to untowarded incidents, identified the impact of task complexity on team coordination patterns, and investigated the linkage between task performance and communication failures. Derived from text

N95-20609# Organisatie voor Toegepast Natuurwetenschappelijk Onderzoek, Soesterberg (Netherlands). Human Factors Research Inst.
A COMPARISON OF DECISION MAKING BEHAVIOUR IN A STATIC AND A DYNAMIC TASK ENVIRONMENT AS A FUNCTION OF TIME PRESSURE Interim Report [EEN VERGELIJKING VAN BESLISGEDRAG IN EEN STATISCHE EN EEN DYNAMISCHE TAAKOMGEVING ALS FUNCTIE VAN TIJDSDRUK]
J. H. Kerstholt and A. R. Pieters 20 May 1994 25 p
(AD-A285389; TNO-TM-1994-B-10; TDCK-94-0052) Avail: CASI HC A03/MF A01

Decision making research shows an increasing interest for time-dependent decisions. In contrast with decision making in static tasks, where, based on the available information, only one decision needs to be made, dynamic environments offer the possibility to adjust incorrect decisions through continuous feedback on the overall system state. It is therefore to be expected that the outcome performance will be better in a dynamic than in a static task environment. Previous research indicates that decision makers adjust their mental activities to the demands of the decision environment. Since dynamic environments offer the possibility for corrective actions, in contrast to static environments, it was predicted that cognitive performance would be worse in a dynamic task, on the assumption that people want to make accurate decisions with minimal mental effort. Furthermore, as it was assumed that the advantages of dynamic environments would reduce as time pressure increased, we predicted that both outcomes and cognitive performance would be more equal in dynamic and static tasks as time pressure increased. In an experiment two versions of a similar diagnosis task were used: a static and a dynamic one. In the dynamic task version subjects decided in real time, and they saw a graph on a computer screen indicating the state of the system. In the static task version, subjects did not get this information and their task was to make one diagnosis per trial. DTIC

N95-20845# Boston Univ., MA.
NEURAL MODELS OF MOTION PERCEPTION Annual Technical Report, 1 Sep. 1993 - 31 Aug. 1994
Stephen Grossberg and Ennio Mingolla Nov. 1994 9 p
(Contract F49620-92-J-0334)
(AD-A286560; AFOSR-94-0720TR) Avail: CASI HC A02/MF A01

Six research projects supported by this grant during the reporting period have resulted in one published book chapter, one refereed article in press, two articles under review, and five conference publications. Areas of research included design and simulation of network architectures for: (1) spatial pooling and perceptual framing by synchronized cortical dynamics; (2)

synthetic aperture radar processing by a multiple scale; (3) formation of cortical maps of ocular dominance and orientation columns; (4) a neuron model with variable ion concentrations; (5) a multi-scale model of brightness perception; and (6) models of motion perception. DTIC

N95-21101# State Univ. of New York, Stony Brook, NY. Dept. of Psychology.
SIGNAL- AND LISTENER- BASED FACTORS IN COMPLEX AUDITORY PATTERN PERCEPTION Final Technical Report, 15 Sep. 1991 - 14 Aug. 1994
Arthur G. Samuel 23 Sep. 1994 13 p
(Grant AF-AFOSR-0378-91)
(AD-A285636; AFOSR-94-0644TR) Avail: CASI HC A03/MF A01

The research project was designed to delineate principles that underlie the perception of complex auditory patterns. During the granting period, nine lines of research were conducted that investigated various aspects of complex auditory perception. These research efforts largely focussed on perception of speech sounds, and provided important information about three aspects of perception. Several of the projects clarified the role that the listener's knowledge of English words can play in decoding speech. Additional studies examined how lower-level representations (spectral patterns, high-frequency sublexical patterns) are processed. Across a number of the research efforts, attentional effects were investigated, to determine how they modulate other processing. Collectively, the research effort made significant progress in clarifying how human listeners decode very complex sounds. DTIC

N95-21192# Wright State Univ., Dayton, OH. Dept. of Psychology.
PERCEPTION AND CONTROL OF LOCOMOTION Annual Technical Report, 1 Sep. 1993 - 31 Aug. 1994
John M. Flach 30 Sep. 1994 12 p
(Contract F49620-93-1-0560)
(AD-A285605; WSU/ATR/662480; AFOSR-94-0648TR) Avail: CASI HC A03/MF A01

This report describes an empirical study to evaluate the ability to track a constant altitude as a function of the structure in optical flow (Manipulated using types of ground texture - splay, depression, dot, and block and the rate of forward motion - global optical flow (GOF) rate). Subjects were asked to track a constant altitude (25 ft) in the face of disturbances to the vertical, lateral, and fore-aft axes. The critical independent variables were texture type and GOF rate. Texture type was manipulated within subjects and GOF rate was manipulated between subjects. Dependent variables included RMS altitude error and correlated control power. The results showed a crossover interaction. For both dependent measures, performance at 0 GOF rate was best with depression angle and poorest with splay angle. The reverse was true at a GOF rate of 3 eyeheights/s. The results are consistent with the hypothesis, suggested by Flach et al. (1992), that the ability to pick-up information about altitude from optic flow depends on the amount of optical flow activity specific to altitude (signal) relative to the flow activity arising from other factors (e.g., motion in the fore-aft and lateral axes) (noise). The optical flow that results from forward motion (GOF rate) is visible in the depression, dot and block textures. This 'noise' makes it more difficult to differentiate the optical activity specific to changes in altitude. With splay texture, there is no change in the flow as a result of forward motion. Therefore, performance with splay texture is independent of GOF rate. DTIC

N95-21284 Technical Research Centre of Finland, Espoo (Finland).
13TH EUROPEAN ANNUAL CONFERENCE ON HUMAN DECISION MAKING AND MANUAL CONTROL
Leena Norros, ed. May 1994 222 p Conference held in Espoo, Finland, 13-14 Jun. 1994
(ISSN 0357-9387)
(PB95-132874; VTT/SYMPOSIUM-146; ISBN-951-38-4097-2) Copyright Avail: Issuing Activity (National Technical Information Service (NTIS))

Contents include the following: Task allocation problems in human-centered automation systems; Use of a questionnaire for the modelization of trust in a man-machine system; Human reliability in civil aviation; Towards a method to analyze cognitive errors during accident management: A taxonomy of cognitive errors; Misdiagnosis is not the only diagnostic error mode; Towards a computer-based decision making system for conceptual design; The COMMONKADS method for the analysis and the modelling of the expertise in a design activity; Decision support for planning rehabilitation in hydro power production systems; Methodology for robotic software design; Computer support for sharing expertise in process disturbances; Towards a new way of presenting information to a supervision system; Design of dynamic display systems for process plants; The integration of peripheral vision concepts into conventional display design; KSM-SUPPORT - A real time, fault diagnosis system for an absorption heat transformer; Fuzzy characterization of the human operator for a decision support system in teleoperation; Conceptual mastery of work, mastery of disturbance handling, and their development among personnel in paper production; Collective activities and reliability; Knowledge acquisition and case-based reasoning: An integrated approach; and A method for analysis of nuclear power plant operators' decision making in simulated disturbance situations. NTIS

N95-21927 Army Aeromedical Research Lab., Fort Rucker, AL.
FACTORS THAT DETERMINE VISUAL ACUITY THROUGH NIGHT VISION GOGGLES FOR EMMETROPES
John C. Kotulak and Stephen E. Morse Apr. 1994 30 p Limited Reproducibility: More than 20% of this document may be affected by microfiche quality
(AD-A279339; USAARL-94-16) Avail: Issuing Activity (Defense Technical Information Center (DTIC))

Many factors which could affect visual acuity (VA) with night vision goggles (NVG's) already have been studied, e.g., night sky condition and target contrast (Levine and Rash, 1989a and 1989b; Wiley, 1989; Kotulak and Rash, 1992), NVG generation (Miller et al., 1984; Kotulak and Rash, 1992), nuclear flashblindness protection (Levine and Rash, 1989a and 1989b), chemical protective masks (Miller et al., 1989; Donohue-Perry, Riegler, and Hausman, 1990), signal-to-noise ratio (Riegler et al., 1991), interpupillary distance misadjustment (King and morse, 1992), and instrument myopia (Kotulak and Morse, 1992, 1994a, and 1994b; Kotulak, Morse, and Wiley, 1993). Another factor which could influence NVG VA is decreased unaided VA, i.e., VA without NVG's; however, relatively little is known about it. DTIC

N95-21968 Army Armament Research, Development and Engineering Center, Watervliet, NY.
HOW THE BRAIN WORKS Final Report
Raymond Scanlon and Mark Johnson Feb. 1994 31 p Limited Reproducibility: More than 20% of this document may be affected by microfiche quality
(AD-A279138; ARCCB-TR-94006) Avail: Issuing Activity (Defense Technical Information Center (DTIC))

The vertebrate brain is explained as an assemblage of neurons, each responsive only to those afferent upon it. Thought is shown to proceed without a homunculus. DTIC

N95-22052# Northwestern Univ., Evanston, IL. Inst. for the Learning Sciences.
MAC/FAC: A MODEL OF SIMILARITY-BASED RETRIEVAL Technical Report, 1 Sep. 1989 - 31 Oct. 1992
Kenneth D. Forbus, Dedre Gentner, and Keith Law Oct. 1994 67 p
(Contract N00014-89-J-1272)
(AD-A286291; TR-59) Avail: CASI HC A04/MF A01

We present a model of similarity-based retrieval that attempts to capture these seemingly contradictory psychological phenomena: (1) structural commonalities are weighed more heavily than surface commonalities in soundness or similarity judgments (when both members are present); (2) superficial similarity is more important in retrieval from long-term memory than is structural similarity; and yet (3) purely structural (analogical) remindings are sometimes experienced. Our model, called MAC/FAC (for many are called but few are chosen) consists of two stages. The first stage (MAC) uses a computationally cheap, nonstructured matcher to filter candidates from a pool of memory items. We redundantly encode structured representations as content vectors, whose dot product yields an estimate of how well the corresponding structural representations will match. The second stage (FAC) uses SME to compute a true structural match between the probe and output from the first stage. MAC/FAC has been fully implemented and tested on dozens of examples. We show that MAC/FAC is capable of modeling patterns of access found in psychological data, and illustrative via sensitivity analyses that these results exhibit the desired dependence on theoretically important factors. The relationship of MAC/FAC to other models of memory is discussed, along with implications and possible extensions. DTIC

N95-22323# Army Medical Research Unit (Europe).
PSYCHOSOCIAL STRESS AND MENTAL HEALTH IN A FORWARD-DEPLOYED MILITARY COMMUNITY
Paul T. Bartone, Mark A. Vaitkus, and Robert C. Williams Jul. 1994 14 p
(AD-A285940; WRAIR-TR-94-0020) Avail: CASI HC A03/MF A01

The impact of perceived stressful experiences on mental health was studied using 1993 survey data from a representative sample (N=5,235) of the Army population in Europe. Regression results show stress in various life areas (personal, job, family) strongly predicts depression. Stress associated with mandated force reductions is also a predictor of depression for soldiers with children and working spouses. This study demonstrates empirically that stress associated with military force reductions is related to negative mental health effects. DTIC

N95-22324# Army Medical Research Unit (Europe).
ASSESSING POST TRAUMATIC STRESS DISORDER AND PTSD SYMPTOMATOLOGY IN US ARMY PERSONNEL
Paul T. Bartone, Mark A. Adler, and Mark A. Vaitkus 11 Jun. 1994 17 p
(AD-A285941; WRAIR-TR-94-0019) Avail: CASI HC A03/MF A01

This poster presentation reports on selected findings from a large-scale survey study of U.S. Army Gulf War veterans, showing that combat exposure is related to PTSD 'caseness' for substantial numbers of soldiers. In defining PTSD, the diagnostic algorithm contained in DSMIII-R was followed, using appropriate self-reported symptoms from two scales in the soldier survey. While this PTSD scale was adequate to the purpose, some of the items were less than exact matches to the DSM3-R listed symptoms. For future work, a more precise set to DSMIII-R (and now, DSMIV) based items are needed. A review of relevant studies shows that DSM-based PTSD checklists perform very well compared to other self report measures (e.g., Mississippi Scale) in identifying clinically diagnosed cases, and in terms of sensitivity and specificity. A team of researchers at the US Army Medical Research Unit-Europe has developed a new PTSD checklist and scoring procedures for use in future soldier studies. The scale is presented along with recommendations for its use. DTIC

N95-22472# Columbia Univ., New York, NY. Dept. of Psychology.
VISUAL PERCEPTION OF ELEVATION Final Report, 1 Jan. 1991 - 30 Jun. 1994
Leonard Matin 29 Aug. 1994 13 p
(Grant AF-AFOSR-0146-91)
(AD-A284938; Rept-003; AFOSR-94-0565TR) Avail: CASI HC A03/MF A01

The work at Columbia has concentrated on 4 matters: (1) Experimental work aimed at determining the aspects of individual lines and combinations of lines in the visual field that generate the substantial influence on the visual perception of eye level (VPEL); (2) Experimental work aimed at determining the aspects of individual lines and combinations of lines on the visual perception of the vertical (VPV) and visually perceived straight ahead (VPSA) and their connections with the VPEL; (3) Experimental work aimed at measuring the involvement of extraretinal control of VPEL including effects of head and eye position; and (4) Theoretical work on a quantitative model of the mechanism controlling the visual influence on VPEL, VPV, and VPSA, the Great Circle Model (GCM). DTIC

N95-22473# California Univ., Berkeley, CA. School of Optometry.
SPATIO-TEMPORAL MASKING IN HUMAN VISION AND ITS APPLICATION TO IMAGE CODING Annual Technical Report
Stanley Klein and D. A. Silverstein Aug. 1994 3 p
(Contract F49620-92-J-0359)
(AD-A284949; AFOSR-94-0555TR) Avail: CASI HC A01/MF A01

Before an image is stored or transmitted, we have access to the original and the distorted versions. The enhanced codec is compared to the original block by block to determine which blocks have been improved by the enhancement. These blocks are then flagged for post-processing in a way that is compliant with the JPEG standard and adds nothing to the compressed image's bandwidth. The end result is a compressed image that can be decompressed on any standard JPEG decompressor, but that can be enhanced by a sophisticated decompressor. For the comparison of the original and enhanced images, we have been developing a new vision model that is specifically tailored to the detection of errors that occur within or between two JPEG codec blocks. Previous filter models have been restricted from using a large number of filters due to computational constraints which we avoid by focusing the model on a tiny spatial area of 8x16 pixels. Further, features of human vision that have been included in previous models (color, temporal, stereo, etc.) are not needed for this more focused problem. Issues that have not been completely addressed by previous models, such as masking effects, are tractable and the model is more applicable to JPEG compression. DTIC

54 MAN/SYSTEM TECHNOLOGY AND LIFE SUPPORT

Includes human engineering; biotechnology; and space suits and protective clothing.

For related information see also *16 Space Transportation.*

N95-20041 Naval Postgraduate School, Monterey, CA.
PERSONAL COMPUTER AND WORKSTATION OPERATING SYSTEMS TUTORIAL M.S. Thesis
Charles E. Frame, Jr. Mar. 1994 154 p Limited Reproducibility: More than 20% of this document may be affected by microfiche quality
(AD-A280132) Avail: CASI HC A08

This thesis is a review and analysis of personal computer and workstation operating systems. The emphasis is placed on UNIX, MS DOS, MS Windows and OS/2 operating systems. UNIX is covered under the U.S. Government POSIX standard, which dictates its use when practical. MS DOS is the most used operating system worldwide. OS/2 was developed to combat some of the shortcomings of MS DOS. Each operating system which is discussed has a design philosophy that fulfills specific user's needs. UNIX was designed for many users sharing a computer system. MS DOS, MS Windows and OS/2 are designed as single user computer systems. All of these operating systems are in use at the Naval Postgraduate School. All of the operating systems are discussed with regard to their: history of development, process management, file system, input and output system, user interface, network capabilities, and advantages and disadvantages. UNIX has a section devoted to the POSIX standard and MS DOS has a section devoted to Windows 3.1. Apple Corporation's System 7 is mentioned throughout the text, but is not covered in detail. DTIC

N95-20276 Technical Research Centre of Finland, Espoo (Finland).
FORCE BASED MOTION CONTROL OF A WALKING MACHINE Ph.D. Thesis
H. Lehtinen 1994 164 p
(PB95-129672; VTT/PUB-179) Copyright Avail: Issuing Activity (National Technical Information Service (NTIS))

Force control of legs of evolving walking machines is assumed to be essential in natural soft and uneven terrain. The large and varying amount of friction in the leg mechanisms while the body is carried and the practical delays and saturation in the hydraulic system increase the complexity of the process to be controlled. The main contributions in the thesis are as follows. The body forces are transformed to the supporting legs in two phases: sets of minimum forces perpendicular to the resultant body force and forces parallel to the same resultant. This method minimizes the possibility of slippage with walking machines, where the desired body force is often close to vertical due to the weight of the body. A load adaptive performance index (PI) force control method for the hydraulic actuation system of MECANT I consisting of an asymmetric cylinder and a symmetrical valve has been developed. The I term of the controller is changed according to the desired load. A rule based altitude controller and a dead-zone and saturation based attitude controller have been designed. The first tests with force controlled vertical actuators show the usability of the method and fast responses to deviations in body orientation. NTIS

N95-20562 Drexel Univ., Philadelphia, PA. Dept. of Electrical and Computer Engineering.
DESIGNING THE ARCHITECTURE OF HIERACHICAL NEURAL NETWORKS MODEL ATTENTION, LEARNING AND GOAL-ORIENTED BEHAVIOR Final Report, 1 Nov. 1988 - 31 Dec. 1993
Allon Guez 31 Dec. 1993 23 p Limited Reproducibility: More than 20% of this document may be affected by microfiche quality
(Grant AF-AFOSR-0010-89)
(AD-A279898; AFOSR-94-0329TR) Avail: Issuing Activity (Defense Technical Information Center (DTIC))

During this period this grant partially supported 6 researchers, and resulted in over 21 publications. This unusually large activity is largely due to the enthusiasm of the researchers and their institution, Drexel University, which indirectly carried some of the financial burden. Neural or other learning architecture for real world, real time applications, necessarily employ feedback and thus deal with the unavoidable dilemma of identification versus stabilization or tracking. The major finding reported focuses on this tradeoff and how to optimally perform it. For linear time invariant finite dimensional systems they are able to perform on-line closed loop identification and tracking. If in addition the learning and tracking cost functions are quadratic they show these costs may be linearly scalarized without loss of optimality. DTIC

N95-20625 Army Research Lab., Aberdeen Proving Ground, MD.
EVALUATION OF STRESS EXPERIENCED BY SOLDIERS WEARING CHEMICAL PROTECTIVE CLOTHING DURING VARYING WORK LOADS IN DESERT OR TROPICAL ENVIRONMENTS Final Report
Gerald A. Hudgens, Louis E. Banderet, and Bruce S. Cadarette Apr. 1994 45 p Limited Reproducibility: More than 20% of this document may be affected by microfiche quality
(AF Proj. B74A)
(AD-A280113; ARL-TR-460) Avail: Issuing Activity (Defense Technical Information Center (DTIC))

A stress evaluation was conducted in a laboratory test in which the physiological and psychological reactions of soldiers were monitored while they wore either the standard battle dress overgarment (MOPPI) or the full complement of chemical protective clothing with mask (MOPPIV) and worked at low, moderate, or high work loads in simulated desert (hot and dry) or tropic (hot and humid) environments. The psychological instruments indicated greater stress responses for soldiers wearing MOPPIV than wearing MOPPI and for soldiers working at a high work load than working at a low work load. DTIC

N95-20768# Naval Command, Control and Ocean Surveillance Center, San Diego, CA. Research, Development, Test and Evaluation Div.
HUMAN PERFORMANCE STUDIES FOR CONTROL OF MULTIPLE REMOTE SYSTEMS Final Report
Steven A. Murray Jul. 1994 43 p
(AD-A286623; NCCOSC/RDT/E-TR-1658) Avail: CASI HC A03/MF A01

Many systems involving multiple remote sensors or machines require a single operator to control more than one device simultaneously. Interface design issues for operator support in such systems can be formidable, as the inherent task complexity creates significant opportunities for operator confusion and overload. A study was conducted to examine some of these issues, using a simulated industrial security environment as the applied setting. The operator task was to designate the number and location of intruders in a simulated building, using video information from remote sensor platforms. The experiment manipulated the number of displays which had to be monitored, event rate, image redundancy and sensor platform mobility. Response time increased significantly for increasing numbers of displays, as expected, but also increased independently for event rate image redundancy and for mobile sensors. Results showed that significant performance penalties may be encountered in multiple platform control, and that these penalties accumulate at seemingly low levels of complexity. DTIC

N95-20973# Logistics Management Engineering, Inc., Warminster, PA. Systems Engineering Group.
HELICOPTER CREWSEAT CUSHION PROGRAM Final Report
Ricky L. Greth Nov. 1994 73 p
(Contract DAAJ02-92-C-0043)
(AD-A286654; USAATCOM-TR-94-D-11) Avail: CASI HC A04/MF A01

A large proportion of Army helicopter pilots suffer back pain caused by flying. Extended missions required during Desert Shield/Desert Storm emphasized this problem. This pain could have an adverse impact on operational readiness, crew effectiveness, and flight safety. Poor posture during flight has been a contributing factor in pilot lower back pain. This program was performed to develop a seat cushion that improves comfort and reduces the incidence of lower back pain without adversely affecting crashworthiness. A literature survey and fact finding study analyzed the problem as it relates to AH-64 pilots. The knowledge and design, however, should be useful in all helicopters, especially in those with crashworthy stroking seats such as the UH-60 and AH-64 and in the future, the Comanche. Conceptual designs were developed which could help alleviate the problem. A survey of materials identified a few foams which were best suited to satisfy most of the requirements identified. Additional laboratory testing of foams was conducted to better compare the final candidates and aid in determining the optimal thickness and density to be used for the bottom cushion. A fit and function evaluation determined appropriate size and range of adjustment required for each postural/comfort aid (thigh, lumbar, and arm support). Prototype cushions were designed and fabricated and were used in dynamic crash test and in an Army-conducted comfort evaluation. Final design modifications were made prior to fabricating the twelve deliverable cushion assemblies. DTIC

N95-21283 Technische Univ., Delft (Netherlands). Dept. of Industrial Design Engineering.
HUMAN FORCE EXERTION IN USER-PRODUCT INTERACTION. BACKGROUNDS FOR DESIGN Ph.D. Thesis
B. J. Daams 26 Apr. 1994 347 p See also AD-A233989
(PB95-132858) Copyright Avail: Issuing Activity (National Technical Information Service (NTIS))

The objective of this project is to suggest how an 'Atlas of Human Force Exertion' for use by designers should be set up, and to assess how far it can contribute to the design of consumer products. In addition, the objective is also to investigate the relations between the forces measured, and between those forces and anthropometric variables. From the nature of the objectives, the emphasis in this research is on the relation between research, results and design, and not so much on the interpretation of the results. The objective of the Atlas of Human Force Exertion is to provide designers with some information to enable them to improve their products on the aspects of force interaction with the user. Further assessment in how far the atlas can contribute to design is necessary to improve the definition of the ambitions, to adjust the expectations of the designers, and to find out whether it is worthwhile to invest time and money to make one. NTIS

N95-21358# Lawrence Livermore National Lab., Livermore, CA.
QUANTITATIVE EVALUATION OF WRIST POSTURE AND TYPING PERFORMANCE: A COMPARATIVE STUDY OF 4 COMPUTER KEYBOARDS
Steve Burastero May 1994 7 p Presented at the 38th Annual Meeting of the Human Factors and Ergonomics Society, Nashville, TN, 24-28 Oct. 1994
(Contract W-7405-eng-48)
(DE95-002392; UCRL-JC-117547; CONF-941086-3) Avail: CASI HC A02/MF A01

The present study focuses on an ergonomic evaluation of 4 computer keyboards, based on subjective analyses of operator comfort and on a quantitative analysis of typing performance and wrist posture during typing. The objectives of this study are (1) to quantify differences in the wrist posture and in typing performance when the four different keyboards are used, and (2) to analyze the subjective preferences of the subjects for alternative keyboards compared to the standard flat keyboard with respect to the quantitative measurements. DOE

N95-21467 National Defence Research Establishment, Stockholm (Sweden). Huvudavdelning foer Maensklig Prestation och Funktion.
NAVIGATION SYSTEM IN COMBAT VEHICLE [NAVIGERINGSSTOED I STRIDSFORDON]
U. Hoerberg Apr. 1994 19 p In SWAHILI

(PB95-131629; FOA-A-50023-5.2) Avail: Issuing Activity (National Technical Information Service (NTIS))

This study investigates the possibility to reduce, by means of different kinds of technical support, the workload of tank crew members, and in that way increase the capacity of the tank. Basic studies indicated that navigation and position location burdened the tank commander to such a degree that other important functions suffered. The effect of a navigation system on the tank commander's workload is therefore investigated here. The results indicate that in order to reduce the workload of the commander, a large part of the navigation and transportation functions have to be delegated to the tank driver. The driver's need for technical support is also discussed in the report. NTIS

N95-21566# Veda, Inc., Dayton, OH.

CREW-CENTERED COCKPIT DESIGN (CCCD) FIELD DEMONSTRATION PROGRAM, VOLUME 1 Interim Report No. 1, Sep. 1992 - Jun. 1993

Roger Andrews, Robert Baltzer, Andrew Boone, Lucy Garcia, and Rick Gier Dec. 1993 138 p
(Contract F33615-92-C-5936)
(AD-A286426; Rept-63819-93U/P60099-Vol-1; AL/CF-TR-1994-0077-Vol-1) Avail: CASI HC A07/MF A02

This is Volume 1 of Interim Technical Report No. 1 for the Crew-Centered Cockpit Design (CCCD) Field Demonstration Program. Volume 1 discusses technical accomplishments and results. Volume 2 contains supplementary material in the form of twelve appendices. The objectives of the CCCD Field Demonstration Program are to upgrade, validate, and transition a new system for cockpit design. The system consists of a crew-centered system design process (CSDP) and a set of computer-aided tools known as the Cockpit Design System (CDS). This report summarizes accomplishments during the period September 1992 through June 1993 that include: development of an improved CSDP; system support and management; design of new tools to manage and trace design progress; conversion and improvements to existing software tools; and restructuring of real-time simulation software. The progress on the first of five field demonstrations, known as the F-16 reconnaissance mission, is described and includes information on planning, crew system analysis tasks, prototyping of design alternatives, and reconfiguration of the real-time simulator. DTIC

N95-21637# Lawrence Livermore National Lab., Livermore, CA.

ERGONOMIC EVALUATION OF THE APPLE ADJUSTABLE KEYBOARD

P. Tittiranonda, S. Burastero, M. Shih, and D. Rempel (California Univ., Richmond, CA.) May 1994 4 p Presented at the International Ergonomics Association Workshop, Toronto, Ontario, 15-19 Aug. 1994
(Contract W-7405-eng-48)
(DE95-002393; UCRL-JC-117548; CONF-940876-2) Avail: CASI HC A01/MF A01

This study presents an evaluation of the Apple Adjustable Keyboard based on subjective preference and observed joint angles during typing. Thirty five keyboard users were asked to use the Apple adjustable keyboard for 7-14 days and rate the various characteristics of the keyboard. Our findings suggest that the most preferred opening angles range from 11-20 deg. The mean ulnar deviation on the Apple Adjustable keyboard is 11 deg, compared to 16 deg on the standard keyboard. The mean extension was decreased from 24 deg to 16 deg when using the adjustable keyboard. When asked to subjectively rate the adjustable keyboard in comparison to the standard, the average subject felt that the Apple Adjustable Keyboard was more comfortable and easier to use than the standard flat keyboard. DOE

N95-21691# CHI Systems, Inc., Spring House, PA.

THE ADVANCED TECHNOLOGY CREW STATION: DEVELOPMENT AND VALIDATION OF A WORKLOAD ASSESSMENT TECHNIQUE FOR COCKPIT FUNCTION ALLOCATION Final Report

Floyd Glenn, James Boardway, Robert Wherry, Jr., David Cohen, and Meghan Carmody 30 Jul. 1993 58 p
(Contract N62269-90-D-0110)
(AD-A279544; NAWCADWAR-93073-60) Avail: CASI HC A04/MF A01

The design of a new severely upgraded aircraft cockpit requires many design decisions to be made, at least tentatively, prior to any opportunities for generation of detailed design specifications and experimentation with prototypes. In considering issues of interface design and function allocation, it is important to develop predictions concerning the effects of the various design alternatives on pilot performance. Task network models and workload estimation techniques are typically used jointly to accomplish this goal. The work described here was conducted in order to refine type of analysis and prediction technique as part of the U.S. Navy's Advanced Tactical Cockpit (ATC) Pilot-Vehicle Interface (PVI) Program. DTIC

N95-21700 Southampton Univ. (England). Inst. of Sound and Vibration Research.

EFFECT OF LAGS ON HUMAN PERFORMANCE WITH HEAD-COUPLED SIMULATORS Final Report, 1 Jul. - 30 Nov. 1992

R. H. So and M. J. Griffin Jun. 1993 90 p Limited Reproducibility: More than 20% of this document may be affected by microfiche quality
(AF Proj. 7184)
(AD-A279577; ISVR-92/33; AL/CF-TR-1993-0101) Avail: Issuing Activity (Defense Technical Information Center (DTIC))

This report reviews factors contributing to the effects of lags in head-coupled systems. A model of head tracking behavior is defined with appropriate feedback loops. The relevant lags and their possible effects on operator performance are defined. Twenty-one head-coupled simulators and operational head-coupled airborne systems are listed and grouped according to their feedback loops. Studies of the effects of lags within individual feedback loops are reviewed. The feedback loops investigated were the head-coupled visual loop, the head-slaved weapon control loop, the manual control loop, the eye-coupled visual loop, and the eye-slaved weapon control loop. The effects of relevant task and simulator variables, such as target velocity and motion cues are also discussed. DTIC

N95-21721# Sandia National Labs., Albuquerque, NM.

TOP TEN LIST OF USER-HOSTILE INTERFACE DESIGN

D. P. Miller 1994 31 p Presented at the 41st Annual American Vacuum Society Symposium, Denver, CO, 24-28 Oct. 1994
(Contract DE-AC04-94AL-85000)
(DE95-001602; SAND-94-2548C; CONF-941001-2) Avail: CASI HC A03/MF A01

This report describes ten of the most frequent ergonomic problems found in human-computer interfaces (HCI's) associated with complex industrial machines. In contrast with being thought of as 'user friendly,' many of these machines are seen as exhibiting 'user-hostile' attributes by the author. The historical lack of consistent application of ergonomic principles in the HCI's has led to a breed of very sophisticated, complex manufacturing equipment that few people can operate without extensive orientation, training, or experience. This design oversight has produced the need for extensive training programs and help documentation, unnecessary machine downtime, and reduced productivity resulting from operator stress and confusion. Ergonomic considerations affect industrial machines in at least three important areas: (1) the physical package including CRT and keyboard, maintenance access areas, and dedicated hardware selection, layout, and labeling; (2) the software by which the user interacts with the computer that controls the equipment; and (3) the supporting documentation. DOE

N95-21866*# Tulane Univ., New Orleans, LA. Dept. of Mechanical Engineering.

A METHOD TO DETERMINE THE KINEMATICS OF THE LOWER LIMBS OF A SUBJECT PEDALING A BICYCLE USING ENCODERS AND ACCELEROMETERS M.S. Thesis

Shih-Ching Liu 1 Apr. 1994 68 p Sponsored by NASA and the American Association of Engineering Education
(NASA-CR-197401; NAS 1.26:197401) Avail: CASI HC A04/MF A01

The goal of this research was to determine kinematic parameters of the lower limbs of a subject pedaling a bicycle. An existing measurement system was used as the basis to develop the model to determine position and acceleration of the limbs. The system consists of an ergometer instrumented to provide position of the pedal (foot), accelerometers to be attached to the lower limbs to measure accelerations, a recorder used for filtering, and a computer instrumented with an A/D board and a decoder board. The system is designed to read and record data from accelerometers and encoders. Software has been developed for data collection, analysis and presentation. Based on the measurement system, a two dimensional analytical model has been developed to determine configuration (position, orientation) and kinematics (velocities, accelerations). The model has been implemented in software and verified by simulation. An error analysis to determine the system's accuracy shows that the expected error is well within the specifications of practical applications. When the physical hardware is completed, NASA researchers hope to use the system developed to determine forces exerted by muscles and forces at articulations. This data will be useful in the development of countermeasures to minimize bone loss experienced by astronauts in microgravity conditions. Author

N95-22045# Army Aeromedical Research Lab., Fort Rucker, AL.

TEMPORARY THRESHOLD SHIFTS PRODUCED BY HIGH INTENSITY FREEFIELD IMPULSE NOISE IN HUMANS WEARING HEARING PROTECTION

James H. Patterson, Jr. and Daniel L. Johnson Aug. 1994 28 p
(DA Proj. 301-62787-A-878)
(AD-A286289; USAARL-94-46) Avail: CASI HC A03/MF A01

Exposure to high intensity impulse noise produced by modern military weapons is known to be hazardous to hearing. Hearing protection is required; however, there is no generally accepted theoretical way to predict whether protection will be adequate for the highest noise levels. This had led us to empirically determine the safe limits of exposure to impulse noise when hearing protection is used by exposing human volunteers under controlled conditions. Over the past 5 years, a series of studies has been conducted to determine the maximum safe exposure to high intensity freefield impulse noise. An exposure was considered to be safe if it produced only a small temporary threshold shift (TTS less than 25 dB) in a small percentage of the volunteers exposed. Three different impulses were used with A-durations of 0.8, 1.4, and 2.9 ms. Both the level and number of impulses were varied to find the maximum tolerable exposure for combinations of these parameters. The peak sound pressure levels ranged up to 196 dB. The number of impulses was varied from 6 to 100. Approximately 60 volunteers were exposed to each type of impulse, allowing high confidence estimates of the exposures which would produce no significant TTS in 95 percent of the exposed population. The hearing protection used was an ear muff which had been modified to simulate a poor fitting protector. The results of these studies indicated that even with a relatively poor hearing protector, combinations of level and number of impulses which far exceed our currently accepted exposure limits could be tolerated by 95 percent of the volunteers. DTIC

N95-22099# Department of the Navy, Washington, DC.

OCCUPANT REACH AND MOBILITY APPARATUS Patent Application

Gary R. Whitman, inventor (to Navy) and David A. Rose, inventor (to Navy) 12 Apr. 1994 12 p
(AD-D016253; US-Patent-Appl-SN-226517) Avail: CASI HC A03/MF A01

A three-dimensional grid is created by a series of panels arranged in a semi-circle about a seated subject. The panels are configured or otherwise arranged to allow the seated subject full range of reach in all directions. The subject may be seated or standing and is placed a distance from the panels. The panels include a plurality of rods which slideably project through the panels in the direction of the seated subject. To determine reach, the subject reaches toward the rods and pushes them with either hand as far away from him/her as possible. Measurements may then be taken from the end of each rod that has been moved. Similarly situated panels, including visual indicia, may be used to evaluate field of view. DTIC

N95-22274# Army Natick Labs., MA.

PERSONAL HYGIENE BODY WIPE Final Report, 1 Oct. 1993 - 30 Sep. 1994

Edmund M. Powers and Mark J. Buller Nov. 1994 71 p
(AD-A286092; Natick/TR-95/002) Avail: CASI HC A04/MF A01

Military doctrine requires a soldier to take a shower at least once every seven days to maintain certain health standards. The objective of the PHBW is to provide the soldier with a temporary means of maintaining personal hygiene and sanitation when water/showers are not available. The PHBW will improve personal hygiene, morale and quality of life of the soldier in the field when water is not available. Statistically designed technical user tests of several typical commercially available wipes were conducted. The wipe selected as the most suitable for the soldier was one of the most effective soil removers, the most cost effective and was readily available from commercial sources. The formulation in the wipe is used on babies and is alcohol free and hypo-allergenic. Ingredients include cocoamphodi-acetate, aloe gel, lanolin, water, propylene glycol, preservatives and an adult fragrance. Toxicity clearance was granted by the Army Materiel Command Surgeon. The size of the wipes will be at least 7.2 x 8.5 and will be packed 12 wipes per package. A resealable label will allow removal of one wipe at a time. The PHBW will be managed by the General Service Agency and will be issued through the Class I distribution system. It will be regulated by revised Commercial Item Description A-A-641B, Hand Cleaner, Body Wipe (Pre-moistened Paper Towelette in a Packet). DTIC

N95-22275# Indiana Univ., Bloomington, IN. Inst. for the Study of Human Capabilies.

[ACTIVITIES OF THE INSTITUTE FOR THE STUDY OF HUMAN CAPABILITIES] Final Technical Report, 1 Jun. 1990 - 31 May 1994

Charles S. Watson 31 May 1994 124 p
(Contract AF-AFOSR-0215-90)
(AD-A286471; AFOSR-94-0721TR) Avail: CASI HC A06/MF A02

During the final year of the award we devoted considerable time to an evaluation of the Institute's activities during its first years of operation. A great deal has been accomplished, as described in this report and the annual reports that preceded it. It was recognized in our final evaluation of the Institute's accomplishments, however, that the central theme of 'human capabilities' too broad to accurately represent the range of research conducted by our associated investigators. There is a need to identify more precisely the specific practical area or areas of science to which our research is applicable. Partly as a result of consultation with one of our visiting scientists, Dr. Gilbert Ricard from Grumman Aircraft Corporation, we have elected to limit the Institute's future research focus to the subject of Human-Computer Interaction (HCI). DTIC

N95-22466# Sandia National Labs., Albuquerque, NM.

FUZZY CLUSTERING OF FACIAL FORM FOR PROTOTYPING ENVIRONMENTAL PROTECTION EQUIPMENT

D. G. Robinson (GRAM, Inc., Albuquerque, NM.) 1994 6 p Presented at the International Joint Conference of the North American Fuzzy Information Processing Society and the Industrial Fuzzy Control and Intelligent Systems Conference and the NASA Joint Workshop on Neural Networks and Fuzzy Logic, San Antonio
(Contract DE-AC04-94AL-85000)
(DE94-014657; SAND-94-1354C; CONF-941219-1) Avail: CASI HC A02/MF A01

Emphasis on the human-to-aircraft interface has magnified in importance as the performance envelope of today's aircraft has continued to expand. A major problem is that there has been a corresponding increase in the need for better fitting protection equipment and unfortunately it has become increasingly difficult for aircrew members to find equipment that will provide this level of fit. While protection equipment has, historically had poor fit characteristics, the issue has grown tremendously with the recent increase in the numbers of minorities and women. Fundamental to this problem are the archaic methods for sizing individual equipment and the methods for establishing a sizing system. This paper documents recent investigations by the author into developing new methods to overcome these problems. Research centered on the development of a new statistically based method for describing form and the application of fuzzy clustering using the new shape descriptors. A sizing system was developed from the application of the research; prototype masks were constructed and the hardware tested under flight conditions. DOE

55 SPACE BIOLOGY

Includes exobiology; planetary biology; and extraterrestrial life.

No abstracts in this category.

59 MATHEMATICAL AND COMPUTER SCIENCES (GENERAL)

No abstracts in this category.

60 COMPUTER OPERATIONS AND HARDWARE

Includes hardware for computer graphics, firmware, and data processing.
For components see *33 Electronics and Electrical Engineering.*

N95-21116 Department of the Navy, Washington, DC.
CIRCUIT MEANS FOR PROVIDING COMPATIBILITY BETWEEN TWO SEPARATE DIGITAL DATA INTERFACES Patent Application
James T. Michell, inventor (to Navy) 4 Mar. 1994 36 p Limited Reproducibility: More than 20% of this document may be affected by microfiche quality
(AD-D016225; US-Patent-Appl-SN-207311) Avail: CASI HC A03

A computing device for providing compatibility between two separate digital interfaces is disclosed. The computing device adapts the power that is available from a first computer to supply the voltage to circuit elements that are interconnected to the two different digital interfaces. A computing device is disclosed that provides communications, in a half-duplex manner, between first and second general purpose computers. The first computer has a digital data interface conforming to the specifications of MIL-STD-1397A (NTDS fast) protocol with NTDS fast voltages, and the second computer is a commercial type having a 'Flag In/Device Flag Out' protocol with complementary transistor logic (CTL) voltages. The computing device provides compatibility for the logic levels of the associated signals, control words, and data words of each of the separate digital data interfaces. Algorithm means are to be installed in the commercial computer which can control said computing device to make its logic components conform to MIL-STD-1397A, and are disclosed. DTIC

N95-21589 Texas A&M Univ., College Station, TX. Engineering Experiment Station.
HARDWARE IMPLEMENTATION OF A DESKTOP SUPERCOMPUTER FOR HIGH PERFORMANCE IMAGE PROCESSING. COLOR IMAGE PROCESSING USING CELLULAR NEURAL NETWORKS Technical Report, 1 Aug. - 1 Nov. 1994
Jose P. DeGyvez Nov. 1994 11 p Limited Reproducibility: More than 20% of this document may be affected by microfiche quality
(Contract N00014-94-1-0516)
(AD-A286455; Rept-93-549/3) Avail: Issuing Activity (Defense Technical Information Center (DTIC))

This report addresses the functional behavior of Cellular Neural Networks (CNN). The impact of variable convergence times on the proper operation of the network is discussed. A test method is presented to determine the functionality of the network. The function fault models assume that the cells are unable to switch between limiting states. The proposed method attains 100% stuck-at fault coverage without any extra hardware for its implementation. Moreover, the required number of test vectors is constant and independent of the array size which makes it suitable for practical implementations. The report discusses the new fault model, presents the algorithmic procedures and shows simulated testing results. DTIC

N95-21607# Oak Ridge National Lab., TN.
PVM A PLATFORM FOR PORTABLE DISTRIBUTED COMPUTING
G. A. Geist 1 Jun. 1994 13 p Presented at the High Performance Computing Conference, Singapore, Singapore, 29-30 Sep. 1994
(Contract DE-AC05-84OR-21400)
(DE94-019156; CONF-9409206-1) Avail: CASI HC A03/MF A01

PVM (Parallel Virtual Machine) is a byproduct of the heterogeneous network research project going on at Oak Ridge National Laboratory and the University of Tennessee. It is a software package that permits a user defined collection of serial, parallel, and vector computers to appear as one large distributed memory computer. PVM's popularity is quickly making it the worldwide de facto standard for distributed computing. Applications, which can be written in FORTRAN or C, can be parallelized by using simple message-passing constructs common to most distributed-memory computers. By sending and receiving messages, subtasks of an application can cooperate to solve a problem in parallel. This paper describes the features of the latest release of PVM (version 3.3) and describes the major new research areas being explored in heterogeneous network computing. The paper explains how PVM version 3 opens many new opportunities in distributed computing, and how several technical and social challenges must be addressed before distributed computing can be taken into the 21st century. DOE

N95-21632# Brookhaven National Lab., Upton, NY.
DOS BASICS
P. OConnor 1994 13 p
(Contract DE-AC02-76CH-00016)
(DE94-018434; BNL-60710) Avail: CASI HC A03/MF A01

DOS is an acronym for Disk Operating System. It is actually a set of programs that allows you to control your personal computer. DOS offers the capabilities to create and manage files; organize and maintain information placed on disks; use application programs such as WordPerfect, Lotus 123, Excel, Windows, etc. In addition, DOS provides the basic utilities needed to copy files from one area to another, delete files and list files. The latest version of DOS also offers more advanced features that include hard disk compression and memory management. Basic DOS commands are discussed. DOE

N95-21871 Technische Univ., Twente (Netherlands). Faculteit der Informatica.
COMPOSITIONAL APPROACH TO SEQUENTIAL CONSISTENCY AND LAZY CACHING
Wil Janssen, Mannes Poel, and Job Zwiers Jun. 1994 36 p
(ISSN 0924-3755)
(PB95-134110; Memo-INF-94-37) Copyright Avail: Issuing Activity (National Technical Information Service (NTIS))

The lazy caching algorithm is explained and formally proven correct by means of compositional methods. The algorithm is decomposed into four simple protocols, that are of interest on their own. A top level proof is given that is to a large extent independent of the particular model used for the more detailed proofs. Detailed proofs are given within a partial order variation of the quiescent trace model. NTIS

N95-22018 Selskapet for Industriell og Teknisk Forskning, Oslo (Norway). Dept. of Instrumentation.
DESIGN OF A 10 BIT 10k Samples/s LOW POWER CMOS ADC
S. A. Tunheim and J. Gakkestad 25 Apr. 1994 28 p
(PB95-110425; STF31-A94020) Avail: Issuing Activity (National Technical Information Service (NTIS))

This technical report describes a 10 bit 10k samples/s low power CMOS analog to digital converter (ADC). The ADC is implemented with a successive approximation architecture with an inherent sample and hold function. A resistor string is used to determine the five most significant bits, while a capacitor array is used to define the five least significant bits (voltage scaling - charge scaling technique). With respect to monotonicity and input capacitance, this method is in many cases favorable compared with other ADC architectures. The ADC has been designed in the AMS 1.2 micron CMOS process (CAE). The accuracy of the ADC is 10 bits at 10 kS/s conversion rate. The maximum power consumption is estimated to be less than 4.1 mW, and the typical power consumption at +27 C is 2.4 mW. NTIS

N95-22082 Technische Univ., Twente (Netherlands). Tele-Informatics and Open Systems Group.
VERIFICATION OF A TIMESTAMP-BASED SLIDING-WINDOW PROTOCOL
A. L. Olah 1994 35 p
(PB95-132759; Memo-INF-94-42) Copyright Avail: Issuing Activity (National Technical Information Service (NTIS))

The authors present the verification and analysis of a sliding-window protocol which uses sequence numbers and timestamps to achieve reliable, flow-controlled data transfer over an unreliable network. The timestamps are used to prevent hazards present in very high-speed networks due to the too fast wrap-around of sequence numbers. The protocol the authors analyze in this paper models the PAWS (protect against wrapped sequence numbers) mechanism, a proposed extension of the Transmission Control Protocol (TCP) of the Internet protocol suite. Some modifications are made on the original proposal to eliminate a possible hazard which was revealed during the formal analysis and to extend it with selective acknowledgements. The protocol is specified as an event-driven system using a system model which is capable to express real-time properties, such as packet lifetimes in the network, maximum transmission rate and clock skew. The authors take into account that both sequence numbers and timestamps are represented as finite numbers and give sufficient conditions for the safe reuse of these identifiers. Informal arguments about the sharpness of the sufficient conditions are also presented. NTIS

N95-22400# Eastman Kodak Co., Rochester, NY.
HIGH SPEED OPTICAL STORAGE TECHNOLOGY Final Report, Apr. 1992 - Aug. 1993
David R. Kaiser, Edward C. Gage, Daniel Sillick, and Michael Meichle Sep. 1994 63 p
(Contract F30602-92-C-0076)
(AD-A285788; RL-TR-94-118) Avail: CASI HC A04/MF A01

The objective of the effort was to investigate and demonstrate by means of a breadboard model, a high performance 14-inch digital optical system with the following specifications: (1) 25 Mbps minimum sustained user data rate; (2) 5.0 GB per side minimum user data capacity; (3) Double-sided media capacity of 10.0 GigaBytes; (4) Magneto-Optic media which is erasable and reusable many times with a design goal of 10,000 write/read/erase cycles; and (5) Effective corrected bit error rate of less than 1 bit in 10(exp 12) bits. In order to achieve a low life cycle cost system, off-the-shelf technology and utilization of commercial developments were employed. This approach was realized in the optical head design and the tracking servo system. Successful completion of this effort has laid the foundation for a next-generation optical jukebox system. DTIC

N95-22431*# Institute for Computer Applications in Science and Engineering, Hampton, VA.
EXPERIMENTAL EVALUATION OF DYNAMIC DATA ALLOCATION STRATEGIES IN A DISTRIBUTED DATABASE WITH CHANGING WORKLOADS Final Report
Anna Brunstrom (College of William and Mary, Williamsburg, VA.), Scott T. Leutenegger (Denver Univ., Denver, CO.), and Rahul Simha (College of William and Mary, Williamsburg, VA.) Jan. 1995 18 p
(Contract NAS1-19480; RTOP 505-90-52-01)
(NASA-CR-195024; NAS 1.26:195024; ICASE-95-2) Avail: CASI HC A03/MF A01

Traditionally, allocation of data in distributed database management systems has been determined by off-line analysis and optimization. This technique works well for static database access patterns, but is often inadequate for frequently changing workloads. In this paper we address how to dynamically reallocate data for partionable distributed databases with changing access patterns. Rather than complicated and expensive optimization algorithms, a simple heuristic is presented and shown, via an implementation study, to improve system throughput by 30 percent in a local area network based system. Based on artificial wide area network delays, we show that dynamic reallocation can improve system throughput by a factor of two and a half for wide area networks. We also show that individual site load must be taken into consideration when reallocating data, and provide a simple policy that incorporates load in the reallocation decision. Author

61 COMPUTER PROGRAMMING AND SOFTWARE

Includes computer programs, routines, alogorithms, and specific applications, e.g., CAD/CAM.

N95-19889# Technische Univ., Eindhoven (Netherlands). Dept. of Mathematics and Computing Science.
K(1,3)-FREE AND W(4)-FREE GRAPHS
T. Kloks May 1994 20 p
(PB95-110573) Avail: CASI HC A03/MF A01

We show that in any claw- and 4-wheel-free graph the number of maximal cliques is polynomial bounded. We show there exists an efficient algorithm to solve the MAXIMUM CLIQUE problem for this class of graphs. We also give an O(ne) recognition algorithm. NTIS

N95-19891# Technische Univ., Eindhoven (Netherlands). Dept. of Mathematics and Computing Science.
INTRODUCTION TO THE FIRE ENGINE: A C++ TOOLKIT FOR FINITE AUTOMATA AND REGULAR EXPRESSIONS
B. W. Watson 17 May 1994 25 p
(PB95-110599) Avail: CASI HC A03/MF A01

This paper is an introduction to the programmer's interface of version 1.1 of the FIRE engine. The FIRE engine is a C++ class library implementing Finite automata and Regular Expression algorithms. The algorithms implemented in the toolkit are almost all of those presented in the taxonomies of finite automata algorithms. None of the implementation details of the library are discussed. The toolkit is unique in providing implementations of all of the known algorithms for constructing finite automata. The implementations, which were developed with efficiency in mind, are intended for use in production quality applications. No shell of graphical user-interface is provided, as the toolkit is intended for integration into applications. The implementations of the algorithms follow directly from the abstract algorithms. As such, the toolkit also serves as an educational example of the implementation of abstract algorithms. NTIS

N95-19905# Technische Univ., Eindhoven (Netherlands).
DOMINOES
T. Kloks, D. Kratsch (Institut de Recherche en Informatique et Systemes Aleatoires, Rennes, France.), and H. Mueller (Friedrich-Schiller Univ., Jena, Germany.) Mar. 1994 24 p
(PB95-110680) Avail: CASI HC A03/MF A01

A graph is called a domino if every vertex is contained in at most two maximal cliques. The class of dominoes properly contains the class of line graphs of bipartite graphs, and is in turn properly contained in the class of claw-free graphs. We give some characterizations of this class of graphs, show that they can be recognized in linear time, give a linear time algorithm for listing all maximal cliques (which implies a linear time algorithm computing a maximum clique of a domino) and show that the pathwidth problem remains NP-complete when restricted to the class of chordal dominoes. NTIS

N95-19908# Technische Univ., Eindhoven (Netherlands). Dept. of Mathematics and Computing Science.
HIERARCHICAL DIAGRAMMATIC REPRESENTATION OF CLASS STRUCTURE
O. S. vanRoosmalen Feb. 1994 32 p
(PB95-110722) Avail: CASI HC A03/MF A01

A method is described to graphically represent class-structure and class-relations in an object-oriented application. This graphical representation can be used for system-design at various levels of abstraction as well as documentation of existing programs. A hierarchical way of ordering class-diagrams is an integral part of the method. NTIS

N95-19928 Rutherford Appleton Lab., Chilton (England). ISIS Science Div.
PRSPLOT6 MANUAL
M. Hagen Aug. 1994 14 p Prepared in cooperation with Science Research Council, Daresbury, England; and Keele Univ., England
(PB95-110862; RAL-94-087) Avail: Issuing Activity (National Technical Information Service (NTIS))

The PRSPLOT6 program can be used to plot data from PRISMA experiments in the form of either extended zone dispersion relations or contour maps and can be used to extract (and plot) data from contour maps. The program is available on the ISISE and ISVS5 VAX VMS computers at the Rutherford Appleton Laboratory (RAL) and on the plotter SUN SPARCcenter (UNIX) computer at Keele. It uses plotting subroutines from the UNIRAS library. For most of the program the code is identical on both the VAX and UNIX systems, however, there is some system dependent code, to do with renaming files, creating sub-processes and the inability of UNIRAS to work properly on a terminal emulating a TEK 4010 on a UNIX system. The program is designed to let the user interactively create a plot at the terminal from data read in from a file(s) and then to get a postscript or color postscript output file. It consists of 11 commands and their qualifiers and parameters. The program can be run on: (1) terminals emulating a vt100 alpha and tektronix 4010 graphics setup (e.g. Pericom or Falco); (2) a color X11 terminal (or workstation, e.g. Vaxstation 3100 or 4000 or color Sun); or (3) a P.C. emulating a tektronix 4200 series color terminal (e.g. the TEEMTALK or EMUTEK emulators). NTIS

N95-19929# Army Research Lab., Fort Monmouth, NJ. Electronics and Power Sources Directorate.
VHDL MODELING OF PRC-70 RADIO ASICs FOR REVERSE ENGINEERING Technical Report, 1991 - 1994
Jared M. Brodsky Aug. 1994 166 p
(AD-A285740; ARL-TR-419) Avail: CASI HC A08/MF A02

Army Research Laboratory has been researching methods to maintain fielded-legacy systems built with technology that is no longer available in the commercial market. One method under examination is using the VHSIC hardware description language (VHDL) to document circuits for future redesign and reengineering for efficient reprocurement of spare electronic components. This report describes a case where structural VHDL modeling methods were studied while documenting the structure of three recently reengineered ASIC's. These three ASIC's form part of an antenna coupler board which is used in the AN/PRC-70 special operation forces radio. The report describes the steps used in setting up the structural models from the technology information models through the cell library models to the overall structure models of each ASIC. Through the description of the creation of the models a reader will be able to understand how the models allow future reengineering of these ASIC's to be technology independent. The report also describes the steps taken to validate the VHDL models and verify them against the actual design drawings using data taken from the results of simulating both. A number of obstacles were revealed during the simulation and verification of the models. An account of those obstacles and the solutions to them are also described. DTIC

N95-19961# Adaptive Solutions, Inc., Beaverton, OR.
HIGH PERFORMANCE HARDWARE AND SOFTWARE FOR PATTERN RECOGNITION AND IMAGE PROCESSING Status Report, 1 Feb. - 30 Apr. 1994
Wendell A. Henry 23 May 1994 6 p
(Contract N00014-93-C-0234)
(AD-A279776) Avail: CASI HC A02/MF A01

Effort on Phase 1 tasks continued and good progress was made during this reporting period. The hardware design of the CNAPS/PC board was completed and five (5) prototype boards were fabricated. Preliminary debug of the boards has been successfully completed. Very good progress was made on the software port and debug of the CNAPS-C compiler and the source-level debugger. Progress was made, but not as much as planned, on the software port and debug of the OEMlib control software to the CNAPS/PC hardware and the DOS/Windows environment. At the time of this report, the project has expenditures and commitments totaling 66% of the funds allocated for Phase 1 of the contract. DTIC

N95-19999# Carnegie-Mellon Univ., Pittsburgh, PA. Software Engineering Inst.
A CONSTRUCT FOR DESCRIBING SOFTWARE DEVELOPMENT RISKS Final Report
David P. Gluch Jul. 1994 38 p
(Contract F19628-90-C-0003)
(AD-A284923; CMU/SEI-94-TR-14; ESC-TR-94-014) Avail: CASI HC A03/MF A01

This report establishes a representation of software risk wherein the risks associated with software-dependent development programs are defined as distinct, manageable risk entities. The risk entities and their descriptive statements of risk are based upon a condition - transition - consequence (CTC) construct. The CTC construct arises out of a systems representation, where time and value are identified as fundamental to the concept of risk. The CTC construct is also shown to provide a common representation for both program risks and program tasks and to fit into a heuristic framework for identifying risks within software-dependent development programs. Examples of risks are used to demonstrate that the approach facilitates the management of risk as an integral part of routine program management. DTIC

N95-20000# Scientific Computing Associates, Inc., New Haven, CT.
DESIGN OF A PARALLEL OBJECT ORIENTED PROGRAMMING LANGUAGE Final Report, 23 Feb. - 27 Sep. 1994
Daya Atapattu 26 Sep. 1994 20 p
(Contract DAAH01-94-C-R089)
(AD-A284924) Avail: CASI HC A03/MF A01

Object-oriented programming techniques have become a vital part of modern software engineering. Most large new commercial software products are designed today using object oriented principles along with supporting development environments and tools. Such methodology is particularly appealing for parallel computing, where there is great need for approaches capable of simplifying the programming task and producing high quality software more quickly. We have carried out research that will lead to a new parallel object-oriented language based on C++. The new language, C++-Linda, is a novel combination of the most widely used object-oriented language and a successful environment for parallel computing that supports a virtual shared memory model for process interaction. This combination is an especially appropriate one because Linda's memory model is naturally object-oriented, enabling a seamless design that is completely consistent with object-oriented methodology. We have carried out research to understand the basic issues underlying parallel object-oriented languages, and we have created a preliminary design for C++-Linda. DTIC

N95-20042# Naval Postgraduate School, Monterey, CA.
SOFTWARE FAULT TREE ANALYSIS OF CONCURRENT Ada PROCESSES M.S. Thesis
William Samual Reid, Jr. Sep. 1994 94 p
(AD-A284979) Avail: CASI HC A05/MF A01

The Automated Code Translation Tool (ACTT) was developed at Naval Postgraduate School to partially automate the translation of Ada programs into software fault trees. The tool works as follows: the Ada parser and lexical analyzer calls the ACTT upon recognition of an Ada statement; the ACTT produces a template representing the statement; the templates are linked together. The tool was lacking in that it only looked at a subset of Ada structures. The problem that this thesis addresses is the implementation of the missing language structures, specifically, concurrency and exception handling, to allow the ACTT to handle all of the Ada structures. The result is a tool that takes the Ada source code and provides the analyst with a sequence of templates, and summary information to assist in incorporating hazard information for generating a fault tree. DTIC

N95-20060 Mei Technology Corp., San Antonio, TX.
DETERMINING THE USABILITY OF DIGITAL VIDEO INTERACTIVE (DVI) TECHNOLOGY IN COMPUTER-BASED INSTRUCTION Final Report, May 1992 - May 1993
William J. Walsh, Elizabeth G. Gibson, Joseph P. Vasile, Albert McLain, and George Vigue Jul. 1994 101 p Limited Reproducibility: More than 20% of this document may be affected by microfiche quality
(Contract F33616-91-D-0651)
(AD-A284717; AL/HR-TP-1994-0018) Avail: CASI HC A06

The use of-advanced multimedia technologies can enhance computer-based instruction (CBI). This research sought to understand the usability of digital video interactive (DVI) for Air Force instructional designers. Findings were expanded to include the development of a model for multimedia development. Task analysis and process description data are also provided. Findings were that DVI technology is very difficult to use and AF users will better be able to employ software multimedia packages currently available. The multimedia development model developed during this project uses job, task, and observational data to provide process descriptions of multimedia development relying on the ISD model as the overall support structure. It is highly recommended this model be validated and automated for use by Air Force CBI developers. DTIC

N95-20070 Analyticon Corp., Rancho Palos Verdes, CA.
ENHANCED VEHICLE AND EVENT TYPING SOFTWARE, PHASE 1 Progress Report
John T. Wagner and Z. E. Schwarzbein 3 Dec. 1993 28 p Limited Reproducibility: More than 20% of this document may be affected by microfiche quality
(Contract N00014-93-C-0182)
(AD-A284862) Avail: CASI HC A03

Analyticon's Phase 1 SBIR effort emphasizes real-time typing of strategic military booster threats (ICBM's and SLBM's) from satellite-based infrared sensor measurements of received radiant intensity from their boost phase rockets. It is crucial to BMC3 planning and commanding of assets for strategic missile defense via boost-phase target interception and for TMD, BMD ground resources (sensor, weaponry) utilization, and early warning (EW) of threats. Accordingly it necessitates properly understanding salient analytical foundations, automating candidate algorithm concepts, and resolving key algorithm-implementation issues. The upshot is an upgraded largely radiometric typing procedure couched entirely in sensor (i.e. focal plane) coordinates, that obviates reliance on formal launch point estimation information, readily uses target motion and all intensity measurements, and expediently combines/amplifies available multi-color data. Our baseline typer entails judicious variants, configured per selected performance criteria/payoffs and input data pre-conditioning, of a decision-making process commonly known as a Fisher technique of cluster analysis for ascertaining the best decision space (i.e. coordinates of a measurement hyperspace), that is combined with a general Likelihood Ratio Test (LRT) of hypotheses testing for the accompanying decision rule (i.e. classification strategy) DTIC

N95-20073# Oak Ridge National Lab., TN.
GUIDELINES FOR THE CREATION AND MANAGEMENT OF GEOGRAPHIC DATA BASES WITHIN A GIS ENVIRONMENT, VERSION 1.0
R. C. Durfee, M. L. Land, R. A. McCord, R. J. Olson, J. K. Thomas, E. P. Tinnel, and L. D. Voorhees Jul. 1994 79 p
(Contract DE-AC05-84OR-21400)
(DE94-019214; ES/ER/TM-56/V1) Avail: CASI HC A05/MF A01

A Geographic Information System (GIS) provides the ability to manage and analyze all types of geographic and environmental information. It performs these functions by providing the tools necessary to capture, access, analyze, and display spatially referenced information in graphic and tabular form. Typical data elements that can be visualized in a map might include roads, buildings, topography, streams, waste areas, monitoring wells, groundwater measurements, soil sample results, landcover, and demography. The intent of this document is to provide data management and quality assurance (QA) guidelines that will aid implementors and users of GIS technology and data bases. These guidelines should be useful in all, phases of GIS activities, including the following: (1) project planning; (2) data collection and generation; (3) data maintenance and management; (4) QA and standards; (5) project implementation; (6) spatial analysis and data interpretation; (7) data transformation and exchange; and (8) output and reporting. The daily use of desktop GIS technologies within Martin Marietta Energy Systems, Inc. (Energy Systems), is a relatively new phenomenon, but usage is increasing rapidly. Large volumes of GIS-related data are now being collected and analyzed for the U.S. Department of Energy (DOE) Oak Ridge Reservation (ORR) and its facilities. It is very important to establish and follow good data management practices for GIS. DOE

N95-20095 University of Southern Mississippi, Bay Saint Louis, MS. Center for Ocean and Atmospheric Modeling.
NOMADS GRAPHICAL USER INTERFACE VERSION 2.0 USER'S MANUAL Final Report
Peter J. Sakalaukus Sep. 1994 19 p Limited Reproducibility: More than 20% of this document may be affected by microfiche quality
(Contract N00014-93-C-6010)
(AD-A286314; COAM-TM-2/95) Avail: CASI HC A03

The Naval Ocean Models and Acoustic Demonstration System (NOMADS) V1.0 is a collection of individual programs accessed through a less-than-optimal screen-menu interface. It is presently being used to test and evaluate the Modular Ocean Data Assimilation System (MODAS). The current NOMADS Graphical User Interface (GUI) V2.0 is mouse (event) driven, which makes it simpler and faster to access and execute the different aspects of the NOMADS software. Additionally, the NOMADS GUI has an increased error-checking ability as well as a near 'bullet-proof' design. The NOMADS GUI V2.0 also has the characteristic that it may be altered or enhanced with additional functions and tools with minimal programming, due to the modular approach that was used in its design. DTIC

N95-20136# Ames Lab., IA.
TRULY DISTRIBUTION-INDEPENDENT ALGORITHMS FOR THE N-BODY PROBLEM
S. Aluru, G. M. Prabhu, and J. Gustafson 1994 23 p Presented at the Supercomputing 1994 Meeting, Washington, DC, 14-18 Nov. 1994
(Contract W-7405-eng-82)
(DE94-014238; IS-M-789; CONF-941118-4) Avail: CASI HC A03/MF A01

The N-body problem is to simulate the motion of N particles under the influence of mutual force fields based on an inverse square law. Greengard's algorithm claims to compute the cumulative force on each particle in O(N) time for a fixed precision irrespective of the distribution of the particles. In this paper, we show that Greengard's algorithm is distribution dependent and has a lower bound of (Omega)(N log(sup 2) N) in two dimensions and (Omega)(N log(sup 4) N) in three dimensions. We analyze the Greengard and Barnes-Hut algorithms and show that they are unbounded for arbitrary distributions. We also present a truly distribution independent algorithm for solving the N-body problem in (Omega)(N log N) time in two dimensions and in (Omega)(N log(sup 2) N) time in three dimensions. DOE

N95-20153# Pacific Northwest Lab., Richland, WA.
SYNTH: A SPECTRUM SYNTHESIZER
W. K. Hensley, A. D. McKinnon, H. S. Miley, M. E. Panisko, and R. M. Savard Jul. 1994 7 p Presented at the Institute of Nuclear Materials Management Annual Meeting, Naples, FL, 17-20 Jul. 1994
(Contract DE-AC06-76RL-01830)
(DE94-015943; PNL-SA-23879; CONF-940748-30) Avail: CASI HC A02/MF A01

A computer code has been written at the Pacific Northwest Laboratory (PNL) to synthesize the results of typical gamma-ray spectroscopy experiments. The code, dubbed SYNTH, allows a user to specify physical characteristics of a gamma-ray source, the quantity of the nuclides producing the radiation, the source-to-detector distance and the type and thickness of absorbers, the size and composition of the detector (Ge or NaI), and the electronic set up used to gather the data. In the process of specifying the parameters needed to synthesize a spectrum, several interesting intermediate results are produced, including a photopeak transmission function vs energy, a detector efficiency curve, and a weighted list of gamma and x rays produced from a set of nuclides. All of these intermediate results are available for graphical inspection and for printing. SYNTH runs on personal computers. It is menu driven and can be customized to user specifications. SYNTH contains robust support for coaxial germanium detectors and some support for sodium iodide detectors. SYNTH is not a finished product. A number of additional developments are planned. However, the existing code has been compared carefully to spectra obtained from National Institute for Standards and Technology (NIST) certified standards with very favorable results. Examples of the use of SYNTH and several spectral results will be presented. DOE

N95-20154# Los Alamos National Lab., NM.
UNIFIED GUI FOR THE LOS ALAMOS RADIATION TRANSPORT CODE SYSTEM
S. R. Lee, D. G. Collins, and J. Anderson (Worcester Polytechnic Inst., MA.) 1994 6 p Presented at the Winter Meeting of the American Nuclear Society, Washington, DC, 13-18 Nov. 1994
(Contract W-7405-eng-36)
(DE94-016088; LA-UR-94-2505; CONF-941102-8) Avail: CASI HC A02/MF A01

Justine is a Unified Graphical User Interface (UGUI) which is used to define geometries using constructive solid geometric (CSG) operations on three-dimensional objects. These user defined geometries, along with other code specific parameters also controlled by Justine, are used by the Los Alamos Radiation Transport Code System (LARTCS), which includes the Radiation Transport Group's (X-6) Monte Carlo and deterministic transport codes. Justine enhances user productivity, aids in code debugging, and enhances the reliability of the LARTCS. DOE

N95-20157 Massachusetts Inst. of Tech., Cambridge, MA. Artificial Intelligence Inst.
VIEW-BASED MODELS OF 3D OBJECT RECOGNITION AND CLASS-SPECIFIC INVARIANCE
Nikos K. Logothetis, Thomas Vetter, Anya Hurlbert, and Tomaso Poggio Apr. 1994 13 p Limited Reproducibility: More than 20% of this document may be affected by microfiche quality
(Contract N00014-93-1-0385)
(AD-A279858; AI-M-1472) Avail: CASI HC A03

This paper describes the main features of a view-based model of object recognition. The model tries to capture general properties to be expected in a biological architecture for object recognition. The basic module is a regularization network in which each of the hidden units is broadly tuned to a specific view of the object to be recognized. DTIC

N95-20165# Los Alamos National Lab., NM.
AN OBJECT-ORIENTED OPTIMIZATION SYSTEMS
G. S. Cunningham, K. M. Hanson, G. R. Jennings, Jr., and D. R. Wolf 1994 8 p Presented at the Institute of Electrical and Electronics Engineers (IEEE) International Conference on Image Processing, Austin, TX, 13-16 Nov. 1994
(Contract W-7405-eng-36)
(DE94-016190; LA-UR-94-2649; CONF-9411104-2) Avail: CASI HC A02/MF A01

We have described the implementation of a graphical programming tool in the object-oriented language, Smalltalk-80, that allows a user to construct a radiographic measurement model. The measurement model can be used to generate the measurements predicted by a given parameterized model of an experimental object. In this paper, we describe extensions to the graphical programming tool that allow it to be used to perform Bayesian inference on very large sets of object parameters, given real experimental data, by optimizing the likelihood or posterior probability of the parameters, given the real data. DOE

N95-20184# Defence Research Establishment Ottawa, Ottawa (Ontario).
EVALUATION OF BORLAND TURBO VISION
David Lee and Andrew Mudry Dec. 1993 21 p
(AD-A279873; DREO-TN-93-37) Avail: CASI HC A03/MF A01

Turbo Vision (Trade Mark), a new application framework for PC DOS-based software development, is evaluated for its effectiveness as a base for computer applications. Turbo Vision provides an object-oriented, text-mode user interface and an event-driven program structure. An overview of the structure and software tools provided by Turbo Vision is presented. Various factors, such as consistency in architectural design, technical support, and ease of use, are considered. DTIC

N95-20255# Lawrence Livermore National Lab., Livermore, CA.
MESHES: THE NEXT GENERATION
M. Christon, D. Hardin, J. Compton, and M. Zosel 29 Aug. 1994 3 p Presented at the Supercomputing 1994 Meeting, Washington, DC, 14-18 Nov. 1994
(Contract W-7405-eng-48)
(DE94-016702; UCRL-JC-118234; CONF-941118-6) Avail: CASI HC A01/MF A01

Building complex meshes for large-scale numerical simulations presents immense difficulties in exploiting high-performance computers. Industry and research leaders will describe the current state of the art for generating meshes for such large scientific problems. This will be followed by a panel and general audience discussion of the algorithmic and architectural issues surrounding the generation of meshes with 10(exp 7) to 10(exp 9) grid points. (Note: The terms 'mesh' and 'grid' are used interchangeably in the literature.) DOE

N95-20258# Technische Univ., Eindhoven (Netherlands). Dept. of Mathematics and Computing Science.
COMPARISON OF WARD AND MELLOR'S TRANSFORMATION SCHEMA WITH STATE- AND ACTIVITYCHARTS
Jan Peleska (Deutsche System-Technik G.m.b.H., Kiel, Germany.), Cornelis Huizing, and Carsta Petersohn (Kiel Univ., Germany.) Mar. 1994 40 p
(PB95-110698) Avail: CASI HC A03/MF A01

A comparison between Structured Methods, as represented by the Essential Model of Ward & Mellor's Transformation Schemas, and the Statemate specification language consisting of State- and Activitycharts, is presented. The comparison is based on the languages' semantic properties. An example from the field of fault-tolerant systems serves as a 'benchmark problem' to investigate the practical applicability of both Transformation Schemas and Statemate in a context of meaningful 'real-world' systems. While the article's contents is founded on formal mathematical concepts, its objective is also to reach the software engineers and CASE tool builders who are not neccessarily experts in the field of Formal Methods. Therefore all the authors' results are presented in an informal natural-language style of reasoning. NTIS

N95-20284# Sandia National Labs., Albuquerque, NM.
ADAPTIVE PATH PLANNING FOR FLEXIBLE MANUFACTURING
Pang C. Chen 1994 7 p Presented at the 1994 International Conference on Computer Integrated Manufacturing and Automation Technology, Troy, NY, 10 Oct. 1994
(Contract DE-AC04-94AL-85000)
(DE94-016561; SAND-94-2005C; CONF-9410167-1) Avail: CASI HC A02/MF A01

Path planning needs to be fast to facilitate real-time robot programming. Unfortunately, current planning techniques are still too slow to be effective, as they often require several minutes, if not hours of computation. To overcome this difficulty, we present an adaptive algorithm that uses past experience to speed up future performance. It is a learning algorithm suitable for automating flexible manufacturing in incrementally-changing environments. The algorithm allows the robot to adapt to its environment by having two experience manipulation schemes: For minor environmental change, we use an object-attached experience abstraction scheme to increase the flexibility of the learned experience; for major environmental change, we use an on-demand experience repair scheme to retain those experiences that remain valid and useful. Using this algorithm, we can effectively reduce the overall robot planning time by re-using the computation result for one task to plan a path for another. DOE

N95-20304 Naval Postgraduate School, Monterey, CA. Dept. of Computer Science.
SOFTWARE MERGE: SEMANTICS OF COMBINING CHANGES TO PROGRAMS Interim Report
Valdis Berzins Dec. 1993 33 p Limited Reproducibility: More than 20% of this document may be affected by microfiche quality
(AD-A279657; NPSCS-93-011) Avail: CASI HC A03

We present a language-independent semantic model of the process of combining changes to programs. This model extends the domains used in denotational semantics (complete partial orders) to Boolean algebras, and represents incompatible modifications as well as compatible extensions. The model is used to define the intended semantics of change merging operations on programs and to establish some general properties of software merging. We determine conditions under which changes to subprograms of a software system can be merged independently and illustrate cases where this is not possible. DTIC

N95-20310 Wickersheimer Engineers, Inc., Champaign, IL.
COMPUTER-AIDED STRUCTURAL ENGINEERING (CASE) PROJECT. USER'S GUIDE: COMPUTER-AIDED STRUCTURAL MODELING (CASM). VERSION 5.00 Final Report
David Wickersheimer, Gene McDermott, Ken Taylor, and Carl Roth Apr. 1994 415 p Limited Reproducibility: More than 20% of this document may be affected by microfiche quality
(Contract DACA39-86-C-0024)
(AD-A279913; WES/IR/ITL-94-2) Avail: Issuing Activity (Defense Technical Information Center (DTIC))

CASM stands for Computer Aided Structural Modeling. It is a program designed to aid the structural engineer in the preliminary design and evaluation of structural building systems by the use of 3-D interactive graphics. Think of this program as a scratch pad for the structural decision process that would have been done on paper before you went to the computer to do the final numerical analysis of structural members. CASM will let you change your mind quickly and give you results that previously might have taken hours to obtain. By allowing quick changes, CASM allows you to make more informed decisions in the initial structural evaluation process. DTIC

N95-20313 Naval Postgraduate School, Monterey, CA.
TOWARDS BETTER QUALITY AND RELIABILITY IN THE SOFTWARE REUSE LIBRARY ENVIRONMENT M.S. Thesis
Kenneth M. Warburton 24 Mar. 1994 103 p Limited Reproducibility: More than 20% of this document may be affected by microfiche quality
(AD-A280013) Avail: Issuing Activity (Defense Technical Information Center (DTIC))

In today's DOD software environment, where systems of enormous size, complexity and cost are the norm, economic conditions are driving DOD system developers to seek ways to increase productivity while decreasing product defects. To achieve its goals, DOD has taken the approach of integrating reuse into the software development process. In 1992, DISA established its Software Reuse Program to serve as a prototype for the DOD-wide reuse initiative. This thesis will look at DISA's effort to support DOD's reuse vision. Specifically, it will discuss DISA's software reuse library management and will introduce a methodology for the collection and analysis of metrics relating to software performance in order to improve library software quality. This thesis concludes that metrics can play a key role in any organization's software quality program. While metrics alone are not a solution to the reuse quality problem, they are a tool to be used prudently by the software quality manager to manage and improve the quality of organizational software. DTIC

N95-20326 Army Research Inst. for the Behavioral and Social Sciences, Alexandria, VA.
MEASURING PRESENCE IN VIRTUAL ENVIRONMENTS Final Report, Jan. 1993 - Apr. 1994
Bob G. Witmer and Michael F. Singer Oct. 1994 54 p Limited Reproducibility: More than 20% of this document may be affected by microfiche quality
(DA Proj. 2Q1-62785-A-790)
(AD-A286183; ARI-TR-1014) Avail: CASI HC A04

A primary argument for the efficacy of virtual environments (VE) applications is that the user is 'present' in the simulated environment. Presence is defined as the subjective experience of being in one environment (there) when physically in another environment (here). Presence may be based on external factors and internal tendencies that support both awareness of the current situation and the transition from the immediate physical location (here) to a remote or artificial environment (there). These factors are labeled as immersive because they may lead to the experience of presence. Some major immersive factors identified in current literature or hypothesized as contributing to presence are briefly reviewed. These concepts and ideas have been used as the basis for two questionnaires. An immersive tendencies questionnaire (ITQ) was developed to investigate possible correlates that may indicate an individual's tendency to experience more or less presence in artificial environments. The presence questionnaire (PQ) addresses different factors or features peculiar to the artificial environment that may affect the experience of presence, or the capability to immerse oneself, in that environment. The results of administration of these questionnaires, in conjunction with an experiment on the performance of basic tasks in VE, are presented. These results should be considered preliminary and interpreted with caution because of the small number of subjects involved. Analyses indicate reasonable reliability values for the ITQ and PQ. DTIC

N95-20351# Lawrence Livermore National Lab., Livermore, CA.
CHOICE OF COMPUTER SOFTWARE FOR ANALYSIS OF SPECTRA FROM THE MULTI-SPECTRAL LOGGING SYSTEM
J. R. Hearst Jul. 1994 7 p
(Contract W-7405-eng-48)
(DE94-019013; UCRL-ID-118023) Avail: CASI HC A02/MF A01

We have investigated the range of software available for determination of elemental concentration from gamma-ray spectra, to learn which are most suitable for use with the Multi-spectral Logging System being developed for the Department of Energy. We believe that the spectrum fitting method will be more satisfactory than the peak-matching method. DOE

N95-20358# Oak Ridge National Lab., TN.
HIGH PERFORMANCE COMPUTING FOR MATERIALS PROCESS MODELING
T. Zacharia, M. A. Bjerke, and S. Simunovic 1993 9 p Presented at the American Welding Society International Conference on Modeling and Control of Joining Processes, Orlando, FL, 8-10 Dec. 1993
(Contract DE-AC05-84OR-21400)
(DE94-017860; CONF-931234-9) Avail: CASI HC A02/MF A01

Advanced mathematical techniques and computer simulation play a major role in providing enhanced understanding of conventional materials processing operations such as welding and joining. Many of these numerical models are highly compute-intensive. It is not unusual for an analysis to require several hours of computational time on current supercomputers despite the simplicity of the models being studied. As computer simulations and materials databases grow in complexity, massively parallel computers have become important tools. This paper briefly describes massively parallel computational research at the ORNL with the objective of providing fundamental insight into the welding process. DOE

N95-20385# Argonne National Lab., IL.
KERNEL MUCKING IN TOP
W. LeFebvre 1994 12 p Presented at the 8th System Administration Conference, San Diego, CA, 21-23 Sep. 1994
(Contract W-31-109-eng-38)
(DE94-017077; ANL/DIS/CP-83108; CONF-9409186-1) Avail: CASI HC A03/MF A01

For many years, the popular program top has aided system administrations in examination of process resource usage on their machines. Yet few are familiar with the techniques involved in obtaining this information. Most of what is displayed by top is available only in the dark recesses of kernel memory. Extracting this information requires familiarity not only with how bytes are read from the kernel, but also what data needs to be read. The wide variety of systems and variants of the Unix operating system in today's marketplace makes writing such a program very challenging. This paper explores the tremendous diversity in kernel information across the many platforms and the solutions employed by top to achieve and maintain ease of portability in the presence of such divergent systems. DOE

N95-20387# Lawrence Livermore National Lab., Livermore, CA.
SYSTEM DESIGN DOCUMENT U-AVLIS CONTROL SYSTEM ARCHITECTURE
P. G. Viebeck 16 Feb. 1994 24 p
(Contract W-7405-eng-48)
(DE94-017297; UCRL-ID-116218) Avail: CASI HC A03/MF A01

This document describes the architecture of the integrated control system for the U-AVLIS process. It includes an overview of the major control system components and their interfaces to one another. Separate documents are utilized to fully describe each component mentioned herein. The purpose of this document is to introduce the reader to the integrated U-AVLIS control system. It describes the philosophy of the control system architecture and how all of the control system components are integrated. While the other System Design Documents describe in detail the design of individual control system components, this document puts those components into their correct context within the entire integrated control system. DOE

N95-20546# Johns Hopkins Univ., Laurel, MD. Applied Physics Lab.
PROCEEDINGS OF THE 4TH SYSTEMS REENGINEERING TECHNOLOGY WORKSHOP
Bruce I. Blum Sep. 1994 412 p Workshop held in Monterey, CA, 8-10 Feb. 1994
(Contract N00039-91-C-0001)
(AD-A285357; JHU/APL-TG-1386) Avail: CASI HC A18/MF A04

The Navy has invested significant resources in the development of large and complex systems that must be modified and extended to respond to changing requirements. However, many of these systems are based on archaic automation technologies that do not support modern hardware and software engineering methodologies or maintenance strategies. Consequently, system modification has become increasingly complex. To reduce the complexity, developers can employ reengineering techniques to create new systems. This report contains the papers presented at the Fourth Systems Reengineering Technology Workshop sponsored by the Naval Surface Warfare Center. The papers discuss theoretical and applied techniques that can be used to facilitate systems reengineering efforts. Specific topics include design issues in systems reengineering, reuse in reengineering and forward engineering, experience reports, reengineering translation and transformation, evaluating a reengineering project, tools for reengineering, engineering science and reengineering, the impact of object orientation, and approaches to reengineering. DTIC

N95-20579 Naval Postgraduate School, Monterey, CA. Dept. of Computer Science.
AUTOMATION SUPPORT FOR CONCURRENT SOFTWARE ENGINEERING M.S. Thesis
Salah Badr Dec. 1993 26 p Limited Reproducibility: More than 20% of this document may be affected by microfiche quality
(AD-A279691; NPS-CS-93-013) Avail: Issuing Activity (Defense Technical Information Center (DTIC))

This paper presents an evolution control system that provide automated assistance for the software evolution process in an uncertain environment where designer tasks and their properties are always changing. We view an Evolution Control System (ECS) as the agent that keeps track of proposed, ongoing, and completed changes to a software system. It provides automated assistance to the software evolution manager to help him/her make the right decisions. It automatically propagates change consequences by constructing the set of possibly affected modules. It also coordinates change implementation activities within the design team in a way that supports teamwork and maintains system integrity, as well as adapting itself to the dynamic nature of the evolution process where new changes arrive randomly and ongoing modifications are themselves subject to change as more information becomes available. DTIC

N95-20595 Texas A&M Univ., College Station, TX. Dept. of Computer Science.
FAULT-TOLERANCE IN DISTRIBUTED AND MULTIPROCESSOR REAL-TIME SYSTEMS Final Report, 1 Sep. 1992 - 31 Aug. 1993
Dhiraj K. Pradhan 31 Aug. 1993 41 p Limited Reproducibility: More than 20% of this document may be affected by microfiche quality
(Contract F49620-92-J-0383)
(AD-A279896; AFOSR-94-0330TR) Avail: Issuing Activity (Defense Technical Information Center (DTIC))

New schemes for fault-tolerance in multiprocessor and distributed systems have been developed in the following areas. We have investigated a number of fault tolerance schemes to evaluate performance, reliability, and availability trade-offs. Fault tolerance schemes are being developed for various fault models (tail-stop model, fail-slow model, and arbitrary failure model) and application areas (applications that are to provide results at the end of computation and applications that are long-running but should also provide results during computation). In the area of software-implemented fault tolerance, we are studying approaches for providing user transparent mechanisms for fault tolerance to design and implement a software library to which the user can link existing application software to achieve the desired level of fault tolerance. We are developing a new tool (Reliable Architecture Characterization Tool--REACT) for evaluating the reliability and availability of distributed multiprocessor systems using various fault tolerance techniques. This tool will facilitate evaluation of the fault tolerance schemes that we develop. DTIC

N95-20622 Carnegie-Mellon Univ., Pittsburgh, PA. School of Computer Science.
MEASURING SOFTWARE DEPENDABILITY BY ROBUSTNESS BENCHMARKING
Arup Mukherjee and Daniel P. Siewiorek May 1994 26 p Sponsored by Computer Sciences Corp. Limited Reproducibility: More than 20% of this document may be affected by microfiche quality
(Contract N00014-91-J-4139)
(AD-A280053; CMU-CS-94-148) Avail: Issuing Activity (Defense Technical Information Center (DTIC))

Inability to identify weaknesses or to quantify advancements in software system robustness frequently hinders the development of robust software systems. Efforts have been made to develop benchmarks of software robustness to address this problem, but they all suffer from significant shortcomings. This paper presents the various features that are desirable in a benchmark of system robustness, and evaluates some existing benchmarks according to these features. A new hierarchically structured approach to building robustness benchmarks, which overcomes many deficiencies of past efforts, is also presented. This approach has been applied to building a hierarchically structured benchmark that tests part of the Unix file and virtual memory systems. The resultant benchmark has successfully been used to identify new response class structures that were not detected in a similar situation by other less organized techniques. DTIC

N95-20623 Carnegie-Mellon Univ., Pittsburgh, PA. School of Computer Science.
MAKING STRUCTURED GRAPHICS AND CONSTRAINTS PRACTICAL FOR LARGE-SCALE APPLICATIONS
Brad A. Myers, Dario A. Giuse, Andrew Mickish, and David S. Kosbie May 1994 26 p Limited Reproducibility: More than 20% of this document may be affected by microfiche quality
(Contract F33615-90-C-1465; ARPA Order 7597)
(AD-A280062; CMU-CS-94-150) Avail: Issuing Activity (Defense Technical Information Center (DTIC))

Providing a structured graphics model and a constraint system makes the programming of graphical applications significantly easier. In a structured graphics model, each graphic element on the screen is represented by a real object in the object system, while a constraint system automatically maintains relationships among the objects. Although many research systems and a few commercial environments provide structured graphics and constraints, none scale up to large interfaces with thousands of objects and thousands of constraints. This paper presents four techniques to overcome this problem: automatic elimination of constraints that depend only on values that do not change, layout hints to help with refresh and hit detection, virtual aggregates that only pretend to allocate objects for their components, and compiling composite aggregates into a single object with a complex draw method. These have been implemented as part of the Garnet environment, and we have demonstrated that together they allow structured graphics and constraints to scale up to applications with tens of thousands of objects and constraints without compromising the ease-of-use. DTIC

N95-20665# Naval Postgraduate School, Monterey, CA.
COMPUTER GRAPHICS TOOLS FOR VISUALIZING GRAVITY GRADIENT TORQUES ON A RIGID SPACECRAFT M.S. Thesis
Jeffrey A. Stewart Sep. 1994 140 p
(AD-A285971) Avail: CASI HC A07/MF A02

This thesis provides students with a set of graphics tools allowing them to better visualize the effects of gravity-gradient torques on a rigid spacecraft in a low earth orbit. It allows the user to select from a variety of rigid bodies of different configurations, place them in any orientation at any altitude, apply the appropriate gravity-gradient moments to the body and immediately see the effect on the rigid body. This is accomplished through interactive computer graphics written to run on Silicon Graphics computers. The thesis includes a presentation of the theory involved in the programming of the physical properties and then discusses the basics of computer graphics including a more detailed look at the specific implementation for this thesis. A detailed user's guide is included to train students to use the tools as expeditiously as possible. It concludes with recommendations for further study in this area. DTIC

N95-20687# Naval Postgraduate School, Monterey, CA.
DESIGN AND IMPLEMENTATION OF VISUAL OBJECT-ORIENTED LOGO USING PROGRAPH M.S. Thesis
Emily M. Black and Thierno Fall Sep. 1994 99 p
(AD-A285977) Avail: CASI HC A05/MF A02

This thesis addresses the problem of how best to teach beginning programmers the necessary skills of object oriented programming. There is no established method of introducing object oriented concepts such as encapsulation, inheritance, and polymorphism, or providing an intuitive progression from simple programs to complex problem solving. The approach was to use two commercially available programming languages which we consider exemplify good object oriented programming techniques, to teach beginners how to program. We selected LOGO, which has been used successfully in the past as a first programming language for children. Then we added the concepts of visual programming through the use of Prograph, a language which provides a visual, object oriented, dataflow environment. The main result of our research is the design and implementation of a prototype language called Visual Object Oriented LOGO (VOOL). VOOL is intended for use at all levels of education to teach problem solving, object oriented concepts, and fundamental programming skills. VOOL was implemented on a Macintosh in the pictorial, iconic language of Prograph and fully supports the goals of this thesis. DTIC

N95-20691*# Odessey Research Associates, Ithaca, NY.
TBell: A MATHEMATICAL TOOL FOR ANALYZING DECISION TABLES Final Report
D. N. Hoover and Zewei Chen 29 Nov. 1994 57 p
(Contract NAS1-18972; RTOP 505-64-50-04)
(NASA-CR-195027; Rept-94-0073; NAS 1.26:195027) Avail: CASI HC A04/MF A01

This paper describes the development of mathematical theory and software to analyze specifications that are developed using decision tables. A decision table is a tabular format for specifying a complex set of rules that chooses one of a number of alternative actions. The report also describes a prototype tool, called TBell, that automates certain types of analysis. Author

N95-20699# Los Alamos National Lab., NM.
EPICS SIMULATION TOOLS FOR CONTROL SYSTEM DEVELOPMENT
R. M. Wright, D. M. Kerstiens, G. D. Vaughn, and R. E. Weiss 1994 4 p Presented at the 17th International LINAC Conference, Tsukuba, Japan, 21-26 Aug. 1994
(Contract W-7405-eng-36)
(DE94-018082; LA-UR-94-2781; CONF-9408125-18) Avail: CASI HC A01/MF A01

When developing control system software there are many times when the ability to simulate the response of the instrumentation can be very useful. Examples are: (1) when the operator interface is being designed and the users want an idea of what the finished system might took like; (2) when the interface hardware is not yet available; (3) when the reaction of the control system to an error condition must be tested, but the actual occurrence of such an error would cause undesirable side effects; (4) when operators are being trained to use the system; (5) when an improvement or bug fix needs to be tested, but the running system cannot be shut down for long. The Experimental Physics and Industrial Control System (EPICS) provides tools for building simple simulations and interfacing to more complex simulations of accelerator hardware. At the lowest level an individual data channel can be switched to take its input from either a simulated data location or from the actual hardware. At a slightly higher level, sequences can be run on the real-time interface processor so that output to the hardware is intercepted and an appropriate substitute value is provided for the corresponding read-back records. At a still higher level a program can use the Channel Access software bus facility of EPICS to control some global aspect of an accelerator or can interface to an external accelerator simulation instead of the actual accelerator. The goal of testing control system software using simulated hardware is to minimize the changes required in shifting between the simulated system and the real system. The degree of success of the EPICS tools in meeting the minimum change goal will be addressed with suggestions for improvements. The implementation of simulated responses using EPICS tools will be discussed and examples of experience using the EPICS tools to create and interface to simulations will be given. DOE

N95-20718# University of Southern California, Marina del Rey, CA. Information Sciences Inst.
MODEL FORMALITY IN HUMAN/COMPUTER COLLABORATION
Brian Harp and Robert Neches Mar. 1994 9 p Presented at the AAAI Symposium, Oct. 1993
(Contract MDA972-90-C-0060)
(AD-A286001; ISI/RR-94-383) Avail: CASI HC A02/MF A01

This paper describes a programming methodology called model-based programming which supports development of systems with complex activities accessing large volumes of data. This methodology utilizes multiple levels of data model formality providing some powerful features for systems that are built using this methodology. For example, unlike most traditional systems, information can be programmed into an application during all phases of the system lifecycle from development through daily use. Second, the way information is entered will dictate how much reasoning the system will perform on it. This provides options for the user when they enter information; they can enter information quickly and get less system management, or they can enter information more formally and the system will take-more responsibility. One important component of this programming environment provides a way for users to enter information that was not anticipated at development time - an important capability of a system is going to grow with it's increasingly expert users. This component called TINT (The Intelligent Note Taker) is explained in detail and issues of human/computer collaboration are discussed in the context of adding unanticipated information to complex systems. DTIC

N95-20721# Mitre Corp., Bedford, MA.
A NEW PROCESS FOR ACQUIRING SOFTWARE ARCHITECTURE Final Report
Thomas F. Saunders, Barry M. Horowitz, and Matt L. Mleziva Sep. 1994 26 p
(Contract F19628-94-C-0001)
(AD-A286012; ESC-TR-94-207) Avail: CASI HC A03/MF A01

This paper presents a process to control software architectures during the procurement of military systems. The proposed process extends from RFP preparation through contract award. Software architecture is defined and its role described in the acquisition of flexible defense systems-systems that must accommodate new missions, threats, and technologies. A series of attachments provide sample wording for Statements of Work, System/Segment Design Documents, Software Development Plans, and Instructions for Proposal Preparation to incorporate the architectural control process into DOD acquisitions. DTIC

N95-20765 Carnegie-Mellon Univ., Pittsburgh, PA. Software Engineering Inst.
A SOFTWARE PROCESS FRAMEWORK FOR THE SOFTWARE ENGINEERING INSTITUTE'S (SEI) CAPABILITY MATURITY MODEL Final Report
Timothy G. Olson, James W. Over, and Neal R. Reizer Sep. 1994 820 p Limited Reproducibility: More than 20% of this document may be affected by microfiche quality
(Contract F19628-90-C-0003)
(AD-A286595; CMU/SEI-94-HB-01) Avail: CASI HC A99

The Software Process Framework (SPF) is a document that provides information contained in the SEI Capability Maturity Model (CMM) for Software v1.1 (Paulk93a) in a format suitable for process definition and improvement. The SPF allows users to determine if their organization's software process documentation is consistent with the recommendations made by the CMM. When organizational software process documentation is found to be inconsistent with the CMM, the SPF provides the ability to make informed decisions regarding the applicability of specific CMM recommendations. DTIC

N95-20776 Naval Postgraduate School, Monterey, CA.
AN EMPIRICAL APPROACH TO LOGICAL CLUSTERING OF SOFTWARE FAILURE REGIONS M.S. Thesis
Alexander E. Hilaris Mar. 1994 190 p Limited Reproducibility: More than 20% of this document may be affected by microfiche quality
(AD-A279863) Avail: CASI HC A09

Previous work showed that faults in a program tend to cluster when viewed by the variables that affect execution and propagation of the fault (structural clustering). However, that study was quite preliminary and local in its investigation. This thesis examines clustering from two other perspectives, taxonomical (type of faults) and functional (area of affected functionality). The hypothesis tested was that faults tend to cluster when viewed from these perspectives. DTIC

N95-20809# Carnegie-Mellon Univ., Pittsburgh, PA. Software Engineering Inst.
SOFTWARE CAPABILITY EVALUATION (SCE), VERSION 2.0 TEAM MEMBERS GUIDE Final Report
Oct. 1994 421 p
(Contract F19628-90-C-0003)
(AD-A286082; CMU/SEI-94-HB02) Avail: CASI HC A18/MF A04

Software Capability Evaluation (SCE) is a method for independently evaluating the software process of an organization to gain insight into its software development capability. The method is defined in the report Software Capability Evaluation Version 2.0 Method Description. This document, the Software Capability Evaluation Version 2.0 Team Member's Guide, is intended for use by members of teams that will be conducting an SCE. The guide provides detailed step-by-step instructions and heuristic information to assist an SCE team in preparing for and conducting an evaluation. The Team Member's Guide is provided as a supplement to the SCE Team Training offered by the Software Engineering Institute. It is intended to be used in conjunction with the Method Description and with the Software Capability Evaluation Version 2.0 Implementation Guide (SCE 93A). The Team Member's Guide provides information to reinforce the training and it will serve as a reference for use after the training. DTIC

N95-20810# Carnegie-Mellon Univ., Pittsburgh, PA. Software Engineering Inst.

RATE MONOTONIC ANALYSIS FOR REAL-TIME SYSTEMS: INSTRUCTORS GUIDE Final Report

Ruth Ravenel and Ray Obenza Sep. 1994 47 p
(Contract F19628-90-C-0003)
(AD-A286083; CMU/SEI-94-EM-11) Avail: CASI HC A03/MF A01

This educational materials package has been developed for instructors of software engineering and, more specifically, real-time systems. This package will help instructors teach rate monotonic analysis (RMA) to graduate and undergraduate software, computer, and electrical engineering students. The package can also be used to teach RMA to continuing education students. The presentation materials and exercises included have been used by Ruth Ravenel in both graduate and undergraduate courses. These educational materials are intended to be used in conjunction with the videotape, An Introduction to Rate Monotonic Analysis, from SEI Technology Series. DTIC

N95-20846 Carnegie-Mellon Univ., Pittsburgh, PA. Dept. of Computer Science.

BACKWARD ERROR RECOVERY IN REDUNDANT DISK ARRAYS

William V. Courtright, II and Garth A. Gibson 27 Sep. 1994 17 p
Limited Reproducibility: More than 20% of this document may be affected by microfiche quality
(Grant NSF ECD-89-07068)
(AD-A286064; CMU-CS-94-193) Avail: CASI HC A03

Redundant disk arrays are single fault tolerant, incorporating a layer of error handling not found in nonredundant disk systems. Recovery from these errors is complex, due in part to the large number of erroneous states the system may reach. The established approach to error recovery in disk systems is to transition directly from an erroneous state to completion. This technique, known as forward error recovery, relies upon the context in which an error occurs to determine the steps required to reach completion, which implies forward error recovery is design specific. Forward error recovery requires the enumeration of all erroneous states the system may reach and the construction of a forward path from each erroneous state. We propose a method of error recovery which does not rely upon the enumeration of erroneous states or the context in which errors occur. When an error is encountered, we advocate mechanized recovery to an error-free state from which an operation may be retried. Using a form of backward error recovery, we are able to manage the complexity of error recovery in redundant disk arrays without sacrificing performance. DTIC

N95-20847# Carnegie-Mellon Univ., Pittsburgh, PA. Dept. of Computer Science.

A TABULAR INTERFACE FOR AUTOMATED VERIFICATION OF EVENT-BASED DIALOGS

Hung-Ming Wang and Gregory Abowd (Georgia Inst. of Tech., Atlanta, GA.) 28 Jul. 1994 37 p
(AD-A286065; CMU-CS-94-189) Avail: CASI HC A03/MF A01

In this report, we investigate the feasibility of a tabular interface for the specification and analysis of event-based dialogues. These dialogues are used to define high-level descriptions of interactive systems, and they are based on Olsen's Propositional Production System (PPS) notation. The simulation of the abstract user-system dialogue is an effective means of matching a design with an expected task model. Monk and Curry have produced a prototype dialogue simulation tool, the Action Simulator, which demonstrates how a tabular paradigm can be used to specify and simulate the dialogue. Further analysis of the dialogue can uncover problems which are not, so easy to detect with simulation. If we view the dialogue as defining a finite state machine, then we can make use of powerful model verification tools, such as Clarke's Symbolic Model Verifier (SMV) tool, to perform more powerful analyses on the dialogue. We also find that the tabular paradigm for input is an interesting alternative to the input language for the SMV tool. We provide in this report a mechanical translation from the tabular dialogue specification into SMV and provide templates or heuristics for various reachability analyses using the Computation Tree Logic (CTL) formalism. This research, therefore, presents the beginnings of two significant contributions. For the HCI community, we show how model verification tools can be used to provide a more powerful analytic technique beyond simulation for the specification and design of interactive dialogues. For the model verification community, we demonstrate the possibility of developing a simpler interface to specify and analyze certain finite state machines. DTIC

N95-20877# Optimization Technology, Inc., Huntsville, AL.

ENVIRONMENT FOR TEST AND ANALYSIS OF DISTRIBUTED SOFTWARE (ETADS) Final Summary Report, 28 Mar. - 27 Sep. 1994

R. C. Cox and B. Allen 27 Sep. 1994 130 p
(Contract DASG60-94-C-0036)
(AD-A285776) Avail: CASI HC A07/MF A02

This final report describes results of the Phase 1 SBIR research effort to develop new software testing techniques capable of satisfying the demands of distributed real-time software environments. Traditional software testing techniques are inadequate for distribute systems due to such complicating factors as non-deterministic execution, real-time timing constraints, task interaction event sequencing, race conditions, etc. During the course of the Phase 1 effort, OTI investigate a wide variety of candidate technique. For each technique, OTI evaluated the feasibility and defined a research and development approach for the technique and required supporting technologies. Detailed comparison-of the attributes of each technique gives the following prioritization of techniques: Deterministic Execution Testing, Timing Analysis, Control Flow Testing, Dependency Analysis, Network Communication Testing, Data Flow Analysis, Problem Tracking Facility, Mutation Analysis, Static Concurrency Testing. OTI's research approach was based on developing new functionality on top of an existing software testing environment to construct the Environment for Test and Analysis of Distributed Software (ETADS). DTIC

N95-20887# Sandia National Labs., Albuquerque, NM. Engineering Sciences Center.

COYOTE II: A FINITE ELEMENT COMPUTER PROGRAM FOR NONLINEAR HEAT CONDUCTION PROBLEMS. PART 1: THEORETICAL BACKGROUND

David K. Gartling and Roy E. Hogan Oct. 1994 62 p
(Contract DE-AC04-94AL-85000)
(DE95-002587; SAND-94-1173-Pt-1) Avail: CASI HC A04/MF A01

The theoretical and numerical background for the finite element computer program, COYOTE II, is presented in detail. COYOTE II is designed for the multi-dimensional analysis of nonlinear heat conduction problems and other types of diffusion problems. A general description of the boundary value problems treated by the program is presented. The finite element formulation and the associated numerical methods used in COYOTE II are also outlined. Instructions for use of the code are documented in SAND94-1179; examples of problems analyzed with the code are provided in SAND94-1180. DOE

N95-20901# Fermi National Accelerator Lab., Batavia, IL.

Xwake 1.0 USER'S MANUAL

G. Saewert, T. Jurgens, and F. Harfoush Jul. 1994 21 p
(Contract DE-AC02-76CH-03000)
(DE95-002528; FNAL-TM-1896) Avail: CASI HC A03/MF A01

Xwake is a user friendly Finite Difference Time Domain (FDTD) code for wake potential and impedance calculations of rotationally symmetric structures. Geometry boundaries are automatically meshed, or modeled, by a choice of either of two approximations, the typical 'stepped edge' modeling, or the new 'contour' modeling. Contouring means geometry boundaries described with curves and angles are not distorted to follow the rectangular grid; rather, the grid is adjusted to follow the contour of the geometry boundaries. It offers computer run time savings for large problems or intricate geometries for a given mesh compared with stepped edge modeling. Using stepped approximations with Xwake, on the other hand, one is able to model materials of any linear media type. Ultimately, three solutions are computed, wake potential versus wake length, wake spectrum versus frequency - a Fourier transform (FFT) of the wake potential, and wake impedance versus frequency. Xwake is an OSF/Motif application providing a graphical user interface (GUI) for ease of use. It is written in ANSI C for portability and currently runs on UNIX platforms. DOE

N95-20910# Loral Federal Systems, Manassa, VA.
REAL-TIME RECONFIGURATION STUDY Final Report
Daniel Searles Aug. 1994 23 p
(Contract N00014-91-C-0129)
(AD-A286060) Avail: CASI HC A03/MF A01

The objective of the real-time reconfiguration study was to implement a physical test bed for testing and evaluating a suite of reconfiguration algorithms. The software architecture was composed of an operating system which supported real-time programming concepts, a set of model tasks, control software, and the suite of reconfiguration procedures. Rate monotonic scheduling was used to schedule the execution of the task set, as well as for testing the schedulability of new configurations. Of primary concern was the execution time of the reconfiguration algorithms. The general problem of reconfiguration is similar to the bin packing problem and is NP-Complete. This suite implements a concept of disturbance, a cost associated with moving a task from one CPU to another, to reduce execution time. The hardware platform was composed of a VME chassis populated with 5 Motorola 68030 CPU's. DTIC

N95-20975 Technische Univ., Eindhoven (Netherlands). Dept. of Mathematics and Computing Science.
STARS OR STRIPES: A COMPARATIVE STUDY OF FINITE AND TRANSFINITE TECHNIQUES FOR SURFACE MODELLING
C. W. A. M. vanOverveld and M. Verhoeven Jun. 1994 41 p Limited Reproducibility: More than 20% of this document may be affected by microfiche quality
(PB95-134979) Avail: CASI HC A03

Most geometric modeling systems employ a surface representation for four-sided patches, such as bi-cubic B-splines, which is based on a matrix of N x M control points for integer N and M. The boundary is defined by the 2N + 2M - 4 outermost control points whereas the remaining MN - 2N - 2M + 4 control points indicate the shape of the interior part of the surface. This is in sharp contrast with conventional hand-drafting techniques for curved surfaces, where only the boundary is drawn as a set of curve segments joining in the corners, and the shape of the interior part is usually left unspecified. The bicubic Coons patches make up a representation scheme for such surface which is much more intuitive in this respect. Yet, bicubic Coons patches seem to be not widely used in geometric modelling when compared with B-spline techniques. In this paper, the authors suggest some causes for this apparent mismatch between intuition and common CAGD (Computer Aided Geometric Design) - practice viz. difficulties of the interactive definition of boundary contours, the specification of cross-boundary derivatives, and a lack of control of the interior shape. Next, the authors propose remedies for all three types of problems. NTIS

N95-20982 Helsinki Univ. of Technology, Espoo (Finland). Dept. of Mathematics and Systems Analysis.
SYSTEMS ANALYSIS LABORATORY. TEN YEARS OF PROGRESS 1984-1994
R. P. Haemaelaeinen 1994 68 p Limited Reproducibility: More than 20% of this document may be affected by microfiche quality
(PB95-104451; ISBN-951-22-2064-4) Avail: CASI HC A04

The activity report celebrates the 10th anniversary of the Systems Analysis Laboratory, of Helsinki University of Technology which was established in 1984 within the professorship of applied mathematics. The laboratory belongs to the Department of Mathematics and Systems Analysis in the Faculty of Information Technology. The goals of the present Systems Analysis Laboratory is to cover the area of systems science comprehensively ranging from the mathematical theories of optimization, control and decision making to algorithms, practical modeling and decision support systems based on modern information technology. The focus of interest in applications is in complex energy, production and environmental systems. The problems are analyzed with a balanced engineering-economic systems approach. The report describes the current courses and research activities. It also summarized output in terms of publications and degree theses during the past ten years. NTIS

N95-20996# University of Southern California, Marina del Rey, CA. Information Sciences Inst.
GENERATING EXAMPLES FOR USE IN TUTORIAL EXPLANATIONS: THE USE OF A SUBSUMPTION BASED CLASSIFIER
Vibhu O. Mittal and Cecile L. Paris Jun. 1994 18 p
(Contract DABT63-91-C-0025; NSF IRI-90-03087)
(AD-A286028; ISI/RR-94-384) Avail: CASI HC A03/MF A01

Examples form an integral and very important part of many descriptions, especially in contexts such as tutoring and documentation generation. Previous computational work on example generation has focused on the issue of generating valid examples in different domains. However, there are a large number of examples that can be generated for a given concept, and it is important that examples intended for tutoring situations illustrate specific features that need to be communicated. There is also a strong interaction between the examples and the accompanying textual description. The number of examples to be presented, the order in which they are to be presented, and the position of the examples with respect to the text are all dependent upon the examples generated for use in the presentation. It is therefore important that the example generator be able to generate a set of suitable examples in response to a tutoring goal in a given situation. In this paper, we present one framework, based on the use of a subsumption classifier, that facilitates the generation of appropriate tutorial examples. We illustrate the working of this framework by describing the generation of examples to illustrate the syntax in the programming language LISP. DTIC

N95-21003 Gesellschaft fuer Mathematik und Datenverarbeitung, Bonn (Germany).
PROCEEDINGS OF THE FOURTH INTERNATIONAL WORKSHOP ON INDUCTIVE LOGIC PROGRAMMING (ILP-94)
Stefan Wrobel, ed. Sep. 1994 424 p Conference held in Bonn, Germany, Sep. 12-14 1994
(ISSN 0170-8120)
(PB95-135273; GMD-237; ISBN-3-88457-237-7) Copyright Avail: Issuing Activity (National Technical Information Service (NTIS))

Contents include the following: Learning Clauses by Tracing Derivations; Specialization of Logic Programs by Pruning SLD-Trees; First-order jk-clausal Theories are PAC-Learnable (Abstract); Inductive Learning of Characteristic Concept Descriptions; Inductive Logic Programming and Philosophy of Science; Inductive Metalogic Programming; An Efficient Subsumption Algorithm for Inductive Logic Programming; GRDT: Enhancing Model-Based Learning for Its Application in Robot Navigation; MILP-a stochastic approach to Inductive Logic Programming; A Learnability Model for Universal Representations; Self-Saturation of Definite Clauses; Effective Algorithmic Debugging for Inductive Logic Programming; Induction of Maximally General Clauses Consistent with Integrity Constraints; Mutagenesis: ILP experiments in a non-determinate biological domain; The Arguments of Newly Invented Predicates in ILP; A Note on Ideal Refinement Operators in Inductive Logic Programming; Learning to Recognize Hand-printed Chinese Characters using Inductive Logic Programming; Learning stage transition rules with Indlog; Applications of a logical discovery engine; Finite Element Mesh Design: An Engineering Domain for ILP Application; Pruning Methods for Rule Learning Algorithms; Relational Learning by Heuristic Evaluation of Ground Data; ILP and Automatic Programming: Towards Three Approaches; A Bidirectional search for clauses; Rulebase Stratification: An approach to theory restructuring; and A three-tiered Confidence Model for Revising Logical Theories. NTIS

N95-21010# Michigan Univ., Ann Arbor, MI. Dept. of Mechanical Engineering.
NEXT GENERATION SOLID MODELLERS FOR ELECTRONIC PROTOTYPING Final Report, 15 Feb. 1993 - 14 Feb. 1994
Debasish Dutta and Gunzburger 26 Jul. 1994 5 p
(Contract F49620-93-1-0149; AF Proj. 2304)
(AD-A286525; AFOSR-94-0745TR) Avail: CASI HC A01/MF A01

In this research project, we are focusing on expanding the geometric coverage of solid modellers such that a wider variety of objects can be modelled accurately. Solid modellers are large computer programs that enable a designer to construct, interrogate and manipulate computer models of physical objects. They are at the core of every computer system for engineering analysis, prototyping, manufacture and inspection. Various manufacturing tasks can be simulated in the computer and electronic mock-ups (i.e., prototypes) can be created prior to actual manufacture. DTIC

N95-21012# North Carolina Univ., Raleigh, NC. Precision Engineering Center.
VIRTUAL REALITY IN PRECISION ENGINEERING RESEARCH Quarterly Report
Thomas A. Dow Oct. 1994 7 p
(Contract N00014-94-J-4099)
(AD-A286528) Avail: CASI HC A02/MF A01

A summary of objectives and approach includes: (1) Develop virtual reality environment for precision fabrication processes and use this environment to study material removal processes and the surface created; (2) Explore computer visualization techniques to enhance the understanding of complicated manufacturing processes; and (3) Develop models for brittle fracture and utilize computed images to visualize the resulting surfaces. DTIC

N95-21021# Technische Univ., Eindhoven (Netherlands). Dept. of Mathematics and Computing Science.
GOLD: A GRAPH ORIENTED LANGUAGE FOR DATABASES
R. Post and P. DeBra Sep. 1993 58 p
(ISSN 0926-4515)
(PB95-127544) Avail: CASI HC A04/MF A01

A simple and powerful graph transformation language for databases is defined whose operations are themselves graphs. It was designed to remedy some of the shortcomings of the Graph-Oriented Object Database (GOOD) language, particularly, its restricted syntax for operations and its dependence on the rather awkward abstraction operator. The new language, Graph Oriented Language for Databases (GOLD), has only one operation; operations of GOOD are included as special cases. Thanks to a new idea, the core pattern, many more forms of node addition can be specified with this one operation; abstraction becomes superfluous. Due to its capability to add multiple nodes at once, GOLD surpasses GOOD in expressive power: queries are always generic, but they are not restricted to be constructive. The simpler forms of the GOLD operation have straightforward interpretations. Instead of imposing syntactic restrictions, the GOLD definition extends the semantics to cover a very broad range of expressions. NTIS

N95-21022# Technische Univ., Eindhoven (Netherlands). Dept. of Mathematics and Computing Science.
CORRECTNESS OF SOME ALGORITHMS TO GENERATE FINITE AUTOMATA FOR REGULAR EXPRESSIONS
H. M. M. tenEikelder and H. P. J. vanGeldrop Sep. 1993 30 p
(ISSN 0926-4515)
(PB95-127551) Avail: CASI HC A03/MF A01

We discuss the method given by Glushkov, McNaughton-Yamada and Berry-Sethi and a related method given by Aho, Sethi and Ullmann to generate a deterministic finite automaton accepting the language of a given regular expression. For both methods a formal description and a simple correctness proof is given. NTIS

N95-21025# Technische Univ., Eindhoven (Netherlands). Dept. of Mathematics and Computing Science.
COMPOSITIONAL PROOF THEORY FOR FAULT TOLERANT REAL-TIME DISTRIBUTED SYSTEMS
Henk Schepers and Rob Gerth 1994 42 p See also PB94-126737 Sponsored by Dutch STW
(ISSN 0926-4515)
(PB95-127601) Avail: CASI HC A03/MF A01

In this report we present a compositional network proof theory to specify and verify fault tolerant real-time distributed systems. Important in such systems is the failure hypothesis that stipulates the class of failures that must be tolerated. In the formalism presented in this report, the failure hypothesis of a system is represented by a predicate which expresses how faults might transform the observable input and output behavior of the system. A proof of correctness of a triple modular redundant system is given to illustrate our approach. NTIS

N95-21033 Center for Mathematics and Computer Science, Amsterdam (Netherlands). Dept. of Numerical Mathematics.
VLUGR3: A VECTORIZABLE ADAPTIVE GRID SOLVER FOR PDEs IN 3D. 2: CODE DESCRIPTION
J. G. Blom and J. G. Verwer Feb. 1994 21 p See also Part 1, PB95-135729
(PB95-135737; CWI-NM-R9405) Copyright Avail: Issuing Activity (National Technical Information Service (NTIS))

The paper describes an ANSI FORTRAN 77 code, VLUGR3, auto-vectorizable on the Cray Y/MP, that is based on an adaptive-grid finite-difference method to solve time-dependent three-dimensional systems of partial differential equations. NTIS

N95-21153# Sandia National Labs., Albuquerque, NM.
DAVE: A PLUG AND PLAY MODEL FOR DISTRIBUTED MULTIMEDIA APPLICATION DEVELOPMENT
R. F. Mines, J. A. Friesen, and C. L. Yang Jul. 1994 15 p Presented at the 8th ACM International Conference on Supercomputing, Manchester, England, 11-15 Jul. 1994
(Contract DE-AC04-94AL-85000)
(DE94-016481; SAND-94-8233; CONF-940756-1) Avail: CASI HC A03/MF A01

This paper presents a model being used for the development of distributed multimedia applications. The Distributed Audio Video Environment (DAVE) was designed to support the development of a wide range of distributed applications. The implementation of this model is described. DAVE is unique in that it combines a simple 'plug and play' programming interface, supports both centralized and fully distributed applications, provides device and media extensibility, promotes object reusability, and supports interoperability and network independence. This model enables application developers to easily develop distributed multimedia applications and create reusable multimedia toolkits. DAVE was designed for developing applications such as video conferencing, media archival, remote process control, and distance learning. DOE

N95-21176 Electronics Research Lab., Salisbury (Australia).
THE iMAPS: GENERAL INFORMATION
Martin Burke Aug. 1994 60 p Limited Reproducibility: More than 20% of this document may be affected by microfiche quality
(AD-A285421; ERL-0826-GD; DODA-AR-008-867) Avail: CASI HC A04

This paper introduces the main ideas of the iMAPS Task which aims to establish an integrated approach to the description, measurement, assessment and prediction of the attributes of software. DTIC

N95-21231 Rutherford Appleton Lab., Oxford (England).
PRSCAL MANUAL
M. Hagen Aug. 1994 26 p Prepared in cooperation with Keele Univ., England
(PB95-130480; RAL-94-084) Avail: Issuing Activity (National Technical Information Service (NTIS))

The PRSCAL program is a 'simulation' version of the PRISMA operating program. The commands in PRSCAL are, as far as is possible, identical to those in the PRISMA program. Therefore command procedures can be tested out before they are tried out on PRISMA itself. A particular example of this would be with the CD (Collect Data) command, where PRSCAL can be used to try out various possible sets of CD values to see which is the best or most appropriate. The PRSCAL program can also provide extra information on the configurations set up with the BR (BRagg) and CD commands which may be useful in planning or interpreting measurements. It also provides routines for calculating the resolution function in different configurations and for plotting the different measuring paths on an appropriate reciprocal space diagram. On the PRISMA microVax the program can be run in the PRSMGR and PRISMA accounts by typing: PRSCAL or PRSCALU. The situation on the ISIS Vax computers ISISE/ISVS5/etc. is that you can run either of these programs, using just the names given above if you have executed the DCL command file PRISMA-GENIE-SETUP.COM. The file sets up the various path names and symbols for PRSCAL/PRSCALU, and also for the PRSPLOT6 program and the PRISMA GENIEINIT.COM file. NTIS

N95-21232 Rutherford Appleton Lab., Oxford (England).
PRISMA OPERATING PROGRAM MANUAL
M. Hagen Aug. 1994 14 p Prepared in cooperation with Keele Univ., England
(PB95-130498; RAL-94-085) Avail: Issuing Activity (National Technical Information Service (NTIS))

The PRISMA spectrometer is controlled from the LA120 terminal in the PRISMA cabin by running a program PRISMA. If the program is not already running then it can be started by logging in to the account PRSMGR on the LA120 and typing PRISMA, at which point the prompt PRS> will appear. The program allows the user to driver (move) or scan detector/analyzer/sample angles and analyzer/detector energies and to position the spectrometer angles (16 detectors, 16 analyzers and sample) for an inelastic scattering measurement by specifying the direction of measurement in reciprocal lattice co-ordinates and the energy transfer to be measured at a specific point along the direction of the measurement. The rest of this section is divided into two sub-sections, the first describes the names used for the different angles involved in defining the spectrometer configuration. The second describes the parameters used to define (1) the motor zero and limit angles, (2) the sample, (3) the analyzer crystals and (4) the time of flight channels. The next and final section describes the control commands in the program. NTIS

N95-21269# Technische Univ., Eindhoven (Netherlands). Dept. of Mathematics and Computing Science.
COMPUTING NEAR-OPTIMAL SCHEDULES
J. K. Lenstra and D. B. Shmoys Jun. 1994 18 p Sponsored by UPS, Sun, Proctor & Gamble, DuPont, and AFOSR
(Grants NSF CCR-88-96272; NSF DMS-89-20550) (ISSN 0926-4493)
(PB95-132072; MEMO-COSOR-94-21) Avail: CASI HC A03/MF A01

We shall survey a number of results on computing near-optimal solutions for NP-hard scheduling problems. For many NP-hard optimization problems, there are polynomial-time approximation algorithms for finding solutions that are probably quite close to the optimum, whereas for others, no such algorithm is known. We will concentrate on results that state that certain performance guarantees are unlikely to be attained, in the sense that if there is such a good algorithm, then P = NP. In particular, we will survey results for multiprocessor scheduling and shop scheduling problems. NTIS

N95-21288# North Carolina State Univ., Raleigh, NC. Electric Power Research Center.
NESTLE: FEW-GROUP NEUTRON DIFFUSION EQUATION SOLVER UTILIZING THE NODAL EXPANSION METHOD FOR EIGENVALUE, ADJOINT, FIXED-SOURCE STEADY-STATE AND TRANSIENT PROBLEMS
Paul J. Turinsky, Rifat M. K. Al-Chalabi, Philippe Engrand, Hisham N. Sarsour, Francois Xaiver Faure, and Weiping Guo Jun. 1994 147 p Prepared for Los Alamos National Lab., NM
(Contracts DE-AC07-76ID-01570; W-7405-eng-36)
(DE95-001903; EGG-NRE-11406) Avail: CASI HC A07/MF A02

NESTLE is a FORTRAN77 code that solves the few-group neutron diffusion equation utilizing the Nodal Expansion Method (NEM). NESTLE can solve the eigenvalue (criticality); eigenvalue adjoint; external fixed-source steady-state; or external fixed-source, or eigenvalue initiated transient problems. The code name NESTLE originates from the multi-problem solution capability, abbreviating Nodal Eigenvalue, Steady-state, Transient, Le core Evaluator. The eigenvalue problem allows criticality searches to be completed, and the external fixed-source steady-state problem can search to achieve a specified power level. Transient problems model delayed neutrons via precursor groups. Several core properties can be input as time dependent. Two or four energy groups can be utilized, with all energy groups being thermal groups(i.e., upscatter exits) if desired. Core geometries modelled include Cartesian and Hexagonal. Three, two and one dimensional models can be utilized with various symmetries. The non-linear iterative strategy associated with the NEM method is employed. An advantage of the non-linear iterative strategy is that NESTLE can be utilized to solve either the nodal or Finite Difference Method representation of the few-group neutron diffusion equation. DOE

N95-21311# Argonne National Lab., Idaho Falls, ID.
VISUAL DISPLAYS AND NEURO-LINGUISTIC PROGRAMMING
S. A. Brown-VanHoozer and W. R. VanHoozer (Tranceformations Unlimited, Rigby, ID.) 1994 3 p Presented at the 8th Annual Idaho National Engineering Laboratory (INEL) Computing Symposium, Idaho Falls, ID, 4-7 Oct. 1994
(Contract W-31-109-eng-38)
(DE95-001454; ANL/IFR/CP-82704; CONF-941054-2) Avail: CASI HC A01/MF A01

Advancement of computer technology is forthcoming at such a rapid pace that the research concerning the interplay of humans and computer technology is lagging far behind. One area of particular concern is the design of visual displays that are pragmatic, 'user friendly,' and 'user assisting.' When engineers design visual displays, they generally do so methodically and logically, but only from within their own individual perspective or 'model of the world.' They select the human aspects which make sense to them and not necessarily to non-engineers, operators, and others. The model design is what the engineer chooses to relate, based on his or her perspective of reality. These choices limit the model design thereby excluding the users' perspective. A set of techniques which can be used to assist the designers in expanding their choices and include the users' model is Neuro-Linguistic Programming (NLP). DOE

N95-21325# Carnegie-Mellon Univ., Pittsburgh, PA. School of Computer Science.
USER INTERFACE SOFTWARE TOOLS
Brad A. Myers Aug. 1994 45 p Supersedes CMU-CS-92-114
(Contract N66001-94-C-6037; ARPA Order B326)
(AD-A286056; CMU-CS-94-182; CMU-HCII-94-107) Avail: CASI HC A03/MF A01

Almost as long as there have been user interfaces, there have been special software systems and tools to help design and implement the user interface software. Many of these tools have demonstrated significant productivity gains for programmers, and have become important commercial products. Others have proven less successful at supporting the kinds of user interfaces people want to build. This article discusses the different kinds of user interface software tools, and investigates why some approaches have worked and others have not. Many examples of commercial and research systems are included. Finally, current research directions and open issues in the field are discussed. DTIC

N95-21344 Technische Univ., Twente (Netherlands). Dept. of Computer Science.
EXPRESSIONS THAT TALK ABOUT THEMSELVES
Maarten Fokkinga Jun. 1994 16 p Limited Reproducibility: More than 20% of this document may be affected by microfiche quality
(ISSN 0924-3755)
(PB95-134060; Memo-INF-94-29) Copyright Avail: Issuing Activity (National Technical Information Service (NTIS))

The note explains how to construct an expression in a formal system that 'does something with itself'. As an application of this procedure we show how to construct a program that writes its own text, lay-out included. NTIS

N95-21349 Direction des Recherches, Etudes et Techniques, Paris (France). Centre de Documentation de l'Armement.
SUPPORT TO THE DEVELOPMENT OF HIGH-LEVEL GRAPHICS SOFTWARE Report, 5 Dec. 1990 - 4 Dec. 1993 [SOUTIEN AU DEVELOPPEMENT DE LOGICIELS GRAPHIQUES DE HAUT NIVEAU]
J. P. Bourguignon 4 Dec. 1993 92 p In FRENCH
(PB95-131686) Avail: Issuing Activity (National Technical Information Service (NTIS))

The objective of the study was to provide data-processing tools suitable for the construction of surface triangulations and the computation of associated discrete geometric quantities; the research performed consisted of two parts: (1) A theoretical part in which, after recalling definitions and existing results in the case of smooth and discrete surfaces, results are presented that make it possible to actually compute the Gauss curvature and the normal vector, when parameterization is available; and (2) An applied part, presenting concrete examples of applications to triangulations calculated by a parameterized mesh-generator developed for this study, and obtained by the digitization of surfaces issued from the medical world. NTIS

N95-21374 Vrije Univ., Amsterdam (Netherlands). Faculteit der Viskunde en Informatica.
HEURISTIC GENETIC ALGORITHMS FOR CONSTRAINED PROBLEMS. PART 1: PRINCIPLES
A. E. Eiben, P. E. Raue, and Z. Ruttkay Dec. 1993 41 p
(PB95-132031) Avail: Issuing Activity (National Technical Information Service (NTIS))

This report is an account of the theoretical issues of our research on the applicability of genetic algorithms (GA's) to solve problems where constraints are essential: constraint satisfaction problems (CSP) and constrained optimization problems (COP). We discuss the requirements and possibilities of defining so-called heuristic GA's (HGA's). Whereas in classical GA's only the selection of parents and survivors is biased by an evaluation of the candidate solutions, HGA's also apply biased choices within the child creation mechanism. This bias can be based on some, probably implicit, statistical analysis of the quality of candidate solutions, as well as on some heuristic information adopted from classical CSP solving techniques or depending on the specific problem at hand. HGA's are expected to be effective and efficient methods to solve CSP's and COP's. Test results are discussed extensively in a separate, second report in detail. In general, the test results justify the application of HGA's. Here we sum up only the main lessons learned from the experiments. Finally, we point out several open questions and further possibilities for defining non-classical GA's. NTIS

N95-21389# Allied-Signal Aerospace Co., Kansas City, MO.
REPRESENTING MANUFACTURING FEATURES TO SUPPORT DESIGN AND PROCESS CHANGES
S. L. Brooks, W. J. Kirk, III, W. R. Simons, C. W. Brown, and R. B. Greenway, Jr. (Kansas Univ., Kansas City, KS.) Sep. 1994 8 p Presented at the Mid-America Conference on Intelligent Systems, Overland Park, KS, 27 Oct. 1994
(Contract DE-AC04-76DP-00613)
(DE94-018587; KCP-613-5496; CONF-9410197-1) Avail: CASI HC A02/MF A01

Today there exists several parametric or variational feature-based solid modeling desip tools that aid the user in productively creating a product desip. However, most of these systems do not address mapping from the desip feature to the manufacturing feature and few, if any, automaticaly link design changes to manufacturing feature and/or process changes. Currently, most systems depend on humans to detect and propagate changes. Towards solving this problem, we are working on a manufacturing feature representation that can detect a desip or process change and correct some or at a minimum flag the manufacturing engineer where the change affects manufacturing operations. We define Manufacturing Features as a collection of faces and edges. It is important that these faces and edges can be uniquely identified in the design feature representation. Each Manufacturing Feature has a Clipping Space that defines the extent of the material removal volume. Because the Clipping Space references the design feature's faces and edges we can propagate a design change. Therefore, a change in the geometry of a face or edge is propagated when the Clipping Space is reevaluated. In this paper we present this new approach for representing manufacturing features and discuss its current and planned implementation. DOE

N95-21411 Technische Univ., Twente (Netherlands). Dept. of Computer Science.
GENERALISED APPROACH TO SOFTWARE STRUCTURE METRICS
P. M. vandenBroel and K. G. vandenBerg Apr. 1994 17 p See also PB93-223832 Limited Reproducibility: More than 20% of this document may be affected by microfiche quality
(PB95-107561; Memo-INF-94-22) Copyright Avail: Issuing Activity (National Technical Information Service (NTIS))

The aim of this paper is to generalize the Fenton-Whitty approach to structure software metrics by considering arbitrary sets of decomposition operations for flowgraphs. In the Fenton-Whitty approach decomposition of flowgraphs is unique, but the number of associated metric functions is not finite and these functions are all independent. In general, the decomposition of flowgraphs is not unique, which leads to constraints on the associated metric functions. Here we derive these constraints explicitly for two special cases, where we consider only the two operations sequencing and nesting as decomposition operations. It is shown that the two resulting classes of structure metrics are contained in the class of structure metrics of the Fenton-Whitty approach. NTIS

N95-21415# Technische Univ., Eindhoven (Netherlands). Dept. of mathematics and Computing Science.
DESIGN AND IMPLEMENTATION OF THE FIRE ENGINE: A C++ TOOLKIT FOR FINITE AUTOMATA AND REGULAR EXPRESSIONS
Bruce W. Watson 17 May 1994 191 p
(ISSN 0926-4515)
(PB95-132924) Avail: CASI HC A09/MF A02

This paper describes the design and implementation of version 1.1 of the FIRE engine. The FIRE engine is a C++ class library implementing finite automata and regular expression algorithms. The algorithms implemented in the toolkit are almost all of those presented in the taxonomies of finite automata algorithms. The reader is assumed to be familiar with the two taxonomies and with advanced C++ programming techniques. The toolkit is implemented largely in an object-oriented style, with finite automata and regular expressions being defined as classes. All of the classes and functions in the toolkit are presented in the same format. For each class (or function) the format includes a short description of its behavior, details of its implementation, and techniques for improving its performance. NTIS

N95-21435 Center for Mathematics and Computer Science, Amsterdam (Netherlands).
VLUGR3: A VECTORIZABLE ADAPTIVE GRID SOLVER FOR PDEs IN 3D. 1: ALGORITHMIC ASPECTS AND APPLICATIONS
J. G. Blom and J. G. Verwer Feb. 1994 29 p See also N94-26772 and Part 2, PB95-135737
(ISSN 0169-0388)
(PB95-135729; CWI-NM-R9404) Copyright Avail: Issuing Activity (National Technical Information Service (NTIS))

The paper describes an adaptive-grid finite-difference solver for time-dependent three-dimensional systems of partial differential equations. The robustness and the efficiency of the solver, both for vector and scalar processors, is illustrated by the application of the code to three example problems. NTIS

N95-21450*# Old Dominion Univ., Norfolk, VA. Dept. of Mechanical Engineering.
CONVERGENCE ACCELERATION OF THE PROTEUS COMPUTER CODE WITH MULTIGRID METHODS Final Report, period ending 15 Jan. 1995
A. O. Demuren and S. O. Ibraheem 15 Jan. 1995 162 p
(Grant NAG3-1329)
(NASA-CR-197677; NAS 1.26:197677) Avail: CASI HC A08/MF A02

This report presents the results of a study to implement convergence acceleration techniques based on the multigrid concept in the two-dimensional and three-dimensional versions of the Proteus computer code. The first section presents a review of the relevant literature on the implementation of the multigrid methods in computer codes for compressible flow analysis. The next two sections present detailed stability analysis of numerical schemes for solving the Euler and Navier-Stokes equations, based on conventional von Neumann analysis and the bi-grid analysis, respectively. The next section presents details of the computational method used in the Proteus computer code. Finally, the multigrid implementation and applications to several two-dimensional and three-dimensional test problems are presented. The results of the present study show that the multigrid method always leads to a reduction in the number of iterations (or time steps) required for convergence. However, there is an overhead associated with the use of multigrid acceleration. The overhead is higher in 2-D problems than in 3-D problems, thus overall multigrid savings in CPU time are in general better in the latter. Savings of about 40-50 percent are typical in 3-D problems, but they are about 20-30 percent in large 2-D problems. The present multigrid method is applicable to steady-state problems and is therefore ineffective in problems with inherently unstable solutions.
Author (revised)

N95-21455 Groningen Rijksuniv. (Netherlands). Computing Science Section.

GRONICs-1994. PROCEEDINGS OF THE 1994 GRONINGEN STUDENT CONFERENCE ON COMPUTER SCIENCE

H. M. Groenboom, H. W. K. Hesselink, and M. M. Lankhorst 1994 155 p Conference was held in Groningen, Netherlands, 1994
(PB95-135620; CS-N-9401) Avail: Issuing Activity (National Technical Information Service (NTIS))

The Contents of this Conference proceedings are: Continuation-Passing-Style as an Intermediate Representation for Compiling Scheme; Design and Implementation of a Multi-mode Hard Real-Time System with Dynamic Task Distribution on Heterogeneous Processors; A Generic, Customizable, Hybrid Structure-Oriented Editor; Using Indexes In Parallel Databases; Using Atomic Actions in Replica Groups to Simplify the Replication Implementation; Stochastic Languages and Stochastic Grammars; Implementing Elements of the Spec-Calculus: An Example; On Computing Annotated Logic Programs; Specification of Production Cell with Stream-Processing Functions; Robotic Hand-Eye Coordination using Multi-Resolution Linear Perceptron Representation; Automatic Improvement of Evaluation Functions; Compressing Sparse Tables using a Genetic Algorithm; On the Automation of Single-Exposure Dual-Energy Computed-Radiography; Modularity in IFAD VDM-SL; A Knowledge Base Clustering Heuristic for Distributed Computations; Music in Time-Based Hypermedia; On Parallel Algorithms for Matrix Multiplication; A New Programming Methodology for Lazy Functional Languages; Parallelization of an Optimal Non-linear State Estimator; Programming and Verifying Real-time Systems; Symbolic Model Checking; An Update Protocol for an Shared Data-Object Model. NTIS

N95-21489 Microelectronics and Computer Technology Corp., Austin, TX.

AN MCM CONCURRENT ENGINEERING SOFTWARE TOOL MARKET STUDY Final Technical Report

1994 117 p Limited Reproducibility: More than 20% of this document may be affected by microfiche quality
(Contract MDA972-92-C-0022)
(AD-A279257) Avail: Issuing Activity (Defense Technical Information Center (DTIC))

This market study has been developed for the Advanced Research Projects Agency (ARPA) under the DICE program contract number MDA972-92-C-0022. This market study is focused on concurrent engineering software technology developed under the DICE program that uses the Rensellaer Object Storage Environment (ROSE). The object of this market study, based on a survey of end-user requirements, is to determine how this technology, referred to as CHOICE, could be further developed and then distributed to the commercial market. To reach our stated objective, an assessment of the current CHOICE technology, how this technology could be positioned in the commercial electronic design automation (EDA) market place, and a proposed product-market launch plan are included. DTIC

N95-21495 Massachusetts Inst. of Tech., Cambridge, MA. Artificial Intelligence Lab.

OBJECT RECOGNITION BY ALIGNMENT USING INVARIANT PROJECTIONS OF PLANAR SURFACES

Kenji Nagao and Eric Grimson Dec. 1994 20 p Limited Reproducibility: More than 20% of this document may be affected by microfiche quality
(Contract N00014-91-J-4038; NSF IRI-89-00276)
(AD-A279841; AI-M-1463) Avail: CASI HC A03

In order to recognize an object in an image, we must determine the best transformation from object model to the image. In this paper, we show that for features from coplanar surfaces which undergo linear transformations in space, there exist projections invariant to the surface motions up to rotations in the image field. To use this property, we propose a new alignment approach to object recognition based on centroid alignment of corresponding feature groups. This method uses only a single pair of 2D model and data. Experimental results show the robustness of the proposed method against perturbations of feature positions. DTIC

N95-21515# Brookhaven National Lab., Upton, NY.

BASIC PROGRAM FOR POWER SPECTRUM ESTIMATION

E. L. Church and P. Z. Takacs May 1994 17 p
(Contract DE-AC02-76CH-00016)
(DE95-002228; BNL-49035-Rev-5/94) Avail: CASI HC A03/MF A01

A standard data set is presented to be used in testing routines that are developed for evaluating the one-dimensional periodogram spectral estimate of a series of uniformly spaced data points representing measurements of a surface profile. These data were generated using the GWBASIC program 'FFTPSD' which is included in the Appendix of this report. The original purpose of this data set was to allow us to test and debug our own periodogram estimation routines, written in various programming, languages, against a standard data set. At the request of numerous individuals, we are making it available to others who may wish to do the same. We have also included a summary explanation of periodogram estimators and the various considerations that go into generating computer algorithms for power spectrum estimation. DOE

N95-21567# Carnegie-Mellon Univ., Pittsburgh, PA. Software Engineering Inst.

BENEFITS OF CMM-BASED SOFTWARE PROCESS IMPROVEMENT: EXECUTIVE SUMMARY OF INITIAL RESULTS Final Report

James Herbsleb, Anita Carleton, James Rozum, Jane Siegel, and David Zubrow Sep. 1994 24 p
(Contract F19628-90-C-0003)
(AD-A286444; CMU/SEI-94-SR-13) Avail: CASI HC A03/MF A01

Data from 13 organizations were collected and analyzed to obtain information on the results of software process improvement efforts that were based on the capability maturity model (CMM). We report the cost and business value of improvement efforts, as well as the yearly improvement in productivity, early defect improvement efforts, time to market, and post-release defect reports. Case studies of improvement efforts and results in five organizations are summarized. We end with conclusions about the results of software process improvement (SPI) efforts. DTIC

N95-21619# Technische Univ., Eindhoven (Netherlands). Dept. of Mathematics and Computing Science.

REGULARITY OF BPa-SYSTEMS IS DECIDABLE

Sjouke Mauw and Hans Mulder May 1994 26 p
(ISSN 0926-4515)
(PB95-135489) Avail: CASI HC A03/MF A01

It is undecidable whether a system in Basic Process Algebra (BPA) is regular with respect to bisimulation semantics. Basic operators in BPA are alternative composition, sequential composition and guarded recursion. A system is regular if the interpretations of all process variables defined in the system have finitely many states. We present an effective method to transform a BPA specification into a linear specification whenever possible. NTIS

N95-21627 Carnegie-Mellon Univ., Pittsburgh, PA. Software Engineering Inst.

INTERIM PROFILE: DEVELOPMENT AND TRIAL OF A METHOD TO RAPIDLY MEASURE SOFTWARE ENGINEERING MATURITY STATUS Final Report

Roselyn Whitney, Elise Nawrocki, Will Hayes, and Jane Siegel Mar. 1994 29 p Limited Reproducibility: More than 20% of this document may be affected by microfiche quality
(Contract F19628-90-C-0003)
(AD-A279074; CMU/SEI-94-TR-4; ESC-94-TR-4) Avail: Issuing Activity (Defense Technical Information Center (DTIC))

Development of an interim profile (IP) method was driven by a business need to rapidly measure an organization's software engineering process maturity between organizational software process assessments (SPA's). This document provides information about the process used to develop the method and a description of the method to software engineering process group (SEPG) members and practitioners responsible for diagnosing software process maturity. This document also addresses the next steps in the further development and use of the interim profile method. DTIC

N95-21654 Selskapet for Industriell og Teknisk Forskning, Oslo (Norway). Dept. of Informatics.

DIFFPACK: SOFTWARE FOR PARTIAL DIFFERENTIAL EQUATIONS

H. P. Langtangen 22 Mar. 1994 19 p Prepared in cooperation with Oslo Univ., Norway

(PB95-110268; STF33-A94020) Copyright Avail: Issuing Activity (National Technical Information Service (NTIS))

Diffpack is a collection of C++ libraries for solving partial differential equations arising in various applications such as fluid flow, heat transfer and structural analysis. An overview of the different parts of the package is given. Thereafter more details of the finite element module are presented. NTIS

N95-21655 Selskapet for Industriell og Teknisk Forskning, Oslo (Norway). Dept. of Ceramics.

OBJECT-ORIENTED DESIGN OF PRECONDITIONED ITERATIVE METHODS

A. M. Bruaset and H. P. Langtangen 13 May 1994 27 p Prepared in cooperation with Oslo Univ., Norway

(PB95-110276; STF33-A94036) Copyright Avail: Issuing Activity (National Technical Information Service (NTIS))

As modern programming methodologies migrate from computer science to scientific computing, developers of numerical software are faced with new possibilities and challenges. Based on experiences from an ongoing project that develops C++ software for the solution of partial differential equations, this paper has its focus on object-oriented design of iterative solvers for linear systems of equations. Special attention is paid to possible conflicts that have to be resolved in order to achieve a very flexible, yet efficient, code. NTIS

N95-21711 Technische Univ., Eindhoven (Netherlands). Dept. of Computer Science.

CAISE 1994 DOCTORAL CONSORTIUM

Gunnar Brataas, ed. and Anne Helga Seltveit, ed. May 1994 58 p Conference held in Utrecht, Netherlands, 6-7 Jun. 1994

(ISSN 0924-3755)

(PB95-135182; Memo-INF-94-24) Copyright Avail: Issuing Activity (National Technical Information Service (NTIS))

This document contains the following topics: The Dependency Manager: A Base Service for Transactional Workflow Management; Policy Resolution--A Framework for Specifying Agent Selection and Agent Coordination in Context of Workflow-Management; Performance Engineering of Task Processing Systems; Conceptual Models of Cooperative Information Systems; An Indirective Approach to Information Requirments Determination in the Development of Executive Information Systems; User Enhanceability for Information Systems; Support for Re-engineering-in-the-large; An Object-Oriented Data Model for Official Statistical Information System Applications; Towards a Calculus of Object Oreintedness; Schema Modification Management for Object-Oriented Databases; Application Domain Languages; An Integrated Approach to Large-Scale IS Development Based on Systematic Complexity Reduction; Domain Modeling in Information Systems Engineering; Conceptual Data Model Mapping; Object-Oriented Modeling and Simulation Software Engineering; Meta-Modeling for Schema Transformation and Code Generation; Consistent Information System Development; Modeling Fuzzy Information in Temporal Databases; Advanced Access Cost Models for Databases; A Visual Query Language for Final Users. NTIS

N95-21713# Brookhaven National Lab., Upton, NY.

DBASE 4 BASICS

P. OConnor 1994 65 p

(Contract DE-AC02-76CH-00016)

(DE94-018323; BNL-60712) Avail: CASI HC A04/MF A01

This is a user's manual for dBASE IV. dBASE IV is a popular software application that can be used on your personal computer to help organize and maintain your database files. It is actually a set of tools with which you can create, organize, select and manipulate data in a simple yet effective manner. dBASE IV offers three methods of working with the product: (1) control center; (2) command line; and (3) programming. DOE

N95-21716 Technische Univ., Eindhoven (Netherlands). Dept. of Computer Science.

PROCEEDINGS OF THE 5TH WORKSHOP ON THE NEXT GENERATION OF CASE TOOLS

Babis Theodoulidis, ed. May 1994 229 p Workshop held in Utrecht, Netherlands, 6-7 Jun. 1994 See also report on 4th workshop, PB94-150372

(ISSN 0924-3755)

(PB95-135208; Memo-INF-94-25) Copyright Avail: Issuing Activity (National Technical Information Service (NTIS))

The contents of this document are: A User-Centered Database Design Environment; An Imprecise Querying Mechanism for the Reuse of Conceptual Schema Components; End User CASE - Specializing Rules in a Secure Environment; CASE Tool Integration: A State of the Art Review; Information Resource Dictionary System Standards and CASE Tools; The Reverse Engineering of Relational Databases; Meanings and motives of method customizations in CASE environments-observations and categorizations from an empirical study; A CASE repository based on a service model to support 'open' CASE environments; MENTOR: A Step Forward in Guidance for Information System Development; Specification of services for high performance networking: validation and verification with formal methods; An Intelligent CASE-tool supporting Integrated Business/IT Strategy Planning; Support for Incremental Method Engineering and MetaCASE; A Graph Theory Metrics Family for Software Assessment; Federated CASE Environment System-Towards the Realization of open CASE Environments; CASE Support for the Localization of Software Products; Process and Methodology Aspects of Development Processes; Human Factors and Modern Software Development; Meta-CASE Capability in non-meta-CASE Environments; Temporal Information Bases for CASE; Integrated Software Development Environments: Requirements for the Next Generation; The New PPP: Its Architecture and Repository Management. NTIS

N95-21744# Oak Ridge National Lab., TN.

QMRPACK USER'S GUIDE

R. W. Freund (Bell Telephone Labs., Inc., Murray Hill, NJ.), N. M. Nachtigal, and J. C. Reeb Oct. 1994 25 p

(Contract DE-AC05-84OR-21400)

(DE95-001770; ORNL/TM-12807) Avail: CASI HC A03/MF A01

QMRPACK is a library of FORTRAN 77 subroutines that may be used to solve linear systems of equations with the quasi-minimal residual (QMR) method and to compute eigenvalue approximations. This User's Guide is designed to be an overview of the codes contained in QMRPACK. Installation information is provided, and the example matrix format is discussed. The relative merits of each algorithm, as well as usage criterion are described. The authors also provide instructions for making the test drivers, as well as test output from several machines. DOE

N95-21829# Argonne National Lab., IL.

EAGLES 1.1: A MICROCOMPUTER SOFTWARE PACKAGE FOR ANALYZING FUEL EFFICIENCY OF ELECTRIC AND GASOLINE VEHICLES

W. M. Marr 15 May 1994 8 p Presented at the Electric, Hybrid and Alternative Fuel Vehicles Conference, Aachen, Germany, 31 Oct. - 4 Nov. 1994

(Contract W-31-109-eng-38)

(DE95-001119; ANL/ES/CP-82394; CONF-9410221-1) Avail: CASI HC A02/MF A01

As part of the U.S. Department of Energy's electric/hybrid vehicle research program, Argonne National Laboratory has developed a computer software package called EAGLES. This paper describes the capability of the software and its many features and potential applications. EAGLES version 1.1 is an interactive microcomputer software package for the analysis of battery performance in electric-vehicle applications, or the estimation of fuel economy for a gasoline vehicle. The principal objective of the electric-vehicle analysis is to enable the prediction of electric-vehicle performance (e.g., vehicle range) on the basis of laboratory test data for batteries. The model provides a second-by-second simulation of battery voltage and current for any specified velocity/time or power/time profile, taking into consideration the effects of battery depth-of-discharge and regenerative braking. Alternatively, the software package can be used to determine the size of the battery needed to satisfy given vehicle mission requirements (e.g., range and driving patterns). For gasoline-vehicle analysis, an empirical model relating fuel economy, vehicle parameters, and driving-cycle characteristics is included in the software package. For both types of vehicles, effects of heating/cooling loads on vehicle performance can be simulated. The software package includes many default data sets for vehicles, driving cycles, and battery technologies. EAGLES 1.1 is written in the FORTRAN language for use on IBM-compatible microcomputers. DOE

N95-21950 Defence Science and Technology Organization, Melbourne (Australia). Airframes and Engines Div.

AN EVALUATION OF THE GEAR AVERAGING SIGNAL PROCESSOR (GASP)

D. M. Blunt Sep. 1994 48 p
(DSTO-TR-0067; AR-008-933) Copyright Avail: Issuing Activity (DSTO Aeronautical and Maritime Research Lab., GPO Box 4331, Melbourne, Victoria 3001, Australia)

The Gear Averaging Signal Processor (GASP) is an IBM PC XT board designed and built by AMRL to calculate synchronous vibration signal averages in real-time. This report describes GASP at an initial stage of development in which it produces a signal averages in a non-real-time mode. To evaluate GASP in this mode of operation, a comparison was made with a PC-based signal averaging system. This comparison shows that GASP works effectively, but is limited by the memory available on the board and the precision of some of its floating point calculations. Author

N95-21971 San Jose State Univ., CA.

THE USE OF FUZZY SET CLASSIFICATION FOR PATTERN RECOGNITION OF THE POLYGRAPH Final Report, 15 Jan. - 31 Dec. 1993

Benjamin Knapp, Mitra Dastmalchi, Eric Jacobs, and Shahab Layeghi Dec. 1993 237 p Limited Reproducibility: More than 20% of this document may be affected by microfiche quality
(Contract N00014-93-1-0570)
(AD-A279148) Avail: Issuing Activity (Defense Technical Information Center (DTIC))

Polygraph tests are a widely used method to distinguish between truth and deception. Polygraph charts are usually analyzed by human interpreters. However, computer algorithms are now being developed to score the tests or verify the results. These methods are based on statistical classification techniques. In this study a number of time, frequency and correlation domain features were selected and used. The fuzzy K-nearest neighbor algorithm was used to classify the polygraph charts, a correct classification of ninety-one percent was obtained for a set of one hundred case files supplied by the NSA. DTIC

N95-21972 Software Productivity Consortium, Herndon, VA.

USING THE CoRE REQUIREMENTS METHOD WITH ADARTS. VERSION 01.00.05

H. Lykins, R. Kirk, and D. Smith Mar. 1994 179 p Limited Reproducibility: More than 20% of this document may be affected by microfiche quality
(Contract MDA972-92-J-1018)
(AD-A279151; SPC-93091-CMC) Avail: Issuing Activity (Defense Technical Information Center (DTIC))

This technical report explains how you can use the Ada-Based Design Approach for Real-Time Systems (ADARTSSM) to build a software design that satisfies software requirements specified using the Consortium Requirements Engineering Method (CoRE). ADARTS is a widely accepted object-oriented method for system and software development that results in a robust design that is well documented, meets timing requirements, can withstand change, and contains many reusable components. CoRE is a new object-oriented approach to software requirements engineering that results in requirements that are precise, testable, complete, consistent, and resilient in the face of change. This report is a supplement to the ADARTS Guidebook (Version 2) and the CoRE Guidebook (Version 1) and discusses: developing a CoRE requirements specification for use with ADARTS; deriving an ADARTS process structure from CoRE requirements; combining ADARTS processes and objects derived from CoRE requirements into an ADARTS software architecture design; and taking advantage of CoRE's precision in the ADARTS process structuring, class structuring, and software architecture design activities. DTIC

N95-21974 Carnegie-Mellon Univ., Pittsburgh, PA. Graduate School of Industrial Administration.

BALANCED 0, + OR - MATRICES. PART 2: RECOGNITION ALGORITHM

Michele Conforti, Gerard Cornuejols, Ajai Kapoor, and Krisina Vuskovi 22 Jan. 1994 36 p Limited Reproducibility: More than 20% of this document may be affected by microfiche quality
(Contract N00014-89-J-1063; NSF DDM-92-01340)
(AD-A279156; MSRR-601-Pt-2) Avail: Issuing Activity (Defense Technical Information Center (DTIC))

In this paper we give a polynomial time recognition algorithm for balanced 0, + or - matrices. This algorithm is based on a decomposition theorem proved in a companion paper. DTIC

N95-21983 Vrije Univ., Amsterdam (Netherlands). Faculteit der Wiskunde en Informatica.

VERIFICATION OF KNOWLEDGE-BASED REASONING MODULES

P. Leemans, J. Treur, and M. Willems Dec. 1993 54 p See also PB92-219575
(PB95-132692) Avail: Issuing Activity (National Technical Information Service (NTIS))

A knowledge-based system is made up out of components, and with each component goes a world description (W). Verification of a knowledge-based system is verifying each component in turn. If all components check out then the knowledge-based system has been verified. The paper introduces a number of properties that can be attributed to a knowledge base (KB) in relation to W, and are interesting for verification. Some are familiar from the literature, such as correctness, consistency, and decisiveness, but others such as completeness, and well-informedness are not often described. The authors show that the usual approach to verification is to check for special cases of these more general notions. Besides what to verify, another important topic is how to discover these potential problems. For this, a tool has been developed within the formal specification language DESIRE (a framework for DEsign and Specification of Interacting REasoning modules) for compositional architectures of knowledge-based systems. This tool DES-CHECK performs some automatic verification and fixing of the errors that are described in this paper. NTIS

N95-21992# Colorado Univ., Boulder, CO. Program in Applied Mathematics.

FAST ALGORITHMS FOR TRANSPORT MODELS

Thomas A. Manteuffel 1994 8 p
(Contract DE-FG02-90ER-25086)
(DE95-001702; DOE/ER-25086/T2) Avail: CASI HC A02/MF A01

This project has developed a multigrid in space algorithm for the solution of the S(sub N) equations with isotropic scattering in slab geometry. The algorithm was developed for the Modified Linear Discontinuous (MLD) discretization in space which is accurate in the thick diffusion limit. It uses a red/black two-cell (mu)-line relaxation. This relaxation solves for all angles on two adjacent spatial cells simultaneously. It takes advantage of the rank-one property of the coupling between angles and can perform this inversion in O(N) operations. A version of the multigrid in space algorithm was programmed on the Thinking Machines Inc. CM-200 located at LANL. It was discovered that on the CM-200 a block Jacobi type iteration was more efficient than the block red/black iteration. Given sufficient processors all two-cell block inversions can be carried out simultaneously with a small number of parallel steps. The bottleneck is the need for sums of N values, where N is the number of discrete angles, each from a different processor. These are carried out by machine intrinsic functions and are well optimized. The overall algorithm has computational complexity O(log(M)), where M is the number of spatial cells. The algorithm is very efficient and represents the state-of-the-art for isotropic problems in slab geometry. For anisotropic scattering in slab geometry, a multilevel in angle algorithm was developed. A parallel version of the multilevel in angle algorithm has also been developed. Upon first glance, the shifted transport sweep has limited parallelism. Once the right-hand-side has been computed, the sweep is completely parallel in angle, becoming N uncoupled initial value ODE's. The author has developed a cyclic reduction algorithm that renders it parallel with complexity O(log(M)). The multilevel in angle algorithm visits log(N) levels, where shifted transport sweeps are performed. The overall complexity is O(log(N)log(M)). DOE

N95-22016 Selskapet for Industriell og Teknisk Forskning, Trondheim (Norway). Div. of Industrial Mathematics.

STANDARD DATA FORMATS FOR SIMULATION

J. Amundsen 25 Apr. 1994 16 p
(PB95-110367; STF10-A94001) Avail: Issuing Activity (National Technical Information Service (NTIS))

This report provides an overview of data formats used in computer simulation. It concentrates on, and compares, object describing formats capable of capturing both the problem data and associated methods. Although no single and obvious candidate emerges from this process, two formats separate from the others. The National Center for Supercomputer Applications (NCSA) HDF format provides a widespread, easy to implement and functionally powerful standard format for implementation, while the International Organization for Standardization (ISO) 10303 Standard for the Exchange of Product Model Data (STEP) provides a standard, relational database oriented, general problem encapsulation mechanism for cross discipline work. NTIS

N95-22029 Vrije Univ., Amsterdam (Netherlands). Faculteit der Wiskunde en Informatica.
INITIAL EXPERIENCE WITH NONCORRECTING SYNTAX ERROR HANDLING
A. vanDeudekom, D. Grune, and P. Kooiman Nov. 1993 11 p See also PB83-107623
(PB95-132700) Avail: Issuing Activity (National Technical Information Service (NTIS))

Noncorrecting error handling is a technique which, when implemented with some caution, guarantees fully reliable syntax error messages. This paper describes a simple but efficient implementation and its incorporation in an existing top-down parser generator. Initial experience with the generated parsers is reported. Two points which require special attention are identified and discussed: handling grammars that are not completely context-free, and obtaining informative error message texts. The implementation is general enough to be incorporated in any parser generator. NTIS

N95-22031 Vrije Univ., Amsterdam (Netherlands). Faculteit der Wiskunde en Informatica.
TOP-DOWN NON-CORRECTING ERROR RECOVERY IN LLGEN
A. vanDeudekom and P. Kooiman Nov. 1993 41 p
(PB95-132718) Avail: Issuing Activity (National Technical Information Service (NTIS))

This paper describes the design and implementation of a parser generator with non-correcting error recovery based on the extended LL(1) parser generator LLgen. It describes a top-down algorithm for implementing this error recovery technique that can handle left-recursive grammars. The parser generator has been tested with several existing ACK-compilers, including C and Modula-2. Various optimizations have been tried and are discussed in this paper. NTIS

N95-22068 Coastal Engineering Research Center, Vicksburg, MS.
NODDS/WOSM INTERFACE USER'S MANUAL Final Report, May - Aug. 1993
Zeki Demirbilek and Steven M. Bratos Apr. 1994 62 p Sponsored by NRL Limited Reproducibility: More than 20% of this document may be affected by microfiche quality
(AD-A279095; CERC-94-4) Avail: Issuing Activity (Defense Technical Information Center (DTIC))

This report describes elements of a graphical user interface system developed between the World Oil Spill Model (WOSM) and the U.S. Navy's Oceanographic Data Distribution System (NODDS) database. Although both the NODDS and WOSM systems are briefly described, the emphasis of this report is on the coupling of these two stand-alone systems. Versatility of the interface is illustrated with three worldwide oil spill scenarios. DTIC

N95-22077# Argonne National Lab., IL. Mathematics and Computer Science Div.
A DAVIS-PUTNAM PROGRAM AND ITS APPLICATION TO FINITE-ORDER MODEL SEARCH: QUASIGROUP EXISTENCE PROBLEMS
W. McCune Sep. 1994 14 p
(Contract W-31-109-eng-38)
(DE95-003014; ANL/MCS-TM-194) Avail: CASI HC A03/MF A01

This document describes the implementation and use of a Davis-Putnam procedure for the propositional satisfiability problem. It also describes code that takes statements in first-order logic with equality and a domain size n then searches for models of size n. The first-order model-searching code transforms the statements into set of propositional clauses such that the first-order statements have a model of size n if and only if the propositional clauses are satisfiable. The propositional set is then given to the Davis-Putnam code; any propositional models that are found can be translated to models of the first-order statements. The first-order model-searching program accepts statements only in a flattened relational clause form without function symbols. Additional code was written to take input statements in the language of OTTER 3.0 and produce the flattened relational form. The program was successfully applied to several open questions on the existence of orthogonal quasigroups. DOE

N95-22081 Technische Univ., Twente (Netherlands). Dept. of Computer Science.
STRUCTURING DESIGN REQUIREMENTS USING YMIR
F. Dikker, P. M. Wognum, L. K. Alberts, and N. J. I. Mars Jul. 1994 58 p
(PB95-132742; Memo-INF-94-41) Copyright Avail: Issuing Activity (National Technical Information Service (NTIS))

The engineering design problem is to find a physically realizable description of an artifact that satisfies a given initial specification. In addition to this product-specific initial specification, many general requirements, like design codes, safety requirements and manufacturing possibilities, play a role in the design process. In this report, a conceptual model for describing these general requirements is presented. The basis of this conceptual model is a basic requirement model consisting of a scope and a restriction. The scope describes the design parts for which the requirement is applicable, the restriction describes the actual requirement. Both scope and restriction are represented on the basis of the general ontology for engineering design called YMIR. It is shown that, in this way, requirements can be used in the design process in an active way. This means that they can be incorporated in the design as soon as they become applicable and that the consequences of applicable requirements are propagated to the description of the design under construction. NTIS

N95-22094# Technische Univ., Eindhoven (Netherlands). Dept. of Mathematics and Computing Science.
FOUNDATIONS OF FUNCTIONAL PROGRAMMING: A PROGRAMMER'S POINT OF VIEW
R. R. Hoogerwoord May 1994 68 p
(ISSN 0926-4515)
(PB95-132932) Avail: CASI HC A04/MF A01

Functional programming is a style of programming where possibly recursive definitions of functions are derived to satisfy a priori given specifications. In this study we provide a mathematical justification for the rules of this game. This study is about the foundations of functional programming, not about the foundations of mathematics in general. The main purpose of this study is to show how simple the rules of the functional programming game are. NTIS

N95-22104 Aeronautical Research Labs., Melbourne (Australia).
AN IBM BASED ARINC INTERFACE
M. Iob Mar. 1993 19 p
(ARL-TR-21; AR-007-096) Copyright Avail: Issuing Activity (Director, Aeronautical Research Lab., 506 Lorimer St., Fishermens Bend, Victoria 3207, Australia)

A general purpose ARINC (Aeronautical Radio, INC) serial interface has been developed for use with an IBM PC or compatible computer. The interface consists of a PC card and software to selectively read, log, time tag and process data read from the ARINC bus. The PC card uses an XT slot and the data is written onto floppy disk or hard disk. The data logging and post-processing software has been configured for ARINC 419/561 but can be readily reconfigured to other ARINC formats. ARINC 419/561 are low speed standards dealing with systems operating at 11 +/- 3.5 kilobits per second. The interface and PC software could readily be adapted to handle much higher speed ARINC and non-ARINC formats. Author

N95-22133# Army Construction Engineering Research Lab., Champaign, IL.
DEVELOPMENT AND EVALUATION OF ALEC MICRO-WAND 3e (TRADENAME) TRAINING Final Report
Scott D. Johnson and Jeffrey G. Kirby Aug. 1994 97 p
(AD-A285863; CERL-TR-TA-94/04) Avail: CASI HC A05/MF A02

For today's fast-paced economy, the U.S. Army is introducing automation to replace time-consuming manual procedures. This report documents examination of potentially efficient methods for training the maintenance force at Army installation Directorates of Engineering and Housing (DEH's) or Directorates of Public Works (DPW's) in automated technology. The study examined change theory and recent views on teaching and learning, and tested the relative effectiveness of two types of instructional workbook. Each workbook provided training for the menu-based barcoding program, Automated Labor and Equipment Card Micro-Wand IIIe TM. Training based on the workbooks was offered at Fort Sam Houston and Fort Lee. At each installation one group learned from the procedural, 'step-by-step' workbook while another group used the 'whole task' scenario-based workbook. A post-training performance exercise assessed the subjects' proficiency with the Micro-Wand IIIe TM. Subjects using the scenario-based workbook performed better on the exercise than those using the procedural workbook. Problems encountered during the study are discussed, which should be helpful to project engineers and trainers involved in technology transfer. Recommendations are made on improving Micro-Wand TM software and training, barcoded service orders, and DEH/DPW's support of technology transfer of labor and equipment automation. DTIC

N95-22159 Technische Univ., Twente (Netherlands). Dept. of Computer Science.
SCOPE 1.5: A SOURCE-CODE OPTIMIZATION PackagEFOR REDUCE 3.5: USER'S MANUAL
J. A. vanHulzen Apr. 1994 102 p
(ISSN 0924-3755)
(PB95-107579; Memo-INF-94-21) Copyright Avail: Issuing Activity (National Technical Information Service (NTIS))

The facilities offered by a Source-Code Optimization Package for REDUCE 3.5 (SCOPE 1.5), are presented. We discuss the user aspects of the package. The algorithmic backgrounds are briefly summarized. Examples of straightforward and more advanced usage are shown, both in algebraic and symbolic mode. Possibilities for a combined use of GENTRAN and SCOPE are presented as well. NTIS

N95-22201# Naval Command, Control and Ocean Surveillance Center, San Diego, CA.
SCALABLE PROGRAMMING ENVIRONMENT Final Report, Sep. 1993 - Sep. 1994
Perry Partow Sep. 1994 68 p
(Proj. RJ1-4-B-41)
(AD-A286390; TR-1672) Avail: CASI HC A04/MF A01

This report describes the Scalable Programming Environment (SPE), which provides programmers with a transparent way of creating scalable parallel applications for large-grained parallel computer architectures. The SPE, which has been designed primarily to support data-flow processing applications, allows programs to be scaled to execute on any number of processing nodes while requiring no changes to the compiled binary code. The user is provided with a set of high-level message-passing routines which can be used to connect multi-instanced heterogeneous programs in a system. The SPE library routines hide the intricacies of how the parallel programs communicate. The details of the connections are specified in text files. The SPE allows individual programs to be coded without knowledge of other parts of the system and thus allows systems to be quickly built, modified, or scaled without program recompilation. DTIC

N95-22302# Technische Univ., Eindhoven (Netherlands). Dept. of Mathematics and Computing Science.
LOGIC PROGRAMMING AND NEGATION: A SURVEY
Krzysztof R. Apt (Amsterdam Univ., Netherlands.) and Roland Bol Feb. 1994 72 p
(PB95-110730) Avail: CASI HC A04/MF A01

We survey various approaches which were proposed to incorporate negation in logic programs. We concentrate on the proof-theoretic and model-theoretic issues and the relationships between them. NTIS

N95-22305# Technische Univ., Eindhoven (Netherlands). Dept. of Mathematics and Computing Science.
ABSTRACT INTERPRETATION OF REACTIVE SYSTEMS: ABSTRACTIONS PRESERVING UNIVERSAL CTL(*), EXISTENTIAL CTL(*) AND CTL(*)
D. Dams, O. Grumberg, and R. Gerth May 1994 36 p
(PB95-110557) Avail: CASI HC A03/MF A01

The need for formal verification of systems on one hand, and the advent of complex reactive systems on the other, calls for the development of automated verification techniques. Model checking is one such technique. The theory of abstract interpretation offers a framework for the definition and justification of property preserving abstractions. However, abstract interpretation has traditionally been focused on abstractions that preserve safety properties of programs, properties that hold in all states along every possible execution path. The authors show how it can be extended to the analysis of different kinds of reactive properties. To this purpose, they introduce two notions of abstraction of nondeterministic systems. One preserves universal computation tree logic (CTL*), the fragment of the branching time logic CTL* which allows only universal path quantification. Another preserves existential CTL*, the fragment only allowing existential path quantification. Furthermore the authors show that a combination of both notions preserves full CTL*. This brings several powerful techniques from abstract interpretation within the reach of model checking, including the construction of abstract models by symbolic execution of programs and the use of approximations to find an optimum between precision and speed. Examples are given to illustrate these. NTIS

N95-22310# Helsinki Univ. of Technology, Espoo (Finland).
ACTORSTUDIO REFERENCE MANUAL. A USER'S GUIDE TO THE ACTORSTUDIO USER INTERFACE EDITOR, VERSION 1.0
J. Ahvo, M. Rankinen, S. Riihiaho, B. Riihinen, and M. R. Koivunen 1993 56 p See also PB92-152636 and PB94-132859
(PB95-127023; TKO-C65) Avail: CASI HC A04/MF A01

ActorStudio is an interactive, graphical user interface (GUI) editor. It provides an easy but flexible way to design new direct manipulation interaction techniques, such as buttons, scroll bars and menus. This manual describes the current implementation of ActorStudio. The editor is implemented for Macintosh using Common Lisp and CLOS. The user interface of the editor is implemented following the general rules of the GUI standards for Macintosh applications. NTIS

N95-22328# Helsinki Univ. of Technology, Espoo (Finland).
COMPUTING SYMMETRIES AND STUBBORN SETS Technical Report
K. Varpaaniemi Apr. 1994 23 p See also PB94-179405
(PB95-127700; Rept-B-12) Avail: CASI HC A03/MF A01

We consider two promising methods for alleviating the state space explosion problem in reachability analysis: the symmetry method and the stubborn set method. We concentrate on the computation of symmetries and stubborn sets. The new algorithms presented help us to save time and space in the symmetry method and to avoid inspecting redundant states in the so called chaos-free failure divergences (CFFD)-preserving stubborn set method. NTIS

N95-22351 Technische Univ., Eindhoven (Netherlands). Dept. of Mathematics and Computing Science.
FORMAL SPECIFICATION AND COMPOSITIONAL VERIFICATION OF AN ATOMIC BROADCAST PROTOCOL
P. Zhou and J. Hooman 26 Jan. 1994 33 p Limited Reproducibility: More than 20% of this document may be affected by microfiche quality
(PB95-110508) Avail: CASI HC A03

We apply formal methods to specify and verify an atomic broadcast protocol. The protocol is implemented by replicating a server process on all processors in a network. We show that the verification of the protocol can be done compositionally by using specifications in which timing is expressed by local clock values. The requirements of the protocol are formally described, underlying communication mechanism, clock synchronization assumption, and failure assumptions are axiomatized. The server process is also represented by a formal specification. We verify that parallel execution of the server processes leads to the desired properties, by proving that the conjunction of all server specifications and axioms about the system implies the requirements of the protocol. NTIS

N95-22372# Helsinki Univ. of Technology, Espoo (Finland).
OVERVIEW OF RAPID PROTOTYPING TECHNOLOGIES IN MANUFACTURING
A. Dolenc 20 Apr. 1994 23 p
(PB95-127122; TKO-B116) Avail: CASI HC A03/MF A01

In this paper we overview a new class of manufacturing processes generally known as Rapid Prototyping Techniques or Technologies (RPT) that build parts by adding material on a layer-by-layer basis, in contrast to conventional methods that remove material. We discuss their basic principles, data transfer, applications, and compare them with their conventional counterparts. NTIS

N95-22386 Massachusetts Inst. of Tech., Cambridge, MA. Artificial Intelligence Lab.
FEATURE EXTRACTION WITHOUT EDGE DETECTION
Ronald D. Chaney Sep. 1993 154 p Limited Reproducibility: More than 20% of this document may be affected by microfiche quality
(Contract N00014-92-J-1879)
(AD-A279842; AI-TR-1434) Avail: Issuing Activity (Defense Technical Information Center (DTIC))

Information representation is a critical issue in machine vision. The representation strategy in the primitive stages of a vision system has enormous implications for the performance in subsequent stages. Existing feature extraction paradigms, like edge detection, provide sparse and unreliable representations of the image information. In this thesis, we propose a novel feature extraction paradigm. The features consist of salient, simple parts of regions bounded by zero-crossings. The features are dense, stable, and robust. The primary advantage of the features is that they have abstract geometric attributes pertaining to their size and shape. To demonstrate the utility of the feature extraction paradigm, we apply it to passive navigation. We argue that the paradigm is applicable to other early vision problems. DTIC

N95-22390 National Inst. of Standards and Technology, Gaithersburg, MD. Systems and Software Technology Div.
QUALITY CHARACTERISTICS AND METRICS FOR REUSABLE SOFTWARE Preliminary Report, Oct. 1992 - Jun. 1994
W. J. Salamon and D. R. Wallace May 1994 43 p Limited Reproducibility: More than 20% of this document may be affected by microfiche quality
(Contracts BMDO-92-A-012; BMDO-OA-005)
(PB94-203437; NISTIR-5459) Avail: CASI HC A03

This report identifies a set of quality characteristics of software and provides a summary of software metrics that are useful in measuring these quality characteristics for software products. The metrics are useful in assessing the reusability of software products. Author

N95-22402# Mitre Corp., Bedford, MA.
INCREMENTAL REDERIVATION OF SOFTWARE ARTIFACTS: FY 1993 Final Report, Oct. 1992 - Sep. 1993
Melissa P. Chase, Howard Reubenstein, and Alexander Yeh Sep. 1994 26 p
(Contract F19628-91-C-0001)
(AD-A285790; RL-TR-94-162) Avail: CASI HC A03/MF A01

Design replay presents a possible enabling technology to the Knowledge-Based Software Assistant specification maintenance and implementation derivation approach to software development. More generally, design replay can also be applied to derivations between a variety of different software description abstraction levels. Radical changes to a software artifact cannot generally be addressed by design replay as they require new design output. Evolutionary changes are more amenable to design replay and often involve incremental changes to derived artifacts. This report describes an approach to rederivation that exploits the incrementality of evolutionary maintenance changes, the state of MITRE's implementation of this approach, and what remains to be done to test this approach. DTIC

N95-22426# Lawrence Livermore National Lab., Livermore, CA.
SADDLE-NODE DYNAMICS FOR EDGE DETECTION
Y. F. Wong Sep. 1994 9 p Presented at the IEEE Workshop on Neural Networks for Signal Processing, Ermioni, Greece, 6-8 Sep. 1994
(Contract W-7405-eng-48)
(DE94-017415; UCRL-JC-116635; CONF-9409192-1) Avail: CASI HC A02/MF A01

The author demonstrates how the formulation of a nonlinear scale-space filter can be used for edge detection and junction analysis. By casting edge-preserving filtering in terms of maximizing information content subject to an average cost function, the computed cost at each pixel location becomes a local measure of edgeness. This computation depends on a single scale parameter and the given image data. Unlike previous approaches which require careful tuning of the filter kernels for various types of edges, this scheme is general enough to be able to handle different edges, such as lines, step edges, corners and junctions. Anisotropy in the data is handled automatically by the nonlinear dynamics. DOE

N95-21537*# Jet Propulsion Lab., California Inst. of Tech., Pasadena, CA.
COMBINING IMAGE-PROCESSING AND IMAGE COMPRESSION SCHEMES
H. Greenspan (California Inst. of Tech., Pasadena, CA.) and M.-C. Lee (Microsoft Corp., Redmond, WA.) *In its* The Telecommunications and Data Acquisition Report 15 Feb. 1995 p 54-76 (For primary document see N95-21532 06-32)
(RTOP 315-91-40-20-36)
Avail: CASI HC A03/MF A03

62 COMPUTER SYSTEMS

Includes computer networks and special application computer systems.

N95-19885* Carnegie-Mellon Univ., Pittsburgh, PA. School of Computer Science.
O(log2 n) TIME EFFICIENT PARALLEL FACTORIZATION OF DENSE, SPARSE SEPARABLE, AND BANDED MATRICES
John H. Reif 11 Apr. 1994 28 p Limited Reproducibility: More than 20% of this document may be affected by microfiche quality
(Contracts NAS5-30428; RTOP 550-63-00; N00014-91-J-1985; N00014-92-C-0182; NSF IRI-81-00681)
(NASA-CR-197356; NAS 1.26:197356; AD-A280052; CMU-CS-94-113)
Avail: Issuing Activity (Defense Technical Information Center (DTIC))

Known polylog parallel algorithms for the solution of linear systems and related problems require computation of the characteristic polynomial or related forms, which are known to be highly unstable in practice. However, matrix factorizations of various types, bypassing computation of the characteristic polynomial, are used extensively in sequential numerical computations and are essential in many applications. DTIC

N95-20013* Institute for Computer Applications in Science and Engineering, Hampton, VA.
DESIGN CONSIDERATIONS FOR PARALLEL GRAPHICS LIBRARIES Final Report
Thomas W. Crockett Jun. 1994 23 p Submitted for publication Limited Reproducibility: More than 20% of this document may be affected by microfiche quality
(Contracts NAS1-18605; NAS1-19480; RTOP 505-90-52-01)
(NASA-CR-194935; NAS 1.26:194935; AD-A283733; ICASE-94-49) Avail: CASI HC A03

Applications which run on parallel supercomputers are often characterized by massive datasets. Converting these vast collections of numbers to visual form has proven to be a powerful aid to comprehension. For a variety of reasons, it may be desirable to provide this visual feedback at runtime. One way to accomplish this is to exploit the available parallelism to perform graphics operations in place. In order to do this, we need appropriate parallel rendering algorithms and library interfaces. This paper provides a tutorial introduction to some of the issues which arise in designing parallel graphics libraries and their underlying rendering algorithms. The focus is on polygon rendering for distributed memory message-passing systems. We illustrate our discussion with examples from PGL, a parallel graphics library which has been developed on the Intel family of parallel systems. DTIC

N95-20056# Technische Univ., Eindhoven (Netherlands). Dept. of Mathematics and Computing Science.
ILIAS: A SEQUENTIAL LANGUAGE FOR PARALLEL MATRIX COMPUTATIONS
L. D. J. C. Loyens (Koninklijke/Shell-Lab., Amsterdam, Netherlands.) and J. Moonen Oct. 1993 29 p
(PB95-110631) Avail: CASI HC A03/MF A01

The ILIAS system consists of a sequential language for matrix computations, a compiler translating a source program into ILIAS pseudo code and a parallel interpreter for this code. The pseudo code is independent of a target architecture; it merely specifies scalar and matrix computations. The authors present the ILIAS language and discuss its implementation on a square torus network of transputers. Subscription of matrices causes data-alignment problems, which are solved by redistributions. To reduce redistribution overhead the authors use a new data distribution called the grid-base distribution. Furthermore, they develop several run-time heuristics that, together with the grid-base distribution, efficiently implement matrix subscription. The feasibility and scalability of the ILIAS system is demonstrated by timing results for two example ILIAS programs, an LU decomposition and a Strassen matrix multiplication, on transputer networks up to 400 processors. NTIS

N95-20123# Sandia National Labs., Albuquerque, NM.
SPLIT-C AND ACTIVE MESSAGES UNDER SUNMOS ON THE INTEL PARAGON
Rolf Reisen and Arthur B. Maccabe (New Mexico Univ., Albuquerque, NM.) Apr. 1994 10 p Presented at the Supercomputing 1994 Meeting, Washington, DC, 14-18 Nov. 1994
(Contract DE-AC04-94AL-85000)
(DE94-011418; SAND-94-1228C; CONF-941118-2) Avail: CASI HC A02/MF A01

The compute power of the individual nodes of massively parallel systems increases steadily, while network latencies and bandwidth have not improved as quickly. Many researches believe that it is necessary to use explicit message passing in order to get the best possible performance out of these systems. High level parallel languages are shunned out of fear they might compromise performance. In this paper we have a look at one such language called Split-C. It fits into a middle ground between efforts such as High Performance Fortran (HPF) and explicit message passing. HPF tries to hide the underlying architecture from the programmer and let the compiler and the run time system make decision about parallelization, location of data, and the mechanisms used to transfer the data from one node to another. On the other hand, explicit message passing leaves all the decision to the programmer. Split-C allows access to a global address space, but leaves the programmer in control of the location of data, and offers a clear cost model for data access. Split-C is based on Active Messages. We have implemented both under the SUNMOS operating system on the Intel Paragon. We will discuss performance issues of Split-C and make direct comparisons to the Thinking Machines CM-5 implementation. We will also scrutinize Active Messages, discuss their properties and drawbacks, and show that other mechanisms can be used to support Split-C. DOE

N95-20150# Sandia National Labs., Albuquerque, NM.
PERFORMANCE ISSUES FOR ENGINEERING ANALYSIS ON MIMD PARALLEL COMPUTERS
H. E. Fang, C. T. Vaughan, and D. R. Gardner 1994 8 p Presented at the American Society of Mechanical Engineers' Winter Annual Meeting, Chicago, IL, 9-11 Nov. 1994
(Contract DE-AC04-94AL-85000)
(DE94-015769; SAND-94-0985C; CONF-941142-17) Avail: CASI HC A02/MF A01

We discuss how engineering analysts can obtain greater computational resolution in a more timely manner from applications codes running on MIMD parallel computers. Both processor speed and memory capacity are important to achieving better performance than a serial vector supercomputer. To obtain good performance, a parallel applications code must be scalable. In addition, the aspect ratios of the subdomains in the decomposition of the simulation domain onto the parallel computer should be of order 1. We demonstrate these conclusions using simulations conducted with the PCTH shock wave physics code running on a Cray Y-MP, a 1024-node nCUBE 2, and an 1840-node Paragon. DOE

N95-20152# Sandia National Labs., Albuquerque, NM.
PARALLEL SOLID MECHANICS CODES AT SANDIA NATIONAL LABORATORIES
M. McGlaun 1994 6 p Presented at the American Society of Mechanical Engineers' Winter Annual Meeting, Chicago, IL, 9-11 Nov. 1994
(Contract DE-AC04-94AL-85000)
(DE94-015770; SAND-94-1925C; CONF-941142-13) Avail: CASI HC A02/MF A01

Computational physicists at Sandia National Laboratories have moved their production codes to distributed memory parallel computers. The codes include the multi-material CTH Eulerian code, structural mechanics code. This presentation discusses our experiences moving the codes to parallel computers and experiences running the codes. Moving large production codes onto parallel computers require developing parallel algorithms, parallel data bases and parallel support tools. We rewrote the Eulerian CTH code for parallel computers. We were able to move both ALEGRA and PRONTO to parallel computers with only a modest number of modifications. We restructured the restart and graphics data bases to make them parallel and minimize the I/O to the parallel computer. We developed mesh decomposition tools to divide a rectangular or arbitrary connectivity mesh into sub-meshes. The sub-meshes map to processors and minimize the communication between processors. We developed new visualization tools to process the very large, parallel data bases. This presentation also discusses our experiences running these codes on Sandia's 1840 compute node Intel Paragon, 1024 processor nCUBE and networked workstations. The parallel version of CTH uses the Paragon and nCUBE for production calculations. The ALEGRA and PRONTO codes are moving off networked workstations onto the Paragon and nCUBE massively parallel computers. DOE

N95-20158# Los Alamos National Lab., NM.
A PRACTICAL GUIDE TO USING MCNP WITH PVM
G. W. McKinney 1994 6 p Presented at the Winter Meeting of the American Nuclear Society, Washington, DC, 13-18 Nov. 1994
(Contract W-7405-eng-36)
(DE94-016162; LA-UR-94-2523; CONF-941102-15) Avail: CASI HC A02/MF A01

The introduction of large workstation clusters and massively parallel computing platforms has lead to an increased interest in the distributed-memory multiprocessing feature of MCNP(trademark). Such systems offer the potential of hundredfold increases in speedup. This paper provides step-by-step instructions on the creation and use of MCNP on such systems. DOE

N95-20305 Texas Univ., Austin, TX.
SYSTEM LEVEL FAULT TOLERANCE IN PARALLEL AND DISTRIBUTED COMPUTING SYSTEMS Final Report, 1 Jul. 1988 - 31 Dec. 1993
31 Dec. 1993 15 p Limited Reproducibility: More than 20% of this document may be affected by microfiche quality
(Contract N00014-88-K-0543)
(AD-A279664) Avail: Issuing Activity (Defense Technical Information Center (DTIC))

The major thrust of our effort was focused on the theory and practice of responsive (fault-tolerant, real-time) computing in parallel and distributed processing environments. New efficient methods of system testing have been developed which shorten a multiprocessor testing time by orders of magnitude and, therefore, can be used at system booting (previous techniques were prohibitively long). A new design framework for responsive computing was designed and is being implemented for validation. This framework is based on consensus which can be used to provide synchronization, reliable communication, fault diagnosis, checkpointing and even scheduling in multiprocessor environments. We have formalized and quantified the space-time tradeoff for efficient fault recovery. The system model is a graph, and we were especially successful in analysis of meshes and hypercubes. We developed a new method called naturally redundant algorithms which allows efficient implementation of application-specific techniques. DTIC

N95-20325 Carnegie-Mellon Univ., Pittsburgh, PA. School of Computer Science.
A SCALABLE VIDEO RATE CAMERA INTERFACE
Jon A. Webb, Thomas Warfel, and Sing B. Kang 26 Sep. 1994 15 p Limited Reproducibility: More than 20% of this document may be affected by microfiche quality
(Contract F19628-93-C-0171; ARPA Order A655)
(AD-A286144; CMU-CS-94-192) Avail: CASI HC A03

We survey the state of the art in high-speed interfaces for video input to high performance computers and note the difficulty of providing video at rates appropriate to modern parallel computers. Most interfaces that have been developed to date are not scalable, required extensive hardware development, and impose a full frame time delay between the moment the camera captures video and the moment it is available for processing. We propose a solution, based on a simple interface we have developed, which has been integrated into the iWarp parallel computer developed by Carnegie Mellon University and Intel Corporation. The interface takes advantage of iWarp's systolic capabilities, does not impose any frame buffer delay time, was simple to design, and is readily scalable to provide up to 32 camera ports, from all of which data can be captured at full video rate, on a system that fits in a 19 inch 6U rack. We have applied the system to multibaseline stereo vision, and provide performance figures. DTIC

N95-20366# Oak Ridge National Lab., TN.
MPI WORKSHOP
G. A. Geist 1993 8 p Presented at the Supercomputing Conference on High Performance Computing and Communications, Portland, OR, 15-19 Nov. 1993
(Contract DE-AC05-84OR-21400)
(DE94-017883; CONF-931115-14) Avail: CASI HC A02/MF A01

This paper presents an overview of MPI, a record standard message passing interface for MIMD distributed memory concurrent computers. The design of MPI has been a collective effort involving researchers in the United States and Europe from many organizations and institutions. MPI includes point-to-point and collective communication routines, as well as support for process groups, communication contexts, and application topologies. While making use of new ideas where appropriate, the MPI standard is based largely on current practice. DOE

N95-20435 Rutherford Appleton Lab., Chilton (England). Computational Modeling Div.
RALPAR-RAL MESH PARTITIONING PROGRAM VERSION 1.1
R. F. Fowler and C. Greenough Aug. 1994 48 p
(PB95-129847; RAL-94-091) Avail: Issuing Activity (National Technical Information Service (NTIS))

This report describes the first release of the Rutherford Appleton Laboratory Mesh Partitioning Program ralpar. Ralpar is a software tool to split up unstructured meshes into subdomains for parallel processing on MIMD type architectures. A wide range of basic decomposition methods have been implemented within this tool. This document describes the methods that have been implemented, how to run the tool and the measures of partition quality that are provided. NTIS

N95-20499# Organisatie voor Toegepast Natuurwetenschappelijk Onderzoek, The Hague (Netherlands). Fysisch en Elektronisch Lab.
A THEORETICAL STUDY ON THE PERFORMANCE OF THE FDTD CODE ON A MASSIVELY PARALLEL COMPUTER
M. G. Brand and L. J. VanEwijk 1 Apr. 1994 31 p
(AD-A285346; FEL-93-B366; TDCK-94-0166) Avail: CASI HC A03/MF A01

In this report we present a theoretical study on the performance of an implementation of the FDTD code on a massively parallel computer. The finite difference time domain (FDTD) method is one of the most popular approaches for the numerical modelling of a wide variety of electromagnetic wave interaction problems. The analysis presented is carried out for radar cross section (RCS) prediction but can, with minor adaptations, be used for other electromagnetic problems. The analysis is applied to a possible implementation on the parsytec GCEL-3/512 of the 'Interdisciplinary Center for Computer Based Complex Systems Research Amsterdam (IC3A)', which is configured as a two-dimensional grid of 512 T805 transputers. Comparisons with the performance of an implementation on a conventional supercomputer, the convex C230 of the physics and electronics laboratory TNO, are presented. DTIC

N95-20500# Carnegie-Mellon Univ., Pittsburgh, PA. School of Computer Science.
TASK PARALLEL PROGRAMMING IN Fx
Jaspal Subhlok, David R. OHallaron, and Thomas Gross Aug. 1994 8 p
(AD-A285136; CMU-CS-94-112) Avail: CASI HC A02/MF A01

Many important applications have a heterogeneous structure, and can be implemented efficiently only with task parallelism. This paper presents a set of extensions to Fortran to build task parallel programs for multicomputers consisting of distinct nodes: either private memory parallel machines, or autonomous computers connected by a high speed network. The design of these extensions is driven by the following objectives: (1) The compiler should handle inter-node communication, not the programmer; (2) The task extensions should be integrated into an existing parallel programming language, so that existing programs can benefit from task parallelism, existing libraries can be used, and the users do not have to learn a new language; and (3) Current compiler technology should be able to produce efficient parallel programs that are competitive with hand parallelized codes. DTIC

N95-20566 Georgia Inst. of Tech., Atlanta, GA. School of Industrial and Systems Engineering.
STOCHASTIC NETWORK PROCESSES Final Technical Report, 1 Nov. 1990 - 31 Oct. 1993
Richard F. Serfozo 31 Oct. 1993 6 p Limited Reproducibility: More than 20% of this document may be affected by microfiche quality
(Grant AF-AFOSR-0013-91)
(AD-A279905; AFOSR-94-0309TR) Avail: Issuing Activity (Defense Technical Information Center (DTIC))

The general theme of the research has been to develop stochastic network processes for modeling the movement of discrete units in networks. Primary examples are the movement of parts and supplies in manufacturing plants and in distribution systems and the movement of data packets and telephone calls in computer and telecommunications networks. The distinguishing feature of the research is the emphasis on the next generation of intelligent networks that will be the backbone of the manufacturing and computer systems. In these networks, the processing of units at the nodes and the routing of units typically depend dynamically on the actual network congestion, and units move concurrently (e.g. batch processing) most of the present theory of stochastic network processes is for unintelligent networks in which the nodes operate independently, the routes of units are independent, and the units move one-at-a-time. The goal is to provide an understanding of these more complex intelligent networks by describing their stochastic behavior. DTIC

N95-20618# Elizabeth City State Univ., NC.
ECSU-AASERT SUMMER RESEARCH PROJECT IN PARALLEL PROCESSING AND COMPUTER VISUALIZATION
Quarterly Report No. 4
Linda Hayden 1994 41 p
(Contract N00014-91-J-1308)
(AD-A285983) Avail: CASI HC A03/MF A01

Future parallel applications will be run on a variety of parallel machines linked with high performance networks. The primary purpose of our research is to exploit these modern systems capabilities to offer human interactive interfaces that can execute simultaneously with a parallel application's computation and storage tasks. DTIC

N95-20888# Yale Univ., New Haven, CT. Dept. of Computer Science.
FUNCTIONAL AND PARA-FUNCTIONAL PARALLEL PROCESSING
1994 12 p
(Contract DE-FG02-86ER-25012)
(DE95-002805; DOE/ER-25012/5) Avail: CASI HC A03/MF A01

For years (about 20, in fact) dataflow researchers have argued for the use of dataflow (a subset of functional) languages for parallel computing, resting their proof on the ability to construct large-scale dataflow machines to realize the inherent parallelism in Functional programs. Unfortunately, such machines have never materialized as commercial products - instead, the market shows a vast variety of parallel multiprocessors that require special skills to program. It may be the case that these machines reflect a wrong direction in computer architecture design, and it may be the case that dataflow machines are the right way to go, but the proof is in the pudding, and thus far there does not exist even a prototype dataflow machine that can prove the 'dataflow thesis'. Under the circumstances it would seem rather foolhardy simply to ignore the commercial parallel machines that are available now, regardless of one's favorite programming methodology or concurrency model. It has been the authors' thesis that one can in fact use such machines effectively, while maintaining the concomitant thesis that functional programming is good for parallel computation. During the last two years the author has made considerable progress to support this two-fold thesis, and is now prepared to extend this work in several ways. The authors' particular interest, and presumably the primary interest to DOE, is to concentrate the work in the area of scientific computing, including functional language features, program development tools, and systems support tailored for scientific computing applications. The authors' desire to do this reflects confidence that this approach really will work for scientific computing - the author has spent two years proving the viability of the ideas, and now it's time to put them into action. DOE

N95-21257# Argonne National Lab., IL. Mathematics and Computer Science Div.
A DIVIDE-AND-CONQUER METHOD FOR TRIDIAGONALIZING SYMMETRIC MATRICES WITH REPEATED EIGENVALUES
Christina H. Bischof and Xiaobai Sun 1994 13 p
(Contract W-31-109-eng-38)
(DE95-002918; ANL/MCS/PP-75731) Avail: CASI HC A03/MF A01

The authors describe a divide-and-conquer tridiagonalization approach for matrices with repeated eigenvalues. The algorithm hinges on the fact that, loosely speaking, a symmetric matrix with bandwidth b and k distinct eigenvalues must be block diagonal with diagonal blocks of size at most bk. A slight modification of the usual orthogonal bandreduction algorithm allows them to reveal this structure, which then leads to parallelism in the form of independent diagonal blocks. Compared to the usual Householder reduction algorithm, the approach allows significantly more scope for the exploitation of parallelism and can reduce the number of floating-point operations by up to 50%. The actual savings depend very much on the number of distinct eigenvalues, but at worst it behaves exactly like the usual tridiagonalization procedure. They also mention how the resulting tridiagonal structure can be employed very advantageously in determining range and nullspaces of symmetric matrices with two distinct eigenvalues, one of which is zero. DOE

N95-21307 Department of the Navy, Washington, DC.
NON-INTRUSIVE SCSI STATUS SENSING SYSTEM Patent Application
Stephen J. Amuro, inventor (to Navy) and Paul J. Giorgio, inventor (to Navy) 29 Mar. 1994 26 p Limited Reproducibility: More than 20% of this document may be affected by microfiche quality
(AD-D016242; US-Patent-Appl-SN-219553) Avail: Issuing Activity (Defense Technical Information Center (DTIC))

An improved Small Computer System Interface (SCSI) controller provides a logical connection between a plurality of host processors using a single SCSI initiator. The controller contains removable host adapters for connection to any type of host processor interface'. When a host processor requests status information of a target device, that status information is passed to the requesting processor and subsequently stored in the controller and made available to all other host processors. In addition, a fault tolerant performance monitoring algorithm, executing within the controller, is scheduled to non-intrusively and periodically check the status of each SCSI target device and to store that status information for all host processors. The advantage to such a controller is that by using a single SCSI initiator, each host processor can independently and logically connect through the controller and SCSI initiator to a target without clearing target status information for other host processors. This is particularly advantageous when adapted to function on a local area network (LAN) arrangement wherein a significant number of host processors are requesting data. DTIC

N95-21341# Argonne National Lab., IL. Mathematics and Science Div.
A FRAMEWORK FOR SYMMETRIC BAND REDUCTION AND TRIDIAGONALIZATION
Christian H. Bischof and Xiaobai Sun 1994 16 p
(Contract W-31-109-eng-38)
(DE95-002919; ANL/MCS/PP-76460) Avail: CASI HC A03/MF A01

This paper develops a framework for bandwidth reduction and tridiagonalization algorithms for symmetric banded matrices. The algorithm family includes the algorithms by Rutishauser and Schwarz, which underlie the EISPACK and LAPACK implementations, and the algorithm recently proposed by Lang. The framework leads to algorithms that require fewer floating-point operations, allow for space-time tradeoffs, enable the use of block orthogonal transformations, and increase the degree of parallelism inherent in the algorithm. DOE

N95-21355# IG Technologies, San Diego, CA.
HPCC TECHNOLOGY AWARENESS PROGRAM: IMPROVED ECONOMIC COMPETITIVENESS THROUGH TECHNOLOGY AWARENESS, TRANSFER AND APPLICATION
Apr. 1994 104 p
(Contract DE-FG03-93ER-25149)
(DE95-002134; DOE/ER-25149/T1) Avail: CASI HC A06/MF A02

A need has been defined by Congress for the DOE National Laboratories to participate in various dual use and technology transfer programs. This requirement has spawned several technology transfer approaches at the DOE laboratories. These programs are designed to encourage large and small business to bring their problems and needs forward, and to allow the labs to transfer effective high performance computing technology to the commercial marketplace. This IG Technologies grant from the DOE was undertaken to address the issues and problems associated with technology transfer between the DOE National Laboratories and commercial industry. The key focus is to gain an understanding of how DOE and industry independently and collectively view the requirements and the missing elements that could allow DOE to facilitate HPCC technology transfer. At issue is HPCC Technology Transfer for the High Performance Computing industry and its relationship to the DOE National Laboratories. Several observations on this are addressed. The issue of a 'Technology Utilization Gap' between the National Laboratories and Independent Software Vendors is discussed. This study addressed the HPCC Technology Transfer plans of all six DOE National Labs. Study team members briefed numerous industrial users of HPCC technology as to the feasibility of technology transfer for various applications. Significant findings of the effort are that the resistance to technology transfer is much higher than anticipated for both the National Labs and industry. Also, HPCC Technology Transfer is observed to be a large company's dominion. Small businesses have a difficult time in addressing the requirements of technology transfer using Cooperative Research and Development Agreements (CRADA's). Large businesses and the DOE National Labs however, often have requirements and objectives which are at cross purposes, making effective technology transfer difficult. DOE

N95-21496 Department of the Navy, Washington, DC.
NETWORK FILE SERVER WITH AUTOMATIC SENSING MEANS Patent Application
Stephen J. Amuro, inventor (to Navy) and Paul J. Giorgio, inventor (to Navy) 29 Mar. 1994 29 p Limited Reproducibility: More than 20% of this document may be affected by microfiche quality
(AD-D016250; US-Patent-Appl-SN-219556) Avail: Issuing Activity (Defense Technical Information Center (DTIC))

A Small Computer System Interface (SCSI) controller adapted as a network file server provides a virtual connection between a plurality of host processors and a single SCSI initiator. The controller contains a removable host adapter for connection to any type of network interface. When a host processor issues a command packet and requests status information of a target device, that status information is passed to the requesting processor and subsequently stored in the controller and made available to all other host processors on the network. A fault tolerant performance monitoring algorithm, executing within the controller, is scheduled to non-intrusively and periodically check the status of each SCSI target device and to store that status information for all host processors. The advantage to such a controller is the expanded number of host processor connections to a single SCSI initiator whereby each host processor can independently and logically connect through the controller and SCSI initiator to a target without clearing target status information for other host processors. DTIC

N95-21504 Department of the Navy, Washington, DC.
SCSI CONTROLLER WITH TARGET STATUS RETRIEVAL Patent Application
Stephen J. Amuro, inventor (to Navy) and Paul J. Giorgio, inventor (to Navy) 29 Mar. 1994 21 p Limited Reproducibility: More than 20% of this document may be affected by microfiche quality
(AD-D016249; US-Patent-Appl-SN-219552) Avail: Issuing Activity (Defense Technical Information Center (DTIC))

An improved Small Computer System Interface (SCSI) controller provides a logical connection between a plurality of host processors using a single SCSI initiator. The controller contains removable host adapters for connection to any type of host processor interface. When a host processor requests status information of a target device, that status information is passed to the requesting processor and subsequently stored in the controller and made available to all other host processors. The advantage to such a controller is the expanded number of host processor connections to a single SCSI initiator whereby each host processor can independently and logically connect through the controller and SCSI initiator to a target without clearing target status information for other host processors. The invention is particularly advantageous when adapted to function in a local area network (LAN) arrangement where a significant number of host processors are requesting data from one mass storage device. DTIC

N95-21505# Sandia National Labs., Livermore, CA.
A SIMULATION STUDY OF TCP PERFORMANCE IN ATM NETWORKS
Chien Fang, Helen Chen, and J. Hutchins 1994 7 p Presented at the GLOBECOM 1994, San Francisco, CA, 27 Nov. - 1 Dec. 1994
(Contract DE-AC04-76DR-00789)
(DE94-016622; SAND-94-8728C; CONF-9411102-1) Avail: CASI HC A02/MF A01

This paper presents a simulation study of TCP performance over congested asynchronous transfer mode (ATM) local area networks (LAN's). We simulated a variety of schemes for congestion control for ATM LAN's, including a simple cell-drop, a credit-based flow control scheme that back-pressures individual virtual circuits (VC's), and two selective cell-drop schemes. Our simulation results for congested ATM LAN's show the following: (1) TCP performance is poor under simple cell-drop, (2) the selective cell-drop schemes increase effective link utilization and result in higher TCP throughputs than the simple cell-drop scheme, and (3) the credit-based flow control scheme eliminates cell loss and achieves maximum performance and effective link utilization. DOE

N95-21556# Oak Ridge National Lab., TN.
PVM 3 BEYOND NETWORK COMPUTING
G. A. Geist 1993 11 p Presented at the 2d International Austrian Conference on Parallel Computing (ACPC), Vienna, Austria, 4-8 Oct. 1993
(Contract DE-AC05-84OR-21400)
(DE94-019115; CONF-9310161-2) Avail: CASI HC A03/MF A01

PVM (Parallel Virtual Machine) is a byproduct of the heterogeneous network research project going on at Oak Ridge National Laboratory and the University of Tennessee. It is a software package that permits a user defined collection of serial, parallel, and vector computers to appear as one large distributed memory computer. PVM's popularity is quickly making it the worldwide de facto standard for distributed computing. Applications, which can be written in FORTRAN or C, can be parallelized by using simple message-passing constructs common to most distributed-memory computers. By sending and receiving messages, subtasks of an application can cooperative to solve a problem in parallel. This paper describes the features of the latest release of PVM (version 3.1) and explains the major new research areas they are beginning to explore in heterogeneous network computing. The new features of PVM version 3 open many new opportunities to go beyond simple network computing, but several technical and social issues must be addressed before one can make the next big leap in distributed computing. DOE

N95-21602# Oak Ridge National Lab., TN.
DONIO: DISTRIBUTED OBJECT NETWORK I/O LIBRARY
E. F. DAzevedo and C. H. Romine Sep. 1994 39 p
(Contract DE-AC05-84OR-21400)
(DE94-019163; ORNL/TM-12743) Avail: CASI HC A03/MF A01

This report describes the use and implementation of DONIO (Distributed Object Network I/O), a library of routines that provide fast file I/O capabilities in the Intel iPSC/860 and Paragon distributed memory parallel environments. DONIO caches a copy of the file in memory distributed across all processors. Disk I/O routines (such as read, write, and lseek) are replaced by calls to DONIO routines, which translate these operations into message communication to update the cached data. Experiments on the Intel Paragon show that the cost of concurrent disk I/O using DONIO for large files can be 15-30 times smaller than using standard disk I/O. DOE

N95-21620# Technische Univ., Twente (Netherlands). Tele-Informatics and Open Systems Group.
DESIGN MODEL FOR OPEN DISTRIBUTED PROCESSING SYSTEMS
Marten vanSinderen, Luis FerreiraPires, Chris A. Vissers, and Joost-Pieter Katoen 1994 35 p
(ISSN 0924-3755)
(PB95-135505; Memo-INF-94-27) Avail: CASI HC A03/MF A01

This paper proposes design concepts that allow the conception, understanding and development of complex technical structures for open distributed systems. The proposed concepts are related to, and partially motivated by, the present work on Open Distributed Processing (ODP). As opposed to the current ODP approach, the concepts are aimed at supporting a design trajectory with several related abstraction levels. Simple examples are used to illustrate the proposed concepts. NTIS

N95-21674 Office of Naval Research, Arlington, VA.
PROGRAMMABLE MODULAR NETWORK INTERFACE Patent Application
Terry R. Clayton, inventor and Andrew W. Lepp, inventor 17 May 1994 14 p Limited Reproducibility: More than 20% of this document may be affected by microfiche quality
(AD-D016505; US-Patent-Appl-SN-063227) Avail: Issuing Activity (Defense Technical Information Center (DTIC))

A modular system for interfacing between a Navy Standard UYK-43 computer and a plurality of workstation consoles connected to a control data bus is provided. A first conversion processor is functionally connected to the computer and functionally connected to a backplane. A second conversion processor is functionally connected to the computer and functionally connected to the backplane. The second conversion processor also includes memory for storing status and action information associated with each of the consoles. A system processor is functionally connected to the backplane and a local area network (LAN) processor is functionally connected to the backplane and to the consoles. DTIC

N95-21698 Carnegie-Mellon Univ., Pittsburgh, PA. Dept. of Computer Science.
ADVANCED COMPUTING SYSTEMS: USABILITY OF KNOWLEDGE-BASED PLANNING SYSTEMS Status Report, 1 Jul. - 30 Sep. 1993
30 Sep. 1993 3 p Limited Reproducibility: More than 20% of this document may be affected by microfiche quality
(Contract N00014-93-1-0934)
(AD-A279573) Avail: Issuing Activity (Defense Technical Information Center (DTIC))

The objective of this research is to assess the value of different usability methods to designing a system as complex as a programming environment for a knowledge-based architecture that learns. As well as traditional empirical methods observing real users, analytic and heuristic methods to assess the usability of complex computer systems in advance of running prototypes are emerging from human-computer interaction (HCI) research. We will demonstrate the effectiveness of these observational, analytic and heuristic usability methods with respect to: (1) The classes of knowledge-based systems to which they can be applied; (2) The types of usability problems they can, and cannot identify; (3) The types of suggestions they can generate for the design of improved knowledge-based systems and the relative value of those suggestions for overall usability of the systems; (4) The expertise of the evaluators necessary to apply the methods; and (5) The effort involved in applying the methods. DTIC

N95-21843# Sandia National Labs., Albuquerque, NM.
A MASSIVELY PARALLEL ALGORITHM FOR GRAND CANONICAL MONTE CARLO COMPUTER SIMULATION WITH THE SHORT-RANGED LENNARD-JONES POTENTIAL
Grant S. Heffelfinger and Martin E. Lewitt (nCUBE Corp., Sandia Park, NM.) 1994 17 p Presented at the Supercomputing 1994 Meeting, Washington, DC, 14-18 Nov. 1994
(Contract DE-AC04-94AL-85000)
(DE94-010396; SAND-94-0989C; CONF-941118-1) Avail: CASI HC A03/MF A01

We present a new massively parallel decomposition for grand canonical Monte Carlo computer simulation (GCMC) suitable for short ranged fluids. Our spatial algorithm relies on the fact that for short-ranged fluids, molecules separated by a greater distance than the reach of the potential act independently, thus different processors can work concurrently in regions of the same system which are sufficiently far apart. Several parallelization issues unique to GCMC are addressed such as the handling of the three different types of Monte Carlo move used in GCMC: the displacement of a molecule, the creation of a molecule, and the destruction of a molecule. The decomposition is shown to scale with system size, making it especially useful for systems where the physical problem dictates the system size, for example, fluid behavior in mesopores. DOE

N95-21869 Technische Univ., Twente (Netherlands). Tele-Informatics and Open Systems Group.
PERFORMANCE ANALYSIS AND TRUE CONCURRENCY SEMANTICS
Ed Brinksma, Joost-Pieter Katoen, Rom Langerak, and Diego Latella (Centro Nazionale Univ. per il Calcolo Elettronico, Pisa, Italy.) 27 Jun. 1994 36 p
(ISSN 0924-3755)
(PB95-134086; Memo-INF-94-39) Copyright Avail: Issuing Activity (National Technical Information Service (NTIS))

The paper addresses the subject of linking functional specifications to performance analysis in a process algebraic context. It presents a timed, probabilistic extension of a process algebraic formalism and its application to performance analysis. More specifically, an extension of a subset of LOTOS is presented equipped with a truly concurrent semantical model based on bundel event structures. It is investigated how semi-Markov chains can be obtained from functional specifications using this semantical model. The use of a true concurrency model enables us to distinguish between non-determinism and parallelism, to reduce the state explosion problem and, moreover, to analyze part of the system without considering other (irrelevant) parts. An example illustrates the proposed approach. NTIS

N95-21925# Los Alamos National Lab., NM. Theoretical Div.
STATUS OF CFDLIB PERFORMANCE TESTS ON THE T3D
Nely T. Padial, Bryan A. Kashiwa, and Douglas B. Kothe 1994 11 p Presented at the Cray User's Group Conference, Tours, France, 10-14 Oct. 1994 Sponsored by DOD, Amoco Oil Co., and Molten Metal Technology, Inc.
(Contract W-7405-eng-36)
(DE95-002708; LA-UR-94-3449; CONF-9410212-3) Avail: CASI HC A03/MF A01

Computational Fluid Dynamics LIBrary (CFDLIB) is a collection of two and three-dimensional computer codes for problems in computational fluid dynamics. The library handles a wide range of flow regimes both single and multiphase, from fully incompressible to hypersonic, chemically reacting or inert materials. The method uses the Implicity Continuous-fluid Eulerian scheme (ICE) which becomes essentially identical to the Marker and Cell (MAC) method in the incompressible limit. The method, a Finite-Volume scheme, with cell-centered state variables, utilizes an Arbitrary-Lagrangian-Eulerian (ALE) split computational cycle in the sense that the mesh is allowed to move in an arbitrary fashion. In addition, CFDLIB employs a multiblock data structure that proved extremely convenient for implementation on parallel computers. CFDLIB is now available in sequential or parallel environments, is written in standard FORTRAN 77, and is highly portable. Results are given for a selection of specialized applications that illustrate the kind of problems of interest to CFDLIB users. Finally, initial results are given for performance studies comparing the Cray Y-MP, T3D, and an IBM workstation cluster. For certain problems, a Y-MP-equivalent real solution time is achieved with less than eight processors on the T3D. DOE

N95-22090 Department of the Navy, Washington, DC.
METHOD OF SENSING TARGET STATUS IN A LOCAL AREA NETWORK Patent Application
Stephen J. Amuro, inventor (to Navy) and Paul J. Giorgio, inventor (to Navy) 29 Mar. 1994 29 p Limited Reproducibility: More than 20% of this document may be affected by microfiche quality
(AD-D016248; US-Patent-Appl-SN-219555) Avail: Issuing Activity (Defense Technical Information Center (DTIC))

A Small Computer System Interface (SCSI) controller adapted as a network file server provides a virtual connection between a plurality of host processors and a single SCSI initiator. The controller contains a removable host adapter for connection to any type of network interface. When a host processor issues a command packet and requests status information of a target device, that status information is passed to the requesting processor and subsequently stored in the controller and made available to all other host processors on the network. A fault tolerant performance monitoring algorithm, executing within the controller, is scheduled to non-intrusively and periodically check the status of each SCSI target device and to store that status information for all host processors. The advantage to such a controller is the expanded number of host processor connections to a single SCSI initiator whereby each host processor can independently and logically connect through the controller and SCSI initiator to a target without clearing target status information for other host processors. DTIC

N95-22108*# Research Inst. for Advanced Computer Science, Moffett Field, CA.
[ACTIVITIES OF THE RESEARCH INSTITUTE FOR ADVANCED COMPUTER SCIENCE] Annual Report, 1994
Joseph Oliger 1994 53 p
(Contract NAS2-13721)
(NASA-CR-197291; NAS 1.26:197291) Avail: CASI HC A04/MF A01

The Research Institute for Advanced Computer Science (RIACS) was established by the Universities Space Research Association (USRA) at the NASA Ames Research Center (ARC) on June 6, 1983. RIACS is privately operated by USRA, a consortium of universities with research programs in the aerospace sciences, under contract with NASA. The primary mission of RIACS is to provide research and expertise in computer science and scientific computing to support the scientific missions of NASA ARC. The research carried out at RIACS must change its emphasis from year to year in response to NASA ARC's changing needs and technological opportunities. Research at RIACS is currently being done in the following areas: (1) parallel computing; (2) advanced methods for scientific computing; (3) high performance networks; and (4) learning systems. RIACS technical reports are usually preprints of manuscripts that have been submitted to research journals or conference proceedings. A list of these reports for the period January 1, 1994 through December 31, 1994 is in the Reports and Abstracts section of this report. Author

N95-22146 Department of the Navy, Washington, DC.
METHOD OF NON-INTRUSIVELY SENSING STATUS IN A COMPUTER PERIPHERAL Patent Application
Stephen J. Amuro, inventor (to Navy) and Paul J. Giorgio, inventor (to Navy) 29 Mar. 1994 26 p Limited Reproducibility: More than 20% of this document may be affected by microfiche quality
(AD-D016241; US-Patent-Appl-SN-219557) Avail: CASI HC A03

An improved method of having a Small Computer System Interface (SCSI) controller provide a logical connection between a plurality of host processors using a single SCSI initiator. The controller contains removable host adapters for connection to any type of host processor interface. When a host processor requests status information of a target device, that status information is passed to the requesting processor and subsequently stored in the controller and made available to all other host processors. In addition, a fault tolerant performance monitoring algorithm, executing within the controller is scheduled to non-intrusively and periodically check the status of each SCSI target device and to store that status information for all host processors. The advantage to such a controller is that by using only a single SCSI initiator, each host processor can independently and logically connect through the controller and SCSI initiator to a target without clearing target status information for other host processors. This is particularly advantageous when adapted to function in a local area network (LAN) arrangement wherein a significant number of host processors are requesting data. DTIC

N95-22228# Computer Sciences Corp., Falls Church, VA.
NETWORK DISTRIBUTED GLOBAL MEMORY FOR TRANSPARENT MESSAGE PASSING ON DISTRIBUTED NETWORKS Progress Report, 1 Nov. 1993 - 7 Mar. 1994
Jerry A. Clarke Oct. 1994 23 p
(Contract DAAL03-89-7C-0088)
(AD-A286096; ARL-CR-173) Avail: CASI HC A03/MF A01

Distributing compute-intensive applications across multiple platforms can significantly reduce the total execution time of the application. Programming such a system typically involves sending explicit messages between cooperating processes. Keeping track of these messages, however, can be a difficult, error-prone task. Shared memory models are typically easier to program. Network Distributed Global Memory (NDGM) allows the programmer to view the physically distributed environment as a single, contiguous address space. Instead of sending an explicit message to another node, processes write and read from a global block of memory. DTIC

N95-22257# Illinois Univ., Urbana, IL. Dept. of Dairy Science.
AN ASSESSMENT OF EUROPEAN PARALLEL SOFTWARE RESEARCH Final Report
Gul Agha 25 Oct. 1994 19 p Sponsored by ONR
(AD-A286357) Avail: CASI HC A03/MF A01

This report summarizes research reviewed during trips to a number of institutions in France, Switzerland and Italy to review the state of research in parallel and distributed software. The report makes note of the research models, current status and organizational difference between the U.S. and these countries. As with any such report, it does not aim to be complete; instead it describes the overall organization and focuses on some salient research efforts. The report is most complete about France but includes some institutions in Switzerland and Italy. DTIC

N95-22406*# Bucknell Univ., Lewisburg, PA. Dept. of Electrical Engineering.
DESIGN OF A MASSIVELY PARALLEL COMPUTER USING BIT SERIAL PROCESSING ELEMENTS
Maurice F. Aburdene, Kamal S. Khouri, Jason E. Piatt, and Jianqing Zheng 24 Jan. 1995 23 p
(Grant NAG5-2509)
(NASA-CR-197365; NAS 1.26:197365) Avail: CASI HC A03/MF A01

A 1-bit serial processor designed for a parallel computer architecture is described. This processor is used to develop a massively parallel computational engine, with a single instruction-multiple data (SIMD) architecture. The computer is simulated and tested to verify its operation and to measure its performance for further development. Author

63 CYBERNETICS

Includes feedback and control theory, artificial intelligence, robotics and expert systems.

For related information see also *54 Man/System Technology and Life Support.*

N95-20005# Navy Personnel Research and Development Center, San Diego, CA.
COMPARISON OF A BACK PROPAGATION ARTIFICIAL NEURAL NETWORK MODEL WITH A LINEAR REGRESSION MODEL FOR PERSONNEL SELECTION Interim Report, 1 Oct. 1990 - 30 Sep. 1991
C. A. Wilkins and W. A. Sands May 1994 16 p
(AD-A280023; NPRDC-TN-94-18) Avail: CASI HC A03/MF A01

This exploratory research examined the usefulness of an Artificial Neural Network-Back Propagation (ANN-BP) model predicting dichotomous criteria in personnel selection. The results are quite encouraging. Under a wide variety of circumstances, the ANN-BP model was superior to the Ordinary Least-Squares-Linear Regression (OLS-LR) model in predicting curvilinear relationships. When the underlying relationship was linear, there were no significant differences. This is somewhat remarkable, given that the OLS-LR model was designed to perform optimally in the linear case. DTIC

N95-20010* Institute for Computer Applications in Science and Engineering, Hampton, VA.
FINITE DIMENSIONAL APPROXIMATION OF A CLASS OF CONSTRAINED NONLINEAR OPTIMAL CONTROL PROBLEMS Final Report
Max D. Gunzburger and L. S. Hou Mar. 1994 50 p Submitted for publication Limited Reproducibility: More than 20% of this document may be affected by microfiche quality
(Contracts NAS1-19480; RTOP 505-90-52-01; N00014-91-J-04933; AF-AFOSR-10061-93; AF-AFOSR-10280-93)
(NASA-CR-194891; NAS 1.26:194891; AD-A280142; ICASE-94-16) Avail: CASI HC A03

An abstract framework for the analysis and approximation of a class of nonlinear optimal control and optimization problems is constructed. Nonlinearities occur in both the objective functional and in the constraints. The framework includes an abstract nonlinear optimization problem posed on infinite dimensional spaces, and approximate problem posed on finite dimensional spaces, together with a number of hypotheses concerning the two problems. The framework is used to show that optimal solutions exist, to show that Lagrange multipliers may be used to enforce the constraints, to derive an optimality system from which optimal states and controls may be deduced, and to derive existence results and error estimates for solutions of the approximate problem. The abstract framework and the results derived from that framework are then applied to three concrete control or optimization problems and their approximation by finite element methods. The first involves the von Karman plate equations of nonlinear elasticity, the second, the Ginzburg-Landau equations of superconductivity, and the third, the Navier-Stokes equations for incompressible, viscous flows. DTIC

N95-20011 Massachusetts Inst. of Tech., Cambridge, MA. Artificial Intelligence Lab.
ROBUST AGENT CONTROL OF AN AUTONOMOUS ROBOT WITH MANY SENSORS AND ACTUATORS
Cynthia Ferrell May 1993 167 p Limited Reproducibility: More than 20% of this document may be affected by microfiche quality
(Contract N00014-91-J-4038)
(AD-A280148; MIT-TR-1443) Avail: Issuing Activity (Defense Technical Information Center (DTIC))

This thesis presents methods for implementing robust hexpod locomotion on an autonomous robot with many sensors and actuators. The controller is based on the Subsumption Architecture and is fully distributed over approximately 1500 simple, concurrent processes. The robot, Hannibal, weighs approximately 6 pounds and is equipped with over 100 physical sensors, 19 degrees of freedom, and 8 on board computers. We investigate the following topics in depth: distributed control of a complex robot, insect-inspired locomotion control for gait generation and rough terrain mobility, and fault tolerance. The controller was implemented, debugged, and tested on Hannibal. Through a series of experiments, we examined Hannibal's gait generation, rough terrain locomotion, and fault tolerance performance. These results demonstrate that Hannibal exhibits robust, flexible, real-time locomotion over a variety of terrain and tolerates a multitude of hardware failures. DTIC

N95-20057# Syracuse Univ., NY. School of Computer and Information Science.
FAULT TOLERANCE OF NEURAL NETWORKS Final Technical Report, Feb. 1992 - Aug. 1993
Jul. 1994 108 p
(Contract F30602-92-C-0031; AF Proj. 2338)
(AD-A285098; RL-TR-94-93) Avail: CASI HC A06/MF A02

This effort studied fault tolerance aspects of artificial neural networks, and resulted in the development of neural learning techniques that more effectively utilize the inherent redundancy and excess of resources over the minimum required found in most classically trained networks. Performance evaluation measures were developed and used to quantify network tolerance to faults such as single link failures, multiple node failures, multiple link failures, and also small degradations in multiple links or nodes. Several variations of the basic back-propagation algorithm were designed and implemented, yielding improvements in fault tolerance. An Addition-Deletion algorithm was designed to successively modify the size of a network by deleting nodes that do not contribute to fault tolerance, and to add new nodes in a way that is assured to improve fault tolerance. The techniques designed in this project were compared to those suggested by others, and were found to improve robustness. Also, a Refine algorithm was defined, which takes a robust network which does not satisfy hardware restrictions and transforms it to another network which does. DTIC

N95-20061# Massachusetts Univ., Amherst, MA.
BIOLOGICAL AND THEORETICAL STUDIES OF ADAPTIVE NETWORKS: THE CONDITIONED RESPONSE Final Technical Report, 1 Aug. 1992 - 31 Jul. 1994
John W. Moore 30 Aug. 1994 15 p
(Contract F49620-92-J-0387)
(AD-A284781; AFOSR-94-0576TR) Avail: CASI HC A03/MF A01

Investigations of adaptive neural networks were conducted using the classically conditioned eyeblink of rabbit, a widely used model system for studies of learning and memory. Our work has focused on processes that mediate adaptive timing of conditioned responses, an important question in the field of learning and motor control. The following experimental projects were conducted: (1) a recording study of the medial geniculate neurons during two-tone differential trace conditioning; (2) a recording study of the ventrolateral pontine reticular formation and pontine nuclei during two-tone differential conditioning; (3) anatomical experiments using WGA-HRP that clarify cerebellar and red nucleus circuits involved in eyeblink conditioning; (4) behavioral experiments examining the role of temporal uncertainty in conditioned response timing and topography; and (5) behavioral experiments on asynchronous bilateral eyelid conditioning in rabbits. DTIC

N95-20083# Maryland Univ., College Park, MD. Inst. for Physical Science and Technology.
A-POSTERIORI ESTIMATION AND ADAPTIVE CONTROL OF THE POLLUTION-ERROR IN THE h-VERSION OF THE FINITE ELEMENT METHOD
I. Babuska, T. Strouboulis (Texas A&M Univ., College Station, TX.), C. S. Upadhyay (Texas A&M Univ., College Station, TX.), and S. K. Gangaraj (Texas A&M Univ., College Station, TX.) Aug. 1994 56 p
(Contract N00014-90-J-1030; NSF CCR-88-20279; NSF MSS-90-25110)
(AD-A285670; TN-BN-1175) Avail: CASI HC A04/MF A01

We studied the pollution-error in the h-version of the finite element method and its effect on the quality of the local error indicators (resp. the quality of the derivatives recovered by local postprocessing) in the interior of the mesh. Here we show that it is possible to construct a-posteriori estimates of the pollution-error in a patch of elements by employing the local error indicators over the entire mesh. We also give an adaptive algorithm for the local control of the pollution-error in a patch of elements of interest. DTIC

N95-20126# Brookhaven National Lab., Upton, NY.
ANALYTIC PERTURBATION ANALYSIS OF DISCRETE EVENT DYNAMIC SYSTEMS
S. Uryasev 1994 6 p Presented at the 1994 International Conference on Computer Integrated Manufacturing and Automation Technology, Troy, NY, 10 Oct. 1994
(Contract DE-AC02-76CH-00016)
(DE94-018635; BNL-60747; CONF-9410167-2) Avail: CASI HC A02/MF A01

This paper considers a new analytic perturbation analysis (APA) approach for discrete event dynamic systems (DEDS) with discontinuous sample-path functions with respect to control parameters. The performance functions for DEDS usually are formulated as mathematical expectations, which can be calculated only numerically. APA is based on new analytic formulas for the gradients of expectations of indicator functions; therefore, it is called an analytic perturbation analysis. The gradient of performance function may not coincide with the expectation of a gradient of sample-path function (i.e., the interchange formula for the gradient and expectation sign may not be valid). Estimates of gradients can be obtained with one simulation run of the models. DOE

N95-20202 Department of the Navy, Washington, DC.
OPTIMAL DISTRIBUTED CONTROL SYSTEM FOR A LINEAR DISTRIBUTED PARAMETER SYSTEM Patent
Allen Moshfegh, inventor (to Navy) 12 Jul. 1994 34 p Filed 29 Aug. 1991
(AD-D016583; US-Patent-5,329,442; US-Patent-Appl-SN-751939; US-Patent-Class-364-149) Avail: US Patent and Trademark Office

An optimal control system for canceling the undesired responses of a linear distributed-parameter system in response to an input stimulus is described. The control system is optimally distributed and its design is based on the extension of the Pontryagin's maximum principle for a lumped-parameter system to a distributed-parameter system. The technique is to transform the stimulus-to-undesired-output transfer function of the distributed-parameter system into a multidimensional discrete state-space model, and to require a performance criterion to be defined. Theorems have been established to give conditions for asymptotic stability of the closed-loop distributed-parameter system, and to set up weighting factors for the performance criterion. An optimal distributed-control system can force the states of the distributed system to behave according to the prescribed performance criterion regardless of the boundary and initial conditions. The optimal control law can be implemented either as a state-feedback or an output-feedback controller. DTIC

N95-20342# Sandia National Labs., Albuquerque, NM.
A NEW MINI BALL GRID ARRAY (mBGA) MULTICHIP MODULE TECHNOLOGY
R. Chanchani, K. Treece, and P. Dressendorfer 1994 7 p Presented at the Meeting on the Revolution in Microelectronics, Boston, MA, 15-17 Nov. 1994
(Contract DE-AC04-94AL-85000)
(DE94-018897; SAND-94-2195C; CONF-941199-1) Avail: CASI HC A02/MF A01

A new die-level packaging technology, mBGA, is reported in this paper. The mBGA enables high circuit packaging density on multichip module (MCM), facilitates die testing to obtain 'known good die,' and allows a cost effective module assembly. We have designed and fabricated a test vehicle to evaluate mBGA multichip module technology. This paper describes the mBGA technology and the test vehicle multichip module and reports preliminary results on the die test and burn-in, thermal performance and reliability studies. DOE

N95-20482 Massa Products Corp., Hingham, MA.
LEGGED VEHICLE FOR UNDERWATER MOBILE OPERATIONS Progress Report
Joseph Ayers 15 Sep. 1994 6 p Limited Reproducibility: More than 20% of this document may be affected by microfiche quality
(Contract N00014-94-C-0078)
(AD-A285043) Avail: CASI HC A02

Work has been done on analyzing the Nitinol to determine how it can be best utilized as an actuator for the robot. Using a wire-wrap gun may lead to a technique in which a piece of solid wire can be attached to the Nitinol so that there won't be fatigue of the wire or overheating damage of soldering. The utilization of small strain gauges with the Nitinol actuator is being investigated as is the use of micro-thermal couples to determine the temperature of the wire. A mechanism is being built to demonstrate the control of three muscle pairs to perform walking motions under the control of the computer program based on the neural outputs produced by the lobster during ambulation. A large number of experiments have been conducted to determine how best to drive the Nitinol with electric currents to heat it and then how best to cool it to allow it to return to its original length. Derived from text

N95-20606# Naval Air Warfare Center, China Lake, CA. Weapons Div.
MULTILAYER PIECEWISE LINEAR NETWORKS Final Report, 1993 - 1994
W. O. Alltop Sep. 1994 57 p
(AD-A285382; NAWC-WPNS-TP-8217) Avail: CASI HC A04/MF A01

Feed-forward layered networks are the simplest neural computers. These networks provide fast compact devices for computing discriminant functions and other mappings applicable to pattern recognition problems. This report treats the problem of weight initialization'/assignment for feed-forward networks with piecewise linear neuron transfer function. Specific transformations are shown to be impossible with a single hidden layer. Techniques are presented for constructing such transformations with two hidden layers. DTIC

N95-20607# Naval Coastal Systems Center, Panama City, FL.
OPTICAL PATTERN RECOGNITION Final Report
M. A. Abushagur and G. L. Henderson Aug. 1994 48 p
(AD-A285384; CSS/TR-94/26) Avail: CASI HC A03/MF A01

This study provides a basic understanding of the fundamentals of optical pattern recognition systems. An emphasis on the capabilities and limitations of such systems is presented. Areas in need of further development are highlighted. Pattern recognition using optical systems can be performed based on either correlator or non-correlator systems. Recognition can be achieved by using linear processing techniques such as wavelet transforms or nonlinear processing using morphological operations or neural networks. The fundamentals of pattern recognition are presented, specifically, Fourier transformation using lenses, and the basic optical correlator architecture. Both the 4-f in-line and joint-transform correlators are described with an emphasis on the advantages and limitations of each. Morphological processors, neural-network and wavelet transform systems are introduced along with their optical implementations. A brief overview of the optical components involved in the design and fabrication of optical pattern recognition systems is discussed. Spatial filter designs used in optical correlator systems are reviewed with particular emphasis on distortion-invariant applications. Discussion of system performance criteria, and a comparison between some of the systems, are included. DTIC

N95-20693# Los Alamos National Lab., NM.
AN INTEGRATED ARCHITECTURE OF ADAPTIVE NEURAL NETWORK CONTROL FOR DYNAMIC SYSTEMS
Liu Ke, R. Tokar, and B. Mcvey 1994 8 p Presented at the Neural Information Processing Systems, Denver, CO, 29 Nov. - 3 Dec. 1994
(Contract W-7405-eng-36)
(DE94-014813; LA-UR-94-1705; CONF-941190-1) Avail: CASI HC A02/MF A01

In this study, an integrated neural network control architecture for nonlinear dynamic systems is presented. Most of the recent emphasis in the neural network control field has no error feedback as the control input which rises the adaptation problem. The integrated architecture in this paper combines feed forward control and error feedback adaptive control using neural networks. The paper reveals the different internal functionality of these two kinds of neural network controllers for certain input styles, e.g., state feedback and error feedback. Feed forward neural network controllers with state feedback establish fixed control mappings which can not adapt when model uncertainties present. With error feedbacks, neural network controllers learn the slopes or the gains respecting to the error feedbacks, which are error driven adaptive control systems. The results demonstrate that the two kinds of control scheme can be combined to realize their individual advantages. Testing with disturbances added to the plant shows good tracking and adaptation. DOE

N95-20812# Los Alamos National Lab., NM.
MODELING AND IDENTIFICATION OF PARALLEL AND FEEDBACK NONLINEAR SYSTEMS
Hai-Wen Chen 1994 18 p Presented at the 33d IEEE Conference on Decision and Control, Orlando, FL, 14-16 Dec. 1994
(Contract W-7405-eng-36)
(DE95-001006; LA-UR-94-3075; CONF-941216-1) Avail: CASI HC A03/MF A01

Structural classification and parameter estimation (SCPE) methods have been used for studying single-input single, output (SISO) parallel and feedback nonlinear system models from input-output (I-O) measurements. The uniqueness of the I-O mappings of different models and parameter uniqueness of the I-O mapping of a given structural model are evaluated. The former aids in defining the conditions under which different model structures may be differentiated from one another. The latter defines the conditions under which a given model parameter can be uniquely estimated from I-O measurements. SCPE methods presented in this paper can be further developed to study more complicated multi-input multi-output (MIMO) block-structured models which will provide useful techniques for modeling and identifying highly complex nonlinear systems. DOE

N95-20828# Michigan Univ., Ann Arbor, MI. Dept. of Electrical Engineering and Computer Science.
DESIGN OF A CONTROLLER FOR A FLEXIBLE POINTING SYSTEM USING H(INFINITY) SYNTHESIS Final Report, Jun. - Sep. 1993
Michael S. Mattice, S. S. Amberkar, N. Sivashankar, and P. P. Khargonekar Oct. 1994 22 p
(Contract AF-AFOSR-0053-90; DAAL03-90-G-0008)
(AD-A286572; ARFSD-TR-94010) Avail: CASI HC A03/MF A01

This report presents the results of a digital controller design implementation using the H-infinity synthesis method on the ATB 1000 test fixture at the Army Research Development Engineering Center (ARDEC), Picatinny Arsenal, NJ. The objective was to design a robust tracking controller to make the beam tip track a reference command applied to the base in the face of nominal disturbances. In this report, the salient features of the design approach will be reviewed and the implementation issues that arose will be discussed at length. DTIC

N95-20837# Oak Ridge National Lab., TN.
AUTOMATIC GENERATION OF FUZZY RULES FOR THE SENSOR-BASED NAVIGATION OF A MOBILE ROBOT
F. G. Pin and Y. Watanabe 1994 9 p Presented at the 5th International Symposium on Robotics and Manufacturing, Maui, HI, 14-18 Aug. 1994
(Contract DE-AC05-84OR-21400)
(DE95-001428; CONF-940859-27) Avail: CASI HC A02/MF A01

A system for automatic generation of fuzzy rules is proposed which is based on a new approach, called 'Fuzzy Behaviorist', and on its associated formalism for rule base development in behavior-based robot control systems. The automated generator of fuzzy rules automatically constructs the set of rules and the associated membership functions that implement reasoning schemes that have been expressed in qualitative terms. The system also checks for completeness of the rule base and independence and/or redundancy of the rules to ensure that the requirements of the formalism are satisfied. Examples of the automatic generation of fuzzy rules for cases involving suppression and/or inhibition of fuzzy behaviors are given and discussed. Experimental results obtained with the automated fuzzy rule generator applied to the domain of sensor-based navigation in a priori unknown environments using one of our autonomous test-bed robots are then presented and discussed to illustrate the feasibility of large-scale automatic fuzzy rule generation using our proposed 'Fuzzy Behaviorist' approach. DOE

N95-20884# Sandia National Labs., Albuquerque, NM.
ADVANCED ROBOTIC TECHNOLOGIES FOR TRANSFER AT SANDIA NATIONAL LABORATORIES
P. C. Bennett 1994 11 p Presented at the 3d International Conference on Heat Transfer: Advanced Computational Methods in Heat Transfer, Southampton, England, 5-7 Sep. 1994
(Contract DE-AC04-94AL-85000)
(DE95-001617; SAND-94-2354C; CONF-940917-1) Avail: CASI HC A03/MF A01

Hazardous operations which have in the past been completed by technicians are under increased scrutiny due to high costs and low productivity associated with providing protective clothing and environments. As a result, remote systems are needed to accomplish many hazardous materials handling tasks such as the clean-up of waste sites in which the exposure of personnel to radiation, chemical, explosive and other hazardous constituents is unacceptable. Computer models augmented by sensing, and structured, modular computing environments are proving effective in automating many unstructured hazardous tasks. Work at Sandia National Laboratories (SNL) has focused on applying flexible automation (robotics) to meet the needs of the U.S. Department of Energy (USDOE). Dismantling facilities, environmental remediation, and materials handling in changing, hazardous environments lead to many technical challenges. Computer planning, monitoring and operator assistance shorten training cycles, reduce errors, and speed execution of operations. Robotic systems that re-use well-understood generic technologies can be much better characterized than robotic systems developed for a particular application, leading to a more reliable and safer systems. Further safety in robotic operations results from use of environmental sensors and knowledge of the task and environment. Collision detection and avoidance is achieved from such sensor integration and model-based control. This paper discusses selected technologies developed at SNL for use within the USDOE complex that have been or are ready for transfer to government and industrial suppliers. These technologies include sensors, sub-systems, and the design philosophy applied to quickly integrate them into a working robotic system. This paper represents the work of many people at the Intelligent Systems and Robotics Center at SNL, to whom the credit belongs. DOE

N95-21185 Massachusetts Inst. of Tech., Cambridge, MA. Artificial Intelligence Lab.
HETEROGENEOUS MULTI-ROBOT COOPERATION
Lynne E. Parker Feb. 1994 244 p Limited Reproducibility: More than 20% of this document may be affected by microfiche quality
(Contracts N00014-85-K-0124; N00014-91-J-4038)
(AD-A279839; AI-TR-1465) Avail: Issuing Activity (Defense Technical Information Center (DTIC))

This report addresses the problem of achieving cooperation within small to medium-sized teams of heterogeneous mobile robots. I describe a software architecture I have developed, called ALLIANCE, that facilitates robust, fault tolerant, reliable, and adaptive cooperative control. In addition, an extended version of ALLIANCE, called L-ALLIANCE, is described, which incorporates a dynamic parameter update mechanism that allows teams of mobile robots to improve the efficiency of their mission performance through learning. A number of experimental results of implementing these architectures on both physical and simulated mobile robot teams are described. In addition, this report presents the results of studies of a number of issues in mobile robot cooperation, including fault tolerant cooperative control, adaptive action selection, distributed control, robot awareness of team member actions, improving efficiency through learning, inter-robot communication, action recognition, and local versus global control. DTIC

N95-21249# Stanford Linear Accelerator Center, CA.
NEURAL NETWORK CONSTRUCTION VIA BACK-PROPAGATION
Thomas T. Burwick Jun. 1994 7 p Presented at the Stanford PDP Research Meeting, Stanford, CA, 23 Jun. 1994
(Contract DE-AC03-76SF-00515)
(DE95-002867; SU-SLAC-PUB-6516; CONF-9406278-1) Avail: CASI HC A02/MF A01

A method is presented that combines back-propagation with multi-layer neural network construction. Back-propagation is used not only to adjust the weights but also the signal functions. Going from one network to an equivalent one that has additional linear units, the non-linearity of these units and thus their effective presence is then introduced via back-propagation (weight-splitting). The back-propagated error causes the network to include new units in order to minimize the error function. We also show how this formalism allows to escape local minima. DOE

N95-21267# Vrije Univ., Amsterdam (Netherlands). Artificial Intelligence Group.
FORMAL MODEL FOR THE DYNAMICS OF COMPOSITIONAL REASONING SYSTEMS
Ioa Gavrila and Jan Treur Dec. 1993 63 p
(PB95-132056; IR-323) Avail: CASI HC A04/MF A01

In this report we introduce a formal model to describe in a generic manner the behavior (or dynamics) of a certain type of reasoning systems, 'compositional reasoning systems'. This model can be used to specify behavior at any desired level of detail. Our formalization is based on partial temporal models, and uses the notions of information states, transitions between them, and traces generated by these transitions. We illustrate these notions for a specific type of compositional reasoning systems, the ones that can be specified using our framework for formal DEsign and Specification of Interacting REasoning modules (DESIRE). It will be shown how various aspects of behavior of DESIRE systems can be described using the formal model for dynamics introduced in this report; it is pointed out how semantics of the dynamics of DESIRE systems can be based on this formal model. NTIS

N95-21271# Technische Univ., Eindhoven (Netherlands). Dept. of Mathematics and Computing Science.
DUALITY AND EQUIVALENCIES IN CLOSED TANDEM QUEUEING NETWORKS
Zhen Liu (Institut National de Recherche d'Informatique et d'Automatique, Sophia Antipolis, France.) and Jacques A. C. Resing Sep. 1993 48 p Sponsored by ESPRIT BRA and Netherlands Organization for Scientific Research
(ISSN 0926-4493)
(PB95-132502; MEMO-COSOR-93-30) Avail: CASI HC A03/MF A01

Equivalence relations between closed tandem queueing networks are established. Four types of models are under consideration: single-server infinite-capacity buffer queues, infinite-server queues with resequencing, single-server unit-capacity buffer queues with blocking before service, and single-server unit-capacity buffer queues with blocking after service. Using a customer/server duality we show that in a network consisting of single-server infinite-capacity-buffer queues, customer-dependent service times and server-dependent service times yield equivalent performance characteristics. We further show that for closed tandem queueing networks, a system consisting of single-server infinite-capacity-buffer queues and a system consisting of single-server unit-capacity-buffer queues with blocking before service have equivalent performance behaviors. As applications of these equivalence properties, we obtain new results on the analysis of symmetric closed tandem networks, where all the service times are independent and identically distributed random variables. In particular, we obtain a closed-form expression for the throughput of networks with unit-capacity-buffer queues and blocking before service when the service times are exponentially distributed. NTIS

N95-21385# Oak Ridge National Lab., TN.
UNKNOWN-TERRAINS NAVIGATION OF A MOBILE ROBOT USING AN ARRAY OF SONARS
N. S.V. Rao 1994 9 p Presented at the Conference on Robotics Motion and Machine Vision, Aachen, Germany, 31 Oct. - 4 Nov. 1994
(Contract DE-AC05-84OR-21400)
(DE94-017902; CONF-9410186-1) Avail: CASI HC A02/MF A01

A mobile robot equipped with an array of sonars is required to navigate to a destination through a planar terrain populated by polygonal obstacles whose locations and shapes are unknown. A navigation method is proposed based on a trapezoidal decomposition of tile terrain for an abstract formulation, where elementary navigational steps consist of following the obstacle edges and turning around the corners. The convergence of an abstract version of the algorithm is first analytically established. Then experimental results on implementing the algorithm on an experimental mobile robot are reported. DOE

N95-21412 Technische Univ., Twente (Netherlands). Dept. of Computer Science.
ELEMENTS OF DELIBERATIVE ROBOT CONTROL
Jan M. Nauta Apr. 1994 36 p
(PB95-107595; Memo-INF-94-18) Copyright Avail: Issuing Activity (National Technical Information Service (NTIS))

In this study of the literature a number of elements of systems for deliberative robot control are discussed. Using the well-known sense-model-plan-act cycle as an analysis tool, these elements can be distinguished clearly. After this analysis, architectures of systems for deliberative control are discussed, and attention is focused on world modeling, task planning, and motion planning. NTIS

N95-21429 National Defence Research Establishment, Stockholm (Sweden). Dept. of Weapon Systems, Effects and Protection.
EXPERT SYSTEM EXPERT: PROGRAM DESCRIPTION [EXPERTSYSTEMET EXPERT: PROGRAMBESKRIVNING]
S. E. Hofmann May 1994 86 p In SWAHILI See also Users Manual, PB95-131579
(PB95-131561; FOA-C-20966-2.1) Avail: Issuing Activity (National Technical Information Service (NTIS))

This report describes how the program code for the general expert system Expert is constructed, its different parts, and the methods used for the system design. Expert is a rule based, real time expert system for use in process control applications. NTIS

N95-21430 National Defence Research Establishment, Stockholm (Sweden). Dept. of Weapon Systems, Effects and Protection.
EXPERT SYSTEM EXPERT: USERS MANUAL [EXPERTSYSTEMET EXPERT: ANVAENDARHANDLEDNING]
S. E. Hofmann May 1994 79 p In SWAHILI See also Program Description, PB95-131561
(PB95-131579; FOA-C-20965-2.1) Avail: Issuing Activity (National Technical Information Service (NTIS))

Expert is a rule based real time expert system for use in process control applications. This report describes its design and use. NTIS

N95-21522# Los Alamos National Lab., NM.
UTILIZING ARTIFICIAL NEURAL NETWORKS IN NETWORK FLOW ANALYSIS: AN ANNOTATED BIBILIOGRAPHY
Varun Madhok Nov. 1994 14 p
(Contract W-7405-eng-36)
(DE95-002453; LA-12856-MS) Avail: CASI HC A03/MF A01

This annotated bibliography reviews research in the development of neural network applications for power systems and for traffic and communications networks. Papers describing neural network techniques for applications such as security assessment, load forecasting, scheduling, and maintenance planning are cited. Some articles that present new algorithms for optimization or pattern analysis with the potential for neural network implementations also have been included. DOE

N95-21613*# Jet Propulsion Lab., California Inst. of Tech., Pasadena, CA.

COMMUNICATIONS AND CONTROL FOR ELECTRIC POWER SYSTEMS: POWER SYSTEM STABILITY APPLICATIONS OF ARTIFICIAL NEURAL NETWORKS

N. Toomarian and H. Kirkham Dec. 1993 42 p Sponsored by NASA
(Contract DE-AI05-79ET-29372)
(NASA-CR-197594; NAS 1.26:197594; DE94-019195; DOE/ET-29372/T3)
Avail: CASI HC A03/MF A01

This report investigates the application of artificial neural networks to the problem of power system stability. The field of artificial intelligence, expert systems and neural networks is reviewed. Power system operation is discussed with emphasis on stability considerations. Real-time system control has only recently been considered as applicable to stability, using conventional control methods. The report considers the use of artificial neural networks to improve the stability of the power system. The networks are considered as adjuncts and as replacements for existing controllers. The optimal kind of network to use as an adjunct to a generator exciter is discussed. DOE

N95-21618# Technische Univ., Eindhoven (Netherlands). Dept. of Mathematics nad Computer Science.

SEMI-GLOBAL STABILIZATION OF LINEAR DISCRETE-TIME SYSTEMS SUBJECT TO INPUT SATURATION VIA LINEAR FEEDBACK: AN ARE-BASED APPROACH

Zongli Lin (State Univ. of New York, Stony Brook, NY.), Ali Saberi (Washington State Univ., Pullman, WA.), and Anton A. Stoorvogel Jun. 1994 17 p
(ISSN 0926-4493)
(PB95-135463; Memo-COSOR-94-17) Avail: CASI HC A03/MF A01

We revisit the problem of semi-global stabilization of linear discrete-time systems subject to input saturation and give a Riccati equation-based approach to the proof of a fact we established earlier, i.e., a linear discrete-time system subject to input saturation is semi-globally stabilizable via linear feedback as long as the linear system in the absence of the saturation is stabilizable and detectable and all its open loop poles are located inside or on the unit circle. Moreover, we drastically relax the requirements on the characteristic of the saturation elements as imposed in our earlier work. NTIS

N95-21669 Technische Hogeschool, Delft (Netherlands). Dept. of Electrical Engineering.

SENSOR BASED FINE MOTION CONTROL Ph.D. Thesis

Cornelis Klomp 14 Jun. 1994 229 p
(PB95-108007; ISBN-90-9007162-8) Copyright Avail: Issuing Activity (National Technical Information Service (NTIS))

The aim of the research was to develop and implement a sensor based control system which allows a robot manipulator to assemble objects. The main test case is the Bosch Turbo-SCARA robot. An overview of control algorithms for performing fine motion tasks is given. Chapter three focuses on the one-dimensional aspects of fine motion control applied to the Bosch robot. This includes the modeling of the one-dimensional sub-system, controller design and verification. The subsequent chapter deals with the multi-dimensional control aspects in a similar way. A general framework for implementing the designed controllers is presented. This framework includes hardware design as well as software design. The sixth chapter describes the application of gripper sensors, like tactile image sensors, for robotic assembly. The results obtained using the implemented task description language in combination with the designed controllers are presented. Finally, the conclusions are drawn and some suggestions for future research are made. NTIS

N95-21710# Los Alamos National Lab., NM.

ADAPTIVE CAPTURE OF EXPERT BEHAVIOR

R. D. Jones, C. L. Barrett, U. Hand, and R. C. Gordon Aug. 1994 28 p
(Contract W-7405-eng-36)
(DE94-018285; LA-UR-94-2825) Avail: CASI HC A03/MF A01

The authors smoothed and captured a set of expert rules with adaptive networks. The motivation for doing this is discussed as follows: (1) Smoothing leads to stabler control actions; (2) For some sets of rules, the evaluation of the rules can be sped up. This is important in large-scale simulations where many intelligent elements are present; (3) Variability of the intelligent elements can be achieved by adjusting the weights in an adaptive network; (4) After capture has occurred, the weights can be adjusted based on performance criteria. The authors thus have the capability of learning a new set of rules that lead to better performance. The set of rules the authors chose to capture were based on a set of threat determining rules for tank commanders. The approach in this paper: (1) They smoothed the rules. The rule set was converted into a simple set of arithmetic statements. Continuous, non-binary inputs, are now permitted; (2) An operational measure of capturability was developed; (3) They chose four candidate networks for the rule set capture: (a) multi-linear network, (b) adaptive partial least squares, (c) connectionist normalized local spline (CNLS) network, and (d) CNLS net with a PLS preprocessor. These networks were able to capture the rule set to within a few percent. For the simple tank rule set, the multi-linear network performed the best. When the rules were modified to include more nonlinear behavior, CNLS net performed better than the other three nets which made linear assumptions; (4) The networks were tested for robustness to input noise. Noise levels of plus or minus 10% had no real effect on the network performance. Noise levels in the plus or minus 30% range degraded performance by a factor of two. Some performance enhancement occurred when the networks were trained with noisy data; (5) The scaling of the evaluation time was calculated; (6) Human variation can be mimicked in all the networks by perturbing the weights. DOE

N95-21741# Oak Ridge National Lab., TN.

LEARNING ALGORITHMS FOR FEEDFORWARD NETWORKS BASED ON FINITE SAMPLES

N. S. V. Rao, V. Protopopescu, R. C. Mann, E. M. Oblow, and S. S. Iyengar Sep. 1994 37 p
(Contract DE-AC05-84OR-21400)
(DE95-001739; ORNL/TM-12819) Avail: CASI HC A03/MF A01

Two classes of convergent algorithms for learning continuous functions (and also regression functions) that are represented by feedforward networks, are discussed. The first class of algorithms, applicable to networks with unknown weights located only in the output layer, is obtained by utilizing the potential function methods of Aizerman et al. The second class, applicable to general feedforward networks, is obtained by utilizing the classical Robbins-Monro style stochastic approximation methods. Conditions relating the sample sizes to the error bounds are derived for both classes of algorithms using martingale-type inequalities. For concreteness, the discussion is presented in terms of neural networks, but the results are applicable to general feedforward networks, in particular to wavelet networks. The algorithms can be directly adapted to concept learning problems. DOE

N95-21913 Drexel Univ., Philadelphia, PA.

DESIGN OF ROBUST OPTIMAL CONTROL SYSTEMS AND STABILITY ANALYSIS OF REAL STRUCTURED UNCERTAINTIES Final Report, Aug. 1990 - Mar. 1994

Bor-Chin Chang and Ajmal Yousuff Mar. 1994 149 p Limited Reproducibility: More than 20% of this document may be affected by microfiche quality
(Contract F33615-90-C-3613)
(AD-A279089; WL-TR-94-3030) Avail: Issuing Activity (Defense Technical Information Center (DTIC))

This report addresses the computational problems arising in the design of robust controllers via H-inf optimization and mu-synthesis and proposes several new controller reduction approaches. Through our discovery of the convexity and monotonicity properties of the general parameter dependent H-inf Riccati equation, a quadratically convergent algorithm which is faster than the other existing search schemes is developed to compute the optimal H-inf norm. It is desired to preserve the closed-loop stability and performance while reducing the order of the controller. A structured truncation technique based on the closed-loop controllability and observability diagrams, an H-inf controller parameterization and reduction method, and an observer-based controller parameterization and reduction procedure are employed to achieve this objective. DTIC

N95-21981 Vrije Univ., Amsterdam (Netherlands).

GENERIC ARCHITECTURE FOR KNOWLEDGE-BASED CONTROL OF PROCESSES IN DYNAMIC ENVIRONMENTS

F. Brazier, D. deKlerk, P. vanLangen, and J. Treur Dec. 1993 41 p
(PB95-132676) Avail: Issuing Activity (National Technical Information Service (NTIS))

In the report the authors explore knowledge-based control of processes in dynamic environments, the main focus being on the design and formal specification of compositional architectures for such complex tasks. After introducing the notions of dynamic environment, process, plan and compositional architecture, the authors present a generic, compositional architecture for knowledge-based control of processes in dynamic environments. Then they describe the dynamic environment of a shipyard, where the processes of interest are pipe installation activities. The authors present the main features of DESIRE (DEsign and Specification of Interacting REasoning modules), the framework for the design and specification of compositional architectures, and show how DESIRE has been used to formally specify the application of the generic architecture to the control of pipe installation activities. Finally, the authors draw some conclusions about the generic architecture for knowledge-based control of processes in dynamic environments. NTIS

N95-22015 Selskapet for Industriell og Teknisk Forskning, Trondheim (Norway). Automatic Control.
DIRECTIVES FOR THE PARTICIPATION IN MiTS FORUM. V3.0
O. JanRodseth 17 Mar. 1994 12 p
(PB95-110342; STF48-A94009) Avail: Issuing Activity (National Technical Information Service (NTIS))

The purpose of the MiTS Forum is to fund the administration, maintenance, and further development of the Maritime Information Technology Standard (MiTS). All interested individuals or companies can participate in MiTS Forum when they pay the appropriate membership fees. Membership and right-to-use fees paid by MiTS Forum members are placed in the MiTS Forum project account. MiTS Forum Steering Committee manages these funds on behalf of the participants in MiTS Forum. The actual administration and maintenance work is done within the scope of a separate project: MiTS Forum Administration. The formal relationship between MiTS Forum, that funds the administration project under control of the MiTS Forum participants, and MiTS Forum Administration is regulated by a contract of which this document is one part. The document gives directions for the organization of MiTS Forum and MiTS Forum Administration. NTIS

N95-22056# Pittsburgh Univ., Pittsburgh, PA. Dept. of Industrial Engineering.
ARTIFICIAL NEURAL NETWORK METAMODELS OF STOCHASTIC COMPUTER SIMULATIONS Final Report, 25 Jun. 1990 - 10 Aug. 1994 Ph.D. Thesis
Robert Allen Kilmer 10 Aug. 1994 254 p Sponsored by Army
(AD-A285951) Avail: CASI HC A12/MF A03

A computer simulation model can be thought of as a relation that connects input parameters to output measures. Since these models can become computationally expensive in terms of processing time and/or memory requirements, there are many reasons why it would be beneficial to be able to approximate these models in a computationally expedient manner. This research examines the use of artificial neural networks (ANN), to develop a metamodel of computer simulations. The development and use of the Baseline ANN Metamodel Approach is provided and is shown to outperform traditional regression approaches. The results provide a solid foundation and methodological direction for developing ANN metamodels to perform complex tasks such as simulation optimization, sensitivity analysis, and simulation aggregation/reduction. DTIC

N95-22139# Technische Univ., Eindhoven (Netherlands). Dept. of Mathematics and Computing Science.
DISCRETE ALGEBRAIC RICCATI EQUATION AND LINEAR MATRIX INEQUALITY
A. A. Stoorvogel and A. Saberi (Washington State Univ., Pullman, WA.) 9 May 1994 35 p Sponsored by Royal Netherlands Academy of Sciences and Arts
(ISSN 0926-4493)
(PB95-133575; MEMO-COSOR-94-16) Avail: CASI HC A03/MF A01

In this paper we study the discrete time algebraic Riccati equation and its connection to the discrete time linear matrix inequality. We show that in general only a subset of the set of rank-minimizing solutions of the linear matrix inequality correspond to the solutions of the associated algebraic Riccati equation, and study under what conditions these sets are equal. In this process we also derive very weak assumptions under which a Riccati equation has a solution. NTIS

N95-22156 Technische Univ., Twente (Netherlands). Dept. of Computer Science.
TOM THUMB ALGORITHM FOR PLANNING SIMPLE VEHICLE MOTIONS
Jan M. Nauta May 1994 27 p See also PB93-223824
(ISSN 0924-3755)
(PB95-107553; Memo-INF-94-23) Copyright Avail: Issuing Activity (National Technical Information Service (NTIS))

An algorithm for planning smooth collision-free paths, together with the velocities along that path, is presented. In this algorithm a search technique, which uses a heuristic rule to guide the search process, is applied. We will use interval arithmetic for checking both collisions and mechanical constraints. The algorithm is demonstrated with a mathematical model of a mobile robot such as constructed in the Mobile Autonomous Robot Twente (MART) project. NTIS

N95-22171*# Jet Propulsion Lab., California Inst. of Tech., Pasadena, CA.
COMMUNICATIONS AND CONTROL FOR ELECTRIC POWER SYSTEMS: POWER SYSTEM STABILITY APPLICATIONS OF ARTIFICIAL NEURAL NETWORKS Final Report
N. Toomarian and Harold Kirkham Apr. 1994 49 p
(Contracts NAS7-918; DE-AI01-79ET-29372)
(NASA-CR-197333; JPL-Publ-94-8; NAS 1.26:197333) Avail: CASI HC A03/MF A01

This report investigates the application of artificial neural networks to the problem of power system stability. The field of artificial intelligence, expert systems, and neural networks is reviewed. Power system operation is discussed with emphasis on stability considerations. Real-time system control has only recently been considered as applicable to stability, using conventional control methods. The report considers the use of artificial neural networks to improve the stability of the power system. The networks are considered as adjuncts and as replacements for existing controllers. The optimal kind of network to use as an adjunct to a generator exciter is discussed. Author

N95-22203# SRI International Corp., Menlo Park, CA.
ADAPTIVE FAULT-RESISTANT SYSTEMS Final Technical Report, Aug. 1992 - Apr. 1994
Jack Goldberg, Ira Greenberg, Raymond Clark, E. D. Jensen, and Kane Kim Oct. 1994 160 p
(Contract F30602-92-C-0098)
(AD-A286406; RL-TR-94-191) Avail: CASI HC A08/MF A02

The combined effects of faults and resource failures, wide swings in service demand, and situation-dependent user requirements, stress a computer's ability to satisfy its service expectations. This is an especially significant problem in distributed systems that employ unreliable communications, and whose components may operate in different and perhaps harsh physical data and usage environments. One of the goals for adaptive design is to allow flexible use of available resources to cover a much wider range of different kinds of environmental variables than could be covered by a fixed, worst-case design. The research focused on the tasks of: (1) developing a theory of adaptive fault-resistant systems and general principles of architectural design; (2) developing specific architectural design techniques; and (3) demonstrating adaptive designs. Three mechanisms were investigated: (1) Adaptive Distributed Recovery Blocks (ADRB's), a multiple-mode scheme for error detection and recovery, useful for both hardware and software faults; (2) adaptive fault tolerance for hybrid faults, an economical technique for tolerating both simple and complex fault types; and (3) adaptive distributed thread integrity, a technique for detecting and repairing thread breaks in a wide range of operating environments using the Alpha programming model. DTIC

N95-22210 Maryland Univ., College Park, MD. Lab. for Plasma Research.
CONNECTIONIST MODELS FOR INTELLIGENT COMPUTATION Final Report, 1 May 1991 - 30 May 1994

H. H. Chen and Y. C. Lee 28 Jul. 1994 9 p Limited Reproducibility: More than 20% of this document may be affected by microfiche quality
(Grant AF-AFOSR-0257-91)
(AD-A286436; AFOSR-94-0747TR) Avail: CASI HC A02

This final report covers the work done by our group of neural network computing at the University of Maryland for the past three years. We studied the neural network's capability of processing temporal or sequential data. Recurrent neural networks were used to perform inference on grammars. An external memory stack was constructed to work with the neural network to perform inferences on context free languages. And finally, a spatially homogeneous locally connected recurrent neural network that could simulate any given turing machine, including the universal Turing machine was devised. It is capable of performing universal computations and demonstrated the universal power of recurrent neural network architectures. To train these sequential neural net machines, we have investigated the forward propagating learning algorithms. DTIC

N95-22213# Rutgers - The State Univ., New Brunswick, NJ. Dept. of Mathematics.
MATHEMATICAL THEORY OF NEURAL NETWORKS Final Report, 1 Aug. 1991 - 31 Jul. 1994
Eduardo D. Sontag and Hector J. Sussmann 31 Aug. 1994 31 p
Sponsored by AF
(AF Proj. 2304)
(AD-A286508; AFOSR-94-0746TR) Avail: CASI HC A03/MF A01

This report provides a summary of the grant work by the principal investigators in the area of neural networks. The topics covered deal with: analysis of networks from the viewpoint of analog computational devices, exploring limitations imposed by resource constraints; questions of parameter identification of recurrent nets; use of feedforward nets for function approximation and interpolation problems; systems theory (observability and other properties) for nets; and the use of neural networks for the control of nonlinear systems. DTIC

N95-22214# Army Missile Command, Redstone Arsenal, AL.
INFORMATION SECURITY FOR UNMANNED SYSTEMS
John R. Coward Jul. 1994 15 p
(AD-A286511; AMSMI-MB-RD-SE-94-1) Avail: CASI HC A03/MF A01

The primary mission of unmanned systems is to perform reconnaissance and gather electronic intelligence. Information gathered by these systems is most often sensitive and steps should be taken to ensure its security and integrity. This report will discuss the role of unmanned systems with respect to intelligence gathering and give an overview of methods which can be used to ensure the security and integrity of the intelligence data gathered by these systems. This will include an introduction to signal scrambling, encryption techniques, and tradeoffs involved in the use of these methods of information security. DTIC

N95-22216# Michigan Univ., Ann Arbor, MI. Dept. of Aerospace Engineering.
ROBUST FIXED-STRUCTURE CONTROL Final Report, 1 Feb. 1992 - 30 Sep. 1994
Dennis S. Bernstein 30 Oct. 1994 27 p
(Contract F49620-92-J-0127)
(AD-A286515; AFOSR-94-0741TR) Avail: CASI HC A03/MF A01

This final report for AFOSR Grant F49620-92-J-0127 summarizes results obtained in five areas, namely, robust control, linear control, sampled-data control, tracking and disturbance rejection, and nonlinear control. Principal results include new bounds for the structured singular value, implementation of structured singular value synthesis using fixed-structure optimization techniques, a more rigorous foundation for the Maximum Entropy control technique, extensions of linear-quadratic control to stable stabilizing controllers, determination of the achievable performance of sampled-data controllers in the presence of sample-rate constraints, control of noise in an acoustic duct, stability theory for second-order systems, a rigorous treatment of Guyan reduction, a deterministic foundation for energy flow theory, a unified treatment of quadratic optimality and servo-compensation, nonlinear control of the spinning top and rotating bodies with known and unknown mass imbalance, global stabilization of the oscillating eccentric rotor using integrator backstepping, and Lyapunov theory for finite-time convergence. DTIC

N95-22226# Carnegie-Mellon Univ., Pittsburgh, PA. Software Engineering Inst.
ARTIFICIAL INTELLIGENCE (AI) AND Ada: INTEGRATING AI WITH MAINSTREAM SOFTWARE ENGINEERING Final Report
Jorge L. Diaz-Herrera Sep. 1994 63 p
(Contract F19628-90-C-0003)
(AD-A286093; CMU/SEI-94-TR-09; ESC-TR-94-009) Avail: CASI HC A04/MF A01

In this report we discuss in detail pragmatic problems posed by the integration of AI with conventional software engineering, and within the framework of current Ada technology. A major objective of this work has been to begin to bridge the gap between the Ada and AI software cultures. The report summarizes survey results from the Association for Computing Machinery (ACM) Special Interest Group for Ada (SIGAda) AI Working Group (AIWG), highlighting lessons learned and sample applications. An interesting observation is that a large percentage of AI code is procedural by nature and that better productivity rates are achieved by using Ada; also, efficiency is much better when compared to traditional AI languages. Although we show favorable results on the use of Ada technology for the implementation of AI software, a total integration remains difficult at the conceptual level. There are some impediments to a completely satisfactory solution, but only a few restrictions are more intrinsically related to the current Ada standard (Ada83); these, however, are being dealt with in the next revision known as Ada9X. DTIC

N95-22233# Naval Postgraduate School, Monterey, CA.
OPTIMAL CONTROL OF A TWO WHEELED MOBILE ROBOT M.S. Thesis
Bryan R. Emond Sep. 1994 163 p
(AD-A286130) Avail: CASI HC A08/MF A02

Feedback control of a two wheeled mobile robot from one point in its configuration space to another presents a challenging problem. The mobile robot belongs to a class of systems with non-integrable motion constraints for which smooth feedback control laws cannot be designed. Recent work has been aimed at developing time-varying feedback control laws and piecewise smooth feedback control laws. These control techniques are, however, not optimal in any sense. In this research, we look into the optimal control of a mobile robot using partial feedback. A solution is obtained by application of Pontryagin's Minimization Principle and solving the associated two point boundary value problem using a numerical relaxation technique. The resulting robot trajectories exhibit optimal behavior for all non-trivial cases. DTIC

N95-22244 Naval Postgraduate School, Monterey, CA.
LAYERED PATH PLANNING FOR AN AUTONOMOUS MOBILE ROBOT M.S. Thesis
Timothy A. Haight Sep. 1994 115 p Limited Reproducibility: More than 20% of this document may be affected by microfiche quality
(AD-A286138) Avail: CASI HC A06

In order to continue to improve the usefulness of robots, it is becoming increasingly important to have them act as autonomous agents. A significant step toward this object is autonomous motion planning. This research was conducted as part of a broader effort to empower Yambico-11, a mobile robot under development at the Naval Postgraduate School, with ability to move autonomously. We believe that this problem is best attacked in layers. This thesis is our proposal for the initial layer. Given a robot's current location and its goal location, we use the homotopy relation to reduce the infinite set of path choices into a more manageable and smaller set of path classes. Specifically, we solve the problem of how to enable a robot to autonomously identify and label these classes of paths. We begin by decomposing the robot's operating environment into a collection of convex pieces called cells. The cells are transformed into a graph by adjacency. We show that every simple path on the graph corresponds to a unique simple homotopy class in the robot's world. We then search the graph to give each class a symbolic representation which also provides intermediate path planning clues. Subsequent layers can use these clues to form a more detailed plan. We implement the cell decomposition, graph transformation, and path class labeling as C programs, and preprocess them on a Unix workstation. This resulting data structures are then compiled and linked into the robot's kernel. All implementation has been integrated into the model-based mobile robot language (mml) used by Yamabico-11. DTIC

N95-22267# Massachusetts Inst. of Tech., Cambridge, MA. Artificial Intelligence Lab.
LEARNING MANEUVERS USING NEURAL NETWORK MODELS Final Report, 1 Apr. 1993 - 31 Mar. 1994
Christopher Atkeson 7 Aug. 1994 128 p
(Contract F49620-93-1-0263)
(AD-A286470; AFOSR-94-0702TR) Avail: CASI HC A07/MF A02

The researchers explored issues involved in implementing robot learning for a challenging dynamic task, using a case study from robot juggling. They used a memory based local modeling approach (locally weighted regression) to represent a learned model of the task to be performed. Statistical tests are given to examine the uncertainty of a model, to optimize its prediction quality, and to deal-with noisy and corrupted data. They developed an exploration algorithm that explicitly deals with prediction accuracy requirements during exploration. Using all these ingredients in combination with methods from optimal control, the robot achieves fast real-time learning of the task within 40 to 100 trials. DTIC

N95-22366# Helsinki Univ. of Technology, Espoo (Finland).
QUADRATIC OPTIMAL CONTROL OF A DELAY EQUATION II: THE UNSTABLE CASE Research Report
O. J. Staffans Jun. 1994 22 p See also PB95-127072
(PB95-127064; RR-A334) Avail: CASI HC A03/MF A01

The authors consider the infinite horizon quadratic cost minimization problem for a certain class of systems with finitely may inputs and outputs. The authors approach is to interpret the system as a delay equation, and to user a transfer function approach. This is the second half of a two-part paper. In the first part the authors have discussed the case where the system is stable, and this part is devoted to an extension of the theory to the unstable case. Out of many possible formulations of the unstable case the authors have chosen a right coprime factorization approach, as this seems to be the most natural and simple one. As in the stable case, the authors are able to reduce the problem to a symmetric Wiener-Hopf factorization problem, and all the authors' main constructions and conclusions for the stable case carry over to the unstable case. NTIS

N95-22367# Helsinki Univ. of Technology, Espoo (Finland).
QUADRATIC OPTIMAL CONTROL OF A DELAY EQUATION I: THE STABLE CASE Research Report
O. J. Staffans Apr. 1994 27 p See also PB95-127064
(PB95-127072; RR-A332) Avail: CASI HC A03/MF A01

The authors consider the infinite horizon quadratic cost minimization problem for a certain class of systems with finitely may inputs and ouputs. This class contains all detectable and stabilizable systems of Pritchard-Salamon type with finitely many inputs and outputs as a proper subclass. The most common approach to treat a problem of this type is to construct a semigroup in an abstract state space, and to use infinite dimensional control theory. However, this approach is less appealing in the case where there are discrete time delays in the transfer function, because such time delays cause the input and output operators to become too unbounded compared to the generator of the semigroup to be comfortably handled. In particular, the system is then no longer of Pritchard-Salamon type. In order to be able to include this case, the authors take an alternative approach, and reduce the problem to a symmetric Weiner-Hopf problem, that can be solved by means of a canonical factorization of the symbol. In a standard delay equation realization of the system, this amounts to factorizations of the Riccati operator and the feedback operator into convolution operators and projections. In particular, the authors show that, under their assumptions, the optimally controlled system is well-posed in every L(sup p)-space, I = or less than p = or less than inifinty, and not just the usual L(sup 2)-space. It is also well-posed in (a subspace of) the space of continuous functions. Part I of this paper deals with the case where the system is stable; the unstable case is discussed in Part II. NTIS

N95-22409# Sandia National Labs., Albuquerque, NM.
SIMULATION OF STRUCTURAL RESPONSE USING A RECURRENT RADIAL BASIS FUNCTION NETWORK
T. L. Paez 1994 10 p Presented at the 1st World Conference on Structural Control, Pasadena, CA, 3-5 Aug. 1994
(Contract DE-AC04-94AL-85000)
(DE94-017342; SAND-94-2079C; CONF-9408141-1) Avail: CASI HC A02/MF A01

System behaviors can be accurately simulated using artificial neural networks (ANN's), and one that performs well in simulation of structural response is the radial basis function network. A specific implementation of this is the connectionist normalized linear spline (CNLS) network, investigated in this study. A useful framework for ANN simulation of structural response is the recurrent network. This framework simulates the response of a structure one step at a time. It requires as inputs some measures of the excitation, and the response at previous times. On output, the recurrent ANN yields the response at some time in the future. This framework is practical to implement because every ANN requires training, and this is executed by showing the ANN examples of correct input/output behavior (exemplars), and requiring the ANN to simulate this behavior. In practical applications, hundreds or, perhaps, thousands, of exemplars are required for ANN training. The usual laboratory and non-neural numerical applications to be simulated by ANN's produce these amounts of information. Once the recurrent ANN is trained, it can be provided with excitation information, and used to propagate structural response, simulating the response it was trained to approximate. The structural characteristics, parameters in the CNLS network, and degree of training influence the accuracy of approximation. This investigation studies the accuracy of structural response simulation for a single-degree-of-freedom (SDF), nonlinear system excited by random vibration loading. The ANN used to simulate structural response is a recurrent CNLS network. We investigate the error in structural system simulation. DOE

N95-22430# Los Alamos National Lab., NM.
A SURVEY OF ARTIFICIAL NEURAL NETWORK APPLICATIONS IN FLOW ANALYSIS OF ENERGY NETWORKS
Varun Madhok Nov. 1994 34 p
(Contract W-7405-eng-36)
(DE95-002452; LA-12855-MS) Avail: CASI HC A03/MF A01

This report presents the results of a literature survey carried out to analyze the work done so far using artificial neural networks (ANN's) in tasks of flow assessment in networked systems. The survey revealed that current implementations developed so far may be classified as pattern analysis and optimization, with a parallel grouping for the types of ANN's used: the feedforward network trained using error backpropagation and the Hopfield network. Pattern analysis has been used in developing ANN's for prediction and system security monitoring, with the Kohonen feature map, as well as the backpropagation type of network, being useful in the latter application. Results have been promising, showing ANN's potential for use in problems of load flow analysis in dense energy networks or in system monitoring in hazardous situations. Problems of the nature of resource scheduling, optimal path search, and so forth, have been handled in general by methods based on Hopfield dynamics. By and large, however, large-scale commercial applications of ANN's are rare. Industry has failed to exploit the technology fully, probably because of a lack of funding and the necessary multifaceted scientific workforce. DOE

64 NUMERICAL ANALYSIS

Includes iteration, difference equations, and numerical approximation.

N95-19892# Technische Univ., Eindhoven (Netherlands). Dept. of Mathematics and Computing Science.
NON INTERLEAVING PROCESS ALGEBRA
J. C. M. Baeten and J. A. Bergstra (Amsterdam Univ., Netherlands.) Oct. 1993 27 p
(PB95-110607) Avail: CASI HC A03/MF A01

We study a non-interleaving subalgebra of a reduct of a model of the Algebra of Communicating Processes (ACP). The model discussed uses step bisimulation semantics. We can derive identities in this model with the help of the (interleaving) ACP calculus with multi-actions. We study the connection with Petri nets, and introduce causalities and a causal state operator. NTIS

N95-19902# Technische Univ., Eindhoven (Netherlands). Dept. of Mathematics and Computing Science.
GENERAL CONSERVATIVE EXTENSION THEOREM IN PROCESS ALGEBRA
C. Verhoef Nov. 1993 26 p
(PB95-110656) Avail: CASI HC A03/MF A01

The authors proved a general conservative extension theorem for transition system based process theories with easy-to-check and reasonable conditions. The core of this result is another general theorem giving sufficient conditions for a system of operational rules and an extension ensuring that outgoing transitions from an original term in the extension are the same as in the original system. As a simple corollary of the conservative extension theorem, the authors proved a completeness theorem. As a first application of their conservativity results, the authors proved a general theorem giving sufficient conditions to reduce the question of ground confluence modulo (some equations for a large term rewriting system associated with an equation process theory) to a small term rewriting system under the condition that the large system is a conservative extension of the small one. The authors proved many other applications to show that the results are useful. The applications include (but are not limited to) various real and discrete time settings in Calculus of Communicating Systems (CCS), Algebra of Communicating Processes (ACP), and Algebra of Timed Processes (ATP), and the notions projection, renaming, state operator, priority, recursion, the silent step, and the empty process. NTIS

N95-19903# Technische Univ., Eindhoven (Netherlands). Dept. of Mathematics and Computing Science.
UPS AND DOWNS OF TYPE THEORY
W. Peremans Mar. 1994 19 p
(PB95-110664) Avail: CASI HC A03/MF A01

The report gives a global historical sketch of the development of formalized type theory in the 20th century. NTIS

N95-19906# Technische Univ., Eindhoven (Netherlands). Dept. of Mathematics and Computing Science.
TESTING PARADIGM APPLIED TO NETWORK STRUCTURE (REVISED)
T. Verhoeff Mar. 1994 44 p
(PB95-110706) Avail: CASI HC A03/MF A01

The testing paradigm provides a simple framework for comparing networks of processes. In this note, we use the testing paradigm to compare structural aspects of process networks. Central to our approach are the following three ingredients: (1) Tests are drawn from the set of process networks; (2) A (global) correctness concern, in the form of a predicate, expresses when a network is correct as an autonomous system; (3) A network passes a test when the composition of two networks involved is a correct (autonomous) system. Our approach has several merits. It allows a uniform treatment of structure and behavior. Structural and behavioral correctness concerns can be varied independently within the same framework. Structural correctness concerns can be made explicit at the very beginning, and need not appear implicitly as an unmotivated afterthought. For one particular choice of (structural) correctness concerns, we work out a model in full detail. We briefly investigate alternative correctness concerns. NTIS

N95-19907# Technische Univ., Eindhoven (Netherlands). Dept. of Mathematics and Computing Science.
PROCESS ALGEBRA WITH PARTIAL CHOICE
J. C. M. Baeten and J. A. Bergstra (Amsterdam Univ., Netherlands.) Mar. 1994 26 p
(PB95-110714) Avail: CASI HC A03/MF A01

The objective of this paper is to bridge the gap between the Algebra of Communicating Processes (ACP) and the Theory of Communicating Sequential Processes (TCSP). To this end, ACP is extended with two non-deterministic choice operators in a setting of bisimulation semantics. With these operators, we can express safety properties of systems without the use of silent steps, and we can verify safety properties in a setting in which no assumption on fairness (or unfairness) has been made. NTIS

N95-19915# Technische Univ., Eindhoven (Netherlands). Dept. of Mathematics and Computing Science.
MULTIGRID WITH MATRIX-DEPENDENT TRANSFER OPERATORS FOR CONVECTION-DIFFUSION PROBLEMS
A. Reusken Jul. 1993 22 p
(PB95-110821; RANA-93-10) Avail: CASI HC A03/MF A01

It was previously proved that for 1D convection-diffusion problems the use of suitable matrix-dependent transfer operators results in a multigrid method which is robust with regard to variation in the amount of convection, even if one uses damped Jacobi for smoothing. The main subject of this paper is a generalization of the 1D approach, resulting in a new multigrid method for 2D convection-diffusion problems. We remain close to the red-black structure of the 1D case. We briefly explain our multigrid method for the case with uniform square grids and standard h to 2h coarsening. Results of numerical experiments again show robustness. NTIS

N95-19916# Technische Univ., Eindhoven (Netherlands). Dept. of Mathematics and Computing Science.
SOLUTIONS OF D(SUP n)D(SUP m)f=0
B. Klein Obbink May 1993 42 p
(PB95-110839; RANA-93-07) Avail: CASI HC A03/MF A01

In the papers of R.W. Hopper and J. de Graaf, there are given some exact solutions of the shape evolution of a two-dimensional piece of viscous matter driven by surface tension on the free boundary. After making some assumptions and approximations, they described such a physical system with a set of the following equations. The derivation of the evolution equation for the change of the shape in time is then based on complex analysis. The starting point is to solve Stoke's equations in terms of holomorphic functions. An analogous treatment of the three-dimensional problem may be based on hypercomplex analysis. The starting point would then be to solve Stokes' equations in three dimensions in terms of left monogenic functions. That is exactly what will be done in the paper: the authors will show that the general solution of Stokes' equations on three-dimensional, special x-normal domains can be represented by two left monogenic functions. NTIS

N95-19917# Technische Univ., Eindhoven (Netherlands).
WEIGHTED STRONGLY ELLIPTIC OPERATORS ON LIE GROUPS
A. F. M. terElst and Derek W. Robinson (Australian National Univ., Canberra, Australia.) Jul. 1993 54 p
(PB95-110847; RANA-93-11) Avail: CASI HC A04/MF A01

Within the general theory of elliptic operators, the twin notions of subelliptic operator and weighted elliptic operator play related but distinct roles. Subellipticity is based on the idea that there is a certain subset of preferred directions, but in the weighted theory all directions are allowed although some have a greater weight, or preference. Both concepts have non-commutative aspects and are naturally described in the setting of Lie groups. In this paper we develop the theory of weighted strongly elliptic operators for Lie groups in analogy with the subelliptic theory. We start with a basis for the Lie algebra, give each direction a weight, define weighted strongly elliptic forms and then introduce weighted strongly elliptic operators associated with an arbitrary strongly continuous or weakly continuous representation of the Lie group on a Banach space. Under a suitable condition on the Lie algebraic structure, we prove that the closure of each such operator generates a continuous semigroup, which has a representation independent kernel. We then derive kernel bounds, regularity and analyticity properties, et cetera. NTIS

N95-19937# Tilburg Univ. (Netherlands). Dept. of Economics.
ORTHOGONAL REPRESENTATIONS OVER FINITE FIELDS AND THE CHROMATIC NUMBER OF GRAPHS
R. Peeters 1994 22 p
(PB95-110953; FEW-622) Avail: CASI HC A03/MF A01

We study the relationship between the minimum dimension of an orthogonal representation of a graph over a finite field and the chromatic number of its complement. It turns out that for some classes of matrices defined by a graph that the 3-colorability problem is equivalent to deciding whether the class defined by the graph has a matrix of rank 3 or not. This implies the NP-hardness of determining the minimum rank of a matrix in such a class. NTIS

N95-19940# Tilburg Univ. (Netherlands).
QUADRATIC FORMS IN DESIGN THEORY
M. J. Coster 12 Jan. 1994 37 p
(PB95-111019; FEW-635) Avail: CASI HC A03/MF A01

This report describes the Grothendieck Group for rational congruence classes of positive definite integral matrices. The main result is an explicit diagonal matrix for each class of this Grothendieck Group. We give some applications in design theory. NTIS

N95-19942# Tilburg Univ. (Netherlands). Dept. of Economics.
UNIQUENESS OF STRONGLY REGULAR GRAPHS HAVING MINIMAL p-RANK
R. Peeters 1994 30 p
(PB95-111043; FEW-626) Avail: CASI HC A03/MF A01

Let Gamma be a strongly regular graph with adjacency matrix A. Let I be the identity matrix and let p be a prime. We study the p-rank of the matrices A + cI for integral c and want to characterize among all strongly regular graphs with a given parameter set those for which a p-rank is minimal. NTIS

N95-19943# Tilburg Univ. (Netherlands). Dept. of Economics.
GRAPHS COSPECTRAL WITH DISTANCE-REGULAR GRAPHS
W. H. Haemers and E. Spence 1994 31 p
(PB95-111050; FEW-623) Avail: CASI HC A03/MF A01

We determine all graphs with the spectrum of a distance-regular graph with at most 30 vertices (except possibly for the Taylor graph on 28 vertices). NTIS

N95-19944# Institut des Hautes Etudes Scientifiques, Bures-sur-Yvette (France).
SHARP DETERMINANTS
V. Baladi and D. Ruelle May 1994 26 p
(PB95-111068; IHES/P/94/34) Avail: CASI HC A03/MF A01

We introduce a sharp trace and a sharp determinant for an algebra of operators M acting on functions of bounded variation on the real line. We show that the zeroes of the sharp determinant describe the discrete spectrum of M. The relationship with weighted zeta functions of interval maps and Milnor-Thurston kneading determinants is explained. This yields a result on convergence of the discrete spectrum of approximated operators. NTIS

N95-20054# Technische Univ., Eindhoven (Netherlands). Dept. of Mathematics and Computing Science.
ABSTRACT REDUCTION AND TOPOLOGY
Walter Ferrer and Paula Severi Oct. 1993 40 p
(PB95-110615) Avail: CASI HC A03/MF A01

If A = less than A, approaches greater than is an abstract reduction system, we use the reduction greater than to introduce a closure operator on the set P(A) of parts of A. We describe the topologies obtained in this way, and establish a bijective correspondence between these topologies and the category of abstract reduction systems with transitive reductions. Hence, we can view and formulate Church-Rosser (and the converse), Strong and Weak Normalization in topological terms. Also, we give topological proofs of some results on abstract reduction systems. NTIS

N95-20055# Technische Univ., Eindhoven (Netherlands). Dept. of Mathematics and Computing Science.
REAL TIME PROCESS ALGEBRA WITH INFINITESIMALS
J. C. M. Baeten and K. A. Bergstra Oct. 1993 49 p
(PB95-110623) Avail: CASI HC A03/MF A01

We consider a model of a real time process algebra on the nonstandard reals. As a subalgebra, we obtain a theory in which the urgent actions of the Algebra of Timed Processes (ATP), Timed Calculus of Communicating Systems (TiCCS), Temporal Calculus of Communicating Systems (TeCCS) can be modeled. NTIS

N95-20141# Sandia National Labs., Albuquerque, NM.
A DOMAIN DECOMPOSITION SCHEME FOR EULERIAN SHOCK PHYSICS CODES
R. L. Bell (Amparo Corp., Albuquerque, NM.) and E. S. Hertel, Jr. 1994 6 p Presented at the American Society of Mechanical Engineers' Winter Annual Meeting, Chicago, IL, 9-11 Nov. 1994
(Contract DE-AC04-94AL-85000)
(DE94-015739; SAND-94-1005C; CONF-941142-14) Avail: CASI HC A02/MF A01

A new algorithm which allows for complex domain decomposition in Eulerian codes was developed at Sandia National Laboratories. This new feature allows a user to customize the zoning for each portion of a calculation and to refine volumes of the computational space of particular interest This option is available in one, two, and three dimensions. The new technique will be described in detail and several examples of the effectiveness of this technique will also be discussed. DOE

N95-20149 Technische Univ., Eindhoven (Netherlands). Dept. of Mathematics and Computing Science.
BEYOND BETA-REDUCTION IN CHURCH'S LAMBDA YIELD
Roel Bloo, Fairouz Kamareddine (Glasgow Univ., Scotland.), and Rob Nederpelt 26 Apr. 1994 29 p Limited Reproducibility: More than 20% of this document may be affected by microfiche quality
(PB95-110565) Avail: CASI HC A03

In the paper, the authors observed that if they change slightly the classical lambda-notation, then they can make more redexes visible. This is useful and is in line with current research on the needed redexes (for normal forms). The authors have shown further that, using item notation (which makes more redexes visible), one is able to stick to the old beta-reduction and just do a simple reshuffling so that these newly visible redexes can be contracted before other redexes. The authors have shown that this reshuffling (which is very simple and can only be enabled in the authors' notation), is correct. In fact, reshuffling does really make all redexes subject to immediate contraction and preserves typing. So, if t has type rho then the reshuffled version of t also has type rho. NTIS

N95-20167# Los Alamos National Lab., NM.
THE NONLINEAR CHARACTERISTIC SCHEME IN X-Y GEOMETRIES
W. F. Walters and T. A. Wareing 1994 7 p Presented at the Winter Meeting of the American Nuclear Society, Washington, DC, 13-18 Nov. 1994
(Contract W-7405-eng-36)
(DE94-016192; LA-UR-94-2644; CONF-941102-16) Avail: CASI HC A02/MF A01

The nonlinear characteristic (NC) scheme for solving the discrete-ordinates form of the transport equation has recently been introduced and used to analyze one-dimensional slab transport problems. The purpose of this paper is to determine the accuracy and positivity of the NC scheme as extended to solve two-dimensional X-Y problems. We compare the results obtained using the NC scheme to those obtained using the bilinear discontinuous (BLD) scheme, the bilinear nodal (BLN) scheme, linear characteristic scheme, and the diamond difference with fixup (DD/F) scheme. As was found in one-dimensional applications, the NC scheme is strictly positive and as accurate or more accurate than the other schemes for all meshes examined. The accuracy of the NC scheme for coarse meshes is particularly outstanding compared to that of the other schemes. DOE

N95-20169 Los Alamos National Lab., NM.
SEMIQUANTUM CHAOS AND THE LARGE N EXPANSION
F. Cooper, S. Habib, Y. Kluger, J. Dawson (New Hampshire Univ., Durham, NH.), D. Meredith (New Hampshire Univ., Durham, NH.), and H. Shepard (New Hampshire Univ., Durham, NH.) 29 Jun. 1994 30 p Presented at the Quantum Complexity in Mesoscopic Systems, Los Alamos, NM, 16-20 May 1994 Limited Reproducibility: More than 20% of this document may be affected by poor print
(Contract W-7405-eng-36)
(DE94-016196; LA-UR-94-2479; CONF-9405204-1) Avail: Issuing Activity (Department of Energy (DOE))

When a classical oscillator is interacting with a purely quantum mechanical oscillator, described by the Lagrangian L = 1/2 x(exp 2) + 1/2 A(exp 2) - 1/2 (m(exp 2) + e(exp 2) A(exp 2)) x(exp 2), where A is a classical variable and x is a quantum operator the relevant degrees of freedom for the quantum oscillator, when (x(t)) = 0, is (x(t)x(t)) = G(t). The classical Hamiltonian dynamics governing the variables A(t), Pi(sub A)(t), G(t), and Pi(sub G)(t) is chaotic so that the results of making measurements on the quantum system at later times are sensitive to initial conditions. We review this system and discuss how this behavior is altered when the quantum fluctuations of the A oscillator are determined exactly and in a 1/N expansion where N is the number of copies of the x oscillator. DOE

N95-20170# Argonne National Lab., IL.
A CONTROL VOLUME METHOD ON AN ICOSAHEDRAL GRID FOR NUMERICAL INTEGRATION OF THE SHALLOW-WATER EQUATIONS ON THE SPHERE
I.-Liang Chern 1994 40 p
(Contract W-31-109-eng-38)
(DE94-016345; ANL/MCS/PP-73014) Avail: CASI HC A03/MF A01

Two versions of a control volume method on a symmetrized icosahedral grid are proposed for solving the shallow-water equations on a sphere. One version expresses the equations in the 3-D Cartersian coordinate system, while the other expresses the equations in the northern/southern polar stereographic coordinate systems. The pole problem is avoided because of these expressions in both versions and the quasi-homogenity of the icosahedral grid. Truncation errors and convergence tests of the numerical gradient and divergent operators associated with this method are studied. A convergence test for a steady zonal flow is demonstrated. Several simulations of Rossby-Haurwitz waves with various numbers are also performed. DOE

N95-20172# Institut des Hautes Etudes Scientifiques, Bures-sur-Yvette (France).
SQUEEZING AND FLOW OF ENERGY FOR NON LINEAR WAVE EQUATIONS
S. B. Kuksin Jul. 1994 34 p
(PB95-111100; IHES/M/94/39) Avail: CASI HC A03/MF A01

The authors study the nonlinear wave equation u'' - delta(sup 2) Delta u + f(u) = 0 under n-dimensional periodic boundary conditions (n = 1, 2, 3) in a Sobolev phase-space H(sup s) = H(sup s) x H(sup s-1)(T(sup n)) = ((u, u')(x)). In another paper by the author, the author interpreted the 'energy transition to higher frequencies' problem for this (and similar) equations as a squeezing: time-t flow maps of the equation with large t 'squeeze' r-balls in H(sup S) to narrow cylinders formed by vector-functions with norms of first Fourier coefficients less then some small gamma. The authors proved also a version of Gromov's squeezing theorem: the phenomenon stated above is impossible for gamma less than r if for H(sup s) is chosen the symplectic phase space of the equation, H(sup s) = H(sup 1/2). In this paper the authors show that in smooth phase spaces H(sup s), s greater than or equal to 5, the squeezing is typical if the dispersion delta is small. The authors use this result and some related statements to obtain a picture of qualitative behavior of solutions of the phi(sup 4) equation u'' - delta(sup 2) Delta u + u(exp 3) = 0. NTIS

N95-20222# Sandia National Labs., Albuquerque, NM.
UNCERTAINTY ESTIMATES FOR DERIVATIVES AND INTERCEPTS
Edward L. Clark Sep. 1994 22 p
(Contract DE-AC04-94AL-85000)
(DE94-018492; SAND-90-2336) Avail: CASI HC A03/MF A01

Straight line least squares fits of experimental data are widely used in the analysis of test results to provide derivatives and intercepts. A method for evaluating the uncertainty in these parameters is described. The method utilizes conventional least squares results and is applicable to experiments where the independent variable is controlled, but not necessarily free of error. A Monte Carlo verification of the method is given. DOE

N95-20259# Institut des Hautes Etudes Scientifiques, Bures-sur-Yvette (France).
CLASSIFICATION OF DIAGONAL COSET MODULAR INVARIANTS
Terry Gannon and Mark A. Walton (Lethbridge Univ., Lethbridge, Alberta.) Jul. 1994 28 p
(PB95-111118; IHES/P/94/41) Avail: CASI HC A03/MF A01

The authors relate in a novel way the modular matrices of GKO (Goddard-Kent-Olive) diagonal cosets without fixed points to those of WZNW tensor products. Using this, the authors classify all modular invariant partition functions of su(3)(sub k)(circle +)su(3)(sub 1)/su(3)(sub k+1) for all positive integer level k, and su(2)(sub k)(circle +)su(2)(sub l)/su(2)(sub k+l) for all k and infinitely many l (in fact, for each k a positive density of l). Of all these classifications, only that for su(2)(sub k)(circle +)su(2)(sub 1)/su(2)(sub k+1) had been known. The authors' lists include many new invariants. NTIS

N95-20266# Brookhaven National Lab., Upton, NY.
EVALUATING IMPEDANCES IN A SACHERER INTEGRAL EQUATION
S. Y. Zhang and W. T. Weng 1994 4 p Presented at the 4th European Particle Accelerator Conference, London, England, 27 Jun. - 1 Jul. 1994
(Contract DE-AC02-76CH-00016)
(DE94-016823; BNL-49826; CONF-940618-62) Avail: CASI HC A01/MF A01

In a Sacherer integral equation, the beam line density is expanded on the phase deviation (phi), generating a Hankel spectrum, rather than on the time, which generates a Fourier spectrum. This is a natural choice to deal with the particle evolution in phase space, however, it causes complications whenever the impedance corresponding to the spectrum has to be evaluated. In this article, the line density expansion on (phi) is shown to be equivalent to a beam time modulation under an acceptable condition. Therefore for a Hankel spectrum, a number of sidebands, and the corresponding impedance as well, will be involved. For wideband resonators, it is shown that the original Sacherer solution is adequate. For narrowband resonators, the solution had been compromised, therefore a modification may be needed. DOE

N95-20273# Institut des Hautes Etudes Scientifiques, Bures-sur-Yvette (France).
BANACH SPACES WITH SMALL SPACES OF OPERATORS
W. T. Gowers and B. Maurey Jul. 1994 32 p
(PB95-111134; IHES/M/94/44) Avail: CASI HC A03/MF A01

A space X was constructed with the property that every operator from a subspace Y to X was of the form lambda i + S, where i is the inclusion map and S is strictly singular. Among the easy consequences of this fact are that X contains no unconditional basic sequence, and, more generally, that X is hereditarily indecomposable: that is, no subspace of X admits any nontrivial projection. Section 2 introduces notation and some basic lemmas. In the third section the authors state and prove the main result of the paper. The applications are given in the fourth section. The fifth and final section contains a discussion of the space with an unconditional basis. The authors also ask some questions about the possibility of removing some of the restrictions needed for the main result. NTIS

N95-20274# Maryland Univ., College Park, MD. Inst. for Physical Science and Technology.
THE METHOD OF AUXILIARY MAPPING FOR THE FINITE ELEMENT SOLUTIONS OF ELASTICITY PROBLEMS CONTAINING SINGULARITIES
Hae-Soo Oh and Ivo M. Babuska Sep. 1994 44 p
(Contract N00014-90-J-1030; NSF DMS-91-20877; NSF ASC-91-13895)
(AD-A285689; TN-BN-1178) Avail: CASI HC A03/MF A01

Babuska and Oh have introduced a new approach called the Method of Auxiliary Mapping (MAM), to deal with elliptic boundary value problems with singularities. In this paper this method is extended so that it can handle the plane elasticity problems containing singularities. In order to show the effectiveness, this method is compared with the conventional approach in the framework of the p-version of the finite element method. Moreover, it is demonstrated that this method yields a reasonable solution for those elasticity problems containing strong singularities which even can not be solved by using the h-p version of the finite element method. DTIC

N95-20423 Center for Mathematics and Computer Science, Amsterdam (Netherlands). Dept. of Numerical Mathematics.
EXPLICIT PARALLEL TWO-STEP RUNGE-KUTTA-NYSTROEM METHODS
Cong NguyenHuu Jan. 1994 18 p
(PB95-135752; CWI-NM-R9401) Copyright Avail: Issuing Activity (National Technical Information Service (NTIS))

The aim of this paper is to design a class of two-step Runge-Kutta-Nystrom methods of arbitrarily high order for the special second-order equation y(sup 2)(t) = f(y(t)) for use on parallel computers. Starting with an s-stage implicit two-step Runge-Kutta-Nystrom method of order p with k = p/2 implicit stages, we apply the highly parallel predictor-corrector iteration process in P(EC)(sup m)E mode. In this way, we obtain an explicit two-step Runge-Kutta-Nystrom method that has order p for all m and that requires k(m+1) righthand side evaluations per step of which each k evaluation can be computed in parallel. By a number of numerical experiments, we show the superiority of the parallel predictor-corrector methods proposed in this paper over both sequential and parallel methods available in the literature. NTIS

N95-20424 Center for Mathematics and Computer Science, Amsterdam (Netherlands). Dept. of Numerical Mathematics.

PARALLELISM ACROSS THE STEPS IN ITERATED RUNGE-KUTTA METHODS FOR STIFF INITIAL VALUE PROBLEMS

P. J. vanderHouwen, B. P. Sommeijer, and W. A. vanderVeen Nov. 1993 18 p

(PB95-135760; CWI-NM-R9322) Copyright Avail: Issuing Activity (National Technical Information Service (NTIS))

For the parallel integration of stiff initial value problems (IVP's), three main approaches can be distinguished: approaches based on 'parallelism across the problem', 'parallelism across the method' and on 'parallelism across the steps'. The first type of parallelism does not require special integration methods and can be exploited within any available IVP solver. The method-parallel approach received some attention in the case of Runge-Kutta based methods. For these methods, the required number of processors is roughly half the order of the generating Runge-Kutta method and the speed-up with respect to a good sequential IVP solver is about a factor 2. The third type of parallelism (step-parallelism) can be achieved in any IVP solver based on predictor-corrector iteration. Most step-parallel methods proposed so far employ a large number of processors, but lack the property of robustness, due to a poor convergence behavior in the iteration process. Hence, the effective speed-up is rather poor. The step-parallel iteration process proposed in the present paper is less massively parallel, but turns out to be sufficiently robust to achieve speed-up factors up to 10 with respect to the best sequential codes. NTIS

N95-20432 Colorado Univ., Denver, CO. Health Sciences Center.

FITTING STOCHASTIC PARTIAL DIFFERENTIAL EQUATIONS TO SPATIAL DATA Final Report, 1 Oct. 1989 - 30 Sep. 1993

Richard H. Jones 30 Sep. 1993 2 p Sponsored by ONR Limited Reproducibility: More than 20% of this document may be affected by microfiche quality

(AD-A279870) Avail: Issuing Activity (Defense Technical Information Center (DTIC))

The research under this project was aimed at developing numerical methods for fitting stochastic partial differential equations to irregularly spaced spatial data. This is related to two dimensional smoothing spline fitting where the partial differential equation is the Laplacian driven by white noise. A class of continuous two dimensional spatial autoregressive, moving average (ARMA) models were investigated and numerical methods developed to implement fitting these models to spatial data. The spatial ARMA models provide a complete class of covariance structures rather than a very limited set of covariance functions that are typically used in Kriging. Since maximum likelihood methods are used to fit the models, methods such as likelihood ratio tests and Akaike's Information Criterion (AIC) can be used for model selection. Prediction maps can then be calculated at a grid of points, and contour maps drawn. Also maps can be drawn of the standard deviation of the predicted fields giving indications of the variability of the predictions. Applications include aquifer heights, coal field depth and thickness and snowfall amounts. Results have been presented in a number of presentations and publications. DTIC

N95-20452 Institut des Hautes Etudes Scientifiques, Bures-sur-Yvette (France).

GROWTH SERIES FOR THE COMMUTATOR SUBGROUP

Mark Pollicott (Warwick Univ., Coventry, England.) and Richard Sharp (Warwick Univ., Coventry, England.) May 1994 8 p Sponsored in cooperation with the Royal Society and the UK SERC Limited Reproducibility: More than 20% of this document may be affected by microfiche quality

(PB95-111092; IHES/M/94/33) Avail: CASI HC A02

The authors study growth series associated to commutator subgroups of surface groups. They conclude that these growth series are not rational. NTIS

N95-20565 Maryland Univ., College Park, MD. Inst. for Physical Science and Technology.

ETA%-SUPERCONVERGENCE OF FINITE ELEMENT APPROXIMATIONS IN THE INTERIOR OF GENERAL MESHES OF TRIANGLES Final Report

I. Babuska, T. Strouboulis (Texas A&M Univ., College Station, TX.), and C. S. Upadhyay (Texas A&M Univ., College Station, TX.) Dec. 1993 193 p Sponsored by ARO and Texas Advanced Research Program Limited Reproducibility: More than 20% of this document may be affected by microfiche quality

(Contract N00014-90-J-1040; NSF CCR-88-20279; NSF MSS-90-25110)

(AD-A279903; BN-1160) Avail: Issuing Activity (Defense Technical Information Center (DTIC))

In this paper we introduce a new definition of superconvergence - the eta%-superconvergence, which generalizes the classical idea of superconvergence to general meshes. We show that this new definition can be employed to determine the regions of least error in any element in the interior of any grid by using a computer-based approach. We present numerical results for the standard displacement finite element method for the scalar equation of orthotropic heat-conduction. The results demonstrate that eta% superconvergence is applicable to the complexgrids which are employed in practical engineering computations. DTIC

N95-20588 Maryland Univ., College Park, MD. Inst. for Physical Science and Technology.

STUDY OF SUPERCONVERGENCE BY A COMPUTER-BASED APPROACH: SUPERCONVERGENCE OF THE GRADIENT OF THE DISPLACEMENT, THE STRAIN AND STRESS IN FINITE ELEMENT SOLUTIONS FOR PLANE ELASTICITY Final Report

I. Babuska, T. Strouboulis (Texas A&M Univ., College Station, TX.), C. S. Upadhyay (Texas A&M Univ., College Station, TX.), and S. K. Gangaraj (Texas A&M Univ., College Station, TX.) Feb. 1994 91 p Sponsored by ARO and Texas Advanced Research Program Limited Reproducibility: More than 20% of this document may be affected by microfiche quality

(Contract N00014-90-J-1030; NSF MSS-90-25110; NSF CCR-88-20279)

(AD-A279885; BN-1166; CMC-94-02) Avail: Issuing Activity (Defense Technical Information Center (DTIC))

we addressed (in part one) the problem of existence of superconvergence points by a computer-based proof and we gave a detailed study of the superconvergence points for the components of the gradient in finite element solutions for Laplace's and Poisson's equations. Here we employ the same approach to study the superconvergence for the gradient of the displacement, the strain and the stress for finite element solutions of the equations of plane elasticity. We give the superconvergence points for the components of the gradient of the displacement, the strain and stress for meshes of triangles and squares of degree p, with 1 less than or equal to p less than or equal to 4. For the meshes of triangles we investigated the effect of the topology of the mesh by considering four mesh-patterns which typically occur in practical meshes, while in the case of square elements we studied the effect of the element-type (tensor-product, serendipity or other). DTIC

N95-20662 Carnegie-Mellon Univ., Pittsburgh, PA. Management Sciences Research Group.

BALANCED MATRICES

Michele Conforti (Padua Univ., Italy.), Gerard Corneujols, Ajai Kapoor, M. R. Rao (Indian Inst. of Management, Bangalore, India.), and Kristina Vuskovic Apr. 1994 45 p Limited Reproducibility: More than 20% of this document may be affected by microfiche quality

(Contract N00014-89-J-1063; NSF DDM-92-01340; NSF DDM-90-01705)

(AD-A280021; MSRR-605) Avail: CASI HC A03

A 0, +/- 1 matrix A is balanced if, in every submatrix with two nonzero entries per row and column, the sum of the entries is a multiple of four. This definition was introduced by Truemper and generalizes the notion of balanced 0,1 matrix introduced by Berge. In this paper, we survey what is currently known about these matrices, including polyhedral results, structural theorems, recognition algorithms and the relation with some problems in logic. DTIC

N95-20701# Oak Ridge National Lab., TN.
THE DESIGN OF A PARALLEL, DENSE LINEAR ALGEBRA SOFTWARE LIBRARY: REDUCTION TO HESSENBERG, TRIDIAGONAL, AND BIDIAGONAL FORM
J. Choi (Tennessee Univ., Knoxville, TN.) and J. J. Dongarra (Tennessee Univ., Knoxville, TN.) 1994 15 p Presented at the Workshop on Environments and Tools for Parallel Scientific Computing, Walland, TN, 26-27 May 1994
(Contract DE-AC05-84OR-21400)
(DE94-018123; CONF-9405221-1) Avail: CASI HC A03/MF A01

This paper discusses issues in the design of ScaLAPACK, a software library for performing dense linear algebra computations on distributed memory concurrent computers. These issues are illustrated using the ScaLAPACK routines for reducing matrices to Hessenberg, tridiagonal, and bidiagonal forms. These routines are important in the solution of eigenproblems. The paper focuses on how building blocks are used to create higher-level library routines. Results are presented that demonstrate the scalability of the reduction routines. The most commonly-used building blocks used in ScaLAPACK are the sequential BLAS, the Parallel Block BLAS (PB-BLAS) and the Basic Linear Algebra Communication Subprograms (BLACS). Each of the matrix reduction algorithms consists of a series of steps in each of which one block column (or panel), and/or block row, of the matrix is reduced, followed by an update of the portion of the matrix that has not been factorized so far. This latter phase is performed using distributed Level 3 BLAS routines, and contains the bulk of the computation. However, the panel reduction phase involves a significant amount of communication. And is important in determining the scalability of the algorithm. The simplest way to parallelize the panel reduction phase is to replace the appropriate Level 2 and Level 3 BLAS routines appearing in the LAPACK routine (mostly matrix-vector and matrix-matrix multiplications) with PB-BLAS routines. DOE

N95-20719# Stanford Univ., CA.
COMPUTING METHODS FOR THE APPROXIMATE SOLUTION OF TIME DEPENDENT PROBLEMS Final Report, Jul. 1989 - Sep. 1993
Joseph Oliger Nov. 1994 6 p
(Contract N00014-89-J-1815)
(AD-A286007) Avail: CASI HC A02/MF A01

The research dealt with computing methods for applications in aerodynamics, geophysics, hydrodynamics, meteorology, and oceanography. Analysis was done of adaptive numerical methods for time-dependent problems in complicated physical domains which can efficiently and reliably approximate singular and near singular features of the solution such as fronts and shocks. Work focused on development of algorithms which could be executed on parallel architectures and upon data structures and language constructs which allow this to be done efficiently and effectively. Author (DTIC)

N95-20734# International Centre for Theoretical Physics, Trieste (Italy).
ON THE DIFFERENTIAL REPRESENTATIONS OF QUANTUM LIE SUPERALGEBRAS
Li Liao and Xing-Chang Song Jan. 1994 6 p
(DE94-629874; IC-94/7) Avail: CASI HC A02/MF A01 (US Sales Only)

In this letter, we study the differential representations of quantum Lie superalgebras. A concrete example of U(sub q)gl(1 verticle bar 1) is given. DOE

N95-20830# Groningen Rijksuniv. (Netherlands). Dept. of Mathematics.
RICCATI EQUATION THEORY FOR PRITCHARD-SALAMON SYSTEMS: A POPOV FUNCTION APPROACH
M. Weiss 1994 67 p
(PB95-137089; W-9404) Avail: CASI HC A04/MF A01

In a 1993 paper by the author (PB94-125341), a general approach to Riccati equation theory was developed for infinite-dimensional systems with bounded input and output operators, extending the finite-dimensional theory in a 1993 paper by Ionescu and Weiss. This paper is a continuation of the first mentioned paper. The results in the cited paper are extended to a larger class of Riccati equations associated to systems with unbounded input and output operators in the so-called Pritchard-Salamon class and, in addition, some new applications of the Popov function approach are presented which are interesting even for the finite dimensional case. NTIS

N95-20875 Rensselaer Polytechnic Inst., Troy, NY.
DECONVOLUTION AND SINGULAR VALUE DECOMPOSITION Final Technical Report, 1 Mar. 1993 - 30 Nov. 1994
Franklin T. Luk 17 Nov. 1994 2 p Limited Reproducibility: More than 20% of this document may be affected by microfiche quality
(Contract N00014-93-1-0396)
(AD-A286582) Avail: CASI HC A01

We explore numerical methods for solving multi-dimensional deconvolution and inverse scattering problems, and are particularly interested in techniques based on the singular value decomposition (SVD) to find low rank matrix approximations. Our emphasis will be on both speed and accuracy. We will develop new techniques for numerical multilinear algebra, in particular for computing the SVD of a compound matrix. We will investigate implementation on parallel hardware, and the actual prototyping of such designs. We will also study fault tolerance issues associated with such special-purpose VLSI processors, and develop methods to detect possible ill-conditioning of the underlying deconvolution problem. DTIC

N95-20920 Maryland Univ., College Park, MD. Inst. for Physical Science and Technology.
A CONVERGENCE ANALYSIS OF AN h-VERSION FINITE ELEMENT METHOD WITH HIGH ORDER ELEMENTS FOR TWO DIMENSIONAL ELASTO-PLASTICITY PROBLEMS Final Report
Y. Li and I. Babuska Jan. 1994 44 p Limited Reproducibility: More than 20% of this document may be affected by microfiche quality
(Contract N00014-90-1-1030; NSF DMS-91-20877)
(AD-A279975; BN-1162) Avail: CASI HC A03

In this paper, we will give an h-version finite element method for a two dimensional nonlinear elasto-plasticity problem. A family of admissible constitutive laws based on the so-called gauge function method is introduced first, and then a high order h-version semi-discretization scheme is presented. The existence and uniqueness of the solution for the semi-discrete problem are guaranteed by using some special properties of the constitutive law, and finally we will show that as the maximum element size h - 0, the solution of the semi-discrete problem will converge to the solution of the continuous problem. The high order h-version discretization scheme introduced here is unusual. If the partition of the spatial space only has rectangles or parallelograms involved, then there would not be any limit on the element degree. However, if the partition of the spatial space has some triangular elements, then only certain combinations of finite element spaces for displacement and stress functions can be used. The discretization scheme also provides useful idea for applications of hp-version or high order h-version finite element methods for two dimensional problems where the elasto-plastic body is not a polygon, such as a disk or an annulus. DTIC

N95-21005 Technische Univ., Delft (Netherlands).
SET FUNCTIONALS IN STOCHASTIC GEOMETRY Ph.D. Thesis
A. J. Cabo 28 Jun. 1994 144 p
(PB95-135372) Copyright Avail: Issuing Activity (National Technical Information Service (NTIS))

The thesis begins with a brief description of stochastic geometry. It then surveys the results known in the literature and the open questions concerning convex hulls, characterization problems, and stereological estimation. Finally, the last section summarizes the new results obtained. NTIS

N95-21023# Technische Univ., Eindhoven (Netherlands). Dept. of Mathematics and Computing Science.
FINDING ALL MINIMAL SEPARATORS OF A GRAPH
T. Kloks and D. Kratsch (Friedrich-Schiller Univ., Jena, Germany.) Aug. 1993 24 p
(ISSN 0926-4515)
(PB95-127585) Avail: CASI HC A03/MF A01

In this paper we give an efficient algorithm to find all minimal vertex separators of an undirected graph. The algorithm needs polynomial time per separator that is found. NTIS

N95-21024# Technische Univ., Eindhoven (Netherlands). Dept. of Mathematics and Computing Science.
MULTI-DIMENSIONAL PETRI NETS

W. M. P. vanderAalst Aug. 1993 38 p See also PB93-191732
(ISSN 0926-4515)
(PB95-127593) Avail: CASI HC A03/MF A01

Petri nets have become a mature modeling and analysis tool applicable in many application domains. Many extensions of the classical Petri net have been proposed. The multi-dimensional Petri net model presented in this paper deals with these extensions in a unifying way. In this model an arbitrary number of dimensions may be identified, e.g. a 'spatial dimension', a 'time dimension', a 'color dimension', etc. This paper also discusses the relations between the multi-dimensional Petri net model and other Petri net based models. Multi-dimensional Petri nets can be analyzed using traditional techniques. Moreover, it is possible to project a multi-dimensional Petri net onto a limited number of dimensions. By analyzing the projected multi-dimensional Petri net we can deduce properties of the original multi-dimensional Petri net. Therefore, multi-dimensional Petri nets are also interesting from an analysis point of view. NTIS

N95-21032 Technische Univ., Twente (Netherlands). Dept. of Computer Science.
MONADIC MAPS AND FOLDS FOR ARBITRARY DATATYPES
Maarten Fokkinga 1 Jun. 1994 30 p Limited Reproducibility: More than 20% of this document may be affected by microfiche quality
(ISSN 0924-3755)
(PB95-134045; Memo-INF-94-28) Copyright Avail: CASI HC A03

Each datatype constructor comes equipped not only with a so-called map and fold (catamorphism), as is widely known, but, under some condition, also with a kind of map and fold that are related to an arbitrary given monad. This result follows from the preservation of initiality under lifting from the category of algebras in a given category to a certain other category of algebras in the Kleisli category related to the monad. NTIS

N95-21266# Brookhaven National Lab., Upton, NY.
THE PROSAIC LAPLACE AND FOURIER TRANSFORM
G. A. Smith 1994 21 p Presented at the Beam Instrumentation Workshop, Vancouver, British Columbia, 2-6 Oct. 1994
(Contract DE-AC02-76CH-00016)
(DE95-002225; BNL-60655; CONF-9410219-3) Avail: CASI HC A03/MF A01

Integral Transform methods play an extremely important role in many branches of science and engineering. The ease with which many problems may be solved using these techniques is well known. In Electrical Engineering especially, Laplace and Fourier Transforms have been used for a long time as a way to change the solution of differential equations into trivial algebraic manipulations or to provide alternate representations of signals and data. These techniques, while seemingly overshadowed by today's emphasis on digital analysis, still form an invaluable basis in the understanding of systems and circuits. A firm grasp of the practical aspects of these subjects provides valuable conceptual tools. This tutorial paper is a review of Laplace and Fourier Transforms from an applied perspective with an emphasis on engineering applications. The interrelationship of the time and frequency domains will be stressed, in an attempt to comfort those who, after living so much of their lives in the time domain, find thinking in the frequency domain disquieting. DOE

N95-21285# Oak Ridge National Lab., TN. Engineering Physics and Mathematics Div.
ERROR ANALYSIS OF THE QUADRATIC NODAL EXPANSION METHOD IN SLAB GEOMETRY
R. C. Penland (North Carolina State Univ., Raleigh, NC.), P. J. Turinsky, and Y. Y. Azmy (North Carolina State Univ., Raleigh, NC.) 1994 7 p Presented at the Winter Meeting of the American Nuclear Society, Washington, DC, 13-18 Nov. 1994
(Contract DE-AC05-84OR-21400)
(DE95-001352; CONF-941102-29) Avail: CASI HC A02/MF A01

As part of an effort to develop an adaptive mesh refinement strategy for use in state-of-the-art nodal diffusion codes, the authors derive error bounds on the solution variables of the quadratic Nodal Expansion Method (NEM) in slab geometry. Closure of the system is obtained through flux discontinuity relationships and boundary conditions. In order to verify the analysis presented, the authors compare the quadratic NEM to the analytic solution of a test problem. The test problem for this investigation is a one-dimensional slab (0,20cm) with L(exp 2) = 6.495sq cm and D = 0.1429cm. The slab has a unit neutron source distributed uniformly throughout and zero flux boundary conditions. The analytic solution to this problem is used to compute the node-average fluxes over a variety of meshes, and these are used to compute the NEM maximum error on each mesh. DOE

N95-21318# Groningen Rijksuniv. (Netherlands). Dept. of Mathematics and Computer Science.
COMPUTATION OF INVARIANT MANIFOLDS
A. J. Homburg, H. M. Osinga, and G. Vegter 1994 22 p See also PB94-111663 Sponsored by Nederlandse Organisatie voor Wetenschappelijk Onderzoek
(Grants NWO-611-307-018; NWO-611-306-523)
(PB95-135687; W-9406) Avail: CASI HC A03/MF A01

We present a method for the numerical computation of invariant manifolds of hyperbolic and pseudohyperbolic fixed points of diffeomorphisms. The derivation of this algorithm is based on well-known properties of (almost) invariant foliations. Numerical results illustrate the performance of our method. NTIS

N95-21371 Technische Univ., Eindhoven (Netherlands). Dept. of Mathematics and Computing Science.
NUMERICAL WAVE SPEED FOR ONE-DIMENSIONAL SCALAR HYPERBOLIC CONSERVATION LAWS WITH SOURCE TERMS
A. C. Berkenbosch, E. F. Kaasschieter, and J. H. M. tenThijeBoonkamp Apr. 1994 34 p See also PB93-194801
(PB95-127536; RANA-94-01) Avail: Issuing Activity (National Technical Information Service (NTIS))

In this paper we consider initial value problems for scalar hyperbolic conservation laws in one space dimension, with source terms. The source terms admit at least two equilibrium states as solutions of the underlying characteristic equation, one unstable and one stable. An essential numerical difficulty for this initial value problem is that numerical reaction waves are propagating at non-physical wave speeds. In this paper we consider two types of model problems, namely the ignition model and the Arrhenius' model. Applications include reactive gas dynamics, where chemical reactions between the constituent gases need to be modeled along with the fluid dynamics. The numerical solution is computed with a first order splitting method. For this method a detailed analysis of the numerical wave speed is given. Expressions are derived for the numerical wave speed, which explain the occurrence of non-physical wave speeds. Furthermore, convergence of the numerical speed to the exact speed is shown. NTIS

N95-21372 Technische Univ., Eindhoven (Netherlands).
SEMANTICS FOR A FINE LAMBDA-CALCULUS WITH DE BRUIJN INDICES
F. Kamareddine and R. Nederpelt 7 Sep. 1993 60 p Prepared in cooperation with Glasgow Univ.
(PB95-127577) Avail: Issuing Activity (National Technical Information Service (NTIS))

The authors' first task in the paper is to get rid of problematic variable names and to establish what they believe is the most precise and fine lambda-calculus, Omega(sub 11). In such a calculus, de Bruijn's indices are used instead of variable names and substitution and reduction are defined in a step-wise fashion which can be directly implemented without having to carry out a lot of book-keeping as is usually the case in the classical lambda-calculus. Most importantly, the substitution in Omega(sub 11) is no longer the implicit substitution but rather it is the explicit one which is long needed in many applications of the lambda-calculus. Such an explicit substitution has been facilitated as a result of the fine structure of lambda-terms that the authors propose in the paper and where item notation plays a dominant role. Furthermore, the species of variable names is cultivated and ordered so that a fine inter-marriage between de Bruijn's indices and variable names takes place. Such a relationship between de Bruijn's indices and variable names will be used to show the consistency of the authors' fine reduction and explicit substitution in terms of the classical lambda-calculus. The authors shall also reflect on the use and necessity of alpha-conversion. NTIS

N95-21421 Leiden Univ. (Netherlands). Div. of Applied Mathematics.
ERROR COMMITTED BY STOPPING THE NEWTON ITERATION IN RUNGE-KUTTA METHODS AND LINEAR MULTISTEP METHODS

J. Groeneweg Nov. 1993 66 p
(PB95-106324; TW-93-13) Avail: Issuing Activity (National Technical Information Service (NTIS))

This paper concerns the numerical solution of stiff initial value problems, for nonlinear ordinary differential equations, by Runge-Kutta methods and linear multistep methods that are implicit. For stiff problems it is common practice to use Newton iteration, or a variant thereof, for solving the system of (algebraic) equations occurring in each time step of such step-by-step methods. In the recent literature the error committed by stopping the Newton-type iteration has been studied mainly theoretically. In the present paper we confirm the theoretical upperbounds for this error, to be found in the literature, by numerical experiments. In some of our experiments even smaller errors appear to be present than is to be expected according to the theory. NTIS

N95-21423 Technische Hogeschool, Eindhoven (Netherlands). Dept. of Mathematics and Computing Science.
POSITIVE ROCKLAND OPERATORS
P. Auscher, A. F. M. terElst, and D. W. Robinson Aug. 1993 24 p Prepared in cooperation with Australian National Univ., Canberra, Australia
(PB95-127510; RANA-93-12) Avail: Issuing Activity (National Technical Information Service (NTIS))

Let G be a homogeneous Lie group with a left Haar measure dg and L the action of G as left translations on L(sub p)(G;dg). Further let H = dL(C) denote a homogeneous operator associated with L. If H is positive and hypoelliptic on L(sub 2) the authors prove that it is closed on each of the L(sub p)-spaces, p included in (1, infinity), and that it generates a semigroup S with a smooth kernel K which, with its derivatives, satisfies Gaussian bounds. The semigroup is holomorphic in the open right half-plane on all the L(sub p)-spaces, p included in (1, infinity). Further extensions of these results to non-homogeneous operators and general representations are also given. NTIS

N95-21434 Center for Mathematics and Computer Science, Amsterdam (Netherlands). Dept. of Numerical Mathematics.
PARALLEL PREDICTOR-CORRECTOR METHODS
P. J. vanderHouwen, B. P. Sommeijer, and J. J. B. deSwart Mar. 1994 24 p See also N93-32396
(ISSN 0169-0388)
(PB95-135711; CWI-NM-R9408) Copyright Avail: Issuing Activity (National Technical Information Service (NTIS))

In this paper we construct predictor-corrector methods using block Runge-Kutta methods as correctors. Like conventional Runge-Kutta methods, these correctors compute stage values at nonuniformly distributed, intermediate points. The predictor-corrector nature of the methods make them suitable for implementation on parallel computers. Comparisons of an 8th-order, 5-processor predictor-corrector method using Radau 2 points with the celebrated 8(7) Runge-Kutta method of Prince and Dormand shows speed-up factors of about 2.7. NTIS

N95-21439# Ames Lab., IA.
DISTRIBUTION-INDEPENDENT HIERARCHICAL N-BODY METHODS Ph.D. Thesis
S. Aluru 27 Jul. 1994 89 p
(Contract W-7405-eng-82)
(DE95-001686; IS-T-1643) Avail: CASI HC A05/MF A01

The N-body problem is to simulate the motion of N particles under the influence of mutual force fields based on an inverse square law. The problem has applications in several domains including astrophysics, molecular dynamics, fluid dynamics, radiosity methods in computer graphics, and numerical complex analysis. Research efforts have focused on reducing the O(N(exp 2)) time per iteration required by the naive algorithm of computing each pairwise interaction. Widely respected among these are the Barnes-Hut and Greengard methods. Greengard claims his algorithm reduces the complexity to O(N) time per iteration. Throughout this thesis, we concentrate on rigorous, distribution-independent, worst-case analysis of the N-body methods. We show that Greengard's algorithm is not O(N), as claimed. Both Barnes-Hut and Greengard's methods depend on the same data structure, which we show is distribution-dependent. For the distribution that results in the smallest running time, we show that Greengard's algorithm is (Omega)(N log(exp 2) N) in two dimensions and (Omega)(N log(exp 4) N) in three dimensions. We have designed a hierarchical data structure whose size depends entirely upon the number of particles and is independent of the distribution of the particles. We show that both Greengard's and Barnes-Hut algorithms can be used in conjunction with this data structure to reduce their complexity. Apart from reducing the complexity of the Barnes-Hut algorithm, the data structure also permits more accurate error estimation. We present two- and three-dimensional algorithms for creating the data structure. The multipole method designed using this data structure has a complexity of O(N log N) in two dimensions and O(N log(exp 2) N) in three dimensions. DOE

N95-21468 Technische Univ., Eindhoven (Netherlands). Dept. of Mathematics and Computing Science.
APPROXIMATION ALGORITHMS FOR THE GENERAL AND THE ASYMMETRIC STACKER-CRANE PROBLEMS
G. Righini and M. Trubian Jun. 1994 55 p Prepared in cooperation with Politecnico di Milano, Italy
(PB95-132098; MEMO-COSOR-94-20) Avail: Issuing Activity (National Technical Information Service (NTIS))

The Stacker-Crane Problem (SCP) consists of finding the minimum length hamiltonian cycle on a mixed graph with oriented arcs and unoriented edges: feasible solutions must traverse all the arcs. Approximation algorithms are known for the case in which the triangle inequality holds. The authors consider the case in which the triangle inequality is violated (General SCP) and the case in which the problem is formulated on a complete digraph (Asymmetric SCP). They show how data-dependent worst-case bounds for the GSCP and the ASCP can be obtained by known approximation algorithms for the SCP with triangle inequality and by a new one. They also discuss the relationship with the Asymmetric Traveling Salesman Problem (ATSP), and they derive sufficient (and meaningful) conditions for ATSP instances to be solvable within constant worst-case bounds equal to 3, 15/7 and 9/5. NTIS

N95-21564# Lawrence Livermore National Lab., Livermore, CA.
PRECONDITIONING VIA ASYMPTOTICALLY-DEFINED DOMAIN DECOMPOSITION
S. F. Ashby, C. T. Kelley (North Carolina State Univ., Raleigh, NC.), J. S. Scroggs (North Carolina State Univ., Raleigh, NC.), and P. E. Saylor (Illinois Univ., Urbana, IL.) Jun. 1994 10 p Presented at the 7th International Conference on Domain Decomposition Methods in Science and Engineering, University Park, PA, 27-30 Oct. 1993
(Contract W-7405-eng-48)
(DE94-019046; UCRL-JC-118073; CONF-9310357-1) Avail: CASI HC A02/MF A01

Asymptotic analysis is used to derive preconditioners based on operator splitting and domain decomposition for the numerical solution of the advection-diffusion equation. Specifically, asymptotics is used to identify subdomains in which the solution is dominated by a certain operator, and this information is used to construct an effective preconditioner. The authors analyze the one-dimensional case in a function space setting and present numerical results for both one and two dimensions. DOE

N95-21574# Technische Univ., Eindhoven (Netherlands). Dept. of Mathematics and Computing Science.
ANALYSIS OF A LOCAL DEFECT CORRECTION APPROACH ON COMPOSITE GRIDS
P. J. J. Ferket Jun. 1994 30 p
(ISSN 0926-4507)
(PB95-135455; RANA-94-09) Avail: CASI HC A03/MF A01

In this paper we consider the problem of discretization on a composite grid that consist of a global uniform coarse grid and a local uniform fine grid. For elliptic problems a local defect correction approach is described. The error of the resulting approximation is analyzed. It follows that in general the accuracy of this approximation is (much) better than the accuracy of an approximation that results from an approach without local defect correction. The use of a buffer zone in the local defect correction approach appears to be essential for several problems. We discuss when such a buffer zone is necessary to obtain satisfactory results. NTIS

N95-21582# Graz Univ. (Austria). Inst. for Mathematics.
INTERNATIONAL CONFERENCE ON CONTROL AND ESTIMATION OF DISTRIBUTED PARAMETER SYSTEMS: NONLINEAR PHENOMENA

W. Desch, F. Kappel, and K. Kunisch 24 Jul. 1993 412 p Conference held in Vorau, Austria, 18-24 Jul. 1993
(AD-A286449) Avail: CASI HC A18/MF A04

This conference formed a platform for the exchange of new ideas and recent results in control, identification, and optimization of nonlinear infinite dimensional systems. It was designed to provide a melting pot for a broad variety of viewpoints, including theoretical aspects like the maximum principle, relaxation and stabilizability as well as numerical algorithms for optimization and applications to elastic structures, flow control, and population dynamics. Contents include: a semigroup formulation of a nonlinear size-structured distributed rate population model; damage detection and characterization in smart material structures; optimality conditions for nonqualified parabolic control problems; convergence of trajectories for a controlled viscous Burgers' equation; optimality conditions for boundary control problems of parabolic type; Pontryagin's principle for optimal control problems governed by semilinear elliptic equations; and invariance of the Hamiltonian in control problems for semilinear parabolic distributed parameter systems. CASI

N95-21622*# National Aeronautics and Space Administration. Langley Research Center, Hampton, VA.
GRID RESOLUTION AND SOLUTION CONVERGENCE FOR MARS PATHFINDER FOREBODY
Heather L. Nettelhorst and Robert A. Mitcheltree Dec. 1994 16 p
(RTOP 242-80-01-01)
(NASA-TM-109173; NAS 1.15:109173) Avail: CASI HC A03/MF A01

As part of the Discovery Program, NASA Plans to launch a series of probes to Mars. The Mars Pathfinder project is the first of this series with a scheduled Mars arrival in July 1997. The entry vehicle will perform a direct entry into the atmosphere and deliver a lander to the surface. Predicting the entry vehicle's flight performance and designing the forebody heatshield requires knowledge of the expected aerothermodynamic environment. Much of this knowledge can be obtained through computational fluid dynamic (CFD) analysis. Author

N95-21648 Rutherford Appleton Lab., Chilton (England). Central Computing Dept.
[REPORT OF THE NUMERICAL ANALYSIS GROUP] Progress Report, Jan. 1991 - Dec. 1993
I. S. Duff Jun. 1994 75 p
(PB95-108163; RAL-94-062) Avail: Issuing Activity (National Technical Information Service (NTIS))

This report covers the period from January 1991 to December 1993 and describes work performed by the Numerical Analysis Group within the Central Computing Department at the Atlas Center in the Rutherford Appleton Laboratory. The main research areas and interests lie in sparse matrix research, nonlinear algebra and optimization, applied mathematics, and numerical linear algebra. Work pertaining to these areas is discussed in Sections 2 to 5, respectively. We group some miscellaneous topics in Section 6. Much of our research and development results in high quality advanced mathematical software for the Harwell Subroutine Library. The organization, maintenance, documentation, and distribution of this Library is reported in Section 7. Lists of seminars, technical reports, and publications are given in Sections 8, 9, and 10, respectively. NTIS

N95-21867 Technische Univ., Twente (Netherlands). Faculteit der Informatica.
DYADS: A GENERALISATION OF MONADS
Maarten Fokkinga Jun. 1994 16 p
(ISSN 0924-3755)
(PB95-134052; Memo-INF-94-30) Copyright Avail: Issuing Activity (National Technical Information Service (NTIS))

The concept of dyad is defined as the least common generalization of monads and co-monads. So, taking some of the ingredients to be the identity, the concept specializes to the concept of monad, and taking other ingredients to be the identity it specializes to co-monads. Except for one axiom, all have a nice ('natural') form. NTIS

N95-21868 Technische Univ., Twente (Netherlands). Faculteit der Informatica.
ADJUNCTIONS
Maarten Fokkinga and Lambert Meertens (Center for Mathematics and Computer Science, Amsterdam, Netherlands.) Jun. 1994 40 p
(ISSN 0924-3755)
(PB95-134078; Memo-INF-94-31) Copyright Avail: Issuing Activity (National Technical Information Service (NTIS))

We present the category-theoretic notion of adjunction in a way that makes it easy to formally calculate with it; an acquaintance with its algebraic properties may greatly help in understanding the notion. It is illustrated by means of a lot of theorems and proofs. We also attempt to provide some intuitive understanding of adjunctions by various discussions. Our intended readership is familiar with the notion of category, functor, and naturality, and either about to learn about adjunctions or interested in a calculational approach to category theory. NTIS

N95-21955# Vrije Univ., Amsterdam (Netherlands). Faculteit der Wiskunde en Informatica.
GRADED DUAL OF THE NON-COMMUTATIVE UNIVERSAL LEIBNIZ HOPF ALGEBRA ZETA
A. C. J. Scholtens Mar. 1994 69 p
(PB95-134532) Avail: CASI HC A04/MF A01

In the paper the authors consider the dual Z and the graded dual M of the universal Leibniz Hopf algebra Z = Z (less than) Z(sub 1), Z(sub 2),...(greater than) (i.e., the free associative (but non-commutative) algebra over Z on the set (Z(sub 1), Z(sub 2),...). The authors shall show that M = Z(EUW) as algebras, where Z(EUW) is the free polynomial ring over Z generated by the set EUW. P.B. Shay showed in his preprint that, without giving generic variables, Z is a formal power series ring over Z. Hence, it easily follows that M is a polynomial ring. The difficult part of proving the authors' statement is that they have to determine the set of (algebraically independent) generic variables, i.e. the set EUW. However, the corollaries to their main result are worth the effort. For instance, it immediately follows that Z is a non-commutative formal group law over Z. Another corollary is that they can give a Z-module basis for the primitive elements of Z. NTIS

N95-21956# Vrije Univ., Amsterdam (Netherlands). Faculteit der Wiskunde en Informatica.
LINEAR INVARIANCE OF LINDELOEF NUMBERS
Jan Baars and Helma Gladdines Mar. 1994 14 p
(PB95-134540) Avail: CASI HC A03/MF A01

Let X and Y be Tychonov spaces and suppose there exists a continuous linear bijection from C(sub P)(X) to C(sub p)(Y). In this paper the authors develop a method that enables them to compare the Lindelof number of Y with the Lindelof number of some dense subset Z of X. As a corollary the authors get that if for perfect spaces X and Y, C(sub p)(X) and C(sub p)(Y) are linearly homeomorphic, then the Lindelof numbers of X and Y are equal. Another result in the paper is the following. Let X and Y be any two zero dimensional metric spaces or any two linearly ordered perfect Tychonov spaces such that C(sub p)(X) and C(sub p)(Y) are linearly homeomorphic. Let P be a topological property that is closed hereditary, closed under taking countable unions and closed under taking continuous images. Then X has property P is and only if Y has. As examples of such properties the authors consider certain cardinal functions. NTIS

N95-21962# Vrije Univ., Amsterdam (Netherlands). Faculteit der Wiskunde en Informatica.
DUALITY BEYOND SOBER SPACES: TOPOLOGICAL SPACES AND OBSERVATION FRAMES
Marcello Bonsangue, Bart Jacobs (Utrecht State Univ., Netherlands.), and Joost N. Kok (Utrecht State Univ., Netherlands.) Jan. 1994 46 p
(PB95-134565) Avail: CASI HC A03/MF A01

The authors introduce observation frames as an extension of ordinary frames. The aim is to give an abstract representation of a mapping from observable predicates to all predicates of a specific system. A full subcategory of the category of observation frames is shown to be dual to the category of Tau(sub 0) topological spaces. This result extends the Stone duality between the full subcategory of spatial frames and sober spaces. Appropriate notions of filters, prime elements, and morphisms are introduced in order to construct points of observation frames. These notions generalize the standard ones. The authors also give a propositional logic of observation frames with both infinite conjunctions and disjunctions, just like there is a geometric logic for (ordinary) frames with infinite disjunctions but only finite conjunctions. This theory is then applied to two situations: firstly to upper power spaces, and secondly the authors restrict the adjunction between the categories of topological spaces and of observation frames in order to obtain dualities for various subcategories of Tau(sub 0) spaces. These involve non sober spaces. NTIS

N95-22026# Army Armament Research, Development and Engineering Center, Watervliet, NY.

EXPONENTS IN LIFETIME AND POWER SPECTRAL DENSITY FORMS IN SELF-ORGANIZED CRITICAL SYSTEMS Final Report

L. V. Meisel and P. J. Cote Aug. 1994 18 p
(AD-A286242; ARCCB-TR-94029) Avail: CASI HC A03/MF A01

Bak, Tang, and Weisenfeld (BTW) established that power-law frequency dependencies in the power spectral density (PSD) and size-effect modified power-law distributions of lifetimes are the fingerprints of self-organized critical systems. Jensen, Christensen, and Fogedby (JCF) clarified the ideas introduced by BTW and established the connection between the distribution of lifetimes and the PSD for the case of exponentially cutoff (size-effect modified) distributions of lifetimes. Here the (JCF) connection between the PSD and the distribution of lifetimes is established for sharp cutoff distributions, which supports the idea that the JCF connection holds for quite general size-effect modified lifetime distributions. The PSD may be expressed in terms of generalized hypergeometric functions in this case. A detailed discussion of the JCF connections is presented for a subset of values of the lifetime distribution exponent for which the generalized hypergeometric functions reduce to Fresnel integrals and sine and cosine integrals, which were the subject of a recent Numerical Recipes column. All calculations were performed in Mathematica. DTIC

N95-22032 Vrije Univ., Amsterdam (Netherlands). Faculteit der Wiskunde en Informatica.

MINIMAL SQUARE SPECTRAL FACTORS

A. C. M. Ran Jan. 1994 18 p
(PB95-132726) Avail: Issuing Activity (National Technical Information Service (NTIS))

Recently there has been renewed interest in the problem of spectral factorization and in particular, the problem of parametrizing all square minimal spectra factors of a given spectrum. For instance, let us mention two recent papers, one of which dealing with more computational aspects of the problem, the other giving a parametrization under additional constraints. The paper is motivated in a large part by the second paper, in fact the authors shall show that a parametrization similar to the one given there can be achieved without one of the additional constraints imposed in the second paper. A secondary aim of this paper is to give an overview of several parametrizations available in the literature. NTIS

N95-22147 Institut des Hautes Etudes Scientifiques, Bures-sur-Yvette (France).

ALMOST KAPPA-WISE INDEPENDENT RANDOM PERMUTATION OF THE CUBE

W. T. Gowers Jul. 1994 15 p Limited Reproducibility: More than 20% of this document may be affected by microfiche quality
(PB95-108098; IHES/M/94/43) Avail: CASI HC A03

In the paper the authors give a very simple construction which converts a random 01-string sigma of length polynomial in given integers n and k less than 2(sup n) into a permutation pi of the cube (0,1)(sup n), which looks random in the sense that, for any sequence x(1),..., x(k) of distinct points in (9,1)(sup n), the images phi(x(1)),..., phi(x(k)) are approximately uniformly distributed among the set of all k-tuples of distinct points in (0,1)(sup n). (The result is interesting mainly when k is small compared with 2(sup n).) It is likely that the permutation is pseudo-random in the technical sense in which case it is known to have applications. For example, it would then be the basis of an extremely secure private-key cryptosystem. The proof that the permutation is almost k-wise independent uses techniques due to Jerrum and Sinclar and Diaconis and Stroock concerning rapidly mixing Markov chains. NTIS

N95-22151# Technische Univ., Eindhoven (Netherlands). Dept. of Mathematics and Computing Science.

HAMILTONIAN STRUCTURE OF THE REVERSIBLE NONSEMISIMPLE 1:1 RESONANCE

J. C. vanderMeer, J. A. Sanders (Vrije Univ., Amsterdam, Netherlands.), and A. Vanderbauwhede (Ghent Univ., Belgium.) Apr. 1994 24 p
(ISSN 0926-4507)
(PB95-127528; RANA-94-02) Avail: CASI HC A03/MF A01

We show that a reversible non-Hamiltonian vector field at nonsemisimple 1:1 resonance can be split into a Hamiltonian and a non-Hamiltonian part in such a way that after reduction to the orbit space for the S(sup 1)-action coming from the semisimple part of the linearized vector field, the non-Hamiltonian part vanishes. As a consequence, the reduced reversible vector field is Hamiltonian. We furthermore show that for vector fields in normal form on the orbit space, being Hamiltonian is equivalent to being reversible. NTIS

N95-22157* Institute for Computer Applications in Science and Engineering, Hampton, VA.

ON THE WAVELET OPTIMIZED FINITE DIFFERENCE METHOD Final Report

Leland Jameson Mar. 1994 48 p Submitted for publication Limited Reproducibility: More than 20% of this document may be affected by microfiche quality
(Contracts NAS1-19480; RTOP 505-90-52-01; N00014-91-J-4016; AF-AFOSR-0090-93; NSF DMS-92-11820)
(NASA-CR-191601; ICASE-94-9; NAS 1.26:191601; AD-A279810) Avail: CASI HC A03

When one considers the effect in the physical space, Daubechies-based wavelet methods are equivalent to finite difference methods with grid refinement in regions of the domain where small scale structure exists. Adding a wavelet basis function at a given scale and location where one has a correspondingly large wavelet coefficient is, essentially, equivalent to adding a grid point, or two, at the same location and at a grid density which corresponds to the wavelet scale. This paper introduces a wavelet optimized finite difference method which is equivalent to a wavelet method in its multiresolution approach but which does not suffer from difficulties with nonlinear terms and boundary conditions, since all calculations are done in the physical space. With this method one can obtain an arbitrarily good approximation to a conservative difference method for solving nonlinear conservation laws. DTIC

N95-22317 Rutherford Appleton Lab., Chilton (England).

ITERATED-SUBSPACE MINIMIZATION METHODS FOR NONLINEAR OPTIMIZATION

A. R. Conn, N. I. M. Gould, A. Sartenaer, and P. L. Toint Jun. 1994 31 p Prepared in cooperation with IBM Watson Research Center, Yorktown Heights, NY; Facultes Univ. Notre-Dame de la Paix, Namur, Belgium; and AFOSR, Bolling AFB, Washington, DC
(Contract F49620-91-C-0079)
(PB95-108171; RAL-94-069) Avail: Issuing Activity (National Technical Information Service (NTIS))

We consider a class of Iterated-Subspace Minimization (ISM) methods for solving large-scale unconstrained minimization problems. At each major iteration of such a method, a low-dimensional manifold, the iterated subspace, is constructed and an approximate minimizer of the objective function in this manifold then determined. The iterated subspace is chosen to contain vectors which ensure global convergence of the overall scheme and may also contain vectors which encourage fast asymptotic convergence. We demonstrate the efficiency of this approach on a collection of large problems and indicate a number of avenues of future research. NTIS

N95-22325*# Institute for Computer Applications in Science and Engineering, Hampton, VA.

ON THE DYNAMICS OF A SHOCK-BUBBLE INTERACTION Final Report

James J. Quirk and Smadar Karni (New York Univ., New York, NY.) Sep. 1994 38 p Submitted for publication Sponsored in part by a Packard Fellowship
(Contracts NAS1-19480; RTOP 505-90-52-01; N00014-92-J-1245; DE-FG02-88ER-25053; NSF DMS-92-03768)
(NASA-CR-194978; NAS 1.26:194978; ICASE-94-75) Avail: CASI HC A03/MF A01

We present a detailed numerical study of the interaction of a weak shock wave with an isolated cylindrical gas inhomogenity. Such interactions have been studied experimentally in an attempt to elucidate the mechanisms whereby shock waves propagating through random media enhance mixing. Our study concentrates on the early phases of the interaction process which are dominated by repeated refractions of acoustic fronts at the bubble interface. Specifically, we have reproduced two of the experiments performed by Haas and Sturtevant : M(sub s) = 1.22 planar shock wave, moving through air, impinges on a cylindrical bubble which contains either helium or Refrigerant 22. These flows are modelled using the two-dimensional, compressible Euler equations for a two component fluid (air-helium or air-Refrigerant 22). Although simulations of shock wave phenomena are now fairly commonplace, they are mostly restricted to single component flows. Unfortunately, multi-component extensions of successful single component schemes often suffer from spurious oscillations which are generated at material interfaces. Here we avoid such problems by employing a novel, nonconservative shock-capturing scheme. In addition, we have utilized a sophisticated adaptive mesh refinement algorithm which enables extremely high resolution simulations to be performed relatively cheaply. Thus we have been able to reproduce numerically all the intricate mechanisms that were observed experimentally (e.g., transitions from regular to irregular refraction, cusp formation and shock wave focusing, multi-shock and Mach shock structures, jet formation, etc.), and we can now present an updated description for the dynamics of a shock-bubble interaction. Author

N95-22327# Technische Univ., Eindhoven (Netherlands).

VERTEX RANKING FOR PERMUTATION AND OTHER GRAPHS

J. S. Deogun (Nebraska Univ., Lincoln, NE.), T. Kloks, D. Kratsch (Friedrich-Schiller Univ., Jena, Germany.), and H. Mueller (Friedrich-Schiller Univ., Jena, Germany.) Sep. 1993 22 p Prepared in cooperation with Nebraska Univ.

(PB95-127569) Avail: CASI HC A03/MF A01

An optimal vertex ranking of a permutation graph can be computed in time O(n to the 6th power), where n is the number of vertices. The demonstrated method can be used for designing polynomial time algorithms computing an optimal vertex ranking on the following classes of well-structured graphs too: circular permutation graphs, interval graphs, circular arc graphs, trapezoid graphs, and co-comparability graphs of bounded dimension. NTIS

N95-22349# Technische Univ., Eindhoven (Netherlands). Dept. of Mathematics and Computing Science.

TIME AND THE ORDER OF ABSTRACT EVENTS IN DISTRIBUTED COMPUTATIONS

Twan Basten, Thomas Kunz (Technische Univ., Darmstadt, Germany.), James Black (Waterloo Univ., Ontario.), Michael Coffin (Waterloo Univ., Ontario.), and David Taylor (Waterloo Univ., Ontario.) Feb. 1994 40 p Prepared in cooperation with Waterloo Univ., Ontario

(PB95-110482) Avail: CASI HC A03/MF A01

An important problem in event-based models of distributed computations is the amount of behavioral information. Even for simple applications, the number of events is large and the causal structure is complex. Event abstraction can be used to reduce the apparent complexity of a distributed computation. The paper discusses one important aspect of event abstraction: causality among abstract events. Logical vector time and a derived notion called reversed vector time can be used to assign two meaningful timestamps to abstract events. These timestamps can be used to efficiently determine causal relationships between arbitrary abstract events. The class of convex abstract events is identified as a subclass of abstract events that is general enough to be widely applicable and restricted enough to simplify timestamping. For this class, ordinary vector time is sufficient to determine causal relationships. At the cost of some extra computational effort, the timestamps derived for convex abstract events can also be used for arbitrary abstract events, overcoming the need for reversed timestamping. NTIS

N95-22353# Institut des Hautes Etudes Scientifiques, Bures-sur-Yvette (France).

LOCAL CONNECTIVITY OF SOME JULIA SETS CONTAINING A CIRCLE WITH AN IRRATIONAL ROTATION

Carsten Lunde Petersen Apr. 1994 52 p

(PB95-109070; IHES/M/94/26) Avail: CASI HC A04/MF A01

Let P(sub theta)(z) := exp(i2(pi)(theta))z + z(sup 2) for theta (epsilon) (0,1) and let J(sub P(sub theta)) denote the Julia set of P(sub theta). We prove that J(sub P(sub theta)) is locally connected and has Lebesque zero whenever theta is of constant type. This provides the first proof of local connectivity of the Julia set for a rational map with a Siegel disc. We prove also that the Julia sets of a certain 'model' family of degree 3 Blaschke products are locally connected. NTIS

N95-22354# Institut des Hautes Etudes Scientifiques, Bures-sur-Yvette (France).

SINGULAR SYMMETRIC MATRICES

Alex Eskin and Yonatan R. Katznelson Apr. 1994 30 p Sponsored by Alfred P. Foundation and Department of Education

(PB95-109088; IHES/M/94/27) Avail: CASI HC A03/MF A01

The varieties, S(sub n, r), of n x n symmetric matrices are studied, with the purpose of estimating the counting function N(T; n, r), which counts the number of integer points whose norm is bounded by T. NTIS

N95-22355# Institut des Hautes Etudes Scientifiques, Bures-sur-Yvette (France).

ELLIPTIC GENERA FOR Z/K-MANIFOLDS I

Jorge A. Devoto Apr. 1994 18 p

(PB95-109096; IHES/M/94/29) Avail: CASI HC A03/MF A01

We define and study, for k an odd number, an elliptic genus Phi(sub k) for Z/k-manifolds. We show that this elliptic genus defines a MSO(sub star)-module epimorphism from oriented bordism with coefficients in Z/k to the ring of mod k-modular forms of Serre and Swinnerton-Dyer. NTIS

N95-22359 Technische Univ., Delft (Netherlands).

MAXIMUM WEIGHTED MATCHING FOR HIGH INDEX DIFFERENTIAL ALGEBRAIC EQUATIONS Thesis

P. Bujakiewicz 1 Apr. 1993 168 p

(PB95-135075; ISBN-90-9007240-3) Avail: Issuing Activity (National Technical Information Service (NTIS))

This thesis is the result of a research which originally started in the area of modelling of combined continuous/discrete-event systems. In chapter 2, some aspects from the theory of DAE's are briefly described. In chapter 3, the numerical solution of DAE's by the BDF method is described. In section 3.8, recent results on the stability of the numerical solution of high index DAE's are summarized. In chapter 4, some classical graph algorithms which we use in chapter 5, are presented. In chapter 5, the article is presented in which we propose the algorithm for determining powers of s in structurally high index DAE's. In chapter 6, simulation results are presented, where the modifications from section 3.7 are applied. These modifications use the knowledge of powers of s determined by the algorithm developed in chapter 5. NTIS

N95-22369# Helsinki Univ. of Technology, Espoo (Finland).

RIGHT INVERSE FOR THE DIVERGENCE OPERATOR IN SPACES OF CONTINUOUS PIECEWISE POLYNOMIALS Research Report

E. Boillat May 1994 19 p See also AD-A136889

(PB95-127080) Avail: CASI HC A03/MF A01

The paper is concerned with the norm of a right inverse for the divergence operator between spaces of piecewise polynomials on triangular elements. More specifically, one tries to construct a right inverse acting from the space W of continuous piecewise polynomials of degree p into the space V of R(exp 2) - valued piecewise polynomials of degree p + 1. Under the hypothesis of quasiuniformity of the triangulation, one proves that this right inverse has an operator norm which grows at most like square root of (ln p) when both W and V are equipped with the H(exp 1) - norm and at most like p(exp 2) square root of (ln p) if W is equipped with the L(exp 2) - norm only. An application of the first of these two results is the approximation of the thermoelasticity equations by the p-version of the finite element methods. One also shows how the second result can be used in the context of higher-order Hood-Taylor method for the Stokes problem. NTIS

N95-22370# Helsinki Univ. of Technology, Espoo (Finland).

LOCKING OF THE FINITE ELEMENT METHOD IN THERMOELASTICITY Research Report

E. Boillat May 1994 20 p See also AD-A187902

(PB95-127098) Avail: CASI HC A03/MF A01

The paper is concerned with the solution mu to the stationary problem of thermoelasticity and with the approximation mu(sub n) of u obtained with a standard Galerkin method. In the incompressible limit, when the Lame coefficient lambda becomes infinite, mu(sub n) is subject to a divergence constraint, div mu(sub n) = P(sub n)T, where Pn is a given approximation operator acting on the temperature field T. This mechanism provokes a locking phenomenon similar to the one observed in elasticity and studied by Babuska and Suri in another paper. The purpose of the work is to give a sufficient and necessary condition on the discrete spaces V(sub n), used in the Galerkin formulation, to avoid locking and get an estimation of the error which is optimal and independant of lambda. The criterion will be used to construct two practical examples of methods free from locking for the usual thermoelasticity problem where the temperature field is solution of a Poisson equation. The first example is based on the h-version of the finite element method, the second one on the p-version. NTIS

N95-22375 Technische Univ., Delft (Netherlands). Faculty of Technical Mathematics and Informatics.
SELF-SIMILAR SOLUTIONS OF A FAST DIFFUSION EQUATION THAT DO NOT CONSERVE MASS
Mark A. Peletier and Hongfei Zhang 1994 26 p
(ISSN 0922-5641)
(PB95-134920) Copyright Avail: Issuing Activity (National Technical Information Service (NTIS))

The equation u(sub t) = del(vector differential operator) dot (u(sup -n)del(vector differential operator)u) (1.1) arises in many areas of applications. The case n = 0 corresponds to the classical heat conduction equation. When n is less than 0, the equation models the flow of a gas in a porous medium. Because the diffusion coefficient u(sup -n) vanishes when u = 0, disturbances of u = 0 propagate at finite speed. Therefore (1.1) with n less than 0 is also known as the slow diffusion equation, and has been the focus of extensive study during the past two decades. In this paper the authors consider the solutions in the case of fast diffusion, i.e. n greater than 0. The authors shall consider equation (1.1) in R(sup N), for a spatial dimension N larger than two, subject to an initial condition u(x,0) = u(sub 0)(x) for x (is a member of) R(sup N) where the initial distribution u(sub 0) is non-negative and u(sub 0)(is a member of) L(sup 1)(R sup N). In particular the authors take N greater than 2 and 2/N less than n less than 1, and seek solutions u of (1.1) which vanish at a finite time T. NTIS

N95-22379# Technische Univ., Eindhoven (Netherlands). Dept. of Mathematics and Computing Science.
FORTRAN SUBROUTINE FOR COLUMN REDUCTION OF POLYNOMIAL MATRICES
A. J. Geurts and C. Praagman (Groningen Rijksuniv., Netherlands.) Jun. 1994 74 p
(ISSN 0167-9708)
(PB95-134987; EUT-94-WSK-01) Avail: CASI HC A04/MF A01

In this report we describe a subroutine that takes an arbitrary polynomial matrix P as input, and yields on output a unimodular polynomial matrix U and a column reduced polynomial matrix R such that PU = R. The subroutine was run on four different computers, with comparable results. We found examples in which the routine behaves well, as well as examples in which the routine performs poorly, if no precautions are taken. We provide both kinds of examples and discuss the cause of the behavior of the routine. From these considerations a guideline for the use of the routine is derived. NTIS

N95-22388 Maryland Univ., College Park, MD. Inst. for Physical Science and Technology.
POLLUTION ERROR IN THE H-VERSION OF THE FINITE ELEMENT METHOD AND THE LOCAL QUALITY OF A-POSTERIORI ERROR ESTIMATORS Final Report
I. Babuska, T. Strouboulis (Texas A&M Univ., College Station, TX.), C. S. Upadhyay (Texas A&M Univ., College Station, TX.), and A. Mathur (Texas A&M Univ., College Station, TX.) Feb. 1994 161 p Limited Reproducibility: More than 20% of this document may be affected by microfiche quality
(Contract N00014-90-J-1030; NSF CCR-88-20279; NSF MSS-90-25110)
(AD-A279868; BN-1163; CMC-94-01) Avail: Issuing Activity (Defense Technical Information Center (DTIC))

In this work we study the pollution-error in the h-version of the finite element method and its effect on the local quality of a-posteriori error estimators. We show that the pollution-effect in an interior subdomain depends on the relationship between the mesh inside and outside the subdomain and the smoothness of the exact solution. We also demonstrate that it is possible to guarantee the quality of local error-estimators in the interior of a finite-element mesh-patch of interest by employing meshes which are sufficiently refined outside the patch. DTIC

N95-22389 Army Research Office, Research Triangle Park, NC.
TRANSACTIONS OF THE ELEVENTH ARMY CONFERENCE ON APPLIED MATHEMATICS AND COMPUTING
Mar. 1994 749 p Conference held in Pittsburgh, PA, 8-10 Jun. 1993
Limited Reproducibility: More than 20% of this document may be affected by microfiche quality
(AD-A279884; ARO-94-1) Avail: CASI HC A99

This is a technical report resulting from the Eleventh Army Conference on Applied Mathematics and Computing. It contains most of the papers in the agenda of this meeting. These treat many Army applied mathematical problems. DTIC

65 STATISTICS AND PROBABILITY

Includes data sampling and smoothing; Monte Carlo method; and stochastic processes.

N95-19914 Technische Univ., Eindhoven (Netherlands). Dept. of Mathematics and Computing Science.
APPLICATION OF MARKOV DECISION PROCESSES TO SEARCH PROBLEMS
Leo B. Hartman (Waterloo Univ., Ontario.) and Kees M. vanHee (Waterloo Univ., Ontario.) Jan. 1994 34 p Limited Reproducibility: More than 20% of this document may be affected by microfiche quality
(PB95-110813) Avail: CASI HC A03

In the paper the authors show how Markov decision processes can be used to guide a random search process. The authors first formulate search problems as a special class of Markov decision processes such that the search space of a search problem is the state space of the Markov decision process. In general it is not possible to compute an optimal control procedure for these Markov decision processes in a reasonable time. The authors, therefore, define several simplifications of the original problem that have much smaller state spaces. For these simplifications, decompositions and abstractions, the authors find optimal strategies and use the exact solutions of these simplified problems to guide a randomized search process. The search process selects states for further search at random with probabilities based on the optimal strategies of the simplified problems. These randomized search procedures are repeated as long as the authors have time to solve the problem. The authors illustrate the approach with two examples: the N-puzzle and job shop scheduling problem. NTIS

N95-19936# Tilburg Univ. (Netherlands). Dept. of Economics.
QUALIFICATION OF THE DEPENDENCE IN THE GENERALIZED EXTREME VALUE CHOICE MODEL
M. R. Jaiebi 1994 21 p
(PB95-110946; FEW-619) Avail: CASI HC A03/MF A01

The Generalized Extreme Value (GEV) model of discrete choice theory is shown to be observationally equivalent to a random utility maximization model with independent utilities and type-1 extreme value distributions. The observational equivalence is not only in terms of choice probabilities, but in terms of the entire joint distribution of choice and achieved utility. NTIS

N95-19938 Tilburg Univ. (Netherlands). Dept. of Economics.
FREQUENT SAMPLING IN DISCRETE CHOICE
M. R. Jaiebi 1994 22 p Limited Reproducibility: More than 20% of this document may be affected by microfiche quality
(PB95-110961; FEW-618) Avail: CASI HC A03

We analyze a discrete choice model based on random utility maximization involving frequent sampling, without restrictions on the stochastic structure (admitting dependence). For large samples, we calculate the (limiting) choice probabilities. They are hit for any size of the sample if and only if the invariance of achieved utility property holds. Examples are the Multinomial Logit model and the Generalized Extreme Value model. NTIS

N95-19945# Institut des Hautes Etudes Scientifiques, Bures-sur-Yvette (France).
COUPLED ANALYTIC MAPS
J. Bricmont (Universite Catholique de Louvain, Belgium.) and A. Kupiainen (Helsinki Univ., Helsinki, Finland.) Jun. 1994 25 p
(Grants EC-SCI-CT91-0695; EC-CHRX-CT93-0695; NSF DMS-92-05296)
(PB95-111076; IHES/P/94/38) Avail: CASI HC A03/MF A01

We consider a lattice of weakly coupled expanding circle maps. We construct, via a cluster expansion of the Perron-Frobenius operator, an invariant measure for these infinite dimensional dynamical systems which exhibits space-time chaos. NTIS

N95-19990# Army Research Lab., Aberdeen Proving Ground, MD.
A MULTIVARIATE MULTISAMPLE RANK TEST FOR STOCHASTIC SIMULATION VALIDATION Final Report, 1 Oct. 1993 - 31 May 1994
Ann E. Brodeen and Malcolm S. Taylor Oct. 1994 36 p
(AD-A285922; ARL-TR-592) Avail: CASI HC A03/MF A01

Nonparametric multivariate statistical methods address a broad class of problems in data analysis in which the assumption of normality is not feasible, and where the data occur naturally as n-tuples (vectors) rather than scalar values. This is the data structure that is most common in the engineering sciences and, coincidentally, the least tractable. A computer-intensive approach to the analysis of these data, usually referred to as randomization or permutation procedures, will be the specific focus of this work. Tests based on permutations of observations are nonparametric tests. This study considers a multivariate extension of the well-known Kruskal-Wallis rank sum test as a method for hypothesis testing, a technique commonly employed for simulation validation. The test statistic investigated is a nonparametric analogue of the classical Hotelling T2 used for the normal theory model. This undertaking is part of a broader based Army research program, the goal of which is to improve the ability of communications networks to deliver critical information on the battlefield when and where it is needed, despite a rapidly changing and often hostile environment. It will also support the ongoing effort to formalize the validation process for network simulation that, in turn, provides the groundwork for exploring alternatives and testing hypotheses throughout the research program. This formalization of the validation process can be readily transmitted to other organizations that rely on network simulations for their analyses. DTIC

N95-20102 Naval Aerospace Medical Research Lab., Pensacola, FL.
ITERATED-BOOTSTRAP CONFIDENCE INTERVALS FOR THE MEAN Special Report
R. R. Stanny 20 Dec. 1993 13 p Limited Reproducibility: More than 20% of this document may be affected by microfiche quality
(AD-A279802; NAMRL-SP-93-6) Avail: Issuing Activity (Defense Technical Information Center (DTIC))

Several reports indicate that nonparametric bootstrap confidence intervals (CI's) produced by the percentile method can yield overly liberal Type I error rates in small samples when the nominal alpha level is .05 or less. In the Monte Carlo simulations described here, percentile-method bootstrap 95% CI's for mu produced higher Type I error rates than standard parametric CI's in Gaussian and exponential samples of 40 or fewer observations. Iterated-bootstrap CI's for mu, however, yielded Type I error rates near alpha = .05 in Gaussian and exponential samples of as few as 10 observations. In exponential samples of 10 or more observations, iterated-bootstrap intervals controlled Type I errors more reliably than parametric intervals and were not obviously inferior to the parametric intervals when the data were Gaussian. Thus, ordinary percentile-method bootstrap CI's for mu may be of questionable accuracy when Type I error rates are to be controlled at values of alpha less than or equal .05 or so. On the other hand, iterated-bootstrap CI's may be preferable to parametric CI's for data that come from a skewed distribution, such as the exponential, provided n is 10 or more. In samples of about 10 observations or more, iterated CI's may yield better Type I error control than parametric CI's when the data are skewed and nearly the same Type I error control when the data are Gaussian. DTIC

N95-20608# Naval Research Lab., Washington, DC.
ON COMMONALITIES IN SIGNAL DESIGN FOR NON-GAUSSIAN CHANNELS Final Report
Nhi-Anh Chu, Nirmal Warke (George Mason Univ., Fairfax, VA.), and Geoffrey C. Orsak (George Mason Univ., Fairfax, VA.) 26 Aug. 1994 46 p
(AD-A285385; NRL/FR/5591-94-9735) Avail: CASI HC A03/MF A01

We derive for additive non-Gaussian white noise channels signal waveforms that are simultaneously optimal with respect to the minimum probability of error, the mini-max, and the Neyman-Pearson criteria. We show that for a large class of non-Gaussian statistics, there exist only two asymptotically optimal signal waveforms; one impulsive while the other is constant in amplitude. The impulsive waveform is optimal when the tails of the noise density fall off faster than the tails of the Gaussian density. We show that under each of the three optimality criteria the asymptotic performance for small signals is essentially determined by the signal energy, while for large signals the performance is determined by a non-Euclidean metric that varies with respect to the tails of the noise density function. To support these results, we offer simulations for a variety of non-Gaussian channels. In each case, the asymptotic theory holds strikingly well even for decidedly nonasymptotic regimes. DTIC

N95-20620 Naval Postgraduate School, Monterey, CA.
ERROR PROBABILITIES OF FFH/BFSK WITH NOISE NORMALIZATION AND SOFT DECISION VITERBI DECODING IN A FADING CHANNEL WITH PARTIAL-BAND JAMMING M.S. Thesis
Anthony Y. Chua Mar. 1994 75 p Limited Reproducibility: More than 20% of this document may be affected by microfiche quality
(AD-A280041) Avail: Issuing Activity (Defense Technical Information Center (DTIC))

An error probability analysis of a communications link employing convolutional coding with soft decision Viterbi decoding implemented on a fast frequency-hopped, binary frequency-shift keying (FFH/BFSK) spread spectrum system is performed. The signal is transmitted through a frequency nonselective, slowly fading channel with partial-band jamming. Noise normalization combining is employed at the receiver to alleviate the effects of partial-band jamming. The received signal amplitude of each hop is modeled as a Rician process, and each hop is assumed to fade independently. It is found that with the implementation of soft decision Viterbi decoding that the performance of the receiver is improved dramatically when the coded bit energy to partial-band noise power spectral density ratio (E(sub b)/N(sub 1)) is greater than 10dB. At higher E(sub b)/N(sub 1), the asymptotic error improves dramatically and varies from 10(exp -6) to 10(exp -12) depending on the constraint length (v), number of hops/bit (L), and the strength of the direct signal (alpha sq/(2 alpha)sq). In addition, nearly worst case jamming occurs when the jammer uses a full band jamming strategy, even when L = 1 and there is a very strong direct signal (alpha sq/(2 alpha)sq) = 100).Due to noncoherent combining losses, when the hopper bit ratio is increased, there is some degradation at moderate E(sub b)/N(sub 1). Furthermore, when a stronger code is used (i.e., the constraint length is longer), performance improves, especially for high E(sub b)/N(sub 1) where the asymptotic error is reduced. Finally, soft decision decoding improves performance over hard decision decoding from 4 to 8 dB at moderate E(sub b)/N(sub 1) depending on the code rate and with a much lower asymptotic error at high E(sub b)/N(sub 1). DTIC

N95-20779# Washington Univ., Seattle, WA.
UNIVERSAL FEATURES OF MULTIPLICITY DISTRIBUTIONS
A. B. Balantekin (Wisconsin Univ., Madison, WI.) 1994 11 p
(Contract DE-FG06-90ER-40561)
(DE94-012854; DOE/ER-40561/142) Avail: CASI HC A03/MF A01

Universal features of multiplicity distributions are studied and combinants, certain linear combinations of ratios of probabilities, are introduced. It is argued that they can be a useful tool in analyzing multiplicity distributions of hadrons emitted in high energy collisions and large scale structure of galaxy distributions. DOE

N95-21219# Army Research Lab., Adelphi, MD.
NONPARAMETRIC ESTIMATION OF THE CYCLIC CROSS-SPECTRUM Final Report, Jan. - May 1994
Brian Sadler Oct. 1994 19 p
(AD-A285756; ARL-TR-464) Avail: CASI HC A03/MF A01

Cyclostationary processes are an important class of nonstationary processes. In this report we consider nonparametric estimation of the cyclic cross-spectrum. A periodogram-based estimator is studied and its asymptotic behavior characterized. This extends the recent univariate work of Dandawate and Giannakis to the multivariate case. The results are useful for a variety of multi-sensor cyclostationary signal processing scenarios, such as bearing estimation. DTIC

N95-21469 Technische Univ., Delft (Netherlands). Dept. of Technical Mathematics and Informatics.
EXPONENTIAL DECONVOLUTION: TWO ASYMPTOTICALLY EQUIVALENT ESTIMATORS
G. Jongbloed 1994 15 p
(PB95-132122) Copyright Avail: Issuing Activity (National Technical Information Service (NTIS))

For two isotonic estimators for the distribution function in the exponential deconvolution problem, the asymptotic behavior is investigated. The first estimator is a least squares projection of a naive estimator for the distribution function on the set of distribution functions. The second estimator is the well known maximum likelihood estimator. It turns out that these estimators at a fixed point are asymptotically equivalent. NTIS

N95-21945 Stanford Univ., CA. Dept. of Statistics.
ON MARKOV CHAIN MONTE CARLO ACCELERATION
Alan E. Gelfand and Sujit K. Sahu 4 Apr. 1994 24 p Limited Reproducibility: More than 20% of this document may be affected by microfiche quality
(Contract N00014-92-J-1264)
(AD-A279393; SU-TR-480) Avail: Issuing Activity (Defense Technical Information Center (DTIC))

Markov chain Monte Carlo (MCMC) methods are currently enjoying a surge of interest within the statistical community. The goal of this work is to formalize and support two distinct adaptive strategies which typically accelerate the convergence of a MCMC algorithm. One approach is through resampling; the other incorporates adaptive switching of the transition kernel. Support is both by analytic arguments and simulation study. Application is envisioned in low dimensional but non-trivial problems. Two pathological illustrations are presented. Connections with reparametrization are discussed as well as possible difficulties with infinitely often adaptation. DTIC

N95-21946 Stanford Univ., CA. Dept. of Statistics.
BAYESIAN ANALYSIS OF SEMIPARAMETRIC PROPORTIONAL HAZARDS MODELS
Alan E. Gelfand and Bani K. Mallick 21 Mar. 1994 24 p Limited Reproducibility: More than 20% of this document may be affected by microfiche quality
(Contract N00014-92-J-1264)
(AD-A279394; SU-TR-479) Avail: Issuing Activity (Defense Technical Information Center (DTIC))

We consider the usual proportional hazards model in the case where the baseline hazard, the covariate link and the covariate coefficients are all unknown. Both the baseline hazard and the covariate link are monotone functions and are characterized nonparametrically using a dense class arising as a mixture of Beta distribution functions. We take a Bayesian approach for fitting such a model. Since interest focuses more upon the likelihood, we consider vague prior specifications including Jeffreys's prior. Computations are carried out using sampling-based methods. Model criticism is also discussed. Finally, a data set studying survival of a sample of lung cancer patients is analyzed. DTIC

N95-21979# Technische Hogeschool, Eindhoven (Netherlands). Dept. of Mathematics and Computing Science.
PROOF OF A CONJECTURE OF NARAYANA ON DOMINANCE REFINEMENTS OF THE SMIRNOV TWO-SAMPLE TEST
A. DiBucchianico and D. Loeb (Bordeaux 1 Univ., Talence, France.) Jun. 1994 13 p Sponsored by PRC Maths-Info.
(Grants NATO-CRG-930554; EC-CHRX-CT93-0400) (ISSN 0926-4493)
(PB95-132650; Memo-COSOR-94-18) Avail: CASI HC A03/MF A01

We prove the following conjecture of Narayana: there are no dominance refinements of the Smirnov two-sample test if and only if the two sample sizes are relatively prime. NTIS

N95-21980# Technische Hogeschool, Eindhoven (Netherlands). Dept. of Mathematics and Computing Science.
PRECEDENCE TESTS AND CONFIDENCE BOUNDS FOR COMPLETE DATA: AN OVERVIEW AND SOME RESULTS
S. Chakraborti (Alabama Univ., Tuscaloosa, AL.) and P. vanderLaan Jun. 1994 40 p
(Grant NATO-CRG-920287) (ISSN 0926-4493)
(PB95-132668; Memo-COSOR-94-19) Avail: CASI HC A03/MF A01

An overview of some nonparametric procedures based on precedence (or exceedance) statistics is given. The procedures include both tests and confidence intervals. In particular, the construction of some simple distribution-free confidence bounds for location difference of two distributions with the same shape is considered and some properties are derived. The asymptotic relative efficiency of an asymptotic form of the corresponding test relative to Wilcoxon's two-sample rank-sum test and the two-sample Student's t-test is given for various cases. Some K-sample problems are discussed where precedence type tests are useful, along with a review of the literature. NTIS

N95-22135# Army Research Lab., Aberdeen Proving Ground, MD.
LATIN HYPERCUBE SAMPLING IN SENSITIVITY ANALYSIS Final Report, Oct. 1992 - May 1994
Joseph C. Collins, III Oct. 1994 32 p
(DA Proj. 1L1-62618-AH-80)
(AD-A285867; ARL-TR-586) Avail: CASI HC A03/MF A01

In practice, production computer simulation models are usually run for a limited number of real input vectors. To make statistical inferences about the model, it is frequently desirable to generate additional realistic inputs for the purpose of obtaining better coverage of the input space. Latin Hypercube Sampling is presented as a method for accomplishing this task. DTIC

66 SYSTEMS ANALYSIS

Includes mathematical modeling; network analysis; and operations research.

N95-19941# Tilburg Univ. (Netherlands).
ASYMPTOTIC ANALYSIS OF NASH EQUILIBRIA IN NONZERO-SUM LINEAR-QUADRATIC DIFFERENTIAL GAMES. THE TWO-PLAYER CASE
A. J. T. M. Weeren, J. M. Schumacher, and J. C. Engwerda 1994 37 p
(PB95-111027; FEW-634) Avail: CASI HC A03/MF A01

In the paper the authors discuss nonzero-sum linear-quadratic differential games. The Nash equilibria for different kinds of information structures were previously studied. Most of the literature on the topic of nonzero-sum linear-quadratic differential games is concerned with games of fixed (finite) duration, i.e. the games are studied over a finite time horizon t(sub f). The authors will study the behavior of Nash equilibria for t(sub f) approaches infinity for two different information structures, the open-loop and the closed-loop perfect state information. In the open-loop case, it is known that the coupled Riccati differential equations describing the Nash equilibrium can be related to alinear dynamical system. Using this linear system, asymptotic properties of the open-loop Nash equilibrium are studied. In the case of closed-loop perfect state information, they will study the so-called feedback Nash equilibrium. The authors show that there exist choices of parameters, for which the asymptotic behavior of the solutions of the Riccati equations depends strongly on the specified terminal values. Finally, they show that, although the feedback Nash equilibrium over any fixed finite horizon is unique, there can exist several different feedback Nash equilibria in stationary strategies for the infinite horizon problem, even when they restrict their attention to Nash equilibria that are stable in the dynamical sense of the word. NTIS

N95-21709 Tilburg Univ. (Netherlands). Faculty of Economics.
NOTE ON THE CHARACTERIZATIONS OF THE COMPROMISE VALUE
G. J. Otten, P. Borm, and S. Tijs May 1994 28 p
(PB95-135117; FEW-655) Avail: Issuing Activity (National Technical Information Service (NTIS))

The compromise value was previously introduced as a solution concept on the class of compromise admissible non-transferable utility (NTU) games. Two characterizations of the compromise value are provided on sub-classes of NTU-games. This note shows that in one of these characterizations the axioms are dependent. It turns out that with a small weakening of the symmetry property the axioms become independent. Moreover, a new characterization of the compromise value is provided. Further, it is shown that these characterizations can be extended to a larger class of NTU-games. Finally, all monotonic, Pareto optimal, and covariant values on the class of NTU-games are described. NTIS

67 THEORETICAL MATHEMATICS

Includes topology and number theory.

N95-21136# Los Alamos National Lab., NM.
UNDERSTANDING THE MECHANISMS OF LENGTH SCALE COMPETITION: THE SINE-GORDAN SOLITON CASE
A. Sanchez, A. R. Bishop, and F. Dominguez-Adame (Universidad Complutense, Madrid, Spain.) 1994 5 p Presented at the Fluctuation Phenomena: Disorder and Nonlinearity Conference, Madrid, Spain, 26-30 Sep. 1994
(Contract W-7405-eng-36)
(DE94-016201; LA-UR-94-2592; CONF-9409182-1) Avail: CASI HC A01/MF A01

We have examined the dynamical behavior of the kink solutions of the one-dimensional sine-Gordon equation in the presence of a spatially periodic parametric perturbation. We report on a novel occurrence of length scale competition in this system and show how it can be understood by means of linear stability analysis. DOE

N95-21592# International Centre for Theoretical Physics, Trieste (Italy).
EXPLICIT ANALYTICAL SOLUTION OF THE NONLINEAR VLASOV POISSON SYSTEM
V. Skarka, S. M. Mahajan, and E. Fijalkow (Centre National de la Recherche Scientifique, Orleans, France.) Oct. 1993 32 p
(DE94-628931; IC-93/339) Avail: CASI HC A03/MF A01 (US Sales Only)

In order to describe the time evolution of an inhomogeneous collisionless plasma the nonlinear Vlasov equation is solved perturbatively, using the subdynamics approach and the diagrammatic techniques. The solution is given in terms of a double perturbation series, one with respect to the nonlinearities and the other with respect to the interaction between particles. The infinite sum of interaction terms can be performed exactly due to the property of dynamical factorization. Following the methodology, the exact solution in each order with respect to nonlinearities is computed. For a choice of initial perturbation the first order exact solution is numerically integrated in order to find the local density excess. The approximate analytical solution is found to be in excellent agreement with exact numerical integration as well as with ab initio numerical simulations. Analytical computation gives a better insight into the problem and it has the advantage to be simpler, and also accessible in some range of parameters where it is difficult to find numerical solutions. DOE

N95-21964 Rutherford Appleton Lab., Oxford (England).
N=1 SUPERCONFORMAL MINIMAL MODEL CORRELATION FUNCTIONS ON THE TORUS
A. Abdurrahman, F. Anton, M. A. Namazie, and C. Nunez Dec. 1993 64 p Prepared in cooperation with Rome Univ., Italy and Oxford Univ., Oxford, England
(PB95-134615; RAL-94-057) Avail: Issuing Activity (National Technical Information Service (NTIS))

The Coulomb gas formalism is employed to construct contour integral representations of two-point correlation functions on the torus for the N = 1 superconformal unitary discrete series, characterized by the single integer p. (For the particular case of the Tricritical Ising Model, these include the energy and vacancy density operators.) Modular and monodromy properties of the superconformal blocks are examined and the generalization to superconformal theories of Verlinde's results on modular transformations and the fusion algebra discussed in some detail. For p odd, the relevant modular matrix is (with respect to a particular basis) symmetric and unitary, as in ordinary rational conformal theory. However, for p even, there appears to be an obstruction due to the Ramond vacuum state. NTIS

70 PHYSICS (GENERAL)

For precision time and time interval (PTTI) see *35 Instrumentation and Photography;* for geophysics, astrophysics or solar physics see *46 Geophysics, 90 Astrophysics,* or *92 Solar Physics.*

N95-20106# Argonne National Lab., IL.
DESIGN AND THERMAL STRESS ANALYSIS OF HIGH POWER X-RAY MONOCHROMATORS COOLED WITH LIQUID NITROGEN
C. S. Rogers and L. Assoufid Jul. 1994 14 p Presented at the International Meeting on Synchrotron Radiation Instrumentation, Stony Brook, NY, 18-22 Jul. 1994
(Contract W-31-109-eng-38)
(DE94-016879; ANL/XFD/CP-82667; CONF-940714-9) Avail: CASI HC A03/MF A01

Cryogenically cooled, single-crystal silicon, x-ray monochromators offer much better thermal performance than room-temperature silicon monochromators. The improved performance can be quantified by a figure-of-merit equal to the ratio of the thermal conductivity to the coefficient of thermal expansion. This ratio increases by about a factor of 50 as the temperature is decreased from 300 K to 100 K. An extensive thermal and structural finite element analysis is presented for an inclined, liquid nitrogen cooled, Si monochromator crystal diffracting 4.2 keV photons from the (111) planes using Undulator A at the Advanced Photon Source. The angular size of the beam accepted on the crystal was chosen to be 50 (mu)rad vertically and 120 (mu)rad horizontally. The deflection parameter, K, was 2.17 for all cases. The peak power density at normal incidence to the beam was calculated to be 139 W/mm(exp 2), and the total power was 750 W at a distance of 30 m from the source for a positron current of 100 mA. The crystal was oriented in the inclined geometry with an inclination angle of 85 degrees for all cases. The performance of the crystal was investigated for beam currents of 100, 200, and 300 mA. The calculated peak slopes of the diffraction plane over the extent of the beam footprint were -1.17, -2.35, and 0.33 (mu)rad, and the peak temperatures were 88.2, 102.6, and 121.4 K, respectively. The variation in the Bragg angle due to change in d-spacing across the beam footprint was less than 1 (mu)rad for all cases. These results indicate that a properly designed, cryogenically cooled, inclined silicon monochromator can deliver the full brilliance of Undulator A at even the highest machine currents. DOE

N95-20129# Oak Ridge National Lab., TN.
GIANT MAGNETORESISTANCE CALCULATED FROM FIRST PRINCIPLES
W. H. Butler, J. M. MacLaren (Tulane Univ., New Orleans, LA.), and X. G. Zhang (Kentucky Univ., Lexington, KY.) 1994 2 p Presented at the Spring Meeting of the Materials Research Society, San Francisco, CA, 12-16 Apr. 1993
(Contract DE-AC05-84OR-21400)
(DE94-018658; CONF-930405-58) Avail: CASI HC A01/MF A01

The Layer Korringa Kohn Rostoker-Coherent Potential Approximation technique was used to calculate the low temperature giant magnetoresistance (GMR) from first principles for Co (vertical bar) Cu and permalloy (vertical bar) Cu superlattices. Our calculations predict large giant magnetoresistance ratios for Co (vertical bar) Cu and extremely large ratios for permalloy (vertical bar) Cu for current perpendicular to the layers. Mechanisms such as spin-orbit coupling which mix spin channels are expected to greatly reduce the GMR effect for permalloy (vertical bar) Cu. DOE

N95-20229# American Inst. of Physics, New York, NY.
JOURNAL OF APPLIED PHYSICS, VOLUME 76, NUMBER 10, PART 2. PROCEEDINGS OF THE 6TH JOINT MAGNETISM AND MAGNETIC MATERIALS-INTERMAG CONFERENCE
W. Yelon, ed., W.-Y. Ching, ed., Y. Idzerda, ed., and F. E. Pinkerton, ed. 23 Jun. 1994 1184 p Conference held in Albuquerque, NM, 20-23 Jun. 1994
(AD-A286364) Avail: CASI HC A99/MF A10

In addition to the usual invited papers, there were eight invited symposia: three on topics relating to magnetic and magneto-optic recording, and one each on magnetic microscopy, magnetic aftereffect, giant magnetoresistance, magneto-impedance, and neutron scattering studies of vortex structures in superconductors. There was also an evening panel discussion on units in magnetism. The journal volume includes 280 contributed papers and 47 invited papers and constitutes the Magnetism and Magnetic Materials (MMM) proceedings for 1994. Derived from text

N95-20241# Argonne National Lab., IL.

POWER-LAW RESISTIVITY, MAGNETIC RELAXATION AND AC SUSCEPTIBILITY

J. Gilchrist (Centre National de la Recherche Scientifique, Grenoble, France.) and C. J. vanderBeek Jul. 1994 3 p Presented at the Meeting on Materials and Mechanisms of Superconductivity: High Temperature Superconductors, Grenoble, 4-9 Jul. 1994
(Contract W-31-109-eng-38)
(DE94-016893; ANL/MSD/CP-83799; CONF-940701-18) Avail: CASI HC A01/MF A01

The nonlinear diffusion of magnetic flux into a superconducting sample can be studied by measuring the relaxation of the magnetization after application of a step field or by measuring the ac susceptibility, chi(sub 1) and its third harmonic, chi(sub 3), or preferably both methods covering different time scales. Each has been analyzed recently for a field-cooled sample of a material whose creep activation energy depends logarithmically on current density, J corresponding to a power-law relation between electric field, E and J. Here, results are compared, using a universal scaling depth. Maximum chi(sub 1)'' and absolute value of chi(sub 3) values occur, and also the magnetization has relaxed to half its initial value when the scaling depth is comparable to the sample half-thickness. DOE

N95-20246# Los Alamos National Lab., NM.

[PHYSICS DIVISION RESEARCH AND DEVELOPMENT] Progress Report, 1 Jan. - 31 Dec. 1993

G. Y. Hollen, comp. and G. T. Schappert, comp. Jul. 1994 153 p
(Contract W-7405-eng-36)
(DE94-017685; LA-12804-PR) Avail: CASI HC A08/MF A02

This report discusses its following topics: Recent Weapons-Physics Experiments on the Pegasus II Pulsed Power Facility; Operation of a Large-Scale Plasma Source Ion Implantation Experiment; Production of Charm and Beauty Mesons at Fermilab Sudbury Neutrino Observatory; P-Division's Essential Role in the Redirected Inertial Confinement Fusion Program; Trident Target Physics Program; Comparative Studies of Brain Activation with Magnetocephalography and Functional Magnetic Resonance Imaging; Cellular Communication, Interaction of G-Proteins, and Single-Photon Detection; Nuclear Magnetic Resonance Studies of Oxygen-doped La2CuO(4+delta) Thermoacoustic Engines; A Shipborne Raman Water-Vapor Lidar for the Central Pacific Experiment; Angara-5 Pinch Temperature Verification with Time-resolved Spectroscopy; Russian Collaborations on Megagauss Magnetic Fields and Pulsed-Power Applications; Studies of Energy Coupling from Underground Explosions; Trapping and Cooling Large Numbers of Antiprotons: A First Step Toward the Measurement of Gravity on Antimatter; and Nuclear-Energy Production Without a Long-Term High-Level Waste Stream. DOE

N95-20725# Oak Ridge National Lab., TN.

MAGNETIC FLOCCULATION OF PARAMAGNETIC PARTICLES

C. Tsouris and T. C. Scott 1994 7 p Presented at the Summer Meeting of the American Institute of Chemical Engineers, Denver, CO, 14-17 Aug. 1994
(Contract DE-AC05-84OR-21400)
(DE94-018144; CONF-940853-9) Avail: CASI HC A02/MF A01

An experimental apparatus has been assembled for the flocculation study of paramagnetic particles under the influence of a strong magnetic field. A magnetic field of strength up to 6 T is generated by a cryogenic magnet operating near liquid helium temperatures. Experimental information is obtained from fluctuation and intensity measurements of light passing through a particle suspension located in a uniform magnetic field. Particle flocculation is described by a Brownian flocculation model in which hydrodynamic, van der Waals, double-layer, and magnetic forces are incorporated for the estimation of the particle flocculation rate. A population-balance model is employed in conjunction with the flocculation model to predict the evolution of the particle size and composition or magnetic susceptibility with time. The effects of magnetic-field strength, magnetic susceptibility of the particles, particle size, and zeta potential are investigated. Results show that particle size and magnetic susceptibility each play an important role in the selective flocculation of particles of different properties. DOE

N95-20731 Department of the Navy, Washington, DC.

TIME CODE INTERFACE Patent

James D. Perry, inventor (to Navy) 13 Sep. 1994 8 p Filed 26 Dec. 1991 Supersedes AD-D015278
(AD-D016535; US-Patent-5,347,645; US-Patent-Appl-SN-813563; US-Patent-Class-395-550) Avail: US Patent and Trademark Office

A modularized Time Code Interface (TCI) used to time tag asynchronous events. Input and output connectors provide modularity in that the TCI may be readily plugged into or removed from a system. The TCI utilizes programmable memory for storing time intervals that are used in producing time of day data associated with the occurrence of an asynchronous event. DTIC

N95-20773# Massachusetts Inst. of Tech., Cambridge, MA. Center for Space Research.

ION HEATING PERPENDICULAR TO THE MAGNETIC FIELD

Mats Andre and Tom Chang 28 Mar. 1994 41 p
(Contract F19628-91-K-0043)
(AD-A286635; PL-TR-94-2139; SR-2) Avail: CASI HC A03/MF A01

Several theories of ion heating perpendicular to the geomagnetic field are briefly reviewed and assessed. Perpendicular heating of ions leading to the formation of ion conics is common in the ionosphere and magnetosphere. Ion conics at altitudes above a few thousand kilometers are often associated with waves around the ion gyrofrequency. It is concluded that the majority of these ion conics that are locally heated or generated over extended altitude regimes, may be best explained by ion cyclotron resonance heating. At lower altitudes, particularly in the region of discrete auroras, energization by turbulence around the lower hybrid frequency seems to be an important heating mechanism. DTIC

N95-20869# Wright Lab., Eglin AFB, FL.

ON THE TAYLOR TEST. PART 3: A CONTINUUM MECHANICS CODE ANALYSIS OF STEADY PLASTIC WAVE PROPAGATION

P. J. Maudlin, J. C. Foster, Jr. (Wright Lab., Eglin AFB, FL.), and S. E. Jones (Alabama Univ., Tuscaloosa, AL.) Nov. 1994 42 p
(Contract W-7405-eng-36)
(DE95-002252; LA-12836-MS) Avail: CASI HC A03/MF A01

Simple conservation relationships ('Jump' conditions) in conjunction with postulated material constitutive behavior are applied to steady plastic strain waves propagating in problems of uniaxial stress and Taylor Cylinder Impact. These problems are simulated with a two-dimensional Lagrangian continuum mechanics code for numerically validating the Jump relationships as an accurate analytical representation of plastic wave propagation. The constitutive behavior used in this effort assumes isotropy and models the thermodynamic response with a Mie-Grunisen Equation-of-State and the mechanical response with the rate-dependent Johnson-Cook and MTS flow stress models. The Jump relationships successfully replicate the results produced by continuum code simulations of plastic wave propagation and provide a methodology for constructing mechanical constitutive models from experimental plastic wave speed information. Comparisons are also presented between experimental speeds from Taylor Cylinder Impact tests with Jump relationships and continuum code predictions, indicating that the above mentioned flow stress models may not accurately capture plastic wave propagation speeds in annealed and hardened copper. DOE

N95-20874# California Univ., Berkeley. Lawrence Berkeley Lab, CA. Materials Sciences Div.

CORRELATED WAVEFUNCTION MONTE CARLO STUDIES OF EXCITATIONS IN THE QUANTUM HALL LIQUIDS

Balazs Kralik, Andrew M. Rappe, and Steven G. Louie Aug. 1994 4 p Presented at the 22th International Conference on Physics of Semiconductors, Vancouver, British Columbia, 15-19 Aug. 1994
(Contract DE-AC03-76SF-00098)
(DE95-002337; LBL-36063; CONF-9408155-10) Avail: CASI HC A01/MF A01

Various excitations in the quantum Hall liquid at different Landau level filling factors are studied using a variational quantum Monte Carlo approach. Quantities calculated include spin-flip energies and dispersion relations for the collective modes (the magnetorotons and magnetoplasmons). The present approach goes beyond the lowest-Landau-level and single-mode approximations commonly used in previous studies. The inclusion of Landau-level mixing along with finite-thickness and donor effects satisfactorily explains values for the (nu) = 1 spin-flip energy that are found in recent photoluminescence experiments on (delta)-doped samples. In the case of the magnetorotons at (nu) = 1/3, the authors show that multiple-mode effects can change the excitation energies significantly, especially for high r(sub s) samples (by nearly 50% at r(sub s) = 20). DOE

N95-21102# Helsinki Univ. of Technology, Espoo (Finland). Electromagnetics Lab.
CLASSIFICATION OF BIANISOTROPIC MEDIA
Ari H. Sihvola and Ismo V. Lindell Apr. 1994 11 p
(ISSN 0784-848X)
(PB95-127635; ISBN-951-22-2079-2) Avail: CASI HC A03/MF A01

The constitutive relations of bianisotropic media contain four dyadic material coefficients with 36 scalar in maximum. Based on the separation of reciprocal and nonreciprocal effects, the paper presents a division of bianisotropic media into basic classes, which all can be interpreted with simple physical ideas. NTIS

N95-21194# Columbia Univ., New York, NY.
STUDY OF IMPROVED CRITICAL CURRENTS AND MECHANICAL PROPERTIES IN THE Y-Ba-Cu-O SUPERCONDUCTOR WITH SILVER OR Y2BaCuO3 OR 211 DISPERSIONS Final Report, 1 Apr. 1992 - 31 Aug. 1994
Siu-Wai Chan Aug. 1994 93 p
(Contract F49620-92-J-0160)
(AD-A285609; AFOSR-94-0651TR) Avail: CASI HC A05/MF A01

The microstructure of the top-seeded, single grain, melted textured YBCO materials with different vol% 211 were investigated. The homogeneity of 211 distribution was greatly improved by using a solution precipitated 211 powder in preparation. Crack spacings and twin spacings were found to decrease with increasing vol% of the 211 particles. The 211 particles were found to be effective in holding crack propagation. Relationship between twin spacing and interparticle spacing was found to depend on the elastic strain energy from the tetragonal to orthorhombic transformation. The accumulative beneficial effects of the 211 addition on Jc are summarized. The highest Jc was 10(exp 4) A/sq cm at 77K 1T. Our transmission electron microscopy of the Au/YBCO interfaces shows well-bonded interfaces with no extraneous phases present with the (001) lattice fringe of YBCO terminated at the interfaces abruptly. Both integral steps of (001) height and multiples of 1/3(001) steps were observed. Our finding supports earlier contact resistivity and XPS results of the Au/YBCO interfaces. Amorphous carbon films were shown to protect superconducting YBCO films from degradation by humidity. The YBCO films with carbon coating were founded to retain critical current densities 4 orders of magnitude higher than the uncoated YBCO films after 2h at 100% relative humidity stressing at room temperature. DTIC

N95-22138 Rutherford Appleton Lab., Oxford (England).
THEORY OF SPIN DYNAMICS IN THE CLASSICAL TWO-DIMENSIONAL HEISENBERG MAGNET
S. W. Lovesay, E. Engdahl, A. Cuccoli, and V. Tognetti Jun. 1994 29 p See also PB92-200203 Prepared in cooperation with Florence Univ., Italy
(PB95-133559; RAL-94-067) Avail: Issuing Activity (National Technical Information Service (NTIS))

The wave vector-dependent spin autocorrelation function of a classical Heisenberg model on a square lattice is calculated from the coupled-mode theory of spin dynamics. This theory is consistent with the spherical model for static spin correlations; as the temperature, T, approaches zero the inverse correlation length kappa approx equals exp(-const./T). For a ferromagnetic exchange coupling, the decay rate of long wavelength fluctuations, Gamma(q), is proportional to q(sup 2)T(sup 1/2) in the limit (q/kappa) yields infinity, whereas in the opposite, hydrodynamic limit Gamma(q) (alpha) q(sup 2) (T ln (kappa/q))(sup 1/2). At the wave vector for incipient antiferromagnetic ordering, the decay rate is proportional to kappa T(sup 1/2), while the corresponding decay rate near the Brillouin zone center is proportional to q(sup 2)T((sup 1/2)/kappa). The coupled-mode equations for ferromagnetically and antiferromagnetically coupled models are solved numerically on a fine grid of wave vectors. The spin autocorrelation function, and its power spectrum, are surveyed over a wide range of temperatures and wave vectors. NTIS

N95-22177# International Centre for Theoretical Physics, Trieste (Italy).
TEMPERATURE DEPENDENCE OF A MAGNETOPOLARON IN A HARMONIC QUANTUM DOT IN RESONANT MAGNETIC FIELDS
Kadi Zhu and Shiwei Gu (Jiaotong Univ., Shanghai, China.) Nov. 1993 18 p
(DE94-629036; IC-93/374) Avail: CASI HC A03/MF A01 (US Sales Only)

The temperature and the size dependence of a magnetopolaron in a harmonic quantum dot are investigated theoretically in the presence of an external magnetic field normal to the plane of the quantum dot. It is shown that in resonant magnetic field, the two cyclotron masses (m(sup *)(sub c+) and m(sup *)(sub c-)) in a harmonic quantum dot are each split into two cyclotron masses, respectively. The upper branches of m(sup *)(sub c+) and m(sup *)(sub c-) are the increasing functions of temperature, while the lower branches of m(sup *)(sub c+) and m(sup *)(sub c-) are the slowly decreasing functions of temperature. The results also show that the resonant magnetic fields are different in the quantum dots of different sizes. DOE

N95-22420# Sandia National Labs., Albuquerque, NM.
SANDIA NATIONAL LABORATORIES ANALYSIS CODE DATA BASE
C. W. Peterson Nov. 1994 203 p
(Contract DE-AC04-94AL-85000)
(DE95-004188; SAND-94-2177) Avail: CASI HC A10/MF A03

Sandia National Laboratories' mission is to solve important problems in the areas of national defense, energy security, environmental integrity, and industrial technology. The laboratories' strategy for accomplishing this mission is to conduct research to provide an understanding of the important physical phenomena underlying any problem, and then to construct validated computational models of the phenomena which can be used as tools to solve the problem. In the course of implementing this strategy, Sandia's technical staff has produced a wide variety of numerical problem-solving tools which they use regularly in the design, analysis, performance prediction, and optimization of Sandia components, systems, and manufacturing processes. This report provides the relevant technical and accessibility data on the numerical codes used at Sandia, including information on the technical competency or capability area that each code addresses, code 'ownership' and release status, and references describing the physical models and numerical implementation. DOE

71 ACOUSTICS

Includes sound generation, transmission and attenuation.
For noise pollution see *45 Environmental Pollution.*

N95-19883 Pennsylvania State Univ., University Park, PA. Materials Research Lab.
MATERIALS FOR ADAPTIVE STRUCTURAL ACOUSTIC CONTROL, VOLUME 2 Annual Report, 1 Feb. 1993 - 31 Jan. 1994
L. E. Cross 11 Apr. 1994 208 p See also AD-A279223 Limited Reproducibility: More than 20% of this document may be affected by microfiche quality
(Contract N00014-92-J-1510)
(AD-A279222) Avail: Issuing Activity (Defense Technical Information Center (DTIC))

The research goals of this ONR sponsored University Research Initiative entitled 'Materials for Adaptive Structural Acoustics Control' relate directly to the sensing and actuating material which must be integrated to function in adaptive control of acoustic structures. This report documents work in the second year of the program and for convenience the activities are grouped under the headings General Summary Papers, Materials Studies, Composite Sensors, Actuator Studies, Integration Issues, Processing Studies, and Thin Film Ferroelectrics. The general papers cover a new comprehensive description of ferroelectric ceramics and their applications, analysis of high temperature piezoelectric sensors and the possible application of nonlinearity in enhancing the smartness of ceramics and composites. Scale effects on ferroics are of increasing interest and the manner in which nano-scale polar regions control the properties of relaxor ferroelectrics is again emphasized. For material studies the detailed examination of the evolution of diffuse, then relaxor behavior in lanthanum modified lead titanate has been completed. Interest in the soft PZT's, relaxor and phase switching materials continues, with a new thrust developing towards a more complete description of domain walls and morphotropic phase boundaries in perovskites. Materials issues in the wear out and fatigue effects in polarization switching systems have been subjected to detailed evaluation and the precautions necessary to fabricate long lasting materials which will stand 109 switches without any fatigue are delineated. DTIC

N95-19911# Texas Univ., Austin, TX. Applied Research Labs.
THE COMBUSTIVE SOUND SOURCE M.S. Thesis
Preston S. Wilson 21 Apr. 1994 80 p
(ARL-TR-94-9) Avail: CASI HC A05/MF A01

This thesis describes a unique type of low frequency underwater sound source, the Combustive Sound Source (CSS). The fundamental operating principle of CSS is the following: Electrolysis of water produces hydrogen and oxygen gas, which is a combustible mixture. The gas mixture is captured in a combustion chamber and ignited with a spark. The ensuing combustion produces expanding gases which in turn produce high intensity, low frequency acoustic pulses. The thesis begins by discussing the background of the project and initial feasibility work. It continues by briefly discussing electrolysis and gas production. Fundamental combustion theory is discussed, along with two experiments that relate the acoustic output of CSS to theory. Additional experiments were conducted in order to compare the first bubble period in the CSS pressure signature with the predictions of the Rayleigh-Willis equation. The dependence of the radiated acoustic waveform on the volume and depth of the bubble was investigated. The first bubble period of the CSS pressure signature agrees with Rayleigh-Willis theory in trend, but not in absolute value. Empirical equations are presented which predict the first bubble period for three different situations, a depth of nine meters for various stoichiometric volumes, a stoichiometric volume of 0.5 STP liters for various depths, and a stoichiometric volume of 500 cubic centimeters for various depths. High speed filming of the CSS bubble is presented. The high speed films confirm that CSS produces a bubble of high temperature combustion products. The bubble oscillates and generates acoustic output. The motion of the bubble is shown to be related to the acoustic output in the classic manner, with pressure peaks associated with minimum bubble volumes. Finally, several other factors that affect the acoustic output of CSS are discussed. These include the shape of the CSS combustion chamber, the ignition source, the oxidizer, the presence of high pressure bubble collapses, and the presence of high frequency components. Derived from text

N95-20019# Oak Ridge National Lab., TN.
WAVELET-BASED ACOUSTIC RECOGNITION OF AIRCRAFT
W. B. Dress and S. W. Kercel 1994 15 p Presented at the Society of Photo-Optical Instrumentation Engineers Conference on Intelligent Information Systems, Orlando, FL, 4-8 Apr. 1994
(Contract DE-AC05-84OR-21400)
(DE94-017701; CONF-940449-15) Avail: CASI HC A03/MF A01

We describe a wavelet-based technique for identifying aircraft from acoustic emissions during take-off and landing. Tests show that the sensor can be a single, inexpensive hearing-aid microphone placed close to the ground the paper describes data collection, analysis by various technique, methods of event classification, and extraction of certain physical parameters from wavelet subspace projections. The primary goal of this paper is to show that wavelet analysis can be used as a divide-and-conquer first step in signal processing, providing both simplification and noise filtering. The idea is to project the original signal onto the orthogonal wavelet subspaces, both details and approximations. Subsequent analysis, such as system identification, nonlinear systems analysis, and feature extraction, is then carried out on the various signal subspaces. DOE

N95-20084# Naval Command, Control and Ocean Surveillance Center, San Diego, CA. Research, Development, Technology and Evaluation Div.
SIGNAL-TO-NOISE GAIN FROM ADAPTIVE MATCHED-FIELD BEAMFORMING OF MULTIDIMENSIONAL ACOUSTIC ARRAYS Final Report, Oct. 1989 - Oct. 1990
Newell O. Booth and Gary L. Mohnkern Sep. 1994 29 p
(AD-A285671; NCCOSC/RDT/E-TR-1661) Avail: CASI HC A03/MF A01

Linear and adaptive matched-field beamforming of multidimensional arrays provide signal-to-noise gain and an estimation of range, depth, and azimuth of the sources of incident signals. Adaptive matched-field beamforming (MFB) with large arrays is predicted to achieve gain equal to the directivity index plus the total input-interference to independent-noise ratio (IINR). An example distribution of received interference levels illustrates that measurements with relatively small volumetric arrays can determine the IINR, enabling an estimation of achievable array gain. Array sidelobe level requirements for adaptive MFB are derived, showing that good performance is obtained with relatively high sidelobes. Adaptive matched-field gain degradation from replica errors is shown to approach the linear matched-field gain degradation at low-output-signal-to-noise ratios. DTIC

N95-20098 California Univ., Berkeley, CA. Dept. of Physics.
JOSEPHSON ACOUSTIC RADIATION IN SUPERFLUID HELIUM Annual Report
Richard Packard 25 May 1994 3 p Limited Reproducibility: More than 20% of this document may be affected by microfiche quality
(Contract N00014-94-1-0043)
(AD-A279809) Avail: Issuing Activity (Defense Technical Information Center (DTIC))

This project is directed towards the detection of an acoustical field generated near a microaperture, by quantized phase slip events in superfluid He-4. The annual report details the accomplishments of the first few months of this work. DTIC

N95-20267# EG and G Rocky Flats, Inc., Golden, CO.
ACOUSTIC EMISSION: THE FIRST HALF CENTURY
Thomas F. Drouillard 1994 13 p Presented at the 12th International Acoustic Emission Symposium, Sapporo, Japan, 21 Oct. 1994
(Contract DE-AC34-90DP-62349)
(DE94-017176; RFP-4875; CONF-9410182-1) Avail: CASI HC A03/MF A01

The technology of acoustic emission (AE) is approaching the half century mark, having had its beginning in 1950 with the work of Joseph Kaiser. During the 1950s and 1960s researchers delved into the fundamentals of acoustic emission, developed instrumentation specifically for AE, and characterized the AE behavior of many materials. AE was starting to be recognized for its unique capabilities as an NDT method for monitoring dynamic processes. In the decade of the 1970s research activities became more coordinated and directed with the formation of the working groups, and its use as an NDT method continued to increase for industrial applications. In the 1980s the computer became a basic component for both instrumentation and data analysis, and today it has sparked a resurgence of opportunities for research and development. Today we are seeing a transition to waveform-based AE analysis and a shift in AE activities with more emphasis on applications than on research. From the beginning, we have been fortunate to have had so many dedicated savants with different fields of expertise contribute in a collective way to bring AE to a mature, fully developed technology and leave a legacy of knowledge recorded in its literature. AE literature has been a key indicator of the amount of activity, the proportion of research to application, the emphasis on what was of current interest, and the direction AE has taken. The following is a brief survey of the history of acoustic emission with emphasis on development of the infrastructure over the past half century. DOE

N95-20272# Naval Command, Control and Ocean Surveillance Center, San Diego, CA.
CHARACTERIZATION AND SIMULATION OF AN ACOUSTIC SOURCE MOVING THROUGH AN OCEANIC WAVEGUIDE Final Report, Sep. 1993 - Sep. 1994
Michael Reuter Sep. 1994 33 p
(Proj. RJ3-5-C-72)
(AD-A285688; NCCOSC/RDT/E-TR-1673) Avail: CASI HC A03/MF A01

This report presents a time-varying linear-systems interpretation of the moving-acoustic-source problem. We present an algorithm that simulates the time series received at a sensor or an array of sensors resulting from the moving source. We then compare simulated data to experimental data to demonstrate the potential of the algorithm. DTIC

N95-20296 Department of the Navy, Washington, DC.
METHOD AND SYSTEM OF MAPPING ACOUSTIC NEAR FIELD Patent
Joseph A. Clark, inventor (to Navy) and Michael A. Sartori, inventor (to Navy) 13 Sep. 1994 10 p Filed 11 Aug. 1993
(AD-D016574; US-Patent-5,347,496; US-Patent-Appl-SN-104707; US-Patent-Class-367-140) Avail: US Patent and Trademark Office

A method and system for mapping the acoustic near field of a stationary axial symmetric structure are provided. The structure is subjected to a rotating excitation energy profile from a plurality of stationary excitation sites located radially around the structure. The acoustic near field of the structure due to the rotating excitation energy profile is measured along at least one line that conforms to a longitudinal surface of the structure. Mapping of the acoustic near field is complete when one rotation of the rotating excitation energy profile is complete. DTIC

N95-20300 Maryland Univ., College Park, MD. Dept. of Mathematics.
HIGHER ORDER CROSSINGS Final Report, 1 Oct. 1988 - 30 Sep. 1993
Benjamin Kedem 30 Sep. 1993 7 p Limited Reproducibility: More than 20% of this document may be affected by microfiche quality
(Grant AF-AFOSR-0049-89)
(AD-A279597; AFOSR-94-0304TR) Avail: CASI HC A02

Progress in the higher order crossings (HOC) method included development of 'contraction mapping' for the estimation of discrete frequencies in noise. Parametric filters allow the estimates to attain high precision. Reports and papers on this technique are listed, and applications to the discrimination of metal plates has begun. DTIC

N95-20724 Department of the Navy, Washington, DC.
CASCADE ORIFICIAL RESISTIVE DEVICE Patent
Nicholas Bitsakis, inventor (to Navy) and James Cassidy, inventor (to Navy) 12 Jul. 1994 6 p Filed 16 Jun. 1992
(AD-D016529; US-Patent-5,327,941; US-Patent-Appl-SN-899520; US-Patent-Class-138-42) Avail: US Patent and Trademark Office

A cascade orificial resistive device for throttling fluid flow which minimizes acoustic noise and internal vibrations is described herein. The device has a hollow body defining a fluid passageway, a plurality of perforated plates mounted within the passageway, a fixed end ring adjacent one end of the perforated plates, and a threadable end ring adjacent an opposite end of the perforated plates to place the plates in compression. Each of the perforated plates is a single piece molded plate having an integral outer ring and an integrally formed center keying mechanism as well as a plurality of orifices. The keying mechanism formed on each plate is designed so that adjacent ones of the plates have their orifices misaligned. In this manner, a pressure drop across each plate is created and the fluid flow through the device is throttled. The device of the present invention has utility in a number of onboard marine vessel systems wherein reduced acoustic noise and internal vibrations are particularly desirable. DTIC

N95-20823# Loyola Univ., Chicago, IL. Hearing Inst.
DETERMINATION OF MULTIPLE SOUND SOURCES Annual Report, 1 Sep. 1993 - 31 Aug. 1994
William A. Yost, Stanley Sheft, and Raymond Dye 31 Aug. 1994 11 p
(Contract F49620-92-J-0489)
(AD-A286563; AFOSR-94-0713TR) Avail: CASI HC A03/MF A01

The results studied showed that the SALT procedure produced weights that were much more consistent with subject reports than threshold measures. That is, the change in weights with increasing stimulus duration for the lateralization task indicated that the tones become more separable (analytic listening) as the overall duration increases. This does not occur with traditional measures of thresholds. In the amplitude modulation task, the modulated tones become more separable (analytic listening) as the modulation rates of the targets and distractor differ. Again traditional measures using thresholds do not show the same trend. Subjects also report that the modulated tones are different when the rates differ. DTIC

N95-20918# Iowa State Univ. of Science and Technology, Ames, IA. Center for Nondestructive Evaluation.
EXPERIMENTAL AND THEORETICAL EVALUATION OF ELASTIC WAVES IN CURVED LAYERED MEDIA Interim Report No. 3
Dale E. Chimenti and Ali Safaeinilli Jul. 1994 73 p
(Contract N61533-91-K-0032)
(AD-A286578) Avail: CASI HC A04/MF A01

This report describes the progress achieved during the third period of the study of elastic wave reflection from the curved and planar media subject to water loading. During the previous period, extensive experimental investigations were initiated to study parametrically the behavior of acoustic beams at curved and planar fluid-solid interfaces. Three types of materials, representative of Navy applications, in two geometries and two sizes, and many values of incident angle and angular or linear coordinates were included in the effort of last year. Simultaneously, an aggressive program of theoretical modeling and experimental verification were mounted and essentially all of the data were compared to predictions of the model. We found, in most cases, very good agreement between model calculations and experimental data. For the theoretical modeling of these effects, the complex source point (CSP) method was used to produce Gaussian line sources to account for the wave-solid interaction for acoustic beams. The scattering problem solved in this work is couched in terms of spectral integrals that are approximated by high-frequency uniform asymptotics. The resulting expressions for the reflected field contain interacting specularly reflected beam and leaky wave contributions which establish the physical basis for the observed phenomena. In addition to the two-dimensional modeling for comparison to experiments, work began to formulate a 3-D beam model within the theoretical framework for this more complicated circumstance as well. In continuation of the efforts of last year, we have extended the two-dimensional model to three dimensions. DTIC

N95-20963 Naval Surface Warfare Center, Dahlgren, VA.
WAVELET TRANSFORMATIONS FOR HELICOPTER IDENTIFICATION VIA ACOUSTIC SIGNATURES
Jeffrey L. Solka, Carey E. Priebe, Halford I. Hayes, and George W. Rogers May 1994 25 p Limited Reproducibility: More than 20% of this document may be affected by microfiche quality
(AD-A279980; NSWCDD/TR-93/169) Avail: CASI HC A03

The ability to classify helicopters based on their acoustic signature has applications to both detection and tracking. The current approach to this problem uses standard signal-processing techniques to extract features based on the fundamental harmonics of the helicopters' blades. This document examines the role that the wavelet transformation might play in this feature extraction process. It addresses ways to use the wavelet transform both to improve the performance of the existing approach and to expand the capabilities of the classification system. DTIC

N95-21119 Department of the Navy, Washington, DC.
MANDREL BASED EMBEDDED PLANAR FIBER-OPTIC INTERFEROMETRIC ACOUSTIC SENSOR Patent Application
Nichols Lagakas, inventor (to Navy) and Joseph A. Bucaro, inventor (to Navy) 28 Feb. 1994 38 p Limited Reproducibility: More than 20% of this document may be affected by microfiche quality
(AD-D016229; US-Patent-Appl-SN-202628) Avail: Issuing Activity (Defense Technical Information Center (DTIC))

This invention is an optimized planar fiber optic sensor utilizing robust design having high acoustic sensitivity and reduced acceleration response over that found in the prior art. A continuous optical fiber sensing arm is wrapped around a plurality of mandrels to reduce acceleration effects. An optical fiber sensing arm is embedded in an epoxy material to effectively eliminate the effects of the acoustic medium on the reference arm. The sensing arm and reference arm, along with input and output couplers, are encapsulated within an elastomer, natural rubber or butyl rubber which is an active element that providing high acoustic sensitivity. The mandrels may be solid compliant mandrels, tubular cylindrical mandrels, and combinations thereof. DTIC

N95-21170*# Georgia Tech Research Inst., Atlanta, GA.
TEMPERATURE EFFECTS ON ACOUSTIC INTERACTIONS BETWEEN ALTITUDE TEST FACILITIES AND JET ENGINE PLUMES Final Report, Feb. 1992 - May 1994
K. K. Ahuja, K. C. Massey, C. K. Tan, and R. R. Jones Oct. 1994 300 p
(Contract NAS1-19061)
(NASA-CR-197638; NAS 1.26:197638; AD-A286058; AEDC-TR-94-10)
Avail: CASI HC A13/MF A03

The overall objective of the present investigation was to determine the mechanisms responsible for engine/test cell resonance observed at the AEDC facility. The specific objective was to determine the effect of heating the jet on its coupling with the diffuser used in a typical engine/test cell facility. This objective was to be accomplished through systematic measurements of cold and heated free and ducted jets using a subscale facility. An additional objective was to analytically examine the behavior of jet instability waves as a function of temperature, and to identify any potential of strong coupling between the jet instabilities and diffuser duct resonance modes directly attributable to heating of the jet. Model cold and heated jet experiments are performed with an axisymmetric convergent nozzle in a test setup that simulates a supersonic jet exhausting into a cylindrical diffuser. The measured data consist of a free and ducted plume for a range of jet exit Mach numbers and four reservoir temperatures: ambient, 400 F, 750 F, and 1,000 F. Analytical results on the growth of instability waves and the duct resonance have been introduced. It is shown that the screech frequency increases with increasing operating temperature ratio. The measured in-duct microphone signatures contain a number of discrete tones, and almost all of them can be associated with duct resonances. The amplitudes increase with increasing Mach number and operating temperature ratios. At certain operating conditions, the acoustic fluctuations associated with these ejector duct modes excite the most amplified wave of the jet. DTIC

N95-21213# Naval Undersea Warfare Center, Newport, RI.
SCATTERING OF AN FM SIGNAL FROM AN ARRAY OF SPHERES Final Report
Theresa A. Baus and Ronald P. Radinski 15 Aug. 1994 16 p
(AD-A285587; NUWC-NPT-TD-10729) Avail: CASI HC A03/MF A01

This document describes the investigation of the dependence of peak target strength on source bandwidth and scatterer spacing using arrays of rigid scatterers and LFM signals at 200-, 400-, and 800-Hz bandwidths. The results demonstrate that, as the bandwidth increases, the average peak target strength increases and shows less aspect dependence (except near 90 degrees) due to more opportunity for coherent addition of the scattering amplitudes. As the spacing between the scatterers was increased, there were more fluctuations in aspect angle due to the greater directivity of the scattering pattern. Misaligning scatterers in a regularly spaced array smoothed the overall response and increased the average peak target strength. DTIC

N95-21863 Pennsylvania State Univ., University Park, PA. Materials Research Lab.
MATERIALS FOR ADAPTIVE STRUCTURAL ACOUSTIC CONTROLS Annual Report, 1 Feb. 1993 - 31 Jan. 1994
L. E. Cross 31 Jan. 1994 156 p Limited Reproducibility: More than 20% of this document may be affected by microfiche quality
(Contract N00014-92-J-1510)
(AD-A279255) Avail: Issuing Activity (Defense Technical Information Center (DTIC))

The research goals of this ONR sponsored University Research Initiative entitled 'Materials for Adaptive Structural Acoustics Control' relate directly to the sensing and actuating material which must be integrated to function in adaptive control of acoustic structures. This report documents work in the second year of the program and for convenience the activities are grouped under the headings General Summary Papers, Materials Studies, Composite Sensors, Actuator Studies, Integration Issues, Processing Studies, and Thin Film Ferroelectrics. The general papers cover a new comprehensive description of ferroelectric ceramics and their applications, analysis of high temperature piezoelectric sensors and the possible application of nonlinearity in enhancing the 'smartness' of ceramics and composites. Scale effects on ferroics are of increasing interest and the manner in which nanoscale polar regions control the properties of relaxor ferroelectrics is again emphasized. DTIC

N95-21888*# General Electric Co., Cincinnati, OH. Aircraft Engines.
ACTIVE CONTROL OF FAN NOISE-FEASIBILITY STUDY. VOLUME 1: FLYOVER SYSTEM NOISE STUDIES Final Report
Robert E. Kraft, B. A. Janardan, G. C. Kontos, and P. R. Gliebe Oct. 1994 42 p
(Contract NAS3-26617; RTOP 538-03-11)
(NASA-CR-195392-Vol-1; E-9170-Vol-1; NAS 1.26:195392-Vol-1) Avail: CASI HC A03/MF A01

A study has been completed to examine the potential reduction of aircraft flyover noise by the method of active noise control (ANC). It is assumed that the ANC system will be designed such that it cancels discrete tones radiating from the engine fan inlet or fan exhaust duct. Thus, without considering the engineering details of the ANC system design, tone levels are arbitrarily removed from the engine component noise spectrum and the flyover noise EPNL levels are compared with and without the presence of tones. The study was conducted for a range of engine cycles, corresponding to fan pressure ratios from 1.3 to 1.75. The major conclusions that can be drawn are that, for a fan pressure ratio of 1.75, ANC of tones gives about the same suppression as acoustic treatment without ANC, and for a fan pressure ratio of 1.45, ANC appears to offer less effectiveness than passive treatment. Additionally, ANC appears to be more effective at sideline and cutback conditions than at approach. Overall EPNL suppressions due to tone removal range from about 1 to 3 dB at takeoff engine speeds and from 1 to 5 db at approach speeds. Studies of economic impact of the installation of an ANC system for the four engine cases indicate increases of DOC ranging from 1 to 2 percent, favoring the lower fan pressure ratio engines. Further study is needed to confirm the results by examining additional engine data, particularly at low fan pressure ratios, and studying the details of the current results to obtain a more complete understanding. Further studies should also include determining the effects of combining passive and active treatment. Author

N95-21930 North Carolina Univ., Raleigh, NC. Dept. of Mechanical and Aerospace Engineering.
LOW FREQUENCY SOUND RADIATION FROM FINITE STIFFENED PLATES
Richard F. Keltie 28 Jul. 1993 23 p Limited Reproducibility: More than 20% of this document may be affected by microfiche quality
(Contract N00014-93-1-0368)
(AD-A279395) Avail: Issuing Activity (Defense Technical Information Center (DTIC))

The purpose of the research effort reported herein was to assess the feasibility of developing efficient low frequency acoustic radiators using flexural vibration of submerged stiffened plates. Candidate radiator geometries were identified at NUWC using an infinite plate model. A finite plate implementation of these models was then examined by the author using an analysis capability previously developed. The purpose of this examination was to study the extent to which infinite plate results could be achieved by a finite radiator, and to obtain an estimate of the effects of plate size and number of attached ribs on the radiation characteristics. DTIC

N95-21984 Materials Research Labs., Ascot Vale (Australia).
MEASUREMENT OF SOUND INTENSITY AND SOUND POWER
Vinh Trinh Feb. 1994 50 p Limited Reproducibility: More than 20% of this document may be affected by microfiche quality
(AD-A279246; MRL-TR-93-32; DODA-AR-008-561) Avail: Issuing Activity (Defense Technical Information Center (DTIC))

In this report the concept of a measurement technique for calculating sound intensity in the frequency domain is discussed and also how such a measurement system can be implemented in practice by using a frequency domain analyzer. The technique described employs a dual-channel FFT analyzer to obtain a cross power spectrum from the two microphones from which sound intensity is calculated. This approach enables a general-purpose FFT analyzer together with a micro-computer to perform the function of a dedicated sound intensity analyzer. The application of sound intensity measurement technique in sound power determination of a reference source is presented. DTIC

N95-22042 Army Research Lab., White Sands Missle Range, NM.
EVALUATION OF SIMPLE SPHERICAL SPREADING MODEL FOR NEAR VERTICAL ACOUSTICAL PROPAGATION Final Report
John M. Noble Aug. 1994 99 p Limited Reproducibility: More than 20% of this document may be affected by microfiche quality
(AD-A286284; ARL-TR-532) Avail: CASI HC A05

A comparison study was performed to evaluate the performance of a simple spherical spreading plus molecular absorption model to a more complex acoustic propagation model for near vertical propagation. The problem of near vertical propagation is important since several acoustic detection systems are being developed for the Army. The operational use of a simple acoustic propagation model in the battlefield will allow for fast computation time providing rapid evaluation of the advantage or disadvantage of using the acoustic detection system. However, simple propagation models can have several limitations. To evaluate the limitations and determine the operational reliability of the simple acoustic propagation model, more complex models must be used that incorporate many effects of the ground and atmosphere on the propagation of sound. This comparison will determine the limitations. DTIC

N95-22071# Brown Univ., Providence, RI.
SURFACES AND THIN FILMS STUDIED BY PICOSECOND ULTRASONICS Annual Progress Report, 1 Dec. 1993 - 30 Nov. 1994
H. J. Maris 1994 8 p
(Contract DE-FG02-86ER-45267)
(DE95-001866; DOE/ER-45267/8) Avail: CASI HC A02/MF A01

We are using picosecond optics techniques to perform ultrasonic and thermal transport measurements on thin films and nanostructures. We are investigating the basic physics of sound and phonon propagation in solids, and also attempting to develop practical techniques for the ultrasonic evaluation of thin-film nanostructures. DOE

N95-22088 Department of the Navy, Washington, DC.
FIBER OPTIC PRESSURE SENSING ARRAY Patent Application
Frank Cuomo, inventor (to Navy), Richard Schmidt, inventor (to Navy), and James Kelly, inventor (to Navy) 22 Feb. 1994 13 p Limited Reproducibility: More than 20% of this document may be affected by microfiche quality
(AD-D016245; US-Patent-Appl-SN-200032) Avail: Issuing Activity (Defense Technical Information Center (DTIC))

An optical pressure sensing array is provided for sensing a high-frequency acoustic energy profile. The array is coupled to a reflector that is responsive to high-frequency acoustic pressure variations. The array transmits and receives light energy to and from the reflector. The received light energy is modulated by the movement of the reflector because of the acoustic field. Each element in the optical array is a closely packed geometrical configuration utilizing a single transmit optical fiber surrounded by six receive fibers, all having the same radius. In this configuration, the receive fibers receive light energy only from their associated transmit fiber resulting in a high-resolution acoustic profile. Furthermore, the geometric configuration permits a center-to-center element spacing that optimally is one-half the wavelength of the ultrasonic beam providing the acoustic energy at the operational frequency. DTIC

N95-22360# Naval Undersea Warfare Center, Newport, RI.
APPLICATIONS OF SONOCHEMISTRY Final Report
George J. Kavarnos, Robert S. Janus, and Harold C. Robinson 26 Oct. 1994 16 p
(Proj. 794-P-76)
(AD-A286388; NUWC-NPT-TR-10759) Avail: CASI HC A03/MF A01

Application of ultrasound can greatly enhance physical and chemical processes. Through the mechanism of cavitation, tremendous amounts of energy are released which can enhance chemical reaction rates, for example. This report reviews several experimental studies of sonochemistry applications with dual-use technology implications. A discussion of potential dual-technology applications, including production of higher powered ultrasonic processors, is presented. DTIC

72 ATOMIC AND MOLECULAR PHYSICS

Includes atomic structure, electron properties, and molecular spectra.

N95-19959# Florida Univ., Gainesville, FL. Quantum Theory Proj.
ATOMIC ORBITAL BASIS SETS FOR MOLECULAR INTERACTIONS Technical Report No. 7
Herbert F. DaCosta and David A. Micha 16 May 1994 21 p
(Contract N00014-93-I-0122)
(AD-A279609) Avail: CASI HC A03/MF A01

In preparation for computational work with molecular orbitals written as linear combinations of atomic orbitals, for first and second row atoms, we have developed a general procedure to parametrize linear combinations of Gaussian orbitals. We used a Gaussian and a Gauss-Legendre quadrature, to express hydrogenic orbitals (with the correct long-range dependence for collisions) as contracted Gaussians, for a general case with varying effective charges. DTIC

N95-19960# Florida Univ., Gainesville, FL. Quantum Theory Proj.
A MODEL FOR ELECTRON NUCLEAR DYNAMICS OF A MONATOMIC CHAIN Technical Report No. 3
Jean-Louis Calais, Erik Deumens, and Yngve Ohrn 16 May 1994 31 p
(Contract N00014-93-I-0122)
(AD-A279652) Avail: CASI HC A03/MF A01

The Electron Nuclear Dynamics (END) approach is developed for a linear chain in a parametrized model inspired by the PPP (Pariser-Parr-Pople) model. Particular attention is given to the model parameters, and the choice of basis functions in this time-dependent theory. The resulting equations of motion include electronic-vibrational couplings. Explicit analysis of the simplest model leads to coupling between the highest frequency longitudinal vibrational mode and the electrons. DTIC

N95-20025# Argonne National Lab., IL.
NEW STRONG INTERACTIONS ABOVE THE ELECTROWEAK SCALE
A. R. White Aug. 1994 32 p Presented at the 8th International Symposium on Very High Energy Cosmic Ray Interactions, Tokyo, Japan, 24-31 Jul. 1994
(Contract W-31-109-eng-38)
(DE94-018385; ANL-HEP-CP-94-46; CONF-9407127-1) Avail: CASI HC A03/MF A01

Theoretical arguments for a new higher-color quark sector, based on Pomeron physics in QCD, are briefly described. The electroweak symmetry-breaking, strong CP conservation, and electroweak scale CP violation, that is naturally produced by this sector is also outlined. A further consequence is that above the electroweak scale there will be a radical change in the strong interaction. Electroweak states, in particular multiple W's and Z's, and new, semi-stable, very massive, baryons, will be commonly produced. The possible correlation of expected phenomena with a wide range of observed cosmic ray effects at and above the primary spectrum knee is described. Related phenomena that might be seen in the highest energy hard scattering events at the Fermilab Tevatron, some of which could be confused with top production, are also briefly discussed. DOE

N95-20026# Sandia National Labs., Albuquerque, NM.
CHARGED PARTICLE DYNAMICS IN THE ACCELERATION GAP OF THE PBFA 2 ION DIODE
J. E. Bailey, A. L. Carlson, and A. B. Filuk et al 1994 4 p Presented at the 10th International Conference on High Power Particle Beams, San Diego, CA, 20-24 Jun. 1994
(Contract DE-AC04-94AL-85000)
(DE94-017347; SAND-93-3837C; CONF-940634-15) Avail: CASI HC A01/MF A01

We are improving the understanding of pulsed-power-driven ion diodes using measurements of the charged particle distributions in the diode anode-cathode (AK) gap. We measure the time- and space-resolved electric field in the AK gap using Stark-shifted Li I 2s-2p emission. The ion density in the gap is determined from the electric field profile and the ion current density. The electron density is inferred by subtracting the net charge density, obtained from the derivative of the electric field profile, from the ion density. The measured electric field and charged particle distributions are compared with results from QUICKSILVER, a 3D particle-in-cell computer code. The comparison validates the fundamental concept of electron build-up in the AK gap. However, the PBFA 2 diode exhibits considerably richer physics than presently contained in the simulation, suggesting improvements both to the experiments and to our understanding of ion diode physics. DOE

N95-20030# Oak Ridge National Lab., TN.
CAVITY-QED ENHANCEMENT OF FLUORESCENCE YIELDS IN MICRODROPLETS
M. D. Barnes, W. B. Whitten, and J. M. Ramsey 1993 18 p Presented at the 1993 Edgewood Research, Development and Engineering Center Science Conference on Obscuration and Aerosol Research, Aberdeen, MD, 21-25 Jun. 1993
(Contract DE-AC05-84OR-21400)
(DE94-018662; CONF-9306210-2) Avail: CASI HC A03/MF A01

Measurements of the integrated fluorescence yield of Rhodamine 6G (R6G) in levitated microdroplets (4 to 16 (mu)m diameter) display a size dependence which is attributed to a decreased probability per excitation cycle of photochemical bleaching as a result of cavity-enhanced spontaneous emission rates. The average number of fluorescence photons detected per molecule in 4 (mu)m droplets (where emission rate enhancement has been previously demonstrated) is shown to be approximately a factor of 2 larger than the yield measured for larger droplets where emission rate enhancement does not occur. Within some simple approximations, these results suggest that essentially no emission rate inhibition occurs in this system. A mechanism based on spectral diffusion is postulated for the apparent absence of cavity-inhibited emission and is illustrated by Monte Carlo calculations using time-dependent lineshape functions. DOE

N95-20034# Stanford Linear Accelerator Center, CA.
COMPLEMENTARITY OF e(+)e(-) AND pp COLLIDERS FOR THE EXPLORATION OF ELECTROWEAK SYMMETRY BREAKING
M. E. Peskin Aug. 1994 17 p Presented at the INS Symposium, Tokyo, Japan, 8-10 Mar. 1994
(Contract DE-AC03-76SF-00515)
(DE94-017397; SU-SLAC-PUB-6582; CONF-9403122-3) Avail: CASI HC A03/MF A01

I review the physics capabilities of the machines proposed for the next generation of high-energy experimentation: in hadron physics, the LHC, and in electron physics, a 500-1500 GeV e(+)e(-) techniques are expected to complement one another in the exploration of the next scale of physics. DOE

N95-20049# Pacific Northwest Lab., Richland, WA.
INTRINSIC BARRIERS FOR H-ATOM TRANSFER REACTIONS
D. M. Camaioni, S. T. Autrey, and J. A. Franz Aug. 1994 9 p Presented at the 208th American Chemical Society National Meeting, Washington, DC, 21-26 Aug. 1994
(Contract DE-AC04-94AL-85000)
(DE94-018914; PNL-SA-24421; CONF-940813-22) Avail: CASI HC A02/MF A01

Hydrogen transfer reactions play a well-recognized role in coal liquefaction. While H-abstraction reactions between radicals and H-donors have been well-studied, understanding of structure-reactivity relationships remains surprisingly incomplete. Another form of hydrogen transfer known as radical hydrogen transfer (radical donation of H to an unsaturated compound) is currently the subject of much speculation. The barriers for identity reactions are key parameters in the Evans-Polanyi equation for estimating reaction barriers and are fundamentally significant for the insight they provide about bond reorganization energies for formation of transition state structures. Although knowable from experiment, relatively few H-abstraction identity barriers and no barriers for hydrocarbon radical hydrogen transfer reactions have been measured. This paper seeks to supplement and extend existing experimental data with results obtained by calculation. The authors have used ab initio and semiempirical molecular orbital methods (MNDO-PM3) to calculate barriers for a series of H-atom abstraction and radical-hydrogen-transfer identity reactions for alkyl, alkenyl, arylalkyl and hydroaryl systems. Details of this methodology and analyses of how barrier heights correlate with reactant and transition state properties will be presented and discussed. DOE

N95-20086# Oak Ridge National Lab., TN.
ELECTRON-IMPACT IONIZATION OF MULTICHARGED IONS AT ORNL: 1985-1992
D. C. Gregory and M. E. Bannister Jul. 1994 152 p
(Contract DE-AC05-84OR-21400)
(DE94-017318; ORNL/TM-12729) Avail: CASI HC A08/MF A02

Absolute cross sections are presented in graphs and tables for single ionization of forty-one ions, multiple ionization of four ions, and for dissociation and ionization of two molecular ions by electron impact. This memo is the third in a series of manuscripts summarizing previously published as well as unpublished ionization cross section measurements at ORNL; contents of the two previous memos are also referenced in this work. All work tabulated in this memo involved ion beams generated in the ORNL-ECR ion source and utilized the ORNL electron-ion crossed beams apparatus. Target ions range from atomic number Z = 8 (oxygen) to Z = 92 (uranium) in initial charge states from +1 to +16. Electron impact energies typically range from threshold to 1500 eV. DOE

N95-20097# Florida Univ., Fort Lauderdale, FL. Quantum Theory Proj.
ELECTRON PROPAGATOR THEORY AND APPLICATION
Ricardo Longo, Benoit Champagne, and Yngve Oehrn 16 May 1994 33 p
(Contract N00014-93-1-0122)
(AD-A279761; TR-2-ONR) Avail: CASI HC A03/MF A01

The electron propagator theory is presented with somewhat of a historical perspective and the working equations are developed with the aim to take advantage of molecular point group symmetry. A new electron propagator code, the vectorized electron propagator program (VEP), is introduced without full details about its structure and capabilities (such details are being published elsewhere). Applications to the (UV) photoelectron spectra of some donor-acceptor complexes of borane with carbon monoxide and water are presented at the level of second-order theory as an illustration of the theory and the VEP code. DTIC

N95-20108# Fermi National Accelerator Lab., Batavia, IL.
J/PSI,PSI(PRIME) YIELDS MU(+)MU(-) AND B YIELDS J/PSI,PSI(PRIME) CROSS SECTIONS
Jun. 1994 13 p Presented at the 27th International Conference on High Energy Physics, Glasgow, Scotland, 21-27 Jul. 1994
(Contract DE-AC02-76CH-03000)
(DE94-017184; FNAL/C-94/136-E; CONF-940722-20) Avail: CASI HC A03/MF A01

This paper presents a measurement of J/(psi),(psi') differential cross sections in p(bar p) collisions at square root of s = 1. 8 TeV. The cross sections are measured above 4 GeV/c in the central region (absolute value of eta lessthan 0.6) using the dimuon decay channel. The fraction of events from B decays is measured, and used to calculate b quark cross sections and direct J/(psi), (psi') cross sections. The direct cross sections are found to be more than an order of magnitude above theoretical expectations. DOE

N95-20110# Fermi National Accelerator Lab., Batavia, IL.
B MESON LIFETIMES AT CDF
J. E. Skarha (Johns Hopkins Univ., Baltimore, MD.) Aug. 1994 8 p Presented at the Meeting of the Division of Particles and Fields of the American Physical Society, Albuquerque, NM, 2-6 Aug. 1994
(Contract DE-AC02-76CH-03000)
(DE95-000564; FNAL/C-94/224-E; CONF-940816-23) Avail: CASI HC A02/MF A01

Measurements of the B(sub u), B(sub d), and B(sub s) meson lifetime using semileptonic B(sub U) yields e(nu)D(0)X, B(sub d) yields e(nu)D* X, B(sub s) yields l(nu)D(sub s)X events and exclusive B(sub u) yields psi(')K(*), B(sub d) yields psi(')K(*,s), B(sub s) yields psi-phi events are presented. These results used the precise position measurements of the CDF SVX silicon vertex detector and were obtained from a 19.3 pb(sup -1) sample of 1.8 TeV (-p)p collisions collected in 1992-93 at the Fermilab Tevatron collider. Comparisons with previous measurements will be shown. DOE

N95-20111# Fermi National Accelerator Lab., Batavia, IL.
HARD DIFFRACTION AND RAPIDITY GAPS
M. G. Albrow Aug. 1994 10 p Presented at the Workshop on Quantum Infrared Physics, Paris, France, Jun. 1994
(Contract DE-AC02-76CH-03000)
(DE95-000565; FNAL/C-94/280-E; CONF-9406248-4) Avail: CASI HC A02/MF A01

I describe the evolution of experiments at hadron colliders on (1) high mass diffraction, (2) double pomeron exchange, from the ISR through the Sp(bar p)S to the Tevatron. I emphasize an experimental approach to the question: 'What is the pomeron?'. DOE

N95-20131# Fermi National Accelerator Lab., Batavia, IL.
CDF TOP RESULTS IN THE LEPTON + JETS CHANNEL
G. Watts (Rochester Univ., NY.) Aug. 1994 8 p Presented at the Meeting of the Division of Particles and Fields of the American Physical Society, Albuquerque, NM, 2-6 Aug. 1994
(Contract DE-AC02-76CH-03000)

(DE95-000641; FNAL/C-94/247-E; CONF-940816-24) Avail: CASI HC A02/MF A01

Results from the 1992-1993 Tevatron run (ran IA) top search at CDF in the lepton+jets channel are reported. The jet-vertexing algorithm tags 6 events on a background of 2.3 plus/minus 0.3 events in the W+ greater than or = 3 jets data sample, and the soft lepton analysis finds T events on a background of 3.1 plus/minus 0.3 events in the same data sample. Jet-vertex and soft-lepton tag correlations are described. Also given are the expected and observed number of tags in the Z+mulitjet control sample. DOE

N95-20132# Fermi National Accelerator Lab., Batavia, IL.

USING SCIENCE CENTERS TO EXPOSE THE GENERAL PUBLIC TO THE MICROWORLD

E. Malamud Aug. 1994 18 p Presented at the Meeting of the Division of Particles and Fields of the American Physical Society, Albuquerque, NM, 2-6 Aug. 1994

(Contract DE-AC02-76CH-03000)

(DE95-000647; FNAL/C-94/264; CONF-940816-26) Avail: CASI HC A03/MF A01

Despite the remarkable progress in the past decades in understanding our Universe, we particle physicists have failed to communicate the wonder, excitement, and beauty of these discoveries to the general public. I am sure all agree there is a need, if our support from public funds is to continue at anywhere approximating the present level, for us collectively to educate and inform the general public of what we are doing and why. Informal science education and especially science and technology centers can play an important role in efforts to raise public awareness of particle physics in particular and of basic research in general. Science Centers are a natural avenue for particle physicists to use to communicate with and gain support from the general public. DOE

N95-20133# Oak Ridge National Lab., TN.

ELECTRON-POSITRON PAIR PRODUCTION IN ULTRARELATIVISTIC ATOMIC COLLISIONS: 6.4 TeV S(SUP 16+) WITH Au, Pd AND Al

S. Datz, C. R. Vane, P. F. Dittner, H. F. Krause, R. Schuch (Stockholm Univ., Sweden.), H. Gao (Stockholm Univ., Sweden.), and R. Hutton (Lund Univ., Sweden.) 1994 29 p Presented at the Atomic Collisions, Oak Ridge, TN, 3-5 Mar. 1994

(Contract DE-AC05-84OR-21400)

(DE95-000690; CONF-9403151-2) Avail: CASI HC A03/MF A01

Angular and momentum distributions have been measured for electron-positron pairs created in peripheral collisions of 6.4 TeV bare sulfur ions with thin targets of Al, Pd, and Au. Singly- and doubly-differential cross sections are presented for 1-17 MeV/c electrons and positrons detected independently and in coincidence as pairs. Various physical parameters are deduced from the coincident electron and positron data, including probability distributions for the pair transverse momentum, the pair total energy, and the positron fraction of the pair energy. DOE

N95-20134# Fermi National Accelerator Lab., Batavia, IL.

SEARCH FOR W PAIR PRODUCTION WITH DILEPTON DECAY MODES AT D0

Nobuaki Oshima Sep. 1994 6 p Presented at the Meeting of the Division of Particles and Fields of the American Physical Society, Albuquerque, NM, 2-6 Aug. 1994

(Contract DE-AC02-76CH-03000)

(DE95-000724; FNAL/C-94/285-E; CONF-940816-29) Avail: CASI HC A02/MF A01

We present the results of a search of 13.5 pb(sup -1) of p(-p) collisions at (radical)s = 1.8 TeV for WW yields dileptons + X using the DO detector. One WW yields e(mu)v(-v) + X candidate was found with an expected background of about 0.96 plus/minus 0.44 events. One WW yields e(mu)v(-v)+ candidate was found with an expected background of about 1.23 plus/minus 0.87 events. The 95% C.L. upper limit for the W pair production cross section is 133 pb without background subtraction. Making the constraint kappa = 1 (Delta(kappa) = 0) implies -2.6 less than or = gamma less than or = 2.7 (95% C.L.) and making the constraint gamma = 0 implies -3.3 less than or = Delta(kappa) less than or = 3.5 (95% C.L.) assuming kappa(sub gamma) = kappa(sub Zeta) and lambda(sub gamma) = lambda(sub Zeta). We also present the contour of excluded couplings when kappa and lambda are allowed to simultaneously vary from their standard model values. DOE

N95-20159# Los Alamos National Lab., NM.

DATA ANALYSIS AND VISUALIZATION IN MCNP (TRADEMARK)

L. S. Waters 1994 4 p Presented at the Winter Meeting of the American Nuclear Society, Washington, DC, 13-18 Nov. 1994

(Contract W-7405-eng-36)

(DE94-016164; LA-UR-94-2521; CONF-941102-11) Avail: CASI HC A01/MF A01

There are many situations where the user may wish to go beyond current MCNP capabilities. For example, data produced by the code may need formatting for input into an external graphics package. Limitations on disk space may hinder writing out large PTRAK files. Specialized data analysis routines may be needed to model complex experimental results. One may wish to produce particle histories in a format not currently available in the code. To address these and other similar concerns a new capability in MCNP is being tested. A number of real, integer, logical and character variables describing the current and past characteristics of a particle are made available online to the user in three subroutines. The type of data passed can be controlled by cards in the INP file. The subroutines otherwise are empty, and the user may code in any desired analysis. A new MCNP executable is produced by compiling these subroutines and linking to a library which contains the object files for the rest of the code. DOE

N95-20160# Los Alamos National Lab., NM.

MCNP (TRADEMARK) ENDF/B-VI IRON BENCHMARK CALCULATIONS

J. D. Court and J. S. Hendricks 1994 5 p Presented at the Winter Meeting of the American Nuclear Society, Washington, DC, 13-18 Nov. 1994

(Contract W-7405-eng-36)

(DE94-016165; LA-UR-94-2520; CONF-941102-14) Avail: CASI HC A01/MF A01

Four iron shielding benchmarks have been calculated for, we believe the first time, with MCNP4A and its new ENDF/B-VI library. These calculations are part of the Hiroshima/Nagasaki dose re-evaluation for the National Academy of Sciences and the Defense Nuclear Agency. We believe these calculations are significant because they validate MCNP and the new ENDF/B-VI libraries. These calculations are compared to ENDF/B-V, experiment, and in some cases the recommended MCNP data library (a T-2 evaluation) and ENDF/IV. DOE

N95-20196# Flinders Univ., Adelaide (Australia). Electronic Structure of Materials Centre.

CONVERGENT CLOSE-COUPLING METHOD FOR CALCULATION OF ELECTRON SCATTERING ON HYDROGEN-LIKE TARGETS

Igor Bray Sep. 1993 46 p Submitted for publication

(DE94-631340; ESM-60) Avail: CASI HC A03/MF A01 (US Sales Only)

The Convergent Close-Coupling (CCC) method for the calculation of electron-hydrogen scattering was extended to hydrogen-like targets, atoms or ions. These include H, Li, Na, and K atoms, as well as the multitude of ions which have the same isoelectronic sequence as these atoms. The reliability of the method is independent of the projectile energy, and its applicability was demonstrated. It shows excellent agreement with a large set of measurements for electron scattering on sodium at projectile energies ranging from 1 to 54.4 eV. These measurements include spin asymmetries, singlet and triplet angular momentum (L) transferred to the atom perpendicular to the scattering plane, reduced Stokes parameters, differential, integrated, and total cross sections, as well as the total ionization spin asymmetry. The method is found to give better agreement with experiment than any other over this entire energy range. DOE

N95-20197# Flinders Univ., Adelaide (Australia). Electronic Structure of Materials Centre.

CALCULATION OF THE TOTAL AND TOTAL IONIZATION CROSS SECTIONS FOR POSITRON SCATTERING ON ATOMIC HYDROGEN

Igor Bray and A. T. Stelbovics Oct. 1993 9 p

(DE94-631341; ESM-62) Avail: CASI HC A02/MF A01 (US Sales Only)

The total and total ionization cross sections for positron scattering on atomic hydrogen are calculated by applying the Convergent Close-Coupling (CCC) method to the model where positronium formation channels are omitted. This model accurately describes the physics of the scattering whenever the positronium formation cross section is negligible, in particular, above 100 eV for this system. The total ionization cross section resulting in this energy region are in excellent agreement with the recent measurements of Jones et al., and so lie below the earlier measurements of Spicher et al., and the recent calculations of Acacia et al.. The total cross section is in very good agreement with the recent measurements of Zhou et al. down to 30 eV. DOE

N95-20198# Flinders Univ., Adelaide (Australia). Electronic Structure of Materials Centre.
THE (e,2e) CALCULATIONS WITH THE FINAL-STATE BOUNDARY CONDITION
D. A. Konovalov and I. E. McCarthy Nov. 1993 6 p
(DE94-631342; ESM-63) Avail: CASI HC A02/MF A01 (US Sales Only)

Calculations explore the use of an auxiliary final-state wave function with the Redmond boundary condition in attempting to describe the absolute cross sections for ionization of helium in coplanar-symmetric kinematics. DOE

N95-20199# Flinders Univ., Adelaide (Australia). Electronic Structure of Materials Centre.
CALCULATION OF ELECTRON SCATTERING ON THE He(+) ION
Igor Bray, I. E. McCarthy, J. Wigley, and A. T. Stelbovics Nov. 1993 10 p
(DE94-631343; ESM-64) Avail: CASI HC A02/MF A01 (US Sales Only)

The Convergent Close-Coupling method is applied to the calculation of electron scattering on the ground state of He(+). The inclusion of the treatment of the continuum, even below the ionization threshold, significantly reduces the calculated 2S cross section. Generally, it shows good agreement with the measurements of the 2S excitation cross section, though in the vicinity of a few eV near threshold the results are characteristically higher than the experiment. Complete quantitative agreement is obtained with the measurement of the total ionization cross section from threshold to 700 eV. DOE

N95-20206# Sandia National Labs., Albuquerque, NM.
DESIGN TRADE-OFF STUDY FOR A LARGE VOLUME SHORT PULSE NEUTRON ASSEMBLY
P. J. Griffin, J. D. Miller, G. A. Harms, E. J. Parma, R. L. Coats, W. C. Fan, and J. P. Petraglia (Battelle Pantex, Amarillo, TX.) 1994 9 p Presented at the Winter Meeting of the American Nuclear Society, Washington, DC, 13-18 Nov. 1994
(Contract DE-AC04-94AL-85000)
(DE94-019175; SAND-94-0796C; CONF-941102-24) Avail: CASI HC A02/MF A01

There is a continuing need within the radiation effects research community for more intense and larger volume pulsed neutron facilities. To fulfill these requirements a study was performed to examine conceptual designs for a neutron assembly that could produce high-intensity, short pulse neutron environments over a large experimental volume. The desired system characteristics were a cylindrical experimental cavity 60 inches long (152.4 cm) with a 24 inch diameter (60.96 cm), a cavity fluence of phi(sub r) = 8 x 10(exp 14) n/cm(exp 2), and a neutron pulse width of tau = 10-20 (mu)s. Attention was focused on booster assemblies which have been studied since the 1950s at Harwell, General Atomic, and at Sandia National Laboratories. Five conceptual designs were developed and evaluated. Only a two-stage coupled core design with a NpO2 primary core assembly was found to meet the design goals. A program is proposed to refine the design and to construct this nuclear assembly. The proposed three-phase effort represents a conservative approach that will yield large increases in the experiment volume even if the final coupled-core design is not realized. DOE

N95-20217# Fermi National Accelerator Lab., Batavia, IL.
SEARCH FOR TOP IN DO USING THE ELECTRON + JETS CHANNEL WITH SOFT MUON TAGGING
R. Raja Sep. 1994 5 p Presented at the 27th International Conference on High Energy Physics, Glasgow, Scotland, 21-27 Jul. 1994
(Contract DE-AC02-76CH-03000)
(DE95-001284; FNAL/C-94/327-E; CONF-940722-26) Avail: CASI HC A01/MF A01

We present preliminary results for the search for the top quark in DO in the electron + jets channel where one of the b quark jets is tagged by means of a soft muon, using 13.5 pb(exp -1) of data. Standard model decay modes for the top quark are assumed. We present the resulting top cross section and error as a function of top mass using this channel combined with the dilepton channel and the untagged lepton + jets channel presented elsewhere in this session. At present, no significant signal for top quark production can be established. DOE

N95-20235# Los Alamos National Lab., NM.
A S2-LIKE ACCELERATION METHOD FOR THE NONLINEAR CHARACTERISTIC TRANSPORT SCHEME
T. A. Wareing, W. F. Walters, and J. E. Morel 1994 6 p Presented at the Winter Meeting of the American Nuclear Society, Washington, DC, 13-18 Nov. 1994
(Contract W-7405-eng-36)
(DE94-016285; LA-UR-94-2397; CONF-941102-13) Avail: CASI HC A02/MF A01

Recently a nonlinear spatial differencing scheme for solving the discrete-ordinate equations was introduced. This scheme, referred to as the Nonlinear Characteristic (NC) scheme, is accurate for both optically thin and optically thick spatial meshes and is strictly positive. The NC discrete-ordinate equations can be solved using the source iteration (SI) method. It is well known that the SI method converges infinitely slowly for optically thick problems with scattering ratios near unity. In this summary, we describe a S2-like acceleration scheme for accelerating the convergence of the SI method as applied to the NC scheme and provide results to show how effective it is. DOE

N95-20236# Los Alamos National Lab., NM.
NEW DATA FOR MCNP (TRADEMARK)
J. S. Hendricks, S. C. Frankle, and J. D. Court 1994 5 p Presented at the Winter Meeting of the American Nuclear Society, Washington, DC, 13-18 Nov. 1994
(Contract W-7405-eng-36)
(DE94-016296; LA-UR-94-2376; CONF-941102-17) Avail: CASI HC A01/MF A01

We report here for the first time the availability of an official set of ENDF/B-VI neutron data for MCNP(trademark). The LANL Radiation Transport group engaged the Nuclear Theory and Applications Group to construct a complete library based on ENDF/B-VI Release in the Spring of 1994. A new and thorough set of quality assurance tests was established and data passing those tests were subject only to a limited set of benchmarking tests. All nuclides were subjected to infinite medium calculations. The fissionable materials were benchmarked against critical assemblies, and 28 nuclides were benchmarked against the LLNL pulsed sphere experiments. DOE

N95-20242# Nebraska Univ., Lincoln, NE. Dept. of Physics and Astronomy.
DYNAMICS OF COLLISION PROCESSES
A. F. Starace Feb. 1994 7 p
(Contract DE-FG02-88ER-13955)
(DE94-017593; DOE/ER-13955/16) Avail: CASI HC A02/MF A01

Investigations have been carried out of one-, two-, and three-photon detachment of the negative hydrogen ion (H(-)) including effects of electron correlations, of two-color detachment of H(-) with excitation of H(n=2), and of the (sup 3pe) state of H(-). Striking effects of long-range dipole field interactions have been demonstrated. Electron correlation effects on detachment cross sections have been quantified. Electric field effects on photodetachment of H(-) above the H(n=2) threshold have also been elucidated. Variational R-matrix calculations of photodetachment of Hand of Li(-) including excitations of the residual atoms up to the n=6 level have provided state-of-the-art agreement with recent experimental results. Furthermore, doubly-excited-state spectra of H(-) and Li(-) have been shown to be remarkably similar. DOE

N95-20254# Los Alamos National Lab., NM.
MCNP (TRADEMARK) DIRECTIONS
J. S. Hendricks 1994 6 p Presented at the Winter Meeting of the American Nuclear Society, Washington, DC, 13-18 Nov. 1994
(Contract W-7405-eng-36)

(DE94-016216; LA-UR-94-2547; CONF-941102-12) Avail: CASI HC A02/MF A01

The MCNP code development program is a relatively large and rapidly changing project in the small and highly-specialized field of radiation transport, specifically radiation protection and shielding. A number of major new MCNP initiatives are described in the subsequent papers in this session. The focus of this paper is the important new developments not described elsewhere and a number of recent developments that have been available since MCNP4A but have gone unnoticed. In particular, we report for the first time a new MCNP quality assurance initiative providing 97% test coverage, a new MCNP feature enabling plotting of nuclear data, and the other new features developed so far for MCNP4B. Finally, an attempt is made to articulate how all these fit together into the overall MCNP development program. DOE

N95-20327 New Orleans Univ., LA. Dept. of Chemistry.
DENSITY FUNCTIONAL STUDIES OF DECOMPOSITION PROCESSES OF ENERGETIC MOLECULES
Peter Politzer, Jorge M. Seminario, and M. E. Grice 3 Nov. 1994 13 p Limited Reproducibility: More than 20% of this document may be affected by microfiche quality
(Contract N00014-91-J-4057)
(AD-A286185) Avail: CASI HC A03

Nonlocal density functional theory is an effective means for determining the energetics and elucidating the mechanisms of the decomposition processes of molecules of real chemical interest and significance. It should be viewed as another practical tool that is available for this purpose, a useful addition to existing experimental techniques, but with the extremely important advantage that it can be applied to proposed molecules that may not yet have been synthesized or isolated. Decomposition energetics of some nitramines and nitrotriazoles are presented and discussed. DTIC

N95-20337# Oak Ridge National Lab., TN.
AMORPHIZATION OF SAPPHIRE DURING ION BEAM MIXING
D. L. Joslin (Tennessee Univ., Knoxville, TN.), C. J. McHargue (Tennessee Univ., Knoxville, TN.), C. W. White, and N. D. Evans (Oak Ridge Inst. for Science and Education, TN.) 1994 9 p Presented at the Nuclear Instruments and Methods in Physics Research on Radiation Effects in Insulators, Nagoya, Japan, 5-10 Sep. 1993
(Contracts DE-AC05-84OR-21400; DE-AC05-76OR-00033)
(DE94-018713; CONF-9309259-6) Avail: CASI HC A02/MF A01

Earlier studies indicated that implantation of zirconium into sapphire at room temperature produced an amorphous layer at a critical composition of approximately 6.5% (cation). Further insight into the amorphization of sapphire has been provided by ion beam mixing studies. Bi-layer couples of approx. 80 nm thick polycrystalline ZrO2 films deposited on the (0001) face of alpha-Al2O3 single crystals were irradiated to 4 x 10(exp 16) ions/sqcm with Kr (475 keV, 20 C), or Cr (340 keV, 20 C or approx. 900 C). Transmission electron microscopy showed the unirradiated couples to have sharp, planar interfaces between the films and substrates. Recoil mixing by both ion species gave Zr concentrations greater than 10% (cation) to depths of 10-20 nm. An amorphous layer containing Zr was present at the interface for samples irradiated at room temperature. The sample mixed at the elevated temperature contained a sharp interface similar to the as-deposited sample. The present results suggest that both irradiation-produced damage (defects) and certain chemical species are required to amorphize sapphire. DOE

N95-20343# Fermi National Accelerator Lab., Batavia, IL.
CDF TOP RESULTS IN THE DILEPTON CHANNEL
J. M. Benlloch (Massachusetts Inst. of Tech., Cambridge, MA.) Sep. 1994 6 p Presented at the Meeting of the Division of Particles and Fields of the American Physical Society, Albuquerque, NM, 2-6 Aug. 1994
(Contract DE-AC02-76CH-03000)
(DE95-000837; FNAL/C-94/326-E; CONF-940816-34) Avail: CASI HC A02/MF A01

The current status of the top quark search at CDF in the dilepton channel is presented. In the 1992-1993 run (Run 1a), with 19.3 pb(exp -1) collected, two e mu events survived all the cuts, including a two-jet cut for high mass top, with a total estimated background of 0.56(sub -0.13)(sup +0.25) events. With approximately 9 pb(exp -1) of data analyzed from the 1993-1994 run (Run 1b) a new e mu event passing all the cuts has been detected. DOE

N95-20344# Fermi National Accelerator Lab., Batavia, IL.
D0 QUANTUM CHROMODYNAMICS: A COMPILATION OF RESULTS PRESENTED AT DPF 1994
S. T. Fahey (Michigan State Univ., East Lansing, MI.) Sep. 1994 49 p Presented at the Meeting of the Division of Particles and Fields of the American Physical Society, Albuquerque, NM, 2-6 Aug. 1994
(Contract DE-AC02-76CH-03000)
(DE95-000838; FNAL/C-94/323-E; CONF-940816) Avail: CASI HC A03/MF A01

This report contains papers on the following topics: direct photon production at D0; direct photon angular distribution at D0; inclusive jet cross sections at the D0 detector; a study of the inclusive jet cross section as a function of jet cone size with the D0 detector; measurement of the triple differential inclusive dijet cross section, d(sup 3) sigma/dE(sub T) d eta(sub 1) d eta(sub 2) in p(bar p) collisions at square root of s = 1.8 TeV; measurement of the jet shapes in p(bar p) collisions at D0; use of a K(sub perpendicular) jet algorithm in p(bar p) collisions at D0; measurement of the strong coupling constant (alpha(sub s)) using W+ jets processes in the D0 detector; measurement of the W/Z P(sub T) distributions at D0; jet production at large rapidity intervals; rapidity gaps between jets at D0; and probing color coherency using high pT W events at the tevatron. DOE

N95-20346# Cornell Univ., Ithaca, NY. Dept. of Chemistry.
MOLECULAR SNAPSHOTS: PRODUCT IMAGING OF DYNAMICS IMPORTANT TO FUNDAMENTAL COMBUSTION PROCESSES
1994 7 p
(Contract DE-FG02-88ER-13934)
(DE94-018595; DOE/ER-13934/6) Avail: CASI HC A02/MF A01

The authors studied the 355 photodissociation of NO2 cooled in a supersonic beam by the method of state-resolved photofragment imaging. In addition, they have studied the state-to-state differential cross-sections for inelastic collisions of NO with Ar in a crossed-beam experiment using time-of-flight ion imaging. DOE

N95-20360# Argonne National Lab., IL.
A TAU-CHARM-FACTORY AT ARGONNE
J. Norem and J. Repond 18 Jul. 1994 8 p Presented at the Workshop on the Future of High Sensitivity Charm Experiments, Batavia, IL, 7-9 Jun. 1994
(Contract W-31-109-eng-38)
(DE94-016913; ANL-HEP-CP-94-39; CONF-9406242-1) Avail: CASI HC A02/MF A01

In this paper we explore the possibility of building a tau-charm-factory at the Argonne National Laboratory. A tau-charm-factory is an e(exp +)e(exp -) collider with a center-of-mass energy between 3.0 GeV and 5.0 GeV and a luminosity of at least 1 x 10(exp 33) cm(exp -2) s(exp -1). Once operational, the facility will produce large samples of tau pairs, charm mesons, and charmonium with either negligible or well understood backgrounds. This will lead to high precision measurements in the second generation quark and the third generation lepton sectors that cannot be done at other facilities. Basic physical properties and processes, such as the tau neutrino mass, rare tau decays, charm decay constants, rare charm meson decays, neutral D(sup 0) -- meson mixing, and many more will be studied with unique precision. An initial design of the collider including the injector system is described. The design shows that a luminosity of at least 1 x 10(exp 33) cm(exp -2) s(exp -1) can be achieved over the entire center-of-mass energy range of the factory. DOE

N95-20367# Los Alamos National Lab., NM.
SEMI-LEPTONIC FORM-FACTORS FROM LATTICE QCD
T. Bhattacharya and R. Gupta 1994 4 p Presented at the Meeting of the Division of Particles and Fields of the American Physical Society, Albuquerque, NM, 2-6 Aug. 1994
(Contract W-7405-eng-36)
(DE95-000871; LA-UR-94-3079; CONF-940816-33) Avail: CASI HC A01/MF A01

We present results for semileptonic form-factors obtained on statistical sample of 63 32(exp 3) x 64 lattices at beta = 6.0 using quenched

Wilson fermions. We find f(sub +)(sup D yields Klv) (q(exp 2) = 0) = 0.73 +/- 0.06, A(sub 2)/A(sub 1)(D yields K(sup *)lv) = 0.79 +/- 0.23, V/A(sub 1)(D(sub s) yields phi lv) = 1.89 +/- 0.04, and A(sub 2)/A(sub 1)(D(sub s) yields phi lv) = 0.70 +/- 0.09, where the error estimate includes statistical errors and errors due to extrapolation to q(exp 2) = 0 and to physical values of (m(sub u) + m(sub d))/2 and m(sub s). The remaining sources of systematic errors are those due to O(a) discretization errors and those due to quenching, which our results indicate may be small. We also comment on the validity of pole-dominance in these form-factors. DOE

N95-20401# Fermi National Accelerator Lab., Batavia, IL.
MASS AND LIFETIME MEASUREMENTS WITH EXCLUSIVE B RECONSTRUCTION AT CDF
J. D. Lewis Jul. 1994 16 p Presented at the Les Rencontres de Physique de la Vallee D'aoste, La Thuile, Italy, 6-12 Mar. 1994
(Contract DE-AC02-76CH-03000)
(DE94-015849; FNAL/C-94/128-E; CONF-9403127-2) Avail: CASI HC A03/MF A01

Lifetimes and masses of B mesons have been measured in exclusively reconstructed decays including J/(psi) yields (mu)(sup +) decays. In 19.3 pb(sup -1) of (bar p)p collisions at s(exp 1/2) = 1.8 TeV taken in 1992-93 at the Fermilab Tevatron collider, approximately 300 B mesons have been fully reconstructed. The measurements require precise determination of the helical track parameters of charged particle tracks. We find M(B(sub S)(sup O)) = 5367.7 +/- 2.4 +/- 4.8 MeV/c(exp 2), tau(B(sup +)) = 1.61 +/- 0.16 +/- 0.05 ps, and tau(B(sup O)) = 1.57 +/- 0.18 +/- 0.08 ps. DOE

N95-20404# Brookhaven National Lab., Upton, NY.
HIGGS DECAY TO BOTTOM QUARKS AT THE TEVATRON
A. Stange, W. Marciano, and S. Willenbrock (Fermi National Accelerator Lab., Batavia, IL.) Oct. 1993 7 p Presented at the Workshop on Physics at Current Accelerators and the Supercollider, Argonne, IL, 2-5 Jun. 1993
(Contract DE-AC02-76CH-00016)
(DE94-016715; BNL-49643; CONF-9306176-24) Avail: CASI HC A02/MF A01

We study the production and detection of the standard-model Higgs boson at the Fermilab Tevatron. The most promising mode is WH and ZH associated production followed by leptonic decay of the weak vector bosons and H yields b(bar b). It may be possible to detect a Higgs boson of mass m(sub H) = 60-80 GeV with 1000 pb(sup -1) of integrated luminosity. DOE

N95-20415# Fermi National Accelerator Lab., Batavia, IL.
MEASUREMENTS OF THE MASS AND WIDTH OF THE W BOSON FROM CDF
Young-Kee Kim (California Univ., Berkeley. Lawrence Berkeley Lab, CA.) 1994 11 p Presented at the 29th Moriond Meeting on Quantum Chromodynamics and High Energy Hadronic Interactions, Les Arcs, France, 12-26 Mar. 1994
(Contract DE-AC02-76CH-03000)
(DE94-015380; FNAL/C-94/169-E; CONF-940327-8) Avail: CASI HC A03/MF A01

We have made a preliminary determination of the W boson mass, M(sub W) = 80.38 +/- 0.23 GeV/c(exp 2) from a combined analysis of W yields e(nu) in (bar p) collisions at s(exp 1/2) = 1.8 TeV. The electron data alone approaches M(sub W) = 80.47 + /- 0.15(stat.) +/- 0.25(syst.) GeV/c(exp 2), while the muon data gives M(sub W) = 80.29 +/- 0.20(stat.) +/- 0.24(syst.) GeV/c(exp 2). Measuring the ratio (sigma)(sub W)(center dot)B(W approaches e(nu)) / (sigma)(sub Z) approaches e(sup +)e(sup -), we have extracted a value for the W width, Gamma(W) = 2.063 +/- 0.061(stat.) +/- 0.060(syst.) GeV and the branching ratio, (Gamma)(W approaches e(nu))/Gamma(W) = 0.1094 +/- 0.0033(stat.) +/- 0.0031(syst.). This allows us to set a decay mode independent limit on the top quark mass, m(sub top) greater than 62 GeV/c(exp 2) at the 95% C.L. DOE

N95-20418# Fermi National Accelerator Lab., Batavia, IL.
NUCLEAR A DEPENDENCE OF EXCLUSIVE VECTOR MESON PRODUCTION IN MUON SCATTERING
Heidi Schellman Jul. 1994 8 p Presented at the 29th Moriond Meeting on Quantum Chromodynamics and High Energy Hadronic Interactions, Les Arc, France, 12-26 Mar. 1994
(Contract DE-AC02-76CH-03000)
(DE95-002248; FNAL/C-94/219-E; CONF-940327-13) Avail: CASI HC A02/MF A01

Results on exclusive vector meson production from Fermilab muon scattering experiment E665 are presented. The A dependence of exclusive vector meson production is studied as a function of Q(exp 2). The data show a significant change in the dependence on A at higher values of Q(exp 2). The observed behavior is consistent with the idea of color transparency. DOE

N95-20422# Oak Ridge National Lab., TN.
NON DESTRUCTIVE CHARACTERIZATION USING PULSED FAST-THERMAL NEUTRONS
P. C. Womble, F. J. Schultz, and G. Vourvopoulos (University of Western Kentucky, Bowling Green, KY.) 1994 15 p Presented at the 13th International Conference on the Application of Accelerators in Research and Industry, Denton, TX, 7-10 Nov. 1994
(Contracts DE-FG22-93PC-93211; DE-AC05-84OR-21400)
(DE95-002601; CONF-941129-7) Avail: CASI HC A03/MF A01

It has been shown that explosives, illicit drugs, and other contraband materials contain various chemical elements in quantities and ratios that differentiate them from each other and from other innocuous substances. In coal, the major chemical elements in it can provide information about various parameters of importance to the coal industry. In both examples, the nondestructive identification of chemical elements can be performed by utilizing incident pulsed fast-thermal neutrons that, through nuclear reactions, excite the nuclei of the various elements. This technique is being currently developed for dismantling of nuclear weapons classified as trainer's, and for on-line coal bulk analysis. DOE

N95-20434 Rutherford Appleton Lab., Chilton (England).
MUON DATA ANALYSIS PROGRAM RUMDA
S. H. Kilcoyne Jul. 1994 34 p
(PB95-129839; RAL-94-080) Avail: Issuing Activity (National Technical Information Service (NTIS))

There are currently two data analysis programs available for muon users at ISIS. Both programs can be used for analyzing MuSR and EMU data and can be run on (MUSR01), (EMU01) or set-up to run on a user's account. RUMDA - 'Reading University Muon Data Analysis' was originally from Reading University and is now controlled at ISIS. At present (mid 1994) this suite of programs is run using VAX/VMS and the ISIS plotting package 'GENIE'. It is possible to fit data to any function with a maximum of 10 variables. UDA - 'mu Data Analysis' is a dashboard driven program which allows the user to plot and fit data files on the screen or as hard copies. It is possible to fit data to a combination of Gaussian and/or Lorentzian line shapes. A manual describing this program can be found in the back of the MuSR User Guide. NTIS

N95-20444# Lawrence Livermore National Lab., Livermore, CA.
PROGRAM WALKMAN: A CODE DESIGNED TO PERFORM ELECTRON SINGLE COLLISION ELASTIC SCATTERING MONTE CARLO CALCULATIONS
D. E. Cullen Aug. 1994 29 p
(Contract W-7405-eng-48)
(DE94-017501; UCRL-ID-118276) Avail: CASI HC A03/MF A01

The computer code WALKMAN performs electron single collision elastic scattering Monte Carlo calculations in spherical or planar geometry. It is intended as a research tool to obtain results that can be compared to the results of condensed history calculations. This code is designed to be self documenting, in the sense that the latest documentation is included as comment lines at the beginning of the code. Printed documentation, such as this document, is periodically published and consists mostly of a copy of the comment lines from the code. The user should be aware that the comment lines within the code are continually updated to reflect the most recent status of the code and these comments should always be considered to be the most recent documentation for the code and may supersede published documentation, such as this document. Therefore, the user is advised to always read the documentation within the actual code. The remainder of this report consists of example results and a listing of the documentation which appears at the beginning of the code. DOE

N95-20451# Washington Univ., Seattle, WA.
DIFFUSION ENHANCES SPONTANEOUS ELECTROWEAK BARYOGENESIS
A. G. Cohen (Boston Univ., MA.), D. B. Kaplan, and A. E. Nelson 1994 15 p
(Contracts DE-FG06-90ER-40561; DE-FG02-91ER-40676)
(DE94-017574; DOE/ER-40561/146; NSF-ITP-94-67) Avail: CASI HC A03/MF A01

We include the effects of diffusion in the electroweak spontaneous baryogenesis scenario and show that it can greatly enhance the resultant baryon density, by as much as a factor of 1/alpha(sub w)(sup 4) approximately equal to 10(exp 6) over previous estimates. Furthermore, the baryon density produced is rather insensitive to parameters characterizing the first order weak phase transition, such as the width and propagation velocity of the phase boundary. DOE

N95-20454 Rutherford Appleton Lab., Chilton (England).
GAJET EXPERIMENT AT THE LHC: THE GAJET COLLABORATION
P. D. Dauncey, T. Nakada, and J. P. Perroud 19 Jul. 1994 33 p Second Workshop on B-Physics at Hadron Machines held in Le Mont Saint Michel, France, 24-29 Apr. 1994 Prepared in cooperation with Science Research Council, Daresbury, England; Paul Scherrer Inst., Villigen, Switzerland; and Lausanne Univ., Switzerland
(PB95-129813; RAL-94-076) Avail: Issuing Activity (National Technical Information Service (NTIS))

CP violation is one of few remaining phenomena which possibly may not be accommodated in the framework of the standard model. Although experiments with kaons will still dominate the scene for a while, the B-meson system provides the cleanest ground to test whether observed violation of CP symmetry is a sign of new physics or not. By the time LHC (Large Hadron Collider) will become fully operational, a CP violation effect in the theoretically cleanest and experimentally simplest decay mode B(sup 0) approaches J/(psi)K(sub s) could well have already been seen elsewhere, for example at e(+)e(-) B-meson factories, by HERA-B and at FNAL. Therefore, the aim of a dedicated B experiment at LHC must be to make precision measurements of all the three angles of the unitarity triangle. This requires a detector capable of identifying particles up to a high momentum, measuring accurately the decay time of the B-meson and triggering on various B-meson decay modes into a few charged particles. In order to realize such an experiment at the LHC, we chose a technique using an internal gas jet target (GAJET). In this paper, we discuss the reason of this choice, the proposed spectrometer, the trigger and the expected physics performance of the experiment. NTIS

N95-20469# Florida Univ., Gainesville, FL. Inst. for Fundamental Theory.
RESEARCH IN THEORETICAL ELEMENTARY PARTICLE PHYSICS AT THE UNIVERSITY OF FLORIDA, TASK A
R. D. Field, P. M. Ramond, P. Sikivie, and C. B. Thorn 1 Nov. 1993 95 p
(Contract DE-FG05-86ER-40272)
(DE94-004373; DOE/ER-40272/194-Task-A; UFIFT-HEP-93-24-Task-A) Avail: CASI HC A05/MF A01

This is the Annual Progress Report of the theoretical particle theory group at the University of Florida under DOE Grant DE-FG05-86ER-40272. At present our group consists of four Full Professors (Field, Ramond, Thorn, Sikivie) and three Assistant Professors (Qiu, Woodard, Kennedy). Dallas Kennedy recently joined our group increasing the Particle Theory faculty to seven. In addition, we have three postdoctoral research associates, an SSC fellow, and eight graduate students. The research of our group covers a broad range of topics in theoretical high energy physics with balance between theory and phenomenology. Included in this report is a summary of the last several years of operation of the group and an outline of our current research program. DOE

N95-20475# Fermi National Accelerator Lab., Batavia, IL.
SEARCH FOR D(+) YIELDS (PI)(+)(MU)(+)(MU)(-)
A. Nguyen et al Jul. 1994 4 p
(Contract DE-AC02-76CH-03000)
(DE94-015538; FNAL/C-94/187-E) Avail: CASI HC A01/MF A01

Flavor-changing neutral current decays are forbidden in lowest order in the Standard Model. The authors present results of a search for the charm changing neutral current decay D(+) (yields) (pi)(+)(mu)(+)(mu)(-) based on the analysis of one third of the data from Fermilab experiment E791, accumulated during the 1991-92 fixed target run with a 500 GeV negative pion beam incident on a segmented target. Assuming that the decay kinematics are the same as for D(+) (yields) K(-)(pi)(+)(pi)(+), they set an upper limit on the branching ratio for this channel, B(D(+) (yields) (pi)(+)(mu)(+)(mu)(-))less than 4.6 x 10(exp -5) at the 90% confidence level. DOE

N95-20476# Fermi National Accelerator Lab., Batavia, IL.
D(SUP 0)-(ANTI-D)(SUP 0) MIXING AND DOUBLY CABIBBO-SUPPRESSED DECAYS OF THE D(+)
M. V. Purohit et al Jul. 1994 11 p
(Contract DE-AC02-76CH-03000)
(DE94-015540; FNAL/C-94/186-E) Avail: CASI HC A03/MF A01

This report summarizes results from Fermilab experiment E791 on D(sup 0)-(anti D)(sup 0) mixing and doubly Cabibbo-suppressed decays of the D(+) meson. In order to search for D(sup 0)-(anti D)(sup 0) mixing, the authors use only D(sup 0) mesons from D(sup *+) decays in which case the charge of the pion from the D(sup *+) decay identifies the charm quantum number of the D(sup 0) at birth. When the D(sup 0) decays, the charge of the kaon identifies the charm quantum number and this way one can tell if mixing has occurred. This kind of search can be carried out by CLEO 2 as well and their conclusion was that there is some evidence of a wrong sign signal (0.77 +/- 0.25 +/- 0.25)% of the right sign signal. However, because of a lack of lifetime information, they cannot distinguish between doubly Cabibbo-suppressed decays which are expected at the level of the observed signal and mixing. They use their excellent lifetime sensitivity to obtain separate limits. During the past year, the authors have been working on extracting D(+) doubly Cabibbo-suppressed decay signals from E791's data sample. These decays are interesting both because they have never been observed and because definite predictions have been made about their rates, based on models of D mesons and their decay mechanisms. Preliminary analyses of 1/3 of the data have now been completed. Figure 3 shows the Cabibbo-favored signal D(+) (yields) K(-) (pi)(+)(pi)(+) and the next figure shows the signal in the doubly Cabibbo-suppressed mode D(+) (yields) K(+)(pi)(-)(pi)(-0). DOE

N95-20477# Brookhaven National Lab., Upton, NY.
A NEW FAMILY OF ANION RECEPTORS AND THEIR EFFECTS ON ION PAIR DISSOCIATION AND CONDUCTIVITY OF LITHIUM SALTS IN NON-AQUEOUS SOLUTIONS
H. S. Lee, X. Q. Yang, J. McBreen, and Y. Okamoto (Polytechnic Univ., Brooklyn, NY.) 1994 13 p Presented at the 4th International Symposium on Polymer Electrolytes, Newport, RI, 19-24 Jun. 1994
(Contract DE-AC02-76CH-00016)
(DE94-016822; BNL-60409; CONF-940690-1) Avail: CASI HC A03/MF A01

A new family of anion receptors based on aza-ether compounds have been synthesized. Since the anion complexation of these compounds is not based on either positively charged sites or hydrogen bonding, they have a potential to be used in lithium batteries as electrolyte additives. When these compounds are added into nonaqueous electrolytes using lithium salts, such as LiCl/BF or LiBr/THF, the ionic conductivity can be dramatically increased. Near Edge X-ray Absorption Fine Structure (NF-XAFS) spectroscopy studies show that Cl(-) anions are completed with the nitrogen groups in these compounds. The increase in ionic conductivity and the degree of complexation, are both related to the number of R=CF3SO2 groups that are used to substitute the amine hydrogen atoms in these aza-ether compounds. DOE

N95-20491# Tennessee Technological Univ., Cookeville, TN. Dept. of Physics.
COMPETING STRUCTURES IN NUCLEI NEAR CLOSED SHELLS
S. J. Robinson Jul. 1994 9 p
(Contract DE-FG05-93ER-40809)
(DE94-017604; DOE/ER-40809/T1) Avail: CASI HC A02/MF A01

This report covers the following topics: (1) GRID lifetime measurements in neodymium 144; (2) fast electronic timing system; and (3) massive neutrino searches. DOE

N95-20496# Fermi National Accelerator Lab., Batavia, IL.
PRODUCTION OF J/(PSI) IN 800 GeV/c p-SI INTERACTIONS
Jul. 1994 8 p
(Contract DE-AC02-76CH-03000)
(DE94-017982; FNAL/C-94/178-E) Avail: CASI HC A02/MF A01

The authors report on the analysis of high mass opposite sign dimuon states produced in pSi interactions at (radical)s = 38.7 GeV. These data have been collected with an open geometry fixed target spectrometer in the Fermilab Experiment E771. J/(psi) and (psi)(2S) total cross section sand J/(psi) x(sub f) and p(sub t) differential cross sections have been measured and compared with extrapolations from data at lower energies. Evidence for (Upsilon) meson production is also presented. DOE

N95-20554# George Washington Univ., Washington, DC. Dept. of Chemistry.
IDENTIFICATION OF RESONANT, TWO-ELECTRON, AND INTER-ATOMIC FEATURES IN K AND L23 NEXAFS SPECTRA Technical Report, Sep. 1993 - Oct. 1994
H. Sambe, X. Qian, David E. Ramaker, and W. E. OGrady Sep. 1994 9 p
(Contract N00014-94-I-0331)
(AD-A285374; TR-69) Avail: CASI HC A02/MF A01

Experimental Cl K NEXAFS spectra for Cl- hydrated in H2O, and on passivated Al electrodes (below and above the pitting potential) have widely different spectral line shapes. Experimental K- and L23-edge NEXAFS data for the alkali halides and rare gas solids are compared with FEFF6 calculated results to optimize code input parameters, test code validity, and identify many-body features in these model systems. Differences are shown to arise from many-body shake-up and charge-transfer excitations. Although relatively small in the model spectra, the latter interatomic excitations are believed to be primarily responsible for the different Cl- line shapes on the passivated Al electrodes. DTIC

N95-20575# California Univ., Berkeley. Lawrence Berkeley Lab, CA.
STRANGE PARTICLE AND ANTIPROTON PRODUCTION IN S + NUCLEUS COLLISIONS AT 200 GeV/NUCLEON
S. Margetis Jun. 1994 6 p Presented at the Meeting of the Division of Particles and Fields of the American Physical Society, Albuquerque, NM, 2-6 Aug. 1994
(Contract DE-AC03-76SF-00098)
(DE95-002348; LBL-36103; CONF-940816-43) Avail: CASI HC A02/MF A01

Central S+S, S+Ag and S+Au collisions at 200 GeV/nucleon were studied in experiment NA35 at the CERN SPS. Recent results on strange particle production as well as the preliminary results on antiproton production are presented and discussed. Enhanced strangeness production relative to the pion and antiproton yields is observed in nucleus-nucleus collisions relative to p-p and p-A. Microscopic string models fail to consistently describe the available set of data. DOE

N95-20585 Wisconsin Univ., Madison, WI. Dept. of Chemistry.
AN ATOMICALLY-RESOLVED STM STUDY OF THE INTERACTION OF PHOSPHINE (PH3) WITH THE SILICON (001) SURFACE Interim Report, 1 Jun. 1993 - 31 May 1994
Y. Wang, J. Bronikowski, and R. J. Hamers 27 May 1994 21 p Limited Reproducibility: More than 20% of this document may be affected by microfiche quality
(Contract N00014-91-J-1629)
(AD-A279819; TR-18) Avail: CASI HC A03

The interaction of phosphine (PH3) with the Si(001) surface has been investigated with scanning tunneling microscopy. At 300 K, PH3 adsorbs molecularly on top of a single Si=Si dimer with the phosphorus atom in a pentacoordinate configuration. Phosphine adsorption is accompanied by occasional ejection of silicon atoms from the substrate onto the surface, creating surface vacancies and Si adatoms. Si atoms are preferentially ejected from defect sites. At high coverage, adsorbed PH3 molecules order into small regions of c(4-by-2) symmetry and the ejected silicon nucleates into small dimer strings. The long-range order of the molecular PH 3 is disrupted by domain boundaries and the ejected silicon. Annealing PH 3- saturated surfaces produces further ejection of silicon onto the surface, resulting in large silicon islands covering approximately 20% of the surface. DTIC

N95-20586 Wisconsin Univ., Madison, WI. Dept. of Chemistry.
ATOMICALLY RESOLVED STRUCTURE AND BONDING OF DELTA-DOPED BORON LAYERS ON SI(001) Interim Report, 1 Jun. 1993 - 31 May 1994
Y. Wang and R. J. Hamers 27 May 1994 10 p Limited Reproducibility: More than 20% of this document may be affected by microfiche quality
(Contract N00014-91-J-1629)
(AD-A279820; TR-19) Avail: Issuing Activity (Defense Technical Information Center (DTIC))

Scanning tunneling microscopy has been used to study the formation of delta-doped layers by thermal decomposition of diborane on Si(001). STM images reveal a number of boron-induced reconstructions which arise from ordered arrangements of three structural subunits. Based on the symmetry of the STM images and the bonding locations of the observed features with respect to the Si(001) lattice, a structural model is proposed with accounts for the observed STM features. The principal structural subunit is shown to be an ordered arrangement of four boron atoms at substitutional sites in the first bulk-like silicon layer, which is then capped with ordered arrangements of silicon dimers and dimer vacancies. DTIC

N95-20621 Bowling Green State Univ., OH. Dept. of Chemistry.
PUBLICATIONS/PATENTS/PRESENTATIONS/HONORS/STUDENT REPORT. INVESTIGATION OF THE ROLE OF VIBRATIONAL EXCITATION IN UNIMOLECULAR REACTIONS
Deanne Snavely 3 Jun. 1994 11 p Limited Reproducibility: More than 20% of this document may be affected by microfiche quality
(Contract N00014-91-J-4130)
(AD-A280044) Avail: Issuing Activity (Defense Technical Information Center (DTIC))

Our overall goal is to investigate the nature of vibrationally energized molecules. Laser vibrational overtone activation produces energized molecules with specific vibrational excitation which undergo subsequent reaction. In these experiments the total pressure, excitation wavelength and collider gas are varied to determine the specific rate coefficient and collisional deactivation rate constants. Vibrational overtone spectroscopy of nonreactive molecules provides evidence of vibrational energy transfer pathways in reactive systems. Vibrational overtone excitation creates a narrow distribution of activated molecules compared to other forms of activation. This unique characteristic has allowed us to investigate the energy dependent reaction rate constant and the attributes of the collisional deactivation distribution in gaseous reactions. We have used laser vibrational excitation. We have determined the experimental specific rate coefficients for this reaction and compared them to the values predicted by RRKM theory. DTIC

N95-20629# California Univ., Berkeley. Lawrence Berkeley Lab, CA.
LASER TRAPPING OF Na-21 ATOMS Ph.D. Thesis
Zheng-Tian Lu Sep. 1994 152 p
(Contract DE-AC03-76SF-00098)
(DE95-002354; LBL-36120) Avail: CASI HC A08/MF A02

This thesis describes an experiment in which about four thousand radioactive (21)Na (t(sub I/2) = 22 sec) atoms were trapped in a magneto-optical trap with laser beams. Trapped (21)Na atoms can be used as a beta source in a precision measurement of the beta-asymmetry parameter of the decay of (21)Na yields (21)Ne + (Beta)(sup +) + v(sub e), which is a promising way to search for an anomalous right-handed current coupling in charged weak interactions. Although the number of trapped atoms that we have achieved is still about two orders of magnitude lower than what is needed to conduct a measurement of the beta-asymmetry parameter at 1% of precision level, the result of this experiment proved the feasibility of trapping short-lived radioactive atoms. In this experiment, (21)Na atoms were produced by bombarding (24)Mg with protons of 25 MeV at the 88 in. Cyclotron of Lawrence Berkeley Laboratory. A few recently developed techniques of laser manipulation of neutral atoms were applied in this experiment. The (21)Na atoms emerging from a heated oven were first transversely cooled. As a result, the on-axis atomic beam intensity was increased by a factor of 16. The atoms in the beam were then slowed down from thermal speed by applying Zeeman-tuned slowing technique, and subsequently loaded into a magneto-optical trap at the end of the slowing path. The last two chapters of this thesis present two studies on the magneto-optical trap of sodium atoms. In particular, the mechanisms of magneto-optical traps at various laser frequencies and the collisional loss mechanisms of these traps were examined. DOE

N95-20667# Cornell Univ., Ithaca, NY.
ION SCATTERING AND DEPOSITION: THE ROLE OF ENERGETIC PARTICLES IN THIN FILM GROWTH Annual Report, 1 Sep. 1993 - 31 Aug. 1994
Barbara H. Cooper 31 Aug. 1994 3 p
(Contract F49620-93-1-0504)
(AD-A285975; AFOSR-94-0675TR) Avail: CASI HC A01/MF A01

Energetic ions or neutrals (in the hyperthermal energy range) have been used in a number of thin film growth applications (e.g., sputtering and plasma deposition techniques, direct ion beam and ion-assisted deposition, etc.). These involve both direct deposition of the film species with an ion beam, and deposition by some other method during simultaneous ion bombardment. Experiments and simulations have shown that energetic ions can lower the substrate temperature required to achieve crystallinity, can change growth morphologies, and influence structure and crystallographic orientation in the film. In many cases, the mechanisms responsible for ion-induced modification of growth are not understood at the atomic level. We have initiated both scattering and scanning tunneling microscopy (STM) studies to probe these mechanisms. DTIC

N95-20732# California Univ., Berkeley. Lawrence Berkeley Lab, CA. Dept. of Physics.
ULTRAFAST MAGNETOEXCITON DYNAMICS IN GaAs
M. A. Mycek, U. Siegner, and D. S. Chemla May 1994 4 p Presented at the International Quantum Electronics Conference, Anaheim, CA, 8-13 May 1994
(Contract DE-AC03-76SF-00098)
(DE94-018175; LBL-35207; CONF-9405219-3) Avail: CASI HC A01/MF A01

A bulk semiconductor provides an excellent system for optically studying the ultrafast dynamics of Coulomb correlated magnetoexcitons. The applications of magnetic field to a 3-D system quantizes the energy levels of states with momentum perpendicular to B and, in contradistinction to experiments performed on 2-D quantum well systems, leaves a 1-D continuum of states with momentum parallel to B. The presence of the continuum states has a dramatic influence on both the linear and nonlinear optical properties. Thus, the experiments described blow track the evolution of the semiconductor from a 3-D to a 1-D system and reveal surprising optical properties not observed in the previously reported studies in quantum wells. Using ultrashort pulsed wave mixing spectroscopy, the authors investigate coherent emission from magnetoexcitons in GaAs. By spectrally resolving the emission, they relate the non periodic beat observed temporally to quantum interferences, which they attribute to Coulomb interactions between magnetoexcitons. Contrary to experiments in quantum wells, these interactions persist for fields strengths up to 10T. DOE

N95-20735# Joint Inst. for Nuclear Research, Dubna (USSR). Lab. of Theoretical Physics.
SYMMETRY, WIGNER FUNCTIONS AND PARTICLE REACTIONS
M. P. Chavlejshvili 1994 14 p Presented at the 3rd International Wigner Symposium: Symmetry in Physics, Oxford, England, 1993
(DE94-629887; JINR-E-2-94-22) Avail: CASI HC A03/MF A01 (US Sales Only)

We consider the great principle of physics - symmetry - and some ideas, connected with it, suggested by a great physicist Eugene Wigner. We will discuss the concept of symmetry and spin, study the problem of separation of kinematics and dynamics in particle reactions. Using Wigner rotation functions (reflecting symmetry properties) in helicity amplitude decomposition and crossing-symmetry between helicity amplitudes (which contains the same Wigner functions) we get convenient general formalism for description of reactions between particles with any masses and spins. We also consider some applications of the formalism. DOE

N95-20737# Tokyo Univ., Tanashi (Japan). Inst. for Nuclear Study.
QUANTIZATION IN CURVILINEAR COORDINATES
Kimihide Nishimura Jan. 1994 13 p
(DE94-770603; INS-1021) Avail: CASI HC A03/MF A01

The general covariant quantization method based on the equivalence principle is proposed. According to this method, it is found that an extra term: -1/3R appears in the Klein-Gordon equation. As a result, the effective mass of an electron, for example, will increase by the ratio of 10(exp -35) at the center of a neutron star. DOE

N95-20738# Tokyo Univ., Tanashi (Japan). Inst. for Nuclear Study.
UNIVERSAL PARAMETRIZATION FOR QUARK AND LEPTON SUBSTRUCTURE
Keiichi Akama (Saitama Univ., Urawa, Japan.) and Hidezumi Terazawa Jan. 1994 13 p
(DE94-770604; INS-1022) Avail: CASI HC A03/MF A01

A universal parametrization for possible quark and lepton substructure is advocated in terms of quark and lepton form factors. It is emphasized that the lower bounds on compositeness scale, (Lambda)(sub c), to be determined experimentally strongly depend on their definitions in composite models. From the recent HERA data, it is estimated to be (Lambda)(sub c) greater than 50 GeV, 0.4 TeV and 10 TeV, depending on the parametrizations with a single-pole form factor, a contact interaction and a logarithmic form factor, respectively. DOE

N95-20756# Tokyo Univ., Tanashi (Japan). Inst. for Nuclear Study.
SEARCH FOR RIGHT-HANDED CURRENTS IN THE DECAY CHAIN OF K(+) YIELDS MUON(+)nu(SUB MUON), MUON(+) YIELDS e(+)nu(SUB e)nu(BAR)(SUB MUON)
M. Aoki, T. Yamazaki, and J. Imazato et al Dec. 1993 65 p
(DE94-770606; INS-1019) Avail: CASI HC A04/MF A01

The asymmetry of positrons in the K(+) yields mu(+)nu, mu(+) yields e(+)nu(sub e) nu-bar(sub mu) decay chain was measured in a search for right-handed weak currents in (Delta)S = 1 semi-leptonic decay. High-intensity low-background monoenergetic polarized muons of 236 MeV/c momentum resulting from kaon decay at rest were directly extracted from a primary production target which was hit by a proton beam of the KEK 12-GeV proton synchrotron. Muons were stopped in a pure-aluminum plate, and the energy-integrated asymmetry of the decay positrons with respect to the incoming muon direction was determined to high precision. The observed asymmetry yielded xi P(sub mu) = -0.9996 +/- 0.0030(stat) +/- 0.0048(sys). This result revealed no evidence of right-handed currents in this kaon-decay chain, and set a stringent bound on the mass of the right-handed weak boson. DOE

N95-20804# Utah Univ., Salt Lake City, UT. Dept. of Chemistry.
ION-MOLECULE CHEMISTRY RELATED TO PLASMA DEPOSITION AND ETCHING OF SILICON Final Report, 16 May 1988 - 16 Dec. 1993
Peter B. Armentrout Feb. 1994 20 p
(Contract F33615-88-C-2833)
(AD-A279749; WL-TR-94-2012) Avail: CASI HC A03/MF A01

During the 5 years of this contract, we used guided ion beam tandem mass spectrometric methods to study a variety of gas-phase ion-molecule reactions relevant to plasma deposition and etching of silicon. Absolute cross sections over a wide range of kinetic energies for reactions involving both atomic and polyatomic ions were measured. The results yielded energy dependent cross sections, temperature dependent rate constants, and thermochemical data, information vital to further understanding of the chemical mechanisms involved in plasma processing. DTIC

N95-20852# Argonne National Lab., IL.
UNBINNED MAXIMUM LIKELIHOOD FIT FOR THE CP CONSERVING COUPLINGS FOR W + PHOTON PRODUCTION AT CDF
K. Lannon (Saint Norbert Coll., De Pere, WI.) 1994 15 p
(Contract W-31-109-eng-38)
(DE95-001471; ANL-HEP-TR-94-57) Avail: CASI HC A03/MF A01

We present an unbinned maximum likelihood fit as an alternative to the currently used fit for the CP conserving couplings W plus photon production studied at CDF. We show that a four parameter double exponential fits the E(sub T) spectrum of the photon very well. We also show that the fit parameters can be related to and by a second order polynomial. Finally, we discuss various conclusions we have reasoned from our results to the fit so far. DOE

N95-20868# Fermi National Accelerator Lab., Batavia, IL.
TRIGGERS FOR A HIGH SENSITIVITY CHARM EXPERIMENT
David C. Christian Jul. 1994 8 p Presented at the Workshop on the Future of High Sensitivity Charm Experiments, Batavia, IL, 7-9 Jun. 1994
(Contract DE-AC02-76CH-03000)
(DE95-002251; FNAL/C-94/213; CONF-9406242-3) Avail: CASI HC A02/MF A01

Any future charm experiment clearly should implement an E(sub T) trigger and a (mu) trigger. In order to reach the 10(exp 8) reconstructed charm level for hadronic final states, a high quality vertex trigger will almost certainly also be necessary. The best hope for the development of an offline quality vertex trigger lies in further development of the ideas of data-driven processing pioneered by the Nevis/U. Mass. group. DOE

N95-20872# California Univ., Berkeley. Lawrence Berkeley Lab, CA. Chemical Sciences Div.
STUDY OF SMALL CARBON AND SEMICONDUCTOR CLUSTERS USING NEGATIVE ION THRESHOLD PHOTODETACHMENT SPECTROSCOPY Ph.D. Thesis
Caroline Chick Arnold Aug. 1994 308 p
(Contract DE-AC03-76SF-00098)
(DE95-002327; LBL-36197) Avail: CASI HC A14/MF A03

The bonding and electronics of several small carbon and semiconductor clusters containing less than ten atoms are probed using negative ion threshold photodetachment (zero electron kinetic energy, or ZEKE) spectroscopy. ZEKE spectroscopy is a particularly advantageous technique for small cluster study, as it combines mass selection with good spectroscopic resolution. The ground and low-lying electronic states of small clusters in general can be accessed by detaching an electron from the ground anion state. The clusters studied using this technique and described in this work are C6(-)/C6, Si(n)(-)/Si(n) (n = 2, 3, 4), Ge2(-)/Ge2, In2P(-)/In2P, InP2(-)/InP2, and Ga2As(-). The total photodetachment cross sections of several other small carbon clusters and the ZEKE spectrum of the I(-)(center dot)CH3I S(N)2 reaction complex are also presented to illustrate the versatility of the experimental apparatus. Clusters with so few atoms do not exhibit bulk properties. However, each specie exhibits bonding properties that relate to the type of bonding found in the bulk. C6, as has been predicted, exhibits a linear cumulenic structure, where double bonds connect all six carbon atoms. This double bonding reflects how important (pi) bonding is in certain phases of pure carbon (graphite and fullerenes). The symmetric stretch frequencies observed in the C6(-) spectra, however, are in poor agreement with the calculated values. Also observed as sharp structure in total photodetachment cross section scans was an excited anion state bound by only (approximately)40/cm relative to the detachment continuum. This excited anion state appears to be a valence bound state, possible because of the high electron affinity of C6, and the open shell of the anion. DOE

N95-20879# Fermi National Accelerator Lab., Batavia, IL.
UNIVERSALITY OF PARTICLE MULTIPLICITIES
K. Goulianos Sep. 1994 12 p Presented at the 3rd Gleb Wataghin School on High Energy Henomenology, Campinas, Brazil, 11-16 Jul. 1994
(Contract DE-AC02-76CH-03000)
(DE95-000727; FNAL/C-94/266-E; CONF-9407134-1) Avail: CASI HC A03/MF A01

We discuss the scaling properties and universality aspects of the rapidity and multiplicity distributions of particles produced in high energy hadronic and e(+)e(-) interactions. This paper is based on material presented in three lectures on pomeron phenomenology, which included a review of traditional soft pomeron physics and selected topics on hard diffraction processes probing the structure function of the pomeron. DOE

N95-20880# Fermi National Accelerator Lab., Batavia, IL.
KINEMATICAL EVIDENCE FOR TOP PAIRS AT THE TEVATRON
H. Grassmann Sep. 1994 5 p Presented at the QCD 1994: Nuclear Physics B, Montpellier, France, 7-13 Jul. 1994
(Contract DE-AC02-76CH-03000)
(DE95-000729; FNAL/C-94/299-E; CONF-9407135-1) Avail: CASI HC A01/MF A01

We present a top search analysis of W(sub +jet) events which combines a study of the kinematic features of the events with a search for bottom quarks. DOE

N95-20893# California Univ., San Diego, CA.
THEORETICAL PARTICLE PHYSICS
1 Sep. 1994 17 p
(Contract DE-FG03-90ER-40546)
(DE95-002447; DOE/ER-40546/T6; UCSD-955220) Avail: CASI HC A03/MF A01

This report discusses the following topics: Large-N Expansion; Semileptonic B Decays; Renormalons; Heavy Quark Chiral Perturbation Theory; Kaon and Pion Condensation; Two-Dimensional Models; Higgs Physics; Fermion Number Production; Defects and Phase Transitions; Discrete Flavor Symmetries; Symmetry Breaking; Rare Decays; Baryon Number Generation; Chiral Gauge Theories; Strongly Interacting Higgs Sectors; Higgs Mass Bound; R(exp 2) Gravity. DOE

N95-20897# Fermi National Accelerator Lab., Batavia, IL.
EVIDENCE FOR t(BAR t) PRODUCTION AT THE TEVATRON: STATISTICAL SIGNIFICANCE AND CROSS SECTION
J. Koningsberg (Harvard Univ., Cambridge, MA.) Sep. 1994 7 p Presented at the Meeting of the Division of Particles and Fields of the American Physical Society, Albuquerque, NM, 2-6 Aug. 1994
(Contract DE-AC02-76CH-03000)
(DE95-002524; FNAL/C-94/314-E; CONF-940816-46) Avail: CASI HC A02/MF A01

We summarize here the results of the 'counting experiments' by the CDF Collaboration in the search of t(bar t) production in p(bar p) collisions at square root of s = 1800 TeV at the Tevatron. We analyze their statistical significance by calculating the probability that the observed excess is a fluctuation of the expected backgrounds, and assuming the excess is from top events, extract a measurement of the t(bar t) production cross-section. DOE

N95-20898# Fermi National Accelerator Lab., Batavia, IL.
CHARMONIUM PRODUCTION, b QUARK AND B MESON PRODUCTION AND b(BAR b) CORRELATIONS AT CDF
K. Byrum (Argonne National Lab., IL.) Sep. 1994 7 p Presented at the 27th International Conference on High Energy Physics, Glasgow, Scotland, 21-27 Jul. 1994
(Contract DE-AC02-76CH-03000)
(DE95-002525; FNAL/C-94/325-E; CONF-940722-30) Avail: CASI HC A02/MF A01

We present results on charmonium production, b quark and B meson production and B(bar B) correlations using data taken with the CDF detector at Fermilab in p(bar p) collisions at square root of s = 1.8 TeV during the 1992-1993 collider run. DOE

N95-20911# Oak Ridge National Lab., TN.
AN ADVANCED ECR ION SOURCE WITH A LARGE UNIFORMLY DISTRIBUTED ECR PLASMA VOLUME FOR MULTIPLY CHARGED ION BEAM GENERATION
G. D. Alton and D. N. Smithe (Mission Research Corp., Newington, VA.) 1994 32 p Presented at the 6th International Symposium on Electron Beam Ion Sources and Their Applications, Stockholm, Sweden, 20-23 Jun. 1994
(Contract DE-AC05-84OR-21400)
(DE95-001078; CONF-9406180-4) Avail: CASI HC A03/MF A01

A new ECR ion source geometry has been conceived which uses a minimum-B magnetic mirror geometry consisting of a multi-cusp, magnetic field, to assist in confining the plasma radially, a flat central field for tuning to the ECR resonant condition, and specially tailored mirror fields in the end zones for confining the plasma in the axial direction. The magnetic field, designed to achieve an axially symmetric plasma 'volume' with constant mod-B, extends over the length of the central field region. This design, which strongly contrasts with 'surface' ECR zones characteristic of conventional ECR ion sources, results in dramatic increases in the adsorption of RF power, thereby increasing the electron temperature and 'hot' electron population within the ionization volume of the source. The ECR zone is concentrated symmetrically around the axis of symmetry and along the length of the plasma volume rather than in thin surface layers located off-axis as is the case in conventional ECR ion sources. The creation of a 'volume' rather than a 'surface' ECR zone and its distribution relative to the optical axis where the ions of interest are extracted is commensurate with the generation of higher beam intensities, higher charge states and a higher degree of ionization. The new ECR ion source concept has been computationally designed through the use of magnet design codes, plasma-dispersion sources, and particle-in-cell codes. A summary of the design attributes of the source is given in this report. DOE

N95-20914# Fermi National Accelerator Lab., Batavia, IL.
RECENT RESULTS FROM E665
Ashutosh V. Kotwal (Harvard Univ., Cambridge, MA.) Sep. 1994 12 p Presented at the 6th Rencontres De Blois: The Heart of the Matter, Orsay, France, 10-25 Jun. 1994
(Contract DE-AC02-76CH-03000)
(DE95-002523; FNAL/C-94/345-E; CONF-9406265-2) Avail: CASI HC A03/MF A01

Preliminary measurements of the structure functions F(sub 2,sup p) and F(sub 2,sup d) and the structure function ratio F(sub 2,sup n)/F(sub 2,sup p), in inelastic mu-N scattering are presented. Preliminary results on nuclear transparency ((sigma)(sup A)/A)/(sigma)(sup H) in incoherent exclusive (rho) production are also presented. The data were obtained by Fermilab experiment 665 using a 465 GeV muon beam and liquid hydrogen, deuterium and carbon, calcium and lead targets. The structure functions are measured in the range x(sub Bj) greater than 8 X 10(exp -4) and Q(sup 2) greater than 0.2 GeV(sup 2). The structure function ratio is presented as a function of x(sub Bj) for x(sub Bj) greater than 10(exp -6). The nuclear transparency in exclusive (rho) production is studied as a function of Q(sup 2) in the range 0.1 less than Q(sup 2) less than 10.0 GeV(sup 2). DOE

N95-20986# Tokyo Univ., Tanashi (Japan). Inst. for Nuclear Study.
CONSTRUCTION OF NON-CRITICAL STRING FIELD THEORY BY TRANSFER MATRIX FORMALISM IN DYNAMICAL TRIANGULATION
Yoshiyuki Watabiki Dec. 1993 67 p
(DE94-770607; INS-1017) Avail: CASI HC A04/MF A01

We propose a new method which analyzes the dynamical triangulation from the viewpoint of the non-critical string field theory. By using the transfer matrix formalism, we construct the non-critical string field theory (including c greater than 1 cases) at the discrete level. For pure quantum gravity, we succeed in taking the continuum limit and obtain the c = 0 non-critical string field theory at the continuous level. We also study about the universality of the non-critical string field theory. DOE

N95-20993 Air Force Systems Command, Tyndall AFB, FL. Environics Directorate.
EVALUATION OF AN IMMOBILIZED CELL BIOREACTOR FOR DEGRADATION OF META- AND PARA-NITROBENZOATE Final Report, Jan. - Aug. 1993
Steven W. Peretti and Stuart M. Thomas 18 Jan. 1994 22 p Limited Reproducibility: More than 20% of this document may be affected by microfiche quality
(AD-A279719; AL/EQ-TR-1994-0012) Avail: Issuing Activity (Defense Technical Information Center (DTIC))

Meta- and para-nitrobenzoic acid are pollutants found in waste streams from metal-stripping processes using cyanide-free solvents. The Kelly AFB industrial Waste Treatment Plant (IWTP) is currently incapable of removing these compounds from its wastewaters because of the presence of significant quantities of ethylenediamine, a preferred substrate and upper limit of 4-5 hours on the hydraulic residence time in the IWTP. This report describes the enrichment and preliminary characterization of a microbial consortium capable of utilizing both Meta- and Para-Nitrobenzoate as sole carbon sources. DTIC

N95-20994 Florida Univ., Gainesville, FL. Quantum Theory Proj.
TEMPORAL REARRANGEMENT OF ELECTRONIC DENSITIES IN SLOW ATOMIC COLLISIONS
D. A. Micha 16 May 1994 20 p Limited Reproducibility: More than 20% of this document may be affected by microfiche quality
(Contract N00014-93-1-0122)
(AD-A279725; TR-6) Avail: Issuing Activity (Defense Technical Information Center (DTIC))

Electronic rearrangement in atomic interactions involve two very different time scales, for nuclear (slow) and electronic (fast) motions. This requires special care when one calculates solutions to the corresponding coupled differential equations. A method has been developed to treat the coupling of very different time scales, based on density operators in Liouville space. Its implementation in terms of density matrices, within an eikonal/TDHF formulation, has allowed us to follow the time-evolution of atomic populations in ion-atom and ion-surface interactions. DTIC

N95-21114# Los Alamos National Lab., NM.
ACTIVE NEUTRON MULTIPLICITY ANALYSIS AND MONTE CARLO CALCULATIONS
M. S. Krick, N. Ensslin, D. G. Langner, M. C. Miller, R. Siebelist, J. E. Stewart, R. N. Ceo (Martin Marietta Energy Systems, Inc., Oak Ridge, TN.), P. K. May (Martin Marietta Energy Systems, Inc., Oak Ridge, TN.), and L. L. Collins, Jr. (Martin Marietta Energy Systems, Inc., Oak Ridge, TN.) 1994 7 p Presented at the Institute of Nuclear Materials Management Annual Meeting, Naples, FL, 17-20 Jul. 1994
(Contract W-7405-eng-36)
(DE94-016178; LA-UR-94-2440; CONF-940748-63) Avail: CASI HC A02/MF A01

Active neutron multiplicity measurements of high-enrichment uranium metal and oxide samples have been made at Los Alamos and Y-12. The data from the measurements of standards at Los Alamos were analyzed to obtain values for neutron multiplication and source-sample coupling. These results are compared to equivalent results obtained from Monte Carlo calculations. An approximate relationship between coupling and multiplication is derived and used to correct doubles rates for multiplication and coupling. The utility of singles counting for uranium samples is also examined. DOE

N95-21120# Florida Univ., Gainesville, FL. Quantum Theory Proj.
ELECTRON-NUCLEAR DYNAMICS OF MOLECULAR SYSTEMS
Agustin Diz and Yngve Ohrn 1994 16 p Sponsored by ONR
(AD-A279649) Avail: CASI HC A03/MF A01

The content of an ab-initio time-dependent theory of quantum molecular dynamics of electrons and atomic nuclei is presented. Employing the time-dependent variational principle and a family of approximate state vectors yields a set of dynamical equations approximating the time-dependent Schrodinger equation. These equations govern the time evolution of the relevant state vector parameters as molecular orbital coefficients, nuclear positions and momenta. This approach does not impose the Born-Oppenheimer approximation, does not use potential energy surfaces and takes into account electron-nuclear coupling. Basic conservation laws are fully obeyed. The simplest model of the theory employs a single determinantal state for the electrons and classical nuclei and is implemented in the computer code ENDyne. Results from this ab-initio theory are reported for ion-atom and ion-molecule collisions. DTIC

N95-21121# Naval Air Warfare Center, China Lake, CA. Weapons Div.
DIELECTRIC MODELS IN ADHESION AND EXTRAPOLATIONS OF MOLECULAR MODELING Report, Jun. 1993 - Feb. 1994
Nancy E. Iwamoto Apr. 1994 40 p
(AD-A279675; NAWC-WPNS-TP-8152) Avail: CASI HC A03/MF A01

In order to separate mechanical mechanisms of adhesion such as surface roughness, chain entanglement, or even chemical reaction from mechanisms based upon the dielectric nature of interface interaction, highlights of dielectric theory dealing with cohesion and adhesion are reviewed. Elements of those theories are applied in order to gain insight into experimental results of adhesive systems taken from the literature. From this analysis dielectric-based explanations are offered for general adhesion trends, including explanations of metal to nonmetal adhesion trends based upon properties of the changing metal and the constituents of the interface. An example of how a dielectric-based explanation could be used to rationalize contributions from both the interface compositions and bulk components is also given. Finally an example of dynamic molecular modeling is given in order to compare current computer models of adhesion. DTIC

N95-21125# Los Alamos National Lab., NM.
THEORIES OF THE ETA-MESON-NUCLEUS INTERACTION
L. C. Liu 1994 9 p Presented at the Mesons and Nuclei at Intermediate Energies, Dubna, Russia, 3-7 May 1994
(Contract W-7405-eng-36)
(DE94-016055; LA-UR-94-2338; CONF-9405202-1) Avail: CASI HC A02/MF A01

It is shown that the pion-nucleon elastic scattering, eta-nucleon scattering length and the cross sections for pion-induced eta production on a nucleon satisfy a set of consistency relations. These relations are used to examine the (eta)N scattering lengths given by the various models. The nature of the threshold (eta)N interaction is discussed and recent advancements in (eta)N interaction is discussed and recent advancements in (eta)-nucleus reaction theory are reviewed. DOE

N95-21126# Colorado Univ., Boulder, CO.
NEW METHODS FOR LARGE SCALE LOCAL AND GLOBAL OPTIMIZATION Final Report, 1 Dec. 1991 - 30 Nov. 1993
Richard Byrd and Robert Schnabel 8 Jul. 1994 9 p
(Grant AF-AFOSR-0109-90)
(AD-A285635; Rept-153-7645; AFOSR-94-0487TR) Avail: CASI HC A02/MF A01

We have pursued all three topics described in the proposal during this research period. A large amount of effort has gone into the development of large scale global optimization methods for molecular configuration problems. We have developed new general purpose methods that combine efficient stochastic global optimization techniques with several new, more deterministic techniques that account for most of the computational effort, and the success, of the methods. We have applied our methods to Lennard-Jones problems with up to 75 atoms, to water clusters with up to 31, molecules, and polymers with up to 58 amino acids. The results appear to be the best so far by general purpose optimization methods, and appear to be leading to some interesting chemistry issues. Our research on the second topic, tensor methods, has addressed several areas. We have designed and implemented tensor methods for large sparse systems of nonlinear equations and nonlinear least squares, and have obtained excellent test results on a wide range of problems. We have also developed new tensor methods for nonlinearly constrained optimization problem, and have obtained promising theoretical and preliminary computational results. Finally, on the third topic, limited memory methods for large scale optimization, we have developed and implemented new, extremely efficient limited memory methods for bound constrained problems, and new limited memory trust regions methods, both using our-recently developed compact representations for quasi-Newton matrices. Computational test results for both methods are promising. DTIC

N95-21127# New Orleans Univ., LA. Dept. of Chemistry.
CALCULATED HEATS OF FORMATION OF SOME PREDICTED STABLE C, N, O, F MOLECULES
Peter Politzer, Pat Lane, and M. E. Grice 20 Oct. 1994 6 p
(Contract N00014-91-J-4057)
(AD-A285957; TR-72) Avail: CASI HC A02/MF A01

Twenty-one potential energetic molecules, containing only C, N, 0, F, were found to have true local energy minimal at the Hartree-Fock 6-31G* computational level. A density functional procedure was used to find their gas phase heats of formation. The nitros group significantly increases Delta H sub f compared to the nitro analogue, while NF2 decreases it. DTIC

N95-21140# Brookhaven National Lab., Upton, NY.
BEHAVIOUR OF SPACE-CHARGE DOMINATED ION BEAMS IN STORAGE RINGS
A. F. Haffmans, D. Maletic, and A. G. Ruggiero 1994 4 p Presented at the 4th European Particle Accelerator Conference, London, England, 27 Jun. - 1 Jul. 1994
(Contract DE-AC02-76CH-00016)
(DE94-015845; BNL-49992; CONF-940618-23) Avail: CASI HC A01/MF A01

The interparticle repulsion, or space charge, limits the density of charged particle beams that can be obtained in storage rings. In this report we study the effect of increasing the space charge, with an exact computation of the lattice parameters using SYNCH. Systematically increasing the ion density by decreasing the emittance with cooling techniques lowers the betatron tune, until the lower half-integral stopband resonance - also induced by the beam is reached. In the simple model described in the report, the amount of 'cooling' is limited by the encountered stopband of the lattice. Therefore, machines with a higher tune and larger periodicity are better suited to store beams with high space charge. DOE

N95-21151# Georgia Inst. of Tech., Atlanta, GA. School of Physics.
ION-MOLECULAR SPIRALING COLLISIONS AND TERMOLECULAR RECOMBINATION Interim Report, 1 Jul. 1989 - 30 Jun. 1994
X. Qi Aug. 1994 189 p
(Grant AF-AFOSR-0426-89)
(AD-A285633; GIT-89-023; AFOSR-94-0643TR) Avail: CASI HC A09/MF A02

A modification is made to the semiclassical adiabatic invariance method for ion-dipole and ion-quadrupole capture collisions. This modification to the adiabatic invariance method includes the effects of coupling of the rotational angular momentum of the target molecule with the orbital angular momentum of the projectile ion. The adiabatic potential energies, cross sections and rate coefficients for capture into rotational eigenstates (J, m) of the target molecule, as well as the thermal averaged rate coefficients are calculated for a number ion-dipole and ion-quadrupole systems for the temperature range 10 less than or - T (deg K) less than or - 1000. DTIC

N95-21174# Lawrence Livermore National Lab., Livermore, CA.
ADVANCED CONCEPTS FOR GAMMA RAY ISOTOPIC ANALYSIS AND INSTRUMENTATION
W. M. Buckley and J. B. Carlson Jul. 1994 5 p Presented at the Institute of Nuclear Materials Management Annual Meeting, Naples, FL, 17-20 Jul. 1994
(Contract W-7405-eng-48)
(DE94-016610; UCRL-JC-116145; CONF-940748-78) Avail: CASI HC A01/MF A01

The Safeguards Technology Program at the Lawrence Livermore National Laboratory is developing actinide isotopic analysis technologies in response to needs that address issues of flexibility of analysis, robustness of analysis, ease-of-use, automation and portability. Recent developments such as the Intelligent Actinide Analysis System (IAAS), begin to address these issues. We are continuing to develop enhancements on this and other instruments that improve ease-of-use, automation and portability. Requests to analyze samples with unusual isotopics, contamination, or containers have made us aware of the need for more flexible and robust analysis. We have modified the MGA program to extend its plutonium isotopic analysis capability to samples with greater Am-241 content or U isotopics. We are looking at methods for dealing with tantalum or lead contamination and contamination with high-energy gamma emitters, such as U-233. We are looking at ways to allow the program to use additional information about the sample to further extend the domain of analyzable samples. These unusual analyses will come from the domain of samples that need to be measured because of complex reconfiguration or environmental cleanup. DOE

N95-21191*# National Aeronautics and Space Administration. Langley Research Center, Hampton, VA.
HEAVY ION TRACK-STRUCTURE CALCULATIONS FOR RADIAL DOSE IN ARBITRARY MATERIALS
Francis A. Cucinotta, Robert Katz (Nebraska Univ., Lincoln, NE.), John W. Wilson, and Rajendra R. Dubey (Old Dominion Univ., Norfolk, VA.) Feb. 1995 21 p
(RTOP 199-45-16-11)
(NASA-TP-3497; L-17424; NAS 1.60:3497) Avail: CASI HC A03/MF A01

The delta-ray theory of track structure is compared with experimental data for the radial dose from heavy ion irradiation. The effects of electron transmission and the angular dependence of secondary electron ejection are included in the calculations. Several empirical formulas for electron range and energy are compared in a wide variety of materials in order to extend the application of the track-structure theory. The model of Rudd for the secondary electron-spectrum in proton collisions, which is based on a modified classical kinematics binary encounter model at high energies and a molecular promotion model at low energies, is employed. For heavier projectiles, the secondary electron spectrum is found by scaling the effective charge. Radial dose calculations for carbon, water, silicon, and gold are discussed. The theoretical data agreed well with the experimental data. Author

N95-21216# Georgia Inst. of Tech., Atlanta, GA. School of Physics.
RECOMBINATION, ION-MOLECULE COLLISIONS AND (LASER ASSISTED) ELECTRON-EXCITED ATOM COLLISIONS Final Report, 1 Jul. 1989 - 30 Jun. 1994

M. R. Flannery Aug. 1994 56 p
(Grant AF-AFOSR-0426-89)
(AD-A285604; GIT-89-024; AFOSR-94-0642TR) Avail: CASI HC A04/MF A01

This final report documents all of the research performed on the project entitled Termolecular Association of Ions in Gases. Theoretical research was completed on (1) termolecular recombination, (2) laser-assisted electron-excited atom collisions, (3) atom-excited atom collisions, (4) ion-molecule collisions, and (5) electron-ion dissociative recombination. DTIC

N95-21220 Rutherford Appleton Lab., Oxford (England).
ANOMALOUS VECTOR-BOSON COUPLINGS IN MAJORANA NEUTRINO MODELS
C. P. Burgess and A. Pilaftsis Jun. 1994 17 p Prepared in cooperation with Neuchatel Univ., Switzerland
(PB95-127460; RAL-94-053) Avail: Issuing Activity (National Technical Information Service (NTIS))

We examine the contributions of Majorana neutrinos to CP-violating WWZ and ZZZ self-couplings, using a model in which sterile neutrinos couple to the W and Z by mixing with a fourth-generation heavy lepton. We find that the induced form factors can be as large as 0.5%. The model satisfies all phenomenological bounds in a natural way, including those due to the strong limits on the neutron and electron electric dipole moments. Anomalous CP-odd couplings of this size are unlikely to be observed at LEP200, but might be detectable at NLC. NTIS

N95-21221 Rutherford Appleton Lab., Oxford (England).
ANTISHADOWING CONTRIBUTION TO THE POMERON STRUCTURE FUNCTION
K. Prytz Jun. 1994 13 p
(PB95-127478; RAL-94-054) Avail: Issuing Activity (National Technical Information Service (NTIS))

In a particular model of the pomeron, its gluon and quark distributions are subject to anti-shadowing, as described by a modified GLR equation recently derived. Inclusion of antishadowing cures the problem of momentum non-conservation previously existing in the GLR equation. A possible outcome of a measurement of the pomeron structure function at HERA is shown in case of DGLAP, GLR and modified GLR parton dynamics. NTIS

N95-21222 Rutherford Appleton Lab., Oxford (England).
WHERE ARE WE GOING WITH BOSE-EINSTEIN: A MINI REVIEW
S. Haywood Jul. 1994 43 p
(PB95-130308; RAL-94-074) Avail: Issuing Activity (National Technical Information Service (NTIS))

In this paper, the author considers the progress (or otherwise) in understanding the Bose-Einstein effect in the context of high energy e(+)e(-) interactions. The agreement between published experimental results is poor, and there are difficulties in explaining the observations theoretically, especially in the light of resonance narrowing. Systems of more than two pions are investigated using event-weights, and the expected distortion of the rho(exp 0) is considered. This paper is written from the perspective of an experimentalist. It seeks to highlight the experimental problems and draw attention to relevant theoretical literature. NTIS

N95-21223 Rutherford Appleton Lab., Oxford (England).
T1F ((1) SIGMA (+)): SOME PRELIMINARY ELECTRONIC STRUCTURE CALCULATIONS
S. Wilson, D. Moncrieff, and J. Kobus Jul. 1994 17 p Workshop on Parity Non-Conservation, Oxford, England, 7-10 Apr. 1994 Prepared in cooperation with Florida State Univ., Tallahassee, FL, and Nicolaus Copernicus Univ., Torun, Poland
(Contract DE-FC05-85ER-25000)
(PB95-130316; RAL-94-082) Avail: Issuing Activity (National Technical Information Service (NTIS))

Some preliminary calculations, using the matrix Hartree-Fock model, for the ground (X singlet Sigma +) state of the thallium fluoride molecule are presented. The convergence of the calculations, carried out within the algebraic approximation, is monitored by employing systematically constructed basis sets of increasing size. The importance of bond centered functions is emphasized. For diatomic molecules containing light atoms, the finite difference method has proved useful in calibrating calculations carried out with finite basis sets. The prospects for finite difference calculations for diatomic systems containing heavy atoms is assessed. NTIS

N95-21224 Rutherford Appleton Lab., Oxford (England).
MUON BEAMLINE AT ISIS
G. H. Eaton, M. A. Clarke-Gayther, C. A. Scott, S. F. J. Cox, and S. H. Kilcoyne Jul. 1994 15 p
(PB95-130324; RAL-94-077) Avail: Issuing Activity (National Technical Information Service (NTIS))

The original pulsed surface muon facility was established at the Rutherford Appleton Laboratory's ISIS in 1987. The facility was then upgraded in 1993 from a single beam line and spectrometer to a triple beam facility with three spectrometers working independently. The layout of ISIS is shown. A plan of the ISIS experimental hall is shown, indicating the respective locations of the neutron beams, the KARMEN neutrino facility and the muon beam line complex. Other topics shown in the report include the following: (1) Muon production; (2) Transport of muons to the experimental areas; (3) Positron elimination from the ISIS muon beam; (4) Creation of three independent beam lines. NTIS

N95-21225 Rutherford Appleton Lab., Oxford (England).
SPIN DEPENDENCE OF DIFFRACTIVE PROCESSES AND IMPLICATIONS FOR THE SMALL x BEHAVIOUR OF g1 AND THE SPIN CONTENT OF THE NUCLEON
F. E. Close and R. G. Roberts Jul. 1994 14 p
(PB95-130332; RAL-94-071) Avail: Issuing Activity (National Technical Information Service (NTIS))

We show that if the Lorentz transformation properties of diffraction are other than scalar, the x approaches 0 behavior of g(sub 1)(x, Q(exp 2) can grow. We compare with new data on g(sub 1, exp p) from SMC, assess implications for sum rules and for future studies of sea polarization. NTIS

N95-21227 Rutherford Appleton Lab., Oxford (England).
NEUTRON MOLELCULAR SPECTROSCOPY: FUTURE PROSPECTS
J. Tomkinson, P. S. R. Krishna, and C. J. Carlile Jul. 1994 11 p Prepared in cooperation with Bhabha Atomic Research Centre, Bombay, India
(PB95-130357; RAL-94-075) Avail: Issuing Activity (National Technical Information Service (NTIS))

The recent revolution in Neutron Molecular Spectroscopy, caused by extending the spectral range, is briefly reviewed. The need to constantly improve the spectral resolution is underlined and the likely benefits are identified. Recent work on improving the energy resolution on TFXA is presented and three future options for TFXA are outlined. Some preliminary high resolution results, from a mock-up spectrometer, are reported. These clearly show that narrow bands are available in solids and improved resolutions can be achieved to observe them. NTIS

N95-21233 Rutherford Appleton Lab., Oxford (England).
MULTIPLE HARD INTERACTIONS IN HERWIG
J. M. Butterworth and J. R. Forshaw Aug. 1994 8 p Presented at the Workshop on Two-Photon Physics at LEP and HERA, Lund, Sweden, May 1994 Prepared in cooperation with Pennsylvania State Univ., State College, PA
(PB95-130548; RAL-94-088) Avail: Issuing Activity (National Technical Information Service (NTIS))

At HERA energies, photoproduction of jets is sensitive to very high parton densities and so the probability of more than one hard partonic scattering occurring in a single photon-proton collision may be significant. This effect has been simulated using an eikonal prescription for the generation of the hard processes and the HERWIG parton showering and hadronization models. The first results on simulated jet cross sections indicate that the effect could be important when interpreting measurements of jet cross sections at HERA, and that the presence of a significant amount of multiple hard interactions could be directly confirmed by experiment. NTIS

N95-21235# Los Alamos National Lab., NM.
PARITY NONCONSERVATION IN RADIOACTIVE ATOMS: AN EXPERIMENTAL PERSPECTIVE

David J. Vieira 1994 7 p Presented at the Antibes Conference on Nuclear Shapes and Nuclear Structure At Low Excitation Energies, Antibes, France, 20-25 Jun. 1994
(Contract W-7405-eng-36)
(DE95-002737; LA-UR-94-3533; CONF-9406212-3) Avail: CASI HC A02/MF A01

The measurement of parity nonconservation (PNC) in atoms constitutes an important test of electroweak interactions in nuclei. Great progress has been made over the last 20 years in performing these measurements with ever increasing accuracies. To date the experimental accuracies have reached a level of 1 to 2%. In all cases, except for cesium, the theoretical atomic structure uncertainties now limit the comparison of these measurements to the predictions of the standard model. New measurements involving the ratio of Stark interference transition rates for a series of Cs or Fr radioisotopes are foreseen as a way of eliminating these atomic structure uncertainties. The use of magneto-optical traps to collect and concentrate the much smaller number of radioactive atoms that are produced is considered to be one of the key steps in realizing these measurements. Plans for how these measurements will be done and progress made to date are outlined. DOE

N95-21237# Los Alamos National Lab., NM.
A NEUTRON BEAM POLARIZER FOR STUDY OF PARITY VIOLATION IN NEUTRON-NUCLEUS INTERACTIONS
S. I. Penttilae, J. D. Bowman, C. M. Frankle, S. J. Seestrom, Yi-Fen Yen, P. P. J. Delheij (Tri-Univ. Meson Facility, Vancouver, British Columbia.), D. G. Haase (North Carolina State Univ., Raleigh, NC.), and H. Postma (Technische Hogeschool, Delft, Netherlands.) 1994 9 p Presented at the International Symposia on High Energy Spin Physics and Polarization Phenomena in Nuclear Physics, Bloomington, IN, 15-22 Sep. 1994
(Contract W-7405-eng-36)
(DE95-002743; LA-UR-94-3579; CONF-9409103-3) Avail: CASI HC A02/MF A01

A dynamically-polarized proton target operating at 5 Tesla and 1 K has been built to, neutron beam for studies of parity violation in compound-nuclear resonances. Nearly 0.9 proton polarization was obtained in an electron-beam irradiated ammonia target. This was used to produce a neutron beam polarization of 0.7 at epithermal energies. The combination of the polarized proton target and the LANSCE spallation neutron source produces the most intense pulsed polarized epithermal neutron beam in the world. The neutron-beam polarizer is described and methods to determine neutron beam polarization are presented. DOE

N95-21248# Stanford Linear Accelerator Center, CA.
MEASURING A(SUB b) WITH POLARIZED BEAMS AT SLC
Thomas R. Junk May 1994 9 p Presented at the 29th Moriond Meeting on Quantum Chromodynamics and High Energy Hadronic Interactions, Les Arcs, France, 12-26 Mar. 1994
(Contract DE-AC03-76SF-00515)
(DE95-002865; SU-SLAC-PUB-6513; CONF-940327-14) Avail: CASI HC A02/MF A01

We present the first direct measurement of the left-right asymmetry of b-quarks from the decay of Z(sup 0) bosons produced in the annihilation of longitudinally polarized electrons and unpolarized positrons in the SLD at the SLC. Two complementary techniques are presented: (1) Z(sup 0) (yields) b(bar b) decays are tagged using track impact parameters measured with a CCD-based vertex detector with b - (bar b) discrimination provided by momentum-weighted track charge; (2) Semileptonic b-decays are tagged using high (P, P(sub T)) muons and electrons with b - (bar b) discrimination provided by the lepton charge. In our 1993 sample of (approximately)50,000 Z(sup 0) decays having a luminosity-weighted average e(-) polarization of (62.6 +/- 1.2)%, we find the following preliminary results: A(sub b)(track charge) = 1.01 +/- 0.12(stat) +/- 0.14(sys), (A sub b)(muons) = 0.94 +/- 0.25(stat) +/- 0.11(sys), and A(sub b)(electrons) 0.99 +/- 0.27(stat) +/- 0.19(sys). DOE

N95-21250# Stanford Linear Accelerator Center, CA.
TOP TEN MODELS CONSTRAINED BY b (YIELDS) s(GAMMA)
J. L. Hewett May 1994 13 p Presented at the 21st Annual SLAC Summer Institute on Particle Physics: Spin Structure in High-energy Processes, Stanford, CA, 26 Jul. - 6 Aug. 1993
(Contract DE-AC03-76SF-00515)
(DE95-002870; SU-SLAC-PUB-6521; CONF-930767-9) Avail: CASI HC A03/MF A01

The radiative decay b (yields) s(gamma) is examined in the Standard Model and in nine classes of models which contain physics beyond the Standard Model. The constraints which may be placed on these models from the recent results of the CLEO Collaboration on both inclusive and exclusive radiative B decays is summarized. Reasonable bounds are found the parameters in some of the models. DOE

N95-21262# California Univ., Berkeley. Lawrence Berkeley Lab, CA.
SOURCES OF AMPLITUDE-DEPENDENT TUNE SHIFT IN THE PEP-2 DESIGN AND THEIR COMPENSATION WITH OCTUPOLES
E. Forest, D. Robin, A. Zholents, M. Donald (Stanford Linear Accelerator Center, CA.), R. Helm (Stanford Linear Accelerator Center, CA.), J. Irwin (Stanford Linear Accelerator Center, CA.), and H. Moshammer (Stanford Linear Accelerator Center, CA.) Jun. 1994 3 p Presented at the 4th European Particle Accelerator Conference, London, England, 27 Jun. - 1 Jul. 1994
(Contract DE-AC03-76SF-00098)
(DE94-018198; LBL-35791; CBP-89; CONF-940618-76) Avail: CASI HC A01/MF A01

Higher order contributions from sextupoles and dipole fringe fields, quadrupole fringe fields, kinematic terms in the Hamiltonian, and systematic or random multipole errors may degrade the dynamic aperture by shifting the particles in the tune plane in an undesired direction. The authors compare the various sources quantitatively and discuss their impact on the dynamic aperture of the PEP-2 low energy ring (LER) lattice. A tunable compensation scheme for the LER lattice which permits an independent control of the tune shift with amplitude in the two transverse planes is presented. DOE

N95-21273# Fermi National Accelerator Lab., Batavia, IL.
A MEASUREMENT OF THE b(BAR b) CROSS SECTION AT CDF
I. Yu (Yale Univ., New Haven, CT.) Aug. 1994 5 p Presented at the Meeting of the Division of Particles and Fields of the American Physical Society, Albuquerque, NM, 2-6 Aug. 1994
(Contract DE-AC02-76CH-03000)
(DE95-000642; FNAL/C-94/241-E; CONF-940816-25) Avail: CASI HC A01/MF A01

We report a measurement of the b(bar b) cross section at CDF from the 1992-1993 run of the Tevatron Collider. Dimuon events from inclusive b yields mu decays of b(bar b) pairs are used to obtain the cross section as a function of P(sub T)(b(sub 1)) and P(sub T)(b(sub 2)). The results are compared to the predictions of next-to-leading order QCD and are found to be consistent. DOE

N95-21276# Toledo Univ., OH. Dept. of Physics and Astronomy.
MEASUREMENTS OF SCATTERING PROCESSES IN NEGATIVE ION: ATOM COLLISIONS
T. J. Kvale 27 Sep. 1994 32 p
(Contract DE-FG05-88ER-13971)
(DE95-000664; DOE/ER-13971/23) Avail: CASI HC A03/MF A01

This report describes the progress made on the research objectives during the past three years of the grant. This research project is designed to study various scattering processes which occur in H(-) collisions with atomic (specifically, noble gas and atomic hydrogen) targets in the intermediate energy region. These processes include: elastic scattering, single- and double-electron detachment, and target excitation/ionization. For the elastic and target inelastic processes where H(-) is scattered intact, the experimental technique of ion energy-loss spectroscopy (IELS) will be employed to identify the final target state(s). In most of the above processes, cross sections are unknown both experimentally and theoretically. The measurements will provide total cross sections (TCS) initially, and once the angular positioning apparatus is installed, will provide angular differential cross sections (ADCS). DOE

N95-21302# State Univ. of New York, Stony Brook, NY.
THE THEORY OF RELATIVISTIC HEAVY ION COLLISIONS
E. Shuryak Jul. 1994 30 p
(Contract DE-FG02-93ER-40768)
(DE95-001805; DOE/ER-40768/2) Avail: CASI HC A03/MF A01

For clarity of presentation, we have divided the topics of interest into the following main topics which are discussed in this report: the dynamics of nuclear collisions at very high energies (RHIC and LHC); electromagnetic probes; the dynamics of nuclear collisions at AGS energies; and non-perturbative QCD and the physics of the phase transition. DOE

N95-21313# Fermi National Accelerator Lab., Batavia, IL.
MEASUREMENT OF THE POLARIZATION IN THE DECAY B(SUP 0) (YIELDS) J/(PSI)K*(SUP 0) IN (BAR p)p COLLISIONS AT (RADICAL)S = 1.8 TeV
Karen E. Ohl (Yale Univ., New Haven, CT.) Aug. 1994 3 p Presented at the Meeting of the Division of Particles and Fields of the American Physical Society, Albuquerque, NM, 2-6 Aug. 1994
(Contract DE-AC02-76CH-03000)
(DE95-002521; FNAL/C-94/216-E; CONF-940816-47) Avail: CASI HC A01/MF A01

We report on a measurement of data of the polarization in the decay B(sup 0) (yields) J/(psi)K*(sup 0) using data collected at the Collider Detector at Fermilab in p(bar p) collisions at (radical)s = 1.8 TeV. B(sup 0) mesons were reconstructed through the decay chain B(sup 0) (yields) J/(psi)K*(sup 0), J/(psi) (yields) (mu)(+)(mu)(-), K*(sup 0) (yields) K(+)(pi)(-). The results, based on a sample of 60 +/- 11 events, is (Gamma)(sub L)/(Gamma) = 0.66 +/- 0.01 (stat) (sub (minus)0.10)(sup +0.08) (sys). DOE

N95-21315 Washington Univ., Seattle, WA. Inst. for Nuclear Theory.
NONPERTURBATIVE ASPECTS OF THE QUARK-PHOTON VERTEX
Michael R. Frank 1994 28 p Limited Reproducibility: More than 20% of this document may be affected by microfiche quality
(Contract DE-FG06-90ER-40561)
(DE94-012846; DOE/ER-40561/131) Avail: CASI HC A03

The electromagnetic interaction with quarks is investigated through a relativistic, electromagnetic gauge-invariant treatment. Gluon dressing of the quark-photon vertex and the quark self-energy functions is described by the inhomogeneous Bethe-Salpeter equation in the ladder approximation and the Schwinger-Dyson equation in the rainbow approximation respectively. Results for the calculation of the quark-photon vertex are presented in both the time-like and space-like regions of photon momentum squared, however emphasis is placed on the space-like region relevant to electron scattering. The treatment presented here simultaneously addresses the role of dynamically generated q(bar-q) vector bound states and the approach to asymptotic behavior. The resulting description is therefore applicable over the entire range of momentum transfers available in electron scattering experiments. Input parameters are limited to the model gluon two-point function which is chosen to reflect confinement and asymptotic freedom and are largely constrained by the obtained bound-state spectrum. DOE

N95-21321# Los Alamos National Lab., NM.
HEAVY ION COLLISIONS
Barbara V. Jacak 1994 11 p Presented at the 27th International Conference on High Energy Physics, Glasgow, United Kingdom, 21-27 Jul. 1994
(Contract W-7405-eng-36)
(DE95-002712; LA-UR-94-3468; CONF-940722-31) Avail: CASI HC A03/MF A01

Heavy ion collisions at very high energies provide an opportunity to recreate in the laboratory the conditions which existed very early in the universe, just after the big bang. We prepare matter at very high energy density and search for evidence that the quarks and gluons are deconfined. I describe the kinds of observables that are experimentally accessible to characterize the system and to search for evidence of new physics. A wealth of information is now available from CERN and BNL heavy ion experiments. I discuss recent results on two particle correlations, strangeness production, and dilepton and direct photon distributions. DOE

N95-21336# Stanford Linear Accelerator Center, CA.
EXCLUSIVE PROCESSES: TESTS OF COHERENT QCD PHENOMENA AND NUCLEON SUBSTRUCTURE AT CEBAF
Stanley J. Brodsky Jul. 1994 16 p Presented at the Workshop on CEBAF At Higher Energies, Newport News, VA, 14-16 Apr. 1994
(Contract DE-AC03-76SF-00515)
(DE95-002892; SU-SLAC-PUB-6570; CONF-9404197-2) Avail: CASI HC A03/MF A01

Measurements of exclusive processes such as electroproduction, photoproduction, and Compton scattering are among the most sensitive probes of proton structure and coherent phenomena in quantum chromodynamics. The continuous electron beam at CEBAF, upgraded in laboratory energy to 10-12 GeV, will allow a systematic study of exclusive, semi-inclusive, and inclusive reactions in a kinematic range well-tuned to the study of fundamental nucleon and nuclear substructure. I also discuss the potential at CEBAF for studying novel QCD phenomena at the charm production threshold, including the possible production of nuclear-bound quarkonium. DOE

N95-21357# California Univ., Berkeley. Lawrence Berkeley Lab, CA.
DILEPTON PRODUCTION FROM p-p TO Ca-Ca AT THE BEVALAC
Howard S. Matis, S. Beedoe (California Univ., Los Angeles, CA.), M. Bougteb (Universite Blaise Pascal, Aubiere, France.), J. Carroll (California Univ., Los Angeles, CA.), W. Christie (Johns Hopkins Univ., Baltimore, MD.), W. Gong, T. Hallman (Johns Hopkins Univ., Baltimore, MD.), L. Heilbronn, H. Huang, and P. N. Kirk (Louisiana State Univ., Baton Rouge, LA.) Jun. 1994 6 p Presented at the Conference on Nucleus-Nucleus Collisions, Catania, Italy, 30 May - 4 Jun. 1994
(Contracts DE-AC03-76SF-00098; DE-FG03-88ER-40424; DE-FG02-88ER-40413; DE-FG05-88ER-40445)
(DE95-002341; LBL-36033; CONF-940509-7) Avail: CASI HC A02/MF A01

The DLS collaboration has recently completed a high statistics study of dilepton production at the Bevalac. In particular, we have measured dielectrons e(+)e(-) from p-p and p-d collisions to understand the basic dilepton production mechanisms in the energy range from 1.05-4.9 GeV. These data can be used to determine the basic processes which contribute to nucleon-nucleon dilepton production such as hadronic bremsstrahlung, vector meson processes, and hadronic Dalitz decay. The data show that a simple elastic bremsstrahlung calculation is insufficient to explain the data. Theoretical models are compared with the data. A new high statistics study of Ca-Ca at 1.05 A(center dot)GeV has been made to study the collectivity of A-A collisions. DOE

N95-21360# Lawrence Livermore National Lab., Livermore, CA.
MAGNETIC X-RAY CIRCULAR DICHROISM IN SPIN-POLARIZED PHOTOELECTRON DIFFRACTION
G. D. Waddill, J. G. Tobin, X. Guo, and S. Y. Tong 12 Jul. 1994 5 p Presented at the 8th International Conference on X-ray Absorption Fine Structure, Berlin, Germany, 8 Aug. - 2 Sep. 1994
(Contracts W-7405-eng-48; DE-FG02-84ER-45076)
(DE95-002394; UCRL-JC-117613; CONF-9408131-4) Avail: CASI HC A01/MF A01

The first structural determination with spin-polarized, energy-dependent photoelectron diffraction using circularly-polarized x rays is reported for Fe films on Cu(001). Circularly-polarized x rays produced spin-polarized photoelectrons from the Fe 2p doublet, and intensity asymmetries in the 2p(sub 3/2) level are observed. Fully spin-specific multiple scattering calculations reproduced the experimentally-determined energy and angular dependences. A new analytical procedure which focuses upon intensity variations due to spin-dependent diffraction is introduced. A sensitivity to local geometric and magnetic structure is demonstrated. DOE

N95-21362# Brookhaven National Lab., Upton, NY. Physics Dept.
PHOTOEMISSION AND FERROMAGNETISM
P. D. Johnson 1994 19 p
(Contract DE-AC02-76CH-00016)
(DE95-002419; BNL-60934) Avail: CASI HC A03/MF A01

Photoemission is a well established technique for the study of the electronic structure of atoms and solids. In particular, angle-resolved photoemission has been used extensively to map the band structure of clean and adsorbate covered surfaces, both metal and semiconductor. Extending the technique by measuring the spin of the photoemitted electrons allows the possibility of examining the exchange split band structures characterizing ferromagnetic systems. Here the technique becomes particularly useful in the study of the magnetic properties of surfaces, thin films and associated interfaces. DOE

N95-21375# Pacific Northwest Lab., Richland, WA.
CALCULATION OF ATOM-CENTERED PARTIAL CHARGES FOR HEME

John I. Manchester, Mark D. Paulsen, and Rick L. Ornstein May 1994 8 p Presented at the 27th Jerusalem Symposium in Quantum Chemistry and Biochemistry, Jerusalem, Israel, 23-26 May 1994
(Contract DE-AC06-76RL-01830)
(DE94-014447; PNL-SA-24303; CONF-9405196-1) Avail: CASI HC A02/MF A01

Atom-centered partial charges are calculated for the Fe-heme in cytochrome P450cam for use in molecular dynamics simulations of polar substrates bound in the active site of the enzyme. Charges are fit to the electrostatic potential produced by ab initio UHF wavefunctions for an Fe-porphine model. Basis set dependence of these charges is observed using the LANL1DZ, LANL2DZ and augmented 6-31G levels of theory. Upon geometry optimization of the enzyme, these charge sets cause varying degrees of distortion of the porphyrin from its crystallographically observed conformation. Scaling the charges calculated from the augmented 6-31G basis by 75% reduces the heme distortion while preserving reasonable interactions with a polar substrate. A comparison of the calculated charges with other published values is presented. DOE

N95-21378# Fermi National Accelerator Lab., Batavia, IL.
A HIGH-RATE FIXED-TARGET CHARM EXPERIMENT
Daniel M. Kaplan (University of Northern Illinois, De Kalb, IL.) Jul. 1994 8 p Presented at the Workshop on the Future of High Sensitivity Charm Experiments, Batavia, IL, 7-9 Jun. 1994
(Contract DE-AC02-76CH-03000)
(DE95-001767; FNAL/C-94/201; CONF-9406242-4) Avail: CASI HC A02/MF A01

In the P865 Letter of Intent, we have proposed a fixed-target experiment aimed at achieving high sensitivity to decays both of charm and of beauty. I describe here a revised version which is somewhat more optimized for charm and less so for beauty. The rationale for this change of emphasis is two-fold: by the time a new fixed-target experiment might run (approximately Year 2000), it is likely that studies of beauty at the level proposed in P865 will no longer be competitive; furthermore, it may well be that charm is even more interesting than beauty since the background to rare processes beyond the Standard Model is so much smaller in charm than in beauty. At this workshop, Pakvasa has emphasized that rare and forbidden processes such as D(sup 0) mixing, charm-changing neutral currents, and lepton-family-violating currents must exist at some level if we are ever to have an understanding of the fermion masses and mixings; some extensions of the Standard Model predict effects detectable at the level of sensitivity discussed here. DOE

N95-21380# California Univ., Berkeley. Lawrence Berkeley Lab, CA.
SIMILARITIES AND DIFFERENCES IN STRANGENESS PRODUCTION AT BNL AND CERN
Grazyna Odyniec Sep. 1994 13 p Presented at the NATO Advanced Research Workshop on Hot Hadronic Matter: Theory and Experiment, Divonne-les-Bains, France, 27 Jun. - 1 Jul. 1994
(Contract DE-AC03-76SF-00098)
(DE95-002343; LBL-36219; CONF-9406274-1) Avail: CASI HC A03/MF A01

Relativistic heavy ion collisions provide, in principle, necessary conditions for the formation of the quark gluon plasma. Strangeness enhancement was among the announced specific signals expected from this new, hypothetical state of nuclear matter. Analysis of the first generation of experiments with light and medium sized ions have been completed. Results on strangeness production become precious handles to study in great detail what is actually happening. The current experimental situation is assessed. The emerging picture is still incomplete: however, open questions constrain requirements on future heavy ion experiments. DOE

N95-21406# Argonne National Lab., IL. Physics Div.
RECENT PHOTOABSORPTION MEASUREMENTS IN THE RARE GASES AND ALKALIS IN THE 3 TO 15 keV PHOTON ENERGY REGION
H. G. Berry 1994 14 p Presented at the Workshop on Atomic Physics at High Brilliance Light Sources, Argonne, IL, 23-24 Apr. 1994
(Contract W-31-109-eng-38)
(DE94-019278; ANL/PHY/CP-84072; CONF-9404198-3) Avail: CASI HC A03/MF A01

The attenuation cross-section of photons in helium in the range 3 to 14 keV has been measured. The results indicate the importance of Compton scattering in this range and show reasonable agreement with theory. The authors have also used a heat-pipe to measure absorption spectra in argon, potassium and rubidium near their respective K-edges and have made identifications using relativistic Hartree-Fock calculations. Some ion spectra near and below the K-edges of argon and potassium are also presented. DOE

N95-21441# Cornell Univ., Ithaca, NY.
EXPERIMENTAL STUDY OF INTERACTIONS OF HIGHLY CHARGED IONS WITH ATOMS AT keV ENERGIES
V. O. Kostroun 27 Apr. 1994 8 p
(Contract DE-FG02-86ER-13519)
(DE95-001807; DOE/ER-13519/8) Avail: CASI HC A02/MF A01

Experimental study of low energy, highly charged ions with other atomic species requires an advanced ion source such as an electron beam ion source (EBIS) or an electron cyclotron ion source (ECRIS). Five years ago we finished the design and construction of the Cornell superconducting solenoid, cryogenic EBIS (CEBIS). Since then, this source has been in continuous operation in a program whose main purpose is the experimental study of interactions of highly charged ions with atoms at keV energies. This progress report for the period February 16, 1993 to April 15, 1994 describes the work accomplished during this time in the form of short abstracts. DOE

N95-21443# Fermi National Accelerator Lab., Batavia, IL.
BORON NEUTRINO FLUX AND THE MSW SOLUTION OF THE SOLAR NEUTRINO PROBLEM
P. I. Krastev (North Carolina Univ., Chapel Hill, NC.) and A. Y. Smirnov (Washington Univ., Seattle, WA.) 1994 19 p
(Contracts DE-FG06-90ER-40561; DE-FG05-85ER-40219)
(DE95-001861; FNAL/Pub-94/179-T; DOE/ER-40561/137) Avail: CASI HC A03/MF A01

There are large uncertainties in the predictions of the boron neutrino flux from the sun which cannot be considered as being of purely statistical origin. We treat the magnitude of this flux, Phi(sub B), as a parameter to be found from experiment. The properties of the MSW solution to the solar neutrino problem for different values of Phi(sub B) are studied. Present data give the bounds: 0.38 less than Phi(sub B)/Phi(sub B)(sup O) less than 3.1 (2 sigma), where Phi(sub B)(sup O) defined as 5.7 x 10(exp 6) cm(exp -2) s(exp -1) is the flux in the reference SSM. The variations of the flux in this interval enlarge the allowed region of mixing angles: sin(exp 2) 2 theta = 8 x 10(exp -4) / 2 x 10(exp -2) (small mixing solutions) and sin(exp 2) 2 theta = 0.2 / 0.85 (large mixing solution). If the value of the original boron neutrino flux is about that measured by Kamiokande, a consistent description of the data is achieved for sin(exp 2) 2 theta approximately (0.8/2) x 10(exp -3) ('very small mixing solution'). The solution is characterized by a strong suppression of the beryllium neutrino line, a weak distortion of the high energy part of the boron neutrino spectrum, and a value of the double ratio (CC/NC)(sup exp)/(CC/NC)(sup SSM) at E greater than 5 MeV close to 1. We comment on the possibility to measure the neutrino parameters and the original boron neutrino flux in future experiments. DOE

N95-21454# Argonne National Lab., IL. Physics Div.
ON THE AHARONOV-BOHM EFFECT WITH NEUTRONS
Murray Peshkin 1994 8 p Presented at the Fundamental Problems in Quantum Theory, College Park, MD, 18-22 Jun. 1994
(Contract W-31-109-eng-38)
(DE95-002985; ANL/PHY/CP-84348; CONF-9406243-2) Avail: CASI HC A02/MF A01

The neutron interferometry phenomenon called scalar Aharonov-Bohm effect (SAB) follows from an ordinary local interaction, contrary to the usual Aharonov-Bohm effect with electrons (AB). I argue that SAB is not a topological effect by any useful definition. SAB in fact measures an apparently novel spin autocorrelation whose operator equations of motion contain the local torque in the magnetic field. The Aharonov-Casher effect shares these properties with SAB. DOE

N95-21484# Brookhaven National Lab., Upton, NY.
STRANGE HADRONIC MATTER
A. Gal (Hebrew Univ., Jerusalem, Israel.) and C. B. Dover Sep. 1994 13 p Presented at the International Conference on Hypernuclear and

Strange Particle Physics, Vancouver, British Columbia, 4-8 Jul. 1994
(Contract DE-AC02-76CH-00016)
(DE94-019345; BNL-60795; CONF-940725-3) Avail: CASI HC A03/MF A01

Recent investigations of regions of stability for multi-strange hadronic systems, made up of nucleons and hyperons (p, n, Lambda, Xi(exp 0), Xi(exp -)) are reviewed. Relativistic mean field calculations, designed to reproduce the observed binding energies of ordinary nuclei and of Lambda, Xi, and Lambda Lambda hypernuclei, predict a large class of such objects which are stable against strong decay, including the bulk limit A approaches infinity, with binding energies as E(sub B)/A approximately -22 MeV, large strangeness per baryon f(sub s) 1-1.2, small charge per baryon f(sub q) approximately -0.1 to 0 and with baryon densities 2-3 times that of ordinary nuclear matter. A straightforward extension of the Bethe-Weizsacker mass formula into the strange domain accounts satisfactorily for all of these features. DOE

N95-21485# Louisiana State Univ., Baton Rouge, LA. Dept. of Physics and Astronomy.
MONOPOLES AND QUARK CONFINEMENT: INTRODUCTION AND OVERVIEW
Ken Yee 20 Feb. 1994 20 p Presented at the Lake Louise Winter Institute Conference, Alberta, 20-26 Feb. 1994
(Contract DE-FG05-91ER-40617)
(DE94-019348; DOE/ER-40617/167; CONF-9402102-1) Avail: CASI HC A03/MF A01

We (try to) pedagogically explain how monopoles arise in QCD, why maximal Abelian (MA) gauge is 'special' for monopole study, the Abelian projection in MA gauge, its resultant degrees of freedom (photons, monopoles and charged matter fields), and the QCD-equivalent action in terms of these degrees of freedom. Then we turn to more recent developments in the subject: Abelian dominance, large N behavior of Abelian projected QCD, mass of the charged matter fields, notion of an effective photon-monopole action obtained by integrating out the charged matter fields, and problems encountered in evaluating this effective action using the microcanonical demon method on the lattice. DOE

N95-21492 Pennsylvania Univ., Philadelphia, PA. Dept. of Chemistry.
QUANTUM SIMULATION OF HETEROGENEOUS ELECTRON TRANSFER FREE ENERGIES AT THE WATER-METAL INTERFACE Technical Report, May 1993 - May 1994
Jay B. Straus and Gregory A. Voth 6 May 1994 38 p Limited Reproducibility: More than 20% of this document may be affected by microfiche quality
(Contract N00014-92-J-1243)
(AD-A279279; TR-10) Avail: Issuing Activity (Defense Technical Information Center (DTIC))

The free energy for electron transfer is studied for the Fe(2+)/Fe(3+) charge transfer system at the water-Pt(111) interface. Classical adiabatic free energy curves are calculated along with an adiabatic curve based on the Anderson-Newns Hamiltonian. Reactive flux calculations are then performed on this curve to determine the effect of recrossings on the classical rate constant. These effects are not found to be large (Kappa approximately 0.6). The solvent model is then extended to a quantum mechanical path integral version and quantum adiabatic free energy curves are calculated. The resulting quantum effects are found to be quite significant, illustrating that the same electrode overpotential does not necessarily result from the same free energy curves for the classical and quantum mechanical solvent models. These results suggest that classical models for water may not be adequate, or at least need to be modified, for accurate simulations of heterogeneous electron transfer. DTIC

N95-21497# Argonne National Lab., IL.
THE DIPHOTON PRODUCTION RATE IN (BAR p)p COLLISIONS AT THE SQUARE ROOT OF s = 1800 GeV
R. Blair Aug. 1994 5 p Presented at the Meeting of the Division of Particles and Fields of the American Physical Society, Albuquerque, NM, 2-6 Aug. 1994
(Contract DE-AC02-76CH-03000)
(DE95-000559; FNAL/C-94/269-E; CONF-940816-20) Avail: CASI HC A01/MF A01

A measurement of the rate of prompt diphoton production in (bar p)p collisions at square root of s = 1800 GeV using the CDF detector is presented. The background from non-prompt sources is estimated using a sample of single photon candidate events. The results are compared to a next-to-leading order calculation by Bailey, et al. Both background and signal take on particular significance as an indicator of our ability to estimate the backgrounds affecting LHC low mass Higgs to diphoton searches. DOE

N95-21498# Fermi National Accelerator Lab., Batavia, IL.
SEARCH FOR THE TOP QUARK USING MULTIVARIATE ANALYSIS TECHNIQUES
P. C. Bhat Aug. 1994 5 p Presented at the Meeting of the Division of Particles and Fields of the American Physical Society, Albuquerque, NM, 2-6 Aug. 1994
(Contract DE-AC02-76CH-03000)
(DE95-000561; FNAL/C-94/261-E; CONF-940816-22) Avail: CASI HC A01/MF A01

The D0 collaboration is developing top search strategies using multivariate analysis techniques. We report here on applications of the H-matrix method to the e mu channel and neural networks to the e+jets channel. DOE

N95-21499# Fermi National Accelerator Lab., Batavia, IL.
NEW SHOWER MAXIMUM TRIGGER FOR ELECTRONS AND PHOTONS AT CDF
D. Gerdes (Michigan Univ., Ann Arbor, MI.) Aug. 1994 6 p Presented at the Meeting of the Division of Particles and Fields of the American Physical Society, Albuquerque, NM, 2-6 Aug. 1994
(Contracts DE-AC02-76CH-03000; DE-AC02-76ER-01112; W-31-109-eng-38)
(DE95-000563; FNAL/C-94/243-E; CONF-940816-21) Avail: CASI HC A02/MF A01

For the 1994 Tevatron collider run, CDF has upgraded the electron and photon trigger hardware to make use of shower position and size information from the central shower maximum detector. For electrons, the upgrade has resulted in a 50% reduction in backgrounds while retaining approximately 90% of the signal. The new trigger also eliminates the background to photon triggers from single-phototube discharge. DOE

N95-21502# Argonne National Lab., IL.
ION CHARGE-STATE PRODUCTION AND PHOTOIONIZATION NEAR THE K EDGE IN ARGON AND POTASSIUM
H. G. Berry, Y. Azuma, P. L. Cowan, D. S. Gemmell, T. LeBrun, and M. Y. Amusia 1994 11 p Presented at the 7th International Conference on Physics of Highly Charged Ions, Vienna, Austria, 19-23 Sep. 1994
(Contract W-31-109-eng-38)
(DE95-001443; ANL/PHY/CP-82766; CONF-940922-3) Avail: CASI HC A03/MF A01

We have measured the time-of-flight charge distributions of ions of argon and potassium following x-ray absorption at energies near their respective K edges. We confirm previously observed enhancements of the higher charge states at energies up to 100 eV below the K edge in argon. The measurements confirm recent calculations suggesting excitation of a virtual 1s state in this energy range. DOE

N95-21506# Brookhaven National Lab., Upton, NY.
QCD CORRECTIONS TO HIGGS BOSON PRODUCTION: AN UPDATE
S. Dawson and R. Kauffman (Franklin and Marshall Coll., Lancaster, PA.) Sep. 1994 5 p Presented at the 27th International Conference on High Energy Physics, Glasgow, Scotland, 21-27 Jul. 1994
(Contract DE-AC02-76CH-00016)
(DE95-000626; BNL-60769; CONF-940722-23) Avail: CASI HC A01/MF A01

We compute analytic results for the QCD corrections to Higgs boson production in hadronic collisions in the limit in which the top quark is much heavier than the Higgs boson. The first nonleading corrections of O(alpha(sub s)(exp 2)M(sub H)(exp 2)/m(sub t)(exp 2)) are given and numerical results presented for the LHC. DOE

N95-21519# Oak Ridge National Lab., TN.
ELECTRON ATTACHMENT TO EXCITED MOLECULES
L. G. Christophorou, L. A. Pinnaduwage, and P. G. Datskos (Tennessee Univ., Knoxville, TN.) 1993 28 p Presented at the NATO Advanced

Study Institute: Linking the Gaseous and Condensed Phases of Matter - the Behavior of Slow Electrons, Patras, Greece, 5-18 Sep. 1993
(Contract DE-AC05-84OR-21400)
(DE94-019124; CONF-930993-3) Avail: CASI HC A03/MF A01

Studies on electron attachment to molecules rotationally/vibrationally excited thermally or via infrared-laser excitation showed that the effect of internal energy of a molecule on its electron attachment properties depends on the mode-dissociative or nondissociative-of electron attachment. They quantified the effect of the internal energy of the molecule on the rate of destruction (by autodissociation or by autodetachment) of its parent transient anion. Generally, increases in ro-vibrational molecular energy increase the cross section for dissociative electron attachment and decrease the effective cross section for parent anion formation due mainly to increased autodetachment. These findings and their understanding are discussed. A discussion is given, also, of recent investigations of electron attachment to electronically excited molecules, especially photoenhanced dissociative electron attachment to long- and short-lived excited electronic states of molecules produced directly or indirectly by laser irradiation. These studies showed that the cross sections for dissociative electron attachment to electronically excited molecules usually are many orders of magnitude larger than those for the ground-state molecules. The new techniques that have been developed for such studies are briefly described also. DOE

N95-21521# Fermi National Accelerator Lab., Batavia, IL.
MEASUREMENT OF W AND Z PRODUCTION CROSS-SECTIONS IN p(BAR p) COLLISIONS AT (RADICAL)S = 1.8 TeV
Paul Z. Quintas Sep. 1994 6 p Presented at the Meeting of the Division of Particles and Fields of the American Physical Society, Albuquerque, NM, 2-6 Aug. 1994
(Contract DE-AC02-76CH-03000)
(DE95-002250; FNAL/C-94/341-E; CONF-940816-40) Avail: CASI HC A02/MF A01

The cross sections for W and Z production in p(bar p) collisions at (radical)s = 1.8 TeV are measured using the DO detector at the Fermilab Tevatron collider. The detected final states are W (yields) ev(sub e), Z (yields) e(+)ɘ(-), W (yields) (mu)v(sub (mu)), and Z (yields) (mu)(+)(mu)(-). In the ratio of these measurements, many common sources of systematic error cancel and we measure R = (sigma),(p(bar p) (yields) W) (center dot) Br(W (yields) lv)/ (sigma),(p(bar p) (yields) Z) (center dot) Br(Z (yields) l(+)l(-). Assuming standard model couplings, this result is used to determine the width of the W bosom and to set a limit on the decay W(+) (yields) t(bar b). DOE

N95-21525# Stanford Linear Accelerator Center, CA.
POLARIZATION OF CHARMONIUM IN PION-NUCLEUS COLLISIONS
Wai-Keung Tang Sep. 1994 3 p Presented at the International Symposia on High Energy Spin Physics and Polarization Phenomena in Nuclear Physics, Bloomington, IN, 15-22 Sep. 1994
(Contract DE-AC03-76SF-00515)
(DE95-002783; SU-SLAC-PUB-6665; CONF-9409103-2) Avail: CASI HC A01/MF A01

Measurements of the polarization of J/(psi) produced in pion-nucleus collisions are in disagreement with leading twist QCD prediction were J/(psi) is observed to have negligible polarization whereas theory predicts substantial polarization. We argue that this discrepancy cannot be due to poorly known structure functions nor the relative production rates of J/(psi) and X(sub J). The disagreement between theory and experiment suggests important higher twist corrections, as has earlier been surmised from the anomalous non-factorized nuclear A-dependence of the J/(psi) cross section. DOE

N95-21551# Brookhaven National Lab., Upton, NY.
LATTICE RESULTS FOR HEAVY LIGHT MATRIX ELEMENTS
A. Soni Sep. 1994 4 p Presented at the 27th International Conference on High Energy Physics, Glasgow, Scotland, 21-27 Jul. 1994
(Contract DE-AC02-76CH-00016)
(DE94-019101; BNL-60828; CONF-940722-22) Avail: CASI HC A01/MF A01

Lattice results for heavy light matrix elements are reviewed and some of their implications are very briefly discussed. Despite the fact that in most cases the lattice results for weak matrix elements at the moment have only a modest accuracy of about 20-30% they already have important phenomenological repercussions; e.g. for V(sub td)/V(sub ts), x(sub s)/x(sub d) and B yields K*(gamma). DOE

N95-21562# Fermi National Accelerator Lab., Batavia, IL.
MEASUREMENT OF THE B MESON DIFFERENTIAL CROSS-SECTIONS IN p(BAR p) COLLISIONS AT (RADICAL)s = 1.8 TeV USING THE EXCLUSIVE DECAYS B(SUP (+-)) (YIELDS) J/(PSI)K(SUP (+-)) AND B(SUP 0) (YIELDS) J/(PSI)K*(SUP 0)
M. W. Bailey Aug. 1994 5 p Presented at the Meeting of the Division of Particles and Fields of the American Physical Society, Albuquerque, NM, 2-6 Aug. 1994
(Contract DE-AC02-76CH-03000)
(DE94-018993; FNAL/C-94/237-E; CONF-940816-17) Avail: CASI HC A01/MF A01

This paper presents the first measurement of the differential B(+/-)and B(exp 0) cross-sections, d(sigma)/d(sub PT) in p(bar-p) collisions at (radical)s = 1.8 TeV. The data sample used represents an integrated luminosity of 19.3 +/- 0.8 pb(exp -1) accumulated by the Collider Detector at Fermilab (CDF). The cross-sections are measured over the PT range 6-15 GeV/c in the central pseudorapidity region (verticle bar)eta(verticle bar) less than 1 by fully reconstructing the B meson decays B(+/-) yields J/psi K(exp *0), where the J/psi is required to decay to two muons, and the K(exp *0) is required to decay to K(+/-)pi(exp +/-). The results are compared to the theoretical QCD prediction calculated at next-to-leading order. DOE

N95-21563# Fermi National Accelerator Lab., Batavia, IL.
SEARCH FOR NEW PARTICLES DECAYING TO DIJETS IN p(BAR p) COLLISIONS AT (RADICAL)s = 1.8 TeV
R. M. Harris Aug. 1994 5 p Presented at the Meeting of the Division of Particles and Fields of the American Physical Society, Albuquerque, NM, 2-6 Aug. 1994
(Contract DE-AC02-76CH-03000)
(DE94-018994; FNAL/C-94/222-E; CONF-940816-15) Avail: CASI HC A01/MF A01

We present a preliminary search for new particles decaying to dijets using CDF data from the 1992-1993 run. We set the highest mass limits on axigluons and excited quarks, and the first mass limit on a color octet technirho. DOE

N95-21587# Missouri Univ., Rolla, MO.
EXPERIMENTAL INVESTIGATIONS OF ELECTRON CAPTURE FROM ATOMIC HYDROGEN AND DEUTERIUM BY ALPHA PARTICLES Final Report, 15 Sep. 1984 - 14 Sep. 1993
T. J. Gay Jun. 1994 8 p
(Contract DE-FG02-84ER-53188)
(DE95-002138; DOE/ER-53188/1) Avail: CASI HC A02/MF A01

The authors have succeeded in making state-selective measurements of charge capture by doubly-ionized helium colliding with ground-state neutral helium atoms, but failed to achieve the primary goal, which was to investigate atomic hydrogen targets. They discuss a number of ancillary experiments and calculations of relevance for fusion energy production that they have done. DOE

N95-21588# Brookhaven National Lab., Upton, NY. Physics Dept.
SUMMARY OF HEAVY ION THEORY
Sean Gavin Sep. 1994 7 p Presented at the Meeting of the Division of Particles and Fields of the American Physical Society, Albuquerque, NM, 2-6 Aug. 1994
(Contract DE-AC02-76CH-00016)
(DE95-002177; BNL-60809; CONF-940816-38) Avail: CASI HC A02/MF A01

Can we study hot QCD using nuclear collisions? Can we learn about metallic hydrogen from the impact of comet Shoemaker-Levy 9 on Jupiter? The answer to both questions may surprise you; I summarize progress in relativistic heavy ion theory reported at DPF '94 in the parallel sessions. DOE

N95-21591# Joint Inst. for Nuclear Research, Dubna (USSR). Lab. of Nuclear Problems.
MUON TRANSFER FROM MUONIC ATOMS OF HYDROGEN ISOTOPES TO He NUCLEI

V. M. Bystritskij 1993 16 p
(DE94-628903; JINR-E-1-93-451) Avail: CASI HC A03/MF A01 (US Sales Only)

All experimental data on muon transfer from (mu)-atoms of hydrogen isotopes to helium nuclei are discussed and compared. The program of further investigations is proposed so as to get more accurate and detailed information on characteristics of (mu)-atomic and (mu)-molecular processes in mixtures of hydrogen and helium isotopes. DOE

N95-21597# Fermi National Accelerator Lab., Batavia, IL.
MEASUREMENT OF THE B CROSS SECTION AT CDF VIA B SEMILEPTONIC DECAYS
Jonathan Lewis Sep. 1994 7 p Presented at the Meeting of the Division of Particles and Fields of the American Physical Society, Albuquerque, NM, 2-6 Aug. 1994
(Contract DE-AC02-76CH-03000)
(DE95-002217; FNAL/C-94/274-E; CONF-940816-41) Avail: CASI HC A02/MF A01

Using data collected during the 1992-1993 collider run at Fermilab, CDF has reconstructed several hundred charmed mesons (D(0), D(+) D*(+) and D(sub s)) in association with leptons from B semileptonic decays. We report on a measurement of the cross section of B and B(sub s) mesons as a function of transverse momentum using this sample. The observation of a charmed meson eliminates many systematic uncertainties in the background subtraction inherent in previous measurements from inclusive lepton samples, and allows the backgrounds to be measured from the data. The B meson p(sub T) range probed by the lepton + charm technique is 18 GeV and above, and thus these measurements complement similar measurements at lower p(sub T) in the fully exclusive channels B yields J/(psi)K and B yields J/(psi)K*. Results are compared to other Tevatron measurements and Next-To-Leading-Order QCD predictions. DOE

N95-21605# Auburn Univ., AL. Dept. of Physics.
THEORETICAL ATOMIC PHYSICS FOR FUSION
M. S. Pindzola 1994 10 p
(Contract DE-FG05-86ER-53217)
(DE94-019196; DOE/ER-53217/T3) Avail: CASI HC A02/MF A01

The understanding of electron-ion collision processes in plasmas remains a key factor in the ultimate development of nuclear fusion as a viable energy source for the nation. The author's 1993-1994 research proposal delineated several areas of research in electron-ion scattering theory. The author summarizes 1994 efforts, covering electron-impact excitation, ionization, and recombination of atomic ions. DOE

N95-21641# Brookhaven National Lab., Upton, NY.
DYNAMICS OF THE CHIRAL TRANSITION
S. Gavin Jul. 1994 6 p Presented at the Intersections of Particle and Nuclear Physics, St. Petersburg, FL, 31 May - 6 Jun. 1994
(Contract DE-AC02-76CH-00016)
(DE94-016813; BNL-60634; CONF-940514-10) Avail: CASI HC A02/MF A01

Measurements of disoriented chiral condensates (DCC) in heavy ion collisions at RHIC can yield fundamental information on the nature of the QCD phase transition. The author reviews theoretical efforts to understand DCC formation and presents work in progress on possible experimental ramifications. DOE

N95-21646# California Univ., Berkeley. Lawrence Berkeley Lab, CA.
DETECTION EFFICIENCY AND DARK PULSE RATE OF ROCKWELL (SSPM) SINGLE PHOTON COUNTERS
P. H. Eberhard, P. G. Kwiat, M. D. Petroff (Rockwell International Corp., Anaheim, CA.), M. G. Stapelbroek (Rockwell International Corp., Anaheim, CA.), and H. H. Hogue (Rockwell International Corp., Anaheim, CA.) Apr. 1994 4 p Presented at the International Conference on Applications of Photonic Technology, Sensing, Signal Processing and Communications, Ottawa, Ontario, 21-23 Jun. 1994
(Contract DE-AC03-76SF-00098)
(DE94-016872; LBL-35444; CONF-9406233-1) Avail: CASI HC A01/MF A01

This paper describes direct photon counting data on several pixels of the Rockwell solid-state photomultipliers (SSPM) detector array, about which absolute single photon detection efficiencies and time responses were reported previously by Kwiat et al. The new data shows a substantially larger efficiency, 85%, and suggests that damage in the optical fiber employed in the earlier data was responsible for the lower number, 70%. When the results of this paper are analyzed using reasonable assumptions, one concludes that several improvements of the SSPM detector are still possible to bring the photon counting efficiency close to or larger than 95%. DOE

N95-21664# Oak Ridge National Lab., TN.
AUGER SPECTROMETRY OF ATOMS AND MOLECULES
M. O. Krause 1994 19 p Presented at the Workshop on Atomic Physics at High Brilliance Light Sources, Argonne, IL, 23-24 Apr. 1994
(Contract DE-AC05-84OR-21400)
(DE94-018052; CONF-9404198-1) Avail: CASI HC A03/MF A01

The author discusses the importance of Auger spectrometry at synchrotron radiation centers. First, he explains how a high energy photon source such as the APS (Advanced Photon Source) could be used to help provide missing spectral information about the shell structure of some elements. The missing data occurs mainly at higher energies in the 1-10 keV ranges as for the K-shells of $Z = 30$ to 60 elements and the L-shells for $Z = 30$ to 100 elements. He explains how even though Auger electron spectrometry does not depend on synchrotron radiation it can greatly benefit from this variable photon source as it allows one to select the Auger line group that is most suitable for a specific purpose. Most significantly, a continuous photon source becomes indispensable when one is interested in threshold effects. Lastly, he discusses coherence effects between different inner-shell vacancy states by way of some recent work done at Daresbury. DOE

N95-21688 Massachusetts Inst. of Tech., Cambridge, MA. Research Lab. of Electronics.
ATOM WAVE INTERFEROMETER Annual Report
D. Pritchard 13 May 1994 5 p Limited Reproducibility: More than 20% of this document may be affected by microfiche quality
(Contract N00014-89-J-1207)
(AD-A279532) Avail: Issuing Activity (Defense Technical Information Center (DTIC))

In the early part of the current grant period we made many improvements to the apparatus. We have used our now reliable separated beam atom interferometer to perform several pioneering measurements. Recent improvements in our fabrication techniques (at NNF) for 200nm period gratings with absolute phase stability over large areas, improvements in sensitivity and time response of our detector, and learning how to stretch thin foils extremely flat over 10 cm lengths have enabled us to operate our interferometer with a metal septum between the two separated components of the atom wave which interferes with itself at the third grating. By taking data in very short time intervals (two or three milliseconds) and improving the frequency response of our servo electronics, we have been able to overcome the effects of vibration, at least up to about 100 Hz, simply by storing the datum of each short period with other data taken at the same position (as measured with the laser interferometer). This has resulted in higher contrast for the fringes. DTIC

N95-21703# Oak Ridge National Lab., TN.
CHARGE DENSITY OF FRACTIONAL CHARGED QUASIPARTICLES IN THE COMPOSITE FERMION PICTURE
X. M. Chen (Tennessee Univ., Knoxville, TN.), X. Xia (Tennessee Univ., Knoxville, TN.), and J. J. Quinn Jul. 1994 5 p Presented at the Conference on the Application of High Magnetic Fields, Cambridge, MA, 8-12 Aug. 1994
(Contract DE-AC05-84OR-21400)
(DE94-018122; CONF-940847-3) Avail: CASI HC A01/MF A01

Two different models for quasiparticles of the nu = 1/3 Laughlin incompressible state are investigated in the Fermion-Chern-Simons picture. In the first model a quasielectron (quasihole) is induced by adiabatically introducing an infinitesimally thin flux tube parallel (antiparallel) to the external magnetic field. The charge density induced is calculated in linear response theory. The quasielectron (quasihole) of the second model is obtained by creating (annihilating) a composite fermion consisting of a real electron with two attached magnetic flux quanta. Both models give a same total charge +/- 1/3e for quasiparticles; but they produce different charge density distributions rho(r). The self-energies (Coulomb) of quasiparticles are discussed. DOE

N95-21704# Oak Ridge National Lab., TN.
INVESTIGATION OF DIRECT PHOTON PRODUCTION IN 200 A GeV S + Au REACTIONS
1994 6 p Presented at the 29th Moriond Meeting on Quantum Chromodynamics and High Energy Hadronic Interactions, Les Arcs, France, 12-26 Mar. 1994
(Contract DE-AC05-84OR-21400)
(DE94-018129; CONF-940327-10) Avail: CASI HC A02/MF A01

Direct thermal photons in the p(sub T) range of 0-5 GeV/c are expected to provide a sensitive probe of the early conditions of the Quark Gluon Plasma which may be formed in relativistic heavy ion collisions. The production of single photons in 200 A GeV S + Au reactions has been investigated using the 3,800 element Pb glass calorimeter of CERN experiment WA80. Neutral pi(exp 0) and eta cross sections have been measured via their two-photon decay branch yields. The measured pi(exp 0) and eta cross sections have been used to calculate the expected inclusive yield of decay photons. Excess photon yield, beyond that attributed to radiative decays and background sources, may be associated with thermal photon emission. Excess, 'direct' photon yields have been extracted from high-statistics S + Au photon data for different event centrality classes. A slight excess photon yield above that which may be accounted for by hadronic decays was observed for central events. DOE

N95-21715# Fermi National Accelerator Lab., Batavia, IL.
STATUS OF THE DO TOP SEARCH
Qizhong Li-Demarteau Sep. 1994 14 p Presented at the 14th Conference on Physics in Collision, Tallahassee, FL, 15-17 Jun. 1994
(Contract DE-AC02-76CH-03000)
(DE95-002214; FNAL/C-94/332; CONF-940693-3) Avail: CASI HC A03/MF A01

Preliminary new results on the top quark search with the DO experiment in (bar p)p collisions at (radical)s = 1.8 TeV for an integrated luminosity of 15.2 +/- 1.8 pb(exp -1) are reported. In this new analysis, which is optimized for high mass top search, a total of seven candidate events in the electron and muon dilepton decay channels (t(bar t) (yields) e(mu), ee and (mu)(mu)), single lepton decay channels (t(bar t) (yields) e + jets and t(bar t) (yields) (mu) + jets) without b tagging and single electron decay channel (t(bar t) (yields) e + jets) with b tagging have been observed. The estimated background is 4.7 +/- 1.0 events. If we assume the top quark has a mass of 180 GeV/c(exp 2), a t(bar t) production cross section of 3.2 +/- 3.9 pb with upper limit of 13 pb at 95% C.L. is obtained. DOE

N95-21727# Stanford Linear Accelerator Center, CA.
A PRELIMINARY, PRECISE MEASUREMENT OF THE AVERAGE B HADRON LIFETIME
Jul. 1994 10 p Presented at the 27th International Conference on High Energy Physics, Glasgow, Scotland, 21-27 Jul. 1994
(Contracts DE-FG02-91ER-40676; DE-FG03-92ER-40701; DE-FG03-91ER-40618; DE-FG03-92ER-40689; DE-FG03-93ER-40788; DE-FG02-92ER-40715; DE-AC02-76ER-03069; DE-FG06-85ER-40224; DE-AC03-76SF-00515; DE-FG05-91ER-40627)
(DE95-001848; SU-SLAC-PUB-6586; CONF-940722-28) Avail: CASI HC A02/MF A01

The average B hadron lifetime was measured using data collected with the SLD detector at the SLC in 1993. From a sample of approximately 50,000 Z(sup 0) events, a sample enriched in Z(sup 0) yields b(bar-b) was selected by applying an impact parameter tag. The lifetime was extracted from the decay length distribution of inclusive vertices reconstructed in three dimensions. A binned maximum likelihood method yielded an average B hadron lifetime of (tau)(sub B) = 1.577 +/- 0.032(stat.) +/- 0.046(syst.) ps. DOE

N95-21747# Temple Univ., Philadelphia, PA.
NUCLEAR RESEARCH WITH THE ELECTROMAGNETIC PROBE
Z. E. Meziani Oct. 1994 10 p
(Contract DE-FG03-88ER-40439)
(DE95-001812; DOE/ER-40439/T2) Avail: CASI HC A02/MF A01

This is the final report on the research carried at Stanford University under contract DE-FG03-88ER-40439. All the work accomplished under this grant is reported in the publications listed as part of the Principal Investigator bibliography at the end of this report. In the last few years our research was directed at some of the forefront questions in nuclear physics. We investigated the nuclear medium effects on the intrinsic properties of bound nucleons, specifically the electromagnetic form factors. For these studies we performed a number of specialized electron scattering experiments with specific sensitivity to nuclear medium effects. At the next level of structure, elementary constituents of matter are quarks and gluons. Defining the energy regime where the quark-gluon description of nuclear systems becomes more relevant than the nucleon-meson description is of great importance in thoroughly understanding the nuclear structure. To explore this transition region, we studied the scaling region in the disintegration of the deuteron, the simplest nuclear system with high energy photons. Finally we focused on the investigation of the nucleon internal spin structure along with the test of the Bjoerken sum rule a fundamental sum rule of QCD. DOE

N95-21856# International Centre for Theoretical Physics, Trieste (Italy).
SECOND ORDER APPROXIMATION FOR OPTICAL POLARON IN THE STRONG COUPLING CASE
N. N. Bogolubov, Jr. Nov. 1993 22 p
(DE94-628997; IC-93/372) Avail: CASI HC A03/MF A01 (US Sales Only)

Here we propose a method of construction second order approximation for ground state energy for class of model Hamiltonian with linear type interaction on Bose operators in strong coupling case. For the application of the above method we have considered polaron model and propose construction set of nonlinear differential equations for definition ground state energy in strong coupling case. We have considered also radial symmetry case. DOE

N95-21857# Oak Ridge National Lab., TN.
ANGULAR AND CHARGE STATE DISTRIBUTIONS OF HIGHLY CHARGED IONS SCATTERED DURING LOW ENERGY SURFACE-CHANNELING INTERACTIONS WITH Au(110)
F. W. Meyer, L. Folkerts, and S. Schippers 1994 18 p Presented at the 10th International Workshop of Inelastic Ion-Surface Collisions, Grand Targhee Resort, WY, 8-12 Aug. 1994
(Contract DE-AC05-84OR-21400)
(DE95-001348; CONF-9408150-2) Avail: CASI HC A03/MF A01

The authors have measured scattered projectile angular and charge state distributions for 3.75 keV/amu O(sup q+) (3 less than or equal to q less than or equal to 8) and 1.2 keV/amu Ar(sup q+) (3 less than or equal to q less than or equal to 14) ions grazingly incident along the zone axes 110 and the zone axes 100 directions of a Au(110) single crystal target. Scattered projectile angular distribution characteristics of surface channeling are observed. For both incident species, the dominant scattered charge fraction is neutral, which varies only by a few percent as a function of incident charge state. Significant O(-) formation is observed, which manifests a distinct velocity threshold. For incident Ar projectiles with open L-shells, the positive scattered charge fractions, while always less than about 10%, increase linearly with increasing number of initial L-shell vacancies. DOE

N95-21860# International Centre for Theoretical Physics, Trieste (Italy).
UNIFORM UPPER BOUNDS IN THE FROEHLICH POLARON THEORY
N. N. Bogolubov, Jr. and A. V. Soldatov (Academy of Sciences, USSR, Moscow, USSR.) Nov. 1993 10 p
(DE94-628998; IC-93/373) Avail: CASI HC A02/MF A01 (US Sales Only)

We present very simple methods to derive upper bounds of the ground state energy for the Froehlich polaron theory. The obtained bounds are proved to be uniform for all values of the interactions parameter. DOE

N95-21878 New Orleans Univ., LA. Dept. of Chemistry.
COMPARATIVE COMPUTATIONAL ANALYSIS OF SOME NITRAMINE AND DIFLUORAMINE STRUCTURES, DISSOCIATION ENERGIES AND HEATS OF FORMATION
Peter Politzer, Pat Lane, M. E. Grice, Monica C. Concha, and Paul C. Redfern 3 Nov. 1994 12 p Limited Reproducibility: More than 20%

of this document may be affected by microfiche quality
(Contract N00014-91-J-4057)
(AD-A286196) Avail: CASI HC A03

Density functional methods have been used to compute the optimized geometries, dissociation energies, and gas phase heats of formation of several difluoramines (in which the -NF2 is attached to a nitrogen) and the corresponding nitramines. The -NF2 groups are found to be pyramidal, in contrast to the planarity of the -NO2. In each instance, one N-F bond length is at least 0.1 A longer than the other, while the N-N bonds are anomalously short. For the molecules and properties studied, the effects of -NO2 and -NF2 (on nitrogen) do not differ dramatically. Replacing -N-NO2 by -N-NF2 affects the dissociation energies of other N-NO2 and C-NO2 bonds only slightly (2-3 kcal/mole); however the N-NF2 bonds are 3-6 kcal/mole stronger than the N-NO2 that were replaced. The difluoramine heats of formation are less positive, by 15-17 kcal/mole, than those of the corresponding nitramines. DTIC

N95-21920# Washington Univ., Seattle, WA.
CONSTRAINTS ON T-ODD AND P-EVEN HADRONIC INTERACTIONS FROM NUCLEON, NUCLEAR, AND ATOMIC ELECTRIC DIPOLE MOMENTS
W. C. Haxton, A. Hoering, and M. J. Musolf (Continuous Electron Beam Accelerator Facility, Newport New, VA.) 1994 33 p
(Contract DE-FG06-90ER-40561)
(DE94-012845; DOE/ER-40561/130) Avail: CASI HC A03/MF A01

We deduce constraints on time-reversal-noninvariant (TRNI), parity-conserving (PC) hadronic interactions from nucleon, nuclear, and atomic electric dipole moment (edm) limits. Such interactions generate edm's through weak radiative corrections. We consider long-ranged mechanisms, i.e., those mediated by meson exchanges in contrast to short-range two-loop mechanisms. We find that the ratio of typical TRNI.PC nuclear matrix elements to those of the strong interaction are approximately less than 10(exp -5), a limit about two orders of magnitude more stringent than those from direct detailed balance studies of such interactions. DOE

N95-21934# Los Alamos National Lab., NM.
TWO-BAND MODEL DESCRIPTION OF ELECTROABSORPTION AND THIRD-HARMONIC GENERATION IN 1-D MX LINEAR CHAINS
Z. Shuai (Mons Univ., Belgium.), J. L. Bredas (Mons Univ., Belgium.), A. Saxena, J. T. Gammel, and A. R. Bishop 1994 3 p Presented at the International Conference on Science and Technology of Synthetic Metals, Seoul, Republic of Korea, 24-29 Jul. 1994
(Contract W-7405-eng-36)
(DE95-000932; LA-UR-94-3206; CONF-9407117-3) Avail: CASI HC A01/MF A01

Within a two-band model, the authors investigate the electroabsorption (EA) and third-harmonic generation (THG) processes in halogen-bridged mixed-valence Pt complexes: PtCl, PtBr and PtI. For PtCl, the theoretical THG spectrum shows three peaks, corresponding to (1) a three-photon resonance at 0.83 eV originating in a M(etal)-M(etal) transition; (2) a two-photon resonance at 1.5 eV from an M-M band-edge transition; and (3) a three-photon resonance at 1.6 eV from an M-X transition. The latter two peaks account well for the twin-peak structure seen experimentally. They show that the twin-peak intensity strongly decreases from PtCl to PtBr and disappears for PtI. They also discuss the theoretical EA spectra due to localized defects (polarons, bipolarons, kinks, and excitons). DOE

N95-21939# Oak Ridge National Lab., TN.
THE STATUS OF MOLECULES
T. Barnes (Tennessee Univ., Knoxville, TN.) 1994 10 p Presented at the 29th Moriond Meeting on Quantum Chromodynamics and High Energy Hadronic Interactions, Les Arcs, France, 12-26 Mar. 1994
(Contract DE-AC05-84OR-21400)
(DE95-000952; RAL-94-056; ORNL-CCIP-9408; CONF-940327-12) Avail: CASI HC A02/MF A01

This report summarizes the experimental and theoretical status of hadronic molecules, which are weakly-bound states of two or more hadrons. We begin with a brief history of the subject and discuss a few good candidates, and then abstract some signatures for molecules which may be of interest in the classification of possible molecule states. Next we argue that a more general understanding of 2 yields 2 hadron-hadron scattering amplitudes will be crucial for molecule searches, and discuss some of our recent work in this area. We conclude with a discussion of a few more recent molecule candidates (notably the f(sub o)(1710)) which are not well established as molecules but satisfy some of the expected signatures. DOE

N95-21940# Oak Ridge National Lab., TN.
CLASSICAL-QUANTUM CORRESPONDENCE FOR IONIZATION IN FAST ION-ATOM COLLISIONS
J. Burgdoerfer (Tennessee Univ., Knoxville, TN.) and C. O. Reinhold 1994 20 p Presented at the Symposium on Two-Center Effects in Ion-atom Collisions, Boulder, CO, 12-15 May 1994
(Contract DE-AC05-84OR-21400)
(DE95-000953; CONF-9405241-1) Avail: CASI HC A03/MF A01

We analyze the interplay between classical and quantum dynamics in ionization of atoms by fast charged particles. The convergence to the classical limit is studied as a function of the momentum transferred to the electron during the collision, the impact parameter, the energy and angle of the emitted electron, and the initial state of the target. One goal is to assess the validity of exact classical (CTMC) methods and approximate classical models such as the Thomson model. Applications to data for electron ejection at large angles are presented. The connection between collisional ionization by charged particles and ionization by half-cycle pulses is discussed. DOE

N95-21965 Rutherford Appleton Lab., Oxford (England).
MARI MINI-MANUAL
S. M. Bennington and R. S. Eccleston 5 Sep. 1994 49 p
(PB95-134649; RAL-94-102) Avail: Issuing Activity (National Technical Information Service (NTIS))

The MARI spectrometer is funded by the Japanese Ministry of Education, Culture and Science (Monbusho) as part of the UK-Japan collaboration in neutron scattering. MARI is a direct geometry chopper spectrometer. It uses a Fermi chopper to monochromatic the incident neutron beam to give incident energies in the range 10 to 2000 meV. It is very similar in design to its sister machine HET, but with a detector bank that continuously covers the angular range from 3 to 135 degrees, MARI is able to map large regions of Q-E space in a single measurement. At present about 600 of the full complement of 1000 detectors are installed. All are 10 bar (3)He gas proportional counters and all come from the same manufacturer, this means that their efficiency and background are almost the same. The beam size at the sample position is 50 by 50 mm, but motorized jaws in the Fermi chopper pit and in the sample tank can be used to reduce this size. Chapter headings are the following: Introduction; The hardware on MARI; Controlling the Instrument; Data Analysis and Visualization; Appendices. NTIS

N95-22051# Tokyo Univ., Tanashi (Japan). Inst. for Nuclear Study.
THE 9TH INS SCIENTIFIC COMPUTATIONAL PROGRAMS
Jun. 1993 55 p
(DE94-770780; INS-T-520) Avail: CASI HC A04/MF A01

Twelve groups were accepted as the 9-th INS scientific Computational Programs (ISCP). This ISCP can use full resources of the INS central computer without an operational limitation. The 9-th ISCP started on June/1/92 and ended on March/30/93. Some results were already published in journals or appeared in physical meetings. This is a sum of the used statistics of the 9-th ISCP and reports presented by groups at the 9-th ISCP. DOE

N95-22058# Los Alamos National Lab., NM.
THERE MIGHT BE TWO KINDS OF DIBARYON
Fan Wang (Nanjing Univ., China.), Jia-lun Ping (Nanjing Univ., China.), and Terrance Goldman 1994 5 p Presented at the Intersections of Particle and Nuclear Physics, Saint Petersburg, FL, 31 May - 6 Jun. 1994
(Contract W-7405-eng-36)
(DE94-014417; LA-UR-94-2147; CONF-940514-3) Avail: CASI HC A01/MF A01

A new quark potential model, the quark delocalization and color screening model, is used for a systematic search of dibaryon candidates in the u, d and s three flavor world. The color screening results from unquenched lattice gauge calculations and quark delocalization similar to electron delocalization in molecular physics are included. Flavor symmetry breaking and channel coupling effects are studied. The model is constrained not only by the baryon ground state property but also by the N-N scattering phase shifts. The deuteron and the zero energy di-nucleon resonance are reproduced qualitatively. The model predicts that there might be two kinds of dibaryon states. Possible high spin dibaryon resonances are emphasized. DOE

N95-22078# Los Alamos National Lab., NM.
SINGLE PARTICLE MEASUREMENTS AND TWO PARTICLE INTERFEROMETRY RESULTS FROM CERN EXPERIMENT NA44
J. Simon-Gillo 1994 6 p Presented at the Meeting of the Division of Particles and Fields of the American Physical Society, Albuquerque, NM, 2-6 Aug. 1994
(Contract W-7405-eng-36)
(DE95-003041; LA-UR-94-3469; CONF-940816-1) Avail: CASI HC A02/MF A01

CERN experiment NA44 is optimized for the study of identified single and multiple particle distributions to p(sub T) = 0 near mid-rapidity. We measure pi(exp+/-), K(exp +/-), p, (bar-p), d and (bar-d), in p + A and A + A collisions at 450 and 20OGeV/u, respectively. Two-particle intensity interferometry results from pi(+)pi(+), K(+)K(+), and K(-)K(-) measurements and single particle distributions are presented. DOE

N95-22122# Fermi National Accelerator Lab., Batavia, IL.
TESTS OF STRUCTURE FUNCTIONS USING LEPTON PAIRS: W-CHARGE ASYMMETRY AT CDF
W. K. Sakumoto (Rochester Univ., NY.) Sep. 1994 4 p Presented at the 6th Rencontres De Blois: The Heart of the Matter, Orsay, France, 10-25 Jun. 1994
(Contract DE-AC02-76CH-03000)
(DE95-000560; FNAL/C-94/265-E; CONF-9406265-1) Avail: CASI HC A01/MF A01

Large asymmetry of W-bosons produced in p(bar-p) collisions has been measured using 19 039 W yields e nu and W yields mu nu decays recorded by the CDF detector during the 1992-1993 Tevatron collider run. The asymmetry is sensitive to the slope of the proton's d/u quark distribution ratio down to x less than 0.01 at Q(exp 2) approximately M(sub w)(exp 2), where nonperturbative QCD effects are minimal. Of recent parton distribution functions, those of Martin, Roberts, and Stirling are favored over those of the CTEQ collaboration. This difference is seen even though both sets agree, at the level of the nuclear shadowing corrections, with the recent NMC measurements of F(sub 2)(sup mu n)/F(sub 2)(sup mu p). DOE

N95-22152# Stanford Linear Accelerator Center, CA.
MEASUREMENT OF THE AVERAGE LIFETIME OF B HADRONS AT SLD
Greg Punkar Sep. 1994 4 p Presented at the Meeting of the Division of Particles and Fields of the American Physical Society, Albuquerque, NM, 2-6 Aug. 1994
(Contracts DE-FG02-91ER-40676; DE-FG03-92ER-40701; DE-FG03-91ER-40618; DE-FG03-92ER-40689; DE-FG03-93ER-40788; DE-FG02-91ER-40672; DE-FG02-91ER-40677; DE-AC03-76SF-00098; DE-FG02-92ER-40715; DE-AC02-76ER-03069)
(DE95-002121; SU-SLAC-PUB-6595; CONF-940816-37) Avail: CASI HC A01/MF A01

The authors present preliminary measurements of the average B hadron lifetime using a sample of 50,000 Z(sup 0) events collected by SLD at the SLC in 1993. Their first technique uses the impact parameter of tracks in jets opposite tagged b jets. They obtain (tau)(sub B)(Sigma (delta)) = 1.617 (+/-) 0.048 (+/-) 0.086 ps, and (tau)(sub B)((Sigma)(delta)) = 1.627 (+/-) 0.054 (+/-) 0.132ps from single and summed impact parameter distributions. The second technique uses inclusive vertices reconstructed in three dimensions. From the decay length distribution, they extract (tau)(sub B) = 1.577 (+/-) 0.032 (+/-) 0.046 ps. DOE

N95-22179# International Centre for Theoretical Physics, Trieste (Italy).
MICROSCOPIC THEORY OF NORMAL LIQUID He-3
N. Nafari and A. Doroudi (Atomic Energy Organization of Iran, Teheran.) Mar. 1994 21 p
(DE94-629047; IC-94/43) Avail: CASI HC A03/MF A01 (US Sales Only)

We have used the self-consistent scheme proposed by Singwi, Tosi, Land and Sjoelander (STLS) to study the properties of normal liquid He-3. By employing the Aziz potential (HFD-B) and some other realistic pairwise interactions, we have calculated the static structure factor, the pair-correlation function, the zero sound frequencies as a function of wave-vector, and the Landau parameter F(sup s)(sub 0) for different densities. Our results show considerable improvement over the Ng-Singwi's model potential of a hard core plus an attractive tail. Agreement between our results and the experimental data for the static structure factor and the zero sound frequencies is fairly good. DOE

N95-22182# International Centre for Theoretical Physics, Trieste (Italy).
THE DYNAMIC STRUCTURE FUNCTION OF BOSE LIQUIDS IN THE DEEP INELASTIC REGIME
A. Belic Nov. 1993 9 p
(DE94-629077; IC-93/395) Avail: CASI HC A02/MF A01 (US Sales Only)

We study the dynamic structure function S(k, (omega)) of Bose liquids in the asymptotic limit k, omega approaches infinity at constant y equivalent to m/k (omega - k(exp 2)/2m), using orthogonal correlated basis of Feynman phonon states. DOE

N95-22188# Brookhaven National Lab., Upton, NY.
INTERFERENCE OF FLUORESCENCE X RAYS AND COHERENT EXCITATION OF CORE LEVELS
Y. Ma (Washington Univ., Seattle, WA.) and M. Blume 1994 8 p Presented at the International Meeting on Synchrotron Radiation Instrumentation, Stony Brook, NY, 18-22 Jul. 1994
(Contract DE-AC02-76CH-00016)
(DE94-016809; BNL-60676; CONF-940714-5) Avail: CASI HC A02/MF A01

The question of coherence in inelastic x-ray absorption and fluorescence processes among identical interacting atoms is studied using a simple diatomic model. Conditions for the coherence are discussed in terms of energy scales, such as the core hole life-time, instrument energy resolutions, and the splitting of the electronic levels. As in the classical Young double-slit experiment, the primary requirement is that it be impossible to determine which atom has undergone the excitation-decay process. DOE

N95-22190# Argonne National Lab., IL.
THERMAL AND DEFORMATION ANALYSES OF A NOVEL CRYOGENICALLY COOLED MONOCHROMATOR FOR AN ADVANCED PHOTON SOURCE BEAMLINE
Zhibi Wang, Wenbing Yun, T. M. Kuzay, and G. Knapp 1994 11 p Presented at the International Meeting on Synchrotron Radiation Instrumentation, Stony Brook, NY, 18-22 Jul. 1994
(Contract W-31-109-eng-38)
(DE94-016914; ANL/XFD/CP-82931; CONF-940714-6) Avail: CASI HC A03/MF A01

The analytical results and design considerations for a novel cryogenically cooled Advanced Photon Source (APS) monochromator are presented. Because the monochromator uses silicon crystal, cryogenic cooling enables one to take advantage of the high conductivity and low thermal expansion coefficient of silicon at cryogenic temperatures. The APS monochromator features a machined slot with variable thickness below the surface. With this configuration, only a fraction of the total undulator power is absorbed by the crystal; the remaining power is transmitted through the crystal and is absorbed by a second element that can be cooled by standard cooling techniques. A variety of analyses have been performed with different parameters and configurations to maximize the performance of the monochromator and minimize the total absorbed power by the crystal. DOE

N95-22194# Fermi National Accelerator Lab., Batavia, IL.
ELECTROWEAK BOSON PAIR PRODUCTION IN p(-p) COLLISIONS AT THE SQUARE ROOT OF s = 1.8 TeV
T. A. Fuess (Argonne National Lab., IL.) 16 Sep. 1994 6 p Presented at the Meeting of the Division of Particles and Fields of the American Physical Society, Albuquerque, NM, 2-6 Aug. 1994
(Contract DE-AC02-76CH-03000)
(DE95-000725; FNAL/C-94/283-E; CONF-940816-28) Avail: CASI HC A02/MF A01

Results from CDF on W(+)W(-), WZ, and W gamma production in square root of s = 1.8 TeV (bar p)-p collisions from the 1992-1993 collider run are presented. Direct limits on WW gamma and WWZ anomalous couplings are obtained. DOE

N95-22196# Fermi National Accelerator Lab., Batavia, IL.
INCLUSIVE B PRODUCTION AT CDF AND D0
K. A. Bazizi Sep. 1994 14 p Presented at the 29th Moriond Meeting on Quantum Chromodynamics and High Energy Hadronic Interactions, Les Arcs, France, 12-26 Mar. 1994
(Contract DE-AC02-76CH-03000)
(DE95-000728; FNAL/C-94/300-E; CONF-940327-11) Avail: CASI HC A03/MF A01

We present the latest results on inclusive b production studies from CDF and D0 collaborations in p(bar p) collisions at square root of s = 1.8 TeV at the Fermilab Tevatron Collider. The results are from recently completed analyses of 1988-1989 data and preliminary analyses of 1992-1993 data. This report includes new b cross section measurements using semileptonic b decays to muons, J/psi production in dimuon events, and a study of b(bar b) correlations in e mu events. The new results from CDF and D0 show no major discrepancies between the Tevatron data and the NLO QCD prediction for p(sub t) values down to 6 GeV. DOE

N95-22197# Fermi National Accelerator Lab., Batavia, IL.
SEARCH FOR SQUARKS AND GLUINOS IN D0
D. R. Claes (State Univ. of New York, Stony Brook, NY.) Sep. 1994 5 p Presented at the Meeting of the Division of Particles and Fields of the American Physical Society, Albuquerque, NM, 2-6 Aug. 1994
(Contracts DE-AC02-76CH-03000; DE-FG02-92ER-40697)
(DE95-000730; FNAL/C-94/290-E; CONF-940816-30) Avail: CASI HC A01/MF A01

Based on 7.1 pb(exp -1) of single interaction event data collected by the DO Detector at Fermilab during the 1992-1993 p(bar p) collider run at square root of s = 1.8 TeV, results are presented of a search for supersymmetric partners of the quark and gluon, the squark and gluino, using missing E(sub T) and jets as the signature. Limits are set on the squark and gluino masses in the context of the Minimal Supersymmetric Standard Model including the effect of cascade decays of the squark and gluino. DOE

N95-22217# International Centre for Theoretical Physics, Trieste (Italy).
UNIVERSAL SPECTRAL CORRELATIONS AT THE MOBILITY EDGE
V. E. Kravtsov, A. G. Aronov, I. V. Lerner (Birmingham Univ., England.), and B. L. Altshuler (Massachusetts Inst. of Tech., Cambridge, MA.) Sep. 1993 13 p
(DE94-629031; IC-93/330) Avail: CASI HC A03/MF A01 (US Sales Only)

The two-point spectral correlation function for a quantum particle in a random potential is calculated in the vicinity of the Anderson transition in d greater than 2 dimensions. Based on this, the variance of the number of states N in a given energy interval with /N/ much greater than 1 (/.../ means the ensemble average) is shown to have a universal behavior, /(N - /N/)(exp 2)/ approximately /N/(exp 2/d), different from that in both metallic and insulator regime. This is much smaller than a naive dimensional estimation would give. The suppression of fluctuations N is due to nontrivial cancellations resulting from the causality and scaling requirements. These cancellations are necessary for the spectral correlation function to satisfy an exact sum rule resulting from the conservation of the total number of states. DOE

N95-22218# International Centre for Theoretical Physics, Trieste (Italy).
TEMPERATURE DEPENDENCE OF MAGNETOPOLARONS IN A PARABOLIC QUANTUM DOT IN ARBITRARY MAGNETIC FIELDS
Ka-Di Zhu and Shi-Wei Gu (Jiaotong Univ., Shanghai, China.) Oct. 1993 18 p
(DE94-629033; IC-93/345) Avail: CASI HC A03/MF A01 (US Sales Only)

The temperature and the size dependence of a magnetopolaron in a harmonic quantum dot with an external magnetic field normal to the plane of the quantum dot are investigated theoretically. For a weak magnetic field (omega(sub c) less than omega(sub LO)), both the cyclotron mass m(sup *)(sub c+) and the cyclotron mass m(sup *)(sub c-) are the increasing functions of temperature, whereas for strong magnetic fields (omega(sub c) greater than omega(sub LO)), the cyclotron mass m(sup *)(sub c+) is the decreasing function of temperature, while the cyclotron mass m(sup *)(sub c-) is the increasing function of temperature. DOE

N95-22222# Lawrence Livermore National Lab., Livermore, CA.
AN ANALYTICAL ELECTRON DISTRIBUTION FUNCTION FOR INELASTIC COLLISIONS IN A UNIFORM GAS WITH TIME VARYING ELECTRIC FIELD
M. Garcia 21 Jul. 1994 24 p
(Contract W-7405-eng-48)
(DE95-003476; UCRL-ID-117952) Avail: CASI HC A03/MF A01

The desire for improved control over electric discharge phenomena in a wide variety of scientific, technological, manufacturing, and waste processing activities spurs the development of non-equilibrium, non-uniform, and time dependent models. This paper addresses the situation of slightly ionized, spatially uniform gas with a time varying electric field, and in which inelastic collisions occur. The purpose here is to present a reasonably consistent, and reasonably accessible analytical result for the electron kinetics in a gas discharge regime of technological interest. This paper will be structured as follows. First, the analytical result for the time dependent electron distribution function is stated. Second, a summary of the solution procedure with its attendant assumptions is given. Lastly, examples of the solution are given for an idealized nitrogen-like gas where the electric field ramps between static conditions, and then for sinusoidal behavior. DOE

N95-22223# Lawrence Livermore National Lab., Livermore, CA.
AN ANALYTICAL, INELASTIC, SPACE AND TIME DEPENDENT ELECTRON DISTRIBUTION FOR ELECTRICALLY EXCITED GASES
M. Garcia 2 Sep. 1994 30 p
(Contract W-7405-eng-48)
(DE95-003478; UCRL-ID-118498) Avail: CASI HC A03/MF A01

An approximate, electron energy distribution function, f((var epsilon), x, t), is obtained for the case of a slightly ionized gas with inelastic electron-molecule collisions, and for an external electric field with both spatial and temporal variation. A previous analysis of the Boltzmann equation, for a slightly ionized gas with time-varying electric field and inelastic collisions, has been extended to include the effect of a spatial gradient in the electric field. This paper describes the spatial variation effect by continuing the discussion on the electron distribution initiated in that previous report. An interesting feature of this analytical distribution function is its explicit dependence on both the magnitude of the field and its gradients. An example is included of the combined effect of field variations in space and time upon the local average electron energy in an idealized N2-like gas. DOE

N95-22239# Stanford Linear Accelerator Center, CA.
CONSTRAINTS ON THE LEFT-RIGHT SYMMETRIC MODEL FROM b YIELDS s GAMMA
T. G. Rizzo Nov. 1994 7 p Presented at the 1994 International Workshop on B Physics, Physics Beyond the Standard Model at the B Factory, Nagoya, Japan, 26-28 Oct. 1994
(Contract DE-AC03-76SF-00515)
(DE95-003469; SU-SLAC-PUB-6719; CONF-9410248-1) Avail: CASI HC A02/MF A01

The recent observation by the CLEO Collaboration of the inclusive decay b yields s gamma with a branching fraction consistent with the expectations of the Standard Model is used to constrain the parameter space of the Left-Right Symmetric Model. Two scenarios are considered: (1) equal left- and right-handed Cabibbo-Kobayashi-Maskawa mixing matrices, V(sub L) = V(sub R)(or V(sub R)*); and (2) the Gronau-Wakaizumi model wherein B-decays proceed only via right-handed currents and V(sub L) and V(sub R) are quite distinct. In the later case the bounds from b yields s gamma are combined with other constraints leaving a parameter range that is very highly restricted and which implies that this model may soon be completely ruled out by improving data. DOE

N95-22265# Oak Ridge National Lab., TN.
THE TWO-ELECTRON PROBLEM AND PROSPECTS FOR ATOMIC COLLISION THEORY ON A NUMERICAL LATTICE
D. R. Schulz 1994 13 p Presented at the Atomic Collisions, Oak Ridge, TN, 3-5 Mar. 1994

(Contract DE-AC05-84OR-21400)
(DE94-017856; CONF-9403151-1) Avail: CASI HC A03/MF A01

An exact numerical treatment of fully correlated two-electron systems is described and placed in context with themes characterizing Chris Bottcher's research regarding time-dependent, lattice approaches to the quantum mechanical solution of atomic collision problems. Tests of the method are summarized in which low-lying bound state are computed and the time-dependence of autoionization is described. Finally, prospects for treating the near-threshold electron-impact ionization of hydrogen and photoionization are discussed, as well as the general prospects for further development of this type of lattice treatment. DOE

N95-22279# Northeastern Univ., Boston, MA.
TOPICS IN GAUGE THEORIES AND THE UNIFICATION OF ELEMENTARY PARTICLE INTERACTIONS Progress Report, 1 Feb. 1993 - - 31 Jan. 1994
Y. N. Srivastava and M. T. Vaughn Feb. 1994 12 p
(Contract DE-FG02-85ER-40233)
(DE94-013485; DOE/ER-40233/9) Avail: CASI HC A03/MF A01

We report on work done by the principal investigators (Y.N. Srivastava and M.T. Vaughn) and their collaborators on: (1) Interference Between Past and Future Events in Neutral Kaon Decays in Phi yields K(-K); (2) Single Top Production at LEP II and at Electron -- Photon Colliders; (3) Renormalization Group Studies of Unified Gauge Theories; (4) Analysis of Classical Field Theories; and (5) Quantum Effects of Strong Classical Electromagnetic Fields. DOE

N95-22280# Los Alamos National Lab., NM.
HELIUM PRODUCTION BY 10 MeV NEUTRONS IN IRON, NICKEL AND COPPER
R. C. Haight, D. W. Kneff (Rockwell International Corp., Canoga Park, CA.), B. M. Oliver (Rockwell International Corp., Canoga Park, CA.), L. R. Greenwood (Pacific Northwest Lab., Richland, WA.), and H. Vonach (Wien Univ., Austria.) 1994 7 p Presented at the International Conference on Nuclear Data for Science and Technology: Nuclear Data for the Twenty-first Century, Gatlinburg, TN, 9-13 May 1994
(Contract W-7405-eng-36)
(DE94-014798; LA-UR-94-1593; CONF-940507-28) Avail: CASI HC A02/MF A01

Helium production cross sections for the elements Fe, Ni, and Cu and for the isotopes (56)Fe, (58)Ni and (60)Ni have been measured for 10-MeV neutrons. Samples were irradiated with an intense neutron source from the (1)H(t,n) reaction using a rotating gas cell. The generated helium was determined by isotope dilution gas mass spectrometry. Induced radioactivities and known cross sections were used together with calculations based on the source reaction to deduce the neutron fluence at each sample position. The results are in fair agreement with literature values for (n, alpha) cross sections measured by alpha-particle detection and integrated over the alpha-particle energies and angular distributions. DOE

N95-22281# Academy of Sciences (USSR), Moscow (USSR).
THESES OF THE PROCEEDINGS OF THE 23D INTERNATIONAL MEETING ON THE PHYSICS OF CHARGED PARTICLE INTERACTION WITH CRYSTALS Abstracts Only
A. F. Tulinov, ed. and V. A. Khodyrev, ed. 1993 148 p In RUSSIAN Meeting held in Moscow, Russia, 31 May - 2 Jun. 1993
(DE94-631501; INIS-RU-377; CONF-9305364) Avail: CASI HC A07/MF A02 (US Sales Only)

Reports containing results on theoretical and experimental studies in the area of orientation problems by charged particles interaction with crystals, their application in nuclear physics, solid matter physics for solving technological and material science tasks are presented. DOE

N95-22283# Academy of Sciences (USSR), Novosibirsk (USSR). Inst. Yadernoj Fiziki.
GAS-DYNAMIC TRAP DIAGNOSTIC COMPLEX FOR STUDY ON PLASMA HEATING AND POWER ATOMIC BEAM INJECTION
P. A. Bagryanskij, V. N. Bocharov, and P. P. Dejchuli et al 1993 44 p In RUSSIAN
(DE94-633377; IYaF-93-70) Avail: CASI HC A03/MF A01 (US Sales Only)

Gas-dynamic trap (GDT) constitutes an open trap with long central part and axial-symmetric MGD-stabilizers at the ends. DOE

N95-22303 Rutherford Appleton Lab., Chilton (England). ISIS Facility.
RADIO-FREQUENCY TECHNIQUES AT THE ISIS PULSED MUON SOURCE
S. P. Cottrell, B. Hitti, and C. A. Scott Sep. 1994 15 p Prepared in cooperation with Science Research Council, Daresbury, England
(PB95-129854; RAL-94-101) Copyright Avail: Issuing Activity (National Technical Information Service (NTIS))

This report describes experiments performed at the ISIS pulsed muon facility with a view to the future development of an RF MuSR facility. After a brief introduction to the principles of the magnetic resonance experiment, the design of the high-power pulsed RF equipment is discussed. Because the longitudinal field strength was limited to approximately 140 G, with the corresponding resonance frequency for muon plus below the base frequency of our power amplifier, studies were restricted to muonium systems with results being presented both for quartz and boron nitride. Finally, both the RF field strength and homogeneity are evaluated using time differential data taken at resonance in the rotating frame. NTIS

N95-22314# Fermi National Accelerator Lab., Batavia, IL.
SEARCH FOR TOP WITH DO DETECTOR IN DILEPTON CHANNEL
K. Genser Sep. 1994 7 p Presented at the Meeting of the Division of Particles and Fields of the American Physical Society, Albuquerque, NM, 2-6 Aug. 1994
(Contract DE-AC02-76CH-03000)
(DE95-000731; FNAL/C-94/288-E; CONF-940816-31) Avail: CASI HC A02/MF A01

Preliminary results from a search for high mass t(bar t) quark pair production in p(bar p) collisions at square root of s = 1.8 TeV with the DO detector in the ee + jets, e mu + jets, and mu mu + jets decay channels are presented. No conclusive evidence for top quark production for an integrated luminosity of 13.5 +/- 1.6 pb(exp -1) is observed. DOE

N95-22315# Sandia National Labs., Albuquerque, NM.
A NEW PARALLEL METHOD FOR MOLECULAR DYNAMICS SIMULATION OF MACROMOLECULAR SYSTEMS
S. Plimpton and B. Hendrickson Aug. 1994 22 p
(Contract DE-AC04-94AL-85000)
(DE94-018621; SAND-94-1862) Avail: CASI HC A03/MF A01

Short-range molecular dynamics simulations of molecular systems are commonly parallelized by replicated-data methods, where each processor stores a copy of all atom positions. This enables computation of bonded 2-, 3-, and 4-body forces within the molecular topology to be partitioned among processors straightforwardly. A drawback to such methods is that the inter-processor communication scales as N, the number of atoms, independent of P, the number of processors. Thus, their parallel efficiency falls off rapidly when large numbers of processors are used. In this paper a new parallel method called force-decomposition for simulating macromolecular or small-molecule systems is presented. Its memory and communication costs scale as N/(radical)P, allowing larger problems to be run faster on greater numbers of processors. Like replicated-data techniques, and in contrast to spatial-decomposition approaches, the new method can be simply load-balanced and performs well even for irregular simulation geometries. The implementation of the algorithm in a prototypical macromolecular simulation code ParBond is also discussed. On a 1024-processor Intel Paragon, ParBond runs a standard benchmark simulation of solvated myoglobin with a parallel efficiency of 61% and at 40 times the speed of a vectorized version of CHARMM running on a single Cray Y-MP processor. DOE

N95-22316# Cornell Univ., Ithaca, NY.
EXPERIMENTAL STUDY OF INTERACTIONS OF HIGHLY CHARGED IONS WITH ATOMS AT keV ENERGIES Progress Report, 16 Apr. - 1 Aug. 1994
V. O. Kostroun 3 Aug. 1994 9 p
(Contract DE-FG02-86ER-13519)
(DE94-018648; DOE/ER-13519/9) Avail: CASI HC A02/MF A01

The objective of this program is the experimental study of interactions of low energy, highly charged ions with other atomic species. The Cornell superconducting solenoid, cryogenic electron beam ion source CEBIS designed and built in our laboratory is the major piece of apparatus used in these investigations. This progress report describes the work accomplished during the period April 16, 1994 and August 1, 1994. This includes both finished experiments and preparatory work for planned future experiments using the source. During this time, we have completed measurements of the angular distributions and energy gains in Ar(q+) (11 less than or equal to q less than or equal to 14) on Ar collisions at 72 qeV laboratory energy. In particular, energy gain spectra at different laboratory scattering angles were obtained for Ar(q-1)(+) projectiles, i.e. projectiles whose final charge state had decreased by one unit. The experimental technique used, and the method of analysis are described elsewhere. The raw spectra are similar to those observed for Ar(8+) and Ar(I0+) on Ar at comparable energies, as well as those described in the last progress report for Ar(I2+) on Ar. DOE

N95-22332 Rutherford Appleton Lab., Oxford (England).
NEUTRON COMPTON SCATTERING
J. Mayers Jul. 1994 16 p See also PB93-225993
(PB95-130290; RAL-94-078) Avail: Issuing Activity (National Technical Information Service (NTIS))

The possibility of measuring atomic momentum distributions in condensed matter systems by neutron scattering is analagous to the measurement of electron momentum distributions by Compton scattering and measurement of nucleon momenta by deep inelastic scattering, and is known as neutron Compton scattering (NCS) or deep inelastic neutron scattering. The electron volt spectrometer at ISIS has been dedicated to the development of the NCS technique during the last five years and now has a full user program which is demonstrating the potential of this new neutron scattering technique for providing unique and detailed information about the atomic wavefunction and atomic kinetic energies in condensed matter. NCS has applications to all areas of neutron science e.g. quantum fluids, molecular science, liquid metals, amorphous and noncrystalline materials, hydrogen bonds, atomic and molecular hydrogen in materials, and many other areas. We discuss the type of information which can be obtained from NCS measurements and give a number of examples of such measurements. NTIS

N95-22339# Fermi National Accelerator Lab., Batavia, IL.
BEAM FLAVOR DEPENDENCE IN THE HADROPRODUCTION OF D(+-) AND D(SUB s)(+-) MESONS
A. Wallace (Yale Univ., New Haven, CT.), G. A. Alves (Centro Brasileiro de Pesquisas Fisicas, Rio de Janeiro.), S. Amato (Centro Brasileiro de Pesquisas Fisicas, Rio de Janeiro.), J. C. Anjos (Centro Brasileiro de Pesquisas Fisicas, Rio de Janeiro.), J. A. Appel, J. Astorga (Tufts Univ., Medford, MA.), S. B. Bracker (Toronto Univ., Ontario.), L. M. Cremaldi (Mississippi Univ., University, MS.), C. L. Darling (Yale Univ., New Haven, CT.), and R. L. Dixson et al Jul. 1994 7 p Presented at ICHEP94, 20-27 Jul. 1994
(Contract DE-AC02-76CH-03000)
(DE94-015541; FNAL/C-94/184-E) Avail: CASI HC A02/MF A01

Fermilab E769, a fixed-target experiment conducted during the 1987-88 running period, yielded large numbers of charm particles. Through collisions of 250 GeV (pi)(sup (+-)), K(sup (+-)), and p on a multifoil target, E769 allows for studies of beam flavor dependence in the hadroproduction of charm. Through the decay modes D(sup +) (yields) K(sup (minus))(pi)(sup +)(pi)(sup +), D(sub s)(sup +) (yields) (phi)(pi)(sup +), and D(sub s)(sup +) (yields) (anti K)(sup *0) K(sup +) (and charge conjugates), the authors have extracted D(sup (+-)) and D(sub s)(sup (+-)) signals for all five beam types. They report preliminary measurements of the beam dependence of the absolute production cross-sections (For Feynman x greater than 0) of the D(sup (+-)) and D(sub s)(sup (+-)). DOE

N95-22340# Fermi National Accelerator Lab., Batavia, IL.
STRUCTURE FUNCTIONS AND STRUCTURE FUNCTION RATIO F(SUP n)2/F(SUP p)2 AT SMALL x(SUB Bj) AND Q2 IN MUON-NUCLEON SCATTERING
P. Spentzouris (Northwestern Univ., Evanston, IL.) Jul. 1994 6 p Presented at the Intersections of Particle and Nuclear Physics, St. Petersburg, FL, 31 May - 6 Jun. 1994
(Contract DE-AC02-76CH-03000)
(DE94-017981; FNAL/C-94/220-E; CONF-940514-12) Avail: CASI HC A02/MF A01

Preliminary results on the measurement of the structure functions F(sub 2)(sup p)(x(sub Bj), Q(sup 2)) and F(sub 2)(sup d)(x(sub Bj), Q(sub 2)) and of the ratio F(sub 2)(sup n)/F(sub 2)(sup p) from experiment E665 are presented. The data were obtained using 465 GeV/c muons scattering off liquid hydrogen and deuterium targets. The dependence of the structure functions on x(sub Bj) and Q(sup 2) is examined in the kinematic range x(sub Bj) greater than 8 x 10(exp -4) and Q(sup 2) greater than 0.2 GeV(sup 2)/c(sup 2). The structure function ratio is presented as a function of x(sub Bj), for x(sub Bj) greater than 10(exp -6). DOE

N95-22392# Brookhaven National Lab., Upton, NY.
PROTON AND PRODUCED PARTICLE DISTRIBUTIONS FROM Au+Au COLLISIONS AT 11.6 A GeV/c
B. Moskowitz 1994 6 p Presented at the Meeting of the Division of Particles and Fields of the American Physical Society, Albuquerque, NM, 2-6 Aug. 1994
(Contract DE-AC02-76CH-00016)
(DE94-018634; BNL-60732; CONF-940816-4) Avail: CASI HC A02/MF A01

The highest net baryon density possible in the laboratory - up to ten times normal nuclear density - is expected in the central region of collisions of heavy nuclei (A approx. 200) at energies near 10 GeV per nucleon. The transverse energy (E(sub T)) distribution, as well as yields of identified particles ((pi)(sup +), K(sup +) and protons), from Au-197 + Au-197 at 11.64A GeV/c are presented. Two key observations are a large degree of proton 'stopping,' indicating multiple scatterings of the incident nucleons, and a proportional relationship of the pion production to the number of participating nucleons. Strangeness enhancement, a proposed signature of the quark-gluon plasma, is studied via the K(sup +)/(pi)(sup +) ratio, which achieves the value of 21% without a strong centrality dependence. Comparisons to similar data taken with a 14.6A GeV/c beam of Si-28 are made. DOE

N95-22435# Los Alamos National Lab., NM.
PARITY VIOLATION IN THE COMPOUND NUCLEUS
J. D. Bowman, C. M. Frankle, and A. A. Green 1994 15 p Presented at the Intersections of Particle and Nuclear Physics; Symmetries in Subatomic Physics, St. Petersburg, FL; Taiwan (China), 31 May - 6 Jun. 1994; 16-18 May 1994
(Contract W-7405-eng-36)
(DE95-002742; LA-UR-94-3563; CONF-940514-16; CONF-9405249-1)
Avail: CASI HC A03/MF A01

The status of parity violation in the compound nucleus is reviewed. The results of previous experimental results obtained by scattering polarized epithermal neutrons from heavy nuclei in the 3-p and 4-p p-wave strength function peaks are presented. Experimental techniques are presented. The extraction of the mean squared matrix element of the parity-violating interaction, M(exp 2), between compound-nuclear levels and the relationship of M(exp 2) to the coupling strengths in the meson exchange weak nucleon-nucleon potential are discussed. The tendency of measured asymmetries to have a common sign and theoretical implications are discussed. New experimental results are presented that show that the common sign phenomenon is not universal, as theoretical models developed up to now would predict. DOE

N95-22471# Cornell Univ., Ithaca, NY. Lab. of Atomic and Solid State Physics.
RESONANT CHARGE TRANSFER IN HYPERTHERMAL ATOMIC AND MOLECULAR ION-SURFACE COLLISIONS Final Report, 1 Jan. 1991 - 30 Jun. 1994
Barbara H. Cooper 23 Aug. 1994 35 p
(Grant AF-AFOSR-0137-91)
(AD-A284937; AFOSR-94-0561TR) Avail: CASI HC A03/MF A01

We have investigated the interactions of hyperthermal (few to several hundred eV) atomic ions with metal surfaces, in particular the dynamics of electron transfer between the particle and surface. Progress is reported in the following areas: (1) construction of a time-of-flight spectrometer for measuring energy- and angle-resolved distributions of neutral and charged alkali atoms; (2) measurements of the magnitude and velocity-dependence of the neutralization probabilities for Li, Na, and K scattered from clean Cu(001); dramatic differences for Li, Na, and K reflect the sensitivity of nonadiabatic charge transfer to the energies and lifetimes of atomic electronic states near the surface; (3) measurements of branching ratios for Li(+), Li(-) and ground- and excited state (Li(2s) and Li(2p)) formation in Li(+) scattering from alkali-covered Cu(001), which provide a test of new multi-state charge transfer models and indicate some of the first evidence of multi-state effects in atom-surface charge transfer; (4) extensions of our multi-state studies to include formation of higher energy excited states of Li and Na, and multiple states in O(+) and O(+2) scattering; (5) observation of trajectory-dependent charge transfer for 50 eV Na(+) scattering from clean Cu(001); evidence is found for modification of the neutralization due to collision-induced defect formation in the surface; (6) preliminary measurements of trapping probabilities for 10-100 eV Na(+) scattering from clean Cu(001), which show a strong nonmonotonic dependence on the incident energy. These studies are part of a new program to investigate the mechanisms by which hyperthermal energy ion beams can be used to modify thin film growth. DTIC

73 NUCLEAR AND HIGH-ENERGY PHYSICS

Includes elementary and nuclear particles; and reactor theory.
For space radiation see *93 Space Radiation.*

N95-19974 Michigan Univ., Ann Arbor, MI. Dept. of Nuclear Engineering.
THEORETICAL AND EXPERIMENTAL STUDIES OF A NOVEL ACCELERATING STRUCTURE Annual Technical Report, 1 May 1993 - 30 Apr. 1994
R. M. Gilgenbach and Y. Y. Lau 17 Aug. 1994 30 p Limited Reproducibility: More than 20% of this document may be affected by microfiche quality
(Contract N00014-91-J-1941)
(AD-A283730) Avail: CASI HC A03

Research during the past year has concentrated on a novel, two-beam accelerator (twobetron). This idea was published in Physical Review Letters and a patent application was filed. Accomplishments include the following: (1) theoretical analysis of the new technique for phase-focusing this new accelerator; (2) theory of e-beam modulation, BBU and other issues; (3) initial generation and transport of an annular electron beam; (4) design and fabrication of model/prototype accelerator cavities; and (5) initial cold tests of accelerator cavities. DTIC

N95-19983# Argonne National Lab., IL.
MODELING THE DYNAMICS OF CHARGED-PARTICLE BEAMS USING A FOKKER-PLANCK APPROACH
C. L. Bohn and J. R. Delayen 1994 3 p Presented at the 17th International LINAC Conference, Tsukuba, Japan, 21-26 Aug. 1994
(Contract W-31-109-eng-38)
(DE95-001458; ANL/TD/CP-84288; CONF-9408125-37) Avail: CASI HC A01/MF A01

At the previous Linac Conference, we introduced a semianalytic Fokker-Planck formalism for calculating the evolution of intense, nonrelativistic, mismatched beams propagating through focusing channels. We have since elaborated on its physical basis and greatly expanded its applicability. In this paper, we implement the model to study the dynamics of a circularly symmetric beam propagating through a linear focusing channel. An example is discussed for an ion beam and accelerator parameters which are representative of high-current spallation neutron sources in which space-charge forces are important. The example illustrates the dynamics of emittance growth and halo formation in the beam. DOE

N95-20015# Lawrence Livermore National Lab., Livermore, CA.
X-RAY IMAGING OF UNIFORM LARGE SCALE-LENGTH PLASMAS CREATED FROM GAS-FILLED TARGETS ON NOVA
D. H. Kalantar, B. J. MacGowan, T. P. Bernat, D. E. Klem, D. S. Montgomery, J. D. Moody, D. H. Munro, G. F. Stone, W. W. Hsing (Los Alamos National Lab., NM.), and B. H. Failor (Physics International Corp., Berkeley, CA.) May 1994 15 p Presented at the 10th Topical Conference on High-Temperature Plasma Diagnostics, Rochester, NY, 8-12 May 1994
(Contract W-7405-eng-48)
(DE94-018339; UCRL-JC-116195; CONF-940552-31) Avail: CASI HC A03/MF A01

We report on the production and characterization of large scale-length plasmas created by illuminating gas-filled thin-walled balloon-like targets using the Nova laser. The targets consisted of a 4-5 000 (angstrom) skin surrounding 1 atm of neopentane which when ionized becomes a plasma with 10(sup 21) electrons/cu cm. Results are presented from x ray imaging used to evaluate the uniformity of the plasma. The most uniform plasmas were produced by illuminating the target with large converging beams that overlapped to cover most of the surface of the gasbag. An alternate focus geometry using small beam spots resulted in a less uniform plasma with low density holes in it. DOE

N95-20021# Brookhaven National Lab., Upton, NY.
TRANSITION-ENERGY CROSSING WITH A GAMMA(SUB t)(-)JUMP
Jie Wei and S. Peggs 1994 4 p Presented at the 4th European Particle Accelerator Conference, London, England, 27 Jun. - 1 Jul. 1994
(Contract DE-AC02-76CH-00016)
(DE94-017315; BNL-49853; CONF-940618-47) Avail: CASI HC A01/MF A01

Expressions for the minimum size and speed of a transition-energy gamma(sub t)(-)jump needed to diminish the chromatic non-linear effect, the self-field mismatch, and the microwave instabilities in the Relativistic Heavy Ion Collider (RHIC) are obtained. A gamma(sub t)(-)jump of 0.8 units is needed to be performed within 60 ms in order to achieve a 'clean' transition crossing. DOE

N95-20120# Lawrence Livermore National Lab., Livermore, CA.
HIGH POWER SPECTRAL AND SPATIAL BEAM CONTROL USING SELF-PHASE MODULATION AND A MULTISEGMENT MONOCHROMATOR
R. Wilcox, D. Pennington, D. Eimerl, T. Weiland, and M. Henesian Jun. 1994 8 p Presented at the Institute for Electrical and Electronics Engineers/Lasers and Electro-Optics Society (IEEE/LEOS) Conference, Amsterdam, Netherlands, 28 Aug. - 2 Sep. 1994
(Contract W-7405-eng-48)
(DE94-016604; UCRL-JC-117490; CONF-9408133-1) Avail: CASI HC A02/MF A01

We present a novel optical system for forming high power beams with spatial separation of selected spectral components. Self-phase modulation in an optical fiber creates multiple wavelengths. A segmented diffraction grating device provides spectral control. DOE

N95-20203# Los Alamos National Lab., NM.
A NEW TOOL FOR ACCELERATOR SYSTEM MODELING AND ANALYSIS
George H. Gillespie (Gillespie, George H. Associates, Inc., Del Mar, CA.), Barry W. Hill (Gillespie, George H. Associates, Inc., Del Mar, CA.), and Robert A. Jameson 1994 5 p Presented at the 17th International LINAC Conference, Tsukuba, Japan, 21-26 Aug. 1994
(Contract W-7405-eng-36)
(DE94-018292; LA-UR-94-2804; CONF-9408125-22) Avail: CASI HC A01/MF A01

A novel computer code is being developed to generate system level designs of radiofrequency ion accelerators. The goal of the Accelerator System Model (ASM) code is to create a modeling and analysis tool that is easy to use, automates many of the initial design calculations, supports trade studies used in assessing alternate designs and yet is flexible enough to incorporate new technology concepts as they emerge. Hardware engineering parameters and beam dynamics are modeled at comparable levels of fidelity. Existing scaling models of accelerator subsystems were used to produce a prototype of ASM (version 1.0) working within the Shell for Particle Accelerator Related Codes (SPARC) graphical user interface. A small user group has been testing and evaluating the prototype for about a year. Several enhancements and improvements are now being developed. The current version (1.1) of ASM is briefly described and an example of the modeling and analysis capabilities is illustrated. DOE

N95-20282# Brookhaven National Lab., Upton, NY.
EFFECT OF SPACE CHARGE TUNE SHIFT ON TRANSVERSE INSTABILITIES
M. Blaskiewicz and W. T. Weng 1994 3 p Presented at the 4th European Particle Accelerator Conference, London, England, 27 Jun. - 1 Jul. 1994
(Contract DE-AC02-76CH-00016)

(DE94-016790; BNL-49820; CONF-940618-42) Avail: CASI HC A01/MF A01

Transverse instabilities in synchrotrons with large space charge tune shift are considered. In particular the variation of the incoherent tune with longitudinal position in the bunch is included. Expansion in an appropriate basis set results in an eigenvalue problem which reduces to previously derived expressions when the space charge tune spread is ignored. The regime where the synchrotron tune is negligible compared to the space charge tune shift is also considered. Under appropriate conditions this results in a significantly smaller growth rate than the ones obtained using the weak coupling formalism. Finally, the effect of octupole induced betatron tune spread is included, resulting in a technique for estimating the maximum stable current. DOE

N95-20336# Brookhaven National Lab., Upton, NY.

RELATIONAL DATABASES FOR RHIC DESIGN AND CONTROL

C. G. Trahern, C. Saltmarsh, T. Satogata, S. Peggs, W. W. Mackay, T. Clifford, M. Hemmer, E. Scholl, T. Shea, and V. Mane 1994 3 p Presented at the 4th European Particle Accelerator Conference, London, England, 27 Jun. - 1 Jul. 1994
(Contract DE-AC02-76CH-00016)
(DE94-016785; BNL-49857; CONF-940618-41) Avail: CASI HC A01/MF A01

The preliminary organization of data via relational databases for the design and control of the Relativistic Heavy Ion Collider (RHIC) is described. DOE

N95-20347# Maryland Univ., College Park, MD. Lab. for Plasma Research.

STUDIES OF LONGITUDINAL INSTABILITY WITH AN ELECTRON BEAM

1994 13 p
(Contract DE-FG02-92ER-54178)
(DE94-018646; DOE/ER-54178/4) Avail: CASI HC A03/MF A01

This progress report covers the research on the 'Study of Longitudinal Instability with an Electron Beam' performed at the University of Maryland during the period from September 1, 1993 to February 28, 1994 of the two-year grant sponsored by the Department of Energy, under Grant No. DEFG02-92ER54178. This research is motivated by the issue of longitudinal instability in induction linacs as drivers for heavy ion inertial fusion. The Fusion Policy Advisory Committee (FPAC) in its final report to DOE (September 1990) identified longitudinal instability as a key physics problem that needs to be solved if an induction linac is to be developed into a successful HIF driver. The FPAC report also stated that 'in parallel' to the design and construction of ILSE 'enhanced theoretical and experimental efforts are required for an improved understanding of potentially serious longitudinal beam instability issues'. The experiment with electron beams in this area is a low-cost way to gain a thorough understanding of the instability and to test computer codes in collaboration with LBL, LLNL, and I. Haber at NRL. The last six months saw the transition of the research activities from phase 1 to phase 2. By the end of last September, the experiments on space-charge waves had been completed. This had fulfilled the first year's goal of this two-year grant. Though the completion of the experiments was one month later than that scheduled and the data analysis still continues up to now, the authors have done much more than was originally proposed. DOE

N95-20388# Stanford Linear Accelerator Center, CA.

HIGH ENERGY PHOTON-PHOTON COLLISIONS

S. J. Brodsky and P. M. Zerwas (Deutsches Elektronen-Synchrotron, Hamburg, Germany.) Jul. 1994 45 p Presented at the Workshop on Gamma-Gamma Colliders, Berkeley, CA, 28-31 Mar. 1994
(Contract DE-AC03-76SF-00515)
(DE94-017494; SU-SLAC-PUB-6571; CONF-940351-1) Avail: CASI HC A03/MF A01

The collisions of high energy photons produced at a electron-positron collider provide a comprehensive laboratory for testing QCD, electroweak interactions and extensions of the standard model. The luminosity and energy of the colliding photons produced by back-scattering laser beams is expected to be comparable to that of the primary e(sup +)e(sup -) collisions. In this overview, we shall focus on tests of electroweak theory in photon-photon annihilation, particularly gamma(gamma) yields W(sup +)W(sup -), gamma(gamma) yields Higgs bosons, and higher-order loop processes, such as gamma(gamma) yields gamma(gamma), Z(gamma) and ZZ. Since each photon can be resolved into a W(sup +)W(sup -) pair, high energy photon-photon collisions can also provide a remarkably background-free laboratory for studying WW collisions and annihilation. We also review high energy gamma(gamma) tests of quantum chromodynamics, such as the scaling of the photon structure function, t(bar t) production, mini-jet processes, and diffractive reactions. DOE

N95-20406# General Electric Co., Richland, WA. Hanford Atomic Products Operation.

AN IMPEDANCE MODEL OF THE RELATIVISTIC HEAVY ION COLLIDER (RHIC)

S. Peggs, V. Mane, W. W. MacKay, M. Blaskiewicz, R. Connolly, D. P. Deng, A. Ratti, J. Rose, T. Shea, and J. Wei 1994 4 p Presented at the 4th European Particle Accelerator Conference, London, England, 27 Jun. - 1 Jul. 1994
(Contract DE-AC02-76CH-00016)
(DE94-016784; BNL-49859; CONF-940618-52) Avail: CASI HC A01/MF A01

This paper is an abbreviated version of a comprehensive and detailed analysis of RHIC instabilities soon to be published as a RHIC project report. It emphasizes longitudinal impedance modeling and design choices in RHIC, while a companion paper emphasizes instability calculations. DOE

N95-20421# Fermi National Accelerator Lab., Batavia, IL.

DERIVATION OF COUPLING IMPEDANCE FROM THE WAKE POTENTIAL OF A FINITE BUNCH

King-Yuen Ng Sep. 1994 3 p
(Contract DE-AC02-76CH-03000)
(DE95-002529; FNAL-TM-94/1903) Avail: CASI HC A01/MF A01

The coupling impedance of the vacuum chamber can be obtained from the wake potential left by a bunch of finite extent. Oftentimes, however, the impedance so obtained violates the condition that its real part must be everywhere non-negative. The proper treatment is derived and discussed. DOE

N95-20494# California Univ., Berkeley. Lawrence Berkeley Lab, CA.

SIX-DIMENSIONAL MODELING OF COHERENT BUNCH INSTABILITIES AND RELATED FEEDBACK SYSTEMS IN STORAGE RINGS WITH POWER-SERIES MAPS FOR THE LATTICE

J. Bengtsson, D. Briggs (Stanford Univ., CA.), and M. Meddahi (European Organization for Nuclear Research, Geneva, Switzerland.) Jun. 1994 3 p Presented at the 4th European Particle Accelerator Conference, London, England, 27 Jun. - 1 Jul. 1994
(Contract DE-AC03-76SF-00098)
(DE94-017965; LBL-35956; CONF-940618-64) Avail: CASI HC A01/MF A01

The authors have developed 6-dimensional phase-space code that tracks macroparticles for the study of coherent bunch instabilities and related feedback systems. The model is based on power-series maps to represent the lattice, and allows for straightforward inclusion of effects such as amplitude dependent tune shift, chromaticity, synchrotron oscillations, and synchrotron radiation. It simulates long range wake fields such as resistive-wall effects as well as the higher order modes in cavities. The model has served to study the dynamics relevant to the transverse feedback system currently being commissioned for the Advanced Light Source (ALS). Current work integrates earlier versions into a modular system that includes models for transverse and longitudinal feedback systems. It is designed to provide a modular approach to the dynamics and diagnostics, allowing a user to modify the model of a storage ring at run-time without recompilation. DOE

N95-20495# California Univ., Berkeley. Lawrence Berkeley Lab, CA.

MODELING OF BEAM DYNAMICS AND COMPARISON WITH MEASUREMENTS FOR THE ADVANCED LIGHT SOURCE (ALS)

J. Bengtsson and M. Meddahi (European Organization for Nuclear Research, Geneva, Switzerland.) Jun. 1994 3 p Presented at the 4th European Particle Accelerator Conference, London, England, 27 Jun. - 1 Jul. 1994
(Contract DE-AC03-76SF-00098)

(DE94-017970; LBL-35959; CONF-940618-65) Avail: CASI HC A01/MF A01

The data collected during the April 1993 ALS commissioning period includes the measured closed orbit as a function of either dipole corrector strength or RF frequency, in addition to turn by turn data for the betatron motion as a function of RF frequency. The sensitivity matrix and dispersion function are extracted from this data by taking differences between orbits, whereas lattice functions and chromaticity are obtained using Fourier analysis and interpolation techniques. Lattice functions are also derived from the sensitivity matrix using a nonlinear least squares fit. The results are then compared with numerical simulations and analytical formulas derived using maps and a Lie product normal form approach. The Lie method is preferred to traditional Hamiltonian perturbation theory because it is easily generalized to the nonlinear case and also leads to a significantly reduced amount of algebra. The computer modeling uses state of the art single particle beam dynamics tools including: Tracy-2, DA-pascal, DA-Library and Lie-Lib. In particular, DA-Pascal allows for a straightforward implementation of a Krakpot style code, based on the 'exact' single particle local Hamiltonian and a symplectic integrator, necessary for correct modeling of the nonlinear chromaticity. DOE

N95-20573# Brookhaven National Lab., Upton, NY.
PHOTOELECTRONS BEAM MEASUREMENT FROM A MAGNESIUM CATHODE IN A RF ELECTRON GUN
X. J. Wang, T. Srinivasan-Rao, K. Batchelor, I. Ben-Zvi, and J. Fischer 1994 3 p Presented at the 16th International Free Electron Laser Conference, Stanford, CA, 21-26 Aug. 1994
(Contract DE-AC02-76CH-00016)
(DE94-017994; BNL-60738; CONF-9408146-1) Avail: CASI HC A01/MF A01

The performance of a magnesium cathode in a one-and-half cell photocathode RF gun measured at the Brookhaven Accelerator Test Facility (ATF). The frequency quadrupled Nd:YAG laser (266 nm) was used to stimulate the photoelectron emissions. For a normal incident laser pulse, the quantum efficiency of the magnesium at 10(exp -7) torr was measured to be 5 x 10(exp -4), which is more than 20 times the value for copper under similar conditions. DOE

N95-20672 Naval Research Lab., Washington, DC.
PRS SCOPING STUDY 1: SCALING LAW ESTIMATES FOR K-SHELL RADIATION YIELDS ON JUPITER-CLASS GENERATORS
J. L. Giuliani, Jr., J. Davis, M. Mulbrandon, K. Whitney, and J. W. Thornhill 31 May 1994 68 p Limited Reproducibility: More than 20% of this document may be affected by microfiche quality
(AD-A279716; NRL/MR/6720-94-7466) Avail: Issuing Activity (Defense Technical Information Center (DTIC))

The radiation output from krypton, argon, and xenon z-pinch loads is calculated for JUPITER-class generators using an amended version of the Whitney, et al., K-shell yield scaling law. The present version, termed J-scaling law, is directed toward JUPITER predictions and includes a dependence on the final radius as well as a smooth yield fall off for weak implosions. When combined with a circuit model and a thin shell model for the plasma pinch dynamics, comparisons and predictions of yields can be made for specific machines. Comparisons with existing aluminum data on DOUBLE EAGLE and SATURN demonstrate the veracity of the J-scaling law. A simple equivalent circuit with variable driving voltage is used to predict the trend of K-shell yield with increasing load current. In general, for JUPITER-class machines (30 - 100 MA)Ar is in the efficient I squared scaling regime, xenon is in the weak I to the 4th power regime, and Kr is a transition radiator. Candidate transmission line circuits for the Linear Inductive Adder (LIA) and the modular Inductive Energy Store (IES) JUPITER designs are investigated in detail. Load currents, voltages, and coupled kinetic energies are calculated as a function of (MR (sub 0))(exp 2). These calculations are then combined with the J-scaling law to predict K-shell yields for the transmission line circuits. Variations of the standard candidate point are also investigated: specifically, the effects of a larger front end inductance, of eliminating a closing switch in the LIA, and of increasing the conduction time on the IES. DTIC

N95-20766# Brookhaven National Lab., Upton, NY. Dept. of Advanced Technology.
CRYSTALLINE BEAMS: THE HORIZONTAL ZIGZAG
A. F. Haffmans, D. Maletic, and A. G. Ruggiero May 1994 17 p
(Contract DE-AC02-76CH-00016)
(DE95-002227; BNL-60876) Avail: CASI HC A03/MF A01

The authors continue their investigation of 'Crystalline Beams' in the ground state. In this paper they study the possibility of storing an intense beam of charged particles in a storage ring where the particles acquire a horizontal zigzag configuration. They define the equilibrium configuration, and examine the confinement and stability conditions. The problem of 'shear' between particles circulating side by side caused by the curvature of the trajectories is examined and solved. DOE

N95-20784# Lawrence Livermore National Lab., Livermore, CA.
RADIATION-DRIVEN TARGETS FOR HEAVY-ION FUSION
D. D. M. Ho, J. A. Harte, and M. Tabak Aug. 1994 13 p Presented at the 15th International Conference on plasma Physics and Controlled Nuclear Fusion Research, Seville, Spain, 26 Sep. - 1 Oct. 1994
(Contract W-7405-eng-48)
(DE95-002264; UCRL-JC-118161; CONF-940933-12) Avail: CASI HC A03/MF A01

The baseline hohlraum configuration for heavy-ion fusion has the radiation converters placed at opposite ends. For a capsule that absorbs about 1 MJ and has an initial radius of 0.234 cm, the minimum initial capsule to hohlraum surface area ratio that can provide an adequate time-dependent symmetry requirement for a capsule implosion is about 0.075, based on calculations using the view factor code GERTIE. The capsule implosion is calculated using the hydrodynamic code HYADES. The energy coupling efficiency between the hohlraum and the capsule is 21%; the peak hohlraum temperature is 260 eV, and the gain of this target system can be as high as 80. By placing the converters outside the hohlraum, the radii of the converters can be varied according to the beam focusing requirements while the hohlraum dimensions remain unchanged. By bending the radiation converters by 90 degrees, one can obtain a hohlraum configuration that requires the ion beams to come in from only one direction. DOE

N95-20885# Fermi National Accelerator Lab., Batavia, IL.
OPTIMIZING THE LENGTH OF THE STORES AND RELATED EFFECTS
E. McCrory Oct. 1994 10 p
(Contract DE-AC02-76CH-03000)
(DE95-002531; FNAL-TM-1878) Avail: CASI HC A02/MF A01

This memo is an attempt to create an accurate analytical model for the luminosity obtained in the Fermilab Tevatron during collider operation. Other people, in particular Alan Hahn and, alledgedly, Vinod Bharadwaj and Gerry Dugan, have addressed this topic and predicted an optimum store duration. The approach taken here is slightly different from Hahn's, in particular, analytic forms for the model are written down and the optima are found directly, through differentiation. Also, specifying the parameters clearly is helpful in understanding the dependencies of this phenomenology. First, the optimum store duration is derived from first principles, and then graphs of this are made and various assumptions on the parameters are analyzed. Finally, some related effects are discussed. DOE

N95-20886# Brookhaven National Lab., Upton, NY.
CONFINEMENT AND STABILITY OF CRYSTALLINE BEAMS IN STORAGE RINGS
A. F. Haffmans 1994 17 p Presented at the Advanced Accelerator Concepts Workshop, Lake Geneva, WI, 13-18 Jun. 1994
(Contract DE-AC02-76CH-00016)
(DE95-002515; BNL-60878; CONF-940681-3) Avail: CASI HC A03/MF A01

We present a fully analytical approach to the study of tile confinement and stability of 'Crystalline Beams' in storage rings, in terms of such fundamental accelerator concepts as tune shift and stopband. We consider a 'Crystalline Beam' consisting of substrings, arranged symmetrically around the reference trajectory, and we examine the motion of a slightly perturbed test particle on one of them. Our approach quite naturally leads to the conclusion, that (1) storage rings need to be operated below the transition energy, and (2) the 'Crystalline Beam' has the same periodicity as the storage ring. Each 'Crystalline Beam' has an upper and lower limit of the spacing between the ions. The upper limit is determined by condition (2), and the lower limit is set by the stability of the test particle motion around the equilibrium. DOE

N95-20891# California Univ., Berkeley. Lawrence Berkeley Lab, CA.
INDUCTION LINACS FOR HEAVY ION FUSION
R. O. Bangerter and A. Faltens Aug. 1994 4 p Presented at the 17th International LINAC Conference, Tsukuba, Japan, 21-26 Aug. 1994
(Contract DE-AC03-76SF-00098)
(DE95-002357; LBL-36067; HIFAN-671; CONF-9408125-38) Avail: CASI HC A01/MF A01

Inertial fusion target physics imposes important constraints on the design of linacs for heavy-ion fusion. The most challenging constraint from a scientific standpoint is the requirement that the accelerator deliver more than 10(exp 14) W of beam power to a small quantity (less than 100 mg) of matter. The most challenging constraint from an engineering standpoint is accelerator cost. This paper explains the target physics requirements and shows how they lead to constraints on the usual accelerator parameters such as kinetic energy, current, and emittance. It will be shown that improvements in the final focusing system would have a beneficial effect on both scientific feasibility and cost. The paper also discusses experiments that are presently underway in the United States, specifically, experiments on high-current injectors, recirculating induction accelerators, transverse beam combining, and a proposed accelerator called ILSE. Hardware development for ILSE is now in progress. DOE

N95-20900# Fermi National Accelerator Lab., Batavia, IL.
EMITTANCE GROWTH DUE TO NEGATIVE-MASS INSTABILITY ABOVE TRANSITION
King-Yuen Ng Aug. 1994 14 p Presented at the Workshop on Beam Instabilities in Storage Rings, Hefei, China, 25-30 Jul. 1994
(Contract DE-AC02-76CH-03000)
(DE95-002527; FNAL/C-94/253; CONF-9407121-4) Avail: CASI HC A03/MF A01

Due to space-charge effect, there is a growth of bunch emittance across transition as a result of negative-mass instability. The models of growth at cutoff frequency and growth from high-frequency Schottky noise are reviewed. The difficulties of performing reliable simulations are discussed. An intuitive self-bunching model for estimating emittance growth is presented. DOE

N95-21208# Lawrence Livermore National Lab., Livermore, CA.
NEUTRONICS AND SHIELDING ANALYSIS OF THE NATIONAL IGNITION FACILITY
J. F. Latkowski, M. T. Tobin, and M. S. Singh Jun. 1994 7 p Presented at the 11th Topical Meeting on the Technology of Fusion Energy, New Orleans, LA, 19-24 Jun. 1994
(Contract W-7405-eng-48)
(DE94-016698; UCRL-JC-115585; CONF-940630-31) Avail: CASI HC A02/MF A01

The Department of Energy (DOE) is proposing to construct the National Ignition Facility (NIF) by the year 2001 to embark on a program to achieve ignition and modest gain in the laboratory. The NIF will use 1.8 MJ of 0.35 (mu)m laser light, nearly a fifty-fold increase in energy over the Nova laser at Lawrence Livermore National Laboratory (LLNL). A 5-m radius spherical aluminum chamber will contain the target experiments and allow access to diagnostics for data collection. Based on a projected maximum annual yield of 385 MJ (1.4 x 10(exp 20) 14 MeV neutrons), prompt annual doses will be less than 1.2 (mu)Sv at the nearest site boundary, less than 0.43 mSv immediately outside the Target Area, and less than 30 (mu)Sv in the war-room and control room. The target chamber material has been selected in a trade-off between its mechanical properties and its neutron activation qualities. External target chamber shielding has been selected such that the total annual occupational dose to Target Area workers will be less than or equal to 5 mSv. Finally, some Target Area systems have been redesigned based on their neutron activation and residual dose rates. The operation of the NIF will have an insignificant impact to workers and the general population. DOE

N95-21209# Lawrence Livermore National Lab., Livermore, CA.
LASER DESIGN BASIS FOR THE NATIONAL IGNITION FACILITY
J. T. Hunt, K. R. Manes, J. R. Murray, P. A. Renard, R. Sawicki, J. B. Trenholme, and W. Williams Jun. 1994 5 p Presented at the 11th Topical Meeting on the Technology of Fusion Energy, New Orleans, LA, 19-24 Jun. 1994
(Contract W-7405-eng-48)
(DE94-016700; UCRL-JC-117399; CONF-940630-35) Avail: CASI HC A01/MF A01

Controlled nuclear fusion initiated by highly intense laser beams has been the subject of experiment for many years. The National Ignition Facility (NIF) represents the culmination of design efforts to provide a laser facility that will successfully demonstrate fusion ignition in the laboratory. In this so-called inertial confinement approach, energetic driver beams (laser, X-ray, or charged particle) heat the outer surface of a spherical capsule containing deuterium and tritium (DT) fuel. As the capsule surface explosively evaporates, reaction pressure compresses the DT fuel causing the central core of the fuel to reach extreme density and temperature. When the central temperature is high enough, DT fusion reactions occur. The energy released from these reactions further heats the compressed fuel, and fusion burn propagates outward through the colder regions of the capsule much more rapidly than the inertially confined capsule can expand. The resulting fusion reactions yield many times more energy than was absorbed from the driver beams. DOE

N95-21236# Los Alamos National Lab., NM. Materials Science and Technology Div.
IN-SITU CAPABILITY OF ION BEAM MODIFICATION AND CHARACTERIZATION OF MATERIALS AT LOS ALAMOS NATIONAL LABORATORY
Ning Yu, Michael Nastasi, Joseph R. Tesmer, Mark G. Hollander, Caleb R. Evans, Carl J. Maggiore, and Timothy E. Levine (Cornell Univ., Ithaca, NY.) 1994 11 p Presented at the 13th International Conference on the Application of Accelerators in Research and Industry, Denton, TX, 7-10 Nov. 1994
(Contract W-7405-eng-36)
(DE95-002738; LA-UR-94-3537; CONF-941129-8) Avail: CASI HC A03/MF A01

The capability of in-situ ion beam modification and characterization of materials developed at Los Alamos National Laboratory is described. A beam-line from a 3 MV tandem accelerator and a beam-line from a 200 kV ion implanter are joined together in an in-situ target chamber. The chamber is equipped with a cold and hot sample stage with a temperature range from -100 to 500 C. The angular (sample spin and basal rotation) motions and translational motions of the sample stage are controlled by a multi-axis goniometer. This chamber provides a unique capability to conduct a temperature dependent experiment of ion irradiation and sequential backscattering and channeling analysis. The efficiency and reliability of in-situ ion beam techniques are demonstrated by two examples, irradiation damage in (100) MgAl2O4 spinel crystals and ion-beam-induced densification of zirconia sol-gel thin films. DOE

N95-21246# Stanford Linear Accelerator Center, CA.
COMPARISON OF CALCULATED WITH MEASURED DYNAMIC APERTURE
F. Zimmermann Jun. 1994 5 p Presented at the 4th European Particle Accelerator Conference, London, United Kingdom, 27 Jun. - 1 Jul. 1994
(Contract DE-AC03-76SF-00515)
(DE95-002863; SU-SLAC-PUB-6504; CONF-940618-87) Avail: CASI HC A01/MF A01

The measured dynamic aperture of the HERA proton ring and the value expected from simulation studies agree within a factor of 2. A better agreement is achieved if a realistic tune modulation is included in the simulation. The approximate threshold of tune-modulation induced diffusion can be calculated analytically. Its value is in remarkable agreement with the dynamic aperture measured. The calculation is based on parameters of resonances through order 11 which are computed using differential-algebra methods and normal-form algorithms. Modulational diffusion in conjunction with drifting machine parameters appears to be the most important transverse diffusion process. DOE

N95-21253# Stanford Linear Accelerator Center, CA.
ISSUES IN MULTI-BUNCH EMITTANCE PRESERVATION IN THE NLC
K. L. F. Bane, C. Adolphsen, K. Kubo, and K. A. Thompson Jul. 1994 3 p Presented at the 4th European Particle Accelerator Conference, London, United Kingdom, 27 Jun. - 1 Jul. 1994

(Contract DE-AC03-76SF-00515)
(DE95-002894; SU-SLAC-PUB-6581; CONF-940618-94) Avail: CASI HC A01/MF A01

In the linac of the SLAC NLC design 1 nC bunches are accelerated in trains 90 bunches long with an interbunch spacing of 42 cm. In this multi-bunch design one important problem that needs to be controlled is the multi-bunch beam break-up instability. One method of controlling this instability is by detuning the transverse modes of the accelerator cavities. This is accomplished by varying the cell dimensions as one proceeds down the structure in such a way that the transverse modes are detuned, while the fundamental, accelerating mode is left unchanged. In a properly designed, gaussian detuned structure the transverse wakefield excited by the first bunch in the train can be made to cancel sufficiently at the positions of bunches 2 to 25, after which it begins to grow again. To accommodate the long NLC bunch train it was suggested to build the linac out of 4 types of structures whose modes are interleaved so that the recoherence of the wake does not begin until after the last bunch has passed. More recently, another way of avoiding the recoherence of the wake is being studied: using only one type of structure and introducing weak damping through a manifold coupled by radial slots. In this paper, however, we will consider only the earlier idea. An important consideration in the NLC linac is the tolerance to accelerator structure misalignments. We present here an approximate analytic calculation that works well for the NLC parameters with 4 structure types. DOE

N95-21254# Stanford Linear Accelerator Center, CA.
SIGNALS FOR TOP QUARK ANOMALOUS CHROMOMAGNETIC MOMENTS AT COLLIDERS
Thomas G. Rizzo Jul. 1994 4 p Presented at the Meeting of the American Physical Society, Division of Particals and Fields (DPF94), Albuquerque, NM, 2-6 Aug. 1994
(Contract DE-AC03-76SF-00515)
(DE95-002896; SU-SLAC-PUB-6590; CONF-940816-48) Avail: CASI HC A01/MF A01

The Tevatron and the Next Linear Collider (NLC) will be excellent tools for probing the detailed nature of the top quark. We perform a preliminary examination of the influence of an anomalous chromomagnetic moment for the top, (kappa), on the characteristics of t(bar t) production at the Tevatron and on the spectrum of gluon radiation associated with t(bar t) production at the NLC. In particular, we analyze the sensitivity of future data to non-zero values of (kappa) and estimate the limits that can be placed on this parameter at the Tevatron and at the NLC with center of mass of energies of (radical)s = 500 and 1000 GeV. Constraints on (kappa) from low energy processes, such as b (yields) s(gamma) are briefly discussed. DOE

N95-21255# Stanford Linear Accelerator Center, CA.
FIRST RESULTS FROM THE FINAL FOCUS TEST BEAM
Peter Tenenbaum (California Univ., Santa Cruz, CA.) Jul. 1994 5 p Presented at the Meeting of the American Physical Society, Division of Particals and Fields (DPF94), Albuquerque, NM, 2-6 Aug. 1994
(Contract DE-AC03-76SF-00515)
(DE95-002897; SU-SLAC-PUB-693; CONF-940816-49) Avail: CASI HC A01/MF A01

We have used the Final Focus Test Beam beamline and associated instrumentation to reduce the 46.6 GeV SLAC electron beam to a vertical size of 70 nm. This represents a reduction from the linac beam size by a factor of 320, comparable to the demagnification required by a TeV-scale linear collider, and addresses the same aberrations predicted in such an environment. The beam dimensions were measured by two novel beam size monitors at the focal point. Details of the optical and hardware design of the beam line, necessary tuning operations, beam size monitor principles, and future plans are discussed. DOE

N95-21278# Sandia National Labs., Albuquerque, NM.
REAL-TIME DYNAMIC SIMULATOR FOR THE TOPAZ II REACTOR POWER SYSTEM
Kwan S. Kwok 1994 8 p Presented at the 15th Aerospace Testing Seminar, Manhattan Beach, CA, 11-13 Oct. 1994
(Contract DE-AC04-94AL-85000)
(DE95-001604; SAND-94-2033C; CONF-9410181-3) Avail: CASI HC A02/MF A01

A dynamic simulator of the TOPAZ II reactor system has been developed for the Nuclear Electric Propulsion Space Test Program. The simulator is a self-contained IBM-PC compatible based system that executes at a speed faster than real-time. The simulator combines first-principle modeling and empirical correlations in its algorithm to attain the modeling accuracy and computational through-put that are required for real-time execution. The overall execution time of the simulator for each time step is 15 ms when no data is written to the disk, and 18 ms when nine double precision data points are written to the disk once in every time step. The simulation program has been tested and it is able to handle a step decrease of $8 worth of reactivity. It also provides simulation of fuel, emitter, collector, stainless steel, and ZrH moderator failures. Presented in this paper are the models used in the calculations, a sample simulation session, and a discussion of the performance and limitations of the simulator. The simulator has been found to provide realistic real-time dynamic response of the TOPAZ II reactor system under both normal and causality conditions. DOE

N95-21281# State Univ. of New York, Albany, NY. Research Foundation.
EXPERIMENTS AT HIGH ENERGY HADRON COLLIDERS AND UNDERGROUND WATER CERENKOV DETECTOR EXPERIMENT
1993 20 p
(Contract DE-FG02-92ER-40697)
(DE95-001804; DOE/ER-40697/3) Avail: CASI HC A03/MF A01

This report discusses experiments ran on the DO detector; the Super-Kamiokande underground water Cherenkov detector; and post-SSC development. DOE

N95-21314# Fermi National Accelerator Lab., Batavia, IL.
SEARCH FOR CENTAURO EVENTS IN THE DO DETECTOR AT FERMILAB COLLIDER
M. V. S. Rao (Tata Inst. of Fundamental Research, Bombay, India.) Sep. 1994 14 p Presented at the 8th International Symposium on Very High Energy Cosmic Ray Interactions, Tokyo, Japan, 24-31 Jul. 1994
(Contract DE-AC02-76CH-03000)
(DE95-002522; FNAL/C-94/343-E; CONF-9407127-2) Avail: CASI HC A03/MF A01

We report preliminary results of a Monte Carlo study to search for Centauro events in the DO Detector at Fermilab. Monte Carlo simulation of minimum bias events are being carried out using the ISAJET and DOGEANT packages to study the detector response for low energy particles and to understand the background. Preliminary indications are that the detector is capable of resolving individual particles. Further work on developing reconstruction algorithms for individual particles is in progress. DOE

N95-21328# Sandia National Labs., Albuquerque, NM.
LIF STANDOFF RESEARCH
C. L. Olson, M. E. Cuneo, M. P. Desjarlais, A. B. Filuk, J. B. Greenly (Cornell Univ., Ithaca, NY.), D. L. Hanson, D. D. Hinshelwood (JAYCOR, Vienna, VA.), R. F. Hubbard (Naval Research Lab., Washington, DC.), M. Lampe (Naval Research Lab., Washington, DC.), and T. R. Lockner et al 1994 8 p Presented at the 10th International Conference on High Power Particle Beams, San Diego, CA, 20-24 Jun. 1994
(Contract DE-AC04-94AL-85000)
(DE94-018744; SAND-93-3892C; CONF-940634-19) Avail: CASI HC A02/MF A01

Present Light Ion Fusion (LIF) target experiments on PBFA 2 use a barrel diode in which the total transport length from the anode to the target is less than or equal to 15 cm. Future LIF development includes high yield applications (LMF) and energy production (ETF and LIBRA power plants) that require standoff - the generation of extracted ion beams and transport of these beams over distances of several meters. Standoff research includes the development of high efficiency extraction diodes (single stage and two-stage), improvements in beam quality (divergence, purity, uniformity, etc.), and the efficient transport and focusing of these beams over distances of several meters to a fusion target. Progress in all of these areas is discussed, as well as a strategy to reduce the divergence from the present 17 mrad for 5 MeV protons on SABRE to the required mrad for 35 MeV Li ions for LMF. The status of experiments is summarized, and future directions are indicated. DOE

N95-21331# Los Alamos National Lab., NM.
MOMENT APPROACH TO HIGH-ORDER ACCELERATOR BEAM OPTICS
W. P. Lysenko 1994 30 p Presented at the 4th International Conference on Charged Particle Optics, Tsukuba, Japan, 3-6 Oct. 1994
(Contract W-7405-eng-36)
(DE95-001018; LA-UR-94-3351; CONF-9410229-1) Avail: CASI HC A03/MF A01

High-current beams must be matched to high order to minimize emittance growth and particle losses. For matching problems, the moment approach, in which the author describes the particle beam by the moments of its distributions, is particularly valuable. A variety of analytical results are available for linear motion. The moment approach is also the basis of the 3-D space-charge simulation code BEDLAM, in which the dynamical variables are the moments. Moment simulation codes are particularly useful for computing beams matched to nonlinear systems. This paper outlines what is known about the moment approach, describes work in progress on new space-charge models, and describes further potential applications of and improvements to moment-method simulations. DOE

N95-21332# Stanford Linear Accelerator Center, CA.
EMITTANCE DILUTION BY IONS IN THE SLC ARCS
P. Emma, T. Raubenheimer, and F. Zimmermann Jun. 1994 3 p Presented at the 4th European Particle Accelerator Conference, London, United Kingdom, 27 Jun. - 1 Jul. 1994
(Contract DE-AC03-76SF-00515)
(DE95-002871; SU-SLAC-PUB-6522; CONF-940618-92) Avail: CASI HC A01/MF A01

Since the start of flat-beam operation in 1993 typical vertical IP spot sizes in the SLC are well below 1 micron, and the luminosity is highly sensitive to dilutions of the vertical emittance. In the arcs, the ionization of the residual gas by the bunch head gives rise to an ion cloud, whose electric field deflects the tail of the bunch and may cause an unrecoverable filamentation in phase space. The effect of the ions is particularly important in regions with large dispersion, due to the strong correlation of energy and longitudinal position within a bunch. Computer simulations of a bunch passage in the presence of ions have been performed to estimate the magnitude of the emittance dilution. DOE

N95-21334# Stanford Linear Accelerator Center, CA.
SIMULATION OF BEAM-BEAM LIFETIME FOR LEP
T. Chen, J. Irwin, and R. Siemann Jun. 1994 4 p Presented at the 4th European Particle Accelerator Conference, London, United Kingdom, 27 Jun. - 1 Jul. 1994
(Contract DE-AC03-76SF-00515)
(DE95-002888; SU-SLAC-PUB-6561; CONF-940618-110) Avail: CASI HC A01/MF A01

A program that uses a new technique to simulate die beam halo in circular e(+)e(-) colliders is applied to the LEP. This technique makes it possible to investigate tail particle in reasonable CPU times. The program now includes four interaction points and errors at or between the IP's. Analytical analysis shows that the errors break the symmetry and introduce extra low-order resonances that are forbidden by symmetry. Simulation results show the expected phenomenon. Another effect, the quadrupole mode coherent motion of the strong beam, is also studied. DOE

N95-21335# Stanford Linear Accelerator Center, CA.
LUMINOSITY POLARIZATION CORRELATION IN THE SLC
F. J. Decker and J. T. Seeman Jun. 1994 4 p Presented at the 4th European Particle Accelerator Conference, London, United Kingdom, 27 Jun. - 1 Jul. 1994
(Contract DE-AC03-76SF-00515)
(DE95-002889; SU-SLAC-PUB-6562; CONF-940618-111) Avail: CASI HC A01/MF A01

In this paper we discuss the correlation between low luminosity and low polarization for off-energy particles in the Stanford Linear Collider (SLC). In the arcs of the SLC the spin of the polarized electrons has a net horizontal precession of about 25 turns. For example, a particle off energy by 1% deviates by 0.25 spin turns or a 90(degrees) rotation from the core. It reduces the average polarization measured by a Compton polarimeter near the interaction point (IP). Since the energy acceptance or bandwidth of the final focus optics is limited to a certain range (approx) +/- 0.5%, these off-energy particles are not focussed as well at the IP and thus contribute less to luminosity. Therefore, the effective polarization at the IP weighted by the luminosity is higher than the measured polarization. Relative corrections of this measured value by +0.5 to 1% for the core and another +1 to 2% for low energy beam tails seems to be necessary for the 1993 run. In 1994, beam shaping with over-compression producing lower energy spreads and smaller tails together with a new arc setup with fewer effective spin turns promise to reduce this effect by an order of magnitude. DOE

N95-21337# Stanford Linear Accelerator Center, CA.
PAIR PRODUCTION AS A PROBE OF COLLIDING BEAM SIZE
Pisin Chen, John Irwin, and Anatoly Spitkovsky Jul. 1994 3 p Presented at the 4th European Particle Accelerator Conference, London, United Kingdom, 27 Jun. - 1 Jul. 1994
(Contract DE-AC03-76SF-00515)
(DE95-002893; SU-SLAC-PUB-6578; CONF-940618-93) Avail: CASI HC A01/MF A01

We propose the use of soft e(+) e(-) pairs as a non-evasive measurement of the colliding beam size. The angular distribution of the pair particles that have different sign of charge from that of the opposing beam, provides the information about the aspect ratio of the beam. The transverse momentum of the other species in the pair, on the other hand, carries information about the horizontal dimension of the beam. Together, one can in principle measure both (sigma)(sub x) and (sigma)(sub y). DOE

N95-21342# Brookhaven National Lab., Upton, NY.
HADRON BEAMS AND ACCELERATORS
Thomas Roser 1994 6 p Presented at the 8th International Symposia on High Energy Spin Physics and Polarization Phenomena in Nuclear Physics, Bloomington, IN, 15-22 Sep. 1994
(Contract DE-AC02-76CH-00016)
(DE95-002932; BNL-60946; CONF-9409103-4) Avail: CASI HC A02/MF A01

There were four sessions on Hadron Beams and Accelerators with 7 talks on Siberian Snakes and spin rotators, 3 talks on polarization build-up of unpolarized beams in storage rings and 5.9, and 3 talks on low, medium, and high energy polarimeters, respectively. In this paper I will briefly describe a few highlights from these sessions, giving emphasis to topics which I think will play an important role in the future. DOE

N95-21407# Argonne National Lab., IL. Materials Science Div.
APPLICATION OF NEW SYNCHROTRON POWDER DIFFRACTION TECHNIQUES TO ANOMALOUS SCATTERING FROM GLASSES
M. A. Beno, G. S. Knapp, P. Armand, D. L. Price, and M. L. Saboungi Aug. 1994 14 p Presented at the International Meeting on Synchrotron Radiation Instrumentation, Stony Brook, NY, 18-22 Jul. 1994
(Contract W-31-109-eng-38)
(DE94-019285; ANL/MSD/CP-82834; CONF-940714-28) Avail: CASI HC A03/MF A01

The authors have applied two synchrotron powder diffraction techniques to the measurement of high quality anomalous scattering diffraction data for amorphous materials. One of these methods, which uses a curved perfect crystal analyzer to simultaneously diffract multiple powder lines into a position sensitive detector has been shown to possess high resolution, low background and very high counting rates. This data measurement technique provides excellent energy resolution while minimizing systematic errors resulting from detector non-linearity. Anomalous scattering data for a cesium germanate glass collected using this technique will be presented. The second powder diffraction technique uses a flat analyzer crystal to deflect multiple diffraction lines out of the equatorial plane. Calculations show that this method possesses sufficient energy resolution for anomalous scattering experiments when a perfect crystal analyzer is used and is experimentally much simpler. Future studies will make use of a rapid sample changer allowing the scattering from the sample and a standard material (a material not containing the anomalous scatterer) to be measured alternately at each angle, reducing systematic errors due to beam instability or sample misalignment. DOE

N95-21418# Brookhaven National Lab., Upton, NY. National Synchrotron Light Source.
EFFECTS OF RF SIDE-BANDS ON SPECTRAL REPRODUCIBILITY FOR INFRARED SYNCHROTRON RADIATION

R. Biscardi, G. Ramirez, G. P. Williams, and C. Zimba (Polaroid Corp., Cambridge, MA.) 1994 11 p Presented at the International Meeting on Synchrotron Radiation Instrumentation, Stony Brook, NY, 18-22 Jul. 1994
(Contract DE-AC02-76CH-00016)
(DE95-002450; BNL-60862; CONF-940714-37) Avail: CASI HC A03/MF A01

We have investigated the effects of audio side-bands from the main RF of the NSLS VUV storage ring on beam motion and specifically on spectral reproducibility in the infra-red region. For this spectral region it is advantageous to use Michelson interferometers because of their high throughput (Jacquinot advantage). A second advantage is that interferometers inherently give a multiplex or Felgett advantage, since one is always looking at all the wavelengths for all of the measuring time, even though there is only one detector. In such instruments it is beneficial to scan the moving mirror at a fast rate so that any mechanical or other low frequency noise shows up as a slow modulation in the interferogram and disappears altogether in the Fourier transform from the spectral region of interest. However, audio frequency side-bands appear from the RF energy restoring cavity as noise on the beam. These always occur at multiples of 60 Hz and can thus be readily identified. They can also be confirmed by changing the mirror velocity which changes where they appear in the spectra in a predictable way. In the present work, we measured spectra while simultaneously reducing and shifting the side bands in the RF and thus were able to correlate the effects and ultimately eliminate them as a source of noise. Ultimately we were able to achieve reproducibilities of less than 1% in 15 seconds of scanning time across the entire spectral region from 800/cm to 4000/cm with a sample throughput of only 10(exp -10) sq m steradians. DOE

N95-21460# Oak Ridge National Lab., TN.
THE ORNL NEUTRON-CAPTURE CROSS SECTION FACILITY
R. R. Spencer, N. M. Larson, J. H. Todd, and L. W. Weston 1994 4 p Presented at the International Conference on Nuclear Data for Science and Technology: Nuclear Data for the Twenty-first Century, Gatlinburg, TN, 9-13 May 1994
(Contract DE-AC05-84OR-21400)
(DE94-019146; CONF-940507-38) Avail: CASI HC A01/MF A01

In order to meet the cross section needs required by astrophysical calculations within recent cosmological models, the neutron-capture cross section facility at the Oak Ridge Electron Linear Accelerator (ORELA) has been improved and restored to operation. Changes to the system include replacement of the C6F6 scintillation detectors with C6D6, reduction of the structural mass near and around the detectors, and incorporation of a new IBM PS/2-based data handler. Preliminary measurements on natural iron samples yield Gamma(sub n) = 61.6 +/- 1.8 meV for the 1.15-keV resonance, using a fixed Gamma(sub gamma) = 574 meV from transmission, compared to the value Gamma(sub n) = 61.7 +/- 0.9 meV obtained from the transmission measurements. DOE

N95-21494 Naval Research Lab., Washington, DC.
PRS SCOPING STUDY. 2: ZPIMP PREDICTIONS FOR RADIATION YIELDS ON A JUPITER-CLASS GENERATOR
J. L. Giuliani, Jr., J. Rogerson, and J. Davis 31 May 1994 37 p Limited Reproducibility: More than 20% of this document may be affected by microfiche quality
(AD-A279823; NRL/MR/6720-94-7472-2) Avail: CASI HC A03

A limited radiation-magnetohydrodynamics simulation code, ZPIMP, is used to predict radiation yields in various energy bins on a JUPITER-class machine. Elements of the simulation code are reviewed and calculations are made to compare the code with experimental K-shell yields from aluminum z-pinches on the SATURN generator. For a chosen viscosity parameter the simulated yields agree remarkably with the data. The same code is applied on an early version of the linear inductive voltage adder, but the projected krypton yields arc disappointing. By increasing the compression through a lower viscosity parameter, the subsequent yields are significantly improved for weak implosions, showing that such a case is highly sensitive to the details of the dynamics. The capabilities of an approximately 60 MA JUPITER-class generator are surveyed with the ZPIMP code and the results for argon, krypton, and xenon are compared against the anticipated required source yields in five energy bins ranging from 0 to 60 keV. In the lowest bins (0-1 and 1-5 keV) JUPITER is well suited to reach the required yields, but in the highest bins (15-30 and 30-60 keV) the present calculations indicate that improvements in load design, understanding, and control are necessary to meet the requirements. Limitations of the ZPIMP calculations and directions for improving the PRS estimates for JUPITER are derived from the present work. DTIC

N95-21503# Argonne National Lab., IL.
BEAM INSTABILITY STUDIES AT THE APS
L. C. Teng 1994 16 p Presented at the Workshop on Beam Instabilities in Storage Rings, Hefei, China, 25-30 Jul. 1994
(Contract W-31-109-eng-38)
(DE95-001448; ANL/ASD/CP-84183; CONF-9407121-3) Avail: CASI HC A03/MF A01

The Argonne Advanced Photon Source, APS, is a 7-GeV positron storage ring with a circumference of 1104 m. It has a 'third generation, DBA or Chasman-Green' lattice composed of 40 sectors each having an approximately 6 m long zero-dispersion straight-section for accommodating insertion devices. Neighboring straight-sections are connected by a 360 deg/40 = 9 deg double-bend-achromatic bending section designed to produce the smallest emittance attainable with reasonable component parameter values and dynamic apertures. Thus, it is a very strongly focusing lattice with v(sub x) = 35.22 and v(sub y) = 14.30. The beam chamber of the storage ring including all rf, vacuum, and photon beam components is designed to ensure that a beam current greater than 100 mA can be stably stored. We expect that the maximum stable beam current could be as high as 300 mA. This paper will give some details of the studies and computations to ensure the stability of such a beam. The discussions will be organized in the following three parts: coupled-bunch instability caused by the higher-order modes (HOM's) of the RF cavities; single-bunch instability due to the resistive wall impedance; and single-bunch instability due to broadband impedances arising from beam chamber irregularities. DOE

N95-21603# Sandia National Labs., Albuquerque, NM.
PROGRESS IN THE LIGHT ION DRIVEN INERTIAL CONFINEMENT FUSION PROGRAM
J. P. Quintenz, T. A. Mehlhorn, R. G. Adams, G. O. Allshouse, J. H. Aubert, L. D. Bacon, J. E. Bailey, D. D. Bloomquist, J. Boyes, and G. A. Chandler et al 1994 8 p Presented at the 15th International Conference on Plasma Physics and Controlled Nuclear Fusion Research, Seville, Spain, 26 Sep. - 1 Oct. 1994
(Contract DE-AC04-94AL-85000)
(DE94-019182; SAND-94-0977C; IAEA-CN-60/B-1-I-6; CONF-940933-2) Avail: CASI HC A02/MF A01

The goal of the light ion inertial confinement fusion (ICF) program is high fusion yield for defense and energy applications. The first lithium-driven hohlraum experiments at 1400 TW/g are reported. The lithium beam intensity is presently limited to 1.4 +/- 0.4 TW/cm(exp 2) (averaged over a 6 mm diameter sphere) due to a combination of beam divergence and limited lithium beam power. Surface contamination in the diode plays an important role in limiting the lithium power. Concepts have been developed for beam transport over several meters. Synergism exists between light- and heavy-ion ICF in areas such as transport and target physics. DOE

N95-21647 Rutherford Appleton Lab., Chilton (England).
PROCEEDINGS OF THE SCHOOL FOR YOUNG HIGH ENERGY PHYSICISTS
F. E. Close, J. Flynn, I. Halliday, and C. Maxwell May 1994 232 p School held in Abingdon, England, 5-17 September 1993 Prepared in cooperation with University Coll. of Swansea, Wales
(PB95-108114; RAL-94-026) Avail: Issuing Activity (National Technical Information Service (NTIS))

The 22nd School for Young High Energy Physicists, which was held at Cosenor's House in Abingdon between the 5th and 17th September 1993, was attended by 43 graduate students all at the end of their first year. The lectures published here concentrated on providing students with a thorough grounding in the foundations of the Standard Model of Particle Physics. The lecture courses given are as follows: Quantum Field Theory: Canonical and Path Integral Approaches; Introduction to Quantum Electrodynamics and Quantum Chromodynamics; The Standard Model and Beyond; and The Physics of Structure. NTIS

N95-21720# Brookhaven National Lab., Upton, NY.
RF BEAM CONTROL FOR THE AGS BOOSTER
J. M. Brennan 26 Sep. 1994 112 p
(Contract DE-AC02-76CH-00016)
(DE95-001485; BNL-52438; AGS/AD-94-6) Avail: CASI HC A06/MF A02

RF beam control systems for hadron synchrotrons have evolved over the past three decades into an essentially standard design. The key difference between hadron and lepton machines is the absence of radiation damping and existence of significant frequency variation in the case of hadrons. Although the motion of the hadron in the potential well of the RF wave is inherently stable it is not strongly damped. Damping must be provided by electronic feedback through the accelerating system. This feedback is typically called the phase loop. The technology of the RF beam control system for the AGS Booster synchrotron is described. First, the overall philosophy of the design is explained in terms of a conventional servo system that regulates the beam horizontal position in the vacuum chamber. The concept of beam transfer functions is fundamental to the mathematics of the design process and is reviewed. The beam transfer functions required for this design are derived from first principles. An overview of the beam signal pick-ups and high level RF equipment is given. The major subsystems, the frequency program, the heterodyne system, and beam feedback loops, are described in detail. Beyond accelerating the beam, the RF system must also synchronize the bunches in the Booster to the buckets in the AGS before transfer. The technical challenge in this process is heightened by the need to accomplish synchronization while the frequency is still changing. Details of the synchronization system are given. This report is intended to serve two purposes. One is to document the hardware and performance of the systems that have been built. The other is to serve as a tutorial vehicle from which the non-expert can not only learn the details of this system but also learn the principles of beam control that have led to the particular design choices made. DOE

N95-21733# Superconducting Super Collider Lab., Dallas, TX.
THE 12-GeV/c BEAM TRANSFER AND ABSORBER LINES FOR THE SUPERCONDUCTING SUPER COLLIDER
N. Mao, J. McGill, R. Gerig, and K. Brown (Stanford Linear Accelerator Center, CA.) Aug. 1994 13 p
(Contract DE-AC35-89ER-40486)
(DE95-002100; SSCL-678) Avail: CASI HC A03/MF A01

The beam optics of the 12-GeV/c proton beam transfer line between the Low Energy Booster (LEB) and the Medium Energy Booster (MEB) at the Superconducting Super Collider is presented. The beam is extracted from the LEB vertically and is injected into the MEB through a vertical Lambertson magnet and a horizontal kicker. The beamline has high flexibility for amplitude and dispersion function matching. Effects of various errors in the transfer line are studied, and a beam position correction scheme is proposed. The beam optics of the 12-GeV/c absorber line transporting the beam from the LEB to an absorber during the LEB commissioning is also presented. DOE

N95-21938# Oak Ridge National Lab., TN.
SELECTION OF RIB TARGETS USING ION IMPLANTATION
G. D. Alton, J. Dellwo, J. A. Chediak, H. K. Carter (Oak Ridge Inst. for Science and Education, TN.), and J. Kormicki (Oak Ridge Inst. for Science and Education, TN.) 1994 3 p Presented at the 4th European Particle Accelerator Conference, London, England, 27 Jun. - 1 Jul. 1994
(Contract DE-AC05-84OR-21400)
(DE95-000951; CONF-940618-81) Avail: CASI HC A01/MF A01

Experimental studies are under way at the Oak Ridge National Laboratory (ORNL) which are designed to measure the time evolution, ionization efficiencies, and release efficiencies of implanted elements diffused from refractory target materials which are candidates for forming radioactive ion beams (RIB's) at the Holifield Radioactive Ion Beam Facility (HRIBF). The diffusion coefficients are derived by comparing experimental data with numerical solutions to a one-dimensional form of Fick's second law for ion implanted distributions. In this report, we describe the experimental arrangement and provide time release data and diffusion coefficients for releasing ion implanted Cl from Zr5Si3 and As(75), Br(79), and Se(78) from Zr5Ge3. DOE

N95-22050# Los Alamos National Lab., NM.
EXPERIENCE AT THE LOS ALAMOS MESON PHYSICS FACILITY WITH THE USE OF ALLOY INCONEL 718 AS AN ENCLOSURE FOR A BEAM DEGRADER AND AS A PROTON BEAM ENTRY WINDOW
W. F. Sommer, P. D. Ferguson, R. D. Brown, C. M. Cedillo, and E. Zimmerman 1994 27 p Presented at the International Conference on Accelerator-driven Transmutation Technologies and Applications, Las Vegas, NV, 25-28 Jul. 1994
(Contract W-7405-eng-36)
(DE94-018289; LA-UR-94-2809; CONF-9407103-24) Avail: CASI HC A03/MF A01

Operation of the Los Alamos Meson Physics Facility (LAMPF) began in 1972 and continues at present. An injector delivers protons to a 0.8 km long line ar accelerator which produces a particle energy of 800 MeV; the protons are then transported to a variety of experimental areas. The proton beam is transported in a vacuum tube, controlled and bent by electromagnets. The highest intensity beam, at a maximum level of 1 mA, is delivered to the experimental area designated as Area A. At the end of the experimental area, the beam is transported through an interface between beamline vacuum and one atmosphere air pressure. This interface is made of metal and is generally referred to as a beam entry window. At LAMPF, after the beam has exited the vacuum tube, it becomes incident on a number of experiments or 'targets.' These include capsules for radiation damage studies, a beam 'degrader' for the long-term neutrino experiment, and as many nine targets in the Isotope Production (IP) stringer system used to produce medically significant isotopes. Following the IP system is a beam stop used for the purpose its name implies. The beam stop also contains a beam entry window, whose purpose is to separate the 250 psig water cooling environment from 1 atmosphere of air. The beam entry window, the beam degrader, and the beam stop window are made of alloy Inconel 718, have endured a lengthy irradiation service time at LAMPF, and are the subject of this report. DOE

N95-22117# Oak Ridge National Lab., TN.
NEW TECHNIQUES IN NEUTRON SCATTERING
John B. Hayter 1994 10 p Presented at the 5th International Symposium on Advanced Nuclear Energy Research, Mito, Japan, 10-12 Mar. 1993
(Contract DE-AC05-84OR-21400)
(DE94-018944; CONF-9303258-1) Avail: CASI HC A02/MF A01

New neutron sources being planned, such as the Advanced Neutron Source (ANS) or the European Spallation Source (ESS), will provide an order of magnitude flux increase over what is available today, but neutron scattering will still remain a signal-limited technique. At the same time, the development of new materials, such as polymer and ceramic composites or a variety of complex fluids, will increasingly require neutron-based research. This paper will discuss some of the new techniques which will allow us to make better use of the available neutrons, either through improved instrumentation or through sample manipulation. Discussion will center primarily on unpolarized neutron techniques since polarized neutrons will be the subject of the next paper. DOE

N95-22155# Stanford Linear Accelerator Center, CA.
PROPOSED EMITTANCE UPGRADE FOR THE SLC DAMPING RINGS
R. Early, T. Limberg, H. Moshammer, T. Raubenheimer, K. Skarpaas, and J. Spencer Jun. 1994 4 p Presented at the 4th European Particle Accelerator Conference, London, United Kingdom, 27 Jun. - 1 Jul. 1994
(Contract DE-AC03-76SF-00515)
(DE95-002887; SU-SLAC-PUB-6559; CONF-940618-109) Avail: CASI HC A01/MF A01

One way to improve luminosity is to reduce transverse emittance by changing damping partitions. We consider the options in relation to the constraints. Besides modifications of the basic DR configuration the options include closed-orbit offsets in the quadrupoles, addition of strong multipoles and replacement of existing rectangular nosepieces on the dipoles (shim angles (phi)(equivalent to)(theta)/2) with rotatable inserts. Measurements indicate the possibility of dynamically tuning (phi) greater than or equal to 45(degrees) with decreases in (tau)(sub x) and (epsilon)(sub x) of greater than or equal to 50%. We discuss damping mechanisms to motivate the desirable field characteristics as well as nonlinear contours to cancel dipole harmonic errors (B greater than 2T here) or to provide chromatic corrections. Such inserts could also be used to make cheaper, more compact rings with better impedance by reducing the number of conventional multipoles without impairing the stability. Estimated hardware costs are $250/dipole end or multipole equivalent. DOE

N95-22192# Fermi National Accelerator Lab., Batavia, IL.
NORMAL FORM ANALYSIS OF THE TEVATRON
J. A. Holt Jul. 1994 5 p Presented at the 4th European Particle Accelerator Conference, London, England, 27 Jun. - 1 Jul. 1994
(Contract DE-AC02-76CH-03000)
(DE94-017172; FNAL/C-94/203; CONF-940618-45) Avail: CASI HC A01/MF A01

A systematic analysis effort is under way to calculate and model the effects of present and future upgrades to the Tevatron. As a first step, using normal form theory, amplitude-dependent tuneshifts for current Tevatron collider operating conditions were calculated. The normal form algorithm was implemented within the frame work of the object-oriented accelerator physics class libraries BEAMLINE and MXYZPTLK under development at Fermilab. DOE

N95-22193# Fermi National Accelerator Lab., Batavia, IL.
DESIGN OF THE READOUT IC FOR THE CDF SVX-2 SILICON STRIP DETECTOR
B. T. Huffman (Pittsburgh Univ., Pittsburgh, PA.) 16 Aug. 1994 10 p Presented at the 3d International Workshop on Vertex Detectors, Lake Monroe, IN, 18 May 1994
(Contract DE-AC02-76CH-03000)
(DE95-000562; FNAL/C-94/257-E; CONF-9405233-1) Avail: CASI HC A02/MF A01

Future colliding beam runs at Fermi National Accelerator Laboratory will involve bunch spacings of protons and antiprotons at 132 ns intervals. Due to finite processing time, a pipelined architecture is needed to store events until a trigger decision can reach the detector. A single ported pipeline design has been implemented in a 1.2 micron rad soft CMOS technology and partially tested. Results are presented of the performance of that design. The chip supports a level 1 accept rate of 5 kHz. Because high statistics B physics experiments will require level 1 accept rates of 50 kHz, a new dual ported pipeline device has been proposed which would make the readout virtually deadtimeless for trigger rates approaching 50 kHz. The operation of the proposed deadtimeless device is explained. DOE

N95-22195# Fermi National Accelerator Lab., Batavia, IL.
PHYSICS AT THE FERMILAB COLLIDER
M. J. Shochet (Chicago Univ., Chicago, IL.) Sep. 1994 26 p Presented at the Meeting of the Division of Particles and Fields of the American Physical Society, Albuquerque, NM, 2-6 Aug. 1994
(Contract DE-AC02-76CH-03000)
(DE95-000726; FNAL/C-94/276-E; CONF-940816-27) Avail: CASI HC A03/MF A01

The CDF and D0 experiments at the Fermilab Tevatron Collider have produced many results from the search for the top quark, the study of both the electroweak and strong interactions, the production and decay of b quarks, and the search for new high mass objects. A sample of recently obtained results are presented. DOE

N95-22243# Los Alamos National Lab., NM.
HIGH PERFORMANCE COMPUTING FOR BEAM PHYSICS APPLICATIONS
R. D. Ryne and S. Habib 1994 7 p Presented at the 2d DOE-Energy Research Power Users Symposium, Rockville, MD, 12 Jul. 1994
(Contract W-7405-eng-36)
(DE94-018312; LA-UR-94-2904; CONF-9407126-2) Avail: CASI HC A02/MF A01

Several countries are now involved in efforts aimed at utilizing accelerator-driven technologies to solve problems of national and international importance. These technologies have both economic and environmental implications. The technologies include waste transmutation, plutonium conversion, neutron production for materials science and biological science research, neutron production for fusion materials testing, fission energy production systems, and tritium production. All of these projects require a high-intensity linear accelerator that operates with extremely low beam loss. This presents a formidable computational challenge: One must design and optimize over a kilometer of complex accelerating structures while taking into account beam loss to an accuracy of 10 parts per billion per meter. Such modeling is essential if one is to have confidence that the accelerator will meet its beam loss requirement, which ultimately affects system reliability, safety and cost. At Los Alamos, the authors are developing a capability to model ultra-low loss accelerators using the CM-5 at the Advanced Computing Laboratory. They are developing PIC, Vlasov/Poisson, and Langevin/Fokker-Planck codes for this purpose. With slight modification, they have also applied their codes to modeling mesoscopic systems and astrophysical systems. In this paper, they will first describe HPC activities in the accelerator community. Then they will discuss the tools they have developed to model classical and quantum evolution equations. Lastly they will describe how these tools have been used to study beam halo in high current, mismatched charged particle beams. DOE

N95-22298# Los Alamos National Lab., NM.
RECENT RESULTS IN ANALYSIS AND SIMULATION OF BEAM HALO
R. D. Ryne and T. P. Wangler 1994 8 p Presented at the International Conference on Accelerator-driven Transmutation Technologies and Applications, Las Vegas, NV, 25-28 Jul. 1994
(Contract W-7405-eng-36)
(DE94-018313; LA-UR-94-2903; CONF-9407103-26) Avail: CASI HC A02/MF A01

Understanding and predicting beam halo is a major issue for accelerator driven transmutation technologies. If strict beam loss requirements are not met, the resulting radioactivation can reduce the availability of the accelerator facility and may lead to the necessity for time-consuming remote maintenance. Recently there has been much activity related to the core-halo model of halo evolution. In this paper the authors will discuss the core-halo model in the context of constant focusing channels and periodic focusing channels. They will present numerical results based on this model and they will show comparisons with results from large scale particle simulations run on a massively parallel computer. They will also present results from direct Vlasov simulations. DOE

N95-22306# Sandia National Labs., Albuquerque, NM. Intense Beam Research Dept.
VERY HIGH-POWER ELECTRON-BEAM TRANSPORT IN LONG GAS CELLS FROM 10(EXP -3) TO 10(EXP 3) TORR N2
T. W. L. Sanford 1994 19 p Presented at the Meeting of the Division of Plasma Physics of the American Physical Society, Minneapolis, MN, 7-11 Nov. 1994
(Contract DE-AC04-94AL-85000)
(DE95-002611; SAND-94-1911C; CONF-941101-1) Avail: CASI HC A03/MF A01

Measurements and analyses show that the 13-TW, pulsed Hermes-III electron beam, with current near the Alfven limit, has two regimes of stable transport: a low-pressure window (between (approximately)1 and (approximately)100 mTorr) that is dominated by propagation in the semi-collisionless IFR (ion-focused regime), and a high-pressure window (between (approximately)1 and (approximately)100 Torr) that is dominated by propagation in the resistive CDR (collision-dominated regime). Propagation in both regimes (the IFR at early time and the CDR at later time) is observed from (approximately)10 to (approximately)100 mTorr. Below (approximately)1 mTorr, there is insufficient ionization to confine the beam. As the pressure increases, two-stream instabilities terminate IFR propagation earlier in time. Above 10 mTorr, this instability is sufficiently quenched by gas collisions that CDR propagation in the beam body occurs. Above (approximately)100 mTorr, the gas breaks down too rapidly for a significant IFR pulse to form, and for higher pressures only a single pulse in the CDR is propagated. Between (approximately)100 mTorr and (approximately)1 Torr, however, the hollowing instability and lack of magnetic confinement limit CDR propagation, and above (approximately)100 Torr, the resistive hose instability again degrades propagation. DOE

N95-22357# Brookhaven National Lab., Upton, NY.
BUNCHED BEAM INSTABILITY WITH FREQUENCY SPREAD
S. Y. Zhang and W. T. Weng 1994 21 p Presented at the Workshop on Beam Instabilities in Storage Rings, Hefei, China, 25-30 Jul. 1994
(Contract DE-AC02-76CH-00016)
(DE94-018632; BNL-60749; CONF-9407121-2) Avail: CASI HC A03/MF A01

The eigenvalue type solution to the bunched beam instability with frequency spread is studied. The approach provides a comprehensive solution to the problem by including all necessary modes. The synchrotron frequency spread is represented by a mode decomposition, the decomposed modes have different inherent frequencies from each other, and the corresponding radial functions are different from the ones without frequency spread. The environmental impedance induced feedback applies to these modes and then creates Landau damping effect. The radial modes and therefore the line densities can be solved throughout the Landau damping, thus providing some insight into the process. Several conceptual and computational problems are discussed, and the method is compared with the conventional Landau damping treatment. Finally, the case of mode coupling is also discussed. DOE

N95-22364 Rutherford Appleton Lab., Oxford (England).
VERTEX DETECTORS AT LINEAR COLLIDERS: PRESENT AND FUTURE
C. J. S. Damerell Sep. 1994 13 p 3rd Workshop on Vertex Detectors, Bloomington, IN, May 1994 See also PB87-124426
(PB95-134656; RAL-94-096) Avail: Issuing Activity (National Technical Information Service (NTIS))

After a brief introduction to the general characteristics of pixel-based vertex detectors (as opposed to those using silicon microstrips) the authors give a general description of the operation of SLD's current CCD-based vertex detector. There follows a description of the design and early prototyping for the SLD upgrade detector, due to be completed during 1995. Finally, the authors discuss ideas for an extremely powerful vertex detector suggested for use at the future e(+)e(-) linear collider. NTIS

N95-22391# Brookhaven National Lab., Upton, NY.
LOW EMITTANCE LATTICES FOR ELECTRON STORAGE RINGS REVISITED
D. Trbojevic and E. Courant 1994 4 p Presented at the 4th European Particle Accelerator Conference, London, England, 27 Jun. - 1 Jul. 1994
(Contract DE-AC02-76CH-00016)
(DE94-017302; BNL-49932; CONF-940618-49) Avail: CASI HC A01/MF A01

Conditions for the lowest possible emittance of the lattice for electron storage rings are obtained by a simplified analytical approach. Examples of electron storage lattices with minimum emittances are presented. A simple graphical presentation in the normalized dispersion space (Floquet's transformation) is used to illustrate the conditions and results. DOE

N95-22410# Los Alamos National Lab., NM.
LOW-LEVEL RF CONTROL FOR THE AFEL
C. Ziomek, J. Kinross-Wright, and J. Plato 1994 5 p Presented at the 16th International Free Electron Laser Conference, Stanford, CA, 21-26 Aug. 1994
(Contract W-7405-eng-36)
(DE94-018295; LA-UR-94-2840; CONF-9408146-2) Avail: CASI HC A01/MF A01

A limiting factor in the performance of the Los Alamos Advanced Free Electron Laser (AFEL) is the stability of the RF accelerating field. A high-performance low-level RF control system has been implemented that uses analog feedback and digital feed forward to regulate the RF field. This low-level RF control system has achieved long-term amplitude and phase stabilities better than +/- 0.25% and +/- 0.33 deg respectively. In order to improve the RF field stability further, a detailed system analysis and design is proceeding. Subsystem measurements are being used to model the system performance, predict the performance-limiting components, and determine possible improvements. Results to-date, modeling analyses, and suggested future improvements are presented. DOE

N95-22469# Lawrence Livermore National Lab., Livermore, CA.
TARGET ALIGNMENT IN THE NATIONAL IGNITION FACILITY
Charles S. Vann, Erlan S. Bliss, and James E. Murray Jun. 1994 6 p Presented at the 11th Topical Meeting on the Technology of Fusion Energy, New Orleans, LA, 19-24 Jun. 1994
(Contract W-7405-eng-48)
(DE94-015559; UCRL-JC-115588; CONF-940630-29) Avail: CASI HC A02/MF A01

Accurate placement of hundreds of focused laser beams on target is necessary to achieve success in the National Ignition Facility (NIF). The current system requirement is less than or equal to 7 micro rad error in output pointing and less than or equal to 1 mm error in focusing. To accommodate several system shots per day, a target alignment system must be able to align the target to chamber center, inject an alignment beam to represent each shot beam, and point and focus the alignment beams onto the target in about one hour. At Lawrence Livermore National Laboratory, we have developed a target alignment concept and built a prototype to validate the approach. The concept comprises three systems: the chamber center reference, target alignment sensor, and target alignment beams. DOE

74 OPTICS

Includes light phenomena; and optical devices.
For lasers see *36 Lasers and Masers.*

N95-19897# State Univ. of New York, Buffalo, NY. Dept. of Chemistry.
DESIGN, SYNTHESIS AND CHARACTERIZATION OF NOVEL NONLINEAR OPTICAL MATERIALS Annual Report, 1 Apr. 1993 - 31 Mar. 1994
Paras N. Prasad 31 Mar. 1994 13 p
(Contract F49620-93-C-0017)
(AD-A285617; AFOSR-94-0649TR) Avail: CASI HC A03/MF A01

This project consisted of four tasks each dealing with a different class of nonlinear optical materials. Task 1 involved second-order material. During the past year we used theoretical and experimental studies to develop a new class of materials in which a commonly used electron donor chromophore was replaced by a thiophene ring. To efficiently pole a second-order ionic chromophore, the use of a bulky counter-ion in order to reduce ionic conductivity was demonstrated. We also investigated the imaginary part of X(2) by electro-absorption. Task 2 covered third-order materials. We synthesized a group of phosphoylides which contain a polarizable P atom. Their X(3) behavior was experimentally investigated using femtosecond Kerr gate. Using our new method of optically heterodyned and phase-tuned Kerr gate method, we investigated both the signs and the magnitudes of the real and the imaginary components of X(3). We showed that in the case of one-photon saturation, the sign of imaginary part is negative, while for two-photon absorption, this sign is positive. A very efficient two-photon induced fluorescence was also found for another nonlinear chromophore, diethylaminonitrostyrene, in the crystalline form. Task 3 investigated photorefractive polymeric composites, while task 4 covered sol-gel processed nonlinear optical materials. DTIC

N95-19968# Argonne National Lab., IL. Materials Science Div.
THE ANL X6B BEAMLINE AT NSLS: A VERSATILE FACILITY
K. G. Huang, M. Ramanathan, and P. A. Montano (Illinois Univ., Chicago, IL.) Jul. 1994 14 p Presented at the International Meeting on Synchrotron Radiation Instrumentation, Stony Brook, NY, 18-22 Jul. 1994
(Contracts W-31-109-eng-38; DE-AC02-76CH-00016)
(DE94-018379; ANL/MSD/CP-82679; CONF-940714-21) Avail: CASI HC A03/MF A01

We have described the x ray optics and beamline performance of the ANL X6B beam line at the NSLS. Considerable flexibility has been built into the beam line to accommodate a wide range of x ray diffraction, scattering, and spectroscopy experiments with various requirements. We presented selected examples of experimental results and showed that with the high intensity, high energy resolution, high-q resolution, and energy tunability, the X6B beam line has become a versatile facility. DOE

N95-19976# National Inst. of Standards and Technology, Boulder, CO. Electromagnetic Technology Div.
TECHNICAL DIGEST: EIGHTH SYMPOSIUM ON OPTICAL FIBER MEASUREMENTS
G. W. Day, ed., D. L. Franzen, ed., and R. K. Hickernell, ed. Sep. 1994 233 p Symposium held in Boulder, CO, 13-15 Sep. 1994; sponsored by IEEE and Optical Society of America See also PB93-102259
(PB94-207636; NIST/SP-864) Avail: CASI HC A11/MF A03; SOD HC

The Digest contains the manuscripts of 50 papers, 10 invited and 40 contributed, presented at the eighth Symposium on Optical Fiber

Measurements, September 13-15, 1994 in Boulder, Colorado. The most significant theme of the symposium is the present importance of polarization measurements. More than 20% of the papers are concerned either with polarization measurements, especially polarization mode dispersion and polarization dependent loss, or the characterization of fibers and components with special polarization properties. Optical time-domain reflectometry (OTDR) measurements are another important theme, as they have been since the first Symposium in 1980, and the characterization of optical fiber amplifiers continues to be important. Nonlinear processes in fibers seem to be a growing interest. Approximately two thirds of the papers come from outside of the United States, up from about half at the seventh Symposium. Ten countries are represented in the program. NTIS

N95-20066# Florida Univ., Gainesville, FL. Dept. of Materials Science and Engineering.
VISIBLE LIGHT EMITTING MATERIALS AND INJECTION DEVICES Quarterly Progress Report, 1 Jun. - 31 Aug. 1994
Paul H. Holloway 31 Aug. 1994 29 p
(Contract N00014-92-J-1895)
(AD-A284796) Avail: CASI HC A03/MF A01

We completed an extensive investigation this quarter into the influence of growth parameters (including dopant source condition) on the free-hole concentration in p-type ZnSe:N epilayers which involved real-time in situ cathodoluminescence intensity measurements during growth as well as ex situ Hall-effect measurements on a number of selected samples. The parameters varied included nitrogen plasma integrated intensity, substrate temperature and II/VI beam equivalent pressure ratio. CL intensity measurements were made in situ during epilayer growth. These measurements could be made in real-time as the various growth parameters were modified. In addition, free-hole concentrations were measured in films growth under particular conditions using the sample configuration. The ohmic contact mesas were deposited in situ through a mechanical mask which was introduced over the sample following the growth of the p-doped epilayer. DTIC

N95-20103# Argonne National Lab., IL.
AN INTENSITY INTERFEROMETER FOR SOFT X-RAYS
L. Yang, I. McNulty, and E. Gluskin 15 Jul. 1994 14 p Presented at the International Meeting on Synchrotron Radiation Instrumentation, Stony Brook, NY, 18-22 Jul. 1994
(Contracts W-31-109-eng-38; DE-AC02-76CH-00016)
(DE94-016370; ANL/XFD/CP-82881; CONF-940714-2) Avail: CASI HC A03/MF A01

We designed and built an intensity interferometer to characterize the spatial coherence of a soft x-ray undulator beam. The beam source size and shape can be determined from the measured coherence function. The instrument is 400 mm long and is mounted on a standard 204-mm diameter flange. This compact design is readily adaptable to other beamlines with sources of sufficient spectral brightness. Details of the interferometer design and performance are presented. We anticipate that when this technique is mature, it will provide a useful diagnostic for high brightness x-ray beams. DOE

N95-20218# Lawrence Livermore National Lab., Livermore, CA.
OPTICAL MULTILAYERS WITH AN AMORPHOUS FLUOROPOLYMER
R. Chow, G. E. Loomis, and E. F. Lindsey Jul. 1994 8 p Presented at the Annual Meeting of the Society of Photo-Optical Instrumentation Engineers, San Diego, CA, 24-29 Jul. 1994
(Contract W-7405-eng-48)
(DE94-017693; UCRL-JC-114328; CONF-940723-17) Avail: CASI HC A02/MF A01

Multilayered coatings were made by physical vapor deposition (PVD) of a perfluorinated amorphous polymer, Teflon AF2400, together with other optical materials. A high reflector at 1064 run was made with ZnS and AF2400. An all-organic 1064-nm reflector was made from AF2400 and polyethylene. Oxide (HfO2, SiO2) compatibility was also tested. Each multilayer system adhered to itself. The multilayers were influenced by coating stress and unintentional temperature rises during PVD deposition. DOE

N95-20231# Rome Lab., Griffiss AFB, NY.
PRELIMINARY EVALUATION OF A DIGITAL OPTICAL SYSTOLIC PROCESSOR IMPLEMENTED WITH ACOUSTO-OPTIC CELLS Report, Jul. 1989 - Dec. 1992
James B. Rosetti, Rebecca J. Bussjager, David R. Christie, Stuart I. Libby, and Joanne H. Maurice Oct. 1994 24 p
(AF Proj. 4600)
(AD-A286377; RL-TR-94-157) Avail: CASI HC A03/MF A01

Two multichannel acoustic-optic cells were imaged onto one another, and the output was optically summed to a linear photodiode array. By sending periodic data streams into this primitive processor and monitoring the output data stream, an evaluation was made as to the potential feasibility of this type of architecture. It was shown that a 630 million logical instructions per second processor was feasible. However, there is considerable overhead in implementing higher order functions such as addition and multiplication which reduced the computational capability to 4.5 million additions per second and 260 thousand multiplications per second. DTIC

N95-20239# Sandia National Labs., Livermore, CA.
CHARACTERIZATION OF AN EXPANDED-FIELD SCHWARZSCHILD OBJECTIVE FOR EXTREME ULTRAVIOLET LITHOGRAPHY
G. D. Kubiak, D. A. Tichenor, and A. K. Ray-Chaudhuri et al 1994 16 p Presented at the Electron Ion and Photon Beams Symposium, New Orleans, LA, Jun. 1994
(Contract DE-AC04-94AL-85000)
(DE94-016780; SAND-94-8619C; CONF-9406231-1) Avail: CASI HC A03/MF A01

The performance of a new 10x-reduction Schwarzschild system for projection imaging at 13.4 nm wavelength is reported. The optical design is optimized to achieve 0.1 (mu)m resolution over a 0.4 mm image field of view, an increase in area of a factor of 100 over previous designs. An off-set aperture, located on the convex primary, defines an unobscured 0.08 numerical aperture. The system is illuminated using extreme ultraviolet (EUV) radiation emitted from a laser plasma source and collected by an ellipsoidal condenser. A 450 turning mirror is used to relay the collected EUV radiation onto a near-normal reflecting mask. Multiple sets of primary and secondary elements were fabricated, matched and clocked to minimize the effects of small figure errors on imaging performance. Optical metrology indicates that the wave-front error within the subaperture used is within a factor of two of the design value. Images recorded in PMMA and ZEP 520 resists reveal good imaging fidelity over much of the 0.4 mm field with equal line/space gratings being resolved to 0.1 (mu)m. DOE

N95-20249 Heriot-Watt Univ., Edinburgh (Scotland).
INTERNATIONAL CONFERENCE ON OPTICAL COMPUTING: TECHNICAL DIGEST
24 Aug. 1994 410 p Conference held in Edinburgh, Scotland, 22-25 Aug. 1994 Limited Reproducibility: More than 20% of this document may be affected by microfiche quality
(Contract N68171-94-M-5839)
(AD-A284293; R/D-7376-EE-02) Avail: Issuing Activity (Defense Technical Information Center (DTIC))

Some topics that were discussed in the conference are: Quantum well smart pixels for optical switching and processing; Large scale integration of LED's and GaAs circuits fabricated through MOSIS; Parallel algorithms for optical processors; Quantum-statistical restrictions on the information transmitting/processing rate in electronic and photonic channels; and Spatial-light-modulator based routing systems. DTIC

N95-20352# Lawrence Livermore National Lab., Livermore, CA.
REFRACTIVE INDEX CHANGE IN DISSOCIATING SHOCKED BENZENE
D. J. Erskine Jun. 1994 23 p
(Contract W-7405-eng-48)
(DE94-019015; UCRL-ID-116660) Avail: CASI HC A03/MF A01

A calculation is made of the refractive index of a shocked solution of hydrocarbon species and spheroidal carbon particles that would be the dissociation products of benzene. The results are evaluated for benzene shocked to 15 GPa, both for an arbitrary endpoint distribution of products and reactant, and for a specific endpoint distribution suggested by a statistical-mechanical calculation. In the case of diamond particles, the refractive index is predicted to decrease by a small amount (from 1.96 to 1.75) as the dissociation proceeds. In the case of graphite particles of large oblateness, the refractive index could increase significantly through the dissociation (from 1.96 to 2.75 for infinitely oblate platelets). Thus the measurement of the time dependent refractive index through the dissociation of shocked benzene can indicate the morphology of the carbon particulates as well as the time scale for this reaction. We propose using the refractive index as a measure of completion of the dissociation reaction. This would allow a determination of the instantaneous amount of carbon in particulate form, information which is valuable in conjunction with Mie scattering experiments for example. DOE

N95-20364# Lawrence Livermore National Lab., Livermore, CA.

HIGH PRECISION WOELTER OPTIC CALIBRATION FACILITY

R. I. Morales, B. A. Remington, and T. Schwinn 2 May 1994 14 p Presented at the 10th Topical Conference on High-Temperature Plasma Diagnostics, Rochester, NY, 8-12 May 1994
(Contract W-7405-eng-48)
(DE94-016973; UCRL-JC-116181; CONF-940552-27) Avail: CASI HC A03/MF A01

We have developed an off-line facility for very precise characterization of the reflectance and spatial resolution of the grazing incidence Woelter Type 1 x-ray optics used at Nova. The primary component of the facility is a high brightness, 'point' x-ray source consisting of a focussed DC electron beam incident onto a precision manipulated target/pinhole array. The data are recorded with a selection of detectors. For imaging measurements we use direct exposure x-ray film modules or an x-ray CCD camera. For energy-resolved reflectance measurements, we use lithium drifted silicon detectors and a proportional counter. An in situ laser alignment system allows precise location and rapid periodic alignment verification of the x-ray point source, the statically mounted Woelter optic, and the chosen detector. DOE

N95-20403# Lawrence Livermore National Lab., Livermore, CA.

FREQUENCY RESPONSE MEASUREMENTS OF INTEGRATED-OPTIC ELECTRODES

K. F Hugenberg, P. D. Sargis, and C. F. McConaghy Jul. 1994 4 p Presented at the Symposium on Optical Fiber Measurements, Boulder, CO, 13-15 Sep. 1994
(Contract W-7405-eng-48)
(DE94-016690; UCRL-JC-117433; CONF-9409180-2) Avail: CASI HC A01/MF A01

The frequency response of electro-optic waveguides can be determined using a variety of testing methods. In this paper, we compare and contrast three measurement techniques used to test our LiNbO3 devices for improving packages and electrode designs. Each method is described and accompanied by typical results and the experimental setup. Finally, we summarize the advantages and disadvantages of each method. DOE

N95-20450# Lawrence Livermore National Lab., Livermore, CA.

OPTICAL PROPERTIES OF SILICON CLUSTERS DEPOSITED ON THE BASAL PLANE OF GRAPHITE

L. N. Dinh, L. L. Chase, M. Balooch, L. J. Terminello, R. J. Tench, and F. Wooten Apr. 1994 12 p Presented at the Spring Meeting of the Materials Research Society, San Francisco, CA, 4-8 Apr. 1994
(Contract W-7405-eng-48)
(DE94-017529; UCRL-JC-116430; CONF-940411-51) Avail: CASI HC A03/MF A01

Laser ablation was used to deposit of silicon on highly oriented pyrolytic graphite surfaces in an ultra high-vacuum environment equipped with Auger electron spectroscopy (AES), scanning tunneling microscopy (STM) and luminescence spectroscopy. For deposition of up to several monolayers, post annealing produced silicon clusters, whose size distribution was determined vs annealing time and temperature using STM. Pure silicon clusters ranging from 1 to 10 nm showed no detectable photoluminescence in visible range. Exposure to oxygen at 10(exp -6) Torr and for up to 8 hours showed adsorption on the surface of the clusters without silicon oxide formation and no detectable luminescence. Hydrogen termination of these clusters was accomplished by exposing them to atomic hydrogen beam but did not result in any photoluminescence. Prolonged exposure of these clusters to ambient air, however, resulted in strong photoluminescence spectra with color ranging from red to greenish-blue depending on average cluster size. Auger electron spectra revealed the existence of partially oxidized silicon clusters. This luminescence could be due to either an oxide phase or to changes in electronic structure of the clusters as a result of quantum confinement effect. DOE

N95-20467 Naval Postgraduate School, Monterey, CA.

ANALYSIS OF DIRECT DETECTION LIGHTWAVE SYSTEMS WITH OPTICAL AMPLIFIERS M.S. Thesis

Enver Kucukerman Jun. 1994 71 p Limited Reproducibility: More than 20% of this document may be affected by microfiche quality
(AD-A284077) Avail: CASI HC A04

We provide a detailed analysis of direct detection lightwave systems employing an optical preamplifier at the receiver and derive the closed form expression for the bit error probability of WDM systems employing on-off keying (OOK) as modulation format. In our analysis, we consider various cases in which the receiver model uses either a finite-time integrator or Fabry-Perot filter operating in a single channel or multi-channel environment. We take into account the optical amplifier noise, the postdetection receiver noise, the shot noise, and the effect of the nonzero laser linewidth. DTIC

N95-20489# Lawrence Livermore National Lab., Livermore, CA.

WHITE-LIGHT SPECTRAL ANALYSIS OF LITHIUM NIOBATE WAVEGUIDES

C. F. McConaghy, K. F. Hugenberg, D. Sweider, M. Lowry, and R. A. Becker (Integrated Optical Circuit Consultants, Cupertino, CA.) Jul. 1994 6 p Presented at the Symposium on Optical Fiber Measurements, Boulder, CO, 13-15 Sep. 1994 Revised
(Contract W-7405-eng-48)
(DE94-016692; UCRL-JC-115292-Rev-1; CONF-9409180-1-Rev-1) Avail: CASI HC A02/MF A01

Optical channel waveguides in lithium niobate are a very useful technique for building a variety of integrated optical components such as modulators, splitters, and frequency doublers. In many of these applications, single mode performance is essential in order to achieve the desired device performance. Determination of single-mode operation can be complicated by the fact that a multimode guide can support lower order modes and can appear single mode if the launch conditions for the light into the guide do not excite any of the higher order modes. Typical measurements often made to assure single-mode operation include optical mode spot imaging, and the 'blink test'. While these measurements are useful, they are strictly qualitative in nature, and thus do not provide the fine detail often desired in practice. In developing waveguide fabrication processes, it is more helpful to know how various process steps affect the wavelength at which the waveguide is single-mode, multi-mode and cut-off. In this paper, we show the usefulness of exciting waveguides with a broadband white-light source and observing the output of the guides over much of the visible and near IR spectrum with a spectrometer. Although this technique is not new, its usefulness in process development and control has not been emphasized. DOE

N95-20501# Physical Optics Corp., Torrance, CA. Applied Technology Div.

RESONANT TUNNELING QUANTUM WELL INTEGRATED OPTICAL WAVEGUIDE MODULATOR/SWITCH Final Report, 1 Dec. 1993 - 31 May 1994

Andrew Kostrzewski Jul. 1994 33 p
(Contract F49620-94-C-0008)
(AD-A285142; AFOSR-94-0573TR) Avail: CASI HC A03/MF A01

In this Phase 1 program, Physical Optics Corporation (POC) has investigated resonant tunneling double barrier quantum wells (RTDBQW) for application to all-optical communication networks. The RTDBQW can be used as a building block in superfast SONET/ATM network. The proposed concept relies on the integration of an optical guided wave modulator with the RTDBQW. Several waveguide modulator architectures have been investigated, including Mach-Zehnder directional couplers. A Mach-Zehnder interferometer has been selected for the final implementation and will provide high performance. The major advantage of the proposed integrated optical waveguide modulators/switch is that it uses low voltage due to the use of the high efficiency RTDBQW diode. This, in turn, increase the theoretical speed limit of the device to the femtosecond regime. One important feature of the RTDBQW device is that its response time is limited by quantum tunneling time, not by the conventional diode transit time, which leads to high speed operation. DTIC

N95-20564 Carnegie-Mellon Univ., Pittsburgh, PA. Robotics Inst.
A FRAMEWORK FOR SEGMENTATION USING PHYSICAL MODELS OF IMAGE FORMATION
Bruce A. Maxwell and Steven A. Shafer 10 Dec. 1993 36 p Limited Reproducibility: More than 20% of this document may be affected by microfiche quality
(Contract F33615-90-C-1465; ARPA Order 7597)
(AD-A279900; CMU-RI-TR-93-29) Avail: Issuing Activity (Defense Technical Information Center (DTIC))

Most approaches to computer image segmentation group sets of pixels according to visible features of an image such as edges, color, brightness, and curvature. Such approaches exploit specialized object properties to obtain satisfactory groupings, which can force those techniques to be domain specific. Furthermore, they do not provide a physical explanation for the image, nor do they group regions that have a single physical structure yet differing visible features. This paper presents a new approach to segmentation using explicit hypotheses about the physics that creates images. We propose an initial segmentation that identifies image regions exhibiting constant color, but possibly varying intensity. For each region, hypotheses are proposed that specifically model the illumination, reflectance, and shape of the 3-D patch which caused that region. An image region may have many hypotheses simultaneously, and each hypothesis represents a distinct, plausible explanation for the color and intensity variation of that patch. Hypotheses for adjacent patches can be compared for similarity and merged when appropriate, resulting in more global hypotheses for grouping elementary regions. This approach to segmentation has the potential to provide a list of possible explanations for a given image; to group together regions with coherent physical properties; and to provide a framework for applying specific operators such as shape-from-shading, color constancy, and roughness evaluation as part of the overall process of low-level vision. However, many profound unsolved problems are raised in determining the most plausible explanations for a given image region. In this paper, we present the approach, working through an example by hand, and discuss the implications of this approach for physics-based vision. DTIC

N95-20598 GTE Labs., Inc., Waltham, MA.
METHODS AND COMPONENTS FOR OPTICAL CONTENTION RESOLUTION IN HIGH SPEED NETWORKS Interim Report, 23 Feb. - 23 May 1994
Han Kim and Paul Melman 23 May 1994 15 p Limited Reproducibility: More than 20% of this document may be affected by microfiche quality
(Contract MDA972-93-C-0057; ARPA Order 9339)
(AD-A280016) Avail: Issuing Activity (Defense Technical Information Center (DTIC))

During the third quarter of the CORD project progress was made in the area of design and development of the various subunits of the system. Test and evaluation of the functional blocks built during the past quarter was the focus of the system group at Stanford University and the optoelectronics group at GTE Laboratories. Detailed Performance estimates were made with respect to signaling and its interference with the information channel. Progress was also made in the construction of the CRO module with detailed evaluation of the WDM components to be used and completion of the development of the high speed header detector module. Development of the logic control for CORD's contention resolution strategy was pursued further. Moreover, a 'Multi-Packet' CORD architecture was developed and shown that it can substantially reduce the packet loss probability. Logic control design was then provided also for this improved version of the CORD. DTIC

N95-20601 Massachusetts Inst. of Tech., Cambridge, MA. Research Lab. of Electronics.
ANALOG PROCESSING OF OPTICAL WAVEFRONT USING INTEGRATED GUIDED-WAVE OPTICS Final Report, 1 Jun. 1990 - 31 Dec. 1993
Robert H. Rediker 30 Mar. 1994 55 p Limited Reproducibility: More than 20% of this document may be affected by microfiche quality
(Contract F49620-90-C-0036)
(AD-A279596; AFOSR-94-0306TR) Avail: Issuing Activity (Defense Technical Information Center (DTIC))

Integrated Guided-Wave Optics has many advantages for the analog processing of optical wavefronts. These include small-size, high-speed, simplicity, reliability and reproducibility. The fabrication technique is similar to that of integrated circuits. The thrust of this program was to develop an integrated guide-wave optic system in GaAs and GaAlAs for use at GaAs laser wavelength, to remove aberrations from a laser beam and to steer the beam. The system would in addition have the capability to appropriately phase the outputs from a multiplicity of power amplifiers or injection locked lasers. It was also the intent of the program to design and build the optical circuits so they are compatible with on-chip electronic circuits in order to minimize the required number of off-chip leads. DTIC

N95-20612# Lawrence Livermore National Lab., Livermore, CA.
DEVELOPMENT, FABRICATION, AND METROLOGY OF THE ELECTRO-OPTICAL BREADBOARD MODEL FOR THE REFLECTION GRATING ARRAY OF THE XMM GRATING SPECTROMETER
T. A. Decker, R. C. Montesanti, J. V. Bixler, C. J. Hailey, and S. M. Kahn (California Univ., Berkeley, CA.) Jul. 1994 11 p Presented at the Annual Meeting of the Society of Photo-Optical Instrumentation Engineers, San Diego, CA, 24-29 Jul. 1994
(Contract W-7405-eng-48)
(DE94-016605; UCRL-JC-117808; CONF-940723-14) Avail: CASI HC A03/MF A01

A prototype array consisting of eight diffraction gratings has been fabricated for the XMM Reflection Grating Spectrometer. A component of the full spectrometer is an array of approximately 200 diffraction gratings. The diffraction gratings were produced using lightweight silicon carbide substrates and a replication technique. The prototype array was developed and assembled using the same tolerances as the flight arrays which have typical tolerances of 3 micrometers in translation and sub-arc seconds in rotation. The metrology applied during inspection and assembly included precision linear measurements, full aperture figure measurements, and angular interferometry. DOE

N95-20728 Department of the Navy, Washington, DC.
CONTROL OF CONTINUOUS PHASE PH USING VISIBLE LIGHT TO ACTIVATE PH-DEPENDENT FIBERS AND GELS IN A CONTROLLED AND REVERSIBLE MANNER Patent
Albert Zirino, inventor (to Navy) 2 Aug. 1994 11 p Filed 27 Aug. 1992
(AD-D016532; US-Patent-5,334,629; US-Patent-Appl-SN-936681; US-Patent-Class-523-137) Avail: US Patent and Trademark Office

A transparent polyelectrolyte fiber or gel, such as crosslinked polyacrylic acid, which contracts and expands upon the addition of an acid or base to an aqueous medium solution, is placed in the same solution with a pH dependent dye, a colored photochromatic indicator dye. The dye preferably has a pAa value that is the same as the pH at a null contraction point of the fiber. By irradiating the solution with light of a wavelength of the absorption band of either the acid or base form of the dye, the solution pH is made to change, and the fiber is made to expand or contract, depending upon the wavelength. Thus, light energy is readily converted to work energy and may be used to power a pump, for example or an artificial muscle can be powered via an optical fiber. DTIC

N95-20798*# Alabama Univ., Huntsville, AL.
X-RAY MICROSCOPE FOR SOLIDIFICATION STUDIES Semiannual Report, 1 Mar. 1994 - 28 Feb. 1995
William Kaukler 28 Feb. 1995 6 p
(Contract NAS8-40185)
(NASA-CR-197375; NAS 1.26:197375) Avail: CASI HC A02/MF A01

This report covers the second 6 month period for the year March 1, 1994 to February 28, 1995. The material outlined in this semi-annual report continues from the previous semi-annual report. The Fein Focus Inc. x-ray source was delivered in September and coincides with the beginning of the second 6 month effort. As a result, and as outlined in the statement of work, this period was dedicated to the evaluation, testing and calibration of the x-ray source. In addition, in this period the modeling effort was continued and extended by the Tigêr series of Monte-Carlo simulation programs for photon and electron interactions with materials obtained from the Oak Ridge RISC Library. Some further calculations were also made with the absorption model. Author

N95-20803# Rockwell International Science Center, Thousand Oaks, CA.
LIGHT-SCATTERING FLUCTUATIONS AND NOISE IN NONLINEAR OPTICAL PROCESSING Final Report, Nov. 1989 - Nov. 1992
Robert L. McGraw Mar. 1994 39 p
(Contract F29601-89-C-0085)
(AD-A279748; SC71022.FR; PL-TR-93-1039) Avail: CASI HC A03/MF A01

This report summarizes the results of a 3-yr investigation into the role of light-scattering noise in nonlinear optical processes. These results span a full range - from physical and mathematical description and prediction of noise properties to experimental verification of the theory and interpretation of measurements. Light-scattering noise fluctuations are shown to set fundamental limits on device size and sensitivity and on beam power requirements for nonlinear optical processes. DTIC

N95-20844# Nottingham Univ. (England). Dept. of Geography.
HIGH CONTRAST ORGANIC CRYSTAL OPTICAL MODULATOR FOR PHASED ARRAY ANTENNA AND OPTICAL SIGNAL PROCESSING Final Report, 1 Sep. 1991 - 31 Aug. 1994
K. R. Stewart, E. P. Boden, C. P. Yakymyshyn, and W. T. Lotshaw 27 Oct. 1994 55 p
(Contract F49620-91-C-0075)
(AD-A286557; AFOSR-94-0749TR) Avail: CASI HC A04/MF A01

The utility of organic salts related to 4-Dimethylamino-N-methyl Stilbazolium Tosylate, DAST, to display very useful optoelectronic properties has been broadly investigated and continues to yield new information. New materials have been developed having improved optical and physical properties. Methods for crystal growth and handling have been developed which allow the design and fabrication of useful optoelectronic devices. Design and fabrication of a linear array of high performance Fabry-Perot etalons is described. DTIC

N95-20876 Oregon Univ., Eugene, OR. Dept. of Chemistry.
S-D HYBRIDIZATION AND ANISOTROPY OF THE OPTICAL SECOND HARMONIC AT LOW FREQUENCIES Technical Report, Jun. 1993 - May 1994
Paul E. Bunson, Roger Haydock, and G. L. Richmond 13 May 1994 18 p Limited Reproducibility: More than 20% of this document may be affected by microfiche quality
(Contract N00014-89-J-1261)
(AD-A279449; TR-10) Avail: CASI HC A03

Recent experiments show that the anisotropy of the optical second harmonic (SHG) response from noble metal surfaces persists at frequencies below those associated with interband transitions and plasma resonances. It is proposed that for noble metals this anisotropy is a consequence of the hybridization between s and d-orbitals. By taking advantage of a moment expansion and related path counting methods, the relative importance of the different contributions to SHG can be identified. To illustrate this result, the nonlinear polarizations are calculated using the recursion method. DTIC

N95-21100 Department of the Navy, Washington, DC.
PASSIVE RANGE MEASUREMENT SYSTEM Patent Application
Walter L. Harriman, inventor (to Navy) 27 Jul. 1992 14 p Limited Reproducibility: More than 20% of this document may be affected by microfiche quality
(AD-D016222; US-Patent-Appl-SN-921863) Avail: Issuing Activity (Defense Technical Information Center (DTIC))

A method and apparatus provides instantaneous passive range measurement onboard an aircraft for determining the range between the aircraft and a target. The target may either be stationary and on the earth's surface, or a slower moving vehicle. Calculation of the desired range is achieved using the formula: Range = (Sin a/Sin b) V; where 'a' = angle from aircraft heading to target, 'b' = turning rate; and 'V' ground velocity. The apparatus consists of an automatic video tracker, a video camera, and a servo controlled aiming platform. A resolver on the aiming platform is utilized to determine the angle from the aircraft axis to the target. This angle is added to the aircraft drift angle to determine the total angle from the aircraft heading to the target. The video tracker is utilized to determine the turning rate of the aiming platform. Using the difference in contrast between the target and the background of the video scene, the tracker provides error signals (azimuth and elevation) to keep the aiming platform pointed at the target. DTIC

N95-21103# Helsinki Univ. of Technology, Espoo (Finland). Electromagnetics Lab.
MAGNETOELECTRIC PROPERTIES OF RECIPROCAL BIANISOTROPIC MATERIALS WITH FOCUS ON THE POLARIZABILITY OF CHIRO-OMEGA SPHERES
Ari H. Sihvola and Ismo V. Lindell May 1994 25 p
(ISSN 0784-848X)
(PB95-127650; ISBN-951-22-2129-2) Avail: CASI HC A03/MF A01

The paper concentrates on magnetoelectric characteristics of bianisotropic materials using the concept of reciprocity as a criterion of classification. A dyadic matrix representation is followed, and the complementary operation for dyadic matrices is introduced which is shown to be a very useful operation in treating material parameters of bianisotropic media. The analysis goes further to treat the polarizability properties of bianisotropic spheres. The polarizability matrix, containing four dyadic elements, is derived in compact matrix form. The distinction between two types of reciprocal magnetoelectric coupling is interpreted in terms of helical and omega-type elements. These account for the symmetric and antisymmetric parts, respectively, of the magnetoelectric material dyadic in the bianisotropic relations. The components of the polarizability dyadics are calculated for an omega sphere and also for a chiro-omega sphere. It is found that the components of the material parameter dyadics become coupled in the polarizability components. The coupling details are described and these are shown to be different for the chiral magnetoelectric effects and the omega effects. NTIS

N95-21392# Lawrence Livermore National Lab., Livermore, CA.
AN IMAGE CANCELLATION APPROACH TO DEPTH-FROM-FOCUS
Shin-Yee Lu and M. Graser (EG and G Energy Measurements, Inc., Pleasanton, CA.) 12 Sep. 1994 11 p Presented at the SPIE International Symposium on Photonic Sensors and Controls for Commercial Applications, Boston, MA, 31 Oct. - 4 Nov. 1994
(Contract W-7405-eng-48)
(DE94-019312; UCRL-JC-116963; CONF-9410154-1) Avail: CASI HC A03/MF A01

Depth calculation of an object allows computer reconstruction of the surface of the object in three dimensions. Such information provides human operators 3D measurements for visualization, diagnostic and manipulation. It can also provide the necessary coordinates for semi or fully automated operations. This paper describes a microscopic imaging system with computer vision algorithms that can obtain the depth information by making use of the shallow depth of field of microscopic lenses. DOE

N95-21465 Department of the Navy, Washington, DC.
NONLINEAR FREQUENCY CONVERSION OPTICAL FILTER Patent
Bruce P. Boczar, inventor (to Navy) 16 Aug. 1994 7 p Filed 20 Sep. 1993 Supersedes AD-D016127
(AD-D016523; US-Patent-5,339,189; US-Patent-Appl-SN-123959; US-Patent-Class-359-326) Avail: US Patent and Trademark Office

The present invention is a method and system for performing optical filtering. Light energy in one frequency band is received in this system. The received light energy is filtered in one frequency band in order to provide filtered light which is applied to a nonlinear optical device. The nonlinear optical device provides frequency conversion preferably by forming a sum frequency or difference frequency. The frequency converted light energy is in a second frequency band. The energy in this second frequency band is applied to a further filter in a different frequency band wherein the two filter frequency bands are selected to prevent light energy from passing through both filters. The received light energy may contain information which is recoverable from the light energy which passes through the second filter. The nonlinear device is a crystal in which the index of refraction may be changed in order to tune the filter. DTIC

N95-21466 Department of the Navy, Washington, DC.
METHOD FOR CHARACTERIZATION OF OPTICAL WAVEGUIDE DEVICES USING PARTIAL COHERENCE INTERFEROMETRY Patent
Matthew N. McLandrich, inventor (to Navy), Donald J. Albares, inventor (to

Navy), and Stephen A. Pappert, inventor (to Navy) 23 Aug. 1994 28 p Filed 15 Jan. 1991
(AD-D016525; US-Patent-5,341,205; US-Patent-Appl-SN-643385; US-Patent-Class-356-73) Avail: US Patent and Trademark Office

An optical system and method includes a short coherence length edge, emitting LED, a fiber optic coupler probe, and a Michelson interferometer to measure the parameter of thickness of optical devices, such as thin silicon substrate samples and to characterize other parameters of optical waveguide devices such as absolute attenuation, effective refractive index, and changes in these parameters with the application of a modulation voltage or an external disturbance. The measurable thickness range from a few to hundreds of microns with a thickness precision exceeding 0.1 micron for a 10 micron sample. In situ localized measurements of samples in an etching chamber are obtainable to control processing and provide for thickness uniformity. DTIC

N95-21509# Sandia National Labs., Albuquerque, NM.
UNLIMITED-BANDWIDTH DISTRIBUTED OPTICAL PHASE MODULATORS AND DETECTORS: DESIGN AND FABRICATION ISSUES
G. A. Vawter, V. M. Hietala, S. H. Kravitz, and M. G. Armendariz 1994 3 p Presented at the Institute of Electrical and Electronics Engineers (IEEE) Microwave Theory and Technology Society and Laser Electro-Optical Society Conference, Ile-de-France (France), 21-23 Nov. 1994
(Contract DE-AC04-94AL-85000)
(DE94-017418; SAND-94-2156C; CONF-9411123-1) Avail: CASI HC A01/MF A01

Practical and theoretical limits on the bandwidth of distributed optical phase modulators and traveling-wave photodetectors are given. For the case of perfect velocity matching, RF transmission losses are the main performance-limiting factor. However, some high-performance modulators require highly-capacitive transmission lines making proper slow-wave operation difficult to achieve. DOE

N95-21510# Lawrence Livermore National Lab., Livermore, CA.
FIBER-OPTIC SENSORS FOR RAPID, INEXPENSIVE CHARACTERIZATION OF SOIL AND GROUND WATER CONTAMINATION
Fred P. Milanovich and Jesse L. Yow, Jr. Aug. 1994 7 p Presented at the Conference and Exposition on Petroleum Hydrocarbons, Houston, TX, 2-4 Nov. 1994
(Contract W-7405-eng-48)
(DE95-002471; UCRL-JC-118432; CONF-941152-1) Avail: CASI HC A02/MF A01

The extent and complexity of worldwide environmental contamination are great enough that characterization, remediation, and performance monitoring will be extremely costly and lengthy. Characterization techniques that are rapid, inexpensive, and simple and that do not generate waste are urgently needed. Towards this end LLNL is developing a fiber-optic chemical sensor technology for use in groundwater and vadose-zone monitoring. We use a colorimetric detection technique, based on an irreversible chemical reaction between a specific reagent and the target compound. The accuracy and sensitivity of the sensor (less than 5 ppb by weight in water, determined by comparison with gas chromatographic standard measurements) are sufficient for environmental monitoring of trichloroethylene (TCE) and chloroform. DOE

N95-21643# Brookhaven National Lab., Upton, NY.
LIGHT OUTPUT AND RADIATION DAMAGE IN A YAlO3:Ce CRYSTAL
J. A. Kierstead, S. P. Stoll, and C. L. Woody 1994 5 p Presented at the Spring Meeting of the Materials Research Society, San Francisco, CA, 4-8 Apr. 1994
(Contract DE-AC02-76CH-00016)
(DE94-016815; BNL-60592; CONF-940411-47) Avail: CASI HC A01/MF A01

The optical absorption, light output, and effects of radiation damage have been studied in a 2.1 x 2.1 x 2.1 cm(exp 3) crystal of YAlO3:Ce. The light yield produces approximately 2867 photoelectrons per MeV on a photomultiplier tube with a bialkali photocathode. The scintillation and light transmission properties of the crystal were characterized before and after exposure to 1 Mrad of Co-60 gamma rays. Significant radiation induced optical absorption was observed near the optical band edge of the crystal, along with an extremely intense phosphorescence after irradiation. Partial spontaneous recovery from the damage occurred at room temperature, and it was possible to induce additional recovery by optical bleaching. DOE

N95-21673 Office of Naval Research, Arlington, VA.
FIBER-OPTIC ROTARY JOINT WITH BUNDLE COLLIMATOR ASSEMBLIES Patent Application
Gregory H. Ames, inventor 8 Aug. 1994 15 p Limited Reproducibility: More than 20% of this document may be affected by microfiche quality
(AD-D016504; US-Patent-Appl-SN-287027) Avail: Issuing Activity (Defense Technical Information Center (DTIC))

There is presented a fiber-optic rotary joint with first and second bundle collimator assemblies, the joint comprising a generally cup-shaped main rotor, a first bundle collimator assembly fixed in a central opening in a bottom wall of the main rotor, a generally cup-shaped stator disposed within the main rotor, the stator having a bottom wall opposed to the main rotor bottom wall, and a second bundle collimator assembly disposed in a central opening in the bottom wall of the stator. The joint further includes a prism mounted in a prism rotor in the joint between the first and second collimator assemblies, and gear means for causing rotation of the main rotor at twice the speed of rotation of the prism rotor. Azimuthal adjustment structure is disposed on one of the first and second collimator assemblies for azimuthal alignment of the one collimator assembly with the other of the collimator assemblies. DTIC

N95-21728# Sandia National Labs., Albuquerque, NM.
HIGH FREQUENCY CURRENT SENSORS USING THE FARADAY EFFECT IN OPTICAL FIBERS
R. W. Cernosek Sep. 1994 239 p
(Contract DE-AC04-94AL-85000)
(DE95-001859; SAND-94-2572) Avail: CASI HC A11/MF A03

This study investigates the high frequency response of Faraday effect optical fiber current sensors that are bandwidth-limited by the transit time of the light in the fiber. Mathematical models were developed for several configurations of planar (collocated turns) and travelling wave (helical turns) singlemode fiber sensor coils, and experimental measurements verified the model predictions. High frequency operation above 500 MHz, with good sensitivity, was demonstrated for several current sensors; this frequency region was not previously considered accessible by fiber devices. Planar fiber coils in three configurations were investigated: circular cross section with the conductor centered coaxially; circular cross section with the conductor noncentered; and noncircular cross section with arbitrary location of the conductor. The helical travelling wave fiber coils were immersed in the dielectric of a coaxial transmission line to improve velocity phase matching between the field and light. Three liquids (propanol, methanol, and water) and air were used as transmission line dielectric. Complete models, which must account for liquid dispersion and waveguide dispersion from the multilayer dielectric in the transmission line, were developed to describe the Faraday response of the travelling wave sensors. Other travelling wave current sensors with potentially greater Faraday sensitivity, wider bandwidth and smaller size are investigated using the theoretical models developed for the singlemode fibers coils. DOE

N95-21825 Department of the Navy, Washington, DC.
FIBER GRATING-BASED DETECTION SYSTEM FOR WAVELENGTH ENCODED FIBER SENSORS Patent Application
Alan D. Kersey, inventor (to Navy), Charles Askins, inventor (to Navy), and E. J. Friebele, inventor (to Navy) 30 Nov. 1993 25 p Limited Reproducibility: More than 20% of this document may be affected by microfiche quality
(AD-D016208; US-Patent-Appl-SN-159169) Avail: Issuing Activity (Defense Technical Information Center (DTIC))

An apparatus for the determination of the wavelength and the detection of wavelength shifts in wavelength-encoded fiber sensors, such as Bragg grating sensors. The apparatus is implemented in fiber and uses a pair of tuned fiber gratings to provide a filter type function that tracks the wavelength component of a signal from a wavelength-encoded sensor. DTIC

N95-21832# Mission Research Corp., Santa Barbara, CA.
HIGH RESOLUTION DESCRIPTIONS OF IRAS 12 AND 25 MICRONS CONFUSED REGIONS Final Report, 9 Jan. 1990 - 30 Sep. 1993
R. M. Kennealy, R. S. Sample, J. P. Kennealy, R. A. Gonsalves (Tufts

Univ., Medford, MA.), and R. Canterna (Wyoming Univ., Laramie, WY.) Apr. 1994 136 p
(Contract F19628-90-C-0110; AF Proj. 7670)
(AD-A285847; PL-TR-94-2197; AD-E202172) Avail: CASI HC A07/MF A02

12 and 25 micron IRAS Survey and AO footprint scan data in the galactic plane have been reprocessed as images for 2-dimensional point source extractions in an effort to provide a point source catalog supplement which is more complete than the IRAS PSC in the regions labeled 'confused' by IRAS. Approximately 3500 square degrees of sky are available as an atlas of high resolution galactic plane images (14.4 in.) pixels. For each region of the sky, there are separate background and point source images. Point source extraction results indicate that the 2-D processing improves completeness over the PSC everywhere in the plane, and increases source counts by a factor of 2-4 over the PSC. DTIC

N95-21870 Technische Univ., Twente (Netherlands). Tele-Informatics and Open Systems Group.
HIGH-CAPACITY OPTICAL MULTICHANNEL VIRTUAL MESH INTERCONNECTION NETWORKS
J. H. Laarhuis and A. M. J. Koonen 1994 12 p See also PB93-214922
(ISSN 0924-3755)
(PB95-134094; TIOS-94-09) Copyright Avail: Issuing Activity (National Technical Information Service (NTIS))

A virtual mesh interconnection architecture results from division of channels and nodes into groups. Nodes may send on any channels from one group and receive one channel from all groups. The implementation extensively reuses resources and employs readily available hardware. NTIS

N95-21882# Naval Postgraduate School, Monterey, CA. Dept. of Electrical and Computer Engineering.
A COMPUTER-BASED MULTIMEDIA PROTOTYPE FOR NIGHT VISION GOGGLES M.S. Thesis
Bobby Bryant and Glenroy E. Day, Jr. Sep. 1994 44 p
(AD-A286208) Avail: CASI HC A03/MF A01

Naval aviators who employ night vision goggles (NVG) face additional risks during nighttime operations. In an effort to reduce these risks, increased training with NVG's is suggested. Our goal was to design a computer-based, interactive multimedia system that would assist in the training of pilots who use NVG's. This thesis details the methods and techniques used in the development of the NVG multimedia prototype. It describes which hardware components and software applications were utilized as well as how the prototype was developed. Several facets of multimedia technology (sound, animation, video, and three dimensional graphics) have been incorporated into the interactive prototype. For a more robust successive prototype, recommendations are submitted for future enhancements that include alternative methodologies as well as expanded interactions. DTIC

N95-21898 Department of the Navy, Washington, DC.
TECHNIQUE FOR INTRACAVITY SUM FREQUENCY GENERATION Patent
Richard Scheps, inventor (to Navy) 26 Jul. 1994 16 p Filed 12 Aug. 1993
(AD-D016478; US-Patent-5,333,142; US-Patent-Appl-SN-108131; US-Patent-Class-372-22) Avail: US Patent and Trademark Office

A means for intracavity sum frequency generation is described in which a laser operates simultaneously at two wavelengths. The laser resonator further contains a sum frequency generating nonlinear crystal which is oriented for efficient sum frequency generation of the two fundamental wavelengths. The optical alignment of the resonator provides a region where both fundamental wavelengths are overlapped and are focused. The nonlinear sum frequency generating crystal is placed near this focus in the region where both wavelengths are spatially superimposed, producing the sum frequency of the two wavelengths. Line narrowing of the individual two fundamental wavelengths produces a line narrowed sum frequency generated output. Mirror coatings on all reflective elements are highly reflective for both fundamental wavelengths to produce a high intracavity fluence at both of these frequencies. Sum frequency generation at 459 nm is demonstrated in a non-critically phase matched type II KTP crystal by operating a Ti:sapphire laser simultaneously at 808 nm and 1.064 microns. In order to achieve simultaneous operation at both wavelengths a 1.064 microns signal may be injected into the resonator from an external source, such as a Nd:YAG laser. A doubled Nd:YAG laser may be used to optically excite the Ti:sapphire laser while simultaneously injecting 1.064 microns radiation into the laser cavity. DTIC

N95-21905 Department of the Navy, Washington, DC.
SUBMICROSECOND, SYNCHRONIZABLE X-RAY SOURCE Patent
Robert R. Whitlock, inventor (to Navy) 2 Aug. 1994 7 p Filed 31 Mar. 1993
(AD-D016497; US-Patent-5,335,258; US-Patent-Appl-SN-041388; US-Patent-Class-378-122) Avail: US Patent and Trademark Office

In the submicrosecond, synchronizable x-ray source a high intensity pulsed laser is focused onto a negatively biased laser target, at high irradiance in a vacuum, producing high temperature plasma from which electrons are emitted. The emitted electrons are accelerated in a electric field formed by impressing a potential difference across a laser target-electron target gap. The positively biased electron target collects the emitted electrons, which upon impact with the electron target cause x-rays to be emitted synchronously with the incident laser pulse. DTIC

N95-21975 Wright Lab., Wright-Patterson AFB, OH.
OPTICAL PROCESSING AND CONTROL Final Report, Oct. 1986 - Sep. 1992
Andrew Suzuki, Dale Stevens, Mike Prairie, James Grote, and Antonio Crespo Jan. 1994 69 p Limited Reproducibility: More than 20% of this document may be affected by microfiche quality
(AD-A279157; WL-TR-94-5005) Avail: Issuing Activity (Defense Technical Information Center (DTIC))

The effort is divided into specific topics applicable to data processing. Those topics include the Dember effect, alignment of a ring laser gyro, measurement of the Fresnel drag coefficient, integrated optical switches, aluminum gallium arsenide waveguides, Fredkin gates, optically reconfigurable superconductive circuits, and an initial investigation into the application of an acoustooptical tunable filter to the interrogation of fiber optic Bragg sensors. DTIC

N95-22002 Messina Univ. (Italy).
THE OPTICAL PROPERTIES OF PARTICLES DEPOSITED ON A SURFACE Final Report
F. Borghese Sep. 1994 29 p Limited Reproducibility: More than 20% of this document may be affected by microfiche quality
(Contract DAJA45-93-C-0043)
(AD-A286258; R/D-7130-EN-09) Avail: CASI HC A03

In recent years the optical properties of particles near or on a plane surface have been the subject of several papers that deal with both the theoretical and the experimental aspects of the problem. This interest from the scientific community can be easily understood because revealing through optical measurements the presence of particles on a surface that is expected to be clean is of great importance both for industry and for medicine. Among the theoretical techniques that have been proposed to deal with the problem the method of the images proved to be the most fruitful when the plane surface is a perfectly reflecting one, a condition that is met to a high degree of accuracy by many polished metallic surfaces. According to the theory of the images the problem of scattering from a particle in the vicinity of a perfectly reflecting plane surface is quite equivalent to the problem of the dependent scattering from the compound object that is composed by the actual particle and by its mirror image when excited by the superposition of the fields that come from the actual source and from its image. Of course, the method of the images is advantageous provided one is able to solve, without undue computational effort, the problem of scattering from the compound scatterer. In fact, the lack of an efficient technique to deal with this problem forced several researchers to solve the problem for limiting cases only, e. g. normal incidence, or through approximations, such as the assumption of smallness of the scattering particle. DTIC

N95-22043# Clemson Univ., SC. Dept. of Ceramic Engineering.
CHARACTERIZATION EQUIPMENT FOR ELECTROOPTICS AND ACTUATORS Final Report, 30 Sep. 1993 - 30 Sep. 1994

Gene Haertling, Eugene Furman, and Feiling Wang 17 Oct. 1994 5 p
(Contract N00014-93-1-1129)
(AD-A286285) Avail: CASI HC A01/MF A01

The goal of the ONR sponsored grant is to enhance the characterization capabilities of the Electroceramic Group in the Ceramics Department of Clemson University in the areas of electrooptics and electromechanical actuators. These are core research areas, so the instrumentation acquired through this grant benefits the majority of current research projects. This report summarizes research which directly benefits from the acquired instrumentation. The new equipment strengthens dielectric, piezoelectric, and electrooptic characterization capabilities for both thin film and bulk devices. Dielectric and piezoelectric characterization of materials is especially useful in current studies of actuator devices such as Rainbow devices. Electrooptic characterization equipment is used mainly to study transparent PLZT thin film ceramics. DTIC

N95-22044# Army Aeromedical Research Lab., Fort Rucker, AL.
FACTORS AFFECTING THE PERCEPTION OF LUNING IN MONOCULAR REGIONS OF PARTIAL BINOCULAR OVERLAP DISPLAYS
Victor Klymenko, Robert W. Verona, John S. Martin, Howard H. Beasley, and William E. McLean Aug. 1994 54 p
(DA Proj. 3E1-62787-A-879)
(AD-A286287; USAARL-94-47) Avail: CASI HC A04/MF A01

Luning is a detrimental visual effect characterized by a subjective darkening of the visual field in the monocular regions of partial binocular overlap displays. The effect of a number of factors on the magnitude of luning was investigated. These factors include: (1) the convergent versus the divergent display modes for presenting a partial binocular overlapping field-of-view; (2) the display luminance level; (3) the placement of either black or white contours versus no (null) contours on the binocular overlap border; and (4) the increasing or decreasing of the luminance of the monocular side regions relative to the binocular overlap region. Eighteen Army student aviators served as subjects in a repeated measures design. The percentage of time luning was seen was the measure of the degree of luning. The results indicated that the divergent display mode systematically induced more luning than the convergent display mode under the null contour condition. Adding black contours reduced luning in both the convergent and divergent display modes, where the convergent mode retained its relatively lower magnitude of luning. The display luminance level had no effect on luning for the null or black contour conditions. DTIC

N95-22074 Oregon Univ., Eugene, OR. Dept. of Chemistry.
APPLICATION OF OPTICAL SECOND HARMONIC GENERATION TO SURFACE ANALYSIS Technical Report, Jun. 1993 - May 1994
G. L. Richmond 13 May 1994 6 p Limited Reproducibility: More than 20% of this document may be affected by microfiche quality
(Contract N00014-89-J-1261)
(AD-A279445; TR-12) Avail: Issuing Activity (Defense Technical Information Center (DTIC))

Understanding surface and interfacial properties remains a challenging task, particularly when these interfacial regions are under relatively reactive conditions. This is particularly true of semiconductor surfaces which can be highly reactive under ambient or processing conditions. One of the studies to be described in this presentation is our recent work on Si electrode surfaces. In recent years significant progress has been made in characterizing the Si/electrolyte interface by infrared reflectance, ultra-high vacuum UHV transfer experiments, and scanning tunneling microscopy STM and AFM imaging. These studies have taken advantage of the relative stability of Si surface prepared in a hydrogen terminated state. The more usual form in either air or in water is a heavily oxidized Si surface for which much less is known because of the inapplicability of many of the above techniques to examining the Si/SiO2 interfacial region. The presence of the oxide can significantly alter the electrochemistry and the electronic properties of the semiconductor. In this paper we discuss our application of optical second harmonic generation (SHG) to studying the Si/electrolyte and Si/SiO2/electrolyte interfaces for which oxides have been photoanalytically grown on the surface. DTIC

N95-22076# Rome Lab., Griffiss AFB, NY.
POLYCRYSTALLINE PLZT/ITO CERAMIC ELECTRO-OPTIC PHASE GRATINGS: ELECTRO-OPTICALLY RECONFIGURABLE DIFFFRACTIVE DEVICES FOR FREE-SPACE AND IN-WAFER INTERCONNECTS Report, Oct. 1992 - Sep. 1993
Pierre J. Talbot and Joanne H. Maurice Sep. 1994 39 p
(AF Proj. 4600)
(AD-A285861; RL-TR-94-123) Avail: CASI HC A03/MF A01

The potential of electro-optically reconfigurable phase-only diffractive devices as a suitable extension to static diffractive elements for optical free-space and waveguide interconnects is investigated through the fabrication, testing and modeling of polycrystalline PLZT/ITO ceramic electro-optic phase-only gratings. DTIC

N95-22089 Department of the Navy, Washington, DC.
OPTICAL FIBER PRESSURE SENSOR FOR LIQUID LEVEL MONITORING Patent Application
Frank Cuomo, inventor (to Navy) 22 Feb. 1994 14 p Limited Reproducibility: More than 20% of this document may be affected by microfiche quality
(AD-D016246; US-Patent-Appl-SN-199868) Avail: CASI HC A03

An apparatus for continuously monitoring changes in a liquid level in accordance with a differential pressure is provided. A sensor body immersed in the liquid supports two thin-filmed metallic diaphragms that are independently, axially responsive to pressure of the liquid. Each diaphragm has a different modulus of elasticity. Two fiber optic pressure sensors are mounted within an air space encased by the sensor body in combination with the two diaphragms. Each of the two fiber optic pressure sensors detects the axial response of one of the two diaphragms. The displacement difference between the two diaphragms is an indication of differential pressure related to the liquid level. DTIC

N95-22140 National Defence Research Establishment, Stockholm (Sweden). Dept. of Weapon Systems, Effects and Protection.
EMBEDDED OPTICAL FIBRES AS STRAIN SENSORS IN POLYMER MATRIX FIBRE COMPOSITES: THE INFLUENCE OF ADHESION IN STRAIN TRANSFER |INBAEDDADE OPTISKA FIBRER SOM TOEJNINGSSENSORER I POLYMERBASERADE FIBERKOMPOSITER: VIDHAEFTNINGENS INVERKAN PA TOEJNINGSOEVERFOERINGEN|
M. Ekroth Jun. 1994 34 p In SWAHILI
(PB95-133617; FOA-C-20983-2.4) Avail: Issuing Activity (National Technical Information Service (NTIS))

Optical fibers can serve as strain sensors embedded in load carrying polymer matrix fiber composites. The aim of the study was to investigate the influence of chemical bonding between the optical fiber, its protective polyimide coating and the surrounding composite, in strain transfer from the composite to the optical fiber. The degree of adhesion was determined by measuring the force during debonding and pull-out of the optical fiber from the composite. Debonding occurred between the quartz fiber and the coating for both untreated and ammonia modified fibers. The PTFE coated fibers debonded between the coating and the composite. The modified fibers debonded at a lower applied load than the untreated fibers. The strain during tensile loading was measured both with conventional resistance strain gages mounted on the specimen surfaces, and optically with a Mach-Zehnder-interferometer. The optically measured strains, obtained with the untreated fiber and the modified fibers, were all in good agreement with the response from the resistance strain gages. It is concluded that the chemical bonding between the quartz fiber/coating/composite consequently has little or no influence on the strain transfer. Internal stresses (mechanical pressure and friction forces) arising from the laminate fabrication process are sufficient for strain transfer. NTIS

N95-22205 Cornell Univ., Ithaca, NY.
DESIGN, FABRICATION, AND CHARACTERIZATION OF REFLECTIVE DIFFRACTIVE OPTICAL ELEMENTS IN SI FOR FREE-SPACE OPTICAL INTERCONNECTS Final Report
Steven M. Shank and Harold G. Craighead Oct. 1994 47 p Limited Reproducibility: More than 20% of this document may be affected by microfiche quality
(Contract F30602-93-C-0061)
(AD-A286416; RL-TR-94-185) Avail: CASI HC A03

Diffractive optical element designs are presented for a free-space focused optical interconnect whereby a 4x4 array of LED's is focused onto a 4x4 array of photodetectors. Process development for highly efficient diffractive elements is presented. Fabrication tolerances for binary level alignment and etch depth are determined. Eight-level diffractive elements are fabricated using electron beam lithography and reactive ion etching. Continuously graded gratings are fabricated using focused ion beam milling. Device fabrication is characterized by scanning electron microscopy and atomic force microscopy, and device performance is determined by measuring diffraction efficiencies. DTIC

N95-22238# California Univ., Berkeley. Lawrence Berkeley Lab, CA.
USERS GUIDE TO NCEMSS, VERSION 2.0
M. A. OKeefe and R. Kilaas Oct. 1994 59 p
(Contract DE-AC03-76SF-00098)
(DE95-003443; LBL-Pub-658-Ver-2.0) Avail: CASI HC A04/MF A01

Image simulation grew out of attempts to explain why electron microscopic images of complex oxides sometimes showed black dots, sometimes white dots. Most simulations today are carried out to relate the image character to known features in the structure; images are simulated from all possible structure models and compared with experimental images. The code NCEMSS is divided into the 3 subprograms: PHSGRT, MSLICE, and IMAGE. DOE

N95-22248 Rome Lab., Griffiss AFB, NY.
FABRICATION OF PLZT/ITO GRATING FOR OPTICAL SWITCHING AND RECONFIGURABLE OPTICAL INTERCONNECT APPLICATIONS Final Report, Oct. 1991 - Sep. 1992
Joanne H. Maurice and Pierre J. Talbot Sep. 1994 23 p Limited Reproducibility: More than 20% of this document may be affected by microfiche quality
(AF Proj. 4600)
(AD-A286389; RL-TR-94-102) Avail: CASI HC A03

A two-dimensional opto-electronic diffraction grating based on PLZT ceramic material for optical switching and reconfigurable optical interconnect applications is demonstrated. Integratable chips are fabricated consisting of numerous fine interleaved transparent indium-tin oxide (ITO) electrodes on a polycrystalline PLZT ceramic substrate. The chips measure one centimeter square. The electrode features are scaled and measure from 12.5 micrometers to 100 micrometers. Reported here are chip material and fabrication details. DTIC

N95-22255# Air Force Inst. of Tech., Wright-Patterson AFB, OH. National Air Intelligence Center.
ELECTRO-OPTIC EFFECT IN THE PESO ACOUSTO-OPTIC MODULATOR
Renzhong Tai, Futun Lu, Shuzhong Yuan, Xin-An Guan, and Bing Li 9 Nov. 1994 15 p Transl. into ENGLISH from Wuli Xuebao (China), v. 41, no. 6, Jun. 1992 p 1012-1018
(AD-A286355; NAIC-ID(RS)T-0395-94) Avail: CASI HC A03/MF A01

With the theory of one-dimensional approximation, combined with the boundary conditions, an inhomogeneous electric field is derived from the fundamental equations of piezoelectric effect. This inhomogeneous electric field will lead to generation of electric grating, and high-order grating can also appear owing to coupling between electric grating and acoustic grating. Linear electro-optics effect in PESO modulator is helpful to the diffraction and modulation of the incident light beam. The experimental results verify our conclusions. Author (DTIC)

N95-20652# Deutsche Aerospace A.G., Munich (Germany). Military Aircraft Div.
OPTICAL BACKPLANE FOR MODULAR AVIONICS
R. Bogenberger and O. Krumpholz *In* AGARD, Advanced Packaging Concepts for Digital Avionics Oct. 1994 6 p (For primary document see N95-20631 06-06)
Copyright Avail: CASI HC A02/MF A03

N95-20654# Bell Telephone Labs., Inc., Whippany, NJ.
THE ROC OPTICAL CONNECTOR
Richard J. Pimpinella and J. Dennis Seals *In* AGARD, Advanced Packaging Concepts for Digital Avionics Oct. 1994 6 p (For primary document see N95-20631 06-06)
(Contract F33615-89-C-1036)
Copyright Avail: CASI HC A02/MF A03

75 PLASMA PHYSICS

Includes magnetohydrodynamics and plasma fusion.
For ionospheric plasmas see *46 Geophysics*. For space plasmas see *90 Astrophysics*.

N95-19977# Australian National Univ., Canberra (Australia). Plasma Research Lab.
COUPLED TEARING MODES IN PLASMAS WITH DIFFERENTIAL ROTATION
R. L. Dewar and M. Persson Aug. 1993 34 p
(DE94-631422; ANU-PRL-TP-93/01) Avail: CASI HC A03/MF A01 (US Sales Only)

The global asymptotic matching equations for multiple coupled resistive modes of arbitrary parity in a cylindrical plasma are derived. Three different variational principles are given for the outer region matching data, while the inner-region analysis features a careful treatment of the symmetry-breaking effect of a gradient in the equilibrium current for a zero-(beta) slab model. It is concluded that the usual constant-(psi) result remains valid and constrains the matrix matching formalism. The dispersion relation is compared with initial value calculations of a double tearing mode when there are small relative rotation velocities between the rational surfaces. In treating differential rotation within the asymptotic matching formalism, flow is ignored in the outer region and is assumed to affect the inner response solely through a Doppler shift. It is shown that the relative rotation can have a strong stabilizing effect by making all but one rational surface effectively ideal. DOE

N95-20029# Science Applications International Corp., San Diego, CA.
TRANSPORT AND DYNAMICS IN TOROIDAL FUSION SYSTEMS
D. D. Schnack May 1994 58 p
(Contract DE-FG03-91ER-54124)
(DE94-018653; SAIC-94/1098; DOE/ER-54124/1) Avail: CASI HC A04/MF A01

In this document the author describes an extension of the spatial gridding techniques to an MHD model suitable for the description of the dynamics of toroidal fusion devices. Since the dominant MHD modes in these devices have relatively long toroidal wavelength, the toroidal coordinate is approximated with finite Fourier series. The unstructured, triangular mesh is used to describe the details of the poloidal geometry. With some exceptions, the hydrodynamic variables are treated in a manner analogous to that used in CFD. These quantities (mass, energy, and momentum) are volume based densities that satisfy scalar or vector conservation laws. The electromagnetic variables (the magnetic flux density B and the electric current density J) are area based densities that satisfy pseudo-vector conservation laws, and have no counterpart in fluid dynamics. These variables are also constrained to remain solenoidal. These quantities are represented on the triangular mesh in a new manner that is an extension of that used on rectangular, structured meshes. In this work the author has chosen to solve the primitive MHD equations in order to make the resulting codes and techniques more generally applicable to problems beyond the narrow scope of tokamak plasmas. The temporal stiffness problems inherent in this description of tokamak dynamics that motivate the reduced MHD model are addressed here with the semi-implicit method of time integration. Finally, the author remarks that, while the present work deals strictly with the MHD equations, other volume based fluid descriptions, such as diffusive transport could easily be adapted to these techniques and coupled with the description of the electromagnetic field presented here. DOE

N95-20037# General Atomics Co., San Diego, CA.
TOWARD A DESIGN FOR THE ITER PLASMA SHAPE AND STABILITY CONTROL SYSTEM
D. A. Humphreys, J. A. Leuer, A. G. Kellman, S. W. Haney (Lawrence Livermore National Lab., Livermore, CA.), R. H. Bulmer (Lawrence Livermore National Lab., Livermore, CA.), L. D. Pearlstein (Lawrence Livermore National Lab., Livermore, CA.), and A. Portone (Japan Atomic Energy Research Inst., Naka, Japan.) Jul. 1994 9 p Presented at the 11th Topical

Meeting on the Technology of Fusion Energy, New Orleans, LA, 19-24 Jun. 1994
(Contracts DE-AC03-89ER-51114; W-7405-eng-48)
(DE94-017516; GA-A-21736; CONF-940630-40) Avail: CASI HC A02/MF A01

A design strategy for an integrated shaping and stability control algorithm for ITER is described. This strategy exploits the natural multivariable nature of the system so that all poloidal field coils are used to simultaneously control all regulated plasma shape and position parameters. A nonrigid, flux-conserving linearized plasma response model is derived using a variational procedure analogous to the ideal MHD Extended Energy Principle. Initial results are presented for the non-rigid plasma response model approach applied to an example DIII-D equilibrium. For this example, the nonrigid model is found to yield a higher passive growth rate than a rigid current-conserving plasma response model. Multivariable robust controller design methods are discussed and shown to be appropriate for the ITER shape control problem. DOE

N95-20038# General Atomics Co., San Diego, CA.
RECENT DIII-D RESULTS
P. I. Petersen Jul. 1994 9 p Presented at the 11th Topical Meeting on the Technology of Fusion Energy, New Orleans, LA, 19-24 Jun. 1994
(Contracts DE-AC03-89ER-51114; W-7405-eng-48; DE-AC05-84OR-21400)
(DE94-017519; GA-A-21743; CONF-940630-38) Avail: CASI HC A02/MF A01

This paper summarizes the recent D3-D experimental results and the development of the relevant hardware systems. The D3-D program focuses on divertor solutions for next generation tokamaks such as International Thermo-nuclear Experimental Reactor (ITER) and Tokamak Physics Experiment (TPX), and on developing configurations with enhanced confinement and stability properties that will lead to a more compact and economical fusion reactor. The D3-D program carries out this research in an integrated fashion. DOE

N95-20075# Sandia National Labs., Albuquerque, NM.
PARTICLE BEAM FUSION Progress Report, 1989
M. A. Sweeney, ed. Aug. 1994 235 p
(Contract DE-AC04-94AL-85000)
(DE95-000711; SAND-91-1556) Avail: CASI HC A11/MF A03

This report summarizes the progress on the pulsed power approach to inertial confinement fusion. In 1989, the authors achieved a proton focal intensity of 5 TW/sq cm on PBFA-2 in a 15-cm-radius applied magnetic-field (applied-B) ion diode. This is an improvement by a factor of 4 compared to previous PBFA-2 experiments. They completed development of the three-dimensional (3-D), electromagnetic, particle-in-cell code QUICKSILVER and obtained the first 3-D simulations of an applied-B ion diode. The simulations, together with analytic theory, suggest that control of electromagnetic instabilities could reduce ion divergence. In experiments using a lithium fluoride source, they delivered 26 kJ of lithium energy to the diode axis. Rutherford-scattered ion diagnostics have been developed and tested using a conical foil located inside the diode. They can now obtain energy density profiles by using range filters and recording ion images on nuclear track recording film. Timing uncertainties in power flow experiments on PBFA-2 have been reduced by a factor of 5. They are investigating three plasma opening switches that use magnetic fields to control and confine the injected plasma. These new switches provide better power flow than the standard plasma erosion switch. Advanced pulsed-power fusion drivers will require extraction-geometry applied-B ion diodes. During this reporting period, progress was made in evaluating the generation, transport, and focus of multiple ion beams in an extraction geometry and in assessing the probable damage to a target chamber first wall. DOE

N95-20112# Wisconsin Univ., Madison, WI. Dept. of Physics.
ANALYSIS METHODS FOR FAST IMPURITY ION DYNAMICS DATA
D. J. DenHartog, A. F. Almagri, S. C. Prager, and R. J. Fonck Aug. 1994 13 p Presented at the 10th Topical Conference on High-Temperature Plasma Diagnostics, Rochester, NY, 8-12 May 1994
(Contract DE-FG02-85ER-53198)
(DE95-000589; DOE/ER-53198/248; CONF-940552-32) Avail: CASI HC A03/MF A01

A high resolution spectrometer has been developed and used on the MST reversed-field pinch (RFP) to measure passively impurity ion temperatures and flow velocities with 10 (mu)s temporal resolution. Such measurements of MHD-scale fluctuations are particularly relevant in the RFP because the flow velocity fluctuation induced transport of current (the 'MHD dynamo') may produce the magnetic field reversal characteristic of an RFP. This instrument will also be used to measure rapid changes in the equilibrium flow velocity, such as occur during locking and H-mode transition. The precision of measurements made to date is less than 0.6 km/s. The authors are developing accurate analysis techniques appropriate to the reduction of this fast ion dynamics data. Moment analysis and curve-fitting routines have been evaluated for noise sensitivity and robustness. Also presented is an analysis method which correctly separates the flux-surface average of the correlated fluctuations in u and B from the fluctuations due to rigid shifts of the plasma column. DOE

N95-20113# Wisconsin Univ., Madison, WI. Dept. of Physics.
FLUCTUATIONS AND TRANSPORT IN THE REVERSED FIELD PINCH: CHARACTERIZATION AND REDUCTION
J. S. Sarff, A. F. Almagri, J. D. Callen, M. Cekic, B. E. Chapman, N. Crocker, D. J. DenHartog, E. Fernandez, G. Fiksel, and R. W. Harvey (General Atomics Co., San Diego, CA.) et al Sep. 1994 11 p Presented at the 15th International Conference on Plasma Physics and Controlled Nuclear Fusion Research, Seville, Spain, 26 Sep. - 1 Oct. 1994
(Contract DE-FG02-85ER-53198)
(DE95-000590; DOE/ER-53198/249; IAEA-CN-60/C-1-I-5; CONF-940933-4) Avail: CASI HC A03/MF A01

Reduction via current profile control of the low frequency, resonant, tearing mode fluctuations responsible for the stochastic magnetic field in the core of the RFP has been demonstrated in MST using auxiliary inductive current drive. In making this reduction, sawteeth are stabilized, and the energy confinement time doubles. To enhance and maintain current profile control and improved confinement, non-inductive current drive is required. Analytical and numerical studies indicate that electrostatic and RF current drive can stabilize the tearing fluctuations. Experiments to test such methods are in preparation on MST. In a second key area relating to RFP confinement, recent theoretical initiatives have found that, in the presence of tearing fluctuations, the growth rates and mode widths of short wavelength turbulence increases. If such turbulence governs transport at the edge of the RFP, then reduction of tearing modes may improve edge confinement as well. DOE

N95-20114# Wisconsin Univ., Madison, WI. Dept. of Physics.
MAGNETIC FLUCTUATION INDUCED TRANSPORT AND EDGE DYNAMO MEASUREMENTS IN THE MST REVERSED-FIELD PINCH
S. Hokin, G. Fiksel, H. Ji, M. Stoneking, A. Almagri, M. Cekic, B. E. Chapman, C.-S. Chiang, N. Crocker, and D. J. DenHartog et al Sep. 1994 11 p Presented at the 15th International Conference on Plasma Physics and Controlled Nuclear Fusion Research, Seville, Spain, 26 Sep. - 1 Oct. 1994
(Contract DE-FG02-85ER-53198)
(DE95-000591; DOE/ER-53198/250; IAEA-CN-60/A6/C-P-8; CONF-940933-3) Avail: CASI HC A03/MF A01

Probe measurements in MST indicate that RFP particle and energy loss is governed by magnetic fluctuations inside r/a = 0.8, with energy carried out convectively by superthermal electrons. The radial loss rate is lower than the Rechester-Rosenbluth level, presumably due to the establishment of a restraining ambipolar potential. Several aspects of these measurements contradict the Kinetic Dynamo Theory, while the MHD dynamo EMF is measured to be large enough to drive the edge current carried by these superthermal electrons. DOE

N95-20143# Sandia National Labs., Albuquerque, NM.
ALT-2 ARMOR TILE DESIGN FOR UPGRADED TEXTOR OPERATION
B. L. Newberry (Michigan Univ., Ann Arbor, MI.), R. T. McGrath, R. D. Watson, W. Kohlhaas (Kernforschungsanlage, Juelich, Germany.), and K. H. Finken (Kernforschungsanlage, Juelich, Germany.) 1994 16 p Presented at the ISFNT-3: 3rd International Symposium on Fusion Nuclear Technology, Los Angeles, CA, 27 Jun. - 1 Jul. 1994
(Contract DE-AC04-94AL-85000)
(DE94-015749; SAND-94-1769C; CONF-940664-21) Avail: CASI HC A03/MF A01

The upgrade of the TEXTOR tokamak at KFA Juelich was recently completed. This upgrade extended the TEXTOR pulse length from 5 seconds

to 10 seconds. The auxiliary heating was increased to a total of 8.0 MW through a combination of neutral beam injection and radio frequency heating. Originally, the inertially cooled armor tiles of the full toroidal belt Advanced Limiter Test-2 (ALT-2) were designed for a 5-second operation with total heating of 6.0 MW. The upgrade of TEXTOR will increase the energy deposited per pulse onto the ALT-2 by abo ut 300%. Consequently, the graphite armor tiles for the ALT-2 had to be redesigned to avoid excessively high graphite armor surface temperatures that would lead to unacceptable contamination of the plasma. This redesign took the form of two major changes in the ALT-2 armor tile geometry. The first design change was an increase of the armor tile thermal mass, primarily by increasing the radial thickness of each tile from 17 mm to 20 mm. This increase in the radial tile dimension reduces the overall pumping efficiency of the ALT-2 pump limiter by about 30%. The reduction in exhaust efficiency is unfortunate, but could be avoided only by active cooling of the ALT-2 armor tiles. The active cooling option was too complicated and expensive to be considered at this time. The second design change involved redefining the plasma facing surface of each armor tile in order to fully utilize the entire surface area. The incident charged particle heat flux was distributed uniformly over the armor tile surfaces by carefully matching the radial, poloidal and toroidal curvature of each tile to the plasma flow in the TEXTOR boundary layer. This geometry redefinition complicates the manufacturing of the armor tiles, but results in significant thermal performance gains. In addition to these geometry upgrades, several material options were analyzed and evaluated.
DOE

N95-20146# General Atomics Co., San Diego, CA.
FLUCTUATIONS IN HIGH BETA(SUB p) PLASMAS IN D3-D
T. A. Casper (Lawrence Livermore National Lab., Livermore, CA.), M. S. Chu, P. Gohil, W. W. Heidbrink (California Univ., Irvine, CA.), A. W. Hyatt, R. A. James (Lawrence Livermore National Lab., Livermore, CA.), R. A. Jong (Lawrence Livermore National Lab., Livermore, CA.), L. L. Lao, M. A. Makowski (Lawrence Livermore National Lab., Livermore, CA.), and W. H. Meyer (Lawrence Livermore National Lab., Livermore, CA.) et al Jul. 1994 4 p Presented at the European Conference on Controlled Fusion and Plasma Physics, Montpellier, France, 27 Jun. - 1 Jul. 1994 Submitted for publication
(Contracts DE-AC03-89ER-51114; W-7405-eng-48; GA Proj. 3466)
(DE94-017510; GA-A-21750; CONF-940635-10) Avail: CASI HC A01/MF A01

In our investigation of improved confinement in high poloidal beta (beta(sub p)= 2 to 4) advanced tokamak experiments, we observe that the internal MHD activity evolves from an m/n = 2/1 to a 3/1 structure coincident with q(sub o) rising above 2, and consistent with the GATO code stability analysis. The plasma eventually evolves to a quiescent state at which time the stored energy increases, mostly as a result of improved particle confinement. The bootstrap fraction rises to 80%. The measured plasma pressure profiles during this time are calculated to be stable to high-n ballooning modes consistent with operation of the core in the second stable regime. The sustained improvement in confinement is ultimately limited by our ability to control the toroidal current profile. DOE

N95-20189# Lawrence Livermore National Lab., Livermore, CA.
NATIONAL IGNITION FACILITY: EXPERIMENTAL PLAN
May 1994 26 p
(Contract W-7405-eng-48)
(DE94-016542; UCRL-ID-117344) Avail: CASI HC A03/MF A01

As part of the Conceptual Design Report (CDR) for the National Ignition Facility (NIF), scientists from Lawrence Livermore National Laboratory (LLNL), Los Alamos National Laboratory (LANL), Sandia National Laboratory (SNL), the University of Rochester's Laboratory for Laser Energetics (UR/LLE), and EG&G formed an NIF Target Diagnostics Working Group. The purpose of the Target Diagnostics Working Group is to prepare conceptual designs of target diagnostics for inclusion in the facility CDR and to determine how these specifications impact the CDR. To accomplish this, a subgroup has directed its efforts at constructing an approximate experimental plan for the ignition campaign of the NIF CDR. The results of this effort are contained in this document, the Experimental Plan for achieving fusion ignition in the NIF. This group initially concentrated on the flow-down requirements of the experimental campaign leading to ignition, which will dominate the initial efforts of the NIF. It is envisaged, however, that before ignition, there will be parallel campaigns supporting weapons physics, weapons effects, and other research. This plan was developed by analyzing the sequence of activities required to finally fire the laser at the level of power and precision necessary to achieve the conditions of an ignition hohlraum target, and to then use our experience in activating and running Nova experiments to estimate the rate of completing these activities.
DOE

N95-20190# Lawrence Livermore National Lab., Livermore, CA.
TARGET AREA ACQUISITION AND CONTROL SYSTEM SURVIVABILITY FOR THE NATIONAL IGNITION FACILITY
K. Hagans, P. Stathis, J. Wiedwald, and D. Campbell Jun. 1994 6 p
Presented at the 11th Topical Meeting on the Technology of Fusion Energy, New Orleans, LA, 19-24 Jun. 1994
(Contract W-7405-eng-48)
(DE94-016549; UCRL-JC-117382; CONF-940630-33) Avail: CASI HC A02/MF A01

The hardening of instruments to survive NIF target emission environments presents a significant challenge. Neutron flux is predicted to be as much as six orders of magnitude greater than the highest achieved neutron flux on NOVA. Not withstanding the high prompt radiation fields, the specifications for the instruments are demanding; requiring high resolution imaging and sub nanosecond transient measurements. We present an analysis of the sensitivity of the proposed NIF instrumentation design to EMP, X-rays, gamma rays, and neutrons. Major components assessed include fiber optic cable transport, high bandwidth cable and charge coupled detector (CCD) imaging systems. DOE

N95-20200# Australian National Univ., Canberra (Australia). Plasma Research Lab.
VARIATIONS OF HELICON WAVE INDUCED RADIAL PLASMA TRANSPORT IN DIFFERENT EXPERIMENTAL CONDITIONS
V. Petrzilka Aug. 1993 15 p
(DE94-631410; ANU-PRL-TP-93/02) Avail: CASI HC A03/MF A01 (US Sales Only)

Variations of the helicon wave induced radial plasma transport are presented in dependence on values of the plasma radius, magnetostatic field, plasma density, frequency of the helicon wave and on the ion charge. DOE

N95-20204# Instituto Tecnologico de Toluca, Toluca (Mexico).
THE CONTROL SYSTEM POSITION TO THE ELECTRIC PROBE IN THE TOKAMAK NOVILLO Ph.D. Thesis [CONTROL DE POSICION DE LA SONDA ELECTRICA EN EL TOKAMAK NOVILLO]
A. M. SanchezGarcia 1993 112 p In SPANISH
(DE94-629938; MFIS-mf-13922) Avail: CASI HC A06/MF A02 (US Sales Only)

An electric probe is used to determine the parameters of electronic temperatures, the electron density and the plasma potential in Tokamak machines. On this machine the electric probes are used only in the plasma edge due to the intensive flow of high energy particles. This is the region in which the plasma density and temperature are relatively low. This work shows the design and construction of an electro mechanic system which is used to control the position of the probe into the discharge chamber. This system is called 'The control system position to the electric probe in the tokamak Novillo'. This controller is a minimum system to rule a step motor by a logic sequence commutation. This is done by sliding the probe in a radial way with millimetric precision into the discharge chamber. To this purpose it is used as step motor, due to its principal characteristic as the control of the end element position without needing a feedback of the error signal. The system function consists of reading, through a board, the data corresponding to the position where it is wanted to place the probe; it also displays by a numeric indicator the position in which the probe is located (in an interval from 0 to 100 mm), and provides the logic sequence commutation for the step motor. The minimum system is consists of the microcontroller 8748-8 that gives precision control of the electric probe position in the Tokamak Novillo, by programming, associated circuits, amplification unit bi-phase unipolar and switching power (they supply the power to the control circuit and to the step motor too), avoiding the destruction of the electric probe. DOE

N95-20205# Oak Ridge National Lab., TN.

EXPERIMENTAL MEASUREMENTS OF ICRF AND EDGE PLASMA INTERACTIONS ON TORE SUPRA

J. H. Harris, C. E. Thomas, Jr., J. T. Hogan, G. R. Haste, S. Tobin, C. C. Klepper, B. Saoutic (European Atomic Energy Community, Saint Paul lez Durance, France.), B. Beaumont (European Atomic Energy Community, Saint Paul lez Durance, France.), A. Becoulet (European Atomic Energy Community, Saint Paul lez Durance, France.), and H. Kuus (European Atomic Energy Community, Saint Paul lez Durance, France.) 1994 4 p Presented at the European Conference on Controlled Fusion and Plasma Physics, Marseilles, France, 26 Jun. - 1 Jul. 1994
(Contract DE-AC05-84OR-21400)
(DE94-019154; CONF-940635-15) Avail: CASI HC A01/MF A01

Experiments to explore the interaction of Ion Cyclotron Range of Frequencies (ICRF) heating with the edge plasmas on the Tore Supra tokamak have been undertaken. The actively cooled, lateral protection (bumper limiters) on the three ICRF antennas in Tore Supra can experience overheating for power levels greater than 2 MW per antenna and pulse lengths greater than 2 seconds (depending on the power level) even when the antennas are operated in dipole mode. It appears that the local power fluxes on the lateral protection may exceed the nominally expected fluxes of 5 MW/m(sup 2). Concentrated heat fluxes can result in hot spots with temperatures greater than 1000 C and can result in damage to the carbon tiles that make up the armor on the lateral protection. Initial experiments with plasmas having I(sub p) = 0.8 - 1.6 MA, q(a) = 3 - 6, and P(sub RF) = 1 - 2 MW have been carried out to characterize the phenomena that could contribute to the overheating and develop the diagnostic tools to be used in more comprehensive studies. DOE

N95-20219# Lawrence Livermore National Lab., Livermore, CA.

TARGET AREA STRUCTURAL SUPPORT SYSTEMS DESIGN TO ACHIEVE THE MICRON-LEVEL STABILITY REQUIREMENT OF THE NATIONAL IGNITION FACILITY (NIF)

D. S. Ng, V. P. Karpenko, and R. Wavrik (Sandia National Labs., Albuquerque, NM.) Jun. 1994 5 p Presented at the 11th Topical Meeting on the Technology of Fusion Energy, New Orleans, LA, 19-23 Jul. 1994
(Contract W-7405-eng-48)
(DE94-017696; UCRL-JC-115586; CONF-9407118-1) Avail: CASI HC A01/MF A01

The Target Area Structural Support (TASS) systems are designed to provide an optically stable support for the target area systems and personnel access platforms for the 192 laser beam configuration. The conceptual design of the TASS systems was an optimum configuration selected from three designs on which performance studies were conducted. The supporting bases for the design selection were the analytical results, operation, and cost effective. DOE

N95-20232# HY-Tech Research Corp., Radford, VA.

SOFT X-RAY INNOVATIVE SOURCE DEVELOPMENT PROGRAM Technical Report, 24 Mar. 1989 - 12 Jul. 1993

Edward J. Yadlowsky, John J. Moschella, Robert C. Hazelton, and Thomas B. Settersten 1 Nov. 1994 96 p
(Contract DNA001-89-C-0029)
(AD-A286380; Rept-015FR; DNA-TR-93-190) Avail: CASI HC A05/MF A01

Recent models predict that individual wires in an array will form heterogeneous current channels when exploded by a current pulse. The resulting nonuniform magnetic forces will cause the outer current carrying corona to implode ahead of the core, in contrast to earlier models where the uniform current channel implodes as a unit. Laser based absorption and holographic techniques have been used to study the explosion characteristics of 33 micrometers C and 25 micrometers Al wire loads and the implosion dynamics of two wire Al loads on a 300 kA generator. X-ray techniques have been used to study the implosion and radiation characteristics of Mg coated Al wire arrays on the 4 MA Double Eagle generator. The high resolution laser diagnostics reveal a coronal plasma that implodes far in advance of the core in the two wire experiments. This preemptive implosion of the corona is exacerbated when a plasma opening switch (POS) shortens the current pulse. The Mg coated Al wire load experiments indicate that only the outer 30-50% of the load mass implodes to radiate in the K-shell. The load straggling implies a softened implosion and reduced radiation efficiency. The results demonstrate the importance of the early time current distribution on the implosion and radiation characteristics of the load and underscore the need for adequate modeling to scale present results up to larger machines. DTIC

N95-20279# General Atomics Co., San Diego, CA.

A METHOD FOR MEASURING THE INDUCTIVE ELECTRIC FIELD PROFILE AND NONINDUCTIVE CURRENT PROFILES ON D3-D

C. B. Forest, T. C. Luce, P. A. Politzer, L. L. Lao, K. Kupfer (Oak Ridge Inst. for Science and Education, TN.), and D. Wroblewski (Lawrence Livermore National Lab., Livermore, CA.) Jul. 1994 4 p Presented at the 21st European Conference on Controlled Fusion and Plasma Physics, Marseilles, France, 26 Jun. - 1 Jul. 1994 Submitted for publication
(Contracts DE-AC03-89ER-51114; W-7405-eng-48; GA Proj. 3466)
(DE94-016683; GA-A-21742; CONF-940635-7) Avail: CASI HC A01/MF A01

A new technique for determining the parallel electric field profile and noninductive current profile in tokamak plasmas has been developed and applied to two DIII-D tokamak discharges. Central to this technique is the determination of the current density profile, J(rho), and poloidal flux, psi(rho), from equilibrium reconstructions. From time sequences of the reconstructions, the flux surface averaged, parallel electric field can be estimated from appropriate derivatives of the poloidal flux. With a model for the conductivity and measurements of T(sub e) and Z(sub eff), the noninductive fraction of the current can be determined. Such a technique gives the possibility of measuring directly the bootstrap current profile and the noninductively driven current from auxiliary heating such as neutral beam injection or fast wave current drive. Furthermore, if the noninductively driven current is small or if the noninductive current profile is assumed to be known, this measurement provides a local test of the conductivity model under various conditions. DOE

N95-20283# Lawrence Livermore National Lab., Livermore, CA.

24TH ANNUAL ANOMALOUS ABSORPTION CONFERENCE Abstracts Only

1994 157 p Conference held in Pacific Grove, CA, 5-10 Jun. 1994
(Contract W-7405-eng-48)
(DE94-016457; CONF-9406152-Absts) Avail: CASI HC A08/MF A02

This report contains abstracts on topics in the following areas: parametric instabilities; hohlraum physics; laser plasma physics with short pulses; and Rayleigh-Taylor instability and hydrodynamics. DOE

N95-20285# General Atomics Co., San Diego, CA.

RECENT RESULTS FROM FAST WAVE CURRENT DRIVE EXPERIMENTS ON DIII-D

R. I. Pinsker, S. C. Chiu, and F. W. Baity (Oak Ridge National Lab., TN.) Jul. 1994 4 p Presented at the European Conference on Controlled Fusion and Plasma Physics, Marseilles, France, 26 Jun. - 1 Jul. 1994
(Contracts DE-AC03-89ER-51114; DE-AC05-84OR-21400; DE-AC02-78ET-51013)
(DE94-016718; GA-A-21759; CONF-940635-8) Avail: CASI HC A01/MF A01

The goal of the ongoing DIII-D Fast Wave Current Drive (FWCD) experiments is to demonstrate fully noninductive sustainment of the tokamak discharge by direct electron absorption of the fast magnetosonic wave. Control of the current density profile obtained by combining FWCD with other noninductive current drive techniques (neutral beam injection, electron cyclotron current drive, bootstrap current) will permit extension to long pulse of the improved confinement regimes that have been obtained transiently in DIII-D by use of current and elongation ramps. DOE

N95-20315# Lawrence Livermore National Lab., Livermore, CA.

A COMPARISON OF KINETIC AND MULTIFLUID SIMULATIONS OF LASER-PRODUCED COLLIDING PLASMAS

P. W. Rambo and R. J. Procassini Sep. 1994 6 p Presented at the 15th International Conference on the Numerical Simulation of Plasmas, Valley Forge, PA, 7-9 Sep. 1994
(Contract W-7405-eng-48)
(DE94-016447; UCRL-JC-117498; CONF-9409105-2) Avail: CASI HC A02/MF A01

The collision and subsequent interaction of counter-streaming plasmas occurs in several areas of laser-plasma research including double foil targets for x ray lasers and the plasma blow-off inside ICF hohlraums. Because a single fluid model allows for only one value of the flow velocity at any one spatial location, interpenetration of the plamas is not allowed resulting in immediate stagnation with complete conversion of the ion-streaming kinetic energy to thermal energy. Multifluid models have been developed which employ multiple ion fluid species that interact through the self-consistent electrostatic field and collisional coupling. Because they are approximations to a kinetic situation, the form of these coupling coefficients is not unique, with various workers using differing approximations. More recently, Larroche has implemented a finite difference approach to the ion Fokker-Planck equation while Jones and co-workers have performed two-dimensional simulations of colliding plasmas using a particle-in-cell code with a new collisional model. Our kinetic modeling also makes use of particle in cell (PIC) techniques with Monte Carlo (MC) particle-particle collisions algorithm that is equivalent to the Fokker-Planck collision operator. We have made direct comparison of this MC-PIC model to multifluid simulations on both simple slowing-down and equilibration problems as well as problems characteristic of laser generated colliding plasmas. These comparisons have established the validity of the multifluid model as well as aided in the development of the kinetic capability for more challenging geometries. DOE

N95-20318# Lawrence Livermore National Lab., Livermore, CA.
NUMERICAL MODELING OF A SMALL RECIRCULATING INDUCTION ACCELERATOR FOR HEAVY-ION FUSION
W. M. Sharp, J. J. Barnard, A. Friedman, D. P. Grote, S. M. Lund, M. A. Newton, T. J. Fessenden (California Univ., Berkeley, CA.), and S. S. Yu (California Univ., Berkeley, CA.) 24 Jun. 1994 5 p Presented at the 4th European Particle Accelerator Conference, London, England, 27 Jun. - 1 Jul. 1994
(Contract W-7405-eng-48)
(DE94-018549; UCRL-JC-115555; CONF-940618-79) Avail: CASI HC A01/MF A01

A series of small-scale experiments has been proposed to study critical physics issues of a circular induction accelerator for heavy-ion fusion. Because the beam dynamics will be dominated by space charge, the experiments require careful design of the lattice and acceleration schedule. A hierarchy of codes has been developed for modeling the experiments at different levels of detail. The codes are discussed briefly, and examples of the output are presented. DOE

N95-20334# General Atomics Co., San Diego, CA.
HELIUM EXHAUST STUDIES IN THE D3-D TOKAMAK
M. R. Wade (Oak Ridge National Lab., TN.), J. T. Hogan (Oak Ridge National Lab., TN.), D. L. Hillis (Oak Ridge National Lab., TN.), M. A. Mahdavi, R. Maingi (Oak Ridge National Lab., TN.), W. P. West, N. H. Brooks, K. H. Burrell, D. F. Finkenthal (California Univ., Berkeley, CA.), and R. J. Groebner et al Jul. 1994 16 p Presented at the 11th International Conference on Plasma Surface Interactions in Controlled Fusion Devices, Mito, Japan, 23-27 May 1994
(Contracts DE-AC03-89ER-51114; DE-AC05-84OR-21400)
(DE94-016682; GA-A-21702; CONF-940580-15) Avail: CASI HC A03/MF A01

Significant exhaust of thermal helium in a diverted, H-mode deuterium plasma has been demonstrated for the first time on the DIII-D tokamak using an in-vessel cryopump conditioned with an argon frost. The helium, introduced via gas puffing, is observed to reach the plasma core and then is readily removed from the plasma with a time constant of (approximately) 8-15 energy confinement times. Detailed analysis of the helium profile evolution indicates that the exhaust rate is limited by the exhaust efficiency of the pump (approximately 5%) and not by the intrinsic helium transport properties of the plasma. Additional studies focusing on the recycling properties of helium relative to deuterium in the divertor region indicate some dependence of the helium concentration in the divertor pumping plenum on the divertor outer strike-point (OSP) position in Ohmic discharges. However, the helium concentration in the plenum appears to have little dependence on OSP position in beam-heated, ELMing H-mode discharges. DOE

N95-20345# George Washington Univ., Washington, DC. Office of Sponsored Research.
NEW HIGH TEMPERATURE PLASMAS AND SAMPLE INTRODUCTION SYSTEMS FOR ANALYTICAL ATOMIC EMISSION AND MASS SPECTROMETRY
A. Montaser 1994 9 p
(Contract DE-FG02-93ER-14320)
(DE94-018580; DOE/ER-14320/2) Avail: CASI HC A02/MF A01

This research follows a multifaceted approach, from theory to practice, to the investigation and development of novel helium plasmas, sample introduction systems, and diagnostic techniques for atomic and mass spectrometries. During the period January 1994 - December 1994, four major sets of challenging research programs were addressed that each included a number of discrete but complementary projects: (1) The first program is concerned with fundamental and analytical investigations of novel atmospheric-pressure helium inductively coupled plasmas (He ICPS) that are suitable for the atomization-excitation-ionization of elements, especially those possessing high excitation and ionization energies, for the purpose of enhancing sensitivity and selectivity of analytical measurements. (2) The second program includes simulation and computer modeling of He ICPS. The aim is to ease the hunt for new helium plasmas by predicting their structure and fundamental and analytical properties, without incurring the enormous cost for extensive experimental studies. (3) The third program involves spectroscopic imaging and diagnostic studies of plasma discharges to instantly visualize their prevailing structures, to quantify key fundamental properties, and to verify predictions by mathematical models. (4) The fourth program entails investigation of new, low-cost sample introduction systems that consume micro- to nanoliter quantity of sample solution in plasma spectrometries. A portion of this research involves development and applications of novel diagnostic techniques suitable for probing key fundamental properties of aerosol prior to and after injection into high-temperature plasmas. These efforts, still in progress, collectively offer promise of solving singularly difficult analytical problems that either exist now or are likely to arise in the future in the various fields of energy generation, environmental pollution, material science, biomedicine and nutrition. DOE

N95-20348# Wisconsin Univ., Madison, WI.
[DESIGN AND CONSTRUCTION OF THE HSX EXPERIMENT] Progress Report
1 May 1994 7 p
(Contract DE-FG02-93ER-54222)
(DE94-018657; DOE/ER-54222/1) Avail: CASI HC A02/MF A01

Brief statements on the progress of the design and construction of the HSX experiment are reported. Topics covered include the modular and auxiliary coil systems, the coil support structure, vacuum vessel, the ECH system, the magnet power supply and site. The proposed budget for Year 2 (August 1, 1994 through July 31, 1995) is presented. The effects of a flat funding profile (based on Year 2 budget level of $1137K) on out-years and the HSX project schedule are discussed. The stretching out of the program to accommodate the reduced funding profile should result in only a slight delay in HSX operations. DOE

N95-20362# Lawrence Livermore National Lab., Livermore, CA.
ION TEMPERATURE MEASUREMENT OF INDIRECTLY-DRIVEN IMPLOSIONS USING A GEOMETRY-COMPENSATED NEUTRON TIME-OF-FLIGHT DETECTOR
T. J. Murphy, R. A. Lerche, C. Bennett, and G. Howe May 1994 15 p Presented at the 10th Topical Conference on High-Temperature Plasma Diagnostics, Rochester, NY, 8-12 May 1994
(Contract W-7405-eng-48)
(DE94-016967; UCRL-JC-116199; CONF-940552-23) Avail: CASI HC A03/MF A01

A geometry-compensated neutron time-of-flight detector has been constructed and used on Nova to measure ion temperatures from indirectly-driven implosions with yields between 2.5 and 5 x 10(exp 9) DD neutrons. The detector, which has an estimated response time of 250 ps, was located 150 cm from the targets. Due to the long decay time of the scintillator, the time-of-flight signal must be unfolded from the measured detector signal. Several methods for determining the width of the neutron energy spectrum from the data have been developed and give similar results. Scattered x rays continue to be a problem for low yield shots, but should be brought under control with adequate shielding. DOE

N95-20363# Lawrence Livermore National Lab., Livermore, CA.
CHARACTERIZATION OF NOVA PLASMAS USING AN X-RAY SPECTROMETER WITH TEMPORAL AND SPATIAL RESOLUTION
C. A. Back, R. L. Kauffman, P. Bell, and J. D. Kilkenny May 1994 13 p Presented at the 10th Topical Conference on High-Temperature Plasma Diagnostics, Rochester, NY, 8-12 May 1994
(Contract W-7405-eng-48)
(DE94-016970; UCRL-JC-116211; CONF-940552-22) Avail: CASI HC A03/MF A01

Spectroscopic diagnostics have great potential to obtain high temperature measurements of plasmas created in ICF targets. The plasmas may be over 1 mm in size and therefore, one of the first steps in making accurate spectroscopic measurements has been to improve the resolution of the instrument. A spectrograph is now available for Nova experiments which takes advantage of gated technology by coupling a Bragg crystal to a microchannel plate that can record data over a 250 ps time frame. The crystal disperses the x-rays, while slits add the ability to image the plasmas in the perpendicular direction. The characteristics of this diagnostic, TSPEC, will be evaluated for laser-produced plasmas. Recent data will be presented from colliding plasmas and large-scale hohlraums which indicate that imaging can greatly enhance the ability to diagnose these plasmas. DOE

N95-20402# General Atomics Co., San Diego, CA.
A NEW ALPHA PARTICLE DIAGNOSTIC USING KNOCK-ON ION TAILS
R. K. Fisher, P. B. Parks, J. M. McChesney, and M. N. Rosenbluth (California Univ., San Diego, CA.) Jun. 1994 14 p Presented at the 10th Topical Conference on High-Temperature Plasma Diagnostics, Rochester, NY, 8-12 May 1994
(Contracts DE-FG03-92ER-54150; DE-AC03-89ER-51114)
(DE94-015856; GA-A-21715; CONF-940552-16) Avail: CASI HC A03/MF A01

We propose a new method of measuring the fast confined ct-particle distribution in a reacting plasma. The presence of ct-particles in a D-T plasma will create a high energy tail on the deuterium and tritium ion energy distributions. A 3.5 MeV alpha can transfer 3.4 MeV to a tritium ion in a single elastic scattering interaction. Calculations of the size of these knock-on tails in tokamaks such as TFTR, JET, and ITER show that it may be possible to measure these tails and provide information on the fast confined alphas. The knock-on tail ions will produce D-T neutrons with energies up to 20.7 MeV, so that D-T neutron spectroscopy can be used to monitor the alpha population. Neutron spectroscopy looks especially attractive for ITER. A collimated array of threshold neutron activation detectors could be used to deduce the confined alpha density profile. Tests of this diagnostic can also be done on TFTR and JET. Existing high energy neutral particle analyzers may allow observation of the ion tails directly via passive and/or active charge exchange. DOE

N95-20411 Ohio State Univ., Columbus, OH. Dept. of Mechanical Engineering.
PLASMA CHEMISTRY OF VIBRATIONALLY NONEQUILIBRIUM MOLECULES Final Report, 9 Jul. 1990 - 8 Jul. 1993
J. W. Rich Nov. 1993 448 p Limited Reproducibility: More than 20% of this document may be affected by microfiche quality
(Contract F33615-90-C-2039)
(AD-A279630; WL-TR-93-2116) Avail: Issuing Activity (Defense Technical Information Center (DTIC))

The present report describes experimental and analytical studies of energy transfer and chemical reaction in diatomic and small polyatomic gases under conditions of extreme disequilibrium of the vibrational modes. Primary emphasis is on collision-dominated environments with relatively low translational/rotational mode temperatures, which are characteristic of a variety of gas discharges, plasma chemical reactors and high enthalpy supersonic gas dynamic expansions. Some additional work has also been directed to the complementary environment in which the translational/rotational mode temperatures are high, and the vibrational mode energy content is initially low. This latter environment is characteristic of strong shock waves in gases, such as occurs during planetary entry of hypersonic aerospace vehicles. The report details vibration-translation (V-T), vibration-electronic (V-E), associative ionization, and dissociation processes in CO and NO. There are some data and rate models for related diatomic and small polyatomic species. Emphasis is placed on energy transfer processes involving high quantum states. DTIC

N95-20425 Center for Mathematics and Computer Science, Amsterdam (Netherlands). Dept. of Numerical Mathematics.
APPROXIMATE RIEMANN SOLVER FOR MAGNETOHYDRODYNAMICS (THAT WORKS IN MORE THAN ONE DIMENSION)
K. G. Powell Mar. 1994 15 p
(PB95-135802; CWI-NM-R9407) Copyright Avail: Issuing Activity (National Technical Information Service (NTIS))

An approximate Riemann solver is developed for the governing equations of ideal magnetohydrodynamics (MHD). The Riemann solver has an eight-wave structure, where seven of the waves are those used in previous work on upwind schemes for MHD, and the eighth wave is related to the divergence of the magnetic field. The structure of the eighth wave is not immediately obvious from the governing equations as they are usually written, but arises from a modification of the equations that is presented in this paper. The addition of the eighth wave allows multi-dimensional MHD problems to be solved without the use of staggered grids or a projection scheme, one or the other of which was necessary in previous work on upwind schemes for MHD. A test problem made up of a shock tube with rotated initial conditions is solved to show that the two-dimensional code yields answers consistent with the one-dimensional methods developed previously. NTIS

N95-20437# Texas Univ., Austin, TX. Inst. for Fusion Studies.
HYBRID MODEL IN GENERAL GEOMETRY
M. Yagi (Japan Atomic Energy Research Inst., Ibaraki, Japan.), T. Tajima, and M. J. Lebrun Sep. 1994 24 p
(Contract DE-FG05-80ET-53088)
(DE95-002614; DOE/ET-53088/667; IFSR-667) Avail: CASI HC A03/MF A01

We propose hybrid model equations in toroidal (or more general) geometry for magnetically confined plasmas. This is suitable for low frequency toroidal modes, for example, the trapped electron and current diffusive ballooning instabilities. This model consists of fluid ions and drift kinetic electrons. We discuss the numerical algorithm of these model equations. The linear dispersion relation of this model equations that defines the requirements of the model for describing these modes is also discussed. DOE

N95-20445# General Atomics Co., San Diego, CA.
PLASMA SHAPE EXPERIMENTS FOR AN OPTIMIZED TOKAMAK
A. W. Hyatt, T. H. Osborne, and E. A. Lazarus (Oak Ridge National Lab., TN.) Jul. 1994 4 p Presented at the European Conference on Controlled Fusion and Plasma Physics, Marseilles, France, 26 Jun. - 1 Jul. 1994
(Contracts DE-AC03-89ER-51114; DE-AC05-84OR-21400)
(DE94-017508; GA-A-21761; CONF-940635-11) Avail: CASI HC A01/MF A01

In this paper we present results from recent experiments at DIII-D which measured the plasma stability and confinement performance product, beta(tau)(sub E), in one previously studied and three new plasma shapes. One important goal of these experiments was to identify performance vs. shape trends which would identify a shape compatible with both high performance and the planned effort to decrease the power flux to the divertor floor using a closed 'slot' divertor geometry. The closed divertor hardware must be designed for a reduced set of plasma shapes, so care must be taken to choose the shape that optimizes beta(tau)(sub E) and divertor performance. The four shapes studied form a matrix of moderate and high elongations (kappa congruent to 1.8 and 2.1) and low and high triangularities (delta congruent to 0.3 and 0.9). All configurations were double-null diverted (DND), held fixed during a shot, with neutral beam heating. The shapes span a range of X-point locations compatible with the envisioned closed divertor. We find that from shape to shape, a shot's transient normalized performance, beta(sub N)H, where beta(sub N) is equivalent to beta/(I(sup p)/aB(sub T)) and H is equivalent to tau(sub E)/tau(sub E)(sup ITER-89P), increases strongly with triangularity, but depends only weakly on elongation. However, the normalized performance during quasi stationary ELMing H-mode, to which these discharges eventually relax, is insensitive to both triangularity and elongation. The moderate elongation, high triangularity DND shape is shown to be near optimum for future studies on DIII-D. DOE

N95-20446# General Atomics Co., San Diego, CA.
WALL STABILIZATION EFFECTS IN D3-D HIGH BETA DISCHARGES
E. J. Strait, T. S. Taylor, A. D. Turnbull, J. R. Ferron, L. L. Lao, S. J. Thompson, B. Rice (Lawrence Livermore National Lab., Livermore, CA.), D. Wroblewski (Lawrence Livermore National Lab., Livermore, CA.), and O. Sauter (Centre de Recherches en Physique des Plasmas, Lausanne, Switzerland.) Jul. 1994 4 p Presented at the European Conference on Controlled Fusion and Plasma Physics, Marseilles, France, 26 Jun. - 1 Jul. 1994
(Contracts DE-AC03-89ER-51114; W-7405-eng-48)
(DE94-017509; GA-A-21754; CONF-940635-9) Avail: CASI HC A01/MF A01

Recent high beta discharges in DIII-D, reaching values up to beta = 12.5%, demonstrate that a resistive wall can stabilize low-n MHD modes in a rotating plasma. The maximum beta values reached in discharges with broad current profiles (internal inductance ell(sub i) approximately equal to 0.7) are up to 40% greater than the limit predicted by ideal MHD stability calculations in the absence of a wall, but are consistent with predicted limits assuming a perfectly conducting wall at the position of the vacuum vessel. This wall stabilization is observed for time scales long compared with the resistive penetration time of the wall. Plasma rotation is essential to the stabilization, and instabilities with characteristics of the predicted 'resistive wall' mode are observed only when the rotation velocity approaches zero at the mode rational surface. DOE

N95-20568# General Atomics Co., San Diego, CA.
POWER BALANCE IN D3-D DURING SINGLE-NULL ELMing H-MODE PLASMAS
A. W. Leonard, C. J. Lasnier (Lawrence Livermore National Lab., Livermore, CA.), and J. W. Cuthbertson (Sandia National Labs., Albuquerque, NM.) Jul. 1994 16 p Presented at the 11th International Conference on Plasma Surface Interactions in Controlled Fusion Devices, Mito, Japan, 23-27 May 1994
(Contracts DE-AC03-89ER-51114; DE-AC04-76DP-00789; W-7405-eng-48)
(DE94-016680; GA-A-21693; CONF-940580-13) Avail: CASI HC A03/MF A01

We account for greater than or equal to 85% of the injected power in DIII-D during single-null diverted ELMing H-mode discharges. Core plasma radiation accounts for less than or equal to 18% with the rest flowing through the scrape-off layer to the inboard and outboard divertors. The total power roughly splits in an in:out ratio of 1:1.3. Of the power entering the outboard divertor 75% leaves as direct heat flux to the divertor target plates with the rest in the form of radiation. In the inboard divertor, however, 75% of the power leaves as radiation with the rest as divertor target plate heat flux and charge exchange losses. The in:out ratio remains constant over a range of injected power and plasma current and even as divertor conditions change due to gas puffing. DOE

N95-20571# General Atomics Co., San Diego, CA.
ENHANCED SCRAPE-OFF LAYER PLASMA IN D3-D DOUBLE-NULL DISCHARGES
J. G. Watkins (Sandia National Labs., Albuquerque, NM.), R. A. Jong (Lawrence Livermore National Lab., Livermore, CA.), and R. A. Moyer (California Univ., Los Angeles, CA.) Jul. 1994 14 p Presented at the 11th International Conference on Plasma Surface Interactions in Controlled Fusion Devices, Mito, Japan, 23-27 May 1994
(Contracts DE-AC03-89ER-51114; DE-FG03-89ER-51121; DE-AC04-94AL-85000; W-7405-eng-48)
(DE94-017977; GA-A-21708; CONF-940580-18) Avail: CASI HC A03/MF A01

In this paper, the authors examine a denser and broader scrape-off layer (SOL) plasma, first seen in VH mode, in the D3-D tokamak. The enhanced SOL appears in many types of double-null (DN) discharges and is not a property of VH-mode only. The DN enhanced SOL density and temperature profiles exhibit a 5-6 cm broad profile outside the separatrix. For DN and single-null (SN) boundary geometry with similar core plasma conditions, the enhanced SOL is only observed in high triangularity discharges. The origin of the enhanced SOL is, however, not yet understood. DOE

N95-20675# Lawrence Livermore National Lab., Livermore, CA.
HYDRODYNAMIC INSTABILITIES IN INERTIAL FUSION
N. M. Hoffman 1994 20 p Presented at the 45th Scottish Universities Summer School in Physics, Fife, Scotland, 7-20 Aug. 1994
(Contract W-7405-eng-36)
(DE94-018079; LA-UR-94-2684; CONF-9408127-2) Avail: CASI HC A03/MF A01

This report discusses topics on hydrodynamics instabilities in inertial confinement: (1) linear analysis of Rayleigh-Taylor instability; (2) ablation-surface instability; (3) bubble rise in late-stage Rayleigh-Taylor instability; and (4) saturation and multimode interactions in intermediate-stage Rayleigh-Taylor instability. DOE

N95-20681# Texas Univ., Austin, TX. Fusion Research Center.
A PORTABLE AND INDEPENDENT EDGE FLUCTUATION DIAGNOSTIC
H. Tsui and A. Wootton 1994 18 p
(Contract DE-FG05-89ER-53295)
(DE94-018254; DOE/ER-53295/T1) Avail: CASI HC A03/MF A01

A compact self contained portable probe system has been designed and developed to diagnose the edge plasma of devices of different sizes and configurations. The system measures both the mean and the fluctuation quantities of density, temperature and potential from a standardized Langmuir probe array using a fast reciprocating probe drive. It can also be used for other fluctuation diagnostics, such as magnetic probes. The data acquisition and analysis is performed on a Macintosh IIfx which provides a user-friendly environment. The results obtained by the signal processing routines are stored in a tabloid format to allow comparative studies. The resulting database is a core part of the portable signal analysis system. To date measurements have been performed on the stellarator ATF, the reversed field pinch ZT40(M), and the tokamaks TEXT, Versator, Phaedrus-T and TFTR. The data are presently being analyzed and the results collected into the database for the purpose of edge turbulence and transport studies. Existing published data are also being included. The edge database, an output of this project, will provide readily available information for other experimental groups to compare their results with, and for theoretical groups to validate (or otherwise) the predictions of their models. DOE

N95-20683# National Inst. for Fusion Science, Nagoya (Japan).
CURRENT DIFFUSIVE BALLOONING MODE IN SECOND STABILITY REGION OF TOKAMAKS
M. Yagi (Japan Atomic Energy Research Inst., Naka, Japan.), K. Itoh, S. Itoh, A. Fukuyama, and M. Azumi Sep. 1993 20 p
(DE94-770690; NIFS-246) Avail: CASI HC A03/MF A01

Stability of the current diffusive ballooning mode in tokamaks with high toroidal mode number is analyzed in the region of second-stability against the ideal magnetohydrodynamic mode. It is found that the growth rate of the current diffusive ballooning mode is decreased by the reduction of the geodesic curvature driving force. The reduction of thermal conductivity in the limit of very weak shear or negative shear in comparison with standard shear is also shown. DOE

N95-20684# Japan Atomic Energy Research Inst., Tokyo (Japan).
SIMULATION OF TEARING MODE STABILIZATION BY USING ECH
Gen-Ichi Kurita (Japan Atomic Energy Research Inst., Naka, Japan.), Takashi Tuda, Masafumi Azumi, and Tatsuoki Takeda Nov. 1993 39 p
(DE94-770700; JAERI-M-93-224) Avail: CASI HC A03/MF A01

Nonlinear simulations based on the reduced set of resistive MHD equations with the transport equation of electron temperature are carried out to investigate the effect of electron temperature perturbation induced by local heating of ECH on a tearing mode activity. Effect of poloidal plasma rotation is also considered in the simulations. It is shown that the local heating can suppress low-m tearing mode instability when O-point of the rotating magnetic island is effectively heated. Large parallel heat conduction causes the radially extending heat deposition profile for small width of magnetic island and magnitude of parallel heat conduction determines the heat power necessary for complete stabilization of the tearing mode. DOE

N95-20686# National Inst. for Fusion Science, Nagoya (Japan).
CHAOTIC PHENOMENA IN PLASMA 3
Y. Kawai (Kyushu Univ., Fukuoka, Japan.) Oct. 1993 129 p In

ENGLISH and JAPANESE
(DE94-770765; NIFS-Memo-12) Avail: CASI HC A07/MF A02

To review the present status of the research on plasma chaos, a working group was organized in 1990 as a collaboration research of National Institute for Fusion Science and ended on March 1993. This is the report on the activity which contains both experimental and theoretical works. DOE

N95-20813# Lawrence Livermore National Lab., Livermore, CA.
OBSERVATION OF STRONG EMISSION FROM NeIX AND NeX TRANSITIONS IN A LASER-DRIVEN PLASMA
John K. Crane, Todd Ditmire, Hoang Nguyen, and Michael D. Perry Jul. 1994 7 p Presented at the 4th International Colloquium on X-ray Lasers, Williamsburg, VA, 16-20 May 1994
(Contract W-7405-eng-48)
(DE95-002265; UCRL-JC-116774; CONF-940592-8) Avail: CASI HC A02/MF A01

The authors observe strong emission from the 1s(exp 2)-1snp Rydberg series in Helium-like neon and from the Lyman-(alpha) transition in Helium -like neon. These emissions are observed when 1.05 micrometers light from a 650 femtosecond laser is focused into the dense, localized output of a pulsed, supersonic nozzle. The maximum focal irradiance of the laser was measured at full power in a vacuum to be 2 x 10(exp 18) W/sq cm. Although emissions from lower charge states such as Ne6(+) and Ne7(+) closely follow rates predicted by tunneling theory, emissions from Ne8(+) and Ne9(+) are observed at irradiances two order of magnitude below tunneling theory estimates (e.g. the He-(alpha) line appears at 2 x 10(exp 17) W/sq cm). They discuss the origins of these anomalously high charge states and the implications to recombination-pumped x rays lasers. DOE

N95-20987# Japan Atomic Energy Research Inst., Tokyo (Japan).
IDEAL MAGNETOHYDRODYNAMIC STABILITIES IN JT-60 AND D3-D TOKAMAK PLASMAS
Takahisa Ozeki (Japan Atomic Energy Research Inst., Naka, Japan.) Oct. 1993 226 p
(DE94-770684; JAERI-M-93-184) Avail: CASI HC A11/MF A03

Magnetohydrodynamic (MHD) instabilities of plasmas with a good (enhanced) energy confinement, obtained in the H-mode or after pellet injection in JT-60 and DIII-D tokamaks, are investigated. In enhanced-confinement plasmas, many kinds of MHD instabilities occurred and they inhibit further improvement. In the present thesis, therefore, the mechanism of MHD stability is investigated by computational analysis, and ways to further improve the confinement by suppression of MHD instabilities are discussed. DOE

N95-20988# National Inst. for Fusion Science, Nagoya (Japan).
ION HEAT PULSE AFTER SAWTOOTH CRASH IN THE JFT-2M TOKAMAK
Y. Miura (Japan Atomic Energy Research Inst., Tokai, Japan.), F. Okano (Japan Atomic Energy Research Inst., Tokai, Japan.), N. Suzuki (Japan Atomic Energy Research Inst., Tokai, Japan.), M. Mori (Japan Atomic Energy Research Inst., Tokai, Japan.), K. Hoshino (Japan Atomic Energy Research Inst., Tokai, Japan.), H. Maeda (Japan Atomic Energy Research Inst., Tokai, Japan.), T. Takizuka (Japan Atomic Energy Research Inst., Tokai, Japan.), K. Itoh, and S. Itoh Aug. 1993 21 p
(DE94-770685; NIFS-240) Avail: CASI HC A03/MF A01

The ion heat pulse after sawtooth crash is studied with the time-of-flight neutral measurement on the JFT-2M tokamak. The rapid change of the bulk ion energy distribution near the edge is observed after sawtooth crash. The delay time is measured and the effective measuring position is estimated by a neutral transport code, then the thermal conductivity, chi(sub i)(exp HP), of about 15 +/- 10 sq m/sec is evaluated for the L-mode plasma. The simple diffusive model with constant chi(sub i)(exp HP), however, does not explain the amplitude of the pulse in the ion energy distribution. DOE

N95-20989# National Inst. for Fusion Science, Nagoya (Japan).
OBSERVATION OF NON DIFFUSIVE TERM OF TOROIDAL MOMENTUM TRANSPORT IN THE JFT-2M TOKAMAK
K. Ida, Y. Miura, T. Matsuda, and K. Itoh Aug. 1993 22 p
(DE94-770686; NIFS-241) Avail: CASI HC A03/MF A01

Toroidal rotation velocity profiles are measured with multi-chord charge-exchange spectroscopy to show that from the discharge the neutral beams are interchanged from parallel (co) to anti-parallel (counter) to the direction of the plasma current. Transport analysis of toroidal momentum in the transient phase suggests the existence of a non-diffusive term in the toroidal momentum transport. This non-diffusive term appears as a spontaneous source of the toroidal momentum in the direction that is anti-parallel to the plasma current. DOE

N95-21013# Boston Univ., MA.
SOURCE MECHANISMS AND RADIO EFFECTS OF IONOSPHERIC PLASMA DISTURBANCES Final Report, 1 Oct. 1991 - 30 Sep. 1994
Min-Chang Lee 30 Sep. 1994 7 p
(Contract F49620-92-J-0001)
(AD-A286529; AFOSR-94-0744TR) Avail: CASI HC A02/MF A01

Research on source mechanisms and radio effects of ionospheric plasma disturbances had been conducted, including theories, field experiments at Arecibo, Puerto Rico, and laboratory experiments with the Versatile Toroidal Facility (VTF) at MIT Plasma Fusion Center. DTIC

N95-21115# Los Alamos National Lab., NM.
CRYOGENIC TARGETS FOR INERTIAL CONFINEMENT FUSION
J. K. Hoffer 1994 8 p Presented at the 45th Scottish Universities Summer School in Physics, Fife, England, 7-20 Aug. 1994
(Contract W-7405-eng-36)
(DE94-016200; LA-UR-94-2595; CONF-9408127-1) Avail: CASI HC A02/MF A01

This report discusses the following topics: Do we really need cryogenic targets; cryogenic fuel layer specifications; and fuel layer techniques. DOE

N95-21134# Sandia National Labs., Albuquerque, NM.
SPICE MACRO MODEL OF A SPRYTON WITH MOSFET'S IN THE AVALANCHE MODE
C. W. Raney 1994 5 p Presented at the 37th Midwest Symposium on Circuits and Systems, Lafayette, LA, 2-5 Aug. 1994
(Contract DE-AC04-94AL-85000)
(DE94-015744; SAND-94-1306C; CONF-9408126-1) Avail: CASI HC A01/MF A01

A SPICE macro model for a triggered vacuum gap, a sprytron, intended for use in rapid discharge circuits such as Exploding Bridge Wire (EBW) applications, is presented. Power MOSFET's in the avalanche mode are utilized as the active switching elements in the model. The macro model is compared for accuracy in predicting the time dependent switching current, switch resistance and voltage drop across the switch using several test circuits. Techniques for extracting model parameters are discussed. DOE

N95-21141# General Atomics Co., San Diego, CA.
EXTENDED THEORY OF MAIN ION AND IMPURITY ROTATION AND BOOTSTRAP CURRENT IN A SHEAR LAYER
Y. B. Kim, F. L. Hinton, H. St.John, T. S. Taylor, D. Wroblewski (Lawrence Livermore National Lab., Livermore, CA.), and J. Kim Nov. 1993 5 p Presented at the IAEA Meeting on H-Mode Physics, Naka, Japan, 15-17 Nov. 1993
(Contracts DE-FG03-92ER-54150; DE-AC03-89ER-51114; W-7405-eng-48; Proj. 3938; Proj. 3466)
(DE94-015857; GA-A-21522; CONF-9311147-10) Avail: CASI HC A01/MF A01

In this paper, standard neoclassical theory has been extended into the shear layer. Main ion and impurity ion rotation velocity and bootstrap current within shear layer in H-mode are discussed. Inside the H-mode shear layer, standard neoclassical theory is not valid since the ion poloidal gyroradius becomes comparable to pressure gradient and electric field gradient scale length. To allow for arbitrary ratio of rho theta(sub i)/L(sub n) and rho theta(sub i)/L(sub Er) a new kinetic theory of main ion species within electric field shear layer has been developed with the assumption that rho theta(sub i)/R(sub o) is still small. As a consequence, both impurity flows and bootstrap current have to be modified. We present modified expressions of impurity flows and bootstrap current are presented neglecting ion temperature gradient. Comparisons with DIII-D measurements are also discussed. DOE

N95-21142# General Atomics Co., San Diego, CA.

INVESTIGATIONS OF VH-MODE IN D3-D AND JET

C. M. Greenfield, K. H. Burrell, B. Balet (Joint European Torus Project, Abingdon, England.), M. S. Chu, J. G. Cordey (Joint European Torus Project, Abingdon, England.), J. C. DeBoo, N. Deliyanakis (Joint European Torus Project, Abingdon, England.), E. J. Doyle (California Univ., Los Angeles, CA.), R. J. Groebner, and G. L. Jackson et al Sep. 1993 15 p Presented at the 20th EPS Conference on Controlled Fusion and Plasma Physics, Lisboa, Portugal, 24-31 Jul. 1993
(Contracts DE-AC03-89ER-51114; DE-FG03-92ER-54150; DE-FC03-86ER-52126; Proj. 3466; Proj. 3938; Proj. 3940)
(DE94-015859; GA-A-21368; CONF-9307169-2) Avail: CASI HC A03/MF A01

The VH-mode regime of high confinement has been observed in both DIII-D and JET. VH-mode is characterized by thermal confinement twice that seen in H-mode, with the edge transport barrier penetrating deeper into the plasma. Two mechanisms have been identified as important in achieving this high level of confinement. Expansion of the E x B velocity shear turbulence suppression zone is important in allowing reductions in local transport, while access to the second ballooning stability regime in the edge allows avoidance or elimination of ELMs which impede the confinement improvement. The high performance phase of these discharges is usually terminated by an MHD event which removes energy from a large portion of the plasma cross-section, and is followed by an H-mode phase. DOE

N95-21159# General Atomics Co., San Diego, CA.

EXPERIMENTAL MEASUREMENTS AND MODELING OF IMPURITY TRANSPORT IN THE DIVERTOR AND BOUNDARY PLASMA OF D3-D

W. P. West, N. H. Brooks, and S. L. Allen (Lawrence Livermore National Lab., Livermore, CA.) Jul. 1994 4 p Presented at the European Conference on Controlled Fusion and Plasma Physics, Marseilles, France, 26 Jun. - 1 Jul. 1994
(Contracts DE-AC03-89ER-51114; W-7405-eng-48; DE-AC04-76DP-00789)
(DE94-016519; GA-A-21762; CONF-940635-5) Avail: CASI HC A01/MF A01

Analysis of trace impurity injection experiments on D3-D during a beam power scan is presented. Spectroscopic measurements indicate that as beam power is increased, and concomitantly ELM frequency and scrape-off-layer thickness increase while energy confinement decreases, the core impurity content decreases only slightly. Modeling of the edge plasma using the UEDGE 2D and NEWT1D plasma fluid codes indicate that as beam power is increased, the parallel forces on an impurity ion increase in the direction from the divertor and toward the core plasma. Experiments using the divertor cryopump to induce higher parallel particle flow toward the divertor demonstrate significant reduction in core impurity content. These results indicate that parallel forces on impurity ions in the scrape off layer are playing a significant role in core impurity content. DOE

N95-21162# China Nuclear Information Centre, Beijing (China).

THE EVOLUTION OF CONFIGURATION FROM q GREATER THAN 1 TO q LESS THAN 1

Peng Zhang (Southwestern Inst. of Physics, Chengdu, China.) Jun. 1993 10 p
(DE94-631396; CNIC-00767; SIP-0063) Avail: CASI HC A02/MF A01
(US Sales Only)

The evolution of configuration from an initial state of tokamak-like plasma to RFP (reversed field pinch) along the trajectory of minimum energy state is studied. The high plasma current allowed in a RFP is expected to be sufficient to heat the plasma to ignition without the need of auxiliary neutral-beam or radio-frequency heating. DOE

N95-21163# General Atomics Co., San Diego, CA.

THE PARAMETRIC DEPENDENCE OF THE SPATIAL STRUCTURE OF THE RADIAL ELECTRIC FIELD AT THE PLASMA EDGE IN THE D3-D TOKAMAK

P. Gohil, K. H. Burrell, R. J. Groebner, J. Kim, and R. P. Seraydarian Jul. 1994 4 p Presented at the European Conference on Controlled Fusion and Plasma Physics, Marseilles, France, 26 Jun. - 1 Jul. 1994
(Contract DE-AC03-89ER-51114)
(DE94-016520; GA-A-21756; CONF-940635-6) Avail: CASI HC A01/MF A01

Much recent theoretical and experimental work has focused on the mechanisms controlling the transition from L-mode to H-mode and the subsequent improvement in transport and confinement. Measurements of the radial electric field, E(sub r), with high spatial and time resolution at the L-H transition have led to an understanding of the improved confinement of the plasma edge in H-mode plasmas based on the stabilization of plasma turbulence by sheared E x B flow. The radial electric field just inside the last closed flux surface (LCFS) changes dramatically at the L-H transition and a well-like structure in E(sub r) forms simultaneously at the transition. At present, there is no accepted theory which gives the spatial structure of E(sub r) near the plasma edge and which can predict its time evolution. Present theories propose mechanisms for the generation of a negative E(sub r) at the L-H transition, the bifurcation conditions for the transition and the stabilization of turbulence by sheared E x B flow. Although the various theories invoke different mechanisms to derive the negative E(sub r) (e.g., ion orbit losses, Stringer spin-up, nonlinear transport theory, self-regulating turbulence) they have as yet to come into full agreement with the observed experimental results and, in particular, the observed behavior of the poloidal rotation and pressure gradient of the main ions at the transition. Furthermore, these theories need to be extended to explain the formation of the spatial structure of E(sub r) at the transition and its temporal development into the H-mode. In order to help development of theories on the E(sub r) profile, we have examined the dependence of the radial profile of E(sub r) on different plasma parameters. DOE

N95-21164# China Nuclear Information Centre, Beijing (China).

NUMERICAL ANALYSIS OF ENERGETIC PARTICLE STABILIZATION OF BALLOONING MODES IN FINITE-ASPECT-RATIO TOKAMAKS

Qibing He (Southwestern Inst. of Physics, Chengdu, China.), Qiyang Peng (Southwestern Inst. of Physics, Chengdu, China.), and Wenxiao Qu (Southwestern Inst. of Physics, Chengdu, China.) Sep. 1993 12 p
(DE94-631397; CNIC-00792; SIP-0067) Avail: CASI HC A03/MF A01
(US Sales Only)

The effect of energetic trapped particles on the stabilization of ballooning modes in finite-aspect-ratio tokamaks is numerically analyzed. The numerical solution of boundary value problem of an integro-differential equation is successfully obtained by RKF integral method with variable step size. The results show that the instability domain of ballooning modes becomes small along with the increase of energetic particles pressure. The energetic trapped particles can partially or completely suppress the instability of ballooning modes. DOE

N95-21165# China Nuclear Information Centre, Beijing (China).

EXPERIMENTAL INVESTIGATION OF MOLECULAR BEAM INJECTION IN HL-1 TOKAMAK

Lianghua Yao (Southwestern Inst. of Physics, Chengdu, China.), Guangyao Diao (Southwestern Inst. of Physics, Chengdu, China.), Zhanhe Wang (Southwestern Inst. of Physics, Chengdu, China.), Huichen Deng (Southwestern Inst. of Physics, Chengdu, China.), Junlin Luo (Southwestern Inst. of Physics, Chengdu, China.), Xuru Duan (Southwestern Inst. of Physics, Chengdu, China.), and Zhengying Cui (Southwestern Inst. of Physics, Chengdu, China.) Jul. 1993 12 p
(DE94-631456; CNIC-00783; SIP-0065) Avail: CASI HC A03/MF A01
(US Sales Only)

A new method of gas puffing is presented. The molecular beam, formed by high pressure deuterium gas through Larval nozzle and skimmer slit, is injected into the HL-1 vacuum vessel. The deuterium molecular current from the nozzle passing through the skimmer is about 3 x 10(exp 20)/s. At the line average electron density of 5.2 x 10(exp 19)/cu m, the beam velocity is about 100 m/s. As the plasma density and temperature increases, the influxes of deuterium particles attenuate quickly. When the molecular beam injection (MBI) just returned to normal gas puffing, the D(sub alpha) emission rapidly decreases, meanwhile, the particles move toward plasma center, the electron density is continuously peaking. The line average electron density rising lasts 45 ms. The thermal energy of plasma and confinement time for particles and energy are also increasing. The MBI is a direct and efficient gas fuelling mode, and the injected particles can reach to inside about 8 cm of plasma and q approximately equals 2 confinement region. Its efficiency of injection is about 50%. After the MBI, the particle recycling coefficient R on the wall is 0.6 which is 10% lower than that of normal gas puffing. DOE

N95-21166# Lawrence Livermore National Lab., Livermore, CA.
PLASMA ELECTRODE POCKELS CELLS FOR THE BEAMLET AND NIF LASERS
M. A. Rhodes, B. Woods, J. DeYoreo, and J. Atherton May 1994 8 p Presented at the 11th Topical Meeting on the Technology of Fusion Energy, New Orleans, LA, 19-24 Jun. 1994
(Contract W-7405-eng-48)
(DE94-016541; UCRL-JC-115579; CONF-940630-37) Avail: CASI HC A02/MF A01

We describe Plasma Electrode Pockels Cells (PEPC) for the Beamlet laser and the proposed National Ignition Facility (NIF) laser. These PEPC's, together with passive polarizers, function as large aperture (greater than 35 x 35 sq cm) optical switches enabling the design of high-energy (greater than 5 kJ), multipass laser amplifiers. In a PEPC, plasma discharges form on both sides of a thin (1 cm) electro-optic crystal (KDP). These plasma discharges produce highly conductive and transparent electrodes that facilitate rapid (less than 100 ns) and uniform charging of the KDP up to the half-wave voltage (17 kV) and back to zero volts. We discuss the operating principles, design, and optical performance of the Beamlet PEPC and briefly discuss our plans to extend PEPC technology for the NIF. DOE

N95-21206# Lawrence Livermore National Lab., Livermore, CA.
USE OF THE NATIONAL IGNITION FACILITY FOR THE DEVELOPMENT OF INERTIAL FUSION ENERGY
M. Tobin, G. Logan, A. Anderson, and T. DeLaRubiaDiaz Jun. 1994 13 p Presented at the 11th Topical Meeting on the Technology of Fusion Energy, New Orleans, LA, 19-24 Jun. 1994
(Contract W-7405-eng-48)
(DE94-016696; UCRL-JC-117395; CONF-940630-36) Avail: CASI HC A03/MF A01

The primary purpose of the workshop was to gather input from the inertial confinement fusion (ICF) laboratories, private industry, and universities on the potential use of the NIF to conduct experiments in support of the development of Inertial Fusion Energy (IFE). To accomplish this, we asked over 60 workshop participants to identify key credibility and development issues for IFE in four areas: Target Physics --Issues related to the design and performance of targets for IFE; Chamber Dynamics -- Issues in IFE chambers resulting from the deposition of x-rays and debris; Inertial Fusion Power Technology -- Issues for energy conversion, tritium breeding and processing, and radiation shielding; interactions of neutrons with materials; and chamber design; Target System -- Issues related to automated, high-production-rate manufacture of low-cost targets for IFE, target handling and transport, target injection, tracking, and beam pointing. These topics are discussed in this report. DOE

N95-21207# Lawrence Livermore National Lab., Livermore, CA.
TARGET AREA DESIGN BASIS AND SYSTEM PERFORMANCE FOR THE NATIONAL IGNITION FACILITY
M. Tobin, V. Karpenko, K. Hagans, A. Anderson, J. Latkowski, R. Warren, R. Wavrik (Sandia National Labs., Albuquerque, NM.), R. Garcia (Sandia National Labs., Albuquerque, NM.), and J. Boyes (Sandia National Labs., Albuquerque, NM.) Jun. 1994 10 p Presented at the 11th Topical Meeting on the Technology of Fusion Energy, New Orleans, LA, 19-24 Jun. 1994
(Contract W-7405-eng-48)
(DE94-016697; UCRL-JC-115583; CONF-940630-32) Avail: CASI HC A02/MF A01

A description of Target Area systems performance shows that the target area conceptual design can meet its performance criteria. Before the shot, the target area provides a vacuum of less than 5 x 10(exp -5) Torr within 2 hours. A target, cryogenic or non-cryogenic, is placed to within 1 cm of chamber center with a positioner that minimizes vibration of the target. The target is then aligned to less than or equal to 7 microns by using the Target Alignment Sensor (TAS) system. The viewers in this system will also determine if the target is ready for illumination. Diagnostics are aligned to the necessary specifications by the alignment viewers. The target is shot and data is collected. Nearly all tritium (if present) is passed through the vacuum system and into the collection system. The analysis that supports the target area design basis is a combination of careful assumptions, data, and calculations. Some uncertainty exists concerning certain aspects of the source terms for x-rays and debris, material responses to this energy flux, and the full consequences of the material responses that do occur. For this reason, we have selected what we believe are conservative values in these areas. Advanced conceptual design activities will improve our understanding of these phenomena and allow a more quantitative assessment of the degree of conservatism inherent to the system. However, the results of this preliminary survey of target area operations indicate an annual shot rate of greater than 600 is feasible for this set of target area systems. DOE

N95-21239# Los Alamos National Lab., NM.
REVIEW OF RECENT D-T EXPERIMENTS FROM TFTR
R. J. Hawryluk (Princeton Univ., NJ.), H. Adler (Princeton Univ., NJ.), P. Alling (Princeton Univ., NJ.), P. Alling (Princeton Univ., NJ.), C. Ancher (Princeton Univ., NJ.), H. Anderson (Princeton Univ., NJ.), J. L. Anderson, J. W. Anderson (Princeton Univ., NJ.), V. Arunasalam (Princeton Univ., NJ.), and G. Ascione (Princeton Univ., NJ.) et al 1994 22 p Presented at the 15th International Conference on Plasma Physics and Controlled Nuclear Fusion Research, Seville, Spain, 26 Sep. - 1 Oct. 1994
(Contract W-7405-eng-36)
(DE95-002755; LA-UR-94-3665; CONF-940933-14) Avail: CASI HC A03/MF A01

An extensive set of deuterium-tritium (D-T) experiments has been carried out on the Tokamak Fusion Test Reactor (TFTR), using nearly equal concentrations of deuterium and tritium. The fusion power has been increased to 9.3 MW, using 34 MW of neutral-beam heating, in a supershot discharge and to 6.7 MW in a high-(beta)(sub p) discharge following a current rampdown. Extensive lithium pellet injection has increased the confinement time to 0.27 s and enabled higher current operation in both supershot and high-(beta)(sub p) discharges. The energy confinement time, (tau)(sub E), was observed to increase in D-T, relative to D plasmas, by 20% and the n(sub i)(0) T(sub i)(0) (tau)(sub E) product by 55%. The improvement in thermal confinement was caused primarily by a decrease in ion heat conductivity in both supershot and limiter-H-mode discharges. ICRF heating of a D-T plasma, using the second harmonic of tritium, has been demonstrated. First measurements of the confined alpha particles have been performed and found to be in good agreement with TRANSP simulations. Initial measurements of the alpha ash profile have been compared with simulations using particle transport coefficients from He gas puffing experiments. The loss of alpha particles to a detector at the bottom of the vessel is well described by the first-orbit loss mechanism. No loss due to alpha-particle-driven instabilities has yet been observed. The TFTR experiments were able to challenge and confirm several of the underlying assumptions of the ITER design. DOE

N95-21240# Los Alamos National Lab., NM.
FUSION POWER PRODUCTION IN TFTR
M. G. Bell (Princeton Univ., NJ.), C. W. Barnes, R. V. Budny (Princeton Univ., NJ.), L. R. Grisham (Princeton Univ., NJ.), R. J. Hawryluk (Princeton Univ., NJ.), D. L. Jassby (Princeton Univ., NJ.), L. C. Johnson (Princeton Univ., NJ.), D. R. Mikkelsen (Princeton Univ., NJ.), C. H. Skinner (Princeton Univ., NJ.), and J. D. Strachan (Princeton Univ., NJ.) et al 1994 14 p Presented at the 15th International Conference on Plasma Physics and Controlled Nuclear Fusion Research, Seville, Spain, 26 Sep. - 1 Oct. 1994
(Contracts W-7405-eng-36; DE-AC02-76CH-03073)
(DE95-002756; LA-UR-94-3667; CONF-940933-13) Avail: CASI HC A03/MF A01

Up to 9.3 MW of fusion power has been produced from deuterium-tritium (DT) fusion reactions in the Tokamak Fusion Test Reactor (TFTR). The total fusion yield from a single plasma pulse has reached 6.5 MJ. The experiments in TFTR with deuterium-tritium plasmas fueled and heated by neutral beam injection span wide ranges in plasma and operating conditions. Through the use of lithium pellet conditioning to control the edge recycling, the plasma confinement in TFTR has been improved to the point where the stability of the plasma to pressure driven modes is limiting the fusion power for plasma currents up to 2.5 MA. The central energy and fusion power densities in these plasmas are comparable to those expected in a thermalized DT reactor, such as ITER. DOE

N95-21242# Los Alamos National Lab., NM.
HEATING AND TRANSPORT IN TFTR D-T PLASMAS
M. C. Zarnstorff (Princeton Univ., NJ.), S. D. Scott (Princeton Univ., NJ.), Cris W. Barnes, R. Bell, C. Bush (Oak Ridge National Lab., TN.), Z. Chang (Wisconsin Univ., Madison, WI.), D. Ernst (Massachusetts Inst. of Tech., Boston, MA.), R. J. Fonck (Wisconsin Univ., Madison, WI.), L. Johnson (Princeton Univ., NJ.), and E. Mazzucato (Princeton Univ., NJ.) et al 1994 22 p Presented at the 15th International Conference on Plasma Physics and Controlled Nuclear Fusion Research, Seville, Spain, 26 Sep. - 1 Oct. 1994
(Contracts DE-AC02-76CH-03073; W-7405-eng-36)
(DE95-002812; LA-UR-94-3666; CONF-940933-15) Avail: CASI HC A03/MF A01

The confinement and heating of supershot plasmas are significantly enhanced with tritium beam injection relative to deuterium injection in TFTR. The global energy confinement and local thermal transport are analyzed for deuterium and tritium fueled plasmas to quantify their dependence on the average mass of the hydrogenic ions. The radial profiles of the deuterium and tritium densities are determined from the DT fusion neutron emission profile. DOE

N95-21244# Argonne National Lab., IL.
MHD PRESSURE DROP IN DUCTS WITH IMPERFECTLY INSULATING COATINGS
Siegfried Malang and Leo Buehler (Kernforschungszentrum G.m.b.H., Karlsruhe, Germany.) Aug. 1994 29 p Sponsored by European Fusion Technology Program
(Contract W-31-109-eng-38)
(DE95-002852; ANL/FPP/TM-269) Avail: CASI HC A03/MF A01

Liquid metal cooled blankets in fusion tokamak's are feasible only with electrically insulating coatings at the coolant channel walls. The requirements of such coatings are investigated and a simple analytical model is developed to determine the influence of imperfections in the coatings on the magneto-hydrodynamic pressure drop. This model is compared with the results of a 3D-MHD code based on the core flow approach. Both methods are in good agreement as long as the imperfections do not increase the pressure drop by more than 20%. The analytical model over-estimates the pressure drop for values larger than 20%. The importance of self-healing of coatings in case of cracking or flaking is quantified and an equation for the equilibrium conditions between the generation of imperfection and the healing of such spots is provided. DOE

N95-21247# Sandia National Labs., Albuquerque, NM.
SHOT-TO-SHOT COMPARISON OF THE FIRST Li-BEAM DRIVEN HOHLRAUM EXPERIMENTS
M. S. Derzon, G. E. Rochau, G. A. Chandler, A. R. Moats, and R. J. Leeper 1994 10 p Presented at the 10th Topical Conference on High-Temperature Plasma Diagnostics, Rochester, NY, 8-12 May 1994
(Contract DE-AC04-94AL-85000)
(DE94-016558; SAND-94-0385C; CONF-940552-17) Avail: CASI HC A02/MF A01

Shot-to-shot comparison of the first Li-beam Hohlraum experiments on PBFA 2 provides an opportunity to measure and determine the factors that affect the on-axis reproducibility of the Li ion beam. Both inner shell and thermal x-ray emission are used to estimate the relative beam power on target from shot to shot. The M- and L-shell Au x-ray yield measurements were made with an array of 11 filtered PIN detectors, and the thermal emission measurements were made with an array of three filtered bolometers. The analysis shows that the beam intensity on target varied by more than a factor of ten during the shot series. By correlating the results of the beam on target with other diagnostics and events, we have identified some potential causes for these variations. A slight difference in top-to-bottom timing appears critical in affecting relative peak power on target. DOE

N95-21290# Edgerton, Germeshausen and Grier, Inc., Idaho Falls, ID. National Engineering Lab.
ASSESSMENT OF DATABASE FOR INTERACTION OF TRITIUM WITH ITER PLASMA FACING MATERIALS
T. J. Dolan and R. A. Anderl Sep. 1994 137 p
(Contract DE-AC07-76ID-01570)
(DE95-002038; EGG-FSP-11348) Avail: CASI HC A07/MF A02

The present work surveys recent literature on hydrogen isotope interactions with Be, SS and Inconels, Cu, C, and V, and alloys of Cu and V. The goals are: (1) to provide input to the International Thermonuclear Experimental Reactor (ITER) team to help with tritium source term estimates for the Early Safety and Environmental Characterization Study and (2) to provide guidance for planning additional research that will be needed to fill gaps in the present materials database. Properties of diffusivity, solubility, permeability, chemical reactions, Soret effect, recombination coefficient, surface effects, trapping, porosity, layered structures, interfaces, and oxides are considered. Various materials data are tabulated, and a matrix display shows an assessment of the quality of the data available for each main property of each material. Recommendations are made for interim values of diffusivity and solubility to be used, pending further discussion by the ITER community. DOE

N95-21299# General Atomics Co., San Diego, CA.
THEORY OF THE L-H TRANSITION
F. L. Hinton Sep. 1994 11 p Presented at the ISPP Workshop on the Theory of Fusion Plasmas, Varenna, Italy, 22-26 Aug. 1994
(Contract DE-AC03-89ER-51114)
(DE95-001389; GA-A-21778; CONF-9408176-1) Avail: CASI HC A03/MF A01

The theory of the L-H transition in tokamaks is discussed. A transport bifurcation model is presented, which predicts reasonably well several properties of the L-H transition in the DIII-D tokamak, including the evolution in time of the density and temperature profiles. A bifurcation in the radial transport occurs because of a nonlinear feedback mechanism involving the radial electric field. A spontaneous transition is predicted when certain conditions are met; no trigger mechanism is necessary. The predicted profile evolution in H-mode can include a transition to VH-mode, with its characteristically wider transport barrier at the plasma edge. Trigger mechanisms are discussed, as well as the idea of considering the L-H transition as a phase transition. DOE

N95-21310# California Univ., Berkeley. Lawrence Berkeley Lab, CA.
PLASMA MODEL FOR CHARGING DAMAGE
M. C. Vella (Electro-Graph, Inc., Carlsbad, CA.), W. Lukaszek (Wafer Charging Monitors, Woodside, CA.), M. I. Current (Applied Materials, Santa Clara, CA.), and N. H. Tripsas (Advanced Micro Devices, Sunnyvale, CA.) Jul. 1994 11 p Presented at the IIT 1994 Conference, Catania, Italy, 13-17 Jun. 1994
(Contract DE-AC03-76SF-00098)
(DE95-000788; LBL-35964; CONF-9406267-1) Avail: CASI HC A03/MF A01

The mechanism responsible for charging damage is treated as beam/plasma driven differences in local floating potentials on the process surface. A cold plasma flood is shown to limit these potential differences. Beam/plasma J-V characteristics obtained with CHARM2 in a high current implanter are fit with the theory. With flood OFF, the fit corresponds to plasma buildup over the target surface. DOE

N95-21345*# General Atomics Co., San Diego, CA.
INVESTIGATION OF SPHERICAL TEARING MODE Final Report, 17 Jan. 1992 - 16 Jan. 1994
John M. Greene and R. L. Miller Jan. 1995 17 p
(Contract NASw-4651; GA Proj. 3936)
(NASA-CR-197284; NAS 1.26:197284; GA-C21932) Avail: CASI HC A03/MF A01

The purpose of this research was to better understand tearing and reconnection in genuinely three-dimensional configurations. We have identified an equilibrium model that should contain the required features. Three papers have been written and a fourth is in preparation. They are listed in the bibliography. Derived from text

N95-21368# Los Alamos National Lab., NM.
LOW DENSITY GAS AND FOAM TARGETS FOR ICF LONG SCALE LENGTH PLASMA EXPERIMENTS: FABRICATION AND CHARACTERIZATION
P. L. Gobby, M. A. Mitchell, N. E. Eliott, M. A. Salazar, J. C. Fermandez, W. W. Hsing, J. E. Moore, and V. M. Gomez 1994 6 p Presented at the Laser Interaction With Matter, Oxford, England, Oct. 1994

(Contract W-7405-eng-36)
(DE95-000935; LA-UR-94-3221; CONF-9410224-1) Avail: CASI HC A02/MF A01

Recent ICF experiments performed by the laser-matter interaction group at Los Alamos using the Nova laser to investigate long scale length plasmas required two types of special targets: gas-filled hohlraums and free-standing low density foams, both with densities in the range of 3-5 mg/cc. The mass in each case was provided by hydrogen and carbon - in the form of polymethylpentyene for the foam case and 2.2-dimethylpropane (i.e., neopentane, C_5H_{12}) at 1 atmosphere for the gas case. Dopants of Cl, Ti, Cr and Mn were added to the foams, while Ti and Cr coated carbon fibers were added to the hohlraums - both for isoelectronic x-ray spectroscopic temperature measurements. DOE

N95-21388# Argonne National Lab., IL.
MHD-FLOW IN SLOTTED CHANNELS WITH CONDUCTING WALLS
I. A. Evtushenko (Efremov, D. V. Scientific Research Inst., Saint Petersburg, Russia.), I. R. Kirillov (Efremov, D. V. Scientific Research Inst., Saint Petersburg, Russia.), and C. B. Reed Jul. 1994 22 p Presented at the ISFNT-3: 3rd International Symposium on Fusion Nuclear Technology, Los Angeles, CA, 27 Jun. - 1 Jul. 1994
(Contract W-31-109-eng-38)
(DE94-018370; ANL/TD/CP-83927; CONF-940664-29) Avail: CASI HC A03/MF A01

A review of experimental results is presented for magnetohydrodynamic (MHD) flow in rectangular channels with conducting walls and high aspect ratios (longer side parallel to the applied magnetic field), which are called slotted channels. The slotted channel concept was conceived at Efremov Institute as a method for reducing MHD pressure drop in liquid metal cooled blanket design. The experiments conducted by the authors were aimed at studying both fully developed MHD-flow, and the effect of a magnetic field on the hydrodynamics of 3-D flows in slotted channels. Tests were carried out on five models of the slotted geometry. A good agreement between test and theoretical results for the pressure drop in slotted channels was demonstrated. Application of a 'one-electrode movable probe' for velocity measurement permitted measurement of the M-shape velocity profiles in the slotted channels. Suppression of 3-D inertial effects in slotted channels of complex geometry was demonstrated based on potential distribution data. DOE

N95-21403# California Univ., Los Angeles, CA. Plasma Physics Group.
COMPUTER SIMULATION OF THE DIOCOTRON INSTABILITY
S. C. Neu and G. J. Morales Oct. 1994 7 p Submitted for publication Sponsored by ONR
(AD-A285655; PPG-1522) Avail: CASI HC A02/MF A01

A particle simulation study demonstrates that an initial-value analysis is essential in understanding the early-time growth of diocotron modes. It is also demonstrated that the equilibrium properties of a rigid rotor (including rotation on both the high and the low frequency branches) are well described by particle simulation. DTIC

N95-21404# California Univ., Los Angeles, CA. Plasma Physics Group.
1994 NONNEUTRAL PLASMA WORKSHOP
G. J. Morales Oct. 1994 14 p Workshop held in Berkeley, CA, 17-20 Jul. 1994 Sponsored by ONR
(AD-A285656; PPG-1524) Avail: CASI HC A03/MF A01

A workshop dedicated to the study of nonneutral plasmas confined in traps addresses frontier topics in the dynamics of vortices, development of self-organization, role of shear, operation of positron traps, and dusty plasmas. A personal perspective is presented. DTIC

N95-21451# Lawrence Livermore National Lab., Livermore, CA.
MTX FINAL REPORT
E. B. Hooper, ed., S. L. Allen, M. D. Brown, J. A. Byers, T. A. Casper, B. I. Cohen, R. H. Cohn, M. E. Fenstermacher, J. H. Foote, and K. Hoshino et al Jan. 1994 437 p
(Contract W-7405-eng-48)
(DE95-002960; UCRL-ID-116263) Avail: CASI HC A19/MF A04

The MTX experiment was proposed in 1986 to apply high frequency microwaves generated by a free-electron laser (FEL) to electron cyclotron resonance heating (ECRH) in a high field, high density tokamak. As the absorption of microwaves at the electron cyclotron resonance requires high frequencies, the opportunity of applying a free-electron laser has appeal as the device is not limited to frequencies in the microwave or long millimeter wavelength regions, in contrast to many other sources. In addition, the FEL is inherently a high power source of microwaves, which would permit single units of 10 MW or more, optimum for reactors. Finally, it was recognized early in the study of the application of the FEL based on the induction linear accelerator, that the nonlinear effects associated with the intense pulses of microwaves naturally generated would offer several unique opportunities to apply ECRH to current drive, MHD control, and other plasma effects. It was consequently decided to adapt the induction accelerator based FEL to heating and controlling the tokamak, and to conduct experiments on the associated physics. To this end, the Alcator C tokamak was moved from the Massachusetts Institute of Technology (MIT) to the Lawrence Livermore National Laboratory where it was installed in Building 431 and operated from March, 1989, until the conclusion of the experiment in October, 1992. The FEL, based on the ETA-11 accelerator and IMP wiggler was brought into operation by the LLNL Electron Beam Group and power injected into the tokamak during an experimental run in the Fall, 1989. Following an upgrade by the MTX group, a second experimental run was made lasting from the Winter, 1992 through the end of the experiment. Significant contributions to the ECRH experiments were made by the Japan Atomic Energy Research Institute (JAERI). DOE

N95-21547# Oak Ridge National Lab., TN.
TIME-RESOLVED DIAGNOSTICS OF EXCIMER LASER-GENERATED ABLATION PLASMAS USED FOR PULSED LASER DEPOSITION
D. B. Geohegan 1994 37 p Presented at the NATO Advanced Study Institute: Linking the Gaseous and Condensed Phases of Matter - the Behavior of Slow Electrons, Patras, Greece, 5-18 Sep. 1993
(Contract DE-AC05-84OR-21400)
(DE94-018950; CONF-930993-4) Avail: CASI HC A03/MF A01

Characteristics of laser plasmas used for pulsed laser deposition (PLD) of thin films are examined with four in situ diagnostic techniques: Optical emission spectroscopy, optical absorption spectroscopy, ion probe studies, and gated ICCD (intensified charge-coupled-device array) fast photography. These four techniques are complementary and permit simultaneous views of the transport of ions, excited states, ground state neutrals and ions, and hot particulates following KrF laser ablation of YBCO, BN, graphite and Si in vacuum and background gases. The implementation and advantages of the four techniques are first described in order to introduce the key features of laser plasmas for pulsed laser deposition. Aspects of the interaction of the ablation plume with background gases (i.e., thermalization, attenuation, shock formation) and the collision of the plasma plume with the substrate heater are then summarized. The techniques of fast ICCD photography and gated photon counting are then applied to investigate the temperature, velocity, and spatial distribution of hot particles generated during KrF ablation of YBCO, BN, Si and graphite. Finally, key features of fast imaging of the laser ablation of graphite into high pressure rare gases are presented in order to elucidate internal reflected shocks within the plume, redeposition of material on a surface, and formation of hot nanoparticles within the plume. DOE

N95-21581# Oak Ridge National Lab., TN.
STELLARATOR TRANSPORT OPTIMIZATION WITH SELF-CONSISTENT ELECTRIC FIELDS
J. F. Lyon, S. L. Painter, L. M. Kovrizhnykh, and K. Gulec 1994 5 p Presented at the European Conference on Controlled Fusion and Plasma Physics, Marseilles, France, 26 Jun. - 1 Jul. 1994
(Contract DE-AC05-84OR-21400)
(DE94-019151; CONF-940635-16) Avail: CASI HC A01/MF A01

Future large stellarators will operate in the low-collisionality regime where neoclassical helical-ripple-induced transport is an important, if not dominant, element in the transport. In this regime, E x B poloidal orbit rotation can drastically change the terms in the 1-D particle and heat flow equations. Usually, values for the electron and ion densities (n(sub e)(rho) and N(sub i)(rho)) and the radial component of the electric field (E(sub r)(rho)) are assumed, and the 1-D heat flow equations are solved for the electron and ion temperatures (T(sub 0)(rho) and T(sub i)(rho)): here (rho) = r/a(sub p) is the normalized plasma radius. Previous studies assumed parabolic potential profiles (E(sub r) is proportional to (rho)) for different assumed profiles for n(rho). Solutions with negative electric field led to a lower temperature and higher density than those with positive electric field, but required more initial hearing to reach ignition. No solutions were possible for some choices of parameters. In this paper, steady-state (1-D) integral-differential equations for the heat and particle fluxes for the ions (D,T) and electrons are solved for n(sub e)(r), n(sub i)(r), T(sub e)(r), T(sub i)(r), and E(sub r)(r). The electric field is determined from the ambipolarity condition. The electric field E enters both through an E/B drift term in the denominators of (chi) and D, and directly through the sign-dependent (del)(phi) term. The volumetric heat sources (and sinks) are the usual alpha-particle hearing, electron-ion heat transfer, and radiation terms. The form for the particle source rate (s) is chosen to represent shallow or deep fueling of the plasma. DOE

N95-21593# Rio Grande do Sul Univ., Porto Alegre (Brazil). Inst. de Fisica.

QUASI-LINEAR EQUATION FOR MAGNETOPLASMA OSCILLATIONS IN THE WEAKLY RELATIVISTIC APPROXIMATION M.S. Thesis

F. B. Rizzato 1985 87 p

(DE94-628932; INIS-BR-3340) Avail: CASI HC A05/MF A01 (US Sales Only)

Some limitations which are present in the dynamical equations for collisionless plasmas are discussed. Some elementary corrections to the linear theories are obtained in a heuristic form, which directly lead to the so-called quasi-linear theories in its non-relativistic and relativistic forms. The effect of the relativistic variation of the gyrofrequency on the diffusion coefficient is examined in a typically perturbative approximation. DOE

N95-21609# Sandia National Labs., Albuquerque, NM.

ATOMIC PROCESSES IN PROCESSING PLASMAS

M. E. Riley, G. A. Hebner, and K. E. Greenberg 1994 4 p Presented at the Department of Energy Basic Energy Sciences Atomic Physics Workshop, Lexington, KY, 14-15 Oct. 1994

(Contract DE-AC04-94AL-85000)

(DE94-019177; SAND-94-2332C; CONF-9410198-1) Avail: CASI HC A01/MF A01

The goal of this project is to gain an understanding of the fundamental mechanisms and processes occurring in low pressure, partially ionized plasmas and their interactions with materials. Emphasis is placed on: understanding the basic atomic and molecular physics that is occurring within the plasma bulk and sheath, understanding the relation of the collective plasma dynamics to the internal atomic processes, developing the ability to perform computer simulations of the plasmas as to both collective dynamics and inclusion of atomic properties, and analyzing the response of the materials to the plasma and how the plasma might be tailored to obtain a given effect at the material surface. DOE

N95-21665# Oak Ridge National Lab., TN.

THE ITER IN-VESSEL SYSTEM

D. C. Lousteau 1994 8 p Presented at the 11th Topical Meeting on the Technology of Fusion Energy, New Orleans, LA, 19-24 Jun. 1994

(Contract DE-AC05-84OR-21400)

(DE94-018053; CONF-940630-44) Avail: CASI HC A02/MF A01

The overall programmatic objective, as defined in the ITER Engineering Design Activities (EDA) Agreement, is to demonstrate the scientific and technological feasibility of fusion energy for peaceful purposes. The ITER EDA Phase, due to last until July 1998, will encompass the design of the device and its auxiliary systems and facilities, including the preparation of engineering drawings. The EDA also incorporates validating research and development (R&D) work, including the development and testing of key components. The purpose of this paper is to review the status of the design, as it has been developed so far, emphasizing the design and integration of those components contained within the vacuum vessel of the ITER device. The components included in the in-vessel systems are divertor and first wall; blanket and shield; plasma heating, fueling, and vacuum pumping equipment; and remote handling equipment. DOE

N95-21668# Los Alamos National Lab., NM.

INTENSE PROTON BEAM SOURCE FOR ITER NEUTRAL-BEAM SPECTROSCOPY DIAGNOSTICS

R. R. Bartsch, H. A. Davis, I. Henins, and J. B. Greenly (Cornell Univ., Ithaca, NY.) 1994 7 p Presented at the 10th International Conference on High Power Particle Beams, San Diego, CA, 20-24 Jun. 1994

(Contract W-7405-eng-36)

(DE94-018092; LA-UR-94-2559; CONF-940634-17) Avail: CASI HC A02/MF A01

An intense proton beam has been developed to evaluate a gas-cell neutralizer for use in an intense-neutral beam source for Tokomak Spectroscopy diagnostics. The allowed energy range of the proton stream is determined to be 50 to 70 keV from neutralization and reionization cross-sections and from the alpha particle charge exchange recombination intensity as a function of energy (baseline diagnostic). The neutralization evaluation source uses a flashover anode, magnetized, ion-diode. Neutral probes sensitive to energetic atomic and molecular hydrogen, developed to evaluate neutralizer performance, show neutral fluence from the ion-diode during the beam pulse. An array of Rogowski current probes, used to study the evolution of the current path, suggests that expansion of the anode plasma along the radial insulating magnetic field leads to impedance collapse. DOE

N95-21702# Oak Ridge National Lab., TN.

EVALUATION OF PUMPING AND FUELING REQUIREMENTS FOR THE ITER EDA

W. A. Houlberg and S. E. Attenberger 1994 21 p Presented at the 11th Topical Meeting on the Technology of Fusion Energy, New Orleans, LA, 19-24 Jun. 1994

(Contract DE-AC05-84OR-21400)

(DE94-018117; CONF-940630-43) Avail: CASI HC A03/MF A01

The relationships between fueling (gas injection and pellets of various sizes and velocities), pumping in the divertor chamber (constrained by fuel processing and divertor design), core density (constrained by the desired fusion power and helium ash accumulation), separatrix density (constrained by divertor operation and density limits) and plasma confinement models are examined for the International Engineering Tokamak Reactor (ITER) Engineering Design Activity (EDA) for guidance in the definition of design requirements for the pumping and fueling systems. Various combinations of gas and pellet injection are found to meet the constraints for operation at 1,500 MW of fusion power and 1 bar(center dot)l/s (5.3 x 10(exp 22) atoms/s) of DT pumping. Very low pumping reduces fuel processing requirements, but can lead to excessive helium accumulation depending on the particle transport properties. Isotopic tailoring of the fuel sources, e.g., 20-30% of the input fuel stream as tritium pellets and the rest as deuterium gas, can maintain the core fuel species mixture in the optimum range for fusion production (at least a 40-60 mixture) while reducing the tritium concentration in the edge region to 20-30%. This should reduce the tritium inventory in the plasma facing components, since that is typically governed by the fuel density mix near the plasma edge. A high density, low temperature ignited regime supported by deep pellet injection is shown to exist under some low confinement conditions. DOE

N95-21724# Massachusetts Inst. of Tech., Cambridge, MA. Plasma Fusion Center.

JOULE HEATING OF THE ITER TF COLD STRUCTURE: EFFECTS OF VERTICAL CONTROL COIL CURRENTS AND ELMS

A. Radovinsky and R. D. Pillsbury, Jr. Nov. 1993 55 p

(Contract DE-FC02-93ER-54186)

(DE95-001817; DOE/ER-54186/T2; PFC/RR-93-7) Avail: CASI HC A04/MF A01

The toroidal field coil and support structures for ITER are maintained at cryogenic temperatures. The time-varying currents in the poloidal field coil system will induce eddy currents in these structures. The associated Joule dissipation will cause local heating and require heat removal which will show up as a load on the cryogenic system. Studies of Joule heating of the ITER TF cold structure (TFCS) due to the currents in the poloidal field coil system are presented. The two regimes considered in this study are the plasma vertical stability control and the Edge Loss Mode (ELM) events. The 3-D, thin-shell, eddy current program, EDDYCUFF was used to analyze the eddy currents and Joule losses in the cold structure. The current versus time scenarios were defined. Four control coil options were studied. All schemes use coils external to the TF cold structure. Analyses of power depositions during the plasma vertical stability control were performed for each of the four options. For each of these options three different recovery times were assumed. The times were 3, 1, and 1/3 seconds. Sets of four sequential ELMs, as well as isolated ELM's have been studied for various sets of active PF coils. The results showed that the lowest average power dissipation in the TF cold structure occurs when a subset of PF2 and PF7 are active, and all the other PF coils are passive. The general conclusion is that to minimize power dissipation in the TF cold structure it is preferable that only coils PF2 and PF7 are active. The other coils (PF3-PF6) should be passive and driven by a condition of constant flux. It is recommended in particular, that coils PF3 and PF5 be allowed to change currents to conserve flux, since they provide the maximum shielding of the TFCS from the fields caused by the active coils. DOE

N95-21847# International Centre for Theoretical Physics, Trieste (Italy).
COLLISIONAL DRIFT WAVES IN THE H-MODE EDGE
S. Sen Jan. 1994 17 p
(DE94-628950; IC-94/41) Avail: CASI HC A03/MF A01 (US Sales Only)

The stability of the collisional drift wave in a sheared slab geometry is found to be severely restricted at the H-mode edge plasma due to the very steep density gradient. However, a radially varying transverse velocity field is found to play the key role in stability. Velocity profiles usually found in the H-mode plasma stabilize drift waves. On the other hand, velocity profiles corresponding to the L-mode render collisional drift waves unstable even though the magnetic shear continues to play its stabilizing role. DOE

N95-21848# International Centre for Theoretical Physics, Trieste (Italy).
ON THE INFLUENCE OF ELECTROMAGNETIC WAVE AND RELATIVISTIC ELECTRON BEAM ON A PLASMA
M. Y. El-Ashry (Suez Canal Univ., Ismailia, Egypt.), V. I. Berezhiani (Academy of Sciences of the Georgian SSR, Tbilisi, Georgia.), and J. L. Javakhishvili (Tbilisi State Univ., USSR.) Aug. 1993 8 p
(DE94-628962; IC-93/257) Avail: CASI HC A02/MF A01 (US Sales Only)

The dynamics of nonlinear waves in plasma under the influence of high-frequency electromagnetic pump and relativistic electron beams are considered. It is shown that the electrons of the beams play the role of the heavy plasma component, the matter which creates a possibility of wave formation of a soliton-type in a pure electron plasma. The wave structure is investigated and the characteristic parameters of the soliton are obtained. DOE

N95-21850# International Centre for Theoretical Physics, Trieste (Italy).
ON THE THEORY OF STRONG ELECTROMAGNETIC WAVES PROPAGATION IN AN ELECTRON-POSITRON-ION PLASMA
V. I. Berezhiani (Academy of Sciences of the Georgian SSR, Tbilisi, Georgia.), M. Y. El-Ashry (Suez Canal Univ., Ismailia, Egypt.), and U. A. Mofiz (Atomic Energy Research Establishment, Dhaka, Bangladesh.) Aug. 1993 10 p
(DE94-628964; IC-93/316) Avail: CASI HC A02/MF A01 (US Sales Only)

Propagation of intense electromagnetic radiation in an admixture of unmagnetized electron-positron-ion plasma is investigated analytically. It is shown, that electromagnetic radiation of arbitrary amplitude in presence of heavy ions, in contrast to the case of pure electron-positron plasma, may be localized with the generation of humped ambipolar potential in the plasma. The later may cause acceleration of particles in such plasma. DOE

N95-21851# International Centre for Theoretical Physics, Trieste (Italy).
LARGE AMPLITUDE LOCALIZED STRUCTURES IN A RELATIVISTIC ELECTRON-POSITRON ION PLASMA
V. I. Berezhiani and S. Mahajan Mar. 1994 18 p
(DE94-628965; IC-94/67) Avail: CASI HC A03/MF A01 (US Sales Only)

The nonlinear propagation of circularly polarized electromagnetic (CPEM) waves with relativistic strong amplitude in an unmagnetized cold electron-positron ion plasma is investigated. The possibility of finding soliton solutions in such a plasma is explored. In one- and two-dimensions it is shown that the presence of a small fraction of massive ions in the plasma lead to stable localized solutions. DOE

N95-21852# International Atomic Energy Agency, Vienna (Austria).
ITER EDA NEWSLETTER. VOLUME 3, NO. 2
Feb. 1994 12 p
(DE94-628980; INIS-mf-13862) Avail: CASI HC A03/MF A01 (US Sales Only)

This issue of the ITER EDA (Engineering Design Activities) Newsletter contains reports on the Fifth ITER Council Meeting held in Garching, Germany, January 27-28, 1994, a visit (January 28, 1994) of an international group of Harvard Fellows to the San Diego Joint Work Site, the Inauguration Ceremony of the EC-hosted ITER joint work site in Garching (January 28, 1994), on an ITER Technical Meeting on Assembly and Maintenance held in Garching, Germany, January 19-26, 1994, and a report on a Technical Committee Meeting on radiation effects on in-vessel components held in Garching, Germany, November 15-19, 1993, as well as an ITER Status Report. DOE

N95-21922# Oak Ridge National Lab., TN.
A SYNCOPATED LEAP-FROG ALGORITHM FOR ORBIT CONSISTENT PLASMA SIMULATION OF MATERIALS PROCESSING REACTORS
J. W. Cobb and J. N. Leboeuf 1994 5 p Presented at the 15th International Conference on the Numerical Simulation of Plasmas, Valley Forge, PA, 7-9 Sep. 1994
(Contract DE-AC05-84OR-21400)
(DE95-000954; CONF-9409105-4) Avail: CASI HC A01/MF A01

The authors present a particle algorithm to extend simulation capabilities for plasma based materials processing reactors. The orbit integrator uses a syncopated leap-frog algorithm in cylindrical coordinates, which maintains second order accuracy, and minimizes computational complexity. Plasma source terms are accumulated orbit consistently directly in the frequency and azimuthal mode domains. Finally they discuss the numerical analysis of this algorithm. Orbit consistency greatly reduces the computational cost for a given level of precision. The computational cost is independent of the degree of time scale separation. DOE

N95-22010# Los Alamos National Lab., NM.
CURRENT STATUS OF FUSION-RELEVANT COVARIANCE DATA
D. W. Muir 12 Sep. 1994 6 p Presented at the Improved Evaluations and Integral Data Testing for FENDL, Garching, Germany, 12-16 Sep. 1994
(Contract W-7405-eng-36)
(DE95-000865; LA-UR-94-3105; CONF-9409221-2) Avail: CASI HC A02/MF A01

The following review of the current status of formatted data covariance files and their multigroup processing is a contribution to the IAEA Advisory Group Meeting on 'Improved Evaluations and Integral Data Testing for FENDL,' to be held at the Max-Planck-Institut fuer Plasmaphysik, Garching, Germany, 12-16 September 1994. The draft agenda of this meeting lists as Item 6 the 'assessment of present status and role of uncertainty files, their processing and sensitivity studies related to FENDL.' We conclude that this is an important and timely topic and recommend needed actions in this field. DOE

N95-22116# Stanford Univ., CA. High Temperature Gasdynamics Lab.
ADVANCED DIAGNOSTICS FOR PLASMA CHEMISTRY
Charles H. Kruger Mar. 1994 13 p
(Contract DE-FG03-88ER-13957)
(DE94-018936; DOE/ER-13957/T1) Avail: CASI HC A03/MF A01

Since July 15, 1992, the High Temperature Gasdynamics Laboratory in the Department of Mechanical Engineering at Stanford University has been engaged in a four-year research program on Advanced Diagnostics for Plasma Chemistry. The goal of this program is to develop state-of-the-art laser-based diagnostics of molecular species in harsh chemical environments, particularly those encountered in plasma synthesis of new materials. Emphasis has been placed on exploiting a new nonlinear spectroscopy, degenerate four wave mixing, as well as linear laser induced fluorescence to accomplish these goals. The present submittal is a proposal for the continuation funding for the third year of this program, from July 15, 1994, until July 14, 1995. Section 2 summarizes the research accomplished during the first eighteen months of the program. Section 3 discusses the plans for continuing research activities. Publications and presentations to date resulting from this program are listed in Section 4. The proposed budget for the third year is given in Section 5. DOE

N95-22120# Texas Univ., Austin, TX. Fusion Research Center.
MEASUREMENTS OF THE AUBURN ECE OPTICAL SYSTEM PARAMETERS FOR TEMPERATURE FLUCTUATION MEASUREMENTS ON TEXT-U
M. Koltonyuk (Columbia Univ., New York, NY.) and C. Watts 29 Aug. 1994 14 p
(Contract DE-FG03-94ER-54241)
(DE94-019217; DOE/ER-54241/134; FRCR-449) Avail: CASI HC A03/MF A01

Calibration measurements were performed on Auburn ECE antenna system to determine the beam waist size and location at several characteristic frequencies typically used in TEXT-U experiments, and compare these with known manufacturer's specifications. A halogen bulb, acting as a microwave source, swept a grid of points in a plane parallel to antenna lens' surface. The intensity of the collected signal was recorded and later fitted to a Gaussian for several values of the radial distance from the lens, thus enabling us to estimate the beam waist size and position. Knowledge of the minimum spot size possible allows us to determine the maximum resolution in measuring the wavelength of the tilde-T(sub e) fluctuations in the plasma. Results indicate that the Auburn optical system produces the beam with the waist size bigger than was originally expected. DOE

N95-22191# Lawrence Livermore National Lab., Livermore, CA.
LABORATORY CHARACTERIZATION OF WOELTER X RAY OPTICS
B. A. Remington and R. I. Morales Apr. 1994 15 p Presented at the 10th Topical Conference on High-Temperature Plasma Diagnostics, Rochester, NY, 8-12 May 1994
(Contract W-7405-eng-48)
(DE94-016969; UCRL-JC-116182; CONF-940552-28) Avail: CASI HC A03/MF A01

We have conducted an extensive series of characterization measurements of a Woelter incidence x-ray microscope. The measurements were carried out on 5% sectors of the Woelter x-ray optic in a laboratory utilizing a high brightness, 'point' x-ray source and fall into two categories. (1) Absolute reflectance measurements as a function of x-ray energy were made with Si(Li) detectors to acquire continuum spectra prior to and after reflecting off the Woelter optic. (2) Spatial resolution measurements were made using back-illuminated pinholes or grids imaged onto film or an x-ray CCD camera. The depth of field was mapped out by varying the distance between the Woelter optic and the backlit grid. DOE

N95-22221# Lawrence Livermore National Lab., Livermore, CA.
HEAT LOSS BY HELICITY INJECTION IN SPHEROMAKS
T. K. Fowler 17 Mar. 1994 24 p
(Contract W-7405-eng-48)
(DE95-003473; UCRL-ID-116975) Avail: CASI HC A03/MF A01

A model is presented for spheromak buildup and decay including thermal diffusivity associated with magnetic turbulence during helicity injection. It is shown that heat loss by magnetic turbulence scales more favorably than gyroBohm transport. Thus gyroBohm scaling for the proposed ignition experiment would be the conservative choice, though present experiments may be dominated by magnetic turbulence. Because of a change in boundary conditions when the gun is turned off, the model may account for the observed increase in electron temperature in CTX after turnoff. DOE

N95-22225# Sandia National Labs., Albuquerque, NM.
APPLICATION OF IRIS TO SEMICONDUCTOR PLASMA PROCESSING Final Technical Report
Pauline Ho, Kevin P. Killeen, Carl F. Melius, and Richard J. Buss Nov. 1994 27 p
(Contract DE-AC04-94AL-85000)
(DE95-003591; SAND-94-2439) Avail: CASI HC A03/MF A01

This report describes technical work done at Sandia National Laboratories (SNL) under CRADA No. 1031, a Technology Transfer Initiative (TTI) collaborative project with Texas Instruments, Inc. (TI). The overall objective of the work was to improve specific semiconductor processing technologies by the use of numerical modeling and in situ sensors. On a technical level, this collaboration was very successful. The project had three parts, unequal in size. The first part involved the use of the IRIS (Imaging of Radicals Interacting with Surfaces) technique to measure the reactivities of radical species at surfaces. The second, and smallest, part of the work involved the evaluation and transfer of sensor technologies for monitoring source stability in MOCVD (metal-organic CVD) of compound semiconductors. The third part of the work involved experimental and theoretical investigations into the chemical reactions occurring during the CVD of SiO2 from TEOS (tetraethoxysilane). DOE

N95-22282# Academy of Sciences (USSR), Novosibirsk (USSR). Inst. Yadernoj Fiziki.
ON CONCEPTION OF A COMPACT NEUTRON SOURCE AND THE POSSIBILITY OF ITS SIMULATION ON THE AMBA-M END TRAP
G. I. Dimov, A. A. Kabantsev, V. G. Sokolov, and S. Yu. Taskaev 1993 13 p In RUSSIAN
(DE94-633373; IYaF-93-89) Avail: CASI HC A03/MF A01 (US Sales Only)

Classical end trap Budker-Post with thermobarriers in traps is proposed to apply for obtaining neutron flux of greater than 500 kW power and 2-3 MW.m(exp -2) density. DOE

N95-22300# Lawrence Livermore National Lab., Livermore, CA.
THE SUPERCONDUCTING MAGNET SYSTEM FOR THE TOKAMAK PHYSICS EXPERIMENT
Dwight D. Lang, R. J. Bulmer, M. R. Chaplin, T. G. OConner, D. S. Slack, R. L. Wong, J. P. Zbasnik, J. H. Schultz, N. Diatchenko, and D. B. Montgomery et al 18 Jun. 1994 9 p Presented at the 11th Topical Meeting on the Technology of Fusion Energy, New Orleans, LA, 19-24 Jun. 1994
(Contract W-7405-eng-48)
(DE94-018329; UCRL-JC-116879; CONF-940630-47) Avail: CASI HC A02/MF A01

The superconducting magnet system for the Tokamak Physics eXperiment (TPX) will be the first all superconducting magnet system for a Tokamak, where the poloidal field coils, in addition to the toroidal field coils are superconducting. The magnet system is designed to operate in a steady state mode, and to initiate the plasma discharge ohmically. The toroidal field system provides a peak field of 4.0 Tesla on the plasma axis at a plasma major radius of 2.25 m. The peak field on the niobium 3-tin, cable-in-conduit (CIC) conductor is 8.4 Tesla for the 16 toroidal field coils. The toroidal field coils must absorb approximately 5 kW due to nuclear heating, eddy currents, and other sources. The poloidal field system provides a total of 18 volt seconds to initiate the plasma and drive a plasma current up to 2 MA. The poloidal field system consists of 14 individual coils which are arranged symmetrically above and below the horizontal mid plane. Four pairs of coils make up the central solenoid, and three paris of poloidal ring coils complete the system. The poloidal field coils all use a cable-in-conduit conductor, using either niobium 3-tin (NB3Sn) or niobium titanium (NbTi) superconducting strands depending on the operating conditions for that coil. All of the coils are cooled by flowing supercritical helium, with inlet and outlet connections made on each double pancake. The superconducting magnet system has gone through a conceptual design review, and is in preliminary design started by the Lawrence Livermore National Laboratory; Massachusetts Institute of Technology; and the Princeton Plasma Physics Laboratory (LLNL/MIT/PPPL) collaboration. A number of changes have been made in the design since the conceptual design review, and are described in this paper. DOE

N95-22377# International Centre for Theoretical Physics, Trieste (Italy).
THE FINAL STATUS OF A METAL SURFACE AFTER MULTIPULSE LASER IRRADIATION IN AN AMBIENT GAS
C. Boulmer-Leborgne (Orleans Univ., France.), J. Hermann (Orleans Univ., France.), B. Dubreuil (Orleans Univ., France.), M. Dinescu (Academia R. P. R., Bucharest, Romania.), N. Chitica (Academia R. P. R., Bucharest, Romania.), I. N. Mihailescu (Academia R. P. R., Bucharest, Romania.), and I. Ursu Nov. 1993 14 p
(DE94-629000; IC-93/390) Avail: CASI HC A03/MF A01 (US Sales Only)

We have investigated the role of the ambient gas nature and pressure, and the influence of the laser pulse total duration and temporal shape in the coupling of the incident laser light of lambda = 10.6 micro m wavelength to a metallic surface at intermediate laser intensities of 10(exp 7) - 10(exp 8) W/sq cm. A plasma is accompanying then the action of the laser pulse. It is acting as an active moderator among laser beam and target thus determining the final status of the contact surface. DOE

N95-22422# California Univ., Berkeley, CA. Electronics Research Lab.
PIC SIMULATION OF SURFACE WAVES Annual Report
Charles K. Birdsall 1993 2 p
(Contract N00014-93-1-1389)
(AD-A285358) Avail: CASI HC A01/MF A01

Surface waves are investigated via electrostatic particle simulation of a warm, unmagnetized, bounded 2 1/2 d plasma. The study focuses on a slab configuration in which the y direction is periodic and the x direction is bounded by grounded conducting walls. In order to further the study of surface waves as a mechanism for sustaining plasma discharges, a Monte Carlo collision code was modified to allow simulation particles to have their own variable weights. Derived from text

76 SOLID-STATE PHYSICS

Includes superconductivity.

For related information, see also *33 Electronics and Electrical Engineering* and *36 Lasers and Masers.*

N95-19886 Materials Research Society, Pittsburg, PA.
PHYSICS AND APPLICATIONS OF DEFECTS IN ADVANCED SEMICONDUCTORS, VOLUME 325 Final Report
John Ballance, M. O. Manasreh, ed. (Wright Lab., Wright-Patterson AFB, OH.), H. J. vonBardeleben, ed. (Paris Univ., France.), G. S. Pomrenke, ed. (Air Force Office of Scientific Research, Bolling AFB, Washington, DC.), M. Lannoo, ed. (Institut Superieur d'Electronique du Nord, Lille, France.), and D. N. Talwar, ed. (Indiana Univ. of Pennsylvania, Indiana, PA.) 1994 538 p Symposium held in Boston, MA, 29 Nov. - 1 Dec. 1993 Limited Reproducibility: More than 20% of this document may be affected by microfiche quality
(Contract F49620-94-1-0062)
(AD-A280059; AFOSR-94-0316TR-Vol-325; ISBN-1-55899-224-3) Avail: Issuing Activity (Defense Technical Information Center (DTIC))

Defect characterization, identifications, and their influence on material properties and device performance are a major subject in the physics and applications of semiconductors. This volume focuses on defects in advanced semiconductors or precisely quantum wells, superlattices, and heterostructures. In Part 1 of this proceedings the invited and contributed papers deal with defects in type 1 and type 2 superlattices based on III-V semiconductors such as GaAs/AlGaAs multiple quantum wells (MQWs). Some of the topics include optical spectroscopy of defects in GaAs/AlGaAs MQWs, defects injections and diffusions in heterostructures and impurity effects on the electronic states in quantum wires and quantum dots. Part 2 deals with defects and impurities in bulk and epitaxial InP and related compounds, for example, the semi-insulating behavior of undoped InP is discussed. Recently, SiGe/Si quantum wells and heterostructures have been the subject of an increasing interest due to their applications in electronic and opto-electric devices. Defects, dislocation distributions, and doping in these heterostructures are discussed in Part 3. DTIC

N95-19925# Brookhaven National Lab., Upton, NY.
MATRIX FORMULATION OF THE PARTICLE MOTION IN CRYSTALLINE BEAMS
A. F. Haffmans, D. Maletic, and A. G. Ruggiero 1994 4 p Presented at the 4th European Particle Accelerator Conference, London, England, 27 Jun. - 1 Jul. 1994
(Contract DE-AC02-76CH-00016)
(DE94-017301; BNL-49993; CONF-940618-54) Avail: CASI HC A01/MF A01

To investigate the properties of crystalline beams in their ground state, the equations of motion of a single ion and the envelope equations are derived. It is possible to express the status of motion with a set of transfer matrices associated to each of the magnet elements of the storage ring. By inspection of the eigenvalues of the total transfer matrix one then determines the onset of crystalline structures and the stability limits. An analytical approach is also possible, based on the estimate of the shifting of the frequencies of oscillation, betatron and longitudinal, and on the approaching of a major half-integral stopband resonance driven by the space charge. DOE

N95-19954# Sandia National Labs., Albuquerque, NM.
OPTIMIZATION OF InAsSb/InGaAs STRAINED-LAYER SUPERLATTICE GROWTH BY METAL-ORGANIC CHEMICAL VAPOR DEPOSITION FOR USE IN INFRARED EMITTERS
R. M. Biefeld, K. C. Baucom, D. M. Follstaedt, and S. R. Kurtz 1994 5 p Presented at the 21st International Symposium on Compound Semiconductors, San Diego, CA, 18-22 Sep. 1994
(Contract DE-AC04-94AL-85000)
(DE94-016557; SAND-94-0864C; CONF-940981-1) Avail: CASI HC A01/MF A01

We have prepared InAsSb/InGaAs strained-layer superlattices (SLSs) by metal-organic chemical vapor deposition using a variety of growth conditions. Presence of an InGaAsSb interface layer was indicated by x-ray diffraction. This interface effect was minimized by optimizing the purge times, reactant flows, and growth conditions. The optimized growth conditions involved the use of low pressure, short purge times between the growth of the layers, and no reactant flow during the purges. Electron diffraction indicates that CuPt-type compositional ordering occurs in InAs(sub 1 - x)Sb(sub x) alloys and SLSs which explains an observed bandgap reduction from previously accepted alloy values. DOE

N95-19978# China Nuclear Information Centre, Beijing (China).
HIGH PRECISION TRACE NEUTRON TRANSMUTATION DOPING OF DETECTOR-GRADE HIGH RESISTANCE ZONE-REFINED SILICON MONO-CRYSTAL
Bingxian Chen (Academia Sinica, Beijing, China.), Jijin Gao (Academia Sinica, Beijing, China.), Xiuqing Gao (Academia Sinica, Beijing, China.), Heqin Dong (Academia Sinica, Beijing, China.), and Shiling Li (Academia Sinica, Beijing, China.) Aug. 1993 8 p
(DE94-631463; CNIC-00776; IAE-0122) Avail: CASI HC A02/MF A01 (US Sales Only)

The technique of high precision trace neutron transmutation doping of detector grade high resistance zone-refined Si mono-crystal is introduced. The key technique is to precisely control the doping element. It includes the determination of rho(sub 0) value according to theoretical calculation and experimental results, the selection of irradiation channel and improvement of irradiation devices, the regulation of doping coefficient K, the simulation experiment of silicon crystal, strict control of irradiation time and the study on mechanism of radiation damage and its elimination. The developed N-type (10 approx. 100) k(Omega)cm NTD FZ Si has excellent uniformity of specific resistance, long life of minority carrier and high-purity of the crystal. DOE

N95-20014# Brookhaven National Lab., Upton, NY.
CRYSTALLINE BEAM IN A STORAGE RING: HOW LONG CAN IT LAST?
Xiao-Ping Li (Biosym Technologies, Inc., San Diego, CA.), A. M. Sessler (Lawrence Livermore National Lab., Livermore, CA.), and Jie Wei 1994 4 p Presented at the 4th European Particle Accelerator Conference, London, England, 27 Jun. - 1 Jul. 1994
(Contract DE-AC02-76CH-00016)
(DE94-017303; BNL-49852; CONF-940618-53) Avail: CASI HC A01/MF A01

The ground state of a crystalline beam in a realistic storage ring is well understood by now. No crystalline beam exists in a constant gradient storage ring, but in an alternating gradient (AG) ring crystalline beams exist at all density as long as the beam energy is smaller than the transition energy. However, since the Hamiltonian is time dependent, the total energy of the beam is not a constant of motion. As a result, the crystalline beam will gradually heat up and eventually melt if not refrigerated. Here, we show that if the frequency due to the AG lattice is lower than twice the betatron frequency, heat will transfer into the system extremely fast so that a crystalline beam can not last a meaningful period of time (except at very low density). On the other hand, if the AG lattice frequency is higher than twice the betatron frequency, the heat transfer is slow, and the crystalline beam can last for a long time. We therefore arrive at the conclusion that in order for a crystalline beam to be conveniently observed, the storage ring should be designed such that the AG lattice frequency is as high as possible while the betatron frequency is kept as low as possible. DOE

N95-20017# Argonne National Lab., IL.
POSITRON ANNIHILATION STUDIES OF ORGANIC SUPERCONDUCTIVITY
H. L. Yen (Missouri Univ., Kansas City, MO.), Y. Lou (Missouri Univ., Kansas City, MO.), E. H. Ali (Missouri Univ., Kansas City, MO.), Y.-N. Xu (Missouri Univ., Kansas City, MO.), W. Y. Ching (Missouri Univ., Kansas City, MO.), Y. C. Jean (Missouri Univ., Kansas City, MO.), H. H. Wang, K. D. Carlson, J. M. Williams, and K. M. OBrien (Texas Univ., Austin, TX.) et al 1994 4 p Presented at the 10th International Conference on Positron Annihilation, Beijing, China, 23-29 May 1994
(Contracts W-31-109-eng-38; DE-FG02-84ER-45170)
(DE94-018371; ANL/CHM/CP-83942; CONF-9405170-7) Avail: CASI HC A01/MF A01

The positron lifetimes of two organic superconductors, (kappa)-(ET)(sub 2)Cu(NCS)(sub 2) and (kappa)-(ET)(sub 2)Cu(N(CN)(sub 2))Br, are measured as a function of temperature across (Tc). A drop of positron lifetime below (Tc) is observed. Positron-electron momentum densities are measured by using 2D-ACAR to search for the Fermi surface in (kappa)-(ET)(sub 2)Cu(N(CN)(sub 2))Br. Positron density distributions and positron-electron overlaps are calculated by using the orthogonalized linear combination atomic orbital (OLCAO) method to interprete the temperature dependence due to the local charge transfer which is inferred to relate to the superconducting transition. 2D-ACAR results in (kappa)-(ET)(sub 2)Cu(N(CN)(sub 2))Br are compared with theoretical band calculations based on a first-principles local density approximation. Importance of performing accurate band calculations for the interpretation of positron annihilation data is emphasized. DOE

N95-20087# Sandia National Labs., Albuquerque, NM.
GENERATION OF MICRO-DOMAINS IN AT-CUT QUARTZ BY THERMAL PROCESSING AND THE EFFECT ON RESONATOR MODES
L. Weisenback, S. J. Martin, G. C. Frye, T. V. Bohuszewicz, and D. H. Doughty 1994 5 p Presented at the Annual Frequency Control Symposium, Boston, MA, 1-3 Jun. 1994
(Contract DE-AC04-94AL-85000)
(DE94-017344; SAND-94-0165C; CONF-9406199-2) Avail: CASI HC A01/MF A01

The fabrication of acoustic sensors with sol-gel selective coatings requires the deposition of thin films on quartz resonators using solution chemistry techniques. Oxide films are spin-cast, then heat treated. A variety of film compositions are deposited, requiring a variety of firing schedules. Network analysis of the untreated AT-cut quartz devices revealed a resonant frequency of 5.0 MHz, corresponding to a pure thickness-shear mode resonance. For devices that were rapidly fired to 400 C and rapidly air cooled, network analysis showed the shear-mode response at 5.0 MHz disappeared, while a predominantly compressional mode response at 7.3 MHz emerged. Structural analysis explored the crystal structure changes induced by processing which resulted in this new mode. DOE

N95-20127# Brookhaven National Lab., Upton, NY.
CARRIER DOPING AND INTERLAYER COUPLING IN HTSC SINGLE CRYSTALS
K. Kishio (Tokyo Univ., Japan.), J. Shimoyama (Tokyo Univ., Japan.), T. Kimura (Tokyo Univ., Japan.), Y. Kotaka (Tokyo Univ., Japan.), K. Kitazawa (Tokyo Univ., Japan.), K. Yamafuji (Kyushu Univ., Fukuoka, Japan.), Q. Li, and M. Suenaga 1994 5 p Presented at the Meeting on Materials and Mechanisms of Superconductivity: High Temperature Superconductors, Grenoble, France, 4-9 Jul. 1994
(Contract DE-AC02-76CH-00016)
(DE94-018637; BNL-60756; CONF-940701-20) Avail: CASI HC A01/MF A01

Experimental results of the effect of carrier doping on the irreversibility lines in (La,Sr)2CuO(4-delta) and Bi2Sr2CaCu2O(8+delta) single crystals are summarized. As a function of Sr or oxygen contents, systematic and dramatic widening of the irreversible regions in the B - T phase diagram was observed in both systems. The present study suggests the critical importance of carrier concentration which directly affects the interlayer coupling strength and dimensionality of the flux line lattice in all the layered HTSC compounds as a universal feature. DOE

N95-20130# Brookhaven National Lab., Upton, NY.
CHIRAL SYMMETRY AND LATTICE GAUGE THEORY
M. Creutz Aug. 1994 12 p Presented at the International Conference on Quark Confinement and the Hadron Spectrum, Como, Italy, 20-24 Jun. 1994
(Contract DE-AC02-76CH-00016)
(DE94-018676; BNL-60750; CONF-9406111-1) Avail: CASI HC A03/MF A01

The problem of formulating chiral symmetry in lattice gauge theory is reviewed. Recent approaches involving an infinite tower of additional heavy states to absorb fermion doublers are discussed. For hadronic physics this provides a natural scheme for taking quark masses to zero without requiring a precise tuning of parameters. A mirror fermion variation provides a possible way of extending the picture to chirally coupled light fermions. DOE

N95-20142# Sandia National Labs., Albuquerque, NM.
THE MODIFIED EMBEDDED ATOM METHOD
M. I. Baskes 1994 13 p Presented at the American Society of Mechanical Engineers' Winter Annual Meeting, Chicago, IL, 9-11 Nov. 1994
(Contract DE-AC04-94AL-85000)
(DE94-015746; SAND-94-8704C; CONF-941142-16) Avail: CASI HC A03/MF A01

Recent modifications have been made to generalize the Embedded Atom Method (EAM) to describe bonding in diverse materials. By including angular dependence of the electron density in an empirical way, the Modified Embedded Atom Method (MEAM) has been able to reproduce the basic energetic and structural properties of 45 elements. This method is ideal for examining interfacial behavior of dissimilar materials. This paper explains in detail the derivation of the method, shows how parameters of MEAM are determined directly from experiment or first principles calculations, and examine the quality of the reproduction of the database. Materials with fcc, bcc, hcp, and diamond cubic crystal structure are discussed. A few simple examples of the application of the MEAM to surfaces and interfaces are presented. Calculations of pullout of a SiC fiber in a diamond matrix as a function of applied stress show nonuniform deformation of the fiber. DOE

N95-20210# Bonn Univ. (Germany).
SECOND EUROPEAN SYMPOSIUM ON X-RAY TOPOGRAPHY AND HIGH RESOLUTION DIFFRACTION: PROGRAMME AND ABSTRACTS
7 Sep. 1994 228 p Symposium held in Berlin, Germany, 5-7 Sep. 1994
(Contract N68171-94-M-5247)
(AD-A286328; R/D-7291-MS-02) Avail: CASI HC A11/MF A03

Partial contents include: early experimental proofs of the dynamical theory; topography in magnetism: domain and phase transition investigations; diffraction topographic investigations of crystals under applied electric fields; dependence of defect arrangement in crystals on surface morphology and on conditions of growth from solution; interaction of slip bands with grain boundaries - observation by white beam SR topography; in-situ x-ray topography studies during the MBE growth process of InGaAs strained layers; double- and triple-crystal x-ray diffraction analysis of semiconductor quantum wires; applications in multiple crystal diffractometry; interpretation of the diffraction profile resulting from strain relaxation in epilayers; and study of thin buried interfaces in III-V compound heterostructures by high resolution x-ray diffraction. DTIC

N95-20240# Edgerton, Germeshausen and Grier, Inc., Idaho Falls, ID.
NONLINEAR FARADAY EFFECT IN CdS SEMICONDUCTOR IN AN ULTRAHIGH MAGNETIC FIELD
V. V. Druzhinin, O. M. Tatsenko, and A. I. Bykov et al 1994 8 p Presented at the 4th International Symposium on Research in High Magnetic Fields, Nijmegen, Netherlands, 29-31 Aug. 1994
(Contract DE-AC08-93NV-11265)
(DE94-016804; EGG-11265-2051; CONF-940831-2) Avail: CASI HC A02/MF A01

A significant nonlinearity in the angle of rotation polarization plane was observed in CdS at wavelengths of 494 in the presence of high magnetic fields (0.5-5 MG). The onset significant nonlinearity also depended on sample temperature. An absorption study with probe wavelength of approximately 494 nm revealed an increase in optical transmission associated with a splitting of the conduction band. Dispersion, field and temperature curves indicate a low conduction electron mass m(sub e) = 0.3 m(sub o). A numerical calculation and interpretation of the observed effects was carried out using band theory. The optical and magnetooptical properties of semiconducting crystals of CdS were studied. This article describes joint American-Russian experiments to study the optical and magnetooptical properties of CdS in ultrahigh fields to approximately 7 MG. DOE

N95-20243# Colorado State Univ., Fort Collins, CO.
PROPERTIES OF MOLECULAR SOLIDS AND FLUIDS AT HIGH PRESSURE AND TEMPERATURE
R. D. Etters Jun. 1994 7 p
(Contract DE-FG02-86ER-45238)
(DE94-017594; DOE/ER-45238/7) Avail: CASI HC A02/MF A01

The main thrust of this work was directed to the task of determining the thermodynamic behavior of condensed solids and fluids containing simple molecules. Properties calculated include specific heats, equations of state, compressibilities, sound velocities, virial coefficients, viscosities, and thermal expansion. In addition, details of the structural, orientational, and magnetic phase transitions were determined. Dynamical quantities calculated include the lattice, libron, and vibron mode frequencies at various pressures and temperatures. Also, we developed new techniques required to meet our objectives. One was a method for accurately calculating the Gibbs free energy of various phases. Another is the multiple-histogram Monte Carlo which can dramatically reduce computing time and can provide a continuous map of thermodynamic averages over a range of some thermodynamical variable. DOE

N95-20244# Oak Ridge National Lab., TN.
SIMULATIONS OF THE DISLOCATION ARRAY AT Ge/Si INTERFACES
T. Kaplan, M. F. Chisholm, and M. Mostoller Dec. 1993 5 p Presented at the Fall Meeting of the Materials Research Society (MRS), Boston, MA, 29 Nov. - 3 Dec. 1993
(Contract DE-AC05-84OR-21400)
(DE94-017680; CONF-931108-104) Avail: CASI HC A01/MF A01

When Ge is grown epitaxially on Si(001), the 4% mismatch between the lattice parameters of Ge and Si can produce a regular two-dimensional grid of (a/2) (1,+/-1,0) edge dislocations at the interface, a checkerboard with a spacing of approximately 100 Angstrom. We have performed classical molecular dynamical simulations of this checkboard in large microcrystals. Results show the expected 5-fold plus 7-fold ring structure at the cores of the individual dislocations, and a new closed symmetric structure of 18 atoms at their intersections. Tetrahedral coordination is everywhere retained, with relatively small changes in the bond lengths of less than 10 and in the bond angles of less than 25%. The energetics and dislocation offset of the system are explored for the Stillinger-Weber and Tersoff potentials. DOE

N95-20245# Oak Ridge National Lab., TN.
SURFACE STRESS, MORPHOLOGICAL DEVELOPMENT, AND DISLOCATION NUCLEATION DURING STRAINED-LAYER EPITAXY
D. E. Jesson, S. J. Pennycook, J. M. Baribeau (National Research Council of Canada, Ottawa, Ontario.), and D. C. Houghton (National Research Council of Canada, Ottawa, Ontario.) Dec. 1993 7 p Presented at the Fall Meeting of the Materials Research Society (MRS), Boston, MA, 29 Nov. - 3 Dec. 1993
(Contract DE-AC05-84OR-21400)
(DE94-017682; CONF-931108-108) Avail: CASI HC A02/MF A01

Utilizing marker layer experiments and Z-contrast imaging, we have observed the formation of surface cusps during Si(x)Ge(1-x) alloy growth. The formation of cusps can be understood in terms of stress-driven surface diffusion, and we consider the large stress build-up at the cusp tip as a potential source for the nucleation of misfit dislocations. DOE

N95-20261# Israel Physical Society, Jerusalem (Israel).
ISRAEL PHYSICAL SOCIETY ANNUAL MEETING 1994
10 May 1994 94 p Meeting held in Haifa, Israel, 10 May 1994
(DE94-630140; INIS-mf-13949; CONF-9405195) Avail: CASI HC A05/MF A01 (US Sales Only)

The publication includes research abstracts in several fields of physics: condensed matter, solid state physics, high energy physics, medical physics, non-linear physics and plasma physics. DOE

N95-20265# Brookhaven National Lab., Upton, NY.
LIGHT OUTPUT AND RADIATION DAMAGE IN A LEAD TUNGSTATE CRYSTAL
J. A. Kierstead, S. P. Stoll, and C. L. Woody 1994 7 p Presented at the Spring Meeting of the Materials Research Society, San Francisco, CA, 4-8 Apr. 1994
(Contract DE-AC02-76CH-00016)
(DE94-016814; BNL-60591; CONF-940411-49) Avail: CASI HC A02/MF A01

The optical absorption, light output and effects of radiation damage have been studied in a 2.2 x 2.2 x 12.8 cm(exp 3) crystal of lead tungstate. The crystal exhibits a longitudinal attenuation length which varies from roughly 13 cm to 1.5 m over the region where the scintillation emission occurs (400--800 nm). The light yield produces approximately 10 photoelectrons per MeV on a photomultiplier tube with a bialkali photocathode. The scintillation and light transmission properties of the crystal were characterized before and after exposure to 1 Mrad of C-60O gamma rays. Significant radiation induced optical absorption was observed in this crystal, along with a considerable amount of phosphorescence after irradiation. Partial spontaneous recovery from the damage occurred at room temperature, and it was possible to induce additional recovery by optical bleaching. DOE

N95-20330 Los Alamos National Lab., NM.
PAIRING ON SMALL CLUSTERS IN THE PEIERLS-HUBBARD MODEL: IMPLICATIONS FOR C60
J. T. Gammel, K. C. Ung (National Taiwan Inst. of Tech., Taipei, Taiwan.), and S. Mazumdar (Arizona Univ., Tucson, AZ.) 1994 7 p Presented at the 185th Electrochemical Society Meeting, San Francisco, CA, 22-27 May 1994 Limited Reproducibility: More than 20% of this document may be affected by microfiche quality
(Contract W-7405-eng-36)
(DE94-016284; LA-UR-94-2388; CONF-940529-21) Avail: CASI HC A02

Inclusion of electron-phonon interactions can substantially modify the conclusions about pairing obtained from models including only electron-electron interactions. The authors study pairing within the Peierls-Hubbard model for electron- and hole-doped analogs of C60 accessible to exact diagonalization techniques (cube, truncated tetrahedron, etc.), and discuss the extrapolation from these small system calculations to C60. DOE

N95-20340# Sandia National Labs., Albuquerque, NM.
IMPEDANCE CHARACTERISTICS OF MULTISTAGE ION DIODES
M. Desjarlais 1994 5 p Presented at the 10th International Conference on High Power Particle Beams, San Diego, CA, 20-24 Jun. 1994
(Contract DE-AC04-94AL-85000)
(DE94-018887; SAND-93-3893C; CONF-940634-20) Avail: CASI HC A01/MF A01

We further develop a theory of multistage diodes that includes the possibility of emission of ions in the final stage. The exact solutions are extremely cumbersome and are not practical for most applications. We have developed approximate solutions that are very accurate, require no integrations, and may be rapidly calculated using a simple iterative scheme. These solutions for the total current as a function of voltage are used in time-dependent modeling of a two-stage diode. DOE

N95-20371# Oak Ridge National Lab., TN.
ENHANCED IONIC CONDUCTION AT THE FILM/SUBSTRATE INTERFACE IN LiI THIN FILMS GROWN ON SAPPHIRE(0001)
D. Lubben and F. A. Modine Dec. 1993 7 p Presented at the Fall Meeting of the Materials Research Society (MRS), Boston, MA, 29 Nov. - 3 Dec. 1993
(Contract DE-AC05-84OR-21400)
(DE94-017884; CONF-931108-107) Avail: CASI HC A02/MF A01

The ionic conductivity of LiI thin films grown on sapphire(0001) substrates has been studied in-situ during deposition as a function of film thickness and deposition conditions. LiI films were produced at room temperature by sublimation in an ultra-high-vacuum system. The conductivity of the LiI parallel to the film/substrate interface was determined from frequency-dependent impedance measurements as a function of film thickness using Au interdigital electrodes deposited on the sapphire surface. The measurements show a conduction of (approximately)5 times the bulk value at the interface which gradually decreases as the film thickness is increased beyond 100 nm. This interfacial enhancement is not stable but anneals out with a characteristic log of time dependence. Fully annealed films have an activation energy for conduction (sigma)T of (approximately)0.47 +/- .03 eV, consistent with bulk measurements. The observed annealing behavior can be fit with a model based on dislocation motion which implies that the increase in conduction near the interface is not due to the formation of a space-charge layer as previously reported but to defects generated during the growth process. This explanation is consistent with the behavior exhibited by CaF2 films grown under similar conditions. DOE

N95-20372# Oak Ridge National Lab., TN.
ENERGY GAP STRUCTURE OF LAYERED SUPERCONDUCTORS
S. H. Liu and R. A. Klemm (Argonne National Lab., IL.) Dec. 1993 13 p Presented at the OE/LASE 1994: Conference on Optics, Electro-Optics, and Laser Applications in Science and Engineering, Los Angeles, CA, 22-29 Jan. 1994
(Contracts DE-AC05-84OR-21400; W-31-109-eng-38)
(DE94-017885; CONF-940142-45) Avail: CASI HC A03/MF A01

We report the energy gap structure and density-of-states (DOS) of a model layered superconductor with one superconducting layer and one normal layer in a unit cell along the c-axis. In the physically interesting parameter range where the interlayer hopping strengths of the quasiparticles are comparable to the critical temperature, the peaks in the DOS curve do not correspond to the order parameter (OP) of the superconducting layer, but depend on the OP and the band dispersion in the c-direction in a complex manner. In contrast to a BCS superconductor, the DOS of layered systems have logarithmic singularities. Our simulated tunneling characteristics bear close resemblance to experimental results. DOE

N95-20382# Brookhaven National Lab., Upton, NY.
POSITRON IMPLANTATION PROFILES IN ELEMENTAL AND MULTILAYER SYSTEMS
V. J. Ghosh 1994 25 p Presented at the 6th International Workshop on Slow-Positron Beam Techniques for Solids and Surfaces (SLOPOS6), Makuhari, Japan, 18-22 May 1994
(Contract DE-AC02-76CH-00016)
(DE94-014876; BNL-60583; CONF-9405198-2) Avail: CASI HC A03/MF A01

Different Monte Carlo schemes for modeling positron and electron implantation in solids have been briefly reviewed. Results (mean depth, backscattered fraction, profile shapes) of the Monte Carlo schemes are compared with experimental data and each other. Qualitatively, results of the different Monte Carlo schemes are the same; the most significant difference is in the value of the mean implantation depth. The scaled profiles (for positron implantation in any material) generated by the different Monte Carlo schemes can be superimposed on a universal curve which can be appropriately parameterized. Shapes of the scaled profiles, and the mean depth parameters A and n, are found to be material-dependent. DOE

N95-20399# Sandia National Labs., Albuquerque, NM.
MEAN FIELD ANALYSIS OF ORIENTATION SELECTIVE GRAIN GROWTH DRIVEN BY INTERFACE-ENERGY ANISOTROPY
J. A. Floro and C. V. Thompson (Massachusetts Inst. of Tech., Cambridge, MA.) 1994 6 p Presented at the Spring Meeting of the Materials Research Society, San Francisco, CA, 4-8 Apr. 1994
(Contract DE-AC04-94AL-85000)
(DE94-015797; SAND-94-0360C; CONF-940411-45) Avail: CASI HC A02/MF A01

Abnormal grain growth is characterized by the lack of a steady state grain size distribution. In extreme cases, the size distribution becomes transiently bimodal, with a few grains growing much larger than the average size. This is known as secondary grain growth. In polycrystalline thin films, the surface energy gammas and film/substrate interfacial energy gammas vary with grain orientation, providing an orientation-selective driving force that can lead to abnormal grain growth. We employ a mean field analysis that incorporates the effect of interface energy anisotropy to predict the evolution of the grain size/orientation distribution. While abnormal grain growth and texture evolution always result when interface energy anisotropy is present, whether secondary grain growth occurs will depend sensitively on the details of the orientation dependence of (gamma)i. DOE

N95-20400# Sandia National Labs., Albuquerque, NM.
CHARACTERISTICS OF OXYNITRIDES GROWN IN N2O
N. S. Saks (Naval Research Lab., Washington, DC.), D. I. Ma (Naval Research Lab., Washington, DC.), M. E. Twigg (Naval Research Lab., Washington, DC.), and D. M. Fleetwood 1994 10 p Presented at the 185th Electrochemical Society Meeting, San Francisco, CA, 22-27 May 1994
(Contract DE-AC04-94AL-85000)
(DE94-015798; SAND-94-1742C; CONF-940529-22) Avail: CASI HC A02/MF A01

MOS oxides have been fabricated by oxidation of silicon in N2O. Processes studied include oxidation in N2O alone, and two-step oxidation in O2 followed by N2O. For both oxides, a nitrogen-rich layer with a peak N concentration of approximately 0.5 at. % is observed at the Si-SiO2 interface with SIMS. Electrical characteristics of N2O oxides, such as breakdown and defect generation, are generally improved, especially for the two-step process. Drawbacks typically associated with NH3-nitrided oxides such as high fixed oxide charge and enhanced electron trapping, are not observed in N2O oxides, which is probably due to their smaller nitrogen content. DOE

N95-20405# Sandia National Labs., Livermore, CA.
FIRST PRINCIPLES SIMULATION OF MATERIALS PROPERTIES
W. A. Shelton, G. M. Stocks, R. G. Jordan (Florida Atlantic Univ., Boca Raton, FL.), Y. Liu (Florida Atlantic Univ., Boca Raton, FL.), L. Qui (Florida Atlantic Univ., Boca Raton, FL.), D. D. Johnson, F. J. Pinski (Cincinnati Univ., OH.), J. B. Staunton (Warwick Univ., Coventry, England.), and B. Ginatempo (Messina Univ., Italy.) 1994 7 p Presented at the Scalable High Performance Computing Conference, Cincinnati, OH, May 1994
(Contracts DE-AC04-94AL-85000; DE-AC05-84OR-21400)
(DE94-016781; SAND-94-8691C; CONF-9405207-1) Avail: CASI HC A02/MF A01

We have developed a hybrid, parallel computer code for calculating the electronic structure of both ordered and substitutionally disordered materials. By using PVM3.3, we can integrate into our local computer environment multiple parallel and vector supercomputers as well as high performance workstations. Without this approach, calculations of materials properties of large systems would be otherwise untenable due to a lack of computer resources. For example, we have determined the short-range order intensity and its electronic origin for the Ag-Mg alloy system, including an estimate of the order-disorder (spinodal) temperature. DOE

N95-20419# Argonne National Lab., IL. Energy Technology Div.
A MECHANISTIC MODEL FOR RADIATION-INDUCED CRYSTALLIZATION AND AMORPHIZATION IN U3Si
J. Rest Jun. 1994 16 p Presented at the 17th Symposium on Effects of Radition on Materials, Sun Valley, ID, 20-23 Jun. 1994
(Contract W-31-109-eng-38)
(DE94-015028; ANL/ET/CP-83313; CONF-940657-2) Avail: CASI HC A03/MF A01

Radiation-induced amorphization is assessed. A rate-theory model is formulated wherein amorphous clusters are formed by the damage event. These clusters are considered centers of expansion (CE), or excess-free-volume zones. Simultaneously, centers of compression (CC) are created in the material. The CC's are local regions of increased density that travel through the material as an elastic (e.g., acoustic) shock wave. The CE's can be annihilated upon contact with CC's (annihilation probability depends on height of the energy barrier), forming either a crystallized region indistinguishable from the host material, or a region with a slight disorientation (recrystallized grain). Recrystallized grains grow by the accumulation of additional CC's. Full amorphization is calculated on the basis of achieving a fuel volume fraction consistent with the close packing of spherical entities. Amorphization of a recrystallized grain is hindered by the grain boundary. Preirradiation of U3Si above the critical temperature for amorphization results in nanometer-size grains. Subsequent reirradiation of these samples at temperatures below the critical level shows that the material has developed a resistance to radiation-induced amorphization (that is, a higher dose is needed to amorphize the preirradiated samples than for those that have not been preirradiated). In the model, it is assumed that grain boundaries act as effective defect sinks, and that enhanced defect annihilation is responsible for retarding amorphization at low temperature. The calculations have been validated against data from ion-irradiation experiments with U3Si. To obtain additional validation, the model has also been applied to the ion-induced motion of the interface between crystalline and amorphous phases of U3Si. Results of this analysis are compared to data and results of calculations for ion bombardment of Si. DOE

N95-20426# Massachusetts Inst. of Tech., Lexington, MA. Lincoln Lab.
SOLID STATE RESEARCH Quarterly Report, 1 May - 31 Jul. 1993
Alan L. McWhorter 15 Aug. 1993 66 p
(Contract F19628-90-C-0002)
(AD-A279662) Avail: CASI HC A04/MF A01

This report covers in detail the research work of the Solid State Division at Lincoln Laboratory for the period 1 May through 31 July 1993. The topics covered are Electrooptical Devices, Quantum Electronics, Materials Research, Submicrometer Technology, High Speed Electronics, Microelectronics, and Analog Device Technology. Funding is provided primarily by the Air Force, with additional support provided by the Army, ARPA, Navy, SDIO, and NASA. DTIC

N95-20448# Lawrence Livermore National Lab., Livermore, CA.
SPIN-SPECIFIC PHOTOELECTRON DIFFRACTION USING MAGNETIC X RAY CIRCULAR DICHROISM
J. G. Tobin, G. D. Waddill, X. Guo (Wisconsin Univ., Milwaukee, WI.), and S. Y. Tong (Wisconsin Univ., Milwaukee, WI.) Apr. 1994 8 p Presented at the Intermag: 6th Joint Conference on Magnetism and Magnetic Materials, Albuquerque, NM, 20-23 Jun. 1994
(Contract W-7405-eng-48)
(DE94-017527; UCRL-JC-115741; CONF-940629-9) Avail: CASI HC A02/MF A01

The first observation of spin-dependent photoelectron diffraction using circularly-polarized x-rays is reported for monolayer ferromagnetic fcc Fe films on Cu(001). Circularly polarized x-rays are used to produce spin polarized photoelectrons from the Fe 2p spin-orbit split doublet, and intensity asymmetries in the 2p3/2 level of approximately 3% are observed. The asymmetry is dependent on the relative orientation of the x-ray polarization vector and the Fe magnetic moment. This spin-dependent technique promises the direct, element-specific determination not only of local atomic structure, but magnetic structure as well. DOE

N95-20449# Lawrence Livermore National Lab., Livermore, CA.
A STRUCTURAL DETERMINATION USING MAGNETIC X RAY CIRCULAR DICHROISM IN SPIN-POLARIZED PHOTOELECTRON DIFFRACTION
G. D. Waddill, J. G. Tobin, X. Guo (Wisconsin Univ., Milwaukee, WI.), and S. Y. Tong (Wisconsin Univ., Milwaukee, WI.) 26 May 1994 11 p Presented at the 4th European Vacuum Conference and the 1st Swedish Vacuum Meeting, Uppsala, Sweden, 13-17 Jun. 1994
(Contracts W-7405-eng-48; DE-FG02-84ER-45076)
(DE94-017528; UCRL-JC-117539; CONF-9406201-2) Avail: CASI HC A03/MF A01

The first structural determination with spin-polarized, energy-dependent photoelectron diffraction using circularly-polarized x-rays is reported for Fe films on Cu(001). Circularly-polarized x-rays produce spin-polarized photoelectrons from the Fe 2p doublet, and intensity asymmetries in the 2p(sup 3/2) level are observed. Fully spin-specific multiple scattering calculations reproduce the experimentally determined energy and angular dependences. A new analytical procedure which focuses upon intensity variations due to spin-dependent diffraction is introduced. DOE

N95-20461 Department of the Navy, Washington, DC.
SUPERCONDUCTING THIN FILM WITH FULLERENES AND METHOD OF MAKING Patent
Walter Eidelloth, inventor (to Navy), Richard J. Gambino, inventor (to Navy), Rodney Ruoff, inventor (to Navy), and Claudia D. Tesche, inventor (to Navy) 27 Sep. 1994 10 p Filed 28 Jul. 1993
(AD-D016580; US-Patent-5,332,723; US-Patent-Appl-SN-098094; US-Patent-Class-505-125) Avail: US Patent and Trademark Office

A method of producing a new high Tc superconducting material using fullerene molecules as artificial pinning sites for any magnetic flux that may enter the material. DTIC

N95-20479# Argonne National Lab., IL. Chemistry and Materials Science Lab.
NEW ET-BASED ORGANIC SUPERCONDUCTORS WITH THE ORGANOMETALLIC ANION Cu(CF3)4(-)
Urs Geiser, John A. Schlueter, K. Douglas Carlson, Jack M. Williams, H. Hau Wang, Wai-Kwong Kwok, Ulrich Welp, John A. Fendrich, James D. Dudek, and Crystal A. Achenbach et al 1994 4 p Presented at the International Conference on Science and Technology of Synthetic Metals, Seoul, Republic of Korea, 24-29 Jul. 1994 Prepared in cooperation with Cologne Univ., Germany, Sandia National labs., Albuquerque, NM, and North Carolina State Univ., Raleigh, NC
(Contracts W-31-109-eng-38; DE-AC04-94AL-85000; DE-FG05-86ER-45259)
(DE94-016904; ANL/CHM/CP-83725; CONF-9407117-1) Avail: CASI HC A01/MF A01

Electrocrystallization of bis(ethylenedithio) tetrathiafulvalene (ET) with (PNP)Cu(CF3)4 in 1,1,2-trichloroethane (TCE) results in two new superconductors, K(sub L)-(ET)2Cu(CF3)4 (TCE), with T(sub c) = 4.0 K, and K(sub H)-(ET)2Cu(CF3)4 (TCE)(x), with T2 = 9.2 K. The first, k(sub L), forms well-developed plate-like crystals whose structure was determined by x-ray crystallography. Its band electronic structure is reported. The K(sub H)-phase forms long, thin needle bundles. DOE

N95-20483# California Univ., Los Angeles, CA. Dept. of Chemistry and Biochemistry.
THE DYNAMICS OF FORMATION AND EVAPORATION OF MIXED ALKALI HALIDE NANOCRYSTALS: A CASE OF COMPARABLE LATTICE ENERGIES
Temer S. Ahmadi and Mostafa A. El-Sayed 21 Sep. 1994 22 p Submitted for publication
(Contract N00014-89-J-1350)
(AD-A285052; TR-79) Avail: CASI HC A03/MF A01

The relative intensity distribution of the (Rb(n)K(14-n)I13)(+) mixed nanocrystals containing a 'magic' number of 14 metal cations and 13 iodide anions is examined. These nanocrystals were generated through sputtering of mixed RbI/KI solids using fast atom bombardment, and analyzed by use of a double-focusing sector-field mass spectrometer. The relative intensities of the observed peaks is found to have a 'bimodal' distribution with a maximum near n=7. This observation is explained by assuming: (1) a rate of formation that is proportional to the number of isomers that can be formed for each mixed nanocrystal, and (2) a rate of dissociation that is insensitive to the composition of the mixed nanocrystal. The later assumption leads to the conclusion that the internal energies of these mixed nanocrystals are similar and independent of their composition. The conclusion is supported by the results of Monte Carlo simulation annealing as well as by the similarity of the known lattice energies of KI and RbI bulk crystals. Author (DTIC)

N95-20492# Oak Ridge National Lab., TN.
ATOMIC-RESOLUTION CHARACTERIZATION OF INTERFACE STRUCTURE AND CHEMISTRY IN THE STEM
N. D. Browning, M. M. McGibbon, A. J. McGibbon, M. F. Chisholm, S. J. Pennycook, V. Ravikumar (Northwestern Univ., Evanston, IL.), and V. P. Dravid (Northwestern Univ., Evanston, IL.) Mar. 1994 3 p Presented at the 13th International Congress on Electron Microscopy, Paris, France, 17-22 Jul. 1994
(Contract DE-AC05-84OR-21400)
(DE94-017753; CONF-940766-8) Avail: CASI HC A01/MF A01

Combination of Z-contrast imaging and EELS (electron energy loss spectroscopy) allows the local structure and chemistry of interfaces to be determined on the atomic scale. In this paper, these two complementary techniques are used to analyze the structure and chemistry of a nominally 25 degree (100) symmetric tilt boundary in an electroceramic SrTiO3 bicrystal. DOE

N95-20544# Wisconsin Univ., Madison, WI. Dept. of Chemistry.
AN ATOMICALLY-RESOLVED STM STUDY OF THE THERMAL DECOMPOSITION OF DISILANE ON Si(001) Interim Report, 1 Jun. 1993 - 31 May 1994

Y. Wang, J. Bronikowski, and R. J. Hamers 27 May 1994 77 p
(Contract N00014-91-J-1629)
(AD-A279818; TR-20) Avail: CASI HC A05/MF A01

Scanning Tunneling Microscopy (STM) has been used to study the adsorption and thermal dissociation of disilane (Si2H6) on the Si(001) surface. At low coverage, disilane adsorbs dissociatively to produce adsorbed SiH3 groups which are randomly distributed on the surface. STM images show that these SiH3 groups spontaneously dissociate into SiH2 and H within several minutes of adsorption at room temperature, and images depicting individual dissociation events have been obtained. Thermal annealing leads to diffusion and dissociation of the SiH2 groups through an intermediate which consists of a hydrogenated dimer which has its dimer axis parallel to those of the underlying substrate, instead of rotated. The structure and chemical identity of the intermediates are discussed in terms of the overall dissociation mechanism. Diffusion of hydrogen atoms leads to the formation of segregated surface phase of clean Si and the Si(001)-(2x1) monohydride structure, and bias-dependent STM imaging permits these species to be identified on a dimer-by-dimer basis. At low temperatures the monohydride distribution is non-statistical, showing a preference for flat terraces over small epitaxial islands. The diffusion, desorption, segregation of hydrogen and its role in blocking diffusion of silicon atom is also discussed. DTIC

N95-20552# Materials Research Society, Pittsburg, PA.
MOLECULARLY DESIGNED ULTRAFINE/NANOSTRUCTURED MATERIALS, VOLUME 351
Kenneth E. Gonsalves, Gan-Moog Chow, Tongsan D. Xiao, and Robert C. Cammarata 8 Apr. 1994 477 p Symposium held in San Francisco, CA, 4-8 Apr. 1994
(Contract N00014-1-94-0067)
(AD-A285370) Avail: CASI HC A21/MF A04

Nanostructured materials are usually defined as having some length scale smaller than 100 nm in at least one dimension. An important subset of this group of materials is powders with particle size less than 100 nm, and polycrystalline materials, made by consolidating these powders in such a way as to retain a grain size below this limit. The choice of 100 nm stems from the fact that many physical, optical, and magnetic properties have characteristic lengths in this range. As grain or particle size is reduced below this characteristic length, the properties associated with these phenomena are radically altered. A frequently cited example is the freezing out of mechanisms for generating glissile dislocations. Another reason for expecting remarkable properties in nanostructured polycrystalline materials is the very high proportion of atoms at, or near, grain boundaries (as high as fifty percent or greater for grain sizes below five or ten nanometers). This leads, for example, to very rapid diffusion coupled with very short diffusion distances. DTIC

N95-20553# George Washington Univ., Washington, DC. Dept. of Chemistry.
TWO-CENTER, TWO ELECTRON EXCITATIONS IDENTIFIED IN NEXAFS FOR SOLID Ne Technical Report, Sep. 1993 - Oct. 1994
H. Sambe, X. Qian, and D. E. Ramaker Sep. 1994 12 p
(Contract N00014-93-I-0331)
(AD-A285373; TR-68) Avail: CASI HC A03/MF A01

Experimental K-edge NEXAFS (near edge X ray absorption fine structure) data for solid Ne are compared with theoretical results. Seven features in the experimental spectrum that are not reproduced by the theoretical results are found to be attributable to two-electron excitations. Five of them are usual one-center excitations, but the remaining two are found to be novel two-center excitations involving resonant orbitals as opposed to the usual bound orbitals. In contrast, two-center, two-electron excitations involving only bound orbitals are found to be absent in the experimental spectrum. DTIC

N95-20594 Wisconsin Univ., Madison, WI. Dept. of Chemistry.
ANTIPHASE BOUNDARIES AS NUCLEATION CENTERS IN LOW-TEMPERATURE EPITAXIAL GROWTH Interim Report, 1 Jun. 1993 - 31 May 1994
Michael J. Bronikowski, Yajun Wang, and Robert J. Hamers 27 May 1994 18 p Limited Reproducibility: More than 20% of this document may be affected by microfiche quality
(Contract N00014-91-J-1629)
(AD-A279895; TR-17-ONR) Avail: CASI HC A03

The epitaxial growth of silicon on Si(001) from disilane at 720 K has been investigated using scanning tunneling microscopy. Epitaxy occurs by island nucleation and growth, with islands nucleating preferentially at antiphase boundaries between different regions on the substrate terraces. These islands begin as a single dimer string which grows to cover the entire antiphase boundary before lateral growth begins. The islands increase in size until they meet on the surface, forming new antiphase boundaries (50% of the time) for nucleation of the next layer. We find that islands nucleated at such boundaries account for approximately 94% of the area of a growing layer, indicating that essentially all epitaxial growth at this temperature occurs by this mechanism. DTIC

N95-20614# North Carolina State Univ., Raleigh, NC.
GROWTH, CHARACTERIZATION AND DEVICE DEVELOPMENT IN MONOCRYSTALLINE DIAMOND FILMS Quarterly Technical Report, 1 Jul. - 30 Sep. 1994
Robert F. Davis, J. T. Glass, and R. J. Nemanich Sep. 1994 28 p
(Contract N00014-93-I-0437)
(AD-A285991) Avail: CASI HC A03/MF A01

Candidate substrate materials for the pseudomorphic growth Cu films as host templates on which to subsequently deposit diamond films have been selected. The selection criteria were: (1) high diamond nucleation density as a bulk substrate; (2) low strain energy density in the interlayer material upon 100% two dimensional matching with the substrate; (3) ease of deposition of the interlayer material; and (4) low solubility at growth temperatures. The most promising interlayer materials were Ni, Si, Hf and Ti. Experimentally, the deposition of 5A of Ti on Cu increased the diamond particle density relative to bare Cu by an order of magnitude. No appreciable diffusion to Ti into Cu occurred and only a thin carbide layer was necessary for diamond nucleation. Raman spectroscopy has been employed to analyze residual compressive stress in four diamond films. The line shape analysis indicated that the Raman band is mostly Lorentzian for all four samples and that the main broadening mechanism is via life-time shortening due to scattering from Si and N impurity concentrations. The line width increased linearly as a function of peak position, indicative of a correlation between the impurities and stress. DTIC

N95-20630# California Univ., Berkeley. Lawrence Berkeley Lab, CA.
PHOTOLUMINESCENCE UNDER PRESSURE AND ANNEALING OF NITROGEN-DOPED ZnSe
A. L. Chen, W. Walukiewicz, and E. E. Haller Jul. 1994 4 p Presented at the 22d International Conference on Physics of Semiconductors, Vancouver, British Columbia, 15-19 Aug. 1994
(Contract DE-AC03-76SF-00098)
(DE95-002355; LBL-35358; CONF-9408155-9) Avail: CASI HC A01/MF A01

The authors report photoluminescence measurement of MBE-grown nitrogen-doped ZnSe under hydrostatic stress. They determined the pressure coefficients of two separate donor-acceptor pair transitions in these samples. The results indicate that the deeper transition is caused by a localized donor that moves further into the band gap with increasing pressure, confirming that it stems from a localized donor. They also show that annealing at temperatures above 325 C produces this donor and results in compensation of the acceptor. DOE

N95-20674# Oak Ridge National Lab., TN.
MICROSCOPY OF STRESS-INDUCED MORPHOLOGICAL DEVELOPMENT AND DISLOCATION NUCLEATION DURING SEMICONDUCTOR EPITAXY
D. E. Jesson, K. Chen, S. J. Pennycook, J.-M. Baribeau, and D. C. Houghton Mar. 1994 3 p Presented at the Microscopy Society of America and Microbeam Analysis Society Joint Meeting, New Orleans, LA, 31 Jul. - 5 Aug. 1994
(Contract DE-AC05-84OR-21400)
(DE94-017869; CONF-940753-22) Avail: CASI HC A01/MF A01

A Z-contrast image of a Si0.5Ge0.5 layer, in which 2 monolayer Ge marker layers were inserted during growth by molecular beam epitaxy, showed cusp-like features. The stress concentration at the cusp tip will continue to accelerate rapidly; there must be some mechanism to relieve this stress, and the most obvious solution is the emission of a dislocation half loop at the cusp tip. DOE

N95-20677# California Univ., Berkeley, CA.
INSTANTANEOUS FREQUENCY DYNAMICS OF COHERENT EMISSION FROM MAGNETOEXCITONS IN GALLIUM ARSENIDE
M. A. Mycek, U. Siegner, and D. S. Chemla May 1994 8 p Presented at the International Quantum Electronics Conference, Anaheim, CA, 8-13 May 1994
(Contract DE-AC03-76SF-00098)
(DE94-018182; LBL-35203; CONF-9405219-2) Avail: CASI HC A02/MF A01

By time resolving the power spectrum of the ultrafast four wave mixing emission from the lowest magnetoexciton in GaAs, the authors determine the origin of the very complicated dynamics observed in the time domain. DOE

N95-20678# California Univ., Berkeley, CA.
TEMPORAL AND SPECTRAL INVESTIGATION OF MULTI-LANDAU LEVEL QUANTUM BEATS IN GaAs
U. Siegner, M. A. Mycek, and D. S. Chemla May 1994 8 p Presented at the International Quantum Electronics Conference, Anaheim, CA, 8-13 May 1994
(Contract DE-AC03-76SF-00098)
(DE94-018189; LBL-35204; CONF-9405219-1) Avail: CASI HC A02/MF A01

By resolving temporally and spectrally transient four-wave-mixing, the authors observe multiple Landau level quantum beating in GaAs under 6T magnetic field. Excitation energy and density dependent quantum interference gives rise to non-periodic beats. DOE

N95-20679# California Univ., Berkeley, CA.
PHASE DYNAMICS OF NON-EQUILIBRIUM DISTRIBUTIONS OF FREE ELECTRON-HOLE PAIRS IN GaAs QUANTUM WELLS
J. Y. Bigot, M. A. Mycek, S. Weiss, and D. S. Chemla May 1994 7 p Presented at the International Quantum Electronics Conference, Anaheim, CA, 8-13 May 1994
(Contract DE-AC03-76SF-00098)
(DE94-018190; LBL-35205; CONF-9405219-4) Avail: CASI HC A02/MF A01

The authors resolve the phase and amplitude of the coherent emission of a non-equilibrium Fermi-Sea in four wave mixing experiments. It exhibits an ultrafast dynamical blue shift, due to Fermi-edge many-body effects. DOE

N95-20696# Los Alamos National Lab., NM.
HASSP AND HEAVY: TOOLS FOR AUTOMATED HEAVY ATOM SEARCHES AND REFINEMENT
T. T. Terwilliger Jun. 1994 11 p Presented at the American Crystallographic Association Meeting, Atlanta, GA, 25 Jun. - 1 Jul. 1994
(Contract W-7405-eng-36)
(DE94-016071; LA-UR-94-2273; CONF-9406225-1) Avail: CASI HC A03/MF A01

In this tutorial, a simple example using model data for one derivative with anomalous information will be used to demonstrate the use of HASSP and HEAVY in heavy atom determination and refinement. The data used here will actually be based on model MAD data that has been converted to MIR format using MADMRG, but the treatment is identical to that for any other SIR+anomalous data. DOE

N95-20714 New Mexico Univ., Albuquerque, NM. Dept. of Chemistry.
SYNTHESIS AND CHARACTERIZATION OF (Zn(SEt)Et)10, FORMED VIA INSERTION OF SULFUR INTO Zn-C BONDS: A NEW CLASS OF WURTZITE-LIKE CLUSTER FRAMEWORK
Mark J. Hampden-Smith, D. Zeng, and Eileen Duesler 6 May 1994 14 p Limited Reproducibility: More than 20% of this document may be affected by microfiche quality
(Contract N00014-91-J-1258)
(AD-A279701; TR-15) Avail: Issuing Activity (Defense Technical Information Center (DTIC))

The reaction of a toluene solution of ZnEt2 with one equivalent of sulfur (1/8 S8) results in dissolution of the sulfur to form a colorless solution. After addition of n-pentane and cooling, colorless crystals of Zn10(SEt)10Et10 were isolated and characterized by a variety of spectroscopic characterization techniques and by single-crystal X-ray diffraction. Crystallographic data for Zn10(SEt)10Et10 at 293K: space group P(bar-I), a = 12.010 (2)A, b = 14.739 (3)A, c = 20.327 (4)A, a = 99.93 (3) deg, beta = 91.62 (3) deg, gamma = 107.79 (3) deg, V = 3362.2 (11) A3, Z = 2, d(calc) = 1.636 g/cu cm, R = 9.41%, Rw = 9.00%. Although the crystal deteriorated during data collection, the structural data show that Zn10(SEt)10Et10 exhibits a unique wurtzite-like ZnS core rather than a sphalerite-like core which is more common to zinc and cadmium alkylthiolate clusters. Thermal decomposition of Zn10(SE)10Et10 was studied by diffraction methods, microscopy, thermal analysis and elemental analysis. These data are consistent with the formation of a crystalline, cubic (sphalerite) ZnS at low temperatures, 250 C, providing evidence that the structure of the molecular precursor does not direct the crystallization of a particular polymorph on solid-state thermolysis in this system. DTIC

N95-20767# Kent State Univ., OH. Liquid Crystal Inst.
OPTICAL POWER LIMITING LIQUID CRYSTAL COMPOSITES Final Report, Jun. 1988 - Jun. 1993
Michael A. Lee, P. Palffy-Muhoray, J. W. West, L. C. Chien, and J. W. Doane 10 Nov. 1994 136 p
(Contract DAAB07-88-C-F421)
(AD-A286605; NV-94-C11) Avail: CASI HC A07/MF A02

This final report covers the experimental and theoretical investigations of optical power limiting in liquid crystal systems. Both pure and composite systems were investigated. Evaluation of a variety of liquid crystal materials for optical power limiting applications is reported. Under this project, optical power limiting of several pure materials was demonstrated in the nanosecond regime, with the cyanobiphenyls being found most effective for passive OPL applications. For CW lasers, polymer dispersed liquid crystals in a polymer matrix were shown to be effective optical power limiters when used in an active configuration. Extensive research on the mechanisms causing optical nonlinear response in liquid crystals is reported. Additional work on a separate subproject to evaluate and develop the shuttering capability of polymer dispersed liquid crystals in the IR is reported. Work on a variety of polymer/liquid crystal materials is reported. Successful shuttering of IR radiation was shown. Author (DTIC)

N95-20793# Brookhaven National Lab., Upton, NY.
CRYSTALLINE BEAMS
Jie Wei, Xiao-Ping Li (Biosym Technologies, Inc., San Diego, CA.), and Andrew M. Sessler (California Univ., Berkeley. Lawrence Berkeley Lab, CA.) Oct. 1994 21 p
(Contract DE-AC02-76CH-00016; NSF DMR-91-15342)
(DE95-002656; BNL-52439) Avail: CASI HC A03/MF A01

The low energy states of a beam of charged particles subject to circumferentially varying guiding and focusing forces are studied by first deriving a Hamiltonian in the rest frame of the circulating reference particle, and then using the molecular dynamics method. In an alternating gradient structure, operating below the transition energy, (but not in a constant gradient ring), the lowest state is ordered. The nature of the ground state depends upon the beam, density and the ring parameters. At very low temperature the crystal remains intact for a long time, but as temperature increases it rapidly gains energy from the lattice. In order for the crystalline beam to last a meaningful length of time, the storage ring should be designed such that the lattice periodicity of the machine is at least twice as high as the betatron frequencies. DOE

N95-20807 Ohio Univ., Athens, OH. Dept. of Physics and Astronomy.
THE IN SITU OBSERVATION OF EPITAXIAL DIAMOND THIN FILM NUCLEATION AND GROWTH USING EMISSION ELECTRON MICROSCOPY Semiannual Report, 1 Jul. - 31 Dec. 1993
Martin E. Kordesch 20 May 1994 28 p Limited Reproducibility: More than 20% of this document may be affected by microfiche quality
(Contract N00014-91-J-1596)
(AD-A279811) Avail: Issuing Activity (Defense Technical Information Center (DTIC))

A method for activation of high resistivity, (100) texture CVD diamond films with gold, to improve low field electron emission is described. A model based on the dielectric breakdown of the diamond film is proposed and a test experiment, which consists of heating the gold layer to a point where the gold forms sub-micron spheroids on the diamond surface, is described which supports the model. The deposition of carbon and sulfur on Mo(310) is characterized with scanning Auger Microscopy. Correlation between Photoelectron emission Microscopy, scanning Auger Microscopy and Auger spectroscopy can be made, so that individual features in PEEM and SAM images can be identified by elemental composition. The initial design of a Seeded Supersonic Molecular Beam system for diamond deposition is described. DTIC

N95-20819# Oak Ridge National Lab., TN.
A MONTE CARLO STUDY OF THE MINUS SIGN PROBLEM IN THE t-J MODEL USING AN INTEL iPSC/860 HYPERCUBE
M. D. Kovarik and T. Barnes 1993 15 p Presented at the Mardi Gras Conference on Concurrent Computing in the Physical Sciences, Baton Rouge, LA, 18-20 Feb. 1993 Prepared in cooperation with Tennessee Univ., Knoxville, TN
(Contract DE-AC05-84OR-21400)
(DE95-001072; CONF-9302112-4) Avail: CASI HC A03/MF A01

We describe a Monte Carlo simulation of the 2-dimensional t-J model on an Intel iPSC/860 hypercube. The problem studied is the determination of the dispersion relation of a dynamical hole in the t-J model of the high temperature superconductors. Since this problem involves the motion of many fermions in more than one spatial dimensions, it is representative of the class of systems that suffer from the 'minus sign problem' of dynamical fermions which has made Monte Carlo simulation very difficult. We demonstrate that for small values of the hole hopping parameter one can extract the entire hole dispersion relation using the GRW Monte Carlo algorithm, which is a simulation of the Euclidean time Schroedinger equation, and present results on 4 x 4 and 6 x 6 lattices. We demonstrate that a qualitative picture at higher hopping parameters may be found by extrapolating weak hopping results where the minus sign problem is less severe. Generalization to physical hopping parameter values will only require use of an improved trial wavefunction for importance sampling. DOE

N95-20820# Oak Ridge National Lab., TN.
Hg-199 AND Cu-(63,65) NMR STUDIES OF MERCURY BASED HIGH-Tc SUPERCONDUCTORS
W. Hoffmann (Freie Univ., Berlin, Germany.), H. Breitzke (Freie Univ., Berlin, Germany.), C. T. Simmons (Freie Univ., Berlin, Germany.), K. Lueders (Freie Univ., Berlin, Germany.), G. Buntkowsky (Freie Univ., Berlin, Germany.), H. H. Limbach (Freie Univ., Berlin, Germany.), E. V. Antipov (Moscow State Univ., Russia.), A. A. Gippius, O. Loebich, and H. R. Khan et al Jul. 1994 19 p Presented at the Ampere Workshop on Magnetic Resonance and Microwave Absorption in the High Tc Superconducting Materials, Poznan, Poland, 10-13 Apr. 1994 Submitted for publication
(Contract DE-AC05-84OR-21400)
(DE95-001073; CONF-9404104-1) Avail: CASI HC A03/MF A01

Hg-oxide ceramic high temperature superconductors were studied with Hg-199- and Cu-63,65-NMR spectroscopy. Room temperature spectra, spin-spin and spin-lattice relaxation times of samples with different superconducting transition temperatures are presented. A spin-lattice relaxation time of T(sub 1) = 35 msec and a spin-spin relaxation time of T(sub 2) = 1.6 msec is found for the Hg-199-NMR. All samples exhibit similar characteristic powder spectra caused by an axially symmetric Hg-199 spin interaction. The isotropic value and t he anisotropy of the tensor relative to solid HgCl2 as a standard substance is estimated. Furthermore results of Cu-63,65-NMR at a temperature of 4.2 K are presented. Also this signal shows a powder line shape (for I = 3/2). DOE

N95-20838# Notre Dame Univ., IN. Radiation Lab.
PHOTOINDUCED CHARGE TRANSFER BETWEEN FULLERENES AND TiO2 SEMICONDUCTOR COLLOIDS
P. V. Kamat, I. Bedja (Quebec Univ., Trois-Riveres, Quebec.), and S. Hotchandani (Quebec Univ., Trois-Riveres, Quebec.) 1994 12 p Presented at the 185th Electrochemical Society Meeting, San Francisco, CA, 22-27 May 1994
(Contract DE-AC02-76ER-00038)
(DE95-001447; DOE/ER-00038/3707; CONF-940529-26) Avail: CASI HC A03/MF A01

A photocatalytic method has been presented to carry out one-electron reduction of C60 and C70 in 50/50 (v/v) benzene/ethanol. The fullerene reduction was carried out in colloidal TiO2 suspension using UV excitation. The charge transfer between the excited TiO2 semiconductor colloid and fullerene molecule occurs with a quantum efficiency of 13% for C70 and 24% for C60. Laser flash photolysis measurements have been carried out to elucidate the mechanism of photocatalytic reduction. DOE

N95-20841# Argonne National Lab., IL.
REACTIVE NANOPHASE OXIDE ADDITIONS TO MELT-PROCESSED HIGH-T(SUB c) SUPERCONDUCTORS
K. C. Goretta, B. P. Brandel, M. T. Lanagan, J. Hu, D. J. Miller, S. Sengupta, J. C. Parker (Nanophase Technologies Corp., Evanston, IL.), M. N. Ali (Nanophase Technologies Corp., Evanston, IL.), and Nan Chen (Illinois Superconductor Corp., Evanston, IL.) Oct. 1994 5 p Presented at the Applied Superconductivity Conference, Boston, MA, 16-21 Oct. 1994
(Contract W-31-109-eng-38)
(DE95-001470; ANL/ET/CP-82340; CONF-941013-2) Avail: CASI HC A01/MF A01

Nanophase TiO2 and Al2O3 powders were synthesized by a vapor-phase process and mechanically mixed with stoichiometric YBa2Cu3O(x) and TlBa2Ca2Cu3O(x) powders in 20 mole % concentrations. Pellets produced from powders with and without nanophase oxides were heated in air or O2 above the peritectic melt temperature and slow-cooled. At 4.2 K, the intragranular critical current density J(sub c)) increased dramatically with the oxide additions. At 35-50 K, effects of the oxide additions were positive, but less pronounced. At 77 K, the additions decreased J(sub c), probably because of inducing a depression of the transition temperature. DOE

N95-20881# Argonne National Lab., IL.
ATMOSPHERE INFLUENCE ON IN SITU ION BEAM ANALYSIS OF THIN FILM GROWTH
Yuping Lin, A. R. Krauss, D. M. Gruen, and R. P. H. Chang (Northwestern Univ., Evanston, IL.) 1994 23 p Presented at the International Conference on Metallurgical Coatings and Thin Films, San Diego, CA, 25-29 Apr. 1994
(Contract W-31-109-eng-38)
(DE95-001507; ANL/CHM/CP-81118; CONF-940440-6) Avail: CASI HC A03/MF A01

In situ, nondestructive surface characterization of thin-film growth processes in an environment of chemically active gas at pressures of several mTorr is required both for the understanding of growth processes in multicomponent films and layered heterostructures and for the improvement of process reproducibility and device reliability. The authors have developed a differentially pumped pulsed ion beam surface analysis system that includes ion scattering spectroscopy (ISS) and direct recoil spectroscopy (DRS), coupled to an automated ion beam sputter-deposition system (IBSD), to study film growth processes in an environment of chemically active gas, such as required for the growth of oxide, nitride, or diamond thin films. The influence of gas-phase scattering and gas-surface interactions on the ISS and DRS signal intensity and peak shape have been studied. From the intensity variation as a function of ambient gas pressure, the authors have calculated the mean free path and the scattering cross-section for a given combination of primary ion species and ambient gas. Depending on the system geometry and the combination of primary beam and background, it is shown that surface-specific data can be obtained during thin-film growth at pressures ranging from a few mtorr to approximately 1 Torr. Detailed information such as surface composition, structure, and film growth mechanism may be obtained in real-time, making ion beam analysis an ideal nondestructive, in situ probe of thin-film growth processes. DOE

N95-20916# Nevada Univ., Reno, NV. Dept. of Chemistry.
PHOTOPHYSICAL PROCESSES ON TRIPLET STATES AND RADICAL IONS IN PURE AND MOLECULARLY DOPED POLYMERS
Ricard D. Burkhart 20 May 1994 7 p
(Contract DE-FG03-92ER-45476)
(DE95-002681; DOE/ER-45476/T1) Avail: CASI HC A02/MF A01

Given here is a brief summary of those projects which have or will shortly result in a publication. The photophysics of phenyldibenzophosphole in fluid solution has been studied and evidence for triplet excimers is presented. Time resolved transient absorption spectroscopy of triplet excimers and radical ions produced by laser photoexcitation of phenyldibenzophosphole in N,N-dimethylformamide has been performed. The photophysics of phenyldibenzophosphole and dibromocarbazole in polymers have been studied. DOE

N95-20964 Stanford Univ., CA. Physics Lab.
SCANNING TUNNELING MICROSCOPY OF SEMICONDUCTOR SURFACES Final Report, 1 Oct. 1991 - 30 Sep. 1993
Calvin F. Quate 30 Sep. 1993 11 p Limited Reproducibility: More than 20% of this document may be affected by microfiche quality
(Contract N00014-90-J-1001)
(AD-A279982; GL-5188) Avail: Issuing Activity (Defense Technical Information Center (DTIC))

In this final report, we discuss our recent results with the structure of metals on semiconductor surfaces. In particular, we focus our study on the use of surfactants for the epitaxial growth of germanium on silicon. A surfactant, such as tellurium, reduces the interfacial energy between the Si and Ge, as well as their surface free energies to change the growth mode to layer by layer, which is necessary to epitaxial growth. In addition to this summary of technical progress, we summarize some of the important events that took place in the Ginzton Lab during the period covered by this grant. These include the introduction of the force microscope and the transfer of this technology to industrial firms in such a way that instrument's based on the designs developed under this grant are now available in commercial form. Finally, we point out that our work on microfabrication of silicon cantilevers can be extended to the construction of parallel arrays where each cantilever is operated independently. Such an array will enable a large increase in speed for the new form of lithography based on patterning silicon with the E-field on the scanning tip. Such patterning can produce lines with widths less than 0.1 micrometer. This range, beyond the limits of optical lithography, is of crucial importance to the future of silicon microcircuits. DTIC

N95-20965 Displaytech, Inc., Boulder, CO.
DEVELOPMENT OF FERROELECTRIC LIQUID CRYSTALS WITH ENHANCED NONLINEAR OPTICAL PROPERTIES Final Report, 15 Jul. 1993 - 15 Apr. 1994
Kenneth E. Arnett 24 Apr. 1994 26 p Limited Reproducibility: More than 20% of this document may be affected by microfiche quality
(Contract F49620-93-C-0045)
(AD-A279988; DTI-156F; AFOSR-94-0324TR) Avail: CASI HC A03

During our Phase 1 research, we advanced materials synthesis and evaluation techniques needed to develop ferroelectric liquid crystals into a useful second-order nonlinear optical material. We developed a technique for determining the second-order nonlinear susceptibility by measuring the electro-optic coefficient r22 at 633 nm, using modulation frequencies between 100 KHz-100 MHz. We evaluated two specially synthesized FLCs by measuring their r22 coefficients: previously existing MX-5679 and recently synthesized W-399, both based on a nitrobenzene hyperpolarizable moiety. Results show an increasing r22 with increasing spontaneous polarization. We also partially evaluated a new FLC material, W-371, with an ortho-situated nitroaniline hyperpolarizable moiety. Since the liquid crystalline and the linear and nonlinear materials parameters FLC's have a temperature dependence, we examined existing FLC polymers for a FLC to glass phase and discovered a polymeric/FLC system that potentially could be used to reduce temperature dependent materials properties. Our FLC synthesis efforts concentrated on synthesis of Hoffman-LaRoche compounds roche 1 and roche 2. Unfortunately, we were unable to duplicate their synthesis and instead developed an alternative core that could yield FLC's with a higher second-order nonlinear susceptibility. DTIC

N95-21145# California Univ., Los Angeles, CA. Dept. of Electrical Engineering.
EPITAXIAL LIFTOFF TECHNOLOGY ONTO PROCESSED SILICON FOUNDRY WAFERS Final Report
Eli Yablonovitch 31 Jan. 1994 2 p
(Contract N00014-93-1-0311)
(AD-A285621) Avail: CASI HC A01/MF A01

The technical objectives are to research the application of liftoff transfer of epitaxial material to foreign substrates including: surface chemistry; electrical, mechanical, thermal and optical properties of Van der Waals bonded materials; III-V devices bonded to silicon circuitry and to other substrates with enhanced optical, electrical or thermal properties; and integrated optical devices incorporating lifted-off material and/or devices with LiNbO3, glass or other substrates. DTIC

N95-21167# Oak Ridge National Lab., TN. Metals and Ceramics Div.
DEPENDENCE OF CRITICAL CURRENT DENSITY ON MICROSTRUCTURE AND PROCESSING OF HIGH-T(c) SUPERCONDUCTORS
A. Goyal, E. D. Specht, Z. L. Wang, D. M. Kroeger, J. A. Sutliff (General Electric Co., Schenectady, NY.), J. E. Tkaczyk (General Electric Co., Schenectady, NY.), J. A. Deluca (General Electric Co., Schenectady, NY.), L. Masur (American Semiconductor Corp., Westborough, MA.), and G. N. Riley, Jr. (American Semiconductor Corp., Westborough, MA.) 1994 19 p Presented at the 123d Annual Meeting of the Minerals, Metals and Materials Society, San Francisco, CA, 27 Feb. - 3 Mar. 1994
(Contract DE-AC05-84OR-21400)
(DE95-000685; CONF-940204-10) Avail: CASI HC A03/MF A01

Microstructural origins for reduced weak-link behavior in high-J(sup c) melt-processed YBCO, spray pyrolyzed thick films of Tl-1223, metallic precursor Y-124 polycrystalline powder-in-tube (PIT) wires and PIT Bi-2212/2223 are discussed. Since the materials studied are the highest J(sub c), polycrystalline, high-T(sub c) superconductors fabricated worldwide, the results provide important guidelines for further improvements in superconducting properties, thereby enabling practical applications of these materials. It is found that strongly linked current flow within domains of melt-processed 123 occurs effectively through a single crystal path. In c-axis oriented, polycrystalline Tl-1223 thick films, local in-plane texture has been found to play a crucial role in the reduced weak-link behavior. Formation of 'colonies' of grains with a common c-axis and modest in-plane misorientation was observed. Furthermore, a colony boundary in general has a varying misorientation along the boundary. Large regions comprised primarily of low angle boundaries were observed. Percolative transport through a network of such small angle boundaries appears to provide the non-weak-linked current path. Although powder-in-tube BSCCO 2212 and 2223 also appear to have a 'colony' microstructure, there are some important differences. Colonies in BSCCO consist of stacks of grains with similar c-axis orientation in contrast to colonies in Tl-1223 films where few grains are stacked on top of one another. In the case of Y-124 wires, weak macroscopic in-plane texture is found. Additional measurements are underway to determine if a sharper, local in-plane texture also exists. It is found that in three of the four types of superconductors studied, reduced weak-link behavior can be ascribed to some degree of biaxial alignment between grains, either on a 'local' or a 'global' scale. DOE

N95-21228 Rutherford Appleton Lab., Oxford (England).
NEW THEORY OF CRITICAL FLOW VELOCITIES IN SUPERFLUID HELIUM
J. Mayers Jul. 1994 13 p
(PB95-130365; RAL-94-079) Avail: Issuing Activity (National Technical Information Service (NTIS))

It is shown that the critical flow velocities of superfluid He-4 through narrow channels can be understood using only simple quantum mechanics. The predicted variation of critical velocity with channel size is in good agreement with experimental data over range of channel sizes covering three orders of magnitude. NTIS

N95-21256# Argonne National Lab., IL. Material Science Div.
INTERLAYER MAGNETIC COUPLING IN EPITAXIAL Fe/Cr(211) AND (100) SUPERLATTICES
Eric E. Fullerton, J. E. Mattson, C. H. Sowers, and S. D. Bader Aug. 1994 12 p Presented at the Novel Magnetic Structures and Properties Conference, Santa Fe, NM, 24-25 Jun. 1994; sponsored by Acta Metallurgica, JEOL USA, Inc., Quantum Design, Inc., and Delaware Univ.
(Contract W-31-109-eng-38)
(DE95-002906; ANL/MSD/CP-83081; CONF-9406204-2) Avail: CASI HC A03/MF A01

The authors present magnetic characterization of epitaxial Fe/Cr(211) and Fe/Cr(100) superlattices grown simultaneously on MgO(110) and (100) substrates, respectively. At room temperature, the coupling for these two orientations oscillates in sign with the same period (18(angstrom)), phase and strength. These results indicate that the long-period oscillation is independent of the nested feature of the Cr Fermi-surface. They examine the temperature dependence of interlayer coupling and find a uniform AF bias develops in the (211) samples upon cooling and observe strongly temperature-dependent biquadratic coupling in the (100) samples. DOE

N95-21279# State Univ. of New York, Buffalo, NY. Dept. of Physics.
X-RAY STUDIES OF MICROSTRUCTURES IN SEMICONDUCTOR AND SUPERCONDUCTING MATERIALS Progress Report
Y. H. Kao May 1994 10 p
(Contract DE-FG02-87ER-45283)
(DE95-001802; DOE/ER-45283/8) Avail: CASI HC A02/MF A01

The author uses various techniques of X-ray spectroscopy to study semiconductor and superconductor materials. The microstructure of Si(1-x)Ge(x) and Ge layers on silicon are reported. The superlattice structure of indium/gallium arsenides and local structure of manganese doped zinc sulfides as well as indium manganese arsenic compounds were investigated. Epilayer growth was studied for germanium on Si(1-x)Ge(x). DOE

N95-21287# Dartmouth Coll., Hanover, NH.
EXCITONS IN SEMICONDUCTING SUPERLATTICES, QUANTUM WELLS, AND TERNARY ALLOYS Technical Report, 15 Sep. 1987 - 31 Jan. 1994
M. D. Sturge, R. E. Nahory (Bell Communications Research, Inc., Red Bank, NJ.), and M. C. Tamargo (Bell Communications Research, Inc., Red Bank, NJ.) Feb. 1994 13 p
(Contract DE-FG02-87ER-45330)
(DE95-001867; DOE/ER-45330/T1) Avail: CASI HC A03/MF A01

Semiconducting layered structures can be fabricated with precisely defined layer thicknesses down to one monolayer; an example is superlattices (SL's), in which two semiconductors with different band gaps are interleaved. Research aims to understand optically excited states in SL's, particularly Type 2 indirect SL's (in which the excited electron and hole are separated both in real and in momentum space); time resolved tunable laser spectroscopy is used. Optical experiments were made in SL's with only a few atomic layers per period, to probe the interface quality. From the study of the exciton spectra of the mixed Type 1-Type 2 CdTe/CdZnTe SL's, the band offset at the CdTe/CdZnTe interface was obtained to high accuracy. Analysis of exciton-phonon coupling at isoelectronic traps, which provide a 3-D analog of the exciton traps formed by well width fluctuations in SL's, has corrected errors and given a self-consistent model of phonon-assisted transitions at these centers. DOE

N95-21297# Oak Ridge National Lab., TN.
NEUTRON DIFFRACTION STUDY OF THE MAGNETIC ORDERING OF BaCuO(2+x)
X. L. Wang, J. A. Fernandez-Baca, Z. R. Wang (Iowa State Univ. of Science and Technology, Ames, IA.), D. Vaknin (Iowa State Univ. of Science and Technology, Ames, IA.), and D. C. Johnston (Iowa State Univ. of Science and Technology, Ames, IA.) Aug. 1994 11 p Presented at the Neutron Scattering, Sendai, Japan, 11-14 Oct. 1994
(Contracts DE-AC05-84OR-21400; W-7405-eng-82)
(DE95-001357; CONF-9410165-8) Avail: CASI HC A03/MF A01

Neutron diffraction measurements have revealed that BaCuO(2+x) orders antiferromagnetically below T(sub N) = (15.0 +/- 0.5) with a magnetic propagating vector (kappa) = (1 1 1). The Cu atoms in the Cu6 ring clusters, located at the (1/4, 1/4, 1/4) positions, order ferromagnetically within these clusters while the clusters themselves order antiferromagnetically. The ordered magnetic moment of each of these Cu atoms is (0.69 +/- 0.05)mu(sub B) at T=4.2K. No evidence of long-range magnetic ordering of the Cu atoms in the Cu18 clusters, located at the (O, O, O) and (1/2, 1/2, 1/2) positions, was found down to a temperature T=2.5K. DOE

N95-21304# Sandia National Labs., Albuquerque, NM.
DEFECT PRODUCTION AND RECOMBINATION DURING LOW-ENERGY ION PROCESSING
B. K. Kellerman, J. A. Floro, E. Chason, D. K. Brice, S. T. Picraux, and J. M. White (Texas Univ., Austin, TX.) 1994 20 p Presented at the 41st Annual American Vacuum Society Symposium, Denver, CO, 24-28 Oct. 1994
(Contract DE-AC04-94AL-85000)
(DE95-001827; SAND-94-1280C; CONF-941001-3) Avail: CASI HC A03/MF A01

Low-energy ion processing produces damaged, microroughened semiconductor surfaces due to the production of point defects. The authors present a study of point defect production and annealing on the Ge(001)-2x1 surface during low-energy inert ion bombardment as a function of ion energy, ion mass and substrate temperature. Ion-induced surface point defect production was quantified experimentally in real time using in situ Reflection High Energy Electron Diffraction. The observed surface defect yield decreased abruptly around room temperature as the substrate temperature was increased from 175 K to 475 K. The authors have developed Monte Carlo simulations of defect diffusion to model defect recombination both in the bulk and on the surface. Bulk defect production statistics generated by a binary collision simulator, TRIMRC, were coupled with our bulk diffusion simulator to predict the number of ion-induced surface defects. A comparison between the experimental results and the simulation predictions indicated that defects produced in the bulk may represent a significant contribution to the observed surface defect yield and suggested that TRIMRC may overestimate the depth distribution of the defects. The simulations further indicated that the abrupt drop in the experimental yield with increasing substrate temperature does not arise from bulk defect recombination. The Monte Carlo simulations of surface diffusion (applicable to any crystalline surface) support a defect annealing mechanism (at low ion fluxes) that involves surface recombination of defects generated within a single cascade. DOE

N95-21408# Argonne National Lab., IL. Materials Science Lab.
DIFFRACTION APPLICATIONS USING THE ENERGY DISPERSIVE BEAMLINE, X6A, AT NSLS
P. L. Lee, M. A. Beno, G. S. Knapp, G. Jennings, and C. M. Ogata (Brookhaven National Lab., Upton, NY.) Aug. 1994 15 p Presented at the International Meeting on Synchrotron Radiation Instrumentation, Stony Brook, NY, 18-22 Jul. 1994
(Contract W-31-109-eng-38)
(DE94-019287; ANL/MSD/CP-82827; CONF-940714-30) Avail: CASI HC A03/MF A01

The energy dispersive beamline X6A, at the National Synchrotron Light Source (NSLS) employs a curved crystal monochromator (polychromator) which focuses a range (approximately 1 keV) of x-ray energies into a narrow (100-120 micron) line image. Although this beamline was constructed primarily for time dependent EXAFS experiments, the authors have begun to explore the use of this instrument for energy dispersive diffraction experiments with different types of sample including macromolecular crystals. The tunability (E = 6.5 keV to 21 keV) and flexibility ((Delta)E = 100-1,000 eV) of the instrument makes the beamline ideal as a test bed for the application of polychromatic single crystal diffraction techniques to different chemical or biological materials. DOE

N95-21419# Sandia National Labs., Albuquerque, NM.
A VERSATILE MASKING PROCESS FOR PLASMA ETCHED BACKSIDE VIA HOLES IN GaAs
A. J. Howard, R. J. Shul, M. L. Lovejoy, and J. C. Word 1994 6 p Presented at the Topical Conference on the Synthesis and Processing of Electronic Materials, San Francisco, CA, 13-18 Nov. 1994
(Contract DE-AC04-94AL-85000)
(DE94-019176; SAND-94-2200C; CONF-9411132-2) Avail: CASI HC A02/MF A01

We have developed a versatile backside via patterning process for a visible transmission modulator application. The vias are processed on mechanically thinned (approximately)100 micrometers thick GaAs using a (approximately)45 micrometers thick, negative tone, photo definable Polyimide mask and Reaction Ion Etch (RIE) plasma etching. The Polyimide masking process was found to be superior in both etch resistance and ease of use (more robust process, thicker, straighter sidewall Profile films, were more easily attained) to masking with standard optical photoresist. With the improved etch resistance (GaAs-to-polyimide etch selectivities of 10:1) we were able to Optimize Cl2-based plasma chemistries and etching conditions to achieve high GaAs etch rates in the RIE exceeding 5.0 micrometers/min. These etch optimization results along with our novel via patterning process are reported in this paper. DOE

N95-21444# Columbia Univ., New York, NY. Radiation Lab.
TRANSLATIONAL-ENERGY-RESOLVED STUDIES OF PHOTOGRAPHED CARRIER-INDUCED REACTIONS ON SEMICONDUCTOR SURFACES
Richard M. Osgood, Jr. and Quingyun Yang Aug. 1994 10 p
(Contract DE-FG02-90ER-14104)
(DE95-002944; DOE/ER-14104/5) Avail: CASI HC A02/MF A01

Enhancement in carrier lifetime has made semiconductors of interest for applications in photocatalysis ranging from solar energy conversion to environmental remediation. The authors have focused recent experimental work on adsorbed methyl halide molecules (CH3X, X = Br,Cl , I) on GaAs(110). They have identified and observed for the first time several chemical processes which control photochemistry on semiconductor surfaces. During this last year, the authors have focused on relating the observed electron transfer processes to the structure of the adsorbate molecular layer. To accomplish this, they have had to expand the experimental work with new measurement techniques. The primary focus of the work has been in determining the orientation of the adsorbates with regard to the underlying surface correlation. An important result of this work has been that the authors have provided for the first time an unequivocal determination of the orientation of physisorbed molecules on semiconductor surfaces. In addition, the work has suggested that photostimulated desorption of energetic neutrals can provide a useful technique for determining adsorbate molecular orientation. The primary experimental technique has involved dynamic studies employing angle-resolved time-of-flight (TOF) mass spectrometry in concert with tunable laser excitation sources, to obtain information regarding the kinetic energy and angular distribution of reaction products. DOE

N95-21449# Sandia National Labs., Albuquerque, NM. Geochemistry Dept.
ANALYSIS OF EXPERIMENTALLY SHOCKED MINERALS BY NMR SPECTROSCOPY
Randall T. Cygan and Mark B. Boslough 1 Oct. 1994 110 p
(Contract DE-AC04-94AL-85000)
(DE95-002955; SAND-94-0294) Avail: CASI HC A06/MF A02

The shock-loading of natural materials by an impact or explosion can result in the formation of modified and altered phases. In order to characterize the resulting material and to evaluate the extent of shock modification, the authors have used nuclear magnetic resonance (NMR) spectroscopy to examine several experimentally shocked minerals. In three related NMR studies, they have (1) examined shocked clinoptilolite, (2) performed a preliminary analysis of shocked quartz, and (3) reproduced shocked quartz results with detailed spectral deconvolutions, and extended it with NMR analysis of shocked feldspar powders. DOE

N95-21474# Argonne National Lab., IL.
STRUCTURE OF IONIC INTERFACES FROM AN ABSOLUTELY CONVERGENT SOLUTION OF THE MADELUNG PROBLEM
D. Wolf Sep. 1994 23 p Presented at the International Symposium on Interfaces in Ionic Materials, Schloss Ringberg, Germany, 6-11 Mar. 1994
(Contract W-31-109-eng-38)
(DE94-019268; ANL/MSD/CP-84189; CONF-9403159-1) Avail: CASI HC A03/MF A01

The classic Madelung problem, i.e., the divergence associated with the r(exp -1) term in the Coulomb potential of condensed ionic systems, was cast into an absolutely convergent form that is readily evaluated by direct lattice summation, revealing a net r(exp -5) range of this potential. The realization that Coulomb interactions in condensed systems can actually be rather short ranged (if the system is overall neutral) permits novel physical insights into their structure and energetics to be gained. As an example, it was demonstrated that an understanding of the range and the nature of the convergence of the Coulomb potential leads naturally to the prediction, verified by computer simulations for rocksalt-structured surfaces, that all surfaces in predominantly ionic materials should be fundamentally reconstructed. The work also provides a conceptual framework for the theoretical treatment of polar surfaces and interfaces, as demonstrated for the case of the (111) stacking fault and of the (111) twin boundary in the rocksalt structure. DOE

N95-21483# Oak Ridge National Lab., TN.
EFFECTS OF NEUTRON IRRADIATION ON THE LONDON PENETRATION DEPTH FOR POLYCRYSTALLINE Bi(1.8)Pb(0.3)Sr2Ca2Cu3O10 SUPERCONDUCTOR
J. G. Ossandon (Talca Univ., Chile), J. R. Thompson (Tennessee Univ., Knoxville, TN.), and Y. R. Sun (Tennessee Univ., Knoxville, TN.) Jul. 1994 7 p Presented at the 4th International Conference and Exhibition of the World Congress on Superconductivity, Orlando, FL, 27 Jun. - 1 Jul. 1994
(Contract DE-AC05-84OR-21400)
(DE94-019335; CONF-940627-5) Avail: CASI HC A02/MF A01

Magnetization studies of polycrystalline Bi(1.8)Pb(0.3)Sr2Ca2Cu3O10 superconductor, prior to and after neutron irradiation, showed an increase in J(sub c) due to irradiation damage. Analysis of the equilibrium magnetization revealed significant increases in other more fundamental properties. In particular, the London penetration depth increased by approximately 15% following irradiation with 8 x 10(exp 16) neutrons/sq cm. Corresponding changes were observed in the upper critical magnetic field H(sub c2). However, the most fundamental thermodynamic property, the superconductive condensation energy F(sub c), was unaffected by the moderate level of neutron-induced damage. DOE

N95-21516# Brookhaven National Lab., Upton, NY.
SURFACE X-RAY SCATTERING AND SCANNING TUNNELING MICROSCOPY STUDIES AT THE Au(111) ELECTRODE
B. M. Ocko, O. M. Magnussen, J. X. Wang, and R. R. Adzic 1993 17 p Presented at the NATO Advanced Study Institute on Vortices in Superconductors, Cargese, France, 19-31 Jul. 1993
(Contract DE-AC02-76CH-00016)
(DE95-002409; BNL-60903; CONF-9307153-1) Avail: CASI HC A03/MF A01

This chapter reviews Surface X-ray Scattering and Scanning Tunneling Microscopy results carried out at the Au(111) surface under electrochemical conditions. Results are presented for the reconstructed surface, and for bromide and thallium monolayers. These examples are used to illustrate the complementary nature of the techniques. DOE

N95-21561# Fermi National Accelerator Lab., Batavia, IL.
STRUCTURE FUNCTIONS AND STRUCTURE FUNCTION RATIO F2(n)/F2(p) AT LOW X(Bj) AND Q2 IN INELASTIC MUON SCATTERING
A. V. Kotwal (Harvard Univ., Cambridge, MA.) Aug. 1994 5 p Presented at the Meeting of the Division of Particles and Fields of the American Physical Society, Albuquerque, NM, 2-6 Aug. 1994
(Contract DE-AC02-76CH-03000)
(DE94-018979; FNAL/C-94/251-E; CONF-940816-14) Avail: CASI HC A01/MF A01

Preliminary measurements of the structure functions F(sub 2)(sup p) and F(sub 2)(sup d),and the structure function ratio F(sub 2)(sup n)/F(sub 2)(sup p), in inelastic mu N scattering are presented. The data were obtained by the Fermilab E665 experiment using a 465 GeV muon beam and liquid hydrogen and deuterium targets. The structure functions are presented in the range (chi)(sub Bj) greater than 8 x 10(exp -4) and Q(sup 2) greater than 0.2 GeV(sup 2)/sq c. This structure function ratio is presented as a function of (chi)(sub Bj) for (chi)(sub Bj) greater than 10(exp -6). DOE

N95-21569# Iowa State Univ. of Science and Technology, Ames, IA.
VORTEX DYNAMICS IN A RING-LIKE IRRADIATED Bi2Sr2CaCu2O8 CRYSTAL
B. Khaykovich (Weizmann Inst. of Science, Rehovot, Israel.), E. Zeldov (Weizmann Inst. of Science, Rehovot, Israel.), D. Majer (Weizmann Inst. of Science, Rehovot, Israel.), M. Konczykowski (Ecole Polytechnique, Palaiseau, France.), and A. I. Larkin (Landau Inst. for Theoretical Physics, Moscow, USSR.) 1994 3 p Presented at the Meeting on Materials and Mechanisms of Superconductivity: High Temperature Superconductors, Grenoble, France, 4-9 Jul. 1994
(Contract W-7405-eng-82)
(DE95-001682; IS-M-797; CONF-940701-21) Avail: CASI HC A01/MF A01

A Bi2Sr2CaCu2O8 crystal selectively irradiated near the edges is studied using a Hall-sensor array. Vortices penetrating into the central J(sub c) = 0 region are 'focused' in the center of the sample on increasing the applied field. In decreasing field, vortices leave the center and a large vortex accumulation is observed on the inner rim of the irradiated region. Spatially resolved magnetization measurements confirm the developed theoretical model. DOE

N95-21570# Iowa State Univ. of Science and Technology, Ames, IA.
MAGNETIC FIELD DEPENDENCE OF THE CORRELATION GAP IN SmB6
J. C. Cooley (Michigan Univ., Ann Arbor, MI.), M. C. Aronson (Michigan Univ., Ann Arbor, MI.), A. Lacerda (Los Alamos National Lab., NM.), P. C. Canfield, and Z. Fisk (Los Alamos National Lab., NM.) 11 Jun. 1994 7 p Presented at the SCES 1994, Amsterdam, Netherlands, Aug. 1994
(Contract W-7405-eng-82)
(DE95-001684; IS-M-803; CONF-9408113-5) Avail: CASI HC A02/MF A01

We have used magnetoresistance measurements to probe the effect of large magnetic fields on the stability of the electronic gap Delta in SmB6. Although the Zeeman splitting in a 18 Telsa field is comparable to the ambient pressure Delta, and even exceeds Delta at 56 kbar, Delta is in both cases almost completely unaffected by the magnetic field. DOE

N95-21599 Missouri Univ., Rolla, MO. Dept. of Chemistry.
NMR RELAXATION BEHAVIOR OF THE HEAD GROUP OF SHBS IN LAMELLAR LIQUID CRYSTALS Technical Report, 1 Jan. 1993 - 23 Apr. 1994
Joseph R. Duke and Frank D. Blum 23 Apr. 1994 28 p Submitted for publication Limited Reproducibility: More than 20% of this document may be affected by microfiche quality
(Contract N00014-91-J-1274)
(AD-A279124; UMR-FDB-38) Avail: Issuing Activity (Defense Technical Information Center (DTIC))

Deuterium NMR relaxation-time constants T1Q and T1Z from spectra of a phenyl-ring-deuterated double-tailed surfactant, sodium 4-(1'-heptylnonyl) benzenesulfonate (SHBS) in liquid crystals formed with water were obtained from 0 to 80 C. The relaxation-time constants were determined for the 15 and 90 degree orientations of the powder sample. This data is compared to predicted relaxation time constants from two different models for molecular reorientation, including: (1) phenyl-rings undergoing uniaxial reorientation about the 1'-4' axis and (2) phenyl-rings rotating rapidly about the 1'-4' axis of a molecule which is reorienting about a space fixed director axis. Both models include an adjustable parameter that describes molecular motion about the 1'-4' axis that results from either strong collisions or small step free rotational diffusion. The results from both models indicate the rate of reorientation about the 1'-4' axis of the phenyl ring is approximately three times the nuclear Larmor frequency of the deuterium nucleus, 30 MHz, at room temperature. This rate increases with increasing temperature. The best fits of the data were determined using model (2). The predicted rate constants for motion about this axis differ slightly for each model, whereas, the type of motion predicted by the two models is very different. Model (1) indicates reorientation about the 1'-4' axis is more like strong collisions. Model (2) indicates that the motion is more like small step rotational diffusion. DTIC

N95-21636 Selskapet for Industriell og Teknisk Forskning, Trondheim (Norway). Div. of Applied Physics.
OVERVIEW OF THE FIELD AND TEMPERATURE DEPENDENCE OF J(c) IN Ag/BSCCO TAPES
M. Karkut 10 May 1994 15 p
(PB95-110318; STF19-A94007) Avail: Issuing Activity (National Technical Information Service (NTIS))

We review the status of the critical current densities in Ag/BSCCO tapes in applied magnetic fields at liquid nitrogen temperatures. We also present our own J(c) measurements on a NKT Ag/BSCCO tape. NTIS

N95-21670# Technische Hogeschool, Delft (Netherlands). Lab. of Materials Science.
STRAIN FIELDS IN CRYSTALLINE MATERIALS: METHODS OF ANALYSIS BASED ON X-RAY DIFFRACTION-LINE BROADENING Ph.D. Thesis [REKVELDEN IN KRISTALLIJNE MATERIALEN: ANALYSEMETHODEN GEBASEERD OP ROENTGENIFFRACTIE-LIJNVERBREDING]
J. G. M. vanBerkum 13 Jun. 1994 199 p
(PB95-108064; ISBN-90-9007196-2) Avail: CASI HC A09/MF A03

The mechanical properties of crystalline materials are often largely determined by the presence of crystal imperfections. All crystal imperfections, including the finite sizes of the grains or crystallites of the material, give rise to broadening of (X-ray) diffraction lines. In this thesis, the attention is concentrated on imperfections that are accompanied by microstrains, i.e. local distortions of the crystalline lattice. Examples of such crystal imperfections are dislocations, precipitates and inclusions. It is easily understood quantitatively that microstrains induce diffraction-line broadening. The aim of this thesis is to develop methods for the analysis of microstrains from (X-ray) diffraction-line broadening. Contents include: Determination of Instrumental Line Broadening; Separation of Size and Strain Broadening; Specific Models for Strain Broadening; and General Model for Strain Broadening. NTIS

N95-21712# Los Alamos National Lab., NM.
ANGLE RESOLVED PHOTOEMISSION ON K(0.3)Mo3, TiTe2 AND Ti(1+x)S2
G. H. Gweon (Michigan Univ., Ann Arbor, MI.), J. W. Allen (Michigan Univ., Ann Arbor, MI.), Y. Zhang (Michigan Univ., Ann Arbor, MI.), R. Claessen (Saarland Univ., Saarbruecken, Germany.), W. P. Ellis, Z. X. Shen (Stanford Univ., CA.), and A. Matsurra (Stanford Univ., CA.) 1994 5 p
(Contracts W-7405-eng-36; DE-FG02-90ER-45416; NSF DMR-91-08015)
(DE94-018300; LA-UR-94-2864) Avail: CASI HC A01/MF A01

The authors have performed high resolution angle resolved photoemission spectroscopy (HRARPES) on samples of K(0.3)MoO3, TiTe2 and Ti(1+x)S2, materials which are a quasi-one dimensional metal, a quasi-two dimensional metal, and a quasi two-dimensional metal (x approaches 0) or semi-conductor (x = 0), respectively. They are interested in looking at these samples using HRARPES as part of the general program to assess the use of photoemission to determine whether a particular system behaves like a Fermi liquid or not. For one dimensional metallic systems, angle integrated photoemission studies to date, e.g., reveal that, contrary to higher dimensional cases where a sharp Fermi cutoff is seen at the Fermi level, there is very little weight at the Fermi level. It seems that there is yet no agreement why this is so. They think that detailed information they get from HRARPES will help them answer this question. The system Ti(1+x)S2 gives the possibility to control the filling of the Ti 3d conduction band by adjusting x. Interest in this system lies in measuring the spectra and the line shape of samples with different stoichiometry and correlating the spectroscopic data with the corresponding transport data. DOE

N95-21723# Ames Lab., IA.
QUANTUM DYNAMICAL PHENOMENA OF INDEPENDENT ELECTRONS IN SEMICONDUCTOR SUPERLATTICES SUBJECT TO A UNIFORM ELECTRIC FIELD Ph.D. Thesis
A. M. Bouchard 27 Jul. 1994 212 p
(Contract W-7405-eng-82)
(DE95-001655; IS-T-1711) Avail: CASI HC A10/MF A03

This report discusses the following topics: Bloch oscillations and other dynamical phenomena of electrons in semiconductor superlattices; solvable dynamical model of an electron in a one-dimensional aperiodic lattice subject to a uniform electric field; and quantum dynamical phenomena of electrons in aperiodic semiconductor superlattices. DOE

N95-21839# Rochester Univ., NY. Dept. of Chemistry.
ULTRAFAST OPTICAL STUDIES OF SURFACE REACTION PROCESSES AT SEMICONDUCTOR INTERFACES
R. J. D. Miller 1994 21 p
(Contract DE-FG02-91ER-14185)
(DE95-001548; DOE/ER-14185/T1) Avail: CASI HC A03/MF A01

The DOE funded research has focused on the development of novel non-linear optical methods for the in situ study of surface reaction dynamics. In particular, the work has concentrated on interfacial charge transfer processes as this is the simplest of all surface reactions, i.e., no bonds are broken and the reaction is derived from nuclear repolarization. Interfacial charge transfer forms the basis for a number of important solar energy conversion strategies. In these studies, semiconductor liquid junctions provide a convenient system in which the interfacial charge transfer can be optically initiated. The all-optical approach necessitates that the dynamics of the charge transfer event itself be put in the proper context of the operating photophysical processes at the surface. There are at least four dynamical processes that are coupled in determining the overall rate of electron flux across the interface. In the limit that interfacial charge transfer approaches strong coupling, the time scale for transport of even field accelerated carriers within the space charge region becomes comparable to the charge transfer dynamics. The transport component needs to be convolved to probes of the carrier population at the surface. The other two dynamical processes, carrier thermalization and surface state trapping, determine the states which ultimately serve as the donor levels to the solution acceptor distribution. In terms of the hot carrier model, these latter two processes compete with direct unthermalized charge transfer. There is a fifth dynamical process which also needs consideration: the solvent modes that are coupled to the reaction coordinate. Ultimately, the dynamics of solvent relaxation determine the upper limit to the charge transfer process. Different optical techniques have been developed to follow all the above dynamical processes in which a real time view of charge transfer dynamics at semiconductor surfaces is emerging. These results are discussed here. DOE

N95-21853# International Centre for Theoretical Physics, Trieste (Italy).
ELECTRONIC STRUCTURE AND ENERGIES OF ALKALINE EARTH OXIDES: MgO, CaO AND SrO
M. Ahmed and A. Mookerjee Jul. 1993 12 p
(DE94-628990; IC-93/214) Avail: CASI HC A03/MF A01 (US Sales Only)

We have used the TB-LMTO scheme to study the electronic structure and the total energies of ceramic oxides MgO, CaO and SrO. All three of them have stable rocksalt structures. We find that although the local density approximation seems to work well for the first two, as the atomic number increases, the approximation begins to fail for SrO. Our calculations tend to show that the last is a metal, whereas experimentally it is as good an insulator as the other two. We suggest that for the larger Z oxides one has to bring in more accurate many-body techniques like the self-interaction correction to get the band gap correctly. DOE

N95-21854# International Centre for Theoretical Physics, Trieste (Italy).
RIGOROUS SPIN-SPIN CORRELATION FUNCTION OF ISING MODEL ON A SPECIAL KIND OF SIERPINSKI CARPETS
Z. R. Yang Oct. 1993 9 p
(DE94-628995; IC-93/342) Avail: CASI HC A02/MF A01 (US Sales Only)

We have exactly calculated the rigorous spin-spin correlation function of Ising model on a special kind of Sierpinski Carpets (SC's) by means of graph expansion and a combinatorial approach and investigated the asymptotic behaviour in the limit of long distance. The result show there is no long range correlation between spins at any finite temperature which indicates no existence of phase transition and thus finally confirms the conclusion produced by the renormalization group method and other physical arguments. DOE

N95-21859# International Centre for Theoretical Physics, Trieste (Italy).
ACOUSTOELECTRIC EFFECT IN SEMICONDUCTOR SUPERLATTICE
S. Y. Mensah, F. K. A. Allotey, and S. K. Adjepong Oct. 1993 5 p
(DE94-628994; IC-93/341) Avail: CASI HC A01/MF A01 (US Sales Only)

Acoustoelectric effect in semiconductor superlattice has been studied for acoustic wave whose wavelength lambda = 2pi/q is smaller than the mean free path of the electrons l (where ql approaches 1). Unlike the homogeneous bulk material where Weinreich relation is independent of the wave number q in the superlattice we observe a dependence on q i.e. spatial dispersion. In the presence of applied constant field E a threshold value was obtained where the acoustoelectric current changes direction. DOE

N95-21916 Aerospace Corp., El Segundo, CA. Technology Operations.
TRANSIENT PHOTOLUMINESCENCE MEASUREMENTS ON GaAs AND AlGaAs DOUBLE HETEROSTRUCTURES
Linda F. Halle, Steven C. Moss, and Dean C. Marvin 15 Aug. 1993 11 p Limited Reproducibility: More than 20% of this document may be affected by microfiche quality
(Contract F04701-88-C-0089)
(AD-A279408; TR-93(3925)-1; SMC-TR-94-26) Avail: Issuing Activity (Defense Technical Information Center (DTIC))

We report a set of transient photoluminescence (TPL) measurements of GaAs and AlGaAs double heterostructure (DH) materials as a function of temperature from 10K to 300K. We also report measurements of the time-integrated photoluminescence spectra of these samples. We observe, in both the spectra and the TPL measurements, evidence that the low-temperature photoluminescence kinetics are affected by additional paths for radiative decay that are not evident at room temperature, but have implications for material qualities measured at room temperature. DTIC

N95-21936# Los Alamos National Lab., NM.
ANISOTROPIC TRANSPORT PROPERTIES OF BSCCO SINGLE CRYSTALS AND Ag-CLAD TAPES IN HIGH MAGNETIC FIELDS
M. P. Maley, J. H. Cho, S. Fleshler, and L. N. Bulaevskii 1994 25 p Presented at the 7th Conference on Superconductivity and Applications, Buffalo, NY, 7-9 Sep. 1994
(Contract W-7405-eng-36)
(DE95-000938; LA-UR-94-3235; CONF-940926-2) Avail: CASI HC A03/MF A01

We report measurements of resistivity and critical current density on single crystals of Bi-2212 with current flow both parallel and perpendicular to the CuO2 planes and in magnetic fields to 18T. For comparison, similar measurements were performed on samples of Bi-2223 tape conductors with the Ag cladding removed. For current flow along the c-axis of the crystals the semiconducting behavior (resistivity increasing with decreasing temperature) is extended to below 50K in a field of 18T, followed by a sharp transition to the superconducting state. From I-V curves of c-axis transport we extract the magnetic field and temperature dependencies of the interlayer critical current density J(sub c,c) and define a decoupling line H(sub D)(T) above which J(sub c,c) vanishes. H(sub D)(T) lies close to but above the irreversibility H(sub irr)(T) obtained from magnetic measurements. We also observe a decoupling induced below H(sub D)(T) by the application of a magnetic field starting from the zero field cooled state, ZFC. The resulting 'pancake vortex' density gradient causes a loss of c-axis phase coherence and produces a c-axis resistance that relaxes logarithmically with time as the magnetization decays. These results are contrasted with similar measurements performed on highly textured Bi-2223 tapes. For current flow along the tape normal (nominal c-axis) the resistivity is metallic and its temperature and field dependence scales with those for in-plane current flow. Similarly critical currents for the two directions show similar field and orientation dependence. These results are consistent with predominant percolative current paths along crystallographic ab planes even for transport normal to the tape plane. DOE

N95-21949 Selskapet for Industriell og Teknisk Forskning, Trondheim (Norway). Div. of Applied Physics.
HOW TO IMPROVE J(c(T)) IN Ag/(BiPb)2Sr2Ca2Cu3O10 TAPES
M. Karkut and K. Fossheim 16 Jun. 1994 16 p
(PB95-110326; STF19-A94010) Avail: Issuing Activity (National Technical Information Service (NTIS))

We consider how to improve the magnetic field dependence of the critical current density J(c) in Ag/BSCCO superconducting tapes. First we look at mechanisms that provide pinning in the oxide superconductors and then consider the special problems that one encounters with Ag/BSCCO tapes. We propose several testable propositions to be performed in collaboration with NKT, Denmark and Tampere University, Finland. NTIS

N95-21991# Sandia National Labs., Albuquerque, NM.
RECIPROCAL SPACE MAPPING OF EPITAXIAL MATERIALS USING POSITION-SENSITIVE X-RAY DETECTION
S. R. Lee, B. L. Doyle, T. J. Drummond, J. W. Medernach, and R. P. Schneider, Jr. 1994 14 p Presented at the 43rd Annual Denver X-ray Conference, Steamboat Spring, CO, 1-5 Aug. 1994
(Contract DE-AC04-94AL-85000)
(DE95-001620; SAND-94-1071C; CONF-9408178-1) Avail: CASI HC A03/MF A01

Reciprocal space mapping can be efficiently carried out using a position-sensitive x-ray detector (PSD) coupled to a traditional double-axis diffractometer. The PSD offers parallel measurement of the total scattering angle of all diffracted x-rays during a single rocking-curve scan. As a result, a two-dimensional reciprocal space map can be made in a very short time similar to that of a one-dimensional rocking-curve scan. Fast, efficient reciprocal space mapping offers numerous routine advantages to the x-ray diffraction analyst. Some of these advantages are the explicit differentiation of lattice strain from crystal orientation effects in strain-relaxed heteroepitaxial layers; the nondestructive characterization of the size, shape and orientation of nanocrystalline domains in ordered-alloy epilayers; and the ability to measure the average size and shape of voids in porous epilayers. Here, the PSD-based diffractometer is described, and specific examples clearly illustrating the advantages of complete reciprocal space analysis are presented. DOE

N95-21995# International Centre for Theoretical Physics, Trieste (Italy).
CRITICAL DYNAMICS AND PLASTIC FLOW IN DISORDERED JOSEPHSON JUNCTION ARRAYS
D. Dominguez Jan. 1994 13 p
(DE94-629074; IC-94/12) Avail: CASI HC A03/MF A01 (US Sales Only)

We present numerical simulations of Josephson junction arrays with positional disorder. We study their IV characteristics and vortex dynamics as a function of disorder. We find that above the critical current i(sub c) there is a plastic flow of vortices and antivortices through channels, characterized by strong fluctuations of the total vorticity. For large currents there is a crossover to homogeneous flow without vortex fluctuations. We also study the dynamical critical behaviour close to i(sub c) in the gauge glass mode, calculating critical exponents for the voltage onset and voltage fluctuations. DOE

N95-21996# International Centre for Theoretical Physics, Trieste (Italy).
BREAKDOWN OF THE LAW OF LARGE NUMBERS IN JOSEPHSON JUNCTION SERIES ARRAYS
D. Dominguez and H. A. Cerdeira Jan. 1994 12 p
(DE94-629075; IC-94/13) Avail: CASI HC A03/MF A01 (US Sales Only)

We study underdamped Josephson junction series arrays that are globally coupled through a resistive shunting load and driven by an RF bias current. We find that they can be an experimental realization of many phenomena currently studied in globally coupled logistic maps. We find coherent, ordered, partially ordered and turbulent phases in the IV characteristics of the array. The ordered phase corresponds to giant Shapiro steps. In the turbulent phase there is a saturation of the broad band noise for a large number of junctions. This corresponds to a break down of the law of large numbers as seen in the globally coupled maps. Coexisting with this, we find an emergence of novel pseudo-steps in the IV characteristics. This effect can be experimentally distinguished from the Shapiro steps, which do not have broad band noise emission. DOE

N95-21997# International Centre for Theoretical Physics, Trieste (Italy).
ORDER AND TURBULENCE IN RF-DRIVEN JOSEPHSON JUNCTION SERIES ARRAYS
D. Dominguez and H. A. Cerdeira Jan. 1994 14 p
(DE94-629076; IC-94/14) Avail: CASI HC A03/MF A01 (US Sales Only)

We study underdamped Josephson junction series arrays that are globally coupled through a resistive shunting load and driven by an RF bias current. We find coherent, ordered, partially ordered and turbulent regimes in the IV characteristics. The ordered regime corresponds to giant Shapiro steps. In the turbulent regime there is a saturation of the broad band noise for a large number of junctions. This corresponds to a breaking of the law of large numbers already seen in globally coupled maps. Coexisting with this, we find an emergence of novel pseudo-steps in the IV characteristics. DOE

N95-21998# International Centre for Theoretical Physics, Trieste (Italy).
VARIATIONAL MONTE CARLO STUDY OF He-4 IN TWO DIMENSIONS
A. Belic and S. Fantoni (International School for Advanced Studies, Trieste, Italy.) Nov. 1993 3 p
(DE94-629078; IC-93/396) Avail: CASI HC A01/MF A01 (US Sales Only)

The study of the ground state of liquid and solid He-4 in two dimensions (2D) and at zero temperature, using Variational Monte Carlo (VMC) method, is presented. The trial wave functions used include the Shadow Wave Function (SWF) and the recently proposed Extended Shadow Wave Function (ESWF), and well as Jastrow (JWF), Jastrow-Nosanow (JNWF) and Jastrow+Triplet Wave Function (JTWF). DOE

N95-22008# Los Alamos National Lab., NM.
EQUILIBRIUM AND SHOT NOISE IN MESOSCOPIC SYSTEMS
T. Martin 1994 17 p Presented at the Rencontred de Moriond Meeting on Gravitation and Astrophysics, Villars-Sur-Ollon, France, 22-29 Jan. 1994
(Contract W-7405-eng-36)
(DE95-000855; LA-UR-94-3149; CONF-940187-2) Avail: CASI HC A03/MF A01

Within the last decade, there has been a resurgence of interest in the study of noise in Mesoscopic devices, both experimentally and theoretically. Noise in solid state devices can have different origins: there is 1/f noise, which is believed to arise from fluctuations in the resistance of the sample due to the motion of impurities. On top of this contribution is a frequency independent component associated with the stochastic nature of electron transport, which will be the focus of this paper. If the sample considered is small enough that dephasing and inelastic effects can be neglected, equilibrium (thermal) and excess noise can be completely described in terms of the elastic scattering properties of the sample. As mentioned above, noise arises as a consequence of random processes governing the transport of electrons. Here, there are two sources of randomness: first, electrons incident on the sample occupy a given energy state with a probability given by the Fermi-Dirac distribution function. Secondly, electrons can be transmitted across the sample or reflected in the same reservoir where they came from with a probability given by the quantum mechanical transmission/reflection coefficients. Equilibrium noise refers to the case where no bias voltage is applied between the leads connected to the sample, where thermal agitation alone allows the electrons close to the Fermi level to tunnel through the sample. In general, equilibrium noise is related to the conductance of the sample via the Johnson-Nyquist formula. In the presence of a bias, in the classical regime, one expects to recover the full shot noise ((Delta)(sup 2)I) = 2I(Delta)(mu) as was observed a long time ago in vacuum diodes. In the Mesoscopic regime, however, excess noise is reduced below the shot noise level. The author introduces a more intuitive picture, where the current passing through the device is a superposition of pulses, or electron wave packets, which can be transmitted or reflected. DOE

N95-22059 Department of the Navy, Washington, DC.
METHOD OF MAKING A SEMICONDUCTOR DEVICE BY FORMING A NANOCHANNEL MASK Patent
Ronald J. Tonucci, inventor (to Navy) and Brian L. Justus, inventor (to Navy) 26 Jul. 1994 18 p Filed 12 Jun. 1992
(AD-D016515; US-Patent-5,332,681; US-Patent-Appl-SN-897630; US-Patent-Class-437-16) Avail: US Patent and Trademark Office

The present invention provides a method for depositing a pattern of deposited material on or within a substrate, comprising the steps of: interposing a glass mask between a source and a substrate, the mask having channels therethrough which are arranged in a pattern and which have an average diameter of less than 1 micron; and depositing a material selected from the group of sources consisting of ions, electrons, photons, metals and semiconductor materials through the glass mask into or onto the substrate. The present invention also provides semiconductor devices made by this method. DTIC

N95-22084# Lawrence Livermore National Lab., Livermore, CA.
FULL POTENTIAL MULTIPLE SCATTERING THEORY
J. M. MacLaren (Tulane Univ., New Orleans, LA.) 20 Oct. 1994 6 p
(Contract W-7405-eng-48)
(DE95-003197; UCRL-CR-116369) Avail: CASI HC A02/MF A01

A practical method for performing self-consistent electronic structure calculations based upon full-potential multiple-scattering theory is presented. Solutions to the single site Schroedinger equation are obtained by solving coupled channel integral equations for a potential which is analytically continued out to the circumscribing sphere. This potential coincides with the full cell potential inside each atomic cell. Scattering matrices and wavefunctions for the full cell potential are obtained from surface Wronskian relations. The charge density is obtained from the single particle Green's function. This Green's function is computed using the cell scattering matrices and wavefunctions using the layer multiple scattering theory. Self consistent solutions require a solution at each iteration to the Poisson equation. The Poisson equation is solved using a variational cellular method. In the approach a local solution to each cell is augmented by adding a series of regular harmonics (solutions to Laplace's equation). Minimizing the coulomb energy, subject to continuity of the potential across all cell boundary provides an expression for the coefficients of the regular harmonics. This method is applied to BCC Nb. Calculated properties converge well in angular momentum and show comparable accuracy to full potential linearized muffin-tin orbital calculations. DOE

N95-22103 Department of the Navy, Washington, DC.
GROWING AND RELEASING DIAMONDS Patent Application
Pehr E. Pehrsson, inventor (to Navy) and Michael J. Marchywka, inventor (to Navy) 23 Apr. 1994 17 p Limited Reproducibility: More than 20% of this document may be affected by microfiche quality
(AD-D016489; US-Patent-Appl-SN-266758) Avail: Issuing Activity (Defense Technical Information Center (DTIC))

A process for making diamond and diamond products includes the steps of implanting ions in a diamond substrate to form a damaged layer of non-diamond carbon below the top surface of the substrate, heating the substrate to about 600-1200 C, growing diamond on the top surface of the heated substrate by chemical vapor deposition, and electrochemically etching the damaged layer to separate the grown diamond from the substrate along the damage layer. The diamond product consists of a first diamond layer and a second diamond layer attached to the first layer. The second layer contains damage caused by ions traversing the second layer. DTIC

N95-22137 Department of the Navy, Washington, DC.
METHOD FOR DETERMINING THE GRANULAR NATURE OF SUPERCONDUCTORS USING PULSED CURRENT Patent
Thomas E. Jones, inventor (to Navy) and Wayne C. McGinnis, inventor (to Navy) 16 Aug. 1994 11 p Filed 28 Jan. 1993
(AD-D016517; US-Patent-5,339,025; US-Patent-Appl-SN-010685; US-Patent-Class-324-71) Avail: US Patent and Trademark Office

The present invention provides a method for determining the granular nature of superconductive materials and devices which includes the steps of: conducting a substantially rectangular current pulse through the superconductive material, maintaining the temperature of the superconductive material at a substantially constant temperature which does not exceed the critical temperature of the superconductive material; determining the amplitude of the current pulse; determining the electrical resistance, R, of the superconductive material resulting from conducting current pulse through the superconductive material; increasing the current until the electrical resistance of the superconductive material becomes saturated; determining the electrical resistance difference, Sigma, between the electrical resistance, R, of the saturated superconductive material and a total normal state electrical resistance of the superconductive material. DTIC

N95-22166 Selskapet for Industriell og Teknisk Forskning, Trondheim (Norway). Div. of Applied Physics.
AC MAGNETIC RESPONSE OF YBa2CuO7 WITH Y2BaCuO5 INCLUSIONS AND OF SINGLE-CRYSTAL YBa2Cu3O7: A COMPARATIVE STUDY
M. G. Karkut, M. Slaski, L. K. Heill, L. T. Sagdahl, and K. Fossheim 20 Jan. 1994 18 p Prepared in cooperation with Birmingham Univ., England; Royal Norwegian Council for Scientific and Industrial Research, Oslo, Norway; and Norges Almenvitenskapelige Forskningsraad, Oslo, Norway
(PB94-207917; STF19-A93014) Copyright Avail: Issuing Activity (National Technical Information Service (NTIS))

We have measured the AC magnetic permeability response function mu=mu(prime) + i(mu)(double prime) in melt-process-melt-growth YBa2Cu3O7 (Y123) with Y2BaCuO5 (Y211) inclusions (MPMG) and in single-crystal YBa2Cu3O7 (SC) in applied magnetic fields up to 8T, oriented either parallel or perpendicular to the crystalline c-axis. The AC response of the two samples has been mapped out as a function of temperature, AC field amplitude and frequency, DC applied field, and field orientation. The peak in the lossy part of the susceptibility mu(double prime) (H,T) is used to probe the flux dynamics in the vicinity of the 'irreversibility' line (IL), defined here as the locus of mu(double prime) maxima in the H-T plane. Results are discussed. NTIS

N95-22168# California Univ., Berkeley. Lawrence Berkeley Lab, CA.
CARRIER DYNAMICS IN InGaAs: QUANTUM WELLS VERSUS BULK
S. R. Bolton, G. Sucha, D. S. Chemla, D. L. Sivco (Bell Telephone Labs., Inc., Murray Hill, NJ.), and A. Y. Cho (Bell Telephone Labs., Inc., Murray Hill, NJ.) May 1994 10 p Presented at the CLEO 1994: Conference on Lasers and Electro-optics, Anaheim, CA, 8-13 May 1994
(Contract DE-AC03-76SF-00098)
(DE94-018205; LBL-35219; CONF-940582-6) Avail: CASI HC A02/MF A01

Using femtosecond infrared continuum, we investigate carrier thermalization in L=100 A, 600 A and 6000 A InGaAs layers. Surprisingly, we find that the thermalization time, (approximately)400 fs, is independent of L. In contrast, the initial dynamics for less than 100fs exhibits significant L-dependence. DOE

N95-22176# International Centre for Theoretical Physics, Trieste (Italy).
ELECTRIC-FIELD EFFECTS ON SHALLOW DONOR IMPURITY IN A HARMONIC QUANTUM DOT
Kadi Zhu and Shiwei Gu (Jiaotong Univ., Shanghai, China.) Oct. 1993 17 p
(DE94-629034; IC-93/346) Avail: CASI HC A03/MF A01 (US Sales Only)

Electric-field effects on shallow donor impurity states in a harmonic quantum dot are investigated theoretically using the effective-mass approximation within the strong confinement regime. It is shown that the transition energies between the ground state and the low-lying excited states shrink with enhancement of electric field strength. The results also indicate that the transition energy allowed for left circular light polarization increases with enhancement of magnetic field strength, while the transition energy allowed for right circular light polarization decreases with increasing magnetic field strength. DOE

N95-22178# International Centre for Theoretical Physics, Trieste (Italy).
THE DOPING EFFECT ON SPIN-PEIERLS INSTABILITY
Zhong-Yi Lu (Academia Sinica, Beijing, China.), Zhao-Bin Su (Academia Sinica, Beijing, China.), and Lu Yu Jan. 1994 11 p
(DE94-629046; IC-94/34) Avail: CASI HC A03/MF A01 (US Sales Only)

We study the effects of doping on spin-Peierls (SP) systems using the unimodular mean-field theory. The impurity spins affect the singlet valence bond field and renormalize the magnetic excitations. The SP transition temperature and the energy gap of magnetic excitations are reduced by factors approximately n(sub i) and approximately n(sub i)(sup 2/3), respectively, with n(sub i) as the impurity density. At certain value of n(sub i), a gapless SP phase occurs, and the interaction between impurities becomes RKKY-like. The recently observed reduction of SP transition temperature upon doping and occurrence of a spin glass phase is interpreted using the proposed theory. DOE

N95-22180# International Centre for Theoretical Physics, Trieste (Italy).
FLUX CREEP WITH LOGARITHMIC U(j) DEPENDENCE
Wei Wang and Jinming Dong (Nanjing Univ., China.) Oct. 1993 16 p
(DE94-629058; IC-93/364) Avail: CASI HC A03/MF A01 (US Sales Only)

In this paper we have studied the flux motion in a high-T(sub c) superconductor. For both field-cooled and zero-field-cooled cases, we have numerically solved the flux motion equations, and calculated various magnetizations M(t) changing with the time t. The scaling behaviour of the magnetization has been obtained. There is a kink in the magnetization curve corresponding to the reaching of the flux front to the middle of the slab sample. The self-organized critical state (SOC) relates to the early time of the flux penetration and the effect of temperature on the SOC has been discussed. DOE

N95-22181# International Centre for Theoretical Physics, Trieste (Italy).
MAGNETIC INTERACTIONS IN THE EMERY MODEL
Minhtien Tran Nov. 1993 25 p
(DE94-629059; IC-93/370) Avail: CASI HC A03/MF A01 (US Sales Only)

The Emery model CuO2 planes in high T(sub c) superconductors is considered. Treating this model by the cell-perturbation method, a singlet-triplet model with effective spin interactions is derived. Both superexchange (SE) and Ruderman-Kittle-Kasuya-Yosida (RKKY) interactions are calculated. It is found that with increasing carrier concentration, the SE interaction decreases, while the RKKY interaction increases. With increasing oxygen transfer both SE and RKKY interactions increase. The SE interaction is dominant, except for a small region of large hole doping where the SE interaction changes its sign. The suppression of the exchange interaction with hole doping is found and it may explain the drop of magnetic order with hole doping. The magnetic frustrations are also calculated and they are found even for zero bandwidth and for the half-filling insular case. DOE

N95-22231# Ibis Associates, Inc., Wellesley, MA.
TECHNICAL COST MODELING APPLIED TO CVD DIAMOND DEPOSITION Quarterly Report No. 3
1994 60 p
(Contract N00014-93-C-2044)
(AD-A286119) Avail: CASI HC A04/MF A01

IBIS Associates has completed its predictive spreadsheet models of chemical vapor deposition (CVD) diamond film fabrication. This report details the capabilities of the models, and shows cost sensitivities to product and process input parameters. The DC arcjet, microwave, and combustion flame CVD diamond deposition models, in addition to the CVD diamond finishing model, have been developed to maximize cost estimation flexibility. In doing so for deposition, inputs such as thermal conductivity, machine power, gas concentration, gas temperature, and reactor pressure have been provided in the model to predict the deposition growth rate, which is critical to the cost calculation. For the finishing model, inputs such as laser power, laser spot size, and laser frequency have been provided in the model to predict the diamond removal rate, which is also critical to the final cost calculation. DTIC

N95-22269# Oak Ridge National Lab., TN.
LOCAL TEXTURE AND STRONGLY LINKED CONDUCTION IN SPRAY-PYROLYZED TlBa2Ca2Cu3O(8+x) DEPOSITS
D. M. Kroeger, A. Goyal, E. D. Specht, Z. L. Wang (National Inst. of Standards and Technology, Gaithersburg, MD.), J. E. Tkaczyk (General Electric Co., Schenectady, NY.), J. A. Sutliff (General Electric Co., Schenectady, NY.), and J. A. Deluca (General Electric Co., Schenectady, NY.) 1993 6 p Presented at the 6th US-Japan Workshop on Superconductivity, Houston, TX, 6-7 Dec. 1993
(Contract DE-AC05-84OR-21400)
(DE94-017887; CONF-931238-4) Avail: CASI HC A02/MF A01

Local texture in polycrystalline TlBa2Ca2 Cu3O(8+x) deposits has been determined from transmission electron microscopy, electron backscatter diffraction patterns and x-ray diffraction. The small-grained deposits had excellent c-axis alignment and contained colonies of grains with similar but not identical a-axis orientations. Most grain boundaries within a colony have small misorientation angles and should not be weak links. It is proposed that long range conduction utilizes a percolative network of small angle grain boundaries at colony intersections. DOE

N95-22272# Oak Ridge National Lab., TN. Metals and Ceramics Div.
AN IMPROVED MONTE CARLO ALGORITHM FOR SIMULATING GRAIN GROWTH
B. Radhakrishnan, T. Zacharia, and A. J. Paul (Concurrent Technologies Corp., Johnstown, PA.) 1994 6 p Presented at The Minerals, Metals and Materials Society Conference, Nemacolin Woods, PA, 20 Jul. 1994
(Contract DE-AC05-84OR-21400)
(DE94-017903; CONF-9407119-1) Avail: CASI HC A02/MF A01

The Monte Carlo algorithm that currently exists in the literature for simulating curvature-driven grain growth has been modified. The grain growth exponent as a function of grain size obtained using the new algorithm approaches the theoretical limit of 0.5 more rapidly than that obtained using the old algorithm. The upper limit of grain size distributions obtained with the new algorithm is significantly lower than that obtained with the old, because the new algorithm eliminates grain coalescence during grain growth. The log-normal function provides an excellent fit to the grain size distribution data obtained with the new algorithm, after taking into account the anisotropy in grain boundary energy. DOE

N95-22276# International Centre for Theoretical Physics, Trieste (Italy).
AN EXACT ENUMERATION OF SELF-AVOIDING LOOPS ON A SQUARE LATTICE
E. Kornilov Nov. 1993 11 p
(DE94-628999; IC-93/382) Avail: CASI HC A03/MF A01 (US Sales Only)

An exact enumeration of self-avoiding loops on a set of finite simple square lattices is performed. The partition function zeroes distribution is shown to be oval-like, in contrast to two intersecting circles, as in the case of the Ising model. An analysis of the partition function zeroes distribution shows the closeness of the critical point of the model to the ferromagnetic one of the Ising model. DOE

N95-22277# International Centre for Theoretical Physics, Trieste (Italy).
BIAXIALITY OF CHIRAL LIQUID CRYSTALS
L. Longa, H. R. Trebin (Stuttgart Univ., Germany.), and W. Fink (Stuttgart Univ., Germany.) Oct. 1993 36 p
(DE94-629032; IC-93/338) Avail: CASI HC A03/MF A01 (US Sales Only)

Using extended deGennes-Ginzburg-Landau free energy expansion in terms of the anisotropic part of the dielectric tensor field Q(sub alpha beta)chi a connection between the phase biaxiality and the stability of various chiral liquid crystalline phases is studied. In particular the cholesteric phase, the cubic Blue Phases and the phases characterized by an icosahedral space group symmetry are analysed in detail. Also a general question concerning the applicability of the mean-field approximation in describing the chiral phases is addressed. By an extensive study of the model over a wide range of the parameters a new class of phenomena, not present in the original deGennes-Ginzburg-Landau model, has been found. These include: (1) re-entrant phase transitions between the cholesteric and the cubic blue phases; and (2) the existence of distinct phases of the same symmetry but of different biaxialities. The phase biaxiality serves here as an extra scalar order parameter. Furthermore, it has been shown that due to the presence of the competing bulk terms in the free energy, the stable phases may acquire a large degree of biaxiality, also in liquid crystalline materials composed of effectively uniaxial molecules. A study of icosahedral space group symmetries gives a partial answer to the question as to whether an icosahedral quasicrystalline liquid could be stabilized in liquid crystals. Although, in general, the stability of icosahedral structures could be enhanced by the extra terms in the free energy no absolutely stable icosahedral phase has been found. DOE

N95-22286# University of Southern Mississippi, Hattiesburg, MS. Dept. of Polymer Science.
SOLID-STATE NMR CHARACTERIZATION OF C- AND N-LABELLED PHTHALIMIDES: MODEL COMPOUNDS FOR STUDYING POLYIMIDES
William L. Jarrett, C. G. Johnson, and Lou J. Mathias 15 Nov. 1994 15 p
(Contract N00014-89-J-1225)
(AD-A286479; TR-77) Avail: CASI HC A03/MF A01

15N CSA spectra were acquired for four isotopically labelled bisphthalimide compounds. The 15N CSA tensor elements (delta 11, delta 22, and delta 33) for the labeled derivatives were determined from CSA line shape analysis. In addition, the CSA spectrum for the 15N-13C labelled N-methylphthalimide was obtained. From CSA lineshape analysis it was determined that delta 33 lies approximately along the N-C bond axis, with delta 22 assumed to be approximately perpendicular to the imide plane. The angles alpha and Beta were found to be 90 deg and 7 deg, respectively. The dipolar coupling constant for 13C-I 5N bond was 883 Hz, corresponding to a bond length of 1.51 A. DTIC

N95-22297# Los Alamos National Lab., NM.
MODELING OF NONLINEAR OPTIC AND ESR RESPONSE OF CDW MX MATERIALS
A. Saxena, Z. Shuai (Mons Univ., Belgium.), J. T. Gammel, I. Batiste (Zagreb Univ., Zagreb, Crotia.), M. Alouani (Ohio State Univ., Columbus, OH.), J. L. Bredas (Mons Univ., Belgium.), and A. R. Bishop 1994 5 p Presented at the International Conference on Science and Technology of Synthetic Metals, Seoul, Republic of Korea, 24-29 Jul. 1994
(Contract W-7405-eng-36)
(DE94-018301; LA-UR-94-2860; CONF-9407117-2) Avail: CASI HC A01/MF A01

We report results on the nonlinear optic and electron spin resonance (ESR) response of the PtX MX chain materials calculated using a discrete, 3/4-filled, two-band, tight-binding Peierls-Hubbard model. We calculated electroabsorption (EA) spectra for the three PtX (X=Cl, Br, 1) charge-density-wave (CDW) materials and find good agreement with the experimental data. We also obtain EA spectra for localized defects in PtBr. In addition, the field orientation dependence of the electron spin resonance spectra associated with the spin carrying defects is calculated for PtX materials and compared with ESR data on photoinduced defects.
DOE

N95-22380# Sao Paulo Univ., Sao Carlos (Brazil). Inst. de Fisica e Quimica.
INTRODUCTION TO THE STRUCTURES DETERMINATION METHODS USING X-RAY DIFFRACTION IN MONOCRYSTALS: APPLICATION TO SOME LANTHANIDES AND TRANSITION METALS COMPLEXES WITH ORGANIC LIGANDS M.S. Thesis
G. Oliva 1983 238 p In PORTUGESE
(DE94-629002; INIS-BR-3344) Avail: CASI HC A11/MF A03 (US Sales Only)

The crystal structure of the complexes Ln (Cl O4)3.6(P O N H2 (C6 H5)2) where Ln = Eu, La, Cu(N H2 (C H3)2 C C O2)2 , Ni Br2.4(As O(C6 H5)3) . 8 H2 O (green), Ni Br2.4(As O (C6 H5)3). 1,5 (C H3 C6 H5).H2 O (orange) and of the ligand P O N H2 (C6 H5)2 have been determined by X-ray diffraction. The complexes involving lanthanide ions refined to final R factors of R(Eu) = 0.125 and R(La) = 0.133 and the following main features were found: the crystal system is cubic; the cation is coordinated to six ligand oxygens in octahedral (Eu) and trigonal anti prismatic (La) configurations with the rate earths on positions of high symmetry (23 for Eu and 3-bar for La); the rest of the structures shows different degrees of disorder. In the light of the geometrical configuration, the occurrence of a strong band (sup 5) D(sub O) - (sup 7) F(sub 2) in the fluorescence spectrum of the Eu complex, forbidden on symmetry grounds, is interpreted as a consequence of vibronic coupling. A splitting of the infrared (nu)(sub P=0) band in the La complex is attributed to the presence of P = 0 groups non-equivalently bonded to the rare earth due to the disorder of this atom.
DOE

N95-20536*# National Aeronautics and Space Administration. Lewis Research Center, Cleveland, OH.
RARE EARTH GARNET SELECTIVE EMITTER
Roland A. Lowe (Kent State Univ., OH.), Donald L. Chubb, Serene C. Farmer, and Brian S. Good *In its* Proceedings of the 13th Space Photovoltaic Research and Technology Conference (SPRAT 13) Sep. 1994 p 335-339 (For primary document see N95-20502 06-33)
Avail: CASI HC A01/MF A04

N95-20537*# National Aeronautics and Space Administration. Lewis Research Center, Cleveland, OH.
InGaAs PV DEVICE DEVELOPMENT FOR TPV POWER SYSTEMS
David M. Wilt (Essential Research, Inc., Cleveland, OH.), Navid S. Fatemi (Essential Research, Inc., Cleveland, OH.), Richard W. Hoffman, Jr. (Essential Research, Inc., Cleveland, OH.), Phillip P. Jenkins (NYMA, Inc., Brook Park, OH.), David J. Brinker (NYMA, Inc., Brook Park, OH.), David Scheiman (NYMA, Inc., Brook Park, OH.), Roland A. Lowe (Kent State Univ., OH.), and Donald Chubb *In its* Proceedings of the 13th Space Photovoltaic Research and Technology Conference (SPRAT 13) Sep. 1994 p 341-351 See also N95-11587 (For primary document see N95-20502 06-33)
Avail: CASI HC A03/MF A04

N95-20542*# Ohio State Univ., Columbus, OH.
EFFECTS OF PLASMA HYDROGENATION ON TRAPPING PROPERTIES OF DISLOCATIONS IN HETEROEPITAXIAL InP/GaAs
S. A. Ringel and B. Chatterjee *In* NASA. Lewis Research Center, Proceedings of the 13th Space Photovoltaic Research and Technology Conference (SPRAT 13) Sep. 1994 p 401-408 (For primary document see N95-20502 06-33)
(Grant NAG3-1461)
Avail: CASI HC A02/MF A04

N95-20543*# Yale Univ., New Haven, CT.
NUCLEATION, GROWTH, AND STRAIN RELAXATION OF LATTICE-MISMATCHED 3-5 SEMICONDUCTOR EPITAXIAL LAYERS
R. E. Welser and L. J. Guido *In* NASA. Lewis Research Center, Proceedings of the 13th Space Photovoltaic Research and Technology Conference (SPRAT 13) Sep. 1994 p 409-418 (For primary document see N95-20502 06-33)
(Grants NGT-50832; NSF ECS-92-53760)
Avail: CASI HC A02/MF A04

77 THERMODYNAMICS AND STATISTICAL PHYSICS

Includes quantum mechanics; theoretical physics; and Bose and Fermi statistics.

For related information see also *25 Inorganic and Physical Chemistry* and *34 Fluid Mechanics and Heat Transfer.*

N95-19947*# Kansas Univ., Lawrence, KS. Dept. of Physics and Astronomy.
CONNECTION WITH DYNAMICS: GENERAL INTRODUCTION
Sergei F. Shandarin 1993 7 p Presented at the Cosmic Velocity Fields Conference, Paris, France, Jul. 1993
(Grants NAGw-2923; NSF AST-90-21414; NSF ORS-92-55223)
(NASA-CR-197617; NAS 1.26:197617) Avail: CASI HC A02/MF A01

This is a brief nontechnical introduction to a few theoretical issues to the density-velocity relation. The aim of this introduction is not an exhaustive analysis of the current theoretical situation but rather setting a stage for the following talks. The selection of topics has been determined by the sequel program.
Author

N95-20028# Westinghouse Savannah River Co., Aiken, SC.
THERMODYNAMIC CHARACTERIZATION OF NEW PALLADIUM ALLOY TRITIDES
J. S. Hoelder and J. R. Wermer Aug. 1994 24 p Presented at the International Symposium on Metal-hydrogen Systems, Fuji-Yoshida, Japan, 6-11 Nov. 1994
(Contract DE-AC09-89SR-18035)
(DE94-018430; WSRC-MS-94-0259; CONF-9411129-1) Avail: CASI HC A03/MF A01

The decay of tritium in a metal tritide generates (3)He in the lattice which tends to degrade the performance of the material over time. It is desired to develop a material which minimizes the tritium aging effects and may be tailored to a particular tritium processing application. Pd alloys with Ni and Co have been investigated, as Pd tritide is known to be resistant to tritium aging effects and alloying provides a means for adjusting the plateau pressure of the metal tritide. Sets of tritium desorption isotherms were acquired at temperatures between 273 and 338 K over the pressure range of 1 to 900 kPa. The thermodynamic parameters of (Delta)H and (Delta)S for the (beta)-(alpha) phase transition of the metal tritides were determined across the plateau regions of the P-C-T curves. The average values of (Delta)H (kJ/mol(center dot)T) and (Delta)S (J/K/mol(center dot)T) were found to be 15.8 and 50.1 for Pd(2.8 wt. %)Ni, 13.7 and 50.3 for Pd(5.2 wt. %)Ni, 15.9 and 51.3 for Pd(2.8 wt. %)Co, and 13.6 and 51.8 for Pd(5.2 wt. %)Co, respectively.
DOE

N95-20271# Argonne National Lab., IL.
THE PARADIGM OF PSEUDODUAL CHIRAL MODELS
C. K. Zachos and T. L. Curtright (Miami Univ., Coral Gables, FL.) 1994 10 p Presented at the Symposium on Particles, Strings and Cosmology, Syracuse, NY, 19-24 May 1994
(Contract W-31-109-eng-38)
(DE94-016386; ANL-HEP-CP-94-33; CONF-9405162-1) Avail: CASI HC A02/MF A01

This is a synopsis and extension of Phys. Rev. D49 5408 (1994). The Pseudodual Chiral Model illustrates 2-dimensional field theories which possess an infinite number of conservation laws but also allow particle production, at variance with naive expectations -- a folk theorem of integrable models. We monitor the symmetries of the pseudodual model, both local and nonlocal, as transmutations of the symmetries of the (very different) usual Chiral Model. We refine the conventional algorithm to more efficiently produce the nonlocal symmetries of the model. We further find the canonical transformation which connects the usual chiral model to its fully equivalent dual model, thus contra-distinguishing the pseudodual theory. DOE

N95-20324 Institut des Hautes Etudes Scientifiques, Bures-sur-Yvette (France).

VON NEUMANN ALGEBRA AUTOMORPHISMS AND TIME-THERMODYNAMICS RELATION IN GENERAL COVARIANT QUANTUM THEORIES

A. Connes and C. Rovelli (Pittsburgh Univ., Pittsburgh, PA.) Jun. 1994 28 p Limited Reproducibility: More than 20% of this document may be affected by microfiche quality
(PB95-111084; IHES/M/94/36) Avail: CASI HC A03

The authors consider the cluster of problems raised by the relation between the notion of time, gravitational theory, quantum theory and thermodynamics; in particular, the authors address the problem of relating the 'timelessness' of the hypothetical fundamental general covariant quantum field theory with the 'evidence' of the flow of time. By using the algebraic formulation of quantum theory, the authors propose a unifying perspective on these problems, based on the hypothesis that in a generally covariant quantum theory the physical time-flow is not a universal property of the mechanical theory, but rather it is determined by the thermodynamical state of the system ('thermal time hypothesis'). The authors implement this hypothesis by using a key structural property of von Neumann algebras; the Tomita-Takesaki theorem, which allows to derive a time-flow, namely a one-parameter group of automorphisms of the observable algebra, from a generic thermal physical state. The authors study this time-flow, its classical limit, and the authors relate it to various characteristic theoretical facts, as the Unruh temperature and the Hawking radiation. The authors also point out the existence of a state-independent notion of 'time'. NTIS

N95-21030 Rutherford Appleton Lab., Chilton (England).

FACTORIZATION IN CLOSED STRING FIELD THEORY

F. Anton, A. Abdurrahman, and J. Bordes Jun. 1994 17 p Prepared in cooperation with Valencia Univ.
(PB95-133542; RAL-94-064) Avail: Issuing Activity (National Technical Information Service (NTIS))

The so long made assumption, that a general closed-string vertex operator V should be built as a product of left- and right-moving vertex operators, rests on the fact that closed-string Fock space is constructed as a tensor product of left- and right-moving open-string Fock spaces. In this letter we will relax this assumption by proving that factorization of closed-string vertices is a general rule. NTIS

N95-21229 Rutherford Appleton Lab., Oxford (England).

CONSTRAINTS ON SUSy-GUT UNIFICATION FROM b YIELDS s-GAMMA DECAY

V. Barger, M. S. Berger, P. Ohmann, and R. J. N. Phillips Jul. 1994 20 p Prepared in cooperation with Wisconsin Univ., Madison, WI
(Contract DE-AC02-76ER-00881)
(PB95-130373; RAL-94-046) Avail: Issuing Activity (National Technical Information Service (NTIS))

The top-quark Yukawa infrared fixed-point solution of the renormalization group equations, with minimal supersymmetry and GUT unification, defines a low-energy spectrum of supersymmetric particle masses in terms of a few GUT-scale parameters assuming universal boundary conditions. The authors give predictions in this model for the inclusive b approaches s(gamma) branching fraction and investigate the impact of non-universal scalar mass boundary conditions. The authors find their results do not depend significantly on the value of the GUT-scale trilinear coupling A(sub G). The small tan beta region favors predictions for the inclusive b approaches s(gamma) branching fraction close to that of the Standard Model value. Nevertheless forthcoming experimental results can eliminate some regions of the GUT parameter space. NTIS

N95-21230 Rutherford Appleton Lab., Oxford (England).

CALCULATION OF Z PLUS FOUR JET PRODUCTION AT THE TEVATRON

V. Barger, E. Mirkes, R. J. N. Phillips, and T. Stelzer Aug. 1994 11 p Prepared in cooperation with Wisconsin Univ., Madison, WI
(Contract DE-AC02-76ER-00881)
(PB95-130472; RAL-94-070) Avail: Issuing Activity (National Technical Information Service (NTIS))

We present the first calculation of Z + 4 jet production with heavy quark flavor identification at the Tevatron P(bar-p) collider. The Z + 4 jet channel is especially interesting as a normalizer for the W + 4 jet background to top quark signals, as a background to a possible t approaches cZ flavor-changing neutral-current (FCNC) decay signal, and as a background to missing-P(sub T) signals from gluino pairs. We also calculate the contributions to W + 4 jet production from all the different heavy-flavor final states. The MADGRAPH program is used to generate all leading order subprocess helicity amplitudes. We present Monte Carlo results with separation and acceptance criteria suitable for the Tevatron experimental analyses. NTIS

N95-21264# Los Alamos National Lab., NM.

QUANTUM DIFFUSION

S. Habib 1994 6 p Presented at the Drexel Conference on Quantum Non Integrability, Philadelphia, PA, Sep. 1994
(Contract W-7405-eng-36)
(DE95-001015; LA-UR-94-3329; CONF-9409228-1) Avail: CASI HC A02/MF A01

We consider a simple quantum system subjected to a classical random force. Under certain conditions it is shown that the noise-averaged Wigner function of the system follows an integro-differential stochastic Liouville equation. In the simple case of polynomial noise-couplings this equation reduces to a generalized Fokker-Planck form. With nonlinear noise injection new 'quantum diffusion' terms rise that have no counterpart in the classical case. Two special examples that are not of a Fokker-Planck form are discussed: the first with a localized noise source and the other with a spatially modulated noise source. DOE

N95-21420# Oak Ridge National Lab., TN.

MOLECULAR-BASED STUDY OF SOLUTIONS IN SUPERCRITICAL SOLVENTS

V. M. Shah (Tennessee Univ., Knoxville, TN.), L. L. Lee (Oklahoma Univ., Norman, OK.), and H. D. Cochran 1994 8 p Presented at the 3rd International Symposium on Supercritical Fluids, Strasbourg, France, 17-19 Oct. 1994
(Contract DE-AC05-84OR-21400)
(DE94-019326; CONF-9410114-1) Avail: CASI HC A02/MF A01

Behavior and properties of solutions in supercritical (SC) solvents are related to microscopic structures, and the structure and properties of typical attractive SC solutions have been well studied both experimentally and theoretically. New and interesting properties, however, have been uncovered in recent studies of dilute repulsive and weakly attractive SC solutions. Such repulsive and weakly attractive solutions are encountered in practice when relatively volatile substances are present in a SC solvent. Specific examples of practical importance include organic molecules in SC water and light gases in SC carbon dioxide. We report a study of the microscopic structure and thermodynamic properties of these less-known repulsive and weakly attractive SC mixtures. Results are based on integral equation calculations for model systems and illustrate the qualitative behaviors that may be expected in practice. The results are based on Ornstein-Zernike integral equation calculations in the Percus-Yevick approximation applied to dilute, binary Lennard-Jones mixtures. The microscopic structures calculated (pair correlation functions) are related to the thermodynamic properties through the fluctuation integrals of Kirkwood-Buff theory. Whether the system behaves as a repulsive mixture or a weakly attractive mixture depends on size of solute molecule and strength of its intermolecular attraction relative to the solvent molecule as well as on the temperature and density of the system relative to the critical temperature and density of the solvent. DOE

N95-21486# Louisiana State Univ., Baton Rouge, LA. Dept. of Physics and Astronomy.

NEW IMPROVED DERIVATIVE EXPANSION FOR FIELD THEORIES WITH SPONTANEOUS SYMMETRY BREAKING

Lai-Him Chan 1994 3 p Presented at the Meeting of the Division of Particles and Fields of the American Physical Society, Albuquerque, NM, 2-6 Aug. 1994

(Contract DE-FG05-91ER-40617)
(DE94-019349; DOE/ER-40617/181; CONF-940816-16) Avail: CASI HC A01/MF A01

Derivative expansion of the effective action for field theories with spontaneous symmetry breaking may be badly divergent. I propose a new expansion series in which the series expansion are simultaneous developed in order of the number of derivatives of the field and in power of the deviation of the field from its ground state value. As examples, I have applied this new method to calculate the quantum correction to the energy of the 1+1 dimension soliton in various models. For the models in which exact solutions have been found, such as the Sine-Gordon soliton, phi(exp 4) soliton, and phi(exp 4) soliton with fermion loop, the improved series can be recognized as well-known analytically summable series. The results of the exact solutions are completely recovered. More importantly, for the cases where exact solutions may not be available, Pade approximant or the Borel summation can be used to give good approximation. DOE

N95-21604# California Univ., Berkeley. Lawrence Berkeley Lab, CA. Materials Sciencs Div.

RESONANT GENERATION OF NONEQUILIBRIUM PHONONS IN GaAs/AlAs QUANTUM WELLS VIA INTERSUBBAND SCATTERING

Z. P. Su, T. Ruf, K. R. Wald, P. Y. Yu, and K. T. Chan (Chinese Univ. of Hong Kong, Shatin, Hong Kong.) Jul. 1994 4 p Presented at the 22th International Conference on Physics of Semiconductors, Vancouver, British Columbia, 15-19 Aug. 1994
(Contract DE-AC03-76SF-00098)
(DE95-002338; LBL-35940; CONF-9408155-11) Avail: CASI HC A01/MF A01

The authors have studied the resonant intersubband scattering of optical phonons or RISOP theoretically and by picosecond scattering. Experimentally, the authors have established a way to determine phonon occupancy in quantum wells. The model calculation shows that a significant amount of long wavelength LO phonons are generated by RISOP in GaAs/AlAs quantum wells. However, they measured a much smaller phonon population than predicted. The discrepancy can be explained by a breakdown of in-plane wave vector conservation due to interface roughness. DOE

N95-21639# International Centre for Theoretical Physics, Trieste (Italy).

THE METHOD OF EVALUATING QUANTUM PARTITION FUNCTION FOR THE HUBBARD MODEL

S. Karnaukhov Aug. 1993 9 p
(DE94-628991; IC-93/277) Avail: CASI HC A02/MF A01 (US Sales Only)

The method of evaluation of quantum partition function (QPF) in some four fermion models is proposed. The calculations are carried out by the path integral method. The integral is evaluated by introducing the additional fields (called Hubbard-Stratanovich transformation in some models), integration over fermionic variables, and considering the finite-dimensional approximation of rest integral over bosonic fields in the infinite limit. The result can be represented as a sum of the functional derivatives with respect to the arbitrary bosonic field of the quantum partition of free fermionic theory in the external bosonic field. This expression can be treated in a mean field approximation in closed form (the determinants corresponding to the arbitrary external field are substituted by its mean values corresponding to the mean value of the external fields). The quantum partition function is represented as the integral representation of the function. The approximation for the QPF of the free theory is considered, and the corresponding answer for QPF is studied. A convenient perturbation expansion for ln Z is developed. DOE

N95-21842# Colorado Univ., Boulder, CO.

PHYSICS OF CORRELATED STUDIES

C. H. Greene 1993 8 p
(Contract DE-FG02-90ER-14145)
(DE95-001204; DOE/ER-14145/T3) Avail: CASI HC A02/MF A01

During the three year period of this grant, a major initiative was started to develop theoretical methods to treat complex open-shell atoms in a manner permitting a simple interpretation of the dynamics. This project has been far more successful than originally hoped, with accurate ground state photoionization cross sections calculated for nine different open-shell atoms in the periodic table. This work culminated in our first application to multichannel autoionizing spectra of a transition metal atom, scandium. These methods were also extended and adapted to permit a description of nonresonant two-photon processes at the perturbative level, and some nonperturbative multiphoton processes. The angular distribution of photoelectrons ejected in resonant multiphoton ionization of magnesium was also successfully calculated. We made headway toward understanding aspects of the diamagnetic quasi-Landau problem, specifically interpreting the observed simplicity of the spectrum when plotted simultaneously versus energy and field. High two-electron excitations of H(-) and Li(-) were treated using R-matrix methods, combined with a time delay analysis to quantitatively test various propensity rules proposed in the literature. These calculations also gave the first accurate description of H(-) experiments at Los Alamos, up to the n = 6 threshold. A new set of computer programs was developed to handle double-Rydberg 'planetary' states of barium and strontium, incorporating long range multipole interactions explicitly. Finally, we studied triply-excited states of H(- -) in an attempt to clarify the question of whether such resonances exist. Each of these projects is described in greater detail below. DOE

N95-21887# International Centre for Theoretical Physics, Trieste (Italy).

EFFECT OF THE ELECTRON-SO-PHONON ON THE IMPURITY STATE ENERGIES IN A SEMICONDUCTOR QUANTUM WELL

Zhongjun Shen Sep. 1993 12 p
(DE94-628993; IC-93/315) Avail: CASI HC A03/MF A01 (US Sales Only)

Using variational technique the change of ground state energy and binding energy of impurity atom with impurity position and well width in GaAs-Ga(0.7)Al(0.3)As quantum well is calculated. In calculation the electron-surface optical (SO) phonon interactions are taken into account. The result is discussed. It is found that the electron-phonon interaction energy not only depends on the width of the well but also depends on the position of the impurity atom in the well. DOE

N95-21928 Rome Lab., Griffiss AFB, NY.

HETEROSTRUCTURE QUANTUM CONFINED STARK EFFECT ELECTROOPTIC MODULATORS OPERATING AT 938 nm Report, May 1992 - May 1993

Michael J. Hayduk, Mark F. Krol, and Raymond K. Boncek Dec. 1993 89 p Limited Reproducibility: More than 20% of this document may be affected by microfiche quality
(AD-A279342; RL-TR-93-259) Avail: Issuing Activity (Defense Technical Information Center (DTIC))

Electro-optics modulators are a necessary component of emerging optical fiber based local area interconnects. One type of modulator, suitable for use in optical interconnects, is an asymmetric Fabry-Perot reflection modulator (ARM). This type of an intensity modulator uses an electro-optic material as the spacer material to balance the normally unequal front and back mirror reflectances. The quantum confined Franz-Keldysh and Stark effects shift the absorption edge of semiconductor multiple quantum well (MQW) materials to longer wavelengths in the presence of an external electric field applied perpendicular to the MQW layers, thereby changing the reflectance of the etalon. The combined coherence effects of the etalon coupled with the quantum effects of the MQW materials result in a large modulation depth and a low insertion loss. P-I-N diode structures using an In Ha As/GaAs MQW structure as the intrinsic region were fabricated for the purpose of characterizing the electro-absorption associated with different applied electric fields. Quantum confined Franz-Keldysh and Stark shifts were observed for applied electric fields as large as 6.58 x 10000 V/cm. The resulting change in the absorption coefficient was found to be -3.7 x 1000 cm to the minus 1st power which is sufficient to design a high-speed ARM with a large modulation depth and a low insertion loss. DTIC

N95-21993# International Centre for Theoretical Physics, Trieste (Italy).

A NEW FHNC SCHEME FOR GUTZWILLER CORRELATED WAVE FUNCTIONS

X. Q. G. Wang, S. Fantoni (SISSA, Trieste, Italy.), E. Tosatti, and L. Yu Nov. 1993 11 p
(DE94-629037; IC-93/383; SISSA-83/93/CM/MB) Avail: CASI HC A03/MF A01 (US Sales Only)

A new set of integral equations in Fermi Hyper-Netted Chain scheme, named GHNC is formulated for Gutzwiller correlated wave functions. The well-known exact analytical results of Vollhardt, Metzner and Gebhard for the one and infinite dimension Gutzwiller paramagnetic wave functions are recovered as a byproduct of the theory. In approximate form, the theory is applicable to arbitrary Gutzwiller correlated wave functions, irrespective of the space dimensionality of the model. DOE

N95-21994# International Centre for Theoretical Physics, Trieste (Italy).
AN ASYMPTOTIC SOLUTION OF THE (INFINITY)-d HUBBARD MODEL
X. Y. Zhang and G. M. Zhang Jan. 1994 11 p
(DE94-629042; IC-94/21) Avail: CASI HC A03/MF A01 (US Sales Only)

We present an asymptotically exact solution of the (infinity) - d Hubbard model at a special interaction strength U(sub T) corresponding to the strong-coupling Fermi-liquid fixed point. This solution is intimately related to the Tolouse limit of the single-impurity Kondo model and the symmetric Anderson model in its strong-coupling limit. DOE

N95-22054# Naval Surface Weapons Center, Dahlgren, VA.
NUMERICAL INVESTIGATION OF ONE-DIMENSIONAL HEAT-FLUX CALCULATIONS
C. F. Boyd and A. Howell 25 Oct. 1994 32 p
(AD-A286293; NSWCDD/TR-94-114) Avail: CASI HC A03/MF A01

New computer codes to determine the heat transfer rate from wind tunnel model surface temperature measurements have been developed for use in the Navy's Hypervelocity Wind Tunnel No. 9 (Tunnel 9). The existing code, which assumes one-dimensional (1D) conduction in a Cartesian coordinate system, accurately predicts 1D heat-flux when applied to flat or nearly flat geometries. Heating rates are overpredicted when the code is applied to cylindrical, spherical, and conical geometries. The over-prediction increases with larger test times and smaller radius of curvature. Heating rates are also over-predicted when the code is applied under a two-dimensional (2D) heating load that varies linearly in space. This over-prediction increases with larger test times and larger spatial gradient of heat-flux but is small for typical Tunnel 9 applications. Two new computer codes, which assume 1D conduction in cylindrical and spherical coordinates, accurately predict 1D heat-flux applied to cylindrical, spherical, and conical geometries. These two codes are online for use as a tool in evaluating heat transfer from Tunnel 9 data. DTIC

N95-22153# National Inst. of Standards and Technology, Boulder, CO. Thermophysics Div.
THERMOPHYSICAL PROPERTIES OF HFC-143a AND HFC-152a Final Report, 1 Apr. 1993 - 30 Jun. 1994
W. M. Haynes Jul. 1994 188 p Prepared for Air-Conditioning and Refrigeration Technology Inst., Inc., Arlington, VA
(Contract DE-FG02-91CE-23810; ARTI-MCLR Proj. 650-50800)
(DE95-002199; DOE/CE-23810/39) Avail: CASI HC A09/MF A02

Numerous fluids have been identified as promising alternative refrigerants, but much of the information needed to predict their behavior as pure fluids and as components in mixtures does not exist. In particular, reliable thermophysical properties data and models are needed to predict the performance of the new refrigerants in heating and cooling equipment and to design and optimize equipment to be reliable and energy efficient. The objective of this fifteen-month project has been to provide highly accurate, selected thermophysical properties data for refrigerants HFC-143a (CH3CF3) and HFC-152a (CH3CHF2) and to use these data to fit complex equations of state and detailed transport property models. The new data have filled gaps in the existing data sets and resolved problems and uncertainties that existed in and between the data sets. DOE

N95-22185# European Organization for Nuclear Research, Geneva (Switzerland).
THE DEVELOPMENT OF SCIENCE DURING THIS CENTURY
V. F. Weisskopf (Massachusetts Inst. of Tech., Cambridge, MA.) 20 Dec. 1993 18 p Presented at the Conference on Disarmament and Arms Limitation Obligations: Problems of Compliance and Enforcement, Geneva, Switzerland, 5-6 Aug. 1993
(DE94-632964; CERN-93-06; CONF-9308209) Avail: CASI HC A03/MF A01 (US Sales Only)

This is a slightly revised version of a talk delivered at the meeting of the American Association for the Advancement of Science, in Boston, on 14 February 1993, and at a CERN Colloquium, on 5 August 1993, entitled 'Science -yesterday, today and tomorrow'. It describes the tremendous growth of scientific knowledge and insights acquired since the beginning of this century. The changes in the character, sociology and support, of science are discussed, including the growing predominance of American science and the recent trend away from basic science towards applied research. DOE

N95-22198# International Centre for Theoretical Physics, Trieste (Italy).
ON THE CONDUCTANCE SUM RULE FOR THE HIERARCHICAL EDGE STATES OF THE FRACTIONAL QUANTUM HALL EFFECT
Zhong-Shui Ma (Academia Sinica, Beijing, China.), Yi-Xin Chen (Zhejiang Univ., China.), and Zhao-Bin Su Sep. 1993 11 p
(DE94-629030; IC-93/329) Avail: CASI HC A03/MF A01 (US Sales Only)

The conductance sum rule for the hierarchical edge channel currents of a fractional quantum Hall effect state is derived analytically within the Haldane-Halperin hierarchy scheme. We provide also an intuitive interpretation for the hierarchical drift velocities of the edge excitations. DOE

N95-22237# California Univ., Berkeley. Lawrence Berkeley Lab, CA.
THEORY OF THE EXCITONIC LINESHAPE IN LOW-DIMENSIONAL STRUCTURES WITH ROUGH INTERFACES
S. Glutsch and F. Bechstedt (Friedrich-Schiller Univ., Jena, Germany.) Aug. 1994 11 p Presented at the 7th International Conference on Superlattices, Microstructures and Microdevices, Banff, Alberta, 22-26 Aug. 1994 Submitted for publication
(Contract DE-AC03-76SF-00098)
(DE95-003434; LBL-36144; CONF-940824-1) Avail: CASI HC A03/MF A01

A quantum mechanical theory of single-particle motion under the influence of a stochastic potential is presented. By solving the Dyson equation, the one-particle Green's function can be determined approximately. Gaussian distribution, an explicit expression is derived for the spectral function. The analytical results are in good agreement with numerically calculated data. The theory is applied to excitons on rough interfaces. The optical absorption of excitons on rough surfaces can be traced back to the one-particle Green's function for the center-of-mass motion. In contrast to the classical treatment, the asymmetry of the lines and the redshift of the maxima can be explained. The coefficients for linewidth and asymmetry can be expressed in terms of the excitonic wavefunction and the binary correlation function of the stochastic potential. DOE

N95-22378# International Centre for Theoretical Physics, Trieste (Italy).
TUNNELING OF SELF-TRAPPED STATES AND FORMATION OF A BAND
K. Yonemitsu Dec. 1993 5 p
(DE94-629001; IC-93/412) Avail: CASI HC A01/MF A01 (US Sales Only)

Tunneling of a self-trapped kink and formation of a band are studied semi classically in the one-dimensional extended Peierls-Hubbard model near half filling, considering up to Gaussian fluctuations around imaginary-time-dependent periodic motion of electrons and phonons on the stationary phase of the action derived using Slater determinants. In the strong-coupling limit of both the Holstein and attractive Hubbard models, it reproduces analytically-known effective hopping of a single bipolaron because the tunneling involves only one in this limit. The method gives new results in other general cases and is easily applied to excited or more complex systems. DOE

N95-22432# Helsinki Univ. of Technology, Espoo (Finland).
PHOTOREFLECTANCE AND X RAY DIFFRACTION STUDY OF SEMICONDUCTOR HETEROSTRUCTURES AND QUANTUM WELLS Ph.D. Thesis
H. Lipsanen 13 May 1994 99 p
(PB95-127049) Avail: CASI HC A05/MF A02

The modulation spectroscopy method of photoreflectance and double crystal X-ray diffraction were used for the characterization and development of III-V compound semiconductor heterostructures and quantum wells. The materials studied were based on the compounds of gallium arsenide and indium phosphide grown by molecular beam epitaxy and metalorganic vapor phase epitaxy. The structure of the grown samples were determined from the X-ray diffraction curves using theoretical calculations based on the dynamical theory of X-ray diffraction. A new procedure was developed for the determination of the period of multiple quantum well structures grown on misoriented substrates. Peculiar below-bandgap features in photoreflectance, such as interference in epitaxial layers and impurity-like transitions were studied and modeled. The effect of photovoltage in noncontact determination of electric field in semiconductor structures was determined in a novel way by studying a p-i-n diode structure. The electronic energy levels of quantum well structures were studied by photoreflectance measurements. Strained layer quantum well structures were applied to the development of high-speed semiconductor lasers. A very high modulation bandwidth of 20 GHz was obtained. NTIS

80 SOCIAL SCIENCES (GENERAL)

Includes educational matters.

N95-22100 Florida State Univ., Tallahassee, FL. Geophysical Fluid Dynamics Inst.

DOD SCIENCE AND ENGINEERING APPRENTICESHIP PROGRAM FOR HIGH SCHOOL STUDENTS Annual Report, 1993-1994

Richard L. Pfeffer May 1994 27 p Limited Reproducibility: More than 20% of this document may be affected by microfiche quality
(Contract N00014-91-J-1825)
(AD-A280371) Avail: CASI HC A03

The 14 students that participated in the twelfth Apprenticeship Program for High School Students are profiled. Further information pertaining to each apprentice is attached at the end of the report. The major project in which the students participated during the summer was the analysis of photographic velocity data from laboratory experiments on the interaction of topography with baroclinic waves, and flows with azimuthally varying lower thermal boundary conditions. The experiments were conducted in a thermally driven rotating annulus of fluid. Derived from text

81 ADMINISTRATION AND MANAGEMENT

Includes management planning and research.

N95-20051# Air Force Inst. of Tech., Wright-Patterson AFB, OH. School of Logistics and Acquisition Management.

THE EFFECTS OF THREE-DIMENSIONAL GRAPHS ON DECISION MAKING M.S. Thesis

Anita E. Latin and Anthony L. Villanueva Sep. 1994 286 p
(AD-A285034; AFIT/GSM/LAS/94S-7) Avail: CASI HC A13/MF A03

The objective of this thesis was to determine whether or not, and by how much, three-dimensional graphs are more accurate and efficient than two-dimensional graphs and tables when presenting alternatives to decision makers. A graphical experiment was designed using a microcomputer. This experiment presented a business scenario to test Air Force Institute of Technology (AFIT) Professional Continuing Education (PCE) students. The experiment attempted to determine how well DoD decision makers accurately and efficiently performed elementary data collection tasks using various graphs or tables. The experiment used a randomized order within-subject factorial design with repeated measures. The factorial experiment was designed to analyze the manipulation of three factors or independent variables, anchoring, mode of presentation, and data-set, to determine their effects on the response variables of degree of accuracy, and response time (efficiency). The results of the accuracy analysis showed that in general, accuracy performance was high for most subjects regardless of the mode of presentation or the task anchoring. The timed response analysis showed that it took subjects longer to interpret three-dimensional line graphs and three-dimensional bar charts for two of the elementary data collection tasks. DTIC

N95-20739*# National Aeronautics and Space Administration, Washington, DC.

READINGS IN PROGRAM CONTROL

Francis T. Hoban, ed., William M. Lawbaugh, ed., and Edward J. Hoffman, ed. Nov. 1994 174 p
(NASA-SP-6103; NAS 1.21:6103) Avail: CASI HC A08/MF A02

Under the heading of Program Control, a number of related topics are discussed: cost estimating methods; planning and scheduling; cost overruns in the defense industry; the history of estimating; the advantages of cost plus award fee contracts; and how program control techniques led to the success of a NASA development project. For individual titles, see N95-20740 through N95-20755.

N95-20740*# National Academy of Public Administration, Washington, DC.

PROGRAM CONTROL IN NASA: NEEDS AND OPPORTUNITIES

William E. Lilly *In* NASA, Washington, Readings in Program Control Nov. 1994 p 1-14 (For primary document see N95-20739 06-81)
Avail: CASI HC A03/MF A02

NASA has successfully managed some of this country's most complex technology and development programs. These successes have included the application of sound program control processes. The impetus for this study arose from the NASA Management Study Group findings that over time, some program control tools and disciplined procedures and processes had weakened. The Study Group recommended that steps be taken to establish a comprehensive training approach in program management, and specifically, in program control functions. This study looks at program control processes within NASA currently in use, defines a 'model' of program control functions, and provides recommendations on program control training needs and opportunities. Derived from text

N95-20741*# National Aeronautics and Space Administration, Washington, DC.

COST ESTIMATING METHODS FOR ADVANCED SPACE SYSTEMS c83

Kelley Cyr *In its* Readings in Program Control Nov. 1994 p 15-24 (For primary document see N95-20739 06-81)
Avail: CASI HC A02/MF A02

NASA is responsible for developing much of the nation's future space technology. Cost estimates for new programs are required early in the planning process so that decisions can be made accurately. Because of the long lead times required to develop space hardware, the cost estimates are frequently required 10 to 15 years before the program delivers hardware. The system design in conceptual phases of a program is usually only vaguely defined and the technology used is so often state-of-the-art or beyond. These factors combine to make cost estimating for conceptual programs very challenging. This paper describes an effort to develop parametric cost estimating methods for space systems in the conceptual design phase. The approach is to identify variables that drive cost such as weight, quantity, development culture, design inheritance and time. The nature of the relationships between the driver variables and cost will be discussed. In particular, the relationship between weight and cost will be examined in detail. A theoretical model of cost will be developed and tested statistically against a historical database of major research and development projects. Derived from text

N95-20742*# National Aeronautics and Space Administration, Washington, DC.

BUT WHAT WILL IT COST? THE HISTORY OF NASA COST ESTIMATING c83

Joseph W. Hamaker *In its* Readings in Program Control Nov. 1994 p 25-37 (For primary document see N95-20739 06-81)
Avail: CASI HC A03/MF A02

Within two years of being chartered in 1958 as an independent agency to conduct civilian pursuits in aeronautics and space, NASA absorbed either wholly or partially the people, facilities, and equipment of several existing organizations. These included the laboratories of the National Advisory Committee of Aeronautics (NACA) at Langley Research Center in Virginia, Ames Research Center in California, and Lewis Research Center in Ohio; the Army Ballistic Missile Agency (ABMA) at Redstone Arsenal Alabama, for which the team of Wernher von Braun worked; and the Department of Defense Advanced Research Projects Agency (ARPA) and their ongoing work on big boosters. These were especially valuable resources to jump start the new agency in light of the shocking success of the Soviet space probe Sputnik in the autumn of the previous year and the corresponding pressure from an impatient American public to produce some response. Along with these inheritances, there came some existing systems engineering and management practices, including project cost estimating

methodologies. This paper will briefly trace the origins of those methods and how they evolved within the agency over the past three decades.
Derived from text

N95-20743*# National Aeronautics and Space Administration, Washington, DC.
IMPROVING COST EFFICIENCY IN LARGE PROGRAMS c83
John D. Hodge *In its* Readings in Program Control Nov. 1994 p 38-48 (For primary document see N95-20739 06-81)
Avail: CASI HC A03/MF A02

This paper examines the question of cost, from the birth of a program to its conclusion, particularly from the point of view of large multi-center programs, and suggests how to avoid some of the traps and pitfalls. Emphasis is given to cost in the systems engineering process, but there is an inevitable overlap with program management. (The terms systems engineering and program management have never been clearly defined.) In these days of vast Federal budget deficits and increasing overseas competition, it is imperative that we get more for each research and development dollar. This is the only way we will retain our leadership in high technology and, in the long run, our way of life. Derived from text

N95-20744*# National Aeronautics and Space Administration, Washington, DC.
ESTIMATING THE COSTS OF HUMAN SPACE EXPLORATION c83
Humboldt C. Mandell, Jr. *In its* Readings in Program Control Nov. 1994 p 49-56 (For primary document see N95-20739 06-81)
Avail: CASI HC A02/MF A02

The plan for NASA's new exploration initiative has the following strategic themes: (1) incremental, logical evolutionary development; (2) economic viability; and (3) excellence in management. The cost estimation process is involved with all of these themes and they are completely dependent upon the engineering cost estimator for success. The purpose is to articulate the issues associated with beginning this major new government initiative, to show how NASA intends to resolve them, and finally to demonstrate the vital importance of a leadership role by the cost estimation community.
Derived from text

N95-20745*# National Aeronautics and Space Administration, Washington, DC.
THE ADVANTAGES OF COST PLUS AWARD FEE CONTRACTS
William C. Keathley *In its* Readings in Program Control Nov. 1994 p 57-61 (For primary document see N95-20739 06-81)
Avail: CASI HC A01/MF A02

A Cost Plus Award Fee contract is the best procurement vehicle for the high-tech, one-of-a-kind, development projects that constitute most of NASA'S projects. The use of this type of contract requires more government and contractor effort than any other forms of contracts. An award fee contract is described as an arrangement whereby the government periodically awards a fee consistent with the cost, schedule and technical performance that is achieved by a contractor during a preset period with preset award fee pools. It's the only contracting method where both the government and contractor goals are closely linked. It also has a built-in mechanism to conveniently alter and emphasize program events in order to current external and internal situations. The award fee process also demands good communication between government and contractor participants.
Derived from text

N95-20746*# National Aeronautics and Space Administration, Washington, DC.
A COST AND PERFORMANCE SYSTEM (CAPS) IN A FEDERAL AGENCY
W. F. Huseonia and P. G. Penton *In its* Readings in Program Control Nov. 1994 p 62-75 (For primary document see N95-20739 06-81)
Avail: CASI HC A03/MF A02

Cost and Performance System (CAPS) is an automated system used from the planning phase through implementation to analysis and documentation. Data is retrievable or available for analysis of cost versus performance anomalies. CAPS provides a uniform system across intra- and international elements. A common system is recommended throughout an entire cost or profit center. Data can be easily accumulated and aggregated into higher levels of tracking and reporting of cost and performance.The level and quality of performance or productivity is indicated in the CAPS model and its process. The CAPS model provides the necessary decision information and insight to the principal investigator/project engineer for a successful project management experience. CAPS provides all levels of management with the appropriate detailed level of data.
Derived from text

N95-20747*# Arabian-American Oil Co. (Saudi Arabia).
PLANNING AND SCHEDULING FOR SUCCESS
Ignacio Manzanera *In* NASA, Washington, Readings in Program Control Nov. 1994 p 76-81 (For primary document see N95-20739 06-81)
Avail: CASI HC A02/MF A02

Planning and scheduling programs are excellent management tools when properly introduced to the project management team and regularly maintained. Communications, creativity, flexibility and accuracy are substantially improved by following a simple set of rules. A planning and scheduling program will work for you if you believe in it, make others in your project team realize its benefits, and make it an extension of your project cost control philosophy. Derived from text

N95-20748*# Defense Systems Management School, Fort Belvoir, VA.
SCHEDULING: A GUIDE FOR PROGRAM MANAGERS
In NASA, Washington, Readings in Program Control Nov. 1994 p 82-112 (For primary document see N95-20739 06-81)
Avail: CASI HC A03/MF A02

The following topics are discussed concerning scheduling: (1) milestone scheduling; (2) network scheduling; (3) program evaluation and review technique; (4) critical path method; (5) developing a network; (6) converting an ugly duckling to a swan; (7) network scheduling problem; (8) (9) network scheduling when resources are limited; (10) multi-program considerations; (11) influence on program performance; (12) line-of-balance technique; (13) time management; (14) recapitulization; and (15) analysis.
Derived from text

N95-20749*# National Aeronautics and Space Administration, Washington, DC.
AN ANALYSIS OF COST OVERRUNS ON DEFENSE ACQUISITION CONTRACTS
David S. Christensen *In its* Readings in Program Control Nov. 1994 p 113-120 (For primary document see N95-20739 06-81)
Avail: CASI HC A02/MF A02

This article examines the history of cost overruns reported on 64 completed defense contracts. Its purpose is to formally test the observation of the Under Secretary. Results confirm the observation at the 95 percent level of confidence, and were generally insensitive to the contract type (price, cost), the contract phase (development, production), the type of weapon system (air, ground, sea), and the armed forces service (Air Force, Army, Navy) that managed the contract. After a review of terminology, concepts, and related research for those unfamiliar with the area, the methodology, results, and managerial implications are described.
Derived from text

N95-20750*# National Aeronautics and Space Administration, Washington, DC.
PROGRAM CONTROL ON THE TROPICAL RAINFALL MEASURING MISSION
Dorothy J. Pennington and Walter Majerowicw *In its* Readings in Program Control Nov. 1994 p 121-136 (For primary document see N95-20739 06-81)
Avail: CASI HC A03/MF A02

The Tropical Rainfall Measuring Mission (TRMM), an integral part of NASA's Mission to Planet Earth, is the first satellite dedicated to measuring tropical rainfall. TRMM will contribute to an understanding of the mechanisms through which tropical rainfall influences global circulation and climate. Goddard Space Flight Center's (GSFC) Flight Projects Directorate is responsible for establishing a Project Office for the TRMM to manage, coordinate, and integrate the various organizations involved in the development and operation of this complex satellite. The TRMM observatory, the largest ever developed and built inhouse at GSFC, includes state-of-the-art hardware. It will carry five scientific instruments designed to determine the rate of rainfall and the total rainfall occurring between the north and south latitudes of 35 deg. As a secondary science objective,

TRMM will also measure the Earth's radiant energy budget and lightning.
Derived from text

N95-20751*# National Aeronautics and Space Administration, Washington, DC.
A STRATEGY OF COST CONTROL FOR MARINER VENUS/MERCURY 1973
John R. Biggs and Walter J. Downhower *In its* Readings in Program Control Nov. 1994 p 137-153 (For primary document see N95-20739 06-81)
Avail: CASI HC A02/MF A02

The spacecraft launched by NASA on November 3, 1973 to explore Venus and Mercury proved a notable success as a development project both in space and on the ground. This article on the development points our management approaches and techniques that kept schedules and controlled costs, the intent being to stimulate thought about how to do the same with future spacecraft and payloads. The Mariner Venus/Mercury '73 (MVM '73) project kept within its originally established goals for schedule, performance, and cost. Underlying this development success was the availability of the Mariner technology. But meeting the goals demanded management determination, planning, and discipline to make optimum use of state-of-the-art technology--on the part of people at NASA, JPL, and The Boeing Co. (the contractor). Derived from text

N95-20752*# National Aeronautics and Space Administration, Washington, DC.
PERFORMANCE MEASUREMENT: A TOOL FOR PROGRAM CONTROL
Nancy Abell *In its* Readings in Program Control Nov. 1994 p 147-153 (For primary document see N95-20739 06-81)
Avail: CASI HC A02/MF A02

Performance measurement is a management tool for planning, monitoring, and controlling as aspects of program and project management--cost, schedule, and technical requirements. It is a means (concept and approach) to a desired end (effective program planning and control). To reach the desired end, however, performance measurement must be applied and used appropriately, with full knowledge and recognition of its power and of its limitations--what it can and cannot do for the project manager. What is the potential of this management tool? What does performance measurement do that a traditional plan vs. actual technique cannot do? Performance measurement provides an improvement over the customary comparison of how much money was spent (actual cost) vs. how much was planned to be spent based on a schedule of activities (work planned). This commonly used plan vs. actual comparison does not allow one to know from the numerical data if the actual cost incurred was for work intended to be done. Derived from text

N95-20753*# National Aeronautics and Space Administration, Washington, DC.
PROGRAM CONTROL FOR MISSION SUCCESS
G. W. Longanecker *In its* Readings in Program Control Nov. 1994 p 154-156 (For primary document see N95-20739 06-81)
Avail: CASI HC A01/MF A02

This article suggests that in order to be able to exercise control over a particular program, the program itself must be controllable. A controllable program therefore, according to the author, is one that has been properly scoped technically, realistically scheduled, and adequately budgeted. The article delves indepth into each of the above aspects of a controllable program and discusses both the pros and cons of each. CASI

N95-20754*# National Aeronautics and Space Administration, Washington, DC.
THE MSFC PROGRAM CONTROL DEVELOPMENT PROGRAM
In its Readings in Program Control Nov. 1994 p 157-166 (For primary document see N95-20739 06-81)
Avail: CASI HC A02/MF A02

It is the policy of the Marshall Space Flight Center (MSFC) that employees be given the opportunity to develop their individual skills and realize their full potential consistent with their selected career path and with the overall Center's needs and objectives. The MSFC Program Control Development Program has been designed to assist individuals who have selected Program Control or Program Analyst Program Control as a career path to achieve their ultimate career goals. Individuals selected to participate in the MSFC Program Control Development Program will be provided with development training in the various Program Control functional areas identified in the NASA Program Control Model. The purpose of the MSFC Program Control Development Program is to develop individual skills in the various Program Control functions by on-the-job and classroom instructional training on the various systems, tools, techniques, and processes utilized in these areas.
Derived from text

N95-20755*# National Aeronautics and Space Administration, Washington, DC.
NASA'S ATTACK ON COSTS
George M. Low *In its* Readings in Program Control Nov. 1994 p 167-168 (For primary document see N95-20739 06-81)
Avail: CASI HC A01/MF A02

This article's concern is regarding the high costs of space travel and the need to minimize or reduce these costs in order to effectively provide the continuation of the space programs and space exploration needs of the future. Discussed is the possibility and need to optimize payloads in order to lower the costs associated with them. Design phase principles and implementation phase points are discussed. CASI

N95-20855# Washington Univ., Seattle, WA. Dept. of Civil Engineering.
THE IMPACT OF PARTNERING ON CONSTRUCTION CONTRACTS M.S. Thesis
Jeffrey R. Eckstein 1994 96 p Sponsored by Army Corps of Engineers
(AD-A286588) Avail: CASI HC A05/MF A01

This thesis presents an analysis of the impact of partnering in construction contracts administered by the Seattle District, U.S. Army Corps of Engineers. Partnering was developed as a method to change the adversarial climate and costly disputes associated with administering construction contracts. Partnering attempts to avoid disputes and to complete a quality project by opening communications while developing a commitment and a shared vision between the contracting parties. This thesis analyzes the impact of partnering by comparing project performance of partnered projects with projects not using partnering. The comparison criteria include time to process modifications, time to process submittals, claims, value engineering change proposals, cost growth, time growth, and general contractor perceptions of partnering. DTIC

N95-21414 Technische Univ., Eindhoven (Netherlands).
DESIGN PRINCIPLES FOR REAL-TIME PROCESS CONTROL SYSTEMS
K. Sima'an 1994 49 p
(ISSN 0922-5641)
(PB95-132890; Rept-94-42) Copyright Avail: Issuing Activity (National Technical Information Service (NTIS))

This text discusses a framework for formal requirements and design specification, and designing of Real-Time process Control systems (RTC-systems). The framework combines axiomatic with operational specification approaches for expressing respectively requirements and design. In addition, a design method is discussed and the principles and necessary instrumentation it assumes are identified. This design method enables the incremental designing of total RTC-systems by interleaved application of top-down and bottom-up designing steps. Since the goal of the text is the identification of the principles, and since it does not concern any specific subclass of RTC-systems' requirements specifications, then the principles are kept as general as possible. When necessary, these general principles can be limited to any chosen subclass of these requirements specifications. NTIS

N95-21427 National Defence Research Establishment, Stockholm (Sweden). Huvudavdelning foer Foersvarsanalys.
[POLICIES CONCERNING MILITARY AND CIVILIAN RESEARCH AND TECHNOLOGY APPLICATIONS] [POLICIES BESTRAEFFANDE FORSKNING OCH TEKNOLOGIFOERSOERJNING, FRAEMST FORSKNING OCH TEKNOLOGI AV MILITAERT INTRESSE, I USA, STORBRITANNIEN, TYSKLAND OCH FRANKRIKE]
J. Foghelin May 1994 52 p In SWAHILI
(PB95-131355; FOA-C-10363-1.3) Avail: Issuing Activity (National Technical Information Service (NTIS))

The report deals with policies concerning research and technology which can be used for military as well as civilian purposes. The following countries are considered: USA, Great Britain, Germany, and France. Descriptions have been put together from (official) documents and/or from points of view given in interviews. NTIS

N95-21645# Oak Ridge National Lab., TN.
TOTAL QUALITY MANAGEMENT PROGRAM PLANNING
P. T. Thornton and K. Spence May 1994 16 p
(Contract DE-AC05-84OR-21400)
(DE94-016862; ORNL/TM-12745) Avail: CASI HC A03/MF A01

As government funding grows scarce, competition between the national laboratories is increasing dramatically. In this era of tougher competition, there is no room for resistance to change. There must instead be a uniform commitment to improving the overall quality of our products (research and technology) and an increased focus on our customers' needs. There has been an ongoing effort to bring the principles of total quality management (TQM) to all Energy Systems employees to help them better prepare for future changes while responding to the pressures on federal budgets. The need exists for instituting a vigorous program of education and training to an understanding of the techniques needed to improve and initiate a change in organizational culture. The TQM facilitator is responsible for educating the work force on the benefits of self-managed work teams, designing a program of instruction for implementation, and thus getting TQM off the ground at the worker and first-line supervisory levels so that the benefits can flow back up. This program plan presents a conceptual model for TQM in the form of a hot air balloon. In this model, there are numerous factors which can individually and collectively impede the progress of TQM within the division and the laboratory. When these factors are addressed and corrected, the benefits of TQM become more visible. As this occurs, it is hoped that workers and management alike will grasp the 'total quality' concept as an acceptable agent for change and continual improvement. TQM can then rise to the occasion and take its rightful place as an integral and valid step in the laboratory's formula for survival. DOE

N95-21982 Vrije Univ., Amsterdam (Netherlands). Faculteit der Wiskunde en Informatica.
INTELLIGENT INTERACTIVE PROJECT MANAGEMENT SYSTEM
F. J. Juengen and W. Kowalczyk Dec. 1993 49 p
(PB95-132684) Avail: Issuing Activity (National Technical Information Service (NTIS))

This paper presents a general framework for developing complex systems for tasks like project management, dynamic scheduling, and design. The framework is based on the concept of interactively solving meta-constraint satisfaction problems, and it uses a number of basic notions from Artificial Intelligence: states, search space, operators that modify the states, revision mechanisms and constraint solving. Within this framework, a generic project management support system has been designed and an instantiation of it to a planning and scheduling system for the building industry is presented. A number of modules have been implemented and configured into a highly interactive scheduling system for network planning. The system can be extended by modules supporting such activities of project management as management of resources and project monitoring. By adding knowledge bases with knowledge related to hierarchical construction of project networks and libraries of realized projects, the usefulness of the system can be increased even further. NTIS

N95-22403# General Accounting Office, Washington, DC. Resources, Community and Economic Development Div.
TECHNOLOGY TRANSFER: IMPROVING THE USE OF COOPERATIVE R/D AGREEMENT AT DOE'S CONTRACTOR-OPERATED LABORATORIES. REPORT TO CONGRESSIONAL REQUESTERS
Apr. 1994 16 p
(GAO/RCED-94-91; B-253616) Avail: CASI HC A03/MF A01; GAO, PO Box 6015, Gaithersburg, MD 20884-6015 HC

A comparison of various approaches made by the Department of Energy to those made by the Army and the Department of Commerce's National Institute of Standards and Technology to implement cooperative research and development agreements is presented. The DOE's process for implementing cooperative research and development agreements was compared to the approaches used by the Army and the Department of Commerce's National Institute of Standards and Technology to determine why some federal laboratories had entered into more agreements than DOE's laboratories. The study compared the different processes for implementing cooperative R&D agreements on the level of laboratory resources available for these agreements and on the time and resources used to implement or begin the collaboration. DOE's centralized funding process for implementing most of its cooperative research and development agreements is examined. This report reflects data collected in early 1993 from the National Institute of Standards and Technology, the Army, and the Department of Energy. DOE officials have recognized the need to improve their processes for implementing cooperative R&D agreements and have taken steps to make these procedures more efficient. For example, in early 1994 DOE began using a simplified model cooperative R&D agreement that it expects will speed up its approval process and initiated a 'block funding' pilot program that will allow more cooperative R&D agreement selections to be made at the laboratory and regional office level. Derived from text

82 DOCUMENTATION AND INFORMATION SCIENCE

Includes information management; information storage and retrieval technology; technical writing; graphic arts; and micrography.

For computer documentation see *61 Computer Programming and Software.*

N95-19904# Technische Univ., Eindhoven (Netherlands). Dept. of Mathematics and Computing Science.
NEW METHOD FOR INTEGRITY CONSTRAINT CHECKING IN DEDUCTIVE DATABASES
R. Seljee Mar. 1994 44 p
(PB95-110672) Avail: CASI HC A03/MF A01

In the literature, several integrity checking methods for updates in deductive databases are described. All of these methods try to instantiate the specified integrity constraints with the update in order to constrain the full check to only a relevant part of the database. Globally, they can be divided in two major classes of methods; methods based on 'induced updates' and methods based on 'potential updates'. In this article a new method will be presented. This method represents also a new class of methods. While in the first two classes one has to generate induced updates and potential updates respectively, even if they are not relevant to any of the constraints, the new method, which will be called the 'method based on inconsistency rules', does not have this drawback. Therefore, the proposed method is potentially far more efficient than any other method based on induced updates or potential updates. NTIS

N95-19956# Naval Postgraduate School, Monterey, CA. Dept. of Computer Science.
EFFICIENT CAPTION-BASED RETRIEVAL OF MULTIMEDIA INFORMATION Progress Report, Oct. 1992 - Sep. 1993
Neil C. Rowe 9 Oct. 1993 18 p
(AD-A279604; NPS-CS-94-008) Avail: CASI HC A03/MF A01

We describe MARIE-1 and MARIE-2, information retrieval systems for multimedia data. They exploit captions on the data and perform natural-language processing of them and English retrieval requests. Some content analysis of the data is also performed to obtain additional descriptive information. The key to getting this approach to work is sufficient fast processing. We achieve this by decomposing the problem into information filters and applying a new theory of optimal information filtering which we have developed. DTIC

N95-20016# Argonne National Lab., IL.
MIGRATING THE FACILITY PROFILE INFORMATION MANAGEMENT SYSTEM INTO THE WORLD WIDE WEB
R. E. Kero and C. E. Swietlik 1994 6 p Presented at the 11th Office Information Technology Conference, Chicago, IL, 23-25 Aug. 1994
(Contract W-31-109-eng-38)
(DE94-018367; ANL/DIS/CP-83918; CONF-940873-2) Avail: CASI HC A02/MF A01

The Department of Energy - Office of Special Projects and Argonne National Laboratory (ANL), along with the Department of Energy - office of Scientific and Technical Information have previously designed and implemented the Environment, Safety and Health Facility Profile Information

Management System (FPIMS) to facilitate greater efficiency in searching, analyzing and disseminating information found within environment, safety and health oversight documents. This information retrieval based system serves as a central repository for full-text electronic oversight documents, as well as a management planning and decision making tool that can assist in trend and root cause analyses. Continuous improvement of environment, safety and health programs are currently aided through this personal computer-based system by providing a means for the open communication of lessons learned across the department. Overall benefits have included reductions in costs and improvements in past information management capabilities. Access to the FPIMS has been possible historically through a headquarters-based local area network equipped with modems. Continued demand for greater accessibility of the system by remote DOE field offices and sites, in conjunction with the Secretary of Energy' s call for greater public accessibility to Department of Energy (DOE) information resources, has been the impetus to expand access through the use of Internet technologies. Therefore, the following paper will discuss reasons for migrating the FPIMS system into the World Wide Web (Web), various lessons learned from the FPIMS migration effort, as well as future plans for enhancing the Web-based FPIMS. DOE

N95-20039 Naval Postgraduate School, Monterey, CA. Dept. of Computer Science.

THE DESIGN AND IMPLEMENTATION OF THE FUNCTIONAL/DAPLEX DATA INTERFACE FOR THE MULTIMODEL AND MULTILINGUAL DATABASE SYSTEM M.S. Thesis

William A. Demers and Jon M. Rogelstad Mar. 1994 197 p Limited Reproducibility: More than 20% of this document may be affected by microfiche quality

(AD-A280131) Avail: Issuing Activity (Defense Technical Information Center (DTIC))

The Multi-Lingual and Multi-Model Database System (MDBS), at the Naval Postgraduate School, is the only database system in which five different database model interfaces operate on a single computer system. The purpose of the MDBS is to prove that multiple database models can coexist and share data within a single computer system. The MDBS provides a platform in which diverse database models can share data, via access to other models' base data, stored in the MDBS common format. The problem was that a Functional database model had not previously been implemented on the MDBS. The goal of this thesis was to provide a Functional/DAPLEX interface for the MDBS. The approach was to design and implement a set of programs to encapsulate the Functional/DAPLEX language as introduced by D.W. Shipman in 1981. It is imperative that the interface maintain the look, feel and characteristics of the Functional data model. The result is a set of programs, written in C, which implement a Functional/DAPLEX interface, thus a sixth interface, for the MDBS. The programs parse DAPLEX data definition language and data manipulation language constructs, convert them to an MDBS common format, store the data with other models' base data and can reconvert MDBS common data back to a functional form. DTIC

N95-20162*# National Aeronautics and Space Administration. Langley Research Center, Hampton, VA.

NASA/DOD AEROSPACE KNOWLEDGE DIFFUSION RESEARCH PROJECT. REPORT 28: THE TECHNICAL COMMUNICATION PRACTICES OF AEROSPACE ENGINEERING AND SCIENCE STUDENTS: RESULTS OF THE PHASE 4 CROSS-NATIONAL SURVEYS

Thomas E. Pinelli, Laura M. Hecht (Indiana Univ., Bloomington, IN.), Rebecca O. Barclay (Rensselaer Polytechnic Inst., Troy, NY.), and John M. Kennedy (Indiana Univ., Bloomington, IN.) Dec. 1994 87 p

(RTOP 505-90-00)

(NASA-TM-109123; NAS 1.15:109123) Avail: CASI HC A05/MF A01

This report describes similarities and differences between undergraduate and graduate aerospace engineering and science students in the context of two general aspects of the educational experience. First, we explore the extent to which students differ regarding the factors that lead to the choice of becoming an aerospace engineer or a scientist, current satisfaction with that choice, and career-related goals and objectives. Second, we look at the technical communication skills, practices, habits, and training of aerospace engineering and science students. The reported data were obtained from a survey of students enrolled in aerospace engineering and science programs at universities in India, Japan, Russia, and the United Kingdom. The surveys were undertaken as part of the NASA/DOD Aerospace Knowledge Diffusion Research Project. Data are reported for the following categories: student demographics; skill importance, skill training, and skill helpfulness; collaborative writing; computer and information technology use and importance, use of electronic networks; use and importance of libraries and library services; use and importance of information sources and products; use of foreign language technical reports; and foreign language (reading and speaking) skills. Author

N95-20163*# National Aeronautics and Space Administration. Langley Research Center, Hampton, VA.

NASA/DOD AEROSPACE KNOWLEDGE DIFFUSION RESEARCH PROJECT. REPORT 31: THE TECHNICAL COMMUNICATIONS PRACTICES OF US AEROSPACE ENGINEERS AND SCIENTISTS: RESULTS OF THE PHASE 1 SME MAIL SURVEY

Thomas E. Pinelli, Rebecca O. Barclay (Rensselaer Polytechnic Inst., Troy, NY.), and John M. Kennedy (Indiana Univ., Bloomington, IN.) Dec. 1994 52 p

(RTOP 505-90-00)

(NASA-TM-109169; NAS 1.15:109169) Avail: CASI HC A08/MF A02

The U.S. government technical report is a primary means by which the results of federally funded research and development (R&D) are transferred to the U.S. aerospace industry. However, little is known about this information product in terms of its actual use, importance, and value in the transfer of federally funded R&D. To help establish a body of knowledge, the U.S. government technical report is being investigated as part of the NASA/DOD Aerospace Knowledge Diffusion Research Project. In this report, we summarize the literature on technical reports and provide a model that depicts the transfer of federally funded aerospace R&D via the U.S. government technical report. We present results from our investigation of aerospace knowledge diffusion vis-a-vis the U.S. government technical communications practices of U.S. aerospace engineers and scientists affiliated with, not necessarily belonging to, the Society of Manufacturing Engineers (SME). Author

N95-20302 Naval Postgraduate School, Monterey, CA. Dept. of Computer Science.

USING LOCAL OPTIMALITY CRITERIA FOR EFFICIENT INFORMATION RETRIEVAL WITH REDUNDANT INFORMATION FILTERS Progress Report, Jan. - Dec. 1993

Neil C. Rowe Mar. 1994 48 p Limited Reproducibility: More than 20% of this document may be affected by microfiche quality

(AD-A279603; NPS-CS-94-004) Avail: CASI HC A03

We consider information retrieval when the data, for instance multimedia, is computationally expensive to fetch. Our approach uses information filters to considerably narrow the universe of possibilities before retrieval. Then decisions must be made about the necessity, order, and concurrent processing of proposed filters (an execution plan). We develop simple polynomial-time local criteria for optimal execution plans, and show that most forms of concurrency are suboptimal with information filters. Although the general problem of finding an optimal execution plan is likely exponential in the numbers of filters, we show experimentally that our local optimality criteria, used in a polynomial-time algorithm, nearly always find the global optimum with 15 filters or less, sufficient number of filters for most applications. Our methods do not require special hardware and avoid the high processor idleness that is characteristic of massive-parallelism solutions to this problem. We apply our ideas to an important application, information retrieval of captioned data using natural-language understanding, a problem for which the natural-language processing can be the bottleneck if not implemented well. DTIC

N95-20309 International Business Machines Corp., San Jose, CA. Almaden Research Center.

TIME DOMAIN SPECTRAL HOLE-BURNING STORAGE Final Report, 30 Sep. 1992 - 29 Dec. 1993

Michael Jefferson 2 May 1994 18 p Limited Reproducibility: More than 20% of this document may be affected by microfiche quality

(Contract F49620-92-C-0066)

(AD-A279912; AFOSR-94-0312TR) Avail: Issuing Activity (Defense Technical Information Center (DTIC))

This work achieved several substantial results. A highly stabilized laser system suitable for many detailed studies of data storage phenomena was constructed and made to work. This laser was essential for the investigations which followed. Using the stabilized laser, a real time correlator was demonstrated, which correctly identified all occurences of a test sequence imbedded in random data. This correlator is the first demonstration of the use of phase modulation to store and retrieve data in time domain hole-burning. In the frequency domain, narrow holes were burned and scanned, and information storage at a spectral density exceeding 50,000 bits per spot was demonstrated, with perfect recall and excellent signal to noise. We have also made the first demonstration of a novel technique for storing and retrieving phase modulated data streams with time domain spectral hole-burning. This demonstration has been disclosed for patent purposes. DTIC

N95-20589 Naval Postgraduate School, Monterey, CA.
DOWNSIZING INFORMATION SYSTEMS: FRAMING THE ISSUES FOR THE OFFICE OF NAVAL INTELLIGENCE (ONI) M.S. Thesis
Peter M. Hutson Mar. 1994 115 p Limited Reproducibility: More than 20% of this document may be affected by microfiche quality
(AD-A279888) Avail: Issuing Activity (Defense Technical Information Center (DTIC))

Downsizing information systems from large and centralized mainframe computing architectures to smaller and distributed desktop systems is one of the most difficult and critical strategic decisions facing both corporate and government organizations. Vendor advertisements and media hype often boast of huge cost savings and greater flexibility while retaining mainframe-strength performance. Cryptic terminology, biased vendor assistance, and rapidly changing technology complicate already difficult decisions. This thesis provides an executive summary for middle and top managers requiring a survey of the major downsizing issues. It provides an overview of architectural trends that are helping to fuel the downsizing process to include an emphasis on the client/server paradigm, the evolving roles of the mainframe and desktop computers, and innovative architectural software tools. An analysis of management and technical risks according to organizational, performance, and cost factors also focuses on such critical considerations as business process reengineering, open systems, flexibility, throughput, security, conversion costs, and life-cycle costs of downsized systems. Finally, this thesis 'frames' the issues for the Office of Naval Intelligence and DOD by highlighting and outlining some general guidelines that may be used to intelligently plan strategy and make key organizational decisions. DTIC

N95-20617# Naval Postgraduate School, Monterey, CA.
TRANSLATION OF THE DATA FLOW QUERY LANGUAGE FOR THE MULTIMODEL, MULTIBACKEND DATABASE SYSTEM M.S. Thesis
Nancy C. Free Sep. 1994 74 p
(AD-A285978) Avail: CASI HC A04/MF A01

This thesis involved the design and translation of the Data Flow Query Language (DFQL) for the Multi-Lingual, Multi-Backend Database System (MDBS). The MDBS is a database system that can effectively support multiple data models and their corresponding data manipulation languages. The problem was that MDBS interfaces are text-based, and not very user-friendly. The approach taken to solve this interface problem was to design and translate the DFQL for implementation on the MDBS. DFQL was designed to improve and extend SQL, the data manipulation language associated with the relational data model. It uses a graphical interface based on the data flow paradigm. This translation would extend the MDBS by allowing a graphical interface to be implemented, whereas currently a user can only access the system with text-based interfaces. The result of this thesis is the development of the DFQL to ABDL translator. The subsequent implementation of this translator on the MDBS would be a user-oriented enhancement to the current system. In addition, further improvements to the MDBS should be made, such as allowing the use of additional data types (currently constrained to string and integer) and the ability to create views. These changes would allow all the benefits from DFQL, such as orthogonality, language extensibility and incremental querying to be achieved and made available to the user. DTIC

N95-20762# Department of Energy, Washington, DC. Office of Science Education and Technical Information.
FEDIX: USER'S GUIDE, VERSION 5.0/RELEASE 3.0
Sep. 1994 55 p
(DE95-002274; DOE/ET-0026) Avail: CASI HC A04/MF A01

FEDIX is an on-line information service that links the education community and the federal government to facilitate research, education, and services. The system provides accurate, timely federal agency information to colleges, universities, and other research organizations. Participating agencies include DOE, FAA, NASA, ONR, AFOSR, DOC, HUD, AID, USDA, and DISA/DARIC. This guide is intended to help users access and utilize the FEDIX system. Because the system is frequently updated, some menus and tables in the text may not exactly match those displayed on the live system. DOE

N95-20774# Phillips Lab., Kirtland AFB, NM.
THE 37TH MILITARY LIBRARIANS WORKSHOP ON GLOBAL INFORMATION: THE SUN NEVER SETS
Lee R. McLaughlin Aug. 1994 339 p Workshop held in Albuquerque, NM, 15-18 Nov. 1993
(AD-A286636; PL-CP-94-1000) Avail: CASI HC A15/MF A03

The Thirty-Seventh Annual Military Librarians Workshop was held in Albuquerque, New Mexico, on 15-18 November 1993. The theme of the Thirty-Seventh Annual Military Librarians Workshop was 'Global Information: The Sun Never Sets.' Discussion topics included Emerging Technologies, New Approaches to Training Information Professionals in the United States and Eastern Europe; International Information Research (Space); Knowledge Diffusion Project (NASA); Federal Library Contracting; The Virtual Library; Developments in Position Classification Standards; Access Russia; Relationships Between Libraries and New Information Entities; and the Library Services Alliance of New Mexico. DTIC

N95-20777# Los Alamos National Lab., NM.
SHAPING THE LIBRARY OF THE FUTURE: DIGITAL LIBRARY DEVELOPMENTS AT LOS ALAMOS NATIONAL LABORATORY'S RESEARCH LIBRARY
R. E. Luce 1994 10 p Presented at the Office of Scientific and Technical Information INFOTECH, Oak Ridge, TN, 25-26 Oct. 1994
(Contract W-7405-eng-36)
(DE95-001008; LA-UR-94-3307; CONF-9410141-2) Avail: CASI HC A02/MF A01

This paper offers an overview of current efforts at the Research Library, Los Alamos National Laboratory, (LANL), to develop digital library services. Current projects of LANL's Library without Walls initiative are described. Although the architecture of digital libraries generally is experimental and subject to debate, one principle of LANL's approach to delivering library information is the use of Mosaic as a client for the Research Library's resources. Several projects under development have significant ramifications for delivering library services over the Internet. Specific efforts via Mosaic include support for preprint databases, providing access to citation databases, and access to a digital image database of unclassified Los Alamos technical reports. DOE

N95-20789# Los Alamos National Lab., NM.
DETERMINING INFORMATION MANAGEMENT NEEDS FOR ENHANCED INTERNATIONAL SAFEGUARDS
Richard V. Badalamente (Battelle Pacific Northwest Labs., Richland, WA.), Sharon M. DeLand (Sandia National Labs., Albuquerque, NM.), Rena Whiteson, and George Anzelon (Lawrence Livermore National Lab., Livermore, CA.) 1994 7 p Presented at the Institute of Nuclear Materials Management Annual Meeting, Naples, FL, 17-20 Jul. 1994
(Contracts W-7405-eng-36; DE-AC04-94AL-85000)
(DE94-015787; LA-UR-94-2082; SAND-94-1910C; CONF-940748-35)
Avail: CASI HC A02/MF A01

The Safeguards Information Management System initiative is a program of the Department of Energy's (DOE) Office of Arms Control and Nonproliferation aimed at supporting the International Atomic Energy Agency's (IAEA) efforts to strengthen safeguards through the enhancement of information management capabilities. The DOE hopes to provide the IAEA with the ability to correlate and analyze data from existing and new sources of information, including publicly available information, information on imports and exports, design information, environmental monitoring data, and non-safeguards information. The first step in this effort is to identify and define IAEA requirements. In support of this, we have created a users' requirements document based on interviews with IAEA staff that describes the information management needs of the end user projected by the IAEA, including needs for storage, retrieval, analysis, communication, and visualization of data. Also included are characteristics of the end user and attributes of the current environment. This paper describes our efforts to obtain the required information. We discuss how to accurately represent user needs and involve users for an international organization with a multi-cultural user population. We describe our approach, our experience in setting up and conducting the interviews and brainstorming sessions, and a brief discussion of what we learned. DOE

N95-20818# Los Alamos National Lab., NM.

THE ENERGY SCIENCE AND TECHNOLOGY DATABASE ON A LOCAL LIBRARY SYSTEM: A CASE STUDY AT THE LOS ALAMOS NATIONAL RESEARCH LIBRARY

I. S. Holtkamp 1994 12 p Presented at the Office of Scientific and Technical Information INFOTECH, Oak Ridge, TN, 25-26 Oct. 1994
(Contract W-7405-eng-36)
(DE95-001009; LA-UR-94-3308; CONF-9410141-3) Avail: CASI HC A03/MF A01

This paper presents an overview of efforts at Los Alamos National Laboratory to acquire and mount the Energy Science and Technology Database (EDB) as a citation database on the Research Library's Geac Advance system. The rationale for undertaking this project and expected benefits are explained. Significant issues explored are loading non-USMARC records into a MARC-based library system, the use of EDB records to replace or supplement in-house cataloging of technical reports, the impact of different cataloging standards and database size on searching and retrieval, and how integrating an external database into the library's online catalog may affect staffing and workflow. DOE

N95-21002# University of Southern California, Marina del Rey, CA. Information Sciences Inst.

KNOWLEDGE REFINEMENT IN A REFLECTIVE ARCHITECTURE

Yolanda Gil Jun. 1994 16 p
(Contract DABT63-91-C-0025)
(AD-A286027; ISI/RR-94-378) Avail: CASI HC A03/MF A01

A knowledge acquisition tool should provide a user with maximum guidance in extending and debugging a knowledge base, by preventing inconsistencies and knowledge gaps that may arise inadvertently. Most current acquisition tools are not very flexible in that they are built for a predetermined inference structure or problem-solving mechanism, and the guidance they provide is specific to that inference structure and hard-coded by their designer. This paper focuses on EXPECT, a reflective architecture that supports knowledge acquisition based on an explicit analysis of the structure of a knowledge-based system, rather than on a fixed set of acquisition guidelines. EXPECT's problem solver is tightly integrated with LOOM, a state-of-art knowledge representation system. Domain facts and goals are represented declaratively, and the problem solver keeps records of their functionality within the task domain. When the user corrects the system's knowledge. EXPECT tracks any possible implications of this change in the overall system and cooperates with the user to correct any potential problems that may arise. The key to flexibility of this knowledge acquisition tool is that it adapts its guidance as the knowledge bases evolve in response to changes introduced by the user. DTIC

N95-21004 Technische Univ., Delft (Netherlands).

USE OF OPERATIONS RESEARCH TECHNIQUES IN DEDUCTIVE DATABASES Thesis

M. D. E. vanderLee 1994 122 p
(PB95-135349; ISBN-90-9007222-5) Copyright Avail: Issuing Activity (National Technical Information Service (NTIS))

The thesis is about deductive databases that use operations research techniques. The interconnection between model based logic programming and operations research will be studied. In the first two chapters we give an introduction to the basics of logic programming and operations research. In the next three chapters three classes of programs are considered. In Chapter 3 we deal with definite programs, i.e. programs containing only Horn rules. In Chapter 4 we concentrate on the class of so called disjunctive programs. In Chapter 5 we concentrate on so called normal programs. For these programs the well-founded model can be computed efficiently, but the stable models are expensive to compute. NTIS

N95-21015*# National Aeronautics and Space Administration. Langley Research Center, Hampton, VA.

NASA/DOD AEROSPACE KNOWLEDGE DIFFUSION RESEARCH PROJECT. REPORT 27: THE TECHNICAL COMMUNICATION PRACTICES OF ENGINEERING AND SCIENCE STUDENTS: RESULTS OF THE PHASE 3 ACADEMIC SURVEYS

Thomas E. Pinelli, Rebecca O. Barclay (Rensselaer Polytechnic Inst., Troy, NY.), Laura M. Hecht (Indiana Univ., Bloomington, IN.), and John M. Kennedy (Indiana Univ., Bloomington, IN.) Dec. 1994 91 p
(RTOP 505-90-00)
(NASA-TM-109122; NAS 1.15:109122) Avail: CASI HC A05/MF A01

This report describes similarities and differences between undergraduate and graduate engineering science students in the context of two general aspects of the educational experience. First, we explore the extent to which students differ regarding the factors that lead to the choice of becoming an engineer or a scientist, current satisfaction with that choice, and career-related goals and objectives. Second, we look at the technical communication practices, habits, and training of engineers and science (Physics) students. The reported data were obtained from a survey of students enrolled in the College of Engineering at the University of Illinois at Urbana-Champaign, Bowling Green State University, and Texas A&M University. The survey was undertaken as part of the NASA/DOD Aerospace Knowledge Diffusion Research Project. Data are reported for the following categories: student demographics; skill importance, skill training, and skill helpfulness; collaborative writing; computer and information technology use and importance, use of electronic networks; use and importance of libraries and library services; use and importance of information sources and products; use of foreign technical reports; and foreign language (reading and speaking) skills. Author

N95-21131# Department of Energy, Washington, DC. Office of Intelligence and National Security.

NUCLEAR TERMS HANDBOOK, 1993

1993 187 p
(DE94-016248; DOE-94016248) Avail: CASI HC A09/MF A02 (US Sales Only)

Based on requests from intelligence agencies, law enforcement officials, foreign service security officers and professional organizations, OTA created this unclassified Nuclear Terms Handbook. Objective of this handbook is to provide a useful, unclassified research instrument to assist a broad range of individuals who are involved in nuclear-related activities, but lack technical expertise about the nuclear arena. This handbook is written in non-technical language to assist intelligence, security, and law enforcement officers to understand the types and uses of materials and processes involved in nuclear operations. Listings and maps of nuclear power plants are included. DOE

N95-21187*# National Aeronautics and Space Administration. Lewis Research Center, Cleveland, OH.

BIBLIOGRAPHY OF LEWIS RESEARCH CENTER TECHNICAL PUBLICATIONS ANNOUNCED IN 1993

Nov. 1994 470 p
(NASA-TM-106666; E-8984; NAS 1.15:106666) Avail: CASI HC A20/MF A04

This compilation of abstracts describes and indexes the technical reporting that resulted from the scientific and engineering work performed and managed by the Lewis Research Center in 1993. All the publications were announced in the 1993 issues of STAR (Scientific and Technical Aerospace Reports) and/or IAA (International Aerospace Abstracts). Included are research reports, journal articles, conference presentations, patents and patent applications, and theses. Author

N95-21189*# National Aeronautics and Space Administration. Langley Research Center, Hampton, VA.

NASA LANGLEY SCIENTIFIC AND TECHNICAL INFORMATION OUTPUT: 1994, VOLUME 1

Marilou S. Phillips, comp. and Susan H. Stewart, comp. Jan. 1995 173 p
(NASA-TM-109170-Vol-1; NAS 1.15:109170-Vol-1) Avail: CASI HC A08/MF A02

This document is a compilation of the scientific and technical information that the Langley Research Center has produced during the calendar year

1994. Included are citations for Formal Reports, High-Numbered Conference Publications, High-Numbered Technical Memorandums, Contractor Reports, Journal Articles and Other Publications, Meeting Presentations, Computer Programs, Tech Briefs, and Patents. Author

N95-21401# Massachusetts Univ., Amherst, MA. Dept. of Mathematics and Statistics.
SECOND INTERNATIONAL CONFERENCE ON ORDINAL DATA ANALYSIS Final Technical Report
Melvin F. Janowitz 1993 38 p Conference held in Amherst, MA, 15-17 Oct. 1993
(Contract N00014-94-1-0794)
(AD-A279756) Avail: CASI HC A03/MF A01

The conference was held October 14-17, 1993. There were a total of 59 participants from 10 different countries. The focus of the conference centered on the following topics: (1) What is the nature of ordinal data?; (2) How does ordinal data arise and what are its uses?; (3) What techniques have been used in the past to help interpret various types of ordinal data?; and (4) What directions should be taken by future research? DTIC

N95-21457*# National Aeronautics and Space Administration. Goddard Space Flight Center, Greenbelt, MD.
ABBREVIATIONS AND ACRONYMS
1994 131 p
(NASA-TM-110506; NAS 1.15:110506) Avail: CASI HC A07/MF A02

This booklet provides a partial list of acronyms, abbreviations, and other short word forms, including their definitions, used in documents at the Goddard Space Flight Center (GSFC). This list does not preclude the use of other short forms of less general usage, as long as these short forms are identified the first time they appear in a document and are defined in a glossary in the document in which they are used. This document supplements information in the GSFC Scientific and Technical Information Handbook (GHB 2200.2/April 1989). It is not intended to contain all short word forms used in GSFC documents; however, it was compiled of actual short forms used in recent GSFC documents. The entries are listed first, alphabetically by the short form, and then again alphabetically by definition. Derived from text

N95-21463 Department of the Navy, Washington, DC.
SELECTIVE POLYGON MAP DISPLAY METHOD Patent
Thomas F. Wescott, inventor (to Navy), Lawrence E. McCleary, inventor (to Navy), and David A. Nation, inventor (to Navy) 23 Aug. 1994 619 p Filed 31 Jan. 1990
(AD-D016518; US-Patent-5,341,463; US-Patent-Appl-SN-473258; US-Patent-Class-395-12.9) Avail: US Patent and Trademark Office

This patent discloses signal transformations of inputted data brought about new subroutines in combination with other subroutines to display world maps or other display items with the unique capability of performing the following functions in complete generality. (1) Arbitrary selection of map center and coverage, including global displays, (2) filling of all land and lake areas defined by polygons composed of an arbitrary number of vertices, (3) clipping of map features and overlays at map boundaries and poles, (4) selection from any of nineteen currently implemented map projections with provision to install any other projection topologically similar to an oblique conic, (5) calculation of latitude longitude for any point on a map without the need for inverse mapping equations, and (6) an efficient method of plotting polyline segments along great circles. These are a number of feature functions provided by this inventive concept. The software could potentially be used with any digital global geographic data base such as World Data Bank II (WDBII), a geographic information system or other data base where polylines are used to depict linear and/or areal features. Polygon (region filled) maps and other display items can be constructed from any data base from which closed polygons can be extracted directly, or constructed via additional processing. DTIC

N95-21862# Oak Ridge National Lab., TN.
INFORMATION MANAGEMENT ARCHITECTURE FOR AN INTEGRATED COMPUTING ENVIRONMENT FOR THE ENVIRONMENTAL RESTORATION PROGRAM. VOLUME 1: INTRODUCTION
Sep. 1994 16 p
(Contract DE-AC05-84OR-21400)
(DE95-001384; ES/ER/TM-120/V1-Vol-1) Avail: CASI HC A03/MF A01

As part of the Environmental Restoration Program at Martin Marietta, IEM (Information Engineering Methodology) was developed as part of a complete and integrated approach to the progressive development and subsequent maintenance of automated data sharing systems. This approach is centered around the organization's objectives, inherent data relationships and business practices. IEM provides the Information Systems community with a tool kit of disciplined techniques supported by automated tools. It includes seven stages: Information Strategy Planning; Business Area Analysis; Business System Design; Technical Design; Construction; Transition; Production. DOE

N95-21948* National Aeronautics and Space Administration, Washington, DC.
NASA PATENT ABSTRACTS BIBLIOGRAPHY: A CONTINUING BIBLIOGRAPHY. SECTION 2: INDEXES (SUPPLEMENT 46)
Jan. 1995 644 p
(NASA-SP-7039(46)-Sect-2; NAS 1.21:7039(46)-Sect-2) Avail: CASI HC A99

A subject index is provided for over 5600 patents and patent applications for the period May 1969 through December 1994. Additional indexes list personal authors, corporate authors, contract numbers, NASA case numbers, U.S. patent class numbers, U.S. patent numbers, and NASA accession numbers. Author

N95-21977*# National Aeronautics and Space Administration. Langley Research Center, Hampton, VA.
NASA/DOD AEROSPACE KNOWLEDGE DIFFUSION RESEARCH PROJECT. PAPER 48: VALUING INFORMATION IN AN INTERACTIVE ENVIRONMENT
Herbert R. Brinberg (Parnassus Associates International, New York, NY.), Thomas E. Pinelli, and Rebecca O. Barclay (Electronic Information Age, Inc., Portsmouth, VA.) May 1995 16 p Presented at the International Congress on the Economics of Information, Lyon, France, 18-20 May 1995; sponsored by the French Higher National School of Information Science and Library
(NASA-TM-110448; NAS 1.15:110448) Avail: CASI HC A03/MF A01

Consideration effort has been devoted over the past 30 years to developing methods and means of assessing the value of information. Two approaches - value in exchange and value in use - dominate; however, neither approach enjoys much practical application because validation schema for decision-making is missing. The approaches fail to measure objectively the real costs of acquiring information and the real benefits that information will yield. Moreover, these approaches collectively fail to provide economic justification to build and/or continue to support an information product or service. In addition, the impact of Cyberspace adds a new dimension to the problem. A new paradigm is required to make economic sense in this revolutionary information environment. In previous work, the authors explored the various approaches to measuring the value of information and concluded that, in large measure, these methods were unworkable concepts and constructs. Instead, they proposed several axioms for valuing information. Most particularly they concluded that the 'value of information cannot be measured in the absence of a specific task, objective, or goal.' This paper builds on those axioms and describes under which circumstances information can be measured in objective and actionable terms. This paper also proposes a methodology for undertaking such measures and validating the results. Author

N95-22053# Naval Undersea Warfare Center, Newport, RI.
INFORMATION CLUSTERING FOR BETTER DECISION-MAKING Final Report
S. S. Kirschenbaum 2 May 1994 24 p
(AD-A286292; NUWC-NPT-TR-10372) Avail: CASI HC A03/MF A01

Chunking of information in memory is one of the distinguishing features of expertise. Thus, it is hypothesized that providing information displays that cluster and integrate information according to the expert decision-maker's task leads to more efficient decision performance. Three information format schemes: alphabetical listing, functional partitioning, and integrative clustering were tested for a complex, time-limited task with conflicting goals. The integrative clustering led to the most efficient performance. Functional partitioning required greater effort for limited performance improvement. Results are discussed in terms of implications for display designers. DTIC

N95-22061# Oak Ridge National Lab., TN.
INFORMATION MANAGEMENT ARCHITECTURE FOR AN INTEGRATED COMPUTING ENVIRONMENT FOR THE ENVIRONMENTAL RESTORATION PROGRAM. VOLUME 2: INTERIM BUSINESS SYSTEMS GUIDANCE
Sep. 1994 44 p
(Contract DE-AC05-84OR-21400)
(DE95-001385; ES/ER/TM-120/V2-Vol-2) Avail: CASI HC A03/MF A01

As part of the Environmental Restoration Program at Martin Marietta, IEM (Information Engineering Methodology) was developed as part of a complete and integrated approach to the progressive development and subsequent maintenance of automated data sharing systems. This approach is centered around the organization's objectives, inherent data relationships, and business practices. IEM provides the Information Systems community with a tool kit of disciplined techniques supported by automated tools. It includes seven stages: Information Strategy Planning; Business Area Analysis; Business System Design; Technical Design; Construction; Transition; and Production. This document focuses on the Business Systems Architecture. DOE

N95-22069 RAND Corp., Santa Monica, CA.
CONFERENCE PROCEEDINGS. DEFENSE MODELING AND SIMULATION OFFICE INFORMATION/DATA BASE (I/DB) TASK GROUP MEETINGS, AND NOTES FROM THE PREVIOUS TWO I/DB MEETINGS
Iris M. Kameny, ed. 1994 998 p Meeting held in Washington, DC, 14-18 Feb. 1994 Limited Reproducibility: More than 20% of this document may be affected by microfiche quality
(Contract MDA903-90-C-0004)
(AD-A279097; CF-114-DMSO) Avail: Issuing Activity (Defense Technical Information Center (DTIC))

The work described here was performed for the Defense Modeling and Simulation Office as part of its initiative to strengthen the use of simulation and modeling throughout DOD. This work should be of interest to those working in the areas of interoperability of information systems, information resource management (IRM), data dictionary systems, resource directories, data modeling and use of IDEF tools, complex data, data verification, validation, and certification (VV&C), data quality, and assessment of data management technology. DTIC

N95-22092# Argonne National Lab., IL.
TAKING AIM: THE MANAGEMENT OF SCIENTIFIC AND TECHNICAL INFORMATION AT ARGONNE NATIONAL LABORATORY
Mark Masek, Maria DiStravolo, and Richard Dominiak 1994 10 p Presented at the Office of Scientific and Technical Information INFOTECH 1994, Oak Ridge, TN, 25-26 Oct. 1994
(Contract W-31-109-eng-38)
(DE94-019279; ANL/IPD/CP-83520; CONF-9410141-1) Avail: CASI HC A02/MF A01

Four years ago, Argonne National Laboratory tracked its publications the old-fashioned way - typing information on index cards, making photocopies of the cards and sorting them according to title, author, report number and keywords. Now, the Argonne Information Management (AIM) system collects document clearance and publication information in an integrated electronic system that tracks the laboratory's publications along with associated cost records, and offers a publicly available interface to the data so authors and divisions can create their own publications lists. This presentation will outline the steps taken to develop this system; the benefits to the overall publication review process; how the system meets the needs of a variety of customers, from Argonne authors to DOE and beyond, and the plans for future enhancements. DOE

N95-22098# Department of the Navy, Washington, DC.
METHOD OF RETRIEVING AND STORING COMPUTER PERIPHERAL DATA Patent Application
Stephen J. Amuro, inventor (to Navy) and Paul J. Giorgio, inventor (to Navy) 29 Mar. 1994 21 p
(AD-D016251; US-Patent-Appl-SN-219554) Avail: CASI HC A03/MF A01

An improved method of having a Small Computer System Interface (SCSI) controller provide a logical connection between a plurality of host processors using a single SCSI initiator is presented. The controller contains removable host adapters for connection to any type of host processor interface. When a host processor requests status information of a target device, that status information is passed to the requesting processor and subsequently stored in the controller and made available to all other host processors. DTIC

N95-22107# Oak Ridge National Lab., TN.
ABBREVIATIONS, ACRONYMS, AND INITIALISMS FREQUENTLY USED BY MARTIN MARIETTA ENERGY SYSTEMS, INC.
Jacqueline T. Miller Sep. 1994 210 p
(Contract DE-AC05-84OR-21400)
(DE95-001069; ES/IMS-1) Avail: CASI HC A10/MF A03

Guidelines are given for using abbreviations, acronyms, and initialisms (AAI's) in documents prepared by US Department of Energy facilities managed by Martin Marietta Energy Systems, Inc., in Oak Ridge, Tennessee. The more than 10,000 AAI's listed represent only a small portion of those found in recent documents prepared by contributing editors of the Information Management Services organization of Oak Ridge National Laboratory, the Oak Ridge K-25 Site, and the Oak Ridge Y-12 Plant. This document expands on AAI's listed in the Document Preparation Guide and is intended as a companion document. DOE

N95-22129# Oak Ridge National Lab., TN. Environmental Information Div.
GUIDELINES FOR THE CREATION AND MANAGEMENT OF GEOGRAPHIC DATA BASES WITHIN A GIS ENVIRONMENT, VERSION 1.0. VOLUME 2. APPENDICES
R. C. Durfee, M. L. Land, R. A. McCord, R. J. Olson, J. K. Thomas, E. P. Tinnel, and L. D. Voorhees Jul. 1994 96 p
(Contract DE-AC05-84OR-21400)
(DE94-019215; ES/ER/TM-56-Vol-2) Avail: CASI HC A05/MF A01

This report is the documentation for the geographic data bases within the GIS environment. The data base is to be used in the Environmental Restoration projects being conducted throughout the United States. DOE

N95-22167# Sandia National Labs., Albuquerque, NM.
A GRADED APPROACH TO ISO 9000 IMPLEMENTATION FOR RECORDS MANAGERS
C. E. Pasterczyk 1994 10 p Presented at the 39th Association of Records Managers and Administrators International Annual Conference, Toronto, Ontario, 25-29 Sep. 1994
(Contract DE-AC04-94AL-85000)
(DE94-017409; SAND-93-2610C; CONF-9409191-1) Avail: CASI HC A02/MF A01

ISO 9000 is a series of quality system standards developed by Technical Committee 176 of the International Standards Organization. The series includes three standards, ISO 9001 'Quality systems-Model for quality assurance in design/development, production, installation and serving,' ISO 9002 'Quality systems-Model for quality assurance in production and installation,' ISO 9003 'Quality systems-Model for quality assurance in final inspection and test,' and two guidelines, ISO 9000 'Quality management and quality assurance standards' and ISO 9004 'Quality management and quality system elements-Guidelines.' In companies with quality programs already in place, the structure of the ISO series lends itself to augmenting those policies, procedures, and instructions where problems exist or where the risks of failure are greater. The objectives of this paper are to provide a basic familiarity to ISO 9000 and quality assurance concepts; provide a higher level of familiarity to the records management and document control portions of the ISO 9000 series; and to discuss a graded approach to meeting the intent of ISO 9000. DOE

N95-22235# California Univ., Berkeley. Lawrence Berkeley Lab, CA.
INTERPRETATION OF HRTEM IMAGES BY IMAGE SIMULATION: AN INTRODUCTION TO THEORY AND PRACTICE
M. A. OKeefe Aug. 1994 84 p Presented at the Microscopy Society of America and Microbeam Analysis Society Joint Meeting, New Orleans, LA, 31 Jul. - 5 Aug. 1994
(Contract DE-AC03-76SF-00098)
(DE95-003422; LBL-35348; CONF-940753-24) Avail: CASI HC A05/MF A01

This tutorial describes the use of image simulation as an aid to interpretation of high-resolution transmission electron microscope images.

Topics include some image processing as well as image simulation. Image processing is the manipulation of experimental images in order to extract some desired information. Image simulation is the generation of a computed or simulated image from a model structure. It requires a detailed knowledge of the process of image formation in the high-resolution transmission electron microscope. This tutorial concentrates on image simulation, with examples of image processing appearing only as required as illustrations. Because this is an introduction, the theory of image simulation is described, but not explored in depth. The practice of image simulation is covered in sufficient detail to enable the student to understand the functions of the various steps in the computations, and the parameters necessary for their evaluation. DOE

N95-22263# Westinghouse Savannah River Co., Aiken, SC.
USING GEOGRAPHICAL DATA BROWSERS IN A NETWORKED ENVIRONMENT
H. E. Mackey, P. J. Bresnaham (South Carolina Univ., Columbia, SC.), D. J. Cowen (South Carolina Univ., Columbia, SC.), G. D. Ehler (South Carolina Univ., Columbia, SC.), E. King (South Carolina Univ., Columbia, SC.), W. L. Shirley (South Carolina Univ., Columbia, SC.), and T. White (South Carolina Univ., Columbia, SC.) 1994 16 p Presented at the International Symposium on Spatial Data Handling, Edinburgh, Scotland, 8 Sep. 1994
(Contract DE-AC09-89SR-18035)
(DE94-017809; WSRC-MS-94-0394; CONF-9409190-1) Avail: CASI HC A03/MF A01

The rapid development of spatial information technology has promoted a large variety of applications. The use of diverse, datasets in these applications has often been limited to single-platform analysis and distribution. Recent improvements in networking capabilities have led to the possibility of cross-platform access to geographical information and improved interoperability. To promote access to various databases and limit unsecured use of datasets across networks, spatial data browsers have been developed to allow simple analysis of data void of permanent update. Furthermore, applicable network configurations have greatly improved dissemination of views of existing data and individual use of distributed heterogeneous databases. Various user interfaces and networking applications can be combined to maximize data flow between storage media and data browsing software. This paper reviews the use of such distributed data browsing systems and the characteristics of platform-specific access and performance. Distinct discussions will review both geographical browser interface and networking services components. The selection of networking and software solutions was based on the development of a data browsing system for a twenty-user environment of mixed platforms (Unix, DOS, and Macintosh). Seventy percent of the user environment, however, was Macintosh-based. DOE

N95-22293 Defense Information Systems Agency, Arlington, VA. Center for Information Management.
DEFENSE DATA REPOSITORY SYSTEM (DDRS). END USER MANUAL
1 Sep. 1994 362 p Limited Reproducibility: More than 20% of this document may be affected by microfiche quality
(AD-A286484) Avail: CASI HC A16

The objective of the End User Manual for the Defense Data Repository System (DDRS) is to provide the end user with the information necessary to use the system effectively. The purpose of the DDRS is to assist the Department of Defense in creating and maintaining a data repository system. DTIC

N95-22331# Vrije Univ., Amsterdam (Netherlands).
UNIVERSITY LIBRARY DOCUMENT CIRCULATION SYSTEM SPECIFIED IN LCM
R. J. Wieringa and R. B. Feenstra Dec. 1993 81 p See also PB95-128005 Sponsored by Nederlandse Organisatie voor Wetenschappelijk Onderzoek, The Hague
(PB95-127957) Avail: CASI HC A05/MF A01

The specification language LCM (Language for Conceptual Modeling) is used to specify a part of the university library document circulation system of the Free University. LCM is version 3 of a language previously called CMSL (Conceptual Model Method for Modeling). The authors draw a number of conclusions about the types of axioms that are encountered in the case study, as well as about the kinds of extensions that should be added to LCM to facilitate easier and more expressive modeling of this case study. NTIS

N95-22334# Tilburg Univ. (Netherlands). Faculty of Economics and Business Administration.
THOUSAND GOLDEN TEN ORBITS
J. C. deVos (Samenwerkingsorgaan Brabantse Univ., Eindhoven, Netherlands.) 1994 98 p
(PB95-135109; FEW-654) Avail: CASI HC A05/MF A02

The report describes the methods used to construct a large database of accurately measured Golden Ten orbits. The contents of this database are fully set out, and from every orbit two illustrative graphs are created. The graphs enable the reader to check the orbits at a glance. NTIS

N95-22416# Naval Postgraduate School, Monterey, CA.
A CONCEPTUAL APPROACH TO OBJECT-ORIENTED DATA MODELING M.S. Thesis
Gerald B. Barnes Sep. 1994 98 p
(AD-A286048) Avail: CASI HC A05/MF A02

Object-oriented data modeling is starting to replace the relational model for many recently emerging database applications. The complex nature of these databases precludes mapping of their data directly into a tabular relational structure. Current object-oriented data modeling lacks the standardization and mathematical soundness of the relational model. This thesis addresses this problem by proposing a conceptual data model called OPERA (Object Paradigm / Entity-Relationship Approach). OPERA incorporates the static features of the Entity-Relationship Model with the dynamic properties of object-orientation. In addition to OPERA, an object-oriented extension to the graphical query language GORDAS (Graph-Oriented Data Selection) is proposed. To demonstrate the effectiveness of the proposed model, we will model a United States combat systems support database, the EWIRDB (Electronic Warfare Integrated Reprogramming Database). We map the EWIRDB from its basic relational format to an object schema and then to an OPERA graph. Finally, this conceptual schema is mapped to a GORDAS schema graph and queries are performed on the database. OPERA is conceptually superior to the ER Model and its object-oriented variant, the Enhanced Entity-Relationship Model (EER) Model. We demonstrate this by representing methods as relationship types, which the ER and EER models are incapable of OPERA also aids in query formulation for visual query languages such as GORDAS by providing a query graph mapping template. DTIC

N95-21750*# Jet Propulsion Lab., California Inst. of Tech., Pasadena, CA.
HIRES AND BEYOND
John W. Fowler and H. H. Aumann *In its* Science with High Spatial Resolution Far-Infrared Data Apr. 1994 p 1-10 (For primary document see N95-21749 06-88)
Avail: CASI HC A02/MF A02

N95-21751*# Drake Univ., Des Moines, IA. Dept. of Physics and Astronomy.
MEM APPLICATION TO IRAS CPC IMAGES
A. P. Marston *In* JPL, Science with High Spatial Resolution Far-Infrared Data Apr. 1994 p 11-16 (For primary document see N95-21749 06-88)
Avail: CASI HC A02/MF A02

N95-21752*# Tata Inst. of Fundamental Research, Bombay (India).
AN ASSESSMENT OF IMAGE RECONSTRUCTION FROM BALLOON-BORNE AND THE IRAS DATA
S. K. Ghosh, B. Das, T. N. Rengarajan, and R. P. Verma *In* JPL, Science with High Spatial Resolution Far-Infrared Data Apr. 1994 p 17-22 (For primary document see N95-21749 06-88)
Avail: CASI HC A02/MF A02

N95-21753*# Groningen Rijksuniv. (Netherlands). Space Research Lab.
IN SEARCH OF RANDOM NOISE
Do Kester and Tj. Romke Bontekoe (European Space Agency. European Space Research and Technology Center, ESTEC, Noordwijk, Netherlands.) *In* JPL, Science with High Spatial Resolution Far-Infrared Data Apr.

1994 p 23-31 (For primary document see N95-21749 06-88)
Avail: CASI HC A02/MF A02

N95-21754*# Texas Univ., Austin, TX. Dept. of Astronomy.
PUSHING THE LIMITS OF SPATIAL RESOLUTION WITH THE KUIPER AIRBORNE OBSERVATORY
Daniel Lester *In* JPL, Science with High Spatial Resolution Far-Infrared Data Apr. 1994 p 33-44 (For primary document see N95-21749 06-88)
Avail: CASI HC A03/MF A02

N95-21755*# Phillips Lab., Hanscom AFB, MA. Geophysics Directorate.
A HIGH RESOLUTION ATLAS OF THE GALACTIC PLANE AT 12 MICRONS AND 25 MICRONS
Stephan D. Price, Rose M. Korte (Mission Research Corp., Nashua, NH.), Rebecca S. Sample (Mission Research Corp., Nashua, NH.), John P. Kennealy (Mission Research Corp., Nashua, NH.), and Robert A. Gonsalves (Tufts Univ., Medford, MA.) *In* JPL, Science with High Spatial Resolution Far-Infrared Data Apr. 1994 p 45-54 (For primary document see N95-21749 06-88)
Avail: CASI HC A02/MF A02

N95-21756*# California Inst. of Tech., Pasadena, CA. Dept. of Physics.
CONSTRAINTS AS A DESTRIPING TOOL FOR HIRES IMAGES
Yu Cao and Thomas A. Prince *In* JPL, Science with High Spatial Resolution Far-Infrared Data Apr. 1994 p 55-60 (For primary document see N95-21749 06-88)
Avail: CASI HC A02/MF A02

N95-21757*# California Univ., San Diego, CA. Center for Astrophysics and Space Science.
BEYOND MAXIMUM ENTROPY: FRACTAL PIXON-BASED IMAGE RECONSTRUCTION
Richard C. Puetter and R. K. Pina *In* JPL, Science with High Spatial Resolution Far-Infrared Data Apr. 1994 p 61-67 Sponsored by NSF (For primary document see N95-21749 06-88)
Avail: CASI HC A02/MF A02

N95-21758*# European Space Agency. European Space Research and Technology Center, ESTEC, Noordwijk (Netherlands). Astrophysics Div.
HIRAS: HIGH-RESOLUTION IRAS IMAGES
Tj. Romke Bontekoe and Do Kester (Groningen Rijksuniv., Netherlands.) *In* JPL, Science with High Spatial Resolution Far-Infrared Data Apr. 1994 p 69-70 (For primary document see N95-21749 06-88)
Avail: CASI HC A01/MF A02

N95-21759*# Jet Propulsion Lab., California Inst. of Tech., Pasadena, CA.
INTERACTING GALAXIES RESOLVED BY IRAS
Joseph M. Mazzarella and Jason A. Surace *In its* Science with High Spatial Resolution Far-Infrared Data Apr. 1994 p 71-79 (For primary document see N95-21749 06-88)
Avail: CASI HC A02/MF A02

N95-21760*# New Mexico State Univ., Las Cruces, NM. Dept. of Astronomy.
AZIMUTHALLY AVERAGED RADIAL S(SUB 100 MICRONS)/S(SUB 60 MICRONS) DUST COLOR TEMPERATURES IN SPIRAL GALAXIES
Nick A. Devereux *In* JPL, Science with High Spatial Resolution Far-Infrared Data Apr. 1994 p 81-85 (For primary document see N95-21749 06-88)
Avail: CASI HC A01/MF A02

N95-21761*# Max-Planck-Inst. fuer Kernphysik, Heidelberg (Germany).
FAR-INFRARED SOURCES AND DIFFUSE EMISSION IN M31
Cong Xu and George Helou (California Inst. of Tech., Pasadena, CA.) *In* JPL, Science with High Spatial Resolution Far-Infrared Data Apr. 1994 p 87-93 (For primary document see N95-21749 06-88)
Avail: CASI HC A02/MF A02

N95-21762*# New Mexico State Univ., Las Cruces, NM.
CORRELATION OF FAR-INFRARED EMISSION AND RADIO CONTINUUM EMISSION ALONG THE MAJOR AXIS OF EDGE-ON SPIRAL GALAXIES
Bryant Heikkila and William R. Webber *In* JPL, Science with High Spatial Resolution Far-Infrared Data Apr. 1994 p 95-100 (For primary document see N95-21749 06-88)
Avail: CASI HC A02/MF A02

N95-21763*# Chicago Univ., Chicago, IL. Dept. of Astronomy and Astrophysics.
FAR-INFRARED MAPPING OF DUSTY ELLIPTICAL GALAXIES
Joanna F. Lees, D. A. Harper, Michael P. Rupen (National Radio Astronomy Observatory, Socorro, NM.), and G. R. Knapp (Princeton Univ., NJ.) *In* JPL, Science with High Spatial Resolution Far-Infrared Data Apr. 1994 p 101-106 (For primary document see N95-21749 06-88)
(Grant NGR14-001-227)
Avail: CASI HC A02/MF A02

N95-21764*# Drake Univ., Des Moines, IA. Dept. of Physics and Astronomy.
EXTENDED FAR-INFRARED EMISSION AND STAR FORMATION IN SEYFERT GALAXIES
A. P. Marston *In* JPL, Science with High Spatial Resolution Far-Infrared Data Apr. 1994 p 107-113 (For primary document see N95-21749 06-88)
Avail: CASI HC A02/MF A02

N95-21765*# Jet Propulsion Lab., California Inst. of Tech., Pasadena, CA.
TWO-DIMENSIONAL MAPS OF THE INFRARED-TO-RADIO RATIO IN SPIRAL GALAXIES
Kenneth A. Marsh and George Helou *In its* Science with High Spatial Resolution Far-Infrared Data Apr. 1994 p 115-120 (For primary document see N95-21749 06-88)
Avail: CASI HC A02/MF A02

N95-21766*# Toledo Univ., OH. Dept. of Physics and Astronomy.
THE VARIATION OF THE DUST TEMPERATURE WITHIN LATE-TYPE SPIRAL GALAXIES
Rhodri H. Evans *In* JP, Science with High Spatial Resolution Far-Infrared Data Apr. 1994 p 121-136 (For primary document see N95-21749 06-88)
Avail: CASI HC A02/MF A02

N95-21767*# Jet Propulsion Lab., California Inst. of Tech., Pasadena, CA.
AN IRAS HIRES STUDY OF LOW MASS STAR FORMATION IN THE TAURUS MOLECULAR RING
Susan Terebey and Jason A. Surace (Hawaii Univ., Honolulu, HI.) *In its* Science with High Spatial Resolution Far-Infrared Data Apr. 1994 p 127-136 (For primary document see N95-21749 06-88)
Avail: CASI HC A02/MF A02

N95-21768*# Amsterdam Univ. (Netherlands). Astronomical Inst.
HIRAS IMAGES OF FOSSIL DUST SHELLS AROUND AGB STARS
L. B. F. M. Waters (Groningen Rijksuniv., Netherlands.), Do J. M. Kester (Groningen Rijksuniv., Netherlands.), Tj. Romke Bontekoe (Groningen Rijksuniv., Netherlands.), and C. Loup (Groningen Rijksuniv., Netherlands.) *In* JPL, Science with High Spatial Resolution Far-Infrared Data Apr. 1994 p 137-142 (For primary document see N95-21749 06-88)
(Grants AF-AFOSR-0140-86; AF-AFOSR-0320-89)
Avail: CASI HC A02/MF A02

N95-21769*# Jet Propulsion Lab., California Inst. of Tech., Pasadena, CA.
WAVELET ANALYSIS APPLIED TO THE IRAS CIRRUS
William D. Langer, Robert W. Wilson (Bell Telephone Labs., Inc., Holmdel, NJ.), and Charles H. Anderson (Washington Univ., Saint Louis, MO.) *In its* Science with High Spatial Resolution Far-Infrared Data Apr. 1994 p 143-155 (For primary document see N95-21749 06-88)
Avail: CASI HC A03/MF A02

N95-21770*# Jet Propulsion Lab., California Inst. of Tech., Pasadena, CA.
A HIRES ANALYSIS OF THE FIR EMISSION OF SUPERNOVA REMNANTS
Zhong Wang *In its* Science with High Spatial Resolution Far-Infrared Data Apr. 1994 p 157-163 (For primary document see N95-21749 06-88)
Avail: CASI HC A02/MF A02

N95-21771*# National Aeronautics and Space Administration. Goddard Space Flight Center, Greenbelt, MD.
ARCMIMUTE SCALE HI AND IRAS OBSERVATIONS TOWARD HIGH LATITUDE CLOUD G86.5+59.6
Peter G. Martin (Toronto Univ., Ontario.), C. Rogers (Herzberg Inst. of Astrophysics, Pentiction, British Columbia.), W. T. Reach, P. E. Dewdney (Herzberg Inst. of Astrophysics, Pentiction, British Columbia.), and C. E. Heiles (California Univ., Berkeley, CA.) *In* JPL, Science with High Spatial Resolution Far-Infrared Data Apr. 1994 p 165-171 (For primary document see N95-21749 06-88)
Avail: CASI HC A02/MF A02

N95-21772*# Jamieson Science and Engineering, Inc., Scotts Valley, CA.
APPLICATION OF MCM IMAGE CONSTRUCTION TO IRAS COMET OBSERVATIONS
Martin F. Schlapfer and Russell G. Walker *In* JPL, Science with High Spatial Resolution Far-Infrared Data Apr. 1994 p 173-176 (For primary document see N95-21749 06-88)
Avail: CASI HC A01/MF A02

N95-21773*# Hawaii Univ., Honolulu, HI. Inst. for Astronomy.
LUMINOUS RADIO-QUIET SOURCES IN THE W3(MAIN) CLOUD CORE
C. Gareth WynnWilliams, E. F. Ladd, James R. Deane, and D. B. Sanders *In* JPL, Science with High Spatial Resolution Far-Infrared Data Apr. 1994 p 177-181 (For primary document see N95-21749 06-88)
(Grant NSF AST-89-19563)
Avail: CASI HC A01/MF A02

83 ECONOMICS AND COST ANALYSIS

Includes cost effectiveness studies.

N95-19939 Tilburg Univ. (Netherlands). Faculty of Economics.
PATTERNS OF FINANCIAL CHANGE IN THE OECD AREA
H. vanGemert and N. Gruijters Feb. 1994 37 p Limited Reproducibility: More than 20% of this document may be affected by microfiche quality
(PB95-110979; FEW-641) Avail: CASI HC A03

This paper measures the nature and degree of global financial change by studying interest rate differentials among OECD (Organization for Economic Cooperation and Development) countries. First, a simple portfolio model illuminates the various determinants of international capital mobility. The framework is used to deduce the characteristics of three fundamentally different but analytically connected patterns of financial change: financial integration, asset substitution and monetary integration. Next, the empirical analysis aims at quantifying these patterns for two regions: the FixWorld and the FlexWorld, which differ as to their exchange rate commitment. The results are discussed against the background of some dominant institutional changes in the countries concerned. The policy implications are presented in a monetary policy conflict triangle. NTIS

N95-20741*# National Aeronautics and Space Administration, Washington, DC.
COST ESTIMATING METHODS FOR ADVANCED SPACE SYSTEMS
Kelley Cyr *In its* Readings in Program Control Nov. 1994 p 15-24 (For primary document see N95-20739 06-81)
Avail: CASI HC A02/MF A02

N95-20742*# National Aeronautics and Space Administration, Washington, DC.
BUT WHAT WILL IT COST? THE HISTORY OF NASA COST ESTIMATING
Joseph W. Hamaker *In its* Readings in Program Control Nov. 1994 p 25-37 (For primary document see N95-20739 06-81)
Avail: CASI HC A03/MF A02

N95-20743*# National Aeronautics and Space Administration, Washington, DC.
IMPROVING COST EFFICIENCY IN LARGE PROGRAMS
John D. Hodge *In its* Readings in Program Control Nov. 1994 p 38-48 (For primary document see N95-20739 06-81)
Avail: CASI HC A03/MF A02

N95-20744*# National Aeronautics and Space Administration, Washington, DC.
ESTIMATING THE COSTS OF HUMAN SPACE EXPLORATION
Humboldt C. Mandell, Jr. *In its* Readings in Program Control Nov. 1994 p 49-56 (For primary document see N95-20739 06-81)
Avail: CASI HC A02/MF A02

84 LAW, POLITICAL SCIENCE AND SPACE POLICY

Includes NASA appropriation hearings; aviation law; space law and policy; international law; international cooperation; and patent policy.

No abstracts in this category.

85 URBAN TECHNOLOGY AND TRANSPORTATION

Includes applications of space technology to urban problems; technology transfer; technology assessment; and surface and mass transportation.

For related information see also *03 Air Transportation and Safety, 16 Space Transportation,* and *44 Energy Production and Conversion.*

N95-21893*# National Aeronautics and Space Administration, Washington, DC.
SPINOFF, 1994
James J. Haggerty 1994 130 p Original contains color illustrations
(NASA-NP-214; NAS 1.83:214; ISBN-0-16-045368-2) Avail: Issuing Activity (Technology Transfer Office, NASA Center for AeroSpace Information, 800 Elkridge Landing Road, Linthicum Heights, MD 21090-2934, please call (301) 621-0245 OR (410) 859-5300 X225); SOD HC; 128 functional color

This publication is intended to foster the aim of the NASA Technology Transfer Program by heightening awareness of the NASA technology available for reapplication and its potential for public benefit. The publication is organized in three main sections. The first section, Aerospace Aims, is an illustrated summary of NASA's major aeronautical and space programs, their goals and directions, their contributions to American scientific and technological growth, and their potential for practical benefit. The second section, Technology Twice Used, is a representative selection of new products and processes adapted from technology originally developed for NASA mainline programs, underlying the broad diversity of spinoff applications and the social/economic benefits they provide. The third section, Technology Transfer, is a description of the mechanisms employed to encourage and facilitate practical application of new technologies developed in the course of NASA activities. Derived from text

88 SPACE SCIENCES (GENERAL)

N95-21749*# Jet Propulsion Lab., California Inst. of Tech., Pasadena, CA.
SCIENCE WITH HIGH SPATIAL RESOLUTION FAR-INFRARED DATA
Susan Terebey, ed. and Joseph M. Mazzarella, ed. Apr. 1994 183 p
Workshop held in Pasadena, CA, 14-16 Jun. 1993
(Contract NAS7-918)
(NASA-CR-197353; JPL-Publ-94-5; NAS 1.26:197353) Avail: CASI HC A09/MF A02

The goal of this workshop was to discuss new science and techniques relevant to high spatial resolution processing of far-infrared data, with particular focus on high resolution processing of IRAS data. Users of the maximum correlation method, maximum entropy, and other resolution enhancement algorithms applicable to far-infrared data gathered at the Infrared Processing and Analysis Center (IPAC) for two days in June 1993 to compare techniques and discuss new results. During a special session on the third day, interested astronomers were introduced to IRAS HIRES processing, which is IPAC's implementation of the maximum correlation method to the IRAS data. Topics discussed during the workshop included: (1) image reconstruction; (2) random noise; (3) imagery; (4) interacting galaxies; (5) spiral galaxies; (6) galactic dust and elliptical galaxies; (7) star formation in Seyfert galaxies; (8) wavelet analysis; and (9) supernova remnants. For individual titles, see N95-21750 through N95-21773.

N95-21750*# Jet Propulsion Lab., California Inst. of Tech., Pasadena, CA.
HIRES AND BEYOND c82
John W. Fowler and H. H. Aumann *In its* Science with High Spatial Resolution Far-Infrared Data Apr. 1994 p 1-10 (For primary document see N95-21749 06-88)
Avail: CASI HC A02/MF A02

The High-Resolution image construction program (HiRes) used at IPAC is based on the Maximum Correlation Method. After HiRes intensity images are constructed from IRAS data, additional images are needed to aid in scientific interpretation. Some of the images that are available for this purpose show the fitting noise, estimates of the achieved resolution, and detector track maps. Two methods have been developed for creating color maps without discarding any more spatial information than absolutely necessary: the 'cross-band simulation' and 'prior-knowledge' methods. These maps are demonstrated using the survey observations of a 2 x 2 degree field centered on M31. Prior knowledge may also be used to achieve super-resolution and to suppress ringing around bright point sources observed against background emission. Tools to suppress noise spikes and for accelerating convergence are also described. Author

N95-21751*# Drake Univ., Des Moines, IA. Dept. of Physics and Astronomy.
MEM APPLICATION TO IRAS CPC IMAGES c82
A. P. Marston *In* JPL, Science with High Spatial Resolution Far-Infrared Data Apr. 1994 p 11-16 (For primary document see N95-21749 06-88)
Avail: CASI HC A02/MF A02

A method for applying the Maximum Entropy Method (MEM) to Chopped Photometric Channel (CPC) IRAS additional observations is illustrated. The original CPC data suffered from problems with repeatability which MEM is able to cope with by use of a noise image, produced from the results of separate data scans of objects. The process produces images of small areas of sky with circular Gaussian beams of approximately 30 in. full width half maximum resolution at 50 and 100 microns. Comparison is made to previous reconstructions made in the far-infrared as well as morphologies of objects at other wavelengths. Some projects with this dataset are discussed. Author

N95-21752*# Tata Inst. of Fundamental Research, Bombay (India).
AN ASSESSMENT OF IMAGE RECONSTRUCTION FROM BALLOON-BORNE AND THE IRAS DATA c82
S. K. Ghosh, B. Das, T. N. Rengarajan, and R. P. Verma *In* JPL, Science with High Spatial Resolution Far-Infrared Data Apr. 1994 p 17-22 (For primary document see N95-21749 06-88)
Avail: CASI HC A02/MF A02

Angular resolution and structural information from the far-infrared mapping of astronomical sources (Galactic star forming regions, spiral galaxies, etc.) made using the TIFR 1 m balloon-borne telescope and the IRAS have been compared. The effective wavelengths of the TIFR two-band photometer are 58 and 150 microns. From IRAS, the survey COADD data, additional observations (AO's) made with the survey detectors with different Macros (DPS, DSD, DPM), as well as the chopped photometric channel (CPC) data have been considered here. The observed signals have been processed using different deconvolution strategies, either based on a maximum entropy method (MEM) developed at TIFR or the HiRes package developed at IPAC. Relative merits of each of these, under different conditions of signal to noise ratio, are highlighted. The following sources have been selected for illustration: Carina complex, W31 region, IRAS 10361-5830 (all Galactic), M101 and M81 (extragalactic). The main conclusions are: far-infrared maps from MEM deconvolution of balloon-borne data have the best angular resolution; MEM deconvolution of IRAS AO's gives resolution comparable to HiRes but with less amount of computation, though the dynamic range in MEM maps is less than in HiRes maps. Author

N95-21753*# Groningen Rijksuniv. (Netherlands). Space Research Lab.
IN SEARCH OF RANDOM NOISE c82
Do Kester and Tj. Romke Bontekoe (European Space Agency. European Space Research and Technology Center, ESTEC, Noordwijk, Netherlands.) *In* JPL, Science with High Spatial Resolution Far-Infrared Data Apr. 1994 p 23-31 (For primary document see N95-21749 06-88)
Avail: CASI HC A02/MF A02

In order to make the best high resolution images of IRAS data it is necessary to incorporate any knowledge about the instrument into a model: the IRAS model. This is necessary since every remaining systematic effect will be amplified by any high resolution technique into spurious artifacts in the images. The search for random noise is in fact the never-ending quest for better quality results, and can only be obtained by better models. The Dutch high-resolution effort has resulted in HIRAS which drives the MEMSYS5 algorithm. It is specifically designed for IRAS image construction. A detailed description of HIRAS with many results is in preparation. In this paper we emphasize many of the instrumental effects incorporated in the IRAS model, including our improved 100 micron IRAS response functions. Author

N95-21754*# Texas Univ., Austin, TX. Dept. of Astronomy.
PUSHING THE LIMITS OF SPATIAL RESOLUTION WITH THE KUIPER AIRBORNE OBSERVATORY c82
Daniel Lester *In* JPL, Science with High Spatial Resolution Far-Infrared Data Apr. 1994 p 33-44 (For primary document see N95-21749 06-88)
Avail: CASI HC A03/MF A02

The study of astronomical objects at high spatial resolution in the far-IR is one of the most serious limitations to our work at these wavelengths, which carry information about the luminosity of dusty and obscured sources. At IR wavelengths shorter than 30 microns, ground based telescopes with large apertures at superb sites achieve diffraction-limited performance close to the seeing limit in the optical. At millimeter wavelengths, ground based interferometers achieve resolution that is close to this. The inaccessibility of the far-IR from the ground makes it difficult, however, to achieve complementary resolution in the far-IR. The 1983 IRAS survey, while extraordinarily sensitive, provides us with a sky map at a spatial resolution that is limited by detector size on a spatial scale that is far larger than that available in other wavelengths on the ground. The survey resolution is of order 4 min in the 100 micron bandpass, and 2 min at 60 microns (IRAS Explanatory Supplement, 1988). Information on a scale of 1' is available on some sources from the CPC. Deconvolution and image resolution using this database is one of the subjects of this workshop. Author

N95-21755*# Phillips Lab., Hanscom AFB, MA. Geophysics Directorate.
A HIGH RESOLUTION ATLAS OF THE GALACTIC PLANE AT 12 MICRONS AND 25 MICRONS c82
Stephan D. Price, Rose M. Korte (Mission Research Corp., Nashua, NH.), Rebecca S. Sample (Mission Research Corp., Nashua, NH.), John P.

Kennealy (Mission Research Corp., Nashua, NH.), and Robert A. Gonsalves (Tufts Univ., Medford, MA.) *In* JPL, Science with High Spatial Resolution Far-Infrared Data Apr. 1994 p 45-54 (For primary document see N95-21749 06-88)
Avail: CASI HC A02/MF A02

High resolution images of the 12 micron and 25 micron IRAS survey data from each HCON crossing the Galactic Plane are being created for those regions that the original IRAS processing labeled as confused. This encompasses the area within 100 deg longitude of the Galactic Center and within 3 deg to 10 deg of the Plane. The procedures used to create the images preserve the spatial resolution inherent in the IRAS instrument. The images are separated into diffuse and point source components and candidate sources are extracted from the point source image after non-linear spatial sharpening. Fluxes are estimated by convolving the candidate sources with the point response function and cross-correlating with the original point source image. A source is considered real if it is seen on at least two HCON's with a rather generous flux match but a stringent position criterion. A number of fields spanning a range of source densities from low to high have been examined. Initial analysis indicates that the imaging and extraction works quite well up to a source density of about 100 sources per square degree or down to roughly 0.8 Janskys. Author

N95-21756*# California Inst. of Tech., Pasadena, CA. Dept. of Physics.
CONSTRAINTS AS A DESTRIPING TOOL FOR HIRES IMAGES c82
Yu Cao and Thomas A. Prince *In* JPL, Science with High Spatial Resolution Far-Infrared Data Apr. 1994 p 55-60 (For primary document see N95-21749 06-88)
Avail: CASI HC A02/MF A02

Images produced from the Maximum Correlation Method sometimes suffer from visible striping artifacts, especially for areas of extended sources. Possible causes are different baseline levels and calibration errors in the detectors. We incorporated these factors into the MCM algorithm, and tested the effects of different constraints on the output image. The result shows significant visual improvement over the standard MCM Method. In some areas the new images show intelligible structures that are otherwise corrupted by striping artifacts, and the removal of these artifacts could enhance performance of object classification algorithms. The constraints were also tested on low surface brightness areas, and were found to be effective in reducing the noise level. Author

N95-21757*# California Univ., San Diego, CA. Center for Astrophysics and Space Science.
BEYOND MAXIMUM ENTROPY: FRACTAL PIXON-BASED IMAGE RECONSTRUCTION c82
Richard C. Puetter and R. K. Pina *In* JPL, Science with High Spatial Resolution Far-Infrared Data Apr. 1994 p 61-67 Sponsored by NSF (For primary document see N95-21749 06-88)
Avail: CASI HC A02/MF A02

We have developed a new Bayesian image reconstruction method that has been shown to be superior to the best implementations of other competing methods, including Goodness-of-Fit methods such as Least-Squares fitting and Lucy-Richardson reconstruction, as well as Maximum Entropy (ME) methods such as those embodied in the MEMSYS algorithms. Our new method is based on the concept of the pixon, the fundamental, indivisible unit of picture information. Use of the pixon concept provides an improved image model, resulting in an image prior which is superior to that of standard ME. Our past work has shown how uniform information content pixons can be used to develop a 'Super-ME' method in which entropy is maximized exactly. Recently, however, we have developed a superior pixon basis for the image, the Fractal Pixon Basis (FPB). Unlike the Uniform Pixon Basis (UPB) of our 'Super-ME' method, the FPB basis is selected by employing fractal dimensional concepts to assess the inherent structure in the image. The Fractal Pixon Basis results in the best image reconstructions to date, superior to both UPB and the best ME reconstructions. In this paper, we review the theory of the UPB and FPB pixon and apply our methodology to the reconstruction of far-infrared imaging of the galaxy M51. The results of our reconstruction are compared to published reconstructions of the same data using the Lucy-Richardson algorithm, the Maximum Correlation Method developed at IPAC, and the MEMSYS ME algorithms. The results show that our reconstructed image has a spatial resolution a factor of two better than best previous methods (and a factor of 20 finer than the width of the point response function), and detects sources two orders of magnitude fainter than other methods. Author

N95-21758*# European Space Agency. European Space Research and Technology Center, ESTEC, Noordwijk (Netherlands). Astrophysics Div.
HIRAS: HIGH-RESOLUTION IRAS IMAGES c82
Tj. Romke Bontekoe and Do Kester (Groningen Rijksuniv., Netherlands.) *In* JPL, Science with High Spatial Resolution Far-Infrared Data Apr. 1994 p 69-70 (For primary document see N95-21749 06-88)
Avail: CASI HC A01/MF A02

We describe a process of pyramid maximum entropy reconstruction of images from the IRAS survey data. Author

N95-21759*# Jet Propulsion Lab., California Inst. of Tech., Pasadena, CA.
INTERACTING GALAXIES RESOLVED BY IRAS c82
Joseph M. Mazzarella and Jason A. Surace *In its* Science with High Spatial Resolution Far-Infrared Data Apr. 1994 p 71-79 (For primary document see N95-21749 06-88)
Avail: CASI HC A02/MF A02

We discuss procedures, limitations and results of high resolution processing of interacting galaxies observed by the Infrared Astronomical Satellite (IRAS). Among 56 potentially resolvable interacting groups selected from the IRAS Bright Galaxy Sample, 22 systems have been resolved yielding fluxes for a total of 51 galaxies. In about 2/3 of the resolved pairs, both galaxies were detected in the far-infrared. A set of isolated non-interacting galaxies was chosen from the Bright Galaxy Sample for comparison with the interacting galaxies. For the current sample, which naturally excludes close pairs and ultraluminous merging systems, the primary conclusions are: (1) It is not possible to distinguish individual interacting galaxies from isolated galaxies of similar luminosity on the basis of infrared properties alone. (2) No direct correlation was found between measures of interaction strength and indicators of enhanced star formation within the resolved systems. (3) Comparison of the interacting and isolated samples indicates statistically significant differences between their distributions of far-infrared color ratios, luminosities, and surface brightnesses. Even during the early stages of interaction spanned by these systems, in a statistical sense, tidal perturbations substantially boost far-infrared indicators of star formation compared to non-interacting systems. We also briefly discuss future prospects for pushing the IRAS data to its limits for additional interacting systems. Author

N95-21760*# New Mexico State Univ., Las Cruces, NM. Dept. of Astronomy.
AZIMUTHALLY AVERAGED RADIAL S(SUB 100 MICRONS)/S(SUB 60 MICRONS) DUST COLOR TEMPERATURES IN SPIRAL GALAXIES c82
Nick A. Devereux *In* JPL, Science with High Spatial Resolution Far-Infrared Data Apr. 1994 p 81-85 (For primary document see N95-21749 06-88)
Avail: CASI HC A01/MF A02

The IRAS S(sub 100 micron)/S(sub 60 micron) dust color temperature profiles are presented for two nearby spiral galaxies M 101 and M 81. The radial dust temperature profiles provided an important constraint on the origin of the far-infrared luminosity. The observed dust temperature is compared with that expected for diffuse interstellar dust heated by the general interstellar radiation field within each galaxy. The implications for the contribution of cirrus to the far-infrared luminosity of M 101 and M 81 are discussed. Author

N95-21761*# Max-Planck-Inst. fuer Kernphysik, Heidelberg (Germany).
FAR-INFRARED SOURCES AND DIFFUSE EMISSION IN M31 c82
Cong Xu and George Helou (California Inst. of Tech., Pasadena, CA.) *In* JPL, Science with High Spatial Resolution Far-Infrared Data Apr. 1994 p 87-93 (For primary document see N95-21749 06-88)
Avail: CASI HC A02/MF A02

A study on the far-infrared (FIR) emission of M31 has been carried out with the High Resolution (HiRes) maps (approx. 1 min) derived from IRAS data. Sixty-eight FIR sources are detected in M31, which in general coincide with optical HII regions, and contribute 15, 23, 29, and 23 percent to the fluxes in 12, 25, 60, and 100 micron bands, respectively. The remaining diffuse emission, which dominates the FIR emission of M31, is studied

using a dust heating model which utilizes the UV and optical photometry maps and the HI maps available in the literature. It is found that the global dust-to-gas ratio in M31 disk is 6.5 10(exp -3), very close to the dust-to-gas ratio in the solar neighborhood. There is a significant galactocentric gradient of the dust-to-HI-gas ratio, with an e-folding scale length of 9 kpc. The diffuse dust correlates tightly with the HI gas. The model indicates that the non-ionizing UV (913-4000A) radiation from massive and intermediate massive stars contributes only about 30 percent of the heating of the diffuse dust, while the optical-NIR (4000-9000A) radiation from the old stellar population is responsible for the most of the heating.
Author

N95-21762*# New Mexico State Univ., Las Cruces, NM.
CORRELATION OF FAR-INFRARED EMISSION AND RADIO CONTINUUM EMISSION ALONG THE MAJOR AXIS OF EDGE-ON SPIRAL GALAXIES **c82**
Bryant Heikkila and William R. Webber *In* JPL, Science with High Spatial Resolution Far-Infrared Data Apr. 1994 p 95-100 (For primary document see N95-21749 06-88)
Avail: CASI HC A02/MF A02

Using new High Resolution far-infrared (FIR) images we have determined FIR flux densities, the FIR luminosity, and intensity profiles along the major axis for eight nearby edge-on spiral galaxies. We present spatial comparisons between the FIR profiles in three of the four IRAS Bands (25, 60, 100 microns). We also present direct spatial comparisons between the 60 micron intensity profiles and intensity profiles from 20 cm radio continuum maps with identical resolution (approx. 60 sec) obtained from J. J. Condon. Using these profiles we have evaluated the 60 micron-to-20 cm ratio Q(sub 60) along the major axis for each galaxy and have compared the results to global Q(sub 60) values. This analysis reveals that a considerable amount of complicated structure exists within the disk of spiral galaxies. Closer examination of this disk structure will make it possible to place further constraints on the well known global far-infrared and radio continuum emission correlation. Author

N95-21763*# Chicago Univ., Chicago, IL. Dept. of Astronomy and Astrophysics.
FAR-INFRARED MAPPING OF DUSTY ELLIPTICAL GALAXIES **c82**
Joanna F. Lees, D. A. Harper, Michael P. Rupen (National Radio Astronomy Observatory, Socorro, NM.), and G. R. Knapp (Princeton Univ., NJ.) *In* JPL, Science with High Spatial Resolution Far-Infrared Data Apr. 1994 p 101-106 (For primary document see N95-21749 06-88)
(Grant NGR14-001-227)
Avail: CASI HC A02/MF A02

Preliminary results from a program to map the thermal far-infrared emission from cool dust in elliptical galaxies using the Yerkes 60-Channel Camera on the Kuiper Airborne Observatory (KAO) are presented. The 160 micron emission from the elliptical NGC 6542 is apparently extended over the optical galaxy whereas the 100 micron emission is unresolved. This implies a dust temperature gradient consistent with that expected for dust with Galactic properties exposed to the general interstellar radiation field of the elliptical galaxy. Observations of the elliptical NGC 5666 and the NGC 7463/4/5 compact group (consisting of the elliptical NGC 7464, the S0 NGC 7465, and the spiral NGC 7463) are also discussed. Author

N95-21764*# Drake Univ., Des Moines, IA. Dept. of Physics and Astronomy.
EXTENDED FAR-INFRARED EMISSION AND STAR FORMATION IN SEYFERT GALAXIES **c82**
A. P. Marston *In* JPL, Science with High Spatial Resolution Far-Infrared Data Apr. 1994 p 107-113 (For primary document see N95-21749 06-88)
Avail: CASI HC A02/MF A02

An investigation into the extended distribution of far-infrared (FIR) emission associated with nearby Seyfert galaxies is made using a set of MEM reconstructions of IRAS Chopped Photometric Channel (CPC) data (Marston 1993). The data is compared to a set of HII/starburst galaxy images similarly processed in order to compare distributions and FIR color properties. It is shown that the central 1 kpc or so of Seyfert galaxies show extended FIR emission. FIR colors suggest that the bulk of this emission is not directly associated with an active nucleus. They further suggest that the origins of the majority of the emission is from heated dust associated with star formation surrounding the nucleus rather than dust heated by the active nucleus. Nearby Seyfert galaxies are shown to have a higher concentration of far-infrared emission from their centers than the HII/starburst galaxies and a number appear to reside in disk galaxies with relatively low ongoing star formation in their disks. An example of this is NGC 7582 which has a smooth disk but an active nucleus/starbust center.
Author

N95-21765*# Jet Propulsion Lab., California Inst. of Tech., Pasadena, CA.
TWO-DIMENSIONAL MAPS OF THE INFRARED-TO-RADIO RATIO IN SPIRAL GALAXIES **c82**
Kenneth A. Marsh and George Helou *In its* Science with High Spatial Resolution Far-Infrared Data Apr. 1994 p 115-120 (For primary document see N95-21749 06-88)
Avail: CASI HC A02/MF A02

We have produced two-dimensional maps of the intensity ratio Q(sub 60) of 60 micron infrared to 20 cm radio continuum emission, for a set of 25 nearby galaxies, mostly spirals. The ratio maps were obtained from infrared images made using Infrared Astronomical Satellite (IRAS) data with the Maximum Correlation Method, and radio images made using VLA data. Before taking the ratio, the radio images were processed so as to have the same resolution properties as the infrared images; the final spatial resolution in all cases is approximately 1 min, corresponding to 1-2 kpc for most galaxies. These images allow us to study the variations for the Q(sub 60) ratio with unprecedented spatial resolution, and thus represents a major improvement over earlier work. Our new high-resolution maps confirm the slow decrease of Q(sub 60) with increasing radial distance from the nucleus, but show additional structure which is probably associated with separate sites of active star formation in the spiral arms. The maps show Q(sub 60) to be more closely related to infrared surface brightness than to the radial distance in the galaxy disk. We expect that the results will provide improved constraints on the evolution (diffusion, decay and escape) of cosmic-ray electrons in the magnetic field of the disks. Author

N95-21766*# Toledo Univ., OH. Dept. of Physics and Astronomy.
THE VARIATION OF THE DUST TEMPERATURE WITHIN LATE-TYPE SPIRAL GALAXIES **c82**
Rhodri H. Evans *In* JP, Science with High Spatial Resolution Far-Infrared Data Apr. 1994 p 121-136 (For primary document see N95-21749 06-88)
Avail: CASI HC A02/MF A02

We use high resolution (HiRes) 60 and 100 micron data to investigate the variation of the dust temperature in a sample of 4 late-type spiral galaxies. We have investigated the radial variation of the azimuthally averaged 60 and 100 micron surface brightness profiles to see how the dust temperature (or, more correctly, the relative strength of the two components) varies as a function of radius within the galaxies. We find strong evidence for a decrease in the dust temperature (or an increase in the relative contribution of the 100 micron flux compared to the 60 micron flux) as a function of radius. We discuss these results in the light of the continuing debate as to whether massive star formation or the general interstellar radiation field is the major heating source of the dust. Author

N95-21767*# Jet Propulsion Lab., California Inst. of Tech., Pasadena, CA.
AN IRAS HIRES STUDY OF LOW MASS STAR FORMATION IN THE TAURUS MOLECULAR RING **c82**
Susan Terebey and Jason A. Surace (Hawaii Univ., Honolulu, HI.) *In its* Science with High Spatial Resolution Far-Infrared Data Apr. 1994 p 127-136 (For primary document see N95-21749 06-88)
Avail: CASI HC A02/MF A02

The Taurus molecular cloud supposedly has no star clusters but only isolated star formation. However, the Infrared Astronomical Satellite (IRAS) shows us that a small star cluster is currently forming in Taurus. Most of the sources are deeply embedded and are probably low-mass protostars. We use High Resolution (HiRes) images of the IRAS data from the Infrared Processing and Analysis Center (IPAC) to look for additional infrared members of the cluster. We also investigate the question of whether the infrared emission matches predictions for protostellar sources by examining whether the dust emission is resolved on scales of one arcminute (approx. 10(exp 17) cm). With the exception of a luminous visible star, HD 29647, we find that the sources L1527, TMC1A, TMC1, TMC1C, tMR1, and IC2087 are unresolved in the HiRes images at 60 microns. Further analysis of IC2087 shows that it is unresolved at all four IRAS wavelengths. Author

N95-21768*# Amsterdam Univ. (Netherlands). Astronomical Inst.
HIRAS IMAGES OF FOSSIL DUST SHELLS AROUND AGB STARS c82
L. B. F. M. Waters (Groningen Rijksuniv., Netherlands.), Do J. M. Kester (Groningen Rijksuniv., Netherlands.), Tj. Romke Bontekoe (Groningen Rijksuniv., Netherlands.), and C. Loup (Groningen Rijksuniv., Netherlands.) *In* JPL, Science with High Spatial Resolution Far-Infrared Data Apr. 1994 p 137-142 (For primary document see N95-21749 06-88)
(Grants AF-AFOSR-0140-86; AF-AFOSR-0320-89)
Avail: CASI HC A02/MF A02

We present high resolution HIRAS 60 and 100 micron images of AGB stars surrounded by fossil dust shells. Resolving the extended emission of the circumstellar dust allows a determination of the mass loss history of the star. We show that the geometry of the 60 micron emission surrounding HR 3126 agrees well with that of the optical reflection nebula. The emission around the carbon star U Hya is resolved into a central point source and a ring of dust, and the mass loss rate in the detached shell is 70 times higher than the current mass loss rate. Author

N95-21769*# Jet Propulsion Lab., California Inst. of Tech., Pasadena, CA.
WAVELET ANALYSIS APPLIED TO THE IRAS CIRRUS c82
William D. Langer, Robert W. Wilson (Bell Telephone Labs., Inc., Holmdel, NJ.), and Charles H. Anderson (Washington Univ., Saint Louis, MO.) *In its* Science with High Spatial Resolution Far-Infrared Data Apr. 1994 p 143-155 (For primary document see N95-21749 06-88)
Avail: CASI HC A03/MF A02

The structure of infrared cirrus clouds is analyzed with Laplacian pyramid transforms, a form of non-orthogonal wavelets. Pyramid and wavelet transforms provide a means to decompose images into their spatial frequency components such that all spatial scales are treated in an equivalent manner. The multiscale transform analysis is applied to IRAS 100 micrometer maps of cirrus emission in the north Galactic pole region to extract features on different scales. In the maps we identify filaments, fragments and clumps by separating all connected regions. These structures are analyzed with respect to their Hausdorff dimension for evidence of the scaling relationships in the cirrus clouds. Author

N95-21770*# Jet Propulsion Lab., California Inst. of Tech., Pasadena, CA.
A HIRES ANALYSIS OF THE FIR EMISSION OF SUPERNOVA REMNANTS c82
Zhong Wang *In its* Science with High Spatial Resolution Far-Infrared Data Apr. 1994 p 157-163 (For primary document see N95-21749 06-88)
Avail: CASI HC A02/MF A02

The high resolution (HiRes) algorithm has been used to analyze the far infrared emission of shocked gas and dust in supernova remnants. In the case of supernova remnant IC 443, we find a very good match between the resolved features in the deconvolved images and the emissions of shocked gas mapped in other wavelengths (lines of H2, CO, HCO+, and HI). Dust emission is also found to be surrounding hot bubbles of supernova remnants which are seen in soft X-ray maps. Optical spectroscopy on the emission of the shocked gas suggests a close correlation between the FIR color and local shock speed, which is a strong function of the ambient (preshock) gas density. These provide a potentially effective way to identify regions of strong shock interaction, and thus facilitate studies of kinematics and energetics in the interstellar medium. Author

N95-21771*# National Aeronautics and Space Administration. Goddard Space Flight Center, Greenbelt, MD.
ARCMIMUTE SCALE HI AND IRAS OBSERVATIONS TOWARD HIGH LATITUDE CLOUD G86.5+59.6 c82
Peter G. Martin (Toronto Univ., Ontario.), C. Rogers (Herzberg Inst. of Astrophysics, Penticton, British Columbia.), W. T. Reach, P. E. Dewdney (Herzberg Inst. of Astrophysics, Penticton, British Columbia.), and C. E. Heiles (California Univ., Berkeley, CA.) *In* JPL, Science with High Spatial Resolution Far-Infrared Data Apr. 1994 p 165-171 (For primary document see N95-21749 06-88)
Avail: CASI HC A02/MF A02

G86.5+59.6 is a degree-sized high latitude cloud originally selected for investigation by Heiles, Reach, and Koo (1988) on the basis of its appearance on the IRAS Skyflux images at 60 and 100 micrometers. Because of the interesting possibility that this is an intermediate velocity cloud colliding with HI in the Galactic plane, we have examined this region further, both at low resolution over an extended field to provide some context and at higher (arcminute) resolution within the cloud. Author

N95-21772*# Jamieson Science and Engineering, Inc., Scotts Valley, CA.
APPLICATION OF MCM IMAGE CONSTRUCTION TO IRAS COMET OBSERVATIONS c82
Martin F. Schlapfer and Russell G. Walker *In* JPL, Science with High Spatial Resolution Far-Infrared Data Apr. 1994 p 173-176 (For primary document see N95-21749 06-88)
Avail: CASI HC A01/MF A02

There is a wealth of IRAS comet data, obtained in both the survey and pointed observations modes. However, these measurements have remained largely untouched due to difficulties in removing instrumental effects from the data. We have developed a version of the Maximum Correlation Method for Image Construction algorithm (MCM) which operates in the moving coordinate system of the comet and properly treats both real cometary motion and apparent motion due to spacecraft parallax. This algorithm has been implemented on a 486/33 PC in FORTRAN and IDL codes. Preprocessing of the IRAS CRDD includes baseline removal, deglitching, and removal of long tails due to dielectric time constants of the detectors. The resulting images are virtually free from instrumental effects and have the highest possible spatial resolution consistent with the data sampling. We present examples of high resolution IRAS images constructed from survey observations of Comets P/Tempel 1 and P/Tempel 2, and pointed observations of IRAS-Araki-Alcock. Author

N95-21773*# Hawaii Univ., Honolulu, HI. Inst. for Astronomy.
LUMINOUS RADIO-QUIET SOURCES IN THE W3(MAIN) CLOUD CORE c82
C. Gareth WynnWilliams, E. F. Ladd, James R. Deane, and D. B. Sanders *In* JPL, Science with High Spatial Resolution Far-Infrared Data Apr. 1994 p 177-181 (For primary document see N95-21749 06-88)
(Grant NSF AST-89-19563)
Avail: CASI HC A01/MF A02

We have resolved 450 micrometer and 800 micrometer emission from the W3(Main) star forming region into three major peaks, using 8 inch - 14 inch beams with the James Clerk Maxwell Telescope on the summit of Mauna Kea. One of the submillimeter sources is identified with W3 - IRS5, a well-known candidate protostar. However, to our surprise, we find that none of the submillimeter peaks coincides with any of the prominent compact HII regions in the area. We estimate that the three submillimeter sources together contribute 30-50 percent of the total bolometric luminosity of the region, and speculate that the contribution of luminous radio-quiet sources to the total luminosity of HII region/molecular cloud complexes may be larger than is often assumed. Author

89 ASTRONOMY

Includes radio, gamma-ray, and infrared astronomy, and astrometry.

N95-22376# Helsinki Univ. of Technology, Espoo (Finland).
LOW NOISE 22 GHz RECEIVER FOR THE RADIOASTRON SATELLITE, PART 2: SPACE QUALIFICATION TESTS
P. Piironen, J. Mallat, and A. Raeisaenen Apr. 1994 74 p See also Part 1, PB95-104410
(PB95-127197; ISBN-951-22-2067-9) Avail: CASI HC A04/MF A01

Radioastron project, initiated in 1985, is an international collaborative mission to launch a space research satellite carrying a 10 meter radio telescope to an elliptical orbit around the Earth. The telescope comprises four two-channel VLBI (very long baseline interferometry) receivers at different frequencies built by project participants. The Radio Laboratory of HUT is responsible for the cooled 22 GHz receiver. Thermal, mechanical, engineering and two flight models have been manufactured in co-operation between the Radio Laboratory, Ylinen Electronics, Co. and the Applied Electronics Laboratory of HUT. The engineering model has been exposed to a full space qualification test program. The flight models were delivered in December 1993 and the other models earlier. The most important receiver design objectives have been low noise, good phase stability and high reliability. A noise temperature of better than 100 K and a phase stability of better than 3 deg were measured. This report presents the space qualification tests of the receiver. NTIS

90 ASTROPHYSICS

Includes cosmology; celestial mechanics; space plasmas; and interstellar and interplanetary gases and dust.

For related information see also *75 Plasma Physics.*

N95-20144# Sandia National Labs., Albuquerque, NM.

EXPERIMENTAL HYPERVELOCITY IMPACT EFFECTS ON SIMULATED PLANETESIMAL MATERIALS

William J. Tedeschi, James F. Schulze, John L. Remo (Quantametrics, Inc., Saint James, NY.), and Raymond P. Young, Jr. (Calspan Field Services, Inc., Arnold AFS, TN.) 1994 28 p Presented at the 1994 Hypervelocity Impact Symposium, Santa Fe, NM, 16-20 Oct. 1994

(Contract DE-AC04-94AL-85000)

(DE94-017290; SAND-93-3901C; CONF-9410131-5) Avail: CASI HC A03/MF A01

Experimental results are presented from a series of hypervelocity impact tests on simulated comet and asteroid materials for the purpose of characterizing their response to hypervelocity kinetic energy impacts. Nine tests were conducted at the Air Force Arnold Engineering Development Center (AEDC) S1 Range Facility on ice, rock, and iron target samples using a spherical 2.39 mm diameter aluminum impactor (0.0192 gm) at impact velocities of from 7.6 to 8.4 km/sec. The test objectives were to collect target response phenomenology data on cratering, momentum deposition and enhancement, target fragmentation, and material response under hypervelocity impact loading conditions. A carefully designed ballistic pendulum was used to measure momentum deposition into the targets. Observations and measurements of the impacted samples provide important insights into the response of these materials to kinetic energy impacts, especially in regards to unexpectedly large measured values of momentum enhancement to some of the targets. Such information is required to allow us to successfully deflect or fragment comets or asteroids which might someday be detected on collision trajectories with Earth. DOE

N95-20145# California Univ., Los Angeles, CA. Inst. of Geophysics and Planetary Physics.

[OVERVIEW OF THE INSTITUTE OF GEOPHYSICS AND PLANETARY PHYSICS AND LAWRENCE LIVERMORE NATIONAL LABORATORY COLLABORATIVE EFFORTS] Annual Report, 1 Oct. 1992 - 30 Sep. 1993

Frederick J. Ryerson, ed. and Christina M. Budwine, ed. 15 Jun. 1994 143 p

(Contract W-7405-eng-48)

(DE94-017300; UCRL-53809-93) Avail: CASI HC A07/MF A02

This report contains brief papers on the research being conducted at the Institute of Geophysics and Planetary Physics in 1993 in Geosciences, High-Pressure sciences, and Astrophysics. DOE

N95-20173# Institut des Hautes Etudes Scientifiques, Bures-sur-Yvette (France).

PREDICTIONS FROM QUANTUM COSMOLOGY

A. Vilenkin May 1994 12 p

(PB95-111126; IHES/P/94/35) Avail: CASI HC A03/MF A01

The world view suggested by quantum cosmology is that eternally inflating universes with all possible values of the fundamental constants are spontaneously created out of nothing. The author explores the consequences of the assumption that we are a 'typical' civilization living in this metauniverse. The conclusions include inflation with an extremely flat potential and low thermalization temperature, structure formation by topological defects, and an appreciable cosmological constant. NTIS

N95-20873# Ludwig-Maximilians-Univ., Munich (Germany). Inst. of Theoretical Physics.

PROPERTIES OF STRANGE-MATTER STARS

Fridolin Weber, Christiane Kettner Kettner, and Norman K. Glendenning (California Univ., Berkeley. Lawrence Berkeley Lab, CA.) Jul. 1994 4 p Presented at the International Conference Nuclei in the Cosmos, Gran Sasso, Italy, 8-13 Jul. 1994

(Contract DE-AC03-76SF-00098)

(DE95-002329; LBL-35929; CONF-9407143-1) Avail: CASI HC A01/MF A01

This paper deals with an investigation of the properties of hypothetical strange-matter stars, which are composed of u, d, s quark matter whose energy per baryon number lies below the one of Fe-56 (Witten's strange matter hypothesis). Observable quantities which allow to distinguish such objects from their 'conventional' counterparts, neutron stars and white dwarfs, are pointed out. DOE

N95-21245# Stanford Linear Accelerator Center, CA.

COSMOLOGICAL STRING SOLUTIONS BY DIMENSIONAL REDUCTION

K. Behrndt and S. Foerste (Hebrew Univ., Jerusalem, Israel.) Dec. 1993 9 p Presented at the 27th International Symposium Ahrenshoop on the Theory of Elementary Particles, Wendisch-Rietz, Germany, 7-11 Sep. 1993 Sponsored by DAAD, and MINERA

(Contract DE-AC03-76SF-00515)

(DE95-002858; SU-SLAC-PUB-6411; CONF-9309429-1) Avail: CASI HC A02/MF A01

We obtain cosmological four dimensional solutions of the low energy effective string theory by reducing a five dimensional black hole, and black hole-de Sitter solution of the Einstein gravity down to four dimensions. The appearance of a cosmological constant in the five dimensional Einstein-Hilbert produces a special dilaton potential in the four dimensional effective string action. Cosmological scenarios implement by our solutions are discussed. DOE

N95-21347 Direction des Recherches, Etudes et Techniques, Paris (France). Centre de Documentation de l'Armement.

TWENTYSIXTH YERAC

1994 59 p Conference held in Les Houches, France, 13-17 Sep. 1993

(PB95-127437) Avail: Issuing Activity (National Technical Information Service (NTIS))

The document contains abstracts of papers which were given at the conference. The papers were grouped into seven sessions. The session headings are the following: Stars and protostars; Galaxies; Instruments and surveys; Data reduction; Masers; Distant objects; Molecular clouds. NTIS

N95-21367# Los Alamos National Lab., NM.

NEO-LISP: DEFLECTING NEAR-EARTH OBJECTS USING HIGH AVERAGE POWER, REPETITIVELY PULSED LASERS

C. R. Phipps and M. M. Michaelis (Natal Univ., Durban, South Africa.) 1994 35 p Presented at the ECLIM 23: Laser Interaction With Matter, Oxford, England, 19-23 Sep. 1994

(Contract W-7405-eng-36)

(DE95-000863; LA-UR-94-3124; CONF-9409226-1) Avail: CASI HC A03/MF A01

Several kinds of Near-Earth objects exist for which one would like to cause modest orbit perturbations, but which are inaccessible to normal means of interception because of their number, distance or the lack of early warning. For these objects, LISP (Laser Impulse Space Propulsion) is an appropriate technique for rapidly applying the required mechanical impulse from a ground-based station. In order of increasing laser energy required, examples are: (1) repositioning specially prepared geosynchronous satellites for an enhanced lifetime; (2) causing selected items of space junk to re-enter and burn up in the atmosphere on a computed trajectory; and (3) safely deflecting Earth-directed comet nuclei and earth-crossing asteroids (ECA's) a few tens of meters in size (the most hazardous size). They will discuss each of these problems in turn and show that each application is best matched by its own matrix of LISP laser pulse width, pulse repetition rate, wavelength and average power. The latter ranges from 100W to 3GW for the cases considered. They will also discuss means of achieving the active beam phase error correction during passage through the atmosphere and very large exit pupil in the optical system which are required in each of these cases. DOE

N95-21479# Lawrence Livermore National Lab., Livermore, CA.
RELATIVISTIC BINARY NEUTRON STAR COALESCENCE
J. R. Wilson and G. J. Mathews 1994 6 p Presented at the 7th Marcel Grossman Meeting on General Relativity, Stanford, CA, 24-29 Jul. 1994
(Contract W-7405-eng-48)
(DE94-019311; UCRL-JC-118330; CONF-9407129-1) Avail: CASI HC A02/MF A01

The authors report on the first results from a (3+1) dimensional general relativistic hydrodynamics code to describe the evolution of a neutron-star binary system. The relativistic field equations are exactly solved at each time slice with a constrain that spatial 3-metric remains conformally flat. The effect of gravitational radiation is introduced by the quadrupole radiation reaction formula. The gravitational radiation signal is also estimated by the quadrupole formula. An illustrative calculation of an orbiting binary is presented. DOE

N95-21577 Ettore Majorana Centre for Scientific Culture, Erice (Italy).
ERICE INTERNATIONAL SEMINARS ON PLANETARY EMERGENCIES. 17TH WORKSHOP: THE COLLISION OF AN ASTEROID OR COMET WITH THE EARTH
4 May 1993 13 p Workshop held in Erice, Italy, 28 Apr. - 4 May 1993
Limited Reproducibility: More than 20% of this document may be affected by microfiche quality
(AD-A280122) Avail: CASI HC A03

Participating papers of this workshop included: K/T Mass Extinctions: Some Astronomical Constraints; The dynamical Properties of Near-Earth Objects; Predicting Close Earth Approaches of Asteroids and Comets; Australasian Near-Earth Object Programs; The Cosmic Impact Hazard: Overview; Large Body Impacts And Mass Extinction Events: Evidence from the Cretaceous/Tertiary Boundary and a Possible General Relationship; Historical Perspectives on Impact Hazards; Research Activities on Asteroids and Comets conducted in Japan; Physical and Chemical Properties of Near-Earth Objects; and Search for Near-Earth Objects with Ground-Based Electro-Optical Deep Space Surveillance (GEODSS) Assets. An abstract of each is contained herein. CASI

N95-21615*# Columbia Univ., New York, NY. Dept. of Astronomy and Physics.
PHYSICS OF SYSTEMS CONTAINING NEUTRON STARS Progress Report, 1 Jan. - 31 Dec. 1994
Jacob Shaham Jan. 1995 15 p
(Grant NAGw-1618)
(NASA-CR-197304; NAS 1.26:197304; CAL-2261) Avail: CASI HC A03/MF A01

This grant deals with several topics related to the dynamics of systems containing a compact object. Most of our research in 1994 dealt with systems containing Neutron Stars (NS's), but we also addressed systems containing a Black Hole (BH) or a White Dwarf (WD) in situations relevant to NS systems. Among the systems were isolated regular pulsars, Millisecond Pulsars (MSP's) that are either Single (SMP's) or in a binary (BMP's) Low Mass X-Ray Binaries (LMX's) and Cataclysmic Variables (CV's). We also dealt with one aspect of NS structure, namely NS superfluidity. A large fraction of our research dealt with irradiation-driven winds from companions. These winds turned out to be of some importance in the evolution of LMXB's and MSP's, be they SMP's or BMP's. While their role during LMXB evolution (i.e. during the accretion phase) is not yet clear, they may play an important role in turning BMP's into SMP's and also in bringing about the formation of planets around MSP's. Author

N95-21679 Phillips Lab., Hanscom AFB, MA.
AN EXPERIMENTAL DETERMINATION OF METEOR DAILY ARRIVAL RATE VARIATION Interim Report
John M. Quinn 2 Dec. 1993 24 p Limited Reproducibility: More than 20% of this document may be affected by microfiche quality
(AD-A279484; AD-E201960; PL-TR-93-2247; ERP-1135) Avail: Issuing Activity (Defense Technical Information Center (DTIC))

This report addresses the day to day variability in the meteor arrival rate over a two-month period on the PL/GP High Latitude Meteor Scatter Test Bed and the PL Mid Latitude Meteor Scatter Test bed. In particular, we present evidence that the meteor arrival variability fits an exponential distribution, thus the duration of the system testing period to estimate the meteor arrival variability can be calculated. The arrival rate data from two different sites show that the day-to-day percent change in the arrival rate, at least in the short term, can be modeled as an exponential distribution with a mean of near 10 percent. This suggests meteor scatter communication testing to evaluate performance should be conducted for 9 to 12 days as a minimum to approximate medium term, 30 to 90 days, day-to-day arrival variation. DTIC

N95-21935# Los Alamos National Lab., NM.
OBSERVATIONS OF COLD MAGNETOSPHERIC IONS AT GEOSYNCHRONOUS ORBIT DURING TIMES OF HIGH ACTIVITY
R. C. Elphic, L. A. Weiss, M. F. Thomsen, D. J. McComas, and S. J. Bame 1994 4 p Presented at the 8th International Symposium on Solar Terrestrial Physics, Sendai, Japan, 6-10 Jun. 1994
(Contract W-7405-eng-36)
(DE95-000936; LA-UR-94-3223; CONF-9406192-4) Avail: CASI HC A01/MF A01

Flowing, cold magnetospheric ions have been observed in conjunction with geosynchronous orbit magnetopause crossings since the earliest ATS and OGO missions. The authors have reported on the occurrence and convection of low-energy (10-100 eV) ions seen by multiple satellites in association with geosynchronous orbit magnetopause and low-latitude boundary layer (LLBL) encounters. More generally, Los Alamos 3-D plasma instruments observe these ions following storm sudden commencements (SSC's), when activity levels are high. The ions appear to be convecting radially outward and usually westward at speeds of a few to several tens of kilometers per second. Often the energy spectra reveal peaks at energies appropriate for cold convecting H(+), He(+) and O(+). The occurrence frequency distribution of these dense cold ions is peaked near 1400 LT, with an overall range from 1000 to beyond 1800 LT. This local time distribution is greatly skewed from the overall plasmaspheric distribution, which peaks closer to 1800 LT. Multisatellite observations show that the ions are seen first at late afternoon local times and then at progressively earlier and earlier local times (though usually no earlier than 1000 LT). This apparent evolution in local time suggests that the late-afternoon plasmaspheric plasma moves out and downward during times of increased magnetospheric activity. The three-satellite observations also allow the authors to track cold plasma convection at multiple points in the magnetosphere, and potentially provide a glimpse of the large-scale convection pattern. DOE

N95-22128# Los Alamos National Lab., NM.
DISTRIBUTION OF LIGHT ELEMENT ISOTOPES IN BENCUBBIN AND WEATHERFORD METEORITES: AN INDICATOR OF HETEROGENEITY IN THE PRIMITIVE SOLAR NEBULA Technical Report, 1 Oct. 1988 - 30 Sep. 1989
J. Blacic, C. Maggiore, J. Taylor, H. Newsom, and K. Marti 1994 4 p
(Contract W-7405-eng-36)
(DE94-019167; LA-SUB-94-125) Avail: CASI HC A01/MF A01

The objective is to study light element isotopes, particularly N-15, in meteorites to elucidate early solar nebula processes. The approach is to use microion beams to induce characteristic nuclear reactions in specific minerals in the meteorites, and to develop isotope imaging techniques by beam rastering. Early results demonstrate the feasibility of the beam rastering technique and we have successfully measured a delta N-15 ratio of about -50 (per thousand) in sinoite (Si2N2O) in an enstatite chondrite. No conclusions can be drawn at this stage of the investigation. Ultimately, the results are important to understanding conditions during planetary formation, and in developing new analytic techniques applicable to a wide range of geophysical problems. DOE

N95-21790*# Osaka Univ., Toyonaka (Japan). Dept. of Earth and Space Sciences.
TRANSPORTATION OF VOLATILE ELEMENTS IN THERMALLY EVOLVING PLANETESIMALS: AN IMPORTANT ROLE OF METALLIC IRON Abstract Only
K. Hashizume and N. Sugiura (Tokyo Univ., Japan.) *In* Lunar and Planetary Inst., Conference on Deep Earth and Planetary Volatiles 1994

p 13 (For primary document see N95-21777 06-46)
Avail: CASI HC A01/MF A01

N95-21798*# California Univ., Los Angeles, CA. Dept. of Earth and Space Sciences.
DYNAMICS OF VOLATILE DELIVERY FROM OUTER TO INNER SOLAR SYSTEM Abstract Only
W. M. Kaula *In* Lunar and Planetary Inst., Conference on Deep Earth and Planetary Volatiles 1994 p 21 (For primary document see N95-21777 06-46)
Avail: CASI HC A01/MF A01

N95-21800*# California Univ., San Diego, La Jolla, CA. Dept. of Chemistry.
NITROGEN ISOTOPIC COMPONENTS IN THE EARLY SOLAR SYSTEM Abstract Only
J. F. Kerridge *In* Lunar and Planetary Inst., Conference on Deep Earth and Planetary Volatiles 1994 p 23-24 (For primary document see N95-21777 06-46)
Avail: CASI HC A01/MF A01

N95-21801*# Lunar and Planetary Inst., Houston, TX.
VOLATILES, RHEOLOGY, AND MANTLE CONVECTION: COMPARING EARTH, VENUS, AND MARS Abstract Only
Walter S. Kiefer *In its* Conference on Deep Earth and Planetary Volatiles 1994 p 25 (For primary document see N95-21777 06-46)
Avail: CASI HC A01/MF A01

N95-21806*# Arizona Univ., Tucson, AZ. Lunar and Planetary Lab.
SOLAR SYSTEM FORMATION AND THE DISTRIBUTION OF VOLATILE SPECIES Abstract Only
Jonathan I. Lunine *In* Lunar and Planetary Inst., Conference on Deep Earth and Planetary Volatiles 1994 p 30-31 Sponsored by NASA (For primary document see N95-21777 06-46)
Avail: CASI HC A01/MF A01

N95-21810*# Hawaii Univ., Honolulu, HI. Inst. for Astronomy.
COMETS, IMPACTS, AND ATMOSPHERES Abstract Only
Tobias Owen and Akiva Bar-Nun (Tel-Aviv Univ., Ramat-Aviv, Tel-Aviv, Israel.) *In* Lunar and Planetary Inst., Conference on Deep Earth and Planetary Volatiles 1994 p 35 (For primary document see N95-21777 06-46)
Avail: CASI HC A01/MF A01

91 LUNAR AND PLANETARY EXPLORATION

Includes planetology; and manned and unmanned flights.

For spacecraft design or space stations see *18 Spacecraft Design, Testing and Performance.*

N95-20797*# Atmospheric and Environmental Research, Inc., Cambridge, MA.
STUDIES OF THE GAS TORI OF TITAN AND TRITON Annual Report, 24 Jan. 1994 - 23 Jan. 1995
William H. Smyth Jan. 1995 13 p
(Contract NASw-4832)
(NASA-CR-197377; P-498; NAS 1.26:197377) Avail: CASI HC A03/MF A01

Progress in the development of the model for the circumplanetary distribution of atomic hydrogen in the Saturn system produced by a Titan source is discussed. Because of the action of the solar radiation acceleration and the obliquity of Saturn, the hydrogen distribution is shown to undergo seasonal changes as the planet moves about the Sun. Preliminary model calculations show that for a continuous Titan source, the H distribution is highly asymmetric about the planet and has a density maximum near the dusk side of Saturn, qualitatively similar to the pattern recently deduced by Shemansky and Hall from observations acquired by the UVS instruments aboard the Voyager spacecrafts. The investigation of these Voyager data will be undertaken in the next project year. Author

N95-21196* National Aeronautics and Space Administration. Lyndon B. Johnson Space Center, Houston, TX.
MOON: OLD AND NEW (Videotape)
1970 Videotape: 25 min. playing time, in color, with sound Awards: Golden Eagle Council on International Nontheatrical Events (CINE) 1971; 5th International Review of Didactic Films, Rome, Italy; and 3d International Review of TV Educational Films, Rome Fair, 1971
(NASA-TM-110511; NASA-JSC-554; NONP-NASA-VT-95-42155) Avail: CASI VHS A02/BETA A22

This video presents the moon as studied by man for more than 20 centuries. It reviews the history of lunar studies before the first moon landing, the major things learned since Apollo II, and closes with a resumes of lunar investigations scientists would like to undertake in the future. Author

N95-21621*# National Aeronautics and Space Administration. Ames Research Center, Moffett Field, CA.
SIMULATED RAREFIED ENTRY OF THE GALILEO PROBE INTO THE ATMOSPHERE OF JUPITER
Brian L. Hass (Eloret Corp., Palo Alto, CA.) and Frank S. Milos [1993] 8 p
(Contract NCC2-582)
(NASA-TM-110507; NAS 1.15:110507) Avail: CASI HC A02/MF A01

Flow properties and aerodynamics are computed with a direct simulation Monte Carlo (DSMC) method for rarefied entry of the Galileo Probe into the atmosphere of Jupiter. Accurate predictions of vehicle drag coefficients are needed in order to assess atmospheric properties from the onboard Atmosphere Structure Experiment where highly-sensitive accelerometers will measure the drag force to within 10-6 barr during the initial entry phase at high altitudes. The corresponding flow rarefraction extends from the free molecule limit to the near continuum transition regime (Re less than 1000). Simulation results indicate that C(sub D) varies from 2.1 at the free molecule limit down to 1.6 at Re(infinity) = 1,000. Temperatures, densities, and internal energies throughout the flow field were also computed at each altitude ranging from 735 km to 353 km above the 1 barr level in the Jovian atmosphere. Surface heating and temperatures of the probe were computed directly in the DSMC code by assuming radiative equilibrium. Material response was re-asssessed accurately during entry by accounting for conductivity, heat capacity, and pyrolysis which led to surface material mass efflux several times that of the freestream mass influx. The simulation also accounted for the quantum nature of the rotational energy mode of the dominant atmospheric species H2 through partial internal excitation in the freestream gas. Author

N95-22338*# Michigan Technological Univ., Houghton, MI. Dept. of Physics.
MODELING OF COLLISION INDUCED ABSORPTION SPECTRA OF CO2-CO2 PAIRS FOR PLANETARY ATMOSPHERE OF VENUS Yearly Progress Report, 1 Apr. 1994 - 31 Mar. 1995
Aleksandra Borysow 31 Mar. 1995 4 p
(Grant NAGw-2974)
(NASA-CR-197373; NAS 1.26:197373) Avail: CASI HC A01/MF A01

The objective of the proposal was to model the rototranslational and rotovibrational collision induced absorption spectral bands of importance for the radiative transfer analysis of the atmosphere of Venus. Our main task has involved CO2 pairs. The approach is not straightforward: whereas computational techniques to compute CIA spectra of small linear molecules exist, and were successfully applied to molecules like H2 or N2, they fail when applied to large molecules like CO2. For small molecules one can safely assume that the interaction potential is isotropic. The same approximation does not work for CO2, and when employed, it gives an incorrect band shape and only 50 percent of the CIA intensity. Derived from text

N95-22419# Los Alamos National Lab., NM.
THE DOUBLE EAGLE SPACE EXPERIMENT (DESE) BEAMLINE DESIGN
A. M. M. Todd, D. Berwald, and D. L. Bruhwiler 1994 5 p Presented at the 17th International LINAC Conference, Tsukuba, Japan, 21-26 Aug. 1994
(Contract W-7405-eng-36)
(DE94-018319; LA-UR-94-2890; CONF-9408125-26) Avail: CASI HC A01/MF A01

The beamline design for the Double Eagle Space Experiment (DESE) is described. DESE seeks to map the lunar surface material composition using an active particle beam probe. The 425 MHz, 11.8 m straight beamline delivers a 13 mA, 5.11 MeV neutral hydrogen beam with an equivalent rms divergence of (approximately)40 micro rad. The authors studied the beam propagation through the output optics components to the lunar surface and find an adequate return signal for the DESE mapping mission. DOE

N95-21785*# Michigan Univ., Ann Arbor, MI. Dept. of Atmospheric, Oceanic and Space Sciences.
ORIGIN AND LOSS OF THE VOLATILES OF THE TERRESTRIAL PLANETS Abstract Only
T. M. Donahue *In* Lunar and Planetary Inst., Conference on Deep Earth and Planetary Volatiles 1994 p 8 (For primary document see N95-21777 06-46)
Avail: CASI HC A01/MF A01

N95-21788*# Potsdam Univ., Potsdam (Germany). General Geophysics Group.
MANTLE DEVOLATILIZATION AND RHEOLOGY IN THE FRAMEWORK OF PLANETARY EVOLUTION Abstract Only
S. Franck and Ch. Bounama *In* Lunar and Planetary Inst., Conference on Deep Earth and Planetary Volatiles 1994 p 11 (For primary document see N95-21777 06-46)
Avail: CASI HC A01/MF A01

N95-21794*# Arizona Univ., Tucson, AZ. Lunar and Planetary Lab.
ATMOSPHERES OF THE MOON AND MERCURY Abstract Only
D. M. Hunten *In* Lunar and Planetary Inst., Conference on Deep Earth and Planetary Volatiles 1994 p 17 (For primary document see N95-21777 06-46)
Avail: CASI HC A01/MF A01

N95-21796*# Colorado Univ., Boulder, CO. Lab. for Atmospheric and Space Physics.
MARS ATMOSPHERIC LOSS AND ISOTOPIC FRACTIONATION BY PICK-UP-ION SPUTTERING AND PHOTOCHEMICAL ESCAPE Abstract Only
B. M. Jakosky, R. O. Pepin (Minnesota Univ., Minneapolis, MN.), R. E. Johnson (Virginia Univ., Charlottesville, VA.), and J. L. Fox (State Univ. of New York, Stony Brook, NY.) *In* Lunar and Planetary Inst., Conference on Deep Earth and Planetary Volatiles 1994 p 19 (For primary document see N95-21777 06-46)
Avail: CASI HC A01/MF A01

N95-21811*# California Univ., Los Angeles, CA. Dept. of Earth and Space Sciences.
POLAR VOLATILES ON MERCURY AND THE MOON Abstract Only
D. A. Paige, S. E. Wood, and A. R. Vasavada (California Inst. of Tech., Pasadena, CA.) *In* Lunar and Planetary Inst., Conference on Deep Earth and Planetary Volatiles 1994 p 36 (For primary document see N95-21777 06-46)
Avail: CASI HC A01/MF A01

N95-21815*# National Aeronautics and Space Administration. Ames Research Center, Moffett Field, CA.
SURFACE ICES IN THE OUTER SOLAR SYSTEM Abstract Only
Ted L. Roush and Dale P. Cruikshank *In* Lunar and Planetary Inst., Conference on Deep Earth and Planetary Volatiles 1994 p 40-41 (For primary document see N95-21777 06-46)
(RTOP 151-01-60-01; RTOP 196-41-67-03)
Avail: CASI HC A01/MF A01

N95-21816*# Tokyo Univ. (Japan). Geological Inst.
DEGASSING HISTORY AND EVOLUTION OF VOLCANIC ACTIVITY OF TERRESTRIAL PLANETS BASED ON RADIOGENIC NOBLE GAS DEGASSING MODELS Abstract Only
S. Sasaki and E. Tajika *In* Lunar and Planetary Inst., Conference on Deep Earth and Planetary Volatiles 1994 p 42 (For primary document see N95-21777 06-46)
Avail: CASI HC A01/MF A01

N95-21818*# Arizona Univ., Tucson, AZ. Lunar and Planetary Lab.
SEMI-VOLATILES AT MERCURY: SODIUM (Na) AND POTASSIUM (K) Abstract Only
A. Sprague *In* Lunar and Planetary Inst., Conference on Deep Earth and Planetary Volatiles 1994 p 44 (For primary document see N95-21777 06-46)
Avail: CASI HC A01/MF A01

N95-21819*# Arizona Univ., Tucson, AZ. Lunar and Planetary Lab.
IMPLICATIONS OF NOBLE GASES IN A RECENTLY RECOGNIZED MARTIAN METEORITE (ALH84001) FOR THE DEGASSING HISTORY OF MARS Abstract Only
T. D. Swindle *In* Lunar and Planetary Inst., Conference on Deep Earth and Planetary Volatiles 1994 p 45 (For primary document see N95-21777 06-46)
Avail: CASI HC A01/MF A01

92 SOLAR PHYSICS

Includes solar activity, solar flares, solar radiation and sunspots. For related information see *93 Space Radiation.*

N95-20147# Washington Univ., Seattle, WA. Inst. for Nuclear Theory.
NEUTRINO MAGNETIC MOMENTS AND THE SOLAR NEUTRINO PROBLEM
E. Kh. Akhmedov 1994 10 p
(Contract DE-FG06-90ER-40561)
(DE94-017579; DOE/ER-40561/153) Avail: CASI HC A02/MF A01

Present status of the neutrino magnetic moment solutions of the solar neutrino problem is reviewed. In particular, we discuss a possibility of reconciling different degrees of suppression and time variation of the signal (or lack of such a variation) observed in different solar neutrino experiments. It is shown that the resonant spin-flavor precession of neutrinos due to the interaction of their transitions magnetic moments with solar magnetic field can account for all the available solar neutrino data. For not too small neutrino mixing angles (sin 2(theta))(sub o) is approximately greater than 0.2, the combined effect of the resonant spin-flavor precession and neutrino oscillations can result in an observable flux of solar (bar (nu))(sub e)'s. DOE

N95-20558*# Smithsonian Astrophysical Observatory, Cambridge, MA.
CORONAGRAPHIC OBSERVATIONS AND ANALYSES OF THE ULTRAVIOLET SOLAR CORONA Semiannual Status Report Nos. 21, 22, 23, and 24, 1 Oct. 1992 - 30 Sep. 1994
John L. Kohl 30 Sep. 1994 14 p
(Grant NAG5-613)
(NASA-CR-197370; NAS 1.26:197370) Avail: CASI HC A03/MF A01

This status report for the period 1 October 1992 to 30 September 1994 covers the final preparation and first observations with the Spartan Ultraviolet Coronal Spectrometer on Spartan 201-1, and the preparation and second flight for Spartan 201-2. Both flights were fully successful and resulted in high quality spectroscopic observations of the extended solar corona out to 3.5 solar radii from Sun-center. The primary focus of this report is the results from Spartan 201-1. There is also a brief description of the evaluation of the quick look data from the second flight. Highlights from the first flight include a discovery that the proton velocity distribution in coronal holes is complex and consists of a central core with elevated high velocity wings compared to a Gaussian shape. Author

N95-20593 New York Univ., New York, NY. Inst. of Mathematical Sciences.
SOLAR FLARE MDH Annual Report, 1 Jan. - 31 Dec. 1993
H. Strauss and E. Hameiri 31 Dec. 1993 9 p Limited Reproducibility: More than 20% of this document may be affected by microfiche quality
(Grant AF-AFOSR-0044-91; AF Proj. 2311)
(AD-A279894; AFOSR-94-0315TR) Avail: Issuing Activity (Defense Technical Information Center (DTIC))

During the past year, several topics were studied which are important for solar MHD. These include: (1) 3D coalescence instability and magnetic reconnection. Magnetic reconnection is fairly well understood in two dimensional theory and numerical simulations in which there is an ignorable coordinate. It is poorly understood in three dimensional line tied magnetic fields, which are the generic case in solar flux loops. The 3D line tied coalescence MHD instability was investigated both analytically and numerically. In the nonlinear stages of the simulation, the instability drives magnetic reconnection. As in earlier 3D forced reconnection simulations, an intense current layer forms where magnetic energy is converted to heat. It was found that while line tying somewhat inhibits reconnection, it does not prevent it; (2) Line tied gravitational ballooning instability. A new two dimensional prominence model was found and its stability was analyzed. This instability might describe the irregular rain falling from prominences. Boundary conditions for the solar corona. It has been the practice to model the effects of the chromosphere and photosphere only through their influence on the boundary conditions imposed at the base of the corona. DTIC

N95-20713# National Geophysical Data Center, Boulder, CO.
SOLAR-GEOPHYSICAL DATA NUMBER 600, AUGUST 1994. PART 1: (PROMPT REPORTS). DATA FOR JULY, JUNE 1994, AND LATE DATA
Helen E. Coffey, ed. Aug. 1994 118 p
(ISSN 0038-0911)
(PB95-104923; SGD-600-Pt-1; LC-79-640375//r81) Avail: CASI HC A06/MF A02

Contents: Detailed Index For 1993-1994; Data For July 1994--Solar-Terrestrial Environment, IUWDS Alert Periods (Advance and Worldwide), Solar Activity Indices, Solar Flares, Solar Radio Emission, Stanford Mean Solar Magnetic Field, GOES-7 Daily Electron Fluence; Data for June 1994--Solar Active Regions, Sudden Ionospheric Disturbances, Solar Radio Spectral Observations, Solar Radioheliograph - 164 MHz - Nancay, Cosmic Ray Measurements by Neutron Monitor, Geomagnetic Indices, Principal Magnetic Storms, Sudden Commencements/Solar Flare Effects. NTIS

N95-20722# National Geophysical Data Center, Boulder, CO.
SOLAR-GEOPHYSICAL DATA NUMBER 600, AUGUST 1994. PART 2: (COMPREHENSIVE REPORTS). DATA FOR FEBRUARY 1994 AND MISCELLANEOUS
Helen E. Coffey, ed. Aug. 1994 59 p
(ISSN 0038-0911)
(PB95-105060; SGD-600-Pt-2; LC-79-640375//r81) Avail: CASI HC A04/MF A01

Contents: Detailed Index for 1993-1994; Data for February 1994--Solar Flares, Solar Radio Bursts at Fixed Frequencies, Solar X-Ray Radiation from GOES Satellite, Mass Ejections from the Sun, Active Prominences and Filaments; Miscellaneous Data--Energetic Particles (GOES-7 Daily Proton Fluence January 1987-July 1994 >1 MeV, >10 MeV, and >100 MeV Channels). NTIS

N95-20829# National Geophysical Data Center, Boulder, CO.
SOLAR-GEOPHYSICAL DATA NUMBER 601, SEPTEMBER 1994. PART 2: (COMPREHENSIVE REPORTS). DATA FOR MARCH 1994, AND MISCELLANEOUS
Helen E. Coffey Sep. 1994 37 p
(PB95-136735; SGD-601-Pt-2) Avail: CASI HC A03/MF A01

Contents include the following: Data for March 1994; Solar Flares; Solar Radio Bursts at Fixed Frequencies; Solar X-Ray Radiation from GOES Satellite Graphs; Mass Ejections from the Sun; and Active Prominences and Filaments. NTIS

N95-20919# National Geophysical Data Center, Boulder, CO.
SOLAR-GEOPHYSICAL DATA NUMBER 601, SEPTEMBER 1994. PART 1: (PROMPT REPORTS). DATA FOR AUGUST, JULY 1994, AND LATE DATA
Helen E. Coffey Sep. 1994 130 p
(PB95-136727; SGD-601-Pt-1) Avail: CASI HC A07/MF A02

Contents include the following: Plots of GOES satellite X-rays, Particles and Magnetometer data with ground-based Boulder Magnetometer and Deep River Neutron Monitor; IUWDS Alert Periods (Advance and Worldwide); Solar Activity Indices; Solar Flares; Solar Radio Emission; and Stanford Mean Solar Magnetic Field. NTIS

N95-21316# Washington Univ., Seattle, WA. Inst. for Nuclear Theory.
THE SOLAR NEUTRINO PROBLEM: NEITHER ASTROPHYSICS NOR OSCILLATIONS?
Alexei Yu. Smirnov (Academy of Sciences, USSR, Moscow, USSR.) 1994 22 p Presented at the International Workshop on Solar Neutrino Problem: Astrophysics or Oscillations, GranSasso, Italy, 28 Feb. - 1 Mar. 1994 Prepared in cooperation with International Centre for Theoretical Physics, Trieste, Italy
(Contract DE-FG06-90ER-40561)
(DE94-012850; DOE/ER-40561/136) Avail: CASI HC A03/MF A01

There is no consistent solar model which can describe all experimental data on the solar neutrinos. The problem can be formulated essentially in a model independent way. The key points are the comparison of the Homestake and the Kamiokande data as well as the comparison of the GALLEX and SAGE results with minimal signal estimated from the solar luminosity. It is argued that in such a comparison one should use the Homestake-II data (only after 1986) with caution. The results of the model independent analysis show strong suppression of the beryllium neutrino flux. The data can be well described by the resonant flavor conversion. For the 'low flux model' which can accommodate the Kamiokande signal, a consistent solution can be found for the neutrino mass squared difference Delta sq m = (0.3 - 1.0) (center dot) 10(exp -5) sq eV and values of mixing angle sin(exp 2) 2(theta) approaches 5 (center dot) 10(exp -5) sq eV and values of mixing angle sin(exp 2) 2(theta) ('very small mixing solution'). DOE

N95-21377# Los Alamos National Lab., NM.
CORONAL MASS EJECTIONS IN THE SOLAR WIND AT HIGH SOLAR LATITUDES: AN OVERVIEW
J. T. Gosling 1994 22 p Presented at the 3rd SOHO Workshop: Solar Dynamic Phenomena and Solar Wind Consequences, Estes Park, CO, Sep. 1994
(Contract W-7405-eng-36)
(DE95-000844; LA-UR-94-3265; CONF-9409232-1) Avail: CASI HC A03/MF A01

Ulysses has provided the first direct measurements of coronal mass ejections, CMES, in the solar wind at high heliographic latitudes. This paper provides an overview of new and unexpected results from the plasma experiment on Ulysses, supplemented with magnetic field measurements, during the spacecraft's first excursion to high solar latitudes. A striking aspect of the high-latitude CME's observed is that they all had high speeds, with the overall average speed being 730 km/s. A new class of forward-reverse shock pairs, associated with expansion of CME's, has been discovered at high latitudes. Of six certain CME's observed at high latitudes, three have associated shock pairs of this nature. Combined Ulysses and Yohkoh observations suggest that the flux rope topology characteristic of some CME's results from reconnection within the legs of neighboring magnetic loops embedded within the escaping CME's. DOE

N95-21929 Harvard Coll. Observatory, Cambridge, MA.
ABSOLUTE, EXTREME-ULTRAVIOLET SOLAR SPECTRAL IRRADIANCE MONITOR (AESSIM) Final Technical Report, 15 Nov. 1989 - 14 Nov. 1993
W. H. Parkinson and Peter L. Smith Apr. 1994 24 p Limited Reproducibility: More than 20% of this document may be affected by microfiche quality
(Grant AF-AFOSR-0063-90)
(AD-A279345; AFOSR-94-0293TR) Avail: Issuing Activity (Defense Technical Information Center (DTIC))

The goal of this research program was development of a method for obtaining daily radiometrically accurately, solar spectral irradiance data at EUV wavelengths. In orbit radiometric instrumentation recalibration is a fundamental requirement for accurate spectral flux measurements. We have studied a low-pressure version of the EUV radiance standard and concluded that a substantial redesign of it would be required if a suitable one is to be developed for in orbit calibration of a solar spectral irradiance monitor. We have reviewed the use, suitability, and the availability of thin film filters for in orbit EUV calibration. In our opinion, the availability of space qualified filters has not been verified. We have evaluated and chosen a design of a 4-spectrograph, flat-field package that provides 0.1 to 0.2 nm resolution in the range 5-175 nm with a total weight including detectors of 1.6 Kg.

Several mission concepts, which involve rocket-borne, calibrated spectrometer underflights to recalibrate the Voyager spacecraft have been considered. DTIC

N95-22064# Washington Univ., Seattle, WA. Inst. for Nuclear Theory.
TESTING THE PRINCIPLE OF EQUIVALENCE BY SOLAR NEUTRINOS
Hisakazu Minakata (Tokyo Metropolitan Univ., Japan.) and Hiroshi Nunokawa (National Lab. for High Energy Physics, Tsukuba, Japan.) Apr. 1994 15 p
(Contract DE-FG06-90ER-40561)
(DE94-014972; DOE/ER-40561/145) Avail: CASI HC A03/MF A01

We discuss the possibility of testing the principle of equivalence with solar neutrinos. If there exists a violation of the equivalence principle, quarks and leptons with different flavors may not universally couple with gravity. The method we discuss employs a quantum mechanical phenomenon of neutrino oscillation to probe into the non-university of the gravitational couplings of neutrinos. We develop an appropriate formalism to deal with neutrino propagation under the weak gravitational fields of the sun in the presence of the flavor mixing. We point out that solar neutrino observation by the next generation water Cherenkov detectors can improve the existing bound on violation of the equivalence principle by 3-4 orders of magnitude if the nonadiabatic Mikheyev-Smirnov-Wolfenstein mechanism is the solution to the solar neutrino problem. DOE

N95-22085# Washington Univ., Seattle, WA. Inst. for Nuclear Theory.
THE SOLAR FLUX OF THERMAL NEUTRINOS AND ANTINEUTRINOS OF ALL FLAVORS
Wei Lin (Massachusetts Inst. of Tech., Cambridge, MA.) and W. C. Haxton (Washington Univ., Seattle, WA.) 1994 17 p Presented at the Workshop on Solar Neutrinos and Neutrino Astrophysics, Seattle, WA, Mar. 1994
(Contracts DE-FG06-90ER-40561; DE-AC02-76ER-03069; DE-FC02-94ER-40818)
(DE95-003204; DOE/ER-40561/165; CONF-9403179-1) Avail: CASI HC A03/MF A01

The authors have calculated the flux of neutrinos and antineutrinos of all flavors from various thermal processes occurring in the solar core. They find that the transition of electrons from free states to atomic bound states accompanied by Z(sup 0) emission, is the dominant mechanism of neutrino pair emission in the keV range. Other processes they investigate include Compton production, plasmon decay, and pair emission from thermally populated nuclear states. Their results add to the terrestrial neutrino spectrum for each flavor a prominent peak at about 1 keV, with a flux density comparable to that of the pp electron neutrino peak. These thermal neutrinos carry important information on the solar core temperature and chemical composition and on heavy-flavor neutrino masses. The authors discuss resonant absorption of electron antineutrinos as a possible detection method. DOE

N95-22384*# National Aeronautics and Space Administration. Goddard Space Flight Center, Greenbelt, MD.
SOLAR WIND COMPOSITION Progress Report
K. W. Ogilvie and M. A. Coplan (Maryland Univ., College Park, MD.) Jan. 1995 32 p
(Grant NAG5-1129)
(NASA-TM-197364; NAS 1.15:197364) Avail: CASI HC A03/MF A01

Advances in instrumentation have resulted in the determination of the average abundances of He, C, N, O, Ne, Mg, Si, S, and Fe in the solar wind to approximately 10%. Comparisons with solar energetic particle (SEP) abundances and galactic cosmic ray abundances have revealed many similarities, especially when compared with solar photospheric abundances. It is now well established that fractionation in the corona results in an overabundance (with respect to the photosphere) of elements with first ionization potentials less than 10 eV. These observations have in turn led to the development of fractionation models that are reasonably successful in reproducing the first ionization (FIP) effect. Under some circumstances it has been possible to relate solar wind observations to particular source regions in the corona. The magnetic topologies of the source regions appear to have a strong influence on the fractionation of elements. Comparisons with spectroscopic data are particularly useful in classifying the different topologies. Ions produced from interstellar neutral atoms are also found in the solar wind. These ions are picked up by the solar wind after ionization by solar radiation or charge exchange and can be identified by their velocity in the solar wind. The pick-up ions provide most of the pressure in the interplanetary medium at large distances. Interstellar abundances can be derived from the observed fluxes of solar wind pick-up ions. Author

93 SPACE RADIATION

Includes cosmic radiation; and inner and outer earth's radiation belts.

For biological effects of radiation see *52 Aerospace Medicine.* For theory see *73 Nuclear and High-Energy Physics.*

N95-20383# Washington Univ., Seattle, WA. Inst. for Nuclear Theory.
NEUTRINO-NEUTRINO SCATTERING AND MATTER-ENHANCED NEUTRINO FLAVOR TRANSFORMATION IN SUPERNOVAE
Yong-Zhong Qian and G. M. Fuller (California Univ., San Diego, CA.) 1994 47 p
(Contract DE-FG06-90ER-40561)
(DE94-017577; DOE/ER-40561/150) Avail: CASI HC A03/MF A01

The authors examine matter-enhanced neutrino flavor transformation (nu(sub tau(mu)) reversible transformation nu(sub e)) in the region above the neutrino sphere in Type 2 supernovae. Their treatment explicitly includes contributions to the neutrino-propagation Hamiltonian from neutrino-neutrino forward scattering. A proper inclusion of these contributions shows that they have a completely negligible effect on the range of nu(sub e)-nu(sub tau(mu)) vacuum mass-squared difference, delta m(exp 2), and vacuum mixing angle, theta, or equivalently sin(exp 2) 2 theta, required for enhanced supernova shock reheating. When neutrino background effects are included, the authors find that r-process nucleosynthesis from neutrino-heated supernova ejecta remains a sensitive probe of the mixing between a light nu(sub e) and a nu(sub tau(mu)) with a cosmologically significant mass. Neutrino-neutrino scattering contributions are found to have a generally small effect on the (delta m(exp 2), sin(exp 2) 2 theta) parameter region probed by r-process nucleosynthesis. They point out that the nonlinear effects of the neutrino background extend the range of sensitivity of reprocess nucleosynthesis to smaller values of delta m(exp 2). DOE

N95-20490# Washington Univ., Seattle, WA.
HAS A STANDARD MODEL SOLUTION TO THE SOLAR NEUTRINO PROBLEM BEEN FOUND?
J. N. Bahcall (Institute for Advanced Study, Princeton, NJ.) and C. A. Barnes (California Inst. of Tech., Pasadena, CA.) 1994 5 p
(Contract DE-FG06-90ER-40561)
(DE94-017580; DOE/ER-40561/154) Avail: CASI HC A01/MF A01

The claim by Dar and Shaviv that they have found a standard model solution to the solar neutrino problem is based upon an incorrect assumption made in extrapolating nuclear cross sections and the selective use of a small fraction of the nuclear physics and of the neutrino data. In addition, five different solar model codes show that the rate obtained for the chlorine experiment using the Dar- Shaviv stated parameters differs by a least 14(sigma) from the observed rate. DOE

N95-21475# Argonne National Lab., IL.
THE ATMOSPHERIC NEUTRINO ANOMALY IN SOUDAN 2
M. C. Goodman 1994 6 p Presented at the Neutrino 1994: 16th International Conference on Neutrino Physics and Astrophysics, Eilat, Israel, 29 May - 3 Jun. 1994
(Contract W-31-109-eng-38)
(DE94-019288; ANL-HEP-PR-94-56; CONF-9405216-2) Avail: CASI HC A02/MF A01

Based on a preliminary analysis of 1.01 fiducial kiloton-years of Soudan 2 data, we measure (track/shower)(sub measured)/(track/shower)(sub predicted) = 0.64 +/- 0.17(stat) +/- 0.09(sys). We discuss the implications of a neutrino oscillation interpretation of the atmospheric neutrino anomaly. DOE

99 GENERAL

N95-20182# Naval Research Lab., Washington, DC.
NRL REVIEW, 1994
Mar. 1994 297 p
(AD-A279832; NRL/PU/5200-94-246) Avail: CASI HC A13/MF A03

Partial contents include: Diamond Surface Chemistry; Computational Materials Science; Self-assembled Molecular Templates: Microtubule-based Controlled Release for Biofouling Control and Medical Applications; Monitoring Whales and Earthquakes by using SOSUS; High-Resolution Underwater Acoustic Imaging; Fiber-Optic Sensor for Detection of Trace Levels of Mercury in Water; Multispectral Infrared Visualization and Processing for Dim Target Detection; Missile Hit-Points on the DDG-53; Secure Information Through Replicated Architecture (SINTRA) Database System; Simulation and Visualization of Ultrasonic Waves in Solids by Using Parallel Processing; Reactive Flows in Ram Accelerators; Sea Surface Temperature Retrievals from Satellite; and High Frequency Approximations to Physical Optics. DTIC

N95-21828# Australian Nuclear Science and Technology Organization, Lucas Heights (Australia).
ANSTO: PROGRAM OF RESEARCH, 1993-1994
1993 85 p
(DE94-631122; INIS-mf-13947) Avail: CASI HC A05/MF A01 (US Sales Only)

The 1993-1994 Program of Research outlines ANSTO's scientific activities in four key research areas: Advanced Materials, Application of Nuclear Physics, Biomedicine and Health and Environmental Science. The effort has been channeled into applied research and development in partnership with industry and appropriate national and international institutions and into interdisciplinary strategic research projects to enhance the scientific base of the key research activities. A list of scientific publications originated from these program areas is also included. DOE

N95-21830# Australian Nuclear Science and Technology Organization, Lucas Heights (Australia).
[ANSTO: MISSION STATEMENT, SIGNIFICANT EVENTS AND ACHIEVEMENTS] Annual Report, 1 Jul. 1992 - 30 Jun. 1993
Nov. 1993 92 p
(DE94-631123; INIS-mf-13948) Avail: CASI HC A05/MF A01 (US Sales Only)

Significant events and achievements highlighted in the Annual Reports include: the Research Reactor Review, increase of external revenues by 12.5%, sales of Australian radioisotopes amounting to $8.5 M, regulatory approval for production of thallium-201 in National Medical Cyclotron, completion of first contracts with Wismut GmbH in Germany, production of a database of content of atmospheric particulate matter in air over NSW, word-wide licence agreement signed for further commercialization of blood clot radiopharmaceuticals, collaborative agreement signed with SURPAC Int. for development of geochemical speciation software, and complete design of rings in HIFAR for silicon doping. DOE

N95-22262# Sandia National Labs., Albuquerque, NM.
MANUFACTURING TECHNOLOGY BULLETIN, JULY 1994
Jul. 1994 8 p
(Contract DE-AC04-94AL-85000)
(DE94-017775; SAND-94-1913) Avail: CASI HC A02/MF A01

The following topics are discussed in this issue: (1) Robotic cleaning safer, faster, more reliable, robots taught how to clean in seconds instead of days; (2) Microporous insulating films can boost microcircuit performance; films display improved dielectric constant, mechanical properties; (3) Life-cycle analysis: the big picture, cradle-to-grave environmental analysis tailored to the needs of defense manufacturing; and (4) New simulation tool predicts properties of forged metal; internal state variable model improves design, speeds development time. DOE

N95-22394# Ain Shams Univ., Cairo (Egypt). Dept. of Chemistry.
INDIAN ACADEMY OF SCIENCES. VOLUME 105, NUMBER 6, DECEMBER 1993. PROCEEDINGS OF THE 2ND INTERNATIONAL CONFERENCE ON SOLAR ENERGY STORAGE APPLIED PHOTOCHEMISTRY
V. Krishnan, ed. and S. Chandrasekaran, ed. Dec. 1993 508 p
Conference held in Cairo, Egypt, 6-11 Jan. 1993
(Contract N00014-93-J-9007) (ISSN 0253-4134)
(AD-A286481) Avail: CASI HC A22/MF A04

Contents include: Strategies for solar fuel generation; Photobiotechnology: Application of photosynthesis to the production of renewable fuels and chemicals; Gold-platinum bimetallic cluster catalysts for visible light-induced hydrogen production from water; Light-induced hydrogen production using waste compounds as sacrificial electron donors; What is new in stereophotolithography; Purification of drinking water by irradiation, a review; Heterogeneous and homogeneous photoassisted wastewater treatment; Kinetics of sunlight photodegradation of 2,3,4,7,8-pentachlorodibenzofuran in natural water; Applied photochemistry in dental science; Supramolecular photochemistry, luminescent and redox active dendritic polynuclear metal complexes. DTIC

SUBJECT INDEX

Typical Subject Index Listing

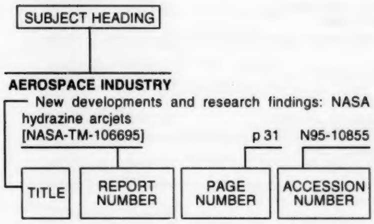

The subject heading is a key to the subject content of the document. Titles, report numbers, and accession numbers of pertinent documents are provided under each subject heading. When the title is insufficiently descriptive of the document content, a title extension is added, separated from the title by three hyphens. The report number helps to indicate the type of document cited (e.g., NASA report, NASA translation, NASA contractor report). The accession number is the number by which the document abstracts are arranged in this journal and by which the document is sold or requested. The page number helps you locate the citation in the abstract section. The titles, with title extensions if present, are arranged under each subject heading in ascending accession number order. The subject headings have been selected from the latest revision of the *NASA Thesaurus.*

A

A-7 AIRCRAFT
Derived gust spectra for the Macchi MB326H
[ARL-TN-3] p 1202 N95-21892

ABBREVIATIONS
Abbreviations and acronyms
[NASA-TM-110506] p 1590 N95-21457
Abbreviations, acronyms, and initialisms frequently used by Martin Marietta Energy Systems, Inc.
[DE95-001069] p 1591 N95-22107

ABERRATION
First results from the final focus test beam
[DE95-002897] p 1535 N95-21255

ABNORMALITIES
Aircraft corrosion study
[AD-A279527] p 1259 N95-21687

ABRASION
Abrasive wear by diesel engine coal-fuel and related particles
[PB95-104915] p 1379 N95-20984

ABRASIVES
Abrasive wear by diesel engine coal-fuel and related particles
[PB95-104915] p 1379 N95-20984

ABSORBENTS
Natural gas cleanup: Evaluation of a molecular sieve carbon as a pressure swing adsorbent for the separation of methane/nitrogen mixtures
[DE94-012263] p 1234 N95-20135

ABSORBERS (MATERIALS)
Polyurethane-epoxy interpenetrating polymer network acoustic damping material
[AD-D016567] p 1266 N95-20293
Polyurethane-acrylic interpenetrating polymer network acoustic damping material
[AD-D016572] p 1266 N95-20294
Test fixture for determination of energy absorbing capabilities of composite materials
[NASA-CASE-LAR-15212-1-CU] p 1229 N95-21008
Accelerated life testing of solar energy materials: Case study of some selective solar absorber coating materials for DHW systems. A report of task 10 solar materials research and development
[PB95-132411] p 1397 N95-22362
Acoustic and vibration attenuation composite material
[AD-D016585] p 1233 N95-22467

ABSORPTION SPECTRA
A new family of anion receptors and their effects on ion pair dissociation and conductivity of lithium salts in non-aqueous solutions
[DE94-016822] p 1512 N95-20477
Visible and near-IR spectroscopic studies of UC1(4) in a basic ambient temperature melt: The observation of a possible geometric distorted UC1(6)(exp 2-) species and the evidence for the hydrogen-bond in the melt
[DE94-017764] p 1237 N95-20493
Control of continuous phase PH using visible light to activate PH-dependent fibers and gels in a controlled and reversible manner
[AD-D016532] p 1543 N95-20728
Novel absorption detection techniques for capillary electrophoresis
[DE95-001673] p 1242 N95-21400
Recent photoabsorption measurements in the rare gases and alkalis in the 3 to 15 keV photon energy region
[DE94-019278] p 1521 N95-21406
Modeling of nonlinear optic and ESR response of CDW MX materials
[DE94-018301] p 1578 N95-22297
Modeling of collision induced absorption spectra of CO2-CO2 pairs for planetary atmosphere of Venus
[NASA-CR-197373] p 1601 N95-22338

ABSORPTION SPECTROSCOPY
Novel absorption detection techniques for capillary electrophoresis
[DE95-001673] p 1242 N95-21400
Time-resolved diagnostics of excimer laser-generated ablation plasmas used for pulsed laser deposition
[DE94-018950] p 1559 N95-21547
Strong interactions studies with medium energy probes
[DE95-001800] p 1245 N95-21745
Vibrational overtone spectroscopy of pyridine and related compounds
[AD-A280105] p 1224 N95-21911

ABSORPTIVITY
Ultraviolet laser emission properties of Ce(3+)-doped LiSrAlF6
[DE94-016364] p 1372 N95-21135

ABSTRACTS
Bibliography of Lewis Research Center technical publications announced in 1993
[NASA-TM-106666] p 1589 N95-21187

ABUNDANCE
Atmospheres of the Moon and Mercury
p 1419 N95-21794
Rates of Earth degassing p 1422 N95-21809
Water abundance and accretion history of terrestrial planets p 1424 N95-21820
Solar wind composition
[NASA-TM-197364] p 1604 N95-22384

AC GENERATORS
Variations observed in the AC generator signal period of a Sea King helicopter
[AD-A284280] p 1206 N95-19963
Brushless Doubly-Fed Machine system development program, phase 3
[DE94-013095] p 1315 N95-20380

ACCELERATED LIFE TESTS
Plastic encapsulated parts
[DE95-001876] p 1332 N95-21729
Protective organic coatings on steel: Accelerated corrosion test method for paint/coatings exposed to water with low conductivity. Nordtest project no. 1010-92. Degradation of organic coatings in fresh water
[PB95-134185] p 1277 N95-21873
Accelerated life testing of solar energy materials: Case study of some selective solar absorber coating materials for DHW systems. A report of task 10 solar materials research and development
[PB95-132411] p 1397 N95-22362

ACCELERATION STRESSES (PHYSIOLOGY)
A method to determine the kinematics of the lower limbs of a subject pedaling a bicycle using encoders and accelerometers
[NASA-CR-197401] p 1453 N95-21866

ACCELERATION TOLERANCE
Command history, 1993
[AD-A279775] p 1446 N95-21989

ACCELERATORS
Approach to compact terawatt CO2 laser system for particle acceleration
[DE95-002170] p 1371 N95-20866
Triggers for a high sensitivity charm experiment
[DE95-002251] p 1515 N95-20868

ACCELEROMETERS
A method to determine the kinematics of the lower limbs of a subject pedaling a bicycle using encoders and accelerometers
[NASA-CR-197401] p 1453 N95-21866

ACCEPTABILITY
The Advanced Avionics Subsystem Technology Demonstration Program p 1209 N95-20636
Military standard: Test requirements for launch, upper-stage, and space vehicles
[AD-A286627] p 1218 N95-20770

ACCESS TIME
Experimental evaluation of dynamic data allocation strategies in a distributed database with changing workloads
[NASA-CR-195024] p 1456 N95-22431

ACCUMULATIONS
Search for D(+) yields (pi)(+)(mu)(+)(mu)(-)
[DE94-015538] p 1512 N95-20475
A Cost and Performance System (CAPS) in a Federal agency p 1584 N95-20746
Measurement of the B meson differential cross-sections in p(bar p) collisions at (radical)s = 1.8 TeV using the exclusive decays B(sup (+-)) (yields) J/(psi)K(sup (+-)) and B(sup 0) (yields) J/(psi)K*(sup 0)
[DE94-018993] p 1523 N95-21562

ACCUMULATORS
ICE BABY: Measurements of concentration fluctuations in a forest area in winter conditions
[PB95-133468] p 1405 N95-21274
Solar collector manufacturing activity 1993
[DE94-017340] p 1398 N95-22429

ACCURACY
Error analysis in wind turbine field testing
[DE94-011864] p 1391 N95-20260
Impact of propagation mechanisms on global navigation satellite system performance p 1298 N95-20950
An in-line ultrasonic viscometer
[DE95-002982] p 1366 N95-21453
Learning maneuvers using neural network models
[AD-A286470] p 1486 N95-22267

ACETIC ACID
Bioconversion of coal derived synthesis gas to liquid fuels
[DE94-018849] p 1314 N95-20339
A direct process for preparing semi-crystalline polyimides
[NASA-CASE-LAR-15020-1] p 1268 N95-20407

ACETONE
Effect of external stress on the transport of fluids in thermoplastic resin systems
[AD-A279993] p 1270 N95-20596

ACETYLENE
Ceramics formed by pyrolysis of either linear or thermosetting carborane (siloxane or silane) acetylene based precursor polymers
[AD-D016563] p 1266 N95-20291
The synthesis and characterization of new mesogenic diacetylene monomers and their polymers
[AD-A286188] p 1267 N95-20328
Conducting thermoset polymers
[AD-A286541] p 1273 N95-21014

ACID RAIN
Assessment of the atmospheric hazards and risks of new chemicals: Procedures to estimate hazard potentials
[PB95-107488] p 1410 N95-22186
ACIDITY
Effects of meteorology on concentrations of acid aerosols
[PB94-209749] p 1400 N95-19965
An investigation of the applicability of the new ion exchange resin, Reillex(TM)-HPQ, in ATW separations
[DE94-016576] p 1274 N95-21234
Acid-site characterization of water-oxidized alumina films by near-edge x-ray absorption and soft x-ray photoemission
[DE95-003355] p 1247 N95-22234
ACOUSTIC ATTENUATION
Polyurethane-epoxy interpenetrating polymer network acoustic damping material
[AD-D016567] p 1266 N95-20293
Polyurethane-acrylic interpenetrating polymer network acoustic damping material
[AD-D016572] p 1266 N95-20294
Higher order crossings
[AD-A279597] p 1504 N95-20300
Cascade orificial resistive device
[AD-D016529] p 1504 N95-20724
Determination of multiple sound sources
[AD-A286563] p 1504 N95-20823
Small antennas for communication over sea ice
[AD-D016206] p 1301 N95-21156
Effect of atmospheric pressure on measured aircraft noise levels
[PB95-130423] p 1207 N95-21425
ACOUSTIC DUCTS
Robust fixed-structure control
[AD-A286515] p 1485 N95-22216
ACOUSTIC EMISSION
Wavelet-based acoustic recognition of aircraft
[DE94-017701] p 1503 N95-20019
Acoustic emission: The first half century
[DE94-017176] p 1503 N95-20267
Experimental and theoretical evaluation of elastic waves in curved layered media
[AD-A286578] p 1504 N95-20918
ACOUSTIC FREQUENCIES
Microscopic theory of normal liquid He-3
[DE94-629047] p 1527 N95-22179
ACOUSTIC IMAGING
Fiber optic pressure sensing array
[AD-D016245] p 1506 N95-22088
ACOUSTIC IMPEDANCE
Acoustic calibration apparatus for calibrating plethysmographic acoustic pressure sensors
[NASA-CASE-LAR-14977-1] p 1443 N95-20763
ACOUSTIC MEASUREMENT
Analysis of low frequency ocean noise. 1: From a long-term experiment across the US East Coast. 2: From the Wake Island Hydrophone Array during northwest Pacific typhoons
[AD-A284975] p 1432 N95-20040
Characterization and simulation of an acoustic source moving through an oceanic waveguide
[AD-A285688] p 1503 N95-20272
Infrasonic observations of the Northridge, California, earthquake
[DE94-018095] p 1413 N95-20289
Data report: Stress measurements in the bottom boundary layer with BASS tripods STRESS 2 1990-1991
[AD-A279875] p 1433 N95-20433
Acoustic calibration apparatus for calibrating plethysmographic acoustic pressure sensors
[NASA-CASE-LAR-14977-1] p 1443 N95-20763
Laser-Induced Thermal Acoustics (LITA): Four-wave mixing measurement of sound speed, thermal diffusivity, and viscosity
[AD-A286524] p 1372 N95-21009
Effect of atmospheric pressure on measured aircraft noise levels
[PB95-130423] p 1207 N95-21425
Materials for adaptive structural acoustic controls
[AD-A279255] p 1505 N95-21863
Measurement of sound intensity and sound power
[AD-A279246] p 1505 N95-21984
Rapid determination of geoacoustic properties of the sea floor by simulated annealing
[AD-A286297] p 1436 N95-22028
ACOUSTIC PROPAGATION
Model-based inversion for a shallow ocean application
[DE94-016968] p 1433 N95-20420
Evaluation of simple spherical spreading model for near vertical acoustical propagation
[AD-A286284] p 1505 N95-22042
Real time system for practical acoustic monitoring of global ocean temperature
[AD-A286435] p 1436 N95-22209
ACOUSTIC PROPERTIES
Materials for adaptive structural acoustic control, volume 2
[AD-A279222] p 1502 N95-19883
Wavelet transformations for helicopter identification via acoustic signatures
[AD-A279980] p 1504 N95-20963
Active control of fan noise-feasibility study. Volume 1: Flyover system noise studies
[NASA-CR-195392-VOL-1] p 1505 N95-21888
Seismic anisothropy and large-scale porosity inthe ocean floor
[AD-A286580] p 1436 N95-22187
ACOUSTIC SCATTERING
Multiple scatter theory of ocean sediments
[AD-A286033] p 1433 N95-20999
Scattering of an FM signal from an array of spheres
[AD-A285587] p 1505 N95-21213
ACOUSTIC VELOCITY
Model-based inversion for a shallow ocean application
[DE94-016968] p 1433 N95-20420
Laser-Induced Thermal Acoustics (LITA): Four-wave mixing measurement of sound speed, thermal diffusivity, and viscosity
[AD-A286524] p 1372 N95-21009
ACOUSTICS
Acoustic climb to cruise test
[NASA-TM-110504] p 1206 N95-20155
Polyurethane-epoxy interpenetrating polymer network acoustic damping material
[AD-D016567] p 1266 N95-20293
Method and system of mapping acoustic near field
[AD-D016574] p 1504 N95-20296
Laser-Induced Thermal Acoustics (LITA): Four-wave mixing measurement of sound speed, thermal diffusivity, and viscosity
[AD-A286524] p 1372 N95-21009
Nonlinear acoustic processes in a solid rocket engine
[AD-A285606] p 1222 N95-21193
A mixed time integration method for large scale acoustic fluid-structure interaction
[DE94-018327] p 1354 N95-21387
ACOUSTO-OPTICS
Preliminary evaluation of a digital optical systolic processor implemented with acousto-optic cells
[AD-A286377] p 1541 N95-20231
Laser-Induced Thermal Acoustics (LITA): Four-wave mixing measurement of sound speed, thermal diffusivity, and viscosity
[AD-A286524] p 1372 N95-21009
Optical processing and control
[AD-A279157] p 1546 N95-21975
Electro-optic effect in the PESO acousto-optic modulator
[AD-A286355] p 1548 N95-22255
ACRYLIC RESINS
Polyurethane-acrylic interpenetrating polymer network acoustic damping material
[AD-D016572] p 1266 N95-20294
Responsive copolymers for enhanced petroleum recovery
[DE94-018822] p 1267 N95-20350
ACTINIDE SERIES
Research in the chemical sciences: Summaries of FY 1994
[DE94-015427] p 1223 N95-20264
ACTIVATED CARBON
Laboratory evaluation of a reactive baffle approach to NOx control
[AD-A283802] p 1400 N95-19921
ACTIVATION
Novel catalysts for methane activation
[DE95-002639] p 1237 N95-20438
ACTIVATION ENERGY
Aerosol-assisted chemical vapor deposition of copper: A liquid delivery approach to metal thin films
[AD-A279702] p 1270 N95-20689
Modeling the effect of water on mantle rheology
p 1417 N95-21783
Oxidation behavior of aluminum nanopowders
[DE95-002721] p 1260 N95-21926
Studies in nonlinear problems of energy
[DE95-001387] p 1356 N95-22148
The enhancement of metallic silver monomer evaporation by the adhesion of polar molecules to silver nanocluster ions
[AD-A284936] p 1281 N95-22470
ACTIVE CONTROL
Optimal distributed control system for a linear distributed parameter system
[AD-D016583] p 1480 N95-20202
Heterogeneous multi-robot cooperation
[AD-A279839] p 1481 N95-21185
Active control of fan noise-feasibility study. Volume 1: Flyover system noise studies
[NASA-CR-195392-VOL-1] p 1505 N95-21888
Experimental investigations of on-demand vortex generators p 1361 N95-22451
Drag reduction strategies p 1361 N95-22453
Optimal active control for Burgers equations
p 1361 N95-22454
ACTIVITY (BIOLOGY)
The Use of Cyanobacteria to Explore Basic Biological Processes
[DE94-019238] p 1440 N95-22066
ACTIVITY CYCLES (BIOLOGY)
Diffusible driving and coupling signals of the biological clock
[AD-A285353] p 1447 N95-22475
ACTS
Cochannel and adjacent-channel interference in nonlinear minimum-shift-keyed satellite system
[NASA-TM-106834] p 1307 N95-21890
ACTUATORS
Materials for adaptive structural acoustic control, volume 2
[AD-A279222] p 1502 N95-19883
Design of power electronics for TVC and EMA systems
[NASA-CR-196540] p 1312 N95-19909
Collocated tunable wavenumber sensor/actuators for smart structures
[AD-A279608] p 1312 N95-19958
Robust agent control of an autonomous robot with many sensors and actuators
[AD-A280148] p 1479 N95-20011
Collocated tunable wavenumber sensor/actuators for smart structures
[AD-A279066] p 1258 N95-21575
Domain processes in ferroelectric ceramics
[AD-A279567] p 1276 N95-21697
Materials for adaptive structural acoustic controls
[AD-A279255] p 1505 N95-21863
Characterization equipment for electrooptics and actuators
[AD-A286285] p 1546 N95-22043
ADA (PROGRAMMING LANGUAGE)
Software fault tree analysis of concurrent Ada processes
[AD-A284979] p 1457 N95-20042
Artificial Intelligence (AI) and Ada: Integrating AI with mainstream software engineering
[AD-A286093] p 1485 N95-22226
ADAPTATION
Passive monitoring for automated MMPP communication systems p 1293 N95-20927
Adaptive fault-resistant systems
[AD-A286406] p 1484 N95-22203
ADAPTIVE CONTROL
Materials for adaptive structural acoustic control, volume 2
[AD-A279222] p 1502 N95-19883
A-posteriori estimation and adaptive control of the pollution-error in the h-version of the finite element method
[AD-A285670] p 1480 N95-20083
An integrated architecture of adaptive neural network control for dynamic systems
[DE94-014813] p 1481 N95-20693
Adaptive error-control scheme for 2-200 MHz Multiple-Mechanism Propagation Paths
p 1293 N95-20926
Electrorheology for smart automotive suspensions
[AD-A285543] p 1380 N95-21157
Heterogeneous multi-robot cooperation
[AD-A279839] p 1481 N95-21185
Adaptive capture of expert behavior
[DE94-018285] p 1483 N95-21710
Materials for adaptive structural acoustic controls
[AD-A279255] p 1505 N95-21863
ADDITIVES
On commonalities in signal design for non-Gaussian channels
[AD-A285385] p 1498 N95-20608
ALCHEMI of Fe-doped B2-ordered NiAl alloys with different doping levels
[DE94-017748] p 1255 N95-20907
Development of an advanced JP-8 fuel
[AD-A285583] p 1283 N95-21161
ADDUCTS
Synthesis and characterization of single-source molecular precursors to binary metal sulphides: Bis(diethyldithiocarbamato) M(2)trialkylphosphine (M = Zn and Cd) adducts
[AD-A279746] p 1248 N95-22385
ADHESION
Effects of ambient conditions on the adhesion of cubic boron nitride films on silicon substrates
[DE94-016779] p 1266 N95-20281
Preclinical investigation of lyophilized platelet preparations
[AD-A286079] p 1443 N95-20851

Dielectric models in adhesion and extrapolations of molecular modeling
[AD-A279675] p 1516 N95-21121
Methods of measuring adhesion for thermally grown oxide scales
[DE94-018177] p 1256 N95-21260
Copper metallization of stainless steels
[DE95-001496] p 1256 N95-21300
Embedded optical fibres as strain sensors in polymer matrix fibre composites: The influence of adhesion in strain transfer
[PB95-133617] p 1547 N95-22140
The enhancement of metallic silver monomer evaporation by the adhesion of polar molecules to silver nanocluster ions
[AD-A284936] p 1281 N95-22470

ADHESIVE BONDING
Vacuum holding fixture and method for fabricating piezoelectric polymer acoustic sensors
[NASA-CASE-LAR-14240-1] p 1268 N95-20410
Joining of dissimilar materials. A review
[PB95-132999] p 1380 N95-21416
Damage tolerant repair techniques for pressurized aircraft fuselages
[AD-A286298] p 1199 N95-22046

ADHESIVES
Dielectric models in adhesion and extrapolations of molecular modeling
[AD-A279675] p 1516 N95-21121

ADIABATIC CONDITIONS
Front-boundary layer models from STORM-FEST observations
[AD-A279907] p 1428 N95-20186
Ion-molecular spiraling collisions and termolecular recombination
[AD-A285633] p 1517 N95-21151

ADMIXTURES
On the theory of strong electromagnetic waves propagation in an electron-positron-ion plasma
[DE94-628964] p 1561 N95-21850

ADRENAL GLAND
Radiopharmaceuticals for diagnosis
[DE95-002200] p 1445 N95-21595

ADSORBENTS
Mercury capture in bench-scale absorbers
[DE94-016910] p 1234 N95-20107
Natural gas cleanup: Evaluation of a molecular sieve carbon as a pressure swing adsorbent for the separation of methane/nitrogen mixtures
[DE94-012263] p 1234 N95-20135

ADSORPTION
Natural gas cleanup: Evaluation of a molecular sieve carbon as a pressure swing adsorbent for the separation of methane/nitrogen mixtures
[DE94-012263] p 1234 N95-20135
An atomically-resolved STM study of the interaction of phosphine (PH3) with the silicon (001) surface
[AD-A279819] p 1513 N95-20585
Time-resolved analytical methods for liquid/solid interfaces
[DE95-002255] p 1240 N95-20780
An advanced ECR ion source with a large uniformly distributed ECR plasma volume for multiply charged ion beam generation
[DE95-001078] p 1515 N95-20911
Translational-energy-resolved studies of photographed carrier-induced reactions on semiconductor surfaces
[DE95-002944] p 1573 N95-21444
Cluster reactions: An approach to understanding the fundamentals of heterogeneous catalysis
[DE95-002947] p 1243 N95-21447
Development and applications of flat ceramic membranes
[PB95-110219] p 1276 N95-21650
Neutron reflectivity study of adsorbed diblock copolymers
[DE95-002740] p 1281 N95-22434

ADVANCED LAUNCH SYSTEM (STS)
STS 63 flight day 4 highlights/MIR-Shuttle rendezvous
[NASA-TM-110512] p 1219 N95-21113

ADVANCED SOLID ROCKET MOTOR (STS)
Radiation from advanced solid rocket motor plumes
[NASA-CR-196554] p 1221 N95-20124

ADVANCED VERY HIGH RESOLUTION RADIOMETER
Ice Processing System software support documentation
[AD-A280030] p 1388 N95-20006

ADVECTION
Balloon tracking for the ASTEX/MAGE Lagrangian experiment
[AD-A280078] p 1430 N95-20969

AERIAL PHOTOGRAPHY
Guidelines for the creation and management of geographic data bases within a GIS environment, version 1.0. Volume 2. Appendices
[DE94-019215] p 1591 N95-22129
A multispectral scanner survey of the Idaho National Engineering Laboratory and the Hanford Reservation
[DE95-003922] p 1391 N95-22398

AERIAL RECONNAISSANCE
Unmanned aerial vehicles
[AD-A286190] p 1206 N95-20329
Lidar technologies for airborne and space-based applications
[DE95-002954] p 1302 N95-21448
Guidelines for the creation and management of geographic data bases within a GIS environment, version 1.0. Volume 2. Appendices
[DE94-019215] p 1591 N95-22129

AEROACOUSTICS
Active control of fan noise-feasibility study. Volume 1: Flyover system noise studies
[NASA-CR-195392-VOL-1] p 1505 N95-21888
Acoustics of laminar boundary layers breakdown
p 1361 N95-22455
A method for obtaining a statistically stationary turbulent free shear flow p 1363 N95-22463

AEROBRAKING
Simulated rarefied entry of the Galileo probe into the atmosphere of Jupiter
[NASA-TM-110507] p 1601 N95-21621

AERODYNAMIC CHARACTERISTICS
Open Skies project computational fluid dynamic analysis
[AD-A285928] p 1200 N95-19991

AERODYNAMIC DRAG
Investigation of a thermal buoyancy effect on the drag of half models tested in the ARA Transonic Wind Tunnel
[ARA-MEMO-407] p 1199 N95-19946
Free shear layers, base pressure and bluff-body drag
[AD-A286316] p 1200 N95-20175
Research on bluff body vortex wakes
[AD-A286319] p 1200 N95-20177
Simulated rarefied entry of the Galileo probe into the atmosphere of Jupiter
[NASA-TM-110507] p 1601 N95-21621

AERODYNAMIC HEATING
A computer code (SKINTEMP) for predicting transient missile and aircraft heat transfer characteristics
[AD-A286044] p 1341 N95-21001
Temperature effects on acoustic interactions between altitude test facilities and jet engine plumes
[NASA-CR-197638] p 1504 N95-21170

AERODYNAMIC INTERFERENCE
Investigation of a thermal buoyancy effect on the drag of half models tested in the ARA Transonic Wind Tunnel
[ARA-MEMO-407] p 1199 N95-19946

AERODYNAMIC LOADS
Prediction of rotor-blade deformations due to unsteady airloads
[AD-A286593] p 1207 N95-20860

AERODYNAMIC NOISE
Active control of fan noise-feasibility study. Volume 1: Flyover system noise studies
[NASA-CR-195392-VOL-1] p 1505 N95-21888
Acoustics of laminar boundary layers breakdown
p 1361 N95-22455

AERODYNAMICS
Advanced wind turbine design studies: Advanced conceptual study
[DE93-000031] p 1394 N95-20985
Aeronautical engineering: A continuing bibliography with indexes (supplement 315)
[NASA-SP-7037(315)] p 1199 N95-21640
Sandia National Laboratories analysis code data base
[DE95-004188] p 1502 N95-22420

AEROELASTICITY
Prediction of rotor-blade deformations due to unsteady airloads
[AD-A286593] p 1207 N95-20860

AEROGELS
Novel electrochemical materials prepared by sol-gel chemistry
[AD-A286310] p 1226 N95-20092

AERONAUTICAL ENGINEERING
Aeronautical engineering: A continuing bibliography with indexes (supplement 315)
[NASA-SP-7037(315)] p 1199 N95-21640

AEROSOLS
Effects of meteorology on concentrations of acid aerosols
[PB94-209749] p 1400 N95-19965
Aerosol-assisted chemical vapor deposition of copper: A liquid delivery approach to metal thin films
[AD-A279702] p 1270 N95-20689
Balloon tracking for the ASTEX/MAGE Lagrangian experiment
[AD-A280078] p 1430 N95-20969
Project Whitefeather
[DE94-016575] p 1415 N95-21184
Evaluation of the technical performance of the Dutch National Air Quality Monitoring Network in 1992
[PB95-131892] p 1405 N95-21327
Monitoring activities in the framework of the Dutch National Air Quality Monitoring Network in 1994
[PB95-131884] p 1406 N95-21351
High resolution properties of the equatorial Pacific marine atmospheric boundary layer from lidar and radiosonde observations
[DE95-001028] p 1426 N95-21875
Confirmatory analysis of SAGE-1, and -2 data
[DE95-003623] p 1427 N95-22240

AEROSPACE ENGINEERING
NASA/DOD Aerospace Knowledge Diffusion Research Project. Report 28: The technical communication practices of aerospace engineering and science students: Results of the phase 4 cross-national surveys
[NASA-TM-109123] p 1587 N95-20162
NASA/DOD Aerospace Knowledge Diffusion Research Project. Report 31: The technical communications practices of US aerospace engineers and scientists: Results of the phase 1 SME mail survey
[NASA-TM-109169] p 1587 N95-20163
Space fundamentals for the war fighter
[AD-A279703] p 1217 N95-20690
Cost estimating methods for advanced space systems
p 1583 N95-20741
Space technology: Force multiplier or false sense of security
[AD-A279726] p 1217 N95-20995
NASA/DOD Aerospace Knowledge Diffusion Research Project. Report 27: The technical communication practices of engineering and science students: Results of the phase 3 academic surveys
[NASA-TM-109122] p 1589 N95-21015
Spinoff, 1994
[NASA-NP-214] p 1594 N95-21893
NASA patent abstracts bibliography: A continuing bibliography. Section 2: Indexes (supplement 46)
[NASA-SP-7039(46)-SECT-2] p 1590 N95-21948
NASA/DOD Aerospace Knowledge Diffusion Research Project. Paper 48: Valuing information in an interactive environment
[NASA-TM-110448] p 1590 N95-21977
Space systems technology working group: Executive report
[AD-A285778] p 1217 N95-22413

AEROSPACE ENVIRONMENTS
Space fundamentals for the war fighter
[AD-A279703] p 1217 N95-20690

AEROSPACE INDUSTRY
The thermal conductivity of carbon-fiber reinforced metal matrix composites
[DE94-017767] p 1226 N95-20125

AEROSPACE MEDICINE
Behavioral effects of tyrosine during sustained wakefulness
[AD-A279789] p 1441 N95-20307
Development and enhancement of a model of performance and decision making under stress in a real life setting
[AD-A285945] p 1449 N95-20393
Modeling platform dynamics and physiological response to short arm centrifugation
[AD-A279640] p 1442 N95-20457
Bibliography of scientific publications 1975-1993
[AD-A279767] p 1444 N95-20977
Effect of increased venous backflow on the release of cardiac hormone. Fine structural, immunohistochemical, and biochemical study
[PB95-130399] p 1445 N95-21424
Aerospace medicine and biology: A continuing bibliography with indexes (supplement 399)
[NASA-SP-7011(399)] p 1446 N95-21947
Command history, 1993
[AD-A279775] p 1446 N95-21989
Age 60 study. Part 1: Bibliographic database
[AD-A286245] p 1446 N95-22027
Age 60 study. Part 2: Airline pilot age and performance. A review of the scientific literature
[AD-A286246] p 1447 N95-22040
Optical radiation: Health based exposure limits for electromagnetic radiation in the wavelength range from 100 nanometer to 1 millimeter
[PB95-132767] p 1447 N95-22083

AEROSPACE SAFETY
Independent review of Aviation Technology and Research Information Analysis System (ATRIAS) database
[AD-A284049] p 1203 N95-21518

AEROSPACE SCIENCES
Bibliography of scientific publications 1975-1993
[AD-A279767] p 1444 N95-20977
Bibliography of Lewis Research Center technical publications announced in 1993
[NASA-TM-106666] p 1589 N95-21187

AEROSPACE SYSTEMS
Space technology: Force multiplier or false sense of security
[AD-A279726] p 1217 N95-20995
Demonstration of multifunctional DNBM corrosion inhibitors in protective coatings for Naval air/weapon systems
[AD-A285869] p 1279 N95-22136
Space systems technology working group: Executive report
[AD-A285778] p 1217 N95-22413

AEROSPACE TECHNOLOGY TRANSFER
NASA/DOD Aerospace Knowledge Diffusion Research Project. Report 31: The technical communications practices of US aerospace engineers and scientists: Results of the phase 1 SME mail survey
[NASA-TM-109169] p 1587 N95-20163
NASA/DOD Aerospace Knowledge Diffusion Research Project. Report 27: The technical communication practices of engineering and science students: Results of the phase 3 academic surveys
[NASA-TM-109122] p 1589 N95-21015
Spinoff, 1994
[NASA-NP-214] p 1594 N95-21893
NASA/DOD Aerospace Knowledge Diffusion Research Project. Paper 48: Valuing information in an interactive environment
[NASA-TM-110448] p 1590 N95-21977

AEROTHERMODYNAMICS
Experimental study of vane heat transfer and aerodynamics at elevated levels of turbulence
[NASA-CR-4633] p 1337 N95-19912
A computer code (SKINTEMP) for predicting transient missile and aircraft heat transfer characteristics
[AD-A286044] p 1341 N95-21001
Grid resolution and solution convergence for Mars Pathfinder forebody
[NASA-TM-109173] p 1494 N95-21622

AFRICAN RIFT SYSTEM
Spatial variation of primordial 3-He in crustal fluids along the East-African Rift system (the Ethiopian and the Kenya Rift section) p 1418 N95-21789

AGE FACTOR
Age 60 study. Part 1: Bibliographic database
[AD-A286245] p 1446 N95-22027
Age 60 study. Part 2: Airline pilot age and performance. A review of the scientific literature
[AD-A286246] p 1447 N95-22040

AGGREGATES
Ultra-high aggregate bandwidth two-dimensional multiple-wavelength diode laser arrays
[AD-A280098] p 1372 N95-21019

AGING (BIOLOGY)
Age 60 study. Part 1: Bibliographic database
[AD-A286245] p 1446 N95-22027
Age 60 study. Part 2: Airline pilot age and performance. A review of the scientific literature
[AD-A286246] p 1447 N95-22040

AGING (MATERIALS)
A test of the Arrhenius extrapolation assumption for a nitrile rubber
[DE94-017337] p 1263 N95-19926
Thermodynamic characterization of new palladium alloy tritides
[DE94-018430] p 1579 N95-20028
The 29th MIL-HDBK-17 Polymer Matrix Composites Coordination Group Meeting
[AD-A279917] p 1269 N95-20578
Aging tests of ethylene contaminated argon/ethane
[DE95-002526] p 1282 N95-20899
Properties of aged metal tritides
[DE95-001787] p 1243 N95-21440

AGREEMENTS
Technology transfer: Improving the use of cooperative R/D agreement at DOE's contractor-operated laboratories. Report to Congressional requesters
[GAO/RCED-94-91] p 1586 N95-22403
Space systems technology working group: Executive report
[AD-A285778] p 1217 N95-22413

AH-64 HELICOPTER
Using the backward transfer paradigm to validate the AH-64 Simulator Training Research Advanced Testbed for Aviation
[AD-A285758] p 1215 N95-19931

AIR CONDITIONING
Proceedings of the 1993 Non-Fluorocarbon Insulation, Refrigeration and Air Conditioning Technology Workshop
[DE94-018333] p 1285 N95-20194

AIR DATA SYSTEMS
Response of the B-1B air data sensor to simulated dust cloud environments
[AD-A286134] p 1213 N95-22036

AIR FLOW
Vapor generator wand
[NASA-CASE-LAR-15058-1] p 1215 N95-20080
Fire experiments in a two dimensional rack storage: BRANDFORSK-project 701-917
[PB95-131538] p 1241 N95-21179

AIR LAND INTERACTIONS
Remote-sensing based technique to account for sub-grid scale variability of land surface properties
[NASA-TM-110501] p 1390 N95-22110

AIR MASSES
Indirect global warming effects of ozone and stratospheric water vapor induced by surface methane emission
[DE94-019016] p 1402 N95-20353

AIR NAVIGATION
Modular CNI avionics system p 1213 N95-20659
The personal aircraft: Status and issues
[NASA-TM-109174] p 1200 N95-20688
Assessment of a non-dedicated GPS receiver system for precise airborne attitude determination
[DE94-019309] p 1205 N95-21520
A real-time algorithm for integrating differential satellite and inertial navigation information during helicopter approach
[NASA-CR-197409] p 1205 N95-21891
Recommendation on transition from primary/secondary radar to secondary-only radar capability
[AD-A286279] p 1308 N95-22005

AIR POLLUTION
Calculation methods for criteria air pollutant emission inventories
[AD-A284675] p 1400 N95-19964
Proceedings of the 1993 Non-Fluorocarbon Insulation, Refrigeration and Air Conditioning Technology Workshop
[DE94-018333] p 1285 N95-20194
An application of wavelet transform for decomposition of millimeter-wave spectroscopic signals
[DE94-018366] p 1402 N95-20247
Energy impacts of controlling carbon dioxide emissions from an integrated gasification/combined-cycle system
[DE94-016878] p 1403 N95-20478
Explicit methods for stiff ODEs from atmospheric Chemistry
[PB95-135794] p 1404 N95-21034
Energy and environmental issues and international opperation in Asia
[DE94-796596] p 1404 N95-21143
Ozone quality control measurements in the Dutch National Air Quality Monitoring Network
[PB95-131900] p 1405 N95-21329
Monitoring activities in the framework of the Dutch National Air Quality Monitoring Network in 1994
[PB95-131884] p 1406 N95-21351
New concepts for refrigerant leak detection and mixture measurement
[DE94-018967] p 1287 N95-21559
Removal of CO2 in closed loop off-gas treatment systems
[DE94-019259] p 1407 N95-21617
Comparison of HFC-134a and the ternary blend, Suva MP39, as replacements for the refrigerant, CGC-12
[MRL-GD-0051] p 1287 N95-21625
Air pollution caused by fireworks during the turn of the year 1992-1993
[PB95-135265] p 1409 N95-21718
Ozone-depleting-substance control and phase-out plan
[DE95-001647] p 1409 N95-21722
Derivation of preliminary maximum permissible concentrations of volatile compounds in air
[PB95-107447] p 1410 N95-22125
Assessment of the atmospheric hazards and risks of new chemicals: Procedures to estimate hazard potentials
[PB95-107488] p 1410 N95-22186
Gas-phase photocatalytic oxidation: Cost comparison with other air pollution control technologies
[DE95-000241] p 1410 N95-22278
Urban air carcinogens and their effects on health
[DE95-002259] p 1447 N95-22285
Current concepts on airborne particles and health
[DE95-002260] p 1447 N95-22287
Micrometeorological methods for measurements of mercury emissions over contaminated soils
[DE94-017679] p 1411 N95-22342

AIR PURIFICATION
Laboratory evaluation of a reactive baffle approach to NOx control
[AD-A283802] p 1400 N95-19921

AIR QUALITY
Atmospheric stability and its influence on air quality in small communities in northern Sweden
[PB95-131652] p 1405 N95-21181
Evaluation of the technical performance of the Duttch National Air Quality Monitoring Network in 1992
[PB95-131892] p 1405 N95-21327
Ozone quality control measurements in the Dutch National Air Quality Monitoring Network
[PB95-131900] p 1405 N95-21329
Monitoring activities in the framework of the Dutch National Air Quality Monitoring Network in 1994
[PB95-131884] p 1406 N95-21351
Ozone-depleting-substance control and phase-out plan
[DE95-001647] p 1409 N95-21722

AIR SAMPLING
Effects of meteorology on concentrations of acid aerosols
[PB94-209749] p 1400 N95-19965

AIR TRAFFIC CONTROL
Crew aiding and automation: A system concept for terminal area operations, and guidelines for automation design
[NASA-CR-4631] p 1204 N95-19950
Data link terminal DLT document
[PB95-110805] p 1205 N95-21369
Recommendation on transition from primary/secondary radar to secondary-only radar capability
[AD-A286279] p 1308 N95-22005

AIR TRANSPORTATION
Census US civil aircraft calendar year 1993
[AD-A286309] p 1199 N95-20091
Commuter/air taxi ditchings and water-related impacts that occurred from 1979 to 1989
[AD-A285691] p 1202 N95-20275
The personal aircraft: Status and issues
[NASA-TM-109174] p 1200 N95-20688

AIR WATER INTERACTIONS
The Surface Wave Dynamics Experiment (SWADE): A retrospective look at the wave modeling activities
[AD-A285612] p 1431 N95-19895
Mississippi State University Center for Air Sea Technology FY 1993 and FY 1994 research program in Navy ocean modeling and prediction
[AD-A286322] p 1432 N95-20209
The vertical distribution of heating in the tropical atmosphere
[AD-A285934] p 1429 N95-20391
Boundary layer cloud studies in support of ASTEX
[AD-A285947] p 1429 N95-20395
A study of westerly wind bursts preceding the 1991-1992 El Nino
[AD-A286570] p 1429 N95-20826
Modelling of microwave propagation and clutter in a maritime environment p 1295 N95-20938
The structure of turbulence and other motions beneath an air-water interface
[AD-A279838] p 1434 N95-21293
High resolution properties of the equatorial Pacific marine atmospheric boundary layer from lidar and radiosonde observations
[DE95-001028] p 1426 N95-21875
A numerical study of wind forcing effects on the California Current System
[AD-A286205] p 1435 N95-21880
The dynamic role of ridges in a beta-plane channel. Towards understanding the dynamics of large scale circulation in the Southern Ocean
[AD-A279390] p 1435 N95-21943
Proceedings: International Symposium on Global Change (IGBP)
[DE94-765351] p 1410 N95-22219
SAR-related stress variability in the Marine Atmospheric Boundary Layer (MABL)
[AD-A286462] p 1431 N95-22393

AIRBORNE EQUIPMENT
Passive range measurement system
[AD-D016222] p 1544 N95-21100
Lidar technologies for airborne and space-based applications
[DE95-002954] p 1302 N95-21448
Assessment of a non-dedicated GPS receiver system for precise airborne attitude determination
[DE94-019309] p 1205 N95-21520

AIRBORNE RADAR
Classical analysis methods for designing and developing downlooking radars
[AD-A285760] p 1302 N95-21405
AN/APS-137 Forward Looking Airborne Radar (FLAR) evaluation, Fall 1992 experiment
[AD-A279526] p 1306 N95-21686

AIRCRAFT ACCIDENTS
Commuter airplane accident data analysis
[AD-A286315] p 1202 N95-20174
Commuter/air taxi ditchings and water-related impacts that occurred from 1979 to 1989
[AD-A285691] p 1202 N95-20275
Age 60 study. Part 2: Airline pilot age and performance. A review of the scientific literature
[AD-A286246] p 1447 N95-22040

Analysis of test criteria for specifying foam firefighting agents for aircraft rescue and firefighting
[AD-A286381] p 1203 N95-22352
Forecasting aircraft mishaps using monthly maintenance reports
[AD-A286049] p 1203 N95-22417

AIRCRAFT COMMUNICATION
Crew aiding and automation: A system concept for terminal area operations, and guidelines for automation design
[NASA-CR-4631] p 1204 N95-19950

AIRCRAFT CONSTRUCTION MATERIALS
Round-robin comparison of heat release apparatus
[AD-A285831] p 1363 N95-20031

AIRCRAFT CONTROL
Crew aiding and automation: A system concept for terminal area operations, and guidelines for automation design
[NASA-CR-4631] p 1204 N95-19950

AIRCRAFT DESIGN
F-16XL interview with Marta Bohn-Meyer
[NASA-TM-110505] p 1200 N95-19996
Parallel calculation of sensitivity derivatives for aircraft design using automatic differentiation
[NASA-TM-110103] p 1206 N95-20370
Why do airlines want and use thrust reversers? A compilation of airline industry responses to a survey regarding the use of thrust reversers on commercial transport airplanes
[NASA-TM-109158] p 1203 N95-20706

AIRCRAFT ENGINES
Turbine design and application
[NASA-SP-290] p 1214 N95-22341

AIRCRAFT EQUIPMENT
FASTPACK: Optimized solutions for modular avionics derived from a parametric study. Part 1: Platform features p 1208 N95-20634
Immersion/two phase cooling p 1211 N95-20648
Composite cases for airborne electronic equipment: A technology study and EMC p 1212 N95-20655
Lightweight electronic enclosures using composite materials p 1213 N95-20656
Modular supplies for a distributed architecture --- avionics packaging p 1213 N95-20657
Modular CNI avionics system p 1213 N95-20659
TIM-SCT cable testing protocol
[AD-A286633] p 1207 N95-20772
Design of a controller for a flexible pointing system using H(infinity) synthesis
[AD-A286572] p 1481 N95-20828
Fuzzy clustering of facial form for prototyping environmental protection equipment
[DE94-014657] p 1454 N95-22466

AIRCRAFT FUELS
Analysis of test criteria for specifying foam firefighting agents for aircraft rescue and firefighting
[AD-A286381] p 1203 N95-22352

AIRCRAFT INDUSTRY
Public-sector aviation issues: Graduate research award papers, 1992-1993
[PB94-217478] p 1199 N95-19967

AIRCRAFT LANDING
Super-heavy aircraft study
[AD-A279602] p 1215 N95-19955
F-15 resource tape
[NASA-TM-110502] p 1206 N95-19994
Minima reduction simulation test results
[AD-A285626] p 1204 N95-21148

AIRCRAFT MAINTENANCE
Why do airlines want and use thrust reversers? A compilation of airline industry responses to a survey regarding the use of thrust reversers on commercial transport airplanes
[NASA-TM-109158] p 1203 N95-20706
Damage tolerant repair techniques for pressurized aircraft fuselages
[AD-A286298] p 1199 N95-22046
Forecasting aircraft mishaps using monthly maintenance reports
[AD-A286049] p 1203 N95-22417

AIRCRAFT MANEUVERS
F-15 resource tape
[NASA-TM-110502] p 1206 N95-19994

AIRCRAFT MODELS
Effects of yaw and pitch motion on model attitude measurements
[NASA-TM-4641] p 1368 N95-22109

AIRCRAFT NOISE
Acoustic climb to cruise test
[NASA-TM-110504] p 1206 N95-20155
Effect of atmospheric pressure on measured aircraft noise levels
[PB95-130423] p 1207 N95-21425

AIRCRAFT PARTS
Electrochemical impedance pattern recognition for detection of hidden chemical corrosion on aircraft components
[AD-A285998] p 1239 N95-20716

AIRCRAFT PERFORMANCE
F-15 resource tape
[NASA-TM-110502] p 1206 N95-19994
Naval aviation: F-14 upgrades are not adequately justified. Report to Congressional Committees
[AD-A286338] p 1206 N95-20212
Why do airlines want and use thrust reversers? A compilation of airline industry responses to a survey regarding the use of thrust reversers on commercial transport airplanes
[NASA-TM-109158] p 1203 N95-20706

AIRCRAFT PILOTS
Effects of bifocal and progressive-addition corrective lenses on aviator target-detection performance
[AD-A279698] p 1442 N95-20710
Age 60 study. Part 1: Bibliographic database
[AD-A286245] p 1446 N95-22027
Age 60 study. Part 2: Airline pilot age and performance. A review of the scientific literature
[AD-A286246] p 1447 N95-22040

AIRCRAFT POWER SUPPLIES
Photovoltaic electric power applied to Unmanned Aerial Vehicles (UAV) p 1321 N95-20530

AIRCRAFT SAFETY
Commuter airplane accident data analysis
[AD-A286315] p 1202 N95-20174
Commuter/air taxi ditchings and water-related impacts that occurred from 1979 to 1989
[AD-A285691] p 1202 N95-20275
Fuselage burnthrough from large exterior fuel fires
[AD-A286295] p 1203 N95-22318
Forecasting aircraft mishaps using monthly maintenance reports
[AD-A286049] p 1203 N95-22417

AIRCRAFT SPECIFICATIONS
Analysis of test criteria for specifying foam firefighting agents for aircraft rescue and firefighting
[AD-A286381] p 1203 N95-22352

AIRCRAFT STRUCTURES
Corrosion of aircraft materials: Correlation between nanometer scale and macroscopic structural damage parameters
[AD-A285930] p 1252 N95-20299
Eddy current for detecting second-layer cracks under installed fasteners
[AD-A279871] p 1382 N95-20414
Electrochemical impedance pattern recognition for detection of hidden chemical corrosion on aircraft components
[AD-A284998] p 1253 N95-20481

AIRCRAFT SURVIVABILITY
Commuter airplane accident data analysis
[AD-A286315] p 1202 N95-20174
Commuter/air taxi ditchings and water-related impacts that occurred from 1979 to 1989
[AD-A285691] p 1202 N95-20275

AIRFOILS
Public-sector aviation issues: Graduate research award papers, 1992-1993
[PB94-217478] p 1199 N95-19967
F-16XL interview with Marta Bohn-Meyer
[NASA-TM-110505] p 1200 N95-19996
Computation of transonic flow on composite overlapping grids in 2 D
[PB95-131348] p 1353 N95-21132
Unstructured-grid large-eddy simulation of flow over an airfoil p 1202 N95-22448

AIRFRAMES
Lift enhancement device
[AD-D016522] p 1201 N95-21864

AIRLINE OPERATIONS
Public-sector aviation issues: Graduate research award papers, 1992-1993
[PB94-217478] p 1199 N95-19967
Test and evaluation report for the Manual Domestic Passive Profiling System (MDPPS)
[AD-A286312] p 1202 N95-20093

AIRPORT SECURITY
Test and evaluation report for the Manual Domestic Passive Profiling System (MDPPS)
[AD-A286312] p 1202 N95-20093

AIRPORTS
Test and Evaluation Plan (TEP) for Improvised Explosive Device Screening Systems (IEDSS)
[AD-A286382] p 1203 N95-22319
Analysis of test criteria for specifying foam firefighting agents for aircraft rescue and firefighting
[AD-A286381] p 1203 N95-22352

AIRSHIPS
CALIOPE and TAISIR airborne experiment platform
[DE94-018328] p 1310 N95-22299

AIRSPEED
A real-time algorithm for integrating differential satellite and inertial navigation information during helicopter approach
[NASA-CR-197409] p 1205 N95-21891

AIRY FUNCTION
Solutions of D(sup n)D(sup m)f=0
[PB95-110839] p 1487 N95-19916

ALBUMINS
Separation of proteins by convective electrophoresis through a porous membrane
[PB95-127130] p 1248 N95-22373

ALCOHOLS
Bioconversion of coal derived synthesis gas to liquid fuels
[DE94-017381] p 1282 N95-19927
Investigation of syngas interaction in alcohol synthesis catalysts
[DE94-018784] p 1236 N95-20349
An improved and facile method for the synthesis of 1,1-bis(4-hydroxyphenyl) 2-phenylethylene and its derivatives
[DE95-001125] p 1240 N95-20836

ALEXANDRITE
Scaling of solid state lasers for satellite power beaming applications
[DE94-016366] p 1368 N95-19986

ALGAE
Effects of increased UV-B radiation on phytoplankton: A preliminary study and research programme
[PB95-133732] p 1439 N95-21884

ALGEBRA
Algebraic semantics of message sequence charts
[PB95-110581] p 1288 N95-19890
Non interleaving process algebra
[PB95-110607] p 1486 N95-19892
General conservative extension theorem in process algebra
[PB95-110656] p 1487 N95-19902
Process algebra with partial choice
[PB95-110714] p 1487 N95-19907
Real time process algebra with infinitesimals
[PB95-110623] p 1488 N95-20055
The design of a parallel, dense linear algebra software library: Reduction to Hessenberg, tridiagonal, and bidiagonal form
[DE94-018123] p 1491 N95-20701
The PROSAIC Laplace and Fourier Transform
[DE95-002225] p 1492 N95-21266
Regularity of BPa-systems is decidable
[PB95-135489] p 1468 N95-21619
Adjunctions
[PB95-134078] p 1494 N95-21868
Performance analysis and true concurrency semantics
[PB95-134086] p 1478 N95-21869
Graded dual of the non-commutative universal Leibniz Hopf algebra zeta
[PB95-134532] p 1494 N95-21955
Discrete algebraic Riccati equation and linear matrix inequality
[PB95-133575] p 1484 N95-22139
Maximum weighted matching for high index differential algebraic equations
[PB95-135075] p 1496 N95-22359

ALGORITHMS
O(log2 n) time efficient parallel factorization of dense, sparse separable, and banded matrices
[NASA-CR-197356] p 1473 N95-19885
K(1,3)-free and W(4)-free graphs
[PB95-110573] p 1456 N95-19889
Introduction to the FIRE engine: A C++ toolkit for Finite automata and Regular Expressions
[PB95-110599] p 1456 N95-19891
Dominoes
[PB95-110680] p 1456 N95-19905
Toward a design for the ITER plasma shape and stability control system
[DE94-017516] p 1548 N95-20037
ILIAS: A sequential language for parallel matrix computations
[PB95-110631] p 1473 N95-20056
Truly distribution-independent algorithms for the N-body problem
[DE94-014238] p 1458 N95-20136
A domain decomposition scheme for Eulerian shock physics codes
[DE94-015739] p 1488 N95-20141
Parallel solid mechanics codes at Sandia National Laboratories
[DE94-015770] p 1474 N95-20152
Adaptive path planning for flexible manufacturing
[DE94-016561] p 1459 N95-20284
Using local optimality criteria for efficient information retrieval with redundant information filters
[AD-A279603] p 1587 N95-20302

Radiative forcing calculations for CH3Cl
[DE94-019018] p 1402 N95-20355
Hybrid model in general geometry
[DE95-002614] p 1553 N95-20437
Computing methods for the approximate solution of time dependent problems
[AD-A286007] p 1491 N95-20719
COYOTE II: A finite element computer program for nonlinear heat conduction problems. Part 1: Theoretical background
[DE95-002587] p 1463 N95-20887
Real-time reconfiguration study
[AD-A286060] p 1464 N95-20910
Superresolution direction finding algorithms for the characterisation of multi-moded HF signals
p 1299 N95-20958
Proceedings of the Fourth International Workshop on Inductive Logic Programming (ILP-94)
[PB95-135273] p 1464 N95-21003
Correctness of some algorithms to generate finite automata for regular expressions
[PB95-127551] p 1465 N95-21022
Finding all minimal separators of a graph
[PB95-127585] p 1491 N95-21023
Attempt to interpret the self-organizing mapping physiologically
[PB95-127783] p 1438 N95-21112
Project Whitefeather
[DE94-016575] p 1415 N95-21184
A divide-and-conquer method for tridiagonalizing symmetric matrices with repeated eigenvalues
[DE95-002918] p 1476 N95-21257
Computing near-optimal schedules
[PB95-132072] p 1466 N95-21269
Real-time dynamic simulator for the Topaz II reactor power system
[DE95-001604] p 1535 N95-21278
Synthetic aperture radar processing with polar formatted subapertures
[DE95-001830] p 1302 N95-21305
Accurate solution algorithms for incompressible multiphase flows
[DE95-002727] p 1353 N95-21317
A framework for symmetric band reduction and tridiagonalization
[DE95-002919] p 1476 N95-21341
Proposal for a tutorial on Minimal Length Encoding (MLE) in molecular biology
[DE94-015076] p 1438 N95-21376
Unknown-terrains navigation of a mobile robot using an array of sonars
[DE94-017902] p 1482 N95-21385
A mixed time integration method for large scale acoustic fluid-structure interaction
[DE94-018327] p 1354 N95-21387
An image cancellation approach to depth-from-focus
[DE94-019312] p 1544 N95-21392
VLUGR3: A vectorizable adaptive grid solver for PDEs in 3D. 1: Algorithmic aspects and applications
[PB95-135729] p 1467 N95-21435
Distribution-independent hierarchical N-body methods
[DE95-001686] p 1493 N95-21439
Approximation algorithms for the general and the asymmetric stacker-crane problems
[PB95-132098] p 1493 N95-21468
Utilizing artificial neural networks in network flow analysis: An annotated bibiliography
[DE95-002453] p 1482 N95-21522
Numerical and symbolic algorithms for application and specific signal processing
[AD-A279802] p 1305 N95-21576
A new Krylov-subspace method for symmetric indefinite linear systems
[DE95-001826] p 1355 N95-21726
Learning algorithms for feedforward networks based on finite samples
[DE95-001739] p 1483 N95-21741
QMRPACK user's guide
[DE95-001770] p 1469 N95-21744
Science with High Spatial Resolution Far-Infrared Data
[NASA-CR-197353] p 1595 N95-21749
Constraints as a destriping tool for Hires images
p 1593 N95-21756
A HIRES analysis of the FIR emission of supernova remnants p 1594 N95-21770
Application of MCM image construction to IRAS comet observations p 1594 N95-21772
A massively parallel algorithm for grand canonical Monte Carlo computer simulation with the short-ranged Lennard-Jones potential
[DE94-010396] p 1477 N95-21843
Compositional approach to sequential consistency and lazy caching
[PB95-134110] p 1455 N95-21871
A real-time algorithm for integrating differential satellite and inertial navigation information during helicopter approach
[NASA-CR-197409] p 1205 N95-21891
A syncopated leap-frog algorithm for orbit consistent plasma simulation of materials processing reactors
[DE95-000954] p 1561 N95-21922
Massively-parallel computational fluid dynamics
[AD-A279389] p 1355 N95-21942
On Markov Chain Monte Carlo acceleration
[AD-A279393] p 1499 N95-21945
Balanced 0, + or - matrices. Part 2: Recognition algorithm
[AD-A279156] p 1470 N95-21974
Fast algorithms for transport models
[DE95-001702] p 1470 N95-21992
Absorbing boundary condition for floating two-dimensional objects in current and waves
[PB95-132882] p 1356 N95-22063
A Davis-Putnam program and its application to finite-order model search: Quasigroup existence problems
[DE95-003014] p 1471 N95-22077
Full potential multiple scattering theory
[DE95-003197] p 1576 N95-22084
Tom Thumb algorithm for planning simple vehicle motions
[PB95-107553] p 1484 N95-22156
Real time system for practical acoustic monitoring of global ocean temperature
[AD-A286435] p 1436 N95-22209
Inverse and control problems in electromagnetics
[AD-A286438] p 1310 N95-22250
Learning maneuvers using neural network models
[AD-A286470] p 1486 N95-22267
An improved Monte Carlo algorithm for simulating grain growth
[DE94-017903] p 1578 N95-22272
Fast parallel tree codes for gravitational and fluid dynamical N-body problems
[AD-A286480] p 1358 N95-22290
A new parallel method for molecular dynamics simulation of macromolecular systems
[DE94-018621] p 1529 N95-22315
Maximum weighted matching for high index differential algebraic equations
[PB95-135075] p 1496 N95-22359
Experimental evaluation of dynamic data allocation strategies in a distributed database with changing workloads
[NASA-CR-195024] p 1456 N95-22431
Direct numerical simulations of on-demand vortex generators: Mathematical formulation
p 1361 N95-22452

ALIGNMENT
Testing of the SAIC facets on the stretched-membrane dish
[DE95-001831] p 1393 N95-20864
Issues in multi-bunch emittance preservation in the NLC
[DE95-002894] p 1534 N95-21253
Object recognition by alignment using invariant projections of planar surfaces
[AD-A279841] p 1468 N95-21495
Magnetostrictive motor system
[AD-D016484] p 1333 N95-21901
Design, fabrication, and characterization of reflective diffractive optical elements in Si for free-space optical interconnects
[AD-A286416] p 1547 N95-22205
Target alignment in the National Ignition Facility
[DE94-015559] p 1540 N95-22469

ALKALI HALIDES
The dynamics of formation and evaporation of mixed alkali halide nanocrystals: A case of comparable lattice energies
[AD-A285052] p 1567 N95-20483
Identification of resonant, two-electron, and inter-atomic features in K and L23 NEXAFS spectra
[AD-A285374] p 1513 N95-20554

ALKALI METALS
The dynamics of formation and evaporation of mixed alkali halide nanocrystals: A case of comparable lattice energies
[AD-A285052] p 1567 N95-20483

ALKALIES
Recent photoabsorption measurements in the rare gases and alkalis in the 3 to 15 keV photon energy region
[DE94-019278] p 1521 N95-21406
Alkali element depletion by core formation and vaporization on the early Earth p 1421 N95-21804
Resonant charge transfer in hyperthermal atomic and molecular ion-surface collisions
[AD-A284937] p 1530 N95-22471

ALKALINITY
Nickel hydroxide electrodes in reduced-alkalinity electrolytes
[DE95-002333] p 1326 N95-20814

ALKANES
Scanning tunneling microscopy studies of self-assembled monolayers of alkanethiols on gold
[AD-A279910] p 1253 N95-20577
Studies of the n-alkane/water interface by total internal reflection second harmonic generation
[AD-A279473] p 1245 N95-21827

ALKENES
Hydrogenation of nitriles on a well-characterized nickel surface: From surface science studies to liquid phase catalytic activity measurements
[DE94-018184] p 1259 N95-21707

ALKYL COMPOUNDS
Polyurethane-acrylic interpenetrating polymer network acoustic damping material
[AD-D016572] p 1266 N95-20294
Novel reagents for chemical vapor deposition of intermetallic alloys
[AD-A286562] p 1271 N95-20815
Restricted mass transport effects on free radical reactions
[DE94-018136] p 1217 N95-21706
Towards tailored interphase formation utilizing surface-bound benzylsulfonium salts as cationic initiators
[AD-A286461] p 1280 N95-22259

ALLOYING
Thermodynamic characterization of new palladium alloy tritides
[DE94-018430] p 1579 N95-20028
Development of superplasticity in 5083 aluminum with additions of Mn and Zr
[DE94-017474] p 1251 N95-20090
Enhancement of corrosion resistance and mechanical properties of light-weight metals through the use of graded nonequilibrium microstructures
[AD-A286320] p 1251 N95-20178
2nd International ADI seminar
[PB95-127734] p 1255 N95-21108
Nitrogen alloyed martensitic steels
[PB95-127791] p 1255 N95-21128
Tribology and surface mechanical properties of excimer laser nitrided titanium
[DE95-002751] p 1255 N95-21238
Atom probe field ion microscopy of type 308 CRE stainless steel welds
[DE94-019162] p 1261 N95-22127

ALLYL COMPOUNDS
Radiation-induced modifications of allylamino-substituted polyphosphazenes
[AD-A279694] p 1268 N95-20428

ALPHA PARTICLES
A new alpha particle diagnostic using knock-on ion tails
[DE94-015856] p 1553 N95-20402
Radioactive check sources for alpha and beta sensitive radiological instrumentation
[DE94-016477] p 1366 N95-21138
Experimental investigations of electron capture from atomic hydrogen and deuterium by alpha particles
[DE95-002138] p 1523 N95-21587
Intense proton beam source for ITER neutral-beam spectroscopy diagnostics
[DE94-018092] p 1560 N95-21668

ALTERNATING CURRENT
Power-law resistivity, magnetic relaxation and ac susceptibility
[DE94-016893] p 1501 N95-20241
A low temperature, ultrahigh vacuum, microwave-frequency-compatible scanning tunneling microscope
[AD-A279869] p 1365 N95-20413
Linear and nonlinear spectroscopy with the tunable AC scanning tunneling microscope
[AD-A285751] p 1241 N95-21217
Small cavity nonresonant tunable microwave-frequency alternating current scanning tunneling microscope
[AD-A285752] p 1328 N95-21218
AC magnetic response of YBa2CuO7 with Y2BaCuO5 inclusions and of single-crystal YBa2Cu3O7: A comparative study
[PB94-207917] p 1577 N95-22166

ALTERNATIVES
Mercury usage and alternatives in the electrical and electronics industries
[PB94-165362] p 1312 N95-19966
The advanced technology crew station: Development and validation of a workload assessment technique for cockpit function allocation
[AD-A279544] p 1453 N95-21691

ALTITUDE TESTS
Temperature effects on acoustic interactions between altitude test facilities and jet engine plumes
[NASA-CR-197638] p 1504 N95-21170
ALUMINATES
High performance YBCO films
[AD-A279560] p 1276 N95-21695
ALUMINIDES
Third Intermetallic Matrix Composites Symposium, volume 350
[NASA-TM-110059] p 1225 N95-20001
Fabrication and properties of alumina matrix composites containing nickel aluminide reinforcements
[DE94-018703] p 1250 N95-20044
Oxide formation on NbAl3 and TiAl due to ion implantation of O-18
[DE94-017874] p 1252 N95-20365
Processing and applications of iron aluminides
[DE94-017855] p 1253 N95-20673
Impact behavior of FeAl alloy FA-350
[DE94-018128] p 1254 N95-20705
Processing and mechanical properties of laminar Al2O3-Ni3Al composites
[DE94-019332] p 1230 N95-21481
Weldability of iron aluminides
[DE94-019114] p 1257 N95-21555
Consequences of oscillatory potentials and angular forces in transition metals and their aluminides
[DE94-019127] p 1258 N95-21600
The development of a super-alpha2 titanium aluminide alloy consolidated by rapid omnidirectional compaction
[AD-A279254] p 1260 N95-21986
Tensile and impact properties of iron-aluminum alloys
[DE94-017750] p 1263 N95-22346
ALUMINUM
A computational study of projectile shape dependence on phase change phenomena with comparisons to experimental data
[DE95-000740] p 1384 N95-20077
A computational study of projectile melt in impact with typical Whipple shields
[DE94-016454] p 1385 N95-20237
Corrosion of aircraft materials: Correlation between nanometer scale and macroscopic structural damage parameters
[AD-A285930] p 1252 N95-20299
The design and manufacturing development of an active silicon substrate MCM p 1211 N95-20645
Polyurethane self-priming topcoats
[AD-D016204] p 1274 N95-21154
Effect of laser radiation on carbon fibre/epoxy composites
[PB95-133526] p 1232 N95-22096
ALUMINUM ALLOYS
Processing and characterization of Ni-Al-Fe-B shape-memory alloy wires produced by rapid solidification
[DE94-017702] p 1250 N95-20020
Development of superplasticity in 5083 aluminum with additions of Mn and Zr
[DE94-017474] p 1251 N95-20090
Enhancement of corrosion resistance and mechanical properties of light-weight metals through the use of graded nonequilibrium microstructures
[AD-A286320] p 1251 N95-20178
Electrochemical impedance pattern recognition for detection of hidden chemical corrosion on aircraft components
[AD-A284998] p 1253 N95-20481
The processing and mechanical properties of high temperature/high performance composites. Book 7: In-situ measurements of stress and damage
[AD-A279814] p 1227 N95-20583
The mechanical property data base from an Air Force/Industry cooperative test program on advanced aluminum alloys
[AD-A280038] p 1386 N95-20615
Processing and applications of iron aluminides
[DE94-017855] p 1253 N95-20673
Electrochemical impedance pattern recognition for detection of hidden chemical corrosion on aircraft components
[AD-A285998] p 1239 N95-20716
ALCHEMI of Fe-doped B2-ordered NiAl alloys with different doping levels
[DE94-017748] p 1255 N95-20907
Electrochemical impedance spectroscopy of trivalent chromium pre-treated aluminum alloy
[AD-A280093] p 1240 N95-20970
Tribology and surface mechanical properties of excimer laser nitrided titanium
[DE95-002751] p 1255 N95-21238
Processing and mechanical properties of laminar Al2O3-Ni3Al composites
[DE94-019332] p 1230 N95-21481
Consequences of oscillatory potentials and angular forces in transition metals and their aluminides
[DE94-019127] p 1258 N95-21600
Relationship between dendrite coherency and castability of some commercial foundry alloys
[PB95-110243] p 1258 N95-21652
Fracture behavior of the Fe-8Al alloy FAP-Y
[DE95-000956] p 1258 N95-21676
Aircraft corrosion study
[AD-A279527] p 1259 N95-21687
Electronic structure and relative stability of icosahedral superatoms in Al-transition-metal alloys
[DE94-628996] p 1260 N95-21855
Demonstration of multifunctional DNBM corrosion inhibitors in protective coatings for Naval air/weapon systems
[AD-A285869] p 1279 N95-22136
Bulk and defect properties of ordered intermetallics
[DE94-017706] p 1262 N95-22344
Processing of intermetallic materials by reaction synthesis
[DE94-017710] p 1263 N95-22345
Tensile and impact properties of iron-aluminum alloys
[DE94-017750] p 1263 N95-22346
Fracture behavior of laminated discontinuously reinforced aluminum material
[DE94-017307] p 1263 N95-22408
ALUMINUM ARSENIDES
Resonant generation of nonequilibrium phonons in GaAs/AlAs quantum wells via intersubband scattering
[DE95-002338] p 1581 N95-21604
ALUMINUM CHLORIDES
Chemistry and electrochemistry in Lewis acid and superacid ionic liquids
[AD-A279396] p 1246 N95-21931
ALUMINUM GALLIUM ARSENIDE LASERS
Semiconductor laser joint study program with Rome Laboratory
[AD-A285858] p 1369 N95-20379
ALUMINUM GALLIUM ARSENIDES
Analog processing of optical wavefront using integrated guided-wave optics
[AD-A279596] p 1543 N95-20601
Transient photoluminescence measurements on GaAs and AlGaAs double heterostructures
[AD-A279408] p 1575 N95-21916
ALUMINUM NITRIDES
Synthesis and studies of organometallic precursors for CVD of thin film electronic materials
[AD-A285834] p 1223 N95-20033
ALUMINUM OXIDES
Comparison of the dynamic fatigue behavior of two monolithic SiC and an Al2O3/SiC composite
[DE94-017751] p 1225 N95-20022
Properties of whisker-reinforced ceramics
[DE94-017759] p 1264 N95-20024
Fabrication and properties of alumina matrix composites containing nickel aluminide reinforcements
[DE94-018703] p 1250 N95-20044
Reactions and microstructure at ceramic/metal interfaces
[DE94-014287] p 1265 N95-20138
Structural performance of cylindrical pressure housings of different ceramic compositions under external pressure loading. Part 1: Isostatically pressed alumina ceramic
[AD-A279669] p 1270 N95-20603
Reactive nanophase oxide additions to melt-processed high-T(sub c) superconductors
[DE95-001470] p 1570 N95-20841
Self-starting femtosecond pulse generation from a Ti:sapphire laser synchronously pumped by a pointing-stabilized mode-locked Nd:YAG laser
[DE94-019319] p 1374 N95-21480
Processing and mechanical properties of laminar Al2O3-Ni3Al composites
[DE94-019332] p 1230 N95-21481
Light output and radiation damage in a YAlO3:Ce crystal
[DE94-016815] p 1545 N95-21643
Directional solidification of the alumina-zirconia ceramic eutectic system
[DE95-001677] p 1277 N95-21735
Creep behavior in SiC whisker-reinforced alumina composite
[DE95-001071] p 1231 N95-21776
Oxidation behavior of aluminum nanopowders
[DE95-002721] p 1260 N95-21926
Structural performance of cylindrical pressure housings of different ceramic compositions under external pressure loading. Part 4: Silicon carbide particulate reinforced alumina ceramic
[AD-A286299] p 1279 N95-22047
Aluminium oxide targets after ballistic impact; fragmentation of the ceramic and the projectile
[PB95-133625] p 1388 N95-22097
Acid-site characterization of water-oxidized alumina films by near-edge x-ray absorption and soft x-ray photoemission
[DE95-003355] p 1247 N95-22234
Measurement of residual stresses on ceramic materials with high spatial resolution
[DE94-017889] p 1280 N95-22270
ALUMINUM SILICATES
A transmission electron microscope characterization of sodium sulfate hot corrosion of silicon carbide fiber-reinforced lithium aluminosilicate glass-ceramic matrix composite
[AD-A286164] p 1231 N95-22038
ALUMINUM-LITHIUM ALLOYS
The mechanical property data base from an Air Force/Industry cooperative test program on advanced aluminum alloys
[AD-A280038] p 1386 N95-20615
AMBIENCE
Effects of meteorology on concentrations of acid aerosols
[PB94-209749] p 1400 N95-19965
Ambient noise and surface wave dissipation in the ocean
[AD-A279650] p 1432 N95-20303
Ultraviolet emission from rocket motor plumes
[DSTO-TR-0002] p 1222 N95-21661
AMBIENT TEMPERATURE
Visible and near-IR spectroscopic studies of UC1(4) in a basic ambient temperature melt: The observation of a possible geometric distorted UC1(6)(exp 2-) species and the evidence for the hydrogen-bond in the melt
[DE94-017764] p 1237 N95-20493
Gas-phase photocatalytic oxidation: Cost comparison with other air pollution control technologies
[DE95-000241] p 1410 N95-22278
AMBIPOLAR DIFFUSION
Stellarator transport optimization with self-consistent electric fields
[DE94-019151] p 1559 N95-21581
AMIDES
Responsive copolymers for enhanced petroleum recovery
[DE94-018822] p 1267 N95-20350
AMINES
Hydrogenation of nitriles on a well-characterized nickel surface: From surface science studies to liquid phase catalytic activity measurements
[DE94-018184] p 1259 N95-21707
AMINO ACIDS
New methods for large scale local and global optimization
[AD-A285635] p 1517 N95-21126
AMMONIA
Monitoring activities in the framework of the Dutch National Air Quality Monitoring Network in 1994
[PB95-131884] p 1406 N95-21351
Development of active-transport membrane devices
[DE94-015947] p 1246 N95-21921
AMMONIUM BROMIDES
Responsive copolymers for enhanced petroleum recovery
[DE94-018822] p 1267 N95-20350
AMMONIUM COMPOUNDS
Thermodynamic and NMR studies of solvent effect on enantiomeric recognition for a chiral organiz ammonium cation by chiral diketopyridino-18-Crown-6 type ligands at 25.0 C
[AD-A279893] p 1223 N95-20592
Neutron molelcular spectroscopy: Future prospects
[PB95-130357] p 1518 N95-21227
AMMONIUM NITRATES
An update of corrosion inhibitors for mild steel exposed to 32-0-0 UAN solution
[DE95-001715] p 1263 N95-22396
AMMUNITION
Evaluation of state-of-the-art high speed deluge systems presently in service at various US Army ammunition plants
[AD-A279102] p 1287 N95-21598
AMORPHOUS MATERIALS
Optical multilayers with an amorphous fluoropolymer
[DE94-017693] p 1541 N95-20218
Amorphization of sapphire during ion beam mixing
[DE94-018713] p 1510 N95-20337
A mechanistic model for radiation-induced crystallization and amorphization in U3Si
[DE94-015028] p 1566 N95-20419
Amorphous silicon thin films: The ultimate lightweight space solar cell p 1318 N95-20515
Application of new synchrotron powder diffraction techniques to anomalous scattering from glasses
[DE94-019285] p 1536 N95-21407
Magnetic properties of the three-dimensional Ising model with an interface amorphization
[DE94-628992] p 1278 N95-21885

Surfaces and thin films studied by picosecond ultrasonics
[DE95-001866] p 1506 N95-22071
Surface technology programme
[PB95-132866] p 1262 N95-22174

AMORPHOUS SILICON
Amorphous silicon thin films: The ultimate lightweight space solar cell p 1318 N95-20515
Investigation of the stability and 1.0 MeV proton radiation resistance of commercially produced hydrogenated amorphous silicon alloy solar cells p 1320 N95-20522
Processing and modeling issues for thin-film solar cell devices
[DE94-011895] p 1394 N95-21294

AMOUNT
Analysis of test criteria for specifying foam firefighting agents for aircraft rescue and firefighting
[AD-A286381] p 1203 N95-22352

AMPHIBOLES
D/H ratios and H2O contents of mantle-derived amphibole megacrysts from Dish Hill, California
p 1416 N95-21781
Subduction of hydrated basalt of the oceanic crust: Implications for recycling of water into the upper mantle and continental growth p 1423 N95-21814

AMPLIFICATION
On FEL integral equation and electron energy loss in intermediate gain regime
[DE94-770631] p 1371 N95-20757
Collisional redistribution effects on x ray laser saturation behavior
[DE94-017308] p 1374 N95-21663
Molecular design concept for multi-kilovolt x-ray amplification
[DE95-001763] p 1374 N95-21743
Pre-amplifier with multi-stage feedback
[AD-D016254] p 1336 N95-22418

AMPLIFIER DESIGN
Hybrid high power amplifier
[AD-D016534] p 1326 N95-20730

AMPLIFIERS
Pasotron(TM) technology
[AD-A279994] p 1314 N95-20311
Plasma Electrode Pockels Cells for the Beamlet and NIF lasers
[DE94-016541] p 1557 N95-21166

AMPLITUDE MODULATION
Determination of multiple sound sources
[AD-A286563] p 1504 N95-20823

AMPLITUDES
Effect of cell size on elliptically polarized radar clutter statistics
[AD-A285789] p 1311 N95-22401

ANAEROBES
Anaerobic Treatment of Municipal Solid Waste and Sludge for Energy Production and Recycling of Nutrients
[DE95-700217] p 1315 N95-20369
Microbiology and physiology of anaerobic fermentations of cellulose
[DE95-002899] p 1438 N95-20917

ANALOG CIRCUITS
Solid state research
[AD-A279662] p 1567 N95-20426

ANALOG TO DIGITAL CONVERTERS
Development of a fast sampling system for estimation of impulse responses of mobile radio channels
p 1296 N95-20943
Non-linear A/D converters for integrated silicon smart sensors
[PB94-208402] p 1330 N95-21590
Design of a 10 bit 10k Samples/s low power CMOS ADC
[PB95-110425] p 1455 N95-22018
SEU and SEL response of the Westinghouse 64K E-2PROM, analog devices AD7876 12-bit ADC, and the Intel 82527 Serial Communications Controller
[DE95-003349] p 1334 N95-22086

ANALOGIES
Role of working memory limitations of retrieval
[AD-A280032] p 1448 N95-20007

ANALYSIS (MATHEMATICS)
Transactions of the Eleventh Army Conference on Applied Mathematics and Computing
[AD-A279884] p 1497 N95-22389

ANALYTIC FUNCTIONS
Solutions of D(sup n)D(sup m)f=0
[PB95-110839] p 1487 N95-19916
Sharp determinants
[PB95-111068] p 1488 N95-19944

ANALYTIC GEOMETRY
Classical analysis methods for designing and developing downlooking radars
[AD-A285760] p 1302 N95-21405

ANALYTICAL CHEMISTRY
Time-resolved analytical methods for liquid/solid interfaces
[DE95-002255] p 1240 N95-20780

ANDROMEDA GALAXY
Far-Infrared sources and diffuse emission in M31
p 1593 N95-21761

ANGLE OF ATTACK
T-45A High Angle of Attack Testing: US Naval Test Pilot School 46th Annual Reunion and Symposium
[AD-A284000] p 1207 N95-20466
Pressure measurements on an F/A-18 twin vertical tail in buffeting flow. Volume 1: Wind tunnel test summary
[AD-A279126] p 1202 N95-21877
Effect of juncture fillets on double-delta wings undergoing sideslip at high angles of attack
[AD-A286165] p 1207 N95-22039

ANGLES (GEOMETRY)
Topography of neutron scattering from diblock copolymer film
[DE95-001457] p 1229 N95-20840

ANGULAR DISTRIBUTION
Pair production as a probe of colliding beam size
[DE95-002893] p 1536 N95-21337
Physics of correlated studies
[DE95-001204] p 1581 N95-21842
Angular and charge state distributions of highly charged ions scattered during low energy surface-channeling interactions with Au(110)
[DE95-001348] p 1525 N95-21857
Residual stress analysis in swage autofrettaged thick-walled cylinders by position-sensitive x-ray diffraction techniques
[AD-A286383] p 1388 N95-22320

ANGULAR MOMENTUM
Ion-molecular spiraling collisions and termolecular recombination
[AD-A285633] p 1517 N95-21151
The energetics and dynamics of free radicals, ions, and clusters
[DE94-018101] p 1244 N95-21701

ANGULAR RESOLUTION
An assessment of image reconstruction from balloon-borne and the IRAS data p 1592 N95-21752

ANGULAR VELOCITY
Effects of yaw and pitch motion on model attitude measurements
[NASA-TM-4641] p 1368 N95-22109

ANHYDRIDES
A direct process for preparing semi-crystalline polyimides
[NASA-CASE-LAR-15020-1] p 1268 N95-20407

ANIMALS
Compilation of 1993 annual reports of the Navy ELF Communications System Ecological Monitoring Program
[AD-A279575] p 1408 N95-21699

ANIONS
Spectroscopic studies of glass structure
[DE94-016551] p 1268 N95-20468
A new family of anion receptors and their effects on ion pair dissociation and conductivity of lithium salts in non-aqueous solutions
[DE94-016822] p 1512 N95-20477
New ET-based organic superconductors with the organometallic anion Cu(CF3)4(-)
[DE94-016904] p 1567 N95-20479
The dynamics of formation and evaporation of mixed alkali halide nanocrystals: A case of comparable lattice energies
[AD-A285052] p 1567 N95-20483
An investigation of the applicability of the new ion exchange resin, Reillex(TM)-HPQ, in ATW separations
[DE94-016576] p 1274 N95-21234
Novel fluorine oxidizers
[AD-A279480] p 1284 N95-21678

ANISOTROPY
Elastic anisotropy in hot-pressed Si3N4 composites: Role of in situ (beta)-Si3N4 grains and added (beta)-Si3N4 whiskers
[DE94-018387] p 1226 N95-20027
Mean field analysis of orientation selective grain growth driven by interface-energy anisotropy
[DE94-015797] p 1566 N95-20399
DC potential anomalies caused by a conducting body in an anisotropic conducting half-space
[PB95-127106] p 1291 N95-20775
The processing and mechanical properties of high temperature/high performance composites. Mechanism-based constitutive laws and design, book 1
[AD-A279736] p 1228 N95-20801
S-D hybridization and anisotropy of the optical second harmonic at low frequencies
[AD-A279449] p 1544 N95-20876
Anisotropic structure of homogeneous turbulence subjected to uniform rotation p 1346 N95-21059
Modelling anisotropy and backscatter effects in the subgrid scale stress tensor p 1349 N95-21077
Ultraviolet laser emission properties of Ce(3+)-doped LiSrAlF6
[DE94-016364] p 1372 N95-21135
Anisotropic transport properties of BSCCO single crystals and Ag-clad tapes in high magnetic fields
[DE95-000938] p 1575 N95-21936
Dielectric mixtures with arbitrarily anisotropic components: Focus on special gyrotropic effects
[PB95-127015] p 1311 N95-22363

ANNEALING
Enhancement of creep resistance of a sintered S3N4 ceramic by microwave annealing
[DE94-017698] p 1265 N95-20220
Electron-irradiated two-terminal, monolithic InP/Ga0.47In0.53As tandem solar cells and annealing of radiation damage p 1319 N95-20519
Radiation effects on p+n InP junctions grown by MOCVD p 1319 N95-20520
Annealing of irradiated n+p InP buried homojunctions
p 1320 N95-20524
Photoluminescence under pressure and annealing of nitrogen-doped ZnSe
[DE95-002355] p 1568 N95-20630
High performance YBCO films
[AD-A286567] p 1326 N95-20824
Defect production and recombination during low-energy ion processing
[DE95-001827] p 1572 N95-21304
Effect of annealing temperature on the texture of rolled tantalum and tantalum-10 wt % tungsten
[DE95-002702] p 1262 N95-22308

ANNIHILATION REACTIONS
D0 quantum chromodynamics: A compilation of results presented at DPF 1994
[DE95-000838] p 1510 N95-20344
High energy photon-photon collisions
[DE94-017494] p 1532 N95-20388
Evidence for t(bar t) production at the Tevatron: Statistical significance and cross section
[DE95-002524] p 1515 N95-20897
Charmonium production, b quark and B meson production and b(bar b) correlations at CDF
[DE95-002525] p 1515 N95-20898
Measuring A(sub b) with polarized beams at SLC
[DE95-002865] p 1519 N95-21248
The diphoton production rate in (bar p)p collisions at the square root of s = 1800 GeV
[DE95-000559] p 1522 N95-21497
Charge density of fractional charged quasiparticles in the composite fermion picture
[DE94-018122] p 1524 N95-21703
Uniform upper bounds in the Froehlich polaron theory
[DE94-628998] p 1525 N95-21860
Tests of structure functions using lepton pairs: W-charge asymmetry at CDF
[DE95-000560] p 1527 N95-22122
Electroweak boson pair production in p(-p) collisions at the square root of s = 1.8 TeV
[DE95-000725] p 1527 N95-22194
Inclusive B production at CDF and D0
[DE95-000728] p 1528 N95-22196

ANNOTATIONS
Utilizing artificial neural networks in network flow analysis: An annotated bibiliography
[DE95-002453] p 1482 N95-21522

ANNUAL VARIATIONS
Climatological data for clouds over the globe from surface observations, 1982-1991: The total cloud edition
[DE95-002537] p 1431 N95-22288

ANNULAR FLOW
Laser anemometry and viscous computation of the flow through an annular turbine cascade
[AD-A280070] p 1341 N95-20968

ANODES
Molten carbonate fuel cell product development test
[DE95-000005] p 1324 N95-20574
Anodic oxygen-transfer electrocatalysis at iron-doped lead dioxide electrodes
[DE95-001653] p 1242 N95-21397

ANODIZING
Aircraft corrosion study
[AD-A279527] p 1259 N95-21687

ANOMALIES
A Cost and Performance System (CAPS) in a Federal agency p 1584 N95-20746
DC potential anomalies caused by a conducting body in an anisotropic conducting half-space
[PB95-127106] p 1291 N95-20775
Anomalous vector-boson couplings in Majorana neutrino models
[PB95-127460] p 1518 N95-21220
The atmospheric neutrino anomaly in Soudan 2
[DE94-019288] p 1604 N95-21475

ANTARCTIC REGIONS
Surface exposure geochronology using cosmogenic nuclides: Applications in Antarctic glacial geology
[AD-A279392] p 1426 N95-21944
Transport, radiative, and dynamical effects of the Antarctic ozone hole: A GFDL SKYHI model experiment
[PB94-192754] p 1409 N95-22101
ANTENNA ARRAYS
A colocated magnetic loop, electric dipole array antenna (preliminary results)
[AD-A285381] p 1290 N95-20556
High contrast organic crystal optical modulator for phased array antenna and optical signal processing
[AD-A286557] p 1544 N95-20844
A method using focal plane analysis to determine the performance of reflector antennas p 1304 N95-21538
Inband scattering from arrays with series feed networks
[AD-A286209] p 1307 N95-21883
ANTENNA COUPLERS
VHDL modeling of PRC-70 radio ASICs for reverse engineering
[AD-A285740] p 1457 N95-19929
ANTENNA DESIGN
The design and analysis of a phased array microstrip antenna for a low earth orbit communication satellite
[AD-A284791] p 1289 N95-20065
Low-cost conical ultra-wideband antenna
[AD-A286569] p 1292 N95-20825
Angle diversity on digital microwave links: Antenna design and experimental results p 1297 N95-20947
Multipath impact on ground-based global positioning system range measurements: Aspects of measurement, modeling, and mitigation p 1297 N95-20949
Small antennas for communication over sea ice
[AD-D016206] p 1301 N95-21156
Design and implementation of a dual-beam printed antenna for a reception in angular diversity on a Hertzien cluster (or bundle)
[PB95-131603] p 1302 N95-21431
Analysis of a microstrip reflectarray antenna for microspacecraft applications p 1305 N95-21541
Analysis of a disk-on-rod surface wave element inside a corrugated horn using the mode-matching technique
p 1305 N95-21543
An 8-meter-long coupled cavity RFQ linac
[DE94-018077] p 1331 N95-21667
Inverse and control problems in electromagnetics
[AD-A286438] p 1310 N95-22250
ANTENNA FEEDS
A method using focal plane analysis to determine the performance of reflector antennas p 1304 N95-21538
Inband scattering from arrays with series feed networks
[AD-A286209] p 1307 N95-21883
ANTENNA RADIATION PATTERNS
Three-dimensional effects for radio frequency antenna modeling
[DE94-019125] p 1303 N95-21459
A method using focal plane analysis to determine the performance of reflector antennas p 1304 N95-21538
Measurements of the Auburn ECE optical system parameters for temperature fluctuation measurements on TEXT-U
[DE94-019217] p 1562 N95-22120
ANTENNAS
Passive surface deployed variable inductance wire antenna statement of government interest
[AD-D016210] p 1307 N95-21910
ANTHROPOMETRY
Human force exertion in user-product interaction. Backgrounds for design
[PB95-132858] p 1452 N95-21283
ANTIBODIES
Monoclonal antibodies directed against surface molecules of multicell spheroids
[NASA-CR-197367] p 1437 N95-20559
ANTIEMETICS AND ANTINAUSEANTS
Acute radiation sickness amelioration analysis
[AD-A279084] p 1445 N95-21629
ANTIFERROMAGNETISM
Neutron diffraction study of the magnetic ordering of BaCuO(2+x)
[DE95-001357] p 1572 N95-21297
ANTIMONIDES
Sputter deposition of multilayer thermoelectric films: An approach to the fabrication of two-dimensional quantum wells
[DE95-002396] p 1272 N95-20892
ANTIMONY
Synthesis and structure of a novel bis-stibole
[AD-A286345] p 1224 N95-22252
ANTIMONY COMPOUNDS
InTISb for long-wavelength infrared photodetectors and arrays
[AD-A280109] p 1331 N95-21660
ANTINEUTRINOS
The solar flux of thermal neutrinos and antineutrinos of all flavors
[DE95-003204] p 1604 N95-22085
ANTIPROTONS
Strange particle and antiproton production in S + nucleus collisions at 200 GeV/nucleon
[DE95-002348] p 1513 N95-20575
Search for new particles decaying to dijets in p(bar p) collisions at (radical)s = 1.8 TeV
[DE94-018994] p 1523 N95-21563
ANTIRADIATION DRUGS
Acute radiation sickness amelioration analysis
[AD-A279084] p 1445 N95-21629
ANTISEPTICS
Disinfection of purified waste water with ultra violet light on a technical scale
[PB95-131926] p 1405 N95-21330
APERTURES
Detection optimization using linear systems analysis of a coded aperture laser sensor system
[DE95-001112] p 1371 N95-20832
Plasma Electrode Pockels Cells for the Beamlet and NIF lasers
[DE94-016541] p 1557 N95-21166
Analytic models for beam propagation and far-field patterns in slab and bow-tie x ray lasers
[DE94-016607] p 1372 N95-21173
Comparison of calculated with measured dynamic aperture
[DE95-002863] p 1534 N95-21246
Sources of amplitude-dependent tune shift in the PEP-2 design and their compensation with octupoles
[DE94-018198] p 1519 N95-21262
Synthetic aperture radar processing with polar formatted subapertures
[DE95-001830] p 1302 N95-21305
Analysis of a microstrip reflectarray antenna for microspacecraft applications p 1305 N95-21541
APEXES
Graphs cospectral with distance-regular graphs
[PB95-111050] p 1488 N95-19943
Factorization in closed string field theory
[PB95-133542] p 1580 N95-21030
Vertex ranking for permutation and other graphs
[PB95-127569] p 1496 N95-22327
APOLLO SPACECRAFT
Moon: Old and new
[NASA-TM-110511] p 1601 N95-21196
APPLICATION SPECIFIC INTEGRATED CIRCUITS
VHDL modeling of PRC-70 radio ASICs for reverse engineering
[AD-A285740] p 1457 N95-19929
The design and manufacturing development of an active silicon substrate MCM p 1211 N95-20645
Design and development SAWAFE peak detector chip
[DE95-001745] p 1332 N95-21742
APPLICATIONS OF MATHEMATICS
Computing methods for the approximate solution of time dependent problems
[AD-A286007] p 1491 N95-20719
Error analysis of the quadratic nodal expansion method in slab geometry
[DE95-001352] p 1492 N95-21285
Method and apparatus for classifying targets
[AD-D016519] p 1303 N95-21464
Foundations of functional programming: A programmer's point of view
[PB95-132932] p 1471 N95-22094
APPLICATIONS PROGRAMS (COMPUTERS)
Introduction to the FIRE engine: A C++ toolkit for Finite automata and Regular Expressions
[PB95-110599] p 1456 N95-19891
Hierarchical diagrammatic representation of class structure
[PB95-110722] p 1456 N95-19908
Computer program for calculation of complex chemical equilibrium compositions and applications. Part 1: Analysis
[NASA-RP-1311] p 1235 N95-20180
Evaluation of Borland Turbo Vision
[AD-A279873] p 1459 N95-20184
A new tool for accelerator system modeling and analysis
[DE94-018292] p 1531 N95-20203
RCS calculation capability
[AD-A286329] p 1289 N95-20211
BACKSCAT lidar simulation version 4.0: Technical documentation and users guide
[AD-A285851] p 1290 N95-20376
Muon data analysis program RUMDA
[PB95-129839] p 1511 N95-20434
Fault-tolerance in distributed and multiprocessor real-time systems
[AD-A279896] p 1461 N95-20595
Software for flow distribution in electronic rack structures
[AD-A285994] p 1325 N95-20715
EPSCoR supplemental grant for an application of neural networks to seismic signal discrimination
[AD-A285846] p 1414 N95-20878
COYOTE II: A finite element computer program for nonlinear heat conduction problems. Part 1: Theoretical background
[DE95-002587] p 1463 N95-20887
Statistical analysis of Turbine Engine Diagnostic (TED) field test data
[AD-A286032] p 1379 N95-20998
A computer code (SKINTEMP) for predicting transient missile and aircraft heat transfer characteristics
[AD-A286044] p 1341 N95-21001
VLUGr3: A vectorizable adaptive grid solver for PDEs in 3D. 2: Code description
[PB95-135737] p 1465 N95-21033
Investigation of shear layer transition using various turbulence models p 1352 N95-21096
Effects of battery technologies, driving patterns, and climate comfort control on the performance of electric vehicles
[DE95-001102] p 1329 N95-21296
SEEK: A FORTRAN optimization program using a feasible directions gradient search
[NASA-CR-4641] p 1380 N95-21359
Operator's manual for the multistation offgas analysis system
[DE95-002060] p 1243 N95-21472
PVM 3 beyond network computing
[DE94-019115] p 1477 N95-21556
The molecular mechanics program DUPLEX: Computing structures of carcinogen modified DNA by surveying the potential energy surface
[DE94-019153] p 1439 N95-21606
Application-oriented architecture for multimedia teleservices
[PB95-135513] p 1306 N95-21623
DOS basics
[DE94-018434] p 1455 N95-21632
The application of a statistical analysis software package to explosive testing
[MRL-TR-93-42] p 1284 N95-21658
Modeling of rolling element bearing mechanics. Computer program user's manual
[NASA-CR-196557] p 1381 N95-21692
Modeling of rolling element bearing mechanics. Theoretical manual
[NASA-CR-196556] p 1381 N95-21705
A user's guide to LUGSAN 1.1: A computer program to calculate and archive lug and sway brace loads for aircraft-carried stores
[DE95-001919] p 1207 N95-21730
EAGLES 1.1: A microcomputer software package for analyzing fuel efficiency of electric and gasoline vehicles
[DE95-001119] p 1469 N95-21829
State of the art in CFD pre- and postprocessing
[PB95-110391] p 1356 N95-22017
Modelling multimedia teleservices with OSI upper layers framework: Short paper
[PB95-132734] p 1308 N95-22080
Users guide to NCEMSS, version 2.0
[DE95-003443] p 1548 N95-22238
Sandia National Laboratories analysis code data base
[DE95-004188] p 1502 N95-22420
APPROACH
A real-time algorithm for integrating differential satellite and inertial navigation information during helicopter approach
[NASA-CR-197409] p 1205 N95-21891
APPROACH CONTROL
Crew aiding and automation: A system concept for terminal area operations, and guidelines for automation design
[NASA-CR-4631] p 1204 N95-19950
APPROACH INDICATORS
Minima reduction simulation test results
[AD-A285626] p 1204 N95-21148
APPROXIMATION
Sharp determinants
[PB95-111068] p 1488 N95-19944
Finite dimensional approximation of a class of constrained nonlinear optimal control problems
[NASA-CR-194891] p 1479 N95-20010
Computing methods for the approximate solution of time dependent problems
[AD-A286007] p 1491 N95-20719
Computing near-optimal schedules
[PB95-132072] p 1466 N95-21269
Diffusion approximations in communication and stochastic theory
[AD-A286440] p 1302 N95-21438

Approximation algorithms for the general and the asymmetric stacker-crane problems [PB95-132098] p 1493 N95-21468

Analysis of a local defect correction approach on composite grids [PB95-135455] p 1493 N95-21574

Electronic structure and energies of alkaline earth oxides: MgO, CaO and SrO [DE94-628990] p 1575 N95-21853

Electronic structure and relative stability of icosahedral superatoms in Al-transition-metal alloys [DE94-628996] p 1260 N95-21855

Second order approximation for optical polaron in the strong coupling case [DE94-628997] p 1525 N95-21856

Single particle measurements and two particle interferometry results from CERN experiment NA44 [DE95-003041] p 1527 N95-22078

Mathematical theory of neural networks [AD-A286508] p 1465 N95-22213

AQUATIC PLANTS

Aquatic plant control research program. Ecological assessment of Kirk Pond [AD-A279090] p 1409 N95-21914

AQUEOUS SOLUTIONS

Direct catalytic decomposition of nitric oxide [DE94-018840] p 1233 N95-20045

Safe conditions for contacting nitric acid or nitrates with Tri-n-Butyl Phosphate (TBP) [DE95-001243] p 1235 N95-20215

Tests of dielectric model descriptions of chemical charge displacements in water [DE94-007530] p 1236 N95-20277

Actinide(IV) and actinide(VI) carbonate speciation studies by PAS and NMR spectroscopies [DE94-016957] p 1236 N95-20361

Theoretical and experimental study of mixed solvent electrolytes [DE94-017605] p 1237 N95-20384

Catalyzed reduction of nitrate in aqueous solutions [DE94-017660] p 1247 N95-22049

AQUIFERS

Degradation of aromatic hydrocarbons in an aquifer during a field experiment demonstrating the feasibility of remediation by natural attenuation [AD-A283809] p 1282 N95-19922

ARC HEATING

Dual active surface heat flux gage probe [NASA-TM-106861] p 1366 N95-21391

ARC MELTING

Plasma arc melting of titanium-tantalum alloys [DE94-016291] p 1252 N95-20331

Plasma arc melting of a 80 weight percent tantalum -20 weight percent titanium alloy [DE95-000846] p 1260 N95-22006

The influence of chemistry and microstructure on the fracture toughness of V-V3Si in-situ composites [DE94-018997] p 1232 N95-22126

ARC WELDING

The origin of acicular ferrite in gas metal arc and submerged arc welds [AD-A286129] p 1377 N95-19984

Fusion welding of advanced borated stainless steels [DE94-019037] p 1378 N95-20053

ARCHITECTURE

Generic architecture for knowledge-based control of processes in dynamic environments [PB95-132676] p 1483 N95-21981

ARCHITECTURE (COMPUTERS)

High-performance packet switching architecture for ATM: Conventional solution and neural network solution [PB95-110920] p 1312 N95-19935

Hindered settling computations using a parallel boundary element method [DE94-014286] p 1339 N95-20137

Preliminary evaluation of a digital optical systolic processor implemented with acousto-optic cells [AD-A286377] p 1541 N95-20231

Kernel mucking in top [DE94-017077] p 1460 N95-20385

System design document U-AVLIS control system architecture [DE94-017297] p 1460 N95-20387

RALPAR-RAL mesh partitioning program version 1.1 [PB95-129847] p 1475 N95-20435

Research in theoretical elementary particle physics at the University of Florida, task A [DE94-004373] p 1512 N95-20469

Downsizing information systems: Framing the issues for the Office of Naval Intelligence (ONI) [AD-A279888] p 1588 N95-20589

Fault-tolerance in distributed and multiprocessor real-time systems [AD-A279896] p 1461 N95-20595

Methods and components for optical contention resolution in high speed networks [AD-A280016] p 1543 N95-20598

The impact of advanced packaging technology on modular avionics architectures p 1208 N95-20632

Standard Hardware Acquisition and Reliability Program (SHARP) advanced SEM-E packaging p 1208 N95-20633

The IEEE scalable coherent interface: An approach for a unified avionics network p 1212 N95-20650

Optical backplane for modular avionics p 1212 N95-20652

High performance backplane components for modular avionics p 1212 N95-20653

An integrated architecture of adaptive neural network control for dynamic systems [DE94-014813] p 1481 N95-20693

A new process for acquiring software architecture [AD-A286012] p 1462 N95-20721

Environment for Test and Analysis of Distributed Software (ETADS) [AD-A285776] p 1463 N95-20877

Functional and para-functional parallel processing [DE95-002805] p 1475 N95-20888

Real-time reconfiguration study [AD-A286060] p 1464 N95-20910

The opportunities for and challenges of common integrated electronics [AD-A279991] p 1327 N95-20966

Preliminary study of HUTSAT microsatellite [PB95-127619] p 1220 N95-21026

Heterogeneous multi-robot cooperation [AD-A279839] p 1481 N95-21185

An object-oriented implementation of the Xpress transfor protocol [DE95-001506] p 1301 N95-21277

Quantitative evaluation of wrist posture and typing performance: A comparative study of 4 computer keyboards [DE95-002392] p 1452 N95-21358

PVM 3 beyond network computing [DE94-019115] p 1477 N95-21556

PVM a platform for portable distributed computing [DE94-019156] p 1455 N95-21607

Application-oriented architecture for multimedia teleservices [PB95-135513] p 1306 N95-21623

Top ten list of user-hostile interface design [DE95-001602] p 1453 N95-21721

High-capacity optical multichannel virtual mesh interconnection networks [PB95-134094] p 1546 N95-21870

Generic architecture for knowledge-based control of processes in dynamic environments [PB95-132676] p 1483 N95-21981

Information Management Architecture for an Integrated Computing Environment for the Environmental Restoration Program. Volume 2: Interim business systems guidance [DE95-001385] p 1591 N95-22061

Modelling multimedia teleservices with OSI upper layers framework: Short paper [PB95-132734] p 1308 N95-22080

Scalable programming environment [AD-A286390] p 1472 N95-22201

Design of a massively parallel computer using bit serial processing elements [NASA-CR-197365] p 1479 N95-22406

TDX: A high-bandwidth crossbar-switched communication paradigm [DE94-017187] p 1311 N95-22407

ARCTIC REGIONS

Atlas of SSM/I satellite ice concentration interpolated to operational ice model domains of the Arctic for 1993 [AD-A280183] p 1432 N95-20012

Propagation measurements on a troposcatter link in the Canadian High Arctic p 1295 N95-20940

Cold regions instrumentation considerations [AD-A279492] p 1367 N95-21680

AREA NAVIGATION

Crew aiding and automation: A system concept for terminal area operations, and guidelines for automation design [NASA-CR-4631] p 1204 N95-19950

ARGON

Helium exhaust studies in the D3-D tokamak [DE94-016682] p 1552 N95-20334

X-ray spectroscopy of xenon [DE95-002132] p 1240 N95-20865

Aging tests of ethylene contaminated argon/ethane [DE95-002526] p 1282 N95-20899

Recent photoabsorption measurements in the rare gases and alkalis in the 3 to 15 keV photon energy region [DE94-019278] p 1521 N95-21406

Experimental study of interactions of highly charged ions with atoms at keV energies [DE95-001807] p 1521 N95-21441

Ion charge-state production and photoionization near the K edge in argon and potassium [DE95-001443] p 1522 N95-21502

Experimental study of interactions of highly charged ions with atoms at keV energies [DE94-018648] p 1529 N95-22316

ARGON ISOTOPES

The ratios of carbon and non-radiogenic helium and argon isotopes in the mantle and crustal rocks p 1421 N95-21805

ARITHMETIC

Packaging the MAMA module p 1209 N95-20639

ARMED FORCES (FOREIGN)

Psychosocial stress and mental health in a forward-deployed military community [AD-A285940] p 1451 N95-22323

ARMED FORCES (UNITED STATES)

Bomber force 2000: Operational concepts for long-range combat aircraft [AD-A279378] p 1206 N95-20181

Assessing post traumatic stress disorder and PTSD symptomatology in US Army personnel [AD-A285941] p 1451 N95-22324

ARMOR

ALT-2 armor tile design for upgraded TEXTOR operation [DE94-015749] p 1549 N95-20143

Tungsten-uranium penetrator target interaction [DE95-000847] p 1387 N95-21364

AROMATIC COMPOUNDS

Restricted mass transport effects on free radical reactions [DE94-018136] p 1217 N95-21706

ARPA COMPUTER NETWORK

Advanced Standard Electronic Modules format-E (SEM-E) processes for rapid prototyping p 1210 N95-20642

ARRAYS

Signal-to-noise gain from adaptive matched-field beamforming of multidimensional acoustic arrays [AD-A285671] p 1503 N95-20084

Investigating the resolution of resistivity arrays using inverse theory [DE94-017760] p 1412 N95-20287

A new mini Ball Grid Array (mBGA) multichip module technology [DE94-018897] p 1480 N95-20342

Field-emitter arrays for RF vacuum microelectronics [AD-A279959] p 1325 N95-20661

InTISb for long-wavelength infrared photodetectors and arrays [AD-A280108] p 1332 N95-21774

Order and turbulence in RF-driven Josephson junction series arrays [DE94-629076] p 1576 N95-21997

ARTIFACTS

Incremental rederivation of software artifacts: FY 1993 [AD-A285790] p 1473 N95-22402

ARTIFICIAL INTELLIGENCE

Intelligent tutoring systems: Past, present, and future [AD-A280011] p 1448 N95-19970

Collected papers of the Soar/IFOR project, Spring 1994 [AD-A280063] p 1216 N95-20624

Automatic generation of fuzzy rules for the sensor-based navigation of a mobile robot [DE95-001428] p 1481 N95-20837

Heterogeneous multi-robot cooperation [AD-A279839] p 1481 N95-21185

13th European Annual Conference on Human Decision Making and Manual Control [PB95-132874] p 1450 N95-21284

Communications and control for electric power systems: Power system stability applications of artificial neural networks [NASA-CR-197594] p 1483 N95-21613

Adaptive capture of expert behavior [DE94-018285] p 1483 N95-21710

Intelligent interactive project management system [PB95-132684] p 1586 N95-21982

Artificial neural network metamodels of stochastic computer simulations [AD-A285951] p 1484 N95-22056

Discovering related DNA sequences via mutual information [DE95-001101] p 1440 N95-22067

Activities of the Research Institute for Advanced Computer Science [NASA-CR-197291] p 1478 N95-22108

Communications and control for electric power systems: Power system stability applications of artificial neural networks [NASA-CR-197333] p 1484 N95-22171

Mathematical theory of neural networks
[AD-A286508] p 1485 N95-22213
Artificial Intelligence (AI) and Ada: Integrating AI with mainstream software engineering
[AD-A286093] p 1485 N95-22226
Logic programming and negation: A survey
[PB95-110730] p 1472 N95-22302
Simulation of structural response using a recurrent radial basis function network
[DE94-017342] p 1486 N95-22409

ARTIFICIAL SATELLITES
Ice Processing System software support documentation
[AD-A280030] p 1388 N95-20006
Angle resolved Auger electron spectroscopy: An alternate tool for identifying electronic excitation processes in solids
[AD-A285375] p 1238 N95-20555
Space fundamentals for the war fighter
[AD-A279703] p 1217 N95-20690

ASIA
Energy and environmental issues and international opperation in Asia
[DE94-796596] p 1404 N95-21143

ASPECT RATIO
Numerical analysis of energetic particle stabilization of ballooning modes in finite-aspect-ratio tokamaks
[DE94-631397] p 1556 N95-21164

ASSAYING
Monoclonal antibodies directed against surface molecules of multicell spheroids
[NASA-CR-197367] p 1437 N95-20559

ASSEMBLIES
Phase E in a water-saturated peridotite system at 9.3 GPa p 1420 N95-21799

ASSESSMENTS
Environmental Hazards Assessment Program
[DE94-019075] p 1406 N95-21565

ASSIMILATION
Real time system for practical acoustic monitoring of global ocean temperature
[AD-A286435] p 1436 N95-22209

ASTEROIDS
Experimental hypervelocity impact effects on simulated planetesimal materials
[DE94-017290] p 1599 N95-20144
Erice International Seminars on Planetary Emergencies. 17th Workshop: The Collision of an Asteroid or Comet with the Earth
[AD-A280122] p 1600 N95-21577

ASTRONAUT LOCOMOTION
STS Flight 64 mission highlights
[NASA-TM-110515] p 1219 N95-22295

ASTRONAUTS
Challenger's night flight
[NASA-TM-110503] p 1217 N95-19995

ASTRONOMICAL MAPS
Hires and beyond p 1592 N95-21750
An assessment of image reconstruction from balloon-borne and the IRAS data p 1592 N95-21752
Far-infrared mapping of dusty elliptical galaxies
p 1593 N95-21763

ASTRONOMICAL MODELS
Predictions from quantum cosmology
[PB95-111126] p 1599 N95-20173
The solar neutrino problem: Neither astrophysics nor oscillations?
[DE94-012850] p 1603 N95-21316
The ORNL Neutron-Capture Cross Section Facility
[DE94-019146] p 1537 N95-21460
In search of random noise p 1592 N95-21753

ASTRONOMICAL SATELLITES
Low noise 22 GHz receiver for the radioastron satellite, part 2: Space qualification tests
[PB95-127197] p 1598 N95-22376

ASTROPHYSICS
Connection with dynamics: General introduction
[NASA-CR-197617] p 1579 N95-19947
Overview of the Institute of Geophysics and Planetary Physics and Lawrence Livermore National Laboratory collaborative efforts
[DE94-017300] p 1599 N95-20145
Israel Physical Society Annual Meeting 1994
[DE94-630140] p 1565 N95-20261
Resonant photon-graviton conversion in EM fields: From earth to heaven
[DE95-002784] p 1301 N95-21241
The solar neutrino problem: Neither astrophysics nor oscillations?
[DE94-012850] p 1603 N95-21316
The ORNL Neutron-Capture Cross Section Facility
[DE94-019146] p 1537 N95-21460
Solar wind composition
[NASA-TM-197364] p 1604 N95-22384

ASYMMETRY
Measuring A(sub b) with polarized beams at SLC
[DE95-002865] p 1519 N95-21248
Magnetic x-ray circular dichroism in spin-polarized photoelectron diffraction
[DE95-002394] p 1520 N95-21360
Approximation algorithms for the general and the asymmetric stacker-crane problems
[PB95-132098] p 1493 N95-21468
Tests of structure functions using lepton pairs: W-charge asymmetry at CDF
[DE95-000560] p 1527 N95-22122
Large-eddy simulation of flow through a plane, asymmetric diffuser p 1360 N95-22449

ASYMPTOTIC GIANT BRANCH STARS
HIRAS images of fossil dust shells around AGB stars
p 1593 N95-21768

ASYMPTOTIC METHODS
Growth series for the commutator subgroup
[PB95-111092] p 1490 N95-20452
Triple flame structure and diffusion flame stabilization
p 1249 N95-21039
Diffusion approximations in communication and stochastic theory
[AD-A286440] p 1302 N95-21438
Rigorous spin-spin correlation function of Ising model on a special kind of Sierpinski Carpets
[DE94-628995] p 1575 N95-21854
An asymptotic solution of the (infinity)-d Hubbard model
[DE94-629042] p 1582 N95-21994

ASYMPTOTIC PROPERTIES
Optimal distributed control system for a linear distributed parameter system
[AD-D016583] p 1480 N95-20202
Exponential deconvolution: Two asymptotically equivalent estimators
[PB95-132122] p 1499 N95-21469

ASYMPTOTIC SERIES
Asymptotic analysis of Nash equilibria in nonzero-sum linear-quadratic differential games. The two-player case
[PB95-111027] p 1499 N95-19941
Preconditioning via asymptotically-defined domain decomposition
[DE94-019046] p 1493 N95-21564

ATMOSPHERIC ATTENUATION
Applicability of the ECMWF rain height and rainfall rate data to the prediction of low-availability rain attenuation in Europe
[PB95-127684] p 1430 N95-21413
Passive millimetre wave imaging: A review
[AD-A279275] p 1303 N95-21491
Evaluation of simple spherical spreading model for near vertical acoustical propagation
[AD-A286284] p 1505 N95-22042

ATMOSPHERIC BOUNDARY LAYER
Front-boundary layer models from STORM-FEST observations
[AD-A279907] p 1428 N95-20186
Boundary layer cloud studies in support of ASTEX
[AD-A285947] p 1429 N95-20395
Real-data tests of a single-Doppler radar assimilation system
[AD-A286638] p 1292 N95-20904
High resolution properties of the equatorial Pacific marine atmospheric boundary layer from lidar and radiosonde observations
[DE95-001028] p 1426 N95-21875
SAR-related stress variability in the Marine Atmospheric Boundary Layer (MABL)
[AD-A286462] p 1431 N95-22393

ATMOSPHERIC CHEMISTRY
An overview of the Evaluation of Oxygen Interactions with Materials 3 Experiment: Space Shuttle Mission 46; July-August, 1992
[NASA-TM-110129] p 1412 N95-20278
Explicit methods for stiff ODEs from atmospheric Chemistry
[PB95-135794] p 1404 N95-21034
An Echelle Grating Spectrometer (EGS) for mid-IR remote chemical detection
[DE94-019310] p 1367 N95-21478
Is xenon eldest? p 1425 N95-21823
Assessment of the atmospheric hazards and risks of new chemicals: Procedures to estimate hazard potentials
[PB95-107488] p 1410 N95-22186
Proceedings: International Symposium on Global Change (IGBP)
[DE94-765351] p 1410 N95-22219

ATMOSPHERIC CIRCULATION
Simulation of stellar speckle imaging
[DE94-016606] p 1412 N95-19985
The vertical distribution of heating in the tropical atmosphere
[AD-A285934] p 1429 N95-20391
Program control on the Tropical Rainfall Measuring Mission p 1584 N95-20750
A study of westerly wind bursts preceding the 1991-1992 El Nino
[AD-A286570] p 1429 N95-20826
Two-micron Laser Atmospheric Wind Sounder (LAWS) pointing/tracking study
[NASA-CR-195012] p 1220 N95-21190
Stability effects on the profiles of vertical velocity and its variance in katabatic flow
[DE95-001126] p 1426 N95-21836
High resolution properties of the equatorial Pacific marine atmospheric boundary layer from lidar and radiosonde observations
[DE95-001028] p 1426 N95-21875
DOD science and engineering apprenticeship program for high school students
[AD-A280371] p 1583 N95-22100
Confirmatory analysis of SAGE-1, and -2 data
[DE95-003623] p 1427 N95-22240
Climatological data for clouds over the globe from surface observations, 1982-1991: The total cloud edition
[DE95-002537] p 1431 N95-22288

ATMOSPHERIC COMPOSITION
Radiative forcing for changes in tropospheric O3
[DE94-019017] p 1413 N95-20354
Radiative forcing calculations for CH3Cl
[DE94-019018] p 1402 N95-20355
The development and evaluation of water-mist fire extinguishing systems
[DE94-019019] p 1286 N95-20356
Studies of the gas tori of Titan and Triton
[NASA-CR-197377] p 1601 N95-20797
Closure on the global carbon cycle
[DE94-018617] p 1404 N95-20991
ICE BABY: Measurements of concentration fluctuations in a forest area in winter conditions
[PB95-133468] p 1405 N95-21274
Definition report on environmental indices in future environmental assessments environmental balance/environmental outlook
[PB95-131876] p 1405 N95-21350
Implications of noble gases in a recently recognized Martian meteorite (ALH84001) for the degassing history of Mars p 1424 N95-21819
He, Xe and Ne isotopes in a steady-state mass transport model and implications about terrestrial volatiles
p 1425 N95-21821
Is xenon eldest? p 1425 N95-21823

ATMOSPHERIC CORRECTION
A comparative survey of current and proposed tropospheric refraction-delay models for DSN radio metric data calibration
[NASA-CR-197338] p 1412 N95-20002

ATMOSPHERIC DENSITY
Electronic structure and energies of alkaline earth oxides: MgO, CaO and SrO
[DE94-628990] p 1575 N95-21853

ATMOSPHERIC DIFFUSION
Study of the fast and slow variations of the power received at VHF links by tropospheric diffusion
p 1293 N95-20929

ATMOSPHERIC EFFECTS
Analysis of mesospheric winds and waves
[AD-A279956] p 1414 N95-20591
Methods for evaluating the effects of conduits at the surface of the sea p 1294 N95-20932
Combined effects of atmosphere and terrain on UHF/microwave paths p 1295 N95-20935
Electric and Hybrid Vehicle Program Site Operator Program
[DE95-002042] p 1333 N95-21960

ATMOSPHERIC ENTRY
Plasma chemistry of vibrationally nonequilibrium molecules
[AD-A279630] p 1553 N95-20411
Simulated rarefied entry of the Galileo probe into the atmosphere of Jupiter
[NASA-TM-110507] p 1601 N95-21621
Grid resolution and solution convergence for Mars Pathfinder forebody
[NASA-TM-109173] p 1494 N95-21622

ATMOSPHERIC GENERAL CIRCULATION MODELS
Completion of spectral rotating shadowband radiometers and analysis of ARM spectral short-wave data
[DE95-000602] p 1412 N95-20116
Monsoons: AMIP simulations of the 1987 and 1988 drought and flood regimes
[DE94-014789] p 1428 N95-20140
A control volume method on an icosahedral grid for numerical integration of the shallow-water equations on the sphere
[DE94-016345] p 1489 N95-20170

Sensitivity of climate models: Comparison of simulated and observed patterns for past climates
[DE95-002257] p 1406 N95-21379
Transport, radiative, and dynamical effects of the Antarctic ozone hole: A GFDL SKYHI model experiment
[PB94-192754] p 1409 N95-22101
Confirmatory analysis of SAGE-1, and -2 data
[DE95-003623] p 1427 N95-22240

ATMOSPHERIC HEATING
Modeling the response of the California Current system to Global Greenhouse Warming
[DE94-018253] p 1408 N95-21708

ATMOSPHERIC MODELS
Front-boundary layer models from STORM-FEST observations
[AD-A279907] p 1428 N95-20186
Radiative forcing for changes in tropospheric O3
[DE94-019017] p 1413 N95-20354
Synthesizing the Gulf Stream thermal structure from XBT data
[AD-A279665] p 1433 N95-20458
Explicit methods for stiff ODEs from atmospheric Chemistry
[PB95-135794] p 1404 N95-21034
Global ionospheric weather
[AD-A285520] p 1430 N95-21177
An integrated cloud observation and modeling investigation in support of the ARM Program
[DE95-002798] p 1430 N95-21527
Remote-sensing based technique to account for sub-grid scale variability of land surface properties
[NASA-TM-110501] p 1390 N95-22110
The applicability of neural networks to ionospheric modeling in support of relocatable Over-the-Horizon radar
[AD-A286114] p 1309 N95-22230
Substorm theories: United they stand, divided they fall
[NASA-CR-197672] p 1427 N95-22326
Modeling of collision induced absorption spectra of CO2-CO2 pairs for planetary atmosphere of Venus
[NASA-CR-197373] p 1601 N95-22338

ATMOSPHERIC MOISTURE
Daytime Raman lidar profiling of atmospheric water vapor
[DE94-015747] p 1413 N95-20397
Methods for evaluating the effects of conduits at the surface of the sea p 1294 N95-20932
Lidar technologies for airborne and space-based applications
[DE95-002954] p 1302 N95-21448
Unified very low stratus cloud/subcloud microphysics model: User's guide
[AD-A286454] p 1430 N95-21586
Response of the B-1B air data sensor to simulated dust cloud environments
[AD-A286134] p 1213 N95-22036

ATMOSPHERIC PHYSICS
The effect of regional-scale soil-moisture deficits on mesoscale atmospheric dynamics that influence fire severity
[DE95-002682] p 1413 N95-20455
Metallic ions and atoms in the upper atmosphere
[AD-A285229] p 1414 N95-20498
Ultraviolet emission from rocket motor plumes
[DSTO-TR-0002] p 1222 N95-21661
Modeling of collision induced absorption spectra of CO2-CO2 pairs for planetary atmosphere of Venus
[NASA-CR-197373] p 1601 N95-22338
The effects of magnetic storm phases on F-layer irregularities from auroral to equatorial latitudes
[AD-A286173] p 1427 N95-22423

ATMOSPHERIC PRESSURE
Effect of atmospheric pressure on measured aircraft noise levels
[PB95-130423] p 1207 N95-21425

ATMOSPHERIC RADIATION
Site Scientific Mission Plan for the Southern Great Plains CART site, July - December 1994
[DE94-017289] p 1401 N95-20193
Effects of microphysics and radiation on mesoscale processes of a midlatitude squall line
[DE94-014732] p 1429 N95-20381
The atmospheric neutrino anomaly in Soudan 2
[DE94-019288] p 1604 N95-21475

ATMOSPHERIC REFRACTION
Combined effects of atmosphere and terrain on UHF/microwave paths p 1295 N95-20935

ATMOSPHERIC SOUNDING
Noise model of the MSX SPIRIT 3 interferometer
[AD-A285837] p 1364 N95-20036
Boundary layer cloud studies in support of ASTEX
[AD-A285947] p 1429 N95-20395
Sounder calibration with backscattering from Losquet Island in the presence of multipaths
p 1300 N95-20961
Two-micron Laser Atmospheric Wind Sounder (LAWS) pointing/tracking study
[NASA-CR-195012] p 1220 N95-21190

ATMOSPHERIC TEMPERATURE
Meso-scale cooling effects of high albedo surfaces: Analysis of meteorological data from White Sands National Monument and White Sands Missile Range
[DE94-018535] p 1429 N95-20782
Sensitivity of climate models: Comparison of simulated and observed patterns for past climates
[DE95-002257] p 1406 N95-21379
Transport, radiative, and dynamical effects of the Antarctic ozone hole: A GFDL SKYHI model experiment
[PB94-192754] p 1409 N95-22101

ATMOSPHERIC TIDES
Analysis of mesospheric winds and waves
[AD-A279956] p 1414 N95-20591

ATMOSPHERIC TURBULENCE
Simulation of stellar speckle imaging
[DE94-016606] p 1412 N95-19985
Simulation of the impact of atmospheric turbulences on millimeter-wave communications systems
p 1295 N95-20939
Stability effects on the profiles of vertical velocity and its variance in katabatic flow
[DE95-001126] p 1426 N95-21836
Threshold detection in the presence of atmospheric turbulence
[AD-A286175] p 1427 N95-22249

ATOLLS
A modal analysis of currents in a Pacific Atoll lagoon
[AD-A283721] p 1431 N95-19971

ATOMIC BEAMS
Time of flight spectroscopy with muonic hydrogen
[DE94-017056] p 1245 N95-21845
Atomic velocity distributions in a hydrogen beam effusing out of an RF discharge dissociator
[AD-A279253] p 1307 N95-21985
Gas-dynamic trap diagnostic complex for study on plasma heating and power atomic beam injection
[DE94-633377] p 1529 N95-22283

ATOMIC CLUSTERS
Pairing on small clusters in the Peierls-Hubbard model: Implications for C60
[DE94-016284] p 1565 N95-20330
Consequences of oscillatory potentials and angular forces in transition metals and their aluminides
[DE94-019127] p 1258 N95-21600

ATOMIC COLLISIONS
Electron-positron pair production in ultrarelativistic atomic collisions: 6.4 TeV S(sup 16+) with Au, Pd and Al
[DE95-000690] p 1508 N95-20133
Convergent Close-Coupling method for calculation of electron scattering on hydrogen-like targets
[DE94-631340] p 1508 N95-20196
Calculation of the total and total ionization cross sections for positron scattering on atomic hydrogen
[DE94-631341] p 1508 N95-20197
The (e,2e) calculations with the final-state boundary condition
[DE94-631342] p 1509 N95-20198
Strange particle and antiproton production in S + nucleus collisions at 200 GeV/nucleon
[DE95-002348] p 1513 N95-20575
Temporal rearrangement of electronic densities in slow atomic collisions
[AD-A279725] p 1516 N95-20994
Recombination, ion-molecule collisions and (laser assisted) electron-excited atom collisions
[AD-A285604] p 1517 N95-21216
Measurements of scattering processes in negative ion: Atom collisions
[DE95-000664] p 1519 N95-21276
Experimental study of interactions of highly charged ions with atoms at keV energies
[DE95-001807] p 1521 N95-21441
The two-electron problem and prospects for atomic collision theory on a numerical lattice
[DE94-017856] p 1528 N95-22265
Experimental study of interactions of highly charged ions with atoms at keV energies
[DE94-018648] p 1529 N95-22316

ATOMIC ENERGY LEVELS
Investigation of laser-induced retinal damage: Wavelength and pulsewidth dependent mechanisms
[AD-A286066] p 1443 N95-20848
Photophysical processes on triplet states and radical ions in pure and molecularly doped polymers
[DE95-002681] p 1570 N95-20916
Auger spectrometry of atoms and molecules
[DE94-018052] p 1524 N95-21664
The solar flux of thermal neutrinos and antineutrinos of all flavors
[DE95-003204] p 1604 N95-22085

ATOMIC EXCITATIONS
Temporal and spectral investigation of multi-Landau level quantum beats in GaAs
[DE94-018189] p 1569 N95-20678
Magnetron power supply at high stability and its application in plasma excitation for the production of ultraviolet radiation
[DE94-629656] p 1326 N95-20733
Electric-field effects on shallow donor impurity in a harmonic quantum dot
[DE94-629034] p 1577 N95-22176
Temperature dependence of a magnetopolaron in a harmonic quantum dot in resonant magnetic fields
[DE94-629036] p 1502 N95-22177
The doping effect on spin-Peierls instability
[DE94-629046] p 1577 N95-22178
Interference of fluorescence x rays and coherent excitation of core levels
[DE94-016809] p 1527 N95-22188

ATOMIC FORCE MICROSCOPY
Gordon Research Conference on Physical Electrochemistry
[AD-A286545] p 1240 N95-20842

ATOMIC INTERACTIONS
A multisite interaction expansion of the total energy in metals
[DE94-017175] p 1262 N95-22313
Experimental study of interactions of highly charged ions with atoms at keV energies
[DE94-018648] p 1529 N95-22316

ATOMIC PHYSICS
Research in the chemical sciences: Summaries of FY 1994
[DE94-015427] p 1223 N95-20264
Temporal rearrangement of electronic densities in slow atomic collisions
[AD-A279725] p 1516 N95-20994
Theoretical atomic physics for fusion
[DE94-019196] p 1524 N95-21605
Atomic processes in processing plasmas
[DE94-019177] p 1560 N95-21609
Auger spectrometry of atoms and molecules
[DE94-018052] p 1524 N95-21664
Formal specification and compositional verification of an atomic broadcast protocol
[PB95-110508] p 1472 N95-22351

ATOMIC SPECTRA
Auger spectrometry of atoms and molecules
[DE94-018052] p 1524 N95-21664

ATOMIC STRUCTURE
Observation of excitonic and band-to-band behavior in ordered InGaP2 alloys
[DE94-018891] p 1314 N95-20341
First principles simulation of materials properties
[DE94-016781] p 1566 N95-20405
New ET-based organic superconductors with the organometallic anion Cu(CF3)4(-)
[DE94-016904] p 1567 N95-20479
An atomically-resolved STM study of the thermal decomposition of disilane on Si(001)
[AD-A279818] p 1567 N95-20544
Angle resolved Auger electron spectroscopy: An alternate tool for identifying electronic excitation processes in solids
[AD-A285375] p 1238 N95-20555
Gordon Research Conference on Physical Electrochemistry
[AD-A286545] p 1240 N95-20842
Anomalous vector-boson couplings in Majorana neutrino models
[PB95-127460] p 1518 N95-21220
Antishadowing contribution to the pomeron structure function
[PB95-127478] p 1518 N95-21221
T1F ((1) sigma (+)): Some preliminary electronic structure calculations
[PB95-130316] p 1518 N95-21223
Spin dependence of diffractive processes and implications for the small x behaviour of g1 and the spin content of the nucleon
[PB95-130332] p 1518 N95-21225
Parity nonconservation in radioactive atoms: An experimental perspective
[DE95-002737] p 1518 N95-21235
Progress in ultrafast scanning probe microscopy
[DE94-018179] p 1373 N95-21261
Photoemission and ferromagnetism
[DE95-002419] p 1520 N95-21362
Theoretical study of the noble metals on semiconductor surfaces and Ti-base shape memory alloys
[DE95-001654] p 1257 N95-21398
Consequences of oscillatory potentials and angular forces in transition metals and their aluminides
[DE94-019127] p 1258 N95-21600
Auger spectrometry of atoms and molecules
[DE94-018052] p 1524 N95-21664

Electronic structure and energies of alkaline earth oxides: MgO, CaO and SrO
[DE94-628990] p 1575 N95-21853

Electronic structure and relative stability of icosahedral superatoms in Al-transition-metal alloys
[DE94-628996] p 1260 N95-21855

Full potential multiple scattering theory
[DE95-003197] p 1576 N95-22084

The dynamic structure function of Bose liquids in the deep inelastic regime
[DE94-629077] p 1527 N95-22182

ATOMIC WEIGHTS

New high temperature plasmas and sample introduction systems for analytical atomic emission and mass spectrometry
[DE94-018580] p 1552 N95-20345

Is xenon eldest? p 1425 N95-21823

ATOMS

Atomic-resolution characterization of interface structure and chemistry in the STEM
[DE94-017753] p 1567 N95-20492

Auger spectrometry of atoms and molecules
[DE94-018052] p 1524 N95-21664

Experimental study of interactions of highly charged ions with atoms at keV energies
[DE94-018648] p 1529 N95-22316

Resonant charge transfer in hyperthermal atomic and molecular ion-surface collisions
[AD-A284937] p 1530 N95-22471

ATTACK AIRCRAFT

Naval aviation: F-14 upgrades are not adequately justified. Report to Congressional Committees
[AD-A286338] p 1206 N95-20212

Design of a controller for a flexible pointing system using H(infinity) synthesis
[AD-A286572] p 1481 N95-20828

ATTENTION

Intermediate levels of visual processing
[AD-A284922] p 1448 N95-19998

ATTENUATION

Degradation of aromatic hydrocarbons in an aquifer during a field experiment demonstrating the feasibility of remediation by natural attenuation
[AD-A283809] p 1282 N95-19922

Acoustic and vibration attenuation composite material
[AD-D016585] p 1233 N95-22467

ATTITUDE (INCLINATION)

Nonlinear dynamics of the planar pitch attitude motion for a gravity-gradient satellite
[AD-A286407] p 1220 N95-22204

ATTITUDE INDICATORS

Assessment of a non-dedicated GPS receiver system for precise airborne attitude determination
[DE94-019309] p 1205 N95-21520

AUDIO EQUIPMENT

FIREDOC users manual, 3rd edition
[PB95-128674] p 1286 N95-21129

AUDITORY PERCEPTION

Determination of multiple sound sources
[AD-A286563] p 1504 N95-20823

Signal- and listener- based factors in complex auditory pattern perception
[AD-A285636] p 1450 N95-21101

AUDITORY SIGNALS

Signal- and listener- based factors in complex auditory pattern perception
[AD-A285636] p 1450 N95-21101

AUDITORY STIMULI

Temporary threshold shifts produced by high intensity freefield impulse noise in humans wearing hearing protection
[AD-A286289] p 1454 N95-22045

AUGER EFFECT

Angle resolved Auger electron spectroscopy: An alternate tool for identifying electronic excitation processes in solids
[AD-A285375] p 1238 N95-20555

Research studies on short wavelength lasers by selective Auger processes
[AD-A285620] p 1372 N95-21144

Micromachined silicon-based analytical microinstruments for space science and planetary exploration
[DE94-019306] p 1367 N95-21507

Auger spectrometry of atoms and molecules
[DE94-018052] p 1524 N95-21664

AUGER SPECTROSCOPY

Optical properties of silicon clusters deposited on the basal plane of graphite
[DE94-017529] p 1542 N95-20450

Angle resolved Auger electron spectroscopy: An alternate tool for identifying electronic excitation processes in solids
[AD-A285375] p 1238 N95-20555

Auger spectrometry of atoms and molecules
[DE94-018052] p 1524 N95-21664

AUGMENTATION

Cavity-QED enhancement of fluorescence yields in microdroplets
[DE94-018662] p 1506 N95-20030

Development and enhancement of a model of performance and decision making under stress in a real life setting
[AD-A285945] p 1449 N95-20393

Performance, defect behavior and carrier enhancement in low energy, proton irradiated p+nn+ InP solar cells
p 1319 N95-20518

Enhancements in the Livermore spectrum analysis package PIXEF
[DE95-002487] p 1272 N95-20895

Modeling tropospheric ducting effects on satellite-to-ground paths p 1295 N95-20936

Translational-energy-resolved studies of photographed carrier-induced reactions on semiconductor surfaces
[DE95-002944] p 1573 N95-21444

AUSTENITE

The effect of oxide inclusions on the kinetics of the austenite to ferrite transformation in low alloy steel weld metal
[DE94-018131] p 1253 N95-20676

AUSTENITIC STAINLESS STEELS

Tritium and decay helium effects on the fracture toughness properties of types 316L, 304L and 21Cr-6Ni-9Mn stainless steels
[DE95-001248] p 1252 N95-20216

Joining dissimilar stainless steels for pressure vessel components
[PB95-133005] p 1380 N95-21446

AUTOCORRELATION

Direct numerical simulation for premixed turbulent combustion modelling p 1249 N95-21082

Theory of spin dynamics in the classical two-dimensional heisenberg magnet
[PB95-133559] p 1502 N95-22138

AUTOIONIZATION

Angle resolved Auger electron spectroscopy: An alternate tool for identifying electronic excitation processes in solids
[AD-A285375] p 1238 N95-20555

Physics of correlated studies
[DE95-001204] p 1581 N95-21842

The two-electron problem and prospects for atomic collision theory on a numerical lattice
[DE94-017856] p 1528 N95-22265

AUTOMATA THEORY

Introduction to the FIRE engine: A C++ toolkit for Finite automata and Regular Expressions
[PB95-110599] p 1456 N95-19891

GPS-Squitter capacity analysis
[AD-A280037] p 1291 N95-20599

Correctness of some algorithms to generate finite automata for regular expressions
[PB95-127551] p 1465 N95-21022

Design and implementation of the FIRE engine: A c++ toolkit for finite automata and regular expressions
[PB95-132924] p 1467 N95-21415

AUTOMATIC CONTROL

High-performance packet switching architecture for ATM: Conventional solution and neural network solution
[PB95-110920] p 1312 N95-19935

Recognition of subsurface defects in machined ceramics by application of neural networks to laser scatter patterns
[DE94-018373] p 1264 N95-20018

Software fault tree analysis of concurrent Ada processes
[AD-A284979] p 1457 N95-20042

Passive monitoring for automated MMPP communication systems p 1293 N95-20927

13th European Annual Conference on Human Decision Making and Manual Control
[PB95-132874] p 1450 N95-21284

Robotic paint stripping cell
[AD-A279158] p 1279 N95-21976

AUTOMATIC PILOTS

Collected papers of the Soar/IFOR project, Spring 1994
[AD-A280063] p 1216 N95-20624

AUTOMATIC REPEAT REQUEST

Adaptive error-control scheme for 2-200 MHz Multiple-Mechanism Propagation Paths
p 1293 N95-20926

AUTOMATIC TEST EQUIPMENT

Development of a tester for evaluation of prototype thermal cells and batteries
[DE95-000540] p 1325 N95-20628

AUTOMATION

Implementation of electronic chain-of-custody, analysis requests, and data verification at Los Alamos National Laboratory
[DE94-018076] p 1407 N95-21666

AUTOMOBILE ENGINES

Natural gas converter performance and durability
[PB95-135554] p 1284 N95-21966

AUTOMOBILES

2nd International ADI seminar
[PB95-127734] p 1255 N95-21108

Electrorheology for smart automotive suspensions
[AD-A285543] p 1380 N95-21157

AUTOMORPHISMS

Classification of diagonal coset modular invariants
[PB95-111118] p 1489 N95-20259

Von Neumann algebra automorphisms and time-thermodynamics relation in general covariant quantum theories
[PB95-111084] p 1580 N95-20324

AUTONOMOUS NAVIGATION

Unknown-terrains navigation of a mobile robot using an array of sonars
[DE94-017902] p 1482 N95-21385

Elements of deliberative robot control
[PB95-107595] p 1482 N95-21412

Tom Thumb algorithm for planning simple vehicle motions
[PB95-107553] p 1484 N95-22156

AUTONOMY

Testing paradigm applied to network structure (revised)
[PB95-110706] p 1487 N95-19906

Robust agent control of an autonomous robot with many sensors and actuators
[AD-A280148] p 1479 N95-20011

Task parallel programming in Fx
[AD-A285136] p 1475 N95-20500

Lidar technologies for airborne and space-based applications
[DE95-002954] p 1302 N95-21448

Layered path planning for an autonomous mobile robot
[AD-A286138] p 1485 N95-22244

AUTOPSIES

Thorium-232 in human tissues: Metabolic parameters and radiation doses
[DE94-019275] p 1441 N95-20074

AUTOREGRESSIVE PROCESSES

EPSCoR supplemental grant for an application of neural networks to seismic signal discrimination
[AD-A285846] p 1414 N95-20878

Application of neural networks to seismic signal discrimination research findings
[AD-A285848] p 1415 N95-21308

AVALANCHES

SPICE macro model of a spryton with MOSFET's in the avalanche mode
[DE94-015744] p 1555 N95-21134

AVIONICS

Advanced Packaging Concepts for Digital Avionics
[AGARD-CP-562] p 1208 N95-20631

The impact of advanced packaging technology on modular avionics architectures p 1208 N95-20632

Standard Hardware Acquisition and Reliability Program (SHARP) advanced SEM-E packaging
p 1208 N95-20633

FASTPACK: Optimized solutions for modular avionics derived from a parametric study. Part 1: Platform features p 1208 N95-20634

FASTPACK: Optimized solutions for modular avionics derived from a parametric study. Part 2: Avionics
p 1209 N95-20635

The Advanced Avionics Subsystem Technology Demonstration Program p 1209 N95-20636

Ultra-Reliable Digital Avionics (URDA) processor
p 1209 N95-20638

MCMs for avionics: Technology selection and intermodule interconnection p 1210 N95-20641

High density monolithic packaging technology for digital/microwave avionics p 1211 N95-20646

High performance backplane components for modular avionics p 1212 N95-20653

Composite cases for airborne electronic equipment: A technology study and EMC p 1212 N95-20655

Modular supplies for a distributed architecture --- avionics packaging p 1213 N95-20657

Modular CNI avionics system p 1213 N95-20659

The opportunities for and challenges of common integrated electronics
[AD-A279991] p 1327 N95-20966

Systems engineering design and technical analyses for Strategic Avionics Crew-station Design Evaluation Facility (SACDEF)
[AD-A286239] p 1213 N95-22024

Evaluation of the Haworth-Newman avionics Display Readability Scale
[AD-A286127] p 1214 N95-22232

AXIAL FLOW TURBINES
Laser anemometry and viscous computation of the flow through an annular turbine cascade
[AD-A280070] p 1341 N95-20968
AXIOMS
Real time process algebra with infinitesimals
[PB95-110623] p 1488 N95-20055
On the Taylor test. Part 3: A continuum mechanics code analysis of steady plastic wave propagation
[DE95-002252] p 1501 N95-20869
Semantics for a fine lambda-calculus with de Bruijn indices
[PB95-127577] p 1492 N95-21372
Note on the characterizations of the compromise value
[PB95-135117] p 1499 N95-21709
Dyads: A generalisation of monads
[PB95-134052] p 1494 N95-21867
Adjunctions
[PB95-134078] p 1494 N95-21868
Formal specification and compositional verification of an atomic broadcast protocol
[PB95-110508] p 1472 N95-22351
AXISYMMETRIC BODIES
A model of an infinite length, axisymmetric, isotropic, forced thick shell
[AD-A285586] p 1386 N95-21212
AXISYMMETRIC FLOW
An advanced ECR ion source with a large uniformly distributed ECR plasma volume for multiply charged ion beam generation
[DE95-001078] p 1515 N95-20911
Direct numerical simulation of incompressible axisymmetric flows p 1363 N95-22464
AZOLES
Density functional studies of decomposition processes of energetic molecules
[AD-A286185] p 1510 N95-20327

B

BACKGROUND NOISE
Adaptive detection in stationary and nonstationary noise environments
[AD-A279581] p 1300 N95-21099
Monolithic low noise preamplifier for piezoelectric sensors
[AD-D016524] p 1333 N95-21865
BACKGROUND RADIATION
Resonant photon-graviton conversion in EM fields: From earth to heaven
[DE95-002784] p 1301 N95-21241
BACKSCATTERING
High energy photon-photon collisions
[DE94-017494] p 1532 N95-20388
Angle resolved Auger electron spectroscopy: An alternate tool for identifying electronic excitation processes in solids
[AD-A285375] p 1238 N95-20555
The effects of multihop HF propagation on the performance of OTH backscatter radars
p 1298 N95-20953
Measurements of radar backscatter from the ocean surface at 94 GHz as a function of wind speed, direction and the modulation by the ocean waves during the SAXON-FPN experiment p 1299 N95-20960
Sounder calibration with backscattering from Losquet Island in the presence of multipaths
p 1300 N95-20961
Multiple scatter theory of ocean sediments
[AD-A286033] p 1433 N95-20999
Analysis of subgrid models using direct and large-eddy simulations of isotropic turbulence p 1348 N95-21071
Modelling anisotropy and backscatter effects in the subgrid scale stress tensor p 1349 N95-21077
Investigation on the backscattering properties of Finnish boreal forests at C- and X-band: A semi-empirical modeling approach
[PB95-127692] p 1389 N95-21105
In-situ capability of ion beam modification and characterization of materials at Los Alamos National Laboratory
[DE95-002738] p 1534 N95-21236
X-band microwave backscattering from ocean waves
[DE94-016719] p 1309 N95-22241
Design and construction of a Ka-band scatterometer
[AD-A286296] p 1368 N95-22322
A dynamic localization model with stochastic backscatter p 1359 N95-22445
Local dynamic subgrid-scale models in channel flow
p 1360 N95-22447
BACKWARD FACING STEPS
Large-eddy simulation of a plane wake
p 1360 N95-22446
BACTERIA
A review of Microbially Induced Corrosion (MIC) of steel and a preliminary investigation to determine its occurrence in naval vessels
[MRL-GD-0048] p 1250 N95-19910
Bacterial luciferase: Determination of the structure by x-ray diffraction
[AD-A279699] p 1437 N95-20711
Microbial degradation of polymers used in electronics
[AD-A286526] p 1273 N95-21011
The Use of Cyanobacteria to Explore Basic Biological Processes
[DE94-019238] p 1440 N95-22066
Electrostatic basis for molecular recognition in photosynthesis
[DE95-002979] p 1440 N95-22075
BACTERIOLOGY
Microbiology and physiology of anaerobic fermentations of cellulose
[DE95-002899] p 1438 N95-20917
BAGGAGE
Test and Evaluation Plan (TEP) for Improvised Explosive Device Screening Systems (IEDSS)
[AD-A286382] p 1203 N95-22319
BALL BEARINGS
Modeling of rolling element bearing mechanics. Computer program user's manual
[NASA-CR-196557] p 1381 N95-21692
Modeling of rolling element bearing mechanics. Theoretical manual
[NASA-CR-196556] p 1381 N95-21705
BALLISTIC MISSILES
Issues in the flight qualification of a space power reactor
[DE95-001606] p 1223 N95-21840
BALLISTICS
Tungsten-uranium penetrator target interaction
[DE95-000847] p 1387 N95-21364
BALLOON FLIGHT
Comparison of meteorological data with fitted values extracted from projectile trajectory
[AD-A285921] p 1428 N95-19989
BALLOON-BORNE INSTRUMENTS
An assessment of image reconstruction from balloon-borne and the IRAS data p 1592 N95-21752
CALIOPE and TAISIR airborne experiment platform
[DE94-018328] p 1310 N95-22299
BALLOONING MODES
Hybrid model in general geometry
[DE95-002614] p 1553 N95-20437
Solar flare MDH
[AD-A279894] p 1602 N95-20593
Current diffusive ballooning mode in second stability region of tokamaks
[DE94-770690] p 1554 N95-20683
Ideal Magnetohydrodynamic stabilities in JT-60 and D3-D tokamak plasmas
[DE94-770684] p 1555 N95-20987
Investigations of VH-mode in D3-D and JET
[DE94-015859] p 1556 N95-21142
Numerical analysis of energetic particle stabilization of ballooning modes in finite-aspect-ratio tokamaks
[DE94-631397] p 1556 N95-21164
BANACH SPACE
Weighted strongly elliptic operators on lie groups
[PB95-110847] p 1487 N95-19917
Sharp determinants
[PB95-111068] p 1488 N95-19944
Banach spaces with small spaces of operators
[PB95-111134] p 1489 N95-20273
BAND STRUCTURE OF SOLIDS
Observation of excitonic and band-to-band behavior in ordered InGaP2 alloys
[DE94-018891] p 1314 N95-20341
Photoreflectance and x ray diffraction study of semiconductor heterostructures and quantum wells
[PB95-127049] p 1582 N95-22432
BANDPASS FILTERS
A technique for increasing the bandwidth of high performance electrical backplanes p 1212 N95-20651
BANDWIDTH
Split-C and active messages under SUNMOS on the Intel Paragon
[DE94-011418] p 1474 N95-20123
Hydrostatic force sensor
[DE94-018923] p 1364 N95-20321
A technique for increasing the bandwidth of high performance electrical backplanes p 1212 N95-20651
LLNL/Lion Precision LVDT amplifier
[DE95-001504] p 1327 N95-20854
Line-of-sight multipath propagation measurements at 15 GHz over 500 MHz bandwidth p 1296 N95-20944
Mitigation of effects of multiple path nulls at super-high frequencies through diversity and networking
p 1297 N95-20948
Ultra-high aggregate bandwidth two-dimensional multiple-wavelength diode laser arrays
[AD-A280098] p 1372 N95-21019
A framework for symmetric band reduction and tridiagonalization
[DE95-002919] p 1476 N95-21341
Unlimited-bandwidth distributed optical phase modulators and detectors: Design and fabrication issues
[DE94-017418] p 1545 N95-21509
TDX: A high-bandwidth crossbar-switched communication paradigm
[DE94-017187] p 1311 N95-22407
BARENTS SEA
Monthly mean sea ice data from the Polar Ice Prediction System, the Regional Polar Ice Prediction System-Barents Sea and the Regional Polar Ice Prediction System-Greenland Sea
[AD-A280095] p 1433 N95-21018
BARIUM ALLOYS
Polyurethane self-priming topcoats
[AD-D016204] p 1274 N95-21154
Polyurethane self-priming topcoats
[AD-D016205] p 1274 N95-21155
BARIUM FLUORIDES
Liquid xenon as a potential laser host medium
[AD-A285365] p 1370 N95-20550
BARIUM OXIDES
Neutron diffraction study of the magnetic ordering of BaCuO(2+x)
[DE95-001357] p 1572 N95-21297
High temperature superconducting films and multilayers for electronics
[AD-A279545] p 1331 N95-21693
High performance YBCO films
[AD-A279560] p 1276 N95-21695
Local texture and strongly linked conduction in spray-pyrolyzed TlBa2Ca2Cu3O(8+x) deposits
[DE94-017887] p 1578 N95-22269
BAROCLINITY
Fourth International Symposium on Stratified Flows, volume 1
[AD-A286450] p 1354 N95-21583
Radar studies of aviation hazards
[AD-A285845] p 1203 N95-21831
BARRIER LAYERS
Improved broadband waveguide pressure window
[AD-D016487] p 1306 N95-21834
BARYONS
Diffusion enhances spontaneous electroweak baryogenesis
[DE94-017574] p 1512 N95-20451
Properties of strange-matter stars
[DE95-002329] p 1599 N95-20873
Strange hadronic matter
[DE94-019345] p 1521 N95-21484
The 9th INS scientific computational programs
[DE94-770780] p 1526 N95-22051
There might be two kinds of dibaryon
[DE94-014417] p 1526 N95-22058
Proton and produced particle distributions from Au+Au collisions at 11.6 A GeV/c
[DE94-018634] p 1530 N95-22392
BASALT
D/H ratios and H2O contents of mantle-derived amphibole megacrysts from Dish Hill, California
p 1416 N95-21781
Solar helium and neon in the Earth
p 1419 N95-21793
The primary carbon and the formation of carbon species in terrestrial magmas p 1420 N95-21797
Solubilities of nitrogen and noble gases in basalt melt
p 1422 N95-21807
Subduction of hydrated basalt of the oceanic crust: Implications for recycling of water into the upper mantle and continental growth p 1423 N95-21814
BASE FLOW
Free shear layers, base pressure and bluff-body drag
[AD-A286316] p 1200 N95-20175
Instability of streamwise vortices in plane channel flows p 1344 N95-21049
Nonlinear interaction between a pair of oblique modes in a supersonic mixing layer: Long-wave limit
[NASA-CR-197380] p 1357 N95-22173
BASE PRESSURE
Free shear layers, base pressure and bluff-body drag
[AD-A286316] p 1200 N95-20175
BASES (CHEMICAL)
Control of continuous phase PH using visible light to activate PH-dependent fibers and gels in a controlled and reversible manner
[AD-D016532] p 1543 N95-20728
BASIC (PROGRAMMING LANGUAGE)
BASIC program for power spectrum estimation
[DE95-002228] p 1468 N95-21515
Regularity of BPa-systems is decidable
[PB95-135489] p 1468 N95-21619

BATCH PROCESSING
Stochastic network processes
[AD-A279905] p 1475 N95-20566
BATHING
Personal hygiene body wipe
[AD-A286092] p 1454 N95-22274
BATHS
The application of electrodialysis to extend the lifetime of commercial electroplating baths
[DE95-000868] p 1246 N95-22012
BATHYMETERS
A modal analysis of currents in a Pacific Atoll lagoon
[AD-A283721] p 1431 N95-19971
Simulation of laser bathymetry for irregular bottoms
[PB95-133518] p 1434 N95-21320
BAUSCHINGER EFFECT
Residual stress analysis in swage autofrettaged thick-walled cylinders by position-sensitive x-ray diffraction techniques
[AD-A286383] p 1388 N95-22320
BAYES THEOREM
An object-oriented optimization systems
[DE94-016190] p 1459 N95-20165
Beyond maximum entropy: Fractal Pixon-based image reconstruction p 1593 N95-21757
Bayesian analysis of semiparametric proportional hazards models
[AD-A279394] p 1499 N95-21946
BAYS (TOPOGRAPHIC FEATURES)
Measurements of radar backscatter from the ocean surface at 94 GHz as a function of wind speed, direction and the modulation by the ocean waves during the SAXON-FPN experiment p 1299 N95-20960
BEAM CURRENTS
Induction linacs for heavy ion fusion
[DE95-002357] p 1534 N95-20891
Emittance growth due to negative-mass instability above transition
[DE95-002527] p 1534 N95-20900
Beam instability studies at the APS
[DE95-001448] p 1537 N95-21503
Very high-power electron-beam transport in long gas cells from 10(exp -3) to 10(exp 3) Torr N2
[DE95-002611] p 1539 N95-22306
Bunched beam instability with frequency spread
[DE94-018632] p 1539 N95-22357
BEAM INJECTION
Transition-energy crossing with a gamma(sub t)(-)jump
[DE94-017315] p 1531 N95-20021
ALT-2 armor tile design for upgraded TEXTOR operation
[DE94-015749] p 1549 N95-20143
A tau-charm-factory at Argonne
[DE94-016913] p 1510 N95-20360
Plasma shape experiments for an optimized tokamak
[DE94-017508] p 1553 N95-20445
Experimental investigation of molecular beam injection in HL-1 tokamak
[DE94-631456] p 1556 N95-21165
Fusion power production in TFTR
[DE95-002756] p 1557 N95-21240
Heating and transport in TFTR D-T plasmas
[DE95-002812] p 1558 N95-21242
The 12-GeV/c beam transfer and absorber lines for the Superconducting Super Collider
[DE95-002100] p 1538 N95-21733
Experience at the Los Alamos Meson Physics Facility with the use of alloy Inconel 718 as an enclosure for a beam degrader and as a proton beam entry window
[DE94-018289] p 1538 N95-22050
Gas-dynamic trap diagnostic complex for study on plasma heating and power atomic beam injection
[DE94-633377] p 1529 N95-22283
Low emittance lattices for electron storage rings revisited
[DE94-017302] p 1540 N95-22391
BEAM INTERACTIONS
Emittance growth due to negative-mass instability above transition
[DE95-002527] p 1534 N95-20900
Simulation of beam-beam lifetime for LEP
[DE95-002888] p 1536 N95-21334
Experience at the Los Alamos Meson Physics Facility with the use of alloy Inconel 718 as an enclosure for a beam degrader and as a proton beam entry window
[DE94-018289] p 1538 N95-22050
Recent results in analysis and simulation of beam halo
[DE94-018313] p 1539 N95-22298
BEAM SPLITTERS
Eigenmode method for electromagnetic synthesis of diffractive elements with three-dimensional profiles
[PB95-127726] p 1301 N95-21107
BEAM SWITCHING
Angle diversity on digital microwave links: Antenna design and experimental results p 1297 N95-20947
BEAM WAVEGUIDES
The efficiency calibration of the DSS-24 34-meter beam-waveguide antenna p 1305 N95-21542
BEAMFORMING
Modeling the dynamics of charged-particle beams using a Fokker-Planck approach
[DE95-001458] p 1531 N95-19983
Crystalline beam in a storage ring: How long can it last?
[DE94-017303] p 1563 N95-20014
Signal-to-noise gain from adaptive matched-field beamforming of multidimensional acoustic arrays
[AD-A285671] p 1503 N95-20084
Analytic models for beam propagation and far-field patterns in slab and bow-tie x ray lasers
[DE94-016607] p 1372 N95-21173
Measurements of the Auburn ECE optical system parameters for temperature fluctuation measurements on TEXT-U
[DE94-019217] p 1562 N95-22120
BEAMS (RADIATION)
Experimental and theoretical evaluation of elastic waves in curved layered media
[AD-A286578] p 1504 N95-20918
Diffraction applications using the energy dispersive beamline, X6A, at NSLS
[DE94-019287] p 1572 N95-21408
Self-starting femtosecond pulse generation from a Ti:sapphire laser synchronously pumped by a pointing-stabilized mode-locked Nd:YAG laser
[DE94-019319] p 1374 N95-21480
RF beam control for the AGS Booster
[DE95-001485] p 1538 N95-21720
BEAMS (SUPPORTS)
Static stability of a three-dimensional space truss p 1220 N95-20533
Vibration analysis of the AN/SPS-67(V)3 surface search radar
[AD-A286050] p 1302 N95-21324
BEARINGS
Fracture analysis of an all-ceramic bearing system
[AD-A285056] p 1269 N95-20486
BEDROCK
VTT test borehole for bedrock investigations
[PB95-132965] p 1427 N95-22095
BEND TESTS
Processing and mechanical properties of laminar Al2O3-Ni3Al composites
[DE94-019332] p 1230 N95-21481
BENDING
Inelastic bending and torsion of steel I-beams
[PB94-208378] p 1384 N95-19975
BENZENE
Refractive index change in dissociating shocked benzene
[DE94-019015] p 1541 N95-20352
Effect of external stress on the transport of fluids in thermoplastic resin systems
[AD-A279993] p 1270 N95-20596
Aromatics oxidation and soot formation in flames
[DE95-001803] p 1241 N95-21280
NMR relaxation behavior of the head group of SHBS in lamellar liquid crystals
[AD-A279124] p 1574 N95-21599
BENZOIC ACID
Evaluation of an immobilized cell bioreactor for degradation of meta- and para-nitrobenzoate
[AD-A279719] p 1516 N95-20993
Polyurethane self-priming topcoats
[AD-D016204] p 1274 N95-21154
Polyurethane self-priming topcoats
[AD-D016205] p 1274 N95-21155
BERYLLIUM COMPOUNDS
Beryllium based multilayers for normal incidence extreme ultraviolet reflectivity
[DE94-015560] p 1274 N95-21175
BETA PARTICLES
Wall stabilization effects in D3-D high beta discharges
[DE94-017509] p 1554 N95-20446
High efficiency GaP power conversion for Betavoltaic applications p 1323 N95-20540
Radioactive check sources for alpha and beta sensitive radiological instrumentation
[DE94-016477] p 1366 N95-21138
BETATRONS
Modeling of beam dynamics and comparison with measurements for the Advanced Light Source (ALS)
[DE94-017970] p 1532 N95-20495
Behaviour of space-charge dominated ion beams in storage rings
[DE94-015845] p 1517 N95-21140
BIAS
A charge distribution analysis instrument for catalysis and material science applications
[DE94-016489] p 1364 N95-20233
Heuristic genetic algorithms for constrained problems. Part 1: Principles
[PB95-132031] p 1467 N95-21374
BIBLIOGRAPHIES
Bibliography of scientific publications 1975-1993
[AD-A279767] p 1444 N95-20977
FIREDOC users manual, 3rd edition
[PB95-128674] p 1286 N95-21129
Bibliography of Lewis Research Center technical publications announced in 1993
[NASA-TM-106666] p 1589 N95-21187
NASA Langley scientific and technical information output: 1994, volume 1
[NASA-TM-109170-VOL-1] p 1589 N95-21189
Utilizing artificial neural networks in network flow analysis: An annotated bibiliography
[DE95-002453] p 1482 N95-21522
Aeronautical engineering: A continuing bibliography with indexes (supplement 315)
[NASA-SP-7037(315)] p 1199 N95-21640
NASA patent abstracts bibliography: A continuing bibliography. Section 2: Indexes (supplement 46)
[NASA-SP-7039(46)-SECT-2] p 1590 N95-21948
Age 60 study. Part 1: Bibliographic database
[AD-A286245] p 1446 N95-22027
Studies in nonlinear problems of energy
[DE95-001387] p 1356 N95-22148
BICRYSTALS
Simulations of the dislocation array at Ge/Si interfaces
[DE94-017680] p 1565 N95-20244
BINARY CODES
Adaptive error-control scheme for 2-200 MHz Multiple-Mechanism Propagation Paths p 1293 N95-20926
Scalable programming environment
[AD-A286390] p 1472 N95-22201
BINARY DATA
Long sequence correlation coprocessor
[AD-D016558] p 1313 N95-20280
Error probabilities of FFH/BFSK with noise normalization and soft decision viterbi decoding in a fading channel with partial-band jamming
[AD-A280041] p 1498 N95-20620
Eigenmode method for electromagnetic synthesis of diffractive elements with three-dimensional profiles
[PB95-127726] p 1301 N95-21107
Design, fabrication, and characterization of reflective diffractive optical elements in Si for free-space optical interconnects
[AD-A286416] p 1547 N95-22205
Synthesis and characterization of single-source molecular precursors to binary metal sulphides: Bis(diethyldithiocarbamato) M(2)trialkylphosphine (M = Zn and Cd) adducts
[AD-A279746] p 1248 N95-22385
BINARY MIXTURES
Molecular-based study of solutions in supercritical solvents
[DE94-019326] p 1580 N95-21420
BINARY STARS
Relativistic binary neutron star coalescence
[DE94-019311] p 1600 N95-21479
BINDERS (MATERIALS)
Polyurethane self-priming topcoats
[AD-D016204] p 1274 N95-21154
Polyurethane self-priming topcoats
[AD-D016205] p 1274 N95-21155
BINOCULAR VISION
Factors affecting the perception of luning in monocular regions of partial binocular overlap displays
[AD-A286287] p 1547 N95-22044
BIOASSAY
Monitoring bioremediation of Volatile Organic Compounds (VOCs) using Fourier Transform Infrared (FT-IR) spectrometry
[AD-A279631] p 1403 N95-20456
Flow cytometry: A powerful technology for measuring biomarkers
[DE94-018284] p 1440 N95-22296
BIOASTRONAUTICS
Annual program analysis of the NASA Space Life Sciences Research and Education Support Program
[NASA-CR-197298] p 1439 N95-21529
BIOCHEMISTRY
Microbiology and physiology of anaerobic fermentations of cellulose
[DE95-002899] p 1438 N95-20917
Potential-of-mean-force description of ionic interactions and structural hydration in biomolecular systems
[DE95-000859] p 1438 N95-21366
Effect of increased venous backflow on the release of cardiac hormone. Fine structural, immunohistochemical, and biochemical study
[PB95-130399] p 1445 N95-21424

Nitrogen control of chloroplast differentiation
[DE95-002797] p 1439 N95-21526

BIOCONVERSION

Bioconversion of coal derived synthesis gas to liquid fuels
[DE94-017381] p 1282 N95-19927

Bioconversion of coal derived synthesis gas to liquid fuels
[DE94-018849] p 1314 N95-20339

Anaerobic Treatment of Municipal Solid Waste and Sludge for Energy Production and Recycling of Nutrients
[DE95-700217] p 1315 N95-20369

Anaerobic digestion analysis model: User's manual
[DE94-011858] p 1437 N95-20471

Producing liquid fuels from biomass
[DE95-717458] p 1398 N95-22425

BIODEGRADABILITY

Investigation on research for degradable plastics
[DE94-796550] p 1277 N95-21714

BIODEGRADATION

A review of Microbially Induced Corrosion (MIC) of steel and a preliminary investigation to determine its occurrence in naval vessels
[MRL-GD-0048] p 1250 N95-19910

Evaluation of an immobilized cell bioreactor for degradation of meta- and para-nitrobenzoate
[AD-A279719] p 1516 N95-20993

Microbial degradation of polymers used in electronics
[AD-A286526] p 1273 N95-21011

BIODYNAMICS

Analysis of musculo-skeletal loading using electromyography and biomechanical modelling
[PB95-135828] p 1444 N95-21007

BIOELECTRICITY

Magnetic source imaging of visually evoked and oscillatory electrical activity of the human brain
[PB95-127205] p 1448 N95-22476

BIOENGINEERING

Seminar on Biomedical Engineering 1993
[PB95-104402] p 1443 N95-20971

Calculation of atom-centered partial charges for heme
[DE94-014447] p 1520 N95-21375

Proposal for a tutorial on Minimal Length Encoding (MLE) in molecular biology
[DE94-015076] p 1438 N95-21376

Command history, 1993
[AD-A279775] p 1446 N95-21989

Life Sciences Division and Center for Human Genome Studies
[DE94-017796] p 1440 N95-22065

BIOGEOCHEMISTRY

Closure on the global carbon cycle
[DE94-018617] p 1404 N95-20991

BIOINSTRUMENTATION

Mechanism of the amperometric response of a proposed glucose sensor based on a polypyrrole-tubule-impregnated membrane
[AD-A279836] p 1365 N95-20431

BIOLOGICAL EFFECTS

Aerospace medicine and biology: A continuing bibliography with indexes (supplement 399)
[NASA-SP-7011(399)] p 1446 N95-21947

The Use of Cyanobacteria to Explore Basic Biological Processes
[DE94-019238] p 1440 N95-22066

Optical radiation: Health based exposure limits for electromagnetic radiation in the wavelength range from 100 nanometer to 1 millimeter
[PB95-132767] p 1447 N95-22083

Urban air carcinogens and their effects on health
[DE95-002259] p 1447 N95-22285

Study of pulsed laser effects on living tissues
[PB95-131330] p 1447 N95-22361

BIOLOGICAL MODELS (MATHEMATICS)

A physiological neural network for saccadic eye movement control
[AD-A279599] p 1441 N95-20301

Modeling platform dynamics and physiological response to short arm centrifugation
[AD-A279640] p 1442 N95-20457

Calculation of atom-centered partial charges for heme
[DE94-014447] p 1520 N95-21375

Discovering related DNA sequences via mutual information
[DE95-001101] p 1440 N95-22067

BIOLUMINESCENCE

Bacterial luciferase: Determination of the structure by x-ray diffraction
[AD-A279699] p 1437 N95-20711

BIOMAGNETISM

Evaluation of superconducting quantum interference devices interfaced with digital signal processing electronics for biomagnetic applications
[DE94-016186] p 1289 N95-20164

Source distribution of visual evoked neuromagnetic responses
[PB95-127643] p 1445 N95-21348

Magnetic source imaging of visually evoked and oscillatory electrical activity of the human brain
[PB95-127205] p 1448 N95-22476

BIOMASS

Assessment of liquefaction and pyrolysis systems
[PB95-129797] p 1236 N95-20290

Radiative forcing calculations for CH3Cl
[DE94-019018] p 1402 N95-20355

Investigation on the backscattering properties of Finnish boreal forests at C- and X-band: A semi-empirical modeling approach
[PB95-127692] p 1389 N95-21105

A low energy continuous reactor separator for the production of ethanol from corn grits/starch and biomass streams
[DE95-002256] p 1283 N95-21356

Hydrothermal conversion of carbohydrates and related compounds
[PB95-134011] p 1396 N95-22175

BIOMASS ENERGY PRODUCTION

Producing liquid fuels from biomass
[DE95-717458] p 1398 N95-22425

BIOMEDICAL DATA

A 3D stereo data visualization and representation
[AD-A284788] p 1449 N95-20064

BIOMETRICS

DSP control of superconducting quantum interference devices
[DE94-016193] p 1313 N95-20168

BIONICS

Analysis of musculo-skeletal loading using electromyography and biomechanical modelling
[PB95-135828] p 1444 N95-21007

BIOPHYSICS

Physics Division research and development
[DE94-017685] p 1501 N95-20246

Israel Physical Society Annual Meeting 1994
[DE94-630140] p 1565 N95-20261

BIOPOLYMERS

Monomer mapping: A PC-based software tool facilitating the determination of monomer compositions from mass spectrometric molecular weight data
[PB95-132155] p 1275 N95-21470

BIOREACTORS

Bioconversion of coal derived synthesis gas to liquid fuels
[DE94-017381] p 1282 N95-19927

Bioconversion of coal derived synthesis gas to liquid fuels
[DE94-018849] p 1314 N95-20339

Evaluation of an immobilized cell bioreactor for degradation of meta- and para-nitrobenzoate
[AD-A279719] p 1516 N95-20993

BIOSYNTHESIS

Nitrogen control of chloroplast differentiation
[DE95-002797] p 1439 N95-21526

The molecular mechanics program DUPLEX: Computing structures of carcinogen modified DNA by surveying the potential energy surface
[DE94-019153] p 1439 N95-21606

BIOT NUMBER

Transport phenomena in the micropores of plug-type phase separators
[NASA-TM-108479] p 1340 N95-20561

BIOTECHNOLOGY

Spinoff, 1994
[NASA-NP-214] p 1594 N95-21893

BIOTITE

Noble gas isotopes and halogens in volatile-rich inclusions in diamonds p 1417 N95-21784

BIPOLAR TRANSISTORS

Physical Si(1-x)Ge(x)/Si heterojunction bipolar transistor model for device and circuit simulation
[PB95-110896] p 1312 N95-19934

Non-linear A/D converters for integrated silicon smart sensors
[PB94-208402] p 1330 N95-21590

BIREFRINGENCE

Physical-chemical studies on rodlike polymer compositions
[AD-A285361] p 1269 N95-20548

3-D TECATE/BREW: Thermal, stress, and birefringent ray-tracing codes for solid-state laser design
[DE95-000330] p 1376 N95-22301

BISMALEIMIDE

Thermo-mechanical fatigue of polymer matrix composites
[AD-A285931] p 1267 N95-20390

BISMUTH

Research on the power generation system with thermoelectric conversion elements
[DE95-714804] p 1397 N95-22309

BISMUTH ALLOYS

A new metallographic procedure for edge retention of enclosed surfaces
[DE94-017549] p 1261 N95-22048

BISMUTH COMPOUNDS

Sputter deposition of multilayer thermoelectric films: An approach to the fabrication of two-dimensional quantum wells
[DE95-002396] p 1272 N95-20892

BISMUTH OXIDES

Effects of neutron irradiation on the London penetration depth for polycrystalline Bi(1.8)Pb(0.3)Sr2Ca2Cu3O10 superconductor
[DE94-019335] p 1573 N95-21483

BIT ERROR RATE

Error probabilities of FFH/BFSK with noise normalization and soft decision viterbi decoding in a fading channel with partial-band jamming
[AD-A280041] p 1498 N95-20620

Turbo codes for deep-space communications
p 1304 N95-21535

High speed optical storage technology
[AD-A285788] p 1456 N95-22400

BITS

Design of a massively parallel computer using bit serial processing elements
[NASA-CR-197365] p 1479 N95-22406

BLACK HOLES (ASTRONOMY)

Cosmological string solutions by dimensional reduction
[DE95-002858] p 1599 N95-21245

BLANKETS (FUSION REACTORS)

MHD pressure drop in ducts with imperfectly insulating coatings
[DE95-002852] p 1558 N95-21244

MHD-flow in slotted channels with conducting walls
[DE94-018370] p 1559 N95-21388

BLOCK COPOLYMERS

Reactive compatibilization of polymer blends
[AD-A284836] p 1263 N95-19893

Hierarchical structure in advanced polymers. Phase behaviour, orientation, properties
[AD-A285938] p 1268 N95-20392

Morphology of highly textured E/EP diblock copolymers
[AD-A279813] p 1269 N95-20582

BLOCKING

Duality and equivalencies in closed tandem queueing networks
[PB95-132502] p 1482 N95-21271

BLOOD

Preclinical investigation of lyophilized platelet preparations
[AD-A286079] p 1443 N95-20851

Solubilities of nitrogen and helium in water and blood at 37 C and pressures of up to 11 ATA
[AD-A286269] p 1446 N95-22003

BLOOD CELLS

Effect of increased venous backflow on the release of cardiac hormone. Fine structural, immunohistochemical, and biochemical study
[PB95-130399] p 1445 N95-21424

BLOOD FLOW

Effect of increased venous backflow on the release of cardiac hormone. Fine structural, immunohistochemical, and biochemical study
[PB95-130399] p 1445 N95-21424

BLOOD PLASMA

Effect of increased venous backflow on the release of cardiac hormone. Fine structural, immunohistochemical, and biochemical study
[PB95-130399] p 1445 N95-21424

Hypervolemia in men from drinking hyperhydration fluids at rest and during exercise
[NASA-TM-4657] p 1439 N95-21544

BLOOD VESSELS

Carboxyhemoglobin formation due to transient exposure to high level carbon monoxide: Experimental results and an explanatory model
[AD-A285476] p 1444 N95-20979

BLOOD VOLUME

Hypervolemia in men from drinking hyperhydration fluids at rest and during exercise
[NASA-TM-4657] p 1439 N95-21544

Intramyocardial blood volume and oxygen exchange
[PB95-108015] p 1445 N95-21580

BLOWDOWN WIND TUNNELS

The dynamic approach to rotor blade research: ARA's oscillatory test facility
[ARA-MEMO-405] p 1200 N95-20758

BLUFF BODIES

Free shear layers, base pressure and bluff-body drag
[AD-A286316] p 1200 N95-20175

Research on bluff body vortex wakes
[AD-A286319] p 1200 N95-20177

BLUNT BODIES
Shock wave interactions in hypervelocity flow [AD-A286507] p 1357 N95-22212
BODY CENTERED CUBIC LATTICES
Metastable bcc phase formation in the Nb-Cr-Ti system [DE94-016212] p 1255 N95-21137
Novel materials and devices from self-assembled periodic structures [AD-A286499] p 1232 N95-22211
BODY KINEMATICS
A method to determine the kinematics of the lower limbs of a subject pedaling a bicycle using encoders and accelerometers [NASA-CR-197401] p 1453 N95-21866
BODY-WING CONFIGURATIONS
Open Skies project computational fluid dynamic analysis [AD-A285928] p 1200 N95-19991
BOILERS
Recent reflux receiver developments under the US DOE program [DE95-001622] p 1393 N95-20861
BOLTZMANN TRANSPORT EQUATION
Numerical investigations of low-density nozzle flow by solving the Boltzmann equation [NASA-TM-110492] p 1354 N95-21675
An analytical, inelastic, space and time dependent electron distribution for electrically excited gases [DE95-003478] p 1528 N95-22223
BOLTZMANN-VLASOV EQUATION
Evaluating impedances in a Sacherer integral equation [DE94-016823] p 1489 N95-20266
Quantum diffusion [DE95-001015] p 1580 N95-21264
Explicit analytical solution of the nonlinear Vlasov Poisson system [DE94-628931] p 1500 N95-21592
BOMBER AIRCRAFT
Bomber force 2000: Operational concepts for long-range combat aircraft [AD-A279378] p 1206 N95-20181
Systems engineering design and technical analyses for Strategic Avionics Crew-station Design Evaluation Facility (SACDEF) [AD-A286239] p 1213 N95-22024
BONDED JOINTS
Attachment methodology for composite cylinder assembly [AD-D016578] p 1227 N95-20459
BONDING
The Modified Embedded Atom Method [DE94-015746] p 1564 N95-20142
Spectroscopic studies of glass structure [DE94-016551] p 1268 N95-20468
Atomically resolved structure and bonding of delta-doped boron layers on Si(001) [AD-A279820] p 1513 N95-20586
Reliability assessment of Multichip Module technologies via the Triservice/NASA RELTECH program p 1210 N95-20643
Assuring Known Good Die (KGD) for reliable, cost effective MCMs p 1210 N95-20644
Selenophene transition metal complexes [DE95-001675] p 1260 N95-21841
Towards tailored interphase formation utilizing surface-bound benzylsulfonium salts as cationic initiators [AD-A286461] p 1280 N95-22259
The Modified Embedded Atom Method [DE94-017958] p 1248 N95-22273
BOOLEAN ALGEBRA
Using local optimality criteria for efficient information retrieval with redundant information filters [AD-A279603] p 1587 N95-20302
BOOMS (EQUIPMENT)
Ohmsett test of NOFI Vee-Sweep and NOFI 600S Oilboom [AD-A279525] p 1408 N95-21685
BOREHOLES
VTT test borehole for bedrock investigations [PB95-132965] p 1427 N95-22095
BORIDES
Magnetic field dependence of the correlation gap in SmB6 [DE95-001684] p 1574 N95-21570
BORON
Processing and characterization of Ni-Al-Fe-B shape-memory alloy wires produced by rapid solidification [DE94-017702] p 1250 N95-20020
Boron carbide-based coatings on graphite for plasma facing components [DE94-017976] p 1269 N95-20570
Atomically resolved structure and bonding of delta-doped boron layers on Si(001) [AD-A279820] p 1513 N95-20586
BORON ALLOYS
Atom probe field ion microscopy of type 308 CRE stainless steel welds [DE94-019162] p 1261 N95-22127
BORON CARBIDES
Boron carbide-based coatings on graphite for plasma facing components [DE94-017976] p 1269 N95-20570
B4C-SiC reaction-sintered coatings on graphite plasma facing components [DE94-019105] p 1230 N95-21553
BORON ISOTOPES
Boron neutrino flux and the MSW solution of the solar neutrino problem [DE95-001861] p 1521 N95-21443
BORON NITRIDES
Effects of ambient conditions on the adhesion of cubic boron nitride films on silicon substrates [DE94-016779] p 1266 N95-20281
Radio-frequency techniques at the ISIS pulsed muon source [PB95-129854] p 1529 N95-22303
BOROSILICATE GLASS
International collaboration program on innovative chemical processing of superior electronic and optical materials [AD-A285122] p 1226 N95-20105
BOSE GEOMETRY
The dynamic structure function of Bose liquids in the deep inelastic regime [DE94-629077] p 1527 N95-22182
BOSONS
CDF top results in the lepton + jets channel [DE95-000641] p 1507 N95-20131
Search for W pair production with dilepton decay modes at D0 [DE95-000724] p 1508 N95-20134
Measurements of the mass and width of the W boson from CDF [DE94-015380] p 1511 N95-20415
Search for right-handed currents in the decay chain of K(+) yields muon(+)nu(sub muon), muon(+) yields e(+)nu(sub e)nu(bar)(sub muon) [DE94-770606] p 1514 N95-20756
Unbinned maximum likelihood fit for the CP conserving couplings for W + photon production at CDF [DE95-001471] p 1514 N95-20852
Calculation of Z plus four jet production at the Tevatron [PB95-130472] p 1580 N95-21230
Measuring A(sub b) with polarized beams at SLC [DE95-002865] p 1519 N95-21248
The 9th INS scientific computational programs [DE94-770780] p 1526 N95-22051
Tests of structure functions using lepton pairs: W-charge asymmetry at CDF [DE95-000560] p 1527 N95-22122
Electroweak boson pair production in p(-p) collisions at the square root of s = 1.8 TeV [DE95-000725] p 1527 N95-22194
Physics at the Fermilab Collider [DE95-000726] p 1539 N95-22195
BOTTLES
Investigation on research for degradable plastics [DE94-796550] p 1277 N95-21714
BOUNDARIES
Hindered settling computations using a parallel boundary element method [DE94-014286] p 1339 N95-20137
Antiphase boundaries as nucleation centers in low-temperature epitaxial growth [AD-A279895] p 1568 N95-20594
BOUNDARY CONDITIONS
Influence of primary boundary conditions on the buckling of shallow cylindrical shells [PB94-208352] p 1384 N95-20003
The (e,2e) calculations with the final-state boundary condition [DE94-631342] p 1509 N95-20198
Continuum transient and frozen startup behavior of conventional and gas-loaded heat pipes [AD-A284297] p 1339 N95-20250
On the sputtering of metals and insulators: A nonlinear evolution problem with nonlinear boundary condition [DE95-001456] p 1254 N95-20792
Numerical simulation of spatially-developing planar jets p 1351 N95-21087
Understanding the mechanisms of length scale competition: The sine-Gordan soliton case [DE94-016201] p 1500 N95-21136
Modeling open boundary conditions by using the optimization approach [AD-A285548] p 1433 N95-21158
Domain processes in ferroelectric ceramics [AD-A279567] p 1276 N95-21697
Absorbing boundary condition for floating two-dimensional objects in current and waves [PB95-132882] p 1356 N95-22063
Inverse and control problems in electromagnetics [AD-A286438] p 1310 N95-22250
Electro-optic effect in the PESO acousto-optic modulator [AD-A286355] p 1548 N95-22255
BOUNDARY ELEMENT METHOD
Analyses of some benchmark cases in fracture mechanics using boundary element method [PB95-110888] p 1384 N95-19930
Hindered settling computations using a parallel boundary element method [DE94-014286] p 1339 N95-20137
BOUNDARY INTEGRAL METHOD
Analyses of some benchmark cases in fracture mechanics using boundary element method [PB95-110888] p 1384 N95-19930
Inverse and control problems in electromagnetics [AD-A286438] p 1310 N95-22250
BOUNDARY LAYER CONTROL
Flow coefficient behavior for boundary layer bleed holes and slots [NASA-TM-106846] p 1338 N95-19953
Supersonic laminar flow control research [NASA-CR-196049] p 1353 N95-21340
Experimental investigations of on-demand vortex generators p 1361 N95-22451
BOUNDARY LAYER FLOW
Role of pressure diffusion in non-homogeneous shear flows p 1345 N95-21053
Simulations of bypass transition for spatially evolving disturbances p 1349 N95-21079
Experiments on the flow field physics of confluent boundary layers for high-lift systems [NASA-CR-197318] p 1201 N95-21343
Acoustics of laminar boundary layers breakdown p 1361 N95-22455
Small-scale behavior in distorted turbulent boundary layers at low Reynolds number p 1362 N95-22456
Numerical study of boundary layer interaction with shocks: Method and code validation p 1362 N95-22461
BOUNDARY LAYER SEPARATION
Direct numerical simulation of 2-D and 3-D instability waves in a laminar separation bubble p 1352 N95-21095
Seismic evidence for volatiles at large depth in the Earth p 1422 N95-21808
BOUNDARY LAYER STABILITY
Numerical study of realistic perturbations in three-dimensional boundary layers p 1351 N95-21091
On subcritical instability of the attachment line boundary layer p 1351 N95-21092
Computational studies of laminar to turbulence transition [AD-A285622] p 1353 N95-21146
Supersonic laminar flow control research [NASA-CR-196049] p 1353 N95-21340
BOUNDARY LAYER TRANSITION
Application of Direct and Large Eddy Simulation to Transition and Turbulence [AGARD-CP-551] p 1346 N95-21061
Numerical study of realistic perturbations in three-dimensional boundary layers p 1351 N95-21091
Spatial direct numerical simulation of boundary layer transition under strong adverse pressure gradient p 1351 N95-21093
Investigation of shear layer transition using various turbulence models p 1352 N95-21096
Computational studies of laminar to turbulence transition [AD-A285622] p 1353 N95-21146
Acoustic receptivity due to weak surface inhomogeneities in adverse pressure gradient boundary layers [NASA-TM-4577] p 1353 N95-21258
Supersonic laminar flow control research [NASA-CR-196049] p 1353 N95-21340
Acoustics of laminar boundary layers breakdown p 1361 N95-22455
BOUNDARY LAYERS
Open Skies project computational fluid dynamic analysis [AD-A285928] p 1200 N95-19991
An evaluation of 915-MHz radar wind profiler/RASS by tower and sodar measurements [DE94-018913] p 1364 N95-20320
Data report: Stress measurements in the bottom boundary layer with BASS tripods STRESS 2 1990-1991 [AD-A279875] p 1433 N95-20433
Numerical simulation of supersonic boundary layer transition p 1348 N95-21074
Direct numerical simulations of leading-edge receptivity for freestream sound p 1351 N95-21090

Spatial direct numerical simulation of boundary layer transition under strong adverse pressure gradient
p 1351 N95-21093

BOUNDARY LUBRICATION

Evaluation of PS 212 coatings under boundary lubrication conditions with an Ester-based oil to 300 C
[NASA-TM-106763] p 1223 N95-19901

Lubricant evaluation and performance, 2
[AD-A279144] p 1278 N95-21969

BOUNDARY VALUE PROBLEMS

Multigrid with matrix-dependent transfer operators for convection-diffusion problems
[PB95-110821] p 1487 N95-19915

Analyses of some benchmark cases in fracture mechanics using boundary element method
[PB95-110888] p 1384 N95-19930

The method of auxiliary mapping for the finite element solutions of elasticity problems containing singularities
[AD-A285689] p 1489 N95-20274

Stabilization and control problems in structural dynamics
[AD-A279996] p 1340 N95-20312

Explicit parallel two-step Runge-Kutta-Nystroem methods
[PB95-135752] p 1489 N95-20423

Parallelism across the steps in iterated Runge-Kutta methods for stiff initial value problems
[PB95-135760] p 1490 N95-20424

COYOTE II: A finite element computer program for nonlinear heat conduction problems. Part 1: Theoretical background
[DE95-002587] p 1463 N95-20887

VLUGr3: A vectorizable adaptive grid solver for PDEs in 3D. 2: Code description
[PB95-135737] p 1465 N95-21033

Numerical analysis of energetic particle stabilization of ballooning modes in finite-aspect-ratio tokamaks
[DE94-631397] p 1556 N95-21164

Numerical wave speed for one-dimensional scalar hyperbolic conservation laws with source terms
[PB95-127536] p 1492 N95-21371

Computer simulation of the diocotron instability
[AD-A285655] p 1559 N95-21403

Error committed by stopping the Newton iteration in Runge-Kutta methods and linear multistep methods
[PB95-106324] p 1492 N95-21421

Positive rockland operators
[PB95-127510] p 1493 N95-21423

Parallel predictor-corrector methods
[PB95-135711] p 1493 N95-21434

VLUGR3: A vectorizable adaptive grid solver for PDEs in 3D. 1: Algorithmic aspects and applications
[PB95-135729] p 1467 N95-21435

Applied mathematical problems in modern electromagnetics
[AD-A286448] p 1303 N95-21462

Uniform upper bounds in the Froehlich polaron theory
[DE94-628998] p 1525 N95-21860

BRAGG ANGLE

X-band microwave backscattering from ocean waves
[DE94-016719] p 1309 N95-22241

BRAGG CELLS

A three-dimensional orthogonal laser velocimeter for the NASA Ames 7- by 10-foot wind tunnel
[NASA-TM-108864] p 1366 N95-21323

BRAIN

Netherlands Institute for Brain Research progress report, 1993
[PB95-135398] p 1445 N95-21352

How the brain works
[AD-A279138] p 1450 N95-21968

Magnetic source imaging of visually evoked and oscillatory electrical activity of the human brain
[PB95-127205] p 1448 N95-22476

BRANCHING (MATHEMATICS)

Direct simulation of tridimensional wake of NACA 0012 profile p 1350 N95-21086

Hamiltonian structure of the reversible nonsemisimple 1:1 resonance
[PB95-127528] p 1495 N95-22151

BRAZING

Strength testing of Ti-vapor-coated silicon nitride braze joints
[DE94-017858] p 1280 N95-22266

BREADBOARD MODELS

Eddy current for detecting second-layer cracks under installed fasteners
[AD-A279871] p 1382 N95-20414

Development, fabrication, and metrology of the electro-optical breadboard model for the reflection grating array of the XMM grating spectrometer
[DE94-016605] p 1543 N95-20612

High speed optical storage technology
[AD-A285788] p 1456 N95-22400

BREATHING APPARATUS

Method and apparatus for non-invasive evaluation of diaphragmatic function
[NASA-CASE-LAR-13888-1] p 1441 N95-20408

BREMSSTRAHLUNG

Dilepton production from p-p to Ca-Ca at the Bevalac
[DE95-002341] p 1520 N95-21357

BRIDGMAN METHOD

Directional solidification of the alumina-zirconia ceramic eutectic system
[DE95-001677] p 1277 N95-21735

BRIGHTNESS

The variation of the dust temperature within late-type spiral galaxies p 1593 N95-21766

BRIGHTNESS TEMPERATURE

Deriving earth science products from SSM/I
[NASA-CR-197299] p 1389 N95-20156

BRITTLE MATERIALS

Analysis of the progressive failure of brittle matrix composites
[NASA-CR-195415] p 1225 N95-19951

The processing and mechanical properties of high temperature/high performance composites. Stress redistribution and notch properties, book 2
[AD-A279737] p 1227 N95-20429

Reliability analysis of uniaxially ground brittle materials
[NASA-TM-106852] p 1386 N95-20790

The processing and mechanical properties of high temperature/high performance composites. Processing/property correlations, book 4
[AD-A279739] p 1228 N95-20802

A study of mechanical processing damage in brittle materials
[DE95-002126] p 1276 N95-21585

The role of microcracking on the crack growth resistance of brittle solids and composites
[DE95-001678] p 1231 N95-21736

BRITTLENESS

Fracture behavior of the Fe-8Al alloy FAP-Y
[DE95-000956] p 1258 N95-21676

BROADBAND

A wideband EMP test system
[DE94-015283] p 1290 N95-20474

A wideband propagation simulator for high speed mobile radio communications p 1295 N95-20934

Line-of-sight multipath propagation measurements at 15 GHz over 500 MHz bandwidth p 1296 N95-20944

Broadband pressure barrier for circular waveguide
[AD-D016503] p 1306 N95-21672

Improved broadband waveguide pressure window
[AD-D016487] p 1306 N95-21834

Breakdown of the law of large numbers in Josephson junction series arrays
[DE94-629075] p 1576 N95-21996

Broadband thermal optical limiter for the protection of eyes and sensors
[AD-D016493] p 1377 N95-22304

BROADCASTING

Passive monitoring for automated MMPP communication systems p 1293 N95-20927

Formal specification and compositional verification of an atomic broadcast protocol
[PB95-110508] p 1472 N95-22351

BROKEN SYMMETRY

New strong interactions above the electroweak scale
[DE94-018385] p 1506 N95-20025

Complementarity of e(+)e(-) and pp colliders for the exploration of electroweak symmetry breaking
[DE94-017397] p 1507 N95-20034

New improved derivative expansion for field theories with spontaneous symmetry breaking
[DE94-019349] p 1580 N95-21486

BROMIDES

Neutron molelcular spectroscopy: Future prospects
[PB95-130357] p 1518 N95-21227

Surface x-ray scattering and scanning tunneling microscopy studies at the Au(111) electrode
[DE95-002409] p 1573 N95-21516

Modeling of nonlinear optic and ESR response of CDW MX materials
[DE94-018301] p 1578 N95-22297

BROMINE ISOTOPES

An investigation of the applicability of the new ion exchange resin, Reillex(TM)-HPQ, in ATW separations
[DE94-016576] p 1274 N95-21234

BROWNIAN MOVEMENTS

Magnetic flocculation of paramagnetic particles
[DE94-018144] p 1501 N95-20725

BRUCITE

Phase E in a water-saturated peridotite system at 9.3 GPa p 1420 N95-21799

BSCCO SUPERCONDUCTORS

Carrier doping and interlayer coupling in HTSC single crystals
[DE94-018637] p 1564 N95-20127

Dependence of critical current density on microstructure and processing of high-T(c) superconductors
[DE95-000685] p 1571 N95-21167

Vortex dynamics in a ring-like irradiated Bi2Sr2CaCu2O8 crystal
[DE95-001682] p 1573 N95-21569

Overview of the field and temperature dependence of J(c) in Ag/BSCCO tapes
[PB95-110318] p 1574 N95-21636

Aligned bismuth, strontium, calcium cuprate coatings on polycrystalline substrates
[AD-D016512] p 1278 N95-21907

Anisotropic transport properties of BSCCO single crystals and Ag-clad tapes in high magnetic fields
[DE95-000938] p 1575 N95-21936

How to improve J(c(T)) in Ag/(BiPb)2Sr2Ca2Cu3O10 tapes
[PB95-110326] p 1575 N95-21949

BUBBLES

The Combustive Sound Source
[ARL-TR-94-9] p 1503 N95-19911

Direct numerical simulation of 2-D and 3-D instability waves in a laminar separation bubble
p 1352 N95-21095

On the dynamics of a shock-bubble interaction
[NASA-CR-194978] p 1495 N95-22325

BUCKLING

Influence of primary boundary conditions on the buckling of shallow cylindrical shells
[PB94-208352] p 1384 N95-20003

BUFFETING

Pressure measurements on an F/A-18 twin vertical tail in buffeting flow. Volume 4, part 1: Buffet cross spectral densities
[AD-A285593] p 1215 N95-21214

Pressure measurements on an F/A-18 twin vertical tail in buffeting flow. Volume 1: Wind tunnel test summary
[AD-A279126] p 1202 N95-21877

BUILDINGS

Global equivalence ratio concept and the prediction of carbon monoxide formation in enclosure fires
[PB94-207511] p 1234 N95-20100

Summaries of BFRL fire research in-house projects and grants, 1994
[PB95-130845] p 1286 N95-21130

Fire smoke ventilation through shafts: Experiments
[PB95-132247] p 1288 N95-21978

BULK ACOUSTIC WAVE DEVICES

Carrier dynamics in InGaAs: Quantum wells versus bulk
[DE94-018205] p 1577 N95-22168

BULK MODULUS

Hydrogen and related materials at high density: Physics, chemistry and planetary implications
p 1418 N95-21791

BUNDLES

Fiber-optic rotary joint with bundle collimator assemblies
[AD-D016504] p 1545 N95-21673

BUOYANCY

Investigation of a thermal buoyancy effect on the drag of half models tested in the ARA Transonic Wind Tunnel
[ARA-MEMO-407] p 1199 N95-19946

The dynamic role of ridges in a beta-plane channel. Towards understanding the dynamics of large scale circulation in the Southern Ocean
[AD-A279390] p 1435 N95-21943

Absorbing boundary condition for floating two-dimensional objects in current and waves
[PB95-132882] p 1356 N95-22063

BURGER EQUATION

Optimal active control for Burgers equations
p 1361 N95-22454

BURN-IN

A new mini Ball Grid Array (mBGA) multichip module technology
[DE94-018897] p 1480 N95-20342

Assuring Known Good Die (KGD) for reliable, cost effective MCMs p 1210 N95-20644

Consortia for Known Good Die (KGD), phase 1
[AD-A279407] p 1383 N95-21933

BURNING RATE

High pressure windowed chamber burned rate determination of liquid propellant XM46
[AD-A283770] p 1282 N95-19920

BURNOUT

Collocated tunable wavenumber sensor/actuators for smart structures
[AD-A279608] p 1312 N95-19958

BUS CONDUCTORS

Augmented thermal bus
[NASA-CASE-LEW-15595-1-C] p 1338 N95-19933

BUTANES

The energetics and dynamics of free radicals, ions, and clusters
[DE94-018101] p 1244 N95-21701

BUTENES
The energetics and dynamics of free radicals, ions, and clusters
[DE94-018101] p 1244 N95-21701
BUTYRIC ACID
Bioconversion of coal derived synthesis gas to liquid fuels
[DE94-018849] p 1314 N95-20339
BY-PRODUCTS
Laboratory evaluation of a reactive baffle approach to NOx control
[AD-A283802] p 1400 N95-19921
Production of S2F10, S2OF10 and S2O2F10 by spark discharges in SF6*
[DE95-001421] p 1243 N95-21500
BYPASSES
Simulations of bypass transition for spatially evolving disturbances p 1349 N95-21079
Direct numerical determination of the minimum bypass Reynolds number in boundary layers
p 1349 N95-21080

C

C (PROGRAMMING LANGUAGE)
Status of CFDLIB performance tests on the T3D
[DE95-002708] p 1478 N95-21925
C++ (PROGRAMMING LANGUAGE)
Introduction to the FIRE engine: A C+ + toolkit for Finite automata and Regular Expressions
[PB95-110599] p 1456 N95-19891
Design of a parallel object oriented programming language
[AD-A284924] p 1457 N95-20000
Design and implementation of the FIRE engine: A c+ + toolkit for finite automata and regular expressions
[PB95-132924] p 1467 N95-21415
Object-oriented design of preconditioned iterative methods
[PB95-110276] p 1469 N95-21655
The navigation toolkit
[NASA-CR-197290] p 1205 N95-22161
CADMIUM SULFIDES
International collaboration program on innovative chemical processing of superior electronic and optical materials
[AD-A285122] p 1226 N95-20105
Polycrystalline thin film cadmium telluride solar cells fabricated by electrodeposition
[DE94-011848] p 1391 N95-20118
Nonlinear Faraday effect in CdS semiconductor in an ultrahigh magnetic field
[DE94-016804] p 1564 N95-20240
Advances in polycrystalline thin-film photovoltaics for space applications p 1318 N95-20514
CADMIUM TELLURIDES
Polycrystalline thin film cadmium telluride solar cells fabricated by electrodeposition
[DE94-011848] p 1391 N95-20118
Polycrystalline CuInSe2 and CdTe solar cells
[DE94-011875] p 1392 N95-20333
Advances in polycrystalline thin-film photovoltaics for space applications p 1318 N95-20514
IR materials producibility
[AD-A280094] p 1328 N95-21017
Processing and modeling issues for thin-film solar cell devices
[DE94-011895] p 1394 N95-21294
Thin-film cadmium telluride photovoltaic cells
[DE94-011886] p 1395 N95-21508
CALCITE
Storage and recycling of water and carbon dioxide in the earth p 1425 N95-21822
CALCIUM OXIDES
Effects of neutron irradiation on the London penetration depth for polycrystalline Bi(1.8)Pb(0.3)Sr2Ca2Cu3O10 superconductor
[DE94-019335] p 1573 N95-21483
Electronic structure and energies of alkaline earth oxides: MgO, CaO and SrO
[DE94-628990] p 1575 N95-21853
Local texture and strongly linked conduction in spray-pyrolyzed TlBa2Ca2Cu3O(8+x) deposits
[DE94-017887] p 1578 N95-22269
CALCULUS
General conservative extension theorem in process algebra
[PB95-110656] p 1487 N95-19902
Real time process algebra with infinitesimals
[PB95-110623] p 1488 N95-20055
Beyond beta-reduction in Church's lambda yield
[PB95-110565] p 1488 N95-20149
Semantics for a fine lambda-calculus with de Bruijn indices
[PB95-127577] p 1492 N95-21372
CALIBRATING
A comparative survey of current and proposed tropospheric refraction-delay models for DSN radio metric data calibration
[NASA-CR-197338] p 1412 N95-20002
Deriving earth science products from SSM/I
[NASA-CR-197299] p 1389 N95-20156
Error analysis in wind turbine field testing
[DE94-011864] p 1391 N95-20260
High precision Woelter optic calibration facility
[DE94-016973] p 1542 N95-20364
16-foot transonic tunnel test section flowfield survey
[NASA-TM-109157] p 1216 N95-20669
The production of calibration specimens for impact testing of subsize Charpy specimens
[DE94-018125] p 1386 N95-20703
The calculation and measurement of Helmholtz coil fields
[AD-A286081] p 1228 N95-20808
Impact of propagation mechanisms on global navigation satellite system performance p 1298 N95-20950
Sounder calibration with backscattering from Losquet Island in the presence of multipaths
p 1300 N95-20961
Radioactive check sources for alpha and beta sensitive radiological instrumentation
[DE94-016477] p 1366 N95-21138
The efficiency calibration of the DSS-24 34-meter beam-waveguide antenna p 1305 N95-21542
CTD calibration and processing methods used at Woods Hole Oceanographic Institution
[AD-A279507] p 1435 N95-21681
Absolute, Extreme-ultraviolet Solar Spectral Irradiance Monitor (AESSIM)
[AD-A279345] p 1603 N95-21929
VTT test borehole for bedrock investigations
[PB95-132965] p 1427 N95-22095
CALIFORNIA
A numerical study of wind forcing effects on the California Current System
[AD-A286205] p 1435 N95-21880
CALORIMETERS
Application of a dimensionless parameter model for Laser Beam Welding
[DE94-018902] p 1378 N95-20048
Monolithic circuits for lead-glass calorimetry
[DE94-019112] p 1330 N95-21554
CAMERAS
A scalable video rate camera interface
[AD-A286144] p 1474 N95-20325
Passive range measurement system
[AD-D016222] p 1544 N95-21100
CANADA
Propagation measurements on a troposcatter link in the Canadian High Arctic p 1295 N95-20940
CANCELLATION
General purpose sidelobe canceller system
[AD-D016560] p 1289 N95-20270
CANCER
Urban air carcinogens and their effects on health
[DE95-002259] p 1447 N95-22285
CANS
Corrosion evaluation of fuel canister crusher rigging
[DE95-002962] p 1257 N95-21452
CANTILEVER BEAMS
Corrosion behavior of landing gear steels
[AD-A285862] p 1261 N95-22132
CAPACITANCE
LLNL/Lion Precision LVDT amplifier
[DE95-001504] p 1327 N95-20854
Surface micromachined capacitive tactile image sensor
[PB95-108031] p 1288 N95-21633
Design of a 10 bit 10k Samples/s low power CMOS ADC
[PB95-110425] p 1455 N95-22018
CAPACITANCE SWITCHES
Sequential shock induced switch tests for Eglin Air Force Base
[DE95-001786] p 1334 N95-22062
CAPACITORS
Monolithic low noise preamplifier for piezoelectric sensors
[AD-D016524] p 1333 N95-21865
Integration of thin film decoupling capacitors
[DE95-001609] p 1333 N95-21881
CAPILLARY FLOW
An augmented Young-Laplace model of an evaporating meniscus in a micro-channel with high heat flux
[NASA-CR-197622] p 1340 N95-20796
CAPTURE EFFECT
The ORNL Neutron-Capture Cross Section Facility
[DE94-019146] p 1537 N95-21460
CARBAMATES (TRADENAME)
Structure of dibis(diethyldithiocarbamato) zinc (2) Mu-bis(diethylphosphino)ethane toluene(2)
[AD-A279792] p 1224 N95-20660
CARBOHYDRATES
A low energy continuous reactor separator for the production of ethanol from corn grits/starch and biomass streams
[DE95-002256] p 1283 N95-21356
Hydrothermal conversion of carbohydrates and related compounds
[PB95-134011] p 1396 N95-22175
Structures and functions of oligosaccharins
[DE95-003195] p 1440 N95-22220
CARBON
The thermal conductivity of carbon coated silicon carbide fibers embedded in a silicon carbide matrix
[DE94-017758] p 1225 N95-20023
Natural gas cleanup:- Evaluation of a molecular sieve carbon as a pressure swing adsorbent for the separation of methane/nitrogen mixtures
[DE94-012263] p 1234 N95-20135
Novel catalysts for methane activation
[DE95-002639] p 1237 N95-20438
Boron carbide-based coatings on graphite for plasma facing components
[DE94-017976] p 1269 N95-20570
Study of small carbon and semiconductor clusters using negative ion threshold photodetachment spectroscopy
[DE95-002327] p 1515 N95-20872
Calculated heats of formation of some predicted stable C, N, O, F molecules
[AD-A285957] p 1517 N95-21127
Nitrogen alloyed martensitic steels
[PB95-127791] p 1255 N95-21128
Friction and wear properties of as-deposited and carbon ion-implanted diamond films
[NASA-TM-106759] p 1274 N95-21252
Corrosion evaluation of fuel canister crusher rigging
[DE95-002962] p 1257 N95-21452
The primary carbon and the formation of carbon species in terrestrial magmas p 1420 N95-21797
The ratios of carbon and non-radiogenic helium and argon isotopes in the mantle and crustal rocks
p 1421 N95-21805
Characterization and performance of DLC films synthesized by plasma and ion beam techniques
[DE94-018287] p 1281 N95-22428
CARBON COMPOUNDS
Computational evaluation of the feasibility of nitrating precursors to C12N12O12
[AD-A285976] p 1239 N95-20668
Studies of the microwave resistivity of kappa-(BEDT-TTF)2Cu(N(CN)2)Cl
[DE95-002980] p 1262 N95-22291
CARBON CYCLE
Closure on the global carbon cycle
[DE94-018617] p 1404 N95-20991
CARBON DIOXIDE
Energy impacts of controlling carbon dioxide emissions from an integrated gasification/combined-cycle system
[DE94-016878] p 1403 N95-20478
Photochemistry of intermolecular C-H bond activation reactions
[DE94-018417] p 1239 N95-20682
The Carnol process for methanol production and utilization with reduced CO2 emissions
[DE94-016808] p 1283 N95-21211
Removal of CO2 in closed loop off-gas treatment systems
[DE94-019259] p 1407 N95-21617
Impact degassing of water and noble gases from silicates p 1416 N95-21780
Origin and loss of the volatiles of the terrestrial planets p 1417 N95-21785
Volatiles in the deep Earth: An experimental study using the laser-heated diamond cell p 1421 N95-21803
The ratios of carbon and non-radiogenic helium and argon isotopes in the mantle and crustal rocks
p 1421 N95-21805
Storage and recycling of water and carbon dioxide in the earth p 1425 N95-21822
Development of active-transport membrane devices
[DE94-015947] p 1246 N95-21921
Numerical study of contaminant effects on combustion of hydrogen, ethane, and methane in air
[NASA-TM-106844] p 1284 N95-22114
Modeling of collision induced absorption spectra of CO2-CO2 pairs for planetary atmosphere of Venus
[NASA-CR-197373] p 1601 N95-22338
CARBON DIOXIDE LASERS
Approach to compact terawatt CO2 laser system for particle acceleration
[DE95-002170] p 1371 N95-20866

Effect of laser radiation on carbon fibre/epoxy composites
[PB95-133526] p 1232 N95-22096

CARBON DISULFIDE
Effect of external stress on the transport of fluids in thermoplastic resin systems
[AD-A279993] p 1270 N95-20596

CARBON FIBERS
The thermal conductivity of carbon coated silicon carbide fibers embedded in a silicon carbide matrix
[DE94-017758] p 1225 N95-20023
The thermal conductivity of carbon-fiber reinforced metal matrix composites
[DE94-017767] p 1226 N95-20125
Thermo-mechanical fatigue of polymer matrix composites
[AD-A285931] p 1267 N95-20390
Wear resistant composite structure of vitreous carbon containing convoluted fibers
[DE95-002254] p 1228 N95-20787
Carbon fiber reinforced superconductor composites
[DE95-002504] p 1229 N95-20913
Damage tolerance of carbon fibre polyetheretherketone laminates
[PB95-131611] p 1230 N95-21432
Effect of laser radiation on carbon fibre/epoxy composites
[PB95-133526] p 1232 N95-22096

CARBON ISOTOPES
The ratios of carbon and non-radiogenic helium and argon isotopes in the mantle and crustal rocks
p 1421 N95-21805

CARBON MONOXIDE
Laboratory evaluation of a reactive baffle approach to NOx control
[AD-A283802] p 1400 N95-19921
Global equivalence ratio concept and the prediction of carbon monoxide formation in enclosure fires
[PB94-207511] p 1234 N95-20100
Bioconversion of coal derived synthesis gas to liquid fuels
[DE94-018849] p 1314 N95-20339
Carboxyhemoglobin formation due to transient exposure to high level carbon monoxide: Experimental results and an explanatory model
[AD-A285476] p 1444 N95-20979
Evaluation of the technical performance of the Duttch National Air Quality Monitoring Network in 1992
[PB95-131892] p 1405 N95-21327
Monitoring activities in the framework of the Dutch National Air Quality Monitoring Network in 1994
[PB95-131884] p 1406 N95-21351
The interaction of localized solutions in a surface reaction
[DE95-002736] p 1248 N95-22433

CARBON STEELS
Theoretical-experimental study on the electroslag remelting technology of high quality steels
[DE94-629216] p 1256 N95-21270
Corrosion evaluation of fuel canister crusher rigging
[DE95-002962] p 1257 N95-21452

CARBON TETRACHLORIDE
Resonance Raman spectroscopy of volatile organics: Carbon tetrachloride
[DE95-000627] p 1233 N95-19980

CARBONACEOUS METEORITES
Primitive Xe in the atmospheres of Earth and mars
p 1419 N95-21795

CARBONATES
Actinide(IV) and actinide(VI) carbonate speciation studies by PAS and NMR spectroscopies
[DE94-016957] p 1236 N95-20361
Multiply manifolded molten carbonate fuel cells
[DE94-017074] p 1392 N95-20480
Molten carbonate fuel cell product development test
[DE95-000005] p 1324 N95-20574
The development of a new plasticizer for poly(ethylene oxide) based polymer electrolyte and the investigation of their ion-pair dissociation effect
[DE94-016821] p 1276 N95-21644
Storage and recycling of water and carbon dioxide in the earth p 1425 N95-21822

CARBONYL COMPOUNDS
Photochemistry of intermolecular C-H bond activation reactions
[DE94-018417] p 1239 N95-20682
Dynamic NMR studies of restricted arene rotation in the chromiu tricarbonyl thiophene and selenophene complexes
[DE95-001656] p 1257 N95-21399

CARBORANE
Ceramics formed by pyrolysis of either linear or thermosetting carborane (siloxane or silane) acetylene based precursor polymers
[AD-D016563] p 1266 N95-20291

CARBOXYHEMOGLOBIN
Carboxyhemoglobin formation due to transient exposure to high level carbon monoxide: Experimental results and an explanatory model
[AD-A285476] p 1444 N95-20979

CARBOXYHEMOGLOBIN TEST
Carboxyhemoglobin formation due to transient exposure to high level carbon monoxide: Experimental results and an explanatory model
[AD-A285476] p 1444 N95-20979

CARBOXYL GROUP
New chiral pyrimidino-crown ether ligands
[AD-A279892] p 1223 N95-20590

CARCINOGENS
The molecular mechanics program DUPLEX: Computing structures of carcinogen modified DNA by surveying the potential energy surface
[DE94-019153] p 1439 N95-21606
Urban air carcinogens and their effects on health
[DE95-002259] p 1447 N95-22285
Cellular responses to environmental DNA damage
[DE94-015606] p 1441 N95-22397

CARDIAC AURICLES
Effect of increased venous backflow on the release of cardiac hormone. Fine structural, immunohistochemical, and biochemical study
[PB95-130399] p 1445 N95-21424

CARDIOVASCULAR SYSTEM
Modeling platform dynamics and physiological response to short arm centrifugation
[AD-A279640] p 1442 N95-20457
Intramyocardial blood volume and oxygen exchange
[PB95-108015] p 1445 N95-21580
The influence of coronary artery disease on +Gz tolerance: A preliminary study
[AD-A279305] p 1446 N95-21941

CARDS
An IBM based ARINC interface
[ARL-TR-21] p 1471 N95-22104

CARRIAGES
A user's guide to LUGSAN 1.1: A computer program to calculate and archive lug and sway brace loads for aircraft-carried stores
[DE95-001919] p 1207 N95-21730

CARRIER DENSITY (SOLID STATE)
Magnetic interactions in the Emery model
[DE94-629059] p 1577 N95-22181

CARRIER FREQUENCIES
Passive monitoring for automated MMPP communication systems p 1293 N95-20927
Development of a fast sampling system for estimation of impulse responses of mobile radio channels
p 1296 N95-20943

CARRIER LIFETIME
Translational-energy-resolved studies of photographed carrier-induced reactions on semiconductor surfaces
[DE95-002944] p 1573 N95-21444
Transient photoluminescence measurements on GaAs and AlGaAs double heterostructures
[AD-A279408] p 1575 N95-21916
The role of point defects and defect complexes in silicon device processing
[DE94-011876] p 1279 N95-22091

CARTESIAN COORDINATES
A control volume method on an icosahedral grid for numerical integration of the shallow-water equations on the sphere
[DE94-016345] p 1489 N95-20170
Quantization in curvilinear coordinates
[DE94-770603] p 1514 N95-20737

CASCADE CONTROL
Pre-amplifier with multi-stage feedback
[AD-D016254] p 1336 N95-22418

CASCADE FLOW
Experimental study of vane heat transfer and aerodynamics at elevated levels of turbulence
[NASA-CR-4633] p 1337 N95-19912
Laser anemometry and viscous computation of the flow through an annular turbine cascade
[AD-A280070] p 1341 N95-20968
Homogeneous turbulence subjected to mean flow with elliptic streamlines p 1345 N95-21056

CASES (CONTAINERS)
Composite cases for airborne electronic equipment: A technology study and EMC p 1212 N95-20655

CASSEGRAIN ANTENNAS
The efficiency calibration of the DSS-24 34-meter beam-waveguide antenna p 1305 N95-21542

CASSINI MISSION
GPHS-RTGs in support of the Cassini Mission
[DE95-001492] p 1222 N95-20853

CAST ALLOYS
Microstructures and tensile properties of as-cast iron-aluminide alloys
[DE94-017868] p 1252 N95-20359
Surface technology programme
[PB95-132866] p 1262 N95-22174

CASTING
Solidification modeling of a spiral casting to determine material fluidity
[DE94-018930] p 1285 N95-20050
Relationship between dendrite coherency and castability of some commercial foundry alloys
[PB95-110243] p 1258 N95-21652

CASTINGS
Improved die castings through plasma surface modification, improved sensors and die soldering prevention
[DE95-002238] p 1253 N95-20417

CATALYSIS
Cluster reactions: An approach to understanding the fundamentals of heterogeneous catalysis
[DE95-002947] p 1243 N95-21447
A catalytic method for the conversion of silanes to stannanes
[AD-A286214] p 1247 N95-22020
Catalyzed reduction of nitrate in aqueous solutions
[DE94-017660] p 1247 N95-22049
Hydrothermal conversion of carbohydrates and related compounds
[PB95-134011] p 1396 N95-22175

CATALYSTS
Direct catalytic decomposition of nitric oxide
[DE94-018840] p 1233 N95-20045
Superior catalysts for selective catalytic reduction of nitric oxide
[DE94-018845] p 1234 N95-20046
Correlations between surface structure and catalytic activity/selectivity
[DE94-019023] p 1234 N95-20052
Selective methane oxidation over promoted oxide catalysts
[DE94-012270] p 1235 N95-20188
Investigation of syngas interaction in alcohol synthesis catalysts
[DE94-018784] p 1236 N95-20349
Novel catalysts for methane activation
[DE95-002639] p 1237 N95-20438
Technology development for cobalt F-T catalysts
[DE94-017363] p 1241 N95-21172
Effects of increased UV-B radiation on phytoplankton: A preliminary study and research programme
[PB95-133732] p 1439 N95-21884
Natural gas converter performance and durability
[PB95-135554] p 1284 N95-21966
Bridging the pressure gap: In situ atomic-level investigations of model platinum catalyst surfaces under reaction conditions by scanning tunneling microscopy
[DE95-002346] p 1246 N95-21990
Lower active metals loading for hydrotreating catalysts
[DE94-018907] p 1261 N95-22119
Transient studies of low temperature catalysts for methane conversion
[DE95-003560] p 1247 N95-22224
Gas-phase photocatalytic oxidation: Cost comparison with other air pollution control technologies
[DE95-000241] p 1410 N95-22278
Catalytic reactions of synthesis gas. Part 3. Determination of reaction kinetics
[PB95-127759] p 1248 N95-22329

CATALYTIC ACTIVITY
Superior catalysts for selective catalytic reduction of nitric oxide
[DE94-018845] p 1234 N95-20046
Technology development for cobalt F-T catalysts
[DE94-017363] p 1241 N95-21172
Hydrogenation of nitriles on a well-characterized nickel surface: From surface science studies to liquid phase catalytic activity measurements
[DE94-018184] p 1259 N95-21707
Bridging the pressure gap: In situ atomic-level investigations of model platinum catalyst surfaces under reaction conditions by scanning tunneling microscopy
[DE95-002346] p 1246 N95-21990
Transient studies of low temperature catalysts for methane conversion
[DE95-003560] p 1247 N95-22224

CATHODES
Photoelectrons beam measurement from a magnesium cathode in a RF electron gun
[DE94-017994] p 1533 N95-20573
Molten carbonate fuel cell product development test
[DE95-000005] p 1324 N95-20574
Applied physics research for innovation in pulsed power
[AD-A285392] p 1324 N95-20610
Field-emitter arrays for RF vacuum microelectronics
[AD-A279959] p 1325 N95-20661
Cathode Life Test Facility
[AD-A286232] p 1334 N95-22023

CATHODIC COATINGS

Characterization and performance of DLC films synthesized by plasma and ion beam techniques
[DE94-018287] p 1281 N95-22428

CATHODOLUMINESCENCE

Visible light emitting materials and injection devices
[AD-A284796] p 1541 N95-20066

CATIONS

Direct catalytic decomposition of nitric oxide
[DE94-018840] p 1233 N95-20045

Spectroscopic studies of glass structure
[DE94-016551] p 1268 N95-20468

The dynamics of formation and evaporation of mixed alkali halide nanocrystals: A case of comparable lattice energies
[AD-A285052] p 1567 N95-20483

Novel fluorine oxidizers
[AD-A279480] p 1284 N95-21678

The energetics and dynamics of free radicals, ions, and clusters
[DE94-018101] p 1244 N95-21701

CAUCHY PROBLEM

Approximate Riemann solver for magnetohydrodynamics (that works in more than one dimension)
[PB95-135802] p 1553 N95-20425

Hybrid Upwind Splitting (HUS) by a field-by-field decomposition
[NASA-TM-106843] p 1355 N95-21957

CAULKING

Frame and edge seal technology: A state of the art survey
[PB95-110334] p 1288 N95-22014

CAVITATION FLOW

Applications of sonochemistry
[AD-A286388] p 1506 N95-22360

CAVITIES

Measurements of shielding effectiveness and cavity characteristics of airplanes
[PB94-210051] p 1289 N95-20191

Improved die castings through plasma surface modification, improved sensors and die soldering prevention
[DE95-002238] p 1253 N95-20417

Large eddy simulation of turbulent flow over a cavity
p 1347 N95-21069

Small cavity nonresonant tunable microwave-frequency alternating current scanning tunneling microscope
[AD-A285752] p 1328 N95-21218

Competition between electromagnetic modes in a free-electron maser
[AD-A279546] p 1374 N95-21694

CAVITY FLOW

DNS of turbulent flow in a driven cavity and their analysis using proper orthogonal decomposition
p 1352 N95-21097

Instabilities in natural-convection flows in cavities
[PB95-107975] p 1354 N95-21578

CAVITY RESONATORS

An 8-meter-long coupled cavity RFQ linac
[DE94-018077] p 1331 N95-21667

CD-ROM

Common mapping system media study
[AD-A279086] p 1390 N95-21912

CELESTIAL MECHANICS

Erice International Seminars on Planetary Emergencies. 17th Workshop: The Collision of an Asteroid or Comet with the Earth
[AD-A280122] p 1600 N95-21577

CELL CATHODES

Photoelectrons beam measurement from a magnesium cathode in a RF electron gun
[DE94-017994] p 1533 N95-20573

CELL MEMBRANES (BIOLOGY)

Cell membrane potentials induced during exposure to EMP fields
[DE94-018952] p 1439 N95-21548

Electrostatic basis for molecular recognition in photosynthesis
[DE95-002979] p 1440 N95-22075

CELLS (BIOLOGY)

Monoclonal antibodies directed against surface molecules of multicell spheroids
[NASA-CR-197367] p 1437 N95-20559

Flow cytometry: A powerful technology for measuring biomarkers
[DE94-018284] p 1440 N95-22296

Cellular responses to environmental DNA damage
[DE94-015606] p 1441 N95-22397

CELLULOSE

Microbiology and physiology of anaerobic fermentations of cellulose
[DE95-002899] p 1438 N95-20917

CENSUS

Census US civil aircraft calendar year 1993
[AD-A286309] p 1199 N95-20091

CENTER OF MASS

Signals for top quark anomalous chromomagnetic moments at colliders
[DE95-002896] p 1535 N95-21254

CENTRAL NERVOUS SYSTEM

A physiological neural network for saccadic eye movement control
[AD-A279599] p 1441 N95-20301

CENTRAL PROCESSING UNITS

Downsizing information systems: Framing the issues for the Office of Naval Intelligence (ONI)
[AD-A279888] p 1588 N95-20589

Fault-tolerance in distributed and multiprocessor real-time systems
[AD-A279896] p 1461 N95-20595

Real-time reconfiguration study
[AD-A286060] p 1464 N95-20910

CENTRIFUGING

Modeling platform dynamics and physiological response to short arm centrifugation
[AD-A279640] p 1442 N95-20457

CERAMIC BONDING

Energetics, bonding mechanism and electronic structure of ceramic/ceramic and metal/ceramic interfaces
[DE95-000601] p 1265 N95-20115

CERAMIC MATRIX COMPOSITES

The environmental durability of fiber reinforced ceramic matrix composites
[AD-A283750] p 1225 N95-19919

The effect of fiber coating thickness on the interfacial properties of a continuous fiber ceramic matrix composite
[DE94-017886] p 1267 N95-20373

The processing and mechanical properties of high temperature/high performance composites. Stress redistribution and notch properties, book 2
[AD-A279737] p 1227 N95-20429

The processing and mechanical properties of high temperature/high performance composites. Fatigue and creep, book 3
[AD-A279738] p 1227 N95-20430

The processing and mechanical properties of high temperature/high performance composites. Book 5: Interface effects
[AD-A279815] p 1228 N95-20584

The processing and mechanical properties of high temperature/high performance composites. Mechanism-based constitutive laws and design, book 1
[AD-A279736] p 1228 N95-20801

Fabrication of ceramic composites: Forced CVI
[DE95-001076] p 1271 N95-20821

Micromechanical approach to transformation toughening in ceramics
[PB95-135422] p 1273 N95-20976

Toughened Silcomp composites for gas turbine engine applications
[DE95-002851] p 1214 N95-21243

The processing and mechanical properties of high temperature/high performance composites. Book 6: Delamination and compressive behavior
[AD-A279780] p 1231 N95-21999

A transmission electron microscope characterization of sodium sulfate hot corrosion of silicon carbide fiber-reinforced lithium aluminosilicate glass-ceramic matrix composite
[AD-A286164] p 1231 N95-22038

Structural performance of cylindrical pressure housings of different ceramic compositions under external pressure loading. Part 4: Silicon carbide particulate reinforced alumina ceramic
[AD-A286299] p 1279 N95-22047

High temperature corrosion and crack growth of SiC/SiC at variable oxygen partial pressures
[DE94-018715] p 1232 N95-22115

CERAMICS

Materials for adaptive structural acoustic control, volume 2
[AD-A279222] p 1502 N95-19883

Recognition of subsurface defects in machined ceramics by application of neural networks to laser scatter patterns
[DE94-018373] p 1264 N95-20018

Comparison of the dynamic fatigue behavior of two monolithic SiC and an Al2O3/SiC composite
[DE94-017751] p 1225 N95-20022

Properties of whisker-reinforced ceramics
[DE94-017759] p 1264 N95-20024

Materials/manufacturing element of the Advanced Turbine System Program
[DE94-017299] p 1378 N95-20085

Energetics, bonding mechanism and electronic structure of ceramic/ceramic and metal/ceramic interfaces
[DE95-000601] p 1265 N95-20115

Reactions and microstructure at ceramic/metal interfaces
[DE94-014287] p 1265 N95-20138

Enhancement of creep resistance of a sintered S3N4 ceramic by microwave annealing
[DE94-017698] p 1265 N95-20220

Ceramics formed by pyrolysis of either linear or thermosetting carborane (siloxane or silane) acetylene based precursor polymers
[AD-D016563] p 1266 N95-20291

Microstructural contributions to the fracture resistance of silicon nitride ceramics
[DE94-018955] p 1267 N95-20323

Fracture analysis of an all-ceramic bearing system
[AD-A285056] p 1269 N95-20486

Biomolecular Materials by Design, volume 330
[AD-A285369] p 1269 N95-20551

Structural performance of cylindrical pressure housings of different ceramic compositions under external pressure loading. Part 1: Isostatically pressed alumina ceramic
[AD-A279669] p 1270 N95-20603

Reliability assessment of Multichip Module technologies via the Triservice/NASA RELTECH program
p 1210 N95-20643

Ferroic materials: Design, preparation and characteristics. Ceramic transactions, volume 43
[AD-A285937] p 1270 N95-20664

Effect of fiber fabric orientation on the monotonic and fatigue behavior of a continuous fiber ceramic composite
[DE94-018121] p 1271 N95-20700

Approaches to the design of structural ceramics incorporating whiskers and particulate phases
[DE94-018126] p 1271 N95-20704

Reliability analysis of uniaxially ground brittle materials
[NASA-TM-106852] p 1386 N95-20790

Hg-199 and Cu-(63,65) NMR studies of mercury based high-Tc superconductors
[DE95-001073] p 1570 N95-20820

Experimental investigation of wave and fracture phenomena in impacted ceramics
[AD-A286589] p 1272 N95-20856

Micromechanical approach to transformation toughening in ceramics
[PB95-135422] p 1273 N95-20976

Microstructural design for tough ceramics
[AD-A285634] p 1273 N95-21152

Comparison of properties of sintered and sintered reaction-bonded silicon nitride fabricated by microwave and conventional heating
[DE95-001426] p 1275 N95-21501

The mechanical behavior of surface-modified ceramics
[DE95-001704] p 1276 N95-21572

A study of mechanical processing damage in brittle materials
[DE95-002126] p 1276 N95-21585

Development and applications of flat ceramic membranes
[PB95-110219] p 1276 N95-21650

Forming of superplastic ceramics
[DE94-017306] p 1276 N95-21662

Domain processes in ferroelectric ceramics
[AD-A279567] p 1276 N95-21697

Directional solidification of the alumina-zirconia ceramic eutectic system
[DE95-001677] p 1277 N95-21735

Electronic structure and energies of alkaline earth oxides: MgO, CaO and SrO
[DE94-628990] p 1575 N95-21853

Tailoring suspension flow for the gelcasting of oxide and nonoxide ceramics
[DE95-001351] p 1277 N95-21861

Materials for adaptive structural acoustic controls
[AD-A279255] p 1505 N95-21863

Cost-effective ceramics program in the United States
[DE95-001425] p 1278 N95-21909

Ceramic technology for advanced heat engines
[DE95-000950] p 1278 N95-21937

Characterization equipment for electrooptics and actuators
[AD-A286285] p 1546 N95-22043

Aluminium oxide targets after ballistic impact; fragmentation of the ceramic and the projectile
[PB95-133625] p 1388 N95-22097

Fabrication of PLZT/ITO grating for optical switching and reconfigurable optical interconnect applications
[AD-A286389] p 1548 N95-22248

Materials support for the development of High Temperature Advanced Furnaces (HITAF): A comparison of selected mechanical properties for three SiC-based ceramics
[DE94-017752] p 1280 N95-22258

Measurement of residual stresses on ceramic materials with high spatial resolution
[DE94-017889] p 1280 N95-22270

Structural performance of cylindrical pressure housings of different ceramic compositions under external pressure loading. Part 3: Sintered reaction bonded silicon nitride ceramic
[AD-A285773] p 1388 N95-22411

CEREBELLUM

Biological and theoretical studies of adaptive networks: The conditioned response
[AD-A284781] p 1479 N95-20061

CEREBROSPINAL FLUID

Diffusible driving and coupling signals of the biological clock
[AD-A285353] p 1447 N95-22475

CERENKOV COUNTERS

Inverse Cerenkov laser acceleration experiment at ATF
[DE94-017990] p 1370 N95-20572

Experiments at high energy hadron colliders and underground water Cerenkov detector experiment
[DE95-001804] p 1535 N95-21281

CERENKOV RADIATION

Inverse Cerenkov laser acceleration experiment at ATF
[DE94-017990] p 1370 N95-20572

Experiments at high energy hadron colliders and underground water Cerenkov detector experiment
[DE95-001804] p 1535 N95-21281

CERIUM COMPOUNDS

Kondo insulators
[DE95-001156] p 1237 N95-20368

CERIUM OXIDES

Microwave sintering of ZrO2-12 mol% CeO2
[DE94-018709] p 1265 N95-20226

CERTIFICATION

An evaluation of Automatic Terminal Information Service (ATIS) flight deck display presentation options
[AD-A280100] p 1204 N95-21020

CESIUM

Parity nonconservation in radioactive atoms: An experimental perspective
[DE95-002737] p 1518 N95-21235

Performance of cesium telluride photocathodes as an electron source for the Los Alamos FEL
[DE94-018302] p 1375 N95-21919

CESIUM COMPOUNDS

Application of new synchrotron powder diffraction techniques to anomalous scattering from glasses
[DE94-019285] p 1536 N95-21407

Photocathodes for free electron lasers
[DE94-018305] p 1376 N95-22242

Fabrication and characterization of cesium telluride photocathodes: A promising electron source for the Los Alamos Advanced FEL
[DE94-018303] p 1377 N95-22348

CESIUM ISOTOPES

Parity nonconservation in radioactive atoms: An experimental perspective
[DE95-002737] p 1518 N95-21235

CHALLENGER (ORBITER)

Challenger's night flight
[NASA-TM-110503] p 1217 N95-19995

CHANNEL FLOW

HIVEL2D: A two-dimensional flow model for high-velocity channels
[AD-A286556] p 1341 N95-20843

Simulation of a turbulent flame in a channel
p 1249 N95-21044

Instability of streamwise vortices in plane channel flows p 1344 N95-21049

A Lagrangian dynamic subgrid-scale model turbulence
p 1344 N95-21051

Modeling near wall effects in second moment closures by elliptic relaxation p 1345 N95-21054

Large-eddy simulation of rotating channel flows using a localized dynamic model p 1346 N95-21064

Direct numerical simulation of turbulent flow in a sudden pipe expansion p 1347 N95-21067

Large-eddy simulation of separated flow in a ribbed duct p 1347 N95-21070

A cheap DNS tool for turbulence models testing
p 1348 N95-21072

Large eddy simulation of channel flow using a vorticity transport subgrid model p 1348 N95-21076

Simulations of bypass transition for spatially evolving disturbances p 1349 N95-21079

High temperature superconducting films and multilayers for electronics
[AD-A279545] p 1331 N95-21693

Large-eddy simulation of a plane wake
p 1360 N95-22446

Local dynamic subgrid-scale models in channel flow
p 1360 N95-22447

Large-eddy simulation of flow through a plane, asymmetric diffuser p 1360 N95-22449

Drag reduction strategies p 1361 N95-22453

CHANNELS

Method of making a semiconductor device by forming a nanochannel mask
[AD-D016515] p 1576 N95-22059

CHANNELS (DATA TRANSMISSION)

White-light spectral analysis of lithium niobate waveguides
[DE94-016692] p 1542 N95-20489

Optical backplane for modular avionics
p 1212 N95-20652

EPICS simulation tools for control system development
[DE94-018082] p 1462 N95-20699

DAMSON: A system to measure multipath dispersion, Doppler spread and Doppler shift on multi-mechanism communications channels p 1299 N95-20955

Programmable modular network interface
[AD-D016505] p 1477 N95-21674

CHAOS

Coupled analytic maps
[PB95-111076] p 1498 N95-19945

Semiquantum chaos and the large N expansion
[DE94-016196] p 1488 N95-20169

Chaotic phenomena in plasma 3
[DE94-770765] p 1554 N95-20686

Time-resolved study of sideband generation and transition to chaos on an infrared FEL
[DE95-002336] p 1374 N95-21528

CHARACTERIZATION

Superior catalysts for selective catalytic reduction of nitric oxide
[DE94-018845] p 1234 N95-20046

Performance specifications for technology development: Application for characterization of volatile organic compounds in the environment
[DE94-016627] p 1401 N95-20234

Characterization and simulation of an acoustic source moving through an oceanic waveguide
[AD-A285688] p 1503 N95-20272

Multiple Mechanism Propagation Paths (MMPPs): Their Characterisation and Influence on System Design
[AGARD-CP-543] p 1292 N95-20921

Fiber-optic sensors for rapid, inexpensive characterization of soil and ground water contamination
[DE95-002471] p 1545 N95-21510

CHARGE CARRIERS

Carrier dynamics in InGaAs: Quantum wells versus bulk
[DE94-018205] p 1577 N95-22168

CHARGE COUPLED DEVICES

Visible light emitting materials and injection devices
[AD-A284796] p 1541 N95-20066

Time-resolved diagnostics of excimer laser-generated ablation plasmas used for pulsed laser deposition
[DE94-018950] p 1559 N95-21547

Time resolved x-ray detection
[AD-A279348] p 1368 N95-22143

Vertex detectors at linear colliders: Present and future
[PB95-134656] p 1540 N95-22364

CHARGE DISTRIBUTION

A charge distribution analysis instrument for catalysis and material science applications
[DE94-016489] p 1364 N95-20233

Ion charge-state production and photoionization near the K edge in argon and potassium
[DE95-001443] p 1522 N95-21502

Modeling of nonlinear optic and ESR response of CDW MX materials
[DE94-018301] p 1578 N95-22297

Image solution for poisson's equation in wedge geometry
[PB95-127171] p 1310 N95-22311

CHARGE EXCHANGE

Power balance in D3-D during single-null ELMing H-mode plasmas
[DE94-016680] p 1554 N95-20568

Observation of non diffusive term of toroidal momentum transport in the JFT-2M tokamak
[DE94-770686] p 1555 N95-20989

Muon transfer from muonic atoms of hydrogen isotopes to He nuclei
[DE94-628903] p 1523 N95-21591

Intense proton beam source for ITER neutral-beam spectroscopy diagnostics
[DE94-018092] p 1560 N95-21668

Magnetic interactions in the Emery model
[DE94-629059] p 1577 N95-22181

CHARGE TRANSFER

A portable and independent edge fluctuation diagnostic
[DE94-018254] p 1554 N95-20681

Photoinduced charge transfer between fullerenes and TiO2 semiconductor colloids
[DE95-001447] p 1570 N95-20838

Quantum simulation of heterogeneous electron transfer free energies at the water-metal interface
[AD-A279279] p 1522 N95-21492

Ultrafast optical studies of surface reaction processes at semiconductor interfaces
[DE95-001548] p 1574 N95-21839

Quantum chemical study of rare gas/halide interactions as a model for high energy density material. 2: The interaction of hydrogen chloride with the rare gas xenon
[AD-A286385] p 1248 N95-22321

Resonant charge transfer in hyperthermal atomic and molecular ion-surface collisions
[AD-A284937] p 1530 N95-22471

CHARGE TRANSFER DEVICES

CTD calibration and processing methods used at Woods Hole Oceanographic Institution
[AD-A279507] p 1435 N95-21681

CHARGED PARTICLES

Modeling the dynamics of charged-particle beams using a Fokker-Planck approach
[DE95-001458] p 1531 N95-19983

ALT-2 armor tile design for upgraded TEXTOR operation
[DE94-015749] p 1549 N95-20143

GAJET experiment at the LHC: The GAJET collaboration
[PB95-129813] p 1512 N95-20454

Current diffusive ballooning mode in second stability region of tokamaks
[DE94-770690] p 1554 N95-20683

Simulation of tearing mode stabilization by using ECH
[DE94-770700] p 1554 N95-20684

Magnetic flocculation of paramagnetic particles
[DE94-018144] p 1501 N95-20725

Ion heat pulse after sawtooth crash in the JFT-2M tokamak
[DE94-770685] p 1555 N95-20988

Observation of non diffusive term of toroidal momentum transport in the JFT-2M tokamak
[DE94-770686] p 1555 N95-20989

Experimental measurements and modeling of impurity transport in the divertor and boundary plasma of D3-D
[DE94-016519] p 1556 N95-21159

Anomalous vector-boson couplings in Majorana neutrino models
[PB95-127460] p 1518 N95-21220

Where are we going with Bose-Einstein: A mini review
[PB95-130308] p 1518 N95-21222

Theory of the L-H transition
[DE95-001389] p 1558 N95-21299

Cluster reactions: An approach to understanding the fundamentals of heterogeneous catalysis
[DE95-002947] p 1243 N95-21447

Monopoles and quark confinement: Introduction and overview
[DE94-019348] p 1522 N95-21485

Structure functions and structure function ratio F2(n)/F2(p) at low X(Bj) and Q2 in inelastic muon scattering
[DE94-018979] p 1573 N95-21561

Classical-quantum correspondence for ionization in fast ion-atom collisions
[DE95-000953] p 1526 N95-21940

Theses of the Proceedings of the 23d International Meeting on the Physics of Charged Particle Interaction with Crystals
[DE94-631501] p 1529 N95-22281

Experimental study of interactions of highly charged ions with atoms at keV energies
[DE94-018648] p 1529 N95-22316

CHARM (PARTICLE PHYSICS)

J/psi,psi(prime) yields mu(+)mu(-) and B yields J/psi,psi(prime) cross sections
[DE94-017184] p 1507 N95-20108

A tau-charm-factory at Argonne
[DE94-016913] p 1510 N95-20360

Triggers for a high sensitivity charm experiment
[DE95-002251] p 1515 N95-20868

Charmonium production, b quark and B meson production and b(bar b) correlations at CDF
[DE95-002525] p 1515 N95-20898

A high-rate fixed-target charm experiment
[DE95-001767] p 1521 N95-21378

Polarization of charmonium in pion-nucleus collisions
[DE95-002783] p 1523 N95-21525

Measurement of the B cross section at CDF via B semileptonic decays
[DE95-002217] p 1524 N95-21597

Strong interactions studies with medium energy probes
[DE95-001800] p 1245 N95-21745

Beam flavor dependence in the hadroproduction of D(+-) and D(sub s)(+-) mesons
[DE94-015541] p 1530 N95-22339

CHARPY IMPACT TEST

The production of calibration specimens for impact testing of subsize Charpy specimens
[DE94-018125] p 1386 N95-20703

Impact behavior of FeAl alloy FA-350
[DE94-018128] p 1254 N95-20705

Effect of neutron irradiation on the impact properties of A533B steel
[DE95-001834] p 1256 N95-21286
Perimeter-yardstick technique for fracture surface fractal analysis
[AD-A286240] p 1387 N95-22025

CHARTS
Common mapping system media study
[AD-A279086] p 1390 N95-21912
The use of fuzzy set classification for pattern recognition of the polygraph
[AD-A279148] p 1470 N95-21971

CHEMICAL ANALYSIS
Experimental investigation of PIC formation during the incineration of recovered CFC-11
[PB94-214772] p 1401 N95-20192
Performance specifications for technology development: Application for characterization of volatile organic compounds in the environment
[DE94-016627] p 1401 N95-20234
ALCHEMI of Fe-doped B2-ordered NiAl alloys with different doping levels
[DE94-017748] p 1255 N95-20907
Methodology for ESCA analysis of electromigration
[AD-A286229] p 1241 N95-21168
An Echelle Grating Spectrometer (EGS) for mid-IR remote chemical detection
[DE94-019310] p 1367 N95-21478
Studies of selenium and xenon in inductively coupled plasma mass spectrometry
[DE95-001676] p 1245 N95-21734

CHEMICAL ATTACK
Evaluation of stress experienced by soldiers wearing chemical protective clothing during varying work loads in desert or tropical environments
[AD-A280113] p 1452 N95-20625

CHEMICAL BONDS
Energetics, bonding mechanism and electronic structure of ceramic/ceramic and metal/ceramic interfaces
[DE95-000601] p 1265 N95-20115
Photochemistry of intermolecular C-H bond activation reactions
[DE94-018417] p 1239 N95-20682
Electronic structure and relative stability of icosahedral superatoms in Al-transition-metal alloys
[DE94-628996] p 1260 N95-21855
Embedded optical fibres as strain sensors in polymer matrix fibre composites: The influence of adhesion in strain transfer
[PB95-133617] p 1547 N95-22140

CHEMICAL CLEANING
Guidelines for qualifying cleaning and verification materials
[NASA-TM-108474] p 1270 N95-20694
A new universal solution for the electrofinishing of metallic materials
[DE95-001681] p 1258 N95-21568

CHEMICAL COMPOSITION
Chemical Structure and Dynamics program
[DE95-001117] p 1403 N95-20834
Gradient index lenses from sol-gel layering
[AD-A285649] p 1242 N95-21402
D/H ratios and H2O contents of mantle-derived amphibole megacrysts from Dish Hill, California
p 1416 N95-21781

CHEMICAL COMPOUNDS
Selection of substances to be considered in the environmental balance/environmental outlook in relation to the dissemination theme
[PB95-132197] p 1407 N95-21635

CHEMICAL EFFECTS
Nitrogen control of chloroplast differentiation
[DE95-002797] p 1439 N95-21526

CHEMICAL ENERGY
Research in the chemical sciences: Summaries of FY 1994
[DE94-015427] p 1223 N95-20264

CHEMICAL ENGINEERING
Research in the chemical sciences: Summaries of FY 1994
[DE94-015427] p 1223 N95-20264
. Initial assessment of the hazards and risks of new chemicals to man and the environment, part 2
[PB95-106407] p 1410 N95-22124
Hydrothermal conversion of carbohydrates and related compounds
[PB95-134011] p 1396 N95-22175

CHEMICAL EQUILIBRIUM
Computer program for calculation of complex chemical equilibrium compositions and applications. Part 1: Analysis
[NASA-RP-1311] p 1235 N95-20180

CHEMICAL LASERS
Chemical lasers emitting in the visible spectrum: Metastable oxygen reactions and YOSHIDA laser
[PB95-104485] p 1372 N95-20983

CHEMICAL PROPERTIES
Monitoring bioremediation of Volatile Organic Compounds (VOCs) using Fourier Transform Infrared (FT-IR) spectrometry
[AD-A279631] p 1403 N95-20456
Nonlinear spectroscopy of multicomponent droplets and two- and three-dimensional measurements in flames
[AD-A279945] p 1238 N95-20581
An initial assessment of the properties of 2,5-dipicryl-1,3,4-oxadiazole: A secondary explosive with high thermal stability
[MRL-TR-93-16] p 1284 N95-21624

CHEMICAL REACTIONS
Chemical and electrochemical interactions on corroding metal surfaces
[DE95-000624] p 1250 N95-19979
Plasma chemistry of vibrationally nonequilibrium molecules
[AD-A279630] p 1553 N95-20411
An atomically-resolved STM study of the thermal decomposition of disilane on Si(001)
[AD-A279818] p 1567 N95-20544
Chemically modified electrodes
[AD-A279821] p 1324 N95-20587
Publications/patents/presentations/honors/student eport. Investigation of the role of vibrational excitation in unimolecular reactions
[AD-A280044] p 1513 N95-20621
Cross-linking reactions for the conversion of polyphosphazenes into useful materials
[AD-A279696] p 1271 N95-20709
An improved and facile method for the synthesis of 1,1-bis(4-hydroxyphenyl) 2-phenylethylene and its derivatives
[DE95-001125] p 1240 N95-20836
Assessment of database for interaction of tritium with ITER plasma facing materials
[DE95-002038] p 1558 N95-21290
Production of S2F10, S2OF10 and S2O2F10 by spark discharges in SF6*
[DE95-001421] p 1243 N95-21500
Fiber-optic sensors for rapid, inexpensive characterization of soil and ground water contamination
[DE95-002471] p 1545 N95-21510
Single-collision studies of energy transfer and chemical reaction
[DE95-002943] p 1244 N95-21517
The energetics and dynamics of free radicals, ions, and clusters
[DE94-018101] p 1244 N95-21701
Restricted mass transport effects on free radical reactions
[DE94-018136] p 1217 N95-21706
Chemical interactions between protein molecules and polymer membrane materials
[DE95-001808] p 1224 N95-21746
Selenophene transition metal complexes
[DE95-001675] p 1260 N95-21841
A catalytic method for the conversion of silanes to stannanes
[AD-A286214] p 1247 N95-22020
Synthesis and structure of a novel bis-stibole
[AD-A286345] p 1224 N95-22252
Applications of sonochemistry
[AD-A286388] p 1506 N95-22360

CHEMICAL REACTORS
Catalytic reactions of synthesis gas. Part 3. Determination of reaction kinetics
[PB95-127759] p 1248 N95-22329

CHEMICAL VAPOR INFILTRATION
Scale-up and modeling of forced chemical vapor infiltration
[DE94-017769] p 1340 N95-20781
Fabrication of ceramic composites: Forced CVI
[DE95-001076] p 1271 N95-20821

CHEMILUMINESCENCE
Compatibility testing of explosives and paints by chemiluminescence techniques
[PB95-133609] p 1275 N95-21275

CHEMISORPTION
Hydrogenation of nitriles on a well-characterized nickel surface: From surface science studies to liquid phase catalytic activity measurements
[DE94-018184] p 1259 N95-21707

CHIPS
Packaging the MAMA module p 1209 N95-20639
MCMs for avionics: Technology selection and intermodule interconnection p 1210 N95-20641
Reliability assessment of Multichip Module technologies via the Triservice/NASA RELTECH program
p 1210 N95-20643
Assuring Known Good Die (KGD) for reliable, cost effective MCMs p 1210 N95-20644

CHIPS (ELECTRONICS)
Materials research for GHz multi-chip modules
[AD-A279661] p 1227 N95-20412
Materials processing and manufacturing technologies for diamond substrates multichip modules
[AD-A285060] p 1315 N95-20488
The design and manufacturing development of an active silicon substrate MCM p 1211 N95-20645
High performance YBCO films
[AD-A286567] p 1326 N95-20824
Monolithic circuits for lead-glass calorimetry
[DE94-019112] p 1330 N95-21554
Non-linear A/D converters for integrated silicon smart sensors
[PB94-208402] p 1330 N95-21590
Design and development SAWAFE peak detector chip
[DE95-001745] p 1332 N95-21742
Consortia for Known Good Die (KGD), phase 1
[AD-A279407] p 1383 N95-21933
Radiation characterization report for the GPS Receiver microcontroller chip
[DE94-019169] p 1335 N95-22165
Radiation tests on service electronics for future multi TeV detectors
[DE94-632822] p 1335 N95-22184
Design of the readout IC for the CDF SVX-2 silicon strip detector
[DE95-000562] p 1539 N95-22193

CHIRAL DYNAMICS
Dynamics of the chiral transition
[DE94-016813] p 1524 N95-21641

CHIRALITY
Chiral symmetry and lattice gauge theory
[DE94-018676] p 1564 N95-20130
The paradigm of Pseudodual Chiral Models
[DE94-016386] p 1579 N95-20271
Biaxiality of chiral liquid crystals
[DE94-629032] p 1578 N95-22277

CHLORIDES
Effect of external stress on the transport of fluids in thermoplastic resin systems
[AD-A279993] p 1270 N95-20596
Modeling of nonlinear optic and ESR response of CDW MX materials
[DE94-018301] p 1578 N95-22297
Quantum chemical study of rare gas/halide interactions as a model for high energy density material. 2: The interaction of hydrogen chloride with the rare gas xenon
[AD-A286385] p 1248 N95-22321

CHLORINE
Experimental investigation of PIC formation during the incineration of recovered CFC-11
[PB94-214772] p 1401 N95-20192
Tests of dielectric model descriptions of chemical charge displacements in water
[DE94-007530] p 1236 N95-20277
Radiative forcing calculations for CH3Cl
[DE94-019018] p 1402 N95-20355
Has a standard model solution to the solar neutrino problem been found?
[DE94-017580] p 1604 N95-20490
Noble gas isotopes and halogens in volatile-rich inclusions in diamonds p 1417 N95-21784
Effects of increased UV-B radiation on phytoplankton: A preliminary study and research programme
[PB95-133732] p 1439 N95-21884

CHLORINE FLUORIDES
Launch safety, toxicity, and environmental effects of the high performance oxidizer ClF(5)
[AD-A286095] p 1284 N95-22227

CHLOROFLUOROCARBONS
Accelerated screening methods for determining chemical and thermal stability of refrigerant-lubricant mixtures. Part 2: Experimental comparisons and verification of methods
[DE95-000743] p 1264 N95-20078
Experimental investigation of PIC formation during the incineration of recovered CFC-11
[PB94-214772] p 1401 N95-20192
The development and evaluation of water-mist fire extinguishing systems
[DE94-019019] p 1286 N95-20356
New concepts for refrigerant leak detection and mixture measurement
[DE94-018967] p 1287 N95-21559
Materials compatibility and lubricants research on CFC-refrigerant substitutes
[DE94-018414] p 1287 N95-21631
Ozone-depleting-substance control and phase-out plan
[DE95-001647] p 1409 N95-21722

CHLOROFORM
Effect of external stress on the transport of fluids in thermoplastic resin systems
[AD-A279993] p 1270 N95-20596

CHLOROPHYLLS
Nitrogen control of chloroplast differentiation
[DE95-002797] p 1439 N95-21526

CHLOROPLASTS
Nitrogen control of chloroplast differentiation
[DE95-002797] p 1439 N95-21526

CHOLESTEROL
The influence of coronary artery disease on +Gz tolerance: A preliminary study
[AD-A279305] p 1446 N95-21941

CHONDRITES
Transportation of volatile elements in thermally evolving planetesimals: An important role of metallic iron
p 1418 N95-21790
Solubilities of nitrogen and noble gases in basalt melt
p 1422 N95-21807
Comets, impacts, and atmospheres
p 1422 N95-21810

CHROMIUM
Modelocking and waveguide amplifiers using Cr:Forsterite and Cr:YAG
[AD-A285857] p 1369 N95-20378
Electrochemical impedance spectroscopy of trivalent chromium pre-treated aluminum alloy
[AD-A280093] p 1240 N95-20970
Nitrogen alloyed martensitic steels
[PB95-127791] p 1255 N95-21128

CHROMIUM ALLOYS
Cr2Nb development
[DE94-018697] p 1250 N95-20043
Microstructures and tensile properties of as-cast iron-aluminide alloys
[DE94-017868] p 1252 N95-20359
Electrochemical impedance spectroscopy of trivalent chromium pre-treated aluminum alloy
[AD-A280093] p 1240 N95-20970
Metastable bcc phase formation in the Nb-Cr-Ti system
[DE94-016212] p 1255 N95-21137
Computational modeling of diffusion-controlled transformations in ternary systems
[DE95-001358] p 1256 N95-21298
Incology alloy 908 data handbook
[DE95-001818] p 1260 N95-22013

CHROMIUM COMPOUNDS
Evaluation of Pd-Cr wires for strain gage application
[NASA-TM-106857] p 1366 N95-21259
Dynamic NMR studies of restricted arene rotation in the chromiu tricarbonyl thiophene and selenophene complexes
[DE95-001656] p 1257 N95-21399

CHROMIUM ISOTOPES
An investigation of the applicability of the new ion exchange resin, Reillex(TM)-HPQ, in ATW separations
[DE94-016576] p 1274 N95-21234

CHROMIUM OXIDES
Selective methane oxidation over promoted oxide catalysts
[DE94-012270] p 1235 N95-20188
Classification of bianisotropic media
[PB95-127635] p 1502 N95-21102

CHROMOPHORES
Design, synthesis and characterization of novel nonlinear optical materials
[AD-A285617] p 1540 N95-19897
Photodegradation and photophysics of laser dyes
[AD-A285105] p 1368 N95-20063
High temperature polymer for second order nonlinear optics for photonic materials
[AD-A279309] p 1280 N95-22141

CHUTES
Corrosion evaluation of fuel canister crusher rigging
[DE95-002962] p 1257 N95-21452

CIRCLES (GEOMETRY)
Coupled analytic maps
[PB95-111076] p 1498 N95-19945
An exact enumeration of self-avoiding loops on a square lattice
[DE94-628999] p 1578 N95-22276
Local connectivity of some Julia sets containing a circle with an irrational rotation
[PB95-109070] p 1496 N95-22353

CIRCUIT BOARDS
High performance hardware and software for pattern recognition and image processing
[AD-A279776] p 1457 N95-19961
Module cooling system
[AD-D016584] p 1315 N95-20436
An automatic placement tool for rapid prototyping of printed circuit boards
[AD-A286029] p 1328 N95-20997

CIRCUIT RELIABILITY
The reliability of laser reflowed Sn-Ag solder joints
[AD-A279787] p 1315 N95-20443

CIRCUITS
Evaluation of superconducting quantum interference devices interfaced with digital signal processing electronics for biomagnetic applications
[DE94-016186] p 1269 N95-20164
A charge distribution analysis instrument for catalysis and material science applications
[DE94-016489] p 1364 N95-20233
Prototype rule-based reliability analysis for VLSI circuit design
[AD-A280065] p 1327 N95-20967
Circuit means for providing compatibility between two separate digital data interfaces
[AD-D016225] p 1455 N95-21116
Quartz resonator fluid monitors for vehicle applications
[DE94-018910] p 1367 N95-21546
SEU and SEL response of the Westinghouse 64K E-2PROM, analog devices AD7876 12-bit ADC, and the Intel 82527 Serial Communications Controller
[DE95-003349] p 1334 N95-22086

CIRCULAR CYLINDERS
Research on bluff body vortex wakes
[AD-A286319] p 1200 N95-20177
The velocity and vorticity fields of the turbulent near wake of a circular cylinder
[NASA-TM-110513] p 1355 N95-21954

CIRCULAR POLARIZATION
A structural determination using magnetic x ray circular dichroism in spin-polarized photoelectron diffraction
[DE94-017528] p 1567 N95-20449
Magnetic x-ray circular dichroism in spin-polarized photoelectron diffraction
[DE95-002394] p 1520 N95-21360
Analysis of a microstrip reflectarray antenna for microspacecraft applications p 1305 N95-21541
Electric-field effects on shallow donor impurity in a harmonic quantum dot
[DE94-629034] p 1577 N95-22176

CIRCULAR WAVEGUIDES
Analysis of a disk-on-rod surface wave element inside a corrugated horn using the mode-matching technique
p 1305 N95-21543
Improved broadband waveguide pressure window
[AD-D016487] p 1306 N95-21834

CIRCULATION
Numerical modeling of a small recirculating induction accelerator for heavy-ion fusion
[DE94-018549] p 1552 N95-20318

CITIES
Propagation of high frequency waves in urban and road tunnel environments p 1294 N95-20933
Environmental cleanup: Too many high priority sites impede DOD's program. Report to the Chairman, Committee on Governmental Affairs, US Senate
[AD-A279511] p 1407 N95-21683
Urban air carcinogens and their effects on health
[DE95-002259] p 1447 N95-22285
Current concepts on airborne particles and health
[DE95-002260] p 1447 N95-22287

CIVIL AVIATION
Census US civil aircraft calendar year 1993
[AD-A286309] p 1199 N95-20091
Test and evaluation report for the Manual Domestic Passive Profiling System (MDPPS)
[AD-A286312] p 1202 N95-20093

CLAMPS
The effect of fiber coating thickness on the interfacial properties of a continuous fiber ceramic matrix composite
[DE94-017886] p 1267 N95-20373

CLASSIFICATIONS
Hierarchical diagrammatic representation of class structure
[PB95-110722] p 1456 N95-19908
Classification of diagonal coset modular invariants
[PB95-111118] p 1489 N95-20259
Modeling and identification of parallel and feedback nonlinear systems
[DE95-001006] p 1481 N95-20812
Classification of bianisotropic media
[PB95-127635] p 1502 N95-21102
Magnetoelectric properties of reciprocal bianisotropic materials with focus on the polarizability of chiro-omega spheres
[PB95-127650] p 1544 N95-21103
The use of fuzzy set classification for pattern recognition of the polygraph
[AD-A279148] p 1470 N95-21971

CLASSIFIERS
Innovative use of DSP technology in space: FORTE event classifier
[DE94-016086] p 1291 N95-20697

CLASSIFYING
Guidelines for qualifying cleaning and verification materials
[NASA-TM-108474] p 1270 N95-20694

CLEAN FUELS
The Carnol process for methanol production and utilization with reduced CO2 emissions
[DE94-016808] p 1283 N95-21211

CLEANERS
Guidelines for qualifying cleaning and verification materials
[NASA-TM-108474] p 1270 N95-20694

CLEANING
Mercury capture in bench-scale absorbers
[DE94-016910] p 1234 N95-20107
Natural gas cleanup: Evaluation of a molecular sieve carbon as a pressure swing adsorbent for the separation of methane/nitrogen mixtures
[DE94-012263] p 1234 N95-20135
Environmental cleanup technology transfer initiatives
[AD-A285059] p 1403 N95-20487
Ceramem filters for removal of particles from hot gas streams
[DE95-001976] p 1275 N95-21354
Environmental cleanup: Too many high priority sites impede DOD's program. Report to the Chairman, Committee on Governmental Affairs, US Senate
[AD-A279511] p 1407 N95-21683

CLIMATE
Monsoons: AMIP simulations of the 1987 and 1988 drought and flood regimes
[DE94-014789] p 1428 N95-20140
Lidar technologies for airborne and space-based applications
[DE95-002954] p 1302 N95-21448

CLIMATE CHANGE
Dust Bowl migration as an analog for possible global warming-induced migration from Mexico
[DE94-017472] p 1401 N95-20089
Site Scientific Mission Plan for the Southern Great Plains CART site, July - December 1994
[DE94-017289] p 1401 N95-20193
Workshop on Uncertainty and Global Climate Change Research
[DE94-016728] p 1401 N95-20238
Daytime Raman lidar profiling of atmospheric water vapor
[DE94-015747] p 1413 N95-20397
Global change integrating factors: Tropical tropopause trends
[DE95-001121] p 1404 N95-20835
Definition report on environmental indices in future environmental assessments environmental balance/environmental outlook
[PB95-131876] p 1405 N95-21350
Sensitivity of climate models: Comparison of simulated and observed patterns for past climates
[DE95-002257] p 1406 N95-21379
Monitoring the response of the upper troposphere/lower stratosphere to a greenhouse gas scenario
[DE95-000982] p 1406 N95-21410
Modeling the response of the California Current system to Global Greenhouse Warming
[DE94-018253] p 1408 N95-21708
Proceedings: International Symposium on Global Change (IGBP)
[DE94-765351] p 1410 N95-22219

CLIMATE MODELS
Workshop on Uncertainty and Global Climate Change Research
[DE94-016728] p 1401 N95-20238
Sensitivity of climate models: Comparison of simulated and observed patterns for past climates
[DE95-002257] p 1406 N95-21379
The message passing version of the parallel Community Climate Model
[DE94-019158] p 1407 N95-21608
Confirmatory analysis of SAGE-1, and -2 data
[DE95-003623] p 1427 N95-22240

CLIMATOLOGY
The initiation of lightning and the growth of electric fields in thunderstorms
[AD-A280033] p 1428 N95-20008
Workshop on Uncertainty and Global Climate Change Research
[DE94-016728] p 1401 N95-20238
Global change integrating factors: Tropical tropopause trends
[DE95-001121] p 1404 N95-20835
Proceedings: International Symposium on Global Change (IGBP)
[DE94-765351] p 1410 N95-22219
Climatological data for clouds over the globe from surface observations, 1982-1991: The total cloud edition
[DE95-002537] p 1431 N95-22288

CLIMBING FLIGHT
Acoustic climb to cruise test
[NASA-TM-110504] p 1206 N95-20155

CLINICAL MEDICINE
Environmental Hazards Assessment Program
[DE94-019075] p 1406 N95-21565

CLOSTRIDIUM
Microbiology and physiology of anaerobic fermentations of cellulose
[DE95-002899] p 1438 N95-20917
CLOSURE LAW
Mapping closures for turbulent combustion
[AD-A279995] p 1238 N95-20597
CLOSURES
Evaluation of Reynolds stress turbulence closures in compressible homogeneous shear flow
[NASA-CR-194892] p 1338 N95-20009
CLOTHING
Governing equations for multiphase heat and mass transfer in hygroscopic porous media with applications to clothing materials
[AD-A286418] p 1357 N95-22206
CLOTTING
Preclinical investigation of lyophilized platelet preparations
[AD-A286079] p 1443 N95-20851
CLOUD COVER
Completion of spectral rotating shadowband radiometers and analysis of ARM spectral short-wave data
[DE95-000602] p 1412 N95-20116
Proceedings of the Cloud Impacts on DOD Operations and Systems 1993 Conference (CIDOS 1993)
[AD-A286658] p 1430 N95-20974
Climatological data for clouds over the globe from surface observations, 1982-1991: The total cloud edition
[DE95-002537] p 1431 N95-22288
CLOUD DISPERSAL
Site Scientific Mission Plan for the Southern Great Plains CART site, July - December 1994
[DE94-017289] p 1401 N95-20193
CLOUD PHYSICS
Effects of microphysics and radiation on mesoscale processes of a midlatitude squall line
[DE94-014732] p 1429 N95-20381
Proceedings of the Cloud Impacts on DOD Operations and Systems 1993 Conference (CIDOS 1993)
[AD-A286658] p 1430 N95-20974
An integrated cloud observation and modeling investigation in support of the ARM Program
[DE95-002798] p 1430 N95-21527
CLOUDS (METEOROLOGY)
Site Scientific Mission Plan for the Southern Great Plains CART site, July - December 1994
[DE94-017289] p 1401 N95-20193
An integrated cloud observation and modeling investigation in support of the ARM Program
[DE95-002798] p 1430 N95-21527
CLUSTER ANALYSIS
An empirical approach to logical clustering of software failure regions
[AD-A279863] p 1462 N95-20776
Saddle-node dynamics for edge detection
[DE94-017415] p 1473 N95-22426
CLUTTER
Detection optimization using linear systems analysis of a coded aperture laser sensor system
[DE95-001112] p 1371 N95-20832
Modelling of microwave propagation and clutter in a maritime environment p 1295 N95-20938
Large bistatic angle clutter depolarization study
p 1296 N95-20941
The effects of multihop HF propagation on the performance of OTH backscatter radars
p 1298 N95-20953
Classical analysis methods for designing and developing downlooking radars
[AD-A285760] p 1302 N95-21405
Probability of detection for a GO CFAR radar processor using envelope detection approximation
[AD-A286211] p 1310 N95-22251
Effect of cell size on elliptically polarized radar clutter statistics
[AD-A285789] p 1311 N95-22401
CMOS
Design of a 10 bit 10k Samples/s low power CMOS ADC
[PB95-110425] p 1455 N95-22018
Defect classes: An overdue paradigm for CMOS IC testing
[DE94-018905] p 1334 N95-22118
Radiation characterization report for the GPS Receiver microcontroller chip
[DE94-019169] p 1335 N95-22165
Design of the readout IC for the CDF SVX-2 silicon strip detector
[DE95-000562] p 1539 N95-22193
COAGULATION
Preclinical investigation of lyophilized platelet preparations
[AD-A286079] p 1443 N95-20851
COAL
Technology development for cobalt F-T catalysts
[DE94-017363] p 1241 N95-21172
Ceramem filters for removal of particles from hot gas streams
[DE95-001976] p 1275 N95-21354
Restricted mass transport effects on free radical reactions
[DE94-018136] p 1217 N95-21706
COAL DERIVED GASES
Bioconversion of coal derived synthesis gas to liquid fuels
[DE94-017381] p 1282 N95-19927
Bioconversion of coal derived synthesis gas to liquid fuels
[DE94-018849] p 1314 N95-20339
COAL DERIVED LIQUIDS
Lower active metals loading for hydrotreating catalysts
[DE94-018907] p 1261 N95-22119
COAL GASIFICATION
Energy impacts of controlling carbon dioxide emissions from an integrated gasification/combined-cycle system
[DE94-016878] p 1403 N95-20478
COAL LIQUEFACTION
Intrinsic barriers for H-atom transfer reactions
[DE94-018914] p 1507 N95-20049
COALESCING
Relativistic binary neutron star coalescence
[DE94-019311] p 1600 N95-21479
COANDA EFFECT
Static investigation of two fluidic thrust-vectoring concepts on a two-dimensional convergent-divergent nozzle
[NASA-TM-4574] p 1199 N95-19913
COASTAL CURRENTS
A numerical study of wind forcing effects on the California Current System
[AD-A286205] p 1435 N95-21880
COASTAL ECOLOGY
Closure on the global carbon cycle
[DE94-018617] p 1404 N95-20991
COASTAL WATER
AN/APS-137 Forward Looking Airborne Radar (FLAR) evaluation, Fall 1992 experiment
[AD-A279526] p 1306 N95-21686
COASTS
Long Time Series Measurements in the Coastal Ocean: A workshop
[AD-A279509] p 1435 N95-21682
AN/APS-137 Forward Looking Airborne Radar (FLAR) evaluation, Fall 1992 experiment
[AD-A279526] p 1306 N95-21686
COATING
The effect of fiber coating thickness on the interfacial properties of a continuous fiber ceramic matrix composite
[DE94-017886] p 1267 N95-20373
Qualification test results for blue-red reflecting solar covers p 1320 N95-20525
Electrochemical impedance spectroscopy of trivalent chromium pre-treated aluminum alloy
[AD-A280093] p 1240 N95-20970
Aircraft corrosion study
[AD-A279527] p 1259 N95-21687
Aligned bismuth, strontium, calcium cuprate coatings on polycrystalline substrates
[AD-D016512] p 1278 N95-21907
COATINGS
The thermal conductivity of carbon coated silicon carbide fibers embedded in a silicon carbide matrix
[DE94-017758] p 1225 N95-20023
Method of making copper-titanium nitride alloy
[AD-D016582] p 1252 N95-20201
UV testing of INTELSAT-7, 7A, and 8 solar cells
p 1320 N95-20526
Boron carbide-based coatings on graphite for plasma facing components
[DE94-017976] p 1269 N95-20570
Aircraft corrosion study
[AD-A279527] p 1259 N95-21687
Protective organic coatings on steel: Accelerated corrosion test method for paint/coatings exposed to water with low conductivity. Nordtest project no. 1010-92. Degradation of organic coatings in fresh water
[PB95-134185] p 1277 N95-21873
Surface technology programme
[PB95-132866] p 1262 N95-22174
Reflective masks for extreme ultraviolet lithography
[DE95-003427] p 1336 N95-22236
Measurement of the thermal properties of electrically conducting fluids using coated transient hot wires
[DE94-017816] p 1357 N95-22264
Defect geometries and laser-induced damage in multilayer coatings
[DE94-017695] p 1377 N95-22343
Accelerated life testing of solar energy materials: Case study of some selective solar absorber coating materials for DHW systems. A report of task 10 solar materials research and development
[PB95-132411] p 1397 N95-22362
COAXIAL CABLES
Proceedings of the International Wire and Cable Symposium
[AD-A279242] p 1403 N95-20465
Analysis of a disk-on-rod surface wave element inside a corrugated horn using the mode-matching technique
p 1305 N95-21543
Current distribution in Cable-In-Conduit Conductors
[DE95-001820] p 1332 N95-21725
Passive surface deployed variable inductance wire antenna statement of government interest
[AD-D016210] p 1307 N95-21910
COBALT
Investigation of syngas interaction in alcohol synthesis catalysts
[DE94-018784] p 1236 N95-20349
Magnetic x ray circular dichroism in Fe Co Pt multilayers
[DE94-017522] p 1253 N95-20447
COBALT ALLOYS
Cr2Nb development
[DE94-018697] p 1250 N95-20043
Hydrogen resistant alloy - NASA 23
[NASA-CASE-MFS-26200-1-SB] p 1251 N95-20068
Giant magnetoresistance calculated from first principles
[DE94-018658] p 1500 N95-20129
Consequences of oscillatory potentials and angular forces in transition metals and their aluminides
[DE94-019127] p 1258 N95-21600
COBALT COMPOUNDS
Technology development for cobalt F-T catalysts
[DE94-017363] p 1241 N95-21172
COCKPITS
Crew-Centered Cockpit Design (CCCD) field demonstration program, volume 1
[AD-A286426] p 1453 N95-21566
The advanced technology crew station: Development and validation of a workload assessment technique for cockpit function allocation
[AD-A279544] p 1453 N95-21691
CODE DIVISION MULTIPLE ACCESS
CDMA with interference cancellation for multiprobe missions p 1304 N95-21536
CODERS
A method to determine the kinematics of the lower limbs of a subject pedaling a bicycle using encoders and accelerometers
[NASA-CR-197401] p 1453 N95-21866
CODES
Time code interface
[AD-D016535] p 1501 N95-20731
CODING
Detection optimization using linear systems analysis of a coded aperture laser sensor system
[DE95-001112] p 1371 N95-20832
Expressions that talk about themselves
[PB95-134060] p 1466 N95-21344
Proposal for a tutorial on Minimal Length Encoding (MLE) in molecular biology
[DE94-015076] p 1438 N95-21376
Subsampling methods for image sequence coding
[PB95-107991] p 1305 N95-21579
Image and video coding using a wavelet decomposition
[PB95-135067] p 1311 N95-22358
COEFFICIENT OF FRICTION
The effect of fiber coating thickness on the interfacial properties of a continuous fiber ceramic matrix composite
[DE94-017886] p 1267 N95-20373
On the origins and modeling of frictional behavior in interfacially-complex sliding contacts
[DE94-019129] p 1381 N95-21601
COEFFICIENTS
Development of ferroelectric liquid crystals with enhanced nonlinear optical properties
[AD-A279988] p 1571 N95-20965
Collisional redistribution effects on x ray laser saturation behavior
[DE94-017308] p 1374 N95-21663
COGNITION
A database for analyzing sequential behavioral data and their associated cognitive models
[AD-A280061] p 1448 N95-19887
COGNITIVE PSYCHOLOGY
MAC/FAC: A model of similarity-based retrieval
[AD-A286291] p 1450 N95-22052

COHERENT RADIATION
Instantaneous frequency dynamics of coherent emission from magnetoexcitons in gallium arsenide
[DE94-018182] p 1569 N95-20677
Coherence properties of high order harmonic radiation
[DE94-016974] p 1377 N95-22312
COHERENT SCATTERING
X-band microwave backscattering from ocean waves
[DE94-016719] p 1309 N95-22241
COHESION
Dielectric models in adhesion and extrapolations of molecular modeling
[AD-A279675] p 1516 N95-21121
COILS
The calculation and measurement of Helmholtz coil fields
[AD-A286081] p 1228 N95-20808
COLD PLASMAS
Plasma model for charging damage
[DE95-000788] p 1558 N95-21310
On the theory of strong electromagnetic waves propagation in an electron-positron-ion plasma
[DE94-628964] p 1561 N95-21850
Large amplitude localized structures in a relativistic electron-positron ion plasma
[DE94-628965] p 1561 N95-21851
Observations of cold magnetospheric ions at geosynchronous orbit during times of high activity
[DE95-000936] p 1600 N95-21935
COLD TOLERANCE
Thermal resistance of the cheek in cold air
[AD-A286257] p 1446 N95-22001
COLD WEATHER TESTS
Cold regions instrumentation considerations
[AD-A279492] p 1367 N95-21680
Thermal resistance of the cheek in cold air
[AD-A286257] p 1446 N95-22001
COLLECTION
Parasitic current collection by solar arrays in LEO
p 1321 N95-20527
COLLIMATORS
Fiber-optic rotary joint with bundle collimator assemblies
[AD-D016504] p 1545 N95-21673
Unique microchannel plate process doubles MCPI resolution
[DE94-017507] p 1337 N95-22427
COLLISION AVOIDANCE
Tom Thumb algorithm for planning simple vehicle motions
[PB95-107553] p 1484 N95-22156
COLLISION PARAMETERS
Measurement of W and Z production cross-sections in p(bar p) collisions at (radical)s = 1.8 TeV
[DE95-002250] p 1523 N95-21521
Correlations for the OH A(sup 2)(Sigma)(sup +)(v(prime)=0) electronic quenching cross-section
[DE95-002591] p 1244 N95-21524
COLLISIONAL PLASMAS
Collisional drift waves in the H-mode edge
[DE94-628950] p 1561 N95-21847
PIC simulation of surface waves
[AD-A285358] p 1563 N95-22422
COLLISIONLESS PLASMAS
Explicit analytical solution of the nonlinear Vlasov Poisson system
[DE94-628931] p 1500 N95-21592
Quasi-linear equation for magnetoplasma oscillations in the weakly relativistic approximation
[DE94-628932] p 1560 N95-21593
On the influence of electromagnetic wave and relativistic electron beam on a plasma
[DE94-628962] p 1561 N95-21848
COLLISIONS
A comparison of kinetic and multifluid simulations of laser-produced colliding plasmas
[DE94-016447] p 1551 N95-20315
Conservative smoothing versus artificial viscosity
[DE95-001108] p 1341 N95-20831
Ion-molecular spiraling collisions and termolecular recombination
[AD-A285633] p 1517 N95-21151
Angular and charge state distributions of highly charged ions scattered during low energy surface-channeling interactions with Au(110)
[DE95-001348] p 1525 N95-21857
Classical-quantum correspondence for ionization in fast ion-atom collisions
[DE95-000953] p 1526 N95-21940
Beam flavor dependence in the hadroproduction of D(+-) and D(sub s)(+-) mesons
[DE94-015541] p 1530 N95-22339
COLLOIDS
Technical Summary for 1993 fall MRS Symposium O, Complex Fluids
[AD-A283722] p 1264 N95-19972
Photoinduced charge transfer between fullerenes and TiO2 semiconductor colloids
[DE95-001447] p 1570 N95-20838
Novel materials and devices from self-assembled periodic structures
[AD-A286499] p 1232 N95-22211
COLOR
Orthogonal representations over finite fields and the chromatic number of graphs
[PB95-110953] p 1487 N95-19937
The synthesis and characterization of new mesogenic diacetylene monomers and their polymers
[AD-A286188] p 1267 N95-20328
Six-dimensional modeling of coherent bunch instabilities and related feedback systems in storage rings with power-series maps for the lattice
[DE94-017965] p 1532 N95-20494
Color control in a multichannel simulator display: The display for advanced research and training
[AD-A279717] p 1216 N95-20992
Search for new particles decaying to dijets in p(bar p) collisions at (radical)s = 1.8 TeV
[DE94-018994] p 1523 N95-21563
Hardware implementation of a desktop supercomputer for high performance image processing. Color image processing using cellular neural networks
[AD-A286455] p 1455 N95-21589
Azimuthally averaged radial S(sub 100 microns)/S(sub 60 microns) dust color temperatures in spiral galaxies
p 1593 N95-21760
European Workshop on Optical Ground Truth Instrumentation for the Validation of Space-Borne Optical Remote Sensing Data of the Marine Environment
[PB95-134144] p 1390 N95-21872
Test and Evaluation Plan (TEP) for Improvised Explosive Device Screening Systems (IEDSS)
[AD-A286382] p 1203 N95-22319
COLOR CODING
Hires and beyond p 1592 N95-21750
COLORIMETRY
Fiber-optic sensors for rapid, inexpensive characterization of soil and ground water contamination
[DE95-002471] p 1545 N95-21510
COMBAT
Bomber force 2000: Operational concepts for long-range combat aircraft
[AD-A279378] p 1206 N95-20181
Navigation system in combat vehicle
[PB95-131629] p 1452 N95-21467
Assessing post traumatic stress disorder and PTSD symptomatology in US Army personnel
[AD-A285941] p 1451 N95-22324
COMBINATORIAL ANALYSIS
Application of Markov decision processes to search problems
[PB95-110813] p 1497 N95-19914
Balanced matrices
[AD-A280021] p 1490 N95-20662
Approximation algorithms for the general and the asymmetric stacker-crane problems
[PB95-132098] p 1493 N95-21468
Rigorous spin-spin correlation function of Ising model on a special kind of Sierpinski Carpets
[DE94-628995] p 1575 N95-21854
COMBUSTIBLE FLOW
Two-dimensional imaging of OH in a lean burning high pressure combustor
[NASA-TM-106854] p 1214 N95-21383
COMBUSTION
The Combustive Sound Source
[ARL-TR-94-9] p 1503 N95-19911
Experimental investigation of PIC formation during the incineration of recovered CFC-11
[PB94-214772] p 1401 N95-20192
Radiative forcing calculations for CH3Cl
[DE94-019018] p 1402 N95-20355
Effect of chemical heat release in a temporally evolving mixing layer p 1249 N95-21037
Two-dimensional imaging of OH in a lean burning high pressure combustor
[NASA-TM-106854] p 1214 N95-21383
Analysis of cost: Combustion flame CVD diamond deposition
[AD-A279153] p 1278 N95-21973
Natural gas combustion chemistry mechanisms research
[PB95-111670] p 1247 N95-22150
COMBUSTION CHAMBERS
The 1993 JANNAF Propulsion Meeting, volume 2
[AD-A279569] p 1221 N95-20708
COMBUSTION CHEMISTRY
Computer program for calculation of complex chemical equilibrium compositions and applications. Part 1: Analysis
[NASA-RP-1311] p 1235 N95-20180
Combustion-related studies using weakly bonded complexes
[DE95-002801] p 1238 N95-20576
Annual Conference on Fire Research: Book of abstracts
[PB95-104964] p 1286 N95-20717
LIEKKI combustion technology
[DE95-700233] p 1242 N95-21282
Correlations for the OH A(sup 2)(Sigma)(sup +)(v(prime)=0) electronic quenching cross-section
[DE95-002591] p 1244 N95-21524
Numerical study of contaminant effects on combustion of hydrogen, ethane, and methane in air
[NASA-TM-106844] p 1284 N95-22114
Natural gas combustion chemistry mechanisms research
[PB95-111670] p 1247 N95-22150
COMBUSTION EFFICIENCY
EAGLES 1.1: A microcomputer software package for analyzing fuel efficiency of electric and gasoline vehicles
[DE95-001119] p 1469 N95-21829
COMBUSTION PHYSICS
Experimental investigation of PIC formation during the incineration of recovered CFC-11
[PB94-214772] p 1401 N95-20192
Molecular snapshots: Product imaging of dynamics important to fundamental combustion processes
[DE94-018595] p 1510 N95-20346
Proceedings of the Zel'Dovich Memorial International Conference on Combustion, Detonation, Shock Waves, volume 2
[AD-A286626] p 1239 N95-20769
LIEKKI combustion technology
[DE95-700233] p 1242 N95-21282
Studies in nonlinear problems of energy
[DE95-001387] p 1356 N95-22148
COMBUSTION PRODUCTS
Laboratory evaluation of a reactive baffle approach to NOx control
[AD-A283802] p 1400 N95-19921
Effects of non-unity Lewis numbers in diffusion flames
p 1249 N95-21036
Summaries of BFRL fire research in-house projects and grants, 1994
[PB95-130845] p 1286 N95-21130
COMETARY COLLISIONS
Experimental hypervelocity impact effects on simulated planetesimal materials
[DE94-017290] p 1599 N95-20144
Erice International Seminars on Planetary Emergencies. 17th Workshop: The Collision of an Asteroid or Comet with the Earth
[AD-A280122] p 1600 N95-21577
COMETS
Experimental hypervelocity impact effects on simulated planetesimal materials
[DE94-017290] p 1599 N95-20144
Erice International Seminars on Planetary Emergencies. 17th Workshop: The Collision of an Asteroid or Comet with the Earth
[AD-A280122] p 1600 N95-21577
Comets, impacts, and atmospheres
p 1422 N95-21810
COMFORT
Helicopter crewseat cushion program
[AD-A286654] p 1452 N95-20973
Quantitative evaluation of wrist posture and typing performance: A comparative study of 4 computer keyboards
[DE95-002392] p 1452 N95-21358
Ergonomic evaluation of the Apple Adjustable Keyboard
[DE95-002393] p 1453 N95-21637
COMMAND AND CONTROL
Advanced Command and Control (C2) applications interfaces to the Advanced Communications Technology Satellite (ACTS)
[AD-A279676] p 1291 N95-20605
Terrain and refractivity effects on non-optical paths
p 1294 N95-20931
Noncoherent transponder standards
[AD-A279512] p 1306 N95-21684
COMMAND LANGUAGES
DBASE 4 basics
[DE94-018323] p 1469 N95-21713
COMMERCE
Advanced Standard Electronic Modules format-E (SEM-E) processes for rapid prototyping
p 1210 N95-20642
User interface software tools
[AD-A286056] p 1466 N95-21325
HPCC technology awareness program: Improved economic competitiveness through technology awareness, transfer and application
[DE95-002134] p 1476 N95-21355

Proceedings of the 4th Annual Major Range and TestFacility Base (MRTFB) Environmental Workshop
[AD-A285779] p 1411 N95-22414

COMMERCIAL AIRCRAFT
Census US civil aircraft calendar year 1993
[AD-A286309] p 1199 N95-20091
Commuter/air taxi ditchings and water-related impacts that occurred from 1979 to 1989
[AD-A285691] p 1202 N95-20275
Why do airlines want and use thrust reversers? A compilation of airline industry responses to a survey regarding the use of thrust reversers on commercial transport airplanes
[NASA-TM-109158] p 1203 N95-20706

COMMONALITY
The opportunities for and challenges of common integrated electronics
[AD-A279991] p 1327 N95-20966

COMMUNICATION
Independent review of Aviation Technology and Research Information Analysis System (ATRIAS) database
[AD-A284049] p 1203 N95-21518

COMMUNICATION EQUIPMENT
System level fault tolerance in parallel and distributed computing systems
[AD-A279664] p 1474 N95-20305
DAMSON: A system to measure multipath dispersion, Doppler spread and Doppler shift on multi-mechanism communications channels p 1299 N95-20955

COMMUNICATION NETWORKS
A multivariate multisample rank test for stochastic simulation validation
[AD-A285922] p 1498 N95-19990
Facsimile transmission standards
[AD-A279911] p 1290 N95-20308
Resonant tunneling quantum well integrated optical waveguide modulator/switch
[AD-A285142] p 1542 N95-20501
Advanced Command and Control (C2) applications interfaces to the Advanced Communications Technology Satellite (ACTS)
[AD-A279676] p 1291 N95-20605
Optical backplane for modular avionics
p 1212 N95-20652
Test and Evaluation Master Plan (TEMP) for the Weather Message Switching Center Replacement (WMSCR)
[AD-A286590] p 1429 N95-20857
Highly survivable communications: Complementary media packet switched networks p 1292 N95-20922
Mitigation of effects of multiple path nulls at super-high frequencies through diversity and networking
p 1297 N95-20948
Polymer based all-optic reconfigurable interconnects
[AD-A279976] p 1272 N95-20962
Routing of unidirectional packet radio for wide-area paging network control and maintenance
[PB95-104428] p 1300 N95-20980
Utilizing artificial neural networks in network flow analysis: An annotated bibiliography
[DE95-002453] p 1482 N95-21522
High-capacity optical multichannel virtual mesh interconnection networks
[PB95-134094] p 1546 N95-21870
Directives for the participation in MiTS forum. V3.0
[PB95-110342] p 1484 N95-22015

COMMUNICATION SATELLITES
The design and analysis of a phased array microstrip antenna for a low earth orbit communication satellite
[AD-A284791] p 1289 N95-20065
Advanced Command and Control (C2) applications interfaces to the Advanced Communications Technology Satellite (ACTS)
[AD-A279676] p 1291 N95-20605
Space fundamentals for the war fighter
[AD-A279703] p 1217 N95-20690
QoS driven routing in packet switched networks of multiple transmission media p 1292 N95-20923

COMMUNICATION THEORY
General conservative extension theorem in process algebra
[PB95-110656] p 1487 N95-19902
Process algebra with partial choice
[PB95-110714] p 1487 N95-19907
Real time process algebra with infinitesimals
[PB95-110623] p 1488 N95-20055

COMMUTATORS
Growth series for the commutator subgroup
[PB95-111092] p 1490 N95-20452

COMMUTER AIRCRAFT
Commuter airplane accident data analysis
[AD-A286315] p 1202 N95-20174

COMPACTING
The development of a super-alpha2 titanium aluminide alloy consolidated by rapid omnidirectional compaction
[AD-A279254] p 1260 N95-21986

COMPATIBILITY
Circuit means for providing compatibility between two separate digital data interfaces
[AD-D016225] p 1455 N95-21116
Compatibility testing of explosives and paints by chemiluminescence techniques
[PB95-133609] p 1275 N95-21275
Materials compatibility and lubricants research on CFC-refrigerant substitutes
[DE94-018414] p 1287 N95-21631

COMPETITION
Competition between electromagnetic modes in a free-electron maser
[AD-A279546] p 1374 N95-21694

COMPILERS
Activities of the Research Institute for Advanced Computer Science
[NASA-CR-197291] p 1478 N95-22108
SCOPE 1.5: A Source-Code Optimization PackagEfor REDUCE 3.5: User's manual
[PB95-107579] p 1472 N95-22159

COMPLETENESS
Quality characteristics and metrics for reusable software
[PB94-203437] p 1473 N95-22390

COMPLEX COMPOUNDS
Combustion-related studies using weakly bonded complexes
[DE95-002801] p 1238 N95-20576
Selenophene transition metal complexes
[DE95-001675] p 1260 N95-21841
Preparation and x-ray structure of $Cp_2Ti(PH_2SiH_2)(PMe_3)$
[AD-A286197] p 1246 N95-21879

COMPLEX SYSTEMS
Proceedings of the 4th Systems Reengineering Technology Workshop
[AD-A285357] p 1460 N95-20546
Chemical Structure and Dynamics program
[DE95-001117] p 1403 N95-20834
Advanced computing systems: Usability of knowledge-based planning systems
[AD-A279573] p 1477 N95-21698
Intelligent interactive project management system
[PB95-132684] p 1586 N95-21982
Abstract interpretation of reactive systems: Abstractions preserving Universal CTL(*), Existential CTL(*) and CTL(*)
[PB95-110557] p 1472 N95-22305

COMPONENT RELIABILITY
Towards better quality and reliability in the software reuse library environment
[AD-A280013] p 1460 N95-20313
Highlights of recent balance of system research and evaluation
[DE95-001626] p 1393 N95-20863

COMPOSITE MATERIALS
Materials for adaptive structural acoustic control, volume 2
[AD-A279222] p 1502 N95-19883
Physics and applications of defects in advanced semiconductors, volume 325
[AD-A280059] p 1563 N95-19886
Materials/manufacturing element of the Advanced Turbine System Program
[DE94-017299] p 1378 N95-20085
Hierarchical structures in biology as a guide for new materials technology
[AD-A286317] p 1265 N95-20176
An application of wavelet transform for decomposition of millimeter-wave spectroscopic signals
[DE94-018366] p 1402 N95-20247
Multi-layered translated rib-stiffened composite hollow cylinder assembly
[AD-D016566] p 1226 N95-20292
Polyurethane-epoxy interpenetrating polymer network acoustic damping material
[AD-D016567] p 1266 N95-20293
Materials research for GHz multi-chip modules
[AD-A279661] p 1227 N95-20412
Dynamic measurement of the hoop modulus of a composite cylinder
[DE94-018958] p 1385 N95-20416
Composite cases for airborne electronic equipment: A technology study and EMC p 1212 N95-20655
Lightweight electronic enclosures using composite materials p 1213 N95-20656
Inorganic-organic polymers and their role in materials science
[AD-A279715] p 1270 N95-20671
Optical power limiting liquid crystal composites
[AD-A286605] p 1569 N95-20767
The processing and mechanical properties of high temperature/high performance composites. Processing/property correlations, book 4
[AD-A279739] p 1228 N95-20802
Detection of environmental deterioration in fiber reinforced composites by FT-Raman spectroscopy, phase 1
[AD-A279763] p 1228 N95-20805
The calculation and measurement of Helmholtz coil fields
[AD-A286081] p 1228 N95-20808
Fabrication of ceramic composites: Forced CVI
[DE95-001076] p 1271 N95-20821
Certain physical properties of lanthanum digermanide
[AD-A286592] p 1229 N95-20859
Test fixture for determination of energy absorbing capabilities of composite materials
[NASA-CASE-LAR-15212-1-CU] p 1229 N95-21008
Strain measurement by diffraction at LANSCE
[DE94-018264] p 1387 N95-21386
B4C-SiC reaction-sintered coatings on graphite plasma facing components
[DE94-019105] p 1230 N95-21553
The role of microcracking on the crack growth resistance of brittle solids and composites
[DE95-001678] p 1231 N95-21736
The role of grain boundary sliding on creep deformation characteristics of discontinuous reinforced composites
[DE95-001671] p 1231 N95-21924
Towards tailored interphase formation utilizing surface-bound benzylsulfonium salts as cationic initiators
[AD-A286461] p 1280 N95-22259
The thermal conductivity of silicon nitride with molybdenum disilicide additions
[DE94-017757] p 1247 N95-22260
Acoustic and vibration attenuation composite material
[AD-D016585] p 1233 N95-22467
Development and demonstration of advanced technologies for direct electrochemical oxidation of hydrocarbons (methanol, methane, propane)
[AD-A285094] p 1224 N95-22474

COMPOSITE PROPELLANTS
The hot fragment conductive ignition test for screening LOVA propellants
[AD-A284259] p 1282 N95-20187

COMPOSITE STRUCTURES
Attachment methodology for composite cylinder assembly
[AD-D016578] p 1227 N95-20459
Ferroic materials: Design, preparation and characteristics. Ceramic transactions, volume 43
[AD-A285937] p 1270 N95-20664
Wear resistant composite structure of vitreous carbon containing convoluted fibers
[DE95-002254] p 1228 N95-20787
Launch vehicle flight control augmentation using smart materials and advanced composites (CDDF Project 93-05)
[NASA-TP-3535] p 1218 N95-21346
Materials for adaptive structural acoustic controls
[AD-A279255] p 1505 N95-21863
Recent developments in low cost stable structures for space
[DE95-000857] p 1231 N95-22009
Attachment methodology for composite cylinder assembly
[AD-D016256] p 1381 N95-22034

COMPOSITION (PROPERTY)
Weld pool phenomena
[DE94-018965] p 1381 N95-21550
Solar helium and neon in the Earth
p 1419 N95-21793
Surface ices in the outer solar system
p 1423 N95-21815
Synthesis and characterization of single-source molecular precursors to binary metal sulphides: Bis(diethyldithiocarbamato) M(2)trialkylphosphine (M = Zn and Cd) adducts
[AD-A279746] p 1248 N95-22385

COMPRESSED GAS
Effect of propane-air on NGVs and vehicle fueling stations
[PB94-210085] p 1282 N95-20253
Experimental investigation of molecular beam injection in HL-1 tokamak
[DE94-631456] p 1556 N95-21165

COMPRESSIBILITY
Carbon fiber reinforced superconductor composites
[DE95-002504] p 1229 N95-20913
The processing and mechanical properties of high temperature/high performance composites. Book 6: Delamination and compressive behavior
[AD-A279780] p 1231 N95-21999

COMPRESSIBILITY EFFECTS
Numerical investigation of supersonic turbulent boundary layers with high wall temperature
p 1344 N95-21050
Effects of turbulence compressibility and unsteadiness in compression corner flow p 1344 N95-21052

COMPRESSIBLE BOUNDARY LAYER
Numerical simulation of supersonic boundary layer transition p 1348 N95-21074
COMPRESSIBLE FLOW
Evaluation of Reynolds stress turbulence closures in compressible homogeneous shear flow [NASA-CR-194892] p 1338 N95-20009
Continuum transient and frozen startup behavior of conventional and gas-loaded heat pipes [AD-A284297] p 1339 N95-20250
Effects of turbulence compressibility and unsteadiness in compression corner flow p 1344 N95-21052
Comparison of DNS and LES of transitional and turbulent compressible flow: Flat plate and mixing layer p 1347 N95-21066
Investigation of shear layer transition using various turbulence models p 1352 N95-21096
Convergence acceleration of the Proteus computer code with multigrid methods [NASA-CR-197677] p 1467 N95-21450
Computations of unsteady viscous compressible flows using adaptive mesh refinement in curvilinear body-fitted grid systems [NASA-TM-106704] p 1356 N95-21959
COMPRESSING
Digital filtering for data compression in telemetry systems [DE94-016611] p 1219 N95-20567
COMPRESSION LOADS
Damage tolerance of carbon fibre polyetheretherketone laminates [PB95-131611] p 1230 N95-21432
COMPRESSION TESTS
Damage tolerance of carbon fibre polyetheretherketone laminates [PB95-131611] p 1230 N95-21432
Characterization of a texture gradient in tantalum plate [DE95-002704] p 1262 N95-22289
COMPRESSIVE STRENGTH
Structural performance of cylindrical pressure housings of different ceramic compositions under external pressure loading. Part 3: Sintered reaction bonded silicon nitride ceramic [AD-A285773] p 1388 N95-22411
COMPRESSORS
Malone-brayton cycle engine/heat pump [AD-D016573] p 1378 N95-20295
COMPTON EFFECT
Exclusive processes: Tests of coherent QCD phenomena and nucleon substructure at CEBAF [DE95-002892] p 1520 N95-21336
Recent photoabsorption measurements in the rare gases and alkalis in the 3 to 15 keV photon energy region [DE94-019278] p 1521 N95-21406
Neutron Compton scattering [PB95-130290] p 1530 N95-22332
COMPUTATION
Computation of invariant manifolds [PB95-135687] p 1492 N95-21318
HPCC technology awareness program: Improved economic competitiveness through technology awareness, transfer and application [DE95-002134] p 1476 N95-21355
Preconditioning via asymptotically-defined domain decomposition [DE94-019046] p 1493 N95-21564
Connectionist models for intelligent computation [AD-A286436] p 1484 N95-22210
Fast parallel tree codes for gravitational and fluid dynamical N-body problems [AD-A286480] p 1358 N95-22290
Time and the order of abstract events in distributed computations [PB95-110482] p 1496 N95-22349
COMPUTATIONAL ASTROPHYSICS
Relativistic binary neutron star coalescence [DE94-019311] p 1600 N95-21479
COMPUTATIONAL CHEMISTRY
Computer program for calculation of complex chemical equilibrium compositions and applications. Part 1: Analysis [NASA-RP-1311] p 1235 N95-20180
T1F ((1) sigma (+)): Some preliminary electronic structure calculations [PB95-130316] p 1518 N95-21223
Comparative computational analysis of some nitramine and difluoramine structures, dissociation energies and heats of formation [AD-A286196] p 1525 N95-21878
Non-local density functional calculations of gas phase heats of formation [AD-A286213] p 1246 N95-22000
COMPUTATIONAL FLUID DYNAMICS
Multigrid with matrix-dependent transfer operators for convection-diffusion problems [PB95-110821] p 1487 N95-19915
Open Skies project computational fluid dynamic analysis [AD-A285928] p 1200 N95-19991
Stabilization and control problems in structural dynamics [AD-A279996] p 1340 N95-20312
Mapping closures for turbulent combustion [AD-A279995] p 1238 N95-20597
HIVEL2D: A two-dimensional flow model for high-velocity channels [AD-A286556] p 1341 N95-20843
Laser anemometry and viscous computation of the flow through an annular turbine cascade [AD-A280070] p 1341 N95-20968
Mixed hp finite element methods for problems in elasticity and stokes flow [PB95-104444] p 1341 N95-20981
Simulation of the injection moulding process [PB94-215555] p 1286 N95-21027
Studying Turbulence Using Numerical Simulation Databases. 5: Proceedings of the 1994 Summer Program [NASA-CR-197362] p 1341 N95-21035
Direct numerical simulations of turbulent non-premixed methane-air flames modeled with reduced kinetics p 1249 N95-21038
Turbulent transport in premixed flames p 1249 N95-21040
The coupling between flame surface dynamics and species mass conservation in premixed turbulent combustion p 1249 N95-21041
Pdf modeling for premixed turbulent combustion based on the properties of iso-concentration surfaces p 1249 N95-21042
Passive turbulent flamelet propagation p 1249 N95-21043
Simulation of a turbulent flame in a channel p 1249 N95-21044
Pressure and higher-order spectra for homogeneous isotropic turbulence p 1343 N95-21045
Statistics of pressure and pressure gradient in homogeneous isotropic turbulence p 1343 N95-21046
Vortex ring instability and its sound p 1344 N95-21048
Numerical investigation of supersonic turbulent boundary layers with high wall temperature p 1344 N95-21050
A Lagrangian dynamic subgrid-scale model turbulence p 1344 N95-21051
Role of pressure diffusion in non-homogeneous shear flows p 1345 N95-21053
Modeling the two-point correlation of the vector stream function p 1345 N95-21055
On the transition towards slow manifold in shallow-water and 3D Euler equations in a rotating frame p 1345 N95-21057
Anisotropic structure of homogeneous turbulence subjected to uniform rotation p 1346 N95-21059
Single point modeling of rotating turbulent flows p 1346 N95-21060
Application of Direct and Large Eddy Simulation to Transition and Turbulence [AGARD-CP-551] p 1346 N95-21061
Developments and applications of dynamic models for large eddy simulation of complex flows p 1346 N95-21062
Large-eddy simulation of rotating channel flows using a localized dynamic model p 1346 N95-21064
The asymptotic state of rotating homogeneous turbulence at high Reynolds numbers p 1347 N95-21065
Direct numerical simulation of turbulent flow in a sudden pipe expansion p 1347 N95-21067
Simulation of separated flows p 1347 N95-21068
Simulation of large scale transitional flows p 1348 N95-21075
Modelling anisotropy and backscatter effects in the subgrid scale stress tensor p 1349 N95-21077
Simulation of pipe flow p 1349 N95-21078
Simulations of bypass transition for spatially evolving disturbances p 1349 N95-21079
Direct numerical determination of the minimum bypass Reynolds number in boundary layers p 1349 N95-21080
Direct numerical simulation for premixed turbulent combustion modelling p 1249 N95-21082
Entrainment in a shear-free turbulent mixing layer p 1350 N95-21083
Numerical study of realistic perturbations in three-dimensional boundary layers p 1351 N95-21091
On subcritical instability of the attachment line boundary layer p 1351 N95-21092
Spatial direct numerical simulation of boundary layer transition under strong adverse pressure gradient p 1351 N95-21093
Navier-Stokes simulations of the effects of suction holes on a flat plate boundary layer p 1352 N95-21094
Investigation of shear layer transition using various turbulence models p 1352 N95-21096
Computational studies of laminar to turbulence transition [AD-A285622] p 1353 N95-21146
Nonlinear acoustic processes in a solid rocket engine [AD-A285606] p 1222 N95-21193
The structure of turbulence and other motions beneath an air-water interface [AD-A279838] p 1434 N95-21293
Application of Navier-Stokes code PAB3D with kappa-epsilon turbulence model to attached and separated flows [NASA-TP-3480] p 1201 N95-21338
Convergence acceleration of the Proteus computer code with multigrid methods [NASA-CR-197677] p 1467 N95-21450
One-dimensional reactive Euler equations [PB95-135430] p 1244 N95-21573
Grid resolution and solution convergence for Mars Pathfinder forebody [NASA-TM-109173] p 1494 N95-21622
DIFFPACK: Software for partial differential equations [PB95-110268] p 1468 N95-21654
Numerical investigations of low-density nozzle flow by solving the Boltzmann equation [NASA-TM-110492] p 1354 N95-21675
Status of CFDLIB performance tests on the T3D [DE95-002708] p 1478 N95-21925
Massively-parallel computational fluid dynamics [AD-A279389] p 1355 N95-21942
Hybrid Upwind Splitting (HUS) by a field-by-field decomposition [NASA-TM-106843] p 1355 N95-21957
Computations of unsteady viscous compressible flows using adaptive mesh refinement in curvilinear body-fitted grid systems [NASA-TM-106704] p 1356 N95-21959
Vortex atoms and vortons [PB95-134599] p 1356 N95-21963
State of the art in CFD pre- and postprocessing [PB95-110391] p 1356 N95-22017
DOD science and engineering apprenticeship program for high school students [AD-A280371] p 1583 N95-22100
Effects of yaw and pitch motion on model attitude measurements [NASA-TM-4641] p 1368 N95-22109
Fluid dynamics of the freeboard in a fluidized bed reactor [PB95-134029] p 1357 N95-22160
On the dynamics of a shock-bubble interaction [NASA-CR-194978] p 1495 N95-22325
Sandia National Laboratories analysis code data base [DE95-004188] p 1502 N95-22420
Turbulence modeling for separated flow p 1359 N95-22443
Notes on rotating turbulence p 1359 N95-22444
Local dynamic subgrid-scale models in channel flow p 1360 N95-22447
Unstructured-grid large-eddy simulation of flow over an airfoil p 1202 N95-22448
Large-eddy simulation of flow through a plane, asymmetric diffuser p 1360 N95-22449
Large-eddy simulation of a boundary layer with concave streamwise curvature p 1360 N95-22450
Direct numerical simulations of on-demand vortex generators: Mathematical formulation p 1361 N95-22452
Drag reduction strategies p 1361 N95-22453
Optimal active control for Burgers equations p 1361 N95-22454
Numerical study of boundary layer interaction with shocks: Method and code validation p 1362 N95-22461
Resolution requirements for velocity gradients in turbulence p 1363 N95-22462
Direct numerical simulation of incompressible axisymmetric flows p 1363 N95-22464
COMPUTATIONAL GEOMETRY
Stars or stripes: A comparative study of finite and transfinite techniques for surface modelling [PB95-134979] p 1464 N95-20975
COMPUTATIONAL GRIDS
Multigrid with matrix-dependent transfer operators for convection-diffusion problems [PB95-110821] p 1487 N95-19915
A control volume method on an icosahedral grid for numerical integration of the shallow-water equations on the sphere [DE94-016345] p 1489 N95-20170

Meshes: The next generation
[DE94-016702] p 1459 N95-20255

RALPAR-RAL mesh partitioning program version 1.1
[PB95-129847] p 1475 N95-20435

Eta%-Superconvergence of Finite Element Approximations in the Interior of General Meshes of Triangles
[AD-A279903] p 1490 N95-20565

Study of superconvergence by a computer-based approach: Superconvergence of the gradient of the displacement, the strain and stress in finite element solutions for plane elasticity
[AD-A279885] p 1490 N95-20588

ALCHEMI of Fe-doped B2-ordered NiAl alloys with different doping levels
[DE94-017748] p 1255 N95-20907

Mixed hp finite element methods for problems in elasticity and stokes flow
[PB95-104444] p 1341 N95-20981

Simulation of the injection moulding process
[PB94-215555] p 1286 N95-21027

VLUGr3: A vectorizable adaptive grid solver for PDEs in 3D. 2: Code description
[PB95-135737] p 1465 N95-21033

Comparison of DNS and LES of transitional and turbulent compressible flow: Flat plate and mixing layer
p 1347 N95-21066

Modelling anisotropy and backscatter effects in the subgrid scale stress tensor p 1349 N95-21077

Simulations of bypass transition for spatially evolving disturbances p 1349 N95-21079

Direct numerical determination of the minimum bypass Reynolds number in boundary layers
p 1349 N95-21080

Support to the development of high-level graphics software
[PB95-131686] p 1466 N95-21349

VLUGR3: A vectorizable adaptive grid solver for PDEs in 3D. 1: Algorithmic aspects and applications
[PB95-135729] p 1467 N95-21435

Convergence acceleration of the Proteus computer code with multigrid methods
[NASA-CR-197677] p 1467 N95-21450

Finite element modelling of creep crack growth in 316 stainless and 9Cr-1Mo steels
[DE94-018977] p 1258 N95-21560

Analysis of a local defect correction approach on composite grids
[PB95-135455] p 1493 N95-21574

Grid resolution and solution convergence for Mars Pathfinder forebody
[NASA-TM-109173] p 1494 N95-21622

Flow and heat transfer simulation in a flash smelting furnace
[PB95-108197] p 1354 N95-21649

Computations of unsteady viscous compressible flows using adaptive mesh refinement in curvilinear body-fitted grid systems
[NASA-TM-106704] p 1356 N95-21959

Absorbing boundary condition for floating two-dimensional objects in current and waves
[PB95-132882] p 1356 N95-22063

Occupant reach and mobility apparatus
[AD-D016253] p 1454 N95-22099

On the wavelet optimized finite difference method
[NASA-CR-191601] p 1495 N95-22157

On the dynamics of a shock-bubble interaction
[NASA-CR-194978] p 1495 N95-22325

Transformation of multichannel magnetocardiographic signals to standard grid form
[PB95-127114] p 1447 N95-22371

A dynamic localization model with stochastic backscatter p 1359 N95-22445

Local dynamic subgrid-scale models in channel flow
p 1360 N95-22447

Unstructured-grid large-eddy simulation of flow over an airfoil p 1202 N95-22448

Large-eddy simulation of a boundary layer with concave streamwise curvature p 1360 N95-22450

COMPUTER AIDED DESIGN

A new tool for accelerator system modeling and analysis
[DE94-018292] p 1531 N95-20203

Numerical controlled polishing program, continued forced wear and part correction experiments
[DE94-018084] p 1285 N95-20288

Computer-Aided Structural Engineering (CASE) project. User's guide: Computer-Aided Structural Modeling (CASM). Version 5.00
[AD-A279913] p 1459 N95-20310

Parallel calculation of sensitivity derivatives for aircraft design using automatic differentiation
[NASA-TM-110103] p 1206 N95-20370

Applications of wavelets to radar, imaging and related problems
[AD-A279909] p 1290 N95-20545

The 29th MIL-HDBK-17 Polymer Matrix Composites Coordination Group Meeting
[AD-A279917] p 1269 N95-20578

Automation support for concurrent software engineering
[AD-A279691] p 1461 N95-20579

Design and implementation of visual object-oriented LOGO using Prograph
[AD-A285977] p 1461 N95-20687

Use of an integrated design tool for weld quality enhancement
[DE94-018135] p 1379 N95-20723

Stars or stripes: A comparative study of finite and transfinite techniques for surface modelling
[PB95-134979] p 1464 N95-20975

Routing of unidirectional packet radio for wide-area paging network control and maintenance
[PB95-104428] p 1300 N95-20980

An automatic placement tool for rapid prototyping of printed circuit boards
[AD-A286029] p 1328 N95-20997

Next generation solid modellers for electronic prototyping
[AD-A286525] p 1464 N95-21010

Proceedings of the NATO-Advanced Study Institute on Computer Aided Analysis of Rigid and Flexible Mechanical Systems. Volume 1: Main lectures
[AD-A286062] p 1380 N95-21171

SEEK: A FORTRAN optimization program using a feasible directions gradient search
[NASA-CR-4641] p 1380 N95-21359

Representing manufacturing features to support design and process changes
[DE94-018587] p 1467 N95-21389

Development of quiet-flow supersonic wind tunnels for laminar-turbulent transition research
[NASA-CR-197286] p 1216 N95-21436

Proceedings of the NATO-Advanced Study Institute on Computer Aided Analysis of Rigid and Flexible Mechanical Systems. Volume 2: Contributed papers
[AD-A286063] p 1381 N95-21488

An MCM concurrent engineering software tool market study
[AD-A279257] p 1468 N95-21489

Crew-Centered Cockpit Design (CCCD) field demonstration program, volume 1
[AD-A286426] p 1453 N95-21566

Directed light fabrication
[DE94-018293] p 1375 N95-21837

Using the CoRE requirements method with ADARTS. Version 01.00.05
[AD-A279151] p 1470 N95-21972

Generic architecture for knowledge-based control of processes in dynamic environments
[PB95-132676] p 1483 N95-21981

Discovering related DNA sequences via mutual information
[DE95-001101] p 1440 N95-22067

Structuring design requirements using YMIR
[PB95-132742] p 1471 N95-22081

Normal form analysis of the Tevatron
[DE94-017172] p 1539 N95-22192

Application of computer-generated holograms to optical transformations
[AD-A286356] p 1368 N95-22256

ActorStudio reference manual. A user's guide to the ActorStudio user interface editor, version 1.0
[PB95-127023] p 1472 N95-22310

Overview of rapid prototyping technologies in manufacturing
[PB95-127122] p 1472 N95-22372

A conceptual approach to object-oriented data modeling
[AD-A286048] p 1592 N95-22416

Fuzzy clustering of facial form for prototyping environmental protection equipment
[DE94-014657] p 1454 N95-22466

Wind Energy Program overview, fiscal year 1993
[DE94-000285] p 1398 N95-22468

COMPUTER AIDED MANUFACTURING

Adaptive path planning for flexible manufacturing
[DE94-016561] p 1459 N95-20284

Applications of wavelets to radar, imaging and related problems
[AD-A279909] p 1290 N95-20545

An automatic placement tool for rapid prototyping of printed circuit boards
[AD-A286029] p 1328 N95-20997

Next generation solid modellers for electronic prototyping
[AD-A286525] p 1464 N95-21010

Virtual reality in precision engineering research
[AD-A286528] p 1465 N95-21012

Representing manufacturing features to support design and process changes
[DE94-018587] p 1467 N95-21389

Directed light fabrication
[DE94-018293] p 1375 N95-21837

Overview of rapid prototyping technologies in manufacturing
[PB95-127122] p 1472 N95-22372

Wind Energy Program overview, fiscal year 1993
[DE94-000285] p 1398 N95-22468

COMPUTER AIDED MAPPING

Selective polygon map display method
[AD-D016518] p 1590 N95-21463

Digital mapping, charting, and geodesy analysis program technical review of Vector Smart Map (VMap) level 1
[AD-A286294] p 1390 N95-22055

Life Sciences Division and Center for Human Genome Studies
[DE94-017796] p 1440 N95-22065

COMPUTER AIDED TOMOGRAPHY

Seminar on Biomedical Engineering 1993
[PB95-104402] p 1443 N95-20971

COMPUTER ASSISTED INSTRUCTION

Intelligent tutoring systems: Past, present, and future
[AD-A280011] p 1448 N95-19970

Determining the usability of Digital Video Interactive (DVI) technology in computer-based instruction
[AD-A284717] p 1457 N95-20060

Computer-Aided Structural Engineering (CASE) project. User's guide: Computer-Aided Structural Modeling (CASM). Version 5.00
[AD-A279913] p 1459 N95-20310

Generating examples for use in tutorial explanations: The use of a subsumption based classifier
[AD-A286028] p 1464 N95-20996

Proposal for a tutorial on Minimal Length Encoding (MLE) in molecular biology
[DE94-015076] p 1438 N95-21376

A computer-based multimedia prototype for night vision goggles
[AD-A286208] p 1546 N95-21882

Development and evaluation of ALEC Micro-Wand 3e (tradename) training
[AD-A285863] p 1471 N95-22133

COMPUTER COMPONENTS

Ergonomic evaluation of the Apple Adjustable Keyboard
[DE95-002393] p 1453 N95-21637

An evaluation of the Gear Averaging Signal Processor (GASP)
[DSTO-TR-0067] p 1470 N95-21950

COMPUTER CONFERENCING

Application-oriented architecture for multimedia teleservices
[PB95-135513] p 1306 N95-21623

COMPUTER GRAPHICS

PRSPLOT6 manual
[PB95-110862] p 1456 N95-19928

Design considerations for parallel graphics libraries
[NASA-CR-194935] p 1473 N95-20013

Unified GUI for the Los Alamos Radiation Transport Code System
[DE94-016088] p 1458 N95-20154

A practical guide to using MCNP with PVM
[DE94-016162] p 1474 N95-20158

Data analysis and visualization in MCNP (trademark)
[DE94-016164] p 1508 N95-20159

An object-oriented optimization systems
[DE94-016190] p 1459 N95-20165

Computer-Aided Structural Engineering (CASE) project. User's guide: Computer-Aided Structural Modeling (CASM). Version 5.00
[AD-A279913] p 1459 N95-20310

Making structured graphics and constraints practical for large-scale applications
[AD-A280062] p 1461 N95-20623

Computer graphics tools for visualizing gravity gradient torques on a rigid spacecraft
[AD-A285971] p 1461 N95-20665

Design and implementation of visual object-oriented LOGO using Prograph
[AD-A285977] p 1461 N95-20687

Use of an integrated design tool for weld quality enhancement
[DE94-018135] p 1379 N95-20723

ALCHEMI of Fe-doped B2-ordered NiAl alloys with different doping levels
[DE94-017748] p 1255 N95-20907

Direct simulation and graphics post-processing of three-dimensional turbulent flows p 1352 N95-21098

DAVE: A plug and play model for distributed multimedia application development
[DE94-016481] p 1465 N95-21153

Support to the development of high-level graphics software
[PB95-131686] p 1466 N95-21349

Selective polygon map display method
[AD-D016518] p 1590 N95-21463

Top ten list of user-hostile interface design
[DE95-001602] p 1453 N95-21721
Tethered satellite: Forces and motion
[NASA-TM-110518] p 1220 N95-21858
MARI mini-manual
[PB95-134649] p 1526 N95-21965
Residual stress analysis in swage autofrettaged thick-walled cylinders by position-sensitive x-ray diffraction techniques
[AD-A286383] p 1388 N95-22320

COMPUTER INFORMATION SECURITY

An abstract model of rogue code insertion into radio frequency wireless networks. The effects of computer viruses on the Program Management Office
[AD-A285759] p 1288 N95-19932
Semaphore network encryption report
[AD-A279294] p 1303 N95-21493
Proceedings of the 5th Workshop on the Next Generation of CASE Tools
[PB95-135208] p 1469 N95-21716

COMPUTER NETWORKS

Testing paradigm applied to network structure (revised)
[PB95-110706] p 1487 N95-19906
A multivariate multisample rank test for stochastic simulation validation
[AD-A285922] p 1498 N95-19990
Migrating the Facility Profile Information Management System into the World Wide Web
[DE94-018367] p 1586 N95-20016
A group communication approach for mobile computing mobile channel: An ISIS tool for mobile services
[AD-A279785] p 1290 N95-20306
MPI workshop
[DE94-017883] p 1475 N95-20366
Stochastic network processes
[AD-A279905] p 1475 N95-20566
Methods and components for optical contention resolution in high speed networks
[AD-A280016] p 1543 N95-20598
ECSU-AASERT summer research project in parallel processing and computer visualization
[AD-A285983] p 1475 N95-20618
The IEEE scalable coherent interface: An approach for a unified avionics network p 1212 N95-20650
High performance backplane components for modular avionics p 1212 N95-20653
Environment for Test and Analysis of Distributed Software (ETADS)
[AD-A285776] p 1463 N95-20877
DAVE: A plug and play model for distributed multimedia application development
[DE94-016481] p 1465 N95-21153
An object-oriented implementation of the Xpress transfor protocol
[DE95-001506] p 1301 N95-21277
Semaphore network encryption report
[AD-A279294] p 1303 N95-21493
Network file server with automatic sensing means
[AD-D016250] p 1476 N95-21496
PVM 3 beyond network computing
[DE94-019115] p 1477 N95-21556
PVM a platform for portable distributed computing
[DE94-019156] p 1455 N95-21607
Massively-parallel computational fluid dynamics
[AD-A279389] p 1355 N95-21942
Activities of the Research Institute for Advanced Computer Science
[NASA-CR-197291] p 1478 N95-22108
Network distributed global memory for transparent message passing on distributed networks
[AD-A286096] p 1478 N95-22228
Using geographical data browsers in a networked environment
[DE94-017809] p 1592 N95-22263

COMPUTER PROGRAM INTEGRITY

New method for integrity constraint checking in deductive databases
[PB95-110672] p 1586 N95-19904

COMPUTER PROGRAMMING

Hierarchical diagrammatic representation of class structure
[PB95-110722] p 1456 N95-19908
Real time process algebra with infinitesimals
[PB95-110623] p 1488 N95-20055
Comparison of Ward and Mellor's transformation schema with State- and Activitycharts
[PB95-110698] p 1459 N95-20258
Software merge: Semantics of combining changes to programs
[AD-A279657] p 1459 N95-20304
Towards better quality and reliability in the software reuse library environment
[AD-A280013] p 1460 N95-20313
A theoretical study on the performance of the FDTD code on a massively parallel computer
[AD-A285346] p 1475 N95-20499
Proceedings of the 4th Systems Reengineering Technology Workshop
[AD-A285357] p 1460 N95-20546
Measuring software dependability by robustness benchmarking
[AD-A280053] p 1461 N95-20622
Computer graphics tools for visualizing gravity gradient torques on a rigid spacecraft
[AD-A285971] p 1461 N95-20665
Model formality in human/computer collaboration
[AD-A286001] p 1462 N95-20718
Software Capability Evaluation (SCE), version 2.0 team members guide
[AD-A286082] p 1462 N95-20809
Rate monotonic analysis for real-time systems: Instructors guide
[AD-A286083] p 1463 N95-20810
Functional and para-functional parallel processing
[DE95-002805] p 1475 N95-20888
Real-time reconfiguration study
[AD-A286060] p 1464 N95-20910
Monadic maps and folds for arbitrary datatypes
[PB95-134045] p 1492 N95-21032
PRSCAL manual
[PB95-130480] p 1465 N95-21231
Expressions that talk about themselves
[PB95-134060] p 1466 N95-21344
GRONICs-1994. Proceedings of the 1994 Groningen Student Conference on Computer Science
[PB95-135620] p 1468 N95-21455
Top-down non-correcting error recovery in LLgen
[PB95-132718] p 1471 N95-22031
Foundations of functional programming: A programmer's point of view
[PB95-132932] p 1471 N95-22094
SCOPE 1.5: A Source-Code Optimization PackagEfor REDUCE 3.5: User's manual
[PB95-107579] p 1472 N95-22159
Incremental rederivation of software artifacts: FY 1993
[AD-A285790] p 1473 N95-22402

COMPUTER PROGRAMS

High performance hardware and software for pattern recognition and image processing
[AD-A279776] p 1457 N95-19961
Ice Processing System software support documentation
[AD-A280030] p 1388 N95-20006
Charged particle dynamics in the acceleration gap of the PBFA 2 ion diode
[DE94-017347] p 1506 N95-20026
Software fault tree analysis of concurrent Ada processes
[AD-A284979] p 1457 N95-20042
Advanced detector development, laboratory simulations, diagnostic development, and data analysis on wake physics
[AD-A284798] p 1364 N95-20069
SYNTH: A spectrum synthesizer
[DE94-015943] p 1458 N95-20153
Nonlinear dynamic fluid-structure interaction calculations with coupled finite element and finite volume programs
[DE94-016204] p 1339 N95-20166
Theoretical prediction of vibrational circular dichroism spectra of R-glyceraldehyde, R-erythrose, and R-threose. Part 2: Development of a procedure to scale the force constant matrix expressed in terms of internal coordinates
[AD-A284305] p 1437 N95-20252
Studies of longitudinal instability with an electron beam
[DE94-018646] p 1532 N95-20347
Choice of computer software for analysis of spectra from the Multi-Spectral Logging System
[DE94-019013] p 1460 N95-20351
First principles simulation of materials properties
[DE94-016781] p 1566 N95-20405
Program WALKMAN: A code designed to perform electron single collision elastic scattering Monte Carlo calculations
[DE94-017501] p 1511 N95-20444
Proceedings of the 4th Systems Reengineering Technology Workshop
[AD-A285357] p 1460 N95-20546
TBell: A mathematical tool for analyzing decision tables
[NASA-CR-195027] p 1462 N95-20691
The design of a parallel, dense linear algebra software library: Reduction to Hessenberg, tridiagonal, and bidiagonal form
[DE94-018123] p 1491 N95-20701
A new process for acquiring software architecture
[AD-A286012] p 1462 N95-20721
Modeling the effect of shroud contact and friction dampers on the mistuned response of turbopumps
[NASA-CR-197285] p 1379 N95-20795
Geometric moire method of strain analysis with displacement discontinuities
[DE95-001114] p 1386 N95-20833
Prediction of rotor-blade deformations due to unsteady airloads
[AD-A286593] p 1207 N95-20860
COYOTE II: A finite element computer program for nonlinear heat conduction problems. Part 1: Theoretical background
[DE95-002587] p 1463 N95-20887
Enhancements in the Livermore spectrum analysis package PIXEF
[DE95-002487] p 1272 N95-20895
ALCHEMI of Fe-doped B2-ordered NiAl alloys with different doping levels
[DE94-017748] p 1255 N95-20907
The opportunities for and challenges of common integrated electronics
[AD-A279991] p 1327 N95-20966
Simulation of the injection moulding process
[PB94-215555] p 1286 N95-21027
Simulation of separated flows p 1347 N95-21066
The iMAPS: General information
[AD-A285421] p 1465 N95-21176
PRSCAL manual
[PB95-130480] p 1465 N95-21231
PRISMA operating program manual
[PB95-130498] p 1466 N95-21232
Multiple hard interactions in HERWIG
[PB95-130548] p 1518 N95-21233
Time-dependent deformation of titanium metal matrix composites
[NASA-CR-195030] p 1230 N95-21363
Data link terminal DLT document
[PB95-110805] p 1205 N95-21369
Generalised approach to software structure metrics
[PB95-107561] p 1467 N95-21411
EXPERT system expert: Program description
[PB95-131561] p 1482 N95-21429
SSME HPOTP post-test diagnostic system enhancement project
[NASA-CR-4643] p 1222 N95-21458
Selective polygon map display method
[AD-D016518] p 1590 N95-21463
Monomer mapping: A PC-based software tool facilitating the determination of monomer compositions from mass spectrometric molecular weight data
[PB95-132155] p 1275 N95-21470
Computer programs for analysis of geophysical data
[DE95-002472] p 1415 N95-21511
BASIC program for power spectrum estimation
[DE95-002228] p 1468 N95-21515
Power systems for future missions. Appendices A-L
[NASA-CR-195320-APP-A-L] p 1395 N95-21530
Analysis of a disk-on-rod surface wave element inside a corrugated horn using the mode-matching technique
p 1305 N95-21543
Unified very low stratus cloud/subcloud microphysics model: User's guide
[AD-A286454] p 1430 N95-21586
Report of the Numerical Analysis Group
[PB95-108163] p 1494 N95-21648
A method to determine the kinematics of the lower limbs of a subject pedaling a bicycle using encoders and accelerometers
[NASA-CR-197401] p 1453 N95-21866
Generic architecture for knowledge-based control of processes in dynamic environments
[PB95-132676] p 1483 N95-21981
Numerical investigation of one-dimensional heat-flux calculations
[AD-A286293] p 1582 N95-22054
NODDS/WOSM interface user's manual
[AD-A279095] p 1471 N95-22068
A Davis-Putnam program and its application to finite-order model search: Quasigroup existence problems
[DE95-003014] p 1471 N95-22077
Regional scale hydrology with a new land surface processes model
[NASA-TM-110500] p 1390 N95-22111
Development and evaluation of ALEC Micro-Wand 3e (tradename) training
[AD-A285863] p 1471 N95-22133
Evaluation of scanners for C-scan imaging for nondestructive inspection of aircraft
[AD-A286398] p 1383 N95-22202
Adaptive fault-resistant systems
[AD-A286406] p 1484 N95-22203
Network distributed global memory for transparent message passing on distributed networks
[AD-A286096] p 1478 N95-22228

Confirmatory analysis of SAGE-1, and -2 data
[DE95-003623] p 1427 N95-22240
High performance computing for beam physics applications
[DE94-018312] p 1539 N95-22243
An assessment of European parallel software research
[AD-A286357] p 1479 N95-22257
3-D TECATE/BREW: Thermal, stress, and birefringent ray-tracing codes for solid-state laser design
[DE95-000330] p 1376 N95-22301
Logic programming and negation: A survey
[PB95-110730] p 1472 N95-22302
A new parallel method for molecular dynamics simulation of macromolecular systems
[DE94-018621] p 1529 N95-22315
Quality characteristics and metrics for reusable software
[PB94-203437] p 1473 N95-22390
Incremental rederivation of software artifacts: FY 1993
[AD-A285790] p 1473 N95-22402
Numerical study of boundary layer interaction with shocks: Method and code validation
p 1362 N95-22461
Databases post-processing in Tensoral
p 1363 N95-22465
Wind Energy Program overview, fiscal year 1993
[DE94-000285] p 1398 N95-22468

COMPUTER STORAGE DEVICES
An IBM based ARINC interface
[ARL-TR-21] p 1471 N95-22104

COMPUTER SYSTEMS DESIGN
High-performance packet switching architecture for ATM: Conventional solution and neural network solution
[PB95-110920] p 1312 N95-19935
The design and implementation of the functional/daplex data interface for the multimodel and multilingual database system
[AD-A280131] p 1587 N95-20039
System level fault tolerance in parallel and distributed computing systems
[AD-A279664] p 1474 N95-20305
A group communication approach for mobile computing mobile channel: An ISIS tool for mobile services
[AD-A279785] p 1290 N95-20306
Measuring software dependability by robustness benchmarking
[AD-A280053] p 1461 N95-20622
The Advanced Avionics Subsystem Technology Demonstration Program p 1209 N95-20636
The IEEE scalable coherent interface: An approach for a unified avionics network p 1212 N95-20650
Environment for Test and Analysis of Distributed Software (ETADS)
[AD-A285776] p 1463 N95-20877
Visual displays and Neuro-Linguistic Programming
[DE95-001454] p 1466 N95-21311
EXPERT system expert: Program description
[PB95-131561] p 1482 N95-21429
Semaphore network encryption report
[AD-A279294] p 1303 N95-21493
Network file server with automatic sensing means
[AD-D016250] p 1476 N95-21496
SCSI controller with target status retrieval
[AD-D016249] p 1476 N95-21504
Independent review of Aviation Technology and Research Information Analysis System (ATRIAS) database
[AD-A284049] p 1203 N95-21518
Design model for open distributed processing systems
[PB95-135505] p 1477 N95-21620
Application-oriented architecture for multimedia teleservices
[PB95-135513] p 1306 N95-21623
Method of retrieving and storing computer peripheral data
[AD-D016251] p 1591 N95-22098
An IBM based ARINC interface
[ARL-TR-21] p 1471 N95-22104
The navigation toolkit
[NASA-CR-197290] p 1205 N95-22161
Formal specification and compositional verification of an atomic broadcast protocol
[PB95-110508] p 1472 N95-22351
TDX: A high-bandwidth crossbar-switched communication paradigm
[DE94-017187] p 1311 N95-22407

COMPUTER SYSTEMS PERFORMANCE
High-performance packet switching architecture for ATM: Conventional solution and neural network solution
[PB95-110920] p 1312 N95-19935
Target area acquisition and control system survivability for the National Ignition Facility
[DE94-016549] p 1550 N95-20190
A theoretical study on the performance of the FDTD code on a massively parallel computer
[AD-A285346] p 1475 N95-20499
Semaphore network encryption report
[AD-A279294] p 1303 N95-21493
A simulation study of TCP performance in ATM networks
[DE94-016622] p 1477 N95-21505
Status of CFDLIB performance tests on the T3D
[DE95-002708] p 1478 N95-21925
A new parallel method for molecular dynamics simulation of macromolecular systems
[DE94-018621] p 1529 N95-22315

COMPUTER SYSTEMS PROGRAMS
The design and implementation of the functional/daplex data interface for the multimodel and multilingual database system
[AD-A280131] p 1587 N95-20039
Towards better quality and reliability in the software reuse library environment
[AD-A280013] p 1460 N95-20313
User interface software tools
[AD-A286056] p 1466 N95-21325
An IBM based ARINC interface
[ARL-TR-21] p 1471 N95-22104

COMPUTER TECHNIQUES
Optimal distributed control system for a linear distributed parameter system
[AD-D016583] p 1480 N95-20202
First principles simulation of materials properties
[DE94-016781] p 1566 N95-20405
Eta%-Superconvergence of Finite Element Approximations in the Interior of General Meshes of Triangles
[AD-A279903] p 1490 N95-20565
Study of superconvergence by a computer-based approach: Superconvergence of the gradient of the displacement, the strain and stress in finite element solutions for plane elasticity
[AD-A279885] p 1490 N95-20588
ECSU-AASERT summer research project in parallel processing and computer visualization
[AD-A285983] p 1475 N95-20618
The IEEE scalable coherent interface: An approach for a unified avionics network p 1212 N95-20650
VLUGr3: A vectorizable adaptive grid solver for PDEs in 3D. 2: Code description
[PB95-135737] p 1465 N95-21033
13th European Annual Conference on Human Decision Making and Manual Control
[PB95-132874] p 1450 N95-21284
Proceedings of the NATO-Advanced Study Institute on Computer Aided Analysis of Rigid and Flexible Mechanical Systems. Volume 2: Contributed papers
[AD-A286063] p 1381 N95-21488
The use of fuzzy set classification for pattern recognition of the polygraph
[AD-A279148] p 1470 N95-21971
Fast algorithms for transport models
[DE95-001702] p 1470 N95-21992
Activities of the Research Institute for Advanced Computer Science
[NASA-CR-197291] p 1478 N95-22108

COMPUTER VIRUSES
An abstract model of rogue code insertion into radio frequency wireless networks. The effects of computer viruses on the Program Management Office
[AD-A285759] p 1288 N95-19932

COMPUTER VISION
Tracking a dynamic set of feature points
[AD-A285124] p 1313 N95-20257
A scalable video rate camera interface
[AD-A286144] p 1474 N95-20325
Integration of segmentation and stereo matching
[PB95-107819] p 1444 N95-21028
Unknown-terrains navigation of a mobile robot using an array of sonars
[DE94-017902] p 1482 N95-21385
An image cancellation approach to depth-from-focus
[DE94-019312] p 1544 N95-21392
Feature extraction without edge detection
[AD-A279842] p 1473 N95-22386

COMPUTERIZED SIMULATION
High-performance packet switching architecture for ATM: Conventional solution and neural network solution
[PB95-110920] p 1312 N95-19935
Simulation of stellar speckle imaging
[DE94-016606] p 1412 N95-19985
Advanced detector development, laboratory simulations, diagnostic development, and data analysis on wake physics
[AD-A284798] p 1364 N95-20069
A computational study of projectile shape dependence on phase change phenomena with comparisons to experimental data
[DE95-000740] p 1384 N95-20077
Performance issues for engineering analysis on MIMD parallel computers
[DE94-015769] p 1474 N95-20150
SYNTH: A spectrum synthesizer
[DE94-015943] p 1458 N95-20153
Unified GUI for the Los Alamos Radiation Transport Code System
[DE94-016088] p 1458 N95-20154
Meshes: The next generation
[DE94-016702] p 1459 N95-20255
Numerical modeling of a small recirculating induction accelerator for heavy-ion fusion
[DE94-018549] p 1552 N95-20318
Simulation of large systems with neural networks
[DE94-018898] p 1428 N95-20319
Measuring presence in virtual environments
[AD-A286183] p 1460 N95-20326
New high temperature plasmas and sample introduction systems for analytical atomic emission and mass spectrometry
[DE94-018580] p 1552 N95-20345
High performance computing for materials process modeling
[DE94-017860] p 1460 N95-20358
BACKSCAT lidar simulation version 4.0: Technical documentation and users guide
[AD-A285851] p 1290 N95-20376
Implementation and performance of a three-dimensional numerical transport model
[PB95-135745] p 1402 N95-20440
Legged vehicle for underwater mobile operations
[AD-A285043] p 1480 N95-20482
Collected papers of the Soar/IFOR project, Spring 1994
[AD-A280063] p 1216 N95-20624
Computer graphics tools for visualizing gravity gradient torques on a rigid spacecraft
[AD-A285971] p 1461 N95-20665
Emitter location via Kalman filtering of signal time difference of arrival
[AD-A285972] p 1291 N95-20666
Simulation of tearing mode stabilization by using ECH
[DE94-770700] p 1554 N95-20684
EPICS simulation tools for control system development
[DE94-018082] p 1462 N95-20699
Use of an integrated design tool for weld quality enhancement
[DE94-018135] p 1379 N95-20723
HIVEL2D: A two-dimensional flow model for high-velocity channels
[AD-A286556] p 1341 N95-20843
Highlights of recent balance of system research and evaluation
[DE95-001626] p 1393 N95-20863
Approach to compact terawatt CO2 laser system for particle acceleration
[DE95-002170] p 1371 N95-20866
Advanced robotic technologies for transfer at Sandia National Laboratories
[DE95-001617] p 1481 N95-20884
COYOTE II: A finite element computer program for nonlinear heat conduction problems. Part 1: Theoretical background
[DE95-002587] p 1463 N95-20887
Performance and cost analysis of monolithic solid oxide fuel cells
[DE95-002511] p 1394 N95-20896
Modelling and simulation of HF/VHF MMPPs
p 1293 N95-20925
Proceedings of the Cloud Impacts on DOD Operations and Systems 1993 Conference (CIDOS 1993)
[AD-A286658] p 1430 N95-20974
Next generation solid modellers for electronic prototyping
[AD-A286525] p 1464 N95-21010
Simulation of the injection moulding process
[PB94-215555] p 1286 N95-21027
Application of Direct and Large Eddy Simulation to Transition and Turbulence
[AGARD-CP-551] p 1346 N95-21061
Developments and applications of dynamic models for large eddy simulation of complex flows
p 1346 N95-21062
Subgrid scale models in finite difference simulations of complex wall bounded flows p 1346 N95-21063
Large-eddy simulation of rotating channel flows using a localized dynamic model p 1346 N95-21064
The asymptotic state of rotating homogeneous turbulence at high Reynolds numbers
p 1347 N95-21065
Comparison of DNS and LES of transitional and turbulent compressible flow: Flat plate and mixing layer
p 1347 N95-21066
Direct numerical simulation of turbulent flow in a sudden pipe expansion p 1347 N95-21067

Simulation of separated flows p 1347 N95-21068
Simulation of large scale transitional flows
p 1348 N95-21075
Simulation of pipe flow p 1349 N95-21078
Simulations of bypass transition for spatially evolving disturbances p 1349 N95-21079
Direct numerical simulation for premixed turbulent combustion modelling p 1249 N95-21082
Entrainment in a shear-free turbulent mixing layer
p 1350 N95-21083
The effect of initial conditions on the development of temporally evolving planar three dimensional incompressible wakes p 1350 N95-21085
Spatial direct numerical simulation of boundary layer transition under strong adverse pressure gradient
p 1351 N95-21093
Direct simulation and graphics post-processing of three-dimensional turbulent flows p 1352 N95-21098
Control of complex multibody spacecraft
[AD-A285623] p 1220 N95-21147
Computer model predictions of the local effects of large, solid-fuel rocket motors on stratospheric ozone
[AD-A285632] p 1404 N95-21150
Simulation of rotor blade element turbulence
[NASA-TM-108862] p 1207 N95-21186
Real-time dynamic simulator for the Topaz II reactor power system
[DE95-001604] p 1535 N95-21278
Effects of battery technologies, driving patterns, and climate comfort control on the performance of electric vehicles
[DE95-001102] p 1329 N95-21296
Defect production and recombination during low-energy ion processing
[DE95-001827] p 1572 N95-21304
Simulation of beam-beam lifetime for LEP
[DE95-002888] p 1536 N95-21334
Calculation of atom-centered partial charges for heme
[DE94-014447] p 1520 N95-21375
Computer simulation of the diocotron instability
[AD-A285655] p 1559 N95-21403
Three-dimensional effects for radio frequency antenna modeling
[DE94-019125] p 1303 N95-21459
Structure of ionic interfaces from an absolutely convergent solution of the Madelung problem
[DE94-019268] p 1573 N95-21474
Simulations of metal dissolution and corrosion
[DE94-019295] p 1257 N95-21476
Unified very low stratus cloud/subcloud microphysics model: User's guide
[AD-A286454] p 1430 N95-21586
Simulated rarefied entry of the Galileo probe into the atmosphere of Jupiter
[NASA-TM-110507] p 1601 N95-21621
Flow and heat transfer simulation in a flash smelting furnace
[PB95-108197] p 1354 N95-21649
The application of a statistical analysis software package to explosive testing
[MRL-TR-93-42] p 1284 N95-21658
A preliminary study of the airwake model used in an existing SH-60B/FFG-7 helicopter/ship simulation program
[DSTO-TR-0015] p 1201 N95-21659
Adaptive capture of expert behavior
[DE94-018285] p 1483 N95-21710
Hires and beyond p 1592 N95-21750
EAGLES 1.1: A microcomputer software package for analyzing fuel efficiency of electric and gasoline vehicles
[DE95-001119] p 1469 N95-21829
Directed light fabrication
[DE94-018293] p 1375 N95-21837
A massively parallel algorithm for grand canonical Monte Carlo computer simulation with the short-ranged Lennard-Jones potential
[DE94-010396] p 1477 N95-21843
Tethered satellite: Forces and motion
[NASA-TM-110518] p 1220 N95-21858
Cochannel and adjacent-channel interference in nonlinear minimum-shift-keyed satellite system
[NASA-TM-106834] p 1307 N95-21890
A syncopated leap-frog algorithm for orbit consistent plasma simulation of materials processing reactors
[DE95-000954] p 1561 N95-21922
Status of CFDLIB performance tests on the T3D
[DE95-002708] p 1478 N95-21925
Critical dynamics and plastic flow in disordered Josephson junction arrays
[DE94-629074] p 1576 N95-21995
Standard data formats for simulation
[PB95-110367] p 1470 N95-22016
Economic feasibility analysis of distributed electric power generation based upon the natural gas-fired fuel cell
[DE94-012277] p 1396 N95-22033
The 9th INS scientific computational programs
[DE94-770780] p 1526 N95-22051
Artificial neural network metamodels of stochastic computer simulations
[AD-A285951] p 1484 N95-22056
Solving the inverse problem in terrain modeling
[AD-A285860] p 1391 N95-22131
Latin hypercube sampling in sensitivity analysis
[AD-A285867] p 1499 N95-22135
Users guide to NCEMSS, version 2.0
[DE95-003443] p 1548 N95-22238
High performance computing for beam physics applications
[DE94-018312] p 1539 N95-22243
Manufacturing Technology Bulletin, July 1994
[DE94-017775] p 1605 N95-22262
Modeling of fundamental phenomena in welds
[DE94-017859] p 1381 N95-22268
An improved Monte Carlo algorithm for simulating grain growth
[DE94-017903] p 1578 N95-22272
On conception of a compact neutron source and the possibility of its simulation on the Amba-M end trap
[DE94-633373] p 1562 N95-22282
Recent results in analysis and simulation of beam halo
[DE94-018313] p 1539 N95-22298
3-D TECATE/BREW: Thermal, stress, and birefringent ray-tracing codes for solid-state laser design
[DE95-000330] p 1376 N95-22301
A new parallel method for molecular dynamics simulation of macromolecular systems
[DE94-018621] p 1529 N95-22315
On the dynamics of a shock-bubble interaction
[NASA-CR-194978] p 1495 N95-22325
Simulation of structural response using a recurrent radial basis function network
[DE94-017342] p 1486 N95-22409
PIC simulation of surface waves
[AD-A285358] p 1563 N95-22422
Experimental evaluation of dynamic data allocation strategies in a distributed database with changing workloads
[NASA-CR-195024] p 1456 N95-22431
Annual research briefs, 1994
[NASA-CR-197352] p 1358 N95-22437
Notes on rotating turbulence p 1359 N95-22444
A dynamic localization model with stochastic backscatter p 1359 N95-22445
Local dynamic subgrid-scale models in channel flow
p 1360 N95-22447
Unstructured-grid large-eddy simulation of flow over an airfoil p 1202 N95-22448
Large-eddy simulation of flow through a plane, asymmetric diffuser p 1360 N95-22449
Large-eddy simulation of a boundary layer with concave streamwise curvature p 1360 N95-22450
Direct numerical simulations of on-demand vortex generators: Mathematical formulation
p 1361 N95-22452
Optimal active control for Burgers equations
p 1361 N95-22454
Numerical study of boundary layer interaction with shocks: Method and code validation
p 1362 N95-22461
Resolution requirements for velocity gradients in turbulence p 1363 N95-22462
A method for obtaining a statistically stationary turbulent free shear flow p 1363 N95-22463
Direct numerical simulation of incompressible axisymmetric flows p 1363 N95-22464
Databases post-processing in Tensoral
p 1363 N95-22465

COMPUTERS
The demise of plastic encapsulated microcircuit myths
p 1209 N95-20640
The opportunities for and challenges of common integrated electronics
[AD-A279991] p 1327 N95-20966
HPCC technology awareness program: Improved economic competitiveness through technology awareness, transfer and application
[DE95-002134] p 1476 N95-21355
Quantitative evaluation of wrist posture and typing performance: A comparative study of 4 computer keyboards
[DE95-002392] p 1452 N95-21358
GRONICs-1994. Proceedings of the 1994 Groningen Student Conference on Computer Science
[PB95-135620] p 1468 N95-21455
Advanced computing systems: Usability of knowledge-based planning systems
[AD-A279573] p 1477 N95-21698
Top ten list of user-hostile interface design
[DE95-001602] p 1453 N95-21721
Evaluation of scanners for C-scan imaging for nondestructive inspection of aircraft
[AD-A286398] p 1383 N95-22202
Adaptive fault-resistant systems
[AD-A286406] p 1484 N95-22203
Time and the order of abstract events in distributed computations
[PB95-110482] p 1496 N95-22349
FORTRAN subroutine for column reduction of polynomial matrices
[PB95-134987] p 1497 N95-22379

CONCATENATED CODES
Adaptive error-control scheme for 2-200 MHz Multiple-Mechanism Propagation Paths
p 1293 N95-20926

CONCENTRATION (COMPOSITION)
Ignition of submarine materials at various oxygen concentrations
[PB95-131371] p 1243 N95-21428
Derivation of preliminary maximum permissible concentrations of volatile compounds in air
[PB95-107447] p 1410 N95-22125

CONCENTRATORS
BMDO photovoltaics program overview
p 1316 N95-20504
An update on the development of a line-focus refractive concentrator array p 1322 N95-20534
An introduction to the Astro Edge solar array
p 1322 N95-20535
Si concentrator solar cell development
[DE95-002314] p 1393 N95-20870
Development of concentrator solar cells
[DE95-002316] p 1394 N95-20871

CONCRETES
Fibre-reinforced high-strength concrete
[PB95-131942] p 1232 N95-22158

CONCURRENT ENGINEERING
Automation support for concurrent software engineering
[AD-A279691] p 1461 N95-20579
An MCM concurrent engineering software tool market study
[AD-A279257] p 1468 N95-21489

CONCURRENT PROCESSING
Non interleaving process algebra
[PB95-110607] p 1486 N95-19892
Using local optimality criteria for efficient information retrieval with redundant information filters
[AD-A279603] p 1587 N95-20302
Multi-dimensional Petri nets
[PB95-127593] p 1491 N95-21024
Regularity of BPa-systems is decidable
[PB95-135489] p 1468 N95-21619
Computing symmetries and stubborn sets
[PB95-127700] p 1472 N95-22328

CONDENSED MATTER PHYSICS
Israel Physical Society Annual Meeting 1994
[DE94-630140] p 1565 N95-20261
Neutron Compton scattering
[PB95-130290] p 1530 N95-22332

CONDENSING
Solar system formation and the distribution of volatile species p 1421 N95-21806

CONDITIONING (LEARNING)
Biological and theoretical studies of adaptive networks: The conditioned response
[AD-A284781] p 1479 N95-20061

CONDUCTING FLUIDS
Role of dielectric constant in electrohydrodynamics of conducting fluids
[NASA-TM-110499] p 1331 N95-21614
Measurement of the thermal properties of electrically conducting fluids using coated transient hot wires
[DE94-017816] p 1357 N95-22264

CONDUCTING POLYMERS
The organic chemistry of conducting polymers
[DE94-018216] p 1270 N95-20680
Conducting thermoset polymers
[AD-A286541] p 1273 N95-21014

CONDUCTION BANDS
Angle resolved photoemission on K(0.3)Mo3, TiTe2 and Ti(1 + x)S2
[DE94-018300] p 1574 N95-21712

CONDUCTIVE HEAT TRANSFER
Simulation of tearing mode stabilization by using ECH
[DE94-770700] p 1554 N95-20684
Meso-scale cooling effects of high albedo surfaces: Analysis of meteorological data from White Sands National Monument and White Sands Missile Range
[DE94-018535] p 1429 N95-20782
An augmented Young-Laplace model of an evaporating meniscus in a micro-channel with high heat flux
[NASA-CR-197622] p 1340 N95-20796

COYOTE II: A finite element computer program for nonlinear heat conduction problems. Part 1: Theoretical background
[DE95-002587] p 1463 N95-20887
Self-similar solutions of a fast diffusion equation that do not conserve mass
[PB95-134920] p 1497 N95-22375

CONDUCTORS
Current distribution in Cable-In-Conduit Conductors
[DE95-001820] p 1332 N95-21725

CONFERENCES
Physics and applications of defects in advanced semiconductors, volume 325
[AD-A280059] p 1563 N95-19886
Technical Summary for 1993 fall MRS Symposium O, Complex Fluids
[AD-A283722] p 1264 N95-19972
Technical digest: Eighth Symposium on Optical Fiber Measurements
[PB94-207636] p 1540 N95-19976
Proceedings of the 1994 DOE/NREL Hydrogen Program Review
[DE94-011835] p 1234 N95-20117
Proceedings of the 1993 Non-Fluorocarbon Insulation, Refrigeration and Air Conditioning Technology Workshop
[DE94-018333] p 1285 N95-20194
Second European Symposium on X-Ray Topography and High Resolution Diffraction: Programme and abstracts
[AD-A286328] p 1564 N95-20210
Proceedings of the 4th International Conference on Electrorheological Fluids
[AD-A286341] p 1266 N95-20227
Journal of Applied Physics, volume 76, number 10, part 2. Proceedings of the 6th Joint Magnetism and Magnetic Materials-INTERMAG Conference
[AD-A286364] p 1500 N95-20229
24th Annual Anomalous Absorption Conference
[DE94-016457] p 1551 N95-20283
The First NREL Conference on Thermophotovoltaic Generation of Electricity: Proceedings
[DE94-011831] p 1391 N95-20332
D0 quantum chromodynamics: A compilation of results presented at DPF 1994
[DE95-000838] p 1510 N95-20344
Anaerobic Treatment of Municipal Solid Waste and Sludge for Energy Production and Recycling of Nutrients
[DE95-700217] p 1315 N95-20369
Proceedings of the International Wire and Cable Symposium
[AD-A279242] p 1403 N95-20465
T-45A High Angle of Attack Testing: US Naval Test Pilot School 46th Annual Reunion and Symposium
[AD-A284000] p 1207 N95-20466
Proceedings of the 13th Space Photovoltaic Research and Technology Conference (SPRAT 13)
[NASA-CP-3278] p 1316 N95-20502
Proceedings of the 4th Systems Reengineering Technology Workshop
[AD-A285357] p 1460 N95-20546
Biomolecular Materials by Design, volume 330
[AD-A285369] p 1269 N95-20551
The 29th MIL-HDBK-17 Polymer Matrix Composites Coordination Group Meeting
[AD-A279917] p 1269 N95-20578
Advanced Packaging Concepts for Digital Avionics
[AGARD-CP-562] p 1208 N95-20631
Annual Conference on Fire Research: Book of abstracts
[PB95-104964] p 1286 N95-20717
Proceedings of the Zel'Dovich Memorial International Conference on Combustion, Detonation, Shock Waves, volume 2
[AD-A286626] p 1239 N95-20769
The 37th Military Librarians Workshop on Global Information: The Sun Never Sets
[AD-A286636] p 1588 N95-20774
Gordon Research Conference on Physical Electrochemistry
[AD-A286545] p 1240 N95-20842
Multiple Mechanism Propagation Paths (MMPPs): Their Characterisation and Influence on System Design
[AGARD-CP-543] p 1292 N95-20921
Seminar on Biomedical Engineering 1993
[PB95-104402] p 1443 N95-20971
Proceedings of the Cloud Impacts on DOD Operations and Systems 1993 Conference (CIDOS 1993)
[AD-A286658] p 1430 N95-20974
Proceedings of the Fourth International Workshop on Inductive Logic Programming (ILP-94)
[PB95-135273] p 1464 N95-21003
Studying Turbulence Using Numerical Simulation Databases. 5: Proceedings of the 1994 Summer Program
[NASA-CR-197362] p 1341 N95-21035
Application of Direct and Large Eddy Simulation to Transition and Turbulence
[AGARD-CP-551] p 1346 N95-21061
Proceedings of the NATO-Advanced Study Institute on Computer Aided Analysis of Rigid and Flexible Mechanical Systems. Volume 1: Main lectures
[AD-A286062] p 1380 N95-21171
13th European Annual Conference on Human Decision Making and Manual Control
[PB95-132874] p 1450 N95-21284
Second International Conference on Ordinal Data Analysis
[AD-A279756] p 1590 N95-21401
GRONICs-1994. Proceedings of the 1994 Groningen Student Conference on Computer Science
[PB95-135620] p 1468 N95-21455
Proceedings of the NATO-Advanced Study Institute on Computer Aided Analysis of Rigid and Flexible Mechanical Systems. Volume 2: Contributed papers
[AD-A286063] p 1381 N95-21488
International Conference on Control and Estimation of Distributed Parameter Systems: Nonlinear Phenomena
[AD-A286449] p 1493 N95-21582
Fourth International Symposium on Stratified Flows, volume 1
[AD-A286450] p 1354 N95-21583
Fourth International Symposium on Stratified Flows, volume 3
[AD-A286452] p 1354 N95-21584
Proceedings of the School for Young High Energy Physicists
[PB95-108114] p 1537 N95-21647
Proceedings of the 5th Workshop on the Next Generation of CASE Tools
[PB95-135208] p 1469 N95-21716
Science with High Spatial Resolution Far-Infrared Data
[NASA-CR-197353] p 1595 N95-21749
Conference on Deep Earth and Planetary Volatiles
[NASA-CR-196944] p 1415 N95-21777
Solar system formation and the distribution of volatile species p 1421 N95-21806
The Use of Cyanobacteria to Explore Basic Biological Processes
[DE94-019238] p 1440 N95-22066
Conference proceedings. Defense Modeling and Simulation Office Information/Data Base (I/DB) Task Group Meetings, and notes from the previous two I/DB meetings
[AD-A279097] p 1591 N95-22069
The role of point defects and defect complexes in silicon device processing
[DE94-011876] p 1279 N95-22091
International Symposium on Advanced Laser Technologies
[AD-A279849] p 1376 N95-22164
Surface technology programme
[PB95-132866] p 1262 N95-22174
Proceedings: International Symposium on Global Change (IGBP)
[DE94-765351] p 1410 N95-22219
Theses of the Proceedings of the 23d International Meeting on the Physics of Charged Particle Interaction with Crystals
[DE94-631501] p 1529 N95-22281
Transactions of the Eleventh Army Conference on Applied Mathematics and Computing
[AD-A279884] p 1497 N95-22389
Indian Academy of Sciences. Volume 105, number 6, December 1993. Proceedings of the 2nd International Conference on Solar Energy Storage Applied Photochemistry
[AD-A286481] p 1605 N95-22394
Cellular responses to environmental DNA damage
[DE94-015606] p 1441 N95-22397
Advanced Materials and Process Technology for Mechanical Failure Prevention (proceedings of the 48th Meeting of the Mechanical Failures Prevention Group
[AD-A285785] p 1233 N95-22399
Proceedings of the 4th Annual Major Range and TestFacility Base (MRTFB) Environmental Workshop
[AD-A285779] p 1411 N95-22414
Fourth International Symposium on Stratified Flows, volume 4
[AD-A286453] p 1358 N95-22424

CONFIDENCE LIMITS
Iterated-bootstrap confidence intervals for the mean
[AD-A279802] p 1498 N95-20102
Search for D(+) yields (pi)(+)(mu)(+)(mu)(-)
[DE94-015538] p 1512 N95-20475
Precedence tests and confidence bounds for complete data: An overview and some results
[PB95-132668] p 1499 N95-21980

CONFIGURATION INTERACTION
D(sup 0)-(anti-D)(sup 0) mixing and doubly Cabibbo-suppressed decays of the D(+)
[DE94-015540] p 1512 N95-20476
The evolution of configuration from q greater than 1 to q less than 1
[DE94-631396] p 1556 N95-21162

CONFINEMENT
Confinement and stability of crystalline beams in storage rings
[DE95-002515] p 1533 N95-20886
Ideal Magnetohydrodynamic stabilities in JT-60 and D3-D tokamak plasmas
[DE94-770684] p 1555 N95-20987
Investigations of VH-mode in D3-D and JET
[DE94-015859] p 1556 N95-21142
Experimental investigation of molecular beam injection in HL-1 tokamak
[DE94-631456] p 1556 N95-21165
Review of recent D-T experiments from TFTR
[DE95-002755] p 1557 N95-21239
Monopoles and quark confinement: Introduction and overview
[DE94-019348] p 1522 N95-21485

CONGRESSIONAL REPORTS
Naval aviation: F-14 upgrades are not adequately justified. Report to Congressional Committees
[AD-A286338] p 1206 N95-20212
Environmental cleanup: Too many high priority sites impede DOD's program. Report to the Chairman, Committee on Governmental Affairs, US Senate
[AD-A279511] p 1407 N95-21683
Technology transfer: Improving the use of cooperative R/D agreement at DOE's contractor-operated laboratories. Report to Congressional requesters
[GAO/RCED-94-91] p 1586 N95-22403

CONGRUENCES
Quadratic forms in design theory
[PB95-111019] p 1487 N95-19940

CONJUGATE GRADIENT METHOD
Iterated-subspace minimization methods for nonlinear optimization
[PB95-108171] p 1495 N95-22317

CONJUGATES
Beam flavor dependence in the hadroproduction of D(+-) and D(sub s)(+-) mesons
[DE94-015541] p 1530 N95-22339

CONNECTORS
A technique for increasing the bandwidth of high performance electrical backplanes p 1212 N95-20651
Ab initio potential energy surface for H + OCS reactions: Extended basis sets and correlation treatment
[AD-A286420] p 1247 N95-22207

CONSERVATION
Unbinned maximum likelihood fit for the CP conserving couplings for W + photon production at CDF
[DE95-001471] p 1514 N95-20852
On the Taylor test. Part 3: A continuum mechanics code analysis of steady plastic wave propagation
[DE95-002252] p 1501 N95-20869
Self-similar solutions of a fast diffusion equation that do not conserve mass
[PB95-134920] p 1497 N95-22375

CONSERVATION EQUATIONS
General conservative extension theorem in process algebra
[PB95-110656] p 1487 N95-19902
The coupling between flame surface dynamics and species mass conservation in premixed turbulent combustion p 1249 N95-21041

CONSERVATION LAWS
Approximate Riemann solver for magnetohydrodynamics (that works in more than one dimension)
[PB95-135802] p 1553 N95-20425
Symmetry, Wigner functions and particle reactions
[DE94-629887] p 1514 N95-20735
Numerical wave speed for one-dimensional scalar hyperbolic conservation laws with source terms
[PB95-127536] p 1492 N95-21371
On the wavelet optimized finite difference method
[NASA-CR-191601] p 1495 N95-22157

CONSISTENCY
The Lorentz reciprocity theorem as a consistency test for propagation models p 1295 N95-20937
Compositional approach to sequential consistency and lazy caching
[PB95-134110] p 1455 N95-21871

CONSTANTS
Natural gas combustion chemistry mechanisms research
[PB95-111670] p 1247 N95-22150

CONSTRAINTS
New method for integrity constraint checking in deductive databases
[PB95-110672] p 1586 N95-19904
Constraints on SUSy-GUT unification from b yields s-gamma decay
[PB95-130373] p 1580 N95-21229

CONSTRUCTION
Design and construction of the HSX experiment
[DE94-018657] p 1552 N95-20348
The impact of partnering on construction contracts
[AD-A286588] p 1585 N95-20855
Neural network construction via back-propagation
[DE95-002867] p 1482 N95-21249
Aeronautical engineering: A continuing bibliography with indexes (supplement 315)
[NASA-SP-7037(315)] p 1199 N95-21640
Environmental Compliance Assessment and Management Program (ECAMP), South Carolina supplement
[AD-A279533] p 1408 N95-21689
CONTACT LOADS
On the origins and modeling of frictional behavior in interfacially-complex sliding contacts
[DE94-019129] p 1381 N95-21601
CONTAMINANTS
Resonance Raman spectroscopy of volatile organics: Carbon tetrachloride
[DE95-000627] p 1233 N95-19980
Surface characterization and contamination analysis
[NASA-CR-197374] p 1238 N95-20557
Evaluation of an immobilized cell bioreactor for degradation of meta- and para-nitrobenzoate
[AD-A279719] p 1516 N95-20993
Numerical study of contaminant effects on combustion of hydrogen, ethane, and methane in air
[NASA-TM-106844] p 1284 N95-22114
Gas-phase photocatalytic oxidation: Cost comparison with other air pollution control technologies
[DE95-000241] p 1410 N95-22278
CONTAMINATION
The in-situ fracture and Auger analysis of Nicalon fibers
[DE94-017771] p 1226 N95-20357
Monitoring bioremediation of Volatile Organic Compounds (VOCs) using Fourier Transform Infrared (FT-IR) spectrometry
[AD-A279631] p 1403 N95-20456
Liquid xenon as a potential laser host medium
[AD-A285365] p 1370 N95-20550
Surface characterization and contamination analysis
[NASA-CR-197374] p 1238 N95-20557
Aging tests of ethylene contaminated argon/ethane
[DE95-002526] p 1282 N95-20899
Fiber-optic sensors for rapid, inexpensive characterization of soil and ground water contamination
[DE95-002471] p 1545 N95-21510
Surface inspection using Fourier Transform Infrared Spectroscopy
[DE95-001699] p 1244 N95-21571
Environmental cleanup: Too many high priority sites impede DOD's program. Report to the Chairman, Committee on Governmental Affairs, US Senate
[AD-A279511] p 1407 N95-21683
D/H ratios and H2O contents of mantle-derived amphibole megacrysts from Dish Hill, California
p 1416 N95-21781
Primitive Xe in the atmospheres of Earth and mars
p 1419 N95-21795
CONTEXT FREE LANGUAGES
Connectionist models for intelligent computation
[AD-A286436] p 1484 N95-22210
CONTINENTAL SHELVES
Long term changes on the continental shelf of the North Sea: Invertebrate trends, 1931-1990
[PB95-135224] p 1435 N95-21717
CONTINUOUS RADIATION
Threshold detection in the presence of atmospheric turbulence
[AD-A286175] p 1427 N95-22249
CONTINUOUS WAVE LASERS
Application of a dimensionless parameter model for Laser Beam Welding
[DE94-018902] p 1378 N95-20048
Optical power limiting liquid crystal composites
[AD-A286605] p 1569 N95-20767
Tunable CW blue, green, orange and red upconversion fiber lasers at room temperature
[DE95-000851] p 1375 N95-22007
CONTINUOUS WAVE RADAR
Millimeter wave front-end figure of merit, part 1
[AD-A279093] p 1307 N95-21915
CONTINUUM FLOW
Continuum transient and frozen startup behavior of conventional and gas-loaded heat pipes
[AD-A284297] p 1339 N95-20250
CONTINUUM MECHANICS
On the Taylor test. Part 3: A continuum mechanics code analysis of steady plastic wave propagation
[DE95-002252] p 1501 N95-20869
CONTINUUM MODELING
Accurate solution algorithms for incompressible multiphase flows
[DE95-002727] p 1353 N95-21317
Domain processes in ferroelectric ceramics
[AD-A279567] p 1276 N95-21697
CONTINUUMS
Correlation of far-infrared emission and radio continuum emission along the major axis of edge-on spiral galaxies
p 1593 N95-21762
Two-dimensional maps of the infrared-to-radio ratio in spiral galaxies p 1593 N95-21765
CONTOURS
Stars or stripes: A comparative study of finite and transfinite techniques for surface modelling
[PB95-134979] p 1464 N95-20975
Visualizing 3D velocity fields near contour surfaces
[DE95-000841] p 1353 N95-21182
N=1 Superconformal minimal model correlation functions on the torus
[PB95-134615] p 1500 N95-21964
CONTRACT MANAGEMENT
An analysis of cost overruns on defense acquisition contracts p 1584 N95-20749
The impact of partnering on construction contracts
[AD-A286588] p 1585 N95-20855
Annual program analysis of the NASA Space Life Sciences Research and Education Support Program
[NASA-CR-197298] p 1439 N95-21529
Technology transfer: Improving the use of cooperative R/D agreement at DOE's contractor-operated laboratories. Report to Congressional requesters
[GAO/RCED-94-91] p 1586 N95-22403
CONTRACT NEGOTIATION
The impact of partnering on construction contracts
[AD-A286588] p 1585 N95-20855
CONTRACTION
Beyond beta-reduction in Church's lambda yield
[PB95-110565] p 1488 N95-20149
CONTRACTORS
The advantages of cost plus award fee contracts
p 1584 N95-20745
CONTRACTS
The impact of partnering on construction contracts
[AD-A286588] p 1585 N95-20855
CONTROL
Automation support for concurrent software engineering
[AD-A279691] p 1461 N95-20579
CONTROL DATA (COMPUTERS)
The GPS Burst Detector W-Sensor
[DE94-017406] p 1204 N95-20269
CONTROL EQUIPMENT
Design of power electronics for TVC and EMA systems
[NASA-CR-196540] p 1312 N95-19909
CONTROL SIMULATION
Control of complex multibody spacecraft
[AD-A285623] p 1220 N95-21147
CONTROL STABILITY
Temporal evolution of turbulence/chemistry interactions in lifted, turbulent-jet flames
[DE95-002481] p 1243 N95-21512
CONTROL SURFACES
Launch vehicle flight control augmentation using smart materials and advanced composites (CDDF Project 93-05)
[NASA-TP-3535] p 1218 N95-21346
Translational-energy-resolved studies of photographed carrier-induced reactions on semiconductor surfaces
[DE95-002944] p 1573 N95-21444
CONTROL SYSTEMS DESIGN
Toward a design for the ITER plasma shape and stability control system
[DE94-017516] p 1548 N95-20037
Force based motion control of a walking machine
[PB95-129672] p 1451 N95-20276
System design document U-AVLIS control system architecture
[DE94-017297] p 1460 N95-20387
Preliminary control system design and analysis for the Space Station Furnace Facility thermal control system
[NASA-TM-108476] p 1365 N95-20560
Design of a controller for a flexible pointing system using H(infinity) synthesis
[AD-A286572] p 1481 N95-20828
Control of complex multibody spacecraft
[AD-A285623] p 1220 N95-21147
Two-micron Laser Atmospheric Wind Sounder (LAWS) pointing/tracking study
[NASA-CR-195012] p 1220 N95-21190
Communications and control for electric power systems: Power system stability applications of artificial neural networks
[NASA-CR-197594] p 1483 N95-21613
Sensor based fine motion control
[PB95-108007] p 1483 N95-21669
Adaptive capture of expert behavior
[DE94-018285] p 1483 N95-21710
RF beam control for the AGS Booster
[DE95-001485] p 1538 N95-21720
Multi-port tester interface
[AD-D016240] p 1332 N95-21775
Design of robust optimal control systems and stability analysis of real structured uncertainties
[AD-A279089] p 1483 N95-21913
Optimal control of a two wheeled mobile robot
[AD-A286130] p 1485 N95-22233
Low-level RF control for the AFEL
[DE94-018295] p 1540 N95-22410
CONTROL THEORY
Summary of a joint program of research into aircraft flight control concepts
[AD-A280012] p 1214 N95-20004
Analytic Perturbation Analysis of Discrete Event Dynamic Systems
[DE94-018635] p 1480 N95-20126
A physiological neural network for saccadic eye movement control
[AD-A279599] p 1441 N95-20301
Performance measurement: A tool for program control
p 1585 N95-20752
Program control for mission success
p 1585 N95-20753
The MSFC Program Control Development Program
p 1585 N95-20754
Riccati equation theory for Pritchard-Salamon systems: A Popov function approach
[PB95-137089] p 1491 N95-20830
International Conference on Control and Estimation of Distributed Parameter Systems: Nonlinear Phenomena
[AD-A286449] p 1493 N95-21582
Semi-global stabilization of linear discrete-time systems subject to input saturation via linear feedback: An ARE-based approach
[PB95-135463] p 1483 N95-21618
Discrete algebraic Riccati equation and linear matrix inequality
[PB95-133575] p 1484 N95-22139
Mathematical theory of neural networks
[AD-A286508] p 1485 N95-22213
Quadratic optimal control of a delay equation II: The unstable case
[PB95-127064] p 1486 N95-22366
Quadratic optimal control of a delay equation I: The stable case
[PB95-127072] p 1486 N95-22367
Pollution error in the H-version of the finite element method and the local quality of A-posteriori error estimators
[AD-A279868] p 1497 N95-22388
Optimal active control for Burgers equations
p 1361 N95-22454
CONTROLLABILITY
Stabilization and control problems in structural dynamics
[AD-A279996] p 1340 N95-20312
CONTROLLED FUSION
Boron carbide-based coatings on graphite for plasma facing components
[DE94-017976] p 1269 N95-20570
Laser design basis for the National Ignition Facility
[DE94-016700] p 1534 N95-21209
CONTROLLERS
A photophysical control mechanism for zeaxanthin-associated radiationless energy dissipation in photosynthesis
[DE94-018383] p 1437 N95-19969
Robust agent control of an autonomous robot with many sensors and actuators
[AD-A280148] p 1479 N95-20011
The control system position to the electric probe in the Tokamak Novillo
[DE94-629938] p 1550 N95-20204
Preliminary control system design and analysis for the Space Station Furnace Facility thermal control system
[NASA-TM-108476] p 1365 N95-20560
Design of a controller for a flexible pointing system using H(infinity) synthesis
[AD-A286572] p 1481 N95-20828
Non-intrusive SCSI status sensing system
[AD-D016242] p 1476 N95-21307
Network file server with automatic sensing means
[AD-D016250] p 1476 N95-21496
SCSI controller with target status retrieval
[AD-D016249] p 1476 N95-21504
Sensor based fine motion control
[PB95-108007] p 1483 N95-21669

SEU and SEL response of the Westinghouse 64K E-2PROM, analog devices AD7876 12-bit ADC, and the Intel 82527 Serial Communications Controller
[DE95-003349] p 1334 N95-22086
Method of sensing target status in a local area network
[AD-D016248] p 1478 N95-22090
Method of non-intrusively sensing status in a computer peripheral
[AD-D016241] p 1478 N95-22146
Radiation characterization report for the GPS Receiver microcontroller chip
[DE94-019169] p 1335 N95-22165
Robust fixed-structure control
[AD-A286515] p 1485 N95-22216

CONVECTION
The initiation of lightning and the growth of electric fields in thunderstorms
[AD-A280033] p 1428 N95-20008
Effects of microphysics and radiation on mesoscale processes of a midlatitude squall line
[DE94-014732] p 1429 N95-20381
Fourth International Symposium on Stratified Flows, volume 1
[AD-A286450] p 1354 N95-21583
Modeling the effect of water on mantle rheology
p 1417 N95-21783
Mantle devolatilization and rheology in the framework of planetary evolution p 1418 N95-21788
Volatiles, rheology, and mantle convection: Comparing Earth, Venus, and Mars p 1420 N95-21801
A simulation of plasma motion in the polar ionosphere
[AD-A286166] p 1426 N95-22019

CONVECTION-DIFFUSION EQUATION
Multigrid with matrix-dependent transfer operators for convection-diffusion problems
[PB95-110821] p 1487 N95-19915

CONVECTIVE HEAT TRANSFER
Rainfall rates and the vertical distribution of diabatic heating components over tropical oceans
[NASA-CR-197603] p 1428 N95-19948
A computer code (SKINTEMP) for predicting transient missile and aircraft heat transfer characteristics
[AD-A286044] p 1341 N95-21001
Instabilities in natural-convection flows in cavities
[PB95-107975] p 1354 N95-21578

CONVERGENCE
Eta%-Superconvergence of Finite Element Approximations in the Interior of General Meshes of Triangles
[AD-A279903] p 1490 N95-20565
A convergence analysis of an h-version finite element method with high order elements for two dimensional elasto-plasticity problems
[AD-A279975] p 1491 N95-20920
Convergence acceleration of the Proteus computer code with multigrid methods
[NASA-CR-197677] p 1467 N95-21450
Structure of ionic interfaces from an absolutely convergent solution of the Madelung problem
[DE94-019268] p 1573 N95-21474
Recycling of volatiles at subduction zones: Noble gas evidence from the Tabar-Lihir-Tanga-Feni arc of papua New Guinea p 1418 N95-21787
Iterated-subspace minimization methods for nonlinear optimization
[PB95-108171] p 1495 N95-22317

CONVERGENT-DIVERGENT NOZZLES
Static investigation of two fluidic thrust-vectoring concepts on a two-dimensional convergent-divergent nozzle
[NASA-TM-4574] p 1199 N95-19913

CONVERSION
Transient studies of low temperature catalysts for methane conversion
[DE95-003560] p 1247 N95-22224

CONVERTERS
Natural gas converter performance and durability
[PB95-135554] p 1284 N95-21966

CONVEXITY
Set functionals in stochastic geometry
[PB95-135372] p 1491 N95-21005
Design of robust optimal control systems and stability analysis of real structured uncertainties
[AD-A279089] p 1483 N95-21913

CONVOLUTION INTEGRALS
Deconvolution and singular value decomposition
[AD-A286582] p 1491 N95-20875
Turbo codes for deep-space communications
p 1304 N95-21535

COOLANTS
Immersion/two phase cooling p 1211 N95-20648
MHD pressure drop in ducts with imperfectly insulating coatings
[DE95-002852] p 1558 N95-21244

COOLING
Solidification modeling of a spiral casting to determine material fluidity
[DE94-018930] p 1285 N95-20050
FASTPACK: Optimized solutions for modular avionics derived from a parametric study. Part 2: Avionics
p 1209 N95-20635
Immersion/two phase cooling p 1211 N95-20648
Meso-scale cooling effects of high albedo surfaces: Analysis of meteorological data from White Sands National Monument and White Sands Missile Range
[DE94-018535] p 1429 N95-20782
Time behavior and frequency response of the microwave propagation channel during multipath propagation
p 1296 N95-20942
Microclimate cooling effect on perceived exertion in four heat/exercise scenarios
[AD-A285549] p 1444 N95-21160
Toughened Silcomp composites for gas turbine engine applications
[DE95-002851] p 1214 N95-21243
Theory and modelling of quench in cable-in-conduit superconducting magnets
[DE95-001819] p 1330 N95-21442
Heat loss by helicity injection in spheromaks
[DE95-003473] p 1562 N95-22221

COOLING FINS
Liquid-metal pin-fin pressure drop by correlation in cross flow
[DE94-017086] p 1338 N95-19923

COOLING SYSTEMS
Module cooling system
[AD-D016584] p 1315 N95-20436
Microclimate cooling effect on perceived exertion in four heat/exercise scenarios
[AD-A285549] p 1444 N95-21160

COORDINATES
SAR image registration in absolute coordinates using GPS carrier phase position and velocity information
[DE94-018738] p 1204 N95-20195

COPOLYMERIZATION
Reactive compatibilization of polymer blends
[AD-A284836] p 1263 N95-19893

COPOLYMERS
Polyurethane-epoxy interpenetrating polymer network acoustic damping material
[AD-D016567] p 1266 N95-20293
Responsive copolymers for enhanced petroleum recovery
[DE94-018822] p 1267 N95-20350
The role of high pressure in the study and applications of the ferroelectric polymer polyvinylidene fluoride and its copolymers
[DE94-015742] p 1268 N95-20396
Topography of neutron scattering from diblock copolymer film
[DE95-001457] p 1229 N95-20840
Neutron reflectivity study of adsorbed diblock copolymers
[DE95-002740] p 1281 N95-22434

COPPER
Direct catalytic decomposition of nitric oxide
[DE94-018840] p 1233 N95-20045
Investigation of syngas interaction in alcohol synthesis catalysts
[DE94-018784] p 1236 N95-20349
Materials research for GHz multi-chip modules
[AD-A279661] p 1227 N95-20412
Spin-specific photoelectron diffraction using magnetic x ray circular dichroism
[DE94-017527] p 1567 N95-20448
Proceedings of the International Wire and Cable Symposium
[AD-A279242] p 1403 N95-20465
Growth, characterization and device development in monocrystalline diamond films
[AD-A285991] p 1568 N95-20614
Aerosol-assisted chemical vapor deposition of copper: A liquid delivery approach to metal thin films
[AD-A279702] p 1270 N95-20689
Copper metallization of stainless steels
[DE95-001496] p 1256 N95-21300
A multisite interaction expansion of the total energy in metals
[DE94-017175] p 1262 N95-22313

COPPER ALLOYS
Mixed-sputter deposition of Ni-Ti-Cu shape memory films
[DE94-017296] p 1250 N95-19900
Giant magnetoresistance calculated from first principles
[DE94-018658] p 1500 N95-20129
Method of making copper-titanium nitride alloy
[AD-D016582] p 1252 N95-20201
Characterization and electrical properties of copper films grown via direct liquid coinjection of (hfac)Cu(TMVS) and TMVS
[DE95-002957] p 1272 N95-20889
New thermodynamic description of the Cu-Zr system
[PB95-127189] p 1263 N95-22374

COPPER COMPOUNDS
Studies of the microwave resistivity of kappa-(BEDT-TTF)2Cu(N(CN)2)Cl
[DE95-002980] p 1262 N95-22291

COPPER FLUORIDES
New ET-based organic superconductors with the organometallic anion Cu(CF3)4(-)
[DE94-016904] p 1567 N95-20479

COPPER ISOTOPES
Helium production by 10 MeV neutrons in iron, nickel and copper
[DE94-014798] p 1529 N95-22280

COPPER OXIDES
Carrier doping and interlayer coupling in HTSC single crystals
[DE94-018637] p 1564 N95-20127
Neutron diffraction study of the magnetic ordering of BaCuO(2+x)
[DE95-001357] p 1572 N95-21297
Effects of neutron irradiation on the London penetration depth for polycrystalline Bi(1.8)Pb(0.3)Sr2Ca2Cu3O10 superconductor
[DE94-019335] p 1573 N95-21483
High temperature superconducting films and multilayers for electronics
[AD-A279545] p 1331 N95-21693
High performance YBCO films
[AD-A279560] p 1276 N95-21695
Magnetic interactions in the Emery model
[DE94-629059] p 1577 N95-22181
Local texture and strongly linked conduction in spray-pyrolyzed TlBa2Ca2Cu3O(8+x) deposits
[DE94-017887] p 1578 N95-22269

COPPER SELENIDES
Polycrystalline CuInSe2 and CdTe solar cells
[DE94-011875] p 1392 N95-20333
Novel thin-film CuInSe2 fabrication
[DE94-011874] p 1268 N95-20472
Processing and modeling issues for thin-film solar cell devices
[DE94-011895] p 1394 N95-21294
Non-H2Se, ultra-thin CuInSe2 devices
[DE94-011894] p 1395 N95-21844

CORE SAMPLING
Descriptions of WHOI sediment cores, volume 8
[AD-A279444] p 1436 N95-22073

CORN
A low energy continuous reactor separator for the production of ethanol from corn grits/starch and biomass streams
[DE95-002256] p 1283 N95-21356

CORNER FLOW
Effects of turbulence compressibility and unsteadiness in compression corner flow p 1344 N95-21052

CORONAL LOOPS
Coronal Mass Ejections in the solar wind at high solar latitudes: An overview
[DE95-000844] p 1603 N95-21377

CORONARY ARTERY DISEASE
The influence of coronary artery disease on +Gz tolerance: A preliminary study
[AD-A279305] p 1446 N95-21941

CORONAS
Solar wind composition
[NASA-TM-197364] p 1604 N95-22384

CORRELATION
Correlations between surface structure and catalytic activity/selectivity
[DE94-019023] p 1234 N95-20052
Long sequence correlation coprocessor
[AD-D016558] p 1313 N95-20280
Charmonium production, b quark and B meson production and b(bar b) correlations at CDF
[DE95-002525] p 1515 N95-20898
Analysis of subgrid models using direct and large-eddy simulations of isotropic turbulence p 1348 N95-21071
Luminosity polarization correlation in the SLC
[DE95-002889] p 1536 N95-21335
Correlations for the OH A(sup 2)(Sigma)(sup +)(v(prime)=0) electronic quenching cross-section
[DE95-002591] p 1244 N95-21524
The method of evaluating quantum partition function for the Hubbard model
[DE94-628991] p 1581 N95-21639
Science with High Spatial Resolution Far-Infrared Data
[NASA-CR-197353] p 1595 N95-21749
Two-dimensional maps of the infrared-to-radio ratio in spiral galaxies p 1593 N95-21765
Primitive Xe in the atmospheres of Earth and mars
p 1419 N95-21795

N=1 Superconformal minimal model correlation functions on the torus
[PB95-134615] p 1500 N95-21964
A new FHNC scheme for Gutzwiller correlated wave functions
[DE94-629037] p 1581 N95-21993
Single particle measurements and two particle interferometry results from CERN experiment NA44
[DE95-003041] p 1527 N95-22078
Microscopic theory of normal liquid He-3
[DE94-629047] p 1527 N95-22179

CORRELATORS
Optical pattern recognition
[AD-A285384] p 1480 N95-20607

CORRIDORS
Long Time Series Measurements in the Coastal Ocean: A workshop
[AD-A279509] p 1435 N95-21682

CORROSION
Chemical and electrochemical interactions on corroding metal surfaces
[DE95-000624] p 1250 N95-19979
FTIR spectroscopy for the determination of water in corrosive gases
[DE94-014658] p 1235 N95-20139
Corrosion of aircraft materials: Correlation between nanometer scale and macroscopic structural damage parameters
[AD-A285930] p 1252 N95-20299
Electrochemical impedance pattern recognition for detection of hidden chemical corrosion on aircraft components
[AD-A284998] p 1253 N95-20481
Electrochemical impedance pattern recognition for detection of hidden chemical corrosion on aircraft components
[AD-A285998] p 1239 N95-20716
VOC compliant wash primer
[AD-A286034] p 1273 N95-21000
Corrosion evaluation of fuel canister crusher rigging
[DE95-002962] p 1257 N95-21452
Aircraft corrosion study
[AD-A279527] p 1259 N95-21687
High temperature corrosion and crack growth of SiC/SiC at variable oxygen partial pressures
[DE94-018715] p 1232 N95-22115
Surface technology programme
[PB95-132866] p 1262 N95-22174
An update of corrosion inhibitors for mild steel exposed to 32-0-0 UAN solution
[DE95-001715] p 1263 N95-22396

CORROSION PREVENTION
Chemical and electrochemical interactions on corroding metal surfaces
[DE95-000624] p 1250 N95-19979
The Materials Corrosion and Environmental Effects Laboratory (MCEL)
[DE94-018268] p 1254 N95-20816
Epoxy lining for shipboard piping systems
[AD-A286228] p 1279 N95-22022
Demonstration of multifunctional DNBM corrosion inhibitors in protective coatings for Naval air/weapon systems
[AD-A285869] p 1279 N95-22136
An update of corrosion inhibitors for mild steel exposed to 32-0-0 UAN solution
[DE95-001715] p 1263 N95-22396

CORROSION RESISTANCE
Chemical and electrochemical interactions on corroding metal surfaces
[DE95-000624] p 1250 N95-19979
Hydrogen resistant alloy - NASA 23
[NASA-CASE-MFS-26200-1-SB] p 1251 N95-20068
Enhancement of corrosion resistance and mechanical properties of light-weight metals through the use of graded nonequilibrium microstructures
[AD-A286320] p 1251 N95-20178
Plasma arc melting of titanium-tantalum alloys
[DE94-016291] p 1252 N95-20331
Processing and applications of iron aluminides
[DE94-017855] p 1253 N95-20673
Feasibility study of power generation system with shape memory alloys
[DE95-714802] p 1254 N95-20890
Electrochemical impedance spectroscopy of trivalent chromium pre-treated aluminum alloy
[AD-A280093] p 1240 N95-20970
Nitrogen alloyed martensitic steels
[PB95-127791] p 1255 N95-21128
Polyurethane self-priming topcoats
[AD-D016204] p 1274 N95-21154
Polyurethane self-priming topcoats
[AD-D016205] p 1274 N95-21155
Joining dissimilar stainless steels for pressure vessel components
[PB95-133005] p 1380 N95-21446
Weldability of iron aluminides
[DE94-019114] p 1257 N95-21555
Corrosion resistance and behavior of construction materials exposed to dilute sulfuric acid at elevated temperatures under static conditions
[DE95-001723] p 1259 N95-21739
Corrosion resistance and behavioral characteristics of metals exposed to 70 percent by weight sulfuric acid at elevated temperatures
[DE95-001724] p 1259 N95-21740
Plasma arc melting of a 80 weight percent tantalum -20 weight percent titanium alloy
[DE95-000846] p 1260 N95-22006

CORROSION TESTS
An overview of the Evaluation of Oxygen Interactions with Materials 3 Experiment: Space Shuttle Mission 46; July-August, 1992
[NASA-TM-110129] p 1412 N95-20278
Corrosion resistance and behavior of construction materials exposed to dilute sulfuric acid at elevated temperatures under static conditions
[DE95-001723] p 1259 N95-21739
Corrosion resistance and behavioral characteristics of metals exposed to 70 percent by weight sulfuric acid at elevated temperatures
[DE95-001724] p 1259 N95-21740
Protective organic coatings on steel: Accelerated corrosion test method for paint/coatings exposed to water with low conductivity. Nordtest project no. 1010-92. Degradation of organic coatings in fresh water
[PB95-134185] p 1277 N95-21873
Corrosion behavior of landing gear steels
[AD-A285862] p 1261 N95-22132

COSMIC DUST
Azimuthally averaged radial S(sub 100 microns)/S(sub 60 microns) dust color temperatures in spiral galaxies
p 1593 N95-21760
Far-Infrared sources and diffuse emission in M31
p 1593 N95-21761
Far-infrared mapping of dusty elliptical galaxies
p 1593 N95-21763
A HIRES analysis of the FIR emission of supernova remnants p 1594 N95-21770

COSMIC PLASMA
The atmospheric neutrino anomaly in Soudan 2
[DE94-019288] p 1604 N95-21475

COSMIC RAY SHOWERS
Search for Centauro events in the DO Detector at Fermilab collider
[DE95-002522] p 1535 N95-21314

COSMIC RAYS
Solar-Geophysical Data number 600, August 1994. Part 2: (Comprehensive reports). Data for February 1994 and miscellaneous
[PB95-105060] p 1603 N95-20722
Search for Centauro events in the DO Detector at Fermilab collider
[DE95-002522] p 1535 N95-21314

COSMIC X RAYS
Solar-Geophysical Data number 600, August 1994. Part 1: (Prompt reports). Data for July, June 1994, and late data
[PB95-104923] p 1603 N95-20713

COSMOLOGY
Connection with dynamics: General introduction
[NASA-CR-197617] p 1579 N95-19947
Predictions from quantum cosmology
[PB95-111126] p 1599 N95-20173
Von Neumann algebra automorphisms and time-thermodynamics relation in general covariant quantum theories
[PB95-111084] p 1580 N95-20324
Cosmological string solutions by dimensional reduction
[DE95-002858] p 1599 N95-21245
The ORNL Neutron-Capture Cross Section Facility
[DE94-019146] p 1537 N95-21460
Surface exposure geochronology using cosmogenic nuclides: Applications in Antarctic glacial geology
[AD-A279392] p 1426 N95-21944

COST ANALYSIS
Progress in the development of recycling processes for electric vehicle batteries
[DE94-015894] p 1324 N95-20626
The personal aircraft: Status and issues
[NASA-TM-109174] p 1200 N95-20688
Readings in program control
[NASA-SP-6103] p 1583 N95-20739
Cost estimating methods for advanced space systems
p 1583 N95-20741
An analysis of cost overruns on defense acquisition contracts p 1584 N95-20749
The impact of partnering on construction contracts
[AD-A286588] p 1585 N95-20855
Performance and cost analysis of monolithic solid oxide fuel cells
[DE95-002511] p 1394 N95-20896
Technical and economic evaluation of natural gas based synthesis gas production technologies
[PB95-130597] p 1242 N95-21426
Power systems for future missions
[NASA-CR-195320] p 1222 N95-21531
Benefits of CMM-based software process improvement: Executive summary of initial results
[AD-A286444] p 1468 N95-21567
Cost-effective ceramics program in the United States
[DE95-001425] p 1278 N95-21909
Analysis of cost: Combustion flame CVD diamond deposition
[AD-A279153] p 1278 N95-21973
Technical cost modeling applied to CVD diamond deposition
[AD-A286119] p 1578 N95-22231

COST EFFECTIVENESS
Naval aviation: F-14 upgrades are not adequately justified. Report to Congressional Committees
[AD-A286338] p 1206 N95-20212
Performance specifications for technology development: Application for characterization of volatile organic compounds in the environment
[DE94-016627] p 1401 N95-20234
Assuring Known Good Die (KGD) for reliable, cost effective MCMs p 1210 N95-20644
Improving cost efficiency in large programs
p 1584 N95-20743
A strategy of cost control for Mariner Venus/Mercury 1973 p 1585 N95-20751
Highlights of recent balance of system research and evaluation
[DE95-001626] p 1393 N95-20863
Cost-effective ceramics program in the United States
[DE95-001425] p 1278 N95-21909
Economic feasibility analysis of distributed electric power generation based upon the natural gas-fired fuel cell
[DE94-012277] p 1396 N95-22033

COST ESTIMATES
Cost estimating methods for advanced space systems
p 1583 N95-20741
Estimating the costs of human space exploration
p 1584 N95-20744

COST REDUCTION
Multiply manifolded molten carbonate fuel cells
[DE94-017074] p 1392 N95-20480
Environmental cleanup technology transfer initiatives
[AD-A285059] p 1403 N95-20487
Reliability assessment of Multichip Module technologies via the Triservice/NASA RELTECH program
p 1210 N95-20643
NASA's attack on costs p 1585 N95-20755
Recent reflux receiver developments under the US DOE program
[DE95-001622] p 1393 N95-20861
The opportunities for and challenges of common integrated electronics
[AD-A279991] p 1327 N95-20966
Research on the promotion measures to introduce new energy and energy-saving technologies with a leasing system
[DE95-714801] p 1375 N95-22079

COSTS
Proceedings of the 13th Space Photovoltaic Research and Technology Conference (SPRAT 13)
[NASA-CP-3278] p 1316 N95-20502
The demise of plastic encapsulated microcircuit myths
p 1209 N95-20640
MCMs for avionics: Technology selection and intermodule interconnection p 1210 N95-20641
Advanced Standard Electronic Modules format-E (SEM-E) processes for rapid prototyping
p 1210 N95-20642
But what will it Cost? The history of NASA cost estimating p 1583 N95-20742
Improving cost efficiency in large programs
p 1584 N95-20743
The advantages of cost plus award fee contracts
p 1584 N95-20745
A Cost and Performance System (CAPS) in a Federal agency p 1584 N95-20746
Development of concentrator solar cells
[DE95-002316] p 1394 N95-20871
Minimax optimal stop rule in reliability checking
[PB95-134557] p 1383 N95-21961

COULOMB POTENTIAL
Structure of ionic interfaces from an absolutely convergent solution of the Madelung problem
[DE94-019268] p 1573 N95-21474

COUNTERMEASURES
Directive optimization of coherent sidelobe canceller systems
[AD-D016513] p 1307 N95-21908

COUNTERS
Uninterrupted, enhanced-rate event sequencer with mixed-speed counter modules
[AD-D016255] p 1334 N95-22030
COUNTING
FTIR spectroscopy for the determination of water in corrosive gases
[DE94-014658] p 1235 N95-20139
Counting methods for the analysis of load time histories
[PB95-132916] p 1388 N95-22093
COUNTING CIRCUITS
Uninterrupted, enhanced-rate event sequencer with mixed-speed counter modules
[AD-D016255] p 1334 N95-22030
Radiation tests on service electronics for future multi TeV detectors
[DE94-632822] p 1335 N95-22184
COUPLED MODES
Coupled tearing modes in plasmas with differential rotation
[DE94-631422] p 1548 N95-19977
Competition between electromagnetic modes in a free-electron maser
[AD-A279546] p 1374 N95-21694
Theory of spin dynamics in the classical two-dimensional heisenberg magnet
[PB95-133559] p 1502 N95-22138
Bunched beam instability with frequency spread
[DE94-018632] p 1539 N95-22357
COUPLING
A model for electron nuclear dynamics of a monatomic chain
[AD-A279652] p 1506 N95-19960
Active neutron multiplicity analysis and Monte Carlo calculations
[DE94-016178] p 1516 N95-21114
COUPLING CIRCUITS
Derivation of coupling impedance from the wake potential of a finite bunch
[DE95-002529] p 1532 N95-20421
Pre-amplifier with multi-stage feedback
[AD-D016254] p 1336 N95-22418
COUPLINGS
Unbinned maximum likelihood fit for the CP conserving couplings for W + photon production at CDF
[DE95-001471] p 1514 N95-20852
Anomalous vector-boson couplings in Majorana neutrino models
[PB95-127460] p 1518 N95-21220
COVARIANCE
Current status of fusion-relevant covariance data
[DE95-000865] p 1561 N95-22010
CRACK CLOSURE
Crack closure and sequential effects in fatigue: A literature survey
[PB95-131637] p 1387 N95-21557
Influence of fatigue crack closure on the growth rate of surface flaws
[AD-A279130] p 1387 N95-21967
CRACK INITIATION
The processing and mechanical properties of high temperature/high performance composites. Mechanism-based constitutive laws and design, book 1
[AD-A279736] p 1228 N95-20801
CRACK OPENING DISPLACEMENT
Finite element modelling of creep crack growth in 316 stainless and 9Cr-1Mo steels
[DE94-018977] p 1258 N95-21560
CRACK PROPAGATION
Analyses of some benchmark cases in fracture mechanics using boundary element method
[PB95-110888] p 1384 N95-19930
Properties of whisker-reinforced ceramics
[DE94-017759] p 1264 N95-20024
The processing and mechanical properties of high temperature/high performance composites. Fatigue and creep, book 3
[AD-A279738] p 1227 N95-20430
Flux-focusing eddy current probe and rotating probe method for flaw detection
[NASA-CASE-LAR-15231-1-SB] p 1383 N95-20764
Experimental investigation of wave and fracture phenomena in impacted ceramics
[AD-A286589] p 1272 N95-20856
Micromechanical approach to transformation toughening in ceramics
[PB95-135422] p 1273 N95-20976
Crack closure and sequential effects in fatigue: A literature survey
[PB95-131637] p 1387 N95-21557
Finite element modelling of creep crack growth in 316 stainless and 9Cr-1Mo steels
[DE94-018977] p 1258 N95-21560
The mechanical behavior of surface-modified ceramics
[DE95-001704] p 1276 N95-21572
The role of microcracking on the crack growth resistance of brittle solids and composites
[DE95-001678] p 1231 N95-21736
Influence of fatigue crack closure on the growth rate of surface flaws
[AD-A279130] p 1387 N95-21967
High temperature corrosion and crack growth of SiC/SiC at variable oxygen partial pressures
[DE94-018715] p 1232 N95-22115
Welding tritium exposed stainless steel
[DE95-003208] p 1382 N95-22356
Fracture behavior of laminated discontinuously reinforced aluminum material
[DE94-017307] p 1263 N95-22408
CRACKING (FRACTURING)
Analysis of the progressive failure of brittle matrix composites
[NASA-CR-195415] p 1225 N95-19951
The processing and mechanical properties of high temperature/high performance composites. Stress redistribution and notch properties, book 2
[AD-A279737] p 1227 N95-20429
The processing and mechanical properties of high temperature/high performance composites. Fatigue and creep, book 3
[AD-A279738] p 1227 N95-20430
Fracture analysis of an all-ceramic bearing system
[AD-A285056] p 1269 N95-20486
Virtual reality in precision engineering research
[AD-A286528] p 1465 N95-21012
Finite element modelling of creep crack growth in 316 stainless and 9Cr-1Mo steels
[DE94-018977] p 1258 N95-21560
Aluminium oxide targets after ballistic impact; fragmentation of the ceramic and the projectile
[PB95-133625] p 1388 N95-22097
Welding tritium exposed stainless steel
[DE95-003208] p 1382 N95-22356
CRACKS
Analyses of some benchmark cases in fracture mechanics using boundary element method
[PB95-110888] p 1384 N95-19930
Analysis of the progressive failure of brittle matrix composites
[NASA-CR-195415] p 1225 N95-19951
An overview of the HSST Full-Thickness Shallow-Crack Clad Beam Testing Program
[DE94-018940] p 1385 N95-20322
Microstructural contributions to the fracture resistance of silicon nitride ceramics
[DE94-018955] p 1267 N95-20323
Eddy current for detecting second-layer cracks under installed fasteners
[AD-A279871] p 1382 N95-20414
Damage tolerance of carbon fibre polyetheretherketone laminates
[PB95-131611] p 1230 N95-21432
Crack closure and sequential effects in fatigue: A literature survey
[PB95-131637] p 1387 N95-21557
A study of mechanical processing damage in brittle materials
[DE95-002126] p 1276 N95-21585
Influence of fatigue crack closure on the growth rate of surface flaws
[AD-A279130] p 1387 N95-21967
Damage tolerant repair techniques for pressurized aircraft fuselages
[AD-A286298] p 1199 N95-22046
CRASH LANDING
Commuter/air taxi ditchings and water-related impacts that occurred from 1979 to 1989
[AD-A285691] p 1202 N95-20275
CRASHES
Commuter airplane accident data analysis
[AD-A286315] p 1202 N95-20174
CRASHWORTHINESS
Commuter airplane accident data analysis
[AD-A286315] p 1202 N95-20174
Commuter/air taxi ditchings and water-related impacts that occurred from 1979 to 1989
[AD-A285691] p 1202 N95-20275
Helicopter crewseat cushion program
[AD-A286654] p 1452 N95-20973
CRATERS
Polar volatiles on Mercury and the Moon
p 1422 N95-21811
CRATONS
Volatiles in the Earth: All shallow and all recycled
p 1416 N95-21779
CRAY COMPUTERS
Implementation and performance of a three-dimensional numerical transport model
[PB95-135745] p 1402 N95-20440
Direct simulation and graphics post-processing of three-dimensional turbulent flows p 1352 N95-21098
Status of CFDLIB performance tests on the T3D
[DE95-002708] p 1478 N95-21925
CREATIVITY
Planning and scheduling for success
p 1584 N95-20747
CREEP ANALYSIS
Creep behavior in SiC whisker-reinforced alumina composite
[DE95-001071] p 1231 N95-21776
CREEP PROPERTIES
Enhancement of creep resistance of a sintered S3N4 ceramic by microwave annealing
[DE94-017698] p 1265 N95-20220
The processing and mechanical properties of high temperature/high performance composites. Stress redistribution and notch properties, book 2
[AD-A279737] p 1227 N95-20429
The processing and mechanical properties of high temperature/high performance composites. Fatigue and creep, book 3
[AD-A279738] p 1227 N95-20430
The reliability of laser reflowed Sn-Ag solder joints
[AD-A279787] p 1315 N95-20443
The processing and mechanical properties of high temperature/high performance composites. Processing/property correlations, book 4
[AD-A279739] p 1228 N95-20802
Finite element modelling of creep crack growth in 316 stainless and 9Cr-1Mo steels
[DE94-018977] p 1258 N95-21560
Mantle devolatilization and rheology in the framework of planetary evolution p 1418 N95-21788
The role of grain boundary sliding on creep deformation characteristics of discontinuous reinforced composites
[DE95-001671] p 1231 N95-21924
The processing and mechanical properties of high temperature/high performance composites. Book 6: Delamination and compressive behavior
[AD-A279780] p 1231 N95-21999
Irradiation creep in structural materials at ITER operating conditions
[DE94-018946] p 1261 N95-22123
Flux creep with logarithmic U(j) dependence
[DE94-629058] p 1577 N95-22180
CREEP RUPTURE STRENGTH
Effect of heat treatment temperature on creep-rupture properties of Fe3Al-based alloys
[DE94-017904] p 1253 N95-20375
Atom probe field ion microscopy of type 308 CRE stainless steel welds
[DE94-019162] p 1261 N95-22127
CREEP STRENGTH
Enhancement of creep resistance of a sintered S3N4 ceramic by microwave annealing
[DE94-017698] p 1265 N95-20220
Creep behavior in SiC whisker-reinforced alumina composite
[DE95-001071] p 1231 N95-21776
CREEP TESTS
Enhancement of creep resistance of a sintered S3N4 ceramic by microwave annealing
[DE94-017698] p 1265 N95-20220
CREW WORKSTATIONS
The advanced technology crew station: Development and validation of a workload assessment technique for cockpit function allocation
[AD-A279544] p 1453 N95-21691
Systems engineering design and technical analyses for Strategic Avionics Crew-station Design Evaluation Facility (SACDEF)
[AD-A286239] p 1213 N95-22024
CREWS
Navigation system in combat vehicle
[PB95-131629] p 1452 N95-21467
CRITERIA
Magnetoelectric properties of reciprocal bianisotropic materials with focus on the polarizability of chiro-omega spheres
[PB95-127650] p 1544 N95-21103
CRITICAL FLOW
New theory of critical flow velocities in superfluid helium
[PB95-130365] p 1571 N95-21228
Critical dynamics and plastic flow in disordered Josephson junction arrays
[DE94-629074] p 1576 N95-21995
CRITICAL PATH METHOD
Scheduling: A guide for program managers
p 1584 N95-20748
CRITICAL POINT
Dependence of critical current density on microstructure and processing of high-T(c) superconductors
[DE95-000685] p 1571 N95-21167

Effects of neutron irradiation on the London penetration depth for polycrystalline Bi(1.8)Pb(0.3)Sr2Ca2Cu3O10 superconductor
|DE94-019335| p 1573 N95-21483
An exact enumeration of self-avoiding loops on a square lattice
|DE94-628999| p 1578 N95-22276

CRITICAL VELOCITY
New theory of critical flow velocities in superfluid helium
|PB95-130365| p 1571 N95-21228

CROSS CORRELATION
Nonparametric estimation of the cyclic cross-spectrum
|AD-A285756| p 1498 N95-21219

CROSS FLOW
Liquid-metal pin-fin pressure drop by correlation in cross flow
|DE94-017086| p 1338 N95-19923
Numerical study of realistic perturbations in three-dimensional boundary layers p 1351 N95-21091
Computational studies of laminar to turbulence transition
|AD-A285622| p 1353 N95-21146

CROSS POLARIZATION
Large bistatic angle clutter depolarization study
p 1296 N95-20941

CROSS SECTIONS
Evidence for t(bar t) production at the Tevatron: Statistical significance and cross section
|DE95-002524| p 1515 N95-20897
Signals for top quark anomalous chromomagnetic moments at colliders
|DE95-002896| p 1535 N95-21254
Measurement of W and Z production cross-sections in p(bar p) collisions at (radical)s = 1.8 TeV
|DE95-002250| p 1523 N95-21521
Structure functions and structure function ratio F2(n)/F2(p) at low X(Bj) and Q2 in inelastic muon scattering
|DE94-018979| p 1573 N95-21561
Measurement of the B meson differential cross-sections in p(bar p) collisions at (radical)s = 1.8 TeV using the exclusive decays B(sup (+-)) (yields) J/(psi)K(sup (+-)) and B(sup 0) (yields) J/(psi)K*(sup 0)
|DE94-018993| p 1523 N95-21562
Measurement of the B cross section at CDF via B semileptonic decays
|DE95-002217| p 1524 N95-21597
Structure functions and structure function ratio F(sup n)2/F(sup p)2 at small x(sub Bj) and Q2 in muon-nucleon scattering
|DE94-017981| p 1530 N95-22340

CROSSINGS
Higher order crossings
|AD-A279597| p 1504 N95-20300
Accuracy problems in the generation of discrete time stochastic processes
|PB95-131397| p 1386 N95-21133

CROSSLINKING
The synthesis and characterization of small molecule and photo-cross-linkable high polymeric phosphazenes bearing cinnamate groups
|AD-A279782| p 1268 N95-20442
Cross-linking reactions for the conversion of polyphosphazenes into useful materials
|AD-A279696| p 1271 N95-20709
Control of continuous phase PH using visible light to activate PH-dependent fibers and gels in a controlled and reversible manner
|AD-D016532| p 1543 N95-20728

CRUDE OIL
Responsive copolymers for enhanced petroleum recovery
|DE94-018822| p 1267 N95-20350

CRUSHERS
Corrosion evaluation of fuel canister crusher rigging
|DE95-002962| p 1257 N95-21452

CRUSHING
Test fixture for determination of energy absorbing capabilities of composite materials
|NASA-CASE-LAR-15212-1-CU| p 1229 N95-21008

CRUSTS
Spatial variation of primordial 3-He in crustal fluids along the East-African Rift system (the Ethiopian and the Kenya Rift section) p 1418 N95-21789
Atmospheres of the Moon and Mercury
p 1419 N95-21794
Alkali element depletion by core formation and vaporization on the early Earth p 1421 N95-21804
The ratios of carbon and non-radiogenic helium and argon isotopes in the mantle and crustal rocks
p 1421 N95-21805
Subduction of hydrated basalt of the oceanic crust: Implications for recycling of water into the upper mantle and continental growth p 1423 N95-21814

CRYOGENIC COOLING
Space power facility readiness for Space Station power system testing
|NASA-TM-106829| p 1218 N95-21384
Thermal and deformation analyses of a novel cryogenically cooled monochromator for an Advanced Photon Source beamline
|DE94-016914| p 1527 N95-22190

CRYOGENIC FLUIDS
Cryogenic targets for inertial confinement fusion
|DE94-016200| p 1555 N95-21115

CRYOGENIC STORAGE
Space power facility readiness for Space Station power system testing
|NASA-TM-106829| p 1218 N95-21384

CRYOGENIC TEMPERATURE
On-wafer, cryogenic characterization of ultra-low noise HEMT devices p 1305 N95-21539

CRYOGENICS
Cryogenic targets for inertial confinement fusion
|DE94-016200| p 1555 N95-21115
Cryogenic pellet laser plasma source targets
|DE95-002488| p 1376 N95-22169

CRYOPUMPING
Helium exhaust studies in the D3-D tokamak
|DE94-016682| p 1552 N95-20334

CRYPTOGRAPHY
Semaphore network encryption report
|AD-A279294| p 1303 N95-21493

CRYSTAL DEFECTS
Strain fields in crystalline materials: Methods of analysis based on x-ray diffraction-line broadening
|PB95-108064| p 1574 N95-21670
Reciprocal space mapping of epitaxial materials using position-sensitive x-ray detection
|DE95-001620| p 1575 N95-21991

CRYSTAL DISLOCATIONS
Post-irradiation deformation characteristics of heavy-ion irradiated 304L SS
|DE94-017462| p 1251 N95-20088

CRYSTAL FIELD THEORY
Lattice results for heavy light matrix elements
|DE94-019101| p 1523 N95-21551

CRYSTAL GROWTH
Radiation effects on p+n InP junctions grown by MOCVD p 1319 N95-20520
Design of high-efficiency, radiation-hard, GaInP/GaAs solar cells p 1319 N95-20521
High contrast organic crystal optical modulator for phased array antenna and optical signal processing
|AD-A286557| p 1544 N95-20844
Characterization and electrical properties of copper films grown via direct liquid coinjection of (hfac)Cu(TMVS) and TMVS
|DE95-002957| p 1272 N95-20889
Dependence of critical current density on microstructure and processing of high-T(c) superconductors
|DE95-000685| p 1571 N95-21167
X-ray studies of microstructures in semiconductor and superconducting materials
|DE95-001802| p 1572 N95-21279
Raman spectra of MOCVD-grown ferroelectric PbTiO3 thin films
|DE94-018964| p 1244 N95-21549
Directional solidification of the alumina-zirconia ceramic eutectic system
|DE95-001677| p 1277 N95-21735
Growing and releasing diamonds
|AD-D016489| p 1577 N95-22103
An improved Monte Carlo algorithm for simulating grain growth
|DE94-017903| p 1578 N95-22272

CRYSTAL LATTICES
The dynamics of formation and evaporation of mixed alkali halide nanocrystals: A case of comparable lattice energies
|AD-A285052| p 1567 N95-20483
InGaAs PV device development for TPV power systems p 1322 N95-20537
Crystalline beams: The horizontal zigzag
|DE95-002227| p 1533 N95-20766
Lattice results for heavy light matrix elements
|DE94-019101| p 1523 N95-21551
Second order approximation for optical polaron in the strong coupling case
|DE94-628997| p 1525 N95-21856
The doping effect on spin-Peierls instability
|DE94-629046| p 1577 N95-22178
The Modified Embedded Atom Method
|DE94-017958| p 1248 N95-22273
An exact enumeration of self-avoiding loops on a square lattice
|DE94-628999| p 1578 N95-22276

CRYSTAL OPTICS
High contrast organic crystal optical modulator for phased array antenna and optical signal processing
|AD-A286557| p 1544 N95-20844
Light output and radiation damage in a YAlO3:Ce crystal
|DE94-016815| p 1545 N95-21643
Thermal and deformation analyses of a novel cryogenically cooled monochromator for an Advanced Photon Source beamline
|DE94-016914| p 1527 N95-22190

CRYSTAL OSCILLATORS
Generation of micro-domains in AT-cut quartz by thermal processing and the effect on resonator modes
|DE94-017344| p 1564 N95-20087

CRYSTAL STRUCTURE
Polycrystalline thin film cadmium telluride solar cells fabricated by electrodeposition
|DE94-011848| p 1391 N95-20118
Pairing on small clusters in the Peierls-Hubbard model: Implications for C60
|DE94-016284| p 1565 N95-20330
Changes in the behavior of magnetic materials undergoing processing in electrical rotating machines
|PB95-104493| p 1325 N95-20702
Crystalline beams
|DE95-002656| p 1569 N95-20793
Plastic deformation of ordered intermetallic alloys: Fundamental aspects
|DE95-001070| p 1256 N95-21265
Structure and stability of hydrous minerals at high pressure p 1417 N95-21786
Hydrogen and related materials at high density: Physics, chemistry and planetary implications
p 1418 N95-21791
Volatiles in the deep Earth: An experimental study using the laser-heated diamond cell p 1421 N95-21803
Reciprocal space mapping of epitaxial materials using position-sensitive x-ray detection
|DE95-001620| p 1575 N95-21991
Electrostatic basis for molecular recognition in photosynthesis
|DE95-002979| p 1440 N95-22075
Gravitational effects on the development of weld-pool and solidification microstructures
|DE94-017772| p 1285 N95-22261
Biaxiality of chiral liquid crystals
|DE94-629032| p 1578 N95-22277
Parallel nanometer scale fabrication
|DE95-002122| p 1336 N95-22284
Characterization of a texture gradient in tantalum plate
|DE95-002704| p 1262 N95-22289
Effect of annealing temperature on the texture of rolled tantalum and tantalum-10 wt % tungsten
|DE95-002702| p 1262 N95-22308
Introduction to the structures determination methods using X-ray diffraction in monocrystals: Application to some lanthanides and transition metals complexes with organic ligands
|DE94-629002| p 1579 N95-22380

CRYSTALLINITY
Matrix formulation of the particle motion in crystalline beams
|DE94-017301| p 1563 N95-19925
Crystalline beam in a storage ring: How long can it last?
|DE94-017303| p 1563 N95-20014
Orientation studies of polyolefins by IR-dichroism
|PB95-104386| p 1236 N95-20256
Morphology of highly textured E/EP diblock copolymers
|AD-A279813| p 1269 N95-20582
Aerosol-assisted chemical vapor deposition of copper: A liquid delivery approach to metal thin films
|AD-A279702| p 1270 N95-20689
Macromolecular and materials design using polyphosphazenes
|AD-A279781| p 1273 N95-20978
Raman spectra of MOCVD-grown ferroelectric PbTiO3 thin films
|DE94-018964| p 1244 N95-21549
Novel materials and devices from self-assembled periodic structures
|AD-A286499| p 1232 N95-22211

CRYSTALLITES
Strain fields in crystalline materials: Methods of analysis based on x-ray diffraction-line broadening
|PB95-108064| p 1574 N95-21670

CRYSTALLIZATION
Gas-phase generation of zinc sulfide particles using a single-source precursor
|AD-A279700| p 1239 N95-20712
Confinement and stability of crystalline beams in storage rings
|DE95-002515| p 1533 N95-20886

CRYSTALLOGRAPHY
Mean field analysis of orientation selective grain growth driven by interface-energy anisotropy
[DE94-015797] p 1566 N95-20399
New ET-based organic superconductors with the organometallic anion Cu(CF3)4(-)
[DE94-016904] p 1567 N95-20479
Synthesis and characterization of (Zn(SEt)Et)10, formed via insertion of sulfur into Zn-C bonds: A new class of Wurtzite-like cluster framework
[AD-A279701] p 1569 N95-20714
A crystallographic model for hydrous wadsleyite (Beta-Mg2SiO4) p 1424 N95-21817
Theses of the Proceedings of the 23d International Meeting on the Physics of Charged Particle Interaction with Crystals
[DE94-631501] p 1529 N95-22281
Synthesis and characterization of single-source molecular precursors to binary metal sulphides: Bis(diethyldithiocarbamato) M(2)trialkylphosphine (M = Zn and Cd) adducts
[AD-A279746] p 1248 N95-22385

CRYSTALS
Light output and radiation damage in a lead tungstate crystal
[DE94-016814] p 1565 N95-20265
Changes in the behavior of magnetic materials undergoing processing in electrical rotating machines
[PB95-104493] p 1325 N95-20702
Synthesis and characterization of (Zn(SEt)Et)10, formed via insertion of sulfur into Zn-C bonds: A new class of Wurtzite-like cluster framework
[AD-A279701] p 1569 N95-20714
Resonant photon-graviton conversion in EM fields: From earth to heaven
[DE95-002784] p 1301 N95-21241
Strain measurement by diffraction at LANSCE
[DE94-018264] p 1387 N95-21386
Application of new synchrotron powder diffraction techniques to anomalous scattering from glasses
[DE94-019285] p 1536 N95-21407
Diffraction applications using the energy dispersive beamline, X6A, at NSLS
[DE94-019287] p 1572 N95-21408
A crystallographic model for hydrous wadsleyite (Beta-Mg2SiO4) p 1424 N95-21817
Electrostatic basis for molecular recognition in photosynthesis
[DE95-002979] p 1440 N95-22075
Magnetic interactions in the Emery model
[DE94-629059] p 1577 N95-22181
Parallel nanometer scale fabrication
[DE95-002122] p 1336 N95-22284

CUBES (MATHEMATICS)
Almost kappa-wise independent random permutation of the cube
[PB95-108098] p 1495 N95-22147

CULTURE TECHNIQUES
Microbial degradation of polymers used in electronics
[AD-A286526] p 1273 N95-21011

CUMULONIMBUS CLOUDS
The initiation of lightning and the growth of electric fields in thunderstorms
[AD-A280033] p 1428 N95-20008

CUMULUS CLOUDS
Boundary layer cloud studies in support of ASTEX
[AD-A285947] p 1429 N95-20395

CURRENT DENSITY
Transport and dynamics in toroidal fusion systems
[DE94-018653] p 1548 N95-20029
A method for measuring the inductive electric field profile and noninductive current profiles on D3-D
[DE94-016683] p 1551 N95-20279
Recent results from Fast Wave Current Drive experiments on DIII-D
[DE94-016718] p 1551 N95-20285
Impedance characteristics of multistage ion diodes
[DE94-018887] p 1565 N95-20340
Electron-irradiated two-terminal, monolithic InP/Ga0.47In0.53As tandem solar cells and annealing of radiation damage p 1319 N95-20519
Field-emitter arrays for RF vacuum microelectronics
[AD-A279959] p 1325 N95-20661
Dependence of critical current density on microstructure and processing of high-T(c) superconductors
[DE95-000685] p 1571 N95-21167
Effects of neutron irradiation on the London penetration depth for polycrystalline Bi(1.8)Pb(0.3)Sr2Ca2Cu3O10 superconductor
[DE94-019335] p 1573 N95-21483
Cell membrane potentials induced during exposure to EMP fields
[DE94-018952] p 1439 N95-21548
Overview of the field and temperature dependence of J(c) in Ag/BSCCO tapes
[PB95-110318] p 1574 N95-21636
RF vacuum microelectronics based on thin film edge-emitter technology
[AD-A279539] p 1331 N95-21690
How to improve J(c(T)) in Ag/(BiPb)2Sr2Ca2Cu3O10 tapes
[PB95-110326] p 1575 N95-21949
Development of practical high temperature superconducting wire for electric power applications
[DE94-017894] p 1336 N95-22271
Effect of cell size on elliptically polarized radar clutter statistics
[AD-A285789] p 1311 N95-22401

CURRENT DISTRIBUTION
Parasitic current collection by solar arrays in LEO
p 1321 N95-20527
Field-emitter arrays for RF vacuum microelectronics
[AD-A279959] p 1325 N95-20661
Fiber-optic control of current filaments in high gain photoconductive semiconductor switches
[DE94-015804] p 1328 N95-21139
Equivalent source current formulation in impedance tomography
[PB95-127627] p 1329 N95-21326
Current distribution in Cable-In-Conduit Conductors
[DE95-001820] p 1332 N95-21725

CURRENTS
High frequency current sensors using the Faraday effect in optical fibers
[DE95-001859] p 1545 N95-21728

CURVATURE
Large-eddy simulation of a boundary layer with concave streamwise curvature p 1360 N95-22450

CURVE FITTING
Uncertainty estimates for derivatives and intercepts
[DE94-018492] p 1489 N95-20222
Fitting stochastic partial differential equations to spatial data
[AD-A279870] p 1490 N95-20432

CUSHIONS
Helicopter crewseat cushion program
[AD-A286654] p 1452 N95-20973

CV-880 AIRCRAFT
Fuselage burnthrough from large exterior fuel fires
[AD-A286295] p 1203 N95-22318

CYANATES
Ferrocyanide safety project Dynamic X-Ray Diffraction studies of sodium nickel ferrocyanide reactions with equimolar nitrate/nitrite salts
[DE94-017396] p 1236 N95-20268
Thermo-mechanical fatigue of polymer matrix composites
[AD-A285931] p 1267 N95-20390

CYANO COMPOUNDS
The organic chemistry of conducting polymers
[DE94-018216] p 1270 N95-20680

CYCLES
High speed optical storage technology
[AD-A285788] p 1456 N95-22400

CYCLIC COMPOUNDS
The synthesis and characterization of small molecule and photo-cross-linkable high polymeric phosphazenes bearing cinnamate groups
[AD-A279782] p 1268 N95-20442
Hydrogenation of nitriles on a well-characterized nickel surface: From surface science studies to liquid phase catalytic activity measurements
[DE94-018184] p 1259 N95-21707

CYCLIC HYDROCARBONS
Direct aromatization of methane
[DE94-017131] p 1233 N95-19924
Use of quantum chemically derived descriptors for QSAR modeling of reductive dehalogenation of aromatic compounds
[PB95-132783] p 1224 N95-22333

CYCLIC LOADS
The processing and mechanical properties of high temperature/high performance composites. Fatigue and creep, book 3
[AD-A279738] p 1227 N95-20430
Structural performance of cylindrical pressure housings of different ceramic compositions under external pressure loading. Part 1: Isostatically pressed alumina ceramic
[AD-A279669] p 1270 N95-20603
Microstructural design for tough ceramics
[AD-A285634] p 1273 N95-21152
Effects of cyclic stress distribution models on fatigue life predictions
[DE95-001619] p 1388 N95-22070

CYCLOTRON RADIATION
Recent results from Fast Wave Current Drive experiments on DIII-D
[DE94-016718] p 1551 N95-20285
MTX final report
[DE95-002960] p 1559 N95-21451

CYCLOTRON RESONANCE
Electrospray ionization Fourier transform ion cyclotron resonance mass spectrometric study of singly and doubly charged organometallic complexes
[AD-A279899] p 1238 N95-20563
Ion heating perpendicular to the magnetic field
[AD-A286635] p 1501 N95-20773
An advanced ECR ion source with a large uniformly distributed ECR plasma volume for multiply charged ion beam generation
[DE95-001078] p 1515 N95-20911
High magnetic field glow discharge ionization source
[AD-A279972] p 1241 N95-21123
1994 Nonneutral Plasma Workshop
[AD-A285656] p 1559 N95-21404
MTX final report
[DE95-002960] p 1559 N95-21451
Plasma-induced-damage of GaAs during etching of refractory metal contacts
[DE95-001525] p 1259 N95-21838
Temperature dependence of magnetopolarons in a parabolic quantum dot in arbitrary magnetic fields
[DE94-629033] p 1526 N95-22216

CYCLOTRON RESONANCE DEVICES
Competition between electromagnetic modes in a free-electron maser
[AD-A279546] p 1374 N95-21694

CYCLOTRONS
Temperature dependence of a magnetopolaron in a harmonic quantum dot in resonant magnetic fields
[DE94-629036] p 1502 N95-22177

CYLINDRICAL BODIES
Multi-layered translated rib-stiffened composite hollow cylinder assembly
[AD-D016566] p 1226 N95-20292
Dynamic measurement of the hoop modulus of a composite cylinder
[DE94-018958] p 1385 N95-20416
Attachment methodology for composite cylinder assembly
[AD-D016578] p 1227 N95-20459
Structural performance of cylindrical pressure housings of different ceramic compositions under external pressure loading. Part 1: Isostatically pressed alumina ceramic
[AD-A279669] p 1270 N95-20603
Broadband pressure barrier for circular waveguide
[AD-D016503] p 1306 N95-21672
Attachment methodology for composite cylinder assembly
[AD-D016256] p 1381 N95-22034
Structural performance of cylindrical pressure housings of different ceramic compositions under external pressure loading. Part 3: Sintered reaction bonded silicon nitride ceramic
[AD-A285773] p 1388 N95-22411

CYLINDRICAL PLASMAS
Coupled tearing modes in plasmas with differential rotation
[DE94-631422] p 1548 N95-19977

CYLINDRICAL SHELLS
Influence of primary boundary conditions on the buckling of shallow cylindrical shells
[PB94-208352] p 1384 N95-20003
A model of an infinite length, axisymmetric, isotropic, forced thick shell
[AD-A285586] p 1386 N95-21212

CYTOCHROMES
Calculation of atom-centered partial charges for heme
[DE94-014447] p 1520 N95-21375
Electrostatic basis for molecular recognition in photosynthesis
[DE95-002979] p 1440 N95-22075
Separation of proteins by convective electrophoresis through a porous membrane
[PB95-127130] p 1248 N95-22373

CYTOMETRY
Life Sciences Division and Center for Human Genome Studies
[DE94-017796] p 1440 N95-22065
Flow cytometry: A powerful technology for measuring biomarkers
[DE94-018284] p 1440 N95-22296

D

DAMAGE
Investigation of laser-induced retinal damage: Wavelength and pulsewidth dependent mechanisms
[AD-A286066] p 1443 N95-20848
A study of mechanical processing damage in brittle materials
[DE95-002126] p 1276 N95-21585
Laser materials processing at Sandia National Laboratories
[DE95-002183] p 1374 N95-21594

Defect geometries and laser-induced damage in multilayer coatings
[DE94-017695] p 1377 N95-22343

DAMAGE ASSESSMENT

Post-flight investigation programmes of recently retrieved solar generators p 1321 N95-20531

Significance of impact velocity for the extent of damage in carbon/epoxy laminates
[PB95-133484] p 1230 N95-21417

Definition report on target and related steering variables of radiation as a part of the environmental balance and environmental outlook investigation
[PB95-135471] p 1409 N95-21846

DAMKOHLER NUMBER

Lewis number and Damkohler number effects in vortex-flame interactions p 1249 N95-22439

DAMPING

Polyurethane-epoxy interpenetrating polymer network acoustic damping material
[AD-D016567] p 1266 N95-20293

Polyurethane-acrylic interpenetrating polymer network acoustic damping material
[AD-D016572] p 1266 N95-20294

Electromagnetic waves in an ultrarelativistically hot and strongly magnetized electron-positron plasma
[DE94-628963] p 1307 N95-21849

Proposed emittance upgrade for the SLC damping rings
[DE95-002887] p 1538 N95-22155

Acoustic and vibration attenuation composite material
[AD-D016585] p 1233 N95-22467

DARKENING

Factors affecting the perception of luning in monocular regions of partial binocular overlap displays
[AD-A286287] p 1547 N95-22044

DATA ACQUISITION

Wavelet-based acoustic recognition of aircraft
[DE94-017701] p 1503 N95-20019

The effects of three-dimensional graphs on decision making
[AD-A285034] p 1583 N95-20051

Target area acquisition and control system survivability for the National Ignition Facility
[DE94-016549] p 1550 N95-20190

Evolution of ground line of sight data field collection techniques
[AD-A285062] p 1204 N95-20497

A portable and independent edge fluctuation diagnostic
[DE94-018254] p 1554 N95-20681

Meso-scale cooling effects of high albedo surfaces: Analysis of meteorological data from White Sands National Monument and White Sands Missile Range
[DE94-018535] p 1429 N95-20782

Software Capability Evaluation (SCE), version 2.0 team members guide
[AD-A286082] p 1462 N95-20809

Airborne Multisensor Pod System (AMPS) data access concept
[DE95-002586] p 1389 N95-20903

Real-time dynamic simulator for the Topaz II reactor power system
[DE95-001604] p 1535 N95-21278

Overview of data fusion work for land electronic warfare
[AD-A279829] p 1301 N95-21292

Monitoring the response of the upper troposphere/lower stratosphere to a greenhouse gas scenario
[DE95-000982] p 1406 N95-21410

The Telecommunications and Data Acquisition Report
[NASA-CR-197390] p 1303 N95-21532

A proposed wind measurement and analysis approach for evaluating a prospective wind plant site
[DE94-019187] p 1395 N95-21611

Materials compatibility and lubricants research on CFC-refrigerant substitutes
[DE94-018414] p 1287 N95-21631

Implementation of electronic chain-of-custody, analysis requests, and data verification at Los Alamos National Laboratory
[DE94-018076] p 1407 N95-21666

CAiSE 1994 Doctoral Consortium
[PB95-135182] p 1469 N95-21711

Variability of total electron content in the high-altitude ionosphere following solar maximum
[AD-A285849] p 1425 N95-21833

Information security for unmanned systems
[AD-A286511] p 1485 N95-22214

DATA BASE MANAGEMENT SYSTEMS

New method for integrity constraint checking in deductive databases
[PB95-110672] p 1586 N95-19904

Calculation methods for criteria air pollutant emission inventories
[AD-A284675] p 1400 N95-19964

Downsizing information systems: Framing the issues for the Office of Naval Intelligence (ONI)
[AD-A279888] p 1588 N95-20589

Determining information management needs for enhanced international safeguards
[DE94-015787] p 1588 N95-20789

Airborne Multisensor Pod System (AMPS) data access concept
[DE95-002586] p 1389 N95-20903

Assessment of database for interaction of tritium with ITER plasma facing materials
[DE95-002038] p 1558 N95-21290

DBASE 4 basics
[DE94-016323] p 1469 N95-21713

Conference proceedings. Defense Modeling and Simulation Office Information/Data Base (I/DB) Task Group Meetings, and notes from the previous two I/DB meetings
[AD-A279097] p 1591 N95-22069

Taking AIM: The management of scientific and technical information at Argonne National Laboratory
[DE94-019279] p 1591 N95-22092

Guidelines for the creation and management of geographic data bases within a GIS environment, version 1.0. Volume 2. Appendices
[DE94-019215] p 1591 N95-22129

Using geographical data browsers in a networked environment
[DE94-017809] p 1592 N95-22263

University library document circulation system specified in LCM
[PB95-127957] p 1592 N95-22331

Experimental evaluation of dynamic data allocation strategies in a distributed database with changing workloads
[NASA-CR-195024] p 1456 N95-22431

DATA BASES

A database for analyzing sequential behavioral data and their associated cognitive models
[AD-A280061] p 1448 N95-19887

New method for integrity constraint checking in deductive databases
[PB95-110672] p 1586 N95-19904

The design and implementation of the functional/daplex data interface for the multimodel and multilingual database system
[AD-A280131] p 1587 N95-20039

Guidelines for the creation and management of geographic data bases within a GIS environment, version 1.0
[DE94-019214] p 1458 N95-20073

The Modified Embedded Atom Method
[DE94-015746] p 1564 N95-20142

Parallel solid mechanics codes at Sandia National Laboratories
[DE94-015770] p 1474 N95-20152

A Hyperspectral Image Data Exploration Workbench for environmental science applications
[DE94-016373] p 1412 N95-20171

Description and flow characterization of hypersonic facilities
[AD-A284291] p 1200 N95-20248

Relational databases for RHIC design and control
[DE94-016785] p 1532 N95-20336

High performance computing for materials process modeling
[DE94-017860] p 1460 N95-20358

Evolution of ground line of sight data field collection techniques
[AD-A285062] p 1204 N95-20497

The mechanical property data base from an Air Force/Industry cooperative test program on advanced aluminum alloys
[AD-A280038] p 1386 N95-20615

Translation of the data flow query language for the multimodel, multibackend database system
[AD-A285978] p 1588 N95-20617

Shaping the library of the future: Digital library developments at Los Alamos National Laboratory's Research Library
[DE95-001008] p 1588 N95-20777

The Energy Science and Technology Database on a local library system: A case study at the Los Alamos National Research Library
[DE95-001009] p 1589 N95-20818

Proceedings of the Cloud Impacts on DOD Operations and Systems 1993 Conference (CIDOS 1993)
[AD-A286658] p 1430 N95-20974

Use of operations research techniques in deductive databases
[PB95-135349] p 1589 N95-21004

GOLD: A Graph Oriented Language for Databases
[PB95-127544] p 1465 N95-21021

Studying Turbulence Using Numerical Simulation Databases. 5: Proceedings of the 1994 Summer Program
[NASA-CR-197362] p 1341 N95-21035

The coupling between flame surface dynamics and species mass conservation in premixed turbulent combustion p 1249 N95-21041

Direct simulation of turbulent flow in a square duct: Reynolds-stress budgets p 1348 N95-21073

FIREDOC users manual, 3rd edition
[PB95-128674] p 1286 N95-21129

Application of neural networks to seismic signal discrimination research findings
[AD-A285848] p 1415 N95-21308

Data link terminal DLT document
[PB95-110805] p 1205 N95-21369

A Hypervelocity Experimental Research Database (HERD): Support for the Wright Laboratory Armament Directorate Code Validation Program (COVAL)
[DE95-001628] p 1387 N95-21396

GRONICs-1994. Proceedings of the 1994 Groningen Student Conference on Computer Science
[PB95-135620] p 1468 N95-21455

Independent review of Aviation Technology and Research Information Analysis System (ATRIAS) database
[AD-A284049] p 1203 N95-21518

Implementation of electronic chain-of-custody, analysis requests, and data verification at Los Alamos National Laboratory
[DE94-018076] p 1407 N95-21666

Proceedings of the 5th Workshop on the Next Generation of CASE Tools
[PB95-135208] p 1469 N95-21716

A user's guide to LUGSAN 1.1: A computer program to calculate and archive lug and sway brace loads for aircraft-carried stores
[DE95-001919] p 1207 N95-21730

Thermochemistry of dense hydrous magnesium silicates p 1416 N95-21782

Variability of total electron content in the high-altitude ionosphere following solar maximum
[AD-A285849] p 1425 N95-21833

Current status of fusion-relevant covariance data
[DE95-000865] p 1561 N95-22010

Digital mapping, charting, and geodesy analysis program technical review of Vector Smart Map (VMap) level 1
[AD-A286294] p 1390 N95-22055

NODDS/WOSM interface user's manual
[AD-A279095] p 1471 N95-22068

Guidelines for the creation and management of geographic data bases within a GIS environment, version 1.0. Volume 2. Appendices
[DE94-019215] p 1591 N95-22129

Defense Data Repository System (DDRS). End user manual
[AD-A286484] p 1592 N95-22293

A conceptual approach to object-oriented data modeling
[AD-A286048] p 1592 N95-22416

Experimental evaluation of dynamic data allocation strategies in a distributed database with changing workloads
[NASA-CR-195024] p 1456 N95-22431

Databases post-processing in Tensoral
p 1363 N95-22465

DATA COMPRESSION

Digital filtering for data compression in telemetry systems
[DE94-016611] p 1219 N95-20567

Combining image-processing and image compression schemes p 1304 N95-21537

Image and video coding using a wavelet decomposition
[PB95-135067] p 1311 N95-22358

Spatio-temporal masking in human vision and its application to image coding
[AD-A284949] p 1451 N95-22473

DATA CONVERSION ROUTINES

BASIC program for power spectrum estimation
[DE95-002228] p 1468 N95-21515

DATA CORRELATION

Hires and beyond p 1592 N95-21750

An assessment of image reconstruction from balloon-borne and the IRAS data p 1592 N95-21752

DATA FLOW ANALYSIS

ILIAS: A sequential language for parallel matrix computations
[PB95-110631] p 1473 N95-20056

Time domain spectral hole-burning storage
[AD-A279912] p 1587 N95-20309

Environment for Test and Analysis of Distributed Software (ETADS)
[AD-A285776] p 1463 N95-20877

Functional and para-functional parallel processing
[DE95-002805] p 1475 N95-20888

Verification of a timestamp-based sliding-window protocol
[PB95-132759] p 1455 N95-22082
Data sampling for a burst mode communications system
[AD-A286098] p 1309 N95-22229
ActorStudio reference manual. A user's guide to the ActorStudio user interface editor, version 1.0
[PB95-127023] p 1472 N95-22310

DATA LINKS
GPS-Squitter capacity analysis
[AD-A280037] p 1291 N95-20599
Advanced Command and Control (C2) applications interfaces to the Advanced Communications Technology Satellite (ACTS)
[AD-A279676] p 1291 N95-20605
Data link terminal DLT document
[PB95-110805] p 1205 N95-21369
Design and modelling of a link monitoring mechanism for the Common Data Link (CDL)
[AD-A286167] p 1309 N95-22245

DATA MANAGEMENT
Guidelines for the creation and management of geographic data bases within a GIS environment, version 1.0
[DE94-019214] p 1458 N95-20073
A Hyperspectral Image Data Exploration Workbench for environmental science applications
[DE94-016373] p 1412 N95-20171
Relational databases for RHIC design and control
[DE94-016785] p 1532 N95-20336
Defense Data Repository System (DDRS). End user manual
[AD-A286484] p 1592 N95-22293
Databases post-processing in Tensoral
p 1363 N95-22465

DATA PROCESSING
Efficient caption-based retrieval of multimedia information
[AD-A279604] p 1586 N95-19956
Data analysis and visualization in MCNP (trademark)
[DE94-016164] p 1508 N95-20159
SAR image registration in absolute coordinates using GPS carrier phase position and velocity information
[DE94-018738] p 1204 N95-20195
Error analysis in wind turbine field testing
[DE94-011864] p 1391 N95-20260
The GPS Burst Detector W-Sensor
[DE94-017406] p 1204 N95-20269
Choice of computer software for analysis of spectra from the Multi-Spectral Logging System
[DE94-019013] p 1460 N95-20351
Kernel mucking in top
[DE94-017077] p 1460 N95-20385
Muon data analysis program RUMDA
[PB95-129839] p 1511 N95-20434
Search for D(+) yields (pi)(+)(mu)(+)(mu)(-)
[DE94-015538] p 1512 N95-20475
Model formality in human/computer collaboration
[AD-A286001] p 1462 N95-20718
Meso-scale cooling effects of high albedo surfaces: Analysis of meteorological data from White Sands National Monument and White Sands Missile Range
[DE94-018535] p 1429 N95-20782
Computer based analysis and synthesis of retinal function
[AD-A286084] p 1443 N95-20811
Enhancements in the Livermore spectrum analysis package PIXEF
[DE95-002487] p 1272 N95-20895
Airborne Multisensor Pod System (AMPS) data access concept
[DE95-002586] p 1389 N95-20903
Statistical properties of geologic fractals
[DE94-019272] p 1414 N95-20908
Development of a fast sampling system for estimation of impulse responses of mobile radio channels
p 1296 N95-20943
Superresolution direction finding algorithms for the characterisation of multi-moded HF signals
p 1299 N95-20958
Overview of data fusion work for land electronic warfare
[AD-A279829] p 1301 N95-21292
Support to the development of high-level graphics software
[PB95-131686] p 1466 N95-21349
Second International Conference on Ordinal Data Analysis
[AD-A279756] p 1590 N95-21401
Orbit determination of highly elliptical Earth orbiters using improved Doppler data-processing modes
p 1218 N95-21533
A proposed wind measurement and analysis approach for evaluating a prospective wind plant site
[DE94-019187] p 1395 N95-21611
Reentry vehicle on-site inspection technology study
[AD-A285960] p 1220 N95-21634
Implementation of electronic chain-of-custody, analysis requests, and data verification at Los Alamos National Laboratory
[DE94-018076] p 1407 N95-21666
CTD calibration and processing methods used at Woods Hole Oceanographic Institution
[AD-A279507] p 1435 N95-21681
MARI mini-manual
[PB95-134649] p 1526 N95-21965
Optical processing and control
[AD-A279157] p 1546 N95-21975
State of the art in CFD pre- and postprocessing
[PB95-110391] p 1356 N95-22017
DOD science and engineering apprenticeship program for high school students
[AD-A280371] p 1583 N95-22100
An IBM based ARINC interface
[ARL-TR-21] p 1471 N95-22104
Interpretation of HRTEM images by image simulation: An introduction to theory and practice
[DE95-003422] p 1591 N95-22235
Confirmatory analysis of SAGE-1, and -2 data
[DE95-003623] p 1427 N95-22240

DATA PROCESSING EQUIPMENT
The impact of advanced packaging technology on modular avionics architectures p 1208 N95-20632

DATA PROCESSING TERMINALS
Space constancy on video display terminals
[AD-A280015] p 1449 N95-20314
Evaluation of the Haworth-Newman avionics Display Readability Scale
[AD-A286127] p 1214 N95-22232

DATA RECORDERS
Investigation of flight data recorder fire test requirements
[AD-A285832] p 1208 N95-20032

DATA REDUCTION
SAR image registration in absolute coordinates using GPS carrier phase position and velocity information
[DE94-018738] p 1204 N95-20195
Uncertainty estimates for derivatives and intercepts
[DE94-018492] p 1489 N95-20222
Fitting stochastic partial differential equations to spatial data
[AD-A279870] p 1490 N95-20432
Enhancements in the Livermore spectrum analysis package PIXEF
[DE95-002487] p 1272 N95-20895
Airborne Multisensor Pod System (AMPS) data access concept
[DE95-002586] p 1389 N95-20903
Statistical properties of geologic fractals
[DE94-019272] p 1414 N95-20908
Laser anemometry and viscous computation of the flow through an annular turbine cascade
[AD-A280070] p 1341 N95-20968
Project Whitefeather
[DE94-016575] p 1415 N95-21184
Twentysixth YERAC
[PB95-127437] p 1599 N95-21347
SSME HPOTP post-test diagnostic system enhancement project
[NASA-CR-4643] p 1222 N95-21458
The ORNL Neutron-Capture Cross Section Facility
[DE94-019146] p 1537 N95-21460
Search for the top quark using multivariate analysis techniques
[DE95-000561] p 1522 N95-21498
Implementation of electronic chain-of-custody, analysis requests, and data verification at Los Alamos National Laboratory
[DE94-018076] p 1407 N95-21666
Numerical investigation of one-dimensional heat-flux calculations
[AD-A286293] p 1582 N95-22054

DATA RETRIEVAL
SCSI controller with target status retrieval
[AD-D016249] p 1476 N95-21504
Method of retrieving and storing computer peripheral data
[AD-D016251] p 1591 N95-22098

DATA SAMPLING
Data sampling for a burst mode communications system
[AD-A286098] p 1309 N95-22229

DATA STORAGE
Time domain spectral hole-burning storage
[AD-A279912] p 1587 N95-20309
Review of GIS applications in hydrologic modeling
[AD-A279076] p 1390 N95-21628
Common mapping system media study
[AD-A279086] p 1390 N95-21912
Standard data formats for simulation
[PB95-110367] p 1470 N95-22016
Taking AIM: The management of scientific and technical information at Argonne National Laboratory
[DE94-019279] p 1591 N95-22092
Method of retrieving and storing computer peripheral data
[AD-D016251] p 1591 N95-22098

DATA STRUCTURES
A multivariate multisample rank test for stochastic simulation validation
[AD-A285922] p 1498 N95-19990
Guidelines for the creation and management of geographic data bases within a GIS environment, version 1.0
[DE94-019214] p 1458 N95-20073
Computing methods for the approximate solution of time dependent problems
[AD-A286007] p 1491 N95-20719
Distribution-independent hierarchical N-body methods
[DE95-001686] p 1493 N95-21439
Standard data formats for simulation
[PB95-110367] p 1470 N95-22016

DATA SYSTEMS
Circuit means for providing compatibility between two separate digital data interfaces
[AD-D016225] p 1455 N95-21116
Programmable modular network interface
[AD-D016505] p 1477 N95-21674
Information Management Architecture for an Integrated Computing Environment for the Environmental Restoration Program. Volume 1: Introduction
[DE95-001384] p 1590 N95-21862
Information Management Architecture for an Integrated Computing Environment for the Environmental Restoration Program. Volume 2: Interim business systems guidance
[DE95-001385] p 1591 N95-22061
NODDS/WOSM interface user's manual
[AD-A279095] p 1471 N95-22068
Conference proceedings. Defense Modeling and Simulation Office Information/Data Base (I/DB) Task Group Meetings, and notes from the previous two I/DB meetings
[AD-A279097] p 1591 N95-22069

DATA TRANSFER (COMPUTERS)
A scalable video rate camera interface
[AD-A286144] p 1474 N95-20325
Non-intrusive SCSI status sensing system
[AD-D016242] p 1476 N95-21307
Network file server with automatic sensing means
[AD-D016250] p 1476 N95-21496
A simulation study of TCP performance in ATM networks
[DE94-016622] p 1477 N95-21505
DONIO: Distributed object network I/O library
[DE94-019163] p 1477 N95-21602
Verification of a timestamp-based sliding-window protocol
[PB95-132759] p 1455 N95-22082
Overview of rapid prototyping technologies in manufacturing
[PB95-127122] p 1472 N95-22372
TDX: A high-bandwidth crossbar-switched communication paradigm
[DE94-017187] p 1311 N95-22407

DATA TRANSMISSION
Proceedings of the International Wire and Cable Symposium
[AD-A279242] p 1403 N95-20465
A technique for increasing the bandwidth of high performance electrical backplanes p 1212 N95-20651
Electromagnetic compatibility effects of advanced packaging configurations p 1213 N95-20658
Innovative use of DSP technology in space: FORTE event classifier
[DE94-016086] p 1291 N95-20697
An object-oriented implementation of the Xpress transfor protocol
[DE95-001506] p 1301 N95-21277
PVM 3 beyond network computing
[DE94-019115] p 1477 N95-21556
The message passing version of the parallel Community Climate Model
[DE94-019158] p 1407 N95-21608
Application-oriented architecture for multimedia teleservices
[PB95-135513] p 1306 N95-21623
Data sampling for a burst mode communications system
[AD-A286098] p 1309 N95-22229
TDX: A high-bandwidth crossbar-switched communication paradigm
[DE94-017187] p 1311 N95-22407

DC 8 AIRCRAFT
Fuselage burnthrough from large exterior fuel fires
[AD-A286295] p 1203 N95-22318

DEACTIVATION

Recommendation on transition from primary/secondary radar to secondary-only radar capability
[AD-A286279] p 1308 N95-22005

DEBONDING (MATERIALS)

The processing and mechanical properties of high temperature/high performance composites. Book 6: Delamination and compressive behavior
[AD-A279780] p 1231 N95-21999

Embedded optical fibres as strain sensors in polymer matrix fibre composites: The influence of adhesion in strain transfer
[PB95-133617] p 1547 N95-22140

DECARBOXYLATION

Hydrothermal conversion of carbohydrates and related compounds
[PB95-134011] p 1396 N95-22175

DECAY RATES

Measurement of the polarization in the decay B(sup 0) (yields) J/(psi)K*(sup 0) in (bar p)p collisions at (radical)s = 1.8 TeV
[DE95-002521] p 1520 N95-21313

Theory of spin dynamics in the classical two-dimensional heisenberg magnet
[PB95-133559] p 1502 N95-22138

DECISION MAKING

The effects of three-dimensional graphs on decision making
[AD-A285034] p 1583 N95-20051

Development and enhancement of a model of performance and decision making under stress in a real life setting
[AD-A285945] p 1449 N95-20393

Designing the architecture of hierachical neural networks model attention, learning and goal-oriented behavior
[AD-A279898] p 1452 N95-20562

A comparison of decision making behaviour in a static and a dynamic task environment as a function of time pressure
[AD-A285389] p 1449 N95-20609

The impact of partnering on construction contracts
[AD-A286588] p 1585 N95-20855

Systems Analysis Laboratory. Ten years of progress 1984-1994
[PB95-104451] p 1464 N95-20982

13th European Annual Conference on Human Decision Making and Manual Control
[PB95-132874] p 1450 N95-21284

Elements of deliberative robot control
[PB95-107595] p 1482 N95-21412

Navigation system in combat vehicle
[PB95-131629] p 1452 N95-21467

NASA/DOD Aerospace Knowledge Diffusion Research Project. Paper 48: Valuing information in an interactive environment
[NASA-TM-110448] p 1590 N95-21977

Information clustering for better decision-making
[AD-A286292] p 1590 N95-22053

DECISION THEORY

Application of Markov decision processes to search problems
[PB95-110813] p 1497 N95-19914

Qualification of the dependence in the generalized extreme value choice model
[PB95-110946] p 1497 N95-19936

TBell: A mathematical tool for analyzing decision tables
[NASA-CR-195027] p 1462 N95-20691

DECODING

Error probabilities of FFH/BFSK with noise normalization and soft decision viterbi decoding in a fading channel with partial-band jamming
[AD-A280041] p 1498 N95-20620

Signal- and listener- based factors in complex auditory pattern perception
[AD-A285636] p 1450 N95-21101

Turbo codes for deep-space communications
p 1304 N95-21535

DECOMPOSITION

Direct catalytic decomposition of nitric oxide
[DE94-018840] p 1233 N95-20045

Accelerated screening methods for determining chemical and thermal stability of refrigerant-lubricant mixtures. Part 2: Experimental comparisons and verification of methods
[DE95-000743] p 1264 N95-20078

A domain decomposition scheme for Eulerian shock physics codes
[DE94-015739] p 1488 N95-20141

An application of wavelet transform for decomposition of millimeter-wave spectroscopic signals
[DE94-018366] p 1402 N95-20247

DNS of turbulent flow in a driven cavity and their analysis using proper orthogonal decomposition
p 1352 N95-21097

Generalised approach to software structure metrics
[PB95-107561] p 1467 N95-21411

Thermal decomposition reactions of HMX and RDX and their importance in predicting cookoff hazards
[DE95-002486] p 1283 N95-21513

Preconditioning via asymptotically-defined domain decomposition
[DE94-019046] p 1493 N95-21564

Bridging the pressure gap: In situ atomic-level investigations of model platinum catalyst surfaces under reaction conditions by scanning tunneling microscopy
[DE95-002346] p 1246 N95-21990

Layered path planning for an autonomous mobile robot
[AD-A286138] p 1485 N95-22244

A multisite interaction expansion of the total energy in metals
[DE94-017175] p 1262 N95-22313

Image and video coding using a wavelet decomposition
[PB95-135067] p 1311 N95-22358

DEEP SPACE

Turbo codes for deep-space communications
p 1304 N95-21535

DEEP SPACE NETWORK

A comparative survey of current and proposed tropospheric refraction-delay models for DSN radio metric data calibration
[NASA-CR-197338] p 1412 N95-20002

The Deep Space Network as an instrument for radio science research
[NASA-CR-197341] p 1302 N95-21456

The Telecommunications and Data Acquisition Report
[NASA-CR-197390] p 1303 N95-21532

DEEP WATER

The Surface Wave Dynamics Experiment (SWADE): A retrospective look at the wave modeling activities
[AD-A285612] p 1431 N95-19895

DEFECTS

Physics and applications of defects in advanced semiconductors, volume 325
[AD-A280059] p 1563 N95-19886

Recognition of subsurface defects in machined ceramics by application of neural networks to laser scatter patterns
[DE94-018373] p 1264 N95-20018

The electronic properties of polysilanes
[DE94-006464] p 1265 N95-20121

Performance, defect behavior and carrier enhancement in low energy, proton irradiated p+nn+ InP solar cells
p 1319 N95-20518

Plastic deformation of ordered intermetallic alloys: Fundamental aspects
[DE95-001070] p 1256 N95-21265

Analysis of a local defect correction approach on composite grids
[PB95-135455] p 1493 N95-21574

Ceramic technology for advanced heat engines
[DE95-000950] p 1278 N95-21937

Minimax optimal stop rule in reliability checking
[PB95-134557] p 1383 N95-21961

Defect classes: An overdue paradigm for CMOS IC testing
[DE94-018905] p 1334 N95-22118

Reflective masks for extreme ultraviolet lithography
[DE95-003427] p 1336 N95-22236

Defect geometries and laser-induced damage in multilayer coatings
[DE94-017695] p 1377 N95-22343

DEFENSE INDUSTRY

Policies concerning military and civilian research and technology applications
[PB95-131355] p 1585 N95-21427

DEFENSE PROGRAM

NRL review, 1994
[AD-A279832] p 1605 N95-20182

Environmental Compliance Assessment and Management Program
[AD-A279605] p 1402 N95-20441

Environmental Compliance Assessment and Management Program (ECAMP), South Carolina supplement
[AD-A279533] p 1408 N95-21689

Environmental Compliance Assessment System (ECAS): Oregon supplement
[AD-A279565] p 1408 N95-21696

Defense Data Repository System (DDRS). End user manual
[AD-A286484] p 1592 N95-22293

DEFLECTION

Determination of layer moduli from falling weight deflectometer measurements
[PB95-129748] p 1286 N95-21333

DEFORMATION

Effect of fiber fabric orientation on the monotonic and fatigue behavior of a continuous fiber ceramic composite
[DE94-018121] p 1271 N95-20700

Approaches to the design of structural ceramics incorporating whiskers and particulate phases
[DE94-018126] p 1271 N95-20704

Geometric moire method of strain analysis with displacement discontinuities
[DE95-001114] p 1386 N95-20833

Prediction of rotor-blade deformations due to unsteady airloads
[AD-A286593] p 1207 N95-20860

Extrudate swell and extrudate distortion of HDPE as a result of different deformation mechanisms during extrusion through capillary dies
[PB95-110227] p 1288 N95-21651

Subduction and volatile recycling in Earth's mantle
p 1421 N95-21802

DEGASSING

Conference on Deep Earth and Planetary Volatiles
[NASA-CR-196944] p 1415 N95-21777

Impact degassing of water and noble gases from silicates p 1416 N95-21780

D/H ratios and H2O contents of mantle-derived amphibole megacrysts from Dish Hill, California
p 1416 N95-21781

Mantle devolatilization and rheology in the framework of planetary evolution p 1418 N95-21788

Rates of Earth degassing p 1422 N95-21809

Surface ices in the outer solar system
p 1423 N95-21815

Degassing history and evolution of volcanic activity of terrestrial planets based on radiogenic noble gas degassing models p 1424 N95-21816

Implications of noble gases in a recently recognized Martian meteorite (ALH84001) for the degassing history of Mars p 1424 N95-21819

Water abundance and accretion history of terrestrial planets p 1424 N95-21820

Degassing mechanisms of noble gases from carbonado diamonds p 1425 N95-21824

DEGENERATION

The preparation of all para-polyphenyls with increased solubility and enhanced third order NLO activity
[AD-A284301] p 1266 N95-20251

DEGRADATION

Degradation of aromatic hydrocarbons in an aquifer during a field experiment demonstrating the feasibility of remediation by natural attenuation
[AD-A283809] p 1282 N95-19922

The use of displacement damage dose to correlate degradation in solar cells exposed to different radiations
p 1320 N95-20523

UV testing of INTELSAT-7, 7A, and 8 solar cells
p 1320 N95-20526

Electromagnetic wave reflection from irregular plasma layers p 1298 N95-20952

Gate oxide shorts in nMOS transistors: Electrical properties and lifetime prediction method
[DE94-018904] p 1330 N95-21545

Performance of Ga(0.47)In(0.53)As cells over a range of proton energies
[NASA-TM-106819] p 1334 N95-22112

DEGREES OF FREEDOM

Three-dimensional laser cooling
[DE94-017963] p 1370 N95-20569

DEHYDRATION

Thermochemistry of dense hydrous magnesium silicates p 1416 N95-21782

Subduction of hydrated basalt of the oceanic crust: Implications for recycling of water into the upper mantle and continental growth p 1423 N95-21814

DEHYDROGENATION

Lower active metals loading for hydrotreating catalysts
[DE94-018907] p 1261 N95-22119

DELAMINATING

The processing and mechanical properties of high temperature/high performance composites. Book 6: Delamination and compressive behavior
[AD-A279780] p 1231 N95-21999

DELETION

Mitigation of effects of multiple path nulls at super-high frequencies through diversity and networking
p 1297 N95-20948

DELTA WINGS

Effect of juncture fillets on double-delta wings undergoing sideslip at high angles of attack
[AD-A286165] p 1207 N95-22039

DEMINERALIZING

Corrosion evaluation of fuel canister crusher rigging
[DE95-002962] p 1257 N95-21452

DEMOGRAPHY
Guidelines for the creation and management of geographic data bases within a GIS environment, version 1.0
[DE94-019214] p 1458 N95-20073
DENDRITIC CRYSTALS
Relationship between dendrite coherency and castability of some commercial foundry alloys
[PB95-110243] p 1258 N95-21652
DENITROGENATION
Lower active metals loading for hydrotreating catalysts
[DE94-018907] p 1261 N95-22119
DENSIFICATION
Processing of intermetallic materials by reaction synthesis
[DE94-017710] p 1263 N95-22345
DENSITY
Connection with dynamics: General introduction
[NASA-CR-197617] p 1579 N95-19947
DENSITY (MASS/VOLUME)
Apparatus and method for determining the mass density of a filament
[NASA-CASE-LAR-14879-1-CU] p 1383 N95-20616
Mixing and dynamics of the Mediterranean outflow
[AD-A279803] p 1434 N95-21306
Gradient index lenses from sol-gel layering
[AD-A285649] p 1242 N95-21402
Quartz resonator fluid monitors for vehicle applications
[DE94-018910] p 1367 N95-21546
DENSITY (NUMBER/VOLUME)
Charge density of fractional charged quasiparticles in the composite fermion picture
[DE94-018122] p 1524 N95-21703
Full potential multiple scattering theory
[DE95-003197] p 1576 N95-22084
DENSITY DISTRIBUTION
Temporal rearrangement of electronic densities in slow atomic collisions
[AD-A279725] p 1516 N95-20994
DENSITY MEASUREMENT
High quality InP-on-Si for solar cell applications
p 1317 N95-20510
Neutron reflectivity study of adsorbed diblock copolymers
[DE95-002740] p 1281 N95-22434
DEOXYRIBONUCLEIC ACID
Biomolecular Materials by Design, volume 330
[AD-A285369] p 1269 N95-20551
Proposal for a tutorial on Minimal Length Encoding (MLE) in molecular biology
[DE94-015076] p 1438 N95-21376
The molecular mechanics program DUPLEX: Computing structures of carcinogen modified DNA by surveying the potential energy surface
[DE94-019153] p 1439 N95-21606
Discovering related DNA sequences via mutual information
[DE95-001101] p 1440 N95-22067
Urban air carcinogens and their effects on health
[DE95-002259] p 1447 N95-22285
Cellular responses to environmental DNA damage
[DE94-015606] p 1441 N95-22397
DEPLETION
The development and evaluation of water-mist fire extinguishing systems
[DE94-019019] p 1286 N95-20356
Application of diode lasers to the isotopically selective determination of uranium in oxides by optogalvanic spectroscopy
[DE94-018045] p 1370 N95-20698
Nitrogen isotopic components in the early solar system p 1420 N95-21800
Alkali element depletion by core formation and vaporization on the early Earth p 1421 N95-21804
Effects of increased UV-B radiation on phytoplankton: A preliminary study and research programme
[PB95-133732] p 1439 N95-21884
DEPLOYMENT
A simple ocean bottom hydrophone with 200 megabyte data capacity
[AD-A279478] p 1434 N95-21677
DEPOLARIZATION
A review of Microbially Induced Corrosion (MIC) of steel and a preliminary investigation to determine its occurrence in naval vessels
[MRL-GD-0048] p 1250 N95-19910
Large bistatic angle clutter depolarization study
p 1296 N95-20941
DEPOSITION
Mixed-sputter deposition of Ni-Ti-Cu shape memory films
[DE94-017296] p 1250 N95-19900
Magnetically controlled deposition of metals using gas plasma
[DE94-018654] p 1251 N95-20128
Rate controlled synthesis of composition modulated, metal-oxide thin films
[DE94-016596] p 1267 N95-20317
Enhanced ionic conduction at the film/substrate interface in LiI thin films grown on sapphire(0001)
[DE94-017884] p 1565 N95-20371
Growth, characterization and device development in monocrystalline diamond films
[AD-A285991] p 1568 N95-20614
Ion scattering and deposition: The role of energetic particles in thin film growth
[AD-A285975] p 1514 N95-20667
Ion-molecule chemistry related to plasma deposition and etching of silicon
[AD-A279749] p 1514 N95-20804
Sputter deposition of multilayer thermoelectric films: An approach to the fabrication of two-dimensional quantum wells
[DE95-002396] p 1272 N95-20892
Use of the National Ignition Facility for the development of inertial fusion energy
[DE94-016696] p 1557 N95-21206
Copper metallization of stainless steels
[DE95-001496] p 1256 N95-21300
Spectroscopic, morphological, and electrical characterization of PdGe ohmic contacts to n-GaAs
[DE95-000738] p 1329 N95-21394
Deposition and properties of novel nitride superlattice coatings
[DE95-002945] p 1230 N95-21445
High performance YBCO films
[AD-A279560] p 1276 N95-21695
Method of making a semiconductor device by forming a nanochannel mask
[AD-D016515] p 1576 N95-22059
Reflective masks for extreme ultraviolet lithography
[DE95-003427] p 1336 N95-22236
Characterization and performance of DLC films synthesized by plasma and ion beam techniques
[DE94-018287] p 1281 N95-22428
DEPOSITS
Atmospheres of the Moon and Mercury
p 1419 N95-21794
Polar volatiles on Mercury and the Moon
p 1422 N95-21811
A new metallographic procedure for edge retention of enclosed surfaces
[DE94-017549] p 1261 N95-22048
DEPTH
An image cancellation approach to depth-from-focus
[DE94-019312] p 1544 N95-21392
Seismic evidence for volatiles at large depth in the Earth p 1422 N95-21808
VTT test borehole for bedrock investigations
[PB95-132965] p 1427 N95-22095
DEPTH MEASUREMENT
Simulation of laser bathymetry for irregular bottoms
[PB95-133518] p 1434 N95-21320
DERIVATION
An improved and facile method for the synthesis of 1,1-bis(4-hydroxyphenyl) 2-phenylethylene and its derivatives
[DE95-001125] p 1240 N95-20836
New improved derivative expansion for field theories with spontaneous symmetry breaking
[DE94-019349] p 1580 N95-21486
Solid-state NMR characterization of C- and N-labelled phthalimides: Model compounds for studying polyimides
[AD-A286479] p 1578 N95-22286
Fully developed turbulent flows
[AD-A286496] p 1358 N95-22294
DESERTIFICATION
Dust Bowl migration as an analog for possible global warming-induced migration from Mexico
[DE94-017472] p 1401 N95-20089
DESIGN
Quadratic forms in design theory
[PB95-111019] p 1487 N95-19940
Si concentrator solar cell development
[DE95-002314] p 1393 N95-20870
DESIGN ANALYSIS
Super-heavy aircraft study
[AD-A279602] p 1215 N95-19955
An intensity interferometer for soft x-rays
[DE94-016370] p 1541 N95-20103
Target Area Structural Support systems design to achieve the micron-level stability requirement of the National Ignition Facility (NIF)
[DE94-017696] p 1551 N95-20219
Characterization of an expanded-field Schwarzschild objective for extreme ultraviolet lithography
[DE94-016780] p 1541 N95-20239
Parallel calculation of sensitivity derivatives for aircraft design using automatic differentiation
[NASA-TM-110103] p 1206 N95-20370
A low temperature, ultrahigh vacuum, microwave-frequency-compatible scanning tunneling microscope
[AD-A279869] p 1365 N95-20413
Legged vehicle for underwater mobile operations
[AD-A285043] p 1480 N95-20482
Goddard Space Flight Center solar array missions, requirements and directions p 1316 N95-20503
Design of high-efficiency, radiation-hard, GaInP/GaAs solar cells p 1319 N95-20521
Preliminary control system design and analysis for the Space Station Furnace Facility thermal control system
[NASA-TM-108476] p 1365 N95-20560
Conceptual design of an RTG Facility Transportation System
[DE94-014443] p 1379 N95-20627
Development of a tester for evaluation of prototype thermal cells and batteries
[DE95-000540] p 1325 N95-20628
Improving Multichip Module (MCM) design and reliability using the Intelligent MCM Analyzer
p 1209 N95-20637
An evaluation of Automatic Terminal Information Service (ATIS) flight deck display presentation options
[AD-A280100] p 1204 N95-21020
Preliminary study of HUTSAT microsatellite
[PB95-127619] p 1220 N95-21026
Proceedings of the NATO-Advanced Study Institute on Computer Aided Analysis of Rigid and Flexible Mechanical Systems. Volume 1: Main lectures
[AD-A286062] p 1380 N95-21171
Heterogeneous multi-robot cooperation
[AD-A279839] p 1481 N95-21185
Development of a portable ice-thickness measuring instrument
[AD-A279472] p 1433 N95-21291
Overview of data fusion work for land electronic warfare
[AD-A279829] p 1301 N95-21292
The Photovoltaic Higher Education National Exemplar Facility (PHENEF)
[DE94-015641] p 1395 N95-21409
Design principles for real-time process control systems
[PB95-132890] p 1585 N95-21414
The advanced technology crew station: Development and validation of a workload assessment technique for cockpit function allocation
[AD-A279544] p 1453 N95-21691
Development of active-transport membrane devices
[DE94-015947] p 1246 N95-21921
Taking AIM: The management of scientific and technical information at Argonne National Laboratory
[DE94-019279] p 1591 N95-22092
Normal form analysis of the Tevatron
[DE94-017172] p 1539 N95-22192
Derivation of a wavenumber filter design for the measurement of turbulent wall pressure fluctuations
[AD-A286421] p 1357 N95-22208
High performance computing for beam physics applications
[DE94-018312] p 1539 N95-22243
CALIOPE and TAISIR airborne experiment platform
[DE94-018328] p 1310 N95-22299
The superconducting magnet system for the Tokamak Physics Experiment
[DE94-018329] p 1562 N95-22300
3-D TECATE/BREW: Thermal, stress, and birefringent ray-tracing codes for solid-state laser design
[DE95-000330] p 1376 N95-22301
Research on the power generation system with thermoelectric conversion elements
[DE95-714804] p 1397 N95-22309
Wave journal bearing. Part 1: Analysis
[NASA-CR-195431-PT-1] p 1382 N95-22404
Design of a massively parallel computer using bit serial processing elements
[NASA-CR-197365] p 1479 N95-22406
DESIGN TO COST
Cost estimating methods for advanced space systems
p 1583 N95-20741
European Workshop on Optical Ground Truth Instrumentation for the Validation of Space-Borne Optical Remote Sensing Data of the Marine Environment
[PB95-134144] p 1390 N95-21872
DESORPTION
Time-resolved analytical methods for liquid/solid interfaces
[DE95-002255] p 1240 N95-20780
International Symposium on Advanced Laser Technologies
[AD-A279849] p 1376 N95-22164
DESTRUCTIVE TESTS
UV testing of INTELSAT-7, 7A, and 8 solar cells
p 1320 N95-20526

The application of a statistical analysis software package to explosive testing
[MRL-TR-93-42] p 1284 N95-21658

DETECTION
Sol-gel-derived silica films with tailored microstructures for applications requiring organic dyes
[DE94-018886] p 1264 N95-20047
The GPS Burst Detector W-Sensor
[DE94-017406] p 1204 N95-20269
Analysis of direct detection lightwave systems with optical amplifiers
[AD-A284077] p 1542 N95-20467
Electrochemical impedance pattern recognition for detection of hidden chemical corrosion on aircraft components
[AD-A285998] p 1239 N95-20716
Modelling of microwave propagation and clutter in a maritime environment p 1295 N95-20938
Adaptive detection in stationary and nonstationary noise environments
[AD-A279581] p 1300 N95-21099
Electron tunneling magnetic field sensor
[AD-D016227] p 1365 N95-21117
Visible fluorescence of weathered lead
[DE95-002454] p 1244 N95-21523
New concepts for refrigerant leak detection and mixture measurement
[DE94-018967] p 1287 N95-21559
Fiber grating-based detection system for wavelength encoded fiber sensors
[AD-D016208] p 1545 N95-21825
Adaptive fault-resistant systems
[AD-A286406] p 1484 N95-22203
Threshold detection in the presence of atmospheric turbulence
[AD-A286175] p 1427 N95-22249

DETECTORS
Materials for adaptive structural acoustic control, volume 2
[AD-A279222] p 1502 N95-19883

DETERIORATION
Test Operations Procedure (TOP) 1-2-616 tropic exposure testing
[AD-A286376] p 1235 N95-20230
Detection of environmental deterioration in fiber reinforced composites by FT-Raman spectroscopy, phase 1
[AD-A279763] p 1228 N95-20805
Evaluation of dried storage of platelets for transfusion: Physiologic integrity and hemostatic functionality
[AD-A286078] p 1443 N95-20850

DETERMINANTS
Patterns of financial change in the OECD area
[PB95-110979] p 1594 N95-19939
Sharp determinants
[PB95-111068] p 1488 N95-19944

DETONATION
Sequential shock induced switch tests for Eglin Air Force Base
[DE95-001786] p 1334 N95-22062

DETONATION WAVES
Proceedings of the Zel'Dovich Memorial International Conference on Combustion, Detonation, Shock Waves, volume 2
[AD-A286626] p 1239 N95-20769
One-dimensional reactive Euler equations
[PB95-135430] p 1244 N95-21573

DEUTERIUM
A new alpha particle diagnostic using knock-on ion tails
[DE94-015856] p 1553 N95-20402
Experimental investigation of molecular beam injection in HL-1 tokamak
[DE94-631456] p 1556 N95-21165
Review of recent D-T experiments from TFTR
[DE95-002755] p 1557 N95-21239
Heating and transport in TFTR D-T plasmas
[DE95-002812] p 1558 N95-21242
Experimental investigations of electron capture from atomic hydrogen and deuterium by alpha particles
[DE95-002138] p 1523 N95-21587
Time of flight spectroscopy with muonic hydrogen
[DE94-017056] p 1245 N95-21845
Structure functions and structure function ratio F(sup n)2/F(sup p)2 at small x(sub Bj) and Q2 in muon-nucleon scattering
[DE94-017981] p 1530 N95-22340

DEUTERIUM PLASMA
Helium exhaust studies in the D3-D tokamak
[DE94-016682] p 1552 N95-20334
Heating and transport in TFTR D-T plasmas
[DE95-002812] p 1558 N95-21242

DEUTERONS
There might be two kinds of dibaryon
[DE94-014417] p 1526 N95-22058
On conception of a compact neutron source and the possibility of its simulation on the Amba-M end trap
[DE94-633373] p 1562 N95-22282

DIAGNOSIS
Mechanisms and diagnostics of ultrashort pulse laser ocular effects
[AD-A285610] p 1373 N95-21195
Proceedings of the NATO-Advanced Study Institute on Computer Aided Analysis of Rigid and Flexible Mechanical Systems. Volume 2: Contributed papers
[AD-A286063] p 1381 N95-21488
Radiopharmaceuticals for diagnosis
[DE95-002200] p 1445 N95-21595
Advanced Materials and Process Technology for Mechanical Failure Prevention (proceedings of the 48th Meeting of the Mechanical Failures Prevention Group
[AD-A285785] p 1233 N95-22399

DIAGRAMS
Hierarchical diagrammatic representation of class structure
[PB95-110722] p 1456 N95-19908

DIAMINES
A direct process for preparing semi-crystalline polyimides
[NASA-CASE-LAR-15020-1] p 1268 N95-20407

DIAMOND FILMS
Growth, characterization and device development in monocrystalline diamond films
[AD-A285991] p 1568 N95-20614
The in situ observation of epitaxial diamond thin film nucleation and growth using emission electron microscopy
[AD-A279811] p 1569 N95-20807
Atmosphere influence on in situ ion beam analysis of thin film growth
[DE95-001507] p 1570 N95-20881
Friction and wear properties of as-deposited and carbon ion-implanted diamond films
[NASA-TM-106759] p 1274 N95-21252
Analysis of cost: Combustion flame CVD diamond deposition
[AD-A279153] p 1278 N95-21973
Growing and releasing diamonds
[AD-D016489] p 1577 N95-22103
Technical cost modeling applied to CVD diamond deposition
[AD-A286119] p 1578 N95-22231

DIAMONDS
Numerical controlled polishing program, continued forced wear and part correction experiments
[DE94-018084] p 1285 N95-20288
Refractive index change in dissociating shocked benzene
[DE94-019015] p 1541 N95-20352
Materials processing and manufacturing technologies for diamond substrates multichip modules
[AD-A285060] p 1315 N95-20488
Conference on Deep Earth and Planetary Volatiles
[NASA-CR-196944] p 1415 N95-21777
Noble gas isotopes and halogens in volatile-rich inclusions in diamonds p 1417 N95-21784
Solar helium and neon in the Earth
p 1419 N95-21793
Volatiles in the deep Earth: An experimental study using the laser-heated diamond cell p 1421 N95-21803
Degassing mechanisms of noble gases from carbonado diamonds p 1425 N95-21824
Growing and releasing diamonds
[AD-D016489] p 1577 N95-22103
Advanced diagnostics for plasma chemistry
[DE94-018936] p 1561 N95-22116
Technical cost modeling applied to CVD diamond deposition
[AD-A286119] p 1578 N95-22231
Materials processing and manufacturing technologies for diamond substrates multichip modules
[AD-A285775] p 1336 N95-22412

DIAPHRAGM (ANATOMY)
Method and apparatus for non-invasive evaluation of diaphragmatic function
[NASA-CASE-LAR-13888-1] p 1441 N95-20408

DIATOMIC GASES
Plasma chemistry of vibrationally nonequilibrium molecules
[AD-A279630] p 1553 N95-20411

DIATOMIC MOLECULES
Plasma chemistry of vibrationally nonequilibrium molecules
[AD-A279630] p 1553 N95-20411
T1F ((1) sigma (+)): Some preliminary electronic structure calculations
[PB95-130316] p 1518 N95-21223
Interference of fluorescence x rays and coherent excitation of core levels
[DE94-016809] p 1527 N95-22188

DIBORANE
Atomically resolved structure and bonding of delta-doped boron layers on Si(001)
[AD-A279820] p 1513 N95-20586

DICHROISM
Theoretical prediction of vibrational circular dichroism spectra of R-glyceraldehyde, R-erythrose, and R-threose. Part 2: Development of a procedure to scale the force constant matrix expressed in terms of internal coordinates
[AD-A284305] p 1437 N95-20252
Orientation studies of polyolefins by IR-dichroism
[PB95-104386] p 1236 N95-20256
Magnetic x ray circular dichroism in Fe Co Pt multilayers
[DE94-017522] p 1253 N95-20447
Spin-specific photoelectron diffraction using magnetic x ray circular dichroism
[DE94-017527] p 1567 N95-20448
A structural determination using magnetic x ray circular dichroism in spin-polarized photoelectron diffraction
[DE94-017528] p 1567 N95-20449
Magnetic x-ray circular dichroism in spin-polarized photoelectron diffraction
[DE95-002394] p 1520 N95-21360

DICTIONARIES
Abbreviations and acronyms
[NASA-TM-110506] p 1590 N95-21457
Glossary of frequency and timing terms and a pictorial representation of terms used in the behavior and analyses of frequency standards
[AD-A286172] p 1310 N95-22247

DIELECTRIC PROPERTIES
The role of high pressure in the study and applications of the ferroelectric polymer polyvinylidene fluoride and its copolymers
[DE94-015742] p 1268 N95-20396

DIELECTRICS
Tests of dielectric model descriptions of chemical charge displacements in water
[DE94-007530] p 1236 N95-20277
Materials research for GHz multi-chip modules
[AD-A279661] p 1227 N95-20412
Reliability assessment of Multichip Module technologies via the Triservice/NASA RELTECH program
p 1210 N95-20643
Ferroic materials: Design, preparation and characteristics. Ceramic transactions, volume 43
[AD-A285937] p 1270 N95-20664
Effect of a solid insulator on the spark yield of S2F10 in SF6(*)
[DE95-001422] p 1326 N95-20791
Low-frequency image theory for a current dipole in front of a permeable sphere
[PB95-127676] p 1300 N95-21104
Dielectric models in adhesion and extrapolations of molecular modeling
[AD-A279675] p 1516 N95-21121
Role of dielectric constant in electrohydrodynamics of conducting fluids
[NASA-TM-110499] p 1331 N95-21614
Localization phenomenon in some random classical systems
[AD-A286514] p 1309 N95-22215
Dielectric mixtures with arbitrarily anisotropic components: Focus on special gyrotropic effects
[PB95-127015] p 1311 N95-22363
Image theory for the unidirectionally conducting screen
[PB95-127031] p 1311 N95-22365
Unique microchannel plate process doubles MCPI resolution
[DE94-017507] p 1337 N95-22427

DIES
Improved die castings through plasma surface modification, improved sensors and die soldering prevention
[DE95-002238] p 1253 N95-20417
Extrudate swell and extrudate distortion of HDPE as a result of different deformation mechanisms during extrusion through capillary dies
[PB95-110227] p 1288 N95-21651
Consortia for Known Good Die (KGD), phase 1
[AD-A279407] p 1383 N95-21933

DIESEL ENGINES
Trimode Power Converter optimizes PV, diesel and battery energy sources
[DE94-015014] p 1313 N95-20262
Abrasive wear by diesel engine coal-fuel and related particles
[PB95-104915] p 1379 N95-20984

DIESEL FUELS
Reducing exhaust gas emissions from Citydiesel busses
[DE95-700245] p 1380 N95-21295

DIFFERENCE EQUATIONS
The Nonlinear Characteristic scheme in X-Y geometries
[DE94-016192] p 1488 N95-20167
Computation of transonic flow on composite overlapping grids in 2 D
[PB95-131348] p 1353 N95-21132
DIFFERENTIAL ABSORPTION LIDAR
Continuously-tunable, narrow-linewidth, Q-switched Cr:LiSAF laser for lidar applications
[DE95-000862] p 1373 N95-21312
Lidar technologies for airborne and space-based applications
[DE95-002954] p 1302 N95-21448
DIFFERENTIAL ANALYZERS
The determination of static and time varying dipole source. Sensor geometry during sea trials using differential global positioning system
[MRL-TN-631] p 1205 N95-21642
DIFFERENTIAL EQUATIONS
Asymptotic analysis of Nash equilibria in nonzero-sum linear-quadratic differential games. The two-player case
[PB95-111027] p 1499 N95-19941
On the differential representations of quantum Lie superalgebras
[DE94-629874] p 1491 N95-20734
On FEL integral equation and electron energy loss in intermediate gain regime
[DE94-770631] p 1371 N95-20757
Temporal rearrangement of electronic densities in slow atomic collisions
[AD-A279725] p 1516 N95-20994
Explicit methods for stiff ODEs from atmospheric Chemistry
[PB95-135794] p 1404 N95-21034
On the transition towards slow manifold in shallow-water and 3D Euler equations in a rotating frame
p 1345 N95-21057
Computation of transonic flow on composite overlapping grids in 2 D
[PB95-131348] p 1353 N95-21132
The PROSAIC Laplace and Fourier Transform
[DE95-002225] p 1492 N95-21266
Structure functions and structure function ratio F2(n)/F2(p) at low X(Bj) and Q2 in inelastic muon scattering
[DE94-018979] p 1573 N95-21561
Measurement of the B meson differential cross-sections in p(bar p) collisions at (radical)s = 1.8 TeV using the exclusive decays B(sup (+-)) (yields) J/(psi)K(sup (+-)) and B(sup 0) (yields) J/(psi)K*(sup 0)
[DE94-018993] p 1523 N95-21562
Preconditioning via asymptotically-defined domain decomposition
[DE94-019046] p 1493 N95-21564
Maximum weighted matching for high index differential algebraic equations
[PB95-135075] p 1496 N95-22359
Self-similar solutions of a fast diffusion equation that do not conserve mass
[PB95-134920] p 1497 N95-22375
DIFFERENTIAL GEOMETRY
Marussi hypothesis in differential geodesy
[AD-A285853] p 1413 N95-20377
DIFFERENTIAL PRESSURE
Optical fiber pressure sensor for liquid level monitoring
[AD-D016246] p 1547 N95-22089
DIFFERENTIATION
Optimizing the length of the stores and related effects
[DE95-002531] p 1533 N95-20885
DIFFRACTION
Hard diffraction and rapidity gaps
[DE95-000565] p 1507 N95-20111
Spin dependence of diffractive processes and implications for the small x behaviour of g1 and the spin content of the nucleon
[PB95-130332] p 1518 N95-21225
Magnetic x-ray circular dichroism in spin-polarized photoelectron diffraction
[DE95-002394] p 1520 N95-21360
Polycrystalline PLZT/ITO ceramic electro-optic phase gratings: Electro-optically reconfigurable difffractive devices for free-space and in-wafer interconnects
[AD-A285861] p 1547 N95-22076
Design, fabrication, and characterization of reflective diffractive optical elements in Si for free-space optical interconnects
[AD-A286416] p 1547 N95-22205
DIFFRACTION PATTERNS
Physical-chemical studies on rodlike polymer compositions
[AD-A285361] p 1269 N95-20548
Angle resolved Auger electron spectroscopy: An alternate tool for identifying electronic excitation processes in solids
[AD-A285375] p 1238 N95-20555
Characterization of a texture gradient in tantalum plate
[DE95-002704] p 1262 N95-22289
DIFFRACTOMETERS
Role of internal stresses in fracture behavior of engineering composites
[DE95-001106] p 1229 N95-20912
Reciprocal space mapping of epitaxial materials using position-sensitive x-ray detection
[DE95-001620] p 1575 N95-21991
DIFFUSE RADIATION
Diffuse reflectance spectra of energetic material
[DSTO-TR-0065] p 1284 N95-21951
DIFFUSERS
Large-eddy simulation of flow through a plane, asymmetric diffuser p 1360 N95-22449
DIFFUSION
Diffusion enhances spontaneous electroweak baryogenesis
[DE94-017574] p 1512 N95-20451
Skeletal muscle ischemia and heat shock proteins
[AD-A285364] p 1442 N95-20549
Preclinical investigation of lyophilized platelet preparations
[AD-A286079] p 1443 N95-20851
Role of pressure diffusion in non-homogeneous shear flows p 1345 N95-21053
Comparison of calculated with measured dynamic aperture
[DE95-002863] p 1534 N95-21246
Quantum diffusion
[DE95-001015] p 1580 N95-21264
NESTLE: Few-group neutron diffusion equation solver utilizing the nodal expansion method for eigenvalue, adjoint, fixed-source steady-state and transient problems
[DE95-001903] p 1466 N95-21288
Computational modeling of diffusion-controlled transformations in ternary systems
[DE95-001358] p 1256 N95-21298
Defect production and recombination during low-energy ion processing
[DE95-001827] p 1572 N95-21304
Loss of solar He and Ne from IDPS in subducting sediment: Diffusion and the effect of phase changes
p 1419 N95-21792
Degassing mechanisms of noble gases from carbonado diamonds p 1425 N95-21824
Selection of RIB targets using ion implantation
[DE95-000951] p 1538 N95-21938
Self-similar solutions of a fast diffusion equation that do not conserve mass
[PB95-134920] p 1497 N95-22375
DIFFUSION COEFFICIENT
Quasi-linear equation for magnetoplasma oscillations in the weakly relativistic approximation
[DE94-628932] p 1560 N95-21593
Loss of solar He and Ne from IDPS in subducting sediment: Diffusion and the effect of phase changes
p 1419 N95-21792
DIFFUSION FLAMES
Heat transfer, fouling, and combustion of supercritical fuels
[AD-A279906] p 1281 N95-19884
Effects of non-unity Lewis numbers in diffusion flames
p 1249 N95-21036
Effect of chemical heat release in a temporally evolving mixing layer p 1249 N95-21037
Triple flame structure and diffusion flame stabilization
p 1249 N95-21039
A flamelet model for turbulent unpremixed combustion
p 1249 N95-21081
DIFFUSION THEORY
Error analysis of the quadratic nodal expansion method in slab geometry
[DE95-001352] p 1492 N95-21285
NESTLE: Few-group neutron diffusion equation solver utilizing the nodal expansion method for eigenvalue, adjoint, fixed-source steady-state and transient problems
[DE95-001903] p 1466 N95-21288
DIFFUSION WELDING
Joining of dissimilar materials. A review
[PB95-132999] p 1380 N95-21416
Forming of superplastic ceramics
[DE94-017306] p 1276 N95-21662
DIFFUSIVITY
Current diffusive ballooning mode in second stability region of tokamaks
[DE94-770690] p 1554 N95-20683
Observation of non diffusive term of toroidal momentum transport in the JFT-2M tokamak
[DE94-770686] p 1555 N95-20989
Assessment of database for interaction of tritium with ITER plasma facing materials
[DE95-002038] p 1558 N95-21290
The permeation of bis(2-fluoro-2,2-dinitroethyl) formal (FEFO), ethyl 4,4-dinitropentanoate (EDNP), ethyl 4-nitropentanoate (ENP), and 1,2,4-trichlorobenzene (TCB) through barrier membranes
[DE95-002492] p 1283 N95-21514
Degassing mechanisms of noble gases from carbonado diamonds p 1425 N95-21824
DIGITAL COMPUTERS
Optimal distributed control system for a linear distributed parameter system
[AD-D016583] p 1480 N95-20202
Long sequence correlation coprocessor
[AD-D016558] p 1313 N95-20280
Circuit means for providing compatibility between two separate digital data interfaces
[AD-D016225] p 1455 N95-21116
DIGITAL DATA
Circuit means for providing compatibility between two separate digital data interfaces
[AD-D016225] p 1455 N95-21116
Subsampling methods for image sequence coding
[PB95-107991] p 1305 N95-21579
Common mapping system media study
[AD-A279086] p 1390 N95-21912
Digital mapping, charting, and geodesy analysis program technical review of Vector Smart Map (VMap) level 1
[AD-A286294] p 1390 N95-22055
DIGITAL ELECTRONICS
Evaluation of superconducting quantum interference devices interfaced with digital signal processing electronics for biomagnetic applications
[DE94-016186] p 1289 N95-20164
Solid state research
[AD-A279662] p 1567 N95-20426
Advanced Packaging Concepts for Digital Avionics
[AGARD-CP-562] p 1208 N95-20631
High density monolithic packaging technology for digital/microwave avionics p 1211 N95-20646
Modular supplies for a distributed architecture --- avionics packaging p 1213 N95-20657
HTS Josephson technology on silicon with application to high speed digital microelectronics
[AD-A285964] p 1328 N95-21178
High temperature superconducting films and multilayers for electronics
[AD-A279545] p 1331 N95-21693
Uninterrupted, enhanced-rate event sequencer with mixed-speed counter modules
[AD-D016255] p 1334 N95-22030
DIGITAL FILTERS
Digital filtering for data compression in telemetry systems
[DE94-016611] p 1219 N95-20567
Saddle-node dynamics for edge detection
[DE94-017415] p 1473 N95-22426
DIGITAL SIMULATION
Preliminary control system design and analysis for the Space Station Furnace Facility thermal control system
[NASA-TM-108476] p 1365 N95-20560
DIGITAL SYSTEMS
Determining the usability of Digital Video Interactive (DVI) technology in computer-based instruction
[AD-A284717] p 1457 N95-20060
DSP control of superconducting quantum interference devices
[DE94-016193] p 1313 N95-20168
Preliminary evaluation of a digital optical systolic processor implemented with acousto-optic cells
[AD-A286377] p 1541 N95-20231
The GPS Burst Detector W-Sensor
[DE94-017406] p 1204 N95-20269
General purpose sidelobe canceller system
[AD-D016560] p 1289 N95-20270
Ultra-Reliable Digital Avionics (URDA) processor
p 1209 N95-20638
Innovative use of DSP technology in space: FORTE event classifier
[DE94-016086] p 1291 N95-20697
Shaping the library of the future: Digital library developments at Los Alamos National Laboratory's Research Library
[DE95-001008] p 1588 N95-20777
Propagation measurements on a troposcatter link in the Canadian High Arctic p 1295 N95-20940
HTS Josephson technology on silicon with application to high speed digital microelectronics
[AD-A285964] p 1328 N95-21178
Surface micromachined capacitive tactile image sensor
[PB95-108031] p 1288 N95-21633
DOD science and engineering apprenticeship program for high school students
[AD-A280371] p 1583 N95-22100
TDX: A high-bandwidth crossbar-switched communication paradigm
[DE94-017187] p 1311 N95-22407

DIGITAL TECHNIQUES
Vibration analysis of the AN/SPS-67(V)3 surface search radar
[AD-A286050] p 1302 N95-21324
Monolithic circuits for lead-glass calorimetry
[DE94-019112] p 1330 N95-21554
DIGITAL TELEVISION
Determining the usability of Digital Video Interactive (DVI) technology in computer-based instruction
[AD-A284717] p 1457 N95-20060
Geometric moire method of strain analysis with displacement discontinuities
[DE95-001114] p 1386 N95-20833
DIISOCYANATES
Polyurethane-acrylic interpenetrating polymer network acoustic damping material
[AD-D016572] p 1266 N95-20294
DILATATIONAL WAVES
A model of an infinite length, axisymmetric, isotropic, forced thick shell
[AD-A285586] p 1386 N95-21212
DILUTION
Emittance dilution by ions in the SLC arcs
[DE95-002871] p 1536 N95-21332
DIMENSIONAL MEASUREMENT
Nonlinear spectroscopy of multicomponent droplets and two- and three-dimensional measurements in flames
[AD-A279945] p 1238 N95-20581
Effects of yaw and pitch motion on model attitude measurements
[NASA-TM-4641] p 1368 N95-22109
DIMENSIONAL STABILITY
Large amplitude localized structures in a relativistic electron-positron ion plasma
[DE94-628965] p 1561 N95-21851
DIMENSIONLESS NUMBERS
Application of a dimensionless parameter model for Laser Beam Welding
[DE94-018902] p 1378 N95-20048
DIMENSIONS
The effects of three-dimensional graphs on decision making
[AD-A285034] p 1583 N95-20051
DIMERS
An atomically-resolved STM study of the thermal decomposition of disilane on Si(001)
[AD-A279818] p 1567 N95-20544
An atomically-resolved STM study of the interaction of phosphine (PH3) with the silicon (001) surface
[AD-A279819] p 1513 N95-20585
Atomically resolved structure and bonding of delta-doped boron layers on Si(001)
[AD-A279820] p 1513 N95-20586
Gas-phase generation of zinc sulfide particles using a single-source precursor
[AD-A279700] p 1239 N95-20712
DIODES
Charged particle dynamics in the acceleration gap of the PBFA 2 ion diode
[DE94-017347] p 1506 N95-20026
Particle beam fusion
[DE95-000711] p 1549 N95-20075
Impedance characteristics of multistage ion diodes
[DE94-018887] p 1565 N95-20340
Application of diode lasers to the isotopically selective determination of uranium in oxides by optogalvanic spectroscopy
[DE94-018045] p 1370 N95-20698
LIF standoff research
[DE94-018744] p 1535 N95-21328
RF vacuum microelectronics based on thin film edge-emitter technology
[AD-A279539] p 1331 N95-21690
DIOPHANTINE EQUATION
Quadratic forms in design theory
[PB95-111019] p 1487 N95-19940
DIPOLE ANTENNAS
A colocated magnetic loop, electric dipole array antenna (preliminary results)
[AD-A285381] p 1290 N95-20556
Small antennas for communication over sea ice
[AD-D016206] p 1301 N95-21156
DIPOLE MOMENTS
Investigation of spherical tearing mode
[NASA-CR-197284] p 1558 N95-21345
The determination of static and time varying dipole source. Sensor geometry during sea trials using differential global positioning system
[MRL-TN-631] p 1205 N95-21642
Constraints on T-odd and P-even hadronic interactions from nucleon, nuclear, and atomic electric dipole moments
[DE94-012845] p 1526 N95-21920
DIPOLES
Investigating the resolution of resistivity arrays using inverse theory
[DE94-017760] p 1412 N95-20287
DIRECT CURRENT
DC potential anomalies caused by a conducting body in an anisotropic conducting half-space
[PB95-127106] p 1291 N95-20775
DIRECT POWER GENERATORS
Trimode Power Converter optimizes PV, diesel and battery energy sources
[DE94-015014] p 1313 N95-20262
DIRECTION FINDING
Superresolution direction finding algorithms for the characterisation of multi-moded HF signals
p 1299 N95-20958
DIRECTIONAL ANTENNAS
Directive optimization of coherent sidelobe canceller systems
[AD-D016513] p 1307 N95-21908
DIRECTIONAL SOLIDIFICATION (CRYSTALS)
Directional solidification of the alumina-zirconia ceramic eutectic system
[DE95-001677] p 1277 N95-21735
The influence of chemistry and microstructure on the fracture toughness of V-V3Si in-situ composites
[DE94-018997] p 1232 N95-22126
DIRICHLET PROBLEM
Analysis of a local defect correction approach on composite grids
[PB95-135455] p 1493 N95-21574
DISCONTINUITY
Geometric moire method of strain analysis with displacement discontinuities
[DE95-001114] p 1386 N95-20833
DISCRETE FUNCTIONS
Qualification of the dependence in the generalized extreme value choice model
[PB95-110946] p 1497 N95-19936
Semi-global stabilization of linear discrete-time systems subject to input saturation via linear feedback: An ARE-based approach
[PB95-135463] p 1483 N95-21618
Discrete algebraic Riccati equation and linear matrix inequality
[PB95-133575] p 1484 N95-22139
On the dynamics of a shock-bubble interaction
[NASA-CR-194978] p 1495 N95-22325
DISCRIMINANT ANALYSIS (STATISTICS)
Multilayer piecewise linear networks
[AD-A285382] p 1480 N95-20606
DISEASES
Netherlands Institute for Brain Research progress report, 1993
[PB95-135398] p 1445 N95-21352
DISILICIDES
Third Intermetallic Matrix Composites Symposium, volume 350
[NASA-TM-110059] p 1225 N95-20001
The thermal conductivity of silicon nitride with molybdenum disilicide additions
[DE94-017757] p 1247 N95-22260
DISK OPERATING SYSTEM (DOS)
Personal computer and workstation operating systems tutorial
[AD-A280132] p 1451 N95-20041
DOS basics
[DE94-018434] p 1455 N95-21632
DISLOCATIONS (MATERIALS)
Microscopy of stress-induced morphological development and dislocation nucleation during semiconductor epitaxy
[DE94-017869] p 1568 N95-20674
Simulations of metal dissolution and corrosion
[DE94-019295] p 1257 N95-21476
DISPERSING
Diffraction applications using the energy dispersive beamline, X6A, at NSLS
[DE94-019287] p 1572 N95-21408
DISPERSION
Three-dimensional laser cooling
[DE94-017963] p 1370 N95-20569
DISPERSIONS
Proceedings of the 4th International Conference on Electrorheological Fluids
[AD-A286341] p 1266 N95-20227
Low emittance lattices for electron storage rings revisited
[DE94-017302] p 1540 N95-22391
DISPLACEMENT
The use of displacement damage dose to correlate degradation in solar cells exposed to different radiations
p 1320 N95-20523
Study of superconvergence by a computer-based approach: Superconvergence of the gradient of the displacement, the strain and stress in finite element solutions for plane elasticity
[AD-A279885] p 1490 N95-20588
Geometric moire method of strain analysis with displacement discontinuities
[DE95-001114] p 1386 N95-20833
LLNL/Lion Precision LVDT amplifier
[DE95-001504] p 1327 N95-20854
DISPLACEMENT MEASUREMENT
LLNL/Lion Precision LVDT amplifier
[DE95-001504] p 1327 N95-20854
DISPLAY DEVICES
A 3D stereo data visualization and representation
[AD-A284786] p 1449 N95-20064
Space constancy on video display terminals
[AD-A280015] p 1449 N95-20314
The impact of advanced packaging technology on modular avionics architectures p 1208 N95-20632
Computer based analysis and synthesis of retinal function
[AD-A286084] p 1443 N95-20811
Seminar on Biomedical Engineering 1993
[PB95-104402] p 1443 N95-20971
Color control in a multichannel simulator display: The display for advanced research and training
[AD-A279717] p 1216 N95-20992
Visual displays and Neuro-Linguistic Programming
[DE95-001454] p 1466 N95-21311
Data link terminal DLT document
[PB95-110805] p 1205 N95-21369
Information clustering for better decision-making
[AD-A286292] p 1590 N95-22053
Evaluation of the Haworth-Newman avionics Display Readability Scale
[AD-A286127] p 1214 N95-22232
DISSIPATION
The GPS Burst Detector W-Sensor
[DE94-017406] p 1204 N95-20269
A cheap DNS tool for turbulence models testing
p 1348 N95-21072
DISSOCIATION
Refractive index change in dissociating shocked benzene
[DE94-019015] p 1541 N95-20352
A new family of anion receptors and their effects on ion pair dissociation and conductivity of lithium salts in non-aqueous solutions
[DE94-016822] p 1512 N95-20477
Electrospray ionization Fourier transform ion cyclotron resonance mass spectrometric study of singly and doubly charged organometallic complexes
[AD-A279899] p 1238 N95-20563
Electron attachment to excited molecules
[DE94-019124] p 1522 N95-21519
Comparative computational analysis of some nitramine and difluoramine structures, dissociation energies and heats of formation
[AD-A286196] p 1525 N95-21878
DISSOLVING
Simulations of metal dissolution and corrosion
[DE94-019295] p 1257 N95-21476
DISTRIBUTED PARAMETER SYSTEMS
Heterogeneous multi-robot cooperation
[AD-A279839] p 1481 N95-21185
International Conference on Control and Estimation of Distributed Parameter Systems: Nonlinear Phenomena
[AD-A286449] p 1493 N95-21582
DISTRIBUTED PROCESSING
System level fault tolerance in parallel and distributed computing systems
[AD-A279664] p 1474 N95-20305
Stochastic network processes
[AD-A279905] p 1475 N95-20566
Fault-tolerance in distributed and multiprocessor real-time systems
[AD-A279896] p 1461 N95-20595
Environment for Test and Analysis of Distributed Software (ETADS)
[AD-A285776] p 1463 N95-20877
Polymer based all-optic reconfigurable interconnects
[AD-A279976] p 1272 N95-20962
GRONICs-1994. Proceedings of the 1994 Groningen Student Conference on Computer Science
[PB95-135620] p 1468 N95-21455
PVM 3 beyond network computing
[DE94-019115] p 1477 N95-21556
PVM a platform for portable distributed computing
[DE94-019156] p 1455 N95-21607
Design model for open distributed processing systems
[PB95-135505] p 1477 N95-21620
Status of CFDLIB performance tests on the T3D
[DE95-002708] p 1478 N95-21925
Massively-parallel computational fluid dynamics
[AD-A279389] p 1355 N95-21942

Modelling multimedia teleservices with OSI upper layers framework: Short paper
[PB95-132734] p 1308 N95-22080
Network distributed global memory for transparent message passing on distributed networks
[AD-A286096] p 1478 N95-22228
Computing symmetries and stubborn sets
[PB95-127700] p 1472 N95-22328
Time and the order of abstract events in distributed computations
[PB95-110482] p 1496 N95-22349
A periodic scheduling heuristic for mapping iterative task graphs onto distributed memory multiprocessors
[AD-A286047] p 1311 N95-22415

DISTRIBUTION FUNCTIONS
Moment approach to high-order accelerator beam optics
[DE95-001018] p 1536 N95-21331
Exponential deconvolution: Two asymptotically equivalent estimators
[PB95-132122] p 1499 N95-21469
Bayesian analysis of semiparametric proportional hazards models
[AD-A279394] p 1499 N95-21946
Exponents in lifetime and power spectral density forms in self-organized critical systems
[AD-A286242] p 1495 N95-22026
Counting methods for the analysis of load time histories
[PB95-132916] p 1388 N95-22093
An analytical electron distribution function for inelastic collisions in a uniform gas with time varying electric field
[DE95-003476] p 1528 N95-22222
An analytical, inelastic, space and time dependent electron distribution for electrically excited gases
[DE95-003478] p 1528 N95-22223

DIURNAL VARIATIONS
Analysis of mesospheric winds and waves
[AD-A279956] p 1414 N95-20591
Climatological data for clouds over the globe from surface observations, 1982-1991: The total cloud edition
[DE95-002537] p 1431 N95-22288

DIVERGENCE
Particle beam fusion
[DE95-000711] p 1549 N95-20075
Structure of ionic interfaces from an absolutely convergent solution of the Madelung problem
[DE94-019268] p 1573 N95-21474
Right inverse for the divergence operator in spaces of continuous piecewise polynomials
[PB95-127080] p 1496 N95-22369
Locking of the finite element method in thermoelasticity
[PB95-127098] p 1496 N95-22370

DIVERTERS
Recent DIII-D results
[DE94-017519] p 1549 N95-20038
Plasma shape experiments for an optimized tokamak
[DE94-017508] p 1553 N95-20445
Power balance in D3-D during single-null ELMing H-mode plasmas
[DE94-016680] p 1554 N95-20568
Experimental measurements and modeling of impurity transport in the divertor and boundary plasma of D3-D
[DE94-016519] p 1556 N95-21159
The ITER in-vessel system
[DE94-018053] p 1560 N95-21665

DIVING (UNDERWATER)
Solubilities of nitrogen and helium in water and blood at 37 C and pressures of up to 11 ATA
[AD-A286269] p 1446 N95-22003

DMSP SATELLITES
Location and characteristics of the reconnection X-line deduced from low-altitude satellite and radar observations
[NASA-TM-110114] p 1413 N95-20453

DOCUMENTATION
Ice Processing System software support documentation
[AD-A280030] p 1388 N95-20006
Program WALKMAN: A code designed to perform electron single collision elastic scattering Monte Carlo calculations
[DE94-017501] p 1511 N95-20444
A software process framework for the Software Engineering Institute's (SEI) capability maturity model
[AD-A286595] p 1462 N95-20765

DOMAIN WALL
Domain processes in ferroelectric ceramics
[AD-A279567] p 1276 N95-21697

DOMAINS
Multi-dimensional Petri nets
[PB95-127583] p 1491 N95-21024

DOMINANCE
Proof of a conjecture of Narayana on dominance refinements of the Smirnov two-sample test
[PB95-132650] p 1499 N95-21979

DOPED CRYSTALS
High precision trace neutron transmutation doping of detector-grade high resistance zone-refined silicon mono-crystal
[DE94-631463] p 1563 N95-19978
Scaling of solid state lasers for satellite power beaming applications
[DE94-016366] p 1368 N95-19986
Processing and characterization of Ni-Al-Fe-B shape-memory alloy wires produced by rapid solidification
[DE94-017702] p 1250 N95-20020
Carrier doping and interlayer coupling in HTSC single crystals
[DE94-018637] p 1564 N95-20127
Radiation effects on p+n InP junctions grown by MOCVD p 1319 N95-20520
Design of high-efficiency, radiation-hard, GaInP/GaAs solar cells p 1319 N95-20521
Photoluminescence under pressure and annealing of nitrogen-doped ZnSe
[DE95-002355] p 1568 N95-20630
Complementary GaAs junction-gated heterostructure field effect transistor fabrication for integrated circuits
[DE95-001522] p 1327 N95-20882
Photophysical processes on triplet states and radical ions in pure and molecularly doped polymers
[DE95-002681] p 1570 N95-20916
Conducting thermoset polymers
[AD-A286541] p 1273 N95-21014
Ultraviolet laser emission properties of Ce(3+)-doped LiSrAlF6
[DE94-016364] p 1372 N95-21135
X-ray studies of microstructures in semiconductor and superconducting materials
[DE95-001802] p 1572 N95-21279
Anodic oxygen-transfer electrocatalysis at iron-doped lead dioxide electrodes
[DE95-001653] p 1242 N95-21397
Light output and radiation damage in a YAlO3:Ce crystal
[DE94-016815] p 1545 N95-21643
InTlSb for long-wavelength infrared photodetectors and arrays
[AD-A280108] p 1332 N95-21774
Tunable CW blue, green, orange and red upconversion fiber lasers at room temperature
[DE95-000851] p 1375 N95-22007
The doping effect on spin-Peierls instability
[DE94-629046] p 1577 N95-22178
Quantum chemical study of rare gas/halide interactions as a model for high energy density material. 2: The interaction of hydrogen chloride with the rare gas xenon
[AD-A286385] p 1248 N95-22321

DOPPLER EFFECT
DAMSON: A system to measure multipath dispersion, Doppler spread and Doppler shift on multi-mechanism communications channels p 1299 N95-20955
Method and apparatus for classifying targets
[AD-D016519] p 1303 N95-21464

DOPPLER NAVIGATION
Orbit determination of highly elliptical Earth orbiters using improved Doppler data-processing modes
p 1218 N95-21533

DOPPLER RADAR
BACKSCAT lidar simulation version 4.0: Technical documentation and users guide
[AD-A285851] p 1290 N95-20376
Real-data tests of a single-Doppler radar assimilation system
[AD-A286638] p 1292 N95-20904
Radar studies of aviation hazards
[AD-A285845] p 1203 N95-21831
Frequency-coded monopulse MTI
[AD-D016495] p 1307 N95-21904

DOSAGE
Thorium-232 in human tissues: Metabolic parameters and radiation doses
[DE94-019275] p 1441 N95-20074
Superresolution direction finding algorithms for the characterisation of multi-moded HF signals
p 1299 N95-20958

DRAG
Low rotational drag in high-temperature superconducting bearings
[DE95-002983] p 1382 N95-22292

DRAG MEASUREMENT
Investigation of a thermal buoyancy effect on the drag of half models tested in the ARA Transonic Wind Tunnel
[ARA-MEMO-407] p 1199 N95-19946
Optical processing and control
[AD-A279157] p 1546 N95-21975

DRAG REDUCTION
Elastic micro-fabricated surface layer for reducing turbulence and drag on an object while it moves through a fluid medium
[AD-D016516] p 1356 N95-22060
Drag reduction strategies p 1361 N95-22453

DRIFT RATE
Radio-science performance analysis software
p 1305 N95-21540

DRILLING
VTT test borehole for bedrock investigations
[PB95-132965] p 1427 N95-22095

DRINKING
Hypervolemia in men from drinking hyperhydration fluids at rest and during exercise
[NASA-TM-4657] p 1439 N95-21544

DROP SIZE
A review of water mist technology for fire suppression
[AD-A285738] p 1202 N95-20071

DROP TESTS
Determination of layer moduli from falling weight deflectometer measurements
[PB95-129748] p 1286 N95-21333

DROPS (LIQUIDS)
Nonlinear spectroscopy of multicomponent droplets and two- and three-dimensional measurements in flames
[AD-A279945] p 1238 N95-20581

DROPSONDES
Resolving velocity profiles with the multi-scale profiler
[AD-A286446] p 1434 N95-21461

DROUGHT
Dust Bowl migration as an analog for possible global warming-induced migration from Mexico
[DE94-017472] p 1401 N95-20089
Monsoons: AMIP simulations of the 1987 and 1988 drought and flood regimes
[DE94-014789] p 1428 N95-20140

DRY FRICTION
On the origins and modeling of frictional behavior in interfacially-complex sliding contacts
[DE94-019129] p 1381 N95-21601

DRYING
Volatiles in the Earth: All shallow and all recycled
p 1416 N95-21779

DUALITY PRINCIPLE
Duality and equivalencies in closed tandem queueing networks
[PB95-132502] p 1482 N95-21271

DUCTED FLOW
Dual active surface heat flux gage probe
[NASA-TM-106861] p 1366 N95-21391

DUCTILE-BRITTLE TRANSITION
Ductile-brittle transition behavior of tungsten under shock loading
[DE94-009913] p 1251 N95-20122
Fracture behavior of the Fe-8Al alloy FAP-Y
[DE95-000956] p 1258 N95-21676

DUCTILITY
Processing and characterization of Ni-Al-Fe-B shape-memory alloy wires produced by rapid solidification
[DE94-017702] p 1250 N95-20020
Fabrication and properties of alumina matrix composites containing nickel aluminide reinforcements
[DE94-018703] p 1250 N95-20044
2nd International ADI seminar
[PB95-127734] p 1255 N95-21108
Fracture behavior of the Fe-8Al alloy FAP-Y
[DE95-000956] p 1258 N95-21676
The development of a super-alpha2 titanium aluminide alloy consolidated by rapid omnidirectional compaction
[AD-A279254] p 1260 N95-21986

DUCTS
Modelling and simulation of HF/VHF MMPPs
p 1293 N95-20925
Modeling tropospheric ducting effects on satellite-to-ground paths p 1295 N95-20936
Large-eddy simulation of separated flow in a ribbed duct p 1347 N95-21070
Direct simulation of turbulent flow in a square duct: Reynolds-stress budgets p 1348 N95-21073
MHD pressure drop in ducts with imperfectly insulating coatings
[DE95-002852] p 1558 N95-21244

DUPLEXERS
Design and modelling of a link monitoring mechanism for the Common Data Link (CDL)
[AD-A286167] p 1309 N95-22245

DURABILITY
The environmental durability of fiber reinforced ceramic matrix composites
[AD-A283750] p 1225 N95-19919
Final results of the advanced photovoltaic experiment
p 1321 N95-20528

The Materials Corrosion and Environmental Effects Laboratory (MCEL)
[DE94-018268] p 1254 N95-20816
Natural gas converter performance and durability
[PB95-135554] p 1284 N95-21966

DUST
The variation of the dust temperature within late-type spiral galaxies p 1593 N95-21766
HIRAS images of fossil dust shells around AGB stars p 1593 N95-21768
Response of the B-1B air data sensor to simulated dust cloud environments
[AD-A286134] p 1213 N95-22036

DYADICS
Classification of bianisotropic media
[PB95-127635] p 1502 N95-21102
Dyads: A generalisation of monads
[PB95-134052] p 1494 N95-21867

DYES
Sol-gel-derived silica films with tailored microstructures for applications requiring organic dyes
[DE94-018886] p 1264 N95-20047
Photodegradation and photophysics of laser dyes
[AD-A285105] p 1368 N95-20063

DYNAMIC CHARACTERISTICS
Connection with dynamics: General introduction
[NASA-CR-197617] p 1579 N95-19947
Transition-energy crossing with a gamma(sub t)(-)jump
[DE94-017315] p 1531 N95-20021
Comparison of the dynamic fatigue behavior of two monolithic SiC and an Al2O3/SiC composite
[DE94-017751] p 1225 N95-20022
Magnetron power supply at high stability and its application in plasma excitation for the production of ultraviolet radiation
[DE94-629656] p 1326 N95-20733
Time behavior and frequency response of the microwave propagation channel during multipath propagation p 1296 N95-20942
Quantum dynamical phenomena of independent electrons in semiconductor superlattices subject to a uniform electric field
[DE95-001655] p 1574 N95-21723
Critical dynamics and plastic flow in disordered Josephson junction arrays
[DE94-629074] p 1576 N95-21995
Determination of the complex elastic moduli of materials using a free-free bar technique
[AD-A279861] p 1281 N95-22387

DYNAMIC CONTROL
Generic architecture for knowledge-based control of processes in dynamic environments
[PB95-132676] p 1483 N95-21981

DYNAMIC MODELS
Development and enhancement of a model of performance and decision making under stress in a real life setting
[AD-A285945] p 1449 N95-20393
Mathematical modeling of a class of multibody flexible spacecraft structures
[NASA-TM-109166] p 1219 N95-20800
Computer based analysis and synthesis of retinal function
[AD-A286084] p 1443 N95-20811
Monthly mean sea ice data from the Polar Ice Prediction System, the Regional Polar Ice Prediction System-Barents Sea and the Regional Polar Ice Prediction System-Greenland Sea
[AD-A280095] p 1433 N95-21018
A Lagrangian dynamic subgrid-scale model turbulence p 1344 N95-21051
Developments and applications of dynamic models for large eddy simulation of complex flows p 1346 N95-21062
Subgrid scale models in finite difference simulations of complex wall bounded flows p 1346 N95-21063
Large-eddy simulation of rotating channel flows using a localized dynamic model p 1346 N95-21064
Comparison of DNS and LES of transitional and turbulent compressible flow: Flat plate and mixing layer p 1347 N95-21066
Rib vortices in round jets: Direct and large eddy simulation p 1351 N95-21088
The method of evaluating quantum partition function for the Hubbard model
[DE94-628991] p 1581 N95-21639
A dynamic localization model with stochastic backscatter p 1359 N95-22445
Large-eddy simulation of a plane wake p 1360 N95-22446
Local dynamic subgrid-scale models in channel flow p 1360 N95-22447
Large-eddy simulation of flow through a plane, asymmetric diffuser p 1360 N95-22449
Large-eddy simulation of a boundary layer with concave streamwise curvature p 1360 N95-22450

DYNAMIC PRESSURE
Pressure measurements on an F/A-18 twin vertical tail in buffeting flow. Volume 1: Wind tunnel test summary
[AD-A279126] p 1202 N95-21877

DYNAMIC PROGRAMMING
Optimal active control for Burgers equations p 1361 N95-22454

DYNAMIC RANGE
LLNL/Lion Precision LVDT amplifier
[DE95-001504] p 1327 N95-20854
Non-linear A/D converters for integrated silicon smart sensors
[PB94-208402] p 1330 N95-21590
A simple ocean bottom hydrophone with 200 megabyte data capacity
[AD-A279478] p 1434 N95-21677

DYNAMIC RESPONSE
Nonlinear dynamic fluid-structure interaction calculations with coupled finite element and finite volume programs
[DE94-016204] p 1339 N95-20166
Stabilization and control problems in structural dynamics
[AD-A279996] p 1340 N95-20312
Instantaneous frequency dynamics of coherent emission from magnetoexcitons in gallium arsenide
[DE94-018182] p 1569 N95-20677
Phase dynamics of non-equilibrium distributions of free electron-hole pairs in GaAs quantum wells
[DE94-018190] p 1569 N95-20679
Dynamic response of pressure measuring systems
[ARL-TR-32] p 1365 N95-20759
Modeling the effect of shroud contact and friction dampers on the mistuned response of turbopumps
[NASA-CR-197285] p 1379 N95-20795
On the influence of electromagnetic wave and relativistic electron beam on a plasma
[DE94-628962] p 1561 N95-21848
Effects of yaw and pitch motion on model attitude measurements
[NASA-TM-4641] p 1368 N95-22109
Wave journal bearing. Part 2: Experimental pressure measurements and fractional frequency whirl threshold for wave and plain journal bearings
[NASA-TM-106848-PT-2] p 1382 N95-22405
Simulation of structural response using a recurrent radial basis function network
[DE94-017342] p 1486 N95-22409

DYNAMIC STABILITY
The doping effect on spin-Peierls instability
[DE94-629046] p 1577 N95-22178

DYNAMIC STRUCTURAL ANALYSIS
Nonlinear dynamic fluid-structure interaction calculations with coupled finite element and finite volume programs
[DE94-016204] p 1339 N95-20166
Stabilization and control problems in structural dynamics
[AD-A279996] p 1340 N95-20312
Ultrafast magnetoexciton dynamics in GaAs
[DE94-018175] p 1514 N95-20732
Modeling the effect of shroud contact and friction dampers on the mistuned response of turbopumps
[NASA-CR-197285] p 1379 N95-20795
Mathematical modeling of a class of multibody flexible spacecraft structures
[NASA-TM-109166] p 1219 N95-20800
Vibration analysis of the AN/SPS-67(V)3 surface search radar
[AD-A286050] p 1302 N95-21324
Generic architecture for knowledge-based control of processes in dynamic environments
[PB95-132676] p 1483 N95-21981
Simulation of structural response using a recurrent radial basis function network
[DE94-017342] p 1486 N95-22409
Sandia National Laboratories analysis code data base
[DE95-004188] p 1502 N95-22420

DYNAMIC TESTS
Effect of atmospheric pressure on measured aircraft noise levels
[PB95-130423] p 1207 N95-21425
Fire smoke ventilation through shafts: Experiments
[PB95-132247] p 1288 N95-21978

DYNAMICAL SYSTEMS
Coupled analytic maps
[PB95-111076] p 1498 N95-19945
Analytic Perturbation Analysis of Discrete Event Dynamic Systems
[DE94-018635] p 1480 N95-20126
Semiquantum chaos and the large N expansion
[DE94-016196] p 1488 N95-20169
Invariant measures of interval maps
[PB95-107835] p 1389 N95-20207
Symmetry, Wigner functions and particle reactions
[DE94-629887] p 1514 N95-20735
Quantization in curvilinear coordinates
[DE94-770603] p 1514 N95-20737
Computation of invariant manifolds
[PB95-135687] p 1492 N95-21318

DYNAMICS
Molecular snapshots: Product imaging of dynamics important to fundamental combustion processes
[DE94-018595] p 1510 N95-20346

DYNAMO THEORY
Magnetic fluctuation induced transport and edge dynamo measurements in the MST reversed-field pinch
[DE95-000591] p 1549 N95-20114

DYNODES
Method of fabricating a microelectronic photomultiplier device with integrated circuitry
[AD-D016530] p 1325 N95-20726

DYSON THEORY
Theory of the excitonic lineshape in low-dimensional structures with rough interfaces
[DE95-003434] p 1582 N95-22237

DYSPROSIUM
The low temperature properties of (Dy(1-x)Er(x))Ni2 alloys
[DE95-001657] p 1260 N95-21923

E

E REGION
The relative importance of meteor burst and other distance polar cap propagation modes in the low VHF band p 1293 N95-20928

EAR PROTECTORS
Temporary threshold shifts produced by high intensity freefield impulse noise in humans wearing hearing protection
[AD-A286289] p 1454 N95-22045

EARTH (PLANET)
Erice International Seminars on Planetary Emergencies. 17th Workshop: The Collision of an Asteroid or Comet with the Earth
[AD-A280122] p 1600 N95-21577

EARTH ALBEDO
Meso-scale cooling effects of high albedo surfaces: Analysis of meteorological data from White Sands National Monument and White Sands Missile Range
[DE94-018535] p 1429 N95-20782
Detection optimization using linear systems analysis of a coded aperture laser sensor system
[DE95-001112] p 1371 N95-20832

EARTH ATMOSPHERE
Daytime Raman lidar profiling of atmospheric water vapor
[DE94-015747] p 1413 N95-20397
Space fundamentals for the war fighter
[AD-A279703] p 1217 N95-20690
Program control on the Tropical Rainfall Measuring Mission p 1584 N95-20750
Continuously-tunable, narrow-linewidth, Q-switched Cr:LiSAF laser for lidar applications
[DE95-000862] p 1373 N95-21312
NEO-LISP: Deflecting near-Earth objects using high average power, repetitively pulsed lasers
[DE95-000863] p 1599 N95-21367
Overview of remote sensing laser development and semiconductor laser technology
[DE94-019103] p 1389 N95-21552
Primitive Xe in the atmospheres of Earth and mars p 1419 N95-21795
Comets, impacts, and atmospheres p 1422 N95-21810
Implications of noble gases in a recently recognized Martian meteorite (ALH84001) for the degassing history of Mars p 1424 N95-21819

EARTH CRUST
Anatomy of the Midcontinent Rift beneath Lake Superior
[DE94-019298] p 1415 N95-21477
Rare gases systematics and mantle structure p 1416 N95-21778

EARTH IONOSPHERE
An overview of the Evaluation of Oxygen Interactions with Materials 3 Experiment: Space Shuttle Mission 46; July-August, 1992
[NASA-TM-110129] p 1412 N95-20278
Innovative use of DSP technology in space: FORTE event classifier
[DE94-016086] p 1291 N95-20697
Ion heating perpendicular to the magnetic field
[AD-A286635] p 1501 N95-20773
A simulation of plasma motion in the polar ionosphere
[AD-A286166] p 1426 N95-22019
The applicability of neural networks to ionospheric modeling in support of relocatable Over-the-Horizon radar
[AD-A286114] p 1309 N95-22230

EARTH MAGNETOSPHERE
Observations of cold magnetospheric ions at geosynchronous orbit during times of high activity
[DE95-000936] p 1600 N95-21935
Substorm theories: United they stand, divided they fall
[NASA-CR-197672] p 1427 N95-22326

EARTH MANTLE
Modeling the effect of water on mantle rheology
p 1417 N95-21783
Structure and stability of hydrous minerals at high pressure p 1417 N95-21786
Nitrogen isotopic components in the early solar system p 1420 N95-21800
Subduction and volatile recycling in Earth's mantle
p 1421 N95-21802
Alkali element depletion by core formation and vaporization on the early Earth p 1421 N95-21804
Hydrogen storage in Earth's mantle and core
p 1423 N95-21813
Water abundance and accretion history of terrestrial planets p 1424 N95-21820
The isotope geochemistry of abyssal peridotites and related rocks
[AD-A279435] p 1435 N95-21918
Source contributions at far-regional distances
[AD-A279405] p 1426 N95-21932

EARTH ORBITAL ENVIRONMENTS
Parasitic current collection by solar arrays in LEO
p 1321 N95-20527
Preliminary results from the flight of the Solar Array Module Plasma Interactions Experiment (SAMPIE)
p 1321 N95-20529
Post-flight investigation programmes of recently retrieved solar generators p 1321 N95-20531
Electrostatic noise in the plasma environment around the shuttle
[NASA-TM-106856] p 1415 N95-21188

EARTH ORBITAL RENDEZVOUS
STS 63 flight day 4 highlights/MIR-Shuttle rendezvous
[NASA-TM-110512] p 1219 N95-21113
STS 63: Post flight presentation
[NASA-TM-110514] p 1219 N95-21558

EARTH ORBITS
The design and analysis of a phased array microstrip antenna for a low earth orbit communication satellite
[AD-A284791] p 1289 N95-20065
Orbit determination of highly elliptical Earth orbiters using improved Doppler data-processing modes
p 1218 N95-21533

EARTH PLANETARY STRUCTURE
Statistical properties of geologic fractals
[DE94-019272] p 1414 N95-20908

EARTH SURFACE
Detection optimization using linear systems analysis of a coded aperture laser sensor system
[DE95-001112] p 1371 N95-20832
Classical analysis methods for designing and developing downlooking radars
[AD-A285760] p 1302 N95-21405
Remote-sensing based technique to account for sub-grid scale variability of land surface properties
[NASA-TM-110501] p 1390 N95-22110
Regional scale hydrology with a new land surface processes model
[NASA-TM-110500] p 1390 N95-22111

EARTHQUAKES
Infrasonic observations of the Northridge, California, earthquake
[DE94-018095] p 1413 N95-20289
The Novaya Zemlya Event of 31 December 1992 and Seismic Identification Issues: 15th Annual Seismic Research Symposium
[AD-A279847] p 1414 N95-20760
Thermochemistry of dense hydrous magnesium silicates p 1416 N95-21782
Source contributions at far-regional distances
[AD-A279405] p 1426 N95-21932

ECHELLE GRATINGS
Fabrication and testing of a silicon immersion grating for infrared spectroscopy
[DE94-017173] p 1237 N95-20386
An Echelle Grating Spectrometer (EGS) for mid-IR remote chemical detection
[DE94-019310] p 1367 N95-21478

ECOLOGY
Compilation of 1993 annual reports of the Navy ELF Communications System Ecological Monitoring Program. Volume 2: Tabs C-F
[AD-A279770] p 1308 N95-21988

ECONOMIC ANALYSIS
Patterns of financial change in the OECD area
[PB95-110979] p 1594 N95-19939
Assessment of liquefaction and pyrolysis systems
[PB95-129797] p 1236 N95-20290
Anaerobic digestion analysis model: User's manual
[DE94-011858] p 1437 N95-20471
An analysis of cost overruns on defense acquisition contracts p 1584 N95-20749
Highlights of recent balance of system research and evaluation
[DE95-001626] p 1393 N95-20863
Technical and economic evaluation of natural gas based synthesis gas production technologies
[PB95-130597] p 1242 N95-21426
Cost-effective ceramics program in the United States
[DE95-001425] p 1278 N95-21909
Economic feasibility analysis of distributed electric power generation based upon the natural gas-fired fuel cell
[DE94-012277] p 1396 N95-22033
Gas-phase photocatalytic oxidation: Cost comparison with other air pollution control technologies
[DE95-000241] p 1410 N95-22278

ECONOMIC DEVELOPMENT
Patterns of financial change in the OECD area
[PB95-110979] p 1594 N95-19939

ECONOMIC FACTORS
Beyond telecommuting: A new paradigm for the effect of telecommunications on travel
[DE95-001224] p 1289 N95-20214
Progress in the development of recycling processes for electric vehicle batteries
[DE94-015894] p 1324 N95-20626
NASA's attack on costs p 1585 N95-20755
Methods and opportunities in the recycling of rare Earth based materials
[DE95-001680] p 1259 N95-21737

ECONOMIC IMPACT
Dust Bowl migration as an analog for possible global warming-induced migration from Mexico
[DE94-017472] p 1401 N95-20089
Energy impacts of controlling carbon dioxide emissions from an integrated gasification/combined-cycle system
[DE94-016878] p 1403 N95-20478

ECONOMICS
Patterns of financial change in the OECD area
[PB95-110979] p 1594 N95-19939
Anaerobic digestion analysis model: User's manual
[DE94-011858] p 1437 N95-20471
Estimating the costs of human space exploration
p 1584 N95-20744
HPCC technology awareness program: Improved economic competitiveness through technology awareness, transfer and application
[DE95-002134] p 1476 N95-21355

ECOSYSTEMS
Definition report on environmental indices in future environmental assessments environmental balance/environmental outlook
[PB95-131876] p 1405 N95-21350
Long term changes on the continental shelf of the North Sea: Invertebrate trends, 1931-1990
[PB95-135224] p 1435 N95-21717
Aquatic plant control research program. Ecological assessment of Kirk Pond
[AD-A279090] p 1409 N95-21914
Proceedings: International Symposium on Global Change (IGBP)
[DE94-765351] p 1410 N95-22219

EDDY CURRENTS
Eddy current for detecting second-layer cracks under installed fasteners
[AD-A279871] p 1382 N95-20414
Flux-focusing eddy current probe and rotating probe method for flaw detection
[NASA-CASE-LAR-15231-1-SB] p 1383 N95-20764
Joule heating of the ITER TF cold structure: Effects of vertical control coil currents and ELMS
[DE95-001817] p 1560 N95-21724
Evaluation of scanners for C-scan imaging for nondestructive inspection of aircraft
[AD-A286398] p 1383 N95-22202

EDDY VISCOSITY
A numerical investigation of energy transfer and subgrid-scale eddy viscosity in homogeneous, isotropic and shear turbulence
[AD-A280005] p 1339 N95-20058
Comparison of DNS and LES of transitional and turbulent compressible flow: Flat plate and mixing layer
p 1347 N95-21066
Modelling anisotropy and backscatter effects in the subgrid scale stress tensor p 1349 N95-21077
Turbulence modeling for separated flow
p 1359 N95-22443
Large-eddy simulation of a plane wake
p 1360 N95-22446

EDGE DETECTION
Feature extraction without edge detection
[AD-A279842] p 1473 N95-22386
Saddle-node dynamics for edge detection
[DE94-017415] p 1473 N95-22426

EDGE DISLOCATIONS
Simulations of the dislocation array at Ge/Si interfaces
[DE94-017680] p 1565 N95-20244

EDGES
A new metallographic procedure for edge retention of enclosed surfaces
[DE94-017549] p 1261 N95-22048
Probability of detection for a GO CFAR radar processor using envelope detection approximation
[AD-A286211] p 1310 N95-22251

EDITING
ActorStudio reference manual. A user's guide to the ActorStudio user interface editor, version 1.0
[PB95-127023] p 1472 N95-22310

EDUCATION
Intelligent tutoring systems: Past, present, and future
[AD-A280011] p 1448 N95-19970
Using science centers to expose the general public to the microworld
[DE95-000647] p 1508 N95-20132
Hindered settling computations using a parallel boundary element method
[DE94-014286] p 1339 N95-20137
NASA/DOD Aerospace Knowledge Diffusion Research Project. Report 28: The technical communication practices of aerospace engineering and science students: Results of the phase 4 cross-national surveys
[NASA-TM-109123] p 1587 N95-20162
Training simulant for Halon 1211 portable extinguishers
[AD-A285403] p 1286 N95-20611
Software Capability Evaluation (SCE), version 2.0 team members guide
[AD-A286082] p 1462 N95-20809
Rate monotonic analysis for real-time systems: Instructors guide
[AD-A286083] p 1463 N95-20810
Microgravity: Teacher's guide with activities for physical science
[NASA-EG-103] p 1285 N95-21322
Development and evaluation of ALEC Micro-Wand 3e (tradename) training
[AD-A285863] p 1471 N95-22133

EFFECTIVE PERCEIVED NOISE LEVELS
Effect of atmospheric pressure on measured aircraft noise levels
[PB95-130423] p 1207 N95-21425
Active control of fan noise-feasibility study. Volume 1: Flyover system noise studies
[NASA-CR-195392-VOL-1] p 1505 N95-21888

EFFICIENCY
Calculation of near optimum design of InP/In(0.53)Ga(0.47)As monolithic tandem solar cells
p 1318 N95-20517
Qualification test results for blue-red reflecting solar covers p 1320 N95-20525
Evaluation of the technical performance of the Duttch National Air Quality Monitoring Network in 1992
[PB95-131892] p 1405 N95-21327
The efficiency calibration of the DSS-24 34-meter beam-waveguide antenna p 1305 N95-21542

EIGENVALUES
Matrix formulation of the particle motion in crystalline beams
[DE94-017301] p 1563 N95-19925
Graphs cospectral with distance-regular graphs
[PB95-111050] p 1488 N95-19943
A divide-and-conquer method for tridiagonalizing symmetric matrices with repeated eigenvalues
[DE95-002918] p 1476 N95-21257
NESTLE: Few-group neutron diffusion equation solver utilizing the nodal expansion method for eigenvalue, adjoint, fixed-source steady-state and transient problems
[DE95-001903] p 1466 N95-21288
Numerical wave speed for one-dimensional scalar hyperbolic conservation laws with source terms
[PB95-127536] p 1492 N95-21371
A new Krylov-subspace method for symmetric indefinite linear systems
[DE95-001826] p 1355 N95-21726
QMRPACK user's guide
[DE95-001770] p 1469 N95-21744
Discrete algebraic Riccati equation and linear matrix inequality
[PB95-133575] p 1484 N95-22139

EIGENVECTORS
Numerical wave speed for one-dimensional scalar hyperbolic conservation laws with source terms
[PB95-127536] p 1492 N95-21371

EL NINO
A study of westerly wind bursts preceding the 1991-1992 El Nino
[AD-A286570] p 1429 N95-20826

ELASTIC ANISOTROPY

Elastic anisotropy in hot-pressed Si3N4 composites: Role of in situ (beta)-Si3N4 grains and added (beta)-Si3N4 whiskers
[DE94-018387] p 1226 N95-20027

ELASTIC BODIES

A mixed time integration method for large scale acoustic fluid-structure interaction
[DE94-018327] p 1354 N95-21387

ELASTIC DEFORMATION

Time-dependent deformation of titanium metal matrix composites
[NASA-CR-195030] p 1230 N95-21363

ELASTIC PROPERTIES

Study of superconvergence by a computer-based approach: Superconvergence of the gradient of the displacement, the strain and stress in finite element solutions for plane elasticity
[AD-A279885] p 1490 N95-20588

Macromolecular and materials design using polyphosphazenes
[AD-A279781] p 1273 N95-20978

Mixed hp finite element methods for problems in elasticity and stokes flow
[PB95-104444] p 1341 N95-20981

Hydrogen and related materials at high density: Physics, chemistry and planetary implications
p 1418 N95-21791

Incology alloy 908 data handbook
[DE95-001818] p 1260 N95-22013

Determination of the complex elastic moduli of materials using a free-free bar technique
[AD-A279861] p 1281 N95-22387

ELASTIC SCATTERING

Program WALKMAN: A code designed to perform electron single collision elastic scattering Monte Carlo calculations
[DE94-017501] p 1511 N95-20444

Theories of the eta-meson-nucleus interaction
[DE94-016055] p 1516 N95-21125

Measurements of scattering processes in negative ion: Atom collisions
[DE95-000664] p 1519 N95-21276

Equilibrium and shot noise in mesoscopic systems
[DE95-000855] p 1576 N95-22008

ELASTIC WAVES

Experimental and theoretical evaluation of elastic waves in curved layered media
[AD-A286578] p 1504 N95-20918

ELASTODYNAMICS

A mixed time integration method for large scale acoustic fluid-structure interaction
[DE94-018327] p 1354 N95-21387

ELASTOMERS

Elastomeric electrical connector
[AD-D016559] p 1325 N95-20663

ELASTOPLASTICITY

Geomaterial models and numerical analysis of softening
[PB95-135380] p 1386 N95-21006

ELECTRIC ARCS

Preliminary results from the flight of the Solar Array Module Plasma Interactions Experiment (SAMPIE)
p 1321 N95-20529

ELECTRIC BATTERIES

Trimode Power Converter optimizes PV, diesel and battery energy sources
[DE94-015014] p 1313 N95-20262

Exploratory Technology Research Program for electrochemical energy storage
[DE95-002651] p 1392 N95-20439

Exploratory Technology Research Program for electrochemical energy storage
[DE95-002652] p 1394 N95-20915

Effects of battery technologies, driving patterns, and climate comfort control on the performance of electric vehicles
[DE95-001102] p 1329 N95-21296

Performance testing of the AC propulsion ELX electric vehicle
[DE95-002049] p 1330 N95-21471

Power systems for future missions. Appendices A-L
[NASA-CR-195320-APP-A-L] p 1395 N95-21530

Electric and Hybrid Vehicles Program
[DE95-001711] p 1332 N95-21738

Electric and Hybrid Vehicle Program Site Operator Program
[DE95-002042] p 1333 N95-21960

ELECTRIC CHARGE

Tests of dielectric model descriptions of chemical charge displacements in water
[DE94-007530] p 1236 N95-20277

Charge density of fractional charged quasiparticles in the composite fermion picture
[DE94-018122] p 1524 N95-21703

Full potential multiple scattering theory
[DE95-003197] p 1576 N95-22084

ELECTRIC CONDUCTORS

Accelerated screening methods for determining chemical and thermal stability of refrigerant-lubricant mixtures. Part 2: Experimental comparisons and verification of methods
[DE95-000743] p 1264 N95-20078

Characterization and electrical properties of copper films grown via direct liquid coinjection of (hfac)Cu(TMVS) and TMVS
[DE95-002957] p 1272 N95-20889

ELECTRIC CONNECTORS

The ROC optical connector p 1212 N95-20654

Elastomeric electrical connector
[AD-D016559] p 1325 N95-20663

ELECTRIC CONTACTS

Polycrystalline thin film cadmium telluride solar cells fabricated by electrodeposition
[DE94-011848] p 1391 N95-20118

Spectroscopic, morphological, and electrical characterization of PdGe ohmic contacts to n-GaAs
[DE95-000738] p 1329 N95-21394

Plasma-induced-damage of GaAs during etching of refractory metal contacts
[DE95-001525] p 1259 N95-21838

ELECTRIC CURRENT

Transport and dynamics in toroidal fusion systems
[DE94-018653] p 1548 N95-20029

Soft X-Ray Innovative Source Development Program
[AD-A286380] p 1551 N95-20232

Fiber-optic control of current filaments in high gain photoconductive semiconductor switches
[DE94-015804] p 1328 N95-21139

The evolution of configuration from q greater than 1 to q less than 1
[DE94-631396] p 1556 N95-21162

Geometric characterization of electromigration voids (A statistical analysis of electromigration voids)
[AD-A286494] p 1328 N95-21169

Acoustoelectric effect in semiconductor superlattice
[DE94-628994] p 1575 N95-21859

Method for determining the granular nature of superconductors using pulsed current
[AD-D016517] p 1577 N95-22137

Estimation of lightning stroke peak current as a function of peak electric field and the normalized amplitude of signal strength: Corrections and improvements
[DE94-016900] p 1335 N95-22189

ELECTRIC DIPOLES

A colocated magnetic loop, electric dipole array antenna (preliminary results)
[AD-A285381] p 1290 N95-20556

Low-frequency image theory for a current dipole in front of a permeable sphere
[PB95-127676] p 1300 N95-21104

Constraints on T-odd and P-even hadronic interactions from nucleon, nuclear, and atomic electric dipole moments
[DE94-012845] p 1526 N95-21920

Image theory for the unidirectionally conducting screen
[PB95-127031] p 1311 N95-22365

ELECTRIC DISCHARGES

Atomic velocity distributions in a hydrogen beam effusing out of an RF discharge dissociator
[AD-A279253] p 1307 N95-21985

ELECTRIC ENERGY STORAGE

Exploratory Technology Research Program for electrochemical energy storage
[DE95-002652] p 1394 N95-20915

ELECTRIC EQUIPMENT TESTS

Fault detection techniques for complex cable shield topologies
[AD-A286632] p 1291 N95-20771

ELECTRIC FIELDS

Physical Si(1-x)Ge(x)/Si heterojunction bipolar transistor model for device and circuit simulation
[PB95-110896] p 1312 N95-19934

The initiation of lightning and the growth of electric fields in thunderstorms
[AD-A280033] p 1428 N95-20008

A method for measuring the inductive electric field profile and noninductive current profiles on D3-D
[DE94-016683] p 1551 N95-20279

Extended theory of main ion and impurity rotation and bootstrap current in a shear layer
[DE94-015857] p 1555 N95-21141

The parametric dependence of the spatial structure of the radial electric field at the plasma edge in the D3-D tokamak
[DE94-016520] p 1556 N95-21163

Equivalent source current formulation in impedance tomography
[PB95-127627] p 1329 N95-21326

Investigation of spherical tearing mode
[NASA-CR-197284] p 1558 N95-21345

Cell membrane potentials induced during exposure to EMP fields
[DE94-018952] p 1439 N95-21548

Stellarator transport optimization with self-consistent electric fields
[DE94-019151] p 1559 N95-21581

Atomic processes in processing plasmas
[DE94-019177] p 1560 N95-21609

Role of dielectric constant in electrohydrodynamics of conducting fluids
[NASA-TM-110499] p 1331 N95-21614

Broadband pressure barrier for circular waveguide
[AD-D016503] p 1306 N95-21672

Quantum dynamical phenomena of independent electrons in semiconductor superlattices subject to a uniform electric field
[DE95-001655] p 1574 N95-21723

Improved broadband waveguide pressure window
[AD-D016487] p 1306 N95-21834

Acoustoelectric effect in semiconductor superlattice
[DE94-628994] p 1575 N95-21859

AC magnetic response of YBa2CuO7 with Y2BaCuO5 inclusions and of single-crystal YBa2Cu3O7: A comparative study
[PB94-207917] p 1577 N95-22166

Electric-field effects on shallow donor impurity in a harmonic quantum dot
[DE94-629034] p 1577 N95-22176

Estimation of lightning stroke peak current as a function of peak electric field and the normalized amplitude of signal strength: Corrections and improvements
[DE94-016900] p 1335 N95-22189

An analytical electron distribution function for inelastic collisions in a uniform gas with time varying electric field
[DE95-003476] p 1528 N95-22222

An analytical, inelastic, space and time dependent electron distribution for electrically excited gases
[DE95-003478] p 1528 N95-22223

Electro-optic effect in the PESO acousto-optic modulator
[AD-A286355] p 1548 N95-22255

Image solution for poisson's equation in wedge geometry
[PB95-127171] p 1310 N95-22311

Large-scale fields and flows in the magnetosphere-ionosphere system
[PB95-134664] p 1427 N95-22368

ELECTRIC GENERATORS

Trimode Power Converter optimizes PV, diesel and battery energy sources
[DE94-015014] p 1313 N95-20262

Feasibility study of power generation system with shape memory alloys
[DE95-714802] p 1254 N95-20890

Economic feasibility analysis of distributed electric power generation based upon the natural gas-fired fuel cell
[DE94-012277] p 1396 N95-22033

ELECTRIC HYBRID VEHICLES

Test and evaluation of electric vehicles
[DE95-001153] p 1313 N95-20213

Electric and Hybrid Vehicle Program: Site Operator Program
[DE95-001925] p 1332 N95-21731

Electric and Hybrid Vehicles Program
[DE95-001711] p 1332 N95-21738

ELECTRIC MOTOR VEHICLES

Test and evaluation of electric vehicles
[DE95-001153] p 1313 N95-20213

Brushless Doubly-Fed Machine system development program, phase 3
[DE94-013095] p 1315 N95-20380

Exploratory Technology Research Program for electrochemical energy storage
[DE95-002651] p 1392 N95-20439

Effects of battery technologies, driving patterns, and climate comfort control on the performance of electric vehicles
[DE95-001102] p 1329 N95-21296

Performance testing of the AC propulsion ELX electric vehicle
[DE95-002049] p 1330 N95-21471

Electric and Hybrid Vehicle Program: Site Operator Program
[DE95-001925] p 1332 N95-21731

Electric and Hybrid Vehicles Program
[DE95-001711] p 1332 N95-21738

EAGLES 1.1: A microcomputer software package for analyzing fuel efficiency of electric and gasoline vehicles
[DE95-001119] p 1469 N95-21829

Electric and Hybrid Vehicle Program Site Operator Program
[DE95-002042] p 1333 N95-21960

Demonstration of zinc/air fuel battery to enhance the range and mission of fleet electric vehicles: Preliminary results in the refueling of a multicell module
[DE95-004206] p 1337 N95-22421

ELECTRIC MOTORS
Design of power electronics for TVC and EMA systems
[NASA-CR-196540] p 1312 N95-19909
Brushless Doubly-Fed Machine system development program, phase 3
[DE94-013095] p 1315 N95-20380

ELECTRIC NETWORKS
Software for flow distribution in electronic rack structures
[AD-A285994] p 1325 N95-20715

ELECTRIC POTENTIAL
Physical Si(1-x)Ge(x)/Si heterojunction bipolar transistor model for device and circuit simulation
[PB95-110896] p 1312 N95-19934
Low electron beam energy CIVA analysis of passivated ICs
[DE94-017421] p 1314 N95-20286
Impedance characteristics of multistage ion diodes
[DE94-018887] p 1565 N95-20340
DC potential anomalies caused by a conducting body in an anisotropic conducting half-space
[PB95-127106] p 1291 N95-20775
Cell membrane potentials induced during exposure to EMP fields
[DE94-018952] p 1439 N95-21548
RF vacuum microelectronics based on thin film edge-emitter technology
[AD-A279539] p 1331 N95-21690
SEU and SEL response of the Westinghouse 64K E-2PROM, analog devices AD7876 12-bit ADC, and the Intel 82527 Serial Communications Controller
[DE95-003349] p 1334 N95-22086

ELECTRIC POWER
Magnetron power supply at high stability and its application in plasma excitation for the production of ultraviolet radiation
[DE94-629656] p 1326 N95-20733

ELECTRIC POWER SUPPLIES
Communications and control for electric power systems: Power system stability applications of artificial neural networks
[NASA-CR-197594] p 1483 N95-21613
Communications and control for electric power systems: Power system stability applications of artificial neural networks
[NASA-CR-197333] p 1484 N95-22171

ELECTRIC PROPULSION
BMDO photovoltaics program overview
p 1316 N95-20504

ELECTRIC PULSES
Method for determining the granular nature of superconductors using pulsed current
[AD-D016517] p 1577 N95-22137

ELECTRIC SPARKS
Effect of a solid insulator on the spark yield of S2F10 in SF6(*)
[DE95-001422] p 1326 N95-20791
Production of S2F10, S2OF10 and S2O2F10 by spark discharges in SF6*
[DE95-001421] p 1243 N95-21500

ELECTRIC TERMINALS
Elastomeric electrical connector
[AD-D016559] p 1325 N95-20663

ELECTRIC WIRE
Soft X-Ray Innovative Source Development Program
[AD-A286380] p 1551 N95-20232

ELECTRICAL FAULTS
Fault detection techniques for complex cable shield topologies
[AD-A286632] p 1291 N95-20771

ELECTRICAL GROUNDING
Analyses of grounded and ungrounded photovoltaic power systems
[DE94-015015] p 1391 N95-20263

ELECTRICAL IMPEDANCE
Derivation of coupling impedance from the wake potential of a finite bunch
[DE95-002529] p 1532 N95-20421
Xwake 1.0 user's manual
[DE95-002528] p 1463 N95-20901
Electrical impedance studies of acid-form NAFION membranes
[AD-A279271] p 1330 N95-21490
Broadband pressure barrier for circular waveguide
[AD-D016503] p 1306 N95-21672
Studies of the microwave resistivity of kappa-(BEDT-TTF)2Cu(N(CN)2)Cl
[DE95-002980] p 1262 N95-22291

ELECTRICAL INSULATION
Effect of a solid insulator on the spark yield of S2F10 in SF6(*)
[DE95-001422] p 1326 N95-20791
Measurement of the thermal properties of electrically conducting fluids using coated transient hot wires
[DE94-017816] p 1357 N95-22264

ELECTRICAL MEASUREMENT
Low electron beam energy CIVA analysis of passivated ICs
[DE94-017421] p 1314 N95-20286
Mechanism of the amperometric response of a proposed glucose sensor based on a polypyrrole-tubule-impregnated membrane
[AD-A279836] p 1365 N95-20431
Field-emitter arrays for RF vacuum microelectronics
[AD-A279959] p 1325 N95-20661
Electrical impedance studies of acid-form NAFION membranes
[AD-A279271] p 1330 N95-21490

ELECTRICAL PROPERTIES
Gate oxide shorts in nMOS transistors: Electrical properties and lifetime prediction method
[DE94-018904] p 1330 N95-21545
Growth and electrical and far-infrared properties of wide electron wells in semiconductors
[AD-A279409] p 1333 N95-21917
Defect classes: An overdue paradigm for CMOS IC testing
[DE94-018905] p 1334 N95-22118

ELECTRICAL RESISTANCE
Evaluation of Pd-Cr wires for strain gage application
[NASA-TM-106857] p 1366 N95-21259
Method for determining the granular nature of superconductors using pulsed current
[AD-D016517] p 1577 N95-22137
Surface technology programme
[PB95-132866] p 1262 N95-22174

ELECTRICAL RESISTIVITY
Properties of whisker-reinforced ceramics
[DE94-017759] p 1264 N95-20024
Power-law resistivity, magnetic relaxation and ac susceptibility
[DE94-016893] p 1501 N95-20241
Investigating the resolution of resistivity arrays using inverse theory
[DE94-017760] p 1412 N95-20287
Characterization and electrical properties of copper films grown via direct liquid coinjection of (hfac)Cu(TMVS) and TMVS
[DE95-002957] p 1272 N95-20889
Study of improved critical currents and mechanical properties in the Y-Ba-Cu-O superconductor with silver or Y2BaCuO3 or 211 dispersions
[AD-A285609] p 1502 N95-21194
Electrical impedance studies of acid-form NAFION membranes
[AD-A279271] p 1330 N95-21490
Structure and stability of hydrous minerals at high pressure p 1417 N95-21786
Breakdown of the law of large numbers in Josephson junction series arrays
[DE94-629075] p 1576 N95-21996
Order and turbulence in RF-driven Josephson junction series arrays
[DE94-629076] p 1576 N95-21997
On the conductance sum rule for the hierarchical edge states of the Fractional Quantum Hall Effect
[DE94-629030] p 1582 N95-22198
Measurement of the thermal properties of electrically conducting fluids using coated transient hot wires
[DE94-017816] p 1357 N95-22264
Development of practical high temperature superconducting wire for electric power applications
[DE94-017894] p 1336 N95-22271
Studies of the microwave resistivity of kappa-(BEDT-TTF)2Cu(N(CN)2)Cl
[DE95-002980] p 1262 N95-22291

ELECTRICITY
Modeling of high efficiency solar cells under laser pulse for power beaming applications p 1318 N95-20516
High efficiency GaP power conversion for Betavoltaic applications p 1323 N95-20540

ELECTRO-OPTICAL EFFECT
Frequency response measurements of integrated-optic electrodes
[DE94-016690] p 1542 N95-20403
Ultrafast optical studies of surface reaction processes at semiconductor interfaces
[DE95-001548] p 1574 N95-21839

ELECTRO-OPTICS
Sol-gel-derived silica films with tailored microstructures for applications requiring organic dyes
[DE94-018886] p 1264 N95-20047
Low temperature synthesis of semiconductor materials
[AD-A285120] p 1226 N95-20081
Program of the 1993 9th Interdisciplinary Laser Science Conference (ILS-9)
[AD-A285131] p 1369 N95-20082
Solid state research
[AD-A279662] p 1567 N95-20426
Development, fabrication, and metrology of the electro-optical breadboard model for the reflection grating array of the XMM grating spectrometer
[DE94-016605] p 1543 N95-20612
High contrast organic crystal optical modulator for phased array antenna and optical signal processing
[AD-A286557] p 1544 N95-20844
Development of ferroelectric liquid crystals with enhanced nonlinear optical properties
[AD-A279988] p 1571 N95-20965
Plasma Electrode Pockels Cells for the Beamlet and NIF lasers
[DE94-016541] p 1557 N95-21166
Heterostructure quantum confined Stark effect electrooptic modulators operating at 938 nm
[AD-A279342] p 1581 N95-21928
Characterization equipment for electrooptics and actuators
[AD-A286285] p 1546 N95-22043
Polycrystalline PLZT/ITO ceramic electro-optic phase gratings: Electro-optically reconfigurable difffractive devices for free-space and in-wafer interconnects
[AD-A285861] p 1547 N95-22076
Electro-optic effect in the PESO acousto-optic modulator
[AD-A286355] p 1548 N95-22255

ELECTROACOUSTICS
Acoustoelectric effect in semiconductor superlattice
[DE94-628994] p 1575 N95-21859

ELECTROCATALYSTS
Anodic oxygen-transfer electrocatalysis at iron-doped lead dioxide electrodes
[DE95-001653] p 1242 N95-21397

ELECTROCHEMICAL CELLS
Exploratory Technology Research Program for electrochemical energy storage
[DE95-002651] p 1392 N95-20439
Exploratory Technology Research Program for electrochemical energy storage
[DE95-002652] p 1394 N95-20915

ELECTROCHEMICAL CORROSION
A review of Microbially Induced Corrosion (MIC) of steel and a preliminary investigation to determine its occurrence in naval vessels
[MRL-GD-0048] p 1250 N95-19910
Simulations of metal dissolution and corrosion
[DE94-019295] p 1257 N95-21476
Corrosion resistance and behavior of construction materials exposed to dilute sulfuric acid at elevated temperatures under static conditions
[DE95-001723] p 1259 N95-21739
Corrosion resistance and behavioral characteristics of metals exposed to 70 percent by weight sulfuric acid at elevated temperatures
[DE95-001724] p 1259 N95-21740

ELECTROCHEMICAL OXIDATION
Mechanism of the amperometric response of a proposed glucose sensor based on a polypyrrole-tubule-impregnated membrane
[AD-A279836] p 1365 N95-20431
Anodic oxygen-transfer electrocatalysis at iron-doped lead dioxide electrodes
[DE95-001653] p 1242 N95-21397
Development and demonstration of advanced technologies for direct electrochemical oxidation of hydrocarbons (methanol, methane, propane)
[AD-A285094] p 1224 N95-22474

ELECTROCHEMISTRY
Chemical and electrochemical interactions on corroding metal surfaces
[DE95-000624] p 1250 N95-19979
Novel electrochemical materials prepared by sol-gel chemistry
[AD-A286310] p 1226 N95-20092
Chemically modified electrodes
[AD-A279821] p 1324 N95-20587
Electrochemical impedance pattern recognition for detection of hidden chemical corrosion on aircraft components
[AD-A285998] p 1239 N95-20716
Gordon Research Conference on Physical Electrochemistry
[AD-A286545] p 1240 N95-20842
Anodic oxygen-transfer electrocatalysis at iron-doped lead dioxide electrodes
[DE95-001653] p 1242 N95-21397
Quantum simulation of heterogeneous electron transfer free energies at the water-metal interface
[AD-A279279] p 1522 N95-21492

Surface x-ray scattering and scanning tunneling microscopy studies at the Au(111) electrode
[DE95-002409] p 1573 N95-21516

Surface second harmonic studies of Si(111)/electrolyte and Si(111)/SiO2/electrolyte interfaces
[AD-A279450] p 1245 N95-21826

Chemistry and electrochemistry in Lewis acid and superacid ionic liquids
[AD-A279396] p 1246 N95-21931

Application of optical second harmonic generation to surface analysis
[AD-A279445] p 1547 N95-22074

Development and demonstration of advanced technologies for direct electrochemical oxidation of hydrocarbons (methanol, methane, propane)
[AD-A285094] p 1224 N95-22474

ELECTRODES

Design and packaging aspects of microwave bandwidth lithium niobate modulators
[DE94-016602] p 1313 N95-20119

A charge distribution analysis instrument for catalysis and material science applications
[DE94-016489] p 1364 N95-20233

Enhanced ionic conduction at the film/substrate interface in LiI thin films grown on sapphire(0001)
[DE94-017884] p 1565 N95-20371

Frequency response measurements of integrated-optic electrodes
[DE94-016690] p 1542 N95-20403

Identification of resonant, two-electron, and inter-atomic features in K and L23 NEXAFS spectra
[AD-A285374] p 1513 N95-20554

Chemically modified electrodes
[AD-A279821] p 1324 N95-20597

Nickel hydroxide electrodes in reduced-alkalinity electrolytes
[DE95-002333] p 1326 N95-20814

Anodic oxygen-transfer electrocatalysis at iron-doped lead dioxide electrodes
[DE95-001653] p 1242 N95-21397

Surface x-ray scattering and scanning tunneling microscopy studies at the Au(111) electrode
[DE95-002409] p 1573 N95-21516

RF vacuum microelectronics based on thin film edge-emitter technology
[AD-A279539] p 1331 N95-21690

Surface second harmonic studies of Si(111)/electrolyte and Si(111)/SiO2/electrolyte interfaces
[AD-A279450] p 1245 N95-21826

Thoriated-tungsten, split-ring, hollow-cathode electrode for discharge devices
[AD-D016508] p 1333 N95-21906

ELECTRODIALYSIS

The application of electrodialysis to extend the lifetime of commercial electroplating baths
[DE95-000868] p 1246 N95-22012

ELECTROHYDRODYNAMICS

Role of dielectric constant in electrohydrodynamics of conducting fluids
[NASA-TM-110499] p 1331 N95-21614

ELECTROLYTES

Theoretical and experimental study of mixed solvent electrolytes
[DE94-017605] p 1237 N95-20384

Surface second harmonic studies of Si(111)/electrolyte and Si(111)/SiO2/electrolyte interfaces
[AD-A279450] p 1245 N95-21826

The application of electrodialysis to extend the lifetime of commercial electroplating baths
[DE95-000868] p 1246 N95-22012

Application of optical second harmonic generation to surface analysis
[AD-A279445] p 1547 N95-22074

ELECTROLYTIC CELLS

Inert gas purification and measuring oxygen partial pressure in gas mixtures with EMF method based on solid electrolyte cell
[PB95-127767] p 1240 N95-21110

ELECTROMAGNETIC ABSORPTION

Light output and radiation damage in a lead tungstate crystal
[DE94-016814] p 1565 N95-20265

Calculation of near optimum design of InP/In(0.53)Ga(0.47)As monolithic tandem solar cells
p 1318 N95-20517

MTX final report
[DE95-002960] p 1559 N95-21451

Time-resolved diagnostics of excimer laser-generated ablation plasmas used for pulsed laser deposition
[DE94-018950] p 1559 N95-21547

Light output and radiation damage in a YAlO3:Ce crystal
[DE94-016815] p 1545 N95-21643

Two-band model description of electroabsorption and third-harmonic generation in 1-D MX linear chains
[DE95-000932] p 1526 N95-21934

ELECTROMAGNETIC COMPATIBILITY

FASTPACK: Optimized solutions for modular avionics derived from a parametric study. Part 2: Avionics
p 1209 N95-20635

Composite cases for airborne electronic equipment: A technology study and EMC p 1212 N95-20655

Electromagnetic compatibility effects of advanced packaging configurations p 1213 N95-20658

ELECTROMAGNETIC FIELDS

Measurements of shielding effectiveness and cavity characteristics of airplanes
[PB94-210051] p 1289 N95-20191

Equivalent source current formulation in impedance tomography
[PB95-127627] p 1329 N95-21326

Three-dimensional effects for radio frequency antenna modeling
[DE94-019125] p 1303 N95-21459

Cell membrane potentials induced during exposure to EMP fields
[DE94-018952] p 1439 N95-21548

Compilation of 1993 annual reports of the Navy ELF Communications System Ecological Monitoring Program
[AD-A279575] p 1408 N95-21699

Compilation of 1993 annual reports of the Navy ELF Communications System Ecological Monitoring Program. Volume 2: Tabs C-F
[AD-A279770] p 1308 N95-21988

Topics in gauge theories and the unification of elementary particle interactions
[DE94-013485] p 1529 N95-22279

Radio-frequency techniques at the ISIS pulsed muon source
[PB95-129854] p 1529 N95-22303

Image theory for the unidirectionally conducting screen
[PB95-127031] p 1311 N95-22365

Low-level RF control for the AFEL
[DE94-018295] p 1540 N95-22410

ELECTROMAGNETIC INTERACTIONS

A theoretical study on the performance of the FDTD code on a massively parallel computer
[AD-A285346] p 1475 N95-20499

Nonperturbative aspects of the quark-photon vertex
[DE94-012846] p 1520 N95-21315

Investigation of direct photon production in 200 A GeV S + Au reactions
[DE94-018129] p 1525 N95-21704

ELECTROMAGNETIC INTERFERENCE

Measurements of shielding effectiveness and cavity characteristics of airplanes
[PB94-210051] p 1289 N95-20191

Electromagnetic interference testing and electrical subsystem: Non-communication
[AD-A286591] p 1292 N95-20858

ELECTROMAGNETIC MEASUREMENT

Measurements of shielding effectiveness and cavity characteristics of airplanes
[PB94-210051] p 1289 N95-20191

Flux-focusing eddy current probe and rotating probe method for flaw detection
[NASA-CASE-LAR-15231-1-SB] p 1383 N95-20764

ELECTROMAGNETIC NOISE

Noise model of the MSX SPIRIT 3 interferometer
[AD-A285837] p 1364 N95-20036

ELECTROMAGNETIC PROPULSION

Superconducting electromagnetic thruster
[AD-D016485] p 1355 N95-21902

ELECTROMAGNETIC PULSES

The GPS Burst Detector W-Sensor
[DE94-017406] p 1204 N95-20269

A wideband EMP test system
[DE94-015283] p 1290 N95-20474

Cell membrane potentials induced during exposure to EMP fields
[DE94-018952] p 1439 N95-21548

ELECTROMAGNETIC RADIATION

Electromagnetic radiation detector utilizing an electromagnetic radiation absorbing element in a mach-zehnder interferometer arrangement
[AD-D016507] p 1306 N95-21835

Electromagnetic waves in an ultrarelativistically hot and strongly magnetized electron-positron plasma
[DE94-628963] p 1307 N95-21849

On the theory of strong electromagnetic waves propagation in an electron-positron-ion plasma
[DE94-628964] p 1561 N95-21850

Large amplitude localized structures in a relativistic electron-positron ion plasma
[DE94-628965] p 1561 N95-21851

Compilation of 1993 annual reports of the Navy ELF Communications System Ecological Monitoring Program. Volume 2: Tabs C-F
[AD-A279770] p 1308 N95-21988

Optical radiation: Health based exposure limits for electromagnetic radiation in the wavelength range from 100 nanometer to 1 millimeter
[PB95-132767] p 1447 N95-22083

Localization phenomenon in some random classical systems
[AD-A286514] p 1309 N95-22215

ELECTROMAGNETIC SCATTERING

Diffraction computation by means of the method of equivalent currents
[AD-A285347] p 1291 N95-20692

Inverse and control problems in electromagnetics
[AD-A286438] p 1310 N95-22250

ELECTROMAGNETIC SHIELDING

Measurements of shielding effectiveness and cavity characteristics of airplanes
[PB94-210051] p 1289 N95-20191

Composite cases for airborne electronic equipment: A technology study and EMC p 1212 N95-20655

Lightweight electronic enclosures using composite materials p 1213 N95-20656

Fault detection techniques for complex cable shield topologies
[AD-A286632] p 1291 N95-20771

TIM-SCT cable testing protocol
[AD-A286633] p 1207 N95-20772

ELECTROMAGNETIC WAVE TRANSMISSION

Measurements of shielding effectiveness and cavity characteristics of airplanes
[PB94-210051] p 1289 N95-20191

A theoretical study on the performance of the FDTD code on a massively parallel computer
[AD-A285346] p 1475 N95-20499

Applications of wavelets to radar, imaging and related problems
[AD-A279909] p 1290 N95-20545

The Lorentz reciprocity theorem as a consistency test for propagation models p 1295 N95-20937

Temporal and spatial comportment of multiple paths in ionospheric propagation in oblique incidence: Fractal measures of perturbations p 1298 N95-20954

Improved broadband waveguide pressure window
[AD-D016487] p 1306 N95-21834

ELECTROMAGNETISM

DC potential anomalies caused by a conducting body in an anisotropic conducting half-space
[PB95-127106] p 1291 N95-20775

Classification of bianisotropic media
[PB95-127635] p 1502 N95-21102

Magnetoelectric properties of reciprocal bianisotropic materials with focus on the polarizability of chiro-omega spheres
[PB95-127650] p 1544 N95-21103

Low-frequency image theory for a current dipole in front of a permeable sphere
[PB95-127676] p 1300 N95-21104

Applied mathematical problems in modern electromagnetics
[AD-A286448] p 1303 N95-21462

Massively-parallel computational fluid dynamics
[AD-A279389] p 1355 N95-21942

Inverse and control problems in electromagnetics
[AD-A286438] p 1310 N95-22250

Dielectric mixtures with arbitrarily anisotropic components: Focus on special gyrotropic effects
[PB95-127015] p 1311 N95-22363

Image theory for the unidirectionally conducting screen
[PB95-127031] p 1311 N95-22365

ELECTROMAGNETS

Compact free electron lasers for medical applications
[AD-A285739] p 1369 N95-20072

ELECTROMECHANICAL DEVICES

Design of power electronics for TVC and EMA systems
[NASA-CR-196540] p 1312 N95-19909

Characterization equipment for electrooptics and actuators
[AD-A286285] p 1546 N95-22043

ELECTROMECHANICS

High density monolithic packaging technology for digital/microwave avionics p 1211 N95-20646

ELECTROMIGRATION

Methodology for ESCA analysis of electromigration
[AD-A286229] p 1241 N95-21168

Geometric characterization of electromigration voids (A statistical analysis of electromigration voids)
[AD-A286494] p 1328 N95-21169

Spectroscopic assessment of the reliability of metal/metal oxide interfaces
[AD-A286131] p 1261 N95-22035

ELECTROMYOGRAPHY

Analysis of musculo-skeletal loading using electromyography and biomechanical modelling
[PB95-135828] p 1444 N95-21007

ELECTRON ACCELERATORS
Theoretical and experimental studies of a novel accelerating structure
[AD-A283730] p 1531 N95-19974
Photocathodes for free electron lasers
[DE94-018305] p 1376 N95-22242
Very high-power electron-beam transport in long gas cells from 10(exp -3) to 10(exp 3) Torr N2
[DE95-002611] p 1539 N95-22306
Low-level RF control for the AFEL
[DE94-018295] p 1540 N95-22410

ELECTRON ATTACHMENT
Electron attachment to excited molecules
[DE94-019124] p 1522 N95-21519

ELECTRON BEAMS
Theoretical and experimental studies of a novel accelerating structure
[AD-A283730] p 1531 N95-19974
Charged particle dynamics in the acceleration gap of the PBFA 2 ion diode
[DE94-017347] p 1506 N95-20026
Low electron beam energy CIVA analysis of passivated ICs
[DE94-017421] p 1314 N95-20286
Studies of longitudinal instability with an electron beam
[DE94-018646] p 1532 N95-20347
High precision Woelter optic calibration facility
[DE94-016973] p 1542 N95-20364
Inverse Cerenkov laser acceleration experiment at ATF
[DE94-017990] p 1370 N95-20572
A URI program for Ultraviolet/extreme ultraviolet research
[AD-A279159] p 1370 N95-20600
On FEL integral equation and electron energy loss in intermediate gain regime
[DE94-770631] p 1371 N95-20757
A neutron beam polarizer for study of parity violation in neutron-nucleus interactions
[DE95-002743] p 1519 N95-21237
First results from the final focus test beam
[DE95-002897] p 1535 N95-21255
Coaxial hybrid wiggler
[AD-D016501] p 1331 N95-21671
Performance of cesium telluride photocathodes as an electron source for the Los Alamos FEL
[DE94-018302] p 1375 N95-21919
A 500 MW annular beam relativistic klystron
[DE95-000867] p 1334 N95-22011
Recent progress of the compact AFEL at Los Alamos
[DE95-002728] p 1376 N95-22154
Design, fabrication, and characterization of reflective diffractive optical elements in Si for free-space optical interconnects
[AD-A286416] p 1547 N95-22205
Experimental study of interactions of highly charged ions with atoms at keV energies
[DE94-018648] p 1529 N95-22316
Low emittance lattices for electron storage rings revisited
[DE94-017302] p 1540 N95-22391

ELECTRON BUNCHING
Derivation of coupling impedance from the wake potential of a finite bunch
[DE95-002529] p 1532 N95-20421
Emittance growth due to negative-mass instability above transition
[DE95-002527] p 1534 N95-20900

ELECTRON CAPTURE
Experimental investigations of electron capture from atomic hydrogen and deuterium by alpha particles
[DE95-002138] p 1523 N95-21587

ELECTRON CYCLOTRON HEATING
Simulation of tearing mode stabilization by using ECH
[DE94-770700] p 1554 N95-20684
MTX final report
[DE95-002960] p 1559 N95-21451

ELECTRON DENSITY (CONCENTRATION)
The Modified Embedded Atom Method
[DE94-015746] p 1564 N95-20142
Global ionospheric weather
[AD-A285520] p 1430 N95-21177
Variability of total electron content in the high-altitude ionosphere following solar maximum
[AD-A285849] p 1425 N95-21833
A simulation of plasma motion in the polar ionosphere
[AD-A286166] p 1426 N95-22019

ELECTRON DIFFRACTION
Correlations between surface structure and catalytic activity/selectivity
[DE94-019023] p 1234 N95-20052
Spin-specific photoelectron diffraction using magnetic x ray circular dichroism
[DE94-017527] p 1567 N95-20448
A structural determination using magnetic x ray circular dichroism in spin-polarized photoelectron diffraction
[DE94-017528] p 1567 N95-20449

ELECTRON DISTRIBUTION
An analytical electron distribution function for inelastic collisions in a uniform gas with time varying electric field
[DE95-003476] p 1528 N95-22222

ELECTRON EMISSION
Electron propagator theory and application
[AD-A279761] p 1507 N95-20097
Semiconductor cold electron emission device
[AD-D016577] p 1314 N95-20298
The in situ observation of epitaxial diamond thin film nucleation and growth using emission electron microscopy
[AD-A279811] p 1569 N95-20807
Emittance growth due to negative-mass instability above transition
[DE95-002527] p 1534 N95-20900

ELECTRON ENERGY
Correlations between surface structure and catalytic activity/selectivity
[DE94-019023] p 1234 N95-20052
Hybrid model in general geometry
[DE95-002614] p 1553 N95-20437
Location and characteristics of the reconnection X-line deduced from low-altitude satellite and radar observations
[NASA-TM-110114] p 1413 N95-20453
Atomic-resolution characterization of interface structure and chemistry in the STEM
[DE94-017753] p 1567 N95-20492
Enhanced scrape-off layer plasma in D3-D double-null discharges
[DE94-017977] p 1554 N95-20571
On FEL integral equation and electron energy loss in intermediate gain regime
[DE94-770631] p 1371 N95-20757
An advanced ECR ion source with a large uniformly distributed ECR plasma volume for multiply charged ion beam generation
[DE95-001078] p 1515 N95-20911
Heavy ion track-structure calculations for radial dose in arbitrary materials
[NASA-TP-3497] p 1517 N95-21191
Measurements of the Auburn ECE optical system parameters for temperature fluctuation measurements on TEXT-U
[DE94-019217] p 1562 N95-22120
An analytical, inelastic, space and time dependent electron distribution for electrically excited gases
[DE95-003478] p 1528 N95-22223

ELECTRON FLUX DENSITY
Low electron beam energy CIVA analysis of passivated ICs
[DE94-017421] p 1314 N95-20286

ELECTRON GUNS
Photoelectrons beam measurement from a magnesium cathode in a RF electron gun
[DE94-017994] p 1533 N95-20573

ELECTRON IMPACT
Electron-impact ionization of multicharged ions at ORNL: 1985-1992
[DE94-017318] p 1507 N95-20086
Theoretical atomic physics for fusion
[DE94-019196] p 1524 N95-21605

ELECTRON IRRADIATION
Electron-irradiated two-terminal, monolithic InP/Ga0.47In0.53As tandem solar cells and annealing of radiation damage p 1319 N95-20519

ELECTRON MICROSCOPES
A low temperature, ultrahigh vacuum, microwave-frequency-compatible scanning tunneling microscope
[AD-A279869] p 1365 N95-20413
Small cavity nonresonant tunable microwave-frequency alternating current scanning tunneling microscope
[AD-A285752] p 1328 N95-21218

ELECTRON MICROSCOPY
Effect of heat treatment temperature on creep-rupture properties of Fe3Al-based alloys
[DE94-017904] p 1253 N95-20375
The in situ observation of epitaxial diamond thin film nucleation and growth using emission electron microscopy
[AD-A279811] p 1569 N95-20807
Evaluation of dried storage of platelets for transfusion: Physiologic integrity and hemostatic functionality
[AD-A286078] p 1443 N95-20850
Parallel nanometer scale fabrication
[DE95-002122] p 1336 N95-22284

ELECTRON MOBILITY
Electron propagator theory and application
[AD-A279761] p 1507 N95-20097
Heavy ion track-structure calculations for radial dose in arbitrary materials
[NASA-TP-3497] p 1517 N95-21191
Quantum dynamical phenomena of independent electrons in semiconductor superlattices subject to a uniform electric field
[DE95-001655] p 1574 N95-21723

ELECTRON ORBITALS
Atomic orbital basis sets for molecular interactions
[AD-A279609] p 1506 N95-19959
Excess energy and structural dependence of the rate of energy redistribution during the photodissociation of iodotoluenes
[AD-A279997] p 1241 N95-21124

ELECTRON PARAMAGNETIC RESONANCE
Conducting thermoset polymers
[AD-A286541] p 1273 N95-21014
Modeling of nonlinear optic and ESR response of CDW MX materials
[DE94-018301] p 1578 N95-22297

ELECTRON PHONON INTERACTIONS
Pairing on small clusters in the Peierls-Hubbard model: Implications for C60
[DE94-016284] p 1565 N95-20330
Effect of the electron-SO-phonon on the impurity state energies in a semiconductor quantum well
[DE94-628993] p 1581 N95-21887
Temperature dependence of magnetopolarons in a parabolic quantum dot in arbitrary magnetic fields
[DE94-629033] p 1528 N95-22218

ELECTRON PLASMA
Experimental investigation of molecular beam injection in HL-1 tokamak
[DE94-631456] p 1556 N95-21165

ELECTRON PROBES
Phase E in a water-saturated peridotite system at 9.3 GPa p 1420 N95-21799

ELECTRON SCATTERING
Convergent Close-Coupling method for calculation of electron scattering on hydrogen-like targets
[DE94-631340] p 1508 N95-20196
Calculation of electron scattering on the He(+) ion
[DE94-631343] p 1509 N95-20199
Program WALKMAN: A code designed to perform electron single collision elastic scattering Monte Carlo calculations
[DE94-017501] p 1511 N95-20444
Nonperturbative aspects of the quark-photon vertex
[DE94-012846] p 1520 N95-21315
Exclusive processes: Tests of coherent QCD phenomena and nucleon substructure at CEBAF
[DE95-002892] p 1520 N95-21336
Recent photoabsorption measurements in the rare gases and alkalis in the 3 to 15 keV photon energy region
[DE94-019278] p 1521 N95-21406
Theoretical atomic physics for fusion
[DE94-019196] p 1524 N95-21605
Strong interactions studies with medium energy probes
[DE95-001800] p 1245 N95-21745
Nuclear research with the electromagnetic probe
[DE95-001812] p 1525 N95-21747
Submicrosecond, synchronizable x-ray source
[AD-D016497] p 1546 N95-21905
An analytical, inelastic, space and time dependent electron distribution for electrically excited gases
[DE95-003478] p 1528 N95-22223
The two-electron problem and prospects for atomic collision theory on a numerical lattice
[DE94-017856] p 1528 N95-22265

ELECTRON SOURCES
RF vacuum microelectronics based on thin film edge-emitter technology
[AD-A279539] p 1331 N95-21690
Performance of cesium telluride photocathodes as an electron source for the Los Alamos FEL
[DE94-018302] p 1375 N95-21919
Photocathodes for free electron lasers
[DE94-018305] p 1376 N95-22242
Fabrication and characterization of cesium telluride photocathodes: A promising electron source for the Los Alamos Advanced FEL
[DE94-018303] p 1377 N95-22348

ELECTRON SPECTROSCOPY
Optical properties of silicon clusters deposited on the basal plane of graphite
[DE94-017529] p 1542 N95-20450
Angle resolved Auger electron spectroscopy: An alternate tool for identifying electronic excitation processes in solids
[AD-A285375] p 1238 N95-20555
Methodology for ESCA analysis of electromigration
[AD-A286229] p 1241 N95-21168

Heavy ion track-structure calculations for radial dose in arbitrary materials
[NASA-TP-3497] p 1517 N95-21191
Micromachined silicon-based analytical microinstruments for space science and planetary exploration
[DE94-019306] p 1367 N95-21507

ELECTRON SPIN
Modeling of nonlinear optic and ESR response of CDW MX materials
[DE94-018301] p 1578 N95-22297

ELECTRON STATES
The electronic properties of polysilanes
[DE94-006464] p 1265 N95-20121
Quantum chemical study of rare gas/halide interactions as a model for high energy density material. 1: Transition properties in HCl
[AD-A285988] p 1239 N95-20613
Study of small carbon and semiconductor clusters using negative ion threshold photodetachment spectroscopy
[DE95-002327] p 1515 N95-20872
Excess energy and structural dependence of the rate of energy redistribution during the photodissociation of iodotoluenes
[AD-A279997] p 1241 N95-21124
Cluster reactions: An approach to understanding the fundamentals of heterogeneous catalysis
[DE95-002947] p 1243 N95-21447

ELECTRON TRANSFER
Solid-state dynamics and quantum transport in novel semiconductor nanostructures
[AD-A285946] p 1315 N95-20394
Gordon Research Conference on Physical Electrochemistry
[AD-A286545] p 1240 N95-20842
Quantum simulation of heterogeneous electron transfer free energies at the water-metal interface
[AD-A279279] p 1522 N95-21492
Equilibrium and shot noise in mesoscopic systems
[DE95-000855] p 1576 N95-22008
Magnetic interactions in the Emery model
[DE94-629059] p 1577 N95-22181
Resonant charge transfer in hyperthermal atomic and molecular ion-surface collisions
[AD-A284937] p 1530 N95-22471

ELECTRON TRANSITIONS
Quantum chemical study of rare gas/halide interactions as a model for high energy density material. 1: Transition properties in HCl
[AD-A285988] p 1239 N95-20613
Electronic structure and relative stability of icosahedral superatoms in Al-transition-metal alloys
[DE94-628996] p 1260 N95-21855
The solar flux of thermal neutrinos and antineutrinos of all flavors
[DE95-003204] p 1604 N95-22085
Electric-field effects on shallow donor impurity in a harmonic quantum dot
[DE94-629034] p 1577 N95-22176
Quantum chemical study of rare gas/halide interactions as a model for high energy density material. 2: The interaction of hydrogen chloride with the rare gas xenon
[AD-A286385] p 1248 N95-22321

ELECTRON TUNNELING
A low temperature, ultrahigh vacuum, microwave-frequency-compatible scanning tunneling microscope
[AD-A279869] p 1365 N95-20413
Electron tunneling magnetic field sensor
[AD-D016227] p 1365 N95-21117
Linear and nonlinear spectroscopy with the tunable AC scanning tunneling microscope
[AD-A285751] p 1241 N95-21217
Tunneling of self-trapped states and formation of a band
[DE94-629001] p 1582 N95-22378

ELECTRON-ION RECOMBINATION
Recombination, ion-molecule collisions and (laser assisted) electron-excited atom collisions
[AD-A285604] p 1517 N95-21216

ELECTRON-POSITRON PAIRS
Complementarity of e(+)e(-) and pp colliders for the exploration of electroweak symmetry breaking
[DE94-017397] p 1507 N95-20034
Electron-positron pair production in ultrarelativistic atomic collisions: 6.4 TeV S(sup 16+) with Au, Pd and Al
[DE95-000690] p 1508 N95-20133
Universality of particle multiplicities
[DE95-000727] p 1515 N95-20879

ELECTRON-POSITRON PLASMAS
Electromagnetic waves in an ultrarelativistically hot and strongly magnetized electron-positron plasma
[DE94-628963] p 1307 N95-21849
On the theory of strong electromagnetic waves propagation in an electron-positron-ion plasma
[DE94-628964] p 1561 N95-21850
Large amplitude localized structures in a relativistic electron-positron ion plasma
[DE94-628965] p 1561 N95-21851

ELECTRONIC COUNTERMEASURES
Directive optimization of coherent sidelobe canceller systems
[AD-D016513] p 1307 N95-21908

ELECTRONIC EQUIPMENT
Acoustic emission: The first half century
[DE94-017176] p 1503 N95-20267
Composite cases for airborne electronic equipment: A technology study and EMC p 1212 N95-20655
Lightweight electronic enclosures using composite materials p 1213 N95-20656
Elastomeric electrical connector
[AD-D016559] p 1325 N95-20663
Electromagnetic interference testing and electrical subsystem: Non-communication
[AD-A286591] p 1292 N95-20858
Study on the reaction kinetics in pulsed RF discharges under RIE conditions
[PB95-107868] p 1300 N95-21029

ELECTRONIC EQUIPMENT TESTS
Electromagnetic interference testing and electrical subsystem: Non-communication
[AD-A286591] p 1292 N95-20858
Assessment of a non-dedicated GPS receiver system for precise airborne attitude determination
[DE94-019309] p 1205 N95-21520
New concepts for refrigerant leak detection and mixture measurement
[DE94-018967] p 1287 N95-21559
The determination of static and time varying dipole source. Sensor geometry during sea trials using differential global positioning system
[MRL-TN-631] p 1205 N95-21642
Underwater Acoustic Generator Phase 2: Sea trial, March 1992
[MRL-TN-640] p 1434 N95-21657
Multi-port tester interface
[AD-D016240] p 1332 N95-21775
Thermal fixture for testing an integrated circuit
[AD-D016483] p 1333 N95-21900
Surfaces and thin films studied by picosecond ultrasonics
[DE95-001866] p 1506 N95-22071
Radiation tests on service electronics for future multi TeV detectors
[DE94-632822] p 1335 N95-22184
The Large Area Pulsed Solar Simulator (LAPSS)
[NASA-CR-197339] p 1397 N95-22336

ELECTRONIC MODULES
Materials research for GHz multi-chip modules
[AD-A279661] p 1227 N95-20412
MCMs for avionics: Technology selection and intermodule interconnection p 1210 N95-20641
Advanced Standard Electronic Modules format-E (SEM-E) processes for rapid prototyping
p 1210 N95-20642
Liquid flow-through cooling of electronic modules
p 1211 N95-20647
Immersion/two phase cooling p 1211 N95-20648
Consortia for Known Good Die (KGD), phase 1
[AD-A279407] p 1383 N95-21933
Uninterrupted, enhanced-rate event sequencer with mixed-speed counter modules
[AD-D016255] p 1334 N95-22030

ELECTRONIC PACKAGING
Design and packaging aspects of microwave bandwidth lithium niobate modulators
[DE94-016602] p 1313 N95-20119
A new mini Ball Grid Array (mBGA) multichip module technology
[DE94-018897] p 1480 N95-20342
High density monolithic packaging technology for digital/microwave avionics p 1211 N95-20646
Liquid flow-through cooling of electronic modules
p 1211 N95-20647
Electromagnetic compatibility effects of advanced packaging configurations p 1213 N95-20658

ELECTRONIC WARFARE
Overview of data fusion work for land electronic warfare
[AD-A279829] p 1301 N95-21292
Systems engineering design and technical analyses for Strategic Avionics Crew-station Design Evaluation Facility (SACDEF)
[AD-A286239] p 1213 N95-22024

ELECTRONS
A model for electron nuclear dynamics of a monatomic chain
[AD-A279652] p 1506 N95-19960
Quantization in curvilinear coordinates
[DE94-770603] p 1514 N95-20737
Electron-nuclear dynamics of molecular systems
[AD-A279649] p 1516 N95-21120
Measuring A(sub b) with polarized beams at SLC
[DE95-002865] p 1519 N95-21248
Luminosity polarization correlation in the SLC
[DE95-002889] p 1536 N95-21335
Photoemission and ferromagnetism
[DE95-002419] p 1520 N95-21362
On the Aharonov-Bohm effect with neutrons
[DE95-002985] p 1521 N95-21454
New shower maximum trigger for electrons and photons at CDF
[DE95-000563] p 1522 N95-21499
Gate oxide shorts in nMOS transistors: Electrical properties and lifetime prediction method
[DE94-018904] p 1330 N95-21545
Quantum dynamical phenomena of independent electrons in semiconductor superlattices subject to a uniform electric field
[DE95-001655] p 1574 N95-21723
Acoustoelectric effect in semiconductor superlattice
[DE94-628994] p 1575 N95-21859
Growth and electrical and far-infrared properties of wide electron wells in semiconductors
[AD-A279409] p 1333 N95-21917
Classical-quantum correspondence for ionization in fast ion-atom collisions
[DE95-000953] p 1526 N95-21940
Tunneling of self-trapped states and formation of a band
[DE94-629001] p 1582 N95-22378

ELECTROPHORESIS
Novel absorption detection techniques for capillary electrophoresis
[DE95-001673] p 1242 N95-21400
Separation of proteins by convective electrophoresis through a porous membrane
[PB95-127130] p 1248 N95-22373

ELECTROPHYSIOLOGY
A physiological neural network for saccadic eye movement control
[AD-A279599] p 1441 N95-20301
Computer based analysis and synthesis of retinal function
[AD-A286084] p 1443 N95-20811

ELECTROPLATING
The application of electrodialysis to extend the lifetime of commercial electroplating baths
[DE95-000868] p 1246 N95-22012

ELECTROPOLISHING
A new universal solution for the electrofinishing of metallic materials
[DE95-001681] p 1258 N95-21568

ELECTRORHEOLOGICAL FLUIDS
Proceedings of the 4th International Conference on Electrorheological Fluids
[AD-A286341] p 1266 N95-20227
Electrorheology for smart automotive suspensions
[AD-A285543] p 1380 N95-21157

ELECTROSLAG REFINING
Theoretical-experimental study on the electroslag remelting technology of high quality steels
[DE94-629216] p 1256 N95-21270

ELECTROSTATIC PROBES
A portable and independent edge fluctuation diagnostic
[DE94-018254] p 1554 N95-20681
Electrostatic noise in the plasma environment around the shuttle
[NASA-TM-106856] p 1415 N95-21188

ELECTROSTATICS
Tests of dielectric model descriptions of chemical charge displacements in water
[DE94-007530] p 1236 N95-20277
Electrostatic noise in the plasma environment around the shuttle
[NASA-TM-106856] p 1415 N95-21188
Electrostatic basis for molecular recognition in photosynthesis
[DE95-002979] p 1440 N95-22075

ELECTROSTRICTION
Laser-Induced Thermal Acoustics (LITA): Four-wave mixing measurement of sound speed, thermal diffusivity, and viscosity
[AD-A286524] p 1372 N95-21009

ELECTROWEAK INTERACTIONS (FIELD THEORY)
New strong interactions above the electroweak scale
[DE94-018385] p 1506 N95-20025
Complementarity of e(+)e(-) and pp colliders for the exploration of electroweak symmetry breaking
[DE94-017397] p 1507 N95-20034
Diffusion enhances spontaneous electroweak baryogenesis
[DE94-017574] p 1512 N95-20451

Parity nonconservation in radioactive atoms: An experimental perspective
[DE95-002737] p 1518 N95-21235

Electroweak boson pair production in p(-p) collisions at the square root of s = 1.8 TeV
[DE95-000725] p 1527 N95-22194

Physics at the Fermilab Collider
[DE95-000726] p 1539 N95-22195

ELECTROWEAK MODEL

Theoretical particle physics
[DE95-002447] p 1515 N95-20893

ELEMENTARY EXCITATIONS

Energy gap structure of layered superconductors
[DE94-017885] p 1566 N95-20372

Charge density of fractional charged quasiparticles in the composite fermion picture
[DE94-018122] p 1524 N95-21703

ELEMENTARY PARTICLE INTERACTIONS

Nonperturbative aspects of the quark-photon vertex
[DE94-012846] p 1520 N95-21315

Strange hadronic matter
[DE94-019345] p 1521 N95-21484

Structure functions and structure function ratio F2(n)/F2(p) at low X(Bj) and Q2 in inelastic muon scattering
[DE94-018979] p 1573 N95-21561

Measurement of the B meson differential cross-sections in p(bar p) collisions at (radical)s = 1.8 TeV using the exclusive decays B(sup (+-)) (yields) J/(psi)K(sup (+-)) and B(sup 0) (yields) J/(psi)K*(sup 0)
[DE94-018993] p 1523 N95-21562

Search for new particles decaying to dijets in p(bar p) collisions at (radical)s = 1.8 TeV
[DE94-018994] p 1523 N95-21563

Status of the DO top search
[DE95-002214] p 1525 N95-21715

The status of molecules
[DE95-000952] p 1526 N95-21939

The 9th INS scientific computational programs
[DE94-770780] p 1526 N95-22051

Single particle measurements and two particle interferometry results from CERN experiment NA44
[DE95-003041] p 1527 N95-22078

Constraints on the left-right symmetric model from b yields s gamma
[DE95-003469] p 1528 N95-22239

Topics in gauge theories and the unification of elementary particle interactions
[DE94-013485] p 1529 N95-22279

ELEMENTARY PARTICLES

Using science centers to expose the general public to the microworld
[DE95-000647] p 1508 N95-20132

ELEMENTS

Lattice results for heavy light matrix elements
[DE94-019101] p 1523 N95-21551

ELEVATION ANGLE

Modeling tropospheric ducting effects on satellite-to-ground paths p 1295 N95-20936

ELLIPTIC DIFFERENTIAL EQUATIONS

Weighted strongly elliptic operators on lie groups
[PB95-110847] p 1487 N95-19917

Role of pressure diffusion in non-homogeneous shear flows p 1345 N95-21053

Modeling near wall effects in second moment closures by elliptic relaxation p 1345 N95-21054

Positive rockland operators
[PB95-127510] p 1493 N95-21423

Stability of pressure and velocity computations for heterogeneous reservoirs
[PB95-110284] p 1354 N95-21656

ELLIPTIC FUNCTIONS

Elliptic genera for Z/K-manifolds I
[PB95-109096] p 1496 N95-22355

ELLIPTICAL GALAXIES

Far-infrared mapping of dusty elliptical galaxies
p 1593 N95-21763

ELLIPTICAL ORBITS

Orbit determination of highly elliptical Earth orbiters using improved Doppler data-processing modes
p 1218 N95-21533

Nonlinear dynamics of the planar pitch attitude motion for a gravity-gradient satellite
[AD-A286407] p 1220 N95-22204

ELLIPTICAL POLARIZATION

Effect of cell size on elliptically polarized radar clutter statistics
[AD-A285789] p 1311 N95-22401

EMBEDDING

The thermal conductivity of carbon coated silicon carbide fibers embedded in a silicon carbide matrix
[DE94-017758] p 1225 N95-20023

The Modified Embedded Atom Method
[DE94-015746] p 1564 N95-20142

An IRAS Hires study of low mass star formation in the Taurus molecular ring p 1593 N95-21767

Embedded optical fibres as strain sensors in polymer matrix fibre composites: The influence of adhesion in strain transfer
[PB95-133617] p 1547 N95-22140

The Modified Embedded Atom Method
[DE94-017958] p 1248 N95-22273

EMERGENCIES

QoS driven routing in packet switched networks of multiple transmission media p 1292 N95-20923

EMISSION

Universal features of multiplicity distributions
[DE94-012854] p 1498 N95-20779

Micrometeorological methods for measurements of mercury emissions over contaminated soils
[DE94-017679] p 1411 N95-22342

EMISSION SPECTRA

Surface characterization and contamination analysis
[NASA-CR-197374] p 1238 N95-20557

Enhancements in the Livermore spectrum analysis package PIXEF
[DE95-002487] p 1272 N95-20895

Two-dimensional imaging of OH in a lean burning high pressure combustor
[NASA-TM-106854] p 1214 N95-21383

EMITTANCE

Qualification test results for blue-red reflecting solar covers p 1320 N95-20525

Angle resolved Auger electron spectroscopy: An alternate tool for identifying electronic excitation processes in solids
[AD-A285375] p 1238 N95-20555

Emittance growth due to negative-mass instability above transition
[DE95-002527] p 1534 N95-20900

Issues in multi-bunch emittance preservation in the NLC
[DE95-002894] p 1534 N95-21253

First results from the final focus test beam
[DE95-002897] p 1535 N95-21255

Emittance dilution by ions in the SLC arcs
[DE95-002871] p 1536 N95-21332

RF vacuum microelectronics based on thin film edge-emitter technology
[AD-A279539] p 1331 N95-21690

Proposed emittance upgrade for the SLC damping rings
[DE95-002887] p 1538 N95-22155

EMITTERS

Optimization of InAsSb/InGaAs strained-layer superlattice growth by metal-organic chemical vapor deposition for use in infrared emitters
[DE94-016557] p 1563 N95-19954

Annealing of irradiated n+p InP buried homojunctions
p 1320 N95-20524

Field-emitter arrays for RF vacuum microelectronics
[AD-A279959] p 1325 N95-20661

Emitter location via Kalman filtering of signal time difference of arrival
[AD-A285972] p 1291 N95-20666

EMPLOYMENT

Beyond telecommuting: A new paradigm for the effect of telecommunications on travel
[DE95-001224] p 1289 N95-20214

EMULSIONS

Novel electrochemical materials prepared by sol-gel chemistry
[AD-A286310] p 1226 N95-20092

ENCAPSULATING

The Photovolatic Manufacturing Technology project (PVMaT) after three years
[DE94-011877] p 1392 N95-20473

Enhancement of cell mediated immunity through non-specific immunostimulation with liposome encapsulated gamma-interferon
[AD-A279667] p 1442 N95-20602

Synthesis of polymeric microcapsule arrays and their use for enzyme immobilization
[AD-A279125] p 1277 N95-21876

ENCLOSURE

Global equivalence ratio concept and the prediction of carbon monoxide formation in enclosure fires
[PB94-207511] p 1234 N95-20100

ENDOTHERMIC REACTIONS

Ferrocyanide safety project Dynamic X-Ray Diffraction studies of sodium nickel ferrocyanide reactions with equimolar nitrate/nitrite salts
[DE94-017396] p 1236 N95-20268

Subduction and volatile recycling in Earth's mantle
p 1421 N95-21802

ENERGETIC PARTICLES

Ion scattering and deposition: The role of energetic particles in thin film growth
[AD-A285975] p 1514 N95-20667

Numerical analysis of energetic particle stabilization of ballooning modes in finite-aspect-ratio tokamaks
[DE94-631397] p 1556 N95-21164

Search for Centauro events in the DO Detector at Fermilab collider
[DE95-002522] p 1535 N95-21314

Solar wind composition
[NASA-TM-197364] p 1604 N95-22384

ENERGY ABSORPTION

Impact behavior of FeAl alloy FA-350
[DE94-018128] p 1254 N95-20705

Method and apparatus for classifying targets
[AD-D016519] p 1303 N95-21464

ENERGY BUDGETS

Radiative forcing calculations for CH3Cl
[DE94-019018] p 1402 N95-20355

ENERGY CONSERVATION

Research on the promotion measures to introduce new energy and energy-saving technologies with a leasing system
[DE95-714801] p 1375 N95-22079

ENERGY CONSUMPTION

Effects of battery technologies, driving patterns, and climate comfort control on the performance of electric vehicles
[DE95-001102] p 1329 N95-21296

Performance testing of the AC propulsion ELX electric vehicle
[DE95-002049] p 1330 N95-21471

Design of a 10 bit 10k Samples/s low power CMOS ADC
[PB95-110425] p 1455 N95-22018

ENERGY CONVERSION

Research in the chemical sciences: Summaries of FY 1994
[DE94-015427] p 1223 N95-20264

Modeling of high efficiency solar cells under laser pulse for power beaming applications p 1318 N95-20516

High efficiency GaP power conversion for Betavoltaic applications p 1323 N95-20540

Approaches to the design of structural ceramics incorporating whiskers and particulate phases
[DE94-018126] p 1271 N95-20704

A fuel cell overview
[DE95-001455] p 1393 N95-20839

Exploratory Technology Research Program for electrochemical energy storage
[DE95-002652] p 1394 N95-20915

Use of the National Ignition Facility for the development of inertial fusion energy
[DE94-016696] p 1557 N95-21206

ENERGY CONVERSION EFFICIENCY

Chemical beam epitaxy for high efficiency photovoltaic devices p 1316 N95-20508

Status of diffused junction p+n InP solar cells for space applications p 1317 N95-20509

Design of high-efficiency, radiation-hard, GaInP/GaAs solar cells p 1319 N95-20521

InGaAs PV device development for TPV power systems p 1322 N95-20537

Pulsed laser illumination of photovoltaic cells
p 1323 N95-20538

High efficiency GaP power conversion for Betavoltaic applications p 1323 N95-20540

Review of solar cell temperature coefficients for space
p 1323 N95-20541

Effects of plasma hydrogenation on trapping properties of dislocations in heteroepitaxial InP/GaAs
p 1323 N95-20542

Cryogenic pellet laser plasma source targets
[DE95-002488] p 1376 N95-22169

Coherence properties of high order harmonic radiation
[DE94-016974] p 1377 N95-22312

ENERGY DISSIPATION

A photophysical control mechanism for zeaxanthin-associated radiationless energy dissipation in photosynthesis
[DE94-018383] p 1437 N95-19969

Magnetic fluctuation induced transport and edge dynamo measurements in the MST reversed-field pinch
[DE95-000591] p 1549 N95-20114

Atomic-resolution characterization of interface structure and chemistry in the STEM
[DE94-017753] p 1567 N95-20492

The use of displacement damage dose to correlate degradation in solar cells exposed to different radiations
p 1320 N95-20523

Parasitic current collection by solar arrays in LEO
p 1321 N95-20527

On FEL integral equation and electron energy loss in intermediate gain regime
[DE94-770631] p 1371 N95-20757

Time of flight spectroscopy with muonic hydrogen
[DE94-017056] p 1245 N95-21845

High performance computing for beam physics applications
[DE94-018312] p 1539 N95-22243

ENERGY DISTRIBUTION
A new alpha particle diagnostic using knock-on ion tails
[DE94-015856] p 1553 N95-20402
Excess energy and structural dependence of the rate of energy redistribution during the photodissociation of iodotoluenes
[AD-A279997] p 1241 N95-21124
Ab initio potential energy surface for H + OCS reactions: Extended basis sets and correlation treatment
[AD-A286420] p 1247 N95-22207

ENERGY GAPS (SOLID STATE)
Optimization of InAsSb/InGaAs strained-layer superlattice growth by metal-organic chemical vapor deposition for use in infrared emitters
[DE94-016557] p 1563 N95-19954
InGaAs PV device development for TPV power systems p 1322 N95-20537
Magnetic field dependence of the correlation gap in SmB6
[DE95-001684] p 1574 N95-21570
Performance of Ga(0.47)In(0.53)As cells over a range of proton energies
[NASA-TM-106819] p 1334 N95-22112

ENERGY LEVELS
Ultrafast magnetoexciton dynamics in GaAs
[DE94-018175] p 1514 N95-20732
Collisional redistribution effects on x ray laser saturation behavior
[DE94-017308] p 1374 N95-21663
Electronic structure and energies of alkaline earth oxides: MgO, CaO and SrO
[DE94-628990] p 1575 N95-21853
Electronic structure and relative stability of icosahedral superatoms in Al-transition-metal alloys
[DE94-628996] p 1260 N95-21855
Universal spectral correlations at the mobility edge
[DE94-629031] p 1528 N95-22217

ENERGY OF FORMATION
IR materials producibility
[AD-A280094] p 1328 N95-21017
Effect of the electron-SO-phonon on the impurity state energies in a semiconductor quantum well
[DE94-628993] p 1581 N95-21887

ENERGY POLICY
Proceedings of the 1994 DOE/NREL Hydrogen Program Review
[DE94-011835] p 1234 N95-20117
Energy and environmental issues and international opperation in Asia
[DE94-796596] p 1404 N95-21143
Research on the promotion measures to introduce new energy and energy-saving technologies with a leasing system
[DE95-714801] p 1375 N95-22079

ENERGY SOURCES
Accelerators for energy production
[DE94-770764] p 1392 N95-20685
The Materials Corrosion and Environmental Effects Laboratory (MCEL)
[DE94-018268] p 1254 N95-20816

ENERGY SPECTRA
Ion temperature measurement of indirectly-driven implosions using a geometry-compensated neutron time-of-flight detector
[DE94-016967] p 1552 N95-20362
On the asymptotic similarity of rotating homogeneous turbulence p 1345 N95-21058
Heavy ion track-structure calculations for radial dose in arbitrary materials
[NASA-TP-3497] p 1517 N95-21191
Physics of correlated studies
[DE95-001204] p 1581 N95-21842
Electronic structure and relative stability of icosahedral superatoms in Al-transition-metal alloys
[DE94-628996] p 1260 N95-21855
Observations of cold magnetospheric ions at geosynchronous orbit during times of high activity
[DE95-000936] p 1600 N95-21935
Experimental study of interactions of highly charged ions with atoms at keV energies
[DE94-018648] p 1529 N95-22316
Notes on rotating turbulence p 1359 N95-22444

ENERGY STORAGE
The Materials Corrosion and Environmental Effects Laboratory (MCEL)
[DE94-018268] p 1254 N95-20816
An overview: Component development for solar thermal systems
[DE95-001623] p 1393 N95-20862
Mars power system concept definition study. Volume 1: Study results
[NASA-CR-195420-VOL-1] p 1396 N95-21952
Mars power system concept definition study. Volume 2: Appendices
[NASA-CR-195420-VOL-2] p 1396 N95-21953
Quantum chemical study of rare gas/halide interactions as a model for high energy density material. 2: The interaction of hydrogen chloride with the rare gas xenon
[AD-A286385] p 1248 N95-22321
Advanced energy systems and technologies research programme
[DE95-717486] p 1397 N95-22337
Indian Academy of Sciences. Volume 105, number 6, December 1993. Proceedings of the 2nd International Conference on Solar Energy Storage Applied Photochemistry
[AD-A286481] p 1605 N95-22394

ENERGY TECHNOLOGY
Energy and Technology Review
[DE94-017686] p 1219 N95-20148
Proceedings of the 1993 Non-Fluorocarbon Insulation, Refrigeration and Air Conditioning Technology Workshop
[DE94-018333] p 1285 N95-20194
Research in the chemical sciences: Summaries of FY 1994
[DE94-015427] p 1223 N95-20264
Energy impacts of controlling carbon dioxide emissions from an integrated gasification/combined-cycle system
[DE94-016878] p 1403 N95-20478
An update on the Department of Energy's photovoltaic program p 1316 N95-20505
Rare earth garnet selective emitter
p 1322 N95-20536
The Energy Science and Technology Database on a local library system: A case study at the Los Alamos National Research Library
[DE95-001009] p 1589 N95-20818
Technical and economic evaluation of natural gas based synthesis gas production technologies
[PB95-130597] p 1242 N95-21426
Applications of ICP magnetic sector multicollector mass spectrometry to basic energy research
[DE95-002600] p 1246 N95-21886
Research on the promotion measures to introduce new energy and energy-saving technologies with a leasing system
[DE95-714801] p 1375 N95-22079
Advanced energy systems and technologies research programme
[DE95-717486] p 1397 N95-22337
Indian Academy of Sciences. Volume 105, number 6, December 1993. Proceedings of the 2nd International Conference on Solar Energy Storage Applied Photochemistry
[AD-A286481] p 1605 N95-22394
Producing liquid fuels from biomass
[DE95-717458] p 1398 N95-22425
Wind Energy Program overview, fiscal year 1993
[DE94-000285] p 1398 N95-22468

ENERGY TRANSFER
A numerical investigation of energy transfer and subgrid-scale eddy viscosity in homogeneous, isotropic and shear turbulence
[AD-A280005] p 1339 N95-20058
Photodegradation and photophysics of laser dyes
[AD-A285105] p 1368 N95-20063
Plasma chemistry of vibrationally nonequilibrium molecules
[AD-A279630] p 1553 N95-20411
State-to-state collisional dynamics of atmospheric species
[AD-A285053] p 1370 N95-20484
Heavy ion track-structure calculations for radial dose in arbitrary materials
[NASA-TP-3497] p 1517 N95-21191
Single-collision studies of energy transfer and chemical reaction
[DE95-002943] p 1244 N95-21517

ENGINE DESIGN
Internal aerodynamics of a generic three-dimensional scramjet inlet at Mach 10
[NASA-TP-3476] p 1340 N95-20619
Turbine design and application
[NASA-SP-290] p 1214 N95-22341

ENGINE INLETS
Active control of fan noise-feasibility study. Volume 1: Flyover system noise studies
[NASA-CR-195392-VOL-1] p 1505 N95-21888

ENGINE NOISE
Active control of fan noise-feasibility study. Volume 1: Flyover system noise studies
[NASA-CR-195392-VOL-1] p 1505 N95-21888

ENGINE PARTS
Evaluation of PS 212 coatings under boundary lubrication conditions with an Ester-based oil to 300 C
[NASA-TM-106763] p 1223 N95-19901
Toughened Silcomp composites for gas turbine engine applications
[DE95-002851] p 1214 N95-21243

ENGINE TESTS
Statistical analysis of Turbine Engine Diagnostic (TED) field test data
[AD-A286032] p 1379 N95-20998
Portable static test facility for small, expendable, turbojet engines, phase 1
[AD-A286337] p 1216 N95-21719

ENGINEERING DRAWINGS
The ITER in-vessel system
[DE94-018053] p 1560 N95-21665

ENGINEERING MANAGEMENT
Improving cost efficiency in large programs
p 1584 N95-20743
Benefits of CMM-based software process improvement: Executive summary of initial results
[AD-A286444] p 1468 N95-21567
Interim profile: Development and trial of a method to rapidly measure software engineering maturity status
[AD-A279074] p 1468 N95-21627

ENRICHMENT
Nitrogen isotopic components in the early solar system p 1420 N95-21800

ENSTATITE
Phase E in a water-saturated peridotite system at 9.3 GPa p 1420 N95-21799

ENTHALPY
Conditional statistics in a turbulent premixed flame derived from direct numerical simulation
p 1249 N95-22438

ENTIRE FUNCTIONS
The method of evaluating quantum partition function for the Hubbard model
[DE94-628991] p 1581 N95-21639

ENTRAINMENT
Entrainment in a shear-free turbulent mixing layer
p 1350 N95-21083
Numerical simulation of spatially-developing planar jets p 1351 N95-21087
Mixing and dynamics of the Mediterranean outflow
[AD-A279803] p 1434 N95-21306
Fourth International Symposium on Stratified Flows, volume 4
[AD-A286453] p 1358 N95-22424

ENTROPY
Digital filtering for data compression in telemetry systems
[DE94-016611] p 1219 N95-20567
Thermodynamic analysis of stable and metastable equilibrium diagrams of the Cu-Cr system
[PB95-127775] p 1255 N95-21111

ENUMERATION
An exact enumeration of self-avoiding loops on a square lattice
[DE94-628999] p 1578 N95-22276

ENVIRONMENT EFFECTS
Dust Bowl migration as an analog for possible global warming-induced migration from Mexico
[DE94-017472] p 1401 N95-20089
Corrosion of aircraft materials: Correlation between nanometer scale and macroscopic structural damage parameters
[AD-A285930] p 1252 N95-20299
The effect of regional-scale soil-moisture deficits on mesoscale atmospheric dynamics that influence fire severity
[DE95-002682] p 1413 N95-20455
Molten carbonate fuel cell product development test
[DE95-000005] p 1324 N95-20574
The Materials Corrosion and Environmental Effects Laboratory (MCEL)
[DE94-018268] p 1254 N95-20816
Computer model predictions of the local effects of large, solid-fuel rocket motors on stratospheric ozone
[AD-A285632] p 1404 N95-21150
Definition report on environmental indices in future environmental assessments environmental balance/environmental outlook
[PB95-131876] p 1405 N95-21350
Environmental Hazards Assessment Program
[DE94-019075] p 1406 N95-21565
Air pollution caused by fireworks during the turn of the year 1992-1993
[PB95-135265] p 1409 N95-21718
Methods and opportunities in the recycling of rare Earth based materials
[DE95-001680] p 1259 N95-21737
Compilation of 1993 annual reports of the Navy ELF Communications System Ecological Monitoring Program. Volume 2: Tabs C-F
[AD-A279770] p 1308 N95-21988
Initial assessment of the hazards and risks of new chemicals to man and the environment, part 2
[PB95-106407] p 1410 N95-22124
Environmental Compliance Assessment System (ECAS): Japan settlement
[AD-A279328] p 1410 N95-22142

Assessment of the atmospheric hazards and risks of new chemicals: Procedures to estimate hazard potentials
[PB95-107488] p 1410 N95-22186
Launch safety, toxicity, and environmental effects of the high performance oxidizer ClF(5)
[AD-A286095] p 1284 N95-22227

ENVIRONMENT MANAGEMENT
Environmental Compliance Assessment and Management Program
[AD-A279605] p 1402 N95-20441
Possible global environmental impacts of solid waste practices
[DE95-000830] p 1406 N95-21487
Selection of substances to be considered in the environmental balance/environmental outlook in relation to the dissemination theme
[PB95-132197] p 1407 N95-21635
Environmental Compliance Assessment and Management Program (ECAMP), South Carolina supplement
[AD-A279533] p 1408 N95-21689
Environmental Compliance Assessment System (ECAS): Japan settlement
[AD-A279328] p 1410 N95-22142

ENVIRONMENT POLLUTION
Mercury usage and alternatives in the electrical and electronics industries
[PB94-165362] p 1312 N95-19966
Performance specifications for technology development: Application for characterization of volatile organic compounds in the environment
[DE94-016627] p 1401 N95-20234
Environmental Compliance Assessment and Management Program
[AD-A279605] p 1402 N95-20441
Environmental cleanup technology transfer initiatives
[AD-A285059] p 1403 N95-20487
Guidelines for qualifying cleaning and verification materials
[NASA-TM-108474] p 1270 N95-20694
Possible global environmental impacts of solid waste practices
[DE95-000830] p 1406 N95-21487
Environmental Hazards Assessment Program
[DE94-019075] p 1406 N95-21565
Spectroscopic studies of hazardous fuel interactions with soils
[AD-A279099] p 1407 N95-21596
Implementation of electronic chain-of-custody, analysis requests, and data verification at Los Alamos National Laboratory
[DE94-018076] p 1407 N95-21666
Launch safety, toxicity, and environmental effects of the high performance oxidizer ClF(5)
[AD-A286095] p 1284 N95-22227

ENVIRONMENT PROTECTION
Calculation methods for criteria air pollutant emission inventories
[AD-A284675] p 1400 N95-19964
Environmental Compliance Assessment and Management Program
[AD-A279605] p 1402 N95-20441
Environmental cleanup technology transfer initiatives
[AD-A285059] p 1403 N95-20487
Environmental Compliance Assessment Protocol - Centers for Disease Control and Prevention (ECAP-CDC), West Virginia supplement
[AD-A286009] p 1403 N95-20720
Energy and environmental issues and international opperation in Asia
[DE94-796596] p 1404 N95-21143
Disinfection of purified waste water with ultra violet light on a technical scale
[PB95-131926] p 1405 N95-21330
Monitoring activities in the framework of the Dutch National Air Quality Monitoring Network in 1994
[PB95-131884] p 1406 N95-21351
Removal of CO2 in closed loop off-gas treatment systems
[DE94-019259] p 1407 N95-21617
Environmental Compliance Assessment and Management Program (ECAMP), South Carolina supplement
[AD-A279533] p 1408 N95-21689
Environmental Compliance Assessment System (ECAS): Oregon supplement
[AD-A279565] p 1408 N95-21696
Ozone-depleting-substance control and phase-out plan
[DE95-001647] p 1409 N95-21722
Compilation of 1993 annual reports of the Navy ELF Communications System Ecological Monitoring Program. Volume 2: Tabs C-F
[AD-A279770] p 1308 N95-21988
Initial assessment of the hazards and risks of new chemicals to man and the environment, part 2
[PB95-106407] p 1410 N95-22124
Derivation of preliminary maximum permissible concentrations of volatile compounds in air
[PB95-107447] p 1410 N95-22125
Guidelines for the creation and management of geographic data bases within a GIS environment, version 1.0. Volume 2. Appendices
[DE94-019215] p 1591 N95-22129
Environmental Compliance Assessment System (ECAS): Japan settlement
[AD-A279328] p 1410 N95-22142
Proceedings of the 4th Annual Major Range and TestFacility Base (MRTFB) Environmental Workshop
[AD-A285779] p 1411 N95-22414
Fuzzy clustering of facial form for prototyping environmental protection equipment
[DE94-014657] p 1454 N95-22466

ENVIRONMENT SIMULATION
Measuring presence in virtual environments
[AD-A286183] p 1460 N95-20326

ENVIRONMENTAL CHEMISTRY
Investigation on research for degradable plastics
[DE94-796550] p 1277 N95-21714

ENVIRONMENTAL ENGINEERING
Long Time Series Measurements in the Coastal Ocean: A workshop
[AD-A279509] p 1435 N95-21682
ANSTO: Program of research, 1993-1994
[DE94-631122] p 1605 N95-21828

ENVIRONMENTAL INDEX
Definition report on environmental indices in future environmental assessments environmental balance/environmental outlook
[PB95-131876] p 1405 N95-21350

ENVIRONMENTAL LABORATORIES
Sustaining the health and performance of soldiers/warfighters deployed to harsh environments
[AD-A286270] p 1446 N95-22004

ENVIRONMENTAL MONITORING
USAF cellular mechanism of turnover of the stress induced protein HSP70
[AD-A285618] p 1441 N95-19898
Environmental Compliance Assessment and Management Program
[AD-A279605] p 1402 N95-20441
Possible global environmental impacts of solid waste practices
[DE95-000830] p 1406 N95-21487
Implementation of electronic chain-of-custody, analysis requests, and data verification at Los Alamos National Laboratory
[DE94-018076] p 1407 N95-21666
Definition report on target and related steering variables of radiation as a part of the environmental balance and environmental outlook investigation
[PB95-135471] p 1409 N95-21846

ENVIRONMENTAL QUALITY
Closure on the global carbon cycle
[DE94-018617] p 1404 N95-20991
Derivation of preliminary maximum permissible concentrations of volatile compounds in air
[PB95-107447] p 1410 N95-22125
Derivation of maximum permissible concentrations for several volatile compounds for water and soil
[PB95-107454] p 1411 N95-22381

ENVIRONMENTAL SURVEYS
Selection of substances to be considered in the environmental balance/environmental outlook in relation to the dissemination theme
[PB95-132197] p 1407 N95-21635
The mechanisms and effects off the plant-activations of chemicals in the environment
[AD-A279388] p 1356 N95-22145

ENVIRONMENTAL TESTS
The environmental durability of fiber reinforced ceramic matrix composites
[AD-A283750] p 1225 N95-19919
Test Operations Procedure (TOP) 1-2-616 tropic exposure testing
[AD-A286376] p 1235 N95-20230
Evaluation of stress experienced by soldiers wearing chemical protective clothing during varying work loads in desert or tropical environments
[AD-A280113] p 1452 N95-20625

ENZYME ACTIVITY
Process strategies in the enzymatic resolution of enantiomers
[PB95-107850] p 1437 N95-20208
A low energy continuous reactor separator for the production of ethanol from corn grits/starch and biomass streams
[DE95-002256] p 1283 N95-21356
Structures and functions of oligosaccharins
[DE95-003195] p 1440 N95-22220

ENZYMES
Process strategies in the enzymatic resolution of enantiomers
[PB95-107850] p 1437 N95-20208
Bacterial luciferase: Determination of the structure by x-ray diffraction
[AD-A279699] p 1437 N95-20711
Calculation of atom-centered partial charges for heme
[DE94-014447] p 1520 N95-21375
Synthesis of polymeric microcapsule arrays and their use for enzyme immobilization
[AD-A279125] p 1277 N95-21876

EPIDEMIOLOGY
Urban air carcinogens and their effects on health
[DE95-002259] p 1447 N95-22285
Current concepts on airborne particles and health
[DE95-002260] p 1447 N95-22287

EPITAXY
Visible light emitting materials and injection devices
[AD-A284796] p 1541 N95-20066
Simulations of the dislocation array at Ge/Si interfaces
[DE94-017680] p 1565 N95-20244
Surface stress, morphological development, and dislocation nucleation during strained-layer epitaxy
[DE94-017682] p 1565 N95-20245
High-efficiency, deep-junction, epitaxial InP solar cells on (100) and (111)B InP substrates
p 1316 N95-20507
P/N InP solar cells on Ge wafers
p 1317 N95-20511
Performance, defect behavior and carrier enhancement in low energy, proton irradiated p+nn+ InP solar cells
p 1319 N95-20518
P/N In(Al) GaAs multijunction laser power converters
p 1323 N95-20539
Effects of plasma hydrogenation on trapping properties of dislocations in heteroepitaxial InP/GaAs
p 1323 N95-20542
Nucleation, growth, and strain relaxation of lattice-mismatched 3-5 semiconductor epitaxial layers
p 1324 N95-20543
Antiphase boundaries as nucleation centers in low-temperature epitaxial growth
[AD-A279895] p 1568 N95-20594
Growth, characterization and device development in monocrystalline diamond films
[AD-A285991] p 1568 N95-20614
The in situ observation of epitaxial diamond thin film nucleation and growth using emission electron microscopy
[AD-A279811] p 1569 N95-20807
Scanning tunneling microscopy of semiconductor surfaces
[AD-A279982] p 1571 N95-20964
Ultra-high aggregate bandwidth two-dimensional multiple-wavelength diode laser arrays
[AD-A280098] p 1372 N95-21019
Epitaxial liftoff technology onto processed silicon foundry wafers
[AD-A285621] p 1571 N95-21145
Interlayer magnetic coupling in epitaxial Fe/Cr(211) and (100) superlattices
[DE95-002906] p 1571 N95-21256
Reciprocal space mapping of epitaxial materials using position-sensitive x-ray detection
[DE95-001620] p 1575 N95-21991

EPOXY MATRIX COMPOSITES
Significance of impact velocity for the extent of damage in carbon/epoxy laminates
[PB95-133484] p 1230 N95-21417
Effect of laser radiation on carbon fibre/epoxy composites
[PB95-133526] p 1232 N95-22096

EPOXY RESINS
VOC compliant wash primer
[AD-A286034] p 1273 N95-21000
Damage tolerance of carbon fibre polyetheretherketone laminates
[PB95-131611] p 1230 N95-21432
Epoxy lining for shipboard piping systems
[AD-A286228] p 1279 N95-22022
Towards tailored interphase formation utilizing surface-bound benzylsulfonium salts as cationic initiators
[AD-A286461] p 1280 N95-22259

EQUATIONS OF MOTION
Matrix formulation of the particle motion in crystalline beams
[DE94-017301] p 1563 N95-19925
Comparison of meteorological data with fitted values extracted from projectile trajectory
[AD-A285921] p 1428 N95-19989
Hybrid model in general geometry
[DE95-002614] p 1553 N95-20437
Three-dimensional laser cooling
[DE94-017963] p 1370 N95-20569

Large eddy simulation of channel flow using a vorticity transport subgrid model p 1348 N95-21076
A model of an infinite length, axisymmetric, isotropic, forced thick shell
[AD-A285586] p 1386 N95-21212
On the Aharonov-Bohm effect with neutrons
[DE95-002985] p 1521 N95-21454
1/f noise in two-dimensional fluids
[DE95-002617] p 1358 N95-22307
Direct numerical simulations of on-demand vortex generators: Mathematical formulation
p 1361 N95-22452

EQUATIONS OF STATE
On the Taylor test. Part 3: A continuum mechanics code analysis of steady plastic wave propagation
[DE95-002252] p 1501 N95-20869
Hydrogen and related materials at high density: Physics, chemistry and planetary implications
p 1418 N95-21791
Storage and recycling of water and carbon dioxide in the earth p 1425 N95-21822
Variational Monte Carlo study of He-4 in two dimensions
[DE94-629078] p 1576 N95-21998
Thermophysical properties of HFC-143a and HFC-152a
[DE95-002199] p 1582 N95-22153

EQUATORIAL REGIONS
Hydrographic data from equatorial Pacific waters near the Galapagos
[AD-A283741] p 1431 N95-19918
Mitigation of the effects of F layer regularities by using multiple paths p 1298 N95-20951
Semi-volatiles at Mercury: Sodium (Na) and potassium (K) p 1424 N95-21818
Exchanges between hemispheres and gyres: A direct approach to the mean circulation of the equatorial Pacific
[NASA-CR-196311] p 1436 N95-22072

EQUILIBRIUM FLOW
Stability of pressure and velocity computations for heterogeneous reservoirs
[PB95-110284] p 1354 N95-21656
Large-eddy simulation of a boundary layer with concave streamwise curvature p 1360 N95-22450

EQUIVALENCE
Duality and equivalencies in closed tandem queueing networks
[PB95-132502] p 1482 N95-21271
Testing the principle of equivalence by solar neutrinos
[DE94-014972] p 1604 N95-22064

ERBIUM
Rare earth garnet selective emitter
p 1322 N95-20536

ERBIUM ALLOYS
The low temperature properties of (Dy(1-x)Er(x))Ni2 alloys
[DE95-001657] p 1260 N95-21923

ERGODIC PROCESS
Invariant measures of interval maps
[PB95-107835] p 1389 N95-20207

ERGOMETERS
A method to determine the kinematics of the lower limbs of a subject pedaling a bicycle using encoders and accelerometers
[NASA-CR-197401] p 1453 N95-21866

EROSION
Aircraft corrosion study
[AD-A279527] p 1259 N95-21687
Dynamics of volatile delivery from outer to inner solar system p 1420 N95-21798

ERROR ANALYSIS
A simple analytical model for asynchronous dense WDM/OOK systems
[AD-A283725] p 1289 N95-19973
A-posteriori estimation and adaptive control of the pollution-error in the h-version of the finite element method
[AD-A285670] p 1480 N95-20083
Iterated-bootstrap confidence intervals for the mean
[AD-A279802] p 1498 N95-20102
Uncertainty estimates for derivatives and intercepts
[DE94-018492] p 1489 N95-20222
Error analysis in wind turbine field testing
[DE94-011864] p 1391 N95-20260
Analysis of direct detection lightwave systems with optical amplifiers
[AD-A284077] p 1542 N95-20467
On commonalities in signal design for non-Gaussian channels
[AD-A285385] p 1498 N95-20608
Error probabilities of FFH/BFSK with noise normalization and soft decision viterbi decoding in a fading channel with partial-band jamming
[AD-A280041] p 1498 N95-20620
An empirical approach to logical clustering of software failure regions
[AD-A279863] p 1462 N95-20776
Geographical diversity combining to exploit multi-mechanism propagation p 1299 N95-20957
Error analysis of the quadratic nodal expansion method in slab geometry
[DE95-001352] p 1492 N95-21285
Error committed by stopping the Newton iteration in Runge-Kutta methods and linear multistep methods
[PB95-106324] p 1492 N95-21421
Orbit determination of highly elliptical Earth orbiters using improved Doppler data-processing modes
p 1218 N95-21533
Analysis of a local defect correction approach on composite grids
[PB95-135455] p 1493 N95-21574
Initial experience with noncorrecting syntax error handling
[PB95-132700] p 1471 N95-22029
LADAR detection statistics in the presence of pointing errors
[AD-A285865] p 1309 N95-22134
Performance of a fast frequency-hopped noncoherent MFSK receiver over Rician fading channels with either partial-band interference or multi-tone interference
[AD-A286168] p 1310 N95-22246
Pollution error in the H-version of the finite element method and the local quality of A-posteriori error estimators
[AD-A279868] p 1497 N95-22388
Simulation of structural response using a recurrent radial basis function network
[DE94-017342] p 1486 N95-22409

ERROR CORRECTING CODES
Fault tolerance of neural networks
[AD-A285098] p 1479 N95-20057
Seamless data-range change using punctured convolutional codes for time-varying signal-to-noise ratios p 1304 N95-21534
Turbo codes for deep-space communications
p 1304 N95-21535

ERROR CORRECTING DEVICES
Analysis of a local defect correction approach on composite grids
[PB95-135455] p 1493 N95-21574

ERROR DETECTION CODES
New method for integrity constraint checking in deductive databases
[PB95-110672] p 1586 N95-19904
Initial experience with noncorrecting syntax error handling
[PB95-132700] p 1471 N95-22029
Top-down non-correcting error recovery in LLgen
[PB95-132718] p 1471 N95-22031
Computing symmetries and stubborn sets
[PB95-127700] p 1472 N95-22328

ERROR FUNCTIONS
Neural network construction via back-propagation
[DE95-002867] p 1482 N95-21249

ERRORS
A-posteriori estimation and adaptive control of the pollution-error in the h-version of the finite element method
[AD-A285670] p 1480 N95-20083
EPICS simulation tools for control system development
[DE94-018082] p 1462 N95-20699
Conservative smoothing versus artificial viscosity
[DE95-001108] p 1341 N95-20831
Backward error recovery in redundant disk arrays
[AD-A286064] p 1463 N95-20846
Multipath impact on ground-based global positioning system range measurements: Aspects of measurement, modeling, and mitigation p 1297 N95-20949
Impact of propagation mechanisms on global navigation satellite system performance p 1298 N95-20950
Geographical diversity combining to exploit multi-mechanism propagation p 1299 N95-20957
Accuracy problems in the generation of discrete time stochastic processes
[PB95-131397] p 1386 N95-21133
Neural network construction via back-propagation
[DE95-002867] p 1482 N95-21249
Design and development SAWAFE peak detector chip
[DE95-001745] p 1332 N95-21742
SEU and SEL response of the Westinghouse 64K E-2PROM, analog devices AD7876 12-bit ADC, and the Intel 82527 Serial Communications Controller
[DE95-003349] p 1334 N95-22086
Adaptive fault-resistant systems
[AD-A286406] p 1484 N95-22203
Pollution error in the H-version of the finite element method and the local quality of A-posteriori error estimators
[AD-A279868] p 1497 N95-22388
A survey of artificial neural network applications in flow analysis of energy networks
[DE95-002452] p 1486 N95-22430

ESTERS
Polyurethane-acrylic interpenetrating polymer network acoustic damping material
[AD-D016572] p 1266 N95-20294
Thermo-mechanical fatigue of polymer matrix composites
[AD-A285931] p 1267 N95-20390

ESTIMATES
Structure and dynamics of turbulent wall layers
[AD-A285360] p 1340 N95-20547
Development of a fast sampling system for estimation of impulse responses of mobile radio channels
p 1296 N95-20943
Nitrogen isotopic components in the early solar system p 1420 N95-21800
Alkali element depletion by core formation and vaporization on the early Earth p 1421 N95-21804

ESTIMATING
Intrinsic barriers for H-atom transfer reactions
[DE94-018914] p 1507 N95-20049
Anaerobic digestion analysis model: User's manual
[DE94-011858] p 1437 N95-20471
Modeling and identification of parallel and feedback nonlinear systems
[DE95-001006] p 1481 N95-20812
Exponential deconvolution: Two asymptotically equivalent estimators
[PB95-132122] p 1499 N95-21469
BASIC program for power spectrum estimation
[DE95-002228] p 1468 N95-21515

ETA-MESONS
Theories of the eta-meson-nucleus interaction
[DE94-016055] p 1516 N95-21125

ETCHING
Study on the reaction kinetics in pulsed RF discharges under RIE conditions
[PB95-107868] p 1300 N95-21029
Plasma-induced-damage of GaAs during etching of refractory metal contacts
[DE95-001525] p 1259 N95-21838
Method for laser-assisted silicon etching using halocarbon ambients
[AD-D016494] p 1375 N95-21903
Design, fabrication, and characterization of reflective diffractive optical elements in Si for free-space optical interconnects
[AD-A286416] p 1547 N95-22205

ETHANE
Structure of dibis(diethyldithiocarbamato) zinc (2) Mu-bis(diethylphosphino)ethane toluene(2)
[AD-A279792] p 1224 N95-20660
Aging tests of ethylene contaminated argon/ethane
[DE95-002526] p 1282 N95-20899
Single-collision studies of energy transfer and chemical reaction
[DE95-002943] p 1244 N95-21517
Numerical study of contaminant effects on combustion of hydrogen, ethane, and methane in air
[NASA-TM-106844] p 1284 N95-22114

ETHERS
Polyurethane-acrylic interpenetrating polymer network acoustic damping material
[AD-D016572] p 1266 N95-20294
A new family of anion receptors and their effects on ion pair dissociation and conductivity of lithium salts in non-aqueous solutions
[DE94-016822] p 1512 N95-20477
New chiral pyrimidino-crown ether ligands
[AD-A279892] p 1223 N95-20590
Towards tailored interphase formation utilizing surface-bound benzylsulfonium salts as cationic initiators
[AD-A286461] p 1280 N95-22259

ETHYL ALCOHOL
Bioconversion of coal derived synthesis gas to liquid fuels
[DE94-018849] p 1314 N95-20339
A low energy continuous reactor separator for the production of ethanol from corn grits/starch and biomass streams
[DE95-002256] p 1283 N95-21356
Producing liquid fuels from biomass
[DE95-717458] p 1398 N95-22425

ETHYL COMPOUNDS
New chiral pyrimidino-crown ether ligands
[AD-A279892] p 1223 N95-20590
Structure of dibis(diethyldithiocarbamato) zinc (2) Mu-bis(diethylphosphino)ethane toluene(2)
[AD-A279792] p 1224 N95-20660
The permeation of bis(2-fluoro-2,2-dinitroethyl) formal (FEFO), ethyl 4,4-dinitropentanoate (EDNP), ethyl 4-nitropentanoate (ENP), and 1,2,4-trichlorobenzene (TCB) through barrier membranes
[DE95-002492] p 1283 N95-21514

ETHYLENE
Aging tests of ethylene contaminated argon/ethane
[DE95-002526] p 1282 N95-20899
The energetics and dynamics of free radicals, ions, and clusters
[DE94-018101] p 1244 N95-21701
Acid-site characterization of water-oxidized alumina films by near-edge x-ray absorption and soft x-ray photoemission
[DE95-003355] p 1247 N95-22234
ETHYLENE COMPOUNDS
Studies of the microwave resistivity of kappa-(BEDT-TTF)2Cu(N(CN)2)Cl
[DE95-002980] p 1262 N95-22291
ETHYLENE OXIDE
The development of a new plasticizer for poly(ethylene oxide) based polymer electrolyte and the investigation of their ion-pair dissociation effect
[DE94-016821] p 1276 N95-21644
ETHYLENEDIAMINE
Evaluation of an immobilized cell bioreactor for degradation of meta- and para-nitrobenzoate
[AD-A279719] p 1516 N95-20993
EULER EQUATIONS OF MOTION
One-dimensional reactive Euler equations
[PB95-135430] p 1244 N95-21573
Fluid dynamics of the freeboard in a fluidized bed reactor
[PB95-134029] p 1357 N95-22160
EULER-LAGRANGE EQUATION
Mathematical modeling of a class of multibody flexible spacecraft structures
[NASA-TM-109166] p 1219 N95-20800
EURECA (ESA)
Post-flight investigation programmes of recently retrieved solar generators p 1321 N95-20531
EUTECTIC ALLOYS
Sputtering of tin and gallium-tin clusters
[DE94-018389] p 1254 N95-20707
EUTECTIC COMPOSITES
The influence of chemistry and microstructure on the fracture toughness of V-V3Si in-situ composites
[DE94-018997] p 1232 N95-22126
EUTECTICS
Directional solidification of the alumina-zirconia ceramic eutectic system
[DE95-001677] p 1277 N95-21735
EUTROPHICATION
Assessment of the atmospheric hazards and risks of new chemicals: Procedures to estimate hazard potentials
[PB95-107488] p 1410 N95-22186
EVALUATION
Evaluation of pumping and fueling requirements for the ITER EDA
[DE94-018117] p 1560 N95-21702
EVAPORATION
The dynamics of formation and evaporation of mixed alkali halide nanocrystals: A case of comparable lattice energies
[AD-A285052] p 1567 N95-20483
An augmented Young-Laplace model of an evaporating meniscus in a micro-channel with high heat flux
[NASA-CR-197622] p 1340 N95-20796
Governing equations for multiphase heat and mass transfer in hygroscopic porous media with applications to clothing materials
[AD-A286418] p 1357 N95-22206
The enhancement of metallic silver monomer evaporation by the adhesion of polar molecules to silver nanocluster ions
[AD-A284936] p 1281 N95-22470
EVAPORATION RATE
An augmented Young-Laplace model of an evaporating meniscus in a micro-channel with high heat flux
[NASA-CR-197622] p 1340 N95-20796
EVAPORATORS
Seawater test results of Open-Cycle Ocean Thermal Energy Conversion (OC-OTEC) components
[DE94-019254] p 1396 N95-21897
EXCIMER LASERS
Sputtering of tin and gallium-tin clusters
[DE94-018389] p 1254 N95-20707
Tribology and surface mechanical properties of excimer laser nitrided titanium
[DE95-002751] p 1255 N95-21238
Time-resolved diagnostics of excimer laser-generated ablation plasmas used for pulsed laser deposition
[DE94-018950] p 1559 N95-21547
Method for laser-assisted silicon etching using halocarbon ambients
[AD-D016494] p 1375 N95-21903
EXCITATION
Cavity-QED enhancement of fluorescence yields in microdroplets
[DE94-018662] p 1506 N95-20030
The electronic properties of polysilanes
[DE94-006464] p 1265 N95-20121
Method and system of mapping acoustic near field
[AD-D016574] p 1504 N95-20296
Observation of excitonic and band-to-band behavior in ordered InGaP2 alloys
[DE94-018891] p 1314 N95-20341
Two-center, two electron excitations identified in NEXAFS for solid Ne
[AD-A285373] p 1568 N95-20553
Angle resolved Auger electron spectroscopy: An alternate tool for identifying electronic excitation processes in solids
[AD-A285375] p 1238 N95-20555
Publications/patents/presentations/honors/student eport. Investigation of the role of vibrational excitation in unimolecular reactions
[AD-A280044] p 1513 N95-20621
Magnetic excitations in modulated PrNi2Si2
[DE95-001077] p 1254 N95-20822
X-ray spectroscopy of xenon
[DE95-002132] p 1240 N95-20865
Correlated wavefunction Monte Carlo studies of excitations in the quantum Hall liquids
[DE95-002337] p 1501 N95-20874
Excess energy and structural dependence of the rate of energy redistribution during the photodissociation of iodotoluenes
[AD-A279997] p 1241 N95-21124
Ultraviolet laser emission properties of Ce(3+)-doped LiSrAlF6
[DE94-016364] p 1372 N95-21135
Studies of selenium and xenon in inductively coupled plasma mass spectrometry
[DE95-001676] p 1245 N95-21734
Molecular design concept for multi-kilovolt x-ray amplification
[DE95-001763] p 1374 N95-21743
Physics of correlated studies
[DE95-001204] p 1581 N95-21842
EXCITONS
Instantaneous frequency dynamics of coherent emission from magnetoexcitons in gallium arsenide
[DE94-018182] p 1569 N95-20677
Temporal and spectral investigation of multi-Landau level quantum beats in GaAs
[DE94-018189] p 1569 N95-20678
Ultrafast magnetoexciton dynamics in GaAs
[DE94-018175] p 1514 N95-20732
Excitons in semiconducting superlattices, quantum wells, and ternary alloys
[DE95-001867] p 1572 N95-21287
Theory of the excitonic lineshape in low-dimensional structures with rough interfaces
[DE95-003434] p 1582 N95-22237
EXERCISE PHYSIOLOGY
Microclimate cooling effect on perceived exertion in four heat/exercise scenarios
[AD-A285549] p 1444 N95-21160
EXHAUST EMISSION
Calculation methods for criteria air pollutant emission inventories
[AD-A284675] p 1400 N95-19964
Reducing exhaust gas emissions from Citydiesel busses
[DE95-700245] p 1380 N95-21295
Analysis of invalid emission testing in the California smog check program
[PB95-128922] p 1406 N95-21373
Two-dimensional imaging of OH in a lean burning high pressure combustor
[NASA-TM-106854] p 1214 N95-21383
EXHAUST FLOW SIMULATION
Radiation from advanced solid rocket motor plumes
[NASA-CR-196554] p 1221 N95-20124
EXHAUST GASES
Helium exhaust studies in the D3-D tokamak
[DE94-016682] p 1552 N95-20334
Reducing exhaust gas emissions from Citydiesel busses
[DE95-700245] p 1380 N95-21295
Ultraviolet emission from rocket motor plumes
[DSTO-TR-0002] p 1222 N95-21661
Gas-phase photocatalytic oxidation: Cost comparison with other air pollution control technologies
[DE95-000241] p 1410 N95-22278
EXHAUST SYSTEMS
Active control of fan noise-feasibility study. Volume 1: Flyover system noise studies
[NASA-CR-195392-VOL-1] p 1505 N95-21888
Natural gas converter performance and durability
[PB95-135554] p 1284 N95-21966
EXOBIOLOGY
Aerospace medicine and biology: A continuing bibliography with indexes (supplement 399)
[NASA-SP-7011(399)] p 1446 N95-21947
EXOTHERMIC REACTIONS
Safe conditions for contacting nitric acid or nitrates with Tri-n-Butyl Phosphate (TBP)
[DE95-001243] p 1235 N95-20215
Ferrocyanide safety project Dynamic X-Ray Diffraction studies of sodium nickel ferrocyanide reactions with equimolar nitrate/nitrite salts
[DE94-017396] p 1236 N95-20268
EXPANSION
Direct numerical simulation of turbulent flow in a sudden pipe expansion p 1347 N95-21067
EXPERIMENT DESIGN
National Ignition Facility: Experimental plan
[DE94-016542] p 1550 N95-20189
Statistical analysis of Turbine Engine Diagnostic (TED) field test data
[AD-A286032] p 1379 N95-20998
ITER EDA Newsletter. Volume 3, no. 2
[DE94-628980] p 1561 N95-21852
Latin hypercube sampling in sensitivity analysis
[AD-A285867] p 1499 N95-22135
Radio-frequency techniques at the ISIS pulsed muon source
[PB95-129854] p 1529 N95-22303
The Double Eagle Space Experiment (DESE) beamline design
[DE94-018319] p 1601 N95-22419
EXPERT SYSTEMS
Tests of an improved oceanographic expert system
[AD-A280123] p 1431 N95-19888
Generating examples for use in tutorial explanations: The use of a subsumption based classifier
[AD-A286028] p 1464 N95-20996
Knowledge refinement in a reflective architecture
[AD-A286027] p 1589 N95-21002
EXPERT system expert: Program description
[PB95-131561] p 1482 N95-21429
EXPERT system expert: Users manual
[PB95-131579] p 1482 N95-21430
SSME HPOTP post-test diagnostic system enhancement project
[NASA-CR-4643] p 1222 N95-21458
Communications and control for electric power systems: Power system stability applications of artificial neural networks
[NASA-CR-197594] p 1483 N95-21613
Advanced computing systems: Usability of knowledge-based planning systems
[AD-A279573] p 1477 N95-21698
Adaptive capture of expert behavior
[DE94-018285] p 1483 N95-21710
Verification of knowledge-based reasoning modules
[PB95-132692] p 1470 N95-21983
Communications and control for electric power systems: Power system stability applications of artificial neural networks
[NASA-CR-197333] p 1484 N95-22171
EXPLOSIONS
Analysis of experimentally shocked minerals by NMR spectroscopy
[DE95-002955] p 1573 N95-21449
EXPLOSIVE DEVICES
Test and Evaluation Plan (TEP) for Improvised Explosive Device Screening Systems (IEDSS)
[AD-A286382] p 1203 N95-22319
EXPLOSIVES
Compatibility testing of explosives and paints by chemiluminescence techniques
[PB95-133609] p 1275 N95-21275
The permeation of bis(2-fluoro-2,2-dinitroethyl) formal (FEFO), ethyl 4,4-dinitropentanoate (EDNP), ethyl 4-nitropentanoate (ENP), and 1,2,4-trichlorobenzene (TCB) through barrier membranes
[DE95-002492] p 1283 N95-21514
Evaluation of state-of-the-art high speed deluge systems presently in service at various US Army ammunition plants
[AD-A279102] p 1287 N95-21598
An initial assessment of the properties of 2,5-dipicryl-1,3,4-oxadiazole: A secondary explosive with high thermal stability
[MRL-TR-93-16] p 1284 N95-21624
The application of a statistical analysis software package to explosive testing
[MRL-TR-93-42] p 1284 N95-21658
Diffuse reflectance spectra of energetic material
[DSTO-TR-0065] p 1284 N95-21951
Sequential shock induced switch tests for Eglin Air Force Base
[DE95-001786] p 1334 N95-22062
EXPONENTIAL FUNCTIONS
Large eddy simulation of turbulent flow over a cavity
p 1347 N95-21069

EXPONENTS
Nonlinear dynamics of the planar pitch attitude motion for a gravity-gradient satellite
[AD-A286407] p 1220 N95-22204
EXPOSURE
The environmental durability of fiber reinforced ceramic matrix composites
[AD-A283750] p 1225 N95-19919
Fracture toughness properties of welded stainless steels for tritium service
[DE95-000755] p 1251 N95-20079
Application of an energy-based life prediction model to bithermal and thermomechanical fatigue
[NASA-TM-106684] p 1385 N95-20179
Test Operations Procedure (TOP) 1-2-616 tropic exposure testing
[AD-A286376] p 1235 N95-20230
Skeletal muscle ischemia and heat shock proteins
[AD-A285364] p 1442 N95-20549
Carboxyhemoglobin formation due to transient exposure to high level carbon monoxide: Experimental results and an explanatory model
[AD-A285476] p 1444 N95-20979
Urban air carcinogens and their effects on health
[DE95-002259] p 1447 N95-22285
EXTINCTION
Temporal evolution of turbulence/chemistry interactions in lifted, turbulent-jet flames
[DE95-002481] p 1243 N95-21512
EXTINGUISHING
A review of water mist technology for fire suppression
[AD-A285738] p 1202 N95-20071
EXTRACTION
Wavelet-based acoustic recognition of aircraft
[DE94-017701] p 1503 N95-20019
Novel catalysts for methane activation
[DE95-002639] p 1237 N95-20438
Feature extraction without edge detection
[AD-A279842] p 1473 N95-22386
EXTRAPOLATION
Has a standard model solution to the solar neutrino problem been found?
[DE94-017580] p 1604 N95-20490
Geometric characterization of electromigration voids (A statistical analysis of electromigration voids)
[AD-A286494] p 1328 N95-21169
EXTRAVEHICULAR ACTIVITY
STS 63: Post flight presentation
[NASA-TM-110514] p 1219 N95-21558
STS Flight 64 mission highlights
[NASA-TM-110515] p 1219 N95-22295
EXTREME ULTRAVIOLET RADIATION
Characterization of an expanded-field Schwarzschild objective for extreme ultraviolet lithography
[DE94-016780] p 1541 N95-20239
A URI program for Ultraviolet/extreme ultraviolet research
[AD-A279159] p 1370 N95-20600
Absolute, Extreme-ultraviolet Solar Spectral Irradiance Monitor (AESSIM)
[AD-A279345] p 1603 N95-21929
Reflective masks for extreme ultraviolet lithography
[DE95-003427] p 1336 N95-22236
Coherence properties of high order harmonic radiation
[DE94-016974] p 1377 N95-22312
EXTREMELY HIGH FREQUENCIES
Design and construction of a Ka-band scatterometer
[AD-A286296] p 1368 N95-22322
EXTREMELY LOW FREQUENCIES
Compilation of 1993 annual reports of the Navy ELF Communications System Ecological Monitoring Program
[AD-A279575] p 1408 N95-21699
Compilation of 1993 annual reports of the Navy ELF Communications System Ecological Monitoring Program. Volume 2: Tabs C-F
[AD-A279770] p 1308 N95-21988
EXTRUDING
Extrudate swell and extrudate distortion of HDPE as a result of different deformation mechanisms during extrusion through capillary dies
[PB95-110227] p 1288 N95-21651
EYE (ANATOMY)
A physiological neural network for saccadic eye movement control
[AD-A279599] p 1441 N95-20301
Space constancy on video display terminals
[AD-A280015] p 1449 N95-20314
Investigation of laser-induced retinal damage: Wavelength and pulsewidth dependent mechanisms
[AD-A286066] p 1443 N95-20848
EYE MOVEMENTS
The spatiotemporal characteristics of visual motion priming
[AD-A284782] p 1449 N95-20062
Space constancy on video display terminals
[AD-A280015] p 1449 N95-20314
Visual perception of elevation
[AD-A284938] p 1451 N95-22472
EYE PROTECTION
Broadband thermal optical limiter for the protection of eyes and sensors
[AD-D016493] p 1377 N95-22304

F

F REGION
Mitigation of the effects of F layer regularities by using multiple paths p 1298 N95-20951
Global ionospheric weather
[AD-A285520] p 1430 N95-21177
The effects of magnetic storm phases on F-layer irregularities from auroral to equatorial latitudes
[AD-A286173] p 1427 N95-22423
F-14 AIRCRAFT
Naval aviation: F-14 upgrades are not adequately justified. Report to Congressional Committees
[AD-A286338] p 1206 N95-20212
F-15 AIRCRAFT
F-15 resource tape
[NASA-TM-110502] p 1206 N95-19994
F-16 AIRCRAFT
F-16XL interview with Marta Bohn-Meyer
[NASA-TM-110505] p 1200 N95-19996
F-18 AIRCRAFT
Pressure measurements on an F/A-18 twin vertical tail in buffeting flow. Volume 1: Wind tunnel test summary
[AD-A279126] p 1202 N95-21877
FABRICATION
Collocated tunable wavenumber sensor/actuators for smart structures
[AD-A279608] p 1312 N95-19958
Fabrication and properties of alumina matrix composites containing nickel aluminide reinforcements
[DE94-018703] p 1250 N95-20044
Polycrystalline CuInSe2 and CdTe solar cells
[DE94-011875] p 1392 N95-20333
Fabrication and testing of a silicon immersion grating for infrared spectroscopy
[DE94-017173] p 1237 N95-20386
Status of diffused junction p+n InP solar cells for space applications p 1317 N95-20509
Development, fabrication, and metrology of the electro-optical breadboard model for the reflection grating array of the XMM grating spectrometer
[DE94-016605] p 1543 N95-20612
Packaging the MAMA module p 1209 N95-20639
The production of calibration specimens for impact testing of subsize Charpy specimens
[DE94-018125] p 1386 N95-20703
Method of fabricating a microelectronic photomultiplier device with integrated circuitry
[AD-D016530] p 1325 N95-20726
Microdynamic devices fabricated on silicon-on-sapphire substrates
[AD-D016531] p 1325 N95-20727
Scale-up and modeling of forced chemical vapor infiltration
[DE94-017769] p 1340 N95-20781
Fabrication of ceramic composites: Forced CVI
[DE95-001076] p 1271 N95-20821
GPHS-RTGs in support of the Cassini Mission
[DE95-001492] p 1222 N95-20853
Complementary GaAs junction-gated heterostructure field effect transistor fabrication for integrated circuits
[DE95-001522] p 1327 N95-20882
HTS Josephson technology on silicon with application to high speed digital microelectronics
[AD-A285964] p 1328 N95-21178
Excitons in semiconducting superlattices, quantum wells, and ternary alloys
[DE95-001867] p 1572 N95-21287
Complementary GaAs junction-gated heterostructure field effect transistor technology
[DE94-018901] p 1329 N95-21390
Comparison of properties of sintered and sintered reaction-bonded silicon nitride fabricated by microwave and conventional heating
[DE95-001426] p 1275 N95-21501
Surface micromachined capacitive tactile image sensor
[PB95-108031] p 1288 N95-21633
Atom wave interferometer
[AD-A279532] p 1524 N95-21688
Design and development SAWAFE peak detector chip
[DE95-001745] p 1332 N95-21742
Application of quaternary phase diagrams to compound semiconductor processing
[DE95-001813] p 1277 N95-21748
Integration of thin film decoupling capacitors
[DE95-001609] p 1333 N95-21881
Performance of cesium telluride photocathodes as an electron source for the Los Alamos FEL
[DE94-018302] p 1375 N95-21919
Development of active-transport membrane devices
[DE94-015947] p 1246 N95-21921
Analysis of cost: Combustion flame CVD diamond deposition
[AD-A279153] p 1278 N95-21973
Design, fabrication, and characterization of reflective diffractive optical elements in Si for free-space optical interconnects
[AD-A286416] p 1547 N95-22205
Fabrication of PLZT/ITO grating for optical switching and reconfigurable optical interconnect applications
[AD-A286389] p 1548 N95-22248
Development of practical high temperature superconducting wire for electric power applications
[DE94-017894] p 1336 N95-22271
Parallel nanometer scale fabrication
[DE95-002122] p 1336 N95-22284
Fabrication and characterization of cesium telluride photocathodes: A promising electron source for the Los Alamos Advanced FEL
[DE94-018303] p 1377 N95-22348
FABRICS
Effect of fiber fabric orientation on the monotonic and fatigue behavior of a continuous fiber ceramic composite
[DE94-018121] p 1271 N95-20700
Zirconia precipitates and zirconia: GeO2 interphase in mullite matrix-SiC woven fabrics composites prepared through a sol-gel route
[PB95-133427] p 1275 N95-21272
FACE (ANATOMY)
Thermal resistance of the cheek in cold air
[AD-A286257] p 1446 N95-22001
FACSIMILE COMMUNICATION
Facsimile transmission standards
[AD-A279911] p 1290 N95-20308
FACTORIZATION
O(log2 n) time efficient parallel factorization of dense, sparse separable, and banded matrices
[NASA-CR-197356] p 1473 N95-19885
Factorization in closed string field theory
[PB95-133542] p 1580 N95-21030
Minimal square spectral factors
[PB95-132726] p 1495 N95-22032
FADING
Angle diversity on digital microwave links: Antenna design and experimental results p 1297 N95-20947
Mitigation of the effects of F layer regularities by using multiple paths p 1298 N95-20951
Performance of a fast frequency-hopped noncoherent MFSK receiver over Rician fading channels with either partial-band interference or multi-tone interference
[AD-A286168] p 1310 N95-22246
FAILURE
Adaptive fault-resistant systems
[AD-A286406] p 1484 N95-22203
Advanced Materials and Process Technology for Mechanical Failure Prevention (proceedings of the 48th Meeting of the Mechanical Failures Prevention Group
[AD-A285785] p 1233 N95-22399
FAILURE ANALYSIS
Physics and applications of defects in advanced semiconductors, volume 325
[AD-A280059] p 1563 N95-19886
Inelastic torsion of steel I-beams
[PB94-208360] p 1384 N95-20101
The numerical integration and 3-D finite element formulation of a viscoelastic model of glass
[DE95-002588] p 1271 N95-20788
Finite element modelling of creep crack growth in 316 stainless and 9Cr-1Mo steels
[DE94-018977] p 1258 N95-21560
Advanced Materials and Process Technology for Mechanical Failure Prevention (proceedings of the 48th Meeting of the Mechanical Failures Prevention Group
[AD-A285785] p 1233 N95-22399
FAILURE MODES
Analysis of the progressive failure of brittle matrix composites
[NASA-CR-195415] p 1225 N95-19951
Advanced Packaging Concepts for Digital Avionics
[AGARD-CP-562] p 1208 N95-20631
Gate oxide shorts in nMOS transistors: Electrical properties and lifetime prediction method
[DE94-018904] p 1330 N95-21545
FALKNER-SKAN EQUATION
Acoustic receptivity due to weak surface inhomogeneities in adverse pressure gradient boundary layers
[NASA-TM-4577] p 1353 N95-21258
FALSE ALARMS
Probability of detection for a GO CFAR radar processor using envelope detection approximation
[AD-A286211] p 1310 N95-22251

FAR FIELDS

Analytic models for beam propagation and far-field patterns in slab and bow-tie x ray lasers
[DE94-016607] p 1372 N95-21173

FAR INFRARED RADIATION

Gordon Research Conference on Physical Electrochemistry
[AD-A286545] p 1240 N95-20842

Signal to noise improvements with a new Far-IR rapid-scan Michelson Interferometer
[DE95-002416] p 1367 N95-21638

Pushing the limits of spatial resolution with the Kuiper Airborne observatory p 1593 N95-21754

Azimuthally averaged radial S(sub 100 microns)/S(sub 60 microns) dust color temperatures in spiral galaxies
p 1593 N95-21760

Far-Infrared sources and diffuse emission in M31
p 1593 N95-21761

Correlation of far-infrared emission and radio continuum emission along the major axis of edge-on spiral galaxies
p 1593 N95-21762

Far-infrared mapping of dusty elliptical galaxies
p 1593 N95-21763

A HIRES analysis of the FIR emission of supernova remnants p 1594 N95-21770

Growth and electrical and far-infrared properties of wide electron wells in semiconductors
[AD-A279409] p 1333 N95-21917

FARADAY EFFECT

Nonlinear Faraday effect in CdS semiconductor in an ultrahigh magnetic field
[DE94-016804] p 1564 N95-20240

High frequency current sensors using the Faraday effect in optical fibers
[DE95-001859] p 1545 N95-21728

FAST FOURIER TRANSFORMATIONS

Simulation of stellar speckle imaging
[DE94-016606] p 1412 N95-19985

Electrochemical impedance pattern recognition for detection of hidden chemical corrosion on aircraft components
[AD-A284998] p 1253 N95-20481

Xwake 1.0 user's manual
[DE95-002528] p 1463 N95-20901

The sharper image: Implementing a Fast Fourier Transform (FFT) to enhance a video-captured image
[AD-A279790] p 1445 N95-21180

Measurement of sound intensity and sound power
[AD-A279246] p 1505 N95-21984

FAST NEUTRONS

Non destructive characterization using pulsed fast-thermal neutrons
[DE95-002601] p 1511 N95-20422

Influence of oxidation on radiation hardness of silicon detectors
[DE95-002466] p 1272 N95-20894

FAST NUCLEAR REACTORS

Reactor pumped laser research at the Sandia National Laboratories pulsed reactor facilities
[DE95-002181] p 1371 N95-20867

FASTENERS

Displaceable spur gear torque controlled driver and method
[NASA-CASE-MSC-22381-1] p 1378 N95-20409

Eddy current for detecting second-layer cracks under installed fasteners
[AD-A279871] p 1382 N95-20414

Attachment methodology for composite cylinder assembly
[AD-D016578] p 1227 N95-20459

Attachment methodology for composite cylinder assembly
[AD-D016256] p 1381 N95-22034

FATIGUE (MATERIALS)

Turbulence descriptors for scaling fatigue loading spectra of wind turbine structural components
[DE94-011833] p 1384 N95-20109

The processing and mechanical properties of high temperature/high performance composites. Fatigue and creep, book 3
[AD-A279738] p 1227 N95-20430

Flux-focusing eddy current probe and rotating probe method for flaw detection
[NASA-CASE-LAR-15231-1-SB] p 1383 N95-20764

2nd International ADI seminar
[PB95-127734] p 1255 N95-21108

Accuracy problems in the generation of discrete time stochastic processes
[PB95-131397] p 1386 N95-21133

Microstructural design for tough ceramics
[AD-A285634] p 1273 N95-21152

Crack closure and sequential effects in fatigue: A literature survey
[PB95-131637] p 1387 N95-21557

Derived gust spectra for the Macchi MB326H
[ARL-TN-3] p 1202 N95-21892

Influence of fatigue crack closure on the growth rate of surface flaws
[AD-A279130] p 1387 N95-21967

FATIGUE LIFE

Application of an energy-based life prediction model to bithermal and thermomechanical fatigue
[NASA-TM-106684] p 1385 N95-20179

Crack closure and sequential effects in fatigue: A literature survey
[PB95-131637] p 1387 N95-21557

Effects of cyclic stress distribution models on fatigue life predictions
[DE95-001619] p 1388 N95-22070

Structural performance of cylindrical pressure housings of different ceramic compositions under external pressure loading. Part 3: Sintered reaction bonded silicon nitride ceramic
[AD-A285773] p 1388 N95-22411

FATIGUE TESTS

The mechanical property data base from an Air Force/Industry cooperative test program on advanced aluminum alloys
[AD-A280038] p 1386 N95-20615

Accuracy problems in the generation of discrete time stochastic processes
[PB95-131397] p 1386 N95-21133

Microstructural design for tough ceramics
[AD-A285634] p 1273 N95-21152

Lubricant evaluation and performance, 2
[AD-A279144] p 1278 N95-21969

FAULT DETECTION

Flux-focusing eddy current probe and rotating probe method for flaw detection
[NASA-CASE-LAR-15231-1-SB] p 1383 N95-20764

Fault detection techniques for complex cable shield topologies
[AD-A286632] p 1291 N95-20771

An empirical approach to logical clustering of software failure regions
[AD-A279863] p 1462 N95-20776

SSME HPOTP post-test diagnostic system enhancement project
[NASA-CR-4643] p 1222 N95-21458

Defect classes: An overdue paradigm for CMOS IC testing
[DE94-018905] p 1334 N95-22118

FAULT TOLERANCE

Fault tolerance of neural networks
[AD-A285098] p 1479 N95-20057

Comparison of Ward and Mellor's transformation schema with State- and Activitycharts
[PB95-110698] p 1459 N95-20258

System level fault tolerance in parallel and distributed computing systems
[AD-A279664] p 1474 N95-20305

A group communication approach for mobile computing mobile channel: An ISIS tool for mobile services
[AD-A279785] p 1290 N95-20306

Fault-tolerance in distributed and multiprocessor real-time systems
[AD-A279896] p 1461 N95-20595

The Advanced Avionics Subsystem Technology Demonstration Program p 1209 N95-20636

Backward error recovery in redundant disk arrays
[AD-A286064] p 1463 N95-20846

Compositional proof theory for fault tolerant real-time distributed systems
[PB95-127601] p 1465 N95-21025

Non-intrusive SCSI status sensing system
[AD-D016242] p 1476 N95-21307

Numerical and symbolic algorithms for application and specific signal processing
[AD-A279902] p 1305 N95-21576

Top-down non-correcting error recovery in LLgen
[PB95-132718] p 1471 N95-22031

Formal specification and compositional verification of an atomic broadcast protocol
[PB95-110508] p 1472 N95-22351

FAULT TREES

Software fault tree analysis of concurrent Ada processes
[AD-A284979] p 1457 N95-20042

FEASIBILITY

Liquid xenon as a potential laser host medium
[AD-A285365] p 1370 N95-20550

FEASIBILITY ANALYSIS

The personal aircraft: Status and issues
[NASA-TM-109174] p 1200 N95-20688

Feasibility study of power generation system with shape memory alloys
[DE95-714802] p 1254 N95-20890

Development of a portable ice-thickness measuring instrument
[AD-A279472] p 1433 N95-21291

Economic feasibility analysis of distributed electric power generation based upon the natural gas-fired fuel cell
[DE94-012277] p 1396 N95-22033

FEDERAL BUDGETS

An update on the Department of Energy's photovoltaic program p 1316 N95-20505

FEED SYSTEMS

The ITER in-vessel system
[DE94-018053] p 1560 N95-21665

FEEDBACK

Six-dimensional modeling of coherent bunch instabilities and related feedback systems in storage rings with power-series maps for the lattice
[DE94-017965] p 1532 N95-20494

A comparison of decision making behaviour in a static and a dynamic task environment as a function of time pressure
[AD-A285389] p 1449 N95-20609

Apparatus and method for determining the mass density of a filament
[NASA-CASE-LAR-14879-1-CU] p 1383 N95-20616

Modeling and identification of parallel and feedback nonlinear systems
[DE95-001006] p 1481 N95-20812

Multiple burn fuel-optimal orbit transfers: Numerical trajectory computation and neighboring optimal feedback guidance
[NASA-CR-197317] p 1222 N95-21616

Effect of lags on human performance with head-coupled simulators
[AD-A279577] p 1453 N95-21700

Monolithic low noise preamplifier for piezoelectric sensors
[AD-D016524] p 1333 N95-21865

FEEDBACK CONTROL

Asymptotic analysis of Nash equilibria in nonzero-sum linear-quadratic differential games. The two-player case
[PB95-111027] p 1499 N95-19941

Optimal distributed control system for a linear distributed parameter system
[AD-D016583] p 1480 N95-20202

A charge distribution analysis instrument for catalysis and material science applications
[DE94-016489] p 1364 N95-20233

Designing the architecture of hierachical neural networks model attention, learning and goal-oriented behavior
[AD-A279898] p 1452 N95-20562

An integrated architecture of adaptive neural network control for dynamic systems
[DE94-014813] p 1481 N95-20693

Riccati equation theory for Pritchard-Salamon systems: A Popov function approach
[PB95-137089] p 1491 N95-20830

Semi-global stabilization of linear discrete-time systems subject to input saturation via linear feedback: An ARE-based approach
[PB95-135463] p 1483 N95-21618

Design of robust optimal control systems and stability analysis of real structured uncertainties
[AD-A279089] p 1483 N95-21913

Optimal control of a two wheeled mobile robot
[AD-A286130] p 1485 N95-22233

Drag reduction strategies p 1361 N95-22453

FEEDFORWARD CONTROL

A neural expert approach to self designing flight control systems
[AD-A279965] p 1215 N95-21122

Learning algorithms for feedforward networks based on finite samples
[DE95-001739] p 1483 N95-21741

Mathematical theory of neural networks
[AD-A286508] p 1485 N95-22213

A survey of artificial neural network applications in flow analysis of energy networks
[DE95-002452] p 1486 N95-22430

FELDSPARS

Analysis of experimentally shocked minerals by NMR spectroscopy
[DE95-002955] p 1573 N95-21449

Semi-volatiles at Mercury: Sodium (Na) and potassium (K) p 1424 N95-21818

FERMENTATION

Bioconversion of coal derived synthesis gas to liquid fuels
[DE94-017381] p 1282 N95-19927

Bioconversion of coal derived synthesis gas to liquid fuels
[DE94-018849] p 1314 N95-20339

Microbiology and physiology of anaerobic fermentations of cellulose
[DE95-002899] p 1438 N95-20917

FERMI LIQUIDS

Angle resolved photoemission on K(0.3)Mo3, TiTe2 and Ti(1+x)S2
[DE94-018300] p 1574 N95-21712

An asymptotic solution of the (infinity)-d Hubbard model
[DE94-629042] p 1582 N95-21994
FERMI SURFACES
Angle resolved photoemission on K(0.3)Mo3, TiTe2 and Ti(1+x)S2
[DE94-018300] p 1574 N95-21712
FERMIONS
Chiral symmetry and lattice gauge theory
[DE94-018676] p 1564 N95-20130
A Monte Carlo study of the minus sign problem in the t-J model using an Intel iPSC/860 hypercube
[DE95-001072] p 1570 N95-20819
A high-rate fixed-target charm experiment
[DE95-001767] p 1521 N95-21378
Charge density of fractional charged quasiparticles in the composite fermion picture
[DE94-018122] p 1524 N95-21703
FERRITES
The origin of acicular ferrite in gas metal arc and submerged arc welds
[AD-A286129] p 1377 N95-19984
The effect of oxide inclusions on the kinetics of the austenite to ferrite transformation in low alloy steel weld metal
[DE94-018131] p 1253 N95-20676
Moessbauer study of the sintered Mn(0.70)Zn(0.23)Fe(2.07)O4
[DE94-631462] p 1255 N95-20909
Classification of bianisotropic media
[PB95-127635] p 1502 N95-21102
FERROELECTRICITY
Materials for adaptive structural acoustic control, volume 2
[AD-A279222] p 1502 N95-19883
The role of high pressure in the study and applications of the ferroelectric polymer polyvinylidene fluoride and its copolymers
[DE94-015742] p 1268 N95-20396
Ferroic materials: Design, preparation and characteristics. Ceramic transactions, volume 43
[AD-A285937] p 1270 N95-20664
Development of ferroelectric liquid crystals with enhanced nonlinear optical properties
[AD-A279988] p 1571 N95-20965
Raman spectra of MOCVD-grown ferroelectric PbTiO3 thin films
[DE94-018964] p 1244 N95-21549
Domain processes in ferroelectric ceramics
[AD-A279567] p 1276 N95-21697
Integration of thin film decoupling capacitors
[DE95-001609] p 1333 N95-21881
FERROMAGNETIC MATERIALS
Changes in the behavior of magnetic materials undergoing processing in electrical rotating machines
[PB95-104493] p 1325 N95-20702
Photoemission and ferromagnetism
[DE95-002419] p 1520 N95-21362
Coaxial hybrid wiggler
[AD-D016501] p 1331 N95-21671
Magnetic properties of the three-dimensional Ising model with an interface amorphization
[DE94-628992] p 1278 N95-21885
FERROMAGNETISM
Photoemission and ferromagnetism
[DE95-002419] p 1520 N95-21362
Theory of spin dynamics in the classical two-dimensional heisenberg magnet
[PB95-133559] p 1502 N95-22138
FIBER COMPOSITES
The environmental durability of fiber reinforced ceramic matrix composites
[AD-A283750] p 1225 N95-19919
Analysis of the progressive failure of brittle matrix composites
[NASA-CR-195415] p 1225 N95-19951
Thermo-mechanical fatigue of polymer matrix composites
[AD-A285931] p 1267 N95-20390
The processing and mechanical properties of high temperature/high performance composites. Stress redistribution and notch properties, book 2
[AD-A279737] p 1227 N95-20429
The processing and mechanical properties of high temperature/high performance composites. Fatigue and creep, book 3
[AD-A279738] p 1227 N95-20430
The processing and mechanical properties of high temperature/high performance composites. Book 7: In-situ measurements of stress and damage
[AD-A279814] p 1227 N95-20583
Effect of fiber fabric orientation on the monotonic and fatigue behavior of a continuous fiber ceramic composite
[DE94-018121] p 1271 N95-20700
Wear resistant composite structure of vitreous carbon containing convoluted fibers
[DE95-002254] p 1228 N95-20787
The processing and mechanical properties of high temperature/high performance composites. Mechanism-based constitutive laws and design, book 1
[AD-A279736] p 1228 N95-20801
Detection of environmental deterioration in fiber reinforced composites by FT-Raman spectroscopy, phase 1
[AD-A279763] p 1228 N95-20805
Carbon fiber reinforced superconductor composites
[DE95-002504] p 1229 N95-20913
Toughened Silcomp composites for gas turbine engine applications
[DE95-002851] p 1214 N95-21243
Significance of impact velocity for the extent of damage in carbon/epoxy laminates
[PB95-133484] p 1230 N95-21417
A transmission electron microscope characterization of sodium sulfate hot corrosion of silicon carbide fiber-reinforced lithium aluminosilicate glass-ceramic matrix composite
[AD-A286164] p 1231 N95-22038
Effect of laser radiation on carbon fibre/epoxy composites
[PB95-133526] p 1232 N95-22096
Embedded optical fibres as strain sensors in polymer matrix fibre composites: The influence of adhesion in strain transfer
[PB95-133617] p 1547 N95-22140
Fibre-reinforced high-strength concrete
[PB95-131942] p 1232 N95-22158
Implementation of the Military Handbook 17 for polymer matrix composites and metal matrix composites
[AD-A285772] p 1233 N95-22395
FIBER OPTICS
Fiber laser amplifiers and oscillators
[AD-A285835] p 1368 N95-20035
Program of the 1993 9th Interdisciplinary Laser Science Conference (ILS-9)
[AD-A285131] p 1369 N95-20082
Proceedings of the International Wire and Cable Symposium
[AD-A279242] p 1403 N95-20465
Optical backplane for modular avionics
p 1212 N95-20652
High performance backplane components for modular avionics p 1212 N95-20653
Detection of environmental deterioration in fiber reinforced composites by FT-Raman spectroscopy, phase 1
[AD-A279763] p 1228 N95-20805
Mandrel based embedded planar fiber-optic interferometric acoustic sensor
[AD-D016229] p 1504 N95-21119
Fiber-optic control of current filaments in high gain photoconductive semiconductor switches
[DE94-015804] p 1328 N95-21139
A three-dimensional orthogonal laser velocimeter for the NASA Ames 7- by 10-foot wind tunnel
[NASA-TM-108864] p 1366 N95-21323
Method for characterization of optical waveguide devices using partial coherence interferometry
[AD-D016525] p 1544 N95-21466
Fiber-optic sensors for rapid, inexpensive characterization of soil and ground water contamination
[DE95-002471] p 1545 N95-21510
Fiber-optic rotary joint with bundle collimator assemblies
[AD-D016504] p 1545 N95-21673
Electromagnetic radiation detector utilizing an electromagnetic radiation absorbing element in a mach-zehnder interferometer arrangement
[AD-D016507] p 1306 N95-21835
Optical processing and control
[AD-A279157] p 1546 N95-21975
Fiber optic pressure sensing array
[AD-D016245] p 1506 N95-22088
FIBER ORIENTATION
Effect of fiber fabric orientation on the monotonic and fatigue behavior of a continuous fiber ceramic composite
[DE94-018121] p 1271 N95-20700
FIBER VOLUME FRACTION
Role of internal stresses in fracture behavior of engineering composites
[DE95-001106] p 1229 N95-20912
Fibre-reinforced high-strength concrete
[PB95-131942] p 1232 N95-22158
FIBER-MATRIX INTERFACES
The processing and mechanical properties of high temperature/high performance composites. Book 5: Interface effects
[AD-A279815] p 1228 N95-20584
Time-dependent deformation of titanium metal matrix composites
[NASA-CR-195030] p 1230 N95-21363
FIBERS
The processing and mechanical properties of high temperature/high performance composites. Book 5: Interface effects
[AD-A279815] p 1228 N95-20584
Apparatus and method for determining the mass density of a filament
[NASA-CASE-LAR-14879-1-CU] p 1383 N95-20616
FIBROBLASTS
Study of pulsed laser effects on living tissues
[PB95-131330] p 1447 N95-22361
FIELD COILS
Joule heating of the ITER TF cold structure: Effects of vertical control coil currents and ELMS
[DE95-001817] p 1560 N95-21724
The superconducting magnet system for the Tokamak Physics Experiment
[DE94-018329] p 1562 N95-22300
FIELD EFFECT TRANSISTORS
Proton irradiation effects on advanced digital and microwave III-V components
[DE94-018742] p 1314 N95-20338
Development of a tester for evaluation of prototype thermal cells and batteries
[DE95-000540] p 1325 N95-20628
Complementary GaAs junction-gated heterostructure field effect transistor fabrication for integrated circuits
[DE95-001522] p 1327 N95-20882
SPICE macro model of a spryton with MOSFET's in the avalanche mode
[DE94-015744] p 1555 N95-21134
Complementary GaAs junction-gated heterostructure field effect transistor technology
[DE94-018901] p 1329 N95-21390
On-wafer, cryogenic characterization of ultra-low noise HEMT devices p 1305 N95-21539
Plastic encapsulated parts
[DE95-001876] p 1332 N95-21729
FIELD EMISSION
Field-emitter arrays for RF vacuum microelectronics
[AD-A279959] p 1325 N95-20661
FIELD OF VIEW
Factors affecting the perception of luning in monocular regions of partial binocular overlap displays
[AD-A286287] p 1547 N95-22044
Occupant reach and mobility apparatus
[AD-D016253] p 1454 N95-22099
FIELD THEORY (ALGEBRA)
Classification of diagonal coset modular invariants
[PB95-111118] p 1489 N95-20259
FIELD THEORY (PHYSICS)
Truly distribution-independent algorithms for the N-body problem
[DE94-014238] p 1458 N95-20136
Von Neumann algebra automorphisms and time-thermodynamics relation in general covariant quantum theories
[PB95-111084] p 1580 N95-20324
Theoretical particle physics
[DE95-002447] p 1515 N95-20893
New improved derivative expansion for field theories with spontaneous symmetry breaking
[DE94-019349] p 1580 N95-21486
The method of evaluating quantum partition function for the Hubbard model
[DE94-628991] p 1581 N95-21639
Second order approximation for optical polaron in the strong coupling case
[DE94-628997] p 1525 N95-21856
Biaxiality of chiral liquid crystals
[DE94-629032] p 1578 N95-22277
FIGHTER AIRCRAFT
Effects of bifocal and progressive-addition corrective lenses on aviator target-detection performance
[AD-A279698] p 1442 N95-20710
FIGURE OF MERIT
Millimeter wave front-end figure of merit, part 1
[AD-A279093] p 1307 N95-21915
FILAMENT WINDING
Multi-layered translated rib-stiffened composite hollow cylinder assembly
[AD-D016566] p 1226 N95-20292
FILE MAINTENANCE (COMPUTERS)
DOS basics
[DE94-018434] p 1455 N95-21632
FILLETS
Effect of juncture fillets on double-delta wings undergoing sideslip at high angles of attack
[AD-A286165] p 1207 N95-22039
FILM THICKNESS
Enhanced ionic conduction at the film/substrate interface in LiI thin films grown on sapphire(0001)
[DE94-017884] p 1565 N95-20371

FILTERS

Using local optimality criteria for efficient information retrieval with redundant information filters [AD-A279603] p 1587 N95-20302

FILTRATION

Ceramem filters for removal of particles from hot gas streams [DE95-001976] p 1275 N95-21354

Development and applications of flat ceramic membranes [PB95-110219] p 1276 N95-21650

FINANCE

Patterns of financial change in the OECD area [PB95-110979] p 1594 N95-19939

FINANCIAL MANAGEMENT

Planning and scheduling for success p 1584 N95-20747

A strategy of cost control for Mariner Venus/Mercury 1973 p 1585 N95-20751

FINE STRUCTURE

A new family of anion receptors and their effects on ion pair dissociation and conductivity of lithium salts in non-aqueous solutions [DE94-016822] p 1512 N95-20477

Semantics for a fine lambda-calculus with de Bruijn indices [PB95-127577] p 1492 N95-21372

FINITE DIFFERENCE THEORY

A S2-like acceleration method for the Nonlinear Characteristic transport scheme [DE94-016285] p 1509 N95-20235

A comparison of kinetic and multifluid simulations of laser-produced colliding plasmas [DE94-016447] p 1551 N95-20315

A theoretical study on the performance of the FDTD code on a massively parallel computer [AD-A285346] p 1475 N95-20499

Xwake 1.0 user's manual [DE95-002528] p 1463 N95-20901

A computer code (SKINTEMP) for predicting transient missile and aircraft heat transfer characteristics [AD-A286044] p 1341 N95-21001

VLUGr3: A vectorizable adaptive grid solver for PDEs in 3D. 2: Code description [PB95-135737] p 1465 N95-21033

Vortex ring instability and its sound p 1344 N95-21048

Subgrid scale models in finite difference simulations of complex wall bounded flows p 1346 N95-21063

Simulation of separated flows p 1347 N95-21068

Analysis of subgrid models using direct and large-eddy simulations of isotropic turbulence p 1348 N95-21071

Computation of transonic flow on composite overlapping grids in 2 D [PB95-131348] p 1353 N95-21132

Computational modeling of diffusion-controlled transformations in ternary systems [DE95-001358] p 1256 N95-21298

VLUGR3: A vectorizable adaptive grid solver for PDEs in 3D. 1: Algorithmic aspects and applications [PB95-135729] p 1467 N95-21435

Numerical investigations of low-density nozzle flow by solving the Boltzmann equation [NASA-TM-110492] p 1354 N95-21675

On the wavelet optimized finite difference method [NASA-CR-191601] p 1495 N95-22157

Local dynamic subgrid-scale models in channel flow p 1360 N95-22447

FINITE ELEMENT METHOD

Inelastic bending and torsion of steel I-beams [PB94-208378] p 1384 N95-19975

Finite dimensional approximation of a class of constrained nonlinear optimal control problems [NASA-CR-194891] p 1479 N95-20010

A-posteriori estimation and adaptive control of the pollution-error in the h-version of the finite element method [AD-A285670] p 1480 N95-20083

Nonlinear dynamic fluid-structure interaction calculations with coupled finite element and finite volume programs [DE94-016204] p 1339 N95-20166

The method of auxiliary mapping for the finite element solutions of elasticity problems containing singularities [AD-A285689] p 1489 N95-20274

Simulation of large systems with neural networks [DE94-018898] p 1428 N95-20319

An overview of the HSST Full-Thickness Shallow-Crack Clad Beam Testing Program [DE94-018940] p 1385 N95-20322

RALPAR-RAL mesh partitioning program version 1.1 [PB95-129847] p 1475 N95-20435

Eta%-Superconvergence of Finite Element Approximations in the Interior of General Meshes of Triangles [AD-A279903] p 1490 N95-20565

Study of superconvergence by a computer-based approach: Superconvergence of the gradient of the displacement, the strain and stress in finite element solutions for plane elasticity [AD-A279885] p 1490 N95-20588

The numerical integration and 3-D finite element formulation of a viscoelastic model of glass [DE95-002588] p 1271 N95-20788

An augmented Young-Laplace model of an evaporating meniscus in a micro-channel with high heat flux [NASA-CR-197622] p 1340 N95-20796

Geometric moire method of strain analysis with displacement discontinuities [DE95-001114] p 1386 N95-20833

COYOTE II: A finite element computer program for nonlinear heat conduction problems. Part 1: Theoretical background [DE95-002587] p 1463 N95-20887

A convergence analysis of an h-version finite element method with high order elements for two dimensional elasto-plasticity problems [AD-A279975] p 1491 N95-20920

Mixed hp finite element methods for problems in elasticity and stokes flow [PB95-104444] p 1341 N95-20981

Simulation of separated flows p 1347 N95-21068

Vibration analysis of the AN/SPS-67(V)3 surface search radar [AD-A286050] p 1302 N95-21324

Finite element modelling of creep crack growth in 316 stainless and 9Cr-1Mo steels [DE94-018977] p 1258 N95-21560

DIFFPACK: Software for partial differential equations [PB95-110268] p 1468 N95-21654

The role of microcracking on the crack growth resistance of brittle solids and composites [DE95-001678] p 1231 N95-21736

Right inverse for the divergence operator in spaces of continuous piecewise polynomials [PB95-127080] p 1496 N95-22369

Locking of the finite element method in thermoelasticity [PB95-127098] p 1496 N95-22370

Multi signal-domain modeling of solid-state transducers: A theoretical framework based on irreversible thermodynamics mixed finite elements and multigrid [PB95-134995] p 1336 N95-22382

Pollution error in the H-version of the finite element method and the local quality of A-posteriori error estimators [AD-A279868] p 1497 N95-22388

Unstructured-grid large-eddy simulation of flow over an airfoil p 1202 N95-22448

FINNISH SPACE PROGRAM

Preliminary study of HUTSAT microsatellite [PB95-127619] p 1220 N95-21026

FIR FILTERS

Digital filtering for data compression in telemetry systems [DE94-016611] p 1219 N95-20567

FIRE CONTROL

Annual Conference on Fire Research: Book of abstracts [PB95-104964] p 1286 N95-20717

FIRE EXTINGUISHERS

A review of water mist technology for fire suppression [AD-A285738] p 1202 N95-20071

The development and evaluation of water-mist fire extinguishing systems [DE94-019019] p 1286 N95-20356

Training simulant for Halon 1211 portable extinguishers [AD-A285403] p 1286 N95-20611

Evaluation of state-of-the-art high speed deluge systems presently in service at various US Army ammunition plants [AD-A279102] p 1287 N95-21598

FIRE FIGHTING

A review of water mist technology for fire suppression [AD-A285738] p 1202 N95-20071

Global equivalence ratio concept and the prediction of carbon monoxide formation in enclosure fires [PB94-207511] p 1234 N95-20100

Training simulant for Halon 1211 portable extinguishers [AD-A285403] p 1286 N95-20611

Evaluation of state-of-the-art high speed deluge systems presently in service at various US Army ammunition plants [AD-A279102] p 1287 N95-21598

Analysis of test criteria for specifying foam firefighting agents for aircraft rescue and firefighting [AD-A286381] p 1203 N95-22352

FIRE PREVENTION

The development and evaluation of water-mist fire extinguishing systems [DE94-019019] p 1286 N95-20356

Annual Conference on Fire Research: Book of abstracts [PB95-104964] p 1286 N95-20717

FIREDOC users manual, 3rd edition [PB95-128674] p 1286 N95-21129

FIRES

Investigation of flight data recorder fire test requirements [AD-A285832] p 1208 N95-20032

Global equivalence ratio concept and the prediction of carbon monoxide formation in enclosure fires [PB94-207511] p 1234 N95-20100

The effect of regional-scale soil-moisture deficits on mesoscale atmospheric dynamics that influence fire severity [DE95-002682] p 1413 N95-20455

Summaries of BFRL fire research in-house projects and grants, 1994 [PB95-130845] p 1286 N95-21130

Fire experiments in a two dimensional rack storage: BRANDFORSK-project 701-917 [PB95-131538] p 1241 N95-21179

Ignition of submarine materials at various oxygen concentrations [PB95-131371] p 1243 N95-21428

Fire smoke ventilation through shafts: Experiments [PB95-132247] p 1288 N95-21978

Fuselage burnthrough from large exterior fuel fires [AD-A286295] p 1203 N95-22318

FIRING (IGNITING)

Thermal decomposition reactions of HMX and RDX and their importance in predicting cookoff hazards [DE95-002486] p 1283 N95-21513

FISCHER-TROPSCH PROCESS

Technology development for cobalt F-T catalysts [DE94-017363] p 1241 N95-21172

FISHERIES

Aquatic plant control research program. Ecological assessment of Kirk Pond [AD-A279090] p 1409 N95-21914

FISHES

Long term changes on the continental shelf of the North Sea: Invertebrate trends, 1931-1990 [PB95-135224] p 1435 N95-21717

FISSION

Reactor pumped laser research at the Sandia National Laboratories pulsed reactor facilities [DE95-002181] p 1371 N95-20867

FIXTURES

Vacuum holding fixture and method for fabricating piezoelectric polymer acoustic sensors [NASA-CASE-LAR-14240-1] p 1268 N95-20410

Test fixture for determination of energy absorbing capabilities of composite materials [NASA-CASE-LAR-15212-1-CU] p 1229 N95-21008

FLAME PROPAGATION

Proceedings of the Zel'Dovich Memorial International Conference on Combustion, Detonation, Shock Waves, volume 2 [AD-A286626] p 1239 N95-20769

Passive turbulent flamelet propagation p 1249 N95-21043

Summaries of BFRL fire research in-house projects and grants, 1994 [PB95-130845] p 1286 N95-21130

Studies in nonlinear problems of energy [DE95-001387] p 1356 N95-22148

Fuselage burnthrough from large exterior fuel fires [AD-A286295] p 1203 N95-22318

Lewis number and Damkohler number effects in vortex-flame interactions p 1249 N95-22439

Fundamental mechanisms in premixed flame propagation via vortex-flame interactions: Numerical simulations p 1249 N95-22440

Triple flames and flame stabilization p 1249 N95-22441

Flame propagation under partially-premixed conditions p 1250 N95-22442

FLAME STABILITY

Triple flame structure and diffusion flame stabilization p 1249 N95-21039

Temporal evolution of turbulence/chemistry interactions in lifted, turbulent-jet flames [DE95-002481] p 1243 N95-21512

Triple flames and flame stabilization p 1249 N95-22441

Flame propagation under partially-premixed conditions p 1250 N95-22442

FLAMES

Global equivalence ratio concept and the prediction of carbon monoxide formation in enclosure fires [PB94-207511] p 1234 N95-20100

Fire experiments in a two dimensional rack storage: BRANDFORSK-project 701-917
[PB95-131538] p 1241 N95-21179
Aromatics oxidation and soot formation in flames
[DE95-001803] p 1241 N95-21280
Temporal evolution of turbulence/chemistry interactions in lifted, turbulent-jet flames
[DE95-002481] p 1243 N95-21512
Analysis of cost: Combustion flame CVD diamond deposition
[AD-A279153] p 1278 N95-21973

FLAMMABILITY
Round-robin comparison of heat release apparatus
[AD-A285831] p 1363 N95-20031
Investigation of flight data recorder fire test requirements
[AD-A285832] p 1208 N95-20032
Summaries of BFRL fire research in-house projects and grants, 1994
[PB95-130845] p 1286 N95-21130
Ignition of submarine materials at various oxygen concentrations
[PB95-131371] p 1243 N95-21428
Fuselage burnthrough from large exterior fuel fires
[AD-A286295] p 1203 N95-22318

FLAT PLATES
Comparison of DNS and LES of transitional and turbulent compressible flow: Flat plate and mixing layer
p 1347 N95-21066
Numerical simulation of supersonic boundary layer transition p 1348 N95-21074
Navier-Stokes simulations of the effects of suction holes on a flat plate boundary layer p 1352 N95-21094
Direct numerical simulation of 2-D and 3-D instability waves in a laminar separation bubble
p 1352 N95-21095
The Photovoltaic Higher Education National Exemplar Facility (PHENEF)
[DE94-015641] p 1395 N95-21409

FLAVOR (PARTICLE PHYSICS)
Neutrino-neutrino scattering and matter-enhanced neutrino flavor transformation in supernovae
[DE94-017577] p 1604 N95-20383
Universal parametrization for quark and lepton substructure
[DE94-770604] p 1514 N95-20738
Theoretical particle physics
[DE95-002447] p 1515 N95-20893
Evidence for t(bar t) production at the Tevatron: Statistical significance and cross section
[DE95-002524] p 1515 N95-20897
Calculation of Z plus four jet production at the Tevatron
[PB95-130472] p 1580 N95-21230
There might be two kinds of dibaryon
[DE94-014417] p 1526 N95-22058
Testing the principle of equivalence by solar neutrinos
[DE94-014972] p 1604 N95-22064
The solar flux of thermal neutrinos and antineutrinos of all flavors
[DE95-003204] p 1604 N95-22085

FLEXIBILITY
The ANL X6B beamline at NSLS: A versatile facility
[DE94-018379] p 1540 N95-19968
Planning and scheduling for success
p 1584 N95-20747

FLEXIBLE BODIES
Proceedings of the NATO-Advanced Study Institute on Computer Aided Analysis of Rigid and Flexible Mechanical Systems. Volume 1: Main lectures
[AD-A286062] p 1380 N95-21171
Proceedings of the NATO-Advanced Study Institute on Computer Aided Analysis of Rigid and Flexible Mechanical Systems. Volume 2: Contributed papers
[AD-A286063] p 1381 N95-21488

FLEXIBLE SPACECRAFT
Mathematical modeling of a class of multibody flexible spacecraft structures
[NASA-TM-109166] p 1219 N95-20800

FLEXING
Effect of fiber fabric orientation on the monotonic and fatigue behavior of a continuous fiber ceramic composite
[DE94-018121] p 1271 N95-20700
Fabrication of ceramic composites: Forced CVI
[DE95-001076] p 1271 N95-20821

FLICKER
Space constancy on video display terminals
[AD-A280015] p 1449 N95-20314

FLIGHT CHARACTERISTICS
T-45A High Angle of Attack Testing: US Naval Test Pilot School 46th Annual Reunion and Symposium
[AD-A284000] p 1207 N95-20466

FLIGHT CONDITIONS
Derived gust spectra for the Macchi MB326H
[ARL-TN-3] p 1202 N95-21892

FLIGHT CONTROL
Summary of a joint program of research into aircraft flight control concepts
[AD-A280012] p 1214 N95-20004
A neural expert approach to self designing flight control systems
[AD-A279965] p 1215 N95-21122
Launch vehicle flight control augmentation using smart materials and advanced composites (CDDF Project 93-05)
[NASA-TP-3535] p 1218 N95-21346

FLIGHT CREWS
Behavioral effects of tyrosine during sustained wakefulness
[AD-A279789] p 1441 N95-20307
Occupant reach and mobility apparatus
[AD-D016253] p 1454 N95-22099

FLIGHT MANAGEMENT SYSTEMS
Crew aiding and automation: A system concept for terminal area operations, and guidelines for automation design
[NASA-CR-4631] p 1204 N95-19950

FLIGHT OPERATIONS
Behavioral effects of tyrosine during sustained wakefulness
[AD-A279789] p 1441 N95-20307

FLIGHT PATHS
Comparison of meteorological data with fitted values extracted from projectile trajectory
[AD-A285921] p 1428 N95-19989

FLIGHT RECORDERS
Investigation of flight data recorder fire test requirements
[AD-A285832] p 1208 N95-20032

FLIGHT SAFETY
Commuter/air taxi ditchings and water-related impacts that occurred from 1979 to 1989
[AD-A285691] p 1202 N95-20275
Helicopter crewseat cushion program
[AD-A286654] p 1452 N95-20973
Age 60 study. Part 2: Airline pilot age and performance. A review of the scientific literature
[AD-A286246] p 1447 N95-22040
Forecasting aircraft mishaps using monthly maintenance reports
[AD-A286049] p 1203 N95-22417

FLIGHT SIMULATION
Summary of a joint program of research into aircraft flight control concepts
[AD-A280012] p 1214 N95-20004
Collected papers of the Soar/IFOR project, Spring 1994
[AD-A280063] p 1216 N95-20624
Minima reduction simulation test results
[AD-A285626] p 1204 N95-21148
A preliminary study of the airwake model used in an existing SH-60B/FFG-7 helicopter/ship simulation program
[DSTO-TR-0015] p 1201 N95-21659

FLIGHT SIMULATORS
Using the backward transfer paradigm to validate the AH-64 Simulator Training Research Advanced Testbed for Aviation
[AD-A285758] p 1215 N95-19931
Summary of a joint program of research into aircraft flight control concepts
[AD-A280012] p 1214 N95-20004
Crew-Centered Cockpit Design (CCCD) field demonstration program, volume 1
[AD-A286426] p 1453 N95-21566

FLIGHT STRESS (BIOLOGY)
Command history, 1993
[AD-A279775] p 1446 N95-21989

FLIGHT TESTS
Open Skies project computational fluid dynamic analysis
[AD-A285928] p 1200 N95-19991
F-15 resource tape
[NASA-TM-110502] p 1206 N95-19994
Acoustic climb to cruise test
[NASA-TM-110504] p 1206 N95-20155
SAR image registration in absolute coordinates using GPS carrier phase position and velocity information
[DE94-018738] p 1204 N95-20195
Assessment of a non-dedicated GPS receiver system for precise airborne attitude determination
[DE94-019309] p 1205 N95-21520

FLIGHT TRAINING
Public-sector aviation issues: Graduate research award papers, 1992-1993
[PB94-217478] p 1199 N95-19967
T-45A High Angle of Attack Testing: US Naval Test Pilot School 46th Annual Reunion and Symposium
[AD-A284000] p 1207 N95-20466
A computer-based multimedia prototype for night vision goggles
[AD-A286208] p 1546 N95-21882

FLOATING
Absorbing boundary condition for floating two-dimensional objects in current and waves
[PB95-132882] p 1356 N95-22063

FLOATING POINT ARITHMETIC
A divide-and-conquer method for tridiagonalizing symmetric matrices with repeated eigenvalues
[DE95-002918] p 1476 N95-21257
A framework for symmetric band reduction and tridiagonalization
[DE95-002919] p 1476 N95-21341

FLOCCULATING
Magnetic flocculation of paramagnetic particles
[DE94-018144] p 1501 N95-20725

FLOODS
Monsoons: AMIP simulations of the 1987 and 1988 drought and flood regimes
[DE94-014789] p 1428 N95-20140

FLOQUET THEOREM
Instability of streamwise vortices in plane channel flows p 1344 N95-21049

FLOW CHARACTERISTICS
Simulation of pipe flow p 1349 N95-21078
Direct numerical determination of the minimum bypass Reynolds number in boundary layers
p 1349 N95-21080
Simulated rarefied entry of the Galileo probe into the atmosphere of Jupiter
[NASA-TM-110507] p 1601 N95-21621
Mantle devolatilization and rheology in the framework of planetary evolution p 1418 N95-21788

FLOW CHARTS
Algebraic semantics of message sequence charts
[PB95-110581] p 1288 N95-19890
Generalised approach to software structure metrics
[PB95-107561] p 1467 N95-21411

FLOW COEFFICIENTS
Flow coefficient behavior for boundary layer bleed holes and slots
[NASA-TM-106846] p 1338 N95-19953

FLOW DEFLECTION
Static investigation of two fluidic thrust-vectoring concepts on a two-dimensional convergent-divergent nozzle
[NASA-TM-4574] p 1199 N95-19913

FLOW DISTRIBUTION
Radiation from advanced solid rocket motor plumes
[NASA-CR-196554] p 1221 N95-20124
Structure and dynamics of turbulent wall layers
[AD-A285360] p 1340 N95-20547
Internal aerodynamics of a generic three-dimensional scramjet inlet at Mach 10
[NASA-TP-3476] p 1340 N95-20619
16-foot transonic tunnel test section flowfield survey
[NASA-TM-109157] p 1216 N95-20669
Software for flow distribution in electronic rack structures
[AD-A285994] p 1325 N95-20715
HIVEL2D: A two-dimensional flow model for high-velocity channels
[AD-A286556] p 1341 N95-20843
Laser anemometry and viscous computation of the flow through an annular turbine cascade
[AD-A280070] p 1341 N95-20968
Wake measurements in a strong adverse pressure gradient
[NASA-CR-197272] p 1201 N95-21031
Effects of non-unity Lewis numbers in diffusion flames
p 1249 N95-21036
Effect of chemical heat release in a temporally evolving mixing layer p 1249 N95-21037
Direct numerical simulations of turbulent non-premixed methane-air flames modeled with reduced kinetics
p 1249 N95-21038
Triple flame structure and diffusion flame stabilization
p 1249 N95-21039
Simulation of a turbulent flame in a channel
p 1249 N95-21044
The decay of axisymmetric homogeneous turbulence
p 1343 N95-21047
Large-eddy simulation of separated flow in a ribbed duct p 1347 N95-21070
Numerical simulation of spatially-developing planar jets p 1351 N95-21087
Rib vortices in round jets: Direct and large eddy simulation p 1351 N95-21088
Nonlinear acoustic processes in a solid rocket engine
[AD-A285606] p 1222 N95-21193
The structure of turbulence and other motions beneath an air-water interface
[AD-A279838] p 1434 N95-21293

Application of Navier-Stokes code PAB3D with kappa-epsilon turbulence model to attached and separated flows [NASA-TP-3480] p 1201 N95-21338
Experiments on the flow field physics of confluent boundary layers for high-lift systems [NASA-CR-197318] p 1201 N95-21343
Triple flames and flame stabilization p 1249 N95-22441
Flame propagation under partially-premixed conditions p 1250 N95-22442
A method for obtaining a statistically stationary turbulent free shear flow p 1363 N95-22463

FLOW EQUATIONS
A control volume method on an icosahedral grid for numerical integration of the shallow-water equations on the sphere [DE94-016345] p 1489 N95-20170
On the transition towards slow manifold in shallow-water and 3D Euler equations in a rotating frame p 1345 N95-21057
Application of Roe's flux-difference splitting for kappa-epsilon turbulence model [PB95-127718] p 1352 N95-21106
Application of Navier-Stokes code PAB3D with kappa-epsilon turbulence model to attached and separated flows [NASA-TP-3480] p 1201 N95-21338
Preconditioning via asymptotically-defined domain decomposition [DE94-019046] p 1493 N95-21564

FLOW MEASUREMENT
Transverse vorticity measurements in the NASA Ames 80 x 120 wind tunnel boundary layer p 1362 N95-22457

FLOW STABILITY
Numerical study of realistic perturbations in three-dimensional boundary layers p 1351 N95-21091
Direct numerical simulation of 2-D and 3-D instability waves in a laminar separation bubble p 1352 N95-21095
Instabilities in natural-convection flows in cavities [PB95-107975] p 1354 N95-21578
Fourth International Symposium on Stratified Flows, volume 1 [AD-A286450] p 1354 N95-21583
Stability effects on the profiles of vertical velocity and its variance in katabatic flow [DE95-001126] p 1426 N95-21836
Nonlinear interaction between a pair of oblique modes in a supersonic mixing layer: Long-wave limit [NASA-CR-197380] p 1357 N95-22173

FLOW THEORY
Robust fixed-structure control [AD-A286515] p 1485 N95-22216

FLOW VELOCITY
A comparison of kinetic and multifluid simulations of laser-produced colliding plasmas [DE94-016447] p 1551 N95-20315
Nonlinear spectroscopy of multicomponent droplets and two- and three-dimensional measurements in flames [AD-A279945] p 1238 N95-20581
Simulation of pipe flow p 1349 N95-21078
Entrainment in a shear-free turbulent mixing layer p 1350 N95-21083
The effect of initial conditions on the development of temporally evolving planar three dimensional incompressible wakes p 1350 N95-21085
Direct simulation of tridimensional wake of NACA 0012 profile p 1350 N95-21086
Direct numerical simulation of 2-D and 3-D instability waves in a laminar separation bubble p 1352 N95-21095
New theory of critical flow velocities in superfluid helium [PB95-130365] p 1571 N95-21228
Mixing and dynamics of the Mediterranean outflow [AD-A279803] p 1434 N95-21306
Resolving velocity profiles with the multi-scale profiler [AD-A286446] p 1434 N95-21461
Stability of pressure and velocity computations for heterogeneous reservoirs [PB95-110284] p 1354 N95-21656

FLOW VISUALIZATION
Visualizing 3D velocity fields near contour surfaces [DE95-000841] p 1353 N95-21182
Effect of juncture fillets on double-delta wings undergoing sideslip at high angles of attack [AD-A286165] p 1207 N95-22039
DOD science and engineering apprenticeship program for high school students [AD-A280371] p 1583 N95-22100
On the dynamics of a shock-bubble interaction [NASA-CR-194978] p 1495 N95-22325
Experimental investigations of on-demand vortex generators p 1361 N95-22451

FLUE GASES
Experimental investigation of PIC formation during the incineration of recovered CFC-11 [PB94-214772] p 1401 N95-20192

FLUENCE
The use of displacement damage dose to correlate degradation in solar cells exposed to different radiations p 1320 N95-20523
Influence of oxidation on radiation hardness of silicon detectors [DE95-002466] p 1272 N95-20894

FLUES
Fire experiments in a two dimensional rack storage: BRANDFORSK-project 701-917 [PB95-131538] p 1241 N95-21179

FLUID BOUNDARIES
Absorbing boundary condition for floating two-dimensional objects in current and waves [PB95-132882] p 1356 N95-22063

FLUID DYNAMICS
Nonlinear dynamic fluid-structure interaction calculations with coupled finite element and finite volume programs [DE94-016204] p 1339 N95-20166
Description and flow characterization of hypersonic facilities [AD-A284291] p 1200 N95-20248
Cascade orificial resistive device [AD-D016529] p 1504 N95-20724
Fluid dynamics of the freeboard in a fluidized bed reactor [PB95-134029] p 1357 N95-22160
Turbine design and application [NASA-SP-290] p 1214 N95-22341
On the dynamics of small-scale vorticity in isotropic turbulence p 1362 N95-22459

FLUID FILMS
An augmented Young-Laplace model of an evaporating meniscus in a micro-channel with high heat flux [NASA-CR-197622] p 1340 N95-20796

FLUID FLOW
Solidification modeling of a spiral casting to determine material fluidity [DE94-018930] p 1285 N95-20050
Proceedings of the 4th International Conference on Electrorheological Fluids [AD-A286341] p 1266 N95-20227
Low flow fluid separator [AD-D016575] p 1339 N95-20297
Cascade orificial resistive device [AD-D016529] p 1504 N95-20724
Application of Direct and Large Eddy Simulation to Transition and Turbulence [AGARD-CP-551] p 1346 N95-21061
Large-eddy simulation of rotating channel flows using a localized dynamic model p 1346 N95-21064
The asymptotic state of rotating homogeneous turbulence at high Reynolds numbers p 1347 N95-21065
Weld pool phenomena [DE94-018965] p 1381 N95-21550
Subduction and volatile recycling in Earth's mantle p 1421 N95-21802
Vortex atoms and vortons [PB95-134599] p 1356 N95-21963
Elastic micro-fabricated surface layer for reducing turbulence and drag on an object while it moves through a fluid medium [AD-D016516] p 1356 N95-22060
Optimal active control for Burgers equations p 1361 N95-22454

FLUID MECHANICS
Oceanographic analysis of the acoustic mid-ocean dynamics experiment [AD-A285907] p 1432 N95-19988
Transactions of the Eleventh Army Conference on Applied Mathematics and Computing [AD-A279884] p 1497 N95-22389

FLUID PRESSURE
Stability of pressure and velocity computations for heterogeneous reservoirs [PB95-110284] p 1354 N95-21656

FLUID-SOLID INTERACTIONS
A mixed time integration method for large scale acoustic fluid-structure interaction [DE94-018327] p 1354 N95-21387

FLUIDICS
Static investigation of two fluidic thrust-vectoring concepts on a two-dimensional convergent-divergent nozzle [NASA-TM-4574] p 1199 N95-19913

FLUIDS
Quartz resonator fluid monitors for vehicle applications [DE94-018910] p 1367 N95-21546

FLUORESCENCE
Cavity-QED enhancement of fluorescence yields in microdroplets [DE94-018662] p 1506 N95-20030
Nonlinear spectroscopy of multicomponent droplets and two- and three-dimensional measurements in flames [AD-A279945] p 1238 N95-20581
Visible fluorescence of weathered lead [DE95-002454] p 1244 N95-21523

FLUORIDES
The role of high pressure in the study and applications of the ferroelectric polymer polyvinylidene fluoride and its copolymers [DE94-015742] p 1268 N95-20396
T1F ((1) sigma (+)): Some preliminary electronic structure calculations [PB95-130316] p 1518 N95-21223

FLUORINE
Experimental investigation of PIC formation during the incineration of recovered CFC-11 [PB94-214772] p 1401 N95-20192
Calculated heats of formation of some predicted stable C, N, O, F molecules [AD-A285957] p 1517 N95-21127
Novel fluorine oxidizers [AD-A279480] p 1284 N95-21678

FLUORO COMPOUNDS
Vibrational overtone spectroscopy of pyridine and related compounds [AD-A280105] p 1224 N95-21911

FLUOROCARBONS
New concepts for refrigerant leak detection and mixture measurement [DE94-018967] p 1287 N95-21559

FLUOROHYDROCARBONS
Materials compatibility and lubricants research on CFC-refrigerant substitutes [DE94-018414] p 1287 N95-21631
Thermophysical properties of HFC-143a and HFC-152a [DE95-002199] p 1582 N95-22153

FLUX DENSITY
Transport and dynamics in toroidal fusion systems [DE94-018653] p 1548 N95-20029
Coaxial hybrid wiggler [AD-D016501] p 1331 N95-21671
N = 1 Superconformal minimal model correlation functions on the torus [PB95-134615] p 1500 N95-21964
The solar flux of thermal neutrinos and antineutrinos of all flavors [DE95-003204] p 1604 N95-22085

FLUX PINNING
How to improve J(c(T)) in Ag/(BiPb)2Sr2Ca2Cu3O10 tapes [PB95-110326] p 1575 N95-21949

FLUX VECTOR SPLITTING
Hybrid Upwind Splitting (HUS) by a field-by-field decomposition [NASA-TM-106843] p 1355 N95-21957

FLYING PERSONNEL
Factors that determine visual acuity through night vision goggles for emmetropes [AD-A279339] p 1450 N95-21927

FLYING PLATFORMS
CALIOPE and TAISIR airborne experiment platform [DE94-018328] p 1310 N95-22299

FOAMS
Low density gas and foam targets for ICF long scale length plasma experiments: Fabrication and characterization [DE95-000935] p 1558 N95-21368
Investigation on research for degradable plastics [DE94-796550] p 1277 N95-21714
Analysis of test criteria for specifying foam firefighting agents for aircraft rescue and firefighting [AD-A286381] p 1203 N95-22352

FOCAL PLANE DEVICES
A method using focal plane analysis to determine the performance of reflector antennas p 1304 N95-21538
InTISb for long-wavelength infrared photodetectors and arrays [AD-A280109] p 1331 N95-21660

FOCUSING
An update on the development of a line-focus refractive concentrator array p 1322 N95-20534
Testing of the SAIC facets on the stretched-membrane dish [DE95-001831] p 1393 N95-20864
Target alignment in the National Ignition Facility [DE94-015559] p 1540 N95-22469

FOILS (MATERIALS)
Atom wave interferometer [AD-A279532] p 1524 N95-21688

FOKKER-PLANCK EQUATION
Modeling the dynamics of charged-particle beams using a Fokker-Planck approach
[DE95-001458] p 1531 N95-19983
Quantum diffusion
[DE95-001015] p 1580 N95-21264
FOLDING STRUCTURES
High-performance, flexible, deployable array development for space applications
p 1322 N95-20532
Static stability of a three-dimensional space truss
p 1220 N95-20533
An introduction to the Astro Edge solar array
p 1322 N95-20535
FOOTPRINTS
High resolution descriptions of IRAS 12 and 25 microns confused regions
[AD-A285847] p 1545 N95-21832
FORCE
The doping effect on spin-Peierls instability
[DE94-629046] p 1577 N95-22178
FORCED CONVECTION
A computer code (SKINTEMP) for predicting transient missile and aircraft heat transfer characteristics
[AD-A286044] p 1341 N95-21001
Governing equations for multiphase heat and mass transfer in hygroscopic porous media with applications to clothing materials
[AD-A286418] p 1357 N95-22206
FORECASTING
Radar studies of aviation hazards
[AD-A285845] p 1203 N95-21831
FORESTS
Large bistatic angle clutter depolarization study
p 1296 N95-20941
Investigation on the backscattering properties of Finnish boreal forests at C- and X-band: A semi-empirical modeling approach
[PB95-127692] p 1389 N95-21105
ICE BABY: Measurements of concentration fluctuations in a forest area in winter conditions
[PB95-133468] p 1405 N95-21274
FORGING
Manufacturing Technology Bulletin, July 1994
[DE94-017775] p 1605 N95-22262
FORM FACTORS
Semi-leptonic form-factors from lattice QCD
[DE95-000871] p 1510 N95-20367
Ultra-Reliable Digital Avionics (URDA) processor
p 1209 N95-20638
Universal parametrization for quark and lepton substructure
[DE94-770604] p 1514 N95-20738
FORMALISM
Ups and downs of type theory
[PB95-110664] p 1487 N95-19903
Physical Si(1-x)Ge(x)/Si heterojunction bipolar transistor model for device and circuit simulation
[PB95-110896] p 1312 N95-19934
TBell: A mathematical tool for analyzing decision tables
[NASA-CR-195027] p 1462 N95-20691
Symmetry, Wigner functions and particle reactions
[DE94-629887] p 1514 N95-20735
Construction of non-critical string field theory by transfer matrix formalism in dynamical triangulation
[DE94-770607] p 1516 N95-20986
Monadic maps and folds for arbitrary datatypes
[PB95-134045] p 1492 N95-21032
Performance analysis and true concurrency semantics
[PB95-134086] p 1478 N95-21869
N=1 Superconformal minimal model correlation functions on the torus
[PB95-134615] p 1500 N95-21964
Testing the principle of equivalence by solar neutrinos
[DE94-014972] p 1604 N95-22064
FORMAT
FASTPACK: Optimized solutions for modular avionics derived from a parametric study. Part 2: Avionics
p 1209 N95-20635
An evaluation of Automatic Terminal Information Service (ATIS) flight deck display presentation options
[AD-A280100] p 1204 N95-21020
Standard data formats for simulation
[PB95-110367] p 1470 N95-22016
FORMING TECHNIQUES
Sheet metal formability
[PB95-110250] p 1258 N95-21653
FORSTERITE
Modelocking and waveguide amplifiers using Cr:Forsterite and Cr:YAG
[AD-A285857] p 1369 N95-20378
FORTRAN
Task parallel programming in Fx
[AD-A285136] p 1475 N95-20500
Software for flow distribution in electronic rack structures
[AD-A285994] p 1325 N95-20715
PRSCAL manual
[PB95-130480] p 1465 N95-21231
SEEK: A FORTRAN optimization program using a feasible directions gradient search
[NASA-CR-4641] p 1380 N95-21359
FORTRAN subroutine for column reduction of polynomial matrices
[PB95-134987] p 1497 N95-22379
FORWARD SCATTERING
Neutrino-neutrino scattering and matter-enhanced neutrino flavor transformation in supernovae
[DE94-017577] p 1604 N95-20383
FOSSILS
HIRAS images of fossil dust shells around AGB stars
p 1593 N95-21768
FOULING
Heat transfer, fouling, and combustion of supercritical fuels
[AD-A279906] p 1281 N95-19884
FOUNDATIONS
Operating manual for hybrid thermosyphons at the Gakona Power Plant, Alaska
[AD-A279068] p 1287 N95-21626
FOUNDRIES
Relationship between dendrite coherency and castability of some commercial foundry alloys
[PB95-110243] p 1258 N95-21652
FOUR-WAVE MIXING
The preparation of all para-polyphenyls with increased solubility and enhanced third order NLO activity
[AD-A284301] p 1266 N95-20251
Instantaneous frequency dynamics of coherent emission from magnetoexcitons in gallium arsenide
[DE94-018182] p 1569 N95-20677
Temporal and spectral investigation of multi-Landau level quantum beats in GaAs
[DE94-018189] p 1569 N95-20678
Phase dynamics of non-equilibrium distributions of free electron-hole pairs in GaAs quantum wells
[DE94-018190] p 1569 N95-20679
Laser-Induced Thermal Acoustics (LITA): Four-wave mixing measurement of sound speed, thermal diffusivity, and viscosity
[AD-A286524] p 1372 N95-21009
Advanced diagnostics for plasma chemistry
[DE94-018936] p 1561 N95-22116
FOURIER ANALYSIS
Modeling of beam dynamics and comparison with measurements for the Advanced Light Source (ALS)
[DE94-017970] p 1532 N95-20495
Analysis of subgrid models using direct and large-eddy simulations of isotropic turbulence p 1348 N95-21071
The sharper image: Implementing a Fast Fourier Transform (FFT) to enhance a video-captured image
[AD-A279790] p 1445 N95-21180
FOURIER SERIES
Transport and dynamics in toroidal fusion systems
[DE94-018653] p 1548 N95-20029
FOURIER TRANSFORMATION
Electrospray ionization Fourier transform ion cyclotron resonance mass spectrometric study of singly and doubly charged organometallic complexes
[AD-A279899] p 1238 N95-20563
Detection of environmental deterioration in fiber reinforced composites by FT-Raman spectroscopy, phase 1
[AD-A279763] p 1228 N95-20805
The PROSAIC Laplace and Fourier Transform
[DE95-002225] p 1492 N95-21266
Synthetic aperture radar processing with polar formatted subapertures
[DE95-001830] p 1302 N95-21305
Surface inspection using Fourier Transform Infrared Spectroscopy
[DE95-001699] p 1244 N95-21571
FRACTALS
Statistical properties of geologic fractals
[DE94-019272] p 1414 N95-20908
Highly survivable communications: Complementary media packet switched networks p 1292 N95-20922
Temporal and spatial comportment of multiple paths in ionospheric propagation in oblique incidence: Fractal measures of perturbations p 1298 N95-20954
Fractal nature and scaling of normal faults, Rio Grande rift, NM: Implications for growth and strain
[DE94-018261] p 1414 N95-20990
Perimeter-yardstick technique for fracture surface fractal analysis
[AD-A286240] p 1387 N95-22025
FRACTIONATION
Primitive Xe in the atmospheres of Earth and mars
p 1419 N95-21795
Mars atmospheric loss and isotopic fractionation by pick-up-ion sputtering and photochemical escape
p 1420 N95-21796
Solar wind composition
[NASA-TM-197364] p 1604 N95-22384
FRACTOGRAPHY
Perimeter-yardstick technique for fracture surface fractal analysis
[AD-A286240] p 1387 N95-22025
FRACTURE MECHANICS
Analyses of some benchmark cases in fracture mechanics using boundary element method
[PB95-110888] p 1384 N95-19930
Analysis of the progressive failure of brittle matrix composites
[NASA-CR-195415] p 1225 N95-19951
Tritium and decay helium effects on the fracture toughness properties of types 316L, 304L and 21Cr-6Ni-9Mn stainless steels
[DE95-001248] p 1252 N95-20216
An overview of the HSST Full-Thickness Shallow-Crack Clad Beam Testing Program
[DE94-018940] p 1385 N95-20322
Fracture analysis of an all-ceramic bearing system
[AD-A285056] p 1269 N95-20486
The 29th MIL-HDBK-17 Polymer Matrix Composites Coordination Group Meeting
[AD-A279917] p 1269 N95-20578
The processing and mechanical properties of high temperature/high performance composites. Book 5: Interface effects
[AD-A279815] p 1228 N95-20584
Effect of external stress on the transport of fluids in thermoplastic resin systems
[AD-A279993] p 1270 N95-20596
The processing and mechanical properties of high temperature/high performance composites. Processing/property correlations, book 4
[AD-A279739] p 1228 N95-20802
Experimental investigation of wave and fracture phenomena in impacted ceramics
[AD-A286589] p 1272 N95-20856
Role of internal stresses in fracture behavior of engineering composites
[DE95-001106] p 1229 N95-20912
The mechanical behavior of surface-modified ceramics
[DE95-001704] p 1276 N95-21572
The role of microcracking on the crack growth resistance of brittle solids and composites
[DE95-001678] p 1231 N95-21736
Influence of fatigue crack closure on the growth rate of surface flaws
[AD-A279130] p 1387 N95-21967
The influence of chemistry and microstructure on the fracture toughness of V-V3Si in-situ composites
[DE94-018997] p 1232 N95-22126
Fracture behavior of laminated discontinuously reinforced aluminum material
[DE94-017307] p 1263 N95-22408
FRACTURE STRENGTH
Cr2Nb development
[DE94-018697] p 1250 N95-20043
Fracture toughness properties of welded stainless steels for tritium service
[DE95-000755] p 1251 N95-20079
Tritium and decay helium effects on the fracture toughness properties of types 316L, 304L and 21Cr-6Ni-9Mn stainless steels
[DE95-001248] p 1252 N95-20216
An overview of the HSST Full-Thickness Shallow-Crack Clad Beam Testing Program
[DE94-018940] p 1385 N95-20322
Microstructural contributions to the fracture resistance of silicon nitride ceramics
[DE94-018955] p 1267 N95-20323
Approaches to the design of structural ceramics incorporating whiskers and particulate phases
[DE94-018126] p 1271 N95-20704
Reliability analysis of uniaxially ground brittle materials
[NASA-TM-106852] p 1386 N95-20790
Processing and mechanical properties of laminar Al2O3-Ni3Al composites
[DE94-019332] p 1230 N95-21481
Fracture behavior of the Fe-8Al alloy FAP-Y
[DE95-000956] p 1258 N95-21676
The role of microcracking on the crack growth resistance of brittle solids and composites
[DE95-001678] p 1231 N95-21736
Incology alloy 908 data handbook
[DE95-001818] p 1260 N95-22013
The influence of chemistry and microstructure on the fracture toughness of V-V3Si in-situ composites
[DE94-018997] p 1232 N95-22126

Low temperature tensile and fracture mechanical strength in mode 1 and mode 2 of fiber reinforced plastics following various irradiation conditions
[DE94-019269] p 1232 N95-22130
Fracture behavior of laminated discontinuously reinforced aluminum material
[DE94-017307] p 1263 N95-22408
Structural performance of cylindrical pressure housings of different ceramic compositions under external pressure loading. Part 3: Sintered reaction bonded silicon nitride ceramic
[AD-A285773] p 1388 N95-22411

FRACTURES (MATERIALS)
The 29th MIL-HDBK-17 Polymer Matrix Composites Coordination Group Meeting
[AD-A279917] p 1269 N95-20578
Perimeter-yardstick technique for fracture surface fractal analysis
[AD-A286240] p 1387 N95-22025

FRACTURING
Ductile-brittle transition behavior of tungsten under shock loading
[DE94-009913] p 1251 N95-20122
The in-situ fracture and Auger analysis of Nicalon fibers
[DE94-017771] p 1226 N95-20357
Effect of heat treatment temperature on creep-rupture properties of Fe3Al-based alloys
[DE94-017904] p 1253 N95-20375
Effect of fiber fabric orientation on the monotonic and fatigue behavior of a continuous fiber ceramic composite
[DE94-018121] p 1271 N95-20700
The processing and mechanical properties of high temperature/high performance composites. Processing/property correlations, book 4
[AD-A279739] p 1228 N95-20802
Experimental investigation of wave and fracture phenomena in impacted ceramics
[AD-A286589] p 1272 N95-20856
The mechanical behavior of surface-modified ceramics
[DE95-001704] p 1276 N95-21572
VTT test borehole for bedrock investigations
[PB95-132965] p 1427 N95-22095

FRAGMENTATION
Aluminium oxide targets after ballistic impact; fragmentation of the ceramic and the projectile
[PB95-133625] p 1388 N95-22097
Cryogenic pellet laser plasma source targets
[DE95-002488] p 1376 N95-22169

FRAMES
Frame and edge seal technology: A state of the art survey
[PB95-110334] p 1288 N95-22014

FRAMES (DATA PROCESSING)
Tracking a dynamic set of feature points
[AD-A285124] p 1313 N95-20257

FREE CONVECTION
Instabilities in natural-convection flows in cavities
[PB95-107975] p 1354 N95-21578

FREE ELECTRON LASERS
Free electron laser program
[AD-A285906] p 1368 N95-19987
Compact free electron lasers for medical applications
[AD-A285739] p 1369 N95-20072
Pulsed laser illumination of photovoltaic cells
p 1323 N95-20538
A URI program for Ultraviolet/extreme ultraviolet research
[AD-A279159] p 1370 N95-20600
MTX final report
[DE95-002960] p 1559 N95-21451
Time-resolved study of sideband generation and transition to chaos on an infrared FEL
[DE95-002336] p 1374 N95-21528
Performance of cesium telluride photocathodes as an electron source for the Los Alamos FEL
[DE94-018302] p 1375 N95-21919
Recent progress of the compact AFEL at Los Alamos
[DE95-002728] p 1376 N95-22154
Photocathodes for free electron lasers
[DE94-018305] p 1376 N95-22242
Fabrication and characterization of cesium telluride photocathodes: A promising electron source for the Los Alamos Advanced FEL
[DE94-018303] p 1377 N95-22348
Low-level RF control for the AFEL
[DE94-018295] p 1540 N95-22410

FREE ELECTRONS
Phase dynamics of non-equilibrium distributions of free electron-hole pairs in GaAs quantum wells
[DE94-018190] p 1569 N95-20679
On FEL integral equation and electron energy loss in intermediate gain regime
[DE94-770631] p 1371 N95-20757
Competition between electromagnetic modes in a free-electron maser
[AD-A279546] p 1374 N95-21694

FREE ENERGY
Quantum simulation of heterogeneous electron transfer free energies at the water-metal interface
[AD-A279279] p 1522 N95-21492
Biaxiality of chiral liquid crystals
[DE94-629032] p 1578 N95-22277

FREE FALL
Microgravity: Teacher's guide with activities for physical science
[NASA-EG-103] p 1285 N95-21322

FREE FLOW
Direct numerical simulation of 2-D and 3-D instability waves in a laminar separation bubble
p 1352 N95-21095
A method for obtaining a statistically stationary turbulent free shear flow p 1363 N95-22463
Direct numerical simulation of incompressible axisymmetric flows p 1363 N95-22464

FREE JETS
Temperature effects on acoustic interactions between altitude test facilities and jet engine plumes
[NASA-CR-197638] p 1504 N95-21170

FREE RADICALS
The energetics and dynamics of free radicals, ions, and clusters
[DE94-018101] p 1244 N95-21701
Restricted mass transport effects on free radical reactions
[DE94-018136] p 1217 N95-21706

FREEZE DRYING
Evaluation of dried storage of platelets for transfusion: Physiologic integrity and hemostatic functionality
[AD-A286078] p 1443 N95-20850

FREEZING
Effect of microgravity on material undergoing melting and freezing: The TES Experiment
[NASA-TM-106845] p 1338 N95-19952

FREON
Experimental investigation of PIC formation during the incineration of recovered CFC-11
[PB94-214772] p 1401 N95-20192

FREQUENCIES
Higher order crossings
[AD-A279597] p 1504 N95-20300
White-light spectral analysis of lithium niobate waveguides
[DE94-016692] p 1542 N95-20489
Modeling of beam dynamics and comparison with measurements for the Advanced Light Source (ALS)
[DE94-017970] p 1532 N95-20495
Instantaneous frequency dynamics of coherent emission from magnetoexcitons in gallium arsenide
[DE94-018182] p 1569 N95-20677
Passive monitoring for automated MMPP communication systems p 1293 N95-20927
Line-of-sight multipath propagation measurements at 15 GHz over 500 MHz bandwidth p 1296 N95-20944
Experimental study of the helicopter-mobile radioelectrical channel and possible extension to the satellite-mobile channel p 1296 N95-20945
The effects of multihop HF propagation on the performance of OTH backscatter radars
p 1298 N95-20953
Glossary of frequency and timing terms and a pictorial representation of terms used in the behavior and analyses of frequency standards
[AD-A286172] p 1310 N95-22247
Inverse and control problems in electromagnetics
[AD-A286438] p 1310 N95-22250
Determination of the complex elastic moduli of materials using a free-free bar technique
[AD-A279861] p 1281 N95-22387

FREQUENCY ANALYZERS
Measurement of sound intensity and sound power
[AD-A279246] p 1505 N95-21984

FREQUENCY CONTROL
Materials processing using a variable frequency microwave furnace
[DE95-001420] p 1271 N95-20761

FREQUENCY CONVERTERS
Solid state frequency conversion technology for remote sensing
[DE94-019102] p 1389 N95-21433
Nonlinear frequency conversion optical filter
[AD-D016523] p 1544 N95-21465

FREQUENCY DISTRIBUTION
1/f noise in two-dimensional fluids
[DE95-002617] p 1358 N95-22307

FREQUENCY DIVISION MULTIPLEXING
A simple analytical model for asynchronous dense WDM/OOK systems
[AD-A283725] p 1289 N95-19973

FREQUENCY HOPPING
A wideband propagation simulator for high speed mobile radio communications p 1295 N95-20934

FREQUENCY MEASUREMENT
Field-emitter arrays for RF vacuum microelectronics
[AD-A279959] p 1325 N95-20661

FREQUENCY MODULATION
Development of an annular electron beam HPM amplifier
[AD-A286646] p 1327 N95-20905
Linear and nonlinear spectroscopy with the tunable AC scanning tunneling microscope
[AD-A285751] p 1241 N95-21217
Millimeter wave front-end figure of merit, part 1
[AD-A279093] p 1307 N95-21915

FREQUENCY RANGES
A MMPP communications system for the frequency range 2-200MHz p 1293 N95-20924
Modelling and simulation of HF/VHF MMPPs
p 1293 N95-20925

FREQUENCY RESPONSE
Frequency response measurements of integrated-optic electrodes
[DE94-016690] p 1542 N95-20403
Dynamic response of pressure measuring systems
[ARL-TR-32] p 1365 N95-20759
Time behavior and frequency response of the microwave propagation channel during multipath propagation
p 1296 N95-20942
Atom wave interferometer
[AD-A279532] p 1524 N95-21688
High frequency current sensors using the Faraday effect in optical fibers
[DE95-001859] p 1545 N95-21728
Multiwire thermocouples: Frequency response
[NASA-TM-110510] p 1367 N95-21889

FREQUENCY SHIFT KEYING
Error probabilities of FFH/BFSK with noise normalization and soft decision viterbi decoding in a fading channel with partial-band jamming
[AD-A280041] p 1498 N95-20620
Cochannel and adjacent-channel interference in nonlinear minimum-shift-keyed satellite system
[NASA-TM-106834] p 1307 N95-21890

FREQUENCY STABILITY
Radio-science performance analysis software
p 1305 N95-21540

FREQUENCY STANDARDS
Glossary of frequency and timing terms and a pictorial representation of terms used in the behavior and analyses of frequency standards
[AD-A286172] p 1310 N95-22247

FRESNEL LENSES
An update on the development of a line-focus refractive concentrator array p 1322 N95-20534

FRICTION FACTOR
Role of internal stresses in fracture behavior of engineering composites
[DE95-001106] p 1229 N95-20912

FRICTION MEASUREMENT
Wear resistant composite structure of vitreous carbon containing convoluted fibers
[DE95-002254] p 1228 N95-20787

FRICTION REDUCTION
Modeling the effect of shroud contact and friction dampers on the mistuned response of turbopumps
[NASA-CR-197285] p 1379 N95-20795

FRONTS (METEOROLOGY)
Front-boundary layer models from STORM-FEST observations
[AD-A279907] p 1428 N95-20186

FUEL CELL POWER PLANTS
A fuel cell overview
[DE95-001455] p 1393 N95-20839

FUEL CELLS
Exploratory Technology Research Program for electrochemical energy storage
[DE95-002651] p 1392 N95-20439
Multiply manifolded molten carbonate fuel cells
[DE94-017074] p 1392 N95-20480
Molten carbonate fuel cell product development test
[DE95-000005] p 1324 N95-20574
A fuel cell overview
[DE95-001455] p 1393 N95-20839
Performance and cost analysis of monolithic solid oxide fuel cells
[DE95-002511] p 1394 N95-20896
Solid oxide fuel cells in the United States
[DE95-002405] p 1395 N95-21361
Electric and Hybrid Vehicles Program
[DE95-001711] p 1332 N95-21738
Economic feasibility analysis of distributed electric power generation based upon the natural gas-fired fuel cell
[DE94-012277] p 1396 N95-22033

Development and demonstration of advanced technologies for direct electrochemical oxidation of hydrocarbons (methanol, methane, propane)
[AD-A285094] p 1224 N95-22474

FUEL COMBUSTION
Heat transfer, fouling, and combustion of supercritical fuels
[AD-A279906] p 1281 N95-19884
LIEKKI combustion technology
[DE95-700233] p 1242 N95-21282
Multiple burn fuel-optimal orbit transfers: Numerical trajectory computation and neighboring optimal feedback guidance
[NASA-CR-197317] p 1222 N95-21616
EAGLES 1.1: A microcomputer software package for analyzing fuel efficiency of electric and gasoline vehicles
[DE95-001119] p 1469 N95-21829
Fuselage burnthrough from large exterior fuel fires
[AD-A286295] p 1203 N95-22318

FUEL INJECTION
Heat transfer, fouling, and combustion of supercritical fuels
[AD-A279906] p 1281 N95-19884
Nonlinear acoustic processes in a solid rocket engine
[AD-A285606] p 1222 N95-21193

FUEL OILS
Producing liquid fuels from biomass
[DE95-717458] p 1398 N95-22425

FUEL PRODUCTION
Assessment of liquefaction and pyrolysis systems
[PB95-129797] p 1236 N95-20290

FUEL SPRAYS
Heat transfer, fouling, and combustion of supercritical fuels
[AD-A279906] p 1281 N95-19884

FUEL SYSTEMS
Effect of propane-air on NGVs and vehicle fueling stations
[PB94-210085] p 1282 N95-20253
Performance and cost analysis of monolithic solid oxide fuel cells
[DE95-002511] p 1394 N95-20896
Solid oxide fuel cells in the United States
[DE95-002405] p 1395 N95-21361
Evaluation of pumping and fueling requirements for the ITER EDA
[DE94-018117] p 1560 N95-21702

FUEL TESTS
Reducing exhaust gas emissions from Citydiesel busses
[DE95-700245] p 1380 N95-21295

FUEL-AIR RATIO
Effect of propane-air on NGVs and vehicle fueling stations
[PB94-210085] p 1282 N95-20253

FULLERENES
Pairing on small clusters in the Peierls-Hubbard model: Implications for C60
[DE94-016284] p 1565 N95-20330
Novel catalysts for methane activation
[DE95-002639] p 1237 N95-20438
Superconducting thin film with fullerenes and method of making
[AD-D016580] p 1567 N95-20461
Photoinduced charge transfer between fullerenes and TiO2 semiconductor colloids
[DE95-001447] p 1570 N95-20838
Aromatics oxidation and soot formation in flames
[DE95-001803] p 1241 N95-21280

FUNCTION SPACE
Linear invariance of Lindeloef numbers
[PB95-134540] p 1494 N95-21956

FUNCTIONAL ANALYSIS
An empirical approach to logical clustering of software failure regions
[AD-A279863] p 1462 N95-20776

FUNCTIONAL DESIGN SPECIFICATIONS
SPACE-R thermionic space nuclear power system: Design and technology demonstration
[DE95-000713] p 1221 N95-20076
Performance specifications for technology development: Application for characterization of volatile organic compounds in the environment
[DE94-016627] p 1401 N95-20234
Goddard Space Flight Center solar array missions, requirements and directions p 1316 N95-20503
Low noise 22 GHz receiver for the radioastron satellite. Part 1: Requirements, design and reliability analysis
[PB95-104410] p 1300 N95-20972
Design principles for real-time process control systems
[PB95-132890] p 1585 N95-21414
Underwater Acoustic Generator Phase 2: Sea trial, March 1992
[MRL-TN-640] p 1434 N95-21657
Evaluation of pumping and fueling requirements for the ITER EDA
[DE94-018117] p 1560 N95-21702
Issues in the flight qualification of a space power reactor
[DE95-001606] p 1223 N95-21840
Performance analysis and true concurrency semantics
[PB95-134086] p 1478 N95-21869
Structuring design requirements using YMIR
[PB95-132742] p 1471 N95-22081
Formal specification and compositional verification of an atomic broadcast protocol
[PB95-110508] p 1472 N95-22351

FUNCTIONAL INTEGRATION
Functional and para-functional parallel processing
[DE95-002805] p 1475 N95-20888

FUNCTIONALS
Set functionals in stochastic geometry
[PB95-135372] p 1491 N95-21005

FUNCTIONS (MATHEMATICS)
Symmetry, Wigner functions and particle reactions
[DE94-629887] p 1514 N95-20735
Recent results from E665
[DE95-002523] p 1516 N95-20914
Structure functions and structure function ratio F2(n)/F2(p) at low X(Bj) and Q2 in inelastic muon scattering
[DE94-018979] p 1573 N95-21561
Dyads: A generalisation of monads
[PB95-134052] p 1494 N95-21867
The dynamic structure function of Bose liquids in the deep inelastic regime
[DE94-629077] p 1527 N95-22182
An exact enumeration of self-avoiding loops on a square lattice
[DE94-628999] p 1578 N95-22276

FUNGI
Microbial degradation of polymers used in electronics
[AD-A286526] p 1273 N95-21011

FURANS
Experimental investigation of PIC formation during the incineration of recovered CFC-11
[PB94-214772] p 1401 N95-20192

FURNACES
Preliminary control system design and analysis for the Space Station Furnace Facility thermal control system
[NASA-TM-108476] p 1365 N95-20560
Impact behavior of FeAl alloy FA-350
[DE94-018128] p 1254 N95-20705
Materials processing using a variable frequency microwave furnace
[DE95-001420] p 1271 N95-20761
Flow and heat transfer simulation in a flash smelting furnace
[PB95-108197] p 1354 N95-21649
Materials support for the development of High Temperature Advanced Furnaces (HITAF): A comparison of selected mechanical properties for three SiC-based ceramics
[DE94-017752] p 1280 N95-22258

FUSELAGES
Damage tolerant repair techniques for pressurized aircraft fuselages
[AD-A286298] p 1199 N95-22046
Fuselage burnthrough from large exterior fuel fires
[AD-A286295] p 1203 N95-22318

FUSION REACTORS
Recent DIII-D results
[DE94-017519] p 1549 N95-20038
Radiation-driven targets for heavy-ion fusion
[DE95-002264] p 1533 N95-20784
Target Area design basis and system performance for the National Ignition Facility
[DE94-016697] p 1557 N95-21207
Laser design basis for the National Ignition Facility
[DE94-016700] p 1534 N95-21209
Review of recent D-T experiments from TFTR
[DE95-002755] p 1557 N95-21239
Fusion power production in TFTR
[DE95-002756] p 1557 N95-21240
Heating and transport in TFTR D-T plasmas
[DE95-002812] p 1558 N95-21242
Irradiation creep in structural materials at ITER operating conditions
[DE94-018946] p 1261 N95-22123

FUSION WELDING
Fusion welding of advanced borated stainless steels
[DE94-019037] p 1378 N95-20053

FUZZY SETS
The use of fuzzy set classification for pattern recognition of the polygraph
[AD-A279148] p 1470 N95-21971

FUZZY SYSTEMS
Automatic generation of fuzzy rules for the sensor-based navigation of a mobile robot
[DE95-001428] p 1481 N95-20837
Fuzzy clustering of facial form for prototyping environmental protection equipment
[DE94-014657] p 1454 N95-22466

G

GALACTIC COSMIC RAYS
Solar wind composition
[NASA-TM-197364] p 1604 N95-22384

GALACTIC EVOLUTION
Connection with dynamics: General introduction
[NASA-CR-197617] p 1579 N95-19947

GALACTIC STRUCTURE
Connection with dynamics: General introduction
[NASA-CR-197617] p 1579 N95-19947
A high resolution atlas of the galactic plane at 12 microns and 25 microns p 1593 N95-21755

GALAXIES
Universal features of multiplicity distributions
[DE94-012854] p 1498 N95-20779
Twentysixth YERAC
[PB95-127437] p 1599 N95-21347
Beyond maximum entropy: Fractal Pixon-based image reconstruction p 1593 N95-21757

GALERKIN METHOD
DNS of turbulent flow in a driven cavity and their analysis using proper orthogonal decomposition
p 1352 N95-21097
Locking of the finite element method in thermoelasticity
[PB95-127098] p 1496 N95-22370

GALILEO PROBE
Simulated rarefied entry of the Galileo probe into the atmosphere of Jupiter
[NASA-TM-110507] p 1601 N95-21621

GALLIUM ARSENIDE LASERS
Analog processing of optical wavefront using integrated guided-wave optics
[AD-A279596] p 1543 N95-20601

GALLIUM ARSENIDES
Optimization of InAsSb/InGaAs strained-layer superlattice growth by metal-organic chemical vapor deposition for use in infrared emitters
[DE94-016557] p 1563 N95-19954
Low temperature synthesis of semiconductor materials
[AD-A285120] p 1226 N95-20081
Proton irradiation effects on advanced digital and microwave III-V components
[DE94-018742] p 1314 N95-20338
GaAs optical circuits
[AD-A285859] p 1369 N95-20389
Development of a lightweight, light-trapped, thin GaAs solar cell for spacecraft applications
p 1318 N95-20513
Design of high-efficiency, radiation-hard, GaInP/GaAs solar cells p 1319 N95-20521
Final results of the advanced photovoltaic experiment
p 1321 N95-20528
Photovoltaic electric power applied to Unmanned Aerial Vehicles (UAV) p 1321 N95-20530
Effects of plasma hydrogenation on trapping properties of dislocations in heteroepitaxial InP/GaAs
p 1323 N95-20542
Nucleation, growth, and strain relaxation of lattice-mismatched 3-5 semiconductor epitaxial layers
p 1324 N95-20543
Analog processing of optical wavefront using integrated guided-wave optics
[AD-A279596] p 1543 N95-20601
Applied physics research for innovation in pulsed power
[AD-A285392] p 1324 N95-20610
Instantaneous frequency dynamics of coherent emission from magnetoexcitons in gallium arsenide
[DE94-018182] p 1569 N95-20677
Temporal and spectral investigation of multi-Landau level quantum beats in GaAs
[DE94-018189] p 1569 N95-20678
Phase dynamics of non-equilibrium distributions of free electron-hole pairs in GaAs quantum wells
[DE94-018190] p 1569 N95-20679
Ultrafast magnetoexciton dynamics in GaAs
[DE94-018175] p 1514 N95-20732
Complementary GaAs junction-gated heterostructure field effect transistor fabrication for integrated circuits
[DE95-001522] p 1327 N95-20882
IR materials producibility
[AD-A280094] p 1328 N95-21017
Fiber-optic control of current filaments in high gain photoconductive semiconductor switches
[DE94-015804] p 1328 N95-21139
Epitaxial liftoff technology onto processed silicon foundry wafers
[AD-A285621] p 1571 N95-21145

Complementary GaAs junction-gated heterostructure field effect transistor technology
[DE94-018901] p 1329 N95-21390

Spectroscopic, morphological, and electrical characterization of PdGe ohmic contacts to n-GaAs
[DE95-000738] p 1329 N95-21394

A versatile masking process for plasma etched backside via holes in GaAs
[DE94-019176] p 1572 N95-21419

Self-starting femtosecond pulse generation from a Ti:sapphire laser synchronously pumped by a pointing-stabilized mode-locked Nd:YAG laser
[DE94-019319] p 1374 N95-21480

Resonant generation of nonequilibrium phonons in GaAs/AlAs quantum wells via intersubband scattering
[DE95-002338] p 1581 N95-21604

InTISb for long-wavelength infrared photodetectors and arrays
[AD-A280108] p 1332 N95-21774

Plasma-induced-damage of GaAs during etching of refractory metal contacts
[DE95-001525] p 1259 N95-21838

Transient photoluminescence measurements on GaAs and AlGaAs double heterostructures
[AD-A279408] p 1575 N95-21916

Heterostructure quantum confined Stark effect electrooptic modulators operating at 938 nm
[AD-A279342] p 1581 N95-21928

Performance of Ga(0.47)In(0.53)As cells over a range of proton energies
[NASA-TM-106819] p 1334 N95-22112

Temperature dependence of a magnetopolaron in a harmonic quantum dot in resonant magnetic fields
[DE94-629036] p 1502 N95-22177

Temperature dependence of magnetopolarons in a parabolic quantum dot in arbitrary magnetic fields
[DE94-629033] p 1528 N95-22218

Photoreflectance and x ray diffraction study of semiconductor heterostructures and quantum wells
[PB95-127049] p 1582 N95-22432

GALLIUM COMPOUNDS

P/N In(Al) GaAs multijunction laser power converters
p 1323 N95-20539

GALLIUM PHOSPHIDES

Low temperature synthesis of semiconductor materials
[AD-A285120] p 1226 N95-20081

Observation of excitonic and band-to-band behavior in ordered InGaP2 alloys
[DE94-018891] p 1314 N95-20341

Design of high-efficiency, radiation-hard, GaInP/GaAs solar cells p 1319 N95-20521

High efficiency GaP power conversion for Betavoltaic applications p 1323 N95-20540

GALLIUM SELENIDES

Polycrystalline CuInSe2 and CdTe solar cells
[DE94-011875] p 1392 N95-20333

Novel thin-film CuInSe2 fabrication
[DE94-011874] p 1268 N95-20472

GAME THEORY

Asymptotic analysis of Nash equilibria in nonzero-sum linear-quadratic differential games. The two-player case
[PB95-111027] p 1499 N95-19941

Note on the characterizations of the compromise value
[PB95-135117] p 1499 N95-21709

Thousand golden ten orbits
[PB95-135109] p 1592 N95-22334

GAMMA RAY BURSTS

Imaging design of the wide field x-ray monitor onboard the HETE satellite
[DE95-002750] p 1221 N95-22436

GAMMA RAY SPECTRA

SYNTH: A spectrum synthesizer
[DE94-015943] p 1458 N95-20153

Unified GUI for the Los Alamos Radiation Transport Code System
[DE94-016088] p 1458 N95-20154

Choice of computer software for analysis of spectra from the Multi-Spectral Logging System
[DE94-019013] p 1460 N95-20351

GAMMA RAY SPECTROMETERS

SYNTH: A spectrum synthesizer
[DE94-015943] p 1458 N95-20153

Choice of computer software for analysis of spectra from the Multi-Spectral Logging System
[DE94-019013] p 1460 N95-20351

GAMMA RAYS

Target area acquisition and control system survivability for the National Ignition Facility
[DE94-016549] p 1550 N95-20190

Advanced concepts for gamma ray isotopic analysis and instrumentation
[DE94-016610] p 1517 N95-21174

Constraints on SUSy-GUT unification from b yields s-gamma decay
[PB95-130373] p 1580 N95-21229

GARNETS

Phase E in a water-saturated peridotite system at 9.3 GPa p 1420 N95-21799

GAS ANALYSIS

Aging tests of ethylene contaminated argon/ethane
[DE95-002526] p 1282 N95-20899

GAS BEARINGS

Wave journal bearing. Part 1: Analysis
[NASA-CR-195431-PT-1] p 1382 N95-22404

GAS CHROMATOGRAPHY

Effect of a solid insulator on the spark yield of S2F10 in SF6(*)
[DE95-001422] p 1326 N95-20791

GAS COMPOSITION

The primary carbon and the formation of carbon species in terrestrial magmas p 1420 N95-21797

GAS DETECTORS

Improved die castings through plasma surface modification, improved sensors and die soldering prevention
[DE95-002238] p 1253 N95-20417

New concepts for refrigerant leak detection and mixture measurement
[DE94-018967] p 1287 N95-21559

GAS DISCHARGES

Effect of a solid insulator on the spark yield of S2F10 in SF6(*)
[DE95-001422] p 1326 N95-20791

Study on the reaction kinetics in pulsed RF discharges under RIE conditions
[PB95-107868] p 1300 N95-21029

Thoriated-tungsten, split-ring, hollow-cathode electrode for discharge devices
[AD-D016508] p 1333 N95-21906

GAS DYNAMICS

Plasma chemistry of vibrationally nonequilibrium molecules
[AD-A279630] p 1553 N95-20411

State-to-state collisional dynamics of atmospheric species
[AD-A285053] p 1370 N95-20484

Numerical wave speed for one-dimensional scalar hyperbolic conservation laws with source terms
[PB95-127536] p 1492 N95-21371

One-dimensional reactive Euler equations
[PB95-135430] p 1244 N95-21573

Gas-dynamic trap diagnostic complex for study on plasma heating and power atomic beam injection
[DE94-633377] p 1529 N95-22283

GAS EXCHANGE

Balloon tracking for the ASTEX/MAGE Lagrangian experiment
[AD-A280078] p 1430 N95-20969

Intramyocardial blood volume and oxygen exchange
[PB95-108015] p 1445 N95-21580

GAS FLOW

Multiply manifolded molten carbonate fuel cells
[DE94-017074] p 1392 N95-20480

One-dimensional reactive Euler equations
[PB95-135430] p 1244 N95-21573

Flow and heat transfer simulation in a flash smelting furnace
[PB95-108197] p 1354 N95-21649

Transportation of volatile elements in thermally evolving planetesimals: An important role of metallic iron
p 1418 N95-21790

Fluid dynamics of the freeboard in a fluidized bed reactor
[PB95-134029] p 1357 N95-22160

GAS GENERATORS

Integral rocket ramjets
[AD-A285135] p 1222 N95-20906

GAS GIANT PLANETS

Hydrogen and related materials at high density: Physics, chemistry and planetary implications
p 1418 N95-21791

Dynamics of volatile delivery from outer to inner solar system p 1420 N95-21798

Solar system formation and the distribution of volatile species p 1421 N95-21806

Comets, impacts, and atmospheres
p 1422 N95-21810

Surface ices in the outer solar system
p 1423 N95-21815

GAS INJECTION

Evaluation of pumping and fueling requirements for the ITER EDA
[DE94-018117] p 1560 N95-21702

GAS IONIZATION

Emittance dilution by ions in the SLC arcs
[DE95-002871] p 1536 N95-21332

The two-electron problem and prospects for atomic collision theory on a numerical lattice
[DE94-017856] p 1528 N95-22265

Very high-power electron-beam transport in long gas cells from 10(exp -3) to 10(exp 3) Torr N2
[DE95-002611] p 1539 N95-22306

GAS LASERS

The effect of reusing laser gas on the fission-fragment pumped 1.73 micron atomic xenon laser output
[DE94-018512] p 1369 N95-20225

Liquid xenon as a potential laser host medium
[AD-A285365] p 1370 N95-20550

Applications for reactor-pumped lasers
[DE95-000536] p 1373 N95-21393

GAS MIXTURES

Effect of propane-air on NGVs and vehicle fueling stations
[PB94-210085] p 1282 N95-20253

Inert gas purification and measuring oxygen partial pressure in gas mixtures with EMF method based on solid electrolyte cell
[PB95-127767] p 1240 N95-21110

Nitrogen isotopic components in the early solar system p 1420 N95-21800

GAS PRESSURE

Forming of superplastic ceramics
[DE94-017306] p 1276 N95-21662

Hydrogen and related materials at high density: Physics, chemistry and planetary implications
p 1418 N95-21791

High temperature corrosion and crack growth of SiC/SiC at variable oxygen partial pressures
[DE94-018715] p 1232 N95-22115

GAS RECOVERY

Development of active-transport membrane devices
[DE94-015947] p 1246 N95-21921

GAS STREAMS

Ceramem filters for removal of particles from hot gas streams
[DE95-001976] p 1275 N95-21354

GAS TEMPERATURE

Fire smoke ventilation through shafts: Experiments
[PB95-132247] p 1288 N95-21978

GAS TUNGSTEN ARC WELDING

Joining dissimilar stainless steels for pressure vessel components
[PB95-133005] p 1380 N95-21446

GAS TURBINE ENGINES

Experimental study of vane heat transfer and aerodynamics at elevated levels of turbulence
[NASA-CR-4633] p 1337 N95-19912

Toughened Silcomp composites for gas turbine engine applications
[DE95-002851] p 1214 N95-21243

GAS TURBINES

Materials/manufacturing element of the Advanced Turbine System Program
[DE94-017299] p 1378 N95-20085

Toughened Silcomp composites for gas turbine engine applications
[DE95-002851] p 1214 N95-21243

GAS-GAS INTERACTIONS

Publications/patents/presentations/honors/student eport. Investigation of the role of vibrational excitation in unimolecular reactions
[AD-A280044] p 1513 N95-20621

GAS-ION INTERACTIONS

Recombination, ion-molecule collisions and (laser assisted) electron-excited atom collisions
[AD-A285604] p 1517 N95-21216

GASEOUS DIFFUSION

Development of active-transport membrane devices
[DE94-015947] p 1246 N95-21921

GASES

The final status of a metal surface after multipulse laser irradiation in an ambient gas
[DE94-629000] p 1562 N95-22377

GASOLINE

Assessment of liquefaction and pyrolysis systems
[PB95-129797] p 1236 N95-20290

GATES (CIRCUITS)

Gate oxide shorts in nMOS transistors: Electrical properties and lifetime prediction method
[DE94-018904] p 1330 N95-21545

Optical processing and control
[AD-A279157] p 1546 N95-21975

GAUGE INVARIANCE

Chiral symmetry and lattice gauge theory
[DE94-018676] p 1564 N95-20130

GAUGE THEORY

Chiral symmetry and lattice gauge theory
[DE94-018676] p 1564 N95-20130

Theoretical particle physics
[DE95-002447] p 1515 N95-20893

Topics in gauge theories and the unification of elementary particle interactions
[DE94-013485] p 1529 N95-22279

GAUSS EQUATION
Atomic orbital basis sets for molecular interactions
[AD-A279609] p 1506 N95-19959
GEARS
Bevel gear driver and method having torque limit selection
[NASA-CASE-MSC-22384-1] p 1378 N95-20151
Displaceable spur gear torque controlled driver and method
[NASA-CASE-MSC-22381-1] p 1378 N95-20409
GELS
High pressure windowed chamber burned rate determination of liquid propellant XM46
[AD-A283770] p 1282 N95-19920
Technical Summary for 1993 fall MRS Symposium O, Complex Fluids
[AD-A283722] p 1264 N95-19972
Sol-gel-derived silica films with tailored microstructures for applications requiring organic dyes
[DE94-018886] p 1264 N95-20047
Novel electrochemical materials prepared by sol-gel chemistry
[AD-A286310] p 1226 N95-20092
Control of continuous phase PH using visible light to activate PH-dependent fibers and gels in a controlled and reversible manner
[AD-D016532] p 1543 N95-20728
Gradient index lenses from sol-gel layering
[AD-A285649] p 1242 N95-21402
Phase E in a water-saturated peridotite system at 9.3 GPa p 1420 N95-21799
Tailoring suspension flow for the gelcasting of oxide and nonoxide ceramics
[DE95-001351] p 1277 N95-21861
GENERAL AVIATION AIRCRAFT
Census US civil aircraft calendar year 1993
[AD-A286309] p 1199 N95-20091
The personal aircraft: Status and issues
[NASA-TM-109174] p 1200 N95-20686
GENERAL OVERVIEWS
Passive millimetre wave imaging: A review
[AD-A279275] p 1303 N95-21491
GENETIC ALGORITHMS
Heuristic genetic algorithms for constrained problems. Part 1: Principles
[PB95-132031] p 1467 N95-21374
GENETIC CODE
Life Sciences Division and Center for Human Genome Studies
[DE94-017796] p 1440 N95-22065
Discovering related DNA sequences via mutual information
[DE95-001101] p 1440 N95-22067
Urban air carcinogens and their effects on health
[DE95-002259] p 1447 N95-22285
GENETICS
Life Sciences Division and Center for Human Genome Studies
[DE94-017796] p 1440 N95-22065
The Use of Cyanobacteria to Explore Basic Biological Processes
[DE94-019238] p 1440 N95-22066
Cellular responses to environmental DNA damage
[DE94-015606] p 1441 N95-22397
GEOCHEMISTRY
Noble gas isotopes and halogens in volatile-rich inclusions in diamonds p 1417 N95-21784
Alkali element depletion by core formation and vaporization on the early Earth p 1421 N95-21804
Solubilities of nitrogen and noble gases in basalt melt p 1422 N95-21807
The isotope geochemistry of abyssal peridotites and related rocks
[AD-A279435] p 1435 N95-21918
GEOCHRONOLOGY
Surface exposure geochronology using cosmogenic nuclides: Applications in Antarctic glacial geology
[AD-A279392] p 1426 N95-21944
GEODESY
Marussi hypothesis in differential geodesy
[AD-A285853] p 1413 N95-20377
Common mapping system media study
[AD-A279086] p 1390 N95-21912
GEODETIC COORDINATES
Marussi hypothesis in differential geodesy
[AD-A285853] p 1413 N95-20377
GEODETIC SURVEYS
Multipath impact on ground-based global positioning system range measurements: Aspects of measurement, modeling, and mitigation p 1297 N95-20949
GEODYNAMICS
Anatomy of the Midcontinent Rift beneath Lake Superior
[DE94-019298] p 1415 N95-21477
GEOGRAPHIC INFORMATION SYSTEMS
Guidelines for the creation and management of geographic data bases within a GIS environment, version 1.0
[DE94-019214] p 1458 N95-20073
Selective polygon map display method
[AD-D016518] p 1590 N95-21463
Review of GIS applications in hydrologic modeling
[AD-A279076] p 1390 N95-21628
GEOGRAPHY
Guidelines for the creation and management of geographic data bases within a GIS environment, version 1.0. Volume 2. Appendices
[DE94-019215] p 1591 N95-22129
Using geographical data browsers in a networked environment
[DE94-017809] p 1592 N95-22263
GEOIDS
Volatiles, rheology, and mantle convection: Comparing Earth, Venus, and Mars p 1420 N95-21801
GEOLOGICAL FAULTS
Fractal nature and scaling of normal faults, Rio Grande rift, NM: Implications for growth and strain
[DE94-018261] p 1414 N95-20990
Anatomy of the Midcontinent Rift beneath Lake Superior
[DE94-019298] p 1415 N95-21477
Source contributions at far-regional distances
[AD-A279405] p 1426 N95-21932
GEOLOGICAL SURVEYS
Anatomy of the Midcontinent Rift beneath Lake Superior
[DE94-019298] p 1415 N95-21477
Descriptions of WHOI sediment cores, volume 8
[AD-A279444] p 1436 N95-22073
A multispectral scanner survey of the Idaho National Engineering Laboratory and the Hanford Reservation
[DE95-003922] p 1391 N95-22398
GEOLOGY
Statistical properties of geologic fractals
[DE94-019272] p 1414 N95-20908
GEOMAGNETISM
Ion heating perpendicular to the magnetic field
[AD-A286635] p 1501 N95-20773
A simulation of plasma motion in the polar ionosphere
[AD-A286166] p 1426 N95-22019
Substorm theories: United they stand, divided they fall
[NASA-CR-197672] p 1427 N95-22326
GEOMETRICAL OPTICS
Diffraction computation by means of the method of equivalent currents
[AD-A285347] p 1291 N95-20692
GEOMETRY
Set functionals in stochastic geometry
[PB95-135372] p 1491 N95-21005
GEOMORPHOLOGY
Anatomy of the Midcontinent Rift beneath Lake Superior
[DE94-019298] p 1415 N95-21477
GEOPHYSICS
Overview of the Institute of Geophysics and Planetary Physics and Lawrence Livermore National Laboratory collaborative efforts
[DE94-017300] p 1599 N95-20145
Investigating the resolution of resistivity arrays using inverse theory
[DE94-017760] p 1412 N95-20287
Solar-Geophysical Data number 600, August 1994. Part 1: (Prompt reports). Data for July, June 1994, and late data
[PB95-104923] p 1603 N95-20713
Solar-Geophysical Data number 600, August 1994. Part 2: (Comprehensive reports). Data for February 1994 and miscellaneous
[PB95-105060] p 1603 N95-20722
Solar-geophysical data number 601, September 1994. Part 1: (Prompt reports). Data for August, July 1994, and late data
[PB95-136727] p 1603 N95-20919
Computer programs for analysis of geophysical data
[DE95-002472] p 1415 N95-21511
VTT test borehole for bedrock investigations
[PB95-132965] p 1427 N95-22095
DOD science and engineering apprenticeship program for high school students
[AD-A280371] p 1583 N95-22100
GEOSYNCHRONOUS ORBITS
Observations of cold magnetospheric ions at geosynchronous orbit during times of high activity
[DE95-000936] p 1600 N95-21935
Magnetospheric Plasma Analyzer (MPA): Plasma observations from geosynchronous orbit
[DE95-002739] p 1427 N95-22477
GEOTECHNICAL ENGINEERING
Geomaterial models and numerical analysis of softening
[PB95-135380] p 1386 N95-21006
GEOTHERMAL ENERGY EXTRACTION
Bridging worlds/charting new courses
[DE95-003808] p 1397 N95-22335
GEOTHERMAL ENERGY UTILIZATION
Geothermal direct-heat utilization assistance
[DE94-011546] p 1391 N95-20104
GEOTHERMAL RESOURCES
Geothermal direct-heat utilization assistance
[DE94-011546] p 1391 N95-20104
GEOTHERMAL TECHNOLOGY
Geothermal direct-heat utilization assistance
[DE94-011546] p 1391 N95-20104
Bridging worlds/charting new courses
[DE95-003808] p 1397 N95-22335
GERMANATES
Application of new synchrotron powder diffraction techniques to anomalous scattering from glasses
[DE94-019285] p 1536 N95-21407
GERMANIDES
Spectroscopic, morphological, and electrical characterization of PdGe ohmic contacts to n-GaAs
[DE95-000738] p 1329 N95-21394
GERMANIUM
Simulations of the dislocation array at Ge/Si interfaces
[DE94-017680] p 1565 N95-20244
P/N InP solar cells on Ge wafers
p 1317 N95-20511
Scanning tunneling microscopy of semiconductor surfaces
[AD-A279982] p 1571 N95-20964
GERMANIUM ALLOYS
Surface stress, morphological development, and dislocation nucleation during strained-layer epitaxy
[DE94-017682] p 1565 N95-20245
Microscopy of stress-induced morphological development and dislocation nucleation during semiconductor epitaxy
[DE94-017869] p 1568 N95-20674
GERMANIUM COMPOUNDS
Physical Si(1-x)Ge(x)/Si heterojunction bipolar transistor model for device and circuit simulation
[PB95-110896] p 1312 N95-19934
Certain physical properties of lanthanum digermanide
[AD-A286592] p 1229 N95-20859
GLACIAL DRIFT
Surface exposure geochronology using cosmogenic nuclides: Applications in Antarctic glacial geology
[AD-A279392] p 1426 N95-21944
GLACIERS
Surface exposure geochronology using cosmogenic nuclides: Applications in Antarctic glacial geology
[AD-A279392] p 1426 N95-21944
GLASS
Spectroscopic studies of glass structure
[DE94-016551] p 1268 N95-20468
Amorphous silicon thin films: The ultimate lightweight space solar cell p 1318 N95-20515
The numerical integration and 3-D finite element formulation of a viscoelastic model of glass
[DE95-002588] p 1271 N95-20788
Experimental investigation of wave and fracture phenomena in impacted ceramics
[AD-A286589] p 1272 N95-20856
Epitaxial liftoff technology onto processed silicon foundry wafers
[AD-A285621] p 1571 N95-21145
Application of new synchrotron powder diffraction techniques to anomalous scattering from glasses
[DE94-019285] p 1536 N95-21407
Lead-indium phosphate glasses for optical applications
[DE94-019333] p 1275 N95-21482
GLASS TRANSITION TEMPERATURE
Determinations of phase transitions in nylon 6-12, nylon-6, polyvinyl chloride and polyethylene terephthalate by positron annihilation spectroscopy
[DE94-629992] p 1239 N95-20736
Lead-indium phosphate glasses for optical applications
[DE94-019333] p 1275 N95-21482
GLINT
Radiance of the ocean horizon
[AD-A285613] p 1431 N95-19896
GLOBAL POSITIONING SYSTEM
GPS-Squitter capacity analysis
[AD-A280037] p 1291 N95-20599
Multipath impact on ground-based global positioning system range measurements: Aspects of measurement, modeling, and mitigation p 1297 N95-20949
Impact of propagation mechanisms on global navigation satellite system performance p 1298 N95-20950

Assessment of a non-dedicated GPS receiver system for precise airborne attitude determination
[DE94-019309] p 1205 N95-21520
The determination of static and time varying dipole source. Sensor geometry during sea trials using differential global positioning system
[MRL-TN-631] p 1205 N95-21642
Variability of total electron content in the high-altitude ionosphere following solar maximum
[AD-A285849] p 1425 N95-21833
Radiation characterization report for the GPS Receiver microcontroller chip
[DE94-019169] p 1335 N95-22165
The effects of magnetic storm phases on F-layer irregularities from auroral to equatorial latitudes
[AD-A286173] p 1427 N95-22423

GLOBAL WARMING
Dust Bowl migration as an analog for possible global warming-induced migration from Mexico
[DE94-017472] p 1401 N95-20089
Indirect global warming effects of ozone and stratospheric water vapor induced by surface methane emission
[DE94-019016] p 1402 N95-20353
Radiative forcing calculations for CH3Cl
[DE94-019018] p 1402 N95-20355
Global change integrating factors: Tropical tropopause trends
[DE95-001121] p 1404 N95-20835
Modeling the response of the California Current system to Global Greenhouse Warming
[DE94-018253] p 1408 N95-21708
Assessment of the atmospheric hazards and risks of new chemicals: Procedures to estimate hazard potentials
[PB95-107488] p 1410 N95-22186

GLONASS
Impact of propagation mechanisms on global navigation satellite system performance p 1298 N95-20950

GLOW DISCHARGES
High magnetic field glow discharge ionization source
[AD-A279972] p 1241 N95-21123

GLUCOSE
Mechanism of the amperometric response of a proposed glucose sensor based on a polypyrrole-tubule-impregnated membrane
[AD-A279836] p 1365 N95-20431

GLUONS
Antishadowing contribution to the pomeron structure function
[PB95-127478] p 1518 N95-21221
Signals for top quark anomalous chromomagnetic moments at colliders
[DE95-002896] p 1535 N95-21254
Nonperturbative aspects of the quark-photon vertex
[DE94-012846] p 1520 N95-21315
Heavy ion collisions
[DE95-002712] p 1520 N95-21321
Search for new particles decaying to dijets in p(bar p) collisions at (radical)s = 1.8 TeV
[DE94-018994] p 1523 N95-21563
Investigation of direct photon production in 200 A GeV S + Au reactions
[DE94-018129] p 1525 N95-21704
Search for squarks and gluinos in D0
[DE95-000730] p 1528 N95-22197

GLYCOLS
New chiral pyrimidino-crown ether ligands
[AD-A279892] p 1223 N95-20590

GOERTLER INSTABILITY
Computational studies of laminar to turbulence transition
[AD-A285622] p 1353 N95-21146

GOGGLES
A computer-based multimedia prototype for night vision goggles
[AD-A286208] p 1546 N95-21882
Factors that determine visual acuity through night vision goggles for emmetropes
[AD-A279339] p 1450 N95-21927

GOLD
Materials research for GHz multi-chip modules
[AD-A279661] p 1227 N95-20412
Scanning tunneling microscopy studies of self-assembled monolayers of alkanethiols on gold
[AD-A279910] p 1253 N95-20577
Theoretical study of the noble metals on semiconductor surfaces and Ti-base shape memory alloys
[DE95-001654] p 1257 N95-21398
Investigation of direct photon production in 200 A GeV S + Au reactions
[DE94-018129] p 1525 N95-21704

GOLD COATINGS
Surface x-ray scattering and scanning tunneling microscopy studies at the Au(111) electrode
[DE95-002409] p 1573 N95-21516

GOLD ISOTOPES
Angular and charge state distributions of highly charged ions scattered during low energy surface-channeling interactions with Au(110)
[DE95-001348] p 1525 N95-21857
Proton and produced particle distributions from Au+Au collisions at 11.6 A GeV/c
[DE94-018634] p 1530 N95-22392

GONIOMETERS
In-situ capability of ion beam modification and characterization of materials at Los Alamos National Laboratory
[DE95-002738] p 1534 N95-21236

GOVERNMENT PROCUREMENT
Technology transfer: Improving the use of cooperative R/D agreement at DOE's contractor-operated laboratories. Report to Congressional requesters
[GAO/RCED-94-91] p 1586 N95-22403

GOVERNMENT/INDUSTRY RELATIONS
Environmental Compliance Assessment and Management Program
[AD-A279605] p 1402 N95-20441
The mechanical property data base from an Air Force/Industry cooperative test program on advanced aluminum alloys
[AD-A280038] p 1386 N95-20615
Policies concerning military and civilian research and technology applications
[PB95-131355] p 1585 N95-21427
ITER EDA Newsletter. Volume 3, no. 2
[DE94-628980] p 1561 N95-21852
Technology transfer: Improving the use of cooperative R/D agreement at DOE's contractor-operated laboratories. Report to Congressional requesters
[GAO/RCED-94-91] p 1586 N95-22403

GRADIENTS
Characterization of a texture gradient in tantalum plate
[DE95-002704] p 1262 N95-22289
Fully developed turbulent flows
[AD-A286496] p 1358 N95-22294

GRAFTING
Neutron reflectivity study of adsorbed diblock copolymers
[DE95-002740] p 1281 N95-22434

GRAIN BOUNDARIES
Overview on superplasticity research on small-grained materials
[DE94-016550] p 1266 N95-20316
Dependence of critical current density on microstructure and processing of high-T(c) superconductors
[DE95-000685] p 1571 N95-21167
Creep behavior in SiC whisker-reinforced alumina composite
[DE95-001071] p 1231 N95-21776
The role of grain boundary sliding on creep deformation characteristics of discontinuous reinforced composites
[DE95-001671] p 1231 N95-21924
The role of point defects and defect complexes in silicon device processing
[DE94-011876] p 1279 N95-22091
An improved Monte Carlo algorithm for simulating grain growth
[DE94-017903] p 1578 N95-22272

GRAIN SIZE
Overview on superplasticity research on small-grained materials
[DE94-016550] p 1266 N95-20316
Mean field analysis of orientation selective grain growth driven by interface-energy anisotropy
[DE94-015797] p 1566 N95-20399
Molecularly Designed Ultrafine/Nanostructured Materials, volume 351
[AD-A285370] p 1568 N95-20552
Oxidation behavior of aluminum nanopowders
[DE95-002721] p 1260 N95-21926
An improved Monte Carlo algorithm for simulating grain growth
[DE94-017903] p 1578 N95-22272

GRAMMARS
Top-down non-correcting error recovery in LLgen
[PB95-132718] p 1471 N95-22031
Connectionist models for intelligent computation
[AD-A286436] p 1484 N95-22210

GRAND UNIFIED THEORY
Constraints on SUSy-GUT unification from b yields s-gamma decay
[PB95-130373] p 1580 N95-21229

GRAPH THEORY
K(1,3)-free and W(4)-free graphs
[PB95-110573] p 1456 N95-19889
Dominoes
[PB95-110680] p 1456 N95-19905
Orthogonal representations over finite fields and the chromatic number of graphs
[PB95-110953] p 1487 N95-19937
Uniqueness of strongly regular graphs having minimal p-rank
[PB95-111043] p 1488 N95-19942
Graphs cospectral with distance-regular graphs
[PB95-111050] p 1488 N95-19943
Finding all minimal separators of a graph
[PB95-127585] p 1491 N95-21023
Regularity of BPa-systems is decidable
[PB95-135489] p 1468 N95-21619
Vertex ranking for permutation and other graphs
[PB95-127569] p 1496 N95-22327
A periodic scheduling heuristic for mapping iterative task graphs onto distributed memory multiprocessors
[AD-A286047] p 1311 N95-22415

GRAPHICAL USER INTERFACE
NOMADS graphical user interface version 2.0 user's manual
[AD-A286314] p 1458 N95-20095
Unified GUI for the Los Alamos Radiation Transport Code System
[DE94-016088] p 1458 N95-20154
Making structured graphics and constraints practical for large-scale applications
[AD-A280062] p 1461 N95-20623
Xwake 1.0 user's manual
[DE95-002528] p 1463 N95-20901
NODDS/WOSM interface user's manual
[AD-A279095] p 1471 N95-22068
ActorStudio reference manual. A user's guide to the ActorStudio user interface editor, version 1.0
[PB95-127023] p 1472 N95-22310

GRAPHITE
Refractive index change in dissociating shocked benzene
[DE94-019015] p 1541 N95-20352
Boron carbide-based coatings on graphite for plasma facing components
[DE94-017976] p 1269 N95-20570
B4C-SiC reaction-sintered coatings on graphite plasma facing components
[DE94-019105] p 1230 N95-21553

GRAPHITE-EPOXY COMPOSITES
Detection of environmental deterioration in fiber reinforced composites by FT-Raman spectroscopy, phase 1
[AD-A279763] p 1228 N95-20805

GRAPHS (CHARTS)
K(1,3)-free and W(4)-free graphs
[PB95-110573] p 1456 N95-19889
Dominoes
[PB95-110680] p 1456 N95-19905
Hierarchical diagrammatic representation of class structure
[PB95-110722] p 1456 N95-19908
The effects of three-dimensional graphs on decision making
[AD-A285034] p 1583 N95-20051
Guidelines for the creation and management of geographic data bases within a GIS environment, version 1.0
[DE94-019214] p 1458 N95-20073
Solar-Geophysical Data number 600, August 1994. Part 1: (Prompt reports). Data for July, June 1994, and late data
[PB95-104923] p 1603 N95-20713
Solar-Geophysical Data number 600, August 1994. Part 2: (Comprehensive reports). Data for February 1994 and miscellaneous
[PB95-105060] p 1603 N95-20722
Vertex ranking for permutation and other graphs
[PB95-127569] p 1496 N95-22327

GRATINGS (SPECTRA)
Development, fabrication, and metrology of the electro-optical breadboard model for the reflection grating array of the XMM grating spectrometer
[DE94-016605] p 1543 N95-20612
Detection optimization using linear systems analysis of a coded aperture laser sensor system
[DE95-001112] p 1371 N95-20832
Eigenmode method for electromagnetic synthesis of diffractive elements with three-dimensional profiles
[PB95-127726] p 1301 N95-21107
Fiber grating-based detection system for wavelength encoded fiber sensors
[AD-D016208] p 1545 N95-21825
Polycrystalline PLZT/ITO ceramic electro-optic phase gratings: Electro-optically reconfigurable difffractive devices for free-space and in-wafer interconnects
[AD-A285861] p 1547 N95-22076
Fabrication of PLZT/ITO grating for optical switching and reconfigurable optical interconnect applications
[AD-A286389] p 1548 N95-22248
Electro-optic effect in the PESO acousto-optic modulator
[AD-A286355] p 1548 N95-22255

GRAVITATION
Fast parallel tree codes for gravitational and fluid dynamical N-body problems
[AD-A286480] p 1358 N95-22290

GRAVITATION THEORY
Von Neumann algebra automorphisms and time-thermodynamics relation in general covariant quantum theories
[PB95-111084] p 1580 N95-20324

GRAVITATIONAL EFFECTS
Connection with dynamics: General introduction
[NASA-CR-197617] p 1579 N95-19947
Modeling platform dynamics and physiological response to short arm centrifugation
[AD-A279640] p 1442 N95-20457
Monoclonal antibodies directed against surface molecules of multicell spheroids
[NASA-CR-197367] p 1437 N95-20559
Computer graphics tools for visualizing gravity gradient torques on a rigid spacecraft
[AD-A285971] p 1461 N95-20665
Microgravity: Teacher's guide with activities for physical science
[NASA-EG-103] p 1285 N95-21322
Tethered satellite: Forces and motion
[NASA-TM-110518] p 1220 N95-21858
Gravitational effects on the development of weld-pool and solidification microstructures
[DE94-017772] p 1285 N95-22261

GRAVITATIONAL FIELDS
Testing the principle of equivalence by solar neutrinos
[DE94-014972] p 1604 N95-22064
Nonlinear dynamics of the planar pitch attitude motion for a gravity-gradient satellite
[AD-A286407] p 1220 N95-22204

GRAVITATIONAL PHYSIOLOGY
Modeling platform dynamics and physiological response to short arm centrifugation
[AD-A279640] p 1442 N95-20457
Monoclonal antibodies directed against surface molecules of multicell spheroids
[NASA-CR-197367] p 1437 N95-20559

GRAVITATIONAL WAVES
Resonant photon-graviton conversion in EM fields: From earth to heaven
[DE95-002784] p 1301 N95-21241

GRAVITONS
Resonant photon-graviton conversion in EM fields: From earth to heaven
[DE95-002784] p 1301 N95-21241

GRAVITY GRADIENT SATELLITES
Nonlinear dynamics of the planar pitch attitude motion for a gravity-gradient satellite
[AD-A286407] p 1220 N95-22204

GRAVITY WAVES
Analysis of mesospheric winds and waves
[AD-A279956] p 1414 N95-20591

GRAZING INCIDENCE
High precision Woelter optic calibration facility
[DE94-016973] p 1542 N95-20364
Topography of neutron scattering from diblock copolymer film
[DE95-001457] p 1229 N95-20840
X-band microwave backscattering from ocean waves
[DE94-016719] p 1309 N95-22241

GREAT CIRCLES
The effects of multihop HF propagation on the performance of OTH backscatter radars
p 1298 N95-20953

GREEN'S FUNCTIONS
Energy gap structure of layered superconductors
[DE94-017885] p 1566 N95-20372
Low-frequency image theory for a current dipole in front of a permeable sphere
[PB95-127676] p 1300 N95-21104
An asymptotic solution of the (infinity)-d Hubbard model
[DE94-629042] p 1582 N95-21994
Absorbing boundary condition for floating two-dimensional objects in current and waves
[PB95-132882] p 1356 N95-22063
Full potential multiple scattering theory
[DE95-003197] p 1576 N95-22084
Theory of the excitonic lineshape in low-dimensional structures with rough interfaces
[DE95-003434] p 1582 N95-22237

GREENHOUSE EFFECT
Workshop on Uncertainty and Global Climate Change Research
[DE94-016728] p 1401 N95-20238
Indirect global warming effects of ozone and stratospheric water vapor induced by surface methane emission
[DE94-019016] p 1402 N95-20353
Global change integrating factors: Tropical tropopause trends
[DE95-001121] p 1404 N95-20835
Monitoring the response of the upper troposphere/lower stratosphere to a greenhouse gas scenario
[DE95-000982] p 1406 N95-21410
Modeling the response of the California Current system to Global Greenhouse Warming
[DE94-018253] p 1408 N95-21708
Proceedings: International Symposium on Global Change (IGBP)
[DE94-765351] p 1410 N95-22219

GRID GENERATION (MATHEMATICS)
Open Skies project computational fluid dynamic analysis
[AD-A285928] p 1200 N95-19991
Meshes: The next generation
[DE94-016702] p 1459 N95-20255
Mixed hp finite element methods for problems in elasticity and stokes flow
[PB95-104444] p 1341 N95-20981
Simulations of bypass transition for spatially evolving disturbances p 1349 N95-21079
Computations of unsteady viscous compressible flows using adaptive mesh refinement in curvilinear body-fitted grid systems
[NASA-TM-106704]. p 1356 N95-21959
State of the art in CFD pre- and postprocessing
[PB95-110391] p 1356 N95-22017
On the dynamics of a shock-bubble interaction
[NASA-CR-194978] p 1495 N95-22325
Unstructured-grid large-eddy simulation of flow over an airfoil p 1202 N95-22448

GRINDING (MATERIAL REMOVAL)
Numerical controlled polishing program, continued forced wear and part correction experiments
[DE94-018084] p 1285 N95-20288
Reliability analysis of uniaxially ground brittle materials
[NASA-TM-106852] p 1386 N95-20790

GROUND STATE
Calculation of electron scattering on the He(+) ion
[DE94-631343] p 1509 N95-20199
Crystalline beams: The horizontal zigzag
[DE95-002227] p 1533 N95-20766
Second order approximation for optical polaron in the strong coupling case
[DE94-628997] p 1525 N95-21856
Uniform upper bounds in the Froehlich polaron theory
[DE94-628998] p 1525 N95-21860
Effect of the electron-SO-phonon on the impurity state energies in a semiconductor quantum well
[DE94-628993] p 1581 N95-21887
Variational Monte Carlo study of He-4 in two dimensions
[DE94-629078] p 1576 N95-21998
There might be two kinds of dibaryon
[DE94-014417] p 1526 N95-22058
Electric-field effects on shallow donor impurity in a harmonic quantum dot
[DE94-629034] p 1577 N95-22176
Microscopic theory of normal liquid He-3
[DE94-629047] p 1527 N95-22179

GROUND STATIONS
GPS-Squitter capacity analysis
[AD-A280037] p 1291 N95-20599
Climatological data for clouds over the globe from surface observations, 1982-1991: The total cloud edition
[DE95-002537] p 1431 N95-22288

GROUND SUPPORT EQUIPMENT
GPHS-RTGs in support of the Cassini Mission
[DE95-001492] p 1222 N95-20853

GROUND TESTS
Description and flow characterization of hypersonic facilities
[AD-A284291] p 1200 N95-20248
Evolution of ground line of sight data field collection techniques
[AD-A285062] p 1204 N95-20497

GROUND TRUTH
Deriving earth science products from SSM/I
[NASA-CR-197299] p 1389 N95-20156
European Workshop on Optical Ground Truth Instrumentation for the Validation of Space-Borne Optical Remote Sensing Data of the Marine Environment
[PB95-134144] p 1390 N95-21872

GROUND WATER
Degradation of aromatic hydrocarbons in an aquifer during a field experiment demonstrating the feasibility of remediation by natural attenuation
[AD-A283809] p 1282 N95-19922
Guidelines for the creation and management of geographic data bases within a GIS environment, version 1.0
[DE94-019214] p 1458 N95-20073
Monitoring bioremediation of Volatile Organic Compounds (VOCs) using Fourier Transform Infrared (FT-IR) spectrometry
[AD-A279631] p 1403 N95-20456
Fiber-optic sensors for rapid, inexpensive characterization of soil and ground water contamination
[DE95-002471] p 1545 N95-21510
Spatial variation of primordial 3-He in crustal fluids along the East-African Rift system (the Ethiopian and the Kenya Rift section) p 1418 N95-21789

GROUP THEORY
New data for MCNP (trademark)
[DE94-016296] p 1509 N95-20236
Positive rockland operators
[PB95-127510] p 1493 N95-21423
A Davis-Putnam program and its application to finite-order model search: Quasigroup existence problems
[DE95-003014] p 1471 N95-22077
Quadratic optimal control of a delay equation I: The stable case
[PB95-127072] p 1486 N95-22367

GRUMMAN AIRCRAFT
Activities of the Institute for the Study of Human Capabilities
[AD-A286471] p 1454 N95-22275

GUIDANCE SENSORS
Assessment of a non-dedicated GPS receiver system for precise airborne attitude determination
[DE94-019309] p 1205 N95-21520

GULF STREAM
Tests of an improved oceanographic expert system
[AD-A280123] p 1431 N95-19888
Synthesizing the Gulf Stream thermal structure from XBT data
[AD-A279665] p 1433 N95-20458

GUN LAUNCHERS
Computational design of Hypervelocity Launchers
[DE95-000744] p 1218 N95-20785

GUST LOADS
Derived gust spectra for the Macchi MB326H
[ARL-TN-3] p 1202 N95-21892

GYRES
Exchanges between hemispheres and gyres: A direct approach to the mean circulation of the equatorial Pacific
[NASA-CR-196311] p 1436 N95-22072

GYROFREQUENCY
Quasi-linear equation for magnetoplasma oscillations in the weakly relativistic approximation
[DE94-628932] p 1560 N95-21593

GYROTROPISM
Dielectric mixtures with arbitrarily anisotropic components: Focus on special gyrotropic effects
[PB95-127015] p 1311 N95-22363

H

H I REGIONS
Arcmimute scale HI and IRAS observations toward high latitude cloud G86.5+59.6 p 1594 N95-21771

H II REGIONS
Luminous radio-quiet sources in the W3(MAIN) cloud core p 1594 N95-21773

H WAVES
Collisional drift waves in the H-mode edge
[DE94-628950] p 1561 N95-21847

H-INFINITY CONTROL
Riccati equation theory for Pritchard-Salamon systems: A Popov function approach
[PB95-137089] p 1491 N95-20830
Design of robust optimal control systems and stability analysis of real structured uncertainties
[AD-A279089] p 1483 N95-21913

HABITATS
Compilation of 1993 annual reports of the Navy ELF Communications System Ecological Monitoring Program
[AD-A279575] p 1408 N95-21699
Compilation of 1993 annual reports of the Navy ELF Communications System Ecological Monitoring Program. Volume 2: Tabs C-F
[AD-A279770] p 1308 N95-21988

HADRONS
Complementarity of e(+)e(-) and pp colliders for the exploration of electroweak symmetry breaking
[DE94-017397] p 1507 N95-20034
Universal features of multiplicity distributions
[DE94-012854] p 1498 N95-20779
Universality of particle multiplicities
[DE95-000727] p 1515 N95-20879
Experiments at high energy hadron colliders and underground water Cerenkov detector experiment
[DE95-001804] p 1535 N95-21281
Hadron beams and accelerators
[DE95-002932] p 1536 N95-21342

Dilepton production from p-p to Ca-Ca at the Bevalac
[DE95-002341] p 1520 N95-21357
Polarization of charmonium in pion-nucleus collisions
[DE95-002783] p 1523 N95-21525
RF beam control for the AGS Booster
[DE95-001485] p 1538 N95-21720
A preliminary, precise measurement of the average B hadron lifetime
[DE95-001848] p 1525 N95-21727
The status of molecules
[DE95-000952] p 1526 N95-21939
Measurement of the average lifetime of B hadrons at SLD
[DE95-002121] p 1527 N95-22152

HALF PLANES
Image solution for poisson's equation in wedge geometry
[PB95-127171] p 1310 N95-22311

HALF SPACES
DC potential anomalies caused by a conducting body in an anisotropic conducting half-space
[PB95-127106] p 1291 N95-20775
Computer programs for analysis of geophysical data
[DE95-002472] p 1415 N95-21511

HALIDES
Translational-energy-resolved studies of photographed carrier-induced reactions on semiconductor surfaces
[DE95-002944] p 1573 N95-21444

HALL EFFECT
Visible light emitting materials and injection devices
[AD-A284796] p 1541 N95-20066
Correlated wavefunction Monte Carlo studies of excitations in the quantum Hall liquids
[DE95-002337] p 1501 N95-20874
Charge density of fractional charged quasiparticles in the composite fermion picture
[DE94-018122] p 1524 N95-21703
On the conductance sum rule for the hierarchical edge states of the Fractional Quantum Hall Effect
[DE94-629030] p 1582 N95-22198

HALOCARBONS
Interspecies extrapolations of halocarbon respiratory and tissue kinetics: Applications to predicting toxicity in different species
[AD-A285055] p 1442 N95-20485
Annual Conference on Fire Research: Book of abstracts
[PB95-104964] p 1286 N95-20717
Method for laser-assisted silicon etching using halocarbon ambients
[AD-D016494] p 1375 N95-21903

HALOGENATION
Use of quantum chemically derived descriptors for QSAR modeling of reductive dehalogenation of aromatic compounds
[PB95-132783] p 1224 N95-22333

HALOGENS
Novel fluorine oxidizers
[AD-A279480] p 1284 N95-21678
Conference on Deep Earth and Planetary Volatiles
[NASA-CR-196944] p 1415 N95-21777
Noble gas isotopes and halogens in volatile-rich inclusions in diamonds p 1417 N95-21784
Method for laser-assisted silicon etching using halocarbon ambients
[AD-D016494] p 1375 N95-21903

HALOS
Simulation of beam-beam lifetime for LEP
[DE95-002888] p 1536 N95-21334
High performance computing for beam physics applications
[DE94-018312] p 1539 N95-22243
Recent results in analysis and simulation of beam halo
[DE94-018313] p 1539 N95-22298

HAMILTONIAN FUNCTIONS
Crystalline beams
[DE95-002656] p 1569 N95-20793
Top ten models constrained by b (yields) s(gamma)
[DE95-002870] p 1519 N95-21250
Simulation of beam-beam lifetime for LEP
[DE95-002888] p 1536 N95-21334
Second order approximation for optical polaron in the strong coupling case
[DE94-628997] p 1525 N95-21856
An asymptotic solution of the (infinity)-d Hubbard model
[DE94-629042] p 1582 N95-21994
Hamiltonian structure of the reversible nonsemisimple 1:1 resonance
[PB95-127528] p 1495 N95-22151
Temperature dependence of a magnetopolaron in a harmonic quantum dot in resonant magnetic fields
[DE94-629036] p 1502 N95-22177

HANDBOOKS
The 29th MIL-HDBK-17 Polymer Matrix Composites Coordination Group Meeting
[AD-A279917] p 1269 N95-20578
Nuclear Terms Handbook, 1993
[DE94-016248] p 1589 N95-21131
Implementation of the military handbook 17 for polymer matrix composites and metal matrix composites
[AD-A285595] p 1229 N95-21215
Incology alloy 908 data handbook
[DE95-001818] p 1260 N95-22013
Implementation of the Military Handbook 17 for polymer matrix composites and metal matrix composites
[AD-A285772] p 1233 N95-22395

HARDNESS
Influence of oxidation on radiation hardness of silicon detectors
[DE95-002466] p 1272 N95-20894

HARDWARE
High performance hardware and software for pattern recognition and image processing
[AD-A279776] p 1457 N95-19961
Hardware implementation of a desktop supercomputer for high performance image processing. Color image processing using cellular neural networks
[AD-A286455] p 1455 N95-21589

HARDWARE DESCRIPTION LANGUAGES
VHDL modeling of PRC-70 radio ASICs for reverse engineering
[AD-A285740] p 1457 N95-19929

HARMONIC ANALYSIS
Counting methods for the analysis of load time histories
[PB95-132916] p 1388 N95-22093

HARMONIC GENERATIONS
Physical-chemical studies on rodlike polymer compositions
[AD-A285361] p 1269 N95-20548
S-D hybridization and anisotropy of the optical second harmonic at low frequencies
[AD-A279449] p 1544 N95-20876
Surface second harmonic studies of Si(111)/electrolyte and Si(111)/SiO2/electrolyte interfaces
[AD-A279450] p 1245 N95-21826
Studies of the n-alkane/water interface by total internal reflection second harmonic generation
[AD-A279473] p 1245 N95-21827
Two-band model description of electroabsorption and third-harmonic generation in 1-D MX linear chains
[DE95-000932] p 1526 N95-21934
Application of optical second harmonic generation to surface analysis
[AD-A279445] p 1547 N95-22074
Coherence properties of high order harmonic radiation
[DE94-016974] p 1377 N95-22312

HARMONIC MOTION
Modeling the effect of shroud contact and friction dampers on the mistuned response of turbopumps
[NASA-CR-197285] p 1379 N95-20795

HARMONIC OSCILLATORS
Self-starting femtosecond pulse generation from a Ti:sapphire laser synchronously pumped by a pointing-stabilized mode-locked Nd:YAG laser
[DE94-019319] p 1374 N95-21480
Temperature dependence of a magnetopolaron in a harmonic quantum dot in resonant magnetic fields
[DE94-629036] p 1502 N95-22177

HARMONIC RADIATION
Coherence properties of high order harmonic radiation
[DE94-016974] p 1377 N95-22312

HARMONICS
Full potential multiple scattering theory
[DE95-003197] p 1576 N95-22084

HARRIER AIRCRAFT
Forecasting aircraft mishaps using monthly maintenance reports
[AD-A286049] p 1203 N95-22417

HARTREE APPROXIMATION
Computational evaluation of the feasibility of nitrating precursors to C12N12O12
[AD-A285976] p 1239 N95-20668
Calculated heats of formation of some predicted stable C, N, O, F molecules
[AD-A285957] p 1517 N95-21127
T1F ((1) sigma (+)): Some preliminary electronic structure calculations
[PB95-130316] p 1518 N95-21223

HAZARDS
Global equivalence ratio concept and the prediction of carbon monoxide formation in enclosure fires
[PB94-207511] p 1234 N95-20100
Environmental cleanup technology transfer initiatives
[AD-A285059] p 1403 N95-20487
Assuring Known Good Die (KGD) for reliable, cost effective MCMs p 1210 N95-20644
Highly survivable communications: Complementary media packet switched networks p 1292 N95-20922
Thermal decomposition reactions of HMX and RDX and their importance in predicting cookoff hazards
[DE95-002486] p 1283 N95-21513
Environmental cleanup: Too many high priority sites impede DOD's program. Report to the Chairman, Committee on Governmental Affairs, US Senate
[AD-A279511] p 1407 N95-21683
Radar studies of aviation hazards
[AD-A285845] p 1203 N95-21831
Initial assessment of the hazards and risks of new chemicals to man and the environment, part 2
[PB95-106407] p 1410 N95-22124

HEALTH
Migrating the Facility Profile Information Management System into the World Wide Web
[DE94-018367] p 1586 N95-20016
Netherlands Institute for Brain Research progress report, 1993
[PB95-135398] p 1445 N95-21352
ANSTO: Program of research, 1993-1994
[DE94-631122] p 1605 N95-21828
Sustaining the health and performance of soldiers/warfighters deployed to harsh environments
[AD-A286270] p 1446 N95-22004

HEALTH PHYSICS
Environmental Hazards Assessment Program
[DE94-019075] p 1406 N95-21565
Comparison of HFC-134a and the ternary blend, Suva MP39, as replacements for the refrigerant, CGC-12
[MRL-GD-0051] p 1287 N95-21625
Optical radiation: Health based exposure limits for electromagnetic radiation in the wavelength range from 100 nanometer to 1 millimeter
[PB95-132767] p 1447 N95-22083
Urban air carcinogens and their effects on health
[DE95-002259] p 1447 N95-22285
Current concepts on airborne particles and health
[DE95-002260] p 1447 N95-22287

HEARING
Temporary threshold shifts produced by high intensity freefield impulse noise in humans wearing hearing protection
[AD-A286289] p 1454 N95-22045

HEART RATE
Microclimate cooling effect on perceived exertion in four heat/exercise scenarios
[AD-A285549] p 1444 N95-21160

HEAT AFFECTED ZONE
Welding tritium exposed stainless steel
[DE95-003208] p 1382 N95-22356

HEAT ENGINES
Cost-effective ceramics program in the United States
[DE95-001425] p 1278 N95-21909
Ceramic technology for advanced heat engines
[DE95-000950] p 1278 N95-21937

HEAT EXCHANGERS
Comparison of the dynamic fatigue behavior of two monolithic SiC and an Al2O3/SiC composite
[DE94-017751] p 1225 N95-20022
Malone-brayton cycle engine/heat pump
[AD-D016573] p 1378 N95-20295
Microchannel heat pipe cooling of modules
p 1211 N95-20649

HEAT FLUX
An augmented Young-Laplace model of an evaporating meniscus in a micro-channel with high heat flux
[NASA-CR-197622] p 1340 N95-20796
Simulation of a turbulent flame in a channel
p 1249 N95-21044
Mixing and dynamics of the Mediterranean outflow
[AD-A279803] p 1434 N95-21306
Dual active surface heat flux gage probe
[NASA-TM-106861] p 1366 N95-21391
Numerical investigation of one-dimensional heat-flux calculations
[AD-A286293] p 1582 N95-22054

HEAT ISLANDS
Meso-scale cooling effects of high albedo surfaces: Analysis of meteorological data from White Sands National Monument and White Sands Missile Range
[DE94-018535] p 1429 N95-20782

HEAT MEASUREMENT
Laser materials processing at Sandia National Laboratories
[DE95-002183] p 1374 N95-21594

HEAT OF FORMATION
Calculated heats of formation of some predicted stable C, N, O, F molecules
[AD-A285957] p 1517 N95-21127
Comparative computational analysis of some nitramine and difluoramine structures, dissociation energies and heats of formation
[AD-A286196] p 1525 N95-21878

Non-local density functional calculations of gas phase heats of formation
[AD-A286213] p 1246 N95-22000

HEAT PIPES
Continuum transient and frozen startup behavior of conventional and gas-loaded heat pipes
[AD-A284297] p 1339 N95-20250
Microchannel heat pipe cooling of modules
p 1211 N95-20649
Recent reflux receiver developments under the US DOE program
[DE95-001622] p 1393 N95-20861

HEAT PUMPS
Augmented thermal bus
[NASA-CASE-LEW-15595-1-C] p 1338 N95-19933
Malone-brayton cycle engine/heat pump
[AD-D016573] p 1378 N95-20295

HEAT RESISTANT ALLOYS
Application of an energy-based life prediction model to bithermal and thermomechanical fatigue
[NASA-TM-106684] p 1385 N95-20179
Methods of measuring adhesion for thermally grown oxide scales
[DE94-018177] p 1256 N95-21260
Plastic deformation of ordered intermetallic alloys: Fundamental aspects
[DE95-001070] p 1256 N95-21265
Weldability of iron aluminides
[DE94-019114] p 1257 N95-21555
Experience at the Los Alamos Meson Physics Facility with the use of alloy Inconel 718 as an enclosure for a beam degrader and as a proton beam entry window
[DE94-018289] p 1538 N95-22050

HEAT SHIELDING
Grid resolution and solution convergence for Mars Pathfinder forebody
[NASA-TM-109173] p 1494 N95-21622

HEAT SINKS
Augmented thermal bus
[NASA-CASE-LEW-15595-1-C] p 1338 N95-19933
The thermal conductivity of carbon-fiber reinforced metal matrix composites
[DE94-017767] p 1226 N95-20125
Module cooling system
[AD-D016584] p 1315 N95-20436

HEAT SOURCES
Weld pool phenomena
[DE94-018965] p 1381 N95-21550

HEAT STORAGE
Effect of microgravity on material undergoing melting and freezing: The TES Experiment
[NASA-TM-106845] p 1338 N95-19952
Mars power system concept definition study. Volume 2: Appendices
[NASA-CR-195420-VOL-2] p 1396 N95-21953

HEAT TRANSFER
Heat transfer, fouling, and combustion of supercritical fuels
[AD-A279906] p 1281 N95-19884
Experimental study of vane heat transfer and aerodynamics at elevated levels of turbulence
[NASA-CR-4633] p 1337 N95-19912
Liquid-metal pin-fin pressure drop by correlation in cross flow
[DE94-017086] p 1338 N95-19923
Investigation of a thermal buoyancy effect on the drag of half models tested in the ARA Transonic Wind Tunnel
[ARA-MEMO-407] p 1199 N95-19946
Round-robin comparison of heat release apparatus
[AD-A285831] p 1363 N95-20031
Solidification modeling of a spiral casting to determine material fluidity
[DE94-018930] p 1285 N95-20050
Site Scientific Mission Plan for the Southern Great Plains CART site, July - December 1994
[DE94-017289] p 1401 N95-20193
Microchannel heat pipe cooling of modules
p 1211 N95-20649
Computational model of drilling with high radiance pulsed lasers
[DE94-018548] p 1371 N95-20783
Recent reflux receiver developments under the US DOE program
[DE95-001622] p 1393 N95-20861
Effect of chemical heat release in a temporally evolving mixing layer p 1249 N95-21037
Triple flame structure and diffusion flame stabilization
p 1249 N95-21039
Turbulent transport in premixed flames
p 1249 N95-21040
NESTLE: Few-group neutron diffusion equation solver utilizing the nodal expansion method for eigenvalue, adjoint, fixed-source steady-state and transient problems
[DE95-001903] p 1466 N95-21288
Theory and modelling of quench in cable-in-conduit superconducting magnets
[DE95-001819] p 1330 N95-21442
Stellarator transport optimization with self-consistent electric fields
[DE94-019151] p 1559 N95-21581
Flow and heat transfer simulation in a flash smelting furnace
[PB95-108197] p 1354 N95-21649
Seawater test results of Open-Cycle Ocean Thermal Energy Conversion (OC-OTEC) components
[DE94-019254] p 1396 N95-21897
Frame and edge seal technology: A state of the art survey
[PB95-110334] p 1288 N95-22014
Shock wave interactions in hypervelocity flow
[AD-A286507] p 1357 N95-22212
Lewis number and Damkohler number effects in vortex-flame interactions p 1249 N95-22439
Fundamental mechanisms in premixed flame propagation via vortex-flame interactions: Numerical simulations p 1249 N95-22440
Flame propagation under partially-premixed conditions
p 1250 N95-22442

HEAT TRANSMISSION
The vertical distribution of heating in the tropical atmosphere
[AD-A285934] p 1429 N95-20391
Alkali element depletion by core formation and vaporization on the early Earth p 1421 N95-21804
Thermal resistance of the cheek in cold air
[AD-A286257] p 1446 N95-22001

HEAT TREATMENT
Fusion welding of advanced borated stainless steels
[DE94-019037] p 1378 N95-20053
Generation of micro-domains in AT-cut quartz by thermal processing and the effect on resonator modes
[DE94-017344] p 1564 N95-20087
Effect of heat treatment temperature on creep-rupture properties of Fe3Al-based alloys
[DE94-017904] p 1253 N95-20375
Ferroic materials: Design, preparation and characteristics. Ceramic transactions, volume 43
[AD-A285937] p 1270 N95-20664
Impact behavior of FeAl alloy FA-350
[DE94-018128] p 1254 N95-20705
2nd International ADI seminar
[PB95-127734] p 1255 N95-21108

HEATING
Vapor generator wand
[NASA-CASE-LAR-15058-1] p 1215 N95-20080
ALT-2 armor tile design for upgraded TEXTOR operation
[DE94-015749] p 1549 N95-20143
Heating and transport in TFTR D-T plasmas
[DE95-002812] p 1558 N95-21242
Loss of solar He and Ne from IDPS in subducting sediment: Diffusion and the effect of phase changes
p 1419 N95-21792

HEAVY ELEMENTS
HASSP and HEAVY: Tools for automated heavy atom searches and refinement
[DE94-016071] p 1569 N95-20696

HEAVY IONS
Numerical modeling of a small recirculating induction accelerator for heavy-ion fusion
[DE94-018549] p 1552 N95-20318
An impedance model of the Relativistic Heavy Ion Collider (RHIC)
[DE94-016784] p 1532 N95-20406
Accelerators for energy production
[DE94-770764] p 1392 N95-20685
Radiation-driven targets for heavy-ion fusion
[DE95-002264] p 1533 N95-20784
Induction linacs for heavy ion fusion
[DE95-002357] p 1534 N95-20891
Heavy ion track-structure calculations for radial dose in arbitrary materials
[NASA-TP-3497] p 1517 N95-21191
The theory of relativistic heavy ion collisions
[DE95-001805] p 1519 N95-21302
Heavy ion collisions
[DE95-002712] p 1520 N95-21321
Similarities and differences in strangeness production at BNL and CERN
[DE95-002343] p 1521 N95-21380
Summary of heavy ion theory
[DE95-002177] p 1523 N95-21588
Dynamics of the chiral transition
[DE94-016813] p 1524 N95-21641
On the theory of strong electromagnetic waves propagation in an electron-positron-ion plasma
[DE94-628964] p 1561 N95-21850
Large amplitude localized structures in a relativistic electron-positron ion plasma
[DE94-628965] p 1561 N95-21851

HEAVY NUCLEI
Parity violation in the compound nucleus
[DE95-002742] p 1530 N95-22435

HEIGHT
Fire experiments in a two dimensional rack storage: BRANDFORSK-project 701-917
[PB95-131538] p 1241 N95-21179

HELICOPTER DESIGN
Helicopter crewseat cushion program
[AD-A286654] p 1452 N95-20973

HELICOPTERS
The personal aircraft: Status and issues
[NASA-TM-109174] p 1200 N95-20688
Experimental study of the helicopter-mobile radioelectrical channel and possible extension to the satellite-mobile channel p 1296 N95-20945
Wavelet transformations for helicopter identification via acoustic signatures
[AD-A279980] p 1504 N95-20963

HELIOSPHERE
Coronal Mass Ejections in the solar wind at high solar latitudes: An overview
[DE95-000844] p 1603 N95-21377
Potential flow downstream of the heliospheric terminal shock: A non-spherical shock
[NASA-TM-110493] p 1426 N95-21874

HELIOSTATS
An overview: Component development for solar thermal systems
[DE95-001623] p 1393 N95-20862

HELIUM
The (e,2e) calculations with the final-state boundary condition
[DE94-631342] p 1509 N95-20198
Helium exhaust studies in the D3-D tokamak
[DE94-016682] p 1552 N95-20334
Analysis of welds on helium-containing restraint test plates
[DE95-001809] p 1257 N95-21303
Recent photoabsorption measurements in the rare gases and alkalis in the 3 to 15 keV photon energy region
[DE94-019278] p 1521 N95-21406
Experimental investigations of electron capture from atomic hydrogen and deuterium by alpha particles
[DE95-002138] p 1523 N95-21587
Muon transfer from muonic atoms of hydrogen isotopes to He nuclei
[DE94-628903] p 1523 N95-21591
Spatial variation of primordial 3-He in crustal fluids along the East-African Rift system (the Ethiopian and the Kenya Rift section) p 1418 N95-21789
Solar helium and neon in the Earth
p 1419 N95-21793
Degassing mechanisms of noble gases from carbonado diamonds p 1425 N95-21824
Solubilities of nitrogen and helium in water and blood at 37 C and pressures of up to 11 ATA
[AD-A286269] p 1446 N95-22003

HELIUM IONS
Calculation of electron scattering on the He(+) ion
[DE94-631343] p 1509 N95-20199
Experimental investigations of electron capture from atomic hydrogen and deuterium by alpha particles
[DE95-002138] p 1523 N95-21587

HELIUM ISOTOPES
Tritium and decay helium effects on the fracture toughness properties of types 316L, 304L and 21Cr-6Ni-9Mn stainless steels
[DE95-001248] p 1252 N95-20216
New theory of critical flow velocities in superfluid helium
[PB95-130365] p 1571 N95-21228
Recent photoabsorption measurements in the rare gases and alkalis in the 3 to 15 keV photon energy region
[DE94-019278] p 1521 N95-21406
Properties of aged metal tritides
[DE95-001787] p 1243 N95-21440
Muon transfer from muonic atoms of hydrogen isotopes to He nuclei
[DE94-628903] p 1523 N95-21591
Spatial variation of primordial 3-He in crustal fluids along the East-African Rift system (the Ethiopian and the Kenya Rift section) p 1418 N95-21789
The ratios of carbon and non-radiogenic helium and argon isotopes in the mantle and crustal rocks
p 1421 N95-21805
He, Xe and Ne isotopes in a steady-state mass transport model and implications about terrestrial volatiles
p 1425 N95-21821
Variational Monte Carlo study of He-4 in two dimensions
[DE94-629078] p 1576 N95-21998
Microscopic theory of normal liquid He-3
[DE94-629047] p 1527 N95-22179

The dynamic structure function of Bose liquids in the deep inelastic regime
[DE94-629077] p 1527 N95-22182

Helium production by 10 MeV neutrons in iron, nickel and copper
[DE94-014798] p 1529 N95-22280

HELIUM PLASMA

New high temperature plasmas and sample introduction systems for analytical atomic emission and mass spectrometry
[DE94-018580] p 1552 N95-20345

HELIUM-NEON LASERS

Recognition of subsurface defects in machined ceramics by application of neural networks to laser scatter patterns
[DE94-018373] p 1264 N95-20018

HELMET MOUNTED DISPLAYS

Factors affecting the perception of luning in monocular regions of partial binocular overlap displays
[AD-A286287] p 1547 N95-22044

HEMOGLOBIN

In vivo distribution of liposome encapsulated hemoglobin studied with imaging radiotracers
[AD-A279774] p 1438 N95-20806

Calculation of atom-centered partial charges for heme
[DE94-014447] p 1520 N95-21375

HERMETIC SEALS

The demise of plastic encapsulated microcircuit myths
p 1209 N95-20640

HETEROCYCLIC COMPOUNDS

The organic chemistry of conducting polymers
[DE94-018216] p 1270 N95-20680

Selenophene transition metal complexes
[DE95-001675] p 1260 N95-21841

HETEROGENEITY

Task parallel programming in Fx
[AD-A285136] p 1475 N95-20500

QoS driven routing in packet switched networks of multiple transmission media p 1292 N95-20923

Cluster reactions: An approach to understanding the fundamentals of heterogeneous catalysis
[DE95-002947] p 1243 N95-21447

D/H ratios and H2O contents of mantle-derived amphibole megacrysts from Dish Hill, California
p 1416 N95-21781

Scalable programming environment
[AD-A286390] p 1472 N95-22201

HETEROJUNCTION DEVICES

Advances in polycrystalline thin-film photovoltaics for space applications p 1318 N95-20514

Photoreflectance and x ray diffraction study of semiconductor heterostructures and quantum wells
[PB95-127049] p 1582 N95-22432

HETEROJUNCTIONS

Physical Si(1-x)Ge(x)/Si heterojunction bipolar transistor model for device and circuit simulation
[PB95-110896] p 1312 N95-19934

Optimization of InAsSb/InGaAs strained-layer superlattice growth by metal-organic chemical vapor deposition for use in infrared emitters
[DE94-016557] p 1563 N95-19954

Semiconductor cold electron emission device
[AD-D016577] p 1314 N95-20298

Sputter deposition of multilayer thermoelectric films: An approach to the fabrication of two-dimensional quantum wells
[DE95-002396] p 1272 N95-20892

Excitons in semiconducting superlattices, quantum wells, and ternary alloys
[DE95-001867] p 1572 N95-21287

Complementary GaAs junction-gated heterostructure field effect transistor technology
[DE94-018901] p 1329 N95-21390

Transient photoluminescence measurements on GaAs and AlGaAs double heterostructures
[AD-A279408] p 1575 N95-21916

Parallel nanometer scale fabrication
[DE95-002122] p 1336 N95-22284

HEURISTIC METHODS

A construct for describing software development risks
[AD-A284923] p 1457 N95-19999

Improving Multichip Module (MCM) design and reliability using the Intelligent MCM Analyzer
p 1209 N95-20637

Software Capability Evaluation (SCE), version 2.0 team members guide
[AD-A286082] p 1462 N95-20809

An automatic placement tool for rapid prototyping of printed circuit boards
[AD-A286029] p 1328 N95-20997

Heuristic genetic algorithms for constrained problems. Part 1: Principles
[PB95-132031] p 1467 N95-21374

Advanced computing systems: Usability of knowledge-based planning systems
[AD-A279573] p 1477 N95-21698

A periodic scheduling heuristic for mapping iterative task graphs onto distributed memory multiprocessors
[AD-A286047] p 1311 N95-22415

Experimental evaluation of dynamic data allocation strategies in a distributed database with changing workloads
[NASA-CR-195024] p 1456 N95-22431

HEXANITROSTILBENE

An initial assessment of the properties of 2,5-dipicryl-1,3,4-oxadiazole: A secondary explosive with high thermal stability
[MRL-TR-93-16] p 1284 N95-21624

HEXENES

Hydrogenation of nitriles on a well-characterized nickel surface: From surface science studies to liquid phase catalytic activity measurements
[DE94-018184] p 1259 N95-21707

HEXYL COMPOUNDS

Characterization and electrical properties of copper films grown via direct liquid coinjection of (hfac)Cu(TMVS) and TMVS
[DE95-002957] p 1272 N95-20889

HIERARCHIES

Hierarchical structures in biology as a guide for new materials technology
[AD-A286317] p 1265 N95-20176

Hierarchical structure in advanced polymers. Phase behaviour, orientation, properties
[AD-A285938] p 1268 N95-20392

Measuring software dependability by robustness benchmarking
[AD-A280053] p 1461 N95-20622

HIGGS BOSONS

Complementarity of e(+)e(-) and pp colliders for the exploration of electroweak symmetry breaking
[DE94-017397] p 1507 N95-20034

Higgs decay to bottom quarks at the Tevatron
[DE94-016715] p 1511 N95-20404

QCD corrections to Higgs boson production: An update
[DE95-000626] p 1522 N95-21506

HIGH ALTITUDE

Photovoltaic electric power applied to Unmanned Aerial Vehicles (UAV) p 1321 N95-20530

Highly survivable communications: Complementary media packet switched networks p 1292 N95-20922

Variability of total electron content in the high-altitude ionosphere following solar maximum
[AD-A285849] p 1425 N95-21833

HIGH CURRENT

The evolution of configuration from q greater than 1 to q less than 1
[DE94-631396] p 1556 N95-21162

HIGH ELECTRON MOBILITY TRANSISTORS

Proton irradiation effects on advanced digital and microwave III-V components
[DE94-018742] p 1314 N95-20338

On-wafer, cryogenic characterization of ultra-low noise HEMT devices p 1305 N95-21539

Sub-millimeterwave semiconductor signal sources
[AD-A279375] p 1335 N95-22144

HIGH ENERGY INTERACTIONS

Transition-energy crossing with a gamma(sub t)(-)jump
[DE94-017315] p 1531 N95-20021

High energy photon-photon collisions
[DE94-017494] p 1532 N95-20388

Research in theoretical elementary particle physics at the University of Florida, task A
[DE94-004373] p 1512 N95-20469

Universal features of multiplicity distributions
[DE94-012854] p 1498 N95-20779

Universality of particle multiplicities
[DE95-000727] p 1515 N95-20879

Theoretical particle physics
[DE95-002447] p 1515 N95-20893

Recent results from E665
[DE95-002523] p 1516 N95-20914

Where are we going with Bose-Einstein: A mini review
[PB95-130308] p 1518 N95-21222

Experiments at high energy hadron colliders and underground water Cerenkov detector experiment
[DE95-001804] p 1535 N95-21281

Heavy ion collisions
[DE95-002712] p 1520 N95-21321

Proceedings of the School for Young High Energy Physicists
[PB95-108114] p 1537 N95-21647

The development of science during this century
[DE94-632964] p 1582 N95-22185

HIGH ENERGY OXIDIZERS

Novel fluorine oxidizers
[AD-A279480] p 1284 N95-21678

HIGH FREQUENCIES

Materials research for GHz multi-chip modules
[AD-A279661] p 1227 N95-20412

Field-emitter arrays for RF vacuum microelectronics
[AD-A279959] p 1325 N95-20661

The relative importance of meteor burst and other distance polar cap propagation modes in the low VHF band p 1293 N95-20928

Propagation of high frequency waves in urban and road tunnel environments p 1294 N95-20933

DAMSON: A system to measure multipath dispersion, Doppler spread and Doppler shift on multi-mechanism communications channels p 1299 N95-20955

Identification of the propagation modes and paths on HF links using a goniopolarimeter p 1299 N95-20956

Geographical diversity combining to exploit multi-mechanism propagation p 1299 N95-20957

Measurements of angles of elevation of HF by a high resolution method using polarization diversity
p 1299 N95-20959

MTX final report
[DE95-002960] p 1559 N95-21451

HIGH LEVEL LANGUAGES

Split-C and active messages under SUNMOS on the Intel Paragon
[DE94-011418] p 1474 N95-20123

HIGH POLYMERS

Cross-linking reactions for the conversion of polyphosphazenes into useful materials
[AD-A279696] p 1271 N95-20709

HIGH POWER LASERS

Reactor pumped laser research at the Sandia National Laboratories pulsed reactor facilities
[DE95-002181] p 1371 N95-20867

Large facilities pilot programme. Access to the VULCAN High Power Laser Facilities at Rutherford Appleton Laboratory
[PB95-130340] p 1373 N95-21226

High average power diode pumped solid state lasers for CALIOPE
[DE94-019248] p 1376 N95-22121

HIGH PRESSURE

High pressure windowed chamber burned rate determination of liquid propellant XM46
[AD-A283770] p 1282 N95-19920

Overview of the Institute of Geophysics and Planetary Physics and Lawrence Livermore National Laboratory collaborative efforts
[DE94-017300] p 1599 N95-20145

Properties of molecular solids and fluids at high pressure and temperature
[DE94-017594] p 1565 N95-20243

The role of high pressure in the study and applications of the ferroelectric polymer polyvinylidene fluoride and its copolymers
[DE94-015742] p 1268 N95-20396

Rare gases systematics and mantle structure
p 1416 N95-21778

Structure and stability of hydrous minerals at high pressure p 1417 N95-21786

Transportation of volatile elements in thermally evolving planetesimals: An important role of metallic iron
p 1418 N95-21790

Subduction and volatile recycling in Earth's mantle
p 1421 N95-21802

Volatiles in the deep Earth: An experimental study using the laser-heated diamond cell p 1421 N95-21803

Bridging the pressure gap: In situ atomic-level investigations of model platinum catalyst surfaces under reaction conditions by scanning tunneling microscopy
[DE95-002346] p 1246 N95-21990

HIGH RESOLUTION

Correlations between surface structure and catalytic activity/selectivity
[DE94-019023] p 1234 N95-20052

Second European Symposium on X-Ray Topography and High Resolution Diffraction: Programme and abstracts
[AD-A286328] p 1564 N95-20210

Investigation on the backscattering properties of Finnish boreal forests at C- and X-band: A semi-empirical modeling approach
[PB95-127692] p 1389 N95-21105

Neutron molelcular spectroscopy: Future prospects
[PB95-130357] p 1518 N95-21227

Progress in ultrafast scanning probe microscopy
[DE94-018179] p 1373 N95-21261

ICE BABY: Measurements of concentration fluctuations in a forest area in winter conditions
[PB95-133468] p 1405 N95-21274

Science with High Spatial Resolution Far-Infrared Data
[NASA-CR-197353] p 1595 N95-21749

Hires and beyond p 1592 N95-21750

In search of random noise p 1592 N95-21753

Two-dimensional maps of the infrared-to-radio ratio in spiral galaxies p 1583 N95-21765

HIRAS images of fossil dust shells around AGB stars
p 1593 N95-21768

Seismic evidence for volatiles at large depth in the Earth p 1422 N95-21808
Polar volatiles on Mercury and the Moon
p 1422 N95-21811
High resolution descriptions of IRAS 12 and 25 microns confused regions
[AD-A285847] p 1545 N95-21832
High resolution properties of the equatorial Pacific marine atmospheric boundary layer from lidar and radiosonde observations
[DE95-001028] p 1426 N95-21875
Fiber optic pressure sensing array
[AD-D016245] p 1506 N95-22088
Resolution requirements for velocity gradients in turbulence p 1363 N95-22462

HIGH REYNOLDS NUMBER
Subgrid scale models in finite difference simulations of complex wall bounded flows p 1346 N95-21063
The asymptotic state of rotating homogeneous turbulence at high Reynolds numbers
p 1347 N95-21065
Experimental and numerical study of the intermittency exponent mu p 1362 N95-22458

HIGH SPEED
Methods and components for optical contention resolution in high speed networks
[AD-A280016] p 1543 N95-20598
Microdynamic devices fabricated on silicon-on-sapphire substrates
[AD-D016531] p 1325 N95-20727
A wideband propagation simulator for high speed mobile radio communications p 1295 N95-20934
Safety issues in high speed machining
[PB95-127411] p 1287 N95-21422
High speed optical storage technology
[AD-A285788] p 1456 N95-22400

HIGH SPEED PHOTOGRAPHY
The Combustive Sound Source
[ARL-TR-94-9] p 1503 N95-19911

HIGH STRENGTH
Nitrogen alloyed martensitic steels
[PB95-127791] p 1255 N95-21128
Noble gas isotopes and halogens in volatile-rich inclusions in diamonds p 1417 N95-21784
Structural performance of cylindrical pressure housings of different ceramic compositions under external pressure loading. Part 3: Sintered reaction bonded silicon nitride ceramic
[AD-A285773] p 1388 N95-22411

HIGH STRENGTH ALLOYS
Hydrogen resistant alloy - NASA 23
[NASA-CASE-MFS-26200-1-SB] p 1251 N95-20068

HIGH STRENGTH STEELS
The effect of oxide inclusions on the kinetics of the austenite to ferrite transformation in low alloy steel weld metal
[DE94-018131] p 1253 N95-20676
Corrosion evaluation of fuel canister crusher rigging
[DE95-002962] p 1257 N95-21452
Perimeter-yardstick technique for fracture surface fractal analysis
[AD-A286240] p 1387 N95-22025
Demonstration of multifunctional DNBM corrosion inhibitors in protective coatings for Naval air/weapon systems
[AD-A285869] p 1279 N95-22136

HIGH TEMPERATURE
Cr2Nb development
[DE94-018697] p 1250 N95-20043
Properties of molecular solids and fluids at high pressure and temperature
[DE94-017594] p 1565 N95-20243
Overview on superplasticity research on small-grained materials
[DE94-016550] p 1266 N95-20316
Oxide formation on NbAl3 and TiAl due to ion implantation of O-18
[DE94-017874] p 1252 N95-20365
Visible and near-IR spectroscopic studies of UC1(4) in a basic ambient temperature melt: The observation of a possible geometric distorted UC1(6)(exp 2-) species and the evidence for the hydrogen-bond in the melt
[DE94-017764] p 1237 N95-20493
Approaches to the design of structural ceramics incorporating whiskers and particulate phases
[DE94-018126] p 1271 N95-20704
The processing and mechanical properties of high temperature/high performance composites. Processing/property correlations, book 4
[AD-A279739] p 1228 N95-20802
Numerical investigation of supersonic turbulent boundary layers with high wall temperature
p 1344 N95-21050
Nitrogen alloyed martensitic steels
[PB95-127791] p 1255 N95-21128
Atmospheric stability and its influence on air quality in small communities in northern Sweden
[PB95-131652] p 1405 N95-21181
Toughened Silcomp composites for gas turbine engine applications
[DE95-002851] p 1214 N95-21243
Solid oxide fuel cells in the United States
[DE95-002405] p 1395 N95-21361
High temperature superconducting films and multilayers for electronics
[AD-A279545] p 1331 N95-21693
Corrosion resistance and behavioral characteristics of metals exposed to 70 percent by weight sulfuric acid at elevated temperatures
[DE95-001724] p 1259 N95-21740
Volatiles in the Earth: All shallow and all recycled
p 1416 N95-21779
Transportation of volatile elements in thermally evolving planetesimals: An important role of metallic iron
p 1418 N95-21790
Volatiles in the deep Earth: An experimental study using the laser-heated diamond cell p 1421 N95-21803
Hydrogen storage in Earth's mantle and core
p 1423 N95-21813
The processing and mechanical properties of high temperature/high performance composites. Book 6: Delamination and compressive behavior
[AD-A279780] p 1231 N95-21999
Atom probe field ion microscopy of type 308 CRE stainless steel welds
[DE94-019162] p 1261 N95-22127
High temperature superconducting microwave device
[AD-A286351] p 1336 N95-22254
Materials support for the development of High Temperature Advanced Furnaces (HITAF): A comparison of selected mechanical properties for three SiC-based ceramics
[DE94-017752] p 1260 N95-22258
Research on the power generation system with thermoelectric conversion elements
[DE95-714804] p 1397 N95-22309

HIGH TEMPERATURE GASES
Temperature effects on acoustic interactions between altitude test facilities and jet engine plumes
[NASA-CR-197638] p 1504 N95-21170
Toughened Silcomp composites for gas turbine engine applications
[DE95-002851] p 1214 N95-21243
Ceramem filters for removal of particles from hot gas streams
[DE95-001976] p 1275 N95-21354

HIGH TEMPERATURE PLASMAS
New high temperature plasmas and sample introduction systems for analytical atomic emission and mass spectrometry
[DE94-018580] p 1552 N95-20345
Characterization of nova plasmas using an x-ray spectrometer with temporal and spatial resolution
[DE94-016970] p 1553 N95-20363
Electromagnetic waves in an ultrarelativistically hot and strongly magnetized electron-positron plasma
[DE94-628963] p 1307 N95-21849
Submicrosecond, synchronizable x-ray source
[AD-D016497] p 1546 N95-21905

HIGH TEMPERATURE SUPERCONDUCTORS
Processing, fabrication, and demonstration of HTS integrated microwave circuits
[AD-A285611] p 1312 N95-19894
Carrier doping and interlayer coupling in HTSC single crystals
[DE94-018637] p 1564 N95-20127
Superconducting thin film with fullerenes and method of making
[AD-D016580] p 1567 N95-20461
A Monte Carlo study of the minus sign problem in the t-J model using an Intel iPSC/860 hypercube
[DE95-001072] p 1570 N95-20819
Hg-199 and Cu-(63,65) NMR studies of mercury based high-Tc superconductors
[DE95-001073] p 1570 N95-20820
Reactive nanophase oxide additions to melt-processed high-T(sub c) superconductors
[DE95-001470] p 1570 N95-20841
Flux creep with logarithmic U(j) dependence
[DE94-629058] p 1577 N95-22180
Magnetic interactions in the Emery model
[DE94-629059] p 1577 N95-22181
Local texture and strongly linked conduction in spray-pyrolyzed TlBa2Ca2Cu3O(8+x) deposits
[DE94-017887] p 1578 N95-22269
Development of practical high temperature superconducting wire for electric power applications
[DE94-017894] p 1336 N95-22271

HIGH TEMPERATURE TESTS
Investigation of flight data recorder fire test requirements
[AD-A285832] p 1208 N95-20032
Moessbauer study of the sintered Mn(0.70)Zn(0.23)Fe(2.07)O4
[DE94-631462] p 1255 N95-20909
Absorption of water and lubricating oils into porous nylon
[NASA-CR-197344] p 1280 N95-22383

HIGH VACUUM
Loss of solar He and Ne from IDPS in subducting sediment: Diffusion and the effect of phase changes
p 1419 N95-21792
Bridging the pressure gap: In situ atomic-level investigations of model platinum catalyst surfaces under reaction conditions by scanning tunneling microscopy
[DE95-002346] p 1246 N95-21990

HIGH VOLTAGES
A charge distribution analysis instrument for catalysis and material science applications
[DE94-016489] p 1364 N95-20233
A wideband EMP test system
[DE94-015283] p 1290 N95-20474
Development of a tester for evaluation of prototype thermal cells and batteries
[DE95-000540] p 1325 N95-20628
Method of fabricating a microelectronic photomultiplier device with integrated circuitry
[AD-D016530] p 1325 N95-20726
Microdynamic devices fabricated on silicon-on-sapphire substrates
[AD-D016531] p 1325 N95-20727

HIGHLANDS
Volatiles, rheology, and mantle convection: Comparing Earth, Venus, and Mars p 1420 N95-21801

HISTOLOGY
Effect of increased venous backflow on the release of cardiac hormone. Fine structural, immunohistochemical, and biochemical study
[PB95-130399] p 1445 N95-21424

HISTORIES
Ups and downs of type theory
[PB95-110664] p 1487 N95-19903
Intelligent tutoring systems: Past, present, and future
[AD-A280011] p 1448 N95-19970
A Clementine collection: Moonglow
[AD-A286360] p 1217 N95-20228
Acoustic emission: The first half century
[DE94-017176] p 1503 N95-20267
Accelerators for energy production
[DE94-770764] p 1392 N95-20685
The personal aircraft: Status and issues
[NASA-TM-109174] p 1200 N95-20688
But what will it Cost? The history of NASA cost estimating p 1583 N95-20742
The problem of space travel: The rocket motor
[NASA-SP-4026] p 1217 N95-21894
The development of science during this century
[DE94-632964] p 1582 N95-22185

HMX
Thermal decomposition reactions of HMX and RDX and their importance in predicting cookoff hazards
[DE95-002486] p 1283 N95-21513

HOHLRAUMS
24th Annual Anomalous Absorption Conference
[DE94-016457] p 1551 N95-20283
A comparison of kinetic and multifluid simulations of laser-produced colliding plasmas
[DE94-016447] p 1551 N95-20315
Radiation-driven targets for heavy-ion fusion
[DE95-002264] p 1533 N95-20784
Effects of plasma physics on capsule implosions in gas-filled hohlraums
[DE95-000923] p 1371 N95-20786
Shot-to-shot comparison of the first Li-beam driven Hohlraum experiments
[DE94-016558] p 1558 N95-21247
Low density gas and foam targets for ICF long scale length plasma experiments: Fabrication and characterization
[DE95-000935] p 1558 N95-21368
Progress in the Light Ion Driven Inertial Confinement Fusion Program
[DE94-019182] p 1537 N95-21603

HOLE BURNING
Free electron laser program
[AD-A285906] p 1368 N95-19987
Time domain spectral hole-burning storage
[AD-A279912] p 1587 N95-20309

HOLE DISTRIBUTION (ELECTRONICS)
Visible light emitting materials and injection devices
[AD-A284796] p 1541 N95-20066
Phase dynamics of non-equilibrium distributions of free electron-hole pairs in GaAs quantum wells
[DE94-018190] p 1569 N95-20679

HOLES (ELECTRON DEFICIENCIES)
Temporal and spectral investigation of multi-Landau level quantum beats in GaAs [DE94-018189] p 1569 N95-20678
Phase dynamics of non-equilibrium distributions of free electron-hole pairs in GaAs quantum wells [DE94-018190] p 1569 N95-20679
A versatile masking process for plasma etched backside via holes in GaAs [DE94-019176] p 1572 N95-21419

HOLES (MECHANICS)
Navier-Stokes simulations of the effects of suction holes on a flat plate boundary layer p 1352 N95-21094
Magnetic interactions in the Emery model [DE94-629059] p 1577 N95-22181

HOLLOW CATHODES
Thoriated-tungsten, split-ring, hollow-cathode electrode for discharge devices [AD-D016508] p 1333 N95-21906

HOLMIUM
Rare earth garnet selective emitter p 1322 N95-20536

HOLOGRAPHY
Application of computer-generated holograms to optical transformations [AD-A286356] p 1368 N95-22256

HOMING DEVICES
Fracture analysis of an all-ceramic bearing system [AD-A285056] p 1269 N95-20486

HOMOGENEOUS TURBULENCE
A numerical investigation of energy transfer and subgrid-scale eddy viscosity in homogeneous, isotropic and shear turbulence [AD-A280005] p 1339 N95-20058
Pressure and higher-order spectra for homogeneous isotropic turbulence p 1343 N95-21045
Statistics of pressure and pressure gradient in homogeneous isotropic turbulence p 1343 N95-21046
The decay of axisymmetric homogeneous turbulence p 1343 N95-21047
Modeling the two-point correlation of the vector stream function p 1345 N95-21055
Homogeneous turbulence subjected to mean flow with elliptic streamlines p 1345 N95-21056
On the transition towards slow manifold in shallow-water and 3D Euler equations in a rotating frame p 1345 N95-21057
On the asymptotic similarity of rotating homogeneous turbulence p 1345 N95-21058
Anisotropic structure of homogeneous turbulence subjected to uniform rotation p 1346 N95-21059
The asymptotic state of rotating homogeneous turbulence at high Reynolds numbers p 1347 N95-21065

HOMOGENIZING
Microstructures and tensile properties of as-cast iron-aluminide alloys [DE94-017868] p 1252 N95-20359

HOMOJUNCTIONS
Status of diffused junction p+n InP solar cells for space applications p 1317 N95-20509
Annealing of irradiated n+p InP buried homojunctions p 1320 N95-20524

HOMOLOGY
Elliptic genera for Z/K-manifolds I [PB95-109096] p 1496 N95-22355

HOMOTOPY THEORY
Layered path planning for an autonomous mobile robot [AD-A286138] p 1485 N95-22244

HORIZON
Radiance of the ocean horizon [AD-A285613] p 1431 N95-19896
Comparative study of C- and K-band propagation mechanisms beyond the horizon p 1297 N95-20946

HORMONES
Effect of increased venous backflow on the release of cardiac hormone. Fine structural, immunohistochemical, and biochemical study [PB95-130399] p 1445 N95-21424

HOT CORROSION
A transmission electron microscope characterization of sodium sulfate hot corrosion of silicon carbide fiber-reinforced lithium aluminosilicate glass-ceramic matrix composite [AD-A286164] p 1231 N95-22038

HOT ELECTRONS
An advanced ECR ion source with a large uniformly distributed ECR plasma volume for multiply charged ion beam generation [DE95-001078] p 1515 N95-20911

HOT-WIRE FLOWMETERS
Transverse vorticity measurements in the NASA Ames 80 x 120 wind tunnel boundary layer p 1362 N95-22457

HOUSINGS
Structural performance of cylindrical pressure housings of different ceramic compositions under external pressure loading. Part 1: Isostatically pressed alumina ceramic [AD-A279669] p 1270 N95-20603
Structural performance of cylindrical pressure housings of different ceramic compositions under external pressure loading. Part 3: Sintered reaction bonded silicon nitride ceramic [AD-A285773] p 1388 N95-22411

HUBBLE SPACE TELESCOPE
Post-flight investigation programmes of recently retrieved solar generators p 1321 N95-20531

HULLS (STRUCTURES)
Set functionals in stochastic geometry [PB95-135372] p 1491 N95-21005

HUMAN BEHAVIOR
13th European Annual Conference on Human Decision Making and Manual Control [PB95-132874] p 1450 N95-21284

HUMAN BEINGS
Carboxyhemoglobin formation due to transient exposure to high level carbon monoxide: Experimental results and an explanatory model [AD-A285476] p 1444 N95-20979

HUMAN FACTORS ENGINEERING
Crew aiding and automation: A system concept for terminal area operations, and guidelines for automation design [NASA-CR-4631] p 1204 N95-19950
A 3D stereo data visualization and representation [AD-A284788] p 1449 N95-20064
Behavioral effects of tyrosine during sustained wakefulness [AD-A279789] p 1441 N95-20307
Measuring presence in virtual environments [AD-A286183] p 1460 N95-20326
An evaluation of Automatic Terminal Information Service (ATIS) flight deck display presentation options [AD-A280100] p 1204 N95-21020
Microclimate cooling effect on perceived exertion in four heat/exercise scenarios [AD-A285549] p 1444 N95-21160
Perception and control of locomotion [AD-A285605] p 1450 N95-21192
Human force exertion in user-product interaction. Backgrounds for design [PB95-132858] p 1452 N95-21283
Visual displays and Neuro-Linguistic Programming [DE95-001454] p 1466 N95-21311
Quantitative evaluation of wrist posture and typing performance: A comparative study of 4 computer keyboards [DE95-002392] p 1452 N95-21358
Independent review of Aviation Technology and Research Information Analysis System (ATRIAS) database [AD-A284049] p 1203 N95-21518
Crew-Centered Cockpit Design (CCCD) field demonstration program, volume 1 [AD-A286426] p 1453 N95-21566
Ergonomic evaluation of the Apple Adjustable Keyboard [DE95-002393] p 1453 N95-21637
Effect of lags on human performance with head-coupled simulators [AD-A279577] p 1453 N95-21700
Adaptive capture of expert behavior [DE94-018285] p 1483 N95-21710
Top ten list of user-hostile interface design [DE95-001602] p 1453 N95-21721
Command history, 1993 [AD-A279775] p 1446 N95-21989
Systems engineering design and technical analyses for Strategic Avionics Crew-station Design Evaluation Facility (SACDEF) [AD-A286239] p 1213 N95-22024
Information clustering for better decision-making [AD-A286292] p 1590 N95-22053
Activities of the Institute for the Study of Human Capabilities [AD-A286471] p 1454 N95-22275
Fuzzy clustering of facial form for prototyping environmental protection equipment [DE94-014657] p 1454 N95-22466

HUMAN FACTORS LABORATORIES
Sustaining the health and performance of soldiers/warfighters deployed to harsh environments [AD-A286270] p 1446 N95-22004

HUMAN PERFORMANCE
The effects of three-dimensional graphs on decision making [AD-A285034] p 1583 N95-20051
Behavioral effects of tyrosine during sustained wakefulness [AD-A279789] p 1441 N95-20307
Development and enhancement of a model of performance and decision making under stress in a real life setting [AD-A285945] p 1449 N95-20393
Modeling platform dynamics and physiological response to short arm centrifugation [AD-A279640] p 1442 N95-20457
The MSFC Program Control Development Program p 1585 N95-20754
Effect of lags on human performance with head-coupled simulators [AD-A279577] p 1453 N95-21700
Aerospace medicine and biology: A continuing bibliography with indexes (supplement 399) [NASA-SP-7011(399)] p 1446 N95-21947
Command history, 1993 [AD-A279775] p 1446 N95-21989
Sustaining the health and performance of soldiers/warfighters deployed to harsh environments [AD-A286270] p 1446 N95-22004
Activities of the Institute for the Study of Human Capabilities [AD-A286471] p 1454 N95-22275

HUMAN TOLERANCES
Evaluation of stress experienced by soldiers wearing chemical protective clothing during varying work loads in desert or tropical environments [AD-A280113] p 1452 N95-20625
Environmental Hazards Assessment Program [DE94-019075] p 1406 N95-21565
The influence of coronary artery disease on +Gz tolerance: A preliminary study [AD-A279305] p 1446 N95-21941

HUMAN-COMPUTER INTERFACE
PRSPLOT6 manual [PB95-110862] p 1456 N95-19928
NOMADS graphical user interface version 2.0 user's manual [AD-A286314] p 1458 N95-20095
Evaluation of Borland Turbo Vision [AD-A279873] p 1459 N95-20184
Measuring presence in virtual environments [AD-A286183] p 1460 N95-20326
Translation of the data flow query language for the multimodel, multibackend database system [AD-A285978] p 1588 N95-20617
ECSU-AASERT summer research project in parallel processing and computer visualization [AD-A285983] p 1475 N95-20618
Making structured graphics and constraints practical for large-scale applications [AD-A280062] p 1461 N95-20623
Model formality in human/computer collaboration [AD-A286001] p 1462 N95-20718
Generating examples for use in tutorial explanations: The use of a subsumption based classifier [AD-A286028] p 1464 N95-20996
DAVE: A plug and play model for distributed multimedia application development [DE94-016481] p 1465 N95-21153
Visual displays and Neuro-Linguistic Programming [DE95-001454] p 1466 N95-21311
CAiSE 1994 Doctoral Consortium [PB95-135182] p 1469 N95-21711
Top ten list of user-hostile interface design [DE95-001602] p 1453 N95-21721
State of the art in CFD pre- and postprocessing [PB95-110391] p 1356 N95-22017
Information clustering for better decision-making [AD-A286292] p 1590 N95-22053
Activities of the Institute for the Study of Human Capabilities [AD-A286471] p 1454 N95-22275
ActorStudio reference manual. A user's guide to the ActorStudio user interface editor, version 1.0 [PB95-127023] p 1472 N95-22310

HUMIDITY
Unified very low stratus cloud/subcloud microphysics model: User's guide [AD-A286454] p 1430 N95-21586

HYBRID STRUCTURES
Trimode Power Converter optimizes PV, diesel and battery energy sources [DE94-015014] p 1313 N95-20262
Forming of superplastic ceramics [DE94-017306] p 1276 N95-21662
Electric and Hybrid Vehicle Program Site Operator Program [DE95-002042] p 1333 N95-21960

HYDRATES
Storage and recycling of water and carbon dioxide in the earth p 1425 N95-21822

HYDRATION
Potential-of-mean-force description of ionic interactions and structural hydration in biomolecular systems [DE95-000859] p 1438 N95-21366

HYDRAULIC EQUIPMENT
Force based motion control of a walking machine
[PB95-129672] p 1451 N95-20276
Input shaping for vibration-damped slewing of a flexible beam using a heavy-lift hydraulic robot
[DE94-015803] p 1379 N95-20695
HYDRAULICS
NESTLE: Few-group neutron diffusion equation solver utilizing the nodal expansion method for eigenvalue, adjoint, fixed-source steady-state and transient problems
[DE95-001903] p 1466 N95-21288
HYDRAZINES
Catalyzed reduction of nitrate in aqueous solutions
[DE94-017660] p 1247 N95-22049
HYDROBROMIC ACID
Combustion-related studies using weakly bonded complexes
[DE95-002801] p 1238 N95-20576
HYDROCARBON COMBUSTION
A flamelet model for turbulent unpremixed combustion
p 1249 N95-21081
HYDROCARBON FUEL PRODUCTION
Bioconversion of coal derived synthesis gas to liquid fuels
[DE94-017381] p 1282 N95-19927
Producing liquid fuels from biomass
[DE95-717458] p 1398 N95-22425
HYDROCARBON FUELS
Spectroscopic studies of hazardous fuel interactions with soils
[AD-A279099] p 1407 N95-21596
Analysis of test criteria for specifying foam firefighting agents for aircraft rescue and firefighting
[AD-A286381] p 1203 N95-22352
HYDROCARBONS
Degradation of aromatic hydrocarbons in an aquifer during a field experiment demonstrating the feasibility of remediation by natural attenuation
[AD-A283809] p 1282 N95-19922
Refractive index change in dissociating shocked benzene
[DE94-019015] p 1541 N95-20352
Novel catalysts for methane activation
[DE95-002639] p 1237 N95-20438
Combustion-related studies using weakly bonded complexes
[DE95-002801] p 1238 N95-20576
A flamelet model for turbulent unpremixed combustion
p 1249 N95-21081
Computer programs for analysis of geophysical data
[DE95-002472] p 1415 N95-21511
New concepts for refrigerant leak detection and mixture measurement
[DE94-018967] p 1287 N95-21559
Development and demonstration of advanced technologies for direct electrochemical oxidation of hydrocarbons (methanol, methane, propane)
[AD-A285094] p 1224 N95-22474
HYDROCHLORIC ACID
Combustion-related studies using weakly bonded complexes
[DE95-002801] p 1238 N95-20576
Quantum chemical study of rare gas/halide interactions as a model for high energy density material. 1: Transition properties in HCl
[AD-A285988] p 1239 N95-20613
The energetics and dynamics of free radicals, ions, and clusters
[DE94-018101] p 1244 N95-21701
HYDROCYANIC ACID
Combustion-related studies using weakly bonded complexes
[DE95-002801] p 1238 N95-20576
HYDRODYNAMICS
Transport and dynamics in toroidal fusion systems
[DE94-018653] p 1548 N95-20029
Computational modeling of physical processes during laser ablation
[DE94-017699] p 1369 N95-20221
A computational study of projectile melt in impact with typical Whipple shields
[DE94-016454] p 1385 N95-20237
Hydrodynamic instabilities in inertial fusion
[DE94-018079] p 1554 N95-20675
Computational design of Hypervelocity Launchers
[DE95-000744] p 1218 N95-20785
Conservative smoothing versus artificial viscosity
[DE95-001108] p 1341 N95-20831
A flamelet model for turbulent unpremixed combustion
p 1249 N95-21081
Relativistic binary neutron star coalescence
[DE94-019311] p 1600 N95-21479
Wave journal bearing. Part 1: Analysis
[NASA-CR-195431-PT-1] p 1382 N95-22404
Wave journal bearing. Part 2: Experimental pressure measurements and fractional frequency whirl threshold for wave and plain journal bearings
[NASA-TM-106848-PT-2] p 1382 N95-22405
HYDROGEN
Intrinsic barriers for H-atom transfer reactions
[DE94-018914] p 1507 N95-20049
Proceedings of the 1994 DOE/NREL Hydrogen Program Review
[DE94-011835] p 1234 N95-20117
Single-collision studies of energy transfer and chemical reaction
[DE95-002943] p 1244 N95-21517
Experimental investigations of electron capture from atomic hydrogen and deuterium by alpha particles
[DE95-002138] p 1523 N95-21587
D/H ratios and H2O contents of mantle-derived amphibole megacrysts from Dish Hill, California
p 1416 N95-21781
Structure and stability of hydrous minerals at high pressure p 1417 N95-21786
Hydrogen and related materials at high density: Physics, chemistry and planetary implications
p 1418 N95-21791
Hydrogen storage in Earth's mantle and core
p 1423 N95-21813
A crystallographic model for hydrous wadsleyite (Beta-Mg2SiO4) p 1424 N95-21817
Water abundance and accretion history of terrestrial planets p 1424 N95-21820
Ab initio potential energy surface for H + OCS reactions: Extended basis sets and correlation treatment
[AD-A286420] p 1247 N95-22207
The two-electron problem and prospects for atomic collision theory on a numerical lattice
[DE94-017856] p 1528 N95-22265
Quantum chemical study of rare gas/halide interactions as a model for high energy density material. 2: The interaction of hydrogen chloride with the rare gas xenon
[AD-A286385] p 1248 N95-22321
HYDROGEN ATOMS
Calculation of the total and total ionization cross sections for positron scattering on atomic hydrogen
[DE94-631341] p 1508 N95-20197
An atomically-resolved STM study of the thermal decomposition of disilane on Si(001)
[AD-A279818] p 1567 N95-20544
Studies of the gas tori of Titan and Triton
[NASA-CR-197377] p 1601 N95-20797
Restricted mass transport effects on free radical reactions
[DE94-018136] p 1217 N95-21706
Atomic velocity distributions in a hydrogen beam effusing out of an RF discharge dissociator
[AD-A279253] p 1307 N95-21985
HYDROGEN BONDS
Visible and near-IR spectroscopic studies of UC1(4) in a basic ambient temperature melt: The observation of a possible geometric distorted UC1(6)(exp 2-) species and the evidence for the hydrogen-bond in the melt
[DE94-017764] p 1237 N95-20493
Siloxanes with strong hydrogen bond donating functionalities
[AD-D016499] p 1279 N95-22057
HYDROGEN COMPOUNDS
Origin and loss of the volatiles of the terrestrial planets p 1417 N95-21785
HYDROGEN EMBRITTLEMENT
Hydrogen resistant alloy - NASA 23
[NASA-CASE-MFS-26200-1-SB] p 1251 N95-20068
Tritium and decay helium effects on the fracture toughness properties of types 316L, 304L and 21Cr-6Ni-9Mn stainless steels
[DE95-001248] p 1252 N95-20216
HYDROGEN FUELS
Numerical study of contaminant effects on combustion of hydrogen, ethane, and methane in air
[NASA-TM-106844] p 1284 N95-22114
HYDROGEN IONS
Dynamics of collision processes
[DE94-017593] p 1509 N95-20242
Measurements of scattering processes in negative ion: Atom collisions
[DE95-000664] p 1519 N95-21276
HYDROGEN ISOTOPES
Muon transfer from muonic atoms of hydrogen isotopes to He nuclei
[DE94-628903] p 1523 N95-21591
HYDROGEN MASERS
Atomic velocity distributions in a hydrogen beam effusing out of an RF discharge dissociator
[AD-A279253] p 1307 N95-21985
HYDROGEN PRODUCTION
Proceedings of the 1994 DOE/NREL Hydrogen Program Review
[DE94-011835] p 1234 N95-20117
HYDROGEN-BASED ENERGY
Proceedings of the 1994 DOE/NREL Hydrogen Program Review
[DE94-011835] p 1234 N95-20117
HYDROGENATION
Investigation of the stability and 1.0 MeV proton radiation resistance of commercially produced hydrogenated amorphous silicon alloy solar cells p 1320 N95-20522
Effects of plasma hydrogenation on trapping properties of dislocations in heteroepitaxial InP/GaAs
p 1323 N95-20542
Hydrogenation of nitriles on a well-characterized nickel surface: From surface science studies to liquid phase catalytic activity measurements
[DE94-018184] p 1259 N95-21707
HYDROGEOLOGY
Review of GIS applications in hydrologic modeling
[AD-A279076] p 1390 N95-21628
HYDROGRAPHY
Hydrographic data from equatorial Pacific waters near the Galapagos
[AD-A283741] p 1431 N95-19918
Mixing and dynamics of the Mediterranean outflow
[AD-A279803] p 1434 N95-21306
Exchanges between hemispheres and gyres: A direct approach to the mean circulation of the equatorial Pacific
[NASA-CR-196311] p 1436 N95-22072
HYDROLOGY
Regional scale hydrology with a new land surface processes model
[NASA-TM-110500] p 1390 N95-22111
Sandia National Laboratories analysis code data base
[DE95-004188] p 1502 N95-22420
HYDROLOGY MODELS
Review of GIS applications in hydrologic modeling
[AD-A279076] p 1390 N95-21628
Regional scale hydrology with a new land surface processes model
[NASA-TM-110500] p 1390 N95-22111
HYDROLYSIS
Safe conditions for contacting nitric acid or nitrates with Tri-n-Butyl Phosphate (TBP)
[DE95-001243] p 1235 N95-20215
Corrosion resistance and behavioral characteristics of metals exposed to 70 percent by weight sulfuric acid at elevated temperatures
[DE95-001724] p 1259 N95-21740
HYDROMETEOROLOGY
Regional scale hydrology with a new land surface processes model
[NASA-TM-110500] p 1390 N95-22111
HYDROPHONES
Analysis of low frequency ocean noise. 1: From a long-term experiment across the US East Coast. 2: From the Wake Island Hydrophone Array during northwest Pacific typhoons
[AD-A284975] p 1432 N95-20040
A simple ocean bottom hydrophone with 200 megabyte data capacity
[AD-A279478] p 1434 N95-21677
HYDROSTATIC PRESSURE
The role of high pressure in the study and applications of the ferroelectric polymer polyvinylidene fluoride and its copolymers
[DE94-015742] p 1268 N95-20396
Attachment methodology for composite cylinder assembly
[AD-D016578] p 1227 N95-20459
Photoluminescence under pressure and annealing of nitrogen-doped ZnSe
[DE95-002355] p 1568 N95-20630
HYDROSTATICS
Hydrostatic force sensor
[DE94-018923] p 1364 N95-20321
HYDROTHERMAL SYSTEMS
Hydrothermal conversion of carbohydrates and related compounds
[PB95-134011] p 1396 N95-22175
HYDROXIDES
Nickel hydroxide electrodes in reduced-alkalinity electrolytes
[DE95-002333] p 1326 N95-20814
Correlations for the OH A(sup 2)(Sigma)(sup +)(v(prime)=0) electronic quenching cross-section
[DE95-002591] p 1244 N95-21524
Acid-site characterization of water-oxidized alumina films by near-edge x-ray absorption and soft x-ray photoemission
[DE95-003355] p 1247 N95-22234
HYDROXYL EMISSION
Two-dimensional imaging of OH in a lean burning high pressure combustor
[NASA-TM-106854] p 1214 N95-21383

HYDROXYL RADICALS

Two-dimensional imaging of OH in a lean burning high pressure combustor
[NASA-TM-106854] p 1214 N95-21383

HYGIENE

Personal hygiene body wipe
[AD-A286092] p 1454 N95-22274

HYGROSCOPICITY

Governing equations for multiphase heat and mass transfer in hygroscopic porous media with applications to clothing materials
[AD-A286418] p 1357 N95-22206

HYPERCUBE MULTIPROCESSORS

A Monte Carlo study of the minus sign problem in the t-J model using an Intel iPSC/860 hypercube
[DE95-001072] p 1570 N95-20819

HYPERGEOMETRIC FUNCTIONS

Exponents in lifetime and power spectral density forms in self-organized critical systems
[AD-A286242] p 1495 N95-22026

HYPERNUCLEI

Strange hadronic matter
[DE94-019345] p 1521 N95-21484

HYPERONS

Strange hadronic matter
[DE94-019345] p 1521 N95-21484

HYPERSONIC FLOW

Application of pressure sensitive paint in hypersonic flows
[NASA-TM-106824] p 1201 N95-20794

Shock wave interactions in hypervelocity flow
[AD-A286507] p 1357 N95-22212

HYPERSONIC HEAT TRANSFER

Numerical investigation of one-dimensional heat-flux calculations
[AD-A286293] p 1582 N95-22054

HYPERSONIC INLETS

Internal aerodynamics of a generic three-dimensional scramjet inlet at Mach 10
[NASA-TP-3476] p 1340 N95-20619

HYPERSONIC SPEED

Internal aerodynamics of a generic three-dimensional scramjet inlet at Mach 10
[NASA-TP-3476] p 1340 N95-20619

HYPERSONIC VEHICLES

Description and flow characterization of hypersonic facilities
[AD-A284291] p 1200 N95-20248

HYPERSONICS

Description and flow characterization of hypersonic facilities
[AD-A284291] p 1200 N95-20248

HYPERTHERMIA

Radiofrequency hyperthermia systems: Experimental and clinical assessment of the feasibility of radiofrequency hyperthermia systems for loco-regional deep heating
[PB94-206885] p 1444 N95-21016

HYPERVELOCITY

A Hypervelocity Experimental Research Database (HERD): Support for the Wright Laboratory Armament Directorate Code Validation Program (COVAL)
[DE95-001628] p 1387 N95-21396

HYPERVELOCITY FLOW

Shock wave interactions in hypervelocity flow
[AD-A286507] p 1357 N95-22212

HYPERVELOCITY IMPACT

Experimental hypervelocity impact effects on simulated planetesimal materials
[DE94-017290] p 1599 N95-20144

A Hypervelocity Experimental Research Database (HERD): Support for the Wright Laboratory Armament Directorate Code Validation Program (COVAL)
[DE95-001628] p 1387 N95-21396

HYPERVELOCITY LAUNCHERS

Chunk projectile launch using the Sandia Hypervelocity Launcher Facility
[DE94-018494] p 1215 N95-20223

Computational design of Hypervelocity Launchers
[DE95-000744] p 1218 N95-20785

HYPERVELOCITY PROJECTILES

Chunk projectile launch using the Sandia Hypervelocity Launcher Facility
[DE94-018494] p 1215 N95-20223

A Hypervelocity Experimental Research Database (HERD): Support for the Wright Laboratory Armament Directorate Code Validation Program (COVAL)
[DE95-001628] p 1387 N95-21396

HYPERVOLEMIA

Hypervolemia in men from drinking hyperhydration fluids at rest and during exercise
[NASA-TM-4657] p 1439 N95-21544

HYPOTHALAMUS

Netherlands Institute for Brain Research progress report, 1993
[PB95-135398] p 1445 N95-21352

HYSTERESIS

Application of an energy-based life prediction model to bithermal and thermomechanical fatigue
[NASA-TM-106684] p 1385 N95-20179

I

I BEAMS

Inelastic bending and torsion of steel I-beams
[PB94-208378] p 1384 N95-19975

Inelastic torsion of steel I-beams
[PB94-208360] p 1384 N95-20101

IBM PERSONAL COMPUTERS

An IBM based ARINC interface
[ARL-TR-21] p 1471 N95-22104

Residual stress analysis in swage autofrettaged thick-walled cylinders by position-sensitive x-ray diffraction techniques
[AD-A286383] p 1388 N95-22320

ICE

ICE BABY: Measurements of concentration fluctuations in a forest area in winter conditions
[PB95-133468] p 1405 N95-21274

Dynamics of volatile delivery from outer to inner solar system p 1420 N95-21798

Surface ices in the outer solar system
p 1423 N95-21815

ICE FORMATION

The initiation of lightning and the growth of electric fields in thunderstorms
[AD-A280033] p 1428 N95-20008

Monthly mean sea ice data from the Polar Ice Prediction System, the Regional Polar Ice Prediction System-Barents Sea and the Regional Polar Ice Prediction System-Greenland Sea
[AD-A280095] p 1433 N95-21018

Development of a portable ice-thickness measuring instrument
[AD-A279472] p 1433 N95-21291

ICE MAPPING

Atlas of SSM/I satellite ice concentration interpolated to operational ice model domains of the Arctic for 1993
[AD-A280183] p 1432 N95-20012

IDEAL GAS

Shock wave interactions in hypervelocity flow
[AD-A286507] p 1357 N95-22212

IDENTIFYING

Wavelet-based acoustic recognition of aircraft
[DE94-017701] p 1503 N95-20019

Angle resolved Auger electron spectroscopy: An alternate tool for identifying electronic excitation processes in solids
[AD-A285375] p 1238 N95-20555

Guidelines for qualifying cleaning and verification materials
[NASA-TM-108474] p 1270 N95-20694

Mantle rare gas relative abundances in a steady-state mass transport model p 1423 N95-21812

IGNEOUS ROCKS

Spatial variation of primordial 3-He in crustal fluids along the East-African Rift system (the Ethiopian and the Kenya Rift section) p 1418 N95-21789

Solar helium and neon in the Earth
p 1419 N95-21793

IGNITERS

Investigation of rocket motors 3 inch number 1 Mk 4
[AD-A284278] p 1221 N95-19962

IGNITION

The hot fragment conductive ignition test for screening LOVA propellants
[AD-A284259] p 1282 N95-20187

National Ignition Facility: Experimental plan
[DE94-016542] p 1550 N95-20189

Proceedings of the Zel'Dovich Memorial International Conference on Combustion, Detonation, Shock Waves, volume 2
[AD-A286626] p 1239 N95-20769

Neutronics and shielding analysis of the National Ignition Facility
[DE94-016698] p 1534 N95-21208

Numerical wave speed for one-dimensional scalar hyperbolic conservation laws with source terms
[PB95-127536] p 1492 N95-21371

Ignition of submarine materials at various oxygen concentrations
[PB95-131371] p 1243 N95-21428

Temporal evolution of turbulence/chemistry interactions in lifted, turbulent-jet flames
[DE95-002481] p 1243 N95-21512

IGNITION LIMITS

Triple flames and flame stabilization
p 1249 N95-22441

IGNITION SYSTEMS

Use of the National Ignition Facility for the development of inertial fusion energy
[DE94-016696] p 1557 N95-21206

IGNITION TEMPERATURE

Ignition of submarine materials at various oxygen concentrations
[PB95-131371] p 1243 N95-21428

ILL-CONDITIONED PROBLEMS (MATHEMATICS)

Applied mathematical problems in modern electromagnetics
[AD-A286448] p 1303 N95-21462

ILLUMINATING

X-ray imaging of uniform large scale-length plasmas created from gas-filled targets on Nova
[DE94-018339] p 1531 N95-20015

ILLUMINATION

Annealing of irradiated n+p InP buried homojunctions
p 1320 N95-20524

Influence of wavelength on transient short-circuit current in polycrystalline silicon solar cells
[DE94-629082] p 1397 N95-22183

IMAGE ANALYSIS

Atlas of SSM/I satellite ice concentration interpolated to operational ice model domains of the Arctic for 1993
[AD-A280183] p 1432 N95-20012

Energy and Technology Review
[DE94-017686] p 1219 N95-20148

View-based models of 3D object recognition and class-specific invariance
[AD-A279858] p 1459 N95-20157

A Hyperspectral Image Data Exploration Workbench for environmental science applications
[DE94-016373] p 1412 N95-20171

Perception and control of locomotion
[AD-A285605] p 1450 N95-21192

Object recognition by alignment using invariant projections of planar surfaces
[AD-A279841] p 1468 N95-21495

Arcmimute scale HI and IRAS observations toward high latitude cloud G86.5+59.6 p 1594 N95-21771

Interpretation of HRTEM images by image simulation: An introduction to theory and practice
[DE95-003422] p 1591 N95-22235

Users guide to NCEMSS, version 2.0
[DE95-003443] p 1548 N95-22238

Saddle-node dynamics for edge detection
[DE94-017415] p 1473 N95-22426

IMAGE CLASSIFICATION

Experimental proof-of-concept of phase derivative based range profile enhancement ATR
[AD-A284921] p 1289 N95-19997

IMAGE CONTRAST

Microscopy of stress-induced morphological development and dislocation nucleation during semiconductor epitaxy
[DE94-017869] p 1568 N95-20674

IMAGE CONVERTERS

An image cancellation approach to depth-from-focus
[DE94-019312] p 1544 N95-21392

IMAGE CORRELATORS

Application of MCM image construction to IRAS comet observations p 1594 N95-21772

IMAGE ENHANCEMENT

The sharper image: Implementing a Fast Fourier Transform (FFT) to enhance a video-captured image
[AD-A279790] p 1445 N95-21180

Synthetic aperture radar processing with polar formatted subapertures
[DE95-001830] p 1302 N95-21305

Combining image-processing and image compression schemes p 1304 N95-21537

Constraints as a destriping tool for Hires images
p 1593 N95-21756

Spatio-temporal masking in human vision and its application to image coding
[AD-A284949] p 1451 N95-22473

IMAGE FILTERS

A framework for segmentation using physical models of image formation
[AD-A279900] p 1543 N95-20564

The sharper image: Implementing a Fast Fourier Transform (FFT) to enhance a video-captured image
[AD-A279790] p 1445 N95-21180

IMAGE INTENSIFIERS

The sharper image: Implementing a Fast Fourier Transform (FFT) to enhance a video-captured image
[AD-A279790] p 1445 N95-21180

Unique microchannel plate process doubles MCPI resolution
[DE94-017507] p 1337 N95-22427

IMAGE PROCESSING

High performance hardware and software for pattern recognition and image processing
[AD-A279776] p 1457 N95-19961

Simulation of stellar speckle imaging
[DE94-016606] p 1412 N95-19985
Ice Processing System software support documentation
[AD-A280030] p 1388 N95-20006
X-ray imaging of uniform large scale-length plasmas created from gas-filled targets on Nova
[DE94-018339] p 1531 N95-20015
A 3D stereo data visualization and representation
[AD-A284788] p 1449 N95-20064
Program of the 1993 9th Interdisciplinary Laser Science Conference (ILS-9)
[AD-A285131] p 1369 N95-20082
Energy and Technology Review
[DE94-017686] p 1219 N95-20148
View-based models of 3D object recognition and class-specific invariance
[AD-A279858] p 1459 N95-20157
SAR image registration in absolute coordinates using GPS carrier phase position and velocity information
[DE94-018738] p 1204 N95-20195
Characterization of an expanded-field Schwarzschild objective for extreme ultraviolet lithography
[DE94-016780] p 1541 N95-20239
Tracking a dynamic set of feature points
[AD-A285124] p 1313 N95-20257
Low electron beam energy CIVA analysis of passivated ICs
[DE94-017421] p 1314 N95-20286
Applications of wavelets to radar, imaging and related problems
[AD-A279909] p 1290 N95-20545
Deconvolution and singular value decomposition
[AD-A286582] p 1491 N95-20875
Integration of segmentation and stereo matching
[PB95-107819] p 1444 N95-21028
Synthetic aperture radar processing with polar formatted subapertures
[DE95-001830] p 1302 N95-21305
An image cancellation approach to depth-from-focus
[DE94-019312] p 1544 N95-21392
Object recognition by alignment using invariant projections of planar surfaces
[AD-A279841] p 1468 N95-21495
Combining image-processing and image compression schemes p 1304 N95-21537
Subsampling methods for image sequence coding
[PB95-107991] p 1305 N95-21579
Hardware implementation of a desktop supercomputer for high performance image processing. Color image processing using cellular neural networks
[AD-A286455] p 1455 N95-21589
Surface micromachined capacitive tactile image sensor
[PB95-108031] p 1288 N95-21633
Hires and beyond p 1592 N95-21750
MEM application to IRAS CPC images
p 1592 N95-21751
An assessment of image reconstruction from balloon-borne and the IRAS data p 1592 N95-21752
Constraints as a destriping tool for Hires images
p 1593 N95-21756
Wavelet analysis applied to the IRAS cirrus
p 1593 N95-21769
A HIRES analysis of the FIR emission of supernova remnants p 1594 N95-21770
Application of MCM image construction to IRAS comet observations p 1594 N95-21772
Thermal imaging systems
[AD-A279146] p 1307 N95-21970
Image and video coding using a wavelet decomposition
[PB95-135067] p 1311 N95-22358
Feature extraction without edge detection
[AD-A279842] p 1473 N95-22386
Imaging design of the wide field x-ray monitor onboard the HETE satellite
[DE95-002750] p 1221 N95-22436
Spatio-temporal masking in human vision and its application to image coding
[AD-A284949] p 1451 N95-22473

IMAGE RECONSTRUCTION
Deconvolution and singular value decomposition
[AD-A286582] p 1491 N95-20875
Three-dimensional ground penetrating radar imaging using multi-frequency diffraction tomography
[DE94-016687] p 1301 N95-21205
Hires and beyond p 1592 N95-21750
MEM application to IRAS CPC images
p 1592 N95-21751
An assessment of image reconstruction from balloon-borne and the IRAS data p 1592 N95-21752
In search of random noise p 1592 N95-21753
Beyond maximum entropy: Fractal Pixon-based image reconstruction p 1593 N95-21757
HIRAS: High-resolution IRAS images
p 1593 N95-21758

IMAGE RESOLUTION
A framework for segmentation using physical models of image formation
[AD-A279900] p 1543 N95-20564
Combining image-processing and image compression schemes p 1304 N95-21537
A high resolution atlas of the galactic plane at 12 microns and 25 microns p 1593 N95-21755
Constraints as a destriping tool for Hires images
p 1593 N95-21756
Beyond maximum entropy: Fractal Pixon-based image reconstruction p 1593 N95-21757
HIRAS: High-resolution IRAS images
p 1593 N95-21758
Unique microchannel plate process doubles MCPI resolution
[DE94-017507] p 1337 N95-22427
Spatio-temporal masking in human vision and its application to image coding
[AD-A284949] p 1451 N95-22473

IMAGE VELOCITY SENSORS
The determination of static and time varying dipole source. Sensor geometry during sea trials using differential global positioning system
[MRL-TN-631] p 1205 N95-21642

IMAGERY
A Hyperspectral Image Data Exploration Workbench for environmental science applications
[DE94-016373] p 1412 N95-20171
Airborne Multisensor Pod System (AMPS) data access concept
[DE95-002586] p 1389 N95-20903
Color control in a multichannel simulator display: The display for advanced research and training
[AD-A279717] p 1216 N95-20992
Common mapping system media study
[AD-A279086] p 1390 N95-21912
Design and modelling of a link monitoring mechanism for the Common Data Link (CDL)
[AD-A286167] p 1309 N95-22245

IMAGES
Propulsion research on the variable tandem mirror plasma rocket
[NASA-CR-196310] p 1221 N95-20059
Low electron beam energy CIVA analysis of passivated ICs
[DE94-017421] p 1314 N95-20286
Interpretation of HRTEM images by image simulation: An introduction to theory and practice
[DE95-003422] p 1591 N95-22235
Users guide to NCEMSS, version 2.0
[DE95-003443] p 1548 N95-22238
Image theory for the unidirectionally conducting screen
[PB95-127031] p 1311 N95-22365
Spatio-temporal masking in human vision and its application to image coding
[AD-A284949] p 1451 N95-22473

IMAGING RADAR
Applications of wavelets to radar, imaging and related problems
[AD-A279909] p 1290 N95-20545

IMAGING SPECTROMETERS
Non-destructive inspection by infrared imaging spectroscopy, phase 1
[AD-A286158] p 1383 N95-22037

IMAGING TECHNIQUES
Characterization of an expanded-field Schwarzschild objective for extreme ultraviolet lithography
[DE94-016780] p 1541 N95-20239
Physics Division research and development
[DE94-017685] p 1501 N95-20246
Corrosion of aircraft materials: Correlation between nanometer scale and macroscopic structural damage parameters
[AD-A285930] p 1252 N95-20299
New high temperature plasmas and sample introduction systems for analytical atomic emission and mass spectrometry
[DE94-018580] p 1552 N95-20345
Molecular snapshots: Product imaging of dynamics important to fundamental combustion processes
[DE94-018595] p 1510 N95-20346
White-light spectral analysis of lithium niobate waveguides
[DE94-016692] p 1542 N95-20489
Atomic-resolution characterization of interface structure and chemistry in the STEM
[DE94-017753] p 1567 N95-20492
An atomically-resolved STM study of the thermal decomposition of disilane on Si(001)
[AD-A279818] p 1567 N95-20544
Applications of wavelets to radar, imaging and related problems
[AD-A279909] p 1290 N95-20545
A framework for segmentation using physical models of image formation
[AD-A279900] p 1543 N95-20564
Nonlinear spectroscopy of multicomponent droplets and two- and three-dimensional measurements in flames
[AD-A279945] p 1238 N95-20581
X-ray microscope for solidification studies
[NASA-CR-197375] p 1543 N95-20798
In vivo distribution of liposome encapsulated hemoglobin studied with imaging radiotracers
[AD-A279774] p 1438 N95-20806
Geometric moire method of strain analysis with displacement discontinuities
[DE95-001114] p 1386 N95-20833
Seminar on Biomedical Engineering 1993
[PB95-104402] p 1443 N95-20971
Integration of segmentation and stereo matching
[PB95-107819] p 1444 N95-21028
The sharper image: Implementing a Fast Fourier Transform (FFT) to enhance a video-captured image
[AD-A279790] p 1445 N95-21180
Three-dimensional ground penetrating radar imaging using multi-frequency diffraction tomography
[DE94-016687] p 1301 N95-21205
Characterization of poly(tetrafluoroethylene) surfaces by atomic force microscopy: Results and artifacts
[DE95-000742] p 1242 N95-21309
Two-dimensional imaging of OH in a lean burning high pressure combustor
[NASA-TM-106854] p 1214 N95-21383
An image cancellation approach to depth-from-focus
[DE94-019312] p 1544 N95-21392
Passive millimetre wave imaging: A review
[AD-A279275] p 1303 N95-21491
MEM application to IRAS CPC images
p 1592 N95-21751
Thermal imaging systems
[AD-A279146] p 1307 N95-21970
Remote-sensing based technique to account for sub-grid scale variability of land surface properties
[NASA-TM-110501] p 1390 N95-22110
Distribution of light element isotopes in Bencubbin and Weatherford meteorites: An indicator of heterogeneity in the primitive solar nebula
[DE94-019167] p 1600 N95-22128
Evaluation of scanners for C-scan imaging for nondestructive inspection of aircraft
[AD-A286398] p 1383 N95-22202
Application of IRIS to semiconductor plasma processing
[DE95-003591] p 1562 N95-22225
Image solution for poisson's equation in wedge geometry
[PB95-127171] p 1310 N95-22311
Imaging design of the wide field x-ray monitor onboard the HETE satellite
[DE95-002750] p 1221 N95-22436
Magnetic source imaging of visually evoked and oscillatory electrical activity of the human brain
[PB95-127205] p 1448 N95-22476

IMINES
Conducting thermoset polymers
[AD-A286541] p 1273 N95-21014

IMMUNITY
Enhancement of cell mediated immunity through non-specific immunostimulation with liposome encapsulated gamma-interferon
[AD-A279667] p 1442 N95-20602

IMMUNOASSAY
Enhancement of cell mediated immunity through non-specific immunostimulation with liposome encapsulated gamma-interferon
[AD-A279667] p 1442 N95-20602

IMMUNOLOGY
Effect of increased venous backflow on the release of cardiac hormone. Fine structural, immunohistochemical, and biochemical study
[PB95-130399] p 1445 N95-21424

IMPACT
Analysis of experimentally shocked minerals by NMR spectroscopy
[DE95-002955] p 1573 N95-21449
Aluminium oxide targets after ballistic impact; fragmentation of the ceramic and the projectile
[PB95-133625] p 1388 N95-22097

IMPACT DAMAGE
Experimental investigation of wave and fracture phenomena in impacted ceramics
[AD-A286589] p 1272 N95-20856
A Hypervelocity Experimental Research Database (HERD): Support for the Wright Laboratory Armament Directorate Code Validation Program (COVAL)
[DE95-001628] p 1387 N95-21396

Significance of impact velocity for the extent of damage in carbon/epoxy laminates
[PB95-133484] p 1230 N95-21417
Safety issues in high speed machining
[PB95-127411] p 1287 N95-21422
Damage tolerance of carbon fibre polyetheretherketone laminates
[PB95-131611] p 1230 N95-21432

IMPACT LOADS
Super-heavy aircraft study
[AD-A279602] p 1215 N95-19955
Experimental hypervelocity impact effects on simulated planetesimal materials
[DE94-017290] p 1599 N95-20144

IMPACT MELTS
A computational study of projectile melt in impact with typical Whipple shields
[DE94-016454] p 1385 N95-20237

IMPACT PREDICTION
Erice International Seminars on Planetary Emergencies. 17th Workshop: The Collision of an Asteroid or Comet with the Earth
[AD-A280122] p 1600 N95-21577

IMPACT STRENGTH
Computational design of Hypervelocity Launchers
[DE95-000744] p 1218 N95-20785
Experimental investigation of wave and fracture phenomena in impacted ceramics
[AD-A286589] p 1272 N95-20856
Effect of neutron irradiation on the impact properties of A533B steel
[DE95-001834] p 1256 N95-21286
Fracture behavior of the Fe-8Al alloy FAP-Y
[DE95-000956] p 1258 N95-21676
Tensile and impact properties of iron-aluminum alloys
[DE94-017750] p 1263 N95-22346

IMPACT TESTING MACHINES
The production of calibration specimens for impact testing of subsize Charpy specimens
[DE94-018125] p 1386 N95-20703

IMPACT TESTS
A computational study of projectile shape dependence on phase change phenomena with comparisons to experimental data
[DE95-000740] p 1384 N95-20077
Experimental hypervelocity impact effects on simulated planetesimal materials
[DE94-017290] p 1599 N95-20144
A computational study of projectile melt in impact with typical Whipple shields
[DE94-016454] p 1385 N95-20237
Dynamic measurement of the hoop modulus of a composite cylinder
[DE94-018958] p 1385 N95-20416
The production of calibration specimens for impact testing of subsize Charpy specimens
[DE94-018125] p 1386 N95-20703
Impact behavior of FeAl alloy FA-350
[DE94-018128] p 1254 N95-20705
Experimental investigation of wave and fracture phenomena in impacted ceramics
[AD-A286589] p 1272 N95-20856
Significance of impact velocity for the extent of damage in carbon/epoxy laminates
[PB95-133484] p 1230 N95-21417

IMPACT TOLERANCES
Damage tolerance of carbon fibre polyetheretherketone laminates
[PB95-131611] p 1230 N95-21432

IMPEDANCE
Evaluating impedances in a Sacherer integral equation
[DE94-016823] p 1489 N95-20266
Effect of space charge tune shift on transverse instabilities
[DE94-016790] p 1531 N95-20282
Impedance characteristics of multistage ion diodes
[DE94-018887] p 1565 N95-20340
An impedance model of the Relativistic Heavy Ion Collider (RHIC)
[DE94-016784] p 1532 N95-20406
Electrochemical impedance pattern recognition for detection of hidden chemical corrosion on aircraft components
[AD-A284998] p 1253 N95-20481
Electrochemical impedance spectroscopy of trivalent chromium pre-treated aluminum alloy
[AD-A280093] p 1240 N95-20970
Equivalent source current formulation in impedance tomography
[PB95-127627] p 1329 N95-21326

IMPEDANCE MEASUREMENT
Enhanced ionic conduction at the film/substrate interface in LiI thin films grown on sapphire(0001)
[DE94-017884] p 1565 N95-20371
Fault detection techniques for complex cable shield topologies
[AD-A286632] p 1291 N95-20771
TIM-SCT cable testing protocol
[AD-A286633] p 1207 N95-20772
Electrical impedance studies of acid-form NAFION membranes
[AD-A279271] p 1330 N95-21490

IMPINGEMENT
Shock wave interactions in hypervelocity flow
[AD-A286507] p 1357 N95-22212

IMPLANTATION
Amorphization of sapphire during ion beam mixing
[DE94-018713] p 1510 N95-20337
Positron implantation profiles in elemental and multilayer systems
[DE94-014876] p 1566 N95-20382

IMPLOSIONS
Soft X-Ray Innovative Source Development Program
[AD-A286380] p 1551 N95-20232
Ion temperature measurement of indirectly-driven implosions using a geometry-compensated neutron time-of-flight detector
[DE94-016967] p 1552 N95-20362
Hydrodynamic instabilities in inertial fusion
[DE94-018079] p 1554 N95-20675
Effects of plasma physics on capsule implosions in gas-filled hohlraums
[DE95-000923] p 1371 N95-20786

IMPULSES
Development of a fast sampling system for estimation of impulse responses of mobile radio channels
p 1296 N95-20943
NEO-LISP: Deflecting near-Earth objects using high average power, repetitively pulsed lasers
[DE95-000863] p 1599 N95-21367
Temporary threshold shifts produced by high intensity freefield impulse noise in humans wearing hearing protection
[AD-A286289] p 1454 N95-22045

IMPURITIES
Analysis methods for fast impurity ion dynamics data
[DE95-000589] p 1549 N95-20112
Experimental measurements and modeling of impurity transport in the divertor and boundary plasma of D3-D
[DE94-016519] p 1556 N95-21159
Properties of aged metal tritides
[DE95-001787] p 1243 N95-21440
Effect of the electron-SO-phonon on the impurity state energies in a semiconductor quantum well
[DE94-628993] p 1581 N95-21887
The role of point defects and defect complexes in silicon device processing
[DE94-011876] p 1279 N95-22091
The influence of chemistry and microstructure on the fracture toughness of V-V3Si in-situ composites
[DE94-018997] p 1232 N95-22126
Electric-field effects on shallow donor impurity in a harmonic quantum dot
[DE94-629034] p 1577 N95-22176
The doping effect on spin-Peierls instability
[DE94-629046] p 1577 N95-22178

IN SITU MEASUREMENT
Resonance Raman spectroscopy of volatile organics: Carbon tetrachloride
[DE95-000627] p 1233 N95-19980
In situ viscometer instrument acceptance test report
[DE94-018507] p 1364 N95-20224
Boundary layer cloud studies in support of ASTEX
[AD-A285947] p 1429 N95-20395
The in situ observation of epitaxial diamond thin film nucleation and growth using emission electron microscopy
[AD-A279811] p 1569 N95-20807
Bridging the pressure gap: In situ atomic-level investigations of model platinum catalyst surfaces under reaction conditions by scanning tunneling microscopy
[DE95-002346] p 1246 N95-21990

INCINERATORS
Ceramem filters for removal of particles from hot gas streams
[DE95-001976] p 1275 N95-21354
Removal of CO2 in closed loop off-gas treatment systems
[DE94-019259] p 1407 N95-21617

INCLUSIONS
The origin of acicular ferrite in gas metal arc and submerged arc welds
[AD-A286129] p 1377 N95-19984
The effect of oxide inclusions on the kinetics of the austenite to ferrite transformation in low alloy steel weld metal
[DE94-018131] p 1253 N95-20676
Solar helium and neon in the Earth
p 1419 N95-21793
Dielectric mixtures with arbitrarily anisotropic components: Focus on special gyrotropic effects
[PB95-127015] p 1311 N95-22363

INCOMPRESSIBLE BOUNDARY LAYER
On subcritical instability of the attachment line boundary layer p 1351 N95-21092

INCOMPRESSIBLE FLOW
Free shear layers, base pressure and bluff-body drag
[AD-A286316] p 1200 N95-20175
Hydrodynamic instabilities in inertial fusion
[DE94-018079] p 1554 N95-20675
Mixed hp finite element methods for problems in elasticity and stokes flow
[PB95-104444] p 1341 N95-20981
Modeling the two-point correlation of the vector stream function p 1345 N95-21055
On the asymptotic similarity of rotating homogeneous turbulence p 1345 N95-21058
Large-eddy simulation of rotating channel flows using a localized dynamic model p 1346 N95-21064
The asymptotic state of rotating homogeneous turbulence at high Reynolds numbers
p 1347 N95-21065
Simulation of separated flows p 1347 N95-21068
Simulation of pipe flow p 1349 N95-21078
Spatial direct numerical simulation of boundary layer transition under strong adverse pressure gradient
p 1351 N95-21093
Accurate solution algorithms for incompressible multiphase flows
[DE95-002727] p 1353 N95-21317
Stability of pressure and velocity computations for heterogeneous reservoirs
[PB95-110284] p 1354 N95-21656
Fast parallel tree codes for gravitational and fluid dynamical N-body problems
[AD-A286480] p 1358 N95-22290
Turbulence modeling for separated flow
p 1359 N95-22443
Direct numerical simulations of on-demand vortex generators: Mathematical formulation
p 1361 N95-22452
Direct numerical simulation of incompressible axisymmetric flows p 1363 N95-22464

INCOMPRESSIBLE FLUIDS
Nonlinear dynamic fluid-structure interaction calculations with coupled finite element and finite volume programs
[DE94-016204] p 1339 N95-20166
Subgrid scale models in finite difference simulations of complex wall bounded flows p 1346 N95-21063
The asymptotic state of rotating homogeneous turbulence at high Reynolds numbers
p 1347 N95-21065
1/f noise in two-dimensional fluids
[DE95-002617] p 1358 N95-22307

INCONEL (TRADEMARK)
Experience at the Los Alamos Meson Physics Facility with the use of alloy Inconel 718 as an enclosure for a beam degrader and as a proton beam entry window
[DE94-018289] p 1538 N95-22050

INDEPENDENT VARIABLES
Graded dual of the non-commutative universal Leibniz Hopf algebra zeta
[PB95-134532] p 1494 N95-21955

INDEXES
NASA Langley scientific and technical information output: 1994, volume 1
[NASA-TM-109170-VOL-1] p 1589 N95-21189

INDEXES (DOCUMENTATION)
Bibliography of Lewis Research Center technical publications announced in 1993
[NASA-TM-106666] p 1589 N95-21187
Aeronautical engineering: A continuing bibliography with indexes (supplement 315)
[NASA-SP-7037(315)] p 1199 N95-21640

INDIUM ALUMINUM ARSENIDES
P/N In(Al) GaAs multijunction laser power converters
p 1323 N95-20539

INDIUM ANTIMONIDES
Optimization of InAsSb/InGaAs strained-layer superlattice growth by metal-organic chemical vapor deposition for use in infrared emitters
[DE94-016557] p 1563 N95-19954
InTlSb for long-wavelength infrared photodetectors and arrays
[AD-A280108] p 1332 N95-21774

INDIUM ARSENIDES
Optimization of InAsSb/InGaAs strained-layer superlattice growth by metal-organic chemical vapor deposition for use in infrared emitters
[DE94-016557] p 1563 N95-19954
Nucleation, growth, and strain relaxation of lattice-mismatched 3-5 semiconductor epitaxial layers
p 1324 N95-20543

An Echelle Grating Spectrometer (EGS) for mid-IR remote chemical detection
[DE94-019310] p 1367 N95-21478
InTlSb for long-wavelength infrared photodetectors and arrays
[AD-A280108] p 1332 N95-21774
Performance of Ga(0.47)In(0.53)As cells over a range of proton energies
[NASA-TM-106819] p 1334 N95-22112

INDIUM COMPOUNDS
Polycrystalline CuInSe2 and CdTe solar cells
[DE94-011875] p 1392 N95-20333
Novel thin-film CuInSe2 fabrication
[DE94-011874] p 1268 N95-20472
Processing and modeling issues for thin-film solar cell devices
[DE94-011895] p 1394 N95-21294
InTlSb for long-wavelength infrared photodetectors and arrays
[AD-A280109] p 1331 N95-21660
Non-H2Se, ultra-thin CuInSe2 devices
[DE94-011894] p 1395 N95-21844
Heterostructure quantum confined Stark effect electrooptic modulators operating at 938 nm
[AD-A279342] p 1581 N95-21928

INDIUM GALLIUM ARSENIDES
Optimization of InAsSb/InGaAs strained-layer superlattice growth by metal-organic chemical vapor deposition for use in infrared emitters
[DE94-016557] p 1563 N95-19954
InGaAs PV device development for TPV power systems p 1322 N95-20537
Optical, electronic and optoelectronic material and device research
[AD-A280111] p 1374 N95-21630
Carrier dynamics in InGaAs: Quantum wells versus bulk
[DE94-018205] p 1577 N95-22168

INDIUM ISOTOPES
In vivo distribution of liposome encapsulated hemoglobin studied with imaging radiotracers
[AD-A279774] p 1438 N95-20806

INDIUM PHOSPHATES
Lead-indium phosphate glasses for optical applications
[DE94-019333] p 1275 N95-21482

INDIUM PHOSPHIDES
Observation of excitonic and band-to-band behavior in ordered InGaP2 alloys
[DE94-018891] p 1314 N95-20341
High-efficiency, deep-junction, epitaxial InP solar cells on (100) and (111)B InP substrates
p 1316 N95-20507
High quality InP-on-Si for solar cell applications
p 1317 N95-20510
P/N InP solar cells on Ge wafers
p 1317 N95-20511
Radiation effects on p+n InP junctions grown by MOCVD p 1319 N95-20520
Design of high-efficiency, radiation-hard, GaInP/GaAs solar cells p 1319 N95-20521
Annealing of irradiated n+p InP buried homojunctions
p 1320 N95-20524
Effects of plasma hydrogenation on trapping properties of dislocations in heteroepitaxial InP/GaAs
p 1323 N95-20542
Sub-millimeterwave semiconductor signal sources
[AD-A279375] p 1335 N95-22144
Photoreflectance and x ray diffraction study of semiconductor heterostructures and quantum wells
[PB95-127049] p 1582 N95-22432

INDUCTANCE
Passive surface deployed variable inductance wire antenna statement of government interest
[AD-D016210] p 1307 N95-21910

INDUSTRIAL PLANTS
Summaries of BFRL fire research in-house projects and grants, 1994
[PB95-130845] p 1286 N95-21130
Evaluation of state-of-the-art high speed deluge systems presently in service at various US Army ammunition plants
[AD-A279102] p 1287 N95-21598

INDUSTRIAL SAFETY
Ferrocyanide safety project Dynamic X-Ray Diffraction studies of sodium nickel ferrocyanide reactions with equimolar nitrate/nitrite salts
[DE94-017396] p 1236 N95-20268
Safety issues in high speed machining
[PB95-127411] p 1287 N95-21422

INDUSTRIAL WASTES
Anaerobic Treatment of Municipal Solid Waste and Sludge for Energy Production and Recycling of Nutrients
[DE95-700217] p 1315 N95-20369
Energy and environmental issues and international operation in Asia
[DE94-796596] p 1404 N95-21143
Possible global environmental impacts of solid waste practices
[DE95-000830] p 1406 N95-21487

INDUSTRIES
The Photovolatic Manufacturing Technology project (PVMaT) after three years
[DE94-011877] p 1392 N95-20473
Standard Hardware Acquisition and Reliability Program (SHARP) advanced SEM-E packaging
p 1208 N95-20633
Recent reflux receiver developments under the US DOE program
[DE95-001622] p 1393 N95-20861
Recent National Solar Thermal Test Facility activities, in partnership with industry
[DE95-001828] p 1394 N95-21353
Ceramem filters for removal of particles from hot gas streams
[DE95-001976] p 1275 N95-21354
HPCC technology awareness program: Improved economic competitiveness through technology awareness, transfer and application
[DE95-002134] p 1476 N95-21355
Space systems technology working group: Executive report
[AD-A285778] p 1217 N95-22413

INELASTIC COLLISIONS
Molecular snapshots: Product imaging of dynamics important to fundamental combustion processes
[DE94-018595] p 1510 N95-20346
An analytical electron distribution function for inelastic collisions in a uniform gas with time varying electric field
[DE95-003476] p 1528 N95-22222
An analytical, inelastic, space and time dependent electron distribution for electrically excited gases
[DE95-003478] p 1528 N95-22223

INELASTIC SCATTERING
Magnetic excitations in modulated PrNi2Si2
[DE95-001077] p 1254 N95-20822
Recent results from E665
[DE95-002523] p 1516 N95-20914
PRISMA operating program manual
[PB95-130498] p 1466 N95-21232
Measurements of scattering processes in negative ion: Atom collisions
[DE95-000664] p 1519 N95-21276
Structure functions and structure function ratio F2(n)/F2(p) at low X(Bj) and Q2 in inelastic muon scattering
[DE94-018979] p 1573 N95-21561
Atomic processes in processing plasmas
[DE94-019177] p 1560 N95-21609
Interference of fluorescence x rays and coherent excitation of core levels
[DE94-016809] p 1527 N95-22188
Neutron Compton scattering
[PB95-130290] p 1530 N95-22332

INELASTIC STRESS
Inelastic bending and torsion of steel I-beams
[PB94-208378] p 1384 N95-19975

INEQUALITIES
Discrete algebraic Riccati equation and linear matrix inequality
[PB95-133575] p 1484 N95-22139

INERTIAL CONFINEMENT FUSION
X-ray imaging of uniform large scale-length plasmas created from gas-filled targets on Nova
[DE94-018339] p 1531 N95-20015
Particle beam fusion
[DE95-000711] p 1549 N95-20075
National Ignition Facility: Experimental plan
[DE94-016542] p 1550 N95-20189
Target Area Structural Support systems design to achieve the micron-level stability requirement of the National Ignition Facility (NIF)
[DE94-017696] p 1551 N95-20219
Physics Division research and development
[DE94-017685] p 1501 N95-20246
Studies of longitudinal instability with an electron beam
[DE94-018646] p 1532 N95-20347
Hydrodynamic instabilities in inertial fusion
[DE94-018079] p 1554 N95-20675
Accelerators for energy production
[DE94-770764] p 1392 N95-20685
Performance of the NIF prototype beamlet
[DE94-018500] p 1371 N95-20817
Induction linacs for heavy ion fusion
[DE95-002357] p 1534 N95-20891
Cryogenic targets for inertial confinement fusion
[DE94-016200] p 1555 N95-21115
Use of the National Ignition Facility for the development of inertial fusion energy
[DE94-016696] p 1557 N95-21206
Target Area design basis and system performance for the National Ignition Facility
[DE94-016697] p 1557 N95-21207
Neutronics and shielding analysis of the National Ignition Facility
[DE94-016698] p 1534 N95-21208
Laser design basis for the National Ignition Facility
[DE94-016700] p 1534 N95-21209
Large facilities pilot programme. Access to the VULCAN High Power Laser Facilities at Rutherford Appleton Laboratory
[PB95-130340] p 1373 N95-21226
Nonperturbative aspects of the quark-photon vertex
[DE94-012846] p 1520 N95-21315
Low density gas and foam targets for ICF long scale length plasma experiments: Fabrication and characterization
[DE95-000935] p 1558 N95-21368
Progress in the Light Ion Driven Inertial Confinement Fusion Program
[DE94-019182] p 1537 N95-21603
The ITER in-vessel system
[DE94-018053] p 1560 N95-21665

INERTIAL FUSION (REACTOR)
Radiation-driven targets for heavy-ion fusion
[DE95-002264] p 1533 N95-20784

INERTIAL NAVIGATION
Assessment of a non-dedicated GPS receiver system for precise airborne attitude determination
[DE94-019309] p 1205 N95-21520
A real-time algorithm for integrating differential satellite and inertial navigation information during helicopter approach
[NASA-CR-197409] p 1205 N95-21891

INFECTIOUS DISEASES
Enhancement of cell mediated immunity through non-specific immunostimulation with liposome encapsulated gamma-interferon
[AD-A279667] p 1442 N95-20602

INFERENCE
Connectionist models for intelligent computation
[AD-A286436] p 1484 N95-22210

INFILTRATION
Absorption of water and lubricating oils into porous nylon
[NASA-CR-197344] p 1280 N95-22383

INFINITY
Asymptotic analysis of Nash equilibria in nonzero-sum linear-quadratic differential games. The two-player case
[PB95-111027] p 1499 N95-19941

INFORMATION DISSEMINATION
Migrating the Facility Profile Information Management System into the World Wide Web
[DE94-018367] p 1586 N95-20016
Mariners Weather Log, volume 38, number 3, summer 1994
[PB94-209541] p 1428 N95-20099
NASA/DOD Aerospace Knowledge Diffusion Research Project. Report 28: The technical communication practices of aerospace engineering and science students: Results of the phase 4 cross-national surveys
[NASA-TM-109123] p 1587 N95-20162
NASA/DOD Aerospace Knowledge Diffusion Research Project. Report 31: The technical communications practices of US aerospace engineers and scientists: Results of the phase 1 SME mail survey
[NASA-TM-109169] p 1587 N95-20163
The 37th Military Librarians Workshop on Global Information: The Sun Never Sets
[AD-A286636] p 1588 N95-20774
Solar Radiation Resource Assessment Project
[DE94-000286] p 1392 N95-20778
NASA/DOD Aerospace Knowledge Diffusion Research Project. Report 27: The technical communication practices of engineering and science students: Results of the phase 3 academic surveys
[NASA-TM-109122] p 1589 N95-21015
Materials compatibility and lubricants research on CFC-refrigerant substitutes
[DE94-018414] p 1287 N95-21631
NASA/DOD Aerospace Knowledge Diffusion Research Project. Paper 48: Valuing information in an interactive environment
[NASA-TM-110448] p 1590 N95-21977
University library document circulation system specified in LCM
[PB95-127957] p 1592 N95-22331

INFORMATION FLOW
Translation of the data flow query language for the multimodel, multibackend database system
[AD-A285978] p 1588 N95-20617
The IEEE scalable coherent interface: An approach for a unified avionics network p 1212 N95-20650

TDX: A high-bandwidth crossbar-switched communication paradigm
[DE94-017187] p 1311 N95-22407

INFORMATION MANAGEMENT

Migrating the Facility Profile Information Management System into the World Wide Web
[DE94-018367] p 1586 N95-20016

Collected papers of the Soar/IFOR project, Spring 1994
[AD-A280063] p 1216 N95-20624

The 37th Military Librarians Workshop on Global Information: The Sun Never Sets
[AD-A286636] p 1588 N95-20774

Determining information management needs for enhanced international safeguards
[DE94-015787] p 1588 N95-20789

Environmental Compliance Assessment System (ECAS): Oregon supplement
[AD-A279565] p 1408 N95-21696

Information Management Architecture for an Integrated Computing Environment for the Environmental Restoration Program. Volume 1: Introduction
[DE95-001384] p 1590 N95-21862

Information Management Architecture for an Integrated Computing Environment for the Environmental Restoration Program. Volume 2: Interim business systems guidance
[DE95-001385] p 1591 N95-22061

Conference proceedings. Defense Modeling and Simulation Office Information/Data Base (I/DB) Task Group Meetings, and notes from the previous two I/DB meetings
[AD-A279097] p 1591 N95-22069

Taking AIM: The management of scientific and technical information at Argonne National Laboratory
[DE94-019279] p 1591 N95-22092

Abbreviations, acronyms, and initialisms frequently used by Martin Marietta Energy Systems, Inc.
[DE95-001069] p 1591 N95-22107

A conceptual approach to object-oriented data modeling
[AD-A286048] p 1592 N95-22416

Experimental evaluation of dynamic data allocation strategies in a distributed database with changing workloads
[NASA-CR-195024] p 1456 N95-22431

INFORMATION PROCESSING (BIOLOGY)

Intermediate levels of visual processing
[AD-A284922] p 1448 N95-19998

Signal- and listener- based factors in complex auditory pattern perception
[AD-A285636] p 1450 N95-21101

MAC/FAC: A model of similarity-based retrieval
[AD-A286291] p 1450 N95-22052

Magnetic source imaging of visually evoked and oscillatory electrical activity of the human brain
[PB95-127205] p 1448 N95-22476

INFORMATION RETRIEVAL

Efficient caption-based retrieval of multimedia information
[AD-A279604] p 1586 N95-19956

Role of working memory limitations of retrieval
[AD-A280032] p 1448 N95-20007

Migrating the Facility Profile Information Management System into the World Wide Web
[DE94-018367] p 1586 N95-20016

Using local optimality criteria for efficient information retrieval with redundant information filters
[AD-A279603] p 1587 N95-20302

FEDIX: User's guide, version 5.0/release 3.0
[DE95-002274] p 1588 N95-20762

Airborne Multisensor Pod System (AMPS) data access concept
[DE95-002586] p 1389 N95-20903

FIREDOC users manual, 3rd edition
[PB95-128674] p 1286 N95-21129

MAC/FAC: A model of similarity-based retrieval
[AD-A286291] p 1450 N95-22052

Using geographical data browsers in a networked environment
[DE94-017809] p 1592 N95-22263

Feature extraction without edge detection
[AD-A279842] p 1473 N95-22386

INFORMATION SYSTEMS

Downsizing information systems: Framing the issues for the Office of Naval Intelligence (ONI)
[AD-A279888] p 1588 N95-20589

Model formality in human/computer collaboration
[AD-A286001] p 1462 N95-20718

FEDIX: User's guide, version 5.0/release 3.0
[DE95-002274] p 1588 N95-20762

Shaping the library of the future: Digital library developments at Los Alamos National Laboratory's Research Library
[DE95-001008] p 1588 N95-20777

Determining information management needs for enhanced international safeguards
[DE94-015787] p 1588 N95-20789

Systems Analysis Laboratory. Ten years of progress 1984-1994
[PB95-104451] p 1464 N95-20982

GOLD: A Graph Oriented Language for Databases
[PB95-127544] p 1465 N95-21021

FIREDOC users manual, 3rd edition
[PB95-128674] p 1286 N95-21129

Independent review of Aviation Technology and Research Information Analysis System (ATRIAS) database
[AD-A284049] p 1203 N95-21518

Aeronautical engineering: A continuing bibliography with indexes (supplement 315)
[NASA-SP-7037(315)] p 1199 N95-21640

CAiSE 1994 Doctoral Consortium
[PB95-135182] p 1469 N95-21711

Proceedings of the 5th Workshop on the Next Generation of CASE Tools
[PB95-135208] p 1469 N95-21716

Information Management Architecture for an Integrated Computing Environment for the Environmental Restoration Program. Volume 1: Introduction
[DE95-001384] p 1590 N95-21862

Directives for the participation in MiTS forum. V3.0
[PB95-110342] p 1484 N95-22015

Conference proceedings. Defense Modeling and Simulation Office Information/Data Base (I/DB) Task Group Meetings, and notes from the previous two I/DB meetings
[AD-A279097] p 1591 N95-22069

A graded approach to ISO 9000 implementation for records managers
[DE94-017409] p 1591 N95-22167

Information security for unmanned systems
[AD-A286511] p 1485 N95-22214

Using geographical data browsers in a networked environment
[DE94-017809] p 1592 N95-22263

INFORMATION THEORY

Using local optimality criteria for efficient information retrieval with redundant information filters
[AD-A279603] p 1587 N95-20302

INFORMATION TRANSFER

The 37th Military Librarians Workshop on Global Information: The Sun Never Sets
[AD-A286636] p 1588 N95-20774

NASA/DOD Aerospace Knowledge Diffusion Research Project. Report 27: The technical communication practices of engineering and science students: Results of the phase 3 academic surveys
[NASA-TM-109122] p 1589 N95-21015

NODDS/WOSM interface user's manual
[AD-A279095] p 1471 N95-22068

INFRARED ABSORPTION

Theoretical prediction of vibrational circular dichroism spectra of R-glyceraldehyde, R-erythrose, and R-threose. Part 2: Development of a procedure to scale the force constant matrix expressed in terms of internal coordinates
[AD-A284305] p 1437 N95-20252

INFRARED ASTRONOMY

Hires and beyond p 1592 N95-21750

MEM application to IRAS CPC images
p 1592 N95-21751

An assessment of image reconstruction from balloon-borne and the IRAS data p 1592 N95-21752

In search of random noise p 1592 N95-21753

Pushing the limits of spatial resolution with the Kuiper Airborne observatory p 1593 N95-21754

A high resolution atlas of the galactic plane at 12 microns and 25 microns p 1593 N95-21755

Interacting galaxies resolved by IRAS
p 1593 N95-21759

Far-Infrared sources and diffuse emission in M31
p 1593 N95-21761

Correlation of far-infrared emission and radio continuum emission along the major axis of edge-on spiral galaxies
p 1593 N95-21762

Wavelet analysis applied to the IRAS cirrus
p 1593 N95-21769

A HIRES analysis of the FIR emission of supernova remnants p 1594 N95-21770

Arcmimute scale HI and IRAS observations toward high latitude cloud G86.5+59.6 p 1594 N95-21771

Application of MCM image construction to IRAS comet observations p 1594 N95-21772

INFRARED ASTRONOMY SATELLITE

Science with High Spatial Resolution Far-Infrared Data
[NASA-CR-197353] p 1595 N95-21749

MEM application to IRAS CPC images
p 1592 N95-21751

In search of random noise p 1592 N95-21753

A high resolution atlas of the galactic plane at 12 microns and 25 microns p 1593 N95-21755

Beyond maximum entropy: Fractal Pixon-based image reconstruction p 1593 N95-21757

HIRAS: High-resolution IRAS images
p 1593 N95-21758

Interacting galaxies resolved by IRAS
p 1593 N95-21759

Far-Infrared sources and diffuse emission in M31
p 1593 N95-21761

Extended far-infrared emission and star formation in Seyfert galaxies p 1593 N95-21764

Two-dimensional maps of the infrared-to-radio ratio in spiral galaxies p 1593 N95-21765

An IRAS Hires study of low mass star formation in the Taurus molecular ring p 1593 N95-21767

Wavelet analysis applied to the IRAS cirrus
p 1593 N95-21769

Arcmimute scale HI and IRAS observations toward high latitude cloud G86.5+59.6 p 1594 N95-21771

Application of MCM image construction to IRAS comet observations p 1594 N95-21772

High resolution descriptions of IRAS 12 and 25 microns confused regions
[AD-A285847] p 1545 N95-21832

INFRARED CIRRUS (ASTRONOMY)

Wavelet analysis applied to the IRAS cirrus
p 1593 N95-21769

INFRARED DETECTORS

Enhanced vehicle and event typing software, phase 1
[AD-A284862] p 1458 N95-20070

State-to-state collisional dynamics of atmospheric species
[AD-A285053] p 1370 N95-20484

Fracture analysis of an all-ceramic bearing system
[AD-A285056] p 1269 N95-20486

InTlSb for long-wavelength infrared photodetectors and arrays
[AD-A280108] p 1332 N95-21774

Electromagnetic radiation detector utilizing an electromagnetic radiation absorbing element in a mach-zehnder interferometer arrangement
[AD-D016507] p 1306 N95-21835

INFRARED IMAGERY

Correlation of far-infrared emission and radio continuum emission along the major axis of edge-on spiral galaxies
p 1593 N95-21762

Two-dimensional maps of the infrared-to-radio ratio in spiral galaxies p 1593 N95-21765

Non-destructive inspection by infrared imaging spectroscopy, phase 1
[AD-A286158] p 1383 N95-22037

INFRARED INSTRUMENTS

An at-sea evaluation of an infrared/resistance temperature device for air/sea-surface temperature measurements
[AD-A279672] p 1365 N95-20604

InTlSb for long-wavelength infrared photodetectors and arrays
[AD-A280109] p 1331 N95-21660

INFRARED INTERFEROMETERS

Noise model of the MSX SPIRIT 3 interferometer
[AD-A285837] p 1364 N95-20036

INFRARED LASERS

Fiber laser amplifiers and oscillators
[AD-A285835] p 1368 N95-20035

The effect of reusing laser gas on the fission-fragment pumped 1.73 micron atomic xenon laser output
[DE94-018512] p 1369 N95-20225

Semiconductor laser joint study program with Rome Laboratory
[AD-A285858] p 1369 N95-20379

State-to-state collisional dynamics of atmospheric species
[AD-A285053] p 1370 N95-20484

INFRARED RADIATION

Free electron laser program
[AD-A285906] p 1368 N95-19987

Radiative forcing calculations for CH3Cl
[DE94-019018] p 1402 N95-20355

Liquid xenon as a potential laser host medium
[AD-A285365] p 1370 N95-20550

Chemical lasers emitting in the visible spectrum: Metastable oxygen reactions and YOSHIDA laser
[PB95-104485] p 1372 N95-20983

Constraints on SUSy-GUT unification from b yields s-gamma decay
[PB95-130373] p 1580 N95-21229

Effects of RF side-bands on spectral reproducibility for infrared synchrotron radiation
[DE95-002450] p 1536 N95-21418

An Echelle Grating Spectrometer (EGS) for mid-IR remote chemical detection
[DE94-019310] p 1367 N95-21478

Time-resolved study of sideband generation and transition to chaos on an infrared FEL
[DE95-002336] p 1374 N95-21528
Ultraviolet emission from rocket motor plumes
[DSTO-TR-0002] p 1222 N95-21661
Two-dimensional maps of the infrared-to-radio ratio in spiral galaxies p 1593 N95-21765
Technique for intracavity sum frequency generation
[AD-D016478] p 1546 N95-21898
Optical radiation: Health based exposure limits for electromagnetic radiation in the wavelength range from 100 nanometer to 1 millimeter
[PB95-132767] p 1447 N95-22083
Recent progress of the compact AFEL at Los Alamos
[DE95-002728] p 1376 N95-22154

INFRARED RADIOMETERS
Non-destructive inspection by infrared imaging spectroscopy, phase 1
[AD-A286158] p 1383 N95-22037

INFRARED SOURCES (ASTRONOMY)
Pushing the limits of spatial resolution with the Kuiper Airborne observatory p 1593 N95-21754
Far-Infrared sources and diffuse emission in M31
p 1593 N95-21761

INFRARED SPECTRA
Chemical lasers emitting in the visible spectrum: Metastable oxygen reactions and YOSHIDA laser
[PB95-104485] p 1372 N95-20983
Hires and beyond p 1592 N95-21750

INFRARED SPECTROMETERS
Fabrication and testing of a silicon immersion grating for infrared spectroscopy
[DE94-017173] p 1237 N95-20386
An Echelle Grating Spectrometer (EGS) for mid-IR remote chemical detection
[DE94-019310] p 1367 N95-21478

INFRARED SPECTROSCOPY
FTIR spectroscopy for the determination of water in corrosive gases
[DE94-014658] p 1235 N95-20139
Orientation studies of polyolefins by IR-dichroism
[PB95-104386] p 1236 N95-20256
Fabrication and testing of a silicon immersion grating for infrared spectroscopy
[DE94-017173] p 1237 N95-20386
Surface inspection using Fourier Transform Infrared Spectroscopy
[DE95-001699] p 1244 N95-21571
Spectroscopic studies of hazardous fuel interactions with soils
[AD-A279099] p 1407 N95-21596
Non-destructive inspection by infrared imaging spectroscopy, phase 1
[AD-A286158] p 1383 N95-22037
Synthesis and characterization of single-source molecular precursors to binary metal sulphides: Bis(diethyldithiocarbamato) M(2)trialkylphosphine (M = Zn and Cd) adducts
[AD-A279746] p 1248 N95-22385

INFRASONIC FREQUENCIES
Infrasonic observations of the Northridge, California, earthquake
[DE94-018095] p 1413 N95-20289

INHIBITORS
An update of corrosion inhibitors for mild steel exposed to 32-0-0 UAN solution
[DE95-001715] p 1263 N95-22396

INHOMOGENEITY
Nitrogen isotopic components in the early solar system p 1420 N95-21800

INITIATION
Towards tailored interphase formation utilizing surface-bound benzylsulfonium salts as cationic initiators
[AD-A286461] p 1280 N95-22259

INJECTION
Review of recent D-T experiments from TFTR
[DE95-002755] p 1557 N95-21239

INJECTION MOLDING
Simulation of the injection moulding process
[PB94-215555] p 1286 N95-21027

INJURIES
Mechanisms and diagnostics of ultrashort pulse laser ocular effects
[AD-A285610] p 1373 N95-21195

INLET FLOW
Internal aerodynamics of a generic three-dimensional scramjet inlet at Mach 10
[NASA-TP-3476] p 1340 N95-20619

INORGANIC COMPOUNDS
Quantitative and qualitative analysis of some inorganic compounds by Raman spectroscopy
[DE94-009757] p 1237 N95-20470

INORGANIC MATERIALS
Inorganic-organic polymers and their role in materials science
[AD-A279715] p 1270 N95-20671

INPUT/OUTPUT ROUTINES
DONIO: Distributed object network I/O library
[DE94-019163] p 1477 N95-21602

INSERTS
Proposed emittance upgrade for the SLC damping rings
[DE95-002887] p 1538 N95-22155

INSPECTION
Analysis of invalid emission testing in the California smog check program
[PB95-128922] p 1406 N95-21373
Reentry vehicle on-site inspection technology study
[AD-A285960] p 1220 N95-21634
Evaluation of scanners for C-scan imaging for nondestructive inspection of aircraft
[AD-A286398] p 1383 N95-22202

INSTALLING
Proceedings of the International Wire and Cable Symposium
[AD-A279242] p 1403 N95-20465

INSTRUCTORS
Rate monotonic analysis for real-time systems: Instructors guide
[AD-A286083] p 1463 N95-20810

INSULATION
MHD pressure drop in ducts with imperfectly insulating coatings
[DE95-002852] p 1558 N95-21244

INSULATORS
Kondo insulators
[DE95-001156] p 1237 N95-20368
Effect of a solid insulator on the spark yield of S2F10 in SF6(*)
[DE95-001422] p 1326 N95-20791

INTEGERS
Data analysis and visualization in MCNP (trademark)
[DE94-016164] p 1508 N95-20159
N=1 Superconformal minimal model correlation functions on the torus
[PB95-134615] p 1500 N95-21964
Singular symmetric matrices
[PB95-109088] p 1496 N95-22354
Elliptic genera for Z/K-manifolds I
[PB95-109096] p 1496 N95-22355

INTEGRAL EQUATIONS
Evaluating impedances in a Sacherer integral equation
[DE94-016823] p 1489 N95-20266
On FEL integral equation and electron energy loss in intermediate gain regime
[DE94-770631] p 1371 N95-20757
Molecular-based study of solutions in supercritical solvents
[DE94-019326] p 1580 N95-21420
A new FHNC scheme for Gutzwiller correlated wave functions
[DE94-629037] p 1581 N95-21993

INTEGRAL ROCKET RAMJETS
Integral rocket ramjets
[AD-A285135] p 1222 N95-20906

INTEGRALS
Quadratic forms in design theory
[PB95-111019] p 1487 N95-19940

INTEGRATED CIRCUITS
Processing, fabrication, and demonstration of HTS integrated microwave circuits
[AD-A285611] p 1312 N95-19894
Design and packaging aspects of microwave bandwidth lithium niobate modulators
[DE94-016602] p 1313 N95-20119
Low electron beam energy CIVA analysis of passivated ICs
[DE94-017421] p 1314 N95-20286
Proton irradiation effects on advanced digital and microwave III-V components
[DE94-018742] p 1314 N95-20338
Ultra-Reliable Digital Avionics (URDA) processor
p 1209 N95-20638
Assuring Known Good Die (KGD) for reliable, cost effective MCMs p 1210 N95-20644
Liquid flow-through cooling of electronic modules
p 1211 N95-20647
Method of fabricating a microelectronic photomultiplier device with integrated circuitry
[AD-D016530] p 1325 N95-20726
Microdynamic devices fabricated on silicon-on-sapphire substrates
[AD-D016531] p 1325 N95-20727
High isolation electronic switch
[AD-D016533] p 1326 N95-20729
Complementary GaAs junction-gated heterostructure field effect transistor fabrication for integrated circuits
[DE95-001522] p 1327 N95-20882
Technologies for highly parallel optoelectronic integrated circuits
[DE95-001607] p 1327 N95-20883
Prototype rule-based reliability analysis for VLSI circuit design
[AD-A280065] p 1327 N95-20967
Unlimited-bandwidth distributed optical phase modulators and detectors: Design and fabrication issues
[DE94-017418] p 1545 N95-21509
Monolithic circuits for lead-glass calorimetry
[DE94-019112] p 1330 N95-21554
Non-linear A/D converters for integrated silicon smart sensors
[PB94-208402] p 1330 N95-21590
Monolithic low noise preamplifier for piezoelectric sensors
[AD-D016524] p 1333 N95-21865
Integration of thin film decoupling capacitors
[DE95-001609] p 1333 N95-21881
Thermal fixture for testing an integrated circuit
[AD-D016483] p 1333 N95-21900
Defect classes: An overdue paradigm for CMOS IC testing
[DE94-018905] p 1334 N95-22118
Sub-millimeterwave semiconductor signal sources
[AD-A279375] p 1335 N95-22144
Plasma processing for integrated circuits
[DE95-001419] p 1335 N95-22149
Radiation tests on service electronics for future multi TeV detectors
[DE94-632822] p 1335 N95-22184
Design of the readout IC for the CDF SVX-2 silicon strip detector
[DE95-000562] p 1539 N95-22193

INTEGRATED LIBRARY SYSTEMS
Introduction to the FIRE engine: A C++ toolkit for Finite automata and Regular Expressions
[PB95-110599] p 1456 N95-19891
Towards better quality and reliability in the software reuse library environment
[AD-A280013] p 1460 N95-20313

INTEGRATED OPTICS
Design and packaging aspects of microwave bandwidth lithium niobate modulators
[DE94-016602] p 1313 N95-20119
GaAs optical circuits
[AD-A285859] p 1369 N95-20389
Analog processing of optical wavefront using integrated guided-wave optics
[AD-A279596] p 1543 N95-20601
Broadband thermal optical limiter for the protection of eyes and sensors
[AD-D016493] p 1377 N95-22304

INTELLIGENCE
Information security for unmanned systems
[AD-A286511] p 1485 N95-22214
Design and modelling of a link monitoring mechanism for the Common Data Link (CDL)
[AD-A286167] p 1309 N95-22245

INTELSAT SATELLITES
UV testing of INTELSAT-7, 7A, and 8 solar cells
p 1320 N95-20526

INTERACTING GALAXIES
Interacting galaxies resolved by IRAS
p 1593 N95-21759

INTERACTIONAL AERODYNAMICS
Nonlinear interaction between a pair of oblique modes in a supersonic mixing layer: Long-wave limit
[NASA-CR-197380] p 1357 N95-22173

INTERACTIVE CONTROL
Intelligent interactive project management system
[PB95-132684] p 1586 N95-21982

INTERCEPTION
Enhanced vehicle and event typing software, phase 1
[AD-A284862] p 1458 N95-20070

INTERFACES
Simulations of the dislocation array at Ge/Si interfaces
[DE94-017680] p 1565 N95-20244
Advanced Command and Control (C2) applications interfaces to the Advanced Communications Technology Satellite (ACTS)
[AD-A279676] p 1291 N95-20605
Time code interface
[AD-D016535] p 1501 N95-20731
Circuit means for providing compatibility between two separate digital data interfaces
[AD-D016225] p 1455 N95-21116
Ultrafast optical studies of surface reaction processes at semiconductor interfaces
[DE95-001548] p 1574 N95-21839
Magnetic properties of the three-dimensional Ising model with an interface amorphization
[DE94-628992] p 1278 N95-21885
NODDS/WOSM interface user's manual
[AD-A279095] p 1471 N95-22068
Application of optical second harmonic generation to surface analysis
[AD-A279445] p 1547 N95-22074

Theory of the excitonic lineshape in low-dimensional structures with rough interfaces
[DE95-003434] p 1582 N95-22237

INTERFACIAL ENERGY

Scanning tunneling microscopy of semiconductor surfaces
[AD-A279982] p 1571 N95-20964

The Modified Embedded Atom Method
[DE94-017958] p 1248 N95-22273

INTERFERENCE IMMUNITY

Cochannel and adjacent-channel interference in nonlinear minimum-shift-keyed satellite system
[NASA-TM-106834] p 1307 N95-21890

INTERFEROMETERS

An intensity interferometer for soft x-rays
[DE94-016370] p 1541 N95-20103

Monitoring the response of the upper troposphere/lower stratosphere to a greenhouse gas scenario
[DE95-000982] p 1406 N95-21410

Effects of RF side-bands on spectral reproducibility for infrared synchrotron radiation
[DE95-002450] p 1536 N95-21418

Atom wave interferometer
[AD-A279532] p 1524 N95-21688

INTERFEROMETRY

Elastic anisotropy in hot-pressed Si3N4 composites: Role of in situ (beta)-Si3N4 grains and added (beta)-Si3N4 whiskers
[DE94-018387] p 1226 N95-20027

Mandrel based embedded planar fiber-optic interferometric acoustic sensor
[AD-D016229] p 1504 N95-21119

Effects of RF side-bands on spectral reproducibility for infrared synchrotron radiation
[DE95-002450] p 1536 N95-21418

On the Aharonov-Bohm effect with neutrons
[DE95-002985] p 1521 N95-21454

Method for characterization of optical waveguide devices using partial coherence interferometry
[AD-D016525] p 1544 N95-21466

Single particle measurements and two particle interferometry results from CERN experiment NA44
[DE95-003041] p 1527 N95-22078

INTERFERON

Enhancement of cell mediated immunity through non-specific immunostimulation with liposome encapsulated gamma-interferon
[AD-A279667] p 1442 N95-20602

INTERIOR BALLISTICS

Chunk projectile launch using the Sandia Hypervelocity Launcher Facility
[DE94-018494] p 1215 N95-20223

Computational design of Hypervelocity Launchers
[DE95-000744] p 1218 N95-20785

INTERLAMINAR STRESS

The influence of ply waviness with nonlinear shear on the stiffness and strength reduction of composite laminates
[AD-A285736] p 1224 N95-19899

INTERLAYERS

Energy gap structure of layered superconductors
[DE94-017885] p 1566 N95-20372

Growth, characterization and device development in monocrystalline diamond films
[AD-A285991] p 1568 N95-20614

Interlayer magnetic coupling in epitaxial Fe/Cr(211) and (100) superlattices
[DE95-002906] p 1571 N95-21256

INTERMETALLICS

Third Intermetallic Matrix Composites Symposium, volume 350
[NASA-TM-110059] p 1225 N95-20001

Fabrication and properties of alumina matrix composites containing nickel aluminide reinforcements
[DE94-018703] p 1250 N95-20044

Oxide formation on NbAl3 and TiAl due to ion implantation of O-18
[DE94-017874] p 1252 N95-20365

The processing and mechanical properties of high temperature/high performance composites. Fatigue and creep, book 3
[AD-A279738] p 1227 N95-20430

Novel reagents for chemical vapor deposition of intermetallic alloys
[AD-A286562] p 1271 N95-20815

ALCHEMI of Fe-doped B2-ordered NiAl alloys with different doping levels
[DE94-017748] p 1255 N95-20907

Plastic deformation of ordered intermetallic alloys: Fundamental aspects
[DE95-001070] p 1256 N95-21265

Processing and mechanical properties of laminar Al2O3-Ni3Al composites
[DE94-019332] p 1230 N95-21481

Bulk and defect properties of ordered intermetallics
[DE94-017706] p 1262 N95-22344

Processing of intermetallic materials by reaction synthesis
[DE94-017710] p 1263 N95-22345

New thermodynamic description of the Cu-Zr system
[PB95-127189] p 1263 N95-22374

INTERMOLECULAR FORCES

Photochemistry of intermolecular C-H bond activation reactions
[DE94-018417] p 1239 N95-20682

Chemical interactions between protein molecules and polymer membrane materials
[DE95-001808] p 1224 N95-21746

Hydrogen and related materials at high density: Physics, chemistry and planetary implications
p 1418 N95-21791

INTERNAL ENERGY

Electron attachment to excited molecules
[DE94-019124] p 1522 N95-21519

INTERNAL FLOW

Experimental study of vane heat transfer and aerodynamics at elevated levels of turbulence
[NASA-CR-4633] p 1337 N95-19912

Internal aerodynamics of a generic three-dimensional scramjet inlet at Mach 10
[NASA-TP-3476] p 1340 N95-20619

INTERNAL PRESSURE

Residual stress analysis in swage autofrettaged thick-walled cylinders by position-sensitive x-ray diffraction techniques
[AD-A286383] p 1388 N95-22320

INTERNAL WAVES

Fourth International Symposium on Stratified Flows, volume 3
[AD-A286452] p 1354 N95-21584

Seismic anisothropy and large-scale porosity inthe ocean floor
[AD-A286580] p 1436 N95-22187

INTERNATIONAL COOPERATION

Patterns of financial change in the OECD area
[PB95-110979] p 1594 N95-19939

INTERPOLATION

Modeling of beam dynamics and comparison with measurements for the Advanced Light Source (ALS)
[DE94-017970] p 1532 N95-20495

Seminar on Biomedical Engineering 1993
[PB95-104402] p 1443 N95-20971

Subsampling methods for image sequence coding
[PB95-107991] p 1305 N95-21579

INTERPROCESSOR COMMUNICATION

Non interleaving process algebra
[PB95-110607] p 1486 N95-19892

Design of a parallel object oriented programming language
[AD-A284924] p 1457 N95-20000

A group communication approach for mobile computing mobile channel: An ISIS tool for mobile services
[AD-A279785] p 1290 N95-20306

The IEEE scalable coherent interface: An approach for a unified avionics network p 1212 N95-20650

Programmable modular network interface
[AD-D016505] p 1477 N95-21674

Method of sensing target status in a local area network
[AD-D016248] p 1478 N95-22090

A new parallel method for molecular dynamics simulation of macromolecular systems
[DE94-018621] p 1529 N95-22315

INTERSTELLAR GAS

A HIRES analysis of the FIR emission of supernova remnants p 1594 N95-21770

Arcminute scale HI and IRAS observations toward high latitude cloud G86.5+59.6 p 1594 N95-21771

INTERSTELLAR RADIATION

Azimuthally averaged radial S(sub 100 microns)/S(sub 60 microns) dust color temperatures in spiral galaxies
p 1593 N95-21760

INVARIANCE

View-based models of 3D object recognition and class-specific invariance
[AD-A279658] p 1459 N95-20157

Classification of diagonal coset modular invariants
[PB95-111118] p 1489 N95-20259

GAJET experiment at the LHC: The GAJET collaboration
[PB95-129813] p 1512 N95-20454

Computation of invariant manifolds
[PB95-135687] p 1492 N95-21318

Object recognition by alignment using invariant projections of planar surfaces
[AD-A279841] p 1468 N95-21495

Constraints on T-odd and P-even hadronic interactions from nucleon, nuclear, and atomic electric dipole moments
[DE94-012845] p 1526 N95-21920

Linear invariance of Lindeloef numbers
[PB95-134540] p 1494 N95-21956

INVENTIONS

Cascade orificial resistive device
[AD-D016529] p 1504 N95-20724

Hybrid high power amplifier
[AD-D016534] p 1326 N95-20730

INVENTORIES

Calculation methods for criteria air pollutant emission inventories
[AD-A284675] p 1400 N95-19964

Origin and loss of the volatiles of the terrestrial planets p 1417 N95-21785

INVERSE SCATTERING

Deconvolution and singular value decomposition
[AD-A286582] p 1491 N95-20875

Inverse and control problems in electromagnetics
[AD-A286438] p 1310 N95-22250

INVERSIONS

Investigating the resolution of resistivity arrays using inverse theory
[DE94-017760] p 1412 N95-20287

Right inverse for the divergence operator in spaces of continuous piecewise polynomials
[PB95-127080] p 1496 N95-22369

INVERTEBRATES

Long term changes on the continental shelf of the North Sea: Invertebrate trends, 1931-1990
[PB95-135224] p 1435 N95-21717

INVERTERS

Design of power electronics for TVC and EMA systems
[NASA-CR-196540] p 1312 N95-19909

INVISCID FLOW

Front-boundary layer models from STORM-FEST observations
[AD-A279907] p 1428 N95-20186

Application of Roe's flux-difference splitting for kappa-epsilon turbulence model
[PB95-127718] p 1352 N95-21106

Nonlinear acoustic processes in a solid rocket engine
[AD-A285606] p 1222 N95-21193

IODIDES

The dynamics of formation and evaporation of mixed alkali halide nanocrystals: A case of comparable lattice energies
[AD-A285052] p 1567 N95-20483

Modeling of nonlinear optic and ESR response of CDW MX materials
[DE94-018301] p 1578 N95-22297

IODINE

Excess energy and structural dependence of the rate of energy redistribution during the photodissociation of iodotoluenes
[AD-A279997] p 1241 N95-21124

ION ACCELERATORS

A new tool for accelerator system modeling and analysis
[DE94-018292] p 1531 N95-20203

An impedance model of the Relativistic Heavy Ion Collider (RHIC)
[DE94-016784] p 1532 N95-20406

Accelerators for energy production
[DE94-770764] p 1392 N95-20685

Induction linacs for heavy ion fusion
[DE95-002357] p 1534 N95-20891

ION ATOM INTERACTIONS

Experimental study of interactions of highly charged ions with atoms at keV energies
[DE95-001807] p 1521 N95-21441

Classical-quantum correspondence for ionization in fast ion-atom collisions
[DE95-000953] p 1526 N95-21940

Experimental study of interactions of highly charged ions with atoms at keV energies
[DE94-018648] p 1529 N95-22316

ION BEAMS

Matrix formulation of the particle motion in crystalline beams
[DE94-017301] p 1563 N95-19925

Modeling the dynamics of charged-particle beams using a Fokker-Planck approach
[DE95-001458] p 1531 N95-19983

Transition-energy crossing with a gamma(sub t)(-)jump
[DE94-017315] p 1531 N95-20021

Relational databases for RHIC design and control
[DE94-016785] p 1532 N95-20336

Ion scattering and deposition: The role of energetic particles in thin film growth
[AD-A285975] p 1514 N95-20667

Accelerators for energy production
[DE94-770764] p 1392 N95-20685

Radiation-driven targets for heavy-ion fusion
[DE95-002264] p 1533 N95-20784

Atmosphere influence on in situ ion beam analysis of thin film growth
[DE95-001507] p 1570 N95-20881

Induction linacs for heavy ion fusion
[DE95-002357] p 1534 N95-20891
An advanced ECR ion source with a large uniformly distributed ECR plasma volume for multiply charged ion beam generation
[DE95-001078] p 1515 N95-20911
Behaviour of space-charge dominated ion beams in storage rings
[DE94-015845] p 1517 N95-21140
In-situ capability of ion beam modification and characterization of materials at Los Alamos National Laboratory
[DE95-002738] p 1534 N95-21236
Shot-to-shot comparison of the first Li-beam driven Hohlraum experiments
[DE94-016558] p 1558 N95-21247
Plasma model for charging damage
[DE95-000788] p 1558 N95-21310
LIF standoff research
[DE94-018744] p 1535 N95-21328
Hadron beams and accelerators
[DE95-002932] p 1536 N95-21342
Progress in the Light Ion Driven Inertial Confinement Fusion Program
[DE94-019182] p 1537 N95-21603
Selection of RIB targets using ion implantation
[DE95-000951] p 1538 N95-21938
Design, fabrication, and characterization of reflective diffractive optical elements in Si for free-space optical interconnects
[AD-A286416] p 1547 N95-22205
Experimental study of interactions of highly charged ions with atoms at keV energies
[DE94-018648] p 1529 N95-22316
Characterization and performance of DLC films synthesized by plasma and ion beam techniques
[DE94-018287] p 1281 N95-22428

ION CONCENTRATION
Advanced detector development, laboratory simulations, diagnostic development, and data analysis on wake physics
[AD-A284798] p 1364 N95-20069

ION CURRENTS
Enhanced ionic conduction at the film/substrate interface in LiI thin films grown on sapphire(0001)
[DE94-017884] p 1565 N95-20371
A new family of anion receptors and their effects on ion pair dissociation and conductivity of lithium salts in non-aqueous solutions
[DE94-016822] p 1512 N95-20477
The development of a new plasticizer for poly(ethylene oxide) based polymer electrolyte and the investigation of their ion-pair dissociation effect
[DE94-016821] p 1276 N95-21644

ION CYCLOTRON RADIATION
Experimental measurements of ICRF and edge plasma interactions on Tore Supra
[DE94-019154] p 1551 N95-20205
Ion heating perpendicular to the magnetic field
[AD-A286635] p 1501 N95-20773
High magnetic field glow discharge ionization source
[AD-A279972] p 1241 N95-21123

ION DENSITY (CONCENTRATION)
Charged particle dynamics in the acceleration gap of the PBFA 2 ion diode
[DE94-017347] p 1506 N95-20026
Behaviour of space-charge dominated ion beams in storage rings
[DE94-015845] p 1517 N95-21140

ION DISTRIBUTION
A new alpha particle diagnostic using knock-on ion tails
[DE94-015856] p 1553 N95-20402
Ion charge-state production and photoionization near the K edge in argon and potassium
[DE95-001443] p 1522 N95-21502

ION EMISSION
Impedance characteristics of multistage ion diodes
[DE94-018887] p 1565 N95-20340

ION ENGINES
SPACE-R thermionic space nuclear power system: Design and technology demonstration
[DE95-000713] p 1221 N95-20076
Power systems for future missions. Appendices A-L
[NASA-CR-195320-APP-A-L] p 1395 N95-21530

ION EXCHANGE MEMBRANE ELECTROLYTES
Electrical impedance studies of acid-form NAFION membranes
[AD-A279271] p 1330 N95-21490

ION EXCHANGE RESINS
An investigation of the applicability of the new ion exchange resin, Reillex(TM)-HPQ, in ATW separations
[DE94-016576] p 1274 N95-21234

ION EXCHANGING
Tests of dielectric model descriptions of chemical charge displacements in water
[DE94-007530] p 1236 N95-20277
An investigation of the applicability of the new ion exchange resin, Reillex(TM)-HPQ, in ATW separations
[DE94-016576] p 1274 N95-21234

ION IMPLANTATION
Physics Division research and development
[DE94-017685] p 1501 N95-20246
Oxide formation on NbAl3 and TiAl due to ion implantation of O-18
[DE94-017874] p 1252 N95-20365
Plasma model for charging damage
[DE95-000788] p 1558 N95-21310
Selection of RIB targets using ion implantation
[DE95-000951] p 1538 N95-21938
Growing and releasing diamonds
[AD-D016489] p 1577 N95-22103
Theses of the Proceedings of the 23d International Meeting on the Physics of Charged Particle Interaction with Crystals
[DE94-631501] p 1529 N95-22281

ION IRRADIATION
Post-irradiation deformation characteristics of heavy-ion irradiated 304L SS
[DE94-017462] p 1251 N95-20088
A mechanistic model for radiation-induced crystallization and amorphization in U3Si
[DE94-015028] p 1566 N95-20419
Ion scattering and deposition: The role of energetic particles in thin film growth
[AD-A285975] p 1514 N95-20667
Sputtering of tin and gallium-tin clusters
[DE94-018389] p 1254 N95-20707
Heavy ion track-structure calculations for radial dose in arbitrary materials
[NASA-TP-3497] p 1517 N95-21191
In-situ capability of ion beam modification and characterization of materials at Los Alamos National Laboratory
[DE95-002738] p 1534 N95-21236
Defect production and recombination during low-energy ion processing
[DE95-001827] p 1572 N95-21304
Vortex dynamics in a ring-like irradiated Bi2Sr2CaCu2O8 crystal
[DE95-001682] p 1573 N95-21569

ION PROBES
Time-resolved diagnostics of excimer laser-generated ablation plasmas used for pulsed laser deposition
[DE94-018950] p 1559 N95-21547

ION SCATTERING
Ion scattering and deposition: The role of energetic particles in thin film growth
[AD-A285975] p 1514 N95-20667
Atmosphere influence on in situ ion beam analysis of thin film growth
[DE95-001507] p 1570 N95-20881
Theses of the Proceedings of the 23d International Meeting on the Physics of Charged Particle Interaction with Crystals
[DE94-631501] p 1529 N95-22281
A multisite interaction expansion of the total energy in metals
[DE94-017175] p 1262 N95-22313
Experimental study of interactions of highly charged ions with atoms at keV energies
[DE94-018648] p 1529 N95-22316
Resonant charge transfer in hyperthermal atomic and molecular ion-surface collisions
[AD-A284937] p 1530 N95-22471

ION SOURCES
An advanced ECR ion source with a large uniformly distributed ECR plasma volume for multiply charged ion beam generation
[DE95-001078] p 1515 N95-20911
High magnetic field glow discharge ionization source
[AD-A279972] p 1241 N95-21123
LIF standoff research
[DE94-018744] p 1535 N95-21328

ION TEMPERATURE
Analysis methods for fast impurity ion dynamics data
[DE95-000589] p 1549 N95-20112
Ion temperature measurement of indirectly-driven implosions using a geometry-compensated neutron time-of-flight detector
[DE94-016967] p 1552 N95-20362

ION TRAPS (INSTRUMENTATION)
On conception of a compact neutron source and the possibility of its simulation on the Amba-M end trap
[DE94-633373] p 1562 N95-22282
Gas-dynamic trap diagnostic complex for study on plasma heating and power atomic beam injection
[DE94-633377] p 1529 N95-22283

IONIC COLLISIONS
Convergent Close-Coupling method for calculation of electron scattering on hydrogen-like targets
[DE94-631340] p 1508 N95-20196
Dynamics of collision processes
[DE94-017593] p 1509 N95-20242
On the sputtering of metals and insulators: A nonlinear evolution problem with nonlinear boundary condition
[DE95-001456] p 1254 N95-20792
Recombination, ion-molecule collisions and (laser assisted) electron-excited atom collisions
[AD-A285604] p 1517 N95-21216
Measurements of scattering processes in negative ion: Atom collisions
[DE95-000664] p 1519 N95-21276
The theory of relativistic heavy ion collisions
[DE95-001805] p 1519 N95-21302
Heavy ion collisions
[DE95-002712] p 1520 N95-21321
Similarities and differences in strangeness production at BNL and CERN
[DE95-002343] p 1521 N95-21380
Experimental study of interactions of highly charged ions with atoms at keV energies
[DE95-001807] p 1521 N95-21441
Summary of heavy ion theory
[DE95-002177] p 1523 N95-21588
Theoretical atomic physics for fusion
[DE94-019196] p 1524 N95-21605
Dynamics of the chiral transition
[DE94-016813] p 1524 N95-21641
Collisional redistribution effects on x ray laser saturation behavior
[DE94-017308] p 1374 N95-21663
Investigation of direct photon production in 200 A GeV S + Au reactions
[DE94-018129] p 1525 N95-21704
Angular and charge state distributions of highly charged ions scattered during low energy surface-channeling interactions with Au(110)
[DE95-001348] p 1525 N95-21857
Very high-power electron-beam transport in long gas cells from 10(exp -3) to 10(exp 3) Torr N2
[DE95-002611] p 1539 N95-22306
Resonant charge transfer in hyperthermal atomic and molecular ion-surface collisions
[AD-A284937] p 1530 N95-22471

IONIC CRYSTALS
Structure of ionic interfaces from an absolutely convergent solution of the Madelung problem
[DE94-019268] p 1573 N95-21474

IONIC REACTIONS
Ion-molecule chemistry related to plasma deposition and etching of silicon
[AD-A279749] p 1514 N95-20804
Ion heat pulse after sawtooth crash in the JFT-2M tokamak
[DE94-770685] p 1555 N95-20988
Potential-of-mean-force description of ionic interactions and structural hydration in biomolecular systems
[DE95-000859] p 1438 N95-21366

IONIZATION
Electron-impact ionization of multicharged ions at ORNL: 1985-1992
[DE94-017318] p 1507 N95-20086
New high temperature plasmas and sample introduction systems for analytical atomic emission and mass spectrometry
[DE94-018580] p 1552 N95-20345
Electrospray ionization Fourier transform ion cyclotron resonance mass spectrometric study of singly and doubly charged organometallic complexes
[AD-A279899] p 1238 N95-20563
High magnetic field glow discharge ionization source
[AD-A279972] p 1241 N95-21123
Experimental investigations of electron capture from atomic hydrogen and deuterium by alpha particles
[DE95-002138] p 1523 N95-21587
Selection of RIB targets using ion implantation
[DE95-000951] p 1538 N95-21938
Classical-quantum correspondence for ionization in fast ion-atom collisions
[DE95-000953] p 1526 N95-21940
Solar wind composition
[NASA-TM-197364] p 1604 N95-22384

IONIZATION CROSS SECTIONS
Electron-impact ionization of multicharged ions at ORNL: 1985-1992
[DE94-017318] p 1507 N95-20086
Calculation of the total and total ionization cross sections for positron scattering on atomic hydrogen
[DE94-631341] p 1508 N95-20197
The (e,2e) calculations with the final-state boundary condition
[DE94-631342] p 1509 N95-20198

Calculation of electron scattering on the He(+) ion
[DE94-631343] p 1509 N95-20199
Intense proton beam source for ITER neutral-beam spectroscopy diagnostics
[DE94-018092] p 1560 N95-21668

IONIZED GASES
An analytical electron distribution function for inelastic collisions in a uniform gas with time varying electric field
[DE95-003476] p 1528 N95-22222
An analytical, inelastic, space and time dependent electron distribution for electrically excited gases
[DE95-003478] p 1528 N95-22223

IONOGRAMS
The effects of multihop HF propagation on the performance of OTH backscatter radars
p 1298 N95-20953

IONOSPHERIC CURRENTS
Substorm theories: United they stand, divided they fall
[NASA-CR-197672] p 1427 N95-22326

IONOSPHERIC DISTURBANCES
Source mechanisms and radio effects of ionospheric plasma disturbances
[AD-A286529] p 1555 N95-21013

IONOSPHERIC HEATING
Ion heating perpendicular to the magnetic field
[AD-A286635] p 1501 N95-20773

IONOSPHERIC PROPAGATION
Temporal and spatial comportment of multiple paths in ionospheric propagation in oblique incidence: Fractal measures of perturbations p 1298 N95-20954
Measurements of angles of elevation of HF by a high resolution method using polarization diversity
p 1299 N95-20959
Source mechanisms and radio effects of ionospheric plasma disturbances
[AD-A286529] p 1555 N95-21013

IONOSPHERIC SOUNDING
The applicability of neural networks to ionospheric modeling in support of relocatable Over-the-Horizon radar
[AD-A286114] p 1309 N95-22230

IONOSPHERIC STORMS
Substorm theories: United they stand, divided they fall
[NASA-CR-197672] p 1427 N95-22326

IONS
Electron-impact ionization of multicharged ions at ORNL: 1985-1992
[DE94-017318] p 1507 N95-20086
Enhanced output of soft x-ray lasers using double slab targets
[DE94-016689] p 1369 N95-20335
Ion heating perpendicular to the magnetic field
[AD-A286635] p 1501 N95-20773
High magnetic field glow discharge ionization source
[AD-A279972] p 1241 N95-21123
Ion-molecular spiraling collisions and termolecular recombination
[AD-A285633] p 1517 N95-21151
Emittance dilution by ions in the SLC arcs
[DE95-002871] p 1536 N95-21332
Dilepton production from p-p to Ca-Ca at the Bevalac
[DE95-002341] p 1520 N95-21357
Potential-of-mean-force description of ionic interactions and structural hydration in biomolecular systems
[DE95-000859] p 1438 N95-21366
Ion charge-state production and photoionization near the K edge in argon and potassium
[DE95-001443] p 1522 N95-21502
The energetics and dynamics of free radicals, ions, and clusters
[DE94-018101] p 1244 N95-21701
Observations of cold magnetospheric ions at geosynchronous orbit during times of high activity
[DE95-000936] p 1600 N95-21935
Experimental study of interactions of highly charged ions with atoms at keV energies
[DE94-018648] p 1529 N95-22316

IRAS-ARAKI-ALCOCK COMET
Application of MCM image construction to IRAS comet observations p 1594 N95-21772

IRIDIUM
Water abundance and accretion history of terrestrial planets p 1424 N95-21820

IRON
MCNP (trademark) ENDF/B-VI iron benchmark calculations
[DE94-016165] p 1508 N95-20160
Magnetic x ray circular dichroism in Fe Co Pt multilayers
[DE94-017522] p 1253 N95-20447
Spin-specific photoelectron diffraction using magnetic x ray circular dichroism
[DE94-017527] p 1567 N95-20448
Processing and applications of iron aluminides
[DE94-017855] p 1253 N95-20673
Transportation of volatile elements in thermally evolving planetesimals: An important role of metallic iron
p 1418 N95-21790

IRON ALLOYS
Processing and characterization of Ni-Al-Fe-B shape-memory alloy wires produced by rapid solidification
[DE94-017702] p 1250 N95-20020
Hydrogen resistant alloy - NASA 23
[NASA-CASE-MFS-26200-1-SB] p 1251 N95-20068
Processing and applications of iron aluminides
[DE94-017855] p 1253 N95-20673
Changes in the behavior of magnetic materials undergoing processing in electrical rotating machines
[PB95-104493] p 1325 N95-20702
Impact behavior of FeAl alloy FA-350
[DE94-018128] p 1254 N95-20705
ALCHEMI of Fe-doped B2-ordered NiAl alloys with different doping levels
[DE94-017748] p 1255 N95-20907
2nd International ADI seminar
[PB95-127734] p 1255 N95-21108
Computational modeling of diffusion-controlled transformations in ternary systems
[DE95-001358] p 1256 N95-21298
Weldability of iron aluminides
[DE94-019114] p 1257 N95-21555
Fracture behavior of the Fe-8Al alloy FAP-Y
[DE95-000956] p 1258 N95-21676
Incology alloy 908 data handbook
[DE95-001818] p 1260 N95-22013
Tensile and impact properties of iron-aluminum alloys
[DE94-017750] p 1263 N95-22346

IRON COMPOUNDS
Calculation of atom-centered partial charges for heme
[DE94-014447] p 1520 N95-21375
Structure and stability of hydrous minerals at high pressure p 1417 N95-21786

IRON ISOTOPES
Properties of strange-matter stars
[DE95-002329] p 1599 N95-20873
Helium production by 10 MeV neutrons in iron, nickel and copper
[DE94-014798] p 1529 N95-22280

IRON OXIDES
Superior catalysts for selective catalytic reduction of nitric oxide
[DE94-018845] p 1234 N95-20046
Selective methane oxidation over promoted oxide catalysts
[DE94-012270] p 1235 N95-20188
Moessbauer study of the sintered Mn(0.70)Zn(0.23)Fe(2.07)O4
[DE94-631462] p 1255 N95-20909
Water abundance and accretion history of terrestrial planets p 1424 N95-21820

IRRADIANCE
Detection optimization using linear systems analysis of a coded aperture laser sensor system
[DE95-001112] p 1371 N95-20832
Effects of increased UV-B radiation on phytoplankton: A preliminary study and research programme
[PB95-133732] p 1439 N95-21884

IRRADIATION
Amorphization of sapphire during ion beam mixing
[DE94-018713] p 1510 N95-20337
The in-situ fracture and Auger analysis of Nicalon fibers
[DE94-017771] p 1226 N95-20357
Performance, defect behavior and carrier enhancement in low energy, proton irradiated p+nn+ InP solar cells
p 1319 N95-20518
Annealing of irradiated n+p InP buried homojunctions
p 1320 N95-20524
UV testing of INTELSAT-7, 7A, and 8 solar cells
p 1320 N95-20526
X-ray spectroscopy of xenon
[DE95-002132] p 1240 N95-20865
Irradiation creep in structural materials at ITER operating conditions
[DE94-018946] p 1261 N95-22123
Low temperature tensile and fracture mechanical strength in mode 1 and mode 2 of fiber reinforced plastics following various irradiation conditions
[DE94-019269] p 1232 N95-22130
Radiation tests on service electronics for future multi TeV detectors
[DE94-632822] p 1335 N95-22184
Helium production by 10 MeV neutrons in iron, nickel and copper
[DE94-014798] p 1529 N95-22280
The final status of a metal surface after multipulse laser irradiation in an ambient gas
[DE94-629000] p 1562 N95-22377

IRREGULARITIES
Mitigation of the effects of F layer regularities by using multiple paths p 1298 N95-20951
The effects of magnetic storm phases on F-layer irregularities from auroral to equatorial latitudes
[AD-A286173] p 1427 N95-22423

ISCHEMIA
Skeletal muscle ischemia and heat shock proteins
[AD-A285364] p 1442 N95-20549

ISING MODEL
Rigorous spin-spin correlation function of Ising model on a special kind of Sierpinski Carpets
[DE94-628995] p 1575 N95-21854
Magnetic properties of the three-dimensional Ising model with an interface amorphization
[DE94-628992] p 1278 N95-21885
N=1 Superconformal minimal model correlation functions on the torus
[PB95-134615] p 1500 N95-21964

ISLAND ARCS
Recycling of volatiles at subduction zones: Noble gas evidence from the Tabar-Lihir-Tanga-Feni arc of papua New Guinea p 1418 N95-21787

ISOCYANATES
Publications/patents/presentations/honors/student eport. Investigation of the role of vibrational excitation in unimolecular reactions
[AD-A280044] p 1513 N95-20621

ISOLATION
High isolation electronic switch
[AD-D016533] p 1326 N95-20729

ISOMERS
Process strategies in the enzymatic resolution of enantiomers
[PB95-107850] p 1437 N95-20208
Excess energy and structural dependence of the rate of energy redistribution during the photodissociation of iodotoluenes
[AD-A279997] p 1241 N95-21124

ISOTHERMAL PROCESSES
Augmented thermal bus
[NASA-CASE-LEW-15595-1-C] p 1338 N95-19933

ISOTHERMS
An investigation of the applicability of the new ion exchange resin, Reillex(TM)-HPQ, in ATW separations
[DE94-016576] p 1274 N95-21234

ISOTONICITY
Exponential deconvolution: Two asymptotically equivalent estimators
[PB95-132122] p 1499 N95-21469

ISOTOPE RATIOS
Spatial variation of primordial 3-He in crustal fluids along the East-African Rift system (the Ethiopian and the Kenya Rift section) p 1418 N95-21789

ISOTOPE SEPARATION
System design document U-AVLIS control system. architecture
[DE94-017297] p 1460 N95-20387
Mars power system concept definition study. Volume 1: Study results
[NASA-CR-195420-VOL-1] p 1396 N95-21952

ISOTOPES
Conference on Deep Earth and Planetary Volatiles
[NASA-CR-196944] p 1415 N95-21777
D/H ratios and H2O contents of mantle-derived amphibole megacrysts from Dish Hill, California
p 1416 N95-21781
Noble gas isotopes and halogens in volatile-rich inclusions in diamonds p 1417 N95-21784
Origin and loss of the volatiles of the terrestrial planets p 1417 N95-21785
Primitive Xe in the atmospheres of Earth and mars
p 1419 N95-21795
Mars atmospheric loss and isotopic fractionation by pick-up-ion sputtering and photochemical escape
p 1420 N95-21796
Nitrogen isotopic components in the early solar system p 1420 N95-21800
Is xenon eldest? p 1425 N95-21823
Distribution of light element isotopes in Bencubbin and Weatherford meteorites: An indicator of heterogeneity in the primitive solar nebula
[DE94-019167] p 1600 N95-22128

ISOTOPIC LABELING
In vivo distribution of liposome encapsulated hemoglobin studied with imaging radiotracers
[AD-A279774] p 1438 N95-20806
Solar helium and neon in the Earth
p 1419 N95-21793
The isotope geochemistry of abyssal peridotites and related rocks
[AD-A279435] p 1435 N95-21918

ISOTROPIC MEDIA
Velocity analysis for transversely isotropic media
[DE95-000643] p 1411 N95-19981

P-wave signatures and parameterization of transversely isotropic media: An overview
[DE95-000644] p 1411 N95-19982

ISOTROPIC TURBULENCE

A numerical investigation of energy transfer and subgrid-scale eddy viscosity in homogeneous, isotropic and shear turbulence
[AD-A280005] p 1339 N95-20058

Mapping closures for turbulent combustion
[AD-A279995] p 1238 N95-20597

Pressure and higher-order spectra for homogeneous isotropic turbulence p 1343 N95-21045

Statistics of pressure and pressure gradient in homogeneous isotropic turbulence p 1343 N95-21046

A Lagrangian dynamic subgrid-scale model turbulence
p 1344 N95-21051

Application of Direct and Large Eddy Simulation to Transition and Turbulence
[AGARD-CP-551] p 1346 N95-21061

Developments and applications of dynamic models for large eddy simulation of complex flows
p 1346 N95-21062

The asymptotic state of rotating homogeneous turbulence at high Reynolds numbers
p 1347 N95-21065

Analysis of subgrid models using direct and large-eddy simulations of isotropic turbulence p 1348 N95-21071

Entrainment in a shear-free turbulent mixing layer
p 1350 N95-21083

Small-scale behavior in distorted turbulent boundary layers at low Reynolds number p 1362 N95-22456

Experimental and numerical study of the intermittency exponent mu p 1362 N95-22458

On the dynamics of small-scale vorticity in isotropic turbulence p 1362 N95-22459

Resolution requirements for velocity gradients in turbulence p 1363 N95-22462

ISOTROPY

Physical-chemical studies on rodlike polymer compositions
[AD-A285361] p 1269 N95-20548

On the Taylor test. Part 3: A continuum mechanics code analysis of steady plastic wave propagation
[DE95-002252] p 1501 N95-20869

The decay of axisymmetric homogeneous turbulence
p 1343 N95-21047

Fast algorithms for transport models
[DE95-001702] p 1470 N95-21992

ITERATION

A S2-like acceleration method for the Nonlinear Characteristic transport scheme
[DE94-016285] p 1509 N95-20235

Error committed by stopping the Newton iteration in Runge-Kutta methods and linear multistep methods
[PB95-106324] p 1492 N95-21421

Iterated-subspace minimization methods for nonlinear optimization
[PB95-108171] p 1495 N95-22317

ITERATIVE SOLUTION

Iterated-bootstrap confidence intervals for the mean
[AD-A279802] p 1498 N95-20102

A domain decomposition scheme for Eulerian shock physics codes
[DE94-015739] p 1488 N95-20141

VLUGR3: A vectorizable adaptive grid solver for PDEs in 3D. 1: Algorithmic aspects and applications
[PB95-135729] p 1467 N95-21435

Distribution-independent hierarchical N-body methods
[DE95-001686] p 1493 N95-21439

Object-oriented design of preconditioned iterative methods
[PB95-110276] p 1469 N95-21655

A new Krylov-subspace method for symmetric indefinite linear systems
[DE95-001826] p 1355 N95-21726

J

JAMMING

General purpose sidelobe canceller system
[AD-D016560] p 1289 N95-20270

Highly survivable communications: Complementary media packet switched networks p 1292 N95-20922

A wideband propagation simulator for high speed mobile radio communications p 1295 N95-20934

Directive optimization of coherent sidelobe canceller systems
[AD-D016513] p 1307 N95-21908

JAPAN

Environmental Compliance Assessment System (ECAS): Japan settlement
[AD-A279328] p 1410 N95-22142

JET AIRCRAFT NOISE

Active control of fan noise-feasibility study. Volume 1: Flyover system noise studies
[NASA-CR-195392-VOL-1] p 1505 N95-21888

JET ENGINE FUELS

Investigation of flight data recorder fire test requirements
[AD-A285832] p 1208 N95-20032

Two-dimensional imaging of OH in a lean burning high pressure combustor
[NASA-TM-106854] p 1214 N95-21383

JET ENGINES

Temperature effects on acoustic interactions between altitude test facilities and jet engine plumes
[NASA-CR-197638] p 1504 N95-21170

JET FLOW

Heat transfer, fouling, and combustion of supercritical fuels
[AD-A279906] p 1281 N95-19884

Numerical simulation of spatially-developing planar jets p 1351 N95-21087

Rib vortices in round jets: Direct and large eddy simulation p 1351 N95-21088

Superconducting electromagnetic thruster
[AD-D016485] p 1355 N95-21902

JET IMPINGEMENT

Numerical simulation of spatially-developing planar jets p 1351 N95-21087

JET MIXING FLOW

Experimental investigations of on-demand vortex generators p 1361 N95-22451

JET THRUST

Static investigation of two fluidic thrust-vectoring concepts on a two-dimensional convergent-divergent nozzle
[NASA-TM-4574] p 1199 N95-19913

JFET

Complementary GaAs junction-gated heterostructure field effect transistor fabrication for integrated circuits
[DE95-001522] p 1327 N95-20882

JOINTS (JUNCTIONS)

Intrinsic barriers for H-atom transfer reactions
[DE94-018914] p 1507 N95-20049

The reliability of laser reflowed Sn-Ag solder joints
[AD-A279787] p 1315 N95-20443

Reliability assessment of Multichip Module technologies via the Triservice/NASA RELTECH program
p 1210 N95-20643

Analysis of a disk-on-rod surface wave element inside a corrugated horn using the mode-matching technique
p 1305 N95-21543

Fiber-optic rotary joint with bundle collimator assemblies
[AD-D016504] p 1545 N95-21673

Attachment methodology for composite cylinder assembly
[AD-D016256] p 1381 N95-22034

Evaluation of scanners for C-scan imaging for nondestructive inspection of aircraft
[AD-A286398] p 1383 N95-22202

JOSEPHSON JUNCTIONS

Josephson acoustic radiation in superfluid helium
[AD-A279809] p 1503 N95-20098

HTS Josephson technology on silicon with application to high speed digital microelectronics
[AD-A285964] p 1328 N95-21178

Critical dynamics and plastic flow in disordered Josephson junction arrays
[DE94-629074] p 1576 N95-21995

Breakdown of the law of large numbers in Josephson junction series arrays
[DE94-629075] p 1576 N95-21996

Order and turbulence in RF-driven Josephson junction series arrays
[DE94-629076] p 1576 N95-21997

JOURNAL BEARINGS

Wave journal bearing. Part 1: Analysis
[NASA-CR-195431-PT-1] p 1382 N95-22404

Wave journal bearing. Part 2: Experimental pressure measurements and fractional frequency whirl threshold for wave and plain journal bearings
[NASA-TM-106848-PT-2] p 1382 N95-22405

JP-8 JET FUEL

Development of an advanced JP-8 fuel
[AD-A285583] p 1283 N95-21161

JUPITER ATMOSPHERE

Simulated rarefied entry of the Galileo probe into the atmosphere of Jupiter
[NASA-TM-110507] p 1601 N95-21621

K

K-EPSILON TURBULENCE MODEL

Effects of turbulence compressibility and unsteadiness in compression corner flow p 1344 N95-21052

Single point modeling of rotating turbulent flows
p 1346 N95-21060

Developments and applications of dynamic models for large eddy simulation of complex flows
p 1346 N95-21062

Application of Roe's flux-difference splitting for kappa-epsilon turbulence model
[PB95-127718] p 1352 N95-21106

Application of Navier-Stokes code PAB3D with kappa-epsilon turbulence model to attached and separated flows
[NASA-TP-3480] p 1201 N95-21338

KALMAN FILTERS

Emitter location via Kalman filtering of signal time difference of arrival
[AD-A285972] p 1291 N95-20666

Brief tutorial on the Kalman filter
[AD-A286571] p 1326 N95-20827

A real-time algorithm for integrating differential satellite and inertial navigation information during helicopter approach
[NASA-CR-197409] p 1205 N95-21891

KAONS

GAJET experiment at the LHC: The GAJET collaboration
[PB95-129813] p 1512 N95-20454

Search for right-handed currents in the decay chain of K(+) yields muon(+)nu(sub muon), muon(+) yields e(+)nu(sub e)nu(bar)(sub muon)
[DE94-770606] p 1514 N95-20756

Single particle measurements and two particle interferometry results from CERN experiment NA44
[DE95-003041] p 1527 N95-22078

KARMAN VORTEX STREET

Forced free-shear layer measurements
p 1362 N95-22460

KELVIN WAVES

A study of westerly wind bursts preceding the 1991-1992 El Nino
[AD-A286570] p 1429 N95-20826

KERNEL FUNCTIONS

Weighted strongly elliptic operators on lie groups
[PB95-110847] p 1487 N95-19917

Kernel mucking in top
[DE94-017077] p 1460 N95-20385

Positive rockland operators
[PB95-127510] p 1493 N95-21423

On Markov Chain Monte Carlo acceleration
[AD-A279393] p 1499 N95-21945

KERR EFFECTS

Ultrafast optical studies of surface reaction processes at semiconductor interfaces
[DE95-001548] p 1574 N95-21839

KERR ELECTROOPTICAL EFFECT

Light-scattering fluctuations and noise in nonlinear optical processing
[AD-A279748] p 1544 N95-20803

KERR MAGNETOOPTICAL EFFECT

Changes in the behavior of magnetic materials undergoing processing in electrical rotating machines
[PB95-104493] p 1325 N95-20702

KEVLAR (TRADEMARK)

Detection of environmental deterioration in fiber reinforced composites by FT-Raman spectroscopy, phase 1
[AD-A279763] p 1228 N95-20805

KINEMATIC EQUATIONS

Mathematical modeling of a class of multibody flexible spacecraft structures
[NASA-TM-109166] p 1219 N95-20800

KINEMATICS

Search for D(+) yields (pi)(+)(mu)(+)(mu)(-)
[DE94-015538] p 1512 N95-20475

Symmetry, Wigner functions and particle reactions
[DE94-629887] p 1514 N95-20735

Kinematical evidence for top pairs at the Tevatron
[DE95-000729] p 1515 N95-20880

Modeling the effect of water on mantle rheology
p 1417 N95-21783

KINETIC ENERGY

Evaluation of Reynolds stress turbulence closures in compressible homogeneous shear flow
[NASA-CR-194892] p 1338 N95-20009

Study of small carbon and semiconductor clusters using negative ion threshold photodetachment spectroscopy
[DE95-002327] p 1515 N95-20872

Correlated wavefunction Monte Carlo studies of excitations in the quantum Hall liquids
[DE95-002337] p 1501 N95-20874

Numerical investigation of supersonic turbulent boundary layers with high wall temperature
p 1344 N95-21050

Effects of turbulence compressibility and unsteadiness in compression corner flow p 1344 N95-21052

The asymptotic state of rotating homogeneous turbulence at high Reynolds numbers
p 1347 N95-21065
Large-eddy simulation of separated flow in a ribbed duct p 1347 N95-21070
Analysis of subgrid models using direct and large-eddy simulations of isotropic turbulence p 1348 N95-21071
A cheap DNS tool for turbulence models testing
p 1348 N95-21072
Application of Roe's flux-difference splitting for kappa-epsilon turbulence model
[PB95-127718] p 1352 N95-21106

KINETIC EQUATIONS
Hybrid model in general geometry
[DE95-002614] p 1553 N95-20437

KINETIC THEORY
Magnetic fluctuation induced transport and edge dynamo measurements in the MST reversed-field pinch
[DE95-000591] p 1549 N95-20114

KINETICS
Chemical Structure and Dynamics program
[DE95-001117] p 1403 N95-20834
Cluster reactions: An approach to understanding the fundamentals of heterogeneous catalysis
[DE95-002947] p 1243 N95-21447

KLEIN-GORDON EQUATION
Quantization in curvilinear coordinates
[DE94-770603] p 1514 N95-20737
Understanding the mechanisms of length scale competition: The sine-Gordan soliton case
[DE94-016201] p 1500 N95-21136

KLYSTRONS
Development of an annular electron beam HPM amplifier
[AD-A286646] p 1327 N95-20905
Development status of an intense beam klystron
[DE95-000745] p 1329 N95-21395
A 500 MW annular beam relativistic klystron
[DE95-000867] p 1334 N95-22011

KNOWLEDGE
NASA/DOD Aerospace Knowledge Diffusion Research Project. Report 28: The technical communication practices of aerospace engineering and science students: Results of the phase 4 cross-national surveys
[NASA-TM-109123] p 1587 N95-20162

KNOWLEDGE BASED SYSTEMS
Generating examples for use in tutorial explanations: The use of a subsumption based classifier
[AD-A286028] p 1464 N95-20996
Knowledge refinement in a reflective architecture
[AD-A286027] p 1589 N95-21002
GRONICs-1994. Proceedings of the 1994 Groningen Student Conference on Computer Science
[PB95-135620] p 1468 N95-21455
Incremental rederivation of software artifacts: FY 1993
[AD-A285790] p 1473 N95-22402

KNOWLEDGE BASES (ARTIFICIAL INTELLIGENCE)
Generating examples for use in tutorial explanations: The use of a subsumption based classifier
[AD-A286028] p 1464 N95-20996
Knowledge refinement in a reflective architecture
[AD-A286027] p 1589 N95-21002
Formal model for the dynamics of compositional reasoning systems
[PB95-132056] p 1482 N95-21267
EXPERT system expert: Program description
[PB95-131561] p 1482 N95-21429
EXPERT system expert: Users manual
[PB95-131579] p 1482 N95-21430
Generic architecture for knowledge-based control of processes in dynamic environments
[PB95-132676] p 1483 N95-21981
Intelligent interactive project management system
[PB95-132684] p 1586 N95-21982
Verification of knowledge-based reasoning modules
[PB95-132692] p 1470 N95-21983
Structuring design requirements using YMIR
[PB95-132742] p 1471 N95-22081

KNOWLEDGE REPRESENTATION
Knowledge refinement in a reflective architecture
[AD-A286027] p 1589 N95-21002
Logic programming and negation: A survey
[PB95-110730] p 1472 N95-22302

KOLMOGOROV THEORY
Simulation of stellar speckle imaging
[DE94-016606] p 1412 N95-19985
Small-scale behavior in distorted turbulent boundary layers at low Reynolds number p 1362 N95-22456
Experimental and numerical study of the intermittency exponent mu p 1362 N95-22458

KONDO EFFECT
Kondo insulators
[DE95-001156] p 1237 N95-20368
An asymptotic solution of the (infinity)-d Hubbard model
[DE94-629042] p 1582 N95-21994

KRYPTON
Is xenon eldest? p 1425 N95-21823

KUIPER AIRBORNE OBSERVATORY
Pushing the limits of spatial resolution with the Kuiper Airborne observatory p 1593 N95-21754

L

LABORATORIES
Parallel solid mechanics codes at Sandia National Laboratories
[DE94-015770] p 1474 N95-20152
The Materials Corrosion and Environmental Effects Laboratory (MCEL)
[DE94-018268] p 1254 N95-20816
Recent reflux receiver developments under the US DOE program
[DE95-001622] p 1393 N95-20861
Reactor pumped laser research at the Sandia National Laboratories pulsed reactor facilities
[DE95-002181] p 1371 N95-20867
Advanced robotic technologies for transfer at Sandia National Laboratories
[DE95-001617] p 1481 N95-20884
Systems Analysis Laboratory. Ten years of progress 1984-1994
[PB95-104451] p 1464 N95-20982
Recent National Solar Thermal Test Facility activities, in partnership with industry
[DE95-001828] p 1394 N95-21353
HPCC technology awareness program: Improved economic competitiveness through technology awareness, transfer and application
[DE95-002134] p 1476 N95-21355
Total quality management program planning
[DE94-016862] p 1586 N95-21645

LAGOONS
A modal analysis of currents in a Pacific Atoll lagoon
[AD-A283721] p 1431 N95-19971

LAGRANGE MULTIPLIERS
A neural expert approach to self designing flight control systems
[AD-A279965] p 1215 N95-21122

LAGRANGIAN FUNCTION
Nonlinear dynamic fluid-structure interaction calculations with coupled finite element and finite volume programs
[DE94-016204] p 1339 N95-20166
On the Taylor test. Part 3: A continuum mechanics code analysis of steady plastic wave propagation
[DE95-002252] p 1501 N95-20869
Balloon tracking for the ASTEX/MAGE Lagrangian experiment
[AD-A280078] p 1430 N95-20969
A Lagrangian dynamic subgrid-scale model turbulence
p 1344 N95-21051

LAKE ERIE
AN/APS-137 Forward Looking Airborne Radar (FLAR) evaluation, Fall 1992 experiment
[AD-A279526] p 1306 N95-21686

LAKE SUPERIOR
Anatomy of the Midcontinent Rift beneath Lake Superior
[DE94-019298] p 1415 N95-21477

LAKES
Fourth International Symposium on Stratified Flows, volume 3
[AD-A286452] p 1354 N95-21584

LAMINAR BOUNDARY LAYER
Navier-Stokes simulations of the effects of suction holes on a flat plate boundary layer p 1352 N95-21094
Direct numerical simulation of 2-D and 3-D instability waves in a laminar separation bubble
p 1352 N95-21095
Acoustic receptivity due to weak surface inhomogeneities in adverse pressure gradient boundary layers
[NASA-TM-4577] p 1353 N95-21258
Supersonic laminar flow control research
[NASA-CR-196049] p 1353 N95-21340
Development of quiet-flow supersonic wind tunnels for laminar-turbulent transition research
[NASA-CR-197286] p 1216 N95-21436
Acoustics of laminar boundary layers breakdown
p 1361 N95-22455

LAMINAR FLOW
Low flow fluid separator
[AD-D016575] p 1339 N95-20297
Software for flow distribution in electronic rack structures
[AD-A285994] p 1325 N95-20715
Homogeneous turbulence subjected to mean flow with elliptic streamlines p 1345 N95-21056
Simulations of bypass transition for spatially evolving disturbances p 1349 N95-21079
Direct numerical determination of the minimum bypass Reynolds number in boundary layers
p 1349 N95-21080
Transient behaviour and stability points of the Poiseuille flow of a KBKZ-fluid
[PB95-132064] p 1353 N95-21268

LAMINATES
The influence of ply waviness with nonlinear shear on the stiffness and strength reduction of composite laminates
[AD-A285736] p 1224 N95-19899
Analysis of the progressive failure of brittle matrix composites
[NASA-CR-195415] p 1225 N95-19951
Superior catalysts for selective catalytic reduction of nitric oxide
[DE94-018845] p 1234 N95-20046
Thermo-mechanical fatigue of polymer matrix composites
[AD-A285931] p 1267 N95-20390
Reliability assessment of Multichip Module technologies via the Triservice/NASA RELTECH program
p 1210 N95-20643
The processing and mechanical properties of high temperature/high performance composites. Mechanism-based constitutive laws and design, book 1
[AD-A279736] p 1228 N95-20801
Significance of impact velocity for the extent of damage in carbon/epoxy laminates
[PB95-133484] p 1230 N95-21417
Damage tolerance of carbon fibre polyetheretherketone laminates
[PB95-131611] p 1230 N95-21432
Processing and mechanical properties of laminar Al2O3-Ni3Al composites
[DE94-019332] p 1230 N95-21481
Damage tolerant repair techniques for pressurized aircraft fuselages
[AD-A286298] p 1199 N95-22046
Fracture behavior of laminated discontinuously reinforced aluminum material
[DE94-017307] p 1263 N95-22408

LAND SURFACE TEMPERATURE
Operating manual for hybrid thermosyphons at the Gakona Power Plant, Alaska
[AD-A279068] p 1287 N95-21626

LANDAU DAMPING
Effect of space charge tune shift on transverse instabilities
[DE94-016790] p 1531 N95-20282
Bunched beam instability with frequency spread
[DE94-018632] p 1539 N95-22357

LANDAU FACTOR
Correlated wavefunction Monte Carlo studies of excitations in the quantum Hall liquids
[DE95-002337] p 1501 N95-20874

LANDAU-GINZBURG EQUATIONS
Biaxiality of chiral liquid crystals
[DE94-629032] p 1578 N95-22277
The interaction of localized solutions in a surface reaction
[DE95-002736] p 1248 N95-22433

LANDING GEAR
Corrosion behavior of landing gear steels
[AD-A285862] p 1261 N95-22132

LANDING LOADS
Super-heavy aircraft study
[AD-A279602] p 1215 N95-19955

LANGMUIR TURBULENCE
A portable and independent edge fluctuation diagnostic
[DE94-018254] p 1554 N95-20681

LANGMUIR-BLODGETT FILMS
Chemical interactions between protein molecules and polymer membrane materials
[DE95-001808] p 1224 N95-21746

LANGUAGE PROGRAMMING
TBell: A mathematical tool for analyzing decision tables
[NASA-CR-195027] p 1462 N95-20691
Visual displays and Neuro-Linguistic Programming
[DE95-001454] p 1466 N95-21311

LANTHANUM
Solid oxide fuel cells in the United States
[DE95-002405] p 1395 N95-21361
High performance YBCO films
[AD-A279560] p 1276 N95-21695

LANTHANUM COMPOUNDS
Certain physical properties of lanthanum digermanide
[AD-A286592] p 1229 N95-20859
Fabrication of PLZT/ITO grating for optical switching and reconfigurable optical interconnect applications
[AD-A286389] p 1548 N95-22248

LANTHANUM OXIDES
Carrier doping and interlayer coupling in HTSC single crystals
[DE94-018637] p 1564 N95-20127
Selective methane oxidation over promoted oxide catalysts
[DE94-012270] p 1235 N95-20188
Transient studies of low temperature catalysts for methane conversion
[DE95-003560] p 1247 N95-22224

LAPLACE TRANSFORMATION
The PROSAIC Laplace and Fourier Transform
[DE95-002225] p 1492 N95-21266
Wavelet analysis applied to the IRAS cirrus
p 1593 N95-21769

LARGE SPACE STRUCTURES
Static stability of a three-dimensional space truss
p 1220 N95-20533

LASER ABLATION
Computational modeling of physical processes during laser ablation
[DE94-017699] p 1369 N95-20221
Optical properties of silicon clusters deposited on the basal plane of graphite
[DE94-017529] p 1542 N95-20450
Time-resolved diagnostics of excimer laser-generated ablation plasmas used for pulsed laser deposition
[DE94-018950] p 1559 N95-21547

LASER ANEMOMETERS
Laser anemometry and viscous computation of the flow through an annular turbine cascade
[AD-A280070] p 1341 N95-20968

LASER ANNEALING
International Symposium on Advanced Laser Technologies
[AD-A279849] p 1376 N95-22164

LASER APPLICATIONS
Compact free electron lasers for medical applications
[AD-A285739] p 1369 N95-20072
Program of the 1993 9th Interdisciplinary Laser Science Conference (ILS-9)
[AD-A285131] p 1369 N95-20082
System design document U-AVLIS control system architecture
[DE94-017297] p 1460 N95-20387
Application of diode lasers to the isotopically selective determination of uranium in oxides by optogalvanic spectroscopy
[DE94-018045] p 1370 N95-20698
Computational model of drilling with high radiance pulsed lasers
[DE94-018548] p 1371 N95-20783
Performance of the NIF prototype beamlet
[DE94-018500] p 1371 N95-20817
Laser-Induced Thermal Acoustics (LITA): Four-wave mixing measurement of sound speed, thermal diffusivity, and viscosity
[AD-A286524] p 1372 N95-21009
Neutronics and shielding analysis of the National Ignition Facility
[DE94-016698] p 1534 N95-21208
Laser design basis for the National Ignition Facility
[DE94-016700] p 1534 N95-21209
Recombination, ion-molecule collisions and (laser assisted) electron-excited atom collisions
[AD-A285604] p 1517 N95-21216
Continuously-tunable, narrow-linewidth, Q-switched Cr:LiSAF laser for lidar applications
[DE95-000862] p 1373 N95-21312
Simulation of laser bathymetry for irregular bottoms
[PB95-133518] p 1434 N95-21320
Applications for reactor-pumped lasers
[DE95-000536] p 1373 N95-21393
Overview of remote sensing laser development and semiconductor laser technology
[DE94-019103] p 1389 N95-21552
Laser materials processing at Sandia National Laboratories
[DE95-002183] p 1374 N95-21594
Molecular design concept for multi-kilovolt x-ray amplification
[DE95-001763] p 1374 N95-21743
Directed light fabrication
[DE94-018293] p 1375 N95-21837
Method for laser-assisted silicon etching using halocarbon ambients
[AD-D016494] p 1375 N95-21903
International Symposium on Advanced Laser Technologies
[AD-A279849] p 1376 N95-22164

LASER ARRAYS
Technologies for highly parallel optoelectronic integrated circuits
[DE95-001607] p 1327 N95-20883
Ultra-high aggregate bandwidth two-dimensional multiple-wavelength diode laser arrays
[AD-A280098] p 1372 N95-21019

LASER BEAMS
High power spectral and spatial beam control using self-phase modulation and a multisegment monochromator
[DE94-016604] p 1531 N95-20120
Enhanced output of soft x-ray lasers using double slab targets
[DE94-016689] p 1369 N95-20335
High energy photon-photon collisions
[DE94-017494] p 1532 N95-20388
Inverse Cerenkov laser acceleration experiment at ATF
[DE94-017990] p 1370 N95-20572
Laser trapping of Na-21 atoms
[DE95-002354] p 1513 N95-20629
Performance of the NIF prototype beamlet
[DE94-018500] p 1371 N95-20817
Large facilities pilot programme. Access to the VULCAN High Power Laser Facilities at Rutherford Appleton Laboratory
[PB95-130340] p 1373 N95-21226
Novel absorption detection techniques for capillary electrophoresis
[DE95-001673] p 1242 N95-21400
Directed light fabrication
[DE94-018293] p 1375 N95-21837
Technique for intracavity sum frequency generation
[AD-D016478] p 1546 N95-21898
Submicrosecond, synchronizable x-ray source
[AD-D016497] p 1546 N95-21905
Effect of laser radiation on carbon fibre/epoxy composites
[PB95-133526] p 1232 N95-22096
LADAR detection statistics in the presence of pointing errors
[AD-A285865] p 1309 N95-22134
3-D TECATE/BREW: Thermal, stress, and birefringent ray-tracing codes for solid-state laser design
[DE95-000330] p 1376 N95-22301
Broadband thermal optical limiter for the protection of eyes and sensors
[AD-D016493] p 1377 N95-22304
Defect geometries and laser-induced damage in multilayer coatings
[DE94-017695] p 1377 N95-22343
Study of pulsed laser effects on living tissues
[PB95-131330] p 1447 N95-22361
Target alignment in the National Ignition Facility
[DE94-015559] p 1540 N95-22469

LASER CAVITIES
Technologies for highly parallel optoelectronic integrated circuits
[DE95-001607] p 1327 N95-20883
Ultra-high aggregate bandwidth two-dimensional multiple-wavelength diode laser arrays
[AD-A280098] p 1372 N95-21019
Technique for intracavity sum frequency generation
[AD-D016478] p 1546 N95-21898

LASER COOLING
Three-dimensional laser cooling
[DE94-017963] p 1370 N95-20569

LASER DAMAGE
Broadband thermal optical limiter for the protection of eyes and sensors
[AD-D016493] p 1377 N95-22304

LASER DOPPLER VELOCIMETERS
Laser anemometry and viscous computation of the flow through an annular turbine cascade
[AD-A280070] p 1341 N95-20968
A three-dimensional orthogonal laser velocimeter for the NASA Ames 7- by 10-foot wind tunnel
[NASA-TM-108864] p 1366 N95-21323

LASER DRILLING
Computational model of drilling with high radiance pulsed lasers
[DE94-018548] p 1371 N95-20783

LASER FUSION
National Ignition Facility: Experimental plan
[DE94-016542] p 1550 N95-20189
Laser design basis for the National Ignition Facility
[DE94-016700] p 1534 N95-21209
Large facilities pilot programme. Access to the VULCAN High Power Laser Facilities at Rutherford Appleton Laboratory
[PB95-130340] p 1373 N95-21226

LASER GYROSCOPES
Optical processing and control
[AD-A279157] p 1546 N95-21975

LASER INDUCED FLUORESCENCE
Observation of strong emission from NeIX and NeX transitions in a laser-driven plasma
[DE95-002265] p 1555 N95-20813
Two-dimensional imaging of OH in a lean burning high pressure combustor
[NASA-TM-106854] p 1214 N95-21383
Advanced diagnostics for plasma chemistry
[DE94-018936] p 1561 N95-22116

LASER INTERFEROMETRY
LLNL/Lion Precision LVDT amplifier
[DE95-001504] p 1327 N95-20854

LASER MATERIALS
Modelocking and waveguide amplifiers using Cr:Forsterite and Cr:YAG
[AD-A285857] p 1369 N95-20378
Reactor pumped laser research at the Sandia National Laboratories pulsed reactor facilities
[DE95-002181] p 1371 N95-20867
Ultraviolet laser emission properties of Ce(3+)-doped LiSrAlF6
[DE94-016364] p 1372 N95-21135
Applications for reactor-pumped lasers
[DE95-000536] p 1373 N95-21393
Lead-indium phosphate glasses for optical applications
[DE94-019333] p 1275 N95-21482
Laser materials processing at Sandia National Laboratories
[DE95-002183] p 1374 N95-21594

LASER MODE LOCKING
Fiber laser amplifiers and oscillators
[AD-A285835] p 1368 N95-20035
Modelocking and waveguide amplifiers using Cr:Forsterite and Cr:YAG
[AD-A285857] p 1369 N95-20378
Self-starting femtosecond pulse generation from a Ti:sapphire laser synchronously pumped by a pointing-stabilized mode-locked Nd:YAG laser
[DE94-019319] p 1374 N95-21480

LASER OUTPUTS
The effect of reusing laser gas on the fission-fragment pumped 1.73 micron atomic xenon laser output
[DE94-018512] p 1369 N95-20225
Enhanced output of soft x-ray lasers using double slab targets
[DE94-016689] p 1369 N95-20335
The reliability of laser reflowed Sn-Ag solder joints
[AD-A279787] p 1315 N95-20443
Pulsed laser illumination of photovoltaic cells
p 1323 N95-20538
P/N In(Al) GaAs multijunction laser power converters
p 1323 N95-20539
Investigation of laser-induced retinal damage: Wavelength and pulsewidth dependent mechanisms
[AD-A286066] p 1443 N95-20848
Chemical lasers emitting in the visible spectrum: Metastable oxygen reactions and YOSHIDA laser
[PB95-104485] p 1372 N95-20983
Ultraviolet laser emission properties of Ce(3+)-doped LiSrAlF6
[DE94-016364] p 1372 N95-21135
Neutronics and shielding analysis of the National Ignition Facility
[DE94-016698] p 1534 N95-21208
EBIT x ray spectroscopy studies for applications to photo-pumped x ray lasers
[DE94-016701] p 1373 N95-21210
NEO-LISP: Deflecting near-Earth objects using high average power, repetitively pulsed lasers
[DE95-000863] p 1599 N95-21367
Self-starting femtosecond pulse generation from a Ti:sapphire laser synchronously pumped by a pointing-stabilized mode-locked Nd:YAG laser
[DE94-019319] p 1374 N95-21480
Collisional redistribution effects on x ray laser saturation behavior
[DE94-017308] p 1374 N95-21663
Technique for intracavity sum frequency generation
[AD-D016478] p 1546 N95-21898
Coherence properties of high order harmonic radiation
[DE94-016974] p 1377 N95-22312

LASER PLASMA INTERACTIONS
Large facilities pilot programme. Access to the VULCAN High Power Laser Facilities at Rutherford Appleton Laboratory
[PB95-130340] p 1373 N95-21226

LASER PLASMAS
X-ray imaging of uniform large scale-length plasmas created from gas-filled targets on Nova
[DE94-018339] p 1531 N95-20015
Characterization of an expanded-field Schwarzschild objective for extreme ultraviolet lithography
[DE94-016780] p 1541 N95-20239
24th Annual Anomalous Absorption Conference
[DE94-016457] p 1551 N95-20283
A comparison of kinetic and multifluid simulations of laser-produced colliding plasmas
[DE94-016447] p 1551 N95-20315

Observation of strong emission from NeIX and NeX transitions in a laser-driven plasma
[DE95-002265] p 1555 N95-20813
Time-resolved diagnostics of excimer laser-generated ablation plasmas used for pulsed laser deposition
[DE94-018950] p 1559 N95-21547
Cryogenic pellet laser plasma source targets
[DE95-002488] p 1376 N95-22169
The final status of a metal surface after multipulse laser irradiation in an ambient gas
[DE94-629000] p 1562 N95-22377

LASER POWER BEAMING
Scaling of solid state lasers for satellite power beaming applications
[DE94-016366] p 1368 N95-19986
Modeling of high efficiency solar cells under laser pulse for power beaming applications p 1318 N95-20516

LASER PUMPING
EBIT x ray spectroscopy studies for applications to photo-pumped x ray lasers
[DE94-016701] p 1373 N95-21210
Self-starting femtosecond pulse generation from a Ti:sapphire laser synchronously pumped by a pointing-stabilized mode-locked Nd:YAG laser
[DE94-019319] p 1374 N95-21480
Tunable CW blue, green, orange and red upconversion fiber lasers at room temperature
[DE95-000851] p 1375 N95-22007
High average power diode pumped solid state lasers for CALIOPE
[DE94-019248] p 1376 N95-22121

LASER SPECTROMETERS
Visible fluorescence of weathered lead
[DE95-002454] p 1244 N95-21523

LASER TARGETS
Target Area Structural Support systems design to achieve the micron-level stability requirement of the National Ignition Facility (NIF)
[DE94-017696] p 1551 N95-20219
Enhanced output of soft x-ray lasers using double slab targets
[DE94-016689] p 1369 N95-20335
High precision Woelter optic calibration facility
[DE94-016973] p 1542 N95-20364
Cryogenic targets for inertial confinement fusion
[DE94-016200] p 1555 N95-21115
Target Area design basis and system performance for the National Ignition Facility
[DE94-016697] p 1557 N95-21207
Neutronics and shielding analysis of the National Ignition Facility
[DE94-016698] p 1534 N95-21208
Large facilities pilot programme. Access to the VULCAN High Power Laser Facilities at Rutherford Appleton Laboratory
[PB95-130340] p 1373 N95-21226
Low density gas and foam targets for ICF long scale length plasma experiments: Fabrication and characterization
[DE95-000935] p 1558 N95-21368
Submicrosecond, synchronizable x-ray source
[AD-D016497] p 1546 N95-21905
Cryogenic pellet laser plasma source targets
[DE95-002488] p 1376 N95-22169
Target alignment in the National Ignition Facility
[DE94-015559] p 1540 N95-22469

LASER WELDING
Application of a dimensionless parameter model for Laser Beam Welding
[DE94-018902] p 1378 N95-20048
Laser materials processing at Sandia National Laboratories
[DE95-002183] p 1374 N95-21594
International Symposium on Advanced Laser Technologies
[AD-A279849] p 1376 N95-22164

LASERS
Photodegradation and photophysics of laser dyes
[AD-A285105] p 1368 N95-20063
Program of the 1993 9th Interdisciplinary Laser Science Conference (ILS-9)
[AD-A285131] p 1369 N95-20082
International collaboration program on innovative chemical processing of superior electronic and optical materials
[AD-A285122] p 1226 N95-20105
Time domain spectral hole-burning storage
[AD-A279912] p 1587 N95-20309
Three-dimensional laser cooling
[DE94-017963] p 1370 N95-20569
Inverse Cerenkov laser acceleration experiment at ATF
[DE94-017990] p 1370 N95-20572
Effects of plasma physics on capsule implosions in gas-filled hohlraums
[DE95-000923] p 1371 N95-20786
Performance of the NIF prototype beamlet
[DE94-018500] p 1371 N95-20817
Detection optimization using linear systems analysis of a coded aperture laser sensor system
[DE95-001112] p 1371 N95-20832
X-ray spectroscopy of xenon
[DE95-002132] p 1240 N95-20865
Plasma Electrode Pockels Cells for the Beamlet and NIF lasers
[DE94-016541] p 1557 N95-21166
Threshold detection in the presence of atmospheric turbulence
[AD-A286175] p 1427 N95-22249
Quantum chemical study of rare gas/halide interactions as a model for high energy density material. 2: The interaction of hydrogen chloride with the rare gas xenon
[AD-A286385] p 1248 N95-22321

LASING
Recent progress of the compact AFEL at Los Alamos
[DE95-002728] p 1376 N95-22154

LATCH-UP
SEU and SEL response of the Westinghouse 64K E-2PROM, analog devices AD7876 12-bit ADC, and the Intel 82527 Serial Communications Controller
[DE95-003349] p 1334 N95-22086
Radiation characterization report for the GPS Receiver microcontroller chip
[DE94-019169] p 1335 N95-22165

LATITUDE
Radiative forcing for changes in tropospheric O3
[DE94-019017] p 1413 N95-20354

LATTICE PARAMETERS
Simulations of the dislocation array at Ge/Si interfaces
[DE94-017680] p 1565 N95-20244
Semi-leptonic form-factors from lattice QCD
[DE95-000871] p 1510 N95-20367
Behaviour of space-charge dominated ion beams in storage rings
[DE94-015845] p 1517 N95-21140

LATTICES (MATHEMATICS)
Coupled analytic maps
[PB95-111076] p 1498 N95-19945
Duality beyond sober spaces: Topological spaces and observation frames
[PB95-134565] p 1494 N95-21962
Full potential multiple scattering theory
[DE95-003197] p 1576 N95-22084
Singular symmetric matrices
[PB95-109088] p 1496 N95-22354

LAUNCH VEHICLES
Space fundamentals for the war fighter
[AD-A279703] p 1217 N95-20690
Military standard: Test requirements for launch, upper-stage, and space vehicles
[AD-A286627] p 1218 N95-20770
Launch vehicle flight control augmentation using smart materials and advanced composites (CDDF Project 93-05)
[NASA-TP-3535] p 1218 N95-21346

LAUNCHING
Challenger's night flight
[NASA-TM-110503] p 1217 N95-19995
Chunk projectile launch using the Sandia Hypervelocity Launcher Facility
[DE94-018494] p 1215 N95-20223
White-light spectral analysis of lithium niobate waveguides
[DE94-016692] p 1542 N95-20489
Computational design of Hypervelocity Launchers
[DE95-000744] p 1218 N95-20785
GPHS-RTGs in support of the Cassini Mission
[DE95-001492] p 1222 N95-20853
Temporal evolution of turbulence/chemistry interactions in lifted, turbulent-jet flames
[DE95-002481] p 1243 N95-21512
Launch safety, toxicity, and environmental effects of the high performance oxidizer ClF(5)
[AD-A286095] p 1284 N95-22227

LAW (JURISPRUDENCE)
Environmental Compliance Assessment and Management Program
[AD-A279605] p 1402 N95-20441
Environmental Compliance Assessment Protocol - Centers for Disease Control and Prevention (ECAP-CDC), West Virginia supplement
[AD-A286009] p 1403 N95-20720
Environmental Compliance Assessment and Management Program (ECAMP), South Carolina supplement
[AD-A279533] p 1408 N95-21689
Environmental Compliance Assessment System (ECAS): Oregon supplement
[AD-A279565] p 1408 N95-21696

LAWS
A convergence analysis of an h-version finite element method with high order elements for two dimensional elasto-plasticity problems
[AD-A279975] p 1491 N95-20920

LEAD ACID BATTERIES
Progress in the development of recycling processes for electric vehicle batteries
[DE94-015894] p 1324 N95-20626

LEAD COMPOUNDS
Lead-indium phosphate glasses for optical applications
[DE94-019333] p 1275 N95-21482

LEAD OXIDES
Anodic oxygen-transfer electrocatalysis at iron-doped lead dioxide electrodes
[DE95-001653] p 1242 N95-21397
Effects of neutron irradiation on the London penetration depth for polycrystalline Bi(1.8)Pb(0.3)Sr2Ca2Cu3O10 superconductor
[DE94-019335] p 1573 N95-21483
Integration of thin film decoupling capacitors
[DE95-001609] p 1333 N95-21881

LEAD SELENIDES
Sputter deposition of multilayer thermoelectric films: An approach to the fabrication of two-dimensional quantum wells
[DE95-002396] p 1272 N95-20892

LEAD TELLURIDES
Sputter deposition of multilayer thermoelectric films: An approach to the fabrication of two-dimensional quantum wells
[DE95-002396] p 1272 N95-20892

LEAD TITANATES
Raman spectra of MOCVD-grown ferroelectric PbTiO3 thin films
[DE94-018964] p 1244 N95-21549

LEAD TUNGSTATES
Light output and radiation damage in a lead tungstate crystal
[DE94-016814] p 1565 N95-20265

LEAD ZIRCONATE TITANATES
Fabrication of PLZT/ITO grating for optical switching and reconfigurable optical interconnect applications
[AD-A286389] p 1548 N95-22248

LEADERSHIP
Estimating the costs of human space exploration
p 1584 N95-20744

LEADING EDGES
Direct numerical simulations of leading-edge receptivity for freestream sound p 1351 N95-21090
Seismic evidence for volatiles at large depth in the Earth p 1422 N95-21808

LEAF AREA INDEX
Remote-sensing based technique to account for sub-grid scale variability of land surface properties
[NASA-TM-110501] p 1390 N95-22110

LEAKAGE
Corrosion evaluation of fuel canister crusher rigging
[DE95-002962] p 1257 N95-21452
The permeation of bis(2-fluoro-2,2-dinitroethyl) formal (FEFO), ethyl 4,4-dinitropentanoate (EDNP), ethyl 4-nitropentanoate (ENP), and 1,2,4-trichlorobenzene (TCB) through barrier membranes
[DE95-002492] p 1283 N95-21514
New concepts for refrigerant leak detection and mixture measurement
[DE94-018967] p 1287 N95-21559

LEARNING
Learning algorithms for feedforward networks based on finite samples
[DE95-001739] p 1483 N95-21741

LEASING
Research on the promotion measures to introduce new energy and energy-saving technologies with a leasing system
[DE95-714801] p 1375 N95-22079

LEAST SQUARES METHOD
Comparison of meteorological data with fitted values extracted from projectile trajectory
[AD-A285921] p 1428 N95-19989
Uncertainty estimates for derivatives and intercepts
[DE94-018492] p 1489 N95-20222
Modeling of beam dynamics and comparison with measurements for the Advanced Light Source (ALS)
[DE94-017970] p 1532 N95-20495
Brief tutorial on the Kalman filter
[AD-A286571] p 1326 N95-20827
New thermodynamic description of the Cu-Zr system
[PB95-127189] p 1263 N95-22374

LEGENDRE FUNCTIONS
Atomic orbital basis sets for molecular interactions
[AD-A279609] p 1506 N95-19959

LEGIBILITY
Evaluation of the Haworth-Newman avionics Display Readability Scale
[AD-A286127] p 1214 N95-22232
LENNARD-JONES POTENTIAL
New methods for large scale local and global optimization
[AD-A285635] p 1517 N95-21126
A massively parallel algorithm for grand canonical Monte Carlo computer simulation with the short-ranged Lennard-Jones potential
[DE94-010396] p 1477 N95-21843
LENS ANTENNAS
Measurements of the Auburn ECE optical system parameters for temperature fluctuation measurements on TEXT-U
[DE94-019217] p 1562 N95-22120
LENSES
Effects of bifocal and progressive-addition corrective lenses on aviator target-detection performance
[AD-A279698] p 1442 N95-20710
Gradient index lenses from sol-gel layering
[AD-A285649] p 1242 N95-21402
Application of computer-generated holograms to optical transformations
[AD-A286356] p 1368 N95-22256
LEPTONS
J/psi,psi(prime) yields mu(+)mu(-) and B yields J/psi,psi(prime) cross sections
[DE94-017184] p 1507 N95-20108
CDF top results in the lepton + jets channel
[DE95-000641] p 1507 N95-20131
Search for W pair production with dilepton decay modes at D0
[DE95-000724] p 1508 N95-20134
CDF top results in the dilepton channel
[DE95-000837] p 1510 N95-20343
Semi-leptonic form-factors from lattice QCD
[DE95-000871] p 1510 N95-20367
Universal parametrization for quark and lepton substructure
[DE94-770604] p 1514 N95-20738
Kinematical evidence for top pairs at the Tevatron
[DE95-000729] p 1515 N95-20880
Evidence for t(bar t) production at the Tevatron: Statistical significance and cross section
[DE95-002524] p 1515 N95-20897
Anomalous vector-boson couplings in Majorana neutrino models
[PB95-127460] p 1518 N95-21220
Heavy ion collisions
[DE95-002712] p 1520 N95-21321
Dilepton production from p-p to Ca-Ca at the Bevalac
[DE95-002341] p 1520 N95-21357
Measurement of W and Z production cross-sections in p(bar p) collisions at (radical)s = 1.8 TeV
[DE95-002250] p 1523 N95-21521
Measurement of the B cross section at CDF via B semileptonic decays
[DE95-002217] p 1524 N95-21597
Status of the DO top search
[DE95-002214] p 1525 N95-21715
Testing the principle of equivalence by solar neutrinos
[DE94-014972] p 1604 N95-22064
Tests of structure functions using lepton pairs: W-charge asymmetry at CDF
[DE95-000560] p 1527 N95-22122
LEVITATION MELTING
Low rotational drag in high-temperature superconducting bearings
[DE95-002983] p 1382 N95-22292
LEWIS NUMBERS
Effects of non-unity Lewis numbers in diffusion flames
p 1249 N95-21036
Direct numerical simulations of turbulent non-premixed methane-air flames modeled with reduced kinetics
p 1249 N95-21038
Lewis number and Damkohler number effects in vortex-flame interactions p 1249 N95-22439
LIBRARIES
Design considerations for parallel graphics libraries
[NASA-CR-194935] p 1473 N95-20013
New data for MCNP (trademark)
[DE94-016296] p 1509 N95-20236
The design of a parallel, dense linear algebra software library: Reduction to Hessenberg, tridiagonal, and bidiagonal form
[DE94-018123] p 1491 N95-20701
The 37th Military Librarians Workshop on Global Information: The Sun Never Sets
[AD-A286636] p 1588 N95-20774
Shaping the library of the future: Digital library developments at Los Alamos National Laboratory's Research Library
[DE95-001008] p 1588 N95-20777
The Energy Science and Technology Database on a local library system: A case study at the Los Alamos National Research Library
[DE95-001009] p 1589 N95-20818
University library document circulation system specified in LCM
[PB95-127957] p 1592 N95-22331
LIE GROUPS
Weighted strongly elliptic operators on lie groups
[PB95-110847] p 1487 N95-19917
On the differential representations of quantum Lie superalgebras
[DE94-629874] p 1491 N95-20734
Positive rockland operators
[PB95-127510] p 1493 N95-21423
LIFE (DURABILITY)
Residual stresses in material processing
[DE94-017888] p 1385 N95-20374
Investigation of the stability and 1.0 MeV proton radiation resistance of commercially produced hydrogenated amorphous silicon alloy solar cells p 1320 N95-20522
Exponents in lifetime and power spectral density forms in self-organized critical systems
[AD-A286242] p 1495 N95-22026
LIFE CYCLE COSTS
Exploratory Technology Research Program for electrochemical energy storage
[DE95-002652] p 1394 N95-20915
Power systems for future missions. Appendices A-L
[NASA-CR-195320-APP-A-L] p 1395 N95-21530
Power systems for future missions
[NASA-CR-195320] p 1222 N95-21531
High speed optical storage technology
[AD-A285788] p 1456 N95-22400
LIFE RAFTS
AN/APS-137 Forward Looking Airborne Radar (FLAR) evaluation, Fall 1992 experiment
[AD-A279526] p 1306 N95-21686
LIFE SCIENCES
Annual program analysis of the NASA Space Life Sciences Research and Education Support Program
[NASA-CR-197298] p 1439 N95-21529
Aerospace medicine and biology: A continuing bibliography with indexes (supplement 399)
[NASA-SP-7011(399)] p 1446 N95-21947
Life Sciences Division and Center for Human Genome Studies
[DE94-017796] p 1440 N95-22065
LIFE SPAN
Optimizing the length of the stores and related effects
[DE95-002531] p 1533 N95-20885
LIFE SUPPORT SYSTEMS
Aerospace medicine and biology: A continuing bibliography with indexes (supplement 399)
[NASA-SP-7011(399)] p 1446 N95-21947
LIFT
Lift enhancement device
[AD-D016522] p 1201 N95-21864
LIFT AUGMENTATION
Experiments on the flow field physics of confluent boundary layers for high-lift systems
[NASA-CR-197318] p 1201 N95-21343
LIFT DEVICES
Wake measurements in a strong adverse pressure gradient
[NASA-CR-197272] p 1201 N95-21031
Experiments on the flow field physics of confluent boundary layers for high-lift systems
[NASA-CR-197318] p 1201 N95-21343
Lift enhancement device
[AD-D016522] p 1201 N95-21864
Experimental investigations of on-demand vortex generators p 1361 N95-22451
LIFTOFF (LAUNCHING)
STS Flight 64 mission highlights
[NASA-TM-110515] p 1219 N95-22295
LIGANDS
New chiral pyrimidino-crown ether ligands
[AD-A279892] p 1223 N95-20590
Thermodynamic and NMR studies of solvent effect on enantiomeric recognition for a chiral organiz ammonium cation by chiral diketopyridino-18-Crown-6 type ligands at 25.0 C
[AD-A279893] p 1223 N95-20592
Time-resolved analytical methods for liquid/solid interfaces
[DE95-002255] p 1240 N95-20780
Introduction to the structures determination methods using X-ray diffraction in monocrystals: Application to some lanthanides and transition metals complexes with organic ligands
[DE94-629002] p 1579 N95-22380
Synthesis and characterization of single-source molecular precursors to binary metal sulphides: Bis(diethyldithiocarbamato) M(2)trialkylphosphine (M = Zn and Cd) adducts
[AD-A279746] p 1248 N95-22385
LIGHT (VISIBLE RADIATION)
Free electron laser program
[AD-A285906] p 1368 N95-19987
LIGHT AMPLIFIERS
Fiber laser amplifiers and oscillators
[AD-A285835] p 1368 N95-20035
Modelocking and waveguide amplifiers using Cr:Forsterite and Cr:YAG
[AD-A285857] p 1369 N95-20378
GaAs optical circuits
[AD-A285859] p 1369 N95-20389
Analysis of direct detection lightwave systems with optical amplifiers
[AD-A284077] p 1542 N95-20467
LIGHT BEAMS
Computational model of drilling with high radiance pulsed lasers
[DE94-018548] p 1371 N95-20783
Investigation of laser-induced retinal damage: Wavelength and pulsewidth dependent mechanisms
[AD-A286066] p 1443 N95-20848
Electro-optic effect in the PESO acousto-optic modulator
[AD-A286355] p 1548 N95-22255
LIGHT ELEMENTS
Distribution of light element isotopes in Bencubbin and Weatherford meteorites: An indicator of heterogeneity in the primitive solar nebula
[DE94-019167] p 1600 N95-22128
LIGHT EMITTING DIODES
Visible light emitting materials and injection devices
[AD-A284796] p 1541 N95-20066
International Conference on Optical Computing: Technical digest
[AD-A284293] p 1541 N95-20249
Design, fabrication, and characterization of reflective diffractive optical elements in Si for free-space optical interconnects
[AD-A286416] p 1547 N95-22205
LIGHT GAS GUNS
Computational design of Hypervelocity Launchers
[DE95-000744] p 1218 N95-20785
LIGHT IONS
LIF standoff research
[DE94-018744] p 1535 N95-21328
Similarities and differences in strangeness production at BNL and CERN
[DE95-002343] p 1521 N95-21380
Progress in the Light Ion Driven Inertial Confinement Fusion Program
[DE94-019182] p 1537 N95-21603
LIGHT MODULATION
High contrast organic crystal optical modulator for phased array antenna and optical signal processing
[AD-A286557] p 1544 N95-20844
Optical, electronic and optoelectronic material and device research
[AD-A280111] p 1374 N95-21630
Application of computer-generated holograms to optical transformations
[AD-A286356] p 1368 N95-22256
LIGHT SCATTERING
Simulation of stellar speckle imaging
[DE94-016606] p 1412 N95-19985
Light-scattering fluctuations and noise in nonlinear optical processing
[AD-A279748] p 1544 N95-20803
Nonlinear frequency conversion optical filter
[AD-D016523] p 1544 N95-21465
The optical properties of particles deposited on a surface
[AD-A286258] p 1546 N95-22002
Electro-optic effect in the PESO acousto-optic modulator
[AD-A286355] p 1548 N95-22255
LIGHT SOURCES
Modeling of beam dynamics and comparison with measurements for the Advanced Light Source (ALS)
[DE94-017970] p 1532 N95-20495
Testing of the SAIC facets on the stretched-membrane dish
[DE95-001831] p 1393 N95-20864
Novel absorption detection techniques for capillary electrophoresis
[DE95-001673] p 1242 N95-21400
Diffraction applications using the energy dispersive beamline, X6A, at NSLS
[DE94-019287] p 1572 N95-21408

LIGHT TRANSMISSION

Light output and radiation damage in a lead tungstate crystal
[DE94-016814] p 1565 N95-20265

Magnetic flocculation of paramagnetic particles
[DE94-018144] p 1501 N95-20725

Unlimited-bandwidth distributed optical phase modulators and detectors: Design and fabrication issues
[DE94-017418] p 1545 N95-21509

Light output and radiation damage in a YAIO3:Ce crystal
[DE94-016815] p 1545 N95-21643

LIGHTHILL GAS MODEL

Acoustics of laminar boundary layers breakdown
p 1361 N95-22455

LIGHTNING

The initiation of lightning and the growth of electric fields in thunderstorms
[AD-A280033] p 1428 N95-20008

Estimation of lightning stroke peak current as a function of peak electric field and the normalized amplitude of signal strength: Corrections and improvements
[DE94-016900] p 1335 N95-22189

LIMITS (MATHEMATICS)

Set functionals in stochastic geometry
[PB95-135372] p 1491 N95-21005

LINE CURRENT

High isolation electronic switch
[AD-D016533] p 1326 N95-20729

Low-frequency image theory for a current dipole in front of a permeable sphere
[PB95-127676] p 1300 N95-21104

LINE OF SIGHT

Evolution of ground line of sight data field collection techniques
[AD-A285062] p 1204 N95-20497

Line-of-sight multipath propagation measurements at 15 GHz over 500 MHz bandwidth p 1296 N95-20944

LINE OF SIGHT COMMUNICATION

Simulation of the impact of atmospheric turbulences on millimeter-wave communications systems
p 1295 N95-20939

LINE SHAPE

Solid-state NMR characterization of C- and N-labelled phthalimides: Model compounds for studying polyimides
[AD-A286479] p 1578 N95-22286

LINE SPECTRA

Identification of resonant, two-electron, and inter-atomic features in K and L23 NEXAFS spectra
[AD-A285374] p 1513 N95-20554

Ultraviolet emission from rocket motor plumes
[DSTO-TR-0002] p 1222 N95-21661

LINEAR ACCELERATORS

Free electron laser program
[AD-A285906] p 1368 N95-19987

Studies of longitudinal instability with an electron beam
[DE94-018646] p 1532 N95-20347

Inverse Cerenkov laser acceleration experiment at ATF
[DE94-017990] p 1370 N95-20572

A URI program for Ultraviolet/extreme ultraviolet research
[AD-A279159] p 1370 N95-20600

Induction linacs for heavy ion fusion
[DE95-002357] p 1534 N95-20891

Issues in multi-bunch emittance preservation in the NLC
[DE95-002894] p 1534 N95-21253

First results from the final focus test beam
[DE95-002897] p 1535 N95-21255

Exclusive processes: Tests of coherent QCD phenomena and nucleon substructure at CEBAF
[DE95-002892] p 1520 N95-21336

An 8-meter-long coupled cavity RFQ linac
[DE94-018077] p 1331 N95-21667

High performance computing for beam physics applications
[DE94-018312] p 1539 N95-22243

Recent results in analysis and simulation of beam halo
[DE94-018313] p 1539 N95-22298

Fabrication and characterization of cesium telluride photocathodes: A promising electron source for the Los Alamos Advanced FEL
[DE94-018303] p 1377 N95-22348

LINEAR AMPLIFIERS

Hybrid high power amplifier
[AD-D016534] p 1326 N95-20730

LINEAR ARRAYS

Design and implementation of a dual-beam printed antenna for a reception in angular diversity on a Hertzien cluster (or bundle)
[PB95-131603] p 1302 N95-21431

LINEAR ENERGY TRANSFER (LET)

Radiation characterization report for the GPS Receiver microcontroller chip
[DE94-019169] p 1335 N95-22165

LINEAR EQUATIONS

Uniqueness of strongly regular graphs having minimal p-rank
[PB95-111043] p 1488 N95-19942

Regularity of BPa-systems is decidable
[PB95-135489] p 1468 N95-21619

Report of the Numerical Analysis Group
[PB95-108163] p 1494 N95-21648

LINEAR QUADRATIC GAUSSIAN CONTROL

Riccati equation theory for Pritchard-Salamon systems: A Popov function approach
[PB95-137089] p 1491 N95-20830

LINEAR SYSTEMS

O(log2 n) time efficient parallel factorization of dense, sparse separable, and banded matrices
[NASA-CR-197356] p 1473 N95-19885

Asymptotic analysis of Nash equilibria in nonzero-sum linear-quadratic differential games. The two-player case
[PB95-111027] p 1499 N95-19941

Detection optimization using linear systems analysis of a coded aperture laser sensor system
[DE95-001112] p 1371 N95-20832

Linear and nonlinear spectroscopy with the tunable AC scanning tunneling microscope
[AD-A285751] p 1241 N95-21217

Semi-global stabilization of linear discrete-time systems subject to input saturation via linear feedback: An ARE-based approach
[PB95-135463] p 1483 N95-21618

Adaptive capture of expert behavior
[DE94-018285] p 1483 N95-21710

A new Krylov-subspace method for symmetric indefinite linear systems
[DE95-001826] p 1355 N95-21726

QMRPACK user's guide
[DE95-001770] p 1469 N95-21744

LINEAR TRANSFORMATIONS

View-based models of 3D object recognition and class-specific invariance
[AD-A279858] p 1459 N95-20157

Object recognition by alignment using invariant projections of planar surfaces
[AD-A279841] p 1468 N95-21495

LINING PROCESSES

Epoxy lining for shipboard piping systems
[AD-A286228] p 1279 N95-22022

LININGS

Epoxy lining for shipboard piping systems
[AD-A286228] p 1279 N95-22022

LIOUVILLE EQUATIONS

Quantum diffusion
[DE95-001015] p 1580 N95-21264

LIPIDS

Enhancement of cell mediated immunity through non-specific immunostimulation with liposome encapsulated gamma-interferon
[AD-A279667] p 1442 N95-20602

LIQUEFACTION

Assessment of liquefaction and pyrolysis systems
[PB95-129797] p 1236 N95-20290

LIQUEFIED GASES

Liquid xenon as a potential laser host medium
[AD-A285365] p 1370 N95-20550

LIQUID ALLOYS

Thermodynamic analysis of stable and metastable equilibrium diagrams of the Cu-Cr system
[PB95-127775] p 1255 N95-21111

LIQUID COOLING

Liquid flow-through cooling of electronic modules
p 1211 N95-20647

Microchannel heat pipe cooling of modules
p 1211 N95-20649

LIQUID CRYSTALS

The synthesis and characterization of new mesogenic diacetylene monomers and their polymers
[AD-A286188] p 1267 N95-20328

Hierarchical structure in advanced polymers. Phase behaviour, orientation, properties
[AD-A285938] p 1268 N95-20392

Optical power limiting liquid crystal composites
[AD-A286605] p 1569 N95-20767

Development of ferroelectric liquid crystals with enhanced nonlinear optical properties
[AD-A279988] p 1571 N95-20965

NMR relaxation behavior of the head group of SHBS in lamellar liquid crystals
[AD-A279124] p 1574 N95-21599

Biaxiality of chiral liquid crystals
[DE94-629032] p 1578 N95-22277

LIQUID FUELS

Bioconversion of coal derived synthesis gas to liquid fuels
[DE94-017381] p 1282 N95-19927

Bioconversion of coal derived synthesis gas to liquid fuels
[DE94-018849] p 1314 N95-20339

Cryogenic targets for inertial confinement fusion
[DE94-016200] p 1555 N95-21115

Producing liquid fuels from biomass
[DE95-717458] p 1398 N95-22425

LIQUID HELIUM

Josephson acoustic radiation in superfluid helium
[AD-A279809] p 1503 N95-20098

New theory of critical flow velocities in superfluid helium
[PB95-130365] p 1571 N95-21228

Microscopic theory of normal liquid He-3
[DE94-629047] p 1527 N95-22179

The dynamic structure function of Bose liquids in the deep inelastic regime
[DE94-629077] p 1527 N95-22182

LIQUID HYDROGEN

Structure functions and structure function ratio F(sup n)2/F(sup p)2 at small x(sub Bj) and Q2 in muon-nucleon scattering
[DE94-017981] p 1530 N95-22340

LIQUID INJECTION

Characterization and electrical properties of copper films grown via direct liquid coinjection of (hfac)Cu(TMVS) and TMVS
[DE95-002957] p 1272 N95-20889

LIQUID LEVELS

Optical fiber pressure sensor for liquid level monitoring
[AD-D016246] p 1547 N95-22089

LIQUID METAL FAST BREEDER REACTORS

Irradiation creep in structural materials at ITER operating conditions
[DE94-018946] p 1261 N95-22123

LIQUID METALS

Liquid-metal pin-fin pressure drop by correlation in cross flow
[DE94-017086] p 1338 N95-19923

Recent reflux receiver developments under the US DOE program
[DE95-001622] p 1393 N95-20861

MHD pressure drop in ducts with imperfectly insulating coatings
[DE95-002852] p 1558 N95-21244

MHD-flow in slotted channels with conducting walls
[DE94-018370] p 1559 N95-21388

LIQUID NITROGEN

Design and thermal stress analysis of high power x-ray monochromators cooled with liquid nitrogen
[DE94-016879] p 1500 N95-20106

LIQUID PHASE EPITAXY

High quality InP-on-Si for solar cell applications
p 1317 N95-20510

LIQUID PHASES

Thermal decomposition reactions of HMX and RDX and their importance in predicting cookoff hazards
[DE95-002486] p 1283 N95-21513

Hydrogenation of nitriles on a well-characterized nickel surface: From surface science studies to liquid phase catalytic activity measurements
[DE94-018184] p 1259 N95-21707

Solar system formation and the distribution of volatile species p 1421 N95-21806

Biaxiality of chiral liquid crystals
[DE94-629032] p 1578 N95-22277

LIQUID ROCKET PROPELLANTS

High pressure windowed chamber burned rate determination of liquid propellant XM46
[AD-A283770] p 1282 N95-19920

LIQUID-LIQUID INTERFACES

Studies of the n-alkane/water interface by total internal reflection second harmonic generation
[AD-A279473] p 1245 N95-21827

LIQUID-SOLID INTERFACES

Time-resolved analytical methods for liquid/solid interfaces
[DE95-002255] p 1240 N95-20780

Nonlinear optical studies of polymer interfaces
[DE94-018199] p 1274 N95-21263

Quantum simulation of heterogeneous electron transfer free energies at the water-metal interface
[AD-A279279] p 1522 N95-21492

LIQUID-VAPOR INTERFACES

Transport phenomena in the micropores of plug-type phase separators
[NASA-TM-108479] p 1340 N95-20561

LIQUIDS

The primary carbon and the formation of carbon species in terrestrial magmas p 1420 N95-21797

Variational Monte Carlo study of He-4 in two dimensions
[DE94-629078] p 1576 N95-21998

LITHIUM

A new family of anion receptors and their effects on ion pair dissociation and conductivity of lithium salts in non-aqueous solutions
[DE94-016822] p 1512 N95-20477
Review of recent D-T experiments from TFTR
[DE95-002755] p 1557 N95-21239
Fusion power production in TFTR
[DE95-002756] p 1557 N95-21240
Shot-to-shot comparison of the first Li-beam driven Hohlraum experiments
[DE94-016558] p 1558 N95-21247
Progress in the Light Ion Driven Inertial Confinement Fusion Program
[DE94-019182] p 1537 N95-21603
Transient studies of low temperature catalysts for methane conversion
[DE95-003560] p 1247 N95-22224

LITHIUM ALLOYS

The mechanical property data base from an Air Force/Industry cooperative test program on advanced aluminum alloys
[AD-A280038] p 1386 N95-20615

LITHIUM CHLORIDES

A new family of anion receptors and their effects on ion pair dissociation and conductivity of lithium salts in non-aqueous solutions
[DE94-016822] p 1512 N95-20477

LITHIUM COMPOUNDS

A transmission electron microscope characterization of sodium sulfate hot corrosion of silicon carbide fiber-reinforced lithium aluminosilicate glass-ceramic matrix composite
[AD-A286164] p 1231 N95-22038

LITHIUM FLUORIDES

Effect of microgravity on material undergoing melting and freezing: The TES Experiment
[NASA-TM-106845] p 1338 N95-19952

LITHIUM NIOBATES

Design and packaging aspects of microwave bandwidth lithium niobate modulators
[DE94-016602] p 1313 N95-20119
White-light spectral analysis of lithium niobate waveguides
[DE94-016692] p 1542 N95-20489
Epitaxial liftoff technology onto processed silicon foundry wafers
[AD-A285621] p 1571 N95-21145

LITHOGRAPHY

Characterization of an expanded-field Schwarzschild objective for extreme ultraviolet lithography
[DE94-016780] p 1541 N95-20239
Radiation-induced modifications of allylamino-substituted polyphosphazenes
[AD-A279694] p 1268 N95-20428
Beryllium based multilayers for normal incidence extreme ultraviolet reflectivity
[DE94-015560] p 1274 N95-21175
Design, fabrication, and characterization of reflective diffractive optical elements in Si for free-space optical interconnects
[AD-A286416] p 1547 N95-22205
Reflective masks for extreme ultraviolet lithography
[DE95-003427] p 1336 N95-22236
Parallel nanometer scale fabrication
[DE95-002122] p 1336 N95-22284

LITHOLOGY

VTT test borehole for bedrock investigations
[PB95-132965] p 1427 N95-22095

LITHOSPHERE

Subduction of hydrated basalt of the oceanic crust: Implications for recycling of water into the upper mantle and continental growth p 1423 N95-21814
Storage and recycling of water and carbon dioxide in the earth p 1425 N95-21822

LOAD DISTRIBUTION (FORCES)

A method to determine the kinematics of the lower limbs of a subject pedaling a bicycle using encoders and accelerometers
[NASA-CR-197401] p 1453 N95-21866

LOAD TESTS

Finite element modelling of creep crack growth in 316 stainless and 9Cr-1Mo steels
[DE94-018977] p 1258 N95-21560

LOADS (FORCES)

Turbulence descriptors for scaling fatigue loading spectra of wind turbine structural components
[DE94-011833] p 1384 N95-20109
Force based motion control of a walking machine
[PB95-129672] p 1451 N95-20276
Hydrostatic force sensor
[DE94-018923] p 1364 N95-20321
Utilizing artificial neural networks in network flow analysis: An annotated bibiliography
[DE95-002453] p 1482 N95-21522
A user's guide to LUGSAN 1.1: A computer program to calculate and archive lug and sway brace loads for aircraft-carried stores
[DE95-001919] p 1207 N95-21730
Breakdown of the law of large numbers in Josephson junction series arrays
[DE94-629075] p 1576 N95-21996
Counting methods for the analysis of load time histories
[PB95-132916] p 1388 N95-22093
Embedded optical fibres as strain sensors in polymer matrix fibre composites: The influence of adhesion in strain transfer
[PB95-133617] p 1547 N95-22140
Wave journal bearing. Part 1: Analysis
[NASA-CR-195431-PT-1] p 1382 N95-22404

LOCAL AREA NETWORKS

An abstract model of rogue code insertion into radio frequency wireless networks. The effects of computer viruses on the Program Management Office
[AD-A285759] p 1288 N95-19932
Non-intrusive SCSI status sensing system
[AD-D016242] p 1476 N95-21307
SCSI controller with target status retrieval
[AD-D016249] p 1476 N95-21504
A simulation study of TCP performance in ATM networks
[DE94-016622] p 1477 N95-21505
Programmable modular network interface
[AD-D016505] p 1477 N95-21674
Method of sensing target status in a local area network
[AD-D016248] p 1478 N95-22090
Method of non-intrusively sensing status in a computer peripheral
[AD-D016241] p 1478 N95-22146
Design and modelling of a link monitoring mechanism for the Common Data Link (CDL)
[AD-A286167] p 1309 N95-22245

LOCOMOTION

Perception and control of locomotion
[AD-A285605] p 1450 N95-21192

LOGARITHMS

O(log2 n) time efficient parallel factorization of dense, sparse separable, and banded matrices
[NASA-CR-197356] p 1473 N95-19885
Flux creep with logarithmic U(j) dependence
[DE94-629058] p 1577 N95-22180

LOGIC CIRCUITS

GaAs optical circuits
[AD-A285859] p 1369 N95-20389
Methods and components for optical contention resolution in high speed networks
[AD-A280016] p 1543 N95-20598
Complementary GaAs junction-gated heterostructure field effect transistor technology
[DE94-018901] p 1329 N95-21390
Radiation tests on service electronics for future multi TeV detectors
[DE94-632822] p 1335 N95-22184
Data sampling for a burst mode communications system
[AD-A286098] p 1309 N95-22229
Design of a massively parallel computer using bit serial processing elements
[NASA-CR-197365] p 1479 N95-22406

LOGIC PROGRAMMING

Proceedings of the Fourth International Workshop on Inductive Logic Programming (ILP-94)
[PB95-135273] p 1464 N95-21003
Use of operations research techniques in deductive databases
[PB95-135349] p 1589 N95-21004
An IBM based ARINC interface
[ARL-TR-21] p 1471 N95-22104
Method of non-intrusively sensing status in a computer peripheral
[AD-D016241] p 1478 N95-22146
Logic programming and negation: A survey
[PB95-110730] p 1472 N95-22302

LOOP ANTENNAS

A colocated magnetic loop, electric dipole array antenna (preliminary results)
[AD-A285381] p 1290 N95-20556

LOOPS

Effect of lags on human performance with head-coupled simulators
[AD-A279577] p 1453 N95-21700
An exact enumeration of self-avoiding loops on a square lattice
[DE94-628999] p 1578 N95-22276

LORENTZ FORCE

Superconducting electromagnetic thruster
[AD-D016485] p 1355 N95-21902

LOSSES

The Lorentz reciprocity theorem as a consistency test for propagation models p 1295 N95-20937
Cell loss analysis of two-class priority generalized knockout switch
[PB95-127742] p 1301 N95-21109
Origin and loss of the volatiles of the terrestrial planets p 1417 N95-21785
Loss of solar He and Ne from IDPS in subducting sediment: Diffusion and the effect of phase changes
p 1419 N95-21792
Mars atmospheric loss and isotopic fractionation by pick-up-ion sputtering and photochemical escape
p 1420 N95-21796

LOVE WAVES

Source contributions at far-regional distances
[AD-A279405] p 1426 N95-21932

LOW ALTITUDE

Modelling of microwave propagation and clutter in a maritime environment p 1295 N95-20938
Atmospheric stability and its influence on air quality in small communities in northern Sweden
[PB95-131652] p 1405 N95-21181

LOW CONCENTRATIONS

Gas-phase photocatalytic oxidation: Cost comparison with other air pollution control technologies
[DE95-000241] p 1410 N95-22278

LOW CONDUCTIVITY

Protective organic coatings on steel: Accelerated corrosion test method for paint/coatings exposed to water with low conductivity. Nordtest project no. 1010-92. Degradation of organic coatings in fresh water
[PB95-134185] p 1277 N95-21873

LOW COST

Wavelet-based acoustic recognition of aircraft
[DE94-017701] p 1503 N95-20019
Si concentrator solar cell development
[DE95-002314] p 1393 N95-20870
Fiber-optic sensors for rapid, inexpensive characterization of soil and ground water contamination
[DE95-002471] p 1545 N95-21510
European Workshop on Optical Ground Truth Instrumentation for the Validation of Space-Borne Optical Remote Sensing Data of the Marine Environment
[PB95-134144] p 1390 N95-21872
High speed optical storage technology
[AD-A285788] p 1456 N95-22400

LOW DENSITY FLOW

Numerical investigations of low-density nozzle flow by solving the Boltzmann equation
[NASA-TM-110492] p 1354 N95-21675

LOW FREQUENCIES

The calculation and measurement of Helmholtz coil fields
[AD-A286081] p 1228 N95-20808
S-D hybridization and anisotropy of the optical second harmonic at low frequencies
[AD-A279449] p 1544 N95-20876
Low-frequency image theory for a current dipole in front of a permeable sphere
[PB95-127676] p 1300 N95-21104
Vibration analysis of the AN/SPS-67(V)3 surface search radar
[AD-A286050] p 1302 N95-21324
Effects of RF side-bands on spectral reproducibility for infrared synchrotron radiation
[DE95-002450] p 1536 N95-21418

LOW NOISE

Evaluation of superconducting quantum interference devices interfaced with digital signal processing electronics for biomagnetic applications
[DE94-016186] p 1289 N95-20164
LLNL/Lion Precision LVDT amplifier
[DE95-001504] p 1327 N95-20854
Low noise 22 GHz receiver for the radioastron satellite. Part 1: Requirements, design and reliability analysis
[PB95-104410] p 1300 N95-20972
Monolithic low noise preamplifier for piezoelectric sensors
[AD-D016524] p 1333 N95-21865
Low noise 22 GHz receiver for the radioastron satellite, part 2: Space qualification tests
[PB95-127197] p 1598 N95-22376

LOW REYNOLDS NUMBER

Direct numerical simulation of turbulent flow in a sudden pipe expansion p 1347 N95-21067
Application of Roe's flux-difference splitting for kappa-epsilon turbulence model
[PB95-127718] p 1352 N95-21106
Small-scale behavior in distorted turbulent boundary layers at low Reynolds number p 1362 N95-22456

LOW SPEED
Damage tolerance of carbon fibre polyetheretherketone laminates
[PB95-131611] p 1230 N95-21432
LOW SPEED WIND TUNNELS
Vapor generator wand
[NASA-CASE-LAR-15058-1] p 1215 N95-20080
LOW TEMPERATURE
Low temperature synthesis of semiconductor materials
[AD-A285120] p 1226 N95-20081
A low temperature, ultrahigh vacuum, microwave-frequency-compatible scanning tunneling microscope
[AD-A279869] p 1365 N95-20413
High density monolithic packaging technology for digital/microwave avionics p 1211 N95-20646
Feasibility study of power generation system with shape memory alloys
[DE95-714802] p 1254 N95-20890
Nitrogen alloyed martensitic steels
[PB95-127791] p 1255 N95-21128
Atmospheric stability and its influence on air quality in small communities in northern Sweden
[PB95-131652] p 1405 N95-21181
LOW TEMPERATURE ENVIRONMENTS
Small antennas for communication over sea ice
[AD-D016206] p 1301 N95-21156
Cold regions instrumentation considerations
[AD-A279492] p 1367 N95-21680
LOW TEMPERATURE TESTS
Moessbauer study of the sintered Mn(0.70)Zn(0.23)Fe(2.07)O4
[DE94-631462] p 1255 N95-20909
LUBRICANT TESTS
Evaluation of PS 212 coatings under boundary lubrication conditions with an Ester-based oil to 300 C
[NASA-TM-106763] p 1223 N95-19901
Comparison of HFC-134a and the ternary blend, Suva MP39, as replacements for the refrigerant, CGC-12
[MRL-GD-0051] p 1287 N95-21625
Materials compatibility and lubricants research on CFC-refrigerant substitutes
[DE94-018414] p 1287 N95-21631
LUBRICANTS
Accelerated screening methods for determining chemical and thermal stability of refrigerant-lubricant mixtures. Part 2: Experimental comparisons and verification of methods
[DE95-000743] p 1264 N95-20078
Comparison of HFC-134a and the ternary blend, Suva MP39, as replacements for the refrigerant, CGC-12
[MRL-GD-0051] p 1287 N95-21625
Lubricant evaluation and performance, 2
[AD-A279144] p 1278 N95-21969
LUBRICATING OILS
Abrasive wear by diesel engine coal-fuel and related particles
[PB95-104915] p 1379 N95-20984
Absorption of water and lubricating oils into porous nylon
[NASA-CR-197344] p 1280 N95-22383
LUBRICATION SYSTEMS
Quartz resonator fluid monitors for vehicle applications
[DE94-018910] p 1367 N95-21546
LUGS
A user's guide to LUGSAN 1.1: A computer program to calculate and archive lug and sway brace loads for aircraft-carried stores
[DE95-001919] p 1207 N95-21730
LUMINANCE
The spatiotemporal characteristics of visual motion priming
[AD-A284782] p 1449 N95-20062
Factors affecting the perception of luning in monocular regions of partial binocular overlap displays
[AD-A286287] p 1547 N95-22044
LUMINESCENCE
Optical properties of silicon clusters deposited on the basal plane of graphite
[DE94-017529] p 1542 N95-20450
Parallel nanometer scale fabrication
[DE95-002122] p 1336 N95-22284
LUMINOSITY
A tau-charm-factory at Argonne
[DE94-016913] p 1510 N95-20360
Optimizing the length of the stores and related effects
[DE95-002531] p 1533 N95-20885
Emittance dilution by ions in the SLC arcs
[DE95-002871] p 1536 N95-21332
Luminosity polarization correlation in the SLC
[DE95-002889] p 1536 N95-21335
Azimuthally averaged radial S(sub 100 microns)/S(sub 60 microns) dust color temperatures in spiral galaxies
p 1593 N95-21760
Correlation of far-infrared emission and radio continuum emission along the major axis of edge-on spiral galaxies
p 1593 N95-21762
Proposed emittance upgrade for the SLC damping rings
[DE95-002887] p 1538 N95-22155
LUMINOUS INTENSITY
Application of pressure sensitive paint in hypersonic flows
[NASA-TM-106824] p 1201 N95-20794
Correlation of far-infrared emission and radio continuum emission along the major axis of edge-on spiral galaxies
p 1593 N95-21762
LUNAR EXPLORATION
Moon: Old and new
[NASA-TM-110511] p 1601 N95-21196
LUNAR MAPS
The Double Eagle Space Experiment (DESE) beamline design
[DE94-018319] p 1601 N95-22419
LUNAR SPACECRAFT
A Clementine collection: Moonglow
[AD-A286360] p 1217 N95-20228
LUNAR SURFACE
The Double Eagle Space Experiment (DESE) beamline design
[DE94-018319] p 1601 N95-22419
LUNGS
Thorium-232 in human tissues: Metabolic parameters and radiation doses
[DE94-019275] p 1441 N95-20074
Urban air carcinogens and their effects on health
[DE95-002259] p 1447 N95-22285
LYMAN ALPHA RADIATION
Observation of strong emission from NeIX and NeX transitions in a laser-driven plasma
[DE95-002265] p 1555 N95-20813
LYSOZYME
Chemical interactions between protein molecules and polymer membrane materials
[DE95-001808] p 1224 N95-21746
Separation of proteins by convective electrophoresis through a porous membrane
[PB95-127130] p 1248 N95-22373

M

MACH NUMBER
Flow coefficient behavior for boundary layer bleed holes and slots
[NASA-TM-106846] p 1338 N95-19953
Advanced detector development, laboratory simulations, diagnostic development, and data analysis on wake physics
[AD-A284798] p 1364 N95-20069
MACH-ZEHNDER INTERFEROMETERS
Electromagnetic radiation detector utilizing an electromagnetic radiation absorbing element in a mach-zehnder interferometer arrangement
[AD-D016507] p 1306 N95-21835
MACHINE LEARNING
Fault tolerance of neural networks
[AD-A285098] p 1479 N95-20057
Adaptive path planning for flexible manufacturing
[DE94-016561] p 1459 N95-20284
Designing the architecture of hierachical neural networks model attention, learning and goal-oriented behavior
[AD-A279898] p 1452 N95-20562
Proceedings of the Fourth International Workshop on Inductive Logic Programming (ILP-94)
[PB95-135273] p 1464 N95-21003
A neural expert approach to self designing flight control systems
[AD-A279965] p 1215 N95-21122
Expressions that talk about themselves
[PB95-134060] p 1466 N95-21344
Elements of deliberative robot control
[PB95-107595] p 1482 N95-21412
Activities of the Research Institute for Advanced Computer Science
[NASA-CR-197291] p 1478 N95-22108
Learning maneuvers using neural network models
[AD-A286470] p 1486 N95-22267
MACHINE TRANSLATION
Software fault tree analysis of concurrent Ada processes
[AD-A284979] p 1457 N95-20042
Translation of the data flow query language for the multimodel, multibackend database system
[AD-A285978] p 1588 N95-20617
TBell: A mathematical tool for analyzing decision tables
[NASA-CR-195027] p 1462 N95-20691
MACHINING
Safety issues in high speed machining
[PB95-127411] p 1287 N95-21422
A study of mechanical processing damage in brittle materials
[DE95-002126] p 1276 N95-21585
MACROMOLECULES
Synthesis and characterization of poly(organophosphazene) interpenetrating polymer networks
[AD-A279872] p 1265 N95-20183
Potential-of-mean-force description of ionic interactions and structural hydration in biomolecular systems
[DE95-000859] p 1438 N95-21366
MACROSCOPIC EQUATIONS
Geographical diversity combining to exploit multi-mechanism propagation p 1299 N95-20957
MAGELLANIC CLOUDS
Twentysixth YERAC
[PB95-127437] p 1599 N95-21347
MAGMA
The primary carbon and the formation of carbon species in terrestrial magmas p 1420 N95-21797
MAGNESIUM
Photoelectrons beam measurement from a magnesium cathode in a RF electron gun
[DE94-017994] p 1533 N95-20573
Conference on Deep Earth and Planetary Volatiles
[NASA-CR-196944] p 1415 N95-21777
Thermochemistry of dense hydrous magnesium silicates p 1416 N95-21782
Hydrogen storage in Earth's mantle and core
p 1423 N95-21813
The isotope geochemistry of abyssal peridotites and related rocks
[AD-A279435] p 1435 N95-21918
MAGNESIUM ALLOYS
First principles simulation of materials properties
[DE94-016781] p 1566 N95-20405
MAGNESIUM OXIDES
Selective methane oxidation over promoted oxide catalysts
[DE94-012270] p 1235 N95-20188
Electronic structure and energies of alkaline earth oxides: MgO, CaO and SrO
[DE94-628990] p 1575 N95-21853
MAGNETIC BEARINGS
Low rotational drag in high-temperature superconducting bearings
[DE95-002983] p 1382 N95-22292
MAGNETIC COILS
Superconducting electromagnetic thruster
[AD-D016485] p 1355 N95-21902
MAGNETIC DIPOLES
A colocated magnetic loop, electric dipole array antenna (preliminary results)
[AD-A285381] p 1290 N95-20556
Low-frequency image theory for a current dipole in front of a permeable sphere
[PB95-127676] p 1300 N95-21104
MAGNETIC DOMAINS
Changes in the behavior of magnetic materials undergoing processing in electrical rotating machines
[PB95-104493] p 1325 N95-20702
MAGNETIC EFFECTS
Neutrino magnetic moments and the solar neutrino problem
[DE94-017579] p 1602 N95-20147
Nonlinear Faraday effect in CdS semiconductor in an ultrahigh magnetic field
[DE94-016804] p 1564 N95-20240
Magnetic field dependence of the correlation gap in SmB6
[DE95-001684] p 1574 N95-21570
Overview of the field and temperature dependence of J(c) in Ag/BSCCO tapes
[PB95-110318] p 1574 N95-21636
How to improve J(c(T)) in Ag/(BiPb)2Sr2Ca2Cu3O10 tapes
[PB95-110326] p 1575 N95-21949
Magnetic interactions in the Emery model
[DE94-629059] p 1577 N95-22181
MAGNETIC EQUATOR
Mitigation of the effects of F layer regularities by using multiple paths p 1298 N95-20951
MAGNETIC FIELD CONFIGURATIONS
Spin-specific photoelectron diffraction using magnetic x ray circular dichroism
[DE94-017527] p 1567 N95-20448
Magnetic x-ray circular dichroism in spin-polarized photoelectron diffraction
[DE95-002394] p 1520 N95-21360
The superconducting magnet system for the Tokamak Physics Experiment
[DE94-018329] p 1562 N95-22300

MAGNETIC FIELD RECONNECTION
Solar flare MDH
[AD-A279894] p 1602 N95-20593
MAGNETIC FIELDS
Particle beam fusion
[DE95-000711] p 1549 N95-20075
Magnetic fluctuation induced transport and edge dynamo measurements in the MST reversed-field pinch
[DE95-000591] p 1549 N95-20114
Magnetically controlled deposition of metals using gas plasma
[DE94-018654] p 1251 N95-20128
Nonlinear Faraday effect in CdS semiconductor in an ultrahigh magnetic field
[DE94-016804] p 1564 N95-20240
Enhanced scrape-off layer plasma in D3-D double-null discharges
[DE94-017977] p 1554 N95-20571
Temporal and spectral investigation of multi-Landau level quantum beats in GaAs
[DE94-018189] p 1569 N95-20678
Magnetic flocculation of paramagnetic particles
[DE94-018144] p 1501 N95-20725
Ultrafast magnetoexciton dynamics in GaAs
[DE94-018175] p 1514 N95-20732
The calculation and measurement of Helmholtz coil fields
[AD-A286081] p 1228 N95-20808
An advanced ECR ion source with a large uniformly distributed ECR plasma volume for multiply charged ion beam generation
[DE95-001078] p 1515 N95-20911
Electron tunneling magnetic field sensor
[AD-D016227] p 1365 N95-21117
High magnetic field glow discharge ionization source
[AD-A279972] p 1241 N95-21123
Resonant photon-graviton conversion in EM fields: From earth to heaven
[DE95-002784] p 1301 N95-21241
Sources of amplitude-dependent tune shift in the PEP-2 design and their compensation with octupoles
[DE94-018198] p 1519 N95-21262
Investigation of spherical tearing mode
[NASA-CR-197284] p 1558 N95-21345
Source distribution of visual evoked neuromagnetic responses
[PB95-127643] p 1445 N95-21348
Monopoles and quark confinement: Introduction and overview
[DE94-019348] p 1522 N95-21485
Vortex dynamics in a ring-like irradiated Bi2Sr2CaCu2O8 crystal
[DE95-001682] p 1573 N95-21569
Magnetic field dependence of the correlation gap in SmB6
[DE95-001684] p 1574 N95-21570
Overview of the field and temperature dependence of J(c) in Ag/BSCCO tapes
[PB95-110318] p 1574 N95-21636
Current distribution in Cable-In-Conduit Conductors
[DE95-001820] p 1332 N95-21725
Collisional drift waves in the H-mode edge
[DE94-628950] p 1561 N95-21847
Electromagnetic waves in an ultrarelativistically hot and strongly magnetized electron-positron plasma
[DE94-628963] p 1307 N95-21849
Anisotropic transport properties of BSCCO single crystals and Ag-clad tapes in high magnetic fields
[DE95-000938] p 1575 N95-21936
How to improve J(c(T)) in Ag/(BiPb)2Sr2Ca2Cu3O10 tapes
[PB95-110326] p 1575 N95-21949
Electric-field effects on shallow donor impurity in a harmonic quantum dot
[DE94-629034] p 1577 N95-22176
Temperature dependence of a magnetopolaron in a harmonic quantum dot in resonant magnetic fields
[DE94-629036] p 1502 N95-22177
Temperature dependence of magnetopolarons in a parabolic quantum dot in arbitrary magnetic fields
[DE94-629033] p 1528 N95-22218
Heat loss by helicity injection in spheromaks
[DE95-003473] p 1562 N95-22221
Large-scale fields and flows in the magnetosphere-ionosphere system
[PB95-134664] p 1427 N95-22368
MAGNETIC FLUX
Transport and dynamics in toroidal fusion systems
[DE94-018653] p 1548 N95-20029
DSP control of superconducting quantum interference devices
[DE94-016193] p 1313 N95-20168
Power-law resistivity, magnetic relaxation and ac susceptibility
[DE94-016893] p 1501 N95-20241
Flux-focusing eddy current probe and rotating probe method for flaw detection
[NASA-CASE-LAR-15231-1-SB] p 1383 N95-20764
Electron tunneling magnetic field sensor
[AD-D016227] p 1365 N95-21117
Coaxial hybrid wiggler
[AD-D016501] p 1331 N95-21671
Charge density of fractional charged quasiparticles in the composite fermion picture
[DE94-018122] p 1524 N95-21703
AC magnetic response of YBa2CuO7 with Y2BaCuO5 inclusions and of single-crystal YBa2Cu3O7: A comparative study
[PB94-207917] p 1577 N95-22166
Electric-field effects on shallow donor impurity in a harmonic quantum dot
[DE94-629034] p 1577 N95-22176
Flux creep with logarithmic U(j) dependence
[DE94-629058] p 1577 N95-22180
MAGNETIC MATERIALS
Journal of Applied Physics, volume 76, number 10, part 2. Proceedings of the 6th Joint Magnetism and Magnetic Materials-INTERMAG Conference
[AD-A286364] p 1500 N95-20229
Magnetic flocculation of paramagnetic particles
[DE94-018144] p 1501 N95-20725
MAGNETIC MEASUREMENT
DSP control of superconducting quantum interference devices
[DE94-016193] p 1313 N95-20168
Magnetic source imaging of visually evoked and oscillatory electrical activity of the human brain
[PB95-127205] p 1448 N95-22476
MAGNETIC MIRRORS
An advanced ECR ion source with a large uniformly distributed ECR plasma volume for multiply charged ion beam generation
[DE95-001078] p 1515 N95-20911
Gas-dynamic trap diagnostic complex for study on plasma heating and power atomic beam injection
[DE94-633377] p 1529 N95-22283
MAGNETIC MOMENTS
Neutrino magnetic moments and the solar neutrino problem
[DE94-017579] p 1602 N95-20147
Signals for top quark anomalous chromomagnetic moments at colliders
[DE95-002896] p 1535 N95-21254
Neutron diffraction study of the magnetic ordering of BaCuO(2+x)
[DE95-001357] p 1572 N95-21297
MAGNETIC PERMEABILITY
Joining dissimilar stainless steels for pressure vessel components
[PB95-133005] p 1380 N95-21446
AC magnetic response of YBa2CuO7 with Y2BaCuO5 inclusions and of single-crystal YBa2Cu3O7: A comparative study
[PB94-207917] p 1577 N95-22166
MAGNETIC PROBES
A portable and independent edge fluctuation diagnostic
[DE94-018254] p 1554 N95-20681
MAGNETIC PROPERTIES
Energetics, bonding mechanism and electronic structure of ceramic/ceramic and metal/ceramic interfaces
[DE95-000601] p 1265 N95-20115
Journal of Applied Physics, volume 76, number 10, part 2. Proceedings of the 6th Joint Magnetism and Magnetic Materials-INTERMAG Conference
[AD-A286364] p 1500 N95-20229
Investigation of syngas interaction in alcohol synthesis catalysts
[DE94-018784] p 1236 N95-20349
Molecularly Designed Ultrafine/Nanostructured Materials, volume 351
[AD-A285370] p 1568 N95-20552
Magnetic excitations in modulated PrNi2Si2
[DE95-001077] p 1254 N95-20822
Photoemission and ferromagnetism
[DE95-002419] p 1520 N95-21362
Magnetic properties of the three-dimensional Ising model with an interface amorphization
[DE94-628992] p 1278 N95-21885
The low temperature properties of (Dy(1-x)Er(x))Ni2 alloys
[DE95-001657] p 1260 N95-21923
Incology alloy 908 data handbook
[DE95-001818] p 1260 N95-22013
MAGNETIC RELAXATION
Power-law resistivity, magnetic relaxation and ac susceptibility
[DE94-016893] p 1501 N95-20241
MAGNETIC RESONANCE
Seminar on Biomedical Engineering 1993
[PB95-104402] p 1443 N95-20971
Radio-frequency techniques at the ISIS pulsed muon source
[PB95-129854] p 1529 N95-22303
MAGNETIC SPECTROSCOPY
Applications of ICP magnetic sector multicollector mass spectrometry to basic energy research
[DE95-002600] p 1246 N95-21886
MAGNETIC STORAGE
Journal of Applied Physics, volume 76, number 10, part 2. Proceedings of the 6th Joint Magnetism and Magnetic Materials-INTERMAG Conference
[AD-A286364] p 1500 N95-20229
MAGNETIC STORMS
Solar-Geophysical Data number 600, August 1994. Part 1: (Prompt reports). Data for July, June 1994, and late data
[PB95-104923] p 1603 N95-20713
Substorm theories: United they stand, divided they fall
[NASA-CR-197672] p 1427 N95-22326
Large-scale fields and flows in the magnetosphere-ionosphere system
[PB95-134664] p 1427 N95-22368
The effects of magnetic storm phases on F-layer irregularities from auroral to equatorial latitudes
[AD-A286173] p 1427 N95-22423
MAGNETIC VARIATIONS
Critical dynamics and plastic flow in disordered Josephson junction arrays
[DE94-629074] p 1576 N95-21995
MAGNETICALLY TRAPPED PARTICLES
1994 Nonneutral Plasma Workshop
[AD-A285656] p 1559 N95-21404
MAGNETITE
Loss of solar He and Ne from IDPS in subducting sediment: Diffusion and the effect of phase changes
p 1419 N95-21792
MAGNETIZATION
Flux creep with logarithmic U(j) dependence
[DE94-629058] p 1577 N95-22180
MAGNETO-OPTICS
Journal of Applied Physics, volume 76, number 10, part 2. Proceedings of the 6th Joint Magnetism and Magnetic Materials-INTERMAG Conference
[AD-A286364] p 1500 N95-20229
Nonlinear Faraday effect in CdS semiconductor in an ultrahigh magnetic field
[DE94-016804] p 1564 N95-20240
Laser trapping of Na-21 atoms
[DE95-002354] p 1513 N95-20629
Instantaneous frequency dynamics of coherent emission from magnetoexcitons in gallium arsenide
[DE94-018182] p 1569 N95-20677
High speed optical storage technology
[AD-A285788] p 1456 N95-22400
MAGNETOACOUSTIC WAVES
Recent results from Fast Wave Current Drive experiments on DIII-D
[DE94-016718] p 1551 N95-20285
MAGNETOACOUSTICS
Approximate Riemann solver for magnetohydrodynamics (that works in more than one dimension)
[PB95-135802] p 1553 N95-20425
MAGNETOCARDIOGRAPHY
Transformation of multichannel magnetocardiographic signals to standard grid form
[PB95-127114] p 1447 N95-22371
MAGNETOELECTRIC MEDIA
Classification of bianisotropic media
[PB95-127635] p 1502 N95-21102
Magnetoelectric properties of reciprocal bianisotropic materials with focus on the polarizability of chiro-omega spheres
[PB95-127650] p 1544 N95-21103
MAGNETOHYDRODYNAMIC FLOW
MHD-flow in slotted channels with conducting walls
[DE94-018370] p 1559 N95-21388
MAGNETOHYDRODYNAMIC STABILITY
Coupled tearing modes in plasmas with differential rotation
[DE94-631422] p 1548 N95-19977
Toward a design for the ITER plasma shape and stability control system
[DE94-017516] p 1548 N95-20037
Particle beam fusion
[DE95-000711] p 1549 N95-20075
Fluctuations and transport in the reversed field pinch: Characterization and reduction
[DE95-000590] p 1549 N95-20113
Fluctuations in high Beta(sub p) plasmas in D3-D
[DE94-017510] p 1550 N95-20146
Soft X-Ray Innovative Source Development Program
[AD-A286380] p 1551 N95-20232
24th Annual Anomalous Absorption Conference
[DE94-016457] p 1551 N95-20283

Plasma shape experiments for an optimized tokamak
[DE94-017508] p 1553 N95-20445
Wall stabilization effects in D3-D high beta discharges
[DE94-017509] p 1554 N95-20446
Solar flare MDH
[AD-A279894] p 1602 N95-20593
Current diffusive ballooning mode in second stability region of tokamaks
[DE94-770690] p 1554 N95-20683
Simulation of tearing mode stabilization by using ECH
[DE94-770700] p 1554 N95-20684
Chaotic phenomena in plasma 3
[DE94-770765] p 1554 N95-20686
Ideal Magnetohydrodynamic stabilities in JT-60 and D3-D tokamak plasmas
[DE94-770684] p 1555 N95-20987
Investigations of VH-mode in D3-D and JET
[DE94-015859] p 1556 N95-21142
Numerical analysis of energetic particle stabilization of ballooning modes in finite-aspect-ratio tokamaks
[DE94-631397] p 1556 N95-21164
Computer simulation of the diocotron instability
[AD-A285655] p 1559 N95-21403
1994 Nonneutral Plasma Workshop
[AD-A285656] p 1559 N95-21404
Quasi-linear equation for magnetoplasma oscillations in the weakly relativistic approximation
[DE94-628932] p 1560 N95-21593

MAGNETOHYDRODYNAMIC WAVES
Approximate Riemann solver for magnetohydrodynamics (that works in more than one dimension)
[PB95-135802] p 1553 N95-20425
Electromagnetic waves in an ultrarelativistically hot and strongly magnetized electron-positron plasma
[DE94-628963] p 1307 N95-21849

MAGNETOHYDRODYNAMICS
Transport and dynamics in toroidal fusion systems
[DE94-018653] p 1548 N95-20029
Magnetic fluctuation induced transport and edge dynamo measurements in the MST reversed-field pinch
[DE95-000591] p 1549 N95-20114
Approximate Riemann solver for magnetohydrodynamics (that works in more than one dimension)
[PB95-135802] p 1553 N95-20425
Solar flare MDH
[AD-A279894] p 1602 N95-20593
Magnetic flocculation of paramagnetic particles
[DE94-018144] p 1501 N95-20725
Ideal Magnetohydrodynamic stabilities in JT-60 and D3-D tokamak plasmas
[DE94-770684] p 1555 N95-20987
Investigations of VH-mode in D3-D and JET
[DE94-015859] p 1556 N95-21142
MHD pressure drop in ducts with imperfectly insulating coatings
[DE95-002852] p 1558 N95-21244
Investigation of spherical tearing mode
[NASA-CR-197284] p 1558 N95-21345
MHD-flow in slotted channels with conducting walls
[DE94-018370] p 1559 N95-21388
PRS scoping study. 2: ZPIMP predictions for radiation yields on a JUPITER-class generator
[AD-A279823] p 1537 N95-21494
A simulation of plasma motion in the polar ionosphere
[AD-A286166] p 1426 N95-22019

MAGNETOMETERS
Evaluation of superconducting quantum interference devices interfaced with digital signal processing electronics for biomagnetic applications
[DE94-016186] p 1289 N95-20164
Source distribution of visual evoked neuromagnetic responses
[PB95-127643] p 1445 N95-21348
Transformation of multichannel magnetocardiographic signals to standard grid form
[PB95-127114] p 1447 N95-22371

MAGNETOPAUSE
Location and characteristics of the reconnection X-line deduced from low-altitude satellite and radar observations
[NASA-TM-110114] p 1413 N95-20453
Investigation of spherical tearing mode
[NASA-CR-197284] p 1558 N95-21345
Observations of cold magnetospheric ions at geosynchronous orbit during times of high activity
[DE95-000936] p 1600 N95-21935
Large-scale fields and flows in the magnetosphere-ionosphere system
[PB95-134664] p 1427 N95-22368
Magnetospheric Plasma Analyzer (MPA): Plasma observations from geosynchronous orbit
[DE95-002739] p 1427 N95-22477

MAGNETORESISTIVITY
Giant magnetoresistance calculated from first principles
[DE94-018658] p 1500 N95-20129
Journal of Applied Physics, volume 76, number 10, part 2. Proceedings of the 6th Joint Magnetism and Magnetic Materials-INTERMAG Conference
[AD-A286364] p 1500 N95-20229
Magnetic field dependence of the correlation gap in SmB6
[DE95-001684] p 1574 N95-21570

MAGNETOSHEATH
Location and characteristics of the reconnection X-line deduced from low-altitude satellite and radar observations
[NASA-TM-110114] p 1413 N95-20453
Investigation of spherical tearing mode
[NASA-CR-197284] p 1558 N95-21345

MAGNETOSPHERE-IONOSPHERE COUPLING
Substorm theories: United they stand, divided they fall
[NASA-CR-197672] p 1427 N95-22326
Large-scale fields and flows in the magnetosphere-ionosphere system
[PB95-134664] p 1427 N95-22368

MAGNETOSTATIC FIELDS
Variations of helicon wave induced radial plasma transport in different experimental conditions
[DE94-631410] p 1550 N95-20200

MAGNETOSTRICTION
Magnetostrictive motor system
[AD-D016484] p 1333 N95-21901

MAGNETRON SPUTTERING
Rate controlled synthesis of composition modulated, metal-oxide thin films
[DE94-016596] p 1267 N95-20317
Magnetic x ray circular dichroism in Fe Co Pt multilayers
[DE94-017522] p 1253 N95-20447
Thin-film cadmium telluride photovoltaic cells
[DE94-011886] p 1395 N95-21508

MAGNETRONS
Magnetron power supply at high stability and its application in plasma excitation for the production of ultraviolet radiation
[DE94-629656] p 1326 N95-20733
Development of an annular electron beam HPM amplifier
[AD-A286646] p 1327 N95-20905

MAINTENANCE
Public-sector aviation issues: Graduate research award papers, 1992-1993
[PB94-217478] p 1199 N95-19967
Analysis of welds on helium-containing restraint test plates
[DE95-001809] p 1257 N95-21303
Analysis of invalid emission testing in the California smog check program
[PB95-128922] p 1406 N95-21373

MAJORITY CARRIERS
Plasma-induced-damage of GaAs during etching of refractory metal contacts
[DE95-001525] p 1259 N95-21838

MAN MACHINE SYSTEMS
Crew aiding and automation: A system concept for terminal area operations, and guidelines for automation design
[NASA-CR-4631] p 1204 N95-19950
Collected papers of the Soar/IFOR project, Spring 1994
[AD-A280063] p 1216 N95-20624
13th European Annual Conference on Human Decision Making and Manual Control
[PB95-132874] p 1450 N95-21284
Crew-Centered Cockpit Design (CCCD) field demonstration program, volume 1
[AD-A286426] p 1453 N95-21566
Aerospace medicine and biology: A continuing bibliography with indexes (supplement 399)
[NASA-SP-7011(399)] p 1446 N95-21947
Systems engineering design and technical analyses for Strategic Avionics Crew-station Design Evaluation Facility (SACDEF)
[AD-A286239] p 1213 N95-22024
Usable, real-time, interactive spoken language systems
[AD-A286349] p 1310 N95-22253
Fuzzy clustering of facial form for prototyping environmental protection equipment
[DE94-014657] p 1454 N95-22466

MANAGEMENT INFORMATION SYSTEMS
Information Management Architecture for an Integrated Computing Environment for the Environmental Restoration Program. Volume 2: Interim business systems guidance
[DE95-001385] p 1591 N95-22061
Taking AIM: The management of scientific and technical information at Argonne National Laboratory
[DE94-019279] p 1591 N95-22092

MANAGEMENT METHODS
Readings in program control
[NASA-SP-6103] p 1583 N95-20739
Program control in NASA: Needs and opportunities
p 1583 N95-20740
But what will it Cost? The history of NASA cost estimating p 1583 N95-20742
Scheduling: A guide for program managers
p 1584 N95-20748
A strategy of cost control for Mariner Venus/Mercury 1973 p 1585 N95-20751
Performance measurement: A tool for program control
p 1585 N95-20752
Program control for mission success
p 1585 N95-20753
Interim profile: Development and trial of a method to rapidly measure software engineering maturity status
[AD-A279074] p 1468 N95-21627
Total quality management program planning
[DE94-016862] p 1586 N95-21645
Implementation of electronic chain-of-custody, analysis requests, and data verification at Los Alamos National Laboratory
[DE94-018076] p 1407 N95-21666

MANAGEMENT PLANNING
Migrating the Facility Profile Information Management System into the World Wide Web
[DE94-018367] p 1586 N95-20016
Materials/manufacturing element of the Advanced Turbine System Program
[DE94-017299] p 1378 N95-20085
Improving cost efficiency in large programs
p 1584 N95-20743
A strategy of cost control for Mariner Venus/Mercury 1973 p 1585 N95-20751
Performance measurement: A tool for program control
p 1585 N95-20752
Program control for mission success
p 1585 N95-20753
A software process framework for the Software Engineering Institute's (SEI) capability maturity model
[AD-A286595] p 1462 N95-20765
Total quality management program planning
[DE94-016862] p 1586 N95-21645

MANAGEMENT SYSTEMS
Migrating the Facility Profile Information Management System into the World Wide Web
[DE94-018367] p 1586 N95-20016
Recognition of subsurface defects in machined ceramics by application of neural networks to laser scatter patterns
[DE94-018373] p 1264 N95-20018
Intelligent interactive project management system
[PB95-132684] p 1586 N95-21982

MANGANESE
Development of superplasticity in 5083 aluminum with additions of Mn and Zr
[DE94-017474] p 1251 N95-20090

MANGANESE ALLOYS
Consequences of oscillatory potentials and angular forces in transition metals and their aluminides
[DE94-019127] p 1258 N95-21600

MANGANESE OXIDES
Selective methane oxidation over promoted oxide catalysts
[DE94-012270] p 1235 N95-20188
Moessbauer study of the sintered Mn(0.70)Zn(0.23)Fe(2.07)O4
[DE94-631462] p 1255 N95-20909
Solid oxide fuel cells in the United States
[DE95-002405] p 1395 N95-21361

MANIFOLDS (MATHEMATICS)
Computation of invariant manifolds
[PB95-135687] p 1492 N95-21318
Iterated-subspace minimization methods for nonlinear optimization
[PB95-108171] p 1495 N95-22317
Elliptic genera for Z/K-manifolds I
[PB95-109096] p 1496 N95-22355

MANIPULATORS
Input shaping for vibration-damped slewing of a flexible beam using a heavy-lift hydraulic robot
[DE94-015803] p 1379 N95-20695
Sensor based fine motion control
[PB95-108007] p 1483 N95-21669

MANUAL CONTROL
13th European Annual Conference on Human Decision Making and Manual Control
[PB95-132874] p 1450 N95-21284

MANUALS
Calculation methods for criteria air pollutant emission inventories
[AD-A284675] p 1400 N95-19964

Personal computer and workstation operating systems tutorial
[AD-A280132] p 1451 N95-20041
Implementation of the military handbook 17 for polymer matrix composites and metal matrix composites
[AD-A285595] p 1229 N95-21215
Operator's manual for the multistation offgas analysis system
[DE95-002060] p 1243 N95-21472

MANUFACTURING
Mercury usage and alternatives in the electrical and electronics industries
[PB94-165362] p 1312 N95-19966
Materials/manufacturing element of the Advanced Turbine System Program
[DE94-017299] p 1378 N95-20085
Residual stresses in material processing
[DE94-017888] p 1385 N95-20374
Proceedings of the International Wire and Cable Symposium
[AD-A279242] p 1403 N95-20465
The Photovolatic Manufacturing Technology project (PVMaT) after three years
[DE94-011877] p 1392 N95-20473
Materials processing and manufacturing technologies for diamond substrates multichip modules
[AD-A285060] p 1315 N95-20488
The design and manufacturing development of an active silicon substrate MCM p 1211 N95-20645
High density monolithic packaging technology for digital/microwave avionics p 1211 N95-20646
Approaches to the design of structural ceramics incorporating whiskers and particulate phases
[DE94-018126] p 1271 N95-20704
Si concentrator solar cell development
[DE95-002314] p 1393 N95-20870
Plasma processing for integrated circuits
[DE95-001419] p 1335 N95-22149
Overview of rapid prototyping technologies in manufacturing
[PB95-127122] p 1472 N95-22372
Materials processing and manufacturing technologies for diamond substrates multichip modules
[AD-A285775] p 1336 N95-22412
Solar collector manufacturing activity 1993
[DE94-017340] p 1398 N95-22429

MANY BODY PROBLEM
Truly distribution-independent algorithms for the N-body problem
[DE94-014238] p 1458 N95-20136
Solid-state dynamics and quantum transport in novel semiconductor nanostructures
[AD-A285946] p 1315 N95-20394
Phase dynamics of non-equilibrium distributions of free electron-hole pairs in GaAs quantum wells
[DE94-018190] p 1569 N95-20679
Distribution-independent hierarchical N-body methods
[DE95-001686] p 1493 N95-21439
Fast parallel tree codes for gravitational and fluid dynamical N-body problems
[AD-A286480] p 1358 N95-22290
A multisite interaction expansion of the total energy in metals
[DE94-017175] p 1262 N95-22313

MAPPING
The method of auxiliary mapping for the finite element solutions of elasticity problems containing singularities
[AD-A285689] p 1489 N95-20274
Evolution of ground line of sight data field collection techniques
[AD-A285062] p 1204 N95-20497
Common mapping system media study
[AD-A279086] p 1390 N95-21912
A periodic scheduling heuristic for mapping iterative task graphs onto distributed memory multiprocessors
[AD-A286047] p 1311 N95-22415

MAPS
Selective polygon map display method
[AD-D016518] p 1590 N95-21463
Digital mapping, charting, and geodesy analysis program technical review of Vector Smart Map (VMap) level 1
[AD-A286294] p 1390 N95-22055

MARINE BIOLOGY
Long term changes on the continental shelf of the North Sea: Invertebrate trends, 1931-1990
[PB95-135224] p 1435 N95-21717
Aquatic plant control research program. Ecological assessment of Kirk Pond
[AD-A279090] p 1409 N95-21914
Derivation of maximum permissible concentrations for several volatile compounds for water and soil
[PB95-107454] p 1411 N95-22381

MARINE ENVIRONMENTS
The vertical distribution of heating in the tropical atmosphere
[AD-A285934] p 1429 N95-20391
European Workshop on Optical Ground Truth Instrumentation for the Validation of Space-Borne Optical Remote Sensing Data of the Marine Environment
[PB95-134144] p 1390 N95-21872
Acoustic Thermometry of Ocean Climate (ATOC): Selection of California source site
[AD-A279295] p 1436 N95-21987

MARINE METEOROLOGY
Mariners Weather Log, volume 38, number 3, summer 1994
[PB94-209541] p 1428 N95-20099
Boundary layer cloud studies in support of ASTEX
[AD-A285947] p 1429 N95-20395
An at-sea evaluation of an infrared/resistance temperature device for air/sea-surface temperature measurements
[AD-A279672] p 1365 N95-20604
Acoustic Thermometry of Ocean Climate (ATOC): Selection of California source site
[AD-A279295] p 1436 N95-21987
SAR-related stress variability in the Marine Atmospheric Boundary Layer (MABL)
[AD-A286462] p 1431 N95-22393

MARINE PROPULSION
Superconducting electromagnetic thruster
[AD-D016485] p 1355 N95-21902

MARINE TECHNOLOGY
Directives for the participation in MiTS forum. V3.0
[PB95-110342] p 1484 N95-22015

MARINER VENUS-MERCURY 1973
A strategy of cost control for Mariner Venus/Mercury 1973 p 1585 N95-20751

MARINER 10 SPACE PROBE
Atmospheres of the Moon and Mercury
p 1419 N95-21794

MARKET RESEARCH
The demise of plastic encapsulated microcircuit myths
p 1209 N95-20640
An MCM concurrent engineering software tool market study
[AD-A279257] p 1468 N95-21489

MARKOV CHAINS
On Markov Chain Monte Carlo acceleration
[AD-A279393] p 1499 N95-21945
Almost kappa-wise independent random permutation of the cube
[PB95-108098] p 1495 N95-22147

MARKOV PROCESSES
Application of Markov decision processes to search problems
[PB95-110813] p 1497 N95-19914

MARS (PLANET)
Volatiles, rheology, and mantle convection: Comparing Earth, Venus, and Mars p 1420 N95-21801
Implications of noble gases in a recently recognized Martian meteorite (ALH84001) for the degassing history of Mars p 1424 N95-21819
Mars power system concept definition study. Volume 2: Appendices
[NASA-CR-195420-VOL-2] p 1396 N95-21953

MARS ATMOSPHERE
Primitive Xe in the atmospheres of Earth and mars
p 1419 N95-21795
Mars atmospheric loss and isotopic fractionation by pick-up-ion sputtering and photochemical escape
p 1420 N95-21796
Comets, impacts, and atmospheres
p 1422 N95-21810
Implications of noble gases in a recently recognized Martian meteorite (ALH84001) for the degassing history of Mars p 1424 N95-21819

MARS SURFACE
Micromachined silicon-based analytical microinstruments for space science and planetary exploration
[DE94-019306] p 1367 N95-21507
Mars power system concept definition study. Volume 1: Study results
[NASA-CR-195420-VOL-1] p 1396 N95-21952

MARTENSITE
Nitrogen alloyed martensitic steels
[PB95-127791] p 1255 N95-21128

MARTENSITIC STAINLESS STEELS
Joining dissimilar stainless steels for pressure vessel components
[PB95-133005] p 1380 N95-21446

MASERS
Competition between electromagnetic modes in a free-electron maser
[AD-A279546] p 1374 N95-21694

MASKING
A versatile masking process for plasma etched backside via holes in GaAs
[DE94-019176] p 1572 N95-21419
Spatio-temporal masking in human vision and its application to image coding
[AD-A284949] p 1451 N95-22473

MASKS
Method of making a semiconductor device by forming a nanochannel mask
[AD-D016515] p 1576 N95-22059
Reflective masks for extreme ultraviolet lithography
[DE95-003427] p 1336 N95-22236

MASS
An IRAS Hires study of low mass star formation in the Taurus molecular ring p 1593 N95-21767

MASS DISTRIBUTION
D(sup 0)-(anti-D)(sup 0) mixing and doubly Cabibbo-suppressed decays of the D(+)
[DE94-015540] p 1512 N95-20476

MASS FLOW
Mixing and dynamics of the Mediterranean outflow
[AD-A279803] p 1434 N95-21306

MASS FLOW RATE
Fire experiments in a two dimensional rack storage: BRANDFORSK-project 701-917
[PB95-131538] p 1241 N95-21179

MASS SPECTRA
Evidence for t(bar t) production at the Tevatron: Statistical significance and cross section
[DE95-002524] p 1515 N95-20897
Emittance growth due to negative-mass instability above transition
[DE95-002527] p 1534 N95-20900

MASS SPECTROMETERS
Micromachined silicon-based analytical microinstruments for space science and planetary exploration
[DE94-019306] p 1367 N95-21507
Applications of ICP magnetic sector multicollector mass spectrometry to basic energy research
[DE95-002600] p 1246 N95-21886

MASS SPECTROSCOPY
New high temperature plasmas and sample introduction systems for analytical atomic emission and mass spectrometry
[DE94-018580] p 1552 N95-20345
Oxide formation on NbAl3 and TiAl due to ion implantation of O-18
[DE94-017874] p 1252 N95-20365
Electrospray ionization Fourier transform ion cyclotron resonance mass spectrometric study of singly and doubly charged organometallic complexes
[AD-A279899] p 1238 N95-20563
Sputtering of tin and gallium-tin clusters
[DE94-018389] p 1254 N95-20707
Ion-molecule chemistry related to plasma deposition and etching of silicon
[AD-A279749] p 1514 N95-20804
High magnetic field glow discharge ionization source
[AD-A279972] p 1241 N95-21123
Monomer mapping: A PC-based software tool facilitating the determination of monomer compositions from mass spectrometric molecular weight data
[PB95-132155] p 1275 N95-21470
Operator's manual for the multistation offgas analysis system
[DE95-002060] p 1243 N95-21472
Thermal decomposition reactions of HMX and RDX and their importance in predicting cookoff hazards
[DE95-002486] p 1283 N95-21513
Studies of selenium and xenon in inductively coupled plasma mass spectrometry
[DE95-001676] p 1245 N95-21734
Time of flight spectroscopy with muonic hydrogen
[DE94-017056] p 1245 N95-21845
Applications of ICP magnetic sector multicollector mass spectrometry to basic energy research
[DE95-002600] p 1246 N95-21886

MASS TRANSFER
Restricted mass transport effects on free radical reactions
[DE94-018136] p 1217 N95-21706
Mantle rare gas relative abundances in a steady-state mass transport model p 1423 N95-21812
Subduction of hydrated basalt of the oceanic crust: Implications for recycling of water into the upper mantle and continental growth p 1423 N95-21814
He, Xe and Ne isotopes in a steady-state mass transport model and implications about terrestrial volatiles
p 1425 N95-21821

MASSACHUSETTS
Large bistatic angle clutter depolarization study
p 1296 N95-20941

MASSIVE STARS
The variation of the dust temperature within late-type spiral galaxies p 1593 N95-21766

MASSIVELY PARALLEL PROCESSORS
Split-C and active messages under SUNMOS on the Intel Paragon
[DE94-011418] p 1474 N95-20123
A practical guide to using MCNP with PVM
[DE94-016162] p 1474 N95-20158
Parallelism across the steps in iterated Runge-Kutta methods for stiff initial value problems
[PB95-135760] p 1490 N95-20424
A theoretical study on the performance of the FDTD code on a massively parallel computer
[AD-A285346] p 1475 N95-20499
The message passing version of the parallel Community Climate Model
[DE94-019158] p 1407 N95-21608
Design of a massively parallel computer using bit serial processing elements
[NASA-CR-197365] p 1479 N95-22406

MATCHED FILTERS
Signal processing in the linear statistical model
[AD-A286255] p 1308 N95-22041
Feature extraction without edge detection
[AD-A279842] p 1473 N95-22386

MATERIAL ABSORPTION
Absorption of water and lubricating oils into porous nylon
[NASA-CR-197344] p 1280 N95-22383

MATERIALS HANDLING
Advanced robotic technologies for transfer at Sandia National Laboratories
[DE95-001617] p 1481 N95-20884
Nuclear Terms Handbook, 1993
[DE94-016248] p 1589 N95-21131

MATERIALS SCIENCE
Materials research for GHz multi-chip modules
[AD-A279661] p 1227 N95-20412
Guidelines for qualifying cleaning and verification materials
[NASA-TM-108474] p 1270 N95-20694
Annual Conference on Fire Research: Book of abstracts
[PB95-104964] p 1286 N95-20717
The Materials Corrosion and Environmental Effects Laboratory (MCEL)
[DE94-018268] p 1254 N95-20816
Crack closure and sequential effects in fatigue: A literature survey
[PB95-131637] p 1387 N95-21557

MATERIALS TESTS
The Materials Corrosion and Environmental Effects Laboratory (MCEL)
[DE94-018268] p 1254 N95-20816
Aging tests of ethylene contaminated argon/ethane
[DE95-002526] p 1282 N95-20899
Ignition of submarine materials at various oxygen concentrations
[PB95-131371] p 1243 N95-21428
Surfaces and thin films studied by picosecond ultrasonics
[DE95-001866] p 1506 N95-22071
Welding tritium exposed stainless steel
[DE95-003208] p 1382 N95-22356
Absorption of water and lubricating oils into porous nylon
[NASA-CR-197344] p 1280 N95-22383

MATHEMATICAL LOGIC
Ups and downs of type theory
[PB95-110664] p 1487 N95-19903
Balanced matrices
[AD-A280021] p 1490 N95-20662
TBell: A mathematical tool for analyzing decision tables
[NASA-CR-195027] p 1462 N95-20691
Abstract interpretation of reactive systems: Abstractions preserving Universal CTL(*), Existential CTL(*) and CTL(*)
[PB95-110557] p 1472 N95-22305

MATHEMATICAL MODELS
Non interleaving process algebra
[PB95-110607] p 1486 N95-19892
Radiance of the ocean horizon
[AD-A285613] p 1431 N95-19896
Dominoes
[PB95-110680] p 1456 N95-19905
Analyses of some benchmark cases in fracture mechanics using boundary element method
[PB95-110888] p 1384 N95-19930
Physical Si(1-x)Ge(x)/Si heterojunction bipolar transistor model for device and circuit simulation
[PB95-110896] p 1312 N95-19934
Qualification of the dependence in the generalized extreme value choice model
[PB95-110946] p 1497 N95-19936
Sharp determinants
[PB95-111068] p 1488 N95-19944
Coupled analytic maps
[PB95-111076] p 1498 N95-19945
A simple analytical model for asynchronous dense WDM/OOK systems
[AD-A283725] p 1289 N95-19973
Simulation of stellar speckle imaging
[DE94-016606] p 1412 N95-19985
Oceanographic analysis of the acoustic mid-ocean dynamics experiment
[AD-A285907] p 1432 N95-19988
Comparison of a back propagation artificial neural network model with a linear regression model for personnel selection
[AD-A280023] p 1479 N95-20005
Noise model of the MSX SPIRIT 3 interferometer
[AD-A285837] p 1364 N95-20036
Polycrystalline thin film cadmium telluride solar cells fabricated by electrodeposition
[DE94-011848] p 1391 N95-20118
Optimal distributed control system for a linear distributed parameter system
[AD-D016583] p 1480 N95-20202
Computational modeling of physical processes during laser ablation
[DE94-017699] p 1369 N95-20221
The paradigm of Pseudodual Chiral Models
[DE94-016386] p 1579 N95-20271
Investigating the resolution of resistivity arrays using inverse theory
[DE94-017760] p 1412 N95-20287
Software merge: Semantics of combining changes to programs
[AD-A279657] p 1459 N95-20304
Computer-Aided Structural Engineering (CASE) project. User's guide: Computer-Aided Structural Modeling (CASM). Version 5.00
[AD-A279913] p 1459 N95-20310
Numerical modeling of a small recirculating induction accelerator for heavy-ion fusion
[DE94-018549] p 1552 N95-20318
New high temperature plasmas and sample introduction systems for analytical atomic emission and mass spectrometry
[DE94-018580] p 1552 N95-20345
High performance computing for materials process modeling
[DE94-017860] p 1460 N95-20358
Solid-state dynamics and quantum transport in novel semiconductor nanostructures
[AD-A285946] p 1315 N95-20394
A mechanistic model for radiation-induced crystallization and amorphization in U3Si
[DE94-015028] p 1566 N95-20419
Model-based inversion for a shallow ocean application
[DE94-016968] p 1433 N95-20420
Hybrid model in general geometry
[DE95-002614] p 1553 N95-20437
Implementation and performance of a three-dimensional numerical transport model
[PB95-135745] p 1402 N95-20440
Modeling platform dynamics and physiological response to short arm centrifugation
[AD-A279640] p 1442 N95-20457
Synthesizing the Gulf Stream thermal structure from XBT data
[AD-A279665] p 1433 N95-20458
Has a standard model solution to the solar neutrino problem been found?
[DE94-017580] p 1604 N95-20490
Metallic ions and atoms in the upper atmosphere
[AD-A285229] p 1414 N95-20498
A theoretical study on the performance of the FDTD code on a massively parallel computer
[AD-A285346] p 1475 N95-20499
Investigation of the stability and 1.0 MeV proton radiation resistance of commercially produced hydrogenated amorphous silicon alloy solar cells p 1320 N95-20522
Transport phenomena in the micropores of plug-type phase seperators
[NASA-TM-108479] p 1340 N95-20561
Designing the architecture of hierachical neural networks model attention, learning and goal-oriented behavior
[AD-A279898] p 1452 N95-20562
Emitter location via Kalman filtering of signal time difference of arrival
[AD-A285972] p 1291 N95-20666
Diffraction computation by means of the method of equivalent currents
[AD-A285347] p 1291 N95-20692
Computing methods for the approximate solution of time dependent problems
[AD-A286007] p 1491 N95-20719
Use of an integrated design tool for weld quality enhancement
[DE94-018135] p 1379 N95-20723
Cost estimating methods for advanced space systems
p 1583 N95-20741
Scale-up and modeling of forced chemical vapor infiltration
[DE94-017769] p 1340 N95-20761
Computational model of drilling with high radiance pulsed lasers
[DE94-018548] p 1371 N95-20783
The numerical integration and 3-D finite element formulation of a viscoelastic model of glass
[DE95-002588] p 1271 N95-20788
An augmented Young-Laplace model of an evaporating meniscus in a micro-channel with high heat flux
[NASA-CR-197622] p 1340 N95-20798
Mathematical modeling of a class of multibody flexible spacecraft structures
[NASA-TM-109166] p 1219 N95-20800
HIVEL2D: A two-dimensional flow model for high-velocity channels
[AD-A286556] p 1341 N95-20843
Optimizing the length of the stores and related effects
[DE95-002531] p 1533 N95-20885
Performance and cost analysis of monolithic solid oxide fuel cells
[DE95-002511] p 1394 N95-20896
Statistical properties of geologic fractals
[DE94-019272] p 1414 N95-20908
Real-time reconfiguration study
[AD-A286060] p 1464 N95-20910
Experimental and theoretical evaluation of elastic waves in curved layered media
[AD-A286578] p 1504 N95-20918
Stars or stripes: A comparative study of finite and transfinite techniques for surface modelling
[PB95-134979] p 1464 N95-20975
Mixed hp finite element methods for problems in elasticity and stokes flow
[PB95-104444] p 1341 N95-20981
Construction of non-critical string field theory by transfer matrix formalism in dynamical triangulation
[DE94-770607] p 1516 N95-20986
Geomaterial models and numerical analysis of softening
[PB95-135380] p 1386 N95-21006
Next generation solid modellers for electronic prototyping
[AD-A286525] p 1464 N95-21010
Explicit methods for stiff ODEs from atmospheric Chemistry
[PB95-135794] p 1404 N95-21034
Role of pressure diffusion in non-homogeneous shear flows p 1345 N95-21053
Modeling near wall effects in second moment closures by elliptic relaxation p 1345 N95-21054
Application of Roe's flux-difference splitting for kappa-epsilon turbulence model
[PB95-127718] p 1352 N95-21106
Dielectric models in adhesion and extrapolations of molecular modeling
[AD-A279675] p 1516 N95-21121
New methods for large scale local and global optimization
[AD-A285635] p 1517 N95-21126
DAVE: A plug and play model for distributed multimedia application development
[DE94-016481] p 1465 N95-21153
Experimental measurements and modeling of impurity transport in the divertor and boundary plasma of D3-D
[DE94-016519] p 1556 N95-21159
Analytic models for beam propagation and far-field patterns in slab and bow-tie x ray lasers
[DE94-016607] p 1372 N95-21173
A model of an infinite length, axisymmetric, isotropic, forced thick shell
[AD-A285586] p 1386 N95-21212
Antishadowing contribution to the pomeron structure function
[PB95-127478] p 1518 N95-21221
Where are we going with Bose-Einstein: A mini review
[PB95-130308] p 1518 N95-21222
Spin dependence of diffractive processes and implications for the small x behaviour of g1 and the spin content of the nucleon
[PB95-130332] p 1518 N95-21225
LIEKKI combustion technology
[DE95-700233] p 1242 N95-21282
NESTLE: Few-group neutron diffusion equation solver utilizing the nodal expansion method for eigenvalue, adjoint, fixed-source steady-state and transient problems
[DE95-001903] p 1466 N95-21288
Computational modeling of diffusion-controlled transformations in ternary systems
[DE95-001358] p 1256 N95-21298
Computation of invariant manifolds
[PB95-135687] p 1492 N95-21318

Vibration analysis of the AN/SPS-67(V)3 surface search radar
[AD-A286050] p 1302 N95-21324

Time-dependent deformation of titanium metal matrix composites
[NASA-CR-195030] p 1230 N95-21363

A Hypervelocity Experimental Research Database (HERD): Support for the Wright Laboratory Armament Directorate Code Validation Program (COVAL)
[DE95-001628] p 1387 N95-21396

Error committed by stopping the Newton iteration in Runge-Kutta methods and linear multistep methods
[PB95-106324] p 1492 N95-21421

VLUGR3: A vectorizable adaptive grid solver for PDEs in 3D. 1: Algorithmic aspects and applications
[PB95-135729] p 1467 N95-21435

Theory and modelling of quench in cable-in-conduit superconducting magnets
[DE95-001819] p 1330 N95-21442

Deposition and properties of novel nitride superlattice coatings
[DE95-002945] p 1230 N95-21445

Structure of ionic interfaces from an absolutely convergent solution of the Madelung problem
[DE94-019268] p 1573 N95-21474

Simulations of metal dissolution and corrosion
[DE94-019295] p 1257 N95-21476

Relativistic binary neutron star coalescence
[DE94-019311] p 1600 N95-21479

New improved derivative expansion for field theories with spontaneous symmetry breaking
[DE94-019349] p 1580 N95-21486

Proceedings of the NATO-Advanced Study Institute on Computer Aided Analysis of Rigid and Flexible Mechanical Systems. Volume 2: Contributed papers
[AD-A286063] p 1381 N95-21488

Correlations for the OH A(sup 2)(Sigma)(sup +)(v(prime)=0) electronic quenching cross-section
[DE95-002591] p 1244 N95-21524

Finite element modelling of creep crack growth in 316 stainless and 9Cr-1Mo steels
[DE94-018977] p 1258 N95-21560

One-dimensional reactive Euler equations
[PB95-135430] p 1244 N95-21573

Analysis of a local defect correction approach on composite grids
[PB95-135455] p 1493 N95-21574

Regularity of BPa-systems is decidable
[PB95-135489] p 1468 N95-21619

The method of evaluating quantum partition function for the Hubbard model
[DE94-628991] p 1581 N95-21639

The application of a statistical analysis software package to explosive testing
[MRL-TR-93-42] p 1284 N95-21658

Domain processes in ferroelectric ceramics
[AD-A279567] p 1276 N95-21697

Charge density of fractional charged quasiparticles in the composite fermion picture
[DE94-018122] p 1524 N95-21703

Modeling the response of the California Current system to Global Greenhouse Warming
[DE94-018253] p 1408 N95-21708

Current distribution in Cable-In-Conduit Conductors
[DE95-001820] p 1332 N95-21725

High frequency current sensors using the Faraday effect in optical fibers
[DE95-001859] p 1545 N95-21728

In search of random noise p 1592 N95-21753

Modeling the effect of water on mantle rheology
p 1417 N95-21783

On the theory of strong electromagnetic waves propagation in an electron-positron-ion plasma
[DE94-628964] p 1561 N95-21850

Electronic structure and energies of alkaline earth oxides: MgO, CaO and SrO
[DE94-628990] p 1575 N95-21853

Rigorous spin-spin correlation function of Ising model on a special kind of Sierpinski Carpets
[DE94-628995] p 1575 N95-21854

Acoustoelectric effect in semiconductor superlattice
[DE94-628994] p 1575 N95-21859

Low frequency sound radiation from finite stiffened plates
[AD-A279395] p 1505 N95-21930

Bayesian analysis of semiparametric proportional hazards models
[AD-A279394] p 1499 N95-21946

A new FHNC scheme for Gutzwiller correlated wave functions
[DE94-629037] p 1581 N95-21993

An asymptotic solution of the (infinity)-d Hubbard model
[DE94-629042] p 1582 N95-21994

Critical dynamics and plastic flow in disordered Josephson junction arrays
[DE94-629074] p 1576 N95-21995

Breakdown of the law of large numbers in Josephson junction series arrays
[DE94-629075] p 1576 N95-21996

Economic feasibility analysis of distributed electric power generation based upon the natural gas-fired fuel cell
[DE94-012277] p 1396 N95-22033

Evaluation of simple spherical spreading model for near vertical acoustical propagation
[AD-A286284] p 1505 N95-22042

Effects of cyclic stress distribution models on fatigue life predictions
[DE95-001619] p 1388 N95-22070

A Davis-Putnam program and its application to finite-order model search: Quasigroup existence problems
[DE95-003014] p 1471 N95-22077

Effects of yaw and pitch motion on model attitude measurements
[NASA-TM-4641] p 1368 N95-22109

Temperature dependence of a magnetopolaron in a harmonic quantum dot in resonant magnetic fields
[DE94-629036] p 1502 N95-22177

Flux creep with logarithmic U(j) dependence
[DE94-629058] p 1577 N95-22180

Magnetic interactions in the Emery model
[DE94-629059] p 1577 N95-22181

Influence of wavelength on transient short-circuit current in polycrystalline silicon solar cells
[DE94-629082] p 1397 N95-22183

Heat loss by helicity injection in spheromaks
[DE95-003473] p 1562 N95-22221

Application of IRIS to semiconductor plasma processing
[DE95-003591] p 1562 N95-22225

Technical cost modeling applied to CVD diamond deposition
[AD-A286119] p 1578 N95-22231

Constraints on the left-right symmetric model from b yields s gamma
[DE95-003469] p 1528 N95-22239

Modeling of fundamental phenomena in welds
[DE94-017859] p 1381 N95-22268

An exact enumeration of self-avoiding loops on a square lattice
[DE94-628999] p 1578 N95-22276

Biaxiality of chiral liquid crystals
[DE94-629032] p 1578 N95-22277

Topics in gauge theories and the unification of elementary particle interactions
[DE94-013485] p 1529 N95-22279

Recent results in analysis and simulation of beam halo
[DE94-018313] p 1539 N95-22298

Image solution for poisson's equation in wedge geometry
[PB95-127171] p 1310 N95-22311

A multisite interaction expansion of the total energy in metals
[DE94-017175] p 1262 N95-22313

A new parallel method for molecular dynamics simulation of macromolecular systems
[DE94-018621] p 1529 N95-22315

Tunneling of self-trapped states and formation of a band
[DE94-629001] p 1582 N95-22378

Solar wind composition
[NASA-TM-197364] p 1604 N95-22384

Fundamental mechanisms in premixed flame propagation via vortex-flame interactions: Numerical simulations p 1249 N95-22440

Turbulence modeling for separated flow
p 1359 N95-22443

Local dynamic subgrid-scale models in channel flow
p 1360 N95-22447

Direct numerical simulations of on-demand vortex generators: Mathematical formulation
p 1361 N95-22452

Optimal active control for Burgers equations
p 1361 N95-22454

MATHEMATICAL PROGRAMMING

TBell: A mathematical tool for analyzing decision tables
[NASA-CR-195027] p 1462 N95-20691

Systems Analysis Laboratory. Ten years of progress 1984-1994
[PB95-104451] p 1464 N95-20982

Heuristic genetic algorithms for constrained problems. Part 1: Principles
[PB95-132031] p 1467 N95-21374

MATRICES (MATHEMATICS)

O(log2 n) time efficient parallel factorization of dense, sparse separable, and banded matrices
[NASA-CR-197356] p 1473 N95-19885

Multigrid with matrix-dependent transfer operators for convection-diffusion problems
[PB95-110821] p 1487 N95-19915

Orthogonal representations over finite fields and the chromatic number of graphs
[PB95-110953] p 1487 N95-19937

Quadratic forms in design theory
[PB95-111019] p 1487 N95-19940

Uniqueness of strongly regular graphs having minimal p-rank
[PB95-111043] p 1488 N95-19942

Graphs cospectral with distance-regular graphs
[PB95-111050] p 1488 N95-19943

ILIAS: A sequential language for parallel matrix computations
[PB95-110631] p 1473 N95-20056

Balanced matrices
[AD-A280021] p 1490 N95-20662

The design of a parallel, dense linear algebra software library: Reduction to Hessenberg, tridiagonal, and bidiagonal form
[DE94-018123] p 1491 N95-20701

Deconvolution and singular value decomposition
[AD-A286582] p 1491 N95-20875

Construction of non-critical string field theory by transfer matrix formalism in dynamical triangulation
[DE94-770607] p 1516 N95-20986

Magnetoelectric properties of reciprocal bianisotropic materials with focus on the polarizability of chiro-omega spheres
[PB95-127650] p 1544 N95-21103

T1F ((1) sigma (+)): Some preliminary electronic structure calculations
[PB95-130316] p 1518 N95-21223

A divide-and-conquer method for tridiagonalizing symmetric matrices with repeated eigenvalues
[DE95-002918] p 1476 N95-21257

A framework for symmetric band reduction and tridiagonalization
[DE95-002919] p 1476 N95-21341

Preconditioning via asymptotically-defined domain decomposition
[DE94-019046] p 1493 N95-21 64

Report of the Numerical Analysis Group
[PB95-108163] p 1494 N95-21648

Balanced 0, + or - matrices. Part 2: Recognition algorithm
[AD-A279156] p 1470 N95-21974

Latin hypercube sampling in sensitivity analysis
[AD-A285867] p 1499 N95-22135

Discrete algebraic Riccati equation and linear matrix inequality
[PB95-133575] p 1484 N95-22139

Singular symmetric matrices
[PB95-109088] p 1496 N95-22354

FORTRAN subroutine for column reduction of polynomial matrices
[PB95-134987] p 1497 N95-22379

MATRIX MATERIALS

The environmental durability of fiber reinforced ceramic matrix composites
[AD-A283750] p 1225 N95-19919

Third Intermetallic Matrix Composites Symposium, volume 350
[NASA-TM-110059] p 1225 N95-20001

Carbon fiber reinforced superconductor composites
[DE95-002504] p 1229 N95-20913

Implementation of the military handbook 17 for polymer matrix composites and metal matrix composites
[AD-A285629] p 1229 N95-21149

Implementation of the military handbook 17 for polymer matrix composites and metal matrix composites
[AD-A285595] p 1229 N95-21215

Directional solidification of the alumina-zirconia ceramic eutectic system
[DE95-001677] p 1277 N95-21735

The role of grain boundary sliding on creep deformation characteristics of discontinuous reinforced composites
[DE95-001671] p 1231 N95-21924

The thermal conductivity of silicon nitride with molybdenum disilicide additions
[DE94-017757] p 1247 N95-22260

The Modified Embedded Atom Method
[DE94-017958] p 1248 N95-22273

MATTER (PHYSICS)

Similarities and differences in strangeness production at BNL and CERN
[DE95-002343] p 1521 N95-21380

Strange hadronic matter
[DE94-019345] p 1521 N95-21484

Monopoles and quark confinement: Introduction and overview
[DE94-019348] p 1522 N95-21485

Investigation of direct photon production in 200 A GeV S + Au reactions
[DE94-018129] p 1525 N95-21704

Vortex atoms and vortons
[PB95-134599] p 1356 N95-21963
Theses of the Proceedings of the 23d International Meeting on the Physics of Charged Particle Interaction with Crystals
[DE94-631501] p 1529 N95-22281

MAXIMUM ENTROPY METHOD
Science with High Spatial Resolution Far-Infrared Data
[NASA-CR-197353] p 1595 N95-21749
MEM application to IRAS CPC images
p 1592 N95-21751
An assessment of image reconstruction from balloon-borne and the IRAS data p 1592 N95-21752
Beyond maximum entropy: Fractal Pixon-based image reconstruction p 1593 N95-21757
HIRAS: High-resolution IRAS images
p 1593 N95-21758
Robust fixed-structure control
[AD-A286515] p 1485 N95-22216

MAXIMUM LIKELIHOOD ESTIMATES
Unbinned maximum likelihood fit for the CP conserving couplings for W + photon production at CDF
[DE95-001471] p 1514 N95-20852
Geographical diversity combining to exploit multi-mechanism propagation p 1299 N95-20957
Superresolution direction finding algorithms for the characterisation of multi-moded HF signals
p 1299 N95-20958
Exponential deconvolution: Two asymptotically equivalent estimators
[PB95-132122] p 1499 N95-21469
Hires and beyond p 1592 N95-21750
An assessment of image reconstruction from balloon-borne and the IRAS data p 1592 N95-21752
Signal processing in the linear statistical model
[AD-A286255] p 1308 N95-22041

MAXWELL EQUATION
On FEL integral equation and electron energy loss in intermediate gain regime
[DE94-770631] p 1371 N95-20757
Massively-parallel computational fluid dynamics
[AD-A279389] p 1355 N95-21942

MEAN
Iterated-bootstrap confidence intervals for the mean
[AD-A279802] p 1498 N95-20102

MEAN FREE PATH
A preliminary study of the airwake model used in an existing SH-60B/FFG-7 helicopter/ship simulation program
[DSTO-TR-0015] p 1201 N95-21659

MEAN SQUARE VALUES
Structure and dynamics of turbulent wall layers
[AD-A285360] p 1340 N95-20547

MEASURING INSTRUMENTS
An evaluation of 915-MHz radar wind profiler/RASS by tower and sodar measurements
[DE94-018913] p 1364 N95-20320
Development of solid state moisture sensors for semiconductor fabrication applications
[DE94-015771] p 1364 N95-20398
Method and apparatus for non-invasive evaluation of diaphragmatic function
[NASA-CASE-LAR-13888-1] p 1441 N95-20408
LLNL/Lion Precision LVDT amplifier
[DE95-001504] p 1327 N95-20854
A convergence analysis of an h-version finite element method with high order elements for two dimensional elasto-plasticity problems
[AD-A279975] p 1491 N95-20920
Advanced concepts for gamma ray isotopic analysis and instrumentation
[DE94-016610] p 1517 N95-21174
Characterization equipment for electrooptics and actuators
[AD-A286285] p 1546 N95-22043

MECHANICAL DEVICES
Proceedings of the NATO-Advanced Study Institute on Computer Aided Analysis of Rigid and Flexible Mechanical Systems. Volume 1: Main lectures
[AD-A286062] p 1380 N95-21171

MECHANICAL DRIVES
Bevel gear driver and method having torque limit selection
[NASA-CASE-MSC-22384-1] p 1378 N95-20151
Magnetostrictive motor system
[AD-D016484] p 1333 N95-21901

MECHANICAL ENGINEERING
Mechanical design of the DO silicon detector
[DE95-002532] p 1365 N95-20902
Proceedings of the NATO-Advanced Study Institute on Computer Aided Analysis of Rigid and Flexible Mechanical Systems. Volume 1: Main lectures
[AD-A286062] p 1380 N95-21171
Proceedings of the NATO-Advanced Study Institute on Computer Aided Analysis of Rigid and Flexible Mechanical Systems. Volume 2: Contributed papers
[AD-A286063] p 1381 N95-21488

MECHANICAL OSCILLATORS
Quartz resonator fluid monitors for vehicle applications
[DE94-018910] p 1367 N95-21546

MECHANICAL PROPERTIES
The influence of ply waviness with nonlinear shear on the stiffness and strength reduction of composite laminates
[AD-A285736] p 1224 N95-19899
Cr2Nb development
[DE94-018697] p 1250 N95-20043
Mechanical behavior of 97.2% W alloy in tension at high temperatures
[AD-A284797] p 1250 N95-20067
Dynamic measurement of the hoop modulus of a composite cylinder
[DE94-018958] p 1385 N95-20416
The processing and mechanical properties of high temperature/high performance composites. Book 7: In-situ measurements of stress and damage
[AD-A279814] p 1227 N95-20583
The processing and mechanical properties of high temperature/high performance composites. Book 5: Interface effects
[AD-A279815] p 1228 N95-20584
Structural performance of cylindrical pressure housings of different ceramic compositions under external pressure loading. Part 1: Isostatically pressed alumina ceramic
[AD-A279669] p 1270 N95-20603
The mechanical property data base from an Air Force/Industry cooperative test program on advanced aluminum alloys
[AD-A280038] p 1386 N95-20615
The processing and mechanical properties of high temperature/high performance composites. Mechanism-based constitutive laws and design, book 1
[AD-A279736] p 1228 N95-20801
The processing and mechanical properties of high temperature/high performance composites. Processing/property correlations, book 4
[AD-A279739] p 1228 N95-20802
Tribology and surface mechanical properties of excimer laser nitrided titanium
[DE95-002751] p 1255 N95-21238
Tungsten-uranium penetrator target interaction
[DE95-000847] p 1387 N95-21364
Ceramic technology for advanced heat engines
[DE95-000950] p 1278 N95-21937
Effect of laser radiation on carbon fibre/epoxy composites
[PB95-133526] p 1232 N95-22096
The influence of chemistry and microstructure on the fracture toughness of V-V3Si in-situ composites
[DE94-018997] p 1232 N95-22126
Corrosion behavior of landing gear steels
[AD-A285862] p 1261 N95-22132
Materials support for the development of High Temperature Advanced Furnaces (HITAF): A comparison of selected mechanical properties for three SiC-based ceramics
[DE94-017752] p 1280 N95-22258
Strength testing of Ti-vapor-coated silicon nitride braze joints
[DE94-017858] p 1280 N95-22266
Bulk and defect properties of ordered intermetallics
[DE94-017706] p 1262 N95-22344

MECHANICS (PHYSICS)
Transactions of the Eleventh Army Conference on Applied Mathematics and Computing
[AD-A279884] p 1497 N95-22389

MECHANIZATION
An evaluation of Automatic Terminal Information Service (ATIS) flight deck display presentation options
[AD-A280100] p 1204 N95-21020

MEDICAL ELECTRONICS
Radiofrequency hyperthermia systems: Experimental and clinical assessment of the feasibility of radiofrequency hyperthermia systems for loco-regional deep heating
[PB94-206885] p 1444 N95-21016

MEDICAL EQUIPMENT
Method and apparatus for non-invasive evaluation of diaphragmatic function
[NASA-CASE-LAR-13888-1] p 1441 N95-20408
Seminar on Biomedical Engineering 1993
[PB95-104402] p 1443 N95-20971
Radiofrequency hyperthermia systems: Experimental and clinical assessment of the feasibility of radiofrequency hyperthermia systems for loco-regional deep heating
[PB94-206885] p 1444 N95-21016

MEDICAL SCIENCE
Development and enhancement of a model of performance and decision making under stress in a real life setting
[AD-A285945] p 1449 N95-20393
Water-soluble polyphosphazenes and their hydrogels
[AD-A279695] p 1269 N95-20580
ANSTO: Program of research, 1993-1994
[DE94-631122] p 1605 N95-21828
Command history, 1993
[AD-A279775] p 1446 N95-21989
Sustaining the health and performance of soldiers/warfighters deployed to harsh environments
[AD-A286270] p 1446 N95-22004

MEDICAL SERVICES
Compact free electron lasers for medical applications
[AD-A285739] p 1369 N95-20072
Command history, 1993
[AD-A279775] p 1446 N95-21989

MELTING
Effect of microgravity on material undergoing melting and freezing: The TES Experiment
[NASA-TM-106845] p 1338 N95-19952
Theoretical-experimental study on the electroslag remelting technology of high quality steels
[DE94-629216] p 1256 N95-21270
Volatiles in the Earth: All shallow and all recycled
p 1416 N95-21779
Structure and stability of hydrous minerals at high pressure p 1417 N95-21786
The primary carbon and the formation of carbon species in terrestrial magmas p 1420 N95-21797
Gravitational effects on the development of weld-pool and solidification microstructures
[DE94-017772] p 1285 N95-22261
Modeling of fundamental phenomena in welds
[DE94-017859] p 1381 N95-22268

MELTS (CRYSTAL GROWTH)
Solubilities of nitrogen and noble gases in basalt melt
p 1422 N95-21807

MEMBRANES
A photophysical control mechanism for zeaxanthin-associated radiationless energy dissipation in photosynthesis
[DE94-018383] p 1437 N95-19969
Mechanism of the amperometric response of a proposed glucose sensor based on a polypyrrole-tubule-impregnated membrane
[AD-A279836] p 1365 N95-20431
Testing of the SAIC facets on the stretched-membrane dish
[DE95-001831] p 1393 N95-20864
The permeation of bis(2-fluoro-2,2-dinitroethyl) formal (FEFO), ethyl 4,4-dinitropentanoate (EDNP), ethyl 4-nitropentanoate (ENP), and 1,2,4-trichlorobenzene (TCB) through barrier membranes
[DE95-002492] p 1283 N95-21514
Development and applications of flat ceramic membranes
[PB95-110219] p 1276 N95-21650
Chemical interactions between protein molecules and polymer membrane materials
[DE95-001808] p 1224 N95-21746
Development of active-transport membrane devices
[DE94-015947] p 1246 N95-21921
Separation of proteins by convective electrophoresis through a porous membrane
[PB95-127130] p 1248 N95-22373

MEMORY
Biological and theoretical studies of adaptive networks: The conditioned response
[AD-A284781] p 1479 N95-20061
MAC/FAC: A model of similarity-based retrieval
[AD-A286291] p 1450 N95-22052

MEMORY (COMPUTERS)
Role of working memory limitations of retrieval
[AD-A280032] p 1448 N95-20007
Performance issues for engineering analysis on MIMD parallel computers
[DE94-015769] p 1474 N95-20150
Parallel solid mechanics codes at Sandia National Laboratories
[DE94-015770] p 1474 N95-20152
MPI workshop
[DE94-017883] p 1475 N95-20366
The design of a parallel, dense linear algebra software library: Reduction to Hessenberg, tridiagonal, and bidiagonal form
[DE94-018123] p 1491 N95-20701
Network distributed global memory for transparent message passing on distributed networks
[AD-A286096] p 1478 N95-22228
TDX: A high-bandwidth crossbar-switched communication paradigm
[DE94-017187] p 1311 N95-22407

A periodic scheduling heuristic for mapping iterative task graphs onto distributed memory multiprocessors [AD-A286047] p 1311 N95-22415

MENISCI

An augmented Young-Laplace model of an evaporating meniscus in a micro-channel with high heat flux [NASA-CR-197622] p 1340 N95-20796

MENTAL HEALTH

Psychosocial stress and mental health in a forward-deployed military community [AD-A285940] p 1451 N95-22323

MENTAL PERFORMANCE

Behavioral effects of tyrosine during sustained wakefulness [AD-A279789] p 1441 N95-20307

A comparison of decision making behaviour in a static and a dynamic task environment as a function of time pressure [AD-A285389] p 1449 N95-20609

MERCURY (METAL)

Mercury usage and alternatives in the electrical and electronics industries [PB94-165362] p 1312 N95-19966

Mercury capture in bench-scale absorbers [DE94-016910] p 1234 N95-20107

Micrometeorological methods for measurements of mercury emissions over contaminated soils [DE94-017679] p 1411 N95-22342

MERCURY (PLANET)

Polar volatiles on Mercury and the Moon p 1422 N95-21811

Semi-volatiles at Mercury: Sodium (Na) and potassium (K) p 1424 N95-21818

MERCURY ATMOSPHERE

Semi-volatiles at Mercury: Sodium (Na) and potassium (K) p 1424 N95-21818

MERCURY COMPOUNDS

Mercury usage and alternatives in the electrical and electronics industries [PB94-165362] p 1312 N95-19966

MERCURY ISOTOPES

Hg-199 and Cu-(63,65) NMR studies of mercury based high-Tc superconductors [DE95-001073] p 1570 N95-20820

MERCURY SURFACE

Semi-volatiles at Mercury: Sodium (Na) and potassium (K) p 1424 N95-21818

MERCURY TELLURIDES

IR materials producibility [AD-A280094] p 1328 N95-21017

MERGING ROUTINES

Software merge: Semantics of combining changes to programs [AD-A279657] p 1459 N95-20304

MESOMETEOROLOGY

Effects of microphysics and radiation on mesoscale processes of a midlatitude squall line [DE94-014732] p 1429 N95-20381

MESON-NUCLEON INTERACTIONS

Hard diffraction and rapidity gaps [DE95-000565] p 1507 N95-20111

Theories of the eta-meson-nucleus interaction [DE94-016055] p 1516 N95-21125

Polarization of charmonium in pion-nucleus collisions [DE95-002783] p 1523 N95-21525

Constraints on T-odd and P-even hadronic interactions from nucleon, nuclear, and atomic electric dipole moments [DE94-012845] p 1526 N95-21920

MESONS

J/psi,psi(prime) yields mu(+)mu(-) and B yields J/psi,psi(prime) cross sections [DE94-017184] p 1507 N95-20108

B meson lifetimes at CDF [DE95-000564] p 1507 N95-20110

Hard diffraction and rapidity gaps [DE95-000565] p 1507 N95-20111

A tau-charm-factory at Argonne [DE94-016913] p 1510 N95-20360

Semi-leptonic form-factors from lattice QCD [DE95-000871] p 1510 N95-20367

Mass and lifetime measurements with exclusive B reconstruction at CDF [DE94-015849] p 1511 N95-20401

D(sup 0)-(anti-D)(sup 0) mixing and doubly Cabibbo-suppressed decays of the D(+) [DE94-015540] p 1512 N95-20476

Charmonium production, b quark and B meson production and b(bar b) correlations at CDF [DE95-002525] p 1515 N95-20898

A measurement of the b(bar b) cross section at CDF [DE95-000642] p 1519 N95-21273

Measurement of the polarization in the decay B(sup 0) (yields) J/(psi)K*(sup 0) in (bar p)p collisions at (radical)s = 1.8 TeV [DE95-002521] p 1520 N95-21313

A high-rate fixed-target charm experiment [DE95-001767] p 1521 N95-21378

Lattice results for heavy light matrix elements [DE94-019101] p 1523 N95-21551

Measurement of the B meson differential cross-sections in p(bar p) collisions at (radical)s = 1.8 TeV using the exclusive decays B(sup (+-)) (yields) J/(psi)K(sup (+-)) and B(sup 0) (yields) J/(psi)K*(sup 0) [DE94-018993] p 1523 N95-21562

Summary of heavy ion theory [DE95-002177] p 1523 N95-21588

Measurement of the B cross section at CDF via B semileptonic decays [DE95-002217] p 1524 N95-21597

The status of molecules [DE95-000952] p 1526 N95-21939

Experience at the Los Alamos Meson Physics Facility with the use of alloy Inconel 718 as an enclosure for a beam degrader and as a proton beam entry window [DE94-018289] p 1538 N95-22050

Constraints on the left-right symmetric model from b yields s gamma [DE95-003469] p 1528 N95-22239

Beam flavor dependence in the hadroproduction of D(+-) and D(sub s)(+-) mesons [DE94-015541] p 1530 N95-22339

Parity violation in the compound nucleus [DE95-002742] p 1530 N95-22435

MESOSCALE PHENOMENA

Mississippi State University Center for Air Sea Technology FY 1993 and FY 1994 research program in Navy ocean modeling and prediction [AD-A286322] p 1432 N95-20209

Effects of microphysics and radiation on mesoscale processes of a midlatitude squall line [DE94-014732] p 1429 N95-20381

The effect of regional-scale soil-moisture deficits on mesoscale atmospheric dynamics that influence fire severity [DE95-002682] p 1413 N95-20455

An integrated cloud observation and modeling investigation in support of the ARM Program [DE95-002798] p 1430 N95-21527

MESOSPHERE

Analysis of mesospheric winds and waves [AD-A279956] p 1414 N95-20591

MESSAGE PROCESSING

Algebraic semantics of message sequence charts [PB95-110581] p 1288 N95-19890

A group communication approach for mobile computing mobile channel: An ISIS tool for mobile services [AD-A279785] p 1290 N95-20306

Test and Evaluation Master Plan (TEMP) for the Weather Message Switching Center Replacement (WMSCR) [AD-A286590] p 1429 N95-20857

Programmable modular network interface [AD-D016505] p 1477 N95-21674

Initial experience with noncorrecting syntax error handling [PB95-132700] p 1471 N95-22029

Network distributed global memory for transparent message passing on distributed networks [AD-A286096] p 1478 N95-22228

MESSAGES

Split-C and active messages under SUNMOS on the Intel Paragon [DE94-011418] p 1474 N95-20123

The message passing version of the parallel Community Climate Model [DE94-019158] p 1407 N95-21608

Initial experience with noncorrecting syntax error handling [PB95-132700] p 1471 N95-22029

Modelling the reassembly buffer in a connectionless server [PB95-132908] p 1308 N95-22087

METABOLISM

Thorium-232 in human tissues: Metabolic parameters and radiation doses [DE94-019275] p 1441 N95-20074

The Use of Cyanobacteria to Explore Basic Biological Processes [DE94-019238] p 1440 N95-22066

METAL BONDING

Energetics, bonding mechanism and electronic structure of ceramic/ceramic and metal/ceramic interfaces [DE95-000601] p 1265 N95-20115

Joining of dissimilar materials. A review [PB95-132999] p 1380 N95-21416

Forming of superplastic ceramics [DE94-017306] p 1276 N95-21662

METAL CLUSTERS

Cluster reactions: An approach to understanding the fundamentals of heterogeneous catalysis [DE95-002947] p 1243 N95-21447

The enhancement of metallic silver monomer evaporation by the adhesion of polar molecules to silver nanocluster ions [AD-A284936] p 1281 N95-22470

METAL COATINGS

Polycrystalline thin film cadmium telluride solar cells fabricated by electrodeposition [DE94-011848] p 1391 N95-20118

Novel reagents for chemical vapor deposition of intermetallic alloys [AD-A286562] p 1271 N95-20815

METAL CRYSTALS

Gravitational effects on the development of weld-pool and solidification microstructures [DE94-017772] p 1285 N95-22261

METAL FATIGUE

Application of an energy-based life prediction model to bithermal and thermomechanical fatigue [NASA-TM-106684] p 1385 N95-20179

The reliability of laser reflowed Sn-Ag solder joints [AD-A279787] p 1315 N95-20443

The mechanical property data base from an Air Force/Industry cooperative test program on advanced aluminum alloys [AD-A280038] p 1386 N95-20615

Moessbauer study of the sintered Mn(0.70)Zn(0.23)Fe(2.07)O4 [DE94-631462] p 1255 N95-20909

Time-dependent deformation of titanium metal matrix composites [NASA-CR-195030] p 1230 N95-21363

Processing and mechanical properties of laminar Al2O3-Ni3Al composites [DE94-019332] p 1230 N95-21481

Welding tritium exposed stainless steel [DE95-003208] p 1382 N95-22356

Fracture behavior of laminated discontinuously reinforced aluminum material [DE94-017307] p 1263 N95-22408

METAL FIBERS

Fibre-reinforced high-strength concrete [PB95-131942] p 1232 N95-22158

METAL FILMS

Mixed-sputter deposition of Ni-Ti-Cu shape memory films [DE94-017296] p 1250 N95-19900

A structural determination using magnetic x ray circular dichroism in spin-polarized photoelectron diffraction [DE94-017528] p 1567 N95-20449

Ferroic materials: Design, preparation and characteristics. Ceramic transactions, volume 43 [AD-A285937] p 1270 N95-20664

Aerosol-assisted chemical vapor deposition of copper: A liquid delivery approach to metal thin films [AD-A279702] p 1270 N95-20689

Copper metallization of stainless steels [DE95-001496] p 1256 N95-21300

Spectroscopic assessment of the reliability of metal/metal oxide interfaces [AD-A286131] p 1261 N95-22035

Surfaces and thin films studied by picosecond ultrasonics [DE95-001866] p 1506 N95-22071

METAL HALIDES

Modeling of nonlinear optic and ESR response of CDW MX materials [DE94-018301] p 1578 N95-22297

METAL HYDRIDES

Structure and stability of hydrous minerals at high pressure p 1417 N95-21786

METAL IONS

Tests of dielectric model descriptions of chemical charge displacements in water [DE94-007530] p 1236 N95-20277

Actinide(IV) and actinide(VI) carbonate speciation studies by PAS and NMR spectroscopies [DE94-016957] p 1236 N95-20361

Metallic ions and atoms in the upper atmosphere [AD-A285229] p 1414 N95-20498

Rare earth garnet selective emitter p 1322 N95-20536

On the sputtering of metals and insulators: A nonlinear evolution problem with nonlinear boundary condition [DE95-001456] p 1254 N95-20792

The application of electrodialysis to extend the lifetime of commercial electroplating baths [DE95-000868] p 1246 N95-22012

The enhancement of metallic silver monomer evaporation by the adhesion of polar molecules to silver nanocluster ions [AD-A284936] p 1281 N95-22470

METAL MATRIX COMPOSITES

Third Intermetallic Matrix Composites Symposium, volume 350 [NASA-TM-110059] p 1225 N95-20001

The thermal conductivity of carbon-fiber reinforced metal matrix composites
[DE94-017767] p 1226 N95-20125

The processing and mechanical properties of high temperature/high performance composites. Stress redistribution and notch properties, book 2
[AD-A279737] p 1227 N95-20429

The processing and mechanical properties of high temperature/high performance composites. Fatigue and creep, book 3
[AD-A279738] p 1227 N95-20430

The processing and mechanical properties of high temperature/high performance composites. Book 7: In-situ measurements of stress and damage
[AD-A279814] p 1227 N95-20583

Wear resistant composite structure of vitreous carbon containing convoluted fibers
[DE95-002254] p 1228 N95-20787

The processing and mechanical properties of high temperature/high performance composites. Mechanism-based constitutive laws and design, book 1
[AD-A279736] p 1228 N95-20801

The processing and mechanical properties of high temperature/high performance composites. Processing/property correlations, book 4
[AD-A279739] p 1228 N95-20802

Implementation of the military handbook 17 for polymer matrix composites and metal matrix composites
[AD-A285629] p 1229 N95-21149

Implementation of the military handbook 17 for polymer matrix composites and metal matrix composites
[AD-A285595] p 1229 N95-21215

Time-dependent deformation of titanium metal matrix composites
[NASA-CR-195030] p 1230 N95-21363

The processing and mechanical properties of high temperature/high performance composites. Book 6: Delamination and compressive behavior
[AD-A279780] p 1231 N95-21999

Surface technology programme
[PB95-132866] p 1262 N95-22174

Implementation of the Military Handbook 17 for polymer matrix composites and metal matrix composites
[AD-A285772] p 1233 N95-22395

METAL OXIDE SEMICONDUCTORS

Characteristics of oxynitrides grown in N2O
[DE94-015798] p 1566 N95-20400

SPICE macro model of a spryton with MOSFET's in the avalanche mode
[DE94-015744] p 1555 N95-21134

METAL OXIDES

Novel electrochemical materials prepared by sol-gel chemistry
[AD-A286310] p 1226 N95-20092

Ferrocyanide safety project Dynamic X-Ray Diffraction studies of sodium nickel ferrocyanide reactions with equimolar nitrate/nitrite salts
[DE94-017396] p 1236 N95-20268

Spectroscopic assessment of the reliability of metal/metal oxide interfaces
[AD-A286131] p 1261 N95-22035

METAL PLATES

Characterization of a texture gradient in tantalum plate
[DE95-002704] p 1262 N95-22289

METAL SHEETS

Sheet metal formability
[PB95-110250] p 1258 N95-21653

METAL SPRAYING

Magnetically controlled deposition of metals using gas plasma
[DE94-018654] p 1251 N95-20128

METAL SURFACES

Chemical and electrochemical interactions on corroding metal surfaces
[DE95-000624] p 1250 N95-19979

Numerical controlled polishing program, continued forced wear and part correction experiments
[DE94-018084] p 1285 N95-20288

S-D hybridization and anisotropy of the optical second harmonic at low frequencies
[AD-A279449] p 1544 N95-20876

Methods of measuring adhesion for thermally grown oxide scales
[DE94-018177] p 1256 N95-21260

Properties of aged metal tritides
[DE95-001787] p 1243 N95-21440

Quantum simulation of heterogeneous electron transfer free energies at the water-metal interface
[AD-A279279] p 1522 N95-21492

A new universal solution for the electrofinishing of metallic materials
[DE95-001681] p 1258 N95-21568

Hydrogenation of nitriles on a well-characterized nickel surface: From surface science studies to liquid phase catalytic activity measurements
[DE94-018184] p 1259 N95-21707

The optical properties of particles deposited on a surface
[AD-A286258] p 1546 N95-22002

The final status of a metal surface after multipulse laser irradiation in an ambient gas
[DE94-629000] p 1562 N95-22377

Resonant charge transfer in hyperthermal atomic and molecular ion-surface collisions
[AD-A284937] p 1530 N95-22471

METAL VAPORS

Thoriated-tungsten, split-ring, hollow-cathode electrode for discharge devices
[AD-D016508] p 1333 N95-21906

METAL WORKING

Weld pool phenomena
[DE94-018965] p 1381 N95-21550

Sheet metal formability
[PB95-110250] p 1258 N95-21653

Directed light fabrication
[DE94-018293] p 1375 N95-21837

METAL-METAL BONDING

The effect of oxide inclusions on the kinetics of the austenite to ferrite transformation in low alloy steel weld metal
[DE94-018131] p 1253 N95-20676

Joining of dissimilar materials. A review
[PB95-132999] p 1380 N95-21416

Joining dissimilar stainless steels for pressure vessel components
[PB95-133005] p 1380 N95-21446

METAL-WATER REACTIONS

Quantum simulation of heterogeneous electron transfer free energies at the water-metal interface
[AD-A279279] p 1522 N95-21492

METALLIZING

Magnetically controlled deposition of metals using gas plasma
[DE94-018654] p 1251 N95-20128

Copper metallization of stainless steels
[DE95-001496] p 1256 N95-21300

METALLOGRAPHY

Application of a dimensionless parameter model for Laser Beam Welding
[DE94-018902] p 1378 N95-20048

Microstructures and tensile properties of as-cast iron-aluminide alloys
[DE94-017868] p 1252 N95-20359

Effect of heat treatment temperature on creep-rupture properties of Fe3Al-based alloys
[DE94-017904] p 1253 N95-20375

A new metallographic procedure for edge retention of enclosed surfaces
[DE94-017549] p 1261 N95-22048

METALLURGY

Fusion welding of advanced borated stainless steels
[DE94-019037] p 1378 N95-20053

METALORGANIC CHEMICAL VAPOR DEPOSITION

High-efficiency, deep-junction, epitaxial InP solar cells on (100) and (111)B InP substrates
p 1316 N95-20507

P/N InP solar cells on Ge wafers
p 1317 N95-20511

Radiation effects on p+n InP junctions grown by MOCVD p 1319 N95-20520

Effects of plasma hydrogenation on trapping properties of dislocations in heteroepitaxial InP/GaAs
p 1323 N95-20542

Nucleation, growth, and strain relaxation of lattice-mismatched 3-5 semiconductor epitaxial layers
p 1324 N95-20543

Application of IRIS to semiconductor plasma processing
[DE95-003591] p 1562 N95-22225

METALS

Scanning tunneling microscopy of semiconductor surfaces
[AD-A279982] p 1571 N95-20964

Monitoring activities in the framework of the Dutch National Air Quality Monitoring Network in 1994
[PB95-131884] p 1406 N95-21351

Simulations of metal dissolution and corrosion
[DE94-019295] p 1257 N95-21476

Corrosion resistance and behavioral characteristics of metals exposed to 70 percent by weight sulfuric acid at elevated temperatures
[DE95-001724] p 1259 N95-21740

A multisite interaction expansion of the total energy in metals
[DE94-017175] p 1262 N95-22313

METAMORPHISM (GEOLOGY)

Thermochemistry of dense hydrous magnesium silicates p 1416 N95-21782

Noble gas isotopes and halogens in volatile-rich inclusions in diamonds p 1417 N95-21784

Transportation of volatile elements in thermally evolving planetesimals: An important role of metallic iron
p 1418 N95-21790

METASTABLE STATE

Chemical lasers emitting in the visible spectrum: Metastable oxygen reactions and YOSHIDA laser
[PB95-104485] p 1372 N95-20983

Thermodynamic analysis of stable and metastable equilibrium diagrams of the Cu-Cr system
[PB95-127775] p 1255 N95-21111

Metastable bcc phase formation in the Nb-Cr-Ti system
[DE94-016212] p 1255 N95-21137

METEORITES

Implications of noble gases in a recently recognized Martian meteorite (ALH84001) for the degassing history of Mars p 1424 N95-21819

Distribution of light element isotopes in Bencubbin and Weatherford meteorites: An indicator of heterogeneity in the primitive solar nebula
[DE94-019167] p 1600 N95-22128

METEORITIC COMPOSITION

Alkali element depletion by core formation and vaporization on the early Earth p 1421 N95-21804

Implications of noble gases in a recently recognized Martian meteorite (ALH84001) for the degassing history of Mars p 1424 N95-21819

He, Xe and Ne isotopes in a steady-state mass transport model and implications about terrestrial volatiles
p 1425 N95-21821

METEOROID CONCENTRATION

An experimental determination of meteor daily arrival rate variation
[AD-A279484] p 1600 N95-21679

METEOROID SHOWERS

The relative importance of meteor burst and other distance polar cap propagation modes in the low VHF band p 1293 N95-20928

METEOROIDS

The relative importance of meteor burst and other distance polar cap propagation modes in the low VHF band p 1293 N95-20928

An experimental determination of meteor daily arrival rate variation
[AD-A279484] p 1600 N95-21679

Atmospheres of the Moon and Mercury
p 1419 N95-21794

METEOROLOGICAL BALLOONS

Comparison of meteorological data with fitted values extracted from projectile trajectory
[AD-A285921] p 1428 N95-19989

METEOROLOGICAL CHARTS

Mariners Weather Log, volume 38, number 3, summer 1994
[PB94-209541] p 1428 N95-20099

METEOROLOGICAL PARAMETERS

Effects of meteorology on concentrations of acid aerosols
[PB94-209749] p 1400 N95-19965

Comparison of meteorological data with fitted values extracted from projectile trajectory
[AD-A285921] p 1428 N95-19989

Meso-scale cooling effects of high albedo surfaces: Analysis of meteorological data from White Sands National Monument and White Sands Missile Range
[DE94-018535] p 1429 N95-20782

Line-of-sight multipath propagation measurements at 15 GHz over 500 MHz bandwidth p 1296 N95-20944

Proceedings of the Cloud Impacts on DOD Operations and Systems 1993 Conference (CIDOS 1993)
[AD-A286658] p 1430 N95-20974

Atmospheric stability and its influence on air quality in small communities in northern Sweden
[PB95-131652] p 1405 N95-21181

Applicability of the ECMWF rain height and rainfall rate data to the prediction of low-availability rain attenuation in Europe
[PB95-127684] p 1430 N95-21413

METEOROLOGICAL RADAR

An evaluation of 915-MHz radar wind profiler/RASS by tower and sodar measurements
[DE94-018913] p 1364 N95-20320

Boundary layer cloud studies in support of ASTEX
[AD-A285947] p 1429 N95-20395

Radar studies of aviation hazards
[AD-A285845] p 1203 N95-21831

METEOROLOGY

Effects of meteorology on concentrations of acid aerosols
[PB94-209749] p 1400 N95-19965

Comparison of meteorological data with fitted values extracted from projectile trajectory
[AD-A285921] p 1428 N95-19989

Monthly mean sea ice data from the Polar Ice Prediction System, the Regional Polar Ice Prediction System-Barents Sea and the Regional Polar Ice Prediction System-Greenland Sea
[AD-A280095] p 1433 N95-21018
Atmospheric stability and its influence on air quality in small communities in northern Sweden
[PB95-131652] p 1405 N95-21181

METHANE
Direct aromatization of methane
[DE94-017131] p 1233 N95-19924
Natural gas cleanup: Evaluation of a molecular sieve carbon as a pressure swing adsorbent for the separation of methane/nitrogen mixtures
[DE94-012263] p 1234 N95-20135
Selective methane oxidation over promoted oxide catalysts
[DE94-012270] p 1235 N95-20188
Indirect global warming effects of ozone and stratospheric water vapor induced by surface methane emission
[DE94-019016] p 1402 N95-20353
Novel catalysts for methane activation
[DE95-002639] p 1237 N95-20438
The Carnol process for methanol production and utilization with reduced CO2 emissions
[DE94-016808] p 1283 N95-21211
Single-collision studies of energy transfer and chemical reaction
[DE95-002943] p 1244 N95-21517
Numerical study of contaminant effects on combustion of hydrogen, ethane, and methane in air
[NASA-TM-106844] p 1284 N95-22114
Natural gas combustion chemistry mechanisms research
[PB95-111670] p 1247 N95-22150
Transient studies of low temperature catalysts for methane conversion
[DE95-003560] p 1247 N95-22224
Development and demonstration of advanced technologies for direct electrochemical oxidation of hydrocarbons (methanol, methane, propane)
[AD-A285094] p 1224 N95-22474

METHOD OF MOMENTS
Moment approach to high-order accelerator beam optics
[DE95-001018] p 1536 N95-21331
Conditional statistics in a turbulent premixed flame derived from direct numerical simulation
p 1249 N95-22438

METHODOLOGY
Methodology for ESCA analysis of electromigration
[AD-A286229] p 1241 N95-21168
The navigation toolkit
[NASA-CR-197290] p 1205 N95-22161

METHYL ALCOHOL
Thermodynamic and NMR studies of solvent effect on enantiomeric recognition for a chiral organiz ammonium cation by chiral diketopyridino-18-Crown-6 type ligands at 25.0 C
[AD-A279893] p 1223 N95-20592
Effect of external stress on the transport of fluids in thermoplastic resin systems
[AD-A279993] p 1270 N95-20596
The Carnol process for methanol production and utilization with reduced CO2 emissions
[DE94-016808] p 1283 N95-21211
Technical and economic evaluation of natural gas based synthesis gas production technologies
[PB95-130597] p 1242 N95-21426
Catalytic reactions of synthesis gas. Part 3. Determination of reaction kinetics
[PB95-127759] p 1248 N95-22329
Development and demonstration of advanced technologies for direct electrochemical oxidation of hydrocarbons (methanol, methane, propane)
[AD-A285094] p 1224 N95-22474

METHYL CHLORIDE
Radiative forcing calculations for CH3Cl
[DE94-019018] p 1402 N95-20355

METHYL COMPOUNDS
Selective methane oxidation over promoted oxide catalysts
[DE94-012270] p 1235 N95-20188
New chiral pyrimidino-crown ether ligands
[AD-A279892] p 1223 N95-20590
Publications/patents/presentations/honors/student eport. Investigation of the role of vibrational excitation in unimolecular reactions
[AD-A280044] p 1513 N95-20621
Structure of dibis(diethyldithiocarbamato) zinc (2) Mu-bis(diethylphosphino)ethane toluene(2)
[AD-A279792] p 1224 N95-20660
Gas-phase generation of zinc sulfide particles using a single-source precursor
[AD-A279700] p 1239 N95-20712
Dynamic NMR studies of restricted arene rotation in the chromiu tricarbonyl thiophene and selenophene complexes
[DE95-001656] p 1257 N95-21399
Translational-energy-resolved studies of photographed carrier-induced reactions on semiconductor surfaces
[DE95-002944] p 1573 N95-21444
Single-collision studies of energy transfer and chemical reaction
[DE95-002943] p 1244 N95-21517

METHYLENE
Effect of external stress on the transport of fluids in thermoplastic resin systems
[AD-A279993] p 1270 N95-20596

METRIC SPACE
Linear invariance of Lindeloef numbers
[PB95-134540] p 1494 N95-21956

METROLOGY
Development, fabrication, and metrology of the electro-optical breadboard model for the reflection grating array of the XMM grating spectrometer
[DE94-016605] p 1543 N95-20612

MEXICO
Dust Bowl migration as an analog for possible global warming-induced migration from Mexico
[DE94-017472] p 1401 N95-20089

MICA
Chemical interactions between protein molecules and polymer membrane materials
[DE95-001808] p 1224 N95-21746

MICE
Enhancement of cell mediated immunity through non-specific immunostimulation with liposome encapsulated gamma-interferon
[AD-A279667] p 1442 N95-20602

MICHELSON INTERFEROMETERS
Effects of RF side-bands on spectral reproducibility for infrared synchrotron radiation
[DE95-002450] p 1536 N95-21418
Method for characterization of optical waveguide devices using partial coherence interferometry
[AD-D016525] p 1544 N95-21466
Signal to noise improvements with a new Far-IR rapid-scan Michelson Interferometer
[DE95-002416] p 1367 N95-21638

MICROANALYSIS
The in-situ fracture and Auger analysis of Nicalon fibers
[DE94-017771] p 1226 N95-20357
Surface inspection using Fourier Transform Infrared Spectroscopy
[DE95-001699] p 1244 N95-21571
A transmission electron microscope characterization of sodium sulfate hot corrosion of silicon carbide fiber-reinforced lithium aluminosilicate glass-ceramic matrix composite
[AD-A286164] p 1231 N95-22038

MICROBALANCES
Generation of micro-domains in AT-cut quartz by thermal processing and the effect on resonator modes
[DE94-017344] p 1564 N95-20087

MICROBIOLOGY
Microbiology and physiology of anaerobic fermentations of cellulose
[DE95-002899] p 1438 N95-20917

MICROCHANNEL PLATES
Unique microchannel plate process doubles MCPI resolution
[DE94-017507] p 1337 N95-22427

MICROCHANNELS
Microchannel heat pipe cooling of modules
p 1211 N95-20649
An augmented Young-Laplace model of an evaporating meniscus in a micro-channel with high heat flux
[NASA-CR-197622] p 1340 N95-20796

MICROCLIMATOLOGY
Microclimate cooling effect on perceived exertion in four heat/exercise scenarios
[AD-A285549] p 1444 N95-21160

MICROCRACKS
Fracture analysis of an all-ceramic bearing system
[AD-A285056] p 1269 N95-20486
The role of microcracking on the crack growth resistance of brittle solids and composites
[DE95-001678] p 1231 N95-21736

MICROCRYSTALS
International collaboration program on innovative chemical processing of superior electronic and optical materials
[AD-A285122] p 1226 N95-20105

MICROELECTRONICS
Solid state research
[AD-A279662] p 1567 N95-20426
The demise of plastic encapsulated microcircuit myths
p 1209 N95-20640
Lightweight electronic enclosures using composite materials p 1213 N95-20656
Method of fabricating a microelectronic photomultiplier device with integrated circuitry
[AD-D016530] p 1325 N95-20726
HTS Josephson technology on silicon with application to high speed digital microelectronics
[AD-A285964] p 1328 N95-21178
RF vacuum microelectronics based on thin film edge-emitter technology
[AD-A279539] p 1331 N95-21690
Surface technology programme
[PB95-132866] p 1262 N95-22174
Manufacturing Technology Bulletin, July 1994
[DE94-017775] p 1605 N95-22262
Parallel nanometer scale fabrication
[DE95-002122] p 1336 N95-22284

MICROGRAVITY
Effect of microgravity on material undergoing melting and freezing: The TES Experiment
[NASA-TM-106845] p 1338 N95-19952
Modeling platform dynamics and physiological response to short arm centrifugation
[AD-A279640] p 1442 N95-20457
Microgravity: Teacher's guide with activities for physical science
[NASA-EG-103] p 1285 N95-21322
Structural performance of cylindrical pressure housings of different ceramic compositions under external pressure loading. Part 3: Sintered reaction bonded silicon nitride ceramic
[AD-A285773] p 1388 N95-22411

MICROINSTRUMENTATION
Micromachined silicon-based analytical microinstruments for space science and planetary exploration
[DE94-019306] p 1367 N95-21507

MICROMACHINING
Micromachined silicon-based analytical microinstruments for space science and planetary exploration
[DE94-019306] p 1367 N95-21507
Surface micromachined capacitive tactile image sensor
[PB95-108031] p 1288 N95-21633

MICROMECHANICS
Microdynamic devices fabricated on silicon-on-sapphire substrates
[AD-D016531] p 1325 N95-20727
Micromechanical approach to transformation toughening in ceramics
[PB95-135422] p 1273 N95-20976
Time-dependent deformation of titanium metal matrix composites
[NASA-CR-195030] p 1230 N95-21363
Surface micromachined capacitive tactile image sensor
[PB95-108031] p 1288 N95-21633

MICROMETEOROLOGY
Effects of microphysics and radiation on mesoscale processes of a midlatitude squall line
[DE94-014732] p 1429 N95-20381
Micrometeorological methods for measurements of mercury emissions over contaminated soils
[DE94-017679] p 1411 N95-22342

MICROPHONES
Wavelet-based acoustic recognition of aircraft
[DE94-017701] p 1503 N95-20019

MICROPOROSITY
Mechanism of the amperometric response of a proposed glucose sensor based on a polypyrrole-tubule-impregnated membrane
[AD-A279836] p 1365 N95-20431
Transport phenomena in the micropores of plug-type phase separators
[NASA-TM-108479] p 1340 N95-20561

MICROPROCESSORS
Non-intrusive SCSI status sensing system
[AD-D016242] p 1476 N95-21307
Method of sensing target status in a local area network
[AD-D016248] p 1478 N95-22090
Method of retrieving and storing computer peripheral data
[AD-D016251] p 1591 N95-22098
Data sampling for a burst mode communications system
[AD-A286098] p 1309 N95-22229

MICROPULSATIONS
Time-resolved study of sideband generation and transition to chaos on an infrared FEL
[DE95-002336] p 1374 N95-21528

MICROSCOPES
X-ray microscope for solidification studies
[NASA-CR-197375] p 1543 N95-20798

Laboratory characterization of Woelter x ray optics
[DE94-016969] p 1562 N95-22191
MICROSCOPY
Microscopic theory of normal liquid He-3
[DE94-629047] p 1527 N95-22179
MICROSEISMS
Computer programs for analysis of geophysical data
[DE95-002472] p 1415 N95-21511
MICROSTRIP ANTENNAS
The design and analysis of a phased array microstrip antenna for a low earth orbit communication satellite
[AD-A284791] p 1289 N95-20065
Analysis of a microstrip reflectarray antenna for microspacecraft applications p 1305 N95-21541
MICROSTRUCTURE
Mixed-sputter deposition of Ni-Ti-Cu shape memory films
[DE94-017296] p 1250 N95-19900
The environmental durability of fiber reinforced ceramic matrix composites
[AD-A283750] p 1225 N95-19919
Recognition of subsurface defects in machined ceramics by application of neural networks to laser scatter patterns
[DE94-018373] p 1264 N95-20018
Properties of whisker-reinforced ceramics
[DE94-017759] p 1264 N95-20024
Cr2Nb development
[DE94-018697] p 1250 N95-20043
Sol-gel-derived silica films with tailored microstructures for applications requiring organic dyes
[DE94-018886] p 1264 N95-20047
Application of a dimensionless parameter model for Laser Beam Welding
[DE94-018902] p 1378 N95-20048
Post-irradiation deformation characteristics of heavy-ion irradiated 304L SS
[DE94-017462] p 1251 N95-20088
Development of superplasticity in 5083 aluminum with additions of Mn and Zr
[DE94-017474] p 1251 N95-20090
Reactions and microstructure at ceramic/metal interfaces
[DE94-014287] p 1265 N95-20138
Enhancement of corrosion resistance and mechanical properties of light-weight metals through the use of graded nonequilibrium microstructures
[AD-A286320] p 1251 N95-20178
Tritium and decay helium effects on the fracture toughness properties of types 316L, 304L and 21Cr-6Ni-9Mn stainless steels
[DE95-001248] p 1252 N95-20216
Microstructural contributions to the fracture resistance of silicon nitride ceramics
[DE94-018955] p 1267 N95-20323
Microstructures and tensile properties of as-cast iron-aluminide alloys
[DE94-017868] p 1252 N95-20359
Effect of heat treatment temperature on creep-rupture properties of Fe3Al-based alloys
[DE94-017904] p 1253 N95-20375
Boron carbide-based coatings on graphite for plasma facing components
[DE94-017976] p 1269 N95-20570
Atomically resolved structure and bonding of delta-doped boron layers on Si(001)
[AD-A279820] p 1513 N95-20586
The processing and mechanical properties of high temperature/high performance composites. Processing/property correlations, book 4
[AD-A279739] p 1228 N95-20802
Role of internal stresses in fracture behavior of engineering composites
[DE95-001106] p 1229 N95-20912
2nd International ADI seminar
[PB95-127734] p 1255 N95-21108
Microstructural design for tough ceramics
[AD-A285634] p 1273 N95-21152
Dependence of critical current density on microstructure and processing of high-T(c) superconductors
[DE95-000685] p 1571 N95-21167
Study of improved critical currents and mechanical properties in the Y-Ba-Cu-O superconductor with silver or Y2BaCuO3 or 211 dispersions
[AD-A285609] p 1502 N95-21194
X-ray studies of microstructures in semiconductor and superconducting materials
[DE95-001802] p 1572 N95-21279
Characterization of poly(tetrafluoroethylene) surfaces by atomic force microscopy: Results and artifacts
[DE95-000742] p 1242 N95-21309
Theoretical study of the noble metals on semiconductor surfaces and Ti-base shape memory alloys
[DE95-001654] p 1257 N95-21398
Molecular-based study of solutions in supercritical solvents
[DE94-019326] p 1580 N95-21420
Creep behavior in SiC whisker-reinforced alumina composite
[DE95-001071] p 1231 N95-21776
Ceramic technology for advanced heat engines
[DE95-000950] p 1278 N95-21937
A new metallographic procedure for edge retention of enclosed surfaces
[DE94-017549] p 1261 N95-22048
The influence of chemistry and microstructure on the fracture toughness of V-V3Si in-situ composites
[DE94-018997] p 1232 N95-22126
Atom probe field ion microscopy of type 308 CRE stainless steel welds
[DE94-019162] p 1261 N95-22127
Surface technology programme
[PB95-132866] p 1262 N95-22174
Gravitational effects on the development of weld-pool and solidification microstructures
[DE94-017772] p 1285 N95-22261
Modeling of fundamental phenomena in welds
[DE94-017859] p 1381 N95-22268
Local texture and strongly linked conduction in spray-pyrolyzed TlBa2Ca2Cu3O(8+x) deposits
[DE94-017887] p 1578 N95-22269
MICROWAVE AMPLIFIERS
Design and construction of the HSX experiment
[DE94-018657] p 1552 N95-20348
Development of an annular electron beam HPM amplifier
[AD-A286646] p 1327 N95-20905
Development status of an intense beam klystron
[DE95-000745] p 1329 N95-21395
A 500 MW annular beam relativistic klystron
[DE95-000867] p 1334 N95-22011
MICROWAVE ATTENUATION
MTX final report
[DE95-002960] p 1559 N95-21451
MICROWAVE CIRCUITS
Processing, fabrication, and demonstration of HTS integrated microwave circuits
[AD-A285611] p 1312 N95-19894
Design and packaging aspects of microwave bandwidth lithium niobate modulators
[DE94-016602] p 1313 N95-20119
High temperature superconducting films and multilayers for electronics
[AD-A279545] p 1331 N95-21693
MICROWAVE EQUIPMENT
Proton irradiation effects on advanced digital and microwave III-V components
[DE94-018742] p 1314 N95-20338
Materials processing using a variable frequency microwave furnace
[DE95-001420] p 1271 N95-20761
High temperature superconducting microwave device
[AD-A286351] p 1336 N95-22254
MICROWAVE FREQUENCIES
An application of wavelet transform for decomposition of millimeter-wave spectroscopic signals
[DE94-018366] p 1402 N95-20247
A low temperature, ultrahigh vacuum, microwave-frequency-compatible scanning tunneling microscope
[AD-A279869] p 1365 N95-20413
Small cavity nonresonant tunable microwave-frequency alternating current scanning tunneling microscope
[AD-A285752] p 1328 N95-21218
Development of a portable ice-thickness measuring instrument
[AD-A279472] p 1433 N95-21291
MICROWAVE IMAGERY
Atlas of SSM/I satellite ice concentration interpolated to operational ice model domains of the Arctic for 1993
[AD-A280183] p 1432 N95-20012
Deriving earth science products from SSM/I
[NASA-CR-197299] p 1389 N95-20156
Passive millimetre wave imaging: A review
[AD-A279275] p 1303 N95-21491
MICROWAVE LANDING SYSTEMS
Minima reduction simulation test results
[AD-A285626] p 1204 N95-21148
MICROWAVE RADIOMETERS
Deriving earth science products from SSM/I
[NASA-CR-197299] p 1389 N95-20156
MICROWAVE SCATTERING
Applied mathematical problems in modern electromagnetics
[AD-A286448] p 1303 N95-21462
X-band microwave backscattering from ocean waves
[DE94-016719] p 1309 N95-22241
Design and construction of a Ka-band scatterometer
[AD-A286296] p 1368 N95-22322
MICROWAVES
Microwave sintering of ZrO2-12 mol% CeO2
[DE94-018709] p 1265 N95-20226
An application of wavelet transform for decomposition of millimeter-wave spectroscopic signals
[DE94-018366] p 1402 N95-20247
Applied physics research for innovation in pulsed power
[AD-A285392] p 1324 N95-20610
Modelling of microwave propagation and clutter in a maritime environment p 1295 N95-20938
Time behavior and frequency response of the microwave propagation channel during multipath propagation
p 1296 N95-20942
Angle diversity on digital microwave links: Antenna design and experimental results p 1297 N95-20947
Investigation on the backscattering properties of Finnish boreal forests at C- and X-band: A semi-empirical modeling approach
[PB95-127692] p 1389 N95-21105
Resonant photon-graviton conversion in EM fields: From earth to heaven
[DE95-002784] p 1301 N95-21241
MTX final report
[DE95-002960] p 1559 N95-21451
Applied mathematical problems in modern electromagnetics
[AD-A286448] p 1303 N95-21462
Comparison of properties of sintered and sintered reaction-bonded silicon nitride fabricated by microwave and conventional heating
[DE95-001426] p 1275 N95-21501
The efficiency calibration of the DSS-24 34-meter beam-waveguide antenna p 1305 N95-21542
Design and modelling of a link monitoring mechanism for the Common Data Link (CDL)
[AD-A286167] p 1309 N95-22245
Studies of the microwave resistivity of kappa-(BEDT-TTF)2Cu(N(CN)2)Cl
[DE95-002980] p 1262 N95-22291
MIGRATION
Migrating the Facility Profile Information Management System into the World Wide Web
[DE94-018367] p 1586 N95-20016
Dust Bowl migration as an analog for possible global warming-induced migration from Mexico
[DE94-017472] p 1401 N95-20089
MILITARY AVIATION
Forecasting aircraft mishaps using monthly maintenance reports
[AD-A286049] p 1203 N95-22417
MILITARY OPERATIONS
Bomber force 2000: Operational concepts for long-range combat aircraft
[AD-A279378] p 1206 N95-20181
Highly survivable communications: Complementary media packet switched networks p 1292 N95-20922
Mitigation of the effects of F layer regularities by using multiple paths p 1298 N95-20951
Sustaining the health and performance of soldiers/warfighters deployed to harsh environments
[AD-A286270] p 1446 N95-22004
MILITARY TECHNOLOGY
NRL review, 1994
[AD-A279832] p 1605 N95-20182
Unmanned aerial vehicles
[AD-A286190] p 1206 N95-20329
Standard Hardware Acquisition and Reliability Program (SHARP) advanced SEM-E packaging
p 1208 N95-20633
Military standard: Test requirements for launch, upper-stage, and space vehicles
[AD-A286627] p 1218 N95-20770
Space technology: Force multiplier or false sense of security
[AD-A279726] p 1217 N95-20995
Policies concerning military and civilian research and technology applications
[PB95-131355] p 1585 N95-21427
Space systems technology working group: Executive report
[AD-A285778] p 1217 N95-22413
MILLIMETER WAVES
An application of wavelet transform for decomposition of millimeter-wave spectroscopic signals
[DE94-018366] p 1402 N95-20247
Simulation of the impact of atmospheric turbulences on millimeter-wave communications systems
p 1295 N95-20939
Measurements of radar backscatter from the ocean surface at 94 GHz as a function of wind speed, direction and the modulation by the ocean waves during the SAXON-FPN experiment p 1299 N95-20960
MTX final report
[DE95-002960] p 1559 N95-21451

Passive millimetre wave imaging: A review
[AD-A279275] p 1303 N95-21491
Millimeter wave front-end figure of merit, part 1
[AD-A279093] p 1307 N95-21915
Design and construction of a Ka-band scatterometer
[AD-A286296] p 1368 N95-22322

MILLING MACHINES
Safety issues in high speed machining
[PB95-127411] p 1287 N95-21422

MIMD (COMPUTERS)
Hindered settling computations using a parallel boundary element method
[DE94-014286] p 1339 N95-20137
Performance issues for engineering analysis on MIMD parallel computers
[DE94-015769] p 1474 N95-20150
MPI workshop
[DE94-017883] p 1475 N95-20366
RALPAR-RAL mesh partitioning program version 1.1
[PB95-129847] p 1475 N95-20435
Direct simulation and graphics post-processing of three-dimensional turbulent flows p 1352 N95-21098
The message passing version of the parallel Community Climate Model
[DE94-019158] p 1407 N95-21608
Fast parallel tree codes for gravitational and fluid dynamical N-body problems
[AD-A286480] p 1358 N95-22290

MIMO (CONTROL SYSTEMS)
Modeling and identification of parallel and feedback nonlinear systems
[DE95-001006] p 1481 N95-20812

MINERALOGY
Implications of noble gases in a recently recognized Martian meteorite (ALH84001) for the degassing history of Mars p 1424 N95-21819

MINERALS
Analysis of experimentally shocked minerals by NMR spectroscopy
[DE95-002955] p 1573 N95-21449
Impact degassing of water and noble gases from silicates p 1416 N95-21780
Modeling the effect of water on mantle rheology
p 1417 N95-21783
Structure and stability of hydrous minerals at high pressure p 1417 N95-21786
Phase E in a water-saturated peridotite system at 9.3 GPa p 1420 N95-21799
Subduction and volatile recycling in Earth's mantle
p 1421 N95-21802
Volatiles in the deep Earth: An experimental study using the laser-heated diamond cell p 1421 N95-21803
Hydrogen storage in Earth's mantle and core
p 1423 N95-21813
Subduction of hydrated basalt of the oceanic crust: Implications for recycling of water into the upper mantle and continental growth p 1423 N95-21814
Distribution of light element isotopes in Bencubbin and Weatherford meteorites: An indicator of heterogeneity in the primitive solar nebula
[DE94-019167] p 1600 N95-22128

MINIMA
Ab initio potential energy surface for H + OCS reactions: Extended basis sets and correlation treatment
[AD-A286420] p 1247 N95-22207

MINIMAL SURFACES
Minimal square spectral factors
[PB95-132726] p 1495 N95-22032

MINIMAX TECHNIQUE
Minimax optimal stop rule in reliability checking
[PB95-134557] p 1383 N95-21961

MINORITY CARRIERS
Physical Si(1-x)Ge(x)/Si heterojunction bipolar transistor model for device and circuit simulation
[PB95-110896] p 1312 N95-19934

MIR SPACE STATION
STS 63 flight day 4 highlights/MIR-Shuttle rendezvous
[NASA-TM-110512] p 1219 N95-21113
STS 63: Post flight presentation
[NASA-TM-110514] p 1219 N95-21558

MIRRORS
Liquid-metal pin-fin pressure drop by correlation in cross flow
[DE94-017086] p 1338 N95-19923
Beryllium based multilayers for normal incidence extreme ultraviolet reflectivity
[DE94-015560] p 1274 N95-21175
Defect geometries and laser-induced damage in multilayer coatings
[DE94-017695] p 1377 N95-22343

MISSILE DEFENSE
Enhanced vehicle and event typing software, phase 1
[AD-A284862] p 1458 N95-20070
Issues in the flight qualification of a space power reactor
[DE95-001606] p 1223 N95-21840

MISSILES
A computer code (SKINTEMP) for predicting transient missile and aircraft heat transfer characteristics
[AD-A286044] p 1341 N95-21001

MISSION PLANNING
Program control on the Tropical Rainfall Measuring Mission p 1584 N95-20750
A strategy of cost control for Mariner Venus/Mercury 1973 p 1585 N95-20751
Program control for mission success
p 1585 N95-20753
STS 63 flight day 4 highlights/MIR-Shuttle rendezvous
[NASA-TM-110512] p 1219 N95-21113
Power systems for future missions
[NASA-CR-195320] p 1222 N95-21531
Electric and Hybrid Vehicle Program: Site Operator Program
[DE95-001925] p 1332 N95-21731
Tethered satellite: Forces and motion
[NASA-TM-110518] p 1220 N95-21858
Common mapping system media study
[AD-A279086] p 1390 N95-21912

MIST
A review of water mist technology for fire suppression
[AD-A285738] p 1202 N95-20071

MIXING LAYERS (FLUIDS)
Effects of non-unity Lewis numbers in diffusion flames
p 1249 N95-21036
Effect of chemical heat release in a temporally evolving mixing layer p 1249 N95-21037
Comparison of DNS and LES of transitional and turbulent compressible flow: Flat plate and mixing layer
p 1347 N95-21066
Direct numerical simulation of turbulent flow in a sudden pipe expansion p 1347 N95-21067
Entrainment in a shear-free turbulent mixing layer
p 1350 N95-21083
Mixing and dynamics of the Mediterranean outflow
[AD-A279803] p 1434 N95-21306
High resolution properties of the equatorial Pacific marine atmospheric boundary layer from lidar and radiosonde observations
[DE95-001028] p 1426 N95-21875
Nonlinear interaction between a pair of oblique modes in a supersonic mixing layer: Long-wave limit
[NASA-CR-197380] p 1357 N95-22173
Forced free-shear layer measurements
p 1362 N95-22460

MIXTURES
Theoretical and experimental study of mixed solvent electrolytes
[DE94-017605] p 1237 N95-20384

MOBILE COMMUNICATION SYSTEMS
A group communication approach for mobile computing mobile channel: An ISIS tool for mobile services
[AD-A279785] p 1290 N95-20306
A wideband propagation simulator for high speed mobile radio communications p 1295 N95-20934
Experimental study of the helicopter-mobile radioelectrical channel and possible extension to the satellite-mobile channel p 1296 N95-20945

MOBILITY
Robust agent control of an autonomous robot with many sensors and actuators
[AD-A280148] p 1479 N95-20011
Optimal control of a two wheeled mobile robot
[AD-A286130] p 1485 N95-22233

MODELS
A framework for segmentation using physical models of image formation
[AD-A279900] p 1543 N95-20564
SPICE macro model of a spryton with MOSFET's in the avalanche mode
[DE94-015744] p 1555 N95-21134
Formal model for the dynamics of compositional reasoning systems
[PB95-132056] p 1482 N95-21267
Consortia for Known Good Die (KGD), phase 1
[AD-A279407] p 1383 N95-21933
Conference proceedings. Defense Modeling and Simulation Office Information/Data Base (I/DB) Task Group Meetings, and notes from the previous two I/DB meetings
[AD-A279097] p 1591 N95-22069
Solving the inverse problem in terrain modeling
[AD-A285860] p 1391 N95-22131

MODEMS
DAMSON: A system to measure multipath dispersion, Doppler spread and Doppler shift on multi-mechanism communications channels p 1299 N95-20955

MODULATION
High power spectral and spatial beam control using self-phase modulation and a multisegment monochromator
[DE94-016604] p 1531 N95-20120
Evaluation of superconducting quantum interference devices interfaced with digital signal processing electronics for biomagnetic applications
[DE94-016186] p 1289 N95-20164
Complementary GaAs junction-gated heterostructure field effect transistor fabrication for integrated circuits
[DE95-001522] p 1327 N95-20882
Problems of coding in multipath channels
p 1294 N95-20930
Development of a fast sampling system for estimation of impulse responses of mobile radio channels
p 1296 N95-20943
Measurements of radar backscatter from the ocean surface at 94 GHz as a function of wind speed, direction and the modulation by the ocean waves during the SAXON-FPN experiment p 1299 N95-20960
Development of ferroelectric liquid crystals with enhanced nonlinear optical properties
[AD-A279988] p 1571 N95-20965
Comparison of calculated with measured dynamic aperture
[DE95-002863] p 1534 N95-21246
Effects of RF side-bands on spectral reproducibility for infrared synchrotron radiation
[DE95-002450] p 1536 N95-21418

MODULATORS
A simple analytical model for asynchronous dense WDM/OOK systems
[AD-A283725] p 1289 N95-19973
Design and packaging aspects of microwave bandwidth lithium niobate modulators
[DE94-016602] p 1313 N95-20119
White-light spectral analysis of lithium niobate waveguides
[DE94-016692] p 1542 N95-20489
Resonant tunneling quantum well integrated optical waveguide modulator/switch
[AD-A285142] p 1542 N95-20501
Applied physics research for innovation in pulsed power
[AD-A285392] p 1324 N95-20610
Heterostructure quantum confined Stark effect electrooptic modulators operating at 938 nm
[AD-A279342] p 1581 N95-21928
Electro-optic effect in the PESO acousto-optic modulator
[AD-A286355] p 1548 N95-22255

MODULES
FASTPACK: Optimized solutions for modular avionics derived from a parametric study. Part 2: Avionics
p 1209 N95-20635
Ultra-Reliable Digital Avionics (URDA) processor
p 1209 N95-20638
Assuring Known Good Die (KGD) for reliable, cost effective MCMs p 1210 N95-20644
Modular supplies for a distributed architecture --- avionics packaging p 1213 N95-20657
Intelligent interactive project management system
[PB95-132684] p 1586 N95-21982
Verification of knowledge-based reasoning modules
[PB95-132692] p 1470 N95-21983
Materials processing and manufacturing technologies for diamond substrates multichip modules
[AD-A285775] p 1336 N95-22412

MODULUS OF ELASTICITY
Determination of layer moduli from falling weight deflectometer measurements
[PB95-129748] p 1286 N95-21333
Determination of the complex elastic moduli of materials using a free-free bar technique
[AD-A279861] p 1281 N95-22387
Structural performance of cylindrical pressure housings of different ceramic compositions under external pressure loading. Part 3: Sintered reaction bonded silicon nitride ceramic
[AD-A285773] p 1388 N95-22411

MOISTURE
FTIR spectroscopy for the determination of water in corrosive gases
[DE94-014658] p 1235 N95-20139
Development of solid state moisture sensors for semiconductor fabrication applications
[DE94-015771] p 1364 N95-20398

MOISTURE CONTENT
The vertical distribution of heating in the tropical atmosphere
[AD-A285934] p 1429 N95-20391

MOISTURE METERS
Conceptual design analyses for Hanford Site deployable remote spectroscopy systems
[DE95-002078] p 1243 N95-21473

MOLECULAR BEAM EPITAXY
Surface stress, morphological development, and dislocation nucleation during strained-layer epitaxy
[DE94-017682] p 1565 N95-20245

Semiconductor laser joint study program with Rome Laboratory
[AD-A285858] p 1369 N95-20379
Photoluminescence under pressure and annealing of nitrogen-doped ZnSe
[DE95-002355] p 1568 N95-20630
InTISb for long-wavelength infrared photodetectors and arrays
[AD-A280108] p 1332 N95-21774
Growth and electrical and far-infrared properties of wide electron wells in semiconductors
[AD-A279409] p 1333 N95-21917
Photoreflectance and x ray diffraction study of semiconductor heterostructures and quantum wells
[PB95-127049] p 1582 N95-22432

MOLECULAR BEAMS
State-to-state collisional dynamics of atmospheric species
[AD-A285053] p 1370 N95-20484
Experimental investigation of molecular beam injection in HL-1 tokamak
[DE94-631456] p 1556 N95-21165

MOLECULAR BIOLOGY
Hierarchical structures in biology as a guide for new materials technology
[AD-A286317] p 1265 N95-20176
Proposal for a tutorial on Minimal Length Encoding (MLE) in molecular biology
[DE94-015076] p 1438 N95-21376
Life Sciences Division and Center for Human Genome Studies
[DE94-017796] p 1440 N95-22065
Structures and functions of oligosaccharins
[DE95-003195] p 1440 N95-22220

MOLECULAR CHAINS
A model for electron nuclear dynamics of a monatomic chain
[AD-A279652] p 1506 N95-19960
The electronic properties of polysilanes
[DE94-006464] p 1265 N95-20121
Orientation studies of polyolefins by IR-dichroism
[PB95-104386] p 1236 N95-20256
Scanning tunneling microscopy studies of self-assembled monolayers of alkanethiols on gold
[AD-A279910] p 1253 N95-20577

MOLECULAR CLOUDS
An IRAS Hires study of low mass star formation in the Taurus molecular ring p 1593 N95-21767
Wavelet analysis applied to the IRAS cirrus
p 1593 N95-21769
Arcmimute scale HI and IRAS observations toward high latitude cloud G86.5+59.6 p 1594 N95-21771
Luminous radio-quiet sources in the W3(MAIN) cloud core p 1594 N95-21773
Solar system formation and the distribution of volatile species p 1421 N95-21806

MOLECULAR CLUSTERS
The energetics and dynamics of free radicals, ions, and clusters
[DE94-018101] p 1244 N95-21701
The enhancement of metallic silver monomer evaporation by the adhesion of polar molecules to silver nanocluster ions
[AD-A284936] p 1281 N95-22470

MOLECULAR COLLISIONS
Recombination, ion-molecule collisions and (laser assisted) electron-excited atom collisions
[AD-A285604] p 1517 N95-21216
Modeling of collision induced absorption spectra of CO2-CO2 pairs for planetary atmosphere of Venus
[NASA-CR-197373] p 1601 N95-22338

MOLECULAR DIFFUSION
Metallic ions and atoms in the upper atmosphere
[AD-A285229] p 1414 N95-20498

MOLECULAR DYNAMICS
A model for electron nuclear dynamics of a monatomic chain
[AD-A279652] p 1506 N95-19960
Density functional studies of decomposition processes of energetic molecules
[AD-A286185] p 1510 N95-20327
Theoretical and experimental study of mixed solvent electrolytes
[DE94-017605] p 1237 N95-20384
Publications/patents/presentations/honors/student eport. Investigation of the role of vibrational excitation in unimolecular reactions
[AD-A280044] p 1513 N95-20621
Crystalline beams
[DE95-002656] p 1569 N95-20793
Electron-nuclear dynamics of molecular systems
[AD-A279649] p 1516 N95-21120
Calculation of atom-centered partial charges for heme
[DE94-014447] p 1520 N95-21375
A new parallel method for molecular dynamics simulation of macromolecular systems
[DE94-018621] p 1529 N95-22315
Modeling of collision induced absorption spectra of CO2-CO2 pairs for planetary atmosphere of Venus
[NASA-CR-197373] p 1601 N95-22338

MOLECULAR EXCITATION
Investigation of laser-induced retinal damage: Wavelength and pulsewidth dependent mechanisms
[AD-A286066] p 1443 N95-20848
Two-dimensional imaging of OH in a lean burning high pressure combustor
[NASA-TM-106854] p 1214 N95-21383
Electron attachment to excited molecules
[DE94-019124] p 1522 N95-21519

MOLECULAR INTERACTIONS
Atomic orbital basis sets for molecular interactions
[AD-A279609] p 1506 N95-19959
Combustion-related studies using weakly bonded complexes
[DE95-002801] p 1238 N95-20576
Quantum chemical study of rare gas/halide interactions as a model for high energy density material. 1: Transition properties in HCl
[AD-A285988] p 1239 N95-20613
Ion-molecule chemistry related to plasma deposition and etching of silicon
[AD-A279749] p 1514 N95-20804
A new parallel method for molecular dynamics simulation of macromolecular systems
[DE94-018621] p 1529 N95-22315

MOLECULAR IONS
Resonant charge transfer in hyperthermal atomic and molecular ion-surface collisions
[AD-A284937] p 1530 N95-22471

MOLECULAR ORBITALS
Atomic orbital basis sets for molecular interactions
[AD-A279609] p 1506 N95-19959
A model for electron nuclear dynamics of a monatomic chain
[AD-A279652] p 1506 N95-19960
Electron-nuclear dynamics of molecular systems
[AD-A279649] p 1516 N95-21120

MOLECULAR OSCILLATIONS
The atmospheric neutrino anomaly in Soudan 2
[DE94-019288] p 1604 N95-21475
Testing the principle of equivalence by solar neutrinos
[DE94-014972] p 1604 N95-22064

MOLECULAR RELAXATION
The role of high pressure in the study and applications of the ferroelectric polymer polyvinylidene fluoride and its copolymers
[DE94-015742] p 1268 N95-20396
NMR relaxation behavior of the head group of SHBS in lamellar liquid crystals
[AD-A279124] p 1574 N95-21599

MOLECULAR SPECTROSCOPY
Neutron molelcular spectroscopy: Future prospects
[PB95-130357] p 1518 N95-21227

MOLECULAR STRUCTURE
Hierarchical structures in biology as a guide for new materials technology
[AD-A286317] p 1265 N95-20176
Hierarchical structure in advanced polymers. Phase behaviour, orientation, properties
[AD-A285938] p 1268 N95-20392
Combustion-related studies using weakly bonded complexes
[DE95-002801] p 1238 N95-20576
Scanning tunneling microscopy studies of self-assembled monolayers of alkanethiols on gold
[AD-A279910] p 1253 N95-20577
Structure of dibis(diethyldithiocarbamato) zinc (2) Mu-bis(diethylphosphino)ethane toluene(2)
[AD-A279792] p 1224 N95-20660
Chemical Structure and Dynamics program
[DE95-001117] p 1403 N95-20834
Electron-nuclear dynamics of molecular systems
[AD-A279649] p 1516 N95-21120
New methods for large scale local and global optimization
[AD-A285635] p 1517 N95-21126
Molecular design concept for multi-kilovolt x-ray amplification
[DE95-001763] p 1374 N95-21743
Selenophene transition metal complexes
[DE95-001675] p 1260 N95-21841
Comparative computational analysis of some nitramine and difluoramine structures, dissociation energies and heats of formation
[AD-A286196] p 1525 N95-21878
Preparation and x-ray structure of Cp2Ti(PH2SiH2)(PMe3)
[AD-A286197] p 1246 N95-21879
Synthesis and structure of a novel bis-stibole
[AD-A286345] p 1224 N95-22252

MOLECULAR WEIGHT
Monomer mapping: A PC-based software tool facilitating the determination of monomer compositions from mass spectrometric molecular weight data
[PB95-132155] p 1275 N95-21470

MOLECULES
Chemical Structure and Dynamics program
[DE95-001117] p 1403 N95-20834
Calculated heats of formation of some predicted stable C, N, O, F molecules
[AD-A285957] p 1517 N95-21127
Ion-molecular spiraling collisions and termolecular recombination
[AD-A285633] p 1517 N95-21151
Electron attachment to excited molecules
[DE94-019124] p 1522 N95-21519
Auger spectrometry of atoms and molecules
[DE94-018052] p 1524 N95-21664
Molecular design concept for multi-kilovolt x-ray amplification
[DE95-001763] p 1374 N95-21743
The status of molecules
[DE95-000952] p 1526 N95-21939
Advanced diagnostics for plasma chemistry
[DE94-018936] p 1561 N95-22116
The enhancement of metallic silver monomer evaporation by the adhesion of polar molecules to silver nanocluster ions
[AD-A284936] p 1281 N95-22470

MOLTEN SALTS
Molten carbonate fuel cell product development test
[DE95-000005] p 1324 N95-20574
Chemistry and electrochemistry in Lewis acid and superacid ionic liquids
[AD-A279396] p 1246 N95-21931

MOLYBDENUM
Reflective masks for extreme ultraviolet lithography
[DE95-003427] p 1336 N95-22236
The thermal conductivity of silicon nitride with molybdenum disilicide additions
[DE94-017757] p 1247 N95-22260

MOLYBDENUM ALLOYS
Lower active metals loading for hydrotreating catalysts
[DE94-018907] p 1261 N95-22119

MOLYBDENUM COMPOUNDS
Third Intermetallic Matrix Composites Symposium, volume 350
[NASA-TM-110059] p 1225 N95-20001

MOLYBDENUM OXIDES
Selective methane oxidation over promoted oxide catalysts
[DE94-012270] p 1235 N95-20188
Angle resolved photoemission on K(0.3)Mo3, TiTe2 and Ti(1+x)S2
[DE94-018300] p 1574 N95-21712

MOMENTUM
Positron annihilation studies of organic superconductivity
[DE94-018371] p 1564 N95-20017
Transport and dynamics in toroidal fusion systems
[DE94-018653] p 1548 N95-20029
Large eddy simulation of channel flow using a vorticity transport subgrid model p 1348 N95-21076

MOMENTUM TRANSFER
Observation of non diffusive term of toroidal momentum transport in the JFT-2M tokamak
[DE94-770686] p 1555 N95-20989
Nonperturbative aspects of the quark-photon vertex
[DE94-012846] p 1520 N95-21315
Classical-quantum correspondence for ionization in fast ion-atom collisions
[DE95-000953] p 1526 N95-21940
The dynamic structure function of Bose liquids in the deep inelastic regime
[DE94-629077] p 1527 N95-22182

MONATOMIC MOLECULES
A model for electron nuclear dynamics of a monatomic chain
[AD-A279652] p 1506 N95-19960

MONITORS
First results from the final focus test beam
[DE95-002897] p 1535 N95-21255
Quartz resonator fluid monitors for vehicle applications
[DE94-018910] p 1367 N95-21546

MONOCHROMATORS
Design and thermal stress analysis of high power x-ray monochromators cooled with liquid nitrogen
[DE94-016879] p 1500 N95-20108
High power spectral and spatial beam control using self-phase modulation and a multisegment monochromator
[DE94-016604] p 1531 N95-20120
Thermal and deformation analyses of a novel cryogenically cooled monochromator for an Advanced Photon Source beamline
[DE94-016914] p 1527 N95-22190

MONOMERS
The synthesis and characterization of new mesogenic diacetylene monomers and their polymers
[AD-A286188] p 1267 N95-20328
The organic chemistry of conducting polymers
[DE94-018216] p 1270 N95-20680
Macromolecular and materials design using polyphosphazenes
[AD-A279781] p 1273 N95-20978
Monomer mapping: A PC-based software tool facilitating the determination of monomer compositions from mass spectrometric molecular weight data
[PB95-132155] p 1275 N95-21470
The enhancement of metallic silver monomer evaporation by the adhesion of polar molecules to silver nanocluster ions
[AD-A284936] p 1281 N95-22470
MONOPOLE ANTENNAS
Low-cost conical ultra-wideband antenna
[AD-A286569] p 1292 N95-20825
MONOPOLES
Monopoles and quark confinement: Introduction and overview
[DE94-019348] p 1522 N95-21485
MONOPULSE RADAR
Frequency-coded monopulse MTI
[AD-D016495] p 1307 N95-21904
MONOTONE FUNCTIONS
Design of robust optimal control systems and stability analysis of real structured uncertainties
[AD-A279089] p 1483 N95-21913
Bayesian analysis of semiparametric proportional hazards models
[AD-A279394] p 1499 N95-21946
MONSOONS
Monsoons: AMIP simulations of the 1987 and 1988 drought and flood regimes
[DE94-014789] p 1428 N95-20140
MONTE CARLO METHOD
Iterated-bootstrap confidence intervals for the mean
[AD-A279802] p 1498 N95-20102
A practical guide to using MCNP with PVM
[DE94-016162] p 1474 N95-20158
MCNP (trademark) ENDF/B-VI iron benchmark calculations
[DE94-016165] p 1508 N95-20160
MCNP (trademark) directions
[DE94-016216] p 1509 N95-20254
Simulation of large systems with neural networks
[DE94-018898] p 1428 N95-20319
Positron implantation profiles in elemental and multilayer systems
[DE94-014876] p 1566 N95-20382
Program WALKMAN: A code designed to perform electron single collision elastic scattering Monte Carlo calculations
[DE94-017501] p 1511 N95-20444
X-ray microscope for solidification studies
[NASA-CR-197375] p 1543 N95-20798
A Monte Carlo study of the minus sign problem in the t-J model using an Intel iPSC/860 hypercube
[DE95-001072] p 1570 N95-20819
Correlated wavefunction Monte Carlo studies of excitations in the quantum Hall liquids
[DE95-002337] p 1501 N95-20874
Active neutron multiplicity analysis and Monte Carlo calculations
[DE94-016178] p 1516 N95-21114
Calculation of Z plus four jet production at the Tevatron
[PB95-130472] p 1580 N95-21230
Multiple hard interactions in HERWIG
[PB95-130548] p 1518 N95-21233
Defect production and recombination during low-energy ion processing
[DE95-001827] p 1572 N95-21304
Search for Centauro events in the DO Detector at Fermilab collider
[DE95-002522] p 1535 N95-21314
The atmospheric neutrino anomaly in Soudan 2
[DE94-019288] p 1604 N95-21475
Simulated rarefied entry of the Galileo probe into the atmosphere of Jupiter
[NASA-TM-110507] p 1601 N95-21621
A preliminary, precise measurement of the average B hadron lifetime
[DE95-001848] p 1525 N95-21727
A massively parallel algorithm for grand canonical Monte Carlo computer simulation with the short-ranged Lennard-Jones potential
[DE94-010396] p 1477 N95-21843
On Markov Chain Monte Carlo acceleration
[AD-A279393] p 1499 N95-21945
Atomic velocity distributions in a hydrogen beam effusing out of an RF discharge dissociator
[AD-A279253] p 1307 N95-21985
Variational Monte Carlo study of He-4 in two dimensions
[DE94-629078] p 1576 N95-21998
An improved Monte Carlo algorithm for simulating grain growth
[DE94-017903] p 1578 N95-22272
An exact enumeration of self-avoiding loops on a square lattice
[DE94-628999] p 1578 N95-22276
MONTMORILLONITE
Spectroscopic studies of hazardous fuel interactions with soils
[AD-A279099] p 1407 N95-21596
MOON
A Clementine collection: Moonglow
[AD-A286360] p 1217 N95-20228
Moon: Old and new
[NASA-TM-110511] p 1601 N95-21196
Atmospheres of the Moon and Mercury
p 1419 N95-21794
Polar volatiles on Mercury and the Moon
p 1422 N95-21811
MORPHOLOGY
Microstructures and tensile properties of as-cast iron-aluminide alloys
[DE94-017868] p 1252 N95-20359
Nucleation, growth, and strain relaxation of lattice-mismatched 3-5 semiconductor epitaxial layers
p 1324 N95-20543
Analysis of mesospheric winds and waves
[AD-A279956] p 1414 N95-20591
Optical pattern recognition
[AD-A285384] p 1480 N95-20607
Spectroscopic, morphological, and electrical characterization of PdGe ohmic contacts to n-GaAs
[DE95-000738] p 1329 N95-21394
Cluster reactions: An approach to understanding the fundamentals of heterogeneous catalysis
[DE95-002947] p 1243 N95-21447
Simulations of metal dissolution and corrosion
[DE94-019295] p 1257 N95-21476
Substorm theories: United they stand, divided they fall
[NASA-CR-197672] p 1427 N95-22326
Magnetospheric Plasma Analyzer (MPA): Plasma observations from geosynchronous orbit
[DE95-002739] p 1427 N95-22477
MORSE POTENTIAL
Microscopic theory of normal liquid He-3
[DE94-629047] p 1527 N95-22179
MORTALITY
Current concepts on airborne particles and health
[DE95-002260] p 1447 N95-22287
MOTION PERCEPTION
Intermediate levels of visual processing
[AD-A284922] p 1448 N95-19998
Neural models of motion perception
[AD-A286560] p 1449 N95-20845
MOTION SICKNESS
Command history, 1993
[AD-A279775] p 1446 N95-21989
MOTION SIMULATION
Simulation of rotor blade element turbulence
[NASA-TM-108862] p 1207 N95-21186
A preliminary study of the airwake model used in an existing SH-60B/FFG-7 helicopter/ship simulation program
[DSTO-TR-0015] p 1201 N95-21659
Occupant reach and mobility apparatus
[AD-D016253] p 1454 N95-22099
MOTION STABILITY
Emittance growth due to negative-mass instability above transition
[DE95-002527] p 1534 N95-20900
Collisional drift waves in the H-mode edge
[DE94-628950] p 1561 N95-21847
MOTOR VEHICLES
Analysis of invalid emission testing in the California smog check program
[PB95-128922] p 1406 N95-21373
MOUNTAINS
Geometric moire method of strain analysis with displacement discontinuities
[DE95-001114] p 1386 N95-20833
MOVING TARGET INDICATORS
Frequency-coded monopulse MTI
[AD-D016495] p 1307 N95-21904
MULLITES
Reactions and microstructure at ceramic/metal interfaces
[DE94-014287] p 1265 N95-20138
Zirconia precipitates and zirconia: GeO2 interphase in mullite matrix-SiC woven fabrics composites prepared through a sol-gel route
[PB95-133427] p 1275 N95-21272
MULTICHANNEL COMMUNICATION
Transformation of multichannel magnetocardiographic signals to standard grid form
[PB95-127114] p 1447 N95-22371
MULTIGRID METHODS
Multigrid with matrix-dependent transfer operators for convection-diffusion problems
[PB95-110821] p 1487 N95-19915
Convergence acceleration of the Proteus computer code with multigrid methods
[NASA-CR-197677] p 1467 N95-21450
MULTIMEDIA
Efficient caption-based retrieval of multimedia information
[AD-A279604] p 1586 N95-19956
Determining the usability of Digital Video Interactive (DVI) technology in computer-based instruction
[AD-A284717] p 1457 N95-20060
Using local optimality criteria for efficient information retrieval with redundant information filters
[AD-A279603] p 1587 N95-20302
DAVE: A plug and play model for distributed multimedia application development
[DE94-016481] p 1465 N95-21153
Application-oriented architecture for multimedia teleservices
[PB95-135513] p 1306 N95-21623
A computer-based multimedia prototype for night vision goggles
[AD-A286208] p 1546 N95-21882
Modelling multimedia teleservices with OSI upper layers framework: Short paper
[PB95-132734] p 1308 N95-22080
MULTIPATH TRANSMISSION
Multiple Mechanism Propagation Paths (MMPPs): Their Characterisation and Influence on System Design
[AGARD-CP-543] p 1292 N95-20921
Adaptive error-control scheme for 2-200 MHz Multiple-Mechanism Propagation Paths
p 1293 N95-20926
Problems of coding in multipath channels
p 1294 N95-20930
A wideband propagation simulator for high speed mobile radio communications p 1295 N95-20934
Time behavior and frequency response of the microwave propagation channel during multipath propagation
p 1296 N95-20942
Line-of-sight multipath propagation measurements at 15 GHz over 500 MHz bandwidth p 1296 N95-20944
Angle diversity on digital microwave links: Antenna design and experimental results p 1297 N95-20947
Mitigation of effects of multiple path nulls at super-high frequencies through diversity and networking
p 1297 N95-20948
Multipath impact on ground-based global positioning system range measurements: Aspects of measurement, modeling, and mitigation p 1297 N95-20949
Temporal and spatial comportment of multiple paths in ionospheric propagation in oblique incidence: Fractal measures of perturbations p 1298 N95-20954
DAMSON: A system to measure multipath dispersion, Doppler spread and Doppler shift on multi-mechanism communications channels p 1299 N95-20955
Sounder calibration with backscattering from Losquet Island in the presence of multipaths
p 1300 N95-20961
MULTIPHASE FLOW
Accurate solution algorithms for incompressible multiphase flows
[DE95-002727] p 1353 N95-21317
Status of CFDLIB performance tests on the T3D
[DE95-002708] p 1478 N95-21925
MULTIPHOTON ABSORPTION
Physics of correlated studies
[DE95-001204] p 1581 N95-21842
MULTIPLEXING
Effects of RF side-bands on spectral reproducibility for infrared synchrotron radiation
[DE95-002450] p 1536 N95-21418
Multi-port tester interface
[AD-D016240] p 1332 N95-21775
MULTIPOLES
A colocated magnetic loop, electric dipole array antenna (preliminary results)
[AD-A285381] p 1290 N95-20556
Sources of amplitude-dependent tune shift in the PEP-2 design and their compensation with octupoles
[DE94-018198] p 1519 N95-21262
Proposed emittance upgrade for the SLC damping rings
[DE95-002887] p 1538 N95-22155
Fast parallel tree codes for gravitational and fluid dynamical N-body problems
[AD-A286480] p 1358 N95-22290

MULTIPROCESSING (COMPUTERS)

The design and implementation of the functional/daplex data interface for the multimodel and multilingual database system
[AD-A280131] p 1587 N95-20039

ILIAS: A sequential language for parallel matrix computations
[PB95-110631] p 1473 N95-20056

System level fault tolerance in parallel and distributed computing systems
[AD-A279664] p 1474 N95-20305

Task parallel programming in Fx
[AD-A285136] p 1475 N95-20500

Packaging the MAMA module p 1209 N95-20639

Functional and para-functional parallel processing
[DE95-002805] p 1475 N95-20888

The message passing version of the parallel Community Climate Model
[DE94-019158] p 1407 N95-21608

A periodic scheduling heuristic for mapping iterative task graphs onto distributed memory multiprocessors
[AD-A286047] p 1311 N95-22415

MULTIPROGRAMMING

Scheduling: A guide for program managers
p 1584 N95-20748

MULTISENSOR APPLICATIONS

Nonparametric estimation of the cyclic cross-spectrum
[AD-A285756] p 1498 N95-21219

MULTISENSOR FUSION

Airborne Multisensor Pod System (AMPS) data access concept
[DE95-002586] p 1389 N95-20903

Overview of data fusion work for land electronic warfare
[AD-A279829] p 1301 N95-21292

MULTISPECTRAL BAND SCANNERS

A multispectral scanner survey of the Idaho National Engineering Laboratory and the Hanford Reservation
[DE95-003922] p 1391 N95-22398

MULTISPECTRAL LINEAR ARRAYS

Line-of-sight multipath propagation measurements at 15 GHz over 500 MHz bandwidth p 1296 N95-20944

MULTISPECTRAL PHOTOGRAPHY

A multispectral scanner survey of the Idaho National Engineering Laboratory and the Hanford Reservation
[DE95-003922] p 1391 N95-22398

MULTISTATIC RADAR

Large bistatic angle clutter depolarization study
p 1296 N95-20941

MULTIVARIATE STATISTICAL ANALYSIS

A multivariate multisample rank test for stochastic simulation validation
[AD-A285922] p 1498 N95-19990

Nonparametric estimation of the cyclic cross-spectrum
[AD-A285756] p 1498 N95-21219

Search for the top quark using multivariate analysis techniques
[DE95-000561] p 1522 N95-21498

MUON SPIN ROTATION

Muon data analysis program RUMDA
[PB95-129839] p 1511 N95-20434

MUONIUM

Radio-frequency techniques at the ISIS pulsed muon source
[PB95-129854] p 1529 N95-22303

MUONS

Search for top in DO using the electron + jets channel with soft muon tagging
[DE95-001284] p 1509 N95-20217

Nuclear A dependence of exclusive vector meson production in muon scattering
[DE95-002248] p 1511 N95-20418

Search for right-handed currents in the decay chain of K(+) yields muon(+)nu(sub muon), muon(+) yields e(+)nu(sub e)nu(bar)(sub muon)
[DE94-770606] p 1514 N95-20756

Recent results from E665
[DE95-002523] p 1516 N95-20914

Muon beamline at ISIS
[PB95-130324] p 1518 N95-21224

A measurement of the b(bar b) cross section at CDF
[DE95-000642] p 1519 N95-21273

Search for Centauro events in the DO Detector at Fermilab collider
[DE95-002522] p 1535 N95-21314

Structure functions and structure function ratio F2(n)/F2(p) at low X(Bj) and Q2 in inelastic muon scattering
[DE94-018979] p 1573 N95-21561

Measurement of the B meson differential cross-sections in p(bar p) collisions at (radical)s = 1.8 TeV using the exclusive decays B(sup (+-)) (yields) J/(psi)K(sup (+-)) and B(sup 0) (yields) J/(psi)K*(sup 0)
[DE94-018993] p 1523 N95-21562

Muon transfer from muonic atoms of hydrogen isotopes to He nuclei
[DE94-628903] p 1523 N95-21591

Measurement of the B cross section at CDF via B semileptonic decays
[DE95-002217] p 1524 N95-21597

Time of flight spectroscopy with muonic hydrogen
[DE94-017056] p 1245 N95-21845

Radio-frequency techniques at the ISIS pulsed muon source
[PB95-129854] p 1529 N95-22303

Structure functions and structure function ratio F(sup n)2/F(sup p)2 at small x(sub Bj) and Q2 in muon-nucleon scattering
[DE94-017981] p 1530 N95-22340

MUSCLES

Skeletal muscle ischemia and heat shock proteins
[AD-A285364] p 1442 N95-20549

MUSCULOSKELETAL SYSTEM

Skeletal muscle ischemia and heat shock proteins
[AD-A285364] p 1442 N95-20549

Analysis of musculo-skeletal loading using electromyography and biomechanical modelling
[PB95-135828] p 1444 N95-21007

MUTAGENS

The mechanisms and effects off the plant-activations of chemicals in the environment
[AD-A279388] p 1356 N95-22145

MUTATIONS

Cellular responses to environmental DNA damage
[DE94-015606] p 1441 N95-22397

MYOCARDIUM

Intramyocardial blood volume and oxygen exchange
[PB95-108015] p 1445 N95-21580

MYOGLOBIN

A new parallel method for molecular dynamics simulation of macromolecular systems
[DE94-018621] p 1529 N95-22315

N

N-P-N JUNCTIONS

Plastic encapsulated parts
[DE95-001876] p 1332 N95-21729

N-TYPE SEMICONDUCTORS

Semiconductor cold electron emission device
[AD-D016577] p 1314 N95-20298

Complementary GaAs junction-gated heterostructure field effect transistor technology
[DE94-018901] p 1329 N95-21390

InTlSb for long-wavelength infrared photodetectors and arrays
[AD-A280108] p 1332 N95-21774

NARROWBAND

QoS driven routing in packet switched networks of multiple transmission media p 1292 N95-20923

NASA PROGRAMS

But what will it Cost? The history of NASA cost estimating p 1583 N95-20742

The MSFC Program Control Development Program
p 1585 N95-20754

Abbreviations and acronyms
[NASA-TM-110506] p 1590 N95-21457

Annual program analysis of the NASA Space Life Sciences Research and Education Support Program
[NASA-CR-197298] p 1439 N95-21529

Spinoff, 1994
[NASA-NP-214] p 1594 N95-21893

NASA patent abstracts bibliography: A continuing bibliography. Section 2: Indexes (supplement 46)
[NASA-SP-7039(46)-SECT-2] p 1590 N95-21948

NATURAL GAS

Proceedings of the 1994 DOE/NREL Hydrogen Program Review
[DE94-011835] p 1234 N95-20117

Natural gas cleanup: Evaluation of a molecular sieve carbon as a pressure swing adsorbent for the separation of methane/nitrogen mixtures
[DE94-012263] p 1234 N95-20135

Effect of propane-air on NGVs and vehicle fueling stations
[PB94-210085] p 1282 N95-20253

A fuel cell overview
[DE95-001455] p 1393 N95-20839

Performance and cost analysis of monolithic solid oxide fuel cells
[DE95-002511] p 1394 N95-20896

Technical and economic evaluation of natural gas based synthesis gas production technologies
[PB95-130597] p 1242 N95-21426

The ratios of carbon and non-radiogenic helium and argon isotopes in the mantle and crustal rocks
p 1421 N95-21805

Natural gas converter performance and durability
[PB95-135554] p 1284 N95-21966

Natural gas combustion chemistry mechanisms research
[PB95-111670] p 1247 N95-22150

NATURAL LANGUAGE (COMPUTERS)

Functional and para-functional parallel processing
[DE95-002805] p 1475 N95-20888

Usable, real-time, interactive spoken language systems
[AD-A286349] p 1310 N95-22253

NATURAL LANGUAGE PROCESSING

Efficient caption-based retrieval of multimedia information
[AD-A279604] p 1586 N95-19956

Collected papers of the Soar/IFOR project, Spring 1994
[AD-A280063] p 1216 N95-20624

NATURAL SATELLITES

Surface ices in the outer solar system
p 1423 N95-21815

NAVIER-STOKES EQUATION

Open Skies project computational fluid dynamic analysis
[AD-A285928] p 1200 N95-19991

Finite dimensional approximation of a class of constrained nonlinear optimal control problems
[NASA-CR-194891] p 1479 N95-20010

A numerical investigation of energy transfer and subgrid-scale eddy viscosity in homogeneous, isotropic and shear turbulence
[AD-A280005] p 1339 N95-20058

Continuum transient and frozen startup behavior of conventional and gas-loaded heat pipes
[AD-A284297] p 1339 N95-20250

Numerical investigation of supersonic turbulent boundary layers with high wall temperature
p 1344 N95-21050

On the asymptotic similarity of rotating homogeneous turbulence p 1345 N95-21058

Simulation of separated flows p 1347 N95-21068

Large eddy simulation of channel flow using a vorticity transport subgrid model p 1348 N95-21076

Spatial direct numerical simulation of boundary layer transition under strong adverse pressure gradient
p 1351 N95-21093

Navier-Stokes simulations of the effects of suction holes on a flat plate boundary layer p 1352 N95-21094

DNS of turbulent flow in a driven cavity and their analysis using proper orthogonal decomposition
p 1352 N95-21097

Direct simulation and graphics post-processing of three-dimensional turbulent flows p 1352 N95-21098

Application of Roe's flux-difference splitting for kappa-epsilon turbulence model
[PB95-127718] p 1352 N95-21106

The structure of turbulence and other motions beneath an air-water interface
[AD-A279838] p 1434 N95-21293

Application of Navier-Stokes code PAB3D with kappa-epsilon turbulence model to attached and separated flows
[NASA-TP-3480] p 1201 N95-21338

Massively-parallel computational fluid dynamics
[AD-A279389] p 1355 N95-21942

Turbulence modeling for separated flow
p 1359 N95-22443

A dynamic localization model with stochastic backscatter p 1359 N95-22445

Unstructured-grid large-eddy simulation of flow over an airfoil p 1202 N95-22448

Large-eddy simulation of flow through a plane, asymmetric diffuser p 1360 N95-22449

Numerical study of boundary layer interaction with shocks: Method and code validation
p 1362 N95-22461

A method for obtaining a statistically stationary turbulent free shear flow p 1363 N95-22463

NAVIGATION

The GPS Burst Detector W-Sensor
[DE94-017406] p 1204 N95-20269

Automatic generation of fuzzy rules for the sensor-based navigation of a mobile robot
[DE95-001428] p 1481 N95-20837

The navigation toolkit
[NASA-CR-197290] p 1205 N95-22161

Feature extraction without edge detection
[AD-A279842] p 1473 N95-22386

NAVIGATION AIDS

GPS-Squitter capacity analysis
[AD-A280037] p 1291 N95-20599

Minima reduction simulation test results
[AD-A285626] p 1204 N95-21148

NAVIGATION INSTRUMENTS

Assessment of a non-dedicated GPS receiver system for precise airborne attitude determination
[DE94-019309] p 1205 N95-21520

NAVIGATION SATELLITES

Impact of propagation mechanisms on global navigation satellite system performance p 1298 N95-20950

NAVY

NRL review, 1994
[AD-A279832] p 1605 N95-20182

Compilation of 1993 annual reports of the Navy ELF Communications System Ecological Monitoring Program
[AD-A279575] p 1408 N95-21699

NEAR FIELDS

Method and system of mapping acoustic near field
[AD-D016574] p 1504 N95-20296

NEAR INFRARED RADIATION

Visible and near-IR spectroscopic studies of UC1(4) in a basic ambient temperature melt: The observation of a possible geometric distorted UC1(6)(exp 2-) species and the evidence for the hydrogen-bond in the melt
[DE94-017764] p 1237 N95-20493

Conceptual design analyses for Hanford Site deployable remote spectroscopy systems
[DE95-002078] p 1243 N95-21473

Study of pulsed laser effects on living tissues
[PB95-131330] p 1447 N95-22361

NEAR WAKES

Free shear layers, base pressure and bluff-body drag
[AD-A286316] p 1200 N95-20175

Research on bluff body vortex wakes
[AD-A286319] p 1200 N95-20177

The velocity and vorticity fields of the turbulent near wake of a circular cylinder
[NASA-TM-110513] p 1355 N95-21954

NEGATIVE FEEDBACK

Logic programming and negation: A survey
[PB95-110730] p 1472 N95-22302

Pre-amplifier with multi-stage feedback
[AD-D016254] p 1336 N95-22418

NEGATIVE IONS

Dynamics of collision processes
[DE94-017593] p 1509 N95-20242

Study of small carbon and semiconductor clusters using negative ion threshold photodetachment spectroscopy
[DE95-002327] p 1515 N95-20872

Measurements of scattering processes in negative ion: Atom collisions
[DE95-000664] p 1519 N95-21276

NEGATIVE MATTER

Emittance growth due to negative-mass instability above transition
[DE95-002527] p 1534 N95-20900

NEODYMIUM ALLOYS

Pulsed laser illumination of photovoltaic cells
p 1323 N95-20538

NEODYMIUM ISOTOPES

Competing structures in nuclei near closed shells
[DE94-017604] p 1512 N95-20491

NEODYMIUM LASERS

High power spectral and spatial beam control using self-phase modulation and a multisegment monochromator
[DE94-016604] p 1531 N95-20120

Large facilities pilot programme. Access to the VULCAN High Power Laser Facilities at Rutherford Appleton Laboratory
[PB95-130340] p 1373 N95-21226

International Symposium on Advanced Laser Technologies
[AD-A279849] p 1376 N95-22164

Coherence properties of high order harmonic radiation
[DE94-016974] p 1377 N95-22312

NEON

Two-center, two electron excitations identified in NEXAFS for solid Ne
[AD-A285373] p 1568 N95-20553

Solar helium and neon in the Earth
p 1419 N95-21793

NEON ISOTOPES

Observation of strong emission from NeIX and NeX transitions in a laser-driven plasma
[DE95-002265] p 1555 N95-20813

He, Xe and Ne isotopes in a steady-state mass transport model and implications about terrestrial volatiles
p 1425 N95-21821

NERVOUS SYSTEM

Radiopharmaceuticals for diagnosis
[DE95-002200] p 1445 N95-21595

NETWORK ANALYSIS

Testing paradigm applied to network structure (revised)
[PB95-110706] p 1487 N95-19906

Environment for Test and Analysis of Distributed Software (ETADS)
[AD-A285776] p 1463 N95-20877

Non-intrusive SCSI status sensing system
[AD-D016242] p 1476 N95-21307

SCSI controller with target status retrieval
[AD-D016249] p 1476 N95-21504

Method of sensing target status in a local area network
[AD-D016248] p 1478 N95-22090

Method of non-intrusively sensing status in a computer peripheral
[AD-D016241] p 1478 N95-22146

A survey of artificial neural network applications in flow analysis of energy networks
[DE95-002452] p 1486 N95-22430

NETWORK CONTROL

A multivariate multisample rank test for stochastic simulation validation
[AD-A285922] p 1498 N95-19990

An integrated architecture of adaptive neural network control for dynamic systems
[DE94-014813] p 1481 N95-20693

Routing of unidirectional packet radio for wide-area paging network control and maintenance
[PB95-104428] p 1300 N95-20980

Network file server with automatic sensing means
[AD-D016250] p 1476 N95-21496

A simulation study of TCP performance in ATM networks
[DE94-016622] p 1477 N95-21505

Verification of a timestamp-based sliding-window protocol
[PB95-132759] p 1455 N95-22082

Communications and control for electric power systems: Power system stability applications of artificial neural networks
[NASA-CR-197333] p 1484 N95-22171

NEURAL NETS

High-performance packet switching architecture for ATM: Conventional solution and neural network solution
[PB95-110920] p 1312 N95-19935

Comparison of a back propagation artificial neural network model with a linear regression model for personnel selection
[AD-A280023] p 1479 N95-20005

Recognition of subsurface defects in machined ceramics by application of neural networks to laser scatter patterns
[DE94-018373] p 1264 N95-20018

Fault tolerance of neural networks
[AD-A285098] p 1479 N95-20057

Biological and theoretical studies of adaptive networks: The conditioned response
[AD-A284781] p 1479 N95-20061

A physiological neural network for saccadic eye movement control
[AD-A279599] p 1441 N95-20301

Simulation of large systems with neural networks
[DE94-018898] p 1428 N95-20319

Designing the architecture of hierachical neural networks model attention, learning and goal-oriented behavior
[AD-A279898] p 1452 N95-20562

Multilayer piecewise linear networks
[AD-A285382] p 1480 N95-20606

Optical pattern recognition
[AD-A285384] p 1480 N95-20607

An integrated architecture of adaptive neural network control for dynamic systems
[DE94-014813] p 1481 N95-20693

Neural models of motion perception
[AD-A286560] p 1449 N95-20845

EPSCoR supplemental grant for an application of neural networks to seismic signal discrimination
[AD-A285846] p 1414 N95-20878

Attempt to interpret the self-organizing mapping physiologically
[PB95-127783] p 1438 N95-21112

A neural expert approach to self designing flight control systems
[AD-A279965] p 1215 N95-21122

Neural network construction via back-propagation
[DE95-002867] p 1482 N95-21249

Application of neural networks to seismic signal discrimination research findings
[AD-A285848] p 1415 N95-21308

GRONICs-1994. Proceedings of the 1994 Groningen Student Conference on Computer Science
[PB95-135620] p 1468 N95-21455

Utilizing artificial neural networks in network flow analysis: An annotated bibiliography
[DE95-002453] p 1482 N95-21522

Hardware implementation of a desktop supercomputer for high performance image processing. Color image processing using cellular neural networks
[AD-A286455] p 1455 N95-21589

Communications and control for electric power systems: Power system stability applications of artificial neural networks
[NASA-CR-197594] p 1483 N95-21613

Adaptive capture of expert behavior
[DE94-018285] p 1483 N95-21710

Learning algorithms for feedforward networks based on finite samples
[DE95-001739] p 1483 N95-21741

How the brain works
[AD-A279138] p 1450 N95-21968

Artificial neural network metamodels of stochastic computer simulations
[AD-A285951] p 1484 N95-22056

Communications and control for electric power systems: Power system stability applications of artificial neural networks
[NASA-CR-197333] p 1484 N95-22171

Connectionist models for intelligent computation
[AD-A286436] p 1484 N95-22210

Mathematical theory of neural networks
[AD-A286508] p 1485 N95-22213

The applicability of neural networks to ionospheric modeling in support of relocatable Over-the-Horizon radar
[AD-A286114] p 1309 N95-22230

Learning maneuvers using neural network models
[AD-A286470] p 1486 N95-22267

Advanced Materials and Process Technology for Mechanical Failure Prevention (proceedings of the 48th Meeting of the Mechanical Failures Prevention Group
[AD-A285785] p 1233 N95-22399

Simulation of structural response using a recurrent radial basis function network
[DE94-017342] p 1486 N95-22409

A survey of artificial neural network applications in flow analysis of energy networks
[DE95-002452] p 1486 N95-22430

NEUROMUSCULAR TRANSMISSION

A physiological neural network for saccadic eye movement control
[AD-A279599] p 1441 N95-20301

NEURONS

Biological and theoretical studies of adaptive networks: The conditioned response
[AD-A284781] p 1479 N95-20061

Neural models of motion perception
[AD-A286560] p 1449 N95-20845

Netherlands Institute for Brain Research progress report, 1993
[PB95-135398] p 1445 N95-21352

How the brain works
[AD-A279138] p 1450 N95-21968

NEUROPHYSIOLOGY

A physiological neural network for saccadic eye movement control
[AD-A279599] p 1441 N95-20301

NEUTRAL BEAMS

ALT-2 armor tile design for upgraded TEXTOR operation
[DE94-015749] p 1549 N95-20143

The evolution of configuration from q greater than 1 to q less than 1
[DE94-631396] p 1556 N95-21162

Review of recent D-T experiments from TFTR
[DE95-002755] p 1557 N95-21239

Fusion power production in TFTR
[DE95-002756] p 1557 N95-21240

Intense proton beam source for ITER neutral-beam spectroscopy diagnostics
[DE94-018092] p 1560 N95-21668

NEUTRAL CURRENTS

Search for D(+) yields (pi)(+)(mu)(+)(mu)(-)
[DE94-015538] p 1512 N95-20475

Search for right-handed currents in the decay chain of K(+) yields muon(+)nu(sub muon), muon(+) yields e(+)nu(sub e)nu(bar)(sub muon)
[DE94-770606] p 1514 N95-20756

Calculation of Z plus four jet production at the Tevatron
[PB95-130472] p 1580 N95-21230

A high-rate fixed-target charm experiment
[DE95-001767] p 1521 N95-21378

NEUTRINOS

Neutrino-neutrino scattering and matter-enhanced neutrino flavor transformation in supernovae
[DE94-017577] p 1604 N95-20383

Has a standard model solution to the solar neutrino problem been found?
[DE94-017580] p 1604 N95-20490

Competing structures in nuclei near closed shells
[DE94-017604] p 1512 N95-20491

Search for right-handed currents in the decay chain of K(+) yields muon(+)nu(sub muon), muon(+) yields e(+)nu(sub e)nu(bar)(sub muon)
[DE94-770606] p 1514 N95-20756

Anomalous vector-boson couplings in Majorana neutrino models
[PB95-127460] p 1518 N95-21220

Muon beamline at ISIS
[PB95-130324] p 1518 N95-21224

Experiments at high energy hadron colliders and underground water Cerenkov detector experiment
[DE95-001804] p 1535 N95-21281
The atmospheric neutrino anomaly in Soudan 2
[DE94-019288] p 1604 N95-21475

NEUTRON BEAMS
Muon beamline at ISIS
[PB95-130324] p 1518 N95-21224
A neutron beam polarizer for study of parity violation in neutron-nucleus interactions
[DE95-002743] p 1519 N95-21237
MARI mini-manual
[PB95-134649] p 1526 N95-21965

NEUTRON COUNTERS
A new alpha particle diagnostic using knock-on ion tails
[DE94-015856] p 1553 N95-20402
Active neutron multiplicity analysis and Monte Carlo calculations
[DE94-016178] p 1516 N95-21114

NEUTRON DIFFRACTION
Role of internal stresses in fracture behavior of engineering composites
[DE95-001106] p 1229 N95-20912
PRSCAL manual
[PB95-130480] p 1465 N95-21231
PRISMA operating program manual
[PB95-130498] p 1466 N95-21232
Neutron diffraction study of the magnetic ordering of BaCuO(2+x)
[DE95-001357] p 1572 N95-21297
Strain measurement by diffraction at LANSCE
[DE94-018264] p 1387 N95-21386

NEUTRON FLUX DENSITY
Target area acquisition and control system survivability for the National Ignition Facility
[DE94-016549] p 1550 N95-20190
On conception of a compact neutron source and the possibility of its simulation on the Amba-M end trap
[DE94-633373] p 1562 N95-22282

NEUTRON IRRADIATION
High precision trace neutron transmutation doping of detector-grade high resistance zone-refined silicon mono-crystal
[DE94-631463] p 1563 N95-19978
Influence of oxidation on radiation hardness of silicon detectors
[DE95-002466] p 1272 N95-20894
Effect of neutron irradiation on the impact properties of A533B steel
[DE95-001834] p 1256 N95-21286
Effects of neutron irradiation on the London penetration depth for polycrystalline Bi(1.8)Pb(0.3)Sr2Ca2Cu3O10 superconductor
[DE94-019335] p 1573 N95-21483

NEUTRON SCATTERING
Magnetic excitations in modulated PrNi2Si2
[DE95-001077] p 1254 N95-20822
Topography of neutron scattering from diblock copolymer film
[DE95-001457] p 1229 N95-20840
PRISMA operating program manual
[PB95-130498] p 1466 N95-21232
Error analysis of the quadratic nodal expansion method in slab geometry
[DE95-001352] p 1492 N95-21285
MARI mini-manual
[PB95-134649] p 1526 N95-21965
New techniques in neutron scattering
[DE94-018944] p 1538 N95-22117
Neutron Compton scattering
[PB95-130290] p 1530 N95-22332
Parity violation in the compound nucleus
[DE95-002742] p 1530 N95-22435

NEUTRON SOURCES
Design trade-off study for a large volume short pulse neutron assembly
[DE94-019175] p 1509 N95-20206
Role of internal stresses in fracture behavior of engineering composites
[DE95-001106] p 1229 N95-20912
New techniques in neutron scattering
[DE94-018944] p 1538 N95-22117
Helium production by 10 MeV neutrons in iron, nickel and copper
[DE94-014798] p 1529 N95-22280
On conception of a compact neutron source and the possibility of its simulation on the Amba-M end trap
[DE94-633373] p 1562 N95-22282

NEUTRON SPECTRA
National Ignition Facility: Experimental plan
[DE94-016542] p 1550 N95-20189
Ion temperature measurement of indirectly-driven implosions using a geometry-compensated neutron time-of-flight detector
[DE94-016967] p 1552 N95-20362
Influence of oxidation on radiation hardness of silicon detectors
[DE95-002466] p 1272 N95-20894

NEUTRON SPECTROMETERS
Ion temperature measurement of indirectly-driven implosions using a geometry-compensated neutron time-of-flight detector
[DE94-016967] p 1552 N95-20362
Neutron molelcular spectroscopy: Future prospects
[PB95-130357] p 1518 N95-21227
PRISMA operating program manual
[PB95-130498] p 1466 N95-21232
New techniques in neutron scattering
[DE94-018944] p 1538 N95-22117

NEUTRON STARS
Properties of strange-matter stars
[DE95-002329] p 1599 N95-20873
Relativistic binary neutron star coalescence
[DE94-019311] p 1600 N95-21479
Physics of systems containing neutron stars
[NASA-CR-197304] p 1600 N95-21615

NEUTRONS
Target area acquisition and control system survivability for the National Ignition Facility
[DE94-016549] p 1550 N95-20190
New data for MCNP (trademark)
[DE94-016296] p 1509 N95-20236
Active neutron multiplicity analysis and Monte Carlo calculations
[DE94-016178] p 1516 N95-21114
Neutron molelcular spectroscopy: Future prospects
[PB95-130357] p 1518 N95-21227
NESTLE: Few-group neutron diffusion equation solver utilizing the nodal expansion method for eigenvalue, adjoint, fixed-source steady-state and transient problems
[DE95-001903] p 1466 N95-21288
On the Aharonov-Bohm effect with neutrons
[DE95-002985] p 1521 N95-21454
The ORNL Neutron-Capture Cross Section Facility
[DE94-019146] p 1537 N95-21460
New techniques in neutron scattering
[DE94-018944] p 1538 N95-22117
Helium production by 10 MeV neutrons in iron, nickel and copper
[DE94-014798] p 1529 N95-22280
Neutron reflectivity study of adsorbed diblock copolymers
[DE95-002740] p 1281 N95-22434
Parity violation in the compound nucleus
[DE95-002742] p 1530 N95-22435

NEWTON METHODS
Error committed by stopping the Newton iteration in Runge-Kutta methods and linear multistep methods
[PB95-106324] p 1492 N95-21421

NICKEL
Fabrication and properties of alumina matrix composites containing nickel aluminide reinforcements
[DE94-018703] p 1250 N95-20044
Ferrocyanide safety project Dynamic X-Ray Diffraction studies of sodium nickel ferrocyanide reactions with equimolar nitrate/nitrite salts
[DE94-017396] p 1236 N95-20268
Hydrogenation of nitriles on a well-characterized nickel surface: From surface science studies to liquid phase catalytic activity measurements
[DE94-018184] p 1259 N95-21707
Acid-site characterization of water-oxidized alumina films by near-edge x-ray absorption and soft x-ray photoemission
[DE95-003355] p 1247 N95-22234

NICKEL ALLOYS
Mixed-sputter deposition of Ni-Ti-Cu shape memory films
[DE94-017296] p 1250 N95-19900
Third Intermetallic Matrix Composites Symposium, volume 350
[NASA-TM-110059] p 1225 N95-20001
Processing and characterization of Ni-Al-Fe-B shape-memory alloy wires produced by rapid solidification
[DE94-017702] p 1250 N95-20020
Hydrogen resistant alloy - NASA 23
[NASA-CASE-MFS-26200-1-SB] p 1251 N95-20068
ALCHEMI of Fe-doped B2-ordered NiAl alloys with different doping levels
[DE94-017748] p 1255 N95-20907
Computational modeling of diffusion-controlled transformations in ternary systems
[DE95-001358] p 1256 N95-21298
Processing and mechanical properties of laminar Al2O3-Ni3Al composites
[DE94-019332] p 1230 N95-21481
Corrosion resistance and behavior of construction materials exposed to dilute sulfuric acid at elevated temperatures under static conditions
[DE95-001723] p 1259 N95-21739
The low temperature properties of (Dy(1-x)Er(x))Ni2 alloys
[DE95-001657] p 1260 N95-21923
Incology alloy 908 data handbook
[DE95-001818] p 1260 N95-22013
Lower active metals loading for hydrotreating catalysts
[DE94-018907] p 1261 N95-22119
Bulk and defect properties of ordered intermetallics
[DE94-017706] p 1262 N95-22344
Processing of intermetallic materials by reaction synthesis
[DE94-017710] p 1263 N95-22345

NICKEL CADMIUM BATTERIES
Progress in the development of recycling processes for electric vehicle batteries
[DE94-015894] p 1324 N95-20626

NICKEL ISOTOPES
Helium production by 10 MeV neutrons in iron, nickel and copper
[DE94-014798] p 1529 N95-22280

NICKEL OXIDES
Nickel hydroxide electrodes in reduced-alkalinity electrolytes
[DE95-002333] p 1326 N95-20814
Transient studies of low temperature catalysts for methane conversion
[DE95-003560] p 1247 N95-22224

NICKEL ZINC BATTERIES
Nickel hydroxide electrodes in reduced-alkalinity electrolytes
[DE95-002333] p 1326 N95-20814

NIGHT FLIGHTS (AIRCRAFT)
Challenger's night flight
[NASA-TM-110503] p 1217 N95-19995
STS 63: Post flight presentation
[NASA-TM-110514] p 1219 N95-21558
A computer-based multimedia prototype for night vision goggles
[AD-A286208] p 1546 N95-21882

NIGHT VISION
Ultra-Reliable Digital Avionics (URDA) processor
p 1209 N95-20638
The sharper image: Implementing a Fast Fourier Transform (FFT) to enhance a video-captured image
[AD-A279790] p 1445 N95-21180
A computer-based multimedia prototype for night vision goggles
[AD-A286208] p 1546 N95-21882
Factors that determine visual acuity through night vision goggles for emmetropes
[AD-A279339] p 1450 N95-21927

NIOBIUM
Enhanced output of soft x-ray lasers using double slab targets
[DE94-016689] p 1369 N95-20335

NIOBIUM ALLOYS
Oxide formation on NbAl3 and TiAl due to ion implantation of O-18
[DE94-017874] p 1252 N95-20365
Metastable bcc phase formation in the Nb-Cr-Ti system
[DE94-016212] p 1255 N95-21137

NITRAMINE PROPELLANTS
Density functional studies of decomposition processes of energetic molecules
[AD-A286185] p 1510 N95-20327
Comparative computational analysis of some nitramine and difluoramine structures, dissociation energies and heats of formation
[AD-A286196] p 1525 N95-21878

NITRATES
Safe conditions for contacting nitric acid or nitrates with Tri-n-Butyl Phosphate (TBP)
[DE95-001243] p 1235 N95-20215
Ferrocyanide safety project Dynamic X-Ray Diffraction studies of sodium nickel ferrocyanide reactions with equimolar nitrate/nitrite salts
[DE94-017396] p 1236 N95-20268
Quantitative and qualitative analysis of some inorganic compounds by Raman spectroscopy
[DE94-009757] p 1237 N95-20470
Catalyzed reduction of nitrate in aqueous solutions
[DE94-017660] p 1247 N95-22049

NITRATION
Computational evaluation of the feasibility of nitrating precursors to C12N12O12
[AD-A285976] p 1239 N95-20668

NITRIC ACID
Safe conditions for contacting nitric acid or nitrates with Tri-n-Butyl Phosphate (TBP)
[DE95-001243] p 1235 N95-20215

NITRIC OXIDE
Direct catalytic decomposition of nitric oxide
[DE94-018840] p 1233 N95-20045

Superior catalysts for selective catalytic reduction of nitric oxide
|DE94-018845| p 1234 N95-20046
Compatibility testing of explosives and paints by chemiluminescence techniques
|PB95-133609| p 1275 N95-21275

NITRIDES
Reactions and microstructure at ceramic/metal interfaces
|DE94-014287| p 1265 N95-20138
Novel materials
|AD-A279693| p 1227 N95-20427
Atmosphere influence on in situ ion beam analysis of thin film growth
|DE95-001507| p 1570 N95-20881
Deposition and properties of novel nitride superlattice coatings
|DE95-002945| p 1230 N95-21445

NITRIDING
Tribology and surface mechanical properties of excimer laser nitrided titanium
|DE95-002751| p 1255 N95-21238
The formation of reaction bonded Si3N4 at low temperatures and in short times
|DE95-001990| p 1275 N95-21289

NITRILES
A test of the Arrhenius extrapolation assumption for a nitrile rubber
|DE94-017337| p 1263 N95-19926
Hydrogenation of nitriles on a well-characterized nickel surface: From surface science studies to liquid phase catalytic activity measurements
|DE94-018184| p 1259 N95-21707

NITRITES
Quantitative and qualitative analysis of some inorganic compounds by Raman spectroscopy
|DE94-009757| p 1237 N95-20470

NITRO COMPOUNDS
Density functional studies of decomposition processes of energetic molecules
|AD-A286185| p 1510 N95-20327

NITROBENZENES
Computational evaluation of the feasibility of nitrating precursors to C12N12O12
|AD-A285976| p 1239 N95-20668

NITROFLUORAMINES
Comparative computational analysis of some nitramine and difluoramine structures, dissociation energies and heats of formation
|AD-A286196| p 1525 N95-21878

NITROGEN
Calculated heats of formation of some predicted stable C, N, O, F molecules
|AD-A285957| p 1517 N95-21127
Nitrogen alloyed martensitic steels
|PB95-127791| p 1255 N95-21128
Tribology and surface mechanical properties of excimer laser nitrided titanium
|DE95-002751| p 1255 N95-21238
Nitrogen control of chloroplast differentiation
|DE95-002797| p 1439 N95-21526
Origin and loss of the volatiles of the terrestrial planets p 1417 N95-21785
Transportation of volatile elements in thermally evolving planetesimals: An important role of metallic iron
p 1418 N95-21790
Nitrogen isotopic components in the early solar system p 1420 N95-21800
Solubilities of nitrogen and noble gases in basalt melt
p 1422 N95-21807
Solubilities of nitrogen and helium in water and blood at 37 C and pressures of up to 11 ATA
|AD-A286269| p 1446 N95-22003
Very high-power electron-beam transport in long gas cells from 10(exp -3) to 10(exp 3) Torr N2
|DE95-002611| p 1539 N95-22306

NITROGEN COMPOUNDS
Studies of the microwave resistivity of kappa-(BEDT-TTF)2Cu(N(CN)2)Cl
|DE95-002980| p 1262 N95-22291

NITROGEN METABOLISM
Nitrogen control of chloroplast differentiation
|DE95-002797| p 1439 N95-21526
The Use of Cyanobacteria to Explore Basic Biological Processes
|DE94-019238| p 1440 N95-22066

NITROGEN OXIDES
Laboratory evaluation of a reactive baffle approach to NOx control
|AD-A283802| p 1400 N95-19921
Evaluation of the technical performance of the Duttch National Air Quality Monitoring Network in 1992
|PB95-131892| p 1405 N95-21327
Monitoring activities in the framework of the Dutch National Air Quality Monitoring Network in 1994
|PB95-131884| p 1406 N95-21351

NITROGEN 15
Distribution of light element isotopes in Bencubbin and Weatherford meteorites: An indicator of heterogeneity in the primitive solar nebula
|DE94-019167| p 1600 N95-22128

NITROSO COMPOUNDS
Calculated heats of formation of some predicted stable C, N, O, F molecules
|AD-A285957| p 1517 N95-21127

NITROUS OXIDES
Characteristics of oxynitrides grown in N2O
|DE94-015798| p 1566 N95-20400
Numerical study of contaminant effects on combustion of hydrogen, ethane, and methane in air
|NASA-TM-106844| p 1284 N95-22114

NOBLE METALS
S-D hybridization and anisotropy of the optical second harmonic at low frequencies
|AD-A279449| p 1544 N95-20876
Theoretical study of the noble metals on semiconductor surfaces and Ti-base shape memory alloys
|DE95-001654| p 1257 N95-21398

NOISE
Adaptive detection in stationary and nonstationary noise environments
|AD-A279581| p 1300 N95-21099

NOISE (SOUND)
Ambient noise and surface wave dissipation in the ocean
|AD-A279650| p 1432 N95-20303
Cascade orificial resistive device
|AD-D016529| p 1504 N95-20724
Safety issues in high speed machining
|PB95-127411| p 1287 N95-21422
1/f noise in two-dimensional fluids
|DE95-002617| p 1358 N95-22307

NOISE GENERATORS
Analysis of low frequency ocean noise. 1: From a long-term experiment across the US East Coast. 2: From the Wake Island Hydrophone Array during northwest Pacific typhoons
|AD-A284975| p 1432 N95-20040
Quantum diffusion
|DE95-001015| p 1580 N95-21264
A method for obtaining a statistically stationary turbulent free shear flow p 1363 N95-22463

NOISE INJURIES
Safety issues in high speed machining
|PB95-127411| p 1287 N95-21422

NOISE INTENSITY
Acoustic climb to cruise test
|NASA-TM-110504| p 1206 N95-20155
Ambient noise and surface wave dissipation in the ocean
|AD-A279650| p 1432 N95-20303
Temporary threshold shifts produced by high intensity freefield impulse noise in humans wearing hearing protection
|AD-A286289| p 1454 N95-22045

NOISE PREDICTION
Light-scattering fluctuations and noise in nonlinear optical processing
|AD-A279748| p 1544 N95-20803

NOISE PROPAGATION
Analysis of low frequency ocean noise. 1: From a long-term experiment across the US East Coast. 2: From the Wake Island Hydrophone Array during northwest Pacific typhoons
|AD-A284975| p 1432 N95-20040
Effect of atmospheric pressure on measured aircraft noise levels
|PB95-130423| p 1207 N95-21425

NOISE REDUCTION
Constraints as a destriping tool for Hires images
p 1593 N95-21756
Active control of fan noise-feasibility study. Volume 1: Flyover system noise studies
|NASA-CR-195392-VOL-1| p 1505 N95-21888

NOISE SPECTRA
Ambient noise and surface wave dissipation in the ocean
|AD-A279650| p 1432 N95-20303
Error probabilities of FFH/BFSK with noise normalization and soft decision viterbi decoding in a fading channel with partial-band jamming
|AD-A280041| p 1498 N95-20620
Breakdown of the law of large numbers in Josephson junction series arrays
|DE94-629075| p 1576 N95-21996
Order and turbulence in RF-driven Josephson junction series arrays
|DE94-629076| p 1576 N95-21997

NOISE TEMPERATURE
On-wafer, cryogenic characterization of ultra-low noise HEMT devices p 1305 N95-21539

NONADIABATIC CONDITIONS
Testing the principle of equivalence by solar neutrinos
|DE94-014972| p 1604 N95-22064

NONAQUEOUS ELECTROLYTES
A new family of anion receptors and their effects on ion pair dissociation and conductivity of lithium salts in non-aqueous solutions
|DE94-016822| p 1512 N95-20477

NONDESTRUCTIVE TESTS
Eddy current for detecting second-layer cracks under installed fasteners
|AD-A279871| p 1382 N95-20414
Non destructive characterization using pulsed fast-thermal neutrons
|DE95-002601| p 1511 N95-20422
The 1993 JANNAF Propulsion Meeting, volume 2
|AD-A279569| p 1221 N95-20708
Flux-focusing eddy current probe and rotating probe method for flaw detection
|NASA-CASE-LAR-15231-1-SB| p 1383 N95-20764
Detection of environmental deterioration in fiber reinforced composites by FT-Raman spectroscopy, phase 1
|AD-A279763| p 1228 N95-20805
Three-dimensional ground penetrating radar imaging using multi-frequency diffraction tomography
|DE94-016687| p 1301 N95-21205
Strain measurement by diffraction at LANSCE
|DE94-018264| p 1387 N95-21386
Non-destructive inspection by infrared imaging spectroscopy, phase 1
|AD-A286158| p 1383 N95-22037
Surfaces and thin films studied by picosecond ultrasonics
|DE95-001866| p 1506 N95-22071
Advanced Materials and Process Technology for Mechanical Failure Prevention (proceedings of the 48th Meeting of the Mechanical Failures Prevention Group
|AD-A285785| p 1233 N95-22399

NONEQUILIBRIUM FLOW
Plasma chemistry of vibrationally nonequilibrium molecules
|AD-A279630| p 1553 N95-20411

NONFLAMMABLE MATERIALS
Ignition of submarine materials at various oxygen concentrations
|PB95-131371| p 1243 N95-21428

NONINTRUSIVE MEASUREMENT
Development of a portable ice-thickness measuring instrument
|AD-A279472| p 1433 N95-21291
Non-intrusive SCSI status sensing system
|AD-D016242| p 1476 N95-21307
Method of non-intrusively sensing status in a computer peripheral
|AD-D016241| p 1478 N95-22146

NONLINEAR EQUATIONS
The Nonlinear Characteristic scheme in X-Y geometries
|DE94-016192| p 1488 N95-20167
Squeezing and flow of energy for non linear wave equations
|PB95-111100| p 1489 N95-20172
Stabilization and control problems in structural dynamics
|AD-A279996| p 1340 N95-20312
COYOTE II: A finite element computer program for nonlinear heat conduction problems. Part 1: Theoretical background
|DE95-002587| p 1463 N95-20887
Explicit analytical solution of the nonlinear Vlasov Poisson system
|DE94-628931| p 1500 N95-21592
Report of the Numerical Analysis Group
|PB95-108163| p 1494 N95-21648

NONLINEAR EVOLUTION EQUATIONS
On the sputtering of metals and insulators: A nonlinear evolution problem with nonlinear boundary condition
|DE95-001456| p 1254 N95-20792

NONLINEAR FEEDBACK
Theory of the L-H transition
|DE95-001389| p 1558 N95-21299

NONLINEAR FILTERS
Saddle-node dynamics for edge detection
|DE94-017415| p 1473 N95-22426

NONLINEAR OPTICS
Design, synthesis and characterization of novel nonlinear optical materials
|AD-A285617| p 1540 N95-19897
Transition-energy crossing with a gamma(sub t)(-)jump
|DE94-017315| p 1531 N95-20021
Program of the 1993 9th Interdisciplinary Laser Science Conference (ILS-9)
|AD-A285131| p 1369 N95-20082

The preparation of all para-polyphenyls with increased solubility and enhanced third order NLO activity
[AD-A284301] p 1266 N95-20251
Optical power limiting liquid crystal composites
[AD-A286605] p 1569 N95-20767
Light-scattering fluctuations and noise in nonlinear optical processing
[AD-A279748] p 1544 N95-20803
Nonlinear optical studies of polymer interfaces
[DE94-018199] p 1274 N95-21263
Nonlinear frequency conversion optical filter
[AD-D016523] p 1544 N95-21465
Technique for intracavity sum frequency generation
[AD-D016478] p 1546 N95-21898
Two-band model description of electroabsorption and third-harmonic generation in 1-D MX linear chains
[DE95-000932] p 1526 N95-21934
High temperature polymer for second order nonlinear optics for photonic materials
[AD-A279309] p 1280 N95-22141
Modeling of nonlinear optic and ESR response of CDW MX materials
[DE94-018301] p 1578 N95-22297
Broadband thermal optical limiter for the protection of eyes and sensors
[AD-D016493] p 1377 N95-22304

NONLINEAR SYSTEMS
Semiquantum chaos and the large N expansion
[DE94-016196] p 1488 N95-20169
Modeling and identification of parallel and feedback nonlinear systems
[DE95-001006] p 1481 N95-20812
A neural expert approach to self designing flight control systems
[AD-A279965] p 1215 N95-21122
Linear and nonlinear spectroscopy with the tunable AC scanning tunneling microscope
[AD-A285751] p 1241 N95-21217
International Conference on Control and Estimation of Distributed Parameter Systems: Nonlinear Phenomena
[AD-A286449] p 1493 N95-21582
Adaptive capture of expert behavior
[DE94-018285] p 1483 N95-21710
Cochannel and adjacent-channel interference in nonlinear minimum-shift-keyed satellite system
[NASA-TM-106834] p 1307 N95-21890
Iterated-subspace minimization methods for nonlinear optimization
[PB95-108171] p 1495 N95-22317
Simulation of structural response using a recurrent radial basis function network
[DE94-017342] p 1486 N95-22409

NONLINEARITY
Inelastic torsion of steel I-beams
[PB94-208360] p 1384 N95-20101
Nonlinear dynamic fluid-structure interaction calculations with coupled finite element and finite volume programs
[DE94-016204] p 1339 N95-20166
A S2-like acceleration method for the Nonlinear Characteristic transport scheme
[DE94-016285] p 1509 N95-20235
Modeling of beam dynamics and comparison with measurements for the Advanced Light Source (ALS)
[DE94-017970] p 1532 N95-20495
Physical-chemical studies on rodlike polymer compositions
[AD-A285361] p 1269 N95-20548
Digital filtering for data compression in telemetry systems
[DE94-016611] p 1219 N95-20567
Optical pattern recognition
[AD-A285384] p 1480 N95-20607
A convergence analysis of an h-version finite element method with high order elements for two dimensional elasto-plasticity problems
[AD-A279975] p 1491 N95-20920
Development of ferroelectric liquid crystals with enhanced nonlinear optical properties
[AD-A279988] p 1571 N95-20965
Eigenmode method for electromagnetic synthesis of diffractive elements with three-dimensional profiles
[PB95-127726] p 1301 N95-21107
Understanding the mechanisms of length scale competition: The sine-Gordan soliton case
[DE94-016201] p 1500 N95-21136
Transient behaviour and stability points of the Poiseuille flow of a KBKZ-fluid
[PB95-132064] p 1353 N95-21268
Domain processes in ferroelectric ceramics
[AD-A279567] p 1276 N95-21697
On the influence of electromagnetic wave and relativistic electron beam on a plasma
[DE94-628962] p 1561 N95-21848
Electromagnetic waves in an ultrarelativistically hot and strongly magnetized electron-positron plasma
[DE94-628963] p 1307 N95-21849
Large amplitude localized structures in a relativistic electron-positron ion plasma
[DE94-628965] p 1561 N95-21851
Breakdown of the law of large numbers in Josephson junction series arrays
[DE94-629075] p 1576 N95-21996
Proposed emittance upgrade for the SLC damping rings
[DE95-002887] p 1538 N95-22155
Nonlinear dynamics of the planar pitch attitude motion for a gravity-gradient satellite
[AD-A286407] p 1220 N95-22204
Novel materials and devices from self-assembled periodic structures
[AD-A286499] p 1232 N95-22211
Robust fixed-structure control
[AD-A286515] p 1485 N95-22216

NONPARAMETRIC STATISTICS
A multivariate multisample rank test for stochastic simulation validation
[AD-A285922] p 1498 N95-19990
Iterated-bootstrap confidence intervals for the mean
[AD-A279802] p 1498 N95-20102
Nonparametric estimation of the cyclic cross-spectrum
[AD-A285756] p 1498 N95-21219
Proof of a conjecture of Narayana on dominance refinements of the Smirnov two-sample test
[PB95-132650] p 1499 N95-21979
Precedence tests and confidence bounds for complete data: An overview and some results
[PB95-132668] p 1499 N95-21980

NORMAL DENSITY FUNCTIONS
Microscopic theory of normal liquid He-3
[DE94-629047] p 1527 N95-22179
Theory of the excitonic lineshape in low-dimensional structures with rough interfaces
[DE95-003434] p 1582 N95-22237

NORMALIZING (STATISTICS)
Geometric characterization of electromigration voids (A statistical analysis of electromigration voids)
[AD-A286494] p 1328 N95-21169

NORTH SEA
Long term changes on the continental shelf of the North Sea: Invertebrate trends, 1931-1990
[PB95-135224] p 1435 N95-21717

NORTHERN HEMISPHERE
Radiative forcing for changes in tropospheric O3
[DE94-019017] p 1413 N95-20354

NORWAY
Ohmsett test of NOFI Vee-Sweep and NOFI 600S Oilboom
[AD-A279525] p 1408 N95-21685

NOTCH SENSITIVITY
The processing and mechanical properties of high temperature/high performance composites. Stress redistribution and notch properties, book 2
[AD-A279737] p 1227 N95-20429

NOZZLE DESIGN
Development of quiet-flow supersonic wind tunnels for laminar-turbulent transition research
[NASA-CR-197286] p 1216 N95-21436

NOZZLE FLOW
Static investigation of two fluidic thrust-vectoring concepts on a two-dimensional convergent-divergent nozzle
[NASA-TM-4574] p 1199 N95-19913
Numerical investigations of low-density nozzle flow by solving the Boltzmann equation
[NASA-TM-110492] p 1354 N95-21675

NUCLEAR BINDING ENERGY
Pairing on small clusters in the Peierls-Hubbard model: Implications for C60
[DE94-016284] p 1565 N95-20330
Effect of the electron-SO-phonon on the impurity state energies in a semiconductor quantum well
[DE94-628993] p 1581 N95-21887

NUCLEAR DEVICES
Performance of the NIF prototype beamlet
[DE94-018500] p 1371 N95-20817

NUCLEAR ELECTRIC PROPULSION
Real-time dynamic simulator for the Topaz II reactor power system
[DE95-001604] p 1535 N95-21278
Issues in the flight qualification of a space power reactor
[DE95-001606] p 1223 N95-21840

NUCLEAR EXPLOSION EFFECT
Nuclear Terms Handbook, 1993
[DE94-016248] p 1589 N95-21131

NUCLEAR EXPLOSIONS
The GPS Burst Detector W-Sensor
[DE94-017406] p 1204 N95-20269

NUCLEAR FUSION
Diffusion enhances spontaneous electroweak baryogenesis
[DE94-017574] p 1512 N95-20451

NUCLEAR INTERACTIONS
Mass and lifetime measurements with exclusive B reconstruction at CDF
[DE94-015849] p 1511 N95-20401
The theory of relativistic heavy ion collisions
[DE95-001805] p 1519 N95-21302

NUCLEAR MAGNETIC RESONANCE
Sol-gel-derived silica films with tailored microstructures for applications requiring organic dyes
[DE94-018886] p 1264 N95-20047
Physics Division research and development
[DE94-017685] p 1501 N95-20246
Investigation of syngas interaction in alcohol synthesis catalysts
[DE94-018784] p 1236 N95-20349
Actinide(IV) and actinide(VI) carbonate speciation studies by PAS and NMR spectroscopies
[DE94-016957] p 1236 N95-20361
Thermodynamic and NMR studies of solvent effect on enantiomeric recognition for a chiral organiz ammonium cation by chiral diketopyridino-18-Crown-6 type ligands at 25.0 C
[AD-A279893] p 1223 N95-20592
Hg-199 and Cu-(63,65) NMR studies of mercury based high-Tc superconductors
[DE95-001073] p 1570 N95-20820
Dynamic NMR studies of restricted arene rotation in the chromiu tricarbonyl thiophene and selenophene complexes
[DE95-001656] p 1257 N95-21399
Analysis of experimentally shocked minerals by NMR spectroscopy
[DE95-002955] p 1573 N95-21449
Radiopharmaceuticals for diagnosis
[DE95-002200] p 1445 N95-21595
NMR relaxation behavior of the head group of SHBS in lamellar liquid crystals
[AD-A279124] p 1574 N95-21599
Selenophene transition metal complexes
[DE95-001675] p 1260 N95-21841
Solid-state NMR characterization of C- and N-labelled phthalimides: Model compounds for studying polyimides
[AD-A286479] p 1578 N95-22286
Synthesis and characterization of single-source molecular precursors to binary metal sulphides: Bis(diethyldithiocarbamato) M(2)trialkylphosphine (M = Zn and Cd) adducts
[AD-A279746] p 1248 N95-22385

NUCLEAR MEDICINE
In vivo distribution of liposome encapsulated hemoglobin studied with imaging radiotracers
[AD-A279774] p 1438 N95-20806
Radiopharmaceuticals for diagnosis
[DE95-002200] p 1445 N95-21595
ANSTO: Program of research, 1993-1994
[DE94-631122] p 1605 N95-21828

NUCLEAR MODELS
A model for electron nuclear dynamics of a monatomic chain
[AD-A279652] p 1506 N95-19960
Anomalous vector-boson couplings in Majorana neutrino models
[PB95-127460] p 1518 N95-21220
New improved derivative expansion for field theories with spontaneous symmetry breaking
[DE94-019349] p 1580 N95-21486

NUCLEAR PHYSICS
Has a standard model solution to the solar neutrino problem been found?
[DE94-017580] p 1604 N95-20490
Nuclear research with the electromagnetic probe
[DE95-001812] p 1525 N95-21747
ANSTO: Program of research, 1993-1994
[DE94-631122] p 1605 N95-21828
Theses of the Proceedings of the 23d International Meeting on the Physics of Charged Particle Interaction with Crystals
[DE94-631501] p 1529 N95-22281

NUCLEAR POWER PLANTS
Nuclear Terms Handbook, 1993
[DE94-016248] p 1589 N95-21131

NUCLEAR POWER REACTORS
Mars power system concept definition study. Volume 1: Study results
[NASA-CR-195420-VOL-1] p 1396 N95-21952

NUCLEAR PUMPED LASERS
Applications for reactor-pumped lasers
[DE95-000536] p 1373 N95-21393

NUCLEAR PUMPING
The effect of reusing laser gas on the fission-fragment pumped 1.73 micron atomic xenon laser output
[DE94-018512] p 1369 N95-20225

NUCLEAR REACTIONS
Non destructive characterization using pulsed fast-thermal neutrons
[DE95-002601] p 1511 N95-20422
The solar neutrino problem: Neither astrophysics nor oscillations?
[DE94-012850] p 1603 N95-21316
Distribution of light element isotopes in Bencubbin and Weatherford meteorites: An indicator of heterogeneity in the primitive solar nebula
[DE94-019167] p 1600 N95-22128
Helium production by 10 MeV neutrons in iron, nickel and copper
[DE94-014798] p 1529 N95-22280
NUCLEAR REACTORS
Real-time dynamic simulator for the Topaz II reactor power system
[DE95-001604] p 1535 N95-21278
Effect of neutron irradiation on the impact properties of A533B steel
[DE95-001834] p 1256 N95-21286
NUCLEAR RESEARCH
Nuclear research with the electromagnetic probe
[DE95-001812] p 1525 N95-21747
NUCLEAR ROCKET ENGINES
Power systems for future missions. Appendices A-L
[NASA-CR-195320-APP-A-L] p 1395 N95-21530
NUCLEAR SCATTERING
Nuclear A dependence of exclusive vector meson production in muon scattering
[DE95-002248] p 1511 N95-20418
Multiple hard interactions in HERWIG
[PB95-130548] p 1518 N95-21233
NUCLEAR SPIN
Spin dependence of diffractive processes and implications for the small x behaviour of g1 and the spin content of the nucleon
[PB95-130332] p 1518 N95-21225
Nuclear research with the electromagnetic probe
[DE95-001812] p 1525 N95-21747
NUCLEAR STRUCTURE
Competing structures in nuclei near closed shells
[DE94-017604] p 1512 N95-20491
Universal parametrization for quark and lepton substructure
[DE94-770604] p 1514 N95-20738
Nuclear research with the electromagnetic probe
[DE95-001812] p 1525 N95-21747
NUCLEAR WEAPONS
The development of science during this century
[DE94-632964] p 1582 N95-22185
NUCLEATION
Nucleation, growth, and strain relaxation of lattice-mismatched 3-5 semiconductor epitaxial layers
p 1324 N95-20543
Antiphase boundaries as nucleation centers in low-temperature epitaxial growth
[AD-A279895] p 1568 N95-20594
Growth, characterization and device development in monocrystalline diamond films
[AD-A285991] p 1568 N95-20614
Microscopy of stress-induced morphological development and dislocation nucleation during semiconductor epitaxy
[DE94-017869] p 1568 N95-20674
The in situ observation of epitaxial diamond thin film nucleation and growth using emission electron microscopy
[AD-A279811] p 1569 N95-20807
NUCLEI (NUCLEAR PHYSICS)
A model for electron nuclear dynamics of a monatomic chain
[AD-A279652] p 1506 N95-19960
Electron-nuclear dynamics of molecular systems
[AD-A279649] p 1516 N95-21120
NUCLEIC ACIDS
Biomolecular Materials by Design, volume 330
[AD-A285369] p 1269 N95-20551
NUCLEON-NUCLEON INTERACTIONS
Dilepton production from p-p to Ca-Ca at the Bevalac
[DE95-002341] p 1520 N95-21357
Constraints on T-odd and P-even hadronic interactions from nucleon, nuclear, and atomic electric dipole moments
[DE94-012845] p 1526 N95-21920
There might be two kinds of dibaryon
[DE94-014417] p 1526 N95-22058
Parity violation in the compound nucleus
[DE95-002742] p 1530 N95-22435
NUCLEONS
Spin dependence of diffractive processes and implications for the small x behaviour of g1 and the spin content of the nucleon
[PB95-130332] p 1518 N95-21225
Exclusive processes: Tests of coherent QCD phenomena and nucleon substructure at CEBAF
[DE95-002892] p 1520 N95-21336
Strange hadronic matter
[DE94-019345] p 1521 N95-21484
Structure functions and structure function ratio F2(n)/F2(p) at low X(Bj) and Q2 in inelastic muon scattering
[DE94-018979] p 1573 N95-21561
Status of the DO top search
[DE95-002214] p 1525 N95-21715
Nuclear research with the electromagnetic probe
[DE95-001812] p 1525 N95-21747
Proton and produced particle distributions from Au+Au collisions at 11.6 A GeV/c
[DE94-018634] p 1530 N95-22392
NUCLIDES
Surface exposure geochronology using cosmogenic nuclides: Applications in Antarctic glacial geology
[AD-A279392] p 1426 N95-21944
NUMBER THEORY
Second International Conference on Ordinal Data Analysis
[AD-A279756] p 1590 N95-21401
NUMERICAL ANALYSIS
A numerical investigation of energy transfer and subgrid-scale eddy viscosity in homogeneous, isotropic and shear turbulence
[AD-A280005] p 1339 N95-20058
RCS calculation capability
[AD-A286329] p 1289 N95-20211
Solid-state dynamics and quantum transport in novel semiconductor nanostructures
[AD-A285946] p 1315 N95-20394
Fitting stochastic partial differential equations to spatial data
[AD-A279870] p 1490 N95-20432
Simulation of tearing mode stabilization by using ECH
[DE94-770700] p 1554 N95-20684
Deconvolution and singular value decomposition
[AD-A286582] p 1491 N95-20875
Laser anemometry and viscous computation of the flow through an annular turbine cascade
[AD-A280070] p 1341 N95-20968
Numerical analysis of energetic particle stabilization of ballooning modes in finite-aspect-ratio tokamaks
[DE94-631397] p 1556 N95-21164
Computation of invariant manifolds
[PB95-135687] p 1492 N95-21318
Report of the Numerical Analysis Group
[PB95-108163] p 1494 N95-21648
Object-oriented design of preconditioned iterative methods
[PB95-110276] p 1469 N95-21655
Critical dynamics and plastic flow in disordered Josephson junction arrays
[DE94-629074] p 1576 N95-21995
Activities of the Research Institute for Advanced Computer Science
[NASA-CR-197291] p 1478 N95-22108
On the wavelet optimized finite difference method
[NASA-CR-191601] p 1495 N95-22157
FORTRAN subroutine for column reduction of polynomial matrices
[PB95-134987] p 1497 N95-22379
Transactions of the Eleventh Army Conference on Applied Mathematics and Computing
[AD-A279884] p 1497 N95-22389
NUMERICAL CONTROL
Target area acquisition and control system survivability for the National Ignition Facility
[DE94-016549] p 1550 N95-20190
The development and evaluation of water-mist fire extinguishing systems
[DE94-019019] p 1286 N95-20356
System design document U-AVLIS control system architecture
[DE94-017297] p 1460 N95-20387
Preliminary control system design and analysis for the Space Station Furnace Facility thermal control system
[NASA-TM-108476] p 1365 N95-20560
An integrated architecture of adaptive neural network control for dynamic systems
[DE94-014813] p 1481 N95-20693
Automatic generation of fuzzy rules for the sensor-based navigation of a mobile robot
[DE95-001428] p 1481 N95-20837
Representing manufacturing features to support design and process changes
[DE94-018587] p 1467 N95-21389
Operator's manual for the multistation offgas analysis system
[DE95-002060] p 1243 N95-21472
RF beam control for the AGS Booster
[DE95-001485] p 1538 N95-21720
NUMERICAL INTEGRATION
A control volume method on an icosahedral grid for numerical integration of the shallow-water equations on the sphere
[DE94-016345] p 1489 N95-20170
The numerical integration and 3-D finite element formulation of a viscoelastic model of glass
[DE95-002588] p 1271 N95-20788
NUMERICAL STABILITY
Parallel predictor-corrector methods
[PB95-135711] p 1493 N95-21434
Convergence acceleration of the Proteus computer code with multigrid methods
[NASA-CR-197677] p 1467 N95-21450
NUMERICAL WEATHER FORECASTING
A control volume method on an icosahedral grid for numerical integration of the shallow-water equations on the sphere
[DE94-016345] p 1489 N95-20170
NUTRITION
Sustaining the health and performance of soldiers/warfighters deployed to harsh environments
[AD-A286270] p 1446 N95-22004
NYLON (TRADEMARK)
Determinations of phase transitions in nylon 6-12, nylon-6, polyvinyl chloride and polyethylene terephthalate by positron annihilation spectroscopy
[DE94-629992] p 1239 N95-20736
Absorption of water and lubricating oils into porous nylon
[NASA-CR-197344] p 1280 N95-22383

O

OBJECT-ORIENTED PROGRAMMING
Hierarchical diagrammatic representation of class structure
[PB95-110722] p 1456 N95-19908
Design of a parallel object oriented programming language
[AD-A284924] p 1457 N95-20000
Evaluation of Borland Turbo Vision
[AD-A279873] p 1459 N95-20184
Making structured graphics and constraints practical for large-scale applications
[AD-A280062] p 1461 N95-20623
Design and implementation of visual object-oriented LOGO using Prograph
[AD-A285977] p 1461 N95-20687
DIFFPACK: Software for partial differential equations
[PB95-110268] p 1468 N95-21654
Object-oriented design of preconditioned iterative methods
[PB95-110276] p 1469 N95-21655
CAiSE 1994 Doctoral Consortium
[PB95-135182] p 1469 N95-21711
Using the CoRE requirements method with ADARTS. Version 01.00.05
[AD-A279151] p 1470 N95-21972
Modelling multimedia teleservices with OSI upper layers framework: Short paper
[PB95-132734] p 1308 N95-22080
The navigation toolkit
[NASA-CR-197290] p 1205 N95-22161
A conceptual approach to object-oriented data modeling
[AD-A286048] p 1592 N95-22416
OBLIQUE SHOCK WAVES
Direct numerical simulation of 2-D and 3-D instability waves in a laminar separation bubble
p 1352 N95-21095
Shock wave interactions in hypervelocity flow
[AD-A286507] p 1357 N95-22212
OBSERVATION
Mariners Weather Log, volume 38, number 3, summer 1994
[PB94-209541] p 1428 N95-20099
Compositional proof theory for fault tolerant real-time distributed systems
[PB95-127601] p 1465 N95-21025
Duality beyond sober spaces: Topological spaces and observation frames
[PB95-134565] p 1494 N95-21962
OBSTACLE AVOIDANCE
Unknown-terrains navigation of a mobile robot using an array of sonars
[DE94-017902] p 1482 N95-21385
OCCURRENCES
An experimental determination of meteor daily arrival rate variation
[AD-A279484] p 1600 N95-21679
OCEAN BOTTOM
Data report: Stress measurements in the bottom boundary layer with BASS tripods STRESS 2 1990-1991
[AD-A279875] p 1433 N95-20433

Multiple scatter theory of ocean sediments [AD-A286033] p 1433 N95-20999

Simulation of laser bathymetry for irregular bottoms [PB95-133518] p 1434 N95-21320

The determination of static and time varying dipole source. Sensor geometry during sea trials using differential global positioning system [MRL-TN-631] p 1205 N95-21642

A simple ocean bottom hydrophone with 200 megabyte data capacity [AD-A279478] p 1434 N95-21677

Volatiles in the Earth: All shallow and all recycled p 1416 N95-21779

Modeling the effect of water on mantle rheology p 1417 N95-21783

Mantle devolatilization and rheology in the framework of planetary evolution p 1418 N95-21788

Subduction and volatile recycling in Earth's mantle p 1421 N95-21802

Subduction of hydrated basalt of the oceanic crust: Implications for recycling of water into the upper mantle and continental growth p 1423 N95-21814

The isotope geochemistry of abyssal peridotites and related rocks [AD-A279435] p 1435 N95-21918

The dynamic role of ridges in a beta-plane channel. Towards understanding the dynamics of large scale circulation in the Southern Ocean [AD-A279390] p 1435 N95-21943

Rapid determination of geoacoustic properties of the sea floor by simulated annealing [AD-A286297] p 1436 N95-22028

Descriptions of WHOI sediment cores, volume 8 [AD-A279444] p 1436 N95-22073

Seismic anisothropy and large-scale porosity inthe ocean floor [AD-A286580] p 1436 N95-22187

OCEAN CURRENTS

A modal analysis of currents in a Pacific Atoll lagoon [AD-A283721] p 1431 N95-19971

Oceanographic analysis of the acoustic mid-ocean dynamics experiment [AD-A285907] p 1432 N95-19988

Ambient noise and surface wave dissipation in the ocean [AD-A279650] p 1432 N95-20303

Fourth International Symposium on Stratified Flows, volume 3 [AD-A286452] p 1354 N95-21584

CTD calibration and processing methods used at Woods Hole Oceanographic Institution [AD-A279507] p 1435 N95-21681

Modeling the response of the California Current system to Global Greenhouse Warming [DE94-018253] p 1408 N95-21708

The dynamic role of ridges in a beta-plane channel. Towards understanding the dynamics of large scale circulation in the Southern Ocean [AD-A279390] p 1435 N95-21943

Exchanges between hemispheres and gyres: A direct approach to the mean circulation of the equatorial Pacific [NASA-CR-196311] p 1436 N95-22072

Seismic anisothropy and large-scale porosity inthe ocean floor [AD-A286580] p 1436 N95-22187

SAR-related stress variability in the Marine Atmospheric Boundary Layer (MABL) [AD-A286462] p 1431 N95-22393

Fourth International Symposium on Stratified Flows, volume 4 [AD-A286453] p 1358 N95-22424

OCEAN DATA ACQUISITIONS SYSTEMS

Resolving velocity profiles with the multi-scale profiler [AD-A286446] p 1434 N95-21461

Climatological data for clouds over the globe from surface observations, 1982-1991: The total cloud edition [DE95-002537] p 1431 N95-22288

OCEAN DYNAMICS

Tests of an improved oceanographic expert system [AD-A280123] p 1431 N95-19888

The Surface Wave Dynamics Experiment (SWADE): A retrospective look at the wave modeling activities [AD-A285612] p 1431 N95-19895

A modal analysis of currents in a Pacific Atoll lagoon [AD-A283721] p 1431 N95-19971

Oceanographic analysis of the acoustic mid-ocean dynamics experiment [AD-A285907] p 1432 N95-19988

Analysis of low frequency ocean noise. 1: From a long-term experiment across the US East Coast. 2: From the Wake Island Hydrophone Array during northwest Pacific typhoons [AD-A284975] p 1432 N95-20040

Model-based inversion for a shallow ocean application [DE94-016968] p 1433 N95-20420

Closure on the global carbon cycle [DE94-018617] p 1404 N95-20991

Monthly mean sea ice data from the Polar Ice Prediction System, the Regional Polar Ice Prediction System-Barents Sea and the Regional Polar Ice Prediction System-Greenland Sea [AD-A280095] p 1433 N95-21018

Mixing and dynamics of the Mediterranean outflow [AD-A279803] p 1434 N95-21306

Fourth International Symposium on Stratified Flows, volume 1 [AD-A286450] p 1354 N95-21583

Fourth International Symposium on Stratified Flows, volume 3 [AD-A286452] p 1354 N95-21584

Modeling the response of the California Current system to Global Greenhouse Warming [DE94-018253] p 1408 N95-21708

High resolution properties of the equatorial Pacific marine atmospheric boundary layer from lidar and radiosonde observations [DE95-001028] p 1426 N95-21875

A numerical study of wind forcing effects on the California Current System [AD-A286205] p 1435 N95-21880

Fourth International Symposium on Stratified Flows, volume 4 [AD-A286453] p 1358 N95-22424

OCEAN MODELS

Tests of an improved oceanographic expert system [AD-A280123] p 1431 N95-19888

The Surface Wave Dynamics Experiment (SWADE): A retrospective look at the wave modeling activities [AD-A285612] p 1431 N95-19895

Radiance of the ocean horizon [AD-A285613] p 1431 N95-19896

A modal analysis of currents in a Pacific Atoll lagoon [AD-A283721] p 1431 N95-19971

Oceanographic analysis of the acoustic mid-ocean dynamics experiment [AD-A285907] p 1432 N95-19988

NOMADS graphical user interface version 2.0 user's manual [AD-A286314] p 1458 N95-20095

Mississippi State University Center for Air Sea Technology FY 1993 and FY 1994 research program in Navy ocean modeling and prediction [AD-A286322] p 1432 N95-20209

Model-based inversion for a shallow ocean application [DE94-016968] p 1433 N95-20420

Closure on the global carbon cycle [DE94-018617] p 1404 N95-20991

Modeling open boundary conditions by using the optimization approach [AD-A285548] p 1433 N95-21158

Sensitivity of climate models: Comparison of simulated and observed patterns for past climates [DE95-002257] p 1406 N95-21379

Modeling the response of the California Current system to Global Greenhouse Warming [DE94-018253] p 1408 N95-21708

A numerical study of wind forcing effects on the California Current System [AD-A286205] p 1435 N95-21880

Seismic anisothropy and large-scale porosity inthe ocean floor [AD-A286580] p 1436 N95-22187

OCEAN SURFACE

The Surface Wave Dynamics Experiment (SWADE): A retrospective look at the wave modeling activities [AD-A285612] p 1431 N95-19895

Radiance of the ocean horizon [AD-A285613] p 1431 N95-19896

Deriving earth science products from SSM/I [NASA-CR-197299] p 1389 N95-20156

Ambient noise and surface wave dissipation in the ocean [AD-A279650] p 1432 N95-20303

Methods for evaluating the effects of conduits at the surface of the sea p 1294 N95-20932

Modelling of microwave propagation and clutter in a maritime environment p 1295 N95-20938

Measurements of radar backscatter from the ocean surface at 94 GHz as a function of wind speed, direction and the modulation by the ocean waves during the SAXON-FPN experiment p 1299 N95-20960

X-band microwave backscattering from ocean waves [DE94-016719] p 1309 N95-22241

SAR-related stress variability in the Marine Atmospheric Boundary Layer (MABL) [AD-A286462] p 1431 N95-22393

OCEAN TEMPERATURE

Long Time Series Measurements in the Coastal Ocean: A workshop [AD-A279509] p 1435 N95-21682

Real time system for practical acoustic monitoring of global ocean temperature [AD-A286435] p 1436 N95-22209

OCEAN THERMAL ENERGY CONVERSION

Seawater test results of Open-Cycle Ocean Thermal Energy Conversion (OC-OTEC) components [DE94-019254] p 1396 N95-21897

OCEANOGRAPHIC PARAMETERS

A modal analysis of currents in a Pacific Atoll lagoon [AD-A283721] p 1431 N95-19971

Mariners Weather Log, volume 38, number 3, summer 1994 [PB94-209541] p 1428 N95-20099

Long Time Series Measurements in the Coastal Ocean: A workshop [AD-A279509] p 1435 N95-21682

NODDS/WOSM interface user's manual [AD-A279095] p 1471 N95-22068

OCEANOGRAPHY

Tests of an improved oceanographic expert system [AD-A280123] p 1431 N95-19888

Oceanographic analysis of the acoustic mid-ocean dynamics experiment [AD-A285907] p 1432 N95-19988

Mississippi State University Center for Air Sea Technology FY 1993 and FY 1994 research program in Navy ocean modeling and prediction [AD-A286322] p 1432 N95-20209

Synthesizing the Gulf Stream thermal structure from XBT data [AD-A279665] p 1433 N95-20458

Monthly mean sea ice data from the Polar Ice Prediction System, the Regional Polar Ice Prediction System-Barents Sea and the Regional Polar Ice Prediction System-Greenland Sea [AD-A280095] p 1433 N95-21018

Modeling open boundary conditions by using the optimization approach [AD-A285548] p 1433 N95-21158

CTD calibration and processing methods used at Woods Hole Oceanographic Institution [AD-A279507] p 1435 N95-21681

Long Time Series Measurements in the Coastal Ocean: A workshop [AD-A279509] p 1435 N95-21682

Modeling the response of the California Current system to Global Greenhouse Warming [DE94-018253] p 1408 N95-21708

Descriptions of WHOI sediment cores, volume 8 [AD-A279444] p 1436 N95-22073

OCEANS

Analysis of low frequency ocean noise. 1: From a long-term experiment across the US East Coast. 2: From the Wake Island Hydrophone Array during northwest Pacific typhoons [AD-A284975] p 1432 N95-20040

Mississippi State University Center for Air Sea Technology FY 1993 and FY 1994 research program in Navy ocean modeling and prediction [AD-A286322] p 1432 N95-20209

Terrain and refractivity effects on non-optical paths p 1294 N95-20931

European Workshop on Optical Ground Truth Instrumentation for the Validation of Space-Borne Optical Remote Sensing Data of the Marine Environment [PB95-134144] p 1390 N95-21872

The dynamic role of ridges in a beta-plane channel. Towards understanding the dynamics of large scale circulation in the Southern Ocean [AD-A279390] p 1435 N95-21943

OFFGASSING

Operator's manual for the multistation offgas analysis system [DE95-002060] p 1243 N95-21472

Removal of CO2 in closed loop off-gas treatment systems [DE94-019259] p 1407 N95-21617

OHMIC DISSIPATION

Joule heating of the ITER TF cold structure: Effects of vertical control coil currents and ELMS [DE95-001817] p 1560 N95-21724

OIL POLLUTION

Ohmsett test of NOFI Vee-Sweep and NOFI 600S Oilboom [AD-A279525] p 1408 N95-21685

OIL SLICKS

Ohmsett test of NOFI Vee-Sweep and NOFI 600S Oilboom [AD-A279525] p 1408 N95-21685

NODDS/WOSM interface user's manual [AD-A279095] p 1471 N95-22068

OILS

Impact behavior of FeAl alloy FA-350 [DE94-018128] p 1254 N95-20705

OLIVINE
Hydrogen storage in Earth's mantle and core
p 1423 N95-21813
ON-LINE SYSTEMS
Daytime Raman lidar profiling of atmospheric water vapor
[DE94-015747] p 1413 N95-20397
FEDIX: User's guide, version 5.0/release 3.0
[DE95-002274] p 1588 N95-20762
FIREDOC users manual, 3rd edition
[PB95-128674] p 1286 N95-21129
Taking AIM: The management of scientific and technical information at Argonne National Laboratory
[DE94-019279] p 1591 N95-22092
ONE DIMENSIONAL FLOW
Multigrid with matrix-dependent transfer operators for convection-diffusion problems
[PB95-110821] p 1487 N95-19915
One-dimensional reactive Euler equations
[PB95-135430] p 1244 N95-21573
Large amplitude localized structures in a relativistic electron-positron ion plasma
[DE94-628965] p 1561 N95-21851
OPEN CIRCUIT VOLTAGE
Status of diffused junction p+n InP solar cells for space applications p 1317 N95-20509
OPENINGS
Geometric moire method of strain analysis with displacement discontinuities
[DE95-001114] p 1386 N95-20833
OPERATING COSTS
An analysis of cost overruns on defense acquisition contracts p 1584 N95-20749
NASA's attack on costs p 1585 N95-20755
Comparison of HFC-134a and the ternary blend, Suva MP39, as replacements for the refrigerant, CGC-12
[MRL-GD-0051] p 1287 N95-21625
OPERATING SYSTEMS (COMPUTERS)
DONIO: Distributed object network I/O library
[DE94-019163] p 1477 N95-21602
OPERATING TEMPERATURE
Temperature effects on acoustic interactions between altitude test facilities and jet engine plumes
[NASA-CR-197638] p 1504 N95-21170
OPERATIONAL AMPLIFIERS
Pre-amplifier with multi-stage feedback
[AD-D016254] p 1336 N95-22418
OPERATIONAL HAZARDS
Safety issues in high speed machining
[PB95-127411] p 1287 N95-21422
OPERATIONS RESEARCH
Use of operations research techniques in deductive databases
[PB95-135349] p 1589 N95-21004
OPERATOR PERFORMANCE
Human performance studies for control of multiple remote systems
[AD-A286623] p 1452 N95-20768
Effect of lags on human performance with head-coupled simulators
[AD-A279577] p 1453 N95-21700
OPERATORS (MATHEMATICS)
Multigrid with matrix-dependent transfer operators for convection-diffusion problems
[PB95-110821] p 1487 N95-19915
Weighted strongly elliptic operators on lie groups
[PB95-110847] p 1487 N95-19917
Abstract reduction and topology
[PB95-110615] p 1488 N95-20054
Banach spaces with small spaces of operators
[PB95-111134] p 1489 N95-20273
On the differential representations of quantum Lie superalgebras
[DE94-629874] p 1491 N95-20734
Monadic maps and folds for arbitrary datatypes
[PB95-134045] p 1492 N95-21032
Positive rockland operators
[PB95-127510] p 1493 N95-21423
Preconditioning via asymptotically-defined domain decomposition
[DE94-019046] p 1493 N95-21564
Right inverse for the divergence operator in spaces of continuous piecewise polynomials
[PB95-127080] p 1496 N95-22369
Self-similar solutions of a fast diffusion equation that do not conserve mass
[PB95-134920] p 1497 N95-22375
OPERATORS (PERSONNEL)
Navigation system in combat vehicle
[PB95-131629] p 1452 N95-21467
OPTICAL ACTIVITY
Perception and control of locomotion
[AD-A285605] p 1450 N95-21192
OPTICAL COMMUNICATION
Optical backplane for modular avionics
p 1212 N95-20652
Eigenmode method for electromagnetic synthesis of diffractive elements with three-dimensional profiles
[PB95-127726] p 1301 N95-21107
Threshold detection in the presence of atmospheric turbulence
[AD-A286175] p 1427 N95-22249
OPTICAL COMPUTERS
Preliminary evaluation of a digital optical systolic processor implemented with acousto-optic cells
[AD-A286377] p 1541 N95-20231
International Conference on Optical Computing: Technical digest
[AD-A284293] p 1541 N95-20249
High performance backplane components for modular avionics p 1212 N95-20653
OPTICAL COUPLING
Semiconductor laser joint study program with Rome Laboratory
[AD-A285858] p 1369 N95-20379
Second order approximation for optical polaron in the strong coupling case
[DE94-628997] p 1525 N95-21856
OPTICAL DATA PROCESSING
Preliminary evaluation of a digital optical systolic processor implemented with acousto-optic cells
[AD-A286377] p 1541 N95-20231
International Conference on Optical Computing: Technical digest
[AD-A284293] p 1541 N95-20249
GaAs optical circuits
[AD-A285859] p 1369 N95-20389
Optical pattern recognition
[AD-A285384] p 1480 N95-20607
High contrast organic crystal optical modulator for phased array antenna and optical signal processing
[AD-A286557] p 1544 N95-20844
OPTICAL DENSITY
Fire smoke ventilation through shafts: Experiments
[PB95-132247] p 1288 N95-21978
OPTICAL DISKS
Common mapping system media study
[AD-A279086] p 1390 N95-21912
OPTICAL EMISSION SPECTROSCOPY
Time-resolved diagnostics of excimer laser-generated ablation plasmas used for pulsed laser deposition
[DE94-018950] p 1559 N95-21547
A HIRES analysis of the FIR emission of supernova remnants p 1594 N95-21770
OPTICAL EQUIPMENT
Characterization of an expanded-field Schwarzschild objective for extreme ultraviolet lithography
[DE94-016780] p 1541 N95-20239
White-light spectral analysis of lithium niobate waveguides
[DE94-016692] p 1542 N95-20489
Epitaxial liftoff technology onto processed silicon foundry wafers
[AD-A285621] p 1571 N95-21145
Twentysixth YERAC
[PB95-127437] p 1599 N95-21347
Nonlinear frequency conversion optical filter
[AD-D016523] p 1544 N95-21465
Method for characterization of optical waveguide devices using partial coherence interferometry
[AD-D016525] p 1544 N95-21466
High-capacity optical multichannel virtual mesh interconnection networks
[PB95-134094] p 1546 N95-21870
High temperature polymer for second order nonlinear optics for photonic materials
[AD-A279309] p 1280 N95-22141
OPTICAL FIBERS
Technical digest: Eighth Symposium on Optical Fiber Measurements
[PB94-207636] p 1540 N95-19976
Control of continuous phase PH using visible light to activate PH-dependent fibers and gels in a controlled and reversible manner
[AD-D016532] p 1543 N95-20728
A three-dimensional orthogonal laser velocimeter for the NASA Ames 7- by 10-foot wind tunnel
[NASA-TM-108864] p 1366 N95-21323
High frequency current sensors using the Faraday effect in optical fibers
[DE95-001859] p 1545 N95-21728
High-capacity optical multichannel virtual mesh interconnection networks
[PB95-134094] p 1546 N95-21870
Heterostructure quantum confined Stark effect electrooptic modulators operating at 938 nm
[AD-A279342] p 1581 N95-21928
Tunable CW blue, green, orange and red upconversion fiber lasers at room temperature
[DE95-000851] p 1375 N95-22007
Optical fiber pressure sensor for liquid level monitoring
[AD-D016246] p 1547 N95-22089
Embedded optical fibres as strain sensors in polymer matrix fibre composites: The influence of adhesion in strain transfer
[PB95-133617] p 1547 N95-22140
OPTICAL FILTERS
A simple analytical model for asynchronous dense WDM/OOK systems
[AD-A283725] p 1289 N95-19973
Methods and components for optical contention resolution in high speed networks
[AD-A280016] p 1543 N95-20598
Nonlinear frequency conversion optical filter
[AD-D016523] p 1544 N95-21465
OPTICAL MATERIALS
Design, synthesis and characterization of novel nonlinear optical materials
[AD-A285617] p 1540 N95-19897
International collaboration program on innovative chemical processing of superior electronic and optical materials
[AD-A285122] p 1226 N95-20105
Optical multilayers with an amorphous fluoropolymer
[DE94-017693] p 1541 N95-20218
The preparation of all para-polyphenyls with increased solubility and enhanced third order NLO activity
[AD-A284301] p 1266 N95-20251
The synthesis and characterization of new mesogenic diacetylene monomers and their polymers
[AD-A286188] p 1267 N95-20328
A URI program for Ultraviolet/extreme ultraviolet research
[AD-A279159] p 1370 N95-20600
Reactor pumped laser research at the Sandia National Laboratories pulsed reactor facilities
[DE95-002181] p 1371 N95-20867
Development of ferroelectric liquid crystals with enhanced nonlinear optical properties
[AD-A279988] p 1571 N95-20965
Optical, electronic and optoelectronic material and device research
[AD-A280111] p 1374 N95-21630
High temperature polymer for second order nonlinear optics for photonic materials
[AD-A279309] p 1280 N95-22141
OPTICAL MEASUREMENT
Technical digest: Eighth Symposium on Optical Fiber Measurements
[PB94-207636] p 1540 N95-19976
Surface characterization and contamination analysis
[NASA-CR-197374] p 1238 N95-20557
Mechanisms and diagnostics of ultrashort pulse laser ocular effects
[AD-A285610] p 1373 N95-21195
International Symposium on Advanced Laser Technologies
[AD-A279849] p 1376 N95-22164
OPTICAL MEASURING INSTRUMENTS
Molecular snapshots: Product imaging of dynamics important to fundamental combustion processes
[DE94-018595] p 1510 N95-20346
State-to-state collisional dynamics of atmospheric species
[AD-A285053] p 1370 N95-20484
Fiber grating-based detection system for wavelength encoded fiber sensors
[AD-D016208] p 1545 N95-21825
Optical processing and control
[AD-A279157] p 1546 N95-21975
OPTICAL MEMORY (DATA STORAGE)
High speed optical storage technology
[AD-A285788] p 1456 N95-22400
OPTICAL POLARIZATION
S-D hybridization and anisotropy of the optical second harmonic at low frequencies
[AD-A279449] p 1544 N95-20876
OPTICAL PROPERTIES
Free electron laser program
[AD-A285906] p 1368 N95-19987
Nonlinear Faraday effect in CdS semiconductor in an ultrahigh magnetic field
[DE94-016804] p 1564 N95-20240
The synthesis and characterization of new mesogenic diacetylene monomers and their polymers
[AD-A286188] p 1267 N95-20328
Optical properties of silicon clusters deposited on the basal plane of graphite
[DE94-017529] p 1542 N95-20450
Physical-chemical studies on rodlike polymer compositions
[AD-A285361] p 1269 N95-20548
Molecularly Designed Ultrafine/Nanostructured Materials, volume 351
[AD-A285370] p 1568 N95-20552
Optical power limiting liquid crystal composites
[AD-A286605] p 1569 N95-20767

S-D hybridization and anisotropy of the optical second harmonic at low frequencies
[AD-A279449] p 1544 N95-20876

Development of ferroelectric liquid crystals with enhanced nonlinear optical properties
[AD-A279988] p 1571 N95-20965

Light output and radiation damage in a YAIO3:Ce crystal
[DE94-016815] p 1545 N95-21643

Optical radiation: Health based exposure limits for electromagnetic radiation in the wavelength range from 100 nanometer to 1 millimeter
[PB95-132767] p 1447 N95-22083

International Symposium on Advanced Laser Technologies
[AD-A279849] p 1376 N95-22164

OPTICAL PUMPING

Continuously-tunable, narrow-linewidth, Q-switched Cr:LiSAF laser for lidar applications
[DE95-000862] p 1373 N95-21312

OPTICAL RADAR

BACKSCAT lidar simulation version 4.0: Technical documentation and users guide
[AD-A285851] p 1290 N95-20376

Daytime Raman lidar profiling of atmospheric water vapor
[DE94-015747] p 1413 N95-20397

Project Whitefeather
[DE94-016575] p 1415 N95-21184

Continuously-tunable, narrow-linewidth, Q-switched Cr:LiSAF laser for lidar applications
[DE95-000862] p 1373 N95-21312

Lidar technologies for airborne and space-based applications
[DE95-002954] p 1302 N95-21448

High resolution properties of the equatorial Pacific marine atmospheric boundary layer from lidar and radiosonde observations
[DE95-001028] p 1426 N95-21875

LADAR detection statistics in the presence of pointing errors
[AD-A285865] p 1309 N95-22134

OPTICAL REFLECTION

The optical properties of particles deposited on a surface
[AD-A286258] p 1546 N95-22002

Defect geometries and laser-induced damage in multilayer coatings
[DE94-017695] p 1377 N95-22343

OPTICAL RESONATORS

Technique for intracavity sum frequency generation
[AD-D016478] p 1546 N95-21898

OPTICAL SCANNERS

Effect of heat treatment temperature on creep-rupture properties of Fe3Al-based alloys
[DE94-017904] p 1253 N95-20375

OPTICAL SWITCHING

International Conference on Optical Computing: Technical digest
[AD-A284293] p 1541 N95-20249

Methods and components for optical contention resolution in high speed networks
[AD-A280016] p 1543 N95-20598

Optical processing and control
[AD-A279157] p 1546 N95-21975

Polycrystalline PLZT/ITO ceramic electro-optic phase gratings: Electro-optically reconfigurable difffractive devices for free-space and in-wafer interconnects
[AD-A285861] p 1547 N95-22076

Novel materials and devices from self-assembled periodic structures
[AD-A286499] p 1232 N95-22211

Fabrication of PLZT/ITO grating for optical switching and reconfigurable optical interconnect applications
[AD-A286389] p 1548 N95-22248

OPTICAL TRACKING

Passive range measurement system
[AD-D016222] p 1544 N95-21100

Thousand golden ten orbits
[PB95-135109] p 1592 N95-22334

OPTICAL WAVEGUIDES

Modelocking and waveguide amplifiers using Cr:Forsterite and Cr:YAG
[AD-A285857] p 1369 N95-20378

Resonant tunneling quantum well integrated optical waveguide modulator/switch
[AD-A285142] p 1542 N95-20501

Methods and components for optical contention resolution in high speed networks
[AD-A280016] p 1543 N95-20598

Analog processing of optical wavefront using integrated guided-wave optics
[AD-A279596] p 1543 N95-20601

Method for characterization of optical waveguide devices using partial coherence interferometry
[AD-D016525] p 1544 N95-21466

Electromagnetic radiation detector utilizing an electromagnetic radiation absorbing element in a mach-zehnder interferometer arrangement
[AD-D016507] p 1306 N95-21835

OPTICS

The 12-GeV/c beam transfer and absorber lines for the Superconducting Super Collider
[DE95-002100] p 1538 N95-21733

OPTIMAL CONTROL

Application of Markov decision processes to search problems
[PB95-110813] p 1497 N95-19914

Finite dimensional approximation of a class of constrained nonlinear optimal control problems
[NASA-CR-194891] p 1479 N95-20010

Optimal distributed control system for a linear distributed parameter system
[AD-D016583] p 1480 N95-20202

International Conference on Control and Estimation of Distributed Parameter Systems: Nonlinear Phenomena
[AD-A286449] p 1493 N95-21582

Inverse and control problems in electromagnetics
[AD-A286438] p 1310 N95-22250

Learning maneuvers using neural network models
[AD-A286470] p 1486 N95-22267

Quadratic optimal control of a delay equation II: The unstable case
[PB95-127064] p 1486 N95-22366

Quadratic optimal control of a delay equation I: The stable case
[PB95-127072] p 1486 N95-22367

Drag reduction strategies p 1361 N95-22453

Optimal active control for Burgers equations
p 1361 N95-22454

OPTIMIZATION

Finite dimensional approximation of a class of constrained nonlinear optimal control problems
[NASA-CR-194891] p 1479 N95-20010

Abstract reduction and topology
[PB95-110615] p 1488 N95-20054

An object-oriented optimization systems
[DE94-016190] p 1459 N95-20165

Using local optimality criteria for efficient information retrieval with redundant information filters
[AD-A279603] p 1587 N95-20302

Parallel calculation of sensitivity derivatives for aircraft design using automatic differentiation
[NASA-TM-110103] p 1206 N95-20370

On commonalities in signal design for non-Gaussian channels
[AD-A285385] p 1498 N95-20608

NASA's attack on costs p 1585 N95-20755

Systems Analysis Laboratory. Ten years of progress 1984-1994
[PB95-104451] p 1464 N95-20982

Modeling open boundary conditions by using the optimization approach
[AD-A285548] p 1433 N95-21158

SEEK: A FORTRAN optimization program using a feasible directions gradient search
[NASA-CR-4641] p 1380 N95-21359

Report of the Numerical Analysis Group
[PB95-108163] p 1494 N95-21648

Note on the characterizations of the compromise value
[PB95-135117] p 1499 N95-21709

SCOPE 1.5: A Source-Code Optimization PackagEfor REDUCE 3.5: User's manual
[PB95-107579] p 1472 N95-22159

Robust fixed-structure control
[AD-A286515] p 1485 N95-22216

Iterated-subspace minimization methods for nonlinear optimization
[PB95-108171] p 1495 N95-22317

Quadratic optimal control of a delay equation II: The unstable case
[PB95-127064] p 1486 N95-22366

OPTOELECTRONIC DEVICES

GaAs optical circuits
[AD-A285859] p 1369 N95-20389

High performance backplane components for modular avionics p 1212 N95-20653

The ROC optical connector p 1212 N95-20654

High contrast organic crystal optical modulator for phased array antenna and optical signal processing
[AD-A286557] p 1544 N95-20844

Optical, electronic and optoelectronic material and device research
[AD-A280111] p 1374 N95-21630

OPTOGALVANIC SPECTROSCOPY

Application of diode lasers to the isotopically selective determination of uranium in oxides by optogalvanic spectroscopy
[DE94-018045] p 1370 N95-20698

ORBIT CALCULATION

A comparative survey of current and proposed tropospheric refraction-delay models for DSN radio metric data calibration
[NASA-CR-197338] p 1412 N95-20002

Orbit determination of highly elliptical Earth orbiters using improved Doppler data-processing modes
p 1218 N95-21533

ORBIT PERTURBATION

NEO-LISP: Deflecting near-Earth objects using high average power, repetitively pulsed lasers
[DE95-000863] p 1599 N95-21367

ORDER-DISORDER TRANSFORMATIONS

First principles simulation of materials properties
[DE94-016781] p 1566 N95-20405

Metastable bcc phase formation in the Nb-Cr-Ti system
[DE94-016212] p 1255 N95-21137

Critical dynamics and plastic flow in disordered Josephson junction arrays
[DE94-629074] p 1576 N95-21995

Order and turbulence in RF-driven Josephson junction series arrays
[DE94-629076] p 1576 N95-21997

Localization phenomenon in some random classical systems
[AD-A286514] p 1309 N95-22215

ORGANIC CHEMISTRY

Biomolecular Materials by Design, volume 330
[AD-A285369] p 1269 N95-20551

The organic chemistry of conducting polymers
[DE94-018216] p 1270 N95-20680

ORGANIC COMPOUNDS

Resonance Raman spectroscopy of volatile organics: Carbon tetrachloride
[DE95-000627] p 1233 N95-19980

Experimental investigation of PIC formation during the incineration of recovered CFC-11
[PB94-214772] p 1401 N95-20192

Performance specifications for technology development: Application for characterization of volatile organic compounds in the environment
[DE94-016627] p 1401 N95-20234

Monitoring bioremediation of Volatile Organic Compounds (VOCs) using Fourier Transform Infrared (FT-IR) spectrometry
[AD-A279631] p 1403 N95-20456

Thermodynamic and NMR studies of solvent effect on enantiomeric recognition for a chiral organiz ammonium cation by chiral diketopyridino-18-Crown-6 type ligands at 25.0 C
[AD-A279893] p 1223 N95-20592

Non-local density functional calculations of gas phase heats of formation
[AD-A286213] p 1246 N95-22000

Derivation of preliminary maximum permissible concentrations of volatile compounds in air
[PB95-107447] p 1410 N95-22125

Derivation of maximum permissible concentrations for several volatile compounds for water and soil
[PB95-107454] p 1411 N95-22381

ORGANIC MATERIALS

Inorganic-organic polymers and their role in materials science
[AD-A279715] p 1270 N95-20671

Protective organic coatings on steel: Accelerated corrosion test method for paint/coatings exposed to water with low conductivity. Nordtest project no. 1010-92. Degradation of organic coatings in fresh water
[PB95-134185] p 1277 N95-21873

ORGANIC SUPERCONDUCTORS

Positron annihilation studies of organic superconductivity
[DE94-018371] p 1564 N95-20017

New ET-based organic superconductors with the organometallic anion Cu(CF3)4(-)
[DE94-016904] p 1567 N95-20479

Studies of the microwave resistivity of kappa-(BEDT-TTF)2Cu(N(CN)2)Cl
[DE95-002980] p 1262 N95-22291

ORGANIZATIONS

Downsizing information systems: Framing the issues for the Office of Naval Intelligence (ONI)
[AD-A279888] p 1588 N95-20589

Summaries of BFRL fire research in-house projects and grants, 1994
[PB95-130845] p 1286 N95-21130

ORGANOMETALLIC COMPOUNDS

Synthesis and studies of organometallic precursors for CVD of thin film electronic materials
[AD-A285834] p 1223 N95-20033

New ET-based organic superconductors with the organometallic anion Cu(CF3)4(-)
[DE94-016904] p 1567 N95-20479

Electrospray ionization Fourier transform ion cyclotron resonance mass spectrometric study of singly and doubly charged organometallic complexes
[AD-A279899] p 1238 N95-20563
Inorganic-organic polymers and their role in materials science
[AD-A279715] p 1270 N95-20671
Photochemistry of intermolecular C-H bond activation reactions
[DE94-018417] p 1239 N95-20682
Dynamic NMR studies of restricted arene rotation in the chromiu tricarbonyl thiophene and selenophene complexes
[DE95-001656] p 1257 N95-21399
Application of IRIS to semiconductor plasma processing
[DE95-003591] p 1562 N95-22225
Synthesis and structure of a novel bis-stibole
[AD-A286345] p 1224 N95-22252
Studies of the microwave resistivity of kappa-(BEDT-TTF)2Cu(N(CN)2)Cl
[DE95-002980] p 1262 N95-22291

ORGANS
Thorium-232 in human tissues: Metabolic parameters and radiation doses
[DE94-019275] p 1441 N95-20074

ORIFICES
Flow coefficient behavior for boundary layer bleed holes and slots
[NASA-TM-106846] p 1338 N95-19953
Cascade orificial resistive device
[AD-D016529] p 1504 N95-20724

ORTHOGONALITY
Orthogonal representations over finite fields and the chromatic number of graphs
[PB95-110953] p 1487 N95-19937

OSCILLATIONS
Six-dimensional modeling of coherent bunch instabilities and related feedback systems in storage rings with power-series maps for the lattice
[DE94-017965] p 1532 N95-20494
Direct simulation of tridimensional wake of NACA 0012 profile p 1350 N95-21086
Quasi-linear equation for magnetoplasma oscillations in the weakly relativistic approximation
[DE94-628932] p 1560 N95-21593
Robust fixed-structure control
[AD-A286515] p 1485 N95-22216

OSCILLATORS
Fiber laser amplifiers and oscillators
[AD-A285835] p 1368 N95-20035
Semiquantum chaos and the large N expansion
[DE94-016196] p 1488 N95-20169
Pasotron(TM) technology
[AD-A279994] p 1314 N95-20311
Competition between electromagnetic modes in a free-electron maser
[AD-A279546] p 1374 N95-21694
Sub-millimeterwave semiconductor signal sources
[AD-A279375] p 1335 N95-22144
Radiation tests on service electronics for future multi TeV detectors
[DE94-632822] p 1335 N95-22184

OUTLET FLOW
Mixing and dynamics of the Mediterranean outflow
[AD-A279803] p 1434 N95-21306

OVER-THE-HORIZON RADAR
The effects of multihop HF propagation on the performance of OTH backscatter radars
p 1298 N95-20953
The applicability of neural networks to ionospheric modeling in support of relocatable Over-the-Horizon radar
[AD-A286114] p 1309 N95-22230

OXAZOLE
An initial assessment of the properties of 2,5-dipicryl-1,3,4-oxadiazole: A secondary explosive with high thermal stability
[MRL-TR-93-16] p 1284 N95-21624

OXIDASE
Mechanism of the amperometric response of a proposed glucose sensor based on a polypyrrole-tubule-impregnated membrane
[AD-A279836] p 1365 N95-20431

OXIDATION
Selective methane oxidation over promoted oxide catalysts
[DE94-012270] p 1235 N95-20188
Oxide formation on NbAl3 and TiAl due to ion implantation of O-18
[DE94-017874] p 1252 N95-20365
Characteristics of oxynitrides grown in N2O
[DE94-015798] p 1566 N95-20400
Influence of oxidation on radiation hardness of silicon detectors
[DE95-002466] p 1272 N95-20894
Aromatics oxidation and soot formation in flames
[DE95-001803] p 1241 N95-21280
Cluster reactions: An approach to understanding the fundamentals of heterogeneous catalysis
[DE95-002947] p 1243 N95-21447
Water abundance and accretion history of terrestrial planets p 1424 N95-21820
Oxidation behavior of aluminum nanopowders
[DE95-002721] p 1260 N95-21926
Spectroscopic assessment of the reliability of metal/metal oxide interfaces
[AD-A286131] p 1261 N95-22035
Acid-site characterization of water-oxidized alumina films by near-edge x-ray absorption and soft x-ray photoemission
[DE95-003355] p 1247 N95-22234
The interaction of localized solutions in a surface reaction
[DE95-002736] p 1248 N95-22433

OXIDATION RESISTANCE
Toughened Silcomp composites for gas turbine engine applications
[DE95-002851] p 1214 N95-21243
Lubricant evaluation and performance, 2
[AD-A279144] p 1278 N95-21969

OXIDATION-REDUCTION REACTIONS
The primary carbon and the formation of carbon species in terrestrial magmas p 1420 N95-21797
Solubilities of nitrogen and noble gases in basalt melt
p 1422 N95-21807

OXIDE FILMS
Generation of micro-domains in AT-cut quartz by thermal processing and the effect on resonator modes
[DE94-017344] p 1564 N95-20087
Oxide formation on NbAl3 and TiAl due to ion implantation of O-18
[DE94-017874] p 1252 N95-20365
Ferroic materials: Design, preparation and characteristics. Ceramic transactions, volume 43
[AD-A285937] p 1270 N95-20664
Methods of measuring adhesion for thermally grown oxide scales
[DE94-018177] p 1256 N95-21260
Characterization and performance of DLC films synthesized by plasma and ion beam techniques
[DE94-018287] p 1281 N95-22428

OXIDES
Reactions and microstructure at ceramic/metal interfaces
[DE94-014287] p 1265 N95-20138
Rate controlled synthesis of composition modulated, metal-oxide thin films
[DE94-016596] p 1267 N95-20317
Oxide formation on NbAl3 and TiAl due to ion implantation of O-18
[DE94-017874] p 1252 N95-20365
The effect of oxide inclusions on the kinetics of the austenite to ferrite transformation in low alloy steel weld metal
[DE94-018131] p 1253 N95-20676
Reactive nanophase oxide additions to melt-processed high-T(sub c) superconductors
[DE95-001470] p 1570 N95-20841
Atmosphere influence on in situ ion beam analysis of thin film growth
[DE95-001507] p 1570 N95-20881
Performance and cost analysis of monolithic solid oxide fuel cells
[DE95-002511] p 1394 N95-20896
Methods of measuring adhesion for thermally grown oxide scales
[DE94-018177] p 1256 N95-21260
Solid oxide fuel cells in the United States
[DE95-002405] p 1395 N95-21361
Gate oxide shorts in nMOS transistors: Electrical properties and lifetime prediction method
[DE94-018904] p 1330 N95-21545
Tailoring suspension flow for the gelcasting of oxide and nonoxide ceramics
[DE95-001351] p 1277 N95-21861

OXIDIZERS
Launch safety, toxicity, and environmental effects of the high performance oxidizer ClF(5)
[AD-A286095] p 1284 N95-22227

OXYFLUORIDES
Production of S2F10, S2OF10 and S2O2F10 by spark discharges in SF6*
[DE95-001421] p 1243 N95-21500
Novel fluorine oxidizers
[AD-A279480] p 1284 N95-21678

OXYGEN
Ferrocyanide safety project Dynamic X-Ray Diffraction studies of sodium nickel ferrocyanide reactions with equimolar nitrate/nitrite salts
[DE94-017396] p 1236 N95-20268
Spectroscopic studies of glass structure
[DE94-016551] p 1268 N95-20468
High performance YBCO films
[AD-A286567] p 1326 N95-20824
Inert gas purification and measuring oxygen partial pressure in gas mixtures with EMF method based on solid electrolyte cell
[PB95-127767] p 1240 N95-21110
Calculated heats of formation of some predicted stable C, N, O, F molecules
[AD-A285957] p 1517 N95-21127
Tribology and surface mechanical properties of excimer laser nitrided titanium
[DE95-002751] p 1255 N95-21238
Ignition of submarine materials at various oxygen concentrations
[PB95-131371] p 1243 N95-21428
Loss of solar He and Ne from IDPS in subducting sediment: Diffusion and the effect of phase changes
p 1419 N95-21792
Water abundance and accretion history of terrestrial planets p 1424 N95-21820
High temperature corrosion and crack growth of SiC/SiC at variable oxygen partial pressures
[DE94-018715] p 1232 N95-22115
Hydrothermal conversion of carbohydrates and related compounds
[PB95-134011] p 1396 N95-22175

OXYGEN ATOMS
An overview of the Evaluation of Oxygen Interactions with Materials 3 Experiment: Space Shuttle Mission 46; July-August, 1992
[NASA-TM-110129] p 1412 N95-20278
Combustion-related studies using weakly bonded complexes
[DE95-002801] p 1238 N95-20576

OXYGEN COMPOUNDS
Computational evaluation of the feasibility of nitrating precursors to C12N12O12
[AD-A285976] p 1239 N95-20668

OXYGEN CONSUMPTION
Intramyocardial blood volume and oxygen exchange
[PB95-108015] p 1445 N95-21580

OXYGEN ISOTOPES
Ignition of submarine materials at various oxygen concentrations
[PB95-131371] p 1243 N95-21428

OXYGEN 18
Oxide formation on NbAl3 and TiAl due to ion implantation of O-18
[DE94-017874] p 1252 N95-20365

OXYNITRIDES
Characteristics of oxynitrides grown in N2O
[DE94-015798] p 1566 N95-20400

OZONE
Indirect global warming effects of ozone and stratospheric water vapor induced by surface methane emission
[DE94-019016] p 1402 N95-20353
Radiative forcing for changes in tropospheric O3
[DE94-019017] p 1413 N95-20354
Compatibility testing of explosives and paints by chemiluminescence techniques
[PB95-133609] p 1275 N95-21275
Evaluation of the technical performance of the Duttch National Air Quality Monitoring Network in 1992
[PB95-131892] p 1405 N95-21327
Ozone quality control measurements in the Dutch National Air Quality Monitoring Network
[PB95-131900] p 1405 N95-21329
Monitoring activities in the framework of the Dutch National Air Quality Monitoring Network in 1994
[PB95-131884] p 1406 N95-21351
Transport, radiative, and dynamical effects of the Antarctic ozone hole: A GFDL SKYHI model experiment
[PB94-192754] p 1409 N95-22101
Confirmatory analysis of SAGE-1, and -2 data
[DE95-003623] p 1427 N95-22240

OZONE DEPLETION
Computer model predictions of the local effects of large, solid-fuel rocket motors on stratospheric ozone
[AD-A285632] p 1404 N95-21150
Definition report on environmental indices in future environmental assessments environmental balance/environmental outlook
[PB95-131876] p 1405 N95-21350
Comparison of HFC-134a and the ternary blend, Suva MP39, as replacements for the refrigerant, CGC-12
[MRL-GD-0051] p 1287 N95-21625
Ozone-depleting-substance control and phase-out plan
[DE95-001647] p 1409 N95-21722
Transport, radiative, and dynamical effects of the Antarctic ozone hole: A GFDL SKYHI model experiment
[PB94-192754] p 1409 N95-22101

Assessment of the atmospheric hazards and risks of new chemicals: Procedures to estimate hazard potentials
[PB95-107488] p 1410 N95-22186

OZONOSPHERE

The development and evaluation of water-mist fire extinguishing systems
[DE94-019019] p 1286 N95-20356

Effects of increased UV-B radiation on phytoplankton: A preliminary study and research programme
[PB95-133732] p 1439 N95-21884

P

P WAVES

Velocity analysis for transversely isotropic media
[DE95-000643] p 1411 N95-19981

P-wave signatures and parameterization of transversely isotropic media: An overview
[DE95-000644] p 1411 N95-19982

Seismic evidence for volatiles at large depth in the Earth p 1422 N95-21808

Parity violation in the compound nucleus
[DE95-002742] p 1530 N95-22435

P-I-N JUNCTIONS

Heterostructure quantum confined Stark effect electrooptic modulators operating at 938 nm
[AD-A279342] p 1581 N95-21928

Photoreflectance and x ray diffraction study of semiconductor heterostructures and quantum wells
[PB95-127049] p 1582 N95-22432

P-N JUNCTIONS

Radiation effects on p+n InP junctions grown by MOCVD p 1319 N95-20520

Annealing of irradiated n+p InP buried homojunctions
p 1320 N95-20524

P/N In(Al) GaAs multijunction laser power converters
p 1323 N95-20539

P-TYPE SEMICONDUCTORS

Visible light emitting materials and injection devices
[AD-A284796] p 1541 N95-20066

Semiconductor cold electron emission device
[AD-D016577] p 1314 N95-20298

Complementary GaAs junction-gated heterostructure field effect transistor technology
[DE94-018901] p 1329 N95-21390

InTISb for long-wavelength infrared photodetectors and arrays
[AD-A280108] p 1332 N95-21774

PACIFIC OCEAN

Hydrographic data from equatorial Pacific waters near the Galapagos
[AD-A283741] p 1431 N95-19918

Loss of solar He and Ne from IDPS in subducting sediment: Diffusion and the effect of phase changes
p 1419 N95-21792

Acoustic Thermometry of Ocean Climate (ATOC): Selection of California source site
[AD-A279295] p 1436 N95-21987

Exchanges between hemispheres and gyres: A direct approach to the mean circulation of the equatorial Pacific
[NASA-CR-196311] p 1436 N95-22072

PACKAGING

Advanced Packaging Concepts for Digital Avionics
[AGARD-CP-562] p 1208 N95-20631

The impact of advanced packaging technology on modular avionics architectures p 1208 N95-20632

Standard Hardware Acquisition and Reliability Program (SHARP) advanced SEM-E packaging
p 1208 N95-20633

FASTPACK: Optimized solutions for modular avionics derived from a parametric study. Part 2: Avionics
p 1209 N95-20635

Ultra-Reliable Digital Avionics (URDA) processor
p 1209 N95-20638

Packaging the MAMA module p 1209 N95-20639

PACKET SWITCHING

High-performance packet switching architecture for ATM: Conventional solution and neural network solution
[PB95-110920] p 1312 N95-19935

A group communication approach for mobile computing mobile channel: An ISIS tool for mobile services
[AD-A279785] p 1290 N95-20306

Cell loss analysis of two-class priority generalized knockout switch
[PB95-127742] p 1301 N95-21109

PACKET TRANSMISSION

Routing of unidirectional packet radio for wide-area paging network control and maintenance
[PB95-104428] p 1300 N95-20980

Modelling the reassembly buffer in a connectionless server
[PB95-132908] p 1308 N95-22087

PACKETS (COMMUNICATION)

Routing of unidirectional packet radio for wide-area paging network control and maintenance
[PB95-104428] p 1300 N95-20980

An object-oriented implementation of the Xpress transfor protocol
[DE95-001506] p 1301 N95-21277

Verification of a timestamp-based sliding-window protocol
[PB95-132759] p 1455 N95-22082

Modelling the reassembly buffer in a connectionless server
[PB95-132908] p 1308 N95-22087

Method of sensing target status in a local area network
[AD-D016248] p 1478 N95-22090

PAINTS

Application of pressure sensitive paint in hypersonic flows
[NASA-TM-106824] p 1201 N95-20794

Compatibility testing of explosives and paints by chemiluminescence techniques
[PB95-133609] p 1275 N95-21275

Robotic paint stripping cell
[AD-A279158] p 1279 N95-21976

PAIR PRODUCTION

Electron-positron pair production in ultrarelativistic atomic collisions: 6.4 TeV S(sup 16+) with Au, Pd and Al
[DE95-000690] p 1508 N95-20133

Search for W pair production with dilepton decay modes at D0
[DE95-000724] p 1508 N95-20134

Signals for top quark anomalous chromomagnetic moments at colliders
[DE95-002896] p 1535 N95-21254

Pair production as a probe of colliding beam size
[DE95-002893] p 1536 N95-21337

Electroweak boson pair production in p(-p) collisions at the square root of s = 1.8 TeV
[DE95-000725] p 1527 N95-22194

Search for top with DO detector in dilepton channel
[DE95-000731] p 1529 N95-22314

PALEOCLIMATOLOGY

Sensitivity of climate models: Comparison of simulated and observed patterns for past climates
[DE95-002257] p 1406 N95-21379

PALLADIUM

Properties of aged metal tritides
[DE95-001787] p 1243 N95-21440

PALLADIUM ALLOYS

Thermodynamic characterization of new palladium alloy tritides
[DE94-018430] p 1579 N95-20028

Natural gas converter performance and durability
[PB95-135554] p 1284 N95-21966

PALLADIUM COMPOUNDS

Evaluation of Pd-Cr wires for strain gage application
[NASA-TM-106857] p 1366 N95-21259

Spectroscopic, morphological, and electrical characterization of PdGe ohmic contacts to n-GaAs
[DE95-000738] p 1329 N95-21394

PANEL METHOD (FLUID DYNAMICS)

Open Skies project computational fluid dynamic analysis
[AD-A285928] p 1200 N95-19991

PARABOLIC BODIES

Experimental study of the helicopter-mobile radioelectrical channel and possible extension to the satellite-mobile channel p 1296 N95-20945

PARABOLIC DIFFERENTIAL EQUATIONS

On the sputtering of metals and insulators: A nonlinear evolution problem with nonlinear boundary condition
[DE95-001456] p 1254 N95-20792

PARABOLIC REFLECTORS

Testing of the SAIC facets on the stretched-membrane dish
[DE95-001831] p 1393 N95-20864

Propagation measurements on a troposcatter link in the Canadian High Arctic p 1295 N95-20940

D/H ratios and H2O contents of mantle-derived amphibole megacrysts from Dish Hill, California
p 1416 N95-21781

PARALLEL COMPUTERS

Performance issues for engineering analysis on MIMD parallel computers
[DE94-015769] p 1474 N95-20150

Parallel solid mechanics codes at Sandia National Laboratories
[DE94-015770] p 1474 N95-20152

A scalable video rate camera interface
[AD-A286144] p 1474 N95-20325

Task parallel programming in Fx
[AD-A285136] p 1475 N95-20500

PVM a platform for portable distributed computing
[DE94-019156] p 1455 N95-21607

Scalable programming environment
[AD-A286390] p 1472 N95-22201

Fast parallel tree codes for gravitational and fluid dynamical N-body problems
[AD-A286480] p 1358 N95-22290

PARALLEL PROCESSING (COMPUTERS)

O(log2 n) time efficient parallel factorization of dense, sparse separable, and banded matrices
[NASA-CR-197356] p 1473 N95-19885

Design considerations for parallel graphics libraries
[NASA-CR-194935] p 1473 N95-20013

ILIAS: A sequential language for parallel matrix computations
[PB95-110631] p 1473 N95-20056

Split-C and active messages under SUNMOS on the Intel Paragon
[DE94-011418] p 1474 N95-20123

Performance issues for engineering analysis on MIMD parallel computers
[DE94-015769] p 1474 N95-20150

A practical guide to using MCNP with PVM
[DE94-016162] p 1474 N95-20158

System level fault tolerance in parallel and distributed computing systems
[AD-A279664] p 1474 N95-20305

Explicit parallel two-step Runge-Kutta-Nystroem methods
[PB95-135752] p 1489 N95-20423

Parallelism across the steps in iterated Runge-Kutta methods for stiff initial value problems
[PB95-135760] p 1490 N95-20424

RALPAR-RAL mesh partitioning program version 1.1
[PB95-129847] p 1475 N95-20435

A theoretical study on the performance of the FDTD code on a massively parallel computer
[AD-A285346] p 1475 N95-20499

Stochastic network processes
[AD-A279905] p 1475 N95-20566

ECSU-AASERT summer research project in parallel processing and computer visualization
[AD-A285983] p 1475 N95-20618

Computing methods for the approximate solution of time dependent problems
[AD-A286007] p 1491 N95-20719

Functional and para-functional parallel processing
[DE95-002805] p 1475 N95-20888

Polymer based all-optic reconfigurable interconnects
[AD-A279976] p 1272 N95-20962

Direct simulation and graphics post-processing of three-dimensional turbulent flows p 1352 N95-21098

New methods for large scale local and global optimization
[AD-A285635] p 1517 N95-21126

A divide-and-conquer method for tridiagonalizing symmetric matrices with repeated eigenvalues
[DE95-002918] p 1476 N95-21257

A framework for symmetric band reduction and tridiagonalization
[DE95-002919] p 1476 N95-21341

Parallel predictor-corrector methods
[PB95-135711] p 1493 N95-21434

GRONICs-1994. Proceedings of the 1994 Groningen Student Conference on Computer Science
[PB95-135620] p 1468 N95-21455

CDMA with interference cancellation for multiprobe missions p 1304 N95-21536

PVM 3 beyond network computing
[DE94-019115] p 1477 N95-21556

DONIO: Distributed object network I/O library
[DE94-019163] p 1477 N95-21602

PVM a platform for portable distributed computing
[DE94-019156] p 1455 N95-21607

The message passing version of the parallel Community Climate Model
[DE94-019158] p 1407 N95-21608

A massively parallel algorithm for grand canonical Monte Carlo computer simulation with the short-ranged Lennard-Jones potential
[DE94-010396] p 1477 N95-21843

Status of CFDLIB performance tests on the T3D
[DE95-002708] p 1478 N95-21925

Massively-parallel computational fluid dynamics
[AD-A279389] p 1355 N95-21942

Activities of the Research Institute for Advanced Computer Science
[NASA-CR-197291] p 1478 N95-22108

High performance computing for beam physics applications
[DE94-018312] p 1539 N95-22243

Recent results in analysis and simulation of beam halo
[DE94-018313] p 1539 N95-22298

A new parallel method for molecular dynamics simulation of macromolecular systems
[DE94-018621] p 1529 N95-22315

Formal specification and compositional verification of an atomic broadcast protocol
[PB95-110508] p 1472 N95-22351
Design of a massively parallel computer using bit serial processing elements
[NASA-CR-197365] p 1479 N95-22406

PARALLEL PROGRAMMING
Design of a parallel object oriented programming language
[AD-A284924] p 1457 N95-20000
Task parallel programming in Fx
[AD-A285136] p 1475 N95-20500

PARALLELOGRAMS
A convergence analysis of an h-version finite element method with high order elements for two dimensional elasto-plasticity problems
[AD-A279975] p 1491 N95-20920

PARAMAGNETISM
Magnetic flocculation of paramagnetic particles
[DE94-018144] p 1501 N95-20725

PARAMETER IDENTIFICATION
Mathematical theory of neural networks
[AD-A286508] p 1485 N95-22213
Biaxiality of chiral liquid crystals
[DE94-629032] p 1578 N95-22277

PARAMETERIZATION
P-wave signatures and parameterization of transversely isotropic media: An overview
[DE95-000644] p 1411 N95-19982
Universal parametrization for quark and lepton substructure
[DE94-770604] p 1514 N95-20738
EPSCoR supplemental grant for an application of neural networks to seismic signal discrimination
[AD-A285846] p 1414 N95-20878
Minimal square spectral factors
[PB95-132726] p 1495 N95-22032

PARAMETRIC AMPLIFIERS
Solid state frequency conversion technology for remote sensing
[DE94-019102] p 1389 N95-21433

PARITY
Parity nonconservation in radioactive atoms: An experimental perspective
[DE95-002737] p 1518 N95-21235
A neutron beam polarizer for study of parity violation in neutron-nucleus interactions
[DE95-002743] p 1519 N95-21237
Parity violation in the compound nucleus
[DE95-002742] p 1530 N95-22435

PARSING ALGORITHMS
Initial experience with noncorrecting syntax error handling
[PB95-132700] p 1471 N95-22029
Top-down non-correcting error recovery in LLgen
[PB95-132718] p 1471 N95-22031

PARTIAL DIFFERENTIAL EQUATIONS
Solutions of D(sup n)D(sup m)f=0
[PB95-110839] p 1487 N95-19916
Squeezing and flow of energy for non linear wave equations
[PB95-111100] p 1489 N95-20172
Stabilization and control problems in structural dynamics
[AD-A279996] p 1340 N95-20312
Fitting stochastic partial differential equations to spatial data
[AD-A279870] p 1490 N95-20432
VLUGr3: A vectorizable adaptive grid solver for PDEs in 3D. 2: Code description
[PB95-135737] p 1465 N95-21033
VLUGR3: A vectorizable adaptive grid solver for PDEs in 3D. 1: Algorithmic aspects and applications
[PB95-135729] p 1467 N95-21435
DIFFPACK: Software for partial differential equations
[PB95-110268] p 1468 N95-21654
Object-oriented design of preconditioned iterative methods
[PB95-110276] p 1469 N95-21655
Locking of the finite element method in thermoelasticity
[PB95-127098] p 1496 N95-22370

PARTIAL PRESSURE
Inert gas purification and measuring oxygen partial pressure in gas mixtures with EMF method based on solid electrolyte cell
[PB95-127767] p 1240 N95-21110
High performance YBCO films
[AD-A279560] p 1276 N95-21695

PARTICLE ACCELERATION
Charged particle dynamics in the acceleration gap of the PBFA 2 ion diode
[DE94-017347] p 1506 N95-20026
Approach to compact terawatt CO2 laser system for particle acceleration
[DE95-002170] p 1371 N95-20866
Confinement and stability of crystalline beams in storage rings
[DE95-002515] p 1533 N95-20886
Theory of the excitonic lineshape in low-dimensional structures with rough interfaces
[DE95-003434] p 1582 N95-22237

PARTICLE ACCELERATOR TARGETS
Accelerators for energy production
[DE94-770764] p 1392 N95-20685
Induction linacs for heavy ion fusion
[DE95-002357] p 1534 N95-20891
Use of the National Ignition Facility for the development of inertial fusion energy
[DE94-016696] p 1557 N95-21206

PARTICLE ACCELERATORS
Relational databases for RHIC design and control
[DE94-016785] p 1532 N95-20336
Optimizing the length of the stores and related effects
[DE95-002531] p 1533 N95-20885
Xwake 1.0 user's manual
[DE95-002528] p 1463 N95-20901
Moment approach to high-order accelerator beam optics
[DE95-001018] p 1536 N95-21331
Normal form analysis of the Tevatron
[DE94-017172] p 1539 N95-22192

PARTICLE BEAMS
Crystalline beam in a storage ring: How long can it last?
[DE94-017303] p 1563 N95-20014
Particle beam fusion
[DE95-000711] p 1549 N95-20075
Crystalline beams: The horizontal zigzag
[DE95-002227] p 1533 N95-20766
Crystalline beams
[DE95-002656] p 1569 N95-20793
Confinement and stability of crystalline beams in storage rings
[DE95-002515] p 1533 N95-20886
Xwake 1.0 user's manual
[DE95-002528] p 1463 N95-20901
Moment approach to high-order accelerator beam optics
[DE95-001018] p 1536 N95-21331
High performance computing for beam physics applications
[DE94-018312] p 1539 N95-22243
Bunched beam instability with frequency spread
[DE94-018632] p 1539 N95-22357
The Double Eagle Space Experiment (DESE) beamline design
[DE94-018319] p 1601 N95-22419

PARTICLE COLLISIONS
J/psi,psi(prime) yields mu(+)mu(-) and B yields J/psi,psi(prime) cross sections
[DE94-017184] p 1507 N95-20108
D0 quantum chromodynamics: A compilation of results presented at DPF 1994
[DE95-000838] p 1510 N95-20344
High energy photon-photon collisions
[DE94-017494] p 1532 N95-20388
Mass and lifetime measurements with exclusive B reconstruction at CDF
[DE94-015849] p 1511 N95-20401
Measurements of the mass and width of the W boson from CDF
[DE94-015380] p 1511 N95-20415
State-to-state collisional dynamics of atmospheric species
[AD-A285053] p 1370 N95-20484
Evidence for t(bar t) production at the Tevatron: Statistical significance and cross section
[DE95-002524] p 1515 N95-20897
Charmonium production, b quark and B meson production and b(bar b) correlations at CDF
[DE95-002525] p 1515 N95-20898
Emittance growth due to negative-mass instability above transition
[DE95-002527] p 1534 N95-20900
Heavy ion track-structure calculations for radial dose in arbitrary materials
[NASA-TP-3497] p 1517 N95-21191
Multiple hard interactions in HERWIG
[PB95-130548] p 1518 N95-21233
Experiments at high energy hadron colliders and underground water Cerenkov detector experiment
[DE95-001804] p 1535 N95-21281
Measurement of the polarization in the decay B(sup 0) (yields) J/(psi)K*(sup 0) in (bar p)p collisions at (radical)s = 1.8 TeV
[DE95-002521] p 1520 N95-21313
1994 Nonneutral Plasma Workshop
[AD-A285656] p 1559 N95-21404
The diphoton production rate in (bar p)p collisions at the square root of s = 1800 GeV
[DE95-000559] p 1522 N95-21497
Measurement of W and Z production cross-sections in p(bar p) collisions at (radical)s = 1.8 TeV
[DE95-002250] p 1523 N95-21521
Polarization of charmonium in pion-nucleus collisions
[DE95-002783] p 1523 N95-21525
Measurement of the B meson differential cross-sections in p(bar p) collisions at (radical)s = 1.8 TeV using the exclusive decays B(sup (+-)) (yields) J/(psi)K(sup (+-)) and B(sup 0) (yields) J/(psi)K*(sup 0)
[DE94-018993] p 1523 N95-21562
Search for new particles decaying to dijets in p(bar p) collisions at (radical)s = 1.8 TeV
[DE94-018994] p 1523 N95-21563
Status of the DO top search
[DE95-002214] p 1525 N95-21715
Single particle measurements and two particle interferometry results from CERN experiment NA44
[DE95-003041] p 1527 N95-22078
Proton and produced particle distributions from Au+Au collisions at 11.6 A GeV/c
[DE94-018634] p 1530 N95-22392

PARTICLE DECAY
J/psi,psi(prime) yields mu(+)mu(-) and B yields J/psi,psi(prime) cross sections
[DE94-017184] p 1507 N95-20108
B meson lifetimes at CDF
[DE95-000564] p 1507 N95-20110
Search for W pair production with dilepton decay modes at D0
[DE95-000724] p 1508 N95-20134
Search for top in DO using the electron + jets channel with soft muon tagging
[DE95-001284] p 1509 N95-20217
CDF top results in the dilepton channel
[DE95-000837] p 1510 N95-20343
Semi-leptonic form-factors from lattice QCD
[DE95-000871] p 1510 N95-20367
Mass and lifetime measurements with exclusive B reconstruction at CDF
[DE94-015849] p 1511 N95-20401
Higgs decay to bottom quarks at the Tevatron
[DE94-016715] p 1511 N95-20404
GAJET experiment at the LHC: The GAJET collaboration
[PB95-129813] p 1512 N95-20454
Constraints on SUSy-GUT unification from b yields s-gamma decay
[PB95-130373] p 1580 N95-21229
Top ten models constrained by b (yields) s(gamma)
[DE95-002870] p 1519 N95-21250
A measurement of the b(bar b) cross section at CDF
[DE95-000642] p 1519 N95-21273
A high-rate fixed-target charm experiment
[DE95-001767] p 1521 N95-21378
Measurement of the B meson differential cross-sections in p(bar p) collisions at (radical)s = 1.8 TeV using the exclusive decays B(sup (+-)) (yields) J/(psi)K(sup (+-)) and B(sup 0) (yields) J/(psi)K*(sup 0)
[DE94-018993] p 1523 N95-21562
Search for new particles decaying to dijets in p(bar p) collisions at (radical)s = 1.8 TeV
[DE94-018994] p 1523 N95-21563
Measurement of the B cross section at CDF via B semileptonic decays
[DE95-002217] p 1524 N95-21597
Status of the DO top search
[DE95-002214] p 1525 N95-21715
A preliminary, precise measurement of the average B hadron lifetime
[DE95-001848] p 1525 N95-21727
Tests of structure functions using lepton pairs: W-charge asymmetry at CDF
[DE95-000560] p 1527 N95-22122
Measurement of the average lifetime of B hadrons at SLD
[DE95-002121] p 1527 N95-22152
Physics at the Fermilab Collider
[DE95-000726] p 1539 N95-22195
Constraints on the left-right symmetric model from b yields s gamma
[DE95-003469] p 1528 N95-22239
Topics in gauge theories and the unification of elementary particle interactions
[DE94-013485] p 1529 N95-22279
Search for top with DO detector in dilepton channel
[DE95-000731] p 1529 N95-22314

PARTICLE DIFFUSION
Positron implantation profiles in elemental and multilayer systems
[DE94-014876] p 1566 N95-20382

PARTICLE ENERGY
Resonant photon-graviton conversion in EM fields: From earth to heaven
[DE95-002784] p 1301 N95-21241

Search for Centauro events in the DO Detector at Fermilab collider
[DE95-002522] p 1535 N95-21314
Luminosity polarization correlation in the SLC
[DE95-002889] p 1536 N95-21335

PARTICLE IMAGE VELOCIMETRY
Visualizing 3D velocity fields near contour surfaces
[DE95-000841] p 1353 N95-21182

PARTICLE IN CELL TECHNIQUE
PIC simulation of surface waves
[AD-A285358] p 1563 N95-22422

PARTICLE INTERACTIONS
A tau-charm-factory at Argonne
[DE94-016913] p 1510 N95-20360
Neutrino-neutrino scattering and matter-enhanced neutrino flavor transformation in supernovae
[DE94-017577] p 1604 N95-20383
Symmetry, Wigner functions and particle reactions
[DE94-629887] p 1514 N95-20735
Recent results from E665
[DE95-002523] p 1516 N95-20914
Construction of non-critical string field theory by transfer matrix formalism in dynamical triangulation
[DE94-770607] p 1516 N95-20986
Heavy ion track-structure calculations for radial dose in arbitrary materials
[NASA-TP-3497] p 1517 N95-21191
A high-rate fixed-target charm experiment
[DE95-001767] p 1521 N95-21378
Explicit analytical solution of the nonlinear Vlasov Poisson system
[DE94-628931] p 1500 N95-21592
Temperature dependence of a magnetopolaron in a harmonic quantum dot in resonant magnetic fields
[DE94-629036] p 1502 N95-22177
Theses of the Proceedings of the 23d International Meeting on the Physics of Charged Particle Interaction with Crystals
[DE94-631501] p 1529 N95-22281

PARTICLE MASS
Constraints on SUSy-GUT unification from b yields s-gamma decay
[PB95-130373] p 1580 N95-21229

PARTICLE MOTION
Matrix formulation of the particle motion in crystalline beams
[DE94-017301] p 1563 N95-19925
Analysis methods for fast impurity ion dynamics data
[DE95-000589] p 1549 N95-20112
Investigation of spherical tearing mode
[NASA-CR-197284] p 1558 N95-21345

PARTICLE PRODUCTION
Search for top in DO using the electron + jets channel with soft muon tagging
[DE95-001284] p 1509 N95-20217
Strange particle and antiproton production in S + nucleus collisions at 200 GeV/nucleon
[DE95-002348] p 1513 N95-20575
Universality of particle multiplicities
[DE95-000727] p 1515 N95-20879
Evidence for t(bar t) production at the Tevatron: Statistical significance and cross section
[DE95-002524] p 1515 N95-20897
Charmonium production, b quark and B meson production and b(bar b) correlations at CDF
[DE95-002525] p 1515 N95-20898
Recent results from E665
[DE95-002523] p 1516 N95-20914
Theories of the eta-meson-nucleus interaction
[DE94-016055] p 1516 N95-21125
A measurement of the b(bar b) cross section at CDF
[DE95-000642] p 1519 N95-21273
Heavy ion collisions
[DE95-002712] p 1520 N95-21321
Dilepton production from p-p to Ca-Ca at the Bevalac
[DE95-002341] p 1520 N95-21357
Similarities and differences in strangeness production at BNL and CERN
[DE95-002343] p 1521 N95-21380
Search for the top quark using multivariate analysis techniques
[DE95-000561] p 1522 N95-21498
QCD corrections to Higgs boson production: An update
[DE95-000626] p 1522 N95-21506
Measurement of W and Z production cross-sections in p(bar p) collisions at (radical)s = 1.8 TeV
[DE95-002250] p 1523 N95-21521
Investigation of direct photon production in 200 A GeV S + Au reactions
[DE94-018129] p 1525 N95-21704
Status of the DO top search
[DE95-002214] p 1525 N95-21715
Physics at the Fermilab Collider
[DE95-000726] p 1539 N95-22195
Inclusive B production at CDF and D0
[DE95-000728] p 1528 N95-22196
Topics in gauge theories and the unification of elementary particle interactions
[DE94-013485] p 1529 N95-22279
Beam flavor dependence in the hadroproduction of D(+-) and D(sub s)(+-) mesons
[DE94-015541] p 1530 N95-22339

PARTICLE SIZE DISTRIBUTION
Magnetic flocculation of paramagnetic particles
[DE94-018144] p 1501 N95-20725
Diffuse reflectance spectra of energetic material
[DSTO-TR-0065] p 1284 N95-21951
Single particle measurements and two particle interferometry results from CERN experiment NA44
[DE95-003041] p 1527 N95-22078

PARTICLE SPIN
Neutrino magnetic moments and the solar neutrino problem
[DE94-017579] p 1602 N95-20147
Hadron beams and accelerators
[DE95-002932] p 1536 N95-21342
Rigorous spin-spin correlation function of Ising model on a special kind of Sierpinski Carpets
[DE94-628995] p 1575 N95-21854

PARTICLE THEORY
Chiral symmetry and lattice gauge theory
[DE94-018676] p 1564 N95-20130
Using science centers to expose the general public to the microworld
[DE95-000647] p 1508 N95-20132
Research in theoretical elementary particle physics at the University of Florida, task A
[DE94-004373] p 1512 N95-20469
Proceedings of the School for Young High Energy Physicists
[PB95-108114] p 1537 N95-21647

PARTICLE TRAJECTORIES
Thousand golden ten orbits
[PB95-135109] p 1592 N95-22334

PARTICLES
Computer simulation of the diocotron instability
[AD-A285655] p 1559 N95-21403
The optical properties of particles deposited on a surface
[AD-A286258] p 1546 N95-22002

PARTICULATE REINFORCED COMPOSITES
Comparison of the dynamic fatigue behavior of two monolithic SiC and an Al2O3/SiC composite
[DE94-017751] p 1225 N95-20022
Structural performance of cylindrical pressure housings of different ceramic compositions under external pressure loading. Part 4: Silicon carbide particulate reinforced alumina ceramic
[AD-A286299] p 1279 N95-22047

PARTICULATES
Low flow fluid separator
[AD-D016575] p 1339 N95-20297
Approaches to the design of structural ceramics incorporating whiskers and particulate phases
[DE94-018126] p 1271 N95-20704
Role of internal stresses in fracture behavior of engineering composites
[DE95-001106] p 1229 N95-20912
Current concepts on airborne particles and health
[DE95-002260] p 1447 N95-22287

PARTITIONS (MATHEMATICS)
Classification of diagonal coset modular invariants
[PB95-111118] p 1489 N95-20259
The method of evaluating quantum partition function for the Hubbard model
[DE94-628991] p 1581 N95-21639
An exact enumeration of self-avoiding loops on a square lattice
[DE94-628999] p 1578 N95-22276

PARTONS
Antishadowing contribution to the pomeron structure function
[PB95-127478] p 1518 N95-21221
Multiple hard interactions in HERWIG
[PB95-130548] p 1518 N95-21233

PASSAGEWAYS
Elastic micro-fabricated surface layer for reducing turbulence and drag on an object while it moves through a fluid medium
[AD-D016516] p 1356 N95-22060

PASSENGER AIRCRAFT
Commuter/air taxi ditchings and water-related impacts that occurred from 1979 to 1989
[AD-A285691] p 1202 N95-20275

PASSENGERS
Test and evaluation report for the Manual Domestic Passive Profiling System (MDPPS)
[AD-A286312] p 1202 N95-20093

PASSIVITY
Low electron beam energy CIVA analysis of passivated ICs
[DE94-017421] p 1314 N95-20286
Status of diffused junction p+n InP solar cells for space applications p 1317 N95-20509
Effects of plasma hydrogenation on trapping properties of dislocations in heteroepitaxial InP/GaAs
p 1323 N95-20542
VOC compliant wash primer
[AD-A286034] p 1273 N95-21000

PASTES
The permeation of bis(2-fluoro-2,2-dinitroethyl) formal (FEFO), ethyl 4,4-dinitropentanoate (EDNP), ethyl 4-nitropentanoate (ENP), and 1,2,4-trichlorobenzene (TCB) through barrier membranes
[DE95-002492] p 1283 N95-21514

PATENT POLICY
NASA patent abstracts bibliography: A continuing bibliography. Section 2: Indexes (supplement 46)
[NASA-SP-7039(46)-SECT-2] p 1590 N95-21948

PATTERN RECOGNITION
High performance hardware and software for pattern recognition and image processing
[AD-A279776] p 1457 N95-19961
Intermediate levels of visual processing
[AD-A284922] p 1448 N95-19998
Recognition of subsurface defects in machined ceramics by application of neural networks to laser scatter patterns
[DE94-018373] p 1264 N95-20018
View-based models of 3D object recognition and class-specific invariance
[AD-A279858] p 1459 N95-20157
Viewer-centered object recognition in monkeys
[AD-A279876] p 1437 N95-20185
Electrochemical impedance pattern recognition for detection of hidden chemical corrosion on aircraft components
[AD-A284998] p 1253 N95-20481
Multilayer piecewise linear networks
[AD-A285382] p 1480 N95-20606
Optical pattern recognition
[AD-A285384] p 1480 N95-20607
Proposal for a tutorial on Minimal Length Encoding (MLE) in molecular biology
[DE94-015076] p 1438 N95-21376
Object recognition by alignment using invariant projections of planar surfaces
[AD-A279841] p 1468 N95-21495
The use of fuzzy set classification for pattern recognition of the polygraph
[AD-A279148] p 1470 N95-21971
Discovering related DNA sequences via mutual information
[DE95-001101] p 1440 N95-22067
Feature extraction without edge detection
[AD-A279842] p 1473 N95-22386

PATTERN REGISTRATION
SAR image registration in absolute coordinates using GPS carrier phase position and velocity information
[DE94-018738] p 1204 N95-20195

PATTERSON MAP
HASSP and HEAVY: Tools for automated heavy atom searches and refinement
[DE94-016071] p 1569 N95-20696

PAVEMENTS
Super-heavy aircraft study
[AD-A279602] p 1215 N95-19955
Determination of layer moduli from falling weight deflectometer measurements
[PB95-129748] p 1286 N95-21333

PAYLOAD DEPLOYMENT & RETRIEVAL SYSTEM
STS 63: Post flight presentation
[NASA-TM-110514] p 1219 N95-21558
Tethered satellite: Forces and motion
[NASA-TM-110518] p 1220 N95-21858
STS Flight 64 mission highlights
[NASA-TM-110515] p 1219 N95-22295

PAYLOADS
Preliminary study of HUTSAT microsatellite
[PB95-127619] p 1220 N95-21026

PEEK
Effect of external stress on the transport of fluids in thermoplastic resin systems
[AD-A279993] p 1270 N95-20596
Damage tolerance of carbon fibre polyetheretherketone laminates
[PB95-131611] p 1230 N95-2143

PELLETS
Review of recent D-T experiments from TFTR
[DE95-002755] p 1557 N95-21239
Fusion power production in TFTR
[DE95-002756] p 1557 N95-21240
Cryogenic pellet laser plasma source targets
[DE95-002488] p 1376 N95-22169

PENDULUMS
The production of calibration specimens for impact testing of subsize Charpy specimens
[DE94-018125] p 1386 N95-20703
PENETRANTS
Effect of external stress on the transport of fluids in thermoplastic resin systems
[AD-A279993] p 1270 N95-20596
PENETRATION
Tungsten-uranium penetrator target interaction
[DE95-000847] p 1387 N95-21364
Flux creep with logarithmic U(j) dependence
[DE94-629058] p 1577 N95-22180
PERCHLORATES
Thermodynamic and NMR studies of solvent effect on enantiomeric recognition for a chiral organiz ammonium cation by chiral diketopyridino-18-Crown-6 type ligands at 25.0 C
[AD-A279893] p 1223 N95-20592
PERFORMANCE PREDICTION
Noise model of the MSX SPIRIT 3 interferometer
[AD-A285837] p 1364 N95-20036
Performance specifications for technology development: Application for characterization of volatile organic compounds in the environment
[DE94-016627] p 1401 N95-20234
An evaluation of 915-MHz radar wind profiler/RASS by tower and sodar measurements
[DE94-018913] p 1364 N95-20320
BACKSCAT lidar simulation version 4.0: Technical documentation and users guide
[AD-A285851] p 1290 N95-20376
Development and enhancement of a model of performance and decision making under stress in a real life setting
[AD-A285945] p 1449 N95-20393
Performance measurement: A tool for program control
p 1585 N95-20752
Performance and cost analysis of monolithic solid oxide fuel cells
[DE95-002511] p 1394 N95-20896
Underwater Acoustic Generator Phase 2: Sea trial, March 1992
[MRL-TN-640] p 1434 N95-21657
Intense proton beam source for ITER neutral-beam spectroscopy diagnostics
[DE94-018092] p 1560 N95-21668
EAGLES 1.1: A microcomputer software package for analyzing fuel efficiency of electric and gasoline vehicles
[DE95-001119] p 1469 N95-21829
Lubricant evaluation and performance, 2
[AD-A279144] p 1278 N95-21969
Effects of cyclic stress distribution models on fatigue life predictions
[DE95-001619] p 1388 N95-22070
PERFORMANCE TESTS
Round-robin comparison of heat release apparatus
[AD-A285831] p 1363 N95-20031
A review of water mist technology for fire suppression
[AD-A285738] p 1202 N95-20071
Test and evaluation of electric vehicles
[DE95-001153] p 1313 N95-20213
In situ viscometer instrument acceptance test report
[DE94-018507] p 1364 N95-20224
A theoretical study on the performance of the FDTD code on a massively parallel computer
[AD-A285346] p 1475 N95-20499
Qualification test results for blue-red reflecting solar covers p 1320 N95-20525
GPS-Squitter capacity analysis
[AD-A280037] p 1291 N95-20599
Field-emitter arrays for RF vacuum microelectronics
[AD-A279959] p 1325 N95-20661
Performance of the NIF prototype beamlet
[DE94-018500] p 1371 N95-20817
Test and Evaluation Master Plan (TEMP) for the Weather Message Switching Center Replacement (WMSCR)
[AD-A286590] p 1429 N95-20857
Si concentrator solar cell development
[DE95-002314] p 1393 N95-20870
Development of concentrator solar cells
[DE95-002316] p 1394 N95-20871
Real-data tests of a single-Doppler radar assimilation system
[AD-A286638] p 1292 N95-20904
Impact of propagation mechanisms on global navigation satellite system performance p 1298 N95-20950
The iMAPS: General information
[AD-A285421] p 1465 N95-21176
Recent National Solar Thermal Test Facility activities, in partnership with industry
[DE95-001828] p 1394 N95-21353
A low energy continuous reactor separator for the production of ethanol from corn grits/starch and biomass streams
[DE95-002256] p 1283 N95-21356
Quantitative evaluation of wrist posture and typing performance: A comparative study of 4 computer keyboards
[DE95-002392] p 1452 N95-21358
An in-line ultrasonic viscometer
[DE95-002982] p 1366 N95-21453
An Echelle Grating Spectrometer (EGS) for mid-IR remote chemical detection
[DE94-019310] p 1367 N95-21478
The efficiency calibration of the DSS-24 34-meter beam-waveguide antenna p 1305 N95-21542
Underwater Acoustic Generator Phase 2: Sea trial, March 1992
[MRL-TN-640] p 1434 N95-21657
The ITER in-vessel system
[DE94-018053] p 1560 N95-21665
Applications of ICP magnetic sector multicollector mass spectrometry to basic energy research
[DE95-002600] p 1246 N95-21886
Performance of cesium telluride photocathodes as an electron source for the Los Alamos FEL
[DE94-018302] p 1375 N95-21919
Electric and Hybrid Vehicle Program Site Operator Program
[DE95-002042] p 1333 N95-21960
Natural gas converter performance and durability
[PB95-135554] p 1284 N95-21966
Cathode Life Test Facility
[AD-A286232] p 1334 N95-22023
Response of the B-1B air data sensor to simulated dust cloud environments
[AD-A286134] p 1213 N95-22036
The Large Area Pulsed Solar Simulator (LAPSS)
[NASA-CR-197339] p 1397 N95-22336
Wave journal bearing. Part 1: Analysis
[NASA-CR-195431-PT-1] p 1382 N95-22404
Wave journal bearing. Part 2: Experimental pressure measurements and fractional frequency whirl threshold for wave and plain journal bearings
[NASA-TM-106848-PT-2] p 1382 N95-22405
Design of a massively parallel computer using bit serial processing elements
[NASA-CR-197365] p 1479 N95-22406
PERIDOTITE
Noble gas isotopes and halogens in volatile-rich inclusions in diamonds p 1417 N95-21784
Phase E in a water-saturated peridotite system at 9.3 GPa p 1420 N95-21799
The isotope geochemistry of abyssal peridotites and related rocks
[AD-A279435] p 1435 N95-21918
PERIPHERAL EQUIPMENT (COMPUTERS)
Non-intrusive SCSI status sensing system
[AD-D016242] p 1476 N95-21307
Network file server with automatic sensing means
[AD-D016250] p 1476 N95-21496
Method of retrieving and storing computer peripheral data
[AD-D016251] p 1591 N95-22098
Method of non-intrusively sensing status in a computer peripheral
[AD-D016241] p 1478 N95-22146
PERMAFROST
Operating manual for hybrid thermosyphons at the Gakona Power Plant, Alaska
[AD-A279068] p 1287 N95-21626
PERMALLOYS (TRADEMARK)
Giant magnetoresistance calculated from first principles
[DE94-018658] p 1500 N95-20129
PERMANENT MAGNETS
Low rotational drag in high-temperature superconducting bearings
[DE95-002983] p 1382 N95-22292
PERMEABILITY
Classification of bianisotropic media
[PB95-127635] p 1502 N95-21102
The permeation of bis(2-fluoro-2,2-dinitroethyl) formal (FEFO), ethyl 4,4-dinitropentanoate (EDNP), ethyl 4-nitropentanoate (ENP), and 1,2,4-trichlorobenzene (TCB) through barrier membranes
[DE95-002492] p 1283 N95-21514
Development and applications of flat ceramic membranes
[PB95-110219] p 1276 N95-21650
PERMEATING
The permeation of bis(2-fluoro-2,2-dinitroethyl) formal (FEFO), ethyl 4,4-dinitropentanoate (EDNP), ethyl 4-nitropentanoate (ENP), and 1,2,4-trichlorobenzene (TCB) through barrier membranes
[DE95-002492] p 1283 N95-21514
PERMISSIVITY
Derivation of maximum permissible concentrations for several volatile compounds for water and soil
[PB95-107454] p 1411 N95-22381
PERMITTIVITY
Dielectric models in adhesion and extrapolations of molecular modeling
[AD-A279675] p 1516 N95-21121
Electrical impedance studies of acid-form NAFION membranes
[AD-A279271] p 1330 N95-21490
Role of dielectric constant in electrohydrodynamics of conducting fluids
[NASA-TM-110499] p 1331 N95-21614
Dielectric mixtures with arbitrarily anisotropic components: Focus on special gyrotropic effects
[PB95-127015] p 1311 N95-22363
PERMUTATIONS
A multivariate multisample rank test for stochastic simulation validation
[AD-A285922] p 1498 N95-19990
Almost kappa-wise independent random permutation of the cube
[PB95-108098] p 1495 N95-22147
Vertex ranking for permutation and other graphs
[PB95-127569] p 1496 N95-22327
PEROVSKITES
Raman spectra of MOCVD-grown ferroelectric PbTiO3 thin films
[DE94-018964] p 1244 N95-21549
PERSONAL COMPUTERS
Personal computer and workstation operating systems tutorial
[AD-A280132] p 1451 N95-20041
PERSONNEL SELECTION
Comparison of a back propagation artificial neural network model with a linear regression model for personnel selection
[AD-A280023] p 1479 N95-20005
PERT
Scheduling: A guide for program managers
p 1584 N95-20748
PERTURBATION
Numerical study of realistic perturbations in three-dimensional boundary layers p 1351 N95-21091
Equivalent source current formulation in impedance tomography
[PB95-127627] p 1329 N95-21326
Explicit analytical solution of the nonlinear Vlasov Poisson system
[DE94-628931] p 1500 N95-21592
Dynamics of volatile delivery from outer to inner solar system p 1420 N95-21798
PERTURBATION THEORY
Analytic Perturbation Analysis of Discrete Event Dynamic Systems
[DE94-018635] p 1480 N95-20126
Theoretical particle physics
[DE95-002447] p 1515 N95-20893
Electromagnetic wave reflection from irregular plasma layers p 1298 N95-20952
PESTICIDES
Use of the carbo-flo process to purify process water contaminated by agricultural pesticides
[PB95-127825] p 1410 N95-22330
PETRI NETS
Multi-dimensional Petri nets
[PB95-127593] p 1491 N95-21024
Design model for open distributed processing systems
[PB95-135505] p 1477 N95-21620
PETROLOGY
D/H ratios and H2O contents of mantle-derived amphibole megacrysts from Dish Hill, California
p 1416 N95-21781
Recycling of volatiles at subduction zones: Noble gas evidence from the Tabar-Lihir-Tanga-Feni arc of papua New Guinea p 1418 N95-21787
PH
Actinide(IV) and actinide(VI) carbonate speciation studies by PAS and NMR spectroscopies
[DE94-016957] p 1236 N95-20361
PH FACTOR
Control of continuous phase PH using visible light to activate PH-dependent fibers and gels in a controlled and reversible manner
[AD-D016532] p 1543 N95-20728
PHARMACOLOGY
Interspecies extrapolations of halocarbon respiratory and tissue kinetics: Applications to predicting toxicity in different species
[AD-A285055] p 1442 N95-20485
ANSTO: Mission statement, significant events and achievements
[DE94-631123] p 1605 N95-21830
PHASE CHANGE MATERIALS
Effect of microgravity on material undergoing melting and freezing: The TES Experiment
[NASA-TM-106845] p 1338 N95-19952

PHASE DETECTORS

Unlimited-bandwidth distributed optical phase modulators and detectors: Design and fabrication issues [DE94-017418] p 1545 N95-21509

PHASE DEVIATION

Josephson acoustic radiation in superfluid helium [AD-A279809] p 1503 N95-20098

Evaluating impedances in a Sacherer integral equation [DE94-016823] p 1489 N95-20266

PHASE DIAGRAMS

Carrier doping and interlayer coupling in HTSC single crystals [DE94-018637] p 1564 N95-20127

Thermodynamic analysis of stable and metastable equilibrium diagrams of the Cu-Cr system [PB95-127775] p 1255 N95-21111

Application of quaternary phase diagrams to compound semiconductor processing [DE95-001813] p 1277 N95-21748

Nonlinear dynamics of the planar pitch attitude motion for a gravity-gradient satellite [AD-A286407] p 1220 N95-22204

New thermodynamic description of the Cu-Zr system [PB95-127189] p 1263 N95-22374

PHASE MATCHING

Technique for intracavity sum frequency generation [AD-D016478] p 1546 N95-21898

PHASE MODULATION

Pasotron(TM) technology [AD-A279994] p 1314 N95-20311

Comparative study of C- and K-band propagation mechanisms beyond the horizon p 1297 N95-20946

Unlimited-bandwidth distributed optical phase modulators and detectors: Design and fabrication issues [DE94-017418] p 1545 N95-21509

PHASE SHIFT

Phase dynamics of non-equilibrium distributions of free electron-hole pairs in GaAs quantum wells [DE94-018190] p 1569 N95-20679

Ultrafast magnetoexciton dynamics in GaAs [DE94-018175] p 1514 N95-20732

PHASE STABILITY (MATERIALS)

Investigation of the stability and 1.0 MeV proton radiation resistance of commercially produced hydrogenated amorphous silicon alloy solar cells p 1320 N95-20522

PHASE TRANSFORMATIONS

Properties of molecular solids and fluids at high pressure and temperature [DE94-017594] p 1565 N95-20243

Hierarchical structure in advanced polymers. Phase behaviour, orientation, properties [AD-A285938] p 1268 N95-20392

The role of high pressure in the study and applications of the ferroelectric polymer polyvinylidene fluoride and its copolymers [DE94-015742] p 1268 N95-20396

The effect of oxide inclusions on the kinetics of the austenite to ferrite transformation in low alloy steel weld metal [DE94-018131] p 1253 N95-20676

Determinations of phase transitions in nylon 6-12, nylon-6, polyvinyl chloride and polyethylene terephthalate by positron annihilation spectroscopy [DE94-629992] p 1239 N95-20736

Moessbauer study of the sintered Mn(0.70)Zn(0.23)Fe(2.07)O4 [DE94-631462] p 1255 N95-20909

Computational modeling of diffusion-controlled transformations in ternary systems [DE95-001358] p 1256 N95-21298

Dynamics of the chiral transition [DE94-016813] p 1524 N95-21641

Biaxiality of chiral liquid crystals [DE94-629032] p 1578 N95-22277

New thermodynamic description of the Cu-Zr system [PB95-127189] p 1263 N95-22374

PHASE VELOCITY

SAR image registration in absolute coordinates using GPS carrier phase position and velocity information [DE94-018738] p 1204 N95-20195

PHASED ARRAYS

The design and analysis of a phased array microstrip antenna for a low earth orbit communication satellite [AD-A284791] p 1289 N95-20065

High contrast organic crystal optical modulator for phased array antenna and optical signal processing [AD-A286557] p 1544 N95-20844

Inband scattering from arrays with series feed networks [AD-A286209] p 1307 N95-21883

PHENOMENOLOGY

Optimizing the length of the stores and related effects [DE95-002531] p 1533 N95-20885

PHENYLS

Low temperature synthesis of semiconductor materials [AD-A285120] p 1226 N95-20081

Photophysical processes on triplet states and radical ions in pure and molecularly doped polymers [DE95-002681] p 1570 N95-20916

Synthesis and structure of a novel bis-stibole [AD-A286345] p 1224 N95-22252

PHONONS

Resonant generation of nonequilibrium phonons in GaAs/AlAs quantum wells via intersubband scattering [DE95-002338] p 1581 N95-21604

Surfaces and thin films studied by picosecond ultrasonics [DE95-001866] p 1506 N95-22071

Tunneling of self-trapped states and formation of a band [DE94-629001] p 1582 N95-22378

PHOSPHATES

Safe conditions for contacting nitric acid or nitrates with Tri-n-Butyl Phosphate (TBP) [DE95-001243] p 1235 N95-20215

Polyurethane self-priming topcoats [AD-D016204] p 1274 N95-21154

Polyurethane self-priming topcoats [AD-D016205] p 1274 N95-21155

PHOSPHAZENE

Synthesis and characterization of poly(organophosphazene) interpenetrating polymer networks [AD-A279872] p 1265 N95-20183

Radiation-induced modifications of allylamino-substituted polyphosphazenes [AD-A279694] p 1268 N95-20428

The synthesis and characterization of small molecule and photo-cross-linkable high polymeric phosphazenes bearing cinnamate groups [AD-A279782] p 1268 N95-20442

Cross-linking reactions for the conversion of polyphosphazenes into useful materials [AD-A279696] p 1271 N95-20709

Macromolecular and materials design using polyphosphazenes [AD-A279781] p 1273 N95-20978

PHOSPHINES

An atomically-resolved STM study of the interaction of phosphine (PH3) with the silicon (001) surface [AD-A279819] p 1513 N95-20585

Structure of dibis(diethyldithiocarbamato) zinc (2) Mu-bis(diethylphosphino)ethane toluene(2) [AD-A279792] p 1224 N95-20660

Photochemistry of intermolecular C-H bond activation reactions [DE94-018417] p 1239 N95-20682

PHOSPHORESCENCE

Application of pressure sensitive paint in hypersonic flows [NASA-TM-106824] p 1201 N95-20794

PHOSPHORIC ACID FUEL CELLS

Research on the power generation system with thermoelectric conversion elements [DE95-714804] p 1397 N95-22309

PHOSPHORUS COMPOUNDS

Photophysical processes on triplet states and radical ions in pure and molecularly doped polymers [DE95-002681] p 1570 N95-20916

PHOSPHORUS POLYMERS

The synthesis and characterization of small molecule and photo-cross-linkable high polymeric phosphazenes bearing cinnamate groups [AD-A279782] p 1268 N95-20442

Water-soluble polyphosphazenes and their hydrogels [AD-A279695] p 1269 N95-20580

PHOTOACOUSTIC SPECTROSCOPY

Actinide(IV) and actinide(VI) carbonate speciation studies by PAS and NMR spectroscopies [DE94-016957] p 1236 N95-20361

Vibrational overtone spectroscopy of pyridine and related compounds [AD-A280105] p 1224 N95-21911

PHOTOCATHODES

Photoelectrons beam measurement from a magnesium cathode in a RF electron gun [DE94-017994] p 1533 N95-20573

Method of fabricating a microelectronic photomultiplier device with integrated circuitry [AD-D016530] p 1325 N95-20726

Performance of cesium telluride photocathodes as an electron source for the Los Alamos FEL [DE94-018302] p 1375 N95-21919

Photocathodes for free electron lasers [DE94-018305] p 1376 N95-22242

Fabrication and characterization of cesium telluride photocathodes: A promising electron source for the Los Alamos Advanced FEL [DE94-018303] p 1377 N95-22348

PHOTOCHEMICAL REACTIONS

Cavity-QED enhancement of fluorescence yields in microdroplets [DE94-018662] p 1506 N95-20030

Photodegradation and photophysics of laser dyes [AD-A285105] p 1368 N95-20063

The synthesis and characterization of small molecule and photo-cross-linkable high polymeric phosphazenes bearing cinnamate groups [AD-A279782] p 1268 N95-20442

Photochemistry of intermolecular C-H bond activation reactions [DE94-018417] p 1239 N95-20682

Cross-linking reactions for the conversion of polyphosphazenes into useful materials [AD-A279696] p 1271 N95-20709

Investigation of laser-induced retinal damage: Wavelength and pulsewidth dependent mechanisms [AD-A286066] p 1443 N95-20848

Translational-energy-resolved studies of photographed carrier-induced reactions on semiconductor surfaces [DE95-002944] p 1573 N95-21444

Mars atmospheric loss and isotopic fractionation by pick-up-ion sputtering and photochemical escape p 1420 N95-21796

International Symposium on Advanced Laser Technologies [AD-A279849] p 1376 N95-22164

Indian Academy of Sciences. Volume 105, number 6, December 1993. Proceedings of the 2nd International Conference on Solar Energy Storage Applied Photochemistry [AD-A286481] p 1605 N95-22394

PHOTOCONDUCTIVITY

Kondo insulators [DE95-001156] p 1237 N95-20368

Fiber-optic control of current filaments in high gain photoconductive semiconductor switches [DE94-015804] p 1328 N95-21139

The role of point defects and defect complexes in silicon device processing [DE94-011876] p 1279 N95-22091

PHOTODETACHMENT

Dynamics of collision processes [DE94-017593] p 1509 N95-20242

Study of small carbon and semiconductor clusters using negative ion threshold photodetachment spectroscopy [DE95-002327] p 1515 N95-20872

PHOTODISSOCIATION

Molecular snapshots: Product imaging of dynamics important to fundamental combustion processes [DE94-018595] p 1510 N95-20346

Excess energy and structural dependence of the rate of energy redistribution during the photodissociation of iodotoluenes [AD-A279997] p 1241 N95-21124

PHOTOELECTRIC EMISSION

Correlations between surface structure and catalytic activity/selectivity [DE94-019023] p 1234 N95-20052

Photoemission and ferromagnetism [DE95-002419] p 1520 N95-21362

Angle resolved photoemission on K(0.3)Mo3, TiTe2 and Ti(1+x)S2 [DE94-018300] p 1574 N95-21712

Acid-site characterization of water-oxidized alumina films by near-edge x-ray absorption and soft x-ray photoemission [DE95-003355] p 1247 N95-22234

PHOTOELECTRON SPECTROSCOPY

Correlations between surface structure and catalytic activity/selectivity [DE94-019023] p 1234 N95-20052

Electron propagator theory and application [AD-A279761] p 1507 N95-20097

Oxide formation on NbAl3 and TiAl due to ion implantation of O-18 [DE94-017874] p 1252 N95-20365

PHOTOELECTRONS

Electron propagator theory and application [AD-A279761] p 1507 N95-20097

Spin-specific photoelectron diffraction using magnetic x ray circular dichroism [DE94-017527] p 1567 N95-20448

A structural determination using magnetic x ray circular dichroism in spin-polarized photoelectron diffraction [DE94-017528] p 1567 N95-20449

Photoelectrons beam measurement from a magnesium cathode in a RF electron gun [DE94-017994] p 1533 N95-20573

Magnetic x-ray circular dichroism in spin-polarized photoelectron diffraction [DE95-002394] p 1520 N95-21360

Physics of correlated studies [DE95-001204] p 1581 N95-21842

PHOTOEXCITATION
Photophysical processes on triplet states and radical ions in pure and molecularly doped polymers
[DE95-002681] p 1570 N95-20916
PHOTOGRAMMETRY
Integration of segmentation and stereo matching
[PB95-107819] p 1444 N95-21028
PHOTOGRAPHIC EQUIPMENT
Cold regions instrumentation considerations
[AD-A279492] p 1367 N95-21680
PHOTOIONIZATION
Sputtering of tin and gallium-tin clusters
[DE94-018389] p 1254 N95-20707
EBIT x ray spectroscopy studies for applications to photo-pumped x ray lasers
[DE94-016701] p 1373 N95-21210
Ion charge-state production and photoionization near the K edge in argon and potassium
[DE95-001443] p 1522 N95-21502
Atmospheres of the Moon and Mercury
p 1419 N95-21794
Physics of correlated studies
[DE95-001204] p 1581 N95-21842
The two-electron problem and prospects for atomic collision theory on a numerical lattice
[DE94-017856] p 1528 N95-22265
PHOTOLITHOGRAPHY
Solid state research
[AD-A279662] p 1567 N95-20426
PHOTOLUMINESCENCE
Observation of excitonic and band-to-band behavior in ordered InGaP2 alloys
[DE94-018891] p 1314 N95-20341
High-efficiency, deep-junction, epitaxial InP solar cells on (100) and (111)B InP substrates
p 1316 N95-20507
Photoluminescence under pressure and annealing of nitrogen-doped ZnSe
[DE95-002355] p 1568 N95-20630
Correlated wavefunction Monte Carlo studies of excitations in the quantum Hall liquids
[DE95-002337] p 1501 N95-20874
Conducting thermoset polymers
[AD-A286541] p 1273 N95-21014
Transient photoluminescence measurements on GaAs and AlGaAs double heterostructures
[AD-A279408] p 1575 N95-21916
PHOTOMASKS
A versatile masking process for plasma etched backside via holes in GaAs
[DE94-019176] p 1572 N95-21419
PHOTOMETERS
Methods and components for optical contention resolution in high speed networks
[AD-A280016] p 1543 N95-20598
Unlimited-bandwidth distributed optical phase modulators and detectors: Design and fabrication issues
[DE94-017418] p 1545 N95-21509
InTISb for long-wavelength infrared photodetectors and arrays
[AD-A280109] p 1331 N95-21660
InTISb for long-wavelength infrared photodetectors and arrays
[AD-A280108] p 1332 N95-21774
Design, fabrication, and characterization of reflective diffractive optical elements in Si for free-space optical interconnects
[AD-A286416] p 1547 N95-22205
PHOTOMETRY
MEM application to IRAS CPC images
p 1592 N95-21751
An assessment of image reconstruction from balloon-borne and the IRAS data p 1592 N95-21752
PHOTOMULTIPLIER TUBES
Method of fabricating a microelectronic photomultiplier device with integrated circuitry
[AD-D016530] p 1325 N95-20726
Detection efficiency and dark pulse rate of Rockwell (SSPM) single photon counters
[DE94-016872] p 1524 N95-21646
PHOTON BEAMS
Beam instability studies at the APS
[DE95-001448] p 1537 N95-21503
PHOTON-ELECTRON INTERACTION
X-ray microscope for solidification studies
[NASA-CR-197375] p 1543 N95-20798
PHOTONS
High energy photon-photon collisions
[DE94-017494] p 1532 N95-20388
Unbinned maximum likelihood fit for the CP conserving couplings for W + photon production at CDF
[DE95-001471] p 1514 N95-20852
Nonperturbative aspects of the quark-photon vertex
[DE94-012846] p 1520 N95-21315
Heavy ion collisions
[DE95-002712] p 1520 N95-21321
Monopoles and quark confinement: Introduction and overview
[DE94-019348] p 1522 N95-21485
The diphoton production rate in (bar p)p collisions at the square root of s = 1800 GeV
[DE95-000559] p 1522 N95-21497
New shower maximum trigger for electrons and photons at CDF
[DE95-000563] p 1522 N95-21499
Detection efficiency and dark pulse rate of Rockwell (SSPM) single photon counters
[DE94-016872] p 1524 N95-21646
Investigation of direct photon production in 200 A GeV S + Au reactions
[DE94-018129] p 1525 N95-21704
PHOTOOXIDATION
Gas-phase photocatalytic oxidation: Cost comparison with other air pollution control technologies
[DE95-000241] p 1410 N95-22278
PHOTOPRODUCTION
Multiple hard interactions in HERWIG
[PB95-130548] p 1518 N95-21233
Exclusive processes: Tests of coherent QCD phenomena and nucleon substructure at CEBAF
[DE95-002892] p 1520 N95-21336
The diphoton production rate in (bar p)p collisions at the square root of s = 1800 GeV
[DE95-000559] p 1522 N95-21497
PHOTORECEPTORS
Computer based analysis and synthesis of retinal function
[AD-A286084] p 1443 N95-20811
PHOTOSPHERE
Solar wind composition
[NASA-TM-197364] p 1604 N95-22384
PHOTOSYNTHESIS
A photophysical control mechanism for zeaxanthin-associated radiationless energy dissipation in photosynthesis
[DE94-018383] p 1437 N95-19969
Nitrogen control of chloroplast differentiation
[DE95-002797] p 1439 N95-21526
The Use of Cyanobacteria to Explore Basic Biological Processes
[DE94-019238] p 1440 N95-22066
Electrostatic basis for molecular recognition in photosynthesis
[DE95-002979] p 1440 N95-22075
PHOTOTHERMAL CONVERSION
InGaAs PV device development for TPV power systems p 1322 N95-20537
PHOTOVOLTAIC CELLS
Analyses of grounded and ungrounded photovoltaic power systems
[DE94-015015] p 1391 N95-20263
InGaAs PV device development for TPV power systems p 1322 N95-20537
Pulsed laser illumination of photovoltaic cells
p 1323 N95-20538
Development of concentrator solar cells
[DE95-002316] p 1394 N95-20871
The Photovoltaic Higher Education National Exemplar Facility (PHENEF)
[DE94-015641] p 1395 N95-21409
Thin-film cadmium telluride photovoltaic cells
[DE94-011886] p 1395 N95-21508
Method of forming a high voltage silicon-on-sapphire photocell array
[AD-D016479] p 1396 N95-21899
Solar collector manufacturing activity 1993
[DE94-017340] p 1398 N95-22429
PHOTOVOLTAIC CONVERSION
Trimode Power Converter optimizes PV, diesel and battery energy sources
[DE94-015014] p 1313 N95-20262
The First NREL Conference on Thermophotovoltaic Generation of Electricity: Proceedings
[DE94-011831] p 1391 N95-20332
The Photovolatic Manufacturing Technology project (PVMaT) after three years
[DE94-011877] p 1392 N95-20473
Proceedings of the 13th Space Photovoltaic Research and Technology Conference (SPRAT 13)
[NASA-CP-3278] p 1316 N95-20502
BMDO photovoltaics program overview
p 1316 N95-20504
An update on the Department of Energy's photovoltaic program p 1316 N95-20505
Europe's space photovoltaics programme
p 1316 N95-20506
High-efficiency, deep-junction, epitaxial InP solar cells on (100) and (111)B InP substrates
p 1316 N95-20507
Chemical beam epitaxy for high efficiency photovoltaic devices p 1316 N95-20508
Advances in polycrystalline thin-film photovoltaics for space applications p 1318 N95-20514
Photovoltaic electric power applied to Unmanned Aerial Vehicles (UAV) p 1321 N95-20530
Rare earth garnet selective emitter
p 1322 N95-20536
Pulsed laser illumination of photovoltaic cells
p 1323 N95-20538
Highlights of recent balance of system research and evaluation
[DE95-001626] p 1393 N95-20863
The Photovoltaic Higher Education National Exemplar Facility (PHENEF)
[DE94-015641] p 1395 N95-21409
Mars power system concept definition study. Volume 2: Appendices
[NASA-CR-195420-VOL-2] p 1396 N95-21953
Bridging worlds/charting new courses
[DE95-003808] p 1397 N95-22335
Advanced energy systems and technologies research programme
[DE95-717486] p 1397 N95-22337
PHOTOVOLTAIC EFFECT
The First NREL Conference on Thermophotovoltaic Generation of Electricity: Proceedings
[DE94-011831] p 1391 N95-20332
InTISb for long-wavelength infrared photodetectors and arrays
[AD-A280109] p 1331 N95-21660
Optical processing and control
[AD-A279157] p 1546 N95-21975
PHYSICAL CHEMISTRY
Thermochemistry of dense hydrous magnesium silicates p 1416 N95-21782
A crystallographic model for hydrous wadsleyite (Beta-Mg2SiO4) p 1424 N95-21817
PHYSICAL EXERCISE
Modeling platform dynamics and physiological response to short arm centrifugation
[AD-A279640] p 1442 N95-20457
Hypervolemia in men from drinking hyperhydration fluids at rest and during exercise
[NASA-TM-4657] p 1439 N95-21544
A method to determine the kinematics of the lower limbs of a subject pedaling a bicycle using encoders and accelerometers
[NASA-CR-197401] p 1453 N95-21866
PHYSICAL OPTICS
Resonant tunneling quantum well integrated optical waveguide modulator/switch
[AD-A285142] p 1542 N95-20501
Diffraction computation by means of the method of equivalent currents
[AD-A285347] p 1291 N95-20692
PHYSICAL PROPERTIES
Lead-indium phosphate glasses for optical applications
[DE94-019333] p 1275 N95-21482
Weld pool phenomena
[DE94-018965] p 1381 N95-21550
An initial assessment of the properties of 2,5-dipicryl-1,3,4-oxadiazole: A secondary explosive with high thermal stability
[MRL-TR-93-16] p 1284 N95-21624
PHYSICAL WORK
Human force exertion in user-product interaction. Backgrounds for design
[PB95-132858] p 1452 N95-21283
PHYSICS
The development of science during this century
[DE94-632964] p 1582 N95-22185
PHYSIOLOGICAL DEFENSES
Monoclonal antibodies directed against surface molecules of multicell spheroids
[NASA-CR-197367] p 1437 N95-20559
PHYSIOLOGICAL EFFECTS
Interspecies extrapolations of halocarbon respiratory and tissue kinetics: Applications to predicting toxicity in different species
[AD-A285055] p 1442 N95-20485
Monoclonal antibodies directed against surface molecules of multicell spheroids
[NASA-CR-197367] p 1437 N95-20559
Influence of oxidation on radiation hardness of silicon detectors
[DE95-002466] p 1272 N95-20894
Helicopter crewseat cushion program
[AD-A286654] p 1452 N95-20973
A method to determine the kinematics of the lower limbs of a subject pedaling a bicycle using encoders and accelerometers
[NASA-CR-197401] p 1453 N95-21866
Command history, 1993
[AD-A279775] p 1446 N95-21989

PHYSIOLOGICAL RESPONSES
Modeling platform dynamics and physiological response to short arm centrifugation
[AD-A279640] p 1442 N95-20457
Monoclonal antibodies directed against surface molecules of multicell spheroids
[NASA-CR-197367] p 1437 N95-20559
PHYSIOLOGICAL TESTS
Evaluation of stress experienced by soldiers wearing chemical protective clothing during varying work loads in desert or tropical environments
[AD-A280113] p 1452 N95-20625
PHYSIOLOGY
Microbiology and physiology of anaerobic fermentations of cellulose
[DE95-002899] p 1438 N95-20917
Compilation of 1993 annual reports of the Navy ELF Communications System Ecological Monitoring Program
[AD-A279575] p 1408 N95-21699
PHYTOPLANKTON
Effects of increased UV-B radiation on phytoplankton: A preliminary study and research programme
[PB95-133732] p 1439 N95-21884
PIEZOELECTRIC CERAMICS
Compositive piezoelectrics utilizing a negative Poisson ratio polymer
[AD-D016579] p 1268 N95-20460
Polycrystalline PLZT/ITO ceramic electro-optic phase gratings: Electro-optically reconfigurable difffractive devices for free-space and in-wafer interconnects
[AD-A285861] p 1547 N95-22076
PIEZOELECTRIC CRYSTALS
Ferroic materials: Design, preparation and characteristics. Ceramic transactions, volume 43
[AD-A285937] p 1270 N95-20664
PIEZOELECTRIC TRANSDUCERS
Transducers with improved signal transfer field of the invention
[AD-D016228] p 1328 N95-21118
PIEZOELECTRICITY
Materials for adaptive structural acoustic control, volume 2
[AD-A279222] p 1502 N95-19883
Vacuum holding fixture and method for fabricating piezoelectric polymer acoustic sensors
[NASA-CASE-LAR-14240-1] p 1268 N95-20410
Ferroic materials: Design, preparation and characteristics. Ceramic transactions, volume 43
[AD-A285937] p 1270 N95-20664
Monolithic low noise preamplifier for piezoelectric sensors
[AD-D016524] p 1333 N95-21865
PIGMENTS
Polyurethane self-priming topcoats
[AD-D016204] p 1274 N95-21154
Polyurethane self-priming topcoats
[AD-D016205] p 1274 N95-21155
PILOT PERFORMANCE
Using the backward transfer paradigm to validate the AH-64 Simulator Training Research Advanced Testbed for Aviation
[AD-A285758] p 1215 N95-19931
The advanced technology crew station: Development and validation of a workload assessment technique for cockpit function allocation
[AD-A279544] p 1453 N95-21691
Age 60 study. Part 1: Bibliographic database
[AD-A286245] p 1446 N95-22027
Age 60 study. Part 2: Airline pilot age and performance. A review of the scientific literature
[AD-A286246] p 1447 N95-22040
PILOT PLANTS
A low energy continuous reactor separator for the production of ethanol from corn grits/starch and biomass streams
[DE95-002256] p 1283 N95-21356
PILOT TRAINING
A computer-based multimedia prototype for night vision goggles
[AD-A286208] p 1546 N95-21882
PILOTLESS AIRCRAFT
Unmanned aerial vehicles
[AD-A286190] p 1206 N95-20329
Photovoltaic electric power applied to Unmanned Aerial Vehicles (UAV) p 1321 N95-20530
PILOTS
The influence of coronary artery disease on +Gz tolerance: A preliminary study
[AD-A279305] p 1446 N95-21941
PINNING
Superconducting thin film with fullerenes and method of making
[AD-D016580] p 1567 N95-20461
PION BEAMS
Polarization of charmonium in pion-nucleus collisions
[DE95-002783] p 1523 N95-21525
PIONS
D(sup 0)-(anti-D)(sup 0) mixing and doubly Cabibbo-suppressed decays of the D(+)
[DE94-015540] p 1512 N95-20476
Strange particle and antiproton production in S + nucleus collisions at 200 GeV/nucleon
[DE95-002348] p 1513 N95-20575
Theories of the eta-meson-nucleus interaction
[DE94-016055] p 1516 N95-21125
Where are we going with Bose-Einstein: A mini review
[PB95-130308] p 1518 N95-21222
Single particle measurements and two particle interferometry results from CERN experiment NA44
[DE95-003041] p 1527 N95-22078
Proton and produced particle distributions from Au+Au collisions at 11.6 A GeV/c
[DE94-018634] p 1530 N95-22392
PIPE FLOW
Continuum transient and frozen startup behavior of conventional and gas-loaded heat pipes
[AD-A284297] p 1339 N95-20250
Direct numerical simulation of turbulent flow in a sudden pipe expansion p 1347 N95-21067
Simulation of pipe flow p 1349 N95-21078
Fluid dynamics of the freeboard in a fluidized bed reactor
[PB95-134029] p 1357 N95-22160
PIPELINING (COMPUTERS)
Software for flow distribution in electronic rack structures
[AD-A285994] p 1325 N95-20715
PIPES (TUBES)
Thermochemistry of dense hydrous magnesium silicates p 1416 N95-21782
Epoxy lining for shipboard piping systems
[AD-A286228] p 1279 N95-22022
PISTONS
Abrasive wear by diesel engine coal-fuel and related particles
[PB95-104915] p 1379 N95-20984
PITCH (INCLINATION)
Visual perception of elevation
[AD-A284938] p 1451 N95-22472
PITCHING MOMENTS
Effects of yaw and pitch motion on model attitude measurements
[NASA-TM-4641] p 1368 N95-22109
PITOT TUBES
Response of the B-1B air data sensor to simulated dust cloud environments
[AD-A286134] p 1213 N95-22036
PITTING
Corrosion of aircraft materials: Correlation between nanometer scale and macroscopic structural damage parameters
[AD-A285930] p 1252 N95-20299
Identification of resonant, two-electron, and inter-atomic features in K and L23 NEXAFS spectra
[AD-A285374] p 1513 N95-20554
PIXELS
A framework for segmentation using physical models of image formation
[AD-A279900] p 1543 N95-20564
PLANAR STRUCTURES
Object recognition by alignment using invariant projections of planar surfaces
[AD-A279841] p 1468 N95-21495
On-wafer, cryogenic characterization of ultra-low noise HEMT devices p 1305 N95-21539
PLANE STRAIN
Morphology of highly textured E/EP diblock copolymers
[AD-A279813] p 1269 N95-20582
PLANE WAVES
Diffraction computation by means of the method of equivalent currents
[AD-A285347] p 1291 N95-20692
PLANETARY ATMOSPHERES
Comets, impacts, and atmospheres
p 1422 N95-21810
Degassing history and evolution of volcanic activity of terrestrial planets based on radiogenic noble gas degassing models p 1424 N95-21816
PLANETARY BOUNDARY LAYER
Front-boundary layer models from STORM-FEST observations
[AD-A279907] p 1428 N95-20186
PLANETARY EVOLUTION
Mantle devolatilization and rheology in the framework of planetary evolution p 1418 N95-21788
Solar system formation and the distribution of volatile species p 1421 N95-21806
Degassing history and evolution of volcanic activity of terrestrial planets based on radiogenic noble gas degassing models p 1424 N95-21816
PLANETARY MAPPING
The Double Eagle Space Experiment (DESE) beamline design
[DE94-018319] p 1601 N95-22419
PLANETARY NEBULAE
Solar system formation and the distribution of volatile species p 1421 N95-21806
Distribution of light element isotopes in Bencubbin and Weatherford meteorites: An indicator of heterogeneity in the primitive solar nebula
[DE94-019167] p 1600 N95-22128
PLANNING
Planning and scheduling for success
p 1584 N95-20747
PLANTS (BOTANY)
Monitoring bioremediation of Volatile Organic Compounds (VOCs) using Fourier Transform Infrared (FT-IR) spectrometry
[AD-A279631] p 1403 N95-20456
Compilation of 1993 annual reports of the Navy ELF Communications System Ecological Monitoring Program
[AD-A279575] p 1408 N95-21699
The mechanisms and effects off the plant-activations of chemicals in the environment
[AD-A279388] p 1356 N95-22145
Structures and functions of oligosaccharins
[DE95-003195] p 1440 N95-22220
PLASMA ANTENNAS
Three-dimensional effects for radio frequency antenna modeling
[DE94-019125] p 1303 N95-21459
PLASMA CHEMISTRY
Plasma chemistry of vibrationally nonequilibrium molecules
[AD-A279630] p 1553 N95-20411
Advanced diagnostics for plasma chemistry
[DE94-018936] p 1561 N95-22116
PLASMA COMPOSITION
Analysis methods for fast impurity ion dynamics data
[DE95-000589] p 1549 N95-20112
Experimental measurements and modeling of impurity transport in the divertor and boundary plasma of D3-D
[DE94-016519] p 1556 N95-21159
PLASMA COMPRESSION
Soft X-Ray Innovative Source Development Program
[AD-A286380] p 1551 N95-20232
PLASMA CONTROL
Recent DIII-D results
[DE94-017519] p 1549 N95-20038
Fluctuations and transport in the reversed field pinch: Characterization and reduction
[DE95-000590] p 1549 N95-20113
Magnetic fluctuation induced transport and edge dynamo measurements in the MST reversed-field pinch
[DE95-000591] p 1549 N95-20114
Fluctuations in high Beta(sub p) plasmas in D3-D
[DE94-017510] p 1550 N95-20146
Helium exhaust studies in the D3-D tokamak
[DE94-016682] p 1552 N95-20334
Hybrid model in general geometry
[DE95-002614] p 1553 N95-20437
Plasma shape experiments for an optimized tokamak
[DE94-017508] p 1553 N95-20445
Boron carbide-based coatings on graphite for plasma facing components
[DE94-017976] p 1269 N95-20570
Enhanced scrape-off layer plasma in D3-D double-null discharges
[DE94-017977] p 1554 N95-20571
Ideal Magnetohydrodynamic stabilities in JT-60 and D3-D tokamak plasmas
[DE94-770684] p 1555 N95-20987
Source mechanisms and radio effects of ionospheric plasma disturbances
[AD-A286529] p 1555 N95-21013
Extended theory of main ion and impurity rotation and bootstrap current in a shear layer
[DE94-015857] p 1555 N95-21141
Investigations of VH-mode in D3-D and JET
[DE94-015859] p 1556 N95-21142
The parametric dependence of the spatial structure of the radial electric field at the plasma edge in the D3-D tokamak
[DE94-016520] p 1556 N95-21163
Experimental investigation of molecular beam injection in HL-1 tokamak
[DE94-631456] p 1556 N95-21165
Fusion power production in TFTR
[DE95-002756] p 1557 N95-21240
Theory of the L-H transition
[DE95-001389] p 1558 N95-21299
1994 Nonneutral Plasma Workshop
[AD-A285656] p 1559 N95-21404
Evaluation of pumping and fueling requirements for the ITER EDA
[DE94-018117] p 1560 N95-21702

Collisional drift waves in the H-mode edge
[DE94-628950] p 1561 N95-21847

On conception of a compact neutron source and the possibility of its simulation on the Amba-M end trap
[DE94-633373] p 1562 N95-22282

PLASMA CURRENTS

A method for measuring the inductive electric field profile and noninductive current profiles on D3-D
[DE94-016683] p 1551 N95-20279

Recent results from Fast Wave Current Drive experiments on DIII-D
[DE94-016718] p 1551 N95-20285

Power balance in D3-D during single-null ELMing H-mode plasmas
[DE94-016680] p 1554 N95-20568

Observation of non diffusive term of toroidal momentum transport in the JFT-2M tokamak
[DE94-770686] p 1555 N95-20989

SPICE macro model of a spryton with MOSFET's in the avalanche mode
[DE94-015744] p 1555 N95-21134

Extended theory of main ion and impurity rotation and bootstrap current in a shear layer
[DE94-015857] p 1555 N95-21141

The evolution of configuration from q greater than 1 to q less than 1
[DE94-631396] p 1556 N95-21162

PLASMA DENSITY

The control system position to the electric probe in the Tokamak Novillo
[DE94-629938] p 1550 N95-20204

Enhanced scrape-off layer plasma in D3-D double-null discharges
[DE94-017977] p 1554 N95-20571

Electrostatic noise in the plasma environment around the shuttle
[NASA-TM-106856] p 1415 N95-21188

Large facilities pilot programme. Access to the VULCAN High Power Laser Facilities at Rutherford Appleton Laboratory
[PB95-130340] p 1373 N95-21226

Explicit analytical solution of the nonlinear Vlasov Poisson system
[DE94-628931] p 1500 N95-21592

Gas-dynamic trap diagnostic complex for study on plasma heating and power atomic beam injection
[DE94-633377] p 1529 N95-22283

PLASMA DIAGNOSTICS

X-ray imaging of uniform large scale-length plasmas created from gas-filled targets on Nova
[DE94-018339] p 1531 N95-20015

Analysis methods for fast impurity ion dynamics data
[DE95-000589] p 1549 N95-20112

National Ignition Facility: Experimental plan
[DE94-016542] p 1550 N95-20189

The control system position to the electric probe in the Tokamak Novillo
[DE94-629938] p 1550 N95-20204

A method for measuring the inductive electric field profile and noninductive current profiles on D3-D
[DE94-016683] p 1551 N95-20279

Ion temperature measurement of indirectly-driven implosions using a geometry-compensated neutron time-of-flight detector
[DE94-016967] p 1552 N95-20362

Characterization of nova plasmas using an x-ray spectrometer with temporal and spatial resolution
[DE94-016970] p 1553 N95-20363

High precision Woelter optic calibration facility
[DE94-016973] p 1542 N95-20364

A new alpha particle diagnostic using knock-on ion tails
[DE94-015856] p 1553 N95-20402

A portable and independent edge fluctuation diagnostic
[DE94-018254] p 1554 N95-20681

Chaotic phenomena in plasma 3
[DE94-770765] p 1554 N95-20686

Observation of non diffusive term of toroidal momentum transport in the JFT-2M tokamak
[DE94-770686] p 1555 N95-20989

Large facilities pilot programme. Access to the VULCAN High Power Laser Facilities at Rutherford Appleton Laboratory
[PB95-130340] p 1373 N95-21226

Intense proton beam source for ITER neutral-beam spectroscopy diagnostics
[DE94-018092] p 1560 N95-21668

Advanced diagnostics for plasma chemistry
[DE94-018936] p 1561 N95-22116

Measurements of the Auburn ECE optical system parameters for temperature fluctuation measurements on TEXT-U
[DE94-019217] p 1562 N95-22120

Plasma processing for integrated circuits
[DE95-001419] p 1335 N95-22149

Laboratory characterization of Woelter x ray optics
[DE94-016969] p 1562 N95-22191

Gas-dynamic trap diagnostic complex for study on plasma heating and power atomic beam injection
[DE94-633377] p 1529 N95-22283

PLASMA DIFFUSION

Variations of helicon wave induced radial plasma transport in different experimental conditions
[DE94-631410] p 1550 N95-20200

Heating and transport in TFTR D-T plasmas
[DE95-002812] p 1558 N95-21242

PLASMA DRIFT

Theory of the L-H transition
[DE95-001389] p 1558 N95-21299

Collisional drift waves in the H-mode edge
[DE94-628950] p 1561 N95-21847

Very high-power electron-beam transport in long gas cells from 10(exp -3) to 10(exp 3) Torr N2
[DE95-002611] p 1539 N95-22306

PLASMA DYNAMICS

Intense proton beam source for ITER neutral-beam spectroscopy diagnostics
[DE94-018092] p 1560 N95-21668

PLASMA ELECTRODES

Plasma Electrode Pockels Cells for the Beamlet and NIF lasers
[DE94-016541] p 1557 N95-21166

PLASMA EQUILIBRIUM

Ideal Magnetohydrodynamic stabilities in JT-60 and D3-D tokamak plasmas
[DE94-770684] p 1555 N95-20987

PLASMA ETCHING

Ion-molecule chemistry related to plasma deposition and etching of silicon
[AD-A279749] p 1514 N95-20804

A versatile masking process for plasma etched backside via holes in GaAs
[DE94-019176] p 1572 N95-21419

PLASMA GUNS

Magnetically controlled deposition of metals using gas plasma
[DE94-018654] p 1251 N95-20128

Plasma processing for integrated circuits
[DE95-001419] p 1335 N95-22149

PLASMA HEATING

Experimental measurements of ICRF and edge plasma interactions on Tore Supra
[DE94-019154] p 1551 N95-20205

Recent results from Fast Wave Current Drive experiments on DIII-D
[DE94-016718] p 1551 N95-20285

Plasma shape experiments for an optimized tokamak
[DE94-017508] p 1553 N95-20445

Simulation of tearing mode stabilization by using ECH
[DE94-770700] p 1554 N95-20684

The evolution of configuration from q greater than 1 to q less than 1
[DE94-631396] p 1556 N95-21162

The ITER in-vessel system
[DE94-018053] p 1560 N95-21665

Gas-dynamic trap diagnostic complex for study on plasma heating and power atomic beam injection
[DE94-633377] p 1529 N95-22283

PLASMA INTERACTIONS

Experimental measurements of ICRF and edge plasma interactions on Tore Supra
[DE94-019154] p 1551 N95-20205

Preliminary results from the flight of the Solar Array Module Plasma Interactions Experiment (SAMPIE)
p 1321 N95-20529

PLASMA JETS

Recent results from Fast Wave Current Drive experiments on DIII-D
[DE94-016718] p 1551 N95-20285

New high temperature plasmas and sample introduction systems for analytical atomic emission and mass spectrometry
[DE94-018580] p 1552 N95-20345

Enhanced scrape-off layer plasma in D3-D double-null discharges
[DE94-017977] p 1554 N95-20571

Kinematical evidence for top pairs at the Tevatron
[DE95-000729] p 1515 N95-20880

Plasma Electrode Pockels Cells for the Beamlet and NIF lasers
[DE94-016541] p 1557 N95-21166

Electrostatic noise in the plasma environment around the shuttle
[NASA-TM-106856] p 1415 N95-21188

Search for new particles decaying to dijets in p(bar p) collisions at (radical)s = 1.8 TeV
[DE94-018994] p 1523 N95-21563

PLASMA LAYERS

Electromagnetic wave reflection from irregular plasma layers p 1298 N95-20952

Experimental measurements and modeling of impurity transport in the divertor and boundary plasma of D3-D
[DE94-016519] p 1556 N95-21159

PLASMA OSCILLATIONS

Fluctuations and transport in the reversed field pinch: Characterization and reduction
[DE95-000590] p 1549 N95-20113

PLASMA PHYSICS

Soft X-Ray Innovative Source Development Program
[AD-A286380] p 1551 N95-20232

Israel Physical Society Annual Meeting 1994
[DE94-630140] p 1565 N95-20261

24th Annual Anomalous Absorption Conference
[DE94-016457] p 1551 N95-20283

Effects of plasma physics on capsule implosions in gas-filled hohlraums
[DE95-000923] p 1371 N95-20786

Source mechanisms and radio effects of ionospheric plasma disturbances
[AD-A286529] p 1555 N95-21013

PRS scoping study. 2: ZPIMP predictions for radiation yields on a JUPITER-class generator
[AD-A279823] p 1537 N95-21494

Theoretical atomic physics for fusion
[DE94-019196] p 1524 N95-21605

Collisional drift waves in the H-mode edge
[DE94-628950] p 1561 N95-21847

On the influence of electromagnetic wave and relativistic electron beam on a plasma
[DE94-628962] p 1561 N95-21848

On the theory of strong electromagnetic waves propagation in an electron-positron-ion plasma
[DE94-628964] p 1561 N95-21850

Large amplitude localized structures in a relativistic electron-positron ion plasma
[DE94-628965] p 1561 N95-21851

Plasma processing for integrated circuits
[DE95-001419] p 1335 N95-22149

PLASMA PINCH

PRS scoping study 1: Scaling law estimates for K-shell radiation yields on JUPITER-class generators
[AD-A279716] p 1533 N95-20672

PLASMA POTENTIALS

The control system position to the electric probe in the Tokamak Novillo
[DE94-629938] p 1550 N95-20204

Electrostatic noise in the plasma environment around the shuttle
[NASA-TM-106856] p 1415 N95-21188

Plasma model for charging damage
[DE95-000788] p 1558 N95-21310

On the theory of strong electromagnetic waves propagation in an electron-positron-ion plasma
[DE94-628964] p 1561 N95-21850

PLASMA POWER SOURCES

Magnetron power supply at high stability and its application in plasma excitation for the production of ultraviolet radiation
[DE94-629656] p 1326 N95-20733

PLASMA PRESSURE

Fluctuations in high Beta(sub p) plasmas in D3-D
[DE94-017510] p 1550 N95-20146

PLASMA PROBES

Plasma model for charging damage
[DE95-000788] p 1558 N95-21310

PLASMA PROPULSION

Propulsion research on the variable tandem mirror plasma rocket
[NASA-CR-196310] p 1221 N95-20059

PLASMA RADIATION

Power balance in D3-D during single-null ELMing H-mode plasmas
[DE94-016680] p 1554 N95-20568

Large facilities pilot programme. Access to the VULCAN High Power Laser Facilities at Rutherford Appleton Laboratory
[PB95-130340] p 1373 N95-21226

PRS scoping study. 2: ZPIMP predictions for radiation yields on a JUPITER-class generator
[AD-A279823] p 1537 N95-21494

PLASMA SHEATHS

Atomic processes in processing plasmas
[DE94-019177] p 1560 N95-21609

PIC simulation of surface waves
[AD-A285358] p 1563 N95-22422

PLASMA SPRAYING

Magnetically controlled deposition of metals using gas plasma
[DE94-018654] p 1251 N95-20128

Improved die castings through plasma surface modification, improved sensors and die soldering prevention
[DE95-002238] p 1253 N95-20417

PLASMA TEMPERATURE
The control system position to the electric probe in the Tokamak Novillo
[DE94-629938] p 1550 N95-20204
Experimental investigation of molecular beam injection in HL-1 tokamak
[DE94-631456] p 1556 N95-21165
PLASMA TURBULENCE
Fluctuations and transport in the reversed field pinch: Characterization and reduction
[DE95-000590] p 1549 N95-20113
Chaotic phenomena in plasma 3
[DE94-770765] p 1554 N95-20686
The parametric dependence of the spatial structure of the radial electric field at the plasma edge in the D3-D tokamak
[DE94-016520] p 1556 N95-21163
PLASMA WAVES
Advanced detector development, laboratory simulations, diagnostic development, and data analysis on wake physics
[AD-A284798] p 1364 N95-20069
Variations of helicon wave induced radial plasma transport in different experimental conditions
[DE94-631410] p 1550 N95-20200
Recent results from Fast Wave Current Drive experiments on DIII-D
[DE94-016718] p 1551 N95-20285
Source mechanisms and radio effects of ionospheric plasma disturbances
[AD-A286529] p 1555 N95-21013
Collisional drift waves in the H-mode edge
[DE94-628950] p 1561 N95-21847
PIC simulation of surface waves
[AD-A285358] p 1563 N95-22422
PLASMAS (PHYSICS)
X-ray imaging of uniform large scale-length plasmas created from gas-filled targets on Nova
[DE94-018339] p 1531 N95-20015
Toward a design for the ITER plasma shape and stability control system
[DE94-017516] p 1548 N95-20037
Fluctuations in high Beta(sub p) plasmas in D3-D
[DE94-017510] p 1550 N95-20146
Computational modeling of physical processes during laser ablation
[DE94-017699] p 1369 N95-20221
Physics Division research and development
[DE94-017685] p 1501 N95-20246
A method for measuring the inductive electric field profile and noninductive current profiles on D3-D
[DE94-016683] p 1551 N95-20279
A comparison of kinetic and multifluid simulations of laser-produced colliding plasmas
[DE94-016447] p 1551 N95-20315
Plasma arc melting of titanium-tantalum alloys
[DE94-016291] p 1252 N95-20331
Power balance in D3-D during single-null ELMing H-mode plasmas
[DE94-016680] p 1554 N95-20568
Boron carbide-based coatings on graphite for plasma facing components
[DE94-017976] p 1269 N95-20570
Enhanced scrape-off layer plasma in D3-D double-null discharges
[DE94-017977] p 1554 N95-20571
Ion scattering and deposition: The role of energetic particles in thin film growth
[AD-A285975] p 1514 N95-20667
A portable and independent edge fluctuation diagnostic
[DE94-018254] p 1554 N95-20681
Current diffusive ballooning mode in second stability region of tokamaks
[DE94-770690] p 1554 N95-20683
Simulation of tearing mode stabilization by using ECH
[DE94-770700] p 1554 N95-20684
Chaotic phenomena in plasma 3
[DE94-770765] p 1554 N95-20686
Magnetron power supply at high stability and its application in plasma excitation for the production of ultraviolet radiation
[DE94-629656] p 1326 N95-20733
An advanced ECR ion source with a large uniformly distributed ECR plasma volume for multiply charged ion beam generation
[DE95-001078] p 1515 N95-20911
Ideal Magnetohydrodynamic stabilities in JT-60 and D3-D tokamak plasmas
[DE94-770684] p 1555 N95-20987
Ion heat pulse after sawtooth crash in the JFT-2M tokamak
[DE94-770685] p 1555 N95-20988
Cryogenic targets for inertial confinement fusion
[DE94-016200] p 1555 N95-21115
The evolution of configuration from q greater than 1 to q less than 1
[DE94-631396] p 1556 N95-21162
The parametric dependence of the spatial structure of the radial electric field at the plasma edge in the D3-D tokamak
[DE94-016520] p 1556 N95-21163
Experimental investigation of molecular beam injection in HL-1 tokamak
[DE94-631456] p 1556 N95-21165
Large facilities pilot programme. Access to the VULCAN High Power Laser Facilities at Rutherford Appleton Laboratory
[PB95-130340] p 1373 N95-21226
Review of recent D-T experiments from TFTR
[DE95-002755] p 1557 N95-21239
Fusion power production in TFTR
[DE95-002756] p 1557 N95-21240
Heating and transport in TFTR D-T plasmas
[DE95-002812] p 1558 N95-21242
Assessment of database for interaction of tritium with ITER plasma facing materials
[DE95-002038] p 1558 N95-21290
Theory of the L-H transition
[DE95-001389] p 1558 N95-21299
Low density gas and foam targets for ICF long scale length plasma experiments: Fabrication and characterization
[DE95-000935] p 1558 N95-21368
Coronal Mass Ejections in the solar wind at high solar latitudes: An overview
[DE95-000844] p 1603 N95-21377
Similarities and differences in strangeness production at BNL and CERN
[DE95-002343] p 1521 N95-21380
Computer simulation of the diocotron instability
[AD-A285655] p 1559 N95-21403
1994 Nonneutral Plasma Workshop
[AD-A285656] p 1559 N95-21404
Atomic processes in processing plasmas
[DE94-019177] p 1560 N95-21609
Investigation of direct photon production in 200 A GeV S + Au reactions
[DE94-018129] p 1525 N95-21704
Studies of selenium and xenon in inductively coupled plasma mass spectrometry
[DE95-001676] p 1245 N95-21734
Plasma-induced-damage of GaAs during etching of refractory metal contacts
[DE95-001525] p 1259 N95-21838
A syncopated leap-frog algorithm for orbit consistent plasma simulation of materials processing reactors
[DE95-000954] p 1561 N95-21922
A simulation of plasma motion in the polar ionosphere
[AD-A286166] p 1426 N95-22019
Plasma processing for integrated circuits
[DE95-001419] p 1335 N95-22149
PLASMASPHERE
Observations of cold magnetospheric ions at geosynchronous orbit during times of high activity
[DE95-000936] p 1600 N95-21935
Magnetospheric Plasma Analyzer (MPA): Plasma observations from geosynchronous orbit
[DE95-002739] p 1427 N95-22477
PLASTIC ANISOTROPY
Plastic deformation of ordered intermetallic alloys: Fundamental aspects
[DE95-001070] p 1256 N95-21265
PLASTIC DEFORMATION
Inelastic torsion of steel I-beams
[PB94-208360] p 1384 N95-20101
Plastic deformation of ordered intermetallic alloys: Fundamental aspects
[DE95-001070] p 1256 N95-21265
Sheet metal formability
[PB95-110250] p 1258 N95-21653
Forming of superplastic ceramics
[DE94-017306] p 1276 N95-21662
Irradiation creep in structural materials at ITER operating conditions
[DE94-018946] p 1261 N95-22123
Characterization of a texture gradient in tantalum plate
[DE95-002704] p 1262 N95-22289
PLASTIC FLOW
Simulation of the injection moulding process
[PB94-215555] p 1286 N95-21027
Critical dynamics and plastic flow in disordered Josephson junction arrays
[DE94-629074] p 1576 N95-21995
PLASTIC PROPERTIES
Attempt to interpret the self-organizing mapping physiologically
[PB95-127783] p 1438 N95-21112
Netherlands Institute for Brain Research progress report, 1993
[PB95-135398] p 1445 N95-21352
PLASTICIZERS
The development of a new plasticizer for poly(ethylene oxide) based polymer electrolyte and the investigation of their ion-pair dissociation effect
[DE94-016821] p 1276 N95-21644
PLASTICS
Plastic encapsulated parts
[DE95-001876] p 1332 N95-21729
PLATEAUS
Thermodynamic characterization of new palladium alloy tritides
[DE94-018430] p 1579 N95-20028
PLATELETS
Refractive index change in dissociating shocked benzene
[DE94-019015] p 1541 N95-20352
Evaluation of dried storage of platelets for transfusion: Physiologic integrity and hemostatic functionality
[AD-A286078] p 1443 N95-20850
Preclinical investigation of lyophilized platelet preparations
[AD-A286079] p 1443 N95-20851
PLATES (STRUCTURAL MEMBERS)
Analyses of some benchmark cases in fracture mechanics using boundary element method
[PB95-110888] p 1384 N95-19930
Low frequency sound radiation from finite stiffened plates
[AD-A279395] p 1505 N95-21930
PLATINUM
Magnetic x ray circular dichroism in Fe Co Pt multilayers
[DE94-017522] p 1253 N95-20447
Bridging the pressure gap: In situ atomic-level investigations of model platinum catalyst surfaces under reaction conditions by scanning tunneling microscopy
[DE95-002346] p 1246 N95-21990
PLATINUM COMPOUNDS
Modeling of nonlinear optic and ESR response of CDW MX materials
[DE94-018301] p 1578 N95-22297
PLETHYSMOGRAPHY
Acoustic calibration apparatus for calibrating plethysmographic acoustic pressure sensors
[NASA-CASE-LAR-14977-1] p 1443 N95-20763
PLOTTING
PRSPLOT6 manual
[PB95-110862] p 1456 N95-19928
ALCHEMI of Fe-doped B2-ordered NiAl alloys with different doping levels
[DE94-017748] p 1255 N95-20907
PLUMES
Temperature effects on acoustic interactions between altitude test facilities and jet engine plumes
[NASA-CR-197638] p 1504 N95-21170
He, Xe and Ne isotopes in a steady-state mass transport model and implications about terrestrial volatiles
p 1425 N95-21821
Launch safety, toxicity, and environmental effects of the high performance oxidizer ClF(5)
[AD-A286095] p 1284 N95-22227
PLUTONIUM
The interaction of localized solutions in a surface reaction
[DE95-002736] p 1248 N95-22433
PLUTONIUM COMPOUNDS
Actinide(IV) and actinide(VI) carbonate speciation studies by PAS and NMR spectroscopies
[DE94-016957] p 1236 N95-20361
PLUTONIUM ISOTOPES
Advanced concepts for gamma ray isotopic analysis and instrumentation
[DE94-016610] p 1517 N95-21174
PLY ORIENTATION
The influence of ply waviness with nonlinear shear on the stiffness and strength reduction of composite laminates
[AD-A285736] p 1224 N95-19899
Nucleation, growth, and strain relaxation of lattice-mismatched 3-5 semiconductor epitaxial layers
p 1324 N95-20543
PODS (EXTERNAL STORES)
Airborne Multisensor Pod System (AMPS) data access concept
[DE95-002586] p 1389 N95-20903
POINCARE PROBLEM
Almost kappa-wise independent random permutation of the cube
[PB95-108098] p 1495 N95-22147
POINT DEFECTS
Defect production and recombination during low-energy ion processing
[DE95-001827] p 1572 N95-21304
The role of point defects and defect complexes in silicon device processing
[DE94-011876] p 1279 N95-22091

Bulk and defect properties of ordered intermetallics
[DE94-017706] p 1262 N95-22344

POINT SOURCES

High precision Woelter optic calibration facility
[DE94-016973] p 1542 N95-20364
In search of random noise p 1592 N95-21753
High resolution descriptions of IRAS 12 and 25 microns confused regions
[AD-A285847] p 1545 N95-21832

POINT TO POINT COMMUNICATION

MPI workshop
[DE94-017883] p 1475 N95-20366
Design and modelling of a link monitoring mechanism for the Common Data Link (CDL)
[AD-A286167] p 1309 N95-22245

POINTS (MATHEMATICS)

Tracking a dynamic set of feature points
[AD-A285124] p 1313 N95-20257

POISSON EQUATION

Analysis of a local defect correction approach on composite grids
[PB95-135455] p 1493 N95-21574
Image solution for poisson's equation in wedge geometry
[PB95-127171] p 1310 N95-22311
Locking of the finite element method in thermoelasticity
[PB95-127098] p 1496 N95-22370

POISSON RATIO

Compositive piezoelectrics utilizing a negative Poisson ratio polymer
[AD-D016579] p 1268 N95-20460

POLAR CAPS

The relative importance of meteor burst and other distance polar cap propagation modes in the low VHF band p 1293 N95-20928

POLAR COORDINATES

A control volume method on an icosahedral grid for numerical integration of the shallow-water equations on the sphere
[DE94-016345] p 1489 N95-20170

POLAR METEOROLOGY

A simulation of plasma motion in the polar ionosphere
[AD-A286166] p 1426 N95-22019

POLAR REGIONS

Mitigation of the effects of F layer regularities by using multiple paths p 1298 N95-20951
DAMSON: A system to measure multipath dispersion, Doppler spread and Doppler shift on multi-mechanism communications channels p 1299 N95-20955
Coronal Mass Ejections in the solar wind at high solar latitudes: An overview
[DE95-000844] p 1603 N95-21377
An experimental determination of meteor daily arrival rate variation
[AD-A279484] p 1600 N95-21679
Arcmimute scale HI and IRAS observations toward high latitude cloud G86.5+59.6 p 1594 N95-21771
Polar volatiles on Mercury and the Moon
p 1422 N95-21811

POLAR SUBSTORMS

Substorm theories: United they stand, divided they fall
[NASA-CR-197672] p 1427 N95-22326

POLARIMETRY

Identification of the propagation modes and paths on HF links using a goniopolarimeter p 1299 N95-20956

POLARIZATION

Magnetoelectric properties of reciprocal bianisotropic materials with focus on the polarizability of chiro-omega spheres
[PB95-127650] p 1544 N95-21103
Ultraviolet laser emission properties of Ce(3+)-doped LiSrAlF6
[DE94-016364] p 1372 N95-21135
Hadron beams and accelerators
[DE95-002932] p 1536 N95-21342

POLARIZATION (CHARGE SEPARATION)

Magnetic flocculation of paramagnetic particles
[DE94-018144] p 1501 N95-20725
Measurement of the polarization in the decay B(sup 0) (yields) J/(psi)K*(sup 0) in (bar p)p collisions at (radical)s = 1.8 TeV
[DE95-002521] p 1520 N95-21313

POLARIZATION (SPIN ALIGNMENT)

Spin dependence of diffractive processes and implications for the small x behaviour of g1 and the spin content of the nucleon
[PB95-130332] p 1518 N95-21225

POLARIZATION (WAVES)

Measurements of angles of elevation of HF by a high resolution method using polarization diversity
p 1299 N95-20959
Polarization of charmonium in pion-nucleus collisions
[DE95-002783] p 1523 N95-21525
Electric-field effects on shallow donor impurity in a harmonic quantum dot
[DE94-629034] p 1577 N95-22176
Image theory for the unidirectionally conducting screen
[PB95-127031] p 1311 N95-22365

POLARIZATION CHARACTERISTICS

Dielectric mixtures with arbitrarily anisotropic components: Focus on special gyrotropic effects
[PB95-127015] p 1311 N95-22363

POLARIZED RADIATION

Technical digest: Eighth Symposium on Optical Fiber Measurements
[PB94-207636] p 1540 N95-19976

POLARIZERS

A neutron beam polarizer for study of parity violation in neutron-nucleus interactions
[DE95-002743] p 1519 N95-21237

POLARONS

Conducting thermoset polymers
[AD-A286541] p 1273 N95-21014
Second order approximation for optical polaron in the strong coupling case
[DE94-628997] p 1525 N95-21856
Uniform upper bounds in the Froehlich polaron theory
[DE94-628998] p 1525 N95-21860
Temperature dependence of a magnetopolaron in a harmonic quantum dot in resonant magnetic fields
[DE94-629036] p 1502 N95-22177
Temperature dependence of magnetopolarons in a parabolic quantum dot in arbitrary magnetic fields
[DE94-629033] p 1528 N95-22218

POLICIES

Patterns of financial change in the OECD area
[PB95-110979] p 1594 N95-19939
Workshop on Uncertainty and Global Climate Change Research
[DE94-016728] p 1401 N95-20238
The MSFC Program Control Development Program
p 1585 N95-20754
Policies concerning military and civilian research and technology applications
[PB95-131355] p 1585 N95-21427
Definition report on target and related steering variables of radiation as a part of the environmental balance and environmental outlook investigation
[PB95-135471] p 1409 N95-21846

POLISHING

Numerical controlled polishing program, continued forced wear and part correction experiments
[DE94-018084] p 1285 N95-20288

POLLUTION CONTROL

Mercury usage and alternatives in the electrical and electronics industries
[PB94-165362] p 1312 N95-19966
Proceedings of the 1993 Non-Fluorocarbon Insulation, Refrigeration and Air Conditioning Technology Workshop
[DE94-018333] p 1285 N95-20194
Environmental Compliance Assessment and Management Program
[AD-A279605] p 1402 N95-20441
Energy impacts of controlling carbon dioxide emissions from an integrated gasification/combined-cycle system
[DE94-016878] p 1403 N95-20478
Progress in the development of recycling processes for electric vehicle batteries
[DE94-015894] p 1324 N95-20626
Energy and environmental issues and international opperation in Asia
[DE94-796596] p 1404 N95-21143
Reducing exhaust gas emissions from Citydiesel busses
[DE95-700245] p 1380 N95-21295
New concepts for refrigerant leak detection and mixture measurement
[DE94-018967] p 1287 N95-21559
Comparison of HFC-134a and the ternary blend, Suva MP39, as replacements for the refrigerant, CGC-12
[MRL-GD-0051] p 1287 N95-21625
Gas-phase photocatalytic oxidation: Cost comparison with other air pollution control technologies
[DE95-000241] p 1410 N95-22278
Use of the carbo-flo process to purify process water contaminated by agricultural pesticides
[PB95-127825] p 1410 N95-22330

POLLUTION MONITORING

Resonance Raman spectroscopy of volatile organics: Carbon tetrachloride
[DE95-000627] p 1233 N95-19980
Proceedings of the 1993 Non-Fluorocarbon Insulation, Refrigeration and Air Conditioning Technology Workshop
[DE94-018333] p 1285 N95-20194
Performance specifications for technology development: Application for characterization of volatile organic compounds in the environment
[DE94-016627] p 1401 N95-20234
An application of wavelet transform for decomposition of millimeter-wave spectroscopic signals
[DE94-018366] p 1402 N95-20247
Environmental Compliance Assessment and Management Program
[AD-A279605] p 1402 N95-20441
Monitoring bioremediation of Volatile Organic Compounds (VOCs) using Fourier Transform Infrared (FT-IR) spectrometry
[AD-A279631] p 1403 N95-20456
Progress in the development of recycling processes for electric vehicle batteries
[DE94-015894] p 1324 N95-20626
Evaluation of the technical performance of the Duttch National Air Quality Monitoring Network in 1992
[PB95-131892] p 1405 N95-21327
Ozone quality control measurements in the Dutch National Air Quality Monitoring Network
[PB95-131900] p 1405 N95-21329
Monitoring activities in the framework of the Dutch National Air Quality Monitoring Network in 1994
[PB95-131884] p 1406 N95-21351
Spectroscopic studies of hazardous fuel interactions with soils
[AD-A279099] p 1407 N95-21596
Removal of CO2 in closed loop off-gas treatment systems
[DE94-019259] p 1407 N95-21617
Current concepts on airborne particles and health
[DE95-002260] p 1447 N95-22287

POLLUTION TRANSPORT

Implementation and performance of a three-dimensional numerical transport model
[PB95-135745] p 1402 N95-20440
Launch safety, toxicity, and environmental effects of the high performance oxidizer ClF(5)
[AD-A286095] p 1284 N95-22227
Current concepts on airborne particles and health
[DE95-002260] p 1447 N95-22287

POLOIDAL FLUX

A method for measuring the inductive electric field profile and noninductive current profiles on D3-D
[DE94-016683] p 1551 N95-20279

POLYACETYLENE

The organic chemistry of conducting polymers
[DE94-018216] p 1270 N95-20680

POLYACRYLONITRILE

Fibre-reinforced high-strength concrete
[PB95-131942] p 1232 N95-22158

POLYAMIDE RESINS

Reactive compatibilization of polymer blends
[AD-A284836] p 1263 N95-19893

POLYATOMIC GASES

Plasma chemistry of vibrationally nonequilibrium molecules
[AD-A279630] p 1553 N95-20411

POLYCHLORINATED BIPHENYLS

The impact of advanced packaging technology on modular avionics architectures p 1208 N95-20632

POLYCRYSTALS

Elastic anisotropy in hot-pressed Si3N4 composites: Role of in situ (beta)-Si3N4 grains and added (beta)-Si3N4 whiskers
[DE94-018387] p 1226 N95-20027
Polycrystalline thin film cadmium telluride solar cells fabricated by electrodeposition
[DE94-011848] p 1391 N95-20118
Polycrystalline CuInSe2 and CdTe solar cells
[DE94-011875] p 1392 N95-20333
Hierarchical structure in advanced polymers. Phase behaviour, orientation, properties
[AD-A285938] p 1268 N95-20392
Mean field analysis of orientation selective grain growth driven by interface-energy anisotropy
[DE94-015797] p 1566 N95-20399
Status of flexible CIS research at ISET
p 1317 N95-20512
Advances in polycrystalline thin-film photovoltaics for space applications p 1318 N95-20514
Molecularly Designed Ultrafine/Nanostructured Materials, volume 351
[AD-A285370] p 1568 N95-20552
Sputtering of tin and gallium-tin clusters
[DE94-018389] p 1254 N95-20707
Dependence of critical current density on microstructure and processing of high-T(c) superconductors
[DE95-000685] p 1571 N95-21167
Deposition and properties of novel nitride superlattice coatings
[DE95-002945] p 1230 N95-21445
Effects of neutron irradiation on the London penetration depth for polycrystalline Bi(1.8)Pb(0.3)Sr2Ca2Cu3O10 superconductor
[DE94-019335] p 1573 N95-21483

Aligned bismuth, strontium, calcium cuprate coatings on polycrystalline substrates
[AD-D016512] p 1278 N95-21907
Polycrystalline PLZT/ITO ceramic electro-optic phase gratings: Electro-optically reconfigurable difffractive devices for free-space and in-wafer interconnects
[AD-A285861] p 1547 N95-22076
Surface technology programme
[PB95-132866] p 1262 N95-22174
Influence of wavelength on transient short-circuit current in polycrystalline silicon solar cells
[DE94-629082] p 1397 N95-22183
Local texture and strongly linked conduction in spray-pyrolyzed TlBa2Ca2Cu3O(8+x) deposits
[DE94-017887] p 1578 N95-22269
Characterization of a texture gradient in tantalum plate
[DE95-002704] p 1262 N95-22289

POLYCYCLIC AROMATIC HYDROCARBONS
Aromatics oxidation and soot formation in flames
[DE95-001803] p 1241 N95-21280

POLYETHYLENE TEREPHTHALATE
Determinations of phase transitions in nylon 6-12, nylon-6, polyvinyl chloride and polyethylene terephthalate by positron annihilation spectroscopy
[DE94-629992] p 1239 N95-20736

POLYETHYLENES
Orientation studies of polyolefins by IR-dichroism
[PB95-104386] p 1236 N95-20256
Morphology of highly textured [illegible]/EP diblock copolymers
[AD-A279813] p 1269 N95-20582
The development of a new plasticizer for poly(ethylene oxide) based polymer electrolyte and the investigation of their ion-pair dissociation effect
[DE94-016821] p 1276 N95-21644
Investigation on research for degradable plastics
[DE94-796550] p 1277 N95-21714
Neutron reflectivity study of adsorbed diblock copolymers
[DE95-002740] p 1281 N95-22434

POLYHEDRONS
Balanced matrices
[AD-A280021] p 1490 N95-20662

POLYIMIDES
Thianthrene containing polyimides with monomer formation via nucleophilic aromatic substitution
[AD-A286313] p 1265 N95-20094
A direct process for preparing semi-crystalline polyimides
[NASA-CASE-LAR-15020-1] p 1268 N95-20407
Embedded optical fibres as strain sensors in polymer matrix fibre composites: The influence of adhesion in strain transfer
[PB95-133617] p 1547 N95-22140
Solid-state NMR characterization of C- and N-labelled phthalimides: Model compounds for studying polyimides
[AD-A286479] p 1578 N95-22286

POLYMER BLENDS
Reactive compatibilization of polymer blends
[AD-A284836] p 1263 N95-19893
Orientation studies of polyolefins by IR-dichroism
[PB95-104386] p 1236 N95-20256

POLYMER CHEMISTRY
Reactive compatibilization of polymer blends
[AD-A284836] p 1263 N95-19893
Technical Summary for 1993 fall MRS Symposium O, Complex Fluids
[AD-A283722] p 1264 N95-19972
Synthesis and characterization of poly(organophosphazene) interpenetrating polymer networks
[AD-A279872] p 1265 N95-20183
Radiation-induced modifications of allylamino-substituted polyphosphazenes
[AD-A279694] p 1268 N95-20428
The organic chemistry of conducting polymers
[DE94-018216] p 1270 N95 20680
Siloxanes with strong hydrogen bond donating functionalities
[AD-D016499] p 1279 N95-22057

POLYMER MATRIX COMPOSITES
Design, synthesis and characterization of novel nonlinear optical materials
[AD-A285617] p 1540 N95-19897
Thermo-mechanical fatigue of polymer matrix composites
[AD-A285931] p 1267 N95-20390
Compositive piezoelectrics utilizing a negative Poisson ratio polymer
[AD-D016579] p 1268 N95-20460
The 29th MIL-HDBK-17 Polymer Matrix Composites Coordination Group Meeting
[AD-A279917] p 1269 N95-20578
Implementation of the military handbook 17 for polymer matrix composites and metal matrix composites
[AD-A285629] p 1229 N95-21149
Implementation of the military handbook 17 for polymer matrix composites and metal matrix composites
[AD-A285595] p 1229 N95-21215
Embedded optical fibres as strain sensors in polymer matrix fibre composites: The influence of adhesion in strain transfer
[PB95-133617] p 1547 N95-22140
Implementation of the Military Handbook 17 for polymer matrix composites and metal matrix composites
[AD-A285772] p 1233 N95-22395

POLYMER PHYSICS
Nonlinear optical studies of polymer interfaces
[DE94-018199] p 1274 N95-21263
Extrudate swell and extrudate distortion of HDPE as a result of different deformation mechanisms during extrusion through capillary dies
[PB95-110227] p 1288 N95-21651
High temperature polymer for second order nonlinear optics for photonic materials
[AD-A279309] p 1280 N95-22141

POLYMERIC FILMS
Thianthrene containing polyimides with monomer formation via nucleophilic aromatic substitution
[AD-A286313] p 1265 N95-20094
Vacuum holding fixture and method for fabricating piezoelectric polymer acoustic sensors
[NASA-CASE-LAR-14240-1] p 1268 N95-20410

POLYMERIZATION
Thianthrene containing polyimides with monomer formation via nucleophilic aromatic substitution
[AD-A286313] p 1265 N95-20094
Synthesis and characterization of poly(organophosphazene) interpenetrating polymer networks
[AD-A279872] p 1265 N95-20183
Polyurethane-acrylic interpenetrating polymer network acoustic damping material
[AD-D016572] p 1266 N95-20294
The synthesis and characterization of new mesogenic diacetylene monomers and their polymers
[AD-A286188] p 1267 N95-20328
Radiation-induced modifications of allylamino-substituted polyphosphazenes
[AD-A279694] p 1268 N95-20428
Macromolecular and materials design using polyphosphazenes
[AD-A279781] p 1273 N95-20978
Tailoring suspension flow for the gelcasting of oxide and nonoxide ceramics
[DE95-001351] p 1277 N95-21861
Synthesis of polymeric microcapsule arrays and their use for enzyme immobilization
[AD-A279125] p 1277 N95-21876
Chemistry and electrochemistry in Lewis acid and superacid ionic liquids
[AD-A279396] p 1246 N95-21931

POLYMERS
The preparation of all para-polyphenyls with increased solubility and enhanced third order NLO activity
[AD-A284301] p 1266 N95-20251
Hierarchical structure in advanced polymers. Phase behaviour, orientation, properties
[AD-A285938] p 1268 N95-20392
Photophysical processes on triplet states and radical ions in pure and molecularly doped polymers
[DE95-002681] p 1570 N95-20916

POLYMETHYL METHACRYLATE
Topography of neutron scattering from diblock copolymer film
[DE95-001457] p 1229 N95-20840
Influence of fatigue crack closure on the growth rate of surface flaws
[AD-A279130] p 1387 N95-21967

POLYNOMIALS
K(1,3)-free and W(4)-free graphs
[PB95-110573] p 1456 N95-19889
Graded dual of the non-commutative universal Leibniz Hopf algebra zeta
[PB95-134532] p 1494 N95-21955
Balanced 0, + or - matrices. Part 2: Recognition algorithm
[AD-A279156] p 1470 N95-21974
Local connectivity of some Julia sets containing a circle with an irrational rotation
[PB95-109070] p 1496 N95-22353
FORTRAN subroutine for column reduction of polynomial matrices
[PB95-134987] p 1497 N95-22379

POLYNUCLEOTIDES
The molecular mechanics program DUPLEX: Computing structures of carcinogen modified DNA by surveying the potential energy surface
[DE94-019153] p 1439 N95-21606

POLYPHENYL ETHER
Lubricant evaluation and performance, 2
[AD-A279144] p 1278 N95-21969

POLYPHENYLS
The preparation of all para-polyphenyls with increased solubility and enhanced third order NLO activity
[AD-A284301] p 1266 N95-20251

POLYPROPYLENE
Orientation studies of polyolefins by IR-dichroism
[PB95-104386] p 1236 N95-20256
Fibre-reinforced high-strength concrete
[PB95-131942] p 1232 N95-22158

POLYPYRROLES
Synthesis of polymeric microcapsule arrays and their use for enzyme immobilization
[AD-A279125] p 1277 N95-21876

POLYSILANES
The electronic properties of polysilanes
[DE94-006464] p 1265 N95-20121

POLYSTYRENE
Topography of neutron scattering from diblock copolymer film
[DE95-001457] p 1229 N95-20840
Investigation on research for degradable plastics
[DE94-796550] p 1277 N95-21714
Neutron reflectivity study of adsorbed diblock copolymers
[DE95-002740] p 1281 N95-22434

POLYTETRAFLUOROETHYLENE
Characterization of poly(tetrafluoroethylene) surfaces by atomic force microscopy: Results and artifacts
[DE95-000742] p 1242 N95-21309

POLYURETHANE RESINS
Polyurethane-epoxy interpenetrating polymer network acoustic damping material
[AD-D016567] p 1266 N95-20293
Microbial degradation of polymers used in electronics
[AD-A286526] p 1273 N95-21011
Polyurethane self-priming topcoats
[AD-D016204] p 1274 N95-21154
Polyurethane self-priming topcoats
[AD-D016205] p 1274 N95-21155

POLYVINYL CHLORIDE
Determinations of phase transitions in nylon 6-12, nylon-6, polyvinyl chloride and polyethylene terephthalate by positron annihilation spectroscopy
[DE94-629992] p 1239 N95-20736

POMERONS
New strong interactions above the electroweak scale
[DE94-018385] p 1506 N95-20025
Hard diffraction and rapidity gaps
[DE95-000565] p 1507 N95-20111
Antishadowing contribution to the pomeron structure function
[PB95-127478] p 1518 N95-21221

PONDS
Aquatic plant control research program. Ecological assessment of Kirk Pond
[AD-A279090] p 1409 N95-21914

PONTRYAGIN PRINCIPLE
Optimal control of a two wheeled mobile robot
[AD-A286130] p 1485 N95-22233

POPULATION THEORY
Environmental Hazards Assessment Program
[DE94-019075] p 1406 N95-21565

POPULATIONS
Environmental cleanup: Too many high priority sites impede DOD's program. Report to the Chairman, Committee on Governmental Affairs, US Senate
[AD-A279511] p 1407 N95-21683

POROSITY
An investigation of the applicability of the new ion exchange resin, Reillex(TM)-HPQ, in ATW separations
[DE94-016576] p 1274 N95-21234
Transportation of volatile elements in thermally evolving planetesimals: An important role of metallic iron
p 1418 N95-21790
Governing equations for multiphase heat and mass transfer in hygroscopic porous media with applications to clothing materials
[AD-A286418] p 1357 N95-22206
Absorption of water and lubricating oils into porous nylon
[NASA-CR-197344] p 1280 N95-22383

POROUS MATERIALS
Governing equations for multiphase heat and mass transfer in hygroscopic porous media with applications to clothing materials
[AD-A286418] p 1357 N95-22206
Separation of proteins by convective electrophoresis through a porous membrane
[PB95-127130] p 1248 N95-22373

PORPHINES
Calculation of atom-centered partial charges for heme
[DE94-014447] p 1520 N95-21375

PORTABLE EQUIPMENT
A portable and independent edge fluctuation diagnostic
[DE94-018254] p 1554 N95-20681

Electromagnetic interference testing and electrical subsystem: Non-communication
[AD-A286591] p 1292 N95-20858
Advanced concepts for gamma ray isotopic analysis and instrumentation
[DE94-016610] p 1517 N95-21174

POSITION (LOCATION)
SAR image registration in absolute coordinates using GPS carrier phase position and velocity information
[DE94-018738] p 1204 N95-20195
The GPS Burst Detector W-Sensor
[DE94-017406] p 1204 N95-20269
Emitter location via Kalman filtering of signal time difference of arrival
[AD-A285972] p 1291 N95-20666
Muon beamline at ISIS
[PB95-130324] p 1518 N95-21224
Localization phenomenon in some random classical systems
[AD-A286514] p 1309 N95-22215
Layered path planning for an autonomous mobile robot
[AD-A286138] p 1485 N95-22244
Inverse and control problems in electromagnetics
[AD-A286438] p 1310 N95-22250
Large-scale fields and flows in the magnetosphere-ionosphere system
[PB95-134664] p 1427 N95-22368

POSITION ERRORS
Orbit determination of highly elliptical Earth orbiters using improved Doppler data-processing modes
p 1218 N95-21533

POSITION SENSING
Unknown-terrains navigation of a mobile robot using an array of sonars
[DE94-017902] p 1482 N95-21385

POSITIONING
Impact of propagation mechanisms on global navigation satellite system performance p 1298 N95-20950

POSITRON ANNIHILATION
Positron annihilation studies of organic superconductivity
[DE94-018371] p 1564 N95-20017
Determinations of phase transitions in nylon 6-12, nylon-6, polyvinyl chloride and polyethylene terephthalate by positron annihilation spectroscopy
[DE94-629992] p 1239 N95-20736
Universality of particle multiplicities
[DE95-000727] p 1515 N95-20879
Where are we going with Bose-Einstein: A mini review
[PB95-130308] p 1518 N95-21222
Muon beamline at ISIS
[PB95-130324] p 1518 N95-21224
The role of point defects and defect complexes in silicon device processing
[DE94-011876] p 1279 N95-22091

POSITRONS
Positron annihilation studies of organic superconductivity
[DE94-018371] p 1564 N95-20017
Calculation of the total and total ionization cross sections for positron scattering on atomic hydrogen
[DE94-631341] p 1508 N95-20197
Positron implantation profiles in elemental and multilayer systems
[DE94-014876] p 1566 N95-20382
Search for right-handed currents in the decay chain of K(+) yields muon(+)nu(sub muon), muon(+) yields e(+)nu(sub e)nu(bar)(sub muon)
[DE94-770606] p 1514 N95-20756
Muon beamline at ISIS
[PB95-130324] p 1518 N95-21224
Measuring A(sub b) with polarized beams at SLC
[DE95-002865] p 1519 N95-21248
1994 Nonneutral Plasma Workshop
[AD-A285656] p 1559 N95-21404
On the theory of strong electromagnetic waves propagation in an electron-positron-ion plasma
[DE94-628964] p 1561 N95-21850

POSTFLIGHT ANALYSIS
Post-flight investigation programmes of recently retrieved solar generators p 1321 N95-20531

POSTURE
Helicopter crewseat cushion program
[AD-A286654] p 1452 N95-20973
Quantitative evaluation of wrist posture and typing performance: A comparative study of 4 computer keyboards
[DE95-002392] p 1452 N95-21358

POTASSIUM
Recent photoabsorption measurements in the rare gases and alkalis in the 3 to 15 keV photon energy region
[DE94-019278] p 1521 N95-21406
Ion charge-state production and photoionization near the K edge in argon and potassium
[DE95-001443] p 1522 N95-21502
Semi-volatiles at Mercury: Sodium (Na) and potassium (K) p 1424 N95-21818

POTASSIUM HYDROXIDES
The application of electrodialysis to extend the lifetime of commercial electroplating baths
[DE95-000868] p 1246 N95-22012

POTASSIUM OXIDES
Angle resolved photoemission on K(0.3)Mo3, TiTe2 and Ti(1+x)S2
[DE94-018300] p 1574 N95-21712

POTENTIAL ENERGY
Modeling of high efficiency solar cells under laser pulse for power beaming applications p 1318 N95-20516
Calculated heats of formation of some predicted stable C, N, O, F molecules
[AD-A285957] p 1517 N95-21127
Consequences of oscillatory potentials and angular forces in transition metals and their aluminides
[DE94-019127] p 1258 N95-21600
The molecular mechanics program DUPLEX: Computing structures of carcinogen modified DNA by surveying the potential energy surface
[DE94-019153] p 1439 N95-21606
Electronic structure and energies of alkaline earth oxides: MgO, CaO and SrO
[DE94-628990] p 1575 N95-21853
Ab initio potential energy surface for H + OCS reactions: Extended basis sets and correlation treatment
[AD-A286420] p 1247 N95-22207
Low rotational drag in high-temperature superconducting bearings
[DE95-002983] p 1382 N95-22292
A multisite interaction expansion of the total energy in metals
[DE94-017175] p 1262 N95-22313

POTENTIAL FLOW
Mixing and dynamics of the Mediterranean outflow
[AD-A279803] p 1434 N95-21306
Potential flow downstream of the heliospheric terminal shock: A non-spherical shock
[NASA-TM-110493] p 1426 N95-21874

POTENTIAL THEORY
Full potential multiple scattering theory
[DE95-003197] p 1576 N95-22084
Image solution for poisson's equation in wedge geometry
[PB95-127171] p 1310 N95-22311

POWDER (PARTICLES)
Method of making copper-titanium nitride alloy
[AD-D016582] p 1252 N95-20201
Molecularly Designed Ultrafine/Nanostructured Materials, volume 351
[AD-A285370] p 1568 N95-20552
Reactive nanophase oxide additions to melt-processed high-T(sub c) superconductors
[DE95-001470] p 1570 N95-20841
Role of internal stresses in fracture behavior of engineering composites
[DE95-001106] p 1229 N95-20912
Application of new synchrotron powder diffraction techniques to anomalous scattering from glasses
[DE94-019285] p 1536 N95-21407
Investigation on research for degradable plastics
[DE94-796550] p 1277 N95-21714

POWDER METALLURGY
The mechanical property data base from an Air Force/Industry cooperative test program on advanced aluminum alloys
[AD-A280038] p 1386 N95-20615
The development of a super-alpha2 titanium aluminide alloy consolidated by rapid omnidirectional compaction
[AD-A279254] p 1260 N95-21986
Surface technology programme
[PB95-132866] p 1262 N95-22174
Processing of intermetallic materials by reaction synthesis
[DE94-017710] p 1263 N95-22345

POWDERED ALUMINUM
The processing and mechanical properties of high temperature/high performance composites. Processing/property correlations, book 4
[AD-A279739] p 1228 N95-20802
Oxidation behavior of aluminum nanopowders
[DE95-002721] p 1260 N95-21926

POWER AMPLIFIERS
Hybrid high power amplifier
[AD-D016534] p 1326 N95-20730
Solid state frequency conversion technology for remote sensing
[DE94-019102] p 1389 N95-21433

POWER BEAMING
Transition-energy crossing with a gamma(sub t)(-)jump
[DE94-017315] p 1531 N95-20021
Modeling of high efficiency solar cells under laser pulse for power beaming applications p 1318 N95-20516
Shot-to-shot comparison of the first Li-beam driven Hohlraum experiments
[DE94-016558] p 1558 N95-21247

POWER CONDITIONING
Space power facility readiness for Space Station power system testing
[NASA-TM-106829] p 1218 N95-21384

POWER CONVERTERS
Trimode Power Converter optimizes PV, diesel and battery energy sources
[DE94-015014] p 1313 N95-20262
P/N In(Al) GaAs multijunction laser power converters
p 1323 N95-20539

POWER EFFICIENCY
P/N In(Al) GaAs multijunction laser power converters
p 1323 N95-20539
Hybrid high power amplifier
[AD-D016534] p 1326 N95-20730
EAGLES 1.1: A microcomputer software package for analyzing fuel efficiency of electric and gasoline vehicles
[DE95-001119] p 1469 N95-21829

POWER FACTOR CONTROLLERS
Communications and control for electric power systems: Power system stability applications of artificial neural networks
[NASA-CR-197594] p 1483 N95-21613

POWER LIMITERS
Optical power limiting liquid crystal composites
[AD-A286605] p 1569 N95-20767

POWER LINES
Fault detection techniques for complex cable shield topologies
[AD-A286632] p 1291 N95-20771
TIM-SCT cable testing protocol
[AD-A286633] p 1207 N95-20772

POWER LOSS
Nickel hydroxide electrodes in reduced-alkalinity electrolytes
[DE95-002333] p 1326 N95-20814
Low rotational drag in high-temperature superconducting bearings
[DE95-002983] p 1382 N95-22292

POWER PLANTS
Trimode Power Converter optimizes PV, diesel and battery energy sources
[DE94-015014] p 1313 N95-20262
Analyses of grounded and ungrounded photovoltaic power systems
[DE94-015015] p 1391 N95-20263
Performance and cost analysis of monolithic solid oxide fuel cells
[DE95-002511] p 1394 N95-20896
Economic feasibility analysis of distributed electric power generation based upon the natural gas-fired fuel cell
[DE94-012277] p 1396 N95-22033

POWER SERIES
Six-dimensional modeling of coherent bunch instabilities and related feedback systems in storage rings with power-series maps for the lattice
[DE94-017965] p 1532 N95-20494
Graded dual of the non-commutative universal Leibniz Hopf algebra zeta
[PB95-134532] p 1494 N95-21955

POWER SPECTRA
Pressure and higher-order spectra for homogeneous isotropic turbulence p 1343 N95-21045
BASIC program for power spectrum estimation
[DE95-002228] p 1468 N95-21515
A preliminary study of the airwake model used in an existing SH-60B/FFG-7 helicopter/ship simulation program
[DSTO-TR-0015] p 1201 N95-21659
Derived gust spectra for the Macchi MB326H
[ARL-TN-3] p 1202 N95-21892
1/f noise in two-dimensional fluids
[DE95-002617] p 1358 N95-22307

POWER SUPPLIES
Analyses of grounded and ungrounded photovoltaic power systems
[DE94-015015] p 1391 N95-20263
Design and construction of the HSX experiment
[DE94-018657] p 1552 N95-20348
Mars power system concept definition study. Volume 2: Appendices
[NASA-CR-195420-VOL-2] p 1396 N95-21953
Radiation tests on service electronics for future multi TeV detectors
[DE94-632822] p 1335 N95-22184

POWER SUPPLY CIRCUITS
Design of power electronics for TVC and EMA systems
[NASA-CR-196540] p 1312 N95-19909

PREAMPLIFIERS

Analysis of direct detection lightwave systems with optical amplifiers
[AD-A284077] p 1542 N95-20467

Monolithic low noise preamplifier for piezoelectric sensors
[AD-D016524] p 1333 N95-21865

Pre-amplifier with multi-stage feedback
[AD-D016254] p 1336 N95-22418

PRECAMBRIAN PERIOD

Volatiles in the Earth: All shallow and all recycled
p 1416 N95-21779

PRECESSION

Luminosity polarization correlation in the SLC
[DE95-002889] p 1536 N95-21335

PRECIPITATES

A direct process for preparing semi-crystalline polyimides
[NASA-CASE-LAR-15020-1] p 1268 N95-20407

Zirconia precipitates and zirconia: GeO2 interphase in mullite matrix-SiC woven fabrics composites prepared through a sol-gel route
[PB95-133427] p 1275 N95-21272

PRECISION

Test reliability and experimental power
[AD-A279607] p 1448 N95-19957

Virtual reality in precision engineering research
[AD-A286528] p 1465 N95-21012

PRECONDITIONING

Preconditioning via asymptotically-defined domain decomposition
[DE94-019046] p 1493 N95-21564

PREDICTION ANALYSIS TECHNIQUES

Atlas of SSM/I satellite ice concentration interpolated to operational ice model domains of the Arctic for 1993
[AD-A280183] p 1432 N95-20012

Application of an energy-based life prediction model to bithermal and thermomechanical fatigue
[NASA-TM-106684] p 1385 N95-20179

Monthly mean sea ice data from the Polar Ice Prediction System, the Regional Polar Ice Prediction System-Barents Sea and the Regional Polar Ice Prediction System-Greenland Sea
[AD-A280095] p 1433 N95-21018

Gate oxide shorts in nMOS transistors: Electrical properties and lifetime prediction method
[DE94-018904] p 1330 N95-21545

Forecasting aircraft mishaps using monthly maintenance reports
[AD-A286049] p 1203 N95-22417

Large-eddy simulation of a boundary layer with concave streamwise curvature p 1360 N95-22450

PREDICTIONS

Residual stresses in material processing
[DE94-017868] p 1385 N95-20374

Geometric moire method of strain analysis with displacement discontinuities
[DE95-001114] p 1386 N95-20833

Thermal decomposition reactions of HMX and RDX and their importance in predicting cookoff hazards
[DE95-002486] p 1283 N95-21513

Fluid dynamics of the freeboard in a fluidized bed reactor
[PB95-134029] p 1357 N95-22160

PREDICTOR-CORRECTOR METHODS

Explicit parallel two-step Runge-Kutta-Nystroem methods
[PB95-135752] p 1489 N95-20423

Parallelism across the steps in iterated Runge-Kutta methods for stiff initial value problems
[PB95-135760] p 1490 N95-20424

Parallel predictor-corrector methods
[PB95-135711] p 1493 N95-21434

PRELAUNCH TESTS

Military standard: Test requirements for launch, upper-stage, and space vehicles
[AD-A286627] p 1218 N95-20770

PREMIXED FLAMES

Direct numerical simulations of turbulent non-premixed methane-air flames modeled with reduced kinetics
p 1249 N95-21038

Turbulent transport in premixed flames
p 1249 N95-21040

The coupling between flame surface dynamics and species mass conservation in premixed turbulent combustion p 1249 N95-21041

Pdf modeling for premixed turbulent combustion based on the properties of iso-concentration surfaces
p 1249 N95-21042

Passive turbulent flamelet propagation
p 1249 N95-21043

Simulation of a turbulent flame in a channel
p 1249 N95-21044

Direct numerical simulation for premixed turbulent combustion modelling p 1249 N95-21082

Conditional statistics in a turbulent premixed flame derived from direct numerical simulation
p 1249 N95-22438

Lewis number and Damkohler number effects in vort ex-flame interactions p 1249 N95-22439

Fundamental mechanisms in premixed flame propagation via vortex-flame interactions: Numerical simulations p 1249 N95-22440

Triple flames and flame stabilization
p 1249 N95-22441

Flame propagation under partially-premixed conditions
p 1250 N95-22442

PREPROCESSING

State of the art in CFD pre- and postprocessing
[PB95-110391] p 1356 N95-22017

PRESENTATION

Rate monotonic analysis for real-time systems: Instructors guide
[AD-A286083] p 1463 N95-20810

PRESERVING

Issues in multi-bunch emittance preservation in the NLC
[DE95-002894] p 1534 N95-21253

PRESSURE DEPENDENCE

Overview of the Institute of Geophysics and Planetary Physics and Lawrence Livermore National Laboratory collaborative efforts
[DE94-017300] p 1599 N95-20145

Properties of molecular solids and fluids at high pressure and temperature
[DE94-017594] p 1565 N95-20243

Solubilities of nitrogen and helium in water and blood at 37 C and pressures of up to 11 ATA
[AD-A286269] p 1446 N95-22003

PRESSURE DISTRIBUTION

Fluctuations in high Beta(sub p) plasmas in D3-D
[DE94-017510] p 1550 N95-20146

Model-based inversion for a shallow ocean application
[DE94-016968] p 1433 N95-20420

Application of pressure sensitive paint in hypersonic flows
[NASA-TM-106824] p 1201 N95-20794

Statistics of pressure and pressure gradient in homogeneous isotropic turbulence p 1343 N95-21046

Effects of turbulence compressibility and unsteadiness in compression corner flow p 1344 N95-21052

Improved broadband waveguide pressure window
[AD-D016487] p 1306 N95-21834

Derivation of a wavenumber filter design for the measurement of turbulent wall pressure fluctuations
[AD-A286421] p 1357 N95-22208

PRESSURE DROP

Liquid-metal pin-fin pressure drop by correlation in cross flow
[DE94-017086] p 1338 N95-19923

PRESSURE EFFECTS

High pressure windowed chamber burned rate determination of liquid propellant XM46
[AD-A283770] p 1282 N95-19920

Influence of primary boundary conditions on the buckling of shallow cylindrical shells
[PB94-208352] p 1384 N95-20003

The role of high pressure in the study and applications of the ferroelectric polymer polyvinylidene fluoride and its copolymers
[DE94-015742] p 1268 N95-20396

Wake measurements in a strong adverse pressure gradient
[NASA-CR-197272] p 1201 N95-21031

Role of pressure diffusion in non-homogeneous shear flows p 1345 N95-21053

Effect of atmospheric pressure on measured aircraft noise levels
[PB95-130423] p 1207 N95-21425

Extrudate swell and extrudate distortion of HDPE as a result of different deformation mechanisms during extrusion through capillary dies
[PB95-110227] p 1288 N95-21651

Stability of pressure and velocity computations for heterogeneous reservoirs
[PB95-110284] p 1354 N95-21656

A visual cell for measuring the solubility of prograde soluble salts in water at high temperatures and pressures
[DE95-002058] p 1245 N95-21732

Atomic velocity distributions in a hydrogen beam effusing out of an RF discharge dissociator
[AD-A279253] p 1307 N95-21985

PRESSURE GAGES

Dynamic response of pressure measuring systems
[ARL-TR-32] p 1365 N95-20759

PRESSURE GRADIENTS

Wake measurements in a strong adverse pressure gradient
[NASA-CR-197272] p 1201 N95-21031

Statistics of pressure and pressure gradient in homogeneous isotropic turbulence p 1343 N95-21046

Numerical study of realistic perturbations in three-dimensional boundary layers p 1351 N95-21091

Spatial direct numerical simulation of boundary layer transition under strong adverse pressure gradient
p 1351 N95-21093

Extended theory of main ion and impurity rotation and bootstrap current in a shear layer
[DE94-015857] p 1555 N95-21141

Acoustic receptivity due to weak surface inhomogeneities in adverse pressure gradient boundary layers
[NASA-TM-4577] p 1353 N95-21258

Large-eddy simulation of flow through a plane, asymmetric diffuser p 1360 N95-22449

PRESSURE MEASUREMENT

Hydrostatic force sensor
[DE94-018923] p 1364 N95-20321

Dynamic response of pressure measuring systems
[ARL-TR-32] p 1365 N95-20759

Acoustic calibration apparatus for calibrating plethysmographic acoustic pressure sensors
[NASA-CASE-LAR-14977-1] p 1443 N95-20763

Application of pressure sensitive paint in hypersonic flows
[NASA-TM-106824] p 1201 N95-20794

Inert gas purification and measuring oxygen partial pressure in gas mixtures with EMF method based on solid electrolyte cell
[PB95-127767] p 1240 N95-21110

Pressure measurements on an F/A-18 twin vertical tail in buffeting flow. Volume 4, part 1: Buffet cross spectral densities
[AD-A285593] p 1215 N95-21214

Ohmsett test of NOFI Vee-Sweep and NOFI 600S Oilboom
[AD-A279525] p 1408 N95-21685

Optical fiber pressure sensor for liquid level monitoring
[AD-D016246] p 1547 N95-22089

Wave journal bearing. Part 2: Experimental pressure measurements and fractional frequency whirl threshold for wave and plain journal bearings
[NASA-TM-106848-PT-2] p 1382 N95-22405

PRESSURE OSCILLATIONS

Derivation of a wavenumber filter design for the measurement of turbulent wall pressure fluctuations
[AD-A286421] p 1357 N95-22208

PRESSURE REDUCTION

A comparison of decision making behaviour in a static and a dynamic task environment as a function of time pressure
[AD-A285389] p 1449 N95-20609

MHD-flow in slotted channels with conducting walls
[DE94-018370] p 1559 N95-21388

PRESSURE SENSORS

Improved die castings through plasma surface modification, improved sensors and die soldering prevention
[DE95-002238] p 1253 N95-20417

Dynamic response of pressure measuring systems
[ARL-TR-32] p 1365 N95-20759

Acoustic calibration apparatus for calibrating plethysmographic acoustic pressure sensors
[NASA-CASE-LAR-14977-1] p 1443 N95-20763

Laser anemometry and viscous computation of the flow through an annular turbine cascade
[AD-A280070] p 1341 N95-20968

Response of the B-1B air data sensor to simulated dust cloud environments
[AD-A286134] p 1213 N95-22036

Fiber optic pressure sensing array
[AD-D016245] p 1506 N95-22088

Optical fiber pressure sensor for liquid level monitoring
[AD-D016246] p 1547 N95-22089

PRESSURE VESSEL DESIGN

The ITER in-vessel system
[DE94-018053] p 1560 N95-21665

PRESSURE VESSELS

An overview of the HSST Full-Thickness Shallow-Crack Clad Beam Testing Program
[DE94-018940] p 1385 N95-20322

Effect of neutron irradiation on the impact properties of A533B steel
[DE95-001834] p 1256 N95-21286

Joining dissimilar stainless steels for pressure vessel components
[PB95-133005] p 1380 N95-21446

PRESSURIZING

Transport phenomena in the micropores of plug-type phase separators
[NASA-TM-108479] p 1340 N95-20561

PRETREATMENT

Mercury capture in bench-scale absorbers
[DE94-016910] p 1234 N95-20107

PREVENTION

Acute radiation sickness amelioration analysis
[AD-A279084] p 1445 N95-21629

Advanced Materials and Process Technology for Mechanical Failure Prevention (proceedings of the 48th Meeting of the Mechanical Failures Prevention Group
[AD-A285785] p 1233 N95-22399

PRIMERS (COATINGS)

VOC compliant wash primer
[AD-A286034] p 1273 N95-21000

PRINTED CIRCUITS

Ultra-Reliable Digital Avionics (URDA) processor
p 1209 N95-20638

An automatic placement tool for rapid prototyping of printed circuit boards
[AD-A286029] p 1328 N95-20997

Integration of thin film decoupling capacitors
[DE95-001609] p 1333 N95-21881

PRIORITIES

Cell loss analysis of two-class priority generalized knockout switch
[PB95-127742] p 1301 N95-21109

PROBABILITY DENSITY FUNCTIONS

Mapping closures for turbulent combustion
[AD-A279995] p 1238 N95-20597

Error probabilities of FFH/BFSK with noise normalization and soft decision viterbi decoding in a fading channel with partial-band jamming
[AD-A280041] p 1498 N95-20620

Pdf modeling for premixed turbulent combustion based on the properties of iso-concentration surfaces
p 1249 N95-21042

Statistics of pressure and pressure gradient in homogeneous isotropic turbulence p 1343 N95-21046

On Markov Chain Monte Carlo acceleration
[AD-A279393] p 1499 N95-21945

Bayesian analysis of semiparametric proportional hazards models
[AD-A279394] p 1499 N95-21946

Remote-sensing based technique to account for sub-grid scale variability of land surface properties
[NASA-TM-110501] p 1390 N95-22110

PROBABILITY DISTRIBUTION FUNCTIONS

Resolution requirements for velocity gradients in turbulence p 1363 N95-22462

PROBABILITY THEORY

Application of Markov decision processes to search problems
[PB95-110813] p 1497 N95-19914

Qualification of the dependence in the generalized extreme value choice model
[PB95-110946] p 1497 N95-19936

Frequent sampling in discrete choice
[PB95-110961] p 1497 N95-19938

Cavity-QED enhancement of fluorescence yields in microdroplets
[DE94-018662] p 1506 N95-20030

An object-oriented optimization systems
[DE94-016190] p 1459 N95-20165

Mapping closures for turbulent combustion
[AD-A279995] p 1238 N95-20597

Universal features of multiplicity distributions
[DE94-012854] p 1498 N95-20779

Modelling of microwave propagation and clutter in a maritime environment p 1295 N95-20938

Dynamics of volatile delivery from outer to inner solar system p 1420 N95-21798

Minimax optimal stop rule in reliability checking
[PB95-134557] p 1383 N95-21961

LADAR detection statistics in the presence of pointing errors
[AD-A285865] p 1309 N95-22134

Threshold detection in the presence of atmospheric turbulence
[AD-A286175] p 1427 N95-22249

Probability of detection for a GO CFAR radar processor using envelope detection approximation
[AD-A286211] p 1310 N95-22251

PROBLEM SOLVING

Eta%-Superconvergence of Finite Element Approximations in the Interior of General Meshes of Triangles
[AD-A279903] p 1490 N95-20565

Design and implementation of visual object-oriented LOGO using Prograph
[AD-A285977] p 1461 N95-20687

Computing methods for the approximate solution of time dependent problems
[AD-A286007] p 1491 N95-20719

Knowledge refinement in a reflective architecture
[AD-A286027] p 1589 N95-21002

A new Krylov-subspace method for symmetric indefinite linear systems
[DE95-001826] p 1355 N95-21726

PROCEDURES

Possible global environmental impacts of solid waste practices
[DE95-000830] p 1406 N95-21487

Environmental Compliance Assessment System (ECAS): Oregon supplement
[AD-A279565] p 1408 N95-21696

PROCESS CONTROL (INDUSTRY)

Magnetically controlled deposition of metals using gas plasma
[DE94-018654] p 1251 N95-20128

Design principles for real-time process control systems
[PB95-132890] p 1585 N95-21414

Generic architecture for knowledge-based control of processes in dynamic environments
[PB95-132676] p 1483 N95-21981

PROCESSING

A syncopated leap-frog algorithm for orbit consistent plasma simulation of materials processing reactors
[DE95-000954] p 1561 N95-21922

PROCUREMENT

The Photovolatic Manufacturing Technology project (PVMaT) after three years
[DE94-011877] p 1392 N95-20473

The Advanced Avionics Subsystem Technology Demonstration Program p 1209 N95-20636

A new process for acquiring software architecture
[AD-A286012] p 1462 N95-20721

The advantages of cost plus award fee contracts
p 1584 N95-20745

PROCUREMENT MANAGEMENT

Improving cost efficiency in large programs
p 1584 N95-20743

PRODUCT DEVELOPMENT

A construct for describing software development risks
[AD-A284923] p 1457 N95-19999

Human force exertion in user-product interaction. Backgrounds for design
[PB95-132858] p 1452 N95-21283

Structuring design requirements using YMIR
[PB95-132742] p 1471 N95-22081

PRODUCTION COSTS

An analysis of cost overruns on defense acquisition contracts p 1584 N95-20749

Analysis of cost: Combustion flame CVD diamond deposition
[AD-A279153] p 1278 N95-21973

Producing liquid fuels from biomass
[DE95-717458] p 1398 N95-22425

PRODUCTION MANAGEMENT

Solar collector manufacturing activity 1993
[DE94-017340] p 1398 N95-22429

PRODUCTIVITY

A Cost and Performance System (CAPS) in a Federal agency p 1584 N95-20746

Advanced robotic technologies for transfer at Sandia National Laboratories
[DE95-001617] p 1481 N95-20884

PROFILES

Test and evaluation report for the Manual Domestic Passive Profiling System (MDPPS)
[AD-A286312] p 1202 N95-20093

PROGRAM VERIFICATION (COMPUTERS)

Software fault tree analysis of concurrent Ada processes
[AD-A284979] p 1457 N95-20042

An empirical approach to logical clustering of software failure regions
[AD-A279863] p 1462 N95-20776

A tabular interface for automated verification of event-based dialogs
[AD-A286065] p 1463 N95-20847

Environment for Test and Analysis of Distributed Software (ETADS)
[AD-A285776] p 1463 N95-20877

Proceedings of the Fourth International Workshop on Inductive Logic Programming (ILP-94)
[PB95-135273] p 1464 N95-21003

Compositional proof theory for fault tolerant real-time distributed systems
[PB95-127601] p 1465 N95-21025

The iMAPS: General information
[AD-A285421] p 1465 N95-21176

Analysis of a disk-on-rod surface wave element inside a corrugated horn using the mode-matching technique
p 1305 N95-21543

The application of a statistical analysis software package to explosive testing
[MRL-TR-93-42] p 1284 N95-21658

Verification of knowledge-based reasoning modules
[PB95-132692] p 1470 N95-21983

Top-down non-correcting error recovery in LLgen
[PB95-132718] p 1471 N95-22031

Verification of a timestamp-based sliding-window protocol
[PB95-132759] p 1455 N95-22082

Abstract interpretation of reactive systems: Abstractions preserving Universal CTL(*), Existential CTL(*) and CTL(*)
[PB95-110557] p 1472 N95-22305

Formal specification and compositional verification of an atomic broadcast protocol
[PB95-110508] p 1472 N95-22351

PROGRAMMERS

Foundations of functional programming: A programmer's point of view
[PB95-132932] p 1471 N95-22094

Scalable programming environment
[AD-A286390] p 1472 N95-22201

PROGRAMMING ENVIRONMENTS

Evaluation of Borland Turbo Vision
[AD-A279873] p 1459 N95-20184

Model formality in human/computer collaboration
[AD-A286001] p 1462 N95-20718

Environment for Test and Analysis of Distributed Software (ETADS)
[AD-A285776] p 1463 N95-20877

Advanced computing systems: Usability of knowledge-based planning systems
[AD-A279573] p 1477 N95-21698

Scalable programming environment
[AD-A286390] p 1472 N95-22201

PROGRAMMING LANGUAGES

The design and implementation of the functional/daplex data interface for the multimodel and multilingual database system
[AD-A280131] p 1587 N95-20039

ILIAS: A sequential language for parallel matrix computations
[PB95-110631] p 1473 N95-20056

Software merge: Semantics of combining changes to programs
[AD-A279657] p 1459 N95-20304

Design and implementation of visual object-oriented LOGO using Prograph
[AD-A285977] p 1461 N95- 0687

Compositional proof theory for fault tolerant real-time distributed systems
[PB95-127601] p 1465 N95-21025

GRONICs-1994. Proceedings of the 1994 Groningen Student Conference on Computer Science
[PB95-135620] p 1468 N95-21455

DBASE 4 basics
[DE94-018323] p 1469 N95-21713

A Davis-Putnam program and its application to finite-order model search: Quasigroup existence problems
[DE95-003014] p 1471 N95-22077

Databases post-processing in Tensoral
p 1363 N95-22465

PROJECT MANAGEMENT

A construct for describing software development risks
[AD-A284923] p 1457 N95-19999

Readings in program control
[NASA-SP-6103] p 1583 N95-20739

Program control in NASA: Needs and opportunities
p 1583 N95-20740

A Cost and Performance System (CAPS) in a Federal agency p 1584 N95-20746

Planning and scheduling for success
p 1584 N95-20747

Performance measurement: A tool for program control
p 1585 N95-20752

Program control for mission success
p 1585 N95-20753

The impact of partnering on construction contracts
[AD-A286588] p 1585 N95-20855

Electric and Hybrid Vehicle Program: Site Operator Program
[DE95-001925] p 1332 N95-21731

ANSTO: Mission statement, significant events and achievements
[DE94-631123] p 1605 N95-21830

Electric and Hybrid Vehicle Program Site Operator Program
[DE95-002042] p 1333 N95-21960

Intelligent interactive project management system
[PB95-132684] p 1586 N95-21982

Directives for the participation in MiTS forum. V3.0
[PB95-110342] p 1484 N95-22015

Information Management Architecture for an Integrated Computing Environment for the Environmental Restoration Program. Volume 2: Interim business systems guidance
[DE95-001385] p 1591 N95-22061

PROJECT PLANNING

Guidelines for the creation and management of geographic data bases within a GIS environment, version 1.0
[DE94-019214] p 1458 N95-20073

Readings in program control [NASA-SP-6103] p 1583 N95-20739
Program control in NASA: Needs and opportunities p 1583 N95-20740
Performance measurement: A tool for program control p 1585 N95-20752
Program control for mission success p 1585 N95-20753
ITER EDA Newsletter. Volume 3, no. 2 [DE94-628980] p 1561 N95-21852

PROJECTILES
Comparison of meteorological data with fitted values extracted from projectile trajectory [AD-A285921] p 1428 N95-19989
A computational study of projectile shape dependence on phase change phenomena with comparisons to experimental data [DE95-000740] p 1384 N95-20077
A computational study of projectile melt in impact with typical Whipple shields [DE94-016454] p 1365 N95-20237
Aluminium oxide targets after ballistic impact; fragmentation of the ceramic and the projectile [PB95-133625] p 1388 N95-22097

PROLOG (PROGRAMMING LANGUAGE)
Logic programming and negation: A survey [PB95-110730] p 1472 N95-22302

PROPAGATION
Electron propagator theory and application [AD-A279761] p 1507 N95-20097

PROPAGATION MODES
Passive monitoring for automated MMPP communication systems p 1293 N95-20927
The relative importance of meteor burst and other distance polar cap propagation modes in the low VHF band p 1293 N95-20928
Study of the fast and slow variations of the power received at VHF links by tropospheric diffusion p 1293 N95-20929
Methods for evaluating the effects of conduits at the surface of the sea p 1294 N95-20932
Identification of the propagation modes and paths on HF links using a goniopolarimeter p 1299 N95-20956

PROPAGATION VELOCITY
Velocity analysis for transversely isotropic media [DE95-000643] p 1411 N95-19981
Numerical study of realistic perturbations in three-dimensional boundary layers p 1351 N95-21091

PROPANE
Effect of propane-air on NGVs and vehicle fueling stations [PB94-210085] p 1282 N95-20253
Development and demonstration of advanced technologies for direct electrochemical oxidation of hydrocarbons (methanol, methane, propane) [AD-A285094] p 1224 N95-22474

PROPELLANT CHEMISTRY
Density functional studies of decomposition processes of energetic molecules [AD-A286185] p 1510 N95-20327

PROPELLANT COMBUSTION
High pressure windowed chamber burned rate determination of liquid propellant XM46 [AD-A283770] p 1282 N95-19920

PROPELLANT DECOMPOSITION
Density functional studies of decomposition processes of energetic molecules [AD-A286185] p 1510 N95-20327

PROPELLANT GRAINS
The 1993 JANNAF Propulsion Meeting, volume 2 [AD-A279569] p 1221 N95-20708

PROPELLANT TESTS
Investigation of rocket motors 3 inch number 1 Mk 4 [AD-A284278] p 1221 N95-19962
The hot fragment conductive ignition test for screening LOVA propellants [AD-A284259] p 1282 N95-20187

PROPELLANTS
The hot fragment conductive ignition test for screening LOVA propellants [AD-A284259] p 1282 N95-20187
Compatibility testing of explosives and paints by chemiluminescence techniques [PB95-133609] p 1275 N95-21275
Evaluation of state-of-the-art high speed deluge systems presently in service at various US Army ammunition plants [AD-A279102] p 1287 N95-21598
Launch safety, toxicity, and environmental effects of the high performance oxidizer ClF(5) [AD-A286095] p 1284 N95-22227

PROPULSION
Propulsion research on the variable tandem mirror plasma rocket [NASA-CR-196310] p 1221 N95-20059
T-45A High Angle of Attack Testing: US Naval Test Pilot School 46th Annual Reunion and Symposium [AD-A284000] p 1207 N95-20466
Space fundamentals for the war fighter [AD-A279703] p 1217 N95-20690
The 1993 JANNAF Propulsion Meeting, volume 2 [AD-A279569] p 1221 N95-20708
Electric and Hybrid Vehicles Program [DE95-001711] p 1332 N95-21738

PROPULSION SYSTEM PERFORMANCE
Computer program for calculation of complex chemical equilibrium compositions and applications. Part 1: Analysis [NASA-RP-1311] p 1235 N95-20180

PROTECTIVE CLOTHING
Evaluation of stress experienced by soldiers wearing chemical protective clothing during varying work loads in desert or tropical environments [AD-A280113] p 1452 N95-20625
Advanced robotic technologies for transfer at Sandia National Laboratories [DE95-001617] p 1481 N95-20884
Microclimate cooling effect on perceived exertion in four heat/exercise scenarios [AD-A285549] p 1444 N95-21160
Aerospace medicine and biology: A continuing bibliography with indexes (supplement 399) [NASA-SP-7011(399)] p 1446 N95-21947
Fuzzy clustering of facial form for prototyping environmental protection equipment [DE94-014657] p 1454 N95-22466

PROTECTIVE COATINGS
Evaluation of PS 212 coatings under boundary lubrication conditions with an Ester-based oil to 300 C [NASA-TM-106763] p 1223 N95-19901
Novel reagents for chemical vapor deposition of intermetallic alloys [AD-A286562] p 1271 N95-20815
Polyurethane self-priming topcoats [AD-D016204] p 1274 N95-21154
Polyurethane self-priming topcoats [AD-D016205] p 1274 N95-21155
B4C-SiC reaction-sintered coatings on graphite plasma facing components [DE94-019105] p 1230 N95-21553
Protective organic coatings on steel: Accelerated corrosion test method for paint/coatings exposed to water with low conductivity. Nordtest project no. 1010-92. Degradation of organic coatings in fresh water [PB95-134185] p 1277 N95-21873
Epoxy lining for shipboard piping systems [AD-A286228] p 1279 N95-22022
Demonstration of multifunctional DNBM corrosion inhibitors in protective coatings for Naval air/weapon systems [AD-A285869] p 1279 N95-22136
Embedded optical fibres as strain sensors in polymer matrix fibre composites: The influence of adhesion in strain transfer [PB95-133617] p 1547 N95-22140

PROTEIN METABOLISM
USAF cellular mechanism of turnover of the stress induced protein HSP70 [AD-A285618] p 1441 N95-19898

PROTEIN SYNTHESIS
USAF cellular mechanism of turnover of the stress induced protein HSP70 [AD-A285618] p 1441 N95-19898
Calculation of atom-centered partial charges for heme [DE94-014447] p 1520 N95-21375

PROTEINS
USAF cellular mechanism of turnover of the stress induced protein HSP70 [AD-A285618] p 1441 N95-19898
Skeletal muscle ischemia and heat shock proteins [AD-A285364] p 1442 N95-20549
Biomolecular Materials by Design, volume 330 [AD-A285369] p 1269 N95-20551
Electrostatic basis for molecular recognition in photosynthesis [DE95-002979] p 1440 N95-22075
Separation of proteins by convective electrophoresis through a porous membrane [PB95-127130] p 1248 N95-22373

PROTOCOL (COMPUTERS)
A database for analyzing sequential behavioral data and their associated cognitive models [AD-A280061] p 1448 N95-19887
Process algebra with partial choice [PB95-110714] p 1487 N95-19907
A group communication approach for mobile computing mobile channel: An ISIS tool for mobile services [AD-A279785] p 1290 N95-20306
High performance backplane components for modular avionics p 1212 N95-20653
An object-oriented implementation of the Xpress transfor protocol [DE95-001506] p 1301 N95-21277
GRONICs-1994. Proceedings of the 1994 Groningen Student Conference on Computer Science [PB95-135620] p 1468 N95-21455
A simulation study of TCP performance in ATM networks [DE94-016622] p 1477 N95-21505
Compositional approach to sequential consistency and lazy caching [PB95-134110] p 1455 N95-21871
Verification of a timestamp-based sliding-window protocol [PB95-132759] p 1455 N95-22082
Formal specification and compositional verification of an atomic broadcast protocol [PB95-110508] p 1472 N95-22351

PROTON BEAMS
Search for right-handed currents in the decay chain of K(+) yields muon(+)nu(sub muon), muon(+) yields e(+)nu(sub e)nu(bar)(sub muon) [DE94-770606] p 1514 N95-20756
Intense proton beam source for ITER neutral-beam spectroscopy diagnostics [DE94-018092] p 1560 N95-21668
The 12-GeV/c beam transfer and absorber lines for the Superconducting Super Collider [DE95-002100] p 1538 N95-21733
Experience at the Los Alamos Meson Physics Facility with the use of alloy Inconel 718 as an enclosure for a beam degrader and as a proton beam entry window [DE94-018289] p 1538 N95-22050

PROTON ENERGY
Performance of Ga(0.47)In(0.53)As cells over a range of proton energies [NASA-TM-106819] p 1334 N95-22112

PROTON IRRADIATION
Proton irradiation effects on advanced digital and microwave III-V components [DE94-018742] p 1314 N95-20338
Investigation of the stability and 1.0 MeV proton radiation resistance of commercially produced hydrogenated amorphous silicon alloy solar cells p 1320 N95-20522

PROTON RESONANCE
Two-band model description of electroabsorption and third-harmonic generation in 1-D MX linear chains [DE95-000932] p 1526 N95-21934

PROTON-PROTON REACTIONS
Complementarity of e(+)e(-) and pp colliders for the exploration of electroweak symmetry breaking [DE94-017397] p 1507 N95-20034
D0 quantum chromodynamics: A compilation of results presented at DPF 1994 [DE95-000838] p 1510 N95-20344
Evidence for t(bar t) production at the Tevatron: Statistical significance and cross section [DE95-002524] p 1515 N95-20897
Charmonium production, b quark and B meson production and b(bar b) correlations at CDF [DE95-002525] p 1515 N95-20898
Antishadowing contribution to the pomeron structure function [PB95-127478] p 1518 N95-21221
Spin dependence of diffractive processes and implications for the small x behaviour of g1 and the spin content of the nucleon [PB95-130332] p 1518 N95-21225
Multiple hard interactions in HERWIG [PB95-130548] p 1518 N95-21233
The diphoton production rate in (bar p)p collisions at the square root of s = 1800 GeV [DE95-000559] p 1522 N95-21497
Tests of structure functions using lepton pairs: W-charge asymmetry at CDF [DE95-000560] p 1527 N95-22122
Electroweak boson pair production in p(-p) collisions at the square root of s = 1.8 TeV [DE95-000725] p 1527 N95-22194
Inclusive B production at CDF and D0 [DE95-000728] p 1528 N95-22196

PROTONS
Particle beam fusion [DE95-000711] p 1549 N95-20075
Performance, defect behavior and carrier enhancement in low energy, proton irradiated p+nn+ InP solar cells p 1319 N95-20518
A neutron beam polarizer for study of parity violation in neutron-nucleus interactions [DE95-002743] p 1519 N95-21237
Comparison of calculated with measured dynamic aperture [DE95-002863] p 1534 N95-21246
Search for new particles decaying to dijets in p(bar p) collisions at (radical)s = 1.8 TeV [DE94-018994] p 1523 N95-21563

Chemistry and electrochemistry in Lewis acid and superacid ionic liquids
[AD-A279396] p 1246 N95-21931
Proton and produced particle distributions from Au+Au collisions at 11.6 A GeV/c
[DE94-018634] p 1530 N95-22392

PROTOPLANETS
Experimental hypervelocity impact effects on simulated planetesimal materials
[DE94-017290] p 1599 N95-20144
Transportation of volatile elements in thermally evolving planetesimals: An important role of metallic iron
p 1418 N95-21790
Dynamics of volatile delivery from outer to inner solar system p 1420 N95-21798
Comets, impacts, and atmospheres
p 1422 N95-21810

PROTOSTARS
Twentysixth YERAC
[PB95-127437] p 1599 N95-21347

PROTOTYPES
Advanced Standard Electronic Modules format-E (SEM-E) processes for rapid prototyping
p 1210 N95-20642
Performance of the NIF prototype beamlet
[DE94-018500] p 1371 N95-20817
A tabular interface for automated verification of event-based dialogs
[AD-A286065] p 1463 N95-20847
Preclinical investigation of lyophilized platelet preparations
[AD-A286079] p 1443 N95-20851
Polymer based all-optic reconfigurable interconnects
[AD-A279976] p 1272 N95-20962
Prototype rule-based reliability analysis for VLSI circuit design
[AD-A280065] p 1327 N95-20967
An automatic placement tool for rapid prototyping of printed circuit boards
[AD-A286029] p 1328 N95-20997
Next generation solid modellers for electronic prototyping
[AD-A286525] p 1464 N95-21010
Vertex detectors at linear colliders: Present and future
[PB95-134656] p 1540 N95-22364
Fuzzy clustering of facial form for prototyping environmental protection equipment
[DE94-014657] p 1454 N95-22466

PROVING
Abstract reduction and topology
[PB95-110615] p 1488 N95-20054
A tabular interface for automated verification of event-based dialogs
[AD-A286065] p 1463 N95-20847
Correctness of some algorithms to generate finite automata for regular expressions
[PB95-127551] p 1465 N95-21022
Compositional proof theory for fault tolerant real-time distributed systems
[PB95-127601] p 1465 N95-21025
Adjunctions
[PB95-134078] p 1494 N95-21868
Compositional approach to sequential consistency and lazy caching
[PB95-134110] p 1455 N95-21871
Proof of a conjecture of Narayana on dominance refinements of the Smirnov two-sample test
[PB95-132650] p 1499 N95-21979

PSYCHOLOGICAL EFFECTS
Interspecies extrapolations of halocarbon respiratory and tissue kinetics: Applications to predicting toxicity in different species
[AD-A285055] p 1442 N95-20485

PSYCHOLOGICAL FACTORS
Neural models of motion perception
[AD-A286560] p 1449 N95-20845

PSYCHOLOGICAL SETS
Test reliability and experimental power
[AD-A279607] p 1448 N95-19957

PSYCHOLOGICAL TESTS
Test reliability and experimental power
[AD-A279607] p 1448 N95-19957

PSYCHOMETRICS
Test reliability and experimental power
[AD-A279607] p 1448 N95-19957

PUBLIC HEALTH
Definition report on target and related steering variables of radiation as a part of the environmental balance and environmental outlook investigation
[PB95-135471] p 1409 N95-21846
Initial assessment of the hazards and risks of new chemicals to man and the environment, part 2
[PB95-106407] p 1410 N95-22124
The mechanisms and effects off the plant-activations of chemicals in the environment
[AD-A279388] p 1356 N95-22145

PULSE COMMUNICATION
A MMPP communications system for the frequency range 2-200MHz p 1293 N95-20924
Numerical and symbolic algorithms for application and specific signal processing
[AD-A279902] p 1305 N95-21576
Data sampling for a burst mode communications system
[AD-A286098] p 1309 N95-22229

PULSE COMPRESSION
Frequency-coded monopulse MTI
[AD-D016495] p 1307 N95-21904

PULSE DURATION
Self-starting femtosecond pulse generation from a Ti:sapphire laser synchronously pumped by a pointing-stabilized mode-locked Nd:YAG laser
[DE94-019319] p 1374 N95-21480
A 500 MW annular beam relativistic klystron
[DE95-000867] p 1334 N95-22011

PULSE GENERATORS
A wideband EMP test system
[DE94-015283] p 1290 N95-20474
LIF standoff research
[DE94-018744] p 1535 N95-21328
Optical, electronic and optoelectronic material and device research
[AD-A280111] p 1374 N95-21630

PULSE HEATING
Ion heat pulse after sawtooth crash in the JFT-2M tokamak
[DE94-770685] p 1555 N95-20988

PULSE RATE
A wideband EMP test system
[DE94-015283] p 1290 N95-20474
Detection efficiency and dark pulse rate of Rockwell (SSPM) single photon counters
[DE94-016872] p 1524 N95-21646

PULSED LASER DEPOSITION
Effects of ambient conditions on the adhesion of cubic boron nitride films on silicon substrates
[DE94-016779] p 1266 N95-20281
Thin-film cadmium telluride photovoltaic cells
[DE94-011886] p 1395 N95-21508

PULSED LASERS
Modeling of high efficiency solar cells under laser pulse for power beaming applications p 1318 N95-20516
Pulsed laser illumination of photovoltaic cells
p 1323 N95-20538
Computational model of drilling with high radiance pulsed lasers
[DE94-018548] p 1371 N95-20783
Research studies on short wavelength lasers by selective Auger processes
[AD-A285620] p 1372 N95-21144
Mechanisms and diagnostics of ultrashort pulse laser ocular effects
[AD-A285610] p 1373 N95-21195
Large facilities pilot programme. Access to the VULCAN High Power Laser Facilities at Rutherford Appleton Laboratory
[PB95-130340] p 1373 N95-21226
Tribology and surface mechanical properties of excimer laser nitrided titanium
[DE95-002751] p 1255 N95-21238
NEO-LISP: Deflecting near-Earth objects using high average power, repetitively pulsed lasers
[DE95-000863] p 1599 N95-21367
Submicrosecond, synchronizable x-ray source
[AD-D016497] p 1546 N95-21905
The final status of a metal surface after multipulse laser irradiation in an ambient gas
[DE94-629000] p 1562 N95-22377

PULSED RADIATION
Design trade-off study for a large volume short pulse neutron assembly
[DE94-019175] p 1509 N95-20206
Muon beamline at ISIS
[PB95-130324] p 1518 N95-21224
Radio-frequency techniques at the ISIS pulsed muon source
[PB95-129854] p 1529 N95-22303
Study of pulsed laser effects on living tissues
[PB95-131330] p 1447 N95-22361

PURIFICATION
Inert gas purification and measuring oxygen partial pressure in gas mixtures with EMF method based on solid electrolyte cell
[PB95-127767] p 1240 N95-21110
Disinfection of purified waste water with ultra violet light on a technical scale
[PB95-131926] p 1405 N95-21330
Removal of CO2 in closed loop off-gas treatment systems
[DE94-019259] p 1407 N95-21617
The application of electrodialysis to extend the lifetime of commercial electroplating baths
[DE95-000868] p 1246 N95-22012
Use of the carbo-flo process to purify process water contaminated by agricultural pesticides
[PB95-127825] p 1410 N95-22330

PYRAMIDS
HIRAS: High-resolution IRAS images
p 1593 N95-21758
Wavelet analysis applied to the IRAS cirrus
p 1593 N95-21769

PYRIDINES
Photochemistry of intermolecular C-H bond activation reactions
[DE94-018417] p 1239 N95-20682
Vibrational overtone spectroscopy of pyridine and related compounds
[AD-A280105] p 1224 N95-21911

PYRIMIDINES
New chiral pyrimidino-crown ether ligands
[AD-A279892] p 1223 N95-20590

PYROLYSIS
Direct aromatization of methane
[DE94-017131] p 1233 N95-19924
Global equivalence ratio concept and the prediction of carbon monoxide formation in enclosure fires
[PB94-207511] p 1234 N95-20100
Assessment of liquefaction and pyrolysis systems
[PB95-129797] p 1236 N95-20290
Ceramics formed by pyrolysis of either linear or thermosetting carborane (siloxane or silane) acetylene based precursor polymers
[AD-D016563] p 1266 N95-20291
Restricted mass transport effects on free radical reactions
[DE94-018136] p 1217 N95-21706

PYROLYTIC GRAPHITE
Optical properties of silicon clusters deposited on the basal plane of graphite
[DE94-017529] p 1542 N95-20450

PYROTECHNICS
Evaluation of state-of-the-art high speed deluge systems presently in service at various US Army ammunition plants
[AD-A279102] p 1287 N95-21598
Air pollution caused by fireworks during the turn of the year 1992-1993
[PB95-135265] p 1409 N95-21718

PYROXENES
Hydrogen storage in Earth's mantle and core
p 1423 N95-21813

PYRROLES
Mechanism of the amperometric response of a proposed glucose sensor based on a polypyrrole-tubule-impregnated membrane
[AD-A279836] p 1365 N95-20431

Q

Q SWITCHED LASERS
High power spectral and spatial beam control using self-phase modulation and a multisegment monochromator
[DE94-016604] p 1531 N95-20120
GaAs optical circuits
[AD-A285859] p 1369 N95-20389
Continuously-tunable, narrow-linewidth, Q-switched Cr:LiSAF laser for lidar applications
[DE95-000862] p 1373 N95-21312

Q VALUES
Measurements of shielding effectiveness and cavity characteristics of airplanes
[PB94-210051] p 1289 N95-20191

QUADRATIC EQUATIONS
Quadratic forms in design theory
[PB95-111019] p 1487 N95-19940

QUADRATURES
Atomic orbital basis sets for molecular interactions
[AD-A279609] p 1506 N95-19959
Probability of detection for a GO CFAR radar processor using envelope detection approximation
[AD-A286211] p 1310 N95-22251

QUADRUPOLES
Ion-molecular spiraling collisions and termolecular recombination
[AD-A285633] p 1517 N95-21151
Sources of amplitude-dependent tune shift in the PEP-2 design and their compensation with octupoles
[DE94-018198] p 1519 N95-21262
An 8-meter-long coupled cavity RFQ linac
[DE94-018077] p 1331 N95-21667
Proposed emittance upgrade for the SLC damping rings
[DE95-002887] p 1538 N95-22155

QUALIFICATIONS

Qualification of the dependence in the generalized extreme value choice model
[PB95-110946] p 1497 N95-19936

Qualification test results for blue-red reflecting solar covers p 1320 N95-20525

Advanced Standard Electronic Modules format-E (SEM-E) processes for rapid prototyping p 1210 N95-20642

QUALITATIVE ANALYSIS

Quantitative and qualitative analysis of some inorganic compounds by Raman spectroscopy
[DE94-009757] p 1237 N95-20470

QUALITY CONTROL

Guidelines for the creation and management of geographic data bases within a GIS environment, version 1.0
[DE94-019214] p 1458 N95-20073

Towards better quality and reliability in the software reuse library environment
[AD-A280013] p 1460 N95-20313

Use of an integrated design tool for weld quality enhancement
[DE94-018135] p 1379 N95-20723

Ozone quality control measurements in the Dutch National Air Quality Monitoring Network
[PB95-131900] p 1405 N95-21329

Benefits of CMM-based software process improvement: Executive summary of initial results
[AD-A286444] p 1468 N95-21567

Interim profile: Development and trial of a method to rapidly measure software engineering maturity status
[AD-A279074] p 1468 N95-21627

Consortia for Known Good Die (KGD), phase 1
[AD-A279407] p 1383 N95-21933

A graded approach to ISO 9000 implementation for records managers
[DE94-017409] p 1591 N95-22167

Quality characteristics and metrics for reusable software
[PB94-203437] p 1473 N95-22390

QUANTITATIVE ANALYSIS

Quantitative and qualitative analysis of some inorganic compounds by Raman spectroscopy
[DE94-009757] p 1237 N95-20470

Enhancements in the Livermore spectrum analysis package PIXEF
[DE95-002487] p 1272 N95-20895

The formation of reaction bonded Si3N4 at low temperatures and in short times
[DE95-001990] p 1275 N95-21289

The energetics and dynamics of free radicals, ions, and clusters
[DE94-018101] p 1244 N95-21701

QUANTUM CHEMISTRY

Quantum chemical study of rare gas/halide interactions as a model for high energy density material. 1: Transition properties in HCl
[AD-A285988] p 1239 N95-20613

Quantum simulation of heterogeneous electron transfer free energies at the water-metal interface
[AD-A279279] p 1522 N95-21492

Use of quantum chemically derived descriptors for QSAR modeling of reductive dehalogenation of aromatic compounds
[PB95-132783] p 1224 N95-22333

QUANTUM CHROMODYNAMICS

New strong interactions above the electroweak scale
[DE94-018385] p 1506 N95-20025

D0 quantum chromodynamics: A compilation of results presented at DPF 1994
[DE95-000838] p 1510 N95-20344

Semi-leptonic form-factors from lattice QCD
[DE95-000871] p 1510 N95-20367

High energy photon-photon collisions
[DE94-017494] p 1532 N95-20388

Production of J/(psi) in 800 GeV/c p-Si interactions
[DE94-017982] p 1513 N95-20496

Strange particle and antiproton production in S + nucleus collisions at 200 GeV/nucleon
[DE95-002348] p 1513 N95-20575

Kinematical evidence for top pairs at the Tevatron
[DE95-000729] p 1515 N95-20880

Theoretical particle physics
[DE95-002447] p 1515 N95-20893

Evidence for t(bar t) production at the Tevatron: Statistical significance and cross section
[DE95-002524] p 1515 N95-20897

Charmonium production, b quark and B meson production and b(bar b) correlations at CDF
[DE95-002525] p 1515 N95-20898

Recent results from E665
[DE95-002523] p 1516 N95-20914

Anomalous vector-boson couplings in Majorana neutrino models
[PB95-127460] p 1518 N95-21220

Antishadowing contribution to the pomeron structure function
[PB95-127478] p 1518 N95-21221

Spin dependence of diffractive processes and implications for the small x behaviour of g1 and the spin content of the nucleon
[PB95-130332] p 1518 N95-21225

Calculation of Z plus four jet production at the Tevatron
[PB95-130472] p 1580 N95-21230

The theory of relativistic heavy ion collisions
[DE95-001805] p 1519 N95-21302

Nonperturbative aspects of the quark-photon vertex
[DE94-012846] p 1520 N95-21315

Exclusive processes: Tests of coherent QCD phenomena and nucleon substructure at CEBAF
[DE95-002892] p 1520 N95-21336

Monopoles and quark confinement: Introduction and overview
[DE94-019348] p 1522 N95-21485

QCD corrections to Higgs boson production: An update
[DE95-000626] p 1522 N95-21506

Polarization of charmonium in pion-nucleus collisions
[DE95-002783] p 1523 N95-21525

Lattice results for heavy light matrix elements
[DE94-019101] p 1523 N95-21551

Structure functions and structure function ratio F2(n)/F2(p) at low X(Bj) and Q2 in inelastic muon scattering
[DE94-018979] p 1573 N95-21561

Measurement of the B meson differential cross-sections in p(bar p) collisions at (radical)s = 1.8 TeV using the exclusive decays B(sup (+-)) (yields) J/(psi)K(sup (+-)) and B(sup 0) (yields) J/(psi)K*(sup 0)
[DE94-018993] p 1523 N95-21562

Search for new particles decaying to dijets in p(bar p) collisions at (radical)s = 1.8 TeV
[DE94-018994] p 1523 N95-21563

Summary of heavy ion theory
[DE95-002177] p 1523 N95-21588

Measurement of the B cross section at CDF via B semileptonic decays
[DE95-002217] p 1524 N95-21597

The method of evaluating quantum partition function for the Hubbard model
[DE94-628991] p 1581 N95-21639

Dynamics of the chiral transition
[DE94-016813] p 1524 N95-21641

Status of the DO top search
[DE95-002214] p 1525 N95-21715

Strong interactions studies with medium energy probes
[DE95-001800] p 1245 N95-21745

Nuclear research with the electromagnetic probe
[DE95-001812] p 1525 N95-21747

Constraints on T-odd and P-even hadronic interactions from nucleon, nuclear, and atomic electric dipole moments
[DE94-012845] p 1526 N95-21920

There might be two kinds of dibaryon
[DE94-014417] p 1526 N95-22058

QUANTUM EFFICIENCY

High-efficiency, deep-junction, epitaxial InP solar cells on (100) and (111)B InP substrates
p 1316 N95-20507

Detection efficiency and dark pulse rate of Rockwell (SSPM) single photon counters
[DE94-016872] p 1524 N95-21646

Non-H2Se, ultra-thin CuInSe2 devices
[DE94-011894] p 1395 N95-21844

Photocathodes for free electron lasers
[DE94-018305] p 1376 N95-22242

Fabrication and characterization of cesium telluride photocathodes: A promising electron source for the Los Alamos Advanced FEL
[DE94-018303] p 1377 N95-22348

QUANTUM ELECTRONICS

Solid state research
[AD-A279662] p 1567 N95-20426

Temperature dependence of magnetopolarons in a parabolic quantum dot in arbitrary magnetic fields
[DE94-629033] p 1528 N95-22218

QUANTUM MECHANICS

Semiquantum chaos and the large N expansion
[DE94-016196] p 1488 N95-20169

On the differential representations of quantum Lie superalgebras
[DE94-629874] p 1491 N95-20734

Quantization in curvilinear coordinates
[DE94-770603] p 1514 N95-20737

Quantum diffusion
[DE95-001015] p 1580 N95-21264

Second order approximation for optical polaron in the strong coupling case
[DE94-628997] p 1525 N95-21856

The development of science during this century
[DE94-632964] p 1582 N95-22185

On the conductance sum rule for the hierarchical edge states of the Fractional Quantum Hall Effect
[DE94-629030] p 1582 N95-22198

Theory of the excitonic lineshape in low-dimensional structures with rough interfaces
[DE95-003434] p 1582 N95-22237

Constraints on the left-right symmetric model from b yields s gamma
[DE95-003469] p 1528 N95-22239

The two-electron problem and prospects for atomic collision theory on a numerical lattice
[DE94-017856] p 1528 N95-22265

QUANTUM NUMBERS

D(sup 0)-(anti-D)(sup 0) mixing and doubly Cabibbo-suppressed decays of the D(+)
[DE94-015540] p 1512 N95-20476

QUANTUM STATISTICS

Where are we going with Bose-Einstein: A mini review
[PB95-130308] p 1518 N95-21222

The dynamic structure function of Bose liquids in the deep inelastic regime
[DE94-629077] p 1527 N95-22182

Universal spectral correlations at the mobility edge
[DE94-629031] p 1528 N95-22217

QUANTUM THEORY

Electron propagator theory and application
[AD-A279761] p 1507 N95-20097

Predictions from quantum cosmology
[PB95-111126] p 1599 N95-20173

Von Neumann algebra automorphisms and time-thermodynamics relation in general covariant quantum theories
[PB95-111084] p 1580 N95-20324

Solid-state dynamics and quantum transport in novel semiconductor nanostructures
[AD-A285946] p 1315 N95-20394

Computational evaluation of the feasibility of nitrating precursors to C12N12O12
[AD-A285976] p 1239 N95-20668

Temporal rearrangement of electronic densities in slow atomic collisions
[AD-A279725] p 1516 N95-20994

Electron-nuclear dynamics of molecular systems
[AD-A279649] p 1516 N95-21120

New improved derivative expansion for field theories with spontaneous symmetry breaking
[DE94-019349] p 1580 N95-21486

Proceedings of the School for Young High Energy Physicists
[PB95-108114] p 1537 N95-21647

Vibrational overtone spectroscopy of pyridine and related compounds
[AD-A280105] p 1224 N95-21911

QUANTUM WELL LASERS

GaAs optical circuits
[AD-A285859] p 1369 N95-20389

QUANTUM WELLS

Physics and applications of defects in advanced semiconductors, volume 325
[AD-A280059] p 1563 N95-19886

International Conference on Optical Computing: Technical digest
[AD-A284293] p 1541 N95-20249

Resonant tunneling quantum well integrated optical waveguide modulator/switch
[AD-A285142] p 1542 N95-20501

Phase dynamics of non-equilibrium distributions of free electron-hole pairs in GaAs quantum wells
[DE94-018190] p 1569 N95-20679

Ultrafast magnetoexciton dynamics in GaAs
[DE94-018175] p 1514 N95-20732

Sputter deposition of multilayer thermoelectric films: An approach to the fabrication of two-dimensional quantum wells
[DE95-002396] p 1272 N95-20892

Excitons in semiconducting superlattices, quantum wells, and ternary alloys
[DE95-001867] p 1572 N95-21287

Resonant generation of nonequilibrium phonons in GaAs/AlAs quantum wells via intersubband scattering
[DE95-002338] p 1581 N95-21604

Optical, electronic and optoelectronic material and device research
[AD-A280111] p 1374 N95-21630

Effect of the electron-SO-phonon on the impurity state energies in a semiconductor quantum well
[DE94-628993] p 1581 N95-21887

Growth and electrical and far-infrared properties of wide electron wells in semiconductors
[AD-A279409] p 1333 N95-21917

Heterostructure quantum confined Stark effect electrooptic modulators operating at 938 nm
[AD-A279342] p 1581 N95-21928

Carrier dynamics in InGaAs: Quantum wells versus bulk
[DE94-018205] p 1577 N95-22168
Photoreflectance and x ray diffraction study of semiconductor heterostructures and quantum wells
[PB95-127049] p 1582 N95-22432

QUARK MODELS
Status of the DO top search
[DE95-002214] p 1525 N95-21715
There might be two kinds of dibaryon
[DE94-014417] p 1526 N95-22058

QUARK PARTON MODEL
Antishadowing contribution to the pomeron structure function
[PB95-127478] p 1518 N95-21221

QUARKS
New strong interactions above the electroweak scale
[DE94-018385] p 1506 N95-20025
J/psi,psi(prime) yields mu(+)mu(-) and B yields J/psi,psi(prime) cross sections
[DE94-017184] p 1507 N95-20108
Search for top in DO using the electron + jets channel with soft muon tagging
[DE95-001284] p 1509 N95-20217
CDF top results in the dilepton channel
[DE95-000837] p 1510 N95-20343
Higgs decay to bottom quarks at the Tevatron
[DE94-016715] p 1511 N95-20404
Universal parametrization for quark and lepton substructure
[DE94-770604] p 1514 N95-20738
Properties of strange-matter stars
[DE95-002329] p 1599 N95-20873
Kinematical evidence for top pairs at the Tevatron
[DE95-000729] p 1515 N95-20880
Charmonium production, b quark and B meson production and b(bar b) correlations at CDF
[DE95-002525] p 1515 N95-20898
Antishadowing contribution to the pomeron structure function
[PB95-127478] p 1518 N95-21221
Calculation of Z plus four jet production at the Tevatron
[PB95-130472] p 1580 N95-21230
Signals for top quark anomalous chromomagnetic moments at colliders
[DE95-002896] p 1535 N95-21254
Nonperturbative aspects of the quark-photon vertex
[DE94-012846] p 1520 N95-21315
Heavy ion collisions
[DE95-002712] p 1520 N95-21321
Strange hadronic matter
[DE94-019345] p 1521 N95-21484
Monopoles and quark confinement: Introduction and overview
[DE94-019348] p 1522 N95-21485
Search for the top quark using multivariate analysis techniques
[DE95-000561] p 1522 N95-21498
Search for new particles decaying to dijets in p(bar p) collisions at (radical)s = 1.8 TeV
[DE94-018994] p 1523 N95-21563
Summary of heavy ion theory
[DE95-002177] p 1523 N95-21588
Investigation of direct photon production in 200 A GeV S + Au reactions
[DE94-018129] p 1525 N95-21704
Status of the DO top search
[DE95-002214] p 1525 N95-21715
There might be two kinds of dibaryon
[DE94-014417] p 1526 N95-22058
Testing the principle of equivalence by solar neutrinos
[DE94-014972] p 1604 N95-22064
Physics at the Fermilab Collider
[DE95-000726] p 1539 N95-22195
Inclusive B production at CDF and D0
[DE95-000728] p 1528 N95-22196
Search for squarks and gluinos in D0
[DE95-000730] p 1528 N95-22197
Search for top with DO detector in dilepton channel
[DE95-000731] p 1529 N95-22314

QUARTZ
Quartz resonator fluid monitors for vehicle applications
[DE94-018910] p 1367 N95-21546
Radio-frequency techniques at the ISIS pulsed muon source
[PB95-129854] p 1529 N95-22303

QUARTZ TRANSDUCERS
Generation of micro-domains in AT-cut quartz by thermal processing and the effect on resonator modes
[DE94-017344] p 1564 N95-20087

QUATERNARY ALLOYS
Application of quaternary phase diagrams to compound semiconductor processing
[DE95-001813] p 1277 N95-21748

QUENCHING (ATOMIC PHYSICS)
Correlations for the OH A(sup 2)(Sigma)(sup +)(v(prime)=0) electronic quenching cross-section
[DE95-002591] p 1244 N95-21524

QUERY LANGUAGES
Translation of the data flow query language for the multimodel, multibackend database system
[AD-A285978] p 1588 N95-20617
GOLD: A Graph Oriented Language for Databases
[PB95-127544] p 1465 N95-21021
Logic programming and negation: A survey
[PB95-110730] p 1472 N95-22302
A conceptual approach to object-oriented data modeling
[AD-A286048] p 1592 N95-22416

QUEUEING THEORY
High-performance packet switching architecture for ATM: Conventional solution and neural network solution
[PB95-110920] p 1312 N95-19935
Stochastic network processes
[AD-A279905] p 1475 N95-20566
Compositional approach to sequential consistency and lazy caching
[PB95-134110] p 1455 N95-21871

R

RABBITS
Biological and theoretical studies of adaptive networks: The conditioned response
[AD-A284781] p 1479 N95-20061

RADAR
Adaptive detection in stationary and nonstationary noise environments
[AD-A279581] p 1300 N95-21099

RADAR ANTENNAS
General purpose sidelobe canceller system
[AD-D016560] p 1289 N95-20270
Inband scattering from arrays with series feed networks
[AD-A286209] p 1307 N95-21883
Millimeter wave front-end figure of merit, part 1
[AD-A279093] p 1307 N95-21915

RADAR BEACONS
GPS-Squitter capacity analysis
[AD-A280037] p 1291 N95-20599
Recommendation on transition from primary/secondary radar to secondary-only radar capability
[AD-A286279] p 1308 N95-22005

RADAR CROSS SECTIONS
RCS calculation capability
[AD-A286329] p 1289 N95-20211
Inband scattering from arrays with series feed networks
[AD-A286209] p 1307 N95-21883
Design and construction of a Ka-band scatterometer
[AD-A286296] p 1368 N95-22322

RADAR DATA
Emitter location via Kalman filtering of signal time difference of arrival
[AD-A285972] p 1291 N95-20666
Real-data tests of a single-Doppler radar assimilation system
[AD-A286638] p 1292 N95-20904
AN/APS-137 Forward Looking Airborne Radar (FLAR) evaluation, Fall 1992 experiment
[AD-A279526] p 1306 N95-21686
The applicability of neural networks to ionospheric modeling in support of relocatable Over-the-Horizon radar
[AD-A286114] p 1309 N95-22230

RADAR DETECTION
BACKSCAT lidar simulation version 4.0: Technical documentation and users guide
[AD-A285851] p 1290 N95-20376
LADAR detection statistics in the presence of pointing errors
[AD-A285865] p 1309 N95-22134
Probability of detection for a GO CFAR radar processor using envelope detection approximation
[AD-A286211] p 1310 N95-22251

RADAR IMAGERY
Experimental proof-of-concept of phase derivative based range profile enhancement ATR
[AD-A284921] p 1289 N95-19997
SAR image registration in absolute coordinates using GPS carrier phase position and velocity information
[DE94-018738] p 1204 N95-20195
Three-dimensional ground penetrating radar imaging using multi-frequency diffraction tomography
[DE94-016687] p 1301 N95-21205
Polar volatiles on Mercury and the Moon
p 1422 N95-21811

RADAR MEASUREMENT
Boundary layer cloud studies in support of ASTEX
[AD-A285947] p 1429 N95-20395
Measurements of radar backscatter from the ocean surface at 94 GHz as a function of wind speed, direction and the modulation by the ocean waves during the SAXON-FPN experiment p 1299 N95-20960

RADAR NAVIGATION
Recommendation on transition from primary/secondary radar to secondary-only radar capability
[AD-A286279] p 1308 N95-22005

RADAR RANGE
Probability of detection for a GO CFAR radar processor using envelope detection approximation
[AD-A286211] p 1310 N95-22251

RADAR RECEIVERS
Processing, fabrication, and demonstration of HTS integrated microwave circuits
[AD-A285611] p 1312 N95-19894

RADAR SCATTERING
Sounder calibration with backscattering from Losquet Island in the presence of multipaths
p 1300 N95-20961
Inband scattering from arrays with series feed networks
[AD-A286209] p 1307 N95-21883

RADAR TARGETS
Experimental proof-of-concept of phase derivative based range profile enhancement ATR
[AD-A284921] p 1289 N95-19997
RCS calculation capability
[AD-A286329] p 1289 N95-20211
Adaptive detection in stationary and nonstationary noise environments
[AD-A279581] p 1300 N95-21099
Method and apparatus for classifying targets
[AD-D016519] p 1303 N95-21464

RADAR TRACKING
Experimental proof-of-concept of phase derivative based range profile enhancement ATR
[AD-A284921] p 1289 N95-19997
Location and characteristics of the reconnection X-line deduced from low-altitude satellite and radar observations
[NASA-TM-110114] p 1413 N95-20453
An integrated cloud observation and modeling investigation in support of the ARM Program
[DE95-002798] p 1430 N95-21527
Noncoherent transponder standards
[AD-A279512] p 1306 N95-21684
Frequency-coded monopulse MTI
[AD-D016495] p 1307 N95-21904

RADIAL DISTRIBUTION
Residual stress analysis in swage autofrettaged thick-walled cylinders by position-sensitive x-ray diffraction techniques
[AD-A286383] p 1388 N95-22320

RADIANCE
Radiance of the ocean horizon
[AD-A285613] p 1431 N95-19896

RADIANT HEATING
Site Scientific Mission Plan for the Southern Great Plains CART site, July - December 1994
[DE94-017289] p 1401 N95-20193
Ion heating perpendicular to the magnetic field
[AD-A286635] p 1501 N95-20773

RADIATION ABSORPTION
Broadband thermal optical limiter for the protection of eyes and sensors
[AD-D016493] p 1377 N95-22304

RADIATION COUNTERS
D0 quantum chromodynamics: A compilation of results presented at DPF 1994
[DE95-000838] p 1510 N95-20344
Mechanical design of the DO silicon detector
[DE95-002532] p 1365 N95-20902
New shower maximum trigger for electrons and photons at CDF
[DE95-000563] p 1522 N95-21499
Detection efficiency and dark pulse rate of Rockwell (SSPM) single photon counters
[DE94-016872] p 1524 N95-21646
Design of the readout IC for the CDF SVX-2 silicon strip detector
[DE95-000562] p 1539 N95-22193

RADIATION DAMAGE
Post-irradiation deformation characteristics of heavy-ion irradiated 304L SS
[DE94-017462] p 1251 N95-20088
Light output and radiation damage in a lead tungstate crystal
[DE94-016814] p 1565 N95-20265
Electron-irradiated two-terminal, monolithic InP/Ga0.47In0.53As tandem solar cells and annealing of radiation damage p 1319 N95-20519

The use of displacement damage dose to correlate degradation in solar cells exposed to different radiations
p 1320 N95-20523

Plasma model for charging damage
[DE95-000788] p 1558 N95-21310

Light output and radiation damage in a YAlO3:Ce crystal
[DE94-016815] p 1545 N95-21643

Optical radiation: Health based exposure limits for electromagnetic radiation in the wavelength range from 1 nanometer to 1 millimeter
[PB95-132767] p 1447 N95-22083

RADIATION DETECTORS

Radioactive check sources for alpha and beta sensitive radiological instrumentation
[DE94-016477] p 1366 N95-21138

Reentry vehicle on-site inspection technology study
[AD-A285960] p 1220 N95-21634

Electromagnetic radiation detector utilizing an electromagnetic radiation absorbing element in a mach-zehnder interferometer arrangement
[AD-D016507] p 1306 N95-21835

RADIATION DISTRIBUTION

Solar Radiation Resource Assessment Project
[DE94-000286] p 1392 N95-20778

Azimuthally averaged radial S(sub 100 microns)/S(sub 60 microns) dust color temperatures in spiral galaxies
p 1593 N95-21760

RADIATION DOSAGE

Post-irradiation deformation characteristics of heavy-ion irradiated 304L SS
[DE94-017462] p 1251 N95-20088

The use of displacement damage dose to correlate degradation in solar cells exposed to different radiations
p 1320 N95-20523

Advanced robotic technologies for transfer at Sandia National Laboratories
[DE95-001617] p 1481 N95-20884

Optical radiation: Health based exposure limits for electromagnetic radiation in the wavelength range from 100 nanometer to 1 millimeter
[PB95-132767] p 1447 N95-22083

RADIATION EFFECTS

Light output and radiation damage in a lead tungstate crystal
[DE94-016814] p 1565 N95-20265

Proton irradiation effects on advanced digital and microwave III-V components
[DE94-018742] p 1314 N95-20338

A mechanistic model for radiation-induced crystallization and amorphization in U3Si
[DE94-015028] p 1566 N95-20419

Radiation-induced modifications of allylamino-substituted polyphosphazenes
[AD-A279694] p 1268 N95-20428

A wideband EMP test system
[DE94-015283] p 1290 N95-20474

Proceedings of the 13th Space Photovoltaic Research and Technology Conference (SPRAT 13)
[NASA-CP-3278] p 1316 N95-20502

Radiation effects on p+n InP junctions grown by MOCVD p 1319 N95-20520

PRS scoping study 1: Scaling law estimates for K-shell radiation yields on JUPITER-class generators
[AD-A279716] p 1533 N95-20672

Reactor pumped laser research at the Sandia National Laboratories pulsed reactor facilities
[DE95-002181] p 1371 N95-20867

Influence of oxidation on radiation hardness of silicon detectors
[DE95-002466] p 1272 N95-20894

Effect of neutron irradiation on the impact properties of A533B steel
[DE95-001834] p 1256 N95-21286

Effects of neutron irradiation on the London penetration depth for polycrystalline Bi(1.8)Pb(0.3)Sr2Ca2Cu3O10 superconductor
[DE94-019335] p 1573 N95-21483

Effects of increased UV-B radiation on phytoplankton: A preliminary study and research programme
[PB95-133732] p 1439 N95-21884

Compilation of 1993 annual reports of the Navy ELF Communications System Ecological Monitoring Program. Volume 2: Tabs C-F
[AD-A279770] p 1308 N95-21988

Effect of laser radiation on carbon fibre/epoxy composites
[PB95-133526] p 1232 N95-22096

Performance of Ga(0.47)In(0.53)As cells over a range of proton energies
[NASA-TM-106819] p 1334 N95-22112

Radiation characterization report for the GPS Receiver microcontroller chip
[DE94-019169] p 1335 N95-22165

Study of pulsed laser effects on living tissues
[PB95-131330] p 1447 N95-22361

RADIATION HARDENING

Target area acquisition and control system survivability for the National Ignition Facility
[DE94-016549] p 1550 N95-20190

Design of high-efficiency, radiation-hard, GaInP/GaAs solar cells p 1319 N95-20521

Influence of oxidation on radiation hardness of silicon detectors
[DE95-002466] p 1272 N95-20894

Polymer based all-optic reconfigurable interconnects
[AD-A279976] p 1272 N95-20962

SEU and SEL response of the Westinghouse 64K E-2PROM, analog devices AD7876 12-bit ADC, and the Intel 82527 Serial Communications Controller
[DE95-003349] p 1334 N95-22086

RADIATION HAZARDS

Definition report on target and related steering variables of radiation as a part of the environmental balance and environmental outlook investigation
[PB95-135471] p 1409 N95-21846

Optical radiation: Health based exposure limits for electromagnetic radiation in the wavelength range from 100 nanometer to 1 millimeter
[PB95-132767] p 1447 N95-22083

RADIATION MEASUREMENT

Site Scientific Mission Plan for the Southern Great Plains CART site, July - December 1994
[DE94-017289] p 1401 N95-20193

Solar Radiation Resource Assessment Project
[DE94-000286] p 1392 N95-20778

RADIATION PROTECTION

MCNP (trademark) directions
[DE94-016216] p 1509 N95-20254

RADIATION SHIELDING

Neutronics and shielding analysis of the National Ignition Facility
[DE94-016698] p 1534 N95-21208

RADIATION SICKNESS

Acute radiation sickness amelioration analysis
[AD-A279084] p 1445 N95-21629

RADIATION SOURCES

Free electron laser program
[AD-A285906] p 1368 N95-19987

PRS scoping study 1: Scaling law estimates for K-shell radiation yields on JUPITER-class generators
[AD-A279716] p 1533 N95-20672

Radioactive check sources for alpha and beta sensitive radiological instrumentation
[DE94-016477] p 1366 N95-21138

PRS scoping study. 2: ZPIMP predictions for radiation yields on a JUPITER-class generator
[AD-A279823] p 1537 N95-21494

Definition report on target and related steering variables of radiation as a part of the environmental balance and environmental outlook investigation
[PB95-135471] p 1409 N95-21846

RADIATION TOLERANCE

Status of diffused junction p+n InP solar cells for space applications p 1317 N95-20509

High quality InP-on-Si for solar cell applications
p 1317 N95-20510

Performance, defect behavior and carrier enhancement in low energy, proton irradiated p+nn+ InP solar cells
p 1319 N95-20518

Investigation of the stability and 1.0 MeV proton radiation resistance of commercially produced hydrogenated amorphous silicon alloy solar cells p 1320 N95-20522

RADIATION TRANSPORT

Unified GUI for the Los Alamos Radiation Transport Code System
[DE94-016088] p 1458 N95-20154

A practical guide to using MCNP with PVM
[DE94-016162] p 1474 N95-20158

Data analysis and visualization in MCNP (trademark)
[DE94-016164] p 1508 N95-20159

MCNP (trademark) ENDF/B-VI iron benchmark calculations
[DE94-016165] p 1508 N95-20160

New data for MCNP (trademark)
[DE94-016296] p 1509 N95-20236

MCNP (trademark) directions
[DE94-016216] p 1509 N95-20254

RADIATIVE LIFETIME

A preliminary, precise measurement of the average B hadron lifetime
[DE95-001848] p 1525 N95-21727

Measurement of the average lifetime of B hadrons at SLD
[DE95-002121] p 1527 N95-22152

RADIATIVE TRANSFER

Radiation from advanced solid rocket motor plumes
[NASA-CR-196554] p 1221 N95-20124

Radiative forcing calculations for CH3Cl
[DE94-019018] p 1402 N95-20355

Effects of microphysics and radiation on mesoscale processes of a midlatitude squall line
[DE94-014732] p 1429 N95-20381

Meso-scale cooling effects of high albedo surfaces: Analysis of meteorological data from White Sands National Monument and White Sands Missile Range
[DE94-018535] p 1429 N95-20782

RADICALS

Intrinsic barriers for H-atom transfer reactions
[DE94-018914] p 1507 N95-20049

Publications/patents/presentations/honors/student eport. Investigation of the role of vibrational excitation in unimolecular reactions
[AD-A280044] p 1513 N95-20621

Structure of dibis(diethyldithiocarbamato) zinc (2) Mu-bis(diethylphosphino)ethane toluene(2)
[AD-A279792] p 1224 N95-20660

Photophysical processes on triplet states and radical ions in pure and molecularly doped polymers
[DE95-002681] p 1570 N95-20916

Application of IRIS to semiconductor plasma processing
[DE95-003591] p 1562 N95-22225

RADII

The variation of the dust temperature within late-type spiral galaxies p 1593 N95-21766

RADIO ASTRONOMY

Solar-Geophysical Data number 600, August 1994. Part 1: (Prompt reports). Data for July, June 1994, and late data
[PB95-104923] p 1603 N95-20713

Twentysixth YERAC
[PB95-127437] p 1599 N95-21347

Science with High Spatial Resolution Far-Infrared Data
[NASA-CR-197353] p 1595 N95-21749

Luminous radio-quiet sources in the W3(MAIN) cloud core p 1594 N95-21773

Low noise 22 GHz receiver for the radioastron satellite, part 2: Space qualification tests
[PB95-127197] p 1598 N95-22376

RADIO COMMUNICATION

An abstract model of rogue code insertion into radio frequency wireless networks. The effects of computer viruses on the Program Management Office
[AD-A285759] p 1288 N95-19932

Modular CNI avionics system p 1213 N95-20659

A wideband propagation simulator for high speed mobile radio communications p 1295 N95-20934

Simulation of the impact of atmospheric turbulences on millimeter-wave communications systems
p 1295 N95-20939

Routing of unidirectional packet radio for wide-area paging network control and maintenance
[PB95-104428] p 1300 N95-20980

Small antennas for communication over sea ice
[AD-D016206] p 1301 N95-21156

RADIO ELECTRONICS

Low noise 22 GHz receiver for the radioastron satellite, part 2: Space qualification tests
[PB95-127197] p 1598 N95-22376

RADIO EMISSION

Correlation of far-infrared emission and radio continuum emission along the major axis of edge-on spiral galaxies
p 1593 N95-21762

Two-dimensional maps of the infrared-to-radio ratio in spiral galaxies p 1593 N95-21765

Luminous radio-quiet sources in the W3(MAIN) cloud core p 1594 N95-21773

RADIO EQUIPMENT

Low-cost conical ultra-wideband antenna
[AD-A286569] p 1292 N95-20825

Radio-science performance analysis software
p 1305 N95-21540

RADIO FREQUENCIES

Modeling of beam dynamics and comparison with measurements for the Advanced Light Source (ALS)
[DE94-017970] p 1532 N95-20495

Pulsed laser illumination of photovoltaic cells
p 1323 N95-20538

Photoelectrons beam measurement from a magnesium cathode in a RF electron gun
[DE94-017994] p 1533 N95-20573

The impact of advanced packaging technology on modular avionics architectures p 1208 N95-20632

High density monolithic packaging technology for digital/microwave avionics p 1211 N95-20646

Field-emitter arrays for RF vacuum microelectronics
[AD-A279959] p 1325 N95-20661

Innovative use of DSP technology in space: FORTE event classifier
[DE94-016086] p 1291 N95-20697

An advanced ECR ion source with a large uniformly distributed ECR plasma volume for multiply charged ion beam generation
[DE95-001078] p 1515 N95-20911

Development of a fast sampling system for estimation of impulse responses of mobile radio channels p 1296 N95-20943
Study on the reaction kinetics in pulsed RF discharges under RIE conditions [PB95-107868] p 1300 N95-21029
Effects of RF side-bands on spectral reproducibility for infrared synchrotron radiation [DE95-002450] p 1536 N95-21418
Three-dimensional effects for radio frequency antenna modeling [DE94-019125] p 1303 N95-21459
Radio-science performance analysis software p 1305 N95-21540
An 8-meter-long coupled cavity RFQ linac [DE94-018077] p 1331 N95-21667
Broadband pressure barrier for circular waveguide [AD-D016503] p 1306 N95-21672
RF vacuum microelectronics based on thin film edge-emitter technology [AD-A279539] p 1331 N95-21690
High temperature superconducting films and multilayers for electronics [AD-A279545] p 1331 N95-21693
RF beam control for the AGS Booster [DE95-001485] p 1538 N95-21720
Improved broadband waveguide pressure window [AD-D016487] p 1306 N95-21834
Atomic velocity distributions in a hydrogen beam effusing out of an RF discharge dissociator [AD-A279253] p 1307 N95-21985
Radio-frequency techniques at the ISIS pulsed muon source [PB95-129854] p 1529 N95-22303
Low-level RF control for the AFEL [DE94-018295] p 1540 N95-22410

RADIO FREQUENCY HEATING
ALT-2 armor tile design for upgraded TEXTOR operation [DE94-015749] p 1549 N95-20143
Experimental measurements of ICRF and edge plasma interactions on Tore Supra [DE94-019154] p 1551 N95-20205
Microwave sintering of ZrO2-12 mol% CeO2 [DE94-018709] p 1265 N95-20226
Radiofrequency hyperthermia systems: Experimental and clinical assessment of the feasibility of radiofrequency hyperthermia systems for loco-regional deep heating [PB94-206885] p 1444 N95-21016
Applied mathematical problems in modern electromagnetics [AD-A286448] p 1303 N95-21462
Comparison of properties of sintered and sintered reaction-bonded silicon nitride fabricated by microwave and conventional heating [DE95-001426] p 1275 N95-21501

RADIO FREQUENCY INTERFERENCE
CDMA with interference cancellation for multiprobe missions p 1304 N95-21536
Cochannel and adjacent-channel interference in nonlinear minimum-shift-keyed satellite system [NASA-TM-106834] p 1307 N95-21890

RADIO RECEIVERS
Low noise 22 GHz receiver for the radioastron satellite. Part 1: Requirements, design and reliability analysis [PB95-104410] p 1300 N95-20972
Design and implementation of a dual-beam printed antenna for a reception in angular diversity on a Hertzien cluster (or bundle) [PB95-131603] p 1302 N95-21431
Low noise 22 GHz receiver for the radioastron satellite, part 2: Space qualification tests [PB95-127197] p 1598 N95-22376

RADIO RELAY SYSTEMS
Design and implementation of a dual-beam printed antenna for a reception in angular diversity on a Hertzien cluster (or bundle) [PB95-131603] p 1302 N95-21431

RADIO SIGNALS
Passive monitoring for automated MMPP communication systems p 1293 N95-20927
Small antennas for communication over sea ice [AD-D016206] p 1301 N95-21156
The Deep Space Network as an instrument for radio science research [NASA-CR-197341] p 1302 N95-21456

RADIO SOURCES (ASTRONOMY)
Luminous radio-quiet sources in the W3(MAIN) cloud core p 1594 N95-21773

RADIO SPECTRA
Passive monitoring for automated MMPP communication systems p 1293 N95-20927
Arcmimute scale HI and IRAS observations toward high latitude cloud G86.5+59.6 p 1594 N95-21771

RADIO TELEMETRY
The Deep Space Network as an instrument for radio science research [NASA-CR-197341] p 1302 N95-21456

RADIO TELESCOPES
Low noise 22 GHz receiver for the radioastron satellite. Part 1: Requirements, design and reliability analysis [PB95-104410] p 1300 N95-20972
Low noise 22 GHz receiver for the radioastron satellite, part 2: Space qualification tests [PB95-127197] p 1598 N95-22376

RADIO TRANSMISSION
Adaptive error-control scheme for 2-200 MHz Multiple-Mechanism Propagation Paths p 1293 N95-20926
Study of the fast and slow variations of the power received at VHF links by tropospheric diffusion p 1293 N95-20929
Problems of coding in multipath channels p 1294 N95-20930
Methods for evaluating the effects of conduits at the surface of the sea p 1294 N95-20932
Propagation of high frequency waves in urban and road tunnel environments p 1294 N95-20933
Combined effects of atmosphere and terrain on UHF/microwave paths p 1295 N95-20935
Propagation measurements on a troposcatter link in the Canadian High Arctic p 1295 N95-20940
The effects of multihop HF propagation on the performance of OTH backscatter radars p 1298 N95-20953
Identification of the propagation modes and paths on HF links using a goniopolarimeter p 1299 N95-20956
Measurements of angles of elevation of HF by a high resolution method using polarization diversity p 1299 N95-20959
Routing of unidirectional packet radio for wide-area paging network control and maintenance [PB95-104428] p 1300 N95-20980
The Deep Space Network as an instrument for radio science research [NASA-CR-197341] p 1302 N95-21456

RADIO WAVES
Combined effects of atmosphere and terrain on UHF/microwave paths p 1295 N95-20935
The effects of multihop HF propagation on the performance of OTH backscatter radars p 1298 N95-20953

RADIOACTIVE DECAY
High efficiency GaP power conversion for Betavoltaic applications p 1323 N95-20540
Laser trapping of Na-21 atoms [DE95-002354] p 1513 N95-20629
Measurement of the polarization in the decay B(sup 0) (yields) J/(psi)K*(sup 0) in (bar p)p collisions at (radical)s = 1.8 TeV [DE95-002521] p 1520 N95-21313

RADIOACTIVE ISOTOPES
Thorium-232 in human tissues: Metabolic parameters and radiation doses [DE94-019275] p 1441 N95-20074
Parity nonconservation in radioactive atoms: An experimental perspective [DE95-002737] p 1518 N95-21235
ANSTO: Mission statement, significant events and achievements [DE94-631123] p 1605 N95-21830

RADIOACTIVE MATERIALS
Selection of substances to be considered in the environmental balance/environmental outlook in relation to the dissemination theme [PB95-132197] p 1407 N95-21635

RADIOACTIVE WASTES
Geometric moire method of strain analysis with displacement discontinuities [DE95-001114] p 1386 N95-20833
Conceptual design analyses for Hanford Site deployable remote spectroscopy systems [DE95-002078] p 1243 N95-21473

RADIOACTIVITY
Parity nonconservation in radioactive atoms: An experimental perspective [DE95-002737] p 1518 N95-21235
Selection of RIB targets using ion implantation [DE95-000951] p 1538 N95-21938

RADIOBIOLOGY
Life Sciences Division and Center for Human Genome Studies [DE94-017796] p 1440 N95-22065

RADIOCHEMISTRY
In vivo distribution of liposome encapsulated hemoglobin studied with imaging radiotracers [AD-A279774] p 1438 N95-20806
Radiopharmaceuticals for diagnosis [DE95-002200] p 1445 N95-21595

RADIOGENIC MATERIALS
Recycling of volatiles at subduction zones: Noble gas evidence from the Tabar-Lihir-Tanga-Feni arc of papua New Guinea p 1418 N95-21787
Degassing history and evolution of volcanic activity of terrestrial planets based on radiogenic noble gas degassing models p 1424 N95-21816
Is xenon eldest? p 1425 N95-21823

RADIOGONIOMETERS
Identification of the propagation modes and paths on HF links using a goniopolarimeter p 1299 N95-20956

RADIOISOTOPE BATTERIES
High efficiency GaP power conversion for Betavoltaic applications p 1323 N95-20540
Conceptual design of an RTG Facility Transportation System [DE94-014443] p 1379 N95-20627
GPHS-RTGs in support of the Cassini Mission [DE95-001492] p 1222 N95-20853

RADIOMETERS
Final results of the advanced photovoltaic experiment p 1321 N95-20528

RAIN
Rainfall rates and the vertical distribution of diabatic heating components over tropical oceans [NASA-CR-197603] p 1428 N95-19948
Program control on the Tropical Rainfall Measuring Mission p 1584 N95-20750
Applicability of the ECMWF rain height and rainfall rate data to the prediction of low-availability rain attenuation in Europe [PB95-127684] p 1430 N95-21413

RAINDROPS
The initiation of lightning and the growth of electric fields in thunderstorms [AD-A280033] p 1428 N95-20008
Aircraft corrosion study [AD-A279527] p 1259 N95-21687

RAMAN SPECTRA
Daytime Raman lidar profiling of atmospheric water vapor [DE94-015747] p 1413 N95-20397
Nonlinear spectroscopy of multicomponent droplets and two- and three-dimensional measurements in flames [AD-A279945] p 1238 N95-20581
Raman spectra of MOCVD-grown ferroelectric PbTiO3 thin films [DE94-018964] p 1244 N95-21549
Resonant generation of nonequilibrium phonons in GaAs/AlAs quantum wells via intersubband scattering [DE95-002338] p 1581 N95-21604

RAMAN SPECTROSCOPY
Resonance Raman spectroscopy of volatile organics: Carbon tetrachloride [DE95-000627] p 1233 N95-19980
Quantitative and qualitative analysis of some inorganic compounds by Raman spectroscopy [DE94-009757] p 1237 N95-20470
Detection of environmental deterioration in fiber reinforced composites by FT-Raman spectroscopy, phase 1 [AD-A279763] p 1228 N95-20805

RAMJET ENGINES
Integral rocket ramjets [AD-A285135] p 1222 N95-20906

RANDOM NOISE
Higher order crossings [AD-A279597] p 1504 N95-20300
Adaptive detection in stationary and nonstationary noise environments [AD-A279581] p 1300 N95-21099
In search of random noise p 1592 N95-21753

RANDOM PROCESSES
Almost kappa-wise independent random permutation of the cube [PB95-108098] p 1495 N95-22147

RANDOM SAMPLING
Latin hypercube sampling in sensitivity analysis [AD-A285867] p 1499 N95-22135

RANDOM VARIABLES
Brief tutorial on the Kalman filter [AD-A286571] p 1326 N95-20827
Duality and equivalencies in closed tandem queueing networks [PB95-132502] p 1482 N95-21271

RANGEFINDING
Multipath impact on ground-based global positioning system range measurements: Aspects of measurement, modeling, and mitigation p 1297 N95-20949
Passive range measurement system [AD-D016222] p 1544 N95-21100

RANGES (FACILITIES)
Proceedings of the 4th Annual Major Range and TestFacility Base (MRTFB) Environmental Workshop [AD-A285779] p 1411 N95-22414

RANK TESTS
A multivariate multisample rank test for stochastic simulation validation
[AD-A285922] p 1498 N95-19990
RANKING
Evaluation of scanners for C-scan imaging for nondestructive inspection of aircraft
[AD-A286398] p 1383 N95-22202
Vertex ranking for permutation and other graphs
[PB95-127569] p 1496 N95-22327
RAPID QUENCHING (METALLURGY)
Processing and characterization of Ni-Al-Fe-B shape-memory alloy wires produced by rapid solidification
[DE94-017702] p 1250 N95-20020
RARE EARTH ALLOYS
Methods and opportunities in the recycling of rare Earth based materials
[DE95-001680] p 1259 N95-21737
RARE EARTH COMPOUNDS
Methods and opportunities in the recycling of rare Earth based materials
[DE95-001680] p 1259 N95-21737
The low temperature properties of (Dy(1-x)Er(x))Ni2 alloys
[DE95-001657] p 1260 N95-21923
RARE GASES
Identification of resonant, two-electron, and inter-atomic features in K and L23 NEXAFS spectra
[AD-A285374] p 1513 N95-20554
Quantum chemical study of rare gas/halide interactions as a model for high energy density material. 1: Transition properties in HCl
[AD-A285988] p 1239 N95-20613
Inert gas purification and measuring oxygen partial pressure in gas mixtures with EMF method based on solid electrolyte cell
[PB95-127767] p 1240 N95-21110
Molecular-based study of solutions in supercritical solvents
[DE94-019326] p 1580 N95-21420
Conference on Deep Earth and Planetary Volatiles
[NASA-CR-196944] p 1415 N95-21777
Rare gases systematics and mantle structure
p 1416 N95-21778
Impact degassing of water and noble gases from silicates p 1416 N95-21780
Noble gas isotopes and halogens in volatile-rich inclusions in diamonds p 1417 N95-21784
Origin and loss of the volatiles of the terrestrial planets p 1417 N95-21785
Recycling of volatiles at subduction zones: Noble gas evidence from the Tabar-Lihir-Tanga-Feni arc of papua New Guinea p 1418 N95-21787
Mars atmospheric loss and isotopic fractionation by pick-up-ion sputtering and photochemical escape
p 1420 N95-21796
The ratios of carbon and non-radiogenic helium and argon isotopes in the mantle and crustal rocks
p 1421 N95-21805
Solubilities of nitrogen and noble gases in basalt melt
p 1422 N95-21807
Rates of Earth degassing p 1422 N95-21809
Mantle rare gas relative abundances in a steady-state mass transport model p 1423 N95-21812
Degassing history and evolution of volcanic activity of terrestrial planets based on radiogenic noble gas degassing models p 1424 N95-21816
Implications of noble gases in a recently recognized Martian meteorite (ALH84001) for the degassing history of Mars p 1424 N95-21819
Is xenon eldest? p 1425 N95-21823
Degassing mechanisms of noble gases from carbonado diamonds p 1425 N95-21824
Quantum chemical study of rare gas/halide interactions as a model for high energy density material. 2: The interaction of hydrogen chloride with the rare gas xenon
[AD-A286385] p 1248 N95-22321
RAREFIED GAS DYNAMICS
Continuum transient and frozen startup behavior of conventional and gas-loaded heat pipes
[AD-A284297] p 1339 N95-20250
Simulated rarefied entry of the Galileo probe into the atmosphere of Jupiter
[NASA-TM-110507] p 1601 N95-21621
RAREFIED GASES
Low density gas and foam targets for ICF long scale length plasma experiments: Fabrication and characterization
[DE95-000935] p 1558 N95-21368
RATES (PER TIME)
Polymer based all-optic reconfigurable interconnects
[AD-A279976] p 1272 N95-20962
High speed optical storage technology
[AD-A285788] p 1456 N95-22400
RAY TRACING
Time behavior and frequency response of the microwave propagation channel during multipath propagation
p 1296 N95-20942
Real time system for practical acoustic monitoring of global ocean temperature
[AD-A286435] p 1436 N95-22209
3-D TECATE/BREW: Thermal, stress, and birefringent ray-tracing codes for solid-state laser design
[DE95-000330] p 1376 N95-22301
RAYLEIGH EQUATIONS
The Combustive Sound Source
[ARL-TR-94-9] p 1503 N95-19911
RAYLEIGH SCATTERING
Nonlinear spectroscopy of multicomponent droplets and two- and three-dimensional measurements in flames
[AD-A279945] p 1238 N95-20581
RAYLEIGH WAVES
Source contributions at far-regional distances
[AD-A279405] p 1426 N95-21932
RDX
The hot fragment conductive ignition test for screening LOVA propellants
[AD-A284259] p 1282 N95-20187
Thermal decomposition reactions of HMX and RDX and their importance in predicting cookoff hazards
[DE95-002486] p 1283 N95-21513
REACTANCE
A colocated magnetic loop, electric dipole array antenna (preliminary results)
[AD-A285381] p 1290 N95-20556
REACTING FLOW
Explicit methods for stiff ODEs from atmospheric Chemistry
[PB95-135794] p 1404 N95-21034
Effect of chemical heat release in a temporally evolving mixing layer p 1249 N95-21037
Direct numerical simulations of turbulent non-premixed methane-air flames modeled with reduced kinetics
p 1249 N95-21038
One-dimensional reactive Euler equations
[PB95-135430] p 1244 N95-21573
REACTION BONDING
Comparison of properties of sintered and sintered reaction-bonded silicon nitride fabricated by microwave and conventional heating
[DE95-001426] p 1275 N95-21501
Hydrogenation of nitriles on a well-characterized nickel surface: From surface science studies to liquid phase catalytic activity measurements
[DE94-018184] p 1259 N95-21707
Angle resolved photoemission on K(0.3)Mo3, TiTe2 and Ti(1+x)S2
[DE94-018300] p 1574 N95-21712
Electric-field effects on shallow donor impurity in a harmonic quantum dot
[DE94-629034] p 1577 N95-22176
REACTION KINETICS
Safe conditions for contacting nitric acid or nitrates with Tri-n-Butyl Phosphate (TBP)
[DE95-001243] p 1235 N95-20215
Density functional studies of decomposition processes of energetic molecules
[AD-A286185] p 1510 N95-20327
The dynamics of formation and evaporation of mixed alkali halide nanocrystals: A case of comparable lattice energies
[AD-A285052] p 1567 N95-20483
Combustion-related studies using weakly bonded complexes
[DE95-002801] p 1238 N95-20576
Publications/patents/presentations/honors/student eport. Investigation of the role of vibrational excitation in unimolecular reactions
[AD-A280044] p 1513 N95-20621
Ion scattering and deposition: The role of energetic particles in thin film growth
[AD-A285975] p 1514 N95-20667
The effect of oxide inclusions on the kinetics of the austenite to ferrite transformation in low alloy steel weld metal
[DE94-018131] p 1253 N95-20676
Photochemistry of intermolecular C-H bond activation reactions
[DE94-018417] p 1239 N95-20682
Time-resolved analytical methods for liquid/solid interfaces
[DE95-002255] p 1240 N95-20780
Ion-molecule chemistry related to plasma deposition and etching of silicon
[AD-A279749] p 1514 N95-20804
Chemical Structure and Dynamics program
[DE95-001117] p 1403 N95-20834
Study on the reaction kinetics in pulsed RF discharges under RIE conditions
[PB95-107868] p 1300 N95-21029
Direct numerical simulations of turbulent non-premixed methane-air flames modeled with reduced kinetics
p 1249 N95-21038
Direct numerical simulation for premixed turbulent combustion modelling p 1249 N95-21082
Attempt to interpret the self-organizing mapping physiologically
[PB95-127783] p 1438 N95-21112
The formation of reaction bonded Si3N4 at low temperatures and in short times
[DE95-001990] p 1275 N95-21289
Simulations of metal dissolution and corrosion
[DE94-019295] p 1257 N95-21476
The energetics and dynamics of free radicals, ions, and clusters
[DE94-018101] p 1244 N95-21701
Oxidation behavior of aluminum nanopowders
[DE95-002721] p 1260 N95-21926
Catalyzed reduction of nitrate in aqueous solutions
[DE94-017660] p 1247 N95-22049
Electrostatic basis for molecular recognition in photosynthesis
[DE95-002979] p 1440 N95-22075
Numerical study of contaminant effects on combustion of hydrogen, ethane, and methane in air
[NASA-TM-106844] p 1284 N95-22114
Natural gas combustion chemistry mechanisms research
[PB95-111670] p 1247 N95-22150
Catalytic reactions of synthesis gas. Part 3. Determination of reaction kinetics
[PB95-127759] p 1248 N95-22329
Use of quantum chemically derived descriptors for QSAR modeling of reductive dehalogenation of aromatic compounds
[PB95-132783] p 1224 N95-22333
Applications of sonochemistry
[AD-A286388] p 1506 N95-22360
REACTION PRODUCTS
An overview of the Evaluation of Oxygen Interactions with Materials 3 Experiment: Space Shuttle Mission 46; July-August, 1992
[NASA-TM-110129] p 1412 N95-20278
Production of S2F10, S2OF10 and S2O2F10 by spark discharges in SF6*
[DE95-001421] p 1243 N95-21500
REACTIVITY
Laboratory evaluation of a reactive baffle approach to NOx control
[AD-A283802] p 1400 N95-19921
An overview of the Evaluation of Oxygen Interactions with Materials 3 Experiment: Space Shuttle Mission 46; July-August, 1992
[NASA-TM-110129] p 1412 N95-20278
Reactive nanophase oxide additions to melt-processed high-T(sub c) superconductors
[DE95-001470] p 1570 N95-20841
Numerical wave speed for one-dimensional scalar hyperbolic conservation laws with source terms
[PB95-127536] p 1492 N95-21371
Deposition and properties of novel nitride superlattice coatings
[DE95-002945] p 1230 N95-21445
One-dimensional reactive Euler equations
[PB95-135430] p 1244 N95-21573
Towards tailored interphase formation utilizing surface-bound benzylsulfonium salts as cationic initiators
[AD-A286461] p 1280 N95-22259
REACTOR DESIGN
Induction linacs for heavy ion fusion
[DE95-002357] p 1534 N95-20891
Use of the National Ignition Facility for the development of inertial fusion energy
[DE94-016696] p 1557 N95-21206
Evaluation of pumping and fueling requirements for the ITER EDA
[DE94-018117] p 1560 N95-21702
REACTOR MATERIALS
Assessment of database for interaction of tritium with ITER plasma facing materials
[DE95-002038] p 1558 N95-21290
Welding tritium exposed stainless steel
[DE95-003208] p 1382 N95-22356
REACTOR TECHNOLOGY
A low energy continuous reactor separator for the production of ethanol from corn grits/starch and biomass streams
[DE95-002256] p 1283 N95-21356
REACTORS
SPACE-R thermionic space nuclear power system: Design and technology demonstration
[DE95-000713] p 1221 N95-20076
READING
Evaluation of the Haworth-Newman avionics Display Readability Scale
[AD-A286127] p 1214 N95-22232

READOUT
Design of the readout IC for the CDF SVX-2 silicon strip detector [DE95-000562] p 1539 N95-22193
REAGENTS
Novel reagents for chemical vapor deposition of intermetallic alloys [AD-A286562] p 1271 N95-20815
REAL TIME OPERATION
Algebraic semantics of message sequence charts [PB95-110581] p 1288 N95-19890
General conservative extension theorem in process algebra [PB95-110656] p 1487 N95-19902
Real time process algebra with infinitesimals [PB95-110623] p 1488 N95-20055
Enhanced vehicle and event typing software, phase 1 [AD-A284862] p 1458 N95-20070
System level fault tolerance in parallel and distributed computing systems [AD-A279664] p 1474 N95-20305
Time domain spectral hole-burning storage [AD-A279912] p 1587 N95-20309
Digital filtering for data compression in telemetry systems [DE94-016611] p 1219 N95-20567
Fault-tolerance in distributed and multiprocessor real-time systems [AD-A279896] p 1461 N95-20595
The impact of advanced packaging technology on modular avionics architectures p 1208 N95-20632
Rate monotonic analysis for real-time systems: Instructors guide [AD-A286083] p 1463 N95-20810
Computer based analysis and synthesis of retinal function [AD-A286084] p 1443 N95-20811
Chemical Structure and Dynamics program [DE95-001117] p 1403 N95-20834
Environment for Test and Analysis of Distributed Software (ETADS) [AD-A285776] p 1463 N95-20877
Real-time reconfiguration study [AD-A286060] p 1464 N95-20910
Compositional proof theory for fault tolerant real-time distributed systems [PB95-127601] p 1465 N95-21025
Real-time dynamic simulator for the Topaz II reactor power system [DE95-001604] p 1535 N95-21278
Design principles for real-time process control systems [PB95-132890] p 1585 N95-21414
EXPERT system expert: Program description [PB95-131561] p 1482 N95-21429
EXPERT system expert: Users manual [PB95-131579] p 1482 N95-21430
A real-time algorithm for integrating differential satellite and inertial navigation information during helicopter approach [NASA-CR-197409] p 1205 N95-21891
Using the CoRE requirements method with ADARTS. Version 01.00.05 [AD-A279151] p 1470 N95-21972
Verification of a timestamp-based sliding-window protocol [PB95-132759] p 1455 N95-22082
Real time system for practical acoustic monitoring of global ocean temperature [AD-A286435] p 1436 N95-22209
Usable, real-time, interactive spoken language systems [AD-A286349] p 1310 N95-22253
RECEIVERS
Recent reflux receiver developments under the US DOE program [DE95-001622] p 1393 N95-20861
An overview: Component development for solar thermal systems [DE95-001623] p 1393 N95-20862
Geographical diversity combining to exploit multi-mechanism propagation p 1299 N95-20957
Design and implementation of a dual-beam printed antenna for a reception in angular diversity on a Hertzien cluster (or bundle) [PB95-131603] p 1302 N95-21431
Assessment of a non-dedicated GPS receiver system for precise airborne attitude determination [DE94-019309] p 1205 N95-21520
The determination of static and time varying dipole source. Sensor geometry during sea trials using differential global positioning system [MRL-TN-631] p 1205 N95-21642
Performance of a fast frequency-hopped noncoherent MFSK receiver over Rician fading channels with either partial-band interference or multi-tone interference [AD-A286168] p 1310 N95-22246
Effect of cell size on elliptically polarized radar clutter statistics [AD-A285789] p 1311 N95-22401
RECEPTION DIVERSITY
Design and implementation of a dual-beam printed antenna for a reception in angular diversity on a Hertzien cluster (or bundle) [PB95-131603] p 1302 N95-21431
Performance of a fast frequency-hopped noncoherent MFSK receiver over Rician fading channels with either partial-band interference or multi-tone interference [AD-A286168] p 1310 N95-22246
RECIPROCITY THEOREM
The Lorentz reciprocity theorem as a consistency test for propagation models p 1295 N95-20937
RECIRCULATIVE FLUID FLOW
Application of Direct and Large Eddy Simulation to Transition and Turbulence [AGARD-CP-551] p 1346 N95-21061
RECOMBINATION REACTIONS
Ion-molecular spiraling collisions and termolecular recombination [AD-A285633] p 1517 N95-21151
RECONNAISSANCE
Information security for unmanned systems [AD-A286511] p 1485 N95-22214
RECONNAISSANCE AIRCRAFT
Unmanned aerial vehicles [AD-A286190] p 1206 N95-20329
Passive range measurement system [AD-D016222] p 1544 N95-21100
RECORDING INSTRUMENTS
A simple ocean bottom hydrophone with 200 megabyte data capacity [AD-A279478] p 1434 N95-21677
RECORDS MANAGEMENT
A graded approach to ISO 9000 implementation for records managers [DE94-017409] p 1591 N95-22167
University library document circulation system specified in LCM [PB95-127957] p 1592 N95-22331
RECRYSTALLIZATION
A mechanistic model for radiation-induced crystallization and amorphization in U3Si [DE94-015028] p 1566 N95-20419
RECTANGLES
A convergence analysis of an h-version finite element method with high order elements for two dimensional elasto-plasticity problems [AD-A279975] p 1491 N95-20920
RECURSIVE FUNCTIONS
S-D hybridization and anisotropy of the optical second harmonic at low frequencies [AD-A279449] p 1544 N95-20876
Foundations of functional programming: A programmer's point of view [PB95-132932] p 1471 N95-22094
RECYCLING
Mercury usage and alternatives in the electrical and electronics industries [PB94-165362] p 1312 N95-19966
Anaerobic Treatment of Municipal Solid Waste and Sludge for Energy Production and Recycling of Nutrients [DE95-700217] p 1315 N95-20369
Progress in the development of recycling processes for electric vehicle batteries [DE94-015894] p 1324 N95-20626
Fusion power production in TFTR [DE95-002756] p 1557 N95-21240
Methods and opportunities in the recycling of rare Earth based materials [DE95-001680] p 1259 N95-21737
Volatiles in the Earth: All shallow and all recycled p 1416 N95-21779
Recycling of volatiles at subduction zones: Noble gas evidence from the Tabar-Lihir-Tanga-Feni arc of papua New Guinea p 1418 N95-21787
Subduction and volatile recycling in Earth's mantle p 1421 N95-21802
Subduction of hydrated basalt of the oceanic crust: Implications for recycling of water into the upper mantle and continental growth p 1423 N95-21814
Storage and recycling of water and carbon dioxide in the earth p 1425 N95-21822
REDUCTION
Semantics for a fine lambda-calculus with de Bruijn indices [PB95-127577] p 1492 N95-21372
REDUCTION (CHEMISTRY)
Catalyzed reduction of nitrate in aqueous solutions [DE94-017660] p 1247 N95-22049
Use of quantum chemically derived descriptors for QSAR modeling of reductive dehalogenation of aromatic compounds [PB95-132783] p 1224 N95-22333
REDUNDANT COMPONENTS
Backward error recovery in redundant disk arrays [AD-A286064] p 1463 N95-20846
REED-SOLOMON CODES
Adaptive error-control scheme for 2-200 MHz Multiple-Mechanism Propagation Paths p 1293 N95-20926
REENTRY SHIELDING
A computational study of projectile melt in impact with typical Whipple shields [DE94-016454] p 1385 N95-20237
REENTRY VEHICLES
Reentry vehicle on-site inspection technology study [AD-A285960] p 1220 N95-21634
REFINING
Degassing mechanisms of noble gases from carbonado diamonds p 1425 N95-21824
REFLECTANCE
Qualification test results for blue-red reflecting solar covers p 1320 N95-20525
Electromagnetic wave reflection from irregular plasma layers p 1298 N95-20952
Beryllium based multilayers for normal incidence extreme ultraviolet reflectivity [DE94-015560] p 1274 N95-21175
Surface inspection using Fourier Transform Infrared Spectroscopy [DE95-001699] p 1244 N95-21571
Recent progress of the compact AFEL at Los Alamos [DE95-002728] p 1376 N95-22154
Laboratory characterization of Woelter x ray optics [DE94-016969] p 1562 N95-22191
Reflective masks for extreme ultraviolet lithography [DE95-003427] p 1336 N95-22236
Neutron reflectivity study of adsorbed diblock copolymers [DE95-002740] p 1281 N95-22434
REFLECTED WAVES
Experimental and theoretical evaluation of elastic waves in curved layered media [AD-A286578] p 1504 N95-20918
REFLECTION
Radiance of the ocean horizon [AD-A285613] p 1431 N95-19896
Studies of the n-alkane/water interface by total internal reflection second harmonic generation [AD-A279473] p 1245 N95-21827
REFLECTOR ANTENNAS
A method using focal plane analysis to determine the performance of reflector antennas p 1304 N95-21538
Analysis of a microstrip reflectarray antenna for microspacecraft applications p 1305 N95-21541
REFLECTORS
Optical multilayers with an amorphous fluoropolymer [DE94-017693] p 1541 N95-20218
Electromagnetic wave reflection from irregular plasma layers p 1298 N95-20952
Diffuse reflectance spectra of energetic material [DSTO-TR-0065] p 1284 N95-21951
REFRACTION
Modeling tropospheric ducting effects on satellite-to-ground paths p 1295 N95-20936
REFRACTIVITY
Refractive index change in dissociating shocked benzene [DE94-019015] p 1541 N95-20352
Terrain and refractivity effects on non-optical paths p 1294 N95-20931
Macromolecular and materials design using polyphosphazenes [AD-A279781] p 1273 N95-20978
Gradient index lenses from sol-gel layering [AD-A285649] p 1242 N95-21402
Lead-indium phosphate glasses for optical applications [DE94-019333] p 1275 N95-21482
Factors that determine visual acuity through night vision goggles for emmetropes [AD-A279339] p 1450 N95-21927
REFRACTORIES
He, Xe and Ne isotopes in a steady-state mass transport model and implications about terrestrial volatiles p 1425 N95-21821
REFRACTORY MATERIALS
Materials/manufacturing element of the Advanced Turbine System Program [DE94-017299] p 1378 N95-20085
Selection of RIB targets using ion implantation [DE95-000951] p 1538 N95-21938

REFRACTORY METALS
Plasma-induced-damage of GaAs during etching of refractory metal contacts
[DE95-001525] p 1259 N95-21838
REFRIGERANTS
Accelerated screening methods for determining chemical and thermal stability of refrigerant-lubricant mixtures. Part 2: Experimental comparisons and verification of methods
[DE95-000743] p 1264 N95-20078
New concepts for refrigerant leak detection and mixture measurement
[DE94-018967] p 1287 N95-21559
Comparison of HFC-134a and the ternary blend, Suva MP39, as replacements for the refrigerant, CGC-12
[MRL-GD-0051] p 1287 N95-21625
Materials compatibility and lubricants research on CFC-refrigerant substitutes
[DE94-018414] p 1287 N95-21631
Thermophysical properties of HFC-143a and HFC-152a
[DE95-002199] p 1582 N95-22153
REFRIGERATING
Proceedings of the 1993 Non-Fluorocarbon Insulation, Refrigeration and Air Conditioning Technology Workshop
[DE94-018333] p 1285 N95-20194
REFUELING
Evaluation of pumping and fueling requirements for the ITER EDA
[DE94-018117] p 1560 N95-21702
Demonstration of zinc/air fuel battery to enhance the range and mission of fleet electric vehicles: Preliminary results in the refueling of a multicell module
[DE95-004206] p 1337 N95-22421
REGIONS
Recycling of volatiles at subduction zones: Noble gas evidence from the Tabar-Lihir-Tanga-Feni arc of papua New Guinea p 1418 N95-21787
Subduction and volatile recycling in Earth's mantle
p 1421 N95-21802
REGRESSION ANALYSIS
Comparison of a back propagation artificial neural network model with a linear regression model for personnel selection
[AD-A280023] p 1479 N95-20005
Learning algorithms for feedforward networks based on finite samples
[DE95-001739] p 1483 N95-21741
Latin hypercube sampling in sensitivity analysis
[AD-A285867] p 1499 N95-22135
REGULARITY
Regularity of BPa-systems is decidable
[PB95-135489] p 1468 N95-21619
REGULATIONS
Analyses of grounded and ungrounded photovoltaic power systems
[DE94-015015] p 1391 N95-20263
Environmental Compliance Assessment and Management Program
[AD-A279605] p 1402 N95-20441
Environmental Compliance Assessment Protocol - Centers for Disease Control and Prevention (ECAP-CDC), West Virginia supplement
[AD-A286009] p 1403 N95-20720
Environmental Compliance Assessment and Management Program (ECAMP), South Carolina supplement
[AD-A279533] p 1408 N95-21689
Environmental Compliance Assessment System (ECAS): Oregon supplement
[AD-A279565] p 1408 N95-21696
Environmental Compliance Assessment System (ECAS): Japan settlement
[AD-A279328] p 1410 N95-22142
REGULATORY MECHANISMS (BIOLOGY)
Structures and functions of oligosaccharins
[DE95-003195] p 1440 N95-22220
REINFORCED PLASTICS
Low temperature tensile and fracture mechanical strength in mode 1 and mode 2 of fiber reinforced plastics following various irradiation conditions
[DE94-019269] p 1232 N95-22130
REINFORCING FIBERS
Third Intermetallic Matrix Composites Symposium, volume 350
[NASA-TM-110059] p 1225 N95-20001
Role of internal stresses in fracture behavior of engineering composites
[DE95-001106] p 1229 N95-20912
Low temperature tensile and fracture mechanical strength in mode 1 and mode 2 of fiber reinforced plastics following various irradiation conditions
[DE94-019269] p 1232 N95-22130
RELATIVISTIC EFFECTS
Investigation of direct photon production in 200 A GeV S + Au reactions
[DE94-018129] p 1525 N95-21704
Electromagnetic waves in an ultrarelativistically hot and strongly magnetized electron-positron plasma
[DE94-628963] p 1307 N95-21849
RELATIVISTIC ELECTRON BEAMS
Development of an annular electron beam HPM amplifier
[AD-A286646] p 1327 N95-20905
Development status of an intense beam klystron
[DE95-000745] p 1329 N95-21395
On the influence of electromagnetic wave and relativistic electron beam on a plasma
[DE94-628962] p 1561 N95-21848
Very high-power electron-beam transport in long gas cells from 10(exp -3) to 10(exp 3) Torr N2
[DE95-002611] p 1539 N95-22306
RELATIVISTIC PARTICLES
Transition-energy crossing with a gamma(sub t)(-)jump
[DE94-017315] p 1531 N95-20021
An impedance model of the Relativistic Heavy Ion Collider (RHIC)
[DE94-016784] p 1532 N95-20406
Quantization in curvilinear coordinates
[DE94-770603] p 1514 N95-20737
Similarities and differences in strangeness production at BNL and CERN
[DE95-002343] p 1521 N95-21380
RELATIVISTIC PLASMAS
Quasi-linear equation for magnetoplasma oscillations in the weakly relativistic approximation
[DE94-628932] p 1560 N95-21593
Large amplitude localized structures in a relativistic electron-positron ion plasma
[DE94-628965] p 1561 N95-21851
RELATIVISTIC THEORY
The theory of relativistic heavy ion collisions
[DE95-001805] p 1519 N95-21302
Relativistic binary neutron star coalescence
[DE94-019311] p 1600 N95-21479
Summary of heavy ion theory
[DE95-002177] p 1523 N95-21588
RELATIVITY
Quantization in curvilinear coordinates
[DE94-770603] p 1514 N95-20737
The development of science during this century
[DE94-632964] p 1582 N95-22185
RELIABILITY
Test reliability and experimental power
[AD-A279607] p 1448 N95-19957
A new mini Ball Grid Array (mBGA) multichip module technology
[DE94-018897] p 1480 N95-20342
Standard Hardware Acquisition and Reliability Program (SHARP) advanced SEM-E packaging
p 1208 N95-20633
Improving Multichip Module (MCM) design and reliability using the Intelligent MCM Analyzer
p 1209 N95-20637
The demise of plastic encapsulated microcircuit myths
p 1209 N95-20640
Advanced Standard Electronic Modules format-E (SEM-E) processes for rapid prototyping
p 1210 N95-20642
Reliability assessment of Multichip Module technologies via the Triservice/NASA RELTECH program
p 1210 N95-20643
Assuring Known Good Die (KGD) for reliable, cost effective MCMs p 1210 N95-20644
Method of fabricating a microelectronic photomultiplier device with integrated circuitry
[AD-D016530] p 1325 N95-20726
Atmosphere influence on in situ ion beam analysis of thin film growth
[DE95-001507] p 1570 N95-20881
Prototype rule-based reliability analysis for VLSI circuit design
[AD-A280065] p 1327 N95-20967
A cheap DNS tool for turbulence models testing
p 1348 N95-21072
Minimax optimal stop rule in reliability checking
[PB95-134557] p 1383 N95-21961
RELIABILITY ANALYSIS
Reliability analysis of uniaxially ground brittle materials
[NASA-TM-106852] p 1386 N95-20790
Prototype rule-based reliability analysis for VLSI circuit design
[AD-A280065] p 1327 N95-20967
Low noise 22 GHz receiver for the radioastron satellite. Part 1: Requirements, design and reliability analysis
[PB95-104410] p 1300 N95-20972
Space power facility readiness for Space Station power system testing
[NASA-TM-106829] p 1218 N95-21384
Radio-science performance analysis software
p 1305 N95-21540
RELIEF MAPS
PRSPLOT6 manual
[PB95-110862] p 1456 N95-19928
RELUCTANCE
Mitigation of the effects of F layer regularities by using multiple paths p 1298 N95-20951
REMOTE CONTROL
Human performance studies for control of multiple remote systems
[AD-A286623] p 1452 N95-20768
Advanced robotic technologies for transfer at Sandia National Laboratories
[DE95-001617] p 1481 N95-20884
Conceptual design analyses for Hanford Site deployable remote spectroscopy systems
[DE95-002078] p 1243 N95-21473
REMOTE SENSING
Tests of an improved oceanographic expert system
[AD-A280123] p 1431 N95-19888
Theoretical prediction of vibrational circular dichroism spectra of R-glyceraldehyde, R-erythrose, and R-threose. Part 2: Development of a procedure to scale the force constant matrix expressed in terms of internal coordinates
[AD-A284305] p 1437 N95-20252
Boundary layer cloud studies in support of ASTEX
[AD-A285947] p 1429 N95-20395
Applications of wavelets to radar, imaging and related problems
[AD-A279909] p 1290 N95-20545
Airborne Multisensor Pod System (AMPS) data access concept
[DE95-002586] p 1389 N95-20903
Measurements of radar backscatter from the ocean surface at 94 GHz as a function of wind speed, direction and the modulation by the ocean waves during the SAXON-FPN experiment p 1299 N95-20960
Investigation on the backscattering properties of Finnish boreal forests at C- and X-band: A semi-empirical modeling approach
[PB95-127692] p 1389 N95-21105
Monitoring the response of the upper troposphere/lower stratosphere to a greenhouse gas scenario
[DE95-000982] p 1406 N95-21410
Solid state frequency conversion technology for remote sensing
[DE94-019102] p 1389 N95-21433
An Echelle Grating Spectrometer (EGS) for mid-IR remote chemical detection
[DE94-019310] p 1367 N95-21478
Visible fluorescence of weathered lead
[DE95-002454] p 1244 N95-21523
Overview of remote sensing laser development and semiconductor laser technology
[DE94-019103] p 1389 N95-21552
European Workshop on Optical Ground Truth Instrumentation for the Validation of Space-Borne Optical Remote Sensing Data of the Marine Environment
[PB95-134144] p 1390 N95-21872
High resolution properties of the equatorial Pacific marine atmospheric boundary layer from lidar and radiosonde observations
[DE95-001028] p 1426 N95-21875
Remote-sensing based technique to account for sub-grid scale variability of land surface properties
[NASA-TM-110501] p 1390 N95-22110
Regional scale hydrology with a new land surface processes model
[NASA-TM-110500] p 1390 N95-22111
Climatological data for clouds over the globe from surface observations, 1982-1991: The total cloud edition
[DE95-002537] p 1431 N95-22288
REMOTE SENSORS
Human performance studies for control of multiple remote systems
[AD-A286623] p 1452 N95-20768
REMOTELY PILOTED VEHICLES
Unmanned aerial vehicles
[AD-A286190] p 1206 N95-20329
RENDEZVOUS SPACECRAFT
STS 63 flight day 4 highlights/MIR-Shuttle rendezvous
[NASA-TM-110512] p 1219 N95-21113
RENORMALIZATION GROUP METHODS
Rigorous spin-spin correlation function of Ising model on a special kind of Sierpinski Carpets
[DE94-628995] p 1575 N95-21854
Topics in gauge theories and the unification of elementary particle interactions
[DE94-013485] p 1529 N95-22279
REPLACING
Mercury usage and alternatives in the electrical and electronics industries
[PB94-165362] p 1312 N95-19966

Proposed emittance upgrade for the SLC damping rings
[DE95-002887] p 1538 N95-22155

REPORTS

NASA/DOD Aerospace Knowledge Diffusion Research Project. Report 31: The technical communications practices of US aerospace engineers and scientists: Results of the phase 1 SME mail survey
[NASA-TM-109169] p 1587 N95-20163
NASA Langley scientific and technical information output: 1994, volume 1
[NASA-TM-109170-VOL-1] p 1589 N95-21189

RESCUE OPERATIONS

Analysis of test criteria for specifying foam firefighting agents for aircraft rescue and firefighting
[AD-A286381] p 1203 N95-22352

RESEARCH

Overview of the Institute of Geophysics and Planetary Physics and Lawrence Livermore National Laboratory collaborative efforts
[DE94-017300] p 1599 N95-20145
NRL review, 1994
[AD-A279832] p 1605 N95-20182
Applications of ICP magnetic sector multicollector mass spectrometry to basic energy research
[DE95-002600] p 1246 N95-21886

RESEARCH AND DEVELOPMENT

Recent DIII-D results
[DE94-017519] p 1549 N95-20038
Energy and Technology Review
[DE94-017686] p 1219 N95-20148
NRL review, 1994
[AD-A279832] p 1605 N95-20182
Acoustic emission: The first half century
[DE94-017176] p 1503 N95-20267
Hydrostatic force sensor
[DE94-018923] p 1364 N95-20321
An update on the Department of Energy's photovoltaic program p 1316 N95-20505
The Energy Science and Technology Database on a local library system: A case study at the Los Alamos National Research Library
[DE95-001009] p 1589 N95-20818
Systems Analysis Laboratory. Ten years of progress 1984-1994
[PB95-104451] p 1464 N95-20982
VOC compliant wash primer
[AD-A286034] p 1273 N95-21000
NASA/DOD Aerospace Knowledge Diffusion Research Project. Report 27: The technical communication practices of engineering and science students: Results of the phase 3 academic surveys
[NASA-TM-109122] p 1589 N95-21015
Development status of an intense beam klystron
[DE95-000745] p 1329 N95-21395
Policies concerning military and civilian research and technology applications
[PB95-131355] p 1585 N95-21427
Investigation on research for degradable plastics
[DE94-796550] p 1277 N95-21714
ANSTO: Program of research, 1993-1994
[DE94-631122] p 1605 N95-21828
ANSTO: Mission statement, significant events and achievements
[DE94-631123] p 1605 N95-21830
Spinoff, 1994
[NASA-NP-214] p 1594 N95-21893
NASA/DOD Aerospace Knowledge Diffusion Research Project. Paper 48: Valuing information in an interactive environment
[NASA-TM-110448] p 1590 N95-21977
Life Sciences Division and Center for Human Genome Studies
[DE94-017796] p 1440 N95-22065
Advanced energy systems and technologies research programme
[DE95-717486] p 1397 N95-22337
Technology transfer: Improving the use of cooperative R/D agreement at DOE's contractor-operated laboratories. Report to Congressional requesters
[GAO/RCED-94-91] p 1586 N95-22403

RESEARCH FACILITIES

Environmental cleanup technology transfer initiatives
[AD-A285059] p 1403 N95-20487
NASA Langley scientific and technical information output: 1994, volume 1
[NASA-TM-109170-VOL-1] p 1589 N95-21189
Neutronics and shielding analysis of the National Ignition Facility
[DE94-016698] p 1534 N95-21206
Laser design basis for the National Ignition Facility
[DE94-016700] p 1534 N95-21209
The Photovoltaic Higher Education National Exemplar Facility (PHENEF)
[DE94-015641] p 1395 N95-21409

RESEARCH MANAGEMENT

Systems Analysis Laboratory. Ten years of progress 1984-1994
[PB95-104451] p 1464 N95-20982
Annual program analysis of the NASA Space Life Sciences Research and Education Support Program
[NASA-CR-197298] p 1439 N95-21529
Directives for the participation in MiTS forum. V3.0
[PB95-110342] p 1484 N95-22015
An assessment of European parallel software research
[AD-A286357] p 1479 N95-22257

RESEARCH PROJECTS

Research in the chemical sciences: Summaries of FY 1994
[DE94-015427] p 1223 N95-20264
Acoustic emission: The first half century
[DE94-017176] p 1503 N95-20267
Systems Analysis Laboratory. Ten years of progress 1984-1994
[PB95-104451] p 1464 N95-20982
Recent National Solar Thermal Test Facility activities, in partnership with industry
[DE95-001828] p 1394 N95-21353
ITER EDA Newsletter. Volume 3, no. 2
[DE94-628980] p 1561 N95-21852

RESERVOIRS

FTIR spectroscopy for the determination of water in corrosive gases
[DE94-014658] p 1235 N95-20139
Stability of pressure and velocity computations for heterogeneous reservoirs
[PB95-110284] p 1354 N95-21656
Rare gases systematics and mantle structure
p 1416 N95-21778
D/H ratios and H2O contents of mantle-derived amphibole megacrysts from Dish Hill, California
p 1416 N95-21781
Noble gas isotopes and halogens in volatile-rich inclusions in diamonds p 1417 N95-21784
Mantle devolatilization and rheology in the framework of planetary evolution p 1418 N95-21788
The ratios of carbon and non-radiogenic helium and argon isotopes in the mantle and crustal rocks
p 1421 N95-21805
Implications of noble gases in a recently recognized Martian meteorite (ALH84001) for the degassing history of Mars p 1424 N95-21819

RESIDUAL GAS

Emittance dilution by ions in the SLC arcs
[DE95-002871] p 1536 N95-21332

RESIDUAL STRESS

The effect of fiber coating thickness on the interfacial properties of a continuous fiber ceramic matrix composite
[DE94-017886] p 1267 N95-20373
Residual stresses in material processing
[DE94-017888] p 1385 N95-20374
The processing and mechanical properties of high temperature/high performance composites. Book 7: In-situ measurements of stress and damage
[AD-A279814] p 1227 N95-20583
The numerical integration and 3-D finite element formulation of a viscoelastic model of glass
[DE95-002588] p 1271 N95-20788
Role of internal stresses in fracture behavior of engineering composites
[DE95-001106] p 1229 N95-20912
Time-dependent deformation of titanium metal matrix composites
[NASA-CR-195030] p 1230 N95-21363
The mechanical behavior of surface-modified ceramics
[DE95-001704] p 1276 N95-21572
A study of mechanical processing damage in brittle materials
[DE95-002126] p 1276 N95-21585
Measurement of residual stresses on ceramic materials with high spatial resolution
[DE94-017889] p 1280 N95-22270
Residual stress analysis in swage autofrettaged thick-walled cylinders by position-sensitive x-ray diffraction techniques
[AD-A286383] p 1388 N95-22320

RESISTANCE HEATING

Joule heating of the ITER TF cold structure: Effects of vertical control coil currents and ELMS
[DE95-001817] p 1560 N95-21724
Welding tritium exposed stainless steel
[DE95-003208] p 1382 N95-22356

RESISTORS

Evaluation of superconducting quantum interference devices interfaced with digital signal processing electronics for biomagnetic applications
[DE94-016186] p 1289 N95-20164
Monolithic low noise preamplifier for piezoelectric sensors
[AD-D016524] p 1333 N95-21865

RESOLUTION

HIRAS images of fossil dust shells around AGB stars
p 1593 N95-21768

RESONANCE

Temperature effects on acoustic interactions between altitude test facilities and jet engine plumes
[NASA-CR-197638] p 1504 N95-21170
A neutron beam polarizer for study of parity violation in neutron-nucleus interactions
[DE95-002743] p 1519 N95-21237
Comparison of calculated with measured dynamic aperture
[DE95-002863] p 1534 N95-21246
Hamiltonian structure of the reversible nonsemisimple 1:1 resonance
[PB95-127528] p 1495 N95-22151
Determination of the complex elastic moduli of materials using a free-free bar technique
[AD-A279861] p 1281 N95-22387

RESONANCE SCATTERING

Resonant generation of nonequilibrium phonons in GaAs/AlAs quantum wells via intersubband scattering
[DE95-002338] p 1581 N95-21604

RESONANT FREQUENCIES

Generation of micro-domains in AT-cut quartz by thermal processing and the effect on resonator modes
[DE94-017344] p 1564 N95-20087
Input shaping for vibration-damped slewing of a flexible beam using a heavy-lift hydraulic robot
[DE94-015803] p 1379 N95-20695
Radio-frequency techniques at the ISIS pulsed muon source
[PB95-129854] p 1529 N95-22303
Determination of the complex elastic moduli of materials using a free-free bar technique
[AD-A279861] p 1281 N95-22387

RESONANT TUNNELING

Resonant tunneling quantum well integrated optical waveguide modulator/switch
[AD-A285142] p 1542 N95-20501

RESONANT VIBRATION

Acoustic and vibration attenuation composite material
[AD-D016585] p 1233 N95-22467

RESONATORS

Generation of micro-domains in AT-cut quartz by thermal processing and the effect on resonator modes
[DE94-017344] p 1564 N95-20087
Evaluating impedances in a Sacherer integral equation
[DE94-016823] p 1489 N95-20266
Quartz resonator fluid monitors for vehicle applications
[DE94-018910] p 1367 N95-21546

RESOURCES MANAGEMENT

Public-sector aviation issues: Graduate research award papers, 1992-1993
[PB94-217478] p 1199 N95-19967

RESPIRATORS

Method and apparatus for non-invasive evaluation of diaphragmatic function
[NASA-CASE-LAR-13888-1] p 1441 N95-20408

RESPIRATORY SYSTEM

Interspecies extrapolations of halocarbon respiratory and tissue kinetics: Applications to predicting toxicity in different species
[AD-A285055] p 1442 N95-20485

RETENTION (PSYCHOLOGY)

Command history, 1993
[AD-A279775] p 1446 N95-21989

RETINA

Computer based analysis and synthesis of retinal function
[AD-A286084] p 1443 N95-20811
Investigation of laser-induced retinal damage: Wavelength and pulsewidth dependent mechanisms
[AD-A286066] p 1443 N95-20848
Mechanisms and diagnostics of ultrashort pulse laser ocular effects
[AD-A285610] p 1373 N95-21195

RETIREMENT

Age 60 study. Part 1: Bibliographic database
[AD-A286245] p 1446 N95-22027
Age 60 study. Part 2: Airline pilot age and performance. A review of the scientific literature
[AD-A286246] p 1447 N95-22040

RETRAINING

The MSFC Program Control Development Program
p 1585 N95-20754

REVERSE ENGINEERING

VHDL modeling of PRC-70 radio ASICs for reverse engineering
[AD-A285740] p 1457 N95-19929
Project Whitefeather
[DE94-016575] p 1415 N95-21184

REVERSE FIELD PINCH
Analysis methods for fast impurity ion dynamics data
[DE95-000589] p 1549 N95-20112
Fluctuations and transport in the reversed field pinch: Characterization and reduction
[DE95-000590] p 1549 N95-20113
Magnetic fluctuation induced transport and edge dynamo measurements in the MST reversed-field pinch
[DE95-000591] p 1549 N95-20114

REYNOLDS EQUATION
Numerical investigation of supersonic turbulent boundary layers with high wall temperature
p 1344 N95-21050
Modelling anisotropy and backscatter effects in the subgrid scale stress tensor p 1349 N95-21077
Application of Roe's flux-difference splitting for kappa-epsilon turbulence model
[PB95-127718] p 1352 N95-21106

REYNOLDS NUMBER
Research on bluff body vortex wakes
[AD-A286319] p 1200 N95-20177
Statistics of pressure and pressure gradient in homogeneous isotropic turbulence p 1343 N95-21046
Simulation of separated flows p 1347 N95-21068
Large eddy simulation of turbulent flow over a cavity
p 1347 N95-21069
A cheap DNS tool for turbulence models testing
p 1348 N95-21072
Direct simulation of turbulent flow in a square duct: Reynolds-stress budgets p 1348 N95-21073
Simulation of pipe flow p 1349 N95-21078
Direct numerical determination of the minimum bypass Reynolds number in boundary layers
p 1349 N95-21080
Direct simulation of a self-similar plane wake
p 1350 N95-21084
The effect of initial conditions on the development of temporally evolving planar three dimensional incompressible wakes p 1350 N95-21085
Rib vortices in round jets: Direct and large eddy simulation p 1351 N95-21088
Acoustic receptivity due to weak surface inhomogeneities in adverse pressure gradient boundary layers
[NASA-TM-4577] p 1353 N95-21258
Experiments on the flow field physics of confluent boundary layers for high-lift systems
[NASA-CR-197318] p 1201 N95-21343
Temporal evolution of turbulence/chemistry interactions in lifted, turbulent-jet flames
[DE95-002481] p 1243 N95-21512
Resolution requirements for velocity gradients in turbulence p 1363 N95-22462

REYNOLDS STRESS
Evaluation of Reynolds stress turbulence closures in compressible homogeneous shear flow
[NASA-CR-194892] p 1338 N95-20009
Turbulent transport in premixed flames
p 1249 N95-21040
Modeling near wall effects in second moment closures by elliptic relaxation p 1345 N95-21054
Homogeneous turbulence subjected to mean flow with elliptic streamlines p 1345 N95-21056
Direct simulation of turbulent flow in a square duct: Reynolds-stress budgets p 1348 N95-21073
Modelling anisotropy and backscatter effects in the subgrid scale stress tensor p 1349 N95-21077
Direct simulation of a self-similar plane wake
p 1350 N95-21084

RHENIUM ALLOYS
Cr2Nb development
[DE94-018697] p 1250 N95-20043

RHENIUM COMPOUNDS
Photochemistry of intermolecular C-H bond activation reactions
[DE94-018417] p 1239 N95-20682

RHEOLOGY
Technical Summary for 1993 fall MRS Symposium O, Complex Fluids
[AD-A283722] p 1264 N95-19972
Proceedings of the 4th International Conference on Electrorheological Fluids
[AD-A286341] p 1266 N95-20227
Conference on Deep Earth and Planetary Volatiles
[NASA-CR-196944] p 1415 N95-21777
Modeling the effect of water on mantle rheology
p 1417 N95-21783
Structure and stability of hydrous minerals at high pressure p 1417 N95-21786
Mantle devolatilization and rheology in the framework of planetary evolution p 1418 N95-21788
Volatiles, rheology, and mantle convection: Comparing Earth, Venus, and Mars p 1420 N95-21801
Subduction and volatile recycling in Earth's mantle
p 1421 N95-21802

RHEOMETERS
Responsive copolymers for enhanced petroleum recovery
[DE94-018822] p 1267 N95-20350

RHO-MESONS
Where are we going with Bose-Einstein: A mini review
[PB95-130308] p 1518 N95-21222

RHODAMINE
Cavity-QED enhancement of fluorescence yields in microdroplets
[DE94-018662] p 1506 N95-20030
Liquid xenon as a potential laser host medium
[AD-A285365] p 1370 N95-20550

RHODIUM ALLOYS
Natural gas converter performance and durability
[PB95-135554] p 1284 N95-21966

RHODIUM COMPOUNDS
Photochemistry of intermolecular C-H bond activation reactions
[DE94-018417] p 1239 N95-20682

RHYTHM (BIOLOGY)
Diffusible driving and coupling signals of the biological clock
[AD-A285353] p 1447 N95-22475

RICCATI EQUATION
Riccati equation theory for Pritchard-Salamon systems: A Popov function approach
[PB95-137089] p 1491 N95-20830
Design of robust optimal control systems and stability analysis of real structured uncertainties
[AD-A279089] p 1483 N95-21913
Discrete algebraic Riccati equation and linear matrix inequality
[PB95-133575] p 1484 N95-22139
Quadratic optimal control of a delay equation II: The unstable case
[PB95-127064] p 1486 N95-22366
Quadratic optimal control of a delay equation I: The stable case
[PB95-127072] p 1486 N95-22367

RIGGING
Corrosion evaluation of fuel canister crusher rigging
[DE95-002962] p 1257 N95-21452

RIGID STRUCTURES
Computer graphics tools for visualizing gravity gradient torques on a rigid spacecraft
[AD-A285971] p 1461 N95-20665
Proceedings of the NATO-Advanced Study Institute on Computer Aided Analysis of Rigid and Flexible Mechanical Systems. Volume 1: Main lectures
[AD-A286062] p 1380 N95-21171
Proceedings of the NATO-Advanced Study Institute on Computer Aided Analysis of Rigid and Flexible Mechanical Systems. Volume 2: Contributed papers
[AD-A286063] p 1381 N95-21488
The dynamic structure function of Bose liquids in the deep inelastic regime
[DE94-629077] p 1527 N95-22182
Nonlinear dynamics of the planar pitch attitude motion for a gravity-gradient satellite
[AD-A286407] p 1220 N95-22204

RING LASERS
Fiber laser amplifiers and oscillators
[AD-A285835] p 1368 N95-20035
Optical processing and control
[AD-A279157] p 1546 N95-21975

RING STRUCTURES
Dynamic measurement of the hoop modulus of a composite cylinder
[DE94-018958] p 1385 N95-20416

RINGS
Abrasive wear by diesel engine coal-fuel and related particles
[PB95-104915] p 1379 N95-20984

RINGS (MATHEMATICS)
Elliptic genera for Z/K-manifolds I
[PB95-109096] p 1496 N95-22355

RISK
A construct for describing software development risks
[AD-A284923] p 1457 N95-19999
Safety issues in high speed machining
[PB95-127411] p 1287 N95-21422
Definition report on target and related steering variables of radiation as a part of the environmental balance and environmental outlook investigation
[PB95-135471] p 1409 N95-21846
Initial assessment of the hazards and risks of new chemicals to man and the environment, part 2
[PB95-106407] p 1410 N95-22124

RIVETING
Damage tolerant repair techniques for pressurized aircraft fuselages
[AD-A286298] p 1199 N95-22046

ROBOT ARMS
Sensor based fine motion control
[PB95-108007] p 1483 N95-21669

ROBOT CONTROL
Robust agent control of an autonomous robot with many sensors and actuators
[AD-A280148] p 1479 N95-20011
Force based motion control of a walking machine
[PB95-129672] p 1451 N95-20276
Adaptive path planning for flexible manufacturing
[DE94-016561] p 1459 N95-20284
Legged vehicle for underwater mobile operations
[AD-A285043] p 1480 N95-20482
Automatic generation of fuzzy rules for the sensor-based navigation of a mobile robot
[DE95-001428] p 1481 N95-20837
Heterogeneous multi-robot cooperation
[AD-A279839] p 1481 N95-21185
Elements of deliberative robot control
[PB95-107595] p 1482 N95-21412
Sensor based fine motion control
[PB95-108007] p 1483 N95-21669
Optimal control of a two wheeled mobile robot
[AD-A286130] p 1485 N95-22233

ROBOT DYNAMICS
Force based motion control of a walking machine
[PB95-129672] p 1451 N95-20276
Legged vehicle for underwater mobile operations
[AD-A285043] p 1480 N95-20482
Input shaping for vibration-damped slewing of a flexible beam using a heavy-lift hydraulic robot
[DE94-015803] p 1379 N95-20695
Unknown-terrains navigation of a mobile robot using an array of sonars
[DE94-017902] p 1482 N95-21385
Sensor based fine motion control
[PB95-108007] p 1483 N95-21669
Tom Thumb algorithm for planning simple vehicle motions
[PB95-107553] p 1484 N95-22156

ROBOTICS
Adaptive path planning for flexible manufacturing
[DE94-016561] p 1459 N95-20284
Advanced robotic technologies for transfer at Sandia National Laboratories
[DE95-001617] p 1481 N95-20884
Heterogeneous multi-robot cooperation
[AD-A279839] p 1481 N95-21185
Unknown-terrains navigation of a mobile robot using an array of sonars
[DE94-017902] p 1482 N95-21385
Sensor based fine motion control
[PB95-108007] p 1483 N95-21669
Robotic paint stripping cell
[AD-A279158] p 1279 N95-21976
Manufacturing Technology Bulletin, July 1994
[DE94-017775] p 1605 N95-22262

ROBOTS
Robust agent control of an autonomous robot with many sensors and actuators
[AD-A280148] p 1479 N95-20011
Force based motion control of a walking machine
[PB95-129672] p 1451 N95-20276
Adaptive path planning for flexible manufacturing
[DE94-016561] p 1459 N95-20284
Legged vehicle for underwater mobile operations
[AD-A285043] p 1480 N95-20482
Input shaping for vibration-damped slewing of a flexible beam using a heavy-lift hydraulic robot
[DE94-015803] p 1379 N95-20695
Automatic generation of fuzzy rules for the sensor-based navigation of a mobile robot
[DE95-001428] p 1481 N95-20837
Proceedings of the Fourth International Workshop on Inductive Logic Programming (ILP-94)
[PB95-135273] p 1464 N95-21003
Unknown-terrains navigation of a mobile robot using an array of sonars
[DE94-017902] p 1482 N95-21385
Sensor based fine motion control
[PB95-108007] p 1483 N95-21669
Robotic paint stripping cell
[AD-A279158] p 1279 N95-21976
Optimal control of a two wheeled mobile robot
[AD-A286130] p 1485 N95-22233
Layered path planning for an autonomous mobile robot
[AD-A286138] p 1485 N95-22244
Learning maneuvers using neural network models
[AD-A286470] p 1486 N95-22267

ROBUSTNESS (MATHEMATICS)
Measuring software dependability by robustness benchmarking
[AD-A280053] p 1461 N95-20622
VLUGR3: A vectorizable adaptive grid solver for PDEs in 3D. 1: Algorithmic aspects and applications
[PB95-135729] p 1467 N95-21435

ROCKET ENGINES
Investigation of rocket motors 3 inch number 1 Mk 4
[AD-A284278] p 1221 N95-19962
Computer program for calculation of complex chemical equilibrium compositions and applications. Part 1: Analysis
[NASA-RP-1311] p 1235 N95-20180
The problem of space travel: The rocket motor
[NASA-SP-4026] p 1217 N95-21894

ROCKET EXHAUST
Radiation from advanced solid rocket motor plumes
[NASA-CR-196554] p 1221 N95-20124
Computer model predictions of the local effects of large, solid-fuel rocket motors on stratospheric ozone
[AD-A285632] p 1404 N95-21150

ROCKET PROPELLANTS
Investigation of rocket motors 3 inch number 1 Mk 4
[AD-A284278] p 1221 N95-19962

ROCKS
Geometric moire method of strain analysis with displacement discontinuities
[DE95-001114] p 1386 N95-20833
Atmospheres of the Moon and Mercury
p 1419 N95-21794

RODS
Input shaping for vibration-damped slewing of a flexible beam using a heavy-lift hydraulic robot
[DE94-015803] p 1379 N95-20695
Magnetostrictive motor system
[AD-D016484] p 1333 N95-21901

ROLL
STS Flight 64 mission highlights
[NASA-TM-110515] p 1219 N95-22295

ROLLER BEARINGS
Modeling of rolling element bearing mechanics. Computer program user's manual
[NASA-CR-196557] p 1381 N95-21692
Modeling of rolling element bearing mechanics. Theoretical manual
[NASA-CR-196556] p 1381 N95-21705

ROLLING CONTACT LOADS
Low rotational drag in high-temperature superconducting bearings
[DE95-002983] p 1382 N95-22292

ROOM TEMPERATURE
The thermal conductivity of carbon coated silicon carbide fibers embedded in a silicon carbide matrix
[DE94-017758] p 1225 N95-20023
Properties of whisker-reinforced ceramics
[DE94-017759] p 1264 N95-20024
Elastic anisotropy in hot-pressed Si3N4 composites: Role of in situ (beta)-Si3N4 grains and added (beta)-Si3N4 whiskers
[DE94-018387] p 1226 N95-20027
Enhanced ionic conduction at the film/substrate interface in LiI thin films grown on sapphire(0001)
[DE94-017884] p 1565 N95-20371
Hg-199 and Cu-(63,65) NMR studies of mercury based high-Tc superconductors
[DE95-001073] p 1570 N95-20820
Interlayer magnetic coupling in epitaxial Fe/Cr(211) and (100) superlattices
[DE95-002906] p 1571 N95-21256
High temperature superconducting microwave device
[AD-A286351] p 1336 N95-22254

ROTARY WINGS
Prediction of rotor-blade deformations due to unsteady airloads
[AD-A286593] p 1207 N95-20860
Simulation of rotor blade element turbulence
[NASA-TM-108862] p 1207 N95-21186

ROTATING BODIES
Mathematical modeling of a class of multibody flexible spacecraft structures
[NASA-TM-109166] p 1219 N95-20800
Safety issues in high speed machining
[PB95-127411] p 1287 N95-21422
Robust fixed-structure control
[AD-A286515] p 1485 N95-22216
Notes on rotating turbulence p 1359 N95-22444

ROTATING FLUIDS
On the transition towards slow manifold in shallow-water and 3D Euler equations in a rotating frame
p 1345 N95-21057
On the asymptotic similarity of rotating homogeneous turbulence p 1345 N95-21058

ROTATING PLASMAS
Coupled tearing modes in plasmas with differential rotation
[DE94-631422] p 1548 N95-19977
Wall stabilization effects in D3-D high beta discharges
[DE94-017509] p 1554 N95-20446

ROTATION
Anisotropic structure of homogeneous turbulence subjected to uniform rotation p 1346 N95-21059
Single point modeling of rotating turbulent flows
p 1346 N95-21060
In-situ capability of ion beam modification and characterization of materials at Los Alamos National Laboratory
[DE95-002738] p 1534 N95-21236
Luminosity polarization correlation in the SLC
[DE95-002889] p 1536 N95-21335
Dynamic NMR studies of restricted arene rotation in the chromiu tricarbonyl thiophene and selenophene complexes
[DE95-001656] p 1257 N95-21399
Stellarator transport optimization with self-consistent electric fields
[DE94-019151] p 1559 N95-21581

ROTATIONAL STATES
Current diffusive ballooning mode in second stability region of tokamaks
[DE94-770690] p 1554 N95-20683
Changes in the behavior of magnetic materials undergoing processing in electrical rotating machines
[PB95-104493] p 1325 N95-20702
Large-eddy simulation of rotating channel flows using a localized dynamic model p 1346 N95-21064
The asymptotic state of rotating homogeneous turbulence at high Reynolds numbers
p 1347 N95-21065
Electron attachment to excited molecules
[DE94-019124] p 1522 N95-21519
Low rotational drag in high-temperature superconducting bearings
[DE95-002983] p 1382 N95-22292

ROTOR AERODYNAMICS
The dynamic approach to rotor blade research: ARA's oscillatory test facility
[ARA-MEMO-405] p 1200 N95-20758

ROTOR BLADES (TURBOMACHINERY)
Prediction of rotor-blade deformations due to unsteady airloads
[AD-A286593] p 1207 N95-20860

ROTOR DYNAMICS
The dynamic approach to rotor blade research: ARA's oscillatory test facility
[ARA-MEMO-405] p 1200 N95-20758

ROTORS
Variations observed in the AC generator signal period of a Sea King helicopter
[AD-A284280] p 1206 N95-19963
Scale-up and modeling of forced chemical vapor infiltration
[DE94-017769] p 1340 N95-20781
Advanced wind turbine design studies: Advanced conceptual study
[DE93-000031] p 1394 N95-20985

ROUTES
Routing of unidirectional packet radio for wide-area paging network control and maintenance
[PB95-104428] p 1300 N95-20980

RUBIDIUM
Recent photoabsorption measurements in the rare gases and alkalis in the 3 to 15 keV photon energy region
[DE94-019278] p 1521 N95-21406

RUN TIME (COMPUTERS)
ILIAS: A sequential language for parallel matrix computations
[PB95-110631] p 1473 N95-20056
Finding all minimal separators of a graph
[PB95-127585] p 1491 N95-21023

RUNGE-KUTTA METHOD
Explicit parallel two-step Runge-Kutta-Nystroem methods
[PB95-135752] p 1489 N95-20423
Parallelism across the steps in iterated Runge-Kutta methods for stiff initial value problems
[PB95-135760] p 1490 N95-20424
Navier-Stokes simulations of the effects of suction holes on a flat plate boundary layer p 1352 N95-21094
Error committed by stopping the Newton iteration in Runge-Kutta methods and linear multistep methods
[PB95-106324] p 1492 N95-21421
Parallel predictor-corrector methods
[PB95-135711] p 1493 N95-21434
Numerical study of boundary layer interaction with shocks: Method and code validation
p 1362 N95-22461

RUNWAYS
Super-heavy aircraft study
[AD-A279602] p 1215 N95-19955

RYDBERG SERIES
Observation of strong emission from NeIX and NeX transitions in a laser-driven plasma
[DE95-002265] p 1555 N95-20813

S

S WAVES
Computer programs for analysis of geophysical data
[DE95-002472] p 1415 N95-21511
Collisional drift waves in the H-mode edge
[DE94-628950] p 1561 N95-21847
Source contributions at far-regional distances
[AD-A279405] p 1426 N95-21932

SACCADIC EYE MOVEMENTS
A physiological neural network for saccadic eye movement control
[AD-A279599] p 1441 N95-20301

SADDLE POINTS
Saddle-node dynamics for edge detection
[DE94-017415] p 1473 N95-22426

SAFETY
GPHS-RTGs in support of the Cassini Mission
[DE95-001492] p 1222 N95-20853
Launch safety, toxicity, and environmental effects of the high performance oxidizer CIF(5)
[AD-A286095] p 1284 N95-22227

SAFETY FACTORS
Analyses of grounded and ungrounded photovoltaic power systems
[DE94-015015] p 1391 N95-20263
Progress in the development of recycling processes for electric vehicle batteries
[DE94-015894] p 1324 N95-20626
The personal aircraft: Status and issues
[NASA-TM-109174] p 1200 N95-20688
The Materials Corrosion and Environmental Effects Laboratory (MCEL)
[DE94-018268] p 1254 N95-20816
Safety issues in high speed machining
[PB95-127411] p 1287 N95-21422
Comparison of HFC-134a and the ternary blend, Suva MP39, as replacements for the refrigerant, CGC-12
[MRL-GD-0051] p 1287 N95-21625
Analysis of test criteria for specifying foam firefighting agents for aircraft rescue and firefighting
[AD-A286381] p 1203 N95-22352

SALTS
Structure of ionic interfaces from an absolutely convergent solution of the Madelung problem
[DE94-019268] p 1573 N95-21474
A visual cell for measuring the solubility of prograde soluble salts in water at high temperatures and pressures
[DE95-002058] p 1245 N95-21732
Demonstration of multifunctional DNBM corrosion inhibitors in protective coatings for Naval air/weapon systems
[AD-A285869] p 1279 N95-22136

SAMARIUM COMPOUNDS
Magnetic field dependence of the correlation gap in SmB6
[DE95-001684] p 1574 N95-21570

SAMPLING
Frequent sampling in discrete choice
[PB95-110961] p 1497 N95-19938
Development of a fast sampling system for estimation of impulse responses of mobile radio channels
p 1296 N95-20943
Subsampling methods for image sequence coding
[PB95-107991] p 1305 N95-21579

SANDWICH STRUCTURES
Carbon fiber reinforced superconductor composites
[DE95-002504] p 1229 N95-20913

SANITATION
Personal hygiene body wipe
[AD-A286092] p 1454 N95-22274

SAPPHIRE
Amorphization of sapphire during ion beam mixing
[DE94-018713] p 1510 N95-20337
Enhanced ionic conduction at the film/substrate interface in LiI thin films grown on sapphire(0001)
[DE94-017884] p 1565 N95-20371
Liquid xenon as a potential laser host medium
[AD-A285365] p 1370 N95-20550
The processing and mechanical properties of high temperature/high performance composites. Book 7: In-situ measurements of stress and damage
[AD-A279814] p 1227 N95-20583
The processing and mechanical properties of high temperature/high performance composites. Book 5: Interface effects
[AD-A279815] p 1228 N95-20584
Microdynamic devices fabricated on silicon-on-sapphire substrates
[AD-D016531] p 1325 N95-20727

SATELLITE ATMOSPHERES
Studies of the gas tori of Titan and Triton
[NASA-CR-197377] p 1601 N95-20797

SATELLITE COMMUNICATION
Facsimile transmission standards
[AD-A279911] p 1290 N95-20308
Preliminary study of HUTSAT microsatellite
[PB95-127619] p 1220 N95-21026
Cochannel and adjacent-channel interference in nonlinear minimum-shift-keyed satellite system
[NASA-TM-106834] p 1307 N95-21890
SATELLITE DESIGN
Preliminary study of HUTSAT microsatellite
[PB95-127619] p 1220 N95-21026
SATELLITE IMAGERY
A Clementine collection: Moonglow
[AD-A286360] p 1217 N95-20228
Analysis of mesospheric winds and waves
[AD-A279956] p 1414 N95-20591
Hires and beyond p 1592 N95-21750
MEM application to IRAS CPC images
p 1592 N95-21751
An assessment of image reconstruction from balloon-borne and the IRAS data p 1592 N95-21752
Remote-sensing based technique to account for sub-grid scale variability of land surface properties
[NASA-TM-110501] p 1390 N95-22110
Imaging design of the wide field x-ray monitor onboard the HETE satellite
[DE95-002750] p 1221 N95-22436
SATELLITE INSTRUMENTS
Imaging design of the wide field x-ray monitor onboard the HETE satellite
[DE95-002750] p 1221 N95-22436
SATELLITE OBSERVATION
Mariners Weather Log, volume 38, number 3, summer 1994
[PB94-209541] p 1428 N95-20099
Location and characteristics of the reconnection X-line deduced from low-altitude satellite and radar observations
[NASA-TM-110114] p 1413 N95-20453
Program control on the Tropical Rainfall Measuring Mission p 1584 N95-20750
Surface ices in the outer solar system
p 1423 N95-21815
SATELLITE POWER TRANSMISSION
Scaling of solid state lasers for satellite power beaming applications
[DE94-016366] p 1368 N95-19986
SATELLITE SOLAR ENERGY CONVERSION
Review of solar cell temperature coefficients for space
p 1323 N95-20541
SATELLITE-BORNE INSTRUMENTS
Program control on the Tropical Rainfall Measuring Mission p 1584 N95-20750
SATELLITE-BORNE PHOTOGRAPHY
A Clementine collection: Moonglow
[AD-A286360] p 1217 N95-20228
SATELLITE-BORNE RADAR
Investigation on the backscattering properties of Finnish boreal forests at C- and X-band: A semi-empirical modeling approach
[PB95-127692] p 1389 N95-21105
SATURATION (CHEMISTRY)
Collisional redistribution effects on x ray laser saturation behavior
[DE94-017308] p 1374 N95-21663
SAWTOOTH WAVEFORMS
Ion heat pulse after sawtooth crash in the JFT-2M tokamak
[DE94-770685] p 1555 N95-20988
SCALARS
Transport and dynamics in toroidal fusion systems
[DE94-018653] p 1548 N95-20029
Classification of bianisotropic media
[PB95-127635] p 1502 N95-21102
Numerical wave speed for one-dimensional scalar hyperbolic conservation laws with source terms
[PB95-127536] p 1492 N95-21371
On the Aharonov-Bohm effect with neutrons
[DE95-002985] p 1521 N95-21454
Fully developed turbulent flows
[AD-A286496] p 1358 N95-22294
SCALE EFFECT
Universality of particle multiplicities
[DE95-000727] p 1515 N95-20879
SCALE MODELS
Geometric moire method of strain analysis with displacement discontinuities
[DE95-001114] p 1386 N95-20833
Subgrid scale models in finite difference simulations of complex wall bounded flows p 1346 N95-21063
Comparison of DNS and LES of transitional and turbulent compressible flow: Flat plate and mixing layer
p 1347 N95-21066
Modelling anisotropy and backscatter effects in the subgrid scale stress tensor p 1349 N95-21077
Regional scale hydrology with a new land surface processes model
[NASA-TM-110500] p 1390 N95-22111
SCALING LAWS
PRS scoping study 1: Scaling law estimates for K-shell radiation yields on JUPITER-class generators
[AD-A279716] p 1533 N95-20672
Fractal nature and scaling of normal faults, Rio Grande rift, NM: Implications for growth and strain
[DE94-018261] p 1414 N95-20990
SCANNERS
Ice Processing System software support documentation
[AD-A280030] p 1388 N95-20006
MEM application to IRAS CPC images
p 1592 N95-21751
High resolution descriptions of IRAS 12 and 25 microns confused regions
[AD-A285847] p 1545 N95-21832
Evaluation of scanners for C-scan imaging for nondestructive inspection of aircraft
[AD-A286398] p 1383 N95-22202
Test and Evaluation Plan (TEP) for Improvised Explosive Device Screening Systems (IEDSS)
[AD-A286382] p 1203 N95-22319
SCANNING ELECTRON MICROSCOPY
Effect of heat treatment temperature on creep-rupture properties of Fe3Al-based alloys
[DE94-017904] p 1253 N95-20375
Advanced Standard Electronic Modules format-E (SEM-E) processes for rapid prototyping
p 1210 N95-20642
SCANNING TUNNELING MICROSCOPY
A low temperature, ultrahigh vacuum, microwave-frequency-compatible scanning tunneling microscope
[AD-A279869] p 1365 N95-20413
Optical properties of silicon clusters deposited on the basal plane of graphite
[DE94-017529] p 1542 N95-20450
Scanning tunneling microscopy studies of self-assembled monolayers of alkanethiols on gold
[AD-A279910] p 1253 N95-20577
Gordon Research Conference on Physical Electrochemistry
[AD-A286545] p 1240 N95-20842
Scanning tunneling microscopy of semiconductor surfaces
[AD-A279982] p 1571 N95-20964
Linear and nonlinear spectroscopy with the tunable AC scanning tunneling microscope
[AD-A285751] p 1241 N95-21217
Small cavity nonresonant tunable microwave-frequency alternating current scanning tunneling microscope
[AD-A285752] p 1328 N95-21218
Progress in ultrafast scanning probe microscopy
[DE94-018179] p 1373 N95-21261
Surface x-ray scattering and scanning tunneling microscopy studies at the Au(111) electrode
[DE95-002409] p 1573 N95-21516
Bridging the pressure gap: In situ atomic-level investigations of model platinum catalyst surfaces under reaction conditions by scanning tunneling microscopy
[DE95-002346] p 1246 N95-21990
SCATTER PROPAGATION
An experimental determination of meteor daily arrival rate variation
[AD-A279484] p 1600 N95-21679
X-band microwave backscattering from ocean waves
[DE94-016719] p 1309 N95-22241
SCATTERING
The ANL X6B beamline at NSLS: A versatile facility
[DE94-018379] p 1540 N95-19968
Calculation of the total and total ionization cross sections for positron scattering on atomic hydrogen
[DE94-631341] p 1508 N95-20197
Application of new synchrotron powder diffraction techniques to anomalous scattering from glasses
[DE94-019285] p 1536 N95-21407
Full potential multiple scattering theory
[DE95-003197] p 1576 N95-22084
Structure functions and structure function ratio F(sup n)2/F(sup p)2 at small x(sub Bj) and Q2 in muon-nucleon scattering
[DE94-017981] p 1530 N95-22340
Effect of cell size on elliptically polarized radar clutter statistics
[AD-A285789] p 1311 N95-22401
SCATTERING AMPLITUDE
The status of molecules
[DE95-000952] p 1526 N95-21939
SCATTERING CROSS SECTIONS
Measurements of scattering processes in negative ion: Atom collisions
[DE95-000664] p 1519 N95-21276
Helium production by 10 MeV neutrons in iron, nickel and copper
[DE94-014798] p 1529 N95-22280
SCATTEROMETERS
Design and construction of a Ka-band scatterometer
[AD-A286296] p 1368 N95-22322
SCENE ANALYSIS
Tracking a dynamic set of feature points
[AD-A285124] p 1313 N95-20257
SCHEDULES
The advantages of cost plus award fee contracts
p 1584 N95-20745
Computing near-optimal schedules
[PB95-132072] p 1466 N95-21269
SCHEDULING
Planning and scheduling for success
p 1584 N95-20747
Scheduling: A guide for program managers
p 1584 N95-20748
Computing near-optimal schedules
[PB95-132072] p 1466 N95-21269
Intelligent interactive project management system
[PB95-132684] p 1586 N95-21982
A periodic scheduling heuristic for mapping iterative task graphs onto distributed memory multiprocessors
[AD-A286047] p 1311 N95-22415
SCHOOLS
Layered path planning for an autonomous mobile robot
[AD-A286138] p 1485 N95-22244
SCHROEDINGER EQUATION
Full potential multiple scattering theory
[DE95-003197] p 1576 N95-22084
SCIENTIFIC VISUALIZATION
A Hyperspectral Image Data Exploration Workbench for environmental science applications
[DE94-016373] p 1412 N95-20171
Computer graphics tools for visualizing gravity gradient torques on a rigid spacecraft
[AD-A285971] p 1461 N95-20665
Design and implementation of visual object-oriented LOGO using Prograph
[AD-A285977] p 1461 N95-20687
SCINTILLATION
Simulation of the impact of atmospheric turbulences on millimeter-wave communications systems
p 1295 N95-20939
SCINTILLATION COUNTERS
Light output and radiation damage in a lead tungstate crystal
[DE94-016814] p 1565 N95-20265
The ORNL Neutron-Capture Cross Section Facility
[DE94-019146] p 1537 N95-21460
SCRUBBERS
Mercury capture in bench-scale absorbers
[DE94-016910] p 1234 N95-20107
SEA BREEZE
Real-data tests of a single-Doppler radar assimilation system
[AD-A286638] p 1292 N95-20904
SEA ICE
Ice Processing System software support documentation
[AD-A280030] p 1388 N95-20006
Atlas of SSM/I satellite ice concentration interpolated to operational ice model domains of the Arctic for 1993
[AD-A280183] p 1432 N95-20012
Monthly mean sea ice data from the Polar Ice Prediction System, the Regional Polar Ice Prediction System-Barents Sea and the Regional Polar Ice Prediction System-Greenland Sea
[AD-A280095] p 1433 N95-21018
Small antennas for communication over sea ice
[AD-D016206] p 1301 N95-21156
SEA SURFACE TEMPERATURE
An at-sea evaluation of an infrared/resistance temperature device for air/sea-surface temperature measurements
[AD-A279672] p 1365 N95-20604
SEA WATER
Small antennas for communication over sea ice
[AD-D016206] p 1301 N95-21156
Seawater test results of Open-Cycle Ocean Thermal Energy Conversion (OC-OTEC) components
[DE94-019254] p 1396 N95-21897
Superconducting electromagnetic thruster
[AD-D016485] p 1355 N95-21902
SEALS (STOPPERS)
Frame and edge seal technology: A state of the art survey
[PB95-110334] p 1288 N95-22014
SEARCH PROFILES
Application of Markov decision processes to search problems
[PB95-110813] p 1497 N95-19914

Efficient caption-based retrieval of multimedia information
[AD-A279604] p 1586 N95-19956

SEARCH RADAR
Vibration analysis of the AN/SPS-67(V)3 surface search radar
[AD-A286050] p 1302 N95-21324

SEAS
Mississippi State University Center for Air Sea Technology FY 1993 and FY 1994 research program in Navy ocean modeling and prediction
[AD-A286322] p 1432 N95-20209
Terrain and refractivity effects on non-optical paths
p 1294 N95-20931
The determination of static and time varying dipole source. Sensor geometry during sea trials using differential global positioning system
[MRL-TN-631] p 1205 N95-21642

SEATS
Helicopter crewseat cushion program
[AD-A286654] p 1452 N95-20973

SECONDARY FLOW
Subgrid scale models in finite difference simulations of complex wall bounded flows p 1346 N95-21063
Direct simulation of turbulent flow in a square duct: Reynolds-stress budgets p 1348 N95-21073
Simulations of bypass transition for spatially evolving disturbances p 1349 N95-21079

SECRETIONS
Effect of increased venous backflow on the release of cardiac hormone. Fine structural, immunohistochemical, and biochemical study
[PB95-130399] p 1445 N95-21424

SECURITY
Utilizing artificial neural networks in network flow analysis: An annotated bibiliography
[DE95-002453] p 1482 N95-21522
Information security for unmanned systems
[AD-A286511] p 1485 N95-22214
A survey of artificial neural network applications in flow analysis of energy networks
[DE95-002452] p 1486 N95-22430

SEDIMENT TRANSPORT
Data report: Stress measurements in the bottom boundary layer with BASS tripods STRESS 2 1990-1991
[AD-A279875] p 1433 N95-20433
Seismic anisothropy and large-scale porosity inthe ocean floor
[AD-A286580] p 1436 N95-22187

SEDIMENTS
Multiple scatter theory of ocean sediments
[AD-A286033] p 1433 N95-20999
Volatiles in the Earth: All shallow and all recycled
p 1416 N95-21779
Loss of solar He and Ne from IDPS in subducting sediment: Diffusion and the effect of phase changes
p 1419 N95-21792
Descriptions of WHOI sediment cores, volume 8
[AD-A279444] p 1436 N95-22073
Derivation of maximum permissible concentrations for several volatile compounds for water and soil
[PB95-107454] p 1411 N95-22381

SEGMENTS
A framework for segmentation using physical models of image formation
[AD-A279900] p 1543 N95-20564

SEISMIC WAVES
Infrasonic observations of the Northridge, California, earthquake
[DE94-018095] p 1413 N95-20289
The Novaya Zemlya Event of 31 December 1992 and Seismic Identification Issues: 15th Annual Seismic Research Symposium
[AD-A279847] p 1414 N95-20760
EPSCoR supplemental grant for an application of neural networks to seismic signal discrimination
[AD-A285846] p 1414 N95-20878
Application of neural networks to seismic signal discrimination research findings
[AD-A285848] p 1415 N95-21308

SEISMOGRAMS
Source contributions at far-regional distances
[AD-A279405] p 1426 N95-21932

SEISMOGRAPHS
The Novaya Zemlya Event of 31 December 1992 and Seismic Identification Issues: 15th Annual Seismic Research Symposium
[AD-A279847] p 1414 N95-20760

SEISMOLOGY
Velocity analysis for transversely isotropic media
[DE95-000643] p 1411 N95-19981
P-wave signatures and parameterization of transversely isotropic media: An overview
[DE95-000644] p 1411 N95-19982
The Novaya Zemlya Event of 31 December 1992 and Seismic Identification Issues: 15th Annual Seismic Research Symposium
[AD-A279847] p 1414 N95-20760
EPSCoR supplemental grant for an application of neural networks to seismic signal discrimination
[AD-A285846] p 1414 N95-20878
Application of neural networks to seismic signal discrimination research findings
[AD-A285848] p 1415 N95-21308
Anatomy of the Midcontinent Rift beneath Lake Superior
[DE94-019298] p 1415 N95-21477
Seismic evidence for volatiles at large depth in the Earth p 1422 N95-21808

SELECTION
Frequent sampling in discrete choice
[PB95-110961] p 1497 N95-19938
Molecularly Designed Ultrafine/Nanostructured Materials, volume 351
[AD-A285370] p 1568 N95-20552
MCMs for avionics: Technology selection and intermodule interconnection p 1210 N95-20641

SELECTIVE FADING
Experimental study of the helicopter-mobile radioelectrical channel and possible extension to the satellite-mobile channel p 1296 N95-20945

SELENIUM
Collisional redistribution effects on x ray laser saturation behavior
[DE94-017308] p 1374 N95-21663
Studies of selenium and xenon in inductively coupled plasma mass spectrometry
[DE95-001676] p 1245 N95-21734

SELENIUM COMPOUNDS
Dynamic NMR studies of restricted arene rotation in the chromiu tricarbonyl thiophene and selenophene complexes
[DE95-001656] p 1257 N95-21399

SELF ADAPTIVE CONTROL SYSTEMS
A neural expert approach to self designing flight control systems
[AD-A279965] p 1215 N95-21122

SELF CONSISTENT FIELDS
Stellarator transport optimization with self-consistent electric fields
[DE94-019151] p 1559 N95-21581

SELF ERECTING DEVICES
High-performance, flexible, deployable array development for space applications
p 1322 N95-20532
An introduction to the Astro Edge solar array
p 1322 N95-20535

SELF EXCITATION
Charge density of fractional charged quasiparticles in the composite fermion picture
[DE94-018122] p 1524 N95-21703

SELF LUBRICATING MATERIALS
Evaluation of PS 212 coatings under boundary lubrication conditions with an Ester-based oil to 300 C
[NASA-TM-106763] p 1223 N95-19901

SELF ORGANIZING SYSTEMS
Attempt to interpret the self-organizing mapping physiologically
[PB95-127783] p 1438 N95-21112
Exponents in lifetime and power spectral density forms in self-organized critical systems
[AD-A286242] p 1495 N95-22026

SEMANTICS
Algebraic semantics of message sequence charts
[PB95-110581] p 1288 N95-19890
Non interleaving process algebra
[PB95-110607] p 1486 N95-19892
General conservative extension theorem in process algebra
[PB95-110656] p 1487 N95-19902
Process algebra with partial choice
[PB95-110714] p 1487 N95-19907
Real time process algebra with infinitesimals
[PB95-110623] p 1488 N95-20055
Comparison of Ward and Mellor's transformation schema with State- and Activitycharts
[PB95-110698] p 1459 N95-20258
Software merge: Semantics of combining changes to programs
[AD-A279657] p 1459 N95-20304
Multi-dimensional Petri nets
[PB95-127593] p 1491 N95-21024
Formal model for the dynamics of compositional reasoning systems
[PB95-132056] p 1482 N95-21267
Semantics for a fine lambda-calculus with de Bruijn indices
[PB95-127577] p 1492 N95-21372
Performance analysis and true concurrency semantics
[PB95-134086] p 1478 N95-21869

SEMICONDUCTOR DEVICES
Semiconductor cold electron emission device
[AD-D016577] p 1314 N95-20298
A new mini Ball Grid Array (mBGA) multichip module technology
[DE94-018897] p 1480 N95-20342
Solid-state dynamics and quantum transport in novel semiconductor nanostructures
[AD-A285946] p 1315 N95-20394
Ultrafast magnetoexciton dynamics in GaAs
[DE94-018175] p 1514 N95-20732
Spectroscopic, morphological, and electrical characterization of PdGe ohmic contacts to n-GaAs
[DE95-000738] p 1329 N95-21394
InTISb for long-wavelength infrared photodetectors and arrays
[AD-A280109] p 1331 N95-21660
Plastic encapsulated parts
[DE95-001876] p 1332 N95-21729
Method of making a semiconductor device by forming a nanochannel mask
[AD-D016515] p 1576 N95-22059
Sub-millimeterwave semiconductor signal sources
[AD-A279375] p 1335 N95-22144

SEMICONDUCTOR JUNCTIONS
Ultrafast optical studies of surface reaction processes at semiconductor interfaces
[DE95-001548] p 1574 N95-21839
Method of forming a high voltage silicon-on-sapphire photocell array
[AD-D016479] p 1396 N95-21899
Equilibrium and shot noise in mesoscopic systems
[DE95-000855] p 1576 N95-22008

SEMICONDUCTOR LASERS
Program of the 1993 9th Interdisciplinary Laser Science Conference (ILS-9)
[AD-A285131] p 1369 N95-20082
Application of diode lasers to the isotopically selective determination of uranium in oxides by optogalvanic spectroscopy
[DE94-018045] p 1370 N95-20698
Ultra-high aggregate bandwidth two-dimensional multiple-wavelength diode laser arrays
[AD-A280098] p 1372 N95-21019
Overview of remote sensing laser development and semiconductor laser technology
[DE94-019103] p 1389 N95-21552
Optical, electronic and optoelectronic material and device research
[AD-A280111] p 1374 N95-21630
High average power diode pumped solid state lasers for CALIOPE
[DE94-019248] p 1376 N95-22121
International Symposium on Advanced Laser Technologies
[AD-A279849] p 1376 N95-22164

SEMICONDUCTOR PLASMAS
Application of IRIS to semiconductor plasma processing
[DE95-003591] p 1562 N95-22225

SEMICONDUCTORS (MATERIALS)
Physics and applications of defects in advanced semiconductors, volume 325
[AD-A280059] p 1563 N95-19886
Low temperature synthesis of semiconductor materials
[AD-A285120] p 1226 N95-20081
FTIR spectroscopy for the determination of water in corrosive gases
[DE94-014658] p 1235 N95-20139
Kondo insulators
[DE95-001156] p 1237 N95-20368
Solid-state dynamics and quantum transport in novel semiconductor nanostructures
[AD-A285946] p 1315 N95-20394
Development of solid state moisture sensors for semiconductor fabrication applications
[DE94-015771] p 1364 N95-20398
Solid state research
[AD-A279662] p 1567 N95-20426
Advances in polycrystalline thin-film photovoltaics for space applications p 1318 N95-20514
P/N In(Al) GaAs multijunction laser power converters
p 1323 N95-20539
Nucleation, growth, and strain relaxation of lattice-mismatched 3-5 semiconductor epitaxial layers
p 1324 N95-20543
Microscopy of stress-induced morphological development and dislocation nucleation during semiconductor epitaxy
[DE94-017869] p 1568 N95-20674
Instantaneous frequency dynamics of coherent emission from magnetoexcitons in gallium arsenide
[DE94-018182] p 1569 N95-20677
Temporal and spectral investigation of multi-Landau level quantum beats in GaAs
[DE94-018189] p 1569 N95-20678

Ultrafast magnetoexciton dynamics in GaAs
[DE94-018175] p 1514 N95-20732

Photoinduced charge transfer between fullerenes and TiO2 semiconductor colloids
[DE95-001447] p 1570 N95-20838

Certain physical properties of lanthanum digermanide
[AD-A286592] p 1229 N95-20859

Study of small carbon and semiconductor clusters using negative ion threshold photodetachment spectroscopy
[DE95-002327] p 1515 N95-20872

Mechanical design of the DO silicon detector
[DE95-002532] p 1365 N95-20902

Scanning tunneling microscopy of semiconductor surfaces
[AD-A279982] p 1571 N95-20964

IR materials producibility
[AD-A280094] p 1328 N95-21017

Fiber-optic control of current filaments in high gain photoconductive semiconductor switches
[DE94-015804] p 1328 N95-21139

X-ray studies of microstructures in semiconductor and superconducting materials
[DE95-001802] p 1572 N95-21279

Excitons in semiconducting superlattices, quantum wells, and ternary alloys
[DE95-001867] p 1572 N95-21287

Defect production and recombination during low-energy ion processing
[DE95-001827] p 1572 N95-21304

Photoemission and ferromagnetism
[DE95-002419] p 1520 N95-21362

Theoretical study of the noble metals on semiconductor surfaces and Ti-base shape memory alloys
[DE95-001654] p 1257 N95-21398

Gradient index lenses from sol-gel layering
[AD-A285649] p 1242 N95-21402

Translational-energy-resolved studies of photographed carrier-induced reactions on semiconductor surfaces
[DE95-002944] p 1573 N95-21444

Thin-film cadmium telluride photovoltaic cells
[DE94-011886] p 1395 N95-21508

Angle resolved photoemission on K(0.3)Mo3, TiTe2 and Ti(1+x)S2
[DE94-018300] p 1574 N95-21712

Quantum dynamical phenomena of independent electrons in semiconductor superlattices subject to a uniform electric field
[DE95-001655] p 1574 N95-21723

Plastic encapsulated parts
[DE95-001876] p 1332 N95-21729

Application of quaternary phase diagrams to compound semiconductor processing
[DE95-001813] p 1277 N95-21748

Ultrafast optical studies of surface reaction processes at semiconductor interfaces
[DE95-001548] p 1574 N95-21839

Acoustoelectric effect in semiconductor superlattice
[DE94-628994] p 1575 N95-21859

Effect of the electron-SO-phonon on the impurity state energies in a semiconductor quantum well
[DE94-628993] p 1581 N95-21887

Growth and electrical and far-infrared properties of wide electron wells in semiconductors
[AD-A279409] p 1333 N95-21917

Method of making a semiconductor device by forming a nanochannel mask
[AD-D016515] p 1576 N95-22059

Surfaces and thin films studied by picosecond ultrasonics
[DE95-001866] p 1506 N95-22071

Application of optical second harmonic generation to surface analysis
[AD-A279445] p 1547 N95-22074

Electric-field effects on shallow donor impurity in a harmonic quantum dot
[DE94-629034] p 1577 N95-22176

Temperature dependence of a magnetopolaron in a harmonic quantum dot in resonant magnetic fields
[DE94-629036] p 1502 N95-22177

Research on the power generation system with thermoelectric conversion elements
[DE95-714804] p 1397 N95-22309

Photoreflectance and x ray diffraction study of semiconductor heterostructures and quantum wells
[PB95-127049] p 1582 N95-22432

SENSITIVITY

Light-scattering fluctuations and noise in nonlinear optical processing
[AD-A279748] p 1544 N95-20803

Triggers for a high sensitivity charm experiment
[DE95-002251] p 1515 N95-20868

Eigenmode method for electromagnetic synthesis of diffractive elements with three-dimensional profiles
[PB95-127726] p 1301 N95-21107

Emittance dilution by ions in the SLC arcs
[DE95-002871] p 1536 N95-21332

SENSORS

A charge distribution analysis instrument for catalysis and material science applications
[DE94-016489] p 1364 N95-20233

SENSORY DEPRIVATION

Command history, 1993
[AD-A279775] p 1446 N95-21989

SEPARATED FLOW

Effects of turbulence compressibility and unsteadiness in compression corner flow p 1344 N95-21052

Single point modeling of rotating turbulent flows
p 1346 N95-21060

Simulation of separated flows p 1347 N95-21068

Large-eddy simulation of separated flow in a ribbed duct p 1347 N95-21070

Application of Navier-Stokes code PAB3D with kappa-epsilon turbulence model to attached and separated flows
[NASA-TP-3480] p 1201 N95-21338

Turbulence modeling for separated flow
p 1359 N95-22443

SEPARATION

Separation of proteins by convective electrophoresis through a porous membrane
[PB95-127130] p 1248 N95-22373

SEPARATORS

Low flow fluid separator
[AD-D016575] p 1339 N95-20297

Transport phenomena in the micropores of plug-type phase separators
[NASA-TM-108479] p 1340 N95-20561

Molten carbonate fuel cell product development test
[DE95-000005] p 1324 N95-20574

Finding all minimal separators of a graph
[PB95-127585] p 1491 N95-21023

A low energy continuous reactor separator for the production of ethanol from corn grits/starch and biomass streams
[DE95-002256] p 1283 N95-21356

SEPTUM

Atom wave interferometer
[AD-A279532] p 1524 N95-21688

SEQUENCING

Algebraic semantics of message sequence charts
[PB95-110581] p 1288 N95-19890

Process algebra with partial choice
[PB95-110714] p 1487 N95-19907

Long sequence correlation coprocessor
[AD-D016558] p 1313 N95-20280

Accuracy problems in the generation of discrete time stochastic processes
[PB95-131397] p 1386 N95-21133

Proposal for a tutorial on Minimal Length Encoding (MLE) in molecular biology
[DE94-015076] p 1438 N95-21376

Uninterrupted, enhanced-rate event sequencer with mixed-speed counter modules
[AD-D016255] p 1334 N95-22030

Sequential shock induced switch tests for Eglin Air Force Base
[DE95-001786] p 1334 N95-22062

Discovering related DNA sequences via mutual information
[DE95-001101] p 1440 N95-22067

Almost kappa-wise independent random permutation of the cube
[PB95-108098] p 1495 N95-22147

SEQUENTIAL ANALYSIS

O(log2 n) time efficient parallel factorization of dense, sparse separable, and banded matrices
[NASA-CR-197356] p 1473 N95-19885

In-situ capability of ion beam modification and characterization of materials at Los Alamos National Laboratory
[DE95-002738] p 1534 N95-21236

SEQUENTIAL CONTROL

A database for analyzing sequential behavioral data and their associated cognitive models
[AD-A280061] p 1448 N95-19887

Multi-port tester interface
[AD-D016240] p 1332 N95-21775

Time and the order of abstract events in distributed computations
[PB95-110482] p 1496 N95-22349

SERIES (MATHEMATICS)

Growth series for the commutator subgroup
[PB95-111092] p 1490 N95-20452

SERIES EXPANSION

Semiquantum chaos and the large N expansion
[DE94-016196] p 1488 N95-20169

New improved derivative expansion for field theories with spontaneous symmetry breaking
[DE94-019349] p 1580 N95-21486

SERPENTINE

Impact degassing of water and noble gases from silicates p 1416 N95-21780

SERUMS

Studies of selenium and xenon in inductively coupled plasma mass spectrometry
[DE95-001676] p 1245 N95-21734

SERVICE LIFE

A test of the Arrhenius extrapolation assumption for a nitrile rubber
[DE94-017337] p 1263 N95-19926

Crack closure and sequential effects in fatigue: A literature survey
[PB95-131637] p 1387 N95-21557

Cathode Life Test Facility
[AD-A286232] p 1334 N95-22023

Effects of cyclic stress distribution models on fatigue life predictions
[DE95-001619] p 1388 N95-22070

SERVOMECHANISMS

Input shaping for vibration-damped slewing of a flexible beam using a heavy-lift hydraulic robot
[DE94-015803] p 1379 N95-20695

SET THEORY

Ups and downs of type theory
[PB95-110664] p 1487 N95-19903

Abstract reduction and topology
[PB95-110615] p 1488 N95-20054

Duality beyond sober spaces: Topological spaces and observation frames
[PB95-134565] p 1494 N95-21962

Computing symmetries and stubborn sets
[PB95-127700] p 1472 N95-22328

Local connectivity of some Julia sets containing a circle with an irrational rotation
[PB95-109070] p 1496 N95-22353

SETTLING

Hindered settling computations using a parallel boundary element method
[DE94-014286] p 1339 N95-20137

SEWAGE TREATMENT

Disinfection of purified waste water with ultra violet light on a technical scale
[PB95-131926] p 1405 N95-21330

SEYFERT GALAXIES

Extended far-infrared emission and star formation in Seyfert galaxies p 1593 N95-21764

SH-3 HELICOPTER

Variations observed in the AC generator signal period of a Sea King helicopter
[AD-A284280] p 1206 N95-19963

SHAFTS (MACHINE ELEMENTS)

Bevel gear driver and method having torque limit selection
[NASA-CASE-MSC-22384-1] p 1378 N95-20151

Fire smoke ventilation through shafts: Experiments
[PB95-132247] p 1288 N95-21978

SHALLOW SHELLS

Influence of primary boundary conditions on the buckling of shallow cylindrical shells
[PB94-208352] p 1384 N95-20003

SHALLOW WATER

Model-based inversion for a shallow ocean application
[DE94-016968] p 1433 N95-20420

On the transition towards slow manifold in shallow-water and 3D Euler equations in a rotating frame
p 1345 N95-21057

SHAPE CONTROL

Toward a design for the ITER plasma shape and stability control system
[DE94-017516] p 1548 N95-20037

SHAPE MEMORY ALLOYS

Mixed-sputter deposition of Ni-Ti-Cu shape memory films
[DE94-017296] p 1250 N95-19900

Processing and characterization of Ni-Al-Fe-B shape-memory alloy wires produced by rapid solidification
[DE94-017702] p 1250 N95-20020

High-performance, flexible, deployable array development for space applications
p 1322 N95-20532

Feasibility study of power generation system with shape memory alloys
[DE95-714802] p 1254 N95-20890

Theoretical study of the noble metals on semiconductor surfaces and Ti-base shape memory alloys
[DE95-001654] p 1257 N95-21398

SHAPES

A computational study of projectile shape dependence on phase change phenomena with comparisons to experimental data
[DE95-000740] p 1384 N95-20077

Plasma shape experiments for an optimized tokamak
[DE94-017508] p 1553 N95-20445

Identification of resonant, two-electron, and inter-atomic features in K and L23 NEXAFS spectra
[AD-A285374] p 1513 N95-20554

Ohmsett test of NOFI Vee-Sweep and NOFI 600S Oilboom [AD-A279525] p 1408 N95-21685

SHEAR FLOW

Evaluation of Reynolds stress turbulence closures in compressible homogeneous shear flow [NASA-CR-194892] p 1338 N95-20009

Role of pressure diffusion in non-homogeneous shear flows p 1345 N95-21053

Modeling the two-point correlation of the vector stream function p 1345 N95-21055

Direct simulation of a self-similar plane wake p 1350 N95-21084

Investigation of shear layer transition using various turbulence models p 1352 N95-21096

Fourth International Symposium on Stratified Flows, volume 1 [AD-A286450] p 1354 N95-21583

Nonlinear interaction between a pair of oblique modes in a supersonic mixing layer: Long-wave limit [NASA-CR-197380] p 1357 N95-22173

Local dynamic subgrid-scale models in channel flow p 1360 N95-22447

Small-scale behavior in distorted turbulent boundary layers at low Reynolds number p 1362 N95-22456

A method for obtaining a statistically stationary turbulent free shear flow p 1363 N95-22463

Direct numerical simulation of incompressible axisymmetric flows p 1363 N95-22464

SHEAR LAYERS

Free shear layers, base pressure and bluff-body drag [AD-A286316] p 1200 N95-20175

Instability of streamwise vortices in plane channel flows p 1344 N95-21049

Role of pressure diffusion in non-homogeneous shear flows p 1345 N95-21053

Direct numerical simulation of turbulent flow in a sudden pipe expansion p 1347 N95-21067

Spatial direct numerical simulation of boundary layer transition under strong adverse pressure gradient p 1351 N95-21093

Investigation of shear layer transition using various turbulence models p 1352 N95-21096

Extended theory of main ion and impurity rotation and bootstrap current in a shear layer [DE94-015857] p 1555 N95-21141

Forced free-shear layer measurements p 1362 N95-22460

SHEAR PROPERTIES

Extrudate swell and extrudate distortion of HDPE as a result of different deformation mechanisms during extrusion through capillary dies [PB95-110227] p 1288 N95-21651

SHEAR STRAIN

Micromechanical approach to transformation toughening in ceramics [PB95-135422] p 1273 N95-20976

SHEAR STRENGTH

Role of internal stresses in fracture behavior of engineering composites [DE95-001106] p 1229 N95-20912

Electrorheology for smart automotive suspensions [AD-A285543] p 1380 N95-21157

Determination of the complex elastic moduli of materials using a free-free bar technique [AD-A279861] p 1281 N95-22387

SHEAR STRESS

The influence of ply waviness with nonlinear shear on the stiffness and strength reduction of composite laminates [AD-A285736] p 1224 N95-19899

Evaluation of Reynolds stress turbulence closures in compressible homogeneous shear flow [NASA-CR-194892] p 1338 N95-20009

Turbulence descriptors for scaling fatigue loading spectra of wind turbine structural components [DE94-011833] p 1384 N95-20109

Direct simulation of turbulent flow in a square duct: Reynolds-stress budgets p 1348 N95-21073

SHELLS (STRUCTURAL FORMS)

Effects of plasma physics on capsule implosions in gas-filled hohlraums [DE95-000923] p 1371 N95-20786

SHIELDING

MCNP (trademark) ENDF/B-VI iron benchmark calculations [DE94-016165] p 1508 N95-20160

SHIFT REGISTERS

Long sequence correlation coprocessor [AD-D016558] p 1313 N95-20280

SHOCK LAYERS

Numerical study of boundary layer interaction with shocks: Method and code validation p 1362 N95-22461

SHOCK LOADS

Ductile-brittle transition behavior of tungsten under shock loading [DE94-009913] p 1251 N95-20122

Analysis of experimentally shocked minerals by NMR spectroscopy [DE95-002955] p 1573 N95-21449

SHOCK TESTS

Sequential shock induced switch tests for Eglin Air Force Base [DE95-001786] p 1334 N95-22062

SHOCK TUBES

Approximate Riemann solver for magnetohydrodynamics (that works in more than one dimension) [PB95-135802] p 1553 N95-20425

SHOCK WAVE INTERACTION

Internal aerodynamics of a generic three-dimensional scramjet inlet at Mach 10 [NASA-TP-3476] p 1340 N95-20619

Shock wave interactions in hypervelocity flow [AD-A286507] p 1357 N95-22212

On the dynamics of a shock-bubble interaction [NASA-CR-194978] p 1495 N95-22325

Numerical study of boundary layer interaction with shocks: Method and code validation p 1362 N95-22461

SHOCK WAVES

A computational study of projectile shape dependence on phase change phenomena with comparisons to experimental data [DE95-000740] p 1384 N95-20077

Ductile-brittle transition behavior of tungsten under shock loading [DE94-009913] p 1251 N95-20122

Infrasonic observations of the Northridge, California, earthquake [DE94-018095] p 1413 N95-20289

Proceedings of the Zel'Dovich Memorial International Conference on Combustion, Detonation, Shock Waves, volume 2 [AD-A286626] p 1239 N95-20769

Potential flow downstream of the heliospheric terminal shock: A non-spherical shock [NASA-TM-110493] p 1426 N95-21874

Sequential shock induced switch tests for Eglin Air Force Base [DE95-001786] p 1334 N95-22062

Shock wave interactions in hypervelocity flow [AD-A286507] p 1357 N95-22212

SHORT CIRCUIT CURRENTS

Electron-irradiated two-terminal, monolithic InP/Ga0.47In0.53As tandem solar cells and annealing of radiation damage p 1319 N95-20519

Influence of wavelength on transient short-circuit current in polycrystalline silicon solar cells [DE94-629082] p 1397 N95-22183

SHOT NOISE

Equilibrium and shot noise in mesoscopic systems [DE95-000855] p 1576 N95-22008

SHRINKAGE

Governing equations for multiphase heat and mass transfer in hygroscopic porous media with applications to clothing materials [AD-A286418] p 1357 N95-22206

SIDEBANDS

Time-resolved study of sideband generation and transition to chaos on an infrared FEL [DE95-002336] p 1374 N95-21528

Recent progress of the compact AFEL at Los Alamos [DE95-002728] p 1376 N95-22154

SIDELOBE REDUCTION

General purpose sidelobe canceller system [AD-D016560] p 1289 N95-20270

Directive optimization of coherent sidelobe canceller systems [AD-D016513] p 1307 N95-21908

SIDESLIP

Pressure measurements on an F/A-18 twin vertical tail in buffeting flow. Volume 1: Wind tunnel test summary [AD-A279126] p 1202 N95-21877

Effect of juncture fillets on double-delta wings undergoing sideslip at high angles of attack [AD-A286165] p 1207 N95-22039

SIGNAL ANALYSIS

Infrasonic observations of the Northridge, California, earthquake [DE94-018095] p 1413 N95-20289

A portable and independent edge fluctuation diagnostic [DE94-018254] p 1554 N95-20681

SIGNAL ANALYZERS

Evaluation of superconducting quantum interference devices interfaced with digital signal processing electronics for biomagnetic applications [DE94-016186] p 1289 N95-20164

The impact of advanced packaging technology on modular avionics architectures p 1208 N95-20632

Innovative use of DSP technology in space: FORTE event classifier [DE94-016086] p 1291 N95-20697

Propagation measurements on a troposcatter link in the Canadian High Arctic p 1295 N95-20940

An evaluation of the Gear Averaging Signal Processor (GASP) [DSTO-TR-0067] p 1470 N95-21950

SIGNAL DETECTION

EPSCoR supplemental grant for an application of neural networks to seismic signal discrimination [AD-A285846] p 1414 N95-20878

Application of neural networks to seismic signal discrimination research findings [AD-A285848] p 1415 N95-21308

Signal processing in the linear statistical model [AD-A286255] p 1308 N95-22041

Threshold detection in the presence of atmospheric turbulence [AD-A286175] p 1427 N95-22249

SIGNAL DETECTORS

Data report: Stress measurements in the bottom boundary layer with BASS tripods STRESS 2 1990-1991 [AD-A279875] p 1433 N95-20433

SIGNAL ENCODING

Problems of coding in multipath channels p 1294 N95-20930

SIGNAL FADING

Error probabilities of FFH/BFSK with noise normalization and soft decision viterbi decoding in a fading channel with partial-band jamming [AD-A280041] p 1498 N95-20620

Problems of coding in multipath channels p 1294 N95-20930

The effects of magnetic storm phases on F-layer irregularities from auroral to equatorial latitudes [AD-A286173] p 1427 N95-22423

SIGNAL GENERATORS

On commonalities in signal design for non-Gaussian channels [AD-A285385] p 1498 N95-20608

Apparatus and method for determining the mass density of a filament [NASA-CASE-LAR-14879-1-CU] p 1383 N95-20616

Sub-millimeterwave semiconductor signal sources [AD-A279375] p 1335 N95-22144

SIGNAL MIXING

D(sup 0)-(anti-D)(sup 0) mixing and doubly Cabibbo-suppressed decays of the D(+) [DE94-015540] p 1512 N95-20476

Light-scattering fluctuations and noise in nonlinear optical processing [AD-A279748] p 1544 N95-20803

Seamless data-range change using punctured convolutional codes for time-varying signal-to-noise ratios p 1304 N95-21534

SIGNAL PROCESSING

Variations observed in the AC generator signal period of a Sea King helicopter [AD-A284280] p 1206 N95-19963

Wavelet-based acoustic recognition of aircraft [DE94-017701] p 1503 N95-20019

Determining the usability of Digital Video Interactive (DVI) technology in computer-based instruction [AD-A284717] p 1457 N95-20060

Signal-to-noise gain from adaptive matched-field beamforming of multidimensional acoustic arrays [AD-A285671] p 1503 N95-20084

Evaluation of superconducting quantum interference devices interfaced with digital signal processing electronics for biomagnetic applications [DE94-016186] p 1289 N95-20164

DSP control of superconducting quantum interference devices [DE94-016193] p 1313 N95-20168

The GPS Burst Detector W-Sensor [DE94-017406] p 1204 N95-20269

Method and system of mapping acoustic near field [AD-D016574] p 1504 N95-20296

Applications of wavelets to radar, imaging and related problems [AD-A279909] p 1290 N95-20545

The impact of advanced packaging technology on modular avionics architectures p 1208 N95-20632

Packaging the MAMA module p 1209 N95-20639

Innovative use of DSP technology in space: FORTE event classifier [DE94-016086] p 1291 N95-20697

Propagation measurements on a troposcatter link in the Canadian High Arctic p 1295 N95-20940

Wavelet transformations for helicopter identification via acoustic signatures [AD-A279980] p 1504 N95-20963

Monolithic circuits for lead-glass calorimetry
[DE94-019112] p 1330 N95-21554
Numerical and symbolic algorithms for application and specific signal processing
[AD-A279902] p 1305 N95-21576
Subsampling methods for image sequence coding
[PB95-107991] p 1305 N95-21579
Multi-port tester interface
[AD-D016240] p 1332 N95-21775
An evaluation of the Gear Averaging Signal Processor (GASP)
[DSTO-TR-0067] p 1470 N95-21950
Signal processing in the linear statistical model
[AD-A286255] p 1308 N95-22041
Image and video coding using a wavelet decomposition
[PB95-135067] p 1311 N95-22358
TDX: A high-bandwidth crossbar-switched communication paradigm
[DE94-017187] p 1311 N95-22407
A periodic scheduling heuristic for mapping iterative task graphs onto distributed memory multiprocessors
[AD-A286047] p 1311 N95-22415

SIGNAL REFLECTION
Development of a portable ice-thickness measuring instrument
[AD-A279472] p 1433 N95-21291

SIGNAL TO NOISE RATIOS
Signal-to-noise gain from adaptive matched-field beamforming of multidimensional acoustic arrays
[AD-A285671] p 1503 N95-20084
Global change integrating factors: Tropical tropopause trends
[DE95-001121] p 1404 N95-20835
Seamless data-range change using punctured convolutional codes for time-varying signal-to-noise ratios p 1304 N95-21534
Signal to noise improvements with a new Far-IR rapid-scan Michelson Interferometer
[DE95-002416] p 1367 N95-21638
Threshold detection in the presence of atmospheric turbulence
[AD-A286175] p 1427 N95-22249

SIGNAL TRANSMISSION
Applications of wavelets to radar, imaging and related problems
[AD-A279909] p 1290 N95-20545
Scattering of an FM signal from an array of spheres
[AD-A285587] p 1505 N95-21213

SIGNATURES
P-wave signatures and parameterization of transversely isotropic media: An overview
[DE95-000644] p 1411 N95-19982
Application of wavelet-filtering techniques to intermittent turbulent and wall pressure events. Part 1: Exploratory results
[AD-A286077] p 1341 N95-20849
Preclinical investigation of lyophilized platelet preparations
[AD-A286079] p 1443 N95-20851

SIGNS AND SYMPTOMS
Conservative smoothing versus artificial viscosity
[DE95-001108] p 1341 N95-20831
Assessing post traumatic stress disorder and PTSD symptomatology in US Army personnel
[AD-A285941] p 1451 N95-22324

SILANES
An atomically-resolved STM study of the thermal decomposition of disilane on Si(001)
[AD-A279818] p 1567 N95-20544
Antiphase boundaries as nucleation centers in low-temperature epitaxial growth
[AD-A279895] p 1568 N95-20594
Preparation and x-ray structure of Cp2Ti(PH2SiH2)(PMe3)
[AD-A286197] p 1246 N95-21879
A catalytic method for the conversion of silanes to stannanes
[AD-A286214] p 1247 N95-22020

SILICATES
Sol-gel-derived silica films with tailored microstructures for applications requiring organic dyes
[DE94-018886] p 1264 N95-20047
Conference on Deep Earth and Planetary Volatiles
[NASA-CR-196944] p 1415 N95-21777
Impact degassing of water and noble gases from silicates p 1416 N95-21780
Thermochemistry of dense hydrous magnesium silicates p 1416 N95-21782
Mantle devolatilization and rheology in the framework of planetary evolution p 1418 N95-21788
Volatiles, rheology, and mantle convection: Comparing Earth, Venus, and Mars p 1420 N95-21801
Hydrogen storage in Earth's mantle and core
p 1423 N95-21813

SILICON
High precision trace neutron transmutation doping of detector-grade high resistance zone-refined silicon mono-crystal
[DE94-631463] p 1563 N95-19978
Computational modeling of physical processes during laser ablation
[DE94-017699] p 1369 N95-20221
Simulations of the dislocation array at Ge/Si interfaces
[DE94-017680] p 1565 N95-20244
Effects of ambient conditions on the adhesion of cubic boron nitride films on silicon substrates
[DE94-016779] p 1266 N95-20281
Fabrication and testing of a silicon immersion grating for infrared spectroscopy
[DE94-017173] p 1237 N95-20386
Optical properties of silicon clusters deposited on the basal plane of graphite
[DE94-017529] p 1542 N95-20450
High quality InP-on-Si for solar cell applications
p 1317 N95-20510
Final results of the advanced photovoltaic experiment
p 1321 N95-20528
An atomically-resolved STM study of the thermal decomposition of disilane on Si(001)
[AD-A279818] p 1567 N95-20544
An atomically-resolved STM study of the interaction of phosphine (PH3) with the silicon (001) surface
[AD-A279819] p 1513 N95-20585
Atomically resolved structure and bonding of delta-doped boron layers on Si(001)
[AD-A279820] p 1513 N95-20586
Antiphase boundaries as nucleation centers in low-temperature epitaxial growth
[AD-A279895] p 1568 N95-20594
The design and manufacturing development of an active silicon substrate MCM p 1211 N95-20645
Microdynamic devices fabricated on silicon-on-sapphire substrates
[AD-D016531] p 1325 N95-20727
Ion-molecule chemistry related to plasma deposition and etching of silicon
[AD-A279749] p 1514 N95-20804
Mechanical design of the DO silicon detector
[DE95-002532] p 1365 N95-20902
Scanning tunneling microscopy of semiconductor surfaces
[AD-A279982] p 1571 N95-20964
Epitaxial liftoff technology onto processed silicon foundry wafers
[AD-A285621] p 1571 N95-21145
HTS Josephson technology on silicon with application to high speed digital microelectronics
[AD-A285964] p 1328 N95-21178
Micromachined silicon-based analytical microinstruments for space science and planetary exploration
[DE94-019306] p 1367 N95-21507
Non-linear A/D converters for integrated silicon smart sensors
[PB94-208402] p 1330 N95-21590
Forming of superplastic ceramics
[DE94-017306] p 1276 N95-21662
Surface second harmonic studies of Si(111)/electrolyte and Si(111)/SiO2/electrolyte interfaces
[AD-A279450] p 1245 N95-21826
Method of forming a high voltage silicon-on-sapphire photocell array
[AD-D016479] p 1396 N95-21899
Method for laser-assisted silicon etching using halocarbon ambients
[AD-D016494] p 1375 N95-21903
Application of optical second harmonic generation to surface analysis
[AD-A279445] p 1547 N95-22074
The role of point defects and defect complexes in silicon device processing
[DE94-011876] p 1279 N95-22091
Influence of wavelength on transient short-circuit current in polycrystalline silicon solar cells
[DE94-629082] p 1397 N95-22183
Reflective masks for extreme ultraviolet lithography
[DE95-003427] p 1336 N95-22236
Parallel nanometer scale fabrication
[DE95-002122] p 1336 N95-22284
Vertex detectors at linear colliders: Present and future
[PB95-134656] p 1540 N95-22364
Multi signal-domain modeling of solid-state transducers: A theoretical framework based on irreversible thermodynamics mixed finite elements and multigrid
[PB95-134995] p 1336 N95-22382

SILICON ALLOYS
Surface stress, morphological development, and dislocation nucleation during strained-layer epitaxy
[DE94-017682] p 1565 N95-20245
Investigation of the stability and 1.0 MeV proton radiation resistance of commercially produced hydrogenated amorphous silicon alloy solar cells p 1320 N95-20522
Microscopy of stress-induced morphological development and dislocation nucleation during semiconductor epitaxy
[DE94-017869] p 1568 N95-20674
Changes in the behavior of magnetic materials undergoing processing in electrical rotating machines
[PB95-104493] p 1325 N95-20702
Theoretical study of the noble metals on semiconductor surfaces and Ti-base shape memory alloys
[DE95-001654] p 1257 N95-21398
Surface micromachined capacitive tactile image sensor
[PB95-108031] p 1288 N95-21633
Relationship between dendrite coherency and castability of some commercial foundry alloys
[PB95-110243] p 1258 N95-21652

SILICON CARBIDES
Comparison of the dynamic fatigue behavior of two monolithic SiC and an Al2O3/SiC composite
[DE94-017751] p 1225 N95-20022
The thermal conductivity of carbon coated silicon carbide fibers embedded in a silicon carbide matrix
[DE94-017758] p 1225 N95-20023
Synthesis and studies of organometallic precursors for CVD of thin film electronic materials
[AD-A285834] p 1223 N95-20033
The in-situ fracture and Auger analysis of Nicalon fibers
[DE94-017771] p 1226 N95-20357
Reliability analysis of uniaxially ground brittle materials
[NASA-TM-106852] p 1386 N95-20790
B4C-SiC reaction-sintered coatings on graphite plasma facing components
[DE94-019105] p 1230 N95-21553
A transmission electron microscope characterization of sodium sulfate hot corrosion of silicon carbide fiber-reinforced lithium aluminosilicate glass-ceramic matrix composite
[AD-A286164] p 1231 N95-22038
Structural performance of cylindrical pressure housings of different ceramic compositions under external pressure loading. Part 4: Silicon carbide particulate reinforced alumina ceramic
[AD-A286299] p 1279 N95-22047
High temperature corrosion and crack growth of SiC/SiC at variable oxygen partial pressures
[DE94-018715] p 1232 N95-22115
Materials support for the development of High Temperature Advanced Furnaces (HITAF): A comparison of selected mechanical properties for three SiC-based ceramics
[DE94-017752] p 1280 N95-22258
The Modified Embedded Atom Method
[DE94-017958] p 1248 N95-22273
Fracture behavior of laminated discontinuously reinforced aluminum material
[DE94-017307] p 1263 N95-22408

SILICON COMPOUNDS
Physical Si(1-x)Ge(x)/Si heterojunction bipolar transistor model for device and circuit simulation
[PB95-110896] p 1312 N95-19934
A mechanistic model for radiation-induced crystallization and amorphization in U3Si
[DE94-015028] p 1566 N95-20419

SILICON DIOXIDE
Sol-gel-derived silica films with tailored microstructures for applications requiring organic dyes
[DE94-018886] p 1264 N95-20047
Selective methane oxidation over promoted oxide catalysts
[DE94-012270] p 1235 N95-20188
Time-resolved analytical methods for liquid/solid interfaces
[DE95-002255] p 1240 N95-20780
Restricted mass transport effects on free radical reactions
[DE94-018136] p 1217 N95-21706
Surface second harmonic studies of Si(111)/electrolyte and Si(111)/SiO2/electrolyte interfaces
[AD-A279450] p 1245 N95-21826

SILICON FILMS
Amorphous silicon thin films: The ultimate lightweight space solar cell p 1318 N95-20515

SILICON ISOTOPES
Sol-gel-derived silica films with tailored microstructures for applications requiring organic dyes
[DE94-018886] p 1264 N95-20047

SILICON NITRIDES
Elastic anisotropy in hot-pressed Si3N4 composites: Role of in situ (beta)-Si3N4 grains and added (beta)-Si3N4 whiskers
[DE94-018387] p 1226 N95-20027

Enhancement of creep resistance of a sintered S3N4 ceramic by microwave annealing
[DE94-017698] p 1265 N95-20220
Microstructural contributions to the fracture resistance of silicon nitride ceramics
[DE94-018955] p 1267 N95-20323
Characterization and electrical properties of copper films grown via direct liquid coinjection of (hfac)Cu(TMVS) and TMVS
[DE95-002957] p 1272 N95-20889
Role of internal stresses in fracture behavior of engineering composites
[DE95-001106] p 1229 N95-20912
The formation of reaction bonded Si3N4 at low temperatures and in short times
[DE95-001990] p 1275 N95-21289
Comparison of properties of sintered and sintered reaction-bonded silicon nitride fabricated by microwave and conventional heating
[DE95-001426] p 1275 N95-21501
The thermal conductivity of silicon nitride with molybdenum disilicide additions
[DE94-017757] p 1247 N95-22260
Strength testing of Ti-vapor-coated silicon nitride braze joints
[DE94-017858] p 1280 N95-22266
Structural performance of cylindrical pressure housings of different ceramic compositions under external pressure loading. Part 3: Sintered reaction bonded silicon nitride ceramic
[AD-A285773] p 1388 N95-22411

SILICON POLYMERS
Ceramics formed by pyrolysis of either linear or thermosetting carborane (siloxane or silane) acetylene based precursor polymers
[AD-D016563] p 1266 N95-20291

SILICONE RUBBER
Elastomeric electrical connector
[AD-D016559] p 1325 N95-20663

SILOXANES
Siloxanes with strong hydrogen bond donating functionalities
[AD-D016499] p 1279 N95-22057

SILVER
Materials research for GHz multi-chip modules
[AD-A279661] p 1227 N95-20412
The reliability of laser reflowed Sn-Ag solder joints
[AD-A279787] p 1315 N95-20443
Study of improved critical currents and mechanical properties in the Y-Ba-Cu-O superconductor with silver or Y2BaCuO3 or 211 dispersions
[AD-A285609] p 1502 N95-21194
Theoretical study of the noble metals on semiconductor surfaces and Ti-base shape memory alloys
[DE95-001654] p 1257 N95-21398
High performance YBCO films
[AD-A279560] p 1276 N95-21695
How to improve J(c(T)) in Ag/(BiPb)2Sr2Ca2Cu3O10 tapes
[PB95-110326] p 1575 N95-21949
The enhancement of metallic silver monomer evaporation by the adhesion of polar molecules to silver nanocluster ions
[AD-A284936] p 1281 N95-22470

SILVER ALLOYS
First principles simulation of materials properties
[DE94-016781] p 1566 N95-20405

SIMD (COMPUTERS)
Design of a massively parallel computer using bit serial processing elements
[NASA-CR-197365] p 1479 N95-22406

SIMULATED ANNEALING
Rapid determination of geoacoustic properties of the sea floor by simulated annealing
[AD-A286297] p 1436 N95-22028

SIMULATION
Truly distribution-independent algorithms for the N-body problem
[DE94-014238] p 1458 N95-20136
Monsoons: AMIP simulations of the 1987 and 1988 drought and flood regimes
[DE94-014789] p 1428 N95-20140
Characterization and simulation of an acoustic source moving through an oceanic waveguide
[AD-A285688] p 1503 N95-20272
A comparison of kinetic and multifluid simulations of laser-produced colliding plasmas
[DE94-016447] p 1551 N95-20315
EPICS simulation tools for control system development
[DE94-018082] p 1462 N95-20699
A tabular interface for automated verification of event-based dialogs
[AD-A286065] p 1463 N95-20847
Modelling and simulation of HF/VHF MMPPs
p 1293 N95-20925
Simulation of the impact of atmospheric turbulences on millimeter-wave communications systems
p 1295 N95-20939
Large eddy simulation of turbulent flow over a cavity
p 1347 N95-21069
Large-eddy simulation of separated flow in a ribbed duct p 1347 N95-21070
Analysis of subgrid models using direct and large-eddy simulations of isotropic turbulence p 1348 N95-21071
A cheap DNS tool for turbulence models testing
p 1348 N95-21072
Direct simulation of turbulent flow in a square duct: Reynolds-stress budgets p 1348 N95-21073
Numerical simulation of supersonic boundary layer transition p 1348 N95-21074
Large eddy simulation of channel flow using a vorticity transport subgrid model p 1348 N95-21076
Direct simulation of a self-similar plane wake
p 1350 N95-21084
Navier-Stokes simulations of the effects of suction holes on a flat plate boundary layer p 1352 N95-21094
Project Whitefeather
[DE94-016575] p 1415 N95-21184
Comparison of calculated with measured dynamic aperture
[DE95-002863] p 1534 N95-21246
Conference proceedings. Defense Modeling and Simulation Office Information/Data Base (I/DB) Task Group Meetings, and notes from the previous two I/DB meetings
[AD-A279097] p 1591 N95-22069
Interpretation of HRTEM images by image simulation: An introduction to theory and practice
[DE95-003422] p 1591 N95-22235
Fast parallel tree codes for gravitational and fluid dynamical N-body problems
[AD-A286480] p 1358 N95-22290
Maximum weighted matching for high index differential algebraic equations
[PB95-135075] p 1496 N95-22359
Multi signal-domain modeling of solid-state transducers: A theoretical framework based on irreversible thermodynamics mixed finite elements and multigrid
[PB95-134995] p 1336 N95-22382
Effect of cell size on elliptically polarized radar clutter statistics
[AD-A285789] p 1311 N95-22401
Large-eddy simulation of a plane wake
p 1360 N95-22446

SIMULATORS
A tabular interface for automated verification of event-based dialogs
[AD-A286065] p 1463 N95-20847
A wideband propagation simulator for high speed mobile radio communications p 1295 N95-20934
Color control in a multichannel simulator display: The display for advanced research and training
[AD-A279717] p 1216 N95-20992
An evaluation of Automatic Terminal Information Service (ATIS) flight deck display presentation options
[AD-A280100] p 1204 N95-21020
Real-time dynamic simulator for the Topaz II reactor power system
[DE95-001604] p 1535 N95-21278
Effect of lags on human performance with head-coupled simulators
[AD-A279577] p 1453 N95-21700

SINE WAVES
Hybrid high power amplifier
[AD-D016534] p 1326 N95-20730

SINGLE CRYSTALS
High precision trace neutron transmutation doping of detector-grade high resistance zone-refined silicon mono-crystal
[DE94-631463] p 1563 N95-19978
Carrier doping and interlayer coupling in HTSC single crystals
[DE94-018637] p 1564 N95-20127
Rare earth garnet selective emitter
p 1322 N95-20536
Growth, characterization and device development in monocrystalline diamond films
[AD-A285991] p 1568 N95-20614
Structure of dibis(diethyldithiocarbamato) zinc (2) Mu-bis(diethylphosphino)ethane toluene(2)
[AD-A279792] p 1224 N95-20660
Ferroic materials: Design, preparation and characteristics. Ceramic transactions, volume 43
[AD-A285937] p 1270 N95-20664
Gas-phase generation of zinc sulfide particles using a single-source precursor
[AD-A279700] p 1239 N95-20712
Synthesis and characterization of (Zn(SEt)Et)10, formed via insertion of sulfur into Zn-C bonds: A new class of Wurtzite-like cluster framework
[AD-A279701] p 1569 N95-20714
Magnetic excitations in modulated PrNi2Si2
[DE95-001077] p 1254 N95-20822
Dependence of critical current density on microstructure and processing of high-T(c) superconductors
[DE95-000685] p 1571 N95-21167
Diffraction applications using the energy dispersive beamline, X6A, at NSLS
[DE94-019287] p 1572 N95-21408
Raman spectra of MOCVD-grown ferroelectric PbTiO3 thin films
[DE94-018964] p 1244 N95-21549
High temperature superconducting films and multilayers for electronics
[AD-A279545] p 1331 N95-21693
Anisotropic transport properties of BSCCO single crystals and Ag-clad tapes in high magnetic fields
[DE95-000938] p 1575 N95-21936
Growing and releasing diamonds
[AD-D016489] p 1577 N95-22103
AC magnetic response of YBa2CuO7 with Y2BaCuO5 inclusions and of single-crystal YBa2Cu3O7: A comparative study
[PB94-207917] p 1577 N95-22166
Gravitational effects on the development of weld-pool and solidification microstructures
[DE94-017772] p 1285 N95-22261
Introduction to the structures determination methods using X-ray diffraction in monocrystals: Application to some lanthanides and transition metals complexes with organic ligands
[DE94-629002] p 1579 N95-22380
Synthesis and characterization of single-source molecular precursors to binary metal sulphides: Bis(diethyldithiocarbamato) M(2)trialkylphosphine (M = Zn and Cd) adducts
[AD-A279746] p 1248 N95-22385

SINGLE EVENT UPSETS
SEU and SEL response of the Westinghouse 64K E-2PROM, analog devices AD7876 12-bit ADC, and the Intel 82527 Serial Communications Controller
[DE95-003349] p 1334 N95-22086
Radiation characterization report for the GPS Receiver microcontroller chip
[DE94-019169] p 1335 N95-22165

SINGULARITY (MATHEMATICS)
The method of auxiliary mapping for the finite element solutions of elasticity problems containing singularities
[AD-A285689] p 1489 N95-20274
Energy gap structure of layered superconductors
[DE94-017885] p 1566 N95-20372
Growth series for the commutator subgroup
[PB95-111092] p 1490 N95-20452

SINKS
Surface ices in the outer solar system
p 1423 N95-21815

SINTERING
Comparison of the dynamic fatigue behavior of two monolithic SiC and an Al2O3/SiC composite
[DE94-017751] p 1225 N95-20022
Enhancement of creep resistance of a sintered S3N4 ceramic by microwave annealing
[DE94-017698] p 1265 N95-20220
Microwave sintering of ZrO2-12 mol% CeO2
[DE94-018709] p 1265 N95-20226
Moessbauer study of the sintered Mn(0.70)Zn(0.23)Fe(2.07)O4
[DE94-631462] p 1255 N95-20909
Comparison of properties of sintered and sintered reaction-bonded silicon nitride fabricated by microwave and conventional heating
[DE95-001426] p 1275 N95-21501
B4C-SiC reaction-sintered coatings on graphite plasma facing components
[DE94-019105] p 1230 N95-21553
Collocated tunable wavenumber sensor/actuators for smart structures
[AD-A279066] p 1258 N95-21575
Tailoring suspension flow for the gelcasting of oxide and nonoxide ceramics
[DE95-001351] p 1277 N95-21861
The thermal conductivity of silicon nitride with molybdenum disilicide additions
[DE94-017757] p 1247 N95-22260
Overview of rapid prototyping technologies in manufacturing
[PB95-127122] p 1472 N95-22372
Structural performance of cylindrical pressure housings of different ceramic compositions under external pressure loading. Part 3: Sintered reaction bonded silicon nitride ceramic
[AD-A285773] p 1388 N95-22411

SISO (CONTROL SYSTEMS)
Modeling and identification of parallel and feedback nonlinear systems
[DE95-001006] p 1481 N95-20812

SITE SELECTION
Acoustic Thermometry of Ocean Climate (ATOC): Selection of California source site
[AD-A279295] p 1436 N95-21987
SIZE (DIMENSIONS)
Scale-up and modeling of forced chemical vapor infiltration
[DE94-017769] p 1340 N95-20781
SIZE DISTRIBUTION
Mean field analysis of orientation selective grain growth driven by interface-energy anisotropy
[DE94-015797] p 1566 N95-20399
SKEWNESS
Fully developed turbulent flows
[AD-A286496] p 1358 N95-22294
SKIN FRICTION
Application of Navier-Stokes code PAB3D with kappa-epsilon turbulence model to attached and separated flows
[NASA-TP-3480] p 1201 N95-21338
Drag reduction strategies p 1361 N95-22453
SKIN TEMPERATURE (BIOLOGY)
Thermal resistance of the cheek in cold air
[AD-A286257] p 1446 N95-22001
SKY SURVEYS (ASTRONOMY)
PRSPLOT6 manual
[PB95-110862] p 1456 N95-19928
Twentysixth YERAC
[PB95-127437] p 1599 N95-21347
MEM application to IRAS CPC images
p 1592 N95-21751
In search of random noise p 1592 N95-21753
SLABS
Analytic models for beam propagation and far-field patterns in slab and bow-tie x ray lasers
[DE94-016607] p 1372 N95-21173
Error analysis of the quadratic nodal expansion method in slab geometry
[DE95-001352] p 1492 N95-21285
Loss of solar He and Ne from IDPS in subducting sediment: Diffusion and the effect of phase changes
p 1419 N95-21792
Seismic evidence for volatiles at large depth in the Earth p 1422 N95-21808
Hydrogen storage in Earth's mantle and core
p 1423 N95-21813
SLAGS
Theoretical-experimental study on the electroslag remelting technology of high quality steels
[DE94-629216] p 1256 N95-21270
SLEEP DEPRIVATION
Behavioral effects of tyrosine during sustained wakefulness
[AD-A279789] p 1441 N95-20307
SLEWING
Input shaping for vibration-damped slewing of a flexible beam using a heavy-lift hydraulic robot
[DE94-015803] p 1379 N95-20695
SLIDING
Overview on superplasticity research on small-grained materials
[DE94-016550] p 1266 N95-20316
The processing and mechanical properties of high temperature/high performance composites. Stress redistribution and notch properties, book 2
[AD-A279737] p 1227 N95-20429
Test fixture for determination of energy absorbing capabilities of composite materials
[NASA-CASE-LAR-15212-1-CU] p 1229 N95-21008
Creep behavior in SiC whisker-reinforced alumina composite
[DE95-001071] p 1231 N95-21776
The role of grain boundary sliding on creep deformation characteristics of discontinuous reinforced composites
[DE95-001671] p 1231 N95-21924
SLIDING FRICTION
Wear resistant composite structure of vitreous carbon containing convoluted fibers
[DE95-002254] p 1228 N95-20787
Friction and wear properties of as-deposited and carbon ion-implanted diamond films
[NASA-TM-106759] p 1274 N95-21252
On the origins and modeling of frictional behavior in interfacially-complex sliding contacts
[DE94-019129] p 1381 N95-21601
SLUDGE
Anaerobic Treatment of Municipal Solid Waste and Sludge for Energy Production and Recycling of Nutrients
[DE95-700217] p 1315 N95-20369
Monitoring bioremediation of Volatile Organic Compounds (VOCs) using Fourier Transform Infrared (FT-IR) spectrometry
[AD-A279631] p 1403 N95-20456
SLURRIES
Tailoring suspension flow for the gelcasting of oxide and nonoxide ceramics
[DE95-001351] p 1277 N95-21861
SMART STRUCTURES
Collocated tunable wavenumber sensor/actuators for smart structures
[AD-A279608] p 1312 N95-19958
Collected papers of the Soar/IFOR project, Spring 1994
[AD-A280063] p 1216 N95-20624
Launch vehicle flight control augmentation using smart materials and advanced composites (CDDF Project 93-05)
[NASA-TP-3535] p 1218 N95-21346
Collocated tunable wavenumber sensor/actuators for smart structures
[AD-A279066] p 1258 N95-21575
Non-linear A/D converters for integrated silicon smart sensors
[PB94-208402] p 1330 N95-21590
Materials for adaptive structural acoustic controls
[AD-A279255] p 1505 N95-21863
SMEAR
Conservative smoothing versus artificial viscosity
[DE95-001108] p 1341 N95-20831
SMELTING
Flow and heat transfer simulation in a flash smelting furnace
[PB95-108197] p 1354 N95-21649
SMOG
Analysis of invalid emission testing in the California smog check program
[PB95-128922] p 1406 N95-21373
Assessment of the atmospheric hazards and risks of new chemicals: Procedures to estimate hazard potentials
[PB95-107488] p 1410 N95-22186
Urban air carcinogens and their effects on health
[DE95-002259] p 1447 N95-22285
SMOKE
Fire smoke ventilation through shafts: Experiments
[PB95-132247] p 1288 N95-21978
SMOKE DETECTORS
Evaluation of state-of-the-art high speed deluge systems presently in service at various US Army ammunition plants
[AD-A279102] p 1287 N95-21598
SMOOTHING
Conservative smoothing versus artificial viscosity
[DE95-001108] p 1341 N95-20831
SOBOLEV SPACE
Squeezing and flow of energy for non linear wave equations
[PB95-111100] p 1489 N95-20172
Right inverse for the divergence operator in spaces of continuous piecewise polynomials
[PB95-127080] p 1496 N95-22369
Locking of the finite element method in thermoelasticity
[PB95-127098] p 1496 N95-22370
SOCIAL FACTORS
Beyond telecommuting: A new paradigm for the effect of telecommunications on travel
[DE95-001224] p 1289 N95-20214
SODAR
An evaluation of 915-MHz radar wind profiler/RASS by tower and sodar measurements
[DE94-018913] p 1364 N95-20320
SODIUM
Ferrocyanide safety project Dynamic X-Ray Diffraction studies of sodium nickel ferrocyanide reactions with equimolar nitrate/nitrite salts
[DE94-017396] p 1236 N95-20268
Tests of dielectric model descriptions of chemical charge displacements in water
[DE94-007530] p 1236 N95-20277
Semi-volatiles at Mercury: Sodium (Na) and potassium (K) p 1424 N95-21818
SODIUM COMPOUNDS
NMR relaxation behavior of the head group of SHBS in lamellar liquid crystals
[AD-A279124] p 1574 N95-21599
SODIUM HYDROXIDES
An investigation of the applicability of the new ion exchange resin, Reillex(TM)-HPQ, in ATW separations
[DE94-016576] p 1274 N95-21234
Catalyzed reduction of nitrate in aqueous solutions
[DE94-017660] p 1247 N95-22049
SODIUM ISOTOPES
Laser trapping of Na-21 atoms
[DE95-002354] p 1513 N95-20629
SODIUM NITRATES
An investigation of the applicability of the new ion exchange resin, Reillex(TM)-HPQ, in ATW separations
[DE94-016576] p 1274 N95-21234
SODIUM SULFATES
The application of electrodialysis to extend the lifetime of commercial electroplating baths
[DE95-000868] p 1246 N95-22012
A transmission electron microscope characterization of sodium sulfate hot corrosion of silicon carbide fiber-reinforced lithium aluminosilicate glass-ceramic matrix composite
[AD-A286164] p 1231 N95-22038
SODIUM SULFUR BATTERIES
Progress in the development of recycling processes for electric vehicle batteries
[DE94-015894] p 1324 N95-20626
SODIUM 22
Determinations of phase transitions in nylon 6-12, nylon-6, polyvinyl chloride and polyethylene terephthalate by positron annihilation spectroscopy
[DE94-629992] p 1239 N95-20736
SOFTWARE ENGINEERING
A construct for describing software development risks
[AD-A284923] p 1457 N95-19999
Software fault tree analysis of concurrent Ada processes
[AD-A284979] p 1457 N95-20042
Evaluation of Borland Turbo Vision
[AD-A279873] p 1459 N95-20184
Comparison of Ward and Mellor's transformation schema with State- and Activitycharts
[PB95-110698] p 1459 N95-20258
Software merge: Semantics of combining changes to programs
[AD-A279657] p 1459 N95-20304
Towards better quality and reliability in the software reuse library environment
[AD-A280013] p 1460 N95-20313
Proceedings of the 4th Systems Reengineering Technology Workshop
[AD-A285357] p 1460 N95-20546
Automation support for concurrent software engineering
[AD-A279691] p 1461 N95-20579
The design of a parallel, dense linear algebra software library: Reduction to Hessenberg, tridiagonal, and bidiagonal form
[DE94-018123] p 1491 N95-20701
A new process for acquiring software architecture
[AD-A286012] p 1462 N95-20721
A software process framework for the Software Engineering Institute's (SEI) capability maturity model
[AD-A286595] p 1462 N95-20765
Software Capability Evaluation (SCE), version 2.0 team members guide
[AD-A286082] p 1462 N95-20809
Rate monotonic analysis for real-time systems: Instructors guide
[AD-A286083] p 1463 N95-20810
Backward error recovery in redundant disk arrays
[AD-A286064] p 1463 N95-20846
Real-time reconfiguration study
[AD-A286060] p 1464 N95-20910
User interface software tools
[AD-A286056] p 1466 N95-21325
Support to the development of high-level graphics software
[PB95-131686] p 1466 N95-21349
Generalised approach to software structure metrics
[PB95-107561] p 1467 N95-21411
Design and implementation of a dual-beam printed antenna for a reception in angular diversity on a Hertzien cluster (or bundle)
[PB95-131603] p 1302 N95-21431
Benefits of CMM-based software process improvement: Executive summary of initial results
[AD-A286444] p 1468 N95-21567
Interim profile: Development and trial of a method to rapidly measure software engineering maturity status
[AD-A279074] p 1468 N95-21627
CAiSE 1994 Doctoral Consortium
[PB95-135182] p 1469 N95-21711
Proceedings of the 5th Workshop on the Next Generation of CASE Tools
[PB95-135208] p 1469 N95-21716
Using the CoRE requirements method with ADARTS. Version 01.00.05
[AD-A279151] p 1470 N95-21972
Artificial Intelligence (AI) and Ada: Integrating AI with mainstream software engineering
[AD-A286093] p 1485 N95-22226
An assessment of European parallel software research
[AD-A286357] p 1479 N95-22257
Incremental rederivation of software artifacts: FY 1993
[AD-A285790] p 1473 N95-22402

SOFTWARE RELIABILITY
Measuring software dependability by robustness benchmarking
[AD-A280053] p 1461 N95-20622
An empirical approach to logical clustering of software failure regions
[AD-A279863] p 1462 N95-20776
Environment for Test and Analysis of Distributed Software (ETADS)
[AD-A285776] p 1463 N95-20877
The iMAPS: General information
[AD-A285421] p 1465 N95-21176
Radio-science performance analysis software
p 1305 N95-21540
A method to determine the kinematics of the lower limbs of a subject pedaling a bicycle using encoders and accelerometers
[NASA-CR-197401] p 1453 N95-21866

SOFTWARE REUSE
Towards better quality and reliability in the software reuse library environment
[AD-A280013] p 1460 N95-20313
Proceedings of the 5th Workshop on the Next Generation of CASE Tools
[PB95-135208] p 1469 N95-21716

SOFTWARE TOOLS
Introduction to the FIRE engine: A C++ toolkit for Finite automata and Regular Expressions
[PB95-110599] p 1456 N95-19891
Facsimile transmission standards
[AD-A279911] p 1290 N95-20308
RALPAR-RAL mesh partitioning program version 1.1
[PB95-129847] p 1475 N95-20435
Improving Multichip Module (MCM) design and reliability using the Intelligent MCM Analyzer
p 1209 N95-20637
Computer graphics tools for visualizing gravity gradient torques on a rigid spacecraft
[AD-A285971] p 1461 N95-20665
TBell: A mathematical tool for analyzing decision tables
[NASA-CR-195027] p 1462 N95-20691
HASSP and HEAVY: Tools for automated heavy atom searches and refinement
[DE94-016071] p 1569 N95-20696
A new process for acquiring software architecture
[AD-A286012] p 1462 N95-20721
The iMAPS: General information
[AD-A285421] p 1465 N95-21176
User interface software tools
[AD-A286056] p 1466 N95-21325
Support to the development of high-level graphics software
[PB95-131686] p 1466 N95-21349
Design and implementation of the FIRE engine: A c++ toolkit for finite automata and regular expressions
[PB95-132924] p 1467 N95-21415
GRONICs-1994. Proceedings of the 1994 Groningen Student Conference on Computer Science
[PB95-135620] p 1468 N95-21455
Monomer mapping: A PC-based software tool facilitating the determination of monomer compositions from mass spectrometric molecular weight data
[PB95-132155] p 1275 N95-21470
An MCM concurrent engineering software tool market study
[AD-A279257] p 1468 N95-21489
Radio-science performance analysis software
p 1305 N95-21540
DBASE 4 basics
[DE94-018323] p 1469 N95-21713
Proceedings of the 5th Workshop on the Next Generation of CASE Tools
[PB95-135208] p 1469 N95-21716
Verification of knowledge-based reasoning modules
[PB95-132692] p 1470 N95-21983
The navigation toolkit
[NASA-CR-197290] p 1205 N95-22161
Quality characteristics and metrics for reusable software
[PB94-203437] p 1473 N95-22390

SOIL EROSION
A multispectral scanner survey of the Idaho National Engineering Laboratory and the Hanford Reservation
[DE95-003922] p 1391 N95-22398

SOIL MAPPING
A multispectral scanner survey of the Idaho National Engineering Laboratory and the Hanford Reservation
[DE95-003922] p 1391 N95-22398

SOIL MECHANICS
Geomaterial models and numerical analysis of softening
[PB95-135380] p 1386 N95-21006

SOIL MOISTURE
The effect of regional-scale soil-moisture deficits on mesoscale atmospheric dynamics that influence fire severity
[DE95-002682] p 1413 N95-20455

SOIL SCIENCE
Spectroscopic studies of hazardous fuel interactions with soils
[AD-A279099] p 1407 N95-21596

SOILS
Monitoring bioremediation of Volatile Organic Compounds (VOCs) using Fourier Transform Infrared (FT-IR) spectrometry
[AD-A279631] p 1403 N95-20456
Geomaterial models and numerical analysis of softening
[PB95-135380] p 1386 N95-21006
Micromachined silicon-based analytical microinstruments for space science and planetary exploration
[DE94-019306] p 1367 N95-21507
Fiber-optic sensors for rapid, inexpensive characterization of soil and ground water contamination
[DE95-002471] p 1545 N95-21510
Descriptions of WHOI sediment cores, volume 8
[AD-A279444] p 1436 N95-22073
Regional scale hydrology with a new land surface processes model
[NASA-TM-110500] p 1390 N95-22111
Micrometeorological methods for measurements of mercury emissions over contaminated soils
[DE94-017679] p 1411 N95-22342
Derivation of maximum permissible concentrations for several volatile compounds for water and soil
[PB95-107454] p 1411 N95-22381

SOL-GEL PROCESSES
Design, synthesis and characterization of novel nonlinear optical materials
[AD-A285617] p 1540 N95-19897
Sol-gel-derived silica films with tailored microstructures for applications requiring organic dyes
[DE94-018886] p 1264 N95-20047
Novel electrochemical materials prepared by sol-gel chemistry
[AD-A286310] p 1226 N95-20092
International collaboration program on innovative chemical processing of superior electronic and optical materials
[AD-A285122] p 1226 N95-20105
Zirconia precipitates and zirconia: GeO2 interphase in mullite matrix-SiC woven fabrics composites prepared through a sol-gel route
[PB95-133427] p 1275 N95-21272
Gradient index lenses from sol-gel layering
[AD-A285649] p 1242 N95-21402

SOLAR ACTIVITY EFFECTS
Variability of total electron content in the high-altitude ionosphere following solar maximum
[AD-A285849] p 1425 N95-21833

SOLAR ARRAYS
Proceedings of the 13th Space Photovoltaic Research and Technology Conference (SPRAT 13)
[NASA-CP-3278] p 1316 N95-20502
Goddard Space Flight Center solar array missions, requirements and directions p 1316 N95-20503
BMDO photovoltaics program overview
p 1316 N95-20504
Europe's space photovoltaics programme
p 1316 N95-20506
Parasitic current collection by solar arrays in LEO
p 1321 N95-20527
Preliminary results from the flight of the Solar Array Module Plasma Interactions Experiment (SAMPIE)
p 1321 N95-20529
Post-flight investigation programmes of recently retrieved solar generators p 1321 N95-20531
High-performance, flexible, deployable array development for space applications
p 1322 N95-20532
Static stability of a three-dimensional space truss
p 1220 N95-20533
An update on the development of a line-focus refractive concentrator array p 1322 N95-20534
An introduction to the Astro Edge solar array
p 1322 N95-20535
The Large Area Pulsed Solar Simulator (LAPSS)
[NASA-CR-197339] p 1397 N95-22336

SOLAR CELLS
Polycrystalline thin film cadmium telluride solar cells fabricated by electrodeposition
[DE94-011848] p 1391 N95-20118
The First NREL Conference on Thermophotovoltaic Generation of Electricity: Proceedings
[DE94-011831] p 1391 N95-20332
Polycrystalline CuInSe2 and CdTe solar cells
[DE94-011875] p 1392 N95-20333
Novel thin-film CuInSe2 fabrication
[DE94-011874] p 1268 N95-20472
Proceedings of the 13th Space Photovoltaic Research and Technology Conference (SPRAT 13)
[NASA-CP-3278] p 1316 N95-20502
Goddard Space Flight Center solar array missions, requirements and directions p 1316 N95-20503
BMDO photovoltaics program overview
p 1316 N95-20504
Europe's space photovoltaics programme
p 1316 N95-20506
High-efficiency, deep-junction, epitaxial InP solar cells on (100) and (111)B InP substrates
p 1316 N95-20507
Chemical beam epitaxy for high efficiency photovoltaic devices p 1316 N95-20508
Status of diffused junction p+n InP solar cells for space applications p 1317 N95-20509
High quality InP-on-Si for solar cell applications
p 1317 N95-20510
P/N InP solar cells on Ge wafers
p 1317 N95-20511
Status of flexible CIS research at ISET
p 1317 N95-20512
Development of a lightweight, light-trapped, thin GaAs solar cell for spacecraft applications
p 1318 N95-20513
Advances in polycrystalline thin-film photovoltaics for space applications p 1318 N95-20514
Amorphous silicon thin films: The ultimate lightweight space solar cell p 1318 N95-20515
Modeling of high efficiency solar cells under laser pulse for power beaming applications p 1318 N95-20516
Calculation of near optimum design of InP/In(0.53)Ga(0.47)As monolithic tandem solar cells
p 1318 N95-20517
Performance, defect behavior and carrier enhancement in low energy, proton irradiated p+nn+ InP solar cells
p 1319 N95-20518
Electron-irradiated two-terminal, monolithic InP/Ga0.47In0.53As tandem solar cells and annealing of radiation damage p 1319 N95-20519
Design of high-efficiency, radiation-hard, GaInP/GaAs solar cells p 1319 N95-20521
Investigation of the stability and 1.0 MeV proton radiation resistance of commercially produced hydrogenated amorphous silicon alloy solar cells p 1320 N95-20522
The use of displacement damage dose to correlate degradation in solar cells exposed to different radiations
p 1320 N95-20523
Annealing of irradiated n+p InP buried homojunctions
p 1320 N95-20524
Qualification test results for blue-red reflecting solar covers p 1320 N95-20525
UV testing of INTELSAT-7, 7A, and 8 solar cells
p 1320 N95-20526
Parasitic current collection by solar arrays in LEO
p 1321 N95-20527
Final results of the advanced photovoltaic experiment
p 1321 N95-20528
Preliminary results from the flight of the Solar Array Module Plasma Interactions Experiment (SAMPIE)
p 1321 N95-20529
Photovoltaic electric power applied to Unmanned Aerial Vehicles (UAV) p 1321 N95-20530
Post-flight investigation programmes of recently retrieved solar generators p 1321 N95-20531
Review of solar cell temperature coefficients for space
p 1323 N95-20541
Effects of plasma hydrogenation on trapping properties of dislocations in heteroepitaxial InP/GaAs
p 1323 N95-20542
Si concentrator solar cell development
[DE95-002314] p 1393 N95-20870
Development of concentrator solar cells
[DE95-002316] p 1394 N95-20871
Processing and modeling issues for thin-film solar cell devices
[DE94-011895] p 1394 N95-21294
Non-H2Se, ultra-thin CuInSe2 devices
[DE94-011894] p 1395 N95-21844
Transient photoluminescence measurements on GaAs and AlGaAs double heterostructures
[AD-A279408] p 1575 N95-21916
The role of point defects and defect complexes in silicon device processing
[DE94-011876] p 1279 N95-22091
Performance of Ga(0.47)In(0.53)As cells over a range of proton energies
[NASA-TM-106819] p 1334 N95-22112
Influence of wavelength on transient short-circuit current in polycrystalline silicon solar cells
[DE94-629082] p 1397 N95-22183
The Large Area Pulsed Solar Simulator (LAPSS)
[NASA-CR-197339] p 1397 N95-22336

Advanced energy systems and technologies research programme
[DE95-717486] p 1397 N95-22337

SOLAR COLLECTORS

An update on the development of a line-focus refractive concentrator array p 1322 N95-20534

An introduction to the Astro Edge solar array
p 1322 N95-20535

An overview: Component development for solar thermal systems
[DE95-001623] p 1393 N95-20862

Accelerated life testing of solar energy materials: Case study of some selective solar absorber coating materials for DHW systems. A report of task 10 solar materials research and development
[PB95-132411] p 1397 N95-22362

Solar collector manufacturing activity 1993
[DE94-017340] p 1398 N95-22429

SOLAR CORONA

Coronagraphic observations and analyses of the ultraviolet solar corona
[NASA-CR-197370] p 1602 N95-20558

SOLAR DYNAMIC POWER SYSTEMS

Effect of microgravity on material undergoing melting and freezing: The TES Experiment
[NASA-TM-106845] p 1338 N95-19952

Mars power system concept definition study. Volume 1: Study results
[NASA-CR-195420-VOL-1] p 1396 N95-21952

Mars power system concept definition study. Volume 2: Appendices
[NASA-CR-195420-VOL-2] p 1396 N95-21953

SOLAR ELECTRIC PROPULSION

CALIOPE and TAISIR airborne experiment platform
[DE94-018328] p 1310 N95-22299

SOLAR ELECTRONS

Coronal Mass Ejections in the solar wind at high solar latitudes: An overview
[DE95-000844] p 1603 N95-21377

SOLAR ENERGY

A photophysical control mechanism for zeaxanthin-associated radiationless energy dissipation in photosynthesis
[DE94-018383] p 1437 N95-19969

Research in the chemical sciences: Summaries of FY 1994
[DE94-015427] p 1223 N95-20264

Recent National Solar Thermal Test Facility activities, in partnership with industry
[DE95-001828] p 1394 N95-21353

Advanced energy systems and technologies research programme
[DE95-717486] p 1397 N95-22337

Indian Academy of Sciences. Volume 105, number 6, December 1993. Proceedings of the 2nd International Conference on Solar Energy Storage Applied Photochemistry
[AD-A286481] p 1605 N95-22394

SOLAR ENERGY ABSORBERS

Accelerated life testing of solar energy materials: Case study of some selective solar absorber coating materials for DHW systems. A report of task 10 solar materials research and development
[PB95-132411] p 1397 N95-22362

SOLAR ENERGY CONVERSION

An update on the development of a line-focus refractive concentrator array p 1322 N95-20534

Translational-energy-resolved studies of photographed carrier-induced reactions on semiconductor surfaces
[DE95-002944] p 1573 N95-21444

Electrostatic basis for molecular recognition in photosynthesis
[DE95-002979] p 1440 N95-22075

SOLAR FLARES

Solar flare MDH
[AD-A279894] p 1602 N95-20593

Solar-Geophysical Data number 600, August 1994. Part 1: (Prompt reports). Data for July, June 1994, and late data
[PB95-104923] p 1603 N95-20713

Solar-Geophysical Data number 600, August 1994. Part 2: (Comprehensive reports). Data for February 1994 and miscellaneous
[PB95-105060] p 1603 N95-20722

Solar-geophysical data number 601, September 1994. Part 2: (Comprehensive reports). Data for March 1994, and miscellaneous
[PB95-136735] p 1603 N95-20829

Solar-geophysical data number 601, September 1994. Part 1: (Prompt reports). Data for August, July 1994, and late data
[PB95-136727] p 1603 N95-20919

Coronal Mass Ejections in the solar wind at high solar latitudes: An overview
[DE95-000844] p 1603 N95-21377

SOLAR FLUX

The solar neutrino problem: Neither astrophysics nor oscillations?
[DE94-012850] p 1603 N95-21316

Boron neutrino flux and the MSW solution of the solar neutrino problem
[DE95-001861] p 1521 N95-21443

The solar flux of thermal neutrinos and antineutrinos of all flavors
[DE95-003204] p 1604 N95-22085

SOLAR GENERATORS

Research on the promotion measures to introduce new energy and energy-saving technologies with a leasing system
[DE95-714801] p 1375 N95-22079

Solar collector manufacturing activity 1993
[DE94-017340] p 1398 N95-22429

SOLAR GRAVITATION

Testing the principle of equivalence by solar neutrinos
[DE94-014972] p 1604 N95-22064

SOLAR HEATING

Accelerated life testing of solar energy materials: Case study of some selective solar absorber coating materials for DHW systems. A report of task 10 solar materials research and development
[PB95-132411] p 1397 N95-22362

SOLAR MAGNETIC FIELD

Neutrino magnetic moments and the solar neutrino problem
[DE94-017579] p 1602 N95-20147

Solar-Geophysical Data number 600, August 1994. Part 1: (Prompt reports). Data for July, June 1994, and late data
[PB95-104923] p 1603 N95-20713

Solar-geophysical data number 601, September 1994. Part 1: (Prompt reports). Data for August, July 1994, and late data
[PB95-136727] p 1603 N95-20919

Coronal Mass Ejections in the solar wind at high solar latitudes: An overview
[DE95-000844] p 1603 N95-21377

SOLAR NEUTRINOS

Neutrino magnetic moments and the solar neutrino problem
[DE94-017579] p 1602 N95-20147

The solar neutrino problem: Neither astrophysics nor oscillations?
[DE94-012850] p 1603 N95-21316

Boron neutrino flux and the MSW solution of the solar neutrino problem
[DE95-001861] p 1521 N95-21443

The 9th INS scientific computational programs
[DE94-770780] p 1526 N95-22051

Testing the principle of equivalence by solar neutrinos
[DE94-014972] p 1604 N95-22064

The solar flux of thermal neutrinos and antineutrinos of all flavors
[DE95-003204] p 1604 N95-22085

SOLAR OSCILLATIONS

The solar neutrino problem: Neither astrophysics nor oscillations?
[DE94-012850] p 1603 N95-21316

SOLAR PHYSICS

Solar-Geophysical Data number 600, August 1994. Part 1: (Prompt reports). Data for July, June 1994, and late data
[PB95-104923] p 1603 N95-20713

Solar-Geophysical Data number 600, August 1994. Part 2: (Comprehensive reports). Data for February 1994 and miscellaneous
[PB95-105060] p 1603 N95-20722

Solar-geophysical data number 601, September 1994. Part 2: (Comprehensive reports). Data for March 1994, and miscellaneous
[PB95-136735] p 1603 N95-20829

Solar-geophysical data number 601, September 1994. Part 1: (Prompt reports). Data for August, July 1994, and late data
[PB95-136727] p 1603 N95-20919

Twentysixth YERAC
[PB95-127437] p 1599 N95-21347

The solar flux of thermal neutrinos and antineutrinos of all flavors
[DE95-003204] p 1604 N95-22085

SOLAR PROPULSION

The 1993 JANNAF Propulsion Meeting, volume 2
[AD-A279569] p 1221 N95-20708

SOLAR PROTONS

Coronagraphic observations and analyses of the ultraviolet solar corona
[NASA-CR-197370] p 1602 N95-20558

SOLAR RADIATION

Radiance of the ocean horizon
[AD-A285613] p 1431 N95-19896

Solar Radiation Resource Assessment Project
[DE94-000286] p 1392 N95-20778

The solar neutrino problem: Neither astrophysics nor oscillations?
[DE94-012850] p 1603 N95-21316

Absolute, Extreme-ultraviolet Solar Spectral Irradiance Monitor (AESSIM)
[AD-A279345] p 1603 N95-21929

Solar wind composition
[NASA-TM-197364] p 1604 N95-22384

SOLAR RADIO BURSTS

Solar-Geophysical Data number 600, August 1994. Part 2: (Comprehensive reports). Data for February 1994 and miscellaneous
[PB95-105060] p 1603 N95-20722

Solar-geophysical data number 601, September 1994. Part 2: (Comprehensive reports). Data for March 1994, and miscellaneous
[PB95-136735] p 1603 N95-20829

SOLAR RADIO EMISSION

Solar-Geophysical Data number 600, August 1994. Part 1: (Prompt reports). Data for July, June 1994, and late data
[PB95-104923] p 1603 N95-20713

Solar-geophysical data number 601, September 1994. Part 1: (Prompt reports). Data for August, July 1994, and late data
[PB95-136727] p 1603 N95-20919

SOLAR REFLECTORS

Qualification test results for blue-red reflecting solar covers p 1320 N95-20525

SOLAR SIMULATORS

The Large Area Pulsed Solar Simulator (LAPSS)
[NASA-CR-197339] p 1397 N95-22336

SOLAR SPECTRA

Absolute, Extreme-ultraviolet Solar Spectral Irradiance Monitor (AESSIM)
[AD-A279345] p 1603 N95-21929

SOLAR SYSTEM

Impact degassing of water and noble gases from silicates p 1416 N95-21780

Dynamics of volatile delivery from outer to inner solar system p 1420 N95-21798

Nitrogen isotopic components in the early solar system p 1420 N95-21800

Solar system formation and the distribution of volatile species p 1421 N95-21806

Comets, impacts, and atmospheres
p 1422 N95-21810

Surface ices in the outer solar system
p 1423 N95-21815

SOLAR THERMAL ELECTRIC POWER PLANTS

Bridging worlds/charting new courses
[DE95-003808] p 1397 N95-22335

SOLAR WIND

Coronal Mass Ejections in the solar wind at high solar latitudes: An overview
[DE95-000844] p 1603 N95-21377

Mars atmospheric loss and isotopic fractionation by pick-up-ion sputtering and photochemical escape
p 1420 N95-21796

Potential flow downstream of the heliospheric terminal shock: A non-spherical shock
[NASA-TM-110493] p 1426 N95-21874

Solar wind composition
[NASA-TM-197364] p 1604 N95-22384

SOLAR X-RAYS

Solar-Geophysical Data number 600, August 1994. Part 2: (Comprehensive reports). Data for February 1994 and miscellaneous
[PB95-105060] p 1603 N95-20722

Solar-geophysical data number 601, September 1994. Part 2: (Comprehensive reports). Data for March 1994, and miscellaneous
[PB95-136735] p 1603 N95-20829

Solar-geophysical data number 601, September 1994. Part 1: (Prompt reports). Data for August, July 1994, and late data
[PB95-136727] p 1603 N95-20919

SOLDERED JOINTS

Survivability of soldered leadless chip carriers after temperature cycling
[DE95-001497] p 1329 N95-21301

Strength testing of Ti-vapor-coated silicon nitride braze joints
[DE94-017858] p 1280 N95-22266

SOLDERING

Survivability of soldered leadless chip carriers after temperature cycling
[DE95-001497] p 1329 N95-21301

SOLDERS

The reliability of laser reflowed Sn-Ag solder joints
[AD-A279787] p 1315 N95-20443

Survivability of soldered leadless chip carriers after temperature cycling
[DE95-001497] p 1329 N95-21301

SOLID CRYOGENS
Two-center, two electron excitations identified in NEXAFS for solid Ne
[AD-A285373] p 1568 N95-20553
Hydrogen and related materials at high density: Physics, chemistry and planetary implications
p 1418 N95-21791
SOLID ELECTROLYTES
Inert gas purification and measuring oxygen partial pressure in gas mixtures with EMF method based on solid electrolyte cell
[PB95-127767] p 1240 N95-21110
The development of a new plasticizer for poly(ethylene oxide) based polymer electrolyte and the investigation of their ion-pair dissociation effect
[DE94-016821] p 1276 N95-21644
SOLID LUBRICANTS
Evaluation of PS 212 coatings under boundary lubrication conditions with an Ester-based oil to 300 C
[NASA-TM-106763] p 1223 N95-19901
SOLID MECHANICS
Parallel solid mechanics codes at Sandia National Laboratories
[DE94-015770] p 1474 N95-20152
Transactions of the Eleventh Army Conference on Applied Mathematics and Computing
[AD-A279884] p 1497 N95-22389
SOLID PHASES
Quantitative and qualitative analysis of some inorganic compounds by Raman spectroscopy
[DE94-009757] p 1237 N95-20470
Thermal decomposition reactions of HMX and RDX and their importance in predicting cookoff hazards
[DE95-002486] p 1283 N95-21513
SOLID PROPELLANT ROCKET ENGINES
Radiation from advanced solid rocket motor plumes
[NASA-CR-196554] p 1221 N95-20124
Computer model predictions of the local effects of large, solid-fuel rocket motors on stratospheric ozone
[AD-A285632] p 1404 N95-21150
Nonlinear acoustic processes in a solid rocket engine
[AD-A285606] p 1222 N95-21193
SOLID PROPELLANTS
Integral rocket ramjets
[AD-A285135] p 1222 N95-20906
SOLID ROCKET PROPELLANTS
The 1993 JANNAF Propulsion Meeting, volume 2
[AD-A279569] p 1221 N95-20708
SOLID SOLUTIONS
The influence of chemistry and microstructure on the fracture toughness of V-V3Si in-situ composites
[DE94-018997] p 1232 N95-22126
New thermodynamic description of the Cu-Zr system
[PB95-127189] p 1263 N95-22374
SOLID STATE
Israel Physical Society Annual Meeting 1994
[DE94-630140] p 1565 N95-20261
Ferrocyanide safety project Dynamic X-Ray Diffraction studies of sodium nickel ferrocyanide reactions with equimolar nitrate/nitrite salts
[DE94-017396] p 1236 N95-20268
Development of solid state moisture sensors for semiconductor fabrication applications
[DE94-015771] p 1364 N95-20398
Applied physics research for innovation in pulsed power
[AD-A285392] p 1324 N95-20610
Solid state frequency conversion technology for remote sensing
[DE94-019102] p 1389 N95-21433
Solid-state NMR characterization of C- and N-labelled phthalimides: Model compounds for studying polyimides
[AD-A286479] p 1578 N95-22286
Multi signal-domain modeling of solid-state transducers: A theoretical framework based on irreversible thermodynamics mixed finite elements and multigrid
[PB95-134995] p 1336 N95-22382
SOLID STATE DEVICES
Solid-state dynamics and quantum transport in novel semiconductor nanostructures
[AD-A285946] p 1315 N95-20394
Equilibrium and shot noise in mesoscopic systems
[DE95-000855] p 1576 N95-22008
SOLID STATE LASERS
Scaling of solid state lasers for satellite power beaming applications
[DE94-016366] p 1368 N95-19986
Modelocking and waveguide amplifiers using Cr:Forsterite and Cr:YAG
[AD-A285857] p 1369 N95-20378
Solid state frequency conversion technology for remote sensing
[DE94-019102] p 1389 N95-21433
High average power diode pumped solid state lasers for CALIOPE
[DE94-019248] p 1376 N95-22121
3-D TECATE/BREW: Thermal, stress, and birefringent ray-tracing codes for solid-state laser design
[DE95-000330] p 1376 N95-22301
SOLID WASTES
Anaerobic Treatment of Municipal Solid Waste and Sludge for Energy Production and Recycling of Nutrients
[DE95-700217] p 1315 N95-20369
Possible global environmental impacts of solid waste practices
[DE95-000830] p 1406 N95-21487
Investigation on research for degradable plastics
[DE94-796550] p 1277 N95-21714
SOLID-SOLID INTERFACES
Energetics, bonding mechanism and electronic structure of ceramic/ceramic and metal/ceramic interfaces
[DE95-000601] p 1265 N95-20115
Nonlinear optical studies of polymer interfaces
[DE94-018199] p 1274 N95-21263
SOLIDIFICATION
Processing and characterization of Ni-Al-Fe-B shape-memory alloy wires produced by rapid solidification
[DE94-017702] p 1250 N95-20020
Solidification modeling of a spiral casting to determine material fluidity
[DE94-018930] p 1285 N95-20050
X-ray microscope for solidification studies
[NASA-CR-197375] p 1543 N95-20798
Metastable bcc phase formation in the Nb-Cr-Ti system
[DE94-016212] p 1255 N95-21137
Weld pool phenomena
[DE94-018965] p 1381 N95-21550
Relationship between dendrite coherency and castability of some commercial foundry alloys
[PB95-110243] p 1258 N95-21652
A new metallographic procedure for edge retention of enclosed surfaces
[DE94-017549] p 1261 N95-22048
Gravitational effects on the development of weld-pool and solidification microstructures
[DE94-017772] p 1285 N95-22261
SOLIDIFIED GASES
Two-center, two electron excitations identified in NEXAFS for solid Ne
[AD-A285373] p 1568 N95-20553
Identification of resonant, two-electron, and inter-atomic features in K and L23 NEXAFS spectra
[AD-A285374] p 1513 N95-20554
SOLIDS
Properties of molecular solids and fluids at high pressure and temperature
[DE94-017594] p 1565 N95-20243
Photoemission and ferromagnetism
[DE95-002419] p 1520 N95-21362
The role of microcracking on the crack growth resistance of brittle solids and composites
[DE95-001678] p 1231 N95-21736
The low temperature properties of (Dy(1-x)Er(x))Ni2 alloys
[DE95-001657] p 1260 N95-21923
Variational Monte Carlo study of He-4 in two dimensions
[DE94-629078] p 1576 N95-21998
Surfaces and thin films studied by picosecond ultrasonics
[DE95-001866] p 1506 N95-22071
Fluid dynamics of the freeboard in a fluidized bed reactor
[PB95-134029] p 1357 N95-22160
SOLIDUS
Fusion welding of advanced borated stainless steels
[DE94-019037] p 1378 N95-20053
SOLITARY WAVES
Understanding the mechanisms of length scale competition: The sine-Gordan soliton case
[DE94-016201] p 1500 N95-21136
New improved derivative expansion for field theories with spontaneous symmetry breaking
[DE94-019349] p 1580 N95-21486
On the influence of electromagnetic wave and relativistic electron beam on a plasma
[DE94-628962] p 1561 N95-21848
Electromagnetic waves in an ultrarelativistically hot and strongly magnetized electron-positron plasma
[DE94-628963] p 1307 N95-21849
SOLUBILITY
The preparation of all para-polyphenyls with increased solubility and enhanced third order NLO activity
[AD-A284301] p 1266 N95-20251
Water-soluble polyphosphazenes and their hydrogels
[AD-A279695] p 1269 N95-20580
Assessment of database for interaction of tritium with ITER plasma facing materials
[DE95-002038] p 1558 N95-21290
A visual cell for measuring the solubility of prograde soluble salts in water at high temperatures and pressures
[DE95-002058] p 1245 N95-21732
Rare gases systematics and mantle structure
p 1416 N95-21778
Solubilities of nitrogen and noble gases in basalt melt
p 1422 N95-21807
Is xenon eldest? p 1425 N95-21823
Solubilities of nitrogen and helium in water and blood at 37 C and pressures of up to 11 ATA
[AD-A286269] p 1446 N95-22003
SOLUTIONS
Control of continuous phase PH using visible light to activate PH-dependent fibers and gels in a controlled and reversible manner
[AD-D016532] p 1543 N95-20728
Molecular-based study of solutions in supercritical solvents
[DE94-019326] p 1580 N95-21420
SOLVATION
Tests of dielectric model descriptions of chemical charge displacements in water
[DE94-007530] p 1236 N95-20277
SOLVENTS
Theoretical and experimental study of mixed solvent electrolytes
[DE94-017605] p 1237 N95-20384
Thermodynamic and NMR studies of solvent effect on enantiomeric recognition for a chiral organiz ammonium cation by chiral diketopyridino-18-Crown-6 type ligands at 25.0 C
[AD-A279893] p 1223 N95-20592
Molecular-based study of solutions in supercritical solvents
[DE94-019326] p 1580 N95-21420
SONAR
Transducers with improved signal transfer field of the invention
[AD-D016228] p 1328 N95-21118
Unknown-terrains navigation of a mobile robot using an array of sonars
[DE94-017902] p 1482 N95-21385
SOOT
Aromatics oxidation and soot formation in flames
[DE95-001803] p 1241 N95-21280
SORBENTS
Laboratory evaluation of a reactive baffle approach to NOx control
[AD-A283802] p 1400 N95-19921
SORPTION
An investigation of the applicability of the new ion exchange resin, Reillex(TM)-HPQ, in ATW separations
[DE94-016576] p 1274 N95-21234
Siloxanes with strong hydrogen bond donating functionalities
[AD-D016499] p 1279 N95-22057
SOS (SEMICONDUCTORS)
Microdynamic devices fabricated on silicon-on-sapphire substrates
[AD-D016531] p 1325 N95-20727
Method of forming a high voltage silicon-on-sapphire photocell array
[AD-D016479] p 1396 N95-21899
SOUND DETECTING AND RANGING
Josephson acoustic radiation in superfluid helium
[AD-A279809] p 1503 N95-20098
Vacuum holding fixture and method for fabricating piezoelectric polymer acoustic sensors
[NASA-CASE-LAR-14240-1] p 1268 N95-20410
Mandrel based embedded planar fiber-optic interferometric acoustic sensor
[AD-D016229] p 1504 N95-21119
Evaluation of simple spherical spreading model for near vertical acoustical propagation
[AD-A286284] p 1505 N95-22042
SOUND FIELDS
Method and system of mapping acoustic near field
[AD-D016574] p 1504 N95-20296
Fiber optic pressure sensing array
[AD-D016245] p 1506 N95-22088
SOUND GENERATORS
The Combustive Sound Source
[ARL-TR-94-9] p 1503 N95-19911
Characterization and simulation of an acoustic source moving through an oceanic waveguide
[AD-A285688] p 1503 N95-20272
Underwater Acoustic Generator Phase 2: Sea trial, March 1992
[MRL-TN-640] p 1434 N95-21657
Acoustic Thermometry of Ocean Climate (ATOC): Selection of California source site
[AD-A279295] p 1436 N95-21987
Annual research briefs, 1994
[NASA-CR-197352] p 1358 N95-22437

SOUND INTENSITY
Measurement of sound intensity and sound power
[AD-A279246] p 1505 N95-21984

SOUND PRESSURE
Measurement of sound intensity and sound power
[AD-A279246] p 1505 N95-21984
Temporary threshold shifts produced by high intensity freefield impulse noise in humans wearing hearing protection
[AD-A286289] p 1454 N95-22045
Fiber optic pressure sensing array
[AD-D016245] p 1506 N95-22088

SOUND PROPAGATION
Low frequency sound radiation from finite stiffened plates
[AD-A279395] p 1505 N95-21930
Surfaces and thin films studied by picosecond ultrasonics
[DE95-001866] p 1506 N95-22071

SOUND TRANSMISSION
Oceanographic analysis of the acoustic mid-ocean dynamics experiment
[AD-A285907] p 1432 N95-19988
Evaluation of simple spherical spreading model for near vertical acoustical propagation
[AD-A286284] p 1505 N95-22042

SOUND WAVES
Development of solid state moisture sensors for semiconductor fabrication applications
[DE94-015771] p 1364 N95-20398
Applications of wavelets to radar, imaging and related problems
[AD-A279909] p 1290 N95-20545
Temperature effects on acoustic interactions between altitude test facilities and jet engine plumes
[NASA-CR-197638] p 1504 N95-21170
Nonlinear acoustic processes in a solid rocket engine
[AD-A285606] p 1222 N95-21193
Scattering of an FM signal from an array of spheres
[AD-A285587] p 1505 N95-21213
Acoustic receptivity due to weak surface inhomogeneities in adverse pressure gradient boundary layers
[NASA-TM-4577] p 1353 N95-21258
Effect of atmospheric pressure on measured aircraft noise levels
[PB95-130423] p 1207 N95-21425
Acoustoelectric effect in semiconductor superlattice
[DE94-628994] p 1575 N95-21859
Low frequency sound radiation from finite stiffened plates
[AD-A279395] p 1505 N95-21930
Surfaces and thin films studied by picosecond ultrasonics
[DE95-001866] p 1506 N95-22071
Localization phenomenon in some random classical systems
[AD-A286514] p 1309 N95-22215
Determination of the complex elastic moduli of materials using a free-free bar technique
[AD-A279861] p 1281 N95-22387

SOURCE PROGRAMS
SCOPE 1.5: A Source-Code Optimization PackagEfor REDUCE 3.5: User's manual
[PB95-107579] p 1472 N95-22159

SPACE BASED RADAR
Classical analysis methods for designing and developing downlooking radars
[AD-A285760] p 1302 N95-21405

SPACE CHARGE
Effect of space charge tune shift on transverse instabilities
[DE94-016790] p 1531 N95-20282
Enhanced ionic conduction at the film/substrate interface in LiI thin films grown on sapphire(0001)
[DE94-017884] p 1565 N95-20371
Emittance growth due to negative-mass instability above transition
[DE95-002527] p 1534 N95-20900
Behaviour of space-charge dominated ion beams in storage rings
[DE94-015845] p 1517 N95-21140

SPACE COMMERCIALIZATION
Space technology: Force multiplier or false sense of security
[AD-A279726] p 1217 N95-20995

SPACE COMMUNICATION
Seamless data-range change using punctured convolutional codes for time-varying signal-to-noise ratios p 1304 N95-21534
Turbo codes for deep-space communications
p 1304 N95-21535
CDMA with interference cancellation for multiprobe missions p 1304 N95-21536

SPACE ERECTABLE STRUCTURES
High-performance, flexible, deployable array development for space applications
p 1322 N95-20532
An introduction to the Astro Edge solar array
p 1322 N95-20535

SPACE EXPLORATION
Estimating the costs of human space exploration
p 1584 N95-20744
NASA's attack on costs p 1585 N95-20755

SPACE FLIGHT
The problem of space travel: The rocket motor
[NASA-SP-4026] p 1217 N95-21894

SPACE MISSIONS
A Clementine collection: Moonglow
[AD-A286360] p 1217 N95-20228

SPACE NAVIGATION
Orbit determination of highly elliptical Earth orbiters using improved Doppler data-processing modes
p 1218 N95-21533

SPACE PERCEPTION
Space constancy on video display terminals
[AD-A280015] p 1449 N95-20314

SPACE PLASMAS
Propulsion research on the variable tandem mirror plasma rocket
[NASA-CR-196310] p 1221 N95-20059
Preliminary results from the flight of the Solar Array Module Plasma Interactions Experiment (SAMPIE)
p 1321 N95-20529
Source mechanisms and radio effects of ionospheric plasma disturbances
[AD-A286529] p 1555 N95-21013
Electrostatic noise in the plasma environment around the shuttle
[NASA-TM-106856] p 1415 N95-21188
Magnetospheric Plasma Analyzer (MPA): Plasma observations from geosynchronous orbit
[DE95-002739] p 1427 N95-22477

SPACE POWER REACTORS
Power systems for future missions. Appendices A-L
[NASA-CR-195320-APP-A-L] p 1395 N95-21530
Issues in the flight qualification of a space power reactor
[DE95-001606] p 1223 N95-21840
Mars power system concept definition study. Volume 1: Study results
[NASA-CR-195420-VOL-1] p 1396 N95-21952
Mars power system concept definition study. Volume 2: Appendices
[NASA-CR-195420-VOL-2] p 1396 N95-21953

SPACE PROGRAMS
NASA's attack on costs p 1585 N95-20755
Spinoff, 1994
[NASA-NP-214] p 1594 N95-21893

SPACE SHUTTLE MAIN ENGINE
SSME HPOTP post-test diagnostic system enhancement project
[NASA-CR-4643] p 1222 N95-21458

SPACE SHUTTLE MISSIONS
STS 63: Post flight presentation
[NASA-TM-110514] p 1219 N95-21558
Tethered satellite: Forces and motion
[NASA-TM-110518] p 1220 N95-21858
STS Flight 64 mission highlights
[NASA-TM-110515] p 1219 N95-22295

SPACE SHUTTLE PAYLOADS
STS 63: Post flight presentation
[NASA-TM-110514] p 1219 N95-21558
STS Flight 64 mission highlights
[NASA-TM-110515] p 1219 N95-22295

SPACE SHUTTLES
STS 63 flight day 4 highlights/MIR-Shuttle rendezvous
[NASA-TM-110512] p 1219 N95-21113
STS 63: Post flight presentation
[NASA-TM-110514] p 1219 N95-21558

SPACE STATION POWER SUPPLIES
Power systems for future missions. Appendices A-L
[NASA-CR-195320-APP-A-L] p 1395 N95-21530
Power systems for future missions
[NASA-CR-195320] p 1222 N95-21531
Mars power system concept definition study. Volume 1: Study results
[NASA-CR-195420-VOL-1] p 1396 N95-21952
Mars power system concept definition study. Volume 2: Appendices
[NASA-CR-195420-VOL-2] p 1396 N95-21953

SPACE STATION STRUCTURES
Static stability of a three-dimensional space truss
p 1220 N95-20533
Space power facility readiness for Space Station power system testing
[NASA-TM-106829] p 1218 N95-21384

SPACE TRANSPORTATION SYSTEM
STS 63: Post flight presentation
[NASA-TM-110514] p 1219 N95-21558
STS Flight 64 mission highlights
[NASA-TM-110515] p 1219 N95-22295

SPACE TRANSPORTATION SYSTEM FLIGHTS
STS 63 flight day 4 highlights/MIR-Shuttle rendezvous
[NASA-TM-110512] p 1219 N95-21113

SPACE VEHICLE CHECKOUT PROGRAM
Military standard: Test requirements for launch, upper-stage, and space vehicles
[AD-A286627] p 1218 N95-20770

SPACEBORNE ASTRONOMY
Solar-geophysical data number 601, September 1994. Part 2: (Comprehensive reports). Data for March 1994, and miscellaneous
[PB95-136735] p 1603 N95-20829
Solar-geophysical data number 601, September 1994. Part 1: (Prompt reports). Data for August, July 1994, and late data
[PB95-136727] p 1603 N95-20919
Science with High Spatial Resolution Far-Infrared Data
[NASA-CR-197353] p 1595 N95-21749
MEM application to IRAS CPC images
p 1592 N95-21751
An assessment of image reconstruction from balloon-borne and the IRAS data p 1592 N95-21752
In search of random noise p 1592 N95-21753
Far-infrared sources and diffuse emission in M31
p 1593 N95-21761

SPACEBORNE EXPERIMENTS
PRSPLOT6 manual
[PB95-110862] p 1456 N95-19928
Effect of microgravity on material undergoing melting and freezing: The TES Experiment
[NASA-TM-106845] p 1338 N95-19952
Challenger's night flight
[NASA-TM-110503] p 1217 N95-19995
An overview of the Evaluation of Oxygen Interactions with Materials 3 Experiment: Space Shuttle Mission 46; July-August, 1992
[NASA-TM-110129] p 1412 N95-20278
Final results of the advanced photovoltaic experiment
p 1321 N95-20528
Preliminary results from the flight of the Solar Array Module Plasma Interactions Experiment (SAMPIE)
p 1321 N95-20529
Microgravity: Teacher's guide with activities for physical science
[NASA-EG-103] p 1285 N95-21322
Micromachined silicon-based analytical microinstruments for space science and planetary exploration
[DE94-019306] p 1367 N95-21507
STS 63: Post flight presentation
[NASA-TM-110514] p 1219 N95-21558
Tethered satellite: Forces and motion
[NASA-TM-110518] p 1220 N95-21858
STS Flight 64 mission highlights
[NASA-TM-110515] p 1219 N95-22295
The Double Eagle Space Experiment (DESE) beamline design
[DE94-018319] p 1601 N95-22419

SPACEBORNE TELESCOPES
Low noise 22 GHz receiver for the radioastron satellite, part 2: Space qualification tests
[PB95-127197] p 1598 N95-22376

SPACECRAFT
Computer graphics tools for visualizing gravity gradient torques on a rigid spacecraft
[AD-A285971] p 1461 N95-20665
Issues in the flight qualification of a space power reactor
[DE95-001606] p 1223 N95-21840

SPACECRAFT ANTENNAS
Analysis of a microstrip reflectarray antenna for microspacecraft applications p 1305 N95-21541
The efficiency calibration of the DSS-24 34-meter beam-waveguide antenna p 1305 N95-21542

SPACECRAFT COMMUNICATION
Innovative use of DSP technology in space: FORTE event classifier
[DE94-016086] p 1291 N95-20697
STS 63 flight day 4 highlights/MIR-Shuttle rendezvous
[NASA-TM-110512] p 1219 N95-21113
The Deep Space Network as an instrument for radio science research
[NASA-CR-197341] p 1302 N95-21456
The Telecommunications and Data Acquisition Report
[NASA-CR-197390] p 1303 N95-21532

SPACECRAFT CONSTRUCTION MATERIALS
Preliminary results from the flight of the Solar Array Module Plasma Interactions Experiment (SAMPIE)
p 1321 N95-20529
Launch vehicle flight control augmentation using smart materials and advanced composites (CDDF Project 93-05)
[NASA-TP-3535] p 1218 N95-21346

Recent developments in low cost stable structures for space
[DE95-000857] p 1231 N95-22009

SPACECRAFT CONTROL
Control of complex multibody spacecraft
[AD-A285623] p 1220 N95-21147

SPACECRAFT DESIGN
Launch vehicle flight control augmentation using smart materials and advanced composites (CDDF Project 93-05)
[NASA-TP-3535] p 1218 N95-21346

SPACECRAFT GUIDANCE
The Telecommunications and Data Acquisition Report
[NASA-CR-197390] p 1303 N95-21532
Multiple burn fuel-optimal orbit transfers: Numerical trajectory computation and neighboring optimal feedback guidance
[NASA-CR-197317] p 1222 N95-21616

SPACECRAFT INSTRUMENTS
The Deep Space Network as an instrument for radio science research
[NASA-CR-197341] p 1302 N95-21456

SPACECRAFT LANDING
Challenger's night flight
[NASA-TM-110503] p 1217 N95-19995
STS Flight 64 mission highlights
[NASA-TM-110515] p 1219 N95-22295

SPACECRAFT MOTION
Mathematical modeling of a class of multibody flexible spacecraft structures
[NASA-TM-109166] p 1219 N95-20800

SPACECRAFT POWER SUPPLIES
Proceedings of the 13th Space Photovoltaic Research and Technology Conference (SPRAT 13)
[NASA-CP-3278] p 1316 N95-20502
Goddard Space Flight Center solar array missions, requirements and directions p 1316 N95-20503
BMDO photovoltaics program overview
p 1316 N95-20504
Development of a lightweight, light-trapped, thin GaAs solar cell for spacecraft applications
p 1318 N95-20513
Final results of the advanced photovoltaic experiment
p 1321 N95-20528
Preliminary results from the flight of the Solar Array Module Plasma Interactions Experiment (SAMPIE)
p 1321 N95-20529
High-performance, flexible, deployable array development for space applications
p 1322 N95-20532
An update on the development of a line-focus refractive concentrator array p 1322 N95-20534
An introduction to the Astro Edge solar array
p 1322 N95-20535
Review of solar cell temperature coefficients for space
p 1323 N95-20541
Power systems for future missions. Appendices A-L
[NASA-CR-195320-APP-A-L] p 1395 N95-21530
Power systems for future missions
[NASA-CR-195320] p 1222 N95-21531

SPACECRAFT STRUCTURES
Mathematical modeling of a class of multibody flexible spacecraft structures
[NASA-TM-109166] p 1219 N95-20800
Control of complex multibody spacecraft
[AD-A285623] p 1220 N95-21147
Recent developments in low cost stable structures for space
[DE95-000857] p 1231 N95-22009

SPACECRAFT TRACKING
The Telecommunications and Data Acquisition Report
[NASA-CR-197390] p 1303 N95-21532

SPACECRAFT TRAJECTORIES
Multiple burn fuel-optimal orbit transfers: Numerical trajectory computation and neighboring optimal feedback guidance
[NASA-CR-197317] p 1222 N95-21616

SPALLING
Methods of measuring adhesion for thermally grown oxide scales
[DE94-018177] p 1256 N95-21260
Aircraft corrosion study
[AD-A279527] p 1259 N95-21687

SPARK GAPS
Investigations into alternate spark gap switching techniques
[AD-A286225] p 1308 N95-22021

SPARTAN SATELLITES
Coronagraphic observations and analyses of the ultraviolet solar corona
[NASA-CR-197370] p 1602 N95-20558

SPATIAL DEPENDENCIES
Qualification of the dependence in the generalized extreme value choice model
[PB95-110946] p 1497 N95-19936
Acoustoelectric effect in semiconductor superlattice
[DE94-628994] p 1575 N95-21859

SPATIAL DISTRIBUTION
Fitting stochastic partial differential equations to spatial data
[AD-A279870] p 1490 N95-20432
Simulations of bypass transition for spatially evolving disturbances p 1349 N95-21079
Spatial variation of primordial 3-He in crustal fluids along the East-African Rift system (the Ethiopian and the Kenya Rift section) p 1418 N95-21789
Characterization of a texture gradient in tantalum plate
[DE95-002704] p 1262 N95-22289
Coherence properties of high order harmonic radiation
[DE94-016974] p 1377 N95-22312

SPATIAL RESOLUTION
LLNL/Lion Precision LVDT amplifier
[DE95-001504] p 1327 N95-20854
Progress in ultrafast scanning probe microscopy
[DE94-018179] p 1373 N95-21261
Science with High Spatial Resolution Far-Infrared Data
[NASA-CR-197353] p 1595 N95-21749
Pushing the limits of spatial resolution with the Kuiper Airborne observatory p 1593 N95-21754
A high resolution atlas of the galactic plane at 12 microns and 25 microns p 1593 N95-21755
Two-dimensional maps of the infrared-to-radio ratio in spiral galaxies p 1593 N95-21765
Laboratory characterization of Woelter x ray optics
[DE94-016969] p 1562 N95-22191
Measurement of residual stresses on ceramic materials with high spatial resolution
[DE94-017889] p 1280 N95-22270

SPECIFICATIONS
The advanced technology crew station: Development and validation of a workload assessment technique for cockpit function allocation
[AD-A279544] p 1453 N95-21691
Incremental rederivation of software artifacts: FY 1993
[AD-A285790] p 1473 N95-22402

SPECKLE HOLOGRAPHY
Simulation of stellar speckle imaging
[DE94-016606] p 1412 N95-19985

SPECKLE PATTERNS
Simulation of stellar speckle imaging
[DE94-016606] p 1412 N95-19985

SPECTRA
Graphs cospectral with distance-regular graphs
[PB95-111050] p 1488 N95-19943
Time domain spectral hole-burning storage
[AD-A279912] p 1587 N95-20309
Nonparametric estimation of the cyclic cross-spectrum
[AD-A285756] p 1498 N95-21219
Semi-volatiles at Mercury: Sodium (Na) and potassium (K) p 1424 N95-21818
Minimal square spectral factors
[PB95-132726] p 1495 N95-22032
Derivation of a wavenumber filter design for the measurement of turbulent wall pressure fluctuations
[AD-A286421] p 1357 N95-22208

SPECTRAL BANDS
Effects of RF side-bands on spectral reproducibility for infrared synchrotron radiation
[DE95-002450] p 1536 N95-21418
Ultraviolet emission from rocket motor plumes
[DSTO-TR-0002] p 1222 N95-21661

SPECTRAL CORRELATION
Universal spectral correlations at the mobility edge
[DE94-629031] p 1528 N95-22217

SPECTRAL EMISSION
Rare earth garnet selective emitter
p 1322 N95-20536

SPECTRAL ENERGY DISTRIBUTION
Signal to noise improvements with a new Far-IR rapid-scan Michelson Interferometer
[DE95-002416] p 1367 N95-21638

SPECTRAL LINE WIDTH
Coherence properties of high order harmonic radiation
[DE94-016974] p 1377 N95-22312

SPECTRAL METHODS
Direct simulation of tridimensional wake of NACA 0012 profile p 1350 N95-21086
Direct numerical simulation of transition to turbulence from a high-symmetry initial condition
p 1351 N95-21089
Derived gust spectra for the Macchi MB326H
[ARL-TN-3] p 1202 N95-21892

SPECTRAL REFLECTANCE
Diffuse reflectance spectra of energetic material
[DSTO-TR-0065] p 1284 N95-21951

SPECTRAL RESOLUTION
Temporal and spectral investigation of multi-Landau level quantum beats in GaAs
[DE94-018189] p 1569 N95-20678
Neutron molelcular spectroscopy: Future prospects
[PB95-130357] p 1518 N95-21227

SPECTRAL SENSITIVITY
Sensitivity of climate models: Comparison of simulated and observed patterns for past climates
[DE95-002257] p 1406 N95-21379
New concepts for refrigerant leak detection and mixture measurement
[DE94-018967] p 1287 N95-21559

SPECTRAL SIGNATURES
Ultraviolet emission from rocket motor plumes
[DSTO-TR-0002] p 1222 N95-21661

SPECTROGRAPHS
Characterization of nova plasmas using an x-ray spectrometer with temporal and spatial resolution
[DE94-016970] p 1553 N95-20363

SPECTROMETERS
Analysis methods for fast impurity ion dynamics data
[DE95-000589] p 1549 N95-20112
Production of J/(psi) in 800 GeV/c p-Si interactions
[DE94-017982] p 1513 N95-20496
Development, fabrication, and metrology of the electro-optical breadboard model for the reflection grating array of the XMM grating spectrometer
[DE94-016605] p 1543 N95-20612
MARI mini-manual
[PB95-134649] p 1526 N95-21965
Radiation tests on service electronics for future multi TeV detectors
[DE94-632822] p 1335 N95-22184

SPECTRORADIOMETERS
Completion of spectral rotating shadowband radiometers and analysis of ARM spectral short-wave data
[DE95-000602] p 1412 N95-20116

SPECTROSCOPIC ANALYSIS
An application of wavelet transform for decomposition of millimeter-wave spectroscopic signals
[DE94-018366] p 1402 N95-20247
An overview of the Evaluation of Oxygen Interactions with Materials 3 Experiment: Space Shuttle Mission 46; July-August, 1992
[NASA-TM-110129] p 1412 N95-20278
Electrochemical impedance pattern recognition for detection of hidden chemical corrosion on aircraft components
[AD-A284998] p 1253 N95-20481
Surface characterization and contamination analysis
[NASA-CR-197374] p 1238 N95-20557
Ultrafast magnetoexciton dynamics in GaAs
[DE94-018175] p 1514 N95-20732
Time-resolved analytical methods for liquid/solid interfaces
[DE95-002255] p 1240 N95-20780
Spectroscopic, morphological, and electrical characterization of PdGe ohmic contacts to n-GaAs
[DE95-000738] p 1329 N95-21394
Spectroscopic studies of hazardous fuel interactions with soils
[AD-A279099] p 1407 N95-21596
Diffuse reflectance spectra of energetic material
[DSTO-TR-0065] p 1284 N95-21951

SPECTROSCOPY
Spectroscopic studies of glass structure
[DE94-016551] p 1268 N95-20468
Atomic-resolution characterization of interface structure and chemistry in the STEM
[DE94-017753] p 1567 N95-20492
Visible and near-IR spectroscopic studies of UC1(4) in a basic ambient temperature melt: The observation of a possible geometric distorted UC1(6)(exp 2-) species and the evidence for the hydrogen-bond in the melt
[DE94-017764] p 1237 N95-20493
Hg-199 and Cu-(63,65) NMR studies of mercury based high-Tc superconductors
[DE95-001073] p 1570 N95-20820
Study of small carbon and semiconductor clusters using negative ion threshold photodetachment spectroscopy
[DE95-002327] p 1515 N95-20872
Atmosphere influence on in situ ion beam analysis of thin film growth
[DE95-001507] p 1570 N95-20881
Electrochemical impedance spectroscopy of trivalent chromium pre-treated aluminum alloy
[AD-A280093] p 1240 N95-20970
Advanced concepts for gamma ray isotopic analysis and instrumentation
[DE94-016610] p 1517 N95-21174
Linear and nonlinear spectroscopy with the tunable AC scanning tunneling microscope
[AD-A285751] p 1241 N95-21217
Analysis of experimentally shocked minerals by NMR spectroscopy
[DE95-002955] p 1573 N95-21449
Conceptual design analyses for Hanford Site deployable remote spectroscopy systems
[DE95-002078] p 1243 N95-21473

Intense proton beam source for ITER neutral-beam spectroscopy diagnostics
[DE94-018092] p 1560 N95-21668

SPECTRUM ANALYSIS
Sharp determinants
[PB95-111068] p 1488 N95-19944
Higher order crossings
[AD-A279597] p 1504 N95-20300
White-light spectral analysis of lithium niobate waveguides
[DE94-016692] p 1542 N95-20489
Phase dynamics of non-equilibrium distributions of free electron-hole pairs in GaAs quantum wells
[DE94-018190] p 1569 N95-20679
Enhancements in the Livermore spectrum analysis package PIXEF
[DE95-002487] p 1272 N95-20895
Chemical lasers emitting in the visible spectrum: Metastable oxygen reactions and YOSHIDA laser
[PB95-104485] p 1372 N95-20983
Friction and wear properties of as-deposited and carbon ion-implanted diamond films
[NASA-TM-106759] p 1274 N95-21252
Application of neural networks to seismic signal discrimination research findings
[AD-A285848] p 1415 N95-21308
Time-resolved study of sideband generation and transition to chaos on an infrared FEL
[DE95-002336] p 1374 N95-21528
The solar flux of thermal neutrinos and antineutrinos of all flavors
[DE95-003204] p 1604 N95-22085

SPEECH
Usable, real-time, interactive spoken language systems
[AD-A286349] p 1310 N95-22253

SPEECH RECOGNITION
Usable, real-time, interactive spoken language systems
[AD-A286349] p 1310 N95-22253

SPEED CONTROL
Brushless Doubly-Fed Machine system development program, phase 3
[DE94-013095] p 1315 N95-20380

SPHERES
Magnetoelectric properties of reciprocal bianisotropic materials with focus on the polarizability of chiro-omega spheres
[PB95-127650] p 1544 N95-21103
Low-frequency image theory for a current dipole in front of a permeable sphere
[PB95-127676] p 1300 N95-21104
Scattering of an FM signal from an array of spheres
[AD-A285587] p 1505 N95-21213
Novel materials and devices from self-assembled periodic structures
[AD-A286499] p 1232 N95-22211

SPHERICAL COORDINATES
Quantization in curvilinear coordinates
[DE94-770603] p 1514 N95-20737

SPHERICAL PLASMAS
Investigation of spherical tearing mode
[NASA-CR-197284] p 1558 N95-21345

SPHEROMAKS
Heat loss by helicity injection in spheromaks
[DE95-003473] p 1562 N95-22221

SPILLING
Ohmsett test of NOFI Vee-Sweep and NOFI 600S Oilboom
[AD-A279525] p 1408 N95-21685

SPIN DYNAMICS
Theory of spin dynamics in the classical two-dimensional heisenberg magnet
[PB95-133559] p 1502 N95-22138
The doping effect on spin-Peierls instability
[DE94-629046] p 1577 N95-22178

SPIN GLASS
The doping effect on spin-Peierls instability
[DE94-629046] p 1577 N95-22178

SPIN-LATTICE RELAXATION
Hg-199 and Cu-(63,65) NMR studies of mercury based high-Tc superconductors
[DE95-001073] p 1570 N95-20820

SPIN-ORBIT INTERACTIONS
A model for electron nuclear dynamics of a monatomic chain
[AD-A279652] p 1506 N95-19960
Constraints on T-odd and P-even hadronic interactions from nucleon, nuclear, and atomic electric dipole moments
[DE94-012845] p 1526 N95-21920

SPIN-SPIN COUPLING
Rigorous spin-spin correlation function of Ising model on a special kind of Sierpinski Carpets
[DE94-628995] p 1575 N95-21854

SPIRAL GALAXIES
Azimuthally averaged radial S(sub 100 microns)/S(sub 60 microns) dust color temperatures in spiral galaxies
p 1593 N95-21760
Correlation of far-infrared emission and radio continuum emission along the major axis of edge-on spiral galaxies
p 1593 N95-21762
Two-dimensional maps of the infrared-to-radio ratio in spiral galaxies p 1593 N95-21765
The variation of the dust temperature within late-type spiral galaxies p 1593 N95-21766

SPLINE FUNCTIONS
Direct numerical simulation of incompressible axisymmetric flows p 1363 N95-22464

SPLINES
Adaptive capture of expert behavior
[DE94-018285] p 1483 N95-21710
Simulation of structural response using a recurrent radial basis function network
[DE94-017342] p 1486 N95-22409

SPORADIC E LAYER
Modelling and simulation of HF/VHF MMPPs
p 1293 N95-20925
The relative importance of meteor burst and other distance polar cap propagation modes in the low VHF band p 1293 N95-20928

SPRAY NOZZLES
Training simulant for Halon 1211 portable extinguishers
[AD-A285403] p 1286 N95-20611

SPRAYERS
Training simulant for Halon 1211 portable extinguishers
[AD-A285403] p 1286 N95-20611

SPRAYING
A review of water mist technology for fire suppression
[AD-A285738] p 1202 N95-20071

SPREAD SPECTRUM TRANSMISSION
A wideband propagation simulator for high speed mobile radio communications p 1295 N95-20934
Performance of a fast frequency-hopped noncoherent MFSK receiver over Rician fading channels with either partial-band interference or multi-tone interference
[AD-A286168] p 1310 N95-22246

SPUTTERING
Mixed-sputter deposition of Ni-Ti-Cu shape memory films
[DE94-017296] p 1250 N95-19900
Enhancement of corrosion resistance and mechanical properties of light-weight metals through the use of graded nonequilibrium microstructures
[AD-A286320] p 1251 N95-20178
Rate controlled synthesis of composition modulated, metal-oxide thin films
[DE94-016596] p 1267 N95-20317
Sputtering of tin and gallium-tin clusters
[DE94-018389] p 1254 N95-20707
On the sputtering of metals and insulators: A nonlinear evolution problem with nonlinear boundary condition
[DE95-001456] p 1254 N95-20792
Atmosphere influence on in situ ion beam analysis of thin film growth
[DE95-001507] p 1570 N95-20881
Sputter deposition of multilayer thermoelectric films: An approach to the fabrication of two-dimensional quantum wells
[DE95-002396] p 1272 N95-20892
Copper metallization of stainless steels
[DE95-001496] p 1256 N95-21300
Deposition and properties of novel nitride superlattice coatings
[DE95-002945] p 1230 N95-21445
Mars atmospheric loss and isotopic fractionation by pick-up-ion sputtering and photochemical escape
p 1420 N95-21796
High temperature superconducting microwave device
[AD-A286351] p 1336 N95-22254

SQUALLS
Effects of microphysics and radiation on mesoscale processes of a midlatitude squall line
[DE94-014732] p 1429 N95-20381

SQUARE WAVES
Ambient noise and surface wave dissipation in the ocean
[AD-A279650] p 1432 N95-20303
Hybrid high power amplifier
[AD-D016534] p 1326 N95-20730

SQUID (DETECTORS)
Evaluation of superconducting quantum interference devices interfaced with digital signal processing electronics for biomagnetic applications
[DE94-016186] p 1289 N95-20164
DSP control of superconducting quantum interference devices
[DE94-016193] p 1313 N95-20168

STABILITY
Six-dimensional modeling of coherent bunch instabilities and related feedback systems in storage rings with power-series maps for the lattice
[DE94-017965] p 1532 N95-20494
Advances in polycrystalline thin-film photovoltaics for space applications p 1318 N95-20514
Hydrodynamic instabilities in inertial fusion
[DE94-018079] p 1554 N95-20675
Current diffusive ballooning mode in second stability region of tokamaks
[DE94-770690] p 1554 N95-20683
Magnetron power supply at high stability and its application in plasma excitation for the production of ultraviolet radiation
[DE94-629656] p 1326 N95-20733
Conservative smoothing versus artificial viscosity
[DE95-001108] p 1341 N95-20831
Geometric moire method of strain analysis with displacement discontinuities
[DE95-001114] p 1386 N95-20833
Confinement and stability of crystalline beams in storage rings
[DE95-002515] p 1533 N95-20886
Numerical simulation of supersonic boundary layer transition p 1348 N95-21074
Thermodynamic analysis of stable and metastable equilibrium diagrams of the Cu-Cr system
[PB95-127775] p 1255 N95-21111
Calculated heats of formation of some predicted stable C, N, O, F molecules
[AD-A285957] p 1517 N95-21127
Understanding the mechanisms of length scale competition: The sine-Gordan soliton case
[DE94-016201] p 1500 N95-21136
Atmospheric stability and its influence on air quality in small communities in northern Sweden
[PB95-131652] p 1405 N95-21181
Transient behaviour and stability points of the Poiseuille flow of a KBKZ-fluid
[PB95-132064] p 1353 N95-21268
Atom wave interferometer
[AD-A279532] p 1524 N95-21688
Conference on Deep Earth and Planetary Volatiles
[NASA-CR-196944] p 1415 N95-21777
Structure and stability of hydrous minerals at high pressure p 1417 N95-21786
Phase E in a water-saturated peridotite system at 9.3 GPa p 1420 N95-21799
Volatiles in the deep Earth: An experimental study using the laser-heated diamond cell p 1421 N95-21803
Solar system formation and the distribution of volatile species p 1421 N95-21806
Polar volatiles on Mercury and the Moon
p 1422 N95-21811
Storage and recycling of water and carbon dioxide in the earth p 1425 N95-21822
Is xenon eldest? p 1425 N95-21823
Ab initio potential energy surface for H + OCS reactions: Extended basis sets and correlation treatment
[AD-A286420] p 1247 N95-22207
Robust fixed-structure control
[AD-A286515] p 1485 N95-22216
Bunched beam instability with frequency spread
[DE94-018632] p 1539 N95-22357
Maximum weighted matching for high index differential algebraic equations
[PB95-135075] p 1496 N95-22359
Quadratic optimal control of a delay equation II: The unstable case
[PB95-127064] p 1486 N95-22366
Quadratic optimal control of a delay equation I: The stable case
[PB95-127072] p 1486 N95-22367

STABILITY AUGMENTATION
Low-level RF control for the AFEL
[DE94-018295] p 1540 N95-22410

STABILITY TESTS
Stability of pressure and velocity computations for heterogeneous reservoirs
[PB95-110284] p 1354 N95-21656
Design of robust optimal control systems and stability analysis of real structured uncertainties
[AD-A279089] p 1483 N95-21913
Wave journal bearing. Part 1: Analysis
[NASA-CR-195431-PT-1] p 1382 N95-22404
Wave journal bearing. Part 2: Experimental pressure measurements and fractional frequency whirl threshold for wave and plain journal bearings
[NASA-TM-106848-PT-2] p 1382 N95-22405

STABILIZATION
Stabilization and control problems in structural dynamics
[AD-A279996] p 1340 N95-20312
Wall stabilization effects in D3-D high beta discharges
[DE94-017509] p 1554 N95-20446

Temporal evolution of turbulence/chemistry interactions in lifted, turbulent-jet flames
[DE95-002481] p 1243 N95-21512
Semi-global stabilization of linear discrete-time systems subject to input saturation via linear feedback: An ARE-based approach
[PB95-135463] p 1483 N95-21618
Communications and control for electric power systems: Power system stability applications of artificial neural networks
[NASA-CR-197333] p 1484 N95-22171
Robust fixed-structure control
[AD-A286515] p 1485 N95-22216

STABILIZERS (FLUID DYNAMICS)
Pressure measurements on an F/A-18 twin vertical tail in buffeting flow. Volume 4, part 1: Buffet cross spectral densities
[AD-A285593] p 1215 N95-21214
Pressure measurements on an F/A-18 twin vertical tail in buffeting flow. Volume 1: Wind tunnel test summary
[AD-A279126] p 1202 N95-21877

STABLE OSCILLATIONS
Radio-science performance analysis software
p 1305 N95-21540

STACKS
Synthesis and structure of a novel bis-stibole
[AD-A286345] p 1224 N95-22252

STAGNATION POINT
Turbulence modeling for separated flow
p 1359 N95-22443

STAINLESS STEELS
Fusion welding of advanced borated stainless steels
[DE94-019037] p 1378 N95-20053
Fracture toughness properties of welded stainless steels for tritium service
[DE95-000755] p 1251 N95-20079
Post-irradiation deformation characteristics of heavy-ion irradiated 304L SS
[DE94-017462] p 1251 N95-20088
Copper metallization of stainless steels
[DE95-001496] p 1256 N95-21300
Analysis of welds on helium-containing restraint test plates
[DE95-001809] p 1257 N95-21303
Corrosion evaluation of fuel canister crusher rigging
[DE95-002962] p 1257 N95-21452
Finite element modelling of creep crack growth in 316 stainless and 9Cr-1Mo steels
[DE94-018977] p 1258 N95-21560
Corrosion resistance and behavior of construction materials exposed to dilute sulfuric acid at elevated temperatures under static conditions
[DE95-001723] p 1259 N95-21739
Atom probe field ion microscopy of type 308 CRE stainless steel welds
[DE94-019162] p 1261 N95-22127
Welding tritium exposed stainless steel
[DE95-003208] p 1382 N95-22356

STANDARD MODEL (PARTICLE PHYSICS)
Search for top in DO using the electron + jets channel with soft muon tagging
[DE95-001284] p 1509 N95-20217
Top ten models constrained by b (yields) s(gamma)
[DE95-002870] p 1519 N95-21250
A high-rate fixed-target charm experiment
[DE95-001767] p 1521 N95-21378
Proceedings of the School for Young High Energy Physicists
[PB95-108114] p 1537 N95-21647
Search for squarks and gluinos in D0
[DE95-000730] p 1528 N95-22197

STANDARDIZATION
Algebraic semantics of message sequence charts
[PB95-110581] p 1288 N95-19890
Military standard: Test requirements for launch, upper-stage, and space vehicles
[AD-A286627] p 1218 N95-20770
TIM-SCT cable testing protocol
[AD-A286633] p 1207 N95-20772

STANDARDS
Standard data formats for simulation
[PB95-110367] p 1470 N95-22016
A graded approach to ISO 9000 implementation for records managers
[DE94-017409] p 1591 N95-22167

STAR CLUSTERS
An IRAS Hires study of low mass star formation in the Taurus molecular ring p 1593 N95-21767

STAR FORMATION
Relativistic binary neutron star coalescence
[DE94-019311] p 1600 N95-21479
Extended far-infrared emission and star formation in Seyfert galaxies p 1593 N95-21764
The variation of the dust temperature within late-type spiral galaxies p 1593 N95-21766
An IRAS Hires study of low mass star formation in the Taurus molecular ring p 1593 N95-21767

STARCHES
A low energy continuous reactor separator for the production of ethanol from corn grits/starch and biomass streams
[DE95-002256] p 1283 N95-21356
Investigation on research for degradable plastics
[DE94-796550] p 1277 N95-21714

STARK EFFECT
Heterostructure quantum confined Stark effect electrooptic modulators operating at 938 nm
[AD-A279342] p 1581 N95-21928

STARS
Simulation of stellar speckle imaging
[DE94-016606] p 1412 N95-19985
Twentysixth YERAC
[PB95-127437] p 1599 N95-21347

STATIC CHARACTERISTICS
The determination of static and time varying dipole source. Sensor geometry during sea trials using differential global positioning system
[MRL-TN-631] p 1205 N95-21642
Microscopic theory of normal liquid He-3
[DE94-629047] p 1527 N95-22179
The dynamic structure function of Bose liquids in the deep inelastic regime
[DE94-629077] p 1527 N95-22182

STATIC FIRING
Investigation of rocket motors 3 inch number 1 Mk 4
[AD-A284278] p 1221 N95-19962

STATIC PRESSURE
Structural performance of cylindrical pressure housings of different ceramic compositions under external pressure loading. Part 1: Isostatically pressed alumina ceramic
[AD-A279669] p 1270 N95-20603

STATIC TESTS
Static investigation of two fluidic thrust-vectoring concepts on a two-dimensional convergent-divergent nozzle
[NASA-TM-4574] p 1199 N95-19913
Portable static test facility for small, expendable, turbojet engines, phase 1
[AD-A286337] p 1216 N95-21719

STATISTICAL ANALYSIS
Ice Processing System software support documentation
[AD-A280030] p 1388 N95-20006
Hindered settling computations using a parallel boundary element method
[DE94-014286] p 1339 N95-20137
The 29th MIL-HDBK-17 Polymer Matrix Composites Coordination Group Meeting
[AD-A279917] p 1269 N95-20578
Analysis of mesospheric winds and waves
[AD-A279956] p 1414 N95-20591
Evidence for t(bar t) production at the Tevatron: Statistical significance and cross section
[DE95-002524] p 1515 N95-20897
Statistical analysis of Turbine Engine Diagnostic (TED) field test data
[AD-A286032] p 1379 N95-20998
Large-eddy simulation of rotating channel flows using a localized dynamic model p 1346 N95-21064
Adaptive detection in stationary and nonstationary noise environments
[AD-A279581] p 1300 N95-21099
Geometric characterization of electromigration voids (A statistical analysis of electromigration voids)
[AD-A286494] p 1328 N95-21169
Ozone quality control measurements in the Dutch National Air Quality Monitoring Network
[PB95-131900] p 1405 N95-21329
Potential-of-mean-force description of ionic interactions and structural hydration in biomolecular systems
[DE95-000859] p 1438 N95-21366
Heuristic genetic algorithms for constrained problems. Part 1: Principles
[PB95-132031] p 1467 N95-21374
Exponential deconvolution: Two asymptotically equivalent estimators
[PB95-132122] p 1499 N95-21469
Simulations of metal dissolution and corrosion
[DE94-019295] p 1257 N95-21476
BASIC program for power spectrum estimation
[DE95-002228] p 1468 N95-21515
The application of a statistical analysis software package to explosive testing
[MRL-TR-93-42] p 1284 N95-21658
The energetics and dynamics of free radicals, ions, and clusters
[DE94-018101] p 1244 N95-21701
LADAR detection statistics in the presence of pointing errors
[AD-A285865] p 1309 N95-22134
Pollution error in the H-version of the finite element method and the local quality of A-posteriori error estimators
[AD-A279868] p 1497 N95-22388
Conditional statistics in a turbulent premixed flame derived from direct numerical simulation
p 1249 N95-22438

STATISTICAL CORRELATION
Rigorous spin-spin correlation function of Ising model on a special kind of Sierpinski Carpets
[DE94-628995] p 1575 N95-21854

STATISTICAL DISTRIBUTIONS
Universal features of multiplicity distributions
[DE94-012854] p 1498 N95-20779
Statistical properties of geologic fractals
[DE94-019272] p 1414 N95-20908
Collisional redistribution effects on x ray laser saturation behavior
[DE94-017308] p 1374 N95-21663
Counting methods for the analysis of load time histories
[PB95-132916] p 1388 N95-22093
Proton and produced particle distributions from Au+Au collisions at 11.6 A GeV/c
[DE94-018634] p 1530 N95-22392

STATISTICAL MECHANICS
Coupled analytic maps
[PB95-111076] p 1498 N95-19945
Rigorous spin-spin correlation function of Ising model on a special kind of Sierpinski Carpets
[DE94-628995] p 1575 N95-21854

STATISTICAL TESTS
Proof of a conjecture of Narayana on dominance refinements of the Smirnov two-sample test
[PB95-132650] p 1499 N95-21979
Precedence tests and confidence bounds for complete data: An overview and some results
[PB95-132668] p 1499 N95-21980
Learning maneuvers using neural network models
[AD-A286470] p 1486 N95-22267

STEADY FLOW
Transient behaviour and stability points of the Poiseuille flow of a KBKZ-fluid
[PB95-132064] p 1353 N95-21268
Multiwire thermocouples: Frequency response
[NASA-TM-110510] p 1367 N95-21889
Shock wave interactions in hypervelocity flow
[AD-A286507] p 1357 N95-22212

STEADY STATE
Properties of whisker-reinforced ceramics
[DE94-017759] p 1264 N95-20024
Mantle rare gas relative abundances in a steady-state mass transport model p 1423 N95-21812
He, Xe and Ne isotopes in a steady-state mass transport model and implications about terrestrial volatiles
p 1425 N95-21821

STEAM
Technical and economic evaluation of natural gas based synthesis gas production technologies
[PB95-130597] p 1242 N95-21426

STEELS
A review of Microbially Induced Corrosion (MIC) of steel and a preliminary investigation to determine its occurrence in naval vessels
[MRL-GD-0048] p 1250 N95-19910
Accelerated screening methods for determining chemical and thermal stability of refrigerant-lubricant mixtures. Part 2: Experimental comparisons and verification of methods
[DE95-000743] p 1264 N95-20078
Fracture toughness properties of welded stainless steels for tritium service
[DE95-000755] p 1251 N95-20079
Inelastic torsion of steel I-beams
[PB94-208360] p 1384 N95-20101
The production of calibration specimens for impact testing of subsize Charpy specimens
[DE94-018125] p 1386 N95-20703
Nitrogen alloyed martensitic steels
[PB95-127791] p 1255 N95-21128
Effect of neutron irradiation on the impact properties of A533B steel
[DE95-001834] p 1256 N95-21286
Damage tolerance of carbon fibre polyetheretherketone laminates
[PB95-131611] p 1230 N95-21432
Protective organic coatings on steel: Accelerated corrosion test method for paint/coatings exposed to water with low conductivity. Nordtest project no. 1010-92. Degradation of organic coatings in fresh water
[PB95-134185] p 1277 N95-21873
Corrosion behavior of landing gear steels
[AD-A285862] p 1261 N95-22132
Fibre-reinforced high-strength concrete
[PB95-131942] p 1232 N95-22158

Residual stress analysis in swage autofrettaged thick-walled cylinders by position-sensitive x-ray diffraction techniques
[AD-A286383] p 1388 N95-22320
An update of corrosion inhibitors for mild steel exposed to 32-0-0 UAN solution
[DE95-001715] p 1263 N95-22396

STEERING
Two-micron Laser Atmospheric Wind Sounder (LAWS) pointing/tracking study
[NASA-CR-195012] p 1220 N95-21190
Definition report on target and related steering variables of radiation as a part of the environmental balance and environmental outlook investigation
[PB95-135471] p 1409 N95-21846

STELLAR ENVELOPES
HIRAS images of fossil dust shells around AGB stars
p 1593 N95-21768

STELLAR EVOLUTION
Relativistic binary neutron star coalescence
[DE94-019311] p 1600 N95-21479
Physics of systems containing neutron stars
[NASA-CR-197304] p 1600 N95-21615
Extended far-infrared emission and star formation in Seyfert galaxies p 1593 N95-21764

STELLAR LUMINOSITY
Interacting galaxies resolved by IRAS
p 1593 N95-21759
Luminous radio-quiet sources in the W3(MAIN) cloud core p 1594 N95-21773

STELLAR MASS
The solar neutrino problem: Neither astrophysics nor oscillations?
[DE94-012850] p 1603 N95-21316

STELLAR MASS EJECTION
Solar-geophysical data number 601, September 1994. Part 2: (Comprehensive reports). Data for March 1994, and miscellaneous
[PB95-136735] p 1603 N95-20829
Coronal Mass Ejections in the solar wind at high solar latitudes: An overview
[DE95-000844] p 1603 N95-21377

STELLAR MODELS
The solar neutrino problem: Neither astrophysics nor oscillations?
[DE94-012850] p 1603 N95-21316
Relativistic binary neutron star coalescence
[DE94-019311] p 1600 N95-21479
Solar wind composition
[NASA-TM-197364] p 1604 N95-22384

STELLAR PHYSICS
Physics of systems containing neutron stars
[NASA-CR-197304] p 1600 N95-21615

STELLARATORS
Design and construction of the HSX experiment
[DE94-018657] p 1552 N95-20348
Stellarator transport optimization with self-consistent electric fields
[DE94-019151] p 1559 N95-21581

STEREOCHEMISTRY
Introduction to the structures determination methods using X-ray diffraction in monocrystals: Application to some lanthanides and transition metals complexes with organic ligands
[DE94-629002] p 1579 N95-22380

STEREOSCOPIC VISION
Intermediate levels of visual processing
[AD-A284922] p 1448 N95-19998
A scalable video rate camera interface
[AD-A286144] p 1474 N95-20325
Integration of segmentation and stereo matching
[PB95-107819] p 1444 N95-21028

STEREOSCOPY
Integration of segmentation and stereo matching
[PB95-107819] p 1444 N95-21028

STIFFNESS
The influence of ply waviness with nonlinear shear on the stiffness and strength reduction of composite laminates
[AD-A285736] p 1224 N95-19899
Fracture behavior of laminated discontinuously reinforced aluminum material
[DE94-017307] p 1263 N95-22408

STIMULATED EMISSION
Tunable CW blue, green, orange and red upconversion fiber lasers at room temperature
[DE95-000851] p 1375 N95-22007

STIRLING CYCLE
Proceedings of the 1993 Non-Fluorocarbon Insulation, Refrigeration and Air Conditioning Technology Workshop
[DE94-018333] p 1285 N95-20194

STIRLING ENGINES
Recent reflux receiver developments under the US DOE program
[DE95-001622] p 1393 N95-20861
Testing of the SAIC facets on the stretched-membrane dish
[DE95-001831] p 1393 N95-20864

STOCHASTIC PROCESSES
Frequent sampling in discrete choice
[PB95-110961] p 1497 N95-19938
A multivariate multisample rank test for stochastic simulation validation
[AD-A285922] p 1498 N95-19990
Analytic Perturbation Analysis of Discrete Event Dynamic Systems
[DE94-018635] p 1480 N95-20126
Higher order crossings
[AD-A279597] p 1504 N95-20300
Fitting stochastic partial differential equations to spatial data
[AD-A279870] p 1490 N95-20432
Structure and dynamics of turbulent wall layers
[AD-A285360] p 1340 N95-20547
Stochastic network processes
[AD-A279905] p 1475 N95-20566
Proceedings of the Fourth International Workshop on Inductive Logic Programming (ILP-94)
[PB95-135273] p 1464 N95-21003
Set functionals in stochastic geometry
[PB95-135372] p 1491 N95-21005
Analysis of subgrid models using direct and large-eddy simulations of isotropic turbulence p 1348 N95-21071
New methods for large scale local and global optimization
[AD-A285635] p 1517 N95-21126
Accuracy problems in the generation of discrete time stochastic processes
[PB95-131397] p 1386 N95-21133
Quantum diffusion
[DE95-001015] p 1580 N95-21264
Duality and equivalencies in closed tandem queueing networks
[PB95-132502] p 1482 N95-21271
Diffusion approximations in communication and stochastic theory
[AD-A286440] p 1302 N95-21438
Learning algorithms for feedforward networks based on finite samples
[DE95-001739] p 1483 N95-21741
Artificial neural network metamodels of stochastic computer simulations
[AD-A285951] p 1484 N95-22056
Counting methods for the analysis of load time histories
[PB95-132916] p 1388 N95-22093
Theory of the excitonic lineshape in low-dimensional structures with rough interfaces
[DE95-003434] p 1582 N95-22237
Optimal active control for Burgers equations
p 1361 N95-22454

STOICHIOMETRY
Reactive nanophase oxide additions to melt-processed high-T(sub c) superconductors
[DE95-001470] p 1570 N95-20841
Triple flame structure and diffusion flame stabilization
p 1249 N95-21039
Fire experiments in a two dimensional rack storage: BRANDFORSK-project 701-917
[PB95-131538] p 1241 N95-21179
Plastic deformation of ordered intermetallic alloys: Fundamental aspects
[DE95-001070] p 1256 N95-21265
Bulk and defect properties of ordered intermetallics
[DE94-017706] p 1262 N95-22344
New thermodynamic description of the Cu-Zr system
[PB95-127189] p 1263 N95-22374

STOKES FLOW
Hindered settling computations using a parallel boundary element method
[DE94-014286] p 1339 N95-20137
Mixed hp finite element methods for problems in elasticity and stokes flow
[PB95-104444] p 1341 N95-20981

STOKES THEOREM (VECTOR CALCULUS)
Solutions of D(sup n)D(sup m)f=0
[PB95-110839] p 1487 N95-19916

STORAGE BATTERIES
Demonstration of zinc/air fuel battery to enhance the range and mission of fleet electric vehicles: Preliminary results in the refueling of a multicell module
[DE95-004206] p 1337 N95-22421

STORAGE RINGS (PARTICLE ACCELERATORS)
Crystalline beam in a storage ring: How long can it last?
[DE94-017303] p 1563 N95-20014
A URI program for Ultraviolet/extreme ultraviolet research
[AD-A279159] p 1370 N95-20600
Crystalline beams: The horizontal zigzag
[DE95-002227] p 1533 N95-20766
Crystalline beams
[DE95-002656] p 1569 N95-20793
Confinement and stability of crystalline beams in storage rings
[DE95-002515] p 1533 N95-20886
Behaviour of space-charge dominated ion beams in storage rings
[DE94-015845] p 1517 N95-21140
Multiple hard interactions in HERWIG
[PB95-130548] p 1518 N95-21233
Sources of amplitude-dependent tune shift in the PEP-2 design and their compensation with octupoles
[DE94-018198] p 1519 N95-21262
Simulation of beam-beam lifetime for LEP
[DE95-002888] p 1536 N95-21334
Hadron beams and accelerators
[DE95-002932] p 1536 N95-21342
Effects of RF side-bands on spectral reproducibility for infrared synchrotron radiation
[DE95-002450] p 1536 N95-21418
Beam instability studies at the APS
[DE95-001448] p 1537 N95-21503
Low emittance lattices for electron storage rings revisited
[DE94-017302] p 1540 N95-22391

STORAGE STABILITY
Beam instability studies at the APS
[DE95-001448] p 1537 N95-21503

STORMS (METEOROLOGY)
Radar studies of aviation hazards
[AD-A285845] p 1203 N95-21831

STRAIN GAGES
Vapor generator wand
[NASA-CASE-LAR-15058-1] p 1215 N95-20080
Evaluation of Pd-Cr wires for strain gage application
[NASA-TM-106857] p 1366 N95-21259

STRAIN MEASUREMENT
Evaluation of Pd-Cr wires for strain gage application
[NASA-TM-106857] p 1366 N95-21259
Strain measurement by diffraction at LANSCE
[DE94-018264] p 1387 N95-21386

STRAIN RATE
Development of superplasticity in 5083 aluminum with additions of Mn and Zr
[DE94-017474] p 1251 N95-20090
The reliability of laser reflowed Sn-Ag solder joints
[AD-A279787] p 1315 N95-20443
Fracture behavior of the Fe-8Al alloy FAP-Y
[DE95-000956] p 1258 N95-21676

STRANGE ATTRACTORS
Similarities and differences in strangeness production at BNL and CERN
[DE95-002343] p 1521 N95-21380

STRANGENESS
Strange particle and antiproton production in S + nucleus collisions at 200 GeV/nucleon
[DE95-002348] p 1513 N95-20575
Heavy ion collisions
[DE95-002712] p 1520 N95-21321
Similarities and differences in strangeness production at BNL and CERN
[DE95-002343] p 1521 N95-21380
Strange hadronic matter
[DE94-019345] p 1521 N95-21484

STRATEGY
Bomber force 2000: Operational concepts for long-range combat aircraft
[AD-A279378] p 1206 N95-20181

STRATIFIED FLOW
Fourth International Symposium on Stratified Flows, volume 1
[AD-A286450] p 1354 N95-21583
Fourth International Symposium on Stratified Flows, volume 3
[AD-A286452] p 1354 N95-21584
Fourth International Symposium on Stratified Flows, volume 4
[AD-A286453] p 1358 N95-22424

STRATOCUMULUS CLOUDS
Balloon tracking for the ASTEX/MAGE Lagrangian experiment
[AD-A280078] p 1430 N95-20969

STRATOSPHERE
Indirect global warming effects of ozone and stratospheric water vapor induced by surface methane emission
[DE94-019016] p 1402 N95-20353
Radiative forcing calculations for CH3Cl
[DE94-019018] p 1402 N95-20355
The development and evaluation of water-mist fire extinguishing systems
[DE94-019019] p 1286 N95-20356
Computer model predictions of the local effects of large, solid-fuel rocket motors on stratospheric ozone
[AD-A285632] p 1404 N95-21150

Definition report on environmental indices in future environmental assessments environmental balance/environmental outlook
[PB95-131876] p 1405 N95-21350
Monitoring the response of the upper troposphere/lower stratosphere to a greenhouse gas scenario
[DE95-000982] p 1406 N95-21410
Transport, radiative, and dynamical effects of the Antarctic ozone hole: A GFDL SKYHI model experiment
[PB94-192754] p 1409 N95-22101

STRATUS CLOUDS
Boundary layer cloud studies in support of ASTEX
[AD-A285947] p 1429 N95-20395
Unified very low stratus cloud/subcloud microphysics model: User's guide
[AD-A286454] p 1430 N95-21586

STREAK CAMERAS
X-ray spectroscopy of xenon
[DE95-002132] p 1240 N95-20865

STREAM FUNCTIONS (FLUIDS)
Modeling the two-point correlation of the vector stream function p 1345 N95-21055

STRESS (PHYSIOLOGY)
USAF cellular mechanism of turnover of the stress induced protein HSP70
[AD-A285618] p 1441 N95-19898
Behavioral effects of tyrosine during sustained wakefulness
[AD-A279789] p 1441 N95-20307
Development and enhancement of a model of performance and decision making under stress in a real life setting
[AD-A285945] p 1449 N95-20393
Evaluation of stress experienced by soldiers wearing chemical protective clothing during varying work loads in desert or tropical environments
[AD-A280113] p 1452 N95-20625
Microclimate cooling effect on perceived exertion in four heat/exercise scenarios
[AD-A285549] p 1444 N95-21160
Psychosocial stress and mental health in a forward-deployed military community
[AD-A285940] p 1451 N95-22323
Assessing post traumatic stress disorder and PTSD symptomatology in US Army personnel
[AD-A285941] p 1451 N95-22324

STRESS (PSYCHOLOGY)
Behavioral effects of tyrosine during sustained wakefulness
[AD-A279789] p 1441 N95-20307
Development and enhancement of a model of performance and decision making under stress in a real life setting
[AD-A285945] p 1449 N95-20393
Evaluation of stress experienced by soldiers wearing chemical protective clothing during varying work loads in desert or tropical environments
[AD-A280113] p 1452 N95-20625
Psychosocial stress and mental health in a forward-deployed military community
[AD-A285940] p 1451 N95-22323
Assessing post traumatic stress disorder and PTSD symptomatology in US Army personnel
[AD-A285941] p 1451 N95-22324

STRESS ANALYSIS
Design and thermal stress analysis of high power x-ray monochromators cooled with liquid nitrogen
[DE94-016879] p 1500 N95-20106
Turbulence descriptors for scaling fatigue loading spectra of wind turbine structural components
[DE94-011833] p 1384 N95-20109
The processing and mechanical properties of high temperature/high performance composites. Book 5: Interface effects
[AD-A279815] p 1228 N95-20584
Geomaterial models and numerical analysis of softening
[PB95-135380] p 1386 N95-21006
Large-eddy simulation of rotating channel flows using a localized dynamic model p 1346 N95-21064
Determination of layer moduli from falling weight deflectometer measurements
[PB95-129748] p 1286 N95-21333
Crack closure and sequential effects in fatigue: A literature survey
[PB95-131637] p 1387 N95-21557
Sheet metal formability
[PB95-110250] p 1258 N95-21653
Effects of cyclic stress distribution models on fatigue life predictions
[DE95-001619] p 1388 N95-22070
Residual stress analysis in swage autofrettaged thick-walled cylinders by position-sensitive x-ray diffraction techniques
[AD-A286383] p 1388 N95-22320

STRESS CONCENTRATION
Microscopy of stress-induced morphological development and dislocation nucleation during semiconductor epitaxy
[DE94-017869] p 1568 N95-20674

STRESS CORROSION CRACKING
Corrosion behavior of landing gear steels
[AD-A285862] p 1261 N95-22132

STRESS DISTRIBUTION
The processing and mechanical properties of high temperature/high performance composites. Stress redistribution and notch properties, book 2
[AD-A279737] p 1227 N95-20429
Effects of cyclic stress distribution models on fatigue life predictions
[DE95-001619] p 1388 N95-22070
Residual stress analysis in swage autofrettaged thick-walled cylinders by position-sensitive x-ray diffraction techniques
[AD-A286383] p 1388 N95-22320

STRESS INTENSITY FACTORS
Analyses of some benchmark cases in fracture mechanics using boundary element method
[PB95-110888] p 1384 N95-19930

STRESS MEASUREMENT
Residual stresses in material processing
[DE94-017888] p 1385 N95-20374
Data report: Stress measurements in the bottom boundary layer with BASS tripods STRESS 2 1990-1991
[AD-A279875] p 1433 N95-20433
Measurement of residual stresses on ceramic materials with high spatial resolution
[DE94-017889] p 1280 N95-22270

STRESS TENSORS
Modelling anisotropy and backscatter effects in the subgrid scale stress tensor p 1349 N95-21077

STRESS-STRAIN RELATIONSHIPS
A model of an infinite length, axisymmetric, isotropic, forced thick shell
[AD-A285586] p 1386 N95-21212

STRESSES
The role of grain boundary sliding on creep deformation characteristics of discontinuous reinforced composites
[DE95-001671] p 1231 N95-21924

STRETCHING
Evaluation of Reynolds stress turbulence closures in compressible homogeneous shear flow
[NASA-CR-194892] p 1338 N95-20009

STRING THEORY
Construction of non-critical string field theory by transfer matrix formalism in dynamical triangulation
[DE94-770607] p 1516 N95-20986
Factorization in closed string field theory
[PB95-133542] p 1580 N95-21030
Cosmological string solutions by dimensional reduction
[DE95-002858] p 1599 N95-21245

STRINGS
Cosmological string solutions by dimensional reduction
[DE95-002858] p 1599 N95-21245

STRONG INTERACTIONS (FIELD THEORY)
Strong interactions studies with medium energy probes
[DE95-001800] p 1245 N95-21745
Uniform upper bounds in the Froehlich polaron theory
[DE94-628998] p 1525 N95-21860
Physics at the Fermilab Collider
[DE95-000726] p 1539 N95-22195

STRONTIUM
Solid oxide fuel cells in the United States
[DE95-002405] p 1395 N95-21361

STRONTIUM OXIDES
Carrier doping and interlayer coupling in HTSC single crystals
[DE94-018637] p 1564 N95-20127
Selective methane oxidation over promoted oxide catalysts
[DE94-012270] p 1235 N95-20188
Effects of neutron irradiation on the London penetration depth for polycrystalline Bi(1.8)Pb(0.3)Sr2Ca2Cu3O10 superconductor
[DE94-019335] p 1573 N95-21483
Electronic structure and energies of alkaline earth oxides: MgO, CaO and SrO
[DE94-628990] p 1575 N95-21853

STRUCTURAL ANALYSIS
Testing paradigm applied to network structure (revised)
[PB95-110706] p 1487 N95-19906
Super-heavy aircraft study
[AD-A279602] p 1215 N95-19955
Inelastic torsion of steel I-beams
[PB94-208360] p 1384 N95-20101
Parallel solid mechanics codes at Sandia National Laboratories
[DE94-015770] p 1474 N95-20152
Simulation of large systems with neural networks
[DE94-018898] p 1428 N95-20319
Hierarchical structure in advanced polymers. Phase behaviour, orientation, properties
[AD-A285938] p 1268 N95-20392
Scanning tunneling microscopy studies of self-assembled monolayers of alkanethiols on gold
[AD-A279910] p 1253 N95-20577
The 29th MIL-HDBK-17 Polymer Matrix Composites Coordination Group Meeting
[AD-A279917] p 1269 N95-20578
Structural performance of cylindrical pressure housings of different ceramic compositions under external pressure loading. Part 1: Isostatically pressed alumina ceramic
[AD-A279669] p 1270 N95-20603
Bacterial luciferase: Determination of the structure by x-ray diffraction
[AD-A279699] p 1437 N95-20711
Military standard: Test requirements for launch, upper-stage, and space vehicles
[AD-A286627] p 1218 N95-20770
ALCHEMI of Fe-doped B2-ordered NiAl alloys with different doping levels
[DE94-017748] p 1255 N95-20907
Statistical properties of geologic fractals
[DE94-019272] p 1414 N95-20908
Moessbauer study of the sintered Mn(0.70)Zn(0.23)Fe(2.07)O4
[DE94-631462] p 1255 N95-20909
Recent results from E665
[DE95-002523] p 1516 N95-20914
Structure functions and structure function ratio F2(n)/F2(p) at low X(Bj) and Q2 in inelastic muon scattering
[DE94-018979] p 1573 N95-21561
Modeling of rolling element bearing mechanics. Computer program user's manual
[NASA-CR-196557] p 1381 N95-21692
Modeling of rolling element bearing mechanics. Theoretical manual
[NASA-CR-196556] p 1381 N95-21705
On the influence of electromagnetic wave and relativistic electron beam on a plasma
[DE94-628962] p 1561 N95-21848
Discovering related DNA sequences via mutual information
[DE95-001101] p 1440 N95-22067

STRUCTURAL BASINS
Anatomy of the Midcontinent Rift beneath Lake Superior
[DE94-019298] p 1415 N95-21477
Fourth International Symposium on Stratified Flows, volume 3
[AD-A286452] p 1354 N95-21584
Semi-volatiles at Mercury: Sodium (Na) and potassium (K) p 1424 N95-21818

STRUCTURAL DESIGN
Cr2Nb development
[DE94-018697] p 1250 N95-20043
Target Area Structural Support systems design to achieve the micron-level stability requirement of the National Ignition Facility (NIF)
[DE94-017696] p 1551 N95-20219
An introduction to the Astro Edge solar array p 1322 N95-20535
Mechanical design of the DO silicon detector
[DE95-002532] p 1365 N95-20902
Methodology for ESCA analysis of electromigration
[AD-A286229] p 1241 N95-21168
Micromachined silicon-based analytical microinstruments for space science and planetary exploration
[DE94-019306] p 1367 N95-21507
Ceramic technology for advanced heat engines
[DE95-000950] p 1278 N95-21937

STRUCTURAL DESIGN CRITERIA
An Echelle Grating Spectrometer (EGS) for mid-IR remote chemical detection
[DE94-019310] p 1367 N95-21478
Structuring design requirements using YMIR
[PB95-132742] p 1471 N95-22081

STRUCTURAL ENGINEERING
Computer-Aided Structural Engineering (CASE) project. User's guide: Computer-Aided Structural Modeling (CASM). Version 5.00
[AD-A279913] p 1459 N95-20310
The 29th MIL-HDBK-17 Polymer Matrix Composites Coordination Group Meeting
[AD-A279917] p 1269 N95-20578
Crack closure and sequential effects in fatigue: A literature survey
[PB95-131637] p 1387 N95-21557

STRUCTURAL FAILURE

Corrosion of aircraft materials: Correlation between nanometer scale and macroscopic structural damage parameters
[AD-A285930] p 1252 N95-20299

Strain measurement by diffraction at LANSCE
[DE94-018264] p 1387 N95-21386

Counting methods for the analysis of load time histories
[PB95-132916] p 1388 N95-22093

STRUCTURAL MEMBERS

Multi-layered translated rib-stiffened composite hollow cylinder assembly
[AD-D016566] p 1226 N95-20292

STRUCTURAL STABILITY

Static stability of a three-dimensional space truss
p 1220 N95-20533

Carbon fiber reinforced superconductor composites
[DE95-002504] p 1229 N95-20913

Electronic structure and energies of alkaline earth oxides: MgO, CaO and SrO
[DE94-628990] p 1575 N95-21853

Electronic structure and relative stability of icosahedral superatoms in Al-transition-metal alloys
[DE94-628996] p 1260 N95-21855

STRUCTURAL VIBRATION

Modeling the effect of shroud contact and friction dampers on the mistuned response of turbopumps
[NASA-CR-197285] p 1379 N95-20795

Two-micron Laser Atmospheric Wind Sounder (LAWS) pointing/tracking study
[NASA-CR-195012] p 1220 N95-21190

Low frequency sound radiation from finite stiffened plates
[AD-A279395] p 1505 N95-21930

STRUCTURED PROGRAMMING

Making structured graphics and constraints practical for large-scale applications
[AD-A280062] p 1461 N95-20623

STUDENTS

NASA/DOD Aerospace Knowledge Diffusion Research Project. Report 28: The technical communication practices of aerospace engineering and science students: Results of the phase 4 cross-national surveys
[NASA-TM-109123] p 1587 N95-20162

SUBCRITICAL FLOW

On subcritical instability of the attachment line boundary layer p 1351 N95-21092

SUBDUCTION (GEOLOGY)

Volatiles in the Earth: All shallow and all recycled
p 1416 N95-21779

D/H ratios and H2O contents of mantle-derived amphibole megacrysts from Dish Hill, California
p 1416 N95-21781

Thermochemistry of dense hydrous magnesium silicates p 1416 N95-21782

Recycling of volatiles at subduction zones: Noble gas evidence from the Tabar-Lihir-Tanga-Feni arc of papua New Guinea p 1418 N95-21787

Subduction and volatile recycling in Earth's mantle
p 1421 N95-21802

Seismic evidence for volatiles at large depth in the Earth p 1422 N95-21808

Subduction of hydrated basalt of the oceanic crust: Implications for recycling of water into the upper mantle and continental growth p 1423 N95-21814

He, Xe and Ne isotopes in a steady-state mass transport model and implications about terrestrial volatiles
p 1425 N95-21821

SUBGROUPS

Growth series for the commutator subgroup
[PB95-111092] p 1490 N95-20452

A crystallographic model for hydrous wadsleyite (Beta-Mg2SiO4) p 1424 N95-21817

SUBLIMATION

Novel catalysts for methane activation
[DE95-002639] p 1237 N95-20438

SUBMERGED BODIES

Legged vehicle for underwater mobile operations
[AD-A285043] p 1480 N95-20482

SUBMERGING

Immersion/two phase cooling p 1211 N95-20648

The permeation of bis(2-fluoro-2,2-dinitroethyl) formal (FEFO), ethyl 4,4-dinitropentanoate (EDNP), ethyl 4-nitropentanoate (ENP), and 1,2,4-trichlorobenzene (TCB) through barrier membranes
[DE95-002492] p 1283 N95-21514

SUBMILLIMETER WAVES

Luminous radio-quiet sources in the W3(MAIN) cloud core p 1594 N95-21773

Sub-millimeterwave semiconductor signal sources
[AD-A279375] p 1335 N95-22144

SUBROUTINE LIBRARIES (COMPUTERS)

DONIO: Distributed object network I/O library
[DE94-019163] p 1477 N95-21602

Report of the Numerical Analysis Group
[PB95-108163] p 1494 N95-21648

DIFFPACK: Software for partial differential equations
[PB95-110268] p 1468 N95-21654

Status of CFDLIB performance tests on the T3D
[DE95-002708] p 1478 N95-21925

SUBROUTINES

PRSPLOT6 manual
[PB95-110862] p 1456 N95-19928

A preliminary study of the airwake model used in an existing SH-60B/FFG-7 helicopter/ship simulation program
[DSTO-TR-0015] p 1201 N95-21659

FORTRAN subroutine for column reduction of polynomial matrices
[PB95-134987] p 1497 N95-22379

SUBSTRATES

Effects of ambient conditions on the adhesion of cubic boron nitride films on silicon substrates
[DE94-016779] p 1266 N95-20281

Materials processing and manufacturing technologies for diamond substrates multichip modules
[AD-A285060] p 1315 N95-20488

Effects of plasma hydrogenation on trapping properties of dislocations in heteroepitaxial InP/GaAs
p 1323 N95-20542

Nucleation, growth, and strain relaxation of lattice-mismatched 3-5 semiconductor epitaxial layers
p 1324 N95-20543

Growth, characterization and device development in monocrystalline diamond films
[AD-A285991] p 1568 N95-20614

The design and manufacturing development of an active silicon substrate MCM p 1211 N95-20645

Microdynamic devices fabricated on silicon-on-sapphire substrates
[AD-D016531] p 1325 N95-20727

Epitaxial liftoff technology onto processed silicon foundry wafers
[AD-A285621] p 1571 N95-21145

Calculation of atom-centered partial charges for heme
[DE94-014447] p 1520 N95-21375

Raman spectra of MOCVD-grown ferroelectric PbTiO3 thin films
[DE94-018964] p 1244 N95-21549

Development and applications of flat ceramic membranes
[PB95-110219] p 1276 N95-21650

Integration of thin film decoupling capacitors
[DE95-001609] p 1333 N95-21881

Method of making a semiconductor device by forming a nanochannel mask
[AD-D016515] p 1576 N95-22059

Growing and releasing diamonds
[AD-D016489] p 1577 N95-22103

Materials processing and manufacturing technologies for diamond substrates multichip modules
[AD-A285775] p 1336 N95-22412

Characterization and performance of DLC films synthesized by plasma and ion beam techniques
[DE94-018287] p 1281 N95-22428

SUBSTRUCTURES

Exclusive processes: Tests of coherent QCD phenomena and nucleon substructure at CEBAF
[DE95-002892] p 1520 N95-21336

SUCTION

Navier-Stokes simulations of the effects of suction holes on a flat plate boundary layer p 1352 N95-21094

SUGARS

Theoretical prediction of vibrational circular dichroism spectra of R-glyceraldehyde, R-erythrose, and R-threose. Part 2: Development of a procedure to scale the force constant matrix expressed in terms of internal coordinates
[AD-A284305] p 1437 N95-20252

SULFATES

A review of Microbially Induced Corrosion (MIC) of steel and a preliminary investigation to determine its occurrence in naval vessels
[MRL-GD-0048] p 1250 N95-19910

Quantitative and qualitative analysis of some inorganic compounds by Raman spectroscopy
[DE94-009757] p 1237 N95-20470

SULFIDATION

Processing and applications of iron aluminides
[DE94-017855] p 1253 N95-20673

SULFIDES

Angle resolved photoemission on K(0.3)Mo3, TiTe2 and Ti(1+x)S2
[DE94-018300] p 1574 N95-21712

Applications of ICP magnetic sector multicollector mass spectrometry to basic energy research
[DE95-002600] p 1246 N95-21886

Synthesis and characterization of single-source molecular precursors to binary metal sulphides: Bis(diethyldithiocarbamato) M(2)trialkylphosphine (M = Zn and Cd) adducts
[AD-A279746] p 1248 N95-22385

SULFONATES

NMR relaxation behavior of the head group of SHBS in lamellar liquid crystals
[AD-A279124] p 1574 N95-21599

SULFUR

Mercury capture in bench-scale absorbers
[DE94-016910] p 1234 N95-20107

Synthesis and characterization of (Zn(SEt)Et)10, formed via insertion of sulfur into Zn-C bonds: A new class of Wurtzite-like cluster framework
[AD-A279701] p 1569 N95-20714

Balloon tracking for the ASTEX/MAGE Lagrangian experiment
[AD-A280078] p 1430 N95-20969

Investigation of direct photon production in 200 A GeV S + Au reactions
[DE94-018129] p 1525 N95-21704

SULFUR DIOXIDES

Combustion-related studies using weakly bonded complexes
[DE95-002801] p 1238 N95-20576

Evaluation of the technical performance of the Dutch National Air Quality Monitoring Network in 1992
[PB95-131892] p 1405 N95-21327

Monitoring activities in the framework of the Dutch National Air Quality Monitoring Network in 1994
[PB95-131884] p 1406 N95-21351

SULFUR FLUORIDES

Effect of a solid insulator on the spark yield of S2F10 in SF6(*)
[DE95-001422] p 1326 N95-20791

Production of S2F10, S2OF10 and S2O2F10 by spark discharges in SF6*
[DE95-001421] p 1243 N95-21500

SULFUR HEXAFLUORIDE

Production of S2F10, S2OF10 and S2O2F10 by spark discharges in SF6*
[DE95-001421] p 1243 N95-21500

SULFURIC ACID

Corrosion resistance and behavior of construction materials exposed to dilute sulfuric acid at elevated temperatures under static conditions
[DE95-001723] p 1259 N95-21739

Corrosion resistance and behavioral characteristics of metals exposed to 70 percent by weight sulfuric acid at elevated temperatures
[DE95-001724] p 1259 N95-21740

SUM RULES

On the conductance sum rule for the hierarchical edge states of the Fractional Quantum Hall Effect
[DE94-629030] p 1582 N95-22198

SUN

Solar-Geophysical Data number 600, August 1994. Part 2: (Comprehensive reports). Data for February 1994 and miscellaneous
[PB95-105060] p 1603 N95-20722

Solar-geophysical data number 601, September 1994. Part 2: (Comprehensive reports). Data for March 1994, and miscellaneous
[PB95-136735] p 1603 N95-20829

Coronal Mass Ejections in the solar wind at high solar latitudes: An overview
[DE95-000844] p 1603 N95-21377

Testing the principle of equivalence by solar neutrinos
[DE94-014972] p 1604 N95-22064

The solar flux of thermal neutrinos and antineutrinos of all flavors
[DE95-003204] p 1604 N95-22085

SUNLIGHT

Modeling of high efficiency solar cells under laser pulse for power beaming applications p 1318 N95-20516

Review of solar cell temperature coefficients for space
p 1323 N95-20541

SUPERCOMPUTERS

Design considerations for parallel graphics libraries
[NASA-CR-194935] p 1473 N95-20013

Performance issues for engineering analysis on MIMD parallel computers
[DE94-015769] p 1474 N95-20150

High performance computing for materials process modeling
[DE94-017860] p 1460 N95-20358

SUPERCONDUCTING DEVICES

Processing, fabrication, and demonstration of HTS integrated microwave circuits
[AD-A285611] p 1312 N95-19894

HTS Josephson technology on silicon with application to high speed digital microelectronics
[AD-A285964] p 1328 N95-21178

High temperature superconducting films and multilayers for electronics
[AD-A279545] p 1331 N95-21693
High temperature superconducting microwave device
[AD-A286351] p 1336 N95-22254
SUPERCONDUCTING FILMS
High performance YBCO films
[AD-A286567] p 1326 N95-20824
Dependence of critical current density on microstructure and processing of high-T(c) superconductors
[DE95-000685] p 1571 N95-21167
High temperature superconducting films and multilayers for electronics
[AD-A279545] p 1331 N95-21693
High performance YBCO films
[AD-A279560] p 1276 N95-21695
SUPERCONDUCTING MAGNETS
Theory and modelling of quench in cable-in-conduit superconducting magnets
[DE95-001819] p 1330 N95-21442
Current distribution in Cable-In-Conduit Conductors
[DE95-001820] p 1332 N95-21725
The superconducting magnet system for the Tokamak Physics Experiment
[DE94-018329] p 1562 N95-22300
SUPERCONDUCTING SUPER COLLIDER
Experiments at high energy hadron colliders and underground water Cerenkov detector experiment
[DE95-001804] p 1535 N95-21281
The 12-GeV/c beam transfer and absorber lines for the Superconducting Super Collider
[DE95-002100] p 1538 N95-21733
SUPERCONDUCTIVITY
Free electron laser program
[AD-A285906] p 1368 N95-19987
Positron annihilation studies of organic superconductivity
[DE94-018371] p 1564 N95-20017
Journal of Applied Physics, volume 76, number 10, part 2. Proceedings of the 6th Joint Magnetism and Magnetic Materials-INTERMAG Conference
[AD-A286364] p 1500 N95-20229
Energy gap structure of layered superconductors
[DE94-017885] p 1566 N95-20372
Superconducting thin film with fullerenes and method of making
[AD-D016580] p 1567 N95-20461
Hg-199 and Cu-(63,65) NMR studies of mercury based high-Tc superconductors
[DE95-001073] p 1570 N95-20820
Gordon Research Conference on Physical Electrochemistry
[AD-A286545] p 1240 N95-20842
Vortex dynamics in a ring-like irradiated Bi2Sr2CaCu2O8 crystal
[DE95-001682] p 1573 N95-21569
High temperature superconducting films and multilayers for electronics
[AD-A279545] p 1331 N95-21693
Superconducting electromagnetic thruster
[AD-D016485] p 1355 N95-21902
SUPERCONDUCTORS (MATERIALS)
Power-law resistivity, magnetic relaxation and ac susceptibility
[DE94-016893] p 1501 N95-20241
Energy gap structure of layered superconductors
[DE94-017885] p 1566 N95-20372
X-ray studies of microstructures in semiconductor and superconducting materials
[DE95-001802] p 1572 N95-21279
Method for determining the granular nature of superconductors using pulsed current
[AD-D016517] p 1577 N95-22137
High temperature superconducting microwave device
[AD-A286351] p 1336 N95-22254
The superconducting magnet system for the Tokamak Physics Experiment
[DE94-018329] p 1562 N95-22300
SUPERCRITICAL FLOW
HIVEL2D: A two-dimensional flow model for high-velocity channels
[AD-A286556] p 1341 N95-20843
SUPERCRITICAL FLUIDS
Heat transfer, fouling, and combustion of supercritical fuels
[AD-A279906] p 1281 N95-19884
Molecular-based study of solutions in supercritical solvents
[DE94-019326] p 1580 N95-21420
SUPERFLUIDITY
Josephson acoustic radiation in superfluid helium
[AD-A279809] p 1503 N95-20098
New theory of critical flow velocities in superfluid helium
[PB95-130365] p 1571 N95-21228
SUPERHIGH FREQUENCIES
Inverse Cerenkov laser acceleration experiment at ATF
[DE94-017990] p 1370 N95-20572
Large bistatic angle clutter depolarization study
p 1296 N95-20941
Comparative study of C- and K-band propagation mechanisms beyond the horizon p 1297 N95-20946
Mitigation of effects of multiple path nulls at super-high frequencies through diversity and networking
p 1297 N95-20948
Investigation on the backscattering properties of Finnish boreal forests at C- and X-band: A semi-empirical modeling approach
[PB95-127692] p 1389 N95-21105
X-band microwave backscattering from ocean waves
[DE94-016719] p 1309 N95-22241
SUPERLATTICES
Physics and applications of defects in advanced semiconductors, volume 325
[AD-A280059] p 1563 N95-19886
Optimization of InAsSb/InGaAs strained-layer superlattice growth by metal-organic chemical vapor deposition for use in infrared emitters
[DE94-016557] p 1563 N95-19954
Giant magnetoresistance calculated from first principles
[DE94-018658] p 1500 N95-20129
Interlayer magnetic coupling in epitaxial Fe/Cr(211) and (100) superlattices
[DE95-002906] p 1571 N95-21256
X-ray studies of microstructures in semiconductor and superconducting materials
[DE95-001802] p 1572 N95-21279
Excitons in semiconducting superlattices, quantum wells, and ternary alloys
[DE95-001867] p 1572 N95-21287
Deposition and properties of novel nitride superlattice coatings
[DE95-002945] p 1230 N95-21445
Quantum dynamical phenomena of independent electrons in semiconductor superlattices subject to a uniform electric field
[DE95-001655] p 1574 N95-21723
Acoustoelectric effect in semiconductor superlattice
[DE94-628994] p 1575 N95-21859
SUPERNOVA REMNANTS
A HIRES analysis of the FIR emission of supernova remnants p 1594 N95-21770
SUPERNOVAE
Neutrino-neutrino scattering and matter-enhanced neutrino flavor transformation in supernovae
[DE94-017577] p 1604 N95-20383
SUPERPLASTIC FORMING
Forming of superplastic ceramics
[DE94-017306] p 1276 N95-21662
SUPERPLASTICITY
Development of superplasticity in 5083 aluminum with additions of Mn and Zr
[DE94-017474] p 1251 N95-20090
Overview on superplasticity research on small-grained materials
[DE94-016550] p 1266 N95-20316
Forming of superplastic ceramics
[DE94-017306] p 1276 N95-21662
SUPERPRESSURE BALLOONS
Balloon tracking for the ASTEX/MAGE Lagrangian experiment
[AD-A280078] p 1430 N95-20969
SUPERSONIC BOUNDARY LAYERS
Numerical investigation of supersonic turbulent boundary layers with high wall temperature
p 1344 N95-21050
Numerical simulation of supersonic boundary layer transition p 1348 N95-21074
Supersonic laminar flow control research
[NASA-CR-196049] p 1353 N95-21340
SUPERSONIC COMBUSTION RAMJET ENGINES
Internal aerodynamics of a generic three-dimensional scramjet inlet at Mach 10
[NASA-TP-3476] p 1340 N95-20619
SUPERSONIC FLOW
Free shear layers, base pressure and bluff-body drag
[AD-A286316] p 1200 N95-20175
Plasma chemistry of vibrationally nonequilibrium molecules
[AD-A279630] p 1553 N95-20411
Application of Navier-Stokes code PAB3D with kappa-epsilon turbulence model to attached and separated flows
[NASA-TP-3480] p 1201 N95-21338
Potential flow downstream of the heliospheric terminal shock: A non-spherical shock
[NASA-TM-110493] p 1426 N95-21874
Nonlinear interaction between a pair of oblique modes in a supersonic mixing layer: Long-wave limit
[NASA-CR-197380] p 1357 N95-22173
Shock wave interactions in hypervelocity flow
[AD-A286507] p 1357 N95-22212
Numerical study of boundary layer interaction with shocks: Method and code validation
p 1362 N95-22461
SUPERSONIC JET FLOW
Temperature effects on acoustic interactions between altitude test facilities and jet engine plumes
[NASA-CR-197638] p 1504 N95-21170
SUPERSONIC NOZZLES
Development of quiet-flow supersonic wind tunnels for laminar-turbulent transition research
[NASA-CR-197286] p 1216 N95-21436
SUPERSONIC SPEED
Flow coefficient behavior for boundary layer bleed holes and slots
[NASA-TM-106846] p 1338 N95-19953
SUPERSONIC WAKES
Free shear layers, base pressure and bluff-body drag
[AD-A286316] p 1200 N95-20175
SUPERSONIC WIND TUNNELS
Supersonic laminar flow control research
[NASA-CR-196049] p 1353 N95-21340
Development of quiet-flow supersonic wind tunnels for laminar-turbulent transition research
[NASA-CR-197286] p 1216 N95-21436
SUPERSYMMETRY
Complementarity of e(+)e(-) and pp colliders for the exploration of electroweak symmetry breaking
[DE94-017397] p 1507 N95-20034
Constraints on SUSy-GUT unification from b yields s-gamma decay
[PB95-130373] p 1580 N95-21229
Search for squarks and gluinos in D0
[DE95-000730] p 1528 N95-22197
SUPPORT SYSTEMS
Application of Markov decision processes to search problems
[PB95-110813] p 1497 N95-19914
Target Area Structural Support systems design to achieve the micron-level stability requirement of the National Ignition Facility (NIF)
[DE94-017696] p 1551 N95-20219
Systems Analysis Laboratory. Ten years of progress 1984-1994
[PB95-104451] p 1464 N95-20982
Intelligent interactive project management system
[PB95-132684] p 1586 N95-21982
SUPPORTS
Joule heating of the ITER TF cold structure: Effects of vertical control coil currents and ELMS
[DE95-001817] p 1560 N95-21724
SURFACE CRACKS
Reliability analysis of uniaxially ground brittle materials
[NASA-TM-106852] p 1386 N95-20790
The mechanical behavior of surface-modified ceramics
[DE95-001704] p 1276 N95-21572
Influence of fatigue crack closure on the growth rate of surface flaws
[AD-A279130] p 1387 N95-21967
SURFACE DEFECTS
Reliability analysis of uniaxially ground brittle materials
[NASA-TM-106852] p 1386 N95-20790
SURFACE DIFFUSION
Simulations of metal dissolution and corrosion
[DE94-019295] p 1257 N95-21476
SURFACE EMITTING LASERS
Semiconductor laser joint study program with Rome Laboratory
[AD-A285858] p 1369 N95-20379
Technologies for highly parallel optoelectronic integrated circuits
[DE95-001607] p 1327 N95-20883
Ultra-high aggregate bandwidth two-dimensional multiple-wavelength diode laser arrays
[AD-A280098] p 1372 N95-21019
SURFACE FINISHING
Defect production and recombination during low-energy ion processing
[DE95-001827] p 1572 N95-21304
A new universal solution for the electrofinishing of metallic materials
[DE95-001681] p 1258 N95-21568
SURFACE LAYERS
Physical-chemical studies on rodlike polymer compositions
[AD-A285361] p 1269 N95-20548
Methods of measuring adhesion for thermally grown oxide scales
[DE94-018177] p 1256 N95-21260
Surface ices in the outer solar system
p 1423 N95-21815

Elastic micro-fabricated surface layer for reducing turbulence and drag on an object while it moves through a fluid medium
[AD-D016516] p 1356 N95-22060

SURFACE NAVIGATION
Navigation system in combat vehicle
[PB95-131629] p 1452 N95-21467

SURFACE PROPERTIES
Correlations between surface structure and catalytic activity/selectivity
[DE94-019023] p 1234 N95-20052
Surface characterization and contamination analysis
[NASA-CR-197374] p 1238 N95-20557
Time-resolved analytical methods for liquid/solid interfaces
[DE95-002255] p 1240 N95-20780
Stars or stripes: A comparative study of finite and transfinite techniques for surface modelling
[PB95-134979] p 1464 N95-20975
Pdf modeling for premixed turbulent combustion based on the properties of iso-concentration surfaces
p 1249 N95-21042
Tribology and surface mechanical properties of excimer laser nitrided titanium
[DE95-002751] p 1255 N95-21238
Nonlinear optical studies of polymer interfaces
[DE94-018199] p 1274 N95-21263
Characterization of poly(tetrafluoroethylene) surfaces by atomic force microscopy: Results and artifacts
[DE95-000742] p 1242 N95-21309
Theoretical study of the noble metals on semiconductor surfaces and Ti-base shape memory alloys
[DE95-001654] p 1257 N95-21398
Simulations of metal dissolution and corrosion
[DE94-019295] p 1257 N95-21476
Surface x-ray scattering and scanning tunneling microscopy studies at the Au(111) electrode
[DE95-002409] p 1573 N95-21516
Surface inspection using Fourier Transform Infrared Spectroscopy
[DE95-001699] p 1244 N95-21571
Bridging the pressure gap: In situ atomic-level investigations of model platinum catalyst surfaces under reaction conditions by scanning tunneling microscopy
[DE95-002346] p 1246 N95-21990
Perimeter-yardstick technique for fracture surface fractal analysis
[AD-A286240] p 1387 N95-22025
Application of optical second harmonic generation to surface analysis
[AD-A279445] p 1547 N95-22074
Remote-sensing based technique to account for sub-grid scale variability of land surface properties
[NASA-TM-110501] p 1390 N95-22110
Acid-site characterization of water-oxidized alumina films by near-edge x-ray absorption and soft x-ray photoemission
[DE95-003355] p 1247 N95-22234
Studies of the microwave resistivity of kappa-(BEDT-TTF)2Cu(N(CN)2)Cl
[DE95-002980] p 1262 N95-22291

SURFACE REACTIONS
A review of Microbially Induced Corrosion (MIC) of steel and a preliminary investigation to determine its occurrence in naval vessels
[MRL-GD-0048] p 1250 N95-19910
Chemical and electrochemical interactions on corroding metal surfaces
[DE95-000624] p 1250 N95-19979
Method of making copper-titanium nitride alloy
[AD-D016582] p 1252 N95-20201
An atomically-resolved STM study of the interaction of phosphine (PH3) with the silicon (001) surface
[AD-A279819] p 1513 N95-20585
Microscopy of stress-induced morphological development and dislocation nucleation during semiconductor epitaxy
[DE94-017869] p 1568 N95-20674
Developments and applications of dynamic models for large eddy simulation of complex flows
p 1346 N95-21062
The formation of reaction bonded Si3N4 at low temperatures and in short times
[DE95-001990] p 1275 N95-21289
Plasma model for charging damage
[DE95-000788] p 1558 N95-21310
Quantum simulation of heterogeneous electron transfer free energies at the water-metal interface
[AD-A279279] p 1522 N95-21492
Ultrafast optical studies of surface reaction processes at semiconductor interfaces
[DE95-001548] p 1574 N95-21839
Regional scale hydrology with a new land surface processes model
[NASA-TM-110500] p 1390 N95-22111
The interaction of localized solutions in a surface reaction
[DE95-002736] p 1248 N95-22433

SURFACE ROUGHNESS
Aircraft corrosion study
[AD-A279527] p 1259 N95-21687

SURFACE TEMPERATURE
Global change integrating factors: Tropical tropopause trends
[DE95-001121] p 1404 N95-20835

SURFACE TREATMENT
Aircraft corrosion study
[AD-A279527] p 1259 N95-21687

SURFACE WATER
Monitoring bioremediation of Volatile Organic Compounds (VOCs) using Fourier Transform Infrared (FT-IR) spectrometry
[AD-A279631] p 1403 N95-20456
Regional scale hydrology with a new land surface processes model
[NASA-TM-110500] p 1390 N95-22111
Use of the carbo-flo process to purify process water contaminated by agricultural pesticides
[PB95-127825] p 1410 N95-22330

SURFACE WAVES
The Surface Wave Dynamics Experiment (SWADE): A retrospective look at the wave modeling activities
[AD-A285612] p 1431 N95-19895
Ambient noise and surface wave dissipation in the ocean
[AD-A279650] p 1432 N95-20303
SAR-related stress variability in the Marine Atmospheric Boundary Layer (MABL)
[AD-A286462] p 1431 N95-22393
PIC simulation of surface waves
[AD-A285358] p 1563 N95-22422

SURFACTANTS
Technical Summary for 1993 fall MRS Symposium O, Complex Fluids
[AD-A283722] p 1264 N95-19972
Scanning tunneling microscopy of semiconductor surfaces
[AD-A279982] p 1571 N95-20964
NMR relaxation behavior of the head group of SHBS in lamellar liquid crystals
[AD-A279124] p 1574 N95-21599
Chemical interactions between protein molecules and polymer membrane materials
[DE95-001808] p 1224 N95-21746

SURVEILLANCE
GPS-Squitter capacity analysis
[AD-A280037] p 1291 N95-20599

SURVEILLANCE RADAR
Recommendation on transition from primary/secondary radar to secondary-only radar capability
[AD-A286279] p 1308 N95-22005

SURVEYS
NASA/DOD Aerospace Knowledge Diffusion Research Project. Report 28: The technical communication practices of aerospace engineering and science students: Results of the phase 4 cross-national surveys
[NASA-TM-109123] p 1587 N95-20162
NASA/DOD Aerospace Knowledge Diffusion Research Project. Report 31: The technical communications practices of US aerospace engineers and scientists: Results of the phase 1 SME mail survey
[NASA-TM-109169] p 1587 N95-20163
Acoustic emission: The first half century
[DE94-017176] p 1503 N95-20267
Computing near-optimal schedules
[PB95-132072] p 1466 N95-21269
High resolution descriptions of IRAS 12 and 25 microns confused regions
[AD-A285847] p 1545 N95-21832
A survey of artificial neural network applications in flow analysis of energy networks
[DE95-002452] p 1486 N95-22430

SURVIVAL
Bayesian analysis of semiparametric proportional hazards models
[AD-A279394] p 1499 N95-21946

SUSPENSION SYSTEMS (VEHICLES)
Electrorheology for smart automotive suspensions
[AD-A285543] p 1380 N95-21157

SWEDEN
ICE BABY: Measurements of concentration fluctuations in a forest area in winter conditions
[PB95-133468] p 1405 N95-21274

SWELLING
Extrudate swell and extrudate distortion of HDPE as a result of different deformation mechanisms during extrusion through capillary dies
[PB95-110227] p 1288 N95-21651

SWEPT WINGS
Computational studies of laminar to turbulence transition
[AD-A285622] p 1353 N95-21146
Lift enhancement device
[AD-D016522] p 1201 N95-21864

SWITCHES
Applied physics research for innovation in pulsed power
[AD-A285392] p 1324 N95-20610
LLNL/Lion Precision LVDT amplifier
[DE95-001504] p 1327 N95-20854
Cell loss analysis of two-class priority generalized knockout switch
[PB95-127742] p 1301 N95-21109
Fiber-optic control of current filaments in high gain photoconductive semiconductor switches
[DE94-015804] p 1328 N95-21139
Plasma Electrode Pockels Cells for the Beamlet and NIF lasers
[DE94-016541] p 1557 N95-21166

SWITCHING
EPICS simulation tools for control system development
[DE94-018082] p 1462 N95-20699
High isolation electronic switch
[AD-D016533] p 1326 N95-20729
Highly survivable communications: Complementary media packet switched networks p 1292 N95-20922
QoS driven routing in packet switched networks of multiple transmission media p 1292 N95-20923
Investigations into alternate spark gap switching techniques
[AD-A286225] p 1308 N95-22021
Sequential shock induced switch tests for Eglin Air Force Base
[DE95-001786] p 1334 N95-22062

SWITCHING CIRCUITS
Design of power electronics for TVC and EMA systems
[NASA-CR-196540] p 1312 N95-19909
High-performance packet switching architecture for ATM: Conventional solution and neural network solution
[PB95-110920] p 1312 N95-19935
High isolation electronic switch
[AD-D016533] p 1326 N95-20729
Polymer based all-optic reconfigurable interconnects
[AD-A279976] p 1272 N95-20962
SPICE macro model of a spryton with MOSFET's in the avalanche mode
[DE94-015744] p 1555 N95-21134

SYMBOLIC PROGRAMMING
Numerical and symbolic algorithms for application and specific signal processing
[AD-A279902] p 1305 N95-21576
Abstract interpretation of reactive systems: Abstractions preserving Universal CTL(*), Existential CTL(*) and CTL(*)
[PB95-110557] p 1472 N95-22305

SYMBOLS
Production of J/(psi) in 800 GeV/c p-Si interactions
[DE94-017982] p 1513 N95-20496
A Monte Carlo study of the minus sign problem in the t-J model using an Intel iPSC/860 hypercube
[DE95-001072] p 1570 N95-20819
Interlayer magnetic coupling in epitaxial Fe/Cr(211) and (100) superlattices
[DE95-002906] p 1571 N95-21256
Pair production as a probe of colliding beam size
[DE95-002893] p 1536 N95-21337

SYMMETRY
Symmetry, Wigner functions and particle reactions
[DE94-629887] p 1514 N95-20735
A crystallographic model for hydrous wadsleyite (Beta-Mg2SiO4) p 1424 N95-21817
Second order approximation for optical polaron in the strong coupling case
[DE94-628997] p 1525 N95-21856
Computing symmetries and stubborn sets
[PB95-127700] p 1472 N95-22328

SYMPTOMOLOGY
Assessing post traumatic stress disorder and PTSD symptomatology in US Army personnel
[AD-A285941] p 1451 N95-22324

SYNCHRONISM
High-performance packet switching architecture for ATM: Conventional solution and neural network solution
[PB95-110920] p 1312 N95-19935
Time code interface
[AD-D016535] p 1501 N95-20731
Modelling the reassembly buffer in a connectionless server
[PB95-132908] p 1308 N95-22087

SYNCHROTRON RADIATION
An intensity interferometer for soft x-rays
[DE94-016370] p 1541 N95-20103

Six-dimensional modeling of coherent bunch instabilities and related feedback systems in storage rings with power-series maps for the lattice
[DE94-017965] p 1532 N95-20494

Gordon Research Conference on Physical Electrochemistry
[AD-A286545] p 1240 N95-20842

Application of new synchrotron powder diffraction techniques to anomalous scattering from glasses
[DE94-019285] p 1536 N95-21407

Diffraction applications using the energy dispersive beamline, X6A, at NSLS
[DE94-019287] p 1572 N95-21408

Effects of RF side-bands on spectral reproducibility for infrared synchrotron radiation
[DE95-002450] p 1536 N95-21418

Auger spectrometry of atoms and molecules
[DE94-018052] p 1524 N95-21664

Bunched beam instability with frequency spread
[DE94-018632] p 1539 N95-22357

SYNCHROTRONS

Effect of space charge tune shift on transverse instabilities
[DE94-016790] p 1531 N95-20282

A URI program for Ultraviolet/extreme ultraviolet research
[AD-A279159] p 1370 N95-20600

Application of new synchrotron powder diffraction techniques to anomalous scattering from glasses
[DE94-019285] p 1536 N95-21407

RF beam control for the AGS Booster
[DE95-001485] p 1538 N95-21720

Hydrogen and related materials at high density: Physics, chemistry and planetary implications
p 1418 N95-21791

SYNOPTIC METEOROLOGY

Climatological data for clouds over the globe from surface observations, 1982-1991: The total cloud edition
[DE95-002537] p 1431 N95-22288

SYNTAX

Comparison of Ward and Mellor's transformation schema with State- and Activitycharts
[PB95-110698] p 1459 N95-20258

GOLD: A Graph Oriented Language for Databases
[PB95-127544] p 1465 N95-21021

Compositional proof theory for fault tolerant real-time distributed systems
[PB95-127601] p 1465 N95-21025

Semantics for a fine lambda-calculus with de Bruijn indices
[PB95-127577] p 1492 N95-21372

Initial experience with noncorrecting syntax error handling
[PB95-132700] p 1471 N95-22029

SYNTHESIS (CHEMISTRY)

Low temperature synthesis of semiconductor materials
[AD-A285120] p 1226 N95-20081

Selective methane oxidation over promoted oxide catalysts
[DE94-012270] p 1235 N95-20188

Method of making copper-titanium nitride alloy
[AD-D016582] p 1252 N95-20201

Research in the chemical sciences: Summaries of FY 1994
[DE94-015427] p 1223 N95-20264

Novel materials
[AD-A279693] p 1227 N95-20427

The synthesis and characterization of small molecule and photo-cross-linkable high polymeric phosphazenes bearing cinnamate groups
[AD-A279782] p 1268 N95-20442

Biomolecular Materials by Design, volume 330
[AD-A285369] p 1269 N95-20551

Water-soluble polyphosphazenes and their hydrogels
[AD-A279695] p 1269 N95-20580

New chiral pyrimidino-crown ether ligands
[AD-A279892] p 1223 N95-20590

Structure of dibis(diethyldithiocarbamato) zinc (2) Mu-bis(diethylphosphino)ethane toluene(2)
[AD-A279792] p 1224 N95-20660

Ferroic materials: Design, preparation and characteristics. Ceramic transactions, volume 43
[AD-A285937] p 1270 N95-20664

Inorganic-organic polymers and their role in materials science
[AD-A279715] p 1270 N95-20671

An improved and facile method for the synthesis of 1,1-bis(4-hydroxyphenyl) 2-phenylethylene and its derivatives
[DE95-001125] p 1240 N95-20836

Macromolecular and materials design using polyphosphazenes
[AD-A279781] p 1273 N95-20978

Aromatics oxidation and soot formation in flames
[DE95-001803] p 1241 N95-21280

Technical and economic evaluation of natural gas based synthesis gas production technologies
[PB95-130597] p 1242 N95-21426

Lead-indium phosphate glasses for optical applications
[DE94-019333] p 1275 N95-21482

An initial assessment of the properties of 2,5-dipicryl-1,3,4-oxadiazole: A secondary explosive with high thermal stability
[MRL-TR-93-16] p 1284 N95-21624

Investigation on research for degradable plastics
[DE94-796550] p 1277 N95-21714

Preparation and x-ray structure of Cp2Ti(PH2SiH2)(PMe3)
[AD-A286197] p 1246 N95-21879

Oxidation behavior of aluminum nanopowders
[DE95-002721] p 1260 N95-21926

Processing of intermetallic materials by reaction synthesis
[DE94-017710] p 1263 N95-22345

SYNTHESIZERS

SYNTH: A spectrum synthesizer
[DE94-015943] p 1458 N95-20153

SYNTHETIC APERTURE RADAR

Neural models of motion perception
[AD-A286560] p 1449 N95-20845

Investigation on the backscattering properties of Finnish boreal forests at C- and X-band: A semi-empirical modeling approach
[PB95-127692] p 1389 N95-21105

Synthetic aperture radar processing with polar formatted subapertures
[DE95-001830] p 1302 N95-21305

SYNTHETIC FUELS

Bioconversion of coal derived synthesis gas to liquid fuels
[DE94-017381] p 1282 N95-19927

Catalytic reactions of synthesis gas. Part 3. Determination of reaction kinetics
[PB95-127759] p 1248 N95-22329

SYNTHETIC RUBBERS

A test of the Arrhenius extrapolation assumption for a nitrile rubber
[DE94-017337] p 1263 N95-19926

SYSTEM IDENTIFICATION

Modular CNI avionics system p 1213 N95-20659

SYSTEMS ANALYSIS

Analytic Perturbation Analysis of Discrete Event Dynamic Systems
[DE94-018635] p 1480 N95-20126

System level fault tolerance in parallel and distributed computing systems
[AD-A279664] p 1474 N95-20305

Detection optimization using linear systems analysis of a coded aperture laser sensor system
[DE95-001112] p 1371 N95-20832

Systems Analysis Laboratory. Ten years of progress 1984-1994
[PB95-104451] p 1464 N95-20982

Multi-dimensional Petri nets
[PB95-127593] p 1491 N95-21024

Proceedings of the NATO-Advanced Study Institute on Computer Aided Analysis of Rigid and Flexible Mechanical Systems. Volume 1: Main lectures
[AD-A286062] p 1380 N95-21171

The Photovoltaic Higher Education National Exemplar Facility (PHENEF)
[DE94-015641] p 1395 N95-21409

Proceedings of the NATO-Advanced Study Institute on Computer Aided Analysis of Rigid and Flexible Mechanical Systems. Volume 2: Contributed papers
[AD-A286063] p 1381 N95-21488

Mars power system concept definition study. Volume 2: Appendices
[NASA-CR-195420-VOL-2] p 1396 N95-21953

Mathematical theory of neural networks
[AD-A286508] p 1485 N95-22213

Low-level RF control for the AFEL
[DE94-018295] p 1540 N95-22410

SYSTEMS COMPATIBILITY

The Materials Corrosion and Environmental Effects Laboratory (MCEL)
[DE94-018268] p 1254 N95-20816

SYSTEMS ENGINEERING

Hierarchical diagrammatic representation of class structure
[PB95-110722] p 1456 N95-19908

SPACE-R thermionic space nuclear power system: Design and technology demonstration
[DE95-000713] p 1221 N95-20076

The First NREL Conference on Thermophotovoltaic Generation of Electricity: Proceedings
[DE94-011831] p 1391 N95-20332

Development of a lightweight, light-trapped, thin GaAs solar cell for spacecraft applications
p 1318 N95-20513

FASTPACK: Optimized solutions for modular avionics derived from a parametric study. Part 1: Platform features p 1208 N95-20634

EPICS simulation tools for control system development
[DE94-018082] p 1462 N95-20699

Highlights of recent balance of system research and evaluation
[DE95-001626] p 1393 N95-20863

Mechanical design of the DO silicon detector
[DE95-002532] p 1365 N95-20902

Exploratory Technology Research Program for electrochemical energy storage
[DE95-002652] p 1394 N95-20915

Multiple Mechanism Propagation Paths (MMPPs): Their Characterisation and Influence on System Design
[AGARD-CP-543] p 1292 N95-20921

A MMPP communications system for the frequency range 2-200MHz p 1293 N95-20924

Low noise 22 GHz receiver for the radioastron satellite. Part 1: Requirements, design and reliability analysis
[PB95-104410] p 1300 N95-20972

Routing of unidirectional packet radio for wide-area paging network control and maintenance
[PB95-104428] p 1300 N95-20980

Advanced wind turbine design studies: Advanced conceptual study
[DE93-000031] p 1394 N95-20985

Preliminary study of HUTSAT microsatellite
[PB95-127619] p 1220 N95-21026

Methodology for ESCA analysis of electromigration
[AD-A286229] p 1241 N95-21168

EXPERT system expert: Program description
[PB95-131561] p 1482 N95-21429

Crew-Centered Cockpit Design (CCCD) field demonstration program, volume 1
[AD-A286426] p 1453 N95-21566

Design model for open distributed processing systems
[PB95-135505] p 1477 N95-21620

Underwater Acoustic Generator Phase 2: Sea trial, March 1992
[MRL-TN-640] p 1434 N95-21657

An 8-meter-long coupled cavity RFQ linac
[DE94-018077] p 1331 N95-21667

Structuring design requirements using YMIR
[PB95-132742] p 1471 N95-22081

Bridging worlds/charting new courses
[DE95-003808] p 1397 N95-22335

SYSTEMS INTEGRATION

System design document U-AVLIS control system architecture
[DE94-017297] p 1460 N95-20387

FASTPACK: Optimized solutions for modular avionics derived from a parametric study. Part 1: Platform features p 1208 N95-20634

SYSTEMS MANAGEMENT

But what will it Cost? The history of NASA cost estimating p 1583 N95-20742

Defense Data Repository System (DDRS). End user manual
[AD-A286484] p 1592 N95-22293

SYSTEMS SIMULATION

A simulation study of TCP performance in ATM networks
[DE94-016622] p 1477 N95-21505

SYSTOLIC ARRAYS

Preliminary evaluation of a digital optical systolic processor implemented with acousto-optic cells
[AD-A286377] p 1541 N95-20231

T

TABLES (DATA)

The effects of three-dimensional graphs on decision making
[AD-A285034] p 1583 N95-20051

Guidelines for the creation and management of geographic data bases within a GIS environment, version 1.0
[DE94-019214] p 1458 N95-20073

TBell: A mathematical tool for analyzing decision tables
[NASA-CR-195027] p 1462 N95-20691

Solar-Geophysical Data number 600, August 1994. Part 1: (Prompt reports). Data for July, June 1994, and late data
[PB95-104923] p 1603 N95-20713

Solar-Geophysical Data number 600, August 1994. Part 2: (Comprehensive reports). Data for February 1994 and miscellaneous
[PB95-105060] p 1603 N95-20722

TACHOMETERS

Variations observed in the AC generator signal period of a Sea King helicopter
[AD-A284280] p 1206 N95-19963

TACTILE SENSORS (ROBOTICS)
Surface micromachined capacitive tactile image sensor
[PB95-108031] p 1288 N95-21633
TAIL ASSEMBLIES
Pressure measurements on an F/A-18 twin vertical tail in buffeting flow. Volume 4, part 1: Buffet cross spectral densities
[AD-A285593] p 1215 N95-21214
Pressure measurements on an F/A-18 twin vertical tail in buffeting flow. Volume 1: Wind tunnel test summary
[AD-A279126] p 1202 N95-21877
TAIL SURFACES
Pressure measurements on an F/A-18 twin vertical tail in buffeting flow. Volume 4, part 1: Buffet cross spectral densities
[AD-A285593] p 1215 N95-21214
Pressure measurements on an F/A-18 twin vertical tail in buffeting flow. Volume 1: Wind tunnel test summary
[AD-A279126] p 1202 N95-21877
TAKEOFF
F-15 resource tape
[NASA-TM-110502] p 1206 N95-19994
Wavelet-based acoustic recognition of aircraft
[DE94-017701] p 1503 N95-20019
TANDEM MIRRORS
Propulsion research on the variable tandem mirror plasma rocket
[NASA-CR-196310] p 1221 N95-20059
TANKS (COMBAT VEHICLES)
Navigation system in combat vehicle
[PB95-131629] p 1452 N95-21467
TANTALUM
Advanced concepts for gamma ray isotopic analysis and instrumentation
[DE94-016610] p 1517 N95-21174
Characterization of a texture gradient in tantalum plate
[DE95-002704] p 1262 N95-22289
TANTALUM ALLOYS
Plasma arc melting of titanium-tantalum alloys
[DE94-016291] p 1252 N95-20331
Corrosion resistance and behavior of construction materials exposed to dilute sulfuric acid at elevated temperatures under static conditions
[DE95-001723] p 1259 N95-21739
Plasma arc melting of a 80 weight percent tantalum -20 weight percent titanium alloy
[DE95-000846] p 1260 N95-22006
Effect of annealing temperature on the texture of rolled tantalum and tantalum-10 wt % tungsten
[DE95-002702] p 1262 N95-22308
TANTALUM OXIDES
Measurement of the thermal properties of electrically conducting fluids using coated transient hot wires
[DE94-017816] p 1357 N95-22264
TARGET ACQUISITION
Effects of bifocal and progressive-addition corrective lenses on aviator target-detection performance
[AD-A279698] p 1442 N95-20710
LADAR detection statistics in the presence of pointing errors
[AD-A285865] p 1309 N95-22134
TARGET RECOGNITION
Experimental proof-of-concept of phase derivative based range profile enhancement ATR
[AD-A284921] p 1289 N95-19997
The spatiotemporal characteristics of visual motion priming
[AD-A284782] p 1449 N95-20062
Method and apparatus for classifying targets
[AD-D016519] p 1303 N95-21464
Definition report on target and related steering variables of radiation as a part of the environmental balance and environmental outlook investigation
[PB95-135471] p 1409 N95-21846
TARGETS
X-ray imaging of uniform large scale-length plasmas created from gas-filled targets on Nova
[DE94-018339] p 1531 N95-20015
Enhanced vehicle and event typing software, phase 1
[AD-A284862] p 1458 N95-20070
A comparison of kinetic and multifluid simulations of laser-produced colliding plasmas
[DE94-016447] p 1551 N95-20315
Rate controlled synthesis of composition modulated, metal-oxide thin films
[DE94-016596] p 1267 N95-20317
Production of J/(psi) in 800 GeV/c p-Si interactions
[DE94-017982] p 1513 N95-20496
Effects of bifocal and progressive-addition corrective lenses on aviator target-detection performance
[AD-A279698] p 1442 N95-20710
Radiation-driven targets for heavy-ion fusion
[DE95-002264] p 1533 N95-20784
In-situ capability of ion beam modification and characterization of materials at Los Alamos National Laboratory
[DE95-002738] p 1534 N95-21236
A neutron beam polarizer for study of parity violation in neutron-nucleus interactions
[DE95-002743] p 1519 N95-21237
Shot-to-shot comparison of the first Li-beam driven Hohlraum experiments
[DE94-016558] p 1558 N95-21247
LIF standoff research
[DE94-018744] p 1535 N95-21328
Tungsten-uranium penetrator target interaction
[DE95-000847] p 1387 N95-21364
A high-rate fixed-target charm experiment
[DE95-001767] p 1521 N95-21378
Fiber-optic sensors for rapid, inexpensive characterization of soil and ground water contamination
[DE95-002471] p 1545 N95-21510
AN/APS-137 Forward Looking Airborne Radar (FLAR) evaluation, Fall 1992 experiment
[AD-A279526] p 1306 N95-21686
Impact degassing of water and noble gases from silicates p 1416 N95-21780
Selection of RIB targets using ion implantation
[DE95-000951] p 1538 N95-21938
Aluminium oxide targets after ballistic impact; fragmentation of the ceramic and the projectile
[PB95-133625] p 1388 N95-22097
LADAR detection statistics in the presence of pointing errors
[AD-A285865] p 1309 N95-22134
Probability of detection for a GO CFAR radar processor using envelope detection approximation
[AD-A286211] p 1310 N95-22251
Materials processing and manufacturing technologies for diamond substrates multichip modules
[AD-A285775] p 1336 N95-22412
TASK COMPLEXITY
Human performance studies for control of multiple remote systems
[AD-A286623] p 1452 N95-20768
TASK PLANNING (ROBOTICS)
Tom Thumb algorithm for planning simple vehicle motions
[PB95-107553] p 1484 N95-22156
TASKS
The MSFC Program Control Development Program
p 1585 N95-20754
TAXONOMY
An empirical approach to logical clustering of software failure regions
[AD-A279863] p 1462 N95-20776
TEARING MODES (PLASMAS)
Coupled tearing modes in plasmas with differential rotation
[DE94-631422] p 1548 N95-19977
Fluctuations and transport in the reversed field pinch: Characterization and reduction
[DE95-000590] p 1549 N95-20113
Simulation of tearing mode stabilization by using ECH
[DE94-770700] p 1554 N95-20684
Investigation of spherical tearing mode
[NASA-CR-197284] p 1558 N95-21345
TECHNETIUM
In vivo distribution of liposome encapsulated hemoglobin studied with imaging radiotracers
[AD-A279774] p 1438 N95-20806
TECHNOLOGIES
The Energy Science and Technology Database on a local library system: A case study at the Los Alamos National Research Library
[DE95-001009] p 1589 N95-20818
TECHNOLOGY ASSESSMENT
Natural gas cleanup: Evaluation of a molecular sieve carbon as a pressure swing adsorbent for the separation of methane/nitrogen mixtures
[DE94-012263] p 1234 N95-20135
Energy and Technology Review
[DE94-017686] p 1219 N95-20148
Beyond telecommuting: A new paradigm for the effect of telecommunications on travel
[DE95-001224] p 1289 N95-20214
Assessment of liquefaction and pyrolysis systems
[PB95-129797] p 1236 N95-20290
Brushless Doubly-Fed Machine system development program, phase 3
[DE94-013095] p 1315 N95-20380
Europe's space photovoltaics programme
p 1316 N95-20506
Status of diffused junction p+n InP solar cells for space applications p 1317 N95-20509
Reliability assessment of Multichip Module technologies via the Triservice/NASA RELTECH program
p 1210 N95-20643
High density monolithic packaging technology for digital/microwave avionics p 1211 N95-20646
Technical and economic evaluation of natural gas based synthesis gas production technologies
[PB95-130597] p 1242 N95-21426
An MCM concurrent engineering software tool market study
[AD-A279257] p 1468 N95-21489
Power systems for future missions. Appendices A-L
[NASA-CR-195320-APP-A-L] p 1395 N95-21530
Power systems for future missions
[NASA-CR-195320] p 1222 N95-21531
An initial assessment of the properties of 2,5-dipicryl-1,3,4-oxadiazole: A secondary explosive with high thermal stability
[MRL-TR-93-16] p 1284 N95-21624
Ceramic technology for advanced heat engines
[DE95-000950] p 1278 N95-21937
Plasma processing for integrated circuits
[DE95-001419] p 1335 N95-22149
TECHNOLOGY TRANSFER
Geothermal direct-heat utilization assistance
[DE94-011546] p 1391 N95-20104
Environmental cleanup technology transfer initiatives
[AD-A285059] p 1403 N95-20487
HPCC technology awareness program: Improved economic competitiveness through technology awareness, transfer and application
[DE95-002134] p 1476 N95-21355
ANSTO: Program of research, 1993-1994
[DE94-631122] p 1605 N95-21828
Bridging worlds/charting new courses
[DE95-003808] p 1397 N95-22335
Technology transfer: Improving the use of cooperative R/D agreement at DOE's contractor-operated laboratories. Report to Congressional requesters
[GAO/RCED-94-91] p 1586 N95-22403
Space systems technology working group: Executive report
[AD-A285778] p 1217 N95-22413
TECHNOLOGY UTILIZATION
Geothermal direct-heat utilization assistance
[DE94-011546] p 1391 N95-20104
Performance specifications for technology development: Application for characterization of volatile organic compounds in the environment
[DE94-016627] p 1401 N95-20234
The First NREL Conference on Thermophotovoltaic Generation of Electricity: Proceedings
[DE94-011831] p 1391 N95-20332
An update on the Department of Energy's photovoltaic program p 1316 N95-20505
Status of flexible CIS research at ISET
p 1317 N95-20512
Development of a lightweight, light-trapped, thin GaAs solar cell for spacecraft applications
p 1318 N95-20513
Advances in polycrystalline thin-film photovoltaics for space applications p 1318 N95-20514
Amorphous silicon thin films: The ultimate lightweight space solar cell p 1318 N95-20515
Calculation of near optimum design of InP/In(0.53)Ga(0.47)As monolithic tandem solar cells
p 1318 N95-20517
Processing and applications of iron aluminides
[DE94-017855] p 1253 N95-20673
Representing manufacturing features to support design and process changes
[DE94-018587] p 1467 N95-21389
Policies concerning military and civilian research and technology applications
[PB95-131355] p 1585 N95-21427
Independent review of Aviation Technology and Research Information Analysis System (ATRIAS) database
[AD-A284049] p 1203 N95-21518
Power systems for future missions. Appendices A-L
[NASA-CR-195320-APP-A-L] p 1395 N95-21530
Spinoff, 1994
[NASA-NP-214] p 1594 N95-21893
Advanced energy systems and technologies research programme
[DE95-717486] p 1397 N95-22337
TECTONICS
Anatomy of the Midcontinent Rift beneath Lake Superior
[DE94-019298] p 1415 N95-21477
TEFLON (TRADEMARK)
Optical multilayers with an amorphous fluoropolymer
[DE94-017693] p 1541 N95-20218
TELECOMMUNICATION
Algebraic semantics of message sequence charts
[PB95-110581] p 1288 N95-19890
Beyond telecommuting: A new paradigm for the effect of telecommunications on travel
[DE95-001224] p 1289 N95-20214

Advanced Command and Control (C2) applications interfaces to the Advanced Communications Technology Satellite (ACTS)
[AD-A279676] p 1291 N95-20605
The demise of plastic encapsulated microcircuit myths p 1209 N95-20640
Passive monitoring for automated MMPP communication systems p 1293 N95-20927
Simulation of the impact of atmospheric turbulences on millimeter-wave communications systems p 1295 N95-20939
Experimental study of the helicopter-mobile radioelectrical channel and possible extension to the satellite-mobile channel p 1296 N95-20945
FIREDOC users manual, 3rd edition
[PB95-128674] p 1286 N95-21129
Application-oriented architecture for multimedia teleservices
[PB95-135513] p 1306 N95-21623
Modelling multimedia teleservices with OSI upper layers framework: Short paper
[PB95-132734] p 1308 N95-22080

TELECONFERENCING
Modelling multimedia teleservices with OSI upper layers framework: Short paper
[PB95-132734] p 1308 N95-22080

TELEMETRY
Digital filtering for data compression in telemetry systems
[DE94-016611] p 1219 N95-20567

TELESCOPES
Pushing the limits of spatial resolution with the Kuiper Airborne observatory p 1593 N95-21754

TELEVISION SYSTEMS
Application of computer-generated holograms to optical transformations
[AD-A286356] p 1368 N95-22256

TELLURIDES
Angle resolved photoemission on K(0.3)Mo3, TiTe2 and Ti(1+x)S2
[DE94-018300] p 1574 N95-21712
Performance of cesium telluride photocathodes as an electron source for the Los Alamos FEL
[DE94-018302] p 1375 N95-21919

TELLURIUM
Scanning tunneling microscopy of semiconductor surfaces
[AD-A279982] p 1571 N95-20964
IR materials producibility
[AD-A280094] p 1328 N95-21017
Research on the power generation system with thermoelectric conversion elements
[DE95-714804] p 1397 N95-22309

TELLURIUM COMPOUNDS
Photocathodes for free electron lasers
[DE94-018305] p 1376 N95-22242
Fabrication and characterization of cesium telluride photocathodes: A promising electron source for the Los Alamos Advanced FEL
[DE94-018303] p 1377 N95-22348

TEMPEL 2 COMET
Application of MCM image construction to IRAS comet observations p 1594 N95-21772

TEMPERATE REGIONS
Effects of microphysics and radiation on mesoscale processes of a midlatitude squall line
[DE94-014732] p 1429 N95-20381
Semi-volatiles at Mercury: Sodium (Na) and potassium (K) p 1424 N95-21818

TEMPERATURE CONTROL
Direct aromatization of methane
[DE94-017131] p 1233 N95-19924
Preliminary control system design and analysis for the Space Station Furnace Facility thermal control system
[NASA-TM-108476] p 1365 N95-20560
Liquid flow-through cooling of electronic modules p 1211 N95-20647
Thermal fixture for testing an integrated circuit
[AD-D016483] p 1333 N95-21900
High average power diode pumped solid state lasers for CALIOPE
[DE94-019248] p 1376 N95-22121

TEMPERATURE DEPENDENCE
A test of the Arrhenius extrapolation assumption for a nitrile rubber
[DE94-017337] p 1263 N95-19926
Post-irradiation deformation characteristics of heavy-ion irradiated 304L SS
[DE94-017462] p 1251 N95-20088
Properties of molecular solids and fluids at high pressure and temperature
[DE94-017594] p 1565 N95-20243
Thermodynamic analysis of stable and metastable equilibrium diagrams of the Cu-Cr system
[PB95-127775] p 1255 N95-21111
In-situ capability of ion beam modification and characterization of materials at Los Alamos National Laboratory
[DE95-002738] p 1534 N95-21236
Overview of the field and temperature dependence of J(c) in Ag/BSCCO tapes
[PB95-110318] p 1574 N95-21636
Corrosion resistance and behavior of construction materials exposed to dilute sulfuric acid at elevated temperatures under static conditions
[DE95-001723] p 1259 N95-21739
Non-H2Se, ultra-thin CuInSe2 devices
[DE94-011894] p 1395 N95-21844
Irradiation creep in structural materials at ITER operating conditions
[DE94-018946] p 1261 N95-22123
Temperature dependence of a magnetopolaron in a harmonic quantum dot in resonant magnetic fields
[DE94-629036] p 1502 N95-22177
Temperature dependence of magnetopolarons in a parabolic quantum dot in arbitrary magnetic fields
[DE94-629033] p 1528 N95-22218
Studies of the microwave resistivity of kappa-(BEDT-TTF)2Cu(N(CN)2)Cl
[DE95-002980] p 1262 N95-22291

TEMPERATURE DISTRIBUTION
Effects of non-unity Lewis numbers in diffusion flames p 1249 N95-21036
Effect of chemical heat release in a temporally evolving mixing layer p 1249 N95-21037

TEMPERATURE EFFECTS
Investigation of a thermal buoyancy effect on the drag of half models tested in the ARA Transonic Wind Tunnel
[ARA-MEMO-407] p 1199 N95-19946
Mechanical behavior of 97.2% W alloy in tension at high temperatures
[AD-A284797] p 1250 N95-20067
Generation of micro-domains in AT-cut quartz by thermal processing and the effect on resonator modes
[DE94-017344] p 1564 N95-20087
Design and thermal stress analysis of high power x-ray monochromators cooled with liquid nitrogen
[DE94-016879] p 1500 N95-20106
Mercury capture in bench-scale absorbers
[DE94-016910] p 1234 N95-20107
Application of an energy-based life prediction model to bithermal and thermomechanical fatigue
[NASA-TM-106684] p 1385 N95-20179
Nonlinear Faraday effect in CdS semiconductor in an ultrahigh magnetic field
[DE94-016804] p 1564 N95-20240
A new mini Ball Grid Array (mBGA) multichip module technology
[DE94-018897] p 1480 N95-20342
Effect of heat treatment temperature on creep-rupture properties of Fe3Al-based alloys
[DE94-017904] p 1253 N95-20375
The role of high pressure in the study and applications of the ferroelectric polymer polyvinylidene fluoride and its copolymers
[DE94-015742] p 1268 N95-20396
Review of solar cell temperature coefficients for space p 1323 N95-20541
Crystalline beams
[DE95-002656] p 1569 N95-20793
Effects of non-unity Lewis numbers in diffusion flames p 1249 N95-21036
Effect of chemical heat release in a temporally evolving mixing layer p 1249 N95-21037
Temperature effects on acoustic interactions between altitude test facilities and jet engine plumes
[NASA-CR-197638] p 1504 N95-21170
Effect of atmospheric pressure on measured aircraft noise levels
[PB95-130423] p 1207 N95-21425
Raman spectra of MOCVD-grown ferroelectric PbTiO3 thin films
[DE94-018964] p 1244 N95-21549
Instabilities in natural-convection flows in cavities
[PB95-107975] p 1354 N95-21578
Non-linear A/D converters for integrated silicon smart sensors
[PB94-208402] p 1330 N95-21590
Modeling the response of the California Current system to Global Greenhouse Warming
[DE94-018253] p 1408 N95-21708
A visual cell for measuring the solubility of prograde soluble salts in water at high temperatures and pressures
[DE95-002058] p 1245 N95-21732
Oxidation behavior of aluminum nanopowders
[DE95-002721] p 1260 N95-21926
Flux creep with logarithmic U(j) dependence
[DE94-629058] p 1577 N95-22180
Effect of annealing temperature on the texture of rolled tantalum and tantalum-10 wt % tungsten
[DE95-002702] p 1262 N95-22308

TEMPERATURE GRADIENTS
Transport phenomena in the micropores of plug-type phase separators
[NASA-TM-108479] p 1340 N95-20561
Instabilities in natural-convection flows in cavities
[PB95-107975] p 1354 N95-21578
Far-infrared mapping of dusty elliptical galaxies p 1593 N95-21763
Phase E in a water-saturated peridotite system at 9.3 GPa p 1420 N95-21799
Stability effects on the profiles of vertical velocity and its variance in katabatic flow
[DE95-001126] p 1426 N95-21836

TEMPERATURE INVERSIONS
Air pollution caused by fireworks during the turn of the year 1992-1993
[PB95-135265] p 1409 N95-21718

TEMPERATURE MEASUREMENT
An at-sea evaluation of an infrared/resistance temperature device for air/sea-surface temperature measurements
[AD-A279672] p 1365 N95-20604
Multiwire thermocouples: Frequency response
[NASA-TM-110510] p 1367 N95-21889
Acoustic Thermometry of Ocean Climate (ATOC): Selection of California source site
[AD-A279295] p 1436 N95-21987
Numerical investigation of one-dimensional heat-flux calculations
[AD-A286293] p 1582 N95-22054
Real time system for practical acoustic monitoring of global ocean temperature
[AD-A286435] p 1436 N95-22209

TEMPERATURE PROBES
Dual active surface heat flux gage probe
[NASA-TM-106861] p 1366 N95-21391

TEMPERATURE PROFILES
Synthesizing the Gulf Stream thermal structure from XBT data
[AD-A279665] p 1433 N95-20458
Enhanced scrape-off layer plasma in D3-D double-null discharges
[DE94-017977] p 1554 N95-20571
Azimuthally averaged radial S(sub 100 microns)/S(sub 60 microns) dust color temperatures in spiral galaxies p 1593 N95-21760

TEMPORAL DISTRIBUTION
Source distribution of visual evoked neuromagnetic responses
[PB95-127643] p 1445 N95-21348

TEMPORAL LOGIC
Abstract interpretation of reactive systems: Abstractions preserving Universal CTL(*), Existential CTL(*) and CTL(*)
[PB95-110557] p 1472 N95-22305

TEMPORAL RESOLUTION
Temporal and spectral investigation of multi-Landau level quantum beats in GaAs
[DE94-018189] p 1569 N95-20678
Progress in ultrafast scanning probe microscopy
[DE94-018179] p 1373 N95-21261
Time resolved x-ray detection
[AD-A279348] p 1368 N95-22143

TENSILE CREEP
Creep behavior in SiC whisker-reinforced alumina composite
[DE95-001071] p 1231 N95-21776

TENSILE PROPERTIES
Microstructures and tensile properties of as-cast iron-aluminide alloys
[DE94-017868] p 1252 N95-20359
The processing and mechanical properties of high temperature/high performance composites. Stress redistribution and notch properties, book 2
[AD-A279737] p 1227 N95-20429
Impact behavior of FeAl alloy FA-350
[DE94-018128] p 1254 N95-20705
Plasma arc melting of a 80 weight percent tantalum -20 weight percent titanium alloy
[DE95-000846] p 1260 N95-22006
Incology alloy 908 data handbook
[DE95-001818] p 1260 N95-22013
Tensile and impact properties of iron-aluminum alloys
[DE94-017750] p 1263 N95-22346

TENSILE STRENGTH
Carbon fiber reinforced superconductor composites
[DE95-002504] p 1229 N95-20913
Fracture behavior of the Fe-8Al alloy FAP-Y
[DE95-000956] p 1258 N95-21676
The development of a super-alpha2 titanium aluminide alloy consolidated by rapid omnidirectional compaction
[AD-A279254] p 1260 N95-21986

Low temperature tensile and fracture mechanical strength in mode 1 and mode 2 of fiber reinforced plastics following various irradiation conditions [DE94-019269] p 1232 N95-22130

TENSILE STRESS

Approaches to the design of structural ceramics incorporating whiskers and particulate phases [DE94-018126] p 1271 N95-20704
The development of a super-alpha2 titanium aluminide alloy consolidated by rapid omnidirectional compaction [AD-A279254] p 1260 N95-21986

TENSILE TESTS

Mechanical behavior of 97.2% W alloy in tension at high temperatures [AD-A284797] p 1250 N95-20067
Development of superplasticity in 5083 aluminum with additions of Mn and Zr [DE94-017474] p 1251 N95-20090

TENSORS

Large eddy simulation of channel flow using a vorticity transport subgrid model p 1348 N95-21076
Solid-state NMR characterization of C- and N-labelled phthalimides: Model compounds for studying polyimides [AD-A286479] p 1578 N95-22286
Databases post-processing in Tensoral p 1363 N95-22465

TEREPHTHALATE

Determinations of phase transitions in nylon 6-12, nylon-6, polyvinyl chloride and polyethylene terephthalate by positron annihilation spectroscopy [DE94-629992] p 1239 N95-20736

TERMINAL BALLISTICS

Significance of impact velocity for the extent of damage in carbon/epoxy laminates [PB95-133484] p 1230 N95-21417
Aluminium oxide targets after ballistic impact; fragmentation of the ceramic and the projectile [PB95-133625] p 1388 N95-22097

TERMINOLOGY

Abbreviations and acronyms [NASA-TM-110506] p 1590 N95-21457
Glossary of frequency and timing terms and a pictorial representation of terms used in the behavior and analyses of frequency standards [AD-A286172] p 1310 N95-22247

TERNARY ALLOYS

Novel materials [AD-A279693] p 1227 N95-20427
Excitons in semiconducting superlattices, quantum wells, and ternary alloys [DE95-001867] p 1572 N95-21287
Tensile and impact properties of iron-aluminum alloys [DE94-017750] p 1263 N95-22346

TERNARY SYSTEMS

Magnetic x ray circular dichroism in Fe Co Pt multilayers [DE94-017522] p 1253 N95-20447
Metastable bcc phase formation in the Nb-Cr-Ti system [DE94-016212] p 1255 N95-21137
Computational modeling of diffusion-controlled transformations in ternary systems [DE95-001358] p 1256 N95-21298

TERRAIN

Evolution of ground line of sight data field collection techniques [AD-A285062] p 1204 N95-20497
Terrain and refractivity effects on non-optical paths p 1294 N95-20931
Combined effects of atmosphere and terrain on UHF/microwave paths p 1295 N95-20935
ICE BABY: Measurements of concentration fluctuations in a forest area in winter conditions [PB95-133468] p 1405 N95-21274
Review of GIS applications in hydrologic modeling [AD-A279076] p 1390 N95-21628
Stability effects on the profiles of vertical velocity and its variance in katabatic flow [DE95-001126] p 1426 N95-21836
Solving the inverse problem in terrain modeling [AD-A285860] p 1391 N95-22131

TERRESTRIAL PLANETS

Conference on Deep Earth and Planetary Volatiles [NASA-CR-196944] p 1415 N95-21777
Impact degassing of water and noble gases from silicates p 1416 N95-21780
Origin and loss of the volatiles of the terrestrial planets p 1417 N95-21785
Degassing history and evolution of volcanic activity of terrestrial planets based on radiogenic noble gas degassing models p 1424 N95-21816
Implications of noble gases in a recently recognized Martian meteorite (ALH84001) for the degassing history of Mars p 1424 N95-21819
Water abundance and accretion history of terrestrial planets p 1424 N95-21820

TEST CHAMBERS

16-foot transonic tunnel test section flowfield survey [NASA-TM-109157] p 1216 N95-20669
Space power facility readiness for Space Station power system testing [NASA-TM-106829] p 1218 N95-21384

TEST FACILITIES

Round-robin comparison of heat release apparatus [AD-A285831] p 1363 N95-20031
Design trade-off study for a large volume short pulse neutron assembly [DE94-019175] p 1509 N95-20206
Description and flow characterization of hypersonic facilities [AD-A284291] p 1200 N95-20248
Inverse Cerenkov laser acceleration experiment at ATF [DE94-017990] p 1370 N95-20572
Testing of the SAIC facets on the stretched-membrane dish [DE95-001831] p 1393 N95-20864
Recent National Solar Thermal Test Facility activities, in partnership with industry [DE95-001828] p 1394 N95-21353
Space power facility readiness for Space Station power system testing [NASA-TM-106829] p 1218 N95-21384
Portable static test facility for small, expendable, turbojet engines, phase 1 [AD-A286337] p 1216 N95-21719
Cathode Life Test Facility [AD-A286232] p 1334 N95-22023
The Large Area Pulsed Solar Simulator (LAPSS) [NASA-CR-197339] p 1397 N95-22336
Proceedings of the 4th Annual Major Range and TestFacility Base (MRTFB) Environmental Workshop [AD-A285779] p 1411 N95-22414

TEST PILOTS

T-45A High Angle of Attack Testing: US Naval Test Pilot School 46th Annual Reunion and Symposium [AD-A284000] p 1207 N95-20466

TEST STANDS

Real-time reconfiguration study [AD-A286060] p 1464 N95-20910

TEST VEHICLES

A new mini Ball Grid Array (mBGA) multichip module technology [DE94-018897] p 1480 N95-20342

TETHERED BALLOONS

CALIOPE and TAISIR airborne experiment platform [DE94-018328] p 1310 N95-22299

TETHERED SATELLITES

Tethered satellite: Forces and motion [NASA-TM-110518] p 1220 N95-21858

TETHERING

Towards tailored interphase formation utilizing surface-bound benzylsulfonium salts as cationic initiators [AD-A286461] p 1280 N95-22259

TETRAHYDROFURAN

The preparation of all para-polyphenyls with increased solubility and enhanced third order NLO activity [AD-A284301] p 1266 N95-20251

TEXTURES

Local texture and strongly linked conduction in spray-pyrolyzed TlBa2Ca2Cu3O(8+x) deposits [DE94-017887] p 1578 N95-22269
Characterization of a texture gradient in tantalum plate [DE95-002704] p 1262 N95-22289
Effect of annealing temperature on the texture of rolled tantalum and tantalum-10 wt % tungsten [DE95-002702] p 1262 N95-22308

THALLIUM

T1F ((1) sigma (+)): Some preliminary electronic structure calculations [PB95-130316] p 1518 N95-21223
Surface x-ray scattering and scanning tunneling microscopy studies at the Au(111) electrode [DE95-002409] p 1573 N95-21516

THALLIUM COMPOUNDS

Dependence of critical current density on microstructure and processing of high-T(c) superconductors [DE95-000685] p 1571 N95-21167
InTlSb for long-wavelength infrared photodetectors and arrays [AD-A280109] p 1331 N95-21660
Local texture and strongly linked conduction in spray-pyrolyzed TlBa2Ca2Cu3O(8+x) deposits [DE94-017887] p 1578 N95-22269

THALLIUM ISOTOPES

ANSTO: Mission statement, significant events and achievements [DE94-631123] p 1605 N95-21830

THEOREMS

General conservative extension theorem in process algebra [PB95-110656] p 1487 N95-19902
Balanced matrices [AD-A280021] p 1490 N95-20662
Adjunctions [PB95-134078] p 1494 N95-21868
Minimal square spectral factors [PB95-132726] p 1495 N95-22032
Local connectivity of some Julia sets containing a circle with an irrational rotation [PB95-109070] p 1496 N95-22353

THEORETICAL PHYSICS

Research in theoretical elementary particle physics at the University of Florida, task A [DE94-004373] p 1512 N95-20469
Theoretical particle physics [DE95-002447] p 1515 N95-20893
Heavy ion collisions [DE95-002712] p 1520 N95-21321
Theoretical atomic physics for fusion [DE94-019196] p 1524 N95-21605
Tethered satellite: Forces and motion [NASA-TM-110518] p 1220 N95-21858
The solar flux of thermal neutrinos and antineutrinos of all flavors [DE95-003204] p 1604 N95-22085
Transactions of the Eleventh Army Conference on Applied Mathematics and Computing [AD-A279884] p 1497 N95-22389

THERAPY

Radiofrequency hyperthermia systems: Experimental and clinical assessment of the feasibility of radiofrequency hyperthermia systems for loco-regional deep heating [PB94-206885] p 1444 N95-21016

THERMAL ANALYSIS

Fusion welding of advanced borated stainless steels [DE94-019037] p 1378 N95-20053
A new mini Ball Grid Array (mBGA) multichip module technology [DE94-018897] p 1480 N95-20342
Synthesizing the Gulf Stream thermal structure from XBT data [AD-A279665] p 1433 N95-20458
The formation of reaction bonded Si3N4 at low temperatures and in short times [DE95-001990] p 1275 N95-21289
Theory and modelling of quench in cable-in-conduit superconducting magnets [DE95-001819] p 1330 N95-21442
An initial assessment of the properties of 2,5-dipicryl-1,3,4-oxadiazole: A secondary explosive with high thermal stability [MRL-TR-93-16] p 1284 N95-21624
Lubricant evaluation and performance, 2 [AD-A279144] p 1278 N95-21969
Frame and edge seal technology: A state of the art survey [PB95-110334] p 1288 N95-22014
High temperature corrosion and crack growth of SiC/SiC at variable oxygen partial pressures [DE94-018715] p 1232 N95-22115
Thermal and deformation analyses of a novel cryogenically cooled monochromator for an Advanced Photon Source beamline [DE94-016914] p 1527 N95-22190

THERMAL BARRIERS (PLASMA CONTROL)

On conception of a compact neutron source and the possibility of its simulation on the Amba-M end trap [DE94-633373] p 1562 N95-22282

THERMAL BATTERIES

Development of a tester for evaluation of prototype thermal cells and batteries [DE95-000540] p 1325 N95-20628

THERMAL CONDUCTIVITY

The thermal conductivity of carbon coated silicon carbide fibers embedded in a silicon carbide matrix [DE94-017758] p 1225 N95-20023
Properties of whisker-reinforced ceramics [DE94-017759] p 1264 N95-20024
Design and thermal stress analysis of high power x-ray monochromators cooled with liquid nitrogen [DE94-016879] p 1500 N95-20106
The thermal conductivity of carbon-fiber reinforced metal matrix composites [DE94-017767] p 1226 N95-20125
Computer program for calculation of complex chemical equilibrium compositions and applications. Part 1: Analysis [NASA-RP-1311] p 1235 N95-20180
Materials processing and manufacturing technologies for diamond substrates multichip modules [AD-A285060] p 1315 N95-20488
Review of recent D-T experiments from TFTR [DE95-002755] p 1557 N95-21239
The thermal conductivity of silicon nitride with molybdenum disilicide additions [DE94-017757] p 1247 N95-22260

Measurement of the thermal properties of electrically conducting fluids using coated transient hot wires
|DE94-017816| p 1357 N95-22264

THERMAL CYCLING TESTS
Thermo-mechanical fatigue of polymer matrix composites
|AD-A285931| p 1267 N95-20390
Carbon fiber reinforced superconductor composites
|DE95-002504| p 1229 N95-20913
Development of an advanced JP-8 fuel
|AD-A285583| p 1283 N95-21161
Survivability of soldered leadless chip carriers after temperature cycling
|DE95-001497| p 1329 N95-21301

THERMAL DECOMPOSITION
An atomically-resolved STM study of the thermal decomposition of disilane on Si(001)
|AD-A279818| p 1567 N95-20544
Atomically resolved structure and bonding of delta-doped boron layers on Si(001)
|AD-A279820| p 1513 N95-20586
Synthesis and characterization of (Zn(SEt)Et)10, formed via insertion of sulfur into Zn-C bonds: A new class of Wurtzite-like cluster framework
|AD-A279701| p 1569 N95-20714
The Carnol process for methanol production and utilization with reduced CO2 emissions
|DE94-016808| p 1283 N95-21211
Thermal decomposition reactions of HMX and RDX and their importance in predicting cookoff hazards
|DE95-002486| p 1283 N95-21513
Restricted mass transport effects on free radical reactions
|DE94-018136| p 1217 N95-21706

THERMAL DEGRADATION
Accelerated screening methods for determining chemical and thermal stability of refrigerant-lubricant mixtures. Part 2: Experimental comparisons and verification of methods
|DE95-000743| p 1264 N95-20078
Detection of environmental deterioration in fiber reinforced composites by FT-Raman spectroscopy, phase 1
|AD-A279763| p 1228 N95-20805

THERMAL DIFFUSIVITY
Laser-Induced Thermal Acoustics (LITA): Four-wave mixing measurement of sound speed, thermal diffusivity, and viscosity
|AD-A286524| p 1372 N95-21009
Heat loss by helicity injection in spheromaks
|DE95-003473| p 1562 N95-22221

THERMAL DISSOCIATION
An atomically-resolved STM study of the thermal decomposition of disilane on Si(001)
|AD-A279818| p 1567 N95-20544

THERMAL EMISSION
Shot-to-shot comparison of the first Li-beam driven Hohlraum experiments
|DE94-016558| p 1558 N95-21247
Far-infrared mapping of dusty elliptical galaxies
p 1593 N95-21763

THERMAL ENERGY
A comparison of kinetic and multifluid simulations of laser-produced colliding plasmas
|DE94-016447| p 1551 N95-20315
Experimental investigation of molecular beam injection in HL-1 tokamak
|DE94-631456| p 1556 N95-21165
Economic feasibility analysis of distributed electric power generation based upon the natural gas-fired fuel cell
|DE94-012277| p 1396 N95-22033

THERMAL ENVIRONMENTS
MCMs for avionics: Technology selection and intermodule interconnection p 1210 N95-20641

THERMAL EXPANSION
Properties of whisker-reinforced ceramics
|DE94-017759| p 1264 N95-20024
Design and thermal stress analysis of high power x-ray monochromators cooled with liquid nitrogen
|DE94-016879| p 1500 N95-20106
The reliability of laser reflowed Sn-Ag solder joints
|AD-A279787| p 1315 N95-20443
High quality InP-on-Si for solar cell applications
p 1317 N95-20510
Lead-indium phosphate glasses for optical applications
|DE94-019333| p 1275 N95-21482
Thermal and deformation analyses of a novel cryogenically cooled monochromator for an Advanced Photon Source beamline
|DE94-016914| p 1527 N95-22190

THERMAL FATIGUE
Thermo-mechanical fatigue of polymer matrix composites
|AD-A285931| p 1267 N95-20390

THERMAL INSTABILITY
Instabilities in natural-convection flows in cavities
|PB95-107975| p 1354 N95-21578

THERMAL INSULATION
Proceedings of the 1993 Non-Fluorocarbon Insulation, Refrigeration and Air Conditioning Technology Workshop
|DE94-018333| p 1285 N95-20194

THERMAL MAPPING
InTISb for long-wavelength infrared photodetectors and arrays
|AD-A280109| p 1331 N95-21660
Thermal imaging systems
|AD-A279146| p 1307 N95-21970

THERMAL NEUTRONS
Non destructive characterization using pulsed fast-thermal neutrons
|DE95-002601| p 1511 N95-20422

THERMAL NOISE
Equilibrium and shot noise in mesoscopic systems
|DE95-000855| p 1576 N95-22008
Performance of a fast frequency-hopped noncoherent MFSK receiver over Rician fading channels with either partial-band interference or multi-tone interference
|AD-A286168| p 1310 N95-22246

THERMAL PROTECTION
Operating manual for hybrid thermosyphons at the Gakona Power Plant, Alaska
|AD-A279068| p 1287 N95-21626

THERMAL RADIATION
Radiation from advanced solid rocket motor plumes
|NASA-CR-196554| p 1221 N95-20124

THERMAL RESISTANCE
Thermal resistance of the cheek in cold air
|AD-A286257| p 1446 N95-22001

THERMAL SHOCK
USAF cellular mechanism of turnover of the stress induced protein HSP70
|AD-A285618| p 1441 N95-19898
Skeletal muscle ischemia and heat shock proteins
|AD-A285364| p 1442 N95-20549

THERMAL STABILITY
Accelerated screening methods for determining chemical and thermal stability of refrigerant-lubricant mixtures. Part 2: Experimental comparisons and verification of methods
|DE95-000743| p 1264 N95-20078
Thianthrene containing polyimides with monomer formation via nucleophilic aromatic substitution
|AD-A286313| p 1265 N95-20094
Development of an advanced JP-8 fuel
|AD-A285583| p 1283 N95-21161
Toughened Silcomp composites for gas turbine engine applications
|DE95-002851| p 1214 N95-21243
Joining dissimilar stainless steels for pressure vessel components
|PB95-133005| p 1380 N95-21446
An initial assessment of the properties of 2,5-dipicryl-1,3,4-oxadiazole: A secondary explosive with high thermal stability
|MRL-TR-93-16| p 1284 N95-21624
Lubricant evaluation and performance, 2
|AD-A279144| p 1278 N95-21969
High temperature polymer for second order nonlinear optics for photonic materials
|AD-A279309| p 1280 N95-22141

THERMAL STRESSES
Design and thermal stress analysis of high power x-ray monochromators cooled with liquid nitrogen
|DE94-016879| p 1500 N95-20106
Geometric moire method of strain analysis with displacement discontinuities
|DE95-001114| p 1386 N95-20833
Recent reflux receiver developments under the US DOE program
|DE95-001622| p 1393 N95-20861
Geometric characterization of electromigration voids (A statistical analysis of electromigration voids)
|AD-A286494| p 1328 N95-21169
Time-dependent deformation of titanium metal matrix composites
|NASA-CR-195030| p 1230 N95-21363
3-D TECATE/BREW: Thermal, stress, and birefringent ray-tracing codes for solid-state laser design
|DE95-000330| p 1376 N95-22301

THERMIONIC CONVERTERS
SPACE-R thermionic space nuclear power system: Design and technology demonstration
|DE95-000713| p 1221 N95-20076

THERMIONIC DIODES
Intense proton beam source for ITER neutral-beam spectroscopy diagnostics
|DE94-018092| p 1560 N95-21668

THERMOCHEMISTRY
Cluster reactions: An approach to understanding the fundamentals of heterogeneous catalysis
|DE95-002947| p 1243 N95-21447
Thermochemistry of dense hydrous magnesium silicates p 1416 N95-21782

THERMOCLINES
Synthesizing the Gulf Stream thermal structure from XBT data
|AD-A279665| p 1433 N95-20458

THERMOCOUPLES
Multiwire thermocouples: Frequency response
|NASA-TM-110510| p 1367 N95-21889

THERMODYNAMIC CYCLES
Malone-brayton cycle engine/heat pump
|AD-D016573| p 1378 N95-20295

THERMODYNAMIC PROPERTIES
Computer program for calculation of complex chemical equilibrium compositions and applications. Part 1: Analysis
|NASA-RP-1311| p 1235 N95-20180
Properties of molecular solids and fluids at high pressure and temperature
|DE94-017594| p 1565 N95-20243
An atomically-resolved STM study of the thermal decomposition of disilane on Si(001)
|AD-A279818| p 1567 N95-20544
Molecular-based study of solutions in supercritical solvents
|DE94-019326| p 1580 N95-21420
The low temperature properties of (Dy(1-x)Er(x))Ni2 alloys
|DE95-001657| p 1260 N95-21923
Incology alloy 908 data handbook
|DE95-001818| p 1260 N95-22013
Materials support for the development of High Temperature Advanced Furnaces (HITAF): A comparison of selected mechanical properties for three SiC-based ceramics
|DE94-017752| p 1280 N95-22258
New thermodynamic description of the Cu-Zr system
|PB95-127189| p 1263 N95-22374

THERMODYNAMICS
Thermodynamic characterization of new palladium alloy tritides
|DE94-018430| p 1579 N95-20028
Von Neumann algebra automorphisms and time-thermodynamics relation in general covariant quantum theories
|PB95-111084| p 1580 N95-20324
Thermo-mechanical fatigue of polymer matrix composites
|AD-A285931| p 1267 N95-20390
Thermodynamic and NMR studies of solvent effect on enantiomeric recognition for a chiral organiz ammonium cation by chiral diketopyridino-18-Crown-6 type ligands at 25.0 C
|AD-A279893| p 1223 N95-20592
Chemical Structure and Dynamics program
|DE95-001117| p 1403 N95-20834
On the Taylor test. Part 3: A continuum mechanics code analysis of steady plastic wave propagation
|DE95-002252| p 1501 N95-20869
Monthly mean sea ice data from the Polar Ice Prediction System, the Regional Polar Ice Prediction System-Barents Sea and the Regional Polar Ice Prediction System-Greenland Sea
|AD-A280095| p 1433 N95-21018
Thermodynamic analysis of stable and metastable equilibrium diagrams of the Cu-Cr system
|PB95-127775| p 1255 N95-21111
Time-dependent deformation of titanium metal matrix composites
|NASA-CR-195030| p 1230 N95-21363
Thermochemistry of dense hydrous magnesium silicates p 1416 N95-21782
Natural gas combustion chemistry mechanisms research
|PB95-111670| p 1247 N95-22150
Turbine design and application
|NASA-SP-290| p 1214 N95-22341
Multi signal-domain modeling of solid-state transducers: A theoretical framework based on irreversible thermodynamics mixed finite elements and multigrid
|PB95-134995| p 1336 N95-22382
The enhancement of metallic silver monomer evaporation by the adhesion of polar molecules to silver nanocluster ions
|AD-A284936| p 1281 N95-22470

THERMOELASTICITY
Right inverse for the divergence operator in spaces of continuous piecewise polynomials
|PB95-127080| p 1496 N95-22369
Locking of the finite element method in thermoelasticity
|PB95-127098| p 1496 N95-22370

THERMOELECTRIC GENERATORS

Conceptual design of an RTG Facility Transportation System
[DE94-014443] p 1379 N95-20627

GPHS-RTGs in support of the Cassini Mission
[DE95-001492] p 1222 N95-20853

THERMOELECTRIC MATERIALS

Sputter deposition of multilayer thermoelectric films: An approach to the fabrication of two-dimensional quantum wells
[DE95-002396] p 1272 N95-20892

THERMOELECTRIC POWER GENERATION

Research on the power generation system with thermoelectric conversion elements
[DE95-714804] p 1397 N95-22309

THERMOELECTRICITY

Multi signal-domain modeling of solid-state transducers: A theoretical framework based on irreversible thermodynamics mixed finite elements and multigrid
[PB95-134995] p 1336 N95-22382

THERMOGRAVIMETRY

Thermal decomposition reactions of HMX and RDX and their importance in predicting cookoff hazards
[DE95-002486] p 1283 N95-21513

High temperature corrosion and crack growth of SiC/SiC at variable oxygen partial pressures
[DE94-018715] p 1232 N95-22115

Synthesis and characterization of single-source molecular precursors to binary metal sulphides: Bis(diethyldithiocarbamato) M(2)trialkylphosphine (M = Zn and Cd) adducts
[AD-A279746] p 1248 N95-22385

THERMONUCLEAR POWER GENERATION

The ITER in-vessel system
[DE94-018053] p 1560 N95-21665

THERMONUCLEAR REACTIONS

National Ignition Facility: Experimental plan
[DE94-016542] p 1550 N95-20189

Laser design basis for the National Ignition Facility
[DE94-016700] p 1534 N95-21209

Evaluation of pumping and fueling requirements for the ITER EDA
[DE94-018117] p 1560 N95-21702

Current status of fusion-relevant covariance data
[DE95-000865] p 1561 N95-22010

THERMOPHYSICAL PROPERTIES

Solidification modeling of a spiral casting to determine material fluidity
[DE94-018930] p 1285 N95-20050

Materials compatibility and lubricants research on CFC-refrigerant substitutes
[DE94-018414] p 1287 N95-21631

Thermophysical properties of HFC-143a and HFC-152a
[DE95-002199] p 1582 N95-22153

THERMOSETTING RESINS

Ceramics formed by pyrolysis of either linear or thermosetting carborane (siloxane or silane) acetylene based precursor polymers
[AD-D016563] p 1266 N95-20291

Conducting thermoset polymers
[AD-A286541] p 1273 N95-21014

THERMOSIPHONS

Operating manual for hybrid thermosyphons at the Gakona Power Plant, Alaska
[AD-A279068] p 1287 N95-21626

THICK FILMS

Effect of external stress on the transport of fluids in thermoplastic resin systems
[AD-A279993] p 1270 N95-20596

Dependence of critical current density on microstructure and processing of high-T(c) superconductors
[DE95-000685] p 1571 N95-21167

Aligned bismuth, strontium, calcium cuprate coatings on polycrystalline substrates
[AD-D016512] p 1278 N95-21907

THICK WALLS

Fabrication of ceramic composites: Forced CVI
[DE95-001076] p 1271 N95-20821

THICKNESS

The effect of fiber coating thickness on the interfacial properties of a continuous fiber ceramic matrix composite
[DE94-017886] p 1267 N95-20373

A model of an infinite length, axisymmetric, isotropic, forced thick shell
[AD-A285586] p 1386 N95-21212

Development of a portable ice-thickness measuring instrument
[AD-A279472] p 1433 N95-21291

Characterization of a texture gradient in tantalum plate
[DE95-002704] p 1262 N95-22289

THIN FILMS

Synthesis and studies of organometallic precursors for CVD of thin film electronic materials
[AD-A285834] p 1223 N95-20033

Sol-gel-derived silica films with tailored microstructures for applications requiring organic dyes
[DE94-018886] p 1264 N95-20047

Thianthrene containing polyimides with monomer formation via nucleophilic aromatic substitution
[AD-A286313] p 1265 N95-20094

Energetics, bonding mechanism and electronic structure of ceramic/ceramic and metal/ceramic interfaces
[DE95-000601] p 1265 N95-20115

Polycrystalline thin film cadmium telluride solar cells fabricated by electrodeposition
[DE94-011848] p 1391 N95-20118

Rate controlled synthesis of composition modulated, metal-oxide thin films
[DE94-016596] p 1267 N95-20317

Polycrystalline CuInSe2 and CdTe solar cells
[DE94-011875] p 1392 N95-20333

Enhanced ionic conduction at the film/substrate interface in LiI thin films grown on sapphire(0001)
[DE94-017884] p 1565 N95-20371

Mean field analysis of orientation selective grain growth driven by interface-energy anisotropy
[DE94-015797] p 1566 N95-20399

Superconducting thin film with fullerenes and method of making
[AD-D016580] p 1567 N95-20461

Novel thin-film CuInSe2 fabrication
[DE94-011874] p 1268 N95-20472

Status of flexible CIS research at ISET
p 1317 N95-20512

Advances in polycrystalline thin-film photovoltaics for space applications p 1318 N95-20514

Amorphous silicon thin films: The ultimate lightweight space solar cell p 1318 N95-20515

Rare earth garnet selective emitter
p 1322 N95-20536

Nucleation, growth, and strain relaxation of lattice-mismatched 3-5 semiconductor epitaxial layers
p 1324 N95-20543

Reliability assessment of Multichip Module technologies via the Triservice/NASA RELTECH program
p 1210 N95-20643

Ferroic materials: Design, preparation and characteristics. Ceramic transactions, volume 43
[AD-A285937] p 1270 N95-20664

Ion scattering and deposition: The role of energetic particles in thin film growth
[AD-A285975] p 1514 N95-20667

Aerosol-assisted chemical vapor deposition of copper: A liquid delivery approach to metal thin films
[AD-A279702] p 1270 N95-20689

The in situ observation of epitaxial diamond thin film nucleation and growth using emission electron microscopy
[AD-A279811] p 1569 N95-20807

Atmosphere influence on in situ ion beam analysis of thin film growth
[DE95-001507] p 1570 N95-20881

Characterization and electrical properties of copper films grown via direct liquid coinjection of (hfac)Cu(TMVS) and TMVS
[DE95-002957] p 1272 N95-20889

Sputter deposition of multilayer thermoelectric films: An approach to the fabrication of two-dimensional quantum wells
[DE95-002396] p 1272 N95-20892

Study on the reaction kinetics in pulsed RF discharges under RIE conditions
[PB95-107868] p 1300 N95-21029

Methodology for ESCA analysis of electromigration
[AD-A286229] p 1241 N95-21168

Processing and modeling issues for thin-film solar cell devices
[DE94-011895] p 1394 N95-21294

Copper metallization of stainless steels
[DE95-001496] p 1256 N95-21300

Photoemission and ferromagnetism
[DE95-002419] p 1520 N95-21362

Thin-film cadmium telluride photovoltaic cells
[DE94-011886] p 1395 N95-21508

Time-resolved diagnostics of excimer laser-generated ablation plasmas used for pulsed laser deposition
[DE94-018950] p 1559 N95-21547

Raman spectra of MOCVD-grown ferroelectric PbTiO3 thin films
[DE94-018964] p 1244 N95-21549

RF vacuum microelectronics based on thin film edge-emitter technology
[AD-A279539] p 1331 N95-21690

Non-H2Se, ultra-thin CuInSe2 devices
[DE94-011894] p 1395 N95-21844

Integration of thin film decoupling capacitors
[DE95-001609] p 1333 N95-21881

Characterization equipment for electrooptics and actuators
[AD-A286285] p 1546 N95-22043

Surfaces and thin films studied by picosecond ultrasonics
[DE95-001866] p 1506 N95-22071

International Symposium on Advanced Laser Technologies
[AD-A279849] p 1376 N95-22164

High temperature superconducting microwave device
[AD-A286351] p 1336 N95-22254

Measurement of the thermal properties of electrically conducting fluids using coated transient hot wires
[DE94-017816] p 1357 N95-22264

THIN WALLS

X-ray imaging of uniform large scale-length plasmas created from gas-filled targets on Nova
[DE94-018339] p 1531 N95-20015

THIOLS

Scanning tunneling microscopy studies of self-assembled monolayers of alkanethiols on gold
[AD-A279910] p 1253 N95-20577

THIOPHENES

Selenophene transition metal complexes
[DE95-001675] p 1260 N95-21841

THORIUM ISOTOPES

Thorium-232 in human tissues: Metabolic parameters and radiation doses
[DE94-019275] p 1441 N95-20074

THORIUM OXIDES

Thoriated-tungsten, split-ring, hollow-cathode electrode for discharge devices
[AD-D016508] p 1333 N95-21906

THREAT EVALUATION

Test and evaluation report for the Manual Domestic Passive Profiling System (MDPPS)
[AD-A286312] p 1202 N95-20093

THREE DIMENSIONAL BOUNDARY LAYER

Numerical study of realistic perturbations in three-dimensional boundary layers p 1351 N95-21091

THREE DIMENSIONAL FLOW

Nonlinear spectroscopy of multicomponent droplets and two- and three-dimensional measurements in flames
[AD-A279945] p 1238 N95-20581

Application of Direct and Large Eddy Simulation to Transition and Turbulence
[AGARD-CP-551] p 1346 N95-21061

Subgrid scale models in finite difference simulations of complex wall bounded flows p 1346 N95-21063

The effect of initial conditions on the development of temporally evolving planar three dimensional incompressible wakes p 1350 N95-21085

Direct simulation of tridimensional wake of NACA 0012 profile p 1350 N95-21086

Spatial direct numerical simulation of boundary layer transition under strong adverse pressure gradient
p 1351 N95-21093

Direct numerical simulation of 2-D and 3-D instability waves in a laminar separation bubble
p 1352 N95-21095

DNS of turbulent flow in a driven cavity and their analysis using proper orthogonal decomposition
p 1352 N95-21097

Direct simulation and graphics post-processing of three-dimensional turbulent flows p 1352 N95-21098

The structure of turbulence and other motions beneath an air-water interface
[AD-A279838] p 1434 N95-21293

Convergence acceleration of the Proteus computer code with multigrid methods
[NASA-CR-197677] p 1467 N95-21450

Forced free-shear layer measurements
p 1362 N95-22460

THREE DIMENSIONAL MODELS

The influence of ply waviness with nonlinear shear on the stiffness and strength reduction of composite laminates
[AD-A285736] p 1224 N95-19899

Solutions of D(sup n)D(sup m)f=0
[PB95-110839] p 1487 N95-19916

Open Skies project computational fluid dynamic analysis
[AD-A285928] p 1200 N95-19991

A 3D stereo data visualization and representation
[AD-A284788] p 1449 N95-20064

View-based models of 3D object recognition and class-specific invariance
[AD-A279858] p 1459 N95-20157

Computer-Aided Structural Engineering (CASE) project. User's guide: Computer-Aided Structural Modeling (CASM). Version 5.00
[AD-A279913] p 1459 N95-20310

Implementation and performance of a three-dimensional numerical transport model
[PB95-135745] p 1402 N95-20440

The effect of regional-scale soil-moisture deficits on mesoscale atmospheric dynamics that influence fire severity
[DE95-002682] p 1413 N95-20455

Use of an integrated design tool for weld quality enhancement
[DE94-018135] p 1379 N95-20723
Simulation of pipe flow p 1349 N95-21078
Visualizing 3D velocity fields near contour surfaces
[DE95-000841] p 1353 N95-21182
Three-dimensional ground penetrating radar imaging using multi-frequency diffraction tomography
[DE94-016687] p 1301 N95-21205
VLUGR3: A vectorizable adaptive grid solver for PDEs in 3D. 1: Algorithmic aspects and applications
[PB95-135729] p 1467 N95-21435
Three-dimensional effects for radio frequency antenna modeling
[DE94-019125] p 1303 N95-21459
Magnetic properties of the three-dimensional Ising model with an interface amorphization
[DE94-628992] p 1278 N95-21885
Influence of wavelength on transient short-circuit current in polycrystalline silicon solar cells
[DE94-629082] p 1397 N95-22183
3-D TECATE/BREW: Thermal, stress, and birefringent ray-tracing codes for solid-state laser design
[DE95-000330] p 1376 N95-22301
Image solution for poisson's equation in wedge geometry
[PB95-127171] p 1310 N95-22311

THRESHOLD VOLTAGE
SEU and SEL response of the Westinghouse 64K E-2PROM, analog devices AD7876 12-bit ADC, and the Intel 82527 Serial Communications Controller
[DE95-003349] p 1334 N95-22086

THRESHOLDS (PERCEPTION)
Determination of multiple sound sources
[AD-A286563] p 1504 N95-20823
Temporary threshold shifts produced by high intensity freefield impulse noise in humans wearing hearing protection
[AD-A286289] p 1454 N95-22045

THROTTLING
Cascade orificial resistive device
[AD-D016529] p 1504 N95-20724

THRUST BEARINGS
Bevel gear driver and method having torque limit selection
[NASA-CASE-MSC-22384-1] p 1378 N95-20151

THRUST REVERSAL
Why do airlines want and use thrust reversers? A compilation of airline industry responses to a survey regarding the use of thrust reversers on commercial transport airplanes
[NASA-TM-109158] p 1203 N95-20706

THRUST VECTOR CONTROL
Design of power electronics for TVC and EMA systems
[NASA-CR-196540] p 1312 N95-19909
Static investigation of two fluidic thrust-vectoring concepts on a two-dimensional convergent-divergent nozzle
[NASA-TM-4574] p 1199 N95-19913

THUNDERSTORMS
The initiation of lightning and the growth of electric fields in thunderstorms
[AD-A280033] p 1428 N95-20008

THYRATRONS
Applied physics research for innovation in pulsed power
[AD-A285392] p 1324 N95-20610

TIDES
Modeling open boundary conditions by using the optimization approach
[AD-A285548] p 1433 N95-21158

TILES
ALT-2 armor tile design for upgraded TEXTOR operation
[DE94-015749] p 1549 N95-20143
Acoustic and vibration attenuation composite material
[AD-D016585] p 1233 N95-22467

TIME
Von Neumann algebra automorphisms and time-thermodynamics relation in general covariant quantum theories
[PB95-111084] p 1580 N95-20324

TIME DEPENDENCE
A numerical investigation of energy transfer and subgrid-scale eddy viscosity in homogeneous, isotropic and shear turbulence
[AD-A280005] p 1339 N95-20058
A comparison of decision making behaviour in a static and a dynamic task environment as a function of time pressure
[AD-A285389] p 1449 N95-20609
Computing methods for the approximate solution of time dependent problems
[AD-A286007] p 1491 N95-20719
Electron-nuclear dynamics of molecular systems
[AD-A279649] p 1516 N95-21120
Time-dependent deformation of titanium metal matrix composites
[NASA-CR-195030] p 1230 N95-21363
Diffraction applications using the energy dispersive beamline, X6A, at NSLS
[DE94-019287] p 1572 N95-21408
Temporal evolution of turbulence/chemistry interactions in lifted, turbulent-jet flames
[DE95-002481] p 1243 N95-21512
Seamless data-range change using punctured convolutional codes for time-varying signal-to-noise ratios p 1304 N95-21534
On the origins and modeling of frictional behavior in interfacially-complex sliding contacts
[DE94-019129] p 1381 N95-21601
Governing equations for multiphase heat and mass transfer in hygroscopic porous media with applications to clothing materials
[AD-A286418] p 1357 N95-22206
An analytical electron distribution function for inelastic collisions in a uniform gas with time varying electric field
[DE95-003476] p 1528 N95-22222
An analytical, inelastic, space and time dependent electron distribution for electrically excited gases
[DE95-003478] p 1528 N95-22223

TIME FUNCTIONS
Semi-global stabilization of linear discrete-time systems subject to input saturation via linear feedback: An ARE-based approach
[PB95-135463] p 1483 N95-21618

TIME MARCHING
Computation of transonic flow on composite overlapping grids in 2 D
[PB95-131348] p 1353 N95-21132

TIME MEASUREMENT
Time code interface
[AD-D016535] p 1501 N95-20731

TIME OF FLIGHT SPECTROMETERS
Ion temperature measurement of indirectly-driven implosions using a geometry-compensated neutron time-of-flight detector
[DE94-016967] p 1552 N95-20362
Sputtering of tin and gallium-tin clusters
[DE94-018389] p 1254 N95-20707
Time of flight spectroscopy with muonic hydrogen
[DE94-017056] p 1245 N95-21845

TIME OPTIMAL CONTROL
Optimal control of a two wheeled mobile robot
[AD-A286130] p 1485 N95-22233

TIME RESPONSE
Time domain spectral hole-burning storage
[AD-A279912] p 1587 N95-20309
Emitter location via Kalman filtering of signal time difference of arrival
[AD-A285972] p 1291 N95-20666
Time-resolved diagnostics of excimer laser-generated ablation plasmas used for pulsed laser deposition
[DE94-018950] p 1559 N95-21547
The determination of static and time varying dipole source. Sensor geometry during sea trials using differential global positioning system
[MRL-TN-631] p 1205 N95-21642

TIME SERIES ANALYSIS
Higher order crossings
[AD-A279597] p 1504 N95-20300
Application of neural networks to seismic signal discrimination research findings
[AD-A285848] p 1415 N95-21308
CTD calibration and processing methods used at Woods Hole Oceanographic Institution
[AD-A279507] p 1435 N95-21681
Long Time Series Measurements in the Coastal Ocean: A workshop
[AD-A279509] p 1435 N95-21682
Signal processing in the linear statistical model
[AD-A286255] p 1308 N95-22041
Time and the order of abstract events in distributed computations
[PB95-110482] p 1496 N95-22349

TIME SHARING
Environment for Test and Analysis of Distributed Software (ETADS)
[AD-A285776] p 1463 N95-20877
Radio-frequency techniques at the ISIS pulsed muon source
[PB95-129854] p 1529 N95-22303

TIME SIGNALS
The GPS Burst Detector W-Sensor
[DE94-017406] p 1204 N95-20269
Passive monitoring for automated MMPP communication systems p 1293 N95-20927

TIN
The reliability of laser reflowed Sn-Ag solder joints
[AD-A279787] p 1315 N95-20443
Sputtering of tin and gallium-tin clusters
[DE94-018389] p 1254 N95-20707

TIN COMPOUNDS
A catalytic method for the conversion of silanes to stannanes
[AD-A286214] p 1247 N95-22020

TISSUES (BIOLOGY)
Hierarchical structures in biology as a guide for new materials technology
[AD-A286317] p 1265 N95-20176
Interspecies extrapolations of halocarbon respiratory and tissue kinetics: Applications to predicting toxicity in different species
[AD-A285055] p 1442 N95-20485
Investigation of laser-induced retinal damage: Wavelength and pulsewidth dependent mechanisms
[AD-A286066] p 1443 N95-20848
Cell membrane potentials induced during exposure to EMP fields
[DE94-018952] p 1439 N95-21548
Study of pulsed laser effects on living tissues
[PB95-131330] p 1447 N95-22361

TITAN
Studies of the gas tori of Titan and Triton
[NASA-CR-197377] p 1601 N95-20797

TITAN LAUNCH VEHICLES
Computer model predictions of the local effects of large, solid-fuel rocket motors on stratospheric ozone
[AD-A285632] p 1404 N95-21150

TITANIUM
Tribology and surface mechanical properties of excimer laser nitrided titanium
[DE95-002751] p 1255 N95-21238
Time-dependent deformation of titanium metal matrix composites
[NASA-CR-195030] p 1230 N95-21363
Spectroscopic assessment of the reliability of metal/metal oxide interfaces
[AD-A286131] p 1261 N95-22035
Strength testing of Ti-vapor-coated silicon nitride braze joints
[DE94-017858] p 1280 N95-22266

TITANIUM ALLOYS
Mixed-sputter deposition of Ni-Ti-Cu shape memory films
[DE94-017296] p 1250 N95-19900
Third Intermetallic Matrix Composites Symposium, volume 350
[NASA-TM-110059] p 1225 N95-20001
Plasma arc melting of titanium-tantalum alloys
[DE94-016291] p 1252 N95-20331
Oxide formation on NbAl3 and TiAl due to ion implantation of O-18
[DE94-017874] p 1252 N95-20365
Electrochemical impedance pattern recognition for detection of hidden chemical corrosion on aircraft components
[AD-A284998] p 1253 N95-20481
Electrochemical impedance pattern recognition for detection of hidden chemical corrosion on aircraft components
[AD-A285998] p 1239 N95-20716
Metastable bcc phase formation in the Nb-Cr-Ti system
[DE94-016212] p 1255 N95-21137
Tribology and surface mechanical properties of excimer laser nitrided titanium
[DE95-002751] p 1255 N95-21238
Theoretical study of the noble metals on semiconductor surfaces and Ti-base shape memory alloys
[DE95-001654] p 1257 N95-21398
The development of a super-alpha2 titanium aluminide alloy consolidated by rapid omnidirectional compaction
[AD-A279254] p 1260 N95-21986
Plasma arc melting of a 80 weight percent tantalum -20 weight percent titanium alloy
[DE95-000846] p 1260 N95-22006
Bulk and defect properties of ordered intermetallics
[DE94-017706] p 1262 N95-22344

TITANIUM COMPOUNDS
The processing and mechanical properties of high temperature/high performance composites. Stress redistribution and notch properties, book 2
[AD-A279737] p 1227 N95-20429
Self-starting femtosecond pulse generation from a Ti:sapphire laser synchronously pumped by a pointing-stabilized mode-locked Nd:YAG laser
[DE94-019319] p 1374 N95-21480
Angle resolved photoemission on K(0.3)Mo3, TiTe2 and Ti(1+x)S2
[DE94-018300] p 1574 N95-21712
Preparation and x-ray structure of Cp2Ti(PH2SiH2)(PMe3)
[AD-A286197] p 1246 N95-21879

TITANIUM NITRIDES
Method of making copper-titanium nitride alloy
[AD-D016582] p 1252 N95-20201
TITANIUM OXIDES
Photoinduced charge transfer between fullerenes and TiO2 semiconductor colloids
[DE95-001447] p 1570 N95-20838
Reactive nanophase oxide additions to melt-processed high-T(sub c) superconductors
[DE95-001470] p 1570 N95-20841
Polyurethane self-priming topcoats
[AD-D016204] p 1274 N95-21154
Polyurethane self-priming topcoats
[AD-D016205] p 1274 N95-21155
Integration of thin film decoupling capacitors
[DE95-001609] p 1333 N95-21881
Lower active metals loading for hydrotreating catalysts
[DE94-018907] p 1261 N95-22119
Gas-phase photocatalytic oxidation: Cost comparison with other air pollution control technologies
[DE95-000241] p 1410 N95-22278
TOKAMAK DEVICES
Toward a design for the ITER plasma shape and stability control system
[DE94-017516] p 1548 N95-20037
Recent DIII-D results
[DE94-017519] p 1549 N95-20038
ALT-2 armor tile design for upgraded TEXTOR operation
[DE94-015749] p 1549 N95-20143
Fluctuations in high Beta(sub p) plasmas in D3-D
[DE94-017510] p 1550 N95-20146
The control system position to the electric probe in the Tokamak Novillo
[DE94-629938] p 1550 N95-20204
Experimental measurements of ICRF and edge plasma interactions on Tore Supra
[DE94-019154] p 1551 N95-20205
A method for measuring the inductive electric field profile and noninductive current profiles on D3-D
[DE94-016683] p 1551 N95-20279
Recent results from Fast Wave Current Drive experiments on DIII-D
[DE94-016718] p 1551 N95-20285
Hybrid model in general geometry
[DE95-002614] p 1553 N95-20437
Plasma shape experiments for an optimized tokamak
[DE94-017508] p 1553 N95-20445
Enhanced scrape-off layer plasma in D3-D double-null discharges
[DE94-017977] p 1554 N95-20571
Current diffusive ballooning mode in second stability region of tokamaks
[DE94-770690] p 1554 N95-20683
Ideal Magnetohydrodynamic stabilities in JT-60 and D3-D tokamak plasmas
[DE94-770684] p 1555 N95-20987
Ion heat pulse after sawtooth crash in the JFT-2M tokamak
[DE94-770685] p 1555 N95-20988
Observation of non diffusive term of toroidal momentum transport in the JFT-2M tokamak
[DE94-770686] p 1555 N95-20989
Investigations of VH-mode in D3-D and JET
[DE94-015859] p 1556 N95-21142
Experimental measurements and modeling of impurity transport in the divertor and boundary plasma of D3-D
[DE94-016519] p 1556 N95-21159
The parametric dependence of the spatial structure of the radial electric field at the plasma edge in the D3-D tokamak
[DE94-016520] p 1556 N95-21163
Review of recent D-T experiments from TFTR
[DE95-002755] p 1557 N95-21239
Fusion power production in TFTR
[DE95-002756] p 1557 N95-21240
Heating and transport in TFTR D-T plasmas
[DE95-002812] p 1558 N95-21242
MHD pressure drop in ducts with imperfectly insulating coatings
[DE95-002852] p 1558 N95-21244
Assessment of database for interaction of tritium with ITER plasma facing materials
[DE95-002038] p 1558 N95-21290
Theory of the L-H transition
[DE95-001389] p 1558 N95-21299
MTX final report
[DE95-002960] p 1559 N95-21451
B4C-SiC reaction-sintered coatings on graphite plasma facing components
[DE94-019105] p 1230 N95-21553
The ITER in-vessel system
[DE94-018053] p 1560 N95-21665
ITER EDA Newsletter. Volume 3, no. 2
[DE94-628980] p 1561 N95-21852
Current status of fusion-relevant covariance data
[DE95-000865] p 1561 N95-22010
The superconducting magnet system for the Tokamak Physics Experiment
[DE94-018329] p 1562 N95-22300
TOLERANCES (MECHANICS)
Toughened Silcomp composites for gas turbine engine applications
[DE95-002851] p 1214 N95-21243
TOLERANCES (PHYSIOLOGY)
Temporary threshold shifts produced by high intensity freefield impulse noise in humans wearing hearing protection
[AD-A286289] p 1454 N95-22045
TOLUENE
Effect of external stress on the transport of fluids in thermoplastic resin systems
[AD-A279993] p 1270 N95-20596
Structure of dibis(diethyldithiocarbamato) zinc (2) Mu-bis(diethylphosphino)ethane toluene(2)
[AD-A279792] p 1224 N95-20660
Aerosol-assisted chemical vapor deposition of copper: A liquid delivery approach to metal thin films
[AD-A279702] p 1270 N95-20689
Synthesis and characterization of (Zn(SEt)Et)10, formed via insertion of sulfur into Zn-C bonds: A new class of Wurtzite-like cluster framework
[AD-A279701] p 1569 N95-20714
Excess energy and structural dependence of the rate of energy redistribution during the photodissociation of iodotoluenes
[AD-A279997] p 1241 N95-21124
Synthesis and characterization of single-source molecular precursors to binary metal sulphides: Bis(diethyldithiocarbamato) M(2)trialkylphosphine (M = Zn and Cd) adducts
[AD-A279746] p 1248 N95-22385
TOMOGRAPHY
Three-dimensional ground penetrating radar imaging using multi-frequency diffraction tomography
[DE94-016687] p 1301 N95-21205
Equivalent source current formulation in impedance tomography
[PB95-127627] p 1329 N95-21326
Computer programs for analysis of geophysical data
[DE95-002472] p 1415 N95-21511
Radiopharmaceuticals for diagnosis
[DE95-002200] p 1445 N95-21595
Volatiles in the Earth: All shallow and all recycled
p 1416 N95-21779
Seismic evidence for volatiles at large depth in the Earth p 1422 N95-21808
Real time system for practical acoustic monitoring of global ocean temperature
[AD-A286435] p 1436 N95-22209
TOOLS
Bevel gear driver and method having torque limit selection
[NASA-CASE-MSC-22384-1] p 1378 N95-20151
TOPOGRAPHY
Second European Symposium on X-Ray Topography and High Resolution Diffraction: Programme and abstracts
[AD-A286328] p 1564 N95-20210
The effect of fiber coating thickness on the interfacial properties of a continuous fiber ceramic matrix composite
[DE94-017886] p 1267 N95-20373
Topography of neutron scattering from diblock copolymer film
[DE95-001457] p 1229 N95-20840
The dynamic role of ridges in a beta-plane channel. Towards understanding the dynamics of large scale circulation in the Southern Ocean
[AD-A279390] p 1435 N95-21943
Solving the inverse problem in terrain modeling
[AD-A285860] p 1391 N95-22131
TOPOLOGY
Abstract reduction and topology
[PB95-110615] p 1488 N95-20054
Invariant measures of interval maps
[PB95-107835] p 1389 N95-20207
MPI workshop
[DE94-017883] p 1475 N95-20366
Duality beyond sober spaces: Topological spaces and observation frames
[PB95-134565] p 1494 N95-21962
Large-scale fields and flows in the magnetosphere-ionosphere system
[PB95-134664] p 1427 N95-22368
TOROIDAL DISCHARGE
Observation of non diffusive term of toroidal momentum transport in the JFT-2M tokamak
[DE94-770686] p 1555 N95-20989
TOROIDAL PLASMAS
Investigation of spherical tearing mode
[NASA-CR-197284] p 1558 N95-21345
Joule heating of the ITER TF cold structure: Effects of vertical control coil currents and ELMS
[DE95-001817] p 1560 N95-21724
TORQUE
Bevel gear driver and method having torque limit selection
[NASA-CASE-MSC-22384-1] p 1378 N95-20151
Displaceable spur gear torque controlled driver and method
[NASA-CASE-MSC-22381-1] p 1378 N95-20409
Computer graphics tools for visualizing gravity gradient torques on a rigid spacecraft
[AD-A285971] p 1461 N95-20665
Nonlinear dynamics of the planar pitch attitude motion for a gravity-gradient satellite
[AD-A286407] p 1220 N95-22204
TORSION
Inelastic bending and torsion of steel I-beams
[PB94-208378] p 1384 N95-19975
Inelastic torsion of steel I-beams
[PB94-208360] p 1384 N95-20101
TORUSES
N=1 Superconformal minimal model correlation functions on the torus
[PB95-134615] p 1500 N95-21964
TOTAL QUALITY MANAGEMENT
Total quality management program planning
[DE94-016862] p 1586 N95-21645
TOUCHDOWN
F-15 resource tape
[NASA-TM-110502] p 1206 N95-19994
TOUGHNESS
Fracture toughness properties of welded stainless steels for tritium service
[DE95-000755] p 1251 N95-20079
Micromechanical approach to transformation toughening in ceramics
[PB95-135422] p 1273 N95-20976
Nitrogen alloyed martensitic steels
[PB95-127791] p 1255 N95-21128
Microstructural design for tough ceramics
[AD-A285634] p 1273 N95-21152
TOWERS
An evaluation of 915-MHz radar wind profiler/RASS by tower and sodar measurements
[DE94-018913] p 1364 N95-20320
An evaluation of Automatic Terminal Information Service (ATIS) flight deck display presentation options
[AD-A280100] p 1204 N95-21020
TOXIC HAZARDS
Production of S2F10, S2OF10 and S2O2F10 by spark discharges in SF6*
[DE95-001421] p 1243 N95-21500
Environmental Hazards Assessment Program
[DE94-019075] p 1406 N95-21565
Assessment of the atmospheric hazards and risks of new chemicals: Procedures to estimate hazard potentials
[PB95-107488] p 1410 N95-22186
Current concepts on airborne particles and health
[DE95-002260] p 1447 N95-22287
TOXICITY
Interspecies extrapolations of halocarbon respiratory and tissue kinetics: Applications to predicting toxicity in different species
[AD-A285055] p 1442 N95-20485
Selection of substances to be considered in the environmental balance/environmental outlook in relation to the dissemination theme
[PB95-132197] p 1407 N95-21635
Derivation of preliminary maximum permissible concentrations of volatile compounds in air
[PB95-107447] p 1410 N95-22125
The mechanisms and effects off the plant-activations of chemicals in the environment
[AD-A279388] p 1356 N95-22145
Launch safety, toxicity, and environmental effects of the high performance oxidizer ClF(5)
[AD-A286095] p 1284 N95-22227
Derivation of maximum permissible concentrations for several volatile compounds for water and soil
[PB95-107454] p 1411 N95-22381
TOXICOLOGY
Current concepts on airborne particles and health
[DE95-002260] p 1447 N95-22287
TRACE CONTAMINANTS
Degradation of aromatic hydrocarbons in an aquifer during a field experiment demonstrating the feasibility of remediation by natural attenuation
[AD-A283809] p 1282 N95-19922
TRACE ELEMENTS
Ultraviolet emission from rocket motor plumes
[DSTO-TR-0002] p 1222 N95-21661

Rare gases systematics and mantle structure
p 1416 N95-21778
Hydrogen storage in Earth's mantle and core
p 1423 N95-21813
The isotope geochemistry of abyssal peridotites and related rocks
[AD-A279435] p 1435 N95-21918

TRAFFIC
Utilizing artificial neural networks in network flow analysis: An annotated bibiliography
[DE95-002453] p 1482 N95-21522

TRAILING EDGE FLAPS
Lift enhancement device
[AD-D016522] p 1201 N95-21864

TRAINING ANALYSIS
Using the backward transfer paradigm to validate the AH-64 Simulator Training Research Advanced Testbed for Aviation
[AD-A285758] p 1215 N95-19931

TRAINING DEVICES
Development and evaluation of ALEC Micro-Wand 3e (tradename) training
[AD-A285863] p 1471 N95-22133

TRAINING EVALUATION
NASA/DOD Aerospace Knowledge Diffusion Research Project. Report 28: The technical communication practices of aerospace engineering and science students: Results of the phase 4 cross-national surveys
[NASA-TM-109123] p 1587 N95-20162
Measuring presence in virtual environments
[AD-A286183] p 1460 N95-20326

TRAINING SIMULATORS
Measuring presence in virtual environments
[AD-A286183] p 1460 N95-20326

TRAJECTORIES
Comparison of meteorological data with fitted values extracted from projectile trajectory
[AD-A285921] p 1428 N95-19989
Tracking a dynamic set of feature points
[AD-A285124] p 1313 N95-20257

TRAJECTORY CONTROL
Layered path planning for an autonomous mobile robot
[AD-A286138] p 1485 N95-22244

TRAJECTORY MEASUREMENT
Thousand golden ten orbits
[PB95-135109] p 1592 N95-22334

TRAJECTORY OPTIMIZATION
Multiple burn fuel-optimal orbit transfers: Numerical trajectory computation and neighboring optimal feedback guidance
[NASA-CR-197317] p 1222 N95-21616

TRAJECTORY PLANNING
Adaptive path planning for flexible manufacturing
[DE94-016561] p 1459 N95-20284
Tom Thumb algorithm for planning simple vehicle motions
[PB95-107553] p 1484 N95-22156
Layered path planning for an autonomous mobile robot
[AD-A286138] p 1485 N95-22244

TRANSDUCERS
Compositive piezoelectrics utilizing a negative Poisson ratio polymer
[AD-D016579] p 1268 N95-20460
Apparatus and method for determining the mass density of a filament
[NASA-CASE-LAR-14879-1-CU] p 1383 N95-20616
Domain processes in ferroelectric ceramics
[AD-A279567] p 1276 N95-21697
Multi signal-domain modeling of solid-state transducers: A theoretical framework based on irreversible thermodynamics mixed finite elements and multigrid
[PB95-134995] p 1336 N95-22382

TRANSFER FUNCTIONS
Multigrid with matrix-dependent transfer operators for convection-diffusion problems
[PB95-110821] p 1487 N95-19915
Optimal distributed control system for a linear distributed parameter system
[AD-D016583] p 1480 N95-20202
Multilayer piecewise linear networks
[AD-A285382] p 1480 N95-20606
Construction of non-critical string field theory by transfer matrix formalism in dynamical triangulation
[DE94-770607] p 1516 N95-20986

TRANSFER OF TRAINING
Using the backward transfer paradigm to validate the AH-64 Simulator Training Research Advanced Testbed for Aviation
[AD-A285758] p 1215 N95-19931
DOD science and engineering apprenticeship program for high school students
[AD-A280371] p 1583 N95-22100

TRANSFER ORBITS
Multiple burn fuel-optimal orbit transfers: Numerical trajectory computation and neighboring optimal feedback guidance
[NASA-CR-197317] p 1222 N95-21616

TRANSFORMATIONS (MATHEMATICS)
Regularity of BPa-systems is decidable
[PB95-135489] p 1468 N95-21619
Uniform upper bounds in the Froehlich polaron theory
[DE94-628998] p 1525 N95-21860
A Davis-Putnam program and its application to finite-order model search: Quasigroup existence problems
[DE95-003014] p 1471 N95-22077
Almost kappa-wise independent random permutation of the cube
[PB95-108098] p 1495 N95-22147
Transformation of multichannel magnetocardiographic signals to standard grid form
[PB95-127114] p 1447 N95-22371

TRANSFORMERS
Recent reflux receiver developments under the US DOE program
[DE95-001622] p 1393 N95-20861

TRANSFUSION
Evaluation of dried storage of platelets for transfusion: Physiologic integrity and hemostatic functionality
[AD-A286078] p 1443 N95-20850

TRANSIENT HEATING
Influence of wavelength on transient short-circuit current in polycrystalline silicon solar cells
[DE94-629082] p 1397 N95-22183

TRANSISTOR CIRCUITS
Complementary GaAs junction-gated heterostructure field effect transistor fabrication for integrated circuits
[DE95-001522] p 1327 N95-20882

TRANSISTOR LOGIC
Radiation tests on service electronics for future multi TeV detectors
[DE94-632822] p 1335 N95-22184

TRANSISTORS
Characteristics of oxynitrides grown in N2O
[DE94-015798] p 1566 N95-20400
Prototype rule-based reliability analysis for VLSI circuit design
[AD-A280065] p 1327 N95-20967
RF vacuum microelectronics based on thin film edge-emitter technology
[AD-A279539] p 1331 N95-21690

TRANSITION FLOW
Application of Direct and Large Eddy Simulation to Transition and Turbulence
[AGARD-CP-551] p 1346 N95-21061
Comparison of DNS and LES of transitional and turbulent compressible flow: Flat plate and mixing layer
p 1347 N95-21066
Simulation of large scale transitional flows
p 1348 N95-21075
Simulations of bypass transition for spatially evolving disturbances p 1349 N95-21079
Direct numerical determination of the minimum bypass Reynolds number in boundary layers
p 1349 N95-21080
Direct numerical simulations of leading-edge receptivity for freestream sound p 1351 N95-21090
Acoustic receptivity due to weak surface inhomogeneities in adverse pressure gradient boundary layers
[NASA-TM-4577] p 1353 N95-21258
Studies in nonlinear problems of energy
[DE95-001387] p 1356 N95-22148

TRANSITION METALS
Consequences of oscillatory potentials and angular forces in transition metals and their aluminides
[DE94-019127] p 1258 N95-21600
Selenophene transition metal complexes
[DE95-001675] p 1260 N95-21841
Catalytic reactions of synthesis gas. Part 3. Determination of reaction kinetics
[PB95-127759] p 1248 N95-22329
Introduction to the structures determination methods using X-ray diffraction in monocrystals: Application to some lanthanides and transition metals complexes with organic ligands
[DE94-629002] p 1579 N95-22380

TRANSITION PROBABILITIES
Quantum chemical study of rare gas/halide interactions as a model for high energy density material. 1: Transition properties in HCl
[AD-A285988] p 1239 N95-20613

TRANSITION TEMPERATURE
Fracture behavior of the Fe-8Al alloy FAP-Y
[DE95-000956] p 1258 N95-21676
The doping effect on spin-Peierls instability
[DE94-629046] p 1577 N95-22178

TRANSLATING
A tabular interface for automated verification of event-based dialogs
[AD-A286065] p 1463 N95-20847

TRANSLATIONAL MOTION
In-situ capability of ion beam modification and characterization of materials at Los Alamos National Laboratory
[DE95-002738] p 1534 N95-21236

TRANSLUCENCE
Recognition of subsurface defects in machined ceramics by application of neural networks to laser scatter patterns
[DE94-018373] p 1264 N95-20018

TRANSMISSION
Propagation measurements on a troposcatter link in the Canadian High Arctic p 1295 N95-20940
Compilation of 1993 annual reports of the Navy ELF Communications System Ecological Monitoring Program
[AD-A279575] p 1408 N95-21699

TRANSMISSION EFFICIENCY
Methods for evaluating the effects of conduits at the surface of the sea p 1294 N95-20932
Performance of Ga(0.47)In(0.53)As cells over a range of proton energies
[NASA-TM-106819] p 1334 N95-22112

TRANSMISSION LINES
A wideband EMP test system
[DE94-015283] p 1290 N95-20474
A technique for increasing the bandwidth of high performance electrical backplanes p 1212 N95-20651
Dynamic response of pressure measuring systems
[ARL-TR-32] p 1365 N95-20759

TRANSMISSION RATE (COMMUNICATIONS)
Electromagnetic compatibility effects of advanced packaging configurations p 1213 N95-20658

TRANSMISSIONS (MACHINE ELEMENTS)
Bevel gear driver and method having torque limit selection
[NASA-CASE-MSC-22384-1] p 1378 N95-20151
Displaceable spur gear torque controlled driver and method
[NASA-CASE-MSC-22381-1] p 1378 N95-20409

TRANSMITTANCE
Qualification test results for blue-red reflecting solar covers p 1320 N95-20525

TRANSMITTER RECEIVERS
Facsimile transmission standards
[AD-A279911] p 1290 N95-20308
High performance backplane components for modular avionics p 1212 N95-20653

TRANSMITTERS
Technologies for highly parallel optoelectronic integrated circuits
[DE95-001607] p 1327 N95-20883
Development of a fast sampling system for estimation of impulse responses of mobile radio channels
p 1296 N95-20943

TRANSMUTATION
High precision trace neutron transmutation doping of detector-grade high resistance zone-refined silicon mono-crystal
[DE94-631463] p 1563 N95-19978
Recent results in analysis and simulation of beam halo
[DE94-018313] p 1539 N95-22298

TRANSONIC FLOW
Computation of transonic flow on composite overlapping grids in 2 D
[PB95-131348] p 1353 N95-21132

TRANSONIC WIND TUNNELS
Investigation of a thermal buoyancy effect on the drag of half models tested in the ARA Transonic Wind Tunnel
[ARA-MEMO-407] p 1199 N95-19946
16-foot transonic tunnel test section flowfield survey
[NASA-TM-109157] p 1216 N95-20669
Testing in the ARA Transonic Wind Tunnel
[ARA-MEMO-395] p 1216 N95-20799

TRANSPARENCE
Control of continuous phase PH using visible light to activate PH-dependent fibers and gels in a controlled and reversible manner
[AD-D016532] p 1543 N95-20728
Scalable programming environment
[AD-A286390] p 1472 N95-22201

TRANSPONDERS
Noncoherent transponder standards
[AD-A279512] p 1306 N95-21684

TRANSPORT AIRCRAFT
Why do airlines want and use thrust reversers? A compilation of airline industry responses to a survey regarding the use of thrust reversers on commercial transport airplanes
[NASA-TM-109158] p 1203 N95-20706

TRANSPORT PROPERTIES

Transport phenomena in the micropores of plug-type phase separators [NASA-TM-108479] p 1340 N95-20561

Effect of external stress on the transport of fluids in thermoplastic resin systems [AD-A279993] p 1270 N95-20596

Simulation of tearing mode stabilization by using ECH [DE94-770700] p 1554 N95-20684

Ion heat pulse after sawtooth crash in the JFT-2M tokamak [DE94-770685] p 1555 N95-20988

Observation of non diffusive term of toroidal momentum transport in the JFT-2M tokamak [DE94-770686] p 1555 N95-20989

Explicit methods for stiff ODEs from atmospheric Chemistry [PB95-135794] p 1404 N95-21034

Experimental measurements and modeling of impurity transport in the divertor and boundary plasma of D3-D [DE94-016519] p 1556 N95-21159

Heating and transport in TFTR D-T plasmas [DE95-002812] p 1558 N95-21242

Evaluation of pumping and fueling requirements for the ITER EDA [DE94-018117] p 1560 N95-21702

Plasma-induced-damage of GaAs during etching of refractory metal contacts [DE95-001525] p 1259 N95-21838

Anisotropic transport properties of BSCCO single crystals and Ag-clad tapes in high magnetic fields [DE95-000938] p 1575 N95-21936

Governing equations for multiphase heat and mass transfer in hygroscopic porous media with applications to clothing materials [AD-A286418] p 1357 N95-22206

TRANSPORT THEORY

MCNP (trademark) ENDF/B-VI iron benchmark calculations [DE94-016165] p 1508 N95-20160

The Nonlinear Characteristic scheme in X-Y geometries [DE94-016192] p 1488 N95-20167

A S2-like acceleration method for the Nonlinear Characteristic transport scheme [DE94-016285] p 1509 N95-20235

Solid-state dynamics and quantum transport in novel semiconductor nanostructures [AD-A285946] p 1315 N95-20394

Extended theory of main ion and impurity rotation and bootstrap current in a shear layer [DE94-015857] p 1555 N95-21141

Theory of the L-H transition [DE95-001389] p 1558 N95-21299

Stellarator transport optimization with self-consistent electric fields [DE94-019151] p 1559 N95-21581

Fast algorithms for transport models [DE95-001702] p 1470 N95-21992

TRANSPORTATION

Beyond telecommuting: A new paradigm for the effect of telecommunications on travel [DE95-001224] p 1289 N95-20214

Approaches to the design of structural ceramics incorporating whiskers and particulate phases [DE94-018126] p 1271 N95-20704

Transportation of volatile elements in thermally evolving planetesimals: An important role of metallic iron p 1418 N95-21790

TRANSVERSE LOADS

The processing and mechanical properties of high temperature/high performance composites. Fatigue and creep, book 3 [AD-A279738] p 1227 N95-20430

TRAPPED PARTICLES

Numerical analysis of energetic particle stabilization of ballooning modes in finite-aspect-ratio tokamaks [DE94-631397] p 1556 N95-21164

Gate oxide shorts in nMOS transistors: Electrical properties and lifetime prediction method [DE94-018904] p 1330 N95-21545

TRAPPING

Development of a lightweight, light-trapped, thin GaAs solar cell for spacecraft applications p 1318 N95-20513

Effects of plasma hydrogenation on trapping properties of dislocations in heteroepitaxial InP/GaAs p 1323 N95-20542

Laser trapping of Na-21 atoms [DE95-002354] p 1513 N95-20629

Tunneling of self-trapped states and formation of a band [DE94-629001] p 1582 N95-22378

TRAVELING WAVE TUBES

Design and packaging aspects of microwave bandwidth lithium niobate modulators [DE94-016602] p 1313 N95-20119

Materials processing using a variable frequency microwave furnace [DE95-001420] p 1271 N95-20761

TRAVELING WAVES

One-dimensional reactive Euler equations [PB95-135430] p 1244 N95-21573

TREES (MATHEMATICS)

Distribution-independent hierarchical N-body methods [DE95-001686] p 1493 N95-21439

Abstract interpretation of reactive systems: Abstractions preserving Universal CTL(*), Existential CTL(*) and CTL(*) [PB95-110557] p 1472 N95-22305

TREMORS

Computer programs for analysis of geophysical data [DE95-002472] p 1415 N95-21511

TRENDS

Global change integrating factors: Tropical tropopause trends [DE95-001121] p 1404 N95-20835

TRIANGULATION

Construction of non-critical string field theory by transfer matrix formalism in dynamical triangulation [DE94-770607] p 1516 N95-20986

Support to the development of high-level graphics software [PB95-131686] p 1466 N95-21349

Right inverse for the divergence operator in spaces of continuous piecewise polynomials [PB95-127080] p 1496 N95-22369

TRIBOLOGY

Tribology and surface mechanical properties of excimer laser nitrided titanium [DE95-002751] p 1255 N95-21238

Friction and wear properties of as-deposited and carbon ion-implanted diamond films [NASA-TM-106759] p 1274 N95-21252

On the origins and modeling of frictional behavior in interfacially-complex sliding contacts [DE94-019129] p 1381 N95-21601

Surface technology programme [PB95-132866] p 1262 N95-22174

Characterization and performance of DLC films synthesized by plasma and ion beam techniques [DE94-018287] p 1281 N95-22428

TRIGGER CIRCUITS

GAJET experiment at the LHC: The GAJET collaboration [PB95-129813] p 1512 N95-20454

Triggers for a high sensitivity charm experiment [DE95-002251] p 1515 N95-20868

New shower maximum trigger for electrons and photons at CDF [DE95-000563] p 1522 N95-21499

Investigations into alternate spark gap switching techniques [AD-A286225] p 1308 N95-22021

TRIMERS

The synthesis and characterization of small molecule and photo-cross-linkable high polymeric phosphazenes bearing cinnamate groups [AD-A279782] p 1268 N95-20442

The organic chemistry of conducting polymers [DE94-018216] p 1270 N95-20680

TRIMETHYL COMPOUNDS

Characterization and electrical properties of copper films grown via direct liquid coinjection of (hfac)Cu(TMVS) and TMVS [DE95-002957] p 1272 N95-20889

TRITIUM

Thermodynamic characterization of new palladium alloy tritides [DE94-018430] p 1579 N95-20028

Fracture toughness properties of welded stainless steels for tritium service [DE95-000755] p 1251 N95-20079

A new alpha particle diagnostic using knock-on ion tails [DE94-015856] p 1553 N95-20402

High efficiency GaP power conversion for Betavoltaic applications p 1323 N95-20540

Target Area design basis and system performance for the National Ignition Facility [DE94-016697] p 1557 N95-21207

Review of recent D-T experiments from TFTR [DE95-002755] p 1557 N95-21239

Assessment of database for interaction of tritium with ITER plasma facing materials [DE95-002038] p 1558 N95-21290

Properties of aged metal tritides [DE95-001787] p 1243 N95-21440

Time of flight spectroscopy with muonic hydrogen [DE94-017056] p 1245 N95-21845

Welding tritium exposed stainless steel [DE95-003208] p 1382 N95-22356

TRITON

Studies of the gas tori of Titan and Triton [NASA-CR-197377] p 1601 N95-20797

TROPICAL METEOROLOGY

Rainfall rates and the vertical distribution of diabatic heating components over tropical oceans [NASA-CR-197603] p 1428 N95-19948

Program control on the Tropical Rainfall Measuring Mission p 1584 N95-20750

A study of westerly wind bursts preceding the 1991-1992 El Nino [AD-A286570] p 1429 N95-20826

TROPICAL REGIONS

Monsoons: AMIP simulations of the 1987 and 1988 drought and flood regimes [DE94-014789] p 1428 N95-20140

Test Operations Procedure (TOP) 1-2-616 tropic exposure testing [AD-A286376] p 1235 N95-20230

The vertical distribution of heating in the tropical atmosphere [AD-A285934] p 1429 N95-20391

Program control on the Tropical Rainfall Measuring Mission p 1584 N95-20750

Global change integrating factors: Tropical tropopause trends [DE95-001121] p 1404 N95-20835

TROPICAL STORMS

A study of westerly wind bursts preceding the 1991-1992 El Nino [AD-A286570] p 1429 N95-20826

TROPOPAUSE

Global change integrating factors: Tropical tropopause trends [DE95-001121] p 1404 N95-20835

TROPOSPHERE

A comparative survey of current and proposed tropospheric refraction-delay models for DSN radio metric data calibration [NASA-CR-197338] p 1412 N95-20002

Indirect global warming effects of ozone and stratospheric water vapor induced by surface methane emission [DE94-019016] p 1402 N95-20353

Radiative forcing for changes in tropospheric O3 [DE94-019017] p 1413 N95-20354

Radiative forcing calculations for CH3Cl [DE94-019018] p 1402 N95-20355

Modelling and simulation of HF/VHF MMPPs p 1293 N95-20925

Terrain and refractivity effects on non-optical paths p 1294 N95-20931

Modeling tropospheric ducting effects on satellite-to-ground paths p 1295 N95-20936

The Lorentz reciprocity theorem as a consistency test for propagation models p 1295 N95-20937

TROPOSPHERIC SCATTERING

Study of the fast and slow variations of the power received at VHF links by tropospheric diffusion p 1293 N95-20929

Propagation measurements on a troposcatter link in the Canadian High Arctic p 1295 N95-20940

Comparative study of C- and K-band propagation mechanisms beyond the horizon p 1297 N95-20946

TRUCKS

Reducing exhaust gas emissions from Citydiesel busses [DE95-700245] p 1380 N95-21295

TRUSSES

Static stability of a three-dimensional space truss p 1220 N95-20533

TUMORS

Radiofrequency hyperthermia systems: Experimental and clinical assessment of the feasibility of radiofrequency hyperthermia systems for loco-regional deep heating [PB94-206885] p 1444 N95-21016

Radiopharmaceuticals for diagnosis [DE95-002200] p 1445 N95-21595

TUNABLE LASERS

Continuously-tunable, narrow-linewidth, Q-switched Cr:LiSAF laser for lidar applications [DE95-000862] p 1373 N95-21312

Tunable CW blue, green, orange and red upconversion fiber lasers at room temperature [DE95-000851] p 1375 N95-22007

TUNGSTEN

Ductile-brittle transition behavior of tungsten under shock loading [DE94-009913] p 1251 N95-20122

Electronic structure and relative stability of icosahedral superatoms in Al-transition-metal alloys [DE94-628996] p 1260 N95-21855

Thoriated-tungsten, split-ring, hollow-cathode electrode for discharge devices
[AD-D016508] p 1333 N95-21906
Spectroscopic assessment of the reliability of metal/metal oxide interfaces
[AD-A286131] p 1261 N95-22035

TUNGSTEN ALLOYS
Mechanical behavior of 97.2% W alloy in tension at high temperatures
[AD-A284797] p 1250 N95-20067
Tungsten-uranium penetrator target interaction
[DE95-000847] p 1387 N95-21364
Effect of annealing temperature on the texture of rolled tantalum and tantalum-10 wt % tungsten
[DE95-002702] p 1262 N95-22308

TUNING
Linear and nonlinear spectroscopy with the tunable AC scanning tunneling microscope
[AD-A285751] p 1241 N95-21217
First results from the final focus test beam
[DE95-002897] p 1535 N95-21255
Recent progress of the compact AFEL at Los Alamos
[DE95-002728] p 1376 N95-22154
Proposed emittance upgrade for the SLC damping rings
[DE95-002887] p 1536 N95-22155

TUNNEL DIODES
Chemical beam epitaxy for high efficiency photovoltaic devices p 1316 N95-20508

TUNNELS
Propagation of high frequency waves in urban and road tunnel environments p 1294 N95-20933

TURBINE BLADES
Modeling the effect of shroud contact and friction dampers on the mistuned response of turbopumps
[NASA-CR-197285] p 1379 N95-20795
Advanced wind turbine design studies: Advanced conceptual study
[DE93-000031] p 1394 N95-20985

TURBINE ENGINES
Evaluation of PS 212 coatings under boundary lubrication conditions with an Ester-based oil to 300 C
[NASA-TM-106762] p 1223 N95-19901
Statistical analysis of Turbine Engine Diagnostic (TED) field test data
[AD-A286032] p 1379 N95-20998
Turbine design and application
[NASA-SP-290] p 1214 N95-22341

TURBINE PUMPS
SSME HPOTP post-test diagnostic system enhancement project
[NASA-CR-4643] p 1222 N95-21458

TURBINES
Scale-up and modeling of forced chemical vapor infiltration
[DE94-017769] p 1340 N95-20781
Turbine design and application
[NASA-SP-290] p 1214 N95-22341

TURBOGENERATORS
An overview: Component development for solar thermal systems
[DE95-001623] p 1393 N95-20862
Seawater test results of Open-Cycle Ocean Thermal Energy Conversion (OC-OTEC) components
[DE94-019254] p 1396 N95-21897

TURBOJET ENGINES
Portable static test facility for small, expendable, turbojet engines, phase 1
[AD-A286337] p 1216 N95-21719

TURBOMACHINE BLADES
Investigation of shear layer transition using various turbulence models p 1352 N95-21096

TURBULENCE
Experimental study of vane heat transfer and aerodynamics at elevated levels of turbulence
[NASA-CR-4633] p 1337 N95-19912
Evaluation of Reynolds stress turbulence closures in compressible homogeneous shear flow
[NASA-CR-194892] p 1338 N95-20009
Structure and dynamics of turbulent wall layers
[AD-A285360] p 1340 N95-20547
Application of wavelet-filtering techniques to intermittent turbulent and wall pressure events. Part 1: Exploratory results
[AD-A286077] p 1341 N95-20849
Studying Turbulence Using Numerical Simulation Databases. 5: Proceedings of the 1994 Summer Program
[NASA-CR-197362] p 1341 N95-21035
Direct numerical simulations of turbulent non-premixed methane-air flames modeled with reduced kinetics
p 1249 N95-21038
Triple flame structure and diffusion flame stabilization
p 1249 N95-21039
The coupling between flame surface dynamics and species mass conservation in premixed turbulent combustion p 1249 N95-21041
Simulation of a turbulent flame in a channel
p 1249 N95-21044
Instability of streamwise vortices in plane channel flows p 1344 N95-21049
Effects of turbulence compressibility and unsteadiness in compression corner flow p 1344 N95-21052
Modeling near wall effects in second moment closures by elliptic relaxation p 1345 N95-21054
Large-eddy simulation of separated flow in a ribbed duct p 1347 N95-21070
A cheap DNS tool for turbulence models testing
p 1348 N95-21072
Simulation of large scale transitional flows
p 1348 N95-21075
Simulations of bypass transition for spatially evolving disturbances p 1349 N95-21079
The effect of initial conditions on the development of temporally evolving planar three dimensional incompressible wakes p 1350 N95-21085
Direct numerical simulation of transition to turbulence from a high-symmetry initial condition
p 1351 N95-21089
Direct numerical simulations of leading-edge receptivity for freestream sound p 1351 N95-21090
Application of Roe's flux-difference splitting for kappa-epsilon turbulence model
[PB95-127718] p 1352 N95-21106
The structure of turbulence and other motions beneath an air-water interface
[AD-A279838] p 1434 N95-21293
Theory of the L-H transition
[DE95-001389] p 1558 N95-21299
Temporal evolution of turbulence/chemistry interactions in lifted, turbulent-jet flames
[DE95-002481] p 1243 N95-21512
Breakdown of the law of large numbers in Josephson junction series arrays
[DE94-629075] p 1576 N95-21996
Order and turbulence in RF-driven Josephson junction series arrays
[DE94-629076] p 1576 N95-21997
Elastic micro-fabricated surface layer for reducing turbulence and drag on an object while it moves through a fluid medium
[AD-D016516] p 1356 N95-22060
Derivation of a wavenumber filter design for the measurement of turbulent wall pressure fluctuations
[AD-A286421] p 1357 N95-22208
Heat loss by helicity injection in spheromaks
[DE95-003473] p 1562 N95-22221
Fully developed turbulent flows
[AD-A286496] p 1358 N95-22294
Annual research briefs, 1994
[NASA-CR-197352] p 1358 N95-22437
Conditional statistics in a turbulent premixed flame derived from direct numerical simulation
p 1249 N95-22438
Notes on rotating turbulence p 1359 N95-22444
A dynamic localization model with stochastic backscatter p 1359 N95-22445
Experimental investigations of on-demand vortex generators p 1361 N95-22451

TURBULENCE EFFECTS
Turbulence descriptors for scaling fatigue loading spectra of wind turbine structural components
[DE94-011833] p 1384 N95-20109
Effects of turbulence compressibility and unsteadiness in compression corner flow p 1344 N95-21052
Single point modeling of rotating turbulent flows
p 1346 N95-21060
Simulation of rotor blade element turbulence
[NASA-TM-108862] p 1207 N95-21186
A preliminary study of the airwake model used in an existing SH-60B/FFG-7 helicopter/ship simulation program
[DSTO-TR-0015] p 1201 N95-21659
Threshold detection in the presence of atmospheric turbulence
[AD-A286175] p 1427 N95-22249

TURBULENCE MODELS
Open Skies project computational fluid dynamic analysis
[AD-A285928] p 1200 N95-19991
Mapping closures for turbulent combustion
[AD-A279995] p 1238 N95-20597
Studying Turbulence Using Numerical Simulation Databases. 5: Proceedings of the 1994 Summer Program
[NASA-CR-197362] p 1341 N95-21035
Turbulent transport in premixed flames
p 1249 N95-21040
The coupling between flame surface dynamics and species mass conservation in premixed turbulent combustion p 1249 N95-21041
Pdf modeling for premixed turbulent combustion based on the properties of iso-concentration surfaces
p 1249 N95-21042
A Lagrangian dynamic subgrid-scale model turbulence
p 1344 N95-21051
Modeling the two-point correlation of the vector stream function p 1345 N95-21055
Homogeneous turbulence subjected to mean flow with elliptic streamlines p 1345 N95-21056
The asymptotic state of rotating homogeneous turbulence at high Reynolds numbers
p 1347 N95-21065
Comparison of DNS and LES of transitional and turbulent compressible flow: Flat plate and mixing layer
p 1347 N95-21066
Direct numerical simulation of turbulent flow in a sudden pipe expansion p 1347 N95-21067
A cheap DNS tool for turbulence models testing
p 1348 N95-21072
Direct simulation of turbulent flow in a square duct: Reynolds-stress budgets p 1348 N95-21073
Modelling anisotropy and backscatter effects in the subgrid scale stress tensor p 1349 N95-21077
Simulation of pipe flow p 1349 N95-21078
Direct numerical determination of the minimum bypass Reynolds number in boundary layers
p 1349 N95-21080
A flamelet model for turbulent unpremixed combustion
p 1249 N95-21081
Direct numerical simulation for premixed turbulent combustion modelling p 1249 N95-21082
Entrainment in a shear-free turbulent mixing layer
p 1350 N95-21083
Direct simulation of a self-similar plane wake
p 1350 N95-21084
Investigation of shear layer transition using various turbulence models p 1352 N95-21096
Application of Roe's flux-difference splitting for kappa-epsilon turbulence model
[PB95-127718] p 1352 N95-21106
Simulation of rotor blade element turbulence
[NASA-TM-108862] p 1207 N95-21186
Annual research briefs, 1994
[NASA-CR-197352] p 1358 N95-22437
Turbulence modeling for separated flow
p 1359 N95-22443
Large-eddy simulation of flow through a plane, asymmetric diffuser p 1360 N95-22449
Large-eddy simulation of a boundary layer with concave streamwise curvature p 1360 N95-22450
Numerical study of boundary layer interaction with shocks: Method and code validation
p 1362 N95-22461
Databases post-processing in Tensoral
p 1363 N95-22465

TURBULENT BOUNDARY LAYER
Application of wavelet-filtering techniques to intermittent turbulent and wall pressure events. Part 1: Exploratory results
[AD-A286077] p 1341 N95-20849
Numerical investigation of supersonic turbulent boundary layers with high wall temperature
p 1344 N95-21050
Developments and applications of dynamic models for large eddy simulation of complex flows
p 1346 N95-21062
Direct numerical determination of the minimum bypass Reynolds number in boundary layers
p 1349 N95-21080
Direct simulation of a self-similar plane wake
p 1350 N95-21084
Large-eddy simulation of a boundary layer with concave streamwise curvature p 1360 N95-22450
Experimental investigations of on-demand vortex generators p 1361 N95-22451
Drag reduction strategies p 1361 N95-22453
Small-scale behavior in distorted turbulent boundary layers at low Reynolds number p 1362 N95-22456
Transverse vorticity measurements in the NASA Ames 80 x 120 wind tunnel boundary layer
p 1362 N95-22457

TURBULENT COMBUSTION
Mapping closures for turbulent combustion
[AD-A279995] p 1238 N95-20597
Direct numerical simulations of turbulent non-premixed methane-air flames modeled with reduced kinetics
p 1249 N95-21038
Turbulent transport in premixed flames
p 1249 N95-21040
The coupling between flame surface dynamics and species mass conservation in premixed turbulent combustion p 1249 N95-21041

Pdf modeling for premixed turbulent combustion based on the properties of iso-concentration surfaces p 1249 N95-21042
Simulation of a turbulent flame in a channel p 1249 N95-21044
A flamelet model for turbulent unpremixed combustion p 1249 N95-21081
Direct numerical simulation for premixed turbulent combustion modelling p 1249 N95-21082
Studies in nonlinear problems of energy [DE95-001387] p 1356 N95-22148
Annual research briefs, 1994 [NASA-CR-197352] p 1358 N95-22437
Conditional statistics in a turbulent premixed flame derived from direct numerical simulation p 1249 N95-22438
Fundamental mechanisms in premixed flame propagation via vortex-flame interactions: Numerical simulations p 1249 N95-22440
Triple flames and flame stabilization p 1249 N95-22441

TURBULENT DIFFUSION
Metallic ions and atoms in the upper atmosphere [AD-A285229] p 1414 N95-20498
The decay of axisymmetric homogeneous turbulence p 1343 N95-21047

TURBULENT FLOW
Turbulence descriptors for scaling fatigue loading spectra of wind turbine structural components [DE94-011833] p 1384 N95-20109
Data report: Stress measurements in the bottom boundary layer with BASS tripods STRESS 2 1990-1991 [AD-A279875] p 1433 N95-20433
Nonlinear spectroscopy of multicomponent droplets and two- and three-dimensional measurements in flames [AD-A279945] p 1238 N95-20581
Mapping closures for turbulent combustion [AD-A279995] p 1238 N95-20597
Software for flow distribution in electronic rack structures [AD-A285994] p 1325 N95-20715
Application of wavelet-filtering techniques to intermittent turbulent and wall pressure events. Part 1: Exploratory results [AD-A286077] p 1341 N95-20849
A computer code (SKINTEMP) for predicting transient missile and aircraft heat transfer characteristics [AD-A286044] p 1341 N95-21001
Studying Turbulence Using Numerical Simulation Databases. 5: Proceedings of the 1994 Summer Program [NASA-CR-197362] p 1341 N95-21035
Turbulent transport in premixed flames p 1249 N95-21040
The coupling between flame surface dynamics and species mass conservation in premixed turbulent combustion p 1249 N95-21041
Passive turbulent flamelet propagation p 1249 N95-21043
Pressure and higher-order spectra for homogeneous isotropic turbulence p 1343 N95-21045
A Lagrangian dynamic subgrid-scale model turbulence p 1344 N95-21051
Role of pressure diffusion in non-homogeneous shear flows p 1345 N95-21053
Modeling the two-point correlation of the vector stream function p 1345 N95-21055
Single point modeling of rotating turbulent flows p 1346 N95-21060
Application of Direct and Large Eddy Simulation to Transition and Turbulence [AGARD-CP-551] p 1346 N95-21061
Developments and applications of dynamic models for large eddy simulation of complex flows p 1346 N95-21062
Subgrid scale models in finite difference simulations of complex wall bounded flows p 1346 N95-21063
Large-eddy simulation of rotating channel flows using a localized dynamic model p 1346 N95-21064
Comparison of DNS and LES of transitional and turbulent compressible flow: Flat plate and mixing layer p 1347 N95-21066
Direct numerical simulation of turbulent flow in a sudden pipe expansion p 1347 N95-21067
Large eddy simulation of turbulent flow over a cavity p 1347 N95-21069
Large-eddy simulation of separated flow in a ribbed duct p 1347 N95-21070
A cheap DNS tool for turbulence models testing p 1348 N95-21072
Direct simulation of turbulent flow in a square duct: Reynolds-stress budgets p 1348 N95-21073
Simulation of pipe flow p 1349 N95-21078
Direct numerical determination of the minimum bypass Reynolds number in boundary layers p 1349 N95-21080
Entrainment in a shear-free turbulent mixing layer p 1350 N95-21083
Direct simulation of a self-similar plane wake p 1350 N95-21084
DNS of turbulent flow in a driven cavity and their analysis using proper orthogonal decomposition p 1352 N95-21097
Direct simulation and graphics post-processing of three-dimensional turbulent flows p 1352 N95-21098
Summaries of BFRL fire research in-house projects and grants, 1994 [PB95-130845] p 1286 N95-21130
Fourth International Symposium on Stratified Flows, volume 1 [AD-A286450] p 1354 N95-21583
Derivation of a wavenumber filter design for the measurement of turbulent wall pressure fluctuations [AD-A286421] p 1357 N95-22208
Fully developed turbulent flows [AD-A286496] p 1358 N95-22294
Annual research briefs, 1994 [NASA-CR-197352] p 1358 N95-22437
Turbulence modeling for separated flow p 1359 N95-22443
Notes on rotating turbulence p 1359 N95-22444
Large-eddy simulation of a plane wake p 1360 N95-22446
Large-eddy simulation of flow through a plane, asymmetric diffuser p 1360 N95-22449
Large-eddy simulation of a boundary layer with concave streamwise curvature p 1360 N95-22450
Drag reduction strategies p 1361 N95-22453
Experimental and numerical study of the intermittency exponent mu p 1362 N95-22458
On the dynamics of small-scale vorticity in isotropic turbulence p 1362 N95-22459
Numerical study of boundary layer interaction with shocks: Method and code validation p 1362 N95-22461
A method for obtaining a statistically stationary turbulent free shear flow p 1363 N95-22463

TURBULENT JETS
Application of Direct and Large Eddy Simulation to Transition and Turbulence [AGARD-CP-551] p 1346 N95-21061
Temporal evolution of turbulence/chemistry interactions in lifted, turbulent-jet flames [DE95-002481] p 1243 N95-21512
Direct numerical simulation of incompressible axisymmetric flows p 1363 N95-22464

TURBULENT MIXING
Entrainment in a shear-free turbulent mixing layer p 1350 N95-21083
Fourth International Symposium on Stratified Flows, volume 4 [AD-A286453] p 1358 N95-22424
Drag reduction strategies p 1361 N95-22453

TURBULENT WAKES
Triple flame structure and diffusion flame stabilization p 1249 N95-21039
Application of Direct and Large Eddy Simulation to Transition and Turbulence [AGARD-CP-551] p 1346 N95-21061
Direct simulation of a self-similar plane wake p 1350 N95-21084
The velocity and vorticity fields of the turbulent near wake of a circular cylinder [NASA-TM-110513] p 1355 N95-21954
Large-eddy simulation of a plane wake p 1360 N95-22446
Direct numerical simulation of incompressible axisymmetric flows p 1363 N95-22464

TWINNING
Post-irradiation deformation characteristics of heavy-ion irradiated 304L SS [DE94-017462] p 1251 N95-20088

TWO DIMENSIONAL BOUNDARY LAYER
On subcritical instability of the attachment line boundary layer p 1351 N95-21092

TWO DIMENSIONAL FLOW
Static investigation of two fluidic thrust-vectoring concepts on a two-dimensional convergent-divergent nozzle [NASA-TM-4574] p 1199 N95-19913
Multigrid with matrix-dependent transfer operators for convection-diffusion problems [PB95-110821] p 1487 N95-19915
Nonlinear spectroscopy of multicomponent droplets and two- and three-dimensional measurements in flames [AD-A279945] p 1238 N95-20581
HIVEL2D: A two-dimensional flow model for high-velocity channels [AD-A286556] p 1341 N95-20843
Direct numerical simulation of 2-D and 3-D instability waves in a laminar separation bubble p 1352 N95-21095
Investigation of shear layer transition using various turbulence models p 1352 N95-21096
DNS of turbulent flow in a driven cavity and their analysis using proper orthogonal decomposition p 1352 N95-21097
Two-dimensional imaging of OH in a lean burning high pressure combustor [NASA-TM-106854] p 1214 N95-21383
Convergence acceleration of the Proteus computer code with multigrid methods [NASA-CR-197677] p 1467 N95-21450
Large amplitude localized structures in a relativistic electron-positron ion plasma [DE94-628965] p 1561 N95-21851
Shock wave interactions in hypervelocity flow [AD-A286507] p 1357 N95-22212
1/f noise in two-dimensional fluids [DE95-002617] p 1358 N95-22307
Direct numerical simulations of on-demand vortex generators: Mathematical formulation p 1361 N95-22452

TWO DIMENSIONAL MODELS
Solutions of D(sup n)D(sup m)f=0 [PB95-110839] p 1487 N95-19916
Analyses of some benchmark cases in fracture mechanics using boundary element method [PB95-110888] p 1384 N95-19930
Open Skies project computational fluid dynamic analysis [AD-A285928] p 1200 N95-19991
The Nonlinear Characteristic scheme in X-Y geometries [DE94-016192] p 1488 N95-20167
Investigating the resolution of resistivity arrays using inverse theory [DE94-017760] p 1412 N95-20287
Theoretical particle physics [DE95-002447] p 1515 N95-20893
Three-dimensional effects for radio frequency antenna modeling [DE94-019125] p 1303 N95-21459
An Echelle Grating Spectrometer (EGS) for mid-IR remote chemical detection [DE94-019310] p 1367 N95-21478
Object recognition by alignment using invariant projections of planar surfaces [AD-A279841] p 1468 N95-21495
A new FHNC scheme for Gutzwiller correlated wave functions [DE94-629037] p 1581 N95-21993

TYROSINE
Behavioral effects of tyrosine during sustained wakefulness [AD-A279789] p 1441 N95-20307

U

ULTRAHIGH FREQUENCIES
Inverse Cerenkov laser acceleration experiment at ATF [DE94-017990] p 1370 N95-20572
Large bistatic angle clutter depolarization study p 1296 N95-20941
Mitigation of effects of multiple path nulls at super-high frequencies through diversity and networking p 1297 N95-20948
Variability of total electron content in the high-altitude ionosphere following solar maximum [AD-A285849] p 1425 N95-21833

ULTRAHIGH VACUUM
A low temperature, ultrahigh vacuum, microwave-frequency-compatible scanning tunneling microscope [AD-A279869] p 1365 N95-20413

ULTRASHORT PULSED LASERS
Fiber laser amplifiers and oscillators [AD-A285835] p 1368 N95-20035
Modelocking and waveguide amplifiers using Cr:Forsterite and Cr:YAG [AD-A285857] p 1369 N95-20378

ULTRASONIC RADIATION
An in-line ultrasonic viscometer [DE95-002982] p 1366 N95-21453

ULTRASONICS
Method and apparatus for non-invasive evaluation of diaphragmatic function [NASA-CASE-LAR-13888-1] p 1441 N95-20408
Surfaces and thin films studied by picosecond ultrasonics [DE95-001866] p 1506 N95-22071
Applications of sonochemistry [AD-A286388] p 1506 N95-22360

ULTRAVIOLET ABSORPTION
Photoinduced charge transfer between fullerenes and TiO2 semiconductor colloids
[DE95-001447] p 1570 N95-20838

ULTRAVIOLET ASTRONOMY
Coronagraphic observations and analyses of the ultraviolet solar corona
[NASA-CR-197370] p 1602 N95-20558

ULTRAVIOLET EMISSION
Ultraviolet emission from rocket motor plumes
[DSTO-TR-0002] p 1222 N95-21661

ULTRAVIOLET LASERS
A URI program for Ultraviolet/extreme ultraviolet research
[AD-A279159] p 1370 N95-20600
Ultraviolet laser emission properties of Ce(3+)-doped LiSrAlF6
[DE94-016364] p 1372 N95-21135
Research studies on short wavelength lasers by selective Auger processes
[AD-A285620] p 1372 N95-21144
Visible fluorescence of weathered lead
[DE95-002454] p 1244 N95-21523

ULTRAVIOLET PHOTOGRAPHY
Imaging design of the wide field x-ray monitor onboard the HETE satellite
[DE95-002750] p 1221 N95-22436

ULTRAVIOLET RADIATION
Free electron laser program
[AD-A285906] p 1368 N95-19987
UV testing of INTELSAT-7, 7A, and 8 solar cells
p 1320 N95-20526
A URI program for Ultraviolet/extreme ultraviolet research
[AD-A279159] p 1370 N95-20600
Magnetron power supply at high stability and its application in plasma excitation for the production of ultraviolet radiation
[DE94-629656] p 1326 N95-20733
Disinfection of purified waste water with ultra violet light on a technical scale
[PB95-131926] p 1405 N95-21330
Optical radiation: Health based exposure limits for electromagnetic radiation in the wavelength range from 100 nanometer to 1 millimeter
[PB95-132767] p 1447 N95-22083

ULTRAVIOLET SPECTRA
Electron propagator theory and application
[AD-A279761] p 1507 N95-20097
The synthesis and characterization of small molecule and photo-cross-linkable high polymeric phosphazenes bearing cinnamate groups
[AD-A279782] p 1268 N95-20442
Ultraviolet emission from rocket motor plumes
[DSTO-TR-0002] p 1222 N95-21661
Coherence properties of high order harmonic radiation
[DE94-016974] p 1377 N95-22312

ULTRAVIOLET SPECTROMETERS
Atmospheres of the Moon and Mercury
p 1419 N95-21794
Absolute, Extreme-ultraviolet Solar Spectral Irradiance Monitor (AESSIM)
[AD-A279345] p 1603 N95-21929

ULTRAVIOLET SPECTROSCOPY
Spectroscopic studies of hazardous fuel interactions with soils
[AD-A279099] p 1407 N95-21596
Cryogenic pellet laser plasma source targets
[DE95-002488] p 1376 N95-22169

UNDERWATER ACOUSTICS
The Combustive Sound Source
[ARL-TR-94-9] p 1503 N95-19911
Oceanographic analysis of the acoustic mid-ocean dynamics experiment
[AD-A285907] p 1432 N95-19988
Analysis of low frequency ocean noise. 1: From a long-term experiment across the US East Coast. 2: From the Wake Island Hydrophone Array during northwest Pacific typhoons
[AD-A284975] p 1432 N95-20040
Signal-to-noise gain from adaptive matched-field beamforming of multidimensional acoustic arrays
[AD-A285671] p 1503 N95-20084
Characterization and simulation of an acoustic source moving through an oceanic waveguide
[AD-A285688] p 1503 N95-20272
Ambient noise and surface wave dissipation in the ocean
[AD-A279650] p 1432 N95-20303
Multiple scatter theory of ocean sediments
[AD-A286033] p 1433 N95-20999
Transducers with improved signal transfer field of the invention
[AD-D016228] p 1328 N95-21118
Underwater Acoustic Generator Phase 2: Sea trial, March 1992
[MRL-TN-640] p 1434 N95-21657
Acoustic Thermometry of Ocean Climate (ATOC): Selection of California source site
[AD-A279295] p 1436 N95-21987
Rapid determination of geoacoustic properties of the sea floor by simulated annealing
[AD-A286297] p 1436 N95-22028
Seismic anisothropy and large-scale porosity inthe ocean floor
[AD-A286580] p 1436 N95-22187

UNDERWATER STRUCTURES
Structural performance of cylindrical pressure housings of different ceramic compositions under external pressure loading. Part 4: Silicon carbide particulate reinforced alumina ceramic
[AD-A286299] p 1279 N95-22047

UNDERWATER VEHICLES
Structural performance of cylindrical pressure housings of different ceramic compositions under external pressure loading. Part 1: Isostatically pressed alumina ceramic
[AD-A279669] p 1270 N95-20603

UNIMOLECULAR STRUCTURES
Publications/patents/presentations/honors/student eport. Investigation of the role of vibrational excitation in unimolecular reactions
[AD-A280044] p 1513 N95-20621

UNIQUENESS
Uniqueness of strongly regular graphs having minimal p-rank
[PB95-111043] p 1488 N95-19942
A convergence analysis of an h-version finite element method with high order elements for two dimensional elasto-plasticity problems
[AD-A279975] p 1491 N95-20920

UNITED STATES
Census US civil aircraft calendar year 1993
[AD-A286309] p 1199 N95-20091

UNIVERSE
Connection with dynamics: General introduction
[NASA-CR-197617] p 1579 N95-19947
Predictions from quantum cosmology
[PB95-111126] p 1599 N95-20173

UNIX (OPERATING SYSTEM)
Personal computer and workstation operating systems tutorial
[AD-A280132] p 1451 N95-20041

UNSTEADY AERODYNAMICS
The dynamic approach to rotor blade research: ARA's oscillatory test facility
[ARA-MEMO-405] p 1200 N95-20758
Prediction of rotor-blade deformations due to unsteady airloads
[AD-A286593] p 1207 N95-20860
Pressure measurements on an F/A-18 twin vertical tail in buffeting flow. Volume 4, part 1: Buffet cross spectral densities
[AD-A285593] p 1215 N95-21214
Pressure measurements on an F/A-18 twin vertical tail in buffeting flow. Volume 1: Wind tunnel test summary
[AD-A279126] p 1202 N95-21877
Direct numerical simulations of on-demand vortex generators: Mathematical formulation
p 1361 N95-22452

UNSTEADY FLOW
Simulation of rotor blade element turbulence
[NASA-TM-108862] p 1207 N95-21186
Transient behaviour and stability points of the Poiseuille flow of a KBKZ-fluid
[PB95-132064] p 1353 N95-21268
The structure of turbulence and other motions beneath an air-water interface
[AD-A279838] p 1434 N95-21293
Multiwire thermocouples: Frequency response
[NASA-TM-110510] p 1367 N95-21889
Computations of unsteady viscous compressible flows using adaptive mesh refinement in curvilinear body-fitted grid systems
[NASA-TM-106704] p 1356 N95-21959
Direct numerical simulations of on-demand vortex generators: Mathematical formulation
p 1361 N95-22452
Acoustics of laminar boundary layers breakdown
p 1361 N95-22455

UPPER ATMOSPHERE
Completion of spectral rotating shadowband radiometers and analysis of ARM spectral short-wave data
[DE95-000602] p 1412 N95-20116
Metallic ions and atoms in the upper atmosphere
[AD-A285229] p 1414 N95-20498
Rare gases systematics and mantle structure
p 1416 N95-21778
Mars atmospheric loss and isotopic fractionation by pick-up-ion sputtering and photochemical escape
p 1420 N95-21796

UPWIND SCHEMES (MATHEMATICS)
Hybrid Upwind Splitting (HUS) by a field-by-field decomposition
[NASA-TM-106843] p 1355 N95-21957

URANIUM
Application of diode lasers to the isotopically selective determination of uranium in oxides by optogalvanic spectroscopy
[DE94-018045] p 1370 N95-20698
Active neutron multiplicity analysis and Monte Carlo calculations
[DE94-016178] p 1516 N95-21114

URANIUM ALLOYS
Tungsten-uranium penetrator target interaction
[DE95-000847] p 1387 N95-21364

URANIUM COMPOUNDS
A mechanistic model for radiation-induced crystallization and amorphization in U3Si
[DE94-015028] p 1566 N95-20419

URANIUM OXIDES
Application of diode lasers to the isotopically selective determination of uranium in oxides by optogalvanic spectroscopy
[DE94-018045] p 1370 N95-20698
Active neutron multiplicity analysis and Monte Carlo calculations
[DE94-016178] p 1516 N95-21114

URANIUM 235
Application of diode lasers to the isotopically selective determination of uranium in oxides by optogalvanic spectroscopy
[DE94-018045] p 1370 N95-20698

USER MANUALS (COMPUTER PROGRAMS)
PRSPLOT6 manual
[PB95-110862] p 1456 N95-19928
Noise model of the MSX SPIRIT 3 interferometer
[AD-A285837] p 1364 N95-20036
NOMADS graphical user interface version 2.0 user's manual
[AD-A286314] p 1458 N95-20095
Computer-Aided Structural Engineering (CASE) project. User's guide: Computer-Aided Structural Modeling (CASM). Version 5.00
[AD-A279913] p 1459 N95-20310
BACKSCAT lidar simulation version 4.0: Technical documentation and users guide
[AD-A285851] p 1290 N95-20376
Anaerobic digestion analysis model: User's manual
[DE94-011858] p 1437 N95-20471
Computer graphics tools for visualizing gravity gradient torques on a rigid spacecraft
[AD-A285971] p 1461 N95-20665
A software process framework for the Software Engineering Institute's (SEI) capability maturity model
[AD-A286595] p 1462 N95-20765
Xwake 1.0 user's manual
[DE95-002528] p 1463 N95-20901
FIREDOC users manual, 3rd edition
[PB95-128674] p 1286 N95-21129
PRSCAL manual
[PB95-130480] p 1465 N95-21231
PRISMA operating program manual
[PB95-130498] p 1466 N95-21232
EXPERT system expert: Users manual
[PB95-131579] p 1482 N95-21430
Unified very low stratus cloud/subcloud microphysics model: User's guide
[AD-A286454] p 1430 N95-21586
Modeling of rolling element bearing mechanics. Computer program user's manual
[NASA-CR-196557] p 1381 N95-21692
DBASE 4 basics
[DE94-018323] p 1469 N95-21713
A user's guide to LUGSAN 1.1: A computer program to calculate and archive lug and sway brace loads for aircraft-carried stores
[DE95-001919] p 1207 N95-21730
QMRPACK user's guide
[DE95-001770] p 1469 N95-21744
MARI mini-manual
[PB95-134649] p 1526 N95-21965
NODDS/WOSM interface user's manual
[AD-A279095] p 1471 N95-22068
SCOPE 1.5: A Source-Code Optimization PackagEfor REDUCE 3.5: User's manual
[PB95-107579] p 1472 N95-22159
Defense Data Repository System (DDRS). End user manual
[AD-A286484] p 1592 N95-22293
ActorStudio reference manual. A user's guide to the ActorStudio user interface editor, version 1.0
[PB95-127023] p 1472 N95-22310

USER REQUIREMENTS
Determining information management needs for enhanced international safeguards
[DE94-015787] p 1588 N95-20789
Accuracy problems in the generation of discrete time stochastic processes
[PB95-131397] p 1386 N95-21133
User interface software tools
[AD-A286056] p 1466 N95-21325
Underwater Acoustic Generator Phase 2: Sea trial, March 1992
[MRL-TN-640] p 1434 N95-21657
Noncoherent transponder standards
[AD-A279512] p 1306 N95-21684
State of the art in CFD pre- and postprocessing
[PB95-110391] p 1356 N95-22017
Economic feasibility analysis of distributed electric power generation based upon the natural gas-fired fuel cell
[DE94-012277] p 1396 N95-22033
Adaptive fault-resistant systems
[AD-A286406] p 1484 N95-22203
UTILIZATION
Processing and applications of iron aluminides
[DE94-017855] p 1253 N95-20673

V

VACUUM
RF vacuum microelectronics based on thin film edge-emitter technology
[AD-A279539] p 1331 N95-21690
Thermal fixture for testing an integrated circuit
[AD-D016483] p 1333 N95-21900
VACUUM CHAMBERS
Derivation of coupling impedance from the wake potential of a finite bunch
[DE95-002529] p 1532 N95-20421
Space power facility readiness for Space Station power system testing
[NASA-TM-106829] p 1218 N95-21384
VACUUM PUMPS
Evaluation of pumping and fueling requirements for the ITER EDA
[DE94-018117] p 1560 N95-21702
VACUUM SYSTEMS
Space power facility readiness for Space Station power system testing
[NASA-TM-106829] p 1218 N95-21384
The ITER in-vessel system
[DE94-018053] p 1560 N95-21665
Evaluation of pumping and fueling requirements for the ITER EDA
[DE94-018117] p 1560 N95-21702
VALUE ENGINEERING
The impact of partnering on construction contracts
[AD-A286588] p 1585 N95-20855
VAN DER WAALS FORCES
Combustion-related studies using weakly bonded complexes
[DE95-002801] p 1238 N95-20576
An augmented Young-Laplace model of an evaporating meniscus in a micro-channel with high heat flux
[NASA-CR-197622] p 1340 N95-20796
VANADIUM
The influence of chemistry and microstructure on the fracture toughness of V-V3Si in-situ composites
[DE94-018997] p 1232 N95-22126
VANADIUM ALLOYS
Tribology and surface mechanical properties of excimer laser nitrided titanium
[DE95-002751] p 1255 N95-21238
VANADIUM COMPOUNDS
The influence of chemistry and microstructure on the fracture toughness of V-V3Si in-situ composites
[DE94-018997] p 1232 N95-22126
VANES
Experimental study of vane heat transfer and aerodynamics at elevated levels of turbulence
[NASA-CR-4633] p 1337 N95-19912
VAPOR DEPOSITION
Optimization of InAsSb/InGaAs strained-layer superlattice growth by metal-organic chemical vapor deposition for use in infrared emitters
[DE94-016557] p 1563 N95-19954
Synthesis and studies of organometallic precursors for CVD of thin film electronic materials
[AD-A285834] p 1223 N95-20033
Enhancement of corrosion resistance and mechanical properties of light-weight metals through the use of graded nonequilibrium microstructures
[AD-A286320] p 1251 N95-20178
Amorphous silicon thin films: The ultimate lightweight space solar cell p 1318 N95-20515
Aerosol-assisted chemical vapor deposition of copper: A liquid delivery approach to metal thin films
[AD-A279702] p 1270 N95-20689
The in situ observation of epitaxial diamond thin film nucleation and growth using emission electron microscopy
[AD-A279811] p 1569 N95-20807
Novel reagents for chemical vapor deposition of intermetallic alloys
[AD-A286562] p 1271 N95-20815
Characterization and electrical properties of copper films grown via direct liquid coinjection of (hfac)Cu(TMVS) and TMVS
[DE95-002957] p 1272 N95-20889
Friction and wear properties of as-deposited and carbon ion-implanted diamond films
[NASA-TM-106759] p 1274 N95-21252
Analysis of cost: Combustion flame CVD diamond deposition
[AD-A279153] p 1278 N95-21973
Siloxanes with strong hydrogen bond donating functionalities
[AD-D016499] p 1279 N95-22057
Growing and releasing diamonds
[AD-D016489] p 1577 N95-22103
Advanced diagnostics for plasma chemistry
[DE94-018936] p 1561 N95-22116
Technical cost modeling applied to CVD diamond deposition
[AD-A286119] p 1578 N95-22231
VAPOR PHASE EPITAXY
Chemical beam epitaxy for high efficiency photovoltaic devices p 1316 N95-20508
High quality InP-on-Si for solar cell applications
p 1317 N95-20510
Photoreflectance and x ray diffraction study of semiconductor heterostructures and quantum wells
[PB95-127049] p 1582 N95-22432
VAPOR PHASES
Gas-phase generation of zinc sulfide particles using a single-source precursor
[AD-A279700] p 1239 N95-20712
Atmosphere influence on in situ ion beam analysis of thin film growth
[DE95-001507] p 1570 N95-20881
Non-local density functional calculations of gas phase heats of formation
[AD-A286213] p 1246 N95-22000
Governing equations for multiphase heat and mass transfer in hygroscopic porous media with applications to clothing materials
[AD-A286418] p 1357 N95-22206
Gas-phase photocatalytic oxidation: Cost comparison with other air pollution control technologies
[DE95-000241] p 1410 N95-22278
VAPOR PRESSURE
Transportation of volatile elements in thermally evolving planetesimals: An important role of metallic iron
p 1418 N95-21790
VAPORIZERS
Vapor generator wand
[NASA-CASE-LAR-15058-1] p 1215 N95-20080
VAPORIZING
Alkali element depletion by core formation and vaporization on the early Earth p 1421 N95-21804
VAPORS
Continuum transient and frozen startup behavior of conventional and gas-loaded heat pipes
[AD-A284297] p 1339 N95-20250
VARIABILITY
An experimental determination of meteor daily arrival rate variation
[AD-A279484] p 1600 N95-21679
Variability of total electron content in the high-altitude ionosphere following solar maximum
[AD-A285849] p 1425 N95-21833
Remote-sensing based technique to account for sub-grid scale variability of land surface properties
[NASA-TM-110501] p 1390 N95-22110
VARIATIONAL PRINCIPLES
Electron-nuclear dynamics of molecular systems
[AD-A279649] p 1516 N95-21120
Second order approximation for optical polaron in the strong coupling case
[DE94-628997] p 1525 N95-21856
Variational Monte Carlo study of He-4 in two dimensions
[DE94-629078] p 1576 N95-21998
VARIATIONS
Light-scattering fluctuations and noise in nonlinear optical processing
[AD-A279748] p 1544 N95-20803
Seamless data-range change using punctured convolutional codes for time-varying signal-to-noise ratios p 1304 N95-21534
VECTOR ANALYSIS
Visualizing 3D velocity fields near contour surfaces
[DE95-000841] p 1353 N95-21182
VECTOR MESONS
Nuclear A dependence of exclusive vector meson production in muon scattering
[DE95-002248] p 1511 N95-20418
Production of J/(psi) in 800 GeV/c p-Si interactions
[DE94-017982] p 1513 N95-20496
Anomalous vector-boson couplings in Majorana neutrino models
[PB95-127460] p 1518 N95-21220
Dilepton production from p-p to Ca-Ca at the Bevalac
[DE95-002341] p 1520 N95-21357
VECTOR PROCESSING (COMPUTERS)
VLUGr3: A vectorizable adaptive grid solver for PDEs in 3D. 2: Code description
[PB95-135737] p 1465 N95-21033
VECTOR SPACES
Linear invariance of Lindeloef numbers
[PB95-134540] p 1494 N95-21956
VECTORS (MATHEMATICS)
Hamiltonian structure of the reversible nonsemisimple 1:1 resonance
[PB95-127528] p 1495 N95-22151
Time and the order of abstract events in distributed computations
[PB95-110482] p 1496 N95-22349
VEGETATION
The effect of regional-scale soil-moisture deficits on mesoscale atmospheric dynamics that influence fire severity
[DE95-002682] p 1413 N95-20455
VEHICLES
Effect of propane-air on NGVs and vehicle fueling stations
[PB94-210085] p 1282 N95-20253
VELOCITY DISTRIBUTION
Velocity analysis for transversely isotropic media
[DE95-000643] p 1411 N95-19981
Passive turbulent flamelet propagation
p 1249 N95-21043
On the transition towards slow manifold in shallow-water and 3D Euler equations in a rotating frame
p 1345 N95-21057
The effect of initial conditions on the development of temporally evolving planar three dimensional incompressible wakes p 1350 N95-21085
Direct simulation of tridimensional wake of NACA 0012 profile p 1350 N95-21086
Rib vortices in round jets: Direct and large eddy simulation p 1351 N95-21088
Direct numerical simulation of transition to turbulence from a high-symmetry initial condition
p 1351 N95-21089
Visualizing 3D velocity fields near contour surfaces
[DE95-000841] p 1353 N95-21182
Resolving velocity profiles with the multi-scale profiler
[AD-A286446] p 1434 N95-21461
A preliminary study of the airwake model used in an existing SH-60B/FFG-7 helicopter/ship simulation program
[DSTO-TR-0015] p 1201 N95-21659
The velocity and vorticity fields of the turbulent near wake of a circular cylinder
[NASA-TM-110513] p 1355 N95-21954
Atomic velocity distributions in a hydrogen beam effusing out of an HF discharge dissociator
[AD-A279253] p 1307 N95-21985
1/f noise in two-dimensional fluids
[DE95-002617] p 1358 N95-22307
Resolution requirements for velocity gradients in turbulence p 1363 N95-22462
VELOCITY MEASUREMENT
A three-dimensional orthogonal laser velocimeter for the NASA Ames 7- by 10-foot wind tunnel
[NASA-TM-108864] p 1366 N95-21323
MHD-flow in slotted channels with conducting walls
[DE94-018370] p 1559 N95-21388
Resolving velocity profiles with the multi-scale profiler
[AD-A286446] p 1434 N95-21461
A preliminary study of the airwake model used in an existing SH-60B/FFG-7 helicopter/ship simulation program
[DSTO-TR-0015] p 1201 N95-21659
VENTILATION
Fire smoke ventilation through shafts: Experiments
[PB95-132247] p 1288 N95-21978
VENUS (PLANET)
Dynamics of volatile delivery from outer to inner solar system p 1420 N95-21798
Volatiles, rheology, and mantle convection: Comparing Earth, Venus, and Mars p 1420 N95-21801

VENUS ATMOSPHERE
Modeling of collision induced absorption spectra of CO2-CO2 pairs for planetary atmosphere of Venus
[NASA-CR-197373] p 1601 N95-22338
VERBAL COMMUNICATION
A database for analyzing sequential behavioral data and their associated cognitive models
[AD-A280061] p 1448 N95-19887
VERMICULITE
Laboratory evaluation of a reactive baffle approach to NOx control
[AD-A283802] p 1400 N95-19921
VERTEBRATES
How the brain works
[AD-A279138] p 1450 N95-21968
VERTICAL AIR CURRENTS
Simulation of rotor blade element turbulence
[NASA-TM-108862] p 1207 N95-21186
Stability effects on the profiles of vertical velocity and its variance in katabatic flow
[DE95-001126] p 1426 N95-21836
VERTICAL DISTRIBUTION
Rainfall rates and the vertical distribution of diabatic heating components over tropical oceans
[NASA-CR-197603] p 1428 N95-19948
The vertical distribution of heating in the tropical atmosphere
[AD-A285934] p 1429 N95-20391
VERTICAL TAKEOFF AIRCRAFT
The personal aircraft: Status and issues
[NASA-TM-109174] p 1200 N95-20688
VERY HIGH FREQUENCIES
The relative importance of meteor burst and other distance polar cap propagation modes in the low VHF band p 1293 N95-20928
Study of the fast and slow variations of the power received at VHF links by tropospheric diffusion
p 1293 N95-20929
VERY LARGE SCALE INTEGRATION
Prototype rule-based reliability analysis for VLSI circuit design
[AD-A280065] p 1327 N95-20967
An automatic placement tool for rapid prototyping of printed circuit boards
[AD-A286029] p 1328 N95-20997
VERY LONG BASE INTERFEROMETRY
Low noise 22 GHz receiver for the radioastron satellite. Part 1: Requirements, design and reliability analysis
[PB95-104410] p 1300 N95-20972
Low noise 22 GHz receiver for the radioastron satellite, part 2: Space qualification tests
[PB95-127197] p 1598 N95-22376
VHSIC (CIRCUITS)
VHDL modeling of PRC-70 radio ASICs for reverse engineering
[AD-A285740] p 1457 N95-19929
VIBRATION
Variations observed in the AC generator signal period of a Sea King helicopter
[AD-A284280] p 1206 N95-19963
Apparatus and method for determining the mass density of a filament
[NASA-CASE-LAR-14879-1-CU] p 1383 N95-20616
Vibration analysis of the AN/SPS-67(V)3 surface search radar
[AD-A286050] p 1302 N95-21324
Determination of the complex elastic moduli of materials using a free-free bar technique
[AD-A279861] p 1281 N95-22387
VIBRATION MEASUREMENT
An evaluation of the Gear Averaging Signal Processor (GASP)
[DSTO-TR-0067] p 1470 N95-21950
VIBRATION TESTS
An Echelle Grating Spectrometer (EGS) for mid-IR remote chemical detection
[DE94-019310] p 1367 N95-21478
VIBRATIONAL SPECTRA
Theoretical prediction of vibrational circular dichroism spectra of R-glyceraldehyde, R-erythrose, and R-threose. Part 2: Development of a procedure to scale the force constant matrix expressed in terms of internal coordinates
[AD-A284305] p 1437 N95-20252
Vibrational overtone spectroscopy of pyridine and related compounds
[AD-A280105] p 1224 N95-21911
VIBRATIONAL STATES
Plasma chemistry of vibrationally nonequilibrium molecules
[AD-A279630] p 1553 N95-20411
Publications/patents/presentations/honors/student eport. Investigation of the role of vibrational excitation in unimolecular reactions
[AD-A280044] p 1513 N95-20621
Changes in the behavior of magnetic materials undergoing processing in electrical rotating machines
[PB95-104493] p 1325 N95-20702
Electron attachment to excited molecules
[DE94-019124] p 1522 N95-21519
VIDEO COMMUNICATION
Subsampling methods for image sequence coding
[PB95-107991] p 1305 N95-21579
VIDEO DATA
Determining the usability of Digital Video Interactive (DVI) technology in computer-based instruction
[AD-A284717] p 1457 N95-20060
A scalable video rate camera interface
[AD-A286144] p 1474 N95-20325
Airborne Multisensor Pod System (AMPS) data access concept
[DE95-002586] p 1389 N95-20903
Subsampling methods for image sequence coding
[PB95-107991] p 1305 N95-21579
VIDEO EQUIPMENT
Color control in a multichannel simulator display: The display for advanced research and training
[AD-A279717] p 1216 N95-20992
Cold regions instrumentation considerations
[AD-A279492] p 1367 N95-21680
Evaluation of the Haworth-Newman avionics Display Readability Scale
[AD-A286127] p 1214 N95-22232
VIDEO SIGNALS
A scalable video rate camera interface
[AD-A286144] p 1474 N95-20325
Passive range measurement system
[AD-D016222] p 1544 N95-21100
Image and video coding using a wavelet decomposition
[PB95-135067] p 1311 N95-22358
VIDEO TAPES
Rate monotonic analysis for real-time systems: Instructors guide
[AD-A286083] p 1463 N95-20810
VINYL POLYMERS
The role of high pressure in the study and applications of the ferroelectric polymer polyvinylidene fluoride and its copolymers
[DE94-015742] p 1268 N95-20396
VINYLIDENE
The role of high pressure in the study and applications of the ferroelectric polymer polyvinylidene fluoride and its copolymers
[DE94-015742] p 1268 N95-20396
VIRTUAL MEMORY SYSTEMS
Design of a parallel object oriented programming language
[AD-A284924] p 1457 N95-20000
VIRTUAL REALITY
Measuring presence in virtual environments
[AD-A286183] p 1460 N95-20326
Virtual reality in precision engineering research
[AD-A286528] p 1465 N95-21012
VISCOELASTICITY
The numerical integration and 3-D finite element formulation of a viscoelastic model of glass
[DE95-002588] p 1271 N95-20788
Transient behaviour and stability points of the Poiseuille flow of a KBKZ-fluid
[PB95-132064] p 1353 N95-21268
VISCOMETERS
In situ viscometer instrument acceptance test report
[DE94-018507] p 1364 N95-20224
An in-line ultrasonic viscometer
[DE95-002982] p 1366 N95-21453
VISCOSITY
Conservative smoothing versus artificial viscosity
[DE95-001108] p 1341 N95-20831
Laser-Induced Thermal Acoustics (LITA): Four-wave mixing measurement of sound speed, thermal diffusivity, and viscosity
[AD-A286524] p 1372 N95-21009
An in-line ultrasonic viscometer
[DE95-002982] p 1366 N95-21453
Quartz resonator fluid monitors for vehicle applications
[DE94-018910] p 1367 N95-21546
Extrudate swell and extrudate distortion of HDPE as a result of different deformation mechanisms during extrusion through capillary dies
[PB95-110227] p 1288 N95-21651
Modeling the effect of water on mantle rheology
p 1417 N95-21783
Volatiles, rheology, and mantle convection: Comparing Earth, Venus, and Mars p 1420 N95-21801
VISCOUS FLOW
Laser anemometry and viscous computation of the flow through an annular turbine cascade
[AD-A280070] p 1341 N95-20968
Experiments on the flow field physics of confluent boundary layers for high-lift systems
[NASA-CR-197318] p 1201 N95-21343
Volatiles, rheology, and mantle convection: Comparing Earth, Venus, and Mars p 1420 N95-21801
Computations of unsteady viscous compressible flows using adaptive mesh refinement in curvilinear body-fitted grid systems
[NASA-TM-106704] p 1356 N95-21959
VISCOUS FLUIDS
Solutions of D(sup n)D(sup m)f=0
[PB95-110839] p 1487 N95-19916
Direct numerical simulations of on-demand vortex generators: Mathematical formulation
p 1361 N95-22452
VISIBILITY
Air pollution caused by fireworks during the turn of the year 1992-1993
[PB95-135265] p 1409 N95-21718
VISIBLE SPECTRUM
Control of continuous phase PH using visible light to activate PH-dependent fibers and gels in a controlled and reversible manner
[AD-D016532] p 1543 N95-20728
Chemical lasers emitting in the visible spectrum: Metastable oxygen reactions and YOSHIDA laser
[PB95-104485] p 1372 N95-20983
Study of pulsed laser effects on living tissues
[PB95-131330] p 1447 N95-22361
VISION
Viewer-centered object recognition in monkeys
[AD-A279876] p 1437 N95-20185
VISUAL ACUITY
The spatiotemporal characteristics of visual motion priming
[AD-A284782] p 1449 N95-20062
Factors that determine visual acuity through night vision goggles for emmetropes
[AD-A279339] p 1450 N95-21927
VISUAL AIDS
Effects of bifocal and progressive-addition corrective lenses on aviator target-detection performance
[AD-A279698] p 1442 N95-20710
FIREDOC users manual, 3rd edition
[PB95-128674] p 1286 N95-21129
VISUAL FIELDS
Source distribution of visual evoked neuromagnetic responses
[PB95-127643] p 1445 N95-21348
Factors affecting the perception of luning in monocular regions of partial binocular overlap displays
[AD-A286287] p 1547 N95-22044
Occupant reach and mobility apparatus
[AD-D016253] p 1454 N95-22099
Visual perception of elevation
[AD-A284938] p 1451 N95-22472
VISUAL OBSERVATION
Reentry vehicle on-site inspection technology study
[AD-A285960] p 1220 N95-21634
Fire smoke ventilation through shafts: Experiments
[PB95-132247] p 1288 N95-21978
VISUAL PERCEPTION
Intermediate levels of visual processing
[AD-A284922] p 1448 N95-19998
The spatiotemporal characteristics of visual motion priming
[AD-A284782] p 1449 N95-20062
A 3D stereo data visualization and representation
[AD-A284788] p 1449 N95-20064
Viewer-centered object recognition in monkeys
[AD-A279876] p 1437 N95-20185
Space constancy on video display terminals
[AD-A280015] p 1449 N95-20314
Perception and control of locomotion
[AD-A285605] p 1450 N95-21192
Effect of lags on human performance with head-coupled simulators
[AD-A279577] p 1453 N95-21700
Factors that determine visual acuity through night vision goggles for emmetropes
[AD-A279339] p 1450 N95-21927
Factors affecting the perception of luning in monocular regions of partial binocular overlap displays
[AD-A286287] p 1547 N95-22044
Visual perception of elevation
[AD-A284938] p 1451 N95-22472
Magnetic source imaging of visually evoked and oscillatory electrical activity of the human brain
[PB95-127205] p 1448 N95-22476
VISUAL SIGNALS
Space constancy on video display terminals
[AD-A280015] p 1449 N95-20314

VITERBI DECODERS

Error probabilities of FFH/BFSK with noise normalization and soft decision viterbi decoding in a fading channel with partial-band jamming [AD-A280041] p 1498 N95-20620

VITON RUBBER (TRADEMARK)

The permeation of bis(2-fluoro-2,2-dinitroethyl) formal (FEFO), ethyl 4,4-dinitropentanoate (EDNP), ethyl 4-nitropentanoate (ENP), and 1,2,4-trichlorobenzene (TCB) through barrier membranes [DE95-002492] p 1283 N95-21514

VITRIFICATION

Removal of CO2 in closed loop off-gas treatment systems [DE94-019259] p 1407 N95-21617

VOICE COMMUNICATION

Usable, real-time, interactive spoken language systems [AD-A286349] p 1310 N95-22253

VOIDS

Scanning tunneling microscopy studies of self-assembled monolayers of alkanethiols on gold [AD-A279910] p 1253 N95-20577

Geometric characterization of electromigration voids (A statistical analysis of electromigration voids) [AD-A286494] p 1328 N95-21169

Reciprocal space mapping of epitaxial materials using position-sensitive x-ray detection [DE95-001620] p 1575 N95-21991

VOLATILITY

Performance specifications for technology development: Application for characterization of volatile organic compounds in the environment [DE94-016627] p 1401 N95-20234

Interspecies extrapolations of halocarbon respiratory and tissue kinetics: Applications to predicting toxicity in different species [AD-A285055] p 1442 N95-20485

Mantle devolatilization and rheology in the framework of planetary evolution p 1418 N95-21788

VOLCANOES

Computer programs for analysis of geophysical data [DE95-002472] p 1415 N95-21511

Degassing history and evolution of volcanic activity of terrestrial planets based on radiogenic noble gas degassing models p 1424 N95-21816

VOLCANOLOGY

Recycling of volatiles at subduction zones: Noble gas evidence from the Tabar-Lihir-Tanga-Feni arc of papua New Guinea p 1418 N95-21787

VOLT-AMPERE CHARACTERISTICS

Order and turbulence in RF-driven Josephson junction series arrays [DE94-629076] p 1576 N95-21997

Estimation of lightning stroke peak current as a function of peak electric field and the normalized amplitude of signal strength: Corrections and improvements [DE94-016900] p 1335 N95-22189

VOLTAGE REGULATORS

Radiation tests on service electronics for future multi TeV detectors [DE94-632822] p 1335 N95-22184

VON KARMAN EQUATION

Finite dimensional approximation of a class of constrained nonlinear optimal control problems [NASA-CR-194891] p 1479 N95-20010

VORTEX BREAKDOWN

Effect of juncture fillets on double-delta wings undergoing sideslip at high angles of attack [AD-A286165] p 1207 N95-22039

VORTEX FILAMENTS

Vortex atoms and vortons [PB95-134599] p 1356 N95-21963

VORTEX GENERATORS

Annual research briefs, 1994 [NASA-CR-197352] p 1358 N95-22437

Experimental investigations of on-demand vortex generators p 1361 N95-22451

Direct numerical simulations of on-demand vortex generators: Mathematical formulation p 1361 N95-22452

VORTEX RINGS

Vortex ring instability and its sound p 1344 N95-21048

VORTEX SHEDDING

Research on bluff body vortex wakes [AD-A286319] p 1200 N95-20177

VORTEX SHEETS

Nonlinear interaction between a pair of oblique modes in a supersonic mixing layer: Long-wave limit [NASA-CR-197380] p 1357 N95-22173

VORTICES

Heat transfer, fouling, and combustion of supercritical fuels [AD-A279906] p 1281 N95-19884

Oceanographic analysis of the acoustic mid-ocean dynamics experiment [AD-A285907] p 1432 N95-19988

Research on bluff body vortex wakes [AD-A286319] p 1200 N95-20177

Synthesizing the Gulf Stream thermal structure from XBT data [AD-A279665] p 1433 N95-20458

Effect of chemical heat release in a temporally evolving mixing layer p 1249 N95-21037

Triple flame structure and diffusion flame stabilization p 1249 N95-21039

Instability of streamwise vortices in plane channel flows p 1344 N95-21049

On the asymptotic similarity of rotating homogeneous turbulence p 1345 N95-21058

Anisotropic structure of homogeneous turbulence subjected to uniform rotation p 1346 N95-21059

Application of Direct and Large Eddy Simulation to Transition and Turbulence [AGARD-CP-551] p 1346 N95-21061

Developments and applications of dynamic models for large eddy simulation of complex flows p 1346 N95-21062

Subgrid scale models in finite difference simulations of complex wall bounded flows p 1346 N95-21063

Large-eddy simulation of rotating channel flows using a localized dynamic model p 1346 N95-21064

The asymptotic state of rotating homogeneous turbulence at high Reynolds numbers p 1347 N95-21065

Comparison of DNS and LES of transitional and turbulent compressible flow: Flat plate and mixing layer p 1347 N95-21066

Simulation of separated flows p 1347 N95-21068

Large eddy simulation of turbulent flow over a cavity p 1347 N95-21069

Large-eddy simulation of separated flow in a ribbed duct p 1347 N95-21070

Analysis of subgrid models using direct and large-eddy simulations of isotropic turbulence p 1348 N95-21071

Rib vortices in round jets: Direct and large eddy simulation p 1351 N95-21088

Direct numerical simulation of transition to turbulence from a high-symmetry initial condition p 1351 N95-21089

Direct numerical simulations of leading-edge receptivity for freestream sound p 1351 N95-21090

Computational studies of laminar to turbulence transition [AD-A285622] p 1353 N95-21146

1994 Nonneutral Plasma Workshop [AD-A285656] p 1559 N95-21404

Vortex dynamics in a ring-like irradiated Bi2Sr2CaCu2O8 crystal [DE95-001682] p 1573 N95-21569

Fourth International Symposium on Stratified Flows, volume 1 [AD-A286450] p 1354 N95-21583

Vortex atoms and vortons [PB95-134599] p 1356 N95-21963

Critical dynamics and plastic flow in disordered Josephson junction arrays [DE94-629074] p 1576 N95-21995

Effect of juncture fillets on double-delta wings undergoing sideslip at high angles of attack [AD-A286165] p 1207 N95-22039

Fast parallel tree codes for gravitational and fluid dynamical N-body problems [AD-A286480] p 1358 N95-22290

Lewis number and Damkohler number effects in vortex-flame interactions p 1249 N95-22439

Fundamental mechanisms in premixed flame propagation via vortex-flame interactions: Numerical simulations p 1249 N95-22440

Notes on rotating turbulence p 1359 N95-22444

A dynamic localization model with stochastic backscatter p 1359 N95-22445

Large-eddy simulation of a plane wake p 1360 N95-22446

Local dynamic subgrid-scale models in channel flow p 1360 N95-22447

Unstructured-grid large-eddy simulation of flow over an airfoil p 1202 N95-22448

Large-eddy simulation of flow through a plane, asymmetric diffuser p 1360 N95-22449

Large-eddy simulation of a boundary layer with concave streamwise curvature p 1360 N95-22450

On the dynamics of small-scale vorticity in isotropic turbulence p 1362 N95-22459

VORTICITY

Effect of chemical heat release in a temporally evolving mixing layer p 1249 N95-21037

Pressure and higher-order spectra for homogeneous isotropic turbulence p 1343 N95-21045

Vortex ring instability and its sound p 1344 N95-21048

Anisotropic structure of homogeneous turbulence subjected to uniform rotation p 1346 N95-21059

Large eddy simulation of channel flow using a vorticity transport subgrid model p 1348 N95-21076

Direct numerical simulation of transition to turbulence from a high-symmetry initial condition p 1351 N95-21089

Direct numerical simulations of leading-edge receptivity for freestream sound p 1351 N95-21090

The dynamic role of ridges in a beta-plane channel. Towards understanding the dynamics of large scale circulation in the Southern Ocean [AD-A279390] p 1435 N95-21943

The velocity and vorticity fields of the turbulent near wake of a circular cylinder [NASA-TM-110513] p 1355 N95-21954

Vortex atoms and vortons [PB95-134599] p 1356 N95-21963

Transverse vorticity measurements in the NASA Ames 80 x 120 wind tunnel boundary layer p 1362 N95-22457

On the dynamics of small-scale vorticity in isotropic turbulence p 1362 N95-22459

Forced free-shear layer measurements p 1362 N95-22460

VULNERABILITY

An abstract model of rogue code insertion into radio frequency wireless networks. The effects of computer viruses on the Program Management Office [AD-A285759] p 1288 N95-19932

W

WAFERS

P/N InP solar cells on Ge wafers p 1317 N95-20511

Assuring Known Good Die (KGD) for reliable, cost effective MCMs p 1210 N95-20644

Epitaxial liftoff technology onto processed silicon foundry wafers [AD-A285621] p 1571 N95-21145

WAKES

Experimental study of vane heat transfer and aerodynamics at elevated levels of turbulence [NASA-CR-4633] p 1337 N95-19912

Advanced detector development, laboratory simulations, diagnostic development, and data analysis on wake physics [AD-A284798] p 1364 N95-20069

Derivation of coupling impedance from the wake potential of a finite bunch [DE95-002529] p 1532 N95-20421

Six-dimensional modeling of coherent bunch instabilities and related feedback systems in storage rings with power-series maps for the lattice [DE94-017965] p 1532 N95-20494

Xwake 1.0 user's manual [DE95-002528] p 1463 N95-20901

Wake measurements in a strong adverse pressure gradient [NASA-CR-197272] p 1201 N95-21031

The effect of initial conditions on the development of temporally evolving planar three dimensional incompressible wakes p 1350 N95-21085

Direct simulation of tridimensional wake of NACA 0012 profile p 1350 N95-21086

Direct numerical simulations of on-demand vortex generators: Mathematical formulation p 1361 N95-22452

Forced free-shear layer measurements p 1362 N95-22460

WALKING MACHINES

Force based motion control of a walking machine [PB95-129672] p 1451 N95-20276

WALL FLOW

Simulation of a turbulent flame in a channel p 1249 N95-21044

Modeling near wall effects in second moment closures by elliptic relaxation p 1345 N95-21054

Subgrid scale models in finite difference simulations of complex wall bounded flows p 1346 N95-21063

Direct numerical simulation of turbulent flow in a sudden pipe expansion p 1347 N95-21067

Large eddy simulation of turbulent flow over a cavity p 1347 N95-21069

Drag reduction strategies p 1361 N95-22453

WALL PRESSURE

Influence of primary boundary conditions on the buckling of shallow cylindrical shells [PB94-208352] p 1364 N95-20003

Application of wavelet-filtering techniques to intermittent turbulent and wall pressure events. Part 1: Exploratory results
[AD-A286077] p 1341 N95-20849

Derivation of a wavenumber filter design for the measurement of turbulent wall pressure fluctuations
[AD-A286421] p 1357 N95-22208

WALL TEMPERATURE

Numerical investigation of supersonic turbulent boundary layers with high wall temperature
p 1344 N95-21050

WALLS

Wall stabilization effects in D3-D high beta discharges
[DE94-017509] p 1554 N95-20446

Structure and dynamics of turbulent wall layers
[AD-A285360] p 1340 N95-20547

WARFARE

Bomber force 2000: Operational concepts for long-range combat aircraft
[AD-A279378] p 1206 N95-20181

WARNING SYSTEMS

The mechanisms and effects off the plant-activations of chemicals in the environment
[AD-A279388] p 1356 N95-22145

Information security for unmanned systems
[AD-A286511] p 1485 N95-22214

WASTE DISPOSAL

Possible global environmental impacts of solid waste practices
[DE95-000830] p 1406 N95-21487

WASTE ENERGY UTILIZATION

Proceedings of the 1994 DOE/NREL Hydrogen Program Review
[DE94-011835] p 1234 N95-20117

Anaerobic Treatment of Municipal Solid Waste and Sludge for Energy Production and Recycling of Nutrients
[DE95-700217] p 1315 N95-20369

WASTE HEAT

Flow and heat transfer simulation in a flash smelting furnace
[PB95-108197] p 1354 N95-21649

WASTE TREATMENT

Anaerobic Treatment of Municipal Solid Waste and Sludge for Energy Production and Recycling of Nutrients
[DE95-700217] p 1315 N95-20369

Environmental cleanup technology transfer initiatives
[AD-A285059] p 1403 N95-20487

Evaluation of an immobilized cell bioreactor for degradation of meta- and para-nitrobenzoate
[AD-A279719] p 1516 N95-20993

Possible global environmental impacts of solid waste practices
[DE95-000830] p 1406 N95-21487

Removal of CO2 in closed loop off-gas treatment systems
[DE94-019259] p 1407 N95-21617

Environmental Compliance Assessment System (ECAS): Japan settlement
[AD-A279328] p 1410 N95-22142

Use of the carbo-flo process to purify process water contaminated by agricultural pesticides
[PB95-127825] p 1410 N95-22330

WASTE WATER

Monitoring bioremediation of Volatile Organic Compounds (VOCs) using Fourier Transform Infrared (FT-IR) spectrometry
[AD-A279631] p 1403 N95-20456

Evaluation of an immobilized cell bioreactor for degradation of meta- and para-nitrobenzoate
[AD-A279719] p 1516 N95-20993

Disinfection of purified waste water with ultra violet light on a technical scale
[PB95-131926] p 1405 N95-21330

Use of the carbo-flo process to purify process water contaminated by agricultural pesticides
[PB95-127825] p 1410 N95-22330

WASTES

Environmental cleanup: Too many high priority sites impede DOD's program. Report to the Chairman, Committee on Governmental Affairs, US Senate
[AD-A279511] p 1407 N95-21683

WATER

A review of water mist technology for fire suppression
[AD-A285738] p 1202 N95-20071

FTIR spectroscopy for the determination of water in corrosive gases
[DE94-014658] p 1235 N95-20139

Indirect global warming effects of ozone and stratospheric water vapor induced by surface methane emission
[DE94-019016] p 1402 N95-20353

Radiative forcing for changes in tropospheric O3
[DE94-019017] p 1413 N95-20354

Water-soluble polyphosphazenes and their hydrogels
[AD-A279695] p 1269 N95-20580

Effect of external stress on the transport of fluids in thermoplastic resin systems
[AD-A279993] p 1270 N95-20596

Training simulant for Halon 1211 portable extinguishers
[AD-A285403] p 1286 N95-20611

Annual Conference on Fire Research: Book of abstracts
[PB95-104964] p 1286 N95-20717

New methods for large scale local and global optimization
[AD-A285635] p 1517 N95-21126

Potential-of-mean-force description of ionic interactions and structural hydration in biomolecular systems
[DE95-000859] p 1438 N95-21366

A visual cell for measuring the solubility of prograde soluble salts in water at high temperatures and pressures
[DE95-002058] p 1245 N95-21732

Conference on Deep Earth and Planetary Volatiles
[NASA-CR-196944] p 1415 N95-21777

Impact degassing of water and noble gases from silicates p 1416 N95-21780

D/H ratios and H2O contents of mantle-derived amphibole megacrysts from Dish Hill, California
p 1416 N95-21781

Thermochemistry of dense hydrous magnesium silicates p 1416 N95-21782

Modeling the effect of water on mantle rheology
p 1417 N95-21783

Phase E in a water-saturated peridotite system at 9.3 GPa p 1420 N95-21799

Volatiles in the deep Earth: An experimental study using the laser-heated diamond cell p 1421 N95-21803

Subduction of hydrated basalt of the oceanic crust: Implications for recycling of water into the upper mantle and continental growth p 1423 N95-21814

Water abundance and accretion history of terrestrial planets p 1424 N95-21820

Storage and recycling of water and carbon dioxide in the earth p 1425 N95-21822

Studies of the n-alkane/water interface by total internal reflection second harmonic generation
[AD-A279473] p 1245 N95-21827

Protective organic coatings on steel: Accelerated corrosion test method for paint/coatings exposed to water with low conductivity. Nordtest project no. 1010-92. Degradation of organic coatings in fresh water
[PB95-134185] p 1277 N95-21873

Solubilities of nitrogen and helium in water and blood at 37 C and pressures of up to 11 ATA
[AD-A286269] p 1446 N95-22003

Numerical study of contaminant effects on combustion of hydrogen, ethane, and methane in air
[NASA-TM-106844] p 1284 N95-22114

Derivation of maximum permissible concentrations for several volatile compounds for water and soil
[PB95-107454] p 1411 N95-22381

Absorption of water and lubricating oils into porous nylon
[NASA-CR-197344] p 1280 N95-22383

WATER FLOW

Resolving velocity profiles with the multi-scale profiler
[AD-A286446] p 1434 N95-21461

Seawater test results of Open-Cycle Ocean Thermal Energy Conversion (OC-OTEC) components
[DE94-019254] p 1396 N95-21897

WATER POLLUTION

Implementation and performance of a three-dimensional numerical transport model
[PB95-135745] p 1402 N95-20440

Monitoring bioremediation of Volatile Organic Compounds (VOCs) using Fourier Transform Infrared (FT-IR) spectrometry
[AD-A279631] p 1403 N95-20456

Ohmsett test of NOFI Vee-Sweep and NOFI 600S Oilboom
[AD-A279525] p 1408 N95-21685

Use of the carbo-flo process to purify process water contaminated by agricultural pesticides
[PB95-127825] p 1410 N95-22330

Derivation of maximum permissible concentrations for several volatile compounds for water and soil
[PB95-107454] p 1411 N95-22381

WATER SPLITTING

The Combustive Sound Source
[ARL-TR-94-9] p 1503 N95-19911

WATER TREATMENT

Use of the carbo-flo process to purify process water contaminated by agricultural pesticides
[PB95-127825] p 1410 N95-22330

WATER TUNNEL TESTS

Effect of juncture fillets on double-delta wings undergoing sideslip at high angles of attack
[AD-A286165] p 1207 N95-22039

WATER VAPOR

Indirect global warming effects of ozone and stratospheric water vapor induced by surface methane emission
[DE94-019016] p 1402 N95-20353

Microstructures and tensile properties of as-cast iron-aluminide alloys
[DE94-017868] p 1252 N95-20359

Daytime Raman lidar profiling of atmospheric water vapor
[DE94-015747] p 1413 N95-20397

Lidar technologies for airborne and space-based applications
[DE95-002954] p 1302 N95-21448

Atmospheres of the Moon and Mercury
p 1419 N95-21794

High resolution properties of the equatorial Pacific marine atmospheric boundary layer from lidar and radiosonde observations
[DE95-001028] p 1426 N95-21875

WATER WAVES

The Surface Wave Dynamics Experiment (SWADE): A retrospective look at the wave modeling activities
[AD-A285612] p 1431 N95-19895

Measurements of radar backscatter from the ocean surface at 94 GHz as a function of wind speed, direction and the modulation by the ocean waves during the SAXON-FPN experiment p 1299 N95-20960

Fourth International Symposium on Stratified Flows, volume 3
[AD-A286452] p 1354 N95-21584

X-band microwave backscattering from ocean waves
[DE94-016719] p 1309 N95-22241

WATERSHEDS

Review of GIS applications in hydrologic modeling
[AD-A279076] p 1390 N95-21628

WAVE DIFFRACTION

Diffraction computation by means of the method of equivalent currents
[AD-A285347] p 1291 N95-20692

Eigenmode method for electromagnetic synthesis of diffractive elements with three-dimensional profiles
[PB95-127726] p 1301 N95-21107

WAVE DISPERSION

PRSPLOT6 manual
[PB95-110862] p 1456 N95-19928

A Monte Carlo study of the minus sign problem in the t-J model using an Intel iPSC/860 hypercube
[DE95-001072] p 1570 N95-20819

WAVE EQUATIONS

Squeezing and flow of energy for non linear wave equations
[PB95-111100] p 1489 N95-20172

A theoretical study on the performance of the FDTD code on a massively parallel computer
[AD-A285346] p 1475 N95-20499

A model of an infinite length, axisymmetric, isotropic, forced thick shell
[AD-A285586] p 1386 N95-21212

A mixed time integration method for large scale acoustic fluid-structure interaction
[DE94-018327] p 1354 N95-21387

WAVE FRONTS

Analog processing of optical wavefront using integrated guided-wave optics
[AD-A279596] p 1543 N95-20601

WAVE FUNCTIONS

The (e,2e) calculations with the final-state boundary condition
[DE94-631342] p 1509 N95-20198

A Monte Carlo study of the minus sign problem in the t-J model using an Intel iPSC/860 hypercube
[DE95-001072] p 1570 N95-20819

Correlated wavefunction Monte Carlo studies of excitations in the quantum Hall liquids
[DE95-002337] p 1501 N95-20874

A new FHNC scheme for Gutzwiller correlated wave functions
[DE94-629037] p 1581 N95-21993

Variational Monte Carlo study of He-4 in two dimensions
[DE94-629078] p 1576 N95-21998

Full potential multiple scattering theory
[DE95-003197] p 1576 N95-22084

Theory of spin dynamics in the classical two-dimensional heisenberg magnet
[PB95-133559] p 1502 N95-22138

WAVE GENERATION

On the influence of electromagnetic wave and relativistic electron beam on a plasma
[DE94-628962] p 1561 N95-21848

WAVE INTERACTION

A theoretical study on the performance of the FDTD code on a massively parallel computer
[AD-A285346] p 1475 N95-20499

Direct numerical simulation of 2-D and 3-D instability waves in a laminar separation bubble
p 1352 N95-21095
Computational studies of laminar to turbulence transition
[AD-A285622] p 1353 N95-21146

WAVE PROPAGATION
P-wave signatures and parameterization of transversely isotropic media: An overview
[DE95-000644] p 1411 N95-19982
Ambient noise and surface wave dissipation in the ocean
[AD-A279650] p 1432 N95-20303
Pasotron(TM) technology
[AD-A279994] p 1314 N95-20311
On the Taylor test. Part 3: A continuum mechanics code analysis of steady plastic wave propagation
[DE95-002252] p 1501 N95-20869
Multiple Mechanism Propagation Paths (MMPPs): Their Characterisation and Influence on System Design
[AGARD-CP-543] p 1292 N95-20921
Propagation of high frequency waves in urban and road tunnel environments p 1294 N95-20933
The effects of multihop HF propagation on the performance of OTH backscatter radars
p 1298 N95-20953
Analytic models for beam propagation and far-field patterns in slab and bow-tie x ray lasers
[DE94-016607] p 1372 N95-21173
Passive millimetre wave imaging: A review
[AD-A279275] p 1303 N95-21491
On the theory of strong electromagnetic waves propagation in an electron-positron-ion plasma
[DE94-628964] p 1561 N95-21850
Large amplitude localized structures in a relativistic electron-positron ion plasma
[DE94-628965] p 1561 N95-21851
Source contributions at far-regional distances
[AD-A279405] p 1426 N95-21932

WAVE REFLECTION
Experimental and theoretical evaluation of elastic waves in curved layered media
[AD-A286578] p 1504 N95-20918
Electromagnetic wave reflection from irregular plasma layers p 1298 N95-20952
Low frequency sound radiation from finite stiffened plates
[AD-A279395] p 1505 N95-21930

WAVE SCATTERING
Electromagnetic wave reflection from irregular plasma layers p 1298 N95-20952
A method using focal plane analysis to determine the performance of reflector antennas p 1304 N95-21538

WAVEFORMS
Applications of wavelets to radar, imaging and related problems
[AD-A279909] p 1290 N95-20545
On commonalities in signal design for non-Gaussian channels
[AD-A285385] p 1498 N95-20608
Performance of a fast frequency-hopped noncoherent MFSK receiver over Rician fading channels with either partial-band interference or multi-tone interference
[AD-A286168] p 1310 N95-22246

WAVEGUIDE ANTENNAS
The efficiency calibration of the DSS-24 34-meter beam-waveguide antenna p 1305 N95-21542
Analysis of a disk-on-rod surface wave element inside a corrugated horn using the mode-matching technique
p 1305 N95-21543

WAVEGUIDE WINDOWS
Improved broadband waveguide pressure window
[AD-D016487] p 1306 N95-21834

WAVEGUIDES
International collaboration program on innovative chemical processing of superior electronic and optical materials
[AD-A285122] p 1226 N95-20105
Characterization and simulation of an acoustic source moving through an oceanic waveguide
[AD-A285688] p 1503 N95-20272
Frequency response measurements of integrated-optic electrodes
[DE94-016690] p 1542 N95-20403
White-light spectral analysis of lithium niobate waveguides
[DE94-016692] p 1542 N95-20489
Resonant tunneling quantum well integrated optical waveguide modulator/switch
[AD-A285142] p 1542 N95-20501
Polymer based all-optic reconfigurable interconnects
[AD-A279976] p 1272 N95-20962
Small antennas for communication over sea ice
[AD-D016206] p 1301 N95-21156
Broadband pressure barrier for circular waveguide
[AD-D016503] p 1306 N95-21672

WAVELENGTH DIVISION MULTIPLEXING
A simple analytical model for asynchronous dense WDM/OOK systems
[AD-A283725] p 1289 N95-19973

WAVELENGTHS
Fiber grating-based detection system for wavelength encoded fiber sensors
[AD-D016208] p 1545 N95-21825
Influence of wavelength on transient short-circuit current in polycrystalline silicon solar cells
[DE94-629082] p 1397 N95-22183

WAVELET ANALYSIS
Wavelet-based acoustic recognition of aircraft
[DE94-017701] p 1503 N95-20019
An application of wavelet transform for decomposition of millimeter-wave spectroscopic signals
[DE94-018366] p 1402 N95-20247
Applications of wavelets to radar, imaging and related problems
[AD-A279909] p 1290 N95-20545
Optical pattern recognition
[AD-A285384] p 1480 N95-20607
Wavelet transformations for helicopter identification via acoustic signatures
[AD-A279980] p 1504 N95-20963
Wavelet analysis applied to the IRAS cirrus
p 1593 N95-21769
On the wavelet optimized finite difference method
[NASA-CR-191601] p 1495 N95-22157
Image and video coding using a wavelet decomposition
[PB95-135067] p 1311 N95-22358

WEAK ENERGY INTERACTIONS
Search for right-handed currents in the decay chain of K(+) yields muon(+)nu(sub muon), muon(+) yields e(+)nu(sub e)nu(bar)(sub muon)
[DE94-770606] p 1514 N95-20756

WEAPON SYSTEMS
An analysis of cost overruns on defense acquisition contracts p 1584 N95-20749
Design of a controller for a flexible pointing system using H(infinity) synthesis
[AD-A286572] p 1481 N95-20828
Demonstration of multifunctional DNBM corrosion inhibitors in protective coatings for Naval air/weapon systems
[AD-A285869] p 1279 N95-22136

WEAR
Numerical controlled polishing program, continued forced wear and part correction experiments
[DE94-018084] p 1285 N95-20288
Abrasive wear by diesel engine coal-fuel and related particles
[PB95-104915] p 1379 N95-20984
Friction and wear properties of as-deposited and carbon ion-implanted diamond films
[NASA-TM-106759] p 1274 N95-21252

WEAR INHIBITORS
Evaluation of PS 212 coatings under boundary lubrication conditions with an Ester-based oil to 300 C
[NASA-TM-106763] p 1223 N95-19901

WEAR RESISTANCE
Wear resistant composite structure of vitreous carbon containing convoluted fibers
[DE95-002254] p 1228 N95-20787
Abrasive wear by diesel engine coal-fuel and related particles
[PB95-104915] p 1379 N95-20984
Friction and wear properties of as-deposited and carbon ion-implanted diamond films
[NASA-TM-106759] p 1274 N95-21252

WEAR TESTS
Numerical controlled polishing program, continued forced wear and part correction experiments
[DE94-018084] p 1285 N95-20288
Abrasive wear by diesel engine coal-fuel and related particles
[PB95-104915] p 1379 N95-20984
Lubricant evaluation and performance, 2
[AD-A279144] p 1278 N95-21969

WEATHER
Mariners Weather Log, volume 38, number 3, summer 1994
[PB94-209541] p 1428 N95-20099
Test and Evaluation Master Plan (TEMP) for the Weather Message Switching Center Replacement (WMSCR)
[AD-A286590] p 1429 N95-20857
Global ionospheric weather
[AD-A285520] p 1430 N95-21177
Air pollution caused by fireworks during the turn of the year 1992-1993
[PB95-135265] p 1409 N95-21718
Radar studies of aviation hazards
[AD-A285845] p 1203 N95-21831
Climatological data for clouds over the globe from surface observations, 1982-1991: The total cloud edition
[DE95-002537] p 1431 N95-22288

WEATHER FORECASTING
Program control on the Tropical Rainfall Measuring Mission p 1584 N95-20750
Real-data tests of a single-Doppler radar assimilation system
[AD-A286638] p 1292 N95-20904
Monthly mean sea ice data from the Polar Ice Prediction System, the Regional Polar Ice Prediction System-Barents Sea and the Regional Polar Ice Prediction System-Greenland Sea
[AD-A280095] p 1433 N95-21018
Sensitivity of climate models: Comparison of simulated and observed patterns for past climates
[DE95-002257] p 1406 N95-21379

WEATHER STATIONS
Climatological data for clouds over the globe from surface observations, 1982-1991: The total cloud edition
[DE95-002537] p 1431 N95-22288

WEATHERING
Test Operations Procedure (TOP) 1-2-616 tropic exposure testing
[AD-A286376] p 1235 N95-20230

WEDGES
Image solution for poisson's equation in wedge geometry
[PB95-127171] p 1310 N95-22311

WEIBULL DENSITY FUNCTIONS
Effects of cyclic stress distribution models on fatigue life predictions
[DE95-001619] p 1388 N95-22070

WELD STRENGTH
Use of an integrated design tool for weld quality enhancement
[DE94-018135] p 1379 N95-20723

WELDABILITY
Joining dissimilar stainless steels for pressure vessel components
[PB95-133005] p 1380 N95-21446
Weldability of iron aluminides
[DE94-019114] p 1257 N95-21555

WELDED JOINTS
The origin of acicular ferrite in gas metal arc and submerged arc welds
[AD-A286129] p 1377 N95-19984
Fusion welding of advanced borated stainless steels
[DE94-019037] p 1378 N95-20053
Use of an integrated design tool for weld quality enhancement
[DE94-018135] p 1379 N95-20723
Analysis of welds on helium-containing restraint test plates
[DE95-001809] p 1257 N95-21303
Atom probe field ion microscopy of type 308 CRE stainless steel welds
[DE94-019162] p 1261 N95-22127
Modeling of fundamental phenomena in welds
[DE94-017859] p 1381 N95-22268

WELDED STRUCTURES
Weld pool phenomena
[DE94-018965] p 1381 N95-21550

WELDING
High performance computing for materials process modeling
[DE94-017860] p 1460 N95-20358
Use of an integrated design tool for weld quality enhancement
[DE94-018135] p 1379 N95-20723
Analysis of welds on helium-containing restraint test plates
[DE95-001809] p 1257 N95-21303
Weld pool phenomena
[DE94-018965] p 1381 N95-21550
Modeling of fundamental phenomena in welds
[DE94-017859] p 1381 N95-22268
Welding tritium exposed stainless steel
[DE95-003208] p 1382 N95-22356

WELLS
Guidelines for the creation and management of geographic data bases within a GIS environment, version 1.0
[DE94-019214] p 1458 N95-20073

WETTABILITY
Processing and mechanical properties of laminar Al2O3-Ni3Al composites
[DE94-019332] p 1230 N95-21481

WHISKER COMPOSITES
Properties of whisker-reinforced ceramics
[DE94-017759] p 1264 N95-20024
Ferroic materials: Design, preparation and characteristics. Ceramic transactions, volume 43
[AD-A285937] p 1270 N95-20664

Creep behavior in SiC whisker-reinforced alumina composite
[DE95-001071] p 1231 N95-21776

WHITE DWARF STARS
Properties of strange-matter stars
[DE95-002329] p 1599 N95-20873

WHITE NOISE
On commonalities in signal design for non-Gaussian channels
[AD-A285385] p 1498 N95-20608

WICKS
Module cooling system
[AD-D016584] p 1315 N95-20436

WIENER HOPF EQUATIONS
Quadratic optimal control of a delay equation II: The unstable case
[PB95-127064] p 1486 N95-22366
Quadratic optimal control of a delay equation I: The stable case
[PB95-127072] p 1486 N95-22367

WIGGLER MAGNETS
Compact free electron lasers for medical applications
[AD-A285739] p 1369 N95-20072
Coaxial hybrid wiggler
[AD-D016501] p 1331 N95-21671
Recent progress of the compact AFEL at Los Alamos
[DE95-002728] p 1376 N95-22154

WIGNER COEFFICIENT
Symmetry, Wigner functions and particle reactions
[DE94-629887] p 1514 N95-20735

WIND (METEOROLOGY)
An evaluation of 915-MHz radar wind profiler/RASS by tower and sodar measurements
[DE94-018913] p 1364 N95-20320
Analysis of mesospheric winds and waves
[AD-A279956] p 1414 N95-20591
A study of westerly wind bursts preceding the 1991-1992 El Nino
[AD-A286570] p 1429 N95-20826

WIND DIRECTION
AN/APS-137 Forward Looking Airborne Radar (FLAR) evaluation, Fall 1992 experiment
[AD-A279526] p 1306 N95-21686

WIND EFFECTS
A numerical study of wind forcing effects on the California Current System
[AD-A286205] p 1435 N95-21880

WIND MEASUREMENT
Deriving earth science products from SSM/I
[NASA-CR-197299] p 1389 N95-20156
Real-data tests of a single-Doppler radar assimilation system
[AD-A286638] p 1292 N95-20904
Project Whitefeather
[DE94-016575] p 1415 N95-21184
Two-micron Laser Atmospheric Wind Sounder (LAWS) pointing/tracking study
[NASA-CR-195012] p 1220 N95-21190
A proposed wind measurement and analysis approach for evaluating a prospective wind plant site
[DE94-019187] p 1395 N95-21611

WIND PROFILES
Comparison of meteorological data with fitted values extracted from projectile trajectory
[AD-A285921] p 1428 N95-19989
Analysis of mesospheric winds and waves
[AD-A279956] p 1414 N95-20591

WIND SHEAR
The dynamic role of ridges in a beta-plane channel. Towards understanding the dynamics of large scale circulation in the Southern Ocean
[AD-A279390] p 1435 N95-21943

WIND TUNNEL APPARATUS
The dynamic approach to rotor blade research: ARA's oscillatory test facility
[ARA-MEMO-405] p 1200 N95-20758
Testing in the ARA Transonic Wind Tunnel
[ARA-MEMO-395] p 1216 N95-20799

WIND TUNNEL CALIBRATION
The dynamic approach to rotor blade research: ARA's oscillatory test facility
[ARA-MEMO-405] p 1200 N95-20758

WIND TUNNEL MODELS
The dynamic approach to rotor blade research: ARA's oscillatory test facility
[ARA-MEMO-405] p 1200 N95-20758
Testing in the ARA Transonic Wind Tunnel
[ARA-MEMO-395] p 1216 N95-20799
Numerical investigation of one-dimensional heat-flux calculations
[AD-A286293] p 1582 N95-22054

WIND TUNNEL TESTS
Static investigation of two fluidic thrust-vectoring concepts on a two-dimensional convergent-divergent nozzle
[NASA-TM-4574] p 1199 N95-19913
Investigation of a thermal buoyancy effect on the drag of half models tested in the ARA Transonic Wind Tunnel
[ARA-MEMO-407] p 1199 N95-19946
Flow coefficient behavior for boundary layer bleed holes and slots
[NASA-TM-106846] p 1338 N95-19953
Internal aerodynamics of a generic three-dimensional scramjet inlet at Mach 10
[NASA-TP-3476] p 1340 N95-20619
16-foot transonic tunnel test section flowfield survey
[NASA-TM-109157] p 1216 N95-20669
The dynamic approach to rotor blade research: ARA's oscillatory test facility
[ARA-MEMO-405] p 1200 N95-20758
Application of pressure sensitive paint in hypersonic flows
[NASA-TM-106824] p 1201 N95-20794
Testing in the ARA Transonic Wind Tunnel
[ARA-MEMO-395] p 1216 N95-20799
Wake measurements in a strong adverse pressure gradient
[NASA-CR-197272] p 1201 N95-21031
Pressure measurements on an F/A-18 twin vertical tail in buffeting flow. Volume 4, part 1: Buffet cross spectral densities
[AD-A285593] p 1215 N95-21214
Experiments on the flow field physics of confluent boundary layers for high-lift systems
[NASA-CR-197318] p 1201 N95-21343
Pressure measurements on an F/A-18 twin vertical tail in buffeting flow. Volume 1: Wind tunnel test summary
[AD-A279126] p 1202 N95-21877
The velocity and vorticity fields of the turbulent near wake of a circular cylinder
[NASA-TM-110513] p 1355 N95-21954
Effects of yaw and pitch motion on model attitude measurements
[NASA-TM-4641] p 1368 N95-22109
Large-eddy simulation of flow through a plane, asymmetric diffuser p 1360 N95-22449
Experimental investigations of on-demand vortex generators p 1361 N95-22451
Small-scale behavior in distorted turbulent boundary layers at low Reynolds number p 1362 N95-22456
Transverse vorticity measurements in the NASA Ames 80 x 120 wind tunnel boundary layer
p 1362 N95-22457
Experimental and numerical study of the intermittency exponent mu p 1362 N95-22458
Forced free-shear layer measurements
p 1362 N95-22460

WIND TUNNEL WALLS
Investigation of a thermal buoyancy effect on the drag of half models tested in the ARA Transonic Wind Tunnel
[ARA-MEMO-407] p 1199 N95-19946

WIND TUNNELS
Application of wavelet-filtering techniques to intermittent turbulent and wall pressure events. Part 1: Exploratory results
[AD-A286077] p 1341 N95-20849
A three-dimensional orthogonal laser velocimeter for the NASA Ames 7- by 10-foot wind tunnel
[NASA-TM-108864] p 1366 N95-21323

WIND TURBINES
Turbulence descriptors for scaling fatigue loading spectra of wind turbine structural components
[DE94-011833] p 1384 N95-20109
Error analysis in wind turbine field testing
[DE94-011864] p 1391 N95-20260
Advanced wind turbine design studies: Advanced conceptual study
[DE93-000031] p 1394 N95-20985
Effects of cyclic stress distribution models on fatigue life predictions
[DE95-001619] p 1388 N95-22070
Wind Energy Program overview, fiscal year 1993
[DE94-000285] p 1398 N95-22468

WIND VARIATIONS
SAR-related stress variability in the Marine Atmospheric Boundary Layer (MABL)
[AD-A286462] p 1431 N95-22393

WIND VELOCITY
Measurements of radar backscatter from the ocean surface at 94 GHz as a function of wind speed, direction and the modulation by the ocean waves during the SAXON-FPN experiment p 1299 N95-20960
AN/APS-137 Forward Looking Airborne Radar (FLAR) evaluation, Fall 1992 experiment
[AD-A279526] p 1306 N95-21686
Stability effects on the profiles of vertical velocity and its variance in katabatic flow
[DE95-001126] p 1426 N95-21836

WIND VELOCITY MEASUREMENT
Analysis of mesospheric winds and waves
[AD-A279956] p 1414 N95-20591

WINDOWS (APERTURES)
Frame and edge seal technology: A state of the art survey
[PB95-110334] p 1288 N95-22014

WINDOWS (COMPUTER PROGRAMS)
Personal computer and workstation operating systems tutorial
[AD-A280132] p 1451 N95-20041
Computer-Aided Structural Engineering (CASE) project. User's guide: Computer-Aided Structural Modeling (CASM). Version 5.00
[AD-A279913] p 1459 N95-20310
Xwake 1.0 user's manual
[DE95-002528] p 1463 N95-20901
The application of a statistical analysis software package to explosive testing
[MRL-TR-93-42] p 1284 N95-21658

WINDOWS (INTERVALS)
Verification of a timestamp-based sliding-window protocol
[PB95-132759] p 1455 N95-22082

WINDPOWER UTILIZATION
Advanced wind turbine design studies: Advanced conceptual study
[DE93-000031] p 1394 N95-20985
A proposed wind measurement and analysis approach for evaluating a prospective wind plant site
[DE94-019187] p 1395 N95-21611
Bridging worlds/charting new courses
[DE95-003808] p 1397 N95-22335
Advanced energy systems and technologies research programme
[DE95-717486] p 1397 N95-22337
Wind Energy Program overview, fiscal year 1993
[DE94-000285] p 1398 N95-22468

WINDPOWERED GENERATORS
Turbulence descriptors for scaling fatigue loading spectra of wind turbine structural components
[DE94-011833] p 1384 N95-20109
Brushless Doubly-Fed Machine system development program, phase 3
[DE94-013095] p 1315 N95-20380

WING LOADING
Derived gust spectra for the Macchi MB326H
[ARL-TN-3] p 1202 N95-21892

WING PROFILES
Direct simulation of tridimensional wake of NACA 0012 profile p 1350 N95-21086

WINTER
ICE BABY: Measurements of concentration fluctuations in a forest area in winter conditions
[PB95-133468] p 1405 N95-21274

WIRE
Processing and characterization of Ni-Al-Fe-B shape-memory alloy wires produced by rapid solidification
[DE94-017702] p 1250 N95-20020
Proceedings of the International Wire and Cable Symposium
[AD-A279242] p 1403 N95-20465
Reliability assessment of Multichip Module technologies via the Triservice/NASA RELTECH program
p 1210 N95-20643
Aging tests of ethylene contaminated argon/ethane
[DE95-002526] p 1282 N95-20899
Small antennas for communication over sea ice
[AD-D016206] p 1301 N95-21156
Evaluation of Pd-Cr wires for strain gage application
[NASA-TM-106857] p 1366 N95-21259
Passive surface deployed variable inductance wire antenna statement of government interest
[AD-D016210] p 1307 N95-21910
Measurement of the thermal properties of electrically conducting fluids using coated transient hot wires
[DE94-017816] p 1357 N95-22264
Development of practical high temperature superconducting wire for electric power applications
[DE94-017894] p 1336 N95-22271

WIRELESS COMMUNICATION
An abstract model of rogue code insertion into radio frequency wireless networks. The effects of computer viruses on the Program Management Office
[AD-A285759] p 1288 N95-19932

WORKING FLUIDS
Malone-brayton cycle engine/heat pump
[AD-D016573] p 1378 N95-20295

WORKLOADS (PSYCHOPHYSIOLOGY)
Navigation system in combat vehicle
[PB95-131629] p 1452 N95-21467
The advanced technology crew station: Development and validation of a workload assessment technique for cockpit function allocation
[AD-A279544] p 1453 N95-21691

WORKSTATIONS
A practical guide to using MCNP with PVM
[DE94-016162] p 1474 N95-20158

An evaluation of Automatic Terminal Information Service (ATIS) flight deck display presentation options
[AD-A280100] p 1204 N95-21020

WOVEN COMPOSITES

Zirconia precipitates and zirconia: GeO2 interphase in mullite matrix-SiC woven fabrics composites prepared through a sol-gel route
[PB95-133427] p 1275 N95-21272

WRIST

Quantitative evaluation of wrist posture and typing performance: A comparative study of 4 computer keyboards
[DE95-002392] p 1452 N95-21358

X

X RAY ABSORPTION

Magnetic x ray circular dichroism in Fe Co Pt multilayers
[DE94-017522] p 1253 N95-20447

Two-center, two electron excitations identified in NEXAFS for solid Ne
[AD-A285373] p 1568 N95-20553

Enhancements in the Livermore spectrum analysis package PIXEF
[DE95-002487] p 1272 N95-20895

Interference of fluorescence x rays and coherent excitation of core levels
[DE94-016809] p 1527 N95-22188

Acid-site characterization of water-oxidized alumina films by near-edge x-ray absorption and soft x-ray photoemission
[DE95-003355] p 1247 N95-22234

X RAY ANALYSIS

Second European Symposium on X-Ray Topography and High Resolution Diffraction: Programme and abstracts
[AD-A286328] p 1564 N95-20210

X-ray studies of microstructures in semiconductor and superconducting materials
[DE95-001802] p 1572 N95-21279

Reciprocal space mapping of epitaxial materials using position-sensitive x-ray detection
[DE95-001620] p 1575 N95-21991

X RAY APPARATUS

X-ray microscope for solidification studies
[NASA-CR-197375] p 1543 N95-20798

Laboratory characterization of Woelter x ray optics
[DE94-016969] p 1562 N95-22191

X RAY ASTRONOMY

Solar-geophysical data number 601, September 1994. Part 1: (Prompt reports). Data for August, July 1994, and late data
[PB95-136727] p 1603 N95-20919

Physics of systems containing neutron stars
[NASA-CR-197304] p 1600 N95-21615

X RAY BINARIES

Physics of systems containing neutron stars
[NASA-CR-197304] p 1600 N95-21615

X RAY DETECTORS

Reciprocal space mapping of epitaxial materials using position-sensitive x-ray detection
[DE95-001620] p 1575 N95-21991

Time resolved x-ray detection
[AD-A279348] p 1368 N95-22143

X RAY DIFFRACTION

The ANL X6B beamline at NSLS: A versatile facility
[DE94-018379] p 1540 N95-19968

Second European Symposium on X-Ray Topography and High Resolution Diffraction: Programme and abstracts
[AD-A286328] p 1564 N95-20210

Ferrocyanide safety project Dynamic X-Ray Diffraction studies of sodium nickel ferrocyanide reactions with equimolar nitrate/nitrite salts
[DE94-017396] p 1236 N95-20268

Bacterial luciferase: Determination of the structure by x-ray diffraction
[AD-A279699] p 1437 N95-20711

Application of new synchrotron powder diffraction techniques to anomalous scattering from glasses
[DE94-019285] p 1536 N95-21407

Diffraction applications using the energy dispersive beamline, X6A, at NSLS
[DE94-019287] p 1572 N95-21408

Strain fields in crystalline materials: Methods of analysis based on x-ray diffraction-line broadening
[PB95-108064] p 1574 N95-21670

Structure and stability of hydrous minerals at high pressure p 1417 N95-21786

Hydrogen and related materials at high density: Physics, chemistry and planetary implications
p 1418 N95-21791

Time resolved x-ray detection
[AD-A279348] p 1368 N95-22143

High temperature superconducting microwave device
[AD-A286351] p 1336 N95-22254

Residual stress analysis in swage autofrettaged thick-walled cylinders by position-sensitive x-ray diffraction techniques
[AD-A286383] p 1388 N95-22320

Introduction to the structures determination methods using X-ray diffraction in monocrystals: Application to some lanthanides and transition metals complexes with organic ligands
[DE94-629002] p 1579 N95-22380

Synthesis and characterization of single-source molecular precursors to binary metal sulphides: Bis(diethyldithiocarbamato) M(2)trialkylphosphine (M = Zn and Cd) adducts
[AD-A279746] p 1248 N95-22385

Photoreflectance and x ray diffraction study of semiconductor heterostructures and quantum wells
[PB95-127049] p 1582 N95-22432

X RAY FLUORESCENCE

Observation of strong emission from NeIX and NeX transitions in a laser-driven plasma
[DE95-002265] p 1555 N95-20813

Interference of fluorescence x rays and coherent excitation of core levels
[DE94-016809] p 1527 N95-22188

X RAY IMAGERY

X-ray imaging of uniform large scale-length plasmas created from gas-filled targets on Nova
[DE94-018339] p 1531 N95-20015

X RAY LASERS

A comparison of kinetic and multifluid simulations of laser-produced colliding plasmas
[DE94-016447] p 1551 N95-20315

Enhanced output of soft x-ray lasers using double slab targets
[DE94-016689] p 1369 N95-20335

Research studies on short wavelength lasers by selective Auger processes
[AD-A285620] p 1372 N95-21144

Analytic models for beam propagation and far-field patterns in slab and bow-tie x ray lasers
[DE94-016607] p 1372 N95-21173

EBIT x ray spectroscopy studies for applications to photo-pumped x ray lasers
[DE94-016701] p 1373 N95-21210

Collisional redistribution effects on x ray laser saturation behavior
[DE94-017308] p 1374 N95-21663

Molecular design concept for multi-kilovolt x-ray amplification
[DE95-001763] p 1374 N95-21743

X RAY OPTICS

The ANL X6B beamline at NSLS: A versatile facility
[DE94-018379] p 1540 N95-19968

Second European Symposium on X-Ray Topography and High Resolution Diffraction: Programme and abstracts
[AD-A286328] p 1564 N95-20210

High precision Woelter optic calibration facility
[DE94-016973] p 1542 N95-20364

Thermal and deformation analyses of a novel cryogenically cooled monochromator for an Advanced Photon Source beamline
[DE94-016914] p 1527 N95-22190

Laboratory characterization of Woelter x ray optics
[DE94-016969] p 1562 N95-22191

X RAY SCATTERING

Surface x-ray scattering and scanning tunneling microscopy studies at the Au(111) electrode
[DE95-002409] p 1573 N95-21516

X RAY SOURCES

Soft X-Ray Innovative Source Development Program
[AD-A286380] p 1551 N95-20232

High precision Woelter optic calibration facility
[DE94-016973] p 1542 N95-20364

X-ray microscope for solidification studies
[NASA-CR-197375] p 1543 N95-20798

Physics of systems containing neutron stars
[NASA-CR-197304] p 1600 N95-21615

Submicrosecond, synchronizable x-ray source
[AD-D016497] p 1546 N95-21905

X RAY SPECTRA

X-ray spectroscopy of xenon
[DE95-002132] p 1240 N95-20865

Enhancements in the Livermore spectrum analysis package PIXEF
[DE95-002487] p 1272 N95-20895

X RAY SPECTROSCOPY

Correlations between surface structure and catalytic activity/selectivity
[DE94-019023] p 1234 N95-20052

Design and thermal stress analysis of high power x-ray monochromators cooled with liquid nitrogen
[DE94-016879] p 1500 N95-20106

Characterization of nova plasmas using an x-ray spectrometer with temporal and spatial resolution
[DE94-016970] p 1553 N95-20363

Oxide formation on NbAl3 and TiAl due to ion implantation of O-18
[DE94-017874] p 1252 N95-20365

X-ray spectroscopy of xenon
[DE95-002132] p 1240 N95-20865

EBIT x ray spectroscopy studies for applications to photo-pumped x ray lasers
[DE94-016701] p 1373 N95-21210

X RAYS

An intensity interferometer for soft x-rays
[DE94-016370] p 1541 N95-20103

Target area acquisition and control system survivability for the National Ignition Facility
[DE94-016549] p 1550 N95-20190

Low electron beam energy CIVA analysis of passivated ICs
[DE94-017421] p 1314 N95-20286

Magnetic x ray circular dichroism in Fe Co Pt multilayers
[DE94-017522] p 1253 N95-20447

Spin-specific photoelectron diffraction using magnetic x ray circular dichroism
[DE94-017527] p 1567 N95-20448

A structural determination using magnetic x ray circular dichroism in spin-polarized photoelectron diffraction
[DE94-017528] p 1567 N95-20449

Approach to compact terawatt CO2 laser system for particle acceleration
[DE95-002170] p 1371 N95-20866

Magnetic x-ray circular dichroism in spin-polarized photoelectron diffraction
[DE95-002394] p 1520 N95-21360

Test and Evaluation Plan (TEP) for Improvised Explosive Device Screening Systems (IEDSS)
[AD-A286382] p 1203 N95-22319

Synthesis and characterization of single-source molecular precursors to binary metal sulphides: Bis(diethyldithiocarbamato) M(2)trialkylphosphine (M = Zn and Cd) adducts
[AD-A279746] p 1248 N95-22385

Imaging design of the wide field x-ray monitor onboard the HETE satellite
[DE95-002750] p 1221 N95-22436

XENON

The effect of reusing laser gas on the fission-fragment pumped 1.73 micron atomic xenon laser output
[DE94-018512] p 1369 N95-20225

Liquid xenon as a potential laser host medium
[AD-A285365] p 1370 N95-20550

Quantum chemical study of rare gas/halide interactions as a model for high energy density material. 1: Transition properties in HCl
[AD-A285988] p 1239 N95-20613

X-ray spectroscopy of xenon
[DE95-002132] p 1240 N95-20865

Research studies on short wavelength lasers by selective Auger processes
[AD-A285620] p 1372 N95-21144

Studies of selenium and xenon in inductively coupled plasma mass spectrometry
[DE95-001676] p 1245 N95-21734

Is xenon eldest? p 1425 N95-21823

Cryogenic pellet laser plasma source targets
[DE95-002488] p 1376 N95-22169

Quantum chemical study of rare gas/halide interactions as a model for high energy density material. 2: The interaction of hydrogen chloride with the rare gas xenon
[AD-A286385] p 1248 N95-22321

XENON ISOTOPES

Comets, impacts, and atmospheres
p 1422 N95-21810

He, Xe and Ne isotopes in a steady-state mass transport model and implications about terrestrial volatiles
p 1425 N95-21821

Y

YAG LASERS

Scaling of solid state lasers for satellite power beaming applications
[DE94-016366] p 1368 N95-19986

Modelocking and waveguide amplifiers using Cr:Forsterite and Cr:YAG
[AD-A285857] p 1369 N95-20378

YAW

Effects of yaw and pitch motion on model attitude measurements
[NASA-TM-4641] p 1368 N95-22109

YBCO SUPERCONDUCTORS

High performance YBCO films
[AD-A286567] p 1326 N95-20824

Carbon fiber reinforced superconductor composites
[DE95-002504] p 1229 N95-20913
Dependence of critical current density on microstructure and processing of high-T(c) superconductors
[DE95-000685] p 1571 N95-21167
Study of improved critical currents and mechanical properties in the Y-Ba-Cu-O superconductor with silver or Y2BaCuO3 or 211 dispersions
[AD-A285609] p 1502 N95-21194
High performance YBCO films
[AD-A279560] p 1276 N95-21695
International Symposium on Advanced Laser Technoiogies
[AD-A279849] p 1376 N95-22164
AC magnetic response of YBa2CuO7 with Y2BaCuO5 inclusions and of single-crystal YBa2Cu3O7: A comparative study
[PB94-207917] p 1577 N95-22166
Low rotational drag in high-temperature superconducting bearings
[DE95-002983] p 1382 N95-22292

YIELD STRENGTH
Plastic deformation of ordered intermetallic alloys: Fundamental aspects
[DE95-001070] p 1256 N95-21265
Fracture behavior of the Fe-8Al alloy FAP-Y
[DE95-000956] p 1258 N95-21676
The development of a super-alpha2 titanium aluminide alloy consolidated by rapid omnidirectional compaction
[AD-A279254] p 1260 N95-21986

YLF LASERS
High power spectral and spatial beam control using self-phase modulation and a multisegment monochromator
[DE94-016604] p 1531 N95-20120

YTTRIA-STABILIZED ZIRCONIA
Forming of superplastic ceramics
[DE94-017306] p 1276 N95-21662

YTTRIUM
Tensile and impact properties of iron-aluminum alloys
[DE94-017750] p 1263 N95-22346

YTTRIUM OXIDES
Selective methane oxidation over promoted oxide catalysts
[DE94-012270] p 1235 N95-20188
Solid oxide fuel cells in the United States
[DE95-002405] p 1395 N95-21361
Light output and radiation damage in a YAlO3:Ce crystal
[DE94-016815] p 1545 N95-21643
High temperature superconducting films and multilayers for electronics
[AD-A279545] p 1331 N95-21693
High performance YBCO films
[AD-A279560] p 1276 N95-21695

YTTRIUM-ALUMINUM GARNET
Rare earth garnet selective emitter
p 1322 N95-20536
Pulsed laser illumination of photovoltaic cells
p 1323 N95-20538

YUKAWA POTENTIAL
Constraints on SUSy-GUT unification from b yields s-gamma decay
[PB95-130373] p 1580 N95-21229

Z

ZENITH
A comparative survey of current and proposed tropospheric refraction-delay models for DSN radio metric data calibration
[NASA-CR-197338] p 1412 N95-20002
Threshold detection in the presence of atmospheric turbulence
[AD-A286175] p 1427 N95-22249

ZETA PINCH
Soft X-Ray Innovative Source Development Program
[AD-A286380] p 1551 N95-20232
PRS scoping study 1: Scaling law estimates for K-shell radiation yields on JUPITER-class generators
[AD-A279716] p 1533 N95-20672

ZINC
Structure of dibis(diethyldithiocarbamato) zinc (2) Mu-bis(diethylphosphino)ethane toluene(2)
[AD-A279792] p 1224 N95-20660
Polyurethane self-priming topcoats
[AD-D016204] p 1274 N95-21154
Polyurethane self-priming topcoats
[AD-D016205] p 1274 N95-21155

ZINC OXIDES
Nickel hydroxide electrodes in reduced-alkalinity electrolytes
[DE95-002333] p 1326 N95-20814

ZINC SELENIDES
Photoluminescence under pressure and annealing of nitrogen-doped ZnSe
[DE95-002355] p 1568 N95-20630

ZINC SULFIDES
Optical multilayers with an amorphous fluoropolymer
[DE94-017693] p 1541 N95-20218
Gas-phase generation of zinc sulfide particles using a single-source precursor
[AD-A279700] p 1239 N95-20712
Synthesis and characterization of (Zn(SEt)Et)10, formed via insertion of sulfur into Zn-C bonds: A new class of Wurtzite-like cluster framework
[AD-A279701] p 1569 N95-20714

ZINC TELLURIDES
Polycrystalline thin film cadmium telluride solar cells fabricated by electrodeposition
[DE94-011848] p 1391 N95-20118

ZINC-OXYGEN BATTERIES
Demonstration of zinc/air fuel battery to enhance the range and mission of fleet electric vehicles: Preliminary results in the refueling of a multicell module
[DE95-004206] p 1337 N95-22421

ZIRCONIUM
Development of superplasticity in 5083 aluminum with additions of Mn and Zr
[DE94-017474] p 1251 N95-20090
Amorphization of sapphire during ion beam mixing
[DE94-018713] p 1510 N95-20337

ZIRCONIUM ALLOYS
Corrosion resistance and behavior of construction materials exposed to dilute sulfuric acid at elevated temperatures under static conditions
[DE95-001723] p 1259 N95-21739

ZIRCONIUM COMPOUNDS
New thermodynamic description of the Cu-Zr system
[PB95-127189] p 1263 N95-22374

ZIRCONIUM NITRIDES
Method of making copper-titanium nitride alloy
[AD-D016582] p 1252 N95-20201

ZIRCONIUM OXIDES
Selective methane oxidation over promoted oxide catalysts
[DE94-012270] p 1235 N95-20188
Microwave sintering of ZrO2-12 mol% CeO2
[DE94-018709] p 1265 N95-20226
Zirconia precipitates and zirconia: GeO2 interphase in mullite matrix-SiC woven fabrics composites prepared through a sol-gel route
[PB95-133427] p 1275 N95-21272
Solid oxide fuel cells in the United States
[DE95-002405] p 1395 N95-21361
Directional solidification of the alumina-zirconia ceramic eutectic system
[DE95-001677] p 1277 N95-21735
Integration of thin film decoupling capacitors
[DE95-001609] p 1333 N95-21881

ZONE MELTING
Volatiles in the Earth: All shallow and all recycled
p 1416 N95-21779

PERSONAL AUTHOR INDEX

SCIENTIFIC AND TECHNICAL AEROSPACE REPORTS VOLUME 33 NUMBER 6

Typical Personal Author Index Listing

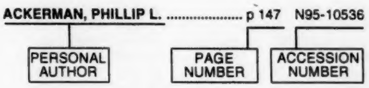

Listings in this index are arranged alphabetically by personal author. The page number helps you locate the citation in the abstract section. The accession number denotes the number by which the citation is identified.

A

AARONS, JULES p 1298 N95-20951
p 1427 N95-22423
AARTS, A. C. T. p 1353 N95-21268
ABADIE, B. p 1447 N95-22361
ABBOUD, R. G. p 1382 N95-22292
ABDOL-HAMID, KHALED S. p 1201 N95-21338
ABDURRAHMAN, A. p 1580 N95-21030
p 1500 N95-21964
ABE, MARY C. p 1220 N95-21634
ABEEL, A. M. p 1247 N95-22260
ABELL, NANCY p 1585 N95-20752
ABEYOUNIS, W. K. p 1216 N95-20669
ABID, R. p 1338 N95-20009
ABOWD, GREGORY p 1463 N95-20847
ABRAHAM, BRUCE M. p 1357 N95-22208
ABRAHAM, JACOB p 1209 N95-20636
ABRUNA, HECTOR D. p 1240 N95-20842
ABURDENE, MAURICE F. p 1479 N95-22406
ABUSHAGUR, M. A. p 1480 N95-20607
ACHENBACH, CRYSTAL A. p 1567 N95-20479
ACKERET, J. R. p 1204 N95-20497
ACKERMAN, CHARLES T. p 1411 N95-22414
ADAMS, GEORGE F. p 1239 N95-20613
p 1248 N95-22321
ADAMS, MICHAEL K. p 1339 N95-20297
ADAMS, N. A. p 1344 N95-21050
p 1348 N95-21074
ADAMS, NIKOLAUS A. p 1362 N95-22461
ADAMS, R. G. p 1537 N95-21603
ADDY, HAROLD E., JR. p 1382 N95-22405
ADJEPONG, S. K. p 1575 N95-21859
ADKINS, D. R. p 1393 N95-20861
ADKINS, JAMES D. p 1279 N95-22022
ADLER, H. p 1557 N95-21239
ADLER, MARK A. p 1451 N95-22324
ADOLPHSEN, C. p 1534 N95-21253
ADRIAN, RONALD J. p 1340 N95-20547
ADZIC, R. R. p 1573 N95-21516
AGARWAL, R. K. p 1209 N95-20640
AGARWALA, VINOD S. p 1240 N95-20970
AGHA, GUL p 1479 N95-22257
AHLFORS, S. p 1447 N95-22371
p 1448 N95-22476
AHLFORS, SEPPO p 1445 N95-21348
AHLFORS, SEPPO P. p 1329 N95-21326
AHMADI, TEMER S. p 1567 N95-20483
AHMED, M. p 1575 N95-21853
AHOKAINEN, T. p 1354 N95-21649
AHUJA, K. K. p 1504 N95-21170
AHUJA, S. p 1285 N95-20050
AHVO, J. p 1472 N95-22310
AKAMA, KEIICHI p 1514 N95-20738
AKBARI, H. p 1429 N95-20782
AKHMEDOV, E. KH. p 1602 N95-20147
AKINWANDE, TAYO p 1331 N95-21690
AKSELVOLL, K. p 1249 N95-21044
p 1346 N95-21062
AL-CHALABI, RIFAT M. K. p 1466 N95-21288
ALAM, T. M. p 1248 N95-22385
ALBARES, DONALD J. p 1544 N95-21466
ALBERSHEIM, P. p 1440 N95-22220
ALBERTS, L. K. p 1471 N95-22081
ALBIN, G. p 1446 N95-22003
ALBRECHT, BRUCE A. p 1429 N95-20395
ALBRECHT, G. F. p 1368 N95-19986
ALBROW, M. G. p 1507 N95-20111
ALDENKAMP, F. J. p 1409 N95-21846
ALDYKIEWICZ, A. J., JR. p 1250 N95-19979
ALEXANDER, D. J. p 1386 N95-20703
p 1254 N95-20705
p 1258 N95-21676
p 1263 N95-22346
ALEXANDER, G. C. p 1315 N95-20380
ALEXANDER, K. B. p 1264 N95-20024
p 1250 N95-20044
p 1271 N95-20704
p 1230 N95-21481
ALFORD, C. p 1274 N95-21175
ALGER, T. p 1367 N95-21478
ALI, E. H. p 1564 N95-20017
ALI, M. N. p 1570 N95-20841
ALKEMADE, ALFONS JOHANNES QUIRINUS
p 1356 N95-21963
ALKHALIFAH, T. p 1411 N95-19981
ALKSNE, R. p 1434 N95-21657
ALLARA, D. L. p 1253 N95-20577
ALLCOCK, HARRY L. p 1270 N95-20671
ALLCOCK, HARRY R. p 1265 N95-20183
p 1269 N95-20580
p 1271 N95-20709
p 1273 N95-20978
ALLEGRE, C. J. p 1416 N95-21778
ALLEN, B. p 1463 N95-20877
ALLEN, DOUGLAS M. p 1316 N95-20504
ALLEN, J. W. p 1574 N95-21712
ALLEN, S. L. p 1556 N95-21159
p 1559 N95-21451
ALLING, P. p 1557 N95-21239
p 1557 N95-21239
ALLISON, S. W. p 1275 N95-21482
ALLMAN, S. L. p 1287 N95-21559
ALLOCK, H. R. p 1268 N95-20428
ALLOTEY, F. K. A. p 1575 N95-21859
ALLSHOUSE, G. O. p 1537 N95-21603
ALLTOP, W. O. p 1480 N95-20606
ALMAGRI, A. p 1549 N95-20114
ALMAGRI, A. F. p 1549 N95-20112
p 1549 N95-20113
ALME, M. L. p 1385 N95-20237
ALONSO, R. G. p 1314 N95-20341
ALOUANI, M. p 1578 N95-22297
ALPER, MARK p 1269 N95-20551
ALTON, G. D. p 1515 N95-20911
p 1538 N95-21938
ALTOZ, FRANK E. p 1315 N95-20436
ALTSHULER, B. L. p 1528 N95-22217
ALURU, S. p 1458 N95-20136
p 1493 N95-21439
ALVAREZ, L. S. p 1305 N95-21542
ALVES, G. A. p 1530 N95-22339
AMATO, S. p 1530 N95-22339
AMBERKAR, S. S. p 1481 N95-20828
AMBROSIO, JORGE A. p 1381 N95-21488
AMBROSIO, JORGE A. C. p 1380 N95-21171
AMES, FORREST E. p 1337 N95-19912
AMES, GREGORY H. p 1545 N95-21673
AMFT, JULIE p 1433 N95-20433
AMUNDSEN, J. p 1470 N95-22016
AMURO, STEPHEN J. p 1476 N95-21307
p 1476 N95-21496
p 1476 N95-21504
p 1478 N95-22090
p 1591 N95-22098
p 1478 N95-22146
AMUSIA, M. Y. p 1522 N95-21502
ANCHER, C. p 1557 N95-21239
ANDERL, R. A. p 1558 N95-21290
ANDERS, SCOTT G. p 1200 N95-20688
ANDERSON, A. p 1200 N95-20248
p 1557 N95-21206
p 1557 N95-21207
ANDERSON, CHARLES E., JR. p 1387 N95-21396
ANDERSON, CHARLES H. p 1593 N95-21769
ANDERSON, DON L. p 1416 N95-21779
ANDERSON, H. p 1557 N95-21239
ANDERSON, I. M. p 1255 N95-20907
ANDERSON, J. p 1458 N95-20154
ANDERSON, J. L. p 1557 N95-21239
ANDERSON, J. W. p 1557 N95-21239
ANDERSON, R. C. p 1214 N95-21383
ANDERSON, VERNON N. p 1431 N95-19918
ANDERSSON, BRODD LEIF p 1353 N95-21132
ANDERSSON, M. p 1312 N95-19934
ANDRAKA, C. E. p 1393 N95-20861
ANDRE, MATS p 1501 N95-20773
ANDREASEN, C. C. p 1425 N95-21833
ANDREAUS, M. p 1205 N95-21642
ANDRESEN, INGER p 1288 N95-22014
ANDREWS, C. p 1252 N95-20299
ANDREWS, MARSHALL p 1383 N95-21933
ANDREWS, ROGER p 1453 N95-21566
ANDRIULLI, J. B. p 1385 N95-20416
ANGELL, THOMAS S. p 1310 N95-22250
ANJOS, J. C. p 1530 N95-22339
ANSOURIAN, P. p 1384 N95-20003
ANTIPOV, E. V. p 1570 N95-20820
ANTOLAK, A. J. p 1272 N95-20895
ANTON, F. p 1580 N95-21030
p 1500 N95-21964
ANTONACOS, JOHN p 1307 N95-21970
ANTWORTH, CHRISTOPHER P. p 1282 N95-19922
ANZELON, GEORGE p 1588 N95-20789
AOKI, M. p 1514 N95-20756
APBLETT, CHRISTOPHER A. p 1272 N95-20889
APPEL, J. A. p 1530 N95-22339
APT, KRZYSZTOF R. p 1472 N95-22302
AQVIST, G. p 1275 N95-21275
ARMAN, M. J. p 1327 N95-20905
p 1329 N95-21395
ARMAND, P. p 1536 N95-21407
ARMENDARIZ, M. G. p 1545 N95-21509
ARMENTROUT, PETER B. p 1514 N95-20804
ARMSTRONG, JOSEPH H. p 1318 N95-20514
p 1322 N95-20532
ARNBERG, L. p 1258 N95-21652
ARNETT, KENNETH E. p 1571 N95-20965
ARNOLD, CAROLINE CHICK p 1515 N95-20872
ARNOLD, JACK H. p 1321 N95-20530
ARONOV, A. G. p 1528 N95-22217
ARONSON, M. C. p 1574 N95-21570
ARUNASALAM, V. p 1557 N95-21239
ARYA, P. V. p 1226 N95-20125
ASBURY, SCOTT C. p 1200 N95-20688
ASCHEHOUG, OEYVIND p 1288 N95-22014
ASCIONE, G. p 1557 N95-21239
ASHBY, H. ANTHONY p 1406 N95-21373
ASHBY, S. F. p 1493 N95-21564
ASHER, SANFORD A. p 1232 N95-22211
ASHLEY, KENNETH R. p 1274 N95-21234
ASHURST, WILLIAM T. p 1249 N95-21043
ASKINS, CHARLES p 1545 N95-21825
ASMAR, S. W. p 1302 N95-21456
p 1305 N95-21540
ASSOUFID, L. p 1338 N95-19923
p 1500 N95-20106
ASTORGA, J. p 1530 N95-22339
ATAC, M. p 1282 N95-20899
ATAPATTU, DAYA p 1457 N95-20000
ATCHER, R. W. p 1240 N95-20836
ATHERTON, J. p 1557 N95-21166
ATKESON, CHRISTOPHER p 1486 N95-22267
ATKINSON, A. p 1256 N95-21260
ATTENBERGER, S. E. p 1560 N95-21702
AUBERT, J. H. p 1537 N95-21603
AUDONE, B. p 1213 N95-20658
AUMANN, CHRISTOPHER E. p 1260 N95-21926
AUMANN, H. H. p 1592 N95-21750
AURAND, J. F. p 1290 N95-20474
AUSCHER, P. p 1493 N95-21423
AUSTIN, THOMAS C. p 1406 N95-21373
AUTREY, S. T. p 1507 N95-20049
AWES, T. C. p 1330 N95-21554

AYERS, JOSEPH .... p 1480 N95-20482
AZMY, Y. Y. .... p 1492 N95-21285
AZUMA, S. .... p 1416 N95-21780
AZUMA, Y. .... p 1522 N95-21502
AZUMI, M. .... p 1554 N95-20683
AZUMI, MASAFUMI .... p 1554 N95-20684

B

BA, B. .... p 1397 N95-22183
BAARS, JAN .... p 1494 N95-21956
BABCOCK, S. R. .... p 1290 N95-20474
BABINE, ALEXEI .... p 1374 N95-21480
BABU, S. S. .... p 1253 N95-20676
p 1261 N95-22127
BABUSKA, I. .... p 1480 N95-20083
p 1490 N95-20565
p 1490 N95-20588
p 1491 N95-20920
p 1497 N95-22388
BABUSKA, IVO M. .... p 1489 N95-20274
BACA, A. G. .... p 1327 N95-20882
p 1328 N95-21139
p 1329 N95-21390
p 1259 N95-21838
BACK, C. A. .... p 1553 N95-20363
BACK, G. G. .... p 1202 N95-20071
BACON, L. D. .... p 1537 N95-21603
BADALAMENTE, RICHARD V. .... p 1588 N95-20789
BADER, S. D. .... p 1571 N95-21256
BADR, SALAH .... p 1461 N95-20579
BAER, T. .... p 1244 N95-21701
BAETEN, J. C. M. .... p 1486 N95-19892
p 1487 N95-19907
p 1488 N95-20055
BAGGERMAN, JACOBUS ANTONIUS GIJSBERTUS
p 1300 N95-21029
BAGRYANSKIJ, P. A. .... p 1529 N95-22283
BAHCALL, J. N. .... p 1604 N95-20490
BAHEI-EL-DIN, Y. A. .... p 1230 N95-21363
BAILEY, J. E. .... p 1506 N95-20026
p 1537 N95-21603
BAILEY, J. M. .... p 1245 N95-21845
BAILEY, M. W. .... p 1523 N95-21562
BAILEY, S. .... p 1317 N95-20509
BAILIN, L. J. .... p 1279 N95-22136
BAITY, F. W. .... p 1551 N95-20285
BAKER, S. M. .... p 1281 N95-22434
BAKHTIARI, S. .... p 1402 N95-20247
BALADI, V. .... p 1488 N95-19944
BALANTEKIN, A. B. .... p 1498 N95-20779
BALARAS, ELIAS .... p 1346 N95-21063
BALDWIN, THOMAS O. .... p 1437 N95-20711
BALET, B. .... p 1556 N95-21142
BALL, JASON .... p 1274 N95-21234
BALLANCE, JOHN .... p 1563 N95-19886
BALLMANN, JOSEF .... p 1207 N95-20860
BALOOCH, M. .... p 1542 N95-20450
BALSA, THOMAS F. .... p 1357 N95-22173
BALTZER, ROBERT .... p 1453 N95-21566
BAME, S. J. .... p 1600 N95-21935
BANANNO, ANTHONY .... p 1228 N95-20805
BANDERET, LOUIS E. .... p 1452 N95-20625
BANDYOPADHYAY, PROMODE R.
p 1356 N95-22060
BANE, K. L. F. .... p 1534 N95-21253
BANFORD, MICHAEL .... p 1215 N95-21214
p 1202 N95-21877
BANGERTER, R. O. .... p 1534 N95-20891
BANKS, DAVE .... p 1289 N95-19997
BANNISTER, M. E. .... p 1507 N95-20086
BAR-NUN, AKIVA .... p 1422 N95-21810
BARANOWSKI, S. .... p 1294 N95-20933
BARBAGELETA, S. .... p 1208 N95-20634
BARBE, M. .... p 1375 N95-21837
BARBEE, T. W., JR. .... p 1272 N95-20892
BARBER, T. E. .... p 1244 N95-21571
BARCLAY, J. .... p 1296 N95-20941
BARCLAY, REBECCA O. .... p 1587 N95-20162
p 1587 N95-20163
p 1589 N95-21015
p 1590 N95-21977
BAREIS, DONNA L. .... p 1445 N95-21629
BARFIELD, WILLIAM L. .... p 1289 N95-20065
BARGER, V. .... p 1580 N95-21229
p 1580 N95-21230
BARIBEAU, J. M. .... p 1565 N95-20245
BARIBEAU, J.-M. .... p 1568 N95-20674
BARINGER, MOLLY O. .... p 1434 N95-21306
BARKER, WALTER R. .... p 1215 N95-19955
BARLETTA, R. E. .... p 1233 N95-19980
BARNARD, H. J. .... p 1311 N95-22358
BARNARD, J. C. .... p 1395 N95-21611
BARNARD, J. J. .... p 1552 N95-20318
BARNES, C. A. .... p 1604 N95-20490
BARNES, C. W. .... p 1557 N95-21240
BARNES, CRIS W. .... p 1558 N95-21242
BARNES, GERALD B. .... p 1592 N95-22416
BARNES, M. D. .... p 1506 N95-20030
BARNES, P. A. .... p 1329 N95-21394
BARNES, P. R. .... p 1439 N95-21544
BARNES, T. .... p 1570 N95-20819
p 1526 N95-21939
BARNETT, ALLEN M. .... p 1318 N95-20513
p 1323 N95-20540
BARNETT, J. M. .... p 1366 N95-21138
BARNETT, S. A. .... p 1230 N95-21445
BARON, A. .... p 1348 N95-21072
BARRET, C. .... p 1218 N95-21346
BARRETT, C. L. .... p 1483 N95-21710
BARRINGTON, L. M. .... p 1221 N95-19962
BARRIOS, AMALIA E. .... p 1294 N95-20931
BARSHICK, C. M. .... p 1370 N95-20698
p 1241 N95-21123
BARTER, J. D. .... p 1309 N95-22241
BARTHES, L. .... p 1298 N95-20954
BARTLETT, DAVID L. .... p 1281 N95-22387
BARTONE, PAUL T. .... p 1451 N95-22323
p 1451 N95-22324
BARTSCH, R. R. .... p 1560 N95-21668
BASFORD, J. A. .... p 1243 N95-21472
BASILAKIS, ROSEMARY .... p 1228 N95-20805
BASKES, M. I. .... p 1564 N95-20142
p 1248 N95-22273
BASOL, B. M. .... p 1317 N95-20512
BASS, B. R. .... p 1385 N95-20322
BASSETT, BARBARA .... p 1388 N95-20006
BASTEN, TWAN .... p 1496 N95-22349
BATCHELOR, D. B. .... p 1303 N95-21459
BATCHELOR, K. .... p 1533 N95-20573
BATES, M. .... p 1310 N95-22253
BATISTE, I. .... p 1578 N95-22297
BATSON, P. J. .... p 1374 N95-21663
BAUCOM, K. C. .... p 1563 N95-19954
BAUER, F. .... p 1268 N95-20396
BAUER, G. .... p 1282 N95-20899
BAUS, THERESA A. .... p 1505 N95-21213
BAUTISTA, J. J. .... p 1305 N95-21539
BAYLEY, HAGAN .... p 1269 N95-20551
BAZIZI, K. A. .... p 1528 N95-22196
BEACH, K. L. .... p 1309 N95-22241
BEACH, R. .... p 1389 N95-21552
BEACH, R. J. .... p 1368 N95-19986
BEARD, L. P. .... p 1412 N95-20287
BEASLEY, HOWARD H. .... p 1547 N95-22044
BEASON, D. G. .... p 1286 N95-20356
BEAUCHAMP, W. T. .... p 1320 N95-20525
BEAUDET, ROBERT A. .... p 1238 N95-20576
BEAUFORT, D. .... p 1297 N95-20947
BEAUMONT, B. .... p 1551 N95-20205
BECHER, P. F. .... p 1264 N95-20024
p 1250 N95-20044
p 1267 N95-20323
p 1271 N95-20704
p 1231 N95-21776
BECHSTEDT, F. .... p 1582 N95-22237
BECKER, R. A. .... p 1313 N95-20119
p 1542 N95-20489
BECKERT, DIETER W. .... p 1240 N95-20970
BECKMAN, D. .... p 1236 N95-20290
BECOULET, A. .... p 1551 N95-20205
BEDJA, I. .... p 1570 N95-20838
BEECHER, S. C. .... p 1225 N95-20023
p 1226 N95-20125
p 1247 N95-22260
BEEDOE, S. .... p 1520 N95-21357
BEENE, JEFFREY K. .... p 1206 N95-20181
BEER, G. A. .... p 1245 N95-21845
BEHRENS, RICHARD JR. .... p 1283 N95-21513
BEHRNDT, K. .... p 1599 N95-21245
BEIERSDORFER, P. .... p 1373 N95-21210
BEISSNER, ROBERT E. .... p 1382 N95-20414
BEKEFI, GEORGE .... p 1369 N95-20072
BELFOR, R. A. F. .... p 1305 N95-21579
BELFORT, G. .... p 1224 N95-21746
BELIC, A. .... p 1576 N95-21998
p 1527 N95-22182
BELL, B. M. .... p 1434 N95-21461
BELL, DAVID R. .... p 1416 N95-21781
BELL, J. BRETT .... p 1312 N95-19909
BELL, M. G. .... p 1557 N95-21240
BELL, P. .... p 1553 N95-20363
BELL, R. .... p 1558 N95-21242
BELL, R. L. .... p 1488 N95-20141
BELL, R. M. .... p 1219 N95-20567
BEN-ZVI, I. .... p 1533 N95-20573
BENCH, G. S. .... p 1272 N95-20895
BENGTSSON, J. .... p 1532 N95-20494
p 1532 N95-20495
BENIGNUS, VERNON A. .... p 1444 N95-20979
BENLLOCH, J. M. .... p 1510 N95-20343
BENNER, JOHN P. .... p 1316 N95-20505
BENNER, WILLIAM .... p 1429 N95-20857
BENNETT, C. .... p 1552 N95-20362
BENNETT, P. C. .... p 1481 N95-20884
BENNINGTON, S. M. .... p 1526 N95-21965
BENO, M. A. .... p 1536 N95-21407
p 1572 N95-21408
BENOCCI, CARLO .... p 1346 N95-21063
p 1351 N95-21087
BENSAOULA, A. .... p 1316 N95-20508
p 1318 N95-20517
BENTLEY, J. .... p 1255 N95-20907
BENYOUSSEF, A. .... p 1278 N95-21885
BERDING, M. A. .... p 1328 N95-21017
BEREZHIANI, V. I. .... p 1561 N95-21848
p 1561 N95-21850
p 1561 N95-21851
BERGEN, D. M. .... p 1226 N95-20292
BERGER, KURT W. .... p 1376 N95-22169
BERGER, M. S. .... p 1580 N95-21229
BERGER, R. C. .... p 1341 N95-20843
BERGSTRA, J. A. .... p 1486 N95-19892
p 1487 N95-19907
BERGSTRA, K. A. .... p 1488 N95-20055
BERKENBOSCH, A. C. .... p 1492 N95-21371
p 1244 N95-21573
BERKOWITZ, J. P. .... p 1202 N95-20093
BERKOWITZ, JACK .... p 1203 N95-22319
BERLIN, S. .... p 1349 N95-21079
BERNARD, PETER S. .... p 1348 N95-21076
BERNAT, T. P. .... p 1531 N95-20015
BERNSTEIN, DENNIS S. .... p 1485 N95-22216
BERRINO, U. .... p 1352 N95-21098
BERRY, G. C. .... p 1269 N95-20548
BERRY, H. G. .... p 1521 N95-21406
p 1522 N95-21502
BERRY, L. A. .... p 1335 N95-22149
BERRY, P. .... p 1282 N95-20187
BERTEL, L. .... p 1293 N95-20929
p 1299 N95-20956
BERTNESS, K. A. .... p 1319 N95-20521
BERTRAND, P. A. .... p 1280 N95-22383
BERWALD, D. .... p 1601 N95-22419
BERZINS, VALDIS .... p 1459 N95-20304
BESMANN, T. M. .... p 1340 N95-20781
p 1271 N95-20821
BESTEK, H. .... p 1351 N95-21093
BEVERIDGE, J. L. .... p 1245 N95-21845
BEWLAY, B. P. .... p 1232 N95-22126
BEYLER, C. L. .... p 1202 N95-20071
BHALLA, A. S. .... p 1270 N95-20664
BHARATHAN, D. .... p 1396 N95-21897
BHAT, P. C. .... p 1522 N95-21498
BHATTACHARYA, T. .... p 1510 N95-20367
BHOL, D. G. .... p 1362 N95-22457
BIANCALANA, V. .... p 1373 N95-21226
BIANCHI, M. A. .... p 1318 N95-20515
BIBLE, D. W. .... p 1271 N95-20761
BICKMORE, TIMOTHY W. .... p 1222 N95-21458
BIDDLE, TEDD B. .... p 1283 N95-21161
BIEFELD, R. M. .... p 1563 N95-19954
BIGELOW, C. A. .... p 1230 N95-21363
BIGGERI, U. .... p 1272 N95-20894
BIGGS, JOHN R. .... p 1585 N95-20751
BIGOT, J. Y. .... p 1569 N95-20679
BILGER, ROBERT W. .... p 1249 N95-22438
BILLMANN, BARRY .... p 1204 N95-21148
BILODEAU, C. .... p 1295 N95-20940
BINER, S. B. .... p 1231 N95-21736
p 1231 N95-21924
BINGERT, SHERRI R. .... p 1262 N95-22308
BIONTA, R. M. .... p 1274 N95-21175
BIRDSALL, CHARLES K. .... p 1563 N95-22422
BIRINGEN, SEDAT .... p 1348 N95-21073
BIRKMIRE, R. W. .... p 1394 N95-21294
BIRMAN, KENNETH P. .... p 1290 N95-20306
BIRTCHER, R. C. .... p 1232 N95-22130
BISCARDI, R. .... p 1536 N95-21418
BISCHOF, C. H. .... p 1206 N95-20370
BISCHOF, CHRISTIAN H. .... p 1476 N95-21341
BISCHOF, CHRISTINA H. .... p 1476 N95-21257
BISHOP, A. R. .... p 1500 N95-21136
p 1526 N95-21934
p 1578 N95-22297
BISHOP, BRUCE A. .... p 1275 N95-21354
BISHOP, G. J. .... p 1297 N95-20949
BISHOP, S. .... p 1339 N95-20166
BISSON, S. E. .... p 1413 N95-20397
BITSAKIS, NICHOLAS .... p 1504 N95-20724
BIXLER, J. V. .... p 1543 N95-20612
BJERKE, M. A. .... p 1460 N95-20358
BLAAUBOER, R. O. .... p 1409 N95-21846
BLACIC, J. .... p 1600 N95-22128
BLACK, EMILY M. .... p 1461 N95-20687
BLACK, JAMES .... p 1496 N95-22349
BLACK, STEPHEN J. .... p 1379 N95-20627

BLAIN, P. p 1291 N95-20697
BLAIR, R. p 1522 N95-21497
BLAISDELL, G. A. p 1345 N95-21056
BLANCHETIERE-CIARLETTI, V. p 1296 N95-20945
BLANCO, J. A. p 1254 N95-20822
BLASKIEWICZ, M. p 1531 N95-20282
p 1532 N95-20406
BLAU, P. J. p 1381 N95-21601
BLEICHER, P. p 1209 N95-20635
BLEIER, A. p 1277 N95-21861
BLISS, ERLAN S. p 1540 N95-22469
BLOM, J. G. p 1465 N95-21033
p 1467 N95-21435
BLOO, ROEL p 1488 N95-20149
BLOOMQUIST, D. D. p 1537 N95-21603
BLUM, BRUCE I. p 1460 N95-20546
BLUM, FRANK D. p 1574 N95-21599
BLUME, M. p 1527 N95-22188
BLUMEN, WILLIAM p 1428 N95-20186
BLUNT, D. M. p 1206 N95-19963
p 1470 N95-21950
BOARDWAY, JAMES p 1453 N95-21691
BOATNER, L. A. p 1275 N95-21482
p 1285 N95-22261
BOBB, LLOYD C. p 1306 N95-21835
BOCHAROV, V. N. p 1529 N95-22283
BOCZAR, BRUCE P. p 1544 N95-21465
BODE, ARTHUR P. p 1443 N95-20850
p 1443 N95-20851
BODEN, E. P. p 1544 N95-20844
BODETTE, D. E. p 1371 N95-20867
BOGENBERGER, R. p 1212 N95-20652
BOGETTI, TRAVIS A. p 1224 N95-19899
BOGGS, J. M. p 1282 N95-19922
BOGGS, S. L. p 1203 N95-21518
BOGOLUBOV, N. N., JR. p 1525 N95-21856
p 1525 N95-21860
BOGUS, KLAUS P. p 1316 N95-20506
BOHN, C. L. p 1531 N95-19983
BOHN, R. G. p 1395 N95-21508
BOHUSZEWICZ, T. V. p 1564 N95-20087
BOILLAT, E. p 1496 N95-22369
p 1496 N95-22370
BOL, ROLAND p 1472 N95-22302
BOLDT, C. p 1277 N95-21735
BOLEY, C. D. p 1371 N95-20783
BOLLA, L. p 1213 N95-20658
BOLTNIEW, E. p 1296 N95-20941
BOLTON, S. R. p 1577 N95-22168
BOMAR, JOHN B., JR. p 1442 N95-20457
BONCEK, RAYMOND K. p 1581 N95-21928
BONN, RUSSELL p 1313 N95-20262
BONSANGUE, MARCELLO p 1494 N95-21962
BONTEKOE, TJ. ROMKE p 1592 N95-21753
p 1593 N95-21758
p 1593 N95-21768
BOOKLESS, WILLIAM A. p 1219 N95-20148
BOONE, ANDREW p 1453 N95-21566
BOOTH, NEWELL O. p 1503 N95-20084
BORATAV, OLUS N. p 1351 N95-21089
BORCHERS, MARY F. p 1278 N95-21969
BORCHI, E. p 1272 N95-20894
BORDEN, BRETT p 1289 N95-19997
BORDES, J. p 1580 N95-21030
BORG, RODNEY A. J. p 1284 N95-21951
BORGHESE, F. p 1546 N95-22002
BORM, P. p 1499 N95-21709
BORYSOW, ALEKSANDRA p 1601 N95-22338
BOSE, KUNAL p 1416 N95-21782
BOSLOUGH, MARK B. p 1573 N95-21449
BOTELHO, ALVIN p 1332 N95-21775
BOTKIN, D. p 1373 N95-21261
BOTROS, SHERIF M. p 1215 N95-21122
BOUCHARD, A. M. p 1574 N95-21723
BOUDJOUK, PHILIP p 1226 N95-20081
BOUGTEB, M. p 1520 N95-21357
BOULMER-LEBORGNE, C. p 1562 N95-22377
BOUMSELLEK, S. p 1367 N95-21507
BOUNAMA, CH. p 1417 N95-21783
p 1418 N95-21788
BOURGUIGNON, J. P. p 1466 N95-21349
BOURKE, M. A. M. p 1387 N95-21386
BOWER, WARD p 1313 N95-20262
p 1391 N95-20263
BOWERS, JAMES S. p 1253 N95-20481
p 1239 N95-20716
BOWERS, L. A. p 1329 N95-21395
BOWERS, LESTER A. p 1327 N95-20905
BOWLING, D. R. p 1290 N95-20556
BOWMAN, CRAIG T. p 1247 N95-22150
BOWMAN, J. D. p 1519 N95-21237
p 1530 N95-22435
BOWMAN, R. R. p 1225 N95-20001
BOYD, C. F. p 1582 N95-22054
BOYER, K. p 1374 N95-21743
BOYES, J. p 1557 N95-21207
p 1537 N95-21603
BRACHT, R. R. p 1313 N95-20168
BRACHT, ROGER R. p 1289 N95-20164
BRACKER, S. B. p 1530 N95-22339
BRADBURY, MORTON p 1440 N95-22065
BRADLEY, E. G. p 1334 N95-22086
BRADSHAW, JERALD S. p 1223 N95-20590
p 1223 N95-20592
BRADY, ROBERT F., JR. p 1279 N95-22022
BRAMKAMP, F. D. p 1362 N95-22457
BRAND, H. R. p 1248 N95-22433
BRAND, M. G. p 1475 N95-20499
BRANDEL, B. P. p 1570 N95-20841
BRANKOVIC, A. p 1344 N95-21052
BRANSTETTER, REAGAN p 1209 N95-20638
BRASKI, D. N. p 1226 N95-20357
BRATAAS, GUNNAR p 1469 N95-21711
BRATOS, STEVEN M. p 1471 N95-22068
BRAUN, HARALD p 1347 N95-21070
BRAX, MATTI p 1220 N95-21026
BRAY, IGOR p 1508 N95-20196
p 1508 N95-20197
p 1509 N95-20199
BRAY, K. N. C. p 1249 N95-21041
p 1249 N95-21042
BRAZIER, F. p 1483 N95-21981
BREDAS, J. L. p 1526 N95-21934
p 1578 N95-22297
BREDER, K. p 1225 N95-20022
p 1280 N95-22258
BREDESEN, R. p 1276 N95-21650
BREITZKE, H. p 1570 N95-20820
BRENNAN, J. J. p 1225 N95-19919
BRENNAN, J. M. p 1538 N95-21720
BRENTNER, KENNETH S. p 1200 N95-20688
BRESNAHAM, P. J. p 1592 N95-22263
BREVICK, J. p 1253 N95-20417
BREWER, J. H. p 1245 N95-21845
BREWSTER, S. B., JR. p 1391 N95-22398
BRICE, D. K. p 1572 N95-21304
BRICKER, T. p 1245 N95-21734
BRICMONT, J. p 1498 N95-19945
BRIDGEMAN, BRUCE p 1449 N95-20314
BRIDGER, K. p 1312 N95-19958
p 1258 N95-21575
BRIDGWATER, T. p 1236 N95-20290
BRIGGS, D. p 1532 N95-20494
BRIGGS, D. A. p 1350 N95-21083
BRILES, S. p 1291 N95-20697
BRINBERG, HERBERT R. p 1590 N95-21977
BRINK, K. H. p 1435 N95-21682
BRINKER, C. J. p 1264 N95-20047
BRINKER, D. J. p 1317 N95-20509
BRINKER, DAVID J. p 1321 N95-20528
p 1322 N95-20537
BRINKGREVE, R. B. J. p 1386 N95-21006
BRINKMAN, C. R. p 1265 N95-20220
BRINKSMA, ED p 1478 N95-21869
BRITCLIFFE, M. J. p 1305 N95-21542
BRITT, J. p 1395 N95-21844
BRITT, P. F. p 1217 N95-21706
BRITTON, C. L., JR. p 1330 N95-21554
BROADWELL, JAMES E. p 1249 N95-22441
BRODA, J. E. p 1436 N95-22073
BRODEEN, ANN E. p 1498 N95-19990
BRODSKY, JARED M. p 1457 N95-19929
BRODSKY, S. J. p 1532 N95-20388
BRODSKY, STANLEY J. p 1520 N95-21336
BROMBERG, PHILLIP A. p 1444 N95-20979
BRONIKOWSKI, J. p 1567 N95-20544
p 1513 N95-20585
BRONIKOWSKI, MICHAEL J. p 1568 N95-20594
BROOK, EDWARD J. p 1426 N95-21944
BROOKS, N. H. p 1552 N95-20334
p 1556 N95-21159
BROOKS, S. L. p 1467 N95-21389
BROTHERS, DANIEL G. p 1377 N95-19984
BROW, R. K. p 1268 N95-20468
BROWN-VANHOOZER, S. A. p 1466 N95-21311
BROWN, C. W. p 1467 N95-21389
BROWN, DANSEN p 1215 N95-21214
p 1202 N95-21877
BROWN, I. M. p 1273 N95-21014
BROWN, K. p 1538 N95-21733
BROWN, M. D. p 1559 N95-21451
BROWN, M. J. p 1409 N95-21722
BROWN, R. D. p 1538 N95-22050
BROWN, S. R. p 1386 N95-20833
BROWNING, N. D. p 1567 N95-20492
BROYDE, S. p 1439 N95-21606
BRUASET, A. M. p 1469 N95-21655
p 1354 N95-21656
BRUCKNER, J. V. p 1442 N95-20485
BRUEMMER, S. M. p 1251 N95-20088
p 1251 N95-20090
BRUHWILER, D. L. p 1601 N95-22419
BRUIN, H. P. p 1389 N95-20207
BRUN, M. K. p 1214 N95-21243
BRUNEAUX, G. p 1249 N95-21044
BRUNSTROM, ANNA p 1456 N95-22431
BRUST, FREDERICK W., JR. p 1258 N95-21560
BRUZZI, M. p 1272 N95-20894
BRYANT, BOBBY p 1546 N95-21882
BRYANT, TIMOTHY D. p 1268 N95-20410
BUCARO, JOSEPH A. p 1504 N95-21119
BUCHANAN, A. C., III p 1217 N95-21706
BUCHANAN, W. A. p 1394 N95-21294
BUCHAU, J. p 1298 N95-20953
BUCHWALD, SEPHEN L. p 1247 N95-22020
BUCHWALD, STEPHEN L. p 1224 N95-22252
BUCKHARDT, GARY L. p 1382 N95-20414
BUCKLEY, W. M. p 1517 N95-21174
BUDIL, K. S. p 1377 N95-22312
BUDNICK, E. K. p 1202 N95-20071
BUDNY, R. V. p 1557 N95-21240
BUDWINE, CHRISTINA M. p 1599 N95-20145
BUEHLER, LEO p 1558 N95-21244
BUFFLEBEN, GEORGE M. p 1283 N95-21514
BUIJS, R. M. p 1445 N95-21352
BUIJSMAN, E. p 1405 N95-21327
p 1406 N95-21351
BUJAKIEWICZ, P. p 1496 N95-22359
BULAEVSKII, L. N. p 1575 N95-21936
BULLER, MARK J. p 1454 N95-22274
BULMER, R. H. p 1548 N95-20037
BULMER, R. J. p 1562 N95-22300
BULUSU, SURYANARAYANA p 1283 N95-21513
BUMM, L. A. p 1241 N95-21217
p 1328 N95-21218
BUNSON, PAUL E. p 1544 N95-20876
BUNTKOWSKY, G. p 1570 N95-20820
BURASTERO, S. p 1453 N95-21637
BURASTERO, STEVE p 1452 N95-21358
BURGDOERFER, J. p 1526 N95-21940
BURGESS, C. P. p 1518 N95-21220
BURGESS, RAYMOND p 1417 N95-21784
BURGETT, S. p 1204 N95-20195
BURKE, A. F. p 1330 N95-21471
BURKE, EDWARD A. p 1317 N95-20511
p 1320 N95-20523
BURKE, MARTIN p 1465 N95-21176
BURKHART, RICARD D. p 1570 N95-20916
BURNLEY, PAMELA p 1416 N95-21782
BURNS, IAN F. p 1199 N95-19946
BURNS, JOHN W. p 1446 N95-21941
BURNS, R. p 1286 N95-20611
BURR, RALPH G. p 1444 N95-21160
BURRELL, K. H. p 1552 N95-20334
p 1556 N95-21142
p 1556 N95-21163
BURTON, R. GAINES p 1228 N95-20787
BURTON, RALPH A. p 1228 N95-20787
BURWICK, THOMAS T. p 1482 N95-21249
BUSH, C. p 1558 N95-21242
BUSHNELL, DENNIS M. p 1200 N95-20688
BUSINGER, STEVEN p 1430 N95-20969
BUSS, RICHARD J. p 1562 N95-22225
BUSSJAGER, REBECCA J. p 1541 N95-20231
BUSSON, P. p 1295 N95-20934
BUTLER, J. M. p 1314 N95-20311
BUTLER, W. H. p 1500 N95-20129
BUTT, D. P. p 1254 N95-20816
BUTTERWORTH, J. M. p 1518 N95-21233
BYERS, J. A. p 1559 N95-21451
BYKOV, A. I. p 1564 N95-20240
BYRD, RICHARD p 1517 N95-21126
BYRUM, K. p 1515 N95-20898
BYSTRITSKIJ, V. M. p 1523 N95-21591

C

CABLE, S. B. p 1358 N95-22307
CABO, A. J. p 1491 N95-21005
CABOT, W. p 1344 N95-21051
CABOT, WILLIAM H. p 1360 N95-22447
CACHEIRO, R. A. p 1326 N95-20791
p 1243 N95-21500
CADARETTE, BRUCE S. p 1452 N95-20625
CAFFREY, M. p 1291 N95-20697
CAGLAYAN, ALPER K. p 1215 N95-21122
CAI, Z. p 1229 N95-20840
CALAHAN, DONALD p 1355 N95-21942
CALAIS, JEAN-LOUIS p 1506 N95-19960
CALAME, J. P. p 1330 N95-21490
CALAWAY, W. F. p 1254 N95-20707
CALLEN, J. D. p 1549 N95-20113
CALZONE, R. F. p 1222 N95-20906
CAMACHOREYES, M. J. p 1239 N95-20736
CAMAIONI, D. M. p 1507 N95-20049
CAMBON, C. p 1346 N95-21059
CAMBON, CLAUDE p 1347 N95-21065
CAMELL, D. G. p 1289 N95-20191

CAMERON, CHRISTOPHER P. p 1394 N95-21353
CAMMARATA, ROBERT C. p 1568 N95-20552
CAMPBELL, D. p 1550 N95-20190
CAMPBELL, J. J. p 1250 N95-20020
CAMPBELL, JOHN H. p 1371 N95-20817
CAMPILLO, ANTHONY J. p 1377 N95-22304
CANADAY, JESSIE W. p 1217 N95-20995
CANDY, J. V. p 1433 N95-20420
CANFIELD, P. C. p 1574 N95-21570
CANNON, M. E. p 1205 N95-21520
CANNON, PAUL S. p 1293 N95-20928
p 1299 N95-20955
CANT, R. S. p 1249 N95-21040
p 1249 N95-21082
CANTERNA, R. p 1545 N95-21832
CANTON, J. H. p 1411 N95-22381
CANTRELL, BEN H. p 1307 N95-21904
CANTRELL, JOHN H. p 1441 N95-20408
CANTWELL, BRIAN J. p 1350 N95-21085
CAO, WENWU p 1276 N95-21697
CAO, YU p 1593 N95-21756
CAPLOT, M. p 1209 N95-20635
p 1212 N95-20655
p 1213 N95-20657
CAPOGNA, C. p 1209 N95-20635
CARANGELO, MARTIN p 1228 N95-20805
CARATI, D. p 1346 N95-21062
CARATI, DANIELE p 1359 N95-22445
CARATORI, J. p 1298 N95-20954
CARBONARO, MARIO p 1201 N95-20794
CARBONELL, J. M. p 1211 N95-20647
CARD, J. M. p 1249 N95-21038
CARDINALE, G. F. p 1266 N95-20281
CAREY, DAVID p 1383 N95-21933
CARLETON, ANITA p 1468 N95-21567
CARLILE, C. J. p 1518 N95-21227
CARLSON, A. L. p 1506 N95-20026
CARLSON, J. B. p 1517 N95-21174
CARLSON, JOHN R. p 1201 N95-21338
CARLSON, K. D. p 1564 N95-20017
p 1262 N95-22291
CARLSON, K. DOUGLAS p 1567 N95-20479
CARLSON, N. W. p 1389 N95-21552
CARLSON, THOMAS R. p 1406 N95-21373
CARLSSON, A. E. p 1258 N95-21600
CARLSSON, BO p 1397 N95-22362
CARLSTEN, B. E. p 1334 N95-22011
CARMICHAEL, C. A. p 1250 N95-20043
CARMODY, MEGHAN p 1453 N95-21691
CARPENTER, S. E. p 1401 N95-20234
CARROLL, J. p 1520 N95-21357
CARROLL, JAMES N. p 1284 N95-21966
CARTER, C. D. p 1244 N95-21524
CARTER, H. K. p 1538 N95-21938
CARTER, K. E. p 1414 N95-20990
CARTER, M. D. p 1303 N95-21459
CARTER, SUSAN V. p 1390 N95-22055
CASARELLA, MARIO J. p 1341 N95-20849
CASPER, T. A. p 1550 N95-20146
p 1559 N95-21451
CASSIDY, JAMES p 1504 N95-20724
CASTILLO, T. p 1332 N95-21729
CASTILLO, V. p 1372 N95-21135
CASTLEMAN, A. W., JR. p 1243 N95-21447
CATCHINGS, ROBERT M. p 1336 N95-22254
CAVENY, LEONARD H. p 1316 N95-20504
CAZEMIER, W. p 1352 N95-21097
CECH, RUSSELL D. p 1334 N95-22062
CEDILLO, C. M. p 1538 N95-22050
CEKIC, M. p 1549 N95-20113
p 1549 N95-20114
CEO, R. N. p 1516 N95-21114
CERCONE, JAMES A. p 1414 N95-20878
p 1415 N95-21308
CERDEIRA, H. A. p 1576 N95-21996
p 1576 N95-21997
CERNOSEK, R. W. p 1367 N95-21546
p 1545 N95-21728
CERUTTI, JOHN H. p 1353 N95-21317
CHABALOWSKI, CARY F. p 1239 N95-20813
p 1247 N95-22207
p 1248 N95-22321
CHAI, B. H. T. p 1372 N95-21135
CHAIKEN, JOSEPH p 1261 N95-22035
CHAKRABORTI, S. p 1499 N95-21980
CHAMBERS, R. S. p 1271 N95-20788
CHAMPAGNE, BENOIT p 1507 N95-20097
CHAN, CHUNG p 1364 N95-20069
CHAN, HELEN M. p 1273 N95-21152
CHAN, K. T. p 1581 N95-21604
CHAN, LAI-HIM p 1580 N95-21486
CHAN, SIU-WAI p 1502 N95-21194
CHAN, Y. C. p 1307 N95-21985
CHANCHANI, R. p 1480 N95-20342
CHANDLER, E. p 1369 N95-20335
CHANDLER, E. A. p 1372 N95-21173
CHANDLER, G. A. p 1558 N95-21247
p 1537 N95-21603
CHANDLER, G. T. p 1257 N95-21303
CHANDLER, N. p 1210 N95-20641
CHANDRASEKARAN, S. p 1605 N95-22394
CHANEY, RONALD D. p 1473 N95-22386
CHANG-DIAZ, F. R. p 1221 N95-20059
CHANG-HASNAIN, CONNIE p 1372 N95-21019
CHANG, ALICE C. p 1268 N95-20407
CHANG, BOR-CHIN p 1483 N95-21913
CHANG, R. P. H. p 1570 N95-20881
CHANG, RICHARD K. p 1238 N95-20581
CHANG, TOM p 1501 N95-20773
CHANG, WEN-HUAN p 1207 N95-22039
CHANG, Z. p 1558 N95-21242
CHAO, KENNETH K. p 1278 N95-21969
CHAPLIN, M. R. p 1562 N95-22300
CHAPLINE, G. C., JR. p 1272 N95-20892
CHAPMAN, B. E. p 1549 N95-20113
p 1549 N95-20114
CHASE, L. L. p 1542 N95-20450
CHASE, MELISSA P. p 1473 N95-22402
CHASE, RONALD J. p 1228 N95-20808
CHASNOV, J. R. p 1343 N95-21047
p 1345 N95-21058
CHASNOV, JEFFREY R. p 1347 N95-21065
CHASON, E. p 1572 N95-21304
CHATTERJEE, B. p 1323 N95-20542
CHAVAND, GENEVIEVE p 1354 N95-21583
p 1354 N95-21584
p 1358 N95-22424
CHAVLEJSHVILI, M. P. p 1514 N95-20735
CHAWLA, N. p 1271 N95-20700
CHEDIAK, J. A. p 1538 N95-21938
CHEIFETZ, MICHAEL G. p 1290 N95-20376
CHELLAPPA, RAMA p 1313 N95-20257
CHEMLA, D. S. p 1569 N95-20677
p 1569 N95-20678
p 1569 N95-20679
p 1514 N95-20732
p 1373 N95-21261
p 1577 N95-22168
CHEN, A. L. p 1568 N95-20630
CHEN, BINGXIAN p 1563 N95-19978
CHEN, C. H. p 1287 N95-21559
CHEN, CHARLES C. p 1202 N95-20275
CHEN, F. C. p 1287 N95-21559
CHEN, GOONG p 1340 N95-20312
CHEN, H. H. p 1484 N95-22210
CHEN, HAI-WEN p 1481 N95-20812
CHEN, HELEN p 1477 N95-21505
CHEN, J. C. p 1305 N95-21543
CHEN, J. H. p 1249 N95-21038
CHEN, J. P. p 1234 N95-20046
CHEN, K. p 1568 N95-20674
CHEN, K. R. p 1369 N95-20221
CHEN, L. D. p 1281 N95-19884
CHEN, NAN p 1570 N95-20841
CHEN, PANG C. p 1459 N95-20284
CHEN, PISIN p 1301 N95-21241
p 1536 N95-21337
CHEN, T. p 1536 N95-21334
CHEN, X. M. p 1524 N95-21703
CHEN, YI-XIN p 1582 N95-22198
CHEN, ZEWEI p 1462 N95-20691
CHENG, A. p 1432 N95-20012
CHENG, C. p 1379 N95-20723
CHERN, I.-LIANG p 1489 N95-20170
CHERN, R. T. p 1268 N95-20428
CHESONIS, KESTUTIS G. p 1273 N95-21000
CHESSA, P. p 1373 N95-21226
CHESTER, A. W. p 1247 N95-22234
CHESTER, DAVID p 1432 N95-19988
CHEUNG, K.-M. p 1304 N95-21534
CHEVRIER, F. p 1293 N95-20929
CHHABILDAS, L. p 1218 N95-20785
CHHABILDAS, LALIT C. p 1215 N95-20223
CHIANG, C.-S. p 1549 N95-20114
CHIAPPETTI, CHARLES F. p 1214 N95-22232
CHIEN, H. T. p 1366 N95-21453
CHIEN, L. C. p 1569 N95-20767
CHIMENTI, DALE E. p 1504 N95-20918
CHIN, HUNG-NENG STEVE p 1429 N95-20381
CHING, W. Y. p 1564 N95-20017
CHING, W.-Y. p 1500 N95-20229
CHISHOLM, M. F. p 1565 N95-20244
p 1567 N95-20492
CHITICA, N. p 1562 N95-22377
CHIU, S. C. p 1551 N95-20285
CHO, A. Y. p 1577 N95-22168
CHO, J. H. p 1575 N95-21936
CHO, KENJIRO p 1290 N95-20306
CHOCOL, C. J. p 1310 N95-22299
CHOI, J. p 1491 N95-20701
CHOI, SUNG R. p 1386 N95-20790
CHOTIROS, NICHOLAS P. p 1433 N95-20999
CHOU, LYNN CHEN p 1354 N95-21675
CHOUDHARI, MEELAN p 1353 N95-21258
CHOW, GAN-MOOG p 1568 N95-20552
CHOW, R. p 1541 N95-20218
p 1377 N95-22343
CHRISTE, KARL O. p 1284 N95-21678
CHRISTENSEN, DAVID S. p 1584 N95-20749
CHRISTENSEN, T. p 1286 N95-21027
CHRISTIAN, DAVID C. p 1515 N95-20868
CHRISTIANSEN, J. H. p 1412 N95-20171
CHRISTIE, DAVID R. p 1541 N95-20231
CHRISTIE, W. p 1520 N95-21357
CHRISTON, M. p 1459 N95-20255
CHRISTON, M. A. p 1354 N95-21387
CHRISTOPHOROU, L. G. p 1522 N95-21519
CHU, H. C. p 1201 N95-21343
CHU, M. S. p 1550 N95-20146
p 1556 N95-21142
CHU, NHI-ANH p 1498 N95-20608
CHUA, ANTHONY Y. p 1498 N95-20620
CHUANG, C.-H. p 1222 N95-21616
CHUBB, DONALD p 1322 N95-20537
CHUBB, DONALD L. p 1322 N95-20536
CHUNG, D. D. L. p 1229 N95-20913
CHURCH, E. L. p 1468 N95-21515
CHUZHOY, L. p 1285 N95-20050
CIARLO, D. R. p 1237 N95-20386
CIESLAK, M. J. p 1378 N95-20053
CIESLAK, MICHAEL J. p 1374 N95-21594
CITERNE, J. p 1295 N95-20934
p 1296 N95-20944
CLAES, D. R. p 1528 N95-22197
CLAESSEN, R. p 1574 N95-21712
CLANCY, R. TODD p 1427 N95-22240
CLAPP, WILLIAM G. p 1217 N95-20690
CLARK, D. L. p 1236 N95-20361
CLARK, EDWARD L. p 1489 N95-20222
CLARK, JOSEPH A. p 1504 N95-20296
CLARK, R. P. p 1324 N95-20626
CLARK, RAYMOND p 1484 N95-22203
CLARK, W. M. p 1415 N95-21308
CLARKE-GAYTHER, M. A. p 1518 N95-21224
CLARKE, JERRY A. p 1478 N95-22228
CLAYTON, TERRY R. p 1477 N95-21674
CLEMENS, M. K. p 1407 N95-21617
CLIFFORD, T. p 1532 N95-20336
CLINE, RAYMOND E., JR. p 1301 N95-21277
CLONTS, L. G. p 1330 N95-21554
CLOSE, F. E. p 1518 N95-21225
p 1537 N95-21647
CLOUD, HARLEY A. p 1327 N95-20966
CLOUGH, R. L. p 1263 N95-19926
COATS, R. L. p 1509 N95-20206
COBB, J. W. p 1561 N95-21922
COBB, STEPHEN p 1274 N95-21234
COCHRAN, H. D. p 1580 N95-21420
COCKROFT, NIGEL J. p 1373 N95-21312
COFFEY, HELEN E. p 1603 N95-20713
p 1603 N95-20722
p 1603 N95-20829
p 1603 N95-20919
COFFIN, MICHAEL p 1496 N95-22349
COFFIN, PAUL p 1227 N95-20459
p 1381 N95-22034
COHEN, A. G. p 1512 N95-20451
COHEN, B. I. p 1559 N95-21451
COHEN, DAVID p 1453 N95-21691
COHEN, MARVIN L. p 1281 N95-22470
COHEN, R. E. p 1269 N95-20582
COHN, R. H. p 1559 N95-21451
COLE, EDWARD I., JR. p 1314 N95-20286
COLE, J. I. p 1251 N95-20088
COLELLA, PHILLIP p 1356 N95-21959
COLEMAN, P. D. p 1329 N95-21395
COLLINS, CURTIS A. p 1431 N95-19918
COLLINS, D. G. p 1458 N95-20154
COLLINS, JOSEPH C., III p 1499 N95-22135
COLLINS, L. L., JR. p 1516 N95-21114
COLLINS, SANDRA R. p 1317 N95-20510
COLLYER, P. D. p 1442 N95-20710
COLOMBAN, P. p 1275 N95-21272
COLSON, S. D. p 1403 N95-20834
COLTON, RICHARD J. p 1365 N95-21117
COMASKEY, B. p 1389 N95-21552
p 1376 N95-22121
COMPAAN, A. D. p 1395 N95-21508
COMPTON, J. p 1459 N95-20255
COMTE, P. p 1348 N95-21075
CONBOY, J. C. p 1245 N95-21827
CONCHA, MONICA C. p 1525 N95-21878
CONCHA, MONICA G. p 1246 N95-22000
CONDE, M. E. p 1374 N95-21528
CONFORTI, MICHELE p 1490 N95-20662
p 1470 N95-21974
CONN, A. R. p 1495 N95-22317
CONNES, A. p 1580 N95-20324

CONNOLLY, R. p 1532 N95-20406
CONNORS, M. P. p 1314 N95-20338
p 1334 N95-22086
COOK, D. R. p 1335 N95-22189
COOK, JOSEPH S., JR. p 1378 N95-20151
p 1378 N95-20409
COOK, W. M. p 1389 N95-21433
COOLEY, J. C. p 1574 N95-21570
COONROD, KURT H. p 1291 N95-20771
p 1207 N95-20772
COOPER, BARBARA H. p 1514 N95-20667
p 1530 N95-22471
COOPER, DANIEL I. p 1426 N95-21875
COOPER, DONALD L. p 1366 N95-21323
COOPER, F. p 1488 N95-20169
COOPER, GENE R. p 1428 N95-19989
COOPER, J. F. p 1337 N95-22421
COOPER, W. E. p 1365 N95-20902
COPLAN, M. A. p 1604 N95-22384
COQUEL, FREDERIC p 1355 N95-21957
CORBIN, JAMES H. p 1432 N95-20209
CORBITT, THOMAS S. p 1270 N95-20689
CORDEY, J. G. p 1556 N95-21142
CORLESS, R. F. p 1259 N95-21838
CORMAN, G. S. p 1214 N95-21243
CORNEUJOLS, GERARD p 1490 N95-20662
CORNUEJOLS, GERARD p 1470 N95-21974
CORNUELLE, BRUCE p 1432 N95-19988
CORRAL, ROQUE p 1349 N95-21080
CORWIN, W. R. p 1386 N95-20703
COSTER, M. J. p 1487 N95-19940
COTAL, H. L. p 1319 N95-20519
COTE, P. J. p 1387 N95-22025
p 1495 N95-22026
COTTRELL, S. P. p 1529 N95-22303
COUGHLIN, K. p 1344 N95-21049
COULTER, R. L. p 1426 N95-21836
COURANT, D. p 1447 N95-22361
COURANT, E. p 1540 N95-22391
COURT, J. D. p 1508 N95-20160
p 1509 N95-20236
COURT, L. p 1447 N95-22361
COURTRIGHT, WILLIAM V., II p 1463 N95-20846
COWAN, P. L. p 1522 N95-21502
COWARD, JOHN R. p 1485 N95-22214
COWEN, D. J. p 1592 N95-22263
COX, R. C. p 1463 N95-20877
COX, S. F. J. p 1518 N95-21224
COX, S. K. p 1406 N95-21410
CRAIGHEAD, HAROLD G. p 1547 N95-22205
CRAM, SCOTT p 1440 N95-22065
CRAMER, P. W. p 1304 N95-21538
CRANE, J. K. p 1377 N95-22312
CRANE, JOHN K. p 1555 N95-20813
CRANE, ROBERT K. p 1297 N95-20946
CRANE, ROGER M. p 1226 N95-20292
p 1227 N95-20459
p 1381 N95-22034
CRAWFIS, ROGER p 1353 N95-21182
CRAWFORD, M. L. p 1289 N95-20191
CRAWFORD, R. A. p 1200 N95-20248
CREEK, EDITH A. p 1382 N95-20414
CREMALDI, L. M. p 1530 N95-22339
CREMERS, D. p 1375 N95-21837
CRESPO, ANTONIO p 1546 N95-21975
CREUTZ, M. p 1564 N95-20130
CROCKER, N. p 1549 N95-20113
p 1549 N95-20114
CROCKETT, THOMAS W. p 1473 N95-20013
CRONYN, WILLARD M. p 1334 N95-22030
CRORY, FREDERICK C. p 1287 N95-21626
CROSLEY, DAVID R. p 1247 N95-22150
CROSS, JON B. p 1412 N95-20278
CROSS, L. E. p 1502 N95-19883
p 1276 N95-21697
p 1505 N95-21863
CROSSON, WILLIAM p 1390 N95-22111
CROSSON, WILLIAM L. p 1390 N95-22110
CROSTON, I. R. p 1210 N95-20641
CROUCH, J. D. p 1351 N95-21091
CRUIKSHANK, DALE P. p 1423 N95-21815
CUA, AGNES p 1437 N95-19969
CUCCOLI, A. p 1502 N95-22138
CUCINOTTA, FRANCIS A. p 1517 N95-21191
CUI, ZHENGYING p 1556 N95-21165
CULLEN, D. E. p 1511 N95-20444
CUMMINGS, ERIC B. p 1372 N95-21009
CUMMINGS, JOHN R. p 1318 N95-20513
CUMMINGS, MARY L. p 1341 N95-21001
CUMMINGS, P. T. p 1237 N95-20384
CUNEO, M. E. p 1535 N95-21328
CUNNINGHAM, G. S. p 1459 N95-20165
CUOMO, FRANK p 1506 N95-22088
p 1547 N95-22089
CURRAN, LAWRENCE J., JR. p 1208 N95-20032
CURRENT, M. I. p 1558 N95-21310
CURTRIGHT, T. L. p 1579 N95-20271
CUTHBERTSON, J. W. p 1554 N95-20568
CYGAN, RANDALL T. p 1573 N95-21449
CYR, KELLEY p 1583 N95-20741

D

DAALAND, O. p 1258 N95-21653
DAAMS, B. J. p 1452 N95-21283
DABABNEH, S. A. p 1330 N95-21545
DACOSTA, HERBERT F. p 1506 N95-19959
DAHLE, A. K. p 1258 N95-21652
DAI, L. p 1281 N95-22434
DAI, S. p 1237 N95-20493
DALE, M. CLARK p 1283 N95-21356
DALLAS, CHAM E. p 1442 N95-20485
DALY, PETER p 1298 N95-20950
DAMERELL, C. J. S. p 1540 N95-22364
DAMKROGER, B. K. p 1387 N95-21364
DAMS, D. p 1472 N95-22305
DANDCKAR, S. p 1298 N95-20953
DANIEL, AARON R. p 1283 N95-21514
DAPP, TIMOTHY L. p 1266 N95-20293
p 1266 N95-20294
DAPPER, R. p 1435 N95-21717
DARLING, C. L. p 1530 N95-22339
DARLING, G. p 1418 N95-21789
DARNELL, M. p 1293 N95-20924
p 1293 N95-20925
p 1293 N95-20926
p 1299 N95-20957
DAS, B. p 1592 N95-21752
DASCHBACH, J. L. p 1245 N95-21826
p 1245 N95-21827
DASGUPTA, S. p 1340 N95-20796
DASHIELL, MICHAEL W. p 1318 N95-20513
DASILVA, L. B. p 1374 N95-21663
DASKIEWICH, DANIEL E. p 1210 N95-20644
DASTMALCHI, MITRA p 1470 N95-21971
DATSKOS, P. G. p 1522 N95-21519
DATYE, A. p 1239 N95-20712
DATZ, S. p 1508 N95-20133
DAUNCEY, P. D. p 1512 N95-20454
DAVE, N. p 1297 N95-20948
DAVENPORT, R. p 1393 N95-20864
DAVID, E. p 1348 N95-21075
DAVID, S. A. p 1253 N95-20676
p 1256 N95-21298
p 1381 N95-21550
p 1261 N95-22127
p 1285 N95-22261
DAVIES, NIGEL C. p 1299 N95-20955
DAVIS, C. J. p 1413 N95-20453
DAVIS, D. O. p 1338 N95-19953
DAVIS, DAVID C. p 1443 N95-20763
DAVIS, H. A. p 1560 N95-21668
DAVIS, HAROLD p 1446 N95-21941
DAVIS, J. p 1533 N95-20672
p 1537 N95-21494
DAVIS, J. M. p 1406 N95-21410
DAVIS, M. M. p 1406 N95-21487
DAVIS, ROBERT F. p 1568 N95-20614
DAVIS, STUART L. p 1291 N95-20771
DAVIS, VICTORIA A. p 1321 N95-20527
DAVIS, WILLIAM M. p 1246 N95-21879
p 1224 N95-22252
DAWSON, J. p 1488 N95-20169
DAWSON, S. p 1522 N95-21506
DAY, G. W. p 1540 N95-19976
DAY, GLENROY E., JR. p 1546 N95-21882
DAY, JOHN p 1316 N95-20503
DAY, M. p 1249 N95-21038
DAY, ROBERT D. p 1285 N95-20288
DAZEVEDO, E. F. p 1477 N95-21602
DEANE, JAMES R. p 1594 N95-21773
DEANGELIS, R. M. p 1428 N95-20099
DEBOO, J. C. p 1556 N95-21142
DEBRA, P. p 1465 N95-21021
DEBROY, T. p 1253 N95-20676
p 1381 N95-21550
DEBROY, T. A. p 1381 N95-22268
DECKER, DWIGHT T. p 1430 N95-21177
DECKER, F. J. p 1536 N95-21335
DECKER, T. A. p 1543 N95-20612
DEFOREST, T. J. p 1406 N95-21487
DEFOUG, S. p 1325 N95-20702
DEGAUQUE, P. p 1294 N95-20933
DEGYVEZ, JOSE P. p 1455 N95-21589
DEIMLER, JIM D. p 1447 N95-22040
DEISSLER, R. J. p 1248 N95-22433
DEIST, DAVID W. p 1426 N95-22019
DEJCHULI, P. P. p 1529 N95-22283
DEJSUPA, C. p 1241 N95-21123
DEKLERK, D. p 1483 N95-21981
DELAHOY, A. E. p 1395 N95-21844
DELAMATER, N. D. p 1371 N95-20786
DELAND, SHARON M. p 1588 N95-20789
DELARUBIADIAZ, T. p 1557 N95-21206
DELAYEN, J. R. p 1531 N95-19983
DELCUL, G. D. p 1237 N95-20493
DELEEUW, F. A. A. M. p 1410 N95-22186
DELHEIJ, P. P. J. p 1519 N95-21237
DELIYANAKIS, N. p 1556 N95-21142
DELLACORTE, CHRISTOPHER p 1223 N95-19901
DELLWO, J. p 1538 N95-21938
DELOOS, M. p 1374 N95-21528
DELUCA, J. A. p 1571 N95-21167
p 1578 N95-22269
DELVINQUIER, J. P. p 1213 N95-20657
DEMERS, WILLIAM A. p 1587 N95-20039
DEMEURE, CEDRIC p 1299 N95-20959
DEMIRBILEK, ZEKI p 1471 N95-22068
DEMUREN, A. O. p 1345 N95-21053
p 1467 N95-21450
DENG, D. P. p 1532 N95-20406
DENG, HUICHEN p 1556 N95-21165
DENG, ZHENG-TAO p 1354 N95-21675
DENHARTOG, D. J. p 1549 N95-20112
p 1549 N95-20113
p 1549 N95-20114
DENIG, W. F. p 1413 N95-20453
DENLINGER, EDGAR J. p 1326 N95-20824
p 1276 N95-21695
DEOGUN, J. S. p 1496 N95-22327
DERZON, M. S. p 1558 N95-21247
DESCH, W. p 1493 N95-21582
DESJARLAIS, M. p 1565 N95-20340
DESJARLAIS, M. P. p 1535 N95-21328
DESOMBRE, E. R. p 1240 N95-20836
DESWART, J. J. B. p 1493 N95-21434
DETROYE, DAVID J. p 1228 N95-20808
DEUMENS, ERIK p 1506 N95-19960
DEVAN, J. H. p 1378 N95-20085
DEVANTIER, BRUCE A. p 1390 N95-21628
DEVEREUX, NICK A. p 1593 N95-21760
DEVOOYS, C. G. N. p 1435 N95-21717
DEVOS, J. C. p 1592 N95-22334
DEVOS, P. W. p 1405 N95-21327
DEVOTO, JORGE A. p 1496 N95-22355
DEWAR, R. L. p 1548 N95-19977
DEWDNEY, P. E. p 1594 N95-21771
DEYOREO, J. p 1557 N95-21166
DHAUSSY, J. C. p 1209 N95-20635
DHERE, N. G. p 1392 N95-20333
DIAO, GUANGYAO p 1556 N95-21165
DIATCHENKO, N. p 1562 N95-22300
DIAZ-HERRERA, JORGE L. p 1485 N95-22226
DIBARI, J. C. p 1406 N95-21487
DIBUCCHIANICO, A. p 1499 N95-21979
DICK, GARY O. p 1409 N95-21914
DICKMAN, O. p 1232 N95-22096
DIEBOLD, J. p 1236 N95-20290
DIEDEREN, H. S. M. A. p 1405 N95-21350
DIKKER, F. p 1471 N95-22081
DILELLA, DANIEL p 1365 N95-21117
DILLMAN, WOLFGANG H. p 1442 N95-20549
DIMOFTE, FLORIN p 1382 N95-22404
p 1382 N95-22405
DIMOS, DUANE p 1333 N95-21881
DIMOV, G. I. p 1562 N95-22282
DINENNO, P. J. p 1202 N95-20071
DINESCU, M. p 1562 N95-22377
DINETTA, LOUIS C. p 1317 N95-20510
p 1318 N95-20513
p 1323 N95-20540
DING, YUNGUI p 1257 N95-21398
DINH, L. N. p 1542 N95-20450
DINWIDDIE, R. B p 1226 N95-20125
DINWIDDIE, R. B. p 1225 N95-20023
p 1247 N95-22260
DISALVO, FRANCIS J. p 1227 N95-20427
DISTRAVOLO, MARIA p 1591 N95-22092
DITARANTO, MARIE p 1228 N95-20805
DITMIRE, T. p 1377 N95-22312
DITMIRE, TODD p 1555 N95-20813
DITTNER, P. F. p 1508 N95-20133
DIVER, R. B. p 1393 N95-20861
DIVSALAR, D. p 1304 N95-21535
p 1304 N95-21536
DIXSON, R. L. p 1530 N95-22339
DIZ, AGUSTIN p 1516 N95-21120
DOANE, J. W. p 1569 N95-20767
DOCTOR, R. D. p 1403 N95-20478
DODD, BRUCE A. p 1314 N95-20286
DODDS, J. N. p 1236 N95-20268
DOERRY, ARMIN W. p 1302 N95-21305
DOHERTY, PATRICIA H. p 1430 N95-21177
DOLAN, N. J. p 1202 N95-20093
DOLAN, T. J. p 1558 N95-21290
DOLENC, A. p 1472 N95-22372
DOMANUS, H. M. p 1285 N95-20050

DOMBROWSKI, MARK .... p 1383 N95-22037
DOMINGUEZ-ADAME, F. .... p 1500 N95-21136
DOMINGUEZ, D. .... p 1576 N95-21995
p 1576 N95-21996
p 1576 N95-21997
DOMINIAK, RICHARD .... p 1591 N95-22092
DONAHUE, T. M. .... p 1417 N95-21785
DONALD, M. .... p 1519 N95-21262
DONALDSON, RALPH S., JR. .... p 1203 N95-21831
DONATO, J. M. .... p 1369 N95-20221
DONG, HEQIN .... p 1563 N95-19978
DONG, JINMING .... p 1577 N95-22180
DONG, YUANJI .... p 1283 N95-21211
DONGARRA, J. J. .... p 1491 N95-20701
DONOHOO, A. .... p 1205 N95-21642
DORMONT, D. .... p 1447 N95-22361
DOROUDI, A. .... p 1527 N95-22179
DOSKEY, P. V. .... p 1401 N95-20234
DOSS, S. K. .... p 1376 N95-22301
DOUGHTY, D. H. .... p 1564 N95-20087
DOUGLAS, J. G. .... p 1237 N95-20470
DOUGLAS, K. .... p 1336 N95-22284
DOVER, C. B. .... p 1521 N95-21484
DOW, THOMAS A. .... p 1465 N95-21012
DOWNER, MICHAEL C. .... p 1374 N95-21480
DOWNHOWER, WALTER J. .... p 1585 N95-20751
DOYLE, B. L. .... p 1575 N95-21991
DOYLE, E. J. .... p 1556 N95-21142
DRAKE, J. B. .... p 1407 N95-21608
DRAVID, V. P. .... p 1567 N95-20492
DREIBUS, G. .... p 1424 N95-21820
DRESS, W. B. .... p 1503 N95-20019
DRESSEL, M. .... p 1262 N95-22291
DRESSELHAUS, ELIOT .... p 1363 N95-22465
DRESSELHAUS, M. S. .... p 1272 N95-20892
DRESSENDORFER, P. .... p 1480 N95-20342
DROUILLARD, THOMAS F. .... p 1503 N95-20267
DRUMMOND, T. J. .... p 1575 N95-21991
DRUZHININ, V. V. .... p 1564 N95-20240
DUAN, XURU .... p 1556 N95-21165
DUAN, YUYING .... p 1255 N95-20909
DUBBELDAY, WADAD B. .... p 1396 N95-21899
DUBEY, RAJENDRA R. .... p 1517 N95-21191
DUBREUIL, B. .... p 1562 N95-22377
DUCROS, F. .... p 1348 N95-21075
DUDEK, JAMES D. .... p 1567 N95-20479
DUENNEBIER, FREDERICK K. .... p 1432 N95-20040
DUESLER, EILEEN .... p 1569 N95-20714
DUFF, I. S. .... p 1494 N95-21648
DUFFY, T. S. .... p 1417 N95-21786
p 1418 N95-21791
DUISENBERG, KEN .... p 1207 N95-21186
DUKE, JOSEPH R. .... p 1574 N95-21599
DUMONT, B. .... p 1212 N95-20655
DUNAGAN, STEPHEN E. .... p 1366 N95-21323
DUNCAN, A. J. .... p 1255 N95-20907
DUNN, P. .... p 1252 N95-20331
DUNN, P. S. .... p 1387 N95-21364
p 1260 N95-22006
DUNN, W. N. .... p 1207 N95-21730
DUPUIS, PAUL .... p 1302 N95-21438
DURANT, J. L., JR. .... p 1244 N95-21524
DURBIN, P. .... p 1345 N95-21053
p 1345 N95-21054
DURBIN, PAUL A. .... p 1359 N95-22443
DURFEE, R. C. .... p 1458 N95-20073
p 1591 N95-22129
DUSEK, J. .... p 1350 N95-21086
DUTTA, DEBASISH .... p 1464 N95-21010
DUWE, R. .... p 1269 N95-20570
DWYER, JOHN P. .... p 1204 N95-19950
DWYER, ROGER F. .... p 1303 N95-21464
DYE, RAYMOND .... p 1504 N95-20823

E

EARLY, JAMES W. .... p 1373 N95-21312
EARLY, R. .... p 1538 N95-22155
EASTERLY, C. E. .... p 1439 N95-21548
EASTMAN, LESTER F. .... p 1369 N95-20379
EASTON, D. S. .... p 1250 N95-20020
EATON, G. H. .... p 1518 N95-21224
EBERHARD, P. H. .... p 1524 N95-21646
ECCLESTON, R. S. .... p 1526 N95-21965
ECKSTEIN, JEFFREY R. .... p 1585 N95-20855
EDJEOU, A. .... p 1299 N95-20956
EGGEN, S. .... p 1288 N95-21651
EGGERT, J. H. .... p 1418 N95-21791
EGGINK, G. J. .... p 1409 N95-21846
EGGLESTON, DEBRA S. .... p 1221 N95-20708
EGUSA, S. .... p 1232 N95-22130
EHLER, G. D. .... p 1592 N95-22263
EIBEN, A. E. .... p 1467 N95-21374
EICHELBERGER, JOHN W., III .... p 1309 N95-22245
EICHINGER, WILLIAM E. .... p 1426 N95-21875
EIDELLOTH, WALTER .... p 1567 N95-20461
EILERS, D. L. .... p 1311 N95-22407
EIMERL, D. .... p 1531 N95-20120
EISLER, R. .... p 1379 N95-20695
EKBERG, S. A. .... p 1236 N95-20361
EKEN, F. .... p 1292 N95-20922
EKROTH, M. .... p 1547 N95-22140
EL-ASHRY, M. Y. .... p 1561 N95-21848
p 1561 N95-21850
EL-SAYED, M. A. .... p 1241 N95-21124
p 1281 N95-22470
EL-SAYED, MOSTAFA A. .... p 1567 N95-20483
ELAMRAOUI, Y. .... p 1278 N95-21885
ELIEZER, ZWY .... p 1252 N95-20201
ELIOTT, N. E. .... p 1558 N95-21368
ELKENZ, A. .... p 1278 N95-21885
ELLINGSON, WILLIAM A. .... p 1264 N95-20018
ELLIOTT, D. C. .... p 1236 N95-20290
ELLIOTT, S. R. .... p 1373 N95-21210
ELLIS, T. W. .... p 1258 N95-21568
p 1259 N95-21737
ELLIS, W. P. .... p 1574 N95-21712
ELORANTA, ESKO H. .... p 1291 N95-20775
ELPHIC, R. C. .... p 1600 N95-21935
ELZEIN, G. .... p 1295 N95-20934
p 1296 N95-20944
EMANUEL, M. .... p 1389 N95-21552
EMERY, M. S. .... p 1330 N95-21554
EMMA, P. .... p 1536 N95-21332
EMOND, BRYAN R. .... p 1485 N95-22233
ENDERLE, JOHN D. .... p 1441 N95-20301
ENDO, T. .... p 1277 N95-21714
ENG, ANTHONY T. .... p 1274 N95-21154
p 1274 N95-21155
ENGDAHL, E. .... p 1502 N95-22138
ENGLE, RANDALL W. .... p 1448 N95-20007
ENGRAND, PHILIPPE .... p 1466 N95-21288
ENGWERDA, J. C. .... p 1499 N95-19941
ENSSLIN, N. .... p 1516 N95-21114
ERBIL, A. .... p 1244 N95-21549
ERDMAN, W. W. .... p 1393 N95-20864
ERICKSON, GARY M. .... p 1427 N95-22326
ERICKSON, M. D. .... p 1401 N95-20234
ERICSON, M. N. .... p 1330 N95-21554
ERM. LINCOLN P. .... p 1201 N95-21659
ERNST, D. .... p 1558 N95-21242
ERSKINE, D. J. .... p 1541 N95-20352
ERTL, A. C. .... p 1439 N95-21544
ERVIN, C. P. .... p 1415 N95-21477
ERVIN, R. D. .... p 1380 N95-21157
ESKIN, ALEX .... p 1496 N95-22354
ESPINOSA, R. J. .... p 1271 N95-20761
ESPINOZA, L. H. .... p 1235 N95-20139
ESTEFAN, J. A. .... p 1412 N95-20002
p 1218 N95-21533
ETTERS, R. D. .... p 1565 N95-20243
EVANS, ANTHONY G. .... p 1227 N95-20429
p 1227 N95-20430
p 1227 N95-20583
p 1228 N95-20584
p 1228 N95-20801
p 1228 N95-20802
p 1231 N95-21999
EVANS, CALEB R. .... p 1534 N95-21236
EVANS, LINDSEY R. .... p 1394 N95-21353
EVANS, M. S. .... p 1364 N95-20321
EVANS, N. D. .... p 1510 N95-20337
EVANS, RHODRI H. .... p 1593 N95-21766
EVERBERG, CARL .... p 1204 N95-21148
EVERLEIGH, C. A. .... p 1271 N95-20761
EVTUSHENKO, I. A. .... p 1559 N95-21388
EYLER, J. R. .... p 1238 N95-20563
p 1241 N95-21123

F

FACY, P. .... p 1445 N95-21424
FADORSEN, G. A. .... p 1287 N95-21598
FAGERQUIST, CLIFTON .... p 1281 N95-22470
FAGHRI, AMIR .... p 1339 N95-20250
FAHEY, S. T. .... p 1510 N95-20344
FAILOR, B. H. .... p 1531 N95-20015
FALL, THIERNO .... p 1461 N95-20687
FALTENS, A. .... p 1534 N95-20891
FAN, W. C. .... p 1509 N95-20206
FANG, CHIEN .... p 1477 N95-21505
FANG, H. E. .... p 1474 N95-20150
FANSLER, KEVIN S. .... p 1428 N95-19989
FANTON, JOHN W. .... p 1446 N95-21941
FANTONI, S. .... p 1581 N95-21993
p 1576 N95-21998
FARAS, F. .... p 1395 N95-21844
FARINA, G. E. .... p 1259 N95-21740
FARLEY, KENNETH .... p 1418 N95-21787
FARMER, J. C. .... p 1272 N95-20892
FARMER, RICHARD C. .... p 1221 N95-20124
FARMER, SERENE C. .... p 1322 N95-20536
FARQUHARSON, STUART .... p 1228 N95-20805
FARRINGTON, GREGORY C. .... p 1226 N95-20092
FASEL, HERMANN F. .... p 1352 N95-21094
FAST, J. D. .... p 1413 N95-20455
FATALE, L. A. .... p 1204 N95-20497
FATEMI, N. S. .... p 1317 N95-20509
FATEMI, NAVID S. .... p 1322 N95-20537
FATHY, ALY .... p 1326 N95-20824
FATICA, M. .... p 1351 N95-21088
FAUR, MARIA .... p 1317 N95-20509
FAUR, MIRCEA .... p 1317 N95-20509
FAURE, FRANCOIS XAIVER .... p 1466 N95-21288
FAYETTE, DANIEL F. .... p 1210 N95-20643
FAYNE, WALTER R. .... p 1327 N95-20905
FAZAH, M. M. .... p 1340 N95-20561
FAZIO, M. V. .... p 1334 N95-22011
FEENSTRA, R. B. .... p 1592 N95-22331
FEGLEY, B., JR. .... p 1421 N95-21804
FEI, Y. .... p 1417 N95-21786
FEISTER, ALAN J. .... p 1445 N95-21629
FELDMAN, ARLEN D. .... p 1390 N95-21628
FELDMAN, URI .... p 1240 N95-20865
FELIZARDO, FRANCIS C. .... p 1432 N95-20303
FELLOWS, MARY M. .... p 1383 N95-21933
FENDRICH, JOHN A. .... p 1567 N95-20479
FENG, JIANREN .... p 1242 N95-21397
FENG, Z. C. .... p 1244 N95-21549
FENIMORE, E. E. .... p 1221 N95-22436
FENSTERMACHER, M. E. .... p 1559 N95-21451
FERBER, M. K. .... p 1378 N95-20085
p 1267 N95-20373
p 1271 N95-20700
FERGUSON, DALE C. .... p 1321 N95-20529
p 1415 N95-21188
FERGUSON, F. J. .... p 1334 N95-22118
FERGUSON, GERALD D. .... p 1333 N95-21906
FERGUSON, P. D. .... p 1538 N95-22050
FERIA, Y. .... p 1304 N95-21534
FERKET, P. J. J. .... p 1493 N95-21574
FERMANDEZ, J. C. .... p 1558 N95-21368
FERNANDEZ-BACA, J. A. .... p 1572 N95-21297
FERNANDEZ, E. .... p 1549 N95-20113
FERNOW, R. .... p 1370 N95-20572
FERREIRAPIRES, LUIS .... p 1477 N95-21620
FERRELL, CYNTHIA .... p 1479 N95-20011
FERREOL, ANNE .... p 1299 N95-20959
FERRER, WALTER .... p 1488 N95-20054
FERRI, M. A. .... p 1332 N95-21725
FERRON, J. R. .... p 1554 N95-20446
FERTIG, TIMOTHY .... p 1211 N95-20646
FERZIGER, J. H. .... p 1249 N95-21044
p 1350 N95-21083
FESSENDEN, T. J. .... p 1552 N95-20318
FETTERER, FLORENCE .... p 1388 N95-20006
FEUDO, CHRISTOPHER V. .... p 1288 N95-19932
FIEBIG, MARTIN .... p 1347 N95-21070
FIELD, J. B. .... p 1281 N95-22434
FIELD, R. D. .... p 1512 N95-20469
FIGOTIN, ALEXANDER .... p 1309 N95-22215
FIJALKOW, E. .... p 1500 N95-21592
FIKSEL, G. .... p 1549 N95-20113
p 1549 N95-20114
FILISKO, F. E. .... p 1380 N95-21157
FILTOPOULOS, E. E. J. .... p 1243 N95-21512
FILUK, A. B. .... p 1506 N95-20026
p 1535 N95-21328
FINCH, STEVE .... p 1213 N95-22024
FINE, MORRIS E. .... p 1252 N95-20201
FINK, W. .... p 1578 N95-22277
FINKEN, K. H. .... p 1549 N95-20143
FINKENTHAL, D. F. .... p 1552 N95-20334
FINLEY, TOM D. .... p 1368 N95-22109
FISCHER, D. S. .... p 1202 N95-20093
FISCHER, DOUGLAS S. .... p 1203 N95-22319
FISCHER, J. .... p 1533 N95-20573
FISCHER, P. R. .... p 1245 N95-21826
FISHER, C. H. .... p 1371 N95-20866
FISHER, E. S. .... p 1226 N95-20027
FISHER, JAY L. .... p 1382 N95-20414
FISHER, PETER W. .... p 1376 N95-22169
FISHER, R. K. .... p 1553 N95-20402
FISHER, RICHARD A. .... p 1224 N95-22252
FISHMAN, B. .... p 1429 N95-20782
FISK, Z. .... p 1237 N95-20368
p 1574 N95-21570
FITTING, J. D. .... p 1280 N95-22270
FITZGERALD, MARK .... p 1316 N95-20505
FLACH, JOHN M. .... p 1450 N95-21192
FLANERY, R. E. .... p 1407 N95-21608
FLANNERY, M. R. .... p 1517 N95-21216
FLEETWOOD, D. M. .... p 1566 N95-20400
FLEMING, D. .... p 1337 N95-22421
FLESHLER, S. .... p 1575 N95-21936
FLESNER, LARRY D. .... p 1396 N95-21899

FLETCHER, LYN E. p 1287 N95-21625
FLEURY, R. p 1300 N95-20961
FLOOD, D. J. p 1317 N95-20509
FLORO, J. A. p 1566 N95-20399
p 1572 N95-21304
FLOYD, THOMAS R. p 1306 N95-21672
p 1306 N95-21834
FLYKT, MIKKO J. p 1291 N95-20775
FLYNN, E. R. p 1313 N95-20168
FLYNN, EDWARD R. p 1289 N95-20164
FLYNN, J. p 1537 N95-21647
FLYTZANI-STEPHANOPOULOS, M.
p 1233 N95-20045
FOBES, J. L. p 1202 N95-20093
FOBES, JAMES L. p 1203 N95-22319
FOCH, J. D. p 1354 N95-21387
FOERSTE, S. p 1599 N95-21245
FOGHELIN, J. p 1585 N95-21427
FOKKINGA, MAARTEN p 1492 N95-21032
p 1466 N95-21344
p 1494 N95-21867
p 1494 N95-21868
FOLKERTS, L. p 1525 N95-21857
FOLLSTAEDT, D. M. p 1563 N95-19954
p 1314 N95-20341
FONCK, R. J. p 1549 N95-20112
p 1558 N95-21242
FONTANELLA, J. J. p 1330 N95-21490
FOOTE, J. H. p 1559 N95-21451
FORBES, JEFFREY M. p 1414 N95-20498
FORBUS, KENNETH D. p 1450 N95-22052
FOREMAN, R. J. p 1272 N95-20892
FOREST, C. B. p 1551 N95-20279
FOREST, E. p 1519 N95-21262
FORNEY, L. J. p 1367 N95-21889
FORSBERG, BERTIL p 1405 N95-21181
FORSHAW, J. R. p 1518 N95-21233
FOSS, COLBY A., JR. p 1324 N95-20587
FOSS, JOHN F. p 1362 N95-22457
FOSSHEIM, K. p 1575 N95-21949
p 1577 N95-22166
FOSTER, C. p 1314 N95-20338
FOSTER, I. T. p 1407 N95-21608
FOSTER, J. C., JR. p 1501 N95-20869
FOSTER, PATRICIA p 1283 N95-21514
FOUNTAIN, A. W., III p 1237 N95-20470
FOURNIER, MICHEL p 1294 N95-20932
FOWLER, JOHN W. p 1592 N95-21750
FOWLER, R. F. p 1475 N95-20435
FOWLER, T. K. p 1562 N95-22221
FOX, J. L. p 1420 N95-21796
FRAAS, LEWIS M. p 1322 N95-20534
FRALICK, G. C. p 1367 N95-21889
FRAME, CHARLES E., JR. p 1451 N95-20041
FRANCK, S. p 1417 N95-21783
p 1418 N95-21788
FRANCO, M. M. p 1305 N95-21542
FRANCOIS, A. p 1445 N95-21424
FRANK, HARRY A. p 1437 N95-19969
FRANK, MICHAEL R. p 1520 N95-21315
FRANK, WILLIAM M. p 1429 N95-20391
FRANKLE, C. M. p 1519 N95-21237
p 1530 N95-22435
FRANKLE, S. C. p 1509 N95-20236
FRANZ, J. A. p 1507 N95-20049
FRANZEN, D. L. p 1540 N95-19976
FRAUNIE, PH. p 1350 N95-21086
FREDELL, ROBERT S. p 1199 N95-22046
FREE, NANCY C. p 1588 N95-20617
FREEMAN, A. J. p 1265 N95-20115
FREI, ULRICH p 1397 N95-22362
FREITAS, JOHN E. p 1241 N95-21124
FRENKLACH, MICHAEL p 1247 N95-22150
FREUND, BEAU J. p 1446 N95-22004
FREUND, F. p 1364 N95-20233
FREUND, HENRY P. p 1331 N95-21671
FREUND, R. W. p 1355 N95-21726
p 1469 N95-21744
FREUNDLICH, A. p 1316 N95-20508
p 1318 N95-20517
FRIBERG, STIG p 1226 N95-20092
FRIEBELE, E. J. p 1545 N95-21825
FRIEDMAN, A. p 1552 N95-20318
FRIEDMAN, H. W. p 1368 N95-19986
FRIEDRICH, R. p 1347 N95-21067
FRIESEN, J. A. p 1465 N95-21153
FRONT, KAI p 1427 N95-22095
FROST, C. A. p 1290 N95-20474
FRY, R. A. p 1238 N95-20555
FRYE, DANIEL E. p 1436 N95-22209
FRYE, G. C. p 1564 N95-20087
FRYE, P. E. p 1395 N95-21530
p 1222 N95-21531
FU, C. L. p 1262 N95-22344
FUCHS, HANS-HELLMUTH p 1299 N95-20960
FUCIARELLI, DAVID A. p 1351 N95-21090
FUERSCHBACH, P. W. p 1378 N95-20048
FUESS, T. A. p 1527 N95-22194
FUJIMOTO, JAMES G. p 1373 N95-21195
FUJIWARA, M. p 1245 N95-21845
FUKUYAMA, A. p 1554 N95-20683
FULLER, G. M. p 1604 N95-20383
FULLER, J. J. p 1415 N95-21308
FULLERTON, ERIC E. p 1571 N95-21256
FULTON, JAMES P. p 1383 N95-20764
FUNG, ADRIAN K. p 1311 N95-22401
FUNG, P. P. p 1439 N95-21544
FUNK, ERIC E. p 1292 N95-20825
FURLANETTO, M. R. p 1244 N95-21524
FURMAN, EUGENE p 1546 N95-22043
FURTAK, T. E. p 1391 N95-20118

G

GABOR, A. M. p 1268 N95-20472
GADDY, EDWARD p 1316 N95-20503
GADOLIN, R. E. p 1446 N95-21989
GAGE, DOUGLAS W. p 1313 N95-20280
GAGE, EDWARD C. p 1456 N95-22400
GAGNON, DAVE p 1289 N95-19997
GAILEY, P. C. p 1439 N95-21548
GAILLOUX, M. p 1260 N95-21923
GAKKESTAD, J. p 1455 N95-22018
GAL, A. p 1521 N95-21484
GALLEGOS, R. R. p 1328 N95-21139
GAMBINO, RICHARD J. p 1567 N95-20461
GAMMEL, J. T. p 1565 N95-20330
p 1526 N95-21934
p 1578 N95-22297
GANDHI, A. p 1349 N95-21078
GANGARAJ, S. K. p 1480 N95-20083
p 1490 N95-20588
GANNON, TERRY p 1489 N95-20259
GAO, H. p 1508 N95-20133
GAO, JIJIN p 1563 N95-19978
GAO, XIUQING p 1563 N95-19978
GARCIA, A. E. p 1438 N95-21366
GARCIA, LUCY p 1453 N95-21566
GARCIA, M. p 1528 N95-22222
p 1528 N95-22223
GARCIA, R. p 1557 N95-21207
GARDIN, D. E. p 1259 N95-21707
GARDINER, WILLIAM C. p 1247 N95-22150
GARDNER, BARBARA M. p 1321 N95-20527
GARDNER, D. R. p 1474 N95-20150
GARDNER, T. J. p 1261 N95-22119
GARINO, TERRY p 1333 N95-21881
GARLAND, JENNIFER p 1217 N95-21894
GARTLING, DAVID K. p 1463 N95-20887
GARTSIDE, JAMES p 1357 N95-22173
GAUL, ERHARD W. p 1374 N95-21480
GAUTHIER, F. p 1300 N95-20961
GAVALER, JOHN R. p 1331 N95-21693
GAVEL, D. T. p 1412 N95-19985
GAVER, ERIC p 1211 N95-20646
GAVIN, S. p 1524 N95-21641
GAVIN, SEAN p 1523 N95-21588
GAVRILA, IOA p 1482 N95-21267
GAY, T. J. p 1523 N95-21587
GEHLING, RUSSELL N. p 1322 N95-20532
GEIS, JACK p 1321 N95-20530
GEISER, URS p 1567 N95-20479
GEIST, G. A. p 1475 N95-20366
p 1477 N95-21556
p 1455 N95-21607
GELFAND, ALAN E. p 1499 N95-21945
p 1499 N95-21946
GELINAS, R. J. p 1376 N95-22301
GEMMELL, D. S. p 1522 N95-21502
GENSER, K. p 1529 N95-22314
GENTNER, DEDRE p 1450 N95-22052
GENTRY, S. M. p 1371 N95-20832
GENTZLINGER, ROBERT C. p 1379 N95-20627
GEOHEGAN, D. B. p 1369 N95-20221
p 1559 N95-21547
GEORGANTOPOULOS, G. A. p 1352 N95-21096
GEORGE, E. P. p 1250 N95-20020
GERDES, D. p 1522 N95-21499
GERIG, R. p 1538 N95-21733
GERSHMAN, V. p 1212 N95-20651
GERSTENBERG, H. p 1232 N95-22130
GERTH, R. p 1472 N95-22305
GERTH, ROB p 1465 N95-21025
GEURTS, A. J. p 1497 N95-22379
GEURTS, BERNARD p 1347 N95-21066
GEYER, H. K. p 1392 N95-20480
GHANBARI, CHERLY p 1394 N95-21353
GHARIB, MORTEZA p 1200 N95-20177
GHOSAL, S. p 1346 N95-21062
GHOSAL, SANDIP p 1359 N95-22445
p 1360 N95-22446
GHOSH, S. K. p 1592 N95-21752
GHOSH, V. J. p 1566 N95-20382
GIBSON, ELIZABETH G. p 1457 N95-20060
GIBSON, GARTH A. p 1463 N95-20846
GIBSON, PHILLIP p 1357 N95-22206
GIER, RICK p 1453 N95-21566
GIERMAN, S. M. p 1376 N95-22154
GIESKE, JOHN H. p 1383 N95-22202
GIFFORD, LISA A. p 1402 N95-20441
p 1408 N95-21689
p 1408 N95-21696
GIL, YOLANDA p 1589 N95-21002
GILCHRIST, J. p 1501 N95-20241
GILG, LARRY p 1383 N95-21933
GILGENBACH, R. M. p 1531 N95-19974
GILL, S. P. p 1395 N95-21530
p 1222 N95-21531
GILLEN, K. T. p 1263 N95-19926
GILLESPIE, GEORGE H. p 1531 N95-20203
GILLESPIE, JOHN W., JR. p 1224 N95-19899
GILMOUR, THOMAS A. p 1378 N95-20295
GINATEMPO, B. p 1566 N95-20405
GIORGIO, PAUL J. p 1476 N95-21307
p 1476 N95-21496
p 1476 N95-21504
p 1478 N95-22090
p 1591 N95-22098
p 1478 N95-22146
GIPPIUS, A. A. p 1570 N95-20820
GIULIANI, J. L., JR. p 1533 N95-20672
p 1537 N95-21494
GIULIETTI, A. p 1373 N95-21226
GIULIETTI, D. p 1373 N95-21226
GIUSE, DARIO A. p 1461 N95-20623
GIZZI, L. A. p 1373 N95-21226
GLADDINES, HELMA p 1494 N95-21956
GLASS, CHRISTOPHER E. p 1200 N95-20688
GLASS, J. T. p 1568 N95-20614
GLASSMAN, ARTHUR J. p 1214 N95-22341
GLENDENNING, NORMAN K. p 1599 N95-20873
GLENN, DENNIS P. p 1433 N95-21291
GLENN, FLOYD p 1453 N95-21691
GLICKMAN, RANDOLPH D. p 1443 N95-20848
GLIEBE, P. R. p 1505 N95-21888
GLUCH, DAVID P. p 1457 N95-19999
GLUSKIN, E. p 1541 N95-20103
GLUTSCH, S. p 1582 N95-22237
GLYNN, G. p 1212 N95-20653
GOBBY, P. L. p 1558 N95-21368
GODWIN, D. S. p 1287 N95-21631
GOEBEL, D. M. p 1314 N95-20311
GOEDEKE, A. D. p 1287 N95-21598
GOHIL, P. p 1550 N95-20146
p 1556 N95-21163
GOLDAK, J. A. p 1381 N95-22268
GOLDBERG, JACK p 1484 N95-22203
GOLDEN, DAVID M. p 1247 N95-22150
GOLDMAN, TERRANCE p 1526 N95-22058
GOLDSMITH, J. E. M. p 1413 N95-20397
GOLDSMITH, ROBERT L. p 1275 N95-21354
GOLDSTEIN, J. C. p 1376 N95-22154
GOLDSTONE, J. A. p 1387 N95-21386
GOMEZ, V. M. p 1558 N95-21368
GONCHAROV, A. p 1418 N95-21791
GONCHARUK, O. B. p 1229 N95-20859
GONG, W. p 1520 N95-21357
GONG, X. G. p 1260 N95-21855
GONIS, A. p 1262 N95-22313
GONSALVES, KENNETH E. p 1568 N95-20552
GONSALVES, R. A. p 1545 N95-21832
GONSALVES, ROBERT A. p 1593 N95-21755
GONZALES-MARTIN, A. p 1252 N95-20299
GONZALEZ, CARLOS R. p 1215 N95-19955
GOOD, BRIAN S. p 1322 N95-20536
GOODFELLOW, R. C. p 1212 N95-20653
GOODMAN, D. W. p 1234 N95-20052
GOODMAN, M. C. p 1604 N95-21475
GOODMAN, STEPHAN p 1415 N95-21308
GOODNER, K. L. p 1241 N95-21123
GOODSON, TROY D. p 1222 N95-21616
GOODWIN, G. M. p 1257 N95-21555
GOODWIN, M. J. p 1212 N95-20653
GOODWIN, MICHAEL J. p 1408 N95-21685
GOODWIN, THOMAS A. p 1317 N95-20510
GOPALAN, K. p 1402 N95-20247
GOPALSAMI, N. p 1402 N95-20247
GORADIA, C. p 1317 N95-20509
GORADIA, M. p 1317 N95-20509
GORDNER, NANNETTE p 1429 N95-20857
GORDON, R. C. p 1483 N95-21710
GORDON, SANFORD p 1235 N95-20180
GORETTA, K. C. p 1570 N95-20841
GORTON, L. C. p 1442 N95-20602
GOSHCHITSKII, B. N. p 1232 N95-22130
GOSLING, J. T. p 1603 N95-21377
GOSNELL, T. R. p 1375 N95-22007

GOSSARD, ARTHUR C. p 1333 N95-21917
GOSZTOLA, DAVID p 1437 N95-19969
GOTOH, T. p 1343 N95-21046
GOUDREAU, G. L. p 1354 N95-21387
GOUGE, MICHAEL J. p 1376 N95-22169
GOULD, N. I. M. p 1495 N95-22317
GOULIANOS, K. p 1515 N95-20879
GOUTELARD, C. p 1294 N95-20930
p 1298 N95-20954
GOUTORBE, T. p 1349 N95-21077
GOUWELEEUW, JOSE M. p 1383 N95-21961
GOVIL, R. p 1374 N95-21528
GOWERS, W. T. p 1489 N95-20273
p 1495 N95-22147
GOYAL, A. p 1571 N95-21167
p 1578 N95-22269
GRABEL, J. V. p 1285 N95-20050
GRACH, PETER p 1241 N95-21168
p 1328 N95-21169
GRAHAM, R. A. p 1268 N95-20396
GRANACKI, JOHN p 1328 N95-20997
GRANT, CHARLES p 1353 N95-21182
GRANT, K. A. p 1402 N95-20353
GRANT, K. E. p 1413 N95-20354
GRANT, KEITH E. p 1402 N95-20355
GRANTHAM, D. D. p 1430 N95-20974
GRASER, M. p 1544 N95-21392
GRASSMANN, H. p 1515 N95-20880
GRASTATARO, C. p 1231 N95-22009
GRATE, JAY W. p 1279 N95-22057
GRAVES, CAROLYN E. p 1257 N95-21452
GRAVES, J. A. p 1225 N95-20001
GRAY, G. T., III p 1251 N95-20122
p 1262 N95-22289
GRAY, J. A. p 1244 N95-21524
GRAY, SIMON p 1301 N95-21277
GREEN, A. A. p 1530 N95-22435
GREEN, D. J. p 1276 N95-21572
GREEN, JOHN E. p 1199 N95-19946
GREEN, JOHN L. p 1250 N95-20067
GREEN, L. L. p 1206 N95-20370
GREENBAUM, S. G. p 1330 N95-21490
GREENBERG, IRA p 1484 N95-22203
GREENBERG, K. E. p 1560 N95-21609
GREENE, C. H. p 1581 N95-21842
GREENE, JOHN M. p 1558 N95-21345
GREENFIELD, C. M. p 1556 N95-21142
GREENHALGH, SAMUEL p 1201 N95-21864
GREENHILL, LYN M. p 1381 N95-21692
p 1381 N95-21705
GREENLEAF, J. E. p 1439 N95-21544
GREENLY, J. B. p 1535 N95-21328
p 1560 N95-21668
GREENOUGH, C. p 1475 N95-20435
GREENSPAN, H. p 1304 N95-21537
GREENWAY, R. B., JR. p 1467 N95-21389
GREENWOOD, L. R. p 1529 N95-22280
GREER, L. C., III p 1366 N95-21259
GREGG, M. C. p 1434 N95-21461
GREGORY, D. C. p 1507 N95-20086
GRELACH, LOTHAR p 1321 N95-20531
GRETH, RICKY L. p 1452 N95-20973
GRETHLEIN, A. p 1314 N95-20339
GRETHLEIN, H. p 1282 N95-19927
GRICE, M. E. p 1510 N95-20327
p 1517 N95-21127
p 1525 N95-21878
p 1246 N95-22000
GRICE, M. EDWARD p 1239 N95-20668
GRIESSHABER, E. p 1418 N95-21789
GRIFFIN, JERRY H. p 1379 N95-20795
GRIFFIN, M. J. p 1453 N95-21700
GRIFFIN, P. J. p 1509 N95-20206
GRIMES, R. W. p 1234 N95-20135
GRIMSON, ERIC p 1468 N95-21495
GRISHAM, L. R. p 1557 N95-21240
GRISSOM, MELISSA p 1274 N95-21234
GROEBNER, R. J. p 1552 N95-20334
p 1556 N95-21142
p 1556 N95-21163
GROENBOOM, H. M. p 1468 N95-21455
GROENEWEG, J. p 1492 N95-21421
GROSS, THOMAS p 1475 N95-20500
GROSS, THOMAS F. p 1433 N95-20433
GROSSBECK, M. L. p 1261 N95-22123
GROSSBERG, STEPHEN p 1449 N95-20845
GROSSMAN, A. S. p 1402 N95-20353
p 1413 N95-20354
GROSSMAN, ALLEN S. p 1402 N95-20355
GROSSMAN, ARTHUR R. p 1440 N95-22066
GROSSMAN, J. W. p 1393 N95-20864
GROTE, D. P. p 1552 N95-20318
GROTE, JAMES p 1546 N95-21975
GROVES-KIRKBY, C. J. p 1212 N95-20653
GRUEN, D. M. p 1570 N95-20881
GRUENER, G. p 1262 N95-22291
GRUIJTERS, N. p 1594 N95-19939
GRUMBERG, O. p 1472 N95-22305
GRUNE, D. p 1471 N95-22029
GRUNE, G. L. p 1268 N95-20428
GRUNTHANER, F. J. p 1367 N95-21507
GU, SHI-WEI p 1528 N95-22218
GU, SHIWEI p 1577 N95-22176
p 1502 N95-22177
GUAN, XIN-AN p 1548 N95-22255
GUENTHER, C. p 1341 N95-20831
GUEZ, ALLON p 1452 N95-20562
GUIDO, L. J. p 1324 N95-20543
GUIDOTTI, RONALD A. p 1325 N95-20628
GUILINGER, T. R. p 1364 N95-20398
GUINEE, E. P. p 1410 N95-22125
GULEC, K. p 1559 N95-21581
GULLIKSON, E. p 1274 N95-21175
GUNDERSEN, MARTIN A. p 1324 N95-20610
GUNNER, M. R. p 1440 N95-22075
GUNZBURGER p 1464 N95-21010
GUNZBURGER, MAX D. p 1479 N95-20010
GUO, WEIPING p 1466 N95-21288
GUO, X. p 1567 N95-20448
p 1567 N95-20449
p 1520 N95-21360
GUO, Y. p 1344 N95-21050
p 1348 N95-21074
GUPTA, R. p 1510 N95-20367
GURAV, A. p 1239 N95-20712
GURMAN, ERNEST B. p 1447 N95-22040
GUST, STEVEN p 1398 N95-22425
GUSTAFSON, J. p 1458 N95-20136
GWEON, G. H. p 1574 N95-21712

H

HAAS, P. A. p 1247 N95-22049
HAASE, D. G. p 1519 N95-21237
HABIB, S. p 1488 N95-20169
p 1580 N95-21264
p 1539 N95-22243
HABIBOLLAHZADEH, DARIUSH p 1246 N95-22000
HACHE, JOSEPH J. p 1310 N95-22251
HACK, J. J. p 1407 N95-21608
HADID, A. H. p 1346 N95-21060
HAEKKINEN, TARJA p 1232 N95-22158
HAEMAELAEINEN, M. p 1263 N95-22374
HAEMAELAEINEN, MARKO p 1255 N95-21111
HAEMAELAEINEN, R. P. p 1464 N95-20982
HAEMERS, W. H. p 1488 N95-19943
HAENNINEN, HANNU p 1255 N95-21128
HAERTLING, GENE p 1546 N95-22043
HAFFMANS, A. F. p 1563 N95-19925
p 1533 N95-20766
p 1533 N95-20886
p 1517 N95-21140
HAFICH, M. J. p 1259 N95-21838
HAGANS, K. p 1550 N95-20190
p 1557 N95-21207
HAGEN, M. p 1456 N95-19928
p 1465 N95-21231
p 1466 N95-21232
HAGERTY, JAMES D. p 1336 N95-22418
HAGGERTY, J. S. p 1275 N95-21289
HAGGERTY, JAMES J. p 1594 N95-21893
HAHN, C. J. p 1431 N95-22288
HAIGHT, R. C. p 1529 N95-22280
HAIGHT, TIMOTHY A. p 1485 N95-22244
HAIGLER, K. J. p 1206 N95-20370
HAILEY, C. J. p 1543 N95-20612
HAKES, CHARLES L. p 1412 N95-20278
HAKIM, E. B. p 1209 N95-20640
HALANI, A. p 1317 N95-20512
HALDAR, PRADEEP p 1336 N95-22271
HALFORD, GARY R. p 1385 N95-20179
HALL, C. M. p 1246 N95-21886
HALL, CLINT A. p 1215 N95-20223
HALL, E. THOMAS, JR. p 1268 N95-20410
HALL, J. P. p 1212 N95-20653
HALL, MELINDA M. p 1433 N95-20458
HALLE, LINDA F. p 1575 N95-21916
HALLER, E. E. p 1568 N95-20630
HALLIDAY, A. N. p 1246 N95-21886
HALLIDAY, I. p 1537 N95-21647
HALLIKAINEN, MARTTI p 1220 N95-21026
HALLMAN, T. p 1520 N95-21357
HALPIN, J. p 1376 N95-22121
HAMAKER, JOSEPH W. p 1583 N95-20742
HAMEIRI, E. p 1602 N95-20593
HAMERS, R. J. p 1567 N95-20544
p 1513 N95-20585
p 1513 N95-20586
HAMERS, ROBERT J. p 1568 N95-20594
HAMILL, T. G. p 1210 N95-20641
HAMILL, THOMAS M. p 1292 N95-20904
HAMILTON, C. H. p 1251 N95-20090
HAMILTON, MARGARET L. p 1256 N95-21286
HAMILTON, W. p 1281 N95-22434
HAMMOND, PAULA T. p 1267 N95-20328
HAMMOND, RUSSELL E. p 1326 N95-20730
HAMPDEN-SMITH, M. p 1248 N95-22385
HAMPDEN-SMITH, M. J. p 1224 N95-20660
HAMPDEN-SMITH, MARK J. p 1270 N95-20689
p 1239 N95-20712
p 1569 N95-20714
HAN, HUAI-YUE p 1380 N95-21446
HANCOCK, J. A. p 1320 N95-20524
HAND, U. p 1483 N95-21710
HANDLER, ROBERT A. p 1348 N95-21076
HANE, THOMAS H. p 1339 N95-20297
HANEY, S. W. p 1548 N95-20037
HANFLAND, M. p 1418 N95-21791
HANKEY, J. p 1212 N95-20653
HANNA-HAWVER, PAMELA D. p 1441 N95-20408
HANNAH, PHILIP R. p 1285 N95-20288
HANNON, MARGARET H. p 1318 N95-20513
HANNULA, S. P. p 1262 N95-22174
HANRAHAN, R. J., JR. p 1252 N95-20365
HANSEN, E. W. M. p 1356 N95-22017
HANSEN, JAMES P. p 1307 N95-21908
HANSON, D. L. p 1535 N95-21328
HANSON, K. M. p 1459 N95-20165
HANSON, L. L. p 1276 N95-21644
HANSON, P. J. p 1411 N95-22342
HANSON, RONALD K. p 1247 N95-22150
HANSSON, S. G. p 1288 N95-21978
HARDIN, D. p 1459 N95-20255
HARDY, R. D. p 1386 N95-20833
HARFOUSH, F. p 1463 N95-20901
HARMAN, WILLIAM H. p 1291 N95-20599
HARMS, G. A. p 1509 N95-20206
HARP, BRIAN p 1462 N95-20718
HARPER, D. A. p 1593 N95-21763
HARRIMAN, WALTER L. p 1544 N95-21100
HARRIS, F. I. p 1203 N95-21831
HARRIS, J. H. p 1551 N95-20205
HARRIS, JOEL M. p 1240 N95-20780
HARRIS, R. M. p 1523 N95-21563
HARRIS, S. E. p 1372 N95-21144
HARRISON, L. p 1412 N95-20116
HARRISON, R. W. p 1378 N95-20085
HARTE, J. A. p 1533 N95-20784
HARTMAN, LEO B. p 1497 N95-19914
HARVEY, R. W. p 1549 N95-20113
HASH, G. L. p 1314 N95-20338
p 1334 N95-22086
HASHIZUME, K. p 1418 N95-21790
HASS, BRIAN L. p 1601 N95-21621
HASSINEN, PERTTI p 1427 N95-22095
HASTE, G. R. p 1551 N95-20205
HATAY, FERHAT F. p 1348 N95-21073
HATCH, DOUGLAS J. p 1285 N95-20288
HAUER, A. p 1371 N95-20786
HAUN, R. p 1252 N95-20331
HAUSLADEN, M. C. p 1234 N95-20046
HAVELAAR, A. H. p 1405 N95-21330
HAWKINS, ANTHONY p 1208 N95-20633
p 1210 N95-20642
HAWKINS, C. F. p 1330 N95-21545
p 1334 N95-22118
HAWLEY, M. p 1287 N95-21631
HAWRYLUK, R. J. p 1557 N95-21239
p 1557 N95-21240
HAWSEY, ROBERT A. p 1336 N95-22271
HAXTON, W. C. p 1526 N95-21920
p 1604 N95-22085
HAYDEN, LINDA p 1475 N95-20618
HAYDOCK, ROGER p 1544 N95-20876
HAYDUK, MICHAEL p 1369 N95-20378
HAYDUK, MICHAEL J. p 1581 N95-21928
HAYES, A. B. p 1243 N95-21472
HAYES, HALFORD I. p 1504 N95-20963
HAYES, WILL p 1468 N95-21627
HAYNES, F. D. p 1287 N95-21626
HAYNES, W. B. p 1334 N95-22011
HAYNES, W. M. p 1582 N95-22153
HAYTER, JOHN B. p 1538 N95-22117
HAYWOOD, S. p 1518 N95-21222
HAZELTON, ROBERT C. p 1551 N95-20232
HAZUCHA, MILAN J. p 1444 N95-20979
HE, QIBING p 1556 N95-21164
HEALY, DENNIS M., JR. p 1290 N95-20545
HEARST, J. R. p 1460 N95-20351
HEATON, HARRY p 1213 N95-22024
HEBNER, G. p 1371 N95-20867
HEBNER, G. A. p 1369 N95-20225
p 1560 N95-21609
HECHT, LAURA M. p 1587 N95-20162
p 1589 N95-21015
HECHT, M. H. p 1367 N95-21507
HEFFELFINGER, GRANT S. p 1477 N95-21843

HEGARTY, JAMES p 1292 N95-20904
HEGEDUS, CHARLES R. p 1274 N95-21154
p 1274 N95-21155
HEGEDUS, S. S. p 1394 N95-21294
HEIDBRINK, W. W. p 1550 N95-20146
HEIJENK, GEERT J. p 1308 N95-22087
HEIKKILA, BRYANT p 1593 N95-21762
HEILBRONN, L. p 1520 N95-21357
HEILES, C. E. p 1594 N95-21771
HEILL, L. K. p 1577 N95-22166
HEISE, J. A. p 1314 N95-20338
HELGESON, W. D. p 1328 N95-21139
HELIE, P. p 1208 N95-20634
HELM, R. p 1519 N95-21262
HELOU, GEORGE p 1593 N95-21761
p 1593 N95-21765
HEMLEY, R. J. p 1417 N95-21786
p 1418 N95-21791
HEMMER, M. p 1532 N95-20336
HENAGER, C. H., JR. p 1232 N95-22115
HENDERSON, CHRISTOPHER L. p 1314 N95-20286
HENDERSON, G. L. p 1480 N95-20607
HENDERSON, LESLIE J., JR. p 1266 N95-20291
HENDRICKS, GERALD K. p 1217 N95-22413
HENDRICKS, J. S. p 1508 N95-20160
p 1509 N95-20236
p 1509 N95-20254
HENDRICKS, K. J. p 1329 N95-21395
HENDRICKS, KYLE J. p 1327 N95-20905
HENDRICKSON, B. p 1529 N95-22315
HENDRICKSON, J. T. p 1207 N95-20772
HENESIAN, M. p 1531 N95-20120
HENINS, I. p 1560 N95-21668
HENNEKE, K. p 1291 N95-20697
HENNINGSON, D. S. p 1349 N95-21079
HENRY, WENDELL A. p 1457 N95-19961
HENSHALL, G. A. p 1232 N95-22126
HENSLEY, W. K. p 1458 N95-20153
HENSON, TAMMY D. p 1302 N95-21448
HERBSLEB, JAMES p 1468 N95-21567
HERMAN, R. G. p 1235 N95-20188
HERMANN, A. M. p 1268 N95-20472
HERMANN, J. p 1562 N95-22377
HERMANS, A. J. p 1356 N95-22063
HEROLD, K. E. p 1211 N95-20647
HERREWYN, J. p 1209 N95-20635
HERTEL, E. S., JR. p 1384 N95-20077
p 1488 N95-20141
HERTEL, EUGENE S., JR. p 1387 N95-21396
HERVIG, RICHARD L. p 1420 N95-21799
HERWIG, LLOYD O. p 1392 N95-20473
HESSELINK, H. W. K. p 1468 N95-21455
HESTER, R. p 1267 N95-20350
HEWETT, J. L. p 1519 N95-21250
HICKERNELL, R. K. p 1540 N95-19976
HICKEY, JOHN R. p 1321 N95-20528
HICKS, D. L. p 1341 N95-20831
HICKS, L. D. p 1272 N95-20892
HICKS, Y. R. p 1214 N95-21383
HIETALA, V. M. p 1545 N95-21509
HIGUERA, F. J. p 1249 N95-21036
p 1249 N95-21037
HIHKIOE, M. p 1275 N95-21275
HILARIS, ALEXANDER E. p 1462 N95-20776
HILDNER, M. L. p 1272 N95-20895
HILL, BARRY W. p 1531 N95-20203
HILL, D. A. p 1289 N95-20191
HILL, D. CHRISTOPHER p 1361 N95-22453
HILLARD, G. BARRY p 1321 N95-20529
HILLIS, D. L. p 1552 N95-20334
HILLS, J. S. p 1320 N95-20524
HILSENBECK, S. p 1258 N95-21568
HINGERTY, B. E. p 1439 N95-21606
HINGST, W. R. p 1338 N95-19953
HINKLEY, JEFFREY A. p 1383 N95-20616
HINRICHSEN, E. L. p 1288 N95-21651
HINSHELWOOD, D. D. p 1535 N95-21328
HINTON, F. L. p 1555 N95-21141
p 1558 N95-21299
HIRSCHMUGL, C. J. p 1367 N95-21638
HIRSCHON, A. S. p 1237 N95-20438
HIRST, DONALD J. p 1274 N95-21154
p 1274 N95-21155
HIRVONEN, J. P. p 1255 N95-21238
p 1262 N95-22174
HIRVONEN, J.-P. p 1281 N95-22428
HITCHCOCK, L. p 1203 N95-21518
HITNEY, HERBERT V. p 1295 N95-20936
HITTI, B. p 1529 N95-22303
HIYAGON, H. p 1416 N95-21780
p 1419 N95-21792
p 1422 N95-21807
p 1425 N95-21824
HJALMARSON, H. P. p 1328 N95-21139
HO, D. D. M. p 1533 N95-20784
HO, L. p 1401 N95-20192
HO, PAULINE p 1562 N95-22225
HOANG, TY p 1205 N95-21891
HOBAN, FRANCIS T. p 1583 N95-20739
HOCHSTEIN, JOHN I. p 1353 N95-21317
HODGE, JOHN D. p 1584 N95-20743
HODGES, WILLIAM T. p 1200 N95-20688
HODKO, D. p 1252 N95-20299
HOELDER, J. S. p 1579 N95-20028
HOERBERG, U. p 1452 N95-21467
HOERING, A. p 1526 N95-21920
HOERING, T. C. p 1416 N95-21781
HOFFENBERG, R. p 1201 N95-21031
HOFFER, J. K. p 1555 N95-21115
HOFFMAN, EDWARD J. p 1583 N95-20739
HOFFMAN, N. M. p 1554 N95-20675
HOFFMAN, RICHARD W., JR. p 1322 N95-20537
HOFFMANN, GUY p 1351 N95-21087
HOFFMANN, W. p 1570 N95-20820
HOFMANN, S. E. p 1482 N95-21429
p 1482 N95-21430
HOGAN, J. T. p 1551 N95-20205
p 1552 N95-20334
HOGAN, ROY E. p 1463 N95-20887
HOGUE, H. H. p 1524 N95-21646
HOKIN, S. p 1549 N95-20114
HOLBOURN, P. E. p 1210 N95-20641
HOLCOMB, R. S. p 1378 N95-20085
HOLLAND, E. A. p 1297 N95-20949
HOLLAND, ELIZABETH p 1425 N95-21833
HOLLAND, SCOTT D. p 1340 N95-20619
HOLLANDER, MARK G. p 1534 N95-21236
HOLLEN, G. Y. p 1501 N95-20246
HOLLOWAY, PAUL H. p 1541 N95-20066
HOLMGREN, M. p 1387 N95-21557
HOLT, J. A. p 1539 N95-22192
HOLTER, G. M. p 1406 N95-21487
HOLTKAMP, I. S. p 1589 N95-20818
HOLY, X. p 1445 N95-21424
HOLZHAUER, DOUGLAS J. p 1209 N95-20637
HOMBURG, A. J. p 1492 N95-21318
HOMER, M. L. p 1367 N95-21507
HONARY, B. p 1293 N95-20926
HONDA, M. p 1419 N95-21793
HONKANEN, J. p 1300 N95-20980
HONNELL, DAVID p 1409 N95-21914
HOOGERWOORD, R. R. p 1471 N95-22094
HOOIE, DIANE TRAUB p 1395 N95-21361
HOOMAN, J. p 1472 N95-22351
HOOPER, E. B. p 1559 N95-21451
HOOPER, J. p 1301 N95-21292
HOOVER, D. N. p 1462 N95-20691
HOPFINGER, EMIL p 1354 N95-21583
p 1354 N95-21584
p 1358 N95-22424
HOPKINS, D. J. p 1327 N95-20854
HOPPER, JAMES p 1213 N95-22024
HORNER, G. S. p 1314 N95-20341
HOROWITZ, BARRY M. p 1462 N95-20721
HORTON, J. A. p 1250 N95-20020
p 1250 N95-20043
HOSHINO, K. p 1555 N95-20988
p 1559 N95-21451
HOSOKAWA, J. p 1277 N95-21714
HOTCHANDANI, S. p 1570 N95-20838
HOU, L. S. p 1479 N95-20010
HOU, P. Y. p 1256 N95-21260
HOUGHTON, D. C. p 1565 N95-20245
p 1568 N95-20674
HOULBERG, W. A. p 1560 N95-21702
HOURAHAN, G. C. p 1287 N95-21631
HOUSER, R. M. p 1393 N95-20864
HOWARD, A. J. p 1327 N95-20882
p 1242 N95-21309
p 1329 N95-21390
p 1329 N95-21394
p 1572 N95-21419
HOWARD, CELESTE M. p 1216 N95-20992
HOWARD, J. B. p 1241 N95-21280
HOWARD, M. E. p 1391 N95-22398
HOWE, BRUCE M. p 1436 N95-21987
HOWE, G. p 1552 N95-20362
HOWELL, A. p 1582 N95-22054
HOWITT, D. G. p 1266 N95-20281
HSING, W. W. p 1531 N95-20015
p 1558 N95-21368
HSU, DONALD P. p 1224 N95-22252
HSUEH, C. H. p 1264 N95-20024
p 1271 N95-20704
HU, J. p 1570 N95-20841
p 1286 N95-21027
HUANG, H. p 1520 N95-21357
HUANG, H. S. p 1234 N95-20107
HUANG, J. p 1305 N95-21541
HUANG, K. G. p 1540 N95-19968
HUANG, YUN-YAO p 1289 N95-19973
HUBBARD, C. R. p 1385 N95-20374
HUBBARD, R. F. p 1535 N95-21328
HUBBE, J. M. p 1364 N95-20320
HUBER, T. M. p 1245 N95-21845
HUDGENS, GERALD A. p 1452 N95-20625
HUFFMAN, B. T. p 1539 N95-22193
HUGDAL, BERIT p 1288 N95-22014
HUGENBERG, K. F p 1542 N95-20403
HUGENBERG, K. F. p 1542 N95-20489
HUGHES, P. p 1394 N95-20985
HUILLIER, A. L. p 1377 N95-22312
HUIZING, CORNELIS p 1459 N95-20258
HULL, ANDREW J. p 1386 N95-21212
HULL, J. R. p 1382 N95-22292
HUMER, K. p 1232 N95-22130
HUMMEL, JOHN R. p 1290 N95-20376
HUMMER, G. p 1438 N95-21366
HUMPHREYS, CAROLINE M. p 1200 N95-20758
HUMPHREYS, D. A. p 1548 N95-20037
HUNLEY, J. D. p 1217 N95-21894
HUNT, J. T. p 1534 N95-21209
HUNT, RICHARD K. p 1231 N95-22038
HUNT, RONALD D. p 1387 N95-21396
HUNTEN, D. M. p 1419 N95-21794
HUNTON, DON E. p 1412 N95-20278
HUPA, M. p 1242 N95-21282
HURLBERT, ANYA p 1459 N95-20157
HURT, TINA M. p 1410 N95-22142
HUSEONIA, W. F. p 1584 N95-20746
HUSER, ASMUND p 1348 N95-21073
HUSTON, ALAN L. p 1377 N95-22304
HUSZTHY, PETER p 1223 N95-20590
HUTCHBY, J. A. p 1316 N95-20507
HUTCHINS, J. p 1477 N95-21505
HUTSON, PETER M. p 1588 N95-20589
HUTTON, R. p 1508 N95-20133
HWANG, HYUN J. p 1241 N95-21124
HWANG, S. L. p 1267 N95-20323
HYATT, A. W. p 1550 N95-20146
p 1553 N95-20445
HYDER, M. p 1235 N95-20215
HYLAND, DIANE T. p 1447 N95-22040
HYNES, MIKE V. p 1426 N95-21875

I

IBRAHEEM, S. O. p 1467 N95-21450
IDA, K. p 1555 N95-20989
IDZERDA, Y. p 1500 N95-20229
IDZERDA, Y. U. p 1238 N95-20555
IGARASHI, G. p 1419 N95-21795
IIJIMA, Y. p 1416 N95-21780
IKEDA, YUTAKA p 1361 N95-22454
ILMONIEMI, R. J. p 1447 N95-22371
ILMONIEMI, RISTO J. p 1329 N95-21326
p 1445 N95-21348
IMAZATO, J. p 1514 N95-20756
IMBRIALE, W. A. p 1304 N95-21538
IMTHURN, GEORGE P. p 1396 N95-21899
INGASON, HAUKUR p 1241 N95-21179
INGBER, M. S. p 1339 N95-20137
INTERRANTE, L. V. p 1223 N95-20033
INTZAND, JEAN J. M. p 1221 N95-22436
IOB, M. p 1471 N95-22104
IRWIN, J. p 1519 N95-21262
p 1536 N95-21334
IRWIN, JOHN p 1536 N95-21337
ISAACS, H. S. p 1250 N95-19979
ISOMAEKI, IIKKA p 1240 N95-21110
ITA, J. J. p 1421 N95-21802
ITOH, K. p 1554 N95-20683
p 1555 N95-20988
p 1555 N95-20989
ITOH, S. p 1554 N95-20683
p 1555 N95-20988
IVES, L. K. p 1379 N95-20984
IWAMOTO, NANCY E. p 1516 N95-21121
IYENGAR, S. S. p 1483 N95-21741
IYER, RAVI p 1209 N95-20636
IZATT, REED M. p 1223 N95-20590
p 1223 N95-20592

J

JACAK, BARBARA V. p 1520 N95-21321
JACKSON, C. G. R. p 1439 N95-21544
JACKSON, G. L. p 1556 N95-21142
JACKSON, H. J. p 1305 N95-21542
JACKSON, KAREN E. p 1229 N95-21008
JACKSON, M. E. p 1365 N95-20560
JACKSON, MITCHELL L. p 1265 N95-20226
JACKSON, ROBERT H. p 1331 N95-21671
JACOBS, BART p 1494 N95-21962
JACOBS, ERIC p 1470 N95-21971
JACOT-GUILLARMOD, R. p 1245 N95-21845

JACQMIN, DAVID ..... p 1338 N95-19952
JADUSZLIWER, B. ..... p 1307 N95-21985
JAGIELSKI, KURT D. ..... p 1400 N95-19964
JAIEBI, M. R. ..... p 1497 N95-19936
p 1497 N95-19938
JAIN, A. ..... p 1402 N95-20353
JAIN, M. K. ..... p 1282 N95-19927
p 1314 N95-20339
JAIN, R. K. ..... p 1319 N95-20518
p 1334 N95-22112
JAIN, RAJ K. ..... p 1318 N95-20516
JAKOSKY, B. M. ..... p 1420 N95-21796
JAMES, R. A. ..... p 1550 N95-20146
JAMESON, LELAND ..... p 1495 N95-22157
JAMESON, ROBERT A. ..... p 1531 N95-20203
JANARDAN, B. A. ..... p 1505 N95-21888
JANKOWSKI, A. F. ..... p 1267 N95-20317
p 1253 N95-20447
JANNEY, MARK A. ..... p 1265 N95-20226
JANNSON, TOMASZ ..... p 1272 N95-20962
JANOWITZ, MELVIN F. ..... p 1590 N95-21401
JANRODSETH, O. ..... p 1484 N95-22015
JANSEN, KENNETH ..... p 1202 N95-22448
JANSSEN, ROGER JOSEPH ANNA
p 1354 N95-21578
JANSSEN, WIL ..... p 1455 N95-21871
JANUS, ROBERT S. ..... p 1506 N95-22360
JARDIEU, RONALD J. ..... p 1334 N95-22023
JARRETT, ANDREW W. ..... p 1233 N95-22467
JARRETT, WILLIAM L. ..... p 1578 N95-22286
JASON, NORA H. ..... p 1286 N95-21129
p 1286 N95-21130
JASSBY, D. L. ..... p 1557 N95-21240
JAVAKHISHVILI, J. L. ..... p 1561 N95-21848
JEAN, Y. C. ..... p 1564 N95-20017
JEANLOZ, RAYMOND ..... p 1421 N95-21803
JEFFERSON, MICHAEL ..... p 1587 N95-20309
JELLISON, JAMES L. ..... p 1374 N95-21594
JENKINS, P. P. ..... p 1317 N95-20509
JENKINS, PHILLIP P. ..... p 1322 N95-20537
p 1323 N95-20538
JENNINGS, G. ..... p 1572 N95-21408
JENNINGS, G. R., JR. ..... p 1459 N95-20165
JENSEN, E. D. ..... p 1484 N95-22203
JENSEN, JAMES O. ..... p 1437 N95-20252
JENSEN, JANET L. ..... p 1437 N95-20252
JENSEN, R. E. ..... p 1431 N95-19895
JERVIS, T. R. ..... p 1255 N95-21238
JESSON, D. E. ..... p 1565 N95-20245
p 1568 N95-20674
JETT, J. H. ..... p 1440 N95-22296
JI, H. ..... p 1549 N95-20114
JIBB, D. J. ..... p 1212 N95-20653
JIMENEZ, J. ..... p 1344 N95-21049
JIMENEZ, JAVIER ..... p 1349 N95-21080
p 1362 N95-22459
p 1363 N95-22462
JOHANSSON, E. M. ..... p 1412 N95-19985
p 1301 N95-21205
JOHANSSON, PER-ERIK ..... p 1405 N95-21181
JOHN, BONNIE E. ..... p 1448 N95-19887
JOHNK, R. T. ..... p 1289 N95-20191
JOHNS, STEVEN ..... p 1369 N95-20378
JOHNSON, A. C. ..... p 1271 N95-20761
JOHNSON, A. K. ..... p 1401 N95-20089
JOHNSON, C. G. ..... p 1578 N95-22286
JOHNSON, D. D. ..... p 1566 N95-20405
JOHNSON, D. R. ..... p 1278 N95-21909
p 1278 N95-21937
JOHNSON, DANIEL L. ..... p 1454 N95-22045
JOHNSON, G. C. ..... p 1250 N95-19900
JOHNSON, KAREN L. ..... p 1303 N95-21493
JOHNSON, L. ..... p 1558 N95-21242
JOHNSON, L. C. ..... p 1557 N95-21240
JOHNSON, LEOPOLD J. ..... p 1326 N95-20730
JOHNSON, MARK ..... p 1450 N95-21968
JOHNSON, MELISSA D. ..... p 1262 N95-22308
JOHNSON, P. D. ..... p 1520 N95-21362
JOHNSON, R. E. ..... p 1420 N95-21796
JOHNSON, R. P. ..... p 1270 N95-20603
p 1388 N95-22411
JOHNSON, RANDY A. ..... p 1265 N95-20094
JOHNSON, RICHARD M. ..... p 1363 N95-20031
JOHNSON, RICHARD P. ..... p 1279 N95-22047
JOHNSON, S. A. ..... p 1392 N95-20480
JOHNSON, SCOTT D. ..... p 1471 N95-22133
JOHNSON, THOMAS A. ..... p 1279 N95-22047
JOHNSON, W. L. ..... p 1216 N95-20624
JOHNSTON, D. C. ..... p 1572 N95-21297
JOKILAAKSO, A. ..... p 1354 N95-21649
JONES, C. D. ..... p 1405 N95-21274
JONES, E. D. ..... p 1314 N95-20341
JONES, GUILFORD, II ..... p 1368 N95-20063
JONES, JACK ..... p 1211 N95-20648
JONES, JAMES R. ..... p 1290 N95-20376
JONES, L. ..... p 1312 N95-19958
p 1258 N95-21575
JONES, L. L. ..... p 1259 N95-21737
JONES, P. ..... p 1286 N95-20611
JONES, R. ..... p 1291 N95-20697
JONES, R. D. ..... p 1483 N95-21710
JONES, R. H. ..... p 1232 N95-22115
JONES, R. R. ..... p 1504 N95-21170
JONES, RANDOLPH M. ..... p 1216 N95-20624
JONES, RICHARD H. ..... p 1490 N95-20432
JONES, S. E. ..... p 1501 N95-20869
JONES, THOMAS E. ..... p 1577 N95-22137
JONG, R. A. ..... p 1550 N95-20146
p 1554 N95-20571
JONGBLOED, G. ..... p 1499 N95-21469
JORDAN, CHRISTINE M. ..... p 1411 N95-22414
JORDAN, DICK ..... p 1216 N95-20799
JORDAN, R. G. ..... p 1566 N95-20405
JOSEPH, JOHN C. ..... p 1433 N95-21291
JOSEPH, PHILIP J. ..... p 1433 N95-21291
JOSLIN, D. L. ..... p 1510 N95-20337
JOSYPENKO, MICHAEL J. ..... p 1306 N95-21672
JOU, JIING-YIH J. ..... p 1389 N95-20903
JUENGEN, F. J. ..... p 1586 N95-21982
JULES, KENOL ..... p 1201 N95-20794
JUNGST, R. G. ..... p 1324 N95-20626
JUNK, THOMAS R. ..... p 1519 N95-21248
JURGENS, T. ..... p 1463 N95-20901
JURISSON, KARL R. ..... p 1207 N95-20772
JURKOVICH, MARK S. ..... p 1200 N95-19991
JUSTUS, BRIAN L. ..... p 1576 N95-22059
p 1377 N95-22304

K

KAASSCHIETER, E. F. ..... p 1492 N95-21371
p 1244 N95-21573
KABANTSEV, A. A. ..... p 1562 N95-22282
KABEYA, H. ..... p 1277 N95-21714
KADIK, A. ..... p 1420 N95-21797
KAHN, MANFRED ..... p 1328 N95-21118
KAHN, S. M. ..... p 1543 N95-20612
KAISER, DAVID R. ..... p 1456 N95-22400
KAJOLA, MATTI ..... p 1445 N95-21348
KALANTAR, D. H. ..... p 1531 N95-20015
KALDELLIS, J. K. ..... p 1352 N95-21096
KALLURI, SREERAMESH ..... p 1385 N95-20179
KALOKITIS, DAVID ..... p 1326 N95-20824
KALTENBACH, HANS-JAKOB ..... p 1360 N95-22449
KAMAREDDINE, F. ..... p 1492 N95-21372
KAMAREDDINE, FAIROUZ ..... p 1488 N95-20149
KAMAT, P. V. ..... p 1570 N95-20838
KAMENY, IRIS M. ..... p 1591 N95-22069
KAMMEL, P. ..... p 1245 N95-21845
KAMMEYER, MARK ..... p 1341 N95-20849
KAMNA, M. M. ..... p 1365 N95-20413
p 1253 N95-20577
p 1241 N95-21217
KANAWATI, GHANI ..... p 1209 N95-20636
KANE, J. E., II ..... p 1366 N95-21138
KANE, M. ..... p 1397 N95-22183
KANG, SING B. ..... p 1474 N95-20325
KANG, SUNG-MO ..... p 1327 N95-20967
KANNARI, F. ..... p 1371 N95-20866
KANNE, W. R., JR. ..... p 1257 N95-21303
p 1382 N95-22356
KAO, Y. H. ..... p 1572 N95-21279
KAPLAN, D. B. ..... p 1512 N95-20451
KAPLAN, DANIEL M. ..... p 1521 N95-21378
KAPLAN, DAVID ..... p 1269 N95-20551
KAPLAN, T. ..... p 1565 N95-20244
KAPOOR, AJAI ..... p 1490 N95-20662
p 1470 N95-21974
KAPPEL, F. ..... p 1493 N95-21582
KAPUR, V. K. ..... p 1317 N95-20512
KARASOPOULOS, HARRY A. ..... p 1220 N95-22204
KARAVASSILIS, N. ..... p 1292 N95-20922
KARHU, SEPPO ..... p 1430 N95-21413
KARKUT, M. ..... p 1574 N95-21636
p 1575 N95-21949
KARKUT, M. G. ..... p 1577 N95-22166
KARLSSON, EDWARD ..... p 1405 N95-21181
KARLSSON, ULF ..... p 1434 N95-21320
KARNAUKHOV, S. ..... p 1581 N95-21639
KARNI, SMADAR ..... p 1495 N95-22325
KARNITZ, M. A. ..... p 1378 N95-20085
KARPENKO, V. ..... p 1557 N95-21207
KARPENKO, V. P. ..... p 1551 N95-20219
KARPPI, RISTO ..... p 1380 N95-21416
KASHIWA, B. A. ..... p 1339 N95-20166
KASHIWA, BRYAN A. ..... p 1478 N95-21925
KASIBHOTLA, V. ..... p 1374 N95-21694
KASINGER, CHARLES DARWIN p 1311 N95-22415
KASSOY, DAVID R. ..... p 1222 N95-21193
KATAYAMA, TAKESHI ..... p 1392 N95-20685
KATILA, T. ..... p 1443 N95-20971
KATOEN, JOOST-PIETER ..... p 1477 N95-21620
p 1478 N95-21869
KATZ, O. M. ..... p 1261 N95-22048
KATZ, ROBERT ..... p 1517 N95-21191
KATZNELSON, YONATAN R. ..... p 1496 N95-22354
KAUFFMAN, R. ..... p 1264 N95-20078
p 1522 N95-21506
KAUFFMAN, R. L. ..... p 1553 N95-20363
KAUKLER, WILLIAM ..... p 1543 N95-20798
KAULA, W. M. ..... p 1420 N95-21798
KAVARNOS, GEORGE J. ..... p 1506 N95-22360
KAWAI, N. ..... p 1221 N95-22436
KAWAI, Y. ..... p 1554 N95-20686
KAWAMOTO, TATSUHIKO ..... p 1420 N95-21799
KAY, EDWIN J. ..... p 1447 N95-22040
KAZEROONI, H. ..... p 1364 N95-20321
KAZI, TAUSEEF ..... p 1328 N95-20997
KE, LIU ..... p 1481 N95-20693
KEATHLEY, WILLIAM C. ..... p 1584 N95-20745
KEDEM, BENJAMIN ..... p 1504 N95-20300
KEENE, L. ..... p 1337 N95-22421
KEENEY, J. A. ..... p 1385 N95-20322
KEIRSEY, DAVID ..... p 1216 N95-20624
KEITH, WILLIAM L. ..... p 1357 N95-22208
KELKAR, ATUL, G. ..... p 1219 N95-20800
KELLER, A. ..... p 1268 N95-20392
KELLER, CHARLES F. ..... p 1426 N95-21875
KELLER, MICHAEL A. ..... p 1278 N95-21969
KELLER, TEDDY M. ..... p 1266 N95-20291
KELLERMAN, B. K. ..... p 1572 N95-21304
KELLEY, C. T. ..... p 1493 N95-21564
KELLEY, N. D. ..... p 1384 N95-20109
KELLMAN, A. G. ..... p 1548 N95-20037
KELLY, J. ..... p 1243 N95-21512
KELLY, JAMES ..... p 1506 N95-22088
KELLY, M. J. ..... p 1364 N95-20398
KELTIE, RICHARD F. ..... p 1505 N95-21930
KENDALL, GAY ..... p 1387 N95-22025
KENNEALY, J. P. ..... p 1545 N95-21832
KENNEALY, JOHN P. ..... p 1593 N95-21755
KENNEALY, R. M. ..... p 1545 N95-21832
KENNEDY, JOHN M. ..... p 1587 N95-20162
p 1587 N95-20163
p 1589 N95-21015
KENNEDY, K. A. ..... p 1251 N95-20178
KENNY, T. W. ..... p 1367 N95-21507
KEPLER, R. G. ..... p 1265 N95-20121
KERCEL, S. W. ..... p 1503 N95-20019
KERO, R. E. ..... p 1586 N95-20016
KERRIDGE, J. F. ..... p 1420 N95-21800
KERSEY, ALAN D. ..... p 1545 N95-21825
KERSTHOLT, J. H. ..... p 1449 N95-20609
KERSTIENS, D. M. ..... p 1462 N95-20699
KESTER, DO ..... p 1592 N95-21753
p 1593 N95-21758
KESTER, DO J. M. ..... p 1593 N95-21768
KETTNER, CHRISTIANE KETTNER
p 1599 N95-20873
KHAN, FERDOUS ..... p 1307 N95-21849
KHAN, H. R. ..... p 1570 N95-20820
KHARGONEKAR, P. P. ..... p 1481 N95-20828
KHAYKOVICH, B. ..... p 1573 N95-21569
KHODYREV, V. A. ..... p 1529 N95-22281
KHOURI, KAMAL S. ..... p 1479 N95-22406
KHURI-YAKUB, B. T. ..... p 1276 N95-21585
KIBBLER, A. E. ..... p 1319 N95-20521
KIEFER, WALTER S. ..... p 1420 N95-21801
KIERSTEAD, J. A. ..... p 1565 N95-20265
p 1545 N95-21643
KIGGANS, J. D. ..... p 1265 N95-20220
KIGGANS, J. O., JR. ..... p 1275 N95-21501
KIKKINIDES, E. S. ..... p 1234 N95-20046
KILAAS, R. ..... p 1548 N95-22238
KILCOYNE, S. H. ..... p 1511 N95-20434
p 1518 N95-21224
KILKENNY, J. D. ..... p 1553 N95-20363
KILLEEN, KEVIN P. ..... p 1562 N95-22225
KILLIAN, JOSEPH W. ..... p 1233 N95-22467
KILMER, NEAL H. ..... p 1430 N95-21586
KILMER, ROBERT ALLEN ..... p 1484 N95-22056
KILPIN, DAVID ..... p 1222 N95-21661
KIM, CHULO ..... p 1328 N95-21118
KIM, D. ..... p 1391 N95-20118
KIM, G. H. ..... p 1370 N95-20572
KIM, HAN ..... p 1543 N95-20598
KIM, J. ..... p 1555 N95-21141
p 1556 N95-21163
KIM, K. H. ..... p 1411 N95-22342
KIM, KANE ..... p 1484 N95-22203
KIM, Y. B. ..... p 1555 N95-21141
KIM, YOUNG-KEE ..... p 1511 N95-20415
KIME, YOLANDA J. ..... p 1241 N95-21168
p 1328 N95-21169
KIMMET, J. S. ..... p 1369 N95-20389
KIMREY, HAL D. ..... p 1265 N95-20226
KIMURA, T. ..... p 1564 N95-20127
KIMURA, W. D. ..... p 1370 N95-20572
p 1371 N95-20866

KINDLE, JOHN C. p 1429 N95-20826
KING, E. p 1592 N95-22263
KING, S. D. p 1421 N95-21802
KINOSHITA, KIM p 1392 N95-20439
p 1394 N95-20915
KINROSS-WRIGHT, J. p 1375 N95-21919
p 1376 N95-22242
p 1540 N95-22410
KINROSS-WRIGHT, J. M. p 1376 N95-22154
KIRBY, JEFFREY G. p 1471 N95-22133
KIRILLOV, I. R. p 1559 N95-21388
KIRK, P. N. p 1520 N95-21357
KIRK, R. p 1470 N95-21972
KIRK, W. J., III p 1467 N95-21389
KIRKHAM, H. p 1483 N95-21613
KIRKHAM, HAROLD p 1484 N95-22171
KIRKKIPN, KADIR p 1222 N95-21193
KIRKPATRICK, THOMAS I. p 1326 N95-20729
KIRSCHENBAUM, S. S. p 1590 N95-22053
KIRSS, REIN U. p 1271 N95-20815
KISER, D. M. p 1332 N95-21731
p 1333 N95-21960
KISHIO, K. p 1564 N95-20127
KISS, Z. p 1395 N95-21844
KITAGAWA, R. p 1277 N95-21714
KITAZAWA, K. p 1564 N95-20127
KJOLLER, K. p 1242 N95-21309
KLAUS, E. J. p 1266 N95-20281
KLEIN, STANLEY p 1451 N95-22473
KLEINMAN, RALPH E. p 1310 N95-22250
KLEISER, L. p 1348 N95-21074
KLEM, D. E. p 1531 N95-20015
KLEM, J. F. p 1327 N95-20882
p 1329 N95-21390
KLEMM, R. A. p 1566 N95-20372
KLEPPER, C. C. p 1551 N95-20205
KLEWICKI, J. G. p 1362 N95-22457
KLIER, K. p 1235 N95-20188
KLINGNER, P. p 1291 N95-20697
KLOKER, M. p 1351 N95-21093
KLOKS, T. p 1456 N95-19889
p 1456 N95-19905
p 1491 N95-21023
p 1496 N95-22327
KLOMP, CORNELIS p 1483 N95-21669
KLUGER, Y. p 1488 N95-20169
KLYMENKO, VICTOR p 1547 N95-22044
KNAPP, BENJAMIN p 1470 N95-21971
KNAPP, G. p 1527 N95-22190
KNAPP, G. R. p 1593 N95-21763
KNAPP, G. S. p 1536 N95-21407
p 1572 N95-21408
KNAUFF, T. L., JR. p 1206 N95-20370
KNEFF, D. W. p 1529 N95-22280
KNOWLES, P. E. p 1245 N95-21845
KNUTH, KURT V. p 1287 N95-21626
KNUUTILA, JUKKA p 1445 N95-21348
KOBUS, J. p 1518 N95-21223
KOCH, J. A. p 1374 N95-21663
KOCH, KARL p 1426 N95-21932
KODALI, P. p 1281 N95-22428
KODAS, T. T. p 1270 N95-20689
KOEHL, MICHAEL p 1397 N95-22362
KOEHLER, J. A. p 1224 N95-21746
KOELSCH, D. E. p 1434 N95-21677
KOFINAS, P. p 1269 N95-20582
KOHL, JOHN L. p 1602 N95-20558
KOHL, PAUL A. p 1227 N95-20412
KOHLASCH, F. L. p 1237 N95-20470
KOHLHAAS, W. p 1549 N95-20143
KOHONEN, TEUVO p 1438 N95-21112
KOIVUNEN, M. R. p 1472 N95-22310
KOK, J. p 1402 N95-20440
KOK, JOOST N. p 1494 N95-21962
KOLLMANN, W. p 1249 N95-21042
KOLODZIEJ, PAUL p 1366 N95-21391
KOLTONYUK, M. p 1562 N95-22120
KONCZYKOWSKI, M. p 1573 N95-21569
KONG, S. H. p 1375 N95-21919
p 1376 N95-22154
p 1376 N95-22242
p 1377 N95-22348
KONINGSBERG, J. p 1515 N95-20897
KONOVALOV, D. A. p 1509 N95-20198
KONTOS, G. C. p 1505 N95-21888
KONY, MICHAEL p 1284 N95-21624
KOOIMAN, P. p 1471 N95-22029
p 1471 N95-22031
KOONEN, A. M. J. p 1546 N95-21870
KOONTZ, STEVEN L. p 1412 N95-20278
KOOPMAN, R. p 1337 N95-22421
KOPPARI, KURT p 1434 N95-21320
KORDESCH, MARTIN E. p 1569 N95-20807
KORMICKI, J. p 1538 N95-21938
KORNILOV, E. p 1578 N95-22276
KORTE, ROSE M. p 1593 N95-21755
KORTRIGHT, J. p 1274 N95-21175
KOSBIE, DAVID S. p 1461 N95-20623
KOSEFF, J. R. p 1350 N95-21083
KOSEK, J. A. p 1224 N95-22474
KOSKINEN, JARKKO p 1281 N95-22428
KOSS, FRANK V. p 1216 N95-20624
KOSTROUN, V. O. p 1521 N95-21441
p 1529 N95-22316
KOSTRZEWSKI, ANDREW p 1542 N95-20501
KOTAKA, Y. p 1564 N95-20127
KOTHE, DOUGLAS B. p 1353 N95-21317
p 1478 N95-21925
KOTULAK, JOHN C. p 1450 N95-21927
KOTWAL, A. V. p 1573 N95-21561
KOTWAL, ASHUTOSH V. p 1516 N95-20914
KOUMOUTSAKOS, PETROS p 1361 N95-22452
KOURNIKAKIS, B. p 1442 N95-20602
KOVARIK, M. D. p 1570 N95-20819
KOVRIZHNYKH, L. M. p 1559 N95-21581
KOWALCZYK, W. p 1586 N95-21982
KOZACZEK, K. J. p 1385 N95-20374
p 1280 N95-22270
KOZLOWSKI, M. R. p 1377 N95-22343
KRAFT, ROBERT E. p 1505 N95-21888
KRALIK, BALAZS p 1501 N95-20874
KRAMER, C. p 1319 N95-20521
KRAMER, W. E. p 1330 N95-21471
KRANER, H. W. p 1272 N95-20894
KRASTEV, P. I. p 1521 N95-21443
KRATSCH, D. p 1456 N95-19905
p 1491 N95-21023
p 1496 N95-22327
KRAUSE, H. F. p 1508 N95-20133
KRAUSE, M. O. p 1524 N95-21664
KRAUSS, A. R. p 1570 N95-20881
KRAVITZ, S. H. p 1545 N95-21509
KRAVTSOV, V. E. p 1528 N95-22217
KREBS, W. K. p 1445 N95-21180
KRENZ, KEVIN D. p 1376 N95-22169
KRETSCHMER, FRANK F., JR. p 1289 N95-20270
KREUTZER, KRISTINA A. p 1246 N95-21879
KRICK, M. S. p 1516 N95-21114
KRIEGSMAN, GREGORY p 1303 N95-21462
KRISHNA, P. S. R. p 1518 N95-21227
KRISHNAN, V. p 1605 N95-22394
KRISHNAPRASAD, P. S. p 1220 N95-21147
KRISHNASWAMY, P. p 1258 N95-21560
KROEGER, D. M. p 1571 N95-21167
p 1578 N95-22269
KROESE, G. W. p 1410 N95-22124
KROL, MARK p 1369 N95-20378
KROL, MARK F. p 1581 N95-21928
KROM, K. R. p 1253 N95-20577
KROOKS, DAVID A. p 1410 N95-22142
KRUER, M. A. p 1318 N95-20515
KRUGER, CHARLES H. p 1561 N95-22116
KRULEVITCH, P. p 1250 N95-19900
KRUMPELT, M. p 1392 N95-20480
p 1393 N95-20839
KRUMPHOLZ, O. p 1212 N95-20652
KRUPKE, B. p 1389 N95-21552
KRUPKE, W. F. p 1372 N95-21135
KRUPPA, G. H. p 1238 N95-20563
KRUT, D. D. p 1393 N95-20870
KRYDER, G. p 1401 N95-20192
KSENDZOV, A. p 1367 N95-21507
KUBIAK, G. D. p 1541 N95-20239
KUBIAK, GLENN D. p 1376 N95-22169
KUBO, K. p 1534 N95-21253
KUBO, T. p 1277 N95-21714
KUCUKERMAN, ENVER p 1542 N95-20467
KUERTEN, HANS p 1347 N95-21066
KUIVALAINEN, P. p 1312 N95-19934
KUKSIN, S. B. p 1489 N95-20172
KUMAR, ARVIND S. p 1256 N95-21286
KUMAR, V. p 1260 N95-21855
KUNG, H. p 1281 N95-22428
KUNG, PANG-JEN p 1289 N95-20164
p 1313 N95-20168
KUNISCH, K. p 1493 N95-21582
KUNZ, THOMAS p 1496 N95-22349
KUPFER, K. p 1551 N95-20279
KUPIAINEN, A. p 1498 N95-19945
KUPPERMAN, D. S. p 1229 N95-20912
KURCHUBASCHE, RAMON R. p 1279 N95-22047
KURITA, GEN-ICHI p 1554 N95-20684
KURKCHUBASCHE, R. R. p 1270 N95-20603
p 1388 N95-22411
KURNIT, N. A. p 1371 N95-20866
KURTZ, S. R. p 1563 N95-19954
KURTZ, SARAH R. p 1319 N95-20521
KURUVILLA, A. K. p 1251 N95-20088
KUSCHE, K. P. p 1370 N95-20572
KUTZBACH, J. p 1406 N95-21379
KUUS, H. p 1551 N95-20205
KUWABATA, SUSUMU p 1365 N95-20431
KUZAY, T. M. p 1338 N95-19923
p 1527 N95-22190
KUZMENKO, P. p 1367 N95-21478
KUZMENKO, P. J. p 1237 N95-20386
KUZNETSOV, V. R. p 1249 N95-21081
KVALE, T. J. p 1519 N95-21276
KWAK, B. S. p 1244 N95-21549
KWAKMAN, P. J. M. p 1409 N95-21846
KWIAT, P. G. p 1524 N95-21646
KWOK, KWAN S. p 1535 N95-21278
KWOK, WAI-KWONG p 1567 N95-20479

L

LAARHUIS, J. H. p 1546 N95-21870
LABAUNE, G. p 1209 N95-20635
p 1212 N95-20655
LABRANCH, ELMER J. p 1444 N95-21160
LACERDA, A. p 1574 N95-21570
LACHENMAIER, RALPH p 1212 N95-20650
LACIAK, D. V. p 1246 N95-21921
LACKRITZ, HILARY S. p 1280 N95-22141
LACONTI, A. B. p 1224 N95-22474
LADD, E. F. p 1594 N95-21773
LAFORET, S. p 1212 N95-20655
LAGAKAS, NICHOLS p 1504 N95-21119
LAI, H. T. p 1284 N95-22114
LAIRD, JOHN E. p 1216 N95-20624
LAKSHMANAN, B. p 1201 N95-21338
LAM, C. p 1284 N95-21658
LAMB, P. J. p 1401 N95-20193
LAMBALLAIS, E. p 1348 N95-21075
LAMMERS, UVE H. W. p 1297 N95-20946
LAMONTIA, MARK A. p 1224 N95-19899
LAMPE, M. p 1535 N95-21328
LANAGAN, M. T. p 1570 N95-20841
LAND, M. L. p 1458 N95-20073
p 1591 N95-22129
LANDIS, GEOFFREY A. p 1318 N95-20516
p 1323 N95-20538
p 1323 N95-20541
LANDUCCI, R. p 1437 N95-20471
LANE, A. L. p 1367 N95-21507
LANE, PAT p 1517 N95-21127
p 1525 N95-21878
LANG, DWIGHT D. p 1562 N95-22300
LANGER, WILLIAM D. p 1593 N95-21769
LANGERAK, ROM p 1478 N95-21869
LANGNER, D. G. p 1516 N95-21114
LANGTANGEN, H. P. p 1468 N95-21654
p 1469 N95-21655
LANKHORST, M. M. p 1468 N95-21455
LANNING, BRUCE R. p 1318 N95-20514
LANNON, K. p 1514 N95-20852
LANNOO, M. p 1563 N95-19886
LAO, L. L. p 1550 N95-20146
p 1551 N95-20279
p 1554 N95-20446
LARA-CURZIO, E. p 1267 N95-20373
p 1271 N95-20700
LARKIN, A. I. p 1573 N95-21569
LARSEN, H. p 1335 N95-22184
LARSON, E. M. p 1224 N95-20660
LARSON, N. M. p 1537 N95-21460
LARSSON, F. p 1230 N95-21432
LASKA, JOSEPH E. p 1325 N95-20663
LASKAR, J. p 1305 N95-21539
LASNIER, C. J. p 1554 N95-20568
LASSILA, D. H. p 1251 N95-20122
LATELLA, DIEGO p 1478 N95-21869
LATHAM, JOHN p 1428 N95-20008
LATIN, ANITA E. p 1583 N95-20051
LATKOWSKI, J. p 1557 N95-21207
LATKOWSKI, J. F. p 1534 N95-21208
LAU, Y. Y. p 1531 N95-19974
LAUF, R. J. p 1271 N95-20761
LAURENCE, D. p 1345 N95-21054
p 1349 N95-21077
LAVENDER, C. A. p 1251 N95-20090
LAVOIE, J. ANDRE p 1229 N95-21008
LAW, KEITH p 1450 N95-22052
LAWBAUGH, WILLIAM M. p 1583 N95-20739
LAWN, BRIAN R. p 1273 N95-21152
LAY, RICHARD J. p 1308 N95-22005
LAYEGHI, SHAHAB p 1470 N95-21971
LAYMON, CHARLES p 1390 N95-22111
LAYMON, CHARLES A. p 1390 N95-22110
LAZANU, S. p 1272 N95-20894
LAZARUS, E. A. p 1553 N95-20445
LE, T. H. p 1347 N95-21068
LEAHY, KEVIN p 1211 N95-20646
LEAR, K. L. p 1327 N95-20883
LEBEDA, CHARLES F. p 1426 N95-21875
LEBLEBICI, YUSUF p 1327 N95-20967
LEBOEUF, J. N. p 1369 N95-20221
p 1561 N95-21922

LEBOEUF, RICHARD L. p 1362 N95-22460
LEBRUN, M. J. p 1553 N95-20437
LEBRUN, T. p 1522 N95-21502
LECHNER, JOHN F. p 1447 N95-22285
LECKIE, FREDERICK A. p 1227 N95-20429
p 1227 N95-20430
p 1227 N95-20583
p 1228 N95-20584
p 1228 N95-20801
p 1228 N95-20802
p 1231 N95-21999
LECUELLET, J. p 1212 N95-20655
LEDSINGER, LAURA A. p 1222 N95-21616
LEE, A. P. p 1250 N95-19900
LEE, DAVID p 1459 N95-20184
LEE, EUN U. p 1261 N95-22132
LEE, H. p 1314 N95-20341
LEE, H. S. p 1512 N95-20477
p 1276 N95-21644
LEE, L. L. p 1580 N95-21420
LEE, M. F. p 1365 N95-20759
LEE, M.-C. p 1304 N95-21537
LEE, MICHAEL A. p 1569 N95-20767
LEE, MIN-CHANG p 1555 N95-21013
LEE, OWEN W. p 1264 N95-20018
LEE, P. H. Y. p 1309 N95-22241
LEE, P. L. p 1572 N95-21408
LEE, R. W. p 1374 N95-21663
LEE, S. L. p 1388 N95-22320
LEE, S. R. p 1458 N95-20154
p 1575 N95-21991
LEE, SEUNGHOON p 1307 N95-21883
LEE, Y. C. p 1484 N95-22210
LEEMANS, P. p 1470 N95-21983
LEEMANS, W. P. p 1374 N95-21528
LEEPER, R. J. p 1558 N95-21247
LEES, A. J. p 1239 N95-20682
LEES, JOANNA F. p 1593 N95-21763
LEFEBVRE, W. p 1460 N95-20385
LEGER, JEFFREY R. p 1390 N95-21912
LEGER, LUBERT J. p 1412 N95-20278
LEGGETT, DAVID B. p 1214 N95-20004
LEHTINEN, H. p 1451 N95-20276
LEI, JIH-FEN p 1366 N95-21259
LEIDHOLM, C. R. p 1317 N95-20512
LEINENWEBER, KURT p 1420 N95-21799
LEINONEN, S. p 1315 N95-20369
LEJANNIC, J. C. p 1293 N95-20929
p 1295 N95-20934
LELE, S. K. p 1345 N95-21053
p 1363 N95-22463
LEMENN, P. p 1296 N95-20945
LEMKE, R. W. p 1329 N95-21395
LEMMON, E. C. p 1251 N95-20128
LENHARDT, B. W. p 1329 N95-21301
LENSTRA, J. K. p 1466 N95-21269
LEONARD, A. W. p 1554 N95-20568
LEONARD, ANTHONY p 1200 N95-20177
LEONARD, JOSEPH T. p 1286 N95-20611
LEONCINI, P. p 1352 N95-21098
LEOPOLD, D. J. p 1273 N95-21014
LEPP, ANDREW W. p 1477 N95-21674
LERCHE, R. A. p 1552 N95-20362
LERNER, I. V. p 1528 N95-22217
LESAOUT, J. Y. p 1300 N95-20961
LESIEUR, M. p 1348 N95-21075
LESTER, CHARLES S. p 1373 N95-21312
LESTER, DANIEL p 1593 N95-21754
LESUER, D. R. p 1276 N95-21662
LEUER, J. A. p 1548 N95-20037
LEUTENEGGER, SCOTT T. p 1456 N95-22431
LEVINE, T. p 1281 N95-22428
LEVINE, TIMOTHY E. p 1534 N95-21236
LEVSKY, L. p 1421 N95-21805
LEVY, M. F. p 1295 N95-20935
LEWANDOWSKI, J. J. p 1225 N95-20001
p 1263 N95-22408
LEWIS, BERNARD L. p 1289 N95-20270
p 1307 N95-21904
LEWIS, G. K. p 1375 N95-21837
LEWIS, J. D. p 1511 N95-20401
LEWIS, JAMES K. p 1433 N95-21158
LEWIS, JONATHAN p 1524 N95-21597
LEWIS, L. K. p 1217 N95-22413
LEWIS, M. W. p 1339 N95-20166
LEWIS, P. S. p 1313 N95-20168
LEWIS, PAUL S. p 1289 N95-20164
LEWITT, MARTIN E. p 1477 N95-21843
LI-DEMARTEAU, QIZHONG p 1525 N95-21715
LI, BING p 1548 N95-22255
LI, DINGZHANG p 1255 N95-20909
LI, F. Y. p 1226 N95-20027
LI, FEI p 1353 N95-21146
LI, M. p 1418 N95-21791
LI, Q. p 1564 N95-20127
LI, SHILING p 1563 N95-19976
LI, W. B. p 1234 N95-20046
LI, XIAO-PING p 1563 N95-20014
p 1569 N95-20793
LI, XIAOYUAN p 1421 N95-21803
LI, Y. p 1491 N95-20920
LI, Z. p 1272 N95-20894
LIAO, LI p 1491 N95-20734
LIAW, GOANG-SHIN p 1354 N95-21675
LIAW, P. K. p 1271 N95-20700
LIAW, Y. P. p 1335 N95-22189
LIBBY, S. I. p 1369 N95-20389
LIBBY, STUART I. p 1541 N95-20231
LIEBERT, CURT H. p 1366 N95-21391
LIENARD, M. p 1294 N95-20933
LIGHART, L. P. p 1297 N95-20947
LILL, T. p 1254 N95-20707
LILLY, WILLIAM E. p 1583 N95-20740
LIMBACH, H. H. p 1570 N95-20820
LIMBERG, T. p 1538 N95-22155
LIN, H. T. p 1264 N95-20024
p 1250 N95-20044
p 1267 N95-20323
p 1271 N95-20704
p 1275 N95-21501
p 1231 N95-21776
LIN, HUA-TAY p 1271 N95-20821
LIN, WEI p 1604 N95-22085
LIN, YUPING p 1570 N95-20881
LIN, ZONGLI p 1483 N95-21618
LINAN, A. p 1249 N95-21036
p 1249 N95-21039
LINDAHL, P. C. p 1401 N95-20234
LINDBERG, S. E. p 1411 N95-22342
LINDELL, I. V. p 1310 N95-22311
p 1311 N95-22365
LINDELL, ISMO V. p 1291 N95-20775
p 1502 N95-21102
p 1544 N95-21103
LINDGREN, REIJO p 1220 N95-21026
LINDMAN, E. L. p 1371 N95-20786
LINDSAY, G. C. p 1446 N95-22004
LINDSEY, E. F. p 1541 N95-20218
LINDWALL, DENNIS p 1436 N95-22028
LINK, H. p 1396 N95-21897
LINKE, J. p 1269 N95-20570
LIOU, MENG-SING p 1355 N95-21957
LIOU, R. p 1374 N95-21694
LIPINSKI, R. J. p 1373 N95-21393
LIPSANEN, H. p 1582 N95-22432
LIPTON, ROSS E. p 1446 N95-22004
LISS, W. E. p 1282 N95-20253
LITTLE, R. C. p 1400 N95-19921
LITTMAN, FRANKLIN D. p 1395 N95-21530
p 1222 N95-21531
p 1396 N95-21952
p 1396 N95-21953
LIU, C. L. p 1369 N95-20221
LIU, C. T. p 1250 N95-20020
p 1250 N95-20043
p 1263 N95-22345
LIU, JUNHUI p 1346 N95-21064
LIU, K. C. p 1265 N95-20220
LIU, L. C. p 1516 N95-21125
LIU, S. H. p 1566 N95-20372
LIU, SHIH-CHING p 1453 N95-21866
LIU, Y. p 1566 N95-20405
p 1370 N95-20572
LIU, YONG p 1255 N95-21128
LIU, ZHEN p 1482 N95-21271
LIVENGOOD, C. D. p 1234 N95-20107
p 1403 N95-20478
LJUNGDAHL, L. G. p 1438 N95-20917
LLOYD, I. K. p 1270 N95-20664
LO, CHING F. p 1353 N95-21340
LOCKE, R. J. p 1214 N95-21383
LOCKNER, T. R. p 1535 N95-21328
LOCKWOOD, M. p 1413 N95-20453
p 1427 N95-22368
LOCKWOOD, STEVE p 1333 N95-21881
LODDERS, K. p 1421 N95-21804
LOEB, D. p 1499 N95-21979
LOEBICH, O. p 1570 N95-20820
LOEHLE, C. p 1414 N95-20908
LOEHMAN, R. E. p 1265 N95-20138
LOFARO, RONALD J. p 1202 N95-20093
p 1203 N95-21518
p 1203 N95-22319
LOGAN, G. p 1557 N95-21206
LOGAN, M. N. p 1264 N95-20047
LOGOTHETIS, NIKOS p 1437 N95-20185
LOGOTHETIS, NIKOS K. p 1459 N95-20157
LOGRASSO, T. A. p 1258 N95-21568
LOHRY, E. J. p 1263 N95-22396
LOKHOV, K. p 1421 N95-21805
LOMBARDI, D. R. p 1237 N95-20470
LONDON, J. p 1431 N95-22288
LONDON, R. A. p 1374 N95-21663
LONG, MARSHALL B. p 1238 N95-20581
LONGA, L. p 1578 N95-22277
LONGANECKER, G. W. p 1585 N95-20753
LONGO, RICARDO p 1507 N95-20097
LONGSTRETH, J. D. p 1401 N95-20089
LONGTIN, DAVID R. p 1290 N95-20376
LOOFTWILSON, R. p 1439 N95-21544
LOOMIS, G. E. p 1541 N95-20218
LOOMIS, WILLIAM R. p 1223 N95-19901
LORD, KENNETH R., II p 1320 N95-20522
LOTJONEN, JYRKI p 1443 N95-20971
LOTSHAW, W. T. p 1544 N95-20844
LOTT, S. E. p 1261 N95-22119
LOU, Y. p 1564 N95-20017
LOU, Z. p 1380 N95-21157
LOUBRIEL, G. M. p 1328 N95-21139
LOUIE, STEVEN G. p 1501 N95-20874
LOULOU, PATRICK p 1363 N95-22464
LOUP, C. p 1593 N95-21768
LOUSTEAU, D. C. p 1560 N95-21665
LOVEJOY, M. L. p 1329 N95-21394
p 1572 N95-21419
p 1259 N95-21838
LOVESAY, S. W. p 1502 N95-22138
LOW, GEORGE M. p 1585 N95-20755
LOWDEN, R. A. p 1225 N95-20023
p 1267 N95-20373
p 1271 N95-20700
p 1247 N95-22260
LOWE, ROLAND A. p 1322 N95-20536
p 1322 N95-20537
p 1323 N95-20538
LOWRY, M. p 1313 N95-20119
p 1542 N95-20489
LOYENS, L. D. J. C. p 1473 N95-20056
LU, FUTUN p 1548 N95-22255
LU, S. Y. p 1313 N95-20119
LU, SHIN-YEE p 1544 N95-21392
LU, ZHENG-TIAN p 1513 N95-20629
LU, ZHONG-YI p 1577 N95-22178
LUBBEN, D. p 1565 N95-20371
LUCE, R. E. p 1588 N95-[illegible]0777
LUCE, T. C. p 1551 N95-20279
LUEDERS, K. p 1570 N95-20820
LUIJKX, GERARDUS CHRISTIANUS ANTONIUS
p 1396 N95-22175
LUJAN, RICHARD E. p 1379 N95-20627
LUK, FRANKLIN T. p 1491 N95-20875
LUKASZEK, W. p 1558 N95-21310
LUKEMEYER, JAMES p 1279 N95-21976
LUND, P. p 1397 N95-22337
LUND, S. M. p 1552 N95-20318
LUND, SAM p 1220 N95-21026
LUND, T. p 1346 N95-21062
LUND, T. S. p 1249 N95-21043
p 1344 N95-21051
LUND, THOMAS S. p 1360 N95-22450
LUNDBLADH, A. p 1349 N95-21079
LUNDEEN, G. N. p 1432 N95-20012
LUNINE, JONATHAN I. p 1421 N95-21806
LUNTAMA, JUHA-PEKKA p 1220 N95-21026
LUO, JUNLIN p 1556 N95-21165
LUTHRA, K. L. p 1214 N95-21243
LYBANON, MATTHEW p 1431 N95-19888
LYKINS, H. p 1470 N95-21972
LYMAN, JOHN L. p 1244 N95-21523
LYON, J. F. p 1559 N95-21581
LYSENKO, W. P. p 1536 N95-21331

M

MA, D. I. p 1566 N95-20400
MA, J. p 1312 N95-19935
MA, JIAN p 1301 N95-21109
MA, Y. p 1527 N95-22188
MA, Z. p 1254 N95-20707
MA, ZHONG-SHUI p 1582 N95-22198
MAASKANT, M. p 1410 N95-22330
MACCABE, ARTHUR B. p 1474 N95-20123
MACCABEE, BRUCE S. p 1333 N95-21901
MACDOWALL, R. D. p 1330 N95-21471
MACGOWAN, B. J. p 1531 N95-20015
p 1374 N95-21663
MACHOL, J. p 1314 N95-20341
MACINTYRE, WILLIAM G. p 1282 N95-19922
MACKAY, W. W. p 1532 N95-20336
p 1532 N95-20406
MACKENZIE, COLIN F. p 1449 N95-20393
MACKENZIE, JOHN D. p 1226 N95-20105
p 1242 N95-21402
MACKEY, H. E. p 1592 N95-22263
MACLAREN, J. M. p 1500 N95-20129
p 1576 N95-22084
MADDOX, S. R. p 1271 N95-20761

MADEY, JOHN M. p 1370 N95-20600
MADHOK, VARUN p 1482 N95-21522
p 1486 N95-22430
MADSEN, JOHN D. p 1409 N95-21914
MAEDA, H. p 1555 N95-20988
MAGELSSEN, G. R. p 1371 N95-20786
MAGGIORE, C. p 1600 N95-22128
MAGGIORE, CARL J. p 1534 N95-21236
MAGNUSSEN, O. M. p 1573 N95-21516
MAHAJAN, S. p 1561 N95-21851
MAHAJAN, S. M. p 1326 N95-20791
p 1243 N95-21500
p 1500 N95-21592
MAHALINGAM, S. p 1249 N95-21038
MAHALOV, A. p 1345 N95-21057
MAHDAVI, M. A. p 1552 N95-20334
MAHLMAN, J. D. p 1409 N95-22101
MAHMOUD, K. E. M. p 1330 N95-21590
MAIMONI, A. p 1337 N95-22421
MAINGI, R. p 1552 N95-20334
MAJER, D. p 1573 N95-21569
MAJEROWICW, WALTER p 1584 N95-20750
MAJUMDAR, S. p 1229 N95-20912
MAKARCHENKO, V. M. p 1229 N95-20859
MAKHOUL, J. p 1310 N95-22253
MAKOWIECKI, D. M. p 1250 N95-19900
p 1274 N95-21175
MAKOWSKI, M. A. p 1550 N95-20146
MALAMUD, E. p 1508 N95-20132
MALANG, SIEGFRIED p 1558 N95-21244
MALETIC, D. p 1563 N95-19925
p 1533 N95-20766
p 1517 N95-21140
MALEY, M. P. p 1575 N95-21936
MALHOTRA, R. p 1237 N95-20438
MALIK, MUJEEB R. p 1353 N95-21146
MALLAT, J. p 1300 N95-20972
p 1598 N95-22376
MALLICK, BANI K. p 1499 N95-21946
MALONE, ROBERT L. p 1203 N95-22319
MALOUVIER, A. p 1445 N95-21424
MANASREH, M. O. p 1563 N95-19886
MANCHESTER, JOHN I. p 1520 N95-21375
MANCINI, T. R. p 1393 N95-20862
MANDELL, HUMBOLDT C., JR. p 1584 N95-20744
MANE, V. p 1532 N95-20336
p 1532 N95-20406
MANES, K. R. p 1534 N95-21209
MANGHNANI, M. H. p 1226 N95-20027
MANLIEF, SCOTT p 1220 N95-21190
MANN, C. K. p 1237 N95-20470
MANN, R. C. p 1483 N95-21741
MANNERS, IAN p 1265 N95-20183
MANSOUR, N. N. p 1338 N95-20009
p 1345 N95-21058
p 1346 N95-21059
p 1346 N95-21060
MANSOUR, NAGI N. p 1347 N95-21065
p 1350 N95-21085
MANTEL, T. p 1249 N95-21041
p 1249 N95-21042
MANTEL, THIERRY p 1249 N95-22438
p 1249 N95-22440
MANTEUFFEL, THOMAS A. p 1470 N95-21992
MANZANERA, IGNACIO p 1584 N95-20747
MAO, H. K. p 1417 N95-21786
p 1418 N95-21791
MAO, N. p 1538 N95-21733
MARCHELLO, JOSEPH M. p 1383 N95-20616
MARCHYWKA, MICHAEL J. p 1577 N95-22103
MARCIANO, W. p 1511 N95-20404
MARCUS, HARRIS L. p 1252 N95-20201
MARGETIS, S. p 1513 N95-20575
MARIAGE, PH. p 1294 N95-20933
MARIS, H. J. p 1506 N95-22071
MARKOVITS, A. S. p 1442 N95-20710
MARKS, G. W. p 1322 N95-20535
MARR, RICHARD A. p 1297 N95-20946
MARR, W. M. p 1469 N95-21829
MARR, WILLIAM W. p 1329 N95-21296
MARRERO-RIVERA, M. p 1244 N95-21571
MARS, N. J. I. p 1471 N95-22081
MARSEE, R. L. p 1306 N95-21686
MARSH, J. S. p 1445 N95-21180
MARSH, KENNETH A. p 1593 N95-21765
MARSHALL, C. D. p 1372 N95-21135
MARSHALL, G. M. p 1245 N95-21845
MARSTON, A. P. p 1592 N95-21751
p 1593 N95-21764
MARTI, K. p 1600 N95-22128
MARTIN, ALAN D. p 1244 N95-21523
MARTIN, C. R. p 1324 N95-20587
MARTIN, CHARLES R. p 1365 N95-20431
p 1277 N95-21876
MARTIN, JOE A. p 1260 N95-21926
MARTIN, JOHN R. p 1414 N95-20878
MARTIN, JOHN S. p 1547 N95-22044
MARTIN, PETER G. p 1594 N95-21771
MARTIN, S. J. p 1564 N95-20087
p 1367 N95-21546
MARTIN, T. p 1576 N95-22008
MARTIN, T. J. p 1426 N95-21836
MARTINEZ, ANDREW O. p 1437 N95-20559
MARVIN, DEAN C. p 1575 N95-21916
MASCARENHAS, A. p 1314 N95-20341
MASEK, MARK p 1591 N95-22092
MASSAM, T. p 1335 N95-22184
MASSEY, K. C. p 1504 N95-21170
MASSOT, V. p 1299 N95-20956
MAST, J. E. p 1301 N95-21205
MASUR, L. p 1571 N95-21167
MATESKI, J. E. p 1203 N95-21518
MATHEWS, G. J. p 1600 N95-21479
MATHIAS, LON J. p 1265 N95-20094
p 1280 N95-22259
MATHIAS, LOU J. p 1578 N95-22286
MATHUR, A. p 1497 N95-22388
MATIN, LEONARD p 1451 N95-22472
MATIS, HOWARD S. p 1520 N95-21357
MATKOWSKY, B. J. p 1356 N95-22148
MATSUDA, T. p 1555 N95-20989
MATSUOKA, M. p 1221 N95-22436
MATSURRA, A. p 1574 N95-21712
MATTHEWS, D. J. p 1374 N95-21663
MATTHEWS, R. K. p 1200 N95-20248
MATTICE, MICHAEL S. p 1481 N95-20828
MATTSON, J. E. p 1571 N95-21256
MAUCHER, ULRICH p 1352 N95-21095
MAUDERLY, JOE L. p 1447 N95-22287
MAUDLIN, P. J. p 1501 N95-20869
MAUREY, B. p 1489 N95-20273
MAURICE, JOANNE H. p 1541 N95-20231
p 1547 N95-22076
p 1548 N95-22248
MAUS, J. R. p 1200 N95-20248
MAUW, S. p 1288 N95-19890
MAUW, SJOUKE p 1468 N95-21619
MAX, NELSON p 1353 N95-21182
MAXWELL, BRUCE A. p 1543 N95-20564
MAXWELL, C. p 1537 N95-21647
MAY, DOUGLAS A. p 1388 N95-20006
MAY, P. K. p 1516 N95-21114
MAYER, K. S. p 1444 N95-20977
p 1446 N95-21989
MAYERS, J. p 1571 N95-21228
p 1530 N95-22332
MAZIASZ, P. J. p 1252 N95-20359
p 1253 N95-20375
p 1257 N95-21555
MAZUMDAR, S. p 1565 N95-20330
MAZZARELLA, JOSEPH M. p 1595 N95-21749
p 1593 N95-21759
MAZZUCATO, E. p 1558 N95-21242
MCAFEE, W. J. p 1385 N95-20322
MCARTHUR, D. A. p 1371 N95-20867
p 1373 N95-21393
MCBRATNEY, W. F. p 1282 N95-19920
MCBREEN, J. p 1512 N95-20477
p 1276 N95-21644
MCBRIDE, BONNIE J. p 1235 N95-20180
MCCANDLESS, B. E. p 1394 N95-21294
MCCARDIE, A. H. p 1441 N95-20307
MCCARTHY, I. E. p 1509 N95-20198
p 1509 N95-20199
MCCARTY, K. F. p 1266 N95-20281
MCCHESNEY, J. M. p 1553 N95-20402
MCCLEARY, LAWRENCE E. p 1590 N95-21463
MCCLURE, E. RAY p 1285 N95-20288
MCCOMAS, D. J. p 1600 N95-21935
p 1427 N95-22477
MCCONAGHY, C. F. p 1313 N95-20119
p 1542 N95-20403
p 1542 N95-20489
MCCONVILLE, G. T. p 1243 N95-21440
MCCORD, R. A. p 1458 N95-20073
p 1591 N95-22129
MCCORMICK, C. p 1267 N95-20350
MCCORMICK, K. S. p 1295 N95-20940
MCCRADY, DENNIS D. p 1204 N95-20269
MCCREERY, CHARLES S. p 1432 N95-20040
MCCRORY, E. p 1533 N95-20885
MCCUNE, W. p 1471 N95-22077
MCCURDY, ALAN H. p 1374 N95-21694
MCDERMOTT, GENE p 1459 N95-20310
MCDOUGALL, I. p 1419 N95-21793
MCFARLAND, R. E. p 1207 N95-21186
MCGIBBON, A. J. p 1567 N95-20492
MCGIBBON, M. M. p 1567 N95-20492
MCGILL, J. p 1538 N95-21733
MCGINNIS, L. D. p 1415 N95-21477
MCGINNIS, WAYNE C. p 1577 N95-22137
MCGLAUN, M. p 1474 N95-20152
MCGOWEN, JOHN A. p 1280 N95-22259
MCGRATH, R. T. p 1549 N95-20143
MCGRAW, ROBERT L. p 1544 N95-20803
MCHARGUE, C. J. p 1510 N95-20337
MCINNES, BRENT p 1418 N95-21787
MCINTOSH, R. L. p 1384 N95-20077
MCINTYRE, BRIAN JAMES p 1246 N95-21990
MCKAMEY, C. G. p 1252 N95-20359
p 1253 N95-20375
MCKAMEY, C. J. p 1257 N95-21555
MCKELVEY, TERESA p 1213 N95-22024
MCKINNEY, G. W. p 1474 N95-20158
MCKINNON, A. D. p 1458 N95-20153
MCLAIN, ALBERT p 1457 N95-20060
MCLANDRICH, MATTHEW N. p 1544 N95-21466
MCLAUGHIN, J. C. p 1271 N95-20821
MCLAUGHLIN, D. J. p 1296 N95-20941
MCLAUGHLIN, J. C. p 1340 N95-20781
MCLAUGHLIN, L. I. p 1261 N95-22119
MCLAUGHLIN, LEE R. p 1588 N95-20774
MCLEAN, WILLIAM E. p 1547 N95-22044
MCLEMORE, DONALD P. p 1291 N95-20771
p 1207 N95-20772
MCLIN, M. G. p 1330 N95-21490
MCNIFF, B. p 1391 N95-20260
MCNULTY, I. p 1541 N95-20103
MCPHERSON, A. p 1374 N95-21743
MCPHERSON, WILLIAM B. p 1251 N95-20068
MCVEY, B. p 1481 N95-20693
MCWHORTER, ALAN L. p 1567 N95-20426
MEADE, C. p 1417 N95-21786
MEDDAHI, M. p 1532 N95-20494
p 1532 N95-20495
MEDELCI, N. p 1316 N95-20508
p 1318 N95-20517
MEDERNACH, J. W. p 1575 N95-21991
MEDLIN, D. L. p 1266 N95-20281
MEERTENS, LAMBERT p 1494 N95-21868
MEHLHORN, T. A. p 1537 N95-21603
MEICHLE, MICHAEL p 1456 N95-22400
MEIER, R. W. p 1339 N95-20166
MEIJER, G. R. p 1410 N95-22124
MEINDL, M. p 1204 N95-20195
MEINDL, M. A. p 1205 N95-21520
MEISEL, L. V. p 1387 N95-22025
p 1495 N95-22026
MEISL, C. J. p 1395 N95-21530
p 1222 N95-21531
MEITZ, HUBERT L. p 1352 N95-21094
MEITZLER, W. D. p 1389 N95-20903
MELANCON, PIERRE p 1296 N95-20943
MELIUS, CARL F. p 1562 N95-22225
MELMAN, PAUL p 1543 N95-20598
MENDELSOHN, M. H. p 1234 N95-20107
MENDILLO, MICHAEL p 1427 N95-22423
MENEVEAU, C. p 1344 N95-21051
MENG, JAMES C. p 1355 N95-21902
MENKE, D. A. p 1243 N95-21440
MENON, S. p 1348 N95-21071
MENSAH, S. Y. p 1575 N95-21859
MERCHANT, DAVID H. p 1381 N95-21692
p 1381 N95-21705
MEREDITH, D. p 1488 N95-20169
MERRILL, R. P. p 1247 N95-22234
MESCHTER, P. J. p 1214 N95-21243
MESMER, R. E. p 1245 N95-21732
MESSENGER, SCOTT R. p 1319 N95-20519
p 1319 N95-20520
p 1320 N95-20523
MESSLER, R. W. p 1315 N95-20443
MESSMORE, J. A. p 1204 N95-20497
METAIS, O. p 1348 N95-21075
METCALF, D. H. p 1237 N95-20493
MEULENBERG, A. p 1320 N95-20526
MEY, G. p 1213 N95-20659
MEYER, F. W. p 1525 N95-21857
MEYER, W. H. p 1550 N95-20146
MEYERS, H. M., III p 1244 N95-21571
MEZIANI, Z. E. p 1525 N95-21747
MICHA, D. A. p 1516 N95-20994
MICHA, DAVID A. p 1506 N95-19959
MICHAELIS, M. M. p 1599 N95-21367
MICHALAKES, J. G. p 1407 N95-21608
MICHALSKY, J. p 1412 N95-20116
MICHELL, JAMES T. p 1455 N95-21116
MICHIE, R. p 1371 N95-20867
MICHIELS, E. p 1308 N95-22080
MICHIELS, EDDIE p 1306 N95-21623
MICKISH, ANDREW p 1461 N95-20623
MIGLIO, J. J. p 1407 N95-21666
MIHAILESCU, I. N. p 1562 N95-22377
MIKKELSEN, D. R. p 1557 N95-21240
MIKKONEN, SEPPO p 1380 N95-21295
MILANOVICH, FRED P. p 1545 N95-21510
MILATOVIC, BORISLAV p 1216 N95-21719
MILESKI, PAUL p 1301 N95-21156
p 1307 N95-21910

MILEWSKI, J. p 1375 N95-21837
MILEY, H. S. p 1458 N95-20153
MILLARD, D. L. p 1315 N95-20443
MILLARD, ROBERT C. p 1435 N95-21681
MILLER, BRIAN H. p 1431 N95-19918
MILLER, CHRISTOPHER E. p 1273 N95-21000
MILLER, D. J. p 1570 N95-20841
MILLER, D. P. p 1453 N95-21721
MILLER, H. V. p 1390 N95-22055
MILLER, J. D. p 1509 N95-20206
MILLER, JACQUELINE T. p 1591 N95-22107
MILLER, KENT L. p 1414 N95-20591
MILLER, M. C. p 1516 N95-21114
MILLER, M. K. p 1261 N95-22127
MILLER, R. J. D. p 1574 N95-21839
MILLER, R. L. p 1558 N95-21345
MILLER, RICHARD A. p 1410 N95-22278
MILLS, P. B. p 1436 N95-22073
MILOS, FRANK S. p 1601 N95-21621
MILOSAVLJEVIC, A. p 1440 N95-22067
MILOSAVLJEVIC, ALEKSANDAR p 1438 N95-21376
MINAKATA, HISAKAZU p 1604 N95-22064
MINES, R. F. p 1465 N95-21153
MINGOLLA, ENNIO p 1449 N95-20845
MINNICK, A. p 1317 N95-20512
MIRDAMADI, M. p 1230 N95-21363
MIRKARIMI, P. B. p 1266 N95-20281
MIRKES, E. p 1580 N95-21230
MISRA, MOHAN S. p 1318 N95-20514
p 1322 N95-20532
MITCHELL, M. A. p 1558 N95-21368
MITCHELL, RALPH p 1273 N95-21011
MITCHELL, RICHARD L. p 1392 N95-20473
MITCHELTREE, ROBERT A. p 1494 N95-21622
MITRA, NIMAI KUMAR p 1347 N95-21070
MITTAL, VIBHU O. p 1464 N95-20996
MIURA, Y. p 1555 N95-20988
p 1555 N95-20989
MIVILLE, FRANK p 1209 N95-20638
MIYAZAKI, A. p 1422 N95-21807
MIYOSHI, KAZUHISA p 1274 N95-21252
MLEZIVA, MATT L. p 1462 N95-20721
MOATS, A. R. p 1558 N95-21247
MOBLEY, C. p 1253 N95-20417
MODIANO, DAVID p 1356 N95-21959
MODINE, F. A. p 1565 N95-20371
MOEHL, DIETER p 1370 N95-20569
MOELLER, KENNETH p 1397 N95-22362
MOFIZ, U. A. p 1307 N95-21849
p 1561 N95-21850
MOHN, J. p 1410 N95-22124
MOHNKERN, GARY L. p 1503 N95-20084
MOIN, P. p 1346 N95-21062
MOIN, PARVIZ p 1355 N95-21954
MOLBURG, J. C. p 1403 N95-20478
MONAGHAN, TIM p 1209 N95-20636
MONCRIEFF, D. p 1518 N95-21223
MONISMITH, S. G. p 1350 N95-21083
MONISMITH, STEPHEN G. p 1434 N95-21293
MONTANO, P. A. p 1540 N95-19968
MONTASER, A. p 1552 N95-20345
MONTELLI, LUCIANNA p 1284 N95-21624
MONTESANTI, R. C. p 1543 N95-20612
MONTGOMERY, D. B. p 1562 N95-22300
MONTGOMERY, D. S. p 1531 N95-20015
MONTICCIOLO, PAUL p 1300 N95-21099
MONTONEN, J. p 1447 N95-22371
MONYAK, JOHN T. p 1379 N95-20998
MOODY, J. D. p 1531 N95-20015
MOOKERJEE, A. p 1575 N95-21853
MOONEN, J. p 1473 N95-20056
MOORE, J. E. p 1558 N95-21368
MOORE, JOHN W. p 1479 N95-20061
MOORE, K. p 1291 N95-20697
MOORE, R. C. p 1245 N95-21732
MOORE, VIRGIL p 1383 N95-22037
MORABITO, D. D. p 1305 N95-21540
MORALES, G. J. p 1559 N95-21403
p 1559 N95-21404
MORALES, R. I. p 1542 N95-20364
p 1562 N95-22191
MORAN, B. p 1376 N95-22121
MORE, K. L. p 1265 N95-20220
MOREAU, A. p 1213 N95-20657
MOREL, J. E. p 1509 N95-20235
MORENO, J. B. p 1393 N95-20861
MORENO, J. C. p 1369 N95-20335
MORGAN, M. p 1251 N95-20079
MORGAN, M. J. p 1252 N95-20216
MORGAN, REED p 1208 N95-20632
MORI, M. p 1555 N95-20988
MORRIS, D. E. p 1236 N95-20361
MORRIS, SHELBY J., JR. p 1200 N95-20668
MORRIS, V. R. p 1395 N95-21611
MORSE, STEPHEN E. p 1450 N95-21927
MORTENSON, L. E. p 1438 N95-20917
MORTON, JOHN p 1229 N95-21008
MOSCHELLA, JOHN J. p 1551 N95-20232
MOSER, G. p 1211 N95-20649
MOSER, R. D. p 1249 N95-21037
p 1344 N95-21049
p 1363 N95-22463
MOSER, ROBERT D. p 1350 N95-21084
MOSHAMMER, H. p 1519 N95-21262
p 1538 N95-22155
MOSHFEGH, ALLEN p 1480 N95-20202
MOSIER, MARY H. p 1208 N95-20633
MOSKOWITZ, B. p 1530 N95-22392
MOSS, STEVEN C. p 1575 N95-21916
MOSS, T. A. p 1393 N95-20861
MOSSO, S. JAY p 1353 N95-21317
MOSTOLLER, M. p 1565 N95-20244
MOTOWIDLO, LESZEK R. p 1336 N95-22271
MOUCHON, E. p 1275 N95-21272
MOULTON, D. S. p 1282 N95-20253
MOYER, R. A. p 1554 N95-20571
MROWKA, S. p 1374 N95-21663
MUDREY, M. G. p 1415 N95-21477
MUDRY, ANDREW p 1459 N95-20184
p 1290 N95-20308
MUEHLHAUSEN, LAUREL A. p 1403 N95-20487
MUELLER, H. p 1456 N95-19905
p 1496 N95-22327
MUELLER, R. L. p 1397 N95-22336
MUELLER, W. p 1351 N95-21093
MUIR, D. W. p 1561 N95-22010
MUKHERJEE, ARUP p 1461 N95-20622
MULBRANDON, M. p 1533 N95-20672
MULCAHY, T. M. p 1382 N95-22292
MULDER, HANS p 1468 N95-21619
MULLER, M. W. p 1328 N95-21017
MULLER, MARK p 1202 N95-20275
MULLIN, SCOTT A. p 1387 N95-21396
MULLIS, CLIFFORD T. p 1308 N95-22041
MUNRO, D. H. p 1531 N95-20015
MURPHY, CINDY p 1383 N95-21933
MURPHY, O. J. p 1252 N95-20299
MURPHY, T. J. p 1552 N95-20362
MURRAY, J. R. p 1534 N95-21209
p 1334 N95-22086
MURRAY, JAMES E. p 1540 N95-22469
MURRAY, JANE S. p 1246 N95-22000
MURRAY, JOHN R. p 1371 N95-20817
MURRAY, STEVEN A. p 1452 N95-20768
MUSOLF, M. J. p 1526 N95-21920
MUTSCHLECNER, J. PAUL p 1413 N95-20289
MYCEK, M. A. p 1569 N95-20677
p 1569 N95-20678
p 1569 N95-20679
p 1514 N95-20732
MYERS, BRAD A. p 1461 N95-20623
p 1466 N95-21325
MYERS, T. P. p 1411 N95-22342
MYRUSKI, BRIAN L. p 1221 N95-20124

N

NACHTIGAL, N. M. p 1355 N95-21726
p 1469 N95-21744
NAFARI, N. p 1527 N95-22179
NAGAO, KENJI p 1468 N95-21495
NAHORMEK, PATRICIA A. p 1441 N95-20408
NAHORY, R. E. p 1572 N95-21287
NAIR, K. M. p 1270 N95-20664
NAKADA, T. p 1512 N95-20454
NAKANISHI, KEITH p 1415 N95-21511
NAKAYAMA, KEN p 1448 N95-19998
NAMAZIAN, M. p 1243 N95-21512
NAMAZIE, M. A. p 1500 N95-21964
NAMKOONG, DAVID p 1338 N95-19952
NAMKUNG, MIN p 1383 N95-20764
NASTASI, M. p 1281 N95-22428
NASTASI, MICHAEL p 1534 N95-21236
NATH, SHRIDHAR C. p 1383 N95-20764
NATION, DAVID A. p 1590 N95-21463
NAUTA, JAN M. p 1482 N95-21412
p 1484 N95-22156
NAVIA, MANUEL p 1269 N95-20551
NAVROTSKY, ALEXANDRA p 1416 N95-21782
NAWROCKI, ELISE p 1468 N95-21627
NEAGLEY, D. p 1291 N95-20697
NEAL, D. R. p 1371 N95-20867
NECHES, ROBERT p 1462 N95-20718
NEDERPELT, R. p 1492 N95-21372
NEDERPELT, ROB p 1488 N95-20149
NEHRKORN, THOMAS p 1292 N95-20904
NELMS, R. MARK p 1312 N95-19909
NELSON, A. E. p 1512 N95-20451
NELSON, J. R. p 1327 N95-20966
NELSON, J. S. p 1314 N95-20341
NELSON, P. A. p 1407 N95-21617
NELSON, R. G. p 1376 N95-22301
NELSON, ROBERT C. p 1201 N95-21343
NELSON, S. G. p 1400 N95-19921
NEMANICH, R. J. p 1568 N95-20614
NEMEC, R. p 1375 N95-21837
NEMETH, NOEL N. p 1386 N95-20790
NENONEN, J. p 1447 N95-22371
NERI, D. F. p 1441 N95-20307
NERNEY, STEVEN p 1426 N95-21874
NESBITT, DAVID J. p 1370 N95-20484
NETTELHORST, HEATHER L. p 1494 N95-21622
NEU, S. C. p 1559 N95-21403
NEUMAN, W. A. p 1389 N95-21433
NEWBERRY, B. L. p 1549 N95-20143
NEWSOM, H. p 1600 N95-22128
NEWTON, CRYSTAL H. p 1229 N95-21149
p 1229 N95-21215
p 1233 N95-22395
NEWTON, M. A. p 1552 N95-20318
NG, D. S. p 1551 N95-20219
NG, KING-YUEN p 1532 N95-20421
p 1534 N95-20900
NG, L. L. p 1351 N95-21091
NG, LIAN p 1353 N95-21258
NGUYEN, A. p 1512 N95-20475
NGUYEN, D. C. p 1376 N95-22154
NGUYEN, D. T. p 1259 N95-21739
p 1259 N95-21740
p 1263 N95-22396
NGUYEN, H. p 1377 N95-22312
NGUYEN, HOANG p 1555 N95-20813
NGUYEN, JEFFREY H. p 1421 N95-21803
NGUYEN, KHANH BAO p 1336 N95-22236
NGUYEN, T. T. p 1282 N95-20187
NGUYENHUU, CONG p 1489 N95-20423
NICHOLS, D. E. p 1263 N95-22396
NICKELS, J. M. p 1409 N95-21722
NICKLOW, R. M. p 1254 N95-20822
NIEH, T. G. p 1266 N95-20316
p 1276 N95-21662
NIELSEN, B. F. p 1354 N95-21656
NIEMCZYK, T. M. p 1235 N95-20139
NIEMEGEERS, IGNAS G. p 1308 N95-22087
NIEMELAE, M. p 1248 N95-22329
NIEMINEN, HANNU p 1444 N95-21007
NIEUWSTAD, T. J. p 1405 N95-21330
NIKOSKINEN, K. I. p 1310 N95-22311
NIKOSKINEN, KEIJO I. p 1291 N95-20775
NILES, J. S. p 1289 N95-20214
NILSEN, J. p 1369 N95-20335
p 1373 N95-21210
NIREUS, K. p 1288 N95-21978
NISHIMURA, KIMIHIDE p 1514 N95-20737
NISHIYAMA, M. p 1277 N95-21714
NOBLE, JOHN M. p 1505 N95-22042
NODDINGS, CHAD p 1383 N95-21933
NOLET, GUUST p 1422 N95-21808
NOORDIJK, H. p 1405 N95-21350
p 1409 N95-21718
NOORDUNG, HERMANN p 1217 N95-21894
NOPONEN, EERO p 1301 N95-21107
NOREM, J. p 1510 N95-20360
NORROS, LEENA p 1450 N95-21284
NORTH, G. L. p 1214 N95-21383
NORTHRUP, M. A. p 1250 N95-19900
NORTON, DOUGLAS p 1369 N95-20378
NOTENBOOM, W. J. G. M. p 1410 N95-22124
NUGUYEN, D. C. p 1375 N95-21919
p 1376 N95-22242
p 1377 N95-22348
NUMMINEN, J. p 1447 N95-22371
NUNEZ, C. p 1500 N95-21964
NUNOKAWA, HIROSHI p 1604 N95-22064
NYREN, K. p 1405 N95-21274

O

OAKLEY, JOHN T. p 1325 N95-20663
OBBINK, B. KLEIN p 1487 N95-19916
OBENZA, RAY p 1463 N95-20810
OBERLACK, M. p 1345 N95-21055
OBERLE, L. G. p 1366 N95-21259
OBLOW, E. M. p 1483 N95-21741
OBRIEN, K. p 1306 N95-21686
OBRIEN, K. M. p 1564 N95-20017
OBRIEN, ROBERT J. p 1400 N95-19964
OCKO, B. M. p 1573 N95-21516
OCKUNZZI, K. A. p 1214 N95-21383
OCONNELL, S. R. p 1442 N95-20710
OCONNER, T. G. p 1562 N95-22300
OCONNOR, P. p 1455 N95-21632
p 1469 N95-21713
ODELL, J. A. p 1268 N95-20392
ODONNELL, N. p 1428 N95-20099
ODYNIEC, GRAZYNA p 1521 N95-21380

OEDING, ROBERT G. p 1213 N95-22036
OEHRN, YNGVE p 1507 N95-20097
OELFKE, J. B. p 1261 N95-22119
OGATA, C. M. p 1572 N95-21408
OGILVIE, K. W. p 1604 N95-22384
OGLESBY, R. J. p 1406 N95-21379
OGLETREE, D. F. p 1373 N95-21261
OGRADY, W. E. p 1513 N95-20554
OH, HAE-SOO p 1489 N95-20274
OHAGAN, P. J. p 1247 N95-22234
OHALLARON, DAVID R. p 1475 N95-20500
OHL, KAREN E. p 1520 N95-21313
OHMANN, P. p 1580 N95-21229
OHRN, YNGVE p 1506 N95-19960
p 1516 N95-21120
OKAMOTO, HIROMI p 1370 N95-20569
OKAMOTO, Y. p 1512 N95-20477
p 1276 N95-21644
OKANO, F. p 1555 N95-20988
OKEEFE, M. A. p 1591 N95-22235
p 1548 N95-22238
OKEEFE, SEAN S. p 1369 N95-20379
OKKO, OLLI p 1427 N95-22095
OLAH, A. L. p 1455 N95-22082
OLIGER, JOSEPH p 1491 N95-20719
p 1478 N95-22108
OLIVA, G. p 1579 N95-22380
OLIVER, B. M. p 1529 N95-22280
OLSON, C. L. p 1535 N95-21328
OLSON, DANIEL p 1209 N95-20636
OLSON, J. M. p 1319 N95-20521
OLSON, R. J. p 1458 N95-20073
p 1591 N95-22129
OLSON, TIMOTHY G. p 1462 N95-20765
OLSSON, P. O. p 1388 N95-22097
OMALLEY, M. W. p 1328 N95-21139
OMATETE, O. O. p 1277 N95-21861
ONDREJKA, A. R. p 1289 N95-20191
ONEILL, MARK J. p 1322 N95-20534
ONG, LAWRENCE p 1355 N95-21954
ONIONS, R. K. p 1422 N95-21809
ONNERMARK, B. p 1243 N95-21428
p 1288 N95-21978
ONSAGER, T. G. p 1413 N95-20453
OPPENHEIM, ALAN V. p 1305 N95-21576
ORAZI, RICHARD J. p 1375 N95-21903
ORKAS, JULKAISU p 1255 N95-21108
ORLANDI, P. p 1249 N95-21036
p 1351 N95-21088
ORLANDO, VINCENT A. p 1291 N95-20599
ORNSTEIN, RICK L. p 1520 N95-21375
OROURKE, CAROLYN p 1402 N95-20441
p 1408 N95-21689
p 1408 N95-21696
ORSAK, GEOFFREY C. p 1498 N95-20608
ORSZAG, S. A. p 1349 N95-21078
OSBORNE, M. C. p 1226 N95-20357
OSBORNE, T. H. p 1553 N95-20445
OSCZEVSKI, R. J. p 1446 N95-22001
OSGOOD, RICHARD M., JR. p 1573 N95-21444
OSHIMA, NOBUAKI p 1508 N95-20134
OSINGA, H. M. p 1492 N95-21318
OSMAN, T. M. p 1263 N95-22408
OSSANDON, J. G. p 1573 N95-21483
OSTERGAARD, JENS p 1293 N95-20928
OSTERMAN, M. D. p 1211 N95-20647
OSTERYOUNG, ROBERT A. p 1246 N95-21931
OSTGAARD, JOHN p 1208 N95-20632
OSULLIVAN, GEORGE p 1313 N95-20262
OTTEN, G. J. p 1499 N95-21709
OUELLETTE, R. p 1286 N95-20611
OVER, JAMES W. p 1462 N95-20765
OVERFELT, P. L. p 1290 N95-20556
OVERLY, JOYCE A. p 1224 N95-21911
OWEN, T. E. p 1205 N95-21520
OWEN, TOBIAS p 1422 N95-21810
OWENS, J. p 1411 N95-22342
OWINGS, T. D. p 1386 N95-20703
OZEKI, TAKAHISA p 1555 N95-20987

P

PACH, O. p 1445 N95-21352
PACHECO, JAMES E. p 1394 N95-21353
PACHECOSOTELO, J. O. p 1326 N95-20733
PACKARD, RICHARD p 1503 N95-20098
PADERNO, YU. B. p 1229 N95-20859
PADIAL, NELY T. p 1478 N95-21925
PAEZ, T. L. p 1428 N95-20319
p 1486 N95-22409
PAIGE, D. A. p 1422 N95-21811
PAINTER, S. L. p 1559 N95-21581
PALFFY-MUHORAY, P. p 1569 N95-20767
PALMA, PILAR p 1246 N95-21879
PALMER, BURTON T. p 1431 N95-19971
PALMER, P. D. p 1236 N95-20361
PALMER, T. N. p 1428 N95-20140
PANCHAL, C. B. p 1396 N95-21897
PANCRATZ, DAVID J. p 1442 N95-20457
PANISKO, M. E. p 1458 N95-20153
PANUNTO, M. J. p 1319 N95-20520
PAPADOPOULOS, K. p 1298 N95-20952
PAPPERT, STEPHEN A. p 1544 N95-21466
PARADOS, THEMIS p 1323 N95-20539
PARES-SIERRA, A. p 1408 N95-21708
PARIKH, A. N. p 1253 N95-20577
PARIS, CECILE L. p 1464 N95-20996
PARKER, G. G. p 1379 N95-20695
PARKER, J. C. p 1570 N95-20841
PARKER, J. E. p 1445 N95-21180
PARKER, LYNNE E. p 1481 N95-21185
PARKER, MICHAEL A. p 1369 N95-20389
PARKINSON, W. H. p 1603 N95-21929
PARKS, P. B. p 1553 N95-20402
PARMA, E. J. p 1509 N95-20206
PARMETER, JOHN E. p 1272 N95-20889
PARRISH, CHRISTOPHER S. p 1444 N95-21160
PARTHASARATHY, RANJANI p 1277 N95-21876
PARTOW, PERRY p 1472 N95-22201
PASTERCZYK, C. E. p 1591 N95-22167
PATTEN, K. O., JR. p 1402 N95-20353
PATTERSON, B. C. p 1384 N95-20077
PATTERSON, D. B. p 1419 N95-21793
PATTERSON, DESMOND p 1418 N95-21787
PATTERSON, JAMES H., JR. p 1454 N95-22045
PATTERSON, R. A. p 1252 N95-20331
p 1260 N95-22006
PATTERSON, W. L. p 1365 N95-20604
PAUL, A. J. p 1379 N95-20723
p 1578 N95-22272
PAUL, D. R. p 1263 N95-19893
PAUL, P. H. p 1244 N95-21524
PAULS, J. p 1437 N95-20185
PAULSEN, MARK D. p 1520 N95-21375
PAULUS, RICHARD A. p 1295 N95-20937
PAXTON, A. T. p 1328 N95-21017
PAYNE, D. A. p 1270 N95-20664
PAYNE, R. C. p 1207 N95-21425
PAYNE, S. A. p 1372 N95-21135
PEAL, K. R. p 1434 N95-21677
PEARCE, K. L. p 1364 N95-20224
PEARLSTEIN, L. D. p 1548 N95-20037
PECHT, M. p 1209 N95-20640
PECK, H. D., JR. p 1438 N95-20917
PEETERS, R. p 1487 N95-19937
p 1488 N95-19942
PEGGS, S. p 1531 N95-20021
p 1532 N95-20336
p 1532 N95-20406
PEHRSSON, PEHR E. p 1577 N95-22103
PEIJNENBURG, W. J. G. M. p 1224 N95-22333
PELESKA, JAN p 1459 N95-20258
PELETIER, MARK A. p 1497 N95-22375
PELLIN, M. J. p 1254 N95-20707
PELZ, RICHARD B. p 1339 N95-20058
p 1351 N95-21089
PENAFIEL, PABLO B. p 1341 N95-20849
PENDLETON, ED p 1215 N95-21214
p 1202 N95-21877
PENDRICK, VALERIE p 1326 N95-20824
PENG, QIYANG p 1556 N95-21164
PENLAND, R. C. p 1492 N95-21285
PENNINGTON, D. p 1531 N95-20120
PENNINGTON, DOROTHY J. p 1584 N95-20750
PENNYCOOK, S. J. p 1565 N95-20245
p 1567 N95-20492
p 1568 N95-20674
PENTON, P. G. p 1584 N95-20746
PENTTILAE, S. I. p 1519 N95-21237
PEPIN, R. O. p 1420 N95-21796
PEREBOLTE, H. p 1410 N95-22330
PEREIRA, J. C. F. p 1347 N95-21069
PEREIRA, MANUEL S. p 1380 N95-21171
p 1381 N95-21488
PEREMANS, W. p 1487 N95-19903
PEREPEZKO, J. H. p 1255 N95-21137
PERETTI, STEVEN W. p 1516 N95-20993
PERKINS, R. A. p 1357 N95-22264
PERKONEN, O. P. M. p 1311 N95-22363
PERKOSKI, EMMETT p 1211 N95-20648
PERROUD, J. P. p 1512 N95-20454
PERRY, JAMES D. p 1501 N95-20731
PERRY, M. D. p 1377 N95-22312
PERRY, MICHAEL D. p 1555 N95-20813
PERSHING, DEAN E. p 1331 N95-21671
PERSSON, M. p 1548 N95-19977
PERUSSE, PATRICK p 1207 N95-20466
PESHKIN, MURRAY p 1521 N95-21454
PESKIN, M. E. p 1507 N95-20034
PETERMAN, K. p 1337 N95-22421
PETERSEN, CARSTEN LUNDE p 1496 N95-22353
PETERSEN, NANCY S. p 1441 N95-19898
PETERSEN, P. I. p 1549 N95-20038
PETERSN, GARY A. p 1272 N95-20889
PETERSOHN, CARSTA p 1459 N95-20258
PETERSON, C. W. p 1502 N95-22420
PETERSON, D. W. p 1364 N95-20398
PETERSON, R. A. p 1400 N95-19921
PETRAGLIA, J. P. p 1509 N95-20206
PETROFF, M. D. p 1524 N95-21646
PETRZILKA, V. p 1550 N95-20200
PETTIT, CHRIS p 1215 N95-21214
p 1202 N95-21877
PETTY, GRANT W. p 1428 N95-19948
PEYGHAMBARIAN, N. p 1369 N95-20082
PFEFFER, RICHARD L. p 1583 N95-22100
PFEIFER, K. B. p 1364 N95-20398
PHELAN, J. p 1379 N95-20695
PHILIPP, BARBARA L. p 1243 N95-21473
PHILIPPART, A. p 1205 N95-21369
PHILIPPS, V. p 1269 N95-20570
PHILLIPS, J. E. p 1394 N95-21294
PHILLIPS, MARILOU S. p 1589 N95-21189
PHILLIPS, MARY ANN p 1386 N95-20615
PHILLIPS, R. p 1258 N95-21600
PHILLIPS, R. J. N. p 1580 N95-21229
p 1580 N95-21230
PHILLIPS, WILLIAM T. p 1438 N95-20806
PHIPPS, C. R. p 1599 N95-21367
PHIPPS, PAUL p 1204 N95-20269
PHOEBUS, PATRICIA A. p 1429 N95-20826
PI, Y. L. p 1384 N95-19975
p 1384 N95-20101
PIATT, JASON E. p 1479 N95-22406
PICKARD, P. S. p 1371 N95-20867
PICONE, PHILIP J. p 1303 N95-21491
PICRAUX, S. T. p 1572 N95-21304
PIEPER, RON J. p 1325 N95-20715
PIERCE, P. E. p 1311 N95-22407
PIETERS, A. R. p 1449 N95-20609
PIIRONEN, P. p 1300 N95-20972
p 1598 N95-22376
PIKAENEN, MIKA p 1220 N95-21026
PILAFTSIS, A. p 1518 N95-21220
PILLSBURY, R. D., JR. p 1560 N95-21724
PIMPINELLA, RICHARD J. p 1212 N95-20654
PIN, F. G. p 1481 N95-20837
PINA, R. K. p 1593 N95-21757
PINDZOLA, M. S. p 1524 N95-21605
PINELLI, THOMAS E. p 1587 N95-20162
p 1587 N95-20163
p 1589 N95-21015
p 1590 N95-21977
PING, JIA-LUN p 1526 N95-22058
PINKEPANK, JAMES A. p 1309 N95-22230
PINKERTON, F. E. p 1500 N95-20229
PINKUS, ALAN R. p 1449 N95-20062
PINNADUWAGE, L. A. p 1522 N95-21519
PINSKER, R. I. p 1551 N95-20285
PINSKI, F. J. p 1566 N95-20405
PINTO, J. P. p 1409 N95-22101
PIOMELLI, UGO p 1346 N95-21064
PIPERIAS, P. p 1202 N95-21892
PISZCZOR, MICHAEL F. p 1322 N95-20534
PITTS, GREG p 1383 N95-21933
PITTS, W. M. p 1234 N95-20100
PLASIL, F. p 1330 N95-21554
PLATO, J. p 1540 N95-22410
PLATO, J. G. p 1376 N95-22154
PLAWSKY, J. p 1340 N95-20796
PLEWA, J. S. p 1374 N95-21694
PLEWA, MICHAEL J. p 1356 N95-22145
PLIMPTON, S. p 1529 N95-22315
PLIVELICH, ROBERT F. p 1326 N95-20814
PLUT, T. A. p 1328 N95-21139
PODBIELSKI, V. p 1395 N95-21409
PODESTA, JOHN p 1326 N95-20827
POEL, MANNES p 1455 N95-21871
POGGIO, TOMASO p 1459 N95-20157
p 1437 N95-20185
POGORELSKY, I. p 1370 N95-20572
POGORELSKY, I. V. p 1371 N95-20866
POHJONEN, H. p 1312 N95-19934
POINSOT, T. p 1249 N95-21039
p 1249 N95-21044
POLANSKY, G. F. p 1223 N95-21840
POLDER, M. D. p 1411 N95-22381
POLING, DAVID A. p 1426 N95-21875
POLITZER, P. A. p 1551 N95-20279
POLITZER, PETER p 1510 N95-20327
p 1239 N95-20668
p 1517 N95-21127
p 1525 N95-21878
p 1246 N95-22000
POLLACK, CLIFFORD p 1369 N95-20378
POLLARA, F. p 1304 N95-21535
POLLICOTT, MARK p 1490 N95-20452

POMRENKE, G. S. .... p 1563 N95-19886
POPE, STEPHEN B. .... p 1238 N95-20597
PORANEN, JOUKO .... p 1255 N95-21108
PORCELLI, D. .... p 1423 N95-21812
p 1425 N95-21821
PORTONE, A. .... p 1548 N95-20037
POSEY, P. G. .... p 1432 N95-20012
p 1433 N95-21018
POST, R. .... p 1465 N95-21021
POSTMA, H. .... p 1519 N95-21237
POULIN, BRAD .... p 1290 N95-20308
POUND, H. C. .... p 1407 N95-21666
POWELL, G. L. .... p 1244 N95-21571
POWELL, K. G. .... p 1553 N95-20425
POWELL, Q. .... p 1239 N95-20712
POWER, G. .... p 1337 N95-22427
POWERS, EDMUND M. .... p 1454 N95-22274
POWERS, LYNN M. .... p 1386 N95-20790
POZOS, ROBERT S. .... p 1444 N95-21160
PRAAGMAN, C. .... p 1497 N95-22379
PRABAKAR, S. .... p 1264 N95-20047
PRABHU, G. M. .... p 1458 N95-20136
PRADHAN, DHIRAJ K. .... p 1461 N95-20595
PRAGER, S. C. .... p 1549 N95-20112
PRAIRIE, MIKE .... p 1546 N95-21975
PRASAD, PARAS N. .... p 1540 N95-19897
PRASKOVSKY, ALEXANDER .... p 1362 N95-22458
PRATT, L. R. .... p 1236 N95-20277
PRELL, W. L. .... p 1406 N95-21379
PRELLER, R. H. .... p 1432 N95-20012
p 1433 N95-21018
PREWITT, CHARLES T. .... p 1423 N95-21813
PRICE, BETSY M. .... p 1247 N95-22207
PRICE, D. L. .... p 1536 N95-21407
PRICE, STEPHAN D. .... p 1593 N95-21755
PRIEBE, CAREY E. .... p 1504 N95-20963
PRINCE, THOMAS A. .... p 1593 N95-21756
PRITCHARD, D. .... p 1524 N95-21688
PROCASSINI, R. J. .... p 1551 N95-20315
PROSSER, REECE .... p 1290 N95-20545
PROTOPOPESCU, V. .... p 1483 N95-21741
PRUPPERS, M. J. M. .... p 1409 N95-21846
PRYTZ, K. .... p 1518 N95-21221
PSOTKA, JOSEPH .... p 1448 N95-19970
PUETTER, RICHARD C. .... p 1593 N95-21757
PUGACZ, EDWARD .... p 1204 N95-21148
PUGH, EVAN .... p 1243 N95-21447
PULLIAINEN, JOUNI T. .... p 1389 N95-21105
PULLIN, D. I. .... p 1343 N95-21045
PUNKAR, GREG .... p 1527 N95-22152
PURDY, G. .... p 1246 N95-22012
PURDY, G. M. .... p 1434 N95-21677
PURETZKY, A. A. .... p 1369 N95-20221
PUROHIT, M. V. .... p 1512 N95-20476
PUSEY, HENRY C. .... p 1233 N95-22399
PUSEY, SALLIE C. .... p 1233 N95-22399
PUTKONEN, JYRI .... p 1220 N95-21026

Q

QI, X. .... p 1517 N95-21151
QIAN, X. .... p 1568 N95-20553
p 1513 N95-20554
QIAN, YONG-ZHONG .... p 1604 N95-20383
QU, WENXIAO .... p 1556 N95-21164
QUADRIO, M. .... p 1348 N95-21072
QUARLES, G. J. .... p 1372 N95-21135
QUATE, CALVIN F. .... p 1571 N95-20964
QUI, L. .... p 1566 N95-20405
QUICK, C. ROBERT .... p 1373 N95-21312
QUINN, J. J. .... p 1524 N95-21703
QUINN, JOHN M. .... p 1600 N95-21679
QUINN, WILLIAM F. .... p 1287 N95-21626
QUINTAS, PAUL Z. .... p 1523 N95-21521
QUINTENZ, J. P. .... p 1537 N95-21603
QUIRK, JAMES J. .... p 1495 N95-22325
QUIRK, WILLIAM J. .... p 1219 N95-20148

R

RABY, PETER .... p 1298 N95-20950
RADDIN, JAMES H., JR. .... p 1442 N95-20457
RADEMAKER, B. C. .... p 1410 N95-22125
RADHAKRISHNAN, B. .... p 1578 N95-22272
RADHAKRISHNAN, V. M. .... p 1385 N95-20179
RADINSKI, RONALD P. .... p 1505 N95-21213
RADOVINSKY, A. .... p 1560 N95-21724
RAEDER, C. H. .... p 1315 N95-20443
RAEISAENEN, A. .... p 1300 N95-20972
p 1598 N95-22376
RAGHAVAN, R. S. .... p 1296 N95-20941
RAHKO, KAUKO .... p 1301 N95-21109
RAJA, R. .... p 1509 N95-20217
RAJAN, S. .... p 1212 N95-20651
RAKELS, J. L. L. .... p 1437 N95-20208
RALPH, MARK E. .... p 1394 N95-21353
RAMAKER, D. E. .... p 1568 N95-20553
RAMAKER, DAVID E. .... p 1513 N95-20554
p 1238 N95-20555
RAMANATHAN, M. .... p 1540 N95-19968
RAMANATHAN, R. .... p 1238 N95-20563
RAMBO, P. W. .... p 1551 N95-20315
RAMIREZ, G. .... p 1536 N95-21418
RAMOND, P. M. .... p 1512 N95-20469
RAMSEY, J. M. .... p 1506 N95-20030
p 1370 N95-20698
RAMSEY, P. B. .... p 1250 N95-19900
RAN, A. C. M. .... p 1495 N95-22032
RANA, D. .... p 1296 N95-20942
RANDALL, CORA E. .... p 1427 N95-22240
RANEY, C. W. .... p 1555 N95-21134
RANKINEN, M. .... p 1472 N95-22310
RAO, M. R. .... p 1490 N95-20662
RAO, M. V. S. .... p 1535 N95-21314
RAO, N. S. V. .... p 1483 N95-21741
RAO, N. S.V. .... p 1482 N95-21385
RAPP, R. P. .... p 1423 N95-21814
RAPPAZ, M. .... p 1381 N95-22268
RAPPE, ANDREW M. .... p 1501 N95-20874
RAPTIS, A. C. .... p 1402 N95-20247
p 1366 N95-21453
RASMUSSEN, JOHN E. .... p 1293 N95-20928
RATHMELL, CLAUDE .... p 1383 N95-21933
RATTI, A. .... p 1532 N95-20406
RAUBENHEIMER, T. .... p 1536 N95-21332
p 1538 N95-22155
RAUE, P. E. .... p 1467 N95-21374
RAUNIG, D. L. .... p 1306 N95-21686
RAVARD, O. .... p 1293 N95-20929
RAVENEL, RUTH .... p 1463 N95-20810
RAVIKUMAR, V. .... p 1567 N95-20492
RAWLINSON, K. SCOTT .... p 1394 N95-21353
RAY-CHAUDHURI, A. K. .... p 1541 N95-20239
RAYMOND, THOMAS D. .... p 1302 N95-21448
RAZEGHI, MANIJEH .... p 1331 N95-21660
p 1332 N95-21774
REACH, W. T. .... p 1594 N95-21771
RECK, R. A. .... p 1404 N95-20835
REDD, J. TY .... p 1223 N95-20590
REDDIX, M. D. .... p 1442 N95-20710
REDFERN, PAUL C. .... p 1525 N95-21878
REDIKER, ROBERT H. .... p 1543 N95-20601
REEB, J. C. .... p 1469 N95-21744
REED, C. B. .... p 1559 N95-21388
REED, HELEN L. .... p 1351 N95-21090
REED, R. P. .... p 1260 N95-22013
REHMANN, ALBERT .... p 1204 N95-21020
REICH, F. R. .... p 1237 N95-20470
p 1243 N95-21473
REID, WILLIAM SAMUAL, JR. .... p 1457 N95-20042
REIF, JOHN H. .... p 1473 N95-19885
REIGLE, T. .... p 1442 N95-20485
REINERT, FRANCIS R. .... p 1325 N95-20663
REINHARDT, BRUCE A. .... p 1266 N95-20251
REINHART, WILLIAM D. .... p 1215 N95-20223
REINHOLD, C. O. .... p 1526 N95-21940
REISEN, ROLF .... p 1474 N95-20123
REISER, C. .... p 1393 N95-20839
REITBERGER, P. H. .... p 1213 N95-20659
REIZER, NEAL R. .... p 1462 N95-20765
REJ, D. J. .... p 1281 N95-22428
REMINGTON, B. A. .... p 1542 N95-20364
p 1562 N95-22191
REMO, JOHN L. .... p 1599 N95-20144
REMPEL, D. .... p 1453 N95-21637
RENARD, P. A. .... p 1534 N95-21209
RENAUD, P. .... p 1316 N95-20508
p 1318 N95-20517
RENGARAJAN, S. R. .... p 1304 N95-21538
RENGARAJAN, T. N. .... p 1592 N95-21752
RENIERS, M. A. .... p 1288 N95-19890
RENTZEPIS, PETER M. .... p 1368 N95-22143
RENZETTI, N. A. .... p 1302 N95-21456
REPOND, J. .... p 1510 N95-20360
RESING, JACQUES A. C. .... p 1482 N95-21271
REST, J. .... p 1566 N95-20419
RETTERER, BERNARD L. .... p 1327 N95-20966
REUBENSTEIN, HOWARD .... p 1473 N95-22402
REUSKEN, A. .... p 1487 N95-19915
REUTER, MICHAEL .... p 1503 N95-20272
REY, J. M. .... p 1213 N95-20657
REYNOLDS, D. .... p 1298 N95-20953
REYNOLDS, E. L. .... p 1223 N95-21840
REYNOLDS, W. C. .... p 1345 N95-21055
RHOADES, C. E., JR. .... p 1385 N95-20237
RHODES, C. K. .... p 1374 N95-21743
RHODES, M. A. .... p 1557 N95-21166
RHODES, PERCY H. .... p 1331 N95-21614
RHODIN, T. N. .... p 1247 N95-22234
RICE, B. .... p 1554 N95-20446
RICH, J. W. .... p 1553 N95-20411
RICH, WILLIAM F. .... p 1205 N95-22161
RICHARDS, DALE W. .... p 1209 N95-20637
RICHARDSON, D. E. .... p 1238 N95-20563
RICHARDSON, LONDE A. .... p 1446 N95-21941
RICHES, MICHAEL R. .... p 1404 N95-20991
RICHMOND, G. L. .... p 1544 N95-20876
p 1245 N95-21826
p 1245 N95-21827
p 1547 N95-22074
RICHTER, J. .... p 1224 N95-22333
RIDE, D. J. .... p 1405 N95-21274
RIDER, WILLIAM J. .... p 1353 N95-21317
RIEGER, D. J. .... p 1327 N95-20882
p 1329 N95-21390
p 1329 N95-21394
p 1259 N95-21838
RIGHINI, G. .... p 1493 N95-21468
RIGHTER, A. W. .... p 1334 N95-22118
RIIHIAHO, S. .... p 1472 N95-22310
RIIHINEN, B. .... p 1472 N95-22310
RILEY, G. N., JR. .... p 1571 N95-21167
RILEY, M. E. .... p 1560 N95-21609
RILEY, N. .... p 1293 N95-20924
RILEY, N. G. .... p 1293 N95-20925
p 1293 N95-20927
RILEY, STUART .... p 1298 N95-20950
RINGEL, S. A. .... p 1323 N95-20542
RIST, ULRICH .... p 1352 N95-21095
RISTOLAINEN, E. O. .... p 1252 N95-20365
RIVERA, DAVID F. .... p 1306 N95-21672
RIZZATO, F. B. .... p 1560 N95-21593
RIZZO, T. G. .... p 1528 N95-22239
RIZZO, THOMAS G. .... p 1535 N95-21254
ROBE, R. Q. .... p 1306 N95-21686
ROBELEN, DAVID B. .... p 1215 N95-20080
ROBERTS, GLYN O. .... p 1331 N95-21614
ROBERTS, R. G. .... p 1518 N95-21225
ROBERTSON, P. J. .... p 1327 N95-20882
p 1329 N95-21390
ROBIN, D. .... p 1519 N95-21262
ROBINETT, R. D. .... p 1379 N95-20695
ROBINO, C. V. .... p 1378 N95-20053
ROBINSON, D. G. .... p 1454 N95-22466
ROBINSON, D. W. .... p 1493 N95-21423
ROBINSON, DEREK W. .... p 1487 N95-19917
ROBINSON, HAROLD C. .... p 1506 N95-22360
ROBINSON, JEMETT L. .... p 1446 N95-21941
ROBINSON, R. A. .... p 1387 N95-21386
ROBINSON, S. J. .... p 1512 N95-20491
ROBINSON, SABINA I. .... p 1445 N95-21629
ROBLESPIEDRAS, EDUARDO FRANCISCO
p 1256 N95-21270
ROCCI, PETER J. .... p 1209 N95-20637
ROCCO, A. G. .... p 1309 N95-22229
ROCHAU, G. E. .... p 1558 N95-21247
ROCHE, M. F. .... p 1392 N95-20480
RODRIQUEZ, DAVID .... p 1306 N95-21834
ROGALLO, R. S. .... p 1343 N95-21045
p 1343 N95-21046
ROGELSTAD, JON M. .... p 1587 N95-20039
ROGER, C. .... p 1270 N95-20689
ROGERS, C. .... p 1594 N95-21771
ROGERS, C. S. .... p 1500 N95-20106
ROGERS, GEORGE W. .... p 1504 N95-20963
ROGERS, M. M. .... p 1345 N95-21055
p 1360 N95-22446
ROGERS, MAX .... p 1207 N95-20466
ROGERS, MICHAEL M. .... p 1350 N95-21084
ROGERSON, J. .... p 1537 N95-21494
ROGIER, JEAN-LUC .... p 1299 N95-20959
ROHWEIN, G. J. .... p 1290 N95-20474
ROMEA, R. D. .... p 1370 N95-20572
ROMINE, C. H. .... p 1477 N95-21602
ROMU, JYRKI .... p 1255 N95-21128
RONDAY, R. .... p 1410 N95-22330
ROOSE, L. D. .... p 1290 N95-20474
ROPER, ROBERT G. .... p 1414 N95-20591
RORIJE, E. .... p 1224 N95-22333
ROSE, DAVID A. .... p 1454 N95-22099
ROSE, J. .... p 1532 N95-20406
ROSEN, W. .... p 1212 N95-20651
ROSENBAUM, S. E. .... p 1335 N95-22144
ROSENBERG, CARLA B. .... p 1285 N95-21322
ROSENBERG, N. J. .... p 1401 N95-20089
ROSENBLUM, B. Z. .... p 1256 N95-21300
ROSENBLUTH, M. N. .... p 1553 N95-20402
ROSENTHAL, PETER .... p 1328 N95-21178
ROSER, THOMAS .... p 1536 N95-21342
ROSETTI, JAMES B. .... p 1541 N95-20231
ROSHKO, A. .... p 1200 N95-20175
ROSHKO, ANATOL .... p 1200 N95-20177
ROSINSKI, STAN T. .... p 1256 N95-21286
ROTH, CARL .... p 1459 N95-20310
ROTH, DAVID .... p 1429 N95-20857
ROTH, J. A. .... p 1318 N95-20515

ROUGHTON, M. G. p 1211 N95-20645
ROUSH, TED L. p 1423 N95-21815
ROUTBORT, J. L. p 1226 N95-20027
ROVELLI, C. p 1580 N95-20324
ROVELSTAD, AMY L. p 1348 N95-21076
ROWE, NEIL C. p 1586 N95-19956
p 1587 N95-20302
ROWE, R. K. p 1235 N95-20139
ROY, GABRIEL D. p 1266 N95-20227
ROYER, T. C. p 1435 N95-21682
ROZHKOV, MIKHAIL p 1415 N95-21511
ROZUM, JAMES p 1468 N95-21567
RUAULT, P. p 1205 N95-21369
RUBIO, ANGEL p 1281 N95-22470
RUBNER, MICHAEL F. p 1267 N95-20328
RUELLE, D. p 1488 N95-19944
RUETSCH, G. p 1249 N95-21039
RUETSCH, G. R. p 1249 N95-21043
RUETSCH, GREGORY R. p 1250 N95-22442
RUF, T. p 1581 N95-21604
RUGGIERO, A. G. p 1563 N95-19925
p 1533 N95-20766
p 1517 N95-21140
RUMPF, A. N. p 1367 N95-21546
RUOFF, RODNEY p 1567 N95-20461
RUOTOISTENMAEKI, A. p 1286 N95-21333
RUPEN, MICHAEL P. p 1593 N95-21763
RUSCH, DAVID W. p 1427 N95-22240
RUSSELL, S. J. p 1376 N95-22154
RUSSELL, STEPHEN D. p 1325 N95-20726
p 1375 N95-21903
RUSSELL, T. P. p 1229 N95-20840
RUSZCZYK, WILLIAM p 1209 N95-20638
RUTH, M. p 1437 N95-20471
RUTLAND, C. J. p 1249 N95-21040
RUTT, H. N. p 1370 N95-20550
RUTTKAY, Z. p 1467 N95-21374
RUUD, C. O. p 1280 N95-22270
RYAN, J. p 1352 N95-21098
RYBICKI, G. C. p 1319 N95-20518
RYDLUND, O. p 1232 N95-22096
RYE, R. R. p 1242 N95-21309
RYERSON, FREDERICK J. p 1599 N95-20145
RYNE, R. D. p 1539 N95-22243
p 1539 N95-22298

S

SABA, COSTANDY S. p 1278 N95-21969
SABER, M. p 1278 N95-21885
SABERI, A. p 1484 N95-22139
SABERI, ALI p 1483 N95-21618
SABOUNGI, M. L. p 1536 N95-21407
SADDOUGHI, SEYED G. p 1361 N95-22451
p 1362 N95-22456
SADDOW, STEPHEN E. p 1292 N95-20825
SADLER, BRIAN p 1498 N95-21219
SAEWERT, G. p 1463 N95-20901
SAFAEINILLI, ALI p 1504 N95-20918
SAGAUT, P. p 1347 N95-21068
SAGDAHL, L. T. p 1577 N95-22166
SAHU, SUJIT K. p 1499 N95-21945
SAILSBURY, H. E. p 1258 N95-21568
SAKALAUKUS, PETER J. p 1458 N95-20095
SAKS, N. S. p 1566 N95-20400
SAKUMOTO, W. K. p 1527 N95-22122
SALAMON, W. J. p 1473 N95-22390
SALAZAR, M. A. p 1558 N95-21368
SALEM, JONATHAN A. p 1386 N95-20790
SALEM, M. A. p 1312 N95-19966
SALES, B. C. p 1275 N95-21482
SALES, G. S. p 1298 N95-20953
SALIERES, P. p 1377 N95-22312
SALIK, M. D. p 1212 N95-20653
SALMERON, M. p 1373 N95-21261
SALMON, JOHN K. p 1358 N95-22290
SALONEN, ERKKI p 1430 N95-21413
SALTMARSH, C. p 1532 N95-20336
SAMANIEGO, JEAN-MICHAEL p 1249 N95-22439
SAMARA, G. A. p 1268 N95-20396
SAMBE, H. p 1568 N95-20553
p 1513 N95-20554
SAMMELLS, ANTHONY F. p 1253 N95-20481
p 1239 N95-20716
SAMPLE, R. S. p 1545 N95-21832
SAMPLE, REBECCA S. p 1593 N95-21755
SAMUEL, ARTHUR G. p 1450 N95-21101
SANCHEZ, A. p 1500 N95-21136
SANCHEZGARCIA, A. M. p 1550 N95-20204
SANDERS, D. B. p 1594 N95-21773
SANDERS, J. A. p 1495 N95-22151
SANDERSON, S. R. p 1357 N95-22212
SANDHAM, N. D. p 1348 N95-21074
SANDOVAL, C. E. p 1314 N95-20338
SANDRECZKI, T. C. p 1273 N95-21014
SANDS, W. A. p 1479 N95-20005
SANFORD, T. B. p 1434 N95-21461
SANFORD, T. W. L. p 1539 N95-22306
SANGER, M. J. p 1257 N95-21399
SANTELLA, M. L. p 1280 N95-22266
SANTINI, DANILO J. p 1329 N95-21296
SANTORU, J. p 1314 N95-20311
SAOUTIC, B. p 1551 N95-20205
SARAVOLAC, E. G. p 1442 N95-20602
SARFF, J. S. p 1549 N95-20113
SARGIS, P. p 1313 N95-20119
SARGIS, P. D. p 1542 N95-20403
SARNO, C. p 1209 N95-20635
p 1213 N95-20656
SAROFIM, A. F. p 1233 N95-20045
SARRAO, J. L. p 1237 N95-20368
SARSOUR, HISHAM N. p 1466 N95-21288
SARTENAER, A. p 1495 N95-22317
SARTORI, MICHAEL A. p 1504 N95-20296
SASAKI, S. p 1424 N95-21816
SASS, B. M. p 1312 N95-19966
SATOGATA, T. p 1532 N95-20336
SAUERS, I. p 1326 N95-20791
p 1243 N95-21500
SAUNDERS, THOMAS F. p 1462 N95-20721
SAUTER, O. p 1554 N95-20446
SAVAGE, M. p 1380 N95-21359
SAVARD, R. M. p 1458 N95-20153
SAWICKI, R. p 1534 N95-21209
SAXENA, A. p 1526 N95-21934
p 1578 N95-22297
SAYLOR, P. E. p 1493 N95-21564
SCANLON, RAYMOND p 1450 N95-21968
SCHAFF, WILLIAM J. p 1369 N95-20379
SCHAPPERT, G. T. p 1501 N95-20246
SCHARF, LOUIS L. p 1308 N95-22041
SCHARLEMANN, T. p 1389 N95-21552
SCHEFER, R. W. p 1243 N95-21512
SCHEFFEY, JOSEPH L. p 1203 N95-22352
SCHEIMAN, D. p 1319 N95-20518
SCHEIMAN, D. A. p 1334 N95-22112
SCHEIMAN, DAVID p 1322 N95-20537
SCHELLMAN, HEIDI p 1511 N95-20418
SCHEPERS, HENK p 1465 N95-21025
SCHEPS, RICHARD p 1546 N95-21898
SCHIPPERS, S. p 1525 N95-21857
SCHLAPFER, MARTIN F. p 1594 N95-21772
SCHLECHTRIEM, STEFAN p 1207 N95-20860
SCHLUETER, JOHN A. p 1567 N95-20479
SCHMID, P. J. p 1349 N95-21079
SCHMIDT, F. A. p 1259 N95-21737
SCHMIDT, G. L. p 1223 N95-21840
SCHMIDT, GREGORY W. p 1439 N95-21526
SCHMIDT, RICHARD p 1506 N95-22088
SCHMITT, D. p 1254 N95-20822
SCHMITT, R. C. p 1285 N95-20050
SCHMITT, RANDAL L. p 1302 N95-21448
SCHNABEL, ROBERT p 1517 N95-21126
SCHNACK, D. D. p 1548 N95-20029
SCHNEIBEL, J. H. p 1250 N95-20044
p 1230 N95-21481
SCHNEIDER, J. M. p 1401 N95-20193
SCHNEIDER, R. P., JR. p 1314 N95-20341
p 1575 N95-21991
SCHNEIDER, S. P. p 1201 N95-21031
SCHNEIDER, STEVEN P. p 1216 N95-21436
SCHNEIDER, WALTER T. p 1333 N95-21900
SCHOENBACHER, H. p 1335 N95-22184
SCHOLL, E. p 1532 N95-20336
SCHOLTENS, A. C. J. p 1494 N95-21955
SCHONBERG, J. A. p 1340 N95-20796
SCHRAGE, DEAN S. p 1338 N95-19933
SCHREIBER, A. L. p 1311 N95-22407
SCHUBERT, LONNIE E. p 1256 N95-21286
SCHUCH, R. p 1508 N95-20133
SCHULTZ, F. J. p 1511 N95-20422
SCHULTZ, J. H. p 1562 N95-22300
SCHULZ, D. R. p 1528 N95-22265
SCHULZ, R. B. p 1278 N95-21909
p 1278 N95-21937
SCHULZE, JAMES F. p 1599 N95-20144
SCHUMACHER, J. M. p 1499 N95-19941
SCHURIG, H. H. p 1318 N95-20515
SCHWANK, J. R. p 1314 N95-20338
p 1334 N95-22086
SCHWARZBEIN, Z. E. p 1458 N95-20070
SCHWETTMAN, H. A. p 1374 N95-21528
SCHWINN, T. p 1542 N95-20364
SCOTT, C. A. p 1518 N95-21224
p 1529 N95-22303
SCOTT, L. p 1205 N95-21642
SCOTT, MICHAEL A. p 1200 N95-20688
SCOTT, S. D. p 1558 N95-21242
SCOTT, T. C. p 1501 N95-20725
SCROGGS, J. S. p 1493 N95-21564
SEAL, SYLVIA p 1388 N95-20006
SEALS, J. DENNIS p 1209 N95-20639
p 1212 N95-20654
SEARLES, DANIEL p 1464 N95-20910
SEARSON, P. C. p 1257 N95-21476
SEEMAN, J. T. p 1536 N95-21335
SEESTROM, S. J. p 1519 N95-21237
SEIBERT, EDWARD J. p 1333 N95-21906
SELJEE, R. p 1586 N95-19904
SELTVEIT, ANNE HELGA p 1469 N95-21711
SEMINARIO, JORGE M. p 1510 N95-20327
SEN, S. p 1561 N95-21847
SENF, H. p 1272 N95-20856
SENGUPTA, S. p 1570 N95-20841
SENSHARMA, DILIP K. p 1281 N95-22470
SERAYDARIAN, R. P. p 1556 N95-21163
SERFOZO, RICHARD F. p 1475 N95-20566
SESSLER, A. M. p 1563 N95-20014
SESSLER, ANDREW M. p 1370 N95-20569
p 1569 N95-20793
SETH, K. K. p 1245 N95-21745
SETTERSTEN, THOMAS B. p 1551 N95-20232
SEVERI, PAULA p 1488 N95-20054
SEVILLANO, EVELIO p 1315 N95-20488
p 1336 N95-22412
SEXTON, DOUGLAS A. p 1325 N95-20727
p 1375 N95-21903
SEXTON, F. W. p 1314 N95-20338
p 1334 N95-22086
SHADARAM, M. p 1212 N95-20651
SHAFARMAN, W. N. p 1394 N95-21294
SHAFER, STEVEN A. p 1543 N95-20564
SHAFF, D. p 1395 N95-21409
SHAFII, B. p 1240 N95-20836
SHAH, V. M. p 1580 N95-21420
SHAHAM, JACOB p 1600 N95-21615
SHAJII, A. p 1330 N95-21442
SHAKER, JOHN F. p 1220 N95-20533
SHANDARIN, SERGEI F. p 1579 N95-19947
SHANEYFELT, M. R. p 1314 N95-20338
SHANK, STEVEN M. p 1547 N95-22205
SHANNY, R. p 1298 N95-20952
SHAPIRO, PHILIP p 1320 N95-20523
SHAPPELL, S. A. p 1441 N95-20307
SHARIFF, K. p 1344 N95-21048
p 1345 N95-21056
SHARP, RICHARD p 1490 N95-20452
SHARP, W. M. p 1552 N95-20318
SHAW, B. A. p 1251 N95-20178
SHAW, KEVIN B. p 1390 N95-22055
SHAW, R. W. p 1370 N95-20698
SHAW, W. J. p 1364 N95-20320
SHEA, T. p 1532 N95-20336
p 1532 N95-20406
SHEARER, JUDY p 1409 N95-21914
SHEEN, S. H. p 1366 N95-21453
SHEFFIELD, R. L. p 1375 N95-21919
p 1376 N95-22154
p 1376 N95-22242
p 1377 N95-22348
SHEFT, STANLEY p 1504 N95-20823
SHELDON, B. W. p 1275 N95-21289
SHELLENBARGER, ZANE A. p 1317 N95-20510
SHELTON, W. A. p 1566 N95-20405
SHELTRY, JOSEPH F. p 1310 N95-22246
SHEN, Y. R. p 1274 N95-21263
SHEN, Z. X. p 1574 N95-21712
SHEN, ZHONGJUN p 1581 N95-21887
SHEPARD, H. p 1488 N95-20169
SHEPHERD, MICHAEL T. p 1312 N95-19909
SHEPODD, TIMOTHY J. p 1283 N95-21514
SHER, A. p 1328 N95-21017
SHERBY, OLEG D. p 1266 N95-20316
SHERIDAN, T. J. p 1314 N95-20338
SHERWIN, M. E. p 1327 N95-20882
p 1329 N95-21390
SHERWIN, R. p 1394 N95-20985
SHERWOOD, B. A. p 1376 N95-22154
p 1377 N95-22348
SHI, CHUNLEI p 1235 N95-20188
SHI, ZHENG-QIANG p 1229 N95-20913
SHIH, M. p 1453 N95-21637
SHIMABUKURO, RANDY L. p 1325 N95-20726
SHIMADA, TSUTOMU p 1373 N95-21312
SHIMOYAMA, J. p 1564 N95-20127
SHINES, J. E. p 1391 N95-22398
SHINN, N. D. p 1247 N95-22234
SHIRER, HAMPTON N. p 1431 N95-22393
SHIRLEY, W. L. p 1592 N95-22263
SHMOYS, D. B. p 1466 N95-21269
SHOCHET, M. J. p 1539 N95-22195
SHORT, R. p 1298 N95-20952
SHOWKATI, H. p 1384 N95-20003
SHUAI, Z. p 1526 N95-21934
p 1578 N95-22297
SHUL, R. J. p 1327 N95-20882
p 1329 N95-21390
p 1329 N95-21394

p 1572 N95-21419
p 1259 N95-21838
SHULMAN, IGOR p 1433 N95-21156
SHURYAK, E. p 1519 N95-21302
SHUTE, VALERIE J. p 1448 N95-19970
SIDERS, CRAIG W. p 1374 N95-21480
SIEBELIST, R. p 1516 N95-21114
SIEGEL, JANE p 1468 N95-21567
p 1468 N95-21627
SIEGNER, U. p 1569 N95-20677
p 1569 N95-20678
p 1514 N95-20732
SIEMANN, R. p 1536 N95-21334
SIEREVOGEL, L. M. p 1356 N95-22063
SIEWIOREK, DANIEL P. p 1461 N95-20622
SIGGIA, ERIC D. p 1358 N95-22294
SIGLER, F. E. p 1376 N95-22154
SIHVOLA, A. H. p 1311 N95-22363
SIHVOLA, ARI H. p 1291 N95-20775
p 1502 N95-21102
p 1544 N95-21103
SIKIVIE, P. p 1512 N95-20469
SIKKA, V. K. p 1252 N95-20359
p 1253 N95-20673
p 1257 N95-21555
p 1263 N95-22346
SILBERMAN, GABRIEL G. p 1307 N95-21915
SILKONEN, T. p 1352 N95-21106
SILLICK, DANIEL p 1456 N95-22400
SILVER, RAE p 1447 N95-22475
SILVERSTEIN, D. A. p 1451 N95-22473
SILVESTRINI, J. p 1348 N95-21075
SIMA'AN, K. p 1585 N95-21414
SIMHA, RAHUL p 1456 N95-22431
SIMMONS, C. T. p 1570 N95-20820
SIMMS, D. p 1391 N95-20260
SIMOLA, JUHA p 1445 N95-21348
SIMON-GILLO, J. p 1527 N95-22078
SIMON, C. p 1276 N95-21650
SIMON, M. K. p 1304 N95-21536
SIMONS, W. R. p 1467 N95-21389
SIMONSON, J. M. p 1245 N95-21732
SIMPSON, D. p 1404 N95-21034
SIMPSON, JOHN W. p 1383 N95-20764
SIMPSON, M. L. p 1330 N95-21554
SIMS, PAUL E. p 1323 N95-20540
SIMUNICH, K. L. p 1412 N95-20171
SIMUNOVIC, S. p 1460 N95-20358
SINCLAIR, R. p 1277 N95-21748
SINGER, MICHAEL F. p 1460 N95-20326
SINGH, D. p 1229 N95-20912
SINGH, J. P. p 1226 N95-20027
p 1229 N95-20912
SINGH, M. S. p 1534 N95-21208
SINGLETON, A. H. p 1241 N95-21172
SISTERSON, D. L. p 1401 N95-20193
p 1335 N95-22189
SIVASHANKAR, N. p 1481 N95-20828
SIVCO, D. L. p 1577 N95-22168
SKAHILL, GEORGE p 1302 N95-21405
SKARHA, J. E. p 1507 N95-20110
SKARKA, V. p 1500 N95-21592
SKARPAAS, K. p 1538 N95-22155
SKIDMORE, J. p 1389 N95-21552
SKINNER, C. H. p 1557 N95-21240
SKOFRONICK, GRETCHEN L. p 1260 N95-21926
SKULINA, K. M. p 1274 N95-21175
SLACK, D. S. p 1562 N95-22300
SLASKI, M. p 1577 N95-22166
SLAVEY, JAMES C. p 1200 N95-19991
SLAYTON, E. M. p 1314 N95-20338
SLINEY, HAROLD E. p 1223 N95-19901
SLOOFF, W. p 1407 N95-21635
SMALLEY, DAVID J. p 1203 N95-21831
SMART, R. M. p 1409 N95-21914
SMIRNOV, A. Y. p 1521 N95-21443
SMIRNOV, ALEXEI YU. p 1603 N95-21316
SMITH, B. p 1246 N95-22012
SMITH, B. G. p 1231 N95-22009
SMITH, BRIAN G. p 1308 N95-22021
SMITH, D. p 1470 N95-21972
SMITH, DON J. p 1415 N95-21308
SMITH, F. R. p 1329 N95-21301
SMITH, G. A. p 1492 N95-21266
SMITH, G. S. p 1281 N95-22434
SMITH, GREGORY P. p 1247 N95-22150
SMITH, HOOVER A. p 1278 N95-21969
SMITH, L. A. p 1312 N95-19966
SMITH, M. F. p 1413 N95-20453
SMITH, M. T. p 1251 N95-20090
SMITH, MARJOLEIN V. p 1444 N95-20979
SMITH, PAUL MARTIN p 1272 N95-20889
SMITH, PETER L. p 1603 N95-21929
SMITH, R. D. p 1259 N95-21687
SMITH, ROGER L. p 1218 N95-21384
SMITH, SHEILDA B. p 1286 N95-20717
SMITH, SHELDON D. p 1221 N95-20124
SMITH, T. I. p 1374 N95-21528
SMITH, TODD p 1368 N95-19987
SMITH, W. H. p 1246 N95-22012
SMITH, WALLACE A. p 1268 N95-20460
SMITHE, D. N. p 1515 N95-20911
SMYRL, N. R. p 1244 N95-21571
SMYTH, J. R. p 1424 N95-21817
SMYTH, WILLIAM H. p 1601 N95-20797
SNAVELY, DEANNE p 1513 N95-20621
p 1224 N95-21911
SNOW, JONATHAN E. p 1435 N95-21918
SNYDER, ROBERT S. p 1331 N95-21614
SO, R. H. p 1453 N95-21700
SOBERING, TIM J. p 1302 N95-21448
SODEN, J. M. p 1330 N95-21545
p 1334 N95-22118
SODEN, JERRY M. p 1314 N95-20286
SOGGE, J. p 1242 N95-21426
SOKOLOV, V. G. p 1562 N95-22282
SOKOLOWSKI, ROBERT S. p 1336 N95-22271
SOLANTAUSTA, Y. p 1236 N95-20290
SOLANTAUSTA, YRJO p 1398 N95-22425
SOLARZ, R. p 1389 N95-21552
SOLDATOV, A. V. p 1525 N95-21860
SOLKA, JEFFREY L. p 1504 N95-20963
SOLOMON, STANLEY C. p 1427 N95-22240
SOMERVILLE, R. C. J. p 1408 N95-21708
SOMMEIJER, B. P. p 1490 N95-20424
p 1402 N95-20440
p 1493 N95-21434
SOMMER, W. F. p 1538 N95-22050
SONDERGAARD, ROLF p 1350 N95-21085
SONG, XING-CHANG p 1491 N95-20734
SONI, A. p 1523 N95-21551
SONTAG, EDUARDO D. p 1485 N95-22213
SOOS, Z. G. p 1265 N95-20121
SOPORI, B. p 1279 N95-22091
SORATHIA, USMAN A. p 1266 N95-20293
p 1266 N95-20294
p 1233 N95-22467
SOUFLI, R. p 1274 N95-21175
SOUMPASIS, D. M. p 1438 N95-21366
SOUSA, J. M. M. p 1347 N95-21069
SOVERS, O. J. p 1412 N95-20002
SOWA, E. C. p 1262 N95-22313
SOWA, M. J. p 1296 N95-20941
SOWERS, C. H. p 1571 N95-21256
SPALART, P. R. p 1351 N95-21091
SPALTENSTEIN, ESTHER p 1246 N95-21879
SPANN, J. R. p 1278 N95-21907
SPECHT, E. D. p 1571 N95-21167
p 1578 N95-22269
SPECK, D. RALPH p 1371 N95-20817
SPEE, R. p 1315 N95-20380
SPEIGHT, T. J. p 1299 N95-20957
SPENCE, B. R. p 1322 N95-20535
SPENCE, E. p 1488 N95-19943
SPENCE, K. p 1586 N95-21645
SPENCER, J. p 1538 N95-22155
SPENCER, R. R. p 1537 N95-21460
SPENCER, THOMAS A. p 1327 N95-20905
SPENTZOURIS, P. p 1530 N95-22340
SPERBER, K. R. p 1428 N95-20140
SPETH, J. A. p 1372 N95-21135
SPEZIALE, C. G. p 1338 N95-20009
SPIESBERGER, JOHN L. p 1436 N95-22209
SPINDT, C. A. p 1325 N95-20661
SPITKOVSKY, ANATOLY p 1536 N95-21337
SPITZ, JOSEPH D. p 1341 N95-20968
SPOONER, CHARLES p 1383 N95-21933
SPOONER, S. p 1385 N95-20374
SPRAGUE, A. p 1424 N95-21818
SPRINGSTEEN, B. p 1401 N95-20192
SPROUL, W. D. p 1230 N95-21445
SPURGEN, W. p 1291 N95-20697
SQUIRES, K. D. p 1345 N95-21058
p 1346 N95-21059
SQUIRES, KYLE D. p 1347 N95-21065
SRIDHAR, S. p 1211 N95-20647
SRINIVASAN-RAO, T. p 1533 N95-20573
SRIVASTAVA, Y. N. p 1529 N95-22279
ST.CLAIR, TERRY L. p 1268 N95-20407
ST.JOHN, H. p 1555 N95-21141
STACEY, C. p 1238 N95-20563
STACHIW, J. D. p 1270 N95-20603
p 1388 N95-22411
STACHIW, JERRY D. p 1279 N95-22047
STAFFANS, O. J. p 1486 N95-22366
p 1486 N95-22367
STAFFORD, CAROLYN p 1440 N95-22065
STAGGS, K. J. p 1286 N95-20356
STALDER, R. E. p 1367 N95-21507
STALLARD, B. R. p 1235 N95-20139
STALLINGS, D. C. p 1303 N95-21459
STAM, G. p 1273 N95-20976
STANGE, A. p 1511 N95-20404
STANNETT, V. T. p 1268 N95-20428
STANNILAND, DENNIS R. p 1199 N95-19946
STANNY, R. R. p 1448 N95-19957
p 1498 N95-20102
p 1441 N95-20307
STAPELBROEK, M. G. p 1524 N95-21646
STAPP, D. C. p 1406 N95-21487
STARACE, A. F. p 1509 N95-20242
STARR, T. L. p 1340 N95-20781
STATHIS, P. p 1550 N95-20190
STATLER, RICHARD p 1320 N95-20523
STAUDACHER, T. p 1416 N95-21778
STAUDIGEL, H. p 1421 N95-21802
STAUFFER, THOMAS B. p 1282 N95-19922
STAUNTON, J. B. p 1566 N95-20405
STECKENRIDER, J. SCOTT p 1264 N95-20018
STEEVES, M. M. p 1260 N95-22013
STEHNEY, A. F. p 1441 N95-20074
STEINBERG, M. p 1283 N95-21211
STEINHAUER, L. C. p 1370 N95-20572
STEINSMO, U. p 1277 N95-21873
STEINTHORSSON, E. p 1356 N95-21959
STEINVALL, OVE p 1434 N95-21320
STELBOVICS, A. T. p 1508 N95-20197
p 1509 N95-20199
STELZER, T. p 1580 N95-21230
STEN, JOHAN C.-E. p 1300 N95-21104
STENBERG, ROLF p 1341 N95-20981
STENGEL, JOHN D. p 1213 N95-22024
STEPANOV, ANDREY p 1374 N95-21480
STEPHENSON, DAVID A. p 1302 N95-21448
STERNE, P. A. p 1253 N95-20447
STEVENS, C. G. p 1237 N95-20386
p 1367 N95-21478
STEVENS, C. O. p 1265 N95-20220
STEVENS, DALE p 1546 N95-21975
STEVENS, J. W. p 1393 N95-20863
STEVENS, R. L. p 1407 N95-21608
STEWART, J. E. p 1516 N95-21114
STEWART, JEFFREY A. p 1461 N95-20665
STEWART, JOHN E., II p 1215 N95-19931
STEWART, K. R. p 1544 N95-20844
STEWART, S. R. p 1305 N95-21542
STEWART, SUSAN H. p 1589 N95-21189
STILL, D. L. p 1445 N95-21180
STINSON, MICHAEL C. p 1264 N95-20018
STOCKS, G. M. p 1566 N95-20405
STOCKSTILL, R. L. p 1341 N95-20843
STOKES, T. I. p 1364 N95-20224
STOKLOSA, MARK J. p 1209 N95-20637
STOLL, S. P. p 1565 N95-20265
p 1545 N95-21643
STONE, DANIEL A. p 1407 N95-21596
STONE, G. F. p 1531 N95-20015
STONEKING, M. p 1549 N95-20114
STOORVOGEL, A. A. p 1484 N95-22139
STOORVOGEL, ANTON A. p 1483 N95-21618
STOUGHTON, R. S. p 1364 N95-20321
STRACHAN, J. D. p 1557 N95-21240
STRAIT, E. J. p 1554 N95-20446
STRAIT, L. H. p 1267 N95-20390
STRANGEWAYS, H. J. p 1299 N95-20958
STRANICK, S. J. p 1365 N95-20413
p 1253 N95-20577
p 1241 N95-21217
STRASSBURGER, E. p 1272 N95-20856
STRAUS, JAY B. p 1522 N95-21492
STRAUSS, H. p 1602 N95-20593
STRAW, TIMOTHY B. p 1333 N95-21865
STRAYER, W. TIMOTHY p 1301 N95-21277
STREET, ROBERT L. p 1434 N95-21293
STREETT, CRAIG p 1353 N95-21258
STRETCH, THOMAS p 1212 N95-20650
STRINGFIELD, R. M. p 1334 N95-22011
STROEM, T. p 1242 N95-21426
STROM, STEPHEN W. p 1205 N95-22161
STROPKI, J. T. p 1259 N95-21687
STROUBOULIS, T. p 1480 N95-20083
p 1490 N95-20565
p 1490 N95-20588
p 1497 N95-22388
STRUM, M. J. p 1232 N95-22126
STUHLINGER, ERNST p 1217 N95-21894
STUMP, BRIAN p 1426 N95-21932
STURGE, M. D. p 1572 N95-21287
STURTEVANT, B. p 1357 N95-22212
SU, Z. P. p 1581 N95-21604
SU, ZHAO-BIN p 1577 N95-22178
p 1582 N95-22198
SUBHLOK, JASPAL p 1475 N95-20500
SUCHA, G. p 1577 N95-22168
SUENAGA, M. p 1564 N95-20127
SUESS, STEVEN T. p 1426 N95-21874
SUGIURA, N. p 1418 N95-21790
p 1422 N95-21807

SUH, H. H. p 1400 N95-19965
SULLIVAN, E. J. p 1433 N95-20420
SULLIVAN, JOHN P. p 1201 N95-21031
SUMMERS, GEOFFREY P. p 1316 N95-20507
p 1319 N95-20519
p 1319 N95-20520
p 1320 N95-20523
p 1320 N95-20524
SUMMERS, L. J. p 1272 N95-20892
SUN, B. p 1237 N95-20470
SUN, H. p 1205 N95-21520
SUN, QUN p 1235 N95-20188
SUN, T. p 1233 N95-20045
SUN, WEISHI p 1327 N95-20967
SUN, XIAOBAI p 1476 N95-21257
p 1476 N95-21341
SUN, Y. R. p 1573 N95-21483
SUN, ZHENG p 1380 N95-21416
p 1380 N95-21446
SUNDSET, T. p 1242 N95-21426
SURACE, JASON A. p 1593 N95-21759
p 1593 N95-21767
SURI, MANIL p 1341 N95-20981
SUSSMANN, HECTOR J. p 1485 N95-22213
SUTHERLAND, H. J. p 1388 N95-22070
SUTLIFF, J. A. p 1571 N95-21167
p 1232 N95-22126
p 1578 N95-22269
SUZUKI, ANDREW p 1546 N95-21975
SUZUKI, N. p 1555 N95-20988
SVENSSON, L. p 1230 N95-21417
p 1232 N95-22096
SVENSSON, THOMAS p 1386 N95-21133
SWAAN, P. p 1405 N95-21327
p 1405 N95-21329
p 1406 N95-21351
SWAB, JEFFREY A. p 1269 N95-20486
SWANSON, P. D. p 1369 N95-20389
SWEENEY, M. A. p 1549 N95-20075
SWEENEY, MARY P. p 1269 N95-20486
SWEET, J. N. p 1364 N95-20398
SWEGLE, J. W. p 1341 N95-20831
SWEIDER, D. p 1542 N95-20489
SWENT, R. L. p 1374 N95-21528
SWIETLIK, C. E. p 1586 N95-20016
SWIFT, W. M. p 1407 N95-21617
SWINDLE, T. D. p 1424 N95-21819
SYAGE, J. A. p 1284 N95-22227
SYLVAIN, M. p 1296 N95-20942
p 1296 N95-20945
SYONO, Y. p 1416 N95-21780
SZANISZLO, ANDREW p 1338 N95-19952
SZYDLIK, P. p 1305 N95-21539
SZYMURSKI, S. R. p 1287 N95-21631

T

TABAK, M. p 1533 N95-20784
TACCETTI, JOSE M. p 1331 N95-21671
TACKET, R. L. p 1442 N95-20485
TAHA, H. p 1429 N95-20782
TAI, RENZHONG p 1548 N95-22255
TAIT, C. D. p 1236 N95-20361
TAJIKA, E. p 1424 N95-21816
TAJIMA, T. p 1553 N95-20437
p 1358 N95-22307
TAKACS, P. Z. p 1468 N95-21515
TAKAO, MASARU p 1371 N95-20757
TAKEDA, TATSUOKI p 1554 N95-20684
TAKIZUKA, T. p 1555 N95-20988
TALBET, JOHN M. p 1364 N95-20069
TALBOT, PIERRE J. p 1547 N95-22076
p 1548 N95-22248
TALISA, S. H. p 1312 N95-19894
TALVACCHIO, J. p 1312 N95-19894
TALVACCHIO, JOHN p 1331 N95-21693
TALWAR, D. N. p 1563 N95-19886
TAMARESIS, J. S. p 1402 N95-20353
TAMARGO, M. C. p 1572 N95-21287
TAMVACLIS, C. p 1292 N95-20923
TAN, C. K. p 1504 N95-21170
TAN, T. Y. p 1279 N95-22091
TANG, WAI-KEUNG p 1523 N95-21525
TAO, RONGJA p 1266 N95-20227
TAPHUOC, LOC p 1347 N95-21068
TARDUCCI, D. p 1213 N95-20658
TASKAEV, S. YU. p 1562 N95-22282
TATSENKO, O. M. p 1564 N95-20240
TATUM, P. A. p 1202 N95-20071
TAURIAINEN, SIMO p 1220 N95-21026
TAWA, G. J. p 1236 N95-20277
TAYLOR, DAVID p 1496 N95-22349
TAYLOR, J. p 1600 N95-22128
TAYLOR, KEN p 1459 N95-20310
TAYLOR, MALCOLM S. p 1498 N95-19990
p 1379 N95-20998
TAYLOR, MARIE E. p 1333 N95-21906
TAYLOR, T. S. p 1554 N95-20446
p 1555 N95-21141
TCHENG, PING p 1368 N95-22109
TEDESCHI, WILLIAM J. p 1599 N95-20144
TEEGARDEN, KENNETH J. p 1368 N95-20035
TEEME, L. A. p 1445 N95-21180
TENCH, R. J. p 1542 N95-20450
p 1377 N95-22343
TENEIKELDER, H. M. M. p 1465 N95-21022
TENENBAUM, PETER p 1535 N95-21255
TENG, CHIN-CHI p 1327 N95-20967
TENG, L. C. p 1537 N95-21503
TENNERY, V. J. p 1225 N95-20022
p 1280 N95-22258
TENTHIJEBOONKAMP, J. H. M. p 1492 N95-21371
TENTHIJEBOONKKAMP, J. H. M. p 1244 N95-21573
TEPPO, O. p 1354 N95-21649
TERAZAWA, HIDEZUMI p 1514 N95-20738
TEREBEY, SUSAN p 1595 N95-21749
p 1593 N95-21767
TERELST, A. F. M. p 1487 N95-19917
p 1493 N95-21423
TERHUNE, R. W. p 1367 N95-21507
TERMINELLO, L. J. p 1542 N95-20450
TERRY, M. D. p 1367 N95-21546
TERWILLIGER, T. T. p 1569 N95-20696
TESCHE, CLAUDIA D. p 1567 N95-20461
TESMER, J. R. p 1255 N95-21238
TESMER, JOSEPH R. p 1534 N95-21236
TESSEREAU, S. p 1302 N95-21431
THAI, J. p 1446 N95-22003
THALER, BARRY p 1326 N95-20824
THANING, LENNART p 1405 N95-21181
THEISS, T. J. p 1385 N95-20322
THEODOULIDIS, BABIS p 1469 N95-21716
THEOFILIS, VASSILIOS p 1351 N95-21092
THIMMAPURAM, P. p 1403 N95-20478
THOMA, D. J. p 1255 N95-21137
p 1375 N95-21837
THOMAS, C. E., JR. p 1551 N95-20205
THOMAS, DAVID J. p 1225 N95-19951
THOMAS, F. O. p 1201 N95-21343
THOMAS, HOLLY p 1392 N95-20473
THOMAS, J. K. p 1458 N95-20073
p 1591 N95-22129
THOMAS, JAMES M. p 1348 N95-21076
THOMAS, JOHN O. p 1226 N95-20092
THOMAS, K. B. p 1217 N95-21706
THOMAS, M. G. p 1393 N95-20863
THOMAS, N. p 1367 N95-21478
THOMAS, S. p 1337 N95-22427
THOMAS, S. R. p 1284 N95-22114
THOMAS, STUART M. p 1516 N95-20993
THOMPSON, C. V. p 1566 N95-20399
THOMPSON, J. D. p 1237 N95-20368
THOMPSON, J. R. p 1573 N95-21483
THOMPSON, K. A. p 1534 N95-21253
THOMPSON, M. D. p 1415 N95-21477
THOMPSON, S. J. p 1554 N95-20446
THOMPSON, STEVEN R. p 1386 N95-20615
THOMPSON, T. C. p 1231 N95-22009
THOMSEN, M. F. p 1600 N95-21935
THOMSON, W. J. p 1236 N95-20268
THORN, C. B. p 1512 N95-20469
THORNHILL, J. W. p 1533 N95-20672
THORNTON, P. T. p 1586 N95-21645
THYHOLT, MARIT p 1288 N95-22014
TICHENOR, D. A. p 1541 N95-20239
TIEDE, D. M. p 1440 N95-22075
TIEE, JOE J. p 1373 N95-21312
TIEGS, T. N. p 1264 N95-20024
p 1265 N95-20220
p 1267 N95-20323
p 1275 N95-21501
TIJS, S. p 1499 N95-21709
TIMMONS, M. L. p 1316 N95-20507
p 1320 N95-20524
TIMSON, STEPHEN F. p 1363 N95-22463
TINNEL, E. P. p 1458 N95-20073
p 1591 N95-22129
TIPTON, TERENCE L. p 1407 N95-21596
TITTIRANONDA, P. p 1453 N95-21637
TJAEDER, T. p 1236 N95-20256
TKACZYK, J. E. p 1571 N95-21167
p 1578 N95-22269
TOBIN, J. G. p 1253 N95-20447
p 1567 N95-20448
p 1567 N95-20449
p 1520 N95-21360
TOBIN, M. p 1557 N95-21206
p 1557 N95-21207
TOBIN, M. T. p 1534 N95-21208
TOBIN, S. p 1551 N95-20205
TODD, A. M. M. p 1601 N95-22419
TODD, J. H. p 1537 N95-21460
TOGNETTI, V. p 1502 N95-22138
TOINT, P. L. p 1495 N95-22317
TOKAR, R. p 1481 N95-20693
TOLBERT, L. M. p 1270 N95-20680
TOMA, L. S. p 1260 N95-22013
TOMAIKO, THOMAS A. p 1302 N95-21324
TOMBOULIDES, A. G. p 1349 N95-21078
TOMKINSON, J. p 1518 N95-21227
TOMSIA, A. P. p 1265 N95-20138
TONG, S. Y. p 1567 N95-20448
p 1567 N95-20449
p 1520 N95-21360
TONN, B. E. p 1401 N95-20238
TONUCCI, RONALD J. p 1576 N95-22059
TOOMARIAN, N. p 1483 N95-21613
p 1484 N95-22171
TOPRAKCIOGLU, C. p 1281 N95-22434
TOSATTI, E. p 1581 N95-21993
TOSTEN, M. p 1252 N95-20216
TOTH, DOUGLAS K. p 1278 N95-21969
TOTH, L. M. p 1237 N95-20493
TOTH, LOUIS E. p 1278 N95-21907
TOUATI, M. p 1296 N95-20944
TRAHAIR, N. S. p 1384 N95-19975
p 1384 N95-20101
TRAHERN, C. G. p 1532 N95-20336
TRAN, MINHTIEN p 1577 N95-22181
TRBOJEVIC, D. p 1540 N95-22391
TREBIN, H. R. p 1578 N95-22277
TREECE, K. p 1480 N95-20342
TREFNY, J. U. p 1391 N95-20118
TRENHOLME, J. B. p 1534 N95-21209
TRESTER, P. W. p 1269 N95-20570
p 1230 N95-21553
TREUR, J. p 1483 N95-21981
p 1470 N95-21983
TREUR, JAN p 1482 N95-21267
TRINH, VINH p 1505 N95-21984
TRIPP, A. C. p 1412 N95-20287
TRIPP, JOHN S. p 1368 N95-22109
TRIPSAS, N. H. p 1558 N95-21310
TROFF, B. p 1347 N95-21068
p 1352 N95-21098
TROHA, WILLIAM A. p 1387 N95-21967
TRONE, DANIEL W. p 1444 N95-21160
TROUVE, A. p 1249 N95-21041
TRUBIAN, M. p 1493 N95-21468
TRUCANO, T. p 1218 N95-20785
TRUCANO, TIMOTHY G. p 1215 N95-20223
p 1376 N95-22169
TSCHEGG, E. K. p 1232 N95-22130
TSOURIS, C. p 1501 N95-20725
TSUI, H. p 1554 N95-20681
TSVANKIN, I. p 1411 N95-19981
p 1411 N95-19982
TUCK, M. R. p 1364 N95-20398
TUDA, TAKASHI p 1554 N95-20684
TUHKURI, J. p 1384 N95-19930
TULINOV, A. F. p 1529 N95-22281
TUNG, SHU-LIN p 1203 N95-21831
TUNHEIM, S. A. p 1455 N95-22018
TUOMINEN, E. p 1397 N95-22337
TURCHI, CRAIG S. p 1410 N95-22278
TURINSKY, P. J. p 1492 N95-21285
TURINSKY, PAUL J. p 1466 N95-21288
TURNBULL, A. D. p 1554 N95-20446
TURNBULL, S. p 1205 N95-21642
TURNER, GRENVILLE p 1417 N95-21784
TURNER, M. H. p 1401 N95-20089
TURUNEN, JARI p 1301 N95-21107
TWIGG, M. E. p 1566 N95-20400
TYLER, S. G. p 1210 N95-20641

U

UHERKA, K. L. p 1382 N95-22292
UMSCHEID, L. J. p 1409 N95-22101
UNDERWOOD, J. p 1274 N95-21175
UNDERWOOD, J. H. p 1374 N95-21663
UNG, K. C. p 1565 N95-20330
UNROE, MARILYN R. p 1266 N95-20251
UPADHYAY, C. S. p 1480 N95-20083
p 1490 N95-20565
p 1490 N95-20588
p 1497 N95-22388
UPPALA, SAKARI p 1430 N95-21413
UPSHER, JOHN F. p 1250 N95-19910
URSU, I. p 1562 N95-22377
URYASEV, S. p 1480 N95-20126

V

VAITKUS, MARK A. p 1451 N95-22323
p 1451 N95-22324

VAKNIN, D. p 1572 N95-21297
VALENTINE, P. G. p 1269 N95-20570
p 1230 N95-21553
VALENTINI, JAMES J. p 1244 N95-21517
VANBERKUM, J. G. M. p 1574 N95-21670
VANBRONKHORST, ERIC p 1289 N95-19997
VANDENBERG, K. G. p 1467 N95-21411
VANDENBROEL, P. M. p 1467 N95-21411
VANDEPLASSCHE, E. J. p 1410 N95-22125
p 1411 N95-22381
VANDERAALST, W. M. P. p 1491 N95-21024
VANDERBAUWHEDE, A. p 1495 N95-22151
VANDERBEEK, C. J. p 1501 N95-20241
VANDERGEER, B. p 1374 N95-21528
VANDERHOFF, J. A. p 1282 N95-19920
VANDERHOUWEN, P. J. p 1490 N95-20424
p 1493 N95-21434
VANDERLAAN, P. p 1499 N95-21980
VANDERLEE, M. D. E. p 1589 N95-21004
VANDERMEER, J. p 1435 N95-21717
VANDERMEER, J. C. p 1495 N95-22151
VANDERPLOEG, C. P. B. p 1445 N95-21580
VANDERVEEN, W. A. p 1490 N95-20424
VANDERVEER, H. W. p 1435 N95-21717
VANDERWOERD, H. p 1405 N95-21350
VANDEUDEKOM, A. p 1471 N95-22029
p 1471 N95-22031
VANDEVEN, A. A. F. p 1353 N95-21268
VANDEWERKEN, G. p 1275 N95-21470
VANDULLEMEN, E. p 1410 N95-22330
VANDUYN, DAVE C. p 1336 N95-22382
VANE, C. R. p 1508 N95-20133
VANELZAKKER, B. G. p 1405 N95-21327
VANEWIJK, L. J. p 1475 N95-20499
p 1291 N95-20692
VANGELDROP, H. P. J. p 1465 N95-21022
VANGEMERT, H. p 1594 N95-19939
VANHEE, KEES M. p 1497 N95-19914
VANHOENACKER, D. p 1295 N95-20939
VANHOOZER, W. R. p 1466 N95-21311
VANHOUTEN, JOHN S. p 1203 N95-22417
VANHULZEN, J. A. p 1472 N95-22159
VANLANGEN, P. p 1483 N95-21981
VANN, CHARLES S. p 1540 N95-22469
VANN, JAMES R. p 1435 N95-21880
VANOVERVELD, C. W. A. M. p 1464 N95-20975
VANRHOON, G. C. p 1444 N95-21016
VANRIJSSEN, E. p 1308 N95-22080
VANRIJSSEN, ERWIN p 1306 N95-21623
VANROOSMALEN, O. S. p 1456 N95-19908
VANSETTEN, D. C. p 1275 N95-21470
VANSINDEREN, MARTEN p 1477 N95-21620
VANSTONE, D. A. p 1400 N95-19921
VANSTRAALEN, D. p 1405 N95-21327
VANVELZE, K. p 1405 N95-21350
VANWONTERGHEM, BRUNO M. p 1371 N95-20817
VANZANDT, T. R. p 1367 N95-21507
VARES, SIRJE p 1232 N95-22158
VARGAS-ABURTO, C. p 1319 N95-20518
VARGASABURTO, C. p 1334 N95-22112
VARPAANIEMI, K. p 1472 N95-22328
VARTULI, C. R. p 1259 N95-21838
VASAVADA, A. R. p 1422 N95-21811
VASHISTA, A. C. p 1440 N95-22075
VASILE, JOSEPH P. p 1457 N95-20060
VASSEUR, H. p 1295 N95-20939
VAUGHAN, C. T. p 1474 N95-20150
VAUGHN, G. D. p 1462 N95-20699
VAUGHN, M. T. p 1529 N95-22279
VAWTER, G. A. p 1545 N95-21509
VAYNER, BORIS V. p 1415 N95-21188
VEBER, G. p 1208 N95-20634
VEEN, ARNOLD p 1439 N95-21884
VEERS, P. S. p 1388 N95-22070
VEGTER, G. p 1492 N95-21318
VELDMAN, A. E. P. p 1352 N95-21097
VELIGDAN, J. T. p 1233 N95-19980
VELLA, M. C. p 1558 N95-21310
VELSKO, S. p 1389 N95-21552
VELSKO, S. P. p 1389 N95-21433
VEMBE, B. E. p 1356 N95-22017
VENDURA, G. J., JR. p 1318 N95-20515
VENHOVENS, P.J. p 1380 N95-21157
VENKATASUBRAMANIAN, R. p 1316 N95-20507
p 1320 N95-20524
VERHOEF, C. p 1487 N95-19902
VERHOEFF, T. p 1487 N95-19906
VERHOEVEN, M. p 1464 N95-20975
VERINK, E. D., JR. p 1252 N95-20365
VERLOOP, WILLEM CORNELIS p 1357 N95-22160
VERMA, R. P. p 1592 N95-21752
VERMEIRE, T. G. p 1410 N95-22124
VERNADSKY, V. I. p 1420 N95-21797
VERNON, STANLEY p 1317 N95-20511
VERONA, ROBERT W. p 1547 N95-22044
VERSTAPPEN, R. W. C. P. p 1352 N95-21097
VERVISCH, L. p 1249 N95-21039
p 1249 N95-21042
VERWEIJ, W. T. P. p 1445 N95-21352
VERWER, J. G. p 1465 N95-21033
p 1404 N95-21034
p 1467 N95-21435
VERZICCO, R. p 1249 N95-21036
p 1344 N95-21048
p 1351 N95-21088
VETRANO, J. S. p 1251 N95-20090
VETTER, THOMAS p 1459 N95-20157
VEYNANTE, D. p 1249 N95-21039
p 1249 N95-21041
VICKERS, T. J. p 1237 N95-20470
VIEBECK, P. G. p 1460 N95-20387
VIEIRA, DAVID J. p 1518 N95-21235
VIGUE, GEORGE p 1457 N95-20060
VILCANS, JANIS p 1308 N95-22005
VILELA, M. F. p 1316 N95-20508
p 1318 N95-20517
VILENKIN, A. p 1599 N95-20173
VILLANUEVA, ANTHONY L. p 1583 N95-20051
VINCENT, C. L. p 1435 N95-21682
VINCENT, DAYTON G. p 1428 N95-19948
VISENTINE, JAMES T. p 1412 N95-20278
VISSCHER, KARYN B. p 1265 N95-20183
VISSER, VANCE P. p 1403 N95-20456
VISSERS, CHRIS A. p 1477 N95-21620
VISWANATHAN, S. p 1252 N95-20359
VITEK, J. M. p 1253 N95-20676
p 1256 N95-21298
p 1381 N95-21550
p 1261 N95-22127
p 1381 N95-22268
VITEK, S. A. p 1256 N95-21298
VOGEL, M. H. p 1295 N95-20938
VOGT, GREGORY L. p 1285 N95-21322
VOISIN, BRUNO p 1354 N95-21583
p 1354 N95-21584
p 1358 N95-22424
VONACH, H. p 1529 N95-22280
VONBARDELEBEN, H. J. p 1563 N95-19886
VONGAS, G. p 1293 N95-20924
p 1293 N95-20925
p 1293 N95-20926
VOORHEES, L. D. p 1458 N95-20073
p 1591 N95-22129
VOS, W. p 1418 N95-21791
VOSS, S. S. p 1223 N95-21840
VOTH, GREGORY A. p 1522 N95-21492
VOURVOPOULOS, G. p 1511 N95-20422
VRBANCICH, J. p 1205 N95-21642
VREMAN, BERT p 1347 N95-21066
VUORINEN, JOUKO J. p 1255 N95-21108
VUORISTO, M. p 1248 N95-22373
VUSKOVI, KRISINA p 1470 N95-21974
VUSKOVIC, KRISTINA p 1490 N95-20662

W

WADDILL, G. D. p 1253 N95-20447
p 1567 N95-20448
p 1567 N95-20449
p 1520 N95-21360
WADE, M. R. p 1552 N95-20334
WADSWORTH, J. p 1266 N95-20316
p 1276 N95-21662
WAENKE, H. p 1424 N95-21820
WAGES, S. p 1281 N95-22434
WAGNER, C. p 1347 N95-21067
WAGNER, G. R. p 1312 N95-19894
WAGNER, JOHN T. p 1458 N95-20070
WAIT, JULIETTE L. p 1441 N95-20408
WAITE, L. p 1211 N95-20645
WALD, JOSEPH K. p 1391 N95-22131
WALD, K. R. p 1581 N95-21604
WALKER, D. W. p 1407 N95-21608
WALKER, DANIEL A. p 1432 N95-20040
WALKER, GILBERT p 1323 N95-20539
WALKER, J. C. p 1204 N95-20497
WALKER, J. W. p 1330 N95-21554
WALKER, JAMES F. p 1382 N95-22405
WALKER, P. p 1293 N95-20924
WALKER, RUSSELL G. p 1594 N95-21772
WALLACE, A. p 1530 N95-22339
WALLACE, A. K. p 1315 N95-20380
WALLACE, D. R. p 1473 N95-22390
WALLACE, JAMES p 1355 N95-21954
WALLURA, E. p 1269 N95-20570
WALSH, WILLIAM J. p 1457 N95-20060
WALTER, K. C. p 1281 N95-22428
WALTER, THERESA p 1211 N95-20646
WALTERS, MICHAEL R. p 1320 N95-20522
WALTERS, ROBERT J. p 1316 N95-20507
p 1319 N95-20519
p 1319 N95-20520
p 1320 N95-20523
p 1320 N95-20524
WALTERS, W. F. p 1488 N95-20167
p 1509 N95-20235
WALTON, MARK A. p 1489 N95-20259
WALUKIEWICZ, W. p 1568 N95-20630
WANG, C. p 1237 N95-20470
WANG, FAN p 1526 N95-22058
WANG, FEILING p 1546 N95-22043
WANG, H. H. p 1564 N95-20017
p 1262 N95-22291
WANG, H. HAU p 1567 N95-20479
WANG, HUNG-MING p 1463 N95-20847
WANG, J. X. p 1573 N95-21516
WANG, KAI-HENG p 1449 N95-20064
WANG, LIPING p 1435 N95-21943
WANG, MENG p 1361 N95-22455
WANG, MICHAEL Q. p 1329 N95-21296
WANG, R. J. p 1226 N95-20027
WANG, TIANJI p 1368 N95-22256
WANG, WEGO p 1260 N95-21986
WANG, WEI p 1577 N95-22180
WANG, X. J. p 1370 N95-20572
p 1533 N95-20573
WANG, X. L. p 1572 N95-21297
WANG, X. Q. G. p 1581 N95-21993
WANG, XUN-LI p 1385 N95-20374
WANG, Y. p 1567 N95-20544
p 1513 N95-20585
p 1513 N95-20586
WANG, YAJUN p 1568 N95-20594
WANG, Z. L. p 1571 N95-21167
p 1578 N95-22269
WANG, Z. R. p 1572 N95-21297
WANG, ZHANHE p 1556 N95-21165
WANG, ZHIBI p 1338 N95-19923
p 1527 N95-22190
WANG, ZHONG p 1594 N95-21770
WANGLER, T. P. p 1539 N95-22298
WARBURTON, KENNETH M. p 1460 N95-20313
WAREING, T. A. p 1488 N95-20167
p 1509 N95-20235
WARFEL, THOMAS p 1474 N95-20325
WARGO, MICHAEL J. p 1285 N95-21322
WARKE, NIRMAL p 1498 N95-20608
WARNER, BENJAMIN J. p 1247 N95-22020
WARNER, BENJAMIN P. p 1224 N95-22252
WARREN, J. F. p 1332 N95-21731
p 1333 N95-21960
WARREN, MICHAEL S. p 1358 N95-22290
WARREN, R. p 1557 N95-21207
WARREN, S. G. p 1431 N95-22288
WARWICK, W. H. p 1264 N95-20024
p 1271 N95-20704
WASIELEWSKI, MICHAEL R. p 1437 N95-19969
WASSERBURG, G. J. p 1423 N95-21812
p 1425 N95-21821
WATABIKI, YOSHIYUKI p 1516 N95-20986
WATANABE, Y. p 1481 N95-20837
WATERS, L. B. F. M. p 1593 N95-21768
WATERS, L. S. p 1508 N95-20159
WATERS, S. B. p 1264 N95-20024
p 1271 N95-20704
WATKINS, J. G. p 1554 N95-20571
WATKINS, T. R. p 1385 N95-20374
WATSON, B. W. p 1456 N95-19891
WATSON, BRUCE W. p 1467 N95-21415
WATSON, CHARLES S. p 1454 N95-22275
WATSON, R. D. p 1549 N95-20143
WATTS, C. p 1562 N95-22120
WATTS, G. p 1507 N95-20131
WAVRIK, R. p 1551 N95-20219
p 1557 N95-21207
WAYNER, P. C., JR. p 1340 N95-20796
WEBB, D. p 1270 N95-20694
WEBB, JON A. p 1474 N95-20325
WEBB, M. S. p 1389 N95-21433
WEBB, T., III p 1406 N95-21379
WEBBER, WILLIAM R. p 1593 N95-21762
WEBER, FRIDOLIN p 1599 N95-20873
WEBER, H. W. p 1232 N95-22130
WEBER, M. E. p 1375 N95-21919
WEBSTER, A. R. p 1296 N95-20942
WEBSTER, HARRY p 1203 N95-22318
WEEREN, A. J. T. M. p 1499 N95-19941
WEI, J. p 1532 N95-20406
WEI, JIE p 1563 N95-20014
p 1531 N95-20021
p 1569 N95-20793
WEIHER, R. p 1401 N95-20238
WEIJERS, B. p 1298 N95-20953
WEILAND, T. p 1531 N95-20120
WEINBERG, I. p 1319 N95-20518
p 1334 N95-22112
WEISE, S. p 1418 N95-21789
WEISENBACK, L. p 1564 N95-20087

WEISS, L. A. p 1600 N95-21935
WEISS, M. p 1491 N95-20830
WEISS, P. S. p 1365 N95-20413
p 1241 N95-21217
p 1328 N95-21218
WEISS, R. E. p 1462 N95-20699
WEISS, S. p 1569 N95-20679
p 1373 N95-21261
WEISSKOPF, V. F. p 1582 N95-22185
WEITZEN, JAY A. p 1293 N95-20928
WELKER, M. F. p 1268 N95-20428
WELLS, MARTIN G. p 1260 N95-21986
WELP, ULRICH p 1567 N95-20479
WELSER, R. E. p 1324 N95-20543
WENDELL, L. L. p 1395 N95-21611
WENG, W. T. p 1489 N95-20266
p 1531 N95-20282
p 1539 N95-22357
WENNEMYR, MAGNUS p 1297 N95-20946
WENTZ, FRANK J. p 1389 N95-20156
WERBLIN, FRANK S. p 1443 N95-20811
WERLING, P. O. p 1243 N95-21428
p 1288 N95-21978
WERMER, J. R. p 1579 N95-20028
WERNAND, MARCEL R. p 1390 N95-21872
WESCOTT, THOMAS F. p 1590 N95-21463
WESSENDORF, K. O. p 1367 N95-21546
WEST, D. S. p 1243 N95-21440
WEST, J. W. p 1569 N95-20767
WEST, W. P. p 1552 N95-20334
p 1556 N95-21159
WESTON, L. W. p 1537 N95-21460
WEYER, ROBERT M. p 1200 N95-19991
WHELAN, DANIEL J. p 1284 N95-21624
WHERRY, ROBERT, JR. p 1453 N95-21691
WHITAKER, RODNEY W. p 1413 N95-20289
WHITE, A. R. p 1506 N95-20025
WHITE, C. J. p 1260 N95-21841
WHITE, C. W. p 1510 N95-20337
WHITE, D. J. p 1290 N95-20556
WHITE, J. M. p 1572 N95-21304
WHITE, JEFF J. p 1284 N95-21966
WHITE, T. p 1592 N95-22263
WHITESON, RENA p 1588 N95-20789
WHITLOCK, ROBERT R. p 1546 N95-21905
WHITMAN, GARY R. p 1454 N95-22099
WHITNEY, K. p 1533 N95-20672
WHITNEY, ROSELYN p 1468 N95-21627
WHITTEN, W. B. p 1506 N95-20030
WICK, RAYMOND V. p 1217 N95-22413
WICKERSHEIMER, DAVID p 1459 N95-20310
WIDYA, I. p 1308 N95-22080
WIDYA, ING p 1306 N95-21623
WIEDWALD, J. p 1550 N95-20190
WIEGEL, J. K. W. p 1438 N95-20917
WIEGMANN, D. L. p 1441 N95-20307
WIERINGA, R. J. p 1592 N95-22331
WIGGINS, DONALD H. p 1403 N95-20720
WIGLEY, J. p 1509 N95-20199
WIJFFELS, SUSAN ELIZABETH p 1436 N95-22072
WILCOX, R. p 1531 N95-20120
WILES, JOHN p 1391 N95-20263
WILHELM, KNUT p 1214 N95-20004
WILKINS, C. A. p 1479 N95-20005
WILLEMS, M. p 1470 N95-21983
WILLENBROCK, S. p 1511 N95-20404
WILLIAMS, ALBERT J., III p 1433 N95-20433
WILLIAMS, D. M. p 1244 N95-21571
WILLIAMS, G. P. p 1536 N95-21418
p 1367 N95-21638
WILLIAMS, J. M. p 1564 N95-20017
p 1262 N95-22291
WILLIAMS, JACK M. p 1567 N95-20479
WILLIAMS, ROBERT C. p 1451 N95-22323
WILLIAMS, W. p 1534 N95-21209
WILLIAMSON, D. L. p 1391 N95-20118
p 1407 N95-21608
WILLIAMSON, MICHELLE p 1274 N95-21234
WILLIAMSON, RICHARD W. p 1291 N95-20666
WILLIS, B. P. p 1338 N95-19953
WILLKENS, C. A. p 1275 N95-21501
WILLOUGHBY, CHRISTOPHER A.
p 1246 N95-21879
WILSON, J. R. p 1600 N95-21479
WILSON, JOHN W. p 1517 N95-21191
WILSON, PRESTON S. p 1503 N95-19911
WILSON, R. B. p 1237 N95-20438
WILSON, ROBERT W. p 1593 N95-21769
WILSON, S. p 1518 N95-21223
WILSON, WILLIAM W. p 1284 N95-21678
WILT, D. M. p 1317 N95-20509
p 1334 N95-22112
WILT, DAVID M. p 1322 N95-20537
WINCHESKI, BUZZ A. p 1383 N95-20764
WINCKELMANS, GREGOIRE S. p 1358 N95-22290
WINDISCH, C. F., JR. p 1232 N95-22115
WINEMAN, S. J. p 1354 N95-21387
WING, DAVID J. p 1199 N95-19913
WINKEL, D. P. p 1434 N95-21461
WINKLER, C. B. p 1380 N95-21157
WINOKUR, P. S. p 1334 N95-22086
WINTENBERG, A. L. p 1330 N95-21554
WINTER, J. p 1269 N95-20570
p 1230 N95-21553
WINTERSGILL, M. C. p 1330 N95-21490
WISE, J. p 1263 N95-19926
WISHERD, P. P. p 1439 N95-21544
WITHERS, J. C. p 1226 N95-20125
WITHROW, S. P. p 1252 N95-20365
WITMER, BOB G. p 1460 N95-20326
WITT, C. EDWIN p 1392 N95-20473
WITTE, J. I. J. p 1435 N95-21717
WITTLIN, G. p 1202 N95-20174
WOGNUM, P. M. p 1471 N95-22081
WOJTCZUK, STEVEN p 1317 N95-20511
p 1323 N95-20539
WOLF, CLARENCE T. p 1270 N95-20596
WOLF, D. p 1573 N95-21474
WOLF, D. R. p 1459 N95-20165
WOLF, E. E. p 1247 N95-22224
WOLFFENBUTTEL, M. R. p 1288 N95-21633
WOLFRUM, EDWARD J. p 1410 N95-22278
WOMBLE, D. E. p 1339 N95-20137
WOMBLE, P. C. p 1511 N95-20422
WONG, J. P. p 1442 N95-20602
WONG, L. G. p 1439 N95-21544
WONG, M. S. p 1230 N95-21445
WONG, R. L. p 1562 N95-22300
WONG, Y. F. p 1473 N95-22426
WOOD, B. P. p 1281 N95-22428
WOOD, BERNARD J. p 1425 N95-21822
WOOD, R. F. p 1369 N95-20221
WOOD, S. E. p 1422 N95-21811
WOODALL, D. M. p 1251 N95-20128
WOODCOCK, ROBERT W. p 1214 N95-20004
WOODING, F. B. p 1434 N95-21677
WOODS, B. p 1557 N95-21166
WOODS, C. M. p 1243 N95-21440
WOODY, C. L. p 1565 N95-20265
p 1545 N95-21643
WOODYARD, JAMES R. p 1320 N95-20522
WOOLERY, G. L. p 1247 N95-22234
WOOTEN, F. p 1542 N95-20450
WOOTTON, A. p 1554 N95-20681
WORCESTER, PETER p 1432 N95-19988
WORD, J. C. p 1572 N95-21419
WORDEN, R. M. p 1282 N95-19927
p 1314 N95-20339
WORKMAN, G. p 1285 N95-22261
WORKMAN, GARY L. p 1238 N95-20557
WORLEY, P. H. p 1407 N95-21608
WORONICK, S. W. p 1247 N95-22234
WOYNA, M. A. p 1412 N95-20171
WRAY, A. A. p 1362 N95-22459
WRIGHT, JOSEPH A. p 1203 N95-22352
WRIGHT, R. M. p 1462 N95-20699
WRIGHT, S. I. p 1262 N95-22289
WRIGHT, STUART I. p 1262 N95-22308
WROBEL, STEFAN p 1464 N95-21003
WROBLEWSKI, D. p 1551 N95-20279
p 1554 N95-20446
p 1555 N95-21141
WU, H. J. p 1237 N95-20438
WU, J. M. p 1234 N95-20107
WU, YEN-YUAN JAMES p 1274 N95-21234
WUEBBLES, D. J. p 1402 N95-20353
p 1413 N95-20354
WUEBBLES, DONALD J. p 1402 N95-20355
WULF, F. p 1335 N95-22184
WYNNE, KENNETH J. p 1268 N95-20442
WYNNWILLIAMS, C. GARETH p 1594 N95-21773

X

XIA, X. p 1524 N95-21703
XIA, Z. p 1312 N95-19934
XIAO, TONGSAN D. p 1568 N95-20552
XIE, PING p 1375 N95-22007
XU, CONG p 1593 N95-21761
XU, Y.-N. p 1564 N95-20017
XUE, Y. p 1242 N95-21400

Y

YABLONOVITCH, ELI p 1571 N95-21145
YADLOWSKY, EDWARD J. p 1551 N95-20232
YAGI, M. p 1553 N95-20437
p 1554 N95-20683
YAKYMYSHYN, C. P. p 1544 N95-20844
YAMAFUJI, K. p 1564 N95-20127
YAMAUCHI, M. p 1221 N95-22436
YAMAZAKI, T. p 1514 N95-20756
YANAGIDA, H. p 1270 N95-20664
YANG, C. L. p 1465 N95-21153
YANG, KEQI p 1435 N95-21681
YANG, L. p 1541 N95-20103
YANG, M.-T. p 1379 N95-20795
YANG, QUINGYUN p 1573 N95-21444
YANG, R. T. p 1234 N95-20046
YANG, T. F. p 1221 N95-20059
YANG, X. Q. p 1512 N95-20477
p 1276 N95-21644
YANG, Y. p 1354 N95-21649
YANG, Z. R. p 1575 N95-21854
YAO, LIANGHUA p 1556 N95-21165
YAO, YI-SHENG p 1313 N95-20257
YARIV, AMNON p 1374 N95-21630
YATER, JANE A. p 1323 N95-20538
YAVUZ, D. p 1292 N95-20922
YAWORSKY, PAUL S. p 1209 N95-20637
YEAGER, WILLIAM L. p 1266 N95-20293
YEE, KEN p 1522 N95-21485
YEH, ALEXANDER p 1473 N95-22402
YELON, W. p 1500 N95-20229
YEN, H. L. p 1564 N95-20017
YEN, YI-FEN p 1519 N95-21237
YESKE, LANNY A. p 1432 N95-20209
YETTER, J. A. p 1216 N95-20669
YETTER, JEFFREY A. p 1203 N95-20706
YEUNG, P. K. p 1348 N95-21071
YODER, MAX N. p 1314 N95-20298
YOKIMCUS, T. A. p 1394 N95-21294
YONEMITSU, K. p 1582 N95-22378
YONEYAMA, MASARU p 1265 N95-20094
YOO, M. H. p 1256 N95-21265
p 1262 N95-22344
YOSHIDA, A. p 1221 N95-22436
YOSHIHARA, K. p 1277 N95-21714
YOST, WILLIAM A. p 1504 N95-20823
YOST, WILLIAM T. p 1441 N95-20408
YOUNG, ANDREW p 1437 N95-19969
YOUNG, DANIEL p 1274 N95-21234
YOUNG, G. R. p 1330 N95-21554
YOUNG, GEORGE S. p 1431 N95-22393
YOUNG, J. P. p 1370 N95-20698
YOUNG, L. M. p 1331 N95-21667
YOUNG, RAYMOND P., JR. p 1599 N95-20144
YOUNG, RIKI G. p 1282 N95-19922
YOUSUFF, AJMAL p 1483 N95-21913
YOW, JESSE L., JR. p 1545 N95-21510
YU, I. p 1519 N95-21273
YU, JOHN p 1307 N95-21890
YU, L. p 1581 N95-21993
YU, LU p 1577 N95-22178
YU, NING p 1534 N95-21236
YU, P. Y. p 1581 N95-21604
YU, S. S. p 1552 N95-20318
YUAN, SHUZHONG p 1548 N95-22255
YUEN, JOSEPH H. p 1303 N95-21532
YUN, WENBING p 1527 N95-22190
YURA, H. T. p 1427 N95-22249
YURA, HAL T. p 1309 N95-22134

Z

ZACHARIA, T. p 1460 N95-20358
p 1379 N95-20723
p 1381 N95-21550
p 1381 N95-22268
p 1578 N95-22272
ZACHARIAS, GREG L. p 1215 N95-21122
ZACHOR, ALEXANDER S. p 1364 N95-20036
ZACHOS, C. K. p 1579 N95-20271
ZAHNLE, K. p 1425 N95-21823
ZANGRANDO, F. p 1396 N95-21897
ZAPOTOSKY, J. E. p 1408 N95-21699
p 1308 N95-21988
ZARNSTORFF, M. C. p 1558 N95-21242
ZASHU, S. p 1425 N95-21824
ZATMAN, M. A. p 1299 N95-20958
ZAVADIL, K. R. p 1329 N95-21394
ZAWADA, D. G. p 1412 N95-20171
ZAWICKI, L. R. p 1329 N95-21301
ZAWODZINSKI, C. p 1246 N95-22012
ZBASNIK, J. P. p 1562 N95-22300
ZEISSE, C. R. p 1431 N95-19896
ZELDOV, E. p 1573 N95-21569
ZELENKA, M. P. p 1400 N95-19965
ZEMAN, O. p 1344 N95-21052
p 1346 N95-21060
ZEMAN, OTTO p 1359 N95-22444
ZEMSCH, STEPHAN p 1201 N95-20794
ZENG, D. p 1224 N95-20660
p 1239 N95-20712
p 1569 N95-20714
p 1248 N95-22385

ZENG, K. .... p 1263 N95-22374
ZENG, KEJUN .... p 1255 N95-21111
ZERATH, E. .... p 1445 N95-21424
ZEROKA, DANIEL .... p 1437 N95-20252
ZERWAS, P. M. .... p 1532 N95-20388
ZHA, C. S. .... p 1418 N95-21791
ZHANG, G. M. .... p 1582 N95-21994
ZHANG, HONGFEI .... p 1254 N95-20792
p 1497 N95-22375
ZHANG, PENG .... p 1556 N95-21162
ZHANG, S. Y. .... p 1489 N95-20266
p 1539 N95-22357
ZHANG, X. G. .... p 1500 N95-20129
ZHANG, X. Y. .... p 1582 N95-21994
ZHANG, XIAN X. .... p 1223 N95-20592
ZHANG, Y. .... p 1233 N95-20045
p 1444 N95-21028
p 1349 N95-21078
p 1574 N95-21712
ZHANG, ZHENLI .... p 1255 N95-20909
ZHAO, QING .... p 1222 N95-21193
ZHENG, JIANQING .... p 1479 N95-22406
ZHENG, SHANFENG .... p 1368 N95-22256
ZHOLENTS, A. .... p 1519 N95-21262
ZHONG, S. .... p 1364 N95-20320
ZHOU, JIANXIN .... p 1340 N95-20312
ZHOU, P. .... p 1472 N95-22351
ZHU, CHENG Y. .... p 1223 N95-20592
ZHU, KA-DI .... p 1528 N95-22218
ZHU, KADI .... p 1577 N95-22176
p 1502 N95-22177
ZIEGLER, MIRIAM M. .... p 1437 N95-20711
ZIMBA, C. .... p 1536 N95-21418
ZIMMERMAN, E. .... p 1538 N95-22050
ZIMMERMANN, F. .... p 1534 N95-21246
p 1536 N95-21332
ZIOMEK, C. .... p 1540 N95-22410
ZIRINO, ALBERT .... p 1543 N95-20728
ZITTEL, P. F. .... p 1404 N95-21150
ZOCCO, T. G. .... p 1255 N95-21238
ZOLL, MICHAEL .... p 1368 N95-22322
ZOLPER, J. C. .... p 1327 N95-20882
p 1329 N95-21390
p 1329 N95-21394
p 1259 N95-21838
ZOSEL, M. .... p 1459 N95-20255
ZOU, J. .... p 1258 N95-21600
ZUBROW, DAVID .... p 1468 N95-21567
ZUCKERWAR, ALLAN J. .... p 1443 N95-20763
ZUND, J. D. .... p 1413 N95-20377
ZUPPARDO, JOSEPH C. .... p 1200 N95-19991
ZUTAVERN, F. J. .... p 1328 N95-21139
ZWEERS, A. J. .... p 1410 N95-22330
ZWIERS, JOB .... p 1455 N95-21871

CORPORATE SOURCE INDEX

SCIENTIFIC AND TECHNICAL AEROSPACE REPORTS VOLUME 33 NUMBER 6

Typical Corporate Source Index Listing

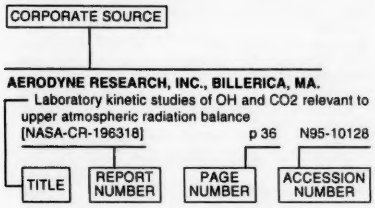
CORPORATE SOURCE
AERODYNE RESEARCH, INC., BILLERICA, MA.
Laboratory kinetic studies of OH and CO2 relevant to upper atmospheric radiation balance
[NASA-CR-196318] p 36 N95-10128
TITLE
REPORT NUMBER
PAGE NUMBER
ACCESSION NUMBER

Listings in this index are arranged alphabetically by corporate source. The title of the document provides the user with a brief description of the subject matter. The report number helps to indicate the type of document cited (e.g., NASA report, translation, NASA contractor report). The accession number denotes the number by which the citation is identified. The page number helps you locate the citation in the abstract section. The titles are arranged under each corporate source in ascending accession number order.

A

ACADEMY OF SCIENCES (USSR), MOSCOW (USSR).

Proceedings of the Zel'Dovich Memorial International Conference on Combustion, Detonation, Shock Waves, volume 2
[AD-A286626] p 1239 N95-20769

The primary carbon and the formation of carbon species in terrestrial magmas p 1420 N95-21797

The ratios of carbon and non-radiogenic helium and argon isotopes in the mantle and crustal rocks
p 1421 N95-21805

International Symposium on Advanced Laser Technologies
[AD-A279849] p 1376 N95-22164

Theses of the Proceedings of the 23d International Meeting on the Physics of Charged Particle Interaction with Crystals
[DE94-631501] p 1529 N95-22281

ACADEMY OF SCIENCES (USSR), NOVOSIBIRSK (USSR).

On conception of a compact neutron source and the possibility of its simulation on the Amba-M end trap
[DE94-633373] p 1562 N95-22282

Gas-dynamic trap diagnostic complex for study on plasma heating and power atomic beam injection
[DE94-633377] p 1529 N95-22283

ADAPTIVE SOLUTIONS, INC., BEAVERTON, OR.

High performance hardware and software for pattern recognition and image processing
[AD-A279776] p 1457 N95-19961

ADVANCED FUEL RESEARCH, INC., EAST HARTFORD, CT.

Detection of environmental deterioration in fiber reinforced composites by FT-Raman spectroscopy, phase 1
[AD-A279763] p 1228 N95-20805

HTS Josephson technology on silicon with application to high speed digital microelectronics
[AD-A285964] p 1328 N95-21178

ADVANCED RESEARCH PROJECTS AGENCY, ARLINGTON, VA.

The Novaya Zemlya Event of 31 December 1992 and Seismic Identification Issues: 15th Annual Seismic Research Symposium
[AD-A279847] p 1414 N95-20760

ADVISORY GROUP FOR AEROSPACE RESEARCH AND DEVELOPMENT, NEUILLY-SUR-SEINE (FRANCE).

Advanced Packaging Concepts for Digital Avionics
[AGARD-CP-562] p 1208 N95-20631

Multiple Mechanism Propagation Paths (MMPPs): Their Characterisation and Influence on System Design
[AGARD-CP-543] p 1292 N95-20921

Application of Direct and Large Eddy Simulation to Transition and Turbulence
[AGARD-CP-551] p 1346 N95-21061

AEROJET-GENERAL CORP., SACRAMENTO, CA.

Modeling of rolling element bearing mechanics. Computer program user's manual
[NASA-CR-196557] p 1381 N95-21692

Modeling of rolling element bearing mechanics. Theoretical manual
[NASA-CR-196556] p 1381 N95-21705

AEROJET TECHNICAL SYSTEMS CO., SACRAMENTO, CA.

SSME HPOTP post-test diagnostic system enhancement project
[NASA-CR-4643] p 1222 N95-21458

AERONAUTICAL RESEARCH INST. OF SWEDEN, BROMMA.

Simulations of bypass transition for spatially evolving disturbances p 1349 N95-21079

AERONAUTICAL RESEARCH LABS., MELBOURNE (AUSTRALIA).

Dynamic response of pressure measuring systems
[ARL-TR-32] p 1365 N95-20759

Derived gust spectra for the Macchi MB326H
[ARL-TN-3] p 1202 N95-21892

An IBM based ARINC interface
[ARL-TR-21] p 1471 N95-22104

AERONAUTICAL SYSTEMS DIV., WRIGHT-PATTERSON AFB, OH.

Open Skies project computational fluid dynamic analysis
[AD-A285928] p 1200 N95-19991

AEROSPACE CORP., EL SEGUNDO, CA.

Computer model predictions of the local effects of large, solid-fuel rocket motors on stratospheric ozone
[AD-A285632] p 1404 N95-21150

Transient photoluminescence measurements on GaAs and AlGaAs double heterostructures
[AD-A279408] p 1575 N95-21916

Atomic velocity distributions in a hydrogen beam effusing out of an RF discharge dissociator
[AD-A279253] p 1307 N95-21985

LADAR detection statistics in the presence of pointing errors
[AD-A285865] p 1309 N95-22134

Launch safety, toxicity, and environmental effects of the high performance oxidizer ClF(5)
[AD-A286095] p 1284 N95-22227

Threshold detection in the presence of atmospheric turbulence
[AD-A286175] p 1427 N95-22249

Absorption of water and lubricating oils into porous nylon
[NASA-CR-197344] p 1280 N95-22383

AIN SHAMS UNIV., CAIRO (EGYPT).

Indian Academy of Sciences. Volume 105, number 6, December 1993. Proceedings of the 2nd International Conference on Solar Energy Storage Applied Photochemistry
[AD-A286481] p 1605 N95-22394

AIR-CONDITIONING AND REFRIGERATION TECHNOLOGY INST., INC., ARLINGTON, VA.

Accelerated screening methods for determining chemical and thermal stability of refrigerant-lubricant mixtures. Part 2: Experimental comparisons and verification of methods
[DE95-000743] p 1264 N95-20078

Materials compatibility and lubricants research on CFC-refrigerant substitutes
[DE94-018414] p 1287 N95-21631

Thermophysical properties of HFC-143a and HFC-152a
[DE95-002199] p 1582 N95-22153

AIR FORCE ENGINEERING AND SERVICES CENTER, TYNDALL AFB, FL.

Spectroscopic studies of hazardous fuel interactions with soils
[AD-A279099] p 1407 N95-21596

AIR FORCE INST. OF TECH., WRIGHT-PATTERSON AFB, OH.

The effects of three-dimensional graphs on decision making
[AD-A285034] p 1583 N95-20051

A 3D stereo data visualization and representation
[AD-A284788] p 1449 N95-20064

Certain physical properties of lanthanum digermanide
[AD-A286592] p 1229 N95-20859

Electro-optic effect in the PESO acousto-optic modulator
[AD-A286355] p 1548 N95-22255

Application of computer-generated holograms to optical transformations
[AD-A286356] p 1368 N95-22256

AIR FORCE MATERIALS LAB., WRIGHT-PATTERSON AFB, OH.

The spatiotemporal characteristics of visual motion priming
[AD-A284782] p 1449 N95-20062

AIR FORCE MATERIEL COMMAND, BROOKS AFB, TX.

Calculation methods for criteria air pollutant emission inventories
[AD-A284675] p 1400 N95-19964

Intelligent tutoring systems: Past, present, and future
[AD-A280011] p 1448 N95-19970

AIR FORCE OFFICE OF SCIENTIFIC RESEARCH, BOLLING AFB, WASHINGTON, DC.

Iterated-subspace minimization methods for nonlinear optimization
[PB95-108171] p 1495 N95-22317

AIR FORCE SYSTEMS COMMAND, TYNDALL AFB, FL.

Evaluation of an immobilized cell bioreactor for degradation of meta- and para-nitrobenzoate
[AD-A279719] p 1516 N95-20993

AIR FORCE SYSTEMS COMMAND, WRIGHT-PATTERSON AFB, OH.

Photovoltaic electric power applied to Unmanned Aerial Vehicles (UAV) p 1321 N95-20530

AIR PRODUCTS AND CHEMICALS, INC., ALLENTOWN, PA.

Development of active-transport membrane devices
[DE94-015947] p 1246 N95-21921

AIRCRAFT RESEARCH ASSOCIATION LTD., BEDFORD (ENGLAND).

Investigation of a thermal buoyancy effect on the drag of half models tested in the ARA Transonic Wind Tunnel
[ARA-MEMO-407] p 1199 N95-19946

The dynamic approach to rotor blade research: ARA's oscillatory test facility
[ARA-MEMO-405] p 1200 N95-20758

Testing in the ARA Transonic Wind Tunnel
[ARA-MEMO-395] p 1216 N95-20799

AKRON UNIV., AKRON, OH.

SEEK: A FORTRAN optimization program using a feasible directions gradient search
[NASA-CR-4641] p 1380 N95-21359

ALABAMA UNIV., HUNTSVILLE, AL.

Surface characterization and contamination analysis
[NASA-CR-197374] p 1238 N95-20557

X-ray microscope for solidification studies
[NASA-CR-197375] p 1543 N95-20798

ALENIA, TURIN (ITALY).

Electromagnetic compatibility effects of advanced packaging configurations p 1213 N95-20658

ALLIED-SIGNAL AEROSPACE CO., KANSAS CITY, MO.

Copper metallization of stainless steels
[DE95-001496] p 1256 N95-21300

Survivability of soldered leadless chip carriers after temperature cycling
[DE95-001497] p 1329 N95-21301

Representing manufacturing features to support design and process changes
[DE94-018587] p 1467 N95-21389

Plastic encapsulated parts
[DE95-001876] p 1332 N95-21729

ALTAMIRA INSTRUMENTS, INC., PITTSBURGH, PA.

Direct aromatization of methane
[DE94-017131] p 1233 N95-19924

AMERICAN ASSOCIATION FOR CANCER RESEARCH, PHILADELPHIA, PA.

Cellular responses to environmental DNA damage
[DE94-015606] p 1441 N95-22397

AMERICAN CERAMIC SOCIETY, WESTERVILLE, OH.

Ferroic materials: Design, preparation and characteristics. Ceramic transactions, volume 43
[AD-A285937] p 1270 N95-20664

AMERICAN INST. OF PHYSICS, NEW YORK, NY.

Journal of Applied Physics, volume 76, number 10, part 2. Proceedings of the 6th Joint Magnetism and Magnetic Materials-INTERMAG Conference
[AD-A286364] p 1500 N95-20229

AMES LAB., IA.

Truly distribution-independent algorithms for the N-body problem
[DE94-014238] p 1458 N95-20136

Theoretical study of the noble metals on semiconductor surfaces and Ti-base shape memory alloys
[DE95-001654] p 1257 N95-21398

Dynamic NMR studies of restricted arene rotation in the chromiu tricarbonyl thiophene and selenophene complexes
[DE95-001656] p 1257 N95-21399

Distribution-independent hierarchical N-body methods
[DE95-001686] p 1493 N95-21439

A new universal solution for the electrofinishing of metallic materials
[DE95-001681] p 1258 N95-21568

Quantum dynamical phenomena of independent electrons in semiconductor superlattices subject to a uniform electric field
[DE95-001655] p 1574 N95-21723

The role of microcracking on the crack growth resistance of brittle solids and composites
[DE95-001678] p 1231 N95-21736

Methods and opportunities in the recycling of rare Earth based materials
[DE95-001680] p 1259 N95-21737

The low temperature properties of (Dy(1-x)Er(x))Ni2 alloys
[DE95-001657] p 1260 N95-21923

The role of grain boundary sliding on creep deformation characteristics of discontinuous reinforced composites
[DE95-001671] p 1231 N95-21924

AMSTERDAM UNIV. (NETHERLANDS).

HIRAS images of fossil dust shells around AGB stars
p 1593 N95-21768

ANALYTICAL SERVICES AND MATERIALS, INC., HAMPTON, VA.

Time-dependent deformation of titanium metal matrix composites
[NASA-CR-195030] p 1230 N95-21363

ANALYTICON CORP., RANCHO PALOS VERDES, CA.

Enhanced vehicle and event typing software, phase 1
[AD-A284862] p 1458 N95-20070

ANKARA UNIV. (TURKEY).

Direct numerical simulation of transition to turbulence from a high-symmetry initial condition
p 1351 N95-21089

APPLIED DATA RESEARCH, INC., NEW YORK, NY.

Aerosol-assisted chemical vapor deposition of copper: A liquid delivery approach to metal thin films
[AD-A279702] p 1270 N95-20689

APPLIED SCIENCE AND TECHNOLOGY, INC., WOBURN, MA.

Materials processing and manufacturing technologies for diamond substrates multichip modules
[AD-A285060] p 1315 N95-20488

Materials processing and manufacturing technologies for diamond substrates multichip modules
[AD-A285775] p 1336 N95-22412

APPLIED SOLAR ENERGY CORP., CITY OF INDUSTRY, CA.

Development of concentrator solar cells
[DE95-002316] p 1394 N95-20871

ARABIAN-AMERICAN OIL CO. (SAUDI ARABIA).

Planning and scheduling for success
p 1584 N95-20747

ARC PROFESSIONAL SERVICE GROUP, INC., ROME, NY.

Cathode Life Test Facility
[AD-A286232] p 1334 N95-22023

ARGONNE NATIONAL LAB., IDAHO FALLS, ID.

Visual displays and Neuro-Linguistic Programming
[DE95-001454] p 1466 N95-21311

ARGONNE NATIONAL LAB., IL.

Liquid-metal pin-fin pressure drop by correlation in cross flow
[DE94-017086] p 1338 N95-19923

The ANL X6B beamline at NSLS: A versatile facility
[DE94-018379] p 1540 N95-19968

A photophysical control mechanism for zeaxanthin-associated radiationless energy dissipation in photosynthesis
[DE94-018383] p 1437 N95-19969

Modeling the dynamics of charged-particle beams using a Fokker-Planck approach
[DE95-001458] p 1531 N95-19983

Migrating the Facility Profile Information Management System into the World Wide Web
[DE94-018367] p 1586 N95-20016

Positron annihilation studies of organic superconductivity
[DE94-018371] p 1564 N95-20017

Recognition of subsurface defects in machined ceramics by application of neural networks to laser scatter patterns
[DE94-018373] p 1264 N95-20018

New strong interactions above the electroweak scale
[DE94-018385] p 1506 N95-20025

Elastic anisotropy in hot-pressed Si3N4 composites: Role of in situ (beta)-Si3N4 grains and added (beta)-Si3N4 whiskers
[DE94-018387] p 1226 N95-20027

Solidification modeling of a spiral casting to determine material fluidity
[DE94-018930] p 1285 N95-20050

Thorium-232 in human tissues: Metabolic parameters and radiation doses
[DE94-019275] p 1441 N95-20074

An intensity interferometer for soft x-rays
[DE94-016370] p 1541 N95-20103

Design and thermal stress analysis of high power x-ray monochromators cooled with liquid nitrogen
[DE94-016879] p 1500 N95-20106

Mercury capture in bench-scale absorbers
[DE94-016910] p 1234 N95-20107

A control volume method on an icosahedral grid for numerical integration of the shallow-water equations on the sphere
[DE94-016345] p 1489 N95-20170

A Hyperspectral Image Data Exploration Workbench for environmental science applications
[DE94-016373] p 1412 N95-20171

Performance specifications for technology development: Application for characterization of volatile organic compounds in the environment
[DE94-016627] p 1401 N95-20234

Power-law resistivity, magnetic relaxation and ac susceptibility
[DE94-016893] p 1501 N95-20241

An application of wavelet transform for decomposition of millimeter-wave spectroscopic signals
[DE94-018366] p 1402 N95-20247

The paradigm of Pseudodual Chiral Models
[DE94-016386] p 1579 N95-20271

A tau-charm-factory at Argonne
[DE94-016913] p 1510 N95-20360

Kernel mucking in top
[DE94-017077] p 1460 N95-20385

A mechanistic model for radiation-induced crystallization and amorphization in U3Si
[DE94-015028] p 1566 N95-20419

Energy impacts of controlling carbon dioxide emissions from an integrated gasification/combined-cycle system
[DE94-016878] p 1403 N95-20478

New ET-based organic superconductors with the organometallic anion Cu(CF3)4(-)
[DE94-016904] p 1567 N95-20479

Multiply manifolded molten carbonate fuel cells
[DE94-017074] p 1392 N95-20480

Sputtering of tin and gallium-tin clusters
[DE94-018389] p 1254 N95-20707

Global change integrating factors: Tropical tropopause trends
[DE95-001121] p 1404 N95-20835

An improved and facile method for the synthesis of 1,1-bis(4-hydroxyphenyl) 2-phenylethylene and its derivatives
[DE95-001125] p 1240 N95-20836

A fuel cell overview
[DE95-001455] p 1393 N95-20839

Topography of neutron scattering from diblock copolymer film
[DE95-001457] p 1229 N95-20840

Reactive nanophase oxide additions to melt-processed high-T(sub c) superconductors
[DE95-001470] p 1570 N95-20841

Unbinned maximum likelihood fit for the CP conserving couplings for W + photon production at CDF
[DE95-001471] p 1514 N95-20852

Atmosphere influence on in situ ion beam analysis of thin film growth
[DE95-001507] p 1570 N95-20881

Statistical properties of geologic fractals
[DE94-019272] p 1414 N95-20908

Role of internal stresses in fracture behavior of engineering composites
[DE95-001106] p 1229 N95-20912

MHD pressure drop in ducts with imperfectly insulating coatings
[DE95-002852] p 1558 N95-21244

Interlayer magnetic coupling in epitaxial Fe/Cr(211) and (100) superlattices
[DE95-002906] p 1571 N95-21256

A divide-and-conquer method for tridiagonalizing symmetric matrices with repeated eigenvalues
[DE95-002918] p 1476 N95-21257

Effects of battery technologies, driving patterns, and climate comfort control on the performance of electric vehicles
[DE95-001102] p 1329 N95-21296

A framework for symmetric band reduction and tridiagonalization
[DE95-002919] p 1476 N95-21341

Proposal for a tutorial on Minimal Length Encoding (MLE) in molecular biology
[DE94-015076] p 1438 N95-21376

MHD-flow in slotted channels with conducting walls
[DE94-018370] p 1559 N95-21388

Recent photoabsorption measurements in the rare gases and alkalis in the 3 to 15 keV photon energy region
[DE94-019278] p 1521 N95-21406

Application of new synchrotron powder diffraction techniques to anomalous scattering from glasses
[DE94-019285] p 1536 N95-21407

Diffraction applications using the energy dispersive beamline, X6A, at NSLS
[DE94-019287] p 1572 N95-21408

An in-line ultrasonic viscometer
[DE95-002982] p 1366 N95-21453

On the Aharonov-Bohm effect with neutrons
[DE95-002985] p 1521 N95-21454

Structure of ionic interfaces from an absolutely convergent solution of the Madelung problem
[DE94-019268] p 1573 N95-21474

The atmospheric neutrino anomaly in Soudan 2
[DE94-019288] p 1604 N95-21475

Anatomy of the Midcontinent Rift beneath Lake Superior
[DE94-019298] p 1415 N95-21477

The diphoton production rate in (bar p)p collisions at the square root of s = 1800 GeV
[DE95-000559] p 1522 N95-21497

Ion charge-state production and photoionization near the K edge in argon and potassium
[DE95-001443] p 1522 N95-21502

Beam instability studies at the APS
[DE95-001448] p 1537 N95-21503

Removal of CO2 in closed loop off-gas treatment systems
[DE94-019259] p 1407 N95-21617

EAGLES 1.1: A microcomputer software package for analyzing fuel efficiency of electric and gasoline vehicles
[DE95-001119] p 1469 N95-21829

Stability effects on the profiles of vertical velocity and its variance in katabatic flow
[DE95-001126] p 1426 N95-21836

Seawater test results of Open-Cycle Ocean Thermal Energy Conversion (OC-OTEC) components
[DE94-019254] p 1396 N95-21897

Discovering related DNA sequences via mutual information
[DE95-001101] p 1440 N95-22067

Electrostatic basis for molecular recognition in photosynthesis
[DE95-002979] p 1440 N95-22075

A Davis-Putnam program and its application to finite-order model search: Quasigroup existence problems
[DE95-003014] p 1471 N95-22077

Taking AIM: The management of scientific and technical information at Argonne National Laboratory
[DE94-019279] p 1591 N95-22092

Low temperature tensile and fracture mechanical strength in mode 1 and mode 2 of fiber reinforced plastics following various irradiation conditions
[DE94-019269] p 1232 N95-22130

Estimation of lightning stroke peak current as a function of peak electric field and the normalized amplitude of signal strength: Corrections and improvements
[DE94-016900] p 1335 N95-22189

Thermal and deformation analyses of a novel cryogenically cooled monochromator for an Advanced Photon Source beamline
[DE94-016914] p 1527 N95-22190

Studies of the microwave resistivity of kappa-(BEDT-TTF)2Cu(N(CN)2)Cl
[DE95-002980] p 1262 N95-22291
Low rotational drag in high-temperature superconducting bearings
[DE95-002983] p 1382 N95-22292

ARIZONA STATE UNIV., TEMPE, AZ.
On the transition towards slow manifold in shallow-water and 3D Euler equations in a rotating frame
p 1345 N95-21057
Direct numerical simulations of leading-edge receptivity for freestream sound p 1351 N95-21090
Phase E in a water-saturated peridotite system at 9.3 GPa p 1420 N95-21799

ARIZONA UNIV., TUCSON, AZ.
Program of the 1993 9th Interdisciplinary Laser Science Conference (ILS-9)
[AD-A285131] p 1369 N95-20082
Navier-Stokes simulations of the effects of suction holes on a flat plate boundary layer p 1352 N95-21094
Atmospheres of the Moon and Mercury
p 1419 N95-21794
Solar system formation and the distribution of volatile species p 1421 N95-21806
Semi-volatiles at Mercury: Sodium (Na) and potassium (K) p 1424 N95-21818
Implications of noble gases in a recently recognized Martian meteorite (ALH84001) for the degassing history of Mars p 1424 N95-21819
Nonlinear interaction between a pair of oblique modes in a supersonic mixing layer: Long-wave limit
[NASA-CR-197380] p 1357 N95-22173

ARMY AEROMEDICAL RESEARCH LAB., FORT RUCKER, AL.
Factors that determine visual acuity through night vision goggles for emmetropes
[AD-A279339] p 1450 N95-21927
Factors affecting the perception of luning in monocular regions of partial binocular overlap displays
[AD-A286287] p 1547 N95-22044
Temporary threshold shifts produced by high intensity freefield impulse noise in humans wearing hearing protection
[AD-A286289] p 1454 N95-22045

ARMY ARMAMENT RESEARCH, DEVELOPMENT AND ENGINEERING CENTER, PICATINNY ARSENAL, NJ.
Brief tutorial on the Kalman filter
[AD-A286571] p 1326 N95-20827
Millimeter wave front-end figure of merit, part 1
[AD-A279093] p 1307 N95-21915
Thermal imaging systems
[AD-A279146] p 1307 N95-21970

ARMY ARMAMENT RESEARCH, DEVELOPMENT AND ENGINEERING CENTER, WATERVLIET, NY.
How the brain works
[AD-A279138] p 1450 N95-21968
Perimeter-yardstick technique for fracture surface fractal analysis
[AD-A286240] p 1387 N95-22025
Exponents in lifetime and power spectral density forms in self-organized critical systems
[AD-A286242] p 1495 N95-22026
Residual stress analysis in swage autofrettaged thick-walled cylinders by position-sensitive x-ray diffraction techniques
[AD-A286383] p 1388 N95-22320

ARMY COLD REGIONS RESEARCH AND ENGINEERING LAB., HANOVER, NH.
Operating manual for hybrid thermosyphons at the Gakona Power Plant, Alaska
[AD-A279068] p 1287 N95-21626

ARMY COLD REGIONS TEST CENTER, FORT GREELY, AK.
Cold regions instrumentation considerations
[AD-A279492] p 1367 N95-21680

ARMY COMMUNICATIONS-ELECTRONICS COMMAND, FORT MONMOUTH, NJ.
Proceedings of the International Wire and Cable Symposium
[AD-A279242] p 1403 N95-20465

ARMY CONSTRUCTION ENGINEERING RESEARCH LAB., CHAMPAIGN, IL.
Environmental Compliance Assessment and Management Program
[AD-A279605] p 1402 N95-20441
Environmental Compliance Assessment Protocol - Centers for Disease Control and Prevention (ECAP-CDC), West Virginia supplement
[AD-A286009] p 1403 N95-20720
Environmental Compliance Assessment and Management Program (ECAMP), South Carolina supplement
[AD-A279533] p 1408 N95-21689
Environmental Compliance Assessment System (ECAS): Oregon supplement
[AD-A279565] p 1408 N95-21696
Development and evaluation of ALEC Micro-Wand 3e (tradename) training
[AD-A285863] p 1471 N95-22133
Environmental Compliance Assessment System (ECAS): Japan settlement
[AD-A279328] p 1410 N95-22142

ARMY ENGINEER WATERWAYS EXPERIMENT STATION, VICKSBURG, MS.
Super-heavy aircraft study
[AD-A279602] p 1215 N95-19955
HIVEL2D: A two-dimensional flow model for high-velocity channels
[AD-A286556] p 1341 N95-20843
Aquatic plant control research program. Ecological assessment of Kirk Pond
[AD-A279090] p 1409 N95-21914

ARMY MEDICAL RESEARCH UNIT (EUROPE).
Psychosocial stress and mental health in a forward-deployed military community
[AD-A285940] p 1451 N95-22323
Assessing post traumatic stress disorder and PTSD symptomatology in US Army personnel
[AD-A285941] p 1451 N95-22324

ARMY MISSILE COMMAND, REDSTONE ARSENAL, AL.
Information security for unmanned systems
[AD-A286511] p 1485 N95-22214

ARMY NATICK LABS., MA.
Personal hygiene body wipe
[AD-A286092] p 1454 N95-22274

ARMY NATICK RESEARCH AND DEVELOPMENT COMMAND, MA.
Governing equations for multiphase heat and mass transfer in hygroscopic porous media with applications to clothing materials
[AD-A286418] p 1357 N95-22206

ARMY RESEARCH INST. FOR THE BEHAVIORAL AND SOCIAL SCIENCES, ALEXANDRIA, VA.
Using the backward transfer paradigm to validate the AH-64 Simulator Training Research Advanced Testbed for Aviation
[AD-A285758] p 1215 N95-19931
Measuring presence in virtual environments
[AD-A286183] p 1460 N95-20326

ARMY RESEARCH INST. OF ENVIRONMENTAL MEDICINE, NATICK, MA.
Sustaining the health and performance of soldiers/warfighters deployed to harsh environments
[AD-A286270] p 1446 N95-22004

ARMY RESEARCH LAB., ABERDEEN PROVING GROUND, MD.
The influence of ply waviness with nonlinear shear on the stiffness and strength reduction of composite laminates
[AD-A285736] p 1224 N95-19899
High pressure windowed chamber burned rate determination of liquid propellant XM46
[AD-A283770] p 1282 N95-19920
Comparison of meteorological data with fitted values extracted from projectile trajectory
[AD-A285921] p 1428 N95-19989
A multivariate multisample rank test for stochastic simulation validation
[AD-A285922] p 1498 N95-19990
Quantum chemical study of rare gas/halide interactions as a model for high energy density material. 1: Transition properties in HCl
[AD-A285988] p 1239 N95-20613
Evaluation of stress experienced by soldiers wearing chemical protective clothing during varying work loads in desert or tropical environments
[AD-A280113] p 1452 N95-20625
Statistical analysis of Turbine Engine Diagnostic (TED) field test data
[AD-A286032] p 1379 N95-20998
Investigations into alternate spark gap switching techniques
[AD-A286225] p 1308 N95-22021
Solving the inverse problem in terrain modeling
[AD-A285860] p 1391 N95-22131
Latin hypercube sampling in sensitivity analysis
[AD-A285867] p 1499 N95-22135
Ab initio potential energy surface for H + OCS reactions: Extended basis sets and correlation treatment
[AD-A286420] p 1247 N95-22207
Quantum chemical study of rare gas/halide interactions as a model for high energy density material. 2: The interaction of hydrogen chloride with the rare gas xenon
[AD-A286385] p 1248 N95-22321

ARMY RESEARCH LAB., ADELPHI, MD.
The calculation and measurement of Helmholtz coil fields
[AD-A286081] p 1228 N95-20808
Low-cost conical ultra-wideband antenna
[AD-A286569] p 1292 N95-20825
Nonparametric estimation of the cyclic cross-spectrum
[AD-A285756] p 1498 N95-21219
Reentry vehicle on-site inspection technology study
[AD-A285960] p 1220 N95-21634
Design and construction of a Ka-band scatterometer
[AD-A286296] p 1368 N95-22322

ARMY RESEARCH LAB., FORT BELVOIR, VA.
VOC compliant wash primer
[AD-A286034] p 1273 N95-21000

ARMY RESEARCH LAB., FORT MONMOUTH, NJ.
VHDL modeling of PRC-70 radio ASICs for reverse engineering
[AD-A285740] p 1457 N95-19929
The demise of plastic encapsulated microcircuit myths
p 1209 N95-20640

ARMY RESEARCH LAB., WATERTOWN, MA.
Mechanical behavior of 97.2% W alloy in tension at high temperatures
[AD-A284797] p 1250 N95-20067
Fracture analysis of an all-ceramic bearing system
[AD-A285056] p 1269 N95-20486
The 29th MIL-HDBK-17 Polymer Matrix Composites Coordination Group Meeting
[AD-A279917] p 1269 N95-20578
The development of a super-alpha2 titanium aluminide alloy consolidated by rapid omnidirectional compaction
[AD-A279254] p 1260 N95-21986

ARMY RESEARCH LAB., WHITE SANDS MISSLE RANGE, NM.
Evaluation of simple spherical spreading model for near vertical acoustical propagation
[AD-A286284] p 1505 N95-22042

ARMY RESEARCH OFFICE, RESEARCH TRIANGLE PARK, NC.
Transactions of the Eleventh Army Conference on Applied Mathematics and Computing
[AD-A279884] p 1497 N95-22389

ARMY TANK-AUTOMOTIVE COMMAND, WARREN, MI.
Electromagnetic interference testing and electrical subsystem: Non-communication
[AD-A286591] p 1292 N95-20858

ARMY TOPOGRAPHIC ENGINEERING CENTER, FORT BELVOIR, VA.
Evolution of ground line of sight data field collection techniques
[AD-A285062] p 1204 N95-20497

ARNOLD ENGINEERING DEVELOPMENT CENTER, ARNOLD AFS, TN.
Description and flow characterization of hypersonic facilities
[AD-A284291] p 1200 N95-20248

ASTON UNIV., BIRMINGHAM (ENGLAND).
Assessment of liquefaction and pyrolysis systems
[PB95-129797] p 1236 N95-20290

ASTRO AEROSPACE CORP., CARPINTERIA, CA.
An introduction to the Astro Edge solar array
p 1322 N95-20535

ASTROPOWER, INC., NEWARK, DE.
High quality InP-on-Si for solar cell applications
p 1317 N95-20510
Development of a lightweight, light-trapped, thin GaAs solar cell for spacecraft applications
p 1318 N95-20513
High efficiency GaP power conversion for Betavoltaic applications p 1323 N95-20540

ATLANTIC ORIENT CORP., NORWICH, VT.
Advanced wind turbine design studies: Advanced conceptual study
[DE93-000031] p 1394 N95-20985

ATMOSPHERIC AND ENVIRONMENTAL RESEARCH, INC., CAMBRIDGE, MA.
Studies of the gas tori of Titan and Triton
[NASA-CR-197377] p 1601 N95-20797
Real-data tests of a single-Doppler radar assimilation system
[AD-A286638] p 1292 N95-20904

ATMOSPHERIC RADIATION CONSULTANTS, ACTON, MA.
Noise model of the MSX SPIRIT 3 interferometer
[AD-A285837] p 1364 N95-20036

AUBURN UNIV., AL.
Design of power electronics for TVC and EMA systems
[NASA-CR-196540] p 1312 N95-19909
Theoretical atomic physics for fusion
[DE94-019196] p 1524 N95-21605

AUSTRALIAN NATIONAL UNIV., CANBERRA (AUSTRALIA).
Coupled tearing modes in plasmas with differential rotation
[DE94-631422] p 1548 N95-19977
Variations of helicon wave induced radial plasma transport in different experimental conditions
[DE94-631410] p 1550 N95-20200
Positive rockland operators
[PB95-127510] p 1493 N95-21423
Solar helium and neon in the Earth
p 1419 N95-21793

AUSTRALIAN NUCLEAR SCIENCE AND TECHNOLOGY ORGANIZATION, LUCAS HEIGHTS (AUSTRALIA).
ANSTO: Program of research, 1993-1994
[DE94-631122] p 1605 N95-21828
ANSTO: Mission statement, significant events and achievements
[DE94-631123] p 1605 N95-21830

B

BALLISTIC MISSILE DEFENSE ORGANIZATION, WASHINGTON, DC.
BMDO photovoltaics program overview
p 1316 N95-20504
BATTELLE COLUMBUS LABS., OH.
Mercury usage and alternatives in the electrical and electronics industries
[PB94-165362] p 1312 N95-19966
Aircraft corrosion study
[AD-A279527] p 1259 N95-21687
BATTELLE MEMORIAL INST., COLUMBUS, OH.
Finite element modelling of creep crack growth in 316 stainless and 9Cr-1Mo steels
[DE94-018977] p 1258 N95-21560
BATTELLE MEMORIAL INST., RESEARCH TRIANGLE PARK, NC.
Theoretical prediction of vibrational circular dichroism spectra of R-glyceraldehyde, R-erythrose, and R-threose. Part 2: Development of a procedure to scale the force constant matrix expressed in terms of internal coordinates
[AD-A284305] p 1437 N95-20252
BATTELLE PACIFIC NORTHWEST LABS., RICHLAND, WA.
Assessment of liquefaction and pyrolysis systems
[PB95-129797] p 1236 N95-20290
BBN SYSTEMS AND TECHNOLOGIES CORP., CAMBRIDGE, MA.
Usable, real-time, interactive spoken language systems
[AD-A286349] p 1310 N95-22253
BELL TELEPHONE LABS., INC., WHIPPANY, NJ.
Packaging the MAMA module p 1209 N95-20639
The ROC optical connector p 1212 N95-20654
BETTIS ATOMIC POWER LAB., WEST MIFFLIN, PA.
A new metallographic procedure for edge retention of enclosed surfaces
[DE94-017549] p 1261 N95-22048
BHABHA ATOMIC RESEARCH CENTRE, BOMBAY (INDIA).
Neutron molelcular spectroscopy: Future prospects
[PB95-130357] p 1518 N95-21227
BIO-PROCESS INNOVATIONS, INC., WEST LAFAYETTE, IN.
A low energy continuous reactor separator for the production of ethanol from corn grits/starch and biomass streams
[DE95-002256] p 1283 N95-21356
BIODYNAMIC RESEARCH CORP., SAN ANTONIO, TX.
Modeling platform dynamics and physiological response to short arm centrifugation
[AD-A279640] p 1442 N95-20457
BIRMINGHAM UNIV. (ENGLAND).
AC magnetic response of YBa2CuO7 with Y2BaCuO5 inclusions and of single-crystal YBa2Cu3O7: A comparative study
[PB94-207917] p 1577 N95-22166
BOEING COMMERCIAL AIRPLANE CO., SEATTLE, WA.
Numerical study of realistic perturbations in three-dimensional boundary layers p 1351 N95-21091
BONN UNIV. (GERMANY).
Second European Symposium on X-Ray Topography and High Resolution Diffraction: Programme and abstracts
[AD-A286328] p 1564 N95-20210
BOSTON COLL., CHESTNUT HILL, MA.
Global ionospheric weather
[AD-A285520] p 1430 N95-21177
BOSTON UNIV., MA.
Photodegradation and photophysics of laser dyes
[AD-A285105] p 1368 N95-20063
Metallic ions and atoms in the upper atmosphere
[AD-A285229] p 1414 N95-20498
Neural models of motion perception
[AD-A286560] p 1449 N95-20845
Mitigation of the effects of F layer regularities by using multiple paths p 1298 N95-20951
Source mechanisms and radio effects of ionospheric plasma disturbances
[AD-A286529] p 1555 N95-21013
Substorm theories: United they stand, divided they fall
[NASA-CR-197672] p 1427 N95-22326
The effects of magnetic storm phases on F-layer irregularities from auroral to equatorial latitudes
[AD-A286173] p 1427 N95-22423
BOWLING GREEN STATE UNIV., OH.
Publications/patents/presentations/honors/student eport. Investigation of the role of vibrational excitation in unimolecular reactions
[AD-A280044] p 1513 N95-20621
BRIGHAM YOUNG UNIV., PROVO, UT.
New chiral pyrimidino-crown ether ligands
[AD-A279892] p 1223 N95-20590
Thermodynamic and NMR studies of solvent effect on enantiomeric recognition for a chiral organiz ammonium cation by chiral diketopyridino-18-Crown-6 type ligands at 25.0 C
[AD-A279893] p 1223 N95-20592
BRISTOL UNIV. (ENGLAND).
Hierarchical structure in advanced polymers. Phase behaviour, orientation, properties
[AD-A285938] p 1268 N95-20392
Storage and recycling of water and carbon dioxide in the earth p 1425 N95-21822
BROOKHAVEN NATIONAL LAB., UPTON, NY.
Matrix formulation of the particle motion in crystalline beams
[DE94-017301] p 1563 N95-19925
Chemical and electrochemical interactions on corroding metal surfaces
[DE95-000624] p 1250 N95-19979
Resonance Raman spectroscopy of volatile organics: Carbon tetrachloride
[DE95-000627] p 1233 N95-19980
Crystalline beam in a storage ring: How long can it last?
[DE94-017303] p 1563 N95-20014
Transition-energy crossing with a gamma(sub t)(-)jump
[DE94-017315] p 1531 N95-20021
Analytic Perturbation Analysis of Discrete Event Dynamic Systems
[DE94-018635] p 1480 N95-20126
Carrier doping and interlayer coupling in HTSC single crystals
[DE94-018637] p 1564 N95-20127
Chiral symmetry and lattice gauge theory
[DE94-018676] p 1564 N95-20130
Light output and radiation damage in a lead tungstate crystal
[DE94-016814] p 1565 N95-20265
Evaluating impedances in a Sacherer integral equation
[DE94-016823] p 1489 N95-20266
Effect of space charge tune shift on transverse instabilities
[DE94-016790] p 1531 N95-20282
Relational databases for RHIC design and control
[DE94-016785] p 1532 N95-20336
Positron implantation profiles in elemental and multilayer systems
[DE94-014876] p 1566 N95-20382
Higgs decay to bottom quarks at the Tevatron
[DE94-016715] p 1511 N95-20404
A new family of anion receptors and their effects on ion pair dissociation and conductivity of lithium salts in non-aqueous solutions
[DE94-016822] p 1512 N95-20477
Inverse Cerenkov laser acceleration experiment at ATF
[DE94-017990] p 1370 N95-20572
Photoelectrons beam measurement from a magnesium cathode in a RF electron gun
[DE94-017994] p 1533 N95-20573
Crystalline beams: The horizontal zigzag
[DE95-002227] p 1533 N95-20766
Crystalline beams
[DE95-002656] p 1569 N95-20793
Approach to compact terawatt CO2 laser system for particle acceleration
[DE95-002170] p 1371 N95-20866
Confinement and stability of crystalline beams in storage rings
[DE95-002515] p 1533 N95-20886
Influence of oxidation on radiation hardness of silicon detectors
[DE95-002466] p 1272 N95-20894
Behaviour of space-charge dominated ion beams in storage rings
[DE94-015845] p 1517 N95-21140
The Carnol process for methanol production and utilization with reduced CO2 emissions
[DE94-016808] p 1283 N95-21211
The PROSAIC Laplace and Fourier Transform
[DE95-002225] p 1492 N95-21266
Hadron beams and accelerators
[DE95-002932] p 1536 N95-21342
Photoemission and ferromagnetism
[DE95-002419] p 1520 N95-21362
Effects of RF side-bands on spectral reproducibility for infrared synchrotron radiation
[DE95-002450] p 1536 N95-21418
Strange hadronic matter
[DE94-019345] p 1521 N95-21484
QCD corrections to Higgs boson production: An update
[DE95-000626] p 1522 N95-21506
BASIC program for power spectrum estimation
[DE95-002228] p 1468 N95-21515
Surface x-ray scattering and scanning tunneling microscopy studies at the Au(111) electrode
[DE95-002409] p 1573 N95-21516
Lattice results for heavy light matrix elements
[DE94-019101] p 1523 N95-21551
Summary of heavy ion theory
[DE95-002177] p 1523 N95-21588
DOS basics
[DE94-018434] p 1455 N95-21632
Signal to noise improvements with a new Far-IR rapid-scan Michelson Interferometer
[DE95-002416] p 1367 N95-21638
Dynamics of the chiral transition
[DE94-016813] p 1524 N95-21641
Light output and radiation damage in a YAlO3:Ce crystal
[DE94-016815] p 1545 N95-21643
The development of a new plasticizer for poly(ethylene oxide) based polymer electrolyte and the investigation of their ion-pair dissociation effect
[DE94-016821] p 1276 N95-21644
DBASE 4 basics
[DE94-018323] p 1469 N95-21713
RF beam control for the AGS Booster
[DE95-001485] p 1538 N95-21720
Interference of fluorescence x rays and coherent excitation of core levels
[DE94-016809] p 1527 N95-22188
Acid-site characterization of water-oxidized alumina films by near-edge x-ray absorption and soft x-ray photoemission
[DE95-003355] p 1247 N95-22234
Bunched beam instability with frequency spread
[DE94-018632] p 1539 N95-22357
Low emittance lattices for electron storage rings revisited
[DE94-017302] p 1540 N95-22391
Proton and produced particle distributions from Au+Au collisions at 11.6 A GeV/c
[DE94-018634] p 1530 N95-22392
BROWN UNIV., PROVIDENCE, RI.
Sensitivity of climate models: Comparison of simulated and observed patterns for past climates
[DE95-002257] p 1406 N95-21379
Diffusion approximations in communication and stochastic theory
[AD-A286440] p 1302 N95-21438
Surfaces and thin films studied by picosecond ultrasonics
[DE95-001866] p 1506 N95-22071
BUCKNELL UNIV., LEWISBURG, PA.
Design of a massively parallel computer using bit serial processing elements
[NASA-CR-197365] p 1479 N95-22406
BURTON TECHNOLOGIES, INC., RALEIGH, NC.
Wear resistant composite structure of vitreous carbon containing convoluted fibers
[DE95-002254] p 1228 N95-20787

C

CALIFORNIA INST. OF TECH., PASADENA, CA.
Free shear layers, base pressure and bluff-body drag
[AD-A286316] p 1200 N95-20175
Research on bluff body vortex wakes
[AD-A286319] p 1200 N95-20177
Laser-Induced Thermal Acoustics (LITA): Four-wave mixing measurement of sound speed, thermal diffusivity, and viscosity
[AD-A286524] p 1372 N95-21009
Optical, electronic and optoelectronic material and device research
[AD-A280111] p 1374 N95-21630
Constraints as a destriping tool for Hires images
p 1593 N95-21756
Volatiles in the Earth: All shallow and all recycled
p 1416 N95-21779
Recycling of volatiles at subduction zones: Noble gas evidence from the Tabar-Lihir-Tanga-Feni arc of papua New Guinea p 1418 N95-21787
Mantle rare gas relative abundances in a steady-state mass transport model p 1423 N95-21812
He, Xe and Ne isotopes in a steady-state mass transport model and implications about terrestrial volatiles
p 1425 N95-21821
Shock wave interactions in hypervelocity flow
[AD-A286507] p 1357 N95-22212

Fast parallel tree codes for gravitational and fluid dynamical N-body problems
[AD-A286480] p 1358 N95-22290

CALIFORNIA POLYTECHNIC STATE UNIV., SAN LUIS OBISPO, CA.

A real-time algorithm for integrating differential satellite and inertial navigation information during helicopter approach
[NASA-CR-197409] p 1205 N95-21891

CALIFORNIA UNIV., BERKELEY, CA.

Josephson acoustic radiation in superfluid helium
[AD-A279809] p 1503 N95-20098

Instantaneous frequency dynamics of coherent emission from magnetoexcitons in gallium arsenide
[DE94-018182] p 1569 N95-20677

Temporal and spectral investigation of multi-Landau level quantum beats in GaAs
[DE94-018189] p 1569 N95-20678

Phase dynamics of non-equilibrium distributions of free electron-hole pairs in GaAs quantum wells
[DE94-018190] p 1569 N95-20679

Computer based analysis and synthesis of retinal function
[AD-A286084] p 1443 N95-20811

Volatiles in the deep Earth: An experimental study using the laser-heated diamond cell p 1421 N95-21803

PIC simulation of surface waves
[AD-A285358] p 1563 N95-22422

Spatio-temporal masking in human vision and its application to image coding
[AD-A284949] p 1451 N95-22473

CALIFORNIA UNIV., BERKELEY. LAWRENCE BERKELEY LAB, CA.

Exploratory Technology Research Program for electrochemical energy storage
[DE95-002651] p 1392 N95-20439

Six-dimensional modeling of coherent bunch instabilities and related feedback systems in storage rings with power-series maps for the lattice
[DE94-017965] p 1532 N95-20494

Modeling of beam dynamics and comparison with measurements for the Advanced Light Source (ALS)
[DE94-017970] p 1532 N95-20495

Three-dimensional laser cooling
[DE94-017963] p 1370 N95-20569

Strange particle and antiproton production in S + nucleus collisions at 200 GeV/nucleon
[DE95-002348] p 1513 N95-20575

Laser trapping of Na-21 atoms
[DE95-002354] p 1513 N95-20629

Photoluminescence under pressure and annealing of nitrogen-doped ZnSe
[DE95-002355] p 1568 N95-20630

Ultrafast magnetoexciton dynamics in GaAs
[DE94-018175] p 1514 N95-20732

Nickel hydroxide electrodes in reduced-alkalinity electrolytes
[DE95-002333] p 1326 N95-20814

Study of small carbon and semiconductor clusters using negative ion threshold photodetachment spectroscopy
[DE95-002327] p 1515 N95-20872

Correlated wavefunction Monte Carlo studies of excitations in the quantum Hall liquids
[DE95-002337] p 1501 N95-20874

Induction linacs for heavy ion fusion
[DE95-002357] p 1534 N95-20891

Exploratory Technology Research Program for electrochemical energy storage
[DE95-002652] p 1394 N95-20915

Methods of measuring adhesion for thermally grown oxide scales
[DE94-018177] p 1256 N95-21260

Progress in ultrafast scanning probe microscopy
[DE94-018179] p 1373 N95-21261

Sources of amplitude-dependent tune shift in the PEP-2 design and their compensation with octupoles
[DE94-018198] p 1519 N95-21262

Nonlinear optical studies of polymer interfaces
[DE94-018199] p 1274 N95-21263

Plasma model for charging damage
[DE95-000788] p 1558 N95-21310

Dilepton production from p-p to Ca-Ca at the Bevalac
[DE95-002341] p 1520 N95-21357

Similarities and differences in strangeness production at BNL and CERN
[DE95-002343] p 1521 N95-21380

Time-resolved study of sideband generation and transition to chaos on an infrared FEL
[DE95-002336] p 1374 N95-21528

Resonant generation of nonequilibrium phonons in GaAs/AlAs quantum wells via intersubband scattering
[DE95-002338] p 1581 N95-21604

Detection efficiency and dark pulse rate of Rockwell (SSPM) single photon counters
[DE94-016872] p 1524 N95-21646

Hydrogenation of nitriles on a well-characterized nickel surface: From surface science studies to liquid phase catalytic activity measurements
[DE94-018184] p 1259 N95-21707

Bridging the pressure gap: In situ atomic-level investigations of model platinum catalyst surfaces under reaction conditions by scanning tunneling microscopy
[DE95-002346] p 1246 N95-21990

Carrier dynamics in InGaAs: Quantum wells versus bulk
[DE94-018205] p 1577 N95-22168

Interpretation of HRTEM images by image simulation: An introduction to theory and practice
[DE95-003422] p 1591 N95-22235

Reflective masks for extreme ultraviolet lithography
[DE95-003427] p 1336 N95-22236

Theory of the excitonic lineshape in low-dimensional structures with rough interfaces
[DE95-003434] p 1582 N95-22237

Users guide to NCEMSS, version 2.0
[DE95-003443] p 1548 N95-22238

CALIFORNIA UNIV., IRVINE, CA.

Time resolved x-ray detection
[AD-A279348] p 1368 N95-22143

CALIFORNIA UNIV., LOS ANGELES, CA.

International collaboration program on innovative chemical processing of superior electronic and optical materials
[AD-A285122] p 1226 N95-20105

Overview of the Institute of Geophysics and Planetary Physics and Lawrence Livermore National Laboratory collaborative efforts
[DE94-017300] p 1599 N95-20145

The dynamics of formation and evaporation of mixed alkali halide nanocrystals: A case of comparable lattice energies
[AD-A285052] p 1567 N95-20483

Excess energy and structural dependence of the rate of energy redistribution during the photodissociation of iodotoluenes
[AD-A279997] p 1241 N95-21124

Epitaxial liftoff technology onto processed silicon foundry wafers
[AD-A285621] p 1571 N95-21145

Gradient index lenses from sol-gel layering
[AD-A285649] p 1242 N95-21402

Computer simulation of the diocotron instability
[AD-A285655] p 1559 N95-21403

1994 Nonneutral Plasma Workshop
[AD-A285656] p 1559 N95-21404

Dynamics of volatile delivery from outer to inner solar system p 1420 N95-21798

Polar volatiles on Mercury and the Moon
p 1422 N95-21811

The enhancement of metallic silver monomer evaporation by the adhesion of polar molecules to silver nanocluster ions
[AD-A284936] p 1281 N95-22470

CALIFORNIA UNIV., SAN DIEGO, CA.

Theoretical particle physics
[DE95-002447] p 1515 N95-20893

Beyond maximum entropy: Fractal Pixon-based image reconstruction p 1593 N95-21757

CALIFORNIA UNIV., SAN DIEGO, LA JOLLA, CA.

Skeletal muscle ischemia and heat shock proteins
[AD-A285364] p 1442 N95-20549

Nitrogen isotopic components in the early solar system p 1420 N95-21800

CALIFORNIA UNIV., SANTA BARBARA, CA.

The processing and mechanical properties of high temperature/high performance composites. Stress redistribution and notch properties, book 2
[AD-A279737] p 1227 N95-20429

The processing and mechanical properties of high temperature/high performance composites. Fatigue and creep, book 3
[AD-A279738] p 1227 N95-20430

The processing and mechanical properties of high temperature/high performance composites. Book 7: In-situ measurements of stress and damage
[AD-A279814] p 1227 N95-20583

The processing and mechanical properties of high temperature/high performance composites. Book 5: Interface effects
[AD-A279815] p 1228 N95-20584

The processing and mechanical properties of high temperature/high performance composites. Mechanism-based constitutive laws and design, book 1
[AD-A279736] p 1228 N95-20801

The processing and mechanical properties of high temperature/high performance composites. Processing/property correlations, bock 4
[AD-A279739] p 1228 N95-20802

Growth and electrical and far-infrared properties of wide electron wells in semiconductors
[AD-A279409] p 1333 N95-21917

The processing and mechanical properties of high temperature/high performance composites. Book 6: Delamination and compressive behavior
[AD-A279780] p 1231 N95-21999

CALIFORNIA UNIV., SANTA CRUZ, CA.

Space constancy on video display terminals
[AD-A280015] p 1449 N95-20314

CAMBRIDGE UNIV., CAMBRIDGE (ENGLAND).

Rates of Earth degassing p 1422 N95-21809

CARNEGIE INSTITUTION OF WASHINGTON, WASHINGTON, DC.

D/H ratios and H2O contents of mantle-derived amphibole megacrysts from Dish Hill, California
p 1416 N95-21781

Structure and stability of hydrous minerals at high pressure p 1417 N95-21786

Hydrogen and related materials at high density: Physics, chemistry and planetary implications
p 1418 N95-21791

Hydrogen storage in Earth's mantle and core
p 1423 N95-21813

CARNEGIE INSTITUTION OF WASHINGTON, STANFORD, CA.

The Use of Cyanobacteria to Explore Basic Biological Processes
[DE94-019238] p 1440 N95-22066

CARNEGIE-MELLON UNIV., PITTSBURGH, PA.

O(log2 n) time efficient parallel factorization of dense, sparse separable, and banded matrices
[NASA-CR-197356] p 1473 N95-19885

A database for analyzing sequential behavioral data and their associated cognitive models
[AD-A280061] p 1448 N95-19887

A construct for describing software development risks
[AD-A284923] p 1457 N95-19999

A scalable video rate camera interface
[AD-A286144] p 1474 N95-20325

Task parallel programming in Fx
[AD-A285136] p 1475 N95-20500

Physical-chemical studies on rodlike polymer compositions
[AD-A285361] p 1269 N95-20548

A framework for segmentation using physical models of image formation
[AD-A279900] p 1543 N95-20564

Measuring software dependability by robustness benchmarking
[AD-A280053] p 1461 N95-20622

Making structured graphics and constraints practical for large-scale applications
[AD-A280062] p 1461 N95-20623

Collected papers of the Soar/IFOR project, Spring 1994
[AD-A280063] p 1216 N95-20624

Balanced matrices
[AD-A280021] p 1490 N95-20662

A software process framework for the Software Engineering Institute's (SEI) capability maturity model
[AD-A286595] p 1462 N95-20765

Modeling the effect of shroud contact and friction dampers on the mistuned response of turbopumps
[NASA-CR-197285] p 1379 N95-20795

Software Capability Evaluation (SCE), version 2.0 team members guide
[AD-A286082] p 1462 N95-20809

Rate monotonic analysis for real-time systems: Instructors guide
[AD-A286083] p 1463 N95-20810

Backward error recovery in redundant disk arrays
[AD-A286064] p 1463 N95-20846

A tabular interface for automated verification of event-based dialogs
[AD-A286065] p 1463 N95-20847

User interface software tools
[AD-A286056] p 1466 N95-21325

Benefits of CMM-based software process improvement: Executive summary of initial results
[AD-A286444] p 1468 N95-21567

Interim profile: Development and trial of a method to rapidly measure software engineering maturity status
[AD-A279074] p 1468 N95-21627

Advanced computing systems: Usability of knowledge-based planning systems
[AD-A279573] p 1477 N95-21698

Balanced 0, + or - matrices. Part 2: Recognition algorithm
[AD-A279156] p 1470 N95-21974

Artificial Intelligence (AI) and Ada: Integrating AI with mainstream software engineering
[AD-A286093] p 1485 N95-22226

CATHOLIC UNIV. OF AMERICA, WASHINGTON, DC.

Application of wavelet-filtering techniques to intermittent turbulent and wall pressure events. Part 1: Exploratory results
[AD-A286077] p 1341 N95-20849

CENTER FOR MATHEMATICS AND COMPUTER SCIENCE, AMSTERDAM (NETHERLANDS).
Explicit parallel two-step Runge-Kutta-Nystroem methods
[PB95-135752] p 1489 N95-20423
Parallelism across the steps in iterated Runge-Kutta methods for stiff initial value problems
[PB95-135760] p 1490 N95-20424
Approximate Riemann solver for magnetohydrodynamics (that works in more than one dimension)
[PB95-135802] p 1553 N95-20425
Implementation and performance of a three-dimensional numerical transport model
[PB95-135745] p 1402 N95-20440
VLUGr3: A vectorizable adaptive grid solver for PDEs in 3D. 2: Code description
[PB95-135737] p 1465 N95-21033
Explicit methods for stiff ODEs from atmospheric Chemistry
[PB95-135794] p 1404 N95-21034
Parallel predictor-corrector methods
[PB95-135711] p 1493 N95-21434
VLUGR3: A vectorizable adaptive grid solver for PDEs in 3D. 1: Algorithmic aspects and applications
[PB95-135729] p 1467 N95-21435

CENTRAL INST. OF AVIATION MOTORS, MOSCOW (RUSSIA).
A flamelet model for turbulent unpremixed combustion
p 1249 N95-21081

CENTRAL IRON AND STEEL RESEARCH INST., BEIJING (CHINA).
Joining of dissimilar materials. A review
[PB95-132999] p 1380 N95-21416

CENTRE D'ELECTRONIQUE DE L'ARMEMENT, BRUZ (FRANCE).
A wideband propagation simulator for high speed mobile radio communications p 1295 N95-20934

CENTRE D'ETUDES ET DE RECHERCHES DE MEDECINE AERONAUTIQUE, PARIS (FRANCE).
Effect of increased venous backflow on the release of cardiac hormone. Fine structural, immunohistochemical, and biochemical study
[PB95-130399] p 1445 N95-21424

CENTRE DE RECHERCHES DU SERVICE DE SANTE DES ARMEES, LA TRONCHE (FRANCE).
Study of pulsed laser effects on living tissues
[PB95-131330] p 1447 N95-22361

CENTRE DE RECHERCHES EN PHYSIQUE DE L'ENVIRONNEMENT, VELIZY (FRANCE).
Time behavior and frequency response of the microwave propagation channel during multipath propagation
p 1296 N95-20942
Experimental study of the helicopter-mobile radioelectrical channel and possible extension to the satellite-mobile channel p 1296 N95-20945

CENTRE NATIONAL D'ETUDES DES TELECOMMUNICATIONS, LANNION (FRANCE).
Sounder calibration with backscattering from Losquet Island in the presence of multipaths
p 1300 N95-20961

CERAMEM CORP., WALTHAM, MA.
Ceramem filters for removal of particles from hot gas streams
[DE95-001976] p 1275 N95-21354

CHARLES RIVER ANALYTICS, INC., CAMBRIDGE, MA.
A neural expert approach to self designing flight control systems
[AD-A279965] p 1215 N95-21122

CHI SYSTEMS, INC., SPRING HOUSE, PA.
The advanced technology crew station: Development and validation of a workload assessment technique for cockpit function allocation
[AD-A279544] p 1453 N95-21691

CHICAGO UNIV., CHICAGO, IL.
Far-infrared mapping of dusty elliptical galaxies
p 1593 N95-21763

CHINA NUCLEAR INFORMATION CENTRE, BEIJING (CHINA).
High precision trace neutron transmutation doping of detector-grade high resistance zone-refined silicon mono-crystal
[DE94-631463] p 1563 N95-19978
Moessbauer study of the sintered Mn(0.70)Zn(0.23)Fe(2.07)O4
[DE94-631462] p 1255 N95-20909
The evolution of configuration from q greater than 1 to q less than 1
[DE94-631396] p 1556 N95-21162
Numerical analysis of energetic particle stabilization of ballooning modes in finite-aspect-ratio tokamaks
[DE94-631397] p 1556 N95-21164
Experimental investigation of molecular beam injection in HL-1 tokamak
[DE94-631456] p 1556 N95-21165

CLARKSON UNIV., POTSDAM, NY.
Novel electrochemical materials prepared by sol-gel chemistry
[AD-A286310] p 1226 N95-20092

CLEMSON UNIV., SC.
Characterization equipment for electrooptics and actuators
[AD-A286285] p 1546 N95-22043

COAST GUARD RESEARCH AND DEVELOPMENT CENTER, GROTON, CT.
AN/APS-137 Forward Looking Airborne Radar (FLAR) evaluation, Fall 1992 experiment
[AD-A279526] p 1306 N95-21686

COASTAL ENGINEERING RESEARCH CENTER, VICKSBURG, MS.
The Surface Wave Dynamics Experiment (SWADE): A retrospective look at the wave modeling activities
[AD-A285612] p 1431 N95-19895
NODDS/WOSM interface user's manual
[AD-A279095] p 1471 N95-22068

COLOGNE UNIV. (GERMANY).
New ET-based organic superconductors with the organometallic anion Cu(CF3)4(-)
[DE94-016904] p 1567 N95-20479

COLORADO SCHOOL OF MINES, GOLDEN, CO.
Velocity analysis for transversely isotropic media
[DE95-000643] p 1411 N95-19981
P-wave signatures and parameterization of transversely isotropic media: An overview
[DE95-000644] p 1411 N95-19982
Polycrystalline thin film cadmium telluride solar cells fabricated by electrodeposition
[DE94-011848] p 1391 N95-20118

COLORADO STATE UNIV., FORT COLLINS, CO.
Properties of molecular solids and fluids at high pressure and temperature
[DE94-017594] p 1565 N95-20243
Mechanism of the amperometric response of a proposed glucose sensor based on a polypyrrole-tubule-impregnated membrane
[AD-A279836] p 1365 N95-20431
Chemically modified electrodes
[AD-A279821] p 1324 N95-20587
Monitoring the response of the upper troposphere/lower stratosphere to a greenhouse gas scenario
[DE95-000982] p 1406 N95-21410
Synthesis of polymeric microcapsule arrays and their use for enzyme immobilization
[AD-A279125] p 1277 N95-21876

COLORADO UNIV., BOULDER, CO.
Front-boundary layer models from STORM-FEST observations
[AD-A279907] p 1428 N95-20186
State-to-state collisional dynamics of atmospheric species
[AD-A285053] p 1370 N95-20484
New methods for large scale local and global optimization
[AD-A285635] p 1517 N95-21126
Nonlinear acoustic processes in a solid rocket engine
[AD-A285606] p 1222 N95-21193
Mars atmospheric loss and isotopic fractionation by pick-up-ion sputtering and photochemical escape
p 1420 N95-21796
A crystallographic model for hydrous wadsleyite (Beta-Mg2SiO4) p 1424 N95-21817
Physics of correlated studies
[DE95-001204] p 1581 N95-21842
· Fast algorithms for transport models
[DE95-001702] p 1470 N95-21992
Signal processing in the linear statistical model
[AD-A286255] p 1308 N95-22041
Confirmatory analysis of SAGE-1, and -2 data
[DE95-003623] p 1427 N95-22240
Parallel nanometer scale fabrication
[DE95-002122] p 1336 N95-22284

COLORADO UNIV., DENVER, CO.
Fitting stochastic partial differential equations to spatial data
[AD-A279870] p 1490 N95-20432

COLUMBIA UNIV., NEW YORK, NY.
Study of improved critical currents and mechanical properties in the Y-Ba-Cu-O superconductor with silver or Y2BaCuO3 or 211 dispersions
[AD-A285609] p 1502 N95-21194
Translational-energy-resolved studies of photographed carrier-induced reactions on semiconductor surfaces
[DE95-002944] p 1573 N95-21444
Single-collision studies of energy transfer and chemical reaction
[DE95-002943] p 1244 N95-21517
Physics of systems containing neutron stars
[NASA-CR-197304] p 1600 N95-21615
Visual perception of elevation
[AD-A284938] p 1451 N95-22472
Diffusible driving and coupling signals of the biological clock
[AD-A285353] p 1447 N95-22475

COMMISSION OF THE EUROPEAN COMMUNITIES, BRUSSELS (BELGIUM).
European Workshop on Optical Ground Truth Instrumentation for the Validation of Space-Borne Optical Remote Sensing Data of the Marine Environment
[PB95-134144] p 1390 N95-21872

COMMUNICATIONS RESEARCH CENTRE, OTTAWA (ONTARIO).
Development of a fast sampling system for estimation of impulse responses of mobile radio channels
p 1296 N95-20943

COMMUNICATIONS SATELLITE CORP., CLARKSBURG, MD.
UV testing of INTELSAT-7, 7A, and 8 solar cells
p 1320 N95-20526

COMPUTER SCIENCES CORP., FALLS CHURCH, VA.
Network distributed global memory for transparent message passing on distributed networks
[AD-A286096] p 1478 N95-22228

CORNELL UNIV., ITHACA, NY.
A group communication approach for mobile computing mobile channel: An ISIS tool for mobile services
[AD-A279785] p 1290 N95-20306
Molecular snapshots: Product imaging of dynamics important to fundamental combustion processes
[DE94-018595] p 1510 N95-20346
Modelocking and waveguide amplifiers using Cr:Forsterite and Cr:YAG
[AD-A285857] p 1369 N95-20378
Semiconductor laser joint study program with Rome Laboratory
[AD-A285858] p 1369 N95-20379
Novel materials
[AD-A279693] p 1227 N95-20427
Mapping closures for turbulent combustion
[AD-A279995] p 1238 N95-20597
Ion scattering and deposition: The role of energetic particles in thin film growth
[AD-A285975] p 1514 N95-20667
Gordon Research Conference on Physical Electrochemistry
[AD-A286545] p 1240 N95-20842
Experimental study of interactions of highly charged ions with atoms at keV energies
[DE95-001807] p 1521 N95-21441
Design, fabrication, and characterization of reflective diffractive optical elements in Si for free-space optical interconnects
[AD-A286416] p 1547 N95-22205
Fully developed turbulent flows
[AD-A286496] p 1358 N95-22294
Experimental study of interactions of highly charged ions with atoms at keV energies
[DE94-018648] p 1529 N95-22316
Resonant charge transfer in hyperthermal atomic and molecular ion-surface collisions
[AD-A284937] p 1530 N95-22471

D

DANIEL DEN HOED CANCER CENTER, ROTTERDAM (NETHERLANDS).
Radiofrequency hyperthermia systems: Experimental and clinical assessment of the feasibility of radiofrequency hyperthermia systems for loco-regional deep heating
[PB94-206885] p 1444 N95-21016

DARTMOUTH COLL., HANOVER, NH.
Applications of wavelets to radar, imaging and related problems
[AD-A279909] p 1290 N95-20545
Excitons in semiconducting superlattices, quantum wells, and ternary alloys
[DE95-001867] p 1572 N95-21287

DASSAULT AVIATION, SAINT-CLOUD (FRANCE).
FASTPACK: Optimized solutions for modular avionics derived from a parametric study. Part 1: Platform features p 1208 N95-20634

DAVID SARNOFF RESEARCH CENTER, PRINCETON, NJ.
High performance YBCO films
[AD-A286567] p 1326 N95-20824
High performance YBCO films
[AD-A279560] p 1276 N95-21695

DAYTON UNIV., OH.
Lubricant evaluation and performance, 2
[AD-A279144] p 1278 N95-21969

DAYTON UNIV. RESEARCH INST., OH.
Color control in a multichannel simulator display: The display for advanced research and training
[AD-A279717] p 1216 N95-20992

DEDICATED ELECTRONICS, INC., CHESTER, NH.
Development of a portable ice-thickness measuring instrument
[AD-A279472] p 1433 N95-21291

DEFENCE AND CIVIL INST. OF ENVIRONMENTAL MEDICINE, DOWNSVIEW (ONTARIO).
Thermal resistance of the cheek in cold air
[AD-A286257] p 1446 N95-22001

DEFENCE RESEARCH AGENCY, MALVERN (ENGLAND).
The relative importance of meteor burst and other distance polar cap propagation modes in the low VHF band p 1293 N95-20928
DAMSON: A system to measure multipath dispersion, Doppler spread and Doppler shift on multi-mechanism communications channels p 1299 N95-20955

DEFENCE RESEARCH ESTABLISHMENT OTTAWA, OTTAWA (ONTARIO).
Evaluation of Borland Turbo Vision
[AD-A279873] p 1459 N95-20184
Facsimile transmission standards
[AD-A279911] p 1290 N95-20308
Overview of data fusion work for land electronic warfare
[AD-A279829] p 1301 N95-21292

DEFENCE RESEARCH ESTABLISHMENT SUFFIELD, RALSTON (ALBERTA).
Enhancement of cell mediated immunity through non-specific immunostimulation with liposome encapsulated gamma-interferon
[AD-A279667] p 1442 N95-20602

DEFENCE SCIENCE AND TECHNOLOGY ORGANIZATION, MELBOURNE (AUSTRALIA).
Investigation of rocket motors 3 inch number 1 Mk 4
[AD-A284278] p 1221 N95-19962
Variations observed in the AC generator signal period of a Sea King helicopter
[AD-A284280] p 1206 N95-19963
A preliminary study of the airwake model used in an existing SH-60B/FFG-7 helicopter/ship simulation program
[DSTO-TR-0015] p 1201 N95-21659
Ultraviolet emission from rocket motor plumes
[DSTO-TR-0002] p 1222 N95-21661
An evaluation of the Gear Averaging Signal Processor (GASP)
[DSTO-TR-0067] p 1470 N95-21950
Diffuse reflectance spectra of energetic material
[DSTO-TR-0065] p 1284 N95-21951

DEFENSE INFORMATION SYSTEMS AGENCY, ARLINGTON, VA.
Defense Data Repository System (DDRS). End user manual
[AD-A286484] p 1592 N95-22293

DEFENSE SYSTEMS MANAGEMENT SCHOOL, FORT BELVOIR, VA.
An abstract model of rogue code insertion into radio frequency wireless networks. The effects of computer viruses on the Program Management Office
[AD-A285759] p 1288 N95-19932
Scheduling: A guide for program managers
p 1584 N95-20748

DELAWARE UNIV., NEWARK, DE.
Inverse and control problems in electromagnetics
[AD-A286438] p 1310 N95-22250

DEPARTMENT OF DEFENSE, WASHINGTON, DC.
Unmanned aerial vehicles
[AD-A286190] p 1206 N95-20329
Military standard: Test requirements for launch, upper-stage, and space vehicles
[AD-A286627] p 1218 N95-20770

DEPARTMENT OF ENERGY, MORGANTOWN, WV.
Performance and cost analysis of monolithic solid oxide fuel cells
[DE95-002511] p 1394 N95-20896
Solid oxide fuel cells in the United States
[DE95-002405] p 1395 N95-21361

DEPARTMENT OF ENERGY, OAK RIDGE, TN.
Research in the chemical sciences: Summaries of FY 1994
[DE94-015427] p 1223 N95-20264

DEPARTMENT OF ENERGY, WASHINGTON, DC.
Beyond telecommuting: A new paradigm for the effect of telecommunications on travel
[DE95-001224] p 1289 N95-20214
FEDIX: User's guide, version 5.0/release 3.0
[DE95-002274] p 1588 N95-20762
Closure on the global carbon cycle
[DE94-018617] p 1404 N95-20991
Nuclear Terms Handbook, 1993
[DE94-016248] p 1589 N95-21131
Electric and Hybrid Vehicles Program
[DE95-001711] p 1332 N95-21738

DEPARTMENT OF THE NAVY, WASHINGTON, DC.
Method of making copper-titanium nitride alloy
[AD-D016582] p 1252 N95-20201
Optimal distributed control system for a linear distributed parameter system
[AD-D016583] p 1480 N95-20202
General purpose sidelobe canceller system
[AD-D016560] p 1289 N95-20270
Long sequence correlation coprocessor
[AD-D016558] p 1313 N95-20280
Ceramics formed by pyrolysis of either linear or thermosetting carborane (siloxane or silane) acetylene based precursor polymers
[AD-D016563] p 1266 N95-20291
Multi-layered translated rib-stiffened composite hollow cylinder assembly
[AD-D016566] p 1226 N95-20292
Polyurethane-epoxy interpenetrating polymer network acoustic damping material
[AD-D016567] p 1266 N95-20293
Polyurethane-acrylic interpenetrating polymer network acoustic damping material
[AD-D016572] p 1266 N95-20294
Malone-brayton cycle engine/heat pump
[AD-D016573] p 1378 N95-20295
Method and system of mapping acoustic near field
[AD-D016574] p 1504 N95-20296
Low flow fluid separator
[AD-D016575] p 1339 N95-20297
Semiconductor cold electron emission device
[AD-D016577] p 1314 N95-20298
Module cooling system
[AD-D016584] p 1315 N95-20436
Attachment methodology for composite cylinder assembly
[AD-D016578] p 1227 N95-20459
Compositive piezoelectrics utilizing a negative Poisson ratio polymer
[AD-D016579] p 1268 N95-20460
Superconducting thin film with fullerenes and method of making
[AD-D016580] p 1567 N95-20461
Elastomeric electrical connector
[AD-D016559] p 1325 N95-20663
Cascade orificial resistive device
[AD-D016529] p 1504 N95-20724
Method of fabricating a microelectronic photomultiplier device with integrated circuitry
[AD-D016530] p 1325 N95-20726
Microdynamic devices fabricated on silicon-on-sapphire substrates
[AD-D016531] p 1325 N95-20727
Control of continuous phase PH using visible light to activate PH-dependent fibers and gels in a controlled and reversible manner
[AD-D016532] p 1543 N95-20728
High isolation electronic switch
[AD-D016533] p 1326 N95-20729
Hybrid high power amplifier
[AD-D016534] p 1326 N95-20730
Time code interface
[AD-D016535] p 1501 N95-20731
Passive range measurement system
[AD-D016222] p 1544 N95-21100
Circuit means for providing compatibility between two separate digital data interfaces
[AD-D016225] p 1455 N95-21116
Electron tunneling magnetic field sensor
[AD-D016227] p 1365 N95-21117
Transducers with improved signal transfer field of the invention
[AD-D016228] p 1328 N95-21118
Mandrel based embedded planar fiber-optic interferometric acoustic sensor
[AD-D016229] p 1504 N95-21119
Polyurethane self-priming topcoats
[AD-D016204] p 1274 N95-21154
Polyurethane self-priming topcoats
[AD-D016205] p 1274 N95-21155
Small antennas for communication over sea ice
[AD-D016206] p 1301 N95-21156
Non-intrusive SCSI status sensing system
[AD-D016242] p 1476 N95-21307
Selective polygon map display method
[AD-D016518] p 1590 N95-21463
Method and apparatus for classifying targets
[AD-D016519] p 1303 N95-21464
Nonlinear frequency conversion optical filter
[AD-D016523] p 1544 N95-21465
Method for characterization of optical waveguide devices using partial coherence interferometry
[AD-D016525] p 1544 N95-21466
Network file server with automatic sensing means
[AD-D016250] p 1476 N95-21496
SCSI controller with target status retrieval
[AD-D016249] p 1476 N95-21504
Multi-port tester interface
[AD-D016240] p 1332 N95-21775
Fiber grating-based detection system for wavelength encoded fiber sensors
[AD-D016208] p 1545 N95-21825
Improved broadband waveguide pressure window
[AD-D016487] p 1306 N95-21834
Electromagnetic radiation detector utilizing an electromagnetic radiation absorbing element in a mach-zehnder interferometer arrangement
[AD-D016507] p 1306 N95-21835
Lift enhancement device
[AD-D016522] p 1201 N95-21864
Monolithic low noise preamplifier for piezoelectric sensors
[AD-D016524] p 1333 N95-21865
Technique for intracavity sum frequency generation
[AD-D016478] p 1546 N95-21898
Method of forming a high voltage silicon-on-sapphire photocell array
[AD-D016479] p 1396 N95-21899
Thermal fixture for testing an integrated circuit
[AD-D016483] p 1333 N95-21900
Magnetostrictive motor system
[AD-D016484] p 1333 N95-21901
Superconducting electromagnetic thruster
[AD-D016485] p 1355 N95-21902
Method for laser-assisted silicon etching using halocarbon ambients
[AD-D016494] p 1375 N95-21903
Frequency-coded monopulse MTI
[AD-D016495] p 1307 N95-21904
Submicrosecond, synchronizable x-ray source
[AD-D016497] p 1546 N95-21905
Thoriated-tungsten, split-ring, hollow-cathode electrode for discharge devices
[AD-D016508] p 1333 N95-21906
Aligned bismuth, strontium, calcium cuprate coatings on polycrystalline substrates
[AD-D016512] p 1278 N95-21907
Directive optimization of coherent sidelobe canceller systems
[AD-D016513] p 1307 N95-21908
Passive surface deployed variable inductance wire antenna statement of government interest
[AD-D016210] p 1307 N95-21910
Uninterrupted, enhanced-rate event sequencer with mixed-speed counter modules
[AD-D016255] p 1334 N95-22030
Attachment methodology for composite cylinder assembly
[AD-D016256] p 1381 N95-22034
Method of making a semiconductor device by forming a nanochannel mask
[AD-D016515] p 1576 N95-22059
Elastic micro-fabricated surface layer for reducing turbulence and drag on an object while it moves through a fluid medium
[AD-D016516] p 1356 N95-22060
Fiber optic pressure sensing array
[AD-D016245] p 1506 N95-22088
Optical fiber pressure sensor for liquid level monitoring
[AD-D016246] p 1547 N95-22089
Method of sensing target status in a local area network
[AD-D016248] p 1478 N95-22090
Method of retrieving and storing computer peripheral data
[AD-D016251] p 1591 N95-22098
Occupant reach and mobility apparatus
[AD-D016253] p 1454 N95-22099
Growing and releasing diamonds
[AD-D016489] p 1577 N95-22103
Method for determining the granular nature of superconductors using pulsed current
[AD-D016517] p 1577 N95-22137
Method of non-intrusively sensing status in a computer peripheral
[AD-D016241] p 1478 N95-22146
Broadband thermal optical limiter for the protection of eyes and sensors
[AD-D016493] p 1377 N95-22304
Pre-amplifier with multi-stage feedback
[AD-D016254] p 1336 N95-22418
Acoustic and vibration attenuation composite material
[AD-D016585] p 1233 N95-22467

DET NORSKE VERITAS, HOVIK (NORWAY).
Direct simulation of turbulent flow in a square duct: Reynolds-stress budgets p 1348 N95-21073

DETROIT DIESEL ALLISON, INDIANAPOLIS, IN.
Experimental study of vane heat transfer and aerodynamics at elevated levels of turbulence
[NASA-CR-4633] p 1337 N95-19912

DEUTSCHE AEROSPACE A.G., MUNICH (GERMANY).
Microchannel heat pipe cooling of modules
p 1211 N95-20649
Optical backplane for modular avionics
p 1212 N95-20652

DEUTSCHE FORSCHUNGSANSTALT FUER LUFT- UND RAUMFAHRT, BRUNSWICK (GERMANY).
Numerical investigation of supersonic turbulent boundary layers with high wall temperature
p 1344 N95-21050

DEUTSCHE FORSCHUNGSANSTALT FUER LUFT- UND RAUMFAHRT, GOETTINGEN (GERMANY).
Numerical simulation of supersonic boundary layer transition p 1348 N95-21074

DIRECTION DES RECHERCHES, ETUDES ET TECHNIQUES, PARIS (FRANCE).
Changes in the behavior of magnetic materials undergoing processing in electrical rotating machines
[PB95-104493] p 1325 N95-20702
Zirconia precipitates and zirconia: GeO2 interphase in mullite matrix-SiC woven fabrics composites prepared through a sol-gel route
[PB95-133427] p 1275 N95-21272
Twentysixth YERAC
[PB95-127437] p 1599 N95-21347
Support to the development of high-level graphics software
[PB95-131686] p 1466 N95-21349
Study of pulsed laser effects on living tissues
[PB95-131330] p 1447 N95-22361

DISPLAYTECH, INC., BOULDER, CO.
Development of ferroelectric liquid crystals with enhanced nonlinear optical properties
[AD-A279988] p 1571 N95-20965

DONMAR LTD., NEWPORT BEACH, CA.
Evaluation of state-of-the-art high speed deluge systems presently in service at various US Army ammunition plants
[AD-A279102] p 1287 N95-21598

DRAKE UNIV., DES MOINES, IA.
MEM application to IRAS CPC images
p 1592 N95-21751
Extended far-infrared emission and star formation in Seyfert galaxies p 1593 N95-21764

DREXEL UNIV., PHILADELPHIA, PA.
Designing the architecture of hierachical neural networks model attention, learning and goal-oriented behavior
[AD-A279898] p 1452 N95-20562
Design of robust optimal control systems and stability analysis of real structured uncertainties
[AD-A279089] p 1483 N95-21913

DUGWAY PROVING GROUND, UT.
Test Operations Procedure (TOP) 1-2-616 tropic exposure testing
[AD-A286376] p 1235 N95-20230

DUKE UNIV., DURHAM, NC.
A URI program for Ultraviolet/extreme ultraviolet research
[AD-A279159] p 1370 N95-20600

E

EAGLE VENTURES, ROCKVILLE, MD.
Independent review of Aviation Technology and Research Information Analysis System (ATRIAS) database
[AD-A284049] p 1203 N95-21518

EAST CAROLINA UNIV., GREENVILLE, NC.
Evaluation of dried storage of platelets for transfusion: Physiologic integrity and hemostatic functionality
[AD-A286078] p 1443 N95-20850
Preclinical investigation of lyophilized platelet preparations
[AD-A286079] p 1443 N95-20851

EASTMAN KODAK CO., ROCHESTER, NY.
High speed optical storage technology
[AD-A285788] p 1456 N95-22400

ECOLE CENTRALE DE LYON (FRANCE).
Modelling anisotropy and backscatter effects in the subgrid scale stress tensor p 1349 N95-21077

ECOLE CENTRALE DE PARIS (FRANCE).
Triple flame structure and diffusion flame stabilization
p 1249 N95-21039

ECOLE POLYTECHNIQUE, PALAISEAU (FRANCE).
Large facilities pilot programme. Access to the VULCAN High Power Laser Facilities at Rutherford Appleton Laboratory
[PB95-130340] p 1373 N95-21226

EDGERTON, GERMESHAUSEN AND GRIER, INC., IDAHO FALLS, ID.
Nonlinear Faraday effect in CdS semiconductor in an ultrahigh magnetic field
[DE94-016804] p 1564 N95-20240
Assessment of database for interaction of tritium with ITER plasma facing materials
[DE95-002038] p 1558 N95-21290
Performance testing of the AC propulsion ELX electric vehicle
[DE95-002049] p 1330 N95-21471
Electric and Hybrid Vehicle Program Site Operator Program
[DE95-002042] p 1333 N95-21960

EG AND G MOUND APPLIED TECHNOLOGIES, MIAMISBURG, OH.
Sequential shock induced switch tests for Eglin Air Force Base
[DE95-001786] p 1334 N95-22062

EG AND G ROCKY FLATS, INC., GOLDEN, CO.
Acoustic emission: The first half century
[DE94-017176] p 1503 N95-20267

ELECTRICITE DE FRANCE, CHATOU (FRANCE).
Modeling near wall effects in second moment closures by elliptic relaxation p 1345 N95-21054

ELECTRONICS RESEARCH LAB., SALISBURY (AUSTRALIA).
The iMAPS: General information
[AD-A285421] p 1465 N95-21176

ELIZABETH CITY STATE UNIV., NC.
ECSU-AASERT summer research project in parallel processing and computer visualization
[AD-A285983] p 1475 N95-20618

ELTRON RESEARCH, INC., BOULDER, CO.
Electrochemical impedance pattern recognition for detection of hidden chemical corrosion on aircraft components
[AD-A284998] p 1253 N95-20481
Electrochemical impedance pattern recognition for detection of hidden chemical corrosion on aircraft components
[AD-A285998] p 1239 N95-20716

ENERGY AND ENVIRONMENTAL RESEARCH CORP., IRVINE, CA.
Experimental investigation of PIC formation during the incineration of recovered CFC-11
[PB94-214772] p 1401 N95-20192

ENERGY INFORMATION ADMINISTRATION, WASHINGTON, DC.
Solar collector manufacturing activity 1993
[DE94-017340] p 1398 N95-22429

ENERGY INTERNATIONAL, INC., PITTSBURGH, PA.
Technology development for cobalt F-T catalysts
[DE94-017363] p 1241 N95-21172

ENGINEERING AND ECONOMICS RESEARCH, INC., VIENNA, VA.
Advanced Command and Control (C2) applications interfaces to the Advanced Communications Technology Satellite (ACTS)
[AD-A279676] p 1291 N95-20605

ENVIRONMENTAL PROTECTION AGENCY, RESEARCH TRIANGLE PARK, NC.
Carboxyhemoglobin formation due to transient exposure to high level carbon monoxide: Experimental results and an explanatory model
[AD-A285476] p 1444 N95-20979
Transport, radiative, and dynamical effects of the Antarctic ozone hole: A GFDL SKYHI model experiment
[PB94-192754] p 1409 N95-22101

ESCUELA TECNICA SUPERIOR DE INGENIEROS AERONAUTICOS, MADRID (SPAIN).
Effects of non-unity Lewis numbers in diffusion flames
p 1249 N95-21036

ETTORE MAJORANA CENTRE FOR SCIENTIFIC CULTURE, ERICE (ITALY).
Erice International Seminars on Planetary Emergencies. 17th Workshop: The Collision of an Asteroid or Comet with the Earth
[AD-A280122] p 1600 N95-21577

EUROCONTROL EXPERIMENTAL CENTRE, BRETIGNY (FRANCE).
Data link terminal DLT document
[PB95-110805] p 1205 N95-21369

EUROPEAN ORGANIZATION FOR NUCLEAR RESEARCH, GENEVA (SWITZERLAND).
Radiation tests on service electronics for future multi TeV detectors
[DE94-632822] p 1335 N95-22184
The development of science during this century
[DE94-632964] p 1582 N95-22185

EUROPEAN SPACE AGENCY. EUROPEAN SPACE RESEARCH AND TECHNOLOGY CENTER, ESTEC, NOORDWIJK (NETHERLANDS).
Europe's space photovoltaics programme
p 1316 N95-20506
Post-flight investigation programmes of recently retrieved solar generators p 1321 N95-20531
HIRAS: High-resolution IRAS images
p 1593 N95-21758

EXXON RESEARCH AND ENGINEERING CO., ANNANDALE, NJ.
Technical Summary for 1993 fall MRS Symposium O, Complex Fluids
[AD-A283722] p 1264 N95-19972

F

FACULTES UNIV. NOTRE-DAME DE LA PAIX, NAMUR (BELGIUM).
Iterated-subspace minimization methods for nonlinear optimization
[PB95-108171] p 1495 N95-22317

FEDERAL AVIATION ADMINISTRATION, ATLANTA, GA.
Fuselage burnthrough from large exterior fuel fires
[AD-A286295] p 1203 N95-22318

FEDERAL AVIATION ADMINISTRATION, ATLANTIC CITY, NJ.
Round-robin comparison of heat release apparatus
[AD-A285831] p 1363 N95-20031
Investigation of flight data recorder fire test requirements
[AD-A285832] p 1208 N95-20032
Test and Evaluation Master Plan (TEMP) for the Weather Message Switching Center Replacement (WMSCR)
[AD-A286590] p 1429 N95-20857
An evaluation of Automatic Terminal Information Service (ATIS) flight deck display presentation options
[AD-A280100] p 1204 N95-21020
Minima reduction simulation test results
[AD-A285626] p 1204 N95-21148

FEDERAL AVIATION ADMINISTRATION, CAMBRIDGE, MA.
Recommendation on transition from primary/secondary radar to secondary-only radar capability
[AD-A286279] p 1308 N95-22005

FEDERAL AVIATION ADMINISTRATION, WASHINGTON, DC.
Census US civil aircraft calendar year 1993
[AD-A286309] p 1199 N95-20091

FERMI NATIONAL ACCELERATOR LAB., BATAVIA, IL.
J/psi,psi(prime) yields mu(+)mu(-) and B yields J/psi,psi(prime) cross sections
[DE94-017184] p 1507 N95-20108
B meson lifetimes at CDF
[DE95-000564] p 1507 N95-20110
Hard diffraction and rapidity gaps
[DE95-000565] p 1507 N95-20111
CDF top results in the lepton + jets channel
[DE95-000641] p 1507 N95-20131
Using science centers to expose the general public to the microworld
[DE95-000647] p 1508 N95-20132
Search for W pair production with dilepton decay modes at D0
[DE95-000724] p 1508 N95-20134
Search for top in DO using the electron + jets channel with soft muon tagging
[DE95-001284] p 1509 N95-20217
CDF top results in the dilepton channel
[DE95-000837] p 1510 N95-20343
D0 quantum chromodynamics: A compilation of results presented at DPF 1994
[DE95-000838] p 1510 N95-20344
Mass and lifetime measurements with exclusive B reconstruction at CDF
[DE94-015849] p 1511 N95-20401
Measurements of the mass and width of the W boson from CDF
[DE94-015380] p 1511 N95-20415
Nuclear A dependence of exclusive vector meson production in muon scattering
[DE95-002248] p 1511 N95-20418
Derivation of coupling impedance from the wake potential of a finite bunch
[DE95-002529] p 1532 N95-20421
Search for D(+) yields (pi)(+)(mu)(+)(mu)(-)
[DE94-015538] p 1512 N95-20475
D(sup 0)-(anti-D)(sup 0) mixing and doubly Cabibbo-suppressed decays of the D(+)
[DE94-015540] p 1512 N95-20476
Production of J/(psi) in 800 GeV/c p-Si interactions
[DE94-017982] p 1513 N95-20496
Triggers for a high sensitivity charm experiment
[DE95-002251] p 1515 N95-20868
Universality of particle multiplicities
[DE95-000727] p 1515 N95-20879
Kinematical evidence for top pairs at the Tevatron
[DE95-000729] p 1515 N95-20880
Optimizing the length of the stores and related effects
[DE95-002531] p 1533 N95-20885
Evidence for t(bar t) production at the Tevatron: Statistical significance and cross section
[DE95-002524] p 1515 N95-20897
Charmonium production, b quark and B meson production and b(bar b) correlations at CDF
[DE95-002525] p 1515 N95-20898
Aging tests of ethylene contaminated argon/ethane
[DE95-002526] p 1282 N95-20899

Emittance growth due to negative-mass instability above transition
[DE95-002527] p 1534 N95-20900
Xwake 1.0 user's manual
[DE95-002528] p 1463 N95-20901
Mechanical design of the DO silicon detector
[DE95-002532] p 1365 N95-20902
Recent results from E665
[DE95-002523] p 1516 N95-20914
A measurement of the b(bar b) cross section at CDF
[DE95-000642] p 1519 N95-21273
Measurement of the polarization in the decay B(sup 0) (yields) J/(psi)K*(sup 0) in (bar p)p collisions at (radical)s = 1.8 TeV
[DE95-002521] p 1520 N95-21313
Search for Centauro events in the DO Detector at Fermilab collider
[DE95-002522] p 1535 N95-21314
A high-rate fixed-target charm experiment
[DE95-001767] p 1521 N95-21378
Boron neutrino flux and the MSW solution of the solar neutrino problem
[DE95-001861] p 1521 N95-21443
Search for the top quark using multivariate analysis techniques
[DE95-000561] p 1522 N95-21498
New shower maximum trigger for electrons and photons at CDF
[DE95-000563] p 1522 N95-21499
Measurement of W and Z production cross-sections in p(bar p) collisions at (radical)s = 1.8 TeV
[DE95-002250] p 1523 N95-21521
Structure functions and structure function ratio F2(n)/F2(p) at low X(Bj) and Q2 in inelastic muon scattering
[DE94-018979] p 1573 N95-21561
Measurement of the B meson differential cross-sections in p(bar p) collisions at (radical)s = 1.8 TeV using the exclusive decays B(sup (+-)) (yields) J/(psi)K(sup (+-)) and B(sup 0) (yields) J/(psi)K*(sup 0)
[DE94-018993] p 1523 N95-21562
Search for new particles decaying to dijets in p(bar p) collisions at (radical)s = 1.8 TeV
[DE94-018994] p 1523 N95-21563
Measurement of the B cross section at CDF via B semileptonic decays
[DE95-002217] p 1524 N95-21597
Status of the DO top search
[DE95-002214] p 1525 N95-21715
Tests of structure functions using lepton pairs: W-charge asymmetry at CDF
[DE95-000560] p 1527 N95-22122
Normal form analysis of the Tevatron
[DE94-017172] p 1539 N95-22192
Design of the readout IC for the CDF SVX-2 silicon strip detector
[DE95-000562] p 1539 N95-22193
Electroweak boson pair production in p(-p) collisions at the square root of s = 1.8 TeV
[DE95-000725] p 1527 N95-22194
Physics at the Fermilab Collider
[DE95-000726] p 1539 N95-22195
Inclusive B production at CDF and D0
[DE95-000728] p 1528 N95-22196
Search for squarks and gluinos in D0
[DE95-000730] p 1528 N95-22197
Search for top with DO detector in dilepton channel
[DE95-000731] p 1529 N95-22314
Beam flavor dependence in the hadroproduction of D(+-) and D(sub s)(+-) mesons
[DE94-015541] p 1530 N95-22339
Structure functions and structure function ratio F(sup n)2/F(sup p)2 at small x(sub Bj) and Q2 in muon-nucleon scattering
[DE94-017981] p 1530 N95-22340

FLINDERS UNIV., ADELAIDE (AUSTRALIA).
Convergent Close-Coupling method for calculation of electron scattering on hydrogen-like targets
[DE94-631340] p 1508 N95-20196
Calculation of the total and total ionization cross sections for positron scattering on atomic hydrogen
[DE94-631341] p 1508 N95-20197
The (e,2e) calculations with the final-state boundary condition
[DE94-631342] p 1509 N95-20198
Calculation of electron scattering on the He(+) ion
[DE94-631343] p 1509 N95-20199

FLORENCE UNIV. (ITALY).
Theory of spin dynamics in the classical two-dimensional heisenberg magnet
[PB95-133559] p 1502 N95-22138

FLORIDA STATE UNIV., TALLAHASSEE, FL.
T1F ((1) sigma (+)): Some preliminary electronic structure calculations
[PB95-130316] p 1518 N95-21223
DOD science and engineering apprenticeship program for high school students
[AD-A280371] p 1583 N95-22100

FLORIDA UNIV., FORT LAUDERDALE, FL.
Electron propagator theory and application
[AD-A279761] p 1507 N95-20097

FLORIDA UNIV., GAINESVILLE, FL.
Atomic orbital basis sets for molecular interactions
[AD-A279609] p 1506 N95-19959
A model for electron nuclear dynamics of a monatomic chain
[AD-A279652] p 1506 N95-19960
Visible light emitting materials and injection devices
[AD-A284796] p 1541 N95-20066
Research in theoretical elementary particle physics at the University of Florida, task A
[DE94-004373] p 1512 N95-20469
Electrospray ionization Fourier transform ion cyclotron resonance mass spectrometric study of singly and doubly charged organometallic complexes
[AD-A279899] p 1238 N95-20563
Temporal rearrangement of electronic densities in slow atomic collisions
[AD-A279725] p 1516 N95-20994
Electron-nuclear dynamics of molecular systems
[AD-A279649] p 1516 N95-21120
High magnetic field glow discharge ionization source
[AD-A279972] p 1241 N95-21123

FORSCHUNGSINSTITUT FUER HOCHFREQUENZPHYSIK, WERTHHOVEN (GERMANY).
Measurements of radar backscatter from the ocean surface at 94 GHz as a function of wind speed, direction and the modulation by the ocean waves during the SAXON-FPN experiment p 1299 N95-20960

FRAUNHOFER-GESELLSCHAFT ZUR FOERDERUNG DER ANGEWANDTEN FORSCHUNG E.V., MUNICH (GERMANY).
Experimental investigation of wave and fracture phenomena in impacted ceramics
[AD-A286589] p 1272 N95-20856

G

GALAXY SCIENTIFIC CORP., PLEASANTVILLE, NJ.
Test and evaluation report for the Manual Domestic Passive Profiling System (MDPPS)
[AD-A286312] p 1202 N95-20093
Commuter airplane accident data analysis
[AD-A286315] p 1202 N95-20174
Commuter/air taxi ditchings and water-related impacts that occurred from 1979 to 1989
[AD-A285691] p 1202 N95-20275
Test and Evaluation Plan (TEP) for Improvised Explosive Device Screening Systems (IEDSS)
[AD-A286382] p 1203 N95-22319

GAS RESEARCH INST., CHICAGO, IL.
Natural gas converter performance and durability
[PB95-135554] p 1284 N95-21966
Natural gas combustion chemistry mechanisms research
[PB95-111670] p 1247 N95-22150

GEC-MARCONI MATERIALS TECHNOLOGY, TOWCESTER (ENGLAND).
High performance backplane components for modular avionics p 1212 N95-20653

GEC-MARCONI RESEARCH CENTRE, GREAT BADDOW (ENGLAND).
MCMs for avionics: Technology selection and intermodule interconnection p 1210 N95-20641

GENERAL ACCOUNTING OFFICE, WASHINGTON, DC.
Naval aviation: F-14 upgrades are not adequately justified. Report to Congressional Committees
[AD-A286338] p 1206 N95-20212
Environmental cleanup: Too many high priority sites impede DOD's program. Report to the Chairman, Committee on Governmental Affairs, US Senate
[AD-A279511] p 1407 N95-21683
Technology transfer: Improving the use of cooperative R/D agreement at DOE's contractor-operated laboratories. Report to Congressional requesters
[GAO/RCED-94-91] p 1586 N95-22403

GENERAL ATOMICS CO., SAN DIEGO, CA.
Toward a design for the ITER plasma shape and stability control system
[DE94-017516] p 1548 N95-20037
Recent DIII-D results
[DE94-017519] p 1549 N95-20038
Fluctuations in high Beta(sub p) plasmas in D3-D
[DE94-017510] p 1550 N95-20146
A method for measuring the inductive electric field profile and noninductive current profiles on D3-D
[DE94-016683] p 1551 N95-20279
Recent results from Fast Wave Current Drive experiments on DIII-D
[DE94-016718] p 1551 N95-20285
Helium exhaust studies in the D3-D tokamak
[DE94-016682] p 1552 N95-20334
A new alpha particle diagnostic using knock-on ion tails
[DE94-015856] p 1553 N95-20402
Plasma shape experiments for an optimized tokamak
[DE94-017508] p 1553 N95-20445
Wall stabilization effects in D3-D high beta discharges
[DE94-017509] p 1554 N95-20446
Power balance in D3-D during single-null ELMing H-mode plasmas
[DE94-016680] p 1554 N95-20568
Boron carbide-based coatings on graphite for plasma facing components
[DE94-017976] p 1269 N95-20570
Enhanced scrape-off layer plasma in D3-D double-null discharges
[DE94-017977] p 1554 N95-20571
Extended theory of main ion and impurity rotation and bootstrap current in a shear layer
[DE94-015857] p 1555 N95-21141
Investigations of VH-mode in D3-D and JET
[DE94-015859] p 1556 N95-21142
Experimental measurements and modeling of impurity transport in the divertor and boundary plasma of D3-D
[DE94-016519] p 1556 N95-21159
The parametric dependence of the spatial structure of the radial electric field at the plasma edge in the D3-D tokamak
[DE94-016520] p 1556 N95-21163
Theory of the L-H transition
[DE95-001389] p 1558 N95-21299
Investigation of spherical tearing mode
[NASA-CR-197284] p 1558 N95-21345
B4C-SiC reaction-sintered coatings on graphite plasma facing components
[DE94-019105] p 1230 N95-21553

GENERAL ELECTRIC CO., CINCINNATI, OH.
Active control of fan noise-feasibility study. Volume 1: Flyover system noise studies
[NASA-CR-195392-VOL-1] p 1505 N95-21888

GENERAL ELECTRIC CO., RICHLAND, WA.
An impedance model of the Relativistic Heavy Ion Collider (RHIC)
[DE94-016784] p 1532 N95-20406

GENERAL ELECTRIC CO., SCHENECTADY, NY.
Toughened Silcomp composites for gas turbine engine applications
[DE95-002851] p 1214 N95-21243

GEORGE WASHINGTON UNIV., WASHINGTON, DC.
New high temperature plasmas and sample introduction systems for analytical atomic emission and mass spectrometry
[DE94-018580] p 1552 N95-20345
Two-center, two electron excitations identified in NEXAFS for solid Ne
[AD-A285373] p 1568 N95-20553
Identification of resonant, two-electron, and inter-atomic features in K and L23 NEXAFS spectra
[AD-A285374] p 1513 N95-20554
Angle resolved Auger electron spectroscopy: An alternate tool for identifying electronic excitation processes in solids
[AD-A285375] p 1238 N95-20555

GEORGETOWN UNIV., WASHINGTON, DC.
The Photovoltaic Higher Education National Exemplar Facility (PHENEF)
[DE94-015641] p 1395 N95-21409

GEORGIA INST. OF TECH., ATLANTA, GA.
Materials research for GHz multi-chip modules
[AD-A279661] p 1227 N95-20412
Stochastic network processes
[AD-A279905] p 1475 N95-20566
The organic chemistry of conducting polymers
[DE94-018216] p 1270 N95-20680
Analysis of subgrid models using direct and large-eddy simulations of isotropic turbulence p 1348 N95-21071
Ion-molecular spiraling collisions and termolecular recombination
[AD-A285633] p 1517 N95-21151
Recombination, ion-molecule collisions and (laser assisted) electron-excited atom collisions
[AD-A285604] p 1517 N95-21216
Multiple burn fuel-optimal orbit transfers: Numerical trajectory computation and neighboring optimal feedback guidance
[NASA-CR-197317] p 1222 N95-21616

GEORGIA TECH RESEARCH INST., ATLANTA, GA.
Temperature effects on acoustic interactions between altitude test facilities and jet engine plumes
[NASA-CR-197638] p 1504 N95-21170

GEORGIA UNIV., ATHENS, GA.

Interspecies extrapolations of halocarbon respiratory and tissue kinetics: Applications to predicting toxicity in different species
[AD-A285055] p 1442 N95-20485

Microbiology and physiology of anaerobic fermentations of cellulose
[DE95-002899] p 1438 N95-20917

Nitrogen control of chloroplast differentiation
[DE95-002797] p 1439 N95-21526

Structures and functions of oligosaccharins
[DE95-003195] p 1440 N95-22220

GESELLSCHAFT FUER MATHEMATIK UND DATENVERARBEITUNG, BONN (GERMANY).

Proceedings of the Fourth International Workshop on Inductive Logic Programming (ILP-94)
[PB95-135273] p 1464 N95-21003

GEZONDHEIDSRAAD, HAGUE (NETHERLANDS).

Optical radiation: Health based exposure limits for electromagnetic radiation in the wavelength range from 100 nanometer to 1 millimeter
[PB95-132767] p 1447 N95-22083

GINER, INC., WALTHAM, MA.

Development and demonstration of advanced technologies for direct electrochemical oxidation of hydrocarbons (methanol, methane, propane)
[AD-A285094] p 1224 N95-22474

GLASGOW UNIV. (SCOTLAND).

Semantics for a fine lambda-calculus with de Bruijn indices
[PB95-127577] p 1492 N95-21372

GRAZ UNIV. (AUSTRIA).

International Conference on Control and Estimation of Distributed Parameter Systems: Nonlinear Phenomena
[AD-A286449] p 1493 N95-21582

GRENOBLE UNIV. (FRANCE).

Fourth International Symposium on Stratified Flows, volume 1
[AD-A286450] p 1354 N95-21583

Fourth International Symposium on Stratified Flows, volume 3
[AD-A286452] p 1354 N95-21584

Fourth International Symposium on Stratified Flows, volume 4
[AD-A286453] p 1358 N95-22424

GRONINGEN RIJKSUNIV. (NETHERLANDS).

Riccati equation theory for Pritchard-Salamon systems: A Popov function approach
[PB95-137089] p 1491 N95-20830

DNS of turbulent flow in a driven cavity and their analysis using proper orthogonal decomposition
p 1352 N95-21097

Computation of invariant manifolds
[PB95-135687] p 1492 N95-21318

GRONICs-1994. Proceedings of the 1994 Groningen Student Conference on Computer Science
[PB95-135620] p 1468 N95-21455

In search of random noise p 1592 N95-21753

GTE LABS., INC., WALTHAM, MA.

Methods and components for optical contention resolution in high speed networks
[AD-A280016] p 1543 N95-20598

H

HARVARD COLL. OBSERVATORY, CAMBRIDGE, MA.

Absolute, Extreme-ultraviolet Solar Spectral Irradiance Monitor (AESSIM)
[AD-A279345] p 1603 N95-21929

HARVARD UNIV., CAMBRIDGE, MA.

Intermediate levels of visual processing
[AD-A284922] p 1448 N95-19998

Microbial degradation of polymers used in electronics
[AD-A286526] p 1273 N95-21011

HAWAII UNIV., HONOLULU, HI.

Analysis of low frequency ocean noise. 1: From a long-term experiment across the US East Coast. 2: From the Wake Island Hydrophone Array during northwest Pacific typhoons
[AD-A284975] p 1432 N95-20040

Luminous radio-quiet sources in the W3(MAIN) cloud core p 1594 N95-21773

Comets, impacts, and atmospheres
p 1422 N95-21810

Seismic anisothropy and large-scale porosity inthe ocean floor
[AD-A286580] p 1436 N95-22187

HELLENIC AIR FORCE ACADEMY, ATHENS (GREECE).

Investigation of shear layer transition using various turbulence models p 1352 N95-21096

HELSINKI UNIV. OF TECHNOLOGY, ESPOO (FINLAND).

Analyses of some benchmark cases in fracture mechanics using boundary element method
[PB95-110888] p 1384 N95-19930

Physical Si(1-x)Ge(x)/Si heterojunction bipolar transistor model for device and circuit simulation
[PB95-110896] p 1312 N95-19934

High-performance packet switching architecture for ATM: Conventional solution and neural network solution
[PB95-110920] p 1312 N95-19935

Orientation studies of polyolefins by IR-dichroism
[PB95-104386] p 1236 N95-20256

DC potential anomalies caused by a conducting body in an anisotropic conducting half-space
[PB95-127106] p 1291 N95-20775

Seminar on Biomedical Engineering 1993
[PB95-104402] p 1443 N95-20971

Low noise 22 GHz receiver for the radioastron satellite. Part 1: Requirements, design and reliability analysis
[PB95-104410] p 1300 N95-20972

Routing of unidirectional packet radio for wide-area paging network control and maintenance
[PB95-104428] p 1300 N95-20980

Mixed hp finite element methods for problems in elasticity and stokes flow
[PB95-104444] p 1341 N95-20981

Systems Analysis Laboratory. Ten years of progress 1984-1994
[PB95-104451] p 1464 N95-20982

Preliminary study of HUTSAT microsatellite
[PB95-127619] p 1220 N95-21026

Classification of bianisotropic media
[PB95-127635] p 1502 N95-21102

Magnetoelectric properties of reciprocal bianisotropic materials with focus on the polarizability of chiro-omega spheres
[PB95-127650] p 1544 N95-21103

Low-frequency image theory for a current dipole in front of a permeable sphere
[PB95-127676] p 1300 N95-21104

Investigation on the backscattering properties of Finnish boreal forests at C- and X-band: A semi-empirical modeling approach
[PB95-127692] p 1389 N95-21105

Application of Roe's flux-difference splitting for kappa-epsilon turbulence model
[PB95-127718] p 1352 N95-21106

Eigenmode method for electromagnetic synthesis of diffractive elements with three-dimensional profiles
[PB95-127726] p 1301 N95-21107

2nd International ADI seminar
[PB95-127734] p 1255 N95-21108

Cell loss analysis of two-class priority generalized knockout switch
[PB95-127742] p 1301 N95-21109

Inert gas purification and measuring oxygen partial pressure in gas mixtures with EMF method based on solid electrolyte cell
[PB95-127767] p 1240 N95-21110

Thermodynamic analysis of stable and metastable equilibrium diagrams of the Cu-Cr system
[PB95-127775] p 1255 N95-21111

Attempt to interpret the self-organizing mapping physiologically
[PB95-127783] p 1438 N95-21112

Nitrogen alloyed martensitic steels
[PB95-127791] p 1255 N95-21128

Equivalent source current formulation in impedance tomography
[PB95-127627] p 1329 N95-21326

Source distribution of visual evoked neuromagnetic responses
[PB95-127643] p 1445 N95-21348

Applicability of the ECMWF rain height and rainfall rate data to the prediction of low-availability rain attenuation in Europe
[PB95-127684] p 1430 N95-21413

Safety issues in high speed machining
[PB95-127411] p 1287 N95-21422

Flow and heat transfer simulation in a flash smelting furnace
[PB95-108197] p 1354 N95-21649

ActorStudio reference manual. A user's guide to the ActorStudio user interface editor, version 1.0
[PB95-127023] p 1472 N95-22310

Image solution for poisson's equation in wedge geometry
[PB95-127171] p 1310 N95-22311

Computing symmetries and stubborn sets
[PB95-127700] p 1472 N95-22328

Catalytic reactions of synthesis gas. Part 3. Determination of reaction kinetics
[PB95-127759] p 1248 N95-22329

Dielectric mixtures with arbitrarily anisotropic components: Focus on special gyrotropic effects
[PB95-127015] p 1311 N95-22363

Image theory for the unidirectionally conducting screen
[PB95-127031] p 1311 N95-22365

Quadratic optimal control of a delay equation II: The unstable case
[PB95-127064] p 1486 N95-22366

Quadratic optimal control of a delay equation I: The stable case
[PB95-127072] p 1486 N95-22367

Right inverse for the divergence operator in spaces of continuous piecewise polynomials
[PB95-127080] p 1496 N95-22369

Locking of the finite element method in thermoelasticity
[PB95-127098] p 1496 N95-22370

Transformation of multichannel magnetocardiographic signals to standard grid form
[PB95-127114] p 1447 N95-22371

Overview of rapid prototyping technologies in manufacturing
[PB95-127122] p 1472 N95-22372

Separation of proteins by convective electrophoresis through a porous membrane
[PB95-127130] p 1248 N95-22373

New thermodynamic description of the Cu-Zr system
[PB95-127189] p 1263 N95-22374

Low noise 22 GHz receiver for the radioastron satellite, part 2: Space qualification tests
[PB95-127197] p 1598 N95-22376

Photoreflectance and x ray diffraction study of semiconductor heterostructures and quantum wells
[PB95-127049] p 1582 N95-22432

Magnetic source imaging of visually evoked and oscillatory electrical activity of the human brain
[PB95-127205] p 1448 N95-22476

HELSINKI UNIV. OF TECHNOLOGY, OTANIEMI (FINLAND).

Advanced energy systems and technologies research programme
[DE95-717486] p 1397 N95-22337

HERCULES DEFENSE ELECTRONICS SYSTEMS, INC., CLEARWATER, FL.

Project Whitefeather
[DE94-016575] p 1415 N95-21184

HERIOT-WATT UNIV., EDINBURGH (SCOTLAND).

International Conference on Optical Computing: Technical digest
[AD-A284293] p 1541 N95-20249

HIGH TECHNOLOGY CORP., HAMPTON, VA.

Computational studies of laminar to turbulence transition
[AD-A285622] p 1353 N95-21146

HILTON SYSTEMS, INC., CHERRY HILL, NJ.

Age 60 study. Part 1: Bibliographic database
[AD-A286245] p 1446 N95-22027

Age 60 study. Part 2: Airline pilot age and performance. A review of the scientific literature
[AD-A286246] p 1447 N95-22040

HIROSHIMA UNIV. (JAPAN).

Primitive Xe in the atmospheres of Earth and mars
p 1419 N95-21795

HONEYWELL, INC., BLOOMINGTON, MN.

RF vacuum microelectronics based on thin film edge-emitter technology
[AD-A279539] p 1331 N95-21690

HONG KONG UNIV. OF SCIENCE AND TECHNOLOGY, KOWLOON (HONG KONG).

The decay of axisymmetric homogeneous turbulence
p 1343 N95-21047

HOUSTON UNIV., TX.

Chemical beam epitaxy for high efficiency photovoltaic devices p 1316 N95-20508

Calculation of near optimum design of InP/In(0.53)Ga(0.47)As monolithic tandem solar cells
p 1318 N95-20517

HOWARD UNIV., WASHINGTON, DC.

High temperature superconducting microwave device
[AD-A286351] p 1336 N95-22254

HUGHES ASSOCIATES, INC., COLUMBIA, MD.

Analysis of test criteria for specifying foam firefighting agents for aircraft rescue and firefighting
[AD-A286381] p 1203 N95-22352

HUGHES RESEARCH LABS., MALIBU, CA.

Pasotron(TM) technology
[AD-A279994] p 1314 N95-20311

Sub-millimeterwave semiconductor signal sources
[AD-A279375] p 1335 N95-22144

HUGHES STX, INC., LEXINGTON, MA.

Radar studies of aviation hazards
[AD-A285845] p 1203 N95-21831

HULL UNIV. (ENGLAND).

A MMPP communications system for the frequency range 2-200MHz p 1293 N95-20924

Modelling and simulation of HF/VHF MMPPs
p 1293 N95-20925

Passive monitoring for automated MMPP communication systems p 1293 N95-20927

Geographical diversity combining to exploit multi-mechanism propagation p 1299 N95-20957

HY-TECH RESEARCH CORP., RADFORD, VA.
Soft X-Ray Innovative Source Development Program
[AD-A286380] p 1551 N95-20232
HYDROLOGIC ENGINEERING CENTER, DAVIS, CA.
Review of GIS applications in hydrologic modeling
[AD-A279076] p 1390 N95-21628

I

IBIS ASSOCIATES, INC., WELLESLEY, MA.
Analysis of cost: Combustion flame CVD diamond deposition
[AD-A279153] p 1278 N95-21973
Technical cost modeling applied to CVD diamond deposition
[AD-A286119] p 1578 N95-22231
IBM WATSON RESEARCH CENTER, YORKTOWN HEIGHTS, NY.
Iterated-subspace minimization methods for nonlinear optimization
[PB95-108171] p 1495 N95-22317
IDAHO NATIONAL ENGINEERING LAB., IDAHO FALLS, ID.
Electric and Hybrid Vehicle Program: Site Operator Program
[DE95-001925] p 1332 N95-21731
A multispectral scanner survey of the Idaho National Engineering Laboratory and the Hanford Reservation
[DE95-003922] p 1391 N95-22398
IDAHO UNIV., MOSCOW, ID.
Magnetically controlled deposition of metals using gas plasma
[DE94-018654] p 1251 N95-20128
IG TECHNOLOGIES SAN DIEGO, CA.
HPCC technology awareness program: Improved economic competitiveness through technology awareness, transfer and application
[DE95-002134] p 1476 N95-21355
IIT RESEARCH INST., CHICAGO, IL.
Compilation of 1993 annual reports of the Navy ELF Communications System Ecological Monitoring Program
[AD-A279575] p 1408 N95-21699
Compilation of 1993 annual reports of the Navy ELF Communications System Ecological Monitoring Program. Volume 2: Tabs C-F
[AD-A279770] p 1308 N95-21988
ILLINOIS UNIV., CHICAGO, IL.
Molecular design concept for multi-kilovolt x-ray amplification
[DE95-001763] p 1374 N95-21743
ILLINOIS UNIV., URBANA, IL.
Structure and dynamics of turbulent wall layers
[AD-A285360] p 1340 N95-20547
Prototype rule-based reliability analysis for VLSI circuit design
[AD-A280065] p 1327 N95-20967
The mechanisms and effects off the plant-activations of chemicals in the environment
[AD-A279388] p 1356 N95-22145
An assessment of European parallel software research
[AD-A286357] p 1479 N95-22257
IMPERIAL COLL. OF SCIENCE AND TECHNOLOGY, LONDON (ENGLAND).
Large facilities pilot programme. Access to the VULCAN High Power Laser Facilities at Rutherford Appleton Laboratory
[PB95-130340] p 1373 N95-21226
INDIANA UNIV., BLOOMINGTON, IN.
Activities of the Institute for the Study of Human Capabilities
[AD-A286471] p 1454 N95-22275
INDUSTRY AND SCIENCE CANADA, OTTAWA (ONTARIO).
Propagation measurements on a troposcatter link in the Canadian High Arctic p 1295 N95-20940
INHALATION TOXICOLOGY RESEARCH INST., ALBUQUERQUE, NM.
Urban air carcinogens and their effects on health
[DE95-002259] p 1447 N95-22285
Current concepts on airborne particles and health
[DE95-002260] p 1447 N95-22287
INNOVASIC, INC., ALBUQUERQUE, NM.
Design and development SAWAFE peak detector chip
[DE95-001745] p 1332 N95-21742
INSTITUT DE MECANIQUE DE GRENOBLE (FRANCE).
Simulation of large scale transitional flows
p 1348 N95-21075
INSTITUT DES HAUTES ETUDES SCIENTIFIQUES, BURES-SUR-YVETTE (FRANCE).
Sharp determinants
[PB95-111068] p 1488 N95-19944
Coupled analytic maps
[PB95-111076] p 1498 N95-19945
Squeezing and flow of energy for non linear wave equations
[PB95-111100] p 1489 N95-20172
Predictions from quantum cosmology
[PB95-111126] p 1599 N95-20173
Classification of diagonal coset modular invariants
[PB95-111118] p 1489 N95-20259
Banach spaces with small spaces of operators
[PB95-111134] p 1489 N95-20273
Von Neumann algebra automorphisms and time-thermodynamics relation in general covariant quantum theories
[PB95-111084] p 1580 N95-20324
Growth series for the commutator subgroup
[PB95-111092] p 1490 N95-20452
Almost kappa-wise independent random permutation of the cube
[PB95-108098] p 1495 N95-22147
Local connectivity of some Julia sets containing a circle with an irrational rotation
[PB95-109070] p 1496 N95-22353
Singular symmetric matrices
[PB95-109088] p 1496 N95-22354
Elliptic genera for Z/K-manifolds I
[PB95-109096] p 1496 N95-22355
INSTITUT FRANCAIS DU PETROLE, PARIS.
The coupling between flame surface dynamics and species mass conservation in premixed turbulent combustion p 1249 N95-21041
Simulation of a turbulent flame in a channel
p 1249 N95-21044
INSTITUT NATIONAL DES SCIENCES APPLIQUEES, RENNES (FRANCE).
Line-of-sight multipath propagation measurements at 15 GHz over 500 MHz bandwidth p 1296 N95-20944
Design and implementation of a dual-beam printed antenna for a reception in angular diversity on a Hertzien cluster (or bundle)
[PB95-131603] p 1302 N95-21431
INSTITUT NATIONAL DES SCIENCES APPLIQUEES, ROUTEN (FRANCE).
Pdf modeling for premixed turbulent combustion based on the properties of iso-concentration surfaces
p 1249 N95-21042
INSTITUT NATIONAL POLYTECHNIQUE, TOULOUSE (FRANCE).
Magnetron power supply at high stability and its application in plasma excitation for the production of ultraviolet radiation
[DE94-629656] p 1326 N95-20733
INSTITUTE FOR COMPUTER APPLICATIONS IN SCIENCE AND ENGINEERING, HAMPTON, VA.
Evaluation of Reynolds stress turbulence closures in compressible homogeneous shear flow
[NASA-CR-194892] p 1338 N95-20009
Finite dimensional approximation of a class of constrained nonlinear optimal control problems
[NASA-CR-194891] p 1479 N95-20010
Design considerations for parallel graphics libraries
[NASA-CR-194935] p 1473 N95-20013
On the wavelet optimized finite difference method
[NASA-CR-191601] p 1495 N95-22157
On the dynamics of a shock-bubble interaction
[NASA-CR-194978] p 1495 N95-22325
Experimental evaluation of dynamic data allocation strategies in a distributed database with changing workloads
[NASA-CR-195024] p 1456 N95-22431
INSTITUTE FOR DEFENSE ANALYSES, ALEXANDRIA, VA.
The opportunities for and challenges of common integrated electronics
[AD-A279991] p 1327 N95-20966
Space systems technology working group: Executive report
[AD-A285778] p 1217 N95-22413
Proceedings of the 4th Annual Major Range and TestFacility Base (MRTFB) Environmental Workshop
[AD-A285779] p 1411 N95-22414
INSTITUTE OF ATOMIC AND MOLECULAR PHYSICS, PISA (ITALY).
Large facilities pilot programme. Access to the VULCAN High Power Laser Facilities at Rutherford Appleton Laboratory
[PB95-130340] p 1373 N95-21226
INSTITUTE OF ENERGY CONVERSION, NEWARK, NJ.
Processing and modeling issues for thin-film solar cell devices
[DE94-011895] p 1394 N95-21294
INSTITUTE OF ENERGY ECONOMICS OF JAPAN, (JAPAN).
Energy and environmental issues and international opperation in Asia
[DE94-796596] p 1404 N95-21143
INSTITUTO SUPERIOR TECNICO, LISBON (PORTUGAL).
Proceedings of the NATO-Advanced Study Institute on Computer Aided Analysis of Rigid and Flexible Mechanical Systems. Volume 1: Main lectures
[AD-A286062] p 1380 N95-21171
Proceedings of the NATO-Advanced Study Institute on Computer Aided Analysis of Rigid and Flexible Mechanical Systems. Volume 2: Contributed papers
[AD-A286063] p 1381 N95-21488
INSTITUTO TECNOLOGICO DE TOLUCA, TOLUCA (MEXICO).
The control system position to the electric probe in the Tokamak Novillo
[DE94-629938] p 1550 N95-20204
INTERNATIONAL ATOMIC ENERGY AGENCY, VIENNA (AUSTRIA).
ITER EDA Newsletter. Volume 3, no. 2
[DE94-628980] p 1561 N95-21852
INTERNATIONAL BUSINESS MACHINES CORP., SAN JOSE, CA.
Time domain spectral hole-burning storage
[AD-A279912] p 1587 N95-20309
INTERNATIONAL CENTRE FOR THEORETICAL PHYSICS, TRIESTE (ITALY).
On the differential representations of quantum Lie superalgebras
[DE94-629874] p 1491 N95-20734
The solar neutrino problem: Neither astrophysics nor oscillations?
[DE94-012850] p 1603 N95-21316
Explicit analytical solution of the nonlinear Vlasov Poisson system
[DE94-628931] p 1500 N95-21592
The method of evaluating quantum partition function for the Hubbard model
[DE94-628991] p 1581 N95-21639
Collisional drift waves in the H-mode edge
[DE94-628950] p 1561 N95-21847
On the influence of electromagnetic wave and relativistic electron beam on a plasma
[DE94-628962] p 1561 N95-21848
Electromagnetic waves in an ultrarelativistically hot and strongly magnetized electron-positron plasma
[DE94-628963] p 1307 N95-21849
On the theory of strong electromagnetic waves propagation in an electron-positron-ion plasma
[DE94-628964] p 1561 N95-21850
Large amplitude localized structures in a relativistic electron-positron ion plasma
[DE94-628965] p 1561 N95-21851
Electronic structure and energies of alkaline earth oxides: MgO, CaO and SrO
[DE94-628990] p 1575 N95-21853
Rigorous spin-spin correlation function of Ising model on a special kind of Sierpinski Carpets
[DE94-628995] p 1575 N95-21854
Electronic structure and relative stability of icosahedral superatoms in Al-transition-metal alloys
[DE94-628996] p 1260 N95-21855
Second order approximation for optical polaron in the strong coupling case
[DE94-628997] p 1525 N95-21856
Acoustoelectric effect in semiconductor superlattice
[DE94-628994] p 1575 N95-21859
Uniform upper bounds in the Froehlich polaron theory
[DE94-628998] p 1525 N95-21860
Magnetic properties of the three-dimensional Ising model with an interface amorphization
[DE94-628992] p 1278 N95-21885
Effect of the electron-SO-phonon on the impurity state energies in a semiconductor quantum well
[DE94-628993] p 1581 N95-21887
A new FHNC scheme for Gutzwiller correlated wave functions
[DE94-629037] p 1581 N95-21993
An asymptotic solution of the (infinity)-d Hubbard model
[DE94-629042] p 1582 N95-21994
Critical dynamics and plastic flow in disordered Josephson junction arrays
[DE94-629074] p 1576 N95-21995
Breakdown of the law of large numbers in Josephson junction series arrays
[DE94-629075] p 1576 N95-21996
Order and turbulence in RF-driven Josephson junction series arrays
[DE94-629076] p 1576 N95-21997
Variational Monte Carlo study of He-4 in two dimensions
[DE94-629078] p 1576 N95-21998
Electric-field effects on shallow donor impurity in a harmonic quantum dot
[DE94-629034] p 1577 N95-22176

Temperature dependence of a magnetopolaron in a harmonic quantum dot in resonant magnetic fields
[DE94-629036] p 1502 N95-22177
The doping effect on spin-Peierls instability
[DE94-629046] p 1577 N95-22178
Microscopic theory of normal liquid He-3
[DE94-629047] p 1527 N95-22179
Flux creep with logarithmic U(j) dependence
[DE94-629058] p 1577 N95-22180
Magnetic interactions in the Emery model
[DE94-629059] p 1577 N95-22181
The dynamic structure function of Bose liquids in the deep inelastic regime
[DE94-629077] p 1527 N95-22182
Influence of wavelength on transient short-circuit current in polycrystalline silicon solar cells
[DE94-629082] p 1397 N95-22183
On the conductance sum rule for the hierarchical edge states of the Fractional Quantum Hall Effect
[DE94-629030] p 1582 N95-22198
Universal spectral correlations at the mobility edge
[DE94-629031] p 1528 N95-22217
Temperature dependence of magnetopolarons in a parabolic quantum dot in arbitrary magnetic fields
[DE94-629033] p 1528 N95-22218
An exact enumeration of self-avoiding loops on a square lattice
[DE94-628999] p 1578 N95-22276
Biaxiality of chiral liquid crystals
[DE94-629032] p 1578 N95-22277
The final status of a metal surface after multipulse laser irradiation in an ambient gas
[DE94-629000] p 1562 N95-22377
Tunneling of self-trapped states and formation of a band
[DE94-629001] p 1582 N95-22378

INTERNATIONAL INST. FOR HYDRAULIC AND ENVIRONMENTAL ENGINEERING, DELFT (NETHERLANDS).
Use of quantum chemically derived descriptors for QSAR modeling of reductive dehalogenation of aromatic compounds
[PB95-132783] p 1224 N95-22333

INTERNATIONAL SOLAR ELECTRIC TECHNOLOGY, INGLEWOOD, CA.
Status of flexible CIS research at ISET
p 1317 N95-20512

IOWA STATE UNIV. OF SCIENCE AND TECHNOLOGY, AMES, IA.
Experimental and theoretical evaluation of elastic waves in curved layered media
[AD-A286578] p 1504 N95-20918
Anodic oxygen-transfer electrocatalysis at iron-doped lead dioxide electrodes
[DE95-001653] p 1242 N95-21397
Novel absorption detection techniques for capillary electrophoresis
[DE95-001673] p 1242 N95-21400
Vortex dynamics in a ring-like irradiated Bi2Sr2CaCu2O8 crystal
[DE95-001682] p 1573 N95-21569
Magnetic field dependence of the correlation gap in SmB6
[DE95-001684] p 1574 N95-21570
Studies of selenium and xenon in inductively coupled plasma mass spectrometry
[DE95-001676] p 1245 N95-21734
Directional solidification of the alumina-zirconia ceramic eutectic system
[DE95-001677] p 1277 N95-21735
Selenophene transition metal complexes
[DE95-001675] p 1260 N95-21841

IOWA UNIV., IOWA CITY, IA.
Heat transfer, fouling, and combustion of supercritical fuels
[AD-A279906] p 1281 N95-19884

ISRAEL PHYSICAL SOCIETY, JERUSALEM (ISRAEL).
Israel Physical Society Annual Meeting 1994
[DE94-630140] p 1565 N95-20261

J

JAMIESON SCIENCE AND ENGINEERING, INC., SCOTTS VALLEY, CA.
Application of MCM image construction to IRAS comet observations p 1594 N95-21772

JAPAN ATOMIC ENERGY RESEARCH INST., TOKYO (JAPAN).
Simulation of tearing mode stabilization by using ECH
[DE94-770700] p 1554 N95-20684
On FEL integral equation and electron energy loss in intermediate gain regime
[DE94-770631] p 1371 N95-20757
Ideal Magnetohydrodynamic stabilities in JT-60 and D3-D tokamak plasmas
[DE94-770684] p 1555 N95-20987

JET PROPULSION LAB., CALIFORNIA INST. OF TECH., PASADENA, CA.
A comparative survey of current and proposed tropospheric refraction-delay models for DSN radio metric data calibration
[NASA-CR-197338] p 1412 N95-20002
The Deep Space Network as an instrument for radio science research
[NASA-CR-197341] p 1302 N95-21456
The Telecommunications and Data Acquisition Report
[NASA-CR-197390] p 1303 N95-21532
Orbit determination of highly elliptical Earth orbiters using improved Doppler data-processing modes
p 1218 N95-21533
Seamless data-range change using punctured convolutional codes for time-varying signal-to-noise ratios p 1304 N95-21534
Turbo codes for deep-space communications
p 1304 N95-21535
CDMA with interference cancellation for multiprobe missions p 1304 N95-21536
Combining image-processing and image compression schemes p 1304 N95-21537
A method using focal plane analysis to determine the performance of reflector antennas p 1304 N95-21538
On-wafer, cryogenic characterization of ultra-low noise HEMT devices p 1305 N95-21539
Radio-science performance analysis software
p 1305 N95-21540
Analysis of a microstrip reflectarray antenna for microspacecraft applications p 1305 N95-21541
The efficiency calibration of the DSS-24 34-meter beam-waveguide antenna p 1305 N95-21542
Analysis of a disk-on-rod surface wave element inside a corrugated horn using the mode-matching technique
p 1305 N95-21543
Communications and control for electric power systems: Power system stability applications of artificial neural networks
[NASA-CR-197594] p 1483 N95-21613
Science with High Spatial Resolution Far-Infrared Data
[NASA-CR-197353] p 1595 N95-21749
Hires and beyond p 1592 N95-21750
Interacting galaxies resolved by IRAS
p 1593 N95-21759
Two-dimensional maps of the infrared-to-radio ratio in spiral galaxies p 1593 N95-21765
An IRAS Hires study of low mass star formation in the Taurus molecular ring p 1593 N95-21767
Wavelet analysis applied to the IRAS cirrus
p 1593 N95-21769
A HIRES analysis of the FIR emission of supernova remnants p 1594 N95-21770
Communications and control for electric power systems: Power system stability applications of artificial neural networks
[NASA-CR-197333] p 1484 N95-22171
The Large Area Pulsed Solar Simulator (LAPSS)
[NASA-CR-197339] p 1397 N95-22336

JOENSUU UNIV. (FINLAND).
Anaerobic Treatment of Municipal Solid Waste and Sludge for Energy Production and Recycling of Nutrients
[DE95-700217] p 1315 N95-20369

JOHNS HOPKINS UNIV., BALTIMORE, MD.
A Lagrangian dynamic subgrid-scale model turbulence
p 1344 N95-21051
Simulations of metal dissolution and corrosion
[DE94-019295] p 1257 N95-21476

JOHNS HOPKINS UNIV., COLUMBIA, MD.
The 1993 JANNAF Propulsion Meeting, volume 2
[AD-A279569] p 1221 N95-20708

JOHNS HOPKINS UNIV., LAUREL, MD.
Proceedings of the 4th Systems Reengineering Technology Workshop
[AD-A285357] p 1460 N95-20546

JOINT INST. FOR NUCLEAR RESEARCH, DUBNA (USSR).
Symmetry, Wigner functions and particle reactions
[DE94-629887] p 1514 N95-20735
Muon transfer from muonic atoms of hydrogen isotopes to He nuclei
[DE94-628903] p 1523 N95-21591

K

KAMAN SCIENCES CORP., ALBUQUERQUE, NM.
Fault detection techniques for complex cable shield topologies
[AD-A286632] p 1291 N95-20771
TIM-SCT cable testing protocol
[AD-A286633] p 1207 N95-20772

KANSAS STATE UNIV., MANHATTAN, KS.
Monitoring bioremediation of Volatile Organic Compounds (VOCs) using Fourier Transform Infrared (FT-IR) spectrometry
[AD-A279631] p 1403 N95-20456

KANSAS UNIV., LAWRENCE, KS.
Connection with dynamics: General introduction
[NASA-CR-197617] p 1579 N95-19947

KAUPPA-JA TEOLLISUUSMINISTERIO, HELSINKI, UUDENMAA (FINLAND).
LIEKKI combustion technology
[DE95-700233] p 1242 N95-21282
Producing liquid fuels from biomass
[DE95-717458] p 1398 N95-22425

KEELE UNIV. (ENGLAND).
PRSPLOT6 manual
[PB95-110862] p 1456 N95-19928
PRSCAL manual
[PB95-130480] p 1465 N95-21231
PRISMA operating program manual
[PB95-130498] p 1466 N95-21232

KENT STATE UNIV., OH.
Optical power limiting liquid crystal composites
[AD-A286605] p 1569 N95-20767

KJT, INC., ROCHESTER, NY.
Fiber laser amplifiers and oscillators
[AD-A285835] p 1368 N95-20035

L

LA SAPIENZA UNIV., ROME (ITALY).
Rib vortices in round jets: Direct and large eddy simulation p 1351 N95-21088

LANCASTER UNIV. (ENGLAND).
Adaptive error-control scheme for 2-200 MHz Multiple-Mechanism Propagation Paths
p 1293 N95-20926

LAUSANNE UNIV. (SWITZERLAND).
GAJET experiment at the LHC: The GAJET collaboration
[PB95-129813] p 1512 N95-20454

LAWRENCE LIVERMORE NATIONAL LAB., LIVERMORE, CA.
Mixed-sputter deposition of Ni-Ti-Cu shape memory films
[DE94-017296] p 1250 N95-19900
Simulation of stellar speckle imaging
[DE94-016606] p 1412 N95-19985
Scaling of solid state lasers for satellite power beaming applications
[DE94-016366] p 1368 N95-19986
X-ray imaging of uniform large scale-length plasmas created from gas-filled targets on Nova
[DE94-018339] p 1531 N95-20015
Recent DIII-D results
[DE94-017519] p 1549 N95-20038
Design and packaging aspects of microwave bandwidth lithium niobate modulators
[DE94-016602] p 1313 N95-20119
High power spectral and spatial beam control using self-phase modulation and a multisegment monochromator
[DE94-016604] p 1531 N95-20120
Ductile-brittle transition behavior of tungsten under shock loading
[DE94-009913] p 1251 N95-20122
Monsoons: AMIP simulations of the 1987 and 1988 drought and flood regimes
[DE94-014789] p 1428 N95-20140
Energy and Technology Review
[DE94-017686] p 1219 N95-20148
National Ignition Facility: Experimental plan
[DE94-016542] p 1550 N95-20189
Target area acquisition and control system survivability for the National Ignition Facility
[DE94-016549] p 1550 N95-20190
Optical multilayers with an amorphous fluoropolymer
[DE94-017693] p 1541 N95-20218
Target Area Structural Support systems design to achieve the micron-level stability requirement of the National Ignition Facility (NIF)
[DE94-017696] p 1551 N95-20219
A computational study of projectile melt in impact with typical Whipple shields
[DE94-016454] p 1385 N95-20237
Meshes: The next generation
[DE94-016702] p 1459 N95-20255
24th Annual Anomalous Absorption Conference
[DE94-016457] p 1551 N95-20283
A comparison of kinetic and multifluid simulations of laser-produced colliding plasmas
[DE94-016447] p 1551 N95-20315
Overview on superplasticity research on small-grained materials
[DE94-016550] p 1266 N95-20316

Rate controlled synthesis of composition modulated, metal-oxide thin films
[DE94-016596] p 1267 N95-20317

Numerical modeling of a small recirculating induction accelerator for heavy-ion fusion
[DE94-018549] p 1552 N95-20318

Plasma arc melting of titanium-tantalum alloys
[DE94-016291] p 1252 N95-20331

Enhanced output of soft x-ray lasers using double slab targets
[DE94-016689] p 1369 N95-20335

Choice of computer software for analysis of spectra from the Multi-Spectral Logging System
[DE94-019013] p 1460 N95-20351

Refractive index change in dissociating shocked benzene
[DE94-019015] p 1541 N95-20352

Indirect global warming effects of ozone and stratospheric water vapor induced by surface methane emission
[DE94-019016] p 1402 N95-20353

Radiative forcing for changes in tropospheric O3
[DE94-019017] p 1413 N95-20354

Radiative forcing calculations for CH3Cl
[DE94-019018] p 1402 N95-20355

The development and evaluation of water-mist fire extinguishing systems
[DE94-019019] p 1286 N95-20356

Ion temperature measurement of indirectly-driven implosions using a geometry-compensated neutron time-of-flight detector
[DE94-016967] p 1552 N95-20362

Characterization of nova plasmas using an x-ray spectrometer with temporal and spatial resolution
[DE94-016970] p 1553 N95-20363

High precision Woelter optic calibration facility
[DE94-016973] p 1542 N95-20364

Effects of microphysics and radiation on mesoscale processes of a midlatitude squall line
[DE94-014732] p 1429 N95-20381

Fabrication and testing of a silicon immersion grating for infrared spectroscopy
[DE94-017173] p 1237 N95-20386

System design document U-AVLIS control system architecture
[DE94-017297] p 1460 N95-20387

Frequency response measurements of integrated-optic electrodes
[DE94-016690] p 1542 N95-20403

Model-based inversion for a shallow ocean application
[DE94-016968] p 1433 N95-20420

Program WALKMAN: A code designed to perform electron single collision elastic scattering Monte Carlo calculations
[DE94-017501] p 1511 N95-20444

Magnetic x ray circular dichroism in Fe Co Pt multilayers
[DE94-017522] p 1253 N95-20447

Spin-specific photoelectron diffraction using magnetic x ray circular dichroism
[DE94-017527] p 1567 N95-20448

A structural determination using magnetic x ray circular dichroism in spin-polarized photoelectron diffraction
[DE94-017528] p 1567 N95-20449

Optical properties of silicon clusters deposited on the basal plane of graphite
[DE94-017529] p 1542 N95-20450

White-light spectral analysis of lithium niobate waveguides
[DE94-016692] p 1542 N95-20489

Development, fabrication, and metrology of the electro-optical breadboard model for the reflection grating array of the XMM grating spectrometer
[DE94-016605] p 1543 N95-20612

Hydrodynamic instabilities in inertial fusion
[DE94-018079] p 1554 N95-20675

Meso-scale cooling effects of high albedo surfaces: Analysis of meteorological data from White Sands National Monument and White Sands Missile Range
[DE94-018535] p 1429 N95-20782

Computational model of drilling with high radiance pulsed lasers
[DE94-018548] p 1371 N95-20783

Radiation-driven targets for heavy-ion fusion
[DE95-002264] p 1533 N95-20784

Observation of strong emission from NeIX and NeX transitions in a laser-driven plasma
[DE95-002265] p 1555 N95-20813

The Materials Corrosion and Environmental Effects Laboratory (MCEL)
[DE94-018268] p 1254 N95-20816

Performance of the NIF prototype beamlet
[DE94-018500] p 1371 N95-20817

LLNL/Lion Precision LVDT amplifier
[DE95-001504] p 1327 N95-20854

Sputter deposition of multilayer thermoelectric films: An approach to the fabrication of two-dimensional quantum wells
[DE95-002396] p 1272 N95-20892

Fractal nature and scaling of normal faults, Rio Grande rift, NM: Implications for growth and strain
[DE94-018261] p 1414 N95-20990

Ultraviolet laser emission properties of Ce(3+)-doped LiSrAlF6
[DE94-016364] p 1372 N95-21135

Plasma Electrode Pockels Cells for the Beamlet and NIF lasers
[DE94-016541] p 1557 N95-21166

Analytic models for beam propagation and far-field patterns in slab and bow-tie x ray lasers
[DE94-016607] p 1372 N95-21173

Advanced concepts for gamma ray isotopic analysis and instrumentation
[DE94-016610] p 1517 N95-21174

Beryllium based multilayers for normal incidence extreme ultraviolet reflectivity
[DE94-015560] p 1274 N95-21175

Visualizing 3D velocity fields near contour surfaces
[DE95-000841] p 1353 N95-21182

Three-dimensional ground penetrating radar imaging using multi-frequency diffraction tomography
[DE94-016687] p 1301 N95-21205

Use of the National Ignition Facility for the development of inertial fusion energy
[DE94-016696] p 1557 N95-21206

Target Area design basis and system performance for the National Ignition Facility
[DE94-016697] p 1557 N95-21207

Neutronics and shielding analysis of the National Ignition Facility
[DE94-016698] p 1534 N95-21208

Laser design basis for the National Ignition Facility
[DE94-016700] p 1534 N95-21209

EBIT x ray spectroscopy studies for applications to photo-pumped x ray lasers
[DE94-016701] p 1373 N95-21210

Continuously-tunable, narrow-linewidth, Q-switched Cr:LiSAF laser for lidar applications
[DE95-000862] p 1373 N95-21312

Quantitative evaluation of wrist posture and typing performance: A comparative study of 4 computer keyboards
[DE95-002392] p 1452 N95-21358

Magnetic x-ray circular dichroism in spin-polarized photoelectron diffraction
[DE95-002394] p 1520 N95-21360

A mixed time integration method for large scale acoustic fluid-structure interaction
[DE94-018327] p 1354 N95-21387

An image cancellation approach to depth-from-focus
[DE94-019312] p 1544 N95-21392

Solid state frequency conversion technology for remote sensing
[DE94-019102] p 1389 N95-21433

MTX final report
[DE95-002960] p 1559 N95-21451

An Echelle Grating Spectrometer (EGS) for mid-IR remote chemical detection
[DE94-019310] p 1367 N95-21478

Relativistic binary neutron star coalescence
[DE94-019311] p 1600 N95-21479

Fiber-optic sensors for rapid, inexpensive characterization of soil and ground water contamination
[DE95-002471] p 1545 N95-21510

Overview of remote sensing laser development and semiconductor laser technology
[DE94-019103] p 1389 N95-21552

Preconditioning via asymptotically-defined domain decomposition
[DE94-019046] p 1493 N95-21564

Ergonomic evaluation of the Apple Adjustable Keyboard
[DE95-002393] p 1453 N95-21637

Forming of superplastic ceramics
[DE94-017306] p 1276 N95-21662

Collisional redistribution effects on x ray laser saturation behavior
[DE94-017308] p 1374 N95-21663

Full potential multiple scattering theory
[DE95-003197] p 1576 N95-22084

High average power diode pumped solid state lasers for CALIOPE
[DE94-019248] p 1376 N95-22121

The influence of chemistry and microstructure on the fracture toughness of V-V3Si in-situ composites
[DE94-018997] p 1232 N95-22126

Laboratory characterization of Woelter x ray optics
[DE94-016969] p 1562 N95-22191

Heat loss by helicity injection in spheromaks
[DE95-003473] p 1562 N95-22221

An analytical electron distribution function for inelastic collisions in a uniform gas with time varying electric field
[DE95-003476] p 1528 N95-22222

An analytical, inelastic, space and time dependent electron distribution for electrically excited gases
[DE95-003478] p 1528 N95-22223

X-band microwave backscattering from ocean waves
[DE94-016719] p 1309 N95-22241

CALIOPE and TAISIR airborne experiment platform
[DE94-018328] p 1310 N95-22299

The superconducting magnet system for the Tokamak Physics Experiment
[DE94-018329] p 1562 N95-22300

3-D TECATE/BREW: Thermal, stress, and birefringent ray-tracing codes for solid-state laser design
[DE95-000330] p 1376 N95-22301

Coherence properties of high order harmonic radiation
[DE94-016974] p 1377 N95-22312

A multisite interaction expansion of the total energy in metals
[DE94-017175] p 1262 N95-22313

Defect geometries and laser-induced damage in multilayer coatings
[DE94-017695] p 1377 N95-22343

Fracture behavior of laminated discontinuously reinforced aluminum material
[DE94-017307] p 1263 N95-22408

Demonstration of zinc/air fuel battery to enhance the range and mission of fleet electric vehicles: Preliminary results in the refueling of a multicell module
[DE95-004206] p 1337 N95-22421

Saddle-node dynamics for edge detection
[DE94-017415] p 1473 N95-22426

Unique microchannel plate process doubles MCPI resolution
[DE94-017507] p 1337 N95-22427

Target alignment in the National Ignition Facility
[DE94-015559] p 1540 N95-22469

LEEDS UNIV. (ENGLAND).

Impact of propagation mechanisms on global navigation satellite system performance p 1298 N95-20950

Superresolution direction finding algorithms for the characterisation of multi-moded HF signals
p 1299 N95-20958

LEHIGH UNIV., BETHLEHEM, PA.

Selective methane oxidation over promoted oxide catalysts
[DE94-012270] p 1235 N95-20188

Microstructural design for tough ceramics
[AD-A285634] p 1273 N95-21152

LEIDEN UNIV. (NETHERLANDS).

Error committed by stopping the Newton iteration in Runge-Kutta methods and linear multistep methods
[PB95-106324] p 1492 N95-21421

LILLE-1 UNIV., VILLENEUVE-D'ASOQ (FRANCE).

Propagation of high frequency waves in urban and road tunnel environments p 1294 N95-20933

LOCKHEED MISSILES AND SPACE CO., PALO ALTO, CA.

Demonstration of multifunctional DNBM corrosion inhibitors in protective coatings for Naval air/weapon systems
[AD-A285869] p 1279 N95-22136

LOGISTICS MANAGEMENT ENGINEERING, INC., WARMINSTER, PA.

Helicopter crewseat cushion program
[AD-A286654] p 1452 N95-20973

LORAL FEDERAL SYSTEMS, MANASSA, VA.

Real-time reconfiguration study
[AD-A286060] p 1464 N95-20910

LOS ALAMOS NATIONAL LAB., NM.

Unified GUI for the Los Alamos Radiation Transport Code System
[DE94-016088] p 1458 N95-20154

A practical guide to using MCNP with PVM
[DE94-016162] p 1474 N95-20158

Data analysis and visualization in MCNP (trademark)
[DE94-016164] p 1508 N95-20159

MCNP (trademark) ENDF/B-VI iron benchmark calculations
[DE94-016165] p 1508 N95-20160

Evaluation of superconducting quantum interference devices interfaced with digital signal processing electronics for biomagnetic applications
[DE94-016186] p 1289 N95-20164

An object-oriented optimization systems
[DE94-016190] p 1459 N95-20165

Nonlinear dynamic fluid-structure interaction calculations with coupled finite element and finite volume programs
[DE94-016204] p 1339 N95-20166

The Nonlinear Characteristic scheme in X-Y geometries
[DE94-016192] p 1488 N95-20167

DSP control of superconducting quantum interference devices
[DE94-016193] p 1313 N95-20168

Semiquantum chaos and the large N expansion
[DE94-016196] p 1488 N95-20169

A new tool for accelerator system modeling and analysis
[DE94-018292] p 1531 N95-20203

A S2-like acceleration method for the Nonlinear Characteristic transport scheme
[DE94-016285] p 1509 N95-20235

New data for MCNP (trademark)
[DE94-016296] p 1509 N95-20236

Physics Division research and development
[DE94-017685] p 1501 N95-20246

MCNP (trademark) directions
[DE94-016216] p 1509 N95-20254

Tests of dielectric model descriptions of chemical charge displacements in water
[DE94-007530] p 1236 N95-20277

Numerical controlled polishing program, continued forced wear and part correction experiments
[DE94-018084] p 1285 N95-20288

Infrasonic observations of the Northridge, California, earthquake
[DE94-018095] p 1413 N95-20289

Pairing on small clusters in the Peierls-Hubbard model: Implications for C60
[DE94-016264] p 1565 N95-20330

Actinide(IV) and actinide(VI) carbonate speciation studies by PAS and NMR spectroscopies
[DE94-016957] p 1236 N95-20361

Semi-leptonic form-factors from lattice QCD
[DE95-000871] p 1510 N95-20367

Kondo insulators
[DE95-001156] p 1237 N95-20368

Conceptual design of an RTG Facility Transportation System
[DE94-014443] p 1379 N95-20627

An integrated architecture of adaptive neural network control for dynamic systems
[DE94-014813] p 1481 N95-20693

HASSP and HEAVY: Tools for automated heavy atom searches and refinement
[DE94-016071] p 1569 N95-20696

Innovative use of DSP technology in space: FORTE event classifier
[DE94-016086] p 1291 N95-20697

EPICS simulation tools for control system development
[DE94-018082] p 1462 N95-20699

Shaping the library of the future: Digital library developments at Los Alamos National Laboratory's Research Library
[DE95-001008] p 1588 N95-20777

Effects of plasma physics on capsule implosions in gas-filled hohlraums
[DE95-000923] p 1371 N95-20786

Determining information management needs for enhanced international safeguards
[DE94-015787] p 1588 N95-20789

Modeling and identification of parallel and feedback nonlinear systems
[DE95-001006] p 1481 N95-20812

The Energy Science and Technology Database on a local library system: A case study at the Los Alamos National Research Library
[DE95-001009] p 1589 N95-20818

Active neutron multiplicity analysis and Monte Carlo calculations
[DE94-016178] p 1516 N95-21114

Cryogenic targets for inertial confinement fusion
[DE94-016200] p 1555 N95-21115

Theories of the eta-meson-nucleus interaction
[DE94-016055] p 1516 N95-21125

Understanding the mechanisms of length scale competition: The sine-Gordan soliton case
[DE94-016201] p 1500 N95-21136

Metastable bcc phase formation in the Nb-Cr-Ti system
[DE94-016212] p 1255 N95-21137

Project Whitefeather
[DE94-016575] p 1415 N95-21184

Parity nonconservation in radioactive atoms: An experimental perspective
[DE95-002737] p 1518 N95-21235

In-situ capability of ion beam modification and characterization of materials at Los Alamos National Laboratory
[DE95-002738] p 1534 N95-21236

A neutron beam polarizer for study of parity violation in neutron-nucleus interactions
[DE95-002743] p 1519 N95-21237

Tribology and surface mechanical properties of excimer laser nitrided titanium
[DE95-002751] p 1255 N95-21238

Review of recent D-T experiments from TFTR
[DE95-002755] p 1557 N95-21239

Fusion power production in TFTR
[DE95-002756] p 1557 N95-21240

Heating and transport in TFTR D-T plasmas
[DE95-002812] p 1558 N95-21242

Quantum diffusion
[DE95-001015] p 1580 N95-21264

NESTLE: Few-group neutron diffusion equation solver utilizing the nodal expansion method for eigenvalue, adjoint, fixed-source steady-state and transient problems
[DE95-001903] p 1466 N95-21288

Accurate solution algorithms for incompressible multiphase flows
[DE95-002727] p 1353 N95-21317

Heavy ion collisions
[DE95-002712] p 1520 N95-21321

Moment approach to high-order accelerator beam optics
[DE95-001018] p 1536 N95-21331

Tungsten-uranium penetrator target interaction
[DE95-000847] p 1387 N95-21364

Potential-of-mean-force description of ionic interactions and structural hydration in biomolecular systems
[DE95-000859] p 1438 N95-21366

NEO-LISP: Deflecting near-Earth objects using high average power, repetitively pulsed lasers
[DE95-000863] p 1599 N95-21367

Low density gas and foam targets for ICF long scale length plasma experiments: Fabrication and characterization
[DE95-000935] p 1558 N95-21368

Coronal Mass Ejections in the solar wind at high solar latitudes: An overview
[DE95-000844] p 1603 N95-21377

Strain measurement by diffraction at LANSCE
[DE94-018264] p 1387 N95-21386

Utilizing artificial neural networks in network flow analysis: An annotated bibiliography
[DE95-002453] p 1482 N95-21522

Visible fluorescence of weathered lead
[DE95-002454] p 1244 N95-21523

Implementation of electronic chain-of-custody, analysis requests, and data verification at Los Alamos National Laboratory
[DE94-018076] p 1407 N95-21666

An 8-meter-long coupled cavity RFQ linac
[DE94-018077] p 1331 N95-21667

Intense proton beam source for ITER neutral-beam spectroscopy diagnostics
[DE94-018092] p 1560 N95-21668

Adaptive capture of expert behavior
[DE94-018285] p 1483 N95-21710

Angle resolved photoemission on K(0.3)Mo3, TiTe2 and Ti(1+x)S2
[DE94-018300] p 1574 N95-21712

Design and development SAWAFE peak detector chip
[DE95-001745] p 1332 N95-21742

Directed light fabrication
[DE94-018293] p 1375 N95-21837

High resolution properties of the equatorial Pacific marine atmospheric boundary layer from lidar and radiosonde observations
[DE95-001028] p 1426 N95-21875

Performance of cesium telluride photocathodes as an electron source for the Los Alamos FEL
[DE94-018302] p 1375 N95-21919

Status of CFDLIB performance tests on the T3D
[DE95-002708] p 1478 N95-21925

Oxidation behavior of aluminum nanopowders
[DE95-002721] p 1260 N95-21926

Two-band model description of electroabsorption and third-harmonic generation in 1-D MX linear chains
[DE95-000932] p 1526 N95-21934

Observations of cold magnetospheric ions at geosynchronous orbit during times of high activity
[DE95-000936] p 1600 N95-21935

Anisotropic transport properties of BSCCO single crystals and Ag-clad tapes in high magnetic fields
[DE95-000938] p 1575 N95-21936

Plasma arc melting of a 80 weight percent tantalum -20 weight percent titanium alloy
[DE95-000846] p 1260 N95-22006

Tunable CW blue, green, orange and red upconversion fiber lasers at room temperature
[DE95-000851] p 1375 N95-22007

Equilibrium and shot noise in mesoscopic systems
[DE95-000855] p 1576 N95-22008

Recent developments in low cost stable structures for space
[DE95-000857] p 1231 N95-22009

Current status of fusion-relevant covariance data
[DE95-000865] p 1561 N95-22010

A 500 MW annular beam relativistic klystron
[DE95-000867] p 1334 N95-22011

The application of electrodialysis to extend the lifetime of commercial electroplating baths
[DE95-000868] p 1246 N95-22012

Experience at the Los Alamos Meson Physics Facility with the use of alloy Inconel 718 as an enclosure for a beam degrader and as a proton beam entry window
[DE94-018289] p 1538 N95-22050

There might be two kinds of dibaryon
[DE94-014417] p 1526 N95-22058

Life Sciences Division and Center for Human Genome Studies
[DE94-017796] p 1440 N95-22065

Single particle measurements and two particle interferometry results from CERN experiment NA44
[DE95-003041] p 1527 N95-22078

Distribution of light element isotopes in Bencubbin and Weatherford meteorites: An indicator of heterogeneity in the primitive solar nebula
[DE94-019167] p 1600 N95-22128

Recent progress of the compact AFEL at Los Alamos
[DE95-002728] p 1376 N95-22154

Radiation characterization report for the GPS Receiver microcontroller chip
[DE94-019169] p 1335 N95-22165

Photocathodes for free electron lasers
[DE94-018305] p 1376 N95-22242

High performance computing for beam physics applications
[DE94-018312] p 1539 N95-22243

Helium production by 10 MeV neutrons in iron, nickel and copper
[DE94-014798] p 1529 N95-22280

Characterization of a texture gradient in tantalum plate
[DE95-002704] p 1262 N95-22289

Flow cytometry: A powerful technology for measuring biomarkers
[DE94-018284] p 1440 N95-22296

Modeling of nonlinear optic and ESR response of CDW MX materials
[DE94-018301] p 1578 N95-22297

Recent results in analysis and simulation of beam halo
[DE94-018313] p 1539 N95-22298

Effect of annealing temperature on the texture of rolled tantalum and tantalum-10 wt % tungsten
[DE95-002702] p 1262 N95-22308

Fabrication and characterization of cesium telluride photocathodes: A promising electron source for the Los Alamos Advanced FEL
[DE94-018303] p 1377 N95-22348

Low-level RF control for the AFEL
[DE94-018295] p 1540 N95-22410

The Double Eagle Space Experiment (DESE) beamline design
[DE94-018319] p 1601 N95-22419

Characterization and performance of DLC films synthesized by plasma and ion beam techniques
[DE94-018287] p 1281 N95-22428

A survey of artificial neural network applications in flow analysis of energy networks
[DE95-002452] p 1486 N95-22430

The interaction of localized solutions in a surface reaction
[DE95-002736] p 1248 N95-22433

Neutron reflectivity study of adsorbed diblock copolymers
[DE95-002740] p 1281 N95-22434

Parity violation in the compound nucleus
[DE95-002742] p 1530 N95-22435

Imaging design of the wide field x-ray monitor onboard the HETE satellite
[DE95-002750] p 1221 N95-22436

Magnetospheric Plasma Analyzer (MPA): Plasma observations from geosynchronous orbit
[DE95-002739] p 1427 N95-22477

LOS ANGELES CITY DEPT. OF WATER AND POWER, CA.

Test and evaluation of electric vehicles
[DE95-001153] p 1313 N95-20213

LOUISIANA STATE UNIV., BATON ROUGE, LA.

Monopoles and quark confinement: Introduction and overview
[DE94-019348] p 1522 N95-21485

New improved derivative expansion for field theories with spontaneous symmetry breaking
[DE94-019349] p 1580 N95-21486

LOYOLA UNIV., CHICAGO, IL.

Determination of multiple sound sources
[AD-A286563] p 1504 N95-20823

LUCAS ELECTRONICS, BIRMINGHAM (ENGLAND).

The design and manufacturing development of an active silicon substrate MCM p 1211 N95-20645

LUDWIG-MAXIMILIANS-UNIV., MUNICH (GERMANY).

Properties of strange-matter stars
[DE95-002329] p 1599 N95-20873

LUNAR AND PLANETARY INST., HOUSTON, TX.

Conference on Deep Earth and Planetary Volatiles [NASA-CR-196944] p 1415 N95-21777

Volatiles, rheology, and mantle convection: Comparing Earth, Venus, and Mars p 1420 N95-21801

LYNNTECH, INC., COLLEGE STATION, TX.

Corrosion of aircraft materials: Correlation between nanometer scale and macroscopic structural damage parameters [AD-A285930] p 1252 N95-20299

M

M-C POWER CORP., BURR RIDGE, IL.

Molten carbonate fuel cell product development test [DE95-000005] p 1324 N95-20574

MANCHESTER COLL. OF SCIENCE AND TECHNOLOGY (ENGLAND).

Direct numerical simulation for premixed turbulent combustion modelling p 1249 N95-21082

MANCHESTER UNIV. (ENGLAND).

The initiation of lightning and the growth of electric fields in thunderstorms [AD-A280033] p 1428 N95-20008

Noble gas isotopes and halogens in volatile-rich inclusions in diamonds p 1417 N95-21784

MAR, INC., ROCKVILLE, MD.

Ohmsett test of NOFI Vee-Sweep and NOFI 600S Oilboom [AD-A279525] p 1408 N95-21685

MARTIN MARIETTA ASTRO SPACE, PHILADELPHIA, PA.

GPHS-RTGs in support of the Cassini Mission [DE95-001492] p 1222 N95-20853

MARTIN MARIETTA CORP., BALTIMORE, MD.

Collocated tunable wavenumber sensor/actuators for smart structures [AD-A279608] p 1312 N95-19958

MARTIN MARIETTA CORP., DENVER, CO.

Advances in polycrystalline thin-film photovoltaics for space applications p 1318 N95-20514

High-performance, flexible, deployable array development for space applications p 1322 N95-20532

MARTIN MARIETTA LABS., BALTIMORE, MD.

Collocated tunable wavenumber sensor/actuators for smart structures [AD-A279066] p 1258 N95-21575

MARYLAND INST. FOR EMERGENCY MEDICAL SERVICES, BALTIMORE, MD.

Development and enhancement of a model of performance and decision making under stress in a real life setting [AD-A285945] p 1449 N95-20393

MARYLAND UNIV., COLLEGE PARK, MD.

A-posteriori estimation and adaptive control of the pollution-error in the h-version of the finite element method [AD-A285670] p 1480 N95-20083

Tracking a dynamic set of feature points [AD-A285124] p 1313 N95-20257

The method of auxiliary mapping for the finite element solutions of elasticity problems containing singularities [AD-A285689] p 1489 N95-20274

Higher order crossings [AD-A279597] p 1504 N95-20300

Studies of longitudinal instability with an electron beam [DE94-018646] p 1532 N95-20347

Eta%-Superconvergence of Finite Element Approximations in the Interior of General Meshes of Triangles [AD-A279903] p 1490 N95-20565

Study of superconvergence by a computer-based approach: Superconvergence of the gradient of the displacement, the strain and stress in finite element solutions for plane elasticity [AD-A279885] p 1490 N95-20588

Liquid flow-through cooling of electronic modules p 1211 N95-20647

A convergence analysis of an h-version finite element method with high order elements for two dimensional elasto-plasticity problems [AD-A279975] p 1491 N95-20920

Electromagnetic wave reflection from irregular plasma layers p 1298 N95-20952

Large-eddy simulation of rotating channel flows using a localized dynamic model p 1346 N95-21064

Control of complex multibody spacecraft [AD-A285623] p 1220 N95-21147

Connectionist models for intelligent computation [AD-A286436] p 1484 N95-22210

Pollution error in the H-version of the finite element method and the local quality of A-posteriori error estimators [AD-A279868] p 1497 N95-22388

MASSA PRODUCTS CORP., HINGHAM, MA.

Legged vehicle for underwater mobile operations [AD-A285043] p 1480 N95-20482

MASSACHUSETTS INST. OF TECH., CAMBRIDGE, MA.

Robust agent control of an autonomous robot with many sensors and actuators [AD-A280148] p 1479 N95-20011

Direct catalytic decomposition of nitric oxide [DE94-018840] p 1233 N95-20045

Propulsion research on the variable tandem mirror plasma rocket [NASA-CR-196310] p 1221 N95-20059

Compact free electron lasers for medical applications [AD-A285739] p 1369 N95-20072

View-based models of 3D object recognition and class-specific invariance [AD-A279858] p 1459 N95-20157

Viewer-centered object recognition in monkeys [AD-A279876] p 1437 N95-20185

Ambient noise and surface wave dissipation in the ocean [AD-A279650] p 1432 N95-20303

The synthesis and characterization of new mesogenic diacetylene monomers and their polymers [AD-A286188] p 1267 N95-20328

Morphology of highly textured E/EP diblock copolymers [AD-A279813] p 1269 N95-20582

Analog processing of optical wavefront using integrated guided-wave optics [AD-A279596] p 1543 N95-20601

Ion heating perpendicular to the magnetic field [AD-A286635] p 1501 N95-20773

Heterogeneous multi-robot cooperation [AD-A279839] p 1481 N95-21185

Mechanisms and diagnostics of ultrashort pulse laser ocular effects [AD-A285610] p 1373 N95-21195

Aromatics oxidation and soot formation in flames [DE95-001803] p 1241 N95-21280

The formation of reaction bonded Si3N4 at low temperatures and in short times [DE95-001990] p 1275 N95-21289

Theory and modelling of quench in cable-in-conduit superconducting magnets [DE95-001819] p 1330 N95-21442

Object recognition by alignment using invariant projections of planar surfaces [AD-A279841] p 1468 N95-21495

Numerical and symbolic algorithms for application and specific signal processing [AD-A279902] p 1305 N95-21576

Atom wave interferometer [AD-A279532] p 1524 N95-21688

Joule heating of the ITER TF cold structure: Effects of vertical control coil currents and ELMS [DE95-001817] p 1560 N95-21724

Current distribution in Cable-In-Conduit Conductors [DE95-001820] p 1332 N95-21725

Preparation and x-ray structure of Cp2Ti(PH2SiH2)(PMe3) [AD-A286197] p 1246 N95-21879

Incology alloy 908 data handbook [DE95-001818] p 1260 N95-22013

A catalytic method for the conversion of silanes to stannanes [AD-A286214] p 1247 N95-22020

Synthesis and structure of a novel bis-stibole [AD-A286345] p 1224 N95-22252

Learning maneuvers using neural network models [AD-A286470] p 1486 N95-22267

Feature extraction without edge detection [AD-A279842] p 1473 N95-22386

MASSACHUSETTS INST. OF TECH., LEXINGTON, MA.

Solid state research [AD-A279662] p 1567 N95-20426

GPS-Squitter capacity analysis [AD-A280037] p 1291 N95-20599

Adaptive detection in stationary and nonstationary noise environments [AD-A279581] p 1300 N95-21099

Data sampling for a burst mode communications system [AD-A286098] p 1309 N95-22229

MASSACHUSETTS UNIV., AMHERST, MA.

Biological and theoretical studies of adaptive networks: The conditioned response [AD-A284781] p 1479 N95-20061

Second International Conference on Ordinal Data Analysis [AD-A279756] p 1590 N95-21401

MATERIALS RESEARCH LABS., ASCOT VALE (AUSTRALIA).

A review of Microbially Induced Corrosion (MIC) of steel and a preliminary investigation to determine its occurrence in naval vessels [MRL-GD-0048] p 1250 N95-19910

The hot fragment conductive ignition test for screening LOVA propellants [AD-A284259] p 1282 N95-20187

An initial assessment of the properties of 2,5-dipicryl-1,3,4-oxadiazole: A secondary explosive with high thermal stability [MRL-TR-93-16] p 1284 N95-21624

Comparison of HFC-134a and the ternary blend, Suva MP39, as replacements for the refrigerant, CGC-12 [MRL-GD-0051] p 1287 N95-21625

The determination of static and time varying dipole source. Sensor geometry during sea trials using differential global positioning system [MRL-TN-631] p 1205 N95-21642

Underwater Acoustic Generator Phase 2: Sea trial, March 1992 [MRL-TN-640] p 1434 N95-21657

The application of a statistical analysis software package to explosive testing [MRL-TR-93-42] p 1284 N95-21658

Measurement of sound intensity and sound power [AD-A279246] p 1505 N95-21984

MATERIALS RESEARCH SOCIETY, PITTSBURG, PA.

Physics and applications of defects in advanced semiconductors, volume 325 [AD-A280059] p 1563 N95-19886

Biomolecular Materials by Design, volume 330 [AD-A285369] p 1269 N95-20551

Molecularly Designed Ultrafine/Nanostructured Materials, volume 351 [AD-A285370] p 1568 N95-20552

MATERIALS SCIENCES CORP., FORT WASHINGTON, PA.

Implementation of the military handbook 17 for polymer matrix composites and metal matrix composites [AD-A285629] p 1229 N95-21149

Implementation of the military handbook 17 for polymer matrix composites and metal matrix composites [AD-A285595] p 1229 N95-21215

Implementation of the Military Handbook 17 for polymer matrix composites and metal matrix composites [AD-A285772] p 1233 N95-22395

MAX-PLANCK-INST. FUER CHEMIE, MAINZ (GERMANY).

Spatial variation of primordial 3-He in crustal fluids along the East-African Rift system (the Ethiopian and the Kenya Rift section) p 1418 N95-21789

Water abundance and accretion history of terrestrial planets p 1424 N95-21820

MAX-PLANCK-INST. FUER KERNPHYSIK, HEIDELBERG (GERMANY).

Far-Infrared sources and diffuse emission in M31 p 1593 N95-21761

MAXWELL LABS., INC., SAN DIEGO, CA.

Parasitic current collection by solar arrays in LEO p 1321 N95-20527

MCDONNELL-DOUGLAS AEROSPACE, LONG BEACH, CA.

Crew aiding and automation: A system concept for terminal area operations, and guidelines for automation design [NASA-CR-4631] p 1204 N95-19950

MCDONNELL-DOUGLAS AEROSPACE, SAINT LOUIS, MO.

Conducting thermoset polymers [AD-A286541] p 1273 N95-21014

Optimal active control for Burgers equations p 1361 N95-22454

Transverse vorticity measurements in the NASA Ames 80 x 120 wind tunnel boundary layer p 1362 N95-22457

MEDICAL UNIV. OF SOUTH CAROLINA, CHARLESTON, SC.

Environmental Hazards Assessment Program [DE94-019075] p 1406 N95-21565

MEI TECHNOLOGY CORP., SAN ANTONIO, TX.

Determining the usability of Digital Video Interactive (DVI) technology in computer-based instruction [AD-A284717] p 1457 N95-20060

MESSINA UNIV. (ITALY).

The optical properties of particles deposited on a surface [AD-A286258] p 1546 N95-22002

MICHIGAN BIOTECHNOLOGY INST., LANSING, MI.

Bioconversion of coal derived synthesis gas to liquid fuels [DE94-017381] p 1282 N95-19927

Bioconversion of coal derived synthesis gas to liquid fuels [DE94-018849] p 1314 N95-20339

MICHIGAN MOLECULAR INST., MIDLAND, MI.
Effect of external stress on the transport of fluids in thermoplastic resin systems
[AD-A279993] p 1270 N95-20596

MICHIGAN TECHNOLOGICAL UNIV., HOUGHTON, MI.
Modeling of collision induced absorption spectra of CO2-CO2 pairs for planetary atmosphere of Venus
[NASA-CR-197373] p 1601 N95-22338

MICHIGAN UNIV., ANN ARBOR, MI.
Theoretical and experimental studies of a novel accelerating structure
[AD-A283730] p 1531 N95-19974
Design of a controller for a flexible pointing system using H(infinity) synthesis
[AD-A286572] p 1481 N95-20828
Next generation solid modellers for electronic prototyping
[AD-A286525] p 1464 N95-21010
Electrorheology for smart automotive suspensions
[AD-A285543] p 1380 N95-21157
Radiopharmaceuticals for diagnosis
[DE95-002200] p 1445 N95-21595
Origin and loss of the volatiles of the terrestrial planets p 1417 N95-21785
Applications of ICP magnetic sector multicollector mass spectrometry to basic energy research
[DE95-002600] p 1246 N95-21886
Massively-parallel computational fluid dynamics
[AD-A279389] p 1355 N95-21942
Robust fixed-structure control
[AD-A286515] p 1485 N95-22216

MICHOACANA UNIV., MORELIA MICHOACAN (MEXICO).
Theoretical-experimental study on the electroslag remelting technology of high quality steels
[DE94-629216] p 1256 N95-21270

MICROELECTRONICS AND COMPUTER TECHNOLOGY CORP., AUSTIN, TX.
An MCM concurrent engineering software tool market study
[AD-A279257] p 1468 N95-21489
Consortia for Known Good Die (KGD), phase 1
[AD-A279407] p 1383 N95-21933

MILAN UNIV. (ITALY).
A cheap DNS tool for turbulence models testing
p 1348 N95-21072

MISSION RESEARCH CORP., SANTA BARBARA, CA.
High resolution descriptions of IRAS 12 and 25 microns confused regions
[AD-A285847] p 1545 N95-21832

MISSISSIPPI STATE UNIV., BAY SAINT LOUIS, MS.
Mississippi State University Center for Air Sea Technology FY 1993 and FY 1994 research program in Navy ocean modeling and prediction
[AD-A286322] p 1432 N95-20209

MISSOURI UNIV., ROLLA, MO.
Experimental investigations of electron capture from atomic hydrogen and deuterium by alpha particles
[DE95-002138] p 1523 N95-21587
NMR relaxation behavior of the head group of SHBS in lamellar liquid crystals
[AD-A279124] p 1574 N95-21599

MITRE CORP., BEDFORD, MA.
RCS calculation capability
[AD-A286329] p 1289 N95-20211
A new process for acquiring software architecture
[AD-A286012] p 1462 N95-20721
Semaphore network encryption report
[AD-A279294] p 1303 N95-21493
Common mapping system media study
[AD-A279086] p 1390 N95-21912
Incremental rederivation of software artifacts: FY 1993
[AD-A285790] p 1473 N95-22402

MOUND LAB., MIAMISBURG, OH.
Properties of aged metal tritides
[DE95-001787] p 1243 N95-21440

N

NATIONAL ACADEMY OF PUBLIC ADMINISTRATION, WASHINGTON, DC.
Program control in NASA: Needs and opportunities
p 1583 N95-20740

NATIONAL AERONAUTICS AND SPACE ADMINISTRATION, WASHINGTON, DC.
Challenger's night flight
[NASA-TM-110503] p 1217 N95-19995
Readings in program control
[NASA-SP-6103] p 1583 N95-20739
Cost estimating methods for advanced space systems
p 1583 N95-20741
But what will it Cost? The history of NASA cost estimating p 1583 N95-20742
Improving cost efficiency in large programs
p 1584 N95-20743
Estimating the costs of human space exploration
p 1584 N95-20744
The advantages of cost plus award fee contracts
p 1584 N95-20745
A Cost and Performance System (CAPS) in a Federal agency p 1584 N95-20746
An analysis of cost overruns on defense acquisition contracts p 1584 N95-20749
Program control on the Tropical Rainfall Measuring Mission p 1584 N95-20750
A strategy of cost control for Mariner Venus/Mercury 1973 p 1585 N95-20751
Performance measurement: A tool for program control
p 1585 N95-20752
Program control for mission success
p 1585 N95-20753
The MSFC Program Control Development Program
p 1585 N95-20754
NASA's attack on costs p 1585 N95-20755
Microgravity: Teacher's guide with activities for physical science
[NASA-EG-103] p 1285 N95-21322
Aeronautical engineering: A continuing bibliography with indexes (supplement 315)
[NASA-SP-7037(315)] p 1199 N95-21640
Spinoff, 1994
[NASA-NP-214] p 1594 N95-21893
The problem of space travel: The rocket motor
[NASA-SP-4026] p 1217 N95-21894
Aerospace medicine and biology: A continuing bibliography with indexes (supplement 399)
[NASA-SP-7011(399)] p 1446 N95-21947
NASA patent abstracts bibliography: A continuing bibliography. Section 2: Indexes (supplement 46)
[NASA-SP-7039(46)-SECT-2] p 1590 N95-21948
Turbine design and application
[NASA-SP-290] p 1214 N95-22341

NATIONAL AERONAUTICS AND SPACE ADMINISTRATION. AMES RESEARCH CENTER, MOFFETT FIELD, CA.
Effect of chemical heat release in a temporally evolving mixing layer p 1249 N95-21037
Pressure and higher-order spectra for homogeneous isotropic turbulence p 1343 N95-21045
Statistics of pressure and pressure gradient in homogeneous isotropic turbulence p 1343 N95-21046
Vortex ring instability and its sound
p 1344 N95-21048
Instability of streamwise vortices in plane channel flows p 1344 N95-21049
Modeling the two-point correlation of the vector stream function p 1345 N95-21055
Homogeneous turbulence subjected to mean flow with elliptic streamlines p 1345 N95-21056
On the asymptotic similarity of rotating homogeneous turbulence p 1345 N95-21058
Anisotropic structure of homogeneous turbulence subjected to uniform rotation p 1346 N95-21059
Single point modeling of rotating turbulent flows
p 1346 N95-21060
Developments and applications of dynamic models for large eddy simulation of complex flows
p 1346 N95-21062
The asymptotic state of rotating homogeneous turbulence at high Reynolds numbers
p 1347 N95-21065
Numerical simulation of supersonic boundary layer transition p 1348 N95-21074
Direct simulation of a self-similar plane wake
p 1350 N95-21084
The effect of initial conditions on the development of temporally evolving planar three dimensional incompressible wakes p 1350 N95-21085
Simulation of rotor blade element turbulence
[NASA-TM-108862] p 1207 N95-21186
A three-dimensional orthogonal laser velocimeter for the NASA Ames 7- by 10-foot wind tunnel
[NASA-TM-108864] p 1366 N95-21323
Hypervolemia in men from drinking hyperhydration fluids at rest and during exercise
[NASA-TM-4657] p 1439 N95-21544
Simulated rarefied entry of the Galileo probe into the atmosphere of Jupiter
[NASA-TM-110507] p 1601 N95-21621
Surface ices in the outer solar system
p 1423 N95-21815
Is xenon eldest? p 1425 N95-21823
The velocity and vorticity fields of the turbulent near wake of a circular cylinder
[NASA-TM-110513] p 1355 N95-21954
Large-eddy simulation of a plane wake
p 1360 N95-22446
On the dynamics of small-scale vorticity in isotropic turbulence p 1362 N95-22459

NATIONAL AERONAUTICS AND SPACE ADMINISTRATION. GODDARD SPACE FLIGHT CENTER, GREENBELT, MD.
Location and characteristics of the reconnection X-line deduced from low-altitude satellite and radar observations
[NASA-TM-110114] p 1413 N95-20453
Goddard Space Flight Center solar array missions, requirements and directions p 1316 N95-20503
Abbreviations and acronyms
[NASA-TM-110506] p 1590 N95-21457
Arcmimute scale HI and IRAS observations toward high latitude cloud G86.5+59.6 p 1594 N95-21771
Solar wind composition
[NASA-TM-197364] p 1604 N95-22384

NATIONAL AERONAUTICS AND SPACE ADMINISTRATION. HUGH L. DRYDEN FLIGHT RESEARCH CENTER, EDWARDS, CA.
F-15 resource tape
[NASA-TM-110502] p 1206 N95-19994
F-16XL interview with Marta Bohn-Meyer
[NASA-TM-110505] p 1200 N95-19996
Acoustic climb to cruise test
[NASA-TM-110504] p 1206 N95-20155

NATIONAL AERONAUTICS AND SPACE ADMINISTRATION. LYNDON B. JOHNSON SPACE CENTER, HOUSTON, TX.
Bevel gear driver and method having torque limit selection
[NASA-CASE-MSC-22384-1] p 1378 N95-20151
An overview of the Evaluation of Oxygen Interactions with Materials 3 Experiment: Space Shuttle Mission 46; July-August, 1992
[NASA-TM-110129] p 1412 N95-20278
Displaceable spur gear torque controlled driver and method
[NASA-CASE-MSC-22381-1] p 1378 N95-20409
STS 63 flight day 4 highlights/MIR-Shuttle rendezvous
[NASA-TM-110512] p 1219 N95-21113
Moon: Old and new
[NASA-TM-110511] p 1601 N95-21196
STS 63: Post flight presentation
[NASA-TM-110514] p 1219 N95-21558
Tethered satellite: Forces and motion
[NASA-TM-110518] p 1220 N95-21858
STS Flight 64 mission highlights
[NASA-TM-110515] p 1219 N95-22295

NATIONAL AERONAUTICS AND SPACE ADMINISTRATION. LANGLEY RESEARCH CENTER, HAMPTON, VA.
Static investigation of two fluidic thrust-vectoring concepts on a two-dimensional convergent-divergent nozzle
[NASA-TM-4574] p 1199 N95-19913
Vapor generator wand
[NASA-CASE-LAR-15058-1] p 1215 N95-20080
NASA/DOD Aerospace Knowledge Diffusion Research Project. Report 28: The technical communication practices of aerospace engineering and science students: Results of the phase 4 cross-national surveys
[NASA-TM-109123] p 1587 N95-20162
NASA/DOD Aerospace Knowledge Diffusion Research Project. Report 31: The technical communications practices of US aerospace engineers and scientists: Results of the phase 1 SME mail survey
[NASA-TM-109169] p 1587 N95-20163
Parallel calculation of sensitivity derivatives for aircraft design using automatic differentiation
[NASA-TM-110103] p 1206 N95-20370
A direct process for preparing semi-crystalline polyimides
[NASA-CASE-LAR-15020-1] p 1268 N95-20407
Method and apparatus for non-invasive evaluation of diaphragmatic function
[NASA-CASE-LAR-13888-1] p 1441 N95-20408
Vacuum holding fixture and method for fabricating piezoelectric polymer acoustic sensors
[NASA-CASE-LAR-14240-1] p 1268 N95-20410
P/N In(Al) GaAs multijunction laser power converters
p 1323 N95-20539
Apparatus and method for determining the mass density of a filament
[NASA-CASE-LAR-14879-1-CU] p 1383 N95-20616
Internal aerodynamics of a generic three-dimensional scramjet inlet at Mach 10
[NASA-TP-3476] p 1340 N95-20619
16-foot transonic tunnel test section flowfield survey
[NASA-TM-109157] p 1216 N95-20669
The personal aircraft: Status and issues
[NASA-TM-109174] p 1200 N95-20688
Why do airlines want and use thrust reversers? A compilation of airline industry responses to a survey regarding the use of thrust reversers on commercial transport airplanes
[NASA-TM-109158] p 1203 N95-20706

Acoustic calibration apparatus for calibrating plethysmographic acoustic pressure sensors
[NASA-CASE-LAR-14977-1] p 1443 N95-20763

Flux-focusing eddy current probe and rotating probe method for flaw detection
[NASA-CASE-LAR-15231-1-SB] p 1383 N95-20764

Mathematical modeling of a class of multibody flexible spacecraft structures
[NASA-TM-109166] p 1219 N95-20800

Test fixture for determination of energy absorbing capabilities of composite materials
[NASA-CASE-LAR-15212-1-CU] p 1229 N95-21008

NASA/DOD Aerospace Knowledge Diffusion Research Project. Report 27: The technical communication practices of engineering and science students: Results of the phase 3 academic surveys
[NASA-TM-109122] p 1589 N95-21015

NASA Langley scientific and technical information output: 1994, volume 1
[NASA-TM-109170-VOL-1] p 1589 N95-21189

Heavy ion track-structure calculations for radial dose in arbitrary materials
[NASA-TP-3497] p 1517 N95-21191

Acoustic receptivity due to weak surface inhomogeneities in adverse pressure gradient boundary layers
[NASA-TM-4577] p 1353 N95-21258

Application of Navier-Stokes code PAB3D with kappa-epsilon turbulence model to attached and separated flows
[NASA-TP-3480] p 1201 N95-21338

Grid resolution and solution convergence for Mars Pathfinder forebody
[NASA-TM-109173] p 1494 N95-21622

NASA/DOD Aerospace Knowledge Diffusion Research Project. Paper 48: Valuing information in an interactive environment
[NASA-TM-110448] p 1590 N95-21977

Effects of yaw and pitch motion on model attitude measurements
[NASA-TM-4641] p 1368 N95-22109

NATIONAL AERONAUTICS AND SPACE ADMINISTRATION. LEWIS RESEARCH CENTER, CLEVELAND, OH.

Evaluation of PS 212 coatings under boundary lubrication conditions with an Ester-based oil to 300 C
[NASA-TM-106763] p 1223 N95-19901

Augmented thermal bus
[NASA-CASE-LEW-15595-1-C] p 1338 N95-19933

Effect of microgravity on material undergoing melting and freezing: The TES Experiment
[NASA-TM-106845] p 1338 N95-19952

Flow coefficient behavior for boundary layer bleed holes and slots
[NASA-TM-106846] p 1338 N95-19953

Third Intermetallic Matrix Composites Symposium, volume 350
[NASA-TM-110059] p 1225 N95-20001

Application of an energy-based life prediction model to bithermal and thermomechanical fatigue
[NASA-TM-106684] p 1385 N95-20179

Computer program for calculation of complex chemical equilibrium compositions and applications. Part 1: Analysis
[NASA-RP-1311] p 1235 N95-20180

Proceedings of the 13th Space Photovoltaic Research and Technology Conference (SPRAT 13)
[NASA-CP-3278] p 1316 N95-20502

Status of diffused junction p+n InP solar cells for space applications p 1317 N95-20509

Modeling of high efficiency solar cells under laser pulse for power beaming applications p 1318 N95-20516

Performance, defect behavior and carrier enhancement in low energy, proton irradiated p+nn+ InP solar cells
p 1319 N95-20518

Final results of the advanced photovoltaic experiment
p 1321 N95-20528

Preliminary results from the flight of the Solar Array Module Plasma Interactions Experiment (SAMPIE)
p 1321 N95-20529

Static stability of a three-dimensional space truss
p 1220 N95-20533

An update on the development of a line-focus refractive concentrator array p 1322 N95-20534

Rare earth garnet selective emitter
p 1322 N95-20536

InGaAs PV device development for TPV power systems p 1322 N95-20537

Pulsed laser illumination of photovoltaic cells
p 1323 N95-20538

Reliability analysis of uniaxially ground brittle materials
[NASA-TM-106852] p 1386 N95-20790

Application of pressure sensitive paint in hypersonic flows
[NASA-TM-106824] p 1201 N95-20794

Bibliography of Lewis Research Center technical publications announced in 1993
[NASA-TM-106666] p 1589 N95-21187

Electrostatic noise in the plasma environment around the shuttle
[NASA-TM-106856] p 1415 N95-21188

Friction and wear properties of as-deposited and carbon ion-implanted diamond films
[NASA-TM-106759] p 1274 N95-21252

Evaluation of Pd-Cr wires for strain gage application
[NASA-TM-106857] p 1366 N95-21259

Two-dimensional imaging of OH in a lean burning high pressure combustor
[NASA-TM-106854] p 1214 N95-21383

Space power facility readiness for Space Station power system testing
[NASA-TM-106829] p 1218 N95-21384

Dual active surface heat flux gage probe
[NASA-TM-106661] p 1366 N95-21391

Multiwire thermocouples: Frequency response
[NASA-TM-110510] p 1367 N95-21889

Cochannel and adjacent-channel interference in nonlinear minimum-shift-keyed satellite system
[NASA-TM-106834] p 1307 N95-21890

Hybrid Upwind Splitting (HUS) by a field-by-field decomposition
[NASA-TM-106843] p 1355 N95-21957

Computations of unsteady viscous compressible flows using adaptive mesh refinement in curvilinear body-fitted grid systems
[NASA-TM-106704] p 1356 N95-21959

Performance of Ga(0.47)In(0.53)As cells over a range of proton energies
[NASA-TM-106819] p 1334 N95-22112

Numerical study of contaminant effects on combustion of hydrogen, ethane, and methane in air
[NASA-TM-106844] p 1284 N95-22114

Wave journal bearing. Part 2: Experimental pressure measurements and fractional frequency whirl threshold for wave and plain journal bearings
[NASA-TM-106848-PT-2] p 1382 N95-22405

NATIONAL AERONAUTICS AND SPACE ADMINISTRATION. MARSHALL SPACE FLIGHT CENTER, HUNTSVILLE, AL.

Hydrogen resistant alloy - NASA 23
[NASA-CASE-MFS-26200-1-SB] p 1251 N95-20068

Preliminary control system design and analysis for the Space Station Furnace Facility thermal control system
[NASA-TM-108476] p 1365 N95-20560

Transport phenomena in the micropores of plug-type phase separators
[NASA-TM-108479] p 1340 N95-20561

Guidelines for qualifying cleaning and verification materials
[NASA-TM-108474] p 1270 N95-20694

Launch vehicle flight control augmentation using smart materials and advanced composites (CDDF Project 93-05)
[NASA-TP-3535] p 1218 N95-21346

Role of dielectric constant in electrohydrodynamics of conducting fluids
[NASA-TM-110499] p 1331 N95-21614

Numerical investigations of low-density nozzle flow by solving the Boltzmann equation
[NASA-TM-110492] p 1354 N95-21675

Potential flow downstream of the heliospheric terminal shock: A non-spherical shock
[NASA-TM-110493] p 1426 N95-21874

Remote-sensing based technique to account for sub-grid scale variability of land surface properties
[NASA-TM-110501] p 1390 N95-22110

Regional scale hydrology with a new land surface processes model
[NASA-TM-110500] p 1390 N95-22111

NATIONAL AEROSPACE LAB., AMSTERDAM (NETHERLANDS).

Counting methods for the analysis of load time histories
[PB95-132916] p 1388 N95-22093

NATIONAL DEFENCE RESEARCH ESTABLISHMENT, LINKOEPING (SWEDEN).

Simulation of laser bathymetry for irregular bottoms
[PB95-133518] p 1434 N95-21320

NATIONAL DEFENCE RESEARCH ESTABLISHMENT, STOCKHOLM (SWEDEN).

Computation of transonic flow on composite overlapping grids in 2 D
[PB95-131348] p 1353 N95-21132

Atmospheric stability and its influence on air quality in small communities in northern Sweden
[PB95-131652] p 1405 N95-21181

Compatibility testing of explosives and paints by chemiluminescence techniques
[PB95-133609] p 1275 N95-21275

Significance of impact velocity for the extent of damage in carbon/epoxy laminates
[PB95-133484] p 1230 N95-21417

Policies concerning military and civilian research and technology applications
[PB95-131355] p 1585 N95-21427

Ignition of submarine materials at various oxygen concentrations
[PB95-131371] p 1243 N95-21428

EXPERT system expert: Program description
[PB95-131561] p 1482 N95-21429

EXPERT system expert: Users manual
[PB95-131579] p 1482 N95-21430

Damage tolerance of carbon fibre polyetheretherketone laminates
[PB95-131611] p 1230 N95-21432

Navigation system in combat vehicle
[PB95-131629] p 1452 N95-21467

Fire smoke ventilation through shafts: Experiments
[PB95-132247] p 1288 N95-21978

Effect of laser radiation on carbon fibre/epoxy composites
[PB95-133526] p 1232 N95-22096

Aluminium oxide targets after ballistic impact; fragmentation of the ceramic and the projectile
[PB95-133625] p 1388 N95-22097

Embedded optical fibres as strain sensors in polymer matrix fibre composites: The influence of adhesion in strain transfer
[PB95-133617] p 1547 N95-22140

NATIONAL DEFENCE RESEARCH ESTABLISHMENT, UMEA (SWEDEN).

ICE BABY: Measurements of concentration fluctuations in a forest area in winter conditions
[PB95-133468] p 1405 N95-21274

NATIONAL GEOPHYSICAL DATA CENTER, BOULDER, CO.

Solar-Geophysical Data number 600, August 1994. Part 1: (Prompt reports). Data for July, June 1994, and late data
[PB95-104923] p 1603 N95-20713

Solar-Geophysical Data number 600, August 1994. Part 2: (Comprehensive reports). Data for February 1994 and miscellaneous
[PB95-105060] p 1603 N95-20722

Solar-geophysical data number 601, September 1994. Part 2: (Comprehensive reports). Data for March 1994, and miscellaneous
[PB95-136735] p 1603 N95-20829

Solar-geophysical data number 601, September 1994. Part 1: (Prompt reports). Data for August, July 1994, and late data
[PB95-136727] p 1603 N95-20919

NATIONAL INST. FOR FUSION SCIENCE, NAGOYA (JAPAN).

Current diffusive ballooning mode in second stability region of tokamaks
[DE94-770690] p 1554 N95-20683

Chaotic phenomena in plasma 3
[DE94-770765] p 1554 N95-20686

Ion heat pulse after sawtooth crash in the JFT-2M tokamak
[DE94-770685] p 1555 N95-20988

Observation of non diffusive term of toroidal momentum transport in the JFT-2M tokamak
[DE94-770686] p 1555 N95-20989

NATIONAL INST. OF STANDARDS AND TECHNOLOGY, BOULDER, CO.

Technical digest: Eighth Symposium on Optical Fiber Measurements
[PB94-207636] p 1540 N95-19976

Measurements of shielding effectiveness and cavity characteristics of airplanes
[PB94-210051] p 1289 N95-20191

Thermophysical properties of HFC-143a and HFC-152a
[DE95-002199] p 1582 N95-22153

Measurement of the thermal properties of electrically conducting fluids using coated transient hot wires
[DE94-017816] p 1357 N95-22264

NATIONAL INST. OF STANDARDS AND TECHNOLOGY, GAITHERSBURG, MD.

Global equivalence ratio concept and the prediction of carbon monoxide formation in enclosure fires
[PB94-207511] p 1234 N95-20100

Annual Conference on Fire Research: Book of abstracts
[PB95-104964] p 1286 N95-20717

Abrasive wear by diesel engine coal-fuel and related particles
[PB95-104915] p 1379 N95-20984

FIREDOC users manual, 3rd edition
[PB95-128674] p 1286 N95-21129

Summaries of BFRL fire research in-house projects and grants, 1994
[PB95-130845] p 1286 N95-21130

Quality characteristics and metrics for reusable software
[PB94-203437] p 1473 N95-22390

NATIONAL MATERIALS ADVISORY BOARD, WASHINGTON, DC.

Hierarchical structures in biology as a guide for new materials technology
[AD-A286317] p 1265 N95-20176

NATIONAL OCEANIC AND ATMOSPHERIC ADMINISTRATION, PRINCETON, NJ.

Transport, radiative, and dynamical effects of the Antarctic ozone hole: A GFDL SKYHI model experiment
[PB94-192754] p 1409 N95-22101

NATIONAL OCEANIC AND ATMOSPHERIC ADMINISTRATION, RESEARCH TRIANGLE PARK, NC.

Effects of meteorology on concentrations of acid aerosols
[PB94-209749] p 1400 N95-19965

NATIONAL OCEANOGRAPHIC DATA CENTER, WASHINGTON, DC.

Mariners Weather Log, volume 38, number 3, summer 1994
[PB94-209541] p 1428 N95-20099

NATIONAL PHYSICAL LAB., TEDDINGTON (ENGLAND).

Effect of atmospheric pressure on measured aircraft noise levels
[PB95-130423] p 1207 N95-21425

NATIONAL RENEWABLE ENERGY LAB., GOLDEN, CO.

Turbulence descriptors for scaling fatigue loading spectra of wind turbine structural components
[DE94-011833] p 1384 N95-20109

Proceedings of the 1994 DOE/NREL Hydrogen Program Review
[DE94-011835] p 1234 N95-20117

Polycrystalline thin film cadmium telluride solar cells fabricated by electrodeposition
[DE94-011848] p 1391 N95-20118

Error analysis in wind turbine field testing
[DE94-011864] p 1391 N95-20260

Assessment of liquefaction and pyrolysis systems
[PB95-129797] p 1236 N95-20290

Assessment of liquefaction and pyrolysis systems
[PB95-129797] p 1236 N95-20290

The First NREL Conference on Thermophotovoltaic Generation of Electricity: Proceedings
[DE94-011831] p 1391 N95-20332

Polycrystalline CuInSe2 and CdTe solar cells
[DE94-011875] p 1392 N95-20333

Anaerobic digestion analysis model: User's manual
[DE94-011858] p 1437 N95-20471

Novel thin-film CuInSe2 fabrication
[DE94-011874] p 1268 N95-20472

The Photovolatic Manufacturing Technology project (PVMaT) after three years
[DE94-011877] p 1392 N95-20473

An update on the Department of Energy's photovoltaic program p 1316 N95-20505

Design of high-efficiency, radiation-hard, GaInP/GaAs solar cells p 1319 N95-20521

Solar Radiation Resource Assessment Project
[DE94-000286] p 1392 N95-20778

Advanced wind turbine design studies: Advanced conceptual study
[DE93-000031] p 1394 N95-20985

Processing and modeling issues for thin-film solar cell devices
[DE94-011895] p 1394 N95-21294

Thin-film cadmium telluride photovoltaic cells
[DE94-011886] p 1395 N95-21508

Non-H2Se, ultra-thin CuInSe2 devices
[DE94-011894] p 1395 N95-21844

The role of point defects and defect complexes in silicon device processing
[DE94-011876] p 1279 N95-22091

Gas-phase photocatalytic oxidation: Cost comparison with other air pollution control technologies
[DE95-000241] p 1410 N95-22278

Wind Energy Program overview, fiscal year 1993
[DE94-000285] p 1398 N95-22468

NAVAL ACADEMY, ANNAPOLIS, MD.

Electrical impedance studies of acid-form NAFION membranes
[AD-A279271] p 1330 N95-21490

NAVAL AEROSPACE MEDICAL RESEARCH LAB., PENSACOLA, FL.

Test reliability and experimental power
[AD-A279607] p 1448 N95-19957

Iterated-bootstrap confidence intervals for the mean
[AD-A279802] p 1498 N95-20102

Behavioral effects of tyrosine during sustained wakefulness
[AD-A279789] p 1441 N95-20307

Effects of bifocal and progressive-addition corrective lenses on aviator target-detection performance
[AD-A279698] p 1442 N95-20710

Bibliography of scientific publications 1975-1993
[AD-A279767] p 1444 N95-20977

The sharper image: Implementing a Fast Fourier Transform (FFT) to enhance a video-captured image
[AD-A279790] p 1445 N95-21180

Command history, 1993
[AD-A279775] p 1446 N95-21989

NAVAL AIR WARFARE CENTER, CHINA LAKE, CA.

Experimental proof-of-concept of phase derivative based range profile enhancement ATR
[AD-A284921] p 1289 N95-19997

A colocated magnetic loop, electric dipole array antenna (preliminary results)
[AD-A285381] p 1290 N95-20556

Multilayer piecewise linear networks
[AD-A285382] p 1480 N95-20606

Dielectric models in adhesion and extrapolations of molecular modeling
[AD-A279675] p 1516 N95-21121

NAVAL AIR WARFARE CENTER, INDIANAPOLIS, IN.

Standard Hardware Acquisition and Reliability Program (SHARP) advanced SEM-E packaging
p 1208 N95-20633

Advanced Standard Electronic Modules format-E (SEM-E) processes for rapid prototyping
p 1210 N95-20642

Immersion/two phase cooling p 1211 N95-20648

NAVAL AIR WARFARE CENTER, WARMINSTER, PA.

The Advanced Avionics Subsystem Technology Demonstration Program p 1209 N95-20636

The IEEE scalable coherent interface: An approach for a unified avionics network p 1212 N95-20650

A technique for increasing the bandwidth of high performance electrical backplanes p 1212 N95-20651

Electrochemical impedance spectroscopy of trivalent chromium pre-treated aluminum alloy
[AD-A280093] p 1240 N95-20970

Corrosion behavior of landing gear steels
[AD-A285862] p 1261 N95-22132

NAVAL COASTAL SYSTEMS CENTER, PANAMA CITY, FL.

Optical pattern recognition
[AD-A285384] p 1480 N95-20607

NAVAL COMMAND, CONTROL AND OCEAN SURVEILLANCE CENTER, SAN DIEGO, CA.

Radiance of the ocean horizon
[AD-A285613] p 1431 N95-19896

Signal-to-noise gain from adaptive matched-field beamforming of multidimensional acoustic arrays
[AD-A285671] p 1503 N95-20084

Characterization and simulation of an acoustic source moving through an oceanic waveguide
[AD-A285688] p 1503 N95-20272

Structural performance of cylindrical pressure housings of different ceramic compositions under external pressure loading. Part 1: Isostatically pressed alumina ceramic
[AD-A279669] p 1270 N95-20603

An at-sea evaluation of an infrared/resistance temperature device for air/sea-surface temperature measurements
[AD-A279672] p 1365 N95-20604

Human performance studies for control of multiple remote systems
[AD-A286623] p 1452 N95-20768

Terrain and refractivity effects on non-optical paths
p 1294 N95-20931

Modeling tropospheric ducting effects on satellite-to-ground paths p 1295 N95-20936

The Lorentz reciprocity theorem as a consistency test for propagation models p 1295 N95-20937

Mitigation of effects of multiple path nulls at super-high frequencies through diversity and networking
p 1297 N95-20948

Structural performance of cylindrical pressure housings of different ceramic compositions under external pressure loading. Part 4: Silicon carbide particulate reinforced alumina ceramic
[AD-A286299] p 1279 N95-22047

Scalable programming environment
[AD-A286390] p 1472 N95-22201

Structural performance of cylindrical pressure housings of different ceramic compositions under external pressure loading. Part 3: Sintered reaction bonded silicon nitride ceramic
[AD-A285773] p 1388 N95-22411

NAVAL FACILITIES ENGINEERING SERVICE CENTER, PORT HUENEME, CA.

Environmental cleanup technology transfer initiatives
[AD-A285059] p 1403 N95-20487

NAVAL HEALTH RESEARCH CENTER, SAN DIEGO, CA.

Microclimate cooling effect on perceived exertion in four heat/exercise scenarios
[AD-A285549] p 1444 N95-21160

NAVAL MEDICAL RESEARCH INST., BETHESDA, MD.

Solubilities of nitrogen and helium in water and blood at 37 C and pressures of up to 11 ATA
[AD-A286269] p 1446 N95-22003

NAVAL POSTGRADUATE SCHOOL, MONTEREY, CA.

Hydrographic data from equatorial Pacific waters near the Galapagos
[AD-A283741] p 1431 N95-19918

Efficient caption-based retrieval of multimedia information
[AD-A279604] p 1586 N95-19956

A modal analysis of currents in a Pacific Atoll lagoon
[AD-A283721] p 1431 N95-19971

A simple analytical model for asynchronous dense WDM/OOK systems
[AD-A283725] p 1289 N95-19973

The origin of acicular ferrite in gas metal arc and submerged arc welds
[AD-A286129] p 1377 N95-19984

The design and implementation of the functional/daplex data interface for the multimodel and multilingual database system
[AD-A280131] p 1587 N95-20039

Personal computer and workstation operating systems tutorial
[AD-A280132] p 1451 N95-20041

Software fault tree analysis of concurrent Ada processes
[AD-A284979] p 1457 N95-20042

The design and analysis of a phased array microstrip antenna for a low earth orbit communication satellite
[AD-A284791] p 1289 N95-20065

Using local optimality criteria for efficient information retrieval with redundant information filters
[AD-A279603] p 1587 N95-20302

Software merge: Semantics of combining changes to programs
[AD-A279657] p 1459 N95-20304

Towards better quality and reliability in the software reuse library environment
[AD-A280013] p 1460 N95-20313

Analysis of direct detection lightwave systems with optical amplifiers
[AD-A284077] p 1542 N95-20467

Automation support for concurrent software engineering
[AD-A279691] p 1461 N95-20579

Downsizing information systems: Framing the issues for the Office of Naval Intelligence (ONI)
[AD-A279888] p 1588 N95-20589

Translation of the data flow query language for the multimodel, multibackend database system
[AD-A285978] p 1588 N95-20617

Error probabilities of FFH/BFSK with noise normalization and soft decision viterbi decoding in a fading channel with partial-band jamming
[AD-A280041] p 1498 N95-20620

Computer graphics tools for visualizing gravity gradient torques on a rigid spacecraft
[AD-A285971] p 1461 N95-20665

Emitter location via Kalman filtering of signal time difference of arrival
[AD-A285972] p 1291 N95-20666

Design and implementation of visual object-oriented LOGO using Prograph
[AD-A285977] p 1461 N95-20687

Software for flow distribution in electronic rack structures
[AD-A285994] p 1325 N95-20715

An empirical approach to logical clustering of software failure regions
[AD-A279863] p 1462 N95-20776

Laser anemometry and viscous computation of the flow through an annular turbine cascade
[AD-A280070] p 1341 N95-20968

A computer code (SKINTEMP) for predicting transient missile and aircraft heat transfer characteristics
[AD-A286044] p 1341 N95-21001

Vibration analysis of the AN/SPS-67(V)3 surface search radar
[AD-A286050] p 1302 N95-21324

A numerical study of wind forcing effects on the California Current System
[AD-A286205] p 1435 N95-21880

A computer-based multimedia prototype for night vision goggles
[AD-A286208] p 1546 N95-21882

Inband scattering from arrays with series feed networks
[AD-A286209] p 1307 N95-21883

A simulation of plasma motion in the polar ionosphere
[AD-A286166] p 1426 N95-22019

A transmission electron microscope characterization of sodium sulfate hot corrosion of silicon carbide fiber-reinforced lithium aluminosilicate glass-ceramic matrix composite
[AD-A286164] p 1231 N95-22038

Effect of juncture fillets on double-delta wings undergoing sideslip at high angles of attack
[AD-A286165] p 1207 N95-22039

The applicability of neural networks to ionospheric modeling in support of relocatable Over-the-Horizon radar
[AD-A286114] p 1309 N95-22230

Evaluation of the Haworth-Newman avionics Display Readability Scale
[AD-A286127] p 1214 N95-22232

Optimal control of a two wheeled mobile robot
[AD-A286130] p 1485 N95-22233

Layered path planning for an autonomous mobile robot
[AD-A286138] p 1485 N95-22244

Design and modelling of a link monitoring mechanism for the Common Data Link (CDL)
[AD-A286167] p 1309 N95-22245

Performance of a fast frequency-hopped noncoherent MFSK receiver over Rician fading channels with either partial-band interference or multi-tone interference
[AD-A286168] p 1310 N95-22246

Probability of detection for a GO CFAR radar processor using envelope detection approximation
[AD-A286211] p 1310 N95-22251

Determination of the complex elastic moduli of materials using a free-free bar technique
[AD-A279861] p 1281 N95-22387

A periodic scheduling heuristic for mapping iterative task graphs onto distributed memory multiprocessors
[AD-A286047] p 1311 N95-22415

A conceptual approach to object-oriented data modeling
[AD-A286048] p 1592 N95-22416

Forecasting aircraft mishaps using monthly maintenance reports
[AD-A286049] p 1203 N95-22417

NAVAL RESEARCH LAB., BAY SAINT LOUIS, MS.

Tests of an improved oceanographic expert system
[AD-A280123] p 1431 N95-19888

Ice Processing System software support documentation
[AD-A280030] p 1388 N95-20006

Atlas of SSM/I satellite ice concentration interpolated to operational ice model domains of the Arctic for 1993
[AD-A280183] p 1432 N95-20012

Monthly mean sea ice data from the Polar Ice Prediction System, the Regional Polar Ice Prediction System-Barents Sea and the Regional Polar Ice Prediction System-Greenland Sea
[AD-A280095] p 1433 N95-21018

Rapid determination of geoacoustic properties of the sea floor by simulated annealing
[AD-A286297] p 1436 N95-22028

Digital mapping, charting, and geodesy analysis program technical review of Vector Smart Map (VMap) level 1
[AD-A286294] p 1390 N95-22055

NAVAL RESEARCH LAB., MONTEREY, CA.

A study of westerly wind bursts preceding the 1991-1992 El Nino
[AD-A286570] p 1429 N95-20826

NAVAL RESEARCH LAB., WASHINGTON, DC.

A review of water mist technology for fire suppression
[AD-A285738] p 1202 N95-20071

NRL review, 1994
[AD-A279832] p 1605 N95-20182

A Clementine collection: Moonglow
[AD-A286360] p 1217 N95-20228

Electron-irradiated two-terminal, monolithic InP/Ga0.47In0.53As tandem solar cells and annealing of radiation damage p 1319 N95-20519

The use of displacement damage dose to correlate degradation in solar cells exposed to different radiations
p 1320 N95-20523

Annealing of irradiated n+p InP buried homojunctions
p 1320 N95-20524

On commonalities in signal design for non-Gaussian channels
[AD-A285385] p 1498 N95-20608

Training simulant for Halon 1211 portable extinguishers
[AD-A285403] p 1286 N95-20611

PRS scoping study 1: Scaling law estimates for K-shell radiation yields on JUPITER-class generators
[AD-A279716] p 1533 N95-20672

X-ray spectroscopy of xenon
[DE95-002132] p 1240 N95-20865

Large eddy simulation of channel flow using a vorticity transport subgrid model p 1348 N95-21076

PRS scoping study. 2: ZPIMP predictions for radiation yields on a JUPITER-class generator
[AD-A279823] p 1537 N95-21494

Epoxy lining for shipboard piping systems
[AD-A286228] p 1279 N95-22022

NAVAL SURFACE WARFARE CENTER, DAHLGREN, VA.

Wavelet transformations for helicopter identification via acoustic signatures
[AD-A279980] p 1504 N95-20963

NAVAL SURFACE WEAPONS CENTER, DAHLGREN, VA.

Numerical investigation of one-dimensional heat-flux calculations
[AD-A286293] p 1582 N95-22054

NAVAL TEST PILOT SCHOOL, PATUXENT RIVER, MD.

T-45A High Angle of Attack Testing: US Naval Test Pilot School 46th Annual Reunion and Symposium
[AD-A284000] p 1207 N95-20466

NAVAL UNDERSEA WARFARE CENTER, NEWPORT, RI.

A model of an infinite length, axisymmetric, isotropic, forced thick shell
[AD-A285586] p 1386 N95-21212

Scattering of an FM signal from an array of spheres
[AD-A285587] p 1505 N95-21213

Information clustering for better decision-making
[AD-A286292] p 1590 N95-22053

Derivation of a wavenumber filter design for the measurement of turbulent wall pressure fluctuations
[AD-A286421] p 1357 N95-22208

Applications of sonochemistry
[AD-A286388] p 1506 N95-22360

NAVAL WAR COLL., NEWPORT, RI.

Bomber force 2000: Operational concepts for long-range combat aircraft
[AD-A279378] p 1206 N95-20181

Space fundamentals for the war fighter
[AD-A279703] p 1217 N95-20690

Space technology: Force multiplier or false sense of security
[AD-A279726] p 1217 N95-20995

NAVY PERSONNEL RESEARCH AND DEVELOPMENT CENTER, SAN DIEGO, CA.

Comparison of a back propagation artificial neural network model with a linear regression model for personnel selection
[AD-A280023] p 1479 N95-20005

NEBRASKA UNIV., LINCOLN, NE.

Dynamics of collision processes
[DE94-017593] p 1509 N95-20242

NEDERLANDS INST. VOOR ONDERZOEK DER ZEE, TEXEL (NETHERLANDS).

Long term changes on the continental shelf of the North Sea: Invertebrate trends, 1931-1990
[PB95-135224] p 1435 N95-21717

NESTE OY, HELSINKI (FINLAND).

Reducing exhaust gas emissions from Citydiesel busses
[DE95-700245] p 1380 N95-21295

NETHERLANDS INST. FOR BRAIN RESEARCH, AMSTERDAM (NETHERLANDS).

Netherlands Institute for Brain Research progress report, 1993
[PB95-135398] p 1445 N95-21352

NEUCHATEL UNIV. (SWITZERLAND).

Anomalous vector-boson couplings in Majorana neutrino models
[PB95-127460] p 1518 N95-21220

NEVADA UNIV., RENO, NV.

Photophysical processes on triplet states and radical ions in pure and molecularly doped polymers
[DE95-002681] p 1570 N95-20916

NEW ENERGY AND INDUSTRIAL TECHNOLOGY DEVELOPMENT ORGANIZATION, TOKYO (JAPAN).

Feasibility study of power generation system with shape memory alloys
[DE95-714802] p 1254 N95-20890

Research on the promotion measures to introduce new energy and energy-saving technologies with a leasing system
[DE95-714801] p 1375 N95-22079

Research on the power generation system with thermoelectric conversion elements
[DE95-714804] p 1397 N95-22309

NEW HAMPSHIRE UNIV., DURHAM, NH.

Location and characteristics of the reconnection X-line deduced from low-altitude satellite and radar observations
[NASA-TM-110114] p 1413 N95-20453

NEW JERSEY INST. OF TECH., NEWARK, NJ.

Applied mathematical problems in modern electromagnetics
[AD-A286448] p 1303 N95-21462

NEW MEXICO STATE UNIV., LAS CRUCES, NM.

Marussi hypothesis in differential geodesy
[AD-A285853] p 1413 N95-20377

Unified very low stratus cloud/subcloud microphysics model: User's guide
[AD-A286454] p 1430 N95-21586

Azimuthally averaged radial S(sub 100 microns)/S(sub 60 microns) dust color temperatures in spiral galaxies
p 1593 N95-21760

Correlation of far-infrared emission and radio continuum emission along the major axis of edge-on spiral galaxies
p 1593 N95-21762

NEW MEXICO UNIV., ALBUQUERQUE, NM.

Structure of dibis(diethyldithiocarbamato) zinc (2) Mu-bis(diethylphosphino)ethane toluene(2)
[AD-A279792] p 1224 N95-20660

Gas-phase generation of zinc sulfide particles using a single-source precursor
[AD-A279700] p 1239 N95-20712

Synthesis and characterization of (Zn(SEt)Et)10, formed via insertion of sulfur into Zn-C bonds: A new class of Wurtzite-like cluster framework
[AD-A279701] p 1569 N95-20714

Synthesis and characterization of single-source molecular precursors to binary metal sulphides: Bis(diethyldithiocarbamato) M(2)trialkylphosphine (M = Zn and Cd) adducts
[AD-A279746] p 1248 N95-22385

NEW ORLEANS UNIV., LA.

Density functional studies of decomposition processes of energetic molecules
[AD-A286185] p 1510 N95-20327

Computational evaluation of the feasibility of nitrating precursors to C12N12O12
[AD-A285976] p 1239 N95-20668

Calculated heats of formation of some predicted stable C, N, O, F molecules
[AD-A285957] p 1517 N95-21127

Comparative computational analysis of some nitramine and difluoramine structures, dissociation energies and heats of formation
[AD-A286196] p 1525 N95-21878

Non-local density functional calculations of gas phase heats of formation
[AD-A286213] p 1246 N95-22000

NEW YORK UNIV., NEW YORK, NY.

Solar flare MDH
[AD-A279894] p 1602 N95-20593

NICOLAUS COPERNICUS UNIV., TORUN (POLAND).

T1F ((1) sigma (+)): Some preliminary electronic structure calculations
[PB95-130316] p 1518 N95-21223

NORGES ALMENVITENSKAPELIGE FORSKNINGSRAAD, OSLO (NORWAY).

AC magnetic response of YBa2CuO7 with Y2BaCuO5 inclusions and of single-crystal YBa2Cu3O7: A comparative study
[PB94-207917] p 1577 N95-22166

NORTH CAROLINA STATE UNIV., RALEIGH, NC.

Solid-state dynamics and quantum transport in novel semiconductor nanostructures
[AD-A285946] p 1315 N95-20394

New ET-based organic superconductors with the organometallic anion Cu(CF3)4(-)
[DE94-016904] p 1567 N95-20479

Growth, characterization and device development in monocrystalline diamond films
[AD-A285991] p 1568 N95-20614

Balloon tracking for the ASTEX/MAGE Lagrangian experiment
[AD-A280078] p 1430 N95-20969

NESTLE: Few-group neutron diffusion equation solver utilizing the nodal expansion method for eigenvalue, adjoint, fixed-source steady-state and transient problems
[DE95-001903] p 1466 N95-21288

Chemistry and electrochemistry in Lewis acid and superacid ionic liquids
[AD-A279396] p 1246 N95-21931

NORTH CAROLINA UNIV., CHAPEL HILL, NC.

The energetics and dynamics of free radicals, ions, and clusters
[DE94-018101] p 1244 N95-21701

NORTH CAROLINA UNIV., CHARLOTTE, NC.

Localization phenomenon in some random classical systems
[AD-A286514] p 1309 N95-22215

NORTH CAROLINA UNIV., RALEIGH, NC.

Virtual reality in precision engineering research
[AD-A286528] p 1465 N95-21012

Low frequency sound radiation from finite stiffened plates
[AD-A279395] p 1505 N95-21930

NORTH DAKOTA STATE UNIV., FARGO, ND.

Low temperature synthesis of semiconductor materials
[AD-A285120] p 1226 N95-20081

A physiological neural network for saccadic eye movement control
[AD-A279599] p 1441 N95-20301

NORTHEASTERN UNIV., BOSTON, MA.

Advanced detector development, laboratory simulations, diagnostic development, and data analysis on wake physics
[AD-A284798] p 1364 N95-20069

Novel reagents for chemical vapor deposition of intermetallic alloys
[AD-A286562] p 1271 N95-20815

Large bistatic angle clutter depolarization study
p 1296 N95-20941

Topics in gauge theories and the unification of elementary particle interactions
[DE94-013485] p 1529 N95-22279

NORTHWEST RESEARCH ASSOCIATES, INC., BELLEVUE, WA.

Variability of total electron content in the high-altitude ionosphere following solar maximum
[AD-A285849] p 1425 N95-21833

NORTHWESTERN UNIV., EVANSTON, IL.

Energetics, bonding mechanism and electronic structure of ceramic/ceramic and metal/ceramic interfaces
[DE95-000601] p 1265 N95-20115

Deposition and properties of novel nitride superlattice coatings
[DE95-002945] p 1230 N95-21445

InTISb for long-wavelength infrared photodetectors and arrays
[AD-A280109] p 1331 N95-21660

Strong interactions studies with medium energy probes
[DE95-001800] p 1245 N95-21745

InTISb for long-wavelength infrared photodetectors and arrays
[AD-A280108] p 1332 N95-21774

MAC/FAC: A model of similarity-based retrieval
[AD-A286291] p 1450 N95-22052

Studies in nonlinear problems of energy
[DE95-001387] p 1356 N95-22148

NOTRE DAME UNIV., IN.

Photoinduced charge transfer between fullerenes and TiO2 semiconductor colloids
[DE95-001447] p 1570 N95-20838

Experiments on the flow field physics of confluent boundary layers for high-lift systems
[NASA-CR-197318] p 1201 N95-21343

Transient studies of low temperature catalysts for methane conversion
[DE95-003560] p 1247 N95-22224

NOTTINGHAM UNIV. (ENGLAND).

High contrast organic crystal optical modulator for phased array antenna and optical signal processing
[AD-A286557] p 1544 N95-20844

NOVUS TECHNOLOGIES, INC., ALBUQUERQUE, NM.

Radiation characterization report for the GPS Receiver microcontroller chip
[DE94-019169] p 1335 N95-22165

NTL, INC., GREENLAWN, NY.

Classical analysis methods for designing and developing downlooking radars
[AD-A285760] p 1302 N95-21405

NYMA, INC., BROOK PARK, OH.

Review of solar cell temperature coefficients for space
p 1323 N95-20541

O

OAK RIDGE INST. FOR SCIENCE AND EDUCATION, TN.

Current distribution in Cable-In-Conduit Conductors
[DE95-001820] p 1332 N95-21725

OAK RIDGE NATIONAL LAB., TN.

Wavelet-based acoustic recognition of aircraft
[DE94-017701] p 1503 N95-20019

Processing and characterization of Ni-Al-Fe-B shape-memory alloy wires produced by rapid solidification
[DE94-017702] p 1250 N95-20020

Comparison of the dynamic fatigue behavior of two monolithic SiC and an Al2O3/SiC composite
[DE94-017751] p 1225 N95-20022

The thermal conductivity of carbon coated silicon carbide fibers embedded in a silicon carbide matrix
[DE94-017758] p 1225 N95-20023

Properties of whisker-reinforced ceramics
[DE94-017759] p 1264 N95-20024

Cavity-QED enhancement of fluorescence yields in microdroplets
[DE94-018662] p 1506 N95-20030

Cr2Nb development
[DE94-018697] p 1250 N95-20043

Fabrication and properties of alumina matrix composites containing nickel aluminide reinforcements
[DE94-018703] p 1250 N95-20044

Guidelines for the creation and management of geographic data bases within a GIS environment, version 1.0
[DE94-019214] p 1458 N95-20073

Materials/manufacturing element of the Advanced Turbine System Program
[DE94-017299] p 1378 N95-20085

Electron-impact ionization of multicharged ions at ORNL: 1985-1992
[DE94-017318] p 1507 N95-20086

The thermal conductivity of carbon-fiber reinforced metal matrix composites
[DE94-017767] p 1226 N95-20125

Giant magnetoresistance calculated from first principles
[DE94-018658] p 1500 N95-20129

Electron-positron pair production in ultrarelativistic atomic collisions: 6.4 TeV S(sup 16+) with Au, Pd and Al
[DE95-000690] p 1508 N95-20133

Proceedings of the 1993 Non-Fluorocarbon Insulation, Refrigeration and Air Conditioning Technology Workshop
[DE94-018333] p 1285 N95-20194

Experimental measurements of ICRF and edge plasma interactions on Tore Supra
[DE94-019154] p 1551 N95-20205

Enhancement of creep resistance of a sintered S3N4 ceramic by microwave annealing
[DE94-017698] p 1265 N95-20220

Computational modeling of physical processes during laser ablation
[DE94-017699] p 1369 N95-20221

Microwave sintering of ZrO2-12 mol% CeO2
[DE94-018709] p 1265 N95-20226

Workshop on Uncertainty and Global Climate Change Research
[DE94-016728] p 1401 N95-20238

Simulations of the dislocation array at Ge/Si interfaces
[DE94-017680] p 1565 N95-20244

Surface stress, morphological development, and dislocation nucleation during strained-layer epitaxy
[DE94-017682] p 1565 N95-20245

Investigating the resolution of resistivity arrays using inverse theory
[DE94-017760] p 1412 N95-20287

An overview of the HSST Full-Thickness Shallow-Crack Clad Beam Testing Program
[DE94-018940] p 1385 N95-20322

Microstructural contributions to the fracture resistance of silicon nitride ceramics
[DE94-018955] p 1267 N95-20323

Amorphization of sapphire during ion beam mixing
[DE94-018713] p 1510 N95-20337

The in-situ fracture and Auger analysis of Nicalon fibers
[DE94-017771] p 1226 N95-20357

High performance computing for materials process modeling
[DE94-017860] p 1460 N95-20358

Microstructures and tensile properties of as-cast iron-aluminide alloys
[DE94-017868] p 1252 N95-20359

Oxide formation on NbAl3 and TiAl due to ion implantation of O-18
[DE94-017874] p 1252 N95-20365

MPI workshop
[DE94-017883] p 1475 N95-20366

Enhanced ionic conduction at the film/substrate interface in LiI thin films grown on sapphire(0001)
[DE94-017884] p 1565 N95-20371

Energy gap structure of layered superconductors
[DE94-017885] p 1566 N95-20372

The effect of fiber coating thickness on the interfacial properties of a continuous fiber ceramic matrix composite
[DE94-017886] p 1267 N95-20373

Residual stresses in material processing
[DE94-017888] p 1385 N95-20374

Effect of heat treatment temperature on creep-rupture properties of Fe3Al-based alloys
[DE94-017904] p 1253 N95-20375

Dynamic measurement of the hoop modulus of a composite cylinder
[DE94-018958] p 1385 N95-20416

Non destructive characterization using pulsed fast-thermal neutrons
[DE95-002601] p 1511 N95-20422

Atomic-resolution characterization of interface structure and chemistry in the STEM
[DE94-017753] p 1567 N95-20492

Visible and near-IR spectroscopic studies of UC1(4) in a basic ambient temperature melt: The observation of a possible geometric distorted UC1(6)(exp 2-) species and the evidence for the hydrogen-bond in the melt
[DE94-017764] p 1237 N95-20493

Processing and applications of iron aluminides
[DE94-017855] p 1253 N95-20673

Microscopy of stress-induced morphological development and dislocation nucleation during semiconductor epitaxy
[DE94-017869] p 1568 N95-20674

The effect of oxide inclusions on the kinetics of the austenite to ferrite transformation in low alloy steel weld metal
[DE94-018131] p 1253 N95-20676

Application of diode lasers to the isotopically selective determination of uranium in oxides by optogalvanic spectroscopy
[DE94-018045] p 1370 N95-20698

Effect of fiber fabric orientation on the monotonic and fatigue behavior of a continuous fiber ceramic composite
[DE94-018121] p 1271 N95-20700

The design of a parallel, dense linear algebra software library: Reduction to Hessenberg, tridiagonal, and bidiagonal form
[DE94-018123] p 1491 N95-20701

The production of calibration specimens for impact testing of subsize Charpy specimens
[DE94-018125] p 1386 N95-20703

Approaches to the design of structural ceramics incorporating whiskers and particulate phases
[DE94-018126] p 1271 N95-20704

Impact behavior of FeAl alloy FA-350
[DE94-018128] p 1254 N95-20705

Use of an integrated design tool for weld quality enhancement
[DE94-018135] p 1379 N95-20723

Magnetic flocculation of paramagnetic particles
[DE94-018144] p 1501 N95-20725

Materials processing using a variable frequency microwave furnace
[DE95-001420] p 1271 N95-20761

Scale-up and modeling of forced chemical vapor infiltration
[DE94-017769] p 1340 N95-20781

Effect of a solid insulator on the spark yield of S2F10 in SF6(*)
[DE95-001422] p 1326 N95-20791

A Monte Carlo study of the minus sign problem in the t-J model using an Intel iPSC/860 hypercube
[DE95-001072] p 1570 N95-20819

Hg-199 and Cu-(63,65) NMR studies of mercury based high-Tc superconductors
[DE95-001073] p 1570 N95-20820

Fabrication of ceramic composites: Forced CVI
[DE95-001076] p 1271 N95-20821

Magnetic excitations in modulated PrNi2Si2
[DE95-001077] p 1254 N95-20822

Automatic generation of fuzzy rules for the sensor-based navigation of a mobile robot
[DE95-001428] p 1481 N95-20837

ALCHEMI of Fe-doped B2-ordered NiAl alloys with different doping levels
[DE94-017748] p 1255 N95-20907

An advanced ECR ion source with a large uniformly distributed ECR plasma volume for multiply charged ion beam generation
[DE95-001078] p 1515 N95-20911

Dependence of critical current density on microstructure and processing of high-T(c) superconductors
[DE95-000685] p 1571 N95-21167

Plastic deformation of ordered intermetallic alloys: Fundamental aspects
[DE95-001070] p 1256 N95-21265

Error analysis of the quadratic nodal expansion method in slab geometry
[DE95-001352] p 1492 N95-21285

Neutron diffraction study of the magnetic ordering of BaCuO(2+x)
[DE95-001357] p 1572 N95-21297

Computational modeling of diffusion-controlled transformations in ternary systems
[DE95-001358] p 1256 N95-21298

Unknown-terrains navigation of a mobile robot using an array of sonars
[DE94-017902] p 1482 N95-21385

Molecular-based study of solutions in supercritical solvents
[DE94-019326] p 1580 N95-21420

Three-dimensional effects for radio frequency antenna modeling
[DE94-019125] p 1303 N95-21459

The ORNL Neutron-Capture Cross Section Facility
[DE94-019146] p 1537 N95-21460

Operator's manual for the multistation offgas analysis system
| DE95-002060 | p 1243 N95-21472

Processing and mechanical properties of laminar Al2O3-Ni3Al composites
| DE94-019332 | p 1230 N95-21481

Lead-indium phosphate glasses for optical applications
| DE94-019333 | p 1275 N95-21482

Effects of neutron irradiation on the London penetration depth for polycrystalline Bi(1.8)Pb(0.3)Sr2Ca2Cu3O10 superconductor
| DE94-019335 | p 1573 N95-21483

Production of S2F10, S2OF10 and S2O2F10 by spark discharges in SF6*
| DE95-001421 | p 1243 N95-21500

Comparison of properties of sintered and sintered reaction-bonded silicon nitride fabricated by microwave and conventional heating
| DE95-001426 | p 1275 N95-21501

Electron attachment to excited molecules
| DE94-019124 | p 1522 N95-21519

Time-resolved diagnostics of excimer laser-generated ablation plasmas used for pulsed laser deposition
| DE94-018950 | p 1559 N95-21547

Cell membrane potentials induced during exposure to EMP fields
| DE94-018952 | p 1439 N95-21548

Raman spectra of MOCVD-grown ferroelectric PbTiO3 thin films
| DE94-018964 | p 1244 N95-21549

Weld pool phenomena
| DE94-018965 | p 1381 N95-21550

Monolithic circuits for lead-glass calorimetry
| DE94-019112 | p 1330 N95-21554

Weldability of iron aluminides
| DE94-019114 | p 1257 N95-21555

PVM 3 beyond network computing
| DE94-019115 | p 1477 N95-21556

New concepts for refrigerant leak detection and mixture measurement
| DE94-018967 | p 1287 N95-21559

Stellarator transport optimization with self-consistent electric fields
| DE94-019151 | p 1559 N95-21581

Consequences of oscillatory potentials and angular forces in transition metals and their aluminides
| DE94-019127 | p 1258 N95-21600

On the origins and modeling of frictional behavior in interfacially-complex sliding contacts
| DE94-019129 | p 1381 N95-21601

DONIO: Distributed object network I/O library
| DE94-019163 | p 1477 N95-21602

The molecular mechanics program DUPLEX: Computing structures of carcinogen modified DNA by surveying the potential energy surface
| DE94-019153 | p 1439 N95-21606

PVM a platform for portable distributed computing
| DE94-019156 | p 1455 N95-21607

The message passing version of the parallel Community Climate Model
| DE94-019158 | p 1407 N95-21608

Total quality management program planning
| DE94-016862 | p 1586 N95-21645

Auger spectrometry of atoms and molecules
| DE94-018052 | p 1524 N95-21664

The ITER in-vessel system
| DE94-018053 | p 1560 N95-21665

Fracture behavior of the Fe-8Al alloy FAP-Y
| DE95-000956 | p 1258 N95-21676

Evaluation of pumping and fueling requirements for the ITER EDA
| DE94-018117 | p 1560 N95-21702

Charge density of fractional charged quasiparticles in the composite fermion picture
| DE94-018122 | p 1524 N95-21703

Investigation of direct photon production in 200 A GeV S + Au reactions
| DE94-018129 | p 1525 N95-21704

Restricted mass transport effects on free radical reactions
| DE94-018136 | p 1217 N95-21706

A new Krylov-subspace method for symmetric indefinite linear systems
| DE95-001826 | p 1355 N95-21726

A visual cell for measuring the solubility of prograde soluble salts in water at high temperatures and pressures
| DE95-002058 | p 1245 N95-21732

Learning algorithms for feedforward networks based on finite samples
| DE95-001739 | p 1483 N95-21741

QMRPACK user's guide
| DE95-001770 | p 1469 N95-21744

Creep behavior in SiC whisker-reinforced alumina composite
| DE95-001071 | p 1231 N95-21776

Angular and charge state distributions of highly charged ions scattered during low energy surface-channeling interactions with Au(110)
| DE95-001348 | p 1525 N95-21857

Tailoring suspension flow for the gelcasting of oxide and nonoxide ceramics
| DE95-001351 | p 1277 N95-21861

Information Management Architecture for an Integrated Computing Environment for the Environmental Restoration Program. Volume 1: Introduction
| DE95-001384 | p 1590 N95-21862

Cost-effective ceramics program in the United States
| DE95-001425 | p 1278 N95-21909

A syncopated leap-frog algorithm for orbit consistent plasma simulation of materials processing reactors
| DE95-000954 | p 1561 N95-21922

Ceramic technology for advanced heat engines
| DE95-000950 | p 1278 N95-21937

Selection of RIB targets using ion implantation
| DE95-000951 | p 1538 N95-21938

The status of molecules
| DE95-000952 | p 1526 N95-21939

Classical-quantum correspondence for ionization in fast ion-atom collisions
| DE95-000953 | p 1526 N95-21940

Catalyzed reduction of nitrate in aqueous solutions
| DE94-017660 | p 1247 N95-22049

Information Management Architecture for an Integrated Computing Environment for the Environmental Restoration Program. Volume 2: Interim business systems guidance
| DE95-001385 | p 1591 N95-22061

Abbreviations, acronyms, and initialisms frequently used by Martin Marietta Energy Systems, Inc.
| DE95-001069 | p 1591 N95-22107

New techniques in neutron scattering
| DE94-018944 | p 1538 N95-22117

Irradiation creep in structural materials at ITER operating conditions
| DE94-018946 | p 1261 N95-22123

Atom probe field ion microscopy of type 308 CRE stainless steel welds
| DE94-019162 | p 1261 N95-22127

Guidelines for the creation and management of geographic data bases within a GIS environment, version 1.0. Volume 2. Appendices
| DE94-019215 | p 1591 N95-22129

Plasma processing for integrated circuits
| DE95-001419 | p 1335 N95-22149

Materials support for the development of High Temperature Advanced Furnaces (HITAF): A comparison of selected mechanical properties for three SiC-based ceramics
| DE94-017752 | p 1280 N95-22258

The thermal conductivity of silicon nitride with molybdenum disilicide additions
| DE94-017757 | p 1247 N95-22260

Gravitational effects on the development of weld-pool and solidification microstructures
| DE94-017772 | p 1285 N95-22261

The two-electron problem and prospects for atomic collision theory on a numerical lattice
| DE94-017856 | p 1528 N95-22265

Strength testing of Ti-vapor-coated silicon nitride braze joints
| DE94-017858 | p 1280 N95-22266

Modeling of fundamental phenomena in welds
| DE94-017859 | p 1381 N95-22268

Local texture and strongly linked conduction in spray-pyrolyzed TlBa2Ca2Cu3O(8 + x) deposits
| DE94-017887 | p 1578 N95-22269

Measurement of residual stresses on ceramic materials with high spatial resolution
| DE94-017889 | p 1280 N95-22270

Development of practical high temperature superconducting wire for electric power applications
| DE94-017894 | p 1336 N95-22271

An improved Monte Carlo algorithm for simulating grain growth
| DE94-017903 | p 1578 N95-22272

Climatological data for clouds over the globe from surface observations, 1982-1991: The total cloud edition
| DE95-002537 | p 1431 N95-22288

Micrometeorological methods for measurements of mercury emissions over contaminated soils
| DE94-017679 | p 1411 N95-22342

Bulk and defect properties of ordered intermetallics
| DE94-017706 | p 1262 N95-22344

Processing of intermetallic materials by reaction synthesis
| DE94-017710 | p 1263 N95-22345

Tensile and impact properties of iron-aluminum alloys
| DE94-017750 | p 1263 N95-22346

OAK RIDGE Y-12 PLANT, TN.

Surface inspection using Fourier Transform Infrared Spectroscopy
| DE95-001699 | p 1244 N95-21571

ODESSEY RESEARCH ASSOCIATES, ITHACA, NY.

TBell: A mathematical tool for analyzing decision tables
| NASA-CR-195027 | p 1462 N95-20691

OFFICE NATIONAL D'ETUDES ET DE RECHERCHES AEROSPATIALES, CHATILLON (FRANCE).

Zirconia precipitates and zirconia: GeO2 interphase in mullite matrix-SiC woven fabrics composites prepared through a sol-gel route
| PB95-133427 | p 1275 N95-21272

OFFICE NATIONAL D'ETUDES ET DE RECHERCHES AEROSPATIALES, PARIS (FRANCE).

Chemical lasers emitting in the visible spectrum: Metastable oxygen reactions and YOSHIDA laser
| PB95-104485 | p 1372 N95-20983

Simulation of separated flows p 1347 N95-21068

Direct simulation and graphics post-processing of three-dimensional turbulent flows p 1352 N95-21098

OFFICE OF NAVAL RESEARCH, ARLINGTON, VA.

Coaxial hybrid wiggler
| AD-D016501 | p 1331 N95-21671

Broadband pressure barrier for circular waveguide
| AD-D016503 | p 1306 N95-21672

Fiber-optic rotary joint with bundle collimator assemblies
| AD-D016504 | p 1545 N95-21673

Programmable modular network interface
| AD-D016505 | p 1477 N95-21674

Siloxanes with strong hydrogen bond donating functionalities
| AD-D016499 | p 1279 N95-22057

OHIO STATE UNIV., COLUMBUS, OH.

Plasma chemistry of vibrationally nonequilibrium molecules
| AD-A279630 | p 1553 N95-20411

Improved die castings through plasma surface modification, improved sensors and die soldering prevention
| DE95-002238 | p 1253 N95-20417

Effects of plasma hydrogenation on trapping properties of dislocations in heteroepitaxial InP/GaAs
p 1323 N95-20542

OHIO UNIV., ATHENS, OH.

The in situ observation of epitaxial diamond thin film nucleation and growth using emission electron microscopy
| AD-A279811 | p 1569 N95-20807

OKLAHOMA UNIV., NORMAN, OK.

Site Scientific Mission Plan for the Southern Great Plains CART site, July - December 1994
| DE94-017289 | p 1401 N95-20193

OLD DOMINION UNIV., HAMPTON, VA.

Role of pressure diffusion in non-homogeneous shear flows p 1345 N95-21053

OLD DOMINION UNIV., NORFOLK, VA.

Convergence acceleration of the Proteus computer code with multigrid methods
| NASA-CR-197677 | p 1467 N95-21450

OPTICAL COATING LAB., INC., SANTA ROSA, CA.

Qualification test results for blue-red reflecting solar covers p 1320 N95-20525

OPTIMIZATION TECHNOLOGY, INC., HUNTSVILLE, AL.

Environment for Test and Analysis of Distributed Software (ETADS)
| AD-A285776 | p 1463 N95-20877

OREGON INST. OF TECH., KLAMATH FALLS, OR.

Geothermal direct-heat utilization assistance
| DE94-011546 | p 1391 N95-20104

OREGON STATE UNIV., CORVALLIS, OR.

Brushless Doubly-Fed Machine system development program, phase 3
| DE94-013095 | p 1315 N95-20380

OREGON UNIV., EUGENE, OR.

S-D hybridization and anisotropy of the optical second harmonic at low frequencies
| AD-A279449 | p 1544 N95-20876

Surface second harmonic studies of Si(111)/electrolyte and Si(111)/SiO2/electrolyte interfaces
| AD-A279450 | p 1245 N95-21826

Studies of the n alkane/water interface by total internal reflection second harmonic generation
| AD-A279473 | p 1245 N95-21827

Application of optical second harmonic generation to surface analysis
| AD-A279445 | p 1547 N95-22074

ORGANISATIE VOOR TOEGEPAST NATUURWETENSCHAPPELIJK ONDERZOEK, SOESTERBERG (NETHERLANDS).

A comparison of decision making behaviour in a static and a dynamic task environment as a function of time pressure
| AD-A285389 | p 1449 N95-20609

ORGANISATIE VOOR TOEGEPAST NATUURWETENSCHAPPELIJK ONDERZOEK, THE HAGUE (NETHERLANDS).

A theoretical study on the performance of the FDTD code on a massively parallel computer
[AD-A285346] p 1475 N95-20499

Diffraction computation by means of the method of equivalent currents
[AD-A285347] p 1291 N95-20692

OSAKA UNIV., TOYONAKA (JAPAN).

Transportation of volatile elements in thermally evolving planetesimals: An important role of metallic iron
p 1418 N95-21790

OSLO UNIV. (NORWAY).

DIFFPACK: Software for partial differential equations
[PB95-110268] p 1468 N95-21654

Object-oriented design of preconditioned iterative methods
[PB95-110276] p 1469 N95-21655

OXFORD UNIV., OXFORD (ENGLAND).

N=1 Superconformal minimal model correlation functions on the torus
[PB95-134615] p 1500 N95-21964

P

PACIFIC NORTHWEST LAB., RICHLAND, WA.

Intrinsic barriers for H-atom transfer reactions
[DE94-018914] p 1507 N95-20049

Post-irradiation deformation characteristics of heavy-ion irradiated 304L SS
[DE94-017462] p 1251 N95-20088

Dust Bowl migration as an analog for possible global warming-induced migration from Mexico
[DE94-017472] p 1401 N95-20089

Development of superplasticity in 5083 aluminum with additions of Mn and Zr
[DE94-017474] p 1251 N95-20090

SYNTH: A spectrum synthesizer
[DE94-015943] p 1458 N95-20153

Ferrocyanide safety project Dynamic X-Ray Diffraction studies of sodium nickel ferrocyanide reactions with equimolar nitrate/nitrite salts
[DE94-017396] p 1236 N95-20268

An evaluation of 915-MHz radar wind profiler/RASS by tower and sodar measurements
[DE94-018913] p 1364 N95-20320

Hydrostatic force sensor
[DE94-018923] p 1364 N95-20321

Chemical Structure and Dynamics program
[DE95-001117] p 1403 N95-20834

Airborne Multisensor Pod System (AMPS) data access concept
[DE95-002586] p 1389 N95-20903

Calculation of atom-centered partial charges for heme
[DE94-014447] p 1520 N95-21375

Possible global environmental impacts of solid waste practices
[DE95-000830] p 1406 N95-21487

A proposed wind measurement and analysis approach for evaluating a prospective wind plant site
[DE94-019187] p 1395 N95-21611

High temperature corrosion and crack growth of SiC/SiC at variable oxygen partial pressures
[DE94-018715] p 1232 N95-22115

PARIS-SUD UNIV., ORSAY (FRANCE).

Problems of coding in multipath channels
p 1294 N95-20930

Temporal and spatial comportment of multiple paths in ionospheric propagation in oblique incidence: Fractal measures of perturbations p 1298 N95-20954

PARIS VI UNIV. (FRANCE).

Rare gases systematics and mantle structure
p 1416 N95-21778

PARIS VII UNIV. (FRANCE).

Rare gases systematics and mantle structure
p 1416 N95-21778

PAUL SCHERRER INST., VILLIGEN (SWITZERLAND).

GAJET experiment at the LHC: The GAJET collaboration
[PB95-129813] p 1512 N95-20454

PDA ENGINEERING, COSTA MESA, CA.

Response of the B-1B air data sensor to simulated dust cloud environments
[AD-A286134] p 1213 N95-22036

PENNSYLVANIA STATE UNIV., STATE COLLEGE, PA.

Multiple hard interactions in HERWIG
[PB95-130548] p 1518 N95-21233

PENNSYLVANIA STATE UNIV., UNIVERSITY PARK, PA.

Materials for adaptive structural acoustic control, volume 2
[AD-A279222] p 1502 N95-19883

Enhancement of corrosion resistance and mechanical properties of light-weight metals through the use of graded nonequilibrium microstructures
[AD-A286320] p 1251 N95-20178

Synthesis and characterization of poly(organophosphazene) interpenetrating polymer networks
[AD-A279872] p 1265 N95-20183

Thermo-mechanical fatigue of polymer matrix composites
[AD-A285931] p 1267 N95-20390

The vertical distribution of heating in the tropical atmosphere
[AD-A285934] p 1429 N95-20391

Boundary layer cloud studies in support of ASTEX
[AD-A285947] p 1429 N95-20395

A low temperature, ultrahigh vacuum, microwave-frequency-compatible scanning tunneling microscope
[AD-A279869] p 1365 N95-20413

Radiation-induced modifications of allylamino-substituted polyphosphazenes
[AD-A279694] p 1268 N95-20428

Scanning tunneling microscopy studies of self-assembled monolayers of alkanethiols on gold
[AD-A279910] p 1253 N95-20577

Water-soluble polyphosphazenes and their hydrogels
[AD-A279695] p 1269 N95-20580

Inorganic-organic polymers and their role in materials science
[AD-A279715] p 1270 N95-20671

Cross-linking reactions for the conversion of polyphosphazenes into useful materials
[AD-A279696] p 1271 N95-20709

Linear and nonlinear spectroscopy with the tunable AC scanning tunneling microscope
[AD-A285751] p 1241 N95-21217

Small cavity nonresonant tunable microwave-frequency alternating current scanning tunneling microscope
[AD-A285752] p 1328 N95-21218

Cluster reactions: An approach to understanding the fundamentals of heterogeneous catalysis
[DE95-002947] p 1243 N95-21447

An integrated cloud observation and modeling investigation in support of the ARM Program
[DE95-002798] p 1430 N95-21527

The mechanical behavior of surface-modified ceramics
[DE95-001704] p 1276 N95-21572

Domain processes in ferroelectric ceramics
[AD-A279567] p 1276 N95-21697

Materials for adaptive structural acoustic controls
[AD-A279255] p 1505 N95-21863

SAR-related stress variability in the Marine Atmospheric Boundary Layer (MABL)
[AD-A286462] p 1431 N95-22393

PENNSYLVANIA UNIV., PHILADELPHIA, PA.

Novel electrochemical materials prepared by sol-gel chemistry
[AD-A286310] p 1226 N95-20092

Quantum simulation of heterogeneous electron transfer free energies at the water-metal interface
[AD-A279279] p 1522 N95-21492

PHILLIPS LAB., HANSCOM AFB, MA.

Location and characteristics of the reconnection X-line deduced from low-altitude satellite and radar observations
[NASA-TM-110114] p 1413 N95-20453

Multipath impact on ground-based global positioning system range measurements: Aspects of measurement, modeling, and mitigation p 1297 N95-20949

The effects of multihop HF propagation on the performance of OTH backscatter radars
p 1298 N95-20953

Proceedings of the Cloud Impacts on DOD Operations and Systems 1993 Conference (CIDOS 1993)
[AD-A286658] p 1430 N95-20974

An experimental determination of meteor daily arrival rate variation
[AD-A279484] p 1600 N95-21679

A high resolution atlas of the galactic plane at 12 microns and 25 microns p 1593 N95-21755

PHILLIPS LAB., KIRTLAND AFB, NM.

The 37th Military Librarians Workshop on Global Information: The Sun Never Sets
[AD-A286636] p 1588 N95-20774

Development of an annular electron beam HPM amplifier
[AD-A286646] p 1327 N95-20905

PHYSICAL OPTICS CORP., TORRANCE, CA.

Resonant tunneling quantum well integrated optical waveguide modulator/switch
[AD-A285142] p 1542 N95-20501

Polymer based all-optic reconfigurable interconnects
[AD-A279976] p 1272 N95-20962

PHYSICS AND ELECTRONICS LAB. TNO, THE HAGUE (NETHERLANDS).

Modelling of microwave propagation and clutter in a maritime environment p 1295 N95-20938

PHYTRON INSTRUMENTS, INC., MOUNTAIN VIEW, CA.

A charge distribution analysis instrument for catalysis and material science applications
[DE94-016489] p 1364 N95-20233

PITTSBURGH UNIV., PITTSBURGH, PA.

The synthesis and characterization of small molecule and photo-cross-linkable high polymeric phosphazenes bearing cinnamate groups
[AD-A279782] p 1268 N95-20442

Macromolecular and materials design using polyphosphazenes
[AD-A279781] p 1273 N95-20978

Artificial neural network metamodels of stochastic computer simulations
[AD-A285951] p 1484 N95-22056

Novel materials and devices from self-assembled periodic structures
[AD-A286499] p 1232 N95-22211

POTSDAM UNIV., POTSDAM (GERMANY).

Modeling the effect of water on mantle rheology
p 1417 N95-21783

Mantle devolatilization and rheology in the framework of planetary evolution p 1418 N95-21788

PRATT AND WHITNEY AIRCRAFT, WEST PALM BEACH, FL.

Effects of turbulence compressibility and unsteadiness in compression corner flow p 1344 N95-21052

Development of an advanced JP-8 fuel
[AD-A285583] p 1283 N95-21161

PRINCETON UNIV., NJ.

Simulation of pipe flow p 1349 N95-21078

Thermochemistry of dense hydrous magnesium silicates p 1416 N95-21782

Seismic evidence for volatiles at large depth in the Earth p 1422 N95-21808

PRINS MAURITS LAB. TNO, RIJSWIJK (NETHERLANDS).

Integral rocket ramjets
[AD-A285135] p 1222 N95-20906

PTT RESEARCH, LEIDSCHENDAM (NETHERLANDS).

Angle diversity on digital microwave links: Antenna design and experimental results p 1297 N95-20947

PURDUE UNIV., WEST LAFAYETTE, IN.

Rainfall rates and the vertical distribution of diabatic heating components over tropical oceans
[NASA-CR-197603] p 1428 N95-19948

Wake measurements in a strong adverse pressure gradient
[NASA-CR-197272] p 1201 N95-21031

Development of quiet-flow supersonic wind tunnels for laminar-turbulent transition research
[NASA-CR-197286] p 1216 N95-21436

Subduction and volatile recycling in Earth's mantle
p 1421 N95-21802

High temperature polymer for second order nonlinear optics for photonic materials
[AD-A279309] p 1280 N95-22141

R

RAND CORP., SANTA MONICA, CA.

Conference proceedings. Defense Modeling and Simulation Office Information/Data Base (I/DB) Task Group Meetings, and notes from the previous two I/DB meetings
[AD-A279097] p 1591 N95-22069

RANGE COMMANDERS COUNCIL, WHITE SANDS MISSILE RANGE, NM.

Noncoherent transponder standards
[AD-A279512] p 1306 N95-21684

Glossary of frequency and timing terms and a pictorial representation of terms used in the behavior and analyses of frequency standards
[AD-A286172] p 1310 N95-22247

REMOTE SENSING SYSTEMS, INC., SANTA ROSA, CA.

Deriving earth science products from SSM/I
[NASA-CR-197299] p 1389 N95-20156

RENNES UNIV. (FRANCE).

Study of the fast and slow variations of the power received at VHF links by tropospheric diffusion
p 1293 N95-20929

Identification of the propagation modes and paths on HF links using a goniopolarimeter p 1299 N95-20956

RENSSELAER POLYTECHNIC INST., TROY, NY.

Synthesis and studies of organometallic precursors for CVD of thin film electronic materials
[AD-A285834] p 1223 N95-20033

The reliability of laser reflowed Sn-Ag solder joints
[AD-A279787] p 1315 N95-20443

An augmented Young-Laplace model of an evaporating meniscus in a micro-channel with high heat flux
[NASA-CR-197622] p 1340 N95-20796
Deconvolution and singular value decomposition
[AD-A286582] p 1491 N95-20875
Chemical interactions between protein molecules and polymer membrane materials
[DE95-001808] p 1224 N95-21746

RESEARCH INST. FOR ADVANCED COMPUTER SCIENCE, MOFFETT FIELD, CA.
Activities of the Research Institute for Advanced Computer Science
[NASA-CR-197291] p 1478 N95-22108

RESEARCH TRIANGLE INST., RESEARCH TRIANGLE PARK, NC.
High-efficiency, deep-junction, epitaxial InP solar cells on (100) and (111)B InP substrates
p 1316 N95-20507

RICHLAND OPERATIONS OFFICE (AEC), WA.
Ozone-depleting-substance control and phase-out plan
[DE95-001647] p 1409 N95-21722

RIJKSINSTITUUT VOOR DE VOLKSGEZONDHEID, BILTHOVEN (NETHERLANDS).
Monomer mapping: A PC-based software tool facilitating the determination of monomer compositions from mass spectrometric molecular weight data
[PB95-132155] p 1275 N95-21470
Selection of substances to be considered in the environmental balance/environmental outlook in relation to the dissemination theme
[PB95-132197] p 1407 N95-21635
Derivation of maximum permissible concentrations for several volatile compounds for water and soil
[PB95-107454] p 1411 N95-22381

RIJKSINSTITUUT VOOR VOLKSGEZONDHEID EN MILIEUHYGIEENE, BILTHOVEN (NETHERLANDS).
Evaluation of the technical performance of the Duttch National Air Quality Monitoring Network in 1992
[PB95-131892] p 1405 N95-21327
Ozone quality control measurements in the Dutch National Air Quality Monitoring Network
[PB95-131900] p 1405 N95-21329
Disinfection of purified waste water with ultra violet light on a technical scale
[PB95-131926] p 1405 N95-21330
Monitoring activities in the framework of the Dutch National Air Quality Monitoring Network in 1994
[PB95-131884] p 1406 N95-21351
Air pollution caused by fireworks during the turn of the year 1992-1993
[PB95-135265] p 1409 N95-21718
Definition report on target and related steering variables of radiation as a part of the environmental balance and environmental outlook investigation
[PB95-135471] p 1409 N95-21846
Effects of increased UV-B radiation on phytoplankton: A preliminary study and research programme
[PB95-133732] p 1439 N95-21884
Initial assessment of the hazards and risks of new chemicals to man and the environment, part 2
[PB95-106407] p 1410 N95-22124
Derivation of preliminary maximum permissible concentrations of volatile compounds in air
[PB95-107447] p 1410 N95-22125
Assessment of the atmospheric hazards and risks of new chemicals: Procedures to estimate hazard potentials
[PB95-107488] p 1410 N95-22186
Use of quantum chemically derived descriptors for QSAR modeling of reductive dehalogenation of aromatic compounds
[PB95-132783] p 1224 N95-22333

RIJKSINSTITUUT VOOR ZUIVERING AFVALWATER, LELYSTAD (NETHERLANDS).
Definition report on environmental indices in future environmental assessments environmental balance/environmental outlook
[PB95-131876] p 1405 N95-21350

RIJKSWATERSTAAT, RIJSWIJK (NETHERLANDS).
Long term changes on the continental shelf of the North Sea: Invertebrate trends, 1931-1990
[PB95-135224] p 1435 N95-21717

RIO GRANDE DO SUL UNIV., PORTO ALEGRE (BRAZIL).
Quasi-linear equation for magnetoplasma oscillations in the weakly relativistic approximation
[DE94-628932] p 1560 N95-21593

ROCHESTER UNIV., NY.
Ultrafast optical studies of surface reaction processes at semiconductor interfaces
[DE95-001548] p 1574 N95-21839

ROCKWELL INTERNATIONAL CORP., CANOGA PARK, CA.
Power systems for future missions. Appendices A-L
[NASA-CR-195320-APP-A-L] p 1395 N95-21530
Power systems for future missions
[NASA-CR-195320] p 1222 N95-21531
Novel fluorine oxidizers
[AD-A279480] p 1284 N95-21678
Mars power system concept definition study. Volume 1: Study results
[NASA-CR-195420-VOL-1] p 1396 N95-21952
Mars power system concept definition study. Volume 2: Appendices
[NASA-CR-195420-VOL-2] p 1396 N95-21953

ROCKWELL INTERNATIONAL SCIENCE CENTER, THOUSAND OAKS, CA.
Light-scattering fluctuations and noise in nonlinear optical processing
[AD-A279748] p 1544 N95-20803

ROCKWELL SPACE OPERATIONS CO., HOUSTON, TX.
The navigation toolkit
[NASA-CR-197290] p 1205 N95-22161

ROHDE AND SCHWARTZ, MUNICH (GERMANY).
Modular CNI avionics system p 1213 N95-20659

ROME LAB., GRIFFISS AFB, NY.
Preliminary evaluation of a digital optical systolic processor implemented with acousto-optic cells
[AD-A286377] p 1541 N95-20231
GaAs optical circuits
[AD-A285859] p 1369 N95-20389
Improving Multichip Module (MCM) design and reliability using the Intelligent MCM Analyzer
p 1209 N95-20637
Reliability assessment of Multichip Module technologies via the Triservice/NASA RELTECH program
p 1210 N95-20643
Assuring Known Good Die (KGD) for reliable, cost effective MCMs p 1210 N95-20644
Heterostructure quantum confined Stark effect electrooptic modulators operating at 938 nm
[AD-A279342] p 1581 N95-21928
Polycrystalline PLZT/ITO ceramic electro-optic phase gratings: Electro-optically reconfigurable difffractive devices for free-space and in-wafer interconnects
[AD-A285861] p 1547 N95-22076
Fabrication of PLZT/ITO grating for optical switching and reconfigurable optical interconnect applications
[AD-A286389] p 1548 N95-22248

ROME LAB., HANSCOM AFB, MA.
Comparative study of C- and K-band propagation mechanisms beyond the horizon p 1297 N95-20946

ROME UNIV. (ITALY).
N=1 Superconformal minimal model correlation functions on the torus
[PB95-134615] p 1500 N95-21964

ROTHE DEVELOPMENT, INC., SAN ANTONIO, TX.
The influence of coronary artery disease on +Gz tolerance: A preliminary study
[AD-A279305] p 1446 N95-21941

ROYAL NORWEGIAN COUNCIL FOR SCIENTIFIC AND INDUSTRIAL RESEARCH, OSLO (NORWAY).
AC magnetic response of YBa2CuO7 with Y2BaCuO5 inclusions and of single-crystal YBa2Cu3O7: A comparative study
[PB94-207917] p 1577 N95-22166

RUHR UNIV., BOCHUM (GERMANY).
Large-eddy simulation of separated flow in a ribbed duct p 1347 N95-21070

RUTGERS - THE STATE UNIV., NEW BRUNSWICK, NJ.
A numerical investigation of energy transfer and subgrid-scale eddy viscosity in homogeneous, isotropic and shear turbulence
[AD-A280005] p 1339 N95-20058
Mathematical theory of neural networks
[AD-A286508] p 1485 N95-22213

RUTHERFORD APPLETON LAB., CHILTON (ENGLAND).
PRSPLOT6 manual
[PB95-110862] p 1456 N95-19928
Muon data analysis program RUMDA
[PB95-129839] p 1511 N95-20434
RALPAR-RAL mesh partitioning program version 1.1
[PB95-129847] p 1475 N95-20435
Location and characteristics of the reconnection X-line deduced from low-altitude satellite and radar observations
[NASA-TM-110114] p 1413 N95-20453
GAJET experiment at the LHC: The GAJET collaboration
[PB95-129813] p 1512 N95-20454
Combined effects of atmosphere and terrain on UHF/microwave paths p 1295 N95-20935
Factorization in closed string field theory
[PB95-133542] p 1580 N95-21030
Proceedings of the School for Young High Energy Physicists
[PB95-108114] p 1537 N95-21647
Report of the Numerical Analysis Group
[PB95-108163] p 1494 N95-21648
Radio-frequency techniques at the ISIS pulsed muon source
[PB95-129854] p 1529 N95-22303
Iterated-subspace minimization methods for nonlinear optimization
[PB95-108171] p 1495 N95-22317

RUTHERFORD APPLETON LAB., OXFORD (ENGLAND).
Anomalous vector-boson couplings in Majorana neutrino models
[PB95-127460] p 1518 N95-21220
Antishadowing contribution to the pomeron structure function
[PB95-127478] p 1518 N95-21221
Where are we going with Bose-Einstein: A mini review
[PB95-130308] p 1518 N95-21222
T1F ((1) sigma (+)): Some preliminary electronic structure calculations
[PB95-130316] p 1518 N95-21223
Muon beamline at ISIS
[PB95-130324] p 1518 N95-21224
Spin dependence of diffractive processes and implications for the small x behaviour of g1 and the spin content of the nucleon
[PB95-130332] p 1518 N95-21225
Large facilities pilot programme. Access to the VULCAN High Power Laser Facilities at Rutherford Appleton Laboratory
[PB95-130340] p 1373 N95-21226
Neutron molelcular spectroscopy: Future prospects
[PB95-130357] p 1518 N95-21227
New theory of critical flow velocities in superfluid helium
[PB95-130365] p 1571 N95-21228
Constraints on SUSy-GUT unification from b yields s-gamma decay
[PB95-130373] p 1580 N95-21229
Calculation of Z plus four jet production at the Tevatron
[PB95-130472] p 1580 N95-21230
PRSCAL manual
[PB95-130480] p 1465 N95-21231
PRISMA operating program manual
[PB95-130498] p 1466 N95-21232
Multiple hard interactions in HERWIG
[PB95-130548] p 1518 N95-21233
N=1 Superconformal minimal model correlation functions on the torus
[PB95-134615] p 1500 N95-21964
MARI mini-manual
[PB95-134649] p 1526 N95-21965
Theory of spin dynamics in the classical two-dimensional heisenberg magnet
[PB95-133559] p 1502 N95-22138
Neutron Compton scattering
[PB95-130290] p 1530 N95-22332
Vertex detectors at linear colliders: Present and future
[PB95-134656] p 1540 N95-22364
Large-scale fields and flows in the magnetosphere-ionosphere system
[PB95-134664] p 1427 N95-22368

S

SAN JOSE STATE UNIV., CA.
The use of fuzzy set classification for pattern recognition of the polygraph
[AD-A279148] p 1470 N95-21971

SANDIA LABS., ALBUQUERQUE, NM.
Low electron beam energy CIVA analysis of passivated ICs
[DE94-017421] p 1314 N95-20286

SANDIA NATIONAL LABS., ALBUQUERQUE, NM.
A test of the Arrhenius extrapolation assumption for a nitrile rubber
[DE94-017337] p 1263 N95-19926
Optimization of InAsSb/InGaAs strained-layer superlattice growth by metal-organic chemical vapor deposition for use in infrared emitters
[DE94-016557] p 1563 N95-19954
Charged particle dynamics in the acceleration gap of the PBFA 2 ion diode
[DE94-017347] p 1506 N95-20026
Sol-gel-derived silica films with tailored microstructures for applications requiring organic dyes
[DE94-018886] p 1264 N95-20047
Application of a dimensionless parameter model for Laser Beam Welding
[DE94-018902] p 1378 N95-20048
Fusion welding of advanced borated stainless steels
[DE94-019037] p 1378 N95-20053
Particle beam fusion
[DE95-000711] p 1549 N95-20075

A computational study of projectile shape dependence on phase change phenomena with comparisons to experimental data
[DE95-000740] p 1384 N95-20077

Generation of micro-domains in AT-cut quartz by thermal processing and the effect on resonator modes
[DE94-017344] p 1564 N95-20087

The electronic properties of polysilanes
[DE94-006464] p 1265 N95-20121

Split-C and active messages under SUNMOS on the Intel Paragon
[DE94-011418] p 1474 N95-20123

Hindered settling computations using a parallel boundary element method
[DE94-014286] p 1339 N95-20137

Reactions and microstructure at ceramic/metal interfaces
[DE94-014287] p 1265 N95-20138

FTIR spectroscopy for the determination of water in corrosive gases
[DE94-014658] p 1235 N95-20139

A domain decomposition scheme for Eulerian shock physics codes
[DE94-015739] p 1488 N95-20141

The Modified Embedded Atom Method
[DE94-015746] p 1564 N95-20142

ALT-2 armor tile design for upgraded TEXTOR operation
[DE94-015749] p 1549 N95-20143

Experimental hypervelocity impact effects on simulated planetesimal materials
[DE94-017290] p 1599 N95-20144

Performance issues for engineering analysis on MIMD parallel computers
[DE94-015769] p 1474 N95-20150

Parallel solid mechanics codes at Sandia National Laboratories
[DE94-015770] p 1474 N95-20152

SAR image registration in absolute coordinates using GPS carrier phase position and velocity information
[DE94-018738] p 1204 N95-20195

Design trade-off study for a large volume short pulse neutron assembly
[DE94-019175] p 1509 N95-20206

Uncertainty estimates for derivatives and intercepts
[DE94-018492] p 1489 N95-20222

Chunk projectile launch using the Sandia Hypervelocity Launcher Facility
[DE94-018494] p 1215 N95-20223

The effect of reusing laser gas on the fission-fragment pumped 1.73 micron atomic xenon laser output
[DE94-018512] p 1369 N95-20225

Trimode Power Converter optimizes PV, diesel and battery energy sources
[DE94-015014] p 1313 N95-20262

Analyses of grounded and ungrounded photovoltaic power systems
[DE94-015015] p 1391 N95-20263

The GPS Burst Detector W-Sensor
[DE94-017406] p 1204 N95-20269

Adaptive path planning for flexible manufacturing
[DE94-016561] p 1459 N95-20284

Simulation of large systems with neural networks
[DE94-018898] p 1428 N95-20319

Proton irradiation effects on advanced digital and microwave III-V components
[DE94-018742] p 1314 N95-20338

Impedance characteristics of multistage ion diodes
[DE94-018887] p 1565 N95-20340

Observation of excitonic and band-to-band behavior in ordered InGaP2 alloys
[DE94-018891] p 1314 N95-20341

A new mini Ball Grid Array (mBGA) multichip module technology
[DE94-018897] p 1480 N95-20342

The role of high pressure in the study and applications of the ferroelectric polymer polyvinylidene fluoride and its copolymers
[DE94-015742] p 1268 N95-20396

Development of solid state moisture sensors for semiconductor fabrication applications
[DE94-015771] p 1364 N95-20398

Mean field analysis of orientation selective grain growth driven by interface-energy anisotropy
[DE94-015797] p 1566 N95-20399

Characteristics of oxynitrides grown in N2O
[DE94-015798] p 1566 N95-20400

Spectroscopic studies of glass structure
[DE94-016551] p 1268 N95-20468

A wideband EMP test system
[DE94-015283] p 1290 N95-20474

New ET-based organic superconductors with the organometallic anion Cu(CF3)4(-)
[DE94-016904] p 1567 N95-20479

Digital filtering for data compression in telemetry systems
[DE94-016611] p 1219 N95-20567

Progress in the development of recycling processes for electric vehicle batteries
[DE94-015894] p 1324 N95-20626

Development of a tester for evaluation of prototype thermal cells and batteries
[DE95-000540] p 1325 N95-20628

Input shaping for vibration-damped slewing of a flexible beam using a heavy-lift hydraulic robot
[DE94-015803] p 1379 N95-20695

Computational design of Hypervelocity Launchers
[DE95-000744] p 1218 N95-20785

The numerical integration and 3-D finite element formulation of a viscoelastic model of glass
[DE95-002588] p 1271 N95-20788

Conservative smoothing versus artificial viscosity
[DE95-001108] p 1341 N95-20831

Detection optimization using linear systems analysis of a coded aperture laser sensor system
[DE95-001112] p 1371 N95-20832

Geometric moire method of strain analysis with displacement discontinuities
[DE95-001114] p 1386 N95-20833

Recent reflux receiver developments under the US DOE program
[DE95-001622] p 1393 N95-20861

An overview: Component development for solar thermal systems
[DE95-001623] p 1393 N95-20862

Highlights of recent balance of system research and evaluation
[DE95-001626] p 1393 N95-20863

Testing of the SAIC facets on the stretched-membrane dish
[DE95-001831] p 1393 N95-20864

Reactor pumped laser research at the Sandia National Laboratories pulsed reactor facilities
[DE95-002181] p 1371 N95-20867

Si concentrator solar cell development
[DE95-002314] p 1393 N95-20870

Development of concentrator solar cells
[DE95-002316] p 1394 N95-20871

Complementary GaAs junction-gated heterostructure field effect transistor fabrication for integrated circuits
[DE95-001522] p 1327 N95-20882

Technologies for highly parallel optoelectronic integrated circuits
[DE95-001607] p 1327 N95-20883

Advanced robotic technologies for transfer at Sandia National Laboratories
[DE95-001617] p 1481 N95-20884

COYOTE II: A finite element computer program for nonlinear heat conduction problems. Part 1: Theoretical background
[DE95-002587] p 1463 N95-20887

Characterization and electrical properties of copper films grown via direct liquid coinjection of (hfac)Cu(TMVS) and TMVS
[DE95-002957] p 1272 N95-20889

SPICE macro model of a spryton with MOSFET's in the avalanche mode
[DE94-015744] p 1555 N95-21134

Fiber-optic control of current filaments in high gain photoconductive semiconductor switches
[DE94-015804] p 1328 N95-21139

DAVE: A plug and play model for distributed multimedia application development
[DE94-016481] p 1465 N95-21153

Shot-to-shot comparison of the first Li-beam driven Hohlraum experiments
[DE94-016558] p 1558 N95-21247

An object-oriented implementation of the Xpress transfor protocol
[DE95-001506] p 1301 N95-21277

Real-time dynamic simulator for the Topaz II reactor power system
[DE95-001604] p 1535 N95-21278

Effect of neutron irradiation on the impact properties of A533B steel
[DE95-001834] p 1256 N95-21286

Defect production and recombination during low-energy ion processing
[DE95-001827] p 1572 N95-21304

Synthetic aperture radar processing with polar formatted subapertures
[DE95-001830] p 1302 N95-21305

Characterization of poly(tetrafluoroethylene) surfaces by atomic force microscopy: Results and artifacts
[DE95-000742] p 1242 N95-21309

LIF standoff research
[DE94-018744] p 1535 N95-21328

Recent National Solar Thermal Test Facility activities, in partnership with industry
[DE95-001828] p 1394 N95-21353

Complementary GaAs junction-gated heterostructure field effect transistor technology
[DE94-018901] p 1329 N95-21390

Applications for reactor-pumped lasers
[DE95-000536] p 1373 N95-21393

Spectroscopic, morphological, and electrical characterization of PdGe ohmic contacts to n-GaAs
[DE95-000738] p 1329 N95-21394

Development status of an intense beam klystron
[DE95-000745] p 1329 N95-21395

A Hypervelocity Experimental Research Database (HERD): Support for the Wright Laboratory Armament Directorate Code Validation Program (COVAL)
[DE95-001628] p 1387 N95-21396

A versatile masking process for plasma etched backside via holes in GaAs
[DE94-019176] p 1572 N95-21419

Lidar technologies for airborne and space-based applications
[DE95-002954] p 1302 N95-21448

Analysis of experimentally shocked minerals by NMR spectroscopy
[DE95-002955] p 1573 N95-21449

Micromachined silicon-based analytical microinstruments for space science and planetary exploration
[DE94-019306] p 1367 N95-21507

Unlimited-bandwidth distributed optical phase modulators and detectors: Design and fabrication issues
[DE94-017418] p 1545 N95-21509

Assessment of a non-dedicated GPS receiver system for precise airborne attitude determination
[DE94-019309] p 1205 N95-21520

Correlations for the OH A(sup 2)(Sigma)(sup +)(v(prime)=0) electronic quenching cross-section
[DE95-002591] p 1244 N95-21524

Gate oxide shorts in nMOS transistors: Electrical properties and lifetime prediction method
[DE94-018904] p 1330 N95-21545

Quartz resonator fluid monitors for vehicle applications
[DE94-018910] p 1367 N95-21546

Laser materials processing at Sandia National Laboratories
[DE95-002183] p 1374 N95-21594

Progress in the Light Ion Driven Inertial Confinement Fusion Program
[DE94-019182] p 1537 N95-21603

Atomic processes in processing plasmas
[DE94-019177] p 1560 N95-21609

Top ten list of user-hostile interface design
[DE95-001602] p 1453 N95-21721

High frequency current sensors using the Faraday effect in optical fibers
[DE95-001859] p 1545 N95-21728

A user's guide to LUGSAN 1.1: A computer program to calculate and archive lug and sway brace loads for aircraft-carried stores
[DE95-001919] p 1207 N95-21730

Plasma-induced-damage of GaAs during etching of refractory metal contacts
[DE95-001525] p 1259 N95-21838

Issues in the flight qualification of a space power reactor
[DE95-001606] p 1223 N95-21840

A massively parallel algorithm for grand canonical Monte Carlo computer simulation with the short-ranged Lennard-Jones potential
[DE94-010396] p 1477 N95-21843

Integration of thin film decoupling capacitors
[DE95-001609] p 1333 N95-21881

Reciprocal space mapping of epitaxial materials using position-sensitive x-ray detection
[DE95-001620] p 1575 N95-21991

Effects of cyclic stress distribution models on fatigue life predictions
[DE95-001619] p 1388 N95-22070

SEU and SEL response of the Westinghouse 64K E-2PROM, analog devices AD7876 12-bit ADC, and the Intel 82527 Serial Communications Controller
[DE95-003349] p 1334 N95-22086

Defect classes: An overdue paradigm for CMOS IC testing
[DE94-018905] p 1334 N95-22118

Lower active metals loading for hydrotreating catalysts
[DE94-018907] p 1261 N95-22119

A graded approach to ISO 9000 implementation for records managers
[DE94-017409] p 1591 N95-22167

Evaluation of scanners for C-scan imaging for nondestructive inspection of aircraft
[AD-A286398] p 1383 N95-22202

Application of IRIS to semiconductor plasma processing
[DE95-003591] p 1562 N95-22225

Acid-site characterization of water-oxidized alumina films by near-edge x-ray absorption and soft x-ray photoemission
[DE95-003355] p 1247 N95-22234
Manufacturing Technology Bulletin, July 1994
[DE94-017775] p 1605 N95-22262
The Modified Embedded Atom Method
[DE94-017958] p 1248 N95-22273
Very high-power electron-beam transport in long gas cells from 10(exp -3) to 10(exp 3) Torr N2
[DE95-002611] p 1539 N95-22306
A new parallel method for molecular dynamics simulation of macromolecular systems
[DE94-018621] p 1529 N95-22315
Bridging worlds/charting new courses
[DE95-003808] p 1397 N95-22335
TDX: A high-bandwidth crossbar-switched communication paradigm
[DE94-017187] p 1311 N95-22407
Simulation of structural response using a recurrent radial basis function network
[DE94-017342] p 1486 N95-22409
Sandia National Laboratories analysis code data base
[DE95-004188] p 1502 N95-22420
Fuzzy clustering of facial form for prototyping environmental protection equipment
[DE94-014657] p 1454 N95-22466

SANDIA NATIONAL LABS., LIVERMORE, CA.
Characterization of an expanded-field Schwarzschild objective for extreme ultraviolet lithography
[DE94-016780] p 1541 N95-20239
Effects of ambient conditions on the adhesion of cubic boron nitride films on silicon substrates
[DE94-016779] p 1266 N95-20281
Daytime Raman lidar profiling of atmospheric water vapor
[DE94-015747] p 1413 N95-20397
First principles simulation of materials properties
[DE94-016781] p 1566 N95-20405
Enhancements in the Livermore spectrum analysis package PIXEF
[DE95-002487] p 1272 N95-20895
Direct numerical simulations of turbulent non-premixed methane-air flames modeled with reduced kinetics
p 1249 N95-21038
Passive turbulent flamelet propagation
p 1249 N95-21043
A simulation study of TCP performance in ATM networks
[DE94-016622] p 1477 N95-21505
Temporal evolution of turbulence/chemistry interactions in lifted, turbulent-jet flames
[DE95-002481] p 1243 N95-21512
Thermal decomposition reactions of HMX and RDX and their importance in predicting cookoff hazards
[DE95-002486] p 1283 N95-21513
The permeation of bis(2-fluoro-2,2-dinitroethyl) formal (FEFO), ethyl 4,4-dinitropentanoate (EDNP), ethyl 4-nitropentanoate (ENP), and 1,2,4-trichlorobenzene (TCB) through barrier membranes
[DE95-002492] p 1283 N95-21514
Cryogenic pellet laser plasma source targets
[DE95-002488] p 1376 N95-22169

SAO PAULO UNIV., SAO CARLOS (BRAZIL).
Introduction to the structures determination methods using X-ray diffraction in monocrystals: Application to some lanthanides and transition metals complexes with organic ligands
[DE94-629002] p 1579 N95-22380

SCIENCE APPLICATIONS INTERNATIONAL CORP., DAYTON, OH.
Systems engineering design and technical analyses for Strategic Avionics Crew-station Design Evaluation Facility (SACDEF)
[AD-A286239] p 1213 N95-22024

SCIENCE APPLICATIONS INTERNATIONAL CORP., MCLEAN, VA.
Acute radiation sickness amelioration analysis
[AD-A279084] p 1445 N95-21629

SCIENCE APPLICATIONS INTERNATIONAL CORP., SAN DIEGO, CA.
Transport and dynamics in toroidal fusion systems
[DE94-018653] p 1548 N95-20029

SCIENCE RESEARCH COUNCIL, DARESBURY (ENGLAND).
PRSPLOT6 manual
[PB95-110862] p 1456 N95-19928
GAJET experiment at the LHC: The GAJET collaboration
[PB95-129813] p 1512 N95-20454
Radio-frequency techniques at the ISIS pulsed muon source
[PB95-129854] p 1529 N95-22303

SCIENTIFIC COMPUTING ASSOCIATES, INC., NEW HAVEN, CT.
Design of a parallel object oriented programming language
[AD-A284924] p 1457 N95-20000

SCITRAN, INC., SANTA BARBARA, CA.
The problem of space travel: The rocket motor
[NASA-SP-4026] p 1217 N95-21894

SCRIPPS INSTITUTION OF OCEANOGRAPHY, LA JOLLA, CA.
Oceanographic analysis of the acoustic mid-ocean dynamics experiment
[AD-A285907] p 1432 N95-19988
Modeling the response of the California Current system to Global Greenhouse Warming
[DE94-018253] p 1408 N95-21708

SECA, INC., HUNTSVILLE, AL.
Radiation from advanced solid rocket motor plumes
[NASA-CR-196554] p 1221 N95-20124

SELSKAPET FOR INDUSTRIELL OG TEKNISK FORSKNING, OSLO (NORWAY).
Development and applications of flat ceramic membranes
[PB95-110219] p 1276 N95-21650
DIFFPACK: Software for partial differential equations
[PB95-110268] p 1468 N95-21654
Object-oriented design of preconditioned iterative methods
[PB95-110276] p 1469 N95-21655
Stability of pressure and velocity computations for heterogeneous reservoirs
[PB95-110284] p 1354 N95-21656
Design of a 10 bit 10k Samples/s low power CMOS ADC
[PB95-110425] p 1455 N95-22018

SELSKAPET FOR INDUSTRIELL OG TEKNISK FORSKNING, TRONDHEIM (NORWAY).
Simulation of the injection moulding process
[PB94-215555] p 1286 N95-21027
Technical and economic evaluation of natural gas based synthesis gas production technologies
[PB95-130597] p 1242 N95-21426
Overview of the field and temperature dependence of J(c) in Ag/BSCCO tapes
[PB95-110318] p 1574 N95-21636
Extrudate swell and extrudate distortion of HDPE as a result of different deformation mechanisms during extrusion through capillary dies
[PB95-110227] p 1288 N95-21651
Relationship between dendrite coherency and castability of some commercial foundry alloys
[PB95-110243] p 1258 N95-21652
Sheet metal formability
[PB95-110250] p 1258 N95-21653
Protective organic coatings on steel: Accelerated corrosion test method for paint/coatings exposed to water with low conductivity. Nordtest project no. 1010-92. Degradation of organic coatings in fresh water
[PB95-134185] p 1277 N95-21873
How to improve J(c(T)) in Ag/(BiPb)2Sr2Ca2Cu3O10 tapes
[PB95-110326] p 1575 N95-21949
Frame and edge seal technology: A state of the art survey
[PB95-110334] p 1288 N95-22014
Directives for the participation in MiTS forum. V3.0
[PB95-110342] p 1484 N95-22015
Standard data formats for simulation
[PB95-110367] p 1470 N95-22016
State of the art in CFD pre- and postprocessing
[PB95-110391] p 1356 N95-22017
AC magnetic response of YBa2CuO7 with Y2BaCuO5 inclusions and of single-crystal YBa2Cu3O7: A comparative study
[PB94-207917] p 1577 N95-22166

SEXTANT AVIONIQUE, VALENCE (FRANCE).
Lightweight electronic enclosures using composite materials p 1213 N95-20656

SFA, INC., LANDOVER, MD.
Radiation effects on p+n InP junctions grown by MOCVD p 1319 N95-20520

SHAPE TECHNICAL CENTER, THE HAGUE (NETHERLANDS).
Highly survivable communications: Complementary media packet switched networks p 1292 N95-20922
QoS driven routing in packet switched networks of multiple transmission media p 1292 N95-20923

SHIKOKU CHEMICAL RESEARCH INDUSTRIES, INC., IBARAGI (JAPAN).
Investigation on research for degradable plastics
[DE94-796550] p 1277 N95-21714

SIERRA RESEARCH, INC., SACRAMENTO, CA.
Analysis of invalid emission testing in the California smog check program
[PB95-128922] p 1406 N95-21373

SMITHSONIAN ASTROPHYSICAL OBSERVATORY, CAMBRIDGE, MA.
Coronagraphic observations and analyses of the ultraviolet solar corona
[NASA-CR-197370] p 1602 N95-20558

SOFTWARE PRODUCTIVITY CONSORTIUM, HERNDON, VA.
Using the CoRE requirements method with ADARTS. Version 01.00.05
[AD-A279151] p 1470 N95-21972

SORBENT TECHNOLOGIES CORP., TWINSBURG, OH.
Laboratory evaluation of a reactive baffle approach to NOx control
[AD-A283802] p 1400 N95-19921

SOUTH CAROLINA UNIV., COLUMBIA, SC.
Role of working memory limitations of retrieval
[AD-A280032] p 1448 N95-20007

SOUTHAMPTON UNIV. (ENGLAND).
Liquid xenon as a potential laser host medium
[AD-A285365] p 1370 N95-20550
Effect of lags on human performance with head-coupled simulators
[AD-A279577] p 1453 N95-21700

SOUTHERN CALIFORNIA GAS CO., LOS ANGELES, CA.
Economic feasibility analysis of distributed electric power generation based upon the natural gas-fired fuel cell
[DE94-012277] p 1396 N95-22033

SOUTHERN METHODIST UNIV., DALLAS, TX.
Source contributions at far-regional distances
[AD-A279405] p 1426 N95-21932

SOUTHWEST RESEARCH INST., SAN ANTONIO, TX.
Effect of propane-air on NGVs and vehicle fueling stations
[PB94-210085] p 1282 N95-20253
Eddy current for detecting second-layer cracks under installed fasteners
[AD-A279871] p 1382 N95-20414
Natural gas converter performance and durability
[PB95-135554] p 1284 N95-21966
Robotic paint stripping cell
[AD-A279158] p 1279 N95-21976

SPACE POWER, INC., SAN JOSE, CA.
SPACE-R thermionic space nuclear power system: Design and technology demonstration
[DE95-000713] p 1221 N95-20076

SPARTA, INC., LEXINGTON, MA.
BACKSCAT lidar simulation version 4.0: Technical documentation and users guide
[AD-A285851] p 1290 N95-20376

SPIRE CORP., BEDFORD, MA.
P/N InP solar cells on Ge wafers
p 1317 N95-20511

SRI INTERNATIONAL CORP., MENLO PARK, CA.
Novel catalysts for methane activation
[DE95-002639] p 1237 N95-20438
Field-emitter arrays for RF vacuum microelectronics
[AD-A279959] p 1325 N95-20661
IR materials producibility
[AD-A280094] p 1328 N95-21017
Natural gas combustion chemistry mechanisms research
[PB95-111670] p 1247 N95-22150
Adaptive fault-resistant systems
[AD-A286406] p 1484 N95-22203

STANFORD LINEAR ACCELERATOR CENTER, CA.
Complementarity of e(+)e(-) and pp colliders for the exploration of electroweak symmetry breaking
[DE94-017397] p 1507 N95-20034
High energy photon-photon collisions
[DE94-017494] p 1532 N95-20388
Resonant photon-graviton conversion in EM fields: From earth to heaven
[DE95-002784] p 1301 N95-21241
Cosmological string solutions by dimensional reduction
[DE95-002858] p 1599 N95-21245
Comparison of calculated with measured dynamic aperture
[DE95-002863] p 1534 N95-21246
Measuring A(sub b) with polarized beams at SLC
[DE95-002865] p 1519 N95-21248
Neural network construction via back-propagation
[DE95-002867] p 1482 N95-21249
Top ten models constrained by b (yields) s(gamma)
[DE95-002870] p 1519 N95-21250
Issues in multi-bunch emittance preservation in the NLC
[DE95-002894] p 1534 N95-21253
Signals for top quark anomalous chromomagnetic moments at colliders
[DE95-002896] p 1535 N95-21254
First results from the final focus test beam
[DE95-002897] p 1535 N95-21255
Emittance dilution by ions in the SLC arcs
[DE95-002871] p 1536 N95-21332
Simulation of beam-beam lifetime for LEP
[DE95-002888] p 1536 N95-21334

Luminosity polarization correlation in the SLC [DE95-002889] p 1536 N95-21335

Exclusive processes: Tests of coherent QCD phenomena and nucleon substructure at CEBAF [DE95-002892] p 1520 N95-21336

Pair production as a probe of colliding beam size [DE95-002893] p 1536 N95-21337

Polarization of charmonium in pion-nucleus collisions [DE95-002783] p 1523 N95-21525

A preliminary, precise measurement of the average B hadron lifetime [DE95-001848] p 1525 N95-21727

Measurement of the average lifetime of B hadrons at SLD [DE95-002121] p 1527 N95-22152

Proposed emittance upgrade for the SLC damping rings [DE95-002887] p 1538 N95-22155

Constraints on the left-right symmetric model from b yields s gamma [DE95-003469] p 1528 N95-22239

STANFORD UNIV., CA.

Free electron laser program [AD-A285906] p 1368 N95-19987

Computing methods for the approximate solution of time dependent problems [AD-A286007] p 1491 N95-20719

Scanning tunneling microscopy of semiconductor surfaces [AD-A279982] p 1571 N95-20964

Ultra-high aggregate bandwidth two-dimensional multiple-wavelength diode laser arrays [AD-A280098] p 1372 N95-21019

Studying Turbulence Using Numerical Simulation Databases. 5: Proceedings of the 1994 Summer Program [NASA-CR-197362] p 1341 N95-21035

Developments and applications of dynamic models for large eddy simulation of complex flows p 1346 N95-21062

The asymptotic state of rotating homogeneous turbulence at high Reynolds numbers p 1347 N95-21065

Entrainment in a shear-free turbulent mixing layer p 1350 N95-21083

Research studies on short wavelength lasers by selective Auger processes [AD-A285620] p 1372 N95-21144

The structure of turbulence and other motions beneath an air-water interface [AD-A279838] p 1434 N95-21293

A study of mechanical processing damage in brittle materials [DE95-002126] p 1276 N95-21585

Application of quaternary phase diagrams to compound semiconductor processing [DE95-001813] p 1277 N95-21748

On Markov Chain Monte Carlo acceleration [AD-A279393] p 1499 N95-21945

Bayesian analysis of semiparametric proportional hazards models [AD-A279394] p 1499 N95-21946

Advanced diagnostics for plasma chemistry [DE94-018936] p 1561 N95-22116

Annual research briefs, 1994 [NASA-CR-197352] p 1358 N95-22437

Conditional statistics in a turbulent premixed flame derived from direct numerical simulation p 1249 N95-22438

Lewis number and Damkohler number effects in vortex-flame interactions p 1249 N95-22439

Fundamental mechanisms in premixed flame propagation via vortex-flame interactions: Numerical simulations p 1249 N95-22440

Triple flames and flame stabilization p 1249 N95-22441

Flame propagation under partially-premixed conditions p 1250 N95-22442

Turbulence modeling for separated flow p 1359 N95-22443

Notes on rotating turbulence p 1359 N95-22444

A dynamic localization model with stochastic backscatter p 1359 N95-22445

Local dynamic subgrid-scale models in channel flow p 1360 N95-22447

Unstructured-grid large-eddy simulation of flow over an airfoil p 1202 N95-22448

Large-eddy simulation of flow through a plane, asymmetric diffuser p 1360 N95-22449

Large-eddy simulation of a boundary layer with concave streamwise curvature p 1360 N95-22450

Experimental investigations of on-demand vortex generators p 1361 N95-22451

Direct numerical simulations of on-demand vortex generators: Mathematical formulation p 1361 N95-22452

Drag reduction strategies p 1361 N95-22453

Acoustics of laminar boundary layers breakdown p 1361 N95-22455

Small-scale behavior in distorted turbulent boundary layers at low Reynolds number p 1362 N95-22456

Experimental and numerical study of the intermittency exponent mu p 1362 N95-22458

Forced free-shear layer measurements p 1362 N95-22460

Numerical study of boundary layer interaction with shocks: Method and code validation p 1362 N95-22461

Resolution requirements for velocity gradients in turbulence p 1363 N95-22462

A method for obtaining a statistically stationary turbulent free shear flow p 1363 N95-22463

Direct numerical simulation of incompressible axisymmetric flows p 1363 N95-22464

Databases post-processing in Tensoral p 1363 N95-22465

STATE UNIV. OF EAST TEXAS, COMMERCE, TX.

An investigation of the applicability of the new ion exchange resin, Reillex(TM)-HPQ, in ATW separations [DE94-016576] p 1274 N95-21234

STATE UNIV. OF NEW YORK, ALBANY, NY.

Completion of spectral rotating shadowband radiometers and analysis of ARM spectral short-wave data [DE95-000602] p 1412 N95-20116

Experiments at high energy hadron colliders and underground water Cerenkov detector experiment [DE95-001804] p 1535 N95-21281

STATE UNIV. OF NEW YORK, BINGHAMTON, NY.

Photochemistry of intermolecular C-H bond activation reactions [DE94-018417] p 1239 N95-20682

STATE UNIV. OF NEW YORK, BUFFALO, NY.

Design, synthesis and characterization of novel nonlinear optical materials [AD-A285617] p 1540 N95-19897

Analysis of the progressive failure of brittle matrix composites [NASA-CR-195415] p 1225 N95-19951

Superior catalysts for selective catalytic reduction of nitric oxide [DE94-018845] p 1234 N95-20046

Carbon fiber reinforced superconductor composites [DE95-002504] p 1229 N95-20913

X-ray studies of microstructures in semiconductor and superconducting materials [DE95-001802] p 1572 N95-21279

STATE UNIV. OF NEW YORK, CORTLAND, NY.

Methodology for ESCA analysis of electromigration [AD-A286229] p 1241 N95-21168

Geometric characterization of electromigration voids (A statistical analysis of electromigration voids) [AD-A286494] p 1328 N95-21169

STATE UNIV. OF NEW YORK, STONY BROOK, NY.

Signal- and listener- based factors in complex auditory pattern perception [AD-A285636] p 1450 N95-21101

The theory of relativistic heavy ion collisions [DE95-001805] p 1519 N95-21302

Subduction of hydrated basalt of the oceanic crust: Implications for recycling of water into the upper mantle and continental growth p 1423 N95-21814

STUTTGART UNIV. (GERMANY).

Spatial direct numerical simulation of boundary layer transition under strong adverse pressure gradient p 1351 N95-21093

Direct numerical simulation of 2-D and 3-D instability waves in a laminar separation bubble p 1352 N95-21095

SUPERCONDUCTING SUPER COLLIDER LAB., DALLAS, TX.

The 12-GeV/c beam transfer and absorber lines for the Superconducting Super Collider [DE95-002100] p 1538 N95-21733

SURFACE OPTICS CORP., SAN DIEGO, CA.

Non-destructive inspection by infrared imaging spectroscopy, phase 1 [AD-A286158] p 1383 N95-22037

SURVEILLANCE RESEARCH LAB., SALISBURY (AUSTRALIA).

Passive millimetre wave imaging: A review [AD-A279275] p 1303 N95-21491

SVERDRUP TECHNOLOGY, INC., BROOK PARK, OH.

Power systems for future missions. Appendices A-L [NASA-CR-195320-APP-A-L] p 1395 N95-21530

Power systems for future missions [NASA-CR-195320] p 1222 N95-21531

SWEDISH INST. FOR MATERIALS TESTING, BORAS (SWEDEN).

Accuracy problems in the generation of discrete time stochastic processes [PB95-131397] p 1386 N95-21133

Fire experiments in a two dimensional rack storage: BRANDFORSK-project 701-917 [PB95-131538] p 1241 N95-21179

Crack closure and sequential effects in fatigue: A literature survey [PB95-131637] p 1387 N95-21557

Accelerated life testing of solar energy materials: Case study of some selective solar absorber coating materials for DHW systems. A report of task 10 solar materials research and development [PB95-132411] p 1397 N95-22362

SYDNEY UNIV. (AUSTRALIA).

Inelastic bending and torsion of steel I-beams [PB94-208378] p 1384 N95-19975

Influence of primary boundary conditions on the buckling of shallow cylindrical shells [PB94-208352] p 1384 N95-20003

Inelastic torsion of steel I-beams [PB94-208360] p 1384 N95-20101

SYNAPSE SCIENCE CENTER/MOSCOW IRIS DATA ANALYSIS CENTER, MOSCOW (RUSSIA).

Computer programs for analysis of geophysical data [DE95-002472] p 1415 N95-21511

SYRACUSE UNIV., NY.

Fault tolerance of neural networks [AD-A285098] p 1479 N95-20057

Spectroscopic assessment of the reliability of metal/metal oxide interfaces [AD-A286131] p 1261 N95-22035

T

TATA INST. OF FUNDAMENTAL RESEARCH, BOMBAY (INDIA).

An assessment of image reconstruction from balloon-borne and the IRAS data p 1592 N95-21752

TECH FOUNDATION, INC., MONTGOMERY, WV.

EPSCoR supplemental grant for an application of neural networks to seismic signal discrimination [AD-A285846] p 1414 N95-20878

Application of neural networks to seismic signal discrimination research findings [AD-A285848] p 1415 N95-21308

TECHNICAL RESEARCH CENTRE OF FINLAND, ESPOO (FINLAND).

Physical Si(1-x)Ge(x)/Si heterojunction bipolar transistor model for device and circuit simulation [PB95-110896] p 1312 N95-19934

Force based motion control of a walking machine [PB95-129672] p 1451 N95-20276

Analysis of musculo-skeletal loading using electromyography and biomechanical modelling [PB95-135828] p 1444 N95-21007

13th European Annual Conference on Human Decision Making and Manual Control [PB95-132874] p 1450 N95-21284

Determination of layer moduli from falling weight deflectometer measurements [PB95-129748] p 1286 N95-21333

Safety issues in high speed machining [PB95-127411] p 1287 N95-21422

Joining dissimilar stainless steels for pressure vessel components [PB95-133005] p 1380 N95-21446

VTT test borehole for bedrock investigations [PB95-132965] p 1427 N95-22095

Fibre-reinforced high-strength concrete [PB95-131942] p 1232 N95-22158

Surface technology programme [PB95-132866] p 1262 N95-22174

TECHNICAL UNIV. OF LISBON (PORTUGAL).

Large eddy simulation of turbulent flow over a cavity p 1347 N95-21069

TECHNISCHE HOCHSCHULE, AACHEN (GERMANY).

Prediction of rotor-blade deformations due to unsteady airloads [AD-A286593] p 1207 N95-20860

TECHNISCHE HOGESCHOOL, DELFT (NETHERLANDS).

Invariant measures of interval maps [PB95-107835] p 1389 N95-20207

Process strategies in the enzymatic resolution of enantiomers [PB95-107850] p 1437 N95-20208

Integration of segmentation and stereo matching [PB95-107819] p 1444 N95-21028

Disinfection of purified waste water with ultra violet light on a technical scale [PB95-131926] p 1405 N95-21330

Instabilities in natural-convection flows in cavities [PB95-107975] p 1354 N95-21578

Subsampling methods for image sequence coding [PB95-107991] p 1305 N95-21579

Intramyocardial blood volume and oxygen exchange [PB95-108015] p 1445 N95-21580

Sensor based fine motion control
[PB95-108007] p 1483 N95-21669
Strain fields in crystalline materials: Methods of analysis based on x-ray diffraction-line broadening
[PB95-108064] p 1574 N95-21670

TECHNISCHE HOGESCHOOL, EINDHOVEN (NETHERLANDS).
Positive rockland operators
[PB95-127510] p 1493 N95-21423
Proof of a conjecture of Narayana on dominance refinements of the Smirnov two-sample test
[PB95-132650] p 1499 N95-21979
Precedence tests and confidence bounds for complete data: An overview and some results
[PB95-132668] p 1499 N95-21980

TECHNISCHE HOGESCHOOL, TWENTE (NETHERLANDS).
Comparison of DNS and LES of transitional and turbulent compressible flow: Flat plate and mixing layer
p 1347 N95-21066

TECHNISCHE HOGESCHOOL TWENTE, ENSCHEDE (NETHERLANDS).
On subcritical instability of the attachment line boundary layer p 1351 N95-21092

TECHNISCHE UNIV., DELFT (NETHERLANDS).
Micromechanical approach to transformation toughening in ceramics
[PB95-135422] p 1273 N95-20976
Use of operations research techniques in deductive databases
[PB95-135349] p 1589 N95-21004
Set functionals in stochastic geometry
[PB95-135372] p 1491 N95-21005
Geomaterial models and numerical analysis of softening
[PB95-135380] p 1386 N95-21006
Radiofrequency hyperthermia systems: Experimental and clinical assessment of the feasibility of radiofrequency hyperthermia systems for loco-regional deep heating
[PB94-206885] p 1444 N95-21016
Study on the reaction kinetics in pulsed RF discharges under RIE conditions
[PB95-107868] p 1300 N95-21029
Human force exertion in user-product interaction. Backgrounds for design
[PB95-132858] p 1452 N95-21283
Exponential deconvolution: Two asymptotically equivalent estimators
[PB95-132122] p 1499 N95-21469
Non-linear A/D converters for integrated silicon smart sensors
[PB94-208402] p 1330 N95-21590
Surface micromachined capacitive tactile image sensor
[PB95-108031] p 1288 N95-21633
Vortex atoms and vortons
[PB95-134599] p 1356 N95-21963
Absorbing boundary condition for floating two-dimensional objects in current and waves
[PB95-132882] p 1356 N95-22063
Fluid dynamics of the freeboard in a fluidized bed reactor
[PB95-134029] p 1357 N95-22160
Hydrothermal conversion of carbohydrates and related compounds
[PB95-134011] p 1396 N95-22175
Image and video coding using a wavelet decomposition
[PB95-135067] p 1311 N95-22358
Maximum weighted matching for high index differential algebraic equations
[PB95-135075] p 1496 N95-22359
Self-similar solutions of a fast diffusion equation that do not conserve mass
[PB95-134920] p 1497 N95-22375
Multi signal-domain modeling of solid-state transducers: A theoretical framework based on irreversible thermodynamics mixed finite elements and multigrid
[PB95-134995] p 1336 N95-22382

TECHNISCHE UNIV., EINDHOVEN (NETHERLANDS).
K(1,3)-free and W(4)-free graphs
[PB95-110573] p 1456 N95-19889
Algebraic semantics of message sequence charts
[PB95-110581] p 1288 N95-19890
Introduction to the FIRE engine: A C++ toolkit for Finite automata and Regular Expressions
[PB95-110599] p 1456 N95-19891
Non interleaving process algebra
[PB95-110607] p 1486 N95-19892
General conservative extension theorem in process algebra
[PB95-110656] p 1487 N95-19902
Ups and downs of type theory
[PB95-110664] p 1487 N95-19903
New method for integrity constraint checking in deductive databases
[PB95-110672] p 1586 N95-19904
Dominoes
[PB95-110680] p 1456 N95-19905
Testing paradigm applied to network structure (revised)
[PB95-110706] p 1487 N95-19906
Process algebra with partial choice
[PB95-110714] p 1487 N95-19907
Hierarchical diagrammatic representation of class structure
[PB95-110722] p 1456 N95-19908
Application of Markov decision processes to search problems
[PB95-110813] p 1497 N95-19914
Multigrid with matrix-dependent transfer operators for convection-diffusion problems
[PB95-110821] p 1487 N95-19915
Solutions of D(sup n)D(sup m)f=0
[PB95-110839] p 1487 N95-19916
Weighted strongly elliptic operators on lie groups
[PB95-110847] p 1487 N95-19917
Abstract reduction and topology
[PB95-110615] p 1488 N95-20054
Real time process algebra with infinitesimals
[PB95-110623] p 1488 N95-20055
ILIAS: A sequential language for parallel matrix computations
[PB95-110631] p 1473 N95-20056
Beyond beta-reduction in Church's lambda yield
[PB95-110565] p 1488 N95-20149
Comparison of Ward and Mellor's transformation schema with State- and Activitycharts
[PB95-110698] p 1459 N95-20258
Stars or stripes: A comparative study of finite and transfinite techniques for surface modelling
[PB95-134979] p 1464 N95-20975
GOLD: A Graph Oriented Language for Databases
[PB95-127544] p 1465 N95-21021
Correctness of some algorithms to generate finite automata for regular expressions
[PB95-127551] p 1465 N95-21022
Finding all minimal separators of a graph
[PB95-127585] p 1491 N95-21023
Multi-dimensional Petri nets
[PB95-127593] p 1491 N95-21024
Compositional proof theory for fault tolerant real-time distributed systems
[PB95-127601] p 1465 N95-21025
Transient behaviour and stability points of the Poiseuille flow of a KBKZ-fluid
[PB95-132064] p 1353 N95-21268
Computing near-optimal schedules
[PB95-132072] p 1466 N95-21269
Duality and equivalencies in closed tandem queueing networks
[PB95-132502] p 1482 N95-21271
Numerical wave speed for one-dimensional scalar hyperbolic conservation laws with source terms
[PB95-127536] p 1492 N95-21371
Semantics for a fine lambda-calculus with de Bruijn indices
[PB95-127577] p 1492 N95-21372
Design principles for real-time process control systems
[PB95-132890] p 1585 N95-21414
Design and implementation of the FIRE engine: A c++ toolkit for finite automata and regular expressions
[PB95-132924] p 1467 N95-21415
Approximation algorithms for the general and the asymmetric stacker-crane problems
[PB95-132098] p 1493 N95-21468
One-dimensional reactive Euler equations
[PB95-135430] p 1244 N95-21573
Analysis of a local defect correction approach on composite grids
[PB95-135455] p 1493 N95-21574
Semi-global stabilization of linear discrete-time systems subject to input saturation via linear feedback: An ARE-based approach
[PB95-135463] p 1483 N95-21618
Regularity of BPa-systems is decidable
[PB95-135489] p 1468 N95-21619
CAiSE 1994 Doctoral Consortium
[PB95-135182] p 1469 N95-21711
Proceedings of the 5th Workshop on the Next Generation of CASE Tools
[PB95-135208] p 1469 N95-21716
Foundations of functional programming: A programmer's point of view
[PB95-132932] p 1471 N95-22094
Discrete algebraic Riccati equation and linear matrix inequality
[PB95-133575] p 1484 N95-22139
Hamiltonian structure of the reversible nonsemisimple 1:1 resonance
[PB95-127528] p 1495 N95-22151
Logic programming and negation: A survey
[PB95-110730] p 1472 N95-22302
Abstract interpretation of reactive systems: Abstractions preserving Universal CTL(*), Existential CTL(*) and CTL(*)
[PB95-110557] p 1472 N95-22305
Vertex ranking for permutation and other graphs
[PB95-127569] p 1496 N95-22327
Time and the order of abstract events in distributed computations
[PB95-110482] p 1496 N95-22349
Formal specification and compositional verification of an atomic broadcast protocol
[PB95-110508] p 1472 N95-22351
FORTRAN subroutine for column reduction of polynomial matrices
[PB95-134987] p 1497 N95-22379

TECHNISCHE UNIV., MUNICH (GERMANY).
Direct numerical simulation of turbulent flow in a sudden pipe expansion p 1347 N95-21067

TECHNISCHE UNIV., TWENTE (NETHERLANDS).
Monadic maps and folds for arbitrary datatypes
[PB95-134045] p 1492 N95-21032
Expressions that talk about themselves
[PB95-134060] p 1466 N95-21344
Generalised approach to software structure metrics
[PB95-107561] p 1467 N95-21411
Elements of deliberative robot control
[PB95-107595] p 1482 N95-21412
Design model for open distributed processing systems
[PB95-135505] p 1477 N95-21620
Application-oriented architecture for multimedia teleservices
[PB95-135513] p 1306 N95-21623
Dyads: A generalisation of monads
[PB95-134052] p 1494 N95-21867
Adjunctions
[PB95-134078] p 1494 N95-21868
Performance analysis and true concurrency semantics
[PB95-134086] p 1478 N95-21869
High-capacity optical multichannel virtual mesh interconnection networks
[PB95-134094] p 1546 N95-21870
Compositional approach to sequential consistency and lazy caching
[PB95-134110] p 1455 N95-21871
Modelling multimedia teleservices with OSI upper layers framework: Short paper
[PB95-132734] p 1308 N95-22080
Structuring design requirements using YMIR
[PB95-132742] p 1471 N95-22081
Verification of a timestamp-based sliding-window protocol
[PB95-132759] p 1455 N95-22082
Modelling the reassembly buffer in a connectionless server
[PB95-132908] p 1308 N95-22087
Tom Thumb algorithm for planning simple vehicle motions
[PB95-107553] p 1484 N95-22156
SCOPE 1.5: A Source-Code Optimization PackagEfor REDUCE 3.5: User's manual
[PB95-107579] p 1472 N95-22159

TEMPLE UNIV., PHILADELPHIA, PA.
Nuclear research with the electromagnetic probe
[DE95-001812] p 1525 N95-21747

TENNESSEE TECHNOLOGICAL UNIV., COOKEVILLE, TN.
Competing structures in nuclei near closed shells
[DE94-017604] p 1512 N95-20491

TENNESSEE UNIV., KNOXVILLE, TN.
Theoretical and experimental study of mixed solvent electrolytes
[DE94-017605] p 1237 N95-20384
A Monte Carlo study of the minus sign problem in the t-J model using an Intel iPSC/860 hypercube
[DE95-001072] p 1570 N95-20819

TENNESSEE UNIV. SPACE INST., TULLAHOMA, TN.
Supersonic laminar flow control research
[NASA-CR-196049] p 1353 N95-21340

TENNESSEE VALLEY AUTHORITY, MUSCLE SHOALS, AL.
Corrosion resistance and behavior of construction materials exposed to dilute sulfuric acid at elevated temperatures under static conditions
[DE95-001723] p 1259 N95-21739
Corrosion resistance and behavioral characteristics of metals exposed to 70 percent by weight sulfuric acid at elevated temperatures
[DE95-001724] p 1259 N95-21740
An update of corrosion inhibitors for mild steel exposed to 32-0-0 UAN solution
[DE95-001715] p 1263 N95-22396

TENNESSEE VALLEY AUTHORITY, NORRIS, TN.
Degradation of aromatic hydrocarbons in an aquifer during a field experiment demonstrating the feasibility of remediation by natural attenuation
[AD-A283809] p 1282 N95-19922

TEST DEVICES, INC., HUDSON, MA.
Portable static test facility for small, expendable, turbojet engines, phase 1
[AD-A286337] p 1216 N95-21719

TEXAS A&M UNIV., COLLEGE STATION, TX.
Correlations between surface structure and catalytic activity/selectivity
[DE94-019023] p 1234 N95-20052
Stabilization and control problems in structural dynamics
[AD-A279996] p 1340 N95-20312
Fault-tolerance in distributed and multiprocessor real-time systems
[AD-A279896] p 1461 N95-20595
Bacterial luciferase: Determination of the structure by x-ray diffraction
[AD-A279699] p 1437 N95-20711
Hardware implementation of a desktop supercomputer for high performance image processing. Color image processing using cellular neural networks
[AD-A286455] p 1455 N95-21589

TEXAS INSTRUMENTS, INC., DALLAS, TX.
Ultra-Reliable Digital Avionics (URDA) processor
p 1209 . N95-20638

TEXAS UNIV., ARLINGTON, TX.
Effect of cell size on elliptically polarized radar clutter statistics
[AD-A285789] p 1311 N95-22401

TEXAS UNIV., AUSTIN, TX.
Reactive compatibilization of polymer blends
[AD-A284836] p 1263 N95-19893
The Combustive Sound Source
[ARL-TR-94-9] p 1503 N95-19911
System level fault tolerance in parallel and distributed computing systems
[AD-A279664] p 1474 N95-20305
Hybrid model in general geometry
[DE95-002614] p 1553 N95-20437
A portable and independent edge fluctuation diagnostic
[DE94-018254] p 1554 N95-20681
On the sputtering of metals and insulators: A nonlinear evolution problem with nonlinear boundary condition
[DE95-001456] p 1254 N95-20792
Multiple scatter theory of ocean sediments
[AD-A286033] p 1433 N95-20999
Self-starting femtosecond pulse generation from a Ti:sapphire laser synchronously pumped by a pointing-stabilized mode-locked Nd:YAG laser
[DE94-019319] p 1374 N95-21480
Pushing the limits of spatial resolution with the Kuiper Airborne observatory p 1593 N95-21754
Measurements of the Auburn ECE optical system parameters for temperature fluctuation measurements on TEXT-U
[DE94-019217] p 1562 N95-22120
1/f noise in two-dimensional fluids
[DE95-002617] p 1358 N95-22307

TEXAS UNIV., SAN ANTONIO, TX.
Monoclonal antibodies directed against surface molecules of multicell spheroids
[NASA-CR-197367] p 1437 N95-20559

TEXAS UNIV. HEALTH SCIENCE CENTER, SAN ANTONIO, TX.
In vivo distribution of liposome encapsulated hemoglobin studied with imaging radiotracers
[AD-A279774] p 1438 N95-20806
Investigation of laser-induced retinal damage: Wavelength and pulsewidth dependent mechanisms
[AD-A286066] p 1443 N95-20848

THOMSON-CSF, GENNEVILLIERS (FRANCE).
Measurements of angles of elevation of HF by a high resolution method using polarization diversity
p 1299 N95-20959

THOMSON-CSF, PARIS (FRANCE).
FASTPACK: Optimized solutions for modular avionics derived from a parametric study. Part 2: Avionics
p 1209 N95-20635
Composite cases for airborne electronic equipment: A technology study and EMC p 1212 N95-20655
Modular supplies for a distributed architecture
p 1213 N95-20657

THOMSON-CSF, VELIZY (FRANCE).
Methods for evaluating the effects of conduits at the surface of the sea p 1294 N95-20932

TILBURG UNIV. (NETHERLANDS).
Qualification of the dependence in the generalized extreme value choice model
[PB95-110946] p 1497 N95-19936
Orthogonal representations over finite fields and the chromatic number of graphs
[PB95-110953] p 1487 N95-19937
Frequent sampling in discrete choice
[PB95-110961] p 1497 N95-19938
Patterns of financial change in the OECD area
[PB95-110979] p 1594 N95-19939
Quadratic forms in design theory
[PB95-111019] p 1487 N95-19940
Asymptotic analysis of Nash equilibria in nonzero-sum linear-quadratic differential games. The two-player case
[PB95-111027] p 1499 N95-19941
Uniqueness of strongly regular graphs having minimal p-rank
[PB95-111043] p 1488 N95-19942
Graphs cospectral with distance-regular graphs
[PB95-111050] p 1488 N95-19943
Note on the characterizations of the compromise value
[PB95-135117] p 1499 N95-21709
Thousand golden ten orbits
[PB95-135109] p 1592 N95-22334

TOKYO UNIV. (JAPAN).
Impact degassing of water and noble gases from silicates p 1416 N95-21780
Loss of solar He and Ne from IDPS in subducting sediment: Diffusion and the effect of phase changes
p 1419 N95-21792
Solubilities of nitrogen and noble gases in basalt melt
p 1422 N95-21807
Degassing history and evolution of volcanic activity of terrestrial planets based on radiogenic noble gas degassing models p 1424 N95-21816
Degassing mechanisms of noble gases from carbonado diamonds p 1425 N95-21824

TOKYO UNIV., TANASHI (JAPAN).
Accelerators for energy production
[DE94-770764] p 1392 N95-20685
Quantization in curvilinear coordinates
[DE94-770603] p 1514 N95-20737
Universal parametrization for quark and lepton substructure
[DE94-770604] p 1514 N95-20738
Search for right-handed currents in the decay chain of K(+) yields muon(+)nu(sub muon), muon(+) yields e(+)nu(sub e)nu(bar)(sub muon)
[DE94-770606] p 1514 N95-20756
Construction of non-critical string field theory by transfer matrix formalism in dynamical triangulation
[DE94-770607] p 1516 N95-20986
The 9th INS scientific computational programs
[DE94-770780] p 1526 N95-22051

TOLEDO UNIV., OH.
Measurements of scattering processes in negative ion: Atom collisions
[DE95-000664] p 1519 N95-21276
Thin-film cadmium telluride photovoltaic cells
[DE94-011886] p 1395 N95-21508
The variation of the dust temperature within late-type spiral galaxies p 1593 N95-21766
Wave journal bearing. Part 1: Analysis
[NASA-CR-195431-PT-1] p 1382 N95-22404

TRANSPORTATION RESEARCH BOARD, WASHINGTON, DC.
Public-sector aviation issues: Graduate research award papers, 1992-1993
[PB94-217478] p 1199 N95-19967

TRI-UNIV. MESON FACILITY, VANCOUVER (BRITISH COLUMBIA).
Time of flight spectroscopy with muonic hydrogen
[DE94-017056] p 1245 N95-21845

TRW SPACE TECHNOLOGY LABS., REDONDO BEACH, CA.
Amorphous silicon thin films: The ultimate lightweight space solar cell p 1318 N95-20515
Two-micron Laser Atmospheric Wind Sounder (LAWS) pointing/tracking study
[NASA-CR-195012] p 1220 N95-21190

TULANE UNIV., NEW ORLEANS, LA.
A method to determine the kinematics of the lower limbs of a subject pedaling a bicycle using encoders and accelerometers
[NASA-CR-197401] p 1453 N95-21866

U

UNITED TECHNOLOGIES RESEARCH CENTER, EAST HARTFORD, CT.
The environmental durability of fiber reinforced ceramic matrix composites
[AD-A283750] p 1225 N95-19919

UNIVERSIDAD AUTONOMA DEL ESTADO DE MEXICO, TOLUCA (MEXICO).
Determinations of phase transitions in nylon 6-12, nylon-6, polyvinyl chloride and polyethylene terephthalate by positron annihilation spectroscopy
[DE94-629992] p 1239 N95-20736

UNIVERSIDAD POLITECNICA DE MADRID (SPAIN).
Direct numerical determination of the minimum bypass Reynolds number in boundary layers
p 1349 N95-21080

UNIVERSITE CATHOLIQUE DE LOUVAIN (BELGIUM).
Simulation of the impact of atmospheric turbulences on millimeter-wave communications systems
p 1295 N95-20939

UNIVERSITIES SPACE RESEARCH ASSOCIATION, COLUMBIA, MD.
Annual program analysis of the NASA Space Life Sciences Research and Education Support Program
[NASA-CR-197298] p 1439 N95-21529

UNIVERSITY COLL. OF SWANSEA (WALES).
Proceedings of the School for Young High Energy Physicists
[PB95-108114] p 1537 N95-21647

UNIVERSITY OF SOUTHERN CALIFORNIA, LOS ANGELES, CA.
Combustion-related studies using weakly bonded complexes
[DE95-002801] p 1238 N95-20576
Applied physics research for innovation in pulsed power
[AD-A285392] p 1324 N95-20610
Competition between electromagnetic modes in a free-electron maser
[AD-A279546] p 1374 N95-21694

UNIVERSITY OF SOUTHERN CALIFORNIA, MARINA DEL REY, CA.
Model formality in human/computer collaboration
[AD-A286001] p 1462 N95-20718
Generating examples for use in tutorial explanations: The use of a subsumption based classifier
[AD-A286028] p 1464 N95-20996
An automatic placement tool for rapid prototyping of printed circuit boards
[AD-A286029] p 1328 N95-20997
Knowledge refinement in a reflective architecture
[AD-A286027] p 1589 N95-21002

UNIVERSITY OF SOUTHERN ILLINOIS, CARBONDALE, IL.
Proceedings of the 4th International Conference on Electrorheological Fluids
[AD-A286341] p 1266 N95-20227

UNIVERSITY OF SOUTHERN MISSISSIPPI, BAY SAINT LOUIS, MS.
NOMADS graphical user interface version 2.0 user's manual
[AD-A286314] p 1458 N95-20095
Modeling open boundary conditions by using the optimization approach
[AD-A285548] p 1433 N95-21158

UNIVERSITY OF SOUTHERN MISSISSIPPI, HATTIESBURG, MS.
Thianthrene containing polyimides with monomer formation via nucleophilic aromatic substitution
[AD-A286313] p 1265 N95-20094
Responsive copolymers for enhanced petroleum recovery
[DE94-018822] p 1267 N95-20350
Towards tailored interphase formation utilizing surface-bound benzylsulfonium salts as cationic initiators
[AD-A286461] p 1280 N95-22259
Solid-state NMR characterization of C- and N-labelled phthalimides: Model compounds for studying polyimides
[AD-A286479] p 1578 N95-22286

UNIVERSITY OF WEST BOHEMIA, PLZEN (CZECHOSLOVAKIA).
Direct simulation of tridimensional wake of NACA 0012 profile p 1350 N95-21086

UPPSALA UNIV. (SWEDEN).
Novel electrochemical materials prepared by sol-gel chemistry
[AD-A286310] p 1226 N95-20092

UTAH STATE UNIV., LOGAN, UT.
Analysis of mesospheric winds and waves
[AD-A279956] p 1414 N95-20591

UTAH UNIV., SALT LAKE CITY, UT.
Time-resolved analytical methods for liquid/solid interfaces
[DE95-002255] p 1240 N95-20780
Ion-molecule chemistry related to plasma deposition and etching of silicon
[AD-A279749] p 1514 N95-20804

V

VALENCIA UNIV. (SPAIN).
Factorization in closed string field theory
[PB95-133542] p 1580 N95-21030

VEDA, INC., DAYTON, OH.
Crew-Centered Cockpit Design (CCCD) field demonstration program, volume 1
[AD-A286426] p 1453 N95-21566

VIBRATION INST., WILLOWBROOK, IL.
Advanced Materials and Process Technology for Mechanical Failure Prevention (proceedings of the 48th Meeting of the Mechanical Failures Prevention Group
[AD-A285785] p 1233 N95-22399

VON KARMAN INST. FOR FLUID DYNAMICS, RHODE-SAINT-GENESE (BELGIUM).
Subgrid scale models in finite difference simulations of complex wall bounded flows p 1346 N95-21063
Numerical simulation of spatially-developing planar jets p 1351 N95-21087

VRIJE UNIV., AMSTERDAM (NETHERLANDS).
Formal model for the dynamics of compositional reasoning systems
[PB95-132056] p 1482 N95-21267
Heuristic genetic algorithms for constrained problems. Part 1: Principles
[PB95-132031] p 1467 N95-21374
Graded dual of the non-commutative universal Leibniz Hopf algebra zeta
[PB95-134532] p 1494 N95-21955
Linear invariance of Lindeloef numbers
[PB95-134540] p 1494 N95-21956
Minimax optimal stop rule in reliability checking
[PB95-134557] p 1383 N95-21961
Duality beyond sober spaces: Topological spaces and observation frames
[PB95-134565] p 1494 N95-21962
Generic architecture for knowledge-based control of processes in dynamic environments
[PB95-132676] p 1483 N95-21981
Intelligent interactive project management system
[PB95-132684] p 1586 N95-21982
Verification of knowledge-based reasoning modules
[PB95-132692] p 1470 N95-21983
Initial experience with noncorrecting syntax error handling
[PB95-132700] p 1471 N95-22029
Top-down non-correcting error recovery in LLgen
[PB95-132718] p 1471 N95-22031
Minimal square spectral factors
[PB95-132726] p 1495 N95-22032
University library document circulation system specified in LCM
[PB95-127957] p 1592 N95-22331

W

WASEDA UNIV., TOKYO (JAPAN).
Proceedings: International Symposium on Global Change (IGBP)
[DE94-765351] p 1410 N95-22219

WASHINGTON UNIV., SAINT LOUIS, MO.
Alkali element depletion by core formation and vaporization on the early Earth p 1421 N95-21804

WASHINGTON UNIV., SEATTLE, WA.
Neutrino magnetic moments and the solar neutrino problem
[DE94-017579] p 1602 N95-20147
Neutrino-neutrino scattering and matter-enhanced neutrino flavor transformation in supernovae
[DE94-017577] p 1604 N95-20383
Diffusion enhances spontaneous electroweak baryogenesis
[DE94-017574] p 1512 N95-20451
Has a standard model solution to the solar neutrino problem been found?
[DE94-017580] p 1604 N95-20490
Universal features of multiplicity distributions
[DE94-012854] p 1498 N95-20779
The impact of partnering on construction contracts
[AD-A286588] p 1585 N95-20855
Nonperturbative aspects of the quark-photon vertex
[DE94-012846] p 1520 N95-21315
The solar neutrino problem: Neither astrophysics nor oscillations?
[DE94-012850] p 1603 N95-21316
Resolving velocity profiles with the multi-scale profiler
[AD-A286446] p 1434 N95-21461
Constraints on T-odd and P-even hadronic interactions from nucleon, nuclear, and atomic electric dipole moments
[DE94-012845] p 1526 N95-21920
Acoustic Thermometry of Ocean Climate (ATOC): Selection of California source site
[AD-A279295] p 1436 N95-21987
Testing the principle of equivalence by solar neutrinos
[DE94-014972] p 1604 N95-22064
The solar flux of thermal neutrinos and antineutrinos of all flavors
[DE95-003204] p 1604 N95-22085

WAYNE STATE UNIV., DETROIT, MI.
Investigation of the stability and 1.0 MeV proton radiation resistance of commercially produced hydrogenated amorphous silicon alloy solar cells p 1320 N95-20522

WESTERN RESEARCH INST., LARAMIE, WY.
Natural gas cleanup: Evaluation of a molecular sieve carbon as a pressure swing adsorbent for the separation of methane/nitrogen mixtures
[DE94-012263] p 1234 N95-20135

WESTINGHOUSE ELECTRIC CORP., BALTIMORE, MD.
High density monolithic packaging technology for digital/microwave avionics p 1211 N95-20646

WESTINGHOUSE HANFORD CO., RICHLAND, WA.
In situ viscometer instrument acceptance test report
[DE94-018507] p 1364 N95-20224
Quantitative and qualitative analysis of some inorganic compounds by Raman spectroscopy
[DE94-009757] p 1237 N95-20470
Radioactive check sources for alpha and beta sensitive radiological instrumentation
[DE94-016477] p 1366 N95-21138
Corrosion evaluation of fuel canister crusher rigging
[DE95-002962] p 1257 N95-21452
Conceptual design analyses for Hanford Site deployable remote spectroscopy systems
[DE95-002078] p 1243 N95-21473

WESTINGHOUSE SAVANNAH RIVER CO., AIKEN, SC.
Thermodynamic characterization of new palladium alloy tritides
[DE94-018430] p 1579 N95-20028
Fracture toughness properties of welded stainless steels for tritium service
[DE95-000755] p 1251 N95-20079
Safe conditions for contacting nitric acid or nitrates with Tri-n-Butyl Phosphate (TBP)
[DE95-001243] p 1235 N95-20215
Tritium and decay helium effects on the fracture toughness properties of types 316L, 304L and 21Cr-6Ni-9Mn stainless steels
[DE95-001248] p 1252 N95-20216
The effect of regional-scale soil-moisture deficits on mesoscale atmospheric dynamics that influence fire severity
[DE95-002682] p 1413 N95-20455
Analysis of welds on helium-containing restraint test plates
[DE95-001809] p 1257 N95-21303
Using geographical data browsers in a networked environment
[DE94-017809] p 1592 N95-22263
Welding tritium exposed stainless steel
[DE95-003208] p 1382 N95-22356

WESTINGHOUSE SCIENCE AND TECHNOLOGY CENTER, PITTSBURGH, PA.
Processing, fabrication, and demonstration of HTS integrated microwave circuits
[AD-A285611] p 1312 N95-19894
High temperature superconducting films and multilayers for electronics
[AD-A279545] p 1331 N95-21693
Vibrational overtone spectroscopy of pyridine and related compounds
[AD-A280105] p 1224 N95-21911

WICKERSHEIMER ENGINEERS, INC., CHAMPAIGN, IL.
Computer-Aided Structural Engineering (CASE) project. User's guide: Computer-Aided Structural Modeling (CASM). Version 5.00
[AD-A279913] p 1459 N95-20310

WINAND STARING CENTRE, WAGENINGEN (NETHERLANDS).
Use of the carbo-flo process to purify process water contaminated by agricultural pesticides
[PB95-127825] p 1410 N95-22330

WISCONSIN UNIV., MADISON, WI.
Analysis methods for fast impurity ion dynamics data
[DE95-000589] p 1549 N95-20112
Fluctuations and transport in the reversed field pinch: Characterization and reduction
[DE95-000590] p 1549 N95-20113
Magnetic fluctuation induced transport and edge dynamo measurements in the MST reversed-field pinch
[DE95-000591] p 1549 N95-20114
Design and construction of the HSX experiment
[DE94-018657] p 1552 N95-20348
An atomically-resolved STM study of the thermal decomposition of disilane on Si(001)
[AD-A279818] p 1567 N95-20544
An atomically-resolved STM study of the interaction of phosphine (PH3) with the silicon (001) surface
[AD-A279819] p 1513 N95-20585
Atomically resolved structure and bonding of delta-doped boron layers on Si(001)
[AD-A279820] p 1513 N95-20586
Antiphase boundaries as nucleation centers in low-temperature epitaxial growth
[AD-A279895] p 1568 N95-20594
Turbulent transport in premixed flames
p 1249 N95-21040
Constraints on SUSy-GUT unification from b yields s-gamma decay
[PB95-130373] p 1580 N95-21229
Calculation of Z plus four jet production at the Tevatron
[PB95-130472] p 1580 N95-21230

WOODS HOLE OCEANOGRAPHIC INST., MA.
Data report: Stress measurements in the bottom boundary layer with BASS tripods STRESS 2 1990-1991
[AD-A279875] p 1433 N95-20433
Synthesizing the Gulf Stream thermal structure from XBT data
[AD-A279665] p 1433 N95-20458
Mixing and dynamics of the Mediterranean outflow
[AD-A279803] p 1434 N95-21306
A simple ocean bottom hydrophone with 200 megabyte data capacity
[AD-A279478] p 1434 N95-21677
CTD calibration and processing methods used at Woods Hole Oceanographic Institution
[AD-A279507] p 1435 N95-21681
Long Time Series Measurements in the Coastal Ocean: A workshop
[AD-A279509] p 1435 N95-21682
The isotope geochemistry of abyssal peridotites and related rocks
[AD-A279435] p 1435 N95-21918
The dynamic role of ridges in a beta-plane channel. Towards understanding the dynamics of large scale circulation in the Southern Ocean
[AD-A279390] p 1435 N95-21943
Surface exposure geochronology using cosmogenic nuclides: Applications in Antarctic glacial geology
[AD-A279392] p 1426 N95-21944
Exchanges between hemispheres and gyres: A direct approach to the mean circulation of the equatorial Pacific
[NASA-CR-196311] p 1436 N95-22072
Descriptions of WHOI sediment cores, volume 8
[AD-A279444] p 1436 N95-22073
Real time system for practical acoustic monitoring of global ocean temperature
[AD-A286435] p 1436 N95-22209

WRIGHT LAB., EGLIN AFB, FL.
On the Taylor test. Part 3: A continuum mechanics code analysis of steady plastic wave propagation
[DE95-002252] p 1501 N95-20869

WRIGHT LAB., WRIGHT-PATTERSON AFB, OH.
Summary of a joint program of research into aircraft flight control concepts
[AD-A280012] p 1214 N95-20004
The preparation of all para-polyphenyls with increased solubility and enhanced third order NLO activity
[AD-A284301] p 1266 N95-20251
The mechanical property data base from an Air Force/Industry cooperative test program on advanced aluminum alloys
[AD-A280038] p 1386 N95-20615
The impact of advanced packaging technology on modular avionics architectures p 1208 N95-20632
Pressure measurements on an F/A-18 twin vertical tail in buffeting flow. Volume 4, part 1: Buffet cross spectral densities
[AD-A285593] p 1215 N95-21214
Pressure measurements on an F/A-18 twin vertical tail in buffeting flow. Volume 1: Wind tunnel test summary
[AD-A279126] p 1202 N95-21877
Influence of fatigue crack closure on the growth rate of surface flaws
[AD-A279130] p 1387 N95-21967
Optical processing and control
[AD-A279157] p 1546 N95-21975
Damage tolerant repair techniques for pressurized aircraft fuselages
[AD-A286298] p 1199 N95-22046
Nonlinear dynamics of the planar pitch attitude motion for a gravity-gradient satellite
[AD-A286407] p 1220 N95-22204

WRIGHT STATE UNIV., DAYTON, OH.
Continuum transient and frozen startup behavior of conventional and gas-loaded heat pipes
[AD-A284297] p 1339 N95-20250
Perception and control of locomotion
[AD-A285605] p 1450 N95-21192

WYOMING UNIV., LARAMIE, WY.
USAF cellular mechanism of turnover of the stress induced protein HSP70
[AD-A285618] p 1441 N95-19898

X

XAVIER UNIV. OF LOUISIANA, NEW ORLEANS, LA.
Investigation of syngas interaction in alcohol synthesis catalysts
[DE94-018784] p 1236 N95-20349

Y

YALE UNIV., NEW HAVEN, CT.
Nucleation, growth, and strain relaxation of lattice-mismatched 3-5 semiconductor epitaxial layers
p 1324 N95-20543
Nonlinear spectroscopy of multicomponent droplets and two- and three-dimensional measurements in flames
[AD-A279945] p 1238 N95-20581
Functional and para-functional parallel processing
[DE95-002805] p 1475 N95-20888

Z

ZETON, INC., BURLINGTON (ONTARIO).
Assessment of liquefaction and pyrolysis systems
[PB95-129797] p 1236 N95-20290

CONTRACT NUMBER INDEX

SCIENTIFIC AND TECHNICAL AEROSPACE REPORTS VOLUME 33 NUMBER 6

Typical Contract Number Index Listing

AF- AFOSR-0090-93 .... p 173 N95-10812

CONTRACT NUMBER | PAGE NUMBER | ACCESSION NUMBER

Listings in this index are arranged alphanumerically by contract number. Under each contract number the accession numbers denoting documents that have been produced as a result of research done under that contract are arranged in ascending order. The page number helps to locate the citation in the abstract section. The accession number denotes the number by which the citation is identified.

AF PROJ. B74A .... p 1452 N95-20625
AF PROJ. 2303 .... p 1266 N95-20251
AF PROJ. 2304 .... p 1340 N95-20312
p 1464 N95-21010
p 1485 N95-22213
p 1309 N95-22215
AF PROJ. 2308 .... p 1221 N95-20059
p 1238 N95-20581
p 1238 N95-20597
AF PROJ. 2311 .... p 1602 N95-20593
AF PROJ. 2313 .... p 1448 N95-19970
p 1449 N95-20314
AF PROJ. 2338 .... p 1479 N95-20057
AF PROJ. 2401 .... p 1215 N95-21214
p 1199 N95-22046
AF PROJ. 2403 .... p 1214 N95-20004
AF PROJ. 3066 .... p 1387 N95-21967
AF PROJ. 3484 .... p 1372 N95-21009
AF PROJ. 4600 .... p 1541 N95-20231
p 1369 N95-20389
p 1547 N95-22076
p 1548 N95-22248
AF PROJ. 6893 .... p 1449 N95-20062
AF PROJ. 7184 .... p 1453 N95-21700
AF PROJ. 7670 .... p 1545 N95-21832
AF PROJ. 7930 .... p 1446 N95-21941
AF PROJ. 9316 .... p 1383 N95-21933
AF-AFOSR-0010-89 .... p 1452 N95-20562
AF-AFOSR-0011-91 .... p 1358 N95-22294
AF-AFOSR-0013-91 .... p 1475 N95-20566
AF-AFOSR-0020-90 .... p 1355 N95-21942
AF-AFOSR-0023-89 .... p 1222 N95-21193
AF-AFOSR-0044-91 .... p 1602 N95-20593
AF-AFOSR-0049-89 .... p 1504 N95-20300
AF-AFOSR-0053-90 .... p 1481 N95-20828
AF-AFOSR-0063-90 .... p 1603 N95-21929
AF-AFOSR-0090-93 .... p 1495 N95-22157
AF-AFOSR-0095-90 .... p 1449 N95-20314
AF-AFOSR-0097-91 .... p 1340 N95-20312
AF-AFOSR-0105-90 .... p 1220 N95-21147
AF-AFOSR-0109-90 .... p 1517 N95-21126
AF-AFOSR-0112-90 .... p 1370 N95-20600
AF-AFOSR-0137-91 .... p 1530 N95-22471
AF-AFOSR-0140-86 .... p 1593 N95-21768
AF-AFOSR-0146-91 .... p 1451 N95-22472
AF-AFOSR-0150-91 .... p 1238 N95-20581
AF-AFOSR-0155-90 .... p 1374 N95-21694
AF-AFOSR-0169-90 .... p 1340 N95-20547
AF-AFOSR-0184-91 .... p 1238 N95-20597
AF-AFOSR-0196-91 .... p 1443 N95-20811
AF-AFOSR-0207-91 .... p 1271 N95-20815
AF-AFOSR-0208-91 .... p 1443 N95-20848
AF-AFOSR-0214-91 .... p 1333 N95-21917
AF-AFOSR-0215-90 .... p 1454 N95-22275
AF-AFOSR-0231-93 .... p 1370 N95-20484
AF-AFOSR-0243-91 .... p 1309 N95-22215
AF-AFOSR-0248-91 .... p 1339 N95-20058
p 1351 N95-21089
AF-AFOSR-0252-91 .... p 1303 N95-21462
AF-AFOSR-0257-91 .... p 1484 N95-22210
AF-AFOSR-0277-91 .... p 1310 N95-22250
AF-AFOSR-0292-90 .... p 1290 N95-20545
AF-AFOSR-0317-91 .... p 1226 N95-20105
AF-AFOSR-0320-89 .... p 1593 N95-21768
AF-AFOSR-0345-89 .... p 1221 N95-20059
AF-AFOSR-0356-91 .... p 1442 N95-20485
AF-AFOSR-0378-91 .... p 1450 N95-21101
AF-AFOSR-0426-89 .... p 1517 N95-21151
p 1517 N95-21216
AF-AFOSR-0432-91 .... p 1356 N95-22145
AF-AFOSR-0433-91 .... p 1276 N95-21697
AF-AFOSR-10061-93 .... p 1479 N95-20010
AF-AFOSR-10280-93 .... p 1479 N95-20010
ARPA ORDER A422 .... p 1313 N95-20257
ARPA ORDER A655 .... p 1474 N95-20325
ARPA ORDER B326 .... p 1466 N95-21325
ARPA ORDER 7597 .... p 1543 N95-20564
p 1461 N95-20623
ARPA ORDER 7932 .... p 1312 N95-19894
ARPA ORDER 8162 .... p 1325 N95-20661
p 1331 N95-21690
ARPA ORDER 8455 .... p 1310 N95-22253
ARPA ORDER 8557 .... p 1328 N95-21017
ARPA ORDER 9339 .... p 1543 N95-20598
ARTI-MCLR PROJ. 650-50800 .... p 1582 N95-22153
BMDO-OA-005 .... p 1473 N95-22390
BMDO-92-A-012 .... p 1473 N95-22390
DA PROJ. 1L1-61102-AH-43 .... p 1239 N95-20613
p 1247 N95-22207
p 1248 N95-22321
DA PROJ. 1L1-61618-AH-43 .... p 1391 N95-22131
DA PROJ. 1L1-62211-A-47-A .... p 1380 N95-21359
DA PROJ. 1L1-62618-AH-80 .... p 1224 N95-19899
p 1499 N95-22135
DA PROJ. 1O1-62622-A-553-C .... p 1437 N95-20252
DA PROJ. 2Q1-62785-A-790 .... p 1460 N95-20326
DA PROJ. 2418 .... p 1386 N95-20615
DA PROJ. 3E1-62787-A-879 .... p 1547 N95-22044
DA PROJ. 301-62787-A-878 .... p 1454 N95-22045
DAAA21-94-C-0013 .... p 1383 N95-22037
DAAB07-88-C-F421 .... p 1569 N95-20767
DAAE07-92-C-R078 .... p 1380 N95-21157
DAAH01-94-C-R032 .... p 1216 N95-21719
DAAH01-94-C-R089 .... p 1457 N95-20000
DAAH04-93-G-0419 .... p 1313 N95-20257
DAAJ02-92-C-0043 .... p 1452 N95-20973
DAAL01-92-K-0200 .... p 1336 N95-22254
DAAL01-93-C-4058 .... p 1228 N95-20805
DAAL01-93-C-4064 .... p 1229 N95-21149
p 1229 N95-21215
p 1233 N95-22395
DAAL03-89-K-0162 .... p 1368 N95-20063
DAAL03-89-7C-0088 .... p 1478 N95-22228
DAAL03-90-G-0008 .... p 1481 N95-20828
DAAL03-91-C-0034 .... p 1437 N95-20252
DAAL03-91-G-0128 .... p 1263 N95-19893
DAAL03-92-C-0011 .... p 1224 N95-22474
DABT63-91-C-0025 .... p 1464 N95-20996
p 1589 N95-21002
DABT65-93-D-0002 .... p 1291 N95-20605
DACA33-91-C-0030 .... p 1433 N95-21291
DACA39-86-C-0024 .... p 1459 N95-20310
DAJA45-89-C-0021 .... p 1268 N95-20392
DAJA45-90-C-0053 .... p 1239 N95-20769
p 1272 N95-20856
DAJA45-93-C-0043 .... p 1546 N95-22002
DAJA45-93-M-0233 .... p 1380 N95-21171
p 1381 N95-21488
DAJA45-93-M-0461 .... p 1376 N95-22164
DAMD17-93-J-3027 .... p 1442 N95-20549
DASG60-94-C-0036 .... p 1463 N95-20877
DASW01-94-C-0054 .... p 1217 N95-22413
p 1411 N95-22414
DE-AC02-76CH-00016 .... p 1563 N95-19925
p 1540 N95-19968
p 1250 N95-19979
p 1233 N95-19980
p 1563 N95-20014
p 1531 N95-20021
p 1541 N95-20103
p 1480 N95-20126
p 1564 N95-20127
p 1564 N95-20130
p 1565 N95-20265
p 1489 N95-20266
p 1531 N95-20282
p 1532 N95-20336
p 1566 N95-20382
p 1511 N95-20404
p 1532 N95-20406
p 1512 N95-20477
p 1370 N95-20572
p 1533 N95-20573
p 1533 N95-20766
p 1569 N95-20793
p 1371 N95-20866
p 1533 N95-20886
p 1272 N95-20894
p 1517 N95-21140
p 1283 N95-21211
p 1492 N95-21266
p 1536 N95-21342
p 1520 N95-21362
p 1536 N95-21418
p 1521 N95-21484
p 1522 N95-21506
p 1468 N95-21515
p 1573 N95-21516
p 1523 N95-21551
p 1523 N95-21588
p 1455 N95-21632
p 1367 N95-21638
p 1524 N95-21641
p 1545 N95-21643
p 1276 N95-21644
p 1469 N95-21713
p 1538 N95-21720
p 1527 N95-22188
p 1247 N95-22234
p 1539 N95-22357
p 1540 N95-22391
p 1530 N95-22392
DE-AC02-76CH-03000 .... p 1507 N95-20108
p 1507 N95-20110
p 1507 N95-20111
p 1507 N95-20131
p 1508 N95-20132
p 1508 N95-20134
p 1509 N95-20217
p 1510 N95-20343
p 1510 N95-20344
p 1511 N95-20401
p 1511 N95-20415
p 1511 N95-20418
p 1532 N95-20421
p 1512 N95-20475
p 1512 N95-20476
p 1513 N95-20496
p 1515 N95-20868
p 1515 N95-20879
p 1515 N95-20880
p 1533 N95-20885
p 1515 N95-20897
p 1515 N95-20898
p 1282 N95-20899
p 1534 N95-20900
p 1463 N95-20901
p 1365 N95-20902
p 1516 N95-20914
p 1519 N95-21273
p 1520 N95-21313
p 1535 N95-21314
p 1521 N95-21378
p 1522 N95-21497
p 1522 N95-21498
p 1522 N95-21499
p 1523 N95-21521
p 1573 N95-21561
p 1523 N95-21562
p 1523 N95-21563
p 1524 N95-21597
p 1525 N95-21715
p 1527 N95-22122
p 1539 N95-22192
p 1539 N95-22193
p 1527 N95-22194
p 1539 N95-22195

p 1528 N95-22196
p 1528 N95-22197
p 1529 N95-22314
p 1530 N95-22339
p 1530 N95-22340
DE-AC02-76CH-03073 .... p 1557 N95-21240
p 1558 N95-21242
DE-AC02-76ER-00038 .... p 1570 N95-20838
DE-AC02-76ER-00881 .... p 1580 N95-21229
p 1580 N95-21230
DE-AC02-76ER-01112 .... p 1522 N95-21499
DE-AC02-76ER-03069 .... p 1525 N95-21727
p 1604 N95-22085
p 1527 N95-22152
DE-AC02-78ET-51013 .... p 1551 N95-20285
DE-AC02-83CH-10093 .... p 1319 N95-20521
DE-AC02-88CE-90027 .... p 1228 N95-20787
DE-AC03-76SF-00098 .... p 1392 N95-20439
p 1532 N95-20494
p 1532 N95-20495
p 1370 N95-20569
p 1513 N95-20575
p 1513 N95-20629
p 1568 N95-20630
p 1569 N95-20677
p 1569 N95-20678
p 1569 N95-20679
p 1514 N95-20732
p 1429 N95-20782
p 1326 N95-20814
p 1515 N95-20872
p 1599 N95-20873
p 1501 N95-20874
p 1534 N95-20891
p 1394 N95-20915
p 1274 N95-21175
p 1256 N95-21260
p 1373 N95-21261
p 1519 N95-21262
p 1274 N95-21263
p 1558 N95-21310
p 1520 N95-21357
p 1521 N95-21380
p 1374 N95-21528
p 1581 N95-21604
p 1524 N95-21646
p 1374 N95-21663
p 1259 N95-21707
p 1246 N95-21990
p 1527 N95-22152
p 1577 N95-22168
p 1591 N95-22235
p 1336 N95-22236
p 1582 N95-22237
p 1548 N95-22238
DE-AC03-76SF-00515 .... p 1507 N95-20034
p 1532 N95-20388
p 1301 N95-21241
p 1599 N95-21245
p 1534 N95-21246
p 1519 N95-21248
p 1482 N95-21249
p 1519 N95-21250
p 1534 N95-21253
p 1535 N95-21254
p 1535 N95-21255
p 1536 N95-21332
p 1536 N95-21334
p 1536 N95-21335
p 1520 N95-21336
p 1536 N95-21337
p 1523 N95-21525
p 1525 N95-21727
p 1538 N95-22155
p 1528 N95-22239
DE-AC03-89ER-51114 .... p 1548 N95-20037
p 1549 N95-20038
p 1550 N95-20146
p 1551 N95-20279
p 1551 N95-20285
p 1552 N95-20334
p 1553 N95-20402
p 1553 N95-20445
p 1554 N95-20446
p 1554 N95-20568
p 1269 N95-20570
p 1554 N95-20571
p 1555 N95-21141
p 1556 N95-21142
p 1556 N95-21159
p 1556 N95-21163
p 1558 N95-21299
p 1230 N95-21553
DE-AC03-91SF-18852 .... p 1222 N95-20853
DE-AC03-92SF-19441 .... p 1221 N95-20076
DE-AC04-76DP-00613 .... p 1256 N95-21300
p 1329 N95-21301
p 1467 N95-21389
p 1332 N95-21729
DE-AC04-76DP-00789 .... p 1266 N95-20281
p 1413 N95-20397
p 1554 N95-20568
p 1556 N95-21159
p 1301 N95-21277
p 1243 N95-21512
DE-AC04-76DR-00789 .... p 1477 N95-21505
DE-AC04-76EV-01013 .... p 1447 N95-22285
p 1447 N95-22287
DE-AC04-88DP-43495 .... p 1243 N95-21440
p 1334 N95-22062
DE-AC04-94AL-85000 .... p 1263 N95-19926
p 1563 N95-19954
p 1506 N95-20026
p 1264 N95-20047
p 1378 N95-20048
p 1507 N95-20049
p 1378 N95-20053
p 1549 N95-20075
p 1384 N95-20077
p 1564 N95-20087
p 1265 N95-20121
p 1474 N95-20123
p 1339 N95-20137
p 1265 N95-20138
p 1235 N95-20139
p 1488 N95-20141
p 1564 N95-20142
p 1549 N95-20143
p 1599 N95-20144
p 1474 N95-20150
p 1474 N95-20152
p 1204 N95-20195
p 1509 N95-20206
p 1489 N95-20222
p 1215 N95-20223
p 1369 N95-20225
p 1541 N95-20239
p 1313 N95-20262
p 1391 N95-20263
p 1204 N95-20269
p 1459 N95-20284
p 1314 N95-20286
p 1428 N95-20319
p 1314 N95-20338
p 1565 N95-20340
p 1314 N95-20341
p 1480 N95-20342
p 1268 N95-20396
p 1364 N95-20398
p 1566 N95-20399
p 1566 N95-20400
p 1566 N95-20405
p 1268 N95-20468
p 1290 N95-20474
p 1567 N95-20479
p 1219 N95-20567
p 1554 N95-20571
p 1324 N95-20626
p 1325 N95-20628
p 1379 N95-20695
p 1218 N95-20785
p 1271 N95-20788
p 1588 N95-20789
p 1341 N95-20831
p 1371 N95-20832
p 1386 N95-20833
p 1393 N95-20861
p 1393 N95-20862
p 1393 N95-20863
p 1393 N95-20864
p 1371 N95-20867
p 1393 N95-20870
p 1394 N95-20871
p 1327 N95-20882
p 1327 N95-20883
p 1481 N95-20884
p 1463 N95-20887
p 1272 N95-20889
p 1272 N95-20895
p 1555 N95-21134
p 1328 N95-21139
p 1465 N95-21153
p 1558 N95-21247
p 1535 N95-21278
p 1256 N95-21286
p 1572 N95-21304
p 1302 N95-21305
p 1242 N95-21309
p 1535 N95-21328
p 1394 N95-21353
p 1387 N95-21364
p 1329 N95-21390
p 1373 N95-21393
p 1329 N95-21394
p 1329 N95-21395
p 1387 N95-21396
p 1572 N95-21419
p 1302 N95-21448
p 1573 N95-21449
p 1367 N95-21507
p 1545 N95-21509
p 1283 N95-21513
p 1283 N95-21514
p 1205 N95-21520
p 1244 N95-21524
p 1330 N95-21545
p 1367 N95-21546
p 1374 N95-21594
p 1537 N95-21603
p 1560 N95-21609
p 1453 N95-21721
p 1545 N95-21728
p 1207 N95-21730
p 1259 N95-21838
p 1223 N95-21840
p 1477 N95-21843
p 1333 N95-21881
p 1575 N95-21991
p 1388 N95-22070
p 1334 N95-22086
p 1334 N95-22118
p 1261 N95-22119
p 1591 N95-22167
p 1376 N95-22169
p 1562 N95-22225
p 1247 N95-22234
p 1605 N95-22262
p 1248 N95-22273
p 1539 N95-22306
p 1529 N95-22315
p 1397 N95-22335
p 1311 N95-22407
p 1486 N95-22409
p 1502 N95-22420
p 1454 N95-22466
DE-AC05-76OR-00033 .... p 1510 N95-20337
p 1332 N95-21725
DE-AC05-84OR-21400 .... p 1503 N95-20019
p 1250 N95-20020
p 1225 N95-20022
p 1225 N95-20023
p 1264 N95-20024
p 1506 N95-20030
p 1549 N95-20038
p 1250 N95-20043
p 1250 N95-20044
p 1458 N95-20073
p 1378 N95-20085
p 1507 N95-20086
p 1226 N95-20125
p 1500 N95-20129
p 1508 N95-20133
p 1285 N95-20194
p 1551 N95-20205
p 1265 N95-20220
p 1369 N95-20221
p 1265 N95-20226
p 1401 N95-20238
p 1565 N95-20244
p 1565 N95-20245
p 1551 N95-20285
p 1412 N95-20287
p 1385 N95-20322
p 1267 N95-20323
p 1552 N95-20334
p 1510 N95-20337
p 1226 N95-20357
p 1460 N95-20358
p 1252 N95-20359
p 1252 N95-20365
p 1475 N95-20366
p 1565 N95-20371
p 1566 N95-20372
p 1267 N95-20373
p 1385 N95-20374
p 1253 N95-20375
p 1566 N95-20405
p 1385 N95-20416
p 1511 N95-20422
p 1553 N95-20445
p 1567 N95-20492
p 1237 N95-20493
p 1253 N95-20673
p 1568 N95-20674
p 1253 N95-20676
p 1370 N95-20698
p 1271 N95-20700
p 1491 N95-20701

p 1386 N95-20703
p 1271 N95-20704
p 1254 N95-20705
p 1379 N95-20723
p 1501 N95-20725
p 1271 N95-20761
p 1340 N95-20781
p 1326 N95-20791
p 1570 N95-20819
p 1570 N95-20820
p 1271 N95-20821
p 1254 N95-20822
p 1481 N95-20837
p 1255 N95-20907
p 1515 N95-20911
p 1571 N95-21167
p 1256 N95-21265
p 1492 N95-21285
p 1572 N95-21297
p 1256 N95-21298
p 1482 N95-21385
p 1580 N95-21420
p 1303 N95-21459
p 1537 N95-21460
p 1230 N95-21481
p 1275 N95-21482
p 1573 N95-21483
p 1243 N95-21500
p 1275 N95-21501
p 1522 N95-21519
p 1559 N95-21547
p 1439 N95-21548
p 1244 N95-21549
p 1381 N95-21550
p 1330 N95-21554
p 1257 N95-21555
p 1477 N95-21556
p 1287 N95-21559
p 1559 N95-21581
p 1258 N95-21600
p 1381 N95-21601
p 1477 N95-21602
p 1439 N95-21606
p 1455 N95-21607
p 1407 N95-21608
p 1586 N95-21645
p 1524 N95-21664
p 1560 N95-21665
p 1258 N95-21676
p 1560 N95-21702
p 1524 N95-21703
p 1525 N95-21704
p 1217 N95-21706
p 1355 N95-21726
p 1245 N95-21732
p 1483 N95-21741
p 1469 N95-21744
p 1231 N95-21776
p 1525 N95-21857
p 1277 N95-21861
p 1590 N95-21862
p 1278 N95-21909
p 1561 N95-21922
p 1278 N95-21937
p 1538 N95-21938
p 1526 N95-21939
p 1526 N95-21940
p 1247 N95-22049
p 1591 N95-22061
p 1591 N95-22107
p 1538 N95-22117
p 1261 N95-22123
p 1261 N95-22127
p 1591 N95-22129
p 1335 N95-22149
p 1280 N95-22258
p 1247 N95-22260
p 1285 N95-22261
p 1528 N95-22265
p 1280 N95-22266
p 1381 N95-22268
p 1578 N95-22269
p 1280 N95-22270
p 1336 N95-22271
p 1578 N95-22272
p 1431 N95-22288
p 1411 N95-22342
p 1262 N95-22344
p 1263 N95-22345
p 1263 N95-22346
DE-AC05-84OS-21400 .... p 1243 N95-21472
p 1244 N95-21571
DE-AC05-840R-21400 .... p 1386 N95-20790
DE-AC06-76RL-01830 .... p 1251 N95-20088
p 1401 N95-20089
p 1251 N95-20090
p 1458 N95-20153
p 1236 N95-20268
p 1364 N95-20320
p 1364 N95-20321
p 1403 N95-20834
p 1389 N95-20903
p 1520 N95-21375
p 1406 N95-21487
p 1395 N95-21611
p 1232 N95-22115
DE-AC06-87RL-10930 .... p 1364 N95-20224
p 1237 N95-20470
p 1366 N95-21138
p 1257 N95-21452
p 1243 N95-21473
DE-AC07-76ID-01570 .... p 1466 N95-21288
p 1558 N95-21290
p 1330 N95-21442
p 1330 N95-21471
p 1332 N95-21731
p 1333 N95-21960
DE-AC08-93NV-11265 .... p 1564 N95-20240
p 1391 N95-22398
DE-AC09-89SR-18035 .... p 1579 N95-20028
p 1251 N95-20079
p 1235 N95-20215
p 1252 N95-20216
p 1413 N95-20455
p 1257 N95-21303
p 1592 N95-22263
p 1382 N95-22356
DE-AC11-93PN-38195 .... p 1261 N95-22048
DE-AC21-89MC-26006 .... p 1394 N95-20896
DE-AC22-92BC-14882 .... p 1267 N95-20350
DE-AC22-92PC-92108 .... p 1241 N95-21172
DE-AC22-92PC-92109 .... p 1233 N95-19924
DE-AC22-92PC-92112 .... p 1237 N95-20438
DE-AC22-92PC-92117 .... p 1282 N95-19927
p 1314 N95-20339
DE-AC34-90DP-62349 .... p 1503 N95-20267
DE-AC35-89ER-40486 .... p 1538 N95-21733
DE-AC36-83CH-10093 .... p 1384 N95-20109
p 1234 N95-20117
p 1391 N95-20118
p 1391 N95-20260
p 1391 N95-20332
p 1392 N95-20333
p 1437 N95-20471
p 1268 N95-20472
p 1392 N95-20473
p 1392 N95-20778
p 1394 N95-20985
p 1394 N95-21294
p 1395 N95-21508
p 1395 N95-21844
p 1279 N95-22091
p 1410 N95-22278
p 1398 N95-22468
DE-AI01-79ET-29372 .... p 1484 N95-22171
DE-AI05-79ET-29372 .... p 1483 N95-21613
DE-AI05-89ER-13992 .... p 1357 N95-22264
DE-A105-83OR-21322 .... p 1379 N95-20984
DE-BI79-90BP-03362 .... p 1315 N95-20380
DE-FC02-92CE-41000 .... p 1214 N95-21243
DE-FC02-93ER-54186 .... p 1330 N95-21442
p 1560 N95-21724
p 1332 N95-21725
p 1260 N95-22013
DE-FC02-94ER-40818 .... p 1604 N95-22085
DE-FC03-86ER-52126 .... p 1556 N95-21142
DE-FC03-90ER-61010 .... p 1408 N95-21708
DE-FC05-85ER-25000 .... p 1518 N95-21223
DE-FC07-94ID-13233 .... p 1253 N95-20417
DE-FC21-86MC-11076 .... p 1234 N95-20135
DE-FC21-92MC-28065 .... p 1324 N95-20574
DE-FC21-92MC-29227 .... p 1396 N95-22033
DE-FC36-89ID-12779 .... p 1246 N95-21921
DE-FG01-91CE-15520 .... p 1229 N95-20913
DE-FG01-92EW-50625 .... p 1406 N95-21565
DE-FG01-94CE-15594 .... p 1283 N95-21356
DE-FG01-94CE-15613 .... p 1228 N95-20787
DE-FG02-84ER-13282 .... p 1241 N95-21280
DE-FG02-84ER-45076 .... p 1567 N95-20449
p 1520 N95-21360
DE-FG02-84ER-45130 .... p 1258 N95-21600
DE-FG02-84ER-45170 .... p 1564 N95-20017
DE-FG02-84ER-53188 .... p 1523 N95-21587
DE-FG02-85ER-40233 .... p 1529 N95-22279
DE-FG02-85ER-53198 .... p 1549 N95-20112
p 1549 N95-20113
p 1549 N95-20114
DE-FG02-85ER-60304 .... p 1406 N95-21379
DE-FG02-86ER-13519 .... p 1521 N95-21441
p 1529 N95-22316
DE-FG02-86ER-25012 .... p 1475 N95-20888
DE-FG02-86ER-45238 .... p 1565 N95-20243
DE-FG02-86ER-45252 .... p 1276 N95-21572
DE-FG02-86ER-45267 .... p 1506 N95-22071
DE-FG02-87ER-25027 .... p 1356 N95-22148
DE-FG02-87ER-40333 .... p 1245 N95-21845
DE-FG02-87ER-40344 .... p 1245 N95-21745
DE-FG02-87ER-45283 .... p 1572 N95-21279
DE-FG02-87ER-45313 .... p 1275 N95-21289
DE-FG02-87ER-45330 .... p 1572 N95-21287
DE-FG02-88ER-13934 .... p 1510 N95-20346
DE-FG02-88ER-13955 .... p 1509 N95-20242
DE-FG02-88ER-25053 .... p 1495 N95-22325
DE-FG02-88ER-40413 .... p 1520 N95-21357
DE-FG02-88ER-45372 .... p 1265 N95-20115
DE-FG02-88ER-60639 .... p 1445 N95-21595
DE-FG02-89ER-14039 .... p 1239 N95-20682
DE-FG02-89ER-14077 .... p 1336 N95-22284
DE-FG02-89ER-14079 .... p 1411 N95-19981
p 1411 N95-19982
DE-FG02-89ER-45388 .... p 1257 N95-21476
DE-FG02-90ER-14104 .... p 1573 N95-21444
DE-FG02-90ER-14114 .... p 1224 N95-21746
DE-FG02-90ER-14135 .... p 1258 N95-21560
DE-FG02-90ER-14145 .... p 1581 N95-21842
DE-FG02-90ER-25086 .... p 1470 N95-21992
DE-FG02-90ER-45416 .... p 1574 N95-21712
DE-FG02-90ER-45434 .... p 1230 N95-21445
DE-FG02-90ER-60931 .... p 1439 N95-21606
DE-FG02-90ER-60970 .... p 1406 N95-21410
DE-FG02-90ER-61071 .... p 1430 N95-21527
DE-FG02-90ER-61072 .... p 1412 N95-20116
DE-FG02-90ER-80896 .... p 1275 N95-21354
DE-FG02-91CE-23810 .... p 1264 N95-20078
p 1287 N95-21631
p 1582 N95-22153
DE-FG02-91ER-12108 .... p 1374 N95-21743
DE-FG02-91ER-14185 .... p 1574 N95-21839
DE-FG02-91ER-14225 .... p 1244 N95-21517
DE-FG02-91ER-40672 .... p 1527 N95-22152
DE-FG02-91ER-40676 .... p 1512 N95-20451
p 1525 N95-21727
p 1527 N95-22152
DE-FG02-91ER-40677 .... p 1527 N95-22152
DE-FG02-92ER-14258 .... p 1243 N95-21447
DE-FG02-92ER-40697 .... p 1535 N95-21281
p 1528 N95-22197
DE-FG02-92ER-40715 .... p 1525 N95-21727
p 1527 N95-22152
DE-FG02-92ER-54178 .... p 1532 N95-20347
DE-FG02-92ER-61370 .... p 1441 N95-22397
DE-FG02-92ER-81461 .... p 1336 N95-22271
DE-FG02-93ER-14320 .... p 1552 N95-20345
DE-FG02-93ER-20112 .... p 1440 N95-22066
DE-FG02-93ER-40768 .... p 1519 N95-21302
DE-FG02-93ER-54222 .... p 1552 N95-20348
DE-FG02-94ER-14412 .... p 1246 N95-21886
DE-FG03-84ER-45085 .... p 1277 N95-21748
DE-FG03-84ER-45157 .... p 1276 N95-21585
DE-FG03-88ER-13957 .... p 1561 N95-22116
DE-FG03-88ER-40424 .... p 1520 N95-21357
DE-FG03-88ER-40439 .... p 1525 N95-21747
DE-FG03-89ER-14053 .... p 1238 N95-20576
DE-FG03-89ER-51121 .... p 1554 N95-20571
DE-FG03-90ER-40546 .... p 1515 N95-20893
DE-FG03-91ER-40618 .... p 1525 N95-21727
p 1527 N95-22152
DE-FG03-91ER-54124 .... p 1548 N95-20029
DE-FG03-91ER-61152 .... p 1440 N95-22067
DE-FG03-92ER-40689 .... p 1525 N95-21727
p 1527 N95-22152
DE-FG03-92ER-40701 .... p 1525 N95-21727
p 1527 N95-22152
DE-FG03-92ER-45476 .... p 1570 N95-20916
DE-FG03-92ER-54150 .... p 1553 N95-20402
p 1555 N95-21141
p 1556 N95-21142
DE-FG03-92SF-19202 .... p 1240 N95-20865
DE-FG03-93ER-14333 .... p 1240 N95-20780
DE-FG03-93ER-25149 .... p 1476 N95-21355
DE-FG03-93ER-40788 .... p 1525 N95-21727
p 1527 N95-22152
DE-FG03-94ER-54241 .... p 1562 N95-22120
DE-FG03-94ER-61856 .... p 1427 N95-22240
DE-FG05-80CS-83014 .... p 1395 N95-21409
DE-FG05-80ET-53088 .... p 1553 N95-20437
p 1358 N95-22307
DE-FG05-85ER-40219 .... p 1521 N95-21443
DE-FG05-85ER-45194 .... p 1270 N95-20680
DE-FG05-86ER-40272 .... p 1512 N95-20469
DE-FG05-86ER-45259 .... p 1567 N95-20479
DE-FG05-86ER-53217 .... p 1524 N95-21605
DE-FG05-88ER-13950 .... p 1244 N95-21701
DE-FG05-88ER-13954 .... p 1234 N95-20052
DE-FG05-88ER-13971 .... p 1519 N95-21276
DE-FG05-88ER-40445 .... p 1520 N95-21357
DE-FG05-89ER-53295 .... p 1554 N95-20681
DE-FG05-91ER-40617 .... p 1522 N95-21485

p 1580 N95-21486
DE-FG05-91ER-40627 .... p 1525 N95-21727
DE-FG05-92ER-40739 .... p 1374 N95-21480
DE-FG05-93ER-40809 .... p 1512 N95-20491
DE-FG05-94ER-14421 .... p 1237 N95-20384
DE-FG06-85ER-40224 .... p 1525 N95-21727
DE-FG06-89ER-75522 .... p 1251 N95-20088
DE-FG06-90ER-40561 .... p 1602 N95-20147
p 1604 N95-20383
p 1512 N95-20451
p 1604 N95-20490
p 1498 N95-20779
p 1520 N95-21315
p 1603 N95-21316
p 1521 N95-21443
p 1526 N95-21920
p 1604 N95-22064
p 1604 N95-22085
DE-FG07-90ID-12942 .... p 1313 N95-20213
DE-FG07-90ID-13040 .... p 1391 N95-20104
DE-FG07-93ID-13220 .... p 1251 N95-20128
DE-FG09-84ER-13188 .... p 1439 N95-21526
DE-FG09-85ER-13425 .... p 1440 N95-22220
DE-FG09-86ER-13614 .... p 1438 N95-20917
DE-FG21-92MC-29228 .... p 1235 N95-20188
DE-FG22-91PC-91293 .... p 1233 N95-20045
DE-FG22-92PC-92529 .... p 1247 N95-22224
DE-FG22-93MT-93010 .... p 1236 N95-20349
DE-FG22-93PC-93211 .... p 1511 N95-20422
DE-FG22-93PC-93217 .... p 1234 N95-20046
DE-FG49-93CE-15566 .... p 1364 N95-20233
DFG-RI-680/1-1 .... p 1352 N95-21095
DGA-91/158 .... p 1350 N95-21086
DNA-MIPR-92-610 .... p 1220 N95-21634
DNA001-89-C-0029 .... p 1551 N95-20232
DNA001-90-C-0111 .... p 1445 N95-21629
DNA001-91-C-0021 .... p 1213 N95-22036
DOT-CG-14-35-0001-30544 .... p 1408 N95-21685
DRET-90-34-473 .... p 1299 N95-20959
DTFA01-93-P-02265 .... p 1203 N95-21518
DTFA01-93-Z-02012 .... p 1291 N95-20599
DTFA02-90-C-90125 .... p 1446 N95-22027
p 1447 N95-22040
DTFA03-89-C-00043 .... p 1202 N95-20174
p 1202 N95-20275
p 1203 N95-22319
DTFA03-91-A-0018 .... p 1383 N95-22202
DTFA03-92-C-0035 .... p 1202 N95-20093
EC-CHRX-CT93-0400 .... p 1499 N95-21979
EC-CHRX-CT93-0695 .... p 1498 N95-19945
EC-SCI-CT91-0695 .... p 1498 N95-19945
EEC-ERBCHDICT930257 .... p 1346 N95-21063
EPA-CR-816740 .... p 1400 N95-19965
EPA-68-CO-0094 .... p 1401 N95-20192
EPA-68-C0-0003 .... p 1312 N95-19966
EPA-68-C1-0079 .... p 1406 N95-21373
ESPRIT 3 PROJ. 6276 .... p 1212 N95-20653
F04611-90-C-0011 .... p 1284 N95-21678
F04701-88-C-0089 .... p 1575 N95-21916
p 1307 N95-21985
p 1309 N95-22134
F04701-93-C-0094 .... p 1404 N95-21150
p 1284 N95-22227
p 1427 N95-22249
F08635-90-C-0053 .... p 1400 N95-19921
F08635-91-C-0217 .... p 1287 N95-21598
F09603-90-D-2217 .... p 1259 N95-21687
F19628-89-K-0044 .... p 1413 N95-20377
F19628-90-C-0002 .... p 1567 N95-20426
p 1291 N95-20599
p 1300 N95-21099
p 1309 N95-22229
F19628-90-C-0003 .... p 1457 N95-19999
p 1462 N95-20765
p 1462 N95-20809
p 1463 N95-20810
p 1468 N95-21567
p 1468 N95-21627
p 1485 N95-22226
F19628-90-C-0110 .... p 1545 N95-21832
F19628-90-C-0171 .... p 1335 N95-22144
F19628-90-K-0003 .... p 1427 N95-22326
F19628-91-C-0001 .... p 1473 N95-22402
F19628-91-C-0011 .... p 1292 N95-20904
F19628-91-C-0093 .... p 1290 N95-20376
F19628-91-K-0013 .... p 1311 N95-22401
F19628-91-K-0016 .... p 1426 N95-21932
F19628-91-K-0019 .... p 1364 N95-20069
F19628-91-K-0039 .... p 1414 N95-20878
p 1415 N95-21308
F19628-91-K-0043 .... p 1501 N95-20773
F19628-92-C-0162 .... p 1425 N95-21833
F19628-93-C-0044 .... p 1364 N95-20036
F19628-93-C-0054 .... p 1203 N95-21831
F19628-93-C-0171 .... p 1474 N95-20325
F19628-93-K-0001 .... p 1430 N95-21177
F19628-94-C-0001 .... p 1462 N95-20721
p 1390 N95-21912
F29601-89-C-0085 .... p 1544 N95-20803
F29601-92-C-0109 .... p 1291 N95-20771
p 1207 N95-20772
F30602-88-D-0028 .... p 1261 N95-22035
F30602-89-D-0028 .... p 1334 N95-22023
F30602-92-C-0031 .... p 1479 N95-20057
F30602-92-C-0069 .... p 1327 N95-20967
F30602-92-C-0076 .... p 1456 N95-22400
F30602-92-C-0080 .... p 1302 N95-21405
F30602-92-C-0084 .... p 1241 N95-21168
F30602-92-C-0098 .... p 1484 N95-22203
F30602-93-C-0003 .... p 1369 N95-20378
F30602-93-C-0020 .... p 1368 N95-20035
F30602-93-C-0061 .... p 1547 N95-22205
F30602-93-C-0083 .... p 1369 N95-20379
F30602-93-C-0167 .... p 1328 N95-21169
F33615-85-D-4510 .... p 1446 N95-21941
F33615-86-C-5044 .... p 1279 N95-21976
F33615-87-C-0531 .... p 1213 N95-22024
F33615-88-C-2817 .... p 1278 N95-21969
F33615-88-C-2820 .... p 1339 N95-20250
F33615-88-C-2833 .... p 1514 N95-20804
F33615-89-C-1036 .... p 1212 N95-20654
F33615-90-C-0005 .... p 1216 N95-20992
F33615-90-C-1465 .... p 1543 N95-20564
p 1461 N95-20623
F33615-90-C-2039 .... p 1553 N95-20411
F33615-90-C-2051 .... p 1283 N95-21161
F33615-90-C-3613 .... p 1483 N95-21913
F33615-90-D-0606 .... p 1441 N95-20301
F33615-91-C-5661 .... p 1382 N95-20414
F33615-92-C-5936 .... p 1453 N95-21566
F33615-93-C-1213 .... p 1383 N95-21933
F33616-91-D-0651 .... p 1457 N95-20060
F41624-93-C-6011 .... p 1442 N95-20457
F49620-89-C-0104 .... p 1368 N95-22143
F49620-90-C-0036 .... p 1543 N95-20601
F49620-91-C-0014 .... p 1353 N95-21146
F49620-91-C-0034 .... p 1331 N95-21693
F49620-91-C-0075 .... p 1544 N95-20844
F49620-91-C-0079 .... p 1495 N95-22317
F49620-92-C-0015 .... p 1314 N95-20311
F49620-92-C-0066 .... p 1587 N95-20309
F49620-92-C-0074 .... p 1273 N95-21014
F49620-92-J-0001 .... p 1555 N95-21013
F49620-92-J-0016 .... p 1448 N95-19998
F49620-92-J-0020 .... p 1428 N95-20008
F49620-92-J-0039 .... p 1273 N95-21152
F49620-92-J-0092 .... p 1414 N95-20498
F49620-92-J-0100 .... p 1341 N95-20981
F49620-92-J-0127 .... p 1485 N95-22216
F49620-92-J-0160 .... p 1502 N95-21194
F49620-92-J-0195 .... p 1447 N95-22475
F49620-92-J-0234 .... p 1441 N95-19898
F49620-92-J-0254 .... p 1273 N95-21011
F49620-92-J-0281 .... p 1269 N95-20548
F49620-92-J-0326 .... p 1246 N95-21931
F49620-92-J-0334 .... p 1449 N95-20845
F49620-92-J-0359 .... p 1451 N95-22473
F49620-92-J-0383 .... p 1461 N95-20595
F49620-92-J-0387 .... p 1479 N95-20061
F49620-92-J-0431 .... p 1226 N95-20081
F49620-92-J-0462 .... p 1281 N95-19884
F49620-92-J-0489 .... p 1504 N95-20823
F49620-92-J-0504 .... p 1370 N95-20550
F49620-93-C-0017 .... p 1540 N95-19897
F49620-93-C-0045 .... p 1571 N95-20965
F49620-93-C-0046 .... p 1272 N95-20962
F49620-93-C-0050 .... p 1215 N95-21122
F49620-93-1-0008 .... p 1232 N95-22211
F49620-93-1-0149 .... p 1464 N95-21010
F49620-93-1-0196 .... p 1270 N95-20596
F49620-93-1-0263 .... p 1486 N95-22267
F49620-93-1-0279 .... p 1302 N95-21438
F49620-93-1-0301 .... p 1373 N95-21195
F49620-93-1-0336 .... p 1448 N95-20007
F49620-93-1-0338 .... p 1372 N95-21009
p 1357 N95-22212
F49620-93-1-0364 .... p 1242 N95-21402
F49620-93-1-0416 .... p 1428 N95-20186
F49620-93-1-0444 .... p 1370 N95-20484
F49620-93-1-0460 .... p 1414 N95-20591
F49620-93-1-0504 .... p 1514 N95-20667
F49620-93-1-0560 .... p 1450 N95-21192
F49620-94-C-0008 .... p 1542 N95-20501
F49620-94-C-0040 .... p 1252 N95-20299
F49620-94-C-0043 .... p 1253 N95-20481
p 1239 N95-20716
F49620-94-1-0062 .... p 1563 N95-19886
GA PROJ. 3466 .... p 1550 N95-20146
p 1551 N95-20279
GA PROJ. 3936 .... p 1558 N95-21345
GRI-5086-293-1848 .... p 1282 N95-20253
p 1284 N95-21966
GRI-5092-260-2454 .... p 1247 N95-22150
MDA903-89-C-0003 .... p 1327 N95-20966
MDA903-90-C-0004 .... p 1591 N95-22069
MDA972-89-C-0043 .... p 1224 N95-19899
MDA972-90-C-0060 .... p 1462 N95-20718
MDA972-91-C-0029 .... p 1325 N95-20661
MDA972-91-C-0030 .... p 1331 N95-21690
MDA972-92-C-0022 .... p 1468 N95-21489
MDA972-92-C-0028 .... p 1265 N95-20176
MDA972-92-C-0053 .... p 1328 N95-21017
MDA972-92-J-1018 .... p 1470 N95-21972
MDA972-93-C-0057 .... p 1543 N95-20598
MDA972-93-1-0003 .... p 1436 N95-21987
MDA972-93-1-0004 .... p 1436 N95-22209
MIPR-0823 .... p 1410 N95-22142
MM-IRD PROJ. D-17R .... p 1318 N95-20514
NAGW-1618 .... p 1600 N95-21615
NAGW-2627 .... p 1427 N95-22326
NAGW-2856 .... p 1427 N95-22326
NAGW-2923 .... p 1579 N95-19947
NAGW-2974 .... p 1601 N95-22338
NAG1-1067 .... p 1383 N95-20616
NAG1-1133 .... p 1216 N95-21436
NAG1-1422 .... p 1352 N95-21094
NAG1-343 .... p 1229 N95-21008
NAG2-819 .... p 1437 N95-20559
NAG2-854 .... p 1201 N95-21031
NAG2-881 .... p 1353 N95-21340
NAG2-905 .... p 1201 N95-21343
NAG3-1047 .... p 1380 N95-21359
NAG3-1329 .... p 1467 N95-21450
NAG3-1370 .... p 1382 N95-22404
p 1382 N95-22405
NAG3-1399 .... p 1340 N95-20796
NAG3-1461 .... p 1323 N95-20542
NAG3-1466 .... p 1316 N95-20502
NAG3-781 .... p 1357 N95-22173
NAG3-862 .... p 1225 N95-19951
NAG5-1129 .... p 1604 N95-22384
NAG5-2509 .... p 1479 N95-22406
NAG5-613 .... p 1602 N95-20558
NAG8-1031 .... p 1428 N95-19948
NAG8-1071 .... p 1238 N95-20557
NAG8-201 .... p 1354 N95-21675
NAG8-921 .... p 1222 N95-21616
NASW-4574 .... p 1415 N95-21777
NASW-4651 .... p 1558 N95-21345
NASW-4714 .... p 1389 N95-20156
NASW-4832 .... p 1601 N95-20797
NAS1-18028 .... p 1204 N95-19950
NAS1-18240 .... p 1353 N95-21258
NAS1-18599 .... p 1353 N95-21258
NAS1-18605 .... p 1473 N95-20013
NAS1-18972 .... p 1462 N95-20691
NAS1-19061 .... p 1504 N95-21170
NAS1-19291 .... p 1220 N95-21190
NAS1-19299 .... p 1338 N95-20009
NAS1-19480 .... p 1338 N95-20009
p 1479 N95-20010
p 1473 N95-20013
p 1495 N95-22157
p 1495 N95-22325
p 1456 N95-22431
NAS1-19592 .... p 1316 N95-20502
NAS1-19708 .... p 1230 N95-21363
NAS2-13721 .... p 1478 N95-22108
NAS3-25266 .... p 1395 N95-21530
p 1222 N95-21531
NAS3-25767 .... p 1223 N95-19901
NAS3-25808 .... p 1396 N95-21952
p 1396 N95-21953
NAS3-25883 .... p 1222 N95-21458
NAS3-25950 .... p 1337 N95-19912
NAS3-26615 .... p 1317 N95-20512
NAS3-26617 .... p 1505 N95-21888
NAS3-26703 .... p 1316 N95-20502
NAS3-27004 .... p 1316 N95-20502
NAS3-27186 .... p 1385 N95-20179
p 1366 N95-21259
p 1214 N95-21383
p 1334 N95-22112
p 1284 N95-22114
NAS5-30428 .... p 1473 N95-19885
NAS7-1260 .... p 1397 N95-22336
NAS7-918 .... p 1412 N95-20002
p 1302 N95-21456
p 1595 N95-21749
p 1484 N95-22171
NAS8-38348 .... p 1379 N95-20795
NAS8-38607 .... p 1381 N95-21692
p 1381 N95-21705
NAS8-39131 .... p 1312 N95-19909
NAS8-39370 .... p 1221 N95-20124
NAS8-40185 .... p 1543 N95-20798
NAS9-18000 .... p 1205 N95-22161
NAS9-18372 .... p 1221 N95-20059

NAS9-18440 p 1439 N95-21529
NATO-CRG-920287 p 1499 N95-21980
NATO-CRG-930554 p 1499 N95-21979
NCC2-460 p 1341 N95-21035
p 1358 N95-22437
NCC2-5003 p 1355 N95-21954
NCC2-582 p 1601 N95-21621
NCC2-775 p 1205 N95-21891
NCC3-233 p 1355 N95-21957
p 1356 N95-21959
NCC3-302 p 1367 N95-21889
NCC8-22 p 1390 N95-22110
p 1390 N95-22111
NGR14-001-227 p 1593 N95-21763
NGT-50832 p 1324 N95-20543
NR PROJ. MM3-3-P-30 p 1441 N95-20307
p 1444 N95-21160
NR PROJ. MM3-3130 p 1445 N95-21180
NR PROJ. M00-96 p 1442 N95-20710
NR PROJ. RH2-1-S-22 p 1202 N95-20071
NR PROJ. SO3-97 p 1388 N95-22411
NR PROJ. S03-97 p 1279 N95-22047
NR PROJ. X05-13 p 1433 N95-21018
NR PROJ. X20-08 p 1432 N95-20012
NR PROJ. 083-004 p 1433 N95-20458
NSF ASC-91-13895 p 1489 N95-20274
NSF AST-89-19563 p 1594 N95-21773
NSF AST-90-21414 p 1579 N95-19947
NSF CCR-88-20279 p 1480 N95-20083
p 1490 N95-20565
p 1490 N95-20588
p 1497 N95-22388
NSF CCR-88-96272 p 1466 N95-21269
NSF DDM-90-01705 p 1490 N95-20662
NSF DDM-92-01340 p 1490 N95-20662
p 1470 N95-21974
NSF DMR-91-08015 p 1574 N95-21712
NSF DMR-91-15342 p 1569 N95-20793
NSF DMS-89-20550 p 1466 N95-21269
NSF DMS-91-20877 p 1489 N95-20274
p 1491 N95-20920
NSF DMS-92-03768 p 1495 N95-22325
NSF DMS-92-05296 p 1498 N95-19945
NSF DMS-92-11820 p 1495 N95-22157
NSF DPP-88-17406 p 1426 N95-21944
NSF DPP-91-17458 p 1426 N95-21944
NSF ECD-89-07068 p 1463 N95-20846
NSF ECS-92-53760 p 1324 N95-20543
NSF III-92-61713 p 1323 N95-20540
NSF IRI-81-00681 p 1473 N95-19885
NSF IRI-89-00276 p 1468 N95-21495
NSF IRI-90-03087 p 1464 N95-20996
NSF MCB-93-04625 p 1440 N95-22066
NSF MSS-90-25110 p 1480 N95-20083
p 1490 N95-20565
p 1490 N95-20588
p 1497 N95-22388
NSF OCE-87-16910 p 1436 N95-22072
NSF OCE-88-00693 p 1436 N95-22073
NSF OCE-89-17628 p 1434 N95-21677
NSF OCE-90-17158 p 1435 N95-21943
NSF OCE-90-19918 p 1434 N95-21677
NSF OCE-91-01734 p 1436 N95-22073
NSF OCE-91-14465 p 1435 N95-21681
NSF OCE-92-24824 p 1435 N95-21682
NSF ORS-92-55223 p 1579 N95-19947
NWO-611-306-523 p 1492 N95-21318
NWO-611-307-018 p 1492 N95-21318
N00014-1-94-0067 p 1568 N95-20552
N00014-82-K-0612 p 1365 N95-20431
p 1324 N95-20587
p 1277 N95-21876
N00014-85-K-0124 p 1481 N95-21185
N00014-86-K-0118 p 1368 N95-19987
N00014-86-K-0690 p 1434 N95-21461
N00014-87-J-1248 p 1238 N95-20563
p 1241 N95-21123
N00014-87-K-0001 p 1433 N95-20458
N00014-87-K-0181 p 1436 N95-22187
N00014-87-K-2001 p 1372 N95-21144
N00014-88-K-0141 p 1341 N95-20849
N00014-88-K-0543 p 1474 N95-20305
N00014-88-K-0612 p 1433 N95-20458
N00014-89-J-1056 p 1433 N95-20458
N00014-89-J-1058 p 1433 N95-20433
N00014-89-J-1063 p 1490 N95-20662
p 1470 N95-21974
N00014-89-J-1070 p 1308 N95-22041
N00014-89-J-1207 p 1524 N95-21688
N00014-89-J-1225 p 1265 N95-20094
p 1280 N95-22259
p 1578 N95-22286
N00014-89-J-1261 p 1544 N95-20876
p 1245 N95-21826
p 1245 N95-21827
p 1547 N95-22074
N00014-89-J-1272 p 1450 N95-22052
N00014-89-J-1350 p 1567 N95-20483
p 1241 N95-21124
p 1281 N95-22470
N00014-89-J-1638 p 1346 N95-21064
N00014-89-J-1754 p 1427 N95-22423
N00014-89-J-1815 p 1491 N95-20719
N00014-90-J-1001 p 1571 N95-20964
N00014-90-J-1030 p 1480 N95-20083
p 1489 N95-20274
p 1490 N95-20588
p 1497 N95-22388
N00014-90-J-1040 p 1490 N95-20565
N00014-90-J-1046 p 1433 N95-20433
N00014-90-J-1108 p 1434 N95-21461
N00014-90-J-1156 p 1226 N95-20092
N00014-90-J-1188 p 1434 N95-21461
N00014-90-J-1474 p 1434 N95-21306
N00014-90-J-1683 p 1432 N95-20040
N00014-90-J-1835 p 1315 N95-20394
N00014-90-J-1976 p 1350 N95-21085
N00014-90-J-4074 p 1324 N95-20610
N00014-90-J-4130 p 1369 N95-20072
N00014-90-1-1030 p 1491 N95-20920
N00014-91-C-0001 p 1221 N95-20708
N00014-91-C-0112 p 1312 N95-19894
N00014-91-C-0129 p 1464 N95-20910
N00014-91-C-0216 p 1326 N95-20824
p 1276 N95-21695
N00014-91-J-04933 p 1479 N95-20010
N00014-91-J-1043 p 1246 N95-21879
p 1247 N95-22020
p 1224 N95-22252
N00014-91-J-1045 p 1269 N95-20582
N00014-91-J-1194 p 1265 N95-20183
p 1268 N95-20428
p 1268 N95-20442
p 1269 N95-20580
p 1270 N95-20671
p 1271 N95-20709
p 1273 N95-20978
N00014-91-J-1195 p 1374 N95-21630
N00014-91-J-1200 p 1434 N95-21293
N00014-91-J-1217 p 1438 N95-20806
N00014-91-J-1258 p 1224 N95-20660
p 1270 N95-20689
p 1239 N95-20712
p 1569 N95-20714
p 1248 N95-22385
N00014-91-J-1269 p 1227 N95-20427
N00014-91-J-1274 p 1574 N95-21599
N00014-91-J-1308 p 1475 N95-20618
N00014-91-J-1381 p 1267 N95-20328
N00014-91-J-1540 p 1449 N95-20393
N00014-91-J-1596 p 1569 N95-20807
N00014-91-J-1629 p 1567 N95-20544
p 1513 N95-20585
p 1513 N95-20586
p 1568 N95-20594
N00014-91-J-1630 p 1365 N95-20413
p 1253 N95-20577
p 1241 N95-21217
p 1328 N95-21218
N00014-91-J-1710 p 1223 N95-20590
p 1223 N95-20592
N00014-91-J-1825 p 1583 N95-22100
N00014-91-J-1917 p 1223 N95-20033
N00014-91-J-1941 p 1531 N95-19974
N00014-91-J-1985 p 1473 N95-19885
N00014-91-J-4008 p 1227 N95-20412
N00014-91-J-4016 p 1495 N95-22157
N00014-91-J-4038 p 1479 N95-20011
p 1481 N95-21185
p 1468 N95-21495
N00014-91-J-4057 p 1510 N95-20327
p 1239 N95-20668
p 1517 N95-21127
p 1525 N95-21878
p 1246 N95-22000
N00014-91-J-4130 p 1513 N95-20621
p 1224 N95-21911
N00014-91-J-4139 p 1461 N95-20622
N00014-91-WX-24079 p 1348 N95-21076
N00014-92-C-0035 p 1310 N95-22253
N00014-92-C-0182 p 1473 N95-19885
N00014-92-C-0214 p 1312 N95-19958
p 1258 N95-21575
N00014-92-C-0216 p 1349 N95-21078
N00014-92-J-1069 p 1429 N95-20391
N00014-92-J-1072 p 1358 N95-22290
N00014-92-J-1243 p 1522 N95-21492
N00014-92-J-1244 p 1443 N95-20850
N00014-92-J-1245 p 1495 N95-22325
N00014-92-J-1264 p 1499 N95-21945
p 1499 N95-21946
N00014-92-J-1285 p 1430 N95-20969
N00014-92-J-1415 p 1280 N95-22141
N00014-92-J-1493 p 1240 N95-20842
N00014-92-J-1510 p 1502 N95-19883
p 1505 N95-21863
N00014-92-J-1611 p 1350 N95-21083
N00014-92-J-1796 p 1349 N95-21078
N00014-92-J-1808 p 1227 N95-20429
p 1227 N95-20430
p 1227 N95-20583
p 1228 N95-20584
p 1228 N95-20801
p 1228 N95-20802
p 1231 N95-21999
N00014-92-J-1866 p 1290 N95-20306
N00014-92-J-1879 p 1473 N95-22386
N00014-92-J-1895 p 1541 N95-20066
N00014-92-J-1900 p 1437 N95-20711
N00014-92-J-4109 p 1432 N95-20209
N00014-92-J-4112 p 1433 N95-21158
N00014-92-K-2015 p 1216 N95-20624
N00014-93-C-0065 p 1225 N95-19919
N00014-93-C-0182 p 1458 N95-20070
N00014-93-C-0234 p 1457 N95-19961
N00014-93-C-2026 p 1315 N95-20488
p 1336 N95-22412
N00014-93-C-2044 p 1278 N95-21973
p 1578 N95-22231
N00014-93-C-6010 p 1458 N95-20095
N00014-93-I-0122 p 1506 N95-19959
p 1506 N95-19960
N00014-93-I-0331 p 1568 N95-20553
N00014-93-I-0385 p 1437 N95-20185
N00014-93-I-0437 p 1568 N95-20614
N00014-93-J-1034 p 1443 N95-20851
N00014-93-J-9007 p 1605 N95-22394
N00014-93-1-0122 p 1507 N95-20097
p 1516 N95-20994
N00014-93-1-0184 p 1348 N95-21076
N00014-93-1-0311 p 1571 N95-21145
N00014-93-1-0316 p 1369 N95-20082
N00014-93-1-0342 p 1348 N95-21071
N00014-93-1-0366 p 1270 N95-20664
N00014-93-1-0368 p 1505 N95-21930
N00014-93-1-0385 p 1459 N95-20157
N00014-93-1-0396 p 1491 N95-20875
N00014-93-1-0409 p 1331 N95-21660
N00014-93-1-0461 p 1432 N95-19988
N00014-93-1-0537 p 1251 N95-20178
N00014-93-1-0558 p 1372 N95-21019
N00014-93-1-0570 p 1470 N95-21971
N00014-93-1-0582 p 1266 N95-20227
N00014-93-1-0686 p 1305 N95-21576
N00014-93-1-0931 p 1332 N95-21774
N00014-93-1-0934 p 1477 N95-21698
N00014-93-1-1129 p 1546 N95-22043
N00014-93-1-1389 p 1563 N95-22422
N00014-94-C-0078 p 1480 N95-20482
N00014-94-C-0261 p 1328 N95-21178
N00014-94-G-0212 p 1225 N95-20001
N00014-94-I-0079 p 1434 N95-21461
N00014-94-I-0331 p 1513 N95-20554
p 1238 N95-20555
N00014-94-J-4099 p 1465 N95-21012
N00014-94-J-9018 p 1354 N95-21583
p 1354 N95-21584
p 1358 N95-22424
N00014-94-1-0043 p 1503 N95-20098
N00014-94-1-0129 p 1264 N95-19972
N00014-94-1-0438 p 1433 N95-20999
N00014-94-1-0516 p 1455 N95-21589
N00014-94-1-0793 p 1200 N95-20175
p 1200 N95-20177
N00014-94-1-0794 p 1590 N95-21401
N00039-91-C-0001 p 1460 N95-20546
N00039-92-C-0100 p 1267 N95-20390
N00039-93-C-0001 p 1408 N95-21699
p 1308 N95-21988
N61533-91-K-0032 p 1504 N95-20918
N62269-89-C-0258 p 1279 N95-22136
N62269-90-D-0110 p 1453 N95-21691
N66001-94-C-6037 p 1466 N95-21325
N68171-94-C-9068 p 1207 N95-20860
N68171-94-M-5247 p 1564 N95-20210
N68171-94-M-5839 p 1541 N95-20249
OSURF PROJ. 729390 p 1253 N95-20417
PAGEIN PROJ. R2031 p 1352 N95-21098
PROJ. M00-99 p 1446 N95-22003
PROJ. RJ1-4-B-41 p 1472 N95-22201
PROJ. RJ3-5-C-72 p 1503 N95-20272
PROJ. SRI-PYH4197 p 1247 N95-22150
PROJ. 3466 p 1555 N95-21141
p 1556 N95-21142
PROJ. 3938 p 1555 N95-21141
p 1556 N95-21142
PROJ. 3940 p 1556 N95-21142
PROJ. 794-P-76 p 1506 N95-22360

RTOP 151-01-60-01 .... p 1423 N95-21815
RTOP 196-41-67-03 .... p 1423 N95-21815
RTOP 199-18-12-07 .... p 1439 N95-21544
RTOP 199-45-16-11 .... p 1517 N95-21191
RTOP 232-01-04-01 .... p 1200 N95-20688
RTOP 233-01-0A .... p 1316 N95-20502
RTOP 233-01-0E .... p 1415 N95-21188
RTOP 233-01-01-03 .... p 1220 N95-21190
RTOP 233-02-0A .... p 1334 N95-22112
RTOP 233-03-0B .... p 1338 N95-19952
RTOP 235-01-03 .... p 1307 N95-21890
RTOP 242-80-01-01 .... p 1494 N95-21622
RTOP 314-30-11-00-10 .... p 1305 N95-21543
RTOP 314-30-11-00-12 .... p 1304 N95-21538
RTOP 314-30-11-10-02 .... p 1305 N95-21539
RTOP 314-30-11-60-02 .... p 1218 N95-21533
RTOP 314-30-21-00-06 .... p 1305 N95-21540
RTOP 314-30-61-02-05 .... p 1304 N95-21534
RTOP 314-30-63-02-04 .... p 1305 N95-21542
RTOP 314-40-31-30-26 .... p 1302 N95-21456
RTOP 315-91-20-20-53 .... p 1304 N95-21535
p 1304 N95-21536
RTOP 315-91-40-20-36 .... p 1304 N95-21537
RTOP 315-91-50-20-04 .... p 1305 N95-21541
RTOP 326-84-00 .... p 1396 N95-21952
p 1396 N95-21953
RTOP 466-05-02 .... p 1201 N95-20794
RTOP 478-83-00 .... p 1218 N95-21384
RTOP 505-59-10-20 .... p 1201 N95-21338
RTOP 505-59-54-02 .... p 1368 N95-22109
RTOP 505-59-54 .... p 1366 N95-21323
RTOP 505-62-10 .... p 1337 N95-19912
RTOP 505-62-30-01 .... p 1199 N95-19913
RTOP 505-62-36 .... p 1380 N95-21359
RTOP 505-62-50 .... p 1366 N95-21259
RTOP 505-62-52 .... p 1338 N95-19953
p 1355 N95-21957
p 1284 N95-22114
RTOP 505-63-5A .... p 1223 N95-19901
p 1274 N95-21252
RTOP 505-63-5B .... p 1385 N95-20179
p 1386 N95-20790
RTOP 505-63-50-04 .... p 1230 N95-21363
RTOP 505-64-13-22 .... p 1204 N95-19950
RTOP 505-64-29 .... p 1207 N95-21186
RTOP 505-64-50-04 .... p 1462 N95-20691
RTOP 505-64-52-01 .... p 1219 N95-20800
RTOP 505-90-00 .... p 1587 N95-20162
p 1587 N95-20163
p 1589 N95-21015
RTOP 505-90-5K .... p 1356 N95-21959
RTOP 505-90-52-01 .... p 1338 N95-20009
p 1479 N95-20010
p 1473 N95-20013
p 1495 N95-22157
p 1495 N95-22325
p 1456 N95-22431
RTOP 506-40-41-02 .... p 1340 N95-20619
RTOP 537-02-21 .... p 1214 N95-21383
RTOP 537-03-23-03 .... p 1353 N95-21258
RTOP 537-04-22 .... p 1225 N95-19951
RTOP 538-03-11 .... p 1505 N95-21888
RTOP 538-05-13-01 .... p 1216 N95-20669
p 1203 N95-20706
RTOP 550-63-00 .... p 1473 N95-19885
RTOP 584-03-11 .... p 1222 N95-21458
RTOP 763-22-21 .... p 1366 N95-21391
RTOP 778-32-21 .... p 1382 N95-22404
p 1382 N95-22405
SRI PROJ. 4069 .... p 1237 N95-20438
SUB93-216 .... p 1390 N95-22110
p 1390 N95-22111
USDA-9301106 .... p 1440 N95-22066
W-31-109-ENG-38 .... p 1338 N95-19923
p 1540 N95-19968
p 1437 N95-19969
p 1531 N95-19983
p 1586 N95-20016
p 1564 N95-20017
p 1264 N95-20018
p 1506 N95-20025
p 1226 N95-20027
p 1285 N95-20050
p 1441 N95-20074
p 1541 N95-20103
p 1500 N95-20106
p 1234 N95-20107
p 1489 N95-20170
p 1412 N95-20171
p 1401 N95-20193
p 1401 N95-20234
p 1501 N95-20241
p 1402 N95-20247
p 1579 N95-20271
p 1510 N95-20360
p 1206 N95-20370
p 1566 N95-20372
p 1460 N95-20385
p 1566 N95-20419
p 1403 N95-20478
p 1567 N95-20479
p 1392 N95-20480
p 1254 N95-20707
p 1254 N95-20792
p 1404 N95-20835
p 1240 N95-20836
p 1393 N95-20839
p 1229 N95-20840
p 1570 N95-20841
p 1514 N95-20852
p 1570 N95-20881
p 1414 N95-20908
p 1229 N95-20912
p 1558 N95-21244
p 1571 N95-21256
p 1476 N95-21257
p 1329 N95-21296
p 1466 N95-21311
p 1476 N95-21341
p 1438 N95-21376
p 1559 N95-21388
p 1521 N95-21406
p 1536 N95-21407
p 1572 N95-21408
p 1366 N95-21453
p 1521 N95-21454
p 1573 N95-21474
p 1604 N95-21475
p 1415 N95-21477
p 1522 N95-21499
p 1522 N95-21502
p 1537 N95-21503
p 1407 N95-21608
p 1407 N95-21617
p 1469 N95-21829
p 1426 N95-21836
p 1396 N95-21897
p 1440 N95-22067
p 1440 N95-22075
p 1471 N95-22077
p 1591 N95-22092
p 1232 N95-22130
p 1335 N95-22189
p 1527 N95-22190
p 1262 N95-22291
p 1382 N95-22292
W-7405-ENG-36 .... p 1458 N95-20154
p 1474 N95-20158
p 1508 N95-20159
p 1508 N95-20160
p 1289 N95-20164
p 1459 N95-20165
p 1339 N95-20166
p 1488 N95-20167
p 1313 N95-20168
p 1488 N95-20169
p 1531 N95-20203
p 1509 N95-20235
p 1509 N95-20236
p 1501 N95-20246
p 1509 N95-20254
p 1236 N95-20277
p 1412 N95-20278
p 1285 N95-20288
p 1413 N95-20289
p 1565 N95-20330
p 1252 N95-20331
p 1236 N95-20361
p 1510 N95-20367
p 1237 N95-20368
p 1379 N95-20627
p 1554 N95-20675
p 1481 N95-20693
p 1569 N95-20696
p 1291 N95-20697
p 1462 N95-20699
p 1588 N95-20777
p 1371 N95-20786
p 1588 N95-20789
p 1481 N95-20812
p 1254 N95-20816
p 1589 N95-20818
p 1501 N95-20869
p 1414 N95-20990
p 1516 N95-21114
p 1555 N95-21115
p 1516 N95-21125
p 1500 N95-21136
p 1255 N95-21137
p 1415 N95-21184
p 1518 N95-21235
p 1534 N95-21236
p 1519 N95-21237
p 1255 N95-21238
p 1557 N95-21239
p 1557 N95-21240
p 1558 N95-21242
p 1580 N95-21264
p 1466 N95-21288
p 1373 N95-21312
p 1353 N95-21317
p 1520 N95-21321
p 1536 N95-21331
p 1387 N95-21364
p 1438 N95-21366
p 1599 N95-21367
p 1558 N95-21368
p 1603 N95-21377
p 1387 N95-21386
p 1482 N95-21522
p 1244 N95-21523
p 1407 N95-21666
p 1331 N95-21667
p 1560 N95-21668
p 1483 N95-21710
p 1574 N95-21712
p 1332 N95-21742
p 1375 N95-21837
p 1426 N95-21875
p 1375 N95-21919
p 1478 N95-21925
p 1260 N95-21926
p 1526 N95-21934
p 1600 N95-21935
p 1575 N95-21936
p 1260 N95-22006
p 1375 N95-22007
p 1576 N95-22008
p 1231 N95-22009
p 1561 N95-22010
p 1334 N95-22011
p 1246 N95-22012
p 1538 N95-22050
p 1526 N95-22058
p 1440 N95-22065
p 1527 N95-22078
p 1600 N95-22128
p 1376 N95-22154
p 1335 N95-22165
p 1376 N95-22242
p 1539 N95-22243
p 1529 N95-22280
p 1262 N95-22289
p 1440 N95-22296
p 1578 N95-22297
p 1539 N95-22298
p 1262 N95-22308
p 1377 N95-22348
p 1540 N95-22410
p 1601 N95-22419
p 1281 N95-22428
p 1486 N95-22430
p 1248 N95-22433
p 1281 N95-22434
p 1530 N95-22435
p 1221 N95-22436
p 1427 N95-22477
W-7405-ENG-48 .... p 1250 N95-19900
p 1412 N95-19985
p 1368 N95-19986
p 1531 N95-20015
p 1548 N95-20037
p 1549 N95-20038
p 1313 N95-20119
p 1531 N95-20120
p 1251 N95-20122
p 1428 N95-20140
p 1599 N95-20145
p 1550 N95-20146
p 1219 N95-20148
p 1550 N95-20189
p 1550 N95-20190
p 1541 N95-20218
p 1551 N95-20219
p 1385 N95-20237
p 1459 N95-20255
p 1551 N95-20279
p 1551 N95-20283
p 1551 N95-20315
p 1266 N95-20316
p 1267 N95-20317
p 1552 N95-20318
p 1369 N95-20335
p 1460 N95-20351
p 1541 N95-20352
p 1402 N95-20353
p 1413 N95-20354
p 1402 N95-20355

p 1286 N95-20356
p 1552 N95-20362
p 1553 N95-20363
p 1542 N95-20364
p 1429 N95-20381
p 1237 N95-20386
p 1460 N95-20387
p 1542 N95-20403
p 1433 N95-20420
p 1511 N95-20444
p 1554 N95-20446
p 1253 N95-20447
p 1567 N95-20448
p 1567 N95-20449
p 1542 N95-20450
p 1542 N95-20489
p 1554 N95-20568
p 1554 N95-20571
p 1543 N95-20612
p 1371 N95-20783
p 1533 N95-20784
p 1555 N95-20813
p 1371 N95-20817
p 1327 N95-20854
p 1272 N95-20892
p 1272 N95-20895
p 1372 N95-21135
p 1555 N95-21141
p 1556 N95-21159
p 1557 N95-21166
p 1372 N95-21173
p 1517 N95-21174
p 1274 N95-21175
p 1353 N95-21182
p 1301 N95-21205
p 1557 N95-21206
p 1557 N95-21207
p 1534 N95-21208
p 1534 N95-21209
p 1373 N95-21210
p 1452 N95-21358
p 1520 N95-21360
p 1354 N95-21387
p 1544 N95-21392
p 1389 N95-21433
p 1559 N95-21451
p 1367 N95-21478
p 1600 N95-21479
p 1545 N95-21510
p 1415 N95-21511
p 1389 N95-21552
p 1493 N95-21564
p 1453 N95-21637
p 1276 N95-21662
p 1374 N95-21663
p 1576 N95-22084
p 1376 N95-22121
p 1232 N95-22126
p 1562 N95-22191
p 1562 N95-22221
p 1528 N95-22222
p 1528 N95-22223
p 1309 N95-22241
p 1310 N95-22299
p 1562 N95-22300
p 1376 N95-22301
p 1377 N95-22312
p 1262 N95-22313
p 1377 N95-22343
p 1263 N95-22408
p 1337 N95-22421
p 1473 N95-22426
p 1337 N95-22427
p 1540 N95-22469
W-7405-ENG-82 .... p 1458 N95-20136
p 1572 N95-21297
p 1242 N95-21397
p 1257 N95-21398
p 1257 N95-21399
p 1242 N95-21400
p 1493 N95-21439
p 1258 N95-21568
p 1573 N95-21569
p 1574 N95-21570
p 1574 N95-21723
p 1245 N95-21734
p 1277 N95-21735
p 1231 N95-21736
p 1259 N95-21737
p 1260 N95-21841
p 1260 N95-21923
p 1231 N95-21924

REPORT NUMBER INDEX

SCIENTIFIC AND TECHNICAL AEROSPACE REPORTS VOLUME 33 NUMBER 6

Typical Report Number Index Listing

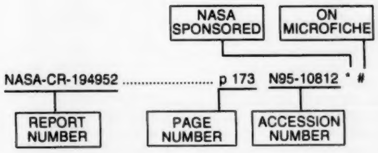

Listings in this index are arranged alphanumerically by report number. The accession number denotes the number by which the citation is identified. The page number helps to locate the citation in the abstract section. An asterisk (*) indicates that the item is a NASA report. A pound sign (#) indicates that the item is available on microfiche.

A-94138 .... p 1439 N95-21544 * #
A-95028 .... p 1207 N95-21186 * #
A-95032 .... p 1366 N95-21323 * #

AD-A091282 .... p 1306 N95-21684
AD-A139805 .... p 1367 N95-21680
AD-A279066 .... p 1258 N95-21575
AD-A279068 .... p 1287 N95-21626
AD-A279074 .... p 1468 N95-21627
AD-A279076 .... p 1390 N95-21628
AD-A279084 .... p 1445 N95-21629
AD-A279086 .... p 1390 N95-21912
AD-A279089 .... p 1483 N95-21913
AD-A279090 .... p 1409 N95-21914
AD-A279093 .... p 1307 N95-21915
AD-A279095 .... p 1471 N95-22068
AD-A279097 .... p 1591 N95-22069
AD-A279099 .... p 1407 N95-21596
AD-A279102 .... p 1287 N95-21598
AD-A279124 .... p 1574 N95-21599
AD-A279125 .... p 1277 N95-21876
AD-A279126 .... p 1202 N95-21877
AD-A279130 .... p 1387 N95-21967
AD-A279138 .... p 1450 N95-21968
AD-A279144 .... p 1278 N95-21969
AD-A279146 .... p 1307 N95-21970
AD-A279148 .... p 1470 N95-21971
AD-A279151 .... p 1470 N95-21972
AD-A279153 .... p 1278 N95-21973
AD-A279156 .... p 1470 N95-21974
AD-A279157 .... p 1546 N95-21975
AD-A279158 .... p 1279 N95-21976
AD-A279159 .... p 1370 N95-20600
AD-A279222 .... p 1502 N95-19883
AD-A279242 .... p 1403 N95-20465
AD-A279246 .... p 1505 N95-21984
AD-A279253 .... p 1307 N95-21985
AD-A279254 .... p 1260 N95-21986
AD-A279255 .... p 1505 N95-21863
AD-A279257 .... p 1468 N95-21489
AD-A279271 .... p 1330 N95-21490
AD-A279275 .... p 1303 N95-21491
AD-A279279 .... p 1522 N95-21492
AD-A279294 .... p 1303 N95-21493
AD-A279295 .... p 1436 N95-21987
AD-A279305 .... p 1446 N95-21941
AD-A279309 .... p 1280 N95-22141
AD-A279328 .... p 1410 N95-22142
AD-A279339 .... p 1450 N95-21927
AD-A279342 .... p 1581 N95-21928
AD-A279345 .... p 1603 N95-21929
AD-A279348 .... p 1368 N95-22143
AD-A279375 .... p 1335 N95-22144
AD-A279378 .... p 1206 N95-20181
AD-A279388 .... p 1356 N95-22145
AD-A279389 .... p 1355 N95-21942
AD-A279390 .... p 1435 N95-21943
AD-A279392 .... p 1426 N95-21944
AD-A279393 .... p 1499 N95-21945
AD-A279394 .... p 1499 N95-21946
AD-A279395 .... p 1505 N95-21930
AD-A279396 .... p 1246 N95-21931
AD-A279405 .... p 1426 N95-21932
AD-A279407 .... p 1383 N95-21933
AD-A279408 .... p 1575 N95-21916
AD-A279409 .... p 1333 N95-21917
AD-A279435 .... p 1435 N95-21918
AD-A279437 .... p 1436 N95-22072 *
AD-A279444 .... p 1436 N95-22073
AD-A279445 .... p 1547 N95-22074
AD-A279449 .... p 1544 N95-20876
AD-A279450 .... p 1245 N95-21826
AD-A279472 .... p 1433 N95-21291
AD-A279473 .... p 1245 N95-21827
AD-A279478 .... p 1434 N95-21677
AD-A279480 .... p 1284 N95-21678
AD-A279484 .... p 1600 N95-21679
AD-A279492 .... p 1367 N95-21680
AD-A279507 .... p 1435 N95-21681
AD-A279509 .... p 1435 N95-21682
AD-A279511 .... p 1407 N95-21683
AD-A279512 .... p 1306 N95-21684
AD-A279525 .... p 1408 N95-21685
AD-A279526 .... p 1306 N95-21686
AD-A279527 .... p 1259 N95-21687
AD-A279532 .... p 1524 N95-21688
AD-A279533 .... p 1408 N95-21689
AD-A279539 .... p 1331 N95-21690
AD-A279544 .... p 1453 N95-21691 #
AD-A279545 .... p 1331 N95-21693
AD-A279546 .... p 1374 N95-21694 #
AD-A279560 .... p 1276 N95-21695
AD-A279565 .... p 1408 N95-21696
AD-A279567 .... p 1276 N95-21697
AD-A279569 .... p 1221 N95-20708
AD-A279573 .... p 1477 N95-21698
AD-A279575 .... p 1408 N95-21699
AD-A279577 .... p 1453 N95-21700
AD-A279581 .... p 1300 N95-21099
AD-A279596 .... p 1543 N95-20601
AD-A279597 .... p 1504 N95-20300
AD-A279599 .... p 1441 N95-20301
AD-A279602 .... p 1215 N95-19955 #
AD-A279603 .... p 1587 N95-20302
AD-A279604 .... p 1586 N95-19956 #
AD-A279605 .... p 1402 N95-20441
AD-A279607 .... p 1448 N95-19957 #
AD-A279608 .... p 1312 N95-19958 #
AD-A279609 .... p 1506 N95-19959 #
AD-A279630 .... p 1553 N95-20411
AD-A279631 .... p 1403 N95-20456
AD-A279640 .... p 1442 N95-20457
AD-A279649 .... p 1516 N95-21120 #
AD-A279650 .... p 1432 N95-20303
AD-A279652 .... p 1506 N95-19960 #
AD-A279657 .... p 1459 N95-20304
AD-A279661 .... p 1227 N95-20412
AD-A279662 .... p 1567 N95-20426 #
AD-A279664 .... p 1474 N95-20305
AD-A279665 .... p 1433 N95-20458
AD-A279667 .... p 1442 N95-20602
AD-A279669 .... p 1270 N95-20603
AD-A279672 .... p 1365 N95-20604
AD-A279675 .... p 1516 N95-21121 #
AD-A279676 .... p 1291 N95-20605
AD-A279691 .... p 1461 N95-20579
AD-A279693 .... p 1227 N95-20427 #
AD-A279694 .... p 1268 N95-20428 #
AD-A279695 .... p 1269 N95-20580
AD-A279696 .... p 1271 N95-20709
AD-A279698 .... p 1442 N95-20710
AD-A279699 .... p 1437 N95-20711
AD-A279700 .... p 1239 N95-20712
AD-A279701 .... p 1569 N95-20714
AD-A279702 .... p 1270 N95-20689
AD-A279703 .... p 1217 N95-20690
AD-A279715 .... p 1270 N95-20671
AD-A279716 .... p 1533 N95-20672
AD-A279717 .... p 1216 N95-20992
AD-A279719 .... p 1516 N95-20993
AD-A279725 .... p 1516 N95-20994
AD-A279726 .... p 1217 N95-20995
AD-A279736 .... p 1228 N95-20801
AD-A279737 .... p 1227 N95-20429 #
AD-A279738 .... p 1227 N95-20430 #
AD-A279739 .... p 1228 N95-20802 #
AD-A279746 .... p 1248 N95-22385
AD-A279748 .... p 1544 N95-20803 #
AD-A279749 .... p 1514 N95-20804 #
AD-A279756 .... p 1590 N95-21401 #
AD-A279761 .... p 1507 N95-20097 #
AD-A279763 .... p 1228 N95-20805 #
AD-A279767 .... p 1444 N95-20977
AD-A279770 .... p 1308 N95-21988 #
AD-A279774 .... p 1438 N95-20806 #
AD-A279775 .... p 1446 N95-21989 #
AD-A279776 .... p 1457 N95-19961 #
AD-A279780 .... p 1231 N95-21999 #
AD-A279781 .... p 1273 N95-20978
AD-A279782 .... p 1268 N95-20442 #
AD-A279785 .... p 1290 N95-20306 #
AD-A279787 .... p 1315 N95-20443 #
AD-A279789 .... p 1441 N95-20307 #
AD-A279790 .... p 1445 N95-21180
AD-A279792 .... p 1224 N95-20660 #
AD-A279802 .... p 1498 N95-20102
AD-A279803 .... p 1434 N95-21306
AD-A279809 .... p 1503 N95-20098
AD-A279810 .... p 1495 N95-22157 *
AD-A279811 .... p 1569 N95-20807
AD-A279813 .... p 1269 N95-20582
AD-A279814 .... p 1227 N95-20583
AD-A279815 .... p 1228 N95-20584
AD-A279818 .... p 1567 N95-20544 #
AD-A279819 .... p 1513 N95-20585
AD-A279820 .... p 1513 N95-20586
AD-A279821 .... p 1324 N95-20587
AD-A279823 .... p 1537 N95-21494
AD-A279829 .... p 1301 N95-21292
AD-A279832 .... p 1605 N95-20182 #
AD-A279836 .... p 1365 N95-20431
AD-A279838 .... p 1434 N95-21293
AD-A279839 .... p 1481 N95-21185
AD-A279841 .... p 1468 N95-21495
AD-A279842 .... p 1473 N95-22386
AD-A279847 .... p 1414 N95-20760
AD-A279849 .... p 1376 N95-22164
AD-A279858 .... p 1459 N95-20157
AD-A279861 .... p 1281 N95-22387
AD-A279863 .... p 1462 N95-20776
AD-A279868 .... p 1497 N95-22388
AD-A279869 .... p 1365 N95-20413
AD-A279870 .... p 1490 N95-20432
AD-A279871 .... p 1382 N95-20414
AD-A279872 .... p 1265 N95-20183 #
AD-A279873 .... p 1459 N95-20184 #
AD-A279875 .... p 1433 N95-20433
AD-A279876 .... p 1437 N95-20185 #
AD-A279884 .... p 1497 N95-22389
AD-A279885 .... p 1490 N95-20588
AD-A279888 .... p 1588 N95-20589
AD-A279892 .... p 1223 N95-20590
AD-A279893 .... p 1223 N95-20592
AD-A279894 .... p 1602 N95-20593
AD-A279895 .... p 1568 N95-20594
AD-A279896 .... p 1461 N95-20595
AD-A279898 .... p 1452 N95-20562
AD-A279899 .... p 1238 N95-20563
AD-A279900 .... p 1543 N95-20564
AD-A279902 .... p 1305 N95-21576
AD-A279903 .... p 1490 N95-20565
AD-A279905 .... p 1475 N95-20566
AD-A279906 .... p 1281 N95-19884
AD-A279907 .... p 1428 N95-20186
AD-A279909 .... p 1290 N95-20545
AD-A279910 .... p 1253 N95-20577
AD-A279911 .... p 1290 N95-20308
AD-A279912 .... p 1587 N95-20309
AD-A279913 .... p 1459 N95-20310
AD-A279917 .... p 1269 N95-20578
AD-A279945 .... p 1238 N95-20581

AD-A279956 .... p 1414 N95-20591
AD-A279959 .... p 1325 N95-20661
AD-A279965 .... p 1215 N95-21122
AD-A279972 .... p 1241 N95-21123
AD-A279975 .... p 1491 N95-20920
AD-A279976 .... p 1272 N95-20962
AD-A279980 .... p 1504 N95-20963
AD-A279982 .... p 1571 N95-20964
AD-A279988 .... p 1571 N95-20965
AD-A279991 .... p 1327 N95-20966
AD-A279993 .... p 1270 N95-20596
AD-A279994 .... p 1314 N95-20311
AD-A279995 .... p 1238 N95-20597
AD-A279996 .... p 1340 N95-20312
AD-A279997 .... p 1241 N95-21124 #
AD-A280005 .... p 1339 N95-20058 #
AD-A280009 .... p 1221 N95-20059 * #
AD-A280011 .... p 1448 N95-19970 #
AD-A280012 .... p 1214 N95-20004 #
AD-A280013 .... p 1460 N95-20313
AD-A280015 .... p 1449 N95-20314
AD-A280016 .... p 1543 N95-20598
AD-A280021 .... p 1490 N95-20662
AD-A280023 .... p 1479 N95-20005 #
AD-A280030 .... p 1388 N95-20006 #
AD-A280032 .... p 1448 N95-20007 #
AD-A280033 .... p 1428 N95-20008 #
AD-A280037 .... p 1291 N95-20599
AD-A280038 .... p 1386 N95-20615
AD-A280041 .... p 1498 N95-20620
AD-A280044 .... p 1513 N95-20621
AD-A280052 .... p 1473 N95-19885 *
AD-A280053 .... p 1461 N95-20622
AD-A280059 .... p 1563 N95-19886
AD-A280061 .... p 1448 N95-19887
AD-A280062 .... p 1461 N95-20623
AD-A280063 .... p 1216 N95-20624
AD-A280065 .... p 1327 N95-20967
AD-A280070 .... p 1341 N95-20968
AD-A280078 .... p 1430 N95-20969
AD-A280093 .... p 1240 N95-20970
AD-A280094 .... p 1328 N95-21017
AD-A280095 .... p 1433 N95-21018
AD-A280098 .... p 1372 N95-21019
AD-A280100 .... p 1204 N95-21020
AD-A280105 .... p 1224 N95-21911 #
AD-A280108 .... p 1332 N95-21774
AD-A280109 .... p 1331 N95-21660 #
AD-A280111 .... p 1374 N95-21630 #
AD-A280113 .... p 1452 N95-20625
AD-A280122 .... p 1600 N95-21577
AD-A280123 .... p 1431 N95-19888
AD-A280131 .... p 1587 N95-20039
AD-A280132 .... p 1451 N95-20041
AD-A280141 .... p 1338 N95-20009 *
AD-A280142 .... p 1479 N95-20010 *
AD-A280148 .... p 1479 N95-20011
AD-A280183 .... p 1432 N95-20012
AD-A280371 .... p 1583 N95-22100
AD-A283721 .... p 1431 N95-19971
AD-A283722 .... p 1264 N95-19972
AD-A283725 .... p 1289 N95-19973
AD-A283730 .... p 1531 N95-19974
AD-A283733 .... p 1473 N95-20013 *
AD-A283741 .... p 1431 N95-19918
AD-A283750 .... p 1225 N95-19919
AD-A283770 .... p 1282 N95-19920
AD-A283802 .... p 1400 N95-19921
AD-A283809 .... p 1282 N95-19922
AD-A284000 .... p 1207 N95-20466
AD-A284049 .... p 1203 N95-21518 #
AD-A284077 .... p 1542 N95-20467
AD-A284259 .... p 1282 N95-20187
AD-A284278 .... p 1221 N95-19962
AD-A284280 .... p 1206 N95-19963 #
AD-A284291 .... p 1200 N95-20248 #
AD-A284293 .... p 1541 N95-20249
AD-A284297 .... p 1339 N95-20250 #
AD-A284301 .... p 1266 N95-20251
AD-A284305 .... p 1437 N95-20252
AD-A284675 .... p 1400 N95-19964 #
AD-A284717 .... p 1457 N95-20060
AD-A284781 .... p 1479 N95-20061 #
AD-A284782 .... p 1449 N95-20062 #
AD-A284788 .... p 1449 N95-20064
AD-A284791 .... p 1289 N95-20065
AD-A284796 .... p 1541 N95-20066 #
AD-A284797 .... p 1250 N95-20067 #
AD-A284798 .... p 1364 N95-20069
AD-A284836 .... p 1263 N95-19893 #
AD-A284862 .... p 1458 N95-20070
AD-A284921 .... p 1289 N95-19997 #
AD-A284922 .... p 1448 N95-19998 #
AD-A284923 .... p 1457 N95-19999 #
AD-A284924 .... p 1457 N95-20000 #
AD-A284936 .... p 1281 N95-22470 #
AD-A284937 .... p 1530 N95-22471 #
AD-A284938 .... p 1451 N95-22472 #
AD-A284949 .... p 1451 N95-22473 #
AD-A284975 .... p 1432 N95-20040 #
AD-A284979 .... p 1457 N95-20042 #
AD-A284984 .... p 1225 N95-20001 * #
AD-A284998 .... p 1253 N95-20481
AD-A285034 .... p 1583 N95-20051 #
AD-A285043 .... p 1480 N95-20482
AD-A285052 .... p 1567 N95-20483 #
AD-A285053 .... p 1370 N95-20484 #
AD-A285055 .... p 1442 N95-20485 #
AD-A285056 .... p 1269 N95-20486 #
AD-A285059 .... p 1403 N95-20487 #
AD-A285060 .... p 1315 N95-20488 #
AD-A285062 .... p 1204 N95-20497 #
AD-A285094 .... p 1224 N95-22474 #
AD-A285098 .... p 1479 N95-20057 #
AD-A285105 .... p 1368 N95-20063 #
AD-A285120 .... p 1226 N95-20081 #
AD-A285122 .... p 1226 N95-20105 #
AD-A285124 .... p 1313 N95-20257 #
AD-A285131 .... p 1369 N95-20082 #
AD-A285135 .... p 1222 N95-20906 #
AD-A285136 .... p 1475 N95-20500 #
AD-A285142 .... p 1542 N95-20501 #
AD-A285229 .... p 1414 N95-20498 #
AD-A285346 .... p 1475 N95-20499 #
AD-A285347 .... p 1291 N95-20692 #
AD-A285353 .... p 1447 N95-22475 #
AD-A285357 .... p 1460 N95-20546 #
AD-A285358 .... p 1563 N95-22422 #
AD-A285360 .... p 1340 N95-20547 #
AD-A285361 .... p 1269 N95-20548 #
AD-A285364 .... p 1442 N95-20549 #
AD-A285365 .... p 1370 N95-20550 #
AD-A285369 .... p 1269 N95-20551 #
AD-A285370 .... p 1568 N95-20552 #
AD-A285373 .... p 1568 N95-20553 #
AD-A285374 .... p 1513 N95-20554 #
AD-A285375 .... p 1238 N95-20555 #
AD-A285381 .... p 1290 N95-20556 #
AD-A285382 .... p 1480 N95-20606 #
AD-A285384 .... p 1480 N95-20607 #
AD-A285385 .... p 1498 N95-20608 #
AD-A285389 .... p 1449 N95-20609 #
AD-A285392 .... p 1324 N95-20610 #
AD-A285403 .... p 1286 N95-20611 #
AD-A285421 .... p 1465 N95-21176
AD-A285476 .... p 1444 N95-20979 #
AD-A285520 .... p 1430 N95-21177 #
AD-A285543 .... p 1380 N95-21157 #
AD-A285548 .... p 1433 N95-21158 #
AD-A285549 .... p 1444 N95-21160 #
AD-A285583 .... p 1283 N95-21161 #
AD-A285586 .... p 1386 N95-21212 #
AD-A285587 .... p 1505 N95-21213 #
AD-A285593 .... p 1215 N95-21214 #
AD-A285595 .... p 1229 N95-21215 #
AD-A285604 .... p 1517 N95-21216 #
AD-A285605 .... p 1450 N95-21192 #
AD-A285606 .... p 1222 N95-21193 #
AD-A285609 .... p 1502 N95-21194 #
AD-A285610 .... p 1373 N95-21195 #
AD-A285611 .... p 1312 N95-19894 #
AD-A285612 .... p 1431 N95-19895 #
AD-A285613 .... p 1431 N95-19896 #
AD-A285617 .... p 1540 N95-19897 #
AD-A285618 .... p 1441 N95-19898 #
AD-A285620 .... p 1372 N95-21144 #
AD-A285621 .... p 1571 N95-21145 #
AD-A285622 .... p 1353 N95-21146 #
AD-A285623 .... p 1220 N95-21147 #
AD-A285626 .... p 1204 N95-21148 #
AD-A285629 .... p 1229 N95-21149 #
AD-A285632 .... p 1404 N95-21150 #
AD-A285633 .... p 1517 N95-21151 #
AD-A285634 .... p 1273 N95-21152 #
AD-A285635 .... p 1517 N95-21126 #
AD-A285636 .... p 1450 N95-21101 #
AD-A285649 .... p 1242 N95-21402 #
AD-A285655 .... p 1559 N95-21403 #
AD-A285656 .... p 1559 N95-21404 #
AD-A285670 .... p 1480 N95-20083 #
AD-A285671 .... p 1503 N95-20084 #
AD-A285688 .... p 1503 N95-20272 #
AD-A285689 .... p 1489 N95-20274 #
AD-A285691 .... p 1202 N95-20275 #
AD-A285736 .... p 1224 N95-19899 #
AD-A285738 .... p 1202 N95-20071 #
AD-A285739 .... p 1369 N95-20072 #
AD-A285740 .... p 1457 N95-19929 #
AD-A285751 .... p 1241 N95-21217 #
AD-A285752 .... p 1328 N95-21218 #
AD-A285756 .... p 1498 N95-21219 #
AD-A285758 .... p 1215 N95-19931 #
AD-A285759 .... p 1288 N95-19932 #
AD-A285760 .... p 1302 N95-21405 #
AD-A285772 .... p 1233 N95-22395 #
AD-A285773 .... p 1388 N95-22411 #
AD-A285775 .... p 1336 N95-22412 #
AD-A285776 .... p 1463 N95-20877 #
AD-A285778 .... p 1217 N95-22413 #
AD-A285779 .... p 1411 N95-22414 #
AD-A285785 .... p 1233 N95-22399 #
AD-A285788 .... p 1456 N95-22400 #
AD-A285789 .... p 1311 N95-22401 #
AD-A285790 .... p 1473 N95-22402 #
AD-A285831 .... p 1363 N95-20031 #
AD-A285832 .... p 1208 N95-20032 #
AD-A285834 .... p 1223 N95-20033 #
AD-A285835 .... p 1368 N95-20035 #
AD-A285837 .... p 1364 N95-20036 #
AD-A285845 .... p 1203 N95-21831 #
AD-A285846 .... p 1414 N95-20878 #
AD-A285847 .... p 1545 N95-21832 #
AD-A285848 .... p 1415 N95-21308 #
AD-A285849 .... p 1425 N95-21833 #
AD-A285851 .... p 1290 N95-20376 #
AD-A285853 .... p 1413 N95-20377 #
AD-A285857 .... p 1369 N95-20378 #
AD-A285858 .... p 1369 N95-20379 #
AD-A285859 .... p 1369 N95-20389 #
AD-A285860 .... p 1391 N95-22131 #
AD-A285861 .... p 1547 N95-22076 #
AD-A285862 .... p 1261 N95-22132 #
AD-A285863 .... p 1471 N95-22133 #
AD-A285865 .... p 1309 N95-22134 #
AD-A285867 .... p 1499 N95-22135 #
AD-A285869 .... p 1279 N95-22136 #
AD-A285906 .... p 1368 N95-19987 #
AD-A285907 .... p 1432 N95-19988 #
AD-A285921 .... p 1428 N95-19989 #
AD-A285922 .... p 1498 N95-19990 #
AD-A285928 .... p 1200 N95-19991 #
AD-A285930 .... p 1252 N95-20299 #
AD-A285931 .... p 1267 N95-20390 #
AD-A285934 .... p 1429 N95-20391 #
AD-A285937 .... p 1270 N95-20664 #
AD-A285938 .... p 1268 N95-20392 #
AD-A285940 .... p 1451 N95-22323 #
AD-A285941 .... p 1451 N95-22324 #
AD-A285945 .... p 1449 N95-20393 #
AD-A285946 .... p 1315 N95-20394 #
AD-A285947 .... p 1429 N95-20395 #
AD-A285951 .... p 1484 N95-22056 #
AD-A285957 .... p 1517 N95-21127 #
AD-A285960 .... p 1220 N95-21634 #
AD-A285964 .... p 1328 N95-21178 #
AD-A285971 .... p 1461 N95-20665 #
AD-A285972 .... p 1291 N95-20666 #
AD-A285975 .... p 1514 N95-20667 #
AD-A285976 .... p 1239 N95-20668 #
AD-A285977 .... p 1461 N95-20687 #
AD-A285978 .... p 1588 N95-20617 #
AD-A285983 .... p 1475 N95-20618 #
AD-A285988 .... p 1239 N95-20613 #
AD-A285991 .... p 1568 N95-20614 #
AD-A285994 .... p 1325 N95-20715 #
AD-A285998 .... p 1239 N95-20716 #
AD-A286001 .... p 1462 N95-20718 #
AD-A286007 .... p 1491 N95-20719 #
AD-A286009 .... p 1403 N95-20720 #
AD-A286012 .... p 1462 N95-20721 #
AD-A286027 .... p 1589 N95-21002 #
AD-A286028 .... p 1464 N95-20996 #
AD-A286029 .... p 1328 N95-20997 #
AD-A286032 .... p 1379 N95-20998 #
AD-A286033 .... p 1433 N95-20999 #
AD-A286034 .... p 1273 N95-21000 #
AD-A286044 .... p 1341 N95-21001 #
AD-A286047 .... p 1311 N95-22415 #
AD-A286048 .... p 1592 N95-22416 #
AD-A286049 .... p 1203 N95-22417 #
AD-A286050 .... p 1302 N95-21324 #
AD-A286056 .... p 1466 N95-21325 #
AD-A286058 .... p 1504 N95-21170 * #
AD-A286060 .... p 1464 N95-20910 #
AD-A286062 .... p 1380 N95-21171 #
AD-A286063 .... p 1381 N95-21488 #
AD-A286064 .... p 1463 N95-20846
AD-A286065 .... p 1463 N95-20847 #
AD-A286066 .... p 1443 N95-20848 #
AD-A286077 .... p 1341 N95-20849 #
AD-A286078 .... p 1443 N95-20850 #
AD-A286079 .... p 1443 N95-20851 #
AD-A286081 .... p 1228 N95-20808
AD-A286082 .... p 1462 N95-20809 #
AD-A286083 .... p 1463 N95-20810 #
AD-A286084 .... p 1443 N95-20811 #
AD-A286092 .... p 1454 N95-22274 #
AD-A286093 .... p 1485 N95-22226 #

AD-A286095 p 1284 N95-22227 #
AD-A286096 p 1478 N95-22228 #
AD-A286098 p 1309 N95-22229 #
AD-A286114 p 1309 N95-22230 #
AD-A286119 p 1578 N95-22231 #
AD-A286127 p 1214 N95-22232 #
AD-A286129 p 1377 N95-19984
AD-A286130 p 1485 N95-22233 #
AD-A286131 p 1261 N95-22035 #
AD-A286134 p 1213 N95-22036 #
AD-A286138 p 1485 N95-22244
AD-A286144 p 1474 N95-20325
AD-A286158 p 1383 N95-22037 #
AD-A286164 p 1231 N95-22038 #
AD-A286165 p 1207 N95-22039
AD-A286166 p 1426 N95-22019 #
AD-A286167 p 1309 N95-22245 #
AD-A286168 p 1310 N95-22246 #
AD-A286172 p 1310 N95-22247 #
AD-A286173 p 1427 N95-22423 #
AD-A286175 p 1427 N95-22249 #
AD-A286183 p 1460 N95-20326
AD-A286185 p 1510 N95-20327
AD-A286188 p 1267 N95-20328
AD-A286190 p 1206 N95-20329
AD-A286196 p 1525 N95-21878
AD-A286197 p 1246 N95-21879 #
AD-A286205 p 1435 N95-21880
AD-A286208 p 1546 N95-21882 #
AD-A286209 p 1307 N95-21883 #
AD-A286211 p 1310 N95-22251 #
AD-A286213 p 1246 N95-22000
AD-A286214 p 1247 N95-22020 #
AD-A286225 p 1308 N95-22021
AD-A286228 p 1279 N95-22022
AD-A286229 p 1241 N95-21168 #
AD-A286232 p 1334 N95-22023 #
AD-A286239 p 1213 N95-22024 #
AD-A286240 p 1387 N95-22025 #
AD-A286242 p 1495 N95-22026 #
AD-A286245 p 1446 N95-22027 #
AD-A286246 p 1447 N95-22040 #
AD-A286255 p 1308 N95-22041 #
AD-A286257 p 1446 N95-22001
AD-A286258 p 1546 N95-22002
AD-A286269 p 1446 N95-22003 #
AD-A286270 p 1446 N95-22004 #
AD-A286279 p 1308 N95-22005 #
AD-A286284 p 1505 N95-22042
AD-A286285 p 1546 N95-22043 #
AD-A286287 p 1547 N95-22044 #
AD-A286289 p 1454 N95-22045 #
AD-A286291 p 1450 N95-22052 #
AD-A286292 p 1590 N95-22053 #
AD-A286293 p 1582 N95-22054 #
AD-A286294 p 1390 N95-22055 #
AD-A286295 p 1203 N95-22318 #
AD-A286296 p 1368 N95-22322 #
AD-A286297 p 1436 N95-22028 #
AD-A286298 p 1199 N95-22046 #
AD-A286299 p 1279 N95-22047
AD-A286309 p 1199 N95-20091
AD-A286310 p 1226 N95-20092
AD-A286312 p 1202 N95-20093
AD-A286313 p 1265 N95-20094
AD-A286314 p 1458 N95-20095
AD-A286315 p 1202 N95-20174 #
AD-A286316 p 1200 N95-20175 #
AD-A286317 p 1265 N95-20176 #
AD-A286319 p 1200 N95-20177
AD-A286320 p 1251 N95-20178 #
AD-A286322 p 1432 N95-20209
AD-A286328 p 1564 N95-20210 #
AD-A286329 p 1289 N95-20211 #
AD-A286337 p 1216 N95-21719 #
AD-A286338 p 1206 N95-20212 #
AD-A286341 p 1266 N95-20227 #
AD-A286345 p 1224 N95-22252 #
AD-A286349 p 1310 N95-22253 #
AD-A286351 p 1336 N95-22254 #
AD-A286355 p 1548 N95-22255 #
AD-A286356 p 1368 N95-22256 #
AD-A286357 p 1479 N95-22257 #
AD-A286360 p 1217 N95-20228 #
AD-A286364 p 1500 N95-20229 #
AD-A286376 p 1235 N95-20230 #
AD-A286377 p 1541 N95-20231 #
AD-A286380 p 1551 N95-20232 #
AD-A286381 p 1203 N95-22352 #
AD-A286382 p 1203 N95-22319 #
AD-A286383 p 1388 N95-22320
AD-A286385 p 1248 N95-22321
AD-A286388 p 1506 N95-22360 #
AD-A286389 p 1548 N95-22248
AD-A286390 p 1472 N95-22201 #
AD-A286398 p 1383 N95-22202 #
AD-A286406 p 1484 N95-22203 #
AD-A286407 p 1220 N95-22204 #
AD-A286416 p 1547 N95-22205
AD-A286418 p 1357 N95-22206 #
AD-A286420 p 1247 N95-22207 #
AD-A286421 p 1357 N95-22208
AD-A286426 p 1453 N95-21566 #
AD-A286435 p 1436 N95-22209
AD-A286436 p 1484 N95-22210
AD-A286438 p 1310 N95-22250
AD-A286440 p 1302 N95-21438
AD-A286444 p 1468 N95-21567 #
AD-A286446 p 1434 N95-21461
AD-A286448 p 1303 N95-21462
AD-A286449 p 1493 N95-21582 #
AD-A286450 p 1354 N95-21583 #
AD-A286452 p 1354 N95-21584 #
AD-A286453 p 1358 N95-22424 #
AD-A286454 p 1430 N95-21586
AD-A286455 p 1455 N95-21589
AD-A286461 p 1280 N95-22259 #
AD-A286462 p 1431 N95-22393
AD-A286470 p 1486 N95-22267 #
AD-A286471 p 1454 N95-22275 #
AD-A286479 p 1578 N95-22286 #
AD-A286480 p 1358 N95-22290 #
AD-A286481 p 1605 N95-22394 #
AD-A286484 p 1592 N95-22293
AD-A286494 p 1328 N95-21169 #
AD-A286496 p 1358 N95-22294 #
AD-A286499 p 1232 N95-22211
AD-A286507 p 1357 N95-22212 #
AD-A286508 p 1485 N95-22213 #
AD-A286511 p 1485 N95-22214 #
AD-A286514 p 1309 N95-22215
AD-A286515 p 1485 N95-22216 #
AD-A286524 p 1372 N95-21009
AD-A286525 p 1464 N95-21010 #
AD-A286526 p 1273 N95-21011 #
AD-A286528 p 1465 N95-21012 #
AD-A286529 p 1555 N95-21013 #
AD-A286541 p 1273 N95-21014 #
AD-A286545 p 1240 N95-20842 #
AD-A286556 p 1341 N95-20843 #
AD-A286557 p 1544 N95-20844 #
AD-A286560 p 1449 N95-20845 #
AD-A286562 p 1271 N95-20815 #
AD-A286563 p 1504 N95-20823 #
AD-A286567 p 1326 N95-20824 #
AD-A286569 p 1292 N95-20825 #
AD-A286570 p 1429 N95-20826 #
AD-A286571 p 1326 N95-20827 #
AD-A286572 p 1481 N95-20828 #
AD-A286578 p 1504 N95-20918 #
AD-A286580 p 1436 N95-22187
AD-A286582 p 1491 N95-20875
AD-A286588 p 1585 N95-20855 #
AD-A286589 p 1272 N95-20856 #
AD-A286590 p 1429 N95-20857 #
AD-A286591 p 1292 N95-20858 #
AD-A286592 p 1229 N95-20859 #
AD-A286593 p 1207 N95-20860 #
AD-A286595 p 1462 N95-20765
AD-A286605 p 1569 N95-20767 #
AD-A286623 p 1452 N95-20768 #
AD-A286626 p 1239 N95-20769
AD-A286627 p 1218 N95-20770 #
AD-A286632 p 1291 N95-20771 #
AD-A286633 p 1207 N95-20772 #
AD-A286635 p 1501 N95-20773 #
AD-A286636 p 1588 N95-20774 #
AD-A286638 p 1292 N95-20904 #
AD-A286646 p 1327 N95-20905 #
AD-A286654 p 1452 N95-20973 #
AD-A286658 p 1430 N95-20974 #

AD-D016204 p 1274 N95-21154
AD-D016205 p 1274 N95-21155
AD-D016206 p 1301 N95-21156
AD-D016208 p 1545 N95-21825
AD-D016210 p 1307 N95-21910
AD-D016222 p 1544 N95-21100
AD-D016225 p 1455 N95-21116
AD-D016227 p 1365 N95-21117
AD-D016228 p 1328 N95-21118
AD-D016229 p 1504 N95-21119
AD-D016240 p 1332 N95-21775
AD-D016241 p 1478 N95-22146
AD-D016242 p 1476 N95-21307
AD-D016245 p 1506 N95-22088
AD-D016246 p 1547 N95-22089
AD-D016248 p 1478 N95-22090
AD-D016249 p 1476 N95-21504
AD-D016250 p 1476 N95-21496
AD-D016251 p 1591 N95-22098 #
AD-D016253 p 1454 N95-22099 #
AD-D016254 p 1336 N95-22418
AD-D016255 p 1334 N95-22030
AD-D016256 p 1381 N95-22034
AD-D016478 p 1546 N95-21898
AD-D016479 p 1396 N95-21899
AD-D016483 p 1333 N95-21900
AD-D016484 p 1333 N95-21901
AD-D016485 p 1355 N95-21902
AD-D016487 p 1306 N95-21834
AD-D016489 p 1577 N95-22103
AD-D016493 p 1377 N95-22304
AD-D016494 p 1375 N95-21903
AD-D016495 p 1307 N95-21904
AD-D016497 p 1546 N95-21905
AD-D016499 p 1279 N95-22057
AD-D016501 p 1331 N95-21671
AD-D016503 p 1306 N95-21672
AD-D016504 p 1545 N95-21673
AD-D016505 p 1477 N95-21674
AD-D016507 p 1306 N95-21835
AD-D016508 p 1333 N95-21906
AD-D016512 p 1278 N95-21907
AD-D016513 p 1307 N95-21908
AD-D016515 p 1576 N95-22059
AD-D016516 p 1356 N95-22060
AD-D016517 p 1577 N95-22137
AD-D016518 p 1590 N95-21463
AD-D016519 p 1303 N95-21464
AD-D016522 p 1201 N95-21864
AD-D016523 p 1544 N95-21465
AD-D016524 p 1333 N95-21865
AD-D016525 p 1544 N95-21466
AD-D016529 p 1504 N95-20724
AD-D016530 p 1325 N95-20726
AD-D016531 p 1325 N95-20727
AD-D016532 p 1543 N95-20728
AD-D016533 p 1326 N95-20729
AD-D016534 p 1326 N95-20730
AD-D016535 p 1501 N95-20731
AD-D016558 p 1313 N95-20280
AD-D016559 p 1325 N95-20663
AD-D016560 p 1289 N95-20270
AD-D016563 p 1266 N95-20291
AD-D016566 p 1226 N95-20292
AD-D016567 p 1266 N95-20293
AD-D016572 p 1266 N95-20294
AD-D016573 p 1378 N95-20295
AD-D016574 p 1504 N95-20296
AD-D016575 p 1339 N95-20297
AD-D016577 p 1314 N95-20298
AD-D016578 p 1227 N95-20459
AD-D016579 p 1268 N95-20460
AD-D016580 p 1567 N95-20461
AD-D016582 p 1252 N95-20201
AD-D016583 p 1480 N95-20202
AD-D016584 p 1315 N95-20436
AD-D016585 p 1233 N95-22467

AD-E201866 p 1284 N95-21678
AD-E201929 p 1426 N95-21932
AD-E201960 p 1600 N95-21679
AD-E202172 p 1545 N95-21832 #
AD-E202186 p 1415 N95-21308 #
AD-E202187 p 1414 N95-20878 #
AD-E501787 p 1327 N95-20966
AD-E501845 p 1217 N95-22413 #
AD-E501847 p 1411 N95-22414 #

AEDC-TR-94-10 p 1504 N95-21170 * #
AEDC-TR-94-8 p 1200 N95-20248 #

AFIT/GCE/ENG/94S-01 p 1449 N95-20064

AFIT/GSM/LAS/94S-7 p 1583 N95-20051 #

AFOSR-94-0284TR p 1370 N95-20600
AFOSR-94-0285TR p 1333 N95-21917
AFOSR-94-0286TR p 1356 N95-22145
AFOSR-94-0293TR p 1603 N95-21929
AFOSR-94-0296TR p 1355 N95-21942
AFOSR-94-0297TR p 1246 N95-21931
AFOSR-94-0303TR p 1368 N95-22143
AFOSR-94-0304TR p 1504 N95-20300
AFOSR-94-0305TR p 1374 N95-21694 #
AFOSR-94-0306TR p 1543 N95-20601
AFOSR-94-0307TR p 1331 N95-21693
AFOSR-94-0308TR p 1276 N95-21697
AFOSR-94-0309TR p 1475 N95-20566
AFOSR-94-0310TR p 1215 N95-21122
AFOSR-94-0311TR p 1314 N95-20311
AFOSR-94-0312TR p 1587 N95-20309
AFOSR-94-0313TR p 1272 N95-20962
AFOSR-94-0314TR p 1270 N95-20596
AFOSR-94-0315TR p 1602 N95-20593
AFOSR-94-0316TR-VOL-325 p 1563 N95-19886
AFOSR-94-0317TR p 1428 N95-20008 #

AFOSR-94-0318TR .... p 1428 N95-20186
AFOSR-94-0319TR .... p 1221 N95-20059 * #
AFOSR-94-0320TR .... p 1238 N95-20581
AFOSR-94-0321TR .... p 1281 N95-19884
AFOSR-94-0323TR .... p 1238 N95-20597
AFOSR-94-0324TR .... p 1571 N95-20965
AFOSR-94-0325TR .... p 1340 N95-20312
AFOSR-94-0329TR .... p 1452 N95-20562
AFOSR-94-0330TR .... p 1461 N95-20595
AFOSR-94-0331TR .... p 1449 N95-20314
AFOSR-94-0332TR .... p 1448 N95-20007 #
AFOSR-94-0333TR .... p 1290 N95-20545
AFOSR-94-0339TR .... p 1339 N95-20058 #
AFOSR-94-0340TR .... p 1414 N95-20591
AFOSR-94-0480TR .... p 1441 N95-19898 #
AFOSR-94-0487TR .... p 1517 N95-21126 #
AFOSR-94-0488TR .... p 1353 N95-21146 #
AFOSR-94-0488TR .... p 1220 N95-21147 #
AFOSR-94-0555TR .... p 1451 N95-22473 #
AFOSR-94-0558TR .... p 1442 N95-20485 #
AFOSR-94-0559TR .... p 1370 N95-20484 #
AFOSR-94-0561TR .... p 1530 N95-22471 #
AFOSR-94-0565TR .... p 1451 N95-22472 #
AFOSR-94-0573TR .... p 1542 N95-20501 #
AFOSR-94-0576TR .... p 1479 N95-20061 #
AFOSR-94-0582TR .... p 1414 N95-20498 #
AFOSR-94-0591TR .... p 1447 N95-22475 #
AFOSR-94-0600TR .... p 1226 N95-20081 #
AFOSR-94-0608TR .... p 1253 N95-20481
AFOSR-94-0617TR .... p 1226 N95-20105 #
AFOSR-94-0621TR .... p 1443 N95-20848 #
AFOSR-94-0622TR .... p 1448 N95-19998 #
AFOSR-94-0634TR .... p 1269 N95-20548 #
AFOSR-94-0642TR .... p 1517 N95-21216 #
AFOSR-94-0643TR .... p 1517 N95-21151 #
AFOSR-94-0644TR .... p 1450 N95-21101 #
AFOSR-94-0648TR .... p 1450 N95-21192 #
AFOSR-94-0649TR .... p 1540 N95-19897 #
AFOSR-94-0651TR .... p 1502 N95-21194 #
AFOSR-94-0652TR .... p 1273 N95-21152 #
AFOSR-94-0653TR .... p 1222 N95-21193 #
AFOSR-94-0656TR .... p 1373 N95-21195 #
AFOSR-94-0657TR .... p 1242 N95-21402 #
AFOSR-94-0673TR .... p 1239 N95-20716 #
AFOSR-94-0674TR .... p 1252 N95-20299 #
AFOSR-94-0675TR .... p 1514 N95-20667 #
AFOSR-94-0676TR .... p 1443 N95-20811 #
AFOSR-94-0702TR .... p 1486 N95-22267 #
AFOSR-94-0703TR .... p 1303 N95-21462
AFOSR-94-0711TR .... p 1273 N95-21014 #
AFOSR-94-0713TR .... p 1504 N95-20823 #
AFOSR-94-0716TR .... p 1358 N95-22294 #
AFOSR-94-0720TR .... p 1449 N95-20845 #
AFOSR-94-0721TR .... p 1454 N95-22275 #
AFOSR-94-0723TR .... p 1271 N95-20815 #
AFOSR-94-0724TR .... p 1273 N95-21011 #
AFOSR-94-0727TR .... p 1357 N95-22212 #
AFOSR-94-0738TR .... p 1372 N95-21009
AFOSR-94-0740TR .... p 1232 N95-22211
AFOSR-94-0741TR .... p 1485 N95-22216 #
AFOSR-94-0742TR .... p 1302 N95-21438
AFOSR-94-0743TR .... p 1310 N95-22250
AFOSR-94-0744TR .... p 1555 N95-21013 #
AFOSR-94-0745TR .... p 1464 N95-21010 #
AFOSR-94-0746TR .... p 1485 N95-22213 #
AFOSR-94-0747TR .... p 1484 N95-22210
AFOSR-94-0748TR .... p 1309 N95-22215
AFOSR-94-0749TR .... p 1544 N95-20844 #
AFOSR-94-101TR .... p 1340 N95-20547 #

AGARD-CP-543 .... p 1292 N95-20921 #
AGARD-CP-551 .... p 1346 N95-21061 #
AGARD-CP-562 .... p 1208 N95-20631 #

AGS/AD-94-6 .... p 1538 N95-21720 #

AI-M-1463 .... p 1468 N95-21495
AI-M-1472 .... p 1459 N95-20157
AI-M-1473 .... p 1437 N95-20185 #

AI-TR-1434 .... p 1473 N95-22386
AI-TR-1465 .... p 1481 N95-21185

AIAA PAPER 94-2330 .... p 1356 N95-21959 * #
AIAA PAPER 94-2613 .... p 1201 N95-21031 * #
AIAA PAPER 95-0031 .... p 1338 N95-19953 * #
AIAA PAPER 95-0173 .... p 1214 N95-21383 * #
AIAA PAPER 95-0614 .... p 1338 N95-19952 * #
AIAA PAPER 95-1944 .... p 1415 N95-21188 * #
AIAA PAPER 95-6097 .... p 1284 N95-22114 * #

AL/AO-TR-1994-0023 .... p 1441 N95-20301

AL/CF-TP-1994-0004 .... p 1446 N95-21941

AL/CF-TR-1993-0101 .... p 1453 N95-21700
AL/CF-TR-1994-0025 .... p 1442 N95-20457
AL/CF-TR-1994-0074 .... p 1213 N95-22024 #
AL/CF-TR-1994-0077-VOL-1 .... p 1453 N95-21566 #
AL/CF-TR-1994-0084 .... p 1449 N95-20062 #

AL/EQ-TR-1993-0007 .... p 1282 N95-19922
AL/EQ-TR-1993-0017 .... p 1400 N95-19921
AL/EQ-TR-1994-0012 .... p 1516 N95-20993

AL/HR-TP-1994-0005 .... p 1448 N95-19970 #
AL/HR-TP-1994-0018 .... p 1457 N95-20060

AL/HR-TR-1994-0024 .... p 1216 N95-20992

AL/OE-TR-1994-0049 .... p 1400 N95-19964 #

AMSMI-MB-RD-SE-94-1 .... p 1485 N95-22214 #

ANL-HEP-CP-94-33 .... p 1579 N95-20271 #
ANL-HEP-CP-94-39 .... p 1510 N95-20360 #
ANL-HEP-CP-94-46 .... p 1506 N95-20025 #

ANL-HEP-PR-94-56 .... p 1604 N95-21475 #

ANL-HEP-TR-94-57 .... p 1514 N95-20852 #

ANL-94/11 .... p 1285 N95-20050 #

ANL/ASD/CP-84183 .... p 1537 N95-21503 #

ANL/BIM/PP-70108 .... p 1441 N95-20074 #

ANL/CHM/CP-80107 .... p 1437 N95-19969 #
ANL/CHM/CP-81118 .... p 1570 N95-20881 #
ANL/CHM/CP-83725 .... p 1567 N95-20479 #
ANL/CHM/CP-83910 .... p 1254 N95-20707 #
ANL/CHM/CP-83942 .... p 1564 N95-20017 #
ANL/CHM/CP-84363 .... p 1262 N95-22291 #

ANL/CHM/PP-75382 .... p 1240 N95-20836 #
ANL/CHM/PP-79997 .... p 1440 N95-22075 #

ANL/CMB/CP-82418 .... p 1438 N95-21376 #

ANL/CMB/PP-81002 .... p 1440 N95-22067 #

ANL/CMT/CP-82692 .... p 1407 N95-21617 #
ANL/CMT/CP-83649 .... p 1392 N95-20480 #
ANL/CMT/CP-84205 .... p 1393 N95-20839 #

ANL/DIS/CP-83108 .... p 1460 N95-20385 #
ANL/DIS/CP-83606 .... p 1412 N95-20171 #
ANL/DIS/CP-83918 .... p 1586 N95-20016 #

ANL/ER/CP-82594 .... p 1426 N95-21836 #

ANL/ER/PP-79069 .... p 1404 N95-20835 #
ANL/ER/PP-79574 .... p 1414 N95-20908 #
ANL/ER/PP-82416 .... p 1335 N95-22189 #

ANL/ER/TM-3 .... p 1401 N95-20234

ANL/ES/CP-82394 .... p 1469 N95-21829 #
ANL/ES/CP-82395 .... p 1329 N95-21296 #
ANL/ES/CP-83738 .... p 1403 N95-20478 #
ANL/ES/CP-83739 .... p 1234 N95-20107 #

ANL/ES/PP-73762 .... p 1396 N95-21897 #
ANL/ES/PP-76517 .... p 1415 N95-21477 #

ANL/ET/CP-80540 .... p 1264 N95-20018 #
ANL/ET/CP-82119 .... p 1382 N95-22292 #
ANL/ET/CP-82224 .... p 1229 N95-20912 #
ANL/ET/CP-82340 .... p 1570 N95-20841 #
ANL/ET/CP-82855 .... p 1366 N95-21453 #
ANL/ET/CP-83313 .... p 1566 N95-20419 #
ANL/ET/CP-83924 .... p 1402 N95-20247 #
ANL/ET/CP-83963 .... p 1226 N95-20027 #

ANL/FPP/TM-269 .... p 1558 N95-21244 #

ANL/IFR/CP-82704 .... p 1466 N95-21311 #

ANL/IPD/CP-83520 .... p 1591 N95-22092 #

ANL/IPNS/PP-79589 .... p 1229 N95-20840 #

ANL/MCS-TM-194 .... p 1471 N95-22077 #

ANL/MCS/CP-82870 .... p 1206 N95-20370 * #

ANL/MCS/PP-71694 .... p 1254 N95-20792 #
ANL/MCS/PP-73014 .... p 1489 N95-20170 #
ANL/MCS/PP-75731 .... p 1476 N95-21257 #
ANL/MCS/PP-76460 .... p 1476 N95-21341 #
ANL/MSD/CP-82679 .... p 1540 N95-19968 #
ANL/MSD/CP-82827 .... p 1572 N95-21408 #
ANL/MSD/CP-82834 .... p 1536 N95-21407 #
ANL/MSD/CP-83081 .... p 1571 N95-21256 #
ANL/MSD/CP-83799 .... p 1501 N95-20241 #
ANL/MSD/CP-84144 .... p 1232 N95-22130 #
ANL/MSD/CP-84189 .... p 1573 N95-21474 #

ANL/PHY/CP-82766 .... p 1522 N95-21502 #
ANL/PHY/CP-84072 .... p 1521 N95-21406 #
ANL/PHY/CP-84348 .... p 1521 N95-21454 #

ANL/TD/CP-83927 .... p 1559 N95-21388 #
ANL/TD/CP-84288 .... p 1531 N95-19983 #

ANL/XFD/CP-82667 .... p 1500 N95-20106 #
ANL/XFD/CP-82881 .... p 1541 N95-20103 #
ANL/XFD/CP-82931 .... p 1527 N95-22190 #
ANL/XFD/CP-82933 .... p 1338 N95-19923 #

ANU-PRL-TP-93/01 .... p 1548 N95-19977 #
ANU-PRL-TP-93/02 .... p 1550 N95-20200 #

APL-UW-TM30-93 .... p 1436 N95-21987

APL-UW-TR-9414 .... p 1434 N95-21461

AR-007-096 .... p 1471 N95-22104
AR-007-104 .... p 1365 N95-20759
AR-007-124 .... p 1202 N95-21892
AR-008-226 .... p 1205 N95-21642
AR-008-241 .... p 1250 N95-19910
AR-008-268 .... p 1434 N95-21657
AR-008-273 .... p 1287 N95-21625
AR-008-281 .... p 1284 N95-21624
AR-008-572 .... p 1284 N95-21658
AR-008-640 .... p 1222 N95-21661
AR-008-644 .... p 1201 N95-21659
AR-008-928 .... p 1284 N95-21951
AR-008-933 .... p 1470 N95-21950

ARA-MEMO-395 .... p 1216 N95-20799 #
ARA-MEMO-405 .... p 1200 N95-20758 #
ARA-MEMO-407 .... p 1199 N95-19946 #

ARCCB-TR-94006 .... p 1450 N95-21968
ARCCB-TR-94028 .... p 1387 N95-22025 #
ARCCB-TR-94029 .... p 1495 N95-22026 #
ARCCB-TR-94031 .... p 1388 N95-22320

ARFSD-SP-94001 .... p 1326 N95-20827 #

ARFSD-TR-93046-PT-1 .... p 1307 N95-21915
ARFSD-TR-93051 .... p 1307 N95-21970
ARFSD-TR-94010 .... p 1481 N95-20828 #

ARI-RR-1666 .... p 1215 N95-19931 #

ARI-TR-1014 .... p 1460 N95-20326

ARL-CR-173 .... p 1478 N95-22228 #
ARL-CR-76 .... p 1336 N95-22254 #
ARL-CR-96 .... p 1430 N95-21586

ARL-MR-190 .... p 1273 N95-21000 #

ARL-TN-35 .... p 1228 N95-20808
ARL-TN-3 .... p 1202 N95-21892

ARL-TR-21 .... p 1471 N95-22104
ARL-TR-302 .... p 1292 N95-20825 #
ARL-TR-32 .... p 1365 N95-20759
ARL-TR-341 .... p 1260 N95-21986
ARL-TR-364 .... p 1368 N95-22322 #
ARL-TR-419 .... p 1457 N95-19929 #
ARL-TR-442 .... p 1282 N95-19920
ARL-TR-460 .... p 1452 N95-20625
ARL-TR-464 .... p 1498 N95-21219 #
ARL-TR-508 .... p 1250 N95-20067 #
ARL-TR-512 .... p 1269 N95-20486 #
ARL-TR-532 .... p 1505 N95-22042
ARL-TR-585 .... p 1224 N95-19899 #
ARL-TR-586 .... p 1499 N95-22135 #
ARL-TR-592 .... p 1498 N95-19990 #
ARL-TR-603 .... p 1428 N95-19989 #
ARL-TR-605 .... p 1391 N95-22131 #
ARL-TR-609 .... p 1239 N95-20613 #
ARL-TR-614 .... p 1379 N95-20998 #
ARL-TR-621 .... p 1248 N95-22321
ARL-TR-623 .... p 1308 N95-22021
ARL-TR-629 .... p 1247 N95-22207 #
ARL-TR-645 .... p 1380 N95-21359 * #
ARL-TR-94-9 .... p 1503 N95-19911 #

ARL/PSU/TR-94-12 .... p 1267 N95-20390 #

ARM-94-002 .... p 1401 N95-20193 #

ARO-94-1 .... p 1497 N95-22389

ASC-TR-94-5027 .... p 1200 N95-19991 #

ATC-214 .... p 1291 N95-20599

ATR-95(5826)-1 .... p 1280 N95-22383 * #

B-253616 .... p 1586 N95-22403 #
B-256676 .... p 1407 N95-21683
B-257718 .... p 1206 N95-20212 #

BN-1160 .... p 1490 N95-20565
BN-1162 .... p 1491 N95-20920
BN-1163 .... p 1497 N95-22388
BN-1166 .... p 1490 N95-20588

BNL-49035-REV-5/94 .... p 1468 N95-21515 #
BNL-49643 .... p 1511 N95-20404 #
BNL-49820 .... p 1531 N95-20282 #
BNL-49826 .... p 1489 N95-20266 #
BNL-49852 .... p 1563 N95-20014 #
BNL-49853 .... p 1531 N95-20021 #
BNL-49857 .... p 1532 N95-20336 #
BNL-49859 .... p 1532 N95-20406 #
BNL-49932 .... p 1540 N95-22391 #
BNL-49992 .... p 1517 N95-21140 #
BNL-49993 .... p 1563 N95-19925 #
BNL-52438 .... p 1538 N95-21720 #
BNL-52439 .... p 1569 N95-20793 #
BNL-60409 .... p 1512 N95-20477 #
BNL-60575 .... p 1283 N95-21211 #
BNL-60583 .... p 1566 N95-20382 #
BNL-60591 .... p 1565 N95-20265 #
BNL-60592 .... p 1545 N95-21643 #
BNL-60634 .... p 1524 N95-21641 #
BNL-60652 .... p 1276 N95-21644 #
BNL-60655 .... p 1492 N95-21266 #
BNL-60676 .... p 1527 N95-22188 #
BNL-60710 .... p 1455 N95-21632 #
BNL-60712 .... p 1469 N95-21713 #
BNL-60732 .... p 1530 N95-22392 #
BNL-60737 .... p 1370 N95-20572 #
BNL-60738 .... p 1533 N95-20573 #
BNL-60747 .... p 1480 N95-20126 #
BNL-60749 .... p 1539 N95-22357 #
BNL-60750 .... p 1564 N95-20130 #
BNL-60755 .... p 1233 N95-19980 #
BNL-60756 .... p 1564 N95-20127 #
BNL-60757 .... p 1250 N95-19979 #
BNL-60769 .... p 1522 N95-21506 #
BNL-60795 .... p 1521 N95-21484 #
BNL-60809 .... p 1523 N95-21588 #
BNL-60826 .... p 1371 N95-20866 #
BNL-60828 .... p 1523 N95-21551 #
BNL-60862 .... p 1536 N95-21418 #
BNL-60876 .... p 1533 N95-20766 #
BNL-60878 .... p 1533 N95-20886 #
BNL-60892 .... p 1367 N95-21638 #
BNL-60903 .... p 1573 N95-21516 #
BNL-60905 .... p 1272 N95-20894 #
BNL-60934 .... p 1520 N95-21362 #
BNL-60946 .... p 1536 N95-21342 #

CAL-2261 .... p 1600 N95-21615 * #

CAR-TR-720 .... p 1313 N95-20257 #

CAST-TR-94-3 .... p 1432 N95-20209

CBCL-95 .... p 1437 N95-20185 #

CBP-102 .... p 1374 N95-21528 #
CBP-89 .... p 1519 N95-21262 #

CERC-94-3 .... p 1431 N95-19895 #
CERC-94-4 .... p 1471 N95-22068

CERL-SR-EC-94/05 .... p 1410 N95-22142
CERL-SR-EC-94/15 .... p 1402 N95-20441
CERL-SR-EC-94/16 .... p 1408 N95-21689
CERL-SR-EC-94/18 .... p 1408 N95-21696
CERL-SR-EC-95/01 .... p 1403 N95-20720 #

CERL-TR-TA-94/04 .... p 1471 N95-22133 #

CERN-93-04 .... p 1335 N95-22184 #
CERN-93-06 .... p 1582 N95-22185 #

CF-114-DMSO .... p 1591 N95-22069

CGR/DC-01/94 .... p 1259 N95-21687
CGR/DC-04/94 .... p 1306 N95-21686
CGR/DC-22/93 .... p 1408 N95-21685

CMC-94-01 .... p 1497 N95-22388
CMC-94-02 .... p 1490 N95-20588

CMU-CS-94-112 .... p 1475 N95-20500 #
CMU-CS-94-113 .... p 1473 N95-19885 *
CMU-CS-94-127 .... p 1448 N95-19887
CMU-CS-94-134 .... p 1216 N95-20624
CMU-CS-94-148 .... p 1461 N95-20622
CMU-CS-94-150 .... p 1461 N95-20623
CMU-CS-94-182 .... p 1466 N95-21325 #
CMU-CS-94-189 .... p 1463 N95-20847 #
CMU-CS-94-192 .... p 1474 N95-20325
CMU-CS-94-193 .... p 1463 N95-20846

CMU-HCII-94-101 .... p 1448 N95-19887
CMU-HCII-94-107 .... p 1466 N95-21325 #

CMU-RI-TR-93-29 .... p 1543 N95-20564

CMU/SEI-94-EM-11 .... p 1463 N95-20810 #
CMU/SEI-94-HB-01 .... p 1462 N95-20765
CMU/SEI-94-HB02 .... p 1462 N95-20809 #
CMU/SEI-94-SR-13 .... p 1468 N95-21567 #
CMU/SEI-94-TR-09 .... p 1485 N95-22226 #
CMU/SEI-94-TR-14 .... p 1457 N95-19999 #
CMU/SEI-94-TR-4 .... p 1468 N95-21627

CNIC-00767 .... p 1556 N95-21162 #
CNIC-00771 .... p 1255 N95-20909 #
CNIC-00776 .... p 1563 N95-19978 #
CNIC-00783 .... p 1556 N95-21165 #
CNIC-00792 .... p 1556 N95-21164 #

COAM-TM-2/95 .... p 1458 N95-20095

COAM-TR-1/95 .... p 1433 N95-21158 #

CONF-890130-6 .... p 1275 N95-21289 #
CONF-9112182 .... p 1441 N95-22397
CONF-9203300 .... p 1410 N95-22219 #
CONF-9208175-SUMM .... p 1279 N95-22091 #
CONF-921049-11 .... p 1391 N95-20260 #
CONF-9211198-3 .... p 1407 N95-21608 #
CONF-9302112-4 .... p 1570 N95-20819 #
CONF-9303258-1 .... p 1538 N95-22117 #
CONF-9303302-1 .... p 1381 N95-22268 #
CONF-9303304-1 .... p 1439 N95-21548 #
CONF-930405-58 .... p 1500 N95-20129 #
CONF-9304112-26 .... p 1303 N95-21459 #
CONF-9304145-4 .... p 1245 N95-21845 #
CONF-930438-32 .... p 1265 N95-20226 #
CONF-930438-33 .... p 1271 N95-20761 #
CONF-9305135-10 .... p 1250 N95-20043 #
CONF-9305135-11 .... p 1257 N95-21555 #
CONF-9305320-2 .... p 1411 N95-22342 #
CONF-9305364 .... p 1529 N95-22281 #
CONF-9305375-ABSTS .... p 1440 N95-22066 #
CONF-9305377-1 .... p 1411 N95-19982 #
CONF-9305377-2 .... p 1411 N95-19981 #
CONF-9306176-24 .... p 1511 N95-20404 #
CONF-9306210-2 .... p 1506 N95-20030 #
CONF-9306367-1 .... p 1261 N95-22123 #
CONF-930685-1 .... p 1280 N95-22270 #
CONF-9307153-1 .... p 1573 N95-21516 #
CONF-9307163-4 .... p 1272 N95-20894 #
CONF-9307169-2 .... p 1556 N95-21142 #
CONF-930767-9 .... p 1519 N95-21250 #
CONF-930802-22 .... p 1263 N95-22396 #
CONF-930803-32 .... p 1385 N95-20322 #
CONF-9308122-19 .... p 1250 N95-20020 #
CONF-9308138-4 .... p 1258 N95-21560 #
CONF-9308209 .... p 1582 N95-22185 #
CONF-9308247-1 .... p 1381 N95-21550 #
CONF-930893-41 .... p 1378 N95-20085 #
CONF-9309259-6 .... p 1510 N95-20337 #
CONF-930928-30 .... p 1269 N95-20570 #
CONF-9309409 .... p 1285 N95-20194 #
CONF-9309429-1 .... p 1599 N95-21245 #
CONF-930993-3 .... p 1522 N95-21519 #
CONF-930993-4 .... p 1559 N95-21547 #
CONF-931009-28 .... p 1263 N95-22346 #
CONF-931009-29 .... p 1262 N95-22344 #
CONF-931009-30 .... p 1250 N95-20044 #
CONF-9310161-2 .... p 1477 N95-21556 #
CONF-9310170-2 .... p 1381 N95-21601 #
CONF-9310191-3 .... p 1287 N95-21559 #
CONF-9310209-2 .... p 1335 N95-22149 #
CONF-9310224-3 .... p 1258 N95-21600 #
CONF-931030-1 .... p 1267 N95-20323 #
CONF-9310328-3 .... p 1278 N95-21937 #
CONF-9310356 .... p 1315 N95-20369 #
CONF-9310357-1 .... p 1493 N95-21564 #
CONF-9310360-1 .... p 1246 N95-22012 #
CONF-931108-104 .... p 1565 N95-20244 #
CONF-931108-106 .... p 1252 N95-20365 #
CONF-931108-107 .... p 1565 N95-20371 #
CONF-931108-108 .... p 1565 N95-20245 #
CONF-931108-110 .... p 1244 N95-21549 #
CONF-9311131-3 .... p 1226 N95-20125 #
CONF-9311131-4 .... p 1225 N95-20023 #
CONF-9311131-5 .... p 1247 N95-22260 #
CONF-9311137-2 .... p 1412 N95-20278 * #
CONF-9311147-10 .... p 1555 N95-21141 #
CONF-931115-14 .... p 1475 N95-20366 #
CONF-931121-39 .... p 1385 N95-20416 #
CONF-9311234-1 .... p 1274 N95-21263 #
CONF-931234-11 .... p 1379 N95-20723 #
CONF-931234-9 .... p 1460 N95-20358 #
CONF-931238-4 .... p 1578 N95-22269 #
CONF-940135-10 .... p 1226 N95-20357 #
CONF-940135-11 .... p 1264 N95-20018 #
CONF-940135-7 .... p 1267 N95-20373 #
CONF-940135-8 .... p 1225 N95-20022 #
CONF-940135-9 .... p 1340 N95-20781 #
CONF-940142-43 .... p 1368 N95-19986 #
CONF-940142-45 .... p 1566 N95-20372 #
CONF-940142-47 .... p 1374 N95-21480 #
CONF-940152-3 .... p 1353 N95-21317 #
CONF-940187-2 .... p 1576 N95-22008 #
CONF-940194-2 .... p 1313 N95-20119 #
CONF-940204-10 .... p 1571 N95-21167 #
CONF-940204-8 .... p 1252 N95-20359 #
CONF-940204-9 .... p 1253 N95-20673 #
CONF-940209-3 .... p 1237 N95-20470 #
CONF-9402102-1 .... p 1522 N95-21485 #
CONF-940226-9 .... p 1372 N95-21135 #
CONF-940286-3 .... p 1253 N95-20375 #
CONF-940286-7 .... p 1254 N95-20705 #
CONF-9403118-2 .... p 1301 N95-21241 #
CONF-9403122-3 .... p 1507 N95-20034 #
CONF-9403127-2 .... p 1511 N95-20401 #
CONF-9403147-SUMM .... p 1401 N95-20238 #
CONF-9403151-1 .... p 1528 N95-22265 #
CONF-9403151-2 .... p 1508 N95-20133 #
CONF-9403159-1 .... p 1573 N95-21474 #
CONF-9403170-1 .... p 1393 N95-20864 #
CONF-9403179-1 .... p 1604 N95-22085 #
CONF-940327-10 .... p 1525 N95-21704 #
CONF-940327-11 .... p 1528 N95-22196 #
CONF-940327-12 .... p 1526 N95-21939 #
CONF-940327-13 .... p 1511 N95-20418 #
CONF-940327-14 .... p 1519 N95-21248 #
CONF-940327-8 .... p 1511 N95-20415 #
CONF-940351-1 .... p 1532 N95-20388 #
CONF-940353-8 .... p 1412 N95-20287 #
CONF-940391-11 .... p 1412 N95-19985 #
CONF-9404104-1 .... p 1570 N95-20820 #
CONF-940411-45 .... p 1566 N95-20399 #
CONF-940411-47 .... p 1545 N95-21643 #
CONF-940411-49 .... p 1565 N95-20265 #
CONF-940411-50 .... p 1253 N95-20447 #
CONF-940411-51 .... p 1542 N95-20450 #
CONF-940411-52 .... p 1264 N95-20047 #
CONF-940411-53 .... p 1230 N95-21481 #
CONF-940411-54 .... p 1275 N95-21501 #
CONF-940411-55 .... p 1277 N95-21861 #
CONF-9404131-3 .... p 1327 N95-20854 #
CONF-9404137-6 .... p 1357 N95-22264 #
CONF-940414-5 .... p 1243 N95-21500 #
CONF-940416-24 .... p 1264 N95-20024 #
CONF-940416-25 .... p 1226 N95-20027 #
CONF-940416-30 .... p 1271 N95-20821 #
CONF-9404162-10 .... p 1310 N95-22299 #
CONF-9404162-11 .... p 1389 N95-21433 #
CONF-9404162-12 .... p 1389 N95-21552 #
CONF-9404162-13 .... p 1376 N95-22121 #
CONF-9404178-1 .... p 1440 N95-22296 #
CONF-9404194 .... p 1234 N95-20117 #
CONF-9404197-2 .... p 1520 N95-21336 #
CONF-9404198-1 .... p 1524 N95-21664 #
CONF-9404198-3 .... p 1521 N95-21406 #
CONF-940426-3 .... p 1283 N95-21211 #
CONF-940440-4 .... p 1266 N95-20281 #
CONF-940440-6 .... p 1570 N95-20881 #
CONF-940449-15 .... p 1503 N95-20019 #
CONF-940507-28 .... p 1529 N95-22280 #
CONF-940507-38 .... p 1537 N95-21460 #
CONF-940509-7 .... p 1520 N95-21357 #
CONF-940514-10 .... p 1524 N95-21641 #
CONF-940514-12 .... p 1530 N95-22340 #
CONF-940514-16 .... p 1530 N95-22435 #
CONF-940514-3 .... p 1526 N95-22058 #
CONF-9405143-8 .... p 1258 N95-21676 #
CONF-9405162-1 .... p 1579 N95-20271 #
CONF-9405170-7 .... p 1564 N95-20017 #
CONF-9405187-2 .... p 1265 N95-20220 #
CONF-9405187-3 .... p 1278 N95-21909 #
CONF-9405193-2 .... p 1266 N95-20316 #
CONF-9405193-3 .... p 1251 N95-20090 #
CONF-9405195 .... p 1565 N95-20261 #
CONF-9405196-1 .... p 1520 N95-21375 #
CONF-9405196-2 .... p 1439 N95-21606 #

CONF-9405198-2 p 1566 N95-20382 #
CONF-9405199-2 p 1330 N95-21554 #
CONF-9405202-1 p 1516 N95-21125 #
CONF-9405204-1 p 1488 N95-20169
CONF-9405207-1 p 1566 N95-20405 #
CONF-9405216-2 p 1604 N95-21475 #
CONF-9405219-1 p 1569 N95-20678 #
CONF-9405219-2 p 1569 N95-20677 #
CONF-9405219-3 p 1514 N95-20732 #
CONF-9405219-4 p 1569 N95-20679 #
CONF-9405220-1 p 1285 N95-22261 #
CONF-9405221-1 p 1491 N95-20701 #
CONF-9405223-1 p 1386 N95-20703 #
CONF-9405229-1 p 1402 N95-20247 #
CONF-9405233-1 p 1539 N95-22193 #
CONF-9405240-2 p 1438 N95-21366 #
CONF-9405241-1 p 1526 N95-21940 #
CONF-9405249-1 p 1530 N95-22435 #
CONF-940529-21 p 1565 N95-20330
CONF-940529-22 p 1566 N95-20400 #
CONF-940529-24 p 1237 N95-20493 #
CONF-940529-26 p 1570 N95-20838 #
CONF-940548-8 p 1395 N95-21611 #
CONF-940552-16 p 1553 N95-20402 #
CONF-940552-17 p 1558 N95-21247 #
CONF-940552-22 p 1553 N95-20363 #
CONF-940552-23 p 1552 N95-20362 #
CONF-940552-27 p 1542 N95-20364 #
CONF-940552-28 p 1562 N95-22191 #
CONF-940552-31 p 1531 N95-20015 #
CONF-940552-32 p 1549 N95-20112 #
CONF-940568-5 p 1276 N95-21644 #
CONF-940580-13 p 1554 N95-20568 #
CONF-940580-15 p 1552 N95-20334 #
CONF-940580-18 p 1554 N95-20571 #
CONF-940580-19 p 1230 N95-21553 #
CONF-940582-6 p 1577 N95-22168 #
CONF-940586-1 p 1369 N95-20221 #
CONF-940592-3 p 1369 N95-20335 #
CONF-940592-4 p 1372 N95-21173 #
CONF-940592-5 p 1373 N95-21210 #
CONF-940592-7 p 1374 N95-21663 #
CONF-940592-8 p 1555 N95-20813 #
CONF-940593-13 p 1377 N95-22312 #
CONF-940602-19 p 1371 N95-20817 #
CONF-9406111-1 p 1564 N95-20130 #
CONF-940613-26 p 1385 N95-20374 #
CONF-9406131-63 p 1275 N95-21354 #
CONF-9406133-3 p 1379 N95-20695 #
CONF-9406143-2 p 1410 N95-22278 #
CONF-9406152-ABSTS p 1551 N95-20283 #
CONF-940618-109 p 1538 N95-22155 #
CONF-940618-110 p 1536 N95-21334 #
CONF-940618-111 p 1536 N95-21335 #
CONF-940618-23 p 1517 N95-21140 #
CONF-940618-41 p 1532 N95-20336 #
CONF-940618-42 p 1531 N95-20282 #
CONF-940618-45 p 1539 N95-22192 #
CONF-940618-47 p 1531 N95-20021 #
CONF-940618-49 p 1540 N95-22391 #
CONF-940618-52 p 1532 N95-20406 #
CONF-940618-53 p 1563 N95-20014 #
CONF-940618-54 p 1563 N95-19925 #
CONF-940618-62 p 1489 N95-20266 #
CONF-940618-64 p 1532 N95-20494 #
CONF-940618-65 p 1532 N95-20495 #
CONF-940618-67 p 1370 N95-20569 #
CONF-940618-76 p 1519 N95-21262 #
CONF-940618-79 p 1552 N95-20318 #
CONF-940618-81 p 1538 N95-21938 #
CONF-940618-87 p 1534 N95-21246 #
CONF-940618-92 p 1536 N95-21332 #
CONF-940618-93 p 1536 N95-21337 #
CONF-940618-94 p 1534 N95-21253 #
CONF-9406180-4 p 1515 N95-20911 #
CONF-9406192-4 p 1600 N95-21935 #
CONF-9406199-2 p 1564 N95-20087 #
CONF-9406201-2 p 1567 N95-20449 #
CONF-9406204-2 p 1571 N95-21256 #
CONF-9406210-3 p 1366 N95-21138 #
CONF-9406212-3 p 1518 N95-21235 #
CONF-9406223-1 p 1384 N95-20109 #
CONF-9406225-1 p 1569 N95-20696 #
CONF-9406229-1 p 1255 N95-21137 #
CONF-9406231-1 p 1541 N95-20239 #
CONF-9406233-1 p 1524 N95-21646 #
CONF-9406239-1 p 1276 N95-21662 #
CONF-9406241-1 p 1433 N95-20420 #
CONF-9406242-1 p 1510 N95-20360 #
CONF-9406242-3 p 1515 N95-20868 #
CONF-9406242-4 p 1521 N95-21378 #
CONF-9406243-2 p 1521 N95-21454 #
CONF-9406244-2 p 1413 N95-20289 #
CONF-9406247-1 p 1256 N95-21260 #
CONF-9406248-4 p 1507 N95-20111 #
CONF-9406261-1 p 1232 N95-22115 #
CONF-9406265-1 p 1527 N95-22122 #
CONF-9406265-2 p 1516 N95-20914 #
CONF-9406267-1 p 1558 N95-21310 #
CONF-9406268-1 p 1242 N95-21309 #
CONF-940627-4 p 1336 N95-22271 #
CONF-940627-5 p 1573 N95-21483 #
CONF-9406274-1 p 1521 N95-21380 #
CONF-9406278-1 p 1482 N95-21249 #
CONF-940629-9 p 1567 N95-20448 #
CONF-940630-29 p 1540 N95-22469 #
CONF-940630-31 p 1534 N95-21208 #
CONF-940630-32 p 1557 N95-21207 #
CONF-940630-33 p 1550 N95-20190 #
CONF-940630-35 p 1534 N95-21209 #
CONF-940630-36 p 1557 N95-21206 #
CONF-940630-37 p 1557 N95-21166 #
CONF-940630-38 p 1549 N95-20038 #
CONF-940630-40 p 1548 N95-20037 #
CONF-940630-43 p 1560 N95-21702 #
CONF-940630-44 p 1560 N95-21665 #
CONF-940630-47 p 1562 N95-22300 #
CONF-940630-48 p 1371 N95-20817 #
CONF-940634-15 p 1506 N95-20026 #
CONF-940634-17 p 1560 N95-21668 #
CONF-940634-19 p 1535 N95-21328 #
CONF-940634-20 p 1565 N95-20340 #
CONF-940635-10 p 1550 N95-20146 #
CONF-940635-11 p 1553 N95-20445 #
CONF-940635-15 p 1551 N95-20205 #
CONF-940635-16 p 1559 N95-21581 #
CONF-940635-5 p 1556 N95-21159 #
CONF-940635-6 p 1556 N95-21163 #
CONF-940635-7 p 1551 N95-20279 #
CONF-940635-8 p 1551 N95-20285 #
CONF-940635-9 p 1554 N95-20446 #
CONF-940650-9 p 1401 N95-20089 #
CONF-940657-2 p 1566 N95-20419 #
CONF-940657-5 p 1251 N95-20088 #
CONF-940657-6 p 1256 N95-21286 #
CONF-940664-21 p 1549 N95-20143 #
CONF-940664-29 p 1559 N95-21388 #
CONF-940671-1 p 1326 N95-20791 #
CONF-940678-7 p 1328 N95-21139 #
CONF-940681-1 p 1371 N95-20866 #
CONF-940681-3 p 1533 N95-20886 #
CONF-940690-1 p 1512 N95-20477 #
CONF-940693-3 p 1525 N95-21715 #
CONF-940701-18 p 1501 N95-20241 #
CONF-940701-20 p 1564 N95-20127 #
CONF-940701-21 p 1573 N95-21569 #
CONF-940704-2 p 1253 N95-20676 #
CONF-940704-4 p 1256 N95-21298 #
CONF-940706-1 p 1370 N95-20698 #
CONF-9407100 p 1391 N95-20332 #
CONF-9407102-2 p 1290 N95-20474 #
CONF-9407103-24 p 1538 N95-22050 #
CONF-9407103-26 p 1539 N95-22298 #
CONF-9407105-1 p 1268 N95-20396 #
CONF-9407106-2 p 1413 N95-20397 #
CONF-940711-18 p 1243 N95-21512 #
CONF-9407112-1 p 1268 N95-20468 #
CONF-9407117-1 p 1567 N95-20479 #
CONF-9407117-2 p 1578 N95-22297 #
CONF-9407117-3 p 1526 N95-21934 #
CONF-9407117-4 p 1262 N95-22291 #
CONF-9407118-1 p 1551 N95-20219 #
CONF-9407119-1 p 1578 N95-22272 #
CONF-9407121-2 p 1539 N95-22357 #
CONF-9407121-3 p 1537 N95-21503 #
CONF-9407121-4 p 1534 N95-20900 #
CONF-9407122-1 p 1263 N95-22345 #
CONF-9407123-2 p 1366 N95-21453 #
CONF-9407126-2 p 1539 N95-22243 #
CONF-9407127-1 p 1506 N95-20025 #
CONF-9407127-2 p 1535 N95-21314 #
CONF-9407129-1 p 1600 N95-21479 #
CONF-9407132-1 p 1261 N95-22127 #
CONF-9407134-1 p 1515 N95-20879 #
CONF-9407135-1 p 1515 N95-20880 #
CONF-940714-16 p 1338 N95-19923 #
CONF-940714-21 p 1540 N95-19968 #
CONF-940714-28 p 1536 N95-21407 #
CONF-940714-2 p 1541 N95-20103 #
CONF-940714-30 p 1572 N95-21408 #
CONF-940714-36 p 1367 N95-21638 #
CONF-940714-37 p 1536 N95-21418 #
CONF-940714-5 p 1527 N95-22188 #
CONF-940714-6 p 1527 N95-22190 #
CONF-940714-9 p 1500 N95-20106 #
CONF-9407143-1 p 1599 N95-20873 #
CONF-9407145-1 p 1281 N95-22434 #
CONF-940722-20 p 1507 N95-20108 #
CONF-940722-22 p 1523 N95-21551 #
CONF-940722-23 p 1522 N95-21506 #
CONF-940722-26 p 1509 N95-20217 #
CONF-940722-28 p 1525 N95-21727 #
CONF-940722-30 p 1515 N95-20898 #
CONF-940722-31 p 1520 N95-21321 #
CONF-940723-13 p 1301 N95-21205 #
CONF-940723-14 p 1543 N95-20612 #
CONF-940723-15 p 1237 N95-20386 #
CONF-940723-17 p 1541 N95-20218 #
CONF-940723-18 p 1377 N95-22343 #
CONF-940723-28 p 1367 N95-21478 #
CONF-940723-29 p 1275 N95-21482 #
CONF-940723-7 p 1267 N95-20317 #
CONF-940725-3 p 1521 N95-21484 #
CONF-940726-14 p 1314 N95-20338 #
CONF-940726-16 p 1334 N95-22086 #
CONF-940731-2 p 1262 N95-22313 #
CONF-940748-30 p 1458 N95-20153 #
CONF-940748-35 p 1588 N95-20789 #
CONF-940748-63 p 1516 N95-21114 #
CONF-940748-78 p 1517 N95-21174 #
CONF-940753-22 p 1568 N95-20674 #
CONF-940753-23 p 1255 N95-20907 #
CONF-940753-24 p 1591 N95-22235 #
CONF-940756-1 p 1465 N95-21153 #
CONF-940766-8 p 1567 N95-20492 #
CONF-940769-7 p 1429 N95-20381 #
CONF-940780-3 p 1234 N95-20107 #
CONF-940780-4 p 1280 N95-22258 #
CONF-940780-5 p 1403 N95-20478 #
CONF-940793-3 p 1261 N95-22048 #
CONF-9408113-4 p 1237 N95-20368 #
CONF-9408113-5 p 1574 N95-21570 #
CONF-9408117-1 p 1438 N95-21376 #
CONF-9408118-3 p 1364 N95-20320 #
CONF-940812-20 p 1392 N95-20473 #
CONF-940812-23 p 1337 N95-22421 #
CONF-9408123-4 p 1283 N95-21513 #
CONF-9408125-18 p 1462 N95-20699 #
CONF-9408125-22 p 1531 N95-20203 #
CONF-9408125-26 p 1601 N95-22419 #
CONF-9408125-34 p 1334 N95-22011 #
CONF-9408125-37 p 1531 N95-19983 #
CONF-9408125-38 p 1534 N95-20891 #
CONF-9408125-8 p 1331 N95-21667 #
CONF-9408126-1 p 1555 N95-21134 #
CONF-9408127-1 p 1555 N95-21115 #
CONF-9408127-2 p 1554 N95-20675 #
CONF-9408129-2 p 1412 N95-20171 #
CONF-940813-18 p 1217 N95-21706 #
CONF-940813-1 p 1236 N95-20277 #
CONF-940813-22 p 1507 N95-20049 #
CONF-9408131-4 p 1520 N95-21360 #
CONF-9408133-1 p 1531 N95-20120 #
CONF-940814-3 p 1309 N95-22241 #
CONF-9408141-1 p 1486 N95-22409 #
CONF-9408146-10 p 1374 N95-21528 #
CONF-9408146-12 p 1376 N95-22154 #
CONF-9408146-1 p 1533 N95-20573 #
CONF-9408146-2 p 1540 N95-22410 #
CONF-9408146-3 p 1375 N95-21919 #
CONF-9408146-4 p 1377 N95-22348 #
CONF-9408146-5 p 1376 N95-22242 #
CONF-9408146-6 p 1370 N95-20572 #
CONF-9408148-1 p 1337 N95-22427 #
CONF-9408150-1 p 1254 N95-20707 #
CONF-9408150-2 p 1525 N95-21857 #
CONF-9408155-10 p 1501 N95-20874 #
CONF-9408155-11 p 1581 N95-21604 #
CONF-9408155-4 p 1314 N95-20341 #
CONF-9408155-9 p 1568 N95-20630 #
CONF-940816-14 p 1573 N95-21561 #
CONF-940816-15 p 1523 N95-21563 #
CONF-940816-16 p 1580 N95-21486 #
CONF-940816-17 p 1523 N95-21562 #
CONF-940816-1 p 1527 N95-22078 #
CONF-940816-20 p 1522 N95-21497 #
CONF-940816-21 p 1522 N95-21499 #
CONF-940816-22 p 1522 N95-21498 #
CONF-940816-23 p 1507 N95-20110 #
CONF-940816-24 p 1507 N95-20131 #
CONF-940816-25 p 1519 N95-21273 #
CONF-940816-26 p 1508 N95-20132 #
CONF-940816-27 p 1539 N95-22195 #
CONF-940816-28 p 1527 N95-22194 #
CONF-940816-29 p 1508 N95-20134 #
CONF-940816-30 p 1528 N95-22197 #
CONF-940816-31 p 1529 N95-22314 #
CONF-940816-33 p 1510 N95-20367 #
CONF-940816-34 p 1510 N95-20343 #
CONF-940816-37 p 1527 N95-22152 #
CONF-940816-38 p 1523 N95-21588 #
CONF-940816-40 p 1523 N95-21521 #
CONF-940816-41 p 1524 N95-21597 #
CONF-940816-43 p 1513 N95-20575 #
CONF-940816-45 p 1365 N95-20902 #
CONF-940816-46 p 1515 N95-20897 #
CONF-940816-47 p 1520 N95-21313 #
CONF-940816-48 p 1535 N95-21254 #

CONF-940816-49 .... p 1535 N95-21255 #
CONF-940816-4 .... p 1530 N95-22392 #
CONF-9408163-1 .... p 1204 N95-20195 #
CONF-940816 .... p 1510 N95-20344 #
CONF-9408174-2 .... p 1244 N95-21571 #
CONF-9408175-1 .... p 1231 N95-21776 #
CONF-9408176-1 .... p 1558 N95-21299 #
CONF-9408178-1 .... p 1575 N95-21991 #
CONF-9408182-1 .... p 1427 N95-22477 #
CONF-940819-4 .... p 1254 N95-20822 #
CONF-940824-1 .... p 1582 N95-22237 #
CONF-940830-2 .... p 1272 N95-20892 #
CONF-940831-2 .... p 1564 N95-20240 #
CONF-940843-8 .... p 1232 N95-22130 #
CONF-940847-3 .... p 1524 N95-21703 #
CONF-940853-9 .... p 1501 N95-20725 #
CONF-940857-1 .... p 1367 N95-21507 #
CONF-940859-26 .... p 1364 N95-20321 #
CONF-940859-27 .... p 1481 N95-20837 #
CONF-940873-2 .... p 1586 N95-20016 #
CONF-940876-2 .... p 1453 N95-21637 #
CONF-940883-1 .... p 1392 N95-20480 #
CONF-9409103-2 .... p 1523 N95-21525 #
CONF-9409103-3 .... p 1519 N95-21237 #
CONF-9409103-4 .... p 1536 N95-21342 #
CONF-9409105-2 .... p 1551 N95-20315 #
CONF-9409105-4 .... p 1561 N95-21922 #
CONF-940917-1 .... p 1481 N95-20884 #
CONF-9409170-1 .... p 1393 N95-20863 #
CONF-9409177-1 .... p 1274 N95-21175 #
CONF-9409177-3 .... p 1376 N95-22169 #
CONF-9409179-3 .... p 1263 N95-22408 #
CONF-9409180-1-REV-1 .... p 1542 N95-20489 #
CONF-9409180-2 .... p 1542 N95-20403 #
CONF-9409181-2 .... p 1263 N95-19926 #
CONF-9409181-5 .... p 1254 N95-20816 #
CONF-9409181-6 .... p 1251 N95-20079 #
CONF-9409182-1 .... p 1500 N95-21136 #
CONF-9409185-1 .... p 1204 N95-20269 #
CONF-9409185-2 .... p 1205 N95-21520 #
CONF-9409186-1 .... p 1460 N95-20385 #
CONF-9409187-1 .... p 1206 N95-20370 * #
CONF-9409190-1 .... p 1592 N95-22263 #
CONF-9409191-1 .... p 1591 N95-22167 #
CONF-9409192-1 .... p 1473 N95-22426 #
CONF-9409196-1 .... p 1281 N95-22428 #
CONF-9409202-1 .... p 1367 N95-21546 #
CONF-9409206-1 .... p 1455 N95-21607 #
CONF-9409207-1 .... p 1261 N95-22119 #
CONF-9409211-2 .... p 1384 N95-20077 #
CONF-9409211-4 .... p 1387 N95-21396 #
CONF-9409215-1 .... p 1407 N95-21617 #
CONF-940922-3 .... p 1522 N95-21502 #
CONF-9409221-2 .... p 1561 N95-22010 #
CONF-9409222-1 .... p 1231 N95-22009 #
CONF-9409225-2 .... p 1373 N95-21393 #
CONF-9409226-1 .... p 1599 N95-21367 #
CONF-9409226-3 .... p 1371 N95-20786 #
CONF-9409227-1 .... p 1256 N95-21265 #
CONF-9409228-1 .... p 1580 N95-21264 #
CONF-9409232-1 .... p 1603 N95-21377 #
CONF-9409236-1 .... p 1301 N95-21277 #
CONF-9409241-1 .... p 1248 N95-22433 #
CONF-9409245-1 .... p 1221 N95-22436 #
CONF-940926-2 .... p 1575 N95-21936 #
CONF-940933-12 .... p 1533 N95-20784 #
CONF-940933-13 .... p 1557 N95-21240 #
CONF-940933-14 .... p 1557 N95-21239 #
CONF-940933-15 .... p 1558 N95-21242 #
CONF-940933-2 .... p 1537 N95-21603 #
CONF-940933-3 .... p 1549 N95-20114 #
CONF-940933-4 .... p 1549 N95-20113 #
CONF-940945-2 .... p 1252 N95-20216 #
CONF-940945-4 .... p 1382 N95-22356 #
CONF-940947-1 .... p 1250 N95-19979 #
CONF-940956-7 .... p 1251 N95-20122 #
CONF-940970-1 .... p 1393 N95-20862 #
CONF-940970-3 .... p 1393 N95-20861 #
CONF-940970-5 .... p 1394 N95-21353 #
CONF-940978-1 .... p 1252 N95-20331 #
CONF-940981-1 .... p 1563 N95-19954 #
CONF-940985-7 .... p 1407 N95-21666 #
CONF-941001-1 .... p 1259 N95-21838 #
CONF-941001-2 .... p 1453 N95-21721 #
CONF-941001-3 .... p 1572 N95-21304 #
CONF-941001-6 .... p 1260 N95-21926 #
CONF-9410114-1 .... p 1580 N95-21420 #
CONF-941013-2 .... p 1570 N95-20841 #
CONF-941013-8 .... p 1382 N95-22292 #
CONF-9410131-4 .... p 1385 N95-20237 #
CONF-9410131-5 .... p 1599 N95-20144 #
CONF-9410131-7 .... p 1218 N95-20785 #
CONF-9410132-2 .... p 1235 N95-20139 #
CONF-9410141-1 .... p 1591 N95-22092 #
CONF-9410141-2 .... p 1588 N95-20777 #
CONF-9410141-3 .... p 1589 N95-20818 #
CONF-9410154-1 .... p 1544 N95-21392 #
CONF-9410156-2 .... p 1302 N95-21305 #
CONF-9410161-1 .... p 1364 N95-20398 #
CONF-9410164-1 .... p 1313 N95-20168 #
CONF-9410164-2 .... p 1289 N95-20164 #
CONF-9410164-3 .... p 1219 N95-20567 #
CONF-9410164-4 .... p 1311 N95-22407 #
CONF-9410164-5 .... p 1291 N95-20697 #
CONF-9410165-3 .... p 1387 N95-21386 #
CONF-9410165-8 .... p 1572 N95-21297 #
CONF-9410167-1 .... p 1459 N95-20284 #
CONF-9410167-2 .... p 1480 N95-20126 #
CONF-9410170-1 .... p 1395 N95-21361 #
CONF-9410181-2 .... p 1223 N95-21840 #
CONF-9410181-3 .... p 1535 N95-21278 #
CONF-9410182-1 .... p 1503 N95-20267 #
CONF-9410184-1 .... p 1271 N95-20700 #
CONF-9410184-3 .... p 1229 N95-20912 #
CONF-9410184-4 .... p 1258 N95-21568 #
CONF-9410184-5 .... p 1259 N95-21737 #
CONF-9410185-1-EXTD-ABST .... p 1285 N95-20288 #
CONF-9410186-1 .... p 1482 N95-21385 #
CONF-9410187-2 .... p 1428 N95-20319 #
CONF-9410189-1 .... p 1371 N95-20783 #
CONF-9410189-2 .... p 1375 N95-21837
CONF-9410189-4 .... p 1378 N95-20048 #
CONF-9410189-5 .... p 1374 N95-21594 #
CONF-9410192-1 .... p 1373 N95-21261 #
CONF-9410194-1 .... p 1334 N95-22118 #
CONF-9410195-1 .... p 1329 N95-21390 #
CONF-9410195-2 .... p 1327 N95-20883 #
CONF-9410196-1 .... p 1414 N95-20990 #
CONF-9410197-1 .... p 1467 N95-21389 #
CONF-9410198-1 .... p 1560 N95-21609 #
CONF-9410199-1 .... p 1330 N95-21545 #
CONF-9410203-1 .... p 1232 N95-22126 #
CONF-9410212-3 .... p 1478 N95-21925 #
CONF-9410213-1 .... p 1387 N95-21364 #
CONF-9410213-2 .... p 1260 N95-22006 #
CONF-9410213-3 .... p 1262 N95-22308 #
CONF-9410217-1 .... p 1393 N95-20839 #
CONF-9410218-1 .... p 1329 N95-21395 #
CONF-9410219-3 .... p 1492 N95-21266 #
CONF-9410221-1 .... p 1469 N95-21829 #
CONF-9410221-2 .... p 1329 N95-21296 #
CONF-9410222-1 .... p 1426 N95-21836 #
CONF-9410224-1 .... p 1558 N95-21368 #
CONF-9410229-1 .... p 1536 N95-21331 #
CONF-9410236-1 .... p 1447 N95-22287 #
CONF-9410236-2 .... p 1447 N95-22285 #
CONF-9410244-1 .... p 1262 N95-22289 #
CONF-9410248-1 .... p 1528 N95-22239 #
CONF-941054-2 .... p 1466 N95-21311 #
CONF-941059-1 .... p 1271 N95-20704 #
CONF-941062-1 .... p 1375 N95-22007 #
CONF-941063-7 .... p 1327 N95-20882 #
CONF-941085-1-REV-1 .... p 1353 N95-21182 #
CONF-941086-3 .... p 1452 N95-21358 #
CONF-941101-1 .... p 1539 N95-22306 #
CONF-941102-11 .... p 1508 N95-20159 #
CONF-941102-12 .... p 1509 N95-20254 #
CONF-941102-13 .... p 1509 N95-20235 #
CONF-941102-14 .... p 1506 N95-20160 #
CONF-941102-15 .... p 1474 N95-20158 #
CONF-941102-16 .... p 1488 N95-20167 #
CONF-941102-17 .... p 1509 N95-20236 #
CONF-941102-24 .... p 1509 N95-20206 #
CONF-941102-29 .... p 1492 N95-21285 #
CONF-941102-31 .... p 1371 N95-20867 #
CONF-941102-8 .... p 1458 N95-20154 #
CONF-9411102-1 .... p 1477 N95-21505 #
CONF-9411104-2 .... p 1459 N95-20165 #
CONF-9411123-1 .... p 1545 N95-21509 #
CONF-9411129-1 .... p 1579 N95-20028 #
CONF-9411132-1 .... p 1329 N95-21394 #
CONF-9411132-2 .... p 1572 N95-21419 #
CONF-941115-1 .... p 1247 N95-22234 #
CONF-941118-1 .... p 1477 N95-21843 #
CONF-941118-2 .... p 1474 N95-20123 #
CONF-941118-4 .... p 1458 N95-20136 #
CONF-941118-6 .... p 1459 N95-20255 #
CONF-941129-6 .... p 1272 N95-20895 #
CONF-941129-7 .... p 1511 N95-20422 #
CONF-941129-8 .... p 1534 N95-21236 #
CONF-941132-1 .... p 1265 N95-20121 #
CONF-941142-10 .... p 1339 N95-20137 #
CONF-941142-13 .... p 1474 N95-20152 #
CONF-941142-14 .... p 1488 N95-20141 #
CONF-941142-15 .... p 1339 N95-20166 #
CONF-941142-16 .... p 1564 N95-20142 #
CONF-941142-17 .... p 1474 N95-20150 #
CONF-941142-18 .... p 1280 N95-22266 #
CONF-941142-20 .... p 1354 N95-21387 #
CONF-941144-1 .... p 1255 N95-21238 #
CONF-941152-1 .... p 1545 N95-21510 #
CONF-941154-1 .... p 1314 N95-20286 #
CONF-941181-1 .... p 1265 N95-20138 #
CONF-941190-1 .... p 1481 N95-20693 #
CONF-941193-1 .... p 1428 N95-20140 #
CONF-941199-1 .... p 1480 N95-20342 #
CONF-941199-2 .... p 1333 N95-21881 #
CONF-941199-3 .... p 1329 N95-21301 #
CONF-941203-5 .... p 1391 N95-20263 #
CONF-941203-6 .... p 1313 N95-20262 #
CONF-941216-1 .... p 1481 N95-20812 #
CONF-941219-1 .... p 1454 N95-22466 #
CONF-941221-1 .... p 1324 N95-20626 #
CONF-950101-1 .... p 1373 N95-21312 #
CONF-950110-1 .... p 1379 N95-20627 #
CONF-950116-1 .... p 1388 N95-22070 #
CONF-950121-1 .... p 1325 N95-20628 #
CONF-950124-1 .... p 1426 N95-21875 #

COO-2197-142 .... p 1245 N95-21845 #

CPIA-PUBL-602-VOL-2 .... p 1221 N95-20708

CRAD-9206-TR-8940 .... p 1204 N95-19950 * #

CRREL-SR-94-3 .... p 1287 N95-21626

CS-N-9401 .... p 1468 N95-21455

CS-TR-3294 .... p 1313 N95-20257 #

CSE-TR-207-94 .... p 1216 N95-20624

CSS/TR-94/26 .... p 1480 N95-20607 #

CT-2-R4921-CT-CT/01 .... p 1336 N95-22254 #

CWI-NM-R9322 .... p 1490 N95-20424
CWI-NM-R9401 .... p 1489 N95-20423
CWI-NM-R9402 .... p 1402 N95-20440
CWI-NM-R9404 .... p 1467 N95-21435
CWI-NM-R9405 .... p 1465 N95-21033
CWI-NM-R9407 .... p 1553 N95-20425
CWI-NM-R9408 .... p 1493 N95-21434
CWI-NM-R9409 .... p 1404 N95-21034

CWP-145P .... p 1411 N95-19981 #
CWP-152P .... p 1411 N95-19982 #

DCIEM-94-47 .... p 1446 N95-22001

DE93-000031 .... p 1394 N95-20985 #
DE94-000285 .... p 1398 N95-22468 #
DE94-000286 .... p 1392 N95-20778 #
DE94-004373 .... p 1512 N95-20469 #
DE94-006464 .... p 1265 N95-20121 #
DE94-007530 .... p 1236 N95-20277 #
DE94-009365 .... p 1412 N95-20278 * #
DE94-009757 .... p 1237 N95-20470 #
DE94-009913 .... p 1251 N95-20122 #
DE94-010396 .... p 1477 N95-21843 #
DE94-011418 .... p 1474 N95-20123 #
DE94-011546 .... p 1391 N95-20104 #
DE94-011831 .... p 1391 N95-20332 #
DE94-011833 .... p 1384 N95-20109 #
DE94-011835 .... p 1234 N95-20117 #
DE94-011848 .... p 1391 N95-20118 #
DE94-011858 .... p 1437 N95-20471 #
DE94-011864 .... p 1391 N95-20260 #
DE94-011874 .... p 1268 N95-20472 #
DE94-011875 .... p 1392 N95-20333 #
DE94-011876 .... p 1279 N95-22091 #
DE94-011877 .... p 1392 N95-20473 #
DE94-011886 .... p 1395 N95-21508 #
DE94-011894 .... p 1395 N95-21844 #
DE94-011895 .... p 1394 N95-21294 #
DE94-012263 .... p 1234 N95-20135 #
DE94-012270 .... p 1235 N95-20188 #
DE94-012277 .... p 1396 N95-22033 #
DE94-012845 .... p 1526 N95-21920 #
DE94-012846 .... p 1520 N95-21315
DE94-012850 .... p 1603 N95-21316 #
DE94-012854 .... p 1498 N95-20779 #
DE94-013095 .... p 1315 N95-20380 #
DE94-013485 .... p 1529 N95-22279 #
DE94-014238 .... p 1458 N95-20136 #
DE94-014286 .... p 1339 N95-20137 #
DE94-014287 .... p 1265 N95-20138 #
DE94-014417 .... p 1526 N95-22058 #
DE94-014443 .... p 1379 N95-20627 #
DE94-014447 .... p 1520 N95-21375 #
DE94-014657 .... p 1454 N95-22466 #
DE94-014658 .... p 1235 N95-20139 #
DE94-014732 .... p 1429 N95-20381 #
DE94-014789 .... p 1428 N95-20140 #
DE94-014798 .... p 1529 N95-22280 #
DE94-014813 .... p 1481 N95-20693 #
DE94-014876 .... p 1566 N95-20382 #

DE94-014972 .... p 1604 N95-22064 #
DE94-015014 .... p 1313 N95-20262 #
DE94-015015 .... p 1391 N95-20263 #
DE94-015028 .... p 1566 N95-20419 #
DE94-015076 .... p 1438 N95-21376 #
DE94-015283 .... p 1290 N95-20474 #
DE94-015380 .... p 1511 N95-20415 #
DE94-015427 .... p 1223 N95-20264 #
DE94-015538 .... p 1512 N95-20475 #
DE94-015540 .... p 1512 N95-20476 #
DE94-015541 .... p 1530 N95-22339 #
DE94-015559 .... p 1540 N95-22469 #
DE94-015560 .... p 1274 N95-21175 #
DE94-015606 .... p 1441 N95-22397
DE94-015641 .... p 1395 N95-21409 #
DE94-015739 .... p 1488 N95-20141 #
DE94-015742 .... p 1268 N95-20396 #
DE94-015744 .... p 1555 N95-21134 #
DE94-015746 .... p 1564 N95-20142 #
DE94-015747 .... p 1413 N95-20397 #
DE94-015749 .... p 1549 N95-20143 #
DE94-015769 .... p 1474 N95-20150 #
DE94-015770 .... p 1474 N95-20152 #
DE94-015771 .... p 1364 N95-20398 #
DE94-015787 .... p 1588 N95-20789 #
DE94-015797 .... p 1566 N95-20399 #
DE94-015798 .... p 1566 N95-20400 #
DE94-015803 .... p 1379 N95-20695 #
DE94-015804 .... p 1328 N95-21139 #
DE94-015845 .... p 1517 N95-21140 #
DE94-015849 .... p 1511 N95-20401 #
DE94-015856 .... p 1553 N95-20402 #
DE94-015857 .... p 1555 N95-21141 #
DE94-015859 .... p 1556 N95-21142 #
DE94-015894 .... p 1324 N95-20626 #
DE94-015943 .... p 1458 N95-20153 #
DE94-015947 .... p 1246 N95-21921 #
DE94-016055 .... p 1516 N95-21125 #
DE94-016071 .... p 1569 N95-20696 #
DE94-016086 .... p 1291 N95-20697 #
DE94-016088 .... p 1458 N95-20154 #
DE94-016162 .... p 1474 N95-20158 #
DE94-016164 .... p 1508 N95-20159 #
DE94-016165 .... p 1508 N95-20160 #
DE94-016178 .... p 1516 N95-21114 #
DE94-016186 .... p 1289 N95-20164 #
DE94-016190 .... p 1459 N95-20165 #
DE94-016192 .... p 1488 N95-20167 #
DE94-016193 .... p 1313 N95-20168 #
DE94-016196 .... p 1488 N95-20169
DE94-016200 .... p 1555 N95-21115 #
DE94-016201 .... p 1500 N95-21136 #
DE94-016204 .... p 1339 N95-20166 #
DE94-016212 .... p 1255 N95-21137 #
DE94-016216 .... p 1509 N95-20254 #
DE94-016248 .... p 1589 N95-21131 #
DE94-016284 .... p 1565 N95-20330
DE94-016285 .... p 1509 N95-20235 #
DE94-016291 .... p 1252 N95-20331 #
DE94-016296 .... p 1509 N95-20236 #
DE94-016345 .... p 1489 N95-20170 #
DE94-016364 .... p 1372 N95-21135 #
DE94-016366 .... p 1368 N95-19986 #
DE94-016370 .... p 1541 N95-20103 #
DE94-016373 .... p 1412 N95-20171 #
DE94-016386 .... p 1579 N95-20271 #
DE94-016447 .... p 1551 N95-20315 #
DE94-016454 .... p 1385 N95-20237 #
DE94-016457 .... p 1551 N95-20283 #
DE94-016477 .... p 1366 N95-21138 #
DE94-016481 .... p 1465 N95-21153 #
DE94-016489 .... p 1364 N95-20233 #
DE94-016519 .... p 1556 N95-21159 #
DE94-016520 .... p 1556 N95-21163 #
DE94-016541 .... p 1557 N95-21166 #
DE94-016542 .... p 1550 N95-20189 #
DE94-016549 .... p 1550 N95-20190 #
DE94-016550 .... p 1266 N95-20316 #
DE94-016551 .... p 1268 N95-20468 #
DE94-016557 .... p 1563 N95-19954 #
DE94-016558 .... p 1558 N95-21247 #
DE94-016561 .... p 1459 N95-20284 #
DE94-016575 .... p 1415 N95-21184 #
DE94-016576 .... p 1274 N95-21234 #
DE94-016596 .... p 1267 N95-20317 #
DE94-016602 .... p 1313 N95-20119 #
DE94-016604 .... p 1531 N95-20120 #
DE94-016605 .... p 1543 N95-20612 #
DE94-016606 .... p 1412 N95-19985 #
DE94-016607 .... p 1372 N95-21173 #
DE94-016610 .... p 1517 N95-21174 #
DE94-016611 .... p 1219 N95-20567 #
DE94-016622 .... p 1477 N95-21505 #
DE94-016627 .... p 1401 N95-20234
DE94-016680 .... p 1554 N95-20568 #
DE94-016682 .... p 1552 N95-20334 #
DE94-016683 .... p 1551 N95-20279 #
DE94-016687 .... p 1301 N95-21205 #
DE94-016689 .... p 1369 N95-20335 #
DE94-016690 .... p 1542 N95-20403 #
DE94-016692 .... p 1542 N95-20489 #
DE94-016696 .... p 1557 N95-21206 #
DE94-016697 .... p 1557 N95-21207 #
DE94-016698 .... p 1534 N95-21208 #
DE94-016700 .... p 1534 N95-21209 #
DE94-016701 .... p 1373 N95-21210 #
DE94-016702 .... p 1459 N95-20255 #
DE94-016715 .... p 1511 N95-20404 #
DE94-016718 .... p 1551 N95-20285 #
DE94-016719 .... p 1309 N95-22241 #
DE94-016728 .... p 1401 N95-20238 #
DE94-016779 .... p 1266 N95-20281 #
DE94-016780 .... p 1541 N95-20239 #
DE94-016781 .... p 1566 N95-20405 #
DE94-016784 .... p 1532 N95-20406 #
DE94-016785 .... p 1532 N95-20336 #
DE94-016790 .... p 1531 N95-20282 #
DE94-016804 .... p 1564 N95-20240 #
DE94-016808 .... p 1283 N95-21211 #
DE94-016809 .... p 1527 N95-22188 #
DE94-016813 .... p 1524 N95-21641 #
DE94-016814 .... p 1565 N95-20265 #
DE94-016815 .... p 1545 N95-21643 #
DE94-016821 .... p 1276 N95-21644 #
DE94-016822 .... p 1512 N95-20477 #
DE94-016823 .... p 1489 N95-20266 #
DE94-016862 .... p 1586 N95-21645 #
DE94-016872 .... p 1524 N95-21646 #
DE94-016878 .... p 1403 N95-20478 #
DE94-016879 .... p 1500 N95-20106 #
DE94-016893 .... p 1501 N95-20241 #
DE94-016894 .... p 1206 N95-20370 * #
DE94-016900 .... p 1335 N95-22189 #
DE94-016904 .... p 1567 N95-20479 #
DE94-016910 .... p 1234 N95-20107 #
DE94-016913 .... p 1510 N95-20360 #
DE94-016914 .... p 1527 N95-22190 #
DE94-016957 .... p 1236 N95-20361 #
DE94-016967 .... p 1552 N95-20362 #
DE94-016968 .... p 1433 N95-20420 #
DE94-016969 .... p 1562 N95-22191 #
DE94-016970 .... p 1553 N95-20363 #
DE94-016973 .... p 1542 N95-20364 #
DE94-016974 .... p 1377 N95-22312 #
DE94-017056 .... p 1245 N95-21845 #
DE94-017074 .... p 1392 N95-20480 #
DE94-017077 .... p 1460 N95-20385 #
DE94-017086 .... p 1338 N95-19923 #
DE94-017131 .... p 1233 N95-19924 #
DE94-017172 .... p 1539 N95-22192 #
DE94-017173 .... p 1237 N95-20386 #
DE94-017175 .... p 1262 N95-22313 #
DE94-017176 .... p 1503 N95-20267 #
DE94-017184 .... p 1507 N95-20108 #
DE94-017187 .... p 1311 N95-22407 #
DE94-017289 .... p 1401 N95-20193 #
DE94-017290 .... p 1599 N95-20144 #
DE94-017296 .... p 1250 N95-19900 #
DE94-017297 .... p 1460 N95-20387 #
DE94-017299 .... p 1378 N95-20085 #
DE94-017300 .... p 1599 N95-20145 #
DE94-017301 .... p 1563 N95-19925 #
DE94-017302 .... p 1540 N95-22391 #
DE94-017303 .... p 1563 N95-20014 #
DE94-017306 .... p 1276 N95-21662 #
DE94-017307 .... p 1263 N95-22408 #
DE94-017308 .... p 1374 N95-21663 #
DE94-017315 .... p 1531 N95-20021 #
DE94-017318 .... p 1507 N95-20086 #
DE94-017337 .... p 1263 N95-19926 #
DE94-017340 .... p 1398 N95-22429 #
DE94-017342 .... p 1486 N95-22409 #
DE94-017344 .... p 1564 N95-20087 #
DE94-017347 .... p 1506 N95-20026 #
DE94-017363 .... p 1241 N95-21172 #
DE94-017381 .... p 1282 N95-19927 #
DE94-017396 .... p 1236 N95-20268 #
DE94-017397 .... p 1507 N95-20034 #
DE94-017406 .... p 1204 N95-20269 #
DE94-017409 .... p 1591 N95-22167 #
DE94-017415 .... p 1473 N95-22426 #
DE94-017418 .... p 1545 N95-21509 #
DE94-017421 .... p 1314 N95-20286 #
DE94-017462 .... p 1251 N95-20088 #
DE94-017472 .... p 1401 N95-20089 #
DE94-017474 .... p 1251 N95-20090 #
DE94-017494 .... p 1532 N95-20388 #
DE94-017501 .... p 1511 N95-20444 #
DE94-017507 .... p 1337 N95-22427 #
DE94-017508 .... p 1553 N95-20445 #
DE94-017509 .... p 1554 N95-20446 #
DE94-017510 .... p 1550 N95-20146 #
DE94-017516 .... p 1548 N95-20037 #
DE94-017519 .... p 1549 N95-20038 #
DE94-017522 .... p 1253 N95-20447 #
DE94-017527 .... p 1567 N95-20448 #
DE94-017528 .... p 1567 N95-20449 #
DE94-017529 .... p 1542 N95-20450 #
DE94-017549 .... p 1261 N95-22048 #
DE94-017574 .... p 1512 N95-20451 #
DE94-017577 .... p 1604 N95-20383 #
DE94-017579 .... p 1602 N95-20147 #
DE94-017580 .... p 1604 N95-20490 #
DE94-017593 .... p 1509 N95-20242 #
DE94-017594 .... p 1565 N95-20243 #
DE94-017604 .... p 1512 N95-20491 #
DE94-017605 .... p 1237 N95-20384 #
DE94-017660 .... p 1247 N95-22049 #
DE94-017679 .... p 1411 N95-22342 #
DE94-017680 .... p 1565 N95-20244 #
DE94-017682 .... p 1565 N95-20245 #
DE94-017685 .... p 1501 N95-20246 #
DE94-017686 .... p 1219 N95-20148 #
DE94-017693 .... p 1541 N95-20218 #
DE94-017695 .... p 1377 N95-22343 #
DE94-017696 .... p 1551 N95-20219 #
DE94-017698 .... p 1265 N95-20220 #
DE94-017699 .... p 1369 N95-20221 #
DE94-017701 .... p 1503 N95-20019 #
DE94-017702 .... p 1250 N95-20020 #
DE94-017706 .... p 1262 N95-22344 #
DE94-017710 .... p 1263 N95-22345 #
DE94-017748 .... p 1255 N95-20907 #
DE94-017750 .... p 1263 N95-22346 #
DE94-017751 .... p 1225 N95-20022 #
DE94-017752 .... p 1280 N95-22258 #
DE94-017753 .... p 1567 N95-20492 #
DE94-017757 .... p 1247 N95-22260 #
DE94-017758 .... p 1225 N95-20023 #
DE94-017759 .... p 1264 N95-20024 #
DE94-017760 .... p 1412 N95-20287 #
DE94-017764 .... p 1237 N95-20493 #
DE94-017767 .... p 1226 N95-20125 #
DE94-017769 .... p 1340 N95-20781 #
DE94-017771 .... p 1226 N95-20357 #
DE94-017772 .... p 1285 N95-22261 #
DE94-017775 .... p 1605 N95-22262 #
DE94-017796 .... p 1440 N95-22065 #
DE94-017809 .... p 1592 N95-22263 #
DE94-017816 .... p 1357 N95-22264 #
DE94-017855 .... p 1253 N95-20673 #
DE94-017856 .... p 1528 N95-22265 #
DE94-017858 .... p 1280 N95-22266 #
DE94-017859 .... p 1381 N95-22268 #
DE94-017860 .... p 1460 N95-20358 #
DE94-017868 .... p 1252 N95-20359 #
DE94-017869 .... p 1568 N95-20674 #
DE94-017874 .... p 1252 N95-20365 #
DE94-017883 .... p 1475 N95-20366 #
DE94-017884 .... p 1565 N95-20371 #
DE94-017885 .... p 1566 N95-20372 #
DE94-017886 .... p 1267 N95-20373 #
DE94-017887 .... p 1578 N95-22269 #
DE94-017888 .... p 1385 N95-20374 #
DE94-017889 .... p 1280 N95-22270 #
DE94-017894 .... p 1336 N95-22271 #
DE94-017902 .... p 1482 N95-21385 #
DE94-017903 .... p 1578 N95-22272 #
DE94-017904 .... p 1253 N95-20375 #
DE94-017958 .... p 1248 N95-22273 #
DE94-017963 .... p 1370 N95-20569 #
DE94-017965 .... p 1532 N95-20494 #
DE94-017970 .... p 1532 N95-20495 #
DE94-017976 .... p 1269 N95-20570 #
DE94-017977 .... p 1554 N95-20571 #
DE94-017981 .... p 1530 N95-22340 #
DE94-017982 .... p 1513 N95-20496 #
DE94-017990 .... p 1370 N95-20572 #
DE94-017994 .... p 1533 N95-20573 #
DE94-018045 .... p 1370 N95-20698 #
DE94-018052 .... p 1524 N95-21664 #
DE94-018053 .... p 1560 N95-21665 #
DE94-018076 .... p 1407 N95-21666 #
DE94-018077 .... p 1331 N95-21667 #
DE94-018079 .... p 1554 N95-20675 #
DE94-018082 .... p 1462 N95-20699 #
DE94-018084 .... p 1285 N95-20288 #
DE94-018092 .... p 1560 N95-21668 #
DE94-018095 .... p 1413 N95-20289 #
DE94-018101 .... p 1244 N95-21701 #
DE94-018117 .... p 1560 N95-21702 #
DE94-018121 .... p 1271 N95-20700 #
DE94-018122 .... p 1524 N95-21703 #
DE94-018123 .... p 1491 N95-20701 #
DE94-018125 .... p 1386 N95-20703 #
DE94-018126 .... p 1271 N95-20704 #
DE94-018128 .... p 1254 N95-20705 #
DE94-018129 .... p 1525 N95-21704 #

DE94-018131 ..... p 1253 N95-20676 #
DE94-018135 ..... p 1379 N95-20723 #
DE94-018136 ..... p 1217 N95-21706 #
DE94-018144 ..... p 1501 N95-20725 #
DE94-018175 ..... p 1514 N95-20732 #
DE94-018177 ..... p 1256 N95-21260 #
DE94-018179 ..... p 1373 N95-21261 #
DE94-018182 ..... p 1569 N95-20677 #
DE94-018184 ..... p 1259 N95-21707 #
DE94-018189 ..... p 1569 N95-20678 #
DE94-018190 ..... p 1569 N95-20679 #
DE94-018198 ..... p 1519 N95-21262 #
DE94-018199 ..... p 1274 N95-21263 #
DE94-018205 ..... p 1577 N95-22168 #
DE94-018216 ..... p 1270 N95-20680 #
DE94-018253 ..... p 1408 N95-21708 #
DE94-018254 ..... p 1554 N95-20681 #
DE94-018261 ..... p 1414 N95-20990 #
DE94-018264 ..... p 1387 N95-21386 #
DE94-018268 ..... p 1254 N95-20816 #
DE94-018284 ..... p 1440 N95-22296 #
DE94-018285 ..... p 1483 N95-21710 #
DE94-018287 ..... p 1281 N95-22428 #
DE94-018289 ..... p 1538 N95-22050 #
DE94-018292 ..... p 1531 N95-20203 #
DE94-018293 ..... p 1375 N95-21837
DE94-018295 ..... p 1540 N95-22410 #
DE94-018300 ..... p 1574 N95-21712 #
DE94-018301 ..... p 1578 N95-22297 #
DE94-018302 ..... p 1375 N95-21919 #
DE94-018303 ..... p 1377 N95-22348 #
DE94-018305 ..... p 1376 N95-22242 #
DE94-018312 ..... p 1539 N95-22243 #
DE94-018313 ..... p 1539 N95-22298 #
DE94-018319 ..... p 1601 N95-22419 #
DE94-018323 ..... p 1469 N95-21713 #
DE94-018327 ..... p 1354 N95-21387 #
DE94-018328 ..... p 1310 N95-22299 #
DE94-018329 ..... p 1562 N95-22300 #
DE94-018333 ..... p 1285 N95-20194 #
DE94-018339 ..... p 1531 N95-20015 #
DE94-018366 ..... p 1402 N95-20247 #
DE94-018367 ..... p 1586 N95-20016 #
DE94-018370 ..... p 1559 N95-21388 #
DE94-018371 ..... p 1564 N95-20017 #
DE94-018373 ..... p 1264 N95-20018 #
DE94-018379 ..... p 1540 N95-19968 #
DE94-018383 ..... p 1437 N95-19969 #
DE94-018385 ..... p 1506 N95-20025 #
DE94-018387 ..... p 1226 N95-20027 #
DE94-018389 ..... p 1254 N95-20707 #
DE94-018414 ..... p 1287 N95-21631 #
DE94-018417 ..... p 1239 N95-20682 #
DE94-018430 ..... p 1579 N95-20028 #
DE94-018434 ..... p 1455 N95-21632 #
DE94-018492 ..... p 1489 N95-20222 #
DE94-018494 ..... p 1215 N95-20223 #
DE94-018500 ..... p 1371 N95-20817 #
DE94-018507 ..... p 1364 N95-20224 #
DE94-018512 ..... p 1369 N95-20225 #
DE94-018535 ..... p 1429 N95-20782 #
DE94-018548 ..... p 1371 N95-20783 #
DE94-018549 ..... p 1552 N95-20318 #
DE94-018580 ..... p 1552 N95-20345 #
DE94-018587 ..... p 1467 N95-21389 #
DE94-018595 ..... p 1510 N95-20346 #
DE94-018617 ..... p 1404 N95-20991 #
DE94-018621 ..... p 1529 N95-22315 #
DE94-018632 ..... p 1539 N95-22357 #
DE94-018634 ..... p 1530 N95-22392 #
DE94-018635 ..... p 1480 N95-20126 #
DE94-018637 ..... p 1564 N95-20127 #
DE94-018646 ..... p 1532 N95-20347 #
DE94-018648 ..... p 1529 N95-22316 #
DE94-018653 ..... p 1548 N95-20029 #
DE94-018654 ..... p 1251 N95-20128 #
DE94-018657 ..... p 1552 N95-20348 #
DE94-018658 ..... p 1500 N95-20129 #
DE94-018662 ..... p 1506 N95-20030 #
DE94-018676 ..... p 1564 N95-20130 #
DE94-018697 ..... p 1250 N95-20043 #
DE94-018703 ..... p 1250 N95-20044 #
DE94-018709 ..... p 1265 N95-20226 #
DE94-018713 ..... p 1510 N95-20337 #
DE94-018715 ..... p 1232 N95-22115 #
DE94-018738 ..... p 1204 N95-20195 #
DE94-018742 ..... p 1314 N95-20338 #
DE94-018744 ..... p 1535 N95-21328 #
DE94-018784 ..... p 1236 N95-20349 #
DE94-018822 ..... p 1267 N95-20350 #
DE94-018840 ..... p 1233 N95-20045 #
DE94-018845 ..... p 1234 N95-20046 #
DE94-018849 ..... p 1314 N95-20339 #
DE94-018886 ..... p 1264 N95-20047 #
DE94-018887 ..... p 1565 N95-20340 #
DE94-018891 ..... p 1314 N95-20341 #
DE94-018897 ..... p 1480 N95-20342 #
DE94-018898 ..... p 1428 N95-20319 #
DE94-018901 ..... p 1329 N95-21390 #
DE94-018902 ..... p 1378 N95-20048 #
DE94-018904 ..... p 1330 N95-21545 #
DE94-018905 ..... p 1334 N95-22118 #
DE94-018907 ..... p 1261 N95-22119 #
DE94-018910 ..... p 1367 N95-21546 #
DE94-018913 ..... p 1364 N95-20320 #
DE94-018914 ..... p 1507 N95-20049 #
DE94-018923 ..... p 1364 N95-20321 #
DE94-018930 ..... p 1285 N95-20050 #
DE94-018936 ..... p 1561 N95-22116 #
DE94-018940 ..... p 1385 N95-20322 #
DE94-018944 ..... p 1538 N95-22117 #
DE94-018946 ..... p 1261 N95-22123 #
DE94-018950 ..... p 1559 N95-21547 #
DE94-018952 ..... p 1439 N95-21548 #
DE94-018955 ..... p 1267 N95-20323 #
DE94-018958 ..... p 1385 N95-20416 #
DE94-018964 ..... p 1244 N95-21549 #
DE94-018965 ..... p 1381 N95-21550 #
DE94-018967 ..... p 1287 N95-21559 #
DE94-018977 ..... p 1258 N95-21560 #
DE94-018979 ..... p 1573 N95-21561 #
DE94-018993 ..... p 1523 N95-21562 #
DE94-018994 ..... p 1523 N95-21563 #
DE94-018997 ..... p 1232 N95-22126 #
DE94-019013 ..... p 1460 N95-20351 #
DE94-019015 ..... p 1541 N95-20352 #
DE94-019016 ..... p 1402 N95-20353 #
DE94-019017 ..... p 1413 N95-20354 #
DE94-019018 ..... p 1402 N95-20355 #
DE94-019019 ..... p 1286 N95-20356 #
DE94-019023 ..... p 1234 N95-20052 #
DE94-019037 ..... p 1378 N95-20053 #
DE94-019046 ..... p 1493 N95-21564 #
DE94-019075 ..... p 1406 N95-21565 #
DE94-019101 ..... p 1523 N95-21551 #
DE94-019102 ..... p 1389 N95-21433 #
DE94-019103 ..... p 1389 N95-21552 #
DE94-019105 ..... p 1230 N95-21553 #
DE94-019112 ..... p 1330 N95-21554 #
DE94-019114 ..... p 1257 N95-21555 #
DE94-019115 ..... p 1477 N95-21556 #
DE94-019124 ..... p 1522 N95-21519 #
DE94-019125 ..... p 1303 N95-21459 #
DE94-019127 ..... p 1258 N95-21600 #
DE94-019129 ..... p 1381 N95-21601 #
DE94-019146 ..... p 1537 N95-21460 #
DE94-019151 ..... p 1559 N95-21581 #
DE94-019153 ..... p 1439 N95-21606 #
DE94-019154 ..... p 1551 N95-20205 #
DE94-019156 ..... p 1455 N95-21607 #
DE94-019158 ..... p 1407 N95-21608 #
DE94-019162 ..... p 1261 N95-22127 #
DE94-019163 ..... p 1477 N95-21602 #
DE94-019167 ..... p 1600 N95-22128 #
DE94-019169 ..... p 1335 N95-22165 #
DE94-019175 ..... p 1509 N95-20206 #
DE94-019176 ..... p 1572 N95-21419 #
DE94-019177 ..... p 1560 N95-21609 #
DE94-019182 ..... p 1537 N95-21603 #
DE94-019187 ..... p 1395 N95-21611 #
DE94-019195 ..... p 1483 N95-21613 * #
DE94-019196 ..... p 1524 N95-21605 #
DE94-019214 ..... p 1458 N95-20073 #
DE94-019215 ..... p 1591 N95-22129 #
DE94-019217 ..... p 1562 N95-22120 #
DE94-019238 ..... p 1440 N95-22066 #
DE94-019248 ..... p 1376 N95-22121 #
DE94-019254 ..... p 1396 N95-21897 #
DE94-019259 ..... p 1407 N95-21617 #
DE94-019268 ..... p 1573 N95-21474 #
DE94-019269 ..... p 1232 N95-22130 #
DE94-019272 ..... p 1414 N95-20908 #
DE94-019275 ..... p 1441 N95-20074 #
DE94-019278 ..... p 1521 N95-21406 #
DE94-019279 ..... p 1591 N95-22092 #
DE94-019285 ..... p 1536 N95-21407 #
DE94-019287 ..... p 1572 N95-21408 #
DE94-019288 ..... p 1604 N95-21475 #
DE94-019295 ..... p 1257 N95-21476 #
DE94-019298 ..... p 1415 N95-21477 #
DE94-019306 ..... p 1367 N95-21507 #
DE94-019309 ..... p 1205 N95-21520 #
DE94-019310 ..... p 1367 N95-21478 #
DE94-019311 ..... p 1600 N95-21479 #
DE94-019312 ..... p 1544 N95-21392 #
DE94-019319 ..... p 1374 N95-21480 #
DE94-019326 ..... p 1580 N95-21420 #
DE94-019332 ..... p 1230 N95-21481 #
DE94-019333 ..... p 1275 N95-21482 #
DE94-019335 ..... p 1573 N95-21483 #
DE94-019345 ..... p 1521 N95-21484 #
DE94-019348 ..... p 1522 N95-21485 #
DE94-019349 ..... p 1580 N95-21486 #
DE94-628903 ..... p 1523 N95-21591 #
DE94-628931 ..... p 1500 N95-21592 #
DE94-628932 ..... p 1560 N95-21593 #
DE94-628950 ..... p 1561 N95-21847 #
DE94-628962 ..... p 1561 N95-21848 #
DE94-628963 ..... p 1307 N95-21849 #
DE94-628964 ..... p 1561 N95-21850 #
DE94-628965 ..... p 1561 N95-21851 #
DE94-628980 ..... p 1561 N95-21852 #
DE94-628990 ..... p 1575 N95-21853 #
DE94-628991 ..... p 1581 N95-21639 #
DE94-628992 ..... p 1278 N95-21885 #
DE94-628993 ..... p 1581 N95-21887 #
DE94-628994 ..... p 1575 N95-21859 #
DE94-628995 ..... p 1575 N95-21854 #
DE94-628996 ..... p 1260 N95-21855 #
DE94-628997 ..... p 1525 N95-21856 #
DE94-628998 ..... p 1525 N95-21860 #
DE94-628999 ..... p 1578 N95-22276 #
DE94-629000 ..... p 1562 N95-22377 #
DE94-629001 ..... p 1582 N95-22378 #
DE94-629002 ..... p 1579 N95-22380 #
DE94-629030 ..... p 1582 N95-22198 #
DE94-629031 ..... p 1528 N95-22217 #
DE94-629032 ..... p 1578 N95-22277 #
DE94-629033 ..... p 1528 N95-22218 #
DE94-629034 ..... p 1577 N95-22176 #
DE94-629036 ..... p 1502 N95-22177 #
DE94-629037 ..... p 1581 N95-21993 #
DE94-629042 ..... p 1582 N95-21994 #
DE94-629046 ..... p 1577 N95-22178 #
DE94-629047 ..... p 1527 N95-22179 #
DE94-629058 ..... p 1577 N95-22180 #
DE94-629059 ..... p 1577 N95-22181 #
DE94-629074 ..... p 1576 N95-21995 #
DE94-629075 ..... p 1576 N95-21996 #
DE94-629076 ..... p 1576 N95-21997 #
DE94-629077 ..... p 1527 N95-22182 #
DE94-629078 ..... p 1576 N95-21998 #
DE94-629082 ..... p 1397 N95-22183 #
DE94-629216 ..... p 1256 N95-21270 #
DE94-629656 ..... p 1326 N95-20733 #
DE94-629874 ..... p 1491 N95-20734 #
DE94-629887 ..... p 1514 N95-20735 #
DE94-629938 ..... p 1550 N95-20204 #
DE94-629992 ..... p 1239 N95-20736 #
DE94-630140 ..... p 1565 N95-20261 #
DE94-631122 ..... p 1605 N95-21828 #
DE94-631123 ..... p 1605 N95-21830 #
DE94-631340 ..... p 1508 N95-20196 #
DE94-631341 ..... p 1508 N95-20197 #
DE94-631342 ..... p 1509 N95-20198 #
DE94-631343 ..... p 1509 N95-20199 #
DE94-631396 ..... p 1556 N95-21162 #
DE94-631397 ..... p 1556 N95-21164 #
DE94-631410 ..... p 1550 N95-20200 #
DE94-631422 ..... p 1548 N95-19977 #
DE94-631456 ..... p 1556 N95-21165 #
DE94-631462 ..... p 1255 N95-20909 #
DE94-631463 ..... p 1563 N95-19978 #
DE94-631501 ..... p 1529 N95-22281 #
DE94-632822 ..... p 1335 N95-22184 #
DE94-632964 ..... p 1582 N95-22185 #
DE94-633373 ..... p 1562 N95-22282 #
DE94-633377 ..... p 1529 N95-22283 #
DE94-765351 ..... p 1410 N95-22219 #
DE94-770603 ..... p 1514 N95-20737 #
DE94-770604 ..... p 1514 N95-20738 #
DE94-770606 ..... p 1514 N95-20756 #
DE94-770607 ..... p 1516 N95-20986 #
DE94-770631 ..... p 1371 N95-20757 #
DE94-770684 ..... p 1555 N95-20987 #
DE94-770685 ..... p 1555 N95-20988 #
DE94-770686 ..... p 1555 N95-20989 #
DE94-770690 ..... p 1554 N95-20683 #
DE94-770700 ..... p 1554 N95-20684 #
DE94-770764 ..... p 1392 N95-20685 #
DE94-770765 ..... p 1554 N95-20686 #
DE94-770780 ..... p 1526 N95-22051 #
DE94-796550 ..... p 1277 N95-21714 #
DE94-796596 ..... p 1404 N95-21143 #
DE95-000005 ..... p 1324 N95-20574 #
DE95-000241 ..... p 1410 N95-22278 #
DE95-000330 ..... p 1376 N95-22301 #
DE95-000536 ..... p 1373 N95-21393 #
DE95-000540 ..... p 1325 N95-20628 #
DE95-000559 ..... p 1522 N95-21497 #
DE95-000560 ..... p 1527 N95-22122 #
DE95-000561 ..... p 1522 N95-21498 #
DE95-000562 ..... p 1539 N95-22193 #
DE95-000563 ..... p 1522 N95-21499 #
DE95-000564 ..... p 1507 N95-20110 #
DE95-000565 ..... p 1507 N95-20111 #
DE95-000589 ..... p 1549 N95-20112 #
DE95-000590 ..... p 1549 N95-20113 #

DE95-000591 p 1549 N95-20114 #
DE95-000601 p 1265 N95-20115 #
DE95-000602 p 1412 N95-20116 #
DE95-000624 p 1250 N95-19979 #
DE95-000626 p 1522 N95-21506 #
DE95-000627 p 1233 N95-19980 #
DE95-000641 p 1507 N95-20131 #
DE95-000642 p 1519 N95-21273 #
DE95-000643 p 1411 N95-19981 #
DE95-000644 p 1411 N95-19982 #
DE95-000647 p 1508 N95-20132 #
DE95-000664 p 1519 N95-21276 #
DE95-000685 p 1571 N95-21167 #
DE95-000690 p 1508 N95-20133 #
DE95-000711 p 1549 N95-20075 #
DE95-000713 p 1221 N95-20076 #
DE95-000724 p 1508 N95-20134 #
DE95-000725 p 1527 N95-22194 #
DE95-000726 p 1539 N95-22195 #
DE95-000727 p 1515 N95-20879 #
DE95-000728 p 1528 N95-22196 #
DE95-000729 p 1515 N95-20880 #
DE95-000730 p 1528 N95-22197 #
DE95-000731 p 1529 N95-22314 #
DE95-000738 p 1329 N95-21394 #
DE95-000740 p 1384 N95-20077 #
DE95-000742 p 1242 N95-21309 #
DE95-000743 p 1264 N95-20078 #
DE95-000744 p 1218 N95-20785 #
DE95-000745 p 1329 N95-21395 #
DE95-000755 p 1251 N95-20079 #
DE95-000788 p 1558 N95-21310 #
DE95-000830 p 1406 N95-21487 #
DE95-000837 p 1510 N95-20343 #
DE95-000838 p 1510 N95-20344 #
DE95-000841 p 1353 N95-21182 #
DE95-000844 p 1603 N95-21377 #
DE95-000846 p 1260 N95-22006 #
DE95-000847 p 1387 N95-21364 #
DE95-000851 p 1375 N95-22007 #
DE95-000855 p 1576 N95-22008 #
DE95-000857 p 1231 N95-22009 #
DE95-000859 p 1438 N95-21366 #
DE95-000862 p 1373 N95-21312 #
DE95-000863 p 1599 N95-21367 #
DE95-000865 p 1561 N95-22010 #
DE95-000867 p 1334 N95-22011 #
DE95-000868 p 1246 N95-22012 #
DE95-000871 p 1510 N95-20367 #
DE95-000923 p 1371 N95-20786 #
DE95-000932 p 1526 N95-21934 #
DE95-000935 p 1558 N95-21368 #
DE95-000936 p 1600 N95-21935 #
DE95-000938 p 1575 N95-21936 #
DE95-000950 p 1278 N95-21937 #
DE95-000951 p 1538 N95-21938 #
DE95-000952 p 1526 N95-21939 #
DE95-000953 p 1526 N95-21940 #
DE95-000954 p 1561 N95-21922 #
DE95-000956 p 1258 N95-21676 #
DE95-000982 p 1406 N95-21410 #
DE95-001006 p 1481 N95-20812 #
DE95-001008 p 1588 N95-20777 #
DE95-001009 p 1589 N95-20818 #
DE95-001015 p 1580 N95-21264 #
DE95-001018 p 1536 N95-21331 #
DE95-001028 p 1426 N95-21875 #
DE95-001069 p 1591 N95-22107 #
DE95-001070 p 1258 N95-21265 #
DE95-001071 p 1231 N95-21776 #
DE95-001072 p 1570 N95-20819 #
DE95-001073 p 1570 N95-20820 #
DE95-001076 p 1271 N95-20821 #
DE95-001077 p 1254 N95-20822 #
DE95-001078 p 1515 N95-20911 #
DE95-001101 p 1440 N95-22067 #
DE95-001102 p 1329 N95-21296 #
DE95-001106 p 1229 N95-20912 #
DE95-001108 p 1341 N95-20831 #
DE95-001112 p 1371 N95-20832 #
DE95-001114 p 1386 N95-20833 #
DE95-001117 p 1403 N95-20834 #
DE95-001119 p 1469 N95-21829 #
DE95-001121 p 1404 N95-20835 #
DE95-001125 p 1240 N95-20836 #
DE95-001126 p 1426 N95-21836 #
DE95-001153 p 1313 N95-20213 #
DE95-001156 p 1237 N95-20368 #
DE95-001204 p 1581 N95-21842 #
DE95-001224 p 1289 N95-20214 #
DE95-001243 p 1235 N95-20215 #
DE95-001248 p 1252 N95-20216 #
DE95-001284 p 1509 N95-20217 #
DE95-001348 p 1525 N95-21857 #
DE95-001351 p 1277 N95-21861 #
DE95-001352 p 1492 N95-21285 #
DE95-001357 p 1572 N95-21297 #
DE95-001358 p 1256 N95-21298 #
DE95-001384 p 1590 N95-21862 #
DE95-001385 p 1591 N95-22061 #
DE95-001387 p 1356 N95-22148 #
DE95-001389 p 1558 N95-21299 #
DE95-001419 p 1335 N95-22149 #
DE95-001420 p 1271 N95-20761 #
DE95-001421 p 1243 N95-21500 #
DE95-001422 p 1326 N95-20791 #
DE95-001425 p 1278 N95-21909 #
DE95-001426 p 1275 N95-21501 #
DE95-001428 p 1481 N95-20837 #
DE95-001443 p 1522 N95-21502 #
DE95-001447 p 1570 N95-20838 #
DE95-001448 p 1537 N95-21503 #
DE95-001454 p 1466 N95-21311 #
DE95-001455 p 1393 N95-20839 #
DE95-001456 p 1254 N95-20792 #
DE95-001457 p 1229 N95-20840 #
DE95-001458 p 1531 N95-19983 #
DE95-001470 p 1570 N95-20841 #
DE95-001471 p 1514 N95-20852 #
DE95-001485 p 1538 N95-21720 #
DE95-001492 p 1222 N95-20853 #
DE95-001496 p 1256 N95-21300 #
DE95-001497 p 1329 N95-21301 #
DE95-001504 p 1327 N95-20854 #
DE95-001506 p 1301 N95-21277 #
DE95-001507 p 1570 N95-20881 #
DE95-001522 p 1327 N95-20882 #
DE95-001525 p 1259 N95-21838 #
DE95-001548 p 1574 N95-21839 #
DE95-001602 p 1453 N95-21721 #
DE95-001604 p 1535 N95-21278 #
DE95-001606 p 1223 N95-21840 #
DE95-001607 p 1327 N95-20883 #
DE95-001609 p 1333 N95-21881 #
DE95-001617 p 1481 N95-20884 #
DE95-001619 p 1388 N95-22070 #
DE95-001620 p 1575 N95-21991 #
DE95-001622 p 1393 N95-20861 #
DE95-001623 p 1393 N95-20862 #
DE95-001626 p 1393 N95-20863 #
DE95-001628 p 1387 N95-21396 #
DE95-001647 p 1409 N95-21722 #
DE95-001653 p 1242 N95-21397 #
DE95-001654 p 1257 N95-21398 #
DE95-001655 p 1574 N95-21723 #
DE95-001656 p 1257 N95-21399 #
DE95-001657 p 1260 N95-21923 #
DE95-001671 p 1231 N95-21924 #
DE95-001673 p 1242 N95-21400 #
DE95-001675 p 1260 N95-21841 #
DE95-001676 p 1245 N95-21734 #
DE95-001677 p 1277 N95-21735 #
DE95-001678 p 1231 N95-21736 #
DE95-001680 p 1259 N95-21737 #
DE95-001681 p 1258 N95-21568 #
DE95-001682 p 1573 N95-21569 #
DE95-001684 p 1574 N95-21570 #
DE95-001686 p 1493 N95-21439 #
DE95-001699 p 1244 N95-21571 #
DE95-001702 p 1470 N95-21992 #
DE95-001704 p 1276 N95-21572 #
DE95-001711 p 1332 N95-21738 #
DE95-001715 p 1263 N95-22396 #
DE95-001723 p 1259 N95-21739 #
DE95-001724 p 1259 N95-21740
DE95-001739 p 1483 N95-21741 #
DE95-001745 p 1332 N95-21742 #
DE95-001763 p 1374 N95-21743 #
DE95-001767 p 1521 N95-21378 #
DE95-001770 p 1469 N95-21744 #
DE95-001786 p 1334 N95-22062 #
DE95-001787 p 1243 N95-21440 #
DE95-001800 p 1245 N95-21745 #
DE95-001802 p 1572 N95-21279 #
DE95-001803 p 1241 N95-21280 #
DE95-001804 p 1535 N95-21281 #
DE95-001805 p 1519 N95-21302 #
DE95-001807 p 1521 N95-21441 #
DE95-001808 p 1224 N95-21746 #
DE95-001809 p 1257 N95-21303 #
DE95-001812 p 1525 N95-21747 #
DE95-001813 p 1277 N95-21748 #
DE95-001817 p 1560 N95-21724 #
DE95-001818 p 1260 N95-22013 #
DE95-001819 p 1330 N95-21442 #
DE95-001820 p 1332 N95-21725 #
DE95-001826 p 1355 N95-21726 #
DE95-001827 p 1572 N95-21304 #
DE95-001828 p 1394 N95-21353 #
DE95-001830 p 1302 N95-21305 #
DE95-001831 p 1393 N95-20864 #
DE95-001834 p 1256 N95-21286 #
DE95-001848 p 1525 N95-21727 #
DE95-001859 p 1545 N95-21728 #
DE95-001861 p 1521 N95-21443 #
DE95-001866 p 1506 N95-22071 #
DE95-001867 p 1572 N95-21287 #
DE95-001876 p 1332 N95-21729 #
DE95-001903 p 1466 N95-21288 #
DE95-001919 p 1207 N95-21730 #
DE95-001925 p 1332 N95-21731 #
DE95-001976 p 1275 N95-21354 #
DE95-001990 p 1275 N95-21289 #
DE95-002038 p 1558 N95-21290 #
DE95-002042 p 1333 N95-21960 #
DE95-002049 p 1330 N95-21471 #
DE95-002058 p 1245 N95-21732 #
DE95-002060 p 1243 N95-21472 #
DE95-002078 p 1243 N95-21473 #
DE95-002100 p 1538 N95-21733 #
DE95-002121 p 1527 N95-22152 #
DE95-002122 p 1336 N95-22284 #
DE95-002126 p 1276 N95-21585 #
DE95-002132 p 1240 N95-20865 #
DE95-002134 p 1476 N95-21355 #
DE95-002138 p 1523 N95-21587 #
DE95-002170 p 1371 N95-20866 #
DE95-002177 p 1523 N95-21588 #
DE95-002181 p 1371 N95-20867 #
DE95-002183 p 1374 N95-21594 #
DE95-002199 p 1582 N95-22153 #
DE95-002200 p 1445 N95-21595 #
DE95-002214 p 1525 N95-21715 #
DE95-002217 p 1524 N95-21597 #
DE95-002225 p 1492 N95-21266 #
DE95-002227 p 1533 N95-20766 #
DE95-002228 p 1468 N95-21515 #
DE95-002238 p 1253 N95-20417 #
DE95-002248 p 1511 N95-20418 #
DE95-002250 p 1523 N95-21521 #
DE95-002251 p 1515 N95-20868 #
DE95-002252 p 1501 N95-20869 #
DE95-002254 p 1228 N95-20787 #
DE95-002255 p 1240 N95-20780 #
DE95-002256 p 1283 N95-21356 #
DE95-002257 p 1406 N95-21379 #
DE95-002259 p 1447 N95-22285 #
DE95-002260 p 1447 N95-22287 #
DE95-002264 p 1533 N95-20784 #
DE95-002265 p 1555 N95-20813 #
DE95-002274 p 1588 N95-20762 #
DE95-002314 p 1393 N95-20870 #
DE95-002316 p 1394 N95-20871 #
DE95-002327 p 1515 N95-20872 #
DE95-002329 p 1599 N95-20873 #
DE95-002333 p 1326 N95-20814 #
DE95-002336 p 1374 N95-21528 #
DE95-002337 p 1501 N95-20874 #
DE95-002338 p 1581 N95-21604 #
DE95-002341 p 1520 N95-21357 #
DE95-002343 p 1521 N95-21380 #
DE95-002346 p 1246 N95-21990 #
DE95-002348 p 1513 N95-20575 #
DE95-002354 p 1513 N95-20629 #
DE95-002355 p 1568 N95-20630 #
DE95-002357 p 1534 N95-20891 #
DE95-002392 p 1452 N95-21358 #
DE95-002393 p 1453 N95-21637 #
DE95-002394 p 1520 N95-21360 #
DE95-002396 p 1272 N95-20892 #
DE95-002405 p 1395 N95-21361 #
DE95-002409 p 1573 N95-21516 #
DE95-002416 p 1367 N95-21638 #
DE95-002419 p 1520 N95-21362 #
DE95-002447 p 1515 N95-20893 #
DE95-002450 p 1536 N95-21418 #
DE95-002452 p 1486 N95-22430 #
DE95-002453 p 1482 N95-21522 #
DE95-002454 p 1244 N95-21523 #
DE95-002466 p 1272 N95-20894 #
DE95-002471 p 1545 N95-21510 #
DE95-002472 p 1415 N95-21511 #
DE95-002481 p 1243 N95-21512 #
DE95-002486 p 1283 N95-21513 #
DE95-002487 p 1272 N95-20895 #
DE95-002488 p 1376 N95-22169 #
DE95-002492 p 1283 N95-21514 #
DE95-002504 p 1229 N95-20913 #
DE95-002511 p 1394 N95-20896 #
DE95-002515 p 1533 N95-20886 #
DE95-002521 p 1520 N95-21313 #
DE95-002522 p 1535 N95-21314 #
DE95-002523 p 1516 N95-20914 #
DE95-002524 p 1515 N95-20897 #
DE95-002525 p 1515 N95-20898 #
DE95-002526 p 1282 N95-20899 #
DE95-002527 p 1534 N95-20900 #
DE95-002528 p 1463 N95-20901 #

DE95-002529 .... p 1532 N95-20421 #
DE95-002531 .... p 1533 N95-20885 #
DE95-002532 .... p 1365 N95-20902 #
DE95-002537 .... p 1431 N95-22288 #
DE95-002586 .... p 1389 N95-20903 #
DE95-002587 .... p 1463 N95-20887 #
DE95-002588 .... p 1271 N95-20788 #
DE95-002591 .... p 1244 N95-21524 #
DE95-002600 .... p 1246 N95-21886 #
DE95-002601 .... p 1511 N95-20422 #
DE95-002611 .... p 1539 N95-22306 #
DE95-002614 .... p 1553 N95-20437 #
DE95-002617 .... p 1358 N95-22307 #
DE95-002639 .... p 1237 N95-20438 #
DE95-002651 .... p 1392 N95-20439 #
DE95-002652 .... p 1394 N95-20915 #
DE95-002656 .... p 1569 N95-20793 #
DE95-002681 .... p 1570 N95-20916 #
DE95-002682 .... p 1413 N95-20455 #
DE95-002702 .... p 1262 N95-22308 #
DE95-002704 .... p 1262 N95-22289 #
DE95-002708 .... p 1478 N95-21925 #
DE95-002712 .... p 1520 N95-21321 #
DE95-002721 .... p 1260 N95-21926 #
DE95-002727 .... p 1353 N95-21317 #
DE95-002728 .... p 1376 N95-22154 #
DE95-002736 .... p 1248 N95-22433 #
DE95-002737 .... p 1518 N95-21235 #
DE95-002738 .... p 1534 N95-21236 #
DE95-002739 .... p 1427 N95-22477 #
DE95-002740 .... p 1281 N95-22434 #
DE95-002742 .... p 1530 N95-22435 #
DE95-002743 .... p 1519 N95-21237 #
DE95-002750 .... p 1221 N95-22436 #
DE95-002751 .... p 1255 N95-21238 #
DE95-002755 .... p 1557 N95-21239 #
DE95-002756 .... p 1557 N95-21240 #
DE95-002783 .... p 1523 N95-21525 #
DE95-002784 .... p 1301 N95-21241 #
DE95-002797 .... p 1439 N95-21526 #
DE95-002798 .... p 1430 N95-21527 #
DE95-002801 .... p 1238 N95-20576 #
DE95-002805 .... p 1475 N95-20888 #
DE95-002812 .... p 1558 N95-21242 #
DE95-002851 .... p 1214 N95-21243 #
DE95-002852 .... p 1558 N95-21244 #
DE95-002858 .... p 1599 N95-21245 #
DE95-002863 .... p 1534 N95-21246 #
DE95-002865 .... p 1519 N95-21248 #
DE95-002867 .... p 1482 N95-21249 #
DE95-002870 .... p 1519 N95-21250 #
DE95-002871 .... p 1536 N95-21332 #
DE95-002887 .... p 1538 N95-22155 #
DE95-002888 .... p 1536 N95-21334 #
DE95-002889 .... p 1536 N95-21335 #
DE95-002892 .... p 1520 N95-21336 #
DE95-002893 .... p 1536 N95-21337 #
DE95-002894 .... p 1534 N95-21253 #
DE95-002896 .... p 1535 N95-21254 #
DE95-002897 .... p 1535 N95-21255 #
DE95-002899 .... p 1438 N95-20917 #
DE95-002906 .... p 1571 N95-21256 #
DE95-002918 .... p 1476 N95-21257 #
DE95-002919 .... p 1476 N95-21341 #
DE95-002932 .... p 1536 N95-21342 #
DE95-002943 .... p 1244 N95-21517 #
DE95-002944 .... p 1573 N95-21444 #
DE95-002945 .... p 1230 N95-21445 #
DE95-002947 .... p 1243 N95-21447 #
DE95-002954 .... p 1302 N95-21448 #
DE95-002955 .... p 1573 N95-21449 #
DE95-002957 .... p 1272 N95-20889 #
DE95-002960 .... p 1559 N95-21451 #
DE95-002962 .... p 1257 N95-21452 #
DE95-002979 .... p 1440 N95-22075 #
DE95-002980 .... p 1262 N95-22291 #
DE95-002982 .... p 1366 N95-21453 #
DE95-002983 .... p 1382 N95-22292 #
DE95-002985 .... p 1521 N95-21454 #
DE95-003014 .... p 1471 N95-22077 #
DE95-003041 .... p 1527 N95-22078 #
DE95-003195 .... p 1440 N95-22220
DE95-003197 .... p 1576 N95-22084 #
DE95-003204 .... p 1604 N95-22085 #
DE95-003208 .... p 1382 N95-22356 #
DE95-003349 .... p 1334 N95-22086 #
DE95-003355 .... p 1247 N95-22234 #
DE95-003422 .... p 1591 N95-22235 #
DE95-003427 .... p 1336 N95-22236 #
DE95-003434 .... p 1582 N95-22237 #
DE95-003443 .... p 1548 N95-22238 #
DE95-003469 .... p 1528 N95-22239 #
DE95-003473 .... p 1562 N95-22221 #
DE95-003476 .... p 1528 N95-22222 #
DE95-003478 .... p 1528 N95-22223 #
DE95-003560 .... p 1247 N95-22224 #
DE95-003591 .... p 1562 N95-22225 #
DE95-003623 .... p 1427 N95-22240 #
DE95-003808 .... p 1397 N95-22335 #
DE95-003922 .... p 1391 N95-22398 #
DE95-004188 .... p 1502 N95-22420 #
DE95-004206 .... p 1337 N95-22421 #
DE95-700217 .... p 1315 N95-20369 #
DE95-700233 .... p 1242 N95-21282 #
DE95-700245 .... p 1380 N95-21295 #
DE95-714801 .... p 1375 N95-22079 #
DE95-714802 .... p 1254 N95-20890 #
DE95-714804 .... p 1397 N95-22309 #
DE95-717458 .... p 1398 N95-22425 #
DE95-717486 .... p 1397 N95-22337 #

DNA-TR-93-131 .... p 1445 N95-21629
DNA-TR-93-164 .... p 1213 N95-22036 #
DNA-TR-93-190 .... p 1551 N95-20232 #
DNA-TR-94-22 .... p 1220 N95-21634 #

DODA-AR-008-522 .... p 1303 N95-21491
DODA-AR-008-545 .... p 1206 N95-19963 #
DODA-AR-008-561 .... p 1505 N95-21984
DODA-AR-008-629 .... p 1282 N95-20187
DODA-AR-008-648 .... p 1221 N95-19962
DODA-AR-008-867 .... p 1465 N95-21176

DOE-94016248 .... p 1589 N95-21131 #

DOE/BC-14882/8 .... p 1267 N95-20350 #

DOE/BP-03362/T1-PHASE-3 .... p 1315 N95-20380 #

DOE/CE-15520/T13 .... p 1229 N95-20913 #
DOE/CE-15566/T3 .... p 1364 N95-20233 #
DOE/CE-15594/T2 .... p 1283 N95-21356 #
DOE/CE-15613/T2 .... p 1228 N95-20787 #
DOE/CE-23810/38C-PT-2 .... p 1264 N95-20078 #
DOE/CE-23810/39 .... p 1582 N95-22153 #
DOE/CE-23810/42 .... p 1287 N95-21631 #
DOE/CE-41000/2 .... p 1214 N95-21243 #

DOE/CH-10093/279 .... p 1398 N95-22468 #

DOE/CS-83014/1 .... p 1395 N95-21409 #

DOE/EE-0026 .... p 1332 N95-21738 #

DOE/EIA-0174(93) .... p 1398 N95-22429 #

DOE/ER-00038/3707 .... p 1570 N95-20838 #
DOE/ER-0144-12 .... p 1223 N95-20264 #
DOE/ER-0620P .... p 1404 N95-20991 #
DOE/ER-0626 .... p 1289 N95-20214 #
DOE/ER-12108/T1 .... p 1374 N95-21743 #
DOE/ER-13188/9 .... p 1439 N95-21526 #
DOE/ER-13282/10 .... p 1241 N95-21280 #
DOE/ER-13425/T4 .... p 1440 N95-22220
DOE/ER-13519/8 .... p 1521 N95-21441 #
DOE/ER-13519/9 .... p 1529 N95-22316 #
DOE/ER-13614/T1 .... p 1438 N95-20917 #
DOE/ER-13934/6 .... p 1510 N95-20346 #
DOE/ER-13950/T3 .... p 1244 N95-21701 #
DOE/ER-13954/T2 .... p 1234 N95-20052 #
DOE/ER-13955/16 .... p 1509 N95-20242 #
DOE/ER-13957/T1 .... p 1561 N95-22116 #
DOE/ER-13971/23 .... p 1519 N95-21276 #
DOE/ER-14039/3 .... p 1239 N95-20682 #
DOE/ER-14053/T6 .... p 1238 N95-20576 #
DOE/ER-14077/T1 .... p 1336 N95-22284 #
DOE/ER-14079/32 .... p 1411 N95-19981 #
DOE/ER-14079/33 .... p 1411 N95-19982 #
DOE/ER-14104/5 .... p 1573 N95-21444 #
DOE/ER-14114/4 .... p 1224 N95-21746 #
DOE/ER-14145/T3 .... p 1581 N95-21842 #
DOE/ER-14185/T1 .... p 1574 N95-21839 #
DOE/ER-14225/3 .... p 1244 N95-21517 #
DOE/ER-14258/2 .... p 1243 N95-21447 #
DOE/ER-14320/2 .... p 1552 N95-20345 #
DOE/ER-14333/T1 .... p 1240 N95-20780 #
DOE/ER-14412/1 .... p 1246 N95-21886 #
DOE/ER-14421/1 .... p 1237 N95-20384 #
DOE/ER-25012/5 .... p 1475 N95-20888 #
DOE/ER-25027/8 .... p 1356 N95-22148 #
DOE/ER-25086/T2 .... p 1470 N95-21992 #
DOE/ER-25149/T1 .... p 1476 N95-21355 #
DOE/ER-40233/9 .... p 1529 N95-22279 #
DOE/ER-40272/194-TASK-A .... p 1512 N95-20469 #
DOE/ER-40333/142 .... p 1245 N95-21845 #
DOE/ER-40344/8 .... p 1245 N95-21745 #
DOE/ER-40439/T2 .... p 1525 N95-21747 #
DOE/ER-40546/T6 .... p 1515 N95-20893 #
DOE/ER-40561/130 .... p 1526 N95-21920 #
DOE/ER-40561/131 .... p 1520 N95-21315
DOE/ER-40561/136 .... p 1603 N95-21316 #
DOE/ER-40561/137 .... p 1521 N95-21443 #
DOE/ER-40561/142 .... p 1498 N95-20779 #
DOE/ER-40561/145 .... p 1604 N95-22064 #
DOE/ER-40561/146 .... p 1512 N95-20451 #
DOE/ER-40561/150 .... p 1604 N95-20383 #
DOE/ER-40561/153 .... p 1602 N95-20147 #
DOE/ER-40561/154 .... p 1604 N95-20490 #
DOE/ER-40561/165 .... p 1604 N95-22085 #
DOE/ER-40617/167 .... p 1522 N95-21485 #
DOE/ER-40617/181 .... p 1580 N95-21486 #
DOE/ER-40697/3 .... p 1535 N95-21281 #
DOE/ER-40768/2 .... p 1519 N95-21302 #
DOE/ER-40809/T1 .... p 1512 N95-20491 #
DOE/ER-45085/T2 .... p 1277 N95-21748 #
DOE/ER-45157/T7 .... p 1276 N95-21585 #
DOE/ER-45194/2 .... p 1270 N95-20680 #
DOE/ER-45238/7 .... p 1565 N95-20243 #
DOE/ER-45252/T6 .... p 1276 N95-21572 #
DOE/ER-45267/8 .... p 1506 N95-22071 #
DOE/ER-45283/8 .... p 1572 N95-21279 #
DOE/ER-45330/T1 .... p 1572 N95-21287 #
DOE/ER-45372/7 .... p 1265 N95-20115 #
DOE/ER-45388/T2 .... p 1257 N95-21476 #
DOE/ER-45434/4 .... p 1230 N95-21445 #
DOE/ER-45476/T1 .... p 1570 N95-20916 #
DOE/ER-53188/1 .... p 1523 N95-21587 #
DOE/ER-53198/248 .... p 1549 N95-20112 #
DOE/ER-53198/249 .... p 1549 N95-20113 #
DOE/ER-53198/250 .... p 1549 N95-20114 #
DOE/ER-53217/T3 .... p 1524 N95-21605 #
DOE/ER-53295/T1 .... p 1554 N95-20681 #
DOE/ER-54124/1 .... p 1548 N95-20029 #
DOE/ER-54178/4 .... p 1532 N95-20347 #
DOE/ER-54186/T2 .... p 1560 N95-21724 #
DOE/ER-54186/T3 .... p 1260 N95-22013 #
DOE/ER-54186/T4 .... p 1330 N95-21442 #
DOE/ER-54186/T5 .... p 1332 N95-21725 #
DOE/ER-54222/1 .... p 1552 N95-20348 #
DOE/ER-54241/134 .... p 1562 N95-22120 #
DOE/ER-60304/10 .... p 1406 N95-21379 #
DOE/ER-60639/6 .... p 1445 N95-21595 #
DOE/ER-60970/3 .... p 1406 N95-21410 #
DOE/ER-61010/T26 .... p 1408 N95-21708 #
DOE/ER-61071/T1 .... p 1430 N95-21527 #
DOE/ER-61072/9 .... p 1412 N95-20116 #
DOE/ER-61370/1 .... p 1441 N95-22397
DOE/ER-61856/T1 .... p 1427 N95-22240 #
DOE/ER-80896/94/C0379 .... p 1275 N95-21354 #

DOE/ET-0026 .... p 1588 N95-20762 #
DOE/ET-29372/T3 .... p 1483 N95-21613 * #
DOE/ET-53088/667 .... p 1553 N95-20437 #
DOE/ET-53088/678 .... p 1358 N95-22307 #

DOE/EW-50625/T18-VOL-4 .... p 1406 N95-21565 #

DOE/ID-12779/1 .... p 1246 N95-21921 #
DOE/ID-12942/1 .... p 1313 N95-20213 #
DOE/ID-13040/T22 .... p 1391 N95-20104 #
DOE/ID-13220/T1 .... p 1251 N95-20128 #
DOE/ID-13233/T1 .... p 1253 N95-20417 #

DOE/MC-11076/3829 .... p 1234 N95-20135 #
DOE/MC-26006/3804 .... p 1394 N95-20896 #
DOE/MC-28065/3880 .... p 1324 N95-20574 #
DOE/MC-29227/3849 .... p 1396 N95-22033 #
DOE/MC-29228/3837 .... p 1235 N95-20188 #

DOE/METC-C/95/7162 .... p 1395 N95-21361 #

DOE/MT-93010/2 .... p 1236 N95-20349 #

DOE/PC-91293/11 .... p 1233 N95-20045 #
DOE/PC-92108/T6 .... p 1241 N95-21172 #
DOE/PC-92109/T5 .... p 1233 N95-19924 #
DOE/PC-92112/T7 .... p 1237 N95-20438 #
DOE/PC-92117/T8 .... p 1282 N95-19927 #
DOE/PC-92117/T9 .... p 1314 N95-20339 #
DOE/PC-92121/T8 .... p 1247 N95-22224 #
DOE/PC-93217/T3 .... p 1234 N95-20046 #

DOE/RL-94-86 .... p 1409 N95-21722 #

DOE/SF-18852/T44 .... p 1222 N95-20853 #
DOE/SF-19202/T1 .... p 1240 N95-20865 #
DOE/SF-19441/T15 .... p 1221 N95-20076 #

DOT-VNTSC-FAA-94-10 .... p 1308 N95-22005 #

DOT/FAA/AM-RN-94/20-PT-1 .... p 1446 N95-22027 #

DOT/FAA/AM-94/21-PT-2 .... p 1447 N95-22040 #

DOT/FAA/CT-TN92/47 .... p 1204 N95-21148 #
DOT/FAA/CT-TN93/25 .... p 1204 N95-21020
DOT/FAA/CT-TN94/23 .... p 1208 N95-20032 #
DOT/FAA/CT-TN94/38 .... p 1429 N95-20857 #

DOT/FAA/CT-TN94/42 .... p 1363 N95-20031 #

DOT/FAA/CT-90-10 .... p 1203 N95-22318 #
DOT/FAA/CT-92/4 .... p 1202 N95-20275 #
DOT/FAA/CT-94/04 .... p 1203 N95-22352 #
DOT/FAA/CT-94/12 .... p 1203 N95-21518 #
DOT/FAA/CT-94/75 .... p 1202 N95-20174 #
DOT/FAA/CT-94/79 .... p 1383 N95-22202 #
DOT/FAA/CT-94/86 .... p 1202 N95-20093
DOT/FAA/CT-94/87 .... p 1203 N95-22319 #

DOT/FAA/NR-94-1 .... p 1308 N95-22005 #

DREO-TN-93-18 .... p 1290 N95-20308
DREO-TN-93-31 .... p 1301 N95-21292
DREO-TN-93-37 .... p 1459 N95-20184 #

DRES-SR-584 .... p 1442 N95-20602

DSMC-TR-4-94 .... p 1288 N95-19932 #

DSTO-GD-0004 .... p 1206 N95-19963 #

DSTO-TR-0002 .... p 1222 N95-21661
DSTO-TR-0015 .... p 1201 N95-21659
DSTO-TR-0017 .... p 1221 N95-19962
DSTO-TR-0065 .... p 1284 N95-21951
DSTO-TR-0067 .... p 1470 N95-21950

DTI-156F .... p 1571 N95-20965

D06209-2-VOL-2 .... p 1308 N95-21988 #

E-5666 .... p 1214 N95-22341 * #
E-8017 .... p 1235 N95-20180 * #
E-8735 .... p 1222 N95-21531 * #
E-8984 .... p 1589 N95-21187 * #
E-9038 .... p 1385 N95-20179 * #
E-9066 .... p 1356 N95-21959 * #
E-9083 .... p 1316 N95-20502 * #
E-9170-VOL-1 .... p 1505 N95-21888 * #
E-9194 .... p 1274 N95-21252 * #
E-9203 .... p 1337 N95-19912 * #
E-9206 .... p 1223 N95-19901 * #
E-9337 .... p 1225 N95-19951 * #
E-9338 .... p 1380 N95-21359 * #
E-9359 .... p 1334 N95-22112 * #
E-9361-VOL-1 .... p 1396 N95-21952 * #
E-9372 .... p 1222 N95-21458 * #
E-9373 .... p 1201 N95-20794 * #
E-9379 .... p 1218 N95-21384 * #
E-9395 .... p 1307 N95-21890 * #
E-9408 .... p 1355 N95-21957 * #
E-9409 .... p 1284 N95-22114 * #
E-9414 .... p 1338 N95-19952 * #
E-9420 .... p 1338 N95-19953 * #
E-9423-PT-1 .... p 1382 N95-22404 * #
E-9424-PT-2 .... p 1382 N95-22405 * #
E-9441 .... p 1386 N95-20790 * #
E-9444 .... p 1214 N95-21383 * #
E-9447 .... p 1415 N95-21188 * #
E-9448 .... p 1366 N95-21259 * #
E-9466 .... p 1366 N95-21391 * #

EEC/NOTE-12/94 .... p 1205 N95-21369

EGG-EP-11237-QTR1 .... p 1332 N95-21731 #
EGG-EP-11237-QTR2 .... p 1333 N95-21960 #
EGG-EP-11320 .... p 1330 N95-21471 #

EGG-FSP-11348 .... p 1558 N95-21290 #

EGG-NRE-11406 .... p 1466 N95-21288 #

EGG-11265-1098 .... p 1391 N95-22398 #
EGG-11265-2051 .... p 1564 N95-20240 #

EOARD-TR-94-06 .... p 1370 N95-20550 #

EPA/420/R-94/003 .... p 1406 N95-21373 #
EPA/600/A-94/168 .... p 1400 N95-19965 #
EPA/600/J-94/308 .... p 1409 N95-22101
EPA/600/R-94/047 .... p 1312 N95-19966 #
EPA/600/R-94/163 .... p 1401 N95-20192 #

ERDEC-TR-112-PT-2 .... p 1437 N95-20252

ERL-0826-GD .... p 1465 N95-21176

ERP-1135 .... p 1600 N95-21679
ERP-1152 .... p 1430 N95-20974 #

ES/ER/TM-120/V1-VOL-1 .... p 1590 N95-21862 #
ES/ER/TM-120/V2-VOL-2 .... p 1591 N95-22061 #
ES/ER/TM-56-VOL-2 .... p 1591 N95-22129 #
ES/ER/TM-56/V1 .... p 1458 N95-20073 #

ES/IMS-1 .... p 1591 N95-22107 #

ESC-TR-93-238 .... p 1300 N95-21099
ESC-TR-93-312 .... p 1390 N95-21912
ESC-TR-94-009 .... p 1485 N95-22226 #
ESC-TR-94-014 .... p 1457 N95-19999 #
ESC-TR-94-207 .... p 1462 N95-20721 #

ESC-94-TR-4 .... p 1468 N95-21627

ESL-TR-90-47 .... p 1407 N95-21596

ESM-60 .... p 1508 N95-20196 #
ESM-62 .... p 1508 N95-20197 #
ESM-63 .... p 1509 N95-20198 #
ESM-64 .... p 1509 N95-20199 #

ETDE/JP-MF-94796550 .... p 1277 N95-21714 #

EUT-94-WSK-01 .... p 1497 N95-22379 #

E19-X20-1 .... p 1367 N95-21889 * #

FAA-APO-94-10 .... p 1199 N95-20091

FEL-93-B366 .... p 1475 N95-20499 #
FEL-94-B195 .... p 1291 N95-20692 #

FEW-618 .... p 1497 N95-19938
FEW-619 .... p 1497 N95-19936 #
FEW-622 .... p 1487 N95-19937 #
FEW-623 .... p 1488 N95-19943 #
FEW-626 .... p 1488 N95-19942 #
FEW-634 .... p 1499 N95-19941 #
FEW-635 .... p 1487 N95-19940 #
FEW-641 .... p 1594 N95-19939
FEW-654 .... p 1592 N95-22334 #
FEW-655 .... p 1499 N95-21709

FNAL-TM-1878 .... p 1533 N95-20885 #
FNAL-TM-1896 .... p 1463 N95-20901 #
FNAL-TM-94/1903 .... p 1532 N95-20421 #

FNAL/C-94/128-E .... p 1511 N95-20401 #
FNAL/C-94/136-E .... p 1507 N95-20108 #
FNAL/C-94/169-E .... p 1511 N95-20415 #
FNAL/C-94/178-E .... p 1513 N95-20496 #
FNAL/C-94/184-E .... p 1530 N95-22339 #
FNAL/C-94/186-E .... p 1512 N95-20476 #
FNAL/C-94/187-E .... p 1512 N95-20475 #
FNAL/C-94/201 .... p 1521 N95-21378 #
FNAL/C-94/203 .... p 1539 N95-22192 #
FNAL/C-94/213 .... p 1515 N95-20868 #
FNAL/C-94/216-E .... p 1520 N95-21313 #
FNAL/C-94/219-E .... p 1511 N95-20418 #
FNAL/C-94/220-E .... p 1530 N95-22340 #
FNAL/C-94/222-E .... p 1523 N95-21563 #
FNAL/C-94/224-E .... p 1507 N95-20110 #
FNAL/C-94/237-E .... p 1523 N95-21562 #
FNAL/C-94/241-E .... p 1519 N95-21273 #
FNAL/C-94/243-E .... p 1522 N95-21499 #
FNAL/C-94/247-E .... p 1507 N95-20131 #
FNAL/C-94/251-E .... p 1573 N95-21561 #
FNAL/C-94/253 .... p 1534 N95-20900 #
FNAL/C-94/257-E .... p 1539 N95-22193 #
FNAL/C-94/261-E .... p 1522 N95-21498 #
FNAL/C-94/264 .... p 1508 N95-20132 #
FNAL/C-94/265-E .... p 1527 N95-22122 #
FNAL/C-94/266-E .... p 1515 N95-20879 #
FNAL/C-94/269-E .... p 1522 N95-21497 #
FNAL/C-94/274-E .... p 1524 N95-21597 #
FNAL/C-94/276-E .... p 1539 N95-22195 #
FNAL/C-94/280-E .... p 1507 N95-20111 #
FNAL/C-94/283-E .... p 1527 N95-22194 #
FNAL/C-94/285-E .... p 1508 N95-20134 #
FNAL/C-94/288-E .... p 1529 N95-22314 #
FNAL/C-94/290-E .... p 1528 N95-22197 #
FNAL/C-94/299-E .... p 1515 N95-20880 #
FNAL/C-94/300-E .... p 1528 N95-22196 #
FNAL/C-94/314-E .... p 1515 N95-20897 #
FNAL/C-94/323-E .... p 1510 N95-20344 #
FNAL/C-94/325-E .... p 1515 N95-20898 #
FNAL/C-94/326-E .... p 1510 N95-20343 #
FNAL/C-94/327-E .... p 1509 N95-20217 #
FNAL/C-94/332 .... p 1525 N95-21715 #
FNAL/C-94/340-E .... p 1282 N95-20899 #
FNAL/C-94/341-E .... p 1523 N95-21521 #
FNAL/C-94/342-E .... p 1365 N95-20902 #
FNAL/C-94/343-E .... p 1535 N95-21314 #
FNAL/C-94/345-E .... p 1516 N95-20914 #

FNAL/PUB-94/179-T .... p 1521 N95-21443 #

FOA-A-20056-2.4 .... p 1230 N95-21432
FOA-A-20057-2.3 .... p 1230 N95-21417
FOA-A-20058-2.4 .... p 1243 N95-21428
FOA-A-20060-2.4 .... p 1232 N95-22096
FOA-A-20061-2.6 .... p 1288 N95-21978
FOA-A-50023-5.2 .... p 1452 N95-21467

FOA-C-10363-1.3 .... p 1585 N95-21427
FOA-C-20965-2.1 .... p 1482 N95-21430
FOA-C-20966-2.1 .... p 1482 N95-21429
FOA-C-20972-2.5 .... p 1353 N95-21132 #
FOA-C-20983-2.4 .... p 1547 N95-22140
FOA-C-20986-2.3 .... p 1275 N95-21275
FOA-C-20987-2.3 .... p 1388 N95-22097
FOA-C-30752-3.1 .... p 1434 N95-21320 #
FOA-C-40320-4.5 .... p 1405 N95-21274 #
FOA-C-40323-4.5 .... p 1405 N95-21181 #

FRCR-449 .... p 1562 N95-22120 #

F19628-90-K-0003 .... p 1427 N95-22326 * #

GA-A-21295 .... p 1269 N95-20570 #
GA-A-21368 .... p 1556 N95-21142 #
GA-A-21522 .... p 1555 N95-21141 #
GA-A-21693 .... p 1554 N95-20568 #
GA-A-21702 .... p 1552 N95-20334 #
GA-A-21708 .... p 1554 N95-20571 #
GA-A-21715 .... p 1553 N95-20402 #
GA-A-21719 .... p 1230 N95-21553 #
GA-A-21736 .... p 1548 N95-20037 #
GA-A-21742 .... p 1551 N95-20279 #
GA-A-21743 .... p 1549 N95-20038 #
GA-A-21750 .... p 1550 N95-20146 #
GA-A-21754 .... p 1554 N95-20446 #
GA-A-21756 .... p 1556 N95-21163 #
GA-A-21759 .... p 1551 N95-20285 #
GA-A-21761 .... p 1553 N95-20445 #
GA-A-21762 .... p 1556 N95-21159 #
GA-A-21778 .... p 1558 N95-21299 #

GA-C21932 .... p 1558 N95-21345 * #

GAO/NSIAD-94-133 .... p 1407 N95-21683
GAO/NSIAD-95-12 .... p 1206 N95-20212 #

GAO/RCED-94-91 .... p 1586 N95-22403 #

GETA-94-04 .... p 1284 N95-21966 #

GIT-89-023 .... p 1517 N95-21151 #
GIT-89-024 .... p 1517 N95-21216 #

GL-5188 .... p 1571 N95-20964

GMD-237 .... p 1464 N95-21003

GRI-94/0158 .... p 1282 N95-20253 #
GRI-94/0269 .... p 1247 N95-22150 #
GRI-94/0314 .... p 1284 N95-21966 #

HAC-REF-J1881 .... p 1335 N95-22144
HAC-REF-J4924 .... p 1314 N95-20311

HEC-TP-144 .... p 1390 N95-21628

HIFAN-671 .... p 1534 N95-20891 #

IAE-0122 .... p 1563 N95-19978 #

IAEA-CN-60/A6/C-P-8 .... p 1549 N95-20114 #
IAEA-CN-60/B-1-I-6 .... p 1537 N95-21603 #
IAEA-CN-60/C-1-I-5 .... p 1549 N95-20113 #

IC-93/214 .... p 1575 N95-21853 #
IC-93/257 .... p 1561 N95-21848 #
IC-93/277 .... p 1581 N95-21639 #
IC-93/304 .... p 1278 N95-21885 #
IC-93/313 .... p 1307 N95-21849 #
IC-93/315 .... p 1581 N95-21887 #
IC-93/316 .... p 1561 N95-21850 #
IC-93/329 .... p 1582 N95-22198 #
IC-93/330 .... p 1528 N95-22217 #
IC-93/338 .... p 1578 N95-22277 #
IC-93/339 .... p 1500 N95-21592 #
IC-93/341 .... p 1575 N95-21859 #
IC-93/342 .... p 1575 N95-21854 #
IC-93/345 .... p 1528 N95-22218 #
IC-93/346 .... p 1577 N95-22176 #
IC-93/348 .... p 1397 N95-22183 #
IC-93/352 .... p 1260 N95-21855 #
IC-93/364 .... p 1577 N95-22180 #
IC-93/370 .... p 1577 N95-22181 #
IC-93/372 .... p 1525 N95-21856 #
IC-93/373 .... p 1525 N95-21860 #
IC-93/374 .... p 1502 N95-22177 #
IC-93/382 .... p 1578 N95-22276 #
IC-93/383 .... p 1581 N95-21993 #
IC-93/390 .... p 1562 N95-22377 #

IC-93/395 ... p 1527 N95-22182 #
IC-93/396 ... p 1576 N95-21998 #
IC-93/412 ... p 1582 N95-22378 #
IC-94/12 ... p 1576 N95-21995 #
IC-94/13 ... p 1576 N95-21996 #
IC-94/14 ... p 1576 N95-21997 #
IC-94/21 ... p 1582 N95-21994 #
IC-94/34 ... p 1577 N95-22178 #
IC-94/41 ... p 1561 N95-21847 #
IC-94/43 ... p 1527 N95-22179 #
IC-94/67 ... p 1561 N95-21851 #
IC-94/7 ... p 1491 N95-20734 #

ICASE-94-16 ... p 1479 N95-20010 *
ICASE-94-17 ... p 1338 N95-20009 *
ICASE-94-49 ... p 1473 N95-20013 *
ICASE-94-75 ... p 1495 N95-22325 * #
ICASE-94-9 ... p 1495 N95-22157 *
ICASE-95-2 ... p 1456 N95-22431 * #

ICOMP-94-17 ... p 1356 N95-21959 * #
ICOMP-95-2 ... p 1355 N95-21957 * #

IDA-D-1490 ... p 1327 N95-20966
IDA-D-1519-REV ... p 1217 N95-22413 #
IDA-D-1537 ... p 1411 N95-22414 #

IDA/HQ-93-44599 ... p 1327 N95-20966
IDA/HQ-94-45640 ... p 1411 N95-22414 #
IDA/HQ-94-45918-REV ... p 1217 N95-22413 #

IEE-SR-251 ... p 1404 N95-21143 #

IFSR-667 ... p 1553 N95-20437 #

IHES/M/94/26 ... p 1496 N95-22353 #
IHES/M/94/27 ... p 1496 N95-22354 #
IHES/M/94/29 ... p 1496 N95-22355 #
IHES/M/94/33 ... p 1490 N95-20452
IHES/M/94/36 ... p 1580 N95-20324
IHES/M/94/39 ... p 1489 N95-20172 #
IHES/M/94/43 ... p 1495 N95-22147
IHES/M/94/44 ... p 1489 N95-20273 #

IHES/P/94/34 ... p 1488 N95-19944 #
IHES/P/94/35 ... p 1599 N95-20173 #
IHES/P/94/38 ... p 1498 N95-19945 #
IHES/P/94/41 ... p 1489 N95-20259 #

INIS-BR-3340 ... p 1560 N95-21593 #
INIS-BR-3344 ... p 1579 N95-22380 #

INIS-JP-019 ... p 1410 N95-22219 #

INIS-MF-13862 ... p 1561 N95-21852 #
INIS-MF-13924 ... p 1239 N95-20736 #
INIS-MF-13927 ... p 1256 N95-21270 #
INIS-MF-13929 ... p 1326 N95-20733 #
INIS-MF-13947 ... p 1605 N95-21828 #
INIS-MF-13948 ... p 1605 N95-21830 #
INIS-MF-13949 ... p 1565 N95-20261 #

INIS-RU-377 ... p 1529 N95-22281 #

INS-T-520 ... p 1526 N95-22051 #

INS-1015 ... p 1392 N95-20685 #
INS-1017 ... p 1516 N95-20986 #
INS-1019 ... p 1514 N95-20756 #
INS-1021 ... p 1514 N95-20737 #
INS-1022 ... p 1514 N95-20738 #

IR-323 ... p 1482 N95-21267 #

IS-M-789 ... p 1458 N95-20136 #
IS-M-795 ... p 1258 N95-21568 #
IS-M-796 ... p 1259 N95-21737 #
IS-M-797 ... p 1573 N95-21569 #
IS-M-803 ... p 1574 N95-21570 #
IS-M-806 ... p 1231 N95-21736 #
IS-M-807 ... p 1231 N95-21924 #

IS-T-1621 ... p 1277 N95-21735 #
IS-T-1643 ... p 1493 N95-21439 #
IS-T-1689 ... p 1257 N95-21398 #
IS-T-1691 ... p 1260 N95-21923 #
IS-T-1696 ... p 1242 N95-21400 #
IS-T-1698 ... p 1257 N95-21399 #
IS-T-1699 ... p 1260 N95-21841 #
IS-T-1701 ... p 1245 N95-21734 #
IS-T-1711 ... p 1574 N95-21723 #
IS-T-1713 ... p 1242 N95-21397 #

ISBN-0-16-045368-2 ... p 1594 N95-21893 * #
ISBN-0-16-045462-X ... p 1217 N95-21894 * #
ISBN-0-309-04638-6 ... p 1265 N95-20176 #
ISBN-0-309-05506-7 ... p 1199 N95-19967 #
ISBN-1-55899-224-3 ... p 1563 N95-19886
ISBN-1-55899-250-2 ... p 1225 N95-20001 * #
ISBN-3-88457-237-7 ... p 1464 N95-21003
ISBN-90-370-0103-3 ... p 1356 N95-21963
ISBN-90-370-0104-1 ... p 1445 N95-21580
ISBN-90-370-0106-8 ... p 1273 N95-20976
ISBN-90-370-0107-6 ... p 1357 N95-22160 #
ISBN-90-407-1002-3 ... p 1396 N95-22175
ISBN-90-5326-016-1 ... p 1311 N95-22358
ISBN-90-5326-017-X ... p 1305 N95-21579
ISBN-90-6275-932-7 ... p 1336 N95-22382
ISBN-90-6275-967-X ... p 1288 N95-21633
ISBN-90-6275-976-9 ... p 1330 N95-21590
ISBN-90-6275-978-5 ... p 1444 N95-21016
ISBN-90-74445-07-1 ... p 1300 N95-21029
ISBN-90-9007034-6 ... p 1386 N95-21006 #
ISBN-90-9007162-8 ... p 1483 N95-21669
ISBN-90-9007196-2 ... p 1574 N95-21670 #
ISBN-90-9007222-5 ... p 1589 N95-21004
ISBN-90-9007240-3 ... p 1496 N95-22359
ISBN-90-9007256-X ... p 1444 N95-21028
ISBN-91-7848-441-3 ... p 1241 N95-21179 #
ISBN-91-7848-483-9 ... p 1386 N95-21133 #
ISBN-92-835-0750-9 ... p 1292 N95-20921 #
ISBN-92-836-0004-5 ... p 1208 N95-20631 #
ISBN-92-836-0006-1 ... p 1346 N95-21061 #
ISBN-951-22-1291-9 ... p 1438 N95-21112 #
ISBN-951-22-1612-4 ... p 1443 N95-20971 #
ISBN-951-22-1783-X ... p 1220 N95-21026 #
ISBN-951-22-1902-6 ... p 1248 N95-22329 #
ISBN-951-22-1923-9 ... p 1255 N95-21111 #
ISBN-951-22-1932-8 ... p 1301 N95-21109 #
ISBN-951-22-1951-4 ... p 1240 N95-21110 #
ISBN-951-22-1985-9 ... p 1291 N95-20775
ISBN-951-22-2038-5 ... p 1301 N95-21107 #
ISBN-951-22-2047-4 ... p 1300 N95-20972
ISBN-951-22-2051-2 ... p 1311 N95-22363 #
ISBN-951-22-2062-8 ... p 1300 N95-20980
ISBN-951-22-2064-4 ... p 1464 N95-20982
ISBN-951-22-2067-9 ... p 1598 N95-22376 #
ISBN-951-22-2079-2 ... p 1502 N95-21102 #
ISBN-951-22-2080-6 ... p 1236 N95-20256 #
ISBN-951-22-2094-6 ... p 1310 N95-22311 #
ISBN-951-22-2122-5 ... p 1329 N95-21326 #
ISBN-951-22-2129-2 ... p 1544 N95-21103 #
ISBN-951-22-2131-4 ... p 1300 N95-21104 #
ISBN-951-22-2135-7 ... p 1255 N95-21128 #
ISBN-951-22-2143-8 ... p 1430 N95-21413
ISBN-951-22-2146-2 ... p 1312 N95-19935 #
ISBN-951-22-2150-0 ... p 1448 N95-22476 #
ISBN-951-22-2154-3 ... p 1312 N95-19934 #
ISBN-951-22-2157-8 ... p 1255 N95-21108 #
ISBN-951-22-2161-6 ... p 1389 N95-21105 #
ISBN-951-22-2162-4 ... p 1384 N95-19930 #
ISBN-951-22-2184-5 ... p 1311 N95-22365
ISBN-951-38-4097-2 ... p 1450 N95-21284
ISBN-951-38-4479-X ... p 1380 N95-21416
ISBN-951-38-4484-6 ... p 1380 N95-21446

ISI/RR-93-388 ... p 1328 N95-20997 #
ISI/RR-94-378 ... p 1589 N95-21002 #
ISI/RR-94-383 ... p 1462 N95-20718 #
ISI/RR-94-384 ... p 1464 N95-20996 #

ISI/SR-94-379 ... p 1216 N95-20624

ISVR-92/33 ... p 1453 N95-21700

IYAF-93-70 ... p 1529 N95-22283 #
IYAF-93-89 ... p 1562 N95-22282 #

JAERI-M-93-184 ... p 1555 N95-20987 #
JAERI-M-93-224 ... p 1554 N95-20684 #
JAERI-M-94-025 ... p 1371 N95-20757 #

JHU/APL-TG-1386 ... p 1460 N95-20546 #

JILA-153-1236 ... p 1370 N95-20484 #

JINR-E-1-93-451 ... p 1523 N95-21591 #
JINR-E-2-94-22 ... p 1514 N95-20735 #

JOY/KT-JULK-105 ... p 1315 N95-20369 #

JPL-PUBL-80-93-REV-1 ... p 1302 N95-21456 * #
JPL-PUBL-93-22-REV-A ... p 1397 N95-22336 * #
JPL-PUBL-94-24 ... p 1412 N95-20002 * #
JPL-PUBL-94-5 ... p 1595 N95-21749 * #
JPL-PUBL-94-8 ... p 1484 N95-22171 * #

JPL-TDA-PR-42-120 ... p 1303 N95-21532 * #

KCP-613-5388 ... p 1329 N95-21301 #
KCP-613-5432 ... p 1332 N95-21729 #
KCP-613-5435 ... p 1256 N95-21300 #
KCP-613-5496 ... p 1467 N95-21389 #

KPT-4/94 ... p 1287 N95-21422

KTM/E-B-153 ... p 1242 N95-21282 #
KTM/E-B-185 ... p 1398 N95-22425 #

L-17162 ... p 1353 N95-21258 * #
L-17347 ... p 1340 N95-20619 * #
L-17350 ... p 1199 N95-19913 * #
L-17354 ... p 1201 N95-21338 * #
L-17381 ... p 1368 N95-22109 * #
L-17424 ... p 1517 N95-21191 * #

LA-SUB-94-105 ... p 1415 N95-21184 #
LA-SUB-94-106 ... p 1274 N95-21234 #
LA-SUB-94-122 ... p 1335 N95-22165 #
LA-SUB-94-125 ... p 1600 N95-22128 #
LA-SUB-94-132 ... p 1332 N95-21742 #

LA-UR-84-3645 ... p 1221 N95-22436 #
LA-UR-94-1593 ... p 1529 N95-22280 #
LA-UR-94-1705 ... p 1481 N95-20693 #
LA-UR-94-1938 ... p 1379 N95-20627 #
LA-UR-94-2082 ... p 1588 N95-20789 #
LA-UR-94-2147 ... p 1526 N95-22058 #
LA-UR-94-2273 ... p 1569 N95-20696 #
LA-UR-94-2338 ... p 1516 N95-21125 #
LA-UR-94-2376 ... p 1509 N95-20236 #
LA-UR-94-2388 ... p 1565 N95-20330
LA-UR-94-2397 ... p 1509 N95-20235 #
LA-UR-94-2409 ... p 1252 N95-20331 #
LA-UR-94-2440 ... p 1516 N95-21114 #
LA-UR-94-2443 ... p 1339 N95-20166 #
LA-UR-94-2479 ... p 1488 N95-20169
LA-UR-94-2505 ... p 1458 N95-20154 #
LA-UR-94-2506 ... p 1291 N95-20697 #
LA-UR-94-2520 ... p 1508 N95-20160 #
LA-UR-94-2521 ... p 1508 N95-20159 #
LA-UR-94-2523 ... p 1474 N95-20158 #
LA-UR-94-2528 ... p 1255 N95-21137 #
LA-UR-94-2547 ... p 1509 N95-20254 #
LA-UR-94-2559 ... p 1560 N95-21668 #
LA-UR-94-2592 ... p 1500 N95-21136 #
LA-UR-94-2595 ... p 1555 N95-21115 #
LA-UR-94-2620 ... p 1289 N95-20164 #
LA-UR-94-2639 ... p 1313 N95-20168 #
LA-UR-94-2644 ... p 1488 N95-20167 #
LA-UR-94-2649 ... p 1459 N95-20165 #
LA-UR-94-2684 ... p 1554 N95-20675 #
LA-UR-94-2686 ... p 1331 N95-21667 #
LA-UR-94-2694 ... p 1407 N95-21666 #
LA-UR-94-2716 ... p 1285 N95-20288 #
LA-UR-94-2731 ... p 1254 N95-20816 #
LA-UR-94-2736 ... p 1387 N95-21386 #
LA-UR-94-2739 ... p 1414 N95-20990 #
LA-UR-94-2770 ... p 1413 N95-20289 #
LA-UR-94-2781 ... p 1462 N95-20699 #
LA-UR-94-2804 ... p 1531 N95-20203 #
LA-UR-94-2809 ... p 1538 N95-22050 #
LA-UR-94-2821 ... p 1281 N95-22428 #
LA-UR-94-2825 ... p 1483 N95-21710 #
LA-UR-94-2831 ... p 1440 N95-22296 #
LA-UR-94-2840 ... p 1540 N95-22410 #
LA-UR-94-2845 ... p 1375 N95-21837
LA-UR-94-2849 ... p 1376 N95-22242 #
LA-UR-94-2850 ... p 1375 N95-21919 #
LA-UR-94-2851 ... p 1377 N95-22348 #
LA-UR-94-2860 ... p 1578 N95-22297 #
LA-UR-94-2864 ... p 1574 N95-21712 #
LA-UR-94-2890 ... p 1601 N95-22419 #
LA-UR-94-2903 ... p 1539 N95-22298 #
LA-UR-94-2904 ... p 1539 N95-22243 #
LA-UR-94-2992 ... p 1237 N95-20368 #
LA-UR-94-3020 ... p 1375 N95-22007 #
LA-UR-94-3075 ... p 1481 N95-20812 #
LA-UR-94-3079 ... p 1510 N95-20367 #
LA-UR-94-3090 ... p 1246 N95-22012 #
LA-UR-94-3101 ... p 1334 N95-22011 #
LA-UR-94-3103 ... p 1426 N95-21875 #
LA-UR-94-3105 ... p 1561 N95-22010 #
LA-UR-94-3124 ... p 1599 N95-21367 #
LA-UR-94-3132 ... p 1373 N95-21312 #
LA-UR-94-3139 ... p 1438 N95-21366 #
LA-UR-94-3144 ... p 1231 N95-22009 #
LA-UR-94-3149 ... p 1576 N95-22008 #
LA-UR-94-3165 ... p 1371 N95-20786 #
LA-UR-94-3206 ... p 1526 N95-21934 #
LA-UR-94-3221 ... p 1558 N95-21368 #
LA-UR-94-3223 ... p 1600 N95-21935 #
LA-UR-94-3235 ... p 1575 N95-21936 #
LA-UR-94-3265 ... p 1603 N95-21377 #
LA-UR-94-3283 ... p 1260 N95-22006 #
LA-UR-94-3284 ... p 1387 N95-21364 #
LA-UR-94-3307 ... p 1588 N95-20777 #
LA-UR-94-3308 ... p 1589 N95-20818 #

LA-UR-94-3329 p 1580 N95-21264 #
LA-UR-94-3351 p 1536 N95-21331 #
LA-UR-94-3413 p 1262 N95-22289 #
LA-UR-94-3431 p 1262 N95-22308 #
LA-UR-94-3449 p 1478 N95-21925 #
LA-UR-94-3468 p 1520 N95-21321 #
LA-UR-94-3469 p 1527 N95-22078 #
LA-UR-94-3499 p 1260 N95-21926 #
LA-UR-94-3529 p 1248 N95-22433 #
LA-UR-94-3533 p 1518 N95-21235 #
LA-UR-94-3537 p 1534 N95-21236 #
LA-UR-94-3552 p 1281 N95-22434 #
LA-UR-94-3554 p 1427 N95-22477 #
LA-UR-94-3563 p 1530 N95-22435 #
LA-UR-94-3579 p 1519 N95-21237 #
LA-UR-94-3611 p 1353 N95-21317 #
LA-UR-94-3624 p 1376 N95-22154 #
LA-UR-94-3656 p 1255 N95-21238 #
LA-UR-94-3665 p 1557 N95-21239 #
LA-UR-94-3666 p 1558 N95-21242 #
LA-UR-94-3667 p 1557 N95-21240 #
LA-UR-94-431 p 1236 N95-20277 #
LA-UR-94-897 p 1412 N95-20278 * #

LA-12754-PR p 1440 N95-22065 #
LA-12804-PR p 1501 N95-20246 #
LA-12820-MS p 1236 N95-20361 #
LA-12836-MS p 1501 N95-20869 #
LA-12855-MS p 1486 N95-22430 #
LA-12856-MS p 1482 N95-21522 #
LA-12865 p 1244 N95-21523 #

LBL-PUB-658-VER-2.0 p 1548 N95-22238 #

LBL-35056 p 1429 N95-20782 #
LBL-35203 p 1569 N95-20677 #
LBL-35204 p 1569 N95-20678 #
LBL-35205 p 1569 N95-20679 #
LBL-35207 p 1514 N95-20732 #
LBL-35219 p 1577 N95-22168 #
LBL-35308 p 1274 N95-21263 #
LBL-35348 p 1591 N95-22235 #
LBL-35358 p 1568 N95-20630 #
LBL-35444 p 1524 N95-21646 #
LBL-35566 p 1392 N95-20439 #
LBL-35567 p 1394 N95-20915 #
LBL-35628 p 1326 N95-20814 #
LBL-35741 p 1256 N95-21260 #
LBL-35791 p 1519 N95-21262 #
LBL-35803 p 1373 N95-21261 #
LBL-35899 p 1370 N95-20569 #
LBL-35914 p 1259 N95-21707 #
LBL-35929 p 1599 N95-20873 #
LBL-35940 p 1581 N95-21604 #
LBL-35956 p 1532 N95-20494 #
LBL-35959 p 1532 N95-20495 #
LBL-35964 p 1558 N95-21310 #
LBL-36033 p 1520 N95-21357 #
LBL-36063 p 1501 N95-20874 #
LBL-36065 p 1246 N95-21990 #
LBL-36067 p 1534 N95-20891 #
LBL-36078 p 1336 N95-22236 #
LBL-36103 p 1513 N95-20575 #
LBL-36109 p 1374 N95-21528 #
LBL-36120 p 1513 N95-20629 #
LBL-36144 p 1582 N95-22237 #
LBL-36197 p 1515 N95-20872 #
LBL-36219 p 1521 N95-21380 #

LC-79-640375//R81 p 1603 N95-20713 #
LC-79-640375//R81 p 1603 N95-20722 #
LC-94-2659 p 1225 N95-20001 * #
LC-94-36645 p 1217 N95-21894 * #
LC-94-67487 p 1214 N95-22341 * #
LC-94-69232 p 1265 N95-20176 #

LMSC-P000457 p 1279 N95-22136 #

LPI-CONTRIB-845 p 1415 N95-21777 * #

LTR94-001 p 1290 N95-20376 #

M-770 p 1218 N95-21346 * #

MDC-94X0025 p 1273 N95-21014 #

MEMO-COSOR-93-30 p 1482 N95-21271 #
MEMO-COSOR-94-16 p 1484 N95-22139 #
MEMO-COSOR-94-17 p 1483 N95-21618 #
MEMO-COSOR-94-18 p 1499 N95-21979 #
MEMO-COSOR-94-19 p 1499 N95-21980 #
MEMO-COSOR-94-20 p 1493 N95-21468
MEMO-COSOR-94-21 p 1466 N95-21269 #

MEMO-INF-94-18 p 1482 N95-21412
MEMO-INF-94-21 p 1472 N95-22159
MEMO-INF-94-22 p 1467 N95-21411
MEMO-INF-94-23 p 1484 N95-22156
MEMO-INF-94-24 p 1469 N95-21711
MEMO-INF-94-25 p 1469 N95-21716
MEMO-INF-94-26 p 1306 N95-21623
MEMO-INF-94-27 p 1477 N95-21620 #
MEMO-INF-94-28 p 1492 N95-21032
MEMO-INF-94-29 p 1466 N95-21344
MEMO-INF-94-30 p 1494 N95-21867
MEMO-INF-94-31 p 1494 N95-21868
MEMO-INF-94-37 p 1455 N95-21871
MEMO-INF-94-39 p 1478 N95-21869
MEMO-INF-94-40 p 1308 N95-22080
MEMO-INF-94-41 p 1471 N95-22081
MEMO-INF-94-42 p 1455 N95-22082

MEMO-SB-80-106-U p 1388 N95-22093 #

MFIS-MF-13922 p 1550 N95-20204 #

MIL-STD-1540B p 1218 N95-20770 #
MIL-STD-1540C p 1218 N95-20770 #

MIT-TR-1012 p 1309 N95-22229 #
MIT-TR-1443 p 1479 N95-20011

MLM-3785 p 1334 N95-22062 #
MLM-3799 p 1243 N95-21440 #

MML-TM-93-23 p 1312 N95-19958 #
MML-TM-94-10 p 1258 N95-21575

MP-94-074 p 1247 N95-22150 #
MP-94B0000022 p 1303 N95-21493
MP-94B0000087 p 1289 N95-20211 #

MRL-GD-0048 p 1250 N95-19910
MRL-GD-0051 p 1287 N95-21625

MRL-TN-631 p 1205 N95-21642
MRL-TN-640 p 1434 N95-21657
MRL-TN-661 p 1282 N95-20187

MRL-TR-93-16 p 1284 N95-21624
MRL-TR-93-32 p 1505 N95-21984
MRL-TR-93-42 p 1284 N95-21658

MSC-TPR-3456/CA07 p 1229 N95-21215 #
MSC-TPR-3457/CA07 p 1233 N95-22395 #
MSC-TPR-3458/CA07-REV p 1229 N95-21149 #

MSRR-601-PT-2 p 1470 N95-21974
MSRR-605 p 1490 N95-20662

MTR-93B0000043 p 1390 N95-21912

NAIC-ID(RS)T-0380-94 p 1368 N95-22256 #
NAIC-ID(RS)T-0395-94 p 1548 N95-22255 #
NAIC-ID(RS)T-0648-94 p 1229 N95-20859 #

NAMRL-SP-93-6 p 1498 N95-20102
NAMRL-SP-93-7 p 1448 N95-19957 #

NAMRL-SR-94-1 p 1445 N95-21180

NAMRL-1390 p 1442 N95-20710
NAMRL-1392 p 1441 N95-20307 #

NAS 1.15:106666 p 1589 N95-21187 * #
NAS 1.15:106684 p 1385 N95-20179 * #
NAS 1.15:106704 p 1356 N95-21959 * #
NAS 1.15:106759 p 1274 N95-21252 * #
NAS 1.15:106763 p 1223 N95-19901 * #
NAS 1.15:106819 p 1334 N95-22112 * #
NAS 1.15:106824 p 1201 N95-20794 * #
NAS 1.15:106829 p 1218 N95-21384 * #
NAS 1.15:106834 p 1307 N95-21890 * #
NAS 1.15:106843 p 1355 N95-21957 * #
NAS 1.15:106844 p 1284 N95-22114 * #
NAS 1.15:106845 p 1338 N95-19952 * #
NAS 1.15:106846 p 1338 N95-19953 * #
NAS 1.15:106848-PT-2 p 1382 N95-22405 * #
NAS 1.15:106852 p 1386 N95-20790 * #
NAS 1.15:106854 p 1214 N95-21383 * #
NAS 1.15:106856 p 1415 N95-21188 * #
NAS 1.15:106857 p 1366 N95-21259 * #
NAS 1.15:106861 p 1366 N95-21391 * #
NAS 1.15:108474 p 1270 N95-20694 * #
NAS 1.15:108476 p 1365 N95-20560 * #
NAS 1.15:108479 p 1340 N95-20561 * #
NAS 1.15:108862 p 1207 N95-21186 * #
NAS 1.15:108864 p 1366 N95-21323 * #
NAS 1.15:109122 p 1589 N95-21015 * #
NAS 1.15:109123 p 1587 N95-20162 * #
NAS 1.15:109157 p 1216 N95-20669 * #
NAS 1.15:109158 p 1203 N95-20706 * #
NAS 1.15:109166 p 1219 N95-20800 * #
NAS 1.15:109169 p 1587 N95-20163 * #
NAS 1.15:109170-VOL-1 p 1589 N95-21189 * #
NAS 1.15:109173 p 1494 N95-21622 * #
NAS 1.15:109174 p 1200 N95-20688 * #
NAS 1.15:110059 p 1225 N95-20001 * #
NAS 1.15:110103 p 1206 N95-20370 * #
NAS 1.15:110114 p 1413 N95-20453 *
NAS 1.15:110129 p 1412 N95-20278 * #
NAS 1.15:110448 p 1590 N95-21977 * #
NAS 1.15:110492 p 1354 N95-21675 * #
NAS 1.15:110493 p 1426 N95-21874 * #
NAS 1.15:110499 p 1331 N95-21614 * #
NAS 1.15:110500 p 1390 N95-22111 * #
NAS 1.15:110501 p 1390 N95-22110 * #
NAS 1.15:110506 p 1590 N95-21457 * #
NAS 1.15:110507 p 1601 N95-21621 * #
NAS 1.15:110510 p 1367 N95-21889 * #
NAS 1.15:110513 p 1355 N95-21954 * #
NAS 1.15:197364 p 1604 N95-22384 * #
NAS 1.15:4574 p 1199 N95-19913 * #
NAS 1.15:4577 p 1353 N95-21258 * #
NAS 1.15:4641 p 1368 N95-22109 * #
NAS 1.15:4657 p 1439 N95-21544 * #
NAS 1.19/4:103 p 1285 N95-21322 * #
NAS 1.21:290 p 1214 N95-22341 * #
NAS 1.21:4026 p 1217 N95-21894 * #
NAS 1.21:6103 p 1583 N95-20739 * #
NAS 1.21:7011(399) p 1446 N95-21947 *
NAS 1.21:7037(315) p 1199 N95-21640 *
NAS 1.21:7039(46)-SECT-2 p 1590 N95-21948 *
NAS 1.26:191601 p 1495 N95-22157 *
NAS 1.26:194891 p 1479 N95-20010 *
NAS 1.26:194892 p 1338 N95-20009 *
NAS 1.26:194935 p 1473 N95-20013 *
NAS 1.26:194978 p 1495 N95-22325 * #
NAS 1.26:195012 p 1220 N95-21190 * #
NAS 1.26:195024 p 1456 N95-22431 * #
NAS 1.26:195027 p 1462 N95-20691 * #
NAS 1.26:195030 p 1230 N95-21363 * #
NAS 1.26:195320-APP-A-L p 1395 N95-21530 * #
NAS 1.26:195320 p 1222 N95-21531 * #
NAS 1.26:195392-VOL-1 p 1505 N95-21888 * #
NAS 1.26:195415 p 1225 N95-19951 * #
NAS 1.26:195420-VOL-1 p 1396 N95-21952 * #
NAS 1.26:195420-VOL-2 p 1396 N95-21953 * #
NAS 1.26:195431-PT-1 p 1382 N95-22404 * #
NAS 1.26:196049 p 1353 N95-21340 * #
NAS 1.26:196310 p 1221 N95-20059 * #
NAS 1.26:196311 p 1436 N95-22072 *
NAS 1.26:196540 p 1312 N95-19909 * #
NAS 1.26:196554 p 1221 N95-20124 * #
NAS 1.26:196556 p 1381 N95-21705 * #
NAS 1.26:196557 p 1381 N95-21692 * #
NAS 1.26:196944 p 1415 N95-21777 * #
NAS 1.26:197272 p 1201 N95-21031 * #
NAS 1.26:197284 p 1558 N95-21345 * #
NAS 1.26:197285 p 1379 N95-20795 * #
NAS 1.26:197286 p 1216 N95-21436 * #
NAS 1.26:197290 p 1205 N95-22161 * #
NAS 1.26:197291 p 1478 N95-22108 * #
NAS 1.26:197298 p 1439 N95-21529 * #
NAS 1.26:197299 p 1389 N95-20156 * #
NAS 1.26:197304 p 1600 N95-21615 * #
NAS 1.26:197317 p 1222 N95-21616 * #
NAS 1.26:197318 p 1201 N95-21343 * #
NAS 1.26:197333 p 1484 N95-22171 * #
NAS 1.26:197338 p 1412 N95-20002 * #
NAS 1.26:197339 p 1397 N95-22336 * #
NAS 1.26:197341 p 1302 N95-21456 * #
NAS 1.26:197344 p 1280 N95-22383 * #
NAS 1.26:197352 p 1358 N95-22437 * #
NAS 1.26:197353 p 1595 N95-21749 * #
NAS 1.26:197356 p 1473 N95-19885 *
NAS 1.26:197362 p 1341 N95-21035 * #
NAS 1.26:197365 p 1479 N95-22406 * #
NAS 1.26:197367 p 1437 N95-20559 * #
NAS 1.26:197370 p 1602 N95-20558 * #
NAS 1.26:197373 p 1601 N95-22338 * #
NAS 1.26:197374 p 1238 N95-20557 * #
NAS 1.26:197375 p 1543 N95-20798 * #
NAS 1.26:197377 p 1601 N95-20797 * #
NAS 1.26:197380 p 1357 N95-22173 * #
NAS 1.26:197390 p 1303 N95-21532 * #
NAS 1.26:197401 p 1453 N95-21866 * #
NAS 1.26:197409 p 1205 N95-21891 * #
NAS 1.26:197594 p 1483 N95-21613 * #
NAS 1.26:197603 p 1428 N95-19948 * #
NAS 1.26:197617 p 1579 N95-19947 * #
NAS 1.26:197622 p 1340 N95-20796 * #
NAS 1.26:197638 p 1504 N95-21170 * #
NAS 1.26:197672 p 1427 N95-22326 * #
NAS 1.26:197677 p 1467 N95-21450 * #
NAS 1.26:4631 p 1204 N95-19950 * #
NAS 1.26:4633 p 1337 N95-19912 * #
NAS 1.26:4641 p 1380 N95-21359 * #

NAS 1.26:4643 p 1222 N95-21458 * #
NAS 1.55:3278 p 1316 N95-20502 * #
NAS 1.60:3476 p 1340 N95-20619 * #
NAS 1.60:3480 p 1201 N95-21338 * #
NAS 1.60:3497 p 1517 N95-21191 * #
NAS 1.60:3535 p 1218 N95-21346 * #
NAS 1.61:1311 p 1235 N95-20180 * #
NAS 1.71:LAR-13888-1 p 1441 N95-20408 * #
NAS 1.71:LAR-14240-1 p 1268 N95-20410 * #
NAS 1.71:LAR-14879-1-CU p 1383 N95-20616 * #
NAS 1.71:LAR-14977-1 p 1443 N95-20763 * #
NAS 1.71:LAR-15020-1 p 1268 N95-20407 * #
NAS 1.71:LAR-15058-1 p 1215 N95-20080 * #
NAS 1.71:LAR-15212-1-CU p 1229 N95-21008 * #
NAS 1.71:LAR-15231-1-SB p 1383 N95-20764 * #
NAS 1.71:LEW-15595-1-C p 1338 N95-19933 * #
NAS 1.71:MFS-26200-1-SB p 1251 N95-20068 * #
NAS 1.71:MSC-22381-1 p 1378 N95-20409 * #
NAS 1.71:MSC-22384-1 p 1378 N95-20151 * #
NAS 1.83:214 p 1594 N95-21893 * #

NASA-ASR-222 p 1217 N95-19995 *

NASA-CASE-LAR-13888-1 p 1441 N95-20408 * #
NASA-CASE-LAR-14240-1 p 1268 N95-20410 * #
NASA-CASE-LAR-14879-1-CU p 1383 N95-20616 * #
NASA-CASE-LAR-14977-1 p 1443 N95-20763 * #
NASA-CASE-LAR-15020-1 p 1268 N95-20407 * #
NASA-CASE-LAR-15058-1 p 1215 N95-20080 * #
NASA-CASE-LAR-15212-1-CU p 1229 N95-21008 * #
NASA-CASE-LAR-15231-1-SB p 1383 N95-20764 * #

NASA-CASE-LEW-15595-1-C p 1338 N95-19933 * #

NASA-CASE-MFS-26200-1-SB p 1251 N95-20068 * #

NASA-CASE-MSC-22381-1 p 1378 N95-20409 * #
NASA-CASE-MSC-22384-1 p 1378 N95-20151 * #

NASA-CP-3278 p 1316 N95-20502 * #

NASA-CR-191601 p 1495 N95-22157 *
NASA-CR-194891 p 1479 N95-20010 *
NASA-CR-194892 p 1338 N95-20009 *
NASA-CR-194935 p 1473 N95-20013 *
NASA-CR-194978 p 1495 N95-22325 * #
NASA-CR-195012 p 1220 N95-21190 * #
NASA-CR-195024 p 1456 N95-22431 * #
NASA-CR-195027 p 1462 N95-20691 * #
NASA-CR-195030 p 1230 N95-21363 * #
NASA-CR-195320-APP-A-L p 1395 N95-21530 * #
NASA-CR-195320 p 1222 N95-21531 * #
NASA-CR-195392-VOL-1 p 1505 N95-21888 * #
NASA-CR-195415 p 1225 N95-19951 * #
NASA-CR-195420-VOL-1 p 1396 N95-21952 * #
NASA-CR-195420-VOL-2 p 1396 N95-21953 * #
NASA-CR-195431-PT-1 p 1382 N95-22404 * #
NASA-CR-196049 p 1353 N95-21340 * #
NASA-CR-196310 p 1221 N95-20059 * #
NASA-CR-196311 p 1436 N95-22072 *
NASA-CR-196540 p 1312 N95-19909 * #
NASA-CR-196554 p 1221 N95-20124 * #
NASA-CR-196556 p 1381 N95-21705 * #
NASA-CR-196557 p 1381 N95-21692 * #
NASA-CR-196944 p 1415 N95-21777 * #
NASA-CR-197272 p 1201 N95-21031 * #
NASA-CR-197284 p 1558 N95-21345 * #
NASA-CR-197285 p 1379 N95-20795 * #
NASA-CR-197286 p 1216 N95-21436 * #
NASA-CR-197290 p 1205 N95-22161 * #
NASA-CR-197291 p 1478 N95-22108 * #
NASA-CR-197298 p 1439 N95-21529 * #
NASA-CR-197299 p 1389 N95-20156 * #
NASA-CR-197304 p 1600 N95-21615 * #
NASA-CR-197317 p 1222 N95-21616 * #
NASA-CR-197318 p 1201 N95-21343 * #
NASA-CR-197333 p 1484 N95-22171 * #
NASA-CR-197338 p 1412 N95-20002 * #
NASA-CR-197339 p 1397 N95-22336 * #
NASA-CR-197341 p 1302 N95-21456 * #
NASA-CR-197344 p 1280 N95-22383 * #
NASA-CR-197352 p 1358 N95-22437 * #
NASA-CR-197353 p 1595 N95-21749 * #
NASA-CR-197356 p 1473 N95-19885 *
NASA-CR-197362 p 1341 N95-21035 * #
NASA-CR-197365 p 1479 N95-22406 * #
NASA-CR-197367 p 1437 N95-20559 * #
NASA-CR-197370 p 1602 N95-20558 * #
NASA-CR-197373 p 1601 N95-22338 * #
NASA-CR-197374 p 1238 N95-20557 * #
NASA-CR-197375 p 1543 N95-20798 * #
NASA-CR-197377 p 1601 N95-20797 * #
NASA-CR-197380 p 1357 N95-22173 * #
NASA-CR-197390 p 1303 N95-21532 * #
NASA-CR-197401 p 1453 N95-21866 * #
NASA-CR-197409 p 1205 N95-21891 * #
NASA-CR-197594 p 1483 N95-21613 * #
NASA-CR-197603 p 1428 N95-19948 * #
NASA-CR-197617 p 1579 N95-19947 * #
NASA-CR-197622 p 1340 N95-20796 * #
NASA-CR-197638 p 1504 N95-21170 * #
NASA-CR-197672 p 1427 N95-22326 * #
NASA-CR-197677 p 1467 N95-21450 * #
NASA-CR-4631 p 1204 N95-19950 * #
NASA-CR-4633 p 1337 N95-19912 * #
NASA-CR-4641 p 1380 N95-21359 * #
NASA-CR-4643 p 1222 N95-21458 * #

NASA-EG-103 p 1285 N95-21322 * #

NASA-JSC-554 p 1601 N95-21196 *

NASA-NP-214 p 1594 N95-21893 * #

NASA-RP-1311 p 1235 N95-20180 * #

NASA-SP-290 p 1214 N95-22341 * #
NASA-SP-4026 p 1217 N95-21894 * #
NASA-SP-6103 p 1583 N95-20739 * #
NASA-SP-7011(399) p 1446 N95-21947 *
NASA-SP-7037(315) p 1199 N95-21640 *
NASA-SP-7039(46)-SECT-2 p 1590 N95-21948 *

NASA-TM-106666 p 1589 N95-21187 * #
NASA-TM-106684 p 1385 N95-20179 * #
NASA-TM-106704 p 1356 N95-21959 * #
NASA-TM-106759 p 1274 N95-21252 * #
NASA-TM-106763 p 1223 N95-19901 * #
NASA-TM-106819 p 1334 N95-22112 * #
NASA-TM-106824 p 1201 N95-20794 * #
NASA-TM-106829 p 1218 N95-21384 * #
NASA-TM-106834 p 1307 N95-21890 * #
NASA-TM-106843 p 1355 N95-21957 * #
NASA-TM-106844 p 1284 N95-22114 * #
NASA-TM-106845 p 1338 N95-19952 * #
NASA-TM-106846 p 1338 N95-19953 * #
NASA-TM-106848-PT-2 p 1382 N95-22405 * #
NASA-TM-106852 p 1386 N95-20790 * #
NASA-TM-106854 p 1214 N95-21383 * #
NASA-TM-106856 p 1415 N95-21188 * #
NASA-TM-106857 p 1366 N95-21259 * #
NASA-TM-106861 p 1366 N95-21391 * #
NASA-TM-108474 p 1270 N95-20694 * #
NASA-TM-108476 p 1365 N95-20560 * #
NASA-TM-108479 p 1340 N95-20561 * #
NASA-TM-108862 p 1207 N95-21186 * #
NASA-TM-108864 p 1366 N95-21323 * #
NASA-TM-109122 p 1589 N95-21015 * #
NASA-TM-109123 p 1587 N95-20162 * #
NASA-TM-109157 p 1216 N95-20669 * #
NASA-TM-109158 p 1203 N95-20706 * #
NASA-TM-109166 p 1219 N95-20800 * #
NASA-TM-109169 p 1587 N95-20163 * #
NASA-TM-109170-VOL-1 p 1589 N95-21189 * #
NASA-TM-109173 p 1494 N95-21622 * #
NASA-TM-109174 p 1200 N95-20688 * #
NASA-TM-110059 p 1225 N95-20001 * #
NASA-TM-110103 p 1206 N95-20370 * #
NASA-TM-110114 p 1413 N95-20453 *
NASA-TM-110129 p 1412 N95-20278 * #
NASA-TM-110448 p 1590 N95-21977 * #
NASA-TM-110492 p 1354 N95-21675 * #
NASA-TM-110493 p 1426 N95-21874 * #
NASA-TM-110499 p 1331 N95-21614 * #
NASA-TM-110500 p 1390 N95-22111 * #
NASA-TM-110501 p 1390 N95-22110 * #
NASA-TM-110502 p 1206 N95-19994 *
NASA-TM-110503 p 1217 N95-19995 *
NASA-TM-110504 p 1206 N95-20155 *
NASA-TM-110505 p 1200 N95-19996 *
NASA-TM-110506 p 1590 N95-21457 * #
NASA-TM-110507 p 1601 N95-21621 * #
NASA-TM-110510 p 1367 N95-21889 * #
NASA-TM-110511 p 1601 N95-21196 *
NASA-TM-110512 p 1219 N95-21113 *
NASA-TM-110513 p 1355 N95-21954 * #
NASA-TM-110514 p 1219 N95-21558 *
NASA-TM-110515 p 1219 N95-22295 *
NASA-TM-110518 p 1220 N95-21858 *
NASA-TM-197364 p 1604 N95-22384 * #
NASA-TM-4574 p 1199 N95-19913 * #
NASA-TM-4577 p 1353 N95-21258 * #
NASA-TM-4641 p 1368 N95-22109 * #
NASA-TM-4657 p 1439 N95-21544 * #

NASA-TP-3476 p 1340 N95-20619 * #
NASA-TP-3480 p 1201 N95-21338 * #
NASA-TP-3497 p 1517 N95-21191 * #
NASA-TP-3535 p 1218 N95-21346 * #

NATICK-TR-95/004 p 1357 N95-22206 #
NATICK/TR-95/002 p 1454 N95-22274 #

NAWC-WPNS-TP-8152 p 1516 N95-21121 #
NAWC-WPNS-TP-8204 p 1289 N95-19997 #
NAWC-WPNS-TP-8212 p 1290 N95-20556 #
NAWC-WPNS-TP-8217 p 1480 N95-20606 #

NAWCADWAR-60-94128 p 1279 N95-22136 #
NAWCADWAR-93073-60 p 1453 N95-21691 #
NAWCADWAR-94001-60 p 1261 N95-22132 #
NAWCADWAR-94014-60 p 1240 N95-20970

NCCOSC/RDT/E-TR-1590-PT-1 p 1270 N95-20603
NCCOSC/RDT/E-TR-1592-PT-3 p 1388 N95-22411 #
NCCOSC/RDT/E-TR-1639 p 1365 N95-20604
NCCOSC/RDT/E-TR-1658 p 1452 N95-20768 #
NCCOSC/RDT/E-TR-1661 p 1503 N95-20084 #
NCCOSC/RDT/E-TR-1673 p 1503 N95-20272 #

NDP-026A p 1431 N95-22288 #

NEDO-P-9323 p 1397 N95-22309 #
NEDO-P-9324 p 1254 N95-20890 #
NEDO-P-9328 p 1375 N95-22079 #

NEI-FI-234 p 1380 N95-21295 #

NFESC-TR-2023-ENV p 1403 N95-20487 #

NHRC-94-7 p 1444 N95-21160 #

NIFS-MEMO-12 p 1554 N95-20686 #

NIFS-240 p 1555 N95-20988 #
NIFS-241 p 1555 N95-20989 #
NIFS-246 p 1554 N95-20683 #

NIOZ-1993-17 p 1435 N95-21717
NIOZ-1994-3 p 1390 N95-21872

NIST/MONO-179 p 1234 N95-20100 #

NIST/SP-864 p 1540 N95-19976 #

NISTIR-5023 p 1289 N95-20191 #
NISTIR-5305 p 1286 N95-21129 #
NISTIR-5459 p 1473 N95-22390
NISTIR-5461 p 1379 N95-20984 #
NISTIR-5499 p 1286 N95-20717 #
NISTIR-5504 p 1286 N95-21130 #

NMAB-464 p 1265 N95-20176 #

NMRI-94-21 p 1446 N95-22003 #

NONP-NASA-VT-95-41114 p 1206 N95-19994 *
NONP-NASA-VT-95-41115 p 1217 N95-19995 *
NONP-NASA-VT-95-41116 p 1206 N95-20155 *
NONP-NASA-VT-95-41117 p 1200 N95-19996 *
NONP-NASA-VT-95-42155 p 1601 N95-21196 *
NONP-NASA-VT-95-42156 p 1219 N95-21113 *
NONP-NASA-VT-95-42494 p 1219 N95-21558 *
NONP-NASA-VT-95-42495 p 1219 N95-22295 *
NONP-NASA-VT-95-42566 p 1220 N95-21858 *

NPL-RSA(EXT)0048 p 1207 N95-21425

NPRDC-TN-94-18 p 1479 N95-20005 #

NPS-CS-93-013 p 1461 N95-20579
NPS-CS-94-004 p 1587 N95-20302
NPS-CS-94-008 p 1586 N95-19956 #

NPS-OC-94-002 p 1431 N95-19918
NPS-OC-94-006 p 1435 N95-21880

NPSCS-93-011 p 1459 N95-20304

NPSEC-94-010 p 1325 N95-20715 #

NRAD-TR-1594-PT-4 p 1279 N95-22047
NRAD-TR-1660 p 1431 N95-19896 #

NREL/CP-413-6186 p 1391 N95-20332 #
NREL/CP-470-6431 p 1234 N95-20117 #

NREL/SP-463-6156 p 1392 N95-20778 #

NREL/TP-411-6639 p 1392 N95-20473 #
NREL/TP-413-7064 p 1279 N95-22091 #
NREL/TP-413-7165 p 1395 N95-21844 #
NREL/TP-421-6331 p 1437 N95-20471 #
NREL/TP-441-7079 p 1391 N95-20260 #
NREL/TP-442-4740 p 1394 N95-20985 #
NREL/TP-442-7035 p 1384 N95-20109 #
NREL/TP-451-6637 p 1392 N95-20333 #

NREL/TP-451-7046 .... p 1391 N95-20118 #
NREL/TP-451-7055 .... p 1268 N95-20472 #
NREL/TP-451-7056 .... p 1394 N95-21294 #
NREL/TP-451-7162 .... p 1395 N95-21508 #
NREL/TP-471-7014 .... p 1410 N95-22278 #

NRL/FR/5591-94-9735 .... p 1498 N95-20608 #
NRL/FR/7531-94-9450 .... p 1429 N95-20826 #

NRL/MR/6120-94-7629 .... p 1279 N95-22022
NRL/MR/6180-94-7615 .... p 1286 N95-20611 #
NRL/MR/6180-94-7624 .... p 1202 N95-20071 #
NRL/MR/6720-94-7466 .... p 1533 N95-20672
NRL/MR/6720-94-7472-2 .... p 1537 N95-21494
NRL/MR/7240-94-7510 .... p 1388 N95-20006 #
NRL/MR/7240-94-7517 .... p 1431 N95-19888
NRL/MR/7322-94-7524 .... p 1432 N95-20012
NRL/MR/7322-94-7525 .... p 1433 N95-21018
NRL/MR/7432-94-7548 .... p 1436 N95-22028 #
NRL/MR/7441-94-7537 .... p 1390 N95-22055 #

NRL/PU/1230-94-261 .... p 1217 N95-20228 #
NRL/PU/5200-94-246 .... p 1605 N95-20182 #

NSF-ITP-94-67 .... p 1512 N95-20451 #

NSWCDD/TR-93/169 .... p 1504 N95-20963
NSWCDD/TR-94-114 .... p 1582 N95-22054 #

NUWC-NPT-TD-10729 .... p 1505 N95-21213 #

NUWC-NPT-TR-10372 .... p 1590 N95-22053 #
NUWC-NPT-TR-10693 .... p 1357 N95-22208
NUWC-NPT-TR-10719 .... p 1386 N95-21212 #
NUWC-NPT-TR-10759 .... p 1506 N95-22360 #

NV-94-C11 .... p 1569 N95-20767 #

NWRA-CR-94-R111 .... p 1425 N95-21833 #

ORNL-CCIP-9408 .... p 1526 N95-21939 #

ORNL-6805 .... p 1285 N95-20194 #
ORNL-6829 .... p 1245 N95-21732 #

ORNL/CDIAC-72 .... p 1431 N95-22288 #

ORNL/M-3704-SUMM .... p 1401 N95-20238 #

ORNL/SUB/83-21322/03 .... p 1379 N95-20984 #

ORNL/TM-12729 .... p 1507 N95-20086 #
ORNL/TM-12743 .... p 1477 N95-21602 #
ORNL/TM-12745 .... p 1586 N95-21645 #
ORNL/TM-12754 .... p 1355 N95-21726 #
ORNL/TM-12800 .... p 1247 N95-22049 #
ORNL/TM-12807 .... p 1469 N95-21744 #
ORNL/TM-12819 .... p 1483 N95-21741 #

P-498 .... p 1601 N95-20797 * #

PB94-165362 .... p 1312 N95-19966 #
PB94-192754 .... p 1409 N95-22101
PB94-203437 .... p 1473 N95-22390
PB94-206885 .... p 1444 N95-21016
PB94-207511 .... p 1234 N95-20100 #
PB94-207636 .... p 1540 N95-19976 #
PB94-207917 .... p 1577 N95-22166
PB94-208352 .... p 1384 N95-20003
PB94-208360 .... p 1384 N95-20101 #
PB94-208378 .... p 1384 N95-19975 #
PB94-208402 .... p 1330 N95-21590
PB94-209541 .... p 1428 N95-20099 #
PB94-209749 .... p 1400 N95-19965 #
PB94-210051 .... p 1289 N95-20191 #
PB94-210085 .... p 1282 N95-20253 #
PB94-214772 .... p 1401 N95-20192 #
PB94-215555 .... p 1286 N95-21027
PB94-217478 .... p 1199 N95-19967 #
PB95-104386 .... p 1236 N95-20256 #
PB95-104402 .... p 1443 N95-20971 #
PB95-104410 .... p 1300 N95-20972
PB95-104428 .... p 1300 N95-20980
PB95-104444 .... p 1341 N95-20981 #
PB95-104451 .... p 1464 N95-20982
PB95-104485 .... p 1372 N95-20983
PB95-104493 .... p 1325 N95-20702
PB95-104915 .... p 1379 N95-20984 #
PB95-104923 .... p 1603 N95-20713 #
PB95-104964 .... p 1286 N95-20717 #
PB95-105060 .... p 1603 N95-20722 #
PB95-106324 .... p 1492 N95-21421
PB95-106407 .... p 1410 N95-22124
PB95-107447 .... p 1410 N95-22125 #
PB95-107454 .... p 1411 N95-22381 #
PB95-107488 .... p 1410 N95-22186 #
PB95-107553 .... p 1484 N95-22156
PB95-107561 .... p 1467 N95-21411
PB95-107579 .... p 1472 N95-22159
PB95-107595 .... p 1482 N95-21412
PB95-107819 .... p 1444 N95-21028
PB95-107835 .... p 1389 N95-20207 #
PB95-107850 .... p 1437 N95-20208 #
PB95-107868 .... p 1300 N95-21029
PB95-107975 .... p 1354 N95-21578 #
PB95-107991 .... p 1305 N95-21579
PB95-108007 .... p 1483 N95-21669
PB95-108015 .... p 1445 N95-21580
PB95-108031 .... p 1288 N95-21633
PB95-108064 .... p 1574 N95-21670 #
PB95-108098 .... p 1495 N95-22147
PB95-108114 .... p 1537 N95-21647
PB95-108163 .... p 1494 N95-21648
PB95-108171 .... p 1495 N95-22317
PB95-108197 .... p 1354 N95-21649
PB95-109070 .... p 1496 N95-22353 #
PB95-109088 .... p 1496 N95-22354 #
PB95-109096 .... p 1496 N95-22355 #
PB95-110219 .... p 1276 N95-21650
PB95-110227 .... p 1288 N95-21651
PB95-110243 .... p 1258 N95-21652
PB95-110250 .... p 1258 N95-21653
PB95-110268 .... p 1468 N95-21654
PB95-110276 .... p 1469 N95-21655
PB95-110284 .... p 1354 N95-21656
PB95-110318 .... p 1574 N95-21636
PB95-110326 .... p 1575 N95-21949
PB95-110334 .... p 1288 N95-22014 #
PB95-110342 .... p 1484 N95-22015
PB95-110367 .... p 1470 N95-22016
PB95-110391 .... p 1356 N95-22017
PB95-110425 .... p 1455 N95-22018
PB95-110482 .... p 1496 N95-22349 #
PB95-110508 .... p 1472 N95-22351
PB95-110557 .... p 1472 N95-22305 #
PB95-110565 .... p 1488 N95-20149
PB95-110573 .... p 1456 N95-19889 #
PB95-110581 .... p 1288 N95-19890 #
PB95-110599 .... p 1456 N95-19891 #
PB95-110607 .... p 1486 N95-19892 #
PB95-110615 .... p 1488 N95-20054 #
PB95-110623 .... p 1488 N95-20055 #
PB95-110631 .... p 1473 N95-20056 #
PB95-110656 .... p 1487 N95-19902 #
PB95-110664 .... p 1487 N95-19903 #
PB95-110672 .... p 1586 N95-19904 #
PB95-110680 .... p 1456 N95-19905 #
PB95-110698 .... p 1459 N95-20258 #
PB95-110706 .... p 1487 N95-19906 #
PB95-110714 .... p 1487 N95-19907 #
PB95-110722 .... p 1456 N95-19908 #
PB95-110730 .... p 1472 N95-22302 #
PB95-110805 .... p 1205 N95-21369
PB95-110813 .... p 1497 N95-19914
PB95-110821 .... p 1487 N95-19915 #
PB95-110839 .... p 1487 N95-19916 #
PB95-110847 .... p 1487 N95-19917 #
PB95-110862 .... p 1456 N95-19928
PB95-110888 .... p 1384 N95-19930 #
PB95-110896 .... p 1312 N95-19934 #
PB95-110920 .... p 1312 N95-19935 #
PB95-110946 .... p 1497 N95-19936 #
PB95-110953 .... p 1487 N95-19937 #
PB95-110961 .... p 1497 N95-19938
PB95-110979 .... p 1594 N95-19939
PB95-111019 .... p 1487 N95-19940 #
PB95-111027 .... p 1499 N95-19941 #
PB95-111043 .... p 1488 N95-19942 #
PB95-111050 .... p 1488 N95-19943 #
PB95-111068 .... p 1488 N95-19944 #
PB95-111076 .... p 1498 N95-19945 #
PB95-111084 .... p 1580 N95-20324
PB95-111092 .... p 1490 N95-20452
PB95-111100 .... p 1489 N95-20172 #
PB95-111118 .... p 1489 N95-20259 #
PB95-111126 .... p 1599 N95-20173 #
PB95-111134 .... p 1489 N95-20273 #
PB95-111670 .... p 1247 N95-22150 #
PB95-127015 .... p 1311 N95-22363 #
PB95-127023 .... p 1472 N95-22310 #
PB95-127031 .... p 1311 N95-22365
PB95-127049 .... p 1582 N95-22432 #
PB95-127064 .... p 1486 N95-22366 #
PB95-127072 .... p 1486 N95-22367 #
PB95-127080 .... p 1496 N95-22369 #
PB95-127098 .... p 1496 N95-22370 #
PB95-127106 .... p 1291 N95-20775
PB95-127114 .... p 1447 N95-22371 #
PB95-127122 .... p 1472 N95-22372 #
PB95-127130 .... p 1248 N95-22373 #
PB95-127171 .... p 1310 N95-22311 #
PB95-127189 .... p 1263 N95-22374 #
PB95-127197 .... p 1598 N95-22376 #
PB95-127205 .... p 1448 N95-22476 #
PB95-127411 .... p 1287 N95-21422
PB95-127437 .... p 1599 N95-21347
PB95-127460 .... p 1518 N95-21220
PB95-127478 .... p 1518 N95-21221
PB95-127510 .... p 1493 N95-21423
PB95-127528 .... p 1495 N95-22151 #
PB95-127536 .... p 1492 N95-21371
PB95-127544 .... p 1465 N95-21021 #
PB95-127551 .... p 1465 N95-21022 #
PB95-127569 .... p 1496 N95-22327 #
PB95-127577 .... p 1492 N95-21372
PB95-127585 .... p 1491 N95-21023 #
PB95-127593 .... p 1491 N95-21024 #
PB95-127601 .... p 1465 N95-21025 #
PB95-127619 .... p 1220 N95-21026 #
PB95-127627 .... p 1329 N95-21326 #
PB95-127635 .... p 1502 N95-21102 #
PB95-127643 .... p 1445 N95-21348 #
PB95-127650 .... p 1544 N95-21103 #
PB95-127676 .... p 1300 N95-21104 #
PB95-127684 .... p 1430 N95-21413
PB95-127692 .... p 1389 N95-21105 #
PB95-127700 .... p 1472 N95-22328 #
PB95-127718 .... p 1352 N95-21106
PB95-127726 .... p 1301 N95-21107 #
PB95-127734 .... p 1255 N95-21108 #
PB95-127742 .... p 1301 N95-21109 #
PB95-127759 .... p 1248 N95-22329 #
PB95-127767 .... p 1240 N95-21110 #
PB95-127775 .... p 1255 N95-21111 #
PB95-127783 .... p 1438 N95-21112 #
PB95-127791 .... p 1255 N95-21128 #
PB95-127825 .... p 1410 N95-22330
PB95-127957 .... p 1592 N95-22331 #
PB95-128674 .... p 1286 N95-21129 #
PB95-128922 .... p 1406 N95-21373 #
PB95-129672 .... p 1451 N95-20276
PB95-129748 .... p 1286 N95-21333
PB95-129797 .... p 1236 N95-20290
PB95-129805 .... p 1413 N95-20453 *
PB95-129813 .... p 1512 N95-20454
PB95-129839 .... p 1511 N95-20434
PB95-129847 .... p 1475 N95-20435
PB95-129854 .... p 1529 N95-22303
PB95-130290 .... p 1530 N95-22332
PB95-130308 .... p 1518 N95-21222
PB95-130316 .... p 1518 N95-21223
PB95-130324 .... p 1518 N95-21224
PB95-130332 .... p 1518 N95-21225
PB95-130340 .... p 1373 N95-21226
PB95-130357 .... p 1518 N95-21227
PB95-130365 .... p 1571 N95-21228
PB95-130373 .... p 1580 N95-21229
PB95-130399 .... p 1445 N95-21424
PB95-130423 .... p 1207 N95-21425
PB95-130472 .... p 1580 N95-21230
PB95-130480 .... p 1465 N95-21231
PB95-130498 .... p 1466 N95-21232
PB95-130548 .... p 1518 N95-21233
PB95-130597 .... p 1242 N95-21426
PB95-130845 .... p 1286 N95-21130 #
PB95-131330 .... p 1447 N95-22361
PB95-131348 .... p 1353 N95-21132 #
PB95-131355 .... p 1585 N95-21427
PB95-131371 .... p 1243 N95-21428
PB95-131397 .... p 1386 N95-21133 #
PB95-131538 .... p 1241 N95-21179 #
PB95-131561 .... p 1482 N95-21429
PB95-131579 .... p 1482 N95-21430
PB95-131603 .... p 1302 N95-21431
PB95-131611 .... p 1230 N95-21432
PB95-131629 .... p 1452 N95-21467
PB95-131637 .... p 1387 N95-21557
PB95-131652 .... p 1405 N95-21181 #
PB95-131686 .... p 1466 N95-21349
PB95-131876 .... p 1405 N95-21350
PB95-131884 .... p 1406 N95-21351
PB95-131892 .... p 1405 N95-21327
PB95-131900 .... p 1405 N95-21329
PB95-131926 .... p 1405 N95-21330
PB95-131942 .... p 1232 N95-22158
PB95-132031 .... p 1467 N95-21374
PB95-132056 .... p 1482 N95-21267 #
PB95-132064 .... p 1353 N95-21268 #
PB95-132072 .... p 1466 N95-21269 #
PB95-132098 .... p 1493 N95-21468
PB95-132122 .... p 1499 N95-21469
PB95-132155 .... p 1275 N95-21470 #
PB95-132197 .... p 1407 N95-21635
PB95-132247 .... p 1288 N95-21978
PB95-132411 .... p 1397 N95-22362
PB95-132502 .... p 1482 N95-21271 #
PB95-132650 .... p 1499 N95-21979 #
PB95-132668 .... p 1499 N95-21980 #

PB95-132676 .... p 1483 N95-21981
PB95-132684 .... p 1586 N95-21982
PB95-132692 .... p 1470 N95-21983
PB95-132700 .... p 1471 N95-22029
PB95-132718 .... p 1471 N95-22031
PB95-132726 .... p 1495 N95-22032
PB95-132734 .... p 1308 N95-22080
PB95-132742 .... p 1471 N95-22081
PB95-132759 .... p 1455 N95-22082
PB95-132767 .... p 1447 N95-22083
PB95-132783 .... p 1224 N95-22333
PB95-132858 .... p 1452 N95-21283
PB95-132866 .... p 1262 N95-22174
PB95-132874 .... p 1450 N95-21284
PB95-132882 .... p 1356 N95-22063
PB95-132890 .... p 1585 N95-21414
PB95-132908 .... p 1308 N95-22087
PB95-132916 .... p 1388 N95-22093 #
PB95-132924 .... p 1467 N95-21415 #
PB95-132932 .... p 1471 N95-22094 #
PB95-132965 .... p 1427 N95-22095
PB95-132999 .... p 1380 N95-21416
PB95-133005 .... p 1380 N95-21446
PB95-133427 .... p 1275 N95-21272
PB95-133468 .... p 1405 N95-21274 #
PB95-133484 .... p 1230 N95-21417
PB95-133518 .... p 1434 N95-21320 #
PB95-133526 .... p 1232 N95-22096
PB95-133542 .... p 1580 N95-21030
PB95-133559 .... p 1502 N95-22138
PB95-133575 .... p 1484 N95-22139 #
PB95-133609 .... p 1275 N95-21275
PB95-133617 .... p 1547 N95-22140
PB95-133625 .... p 1388 N95-22097
PB95-133732 .... p 1439 N95-21884 #
PB95-134011 .... p 1396 N95-22175
PB95-134029 .... p 1357 N95-22160 #
PB95-134045 .... p 1492 N95-21032
PB95-134052 .... p 1494 N95-21867
PB95-134060 .... p 1466 N95-21344
PB95-134078 .... p 1494 N95-21868
PB95-134086 .... p 1478 N95-21869
PB95-134094 .... p 1546 N95-21870
PB95-134110 .... p 1455 N95-21871
PB95-134144 .... p 1390 N95-21872
PB95-134185 .... p 1277 N95-21873
PB95-134532 .... p 1494 N95-21955 #
PB95-134540 .... p 1494 N95-21956 #
PB95-134557 .... p 1383 N95-21961 #
PB95-134565 .... p 1494 N95-21962 #
PB95-134599 .... p 1356 N95-21963
PB95-134615 .... p 1500 N95-21964
PB95-134649 .... p 1526 N95-21965
PB95-134656 .... p 1540 N95-22364
PB95-134664 .... p 1427 N95-22368
PB95-134920 .... p 1497 N95-22375
PB95-134979 .... p 1464 N95-20975
PB95-134987 .... p 1497 N95-22379 #
PB95-134995 .... p 1336 N95-22382
PB95-135067 .... p 1311 N95-22358
PB95-135075 .... p 1496 N95-22359
PB95-135109 .... p 1592 N95-22334 #
PB95-135117 .... p 1499 N95-21709
PB95-135182 .... p 1469 N95-21711
PB95-135208 .... p 1469 N95-21716
PB95-135224 .... p 1435 N95-21717
PB95-135265 .... p 1409 N95-21718
PB95-135273 .... p 1464 N95-21003
PB95-135349 .... p 1589 N95-21004
PB95-135372 .... p 1491 N95-21005
PB95-135380 .... p 1386 N95-21006 #
PB95-135398 .... p 1445 N95-21352 #
PB95-135422 .... p 1273 N95-20976
PB95-135430 .... p 1244 N95-21573 #
PB95-135455 .... p 1493 N95-21574 #
PB95-135463 .... p 1483 N95-21618 #
PB95-135471 .... p 1409 N95-21846
PB95-135489 .... p 1468 N95-21619 #
PB95-135505 .... p 1477 N95-21620 #
PB95-135513 .... p 1306 N95-21623
PB95-135554 .... p 1284 N95-21966 #
PB95-135620 .... p 1468 N95-21455
PB95-135687 .... p 1492 N95-21318 #
PB95-135711 .... p 1493 N95-21434
PB95-135729 .... p 1467 N95-21435
PB95-135737 .... p 1465 N95-21033
PB95-135745 .... p 1402 N95-20440
PB95-135752 .... p 1489 N95-20423
PB95-135760 .... p 1490 N95-20424
PB95-135794 .... p 1404 N95-21034
PB95-135802 .... p 1553 N95-20425
PB95-135828 .... p 1444 N95-21007
PB95-136727 .... p 1603 N95-20919 #
PB95-136735 .... p 1603 N95-20829 #
PB95-137089 .... p 1491 N95-20830 #

PDA-TR-1754-02-01 .... p 1213 N95-22036 #

PFC/RR-93-7 .... p 1560 N95-21724 #
PFC/RR-94-1 .... p 1221 N95-20059 * #
PFC/RR-94-2 .... p 1260 N95-22013 #
PFC/RR-94-5 .... p 1330 N95-21442 #
PFC/RR-94-6 .... p 1332 N95-21725 #

PL-CP-94-1000 .... p 1588 N95-20774 #

PL-TR-93-1039 .... p 1544 N95-20803 #
PL-TR-93-1110 .... p 1207 N95-20772 #
PL-TR-93-1111 .... p 1291 N95-20771 #
PL-TR-93-2247 .... p 1600 N95-21679
PL-TR-93-3058 .... p 1284 N95-21678
PL-TR-94-1065 .... p 1327 N95-20905 #
PL-TR-94-2018 .... p 1426 N95-21932
PL-TR-94-2078 .... p 1425 N95-21833 #
PL-TR-94-2122 .... p 1415 N95-21308 #
PL-TR-94-2139 .... p 1501 N95-20773 #
PL-TR-94-2141-REV .... p 1364 N95-20036 #
PL-TR-94-2146 .... p 1203 N95-21831 #
PL-TR-94-2147 .... p 1430 N95-21177 #
PL-TR-94-2170 .... p 1290 N95-20376 #
PL-TR-94-2178 .... p 1414 N95-20878 #
PL-TR-94-2188 .... p 1430 N95-20974 #
PL-TR-94-2197 .... p 1545 N95-21832 #
PL-TR-94-2199 .... p 1292 N95-20904 #
PL-TR-94-2205 .... p 1364 N95-20069
PL-TR-94-2207 .... p 1413 N95-20377 #

PML-1994-B29 .... p 1222 N95-20906 #

PNL-SA-23032 .... p 1251 N95-20090 #
PNL-SA-23641 .... p 1251 N95-20088 #
PNL-SA-23879 .... p 1458 N95-20153 #
PNL-SA-23891 .... p 1401 N95-20089 #
PNL-SA-24143 .... p 1395 N95-21611 #
PNL-SA-24303 .... p 1520 N95-21375 #
PNL-SA-24421 .... p 1507 N95-20049 #
PNL-SA-24487 .... p 1364 N95-20320 #
PNL-SA-24676 .... p 1364 N95-20321 #
PNL-SA-24865 .... p 1232 N95-22115 #

PNL-10050 .... p 1236 N95-20268 #
PNL-10149 .... p 1406 N95-21487 #
PNL-10197 .... p 1389 N95-20903 #
PNL-9445 .... p 1403 N95-20834 #

PPG-1522 .... p 1559 N95-21403 #
PPG-1524 .... p 1559 N95-21404 #

PWA-FR23047 .... p 1283 N95-21161 #

R-679 .... p 1384 N95-20101 #
R-683 .... p 1384 N95-19975 #
R-684 .... p 1384 N95-20003

R/D-6011-MS-01 .... p 1268 N95-20392 #
R/D-6472-MS-01 .... p 1272 N95-20856 #
R/D-7022-MA-02-VOL-1 .... p 1380 N95-21171 #
R/D-7022-MA-02-VOL-2 .... p 1381 N95-21488 #
R/D-7130-EN-09 .... p 1546 N95-22002
R/D-7213-AN-01 .... p 1207 N95-20860 #
R/D-7234-EE-02 .... p 1376 N95-22164
R/D-7291-MS-02 .... p 1564 N95-20210 #
R/D-7376-EE-02 .... p 1541 N95-20249
R/D-7432-AN-02 .... p 1239 N95-20769

RAL-94-026 .... p 1537 N95-21647
RAL-94-046 .... p 1580 N95-21229
RAL-94-053 .... p 1518 N95-21220
RAL-94-054 .... p 1518 N95-21221
RAL-94-056 .... p 1526 N95-21939 #
RAL-94-057 .... p 1500 N95-21964
RAL-94-060 .... p 1373 N95-21226
RAL-94-062 .... p 1494 N95-21648
RAL-94-064 .... p 1580 N95-21030
RAL-94-067 .... p 1502 N95-22138
RAL-94-069 .... p 1495 N95-22317
RAL-94-070 .... p 1580 N95-21230
RAL-94-071 .... p 1518 N95-21225
RAL-94-074 .... p 1518 N95-21222
RAL-94-075 .... p 1518 N95-21227
RAL-94-076 .... p 1512 N95-20454
RAL-94-077 .... p 1518 N95-21224
RAL-94-078 .... p 1530 N95-22332
RAL-94-079 .... p 1571 N95-21228
RAL-94-080 .... p 1511 N95-20434
RAL-94-081 .... p 1413 N95-20453 *
RAL-94-082 .... p 1518 N95-21223
RAL-94-084 .... p 1465 N95-21231
RAL-94-085 .... p 1466 N95-21232
RAL-94-087 .... p 1456 N95-19928
RAL-94-088 .... p 1518 N95-21233
RAL-94-091 .... p 1475 N95-20435
RAL-94-096 .... p 1540 N95-22364
RAL-94-097 .... p 1427 N95-22368
RAL-94-101 .... p 1529 N95-22303
RAL-94-102 .... p 1526 N95-21965

RANA-93-07 .... p 1487 N95-19916 #
RANA-93-10 .... p 1487 N95-19915 #
RANA-93-11 .... p 1487 N95-19917 #
RANA-93-12 .... p 1493 N95-21423
RANA-94-01 .... p 1492 N95-21371
RANA-94-02 .... p 1495 N95-22151 #
RANA-94-07 .... p 1244 N95-21573 #
RANA-94-09 .... p 1493 N95-21574 #
RANA-94-10 .... p 1353 N95-21268 #

RCC-214-94 .... p 1310 N95-22247 #
RCC-254-94 .... p 1306 N95-21684

REPT-B-12 .... p 1472 N95-22328 #

REPT-003 .... p 1451 N95-22472 #
REPT-015FR .... p 1551 N95-20232 #
REPT-153-7645 .... p 1517 N95-21126 #
REPT-63819-93U/P60099-VOL-1 p 1453 N95-21566 #
REPT-93-549/3 .... p 1455 N95-21589
REPT-94-0073 .... p 1462 N95-20691 * #
REPT-94-42 .... p 1585 N95-21414
REPT-94-9SL2-LAFIL-R1 .... p 1312 N95-19894 #

RFP-4875 .... p 1503 N95-20267 #

RI/RD-93-176 .... p 1284 N95-21678

RIVM-343605002 .... p 1275 N95-21470 #
RIVM-482516002 .... p 1407 N95-21635
RIVM-610055001 .... p 1409 N95-21846
RIVM-679101-008 .... p 1411 N95-22381 #
RIVM-679101-009 .... p 1410 N95-22125 #
RIVM-679102017 .... p 1410 N95-22186 #
RIVM-679102018 .... p 1410 N95-22124
RIVM-719101015 .... p 1224 N95-22333
RIVM-722103001 .... p 1409 N95-21718
RIVM-723101001 .... p 1405 N95-21329
RIVM-723102003 .... p 1405 N95-21327
RIVM-723102004 .... p 1406 N95-21351
RIVM-723308001 .... p 1405 N95-21350
RIVM-731054001 .... p 1439 N95-21884 #

RL-TR-93-259 .... p 1581 N95-21928
RL-TR-94-102 .... p 1548 N95-22248
RL-TR-94-103 .... p 1369 N95-20389 #
RL-TR-94-112 .... p 1368 N95-20035 #
RL-TR-94-113 .... p 1302 N95-21405 #
RL-TR-94-118 .... p 1456 N95-22400 #
RL-TR-94-120 .... p 1369 N95-20378 #
RL-TR-94-123 .... p 1547 N95-22076 #
RL-TR-94-13 .... p 1335 N95-22144
RL-TR-94-157 .... p 1541 N95-20231 #
RL-TR-94-162 .... p 1473 N95-22402 #
RL-TR-94-163 .... p 1369 N95-20379 #
RL-TR-94-172 .... p 1311 N95-22401 #
RL-TR-94-180 .... p 1334 N95-22023 #
RL-TR-94-185 .... p 1547 N95-22205
RL-TR-94-187 .... p 1241 N95-21168 #
RL-TR-94-189 .... p 1261 N95-22035 #
RL-TR-94-190 .... p 1328 N95-21169 #
RL-TR-94-191 .... p 1484 N95-22203 #
RL-TR-94-23 .... p 1327 N95-20967
RL-TR-94-93 .... p 1479 N95-20057 #

RN-8025-1A-PT-2 .... p 1447 N95-22040 #

RPI/CHE/NASA-5-23390-5 .... p 1340 N95-20796 * #

RR-A332 .... p 1486 N95-22367 #
RR-A334 .... p 1486 N95-22366 #

RSS-MEMO-010395 .... p 1389 N95-20156 * #

R93081 .... p 1215 N95-21122

SAIC-94/1098 .... p 1548 N95-20029 #

SAND-90-2336 .... p 1489 N95-20222 #
SAND-91-1556 .... p 1549 N95-20075 #
SAND-93-0992 .... p 1397 N95-22335 #
SAND-93-1157 .... p 1386 N95-20833 #
SAND-93-1306C .... p 1265 N95-20138 #
SAND-93-2610C .... p 1591 N95-22167 #
SAND-93-3837C .... p 1506 N95-20026 #
SAND-93-3892C .... p 1535 N95-21328 #
SAND-93-3893C .... p 1565 N95-20340 #
SAND-93-3901C .... p 1599 N95-20144 #
SAND-93-3909C .... p 1218 N95-20785 #
SAND-93-3981 .... p 1378 N95-20053 #
SAND-93-4010C .... p 1264 N95-20047 #

SAND-94-0024 .... p 1302 N95-21448 #
SAND-94-0060C .... p 1384 N95-20077 #
SAND-94-0165C .... p 1564 N95-20087 #
SAND-94-0198C .... p 1265 N95-20121 #
SAND-94-0205C .... p 1314 N95-20338 #
SAND-94-0294 .... p 1573 N95-21449 #
SAND-94-0349 .... p 1371 N95-20832 #
SAND-94-0360C .... p 1566 N95-20399 #
SAND-94-0378C .... p 1387 N95-21396 #
SAND-94-0385C .... p 1558 N95-21247 #
SAND-94-0428C .... p 1328 N95-21139 #
SAND-94-0449C .... p 1334 N95-22086 #
SAND-94-0796C .... p 1509 N95-20206 #
SAND-94-0864C .... p 1563 N95-19954 #
SAND-94-0977C .... p 1537 N95-21603 #
SAND-94-0985C .... p 1474 N95-20150 #
SAND-94-0989C .... p 1477 N95-21843 #
SAND-94-1005C .... p 1488 N95-20141 #
SAND-94-1071C .... p 1575 N95-21991 #
SAND-94-1075C .... p 1311 N95-22407 #
SAND-94-1129C .... p 1242 N95-21309 #
SAND-94-1136C .... p 1205 N95-21520 #
SAND-94-1167C .... p 1314 N95-20286 #
SAND-94-1173-PT-1 .... p 1463 N95-20887 #
SAND-94-1205C .... p 1378 N95-20048 #
SAND-94-1228C .... p 1474 N95-20123 #
SAND-94-1245C .... p 1393 N95-20864 #
SAND-94-1273 .... p 1215 N95-20223 #
SAND-94-1280C .... p 1572 N95-21304 #
SAND-94-1302C .... p 1329 N95-21390 #
SAND-94-1306C .... p 1555 N95-21134 #
SAND-94-1318C .... p 1259 N95-21838 #
SAND-94-1354C .... p 1454 N95-22466 #
SAND-94-1375C .... p 1302 N95-21305 #
SAND-94-1396C .... p 1339 N95-20137 #
SAND-94-1417C .... p 1204 N95-20195 #
SAND-94-1533C .... p 1364 N95-20398 #
SAND-94-1539C .... p 1256 N95-21286 #
SAND-94-1554C .... p 1235 N95-20139 #
SAND-94-1607 .... p 1271 N95-20788 #
SAND-94-1670C .... p 1327 N95-20882 #
SAND-94-1702C .... p 1379 N95-20695 #
SAND-94-1716 .... p 1272 N95-20889 #
SAND-94-1742C .... p 1566 N95-20400 #
SAND-94-1758C .... p 1393 N95-20861 #
SAND-94-1769C .... p 1549 N95-20143 #
SAND-94-1774C .... p 1391 N95-20263 #
SAND-94-1775C .... p 1313 N95-20262 #
SAND-94-1781C .... p 1290 N95-20474 #
SAND-94-1826 .... p 1207 N95-21730 #
SAND-94-1853 .... p 1341 N95-20831 #
SAND-94-1862 .... p 1529 N95-22315 #
SAND-94-1910C .... p 1588 N95-20789 #
SAND-94-1911C .... p 1539 N95-22306 #
SAND-94-1913 .... p 1605 N95-22262 #
SAND-94-1925C .... p 1474 N95-20152 #
SAND-94-1926C .... p 1268 N95-20396 #
SAND-94-1929C .... p 1268 N95-20468 #
SAND-94-1944C .... p 1324 N95-20626 #
SAND-94-1978C .... p 1371 N95-20867 #
SAND-94-1998 .... p 1369 N95-20225 #
SAND-94-1999C .... p 1367 N95-21546 #
SAND-94-2005C .... p 1459 N95-20284 #
SAND-94-2008C .... p 1330 N95-21545 #
SAND-94-2009C .... p 1334 N95-22118 #
SAND-94-2033C .... p 1535 N95-21278 #
SAND-94-2035C .... p 1263 N95-19926 #
SAND-94-2065C .... p 1314 N95-20341 #
SAND-94-2068 .... p 1394 N95-20871 #
SAND-94-2079C .... p 1486 N95-22409 #
SAND-94-2130C .... p 1204 N95-20269 #
SAND-94-2156C .... p 1545 N95-21509 #
SAND-94-2177 .... p 1502 N95-22420 #
SAND-94-2195C .... p 1480 N95-20342 #
SAND-94-2200C .... p 1572 N95-21419 #
SAND-94-2201C .... p 1329 N95-21394 #
SAND-94-2222C .... p 1261 N95-22119 #
SAND-94-2239C .... p 1333 N95-21881 #
SAND-94-2293C .... p 1367 N95-21507 #
SAND-94-2314C .... p 1428 N95-20319 #
SAND-94-2332C .... p 1560 N95-21609 #
SAND-94-2334C .... p 1388 N95-22070 #
SAND-94-2349C .... p 1327 N95-20883 #
SAND-94-2354C .... p 1481 N95-20884 #
SAND-94-2376C .... p 1223 N95-21840 #
SAND-94-2431C .... p 1393 N95-20862 #
SAND-94-2437C .... p 1394 N95-21353 #
SAND-94-2439 .... p 1562 N95-22225 #
SAND-94-2453 .... p 1393 N95-20870 #
SAND-94-2469C .... p 1373 N95-21393 #
SAND-94-2472C .... p 1325 N95-20628 #
SAND-94-2498C .... p 1393 N95-20863 #
SAND-94-2542C .... p 1329 N95-21395 #
SAND-94-2548C .... p 1453 N95-21721 #
SAND-94-2572 .... p 1545 N95-21726 #
SAND-94-2676C .... p 1374 N95-21594 #
SAND-94-2716C .... p 1247 N95-22234 #
SAND-94-8233 .... p 1465 N95-21153 #
SAND-94-8239 .... p 1283 N95-21514 #
SAND-94-8244 .... p 1244 N95-21524 #
SAND-94-8613C .... p 1219 N95-20567 #
SAND-94-8619C .... p 1541 N95-20239 #
SAND-94-8620C .... p 1266 N95-20281 #
SAND-94-8691C .... p 1566 N95-20405 #
SAND-94-8704C .... p 1564 N95-20142 #
SAND-94-8704 .... p 1248 N95-22273 #
SAND-94-8709C .... p 1283 N95-21513 #
SAND-94-8715C .... p 1413 N95-20397 #
SAND-94-8718C .... p 1301 N95-21277 #
SAND-94-8728C .... p 1477 N95-21505 #
SAND-94-8730C .... p 1243 N95-21512 #
SAND-95-8424C .... p 1272 N95-20895 #
SAND-95-8426C .... p 1376 N95-22169 #

SC71022.FR .... p 1544 N95-20803 #

SECA-FR-94-18 .... p 1221 N95-20124 * #

SER-A-94-A15 .... p 1352 N95-21106

SGD-600-PT-1 .... p 1603 N95-20713 #
SGD-600-PT-2 .... p 1603 N95-20722 #
SGD-601-PT-1 .... p 1603 N95-20919 #
SGD-601-PT-2 .... p 1603 N95-20829 #

SIP-0063 .... p 1556 N95-21162 #
SIP-0065 .... p 1556 N95-21165 #
SIP-0067 .... p 1556 N95-21164 #

SISSA-83/93/CM/MB .... p 1581 N95-21993 #

SMC-TR-94-26 .... p 1575 N95-21916
SMC-TR-94-36 .... p 1404 N95-21150 #
SMC-TR-94-38 .... p 1284 N95-22227 #
SMC-TR-94-39 .... p 1309 N95-22134 #
SMC-TR-94-40 .... p 1427 N95-22249 #
SMC-TR-99-22 .... p 1307 N95-21985

SOC-R875-003-1094 .... p 1383 N95-22037 #

SP-RAPP-1993:56 .... p 1241 N95-21179 #
SP-RAPP-1994:24 .... p 1386 N95-21133 #

SP-RAPPORT-1994:20 .... p 1387 N95-21557

SPC-93091-CMC .... p 1470 N95-21972

SR-1-REV .... p 1364 N95-20036 #
SR-1 .... p 1430 N95-21177 #
SR-1 .... p 1203 N95-21831 #
SR-1 .... p 1425 N95-21833 #
SR-1 .... p 1426 N95-21932
SR-2 .... p 1501 N95-20773 #
SR-3 .... p 1414 N95-20878 #
SR-5 .... p 1292 N95-20904 #
SR-7 .... p 1413 N95-20377 #
SR-8 .... p 1290 N95-20376 #

SRL-0144-RR .... p 1303 N95-21491

SRTC-MTS-94-3017 .... p 1251 N95-20079 #
SRTC-MTS-94-3036 .... p 1252 N95-20216 #

SSCL-678 .... p 1538 N95-21733 #

STF10-A94001 .... p 1470 N95-22016
STF15-A94004 .... p 1356 N95-22017
STF19-A93014 .... p 1577 N95-22166
STF19-A94007 .... p 1574 N95-21636
STF19-A94010 .... p 1575 N95-21949
STF20-A93218 .... p 1286 N95-21027
STF21-A93106 .... p 1242 N95-21426
STF24-A94025 .... p 1276 N95-21650
STF24-A94039 .... p 1288 N95-21651
STF24-A94558 .... p 1258 N95-21652
STF24-A94568 .... p 1277 N95-21873
STF24-A94572 .... p 1258 N95-21653
STF31-A94020 .... p 1455 N95-22018
STF33-A94020 .... p 1468 N95-21654
STF33-A94031 .... p 1354 N95-21656
STF33-A94036 .... p 1469 N95-21655
STF48-A94009 .... p 1484 N95-22015
STF62-A94004 .... p 1288 N95-22014 #

SU-EFML-94-1 .... p 1434 N95-21293

SU-SLAC-PUB-6411 .... p 1599 N95-21245 #
SU-SLAC-PUB-6504 .... p 1534 N95-21246 #
SU-SLAC-PUB-6513 .... p 1519 N95-21248 #
SU-SLAC-PUB-6516 .... p 1482 N95-21249 #
SU-SLAC-PUB-6521 .... p 1519 N95-21250 #
SU-SLAC-PUB-6522 .... p 1536 N95-21332 #
SU-SLAC-PUB-6559 .... p 1538 N95-22155 #
SU-SLAC-PUB-6561 .... p 1536 N95-21334 #
SU-SLAC-PUB-6562 .... p 1536 N95-21335 #
SU-SLAC-PUB-6570 .... p 1520 N95-21336 #
SU-SLAC-PUB-6571 .... p 1532 N95-20388 #
SU-SLAC-PUB-6578 .... p 1536 N95-21337 #
SU-SLAC-PUB-6581 .... p 1534 N95-21253 #
SU-SLAC-PUB-6582 .... p 1507 N95-20034 #
SU-SLAC-PUB-6586 .... p 1525 N95-21727 #
SU-SLAC-PUB-6590 .... p 1535 N95-21254 #
SU-SLAC-PUB-6595 .... p 1527 N95-22152 #
SU-SLAC-PUB-6665 .... p 1523 N95-21525 #
SU-SLAC-PUB-6666 .... p 1301 N95-21241 #
SU-SLAC-PUB-6719 .... p 1528 N95-22239 #
SU-SLAC-PUB-693 .... p 1535 N95-21255 #

SU-TR-479 .... p 1499 N95-21946
SU-TR-480 .... p 1499 N95-21945

SU-0001 .... p 1255 N95-20909 #

SWRI-17-4665 .... p 1382 N95-20414
SWRI-3178-4.23 .... p 1284 N95-21966 #
SWRI-3178-4.8 .... p 1282 N95-20253 #

TDCK-93-2570 .... p 1222 N95-20906 #
TDCK-94-0052 .... p 1449 N95-20609 #
TDCK-94-0166 .... p 1475 N95-20499 #
TDCK-94-1395 .... p 1291 N95-20692 #

TIOS-94-09 .... p 1546 N95-21870
TIOS-94/13 .... p 1308 N95-22087

TKK-F-A726 .... p 1301 N95-21107 #
TKK-F-A727 .... p 1447 N95-22371 #
TKK-F-A728 .... p 1329 N95-21326 #
TKK-F-A729 .... p 1445 N95-21348 #

TKK-F-B151 .... p 1443 N95-20971 #

TKK-NEMO-25 .... p 1397 N95-22337 #

TKK-V-B87 .... p 1255 N95-21111 #
TKK-V-B88 .... p 1263 N95-22374 #
TKK-V-B90 .... p 1240 N95-21110 #
TKK-V-B94 .... p 1354 N95-21649

TKO-B116 .... p 1472 N95-22372 #

TKO-C65 .... p 1472 N95-22310 #

TL-AS-94-07 .... p 1433 N95-20999 #

TN-BN-1175 .... p 1480 N95-20083 #
TN-BN-1178 .... p 1489 N95-20274 #

TNO-TM-1994-B-10 .... p 1449 N95-20609 #

TOP-1-1-004 .... p 1367 N95-21680
TOP-1-2-616 .... p 1235 N95-20230 #
TOP-2-2-613 .... p 1292 N95-20858 #

TR-10 .... p 1544 N95-20876
TR-10 .... p 1522 N95-21492
TR-11 .... p 1245 N95-21827
TR-12 .... p 1253 N95-20577
TR-12 .... p 1270 N95-20689
TR-12 .... p 1547 N95-22074
TR-13 .... p 1239 N95-20712
TR-14 .... p 1224 N95-21911 #
TR-15 .... p 1365 N95-20413
TR-15 .... p 1569 N95-20714
TR-1672 .... p 1472 N95-22201 #
TR-17-ONR .... p 1568 N95-20594
TR-17 .... p 1265 N95-20183 #
TR-18 .... p 1268 N95-20428 #
TR-18 .... p 1513 N95-20585
TR-19 .... p 1513 N95-20586
TR-19 .... p 1270 N95-20671
TR-2-ONR .... p 1507 N95-20097 #
TR-20 .... p 1567 N95-20544 #
TR-20 .... p 1269 N95-20580
TR-20 .... p 1241 N95-21217 #
TR-21 .... p 1268 N95-20442 #
TR-21 .... p 1328 N95-21218 #
TR-22 .... p 1273 N95-20978
TR-23 .... p 1271 N95-20709
TR-28-ONR .... p 1223 N95-20590
TR-30-ONR .... p 1223 N95-20592
TR-44-ONR .... p 1238 N95-20563
TR-59 .... p 1450 N95-22052 #
TR-67 .... p 1238 N95-20555 #
TR-68 .... p 1568 N95-20553 #
TR-69 .... p 1513 N95-20554 #
TR-6 .... p 1516 N95-20994
TR-6 .... p 1330 N95-21490

TR-6 .... p 1224 N95-22252 #
TR-71 .... p 1239 N95-20668 #
TR-72 .... p 1517 N95-21127 #
TR-75 .... p 1265 N95-20094
TR-77 .... p 1241 N95-21124 #
TR-77 .... p 1578 N95-22286 #
TR-78 .... p 1280 N95-22259 #
TR-78 .... p 1281 N95-22470 #
TR-79 .... p 1567 N95-20483 #
TR-7 .... p 1246 N95-21879 #
TR-93(3505)-1 .... p 1309 N95-22134 #
TR-93(3925)-1 .... p 1575 N95-21916
TR-93(3925)-6 .... p 1307 N95-21985
TR-937 .... p 1300 N95-21099
TR-94(4231)-4 .... p 1284 N95-22227 #
TR-94(4231)-9 .... p 1404 N95-21150 #
TR-94(4911)-1 .... p 1427 N95-22249 #
TR-94-1424 .... p 1290 N95-20306 #
TR-94 .... p 1365 N95-20431
TR-95 .... p 1324 N95-20587
TR-9 .... p 1245 N95-21826

TRB/TRR-1428 .... p 1199 N95-19967 #

TW-93-13 .... p 1492 N95-21421

UCRL-CR-116369 .... p 1576 N95-22084 #
UCRL-CR-117680 .... p 1309 N95-22241 #
UCRL-CR-117756 .... p 1415 N95-21511 #

UCRL-ID-115123 .... p 1376 N95-22301 #
UCRL-ID-115719 .... p 1250 N95-19900 #
UCRL-ID-116218 .... p 1460 N95-20387 #
UCRL-ID-116263 .... p 1559 N95-21451 #
UCRL-ID-116660 .... p 1541 N95-20352 #
UCRL-ID-116975 .... p 1562 N95-22221 #
UCRL-ID-117344 .... p 1550 N95-20189 #
UCRL-ID-117952 .... p 1528 N95-22222 #
UCRL-ID-118023 .... p 1460 N95-20351 #
UCRL-ID-118061 .... p 1402 N95-20353 #
UCRL-ID-118063 .... p 1413 N95-20354 #
UCRL-ID-118065 .... p 1402 N95-20355 #
UCRL-ID-118068 .... p 1286 N95-20356 #
UCRL-ID-118276 .... p 1511 N95-20444 #
UCRL-ID-118498 .... p 1528 N95-22223 #

UCRL-JC-114328 .... p 1541 N95-20218 #
UCRL-JC-114400 .... p 1368 N95-19986 #
UCRL-JC-114511 .... p 1428 N95-20140 #
UCRL-JC-115104 .... p 1412 N95-19985 #
UCRL-JC-115131 .... p 1433 N95-20420 #
UCRL-JC-115148 .... p 1372 N95-21135 #
UCRL-JC-115292-REV-1 .... p 1542 N95-20489 #
UCRL-JC-115364 .... p 1253 N95-20447 #
UCRL-JC-115555 .... p 1552 N95-20318 #
UCRL-JC-115579 .... p 1557 N95-21166 #
UCRL-JC-115580 .... p 1371 N95-20817 #
UCRL-JC-115583 .... p 1557 N95-21207 #
UCRL-JC-115585 .... p 1534 N95-21208 #
UCRL-JC-115586 .... p 1551 N95-20219 #
UCRL-JC-115588 .... p 1540 N95-22469 #
UCRL-JC-115676 .... p 1313 N95-20119 #
UCRL-JC-115741 .... p 1567 N95-20448 #
UCRL-JC-115990 .... p 1429 N95-20381 #
UCRL-JC-116145 .... p 1517 N95-21174 #
UCRL-JC-116181 .... p 1542 N95-20364 #
UCRL-JC-116182 .... p 1562 N95-22191 #
UCRL-JC-116195 .... p 1531 N95-20015 #
UCRL-JC-116199 .... p 1552 N95-20362 #
UCRL-JC-116211 .... p 1553 N95-20363 #
UCRL-JC-116231-REV-1 .... p 1353 N95-21182 #
UCRL-JC-116339 .... p 1251 N95-20122 #
UCRL-JC-116340 .... p 1301 N95-21205 #
UCRL-JC-116430 .... p 1542 N95-20450 #
UCRL-JC-116598 .... p 1385 N95-20237 #
UCRL-JC-116635 .... p 1473 N95-22426 #
UCRL-JC-116774 .... p 1555 N95-20813 #
UCRL-JC-116836 .... p 1373 N95-21210 #
UCRL-JC-116838 .... p 1337 N95-22427 #
UCRL-JC-116879 .... p 1562 N95-22300 #
UCRL-JC-116927 .... p 1369 N95-20335 #
UCRL-JC-116930 .... p 1327 N95-20854 #
UCRL-JC-116963 .... p 1544 N95-21392 #
UCRL-JC-117078 .... p 1371 N95-20783 #
UCRL-JC-117162 .... p 1263 N95-22408 #
UCRL-JC-117168 .... p 1276 N95-21662 #
UCRL-JC-117330 .... p 1377 N95-22312 #
UCRL-JC-117382 .... p 1550 N95-20190 #
UCRL-JC-117395 .... p 1557 N95-21206 #
UCRL-JC-117399 .... p 1534 N95-21209 #
UCRL-JC-117433 .... p 1542 N95-20403 #
UCRL-JC-117440 .... p 1274 N95-21175 #
UCRL-JC-117490 .... p 1531 N95-20120 #
UCRL-JC-117498 .... p 1551 N95-20315 #
UCRL-JC-117539 .... p 1567 N95-20449 #
UCRL-JC-117547 .... p 1452 N95-21358 #
UCRL-JC-117548 .... p 1453 N95-21637 #
UCRL-JC-117584 .... p 1262 N95-22313 #
UCRL-JC-117600 .... p 1266 N95-20316 #
UCRL-JC-117602 .... p 1272 N95-20892 #
UCRL-JC-117604 .... p 1267 N95-20317 #
UCRL-JC-117613 .... p 1520 N95-21360 #
UCRL-JC-117630 .... p 1232 N95-22126 #
UCRL-JC-117793 .... p 1374 N95-21663 #
UCRL-JC-117795 .... p 1372 N95-21173 #
UCRL-JC-117808 .... p 1543 N95-20612 #
UCRL-JC-117810 .... p 1237 N95-20386 #
UCRL-JC-117820 .... p 1354 N95-21387 #
UCRL-JC-117946 .... p 1337 N95-22421 #
UCRL-JC-118073 .... p 1493 N95-21564 #
UCRL-JC-118148 .... p 1376 N95-22121 #
UCRL-JC-118149 .... p 1389 N95-21552 #
UCRL-JC-118150 .... p 1389 N95-21433 #
UCRL-JC-118161 .... p 1533 N95-20784 #
UCRL-JC-118203 .... p 1377 N95-22343 #
UCRL-JC-118226 .... p 1367 N95-21478 #
UCRL-JC-118234 .... p 1459 N95-20255 #
UCRL-JC-118289 .... p 1310 N95-22299 #
UCRL-JC-118330 .... p 1600 N95-21479 #
UCRL-JC-118432 .... p 1545 N95-21510 #

UCRL-52000-94-6 .... p 1219 N95-20148 #
UCRL-53809-93 .... p 1599 N95-20145 #

UCSB-08-075892 .... p 1333 N95-21917

UCSD-955220 .... p 1515 N95-20893 #

UDR-TR-93-81-2 .... p 1278 N95-21969

UFIFT-HEP-93-24-TASK-A .... p 1512 N95-20469 #

UMIST/PHYS/2 .... p 1428 N95-20008 #

UMR-FDB-38 .... p 1574 N95-21599

UMTRI-94-15 .... p 1380 N95-21157 #

US-PATENT-APPL-SN-010685 ..... p 1577 N95-22137
US-PATENT-APPL-SN-014928 ..... p 1266 N95-20291
US-PATENT-APPL-SN-016324 ..... p 1355 N95-21902
US-PATENT-APPL-SN-025952 ..... p 1289 N95-20270
US-PATENT-APPL-SN-041388 ..... p 1546 N95-21905
US-PATENT-APPL-SN-045143 ..... p 1333 N95-21865
US-PATENT-APPL-SN-062864 ..... p 1274 N95-21155
US-PATENT-APPL-SN-063227 ..... p 1477 N95-21674
US-PATENT-APPL-SN-066745 ..... p 1375 N95-21903
US-PATENT-APPL-SN-067763 ..... p 1201 N95-21864
US-PATENT-APPL-SN-069820 ..... p 1356 N95-22060
US-PATENT-APPL-SN-081712 ..... p 1315 N95-20436
US-PATENT-APPL-SN-081891 ..... p 1338 N95-19933 * #
US-PATENT-APPL-SN-086079 ..... p 1326 N95-20730
US-PATENT-APPL-SN-098094 ..... p 1567 N95-20461
US-PATENT-APPL-SN-104707 ..... p 1504 N95-20296
US-PATENT-APPL-SN-104952 ..... p 1252 N95-20201
US-PATENT-APPL-SN-107431 ..... p 1325 N95-20663
US-PATENT-APPL-SN-108131 ..... p 1546 N95-21898
US-PATENT-APPL-SN-123959 ..... p 1544 N95-21465
US-PATENT-APPL-SN-127567 ..... p 1378 N95-20295
US-PATENT-APPL-SN-128508 ..... p 1314 N95-20298
US-PATENT-APPL-SN-128785 ..... p 1226 N95-20292
US-PATENT-APPL-SN-128786 ..... p 1227 N95-20459
US-PATENT-APPL-SN-130940 ..... p 1301 N95-21156
US-PATENT-APPL-SN-130941 ..... p 1307 N95-21910
US-PATENT-APPL-SN-134444 ..... p 1383 N95-20764 * #
US-PATENT-APPL-SN-147238 ..... p 1303 N95-21464
US-PATENT-APPL-SN-156192 ..... p 1325 N95-20726
US-PATENT-APPL-SN-159169 ..... p 1545 N95-21825
US-PATENT-APPL-SN-170962 ..... p 1278 N95-21907
US-PATENT-APPL-SN-193688 ..... p 1328 N95-21118
US-PATENT-APPL-SN-193690 ..... p 1365 N95-21117
US-PATENT-APPL-SN-194600 ..... p 1332 N95-21775
US-PATENT-APPL-SN-195500 ..... p 1441 N95-20408 * #
US-PATENT-APPL-SN-199868 ..... p 1547 N95-22089
US-PATENT-APPL-SN-200032 ..... p 1506 N95-22088
US-PATENT-APPL-SN-202628 ..... p 1504 N95-21119
US-PATENT-APPL-SN-207311 ..... p 1455 N95-21116
US-PATENT-APPL-SN-207445 ..... p 1274 N95-21154
US-PATENT-APPL-SN-209345 ..... p 1333 N95-21906
US-PATENT-APPL-SN-215879 ..... p 1336 N95-22418
US-PATENT-APPL-SN-219552 ..... p 1476 N95-21504
US-PATENT-APPL-SN-219553 ..... p 1476 N95-21307
US-PATENT-APPL-SN-219554 ..... p 1591 N95-22098 #
US-PATENT-APPL-SN-219555 ..... p 1478 N95-22090
US-PATENT-APPL-SN-219556 ..... p 1476 N95-21496
US-PATENT-APPL-SN-219557 ..... p 1478 N95-22146
US-PATENT-APPL-SN-226517 ..... p 1454 N95-22099 #
US-PATENT-APPL-SN-243665 ..... p 1443 N95-20763 * #
US-PATENT-APPL-SN-248611 ..... p 1251 N95-20068 * #
US-PATENT-APPL-SN-250768 ..... p 1279 N95-22057
US-PATENT-APPL-SN-251146 ..... p 1377 N95-22304
US-PATENT-APPL-SN-266758 ..... p 1577 N95-22103
US-PATENT-APPL-SN-274183 ..... p 1331 N95-21671
US-PATENT-APPL-SN-287023 ..... p 1306 N95-21672
US-PATENT-APPL-SN-287026 ..... p 1306 N95-21834
US-PATENT-APPL-SN-287027 ..... p 1545 N95-21673
US-PATENT-APPL-SN-288102 ..... p 1378 N95-20151 * #
US-PATENT-APPL-SN-288112 ..... p 1378 N95-20409 * #
US-PATENT-APPL-SN-299385 ..... p 1268 N95-20407 * #
US-PATENT-APPL-SN-306556 ..... p 1229 N95-21008 * #
US-PATENT-APPL-SN-316708 ..... p 1383 N95-20616 * #
US-PATENT-APPL-SN-319142 ..... p 1268 N95-20410 * #
US-PATENT-APPL-SN-343740 ..... p 1383 N95-20764 * #
US-PATENT-APPL-SN-359320 ..... p 1215 N95-20080 * #
US-PATENT-APPL-SN-473258 ..... p 1590 N95-21463
US-PATENT-APPL-SN-528194 ..... p 1307 N95-21908
US-PATENT-APPL-SN-643385 ..... p 1544 N95-21466
US-PATENT-APPL-SN-643632 ..... p 1333 N95-21901
US-PATENT-APPL-SN-707465 ..... p 1307 N95-21904
US-PATENT-APPL-SN-751939 ..... p 1480 N95-20202
US-PATENT-APPL-SN-752248 ..... p 1266 N95-20293
US-PATENT-APPL-SN-758972 ..... p 1266 N95-20294
US-PATENT-APPL-SN-772059 ..... p 1313 N95-20280
US-PATENT-APPL-SN-809349 ..... p 1334 N95-22030
US-PATENT-APPL-SN-813563 ..... p 1501 N95-20731
US-PATENT-APPL-SN-854112 ..... p 1326 N95-20729
US-PATENT-APPL-SN-864794 ..... p 1381 N95-22034
US-PATENT-APPL-SN-866920 ..... p 1333 N95-21900
US-PATENT-APPL-SN-897630 ..... p 1576 N95-22059
US-PATENT-APPL-SN-899520 ..... p 1504 N95-20724
US-PATENT-APPL-SN-921863 ..... p 1544 N95-21100
US-PATENT-APPL-SN-932430 ..... p 1325 N95-20727
US-PATENT-APPL-SN-936681 ..... p 1543 N95-20728
US-PATENT-APPL-SN-938920 ..... p 1396 N95-21899
US-PATENT-APPL-SN-954521 ..... p 1306 N95-21835
US-PATENT-APPL-SN-954805 ..... p 1233 N95-22467
US-PATENT-APPL-SN-976033 ..... p 1339 N95-20297
US-PATENT-APPL-SN-985988 ..... p 1268 N95-20460

US-PATENT-CLASS-138-174 .... p 1226 N95-20292
US-PATENT-CLASS-138-42 .... p 1504 N95-20724
US-PATENT-CLASS-148-237 .... p 1252 N95-20201
US-PATENT-CLASS-156-345 .... p 1375 N95-21903
US-PATENT-CLASS-165-32 .... p 1315 N95-20436
US-PATENT-CLASS-210-519 .... p 1339 N95-20297
US-PATENT-CLASS-244-21 .... p 1201 N95-21864
US-PATENT-CLASS-250-207 .... p 1325 N95-20726
US-PATENT-CLASS-257-10 .... p 1314 N95-20298
US-PATENT-CLASS-285-370 .... p 1381 N95-22034
US-PATENT-CLASS-29-434 .... p 1227 N95-20459
US-PATENT-CLASS-307-241 .... p 1326 N95-20729
US-PATENT-CLASS-310-26 .... p 1333 N95-21901
US-PATENT-CLASS-310-358 .... p 1268 N95-20460
US-PATENT-CLASS-310-40 .... p 1325 N95-20727
US-PATENT-CLASS-324-158 .... p 1333 N95-21900
US-PATENT-CLASS-324-71 .... p 1577 N95-22137
US-PATENT-CLASS-330-251 .... p 1326 N95-20730
US-PATENT-CLASS-342-160 .... p 1307 N95-21904
US-PATENT-CLASS-342-378 .... p 1307 N95-21908
US-PATENT-CLASS-342-384 .... p 1289 N95-20270
US-PATENT-CLASS-356-345 .... p 1306 N95-21835
US-PATENT-CLASS-356-73 .... p 1544 N95-21466
US-PATENT-CLASS-359-326 .... p 1544 N95-21465
US-PATENT-CLASS-364-149 .... p 1480 N95-20202
US-PATENT-CLASS-364-728.03 .. p 1313 N95-20280
US-PATENT-CLASS-367-135 .... p 1333 N95-21865
US-PATENT-CLASS-367-140 .... p 1504 N95-20296
US-PATENT-CLASS-367-1 .... p 1233 N95-22467
US-PATENT-CLASS-372-22 .... p 1546 N95-21898
US-PATENT-CLASS-372-84 .... p 1333 N95-21906
US-PATENT-CLASS-377-44 .... p 1334 N95-22030
US-PATENT-CLASS-378-122 .... p 1546 N95-21905
US-PATENT-CLASS-395-12.9 ...... p 1590 N95-21463
US-PATENT-CLASS-395-550 .... p 1501 N95-20731
US-PATENT-CLASS-428-156 .... p 1356 N95-22060
US-PATENT-CLASS-437-16 .... p 1576 N95-22059
US-PATENT-CLASS-437-2 .... p 1396 N95-21899
US-PATENT-CLASS-439-91 .... p 1325 N95-20663
US-PATENT-CLASS-501-92 .... p 1266 N95-20291
US-PATENT-CLASS-505-125 .... p 1567 N95-20461
US-PATENT-CLASS-505-238 .... p 1278 N95-21907
US-PATENT-CLASS-523-137 .... p 1543 N95-20728
US-PATENT-CLASS-525-123 .... p 1266 N95-20294
US-PATENT-CLASS-525-454 .... p 1266 N95-20293
US-PATENT-CLASS-60-221 .... p 1355 N95-21902
US-PATENT-CLASS-62-467 .... p 1378 N95-20295

US-PATENT-5,288,114 .... p 1381 N95-22034
US-PATENT-5,301,219 .... p 1334 N95-22030
US-PATENT-5,325,913 .... p 1315 N95-20436
US-PATENT-5,326,474 .... p 1339 N95-20297
US-PATENT-5,327,745 .... p 1378 N95-20295
US-PATENT-5,327,941 .... p 1504 N95-20724
US-PATENT-5,328,957 .... p 1266 N95-20294
US-PATENT-5,329,110 .... p 1325 N95-20726
US-PATENT-5,329,245 .... p 1326 N95-20730
US-PATENT-5,329,442 .... p 1480 N95-20202
US-PATENT-5,330,918 .... p 1396 N95-21899

US-PATENT-5,331,062 .... p 1266 N95-20293
US-PATENT-5,331,236 .... p 1325 N95-20727
US-PATENT-5,331,273 .... p 1333 N95-21900
US-PATENT-5,332,681 .... p 1576 N95-22059
US-PATENT-5,332,723 .... p 1567 N95-20461
US-PATENT-5,333,142 .... p 1546 N95-21898
US-PATENT-5,333,444 .... p 1355 N95-21902
US-PATENT-5,334,629 .... p 1543 N95-20728
US-PATENT-5,334,853 .... p 1314 N95-20298
US-PATENT-5,334,881 .... p 1326 N95-20729
US-PATENT-5,334,903 .... p 1268 N95-20460
US-PATENT-5,335,258 .... p 1546 N95-21905
US-PATENT-5,335,886 .... p 1201 N95-21864
US-PATENT-5,337,053 .... p 1303 N95-21464
US-PATENT-5,337,288 .... p 1233 N95-22467
US-PATENT-5,338,374 .... p 1252 N95-20201
US-PATENT-5,339,025 .... p 1577 N95-22137
US-PATENT-5,339,189 .... p 1544 N95-21465
US-PATENT-5,339,285 .... p 1333 N95-21865
US-PATENT-5,341,056 .... p 1333 N95-21901
US-PATENT-5,341,205 .... p 1544 N95-21466
US-PATENT-5,341,463 .... p 1590 N95-21463
US-PATENT-5,346,745 .... p 1356 N95-22060
US-PATENT-5,347,281 .... p 1307 N95-21904
US-PATENT-5,347,496 .... p 1504 N95-20296
US-PATENT-5,347,645 .... p 1501 N95-20731
US-PATENT-5,348,052 .... p 1226 N95-20292
US-PATENT-5,348,609 .... p 1375 N95-21903
US-PATENT-5,348,917 .... p 1266 N95-20291
US-PATENT-5,348,937 .... p 1278 N95-21907
US-PATENT-5,349,437 .... p 1306 N95-21835
US-PATENT-5,349,550 .... p 1313 N95-20280
US-PATENT-5,349,738 .... p 1227 N95-20459
US-PATENT-5,350,308 .... p 1325 N95-20663
US-PATENT-5,351,057 .... p 1307 N95-21908
US-PATENT-5,351,058 .... p 1289 N95-20270
US-PATENT-5,351,260 .... p 1333 N95-21906

USAARL-94-16 .... p 1450 N95-21927
USAARL-94-46 .... p 1454 N95-22045 #
USAARL-94-47 .... p 1547 N95-22044 #

USAATCOM-TR-94-D-11 .... p 1452 N95-20973 #

USARIEM-TN95-2 .... p 1446 N95-22004 #

USATEC-R-240 .... p 1204 N95-20497 #

USCG-D-04-94 .... p 1408 N95-21685
USCG-D-05-94 .... p 1259 N95-21687
USCG-D-07-94 .... p 1306 N95-21686

UTHSCSA-OPH-94-01 .... p 1443 N95-20848 #

UTRC-R94-970439-2 .... p 1225 N95-19919

VTT/PUB-160 .... p 1232 N95-22158
VTT/PUB-179 .... p 1451 N95-20276
VTT/PUB-180 .... p 1444 N95-21007

VTT/RN-1538 .... p 1427 N95-22095
VTT/RN-1545, ... p 1380 N95-21416
VTT/RN-1550 .... p 1380 N95-21446
VTT/RN-1552 .... p 1286 N95-21333
VTT/RN-1573 .... p 1236 N95-20290

VTT/SYMPOSIUM-140 .... p 1262 N95-22174
VTT/SYMPOSIUM-146 .... p 1450 N95-21284

W-9404 .... p 1491 N95-20830 #
W-9406 .... p 1492 N95-21318 #

WAPD-T-3033 .... p 1261 N95-22048 #

WCTC-94-9SL2-SUPER-R1 .... p 1331 N95-21693

WES/IR/ITL-94-2 .... p 1459 N95-20310

WES/MP/EL-A-94-1 .... p 1409 N95-21914

WES/TR/GL-94-12 .... p 1215 N95-19955 #

WES/TR/REMR-HY-12 .... p 1341 N95-20843 #

WHC-SA-2098 .... p 1237 N95-20470 #
WHC-SA-2518 .... p 1366 N95-21138 #

WHC-SD-SNF-ER-004 .... p 1257 N95-21452 #

WHC-SD-WM-ATR-089 .... p 1364 N95-20224 #

WHC-SD-WM-TA-158 .... p 1243 N95-21473 #

WHOI-CONTRIB-8394 .... p 1433 N95-20458

WHOI-93-19-VOL-8 .... p 1436 N95-22073

WHOI-93-31 .... p 1434 N95-21677
WHOI-93-36 .... p 1435 N95-21918
WHOI-93-38 .... p 1435 N95-21943
WHOI-93-42 .... p 1436 N95-22072 *
WHOI-93-44 .... p 1435 N95-21681
WHOI-93-48 .... p 1433 N95-20433
WHOI-93-49 .... p 1435 N95-21682
WHOI-93-50 .... p 1426 N95-21944
WHOI-93-52 .... p 1434 N95-21306

WL-TM-94-3039-VOL-1 .... p 1202 N95-21877
WL-TM-94-3112-VOL-4-PT-1 .... p 1215 N95-21214 #

WL-TR-92-2032 .... p 1387 N95-21967
WL-TR-93-2116 .... p 1553 N95-20411
WL-TR-93-2126-2 .... p 1278 N95-21969
WL-TR-93-3510 .... p 1287 N95-21598
WL-TR-93-4125 .... p 1382 N95-20414
WL-TR-93-8029 .... p 1279 N95-21976
WL-TR-94-2012 .... p 1514 N95-20804 #
WL-TR-94-2033 .... p 1283 N95-21161 #
WL-TR-94-2044 .... p 1339 N95-20250 #
WL-TR-94-3030 .... p 1483 N95-21913
WL-TR-94-3039 .... p 1214 N95-20004 #
WL-TR-94-3123 .... p 1220 N95-22204 #
WL-TR-94-3134 .... p 1199 N95-22046 #
WL-TR-94-4014 .... p 1386 N95-20615
WL-TR-94-4070 .... p 1266 N95-20251
WL-TR-94-5005 .... p 1546 N95-21975
WL-TR-94-5008 .... p 1383 N95-21933

WRAIR-TR-94-0019 .... p 1451 N95-22324 #
WRAIR-TR-94-0020 .... p 1451 N95-22323 #

WSRC-MS-94-0101P .... p 1382 N95-22356 #
WSRC-MS-94-0259 .... p 1579 N95-20028 #
WSRC-MS-94-0394 .... p 1592 N95-22263 #

WSRC-TR-94-0449 .... p 1257 N95-21303 #
WSRC-TR-94-0468 .... p 1413 N95-20455 #
WSRC-TR-94-059 .... p 1235 N95-20215 #

WSU/ATR/662480 .... p 1450 N95-21192 #

Y/DW-1332 .... p 1243 N95-21472 #

Y/DZ-1113/R1 .... p 1244 N95-21571 #

Z-332 .... p 1259 N95-21739 #
Z-333 .... p 1259 N95-21740
Z-337 .... p 1263 N95-22396 #

APPENDIX

NASA SCIENTIFIC AND TECHNICAL INFORMATION OFFICE PRODUCTS AND SERVICES

The NASA Scientific and Technical Information (STI) Office provides for the collection and announcement of aerospace-related reports and literature obtained worldwide through agreements and exchanges. The result of the collection is the comprehensive NASA STI Database that covers aeronautics, space, and supporting disciplines.

The STI Database, documents generated or obtained by NASA, and products and services derived from or supporting the database are made available to the NASA research community and to the public. Descriptions and sources of these items are presented in the following pages.

Scientific and Technical Aerospace Reports (STAR) is an abstract journal, listing citations with abstracts for aerospace-related reports obtained from worldwide sources. *STAR* is issued on the first of each month, and announces current documents that have been entered into the NASA STI Database during the previous month. The reports are of the following types:

- NASA, NASA contractor, and NASA grantee reports;
- Reports issued by other U.S. Government agencies, domestic and foreign institutions, universities, and private firms;
- Translations in report form;
- NASA-owned patents and patent applications
- Other U.S. Government agency and foreign patents and patent applications
- Domestic and foreign dissertations and theses.

Journal, book, and conference literature, journal translations, and certain foreign dissertations having the same subject scope as *STAR* are announced in a companion journal, *NASA Open Volumes on Aerospace (NOVA). NOVA* is issued on the 15th of each month and is available from the NASA Center for AeroSpace Information, at the address below.

ELIGIBILITY AND REGISTRATION FOR NASA STI PRODUCTS AND SERVICES

Organizations of the type listed below that have registered with NASA can receive products and services.

- NASA offices and installations, contractors, subcontractors, grantees, and consultants;
- Other U.S. Government agencies and their contractors;
- Libraries in the United States that have arrangements with NASA to maintain collections of NASA documents for public reference;
- Other organizations in the United States having a need for NASA documents in work related to aeronautics and space research;
- Organizations abroad that have established reciprocal documents exchange arrangements with NASA.

The central service points—central points of document acquisition and control within qualified organizations—or individuals are eligible to register for NASA STI products and services. Domestic organizations or individuals may be eligible to receive various classes of NASA publications and services and should address their requests for registration or further information to:

ATTN: Registration Services
NASA Center for AeroSpace Information
800 Elkridge Landing Road
Linthicum Heights, MD 21090-2934
301-621-0390

Organizations abroad should direct requests to:

National Aeronautics and Space Administration
Scientific and Technical Information Office (JT)
International STI Office
Washington, DC 20546-0001
USA
703-271-5640

SUBJECT SCOPE

The subject scope of *STAR* and *NOVA* includes all aspects of aeronautics and space research and development, supporting basic and applied research, and applications. Aerospace aspects of Earth resources, energy development, conservation, oceanography, environmental protection, urban transportation, and other topics of high national priority are also covered.

HOW TO USE *STAR* SUBJECT CATEGORIES

Abstracts in *STAR* are categorized by 10 major subject divisions that are divided further into 76 specific subject categories. The subject divisions and categories are listed in the Table of Contents together with a note for each that defines its scope and provides any cross-references. For example:

> **16 SPACE TRANSPORTATION**
>
> Includes passenger and cargo space transportation, e.g., shuttle operations; and space rescue techniques. For related information see also *03 Air Transportation and Safety* and *18 Spacecraft Design, Testing and Performance.* For space suits see *54 Man/System Technology and Life Support.*

CROSS-REFERENCES

Individual *STAR* abstracts are not ordinarily cross-referenced, except for certain conference reports or book translations that have had separate abstracts written for their component papers or chapters. Citations and abstracts of the components follow immediately after those of the parent document. When the subject content of a component differs sufficiently from the general content of the parent, a cross-reference citation also is printed at the end of the category to which it normally would have been assigned if it were independent.

DOCUMENTS ON MICROFICHE

Documents available on microfiche are designated by a pound sign (#) following the accession number.

LIMITED REPRODUCIBILITY

A note of limited reproducibility appears in the citation, if there are factors affecting the reproducibility of more than 20% of the document. These factors include faint or broken type, color photographs, black and white photographs, foldouts, dot matrix print, or some other factor that limits the reproducibility of the document. This notation also appears on the microfiche header.

NASA PATENTS AND PATENT APPLICATIONS

Patents and patent applications owned by NASA are announced in *STAR* under appropriate subject categories and are referenced in the *STAR* indexes. In the Report Number Index, patents are indexed by the NASA Case Number, and the U.S. Patent Class. Patent applications are indexed by the NASA Case Number and the U.S. Patent Application Serial Number.

Printed copies of patents (which are not microfiched) are available for purchase from the U.S. Patent and Trademark Office.

When ordering patents, the U.S. Patent Number should be used, and payment must be remitted in advance, by money order or check payable to the Commissioner of Patents and Trademarks. Prepaid purchase coupons for ordering are also available from the U.S. Patent and Trademark Office.

NASA patent application specifications are sold in both paper copy and microfiche by the NASA Center for AeroSpace Information (CASI). The N accession number should be used in ordering either paper copy or microfiche from CASI.

The patents and patent applications announced in *STAR* are owned by NASA and are available for royalty-free licensing. Requests for licensing terms and further information should be addressed to:

National Aeronautics and Space Administration
Associate General Counsel for Intellectual Property
Code GP
Washington, DC 20546-0001

SOURCES FOR DOCUMENTS

One or more sources from which a document announced in *STAR* is available to the public is ordinarily given on the last line of the citation. The most commonly indicated sources and their acronyms or abbreviations are listed below, and their addresses are listed on page A-6. If the publication is available from a source other than those listed, the publisher and his address will be displayed on the availability line or in combination with the corporate source line.

Avail: CASI. Sold by the NASA Center for AeroSpace Information. Prices for hard copy (HC) and microfiche (MF) are indicated by a price code following the letters HC or MF in the *STAR* citation. Current values for the price codes are given in the tables on page A-7.

NOTE ON ORDERING DOCUMENTS: When ordering publications from NASA CASI, use the N accession number or other report number. It is also advisable to cite the title and other bibliographic identification.

Avail: SOD (or GPO). Sold by the Superintendent of Documents, U.S. Government Printing Office, in hard copy.

Avail: BLL (formerly NLL): British Library Lending Division, Boston Spa, Wetherby, Yorkshire, England. Photocopies available from this organization at the price shown. (If none is given, inquiry should be addressed to the BLL.)

Avail: DOE Depository Libraries. Organizations in U.S. cities and abroad that maintain collections of Department of Energy reports, usually in microfiche form, are listed in *Energy Research Abstracts*. Services available from the DOE and its depositories are described in a booklet, *DOE Technical Information Center - Its Functions and Services* (TID-4660), which may be obtained without charge from the DOE Technical Information Center.

Avail: ESDU. Pricing information on specific data, computer programs, and details on Engineering Sciences Data Unit (ESDU) topic categories can be obtained from ESDU International Ltd. Requesters in North America should use the Virginia address while all other requesters should use the London address, both of which are on page A-6.

Avail: Fachinformationszentrum Karlsruhe. Gesellschaft für wissenschaftlich-technische Information mbH 76344 Eggenstein-Leopoldshafen, Germany.

Avail: HMSO. Publications of Her Majesty's Stationery Office are sold in the U.S. by Pendragon House, Inc. (PHI), Redwood City, CA. The U.S. price (including a service and mailing charge) is given, or a conversion table may be obtained from PHI.

Avail: Issuing Activity, or Corporate Author, or no indication of availability. Inquiries as to the availability of these documents should be addressed to the organization shown in the citation as the corporate author of the document.

Avail: NASA Public Document Rooms. Documents so indicated may be examined at or purchased from the National Aeronautics and Space Administration (JBD-4), Public Documents Room (Room 1H23), Washington, DC 20546-0001, or public document rooms located at NASA installations, and the NASA Pasadena Office at the Jet Propulsion Laboratory.

Avail: NTIS. Sold by the National Technical Information Service. Initially distributed microfiche under the NTIS SRIM (Selected Research in Microfiche) are available. For information concerning this service, consult the NTIS Subscription Section, Springfield, VA 22161.

Avail: Univ. Microfilms. Documents so indicated are dissertations selected from *Dissertation Abstracts* and are sold by University Microfilms as xerographic copy (HC) and microfilm. All requests should cite the author and the Order Number as they appear in the citation.

Avail: US Patent and Trademark Office. Sold by Commissioner of Patents and Trademarks, U.S. Patent and Trademark Office, at the standard price of $1.50 each, postage free. (See discussion of NASA patents and patent applications on page A-3.)

Avail: (US Sales Only). These foreign documents are available to users within the United States from the National Technical Information Service (NTIS). They are available to users outside the United States through the International Nuclear Information Service (INIS) representative in their country, or by applying directly to the issuing organization.

Avail: USGS. Originals of many reports from the U.S. Geological Survey, which may contain color illustrations, or otherwise may not have the quality of illustrations preserved in the microfiche or facsimile reproduction, may be examined by the public at the libraries of the USGS field offices whose addresses are listed on page A-6. The libraries may be queried concerning the availability of specific documents and the possible utilization of local copying services, such as color reproduction.

FEDERAL DEPOSITORY LIBRARY PROGRAM

In order to provide the general public with greater access to U.S. Government publications, Congress established the Federal Depository Library Program under the Government Printing Office (GPO), with 53 regional depositories responsible for permanent retention of material, inter-library loan, and reference services. At least one copy of nearly every NASA and NASA-sponsored publication, either in printed or microfiche format, is received and retained by the 53 regional depositories. A list of the regional GPO libraries, arranged alphabetically by state, appears on page A-8. These libraries are *not* sales outlets. A local library can contact a regional depository to help locate specific reports, or direct contact may be made by an individual.

PUBLIC COLLECTION OF NASA DOCUMENTS

An extensive collection of NASA and NASA-sponsored publications is maintained by the British Library Lending Division, Boston Spa, Wetherby, Yorkshire, England for public access. The British Library Lending Division also has available many of the non-NASA publications cited in *STAR*. European requesters may purchase facsimile copy or microfiche of NASA and NASA-sponsored documents, those identified by both the symbols # and * from ESA — Information Retrieval Service European Space Agency, 8-10 rue Mario-Nikis, 75738 CEDEX 15, France.

SUBMITTING DOCUMENTS

All users of this abstract service are urged to forward reports to be considered for announcement in *STAR*. This will aid NASA in its efforts to provide the fullest possible coverage of all scientific and technical publications that might support aeronautics and space research and development. If you have prepared relevant reports (other than those you will transmit to NASA, DOD, or DOE through the usual contract- or grant-reporting channels), please send them for consideration to the NASA Center for AeroSpace Information, 800 Elkridge Landing Road, Linthicum Heights, MD 21090-2934.

Reprints of journal articles, book chapters, and conference papers are also welcome. These will be considered for announcement in *STAR's* companion journal, *NOVA*.

You may specify a particular source to be included in a report announcement if you wish; otherwise the report will be placed on a public sale at the NASA Center for AeroSpace Information. Copyrighted publications will be announced but not distributed or sold.

PURCHASE OF *STAR*

STAR is publicly available on annual subscription from the NASA Center for AeroSpace Information (CASI). 1995 *STAR* subscription prices are $100.00/domestic and $125.00/foreign. Single copy prices: $33.00/domestic, $41.00/foreign.

An annual, cumulative *STAR Index* is also available at $70.00/domestic and foreign.

STAR is available to registered users on annual subscription from the NASA Center for AeroSpace Information, ATTN: Registration Services, 800 Elkridge Landing Road, Linthicum Heights, MD 21090-2934.

ADDRESSES OF ORGANIZATIONS

British Library Lending Division
Boston Spa, Wetherby, Yorkshire
England

Commissioner of Patents and Trademarks
U.S. Patent and Trademark Office
Washington, DC 20231

Department of Energy
Technical Information Center
P.O. Box 62
Oak Ridge, TN 37830

European Space Agency-
Information Retrieval Service ESRIN
Via Galileo Galilei
00044 Frascati (Rome) Italy

Engineering Sciences Data Unit International
P.O. Box 1633
Manassas, VA 22110

Engineering Sciences Data Unit
International, Ltd.
251-259 Regent Street
London, W1R 7AD, England

Fachinformationszentrum Karlsruhe
Gesellschaft für wissenschaftlich-technische
Information mbH
76344 Eggenstein-Leopoldshafen, Germany

Her Majesty's Stationery Office
P.O. Box 569, S.E. 1
London, England

NASA Center for AeroSpace Information
800 Elkridge Landing Road
Linthicum Heights, MD 21090-2934

National Aeronautics and Space Administration
Scientific and Technical Information Office
(JT)
Washington, DC 20546-0001

National Technical Information Service
5285 Port Royal Road
Springfield, VA 22161

Pendragon House, Inc.
899 Broadway Avenue
Redwood City, CA 94063

Superintendent of Documents
U.S. Government Printing Office
Washington, DC 20402

University Microfilms
A Xerox Company
300 North Zeeb Road
Ann Arbor, MI 48106

University Microfilms, Ltd.
Tylers Green
London, England

U.S. Geological Survey Library National Center
MS 950
12201 Sunrise Valley Drive
Reston, VA 22092

U.S. Geological Survey Library
2255 North Gemini Drive
Flagstaff, AZ 86001

U.S. Geological Survey
345 Middlefield Road
Menlo Park, CA 94025

U.S. Geological Survey Library
Box 25046
Denver Federal Center, MS914
Denver, CO 80225

NASA CASI PRICE CODE TABLE

(Effective January 1, 1995)

CASI PRICE CODE	NORTH AMERICAN PRICE	FOREIGN PRICE
A01	$ 6.00	$ 12.00
A02	9.00	18.00
A03	17.50	35.00
A04-A05	19.50	39.00
A06-A09	27.00	54.00
A10-A13	36.50	73.00
A14-A17	44.50	89.00
A18-A21	52.00	104.00
A22-A25	61.00	122.00
A99	Call For Price	Call For Price

IMPORTANT NOTICE

For users not registered at the NASA CASI, prepayment is required. Additionally, a shipping and handling fee of $1.00 per document for delivery within the United States and $9.00 per document for delivery outside the United States is charged.

For users registered at the NASA CASI, document orders may be invoiced at the end of the month, charged against a deposit account, or paid by check or credit card. NASA CASI accepts American Express, Diners' Club, MasterCard, and VISA credit cards. There are no shipping and handling charges. To register at the NASA CASI, please request a registration form through the NASA Access Help Desk at the address or numbers below.

NASA Center for AeroSpace Information
800 Elkridge Landing Road
Linthicum Heights, MD 21090-2934
Telephone: (301) 621-0390
E-mail: help@sti.nasa.gov
Fax: (301) 621-0134

Rev. 1/95

FEDERAL REGIONAL DEPOSITORY LIBRARIES

ALABAMA

AUBURN UNIV. AT MONTGOMERY LIBRARY
Documents Dept.
7300 University Dr.
Montgomery, AL 36117-3596
(205) 244-3650 Fax: (205) 244-0678

UNIV. OF ALABAMA
Amelia Gayle Gorgas Library
Govt. Documents
P.O. Box 870266
Tuscaloosa, AL 35487-0266
(205) 348-6046 Fax: (205) 348-0760

ARIZONA

DEPT. OF LIBRARY, ARCHIVES, AND PUBLIC RECORDS
Research Division
Third Floor, State Capitol
1700 West Washington
Phoenix, AZ 85007
(602) 542-3701 Fax: (602) 542-4400

ARKANSAS

ARKANSAS STATE LIBRARY
State Library Service Section
Documents Service Section
One Capitol Mall
Little Rock, AR 72201-1014
(501) 682-2053 Fax: (501) 682-1529

CALIFORNIA

CALIFORNIA STATE LIBRARY
Govt. Publications Section
P.O. Box 942837 - 914 Capitol Mall
Sacramento, CA 94337-0091
(916) 654-0069 Fax: (916) 654-0241

COLORADO

UNIV. OF COLORADO - BOULDER
Libraries - Govt. Publications
Campus Box 184
Boulder, CO 80309-0184
(303) 492-8834 Fax: (303) 492-1881

DENVER PUBLIC LIBRARY
Govt. Publications Dept. BSG
1357 Broadway
Denver, CO 80203-2165
(303) 640-8846 Fax: (303) 640-8817

CONNECTICUT

CONNECTICUT STATE LIBRARY
231 Capitol Avenue
Hartford, CT 06106
(203) 566-4971 Fax: (203) 566-3322

FLORIDA

UNIV. OF FLORIDA LIBRARIES
Documents Dept.
240 Library West
Gainesville, FL 32611-2048
(904) 392-0366 Fax: (904) 392-7251

GEORGIA

UNIV. OF GEORGIA LIBRARIES
Govt. Documents Dept.
Jackson Street
Athens, GA 30602-1645
(706) 542-8949 Fax: (706) 542-4144

HAWAII

UNIV. OF HAWAII
Hamilton Library
Govt. Documents Collection
2550 The Mall
Honolulu, HI 96822
(808) 948-8230 Fax: (808) 956-5968

IDAHO

UNIV. OF IDAHO LIBRARY
Documents Section
Rayburn Street
Moscow, ID 83844-2353
(208) 885-6344 Fax: (208) 885-6817

ILLINOIS

ILLINOIS STATE LIBRARY
Federal Documents Dept.
300 South Second Street
Springfield, IL 62701-1796
(217) 782-7596 Fax: (217) 782-6437

INDIANA

INDIANA STATE LIBRARY
Serials/Documents Section
140 North Senate Avenue
Indianapolis, IN 46204-2296
(317) 232-3679 Fax: (317) 232-3728

IOWA

UNIV. OF IOWA LIBRARIES
Govt. Publications
Washington & Madison Streets
Iowa City, IA 52242-1166
(319) 335-5926 Fax: (319) 335-5900

KANSAS

UNIV. OF KANSAS
Govt. Documents & Maps Library
6001 Malott Hall
Lawrence, KS 66045-2800
(913) 864-4660 Fax: (913) 864-3855

KENTUCKY

UNIV. OF KENTUCKY
King Library South
Govt. Publications/Maps Dept.
Patterson Drive
Lexington, KY 40506-0039
(606) 257-3139 Fax: (606) 257-3139

LOUISIANA

LOUISIANA STATE UNIV.
Middleton Library
Govt. Documents Dept.
Baton Rouge, LA 70803-3312
(504) 388-2570 Fax: (504) 388-6992

LOUISIANA TECHNICAL UNIV.
Prescott Memorial Library
Govt. Documents Dept.
Ruston, LA 71272-0046
(318) 257-4962 Fax: (318) 257-2447

MAINE

UNIV. OF MAINE
Raymond H. Fogler Library
Govt. Documents Dept.
Orono, ME 04469-5729
(207) 581-1673 Fax: (207) 581-1653

MARYLAND

UNIV. OF MARYLAND - COLLEGE PARK
McKeldin Library
Govt. Documents/Maps Unit
College Park, MD 20742
(301) 405-9165 Fax: (301) 314-9416

MASSACHUSETTS

BOSTON PUBLIC LIBRARY
Govt. Documents
666 Boylston Street
Boston, MA 02117-0286
(617) 536-5400, ext. 226
Fax: (617) 536-7758

MICHIGAN

DETROIT PUBLIC LIBRARY
5201 Woodward Avenue
Detroit, MI 48202-4093
(313) 833-1025 Fax: (313) 833-0156

LIBRARY OF MICHIGAN
Govt. Documents Unit
P.O. Box 30007
717 West Allegan Street
Lansing, MI 48909
(517) 373-1300 Fax: (517) 373-3381

MINNESOTA

UNIV. OF MINNESOTA
Govt. Publications
409 Wilson Library
309 19th Avenue South
Minneapolis, MN 55455
(612) 624-5073 Fax: (612) 626-9353

MISSISSIPPI

UNIV. OF MISSISSIPPI
J.D. Williams Library
106 Old Gym Bldg.
University, MS 38677
(601) 232-5857 Fax: (601) 232-7465

MISSOURI

UNIV. OF MISSOURI - COLUMBIA
106B Ellis Library
Govt. Documents Sect.
Columbia, MO 65201-5149
(314) 882-6733 Fax: (314) 882-8044

MONTANA

UNIV. OF MONTANA
Mansfield Library
Documents Division
Missoula, MT 59812-1195
(406) 243-6700 Fax: (406) 243-2060

NEBRASKA

UNIV. OF NEBRASKA - LINCOLN
D.L. Love Memorial Library
Lincoln, NE 68588-0410
(402) 472-2562 Fax: (402) 472-5131

NEVADA

THE UNIV. OF NEVADA LIBRARIES
Business and Govt. Information Center
Reno, NV 89557-0044
(702) 784-6579 Fax: (702) 784-1751

NEW JERSEY

NEWARK PUBLIC LIBRARY
Science Div. - Public Access
P.O. Box 630
Five Washington Street
Newark, NJ 07101-7812
(201) 733-7782 Fax: (201) 733-5648

NEW MEXICO

UNIV. OF NEW MEXICO
General Library
Govt. Information Dept.
Albuquerque, NM 87131-1466
(505) 277-5441 Fax: (505) 277-6019

NEW MEXICO STATE LIBRARY
325 Don Gaspar Avenue
Santa Fe, NM 87503
(505) 827-3824 Fax: (505) 827-3888

NEW YORK

NEW YORK STATE LIBRARY
Cultural Education Center
Documents/Gift & Exchange Section
Empire State Plaza
Albany, NY 12230-0001
(518) 474-5355 Fax: (518) 474-5786

NORTH CAROLINA

UNIV. OF NORTH CAROLINA - CHAPEL HILL
Walter Royal Davis Library
CB 3912, Reference Dept.
Chapel Hill, NC 27514-8890
(919) 962-1151 Fax: (919) 962-4451

NORTH DAKOTA

NORTH DAKOTA STATE UNIV. LIB.
Documents
P.O. Box 5599
Fargo, ND 58105-5599
(701) 237-8886 Fax: (701) 237-7138

UNIV. OF NORTH DAKOTA
Chester Fritz Library
University Station
P.O. Box 9000 - Centennial and University Avenue
Grand Forks, ND 58202-9000
(701) 777-4632 Fax: (701) 777-3319

OHIO

STATE LIBRARY OF OHIO
Documents Dept.
65 South Front Street
Columbus, OH 43215-4163
(614) 644-7051 Fax: (614) 752-9178

OKLAHOMA

OKLAHOMA DEPT. OF LIBRARIES
U.S. Govt. Information Division
200 Northeast 18th Street
Oklahoma City, OK 73105-3298
(405) 521-2502, ext. 253
Fax: (405) 525-7804

OKLAHOMA STATE UNIV.
Edmon Low Library
Stillwater, OK 74078-0375
(405) 744-6546 Fax: (405) 744-5183

OREGON

PORTLAND STATE UNIV.
Branford P. Millar Library
934 Southwest Harrison
Portland, OR 97207-1151
(503) 725-4123 Fax: (503) 725-4524

PENNSYLVANIA

STATE LIBRARY OF PENN.
Govt. Publications Section
116 Walnut & Commonwealth Ave.
Harrisburg, PA 17105-1601
(717) 787-3752 Fax: (717) 783-2070

SOUTH CAROLINA

CLEMSON UNIV.
Robert Muldrow Cooper Library
Public Documents Unit
P.O. Box 343001
Clemson, SC 29634-3001
(803) 656-5174 Fax: (803) 656-3025

UNIV. OF SOUTH CAROLINA
Thomas Cooper Library
Green and Sumter Streets
Columbia, SC 29208
(803) 777-4841 Fax: (803) 777-9503

TENNESSEE

UNIV. OF MEMPHIS LIBRARIES
Govt. Publications Dept.
Memphis, TN 38152-0001
(901) 678-2206 Fax: (901) 678-2511

TEXAS

TEXAS STATE LIBRARY
United States Documents
P.O. Box 12927 - 1201 Brazos
Austin, TX 78701-0001
(512) 463-5455 Fax: (512) 463-5436

TEXAS TECH. UNIV. LIBRARIES
Documents Dept.
Lubbock, TX 79409-0002
(806) 742-2282 Fax: (806) 742-1920

UTAH

UTAH STATE UNIV.
Merrill Library Documents Dept.
Logan, UT 84322-3000
(801) 797-2678 Fax: (801) 797-2677

VIRGINIA

UNIV. OF VIRGINIA
Alderman Library
Govt. Documents
University Ave. & McCormick Rd.
Charlottesville, VA 22903-2498
(804) 824-3133 Fax: (804) 924-4337

WASHINGTON

WASHINGTON STATE LIBRARY
Govt. Publications
P.O. Box 42478
16th and Water Streets
Olympia, WA 98504-2478
(206) 753-4027 Fax: (206) 586-7575

WEST VIRGINIA

WEST VIRGINIA UNIV. LIBRARY
Govt. Documents Section
P.O. Box 6069 - 1549 University Ave.
Morgantown, WV 26506-6069
(304) 293-3051 Fax: (304) 293-6638

WISCONSIN

ST. HIST. SOC. OF WISCONSIN LIBRARY
Govt. Publication Section
816 State Street
Madison, WI 53706
(608) 264-6525 Fax: (608) 264-6520

MILWAUKEE PUBLIC LIBRARY
Documents Division
814 West Wisconsin Avenue
Milwaukee, WI 53233
(414) 286-3073 Fax: (414) 286-8074

★U.S. GOVERNMENT PRINTING OFFICE: 1995-387-253/20008

SCAN Goes Electronic!

If you have NASA Mail or if you can access the Internet, you can get biweekly issues of *SCAN* delivered to your desk—top absolutely free!

Electronic SCAN takes advantage of computer technology to alert you to the latest aerospace-related, worldwide scientific and technical information that has been published.

No more waiting while the paper copy is printed and mailed to you. You can review *Electronic SCAN* the same day it is released! And you get all 191—or any combination of—subject areas of announcements with abstracts to browse at your leisure. When you locate a publication of interest, you can print the announcement or electronically add it to your publication order list.

Electronic SCAN
Timely
Flexible
Complete
Free!

Start your free access to *Electronic SCAN* today. Over 1,000 announcements of new reports, books, conference proceedings, journal articles . . . and more—delivered to your computer every two weeks.

For instant access via Internet:
ftp.sti.nasa.gov
gopher.sti.nasa.gov
listserv@sti.nasa.gov

For additional information:
e-mail: help@sti.nasa.gov
scan@sti.nasa.gov

(Enter this address on the "To" line. Leave the subject line blank and send. You will receive an automatic reply with instructions in minutes.)

Phone: (301) 621-0390 **Fax:** (301) 621-0134

Write: NASA Access Help Desk
NASA STI Office
NASA Center for AeroSpace Information
800 Elkridge Landing Road
Linthicum Heights, MD 21090-2934

National Aeronautics and Space Administration
Scientific and Technical Information Office

4/95

National Aeronautics and
Space Administration
Code JT
Washington, DC 20546-0001